SAE TRANSACTIONS

1958

BENDIX AVIATION
CORPORATION
RESEARCH LABORATORIES
LIBRARY

RELEASED
BY
BENDIX RESEARCH LABORATORIES
LIBRARY
DATE
LIBRARIAN

TL
1
56
Vol. 66

SAE TRANSACTIONS

BENDIX AVIATION
CORPORATION
RESEARCH LABORATORIES
LIBRARY

Society of Automotive Engineers, Inc.
485 Lexington Avenue New York 17, New York

William K. Creson
President

John A. C. Warner
Secretary and General Manager

B. B. Bachman
Treasurer

E. D. Allen
Editor

All articles appearing in SAE Transactions are indexed by Engineering Index, Inc.

Copyright 1958, Society of Automotive Engineers, Inc.

Price: $3 to members, $7 to public and college libraries and U.S. Government Agencies, $10 to nonmembers. Foreign: $3 to members, $8 to public and college libraries, $11 to nonmembers.

Photolithographed reproductions are available of any article published in SAE Transactions. Prices, on quantities of 100 copies or more, varying with number of pages and illustrations, can be obtained upon request from SAE Special Publications Department, 485 Lexington Avenue, New York 17, N.Y.

— CONTENTS

	Page
Bearing Applications for Heavy-Duty Axles—**R. M. Riblet and C. M. Kitson**	5
Shell Molded Cast Crankshafts—**H. N. Bogart and H. C. Grant**	32
The MWM Balanced-Pressure Precombustion Chamber System for High-Speed Diesel Engines—**Hans L. Hockel**	38
Effects of Radiation on Materials—**Michael Ference, Jr.**	47
Bifuel Approach to Burning Residual Fuels in Diesel Engines—**W. C. Arnold, R. H. Beadle, R. L. Logelin, and H. D. Young**	54
Automotive Gasoline Injection—**C. H. Nystrom**	65
Resilient Face Seals for Tractor Final Drives—**F. S. Engelking and M. C. Keys**	75
Some Metallurgical Aspects of Pontiac V-8 Engine Pearlitic Malleable Iron Crankshaft—**K. B. Valentine**	81
The Cadillac Frame: A New Design Concept for Lower Cars—**S. L. Milliken and J. R. Parker**	86
Turbocharging the Series 71 Engine—**J. J. May and V. C. Reddy**	100
Problems in the Application of High-Strength Steel Alloys in the Design of Supersonic Aircraft—**A. F. Ensrud**	118
The Beam Strength of Modern Gear-Tooth Design—**B. W. Kelley and R. Pederson**	137
Chrysler TorqueFlite Transmission—**S. D. Jeffe and B. W. Cartwright**	158
Chevrolet Turboglide Transmission—**F. J. Winchell, W. D. Route, and O. K. Kelley**	167
Autoignition Associated with Hot Starting—**F. W. Bowditch and R. F. Stebar**	179
High-Temperature Properties of Vacuum-Melted Superalloys—**F. M. Richmond**	193
Torque Converters Can Be Different—**J. B. Black and M. W. Dundore**	200
Aircooled Diesel-Engine Appraisal—**C. F. Bachle**	213
Rear-Engine Motor Cars—The European Point of View—**Fernand Picard**	226
Valve Train Wear as Affected by Metallurgy, Driving Conditions, and Lubricants—**V. Ayres, J. B. Bidwell, A. C. Pilger, Jr., and R. K. Williams**	242
Visual Avoidance of Mid-Air Collisions—**W. D. Howell and R. B. Fisher**	252
Design Features of the New Ford Axle—**Bain Griffith**	257
The Improvement of Welded Structures by Subsequent Forging Operations—**W. R. Wollering and E. H. Lundby**	261
Designing Materials for Future Aerial Vehicles—**N. E. Promisel**	267
Combustion-Chamber Deposits—A Radiotracer Study—**L. B. Shore and K. F. Ockert**	285
Chrysler Torsion-Aire Suspension—Across the Board—**O. D. Dillman and R. R. Love**	295
The Future of the Free-Piston Engine in Commercial Vehicles—**O. B. Noren and R. L. Erwin**	305
Large Lightweight Turbojet Engines—**C. A. Grinyer**	315
Vapor-Locking Tendencies of Fuels—A Practical Approach—**J. D. Caplan and C. J. Brady**	327
Mathematical Correction for Stress in Removed Layers in X-Ray Diffraction Residual Stress Analysis—**M. G. Moore and W. P. Evans**	340
Cadillac's Air Suspension for the Eldorado Brougham—**V. D. Polhemus, L. J. Kehoe, Jr., F. H. Cowin, and S. L. Milliken**	346
Thrust Measurement for Jet Transport Operation—**M. J. Saari**	357

BENDIX AVIATION CORPORATION RESEARCH LABORATORIES LIBRARY

VOL. 66, 1958 —

	Page
Rear Axles—Today—Tomorrow—**R. P. Lewis and L. J. O'Brien**	364
Automotive Exhaust Hydrocarbon Reduction During Deceleration by Induction System Devices—**Induction System Task Group, Automobile Manufacturers Association**	383
Truck Performance—Computed versus Measured Data—**A. F. Stamm**	397
Designing with Steel for Lighter Aircraft—**Bruce Mitchell**	407
Mercedes-Benz Racing Cars—Design and Experience—**H. Scherenberg**	414
Use of Temperature-Density for Measuring Antiknock Quality—**Bruno R. Siegel**	421
Loop Scavenging versus Through Scavenging of Two-Stroke Engines—**C. F. Taylor, A. R. Rogowski, A. L. Hagen, and J. D. Koppernaes**	444
Behavior of Aircraft Structures under Thermal Stress—**G. H. Sprague and P. C. Huang**	457
The Buick Air-Poise Suspension—**Forest R. McFarland, E. G. Peckham, and Eric Dietrich**	466
The Air Coil Spring—A New Factor in Rambler Suspension—**W. S. Berry**	471
The Ford Approach to Air Suspension—**C. F. O'Shea**	475
1958 Chevrolet Level Air Suspension—**K. H. Hansen, J. F. Bertsch, and R. E. Denzer**	483
Oldsmobile New-Matic Ride—**R. W. Perkins**	491
Requirements, Parameters, and Design Considerations for Pneumatic Inlet Control Systems—**R. E. Matzdorff and C. F. Newberry**	496
Principles of Noise Reduction—**L. M. Ball**	515
Diesel Cylinder Heat Transfer Design Criteria—**D. H. Brown**	522
The Effects of Machine and Foundation Resilience and of Wave Propagation on the Isolation Provided by Vibration Mounts—**A. O. Sykes**	532
Investigating Combustion Phenomena in Unmodified Engines—**J. A. Robison, M. D. Behrens, R. G. Mosher, and J. M. Chandler**	549
Engineering the Edsel—**N. L. Blume**	557
Metallurgical Design Considerations for Precipitation-Hardening Steels up to 1200 F—**F. K. Lampson**	565
Fumigation Kills Smoke—Improves Diesel Performance—**M. Alperstein, W. B. Swim, and P. H. Schweitzer**	574
Protective Atmospheres for High-Temperature Bearing Operation—**C. H. Bailey, S. S. Sorem, and A. G. Cattaneo**	596
Continuous Radiotracer Monitoring Shows How Piston Rings Wear in Service—**J. S. Batzold, J. V. Clark, Jr., and J. F. Kunc**	602
Tractor Hydraulics, Good Field, No Hit—**G. L. Hershman**	612
Considerations of Some Jet-Deflection Principles for Directional Control and for Lift—**U. H. von Glahn and J. H. Povolny**	620
Bio-Technical Aspects of Driver Safety and Comfort—**R. A. McFarland and R. G. Domey**	630
Determination of True Engine Friction—**R. E. Gish, J. D. McCullough, J. B. Retzloff, and H. T. Mueller**	649
Simulation of a Free-Piston Engine with a Digital Computer—**D. R. Olson**	668
Measurement of Gas Temperature in an Engine by the Velocity of Sound Method—**J C. Livengood, C. F. Taylor, and P. C. Wu**	683
Complete Author and Subject Index	700

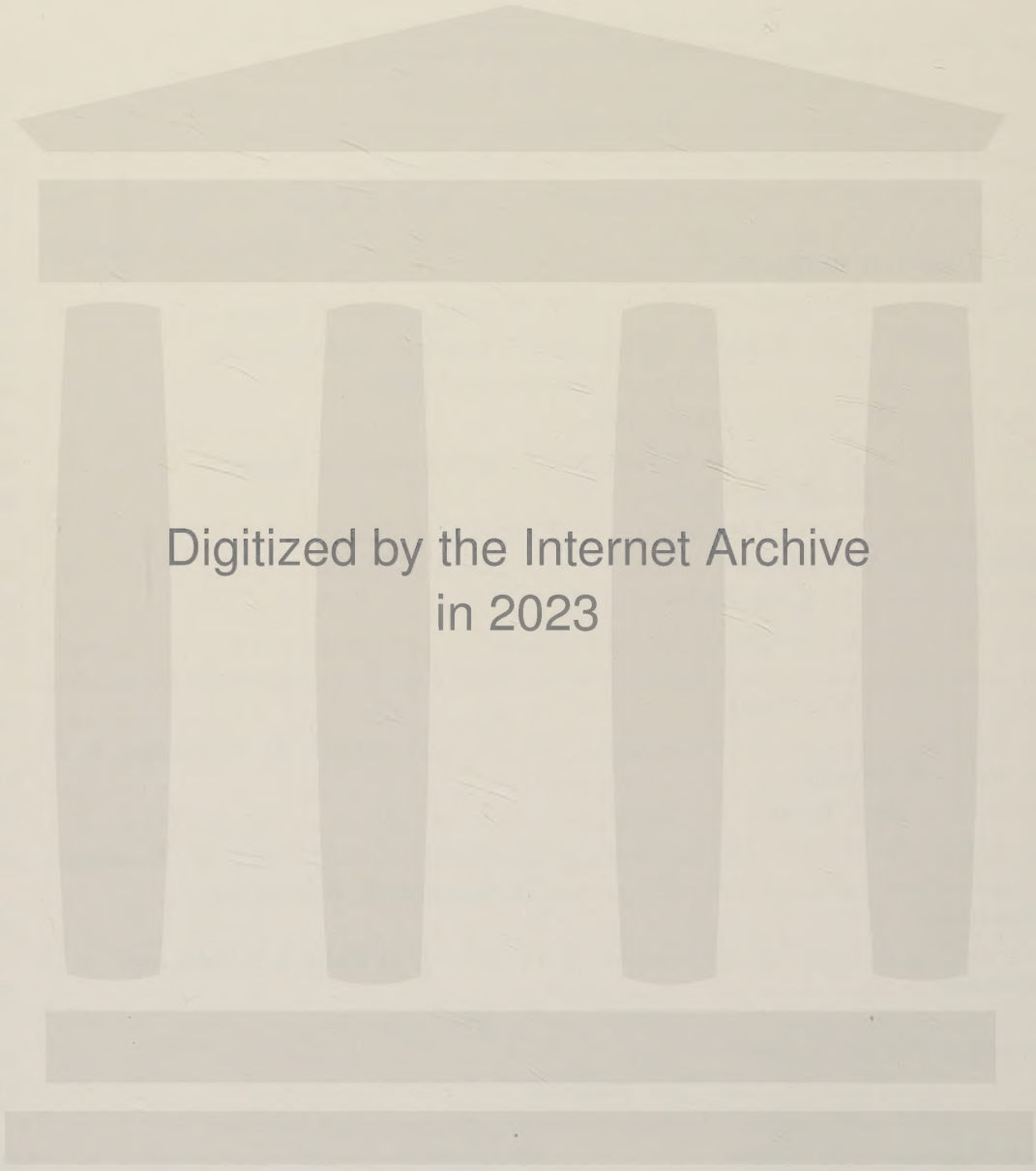

Digitized by the Internet Archive
in 2023

https://archive.org/details/sae-transactions_1958_66

BENDIX AVIATION
CORPORATION
RESEARCH LABORATORIES
LIBRARY

Bearing Applications For Heavy-Duty Axles

Robert M. Riblet and Charles M. Kitson,
The Timken Roller Bearing Co.

This paper was presented during the SAE National Transportation and Diesel-Engine Meetings, at a session sponsored by the SAE Cleveland Section, Cleveland, Nov. 5, 1957.

TRUCKING is a fundamental segment of our entire commercial and industrial transportation picture. Highway trucks, at some time, haul practically every commodity which we use in our daily living. Off-highway trucks are moving mountains of earth and minerals. Military trucks are constantly being developed and improved for present military use as well as for some future emergency. Each of these fields requires that the axles be designed or adapted for its particular purpose. Axles for highway trucks carry a load which has its maximum regulated by State laws, operate at high speeds for long periods of time, and function in what is classed as a reasonably clean environment. Axles for off-highway trucks, on the other hand, are heavily loaded and operate at lower speeds, on steeper grades, and under adverse conditions. Military vehicles are usually equipped with multiple-drive axles which require a maximum interchangeability of component parts and operate under an extremely wide range of conditions.

Industry-wide there is a constant search for new and better materials, methods, and personnel to meet the demands created by this competitive market. It is a real challenge to the young engineers of today to endeavor to match the strides of the last generation of engineers and mechanics in this field.

Heavy-Duty Truck Axles and Antifriction Bearings

Let's define the subjects of our discussion, heavy-duty truck axles and antifriction bearings, so that we will all be thinking in terms of the same applications, load magnitude, and nomenclature.

Heavy-Duty Truck Axle—A heavy-duty axle is used on trucks with a loaded gross vehicle weight in the range of 18,000 lb and up. The axle has two major functions: to carry the load and, in the case of a driving axle, to convert torque to tractive effort. The front steering axle may be a combined power-transmitting and weight-carrying axle or it may function only to carry the load. Trailer wheels are strictly load-carrying axles. The rear axles both transmit power and carry load. The rear-axle centers can be generally classed in three groups: single-

IN this fourth L. Ray Buckendale Lecture, the authors discuss the application of tapered roller bearings to heavy-duty axles, with emphasis on bearing selection, mounting, adjustment, and lubrication.

The lecture defines heavy-duty axles and their function, and the basic types of antifriction bearings. Tapered roller bearing design, nomenclature, and basic rating are discussed.

Numerous typical bearing applications in wheels and axle centers are covered. The calculations for selecting bearings for a typical heavy-duty front axle and a hypoid rear-axle center are shown in detail. The effect of bearing alignment and machining practice on bearing life is emphasized. Proper bearing fitting with recommended fits is also discussed.

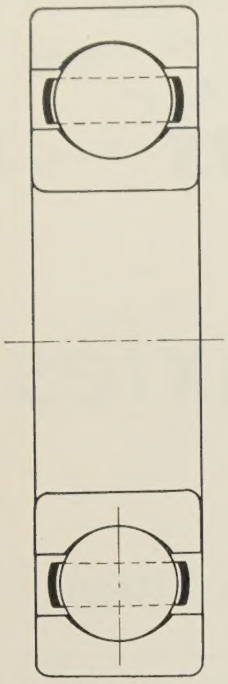

Fig. 1

Fig. 2

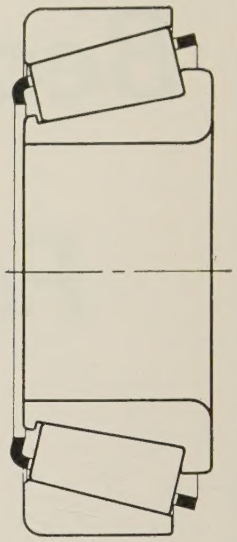

Fig. 3

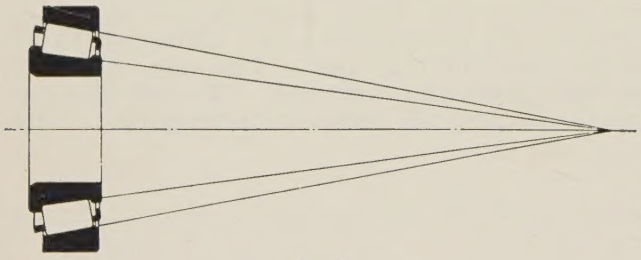

Fig. 4

reduction, dual-reduction, and 2-speed units. They may be either front mounted or top mounted relative to the axle housing. Rear axles are often mounted in tandem with or without interaxle differentials built integral with the forward-axle center or in a separate transfer case.

The function of the antifriction bearing in the wheel application is to carry the vehicle load. In the axle center the bearing application must hold the gear trains to the prescribed deflection limits and be reasonably adaptable to high-production techniques.

Antifriction Bearings—There are three basic designs of antifriction bearings used in heavy-duty truck applications: ball bearings, straight roller bearings, and tapered roller bearings. Fig. 1 shows a ball bearing which consists of an inner race, outer race, balls, cage or ball retainer. It may have closure seals assembled at either or both ends. It has the capacity to carry load perpendicular to the axis and some thrust. The straight roller bearing (shown in Fig. 2) consists of an inner race with or without ribs, an outer race with or without ribs, and cylindrical rollers. It is made either with or without a cage. This design carries only radial loads. Fig. 3 shows a single-row tapered roller bearing which consists of a conical inner race with ribs, an outer race, tapered rollers, and a cage. This bearing carries both radial and thrust or any combination of loadings.

The material covered in this paper is going to be concentrated on tapered roller bearings and their application to heavy-duty truck and trailer axles. The wide range of bearing applications in today's heavy-duty truck axles, both friction and antifriction, makes it impossible to cover adequately the entire field of bearing applications. For instance, in the antifriction bearing field alone, the various bearing manufacturers use different methods of rating, calculating, selecting and mounting which are adaptable to their own particular product.

Tapered Roller Bearings

Bearing Design—Fig. 4 shows a tapered roller bearing as one in which all the rolling elements and raceways are conical in shape. The apexes of the tapered surfaces of the rollers, the inner race, and the outer race all coincide at a common point on the axis of the bearing. Thus a true rolling action results from this design. The tapered roller-bearing design will handle all types of loads: radial, thrust, or both in any combination. The angles of the rollers and races determine the relative radial and thrust load carrying capacity. By changing these

angles a few degrees, a more suitable bearing is provided for a particular application. The shallow-angle bearings are more adapted for carrying heavy radial loads, while the steeper-angle bearings are designed for carrying heavier thrust loads.

The wide area contact between the ends of the rollers and the cone back face rib on a tapered roller bearing keeps the rollers in alignment. The cage merely spaces the rollers properly around the cone and holds the cone roller assembly together as a unit. Perfect alignment of the rollers results in full line contact between the rollers and the races and permits the distribution of the unit pressure over the entire length of each roller.

Tapered roller bearings can be adjusted through either cup or cone and are mounted in pairs.

Bearing Nomenclature—Fig. 5 shows the four parts of a tapered roller bearing, which are the cup, cone, rollers, and cage.

Fig. 6 shows the industry-wide nomenclature for tapered roller bearings.

Fig. 7 explains the terms of "indirect" and "direct" bearing mounting. The indirect bearing mounting is one in which the bearings are applied with the small ends of the rollers in each bearing pointing in toward each other. The direct mounting is one in which the bearings are applied with the large ends of the rollers pointing in toward each other.

Bearing Rating—The base ratings of tapered roller bearings are made upon a B-10 life expectancy of 3000 hr at 500 rpm. The term "B-10 life" is used to express the bearing rating at which 90% or more of a large group of identically loaded bearings will still be operating at the end of a specified time. Average bearing life is approximately five times the B-10 life. All rotating bearings are subject to repeated stress as the rollers pass around the raceways; hence, they are subject to the type of failure of metal known as fatigue. Fatigue is the progressive failure within the crystals of metal due to the repeated application of the stress cycle below the ultimate strength of the material. The number of stress applications a specimen will withstand is dependent upon a number of factors: the range and magnitude of the applied stress, metallurgical and physical characteristics of the material, uniformity of the material, bearing design, geometric accuracy of manufacture, surface stresses left in manufacture, and the surface finish of the material. Plotting the

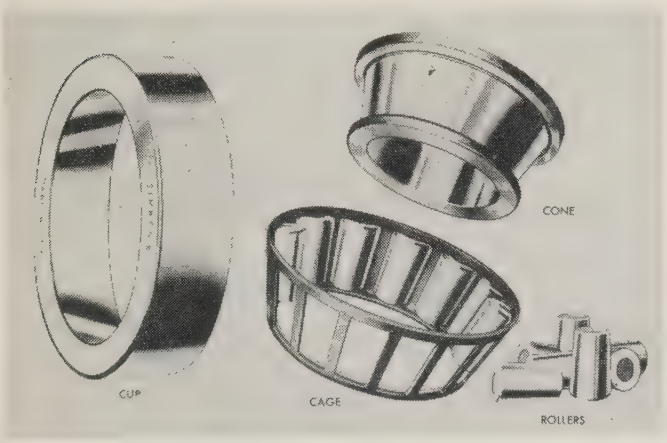

Fig. 5

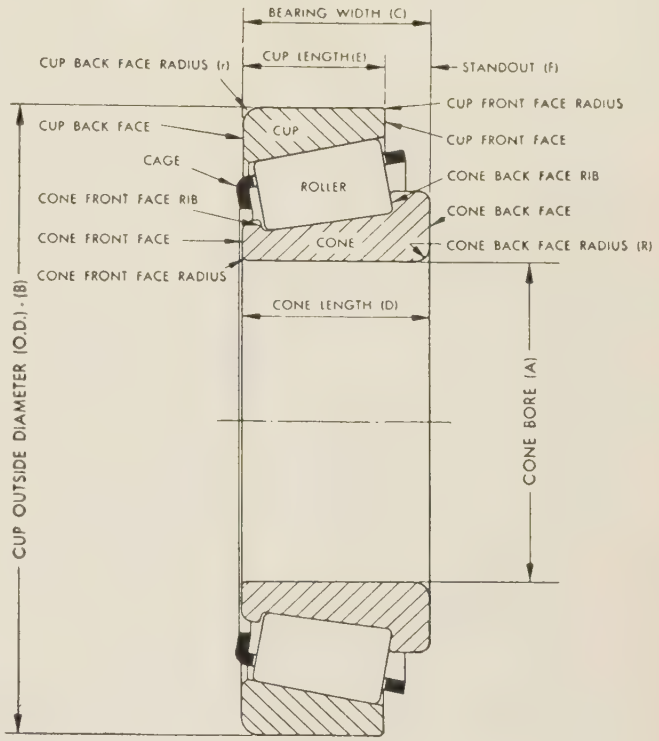

Fig. 6

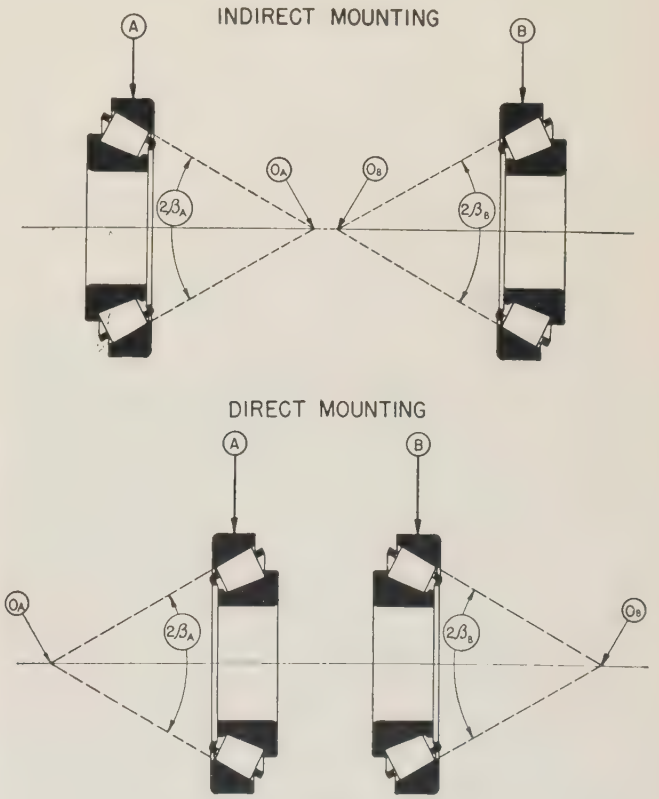

Fig. 7

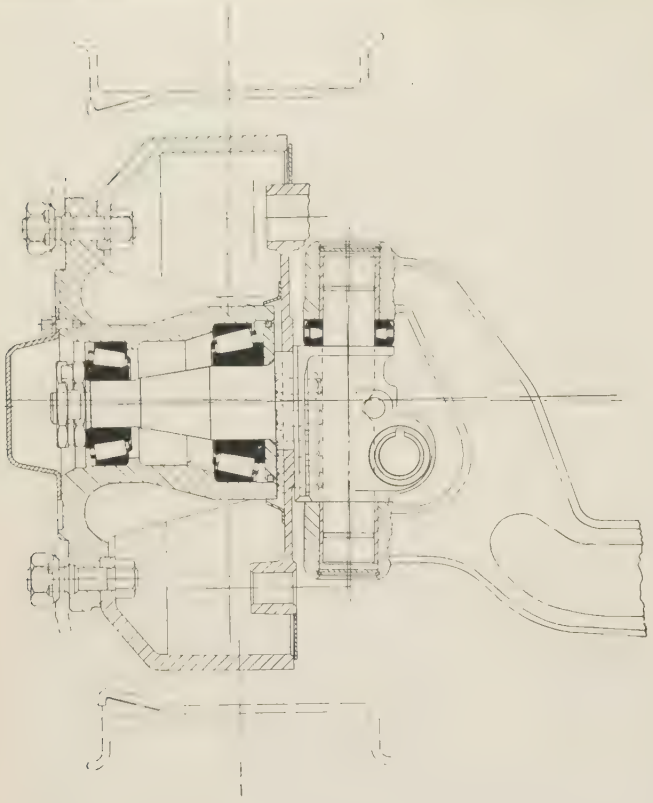

Fig. 8

results of fatigue tests of a large number of identical specimens at different magnitudes of stress will show a scatter of points following a general trend. Prediction of the life within a narrow limit band can, therefore, be made. Fatigue formulas are developed from this theoretical consideration of stress intensity and stress repetition.

The life expectancy of the bearing will vary with the load and speed. By doubling the rpm for a given load the hours life expectancy is cut in two, while doubling the load at a fixed speed cuts the life expectancy by approximately ten.

Typical Wheel Bearing Applications

The prime function of the tapered roller bearing in all wheel bearing applications is to carry the load on the axle. In driving-axle designs it also has a second function of carrying the reaction load resulting from the tractive effort of the wheel with the ground. On highway vehicles this tractive-effort reaction force is negligible in so far as the driving-wheel bearing selection is concerned. On off-highway vehicles, though, it is of such magnitude that it is considered in the calculations of the driving-wheel bearings and steering-pivot bearing loading.

The bearing spread, center of roller to center of roller, should be at least 10% of the tire diameter in order to obtain proper wheel stability.

On heavy-duty truck wheel applications, the tapered roller bearings are indirectly mounted. The wheel hub into which the cups are fit is the rotating member. The spindle upon which the cones are mounted is the stationary member.

Nondriving Front Wheels and Steering Pivots—On front-wheel tapered roller bearing applications, the load reaction line is usually located close to the inner bearing to bring the plane of the wheel closer to the plane of the steering-pivot pin, which reduces steering effort. Placing the majority of the radial load over the inner bearing results in a relatively low radial load on the outer bearing; however, combined with this low radial load is also the induced thrust loading from the inner bearing.

The steering-pivot bearing is an oscillating bearing application. Practically all of the load on the spindle is carried on this self-contained tapered roller thrust bearing. Plain bearings are used in the king-pin mounting to stabilize the overturning forces resulting from the load on the spindle.

Fig. 8 is an Elliott-type steering-head front axle. The axle beam has a yoke forged at each end. The spindle and knuckle are forged T shape in order to form a flange upon which to mount the brake anchor plate. The wheel bearing adjustment is made and secured with double locknuts and a "D" washer. An OD-type lubricant seal is shown. The thrust bearing is located between the steering knuckle and the upper arm of the axle beam yoke.

Fig. 9 is a reversed Elliott-type steering-head front axle. The yoke is integral with the spindle rather than on the ends of the axle beam. Double locknuts and a tongued washer are shown as a means of obtaining and securely locking the wheel bearing adjustment. An ID-type lubricant seal is shown. The steering-pivot thrust bearing is located between the end of the axle and the lower arm of the spindle yoke.

Fig. 10 is another reversed Elliott-type steering-head front axle. The wheel bearing adjustment is accomplished in this case with a hardened "D" washer used in conjunction with an especially designed split nut. A bolt located axially into a split nut locks the nut relative to the "D" washer with a nib which projects into one of the holes provided for it in the hardened washer. The wheel bearing lubricant is sealed into the hub with an OD-type seal. The load from the spindle yoke is carried on the thrust bearing.

Driving Front Wheels and Steering Pivots—Front-driving steering axles for heavy-duty trucks have two bearing applications: the front-wheel bearing application and the steering-pivot application.

Fig. 11 shows a front-wheel-drive bearing application in which the ends of the axle housing are flanged out to a spherical shape. The steering-pivot steep-angle tapered roller-bearing cones are mounted on pins welded into the OD of this half sphere on or near its vertical axis. The adjustable cups are mounted in the steering-pivot housing to which is bolted the flanged tubular wheel spindle. The axle universal joint is mounted in this housing with its center in the plane of the steering-pivot axis. The wheel bearings are both mounted on the tubular wheel spindle. The wheel bearing adjustment is accomplished by a double nut and tongued washer on the spindle tube OD. The axle torque is transmitted to the wheel through the axle drive flange by a stub shaft which is also part of the universal joint and drive line. An external-type seal is shown for retaining the wheel bearing grease. The steering-pivot bearings and universal joint use the same lubrication as the axle center.

The planetary front-wheel-drive bearing shown in Fig. 12 has the same steering-pivot bearing mount-

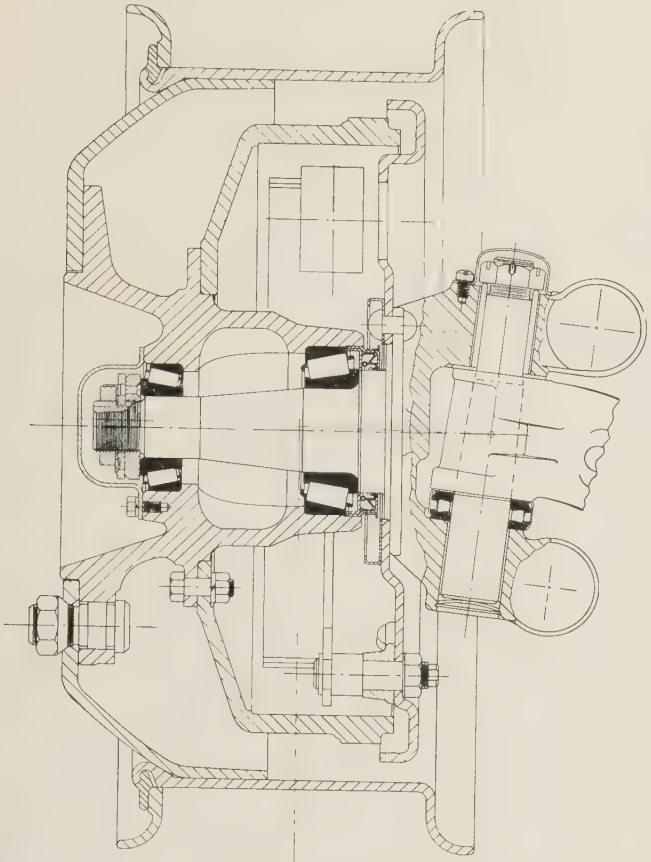

Fig. 9

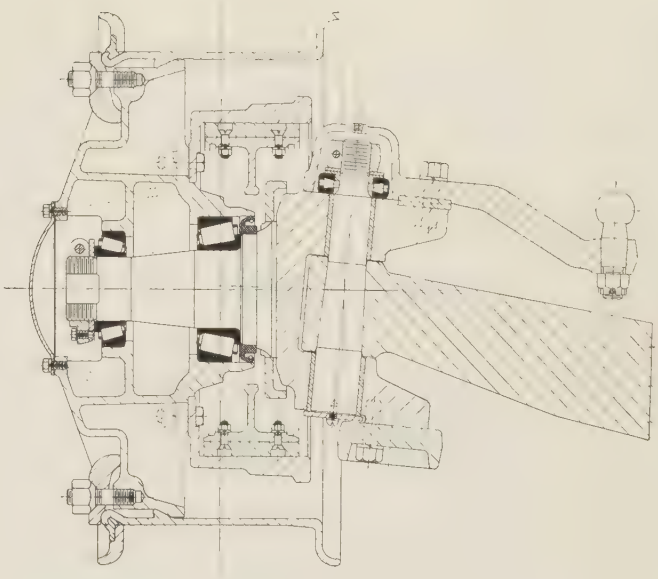

Fig. 10

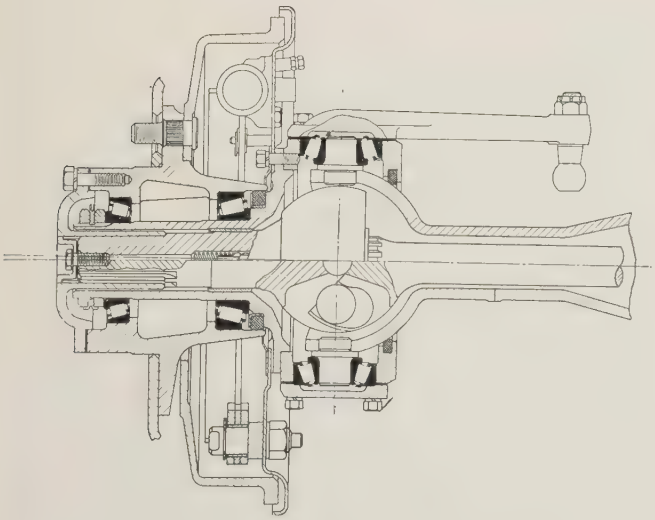

Fig. 11

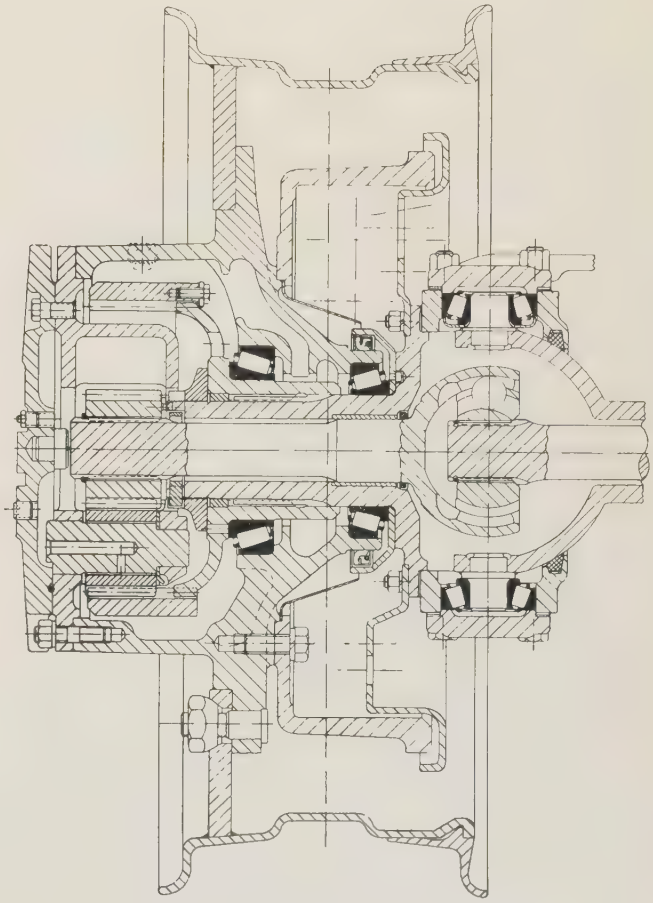

Fig. 12

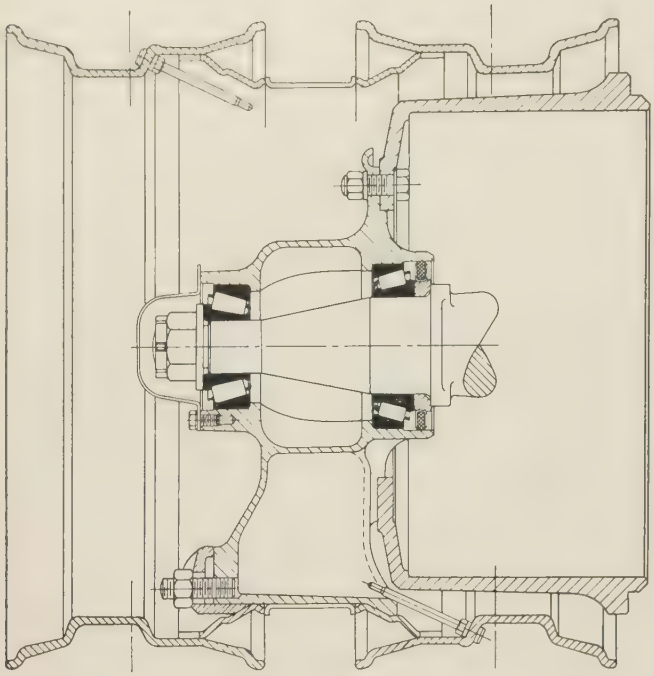

Fig. 13

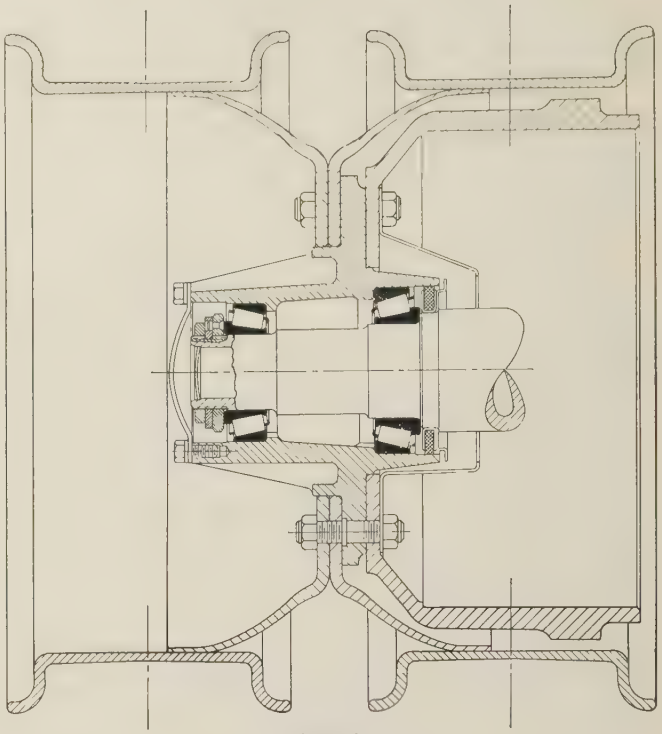

Fig. 14

ing as shown in Fig. 11. On the wheel bearing application the inner cone is mounted on the tubular flanged wheel spindle while the outer cone is mounted on the shank of the internal gear carrier of the planetary system. This, in turn, is mounted on a spline on the tubular flanged wheel spindle. A special adjusting nut and locking device secure the bearing adjustment. The wheel bearings and planetary gears are oil lubricated. The wheel bearing lubricant is contained with internal-type oil seals. The steering-pivot bearings are grease lubricated. There is an oil seal (not shown in this picture) between the axle center and the universal-joint housing, which serves to keep the axle-center lubricant separated from that of the universal joint.

Trailer wheels—Heavy-duty trailer axles function primarily as load-carrying units—tapered roller bearings are used in the wheel application.

Fig. 13 shows a heavy-duty trailer wheel bearing application. It has a solid axle shaft and cast wheel. Adjustment is accomplished by the use of a slotted nut and cotter pin. An external-type lubricant seal to retain the grease is shown.

Fig. 14 shows another trailer wheel bearing application. You will notice that it has a tubular axle and a steel hub designed for a stamped wheel. Adjustment is obtained and secured by a double locknut and tongued washer. An external-type seal is shown and the end of the axle tube is plugged to retain the lubricant in the wheel hub.

Rear Wheels—The rear axle is normally the load-carrying and power-transmitting axle. The weight of the vehicle is carried on tapered roller bearings mounted on the axle-housing tube so that the only function of the full-floating axle shaft is to transmit torque. The wheel bearings, once mounted and adjusted, need not be disturbed when replacing the axle shaft.

Fig. 15 illustrates a typical highway rear-wheel design with a flanged-type full-floating rear-axle shaft. Bearing adjustment is secured and locked by double locknuts and tongued washer. A seal is located at the outer end of the axle tube between the wheel hub and the axle tube to keep the axle-center lubricant from mixing with the wheel-bearing grease. An internal-type seal is shown at the wheel inner position.

Fig. 16 is a typical off-highway planetary rear-wheel design with a full-floating axle shaft. The planetary gear reduction of the rear wheel is designed to meet the needs of the numerically large total gear reductions necessary on off-highway equipment. Bearing adjustment is made through an adjusting and locking nut on the axle tube OD. The inner bearing is grease lubricated while the outer bearing is lubricated by the axle-center lubricant. A seal between the two bearings serves to separate the two lubricants.

Fig. 17 is another planetary rear-wheel bearing application. It is similar to the preceding illustration. The inner cone is mounted on the stationary axle tube while the bearing adjustment is made through the outer cone, which is mounted on the planetary internal-gear carrier hub. This hub, in turn, is mounted on a spline machined on the axle tube. The bearing adjustment is made and secured by a double locknut and tongued lock washer. An internal seal and adapter are mounted at the wheel

inner position. This entire unit is lubricated by the axle-center lubricant.

Axle-Center Bearing Applications

A major function of the tapered roller bearing in the rear-axle center is to hold the gears in proper alignment under all loads imposed upon them while transmitting and converting the torque of the engine into tractive effort of the wheel at the ground.

Before presenting a series of axle-center bearing application illustrations, a few of the more common bearing mountings used in axle centers will be presented in some detail.

Straddle Mounted Pinions (*Fig. 18*)—With a straddle-mounted pinion design, the pinion is mounted between a straight roller bearing at the inner position on a projection on the nose of the

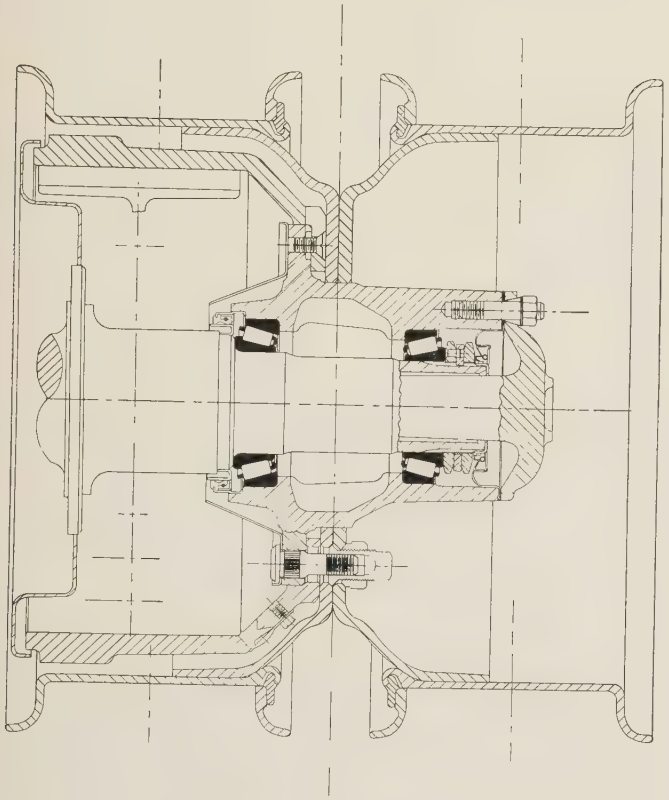

Fig. 15

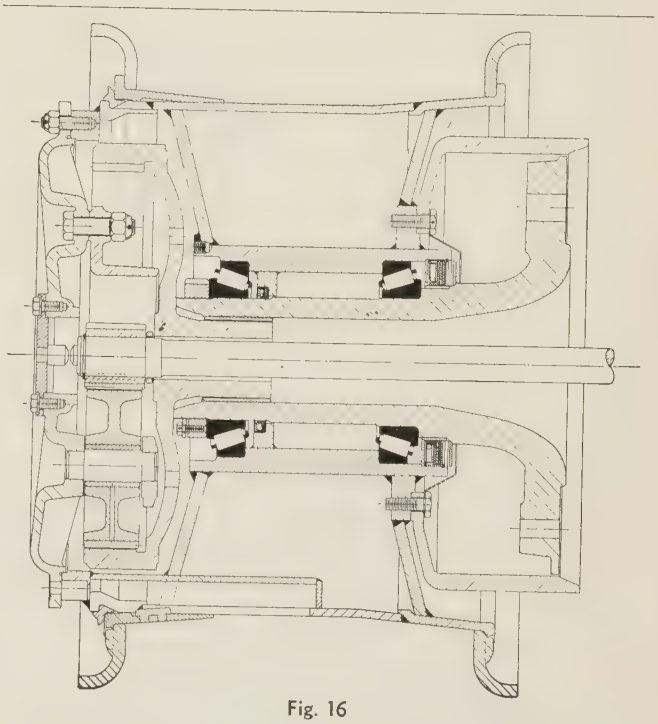

Fig. 16

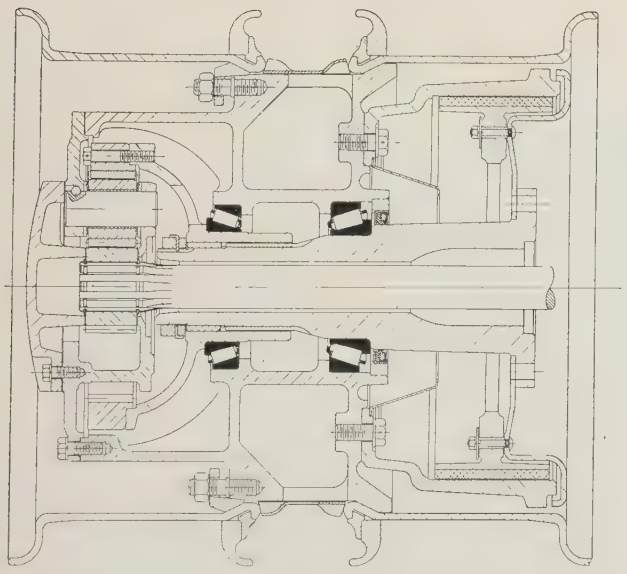

Fig. 17

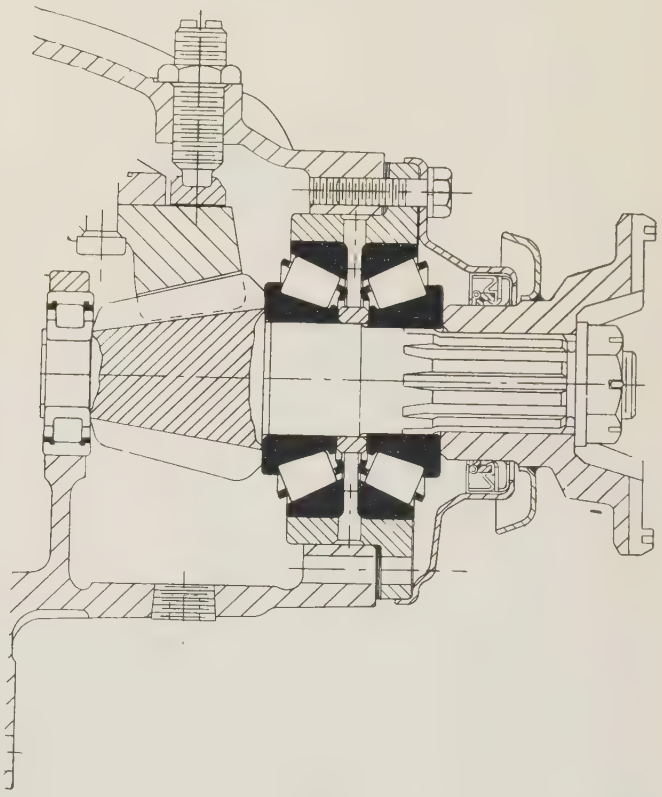

Fig. 18

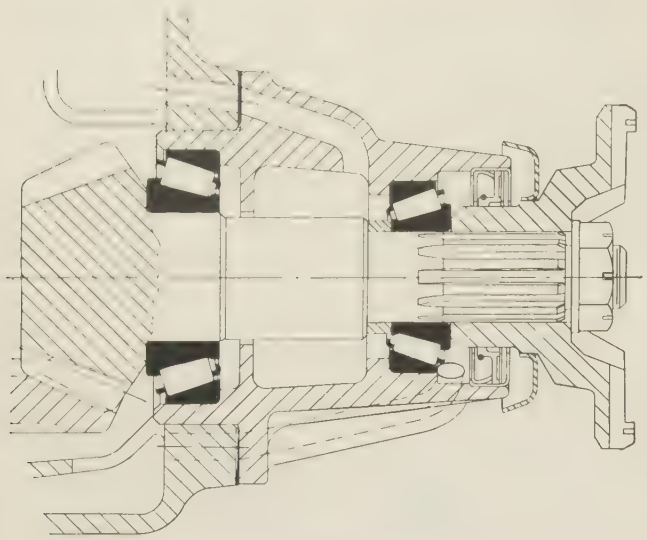

Fig. 19

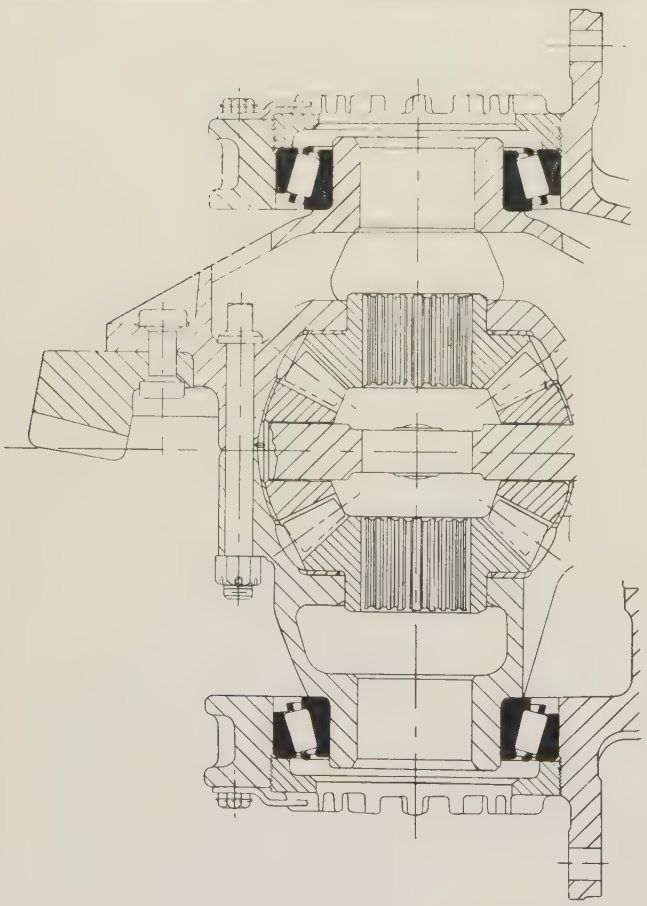

Fig. 20

pinion head and two indirectly mounted steep-angle tapered roller bearings at the pinion outer position. The straight roller bearing on the pinion nose is supported by a pedestal leg cast integral with the housing, and is designed to carry radial loads only. The cups of the outer pinion bearings are usually mounted in a flanged sleeve. The cones are assembled on the pinion shaft and the shaft assembly is mounted into this pinion-carrying sleeve as a bench assembly. Bearing adjustment is obtained with a selective spacer, spacer and shims, or shims between the cone front faces. The flanged pinion sleeve assembly is mounted into a bore in the axle-center housing with the proper amount of shims between the flange of the sleeve and the axle housing to locate the pinion properly. Provisions are made in the axle-center housing and in the pinion-carrying sleeve to intercept and channel lubricant to between the pinion bearings. An oil return is provided between the outer tapered roller bearing and the seal to circulate the oil and to avoid any pressure buildup against the seal which could cause seal leakage.

Overhung-Type Pinions (*Fig. 19*)—The overhung pinion mounting, as the name implies, has the pinion head overhanging the indirectly mounted tapered roller bearings upon which the pinion shaft is mounted. The bearing spread should be at least two times the overhang of the pinion. These measurements are taken from the center of the rollers of the bearings and from the inner-bearing center of roller to the mean pitch diameter of the gear intersection with the pinion axis. The axle-center housing is extended and ribbed to provide for proper bearing spread and rigidity. The pinion shaft may be tapered between the cone seats, in which case a selective spacer or spacer and shims are used to establish the bearing adjustment; or the pinion shaft may be stepped, in which case the bearing adjustment is controlled with either a short spacer or shims between the shoulder on the shaft and the outer cone front face. When the overhung pinion mounting cup seats are machined into the axle housing, the pinion location is controlled either by shims or by a spacer between the inner cup back face and the housing or by shims or a spacer located between the pinion head and the inner cone back face. When the overhung pinion bearings are mounted in a separate pinion carrier, shims between the pinion carrier flange and the axle housing are used to locate the pinion. Provisions are made in the pinion housing to channel the lubricant to the small end of the rollers of the outer pinion bearing. An oil return is located between the outer bearing and the seal.

Pedestal Leg Differential Mounting (*Fig. 20*)—Pedestal leg differential bearing mountings are generally used in conjunction with banjo-type axle housings. The axle center, being a bench-assembled self-contained unit, it is bolted to the face of the axle housing. In this design the pedestal legs, which later form one-half of the differential bearing cup seat, are cast integral with the axle carrier. Pedestal caps are bolted to these pedestal legs, after which both cup seats are bored and either threaded to receive cup adjusting nuts or grooved to receive adjusting rings. The differential case assembly is supported on two directly mounted single-row bearings. The bearings and ring gear are adjusted by means of threaded nuts mounted in the pedestal legs, which are locked after correct bearing adjustment and gear mesh have been obtained.

Carrier-Type Differential Mounting (*Fig. 21*)—In the carrier-type axle-center housing, the axle tubes are pressed into and welded securely to the carrier housing. The differential case is supported on two single-row directly mounted bearings. The cup backing is integral with the carrier housing. Shims between the cone back faces and the shoulder on the

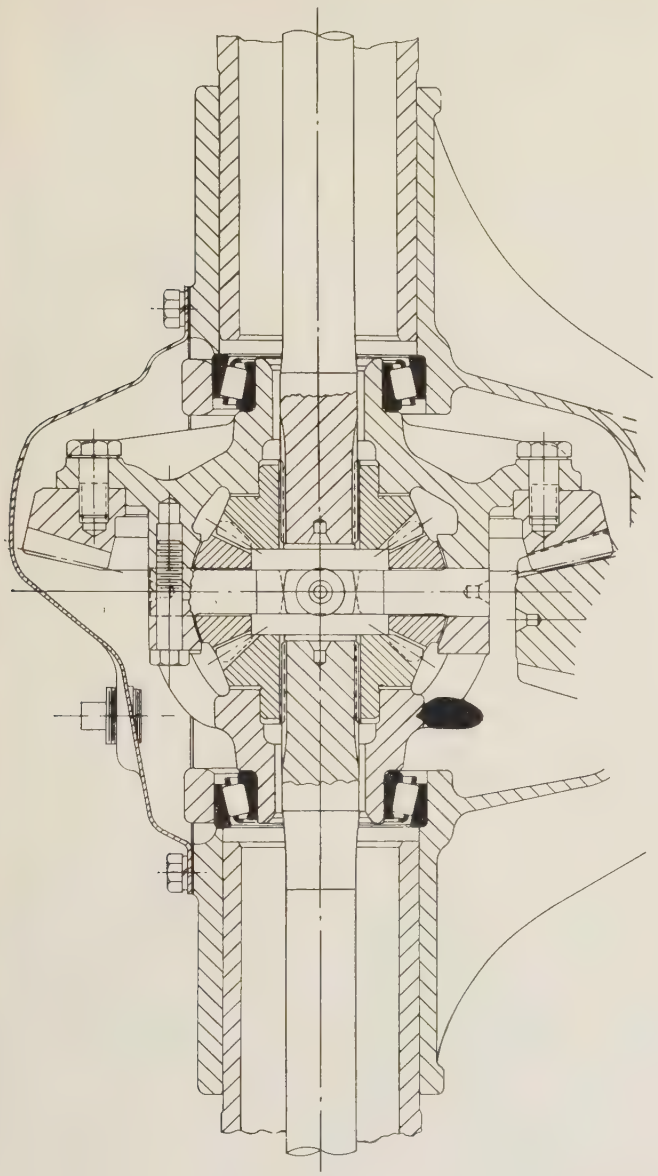

Fig. 21

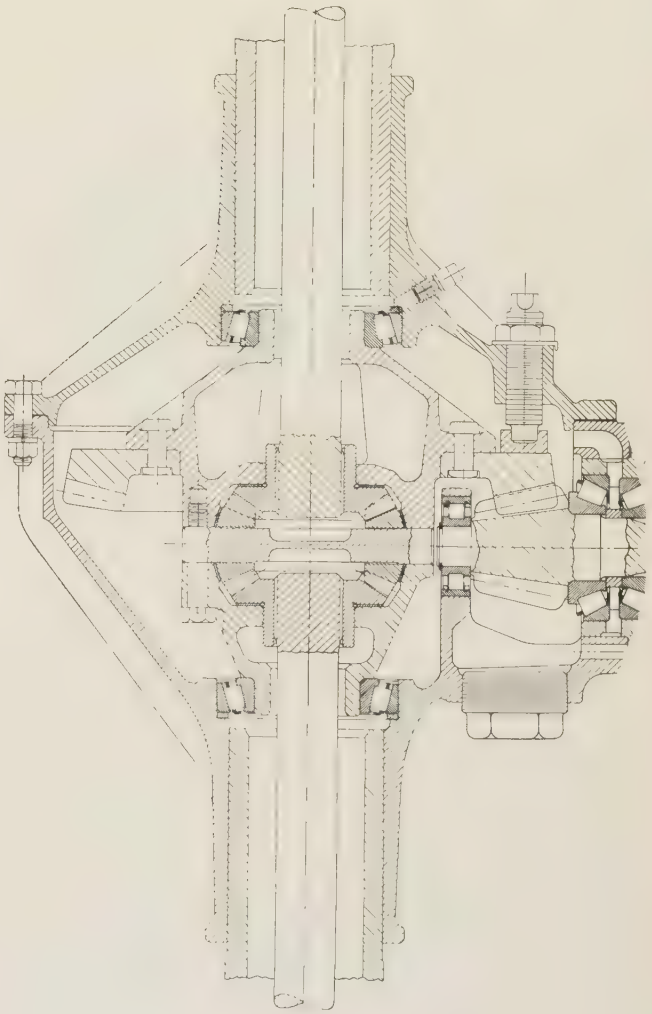

Fig. 22

differential case are used for locating the gear properly and providing bearing adjustment.

Trumpet-Type Differential Mounting (*Fig. 22*)—When assembled, the two halves of the rear-axle housing, trumpet-like in shape, are piloted and securely bolted together. The differential cup seats are machined into each half of the axle housing. Selective spacers behind the differential cups are used to locate the gear and to provide the proper bearing adjustment.

Typical Axle-Center Bearing Application

Single-Reduction Axles—The first series of illustrations will show various designs of single-reduction axles and bearing applications for each axle, as used on heavy-duty trucks. Single-reduction axles are identifiable by their single-step reduction.

Fig. 23 is a typical rear-axle center with a spiral-bevel straddle-mounted pinion and pedestal leg differential bearing mounting. The adjustable thrust block adjacent to the point of gear mesh is used to limit extreme shock deflections. Under normal load-

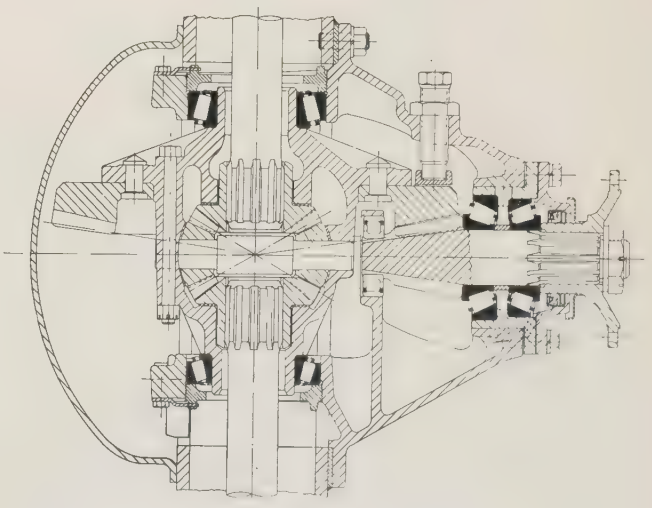

Fig. 23

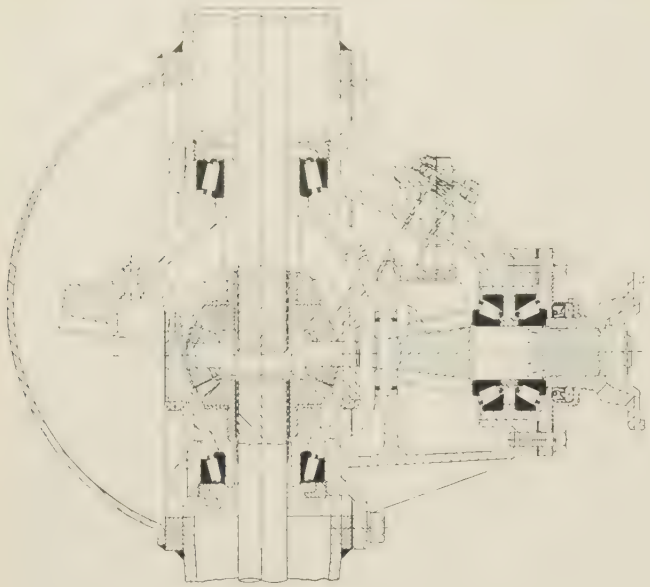

Fig. 24

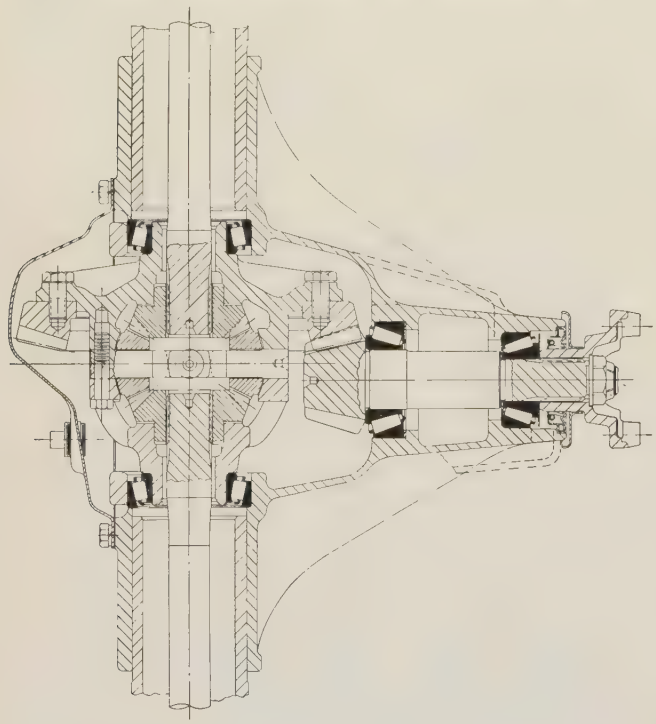

Fig. 25

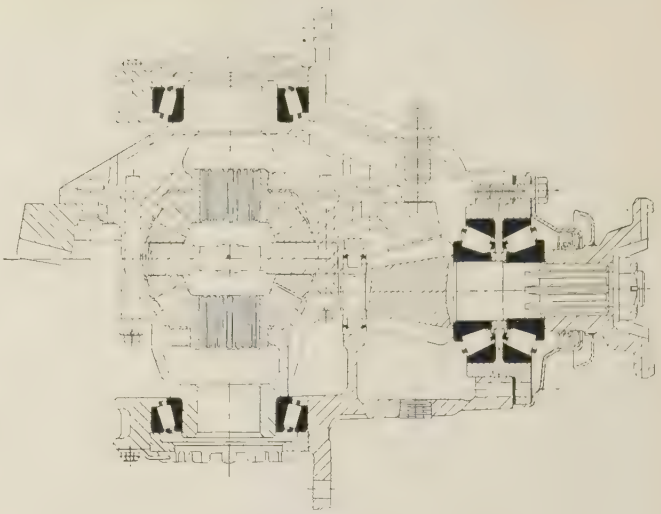

Fig. 26

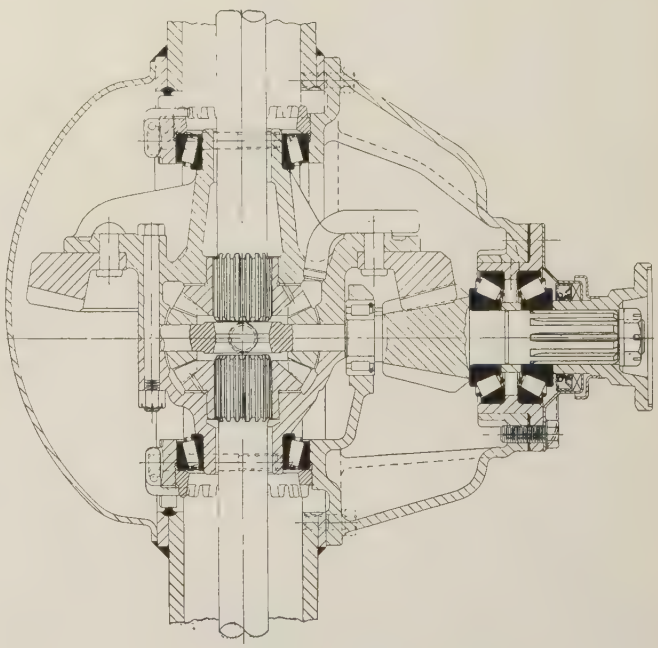

Fig. 27

ing there is a running clearance between the gear and this thrust block.

Fig. 24 is another spiral-bevel straddle-mounted pinion and pedestal leg differential bearing mounting. It is the same as the previous illustration except both pinion front bearings are identical. It also shows an oil scoop used to pick up and channel lubricant to the pinion bearing.

The carrier-type housing of Fig. 25 is more prevalent in the light or medium-duty truck axles than it is in the heavy-duty truck axles. It is shown here to illustrate this type of pinion and gear mounting. It has an overhung pinion mounting with a stepped pinion shaft design and a carrier-type differential bearing mounting.

Fig. 26 is an illustration of a rear-axle center with a hypoid straddle-mounted pinion bearing application and a pedestal-type differential bearing mounting.

Fig. 27 is another rear-axle center with a hypoid straddle-mounted pinion. The differential mounting is again a pedestal-leg type. An oil scoop is used to introduce oil into the differential case. It also shows the pedestal legs backed against the axle housing; this controls the spread of the pedestal legs.

The hypoid straddle-mounted pinion bearing application is shown in Fig. 28 in a trumpet-type axle housing. It shows a trumpet-type differential bearing mounting. This is a good illustration of an internally ribbed differential case. A large plug

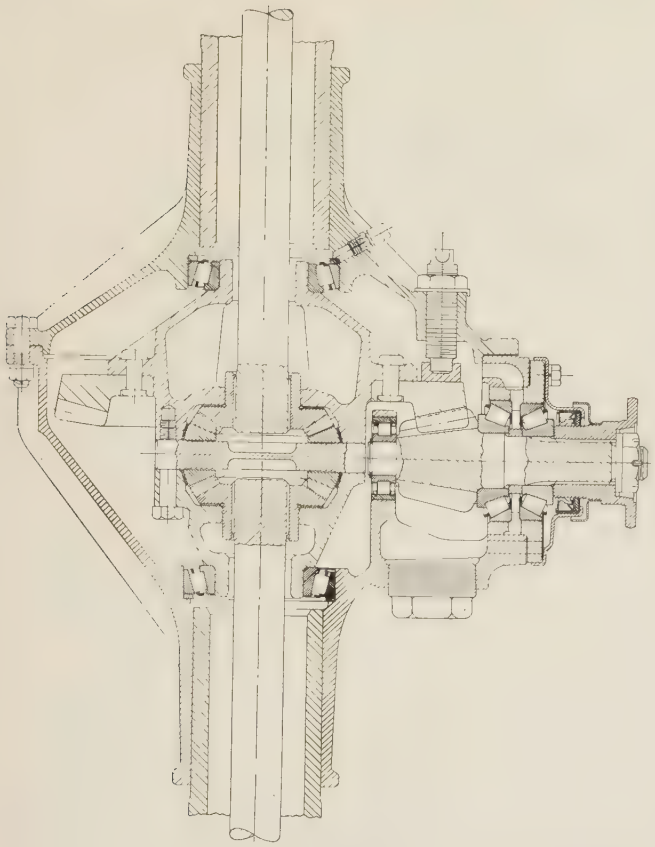

Fig. 28

threaded into the side of the pinion housing opposite the pinion provides for gear inspection.

Double-Reduction Axle—Double-reduction axles are designed to expand the ratio range beyond the practical limits of a single-reduction axle unit by introducing a second set of gears behind the customary bevel or hypoid gear set. These final-drive gears may be herringbone, helical, or spur gears.

Fig. 29 shows a dual-reduction rear-axle center with a spiral-bevel overhung pinion. The pinion shaft has a step design and is mounted in a pinion carrier which, in turn, is piloted into the axle-center carrier. The cross shaft is a direct bearing mounting on two single-row tapered roller bearings. The cones are located against the shoulders on the cross shaft. The right-hand cross-shaft cup is mounted directly into the housing and located by a cup follower. The left-hand cross-shaft cup is mounted in a cup adapter which, in turn, is mounted in the housing. Shims located between the axle housing and the flanges of the cup follower and cup adapter are used to locate the spiral-bevel gear and also to provide bearing adjustment. The herringbone final-drive pinion is integral with the cross shaft and the spiral-bevel gear is splined and bolted to the gear mounting flange on the cross shaft. The differential is mounted on two straight roller bearings. Their mounting is such as to allow free lateral movement of the herringbone final-drive gear, permitting it to seek its own operating position.

Two-Speed Axle Centers—The next two illustrations are two different design approaches to the 2-speed-axle center. One is a double-reduction axle

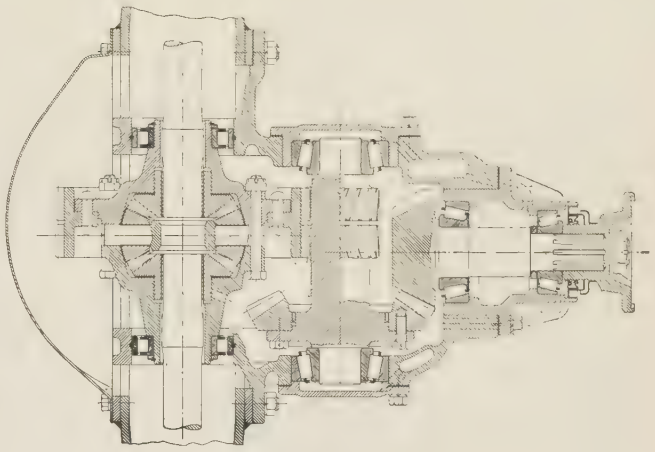

Fig. 29

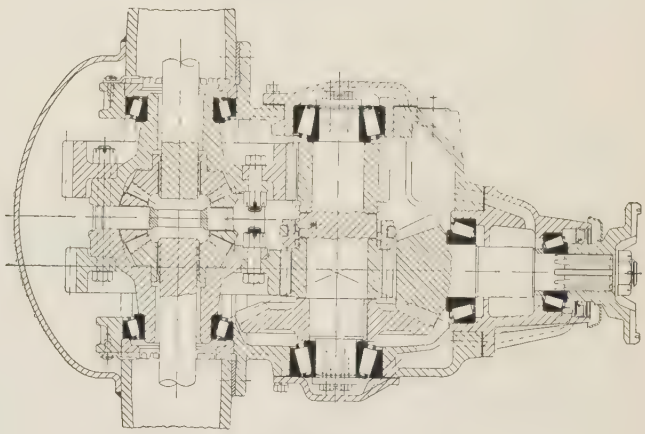

Fig. 30

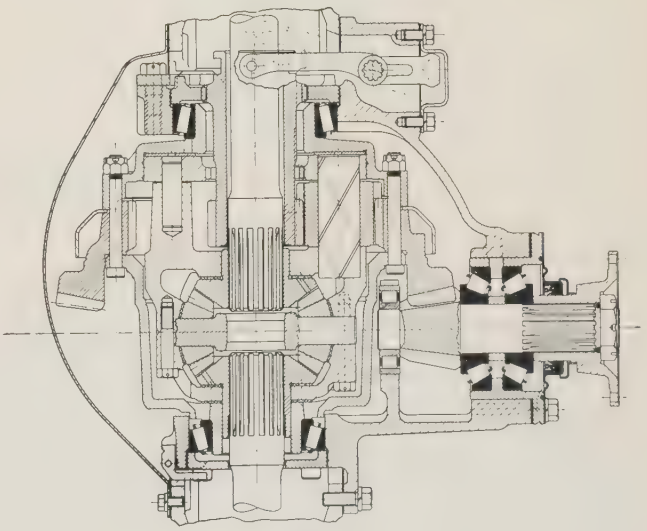

Fig. 31

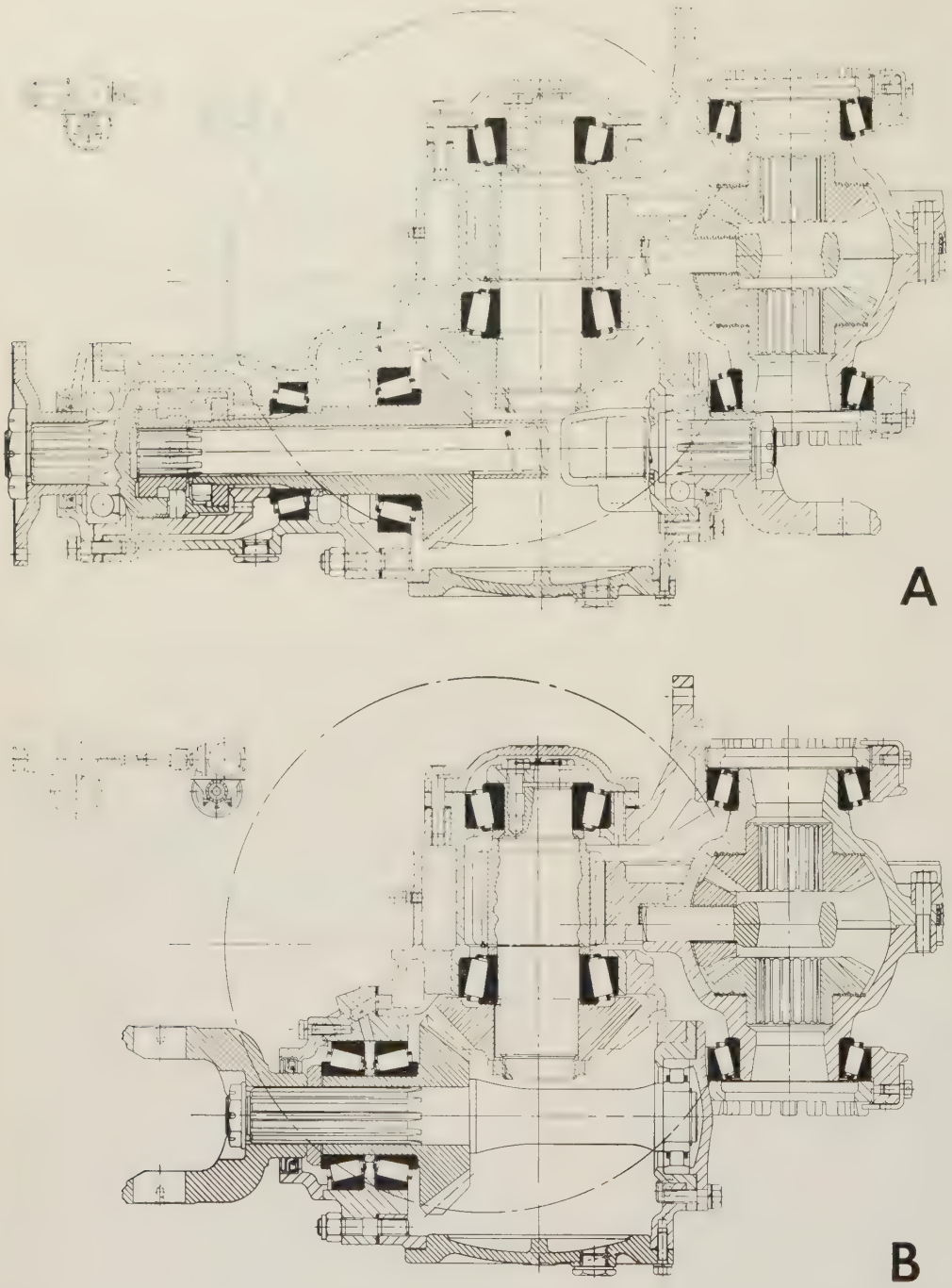

Fig. 32

with two sets of second-reduction or final-drive gears. The second is a two-speed axle combining a planetary gear arrangement in the differential case assembly.

Fig. 30 is a 2-speed dual-reduction axle center with a hypoid overhung pinion. The pinion shaft has a step design. It is indirectly mounted and spacer adjusted on tapered roller bearings in a pinion carrier. Shims mounted between the axle center and the pinion carrier flange are used to obtain pinion location. An intermediate shaft with two rows of clutch teeth integral with the shaft carries the hypoid gear (which is keyed and pressed onto the shaft), a shifting ring, and two different ratio final-drive helical pinions. These helical pinions are free to turn on the intermediate shaft unless they are individually clutched to the integral clutch teeth on the shaft by the shifting ring. The intermediate shaft mounting is a direct roller-bearing mounting. The right-hand intermediate shaft cup is mounted directly into the axle housing and located by a cup follower. The left-hand cup is mounted in a cup adapter. Shims

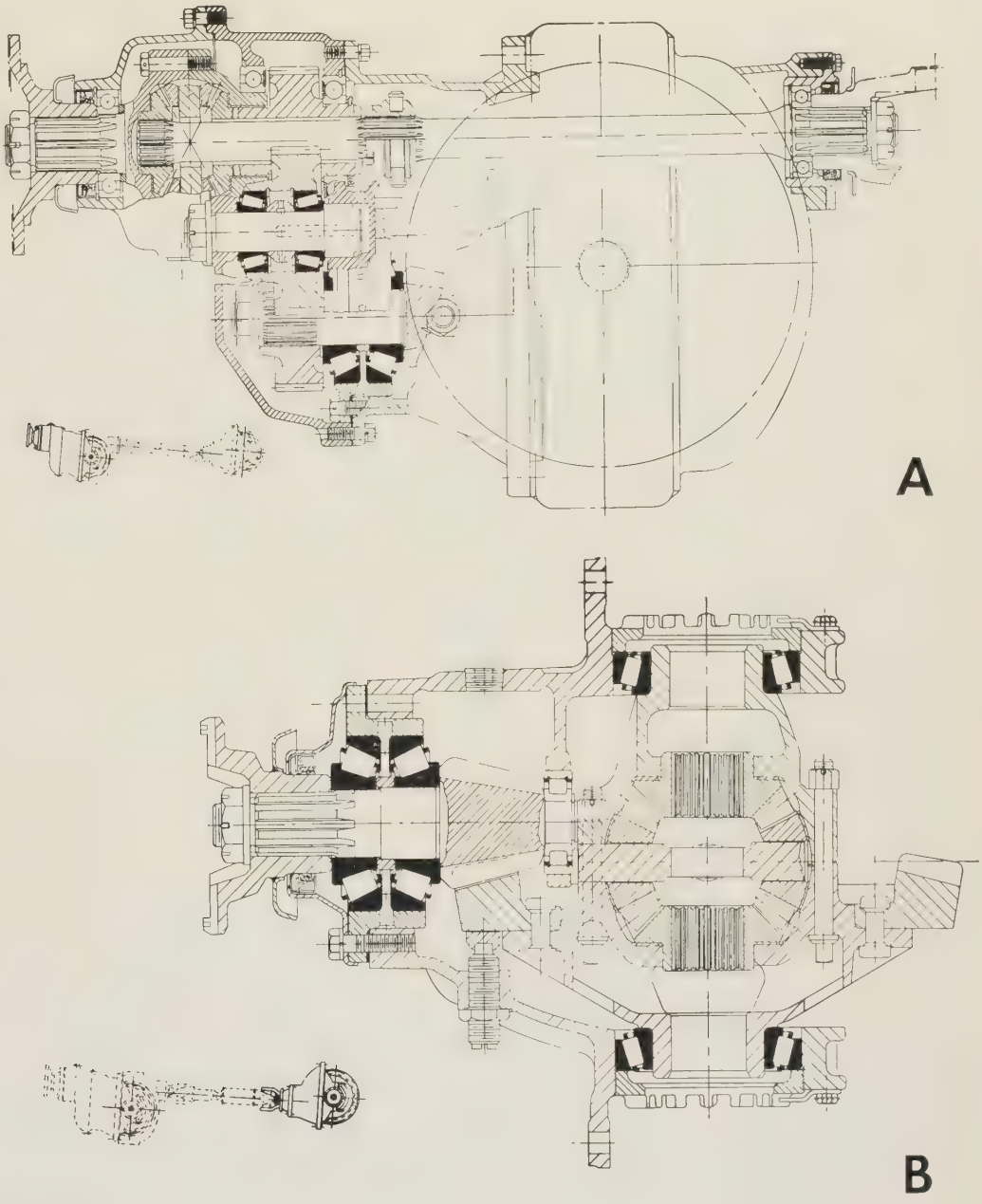

Fig. 33

located between the axle housing and the flanges of the cup follower and cup carrier are used to locate the hypoid gear and to obtain bearing adjustment. The left-hand cone is mounted on the shaft against a shoulder on the shaft, allowing axial running clearance for the helical pinion. It is clamped with an end plate and bolts. On the right side the hypoid gear is keyed and pressed onto the shaft against a shoulder, allowing axial running clearance for the other helical pinion. This cone is also pressed tight against the hypoid gear and clamped securely. The differential mounting is consistent with the standard practice for pedestal-type differentials.

The 2-speed planetary axle center shown in Fig. 31 has a straddle-mounted input pinion, assembled in a flanged pinion carrier, which is installed in a bore in the axle-center housing. The internal gear of the planetary system is combined with the bevel gear, which instead of being mounted on the housing of the differential gears is bolted to an outer case. The differential bearings are a direct mounting on this outer case. This outer case encloses the planetary system and differential case as a self-contained unit. When the planetary gear is in action, the sun gear is held from rotation by means of clutch teeth on the sun-gear shifting sleeve and the left-hand bearing

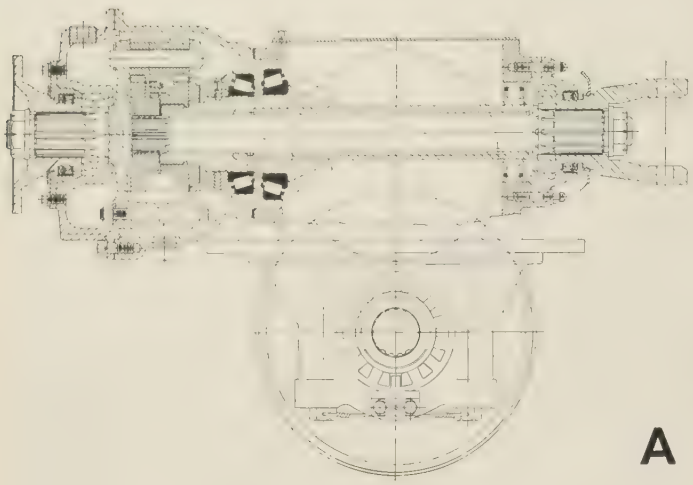

A

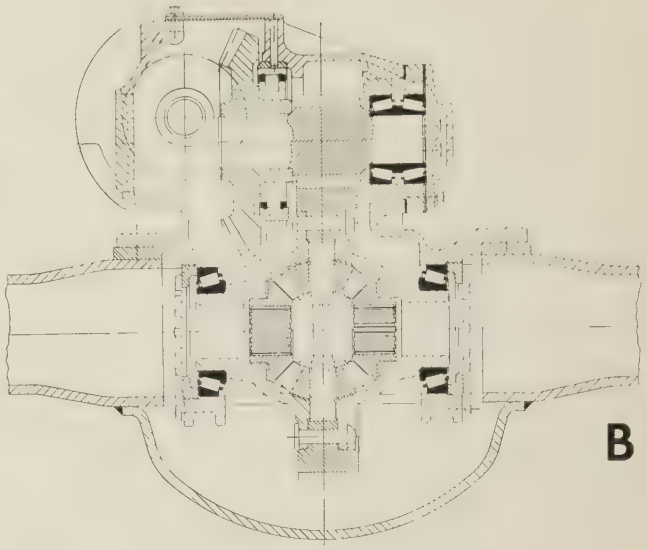

B

Fig. 34

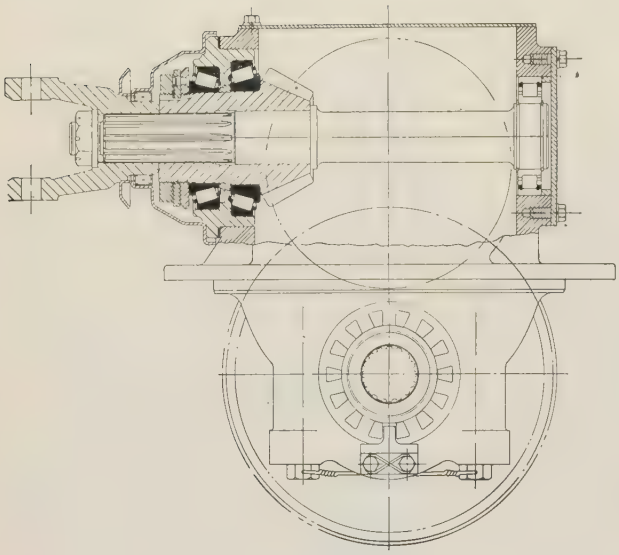

C

adjustment nut. When the sun gear is located as shown by the dotted lines in this layout, it is out of action locking the planets and the planet carrier into one unit and disengaging the clutch teeth; therefore, the power is transmitted only through the bevel-gear ratio. The differential bearings are shown in a pedestal leg-type mounting.

Tandem Axle Centers with Power Dividing Interaxle Differential—A number of current designs of tandem axle centers with single drive lines will be shown next. A single driveshaft introduces torque to the interaxle differential power-divider unit for distribution between the forward rear and rear rear axles. The interaxle differential unit is mounted on, or incorporated with, the forward rear-axle center of the tandem unit.

Fig. 32A shows a forward rear-axle center of a top-mounted, spiral-bevel, dual-reduction, tandem unit with an interaxle differential and power divider. It has a cam, plunger type of interaxle differential. This overhung-type pinion mounting, with a stepped pinion shaft, has the indirectly mounted tapered roller bearings assembled on the pinion shaft. The entire pinion interaxle differential assembly is mounted in a flanged pinion carrier housing. The intermediate or cross shaft carrying the bevel gear and helical pinion is mounted in a flanged sleeve bolted into the axle-center carrier. The spiral-bevel gear is on overhung mounting while the helical-gear pinion is a straddle mounting on two indirectly mounted tapered roller bearings. The cups are mounted in the flanged sleeve. The inner left-hand cone is pressed against the spacer and shoulder to position the bevel gear relative to the cross shaft. The bevel gear is keyed and pressed on the shaft and secured by a nut and locking device. The bearing adjustment is obtained by a spacer between the outer cone face and a shoulder on the cross shaft. The outer cone is secured by a plate bolted onto the end of the shaft. The spiral-bevel gear is located by shims between the axle housing and the sleeve flange. The differential bearing mounting is the conventional pedestal leg type. Ball bearings are shown on the input and the output shafts.

Fig. 32B shows the rear rear-axle center. It is similar to the forward rear-axle center except for the pinion shaft. In this layout the tapered roller bearings are indirectly mounted on the shank of the pinion. The pinion bore is splined and is pressed onto an extended pinion shaft, which is supported at the rear by a straight roller bearing. This results in a wide-spread straddle-mounted pinion.

Fig. 33A shows forward rear-axle center of a front-mounted, hypoid-pinion, single-reduction, tandem unit with a bevel-gear interaxle differential and power divider. The input shaft interaxle differential case unit is straddle mounted on two ball bear-

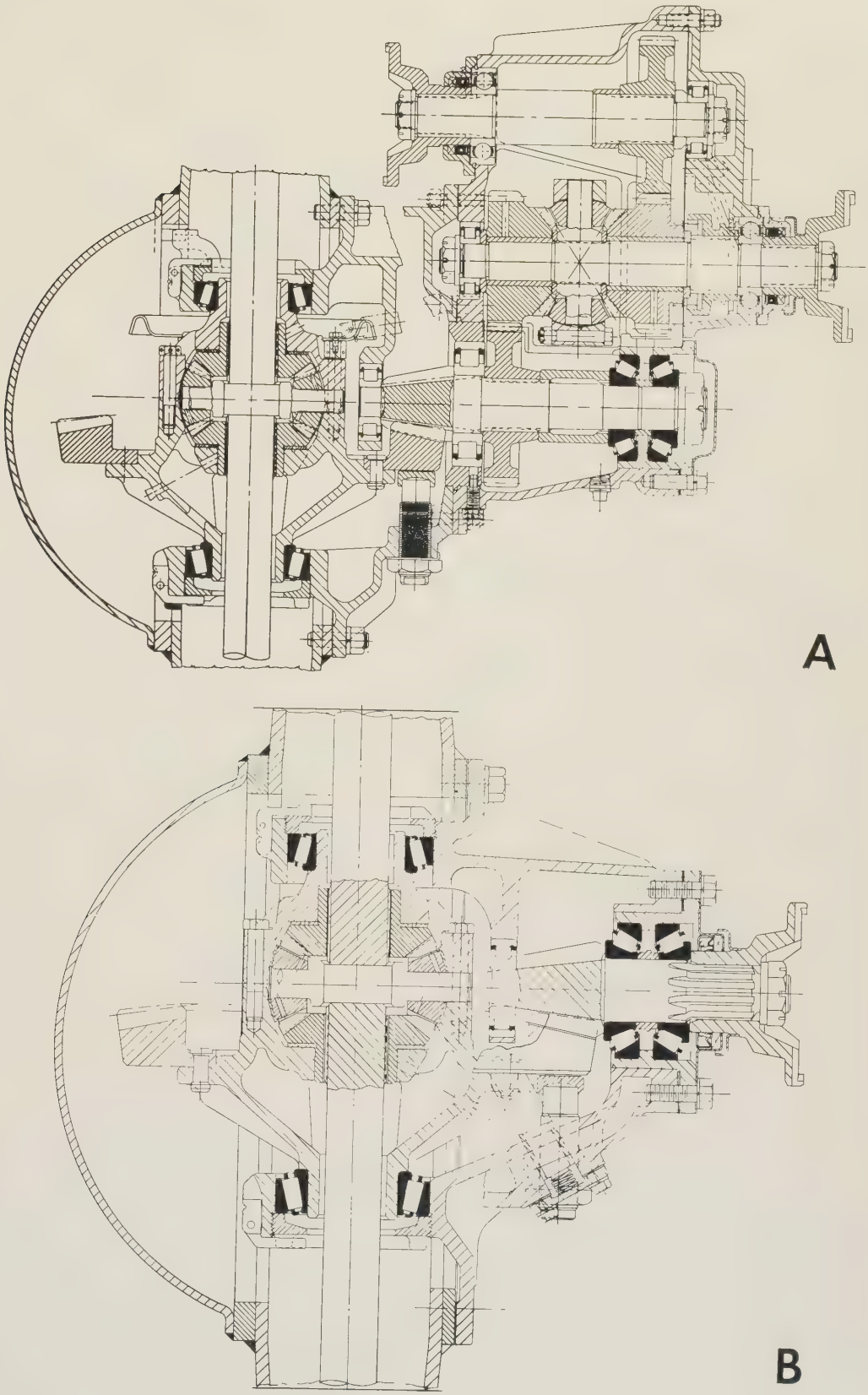

Fig. 35

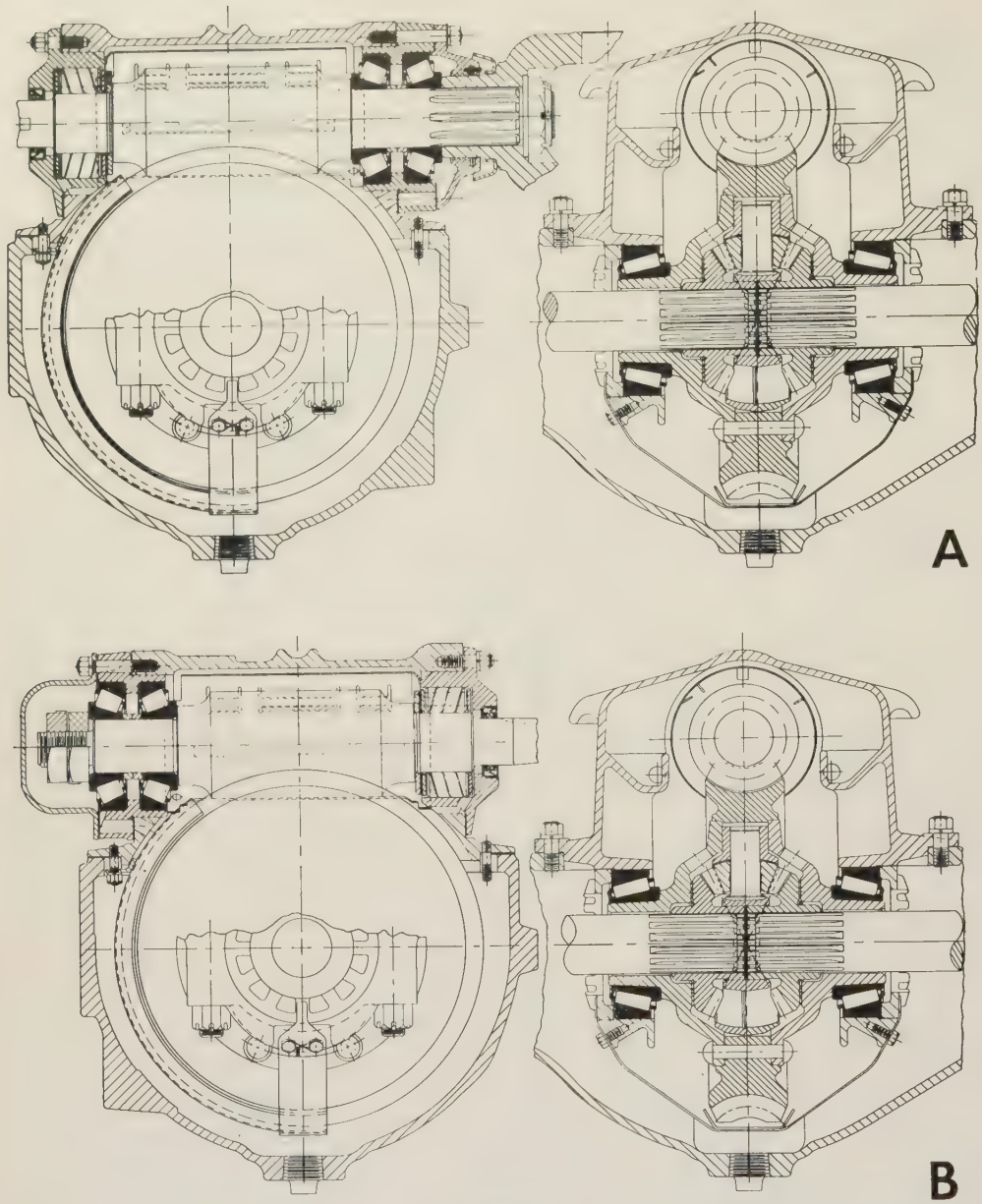

Fig. 36

ings. The input helical gear to the forward rear axle is straddle mounted, being supported at the front in the interaxle differential housing and at the rear on a single-row ball bearing. The idler gear is a dead-shaft application on two indirectly mounted tapered roller bearings. The cups are mounted in the idler gear and the cones are fit on the dead shaft. The bearing adjustment is secured through the use of a selective spacer located between the two cone front faces. Lubrication is introduced to the bearings through holes cross drilled in the shaft and a groove and holes in the spacer. The bearing application for the hypoid pinion is similar to the conventional straddle-mounted pinion except it has a helical gear mounted on the splines of the pinion shank as an overhung mounting. The differential is the standard pedestal leg type.

The rear rear-axle center of this tandem unit is a straight-forward, single-reduction, straddle-mounted, hypoid-pinion axle center as shown in Fig. 33B.

Fig. 34A is the side view of a forward rear-axle top-mounted center of a straddle-mounted, hypoid-pinion, double-reduction, tandem unit, with a spur-gear interaxle differential and power divider. The interaxle differential assembly is straddle-mounted between a double-row ball bearing on the input shaft and the three gears of the interaxle differential meshing with the sun gear mounted on the shank of the pinion shaft. The pinion of the forward rear

axle is a wide-spread, straddle-mounted, pinion bearing mounting with two indirectly mounted tapered roller bearings at the front, and a straight roller bearing at the rear on a tubular extension which has been pressed into the nose of the pinion. The pinion bearing cups are fit into the interaxle differential housing and pinion carrier. The bearings are spacer adjusted and the pinion location is secured by shims between the pinion carrier and the axle housing. The rear rear output shaft is supported at the forward end in the interaxle differential sun gear and at the rear on a single-row ball bearing.

Fig. 34B shows that the cross shaft carries the hypoid gear as an overhung load, and the helical pinion as a straddle-mounted load, between a straight roller bearing in the inner position and two single-row, directly mounted, tapered roller bearings at the outer position. The straight roller bearing is mounted on the shank of the hypoid gear which, in turn, is keyed and pressed onto the cross shaft against the shoulder. The helical pinion is integral with the shaft. The two tapered roller-bearing cones are mounted on the shaft and clamped securely against the shoulder on the shaft by an end plate and bolts into the end of the shaft. A flanged cup adapter carries the directly mounted tapered roller-bearing cups which are the adjustable members. This bearing adjustment is made with an end cap and shims. The hypoid-gear location is obtained by shims between the axle housing and the flange of the cup adapter. The differential tapered roller-bearing mounting is the conventional pedestal leg type.

Fig. 34C shows a side view of the rear rear axle of this unit. The cross shaft and axle-center differential mounting are identical with that of the forward rear axle. The axle-center housing is also the same, the only modification being in the pinion shaft and its mounting. In this rear rear axle the pinion is splined and pressed on the solid pinion shaft to make a shaft unit which, in turn, is straddle mounted on two indirectly mounted tapered roller bearings at the front and a straight roller bearing at the pinion rear position. Pinion adjustment is obtained by the use of shims between the pinion carrier and the axle housing. A selective spacer between the cone front faces is used for controlling bearing adjustment.

Fig. 35A shows the forward rear axle of a tandem unit, which has a helical-gear power-dividing interaxle differential unit mounted on the front of the forward rear-axle housing. This interaxle differential is set at such an angle as to allow the interaxle driveshaft to the rear rear axle to clear the front rear-axle housing when transmitting the drive from the power-divider output shaft. The input shaft carries the interaxle differential unit and helical gears as a straddle mounting between a straight roller bearing at the rear and a ball bearing at the front. The forward rear-axle spiral-bevel pinion is integral with the lower output shaft of the power divider. The spiral-bevel pinion is a straddle mounting between two straight roller bearings, while the helical gear on the same shaft is a straddle mounting between the straight roller bearing on the pinion rear position and the two steep-angle tapered roller bearings in the pinion front position. The pinion front bearings are mounted in a flanged adapter. Shims between the axle housing and the flange of this adapter are used to obtain pinion adjustment. Adjustment of the tapered roller bearings on the pinion shaft is accomplished by the use of a selective spacer between the cone front faces. The helical gear on the output shaft to the rear axle is straddle mounted with a straight roller bearing at the front and a ball bearing at the rear. In the design of this unit, the pinion shaft rotation is counterclockwise for forward drive, which requires that the bevel gear be mounted to the right of the pinion. The differential bearings of this unit are mounted in the conventional manner for a pedestal leg-type design.

Fig. 35B shows the rear rear axle of this tandem unit. This rear rear axle has a counterclockwise input rotation; therefore, the ring gear is mounted on the right of the pinion. The axle center is front mounted in a banjo-type housing. In all other respects, it is a conventional, single-reduction, straddle-mounted, pinion axle center with a pedestal-type differential bearing mounting.

Tandem Axle Center, Worm Drive—Worm and wormwheel gearing have been used in many of the tandem axles. It gives a large gear reduction in a single step and with a straight-line drive.

Fig. 36A shows the forward rear axle of the tandem with an overhead or top-mounted worm drive for heavy-duty trucks. Two single tapered roller bearings indirectly mounted are shown at the front of the worm-gear shaft. They carry the thrust load of the worm in either direction and also a portion of the radial load. The straight roller bearing at the opposite end of the worm carries radial load only The tapered roller bearings are cone adjusted with spacers between the cone front faces and are clamped securely to the worm gear through the companion flange. The cups are mounted into a flanged-cup adapter, which is, in turn, bolted to the face of the housing. This unit uses a conventional pedestal-type differential bearing mounting.

Fig. 36B shows the rear rear axle of a tandem with a top-mounted worm drive. This design is essentially the same as the forward rear axle except that the bearing positions on the worm gear have been reversed. The straight roller bearing is in the forward position and the two steep-angle tapered roller bearings are in the rear position. Double locknuts and a lock washer securely clamp the cones to the worm shaft after proper adjustment has been obtained with cone spacers located between the cone front faces.

Bearing Selection[1]

Bearings for heavy-duty truck applications are selected on the basis of the loads imposed on the bearings, their operating speeds and application, and the economic factors involved.

The loads on nondriving members, such as wheels, require that the bearings carry the axle load, so that the resultant loading on the bearings is the function of the gross load on the axle less the weight of the wheel assembly.

In calculating the bearing loads for the driving axles, the gear forces derived from the tractive effort

[1] Based on "Timken Roller Bearing Co. Engineering Journal," 1957.

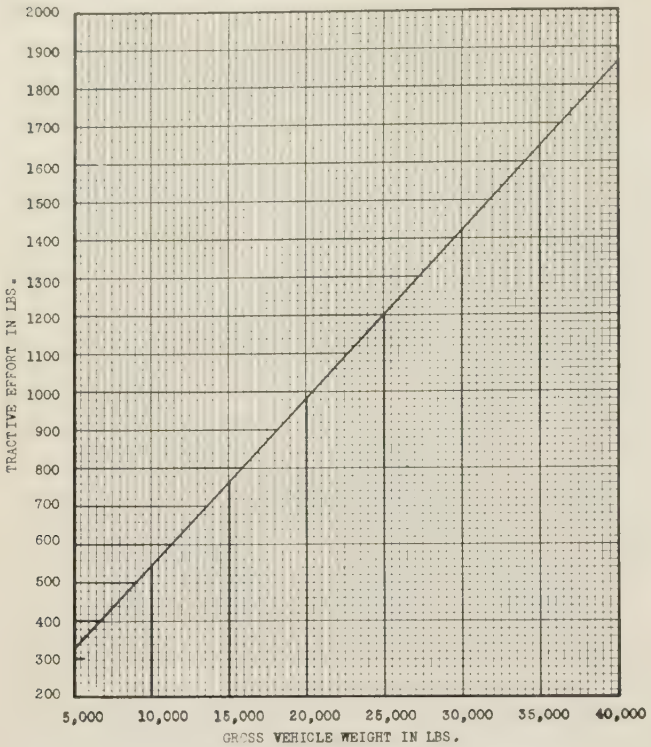

Fig. 37—Tractive effort curve for trucks and buses

of the vehicle wheel at the ground are used for a basis of bearing calculation.

Tractive Effort—Tractive effort (TE) is a function of the gross vehicle weight and the weighted equivalent grade of a highway truck. The weighted equivalent grade includes consideration for actual average grade, rolling resistance, frictional resistance, wind resistance, and acceleration forces.

The truck tractive effort curve (shown in Fig. 37) was developed in order to obtain an average traction at the ground on the basis of gross vehicle weight for highway vehicles for average speeds.

The slope of the curve has a value of:

$$\left(\frac{\text{gvw}}{1000} \times 43.75\right) + 110 = \text{TE}$$

where:

gvw = Gross vehicle weight
43.75 = Slope of curve
110 = Constant

Factors—There are a number of factors which must be considered when calculating the bearing loading prior to the selection of a bearing: the dimensional limitations, the type of application, the average speed of operation, and the type of mounting. An explanation of these essential factors follows:

Application factor—This is a factor which compensates for a variation of operating conditions, such as shocks, continuous duty, and inequality of loading.

Life factor—a life factor of 1.0 is used for all automotive applications; therefore, 100% bearing loading is equivalent to 3000 hr B-10 life.

Speed factor—The speed factor compensates for the deviations from 1.0 for 500 rpm, at which the bearing is rated, to any given operating speed.

$$\left(\frac{\text{500 rpm bearing rated speed}}{\text{operating speed}}\right)^{0.3} = \text{speed factor}$$

Rotation factor—There is a rotation factor for applications where the cone is stationary and the cup rotates under radial loading. Theoretical consideration and experience indicate that a 1.25 factor on the radial portion of the load only, must be used as a basis when calculating radial equivalent load. The rotation factor for a cone rotating application is 1.0.

Fundamental Formulas—Once tentative bearings are selected (based on similar applications, required bore size and other dimensional characteristics, and type of application) tentative effective spread centers are established. The calculation of the radial loading on these established effective spread centers is a straightforward application of known gear formulas and applied mechanics. The application of formulas pertaining to tapered roller bearings is then used to combine all the radial and thrust loadings and to put them into the same terms as the bearing rating.

As mentioned above, the life factor of 1.0 means that for 100% bearing loading, the bearings will give 3000 hr of B-10 life.

$$\%\ \text{load} = \frac{\text{RRR}}{\text{BRR}} \qquad (1)$$

where:

BRR = Basic radial rating of the bearing at 500 rpm
RRR = Required radial rating of the bearing at 500 rpm

Required radial rating (RRR) is a step which converts the actual radial equivalent (RE) load on the bearing at the actual average speed of operation into the same terms as the basic radial rating (BRR) of the bearing at 500 rpm.

$$\text{RRR} = \frac{\text{RE} \times \text{AF}}{\text{SF}} \qquad (2)$$

where:

RE = Radial equivalent load, which is an imaginary radial load that, if applied, would result in the same endurance life to the bearing as would be obtained from the actual radial and thrust loads acting simultaneously.

AF = Application factor as used to compensate for the variation in operating conditions such as shock, continuous duty, inequality of load, and deflection.

SF = Speed factor. Tapered roller bearings are rated at 500 rpm; therefore, the speed factor is 1.0 for 500 rpm. For any other speed, a speed factor of $(500 \div \text{actual operating speed})^{0.3}$ is used to modify the radial equivalent load in order to obtain the required rating in the same terms as the bearing basic radial rating.

Before proceeding with the discussion of the radial equivalent load formula, which gives the necessary steps to combine radial loads on the bearing

with either thrust or induced thrust loads, let us consider the K factor of the tapered roller bearing.

$$K = \frac{\text{BRR}}{\text{BTR}} \tag{3}$$

where:

BTR = Basic thrust rating at 500 rpm

The K factor is the relationship of the basic radial and the basic thrust rating. This factor plays a large part in determining the induced thrust and subsequently the radial equivalent loads.

The development of a radial equivalent load formula necessitates an analysis of the thrust reaction that is induced whenever a tapered roller bearing is loaded radially. This thrust reaction is expressed by:

$$T_r = \frac{0.47 \times R}{K} \tag{4}$$

where:

T_r = Thrust reaction due to a radial load on the bearing
R = Radial load on the bearing
K = K factor due to cup angle
0.47 = Constant

This formula develops from a summation of the thrust components from the individual rollers supporting the radial load. The T_r is available to oppose an externally applied thrust imposed on the bearing or from the induced thrust of an opposing bearing on the shaft. Therefore, if a bearing is subjected to an externally applied thrust T while supporting a radial load R, the effective thrust on the bearing is evaluated by:

$$T_e = T - \frac{0.47R}{K} \tag{5}$$

where:

T_e = Effective thrust
T = Applied or imposed thrust on the bearing axially

The relative fatigue relationship between the radial and thrust capacity of a tapered roller bearing was expressed by the factor K and, accordingly, the radial load that is equivalent to the effective thrust (T_e) can be expressed by:

$$R' = K \times T_e \tag{6}$$

where:

R' = Radial load equivalent to the effective thrust (T_e)

We can now write the radial equivalent load basic formula for a rotating cone. (Rotation factor for cone rotating application = 1.0), bearing as is shown in:

$$\text{RE} = R + K\left(T - \frac{0.47R}{K}\right) \tag{7}$$

or:

$$0.53R + KT$$

Since tapered roller bearings are generally mounted in pairs, that is, two bearings with tapers opposed, equation 7 can be expanded to:

$$\text{RE}_a = R_a + K_a\left(T_a + \frac{0.47R_b}{K_b} - \frac{0.47R_a}{K_a}\right) \tag{8}$$

or:

$$\text{RE}_a = 0.53R_a + K_a\left(T_a + \frac{0.47R_b}{K_b}\right)$$

where:

RE_a = Radial equivalent on bearing (a)
R_a = Radial load on bearing (a)
R_b = Radial load on bearing (b)
K_a = K factor for bearing (a)
K_b = K factor for bearing (b)
T_a = Axially applied thrust load on bearing (a)

For a bearing under a given radial load the greatest stress occurs on the roller in the center of the load zone; however, because of the curvatures involved, the stress is greater between the cone and roller. Thus, with a stationary cone one portion of the cone is always submitted to the highest stress. Since the stress between the cone and roller is the greatest, cup rotation gives a reduced rating for the bearing. Therefore, a rotating cup factor of 1.25 is used in the radial equivalent (RE) formula to modify the bearing load.

$$\text{RE} = 1.25 \times R \tag{9}$$

It may be said here that for a bearing carrying strictly thrust loading, the equivalent load is identical for either cup or cone rotation.

For a combined radial and thrust bearing loading on a stationary cone mounting, the radial equivalent (RE) load will be shown by:

$$\text{RE} = 1.25R + K\left(T - \frac{0.47R}{K}\right) \tag{10}$$

or:

$$0.78R + KT$$

Equation 10 can be expanded into the form of equation 8 for two opposed bearings with rotating cups having different K factors as:

$$\text{RE} = 0.78R_a + K_a\left(T_a + \frac{0.47R_b}{K_b}\right) \tag{11}$$

The formulas discussed are the basis for the radial equivalent (RE) or combined loading of any condition of single-row bearings with either cone rotating or cup rotating members.

When the calculated radial equivalent (RE) load

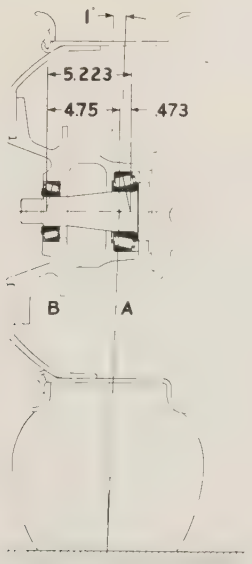

Fig. 38

Table 1—Modifications of Basic Induced Thrust Formulas

single-row bearings

design	thrust condition	rotating cone or "rotating cup with rotating cone"	rotating cup (stationary cone)
		equation	equation
no external thrust load			
		identical series	
	$0.47R_A < 0.47R_B$	$RE_A = 0.53R_A + 0.47R_B$ $RE_B = R_B$	$RE_A = 0.78R_A + 0.47R_B$ $RE_B = 1.25R_B$
	$0.47R_A > 0.47R_B$	$RE_A = R_A$ $RE_B = 0.53R_B + 0.47R_A$	$RE_A = 1.25R_A$ $RE_B = 0.78R_B + 0.47R_A$
		dissimilar series	
	$\frac{0.47R_A}{K_A} < \frac{0.47R_B}{K_B}$	$RE_A = 0.53R_A + \frac{0.47R_B K_A}{K_B}$ $RE_B = R_B$	$RE_A = 0.78R_A + \frac{0.47R_B K_A}{K_B}$ $RE_B = 1.25R_B$
	$\frac{0.47R_A}{K_A} > \frac{0.47R_B}{K_B}$	$RE_A = R_A$ $RE_B = 0.53R_B + \frac{0.47R_A K_B}{K_A}$	$RE_A = 1.25R_A$ $RE_B = 0.78R_B + \frac{0.47R_A K_B}{K_A}$
with external thrust load			
		identical series	
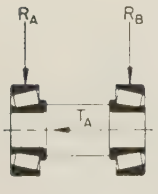	$\frac{0.47R_A}{K_A} < \left(\frac{0.47R_B}{K_B} + T_A\right)$	$RE_A = 0.53R_A + 0.47R_B + K_A T_A$ $RE_B = R_B$	$RE_A = 0.78R_A + 0.47R_B + K_A T_A$ $RE_B = 1.25R_B$
	$\frac{0.47R_A}{K_A} > \left(\frac{0.47R_B}{K_B} + T_A\right)$	$RE_A = R_A$ $RE_B = 0.53R_B + 0.47R_A - K_B T_A$	$RE_A = 1.25R_A$ $RE_B = 0.78R_B + 0.47R_A - K_B T_A$
		dissimilar series	
	$\frac{0.47R_A}{K_A} < \left(\frac{0.47R_B}{K_B} + T_A\right)$	$RE_A = 0.53R_A + K_A\left(\frac{0.47R_B}{K_B} + T_A\right)$ $RE_B = R_B$	$RE_A = 0.78R_A + K_A\left(\frac{0.47R_B}{K_B} + T_A\right)$ $RE_B = 1.25R_B$
	$\frac{0.47R_A}{K_A} > \left(\frac{0.47R_B}{K_B} + T_A\right)$	$RE_A = R_A$ $RE_B = 0.53R_B + K_B\left(\frac{0.47R_A}{K_A} - T_A\right)$	$RE_A = 1.25R_A$ $RE_B = 0.78R_B + K_B\left(\frac{0.47R_A}{K_A} - T_A\right)$

two-row bearings

design	thrust condition	rotating cone or "rotating cup with rotating cone"	rotating cup (stationary cone)
		identical series	
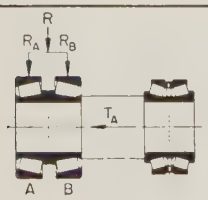	$T_A < \frac{0.47R}{K_A}$	$RE_A = \frac{R}{2} + 1.064K_A T_A$ $RE_B = \frac{R}{2} - 1.064K_A T_A$	$RE_A = 0.625R + 1.33K_A T_A$ $RE_B = 0.625R - 1.33K_A T_A$
	$T_A > \frac{0.47R}{K_A}$	$RE_A = 0.53R + K_A T_A$ $RE_B = 0$	$RE_A = 0.78R + K_A T_A$ $RE_B = 0$
		dissimilar series	
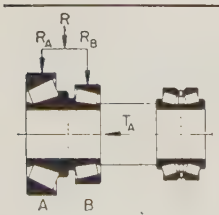	$T_A < \frac{0.47R}{K_A}$	$RE_A = \frac{K_A}{K_B + K_A}(R + 2.13T_A K_B)$ $RE_B = \frac{K_B}{K_B + K_A}(R - 2.13T_A K_A)$	$RE_A = \frac{1.25K_A}{K_B + K_A}(R + 2.13T_A K_B)$ $RE_B = \frac{1.25K_B}{K_B + K_A}(R - 2.13T_A K_A)$
	$T_A > \frac{0.47R}{K_A}$	$RE_A = 0.53R + K_A T_A$ $RE_B = 0$	$RE_A = 0.78R + K_A T_A$ $RE_B = 0$

is less than the actual radial (R) load, the bearing is selected on the basis of the radial load only and the radial equivalent load is calculated for the opposed bearing of the set. After the loads are calculated, the percentage loads on the bearings should not exceed 100%.

Table 1 shows all the various modifications of the basic induced thrust formulas.

Sample Calculation for a Front Wheel (Stationary Cone, Rotating Cup Condition)—The selection of front-wheel bearings is a matter of hub and spindle design and proper bearing combination. The bearing loads are calculated on the basis of one-half of the gross axle load on the tires at the ground, less the weight of the tire, wheel, and rim assembly. (See Fig. 38.)

Given Conditions:

Type of vehicle—truck
Gross weight on front axle—10,000 lb
Tire rolling diameter—39 in.
Camber angle—1 deg
Weight per wheel and tire—450 lb
Bearing spacing on effective spread basis
Desired shaft diameter at bearing seats:
Front wheel inner—position A—2.2500 in.
Front wheel outer—position B—1.500 in.

The effective spread centers of the bearing lie at the intersection of a line projected perpendicularly to the cup angle halfway down the roller slant length and the bearing axis. This is considered the true center of pressure of all the resisting forces set up by the rollers in the bearing. These effective spread centers are used in taking moments about the bearings.

Analysis:

Locate load reaction line from wheel camber angle
Wheel speed—345 rpm

The wheel speed is established from the rolling diameter of the tire on the basis of an average truck speed of 40 mph.

Speed factor (SF)—1.118

Tapered roller bearings are rated at 500 rpm. Therefore, the base is 1.0 for 500 rpm. For the effect on bearing life at any other speed, a speed factor of (500/actual operating speed)$^{0.3}$ is used to modify the radial equivalent load in order to obtain the required radial rating in the same terms as the bearing basic radial rating.

Application factor (AF)—1.35

The application factor is used to compensate for the variation in operating conditions such as shock, continuous duty, and inequality of loading.

Rotating cup factor—1.25

Theoretical consideration and experience indicate that a 1.25 factor on the radial portion of the bearing load should be used when calculating radial equivalent loads.

$$\text{Load per hub} = \left(\frac{\text{gross weight per axle}}{2}\right) - \text{weight of wheel and tire}$$

$$= \frac{10000}{2} - 450 = 4550 \text{ lb}$$

Bearing Selections (tentative):

These selections are made on the basis of dimensional requirements and K factor range. The K factor range for this application is from 1.10 to 1.90.

Position	Cone No.	Cup No.	BRR	K Factor
Front wheel A				
Inner	623	612	6750	1.62
Front wheel B				
Outer	444	432	3910	1.79

Bearing radial loads (R):

$R_A = 4550 \times 4.750/5.223 = 4140$ lb
$R_B = 4550 \times 0.473/5.223 = 410$ lb

Bearing radial equivalent loads (RE):

$$RE_A = 1.25 \times 4140 = 5180 \text{ lb}$$

$$RE_B = 0.78 \times 410 + 1.79 \frac{0.47 \times 4140}{1.62} = 2470 \text{ lb}$$

The radial equivalent load (RE) is an imaginary radial load that, if applied, would result in the same endurance life to the bearing as would be obtained from the actual radial and thrust loads acting simultaneously. When series of the opposed bearings differ or when one bearing carries most of the radial load, the induced excess thrust reaction must be carried by the other bearing, in this case, the outer bearing.

A radial load applied to a single bearing induces a thrust load in the magnitude of (0.47 × radial load/K factor) in which the K factor equals the (BRR of the bearing/BTR of the bearing) and the 0.47 equals a constant derived from the summation of the thrust components from the individual rollers supporting the load. By observation it can be seen that the induced thrust caused by the radial load on A is far greater than the induced thrust resulting from the radial load on B.

$$\frac{0.47 \times R_A}{K_A} \text{ is greater than } \frac{0.47 \times R_B}{K_B}$$

$$\frac{0.47 \times 4140}{1.62} \text{ is greater than } \frac{0.47 \times 410}{1.79}$$

1200 lb is greater than 108 lb

Therefore, the B bearing must carry a combined radial and thrust load, while A bearing carries only a radial loading.

The rotating cup factor of 1.25 modifies the radial loads only on the bearings; therefore, we have the following:

$$RE_A = 1.25 \times R_A = 1.25 \times 4140 = 5180 \text{ lb}$$

$$RE_B = 1.25\, R_B + K_B \left(T_A - \frac{0.47\, R_B}{K_B}\right)$$

$$= 1.25 \times 410 + 1.79 \left(1200 - \frac{0.47 \times 410}{1.79}\right) = 2470 \text{ lb}$$

or simplified to:

$$= 0.78\, R_B + K_B \left(\frac{0.47 \times R_A}{K_A}\right)$$

$$= 0.78 \times 410 + 1.79 \left(\frac{0.47 \times 4140}{1.62}\right) = 2470 \text{ lb}$$

Bearing required radial ratings (RRR):

$RRR_A = RE_A \times AF/SF = 5180 \times 1.35/1.118 = 6260$ lb
$RRR_B = RE_B \times AF/SF = 2470 \times 1.35/1.118 = 2980$ lb

The calculation for the required radial rating is a step which converts the actual load on the bearing at an actual average speed into the same terms as the bearing basic radial rating at 500 rpm, so that

a direct comparison can be made. This step also takes into consideration the type of application by the use of a predetermined application factor (AF).

Bearing Loading Analysis:

Position	Cone No.	Cup No.	Rpm	RRR	BRR	% Load
Front wheel A Inner	623	612	345	6260	6750	93
Front wheel B Outer	444	432	345	2980	3910	76

Required radial rating/basic radial rating = % bearing loading. In automotive practice we endeavor to hold the loading for average operating conditions to 100%.

Sample Calculation for a Rear-Axle Center—At this point it seems appropriate to inject a typical bearing loading calculation of a heavy-duty, single-reduction, hypoid rear-axle center. (See Fig. 39.)

Given Conditions:

Type of vehicle—highway truck
Gross vehicle weight—29,500 lb
Tire rolling diameter—44.2 in.
Axle ratio (m)—7.4
Pinion rotation in forward drive—clockwise
Bearing spacing on effective spread basis
Desired shaft diameter at the bearing seats:
Differential right hand and left hand—F & G—3.6250 in.
Pinion front inner and outer—H_o & H_i—2.4375 in.

The effective spread centers of the bearing lie at the intersection of a line projected perpendicularly to the cup angle, halfway down the roller slant length and the bearing axis. This is considered the true center of pressure of all the resisting forces set up by the rollers in the bearing. These effective spread centers are used in taking moments about the bearings.

The hypoid pinion and gear have no pitch angles because the pitch surfaces are hyperboloids; therefore, the face angle of the pinion and the root angle of the gear are the generally accepted surfaces used in considering the theoretical gear loads.

Hypoid gear data:

Pitch diameter of gear ($D_P{}^G$)—16.625 in.
Face width of gear (F^G)—2.00 in.
Root angle of gear (γ^G)—75 deg 45 min
sin (γ^G) = 0.969 cos (γ^G) = 0.246
Spiral angle of gear (ψ^G)—33 deg 54 min
sin (ψ^G) = 0.558 cos (ψ^G) = 0.830
Pressure angle drive (ϕ)—23 deg 15 min
tan (ϕ) = 0.430
Pressure angle coast (ϕ_c)—21 deg 45 min
tan (ϕ_c) = 0.399
Face angle of pinion (γ^P)—13 deg 52 min
sin (γ^P) = 0.240 cos (γ^P) = 0.971
Spiral angle of pinion (ψ^P)—47 deg 33 min
sin (ψ^P) = 0.738 cos (ψ^P) = 0.675
Hand of pinion spiral angle—left hand
Pinion offset—1.75 in.

Analysis:

Wheel and differential speed—304 rpm
Pinion speed—304 × 7.4 = 2250 rpm

Wheel speed is established from the rolling diameter of the tire on the basis of an average truck speed of 40 mph. Pinion speed equals the wheel speed times the axle ratio.

Differential speed factor (SF)—1.160
Pinion speed factor (SF)—0.637

Tapered roller bearings are rated at a speed of 500 rpm. Thus, the speed factor is 1.0 at 500 rpm. For the effect on bearing life at any other speed, a speed factor of (500 divided by the actual operating speed)$^{0.3}$ is used to modify the radial equivalent load in order to obtain the required radial rating in the same terms as the bearing basic radial rating.

Application factor (AF)
Differential bearings—1.65
Pinion bearings—1.0

The application factors are used to compensate for the variation in operating conditions such as shock, continuous duty, and inequality of loading.

Rotation factor, cone—1.0

In this application the cones are the rotating members, therefore, there is no modification.

Tractive effort (TE)—1400 lb

Tractive effort (TE) is a function of the gross vehicle weight and equivalent grade for this truck. This equivalent grade includes consideration for actual average grade, frictional resistance, rolling resistance, wind resistance, and accelerating forces. The tractive effort is taken from the curve shown in Fig. 37.

Mean pitch diameter of hypoid gear ($D_M{}^G$)
$D_M{}^G = D_P{}^G - (F_G \times \sin \text{ root angle of gear})$
$= 16.625 - (2.0 \times .969) = 14.68$ in.
Mean pitch radius of the hypoid gear
$= (1/2\ D_M{}^G) = 7.34$ in.

On hypoid gears the generally accepted mean pitch diameter is taken half-way down the gear tooth face on the gear root angle.

Mean pitch diameter of the hypoid pinion ($D_M{}^P$)

$$D_M{}^P = \frac{D_M{}^G}{\text{axle ratio}} \times \frac{\cos \text{ spiral angle gear}}{\cos \text{ spiral angle pinion}}$$

$$= \frac{14.68}{7.4} \times \frac{0.830}{0.675} = 2.44 \text{ in.}$$

Mean pitch radius of hypoid pinion ($1/2\ D_M{}^P$)
$= 1.22$ in.

On hypoid pinions the generally accepted mean pitch diameter is taken at the intersection of the mean pitch radius of the gear and the offset axis of the pinion. It is a function of the mean pitch diameter of the gear, the ratio, the spiral angle of the gear, and the spiral angle of the pinion.

Tangential force on the hypoid gear (TF^G)

$$TF^G = \frac{TE \times \text{tire diameter}}{D_M{}^G} = \frac{1400 \times 44.2}{14.68} = 4220 \text{ lb}$$

The tangential force on the gear is the result of the tractive effort on the rolling diameter of the tire resolved to the mean pitch diameter of the ring gear.

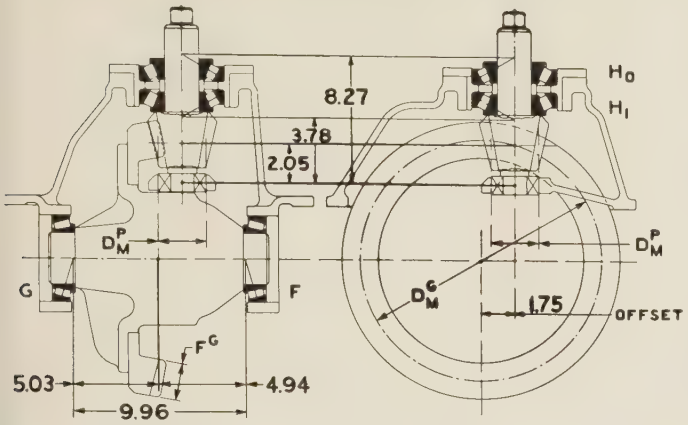

Fig. 39

Tangential force on the hypoid pinion (TF^P)

$$TF^P = TF^G \times \frac{\text{cos spiral angle pinion}}{\text{cos spiral angle gear}}$$
$$= 4220 \times 0.675/0.830 = 3430 \text{ lb}$$

The tangential force on the pinion is the tangential force on the gear converted to a force perpendicular to the spiral angle of the gear at the mean pitch circle, then converted to a tangential force on the pinion shaft perpendicular to the pinion axis.

Tangential force on the hypoid pinion in coast (TF_C^P)

$$TF_C^P = 70\% \ TF^P$$
$$= 70\% \times 3430 = 2400 \text{ lb}$$

Hypoid gear loads:

Gear thrust drive (T_{TF}^G)

$$T_{TF}^G = \frac{4220}{0.830} \times (0.430 \times 0.969 - 0.558 \times 0.246) = 1425 \text{ lb}$$

Gear radial drive (S_{TF}^G)

$$S_{TF}^G = \frac{4220}{0.830} \times (0.430 \times 0.246 + 0.558 \times 0.969) = 3290 \text{ lb}$$

Pinion thrust coast ($T_{TF_C}^P$)

$$T_{TF_C}^P = \frac{2400}{0.675} \times (0.399 \times 0.240 - 0.738 \times 0.971) = -2200 \text{ lb}$$

Pinion radial coast ($S_{TF_C}^P$)

$$S_{TF_C}^P = \frac{2400}{0.675} \times (0.399 \times 0.971 + 0.738 \times 0.240) = 2010 \text{ lb}$$

Pinion thrust drive (T_{TF}^P)

$$T_{TF}^P = \frac{3430}{0.675} \times (0.430 \times 0.240 + 0.738 \times 0.971) = 4160 \text{ lb}$$

Pinion radial drive (S_{TF}^P)

$$S_{TF}^P = \frac{3430}{0.675} \times (0.430 \times 0.971 - 0.738 \times 0.240) = 1225 \text{ lb}$$

Formulas for the values of the axial thrust and the separating component of the radial load for both driving and driven gear members are well established in reference material for both left- and right-hand spiral-angle hypoid gears, as shown in Table 2.

Bearing Selections (tentative):

The selections are tentatively made on the basis of dimensional requirements and K factor range. The K factor range for the differential positions is from 1.0 to 1.70 and for the pinion positions from 0.55 to 1.05.

Position	Cone No.	Cup No.	BRR	K
Differential right hand—F	47890	47820	7300	1.14
Differential left hand—G	47890	47820	7300	1.14
Pinion front outer—H_O	H913842	H913810	6850	0.65
Pinion front inner—H_I	H913842	H913810	6850	0.65

Bearing radial loads:

$$R_F = \sqrt{\left(\frac{4220 \times 5.03}{9.96}\right)^2 + \left(\frac{3920 \times 5.03}{9.96} - \frac{1425 \times 7.34}{9.96}\right)^2} = 2215 \text{ lb}$$

$$R_G = \sqrt{\left(\frac{4220 \times 4.93}{9.96}\right)^2 + \left(\frac{3290 \times 4.93}{9.96} + \frac{1425 \times 7.34}{9.96}\right)^2} = 3400 \text{ lb}$$

$$R_{C^HO} = \sqrt{\left(\frac{2400 \times 2.05}{8.27}\right)^2 + \left(\frac{2010 \times 2.05}{8.27} - \frac{2200 \times 1.22}{8.27}\right)^2} = 620 \text{ lb}$$

$$R_{H_I} = \sqrt{\left(\frac{3420 \times 2.05}{3.78}\right)^2 + \left(\frac{1225 \times 2.05}{3.78} + \frac{4160 \times 1.22}{3.78}\right)^2} = 2745 \text{ lb}$$

The bearing radial loads are based on the effective spread centers of the tentatively selected bearings.

Bearing radial equivalent loads:

$$RE_F = R_F = 2215 \text{ lb}$$

$$RE_G = 0.53 \times 3400 + 1.14 \ (0.47 \times 2215/1.14 + 1425) = 4470 \text{ lb}$$

$$RE_{C^HO} = 0.53 \times 620 + 0.65 \times 2200 = 1760 \text{ lb}$$

$$RE_{H_I} = 0.53 \times 2745 + 0.65 \times 4160 = 4155 \text{ lb}$$

The radial equivalent load (RE) is an imaginary radial load which would result in the same endurance life to the bearing as would be obtained from the actual radial and thrust loads acting simultaneously. When the series of the opposed bearings are the same but one bearing carries most of the radial load, the induced thrust reaction must be carried by the other bearing, in this case the G bearing. In the case of the H_I drive and H_O coast, the applied thrust from the pinion is great enough to overcome the induced thrust and to seat the bearings definitely (the inner bearing in drive and the outer bearing in coast); therefore, the applied thrust is combined with the radial load to form a radial equivalent (RE) load.

A radial load applied to a single tapered roller bearing induces a thrust load in the magnitude of $\left(\frac{0.47 \times \text{radial load}}{K \text{ Factor}}\right)$ in which the K factor equals the basic radial rating divided by the basic thrust rating of the bearing, and the 0.47 equals a constant derived

Table 2—Formulas for Values of Axial Thrust and Separating Component of Radial Load

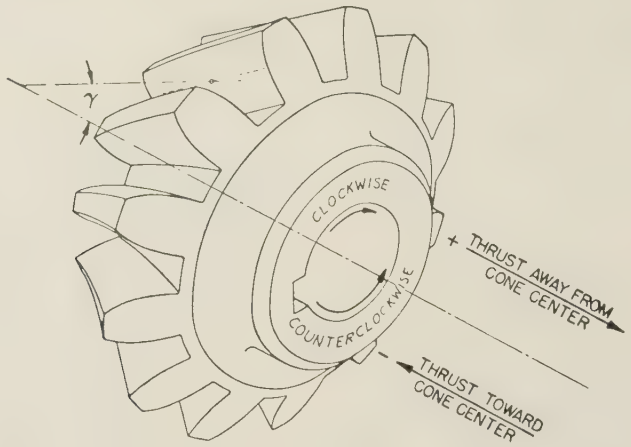

driving member rotation	value of axial thrust	value of separating component of radial load
RH Spiral—Clockwise or LH Spiral—Counterclockwise	**driving member** $T_{TF} = \frac{TF}{\cos\psi}\left(\tan\phi\sin\gamma - \sin\psi\cos\gamma\right)$	**driving member** $S_{TF} = -\frac{TF}{\cos\psi}\left(\tan\phi\cos\gamma + \sin\psi\sin\gamma\right)$
	driven member $T_{TF} = \frac{TF}{\cos\psi}\left(\tan\phi\sin\gamma + \sin\psi\cos\gamma\right)$	**driven member** $S_{TF} = -\frac{TF}{\cos\psi}\left(\tan\phi\cos\gamma - \sin\psi\sin\gamma\right)$
RH Spiral—Counterclockwise or LH Spiral—Clockwise	**driving member** $T_{TF} = \frac{TF}{\cos\psi}\left(\tan\phi\sin\gamma + \sin\psi\cos\gamma\right)$	**driving member** $S_{TF} = -\frac{TF}{\cos\psi}\left(\tan\phi\cos\gamma - \sin\psi\sin\gamma\right)$
	driven member $T_{TF} = \frac{TF}{\cos\psi}\left(\tan\phi\sin\gamma - \sin\psi\cos\gamma\right)$	**driven member** $S_{TF} = \frac{TF}{\cos\psi}\left(\tan\phi\cos\gamma + \sin\psi\sin\gamma\right)$

note: (Use the value of the angles ψ, ϕ and γ for the particular gear for which the force is determined.)

where

TF = tangential force.

T_{TF} = axial thrust load.

S_{TF} = separating component of radial load.

ϕ = normal pressure angle taken on the driving side of the tooth.

ψ = spiral angle.

γ = pitch angle on spiral gears but in hypoid gears it is taken as the face angle of the pinion or root angle of the gear.

In straight, zerol and spiral bevel gearing the pinion tangential force, TF^P, is equal to the gear tangential force, TF^G. However, in hypoid gearing the tangential force on the pinion, TF^P, is determined from the following equation:

$$TF^P = \frac{TF^G \cos\psi^P}{\cos\psi^G}$$

where: ψ^P = pinion spiral angle.

ψ^G = gear spiral angle.

The mean working diameter of a hypoid pinion, D_M^P, is calculated from the mean working diameter of the gear, D_M^G, as follows

$$D_M^P = D_M^G \times \frac{N^P}{N^G} \times \frac{\cos\psi^G}{\cos\psi^P}$$

where:

N^P = number of teeth in pinion.

N^G = number of teeth in gear.

ψ^G and ψ^P are spiral angles of gear and pinion, respectively.

from the summation of the thrust component from the individual rollers supporting the radial load. By observation it can be seen that the induced thrust and applied thrust loading on bearing G is greater than on bearing F.

$$\frac{0.47 \times R_G}{K_G} + \text{applied thrust } (T_{TF}{}^G) \text{ is greater than } \frac{0.47 \times R_F}{K_F}$$

or:

$$\frac{0.47 \times 3400}{1.14} + 1425 \text{ is greater than } \frac{0.47 \times 2215}{1.14}$$

or:

$$1400 + 1425 = 2825 \text{ lb is greater than } 915 \text{ lb}$$

Therefore, G must carry a combined radial and thrust loading while F carries only the radial loading.

The rotation factor for the rotating cones in this application is 1.0, which means that it will have no effect on the RE loadings.

The bearing F, which does not carry the resultant thrust loading is calculated on strictly its radial loading.

The G bearing, which carries both the induced thrust from F and the applied thrust from $T_{TF}{}^G$, is calculated on its combined loading. According to the basic formula: $0.53 \times R_G + K_G \times$ thrust on G (which includes induced thrust from F and applied thrust) $= RE_G$, the calculation is made as follows:

$$RE_G = 0.53 \times R_G + K_G \left(\frac{0.47 \times R_F}{K_F} + T_G \right)$$

$$= 0.53 \times 3400 + 1.14 \left(\frac{0.47 \times 2215}{1.14} + 1425 \right)$$

$$= 4470 \text{ lb}$$

The straddle-mounted pinion bearing mounting presents two cases, one in drive and one in coast, where the applied thrust is greater than the induced thrust as follows:

$$0.53 \times R_{H_O} + K_{H_O} \times T_{TF_C}{}^P = RE_{C^{H_O}} \text{ (in coast)}$$

$$0.53 \times 620 + 0.65 \times 2200 = 1760 \text{ lb}$$

$$0.53 \times R_{H_I} + K_{H_I} \times T_{TF}{}^P = RE_{H_I} \text{ (in drive)}$$

$$0.53 \times 2745 + 0.65 \times 4160 = 4155 \text{ lb}$$

All the various modifications of the basic radial equivalent load formula for both rotating cone and for rotating cup applications are shown in Table 1.

$$\text{Bearing required radial ratings (RRR)} = \frac{RE \times AF}{SF}$$

$$RRR_F = 2215 \times 1.65/1.160 = 3150 \text{ lb}$$

$$RRR_G = 4470 \times 1.65/1.160 = 6350 \text{ lb}$$

$$RRR_{C^{H_O}} = 1760 \times 1.0/0.637 = 2760 \text{ lb}$$

$$RRR_{H_I} = 4155 \times 1.0/0.637 = 6520 \text{ lb}$$

The calculation for the required radial rating is a step which converts the actual load on the bearing at an actual average speed into the same terms as the basic radial rating at 500 rpm, so that a direct comparison can be made. This step also takes into consideration the type of application by the use of a predetermined application factor (AF).

Bearing Loading Analysis:

Position	Cone No.	Cup No.	Rpm	RRR	BRR	% Load
Differential right hand F	47890	47820	304	3150	7300	43
Differential left hand G	47890	47820	304	6350	7300	87
Pinion front Outer H_O	H913842	H913810	2250	2760	6850	40
Pinion front Inner H_I	H913842	H913810	2250	6520	6850	95

Required radial rating/basic radial rating = % bearing loading. In automotive practice we endeavor to hold the loading for average operating conditions to 100%.

Bearing Mounting

Mounting the tapered roller bearing properly has much to do with its life expectancy. A number of factors contribute to a good bearing mounting regardless of whether it is a direct or indirect type. These factors are alignment, bearing seat finishes, fits of cone on the shaft and cup in the housing, and proper adjustment.

Bearing Alignment—Tapered roller bearing cone and cup seats must be properly aligned. A total indicator reading or runout of 0.001 in. per in. of bearing spread is the maximum acceptable limit. It should be remembered that runout is twice the eccentricity; therefore, the maximum accepted eccentricity is 0.0005 in. per in. of bearing spread. The bearing spread is measured from center of roller to center of roller. Misalignment reduces bearing capacity and life because the rollers are not properly seated, resulting in roller end loading. The concentration of a heavy load on small areas of cups and cones results in early fatigue failures, while the concentration of loads on the roller ends results in chipping and early failure of the bearing. The major causes of misalignment, as shown in Fig. 40, are that the cup bores are parallel but out of line, the bores are off parallel, or that the shoulder of the cup seat or cone shaft shoulder are not square with the bear-

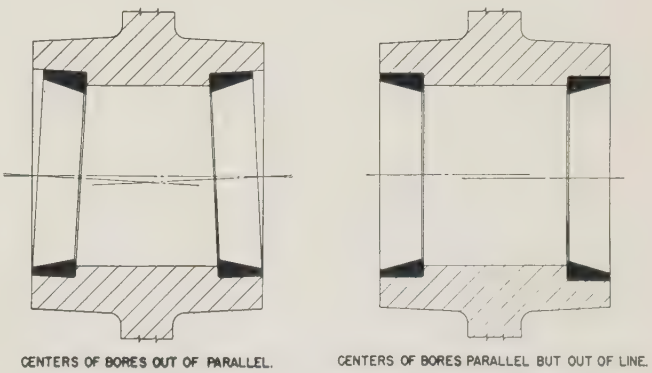

CENTERS OF BORES OUT OF PARALLEL. CENTERS OF BORES PARALLEL BUT OUT OF LINE.

Fig. 40

Table 3—Recommended Fits for Automotive Applications

recommended cone fitting practice

industry	type of application		cone bore					
			5/8" to 2 1/2" inclusive			over 2 1/2"		
			tolerance	recommended fit	cone seat equals nominal cone bore	tolerance	recommended fit	cone seat equals nominal cone bore
automotive rotating shafts	pinion, transmission, rear wheels, cross shaft, transfer case	adj. cones	+.0005 —.0000	.0010 tight .0000 tight	+.0010 max. +.0005 min.	+.0010 —.0000	.0015 tight .0005 loose	+.0015 max. +.0005 min.
		non-adj. cones	+.0005 —.0000	.0015 tight .0005 tight	+.0015 max. +.0010 min.	+.0010 —.0000	.0025 tight .0005 tight	+.0025 max. +.0015 min.
	differential	non-adj. cones	+.0005 —.0000	.0025 tight .0010 tight	+.0025 max. +.0015 min.	+.0010 —.0000	.0035 tight .0015 tight	+.0035 max. +.0025 min.
automotive stationary shafts	front wheels, full floating rear wheels, etc., trailer wheels	adj. cones	+.0005 —.0000	.0002 loose .0012 loose	—.0002 max. —.0007 min.	+.0010 —.0000	.0002 loose .0022 loose	—.0002 max. —.0012 min.

recommended cup fitting practice

industry	type of application		cup outside diameter								
			less than 3"			3" to 5" inclusive			over 5"		
			tolerance	recommended fit	cup seat equals nominal cup o.d.	tolerance	recommended fit	cup seat equals nominal cup o.d.	tolerance	recommended fit	cup seat equals nominal cup o.d.
automotive	front wheels, full floating rear wheels, pinion, differential	non-adj. cups	+.0010 —.0000	.0005 tight .0025 tight	—.0005 max. —.0015 min.	+.0010 —.0000	.0010 tight .0030 tight	—.0010 max. —.0020 min.	+.0010 —.0000	.0010 tight .0040 tight	—.0010 max. —.0030 min.
	differential	adj. cups	+.0010 —.0000	.0020 loose .0000 loose	+.0020 max. +.0010 min.	+.0010 —.0000	.0020 loose .0000 loose	+.0020 max. +.0010 min.	+.0010 —.0000	.0020 loose .0010 tight	+.0020 max. +.0000 min.
	rear wheels, transmission, cross shaft, other applications	adj. cups	+.0010 —.0000	.0010 loose .0010 tight	+.0010 max. +.0000 min.	+.0010 —.0000	.0010 loose .0010 tight	+.0010 max. +.0000 min.	+.0010 —.0000	.0020 loose .0010 tight	+.0020 max. +.0000 min.

ing axis. Fig. 41 shows how burrs or damage to the bearing seats also cause misalignment. Fig. 42 shows why life is reduced since the load is carried on only a small portion of the rollers and race.

Machine Finishes for Shafts and Housings—The cup and cone seats should be smooth and within specified tolerances for size, roundness, and taper. Ground finish is usually recommended for shafts wherever possible. The recommended finishes in micro-inches for ground cone and turned cup seat surfaces are as follows:

1. Ground cone seat—50 micro-in. rms maximum.
2. Turned cup seats—150 micro-in. rms maximum.

Bearing Seats—Careful study should have always be given to the selection of proper cone and cup fitting practice. Table 3 shows recommended fits for automotive applications. The table is self-explanatory. It is set up by application, size of cone or cup, whether the application is cone or cup adjusted, and whether the cone or cup is the rotating or stationary member. The table is for ground cone bores and turned cup seats in steel or malleable iron.

If the application requires that the cups be pressed into aluminum, the following procedure should be used. Cups should not be pressed into aluminum housings without contracting cups by freezing or expanding housing by heating or both, unless a special lubricant containing oil and graphite is used to coat the cup outside diameter and cup seat. If this is not done, the metal may be picked up as the cup is pressed into place, resulting in an unsatisfactory fit or off-square shoulder. Where the cups are mounted directly into aluminum, it is recommended that a minimum fit of 0.001 in. per in. of diameter be used.

Bearing Adjustment—One of the important advantages of tapered roller bearings is that they can be adjusted to suit the needs of the application and

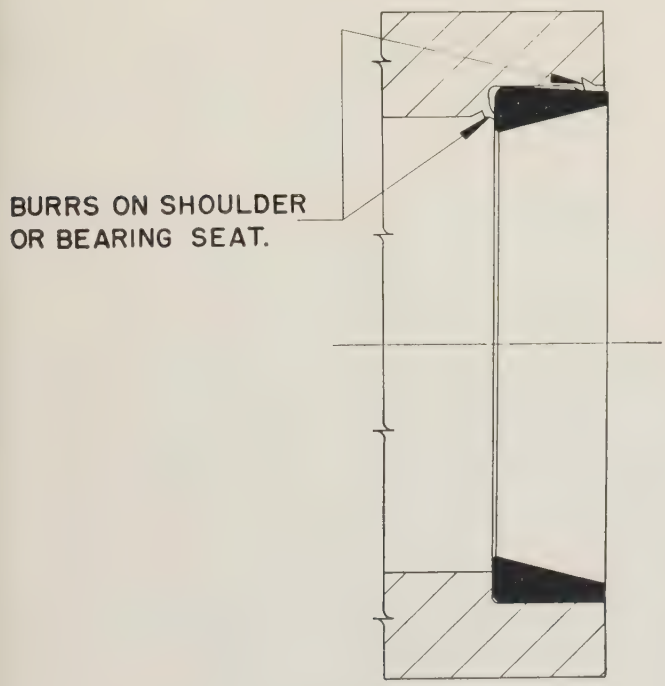

Fig. 41

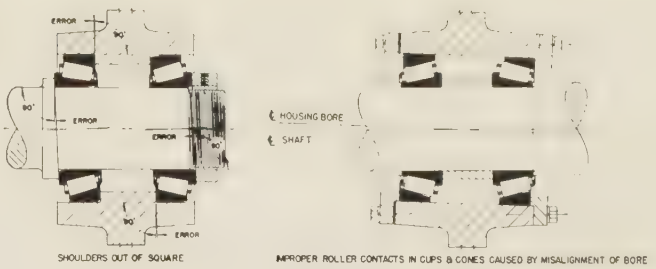

Fig. 42

to get the best all-around performance for the particular unit in which they are used. As far as the bearings themselves are concerned, the best setting is a free-running clearance with no appreciable end play. However, it is often necessary to hold shafts, gears, or spindles absolutely rigid to obtain satisfactory performance; in these cases the bearings can be seated with the necessary preload without penalizing the bearing. The amount of preload or the amount of end play in the bearings depends on the particular application in which the bearings are used. As a general rule, preloading of rotating bearing applications is not recommended where grease lubrication is used.

Lubrication and Seals

Lubrication—In tapered roller bearing applications, the lubricant serves several definite functions: it lubricates and reduces friction; it protects the bearing from corrosion and rust; it reduces operating temperature; and it aids the seal in excluding foreign matter from the bearing application. The design of the bearing and gear application and the environment and speed of their operation dictate the lubricant to be used.

Seals—The function of a lubricant seal is to keep the lubricant in the bearing application while excluding dirt and water. In dirty conditions, multiple seal units are often used.

Conclusion

Bearing mountings of a number of bearing applications have been shown. Some basic bearing formulas for tapered roller bearings have been presented and bearing mountings have been discussed.

Each type of antifriction bearing mounting has its own particular problems and the manufacturer should be consulted as to its proper application.

The importance of proper bearing selection, mounting, and lubrication in the application of antifriction bearings in heavy-duty axles cannot be emphasized too strongly.

Acknowledgment

We wish to give acknowledgment to the following companies for permission to use their axle prints in preparing mounting illustrations for this paper: Clark Equipment Co.; Dana Corp., Toledo Division; Eaton Mfg. Co.; Fruehauf Trailer Co.; General Motors Corp., Euclid Division; International Harvester Co.; Mack Trucks, Inc.; Shuler Axle Co., Inc.; Rockwell Spring and Axle Co., Timken-Detroit Axle Division, Wisconsin Axle Dixision; White Motor Co.

SHELL MOLDED

AMONG the many outstanding advantages of the shell molding process of casting crankshafts, as described here, are the following:

1. Manner in which entire process responds to a high degree of automation.
2. Close tolerances that can be maintained from casting to casting.
3. Raw sand requirements are reduced from 125 lb (previous method) to 20 lb.
4. Results in 70% reduction in weight of chips produced.
5. Resulting crankshafts have highest wear resistance and exceptional endurance.
6. Gives additional design leeway:
   - Allowing the most efficient distribution of weight.
   - Contributing to engine compactness by varying the casting contour to prevent potential interferences.

TO GAIN a complete perspective of the present use of shell molded crankshafts at Ford, it is necessary to go back to 1933, when the company introduced its first cast automotive crankshaft. Then, as now, the automotive industry was interested in manufacturing economies which, by virtue of the automotive volume, could be translated into substantial dollar savings. It was for this reason that the original cast crankshaft was conceived and that the two-step evolution from forged to shell molded crankshaft began.

Traditionally, the crankshaft had been made by conventional forging techniques, and we had accumulated extensive manufacturing skill and facilities for forging of crankshafts. However, it became apparent that this method of obtaining the rough crankshaft, that is, forging, imposed severe requirements on the finishing (machining) operations. These included machining all surfaces, functional and nonfunctional alike, several straightening operations required to maintain bearing alignment during machining, and hardening operations to improve the wear resistance of any forgeable material.

It was with these primary considerations in mind that the cast crankshaft was contemplated. The prospect of greater design flexibility was another incentive. The casting first won engineering support when it was demonstrated that it was possible to counterweight more completely for couple balance, and to cast lightener holes in the bearings for improved rotational characteristics. Engineering support was further increased when subsequent tests demonstrated the greatly improved wear resistance and damping qualities characteristic of the crankshafts made by the new process.

Molding Using Stacked Slab Cores

A dry sand molding method was adopted after extensive investigation had led to the rejection of both green sand mold and permanent mold methods. As may be seen in Fig. 1, the method developed for obtaining four castings with a single set of foundry operations was ingenious enough to merit some description here.

In the pattern development, four vertical crankshaft patterns were grouped symmetrically about a central sprue. A series of horizontal cuts through the assembly yielded pattern subsections that were fastened and located in 16 metal core boxes in such a way that assemblies of cores produced from these boxes accurately reproduced a mold cavity for a crankshaft. From these patterns, oil bonded sand slab cores were made, baked, coated, and assembled in a partially mechanized setup.

A specially designed 1.5% carbon ferrous alloy was ladled from the electric melting furnaces to the central sprue formed in the stacked cores. The four castings so produced were automatically conveyed through a series of conventional cleaning operations to the heat-treat area. Here a unique 6-hr normalizing and spheroidizing heat-treatment relieved stresses and produced a microstructure consisting of a steely matrix with interspersed aggregates of graphite particles. As will be noted later, these graphite discontinuities acted as chip breakers to improve the machinability and imparted a certain self-lubricating quality to the bearing surfaces that reduced journal wear in service.

Our machine shops immediately benefited through the elimination of straightening and heat-treating operations as well as a drastic reduction in a number of machining operations. A battery of cheeking machines was eliminated and the finish stock removal dropped from 18 lb to 9.5 lb with a minute cost reduction of 20 min per crankshaft.[1] Tool consumption was sharply reduced as were floor space requirements.

Of equal importance were the many engineering advances resulting from the unique combination of this, then new, casting method and new engineering material. In many different areas, greater design

[1] SAE *Journal*, May, 1936, pp. 21–24, "How Ford V-8 Crankshafts are Cast and Machined," by W. F. Pioch.

CAST CRANKSHAFTS

H. N. Bogart and H. C. Grant, Ford Motor Co.

This paper was presented at the SAE Annual Meeting, Detroit, Jan. 15, 1957.

flexibility was made available to the engineer. These included:

- Lightening the bearings by coring to improve rotational characteristics and to eliminate the equivalent counterweighting mass.
- Couple balance for smoother engine operation through full counterweighting.
- Redistribution and reduction of weight by making counterweights thicker at their maximum distance from the axis of rotation.
- A wide range in the selection of bearing insert material as a result of the self-lubricating properties of the alloy.

The cast crankshaft process introduced in 1933 indeed represented a major technical advancement in the field of metallurgy and foundry engineering. Experience gained in the more than 15 years of operating this process pointed the way to certain major refinements in further improving the cast crankshaft as an engineered part.

Desired refinements to the process included:

- Providing a continuous supply of molten metal as a replacement for the batch process.
- A further reduction in the machining allowances which were typical of those required in normal casting operations.

As a result of these and other limitations, the process was periodically reviewed in the light of the more recent technical advances in the foundry. It was not unnatural then, that, when pilot work for casting the automotive valve in shell molds had demonstrated that castings could be produced with as little as 0.003–.007-in. finish stock on the stem diameter, and that completely automated operations could be envisioned, experiments would be initiated to extend this method to the production of crankshafts.

Shell Molding Process

The shell molding process itself consists of the following operations: A mixture of sand and thermosetting resin is emplaced on a preheated pattern. This mixture is allowed to remain in contact with the warm pattern until the resin has melted to form a rather gummy plastic mass. The excess unmelted sand mixture is then removed. To complete the curing of the resin, additional heat is applied until a hard thin shell is formed; this shell is removed from the warm pattern by some stripping mechanism. Stripping the rigid shell at this point results in a precise, reproducible mold component, upon which the close precision of the resultant castings are based. After the shells have been removed from the pattern, they are assembled and supported in a flask in such a manner as to give sufficient strength

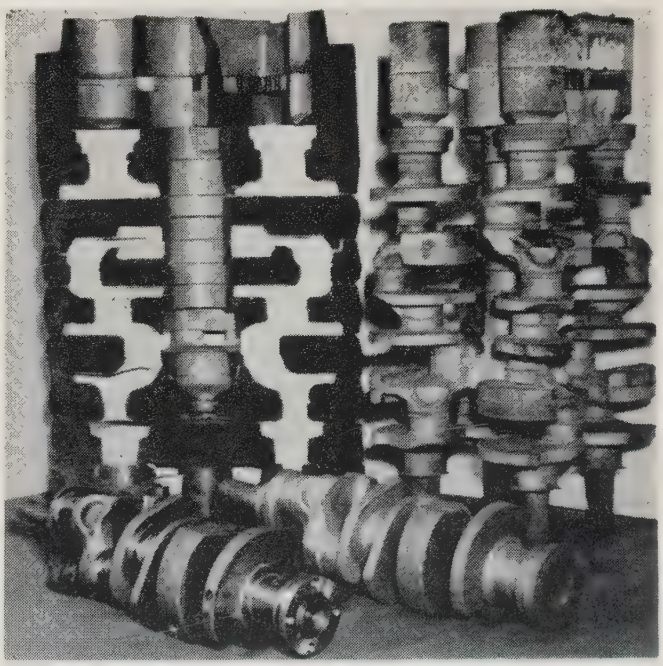

Fig. 1—Crankshafts made from stacked slab cores

Fig. 2—Shell-making turntable

Fig. 3—Raising dump box to heated pattern

to the shell to resist the pressure of the molten iron. We have used the so-called dump box adaptation of these shell molding procedures.

Shell molds for crankshafts are made on individual shell-making machines so mounted on a large turntable that the entire shell-making operation can be performed during a single rotation of the table.

Six individually activated shell molding machines are mounted about the periphery of this turntable, as shown in Fig. 2. The patterns are continuously cycled through the various stations, including preheating of the patterns, application of liquid parting agent, and dump coating the pattern with a mixture of sand and resin to form a 3/16-in. semiplastic shell. The coating and dumping operation is made possible by trunnion-mounting the pattern to allow it to rotate on a horizontal axis independent of the turntable rotation. (See Figs. 3 and 4.)

Final cure of the thin shell is accomplished as the shell-making machine is rotated under a radiant heater, as shown in Fig. 5.

The shell is automatically stripped from the pattern and manually transferred to the assembly table, as shown in Fig. 6.

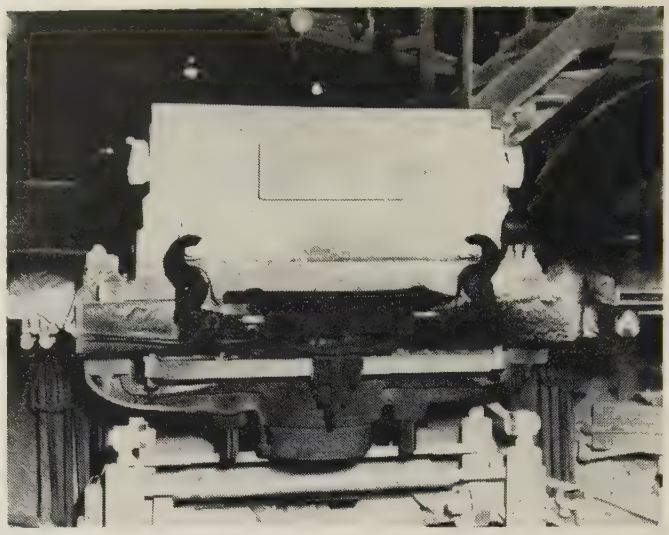

Fig. 4—Inverted dump box emplaces sand-resin mix on hot pattern

Since each pair of shells produces two crankshafts, each turntable rotation, requiring 2 min, makes shells for six crankshafts.

Unique pattern design allows complete interchangeability of all patterns for identical crankshafts. The casting symmetry is such that by mounting both pattern segments as right- and left-hand members of the pattern assembly, a single pattern can be used for both halves of a completed assembly. (See Fig. 7.)

In assembly, two randomly selected shells are joined together by spring-loaded clips and inserted into an open-top, bottom-hinged, basically rectangular flask mounted on the pouring line. (See Fig. 8.)

The flask is conveyed to the loading station, where an overhead gravity hopper drops commercial cleaning shot into the flask cavities to support the thin shell mold against the internal pressure of the molten iron. The flask is then advanced to the pouring station, where previously prepared molten nodular iron is poured into the molds.

The castings continue on the pouring line for an additional 30 min until they reach the shakeout station where the castings, plus gates and risers, are transferred to a cooling conveyor on which the castings proceed through a cleaning operation, break-off and inspection operations until they are delivered to the shipping station.

By comparison with conventional sand castings or the previous cast crankshaft, cleaning costs are at a minimum. While retaining all of the advantages of the previous casting method, additional process advantages have been realized by this new founding technique. Analysis of these advantages can be facilitated by separate examination of the advancements in the foundry and in the machine shop.

Advantages of Shell Molded Crankshafts

The outstanding advantage of the shell molded crankshaft as far as the foundry is concerned is the manner in which the entire process responds to a high degree of automation. The adaptation of automation begins in the melting area where nodular iron is produced continuously from advanced design cupolas and continues throughout the molding,

cleaning, and inspection operations. As demonstrated, the operations are so divided that an effective combination of mechanical activation and manual labor is possible.

Another major advantage relates to the very close tolerances that are maintained from casting to casting. This improved uniformity not only produces dimensionally near-perfect crankshafts, but allows effective use of quality control procedures for inspection, gaging, and metallurgical examination. This is particularly important in that no qualification of the locating points used in the machining operations is necessary.

Raw sand requirements for crankshaft manufacture have been reduced from 125 lb per casting in the previous casting method to 20 lb per casting using shell molding. This not only conserves what is becoming a near strategic mineral, that is, good foundry sand, but also greatly simplifies the problem of refuse sand disposal, with or without sand reclamation.

Of equal importance are several secondary considerations which allow more effective utilization of skilled foundry engineers. As we employ the process, uniform feeding characteristics are obtained. As a result, sound shrink-and-defect-free castings are consistently produced, and no major changes in pattern gating have been required during the last four years. Further, foundry engineering required to meet quality standards during model change-over has been substantially eliminated. Similarly, our experience has shown the process to require less pattern maintenance. None of the many patterns used in casting camshafts, crankshafts, and valves have been replaced because of excessive foundry wear.

A further very important benefit of shell molding to our specialty foundry, where shell molding is used exclusively, has been to provide vastly improved foundry conditions. Reduction in hard manual labor minimizing the amount of sand required in the molding system and the general cleanliness of the castings have contributed much to a cleaner, less fatiguing, quieter, safer, and healthier operation.

As a result of the many foundry advantages enumerated, the rough crankshaft as delivered to the machining operation is distinctly superior to that available from any other fabrication method. As

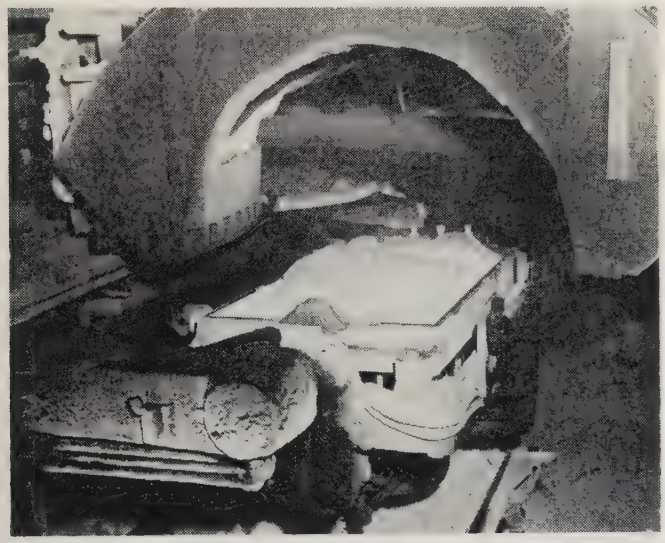

Fig. 5—Final cure of shell

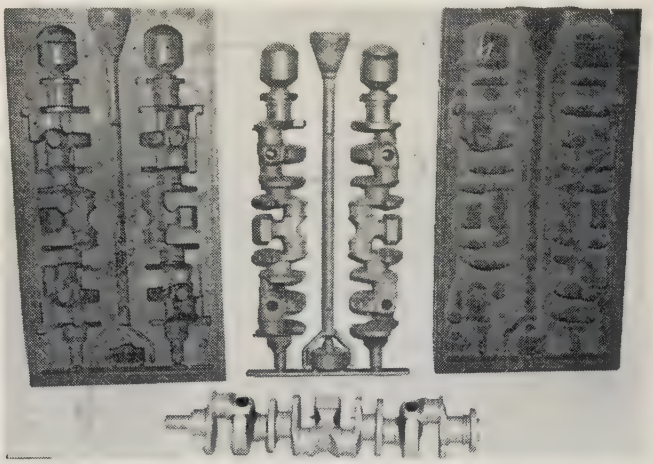

Fig. 7—Pattern gating

Fig. 6—Stripping and removing cured shell

Fig. 8—Loading of shell assemblies into flasks

in our previous practice, our manufacturing engineers have been able to utilize these process characteristics to reduce manufacturing cost even further. The increased precision of the casting has resulted in a reduction in the finish stock from 9.5 lb in the previous casting practice to 5.5 lb in the shell molding process. Thus, the complete transition from the forged shaft to the shell molded shaft has resulted in a 70% reduction in the weight of the chips produced. The influence of this spectacular reduction in total machining on machine cycle time and minute cost is obvious.

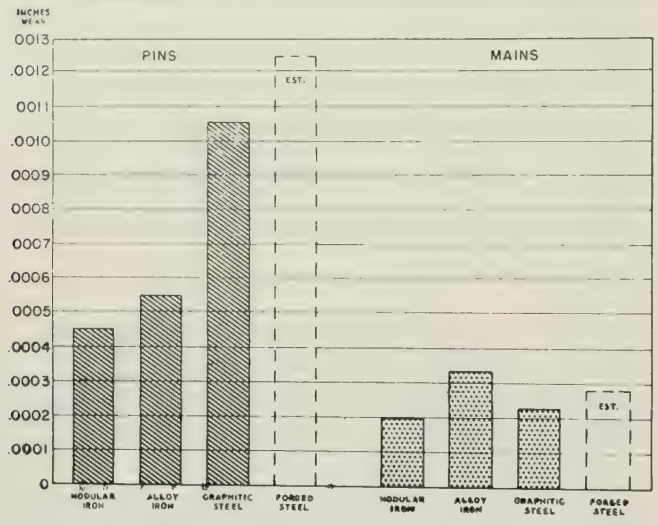

Fig. 9—Comparative wear on crankshaft journals (200 hr at 4000 rpm)

In the same area, moreover, additional advantages have accrued. Specifically, the increased precision with the absence of warpage allows fast traverse in many machining operations until actual contact is made between the tool and the work piece.

The closer tolerances available in this casting procedure also improve the balancing operation. Here, by very close control of the balance weight location, preliminary balance has been eliminated and final balance has been typically limited to drilling a $\frac{7}{8}$-in. diameter hole less than 1 in. deep into the two end counterweights.

Similarly, the centering operation itself has been so simplified by this careful control of mass location that the need for mass centering machines has been eliminated. Present practice uses geometric centering 100%.

The close tolerances to which these castings are held may be illustrated by reference to a recent model year where over one million crankshafts with an allowable 0.0285-in. clearance between the crank cheek outside diameter and the camshaft distributor gear were assembled into engines without machin-

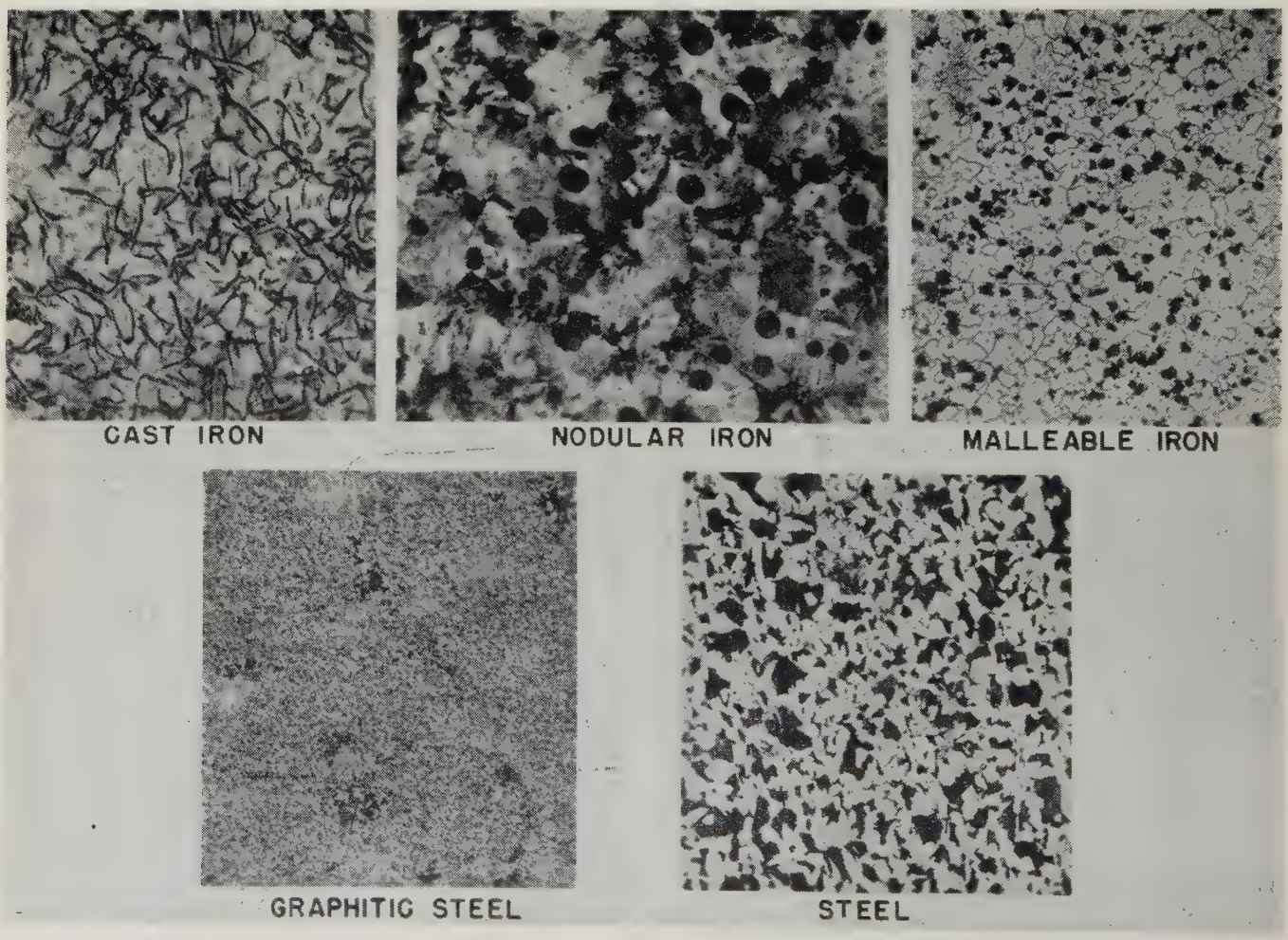

Fig. 10—Typical photomicrographs of ferrous cast materials (reduced from photomicrographs taken at 100x)

ing at this location. No single instance of interference was encountered.

A further benefit growing out of the very precise location of all portions of the casting has been a reduction of maintenance expenses due to tool and machine tool damage resulting from inadequate clearance during the machining operations.

It is obvious that each of these many advantages has contributed substantially to the reduction of cost in the machining area, especially as it affects the tool cost.

Another potent factor that influences tool cost—fortunately in the right direction—has been the absence of small sand particles in the casting skin as has been evidenced in many conventionally cast components.

As important as all of these processing advantages are, they have been accomplished with no sacrifice of engineering properties. In fact, many additional engineering advantages are available through this unique combination of nodular iron and shell molding.

The outstanding engineering property of the shell molded crankshaft is its wear resistance as shown in Fig. 9.

The shell molded crankshaft has the best wear resistance of any of the materials that have been historically used in our automotive crankshaft manufacture. This wear resistance is attributable to the self-lubricating property of the free graphite on the bearing surface, as shown in the photomicrographs (Fig. 10), which compare nodular iron with other commercial alloys. These advantages are achieved in a material whose physical properties compare in many ways to those of steel.

Detailed examination of Table 1 shows the comparison between typical minimum properties obtained from specimens from actual nodular iron crankshaft castings and separately cast specimens of cast iron, malleable iron, graphitic steel, and steel.

The typical chemical analysis in our crankshaft production is:

C	4.00%
Si	2.50%
Mn	0.50%
Cr	0.10%
S	0.010%
P	0.05%
Mg	0.019%

Data illustrating the consistent physical properties obtained with nodular iron are shown in Figure 11. These data are a tabulation of 125 quality determinations from samples machined from actual crankshafts. A second important engineering characteristic is the exceptional endurance of the shell mold crankshafts, based on simulated service tests and field results. These outstanding results are an outgrowth of a combination of factors including the improved damping characteristics of the graphite-rich material, the absence of casting defects such as shrinkages and blows, and the combination of sound design with good manufacturing procedure.

A third valuable engineering advantage is the additional design leeway that the precison cast crankshaft gives:

- Allowing the most efficient distribution of weight.
- Contributing to engine compactness by varying the casting contour to prevent potential interferences.

A fourth advantage has been in the improved, consistent balance attainable at a minimum cost. This eliminates drilling balance holes, or grinding for balance, in critical areas without adequate care to prevent weakening the entire component, leading, and other salvage expedients used to obtain physical balance.

Conclusion

The entire history of the cast crankshaft within our company has been one of active cooperation between manufacturing and product engineering and illustrates the benefits available through the intelligent use of advanced and improved manufacturing technology guided by the sound principles of engineering.

Without an awareness of the advantages of such new manufacturing processes on the part of the product engineer and designer, and a desire to assist in such approaches as were necessary to bring this development to complete fruition, the progress to date would not have been possible. In this area, as in many others, we are merely at the threshold of new manufacturing techniques. The rate at which we will advance from our present skill is not only dependent upon the ingenuity of production and manufacturing engineering personnel, but also to a considerable extent upon the ability of manufacturing and product engineering groups to weld their own ideas and objectives into a common goal.

Table 1—Chemical and Physical Properties of Ferrous Cast Materials

	Cast Iron (Flake Graphite)	Nodular Iron (Nodular Graphite)	Malleable Iron	Graphitic Steel	Steel
Chemical Analysis:					
Carbon	3.50	3.50	2.50	1.50	0.30
Manganese	0.70	0.70	0.35	0.80	0.70
Silicon	2.50	2.50	1.25	1.00	0.40
Magnesium		.020			
Physical Properties:					
Yield Point, psi		65,000	32,500	80,000	35,000
Tensile Strength psi	30,000	90,000	50,000	105,000	65,000
Elongation, %		2	10	3	24
Modulus of Elasticity, psi	17,000,000	22,500,000	25,000,000	28,500,000	30,000,000

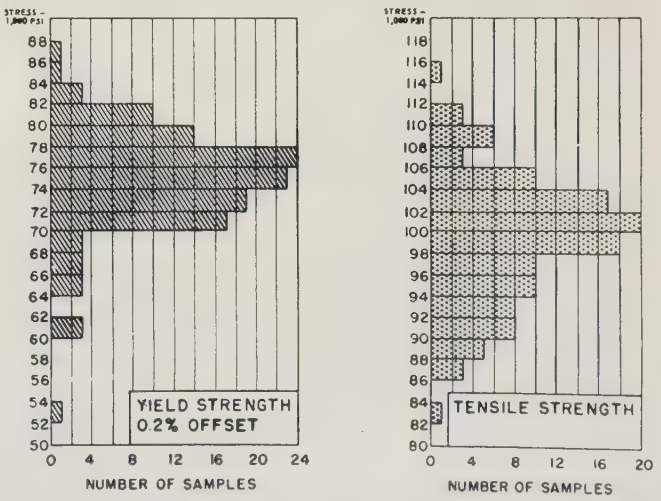

Fig. 11—Mechanical properties of nodular iron (125 samples taken from crankshafts as cast over 25-week period)

THE MWM . . . Balanced-Pressure for High-Speed

IT SEEMS very essential that the economic advantages of the diesel engine be secured and increased by achieving a considerable tolerance in variation of fuel. By means of the Motoren-Werke Mannheim balanced-pressure precombustion-chamber system it has been possible to obtain a considerable tolerance in variation of fuel for both aircooled and water-cooled engines. In addition, and more particularly for aircooled diesel engines, diesel knock has been eliminated, thus contributing to greatly improved quietness of operation. The new combustion system allows a low fuel consumption of an engine with direct injection of fuel as well as excellent starting qualities down to lowest temperatures.

General Requirements of High-Speed Diesel Engines

High-speed engines are sensitive to fuel quality because of their higher speed and the resultant shorter period required for induction and mixing of air and fuel.

An increase in the consumption of diesel fuel and turbine fuel (a fraction of the latter belongs partly to the field of diesel fuel) makes it desirable to enlarge the gain by extending the diesel fraction both to a higher boiling point and to the more volatile fuels. There is little doubt that the most economical fuel would be one which yields all kinds of fuels from volatile gasolines to heavy oils by distillation to approximately 950 F. This can be achieved only if the high-speed diesel engine is able to operate without loss of capacity or other disadvantages. For further development, therefore, it may reasonably be claimed that diesel engines, including high-speed diesel engines, be made to a large extent independent of fuel requirements.

The tolerance for variation in fuel quality should under no circumstances increase running noise or engine wear. Attempts should be made to avoid, if possible, diesel knock with all its attendant drawbacks by introducing measures regarding combustion and technical procedure.

Most Important Combustion Systems

There are two main problems in the development of high-speed diesel engines: combustion and the mixture of fuel and air. The high air speeds caused by higher rpm greatly facilitate mixing of fuel and air. For this reason the development of high-speed engines has taken various different paths, two of which are clearly distinguishable: First, controlling primarily the mixture formation and through it the combustion process (direct-injection system); secondly, direct control over the combustion process of a mixture already formed (precombustion-chamber system). The present swirl-chamber system can be regarded as a combination of individual characteristics of the two previously mentioned systems.

The fuel injected into the precombustion chamber, which is separated from the main combustion chamber, is ignited by the heat reflected from the walls and creates a rise in pressure. This rise in pressure drives the main part of the still unburned fuel through relatively narrow bores into the main combustion chamber, where it is mixed with the available oxygen of the combustion air and almost completely burned. Without going into details concerning the oxidation process, it can be said that mixing

Precombustion Chamber System Diesel Engines

Hans L. Hockel, Motoren-Werke Mannheim AG, Germany

This paper was presented at the SAE Summer Meeting, Atlantic City, June 7, 1957.

THE PROBLEM of using light and heavy fuels other than diesel in diesel engines is becoming increasingly important. With the hitherto known combustion systems it has not always been practicable to use the heavy fractions or the highly volatile fuels such as high-octane gasoline in high-speed diesels.

This article describes the MWM balanced-pressure precombustion system, which has been designed especially to tolerate a wide variety of fuels. The author examines the performance of three systems (direct injection, swirl chamber, and the MWM system) in relation to combustion and fuel influence.

According to the author, the advantages of the MWM balanced-pressure precombustion chamber are: (1) Relatively simple construction, adaptable to both aircooled and water-cooled engines; (2) controlled and thus smoother combustion with moderate firing pressure, enabling higher output even when bearing load remains the same; (3) quiet running by elimination of diesel knock; (4) favorable fuel consumption with excellent part-load performance; (5) cold-starting properties are virtually the same as in engines with direct injection; (6) nearly the same output and same fuel consumption independent of type and quality of fuel.

of fuel and air results not only from the mechanical mixing of the liquid fuel molecules with air, but also from a reinforcement of diffusion caused by thermo and chemical processes. This process can be called a mechanical and thermal mixture of fuel and air. Generally, induction periods are shorter than on engines with direct injection. It is known that the performance of diesel engines equipped with this combustion system is smooth and quiet with a relatively low rise in pressure. They are more

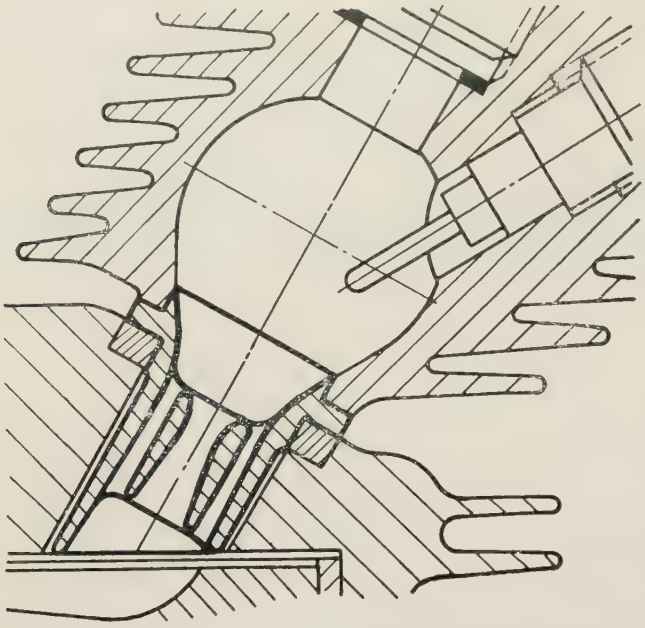

Fig. 1—Design features of new MWM balanced-pressure precombustion chamber for aircooled diesel engine

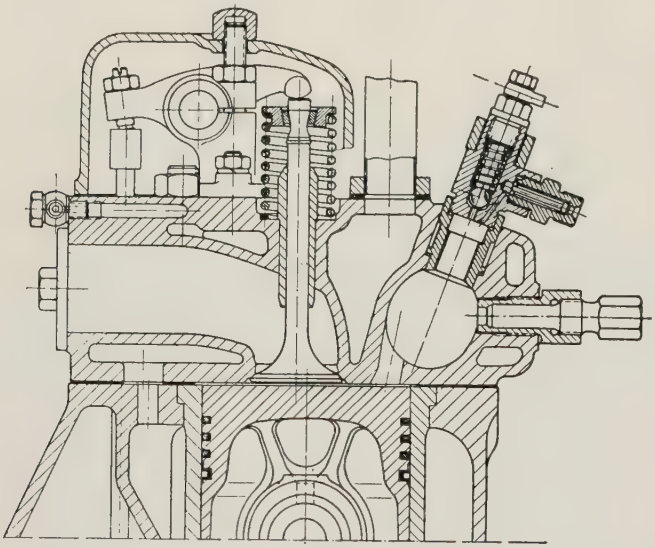

Fig. 2—Section through combustion chamber of water-cooled swirl-chamber engine (W) type KD 12

tolerant with regard to fuel quality than engines with direct injection and can, in addition, bear heavier loads and have favorable exhaust gas behavior. They are more suitable for higher rpm, since the combustion process can be controlled easily. The most striking disadvantage in the precombustion-chamber system is the generally higher fuel consumption. The rather inferior cold-starting properties can be offset by easily insertable glow plugs or ignition paper inserts. In contrast to the precombustion-chamber system, the fuel jet is injected directly into the main combustion chamber in the direct-injection system. In this way the most suitable and best possible atomization of the fuel jet is achieved. Self-ignition takes place after a relatively long ignition lag following thorough mixing of the particles of fuel with the combustion air, the process of mixing fuel and air here being purely mechanical. The large quantity of fuel injected during ignition lag burns at a higher rate when pressure rise increases. The rate of pressure rise and the firing pressure become more unfavorable as the control over injection becomes less, that is, the higher the rpm, the shorter the available time. Not only does the high pressure rise increase stress on nearly all moving parts, but vibration and noisy running cannot be eliminated. The main advantages of this system are low fuel consumption and easy starting without additional aid.

The swirl-chamber system embodies certain individual characteristics and functions of both systems. Output and consumption values lie roughly between those of the two systems, although ignition lag, combustion process, and smooth running are similar to the direct-injection system.

MWM System

The air-compressing system with self-ignition combustion is usually influenced by injecting only a small quantity of fuel during the induction period. The reaction causes a temperature rise which then starts a further reaction in the remaining fuel. The induction periods depend on the structure of the fuel and differ considerably with the employment of the various fuels produced by crude oil distillation. The use of these fuels in an engine operating under approximately the same conditions of combustion and working efficiency presupposes a similar performance of the various fuels in relation to the induction period and speed of reaction.

The induction period and the speed of reaction represent not only structural values, but also can be greatly influenced by fuel concentration and composition and particularly by temperature. The application of the knowledge gained hereby resulted in a combustion system which will be discussed in this paper. By comparing the various combustion systems an attempt will be made to justify the views already expressed.

The system can be appropriately designed to suit water-cooled and aircooled engines with high rpm. Fig. 1 shows the combustion chamber of an aircooled diesel engine (bore = 3.86 in., stroke = 4.72 in.) with an engine speed of 2600 rpm. The combustion chamber is divided into two parts: (a) the part above the piston and (b) the precombustion chamber proper. The precombustion chamber is fitted in the cylinder head and connected to it by only a comparatively small heat-conducting conduit. Thus, the heating of the cylinder head is reduced to a minimum. The precombustion chamber is connected with the main combustion chamber by an inserted burner. The internal diameter of the burner is wide enough to avoid any appreciable choking or back pressure. The through-flow passage of the burner is divided into interior and exterior parts, proportionate to one another. This construction enables simple design of the cylinder head and

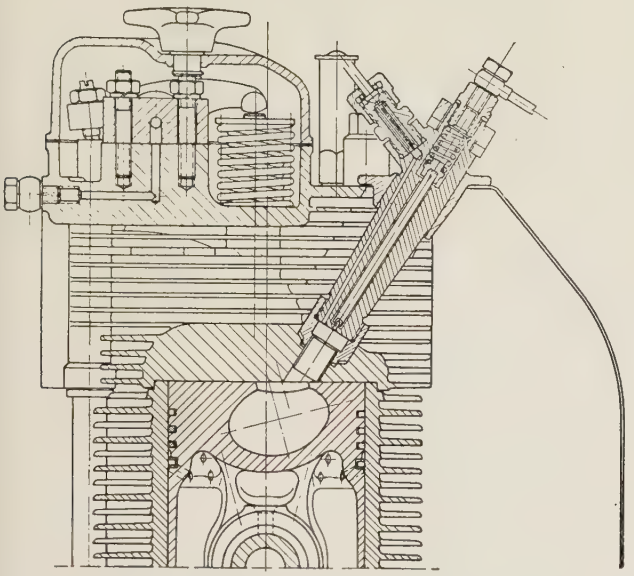

Fig. 3—Section through combustion chamber of aircooled diesel engine with direct fuel injection (K) type AKD 12

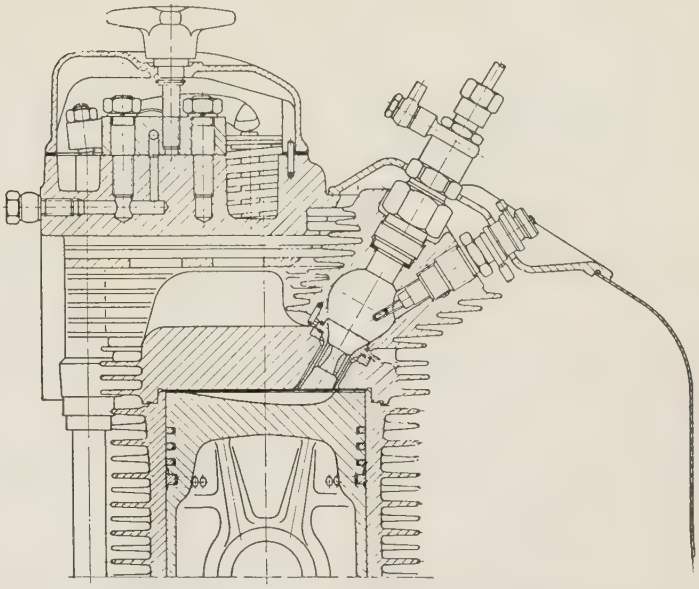

Fig. 4—Section through combustion chamber of aircooled diesel engine with MWM balanced-pressure precombustion chamber (GV)

the piston. The heat dissipation properties in the piston enable it to be highly overcharged, thus increasing working efficiency.

Without going into details, the function can be explained in the following manner. During compression, the air flows at a moderate speed through the exterior passages of the burner into the precombustion chamber. The fuel is injected through the interior bore of the burner, which has a certain temperature. A very short time after contacting the interior wall of the burner, the fuel undergoes a simultaneous evaporation and partial reaction, which starts the main combustion process. The process of mixing is assisted greatly by intensive fuel evaporation and increased diffusion. Almost smokeless combustion results. It is noteworthy that the combustion process begins after a very short induction period without unfavorably influencing the thermodynamic efficiency or the fuel consumption. This is explained by the fact that the combustion process in the combustion zone is undisturbed by air currents. The CO_2 thus generated is very important because of its ability to slow down reaction. The extremely smooth combustion process can be best understood by reference to the indicated diagram discussed later in the paper. The rate of pressure rise is somewhat lower than the compression values. The performance of the engine when using various fuels and the starting properties will be outlined later.

Combustion Process of Different Combustion Systems

The essential difference in combustion can best be demonstrated by examining three diesel engines fitted with swirl chamber, direct injection, and with the new combustion system. Data concerning each engine are as follows:

Swirl chamber (W)—bore 3.75 in., stroke 4.72 in., water-cooled.

Direct injection (K)—(piston combustion chamber)—bore 3.86 in., stroke 4.72 in., aircooled.

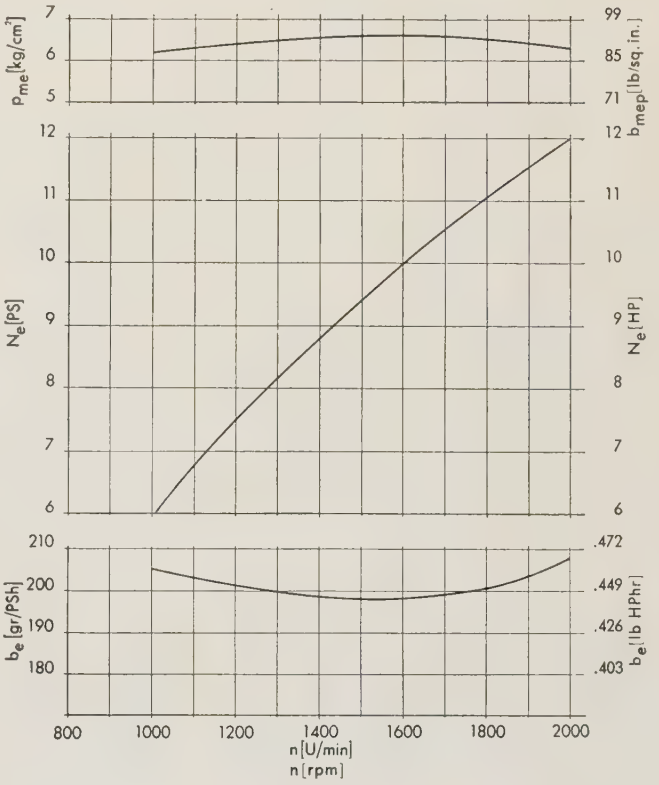

Fig. 5—Output and fuel consumption data of engine W in Fig. 2

Balanced-pressure precombustion chamber (GV)—bore 3.86 in., stroke 4.72 in., aircooled.

Figs. 2–4 show the construction of the combustion chambers in each case. The test was carried out on single-cylinder engines running up to 2200 rpm. The different output and consumption data may be

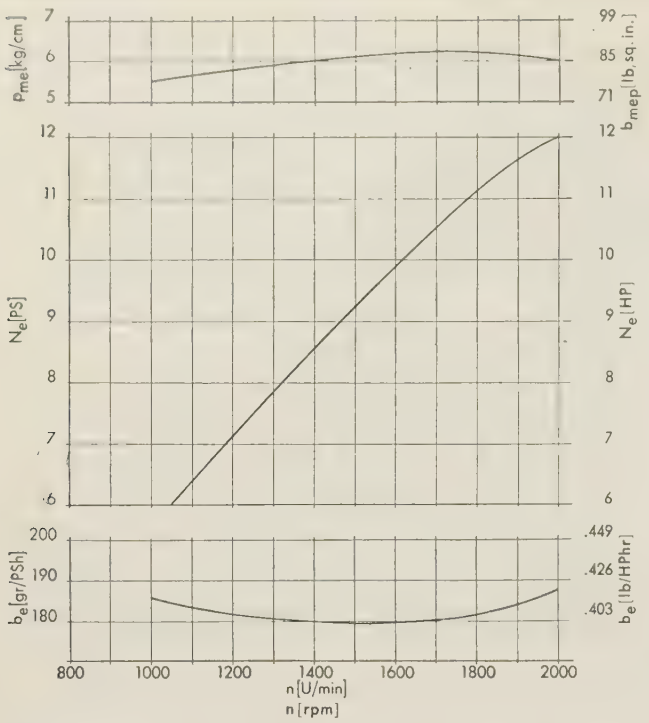

Fig. 6—Ouptut and fuel consumption data of engine K according to Fig. 3

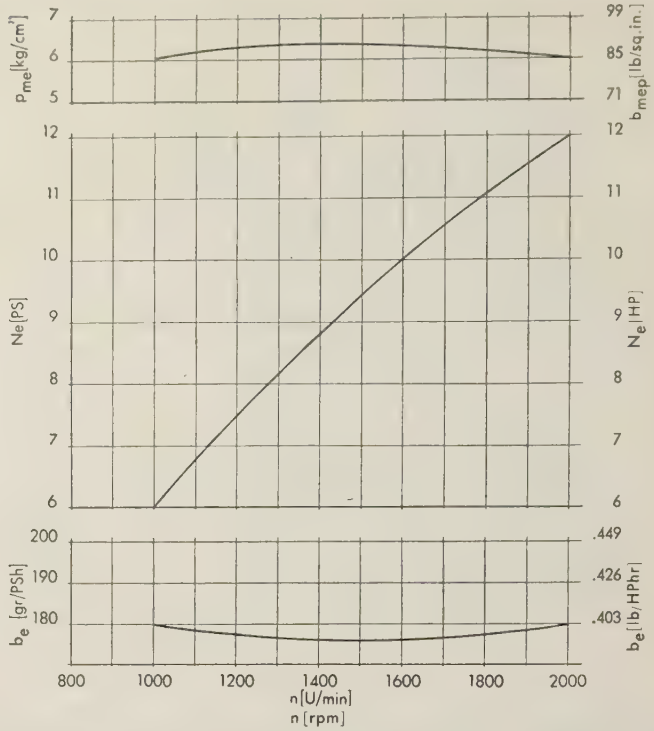

Fig. 7—Output and fuel consumption data of engine GV according to Fig. 4

seen in Figs. 5–7, working at the same degree of mechanical efficiency ($\eta = 0.72$) in all three engines. The result was that fuel consumption in an engine with balanced-pressure precombustion chamber was not only the same but even slightly lower than that in an engine with direct injection. On the other hand, the specific consumption in an engine with swirl chamber is rather higher. In an engine with the balanced-pressure precombustion-chamber system operating at the above mechanical efficiency and at 2000 rpm, the Saurer-Bosch apparatus measured approximately 32% discoloring of exhaust gas. The oscillograms in Fig. 8 show the following data for the three combustion systems:

Speed (n) = 2000 rpm
Bmep = 85 psi
Bmip = 120 psi

In each illustration the indicator diagram for diesel fuel and Mogas 80/86[1] is shown at the top, the rate of pressure rise ($dp/d\phi$) shown in the center, and the body noise measured at the same time appears below. By observing equal technical conditions of measurement, the inductive transmitter, which can be statically gaged, was installed in the main combustion chamber in such a manner that interfering influences were eliminated. The indicator diagram for the three systems shows appreciable differences when diesel fuel is used. The engine with direct injection has the highest firing pressure, as shown clearly in the indicator diagram. Firing pressure in the swirl-chamber engine is somewhat less; the diagram of the balanced-pressure precombustion-chamber engine, however, is quite different from the others, and a rise of pressure caused by combustion is hardly visible. When Mogas 80/86 (OZ 86, CaZ 15) is used, the performance figures differ even more noticeably. In all three cases, the engine had the same injection setting for both Mogas and diesel fuel.

Engines with the direct-injection or swirl-chamber system show a rate of pressure rise and firing pressure intolerable in normal operation. Engines with the balanced-pressure precombustion chamber system show scarcely any rise in firing pressure, nor does the rate of pressure rise show any appreciably higher values than those resulting from the combustion process. For the same injection setting as for diesel fuel the diagram shows only a somewhat longer induction period. There is a close connection between combustion noise and rate of pressure rise. It is this sudden rise of pressure which causes the well-known and disagreeable diesel knock on air-cooled engines not fitted with a muffling water jacket. The influence of the system and of the fuel is seen in Fig. 8 showing body noise. Fig. 9 shows the relationship between combustion noise and the noise of the engine itself. Table 1 compiles characteristic data relating to the combustion process for the three systems using diesel fuel and Mogas 80/86. It is evident that a firing pressure (p_z) in engines with direct injection rises from the relatively high figure of approximately 1100 psi when diesel fuel is used to more than 1400 psi when Mogas is used. The rate of pressure rise increases from 120 psi to more than 280 psi crank angle, while ignition assumes explosives characteristics.

The swirl-chamber system performs more favora-

[1] Mogas (motor gasoline) indicates fuel specified by U. S. Army as MIL-F 5572 A and MIL-F 25172 (7). Numbers 80/86 refer to octane-number range.

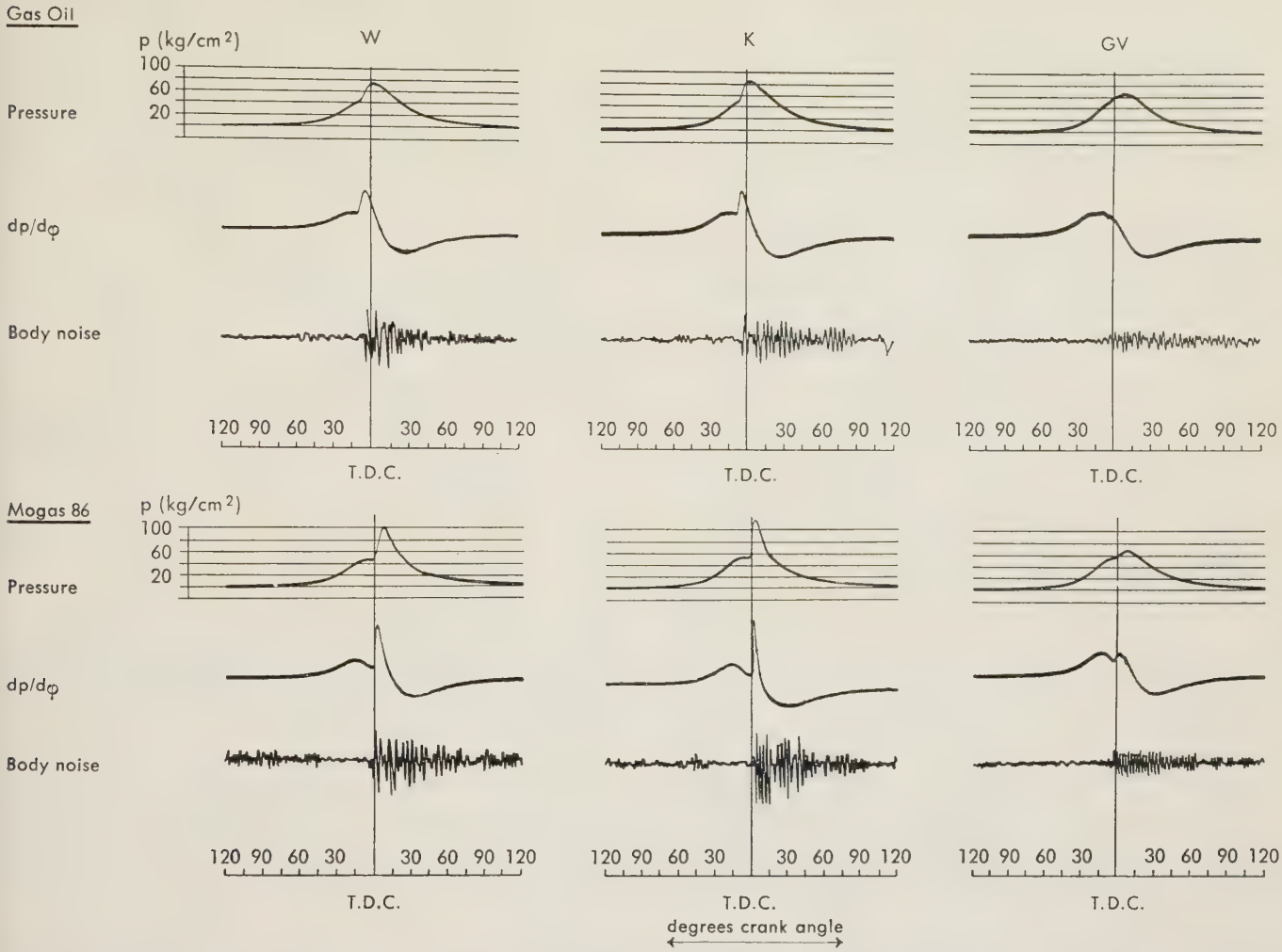

Fig. 8—Comparison of indicator diagrams, rates of pressure rise, and body noise as to the three combustion systems when diesel fuel and Mogas 86 are used (2000 rpm, bmep = 85 psi)

Table 1—Data for Firing Pressure, Rate of Pressure Rise, and Relative Ignition Lag for the Three Combustion Systems when Diesel Fuel and Mogas 86 are Used

(2000 rpm, bmep = 85 psi)

Combustion System	Fuel	Firing Pressure (p_z), kg/cm²	Rate of Pressure Rise $\left(\frac{dp}{d\phi}\right)$ atmospheres/deg crank angle	Relative Ignition Lag (Z_v/Z_{vB})* for Diesel Fuel
W	Diesel fuel	74	6.5	1.25
K	Diesel fuel	80	8.5	1.50
GV	Diesel fuel	64	~ 1.8	1.0
W	Mogas 80/86	100	9.7	3.38
K	Mogas 80/86	105	20–25	3.54
GV	Mogas 80/86	64	~ 1.8	2.08

* Z_v = Ignition lag for the respective temperaeure.
Z_{vB} = Ignition lag for normal running temperature.

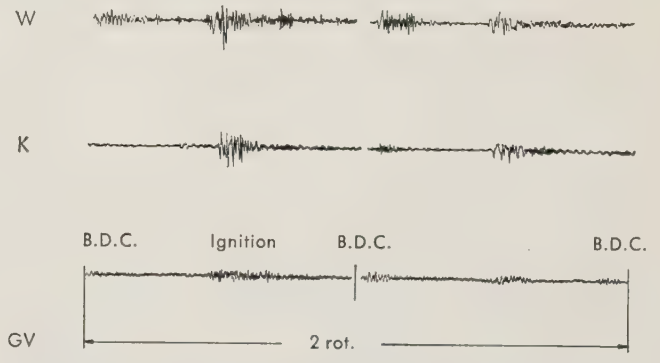

Fig. 9—Combustion noise compared with noise of engine gear of the three combustion systems (2000 rpm, bmep = 85 psi)

bly, but its high firing pressure does not guarantee a safe and quiet engine operation. The performance of an engine with the new combustion system is quite different, as clearly indicated in the data. Engines running on Mogas 86 or diesel fuel have the same firing pressure. The lower figures of the rate in pressure rise are also almost those of an engine with equal pressure combustion. The ignition lag is simply a little higher, which shows that another type of fuel has been used.

Performance of Engine When Different Fuels are Used

The extremely favorable combustion properties of a balanced-pressure precombustion chamber engine

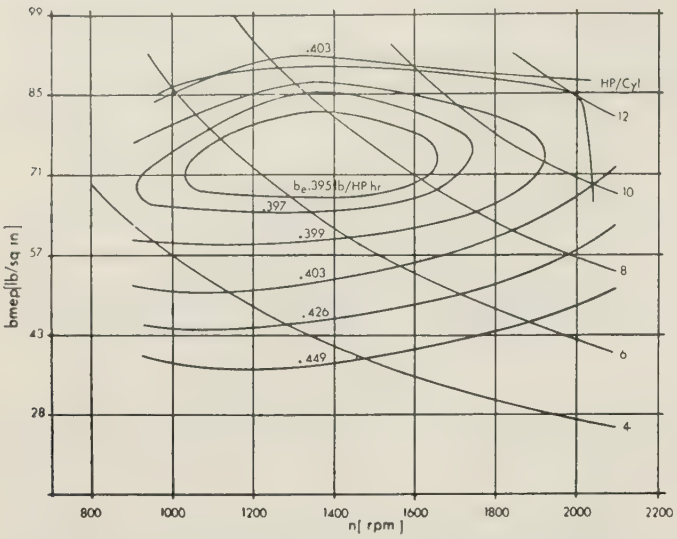

Fig. 10—Output and consumption curves of engine with balanced-pressure precombustion chamber (type AKD 312) when using diesel fuel

Speed n[rpm]	2000	1800	1600
bmep [kg/cm²]	6	6.35	6.4
Exhaust gas discoloring R[%]	30	33	35
Speed n[rpm]	1400	1200	1000
bmep [kg/cm²]	6.55	6.5	6.3
Exhaust gas discoloring R[%]	35	36	40

Fig. 11—Data concerning exhaust gas discoloring and smoke test at various rpm

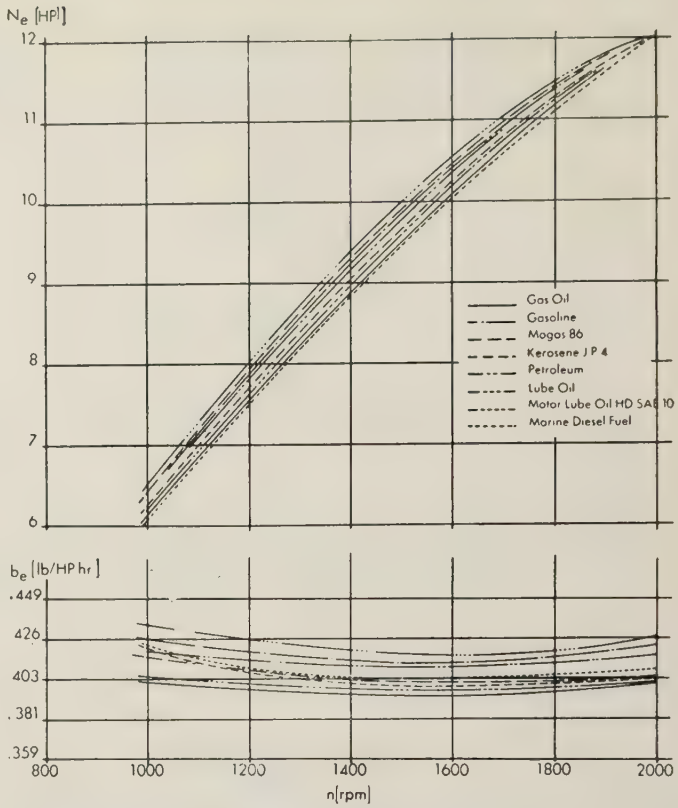

Fig. 12—Output and consumption curves of engine fitted with MWM balanced-pressure precombustion chamber (type AKD 312 E) when using various fuels

resulted in early experiments being made with volatile fuels of crude oil distillation, such as petroleum and turbine fuel kerosene JP4. The injection timing remained unchanged, and it was found that the results of experiments made with these fuels scarcely differed from those made with diesel fuel—a result which could not be obtained with the other combustion systems. These favorable results led to subsequent experiments to ascertain the reaction of the engine to gasoline and the higher fractions up to vacuum distillation. Table 2 shows the essential characteristics of some of the examined fuels.

The results of the balanced-pressure precombustion-chamber engine using the various fuels, as described below, were all obtained without any addition of ignition aids, lubricating oil, or diesel fuel. The fuel injection pump has a fuel leakage seal which prevents excessive fuel leakage and guarantees a certain degree of lubrication of the fuel injection pump. No difficulties were encountered with the pumps. Fig. 10 reproduces the performance curves of the engine with the balanced-pressure precombustion chamber (type AKD 312) for diesel fuel. Particularly striking is the very low variation in consumption between high and the lowest rpm and the very favorable reaction under part load. The greatest part of the diagram is given to the 0.40 lb per hp line. Exhaust smoke discoloring amounts to approximately 30% under full load. Fig. 11 shows data concerning exhaust gas discoloring and smoke test for the full-load range or measured by the Saurer-Bosch apparatus.

Fig. 12 shows the output and consumption data when using various fuels. The quantity injected was adjusted in relation to the specific gravity and the heat value or the special reaction of the corresponding fuel in such a way that the full-load output was the same in all cases. Hereby, the exhaust gas discoloring when using all fuels was lower or at least similar to that when using diesel fuel. The exhaust temperatures varied between 18 and 36 F when using various fuels, but this only slightly affected the total thermal stress. Thus, the engine runs on all fuels without any loss of output, and difference in fuel consumption only amounts to 0.02 lb per hp-hr.

Obviously, it is also possible to mix fuels to any required proportion. The conformity or dependence of consumption in the use of various fuels on their properties such as heat value, specific gravity, composition, and cetane numbers is not ascertained.

The tolerance of the system for variation of fuel is shown clearly in the diagrams and in their differentiations, that is, in the rate of pressure rise (Fig. 13). Also here one observes a pressure rise for all kinds of fuel which is, for a high-speed diesel engine, unusually gradual. Rate of pressure rise and firing pressure are practically independent of the type of fuel used, and they require no alteration or adjustment. This can be observed with each type of fuel, whether under higher loads or with an idling engine, so that no misfires occur even after idle running of

Table 2—Essential Characteristics of Some Examined Fuels

Fuel	Boiling Range, C	C, %	H, %	S, %	Heat Content, $\frac{kcal}{kg}$	Specific Weight (ϕ)	Cetane Number (Caz)	Octane Number (OZ)	Tel, Volume %
Mogas 80/86	32 200	84.2	14.1	0.04	10350	0.726	~ 15	86	0.08
Gasoline	30 180	86.0	14.0	0.06	10500	0.720	~ 15	88	0.04
Kerosene JP 4	100 295	84.6	14.3	0.15	10380	0.730	46		
Petroleum	160 270	85.8	14.2	0.19	10290	0.790	53		
Diesel-fuel	200 360	86.9	12.4	0.65	10180	0.835	60		
Marine diesel fuel	220 365	85.5	12.4	1.52	10100	0.880	47		
Lube oil	260 370	85.2	12.6	1.40	10140	0.890	47		
Heavy-duty motor lube oil (SAE 10)	~ 360 520			1.00	10200	0.876	53		

Table 3—Data Concerning Firing Pressure, Rate of Pressure Rise, and Relative Ignition Lag when Using Various Fuels

(2000 rpm, bmep = 85 psi)

Fuel	Firing Pressure (p_z), kg/cm²	Rate of Pressure Rise $\left(\frac{dp}{d\phi}\right)$ atmospheres/deg crank angle	Relative Ignition Lag (Z_v/Z_{VDK})*	Cetane Number
Mogas 80/86	64	~ 1.8	2.08	~ 15
Gasoline	64–66	1.8–2.0	2.49	~ 15
Kerosene JP 4	64	~ 1.8	1.25	46
Petroleum	62–64	~ 1.8	1.10	53
Diesel fuel	64	~ 1.8	1.0	60
Marine diesel fuel	64	~ 1.8	1.0	47
Lube oil	64	~ 1.8	1.0	47
Heavy-duty motor lube oil (SAE 10)	64	~ 1.8	1.0	53

* Z_v = Ignition lag for the respective temperature.
Z_{VDK} = Ignition lag for the temperature of the diesel fuel.

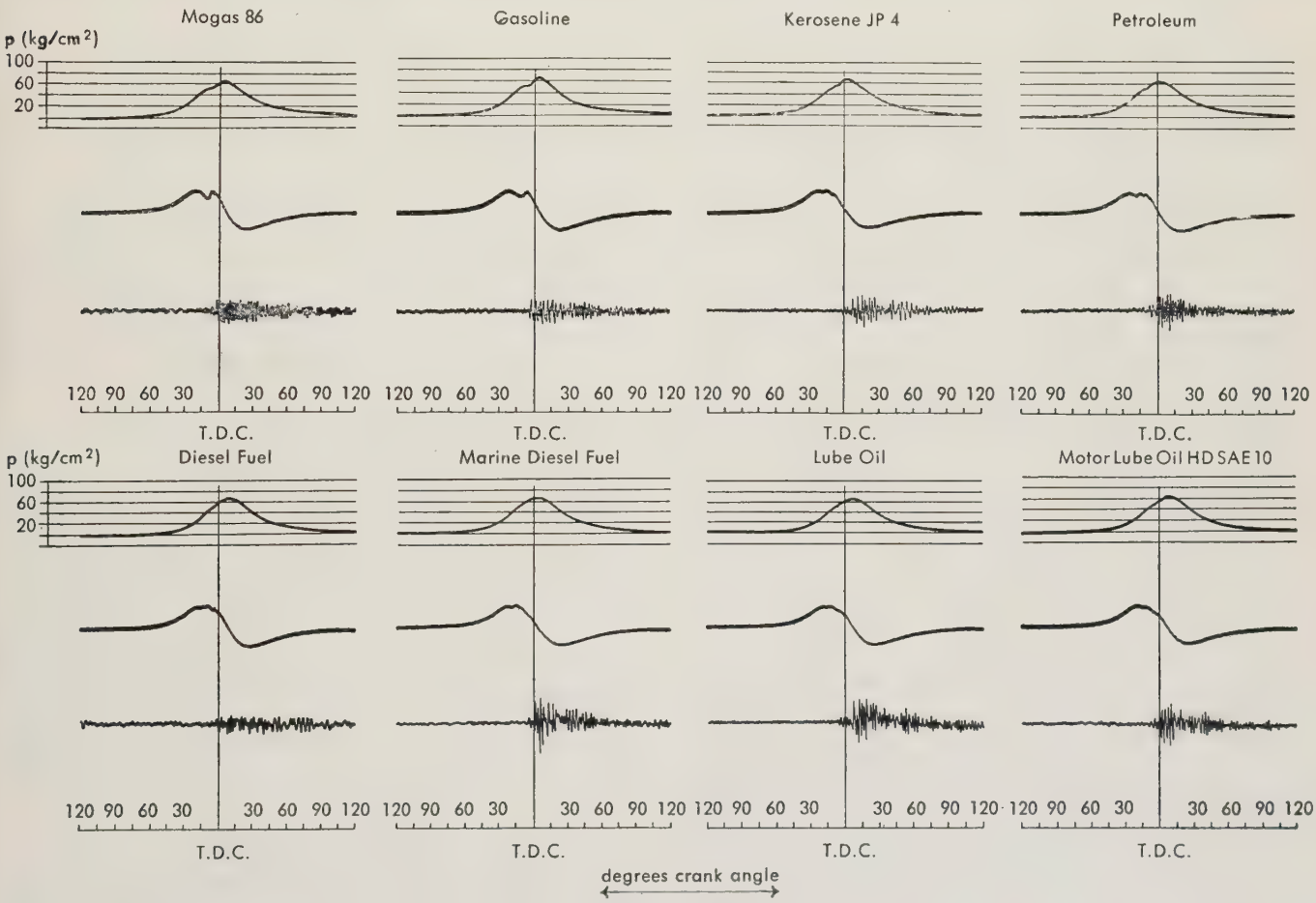

Fig. 13—Pressure rise, rate of pressure rise, and body noise when using various fuels (2000 rpm, bmep = 85 psi)

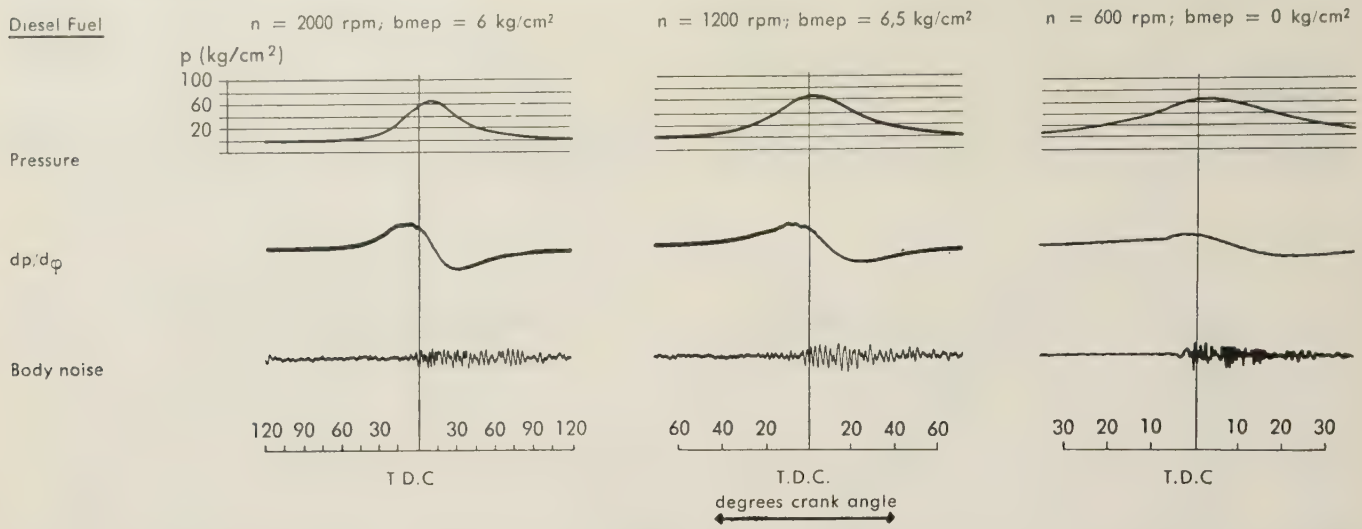

Fig. 14—Pressure rise, rate of pressure rise, and body noise in engine fitted with MWM balanced-pressure precombustion chamber under various loads

several hours. For comparison purposes, Fig. 14 represents two full-load diagrams at 2000 and 1200 rpm and a diagram representing long idling at 600 rpm for diesel fuel and Mogas 86. Table 3 summarizes firing presure, rate of pressure rise, and ignition lag in relation to diesel fuel. This table shows very clearly the amount of tolerance for variation of fuel. It can be said that an engine with the MWM balanced-pressure precombustion-chamber system operates efficiently regardless of the type of fuel (whether distillates, residual oil, or gasoline up to high octane numbers).

The gradual pressure rise, as shown clearly in the data, completely avoids diesel knock—especially important for aircooled engines. Diesel knock is caused by air vibrations following a sudden rise in pressure, and in consequence this knock is radiated unmuffled as body noise in every direction and is particularly unpleasant when the engine is idling.

Fig. 15 shows a sound track of two idling aircooled engines installed in a tractor, one of the engines equipped with direct injection and the other with the MWM balanced-pressure precombustion chamber. Here it was observed that the intensity of the unpleasant metallic noise of the higher frequencies is greatly reduced. The performance at higher rpm and load is even more favorable, as the volume of engine noise produced by gears, valves, piston, and blower equals or even exceeds combustion noise.

Cold-starting properties, which are extremely important for the diesel engine, are assured without particular effort in an engine equipped with the MWM balanced-pressure precombustion chamber. The combustion process in a cold engine naturally differs from that in an engine which has attained the necessary temperature. The excellent starting properties of an engine with high compression ratio using direct injection are achieved by injecting a somewhat larger initial quantity of fuel than usual through the burner insert. With the aid of the low heat capacity of the burner, which can be regarded as a kind of preparation path, sufficient temperature for normal controlled combustion is reached after a very short time. Low-temperature starting is assisted by glow plugs or ignition paper.

Practical results indicate that cold starting at temperatures down to 14 F is possible after a few turns without any starting aid. With the aid of glow plugs or ignition paper starting is possible at temperatures down to – 4 F, and single- and twin-cylinder tractor engines can even be started by hand cranking.

As mentioned earlier in this article, the system can be applied for both aircooled and water-cooled engines. Experiments show that the same output and fuel consumption can be obtained, if the necessary construction and adjustments are provided.

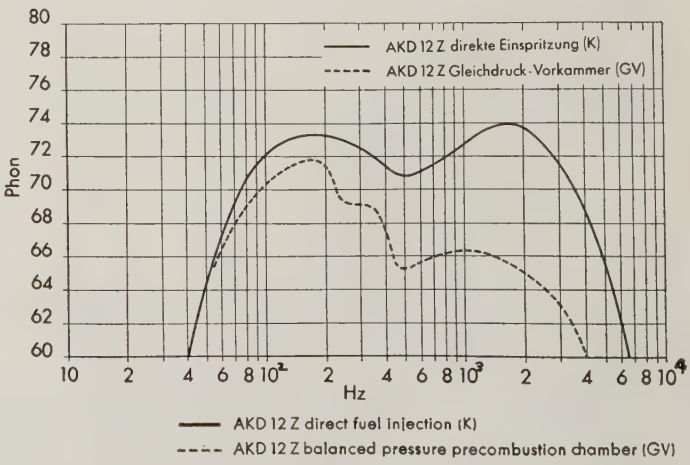

Fig. 15—Sound track of two idling aircooled diesel engines installed in tractor, one equipped with direct injection (K) and the other with MWM balanced-pressure precombustion chamber (GV)

EFFECTS OF RADIATION ON MATERIALS

Michael Ference, Jr., Ford Motor Co.

This paper was presented at the SAE Annual Meeting, Detroit, Jan. 14, 1957.

ALTHOUGH the effects of high-energy radiation on materials have been the subject of study since the discovery of X-rays by Roentgen and of radioactivity by Becquerel at the turn of the century, this field received its greatest stimulus from the wartime research on atomic energy and since then by the availability of unusually intense sources of radiation from both reactors and particle accelerators.

Whereas a curie of radiation was once considered to be a rather intense radioactive source (a curie represents 3.7×10^{10} disintegration per sec, the activity of one gram of radium), today we think in terms of millions of curies. Moreover, when the large number of nuclear-power reactors planned for the immediate future are built, radiation sources of the order of a billion curies will be potentially available. In addition, there exist possibilities for irradiating materials with integrated neutron fluxes of the order of 10^{22} neutrons per cm^2. With such sources clearly on the horizon, it becomes important to ascertain the effect of intense high-energy radiation on matter. Wigner[1] was one of the first to realize that intense fluxes of high-energy neutrons would be able to displace atoms from equilibrium positions in crystal lattices, and hence would give rise to possible deleterious effects on many properties of engineering materials.

It is the purpose of this paper to point out the nature of the changes that occur in the physical and mechanical properties of materials subjected to various types of radiation, and to discuss the results of some recent experiments on the effect of radiation on chemical systems.

Nature of Radiation

We shall first consider the kinds of radiation that are useful in such studies. Natural radioactive materials are sources of alpha particles (helium nuclei with a double positive charge), beta particles (negatively charged electrons), or gamma rays (electromagnetic waves of photons with no charge and negligible mass). In addition, there are energetic protons which are hydrogen nuclei with a single positive charge, and neutrons, which have no charge and a mass nearly that of the proton. Radioactive isotopes created in the nuclear-reactor and spent-reactor fuel elements are useful sources for such radiation. Radiation may also be produced in high-energy accelerators as, for example, cyclotrons, betatrons, synchrotrons, linear accelerators, resonant transformers, or Van de Graaff accelerators. As a matter of fact, some of these accelerators are uniquely suited as sources for high-energy electrons for irradiation purposes.

Although the energies of these radiations can vary over wide ranges, it is the high-energy radiation of the order of 1–5 million electron volts (1–5 mev) that will be of primary interest to this discussion. For comparison, the average kinetic energy of a gas molecule at room temperature is approximately 0.025 electron volts (ev). About 24 ev are required to ionize helium.

Attenuation of Radiation by Materials

We shall discuss the problem of the irradiation of material from three points of view. First, we will consider the effectiveness of various materials in absorbing radiation without any special emphasis on the precise nature of any induced radiation damage. This is an important practical consideration for the shielding of nuclear reactors, be they large stationary power reactors or mobile propulsion reactors.

A second point of view is the study of the basic mechanisms of the interaction of radiation and matter in order to determine the changes brought about in such mechanical properties of materials as tensile strength, ductility, hardness, creep; in such

[1] *Journal of Applied Physics*, Vol. 17, November, 1946, pp. 857–863; "Theoretical Physics in Metallurgical Laboratory of Chicago," by E. P. Wigner.

IT is only since World War II that extensive study has been made of the effects of high-energy radiation on materials. However, a lack of fundamental data still prevents the making of any generalizations or detailed calculations of the effects of radiation-induced defects on the bulk properties of metals.

The author discusses the problem from three points of view:

1. The effectiveness of materials in absorbing radiation.
2. The basic mechanisms of the interaction of radiation and matter—in order to determine the changes on the mechanical properties of materials.
3. Radiation as a convenient and economical source of energy for irradiation of chemical systems.

The author thinks, on the basis of the limited data available, that one of the most useful effects of radiation on matter has been the use of ionizing radiation to bring about chemical reactions, especially in organic compounds.

Table 1—Approximate Ranges of Charged Particles in Aluminum

Radiation	Energy, mev	Range, microns
Proton (H^+)	5	190
	1	13
Alpha particle (He^{++})	5	20
	1	3
Deuteron (D^+)	5	115
	1	8
Electron (e^-)	5	10^4
	1	6×10^3

Table 2—Absorption Coefficients for Gamma Rays

Energy, mev	Water	Aluminum		Lead	
	μ cm^{-1}	μ cm^{-1}	μ/ρ, cm/g	μ cm^{-1}	μ/ρ, g/cm
0.5	0.090	0.23	0.085	1.7	0.15
1.0	0.067	0.16	0.059	0.77	0.068
2.0	0.048	0.12	0.044	0.51	0.045
4.0	0.033	0.08	0.030	0.40	0.042

chemical properties as corrosion resistance; and such physical properties as thermal and electrical conductivities. This is the area of study broadly called "radiation damage," although all the effects need not be deleterious.

Finally, we shall examine radiation as a convenient and, hopefully, an economical source of energy for the irradiation of chemical systems.

The energy of a charged particle is transferred to the medium through which it is moving by either of several mechanisms: ionization, atomic displacement, or thermal spikes. By frequent collisions and intense interaction with the electrical fields of the atoms of the medium, the charged particle is quickly brought to rest at some site in the lattice. The range of such particles depends predominantly upon the initial energy, but the charge and mass of the particle and the nature of the medium are also important. For alpha, beta, and protonic particles with energies of about 5 mev, the range varies approximately as E^n, where n is somewhere between 1 and 2.

Significantly, for heavy particles these ranges are rather short, of the order of a few microns, as shown in Table 1. For a 5-mev electron, however, the range is approximately 1 cm. From a shielding point of view, such radiations are not considered important. However, heavy-particle radiation is important because of the marked surface effects that are possible and the severe radiation damage that may result if such particles are produced internally through fission or neutron interaction.

The deep penetration possible with gamma rays, high-energy X-rays, and neutrons poses a shielding problem of a different order of magnitude. A gamma ray of energy 2–3 mev traversing a material interacts only weakly with the electrons of the medium. Absorption of gamma rays is a complicated process producing photoelectrons, Compton recoil electrons, and electron-positron pairs. The overall effect, however, can be estimated in terms of an absorption coefficient μ. If I_0 is the initial intensity of a collimated beam of monoenergetic gamma rays, then the intensity I_x after traversing a distance x in a material whose absorption coefficient is μ is given by the well-known relation:

$$I_x = I_0 e - \mu x \qquad (1)$$

By dividing μ by the density of the material ρ, the mass-absorption coefficient is obtained, μ/ρ. Equation (1) becomes:

$$I_x = I_0 e - (\mu/\rho)\, x\rho \qquad (2)$$

Values for this coefficient are shown in Table 2. It is apparent that the mass-absorption coefficient in the 1-mev range is approximately constant. About 70 cm of water are required to decrease the intensity of 1-mev gamma rays to 1% the initial value. For beta particles or electrons of this energy the range is 0.4 cm, and for alpha particles about 0.0004 cm.

The relatively poor absorption of gamma rays by even very dense materials places an immediate restriction on automotive applications of nuclear power, as shown by the following simple considerations.

It has been suggested that the maximum permissible human exposure to 2-mev gamma rays should amount to about 2000 photons per cm^2 per sec. Based on this tolerance, a nuclear powerplant for an automobile delivering 300 hp would require shielding of the order of 80,000 lb, the exact value depending upon the geometry assumed for the reactor. This enormous mass is a basic technological barrier to the development of practical automotive application. Because of the exponential attenuation just noted, the weight of shielding does not increase linearly with the strength of the radiation source. In the case of aircraft propulsion, the horsepower crossover point at which a shielded nuclear engine can usefully carry its own weight has been variously estimated[2] to be of the order of 20,000 to 70,000 hp.

[2] *SAE Journal*, Vol. 62, December, 1954, pp. 17–20: "Radiation Rules Out Reactors for Small Planes and Autos," by K. Kasschau.

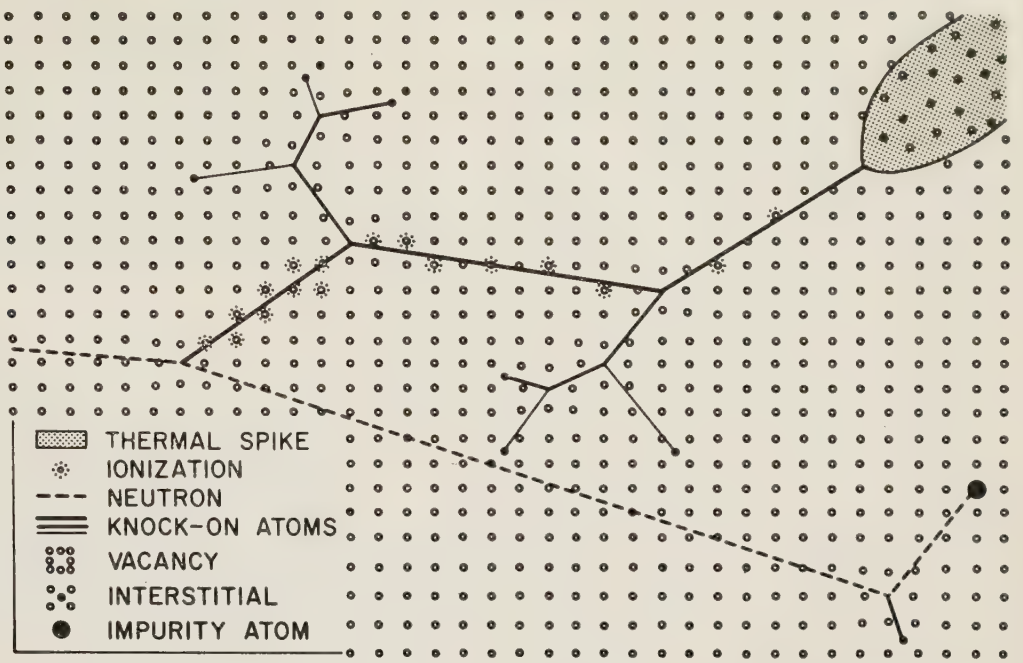

Fig. 1—Schematic representation of radiation damage in a solid, showing ionization, thermal spikes, displacement atoms, and cascading of knock-on atoms

Since large powerplants are an intrinsic requirement for marine and aircraft applications, nuclear power is feasible in these cases.

Mechanisms for Radiation Damage

An early theoretical analysis by Seitz[3] pointed out the defects that would occur in a material when irradiated with high-energy particles. Subsequent experimental work by many investigators has confirmed some of these early ideas and has provided some quantitative data on radiation damage. We shall examine some of these data as they relate to engineering materials. As background for this evaluation, however, it is useful to consider briefly the mechanisms that have been proposed for radiation damage.

Since a neutron has no charge it will not interact with the electrons of the atoms of a solid, as in the case of a charged particle, but will proceed until it collides with an atomic nucleus, ejecting an energetic atom and creating a vacancy in the lattice. A neutron can travel long distances—in the range of several centimeters—before it is finally captured by some nucleus. The amount of energy that the neutron imparts to a knock-on atom will vary considerably and will depend, for example, on the energy of the neutron and the mass of the knock-on atom. The maximum energy that a heavy particle of mass m and energy E can impart to a mass M at rest is given by:

$$E_{\max} = \frac{4mM}{(m+M)^2} E \qquad (3)$$

For a 2-mev neutron, average energies of knock-on atoms are about 280,000 ev for carbon, 130,000 ev for aluminum, 60,000 ev for copper, and about 15,000 ev for uranium. The average energy required to eject an atom from an atomic site is about 30 ev.

The primary high-energy knock-on atom with its accompanying electronic field strongly interacts with the other atoms of the lattice, producing intense ionization along its path. A large part of the energy of the moving particle is lost in this way. In addition, the knock-on atoms can collide elastically to displace more atoms from the solid which, in turn, displaces atoms in a cascade process until the energy of the knock-on atoms appear as thermal energy of the solid. The various displaced atoms will lodge as interstitials within the lattice, provided they do not immediately recombine with a nearby vacancy.

The neutron that is finally captured by an atomic nucleus may render the nucleus radioactive and subsequently eject impurity atoms into the lattice. For example, if the material contains some B^{10}, absorption of neutrons by the boron will create unstable nuclei which will disintegrate, producing energetic helium and lithium nuclei which, in turn, will eject other atoms from the medium.

Together with the effects described, energy from a fast knock-on atom may be transmitted to many atoms near the path of the oncoming particle, setting up intense localized lattice oscillations. This results in the formation of a thermal spike, a region of localized heating. Calculations indicate that several thousand atoms may be raised to temperatures of the order of 2000 K for a duration of about 10^{-10} sec. In these short time intervals it is assumed that melting and some turbulent flow occur. It has also been suggested that strains in the surrounding areas of thermal spikes would produce dislocation rings. Radiation apparently can induce dislocations in materials.

In summary, in traversing a solid energetic particles produce vacancies, ionization, interstitials, impurity atoms, and thermal spikes. These effects are shown schematically in Fig. 1.

Such defects produced by radiation in solids are

[3] *Discussions of the Faraday Society*, No. 5, 1949, pp. 271–282: "On Disordering of Solids by Action of Fast Massive Particles," by F. Seitz.

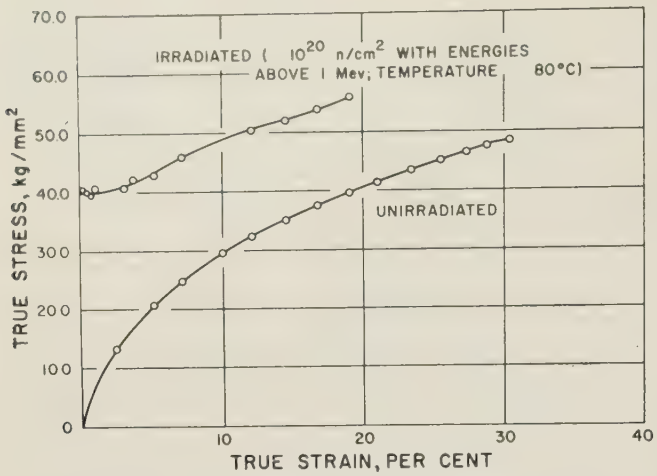

Fig. 2—Effect of reactor exposure on stress-strain curve of nickel

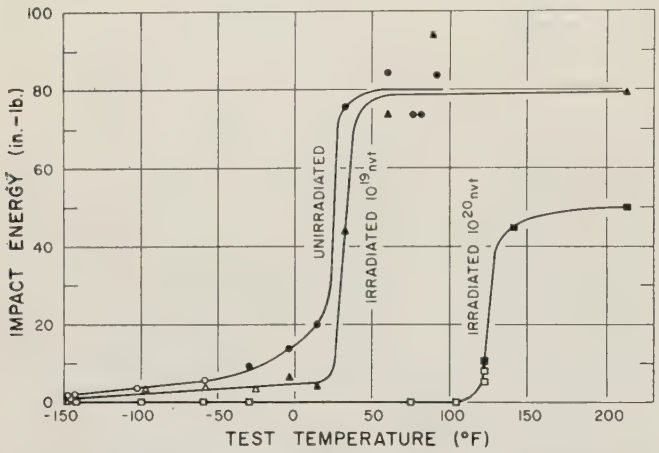

Fig. 3—Impact energy absorbed by normalized ASTM A-212 grade B steel. Temperature of ductile to brittle fracture increases with increasing irradiation

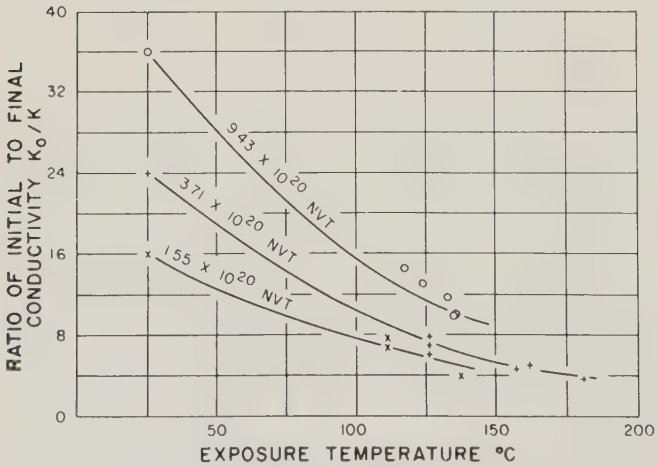

Fig. 4—Variation in thermal conductivity of graphite with temperature

responsible for the observed changes in properties. In the case of metals, these defects serve as scattering centers for electrons, causing changes in the electrical and thermal conductivities of the material. Also, defects, including dislocation formation and movement, will affect the mechanical properties of metals. In the case of metals, ionization effects are not important. On the other hand, ionization and electronic excitation in nonmetals are of paramount importance, for these lead to bond fracture and free radical formation. We shall discuss this at a later point.

Effects on Metals

The radiation defects produced by neutron bombardment of metals are confined to more or less localized areas; nevertheless, under accumulated neutron radiation of the order of 10^{21} nvt[4] rather significant changes in the mechanical properties can occur. Many metals show an increase in hardness after irradiation, an increase in ultimate tensile strength and yield strength (particularly if the temperature of bombardment is low compared to the melting point), decrease in elongation, and, in the case of carbon steels, an increase in fracture-transition temperature.

On the other hand, most metals show very small changes at room temperature in such properties density and creep rates.

In the case of single crystals of copper, Blewitt and Coltman[5] observed a substantial change in the critical shear stress from 0.2 kg per mm^2 for unirradiated copper to 1.94 kg per mm^2 when irradiated with a total flux of 1.8×10^{18} fast neutrons.

Some of the significant changes observed in the stress-strain curves of nickel,[6] as representative of metal, are shown in Fig. 2.

Changes induced in some common engineering metals on irradiation with neutrons are summarized[7] in Tables 3 and 4. In the case of carbon steels, an increase in yield strength with accumulated irradiation has been observed and is shown in Table 4. Of considerable importance is the effect of irradiation on the notch-impact properties of normalized carbon-silicon steel. This is shown in Fig. 3.[8]

The permanency of the changes in properties of the crystalline solids produced by irradiation is dependent upon the temperature at which irradiation took place, subsequent annealing, and the value of the integrated irradiating flux. For example, metals heated above their recrystallization temperature show no permanent effects.

Although the mechanisms of radiation effects are understood qualitatively, there is no satisfactory quantitative theory available for engineering calculations. Also, with the exception of a few materials, there is a lack of comprehensive experimental data

[4] The symbol nvt is used to denote time integrated neutron fluxes, representing the amount of bombardment in neutrons per sq cm.

[5] *Physical Review*, Vol. 82, June 1, 1951, p. 769: "Effect of Pile Irradiation on Stress-Strain Curve of Copper," by T. H. Blewitt and R. R. Coltman.

[6] Proceedings of the International Conference on the Peaceful Uses of Atomic Energy, 1955. Vol. 7, pp. 484–489: "Effects of Irradiation on Structural Materials," by F. E. Faris. United Nations, New York, 1956.

[7] *Journal of Metals*, Vol. 8, May, 1956, pp. 665–672: "Effect of Nuclear Radiation on Structural Materials," by J. C. Wilson and D. S. Billington.

[8] See footnote 7, p. 670.

on the effect of intense radiation on metals. Broadly speaking, for large neutron doses of the order of 10^{20} nvt, hardness increases have been observed of about 40% for carbon steels, 100% for stainless, 140% for nickel, and 100% for zirconium. Ultimate tensile-strength increases have been observed of 10% for carbon steels, 20% stainless, 40% nickel, and 5% for zirconium.[9] At this writing, there is no good experimental evidence that radiation will produce any beneficial changes in the bulk properties of metals that cannot be obtained by conventional metallurgical methods.

Effects of Radiation on Nonmetals

The degree of damage and the resulting changes in physical properties of nonmetallic solids under equivalent irradiation are much greater than for metals. In the case of organic solids, the effect of bond breaking and ionization are quite important.

The physical characteristics of the refractory nonmetallic solids are influenced by the degree of ionic and covalent bonding and the type of crystal structures of the ceramic matrix. Most of the studies of ceramic materials have been confined to the effects of neutron bombardment of the crystal components of the ceramic.

As has been predicted, those crystals that are characterized by covalent bonding appear to be most susceptible to dimensional changes on irradiation. In the case of silica structures, quartz showed[10] a density decrease of 14.7% for an exposure of 2×10^{20} nvt. The unaltered quartz lattice is a network of linked tetrahedrons of SiO_4. Two bonds need be broken to displace an oxygen atom and four bonds to displace a silicon atom. In addition, oxygen atoms need be displaced only a short distance to find an interstitial hole. In quartz the internal structure became amorphous under intense exposures, but, interestingly enough, no macroscopic defects such as cracks or bubbles were observed. The temperature required to anneal this lattice damage appreciably in the single crystal is of the order of 1500 C. The effects on the oxides of beryllium, aluminum, and zirconium are similar though less severe, the oxide of beryllium being the most stable.

In the case of diamonds, a density decrease of 4% was obtained for a neutron irradiation dose of about 10^{21} nvt, indicating that a large number of atomic displacements are produced in diamonds. Clear crystals of diamonds become black after an irradiation of only 10^{17} nvt. The damaged structure will recover some 70% of its density change on annealing for 2 hr at 1600 C.

Graphite has been extensively studied as a structural material for nuclear reactors and, as a consequence, a good deal of radiation damage information is available. Under intense irradiation the crystal lattice of graphite is significantly distorted with an eventual destruction of the crystal into an amorphous form. The distortion is due to the expansion

Table 3—Pre- and Postirradiation Values of Hardness, Yield, and Tensile Strength of Various Alloys

	Rockwell Hardness No.		Yield Strength 10^3, psi		Tensile Strength 10^3, psi		Ratio of Yield Strength to Tensile Strength	
	Pre	Post	Pre	Post	Pre	Post	Pre	Post
2SH14 Aluminum	8 F	40 F	18	23	20	27	0.9	0.85
2S0 Aluminum	—	—	7	17	17.3	26	0.51	0.65
High Purity Iron	—	—	18	31	36	37	0.5	0.84
Normalized Carbon Steel			50	93	75	97	0.67	0.96
Hardened and Tempered Alloy Steel	—	—	153	196	164	198	0.93	0.99
Austenitic Stainless Steel	81 B	99 B	37	97	98	115	0.38	0.84

Table 4—Effect of Irradiation on Mechanical Properties of ASTM A-212 Grade B Carbon Silicon Steel

	Yield Strength 10^3, psi	Tensile Strength 10^3, psi	Reduction of Area, %	Uniform Elongation, to Necking, %
Unirradiated	50	75	64	22
Irradiated 10^{19}nvt at 140 F	65	81	68	18
Irradiated 10^{19}nvt at 570 F	57	84	57	12
Irradiated 10^{20}nvt at 175 F	94	97	26	5

of the interplanar dimensions of the lamellar structure by the displacement of carbon from normal positions in the lattice. The result is a marked change (though not necessarily deleterious) in the physical, mechanical, and electrical properties of graphite. Some of the mechanical properties are improved; for example, compression strength can be doubled. Irradiated graphite produces a tougher, harder graphite which is somewhat more difficult to machine. The thermal and electrical conductivities decrease[11] with radiation in the case of thermal conductivity as much as 36-fold. (See Fig. 4.)

Another interesting effect resulting from the irradiation of graphite is the anomalous increase in energy content of the crystal. This increase is referred to as "stored energy" and represents an increase in enthalpy. It is observed experimentally as an increase in the heat of combustion of the material; this energy can be released by heating the graphite to 1000 C. The amount of energy stored can be large, of the order of 500 cal per gram after exposure to 2×10^{21} n per cm^2. The stored-energy release can be sufficiently high to give an apparent negative specific heat for graphite, that is, the sample spontaneously increases in temperature.

Radiation as a Source of Energy for Chemical Reactions

Perhaps one of the most useful effects of radiation on matter has been the use of ionizing radiation to bring about chemical reactions in solids, liquids, and gases. The use of gamma rays and beta rays from radioactive sources and of high-energy electrons from accelerators has been responsible for rapid development in the radiation chemistry of organic compounds.

In evaluating the usefulness of radiation for chemical reactions, it is necessary to know not only the amount of radiation available but also the efficiency with which radiation can be used to initiate reactions. The criterion used as an efficiency index is the g value of the reaction, which can be defined

[9] *Advances in Physics*, Vol. 4, October, 1955, pp. 381–478: "Survey of Irradiation Effects in Metal," by J. W. Glen.

[10] *Physical Review*, Vol. 89, Feb. 1, 1953, pp. 656–657: "Lattice Expansion of Quartz Due to Fast Neutron Bombardment," by M. C. Whittels.

[11] Proceedings of the International Conference on the Peaceful Uses of Atomic Energy, 1955. Vol. 7, pp. 455–471: "Irradiation Damage to Artificial Graphite," by W. K. Wood, L. P. Bupp, J. F. Fletcher. United Nations, New York, 1956.

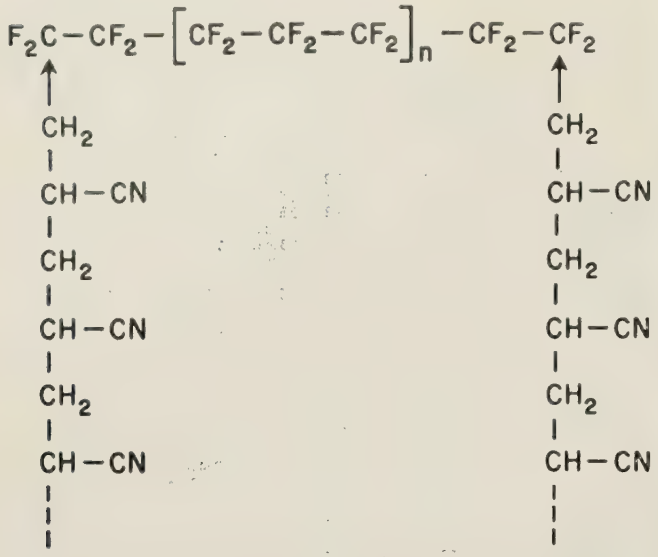

Fig. 5—Formation of graft copolymer system, polyacrylonitrile to polytetrafluoroethylene

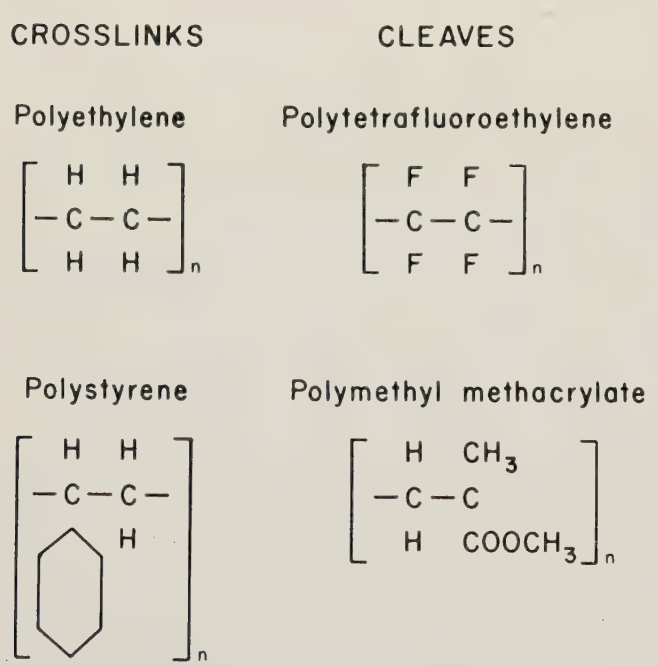

Fig. 6—Structures of polymers that cross-link and those that cleave after exposure to radiation

as the number of free radicals or chemical bonds modified for each 100 ev absorbed. The g values vary over a wide range depending on the nature of the radiation; for example, for benzene g is about 1, ether about 17, acetone 40, cross-linking of solid polyethylene about 3, and for certain chain reactions g can have values of many thousands.

The dosage applied to a chemical system is measured by the amount of energy absorbed per gram of material irradiated, be the radiation gamma rays or electrons. The unit of dosage is the rad equal to 100 ergs per gram. At radiation doses of 1000 megarads (10^9) polyethylene becomes glass-like.

Because of the relatively low g values of many reactions and hence low potential output, the use of radiation for conventional synthesis does not appear feasible except for rather special cases. In the case of chain reactions induced by radiation such as polymerization and chlorination, the economics are more favorable.

In conventional chemical practice, polymerization of monomers is usually initiated by the presence of highly reactive chemical radicals promoted by some type of catalyst. One of the important effects of gamma radiation on organic systems is the breaking of chemical bonds and the formation of free radicals. Radiation, therefore, can initiate polymerization and start a chemical chain reaction. One of the advantages of radiation-induced polymerization is that free radicals can be produced at almost any temperature and in either the liquid or solid phase, whereas chemical polymerization is generally dependent upon temperature. It has been found that in many cases radiation-produced polymers are superior to catalyst-produced polymers. For example, in the case of the polymerization of ethylene by radiation, the polyethylene polymer produced was much more crystalline and tougher than that produced at high temperature and high pressure. Also, polymerization of ethylene is a chain reaction with g values of about 12,000.

It has recently been shown[12] that it is possible to radiation-graft one polymer onto another in such a manner as to control the properties of the grafted copolymer. If a polymer A_n such as polyethylene is added to a monomer B such as methyl methacrylate and the mixture irradiated, part of the monomer B will polymerize as polymer B_m and part as a grafted copolymer A_nB_m. By the proper choice of experimental conditions, it is possible to increase the formation of the grafted polymer at the expense of the polymer B_m. Radiation grafting may be carried out on finished or semifinished materials. The technique of combining in a controlled manner the physical properties of two different polymers has considerable practical interest. For example, the surface characteristics of polytetrafluoroethylene, an extraordinarily inert polymer, may be altered considerably by introducing "grafts" of polyacrylonitrile at intervals along the chain as shown in Fig. 5. The new material exhibits increased adhesive properties, and displays pronounced reactivity.

The mechanical properties of long-chain molecules in the form of a solid can be greatly modified by exposure to radiation. Irradiation of thermoplastics may result in cross-linking of the polymer chain or may result in cleavage of the main chain and hence degradation of the material. In some materials, a fissure of side chains may also take place. Not many cross-links per chain are required to effect important changes in properties. For example, in the case of polyethylene one additional bond per 2000 carbon atoms will change the properties. Polymers such as polyethylene and polystyrene are cross-linked on irradiation. Polymers such as polytetrafluoroethylene and polymethyl methacrylate are degraded by fission of the carbon-carbon bonds. Structures of the monomer forms of these materials are shown in Fig. 6.

[12] Proceedings of the International Conference on the Peaceful Uses of Atomic Energy, 1955. Vol. 7, pp. 526–537: "Chemical Reactions Induced by Ionizing Radiation in Various Organic Substances," by L. Bouby, A. Chapiro, et al. United Nations, New York, 1956.

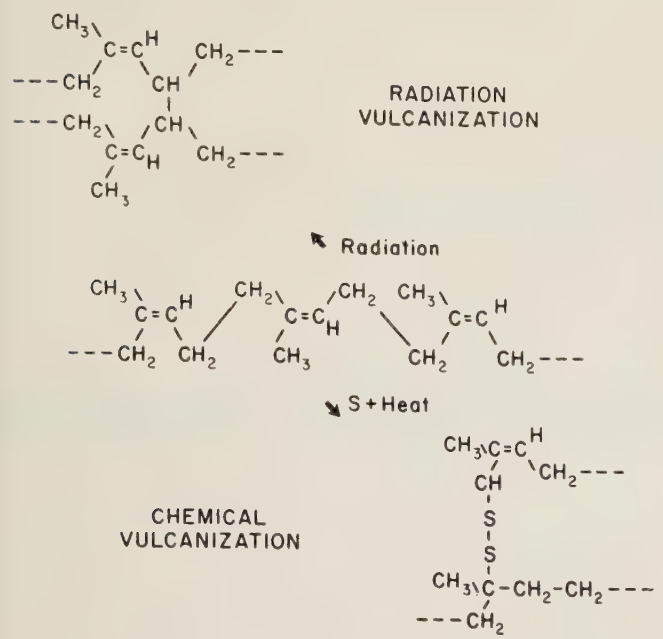

Fig. 7—Vulcanization by chemical means and irradiation by gamma rays

Normal polyethylene can be cold drawn and begins to soften at about 70 C, becoming a viscous liquid at about 115 C. After irradiation with dosages of the order of 50 megarads cross-linking takes place, transforming it partly into a three-dimensional network. As a result, instead of becoming a viscous liquid on heating, the polymer takes on rubber-like elastic properties, that is, becomes an elastomer. Both the tensile strengths and elastic moduli increase. At very high dosages of the order of 1000 megarads, however, the polymer becomes glass-like.

Polystyrene requires 50 times the dosage of polyethylene to start cross-linking due to the presence of the benzene ring in styrene. Such a side-chain ring stabilizes many organic compounds against radiation damage.

In the case of polytetrafluoroethylene, even light irradiation tends to fragment the chain-producing, short random chains that eventually evolve as CF_4. Polymethyl methacrylate degrades rapidly under light dosages of less than one megarad.

Vulcanization of Rubber

Vulcanization changes the natural-rubber polymer from a soft, sticky, plastic to a nonplastic highly elastic substance. A single rubber molecule may consist of several thousand monomers (C_5H_8) joined end to end. The change in properties by vulcanization is brought about by cross-linking these long rubber molecules by the presence of sulfur. The number of cross-links are relatively few, of the order of one per several hundred monomer units. The cross-linking of the long rubber chain can also be induced by radiation with gamma rays without the presence of sulfur. Here the cross-linking is between carbon atoms rather than through sulfur-sulfur atoms. This is shown in Fig. 7. Bonds between the carbon atoms are stronger than those between sulfur atoms and it is expected, therefore, that radiation-vulcanized rubber would be more heat stable than sulfur vulcanization. The smearing temperatures[13] for gamma-ray vulcanization of rubber and carbon black were about 500 F as compared to 400 F for ordinary vulcanizates.

To obtain proper cures through radiation cross-linking requires rather large doses of the order of 50 megarads and because of this very low g value is rather costly to produce. Although it is difficult to visualize radiation vulcanization of natural rubber for passenger-car tires, irradiation may be justified in order to obtain valuable new properties of synthetic rubber, for example, or to cold-vulcanize unusual shapes in situ.

Summary

Radiation can produce significant changes in the properties of materials. However, a lack of fundamental data and theory prohibits engineering calculation of the effect of radiation-induced point defects on the bulk properties of metals. Furthermore, there is no economic advantage at present to irradiate metals in the bulk for possible beneficial effects. Most plastics degrade rapidly in intense-radiation fields; although in the case of polyethylene, improvements in properties have been noted under moderate radiation doses.[14] On the other hand, there is real promise in the use of radiation for initiating novel chemical reactions. For example, radiation grafted copolymers offer the possibility of a new class of engineering materials with prescribed properties.

DISCUSSION

Emphasizes Lack of Data On Effects of Radiation on Metals

—J. B. Austin
United States Steel Corp.

ANYONE who has had occasion to go through the extensive, and confusing, literature on the effect of radiation on materials will realize how lucidly Dr. Ference has summarized the salient results in this field. He has also included a warning which I should like to emphasize. It is that there is still a lack of fundamental data and theory to serve as a basis for calculating the effect of radiation-induced defects on the bulk properties of metals.

Many of the experimental results which have been reported were aimed at answering some specific and limited question. The specimens used have, in the main, not been of standard shape or size, but have been made to fit available space in a reactor. Widely different times of exposure have been used and inadequate attention has often been given to saturation effects, to self-annealing, or to over-aging. For these reasons, comparisons among various investigations are often unsatisfactory.

I have no wish to disparage the efforts of many investigators who have pioneered under difficult conditions. Their work has given us a significant insight into the effects of radiation on metals. But we must still be extremely cautious about making too broad generalizations or too detailed inferences from the data now available.

[13] A Forum Report, No. 7. Commercial and International Developments in Atomic Energy. Meeting held by Atomic Industrial Forum, Washington, September, 1955. Pp. 77–84: "Vulcanization of Rubber by Gamma Rays," by S. D. Gehman and I. Auerback.

[14] *Nucleonics*, Vol. 14, September, 1956, pp. 53–88: "How Radiation Affects Materials," a group of articles by D. S. Billington, O. Sisman, et al.

BIFUEL APPROACH TO BURNING RESIDUAL FUELS

WORK on the bifuel combustion process[1] began in early 1948. At that time the Sinclair laboratories were engaged in an extensive cold-room test program directed towards evaluation of fluid-type starting aids for starting diesel engines in cold weather.

In the course of these studies it was observed that certain of the aids being tested were effective in smoothing out combustion shock and could be used to boost power output substantially when continually applied, along with the primary or regularly injected diesel fuel, during load operation. Continuing investigation of this subject in both single-cylinder and multicylinder engines further established that engine deposits, wear, and exhaust smoke were likewise beneficially affected by the introduction of auxiliary fuels of certain composition types into the cylinder before, or at the start of, the compression stroke of the engine cycle. The encouraging results of these early exploratory experiments suggested a fresh approach to burning fuels in medium- and high-speed diesel engines, which to our knowledge had not been previously considered.

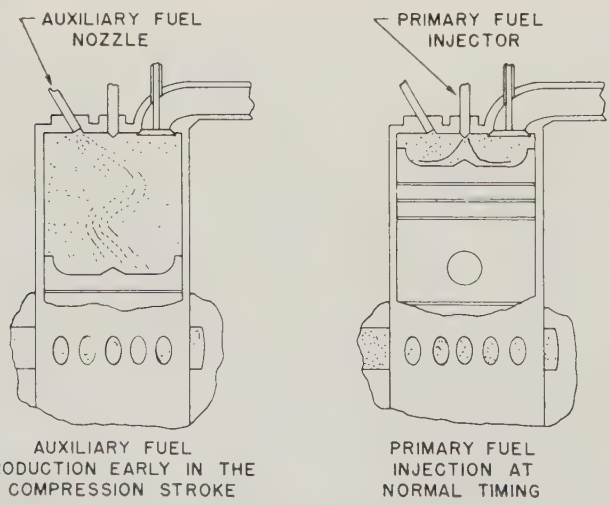

Fig. 1—Bifuel combustion process

Results of experiments covering the burning of low-cetane-number distillates and high-octane-number fuels in the gasoline boiling range will be touched upon in this paper for purposes of defining the versatility of the process. The major emphasis, however, is directed towards use of the process for burning heavy distillates and residual-type fuels more effectively in diesel engines. To date, it is considered that the greatest potential of the bifuel process lies in its application to diesel engines of the stationary type.

Bifuel Combustion Process

As previously inferred, the bifuel process embodies a two-fuel combustion system whereby a

[1] Covered by U.S. Patent No. 2,811,145, Oct. 29, 1957.

IN DIESEL ENGINES

W. C. Arnold and R. H. Beadle, Fairbanks, Morse and Co.
R. L. Logelin and H. D. Young, Sinclair Research Laboratories, Inc.

This paper was presented at the SAE Annual Meeting, Detroit, Jan. 16, 1957.

small percentage of a suitable auxiliary fuel is introduced into the engine cylinder either during the intake stroke or early in the compression stroke of the cycle, but substantially prior to the normal injection of the primary diesel fuel. The process is illustrated schematically in Fig. 1.

In the case of the 2-stroke engine, the auxiliary fuel is preferably introduced directly into the cylinder by means of a properly timed second nozzle. In a 4-stroke engine the auxiliary fuel can be introduced immediately ahead of the air-intake valves by means of individual low-pressure nozzles. Depending upon the volatility characteristics of the auxiliary fuel, another method has been successfully employed in application of the process to high-speed, automotive-type, multicylinder engines. This method introduces the fuel into the air-intake manifold by means of a single nozzle.

During the compression stroke the auxiliary fuel has ample time to become dispersed throughout the cylinder. On the basis of the work reported by various investigators on precombustion reactions, it is speculated that this fuel undergoes preflame oxidation (but not ignition) when properly proportioned with the air charge. A favorable cylinder environment is thus created which serves to trigger ignition of the primary fuel when introduced in the conventional manner. Consequently, the ignition delay of the primary fuel is materially reduced, and in some cases virtually eliminated.

An insight as to how the bifuel process apparently functions is indicated in Fig. 2. The right-hand portion of this outline of the combustion sequence

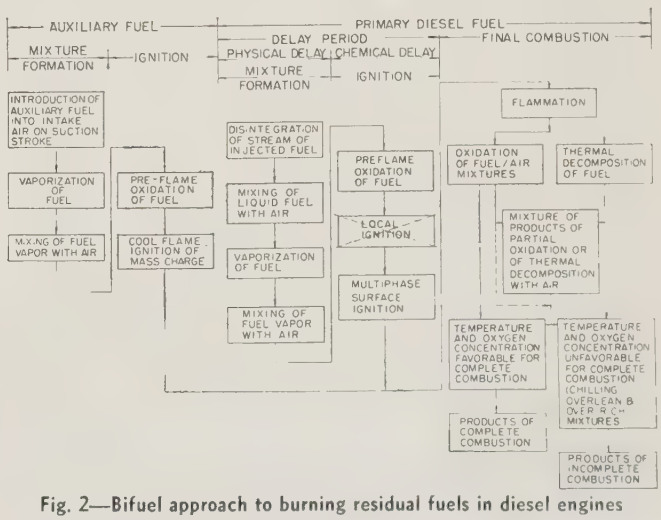

Fig. 2—Bifuel approach to burning residual fuels in diesel engines

THIS paper describes the Sinclair bifuel combustion process, a process basically different from either the dual-fuel gas or dual-fuel residual oil systems in its method of fuel utilization as well as its effect on engine operation.

The benefits of the bifuel process are not the same for all types of engines. However, the authors report that the following favorable performance results have been observed in tests run in one or more of several engine types:

1. Permits low-quality fuels to be effectively burned under conventional engine operating conditions and at an acceptable exhaust-smoke level.
2. Reduces wear and deposits to a level considerably below that generally obtained with low-quality fuels.
3. Allows the smoke-limited power output of an engine to be increased.
4. Allows operation on fuels normally not considered feasible or practicable in conventional diesel engines.

of diesel fuel was taken from Elliott.[2] A left-hand portion has been added to the outline to indicate the role the addition an auxiliary fuel possibly plays in the overall combustion process.

The reacting nature of the auxiliary fuel is indicated in Fig. 3, which shows the pressure-time diagram obtained when 1.5 cc of a 50-cetane-number kerosene employed as an auxiliary fuel is introduced into an engine cylinder. The compression diagram of the cylinder is superimposed and shown for comparison. These data were obtained in a single-cylinder, open-chamber, fixed compression ratio engine having a bore and stroke of $3\frac{1}{4} \times 4\frac{1}{2}$ in. Engine speed was 900 rpm. If the engine had been operating normally on conventional diesel fuel, the quantity of auxiliary fuel would have amounted to 10% of total fuel for smoke-limited power output. The engine could not be run under its own power on this amount of auxiliary fuel and, judging from the small magnitude of the pressure rise (about 20 psi) the fuel was undergoing oxidation but not inflammation.

The optimum quantity of auxiliary fuel required for a given engine is best determined by experiment. It is dependent upon a number of factors, namely: (1) type and size of engine, (2) characteristics of the auxiliary-fuel induction system, (3) combustion-chamber configuration (open, precup, or turbulent), (4) composition and related properties of the primary fuel, (5) type of auxiliary fuel selected for use, and (6) engine speed.

Ordinarily, 5–15% (by volume) of the auxiliary fuel is sufficient to obtain desirable operation on residual fuels, low-cetane-number distillates, and high-octane-number fuels in the gasoline boiling range. Nearly complete absence of combustion noise and/or shock loading has been achieved by introducing 25% (by volume) auxiliary fuel, based on total fuel input, to a single-cylinder, turbulence-chamber ASTM cetane engine. The exhaust-smoke-limited power output of the same type of engine connected to an electric dynamometer can be increased 30–40% while operating on a light residual fuel, when aided by about 20% (by volume) auxiliary fuel.

Exploratory Studies

Test Equipment—Three types of engines were used in evaluating the bifuel combustion process during the initial phase of these studies. These were: (1) the single-cylinder, variable compression ratio, turbulence-chamber, ASTM cetane engine, (2) a single-cylinder, fixed compression ratio, open-chamber engine, and (3) a 2-stroke, General Motors model 2-71 engine.

The normally aspirated ASTM cetane engine is coupled to a synchronous induction motor and operated at 900 rpm. Experiments were also carried out on this same engine coupled to a variable-speed, electric, cradled dynamometer.

The single-cylinder, fixed compression ratio engine represented an adaptation of the ASTM cetane engine. This engine was equipped with an experimental open-chamber head provided by the Waukesha Motor Co. The nominal operating compression ratio of the engine was 16/1. The synchronous induction motor employed on the cetane engine was used for loading.

In both the single-cylinder 4-stroke test engines, the auxiliary fuel was introduced into the air-intake manifold ahead of the intake valve by means of a Bosch pintle-type nozzle. Injection pressure for the auxiliary fuel was 1500 psi. A separate injection pump used for the auxiliary fuel was timed to inject fuel at 25 deg atdc on the intake stroke.

The instrumentation employed on the single-cylinder engines was comprised of a Li pressure pickup, model EP-3000 (Control Engineering Corp.) mounted in the cylinder head. This was connected to associated electronic equipment so that pressure phenomena occurring in the combustion chamber throughout the cycle could be studied. A Du Mont oscillograph record-camera, type 321-A, was employed to obtain a permanent record of the events observed. An Electro Products Laboratories, Inc., Synchromarker connected to the crankshaft of the engine was used for orienting the sequence of events.

The 2-stroke GM engine was coupled to an a-c generator and operated at a governed speed of 1200 rpm. Auxiliary fuel to this engine was introduced directly into the intake manifold through a single low-pressure nozzle supplied by a separately driven pump.

Range of Primary Fuels Employed—The bifuel combustion process allows a wide range of residual and distillate fuels, as well as high-octane stocks in the gasoline boiling range, to be burned. A large number of heavy or highly aromatic fuels having API gravities down to 4 and cetane numbers as low as 10 have been successfully burned at normal compression ratios, that is, 13/1 to 17/1, in the engines described above. Materials, such as premium-grade

[2] "Combustion of Diesel Fuel," by M. A. Elliott. SAE *Quarterly* Transactions, Vol. 3, July, 1949, pp. 490–515.

gasoline of 97 Research octane number and benzene, having critical compression ratios of about 24/1 and 28/1, respectively, have been readily burned at 16/1 compression ratio in both the turbulent and open-chamber single-cylinder engines with the aid of the bifuel combustion process.

Nature and Types of Auxiliary Fuels Used—Useful auxiliary fuels appear to exhibit, at least to some degree, certain basic characteristics: (1) low spontaneous ignition temperature in the neighborhood of 500 F or below, (2) cetane number of 50 and above, and (3) marked preflame oxidation characteristics.

It is pointed out that these characteristics represent observed properties of auxiliary fuels that have been successfully used. They may not fully explain the reasons for their effectiveness. Such materials as highly aromatic naphthas, catallytically cracked gasoline, and distillates, all of which have high spontaneous ignition temperatures and low cetane numbers, have not been found suitable as auxiliary fuels. On the other hand, refinery stocks highly paraffinic in character and having good cetane numbers have been found most effective. Volatility does not appear to be a prime factor in the function of an auxiliary fuel. Volatility can be important, however, with respect to handling characteristics.

Examples of auxiliary fuels that have been found effective are listed in Table 1.

Bifuel Effect on the Combustion Process—A typical composited pressure-time diagram obtained on the ASTM cetane engine equipped with the open-chamber head when burning a straight-run ASTM 2-D grade fuel with and without auxiliary fuel is shown in Fig. 4. The auxiliary fuel, which amounted to 10% of total fuel input to the engine, was a 50-cetane-number kerosene. The superimposed cards of compression pressure, reaction characteristics of auxiliary fuel, and the burning of the primary fuel with and without auxiliary fuel were taken in the sequence mentioned. It will be noted that the maximum cylinder pressure rise due to introduction of auxiliary fuel alone amounts to 15 psi over that obtained for compression. The symmetry of this trace is similar to that of the compression trace. This, in our opinion, indicates fuel oxidation, but not inflammation.

It will be noted also that when the primary fuel is burned with the auxiliary fuel, considerable smoothing out of the combustion pattern results. Peak pressure is also increased by some 45 psi compared with that obtained on the straight-run fuel alone. The rate of pressure rise when burning the primary fuel amounted to 54 psi per deg of crank angle. Upon addition of 10% auxiliary fuel this rate of pressure rise dropped to 42 psi per deg of crank angle.

Fig. 5 shows another composite diagram for a catalytically cracked distillate of 26 cetane number. Here again the combustion pattern smooths out when 10% kerosene is used; peak pressure is increased (about 20 psi); and a lower rate of pressure rise results, 111 psi per deg of crank angle versus 163 psi for the primary fuel alone. A slight pressure rise of 10 psi over compression pressure is noted for the auxiliary fuel.

Similar diagrams are obtained on this same primary fuel when using an ASTM 1-D and 2-D grade (straight-run) auxiliary fuel. These traces are

Table 1—Effective Auxiliary Fuels

1. Normal hexane (156 F boiling point)
2. Normal heptane[a] (209 F boiling point)
3. Normal octane (258 F boiling point)
4. Normal nonane (303 F boiling point)
5. Normal decane (345 F boiling point)
6. Normal cetane (567 F boiling point)
7. Di ethyl ether[a] (94 F boiling point)
8. Kerosene[a]
9. Kerosene plus amyl nitrate (⅛-¾% by volume)
10. ASTM 1-D grade straight-run diesel fuel[a]
11. ASTM 2-D grade straight-run diesel fuel[a]
12. Petroleum naphtha (300–400 F boiling range)
13. Pennsylvania lubricating oil

[a] Used extensively in all exploratory test work.

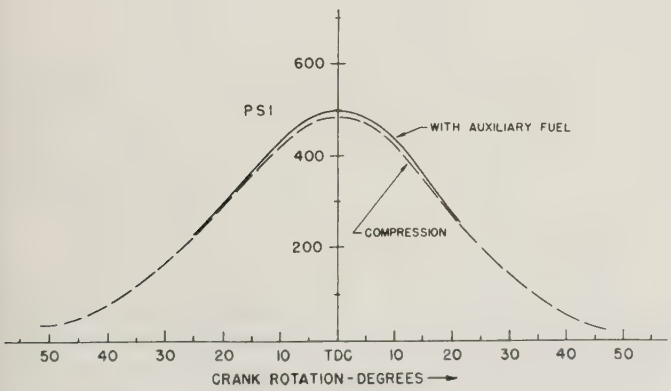

Fig. 3—Pressure-time diagram showing bifuel effect on combustion. ASTM cetane engine with open combustion chamber, compression ratio —16/1, speed—900 rpm, auxiliary fuel—1.5 cc per min kerosene

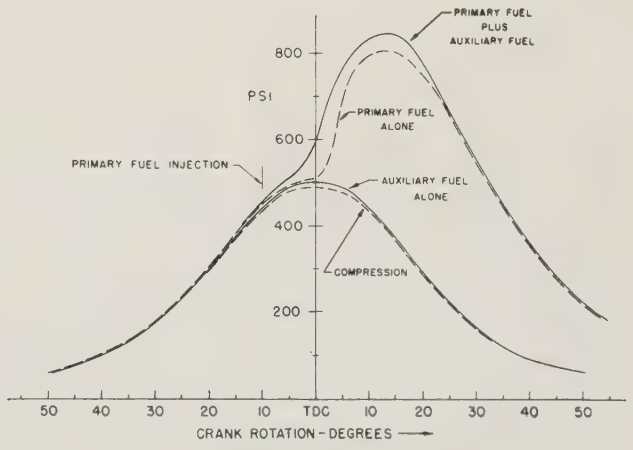

Fig. 4—Pressure-time diagram under same conditions as given in Fig. 3, except: primary fuel—13.0 cc per min ASTM 2-D grade fuel, auxiliary fuel—1.5 cc per min kerosene

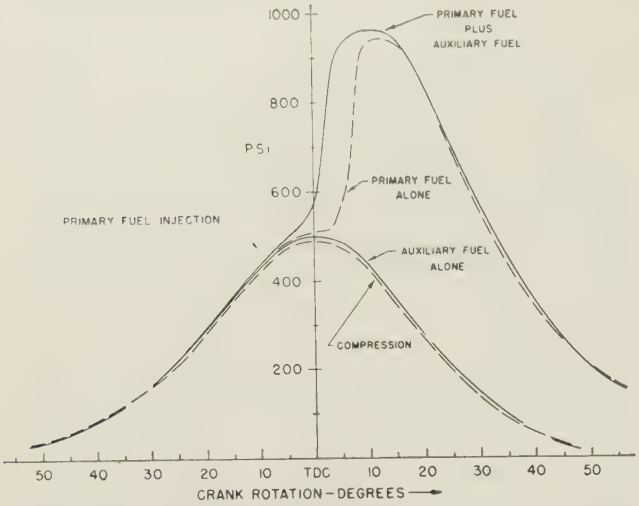

Fig. 5—Pressure-time diagram under same conditions as given in Fig. 3, except: primary fuel—13.0 cc per min catalytically cracked distillate, auxiliary fuel—1.5 cc per min kerosene

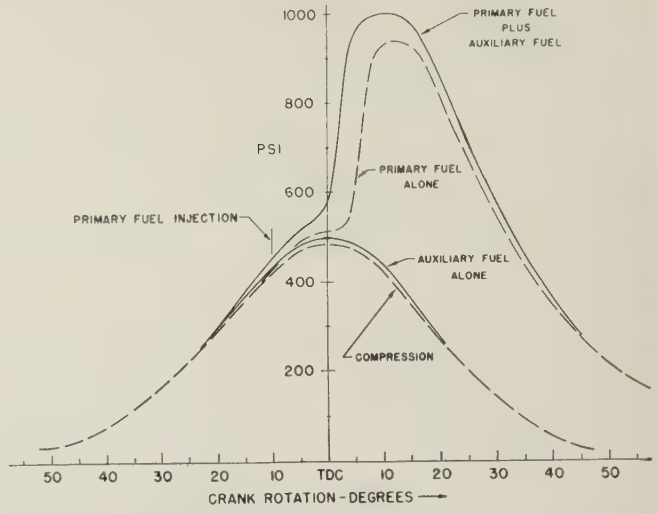

Fig. 6—Pressure-time diagram under same condition as given in Fig. 3, except: primary fuel—13.0 cc per min catalytically cracked distillate, auxiliary fuel—1.5 cc per min ASTM 1-D grade fuel

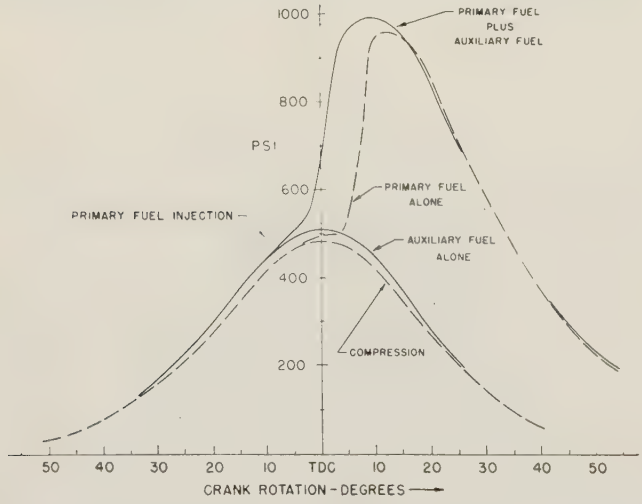

Fig. 7—Pressure-time diagram under same conditions as given in Fig. 3, except: primary fuel—13.0 cc per min catalytically cracked distillate, auxiliary fuel—ASTM 2-D grade fuel

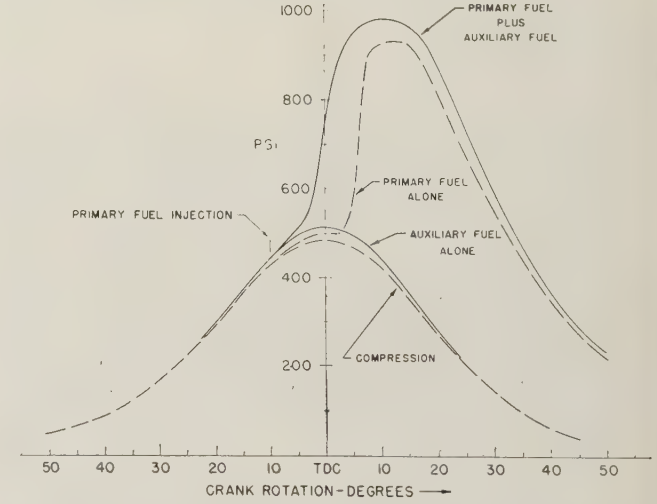

Fig. 8—Pressure-time diagram under same conditions as given in Fig. 3, except: primary fuel—13.0 cc per min catalytically cracked distillate, auxiliary fuel—1.5 cc per min Pennsylvania lubricating oil

shown in Figs. 6 and 7. Fig. 8 shows the composite traces for the same fuel but using a 72 viscosity (SUS at 100 F) Pennsylvania lubricating oil as the auxiliary fuel. Fig. 9 shows the results obtained on a 97 viscosity (SUS at 100 F) light No. 5 residual as primary fuel and 10% kerosene as auxiliary fuel. This was obtained on the ASTM cetane engine.

Figs. 10 and 11 show the rather peculiar traces obtained on a 97 Research octane number gasoline and on benzene as primary fuels when using 22% kerosene in the first instance and 20% in the second as the auxiliary fuel. Neither of these primary fuels could be run alone in the open-chamber engine at its fixed compression ratio of 16/1.

Similar experimental data have been obtained in the ASTM cetane engine run at various speeds and loads. The quantity of auxiliary fuel required by a given engine for successful operation is fairly constant, irrespective of speed and load. Consequently, on a total fuel input basis the amount of auxiliary fuel to primary fuel will vary considerably percentagewise.

The laboratory analyses of the primary and auxiliary fuels used in obtaining these diagrams are given in Table 2.

An analysis of the pressure-time diagrams indicates the following: 1. Oxidation of the auxiliary fuel occurs during the compression stroke. 2. The use of an auxiliary fuel advances the start of the primary-fuel combustion (shortens ignition delay). 3. Higher peak pressures, with somewhat lower rates of pressure rise, are encountered using an auxiliary fuel.

Reduction in Engine Compression Ratio—It is possible, through use of the bifuel combustion Process, to operate an engine successfully on a low-

Table 2—Analysis of Primary and Auxiliary Fuels Used in Combustion Studies

	Primary Fuels					Auxiliary Fuel			
Fuel No.	1	2	3	4	5	6	7	8	9
Type	Straight-Run ASTM 2-D Grade Fuel	Catalytically Cracked Distillate	Light No. 5 Residual Fuel Oil	Premium Gasoline	Benzene	Kerosene	Straight-Run ASTM 1-D Grade Fuel	Straight-Run ASTM 2-D Grade Fuel	Pennsylvania Lubricating Oil
Gravity, deg API	38.5	25.2	21.4	59.6	28.6	42.7	42.1	Same as Fuel No. 1	31.9
Kinematic Viscosity at 100 F, cs	2.92	2.55	97.2 SUS	0.55	—	1.63	1.78		72 SUS
Sulfur, %	0.13	0.56	0.84	0.02	—	0.06	0.05		0.1
Carbon Residue (10% Residue), %	0.12	0.34	4.91 (whole sample)	—	—	0.06	0.07		0.02
Aniline Point, F	163.2	81.7	—	—	—	147.9	151.1		190.4
Olefins, %	3.6	20.4	—	—	—	0.1	1.4		—
Aromatics, %	11.9	43.6	—	—	—	13.4	11.6		—
Distillation									
Ibp	380	442	420[a]	85	—	340	342		—
10%	434	482	500	107	—	375	373		—
50%	514	505	582	215	176	427	445		—
90%	609	551	70% 635	312	—	487	537		—
Ep	658	590	73% 702	388	—	519	571		—
Cetane No.	56	26	59	—	Below 0	50	50		—
Research Octane No.	—	—	—	97.0		—	—		—

[a] ASTM vacuum distillation.

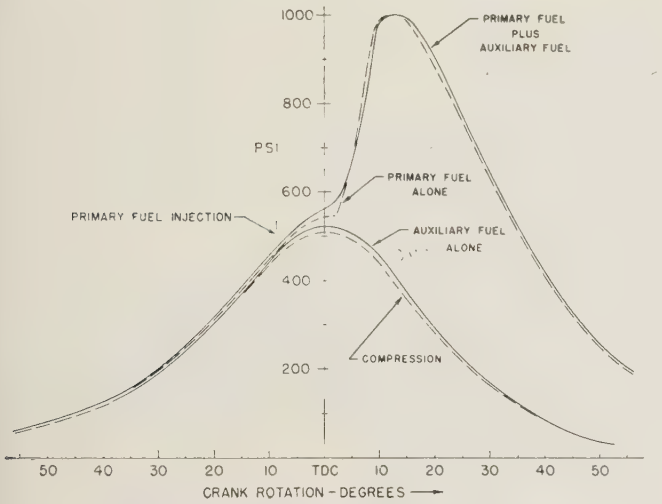

Fig. 9—Pressure-time diagram under same conditions as given in Fig. 3, except: primary fuel—13.0 cc per min light No. 5 residual fuel oil, auxiliary fuel—1.5 cc per min kerosene

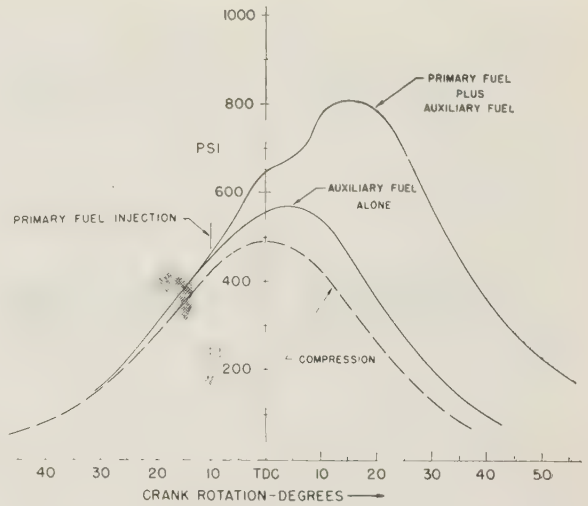

Fig. 10—Pressure-time diagram under same conditions as given in Fig. 3, except: primary fuel—13.0 cc per min premium gasoline, auxiliary fuel —3.7 cc per min kerosene

Table 3—Analysis of Primary Fuels Employed in Experiments on Reduction in Compression Ratio

Fuel No.	10	11	12	13	14
Type	Blend of Catalytically and Thermally Cracked Stocks	Thermally Cracked Distillate	Aromatic Naphtha	Catalytically Cracked Distillate	Benzene[a]
Gravity, API	23.0	20.2	34.2	25.1	28.6
Kinematic Viscosity at 100 F, cs	2.221	2.580	0.895	3.245	
Cetane No.	22.5	16.7	16.5	26.8	Below 0
Distillation, F					
Ibp	334	436	331	442	
10%	446	466	337	489	
50%	495	492	345	518	176
90%	551	542	361	594	
Ep	606	602	386	660	

[a] Nitration grade.

cetane-number primary fuel at a compression ratio substantially below that required for operation on the primary fuel alone. This is evidenced by the results obtained on the ASTM cetane engine when using a series of primary fuels having cetane numbers which ranged from below 0 to 26.8. The identities of the primary fuels tested, together with a listing of their pertinent properties, are given in Table 3. Three of these fuels were cracked distil-

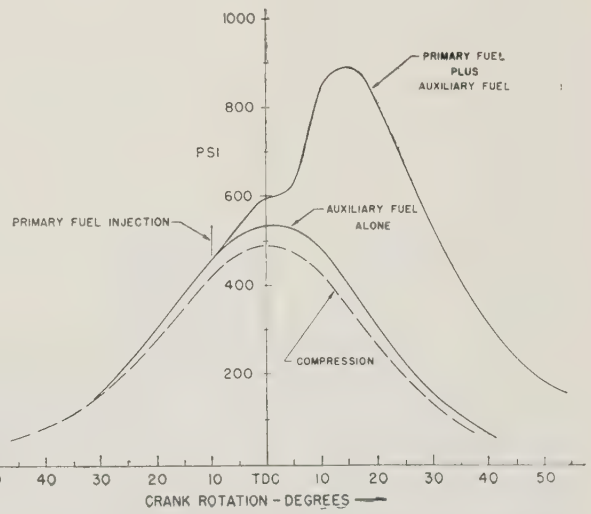

Fig. 11—Pressure-time diagram under same conditions as given in Fig. 3, except: primary fuel—13.0 cc per min benzene, auxiliary fuel—3.3 cc per min kerosene

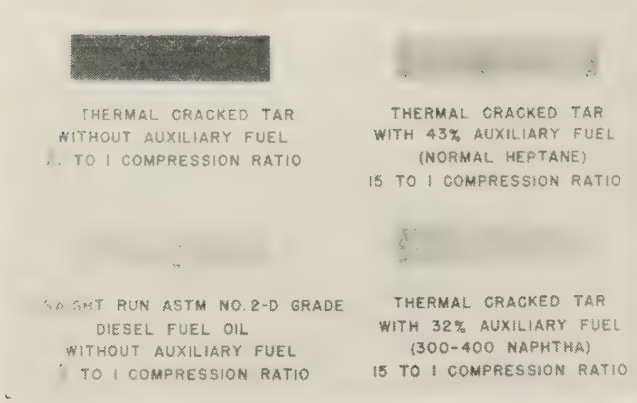

Fig. 12—Reduction in exhaust smoke through use of bifuel process

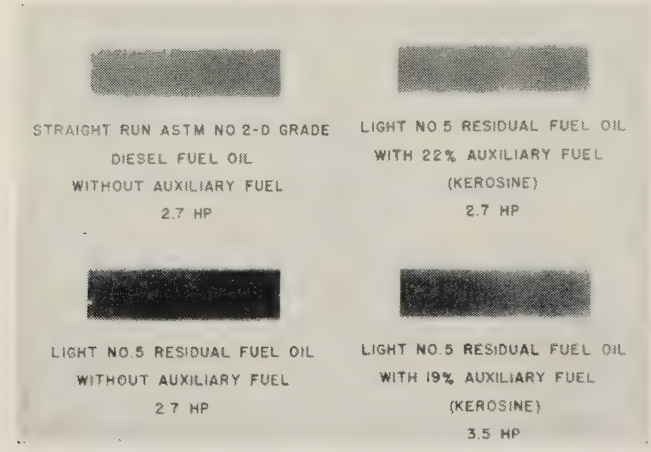

Fig. 13—Effect on exhaust-smoke-limited power output through use of bifuel process

lates whose volatilities identified them as ASTM 2-D types. The fourth fuel represented a close-cut aromatic naphtha having a 331–386 F boiling range. The fifth fuel was nitration-grade benzene, boiling at 176 F. The cetane number of the latter fuel was so low that it could not be established, because its rating fell outside the limits of the ASTM primary reference fuel scale used for determining cetane number.

The reduction in compression ratio that could be realized with these five primary fuels when employing 13% (by volume) reference-grade normal heptane as the auxiliary fuel is shown in Table 4. The percentage of auxiliary fuel used is based on the total fuel injected (primary plus auxiliary).

The data show that a reduction of from 2.2 to 12 compression ratios below the ratios normally required for engine operation on the primary fuels alone could be obtained by means of the bi-fuel process. The compression ratios shown are for steady engine operation in all instances, excepting benzene. This fuel could not be made to burn smoothly at 28/1 compression ratio. Smooth operation was obtained at 16.1/1, however, by means of auxiliary fuel. The variation in compression ratio reduction between the different primary fuels is of

Table 4—Effect of Bifuel Combustion Process on Reduction in Engine Compression Ratios for Steady Combustion

Primary Fuel	Cetane No.	Operating Compression Ratio without Auxiliary Fuel	Operating Compression Ratio with Auxiliary Fuel As n-Heptane	Reduction in Compression Ratio	Vol. % Auxiliary Fuel Based on Total Fuel Input
10	22.5	15.9	13.2	2.7	13.0
11	16.7	23.2	11.6	11.6	13.0
12	16.5	22.8	14.8	8.0	13.0
13	26.8	16.4	14.2	2.2	13.0
14	Below 0	28.0[a]	16.1	11.9	13.0

[a] Erratic operation.

interest. There is some indication that this may be tied in with the aromaticity of the fuel. This is not a proved observation, however.

In these experiments the engine was operated at the test conditions normally used for the ASTM cetane rating procedure, except for air-intake temperature, namely: speed 900 rpm; injection advance, 13 deg btdc; tdc start of combustion; 13 cc per min injection rate of the primary fuel. The air-intake temperature was held at 80–85 F. The auxiliary fuel rate amounted to 2.0 cc per min. The auxiliary fuel was aspirated into the intake manifold of the engine and borne to the cylinder by the intake air charge.

Reduction in Exhaust Smoke—Further studies carried out on the ASTM cetane engine coupled to an electric dynamometer indicate the bifuel process to have merit in reducing exhaust smoke. For example, in one of a series of experiments on this subject, a fairly heavy thermally cracked tar was employed as the primary fuel. This material possessed the following properties:

Gravity, API	4.3
Viscosity at 100 F, SUS	110
Sulfur, %	3.62
Carbon Residue, %	3.3
Cetane Number	15

With the test engine operating at a speed of 1000 rpm, a compression ratio of 21/1, 13 deg btdc injection advance, and 13 cc per min primary-fuel injection rate, the smoke strip shown in the upper left of Fig. 12 was obtained. A Von Brand filtering-type, recording smokemeter was used in obtaining the smoke strips shown in the figure. The instrument was operated at a tape speed of 2 in. per min, an exhaust-line back pressure of 1 in. of H_2O, and a vacuum across the tape of 2 in. of Hg. The smokemeter probe was installed approximately 24 in. down the exhaust line from the engine.

The smoke strip shown in the upper right of this figure is for the same primary fuel plus normal heptane as auxiliary fuel. The normal heptane amounted to 43% (by volume) of total fuel input to the engine. The operating compression ratio of the engine when using auxiliary fuel was 15/1 rather than 21/1, as previously required for the primary fuel alone.

The smoke strip in the lower right was obtained when using 32% (by volume) of petroleum naphtha of 42 cetane number as the auxiliary fuel.

For comparative purposes, the smoke strip for a

straight-run ASTM 2-D grade fuel without auxiliary fuel is shown in the lower left. The similarity in exhaust-smoke density shown on this strip with that obtained on the thermally cracked tar plus auxiliary fuel is apparent. Total fuel input to the engine in all instances was the same, that is, 13 cc per min.

Effect on Exhaust-Smoke-Limited Power Output—A series of experiments carried out on the single-cylinder laboratory engines indicate that the exhaust-smoke-limited power output of engines of this type can be increased by means of the bifuel process. An example of this is shown in Fig. 13. The exhaust-smoke strips shown in this chart were obtained from an ASTM cetane engine. The engine was operated at 1000 rpm at a compression ratio of 15/1. Injection advance was 13 deg btc. A Von Brand smokemeter operated under the procedure previously described was used for obtaining the exhaust-smoke densities.

The smoke strip in the upper left of this chart was obtained on a straight-run ASTM 2-D grade fuel of 54 cetane number. No auxiliary fuel was employed. It will be noted that the output of the engine was 2.7 hp. This was obtained with a fuel-injection rate of 15.8 cc per min.

The strip in the lower left was obtained with the engine operating on a light No. 5 residual fuel, also without auxiliary fuel. In this instance, fuel input was adjusted to give the same hp as obtained on the previous fuel. This input amounted to 16.0 cc per min.

The increased blackness or opacity of this strip compared to the one obtained on the 54-cetane-number distillate is evident.

The smoke strip shown in the upper right was obtained on the residual fuel plus 22% (by volume) kerosene as auxiliary fuel. In this instance also, the power output was held at the same level as before. Total fuel input amounted to 15.8 cc per min. However, input of primary fuel amounted to 12.3 cc per min and that of the auxiliary, 3.5 cc per min.

The improvement in exhaust-smoke density over that obtained when operating on light No. 5 residual without auxiliary fuel is apparent.

The lower right-hand strip shows the resulting exhaust-smoke density when the engine was operated at a 30% higher horsepower output on residual fuel plus 19% (by volume) kerosene as auxiliary fuel. In this test the input of residual fuel to the engine amounted to 15.0 cc per min while the input of auxiliary fuel amounted to 3.5 cc per min.

Under these higher power output conditions the exhaust-smoke density level was reasonably comparable with that obtained on the straight-run ASTM 2-D grade fuel at a lower power output (smoke strip in the upper left).

The laboratory inspections on the two primary fuels used in these particular studies are given in Table 5.

Performance Tests in Small Engines—A number of 80- and 100-hr tests have been run in small engines in order to establish the feasibility of running such engines for extended periods on low-grade fuels using the bifuel process.

In one series of tests, five fuels were run for a period of 80 hr each in a GM model 2-71 diesel engine. The bifuel process was used in burning fuels 15, 16, 17, and 18. These were low-cetane-number distillates. The fifth fuel 19, was straight-run ASTM 2-D grade fuel which was run for comparative purposes. Table 6 gives the laboratory analysis on the five fuels tested.

The 80-hr test period was established on the basis of the time required for the engine to consume approximately one drum of fuel (55 gal) under the test conditions employed. The engine was loaded by an a-c generator. The governed operating speed of the engine was 1200 rpm. The load maintained throughout the test was 25% of full load. The engine was run at a jacket outlet temperature of 135 F and a lubricating oil temperature of 165 F. An SAE 30 grade straight mineral lubricating oil was used throughout. Normal heptane was used as the auxiliary fuel during the tests on the four low-cetane-number primary fuels. This was introduced into the intake airstream in a quantity amounting to 12% (by volume) of the total fuel used.

All four low-cetane-number fuels ran quite successfully with the aid of auxiliary fuel in the engine under the test conditions employed. Little difference could be noted between the performance of these fuels and that obtained on the straight-run ASTM 2-D grade fuel in respect to deposits and wear. It should be pointed out that the engine could not be started at room temperature on any of the low-cetane-number fuels without assistance of auxiliary fuel.

Tests similar to the above, except that kerosene was used as the auxiliary fuel, were run in a single-cylinder ASTM cetane engine for periods of 100 hr. Laboratory inspection data on the primary fuels used in the two long-time tests on this engine are

Table 5—Primary Fuels Used in Experiments Studying Effect of Bifuel Process on Exhaust-Smoke-Limited Power Output

	Straight-Run ASTM 2-D Grade	Light No. 5 Residual Fuel
Gravity, deg API	39.0	22.7
Flash, F	160	208
Viscosity at 100 F, SUS	38.4	102.3
Sulfur, %	0.20	0.61
Carbon Residue, Conradson, %	—	5.44
Cetane No.	54.0	26

Table 6—Analysis of Primary Fuels Used in 80-Hr Performance Tests on GM 2-71 Engine

Fuel No.	15	16	17	18	19
Type	50% Alkylate Bottoms 50% Alpha Methyl-naphthalene	Alkylate Bottoms	Catalytically Cracked Distillate	Gasoline	Straight-Run ASTM 2-D Grade Fuel
Gravity, deg API	26.9	51.6	21.9	52.4	39.0
Viscosity at 100 F, SUS	30.9	30.8	39.9	—	38.4
Sulfur, %	0.64	0.05	0.73	—	0.20
Aniline Point, F	98.6	—	101.1	—	158.0
Olefins, %	2.5	3.6	12.8	—	5.0
Aromatics, %	58.5	2.4	44.2	—	14.0
Distillation, F					
Ibp	362	357	464	105	365
10%	394	369	481	172	421
50%	428	383	516	244	499
90%	465	468	617	301	593
Ep	526	611	645	350	645
Cetane No.	12	24	31.8	—	54.3
Octane No.	—	—	—	86.4	—
Reid Bapor Pressure, psi	—	—	—	6.9	—

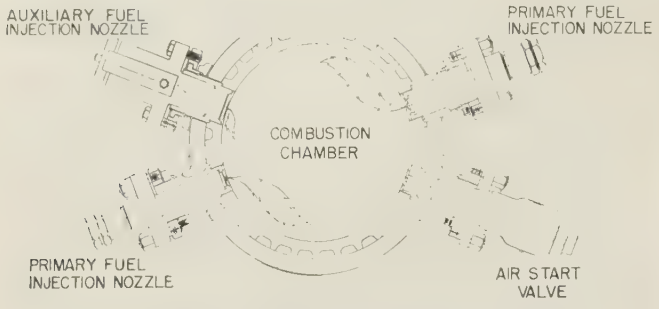

Fig. 14—Bifuel combustion system design arrangement

Table 7—Analysis of Primary Fuels Used in 100-Hr Performance Tests on ASTM Cetane Engine

Fuel No.	20	21
Type	No. 6 Residual Fuel	Aromatic Extract from SO_2 Treat
Gravity, deg API	12.2	26.8
Viscosity at 100 F, SUS	2700.0	30.0
Sulfur, %	2.5	4.0
Carbon Residue, Conradson, %	10.87	—
Aromatics, %	—	81.0
Distillation, F		
Ibp	425[a]	350
10%	652	375
50%	915	442
90%	—	526
Ep	—	543
Cetane No.	35	10

[a] Vacuum distillation.

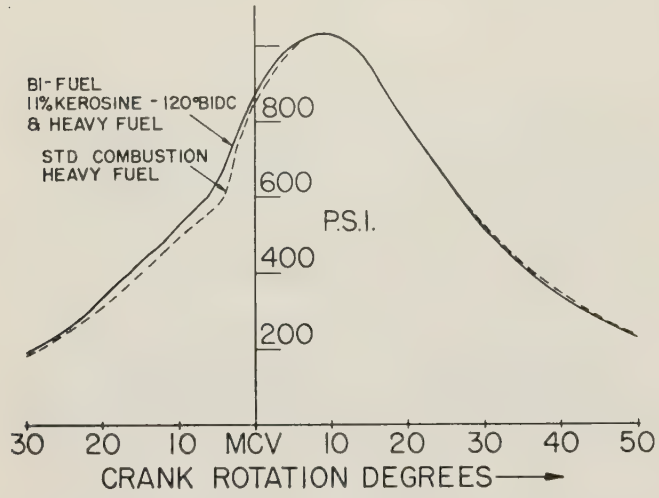

Fig. 15A—Bifuel versus standard combustion. Pressure-time diagram at 100% load and 720 rpm. Proper application of bifuel process.

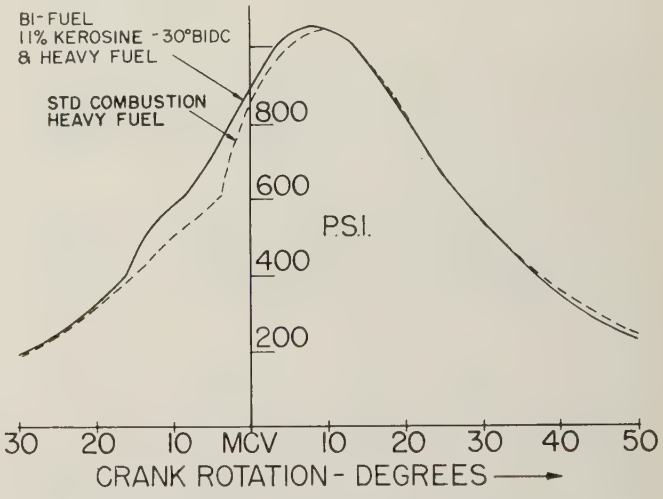

Fig. 15B—Bifuel versus standard combustion. Pressure-time diagram at 100% load and 720 rpm. Late injection of auxiliary fuel.

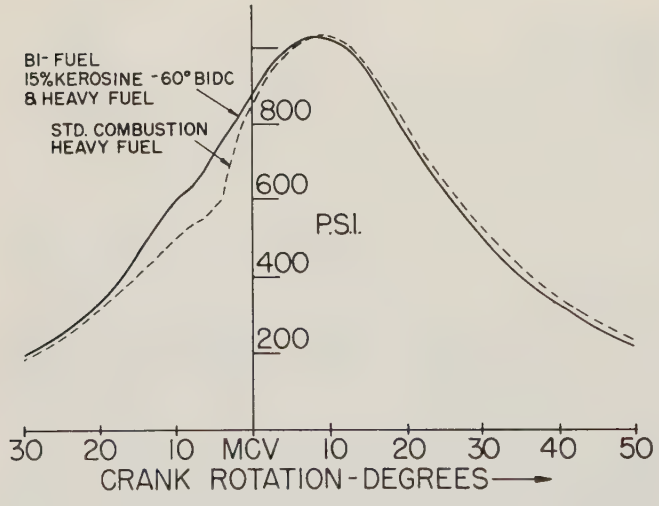

Fig. 15C—Bifuel versus standard combustion. Pressure-time diagram at 100% load and 720 rpm. Injection of too much auxiliary fuel.

given in Table 7. The engine was operated at 13/1 compression ratio at a speed of 1000 rpm. Load was adjusted to 75% of maximum power at this speed. Input of auxiliary fuel amounted to 12% of total fuel. The auxiliary fuel was injected into the air intake at 15 deg before closure of the intake valve.

No operating difficulties whatsoever were encountered with either of these fuels.

Laboratory Tests in a Large Full-Scale Engine

Further work on the development of the bifuel combustion system required testing with larger-size engines than the ones used for the exploratory studies previously discussed. Fairbanks, Morse and Co., in conjunction with Sinclair Research Laboratories, Inc., decided to conduct a series of tests on a commercial engine.

The residual-fuel-burning engine chosen for this test work was the four-cyl model 38D 8⅛. This is a 2-stroke, opposed-piston engine of blower-scavenger design. The bore is 8⅛ in. and the stroke of each crankshaft is 10 in., giving a combined stroke of 20 in. The engine operates at 720 rpm and is rated at 160 bhp per cylinder. The air-intake ports are near the upper end of the cylinder and the exhaust ports near the bottom. Primary fuel is injected through two nozzles installed diametrically opposite each other in the sides of the cylinders, approximately midway between the air and exhaust ports.

The first problem was one of designing and applying components necessary for admitting auxiliary fuel to the cylinders. The requirements of this sys-

tem included: (1) admission of the auxiliary fuel once per revolution at the desired point in the cycle; (2) metering accurate fuel quantities to the cylinder; (3) atomization and distribution of fuel in the cylinders; and (4) injection of fuel at a constant timing. Various means of accomplishing these requirements were possible. For expediency, a unit injector was made which operated off the standard gas valve tappet linkage used on the gas-burning version of this engine. The injector was installed in one of the four adapter holes located at the middle of the cylinder liner. This arrangement is shown in Fig. 14. This drawing also shows the location of the primary-fuel nozzles as well as the direction of air swirl obtained by the skewed position of the air-port bridges. Three different capacity plungers were made for these unit injectors. This allowed testing auxiliary fuel quantities of 8, 11, and 15% (by volume) of the full-load primary-fuel input. The auxiliary-fuel injection timing could be set at any point desired in the engine cycle.

Tests to determine the effect of auxiliary-fuel quantity showed that 15% (by volume) auxiliary fuel ignited prior to the primary-fuel injection point. Audible knocking resulted. Auxiliary-fuel quantities of 11 and 8% (by volume) appeared to give the required results for bifuel combustion.

The effect of auxiliary-fuel injection timing was also studied. If auxiliary-fuel injection occurred late in the compression stroke, 30 deg before inner dead center (bidc) or later, ignition of the auxiliary fuel took place prior to the injection of the primary fuel. At earlier ignition timings, between 60 and 120 deg bidc, preflame oxidation appeared to take place without completing the ignition process. This is, of course, the desired result, as pointed out earlier in the discussion. Point-by-point cylinder-pressure-time diagrams were taken while conducting these tests. Fig. 15 shows combustion without auxiliary fuel compared to: (1) injection of 11% (by volume) auxiliary fuel at 120 deg bidc (A); (2) injection of 11% (by volume) auxiliary fuel at 300 deg bidc (B); and (3) injection of 15 % (by volume) auxiliary fuel at 60 deg bidc (C). The reduction of maximum rate of pressure rise brought about by proper application of the bifuel combustion process can be seen in Fig. 15A. The traces in Figs. 15B and 15C point out the uncontrolled and early combustion of auxiliary fuel caused by late injection (B) or by introduction of too large a quantity of auxiliary fuel (C).

Engine performance was determined when operating with and without bifuel combustion. Comparable results are shown in Fig. 16. It is interesting to note that engine economy d'd not change under the two test conditions except at the lower loads. These data strongly indicate that primary-fuel combustion occurs at increased efficiency when operating with the bifuel process. This increased efficiency makes up for all power losses caused by auxiliary fuel preflame oxidations occuring prior to minimum clearance volume.

Upon completion of combustion evaluation tests, a series of wear tests was conducted. The bifuel combustion process was set up for kerosene auxiliary fuel injection at 120 deg btdc. The primary fuel was a No. 6 residual fuel oil. The analysis given in Table 8 shows the range of fuel characteristics encountered. This fuel was prepared for burning in the engine by heating to a temperature to give a Saybolt viscosity of about 100 at the nozzles, centrifuging, and by 2-stage filtration. After a breakin period of 235 hr a complete engine inspection was made for base-line wear data. The engine was then operated 500 hr at rated speed and load. All wear data were based on the latter 500 hr of test. This test procedure was repeated four times. The fourth test was extended to 1030 hr of operation. Fig. 17 shows the

Table 8—No. 6 Residual Fuel Analysis

	Min	Max
Gravity, deg API	11.8	18.0
Viscosity at 210 F, SUS	93.4	123.2
Bottom Sediment and Water, %	Trace	0.5
Pour Point, F	0	75
Sulfur, %	1.55	2.66
Conradson Carbon Residue, %	7.37	10.97
Ash, %	0.0024	0.66
Cetane No. (Blended Value)	35	35
Vacuum Distillation (Corrected to Standard Conditions)		
Initial Boiling Point, F	405	460
50%, F	891	930
Recovery, %	50	65
Vanadium, ppm	23.5	54.3
Sodium, ppm	3.4	41.9

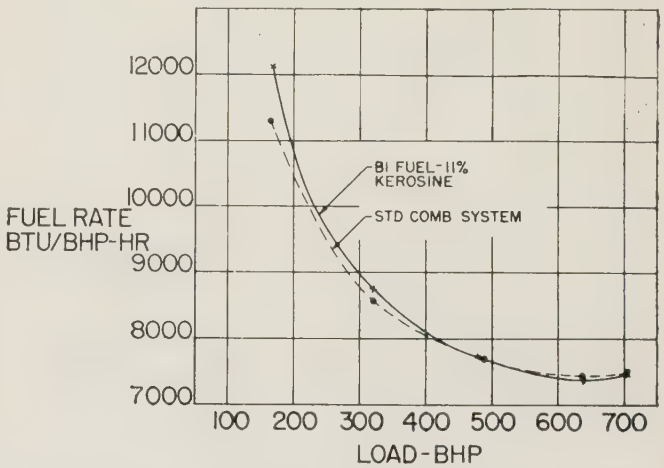

Fig. 16—Fuel consumption, bifuel system versus standard system

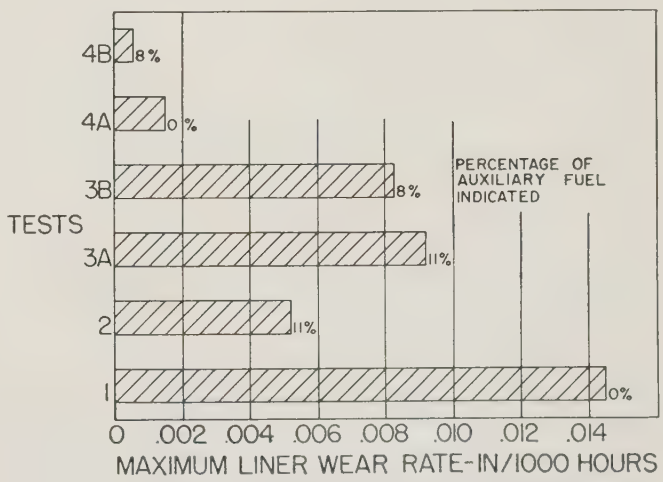

Fig. 17—Maximum cylinder-liner wear rates, heavy fuel and bifuel operation

cylinder-liner wear results obtained. The engine was operated on the No. 6 residual fuel without the aid of the bifuel combustion process in test 1. In test 2 the bifuel process was used and employed 11% auxiliary fuel. A split bifuel process engine was used in the third test where two of the cylinders operated with 11% auxiliary fuel (test 3A), while the other two cylinders operated with 8% auxiliary fuel (test 3B). Again in the last test a split engine was used, but this time two of the cylinders operated on No. 6 residual fuel (test 4A), while the other two cylinders were aided by the bifuel process employing 8% auxiliary fuel (test 4B). The large reduction in wear rate from the first test to the fourth test is mainly due to changes in other engine and test variables. The percentage of auxiliary fuel used in each test is indicated above the bars. Note that the two tests are split engine tests where one-half the cylinders had either a different quantity of auxiliary fuel than the other half or none at all. This was done in an effort to minimize any effects due to changing residual-fuel properties during the course of the tests. The graph shows that no appreciable difference in wear rate results between 11% and 8% (by volume) auxiliary fuel, but the wear rate ratio of 1 to 3 when using either quantity as compared to standard combustion is readily evident.

Fig. 18 is a view of cut-up cylinder liners used in tests 1 and 2. The major reduction in chrome surface corrosion that was obtained when operating with the bifuel combustion process can be easily noted.

An economic study of the bifuel combustion process as used on the Fairbanks, Morse & Co. $8\frac{1}{8} \times 10$ opposed piston engine shows that the increased fuel cost due to using 8% (by volume) kerosene can be turned into an overall saving by reducing part replacement and maintenance costs. The break-even point must be determined for each residual oil under consideration, as well as for the engine load factor, application, lubricating oil used, and other deciding factors.

Conclusion

The results of all the tests carried out to date can be summarized as follows: First, the process described widens the usable range of fuel quality for diesel engines of various types and sizes. Also, there are several commercial auxiliary fuels that can be used to satisfy the requirements of the process. Secondly, and more specifically for particular engines, the process will reduce exhaust-smoke density, increase the exhaust-smoke-limited power output, reduce deposit formation, and reduce power parts wear rates.

In realizing the advantages of the bifuel process, several disadvantages are evident, namely: the cost of the added equipment required, adaptability of the process to new and existing engines, and requirement of a two-fuel system.

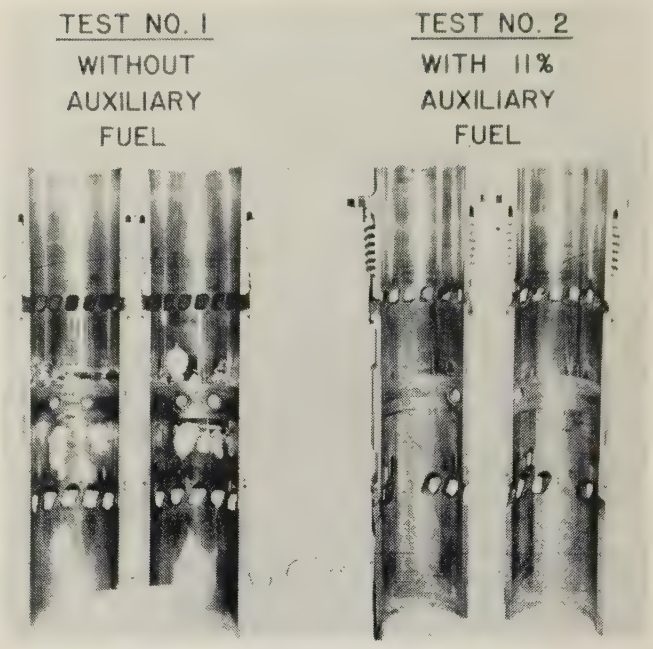

Fig. 18—Cylinder liners used in tests with bifuel process and standard system

Additional References

1. "Precombustion Reactions in a Motored Engine," by D. L. Pastell. SAE *Quarterly* Transactions, Vol. 4, Oct., 1950, pp. 571–587.

2. "Ignition of Fuels by Rapid Compression," by C. F. Taylor, E. S. Taylor, J. C. Livengood, W. A. Russell, W. A. Leary. SAE *Quarterly* Transactions, Vol. 4, April 1950, pp. 232–274.

3. "Early Combustion Reactions in Engine Operation," by E. B. Rifkin, C. Walcutt, G. W. Betker, Jr. SAE *Quarterly* Transactions, Vol. 6, July, 1952, pp. 472–487.

4. "Reaction Processes Leading to Spontaneous Ignition of Hydrocarbons," by C. E. Frank, A. U. Blackham. NACA Technical Note No. 2958, June 1953.

5. "Spontaneous Ignition Temperatures of Pure Hydrocarbons and Commercial Fluids," by J. L. Jackson. NACA Research Memorandum No. E 50J10, Dec. 1950.

6. "A Study of the Autoignition Properties of Certain Diesel Fuels," by J. E. Johnson, J. W. Crellin, H. W. Carhart. Naval Research Laboratory Report No. 3859, Dec. 21, 1951.

7. "Power Booster Fuels for Diesels," by E. J. McLaughlin, P. L. Pinotti, H. W. Sigworth. SAE Preprint No. 682. Presented at SAE National Fuels and Lubricants Meeting, Chicago, Oct. 29–Nov. 1, 1951.

8. "Secondary Fuels for Diesel Engines," by W. G. Ainsley, H. D. Young. Presented at Bureau of Mines Diesel Conference, May 17–18, 1951.

9. "The Effects of Supplementary Fuel Addition by Fumigation Through the Inlet Manifold on Diesel Engine Performance," by P. H. Schweitzer. Pennsylvania State University, Department of Engineering, Research Technical Report, May, 1956.

THIS paper on automotive gasoline injection covers:

1. The basic engine requirements for the gasoline-injection system.

2. The principal advantages achieved with fuel injection for passenger-car and truck engines. There is a report on the successful field test of a gasoline-injection car entered in a transcontinental economy run.

3. A detailed description of the components and operation of the American Bosch injection system.

Automotive Gasoline Injection

C. H. Nystrom, American Bosch Division, American Bosch Arma Corp.

This paper was presented at a meeting of the SAE Cleveland Section, Cleveland, Jan. 21, 1957.

WE have been manufacturing fuel-injection equipment for diesel engines for well over 25 years and electrical equipment for automotive engines for well over 40 years. It was only natural that, since we were manufacturing fuel-injection equipment for diesel engines, we would be interested in the application of an injection pump for the gasoline engine.

Some 20 years ago our company began experimental and research work in the field of handling gasoline in connection with an Air Force contract and the development of a 12-cyl injection pump. During World War II we designed and built a gasoline-injection system for the Wright 3350 engine used on the B-29 bomber. During 1950–1951 we used some of our diesel pumps for metering of gasoline on a 6-cyl truck engine. Although the tests were successful, it was apparent that this injection equipment would be too expensive for the application.

Shortly afterwards we felt that the automobile manufacturer would soon be considering fuel injection for his engine. With this in mind we started a development program to design a very small, compact, and simplified low-cost injection pump. We studied the various designs of single plunger pumps which we were building for diesel engines, and took from these pumps the best features which are today the basic design of the injection pump.

Requirements for Gasoline-Injection System

We made a study of the fuel system required by the modern gasoline engine, whether it be a carburetor or fuel injection, and there are certain basic engine requirements which I would like to discuss:

1. Optimum air–fuel ratio under varying loads and speeds.

2. Starting enrichment, tapering off during warmup.

In the case of carburetion, the cold starting and warmup require substantial amounts of fuel to provide the initial wetting of the manifolds; yet still have adequate liquid and vaporized fuel for the cylinders to insure firing. In our tests on cold-starting carbureted engines, we found that at full choke the engine used as much as 16–20 times full-load fuel quantity; whereas the injection system only required 3–4 times full-load fuel quantity. Naturally this high fuel flow adversely affects fuel economy and increases air pollution.

3. Idling enrichment to compensate for exhaust gas dilution.

With a modern high-speed V-8 engine we do have considerable valve overlap and, consequently, exhaust gas dilution. In the case of a carburetor, this requires considerable idle enrichment. In tests with our fuel-injection system we found we could use less enrichment during idle.

4. Load enrichment for full power at full throttle.

It is quite true that even with an injection system there is an enrichment necessary for full power, but it is less than with a carbureted engine.

5. Acceleration enrichment to avoid momentary lean-out.

All present-day carburetors are provided with acceleration pumps which add fuel during acceleration. With our injection system we found that this acceleration fuel was not necessary to get good acceleration without faltering.

6. Fast idle during warmup.

In the case of carburetion with its exhaust manifold heat crossover, which is necessary to get good vaporization of the fuel, the engine is allowed to run with a fast idle for a considerable length of time during cold weather. With gasoline injection, tests have proved that the fast-idle speed can be set much lower than with the carburetor. The time requirement for this fast idle is very short, because we atomize and spray the fuel just outside the intake valve, and presumably get a better mixture when the engine is cold.

In addition to these, there are other desirable

features which should be incorporated, if possible:

1. Altitude compensation.
2. Temperature compensation.
3. Fuel cutoff during deceleration.

We recently incorporated these features in our injection equipment. For the first, a small bellows was installed in the link between the control piston and the operating lever which moves the sleeve. In this way, we were able to lean out the mixture automatically as altitude increased. For temperature compensation we put a small bimetallic spring on the underside of the operating lever, which gave satisfactory results over the normal ambient operating temperatures.

Fuel cutoff during deceleration has been accomplished by an auxiliary piston on the top of our main control piston. When engine vacuum goes above 23 in. of Hg vacuum, fuel is cut off. We were able to accomplish this very simply because of the small force necessary to move the control sleeve of the pump.

This fuel cutoff is extremely important in certain sections of the country. For example, a great deal of the Los Angeles smog is attributed to unburned gases pouring from vehicle exhausts during deceleration. Our fuel cutoff, if installed in all automobiles, could help this situation immeasurably.

4. Elimination of carburetor icing.

This is a very real problem with carburetors. Under certain atmospheric and temperature conditions, ice formation on carburetor throttles can be very annoying. With our gasoline-injection system, there is no fuel being vaporized across the throttle body and we do not have any ice problem.

5. Reduce vapor lock.

People in the northern part of the United States do not experience vapor lock nearly as much as those living in the South and Southwest, where it can really be a problem. We conducted tests at our plant during a very hot spell last summer, taking two identical vehicles, one with a carburetor and one with our fuel injection. Both vehicles were run until the engines were boiling hot. Both were then soaked in this condition for about 30 min, after which restarts were tried. With our injection system we obtained satisfactory restarts in 6–7 sec. But in the case of the carbureted car we had to wait a considerable length of time before a restart could be made.

Principal Advantages

With fuel injection, we have been able to meet all the basic engine requirements, as well as to incorporate additional features. At the same time we have accomplished certain definite advantages with fuel injection as compared to the carburetor. These are as follows:

1. Increased power.
2. Higher torque.
3. Improved fuel economy.
4. Quicker cold starting and warmup.
5. No need for manifold heat.
6. Lower intake temperatures.

These advantages are important for both passenger-car and truck applications, but I believe most important for truck engines. When the system is considered for the modern passenger car, there are still additional advantages—styling and advertising. Incidentally, the latter advantages in some cases are the most important.

About a year and a half ago, we announced our gasoline-injection system for use in truck and passenger cars. It has now been tested in a number of different engines, on dynamometers, and in installations of various passenger cars and trucks by different manufacturers, as well as by various oil companies in the country. We are road testing continuously four cars equipped with fuel injection for evaluation of basic design components and new experimental features.

Since most of our testing was conducted in the New England area, it was decided last spring to participate in the Mobilgas economy run in Los Angeles. Arrangements were made through combined efforts of American Bosch, General Petroleum Co. of California, and du Pont. General Petroleum thought it would be of great interest to people in this country to include a gasoline-injection car in the Mobilgas economy run. Of course, this entry had to be unofficial, as all cars entered in this race are standard stock cars.

The trip provided us with an excellent opportunity to evaluate our fuel-injection equipment. This car, traveling some 13,000 miles, would be subjected to hot and cold weather, dusty desert conditions, high speeds, hill climbing, and altitude conditions of the far West.

One of our test drivers made the trip across the United States to Los Angeles, from there to Colorado Springs and back to Los Angeles, then up to San Francisco and, from there, home. Altitude ranged from 203 ft below sea level to the 11,312 ft encountered at Continental Divide at Monarch Pass.

The results of the economy run have been publicized on radio and television, as well as in newspapers and magazines. No one lost and everyone won. We were the undisputed winner in our class without really attempting to drive for close economy. Of course, there were no other cars running with fuel injection.

Unfortunately, the carbureted Lincoln was withdrawn shortly before the race started. This left us no means of comparison.

We incorporated various types of testing during the run. These included running stretches with excessively rich setting, using three drivers, demonstrations at impound areas, 0–60 mph acceleration checks, and just plain transportation. General Petroleum used our car to demonstrate that they were prepared with their present stocks of fuel and oil to service American Bosch gasoline-injection equipment. Our system amazed and pleased everyone who saw and drove the car. The performance and simplicity were, without exception, highly regarded by all.

On the return trip to Springfield, we had an opportunity to drive strictly economy-run style at times, and obtained mileages a good 10, 15, and even 20% better than those of the same car equipped with a carburetor.

When the car left Springfield on March 3, 1956, we were prepared for any eventuality. The trunk of the Lincoln contained a complete set of service tools for almost any part of the engine or injection system. Extra copper tubings, bundyweld tubing for injection lines, spare gas lines, and spares of all in-

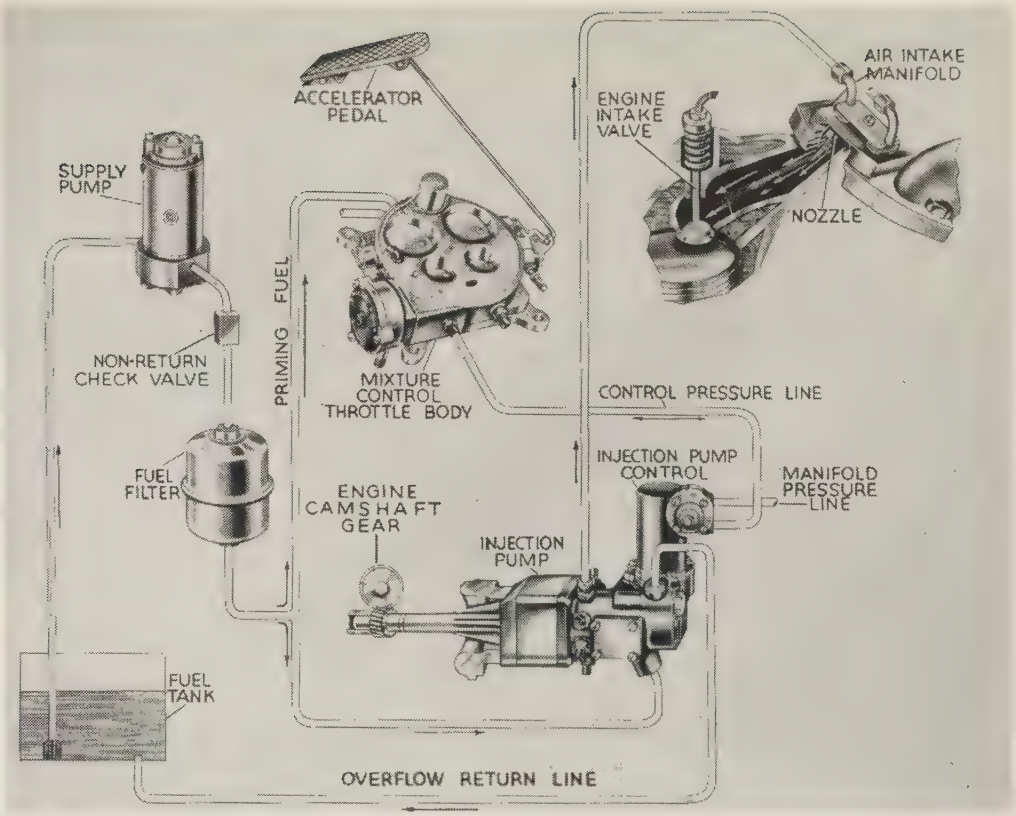

Fig. 1—Gasoline-injection system

jection system components were also carefully packed because we would be 3000 miles away from replacements, if they were needed.

I believe it is significant to state that all this equipment, so carefully inventoried in the luggage space, remained as luggage throughout the entire trip. It was unpacked and replaced in stock the day the car was returned to Springfield.

American Bosch Fuel-Injection System

I will discuss some illustrations which I believe will explain the American Bosch fuel-injection system.

Fuel drawn from the fuel tank by an electric supply pump is first filtered through a micronic fuel filter, as shown in Fig. 1. Then it is delivered to the injection pump, where supply pressure is maintained at a constant 20 psi by a pressure-regulating valve built in the injection pump. Since the output of the supply pump is in excess of the maximum fuel delivery of the injection pump, the overflow fuel is piped back to the tank.

The injection pump, driven at half engine speed, meters and delivers fuel through eight outlets located on the pump periphery. Each of the pump outlets is connected to a nozzle which injects the fuel into the airstream, just before the intake valve at the beginning of the intake stroke. The end of injection occurs before the closing of the intake valve, thus providing ample time for induction and thorough mixing of the fuel charge.

The injection pump control, which is an air piston linked to the control shaft of the pump, receives control pressure from the mixture control unit, and adjusts the fuel delivery of the injection pump in relation to the engine load over the entire operating range.

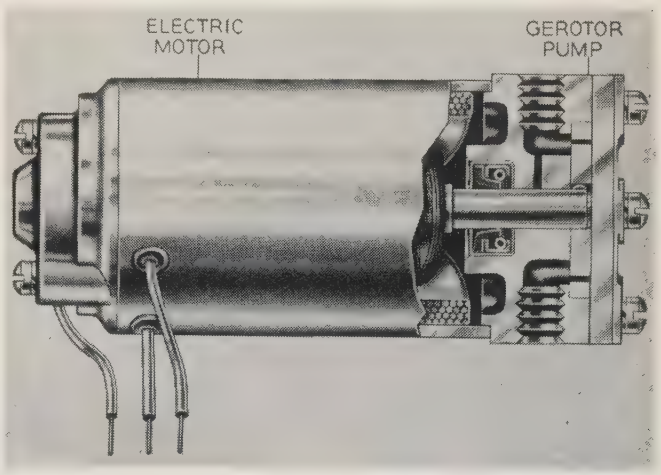

Fig. 2—Fuel supply pump

The mixture control unit, mounted on the intake manifold in place of the carburetor, also contains the conventional throttle blades, the idle speed adjustment screw, and the idle mixture adjustment screw. For cold operation during engine warmup a modulating valve, operated by a temperature-sensitive element, modifies the control pressure to provide a rich mixture to the engine until the engine reaches normal operating temperature. A solenoid-actuated internal priming valve, fed at fuel supply pressure, provides excess fuel for cold starting.

Fuel Supply Pump—The fuel supply pump consists of an electric-motor-driven gerotor pump capable of supplying fuel at over 200 lb/hr at a pressure of 20 psi with a 12-v, 3.3-amp input, as shown in Fig. 2. A pressure regulating valve built in the

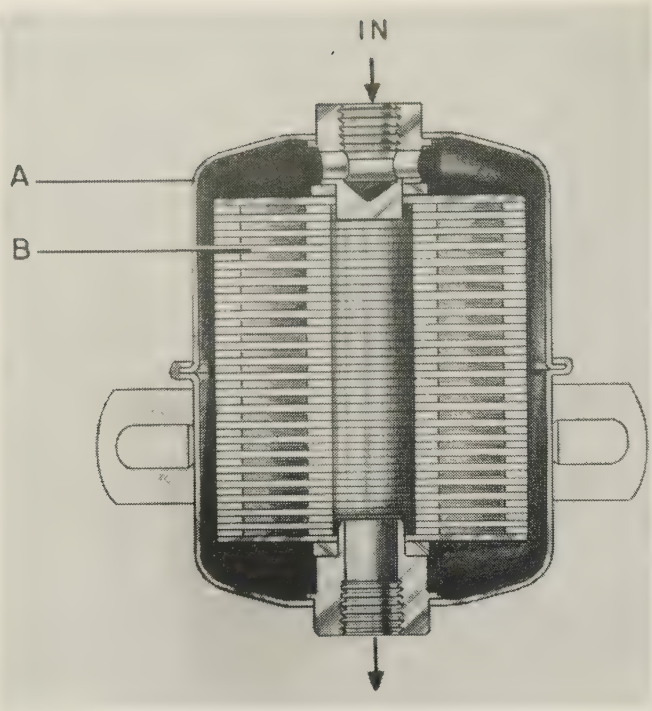

Fig. 3—Fuel filter

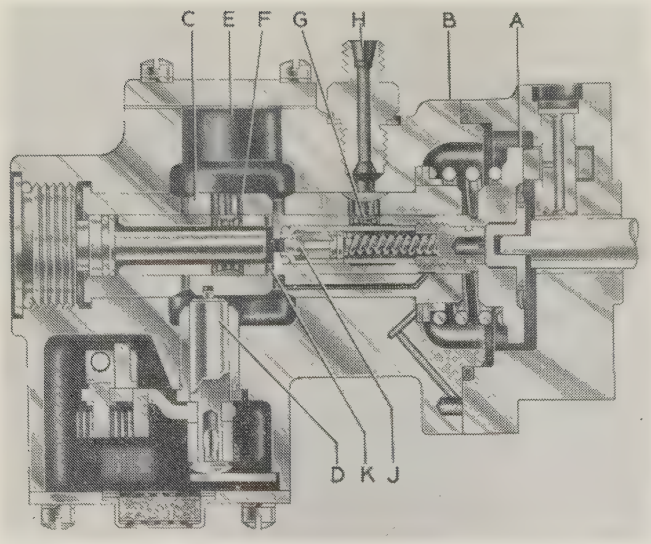

Fig. 4—Injection pump—general construction

injection pump maintains system pressure to a nominal 20 psi, which is well over the service vapor pressure of the fuel. A discharge check valve located between the supply pump and injection pump prevents the decay of supply pressure in the system during temporary engine shutdown.

Fuel Filter—The fuel filter (Fig. 3) is especially designed for gasoline use and consists of a steel enclosure and filter element. The filter element is built up of alternate layers of resin, impregnated filter paper, and fiber spacers to provide 5-micron filtration of the fuel. This element is of the same type that has been widely used with diesel engines.

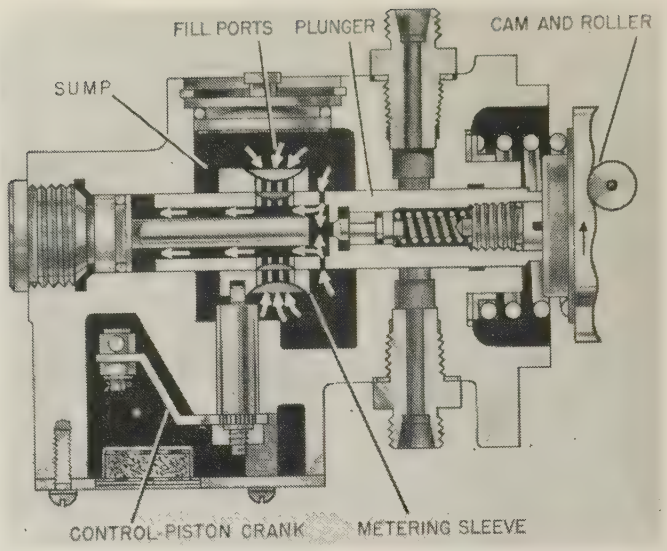

Fig. 5—Injection pump operation showing fuel intake

Service life of the filter is approximately 30,000 miles.

Injection Pump—The injection pump shown in Fig. 4 is comprised of an integral 8-lobe face-cam and plunger *A* reciprocating and rotating within its housing *B*. A metering sleeve *C* is fitted to the plunger to control the fuel spill point and is adjusted for metering position by the eccentric shaft *D*. The metering sleeve is keyed to prevent rotation and can only move axially, relative to the position shown.

In operation, supply fuel enters sump *E* and fills the internal volume of the plunger through fill ports *F* in both plunger and sleeve that have come into registry at the beginning of the suction stroke. As the plunger turns, the fill ports are covered at the end of the suction stroke and a distributing slot *G* registers with one of the outlets *H*. At the start of the pumping stroke, the fuel trapped in the plunger is forced out of the plunger through spill ports *K* back into the sump, until the spill port is covered by the metering sleeve. The fuel is then forced past the delivery valve *J* and through the distributing slot *G* to a nozzle line. Injection continues to the end of the stroke, and the cycle repeats for an adjacent outlet.

Pumping Cycle—Figs. 5–7 illustrate more clearly the three phases of the pumping cycle, namely the fuel intake, the spill, and the fuel delivery.

During the intake or suction stroke, flooding of the internal volume of the plunger occurs through the fill ports, as shown in Fig. 5. The pump control has positioned the metering sleeve with respect to the spill ports.

As the plunger rotates (Fig. 6), the fill ports close and a distributing slot, not shown, starts to register with one of the discharge ports to the nozzle line. The pumping stroke now starts, and fuel trapped in the plunger is forced out of the spill ports into the sump.

As the plunger continues its pump stroke, the sleeve covers the spill ports, and the remaining fuel is forced through the delivery valve, out through the distributing slot to the nozzle line feeding the

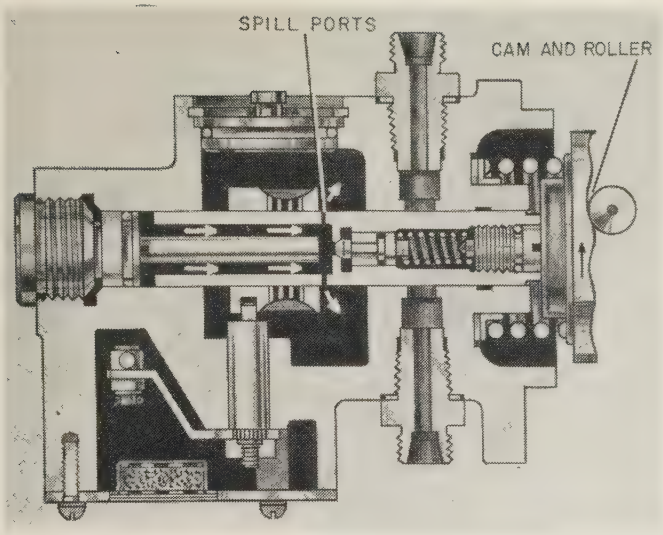

Fig. 6—Injection pump operation showing spill

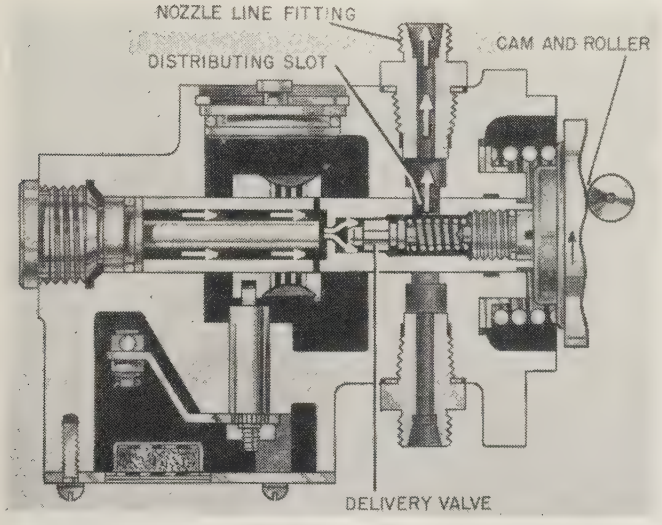

Fig. 7—Injection pump operation showing fuel delivery

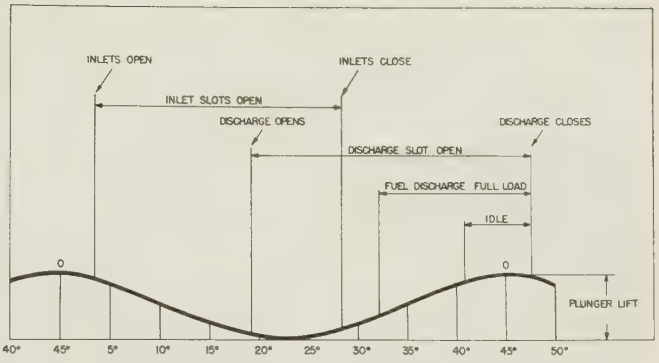

Fig. 8—Plunger lift and porting

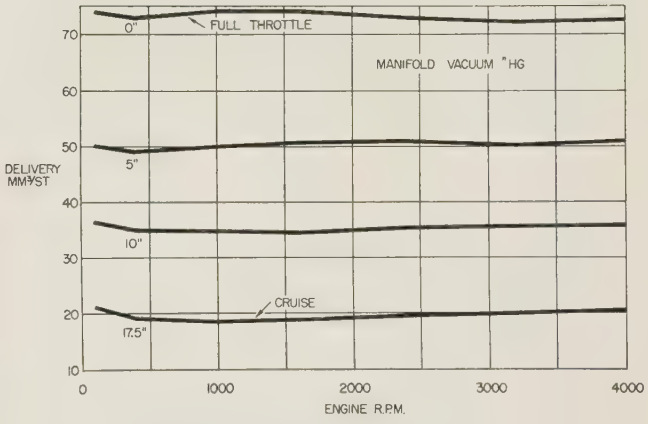

Fig. 9—Injection pump delivery characteristic curve

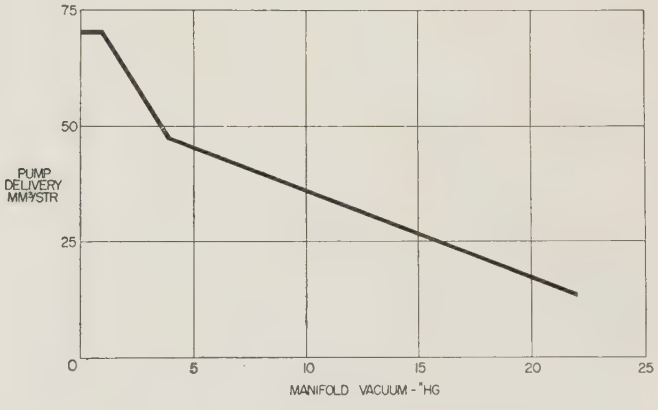

Fig. 10—Typical engine fuel requirement curve

cylinder, as shown in Fig. 7. Injection continues to the end of the stroke.

With an 8-cyl engine, this cycle repeats eight times per pump revolution. At an engine speed of 4000 rpm, the plunger is reciprocating at 16,000 strokes per min or approximately 266 strokes per sec.

Plunger Lift and Porting—Fig. 8 shows the fuel intake, spill, and discharge as the roller follows the cam during its rotation. The inlet slot and the discharge slot are open at the bottom of the stroke. We are able to do this because our spring-loaded delivery prevents fuel from going out through the discharge port.

Pump Delivery Characteristic Curve—With a speed-density type of metering control, the pump delivery characteristic per stroke is basically constant throughout the speed range with fuel quantity change being a function of manifold pressure change, as shown in Fig. 9. The total fuel flow per unit time is, therefore, a function of engine speed and manifold pressure.

Typical Engine Fuel Requirement Curve—Fig. 10 shows a typical fuel delivery requirement of an engine at a constant speed, plotting fuel delivery per stroke against manifold vacuum. Since the change of fuel delivery is linear with respect to change of manifold pressure, a comparatively simple pump control, sensitive to changes in manifold pressure,

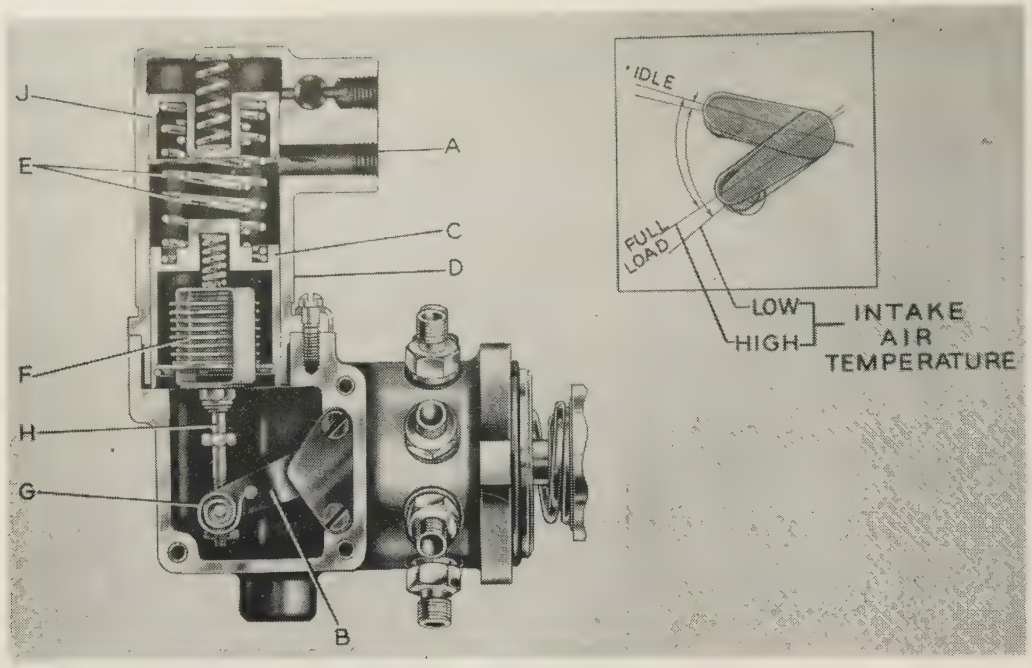

Fig. 11—Injection pump control

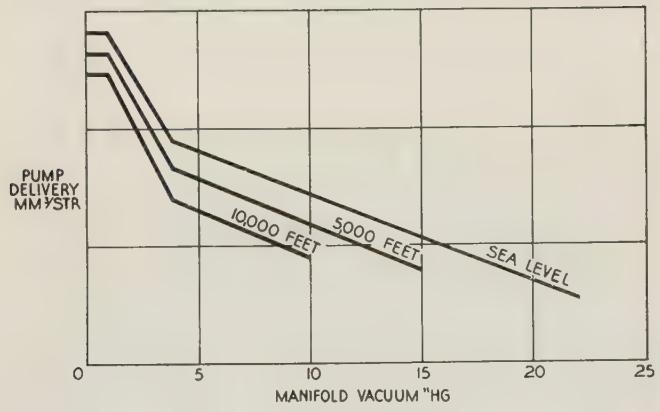

Fig. 12—Altitude compensation

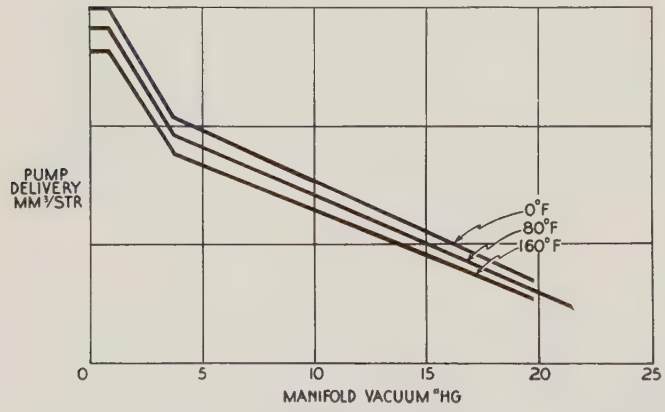

Fig. 13—Temperature compensation

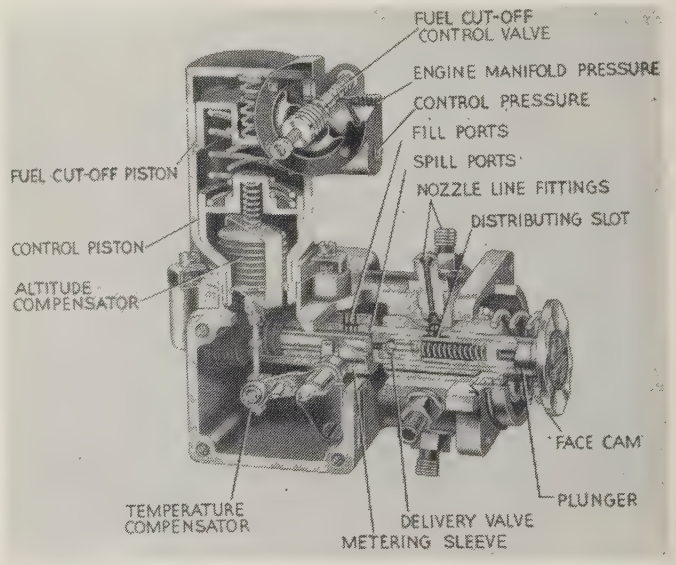

Fig. 14—Sectional view of gasoline injection pump

can be utilized to govern pump setting with respect to engine load.

Pump Control—The pump control (Fig. 11) mounted directly on the injection pump receives control pressure from the mixture control unit through inlet *A* and translates it into angular movement at the metering shaft of the injection pump. The control consists of a piston *C* operating in housing *D* and biased by inner and outer springs *E*. Piston *C* is indirectly linked to metering control lever *B* by link *H* and aneroid bellows *F*. At a high control pressure corresponding to low manifold vacuum (wide-open throttle), the piston is moved toward maximum fuel position (as shown) by the outer spring. As speed increases, the control pressure is reduced. The piston moves upward against the outer spring at a constant rate until the inner spring reaches its seat, at which time the combined spring rate reduces piston travel rate with change in control pressure.

Altitude compensation is obtained by inserting an aneroid bellows between piston *C* and link *H*. The assembly is fixed to the piston and moves with it during normal operation. With an increase in altitude, the bellows expand upward and, in effect,

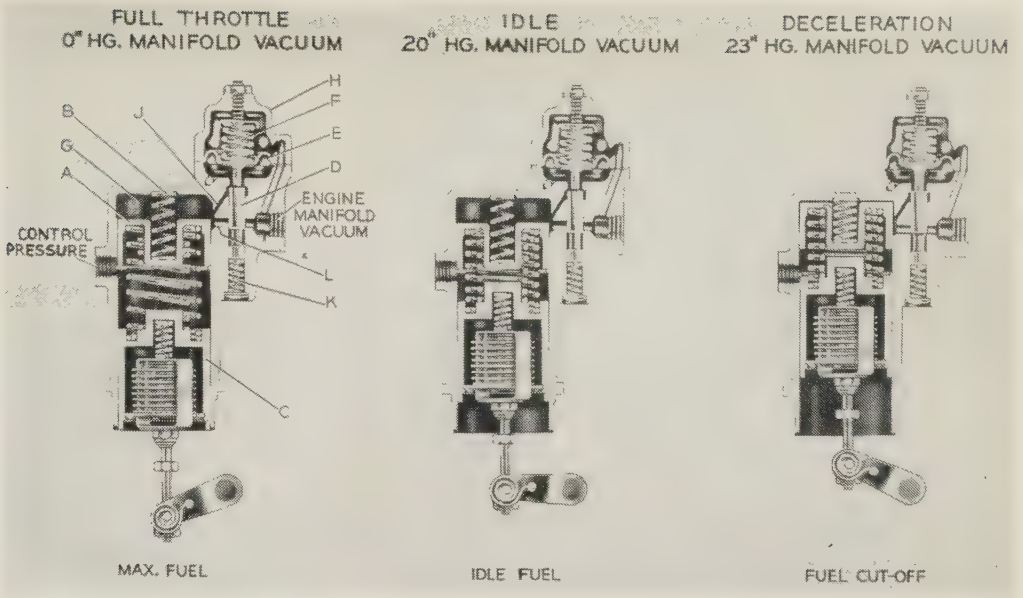

Fig. 15—Fuel cutoff device

shorten the link length between the piston and metering lever. Thus the pump delivery is reduced throughout the entire operating range. Fig. 12 shows a typical fuel delivery requirement at sea level and readjusted pump delivery outputs at 5000- and 10,000-ft altitudes that are obtained with altitude compensation.

Temperature compensation, where required, is provided by coupling lever *B* to link *H* with a temperature sensitive bimetal *G*. The pivot block to which the link is clamped rotates eccentrically on the metering shaft lever *B*. The eccentric is designed to provide an increasing rate of metering lever angular movement per unit movement of the control piston as the latter moves from idle to full load position. This feature permits a constant percentage increase or decrease of fuel delivery with change in temperature. Fig. 13 shows the adjusted pump delivery curves with varying intake air temperature.

Pump and Control Assembly—Fig. 14 shows the interrelation of the control piston and the metering sleeve. The altitude and temperature compensators serve as variable length links which readjust sleeve position with respect to a fixed control piston position.

Fuel Cutoff Device—Attention has recently been directed to the unburned hydrocarbons present in the exhaust of a decelerating engine. There is considerable evidence to indicate that these exhaust products may contribute to the formation of smog. Certainly these unburned gases are wasteful of fuel.

Full cutoff of fuel flow during deceleration can be automatically accomplished in the gasoline system by several methods. During deceleration, manifold vacuum will increase to a value higher than is obtained at idling. For example, with a normal manifold of 20 in. of Hg at idle, the same engine will develop a manifold vacuum up to 25 in. of Hg during deceleration. This narrow range of manifold vacuum above idle can be utilized to sense deceleration conditions and provide the force required to operate a fuel cutoff means.

One such device is shown in Fig. 15 and represents complete fuel cutoff at 23 in. of Hg. It consists of an auxiliary piston *A* biased by a low rate spring *B* and operated by pressure in chamber *G*. Deceleration sensor *H* consists of a two-way shuttle valve *D* operated by differential pressure across diaphragm *E*. Spring *F* is biased by manifold vacuum in the chamber above the diaphragm and by valve return spring *K*. During operation between idle and wide-open throttle, spring *F* positions valve *D* so that atmospheric pressure below the diaphragm is fed to chamber *G* through duct *J*. Auxiliary piston *A* is held against its stop and movement of control piston *C* is limited to its normal operating range.

When manifold vacuum exceeds 23 in. of Hg during deceleration, spring load *F* is unbalanced by the high vacuum and the shuttle valve shuts off duct *J* and opens duct *L*, feeding manifold vacuum to chamber *G*. Piston *A* moves upward reducing the spring load on piston *C*, allowing it to move into full cutoff at 23 in. of Hg. Fuel delivery resumes when idle vacuum values are restored.

Fuel Cutoff Curve—Fig. 16 shows graphically what is explained in Fig. 15: that as the manifold vacuum

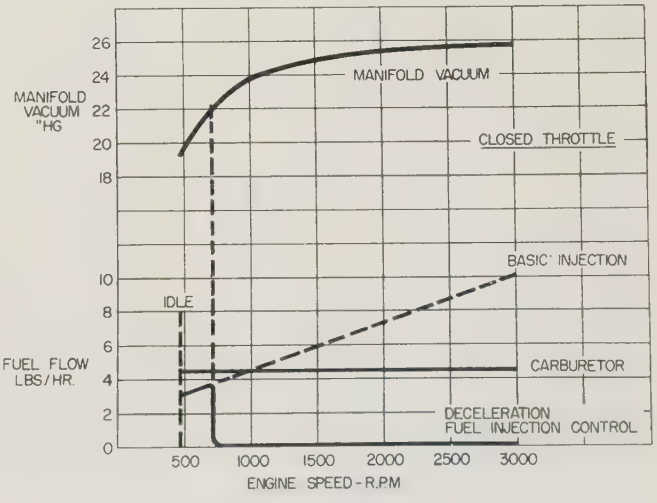

Fig. 16—Fuel cutoff curve

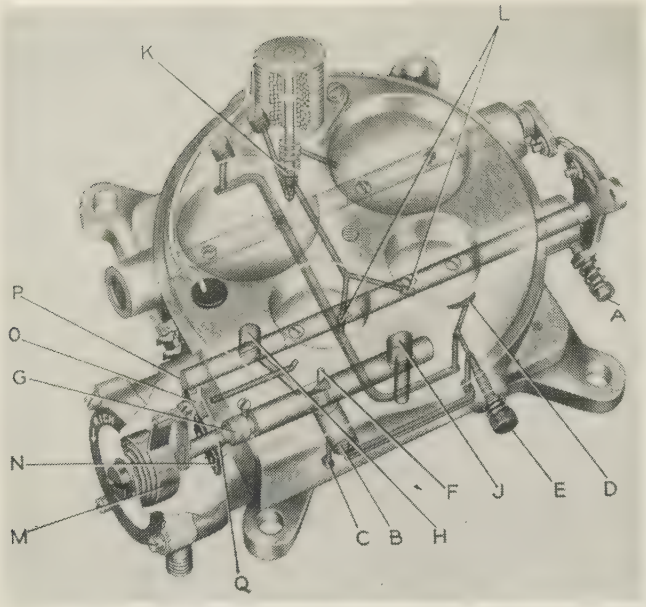

Fig. 17—Mixture control

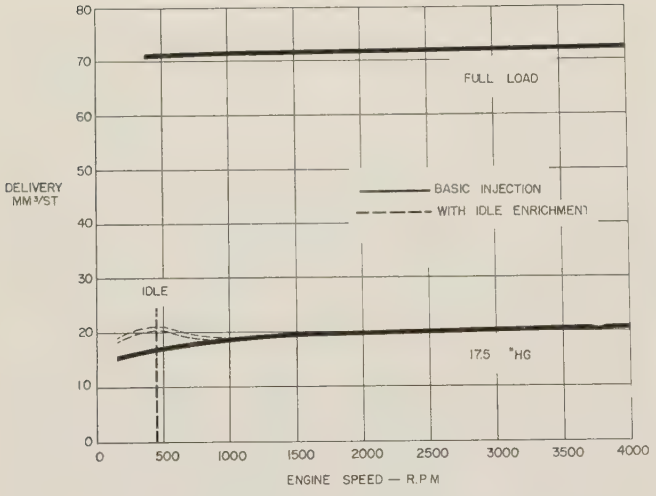

Fig. 18—Idle fuel compensation

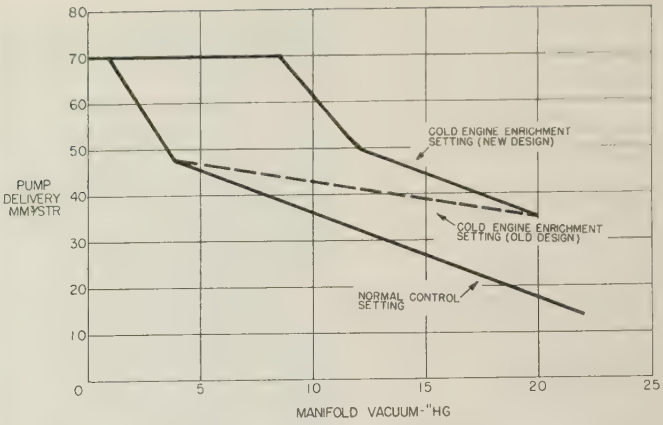

Fig. 19—Enrichment fuel flow control

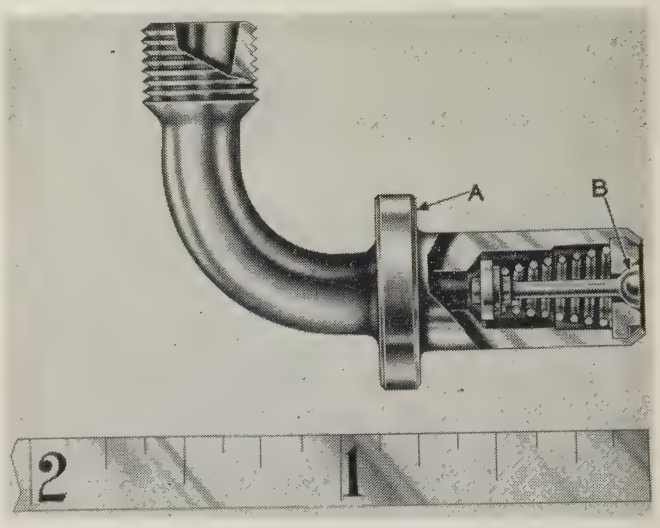

Fig. 20—Injection nozzle

increases during deceleration, it cuts back the fuel flow to zero.

Mixture Control—The mixture control (Fig. 17) contains the conventional throttle blades which are operated by the accelerator pedal and adjusted for idle speed by idle adjustment screw *A*.

Since our system operates to a speed-density principle, the control pressure which operates the pump control is basically manifold pressure throughout the entire range, except at idle and during cold operation. A control pressure chamber *B* receives manifold pressure through duct *C* and feeds the pressure to the injection pump control. During idle, a richer mixture is required to compensate for exhaust gas dilution. A slot *D* milled above the throttle blade at idle position, bleeds intake air pressure to the control chamber and raises the control pressure for a richer pump setting. At above idle position, the throttle blade edge rises above the idle slot, the slot becomes manifold pressure, and idle adjustment screw *E* has no effect on the engine mixture. (See Fig. 18.)

A cold engine requires excess fuel during the warmup period with enrichment gradually tapering off as the engine approaches normal operating temperature. Since the pump meters to a control pressure curve, the control pressure must be raised to increase the pump delivery. This is accomplished as follows:

A drilled orifice *F* connects the control pressure chamber *B* to atmosphere and is closed by modulating valve *G* during normal operation. The valve, operated by thermo responsive element *M*, is rotated during cold operation so that the orifice is uncovered. This feeds atmospheric pressure to the control pressure chamber and raises the control pressure to a higher value. An auxiliary orifice *H* is uncovered by the throttle shaft at above idle setting and supplements the original orifice. This variable orifice is required to maintain a constant differential between manifold pressure and control pressure throughout the entire operating range. As the engine warms up, the modulating valve is rotated gradually until both bleeds are closed. (See Fig. 19.)

In order to insure good cold starting of the engine, a fuel flow two to three times full load value is required. Since supply fuel at a pressure of 20 psi is available as soon as the ignition key is turned on, this convenient source of pressurized fuel is utilized for priming. A solenoid-operated valve *K*, energized by the starter circuit, controls the priming

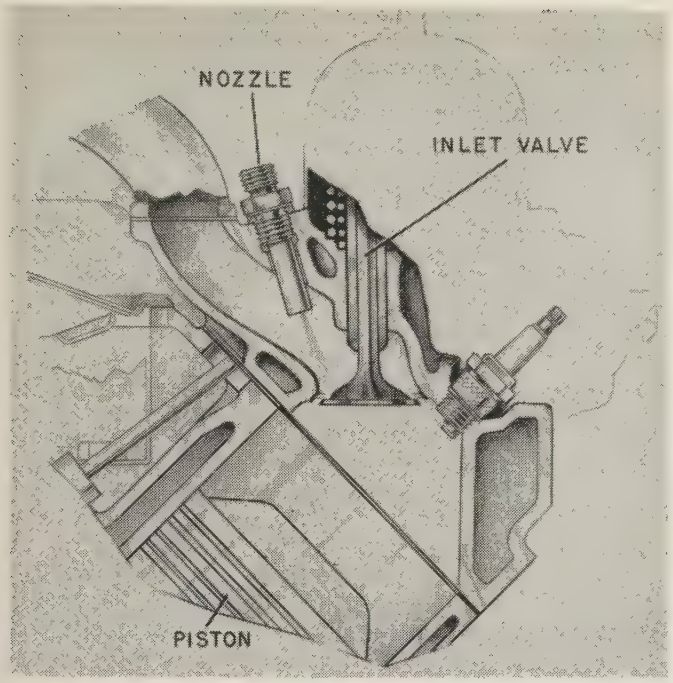

Fig. 21—Nozzle installation

fuel which is sprayed into the manifold through jets *L* located in each of the primary barrels.

During hot re-starts and in the event of flooding, it is desirable to cut off the flow of priming fuel. A microswitch *N*, connected in series in the priming circuit, is actuated by arm *O*, which contacts integral cams *P* and *Q* on throttle shaft and modulating valve, respectively. When either the throttle blades are rotated to wide-open position or the modulating valve is rotated to warm operation position, the switch is opened and priming fuel flow is cut off.

Injection Nozzle—The spray nozzle (Fig. 20) is a simple outwardly opening poppet-type consisting of a seat rolled into a holder, which is available in several lengths to satisfy the various engine and manifold requirements. Opening pressure is 75 psi, and atomization is very good at all quantities due to the floating and self-aligning pintle action.

Nozzle Installation—Fig. 21 shows a typical installation of a gasoline injection nozzle, showing port injection in which the fuel is sprayed towards the back of the inlet valve and is carried into the cylinder by the air during the intake stroke.

Comparative Torque and BSFC Curves—The data for the comparison shown in Fig. 22 was obtained by running the same 300 cu in. V-8 engine with carburetor and with our injection system. You will note that peak torque is higher and also that the same torque is obtained at 500 rpm lower with the injection system than with the carburetor. This explains the livelier throttle response with injection.

Improved fuel economy comparison shown in bsfc between carburetor and injection system is attributed to more uniform distribution.

Road-Load Performance—The data for this comparison was obtained by running the same 300 cu in. V-8 engine in same vehicle with both carburetor and injection system. You will note an improvement of 5 to 15% in mpg can be realized in road-load performance. Again, this is attributed to more

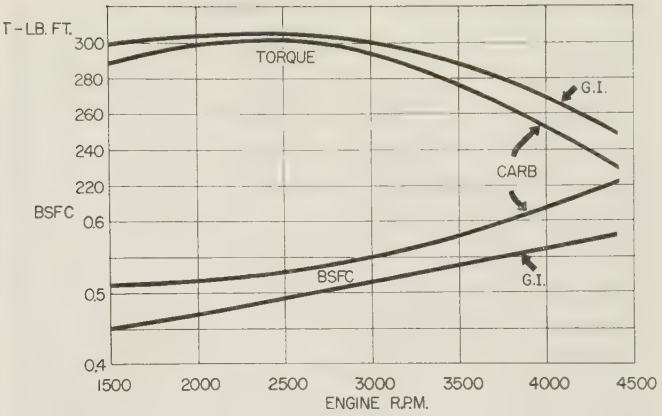

Fig. 22—Comparative torque and bsfc curves for 300 cu in. V-8 engine. Full trottle

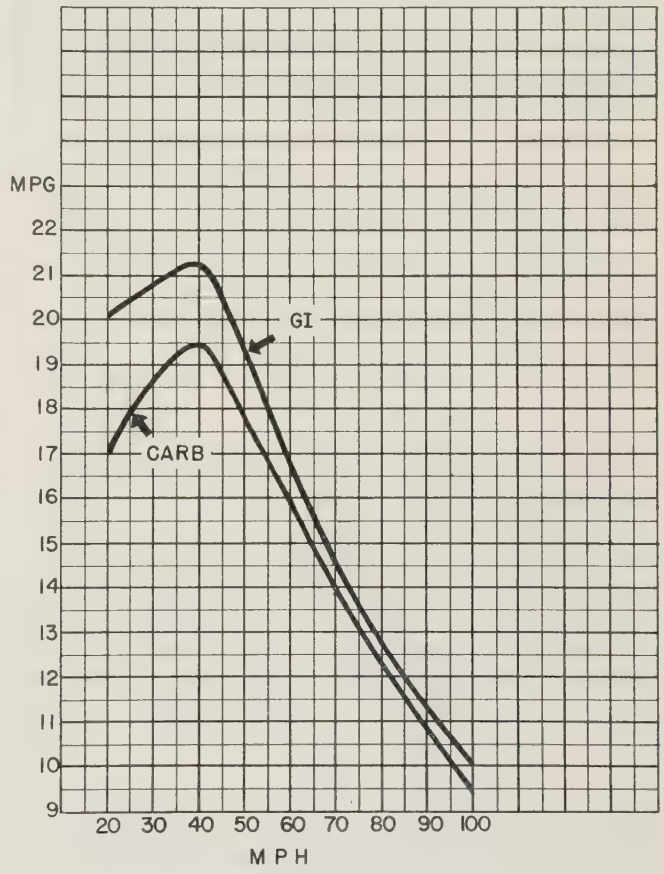

Fig. 23—Road-load performance of 300 cu in. V-8 engine

uniform distribution, no manifold heat, and fuel cutoff during deceleration. (See Fig. 23.)

Installation of System in a 1956 Lincoln—Fig. 24 shows the various components of the complete injection system as installed in a 1956 Lincoln. The pump is driven by a timing belt from the crankshaft at camshaft speed. The mixture control is mounted on the manifold in place of the carburetor and the nozzle is shown in flange of intake manifold, spraying fuel toward the back side of this intake valve.

The supply pump is not visible in the photo as it is mounted underneath the car near the gasoline

Fig. 24—Installation of system in 1956 Lincoln

tank. The bottom of the filter is just visible in upper right-hand side.

It can be seen that if a vertical shaft drive on the centerline of the engine in the front were provided for the injection pump, it would be a much neater installation. This would require relocation of water hose and oil filler cap.

Conclusion

I have often been asked, "What is the future of gasoline injection on the present-day reciprocating engine?" Today we have two basic types of systems to consider, timed versus constant flow.

In the case of timed injection, we have the American Bosch system—which I have described here, and the Borg-Warner system, which is similar to the American Bosch system in that it is timed injection and its control is the speed-density type. Then there is the Bendix Electrojector system, which uses an electronic type of control. There is also the Lucas system, which uses a shuttle-type valve instead of a reciprocating plunger, but uses a basic speed-density-type control. It is my understanding that Holly Carburetor Co. has a license for this system and will carry on the development in this country.

There is the ramjet constant-flow system, which has been announced by General Motors, and is being used by Chevrolet and Pontiac. During the development of the American Bosch metered gasoline-injection system, we studied various carburetion systems, including conventional carburetors, pressure carburetors, and multinozzle constant-flow arrangements. We built such a constant-flow system and it was dynamometer and road tested. In fact, it was quite similar to the present General Motors system. But in our analysis of this system versus timed-metered injection system, we felt that the latter offered the greater potential and the most advantages, not only for application on existing engines but for future engines.

There probably are a number of other carburetor companies, as well as automobile manufacturers, which are working on this constant-flow system.

As for the type of system which will be used in passenger cars of the future, only time will tell. We believe that the time-metered injection system is the right one. It seems to offer the greatest potential. It does seem that the next move would be up to the engine manufacturer. Since we are only accessory manufacturers we do not get into the redesign of engines, combustion chambers, manifolds, or camshafts. We feel that a great deal of work has yet to be done to utilize completely the benefits of gasoline injection to its fullest. By this I mean the redesign of manifolds to incorporate ram effect, as well as the possible use of direct injection into the combustion chamber. This should provide better starting and better acceleration. By proper redesign of the combustion chamber we could obtain better internal cooling, thus permitting higher compression and better volumetric efficiency.

A great deal of work has been done by the Mercedes-Benz Co. in Germany, in using timed injection directly in the combustion chamber. Their engine is designed for fuel-injection use. In this country the engine is designed for a carburetor, and then the fuel-injection system is applied.

I think that the timed injection system, whether it be port or direct injection, allows the oil companies to consider the use of fuels, other than the present ones we are using. Perhaps such things as higher-vapor-pressure fuels could be utilized, and it may be possible eventually to use fuel of a wider boiling range. Study and work on this part of the program is now being carried on by various oil companies in the country who have obtained our injection system and have adapted it to existing cars.

We believe also that the timed injection system has a great potential in the 2-cycle engine. Considerable work along this line is being done in Europe. At the present time in this country outboard motor companies have shown some interest. With some redesigning of engines, I believe that injection can be applied to these engines, resulting in increased power for the same weight engine.

In the case of supercharging, we believe that it will be considerably simpler to apply supercharging to injection than it would be to carburetion.

Still further into the future, I believe something will develop along the lines of controlled combustion—that is, a multifuel type of engine. The Texas Co., I believe, pioneered in this development. There is continuing development along these lines by various universities, oil companies, and engine companies. If someone should be successful in this development, it would greatly increase the use of fuel injection.

In summarizing, I believe that the gasoline-injection system is a new tool with which the automotive engine manufacturer can consider the redesign of the present engine—to take advantage of the injection system. The present engine is now, and has been, designed around the carburetor.

I am often asked, "Why bother with the reciprocating engine when very soon we will be using a gas turbine?" I confidently believe that the gas turbine is a long way off from the reality of six to seven million trucks and cars per year, and that the piston engine will be with us for many years to come.

RESILIENT FACE SEALS

FOR TRACTOR FINAL DRIVES

F. S. Engelking and M. C. Keys, Caterpillar Tractor Co.

This paper was presented at the SAE Annual Meeting, Detroit, Jan. 15, 1957

TRACTOR final-drive seals have to perform their functions under a variety of unusually severe conditions. In most dry operations, they are surrounded by an atmosphere in which dust is highly concentrated. In wet operations, mud may become packed around the seals. In swamps, the seals may have to operate totally submerged in muddy water. Under all these conditions, the seals must keep oil in and mud out.

The seals are located on each side of the sprocket. (See Fig. 1.) They are large and operate at low rotational speeds with a surface speed in the range of 35–175 fpm. They protect the large final-drive gears and the tapered roller bearings. In this final-drive compartment, transmission oil is maintained at a level near the centerline of the shaft.

The very early tractors used a packing-type seal around the shaft. The first seal, consisting of a bellows with a sealing face, appeared in the early 1930s. Since then, as our understanding of the functioning of the seal has grown, many improvements have been made. This paper will discuss these improvements and their effect on the performance of the seal. The function of each part of the sealing system will be analyzed separately and the performance of the entire seal will be evaluated as a unit.

For many years the bellows was formed of brass

TRACTORS operate in a wide range of conditions, from desert to swamp. At all times, the final-drive seals must keep the oil in and the dirt out. In this paper, the authors discuss the latest developments in seal design and the resulting improvements in performance.

Efficient performance of a tractor final-drive seal depends upon a number of factors, including: bellows and bellows-boot operation, seal load and area, seal material, wear washer, and gasket structures.

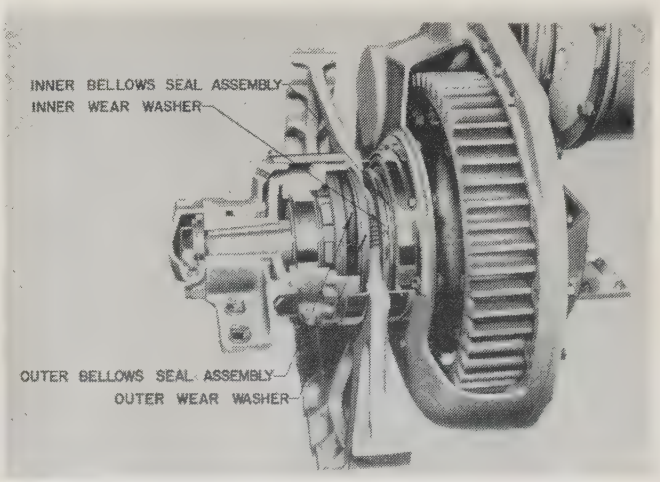

Fig. 1—Tractor final-drive assembly

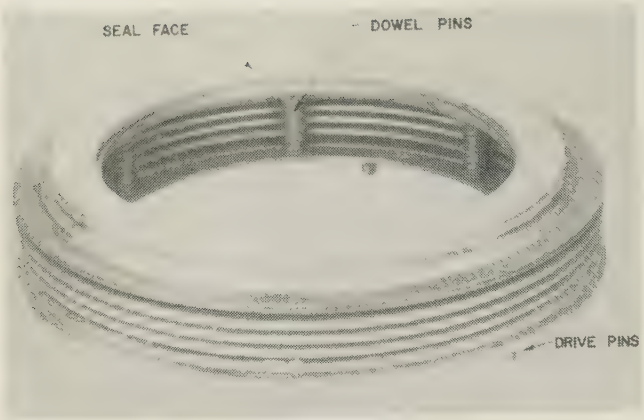

Fig. 2—Brass bellows seal

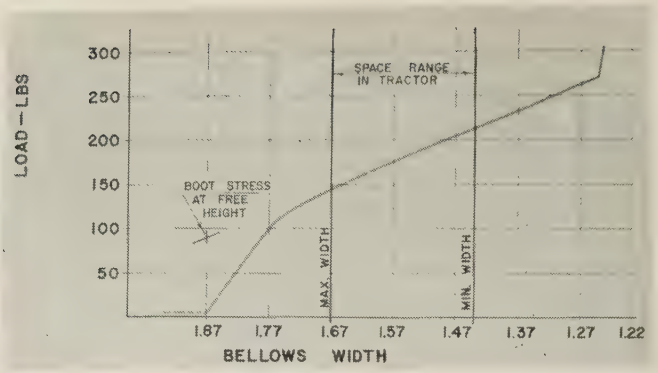

Fig. 4—Bellows width versus load

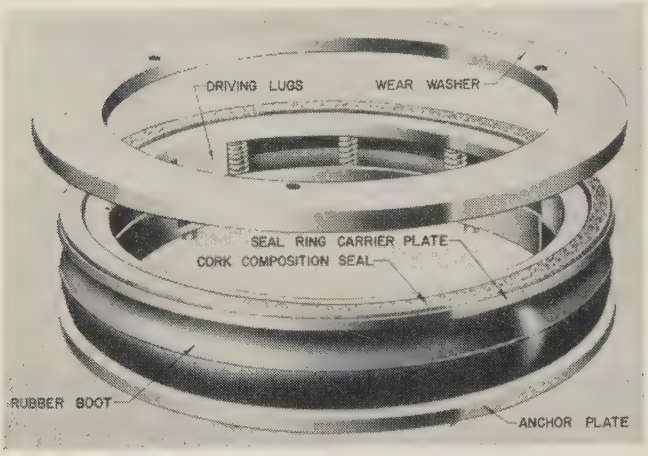

Fig. 3—Bellows seal and wear washer

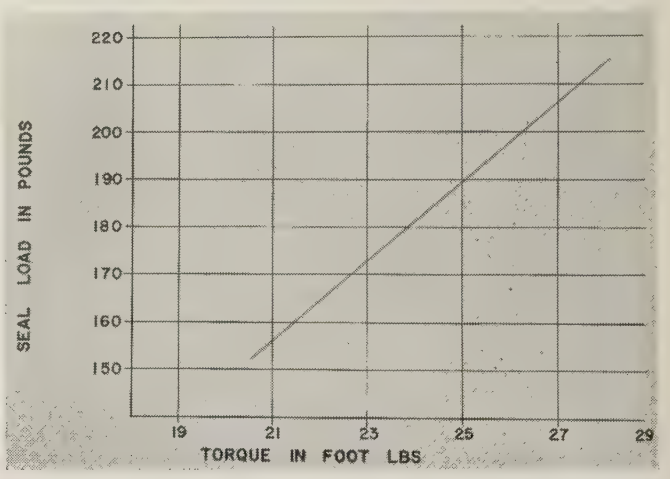

Fig. 5—Seal load versus torque

(Fig. 2). This was attached by solder to a steel backing plate on one side and to a steel seal retainer on the other side. Driving torque was transmitted by seven steel dowel pins attached to the retainer and sliding in holes in the mounting plate. Around each dowel was a small coil spring designed to expand the bellows, which is always static and does not rotate. A gasket is used between the bellows and the final-drive housing. Early gaskets were made in a three-layer design which consisted of 1/16-in. layer of leather bonded between two 1/32-in. layers of cork composition. A single thick cork gasket was not adequate, as mud could force the gasket radially out of position. The metal adhesives available at that time could not prevent this radial movement. Instead, dowel pins positioned the leather layer and the cork did the sealing. We could bond cork to leather satisfactorily. The low bellows force of 120–180 lb required the use of soft cork composition for the gasket. However, the brass bellows had two defects. The outside of the bellows could be packed with mud and become inoperative, and the brass could also crack at the folds. These problems stimulated the development of the present zinc die-casting-rubber bellows assembly.

Fig. 3 shows the present bellows-seal assembly with its washer. The bellows assembly consists of two telescoping metal parts, a rubber boot, springs, a molded rubber gasket, and a cork composition seal. The anchor plate has integrally cast pins which link this member to the final-drive housing. Telescoping driving lugs connect this anchor plate to the seal-ring carrier plate. The outer surface of the seal-ring carrier plate is not flat, but is dished so as to insure greater contact pressure at the OD of the seal. The seal is as near the outer edge of the bellows assembly as is possible. The forces due to mud which tend to separate the seal from the wear washer are thereby minimized. The rigidity of the seal-ring carrier plate is important, as is the precise location of the 12 coil springs. Together they achieve very uniform loading of the seal without distortions. A molded synthetic-rubber boot couples the two die-cast metal parts together. The boot is of sufficient thickness to minimize tearing, but is not so thick as to appreciably decrease the spring rate of the total bellows assembly. The boot is attached to each metal member by crimping the metal over the thickened ends of the rubber.

The three driving lugs must not bind when the bellows flexes and, in addition, must transmit torque in the range of 2–30 ft-lb. Between the bellows assembly and the final-drive housing is a molded rubber gasket. A pair of circular raised ridges in the rubber have sufficient compressibility to achieve sealing. The driving pins, which go through these holes in the gasket, and the formed edge, which encloses the metal part, prevent shifting of the gasket. No adhesive is used or is needed.

In redesigning a part such as this, it is desirable

to make the improved part available to customers with older machines. In addition, there is the ever-present problem of space limitations. Fig. 4 shows that a 1⅞-in. thick seal assembly has a designed space range of 0.23 in. This space range is the difference between the minimum thickness, 1.44 in., and the maximum thickness, 1.67 in., in the tractor. This space range gives the bellows load needed for proper operation of the seal. There is a little over ⅝-in. movement of the bellows between no load and solid height. It is preferred not to allow the seal to operate in the first 0.2 in. of bellows movement because of leakage. The last 0.2 in. of movement is forbidden in order to prevent compression of the seal to solid height. This large bellows movement is necessary because the sprocket is pressed onto a tapered, splined shaft and no adjustment of compressed seal height is possible. As the sprocket is pressed farther on the shaft, the inner seal is compressed more and the outer seal loses compression (Fig. 1). The opposite case, of course, occurs when the sprocket is pressed part way on the tapered shaft, which allows a low bellows force on the inner seal and a high bellows force on the outer seal. Thus, the large bellows movement prevents the possibility of the bellows on one side of the sprocket being compressed to solid height and the bellows on the other side of the sprocket being unloaded.

Fig. 5 shows the driving torque required for a large seal such as is used in a D9 tractor. The friction may seem high, but the rotational speed is very low. The friction is insignificant when it is considered that over 70,000 ft-lb of torque is available at 14 rpm in this large D9 tractor. In some of the smaller machines, the frictional torque may be as low as 2 ft-lb.

The Seal

The seal is attached by an adhesive to the bellows. At present, the seal is a cork composition material, while its predecessor was leather. Some cork-Buna-N compositions have been tested. High compressibility of the seal material is important. It will be noticed in Fig. 6 that cork-rubber has both the greatest compression and the least compression of these materials. This is dependent upon the percentage of rubber in the mix. Cork composition, specification G2214, has adequate compressibility for this job. A sponged rubber-cork mixture would not be desirable due to its seepage of oil through the pores. Resilience is also an important requirement of the seal, since the seal must follow the waviness of the washer during rotation. If the seal material is compressed by a high spot on the washer it must spring back quickly in order to stay in contact in the valleys. For two peaks 120 deg apart on the surface of the washer, the recovery time of peak to valley may be as short as 300 millisec. This points out an advantage of cork-rubber composition over cork composition.

Besides resilience, low friction is a desirable quality in a seal. Fig. 7 shows temperatures measured in a bench test with various seal materials. These temperatures are indicative only of the relative amounts of friction among materials. Due to the large mass of metal and oil in a tractor final-drive compartment, seal temperatures are considerably lower than these figures indicate. As far as minimum operating temperature is concerned, leather is the most desirable of these materials. However, it has lower compressibility than any of the cork composition materials. In oil, cork will generally stand higher temperatures without decomposition than will leather.

Decreasing either the area of the seal or the force on the seal will lower the amount of generated heat (Fig. 8). A reduction in area also increases the seal wear rate at the same bellows force, while de-

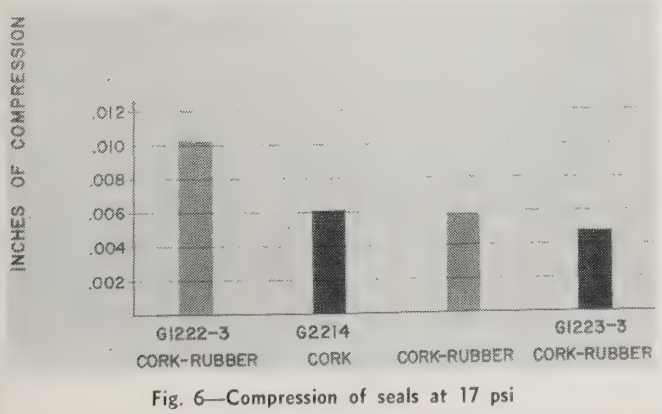

Fig. 6—Compression of seals at 17 psi

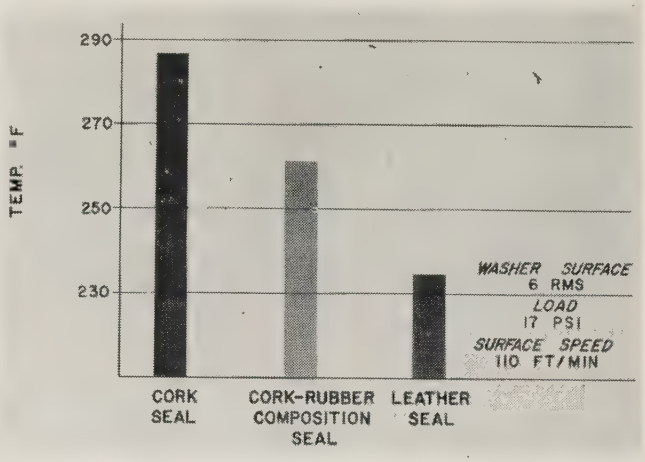

Fig. 7—Generated temperature of seal materials

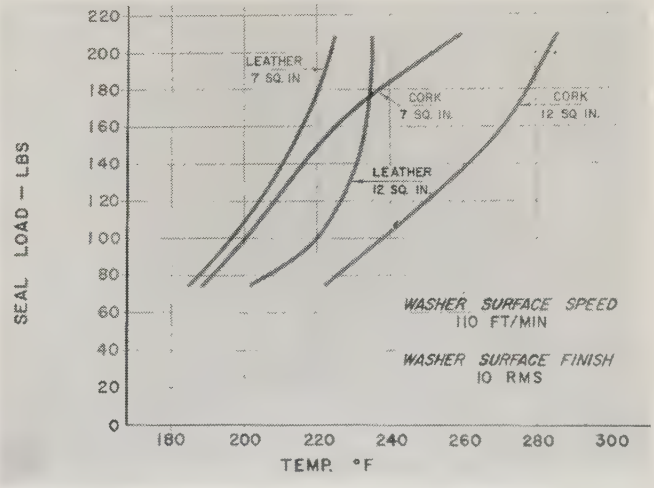

Fig. 8—Reduced seal area versus temperature

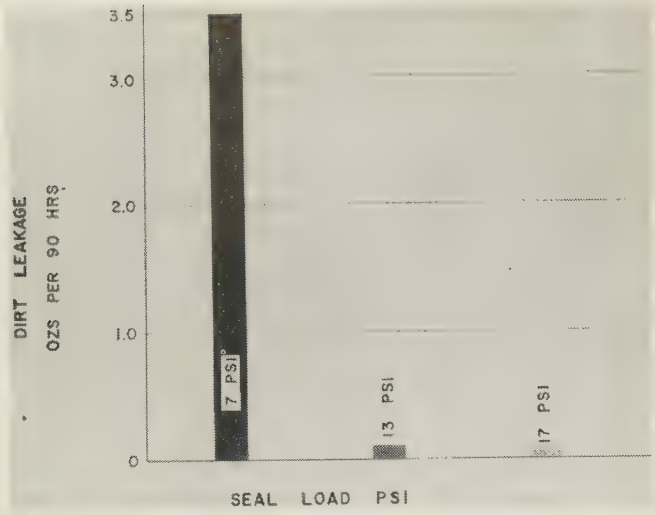

Fig. 9——Load versus dirt leakage (cork seal)

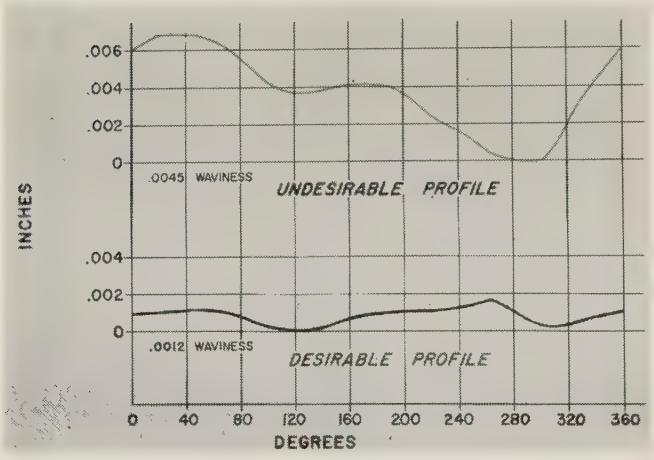

Fig. 10—Profile of washer surface—no load

creasing the bellows force invites poor sealing. Fig. 9 shows the effect of bellows load on leakage. These data were obtained on a machine run on a test in a "mud" bath. This so-called mud was a water mixture of sand, bentonite clay, and a dispersant. It may be seen that a low bellows load of 7 psi allows a large leakage of dirt. At least a 13-psi bellows load is necessary to achieve sufficient sealing.

Before installation in the tractor, a seal assembly is given a spherical grinding on the sealing surface. This spherical grinding facilitates sealing but does not guarantee sealing at low bellows loads.

Wear Washer and Gasket

The wear washer and its gasket are very important parts of the final-drive seal. The washer provides a hard, wear-resistant surface for the seal to run against. The gasket with its liquid sealant provides a mount that holds the washer in a flattened position and seals behind the washer. Torque is transmitted by three dowel pins. Several materials for the washer have been tested: carburized steel, cast iron, sintered bronze, and chromium-plated steel. The wear rates of all these materials, except chromium-plated steel, exceed that of SAE 1018 carburized steel. The temporary advantage of plated steel does not justify the additional cost.

The materials tested for the gasket include cork compositions, cork-rubber compositions, and a plant-fiber mix containing a rubber binder. The soft cork composition is not uniform in thickness and does not reduce washer waviness. The cork-rubber composition is made by the so-called Black Rock process. In this process, the cork-rubber gasket is sliced from a thick-walled tube. Gaskets so prepared are varied in thickness. After cutting, special processing is required to achieve the necessary uniformity of thickness. The mixture of rubber and plant fiber produced by the "beater-saturated" process is rolled by paper-making machines to a uniform thickness, which allows waviness reduction. Unlike cork composition, this plant-fiber material is water and fungus resistant. The plant-fiber material can be used with many adhesives, as it absorbs the solvent to form a fast bond.

The size of the washer is limited by the available space in the assembly. The washers are stamped from soft sheet stock, 7/32 in. thick, of SAE 1018 steel, carburizing grade. They are then carburized and heat-treated to give hardness of Rc 62–65. They are then ground on Blanchard grinders with a light load. The washers must be turned over frequently to remove stock at approximately the same rate from both sides. This prevents warping and makes the two sides very nearly parallel. The surface finish is about 15 microin. Flatness is checked by lightly pressing the washer against a flat surface plate and inserting a feeler gage between the washer and the plate. Finger pressure against the washer must be very light in order to minimize washer deflections. The washers are next Parkerized, which gives some anticorrosion protection and a good surface for adhesion. A soft spot on the surface of a carburized and hardened washer is visually revealed by Parkerizing. This is an effective aid in quality control.

The test for flatness previously described is a measure of the depth of the valleys in the wavy surface of a washer. This may also be described as the vertical distance from the bottom of a valley to the top of one of the three ridges which will contact a

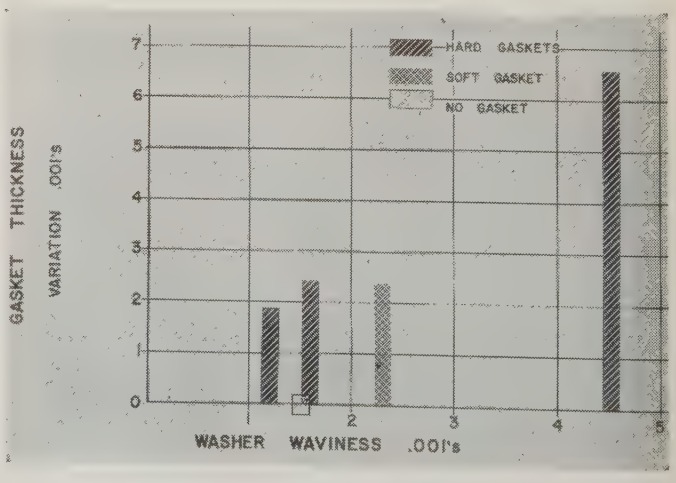

Fig. 11—Effect of gasket thickness variation on waviness of loaded washer

plane. This distance is the washer waviness that must be filled by a compressible seal material to prevent leakage. Constant improvements in production techniques presently enable us to make washers 10 in. in diameter flat within 0.0025 in. consistently. Parallelism of the two sides is always quite good.

Fig. 10 shows the profile of two different washer surfaces. The profile labeled as undesirable has a waviness of 0.0045 in. At first glance it appears that the waviness is almost 0.007 in. However, the washer surface contacts a plane at three points—20, 50, and 175 deg. This tilts the washer and gives the 0.0045-in. waviness as stated. These profiles are shown where there is no load on the washer. A washer with a desirable profile is also shown in Fig. 10. Its waviness is 0.0012 in. and it will seal quite well in the tractor. These profiles in Fig. 10 are shown with no load on the washer. This condition should never exist in a tractor.

The gasket between the wear washer and the sprocket is an important part of this sealing system. It is quite easy to machine the surface of the sprocket hub flat within 0.001 in. This flat sprocket surface improves the performance of the seal, as will be shown. By having a flat sprocket surface and a gasket of uniform thickness, the wear washer can be flattened to a considerable degree. Fig. 11 shows the effect of 135-lb bellows load forcing a 0.0064-in. wavy washer against a gasketed plane surface. A gasket with a thickness variation of 0.006 in. has little beneficial effect on the flatness of the washer. Chance orientation of the thick spots in this gasket with the valleys and ridges of the washer may improve the washer flatness or make it worse. Since the gasket load may be as low as 10 psi, even the softest impermeable gasket will not have enough deflection to help. It is obvious that the most important property is uniform thickness. If we use no gasket in this application, as is shown in Fig. 11, we will have no undesirable distortion of the washer. When no gasket is used, there is some flattening effect on the washer. This is because the washer is pressed against a very flat sprocket hub. The waviness of the washer can be reduced by forcing the washer against a flat sprocket. This shows the flexibility of this 0.200-in. thick steel wear washer. Commercial tolerance for thickness of gasket materials

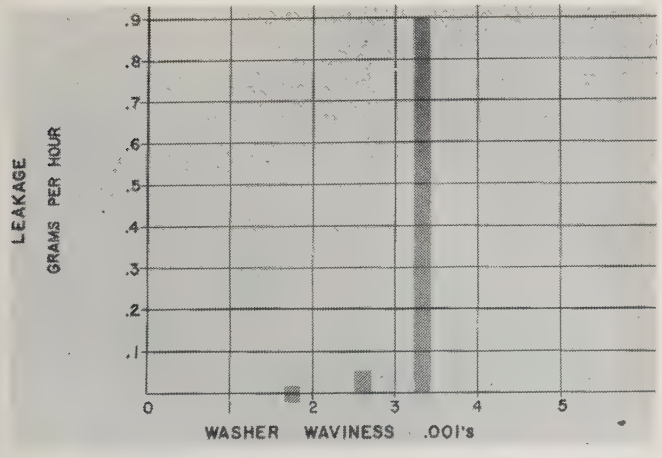

Fig. 12—Effect of washer waviness on leakage

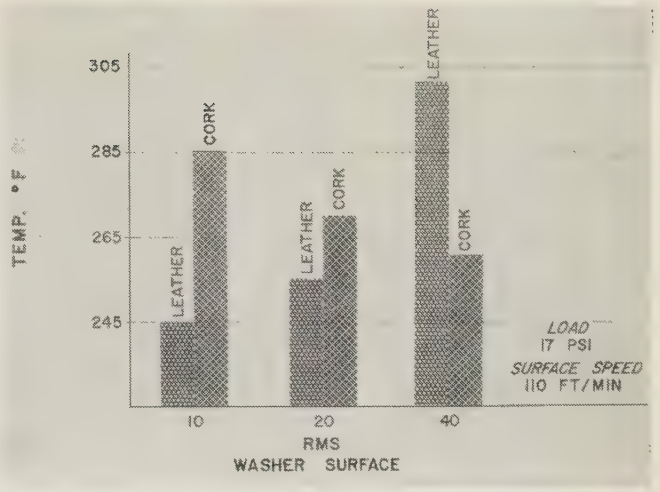

Fig. 13—Washer surface versus generated temperature

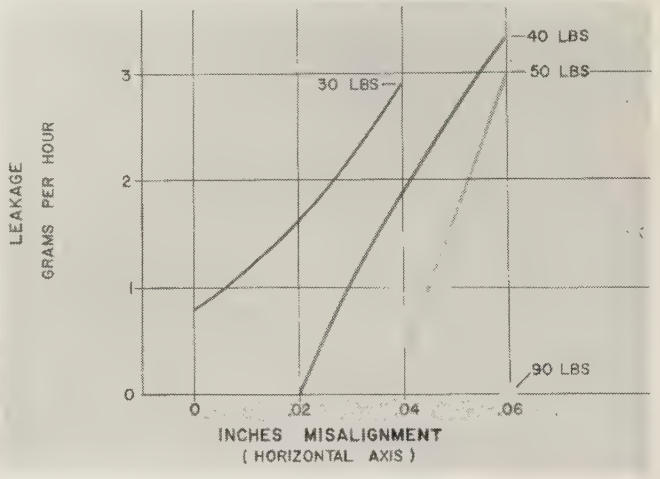

Fig. 14—Misalignment versus leakage

made from cork composition is ± 0.015 in. Gaskets for this application are ground to a special tolerance.

Because of the low compressive pressures involved, no impermeable gasket material will seal without an auxiliary liquid or paste sealant. A rosin-base sealant of the nonhardening variety is used on both sides of the gasket. The reason for interest in the waviness of the washer is shown in Fig. 12. Oil loss becomes severe if the waviness of the washer exceeds about 0.0025 in. If the waviness of the washer under load is held at less than 0.002 in., there will be no leakage.

The surface finish of the washer is also of some interest. Fig. 13 shows the effect of various washer-surface finishes on the heat generated by the seal. These tests were run in a test machine and not on a tractor and thus do not indicate the surface temperature attained in tractor operation. Leather apparently likes to rub against a smooth surface, whereas cork does not. Fig. 14 shows the effect of shaft misalignment on leakage of oil by the seal. Manufacturing tolerance would not allow even 0.010-in. axial misalignment. However, a tractor going over logs or rocks may have axial deflections in this range. Misalignment or deflection is no problem at

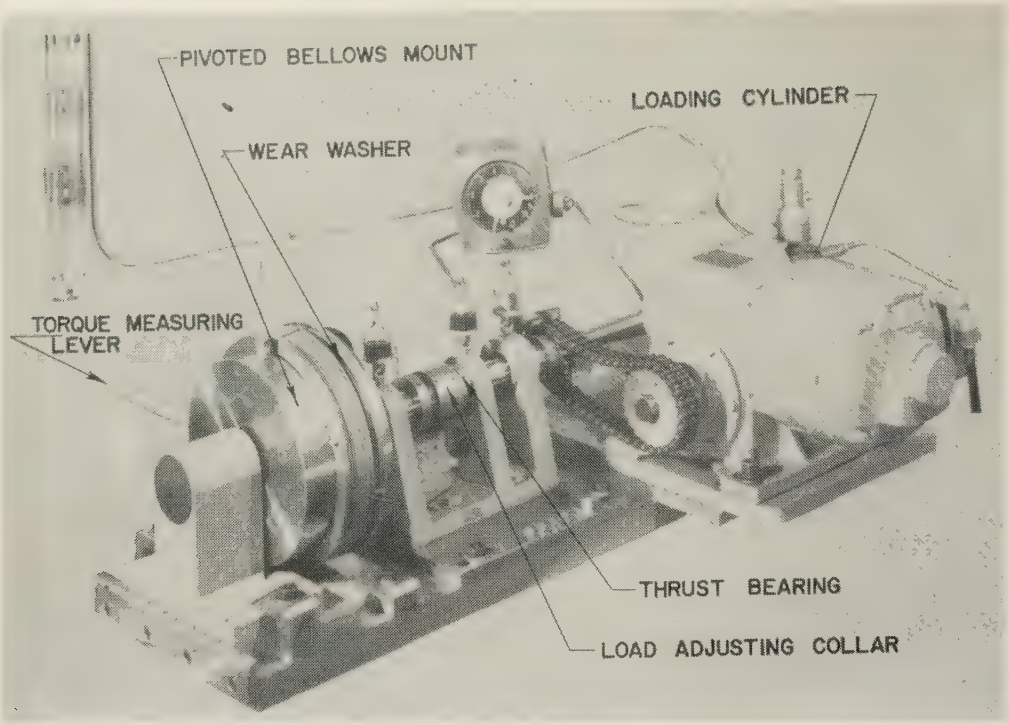

Fig. 15—Test machine

normal bellows seal loads. It is shown in Fig. 14 that with a 90-lb bellows load misalignments as great as 0.060 in. could be tolerated. This 90-lb bellows load is well under the expected 150-lb minimum bellows load which a D4 tractor would have.

All of the data in this paper were obtained in the laboratory test machine. One of them is shown in Fig. 15. Oil leakage, temperatures, load, waviness, torque, and misalignment data were obtained on this machine. The machine can also be used for measuring the washer profile under load and while rotating. This is accomplished by a miniature differential transformer whose movable core acts as a foot moving on the washer surface. The signal is amplified and recorded on a Brush analyzer. A very useful fixture for measuring the profile or waviness of the wear washer is shown in Fig. 16. This fixture was made in our laboratory. It is unique in that it can quickly measure the profile of a washer surface with a contact plane as a reference point. Out-of-parallelism or washer deflections do not affect the measurements.

Development of a seal such as this one involves a comprehensive study of each part and its function. In some cases it is hard to isolate variables. It has been shown that there is much interdepencence of one part or another for proper performance. For a tractor final-drive seal to perform efficiently the following things must be done:

1. There must be ample space allotted to permit enough bellows movement.
2. The bellows must transmit torque without sticking or binding within the bellows and present a seal surface which is uniformly loaded by this bellows.
3. The bellows-boot material must be immune to flexing and abrasion and must not reduce the spring load while operating in the normal space range.
4. The seal load must be high enough to achieve sealing and the materials must be chosen so as not to generate destructive temperatures.
5. The seal area must be small enough to give high unit pressures for good sealing. The area must be large enough for a long wear life.
6. The cork-composition seal material should be as near the OD of the seal-ring carrier plate as possible and should have a spherical grinding at the time of assembly. This seal material should have good compressibility and resilience and be nonporous.
7. The wear washer should be wear resistant, smooth and as flat as possible.
8. The gasket between the wear washer and sprocket must be uniform in thickness primarily The hardness of the gasket is secondary. A sealant must be used on both sides of the gasket.

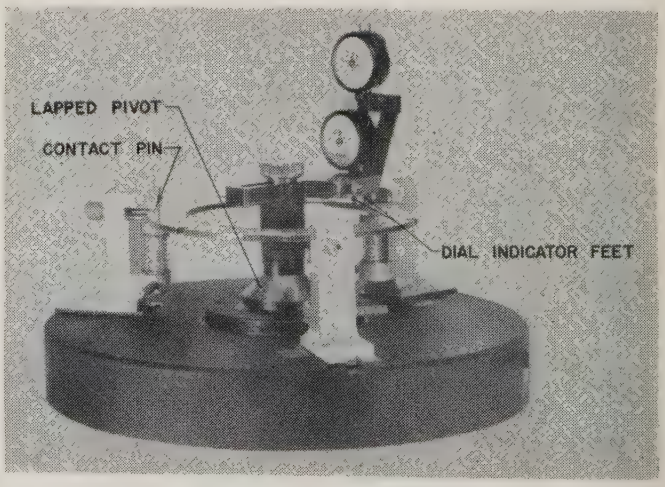

Fig. 16—Fixture for profile measuring

some metallurgical aspects of . . .

Pontiac V-8 Engine Pearlitic Malleable Iron Crankshaft

K. B. Valentine, General Motors Corp.

This paper was presented at the SAE Annual Meeting, Detroit, Jan. 15, 1957.

PEARLITIC MALLEABLE iron is a generic term used to differentiate such metal from the older and better known standard malleable iron. The matrix of pearlitic malleable iron is essentially pearlite or martensite decomposition products; the matrix of standard malleable iron is predominantly ferrite. All pearlitic malleable iron is produced from white iron castings. Subsequent thermal treatments convert the white iron into pearlitic malleable iron.

Three different methods of production are used in the United States today. One method utilizes alloy additions (such as manganese) in the melt. Such additions, employed in conjunction with suitable section size and annealing practice result in a microstructure of temper carbon in a matrix of pearlite and spheroidized cementite.

Another method consists of reheating ferritic malleable iron above the critical temperature, then quenching and tempering. This practice results in a structure of temper carbon in a matrix of tempered martensite.

Table 1—Physical Properties of Commercially Available Pearlitic Malleable Irons

Ultimate Strength, psi	Yield Strength, psi	Elongation, % in 2 in.	Brinell Hardness	Modulus of Elasticity, psi
65,000 to 100,000	45,000 to 80,000	2 to 10	163 to 269	26,000,000 to 28,000,000

A third method consists of adjusting the annealing cycle to control the degree of graphitization. Coupled with aircooling and tempering, this process results in a structure of temper carbon in a matrix of pearlite.

Physical properties of the pearlitic malleable irons mentioned will vary depending on the foundry practice and treatment employed. Table 1 lists the range of physical properties which are associated with commercially available castings.[1, 2, 3]

The third method mentioned (controlled annealing coupled with aircooling and tempering) was used to produce the 1956 Pontiac V-8 engine crankshaft castings.

The use of pearlitic malleable iron for automotive purposes is not new. Rocker arms, transmission parts, and camshafts made from pearlitic malleable

[1] American Foundrymen's Society *Transactions*, Vol. 63, 1955, pp. 244–250, "Pearlitic Malleable Iron—Interrelation of Heat-Treatment, Mechanical Properties, and Machinability," by J. E. Kruse.
[2] American Foundrymen's Society Preprint 56–84, "Comparison of Liquid- and Air-Quenched Pearlitic Malleable Irons."
[3] "Metals Handbook." Pub. by ASM, 1948 edition.

PEARLITIC malleable iron crankshafts are being used in the new Pontiac engine as a result of recent developments.

This paper discusses the physical properties of pearlitic malleable iron such as elastic modulus, fatigue endurance, and tensile strength.

According to the author, definite machining economies result from using pearlitic malleable iron crankshafts.

iron have been used for about 20 years. As will be noted, these parts are all small section-size castings.

Pearlitic Malleable Iron Crankshaft

The recent development of bismuth additions,[4] to molten iron to increase the section-size of castings which can be cast in the white condition, coupled with the development of boron additions to facilitate precipitation of temper carbon, has extended the use of pearlitic malleable iron to include larger section sizes than previously practical. These developments, in conjunction with recent advances made in shell-molding techniques, resulted in an investigation into the suitability of pearlitic malleable iron crankshafts for our 316-cu in. displacement, 8.9/1 compression ratio V-8 Engine.

As a casting this crankshaft would weigh 64 lb, be 26⅛ in. long, and have a maximum section-size of 3½ in.

Engineering and Metallurgical Properties

Engineering factors such as modulus and notch sensitivity, and manufacturing items such as machinability and tolerances must be considered when selecting a crankshaft material. However, all these items are resolved into two major considerations:

1. The crankshaft must function properly in the engine.
2. The crankshaft must be economically competitive with other materials and practices.

Engineering and metallurgical considerations such as modulus of elasticity, fatigue properties, notch sensitivity, static strength, hardness and wear-resistance of pearlitic malleable iron crankshafts, were investigated by us. Results of these tests are herewith presented. Inasmuch as our prior crankshaft experience had been with forged SAE 1046 steel, water-quenched and tempered to 228–269 Brinell, information relative to this material is also included for comparison purposes.

Modulus of Elasticity—Test pieces 3/16 in. thick, ½ in. wide, and 2½ in. long were machined from various positions of finished crankshafts and used for determining elastic modulus. These test pieces were submitted to General Motors Research Laboratories Division, where moduli determinations, utilizing the symmetrically loaded beam-section technique, were ascertained. Table 2 lists results of these elastic moduli determinations. Each modulus figure listed is the average of two determinations made on a single test bar.

When compared with a modulus of 29,500,000 psi for steel, these figures denote a lower modulus for pearlitic malleable iron. In order to obtain maximum machining benefits from a casting made by the shell-molding process, our pearlitic malleable iron crankshaft design varied from the forged crankshaft design. Consequently, a direct comparison of the effects of moduli on torsional vibration characteristics of identically designed crankshafts is not available.

However, the forged steel crankshaft and the pearlitic malleable iron crankshaft (with design modifications) possess similar torsional vibration characteristics as illustrated by typical curves in Fig. 1. The appearance of critical vibration cycles at lower engine speed for the pearlitic malleable iron crankshaft can readily be observed. This feature is commensurate with the moduli of the materials involved.

During the first few months of 1956 production, both cast and forged crankshafts were used in our engine. To facilitate this dual crankshaft material usage, a harmonic balancer was designed to accommodate both types of crankshafts. Fig. 2 compares torsional vibration characteristics of forged crankshaft with harmonic balancer to cast crankshaft with harmonic balancer. The similarity of these curves denotes that with adequate design consideration, the lower modulus of pearlitic malleable iron is no detriment to smoothness of engine operation at normal car driving speed.

Fatigue Properties—Dynamometer tests and 100,000-mile car tests showed comparable endurance of forged and cast crankshafts. One year's field experience has substantiated these results.

A series of fatigue tests were run to obtain information concerning the effect of notch sharpness on fatigue properties of pearlitic malleable iron. Test bars similar to Izod bars, except possessing notches of 10, 20, or 30 deg were machined from crankshaft counterweights and used as test specimens for this series of tests. The specimens were subjected to cycles of impact loading a 3-lb weight dropping 1 in.

Fig. 3 illustrates arrangement of machine used. The weight was raised by the cam and fell by gravity on an anvil and roller assembly. The anvil kept the roller positioned directly over the notch, and suitable guides correctly located the bar at all times. Supports for the test bar were equidistant from the notch (⅝ in.). The machine operated at 8400 cycles per hour and was equipped with an electric timer and automatic shut-off switch.

Results of these fatigue tests are listed in Table 3.

Table 2—Results of Elastic Modulus Determinations

Specimen Number	Elastic Modulus, psi
1	26,200,000
2	24,300,000
3	25,400,000
4	25,200,000
5	26,700,000

[4] General Motors U. S. Patent 2370225.

No effect of variations in notch sharpness on fatigue properties can be discerned.

Tensile Strength—Standard ASTM 505-in. tensile test bars, machined from journals and counterweights of pearlitic malleable iron crankshafts, showed 96,000 psi tensile strength at 228 Brinell hardness. This compares with 114,000 psi obtained on test bars machined from SAE 1046 steel-forged crankshafts at 228 Brinell hardness.

Hardness—Pin and journal sections of pearlitic malleable iron crankshafts are reasonably uniform with regard to Brinell hardness. Fig. 4 lists results of hardness tests run on five crankshafts cast on different days. Periodic hardness tests subsequently run on production crankshafts have revealed similar hardness pattern.

Brinell hardness of journal cross-section of forged crankshafts generally was 217–229 from center to surface.

Wear Characteristics—Resistance of pin and journal surfaces to wear is required for crankshaft longevity. No accurate laboratory tests have been developed by us which suitably determine this property. Consequently, data presented relative to wear are

Table 3—Results of Fatigue Tests Run on Test Bars with Various Notch Contours (Hardness of Test Bars Was 207-217 Brinell)

Notch Radius, deg	Cycles to Failure
10	6720
10	7560
10	7560
10	8400
20	14,280
20	11,760
20	6720
20	6720
20	6720
20	6720
20	5880
30	7560
30	6720
30	6720
30	5880
30	10,920
30	9240
30	8400

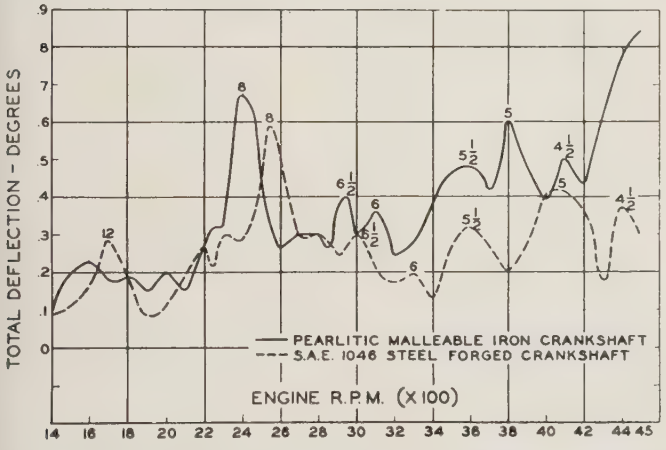

Fig. 1—Torsional vibration curves of pearlitic malleable iron crankshaft and forged SAE 1046 steel crankshaft

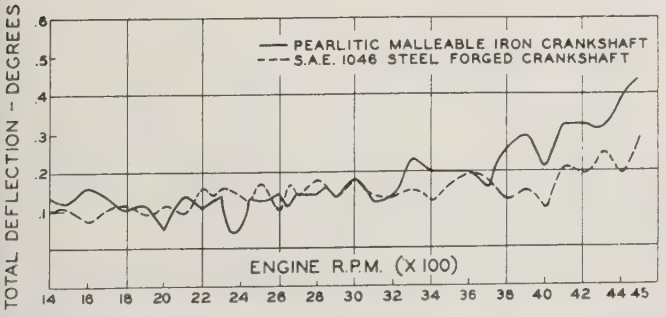

Fig. 2—Torsional vibration curves of pearlitic malleable iron crankshaft with balancer and forged SAE steel crankshaft with balancer

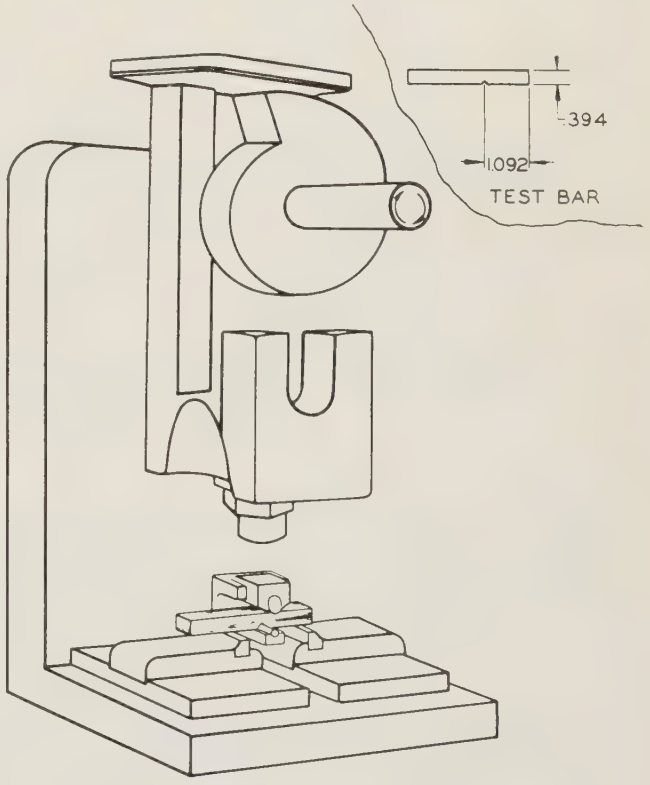

Fig. 3—Notched bar impact-fatigue arrangement

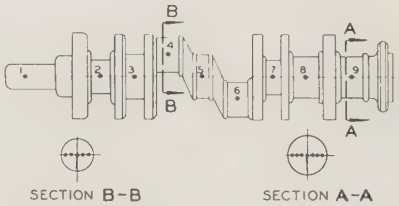

CRANK SHAFT	SURFACE POSITION									SECTION B-B					SECTION A-A						
	1	2	3	4	5	6	7	8	9	1	2	3	4	5	1	2	3	4	5	6	7
1	241	229	229	255	255	255	229	229	241	241	255	241	241	241	255	255	241	241	229	241	241
2	255	241	255	241	255	235	262	241	241	229	229	229	241	229	269	269	255	269	269	269	255
3	255	241	229	241	255	255	228	255	229	217	229	217	229	217	229	217	229	229	241	229	241
4	269	269	229	241	229	223	229	255	241	217	229	241	241	241	255	255	255	255	255	255	255
5	255	255	241	255	269	255	241	255	229	241	241	241	241	241	241	241	229	255	229	241	229

Fig. 4—Brinell hardness values at various positions of five pearlitic malleable iron crankshafts

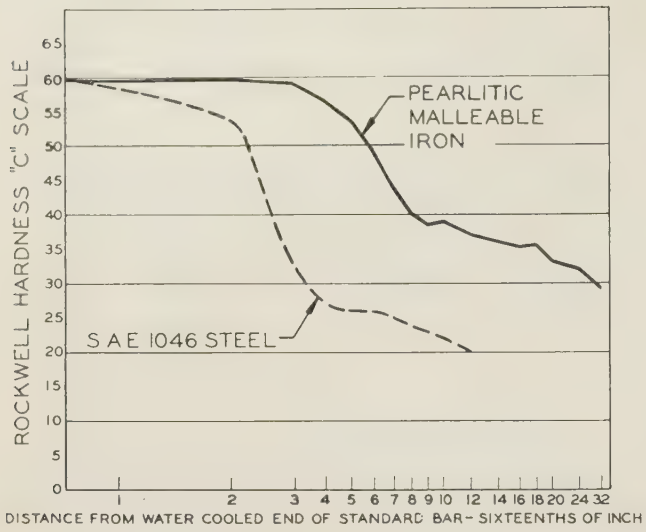

Fig. 5—Hardenability curves for SAE 1046 steel and pearlitic malleable iron

Table 4—Results of Crankshaft Wear Tests

	50,000 Mile (Synchromesh Transmission)		50,000 Mile (Hydra-Matic Transmission)		100,000 Mile (Hydra-Matic Transmission)	
	Minimum	Maximum	Minimum	Maximum	Minimum	Maximum
	(3 Engines)		(5 Engines)		(1 Engine)	
Crankshaft (Cast) Main Journal OD Decrease, in.	0	0.0003	0	0.0005	0	0
Rod Journal OD Decrease, in.	0	0.0005	0	0.0004	0	0.0002
Crankshaft (Forged)	(1 Engine)		(1 Engine)		(2 Engines)	
Main Journal OD Decrease, in.	0.0003	0.0006	0.0002	0.0005	0.0001	0.0004
Rod Journal OD Decrease, in.	0.0004	0.0006	0.0001	0.0002	0.0001	0.0003

the result of many different engine tests. Table 4 lists results of measurements taken on crankshafts prior to and subsequent to car testing. No appreciable difference in pin and journal wear of cast crankshafts as compared to forged crankshafts can be noted.

Measurements taken on main bearings and connecting-rod bearings before and after car testing showed that bearing wear was about the same in engines that operated with forged crankshafts as in engines that operated with pearlitic malleable iron crankshafts.

Other items such as type of bearing material and surface finish of pins and journals were controlled during these wear tests. Connecting rod bearings made of lead base babbitt specification GM 4915 (10% Sn, 15% Sb) or Durex 100A with GM 4167 babbitt (4¼% Sn, 3½% Sb) overlay, functioned satisfactorily with either crankshaft material. Crankshaft main bearings made of Durex 100A with GM 4167 babbitt overlay performed satisfactorily with either type of crankshaft material.

Machining Experiences

A modern automobile engine crankshaft is a combination of drilled holes, flanges, pins, fillets, and the like, all requiring the accuracy of a gargantuan watch. Consequently, machinability is of paramount importance when considering crankshaft material.

In our opinion, results of large quantity production runs are the best criteria for determining machining characteristics of a material. Therefore, in order to present information anent machinability of pearlitic malleable iron crankshafts, as compared to SAE 1046 steel crankshafts, excerpts from production department reports were herewith listed. These tests represent 2-months production; one month when 59,000 forged steel crankshafts were machined and one month when 49,000 pearlitic malleable iron crankshafts were machined.

1. Operation 10: tool life increased 56% with castings.

2. Operation 20: 21 tools required for forgings as compared to 6 tools for castings.

3. Operation 40: 58% better tool life wth castings.

4. Life of 0.246-in. drill increased 147% with use of cast crankshafts.

Life of 0.250-in. drill increased 267% with use of cast crankshafts.

5. Tap life increased 217% with use of cast crankshaft.

6. Operation 150: 47 wheels used to grind 59,000 forged crankshafts, and 27 wheels used to grind 49,000 pearlitic malleable iron crankshafts.

7. Feed rate of several machines increased.

These test results denote our favorable machining experience with pearlitic malleable iron crankshafts.

The crankshaft forging weighed 77½ lb as received and 59½ lb when machined, whereas the casting weighed 64 lb as received and 54 lb when machined. As can be determined from these weight figures, it was necessary to remove more metal from the forging than the casting.

Table 5—Effect of Cold Work on Impact-Fatigue Property of Pearlitic Malleable Iron

Treatment	Cycles to Failure
(1) Air Quenched and Tempered	6720
	7560
	7560
	8400
Same as (1) above except test bar notch coined 0.001 in.	14,100
	42,840
	55,440
	42,000
(2) Oil-Quenched and Tempered	10,080
	11,760
	10,920
	7560
Same as (2) above except test bar notch coined 0.001 in.	14,280
	23,520
	19,320
	11,760

Supplementary Properties of Pearlitic Malleable Iron

Data previously presented concerning pearlitic malleable iron was obtained from, and is applicable only to air-quenched and tempered crankshafts as used for our 1956 production.

However, in order to obtain additional information, it was decided to investigate the effect of other metallurgical practices on pearlitic malleable iron.

Oil-quenching and tempering small section-size parts made of pearlitic malleable iron has been common practice. Consequently, it was decided to investigate the effect of this treatment on some of the properties of pearlitic malleable iron crankshafts.

One of the important factors associated with quenching and tempering a ferrous material is hardenability. Jominy hardenability bars machined from crankshafts were used to obtain hardenability data. Fig. 5 illustrates typical hardenability curve obtained for pearlitic malleable iron as compared with SAE 1046 steel. Other hardenability tests indicate that about 1550 F was the minimum temperature that could be used for quenching pearlitic malleable iron.

Due to presence of temper graphite, the Rockwell C hardness readings conceivably are of questionable accuracy. However, our hardenability tests indicated that pearlitic malleable iron possesses good hardening potential for rather large section-size. This characteristic was confirmed by hardness survey of crankshafts that had been quenched into oil from 1600 F and tempered at 1200 F. Fig. 6 lists hardness values obtained for three crankshafts heat-treated in this manner.

Preliminary investigation into the effects of oil-quenching and tempering of pearlitic malleable iron upon fatigue properties was accomplished with the aid of test bars and impact-fatigue machine previously described. These tests indicated that for the same hardness level, oil-quenched and tempered pearlitic malleable iron possesses slightly better fatigue properties than air-quenched and tempered pearlitic malleable iron.

Cold Work—The effect of cold work on the fatigue properties of pearlitic malleable iron was also investigated with the aid of an impact-fatigue test machine. For these tests Izod impact test bars were machined with a depth of the notches 0.001-in. undersize. Subsequently, the notches were coined in the specified depth. This coining imparted cold work at the bottom of the notch which resulted in a marked increase in fatigue property as illustrated in Table 5.

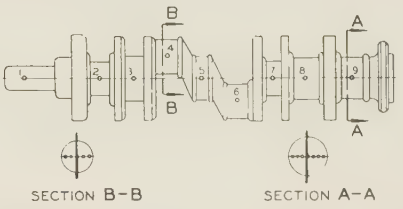

CRANK-SHAFT	SURFACE POSITION									SECTION B-B					SECTION A-A						
	1	2	3	4	5	6	7	8	9	1	2	3	4	5	1	2	3	4	5	6	7
1	214	217	229	229	241	241	217	241	217	241	241	241	229	229	255	255	255	241	269	255	241
2	229	229	217	217	229	217	217	217	207	229	229	229	229	229	229	229	241	229	229	241	229
3	229	255	229	229	255	217	217	241	241	255	241	255	255	255	241	241	241	255	269	255	255

Fig. 6—Results of hardness survey run on oil-quenched and tempered crankshafts

Based on these test results, cranksshafts with the pin and journal fillets cold worked (via fillet rolling) have been made and are on test. Results of these tests are not yet available.

Conclusions

1. Pearlitic malleable iron crankshafts have functioned successfully for Pontiac's 316-cu in. displacement, 8.9/1 compression ratio V-8 engine.

2. Definite machining economies resulted from use of pearlitic malleable iron crankshafts.

DISCUSSION

Thinks Castings Make For Better Crankshafts

—W. G. Ferrell
Auto Specialties Mfg. Co.

CAST material can be made just as sound as any other known material, and only by the cast method can you get the proper material for motor operation. The question of compact engine design, and that when castings are used engines must be longer.

If you wish to machine the crankshaft all over, any material can be used by coring out the pin bearings, and you can hold the same length. Today with the high cost of materials and labor, you are wasting 30% of both by staying with old-fashioned forged design. Nothing on our present modern car has been held back as badly by material as crankshafts. Yet, by using cast method your design is unlimited. Should you wish to save first, machine tools and labor and 20% of material, the casting method is the way. Add ¾ to the length of standard V-8 motors for check clearance, and it can be done without costly checking.

Mr. Valentine's paper brings out some of these important engineering advancements, and there are yet a great many more should the motor engineer start with crankshaft design having no restrictions.

In the past 10 years we have made a large number of tests on the dynamometer and road with bearing wear up to 100,000 miles using Toco hardened forged again No. 80 cast material. This was done by Twin Coach Fagel Co., Detroit, using 25 motors. These tests proved that material of this chemistry will allow designing of motors using castings that will effect vast savings without Toco hardening bearings.

One more point before closing, our past figures of 30,000,000 modules necessary for crankshaft design, should be looked at very closely. Three years ago one of our large manufacturers designed a large motor around forging material. This motor failed to pass dynamometer testing. Material was changed to 4340 with the increased physicals, and these also failed. Yet, the same spacing of bearings with a cast design by coring out rod and main bearings was given an OK in both No. 80 and alloy cast iron. This is just a case of removing the stresses from the critical fillets, and of having your material without straight line fibers.

THE CADILLAC

A New Design Concept for

S. L. Milliken
General Motors Corp.

J. R. Parker
A. O. Smith Corp.

This paper was presented at the SAE Annual Meeting, Detroit, Jan. 16, 1957.

Part I

by S. L. Milliken

VERY OFTEN, a new design to satisfy a specific sales requirement, creates a compromise of other features of the car. In the past, the continual demand for a lower overall height has sometimes caused sacrifices in weight, rigidity, and comfort.

This trend toward lower-car styling has persisted slowly through all our automotive history as our roads, materials, and mechanical and styling designs have improved. The few experiments in attempting to stabilize the height of cars have shown that the buying public does not feel that the added chair height and headroom possible in a higher car is as desirable as the lower and longer silhouette. The constantly increasing millions of cars that have been built to the lower silhouettes by all manufacturers is certain proof that this is one phase of providing a more attractive product for our customers.

The many European manufacturers, even with their pronounced independence of thought on design, have followed the American trend. Their dependence on export sales in other parts of the world leads them to build cars that will be competitive in those markets, and with customers in South America, South Africa, and other free markets showing a preference for our styling the trend to lower cars is worldwide.

We have, of course, been a part of this trend. The "60 Special" in 1938 was truly a "special" car for us. It was 2½ in. lower than the other Cadillac cars of that year. (See Fig. 1.) The new styling made possible by this marked reduction in height was well received and established the direction in car heights for Cadillac's future designs. This 1938 "low car" was 65 in. high, and the tremendous amount of engineering and testing required to meet this height seemed to rule out almost any further lowering of cars. But we have lowered them with every new design, and now the 1957 Eldorado Brougham is only 55½ in. high (Fig. 2), a reduction

THE 1957 Cadillac frame is a significant step in design progress toward the ever lower passenger cars demanded by customers and, therefore, car manufacturers. Stemming from tests and experimental designs in process since 1950, this frame combines reduction in height with a slight increase in structural efficiency. It reverses the trend toward the more costly and heavier structures usually associated with lower cars.

Mr. Milliken discusses in Part I the steps Cadillac has taken in the last 19 years to reduce the height 9½ in. to 55½ in. The "Tubular Center-X" frame of the 1957 Eldorado Brougham was the latest and most successful answer to the problem.

In Part II Mr. Parker describes the A. O. Smith Corp.'s development of the basic idea and the experimental phases and testing which led to the production designs.

FRAME:

Lower Cars

Fig. 1—Cadillac "60 Special" of 1938

Fig. 2—Cadillac 1957 Eldorado Brougham

of 9½ in. during these 19 years. And the 55½-in. height is maintained for all load conditions from curb to full-load-plus-baggage, thanks to the constant-height feature of the air suspension.

Preliminary studies of the proposed 1957 cars showed the customer appeal possible if the usual series of cars could be reduced in height from the 62 in. of 1956 to 59 in. for the sedan and 57¾ in. for the standard coupe.

This is a further step in the styling trend that has persisted through the past years (Fig. 3). Overall height is lower. Along with this, the windshields are higher and are wrapped around the car until the windshield pillar is vertical or even reversed in slope. The offset in the front pillar is greater. The center pillar has been reduced in size, then has disappeared entirely. Back lights are larger and are carried around the top, reducing the area of the quarter panel. Window areas are greater.

The roof rails and heavy pillars in earlier cars contributed to the structure but much of this has been lost in the trend to wraparound windshields and back lights and the 4-door hardtop styling. And bodies have progressively become heavier as more glass, more conveniences, and more accessories have been added to our automobiles.

All of these changes have progressively imposed a greater portion of the load-resistant structure into the lower part of the car while room for frame members has decreased.

The engineer's continuing job has been to provide a frame and a chassis that would accommodate the lower bodies. Many different approaches have been made to the problem, and hundreds of experimental frames have been built and tested. There has been continuous study, on paper and in steel, of various frames and frame/body combinations that might give more efficient use of materials and space.

This shallow box-section, ladder-type frame (Fig.

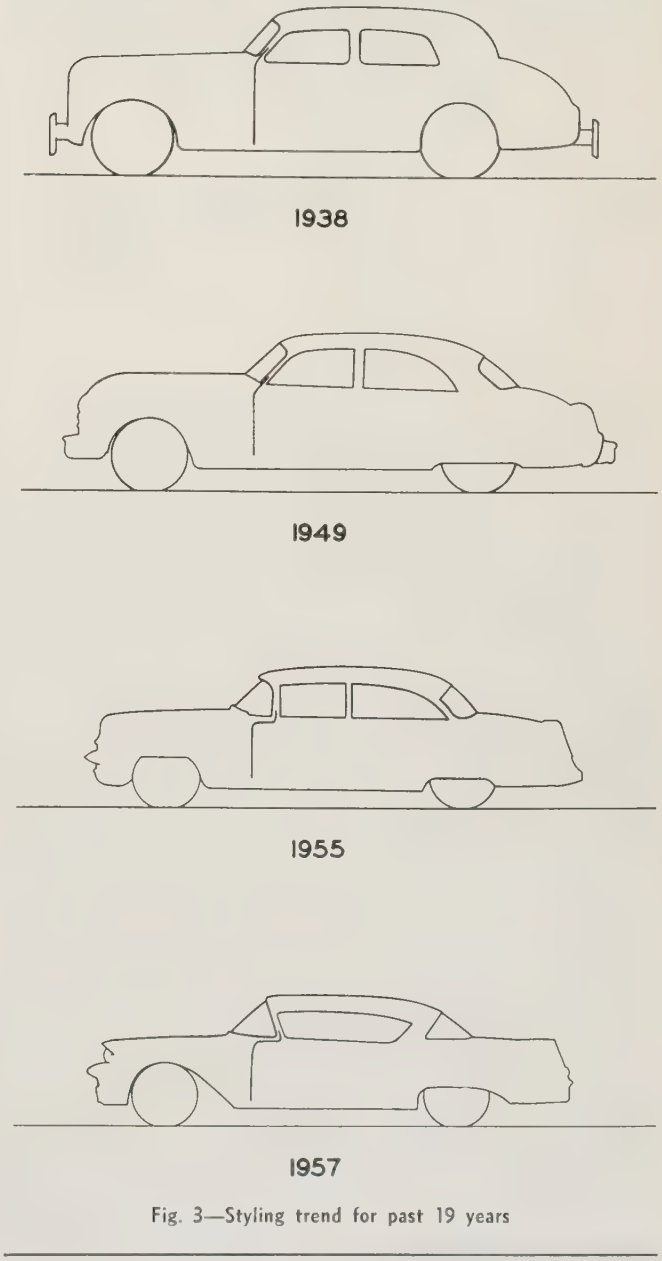

Fig. 3—Styling trend for past 19 years

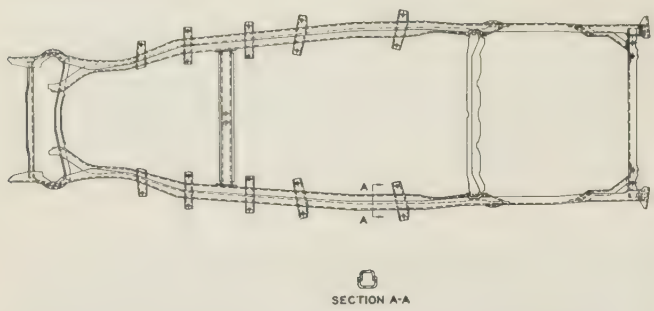

Fig. 4—Box-section frame of 1950 car

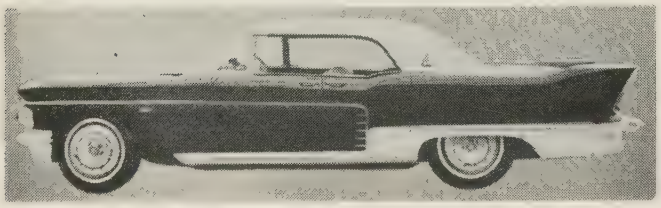

Fig. 5—New Eldorado Brougham

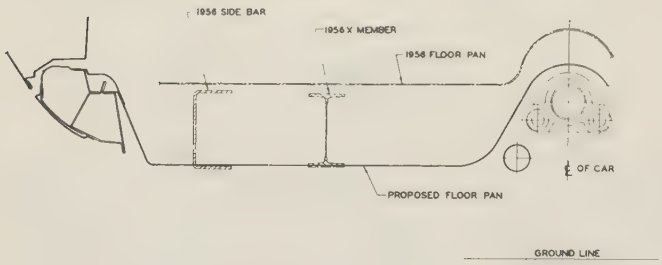

Fig. 6—Section through Eldorado Brougham rear floor

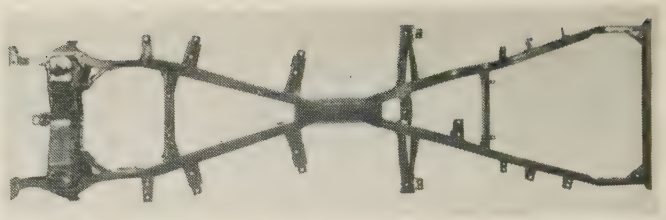

Fig. 7—Frame design of Eldorado Brougham

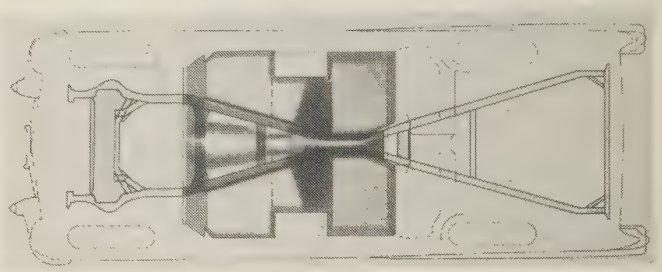

Fig. 8—Frame of 1957 car in 1957 Series 62 body outline

4) was built experimentally in 1950 for use with an extremely low Cadillac "Dream Car" for the General Motors Motorama.

A similar frame was built later to convertible-car proportions. Although the weight was equivalent to that of a product convertible frame (550 lb), the torsional rigidity was but 16% of that of the production frame. When assembled in a car the results were poor, and a variety of braces and struts from cowl to frame would not reduce cowl shake sufficiently. Only when "X" members were added between the side bars, was the frame strong enough to make the automobile acceptable. This experiment did, however, confirm again the importance of the "X" member design with bodies with little or no top structure.

The convertible body models have always been the first consideration in our experimental designing and testing of new frames. If the new frame provides sufficient support for the convertible bodies, there is no difficulty in adapting it to the closed models.

Integral frame/body designs have been studied and have been built experimentally, but have not shown sufficient advantage in weight or height to balance the problems of cost, road noise, and non-interchangeability. All of our studies have indicated that, with present requirements, any advantage of integral construction applies only to the smaller cars of shorter wheelbase and where one body model is used for the major share of the production and over a longer period of years.

Integral frame/body designs are not adaptable, economically, to a variety of wheelbases and body styles. Several of our divisions often use the same basic body shell, with modified or different floor pans to meet the various wheelbase and chassis requirements. The more complicated structure of integral construction would certainly be more expensive to modify to the different needs. The structure is made up of many intricate parts that require expensive tooling and assembly. Bodies made from production tools sometimes vary considerably from the handmade experimental bodies used in the test program. Corrective measures are then costly and time-consuming.

The structure is partly concealed in the body and is involved with many other intricate parts. This makes "tuning" of a car more difficult than with the separate-frame construction. The separate frame can be strengthened or weakened in any area to give the exact tuning required for the particular body and load requirements of that model. This can be done quickly during the test program and without excessive delay even after production has started.

The separate frame construction also makes possible a commercial chassis that can be assembled complete and tested as an operating unit before it is shipped to the custom body builder. The custom body builders have told us that they could not afford to design and build integral frame/body vehicles in the limited volume but great variety of models involved. So for all of these reasons, we have continued with separate frame construction in our studies of future styling.

In addition to our regular series for 1957, the new Eldorado Brougham was proposed with a height of 55½ in. (Fig. 5). This new model is a further development of the Cadillac "Dream Cars" that were shown at the General Motors Motorama in New York City in 1955 and in 1956. All of the styling

features of the regular series are accentuated in the Eldorado Brougham.

It was obvious that only a coordinated design of frame and body would produce the necessary strength for these new automobiles.

Head room was not to be reduced in either the front or rear seats, so seat-chair height and cushion thickness could be maintained only if a more efficient floor pan cross section could be developed. This led us again to the relation between the floor pan and the frame.

This cross section (Fig. 6) through the rear floor pan shows the side bar and "X" member of the 1956 frame in relation to the proposed floor pan for the Eldorado Brougham. The floor pan for the 1957 conventional 4-door sedan is 2 in. higher than this, but the impossibility of using the former type of frame in either model is apparent. So the development of the new frame started with these requirements.

The general dimensions of the frame were dictated by the fixed location of the usual chassis and body components. Between these generally fixed points was to be a frame of maximum efficiency.

This is the frame design (Fig. 7) that satisfied these requirements so thoroughly and made possible the new and radically lower bodies without encroaching on the passengers' room. The basic design of this frame evolved from research work and experimental testing carried on over a number of years by Cadillac and the A. O. Smith Corp.

The basic shape of the frame was attractive to us in that the disposition of the main structural members did allow the lower bodies and lower floor pans required by our new styling. Further study and experimental testing proved that the basic design could be modified to the needs of our different bodies and wheelbases. In addition, the new frame offered more beam stiffness and torsional rigidity without a penalty in weight, even in the longer wheelbases.

Much experimental design and testing was involved in the location and the length of the tubular section at the center of the frame. Earlier designs had the junction under the front seat and with the front and rear extending beams in line. This followed the practice of former frames in utilizing the height available under the front seat. But the spread of the rear extended beams brought the frame into the floor pan well, as occurred on the former type frame shown in Fig. 6.

Further study and experimental testing showed that the junction could be moved rearward and lengthened into a tubular section (Fig. 8). This allows a narrow tunnel in the rear floor pan, even in the 8-passenger models where the rear seat is 28½ in. farther from the front-seat back than in a coupe. This flexibility in design, with no impairment of strength, is one of the marked advantages of the "Tubular Center-X" frame.

With this new frame, the tunnel over the propeller shaft (Fig. 9) is only 0.4 in. higher (in relation to the propeller shaft) than for the former "X" type frame and is 3 in. wider at the base. This is for the 4-door sedan body. The additional tunnel width is on the centerline of the car and between the feet of the rear-seat middle passenger where it does not bother. This floor pan allows a better rear-seat chair height than we had in the 1956 4-door sedan, without impairment of headroom. The 1956 entrance heights, from seat cushion to door-opening windcord, and from floor pan to windcord were also maintained in the 1957 4-door sedan, in spite of the 3-in. reduction in overall height.

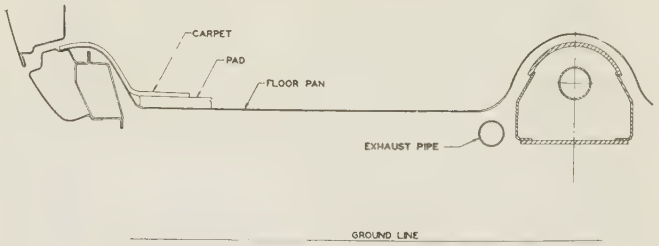

Fig. 9—Section through rear floor, 4-door sedan

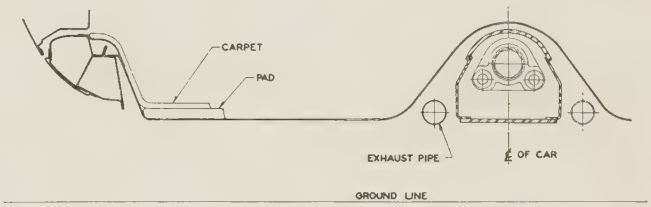

Fig. 10—Rear floor pan of Eldorado Brougham

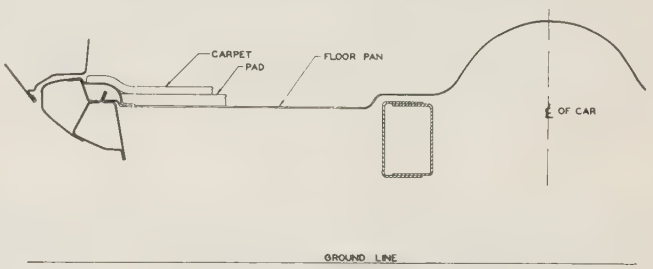

Fig. 11—Section through front floor

On the Eldorado Brougham, with its lower floor pan, the tunnel must clear the exhaust pipe also (Fig. 10) so it is wider. However, as the rear seat of this car is designed for two passengers, and has a center armrest over the propeller-shaft tunnel, the greater width does not bother.

Because there is no side bar to clear at the body rocker sill, the ledge is only 6 in. wide and is stepped over easily in entering or leaving the car.

The ledge at the rocker sill is narrow at the front doors also, and this improves the ease of entrance. Fig. 11 shows the floor cross-section at the 20-in. line (the passenger's feet) in the front compartment. This section is for the Eldorado Brougham, but it is typical of all the bodies.

The frame-member shape was modified in this front floor area by making it wider and shallower than the normal proportions. Tests showed that this did not impair the strength of the frame, and it does allow a lower plateau for the accelerator mounting.

With all the frame structure at the centerline of

the car, there is more height and width available out at the body rocker panel for the attachment of floor-pan cross bars. Fig. 12 shows a cross-section of the floor pan in the center-pillar area, just forward of the depressed well in the rear-compartment floor. The floor-pan cross bar is deeper and has a better attachment to the rocker sill than was possible with the former type of frame shown above. The anchorage for the stub pillar on 4-door hardtop models is also stronger and is reduced in size.

The tubular section of the frame provides a solid, and protected, mounting for the propeller-shaft intermediate support. (See Fig. 13.) This is simple, light, and inexpensive, compared to the cross-member that has been required with a ladder-type frame. The rubber-insulated mounting is shown and also the weld joint between the front and rear extending beams on all frames, but the Eldorado Brougham. The beams for that frame are made 1-piece, as they are not interchangeable with the other frames.

The bulkhead at the front of the tubular section contributes to the strength of the junction. Another transverse member is just behind the tubular section, and between the rearward extending beams. It is in line with the No. 4 body brackets and is arched to clear the propeller shaft at bump position.

This type of frame is adaptable to our full range in wheelbases by merely lengthening the tubular center, so there is good interchangeability of frame tools and parts through our established series of cars. (See Fig. 14.) The Series 62 with 129½-in. wheelbase, the Series 60 with 133-in. wheelbase, the 8-passenger Series 75, with 150-in. wheelbase, and the commercial chassis of 156-in. wheelbase all use the same frame-forming tools for the front and rear extending beams of the frame. As the tubular por-

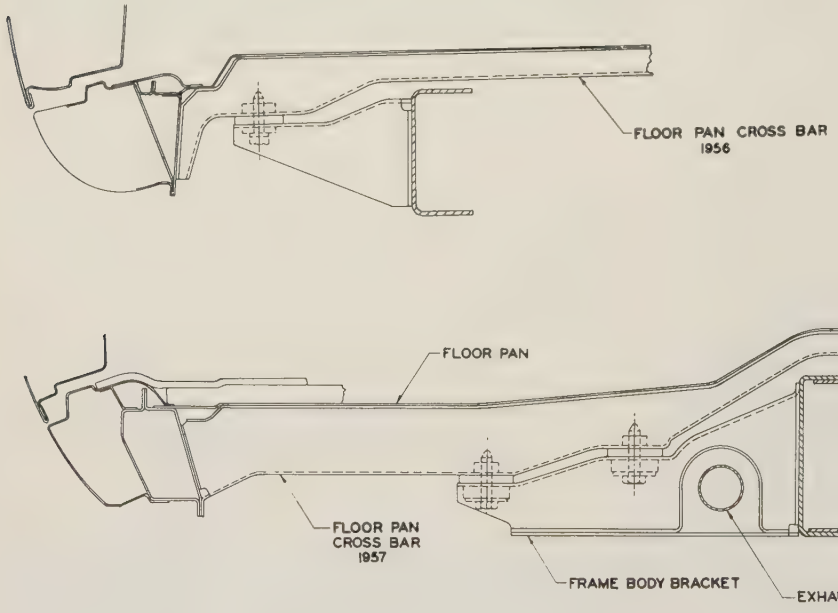

Fig. 12—Section through floor at center pillar

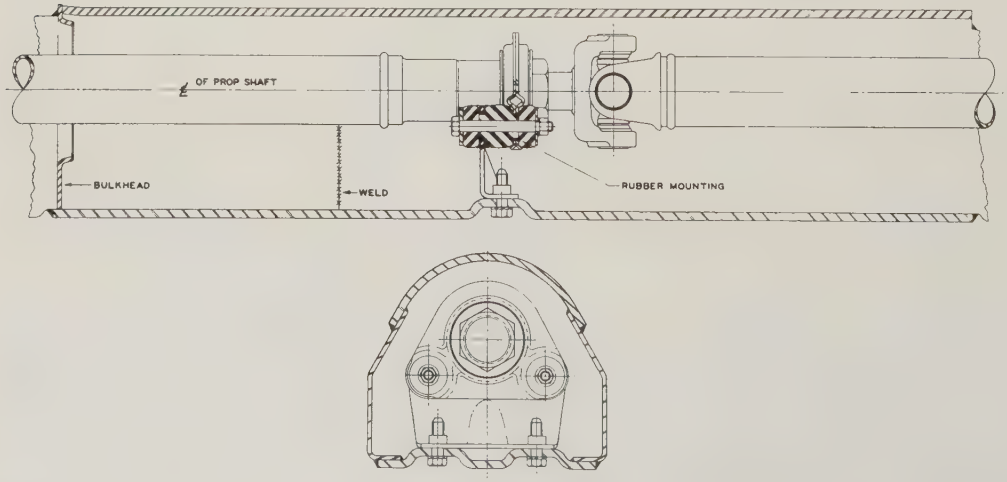

Fig. 13—Mounting of propeller shaft in frame

tion is uniform in cross-section, the same forming tools can be used for all the lengths. The additional length in the longer frames incurs less penalty in weight than we had in the former-type frames. The Series 75 frame, for the 8-passenger body, weighs 3½% less than in 1956, yet the torsional rigidity is improved 18% and the beam stiffness 16%.

The stock thickness is increased for some parts in the longer frames, but this was anticipated in the tooling program, so the tools are interchangeable.

The frame for the convertible models (built on the 129½-in. wheelbase chassis) has some components of increased metal thickness. In addition, straps 2 in. wide by ½ in. thick are welded to the bottoms of the frame members forward from the tubular section and rearward to the start of the kickup.

While the 1957 convertible frame, at 549 lb. weighs 6 lb less than the 1956 convertible frame, it has equal torsional rigidity from front to rear axles. The distribution of rigidity was improved, with more strength in the body area from dash to rear axle. The maximum beaming deflection is 0.058 in. which is 100% stiffer than in 1956.

For equal weight, all of the frames showed increases in torsional rigidity and beam stiffness over our former designs. The exceptionally high beaming stiffness is easily "tuned" to the desired beam stiffness for the complete car by merely changing the stock thickness of the body mounting brackets. This was combined with variations in the stock thickness of the body rocker sills for complete car tuning.

A heavier rocker-sill inner panel and an added reinforcement is used with all bodies mounted on the new frame. These panels contribute to the

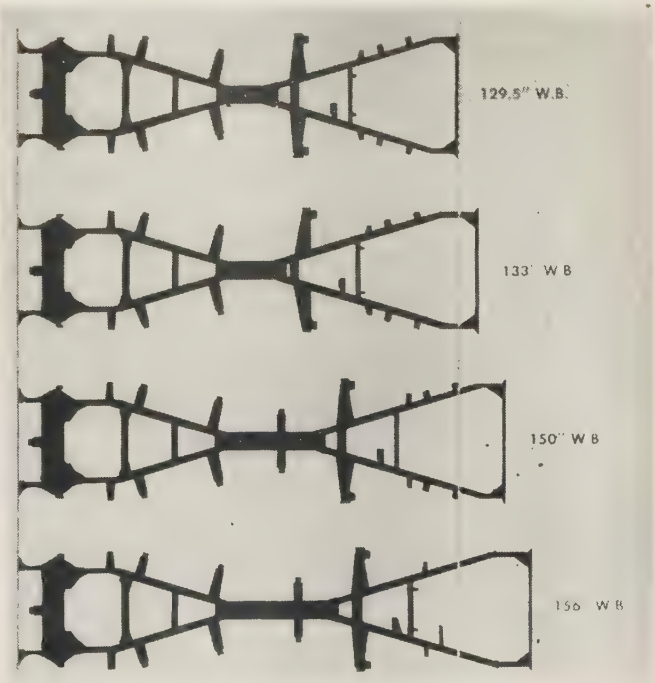

Fig. 14—Car frames showing different lengths

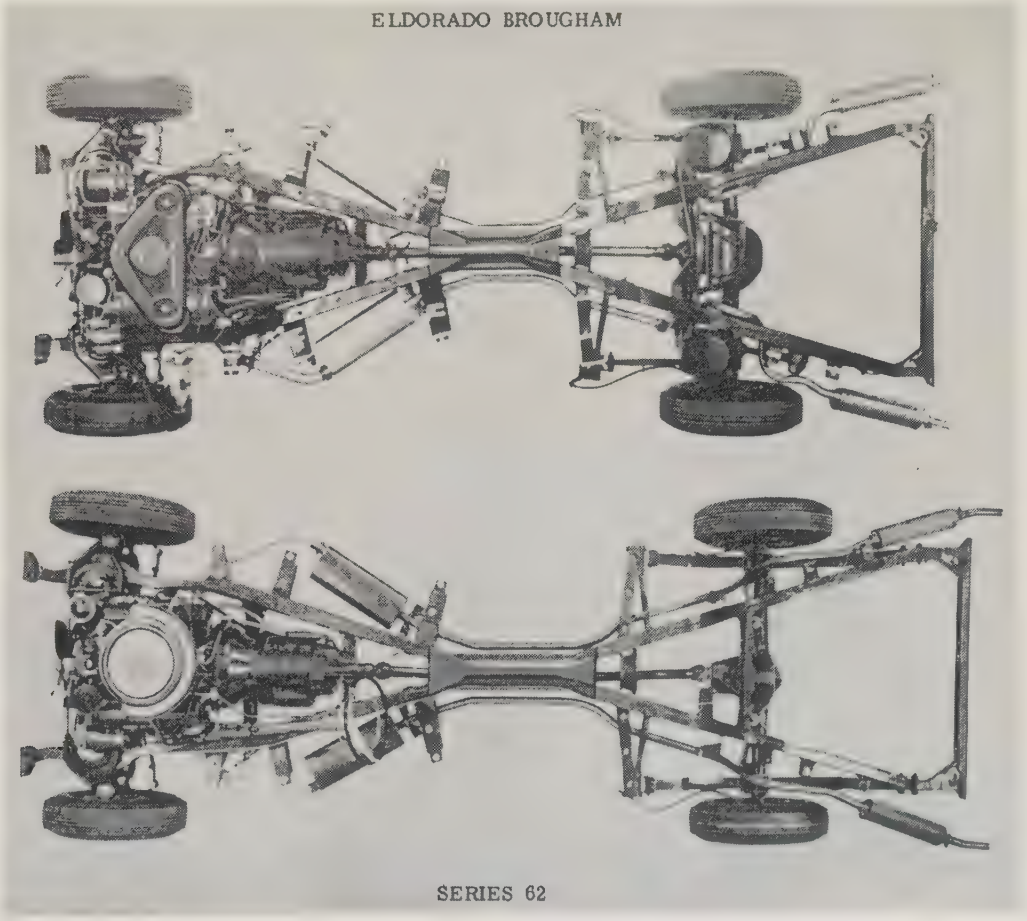

Fig. 15—Comparison of Eldorado Brougham and Series 62 wheelbases

torsional rigidity of the body also, so variations in their thickness help determine the tuning of the car. They may be lightened or eliminated on later bodies as we gain experience in field service performance over a longer period of time.

Variation in torsional rigidity of the complete car is obtained easily, of course, by changing the stock thickness of the proper frame structural component.

The adaptability of the basic frame design was proved on the Eldorado Brougham. The car is entirely different from the other models. (See Fig. 15.)

The wheelbase is 126 in., or 3½ in. shorter than that of the Series 62. The body and all sheet metal parts are different. The body is a true 4-door pillarless design with the rear doors hinged from the rear. The frame is ¾ in. lower than that of the Series 62. The overall height is 55½ in., or 3½ in. lower than the Series 62. Air suspension is used, front and rear, rather than the conventional coil and leaf springs used on the other series.

The "Tubular Center-X" frame meets the requirements of these different features very well. The same basic design is used, with some changes at the rear to accommodate the air suspension and the trunk-compartment floor of the special body. The air chambers are bolted to brackets welded to the frame member. The radius arms for the rear axle are pivoted from the frame outrigger that carries the No. 4 body bolt. This same outrigger is used for the front anchorage of the leaf spring on the conventionally sprung series. The front crossmember is interchangeable for all frames and both types of suspensions. There is also some interchangeability of body brackets between all the frames.

The location of the mufflers and pipes of the exhaust systems is also shown on this picture. (One advantage of the new frame that we had not anticipated developed on the chassis assembly line. Installation of the engine, propeller shaft, exhaust system and other parts is much easier than with the former frames. They do not have to reach over the side bars to install the parts.)

The Eldorado Brougham frame has torsional rigidity 15% higher than that of the frame for the 1956 4-door hardtop. The beaming stiffness is 100% better. The Eldorado Brougham frame weighs 410 lb, while the 1956 frame weighed 391 lb.

The thoroughly coordinated design of frame and body for this Eldorado Brougham resulted in a much stronger car. The frame/body combination is 32% better in torsional rigidity than the comparably-styled 4-door hardtop model of 1956. The beaming stiffness is equal to that of the 4-door sedan of 1956.

This was achieved despite a 55% larger windshield opening, a 50% greater offset in the No. 1 pillar, a flatter rear-light opening, hardtop styling, and an 11% heavier body.

The extreme lowness of the Eldorado Brougham accents the improvement in car handling that comes with lower cars. As cars become lower, they tend to "hug" the road better, particularly on turns and under cross-wind conditions. This makes a car safer because it is easier to handle. While this improvement has been constant with the gradual lowering of cars through the years, it is particularly noticeable in the Eldorado Brougham. We believe that the customer will sense the gain even though he may not be aware of the cause.

We feel that this basic frame design has potential of further improvement in weight and cost reduction as we gain more experience with it. The present design represents much co-ordinated effort between Cadillac and the A. O. Smith Corp. The frame had to be developed with the proper shape and strength to complement the bodies and had to be designed for efficient production at an acceptable cost.

The new-type frame with its "Tubular Center-X" has permitted much lower bodies and a fresh concept of styling. This has been done with very little weight and cost increase, while the frame/body combination is stronger.

Part II

by J. R. Parker

THE 1957 Cadillac frame represents a new solution, based on a fresh approach, to the problem of providing automotive structures which are satisfactory from both the performance and economic standpoint without interfering with those styling and passenger space features which improve the utility and salability of the end product. We believe Cadillac's solution to be particularly noteworthy because it permits a substantial reduction in floor height and at the same time allows an increase rather than a decrease in permissible dimensions of structural members.

The use of a backbone structural arrangement in automobiles is not, of itself, a new thought. It has been a feature of a number of European cars, and it has also been given consideration in this country. The adaptation of this structure to the design and manufacturing problems of today's American automobiles is new, however, and has proved very successful in this case.

Our company has long maintained a product research organization which directs its activities toward developing possible solutions for the structural problems facing the automobile industry. Often we do this by studying performance and manufacturability of alternative designs by incorporating them into existing vehicles. One of the cars selected for study back in 1948 was the Hudson. That car had a floor depressed below the sill structure, and we wished to explore the possibility of accomplishing a similar result with what we felt could be a more economical, separate frame construction.

One of the designs we considered was that of placing the side members in a long "X" arrangement crossing the "X" at the front of the rear compartment floor. This frame differed from the conventional "X" member frame design in two important ways. First, the crossing point of the "X" was moved rearward from its customary position under the front seat to a point just behind the front seat in the rear compartment floor. Secondly, the parallel side members used in the conventional frame were eliminated entirely, and the "X" member itself was designed to provide their function. It was found that the frame width and height in

he area of the rear-compartment floor could be nade less than that of the existing propellor shaft unnel for most of its length. Frame depth in this mportant mid-section could be 6½ in., a tremendous gain from the 4½ in. to 5 in. available at that ime in more conventional frames. Section depth dimensions in other parts of the frame could also oe quite satisfactory since, in the front floor compartment, these sections were near the transmission and could take advantage of the crown in the floor necessary to provide clearance for that unit.

So far as the chassis itself was concerned, the "X" type frame was by far the most attractive of he alternatives studied. Section dimensions were excellent, and the main structural parts were generally in good alignment; such offsets as were required could be readily supported by cross frame oracing. Fig. 16 shows this original design and demonstrates the relatively good alignment and adequate section sizes. In Fig. 17 is shown the way n which the frame of this design allowed clearance for the depressed floor. In Fig. 18, we have indicated typical section properties obtained with the experimental design in comparison with the properties of a conventional box section frame of the same vintage. The conventional box frame would not have accommodated the desired floor; the experimental frame did provide clearance and yet accomplished this with an improvement rather than a reduction in section properties.

It was apparent from the design study that the frame itself could be quite efficient. Granting this, however, the performance of the complete vehicle was subject to question. A large share of the structural stiffness of a passenger car is contributed by the body structure and particularly by the body roof. Whether this kind of frame could be designed to cooperate effectively with the body structure was problematical because of the increased lateral distance between major chassis and body members.

An experiment was set up to evaluate this question. The chassis frame for a typical 1950 car was redesigned and built in such a manner that it could be easily modified to represent several variations of this basic construction, and the production body was reworked to suit. Static tests were made on the frame, the body, and the combination with each of the frame design variations. As expected, the frame itself was very efficient providing excellent stiffness both in torsion and in beaming. We had been less confident that the frame and body combination would prove satisfactory but were pleased to find that the combination reflected the same stiffness improvements inherent in the frame itself. In other words, the experimental combination utilized the structural stiffness of the body shell as effectively as did the conventional design.

We would like to discuss the reason we had hoped this type of frame might cooperate efficiently with the body structure since this test, as well as others we have made since, seems to justify this reasoning. While frame and body must resist both torsional and bending loads, we will talk in terms of bending resistance only since it is easier to depict and the principles are the same.

For purposes of this discussion, we will also differentiate between the under structure of the vehicle and the superstructure. We will consider that the understructure consists of the frame, whether separable as a chassis frame or welded to the body as an integral unit, the underbody structural members such as rocker sills and floor cross-members, and the floor itself with its stamped formations. The superstructure, then, will consist of the remaining features of the car serving overall structural functions, namely, the body roof, the body side frames and panels, the firewall, front end sheet metal, and the like.

Thus, we will be discussing the way in which the understructure is reinforced by the superstructure in resisting bending loads.

The ideal way, from a weight and stiffness stand-

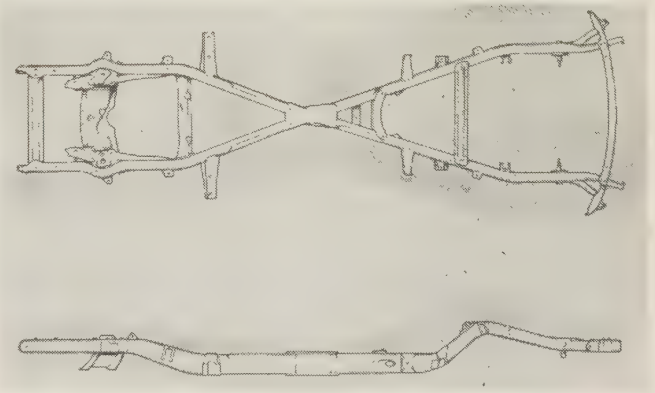

Fig. 16—"X" type frame for 1951 experimental car

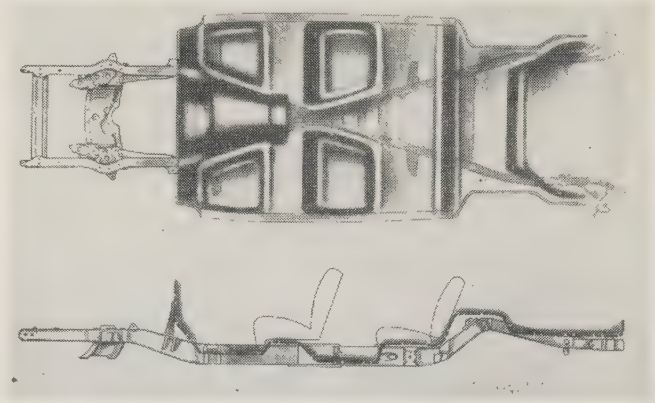

Fig. 17—"X" type frame and body floor for 1951 car

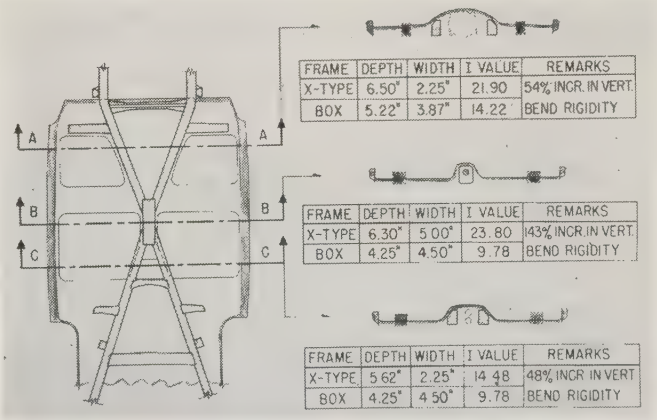

FRAME	DEPTH	WIDTH	I VALUE	REMARKS
X-TYPE	6.50"	2.25"	21.90	54% INCR. IN VERT.
BOX	5.22"	3.87"	14.22	BEND RIGIDITY

FRAME	DEPTH	WIDTH	I VALUE	REMARKS
X-TYPE	6.30"	5.00"	23.80	143% INCR. IN VERT.
BOX	4.25"	4.50"	9.78	BEND RIGIDITY

FRAME	DEPTH	WIDTH	I VALUE	REMARKS
X-TYPE	5.62"	2.25"	14.48	48% INCR. IN VERT.
BOX	4.25"	4.50"	9.78	BEND RIGIDITY

Fig. 18—Comparison of section properties of 1951 "X" type frame versus conventional box frame

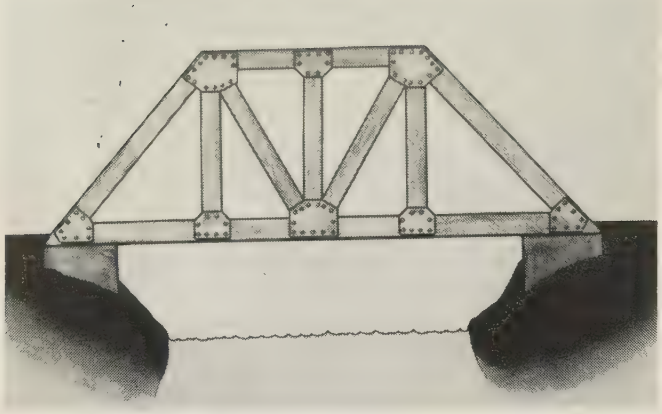

Fig. 19—Familiar example of bridge truss principle

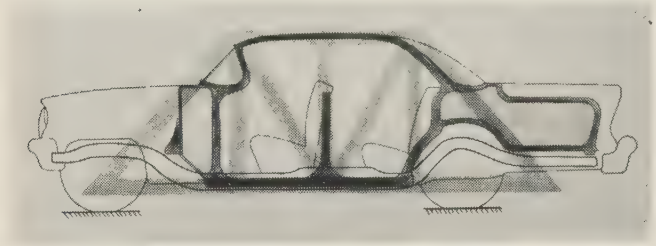

Fig. 20—Analogy of car body and truss

point, to carry bending loads is with a truss structure as shown in Fig. 19. Each of the members is called upon to carry only axial loads, either tension or compression; the large overall dimension of the assembly reduces the magnitude of these loads and results in high rigidity.

In actual practice, however, the application of this ideal structure to the passenger automobile is rather difficult. Limitations imposed by the clearance requirements for the various parts of the vehicle, by the space and visibility requirements of the passengers, by the desire to make the car look like a thing of motion, and by the necessity for doors, result in a structural compromise quite unlike the ideal. Fig. 20 indicates this compromise by showing a typical modern passenger car with the bridge truss superimposed upon it. It is apparent that a good many of the elements do not exist at all and that most of those which do exist are curved and loaded eccentrically. Each of the members must resist bending loads in varying degrees as well as direct axial loads.

While the body roof, because of its favorable placement, can and does contribute importantly to the structural rigidity of the vehicle, it is far from being equivalent to the top chord of our bridge truss. In this respect, the passenger car differs greatly from the airplane or the highway bus. These latter vehicles can be practically designed as monocoque or stressed skin structures but the passenger car cannot. Furthermore, the trend is toward lighter, smaller, and thus less effective roofs.

In the case of the passenger car, the understructure is the principal load-carrying member, and the superstructure serves to reinforce it to the extent allowed by its own limitations and the limitations of its attachment. The reinforcing effect of the

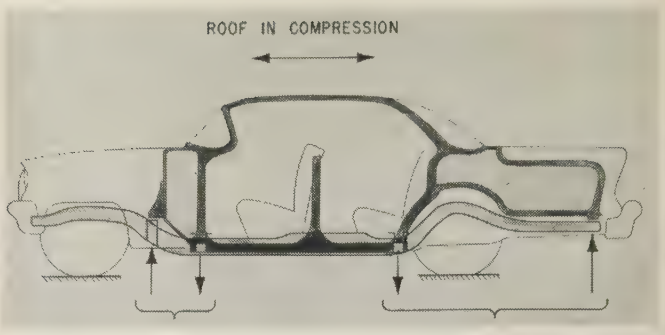

Fig. 21—Forces acting on car frame

superstructure is accomplished in the manner shown in Fig. 21. The understructure, functioning as a beam, attempts to rotate in the front and rear areas. This deflection is resisted by couples in the body side structure and by compression in the body roof. Since the roof itself is light and shallow, it offers little resistance to bending, but it can take compression to resist the bending loads on the understructure and, similarly, it can carry shear to resist twisting loads. The center pillar, when it exists on sedan bodies, is important mainly in stabilizing the roof to prevent its buckling under compression. Thus, through the midsection of the body, attachment between chassis frame and body serves only to reinforce the body floor for local loadings and contributes little to the utilization of the roof in resisting overall loads.

The above analysis can then be resolved into two key points. The first of these is that the understructure functions as the principal load carrying member which is reinforced by the super-structure to whatever extent the capability of the superstructure will permit. This is illustrated in Fig. 22 as a caricature. Here we see that the bridge truss can be a fair representation of the appropriate structural approach to a bus but that, in the case of a passenger car, the demands of styling and the space relationships of the various parts suggests the need of a rigid under structure.

The second key point in the analysis is that the full reinforcing effect of the body superstructure can be achieved so long as firm attachments are made at a few key locations. In order to transmit the resisting moment offered by the body roof through the side walls and inboard to the location of the "Tubular Center-X" frame, it is necessary to have rigid cross-structure at only four points. Such cross-structure already exists or can be provided readily as shown in Fig. 23.

The body-dash serves as an admirable cross member to translate loads from the frame location to the front of the cowl. At the front door pillar, we wish to achieve a downward load on the body, and we can attain this by a substantial outrigger bracket under the toe board with double mounting to the body. At the rear door latch pillar, another location at which the frame must load the body downward, a body cross-member can be provided under the rear seat or the structure of the back of the seat can be effectively utilized. At the rear end, frame and body structure can be brought together for suitably rigid attachments. In addition to these four main connections, additional attachments between chassis frame and underbody can be made as

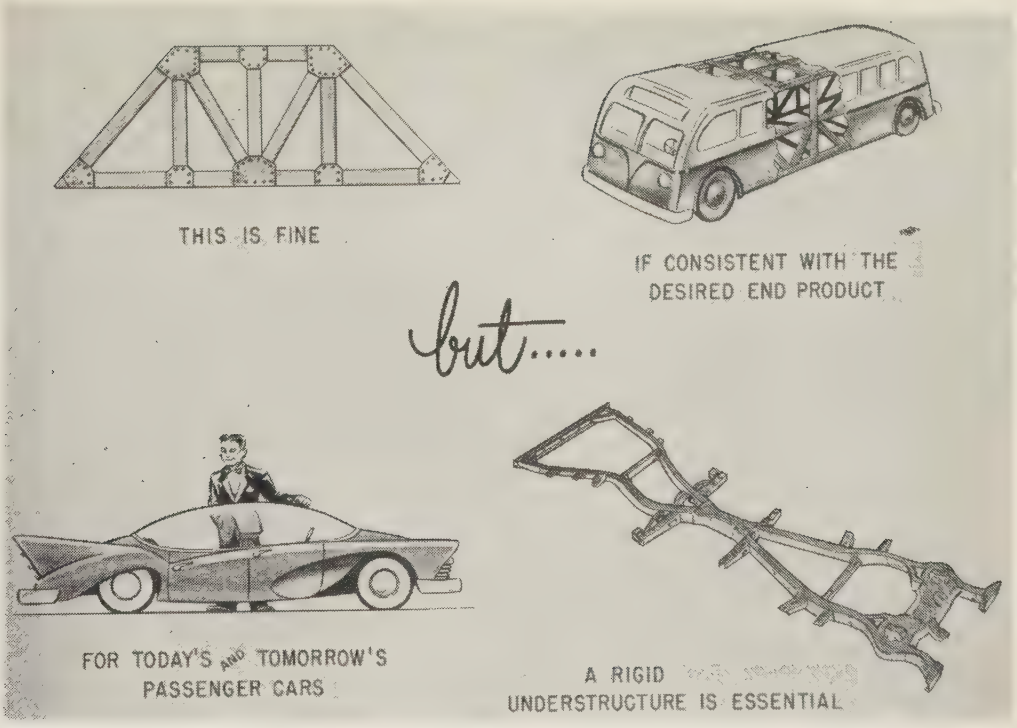

Fig. 22—Structural approach depends on requirements

and if required to reinforce the floor for local loadings or to carry loads imposed by stub pillars on hardtop models.

The front fender structure can be so attached as to transmit a greater or lesser amount of load from the front section of the frame into the body cowl depending upon the degree of stiffness desired and the amount of engine noise pickup and front end harshness considered tolerable.

Subsequent tests on a number of vehicles have confirmed the fact that frame to body attachment efficiency with this style of frame can be equal to previous conventional practice. That is, a given body structure does reinforce the frame against overall bending and torsional loads to about the same degree as the same body reinforces typical frames used in the past.

Having concluded our static structural tests on the 1950 body and experimental frame, we were encouraged to complete the buildup for road performance comparisons with a conventional car of the same model. Road tests proved to be equally encouraging. No objectionable characteristics peculiar to this type of design were experienced; the car felt firm yet not harsh, and road and mechanical noise levels were low.

Data from this original experimental car and from another more refined buildup which we completed in 1954, proved useful to Cadillac in their design of the 1957 models. Fig. 24 is a photograph of the underside of this second experimental car showing the relationship of the floor and the frame. The underbody of this car was rebuilt to be structurally equivalent to conventional practice of that period having rocker sills and body cross members of conventional dimensions. You will note that the positioning of the narrowest part of the frame just behind the front seat pan and the absence of a straight tubular section such as is used on the 1957 Cadillac resulted in a diverging tunnel in the rear

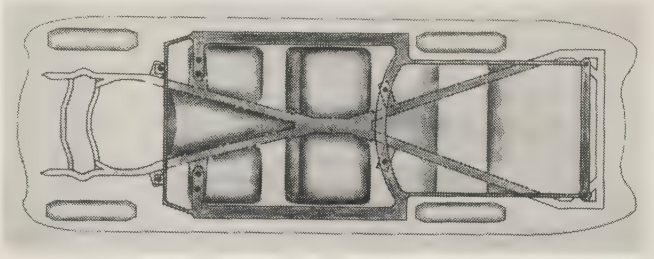

Fig. 23—Effective cross structure in body to frame tie-up

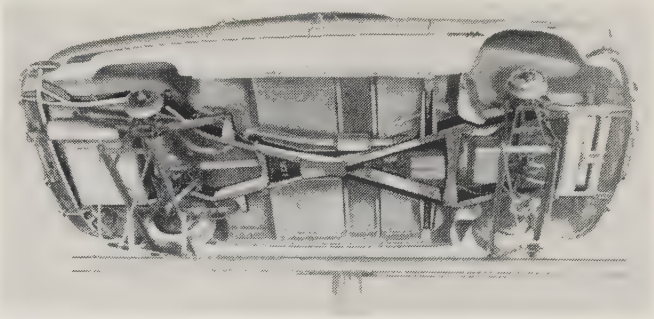

Fig. 24—Bottom view of 1951 experimental car

passenger compartment. While this was not too objectionable because it was minimized by modifications to the contour of the upper part of the frame, later study has proved that it was an unnecessary compromise. The complete car was 42% more rigid in torsion than the production car from which it was rebuilt having a static deflection rate of 7040 lb-ft per deg of twist over the wheelbase. It was 270% more rigid in bending than the production car. Weight had been increased by 18 lb. It should be noted that these great stiffness increases were not necessarily desired; we set out to

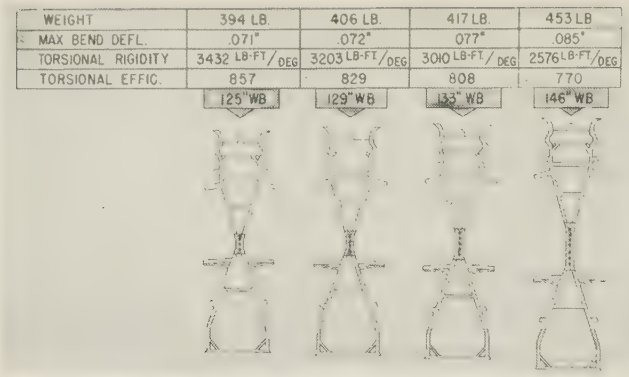

Fig. 25—Results of tests for effect of wheelbase variation

Table 1—Structural Performance Data (Frame and Complete Car Comparison)

Car Name	Complete Car		Frame		
Year and Body Type	Torsional Rigidity, lb-ft per deg	Maximum Bend Deflection, in.	Weight, lb	Torsional Rigidity, lb-ft per deg	Maximum Bend Deflection, in.
1957 Cadillac Sedan De Ville	5560	0.047	410	2900	0.102
1956 Cadillac Sedan De Ville	5200	0.084	393	2700	0.144
1956 Cadillac 4-Door Sedan	5500	0.062	369	2590	0.160
1956 Car "A" 4-Door Sedan	5300	0.050	330	1860	0.171
1956 Car "B" 4-Door Sedan	4160	0.047	325	1450	0.152
1956 Car "C" 4-Door Sedan	4750	0.031	377	1880	0.121

build a car of about the same weight so that stiffness changes would represent design efficiency.

During the period that our research program was in progress, Cadillac Engineering began exploring design possibilities for the Eldorado Brougham. They felt that our test results, to that point, were encouraging enough to warrant further study, and they adapted the design to several special development vehicles including some of their "Dream Cars" in the Motorama Shows. By early 1954, Cadillac's experience with these cars convinced them that they would be able to create a satisfactory design, not only for the Brougham but also for the regular line of 1957 automobiles, and a joint program was started to explore this construction from the standpoint of the many problems and requirements special to that end result.

One of the first and most important matters to be considered in the application of this basic design to Cadillac's production was the matter of varying wheelbases. Cadillac's normal compliment of models involves wheelbases of 129½, 133, 150, and 156 in. Since some of these models were produced in limited numbers, it would have been impractical to provide special tooling for each wheelbase as would have been required if the original concept of the frame of "X" formation were used. If, on the other hand, the midsections could be lengthened to provide for the increased wheelbase, the same basic tooling would suffice for all models. A test program was inaugurated to explore the loss in efficiency which might result from departing from a common intersection point of the four "X" member legs. Fig. 25 shows the dimensions and plan view shapes of the frames tested in this experiment. Above each frame is shown the stiffness and weight. Thus it was established that extending the central tunnel section would not greatly harm stiffness and that the changes which did result could easily be compensated by modest changes in gage in the principal parts. The tools for the higher volume models could be inserted to allow for the gage changes without any substantial cost penalty. As previously mentioned, the final design of the 1957 model-75 frame for the 150-in. wheelbase 8-passenger car is lighter and considerably more rigid than its 1956 counterpart. The results of the above tests on extending the length of the center tunnel, indicated that the frame need not be a true "X" and should more properly be called a "Tubular Center-X" type frame. These tests also showed that, since it was not necessary to widen the rear of the propellor shaft tunnel to allow the rear legs to diverge from a point at the center of the frame, the minimum size tunnel desired by Cadillac could be achieved without penalty.

Several other design features were discovered during the development tests made for Cadillac. Two of these may be worthy of reporting. The contour of the tubular center section, particularly in the region in which it branches out to merge with the extending legs, was found to be a very important factor in the rigidity of the entire frame. In one of the tests, an increase in torsional stiffness of the complete frame of more than 20% was achieved through a change in contour of the top tunnel member without any increase in section size, material thickness, or weight. Bulkheads or shear plates at the ends of the tunnel section were also found to be very desirable in terms of the increase in torsional efficiency they produce. In the 1957 Cadillac frame, a bulkhead was applied at the front end of the tunnel, and a short cross member just rearward of the tunnel to achieve the same effect.

Both the external contour and the bulkhead are effective because of the action of this portion of the frame in resisting overall torsional loads. When torsional loading is applied to the frame, one front beam and the diagonal rear beam are loaded downward while the opposite members are loaded up ward. This results in a combination of cantilever bending and torsion in the legs themselves and a condition of almost true torsion at the center of the tubular section. The stresses in the extending beams must be transmitted into the tubular center section with a minimum of buckling or other secondary distortions in order to provide optimum rigidity. Fig. 26 shows three of the tunnel shapes studied. The first proved structurally effective but required too much space in the rear passenger com-

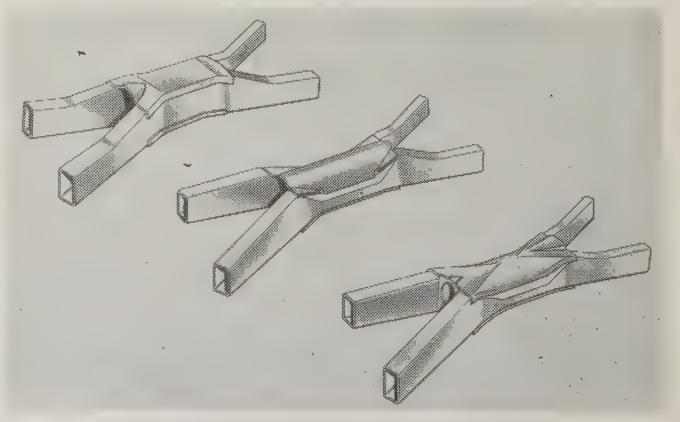

Fig. 26—Evolution of frame tunnel contours

partment. The second shape was satisfactory for space, but its formation resulted in high deflections. The third shape is the one which was finally released for production since it proved optimum both from the standpoint of space required and performance.

The distribution of metal within the center section was also studied as shown in Fig. 27. Since the extreme fiber material is the most effective, the third section proved best. This construction is simple and straightforward from a manufacturing standpoint and provides for a minimum tunnel size in the body floor. It requires an increase in tunnel size of not more than $\frac{5}{8}$ in. radially beyond that which would be needed for the propellor shaft clearance alone if the frame structure were located elsewhere. Space for the frame in the front compartment has not proven to be a particularly serious problem. The front floor is normally higher than the rear floor by several inches because of the difference in seating requirements and headroom for the front-seat passengers and because of clearance needed for the transmission. Furthermore, the high degree of rigidity in the center of the frame has allowed for a frame depth reduction in the front seat area without a loss in efficiency of the overall unit.

Cost is always a subject of great interest and importance in automotive design. Comparisons between different designs are somewhat difficult to make because the detail requirements of each vehicle have a considerable effect on costs. Detail evaluations of a number of comparable frames have proved to our satisfaction that this basic design is little, if any, more expensive for a given end result than conventional frames of the recent past. Further, it appears to be less costly than any of the alternative designs proposed to date for very low floors. The increased structural efficiency generally allows a weight reduction, if no increase in stiffness is desired. It is up to the automobile manufacturer to determine whether he wishes to take advantage of this efficiency improvement in the form of better performance, lower weight, or perhaps compensation for a less effective body superstructure resulting from greater window areas, smaller pillars or other styling features.

In the case of Cadillac, the "Tubular Center-X" frame design was competing with their 1956 model which had the highest structural efficiency of any passenger car frame in the industry, in terms of stiffness per pound of weight adjusted for wheelbase. The 1957 frame is actually slightly heavier than the 1956 (4½%) but it is also considerably more rigid (41% bending, 7½% torsion). If the rigidity had been maintained at the 1956 level, the frame could have been more than 10% lighter than the comparable 1956 model. Structural performance is considered to have been improved correspondingly.

In spite of the potential for further improvement which we believe still exists, we consider that the data in Table 1 is most satisfactory. This table displays comparative weights and stiffnesses in bending and torsional loadings for the 1957 Cadillac Model 62 4-door hardtop sedan in comparison with the equivalent 1956 model as well as the 1956 Cadillac conventional sedan and a number of other 1956 conventional sedans of about the same size.

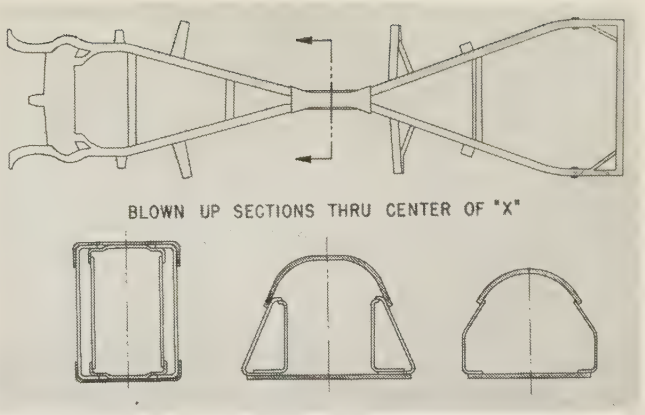

Fig. 27—Evolution of frame tunnel cross-sections

Summing up then, we feel that the structural design of the 1957 Cadillac represents an important degree of progress. It permits the car manufacturer to reduce the height of the vehicle for greater safety, sales appeal, and better performance, without harming the space available for the passengers. It accomplishes this with an increase rather than a reduction in structural efficiency, and thus a reversal in the trend toward more costly and heavy structures usually associated with lower cars. It retains the advantages in cost, design flexibility, and insulation between chassis and body which are inherent in the separate frame construction.

Of course, other design possibilities for low cars exist, both in production and in the development organizations of the industry. As development progresses, or as the functional and spatial requirements of passenger cars change, so, too, may the relative merits of these designs change. From today's perspective, however, the "Tubular Center-X" type frame has much to recommend it as a solution to tomorrow's structural design problems.

We feel that Cadillac Engineering is to be commended for having had the vision and engineering skill to develop this construction into a satisfactory production reality, and we, ourselves, are proud to have had a part in this development.

DISCUSSION

Comments on Frame Designs

—W. E. Liesman
Dana Corp.

AT THE outset, I wish to mention that these comments are a joint effort of John Leggat, formerly of Pontiac Motor Division and now an Engineering Consultant for Dana Corp., and myself. We wish to commend Messrs. Milliken and Parker on their paper. The application of this frame design to the 1957-model Cadillac is the culmination of a long period of development and testing by both Cadillac Division and A. O. Smith Corp.

We must agree with the authors that the styling trend to lower cars must be acceded to in light of its desirability from a sales viewpoint alone—if for no other reason. Consequently, the problems that are a byproduct of low-car styling must be surmounted. The "Tubular Center-X"

type frame is certainly one method of solving a portion of these problems.

Current frame designs are bearing a somewhat greater share of the strength requirements for the entire car than previous designs. Generally, decreased body strength has resulted from larger window openings, decrease in size or elimination of center pillars, and changing of pillars from structural members of a beam design to those having a considerable amount of contour and change in section to meet the needs for the door and window openings. The fact that this frame design provides greater beaming and torsional strength to meet such requirements is of great value.

It must be remembered that stiffness and rigidity factors for the frame must often be adjusted to obtain the desired ride characteristics. An overly rigid automobile will give an unpleasant harshness; an overly flexible car will result in equally unpleasant shake—in other words, a "balanced" or "tuned" car is needed to meet the current "ride" criteria. The variation of the "X" members of this frame design provides some of the flexibility required to meet these demands.

The vulnerability to side collision of this type of frame design, as compared to other designs, has not been mentioned here. We would like to ask the authors whether such studies have been made or are contemplated. Conventional side-rail and body-sill design would have certain deceleration values for side impact, and we ask whether these same factors have been evaluated for this design. Certainly, passenger safety is one of the primary problems in overall car design.

Two of the disadvantages that we can see in this design are the increased amount of body material required by the heavier and reinforced body sills necessary and the wide tunnel area needed to clear the "Tubular Center-X" member. One of the advantages is the narrow section for the passengers to step across on entry or exit from the vehicle.

We cannot state at this time that the manufacturing costs for this design are considerably different than other frame designs of equal weight. We believe, however, that there are some penalties involved for fixturing and tooling in order to maintain alignment of this design during manufacture.

In conclusion, the "Tubular Center-X" type frame is one means of solving the problems which confront the frame and automobile designer.

Discusses Structural Members of New Cars

—N. T. Dietrich, Sr.
Midland Steel Co.

IT HAS very often been said, "There is nothing new under the sun." However, we all recognize that a great deal can be accomplished by taking any basic idea and going to work on it, to develop it, to realize the possibilities that it holds.

It is quite apparent that a great deal of time, effort, and expense has gone into the work in developing this center tube "X" frame. Besides the time, effort, and expense, or may we better say, as a part of it, has been the study, thought, and experimenting, which has resulted in a unique and efficient way of accomplishing the purpose that lay before them.

We have done a considerable amount of laboratory work involving the testing of frames and components of frames for many years. For the past three years, under the direction of our chief engineer, L. F. McNitt, it has been considerably accelerated. We, like our friends and competitors, have sought better ways to design and build frames. We feel that there are many factors that spell out the need for a frame in the modern car of today and in the car of tomorrow. Some of these have received notice and mention by both Mr. Milliken and Mr. Parker. With the automobile becoming more and more a thing of beauty, our engineers and designers have been compelled to sacrifice the straight line for the curved one—and, certainly, we can't quarrel with that. But, as has been said, with lower roof, larger glass area both in front and in rear, curved A post, absence of the B post in some models, such as the hardtops, relatively poor tie for the roof with the rear quarter panel, and thinner roof section or reduction in roof sills or roof rails, we must look to the understructure for compensating strength. The strength which has been attained in this center tube "X" frame is highly gratifying. From the strength and efficiency standpoint it certainly deserves a very high mark and no apology whatever. The figures which we have been given on the charts show conclusively the efficacy of the design.

To obtain a torsional rigidity of 2900 ft-lb per deg and similar results in beam stiffness in a frame weighing 410 lb is a real accomplishment. We may say that our own tests, on a comparative basis, substantiate these results.

However, we would like to discuss the comparative aspects of this frame with a design that would do, perhaps, about the same thing. With the absence of side rails through the center section of the car, one must provide outboard body mounting brackets. These can be, and likely need to be, quite strong and, therefore, may be on the costly side. With no side rail through the center section, it may be necessary, as our friends at Cadillac have done, to reinforce the rocker sill to give added strength. This brings to mind the general idea of crash or collision protection. The absence of side rails must lower the protection offered against car side impacts.

To lower the floor panel and keep the side rail, this section, which we feel should be boxed by means of a channel reinforcement joined to the side rail by suitable welding, must be moved outward or into a position close to the body rocker sill or rocker panel, as it is sometimes called. The stepover can be held to a respectable or reasonable distance. This, of course, makes for more floor space or foot room in the car and ease of stepping over the threshold in entering or leaving the car. The threshold cannot be lowered appreciably, most engineers and designers feel, below present elevation due to curb heights and the sidewalk levels which can prevent the opening of doors.

With boxed side rails and a good boxed cross member under the front-seat location to give torsional rigidity and strength, the clearances over and at the sides of the propeller shaft can be held to an absolute minimum. The situation, design-wise, is helped by an added center bearing. This will reduce the center tunnel in the floor to the very minimum. Keeping the tunnel in the floor panel to a minimum in width might, by some designers, be considered most desirable.

It is obvious that a boxed side rail will require some room or space. What we mean to say is that it can be placed quite close to the rocker panel of the body and attachment of the floor panel to the frame side rail can be accomplished through short or stub body brackets, which can be worked out on both the outboard and inboard of the side rail or even through the top surface of the side-rail box section.

Although we have not run costs on the center tube "X" frame, and perhaps it would not be wise to hazard a guess, it would seem that for a given wheelbase the cost advantage might be with a box-section side rail of more conventional design.

If we were to match the high torsional and beam strength of the center tube "X" frame, that would be a man-sized job. Yet, as we know, not all cars are of the price class for which this design has been worked out. A frame and body combination may very well be developed that will give very satisfactory performance with somewhat less cost, using the boxed side rail in the frame.

As we have said, our testing of the center tube "X" frame under discussion has shown it to be very good. Perhaps "very good" are hardly the words to describe it. Yet when one checks the torsional strength from the dash forward which has always been considered a very critical

area, we find the more conventional boxed side-rail frame shows up better than it does in overall torsion or beam strength.

For instance, on a foot-pounds per degree of twist per pound of frame weight, we have found in our testing that the plain boxed side-rail frame without "X" member checks 103% of an open channel side-rail frame with "X" member and forward channel extension which boxes the side rail only at the steering gear area.

The center tube "X" frame when checked against the same frame shows only 86% of the dash forward strength, torsionally. In every other test that we made in the comparative study of the different general types of frames, the center tube "X" frame checked very favorably.

In the beginning we said that it is often stated that there is nothing new under the sun. This brings to mind the great procession of changes that we have witnessed in cars. Some of us have become tremendously interested in old cars, the forerunners of today's beautiful and efficient automobile with its safety, speed, and comfort. Among these might be found the Tatra, which was built in Czechoslovakia in the late 1920's or early 1930's, with the so-called backbone or center tube construction. About that time or a little later, our friends of the Leaf Spring Institute, Messrs. Probst and Shoemaker, designed a frame that followed the center "X" design, without side rails at the center section. Although the frames of that day were not much when measured for torsional and beam stiffness, as compared with present-day frames, this frame was not exceptional as we recall it. One of the most important changes in frames has resulted from the adoption of the box section. This increased the cost of the frames without question, but it also did wonders for the frame strength-wise.

Mostly out of a desire to simplify or clean up the chassis, as we saw the picture, one of our larger makers some years ago gave up the "X" member and went to a plain boxed side rail, employing full length reinforcement or subside-member. The beam strength of the frame was increased, and the torsional strength overall was about the same. However, the dash forward strength was increased torsion-wise.

In testing specimen channels versus boxed section of the same weight per foot or of the same cross-sectional area, speaking of the actual area of the steel itself, it has been found that the boxed section will test approximately 20 times as strong in torsion as the plain open channel.

Here we have the secret of the surprising strength that boxed sections deliver when employed in side rails and in cross-members and in side rails such as are employed in the center tube "X" frame.

With the center "X" member as recently and presently employed by many manufacturers, the legs of the "X" member have the full depth of the side rails or nearly so, and are very efficient in transmitting torsional loads thrown into the car and the frame, from one side to the other, as beam loads, working through the "X" member as a system of cantilevers. When we remove the "X" member, we are then compelled to handle these loads as pure torsion, as outlined by Mr. Parker. It is here that we find the boxed cross-member quite effective in handling the loads just mentioned.

At the same time we find the center tube a most efficient member, and when reinforced with shear plates or bulkheads as it has been in the Cadillac frame it represents the ultimate in handling pure torsion loads.

With these considerations of the values of the main utensils at our disposal in designing a frame for a particular car, we can choose the things we wish to have or not to have. However, it is only natural that others will find another way, if not better, then a different way of doing the job. In closing we will again say that in this frame development a great job has been done in reducing tooling and production costs over a wide range of basic models, changing mostly in wheelbase except for the Eldorado Brougham. At the same time the means has been preserved of controlling sound and tuning. This frame development gives much that is desirable and good, but among these is that of flexibility, to serve the multiple models that Cadillac produces.

Author's Closure To Discussion

WE gave the frame of the car much thought, of course. And we think that the new "Tubular Center-X" frame/body combination is as safe, collision-wise, as our former cars.

The type and severity of accidents varies greatly—it is hard to design for them and to make tests that will be comparable for different types of accidents.

The complex structure of body rocker sill, body mountings, and frame structure does not permit precise mathematical analysis of the assembly. The rocker sill is about 12% stiffer than the 1956 in beam loading. There are more body bolts in the center area, and the body brackets are heavier.

If a car is hit broadside, the blow is usually well above the frame and body sill. The blow is taken by the door and center pillar until there is considerable penetration, as the frame is usually 12 to 16 in. from the outside of the body. The strength of the center pillar fastening is, therefore, very important.

The center pillar, anchored to the reinforced body sill, deeper floor-pan cross bar, and to the stiff outrigger backed up by the heavy frame structure at the center line, would seem to be stronger than with the former construction.

The floor-pan structure, with the deep cross bar and the stiffer body sill is certainly as strong as that of the integral body constructions, and they have not shown weakness in collisions.

One of the A. O. Smith convertibles with this type of frame was involved in an accident with three big trucks, and the damage was less than that for a car with the former type of frame. It is our opinion that this construction is as safe as any we know of to date.

ORAL DISCUSSION

Reported by C. A. Rasmussen

General Motors Corp.

L. H. Nagler, American Motors Corp.: What has been the experience with this new frame, both in jacking and in raising the car on various types of shop hoists, especially in raising the car on the single-post frame—contact type of hoist?

Mr. Milliken: Extensive jacking tests had been run in the development of the 1957 car and frame, and there were no special problems with regard to jacking. Such things as body deflections and door clearances were kept well in control. The frame does require special provisions to be used when raised on a frame-contact hoist.

C. F. Arnold, General Motors Corp.: A joint meeting of industry executives and representatives of the API Service Station Advisory Committee held on May 14, 1956, discussed various types of hoists. It was brought out that many engineers prefer the drive-on rail or the twin-post type if free access to the wheels is required. The reason for this preference is the risk of possible damage to brake lines, fuel lines, and exhaust systems when lifting a car by frame contact. However, at Cadillac we do not use frame-contact hoists but prefer to see cars lifted by their suspension systems or by the drive-on-type hoist. The new frame was designed with these methods in mind.

A. T. Brown, Globe Hoist Co.: Cadillac has outlined the provisions for the use of a frame-contact hoist and had approved its use with these provisions. The frame-contact hoist has and will handle cars satisfactorily, and they will handle the new type frame as well. Car manufacturers have an obligation to design cars to fit all of the service tools in use, and a number of service stations still use the frame-contact-type of hoist because of its simplicity.

TURBOCHARGING

DISCUSSED in this paper are some of the problems of turbocharging the 2-stroke diesel engine, with particular emphasis on the effects produced by the variable nozzle, the fuel modulating governor, and altitude, among other factors.

Although a turbocharged 2-stroke engine is difficult to rate, the authors' tests appear to demonstrate its practicality through gains in power and economy and to indicate increased future application to automotive diesels.

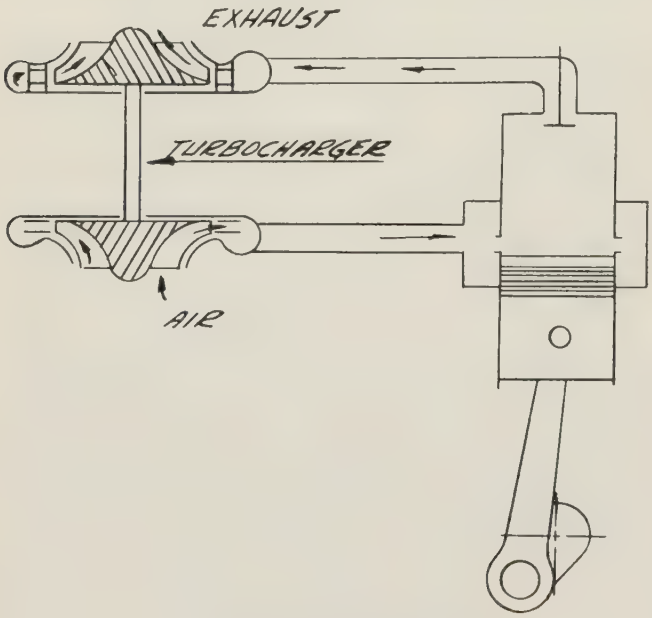

Fig. 1—Diesel with pure turbocharging

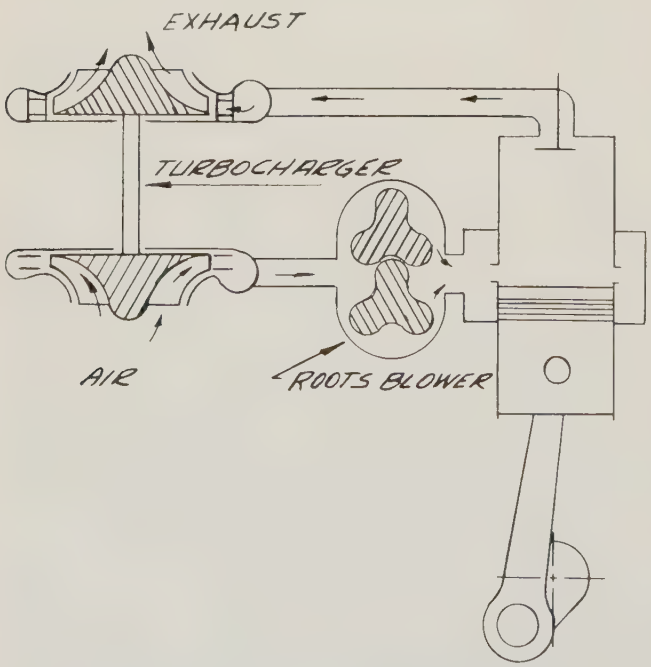

Fig. 2—Turbocharger in series with Roots blower

ALMOST every mechanical development that has reached the point of wide public acceptance has had its origin many years before. The name of the individual who first conceived the idea of using a turbocharger to increase the efficiency of an internal-combustion engine is probably unknown, but certainly the work of Dr. Alfred Buchi of Switzerland proved the practicability of the turbocharged 4-stroke diesel. This knowledge has been available for over 40 years, but the acceptance of this extended work cycle via the turbocharger has certainly not been spontaneous. There are still a tremendous number of nonturbocharged engines being built.

The adaptation of the turbocharger to large engines, that is, those not suitable for installation in automotive vehicles, has been far more rapid in the 4-stroke field than in the 2-stroke field. Turbocharged 4-stroke diesel engines in these larger sizes have been available for over a decade.

The development of turbocharged 2-stroke diesels has been considerably slower, and until recently only a few European engines of relatively large size have been available. Perhaps 2-stroke engineers have felt that the 2-stroke engine provided sufficient development problems without adding those presented by turbocharging. However, the application of turbochargers to automotive diesels waited on the development of small inexpensive turbochargers with reasonable overall efficiency. The development of commercially available turbochargers suitable for automotive diesels has been quite recent and has been expanding rapidly. Automotive diesel-engine manufacturers have followed this develop-

THE SERIES 71 ENGINE

J. J. May and V. C. Reddy, Detroit Diesel-Engine Division, GMC

This paper was presented at the SAE Annual Meeting, Detroit, Jan. 17, 1957.

ment, and at the present time it appears that most manufacturers are either producing or developing turbocharged engines.

A number of years ago an investigation was made at the Detroit Diesel-Engine Division to determine the power that could be recovered from the exhaust of a Model 6-71 engine. Some tests were made but the results were not promising, and the project was temporarily shelved because of projects associated with military applications.

Tests were run on a single-cylinder 71 engine by the U. S. Navy simulating turbocharging. A great deal of information was obtained from these tests, and the results indicated that turbocharging offered definite performance improvement possibilities. This work was reported in an SAE paper by H. T. Smith of the Marine Corps in October, 1954. In 1952 the Lanova Corp. accepted a Bureau of Ships contract to turbocharge a Model 64HN9 engine, a 6-71 marine engine of World War II vintage. The Lanova Corp. did some excellent work and by May of 1953 they had conclusively proved that very appreciable gains in power and economy could be obtained. During this period our engineers negotiated with the Elliott Co. to obtain two turbochargers of a size we hoped would be suitable for the 6-71 engine.

While waiting delivery of the turbochargers, four possibilities of using the turbocharger were considered.

1. The turbocharger as the only source of air, or what might be called pure turbocharging, is shown schematically in Fig. 1.

2. A positive displacement blower in series with the turbocharger (Fig. 2).

3. A positive displacement blower in parallel with the turbocharger (Fig. 3).

4. The turbocharger compounded with the engine,

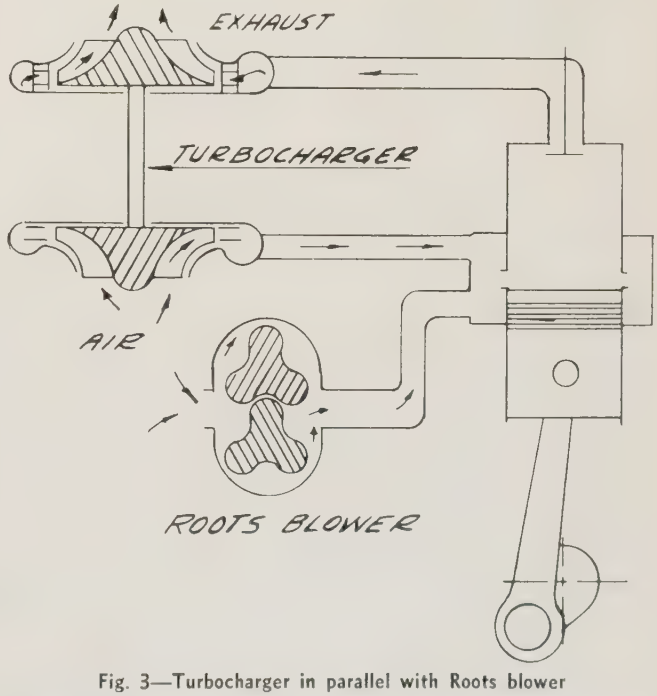

Fig. 3—Turbocharger in parallel with Roots blower

as illustrated in Fig. 4.

These schematic diagrams are self-explanatory.

A surprisingly short test indicated that the engine was certainly not going to operate with pure turbocharging, and the possibilities of operating with a parallel system appeared equally remote. On the second day of the test the engine was operating with the Roots blower in series with the turbocharger, the air delivery of the turbocompressor being used to supercharge the inlet of the engine-driven blower. This appeared at that time to be the most satisfactory combination for our purpose and with modifications it still is. The results of this test, with the turbocharger applied to a standard engine, indicated several items:

1. The maximum permissible speed of the turbocharger was a controlling factor in the output and speed limitations of the engine.
2. The back pressure caused by the turbine nozzle resulted in a definite loss in light load performance.
3. Though power output could be definitely increased, no great improvement in average economy was to be expected.

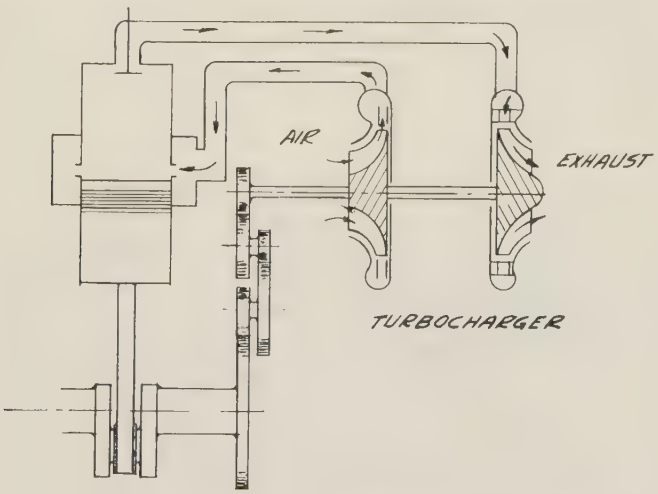

Fig. 4—Turbocharger compounded with engine

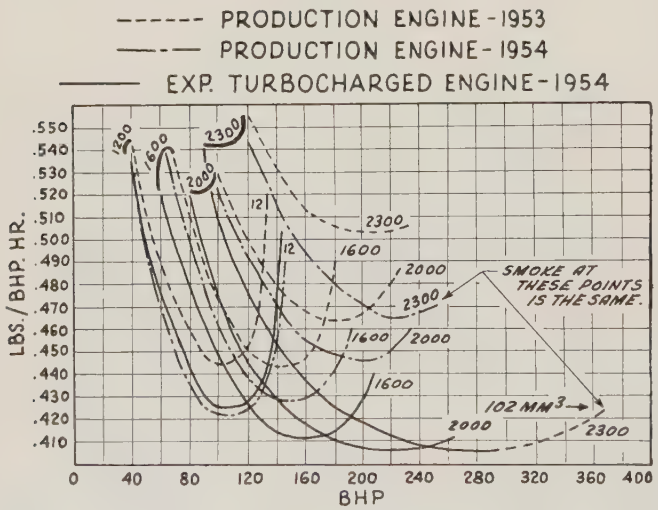

Fig. 5—Performance of 6-71 engines with 80 cu mm injectors. Turbocharged engine has turbocharger, larger intake ports, revised combustion chamber, four-valve cylinder head, smaller Roots blower

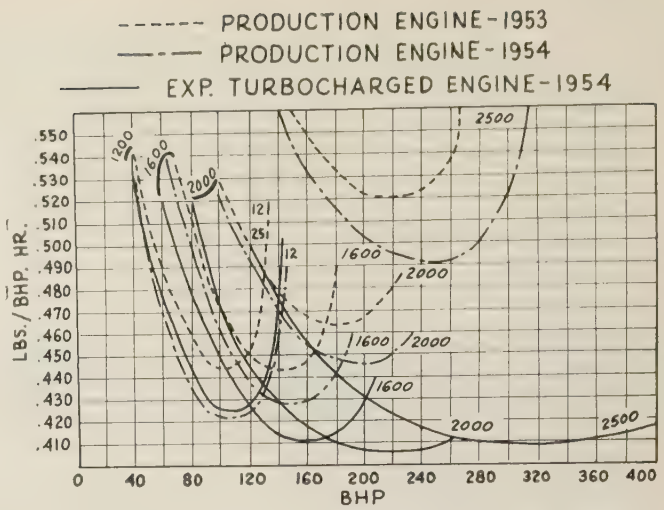

Fig. 6—Maximum output of 6-71 engines with 100 cu mm injectors at 2500 rpm. Turbocharged engine has turbocharger, larger intake ports, revised combustion chamber, four-valve cylinder head, smaller Roots blower

4. The engine apparently needed greater breathing capacity.
5. The peak combustion pressures were higher than desired.

A 50% reduction in Roots blower capacity bracketed the air requirements. The reduction was obviously too great. A 33% reduction in Roots blower capacity produced more satisfactory results.

Experimental parts were available to increase the breathing capacity of the engine. Development work on this project had been in progress prior to the start of the turbocharging program. Liners with intake ports providing an increase of 33% in time area and a cylinder head with four exhaust valves which increased the exhaust time area 27% were installed for successive tests. The performance obtained was quite satisfactory, as shown in Figs. 5 and 6.

The results of the preliminary performance tests were so encouraging, a comprehensive program was established for a complete investigation of the turbocharging process and its effect on engine life and operating conditions. In addition, a more complete investigation into the characteristics of several different turbochargers was scheduled.

Needed was: (1) a calibration chart of the compressor, (2) the air requirements of the engine with the new combination of intake and exhaust areas, (3) a series of turbine nozzles to cover a fairly wide range of areas, (4) the effect of turbocharging on engine life, (5) possible production engine ratings.

Compressor Calibration

A test was set up to calibrate the turbocompressor using the engine as a gas producer for the turbine and discharging the compressor air into a plenum chamber. By controlling engine speed and load the turbine speed could be controlled and the compressor calibrated.

The calibration chart obtained is shown in Fig. 7. The location of the engine work line is shown by line A-A, which can be considered as a satisfactory matching of engine and turbocharger. Lines B-B and C-C represent two types of unsatisfactory engine-turbocharger combinations. Line B-B repre-

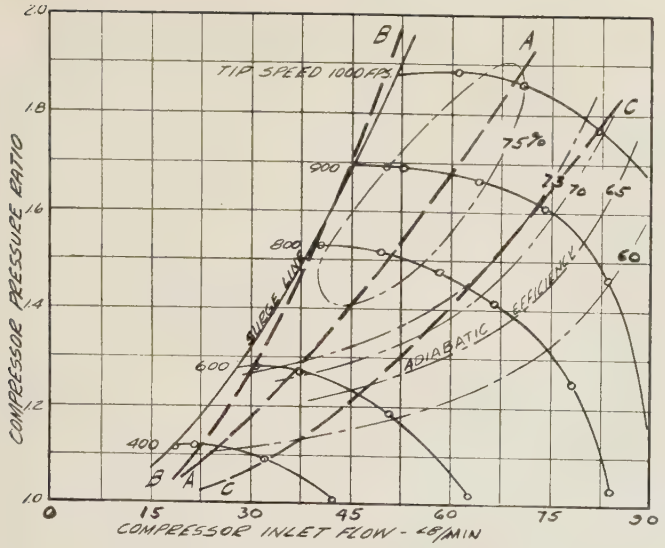

Fig. 7—Compressor thermodynamic performance

sents operation too close to the surge line, which represents the limit of stable operation. Line C-C illustrates incorrect matching of the turbocharger to the engine where the compressor is operating in a range of low adiabatic efficiency. The matching as represented by line A-A can be considered optimum.

This test also provided information as to the power available from the turbine for either compounding or to drive engine accessories. The maximum turbine output obtained was 43 bhp at 2500 engine rpm. However, as a method of improving engine performance it could not be considered. The high exhaust back pressure created by the turbine nozzle seriously increased the Roots blower power requirements and decreased the engine output. Even with full utilization of turbine power, only at high speed and load could the turbine output offset the loss in engine output. This does not include the additional losses that would result from the reduction gearing necessary for either compounding or driving engine accessories. With turbochargers in this efficiency range compounding or utilization of turbine power for driving accessories does not appear practical.

Minimum Air Requirements

At the same time the turbocharger was being calibrated, a similar nonturbocharged engine was tested with a series of blower drive ratios which permitted a range of scavenging ratios from 0.55 to 1.5, or as is frequently used in two-stroke work, from a negative 45% to a positive 50% excess air ratio. In other words, the ratio of the volume of free air pumped to the amount displaced by the engine cylinders was varied from 0.55 to 1.5 to determine the minimum air requirements of the engine.

The results are shown in Fig. 8. These characteristic curves show that even with a scavenging air ratio of less than 1, no loss in minimum fuel economy resulted. Similar results were obtained throughout the speed range. On an indicated basis using motoring friction to determine the indicated power the minimum fuel economy was only very slightly affected by the lower scavenging ratios, as shown in Fig. 9.

These curves also indicated that no major change in scavenging efficiency resulted from the decreased air supply. The ability to accelerate, however, started to deteriorate at the 1.075 scavenging ratio but was considered satisfactory with the 1.19 ratio. With a negative excess air of 45% rapid opening of the throttle would cause misfiring and occasionally complete stalling of the engine. With careful throttle control complete performance curves were obtained. The exhaust condition was satisfactory with all blower drive ratios as long as the overall air-fuel ratio was 30/1 or above. The blower drive ratio which provided 19% excess air was selected for the turbocharged engines and proved optimum for turbochargers with an overall efficiency in the 50% range.

The desired capacity of the Roots blower could be obtained by using shorter rotors and maintaining the original drive ratio of 2/1 or by reducing the

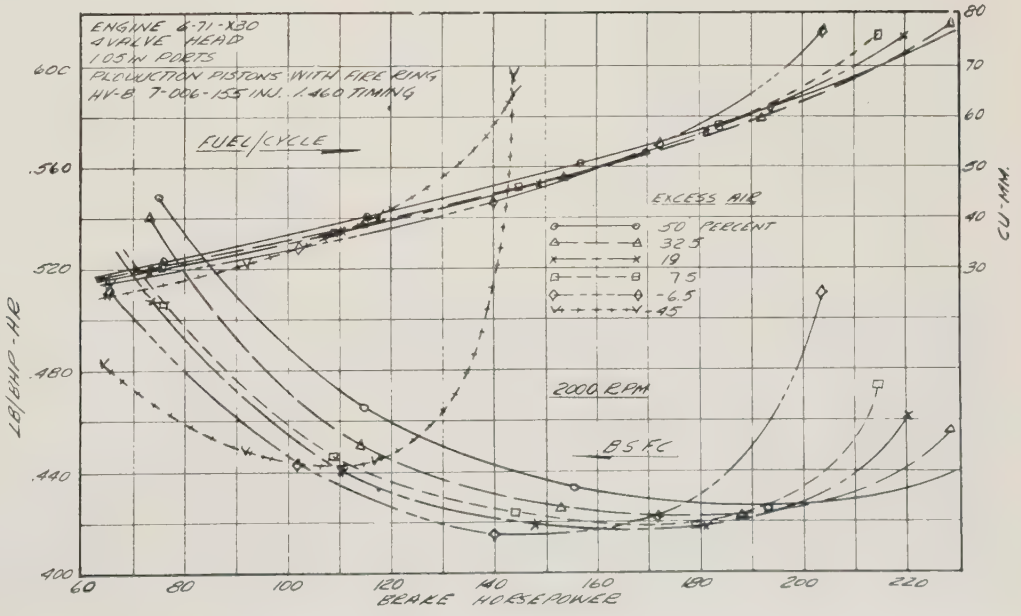

Fig. 8—Effect of reduced airflow on engine brake performance

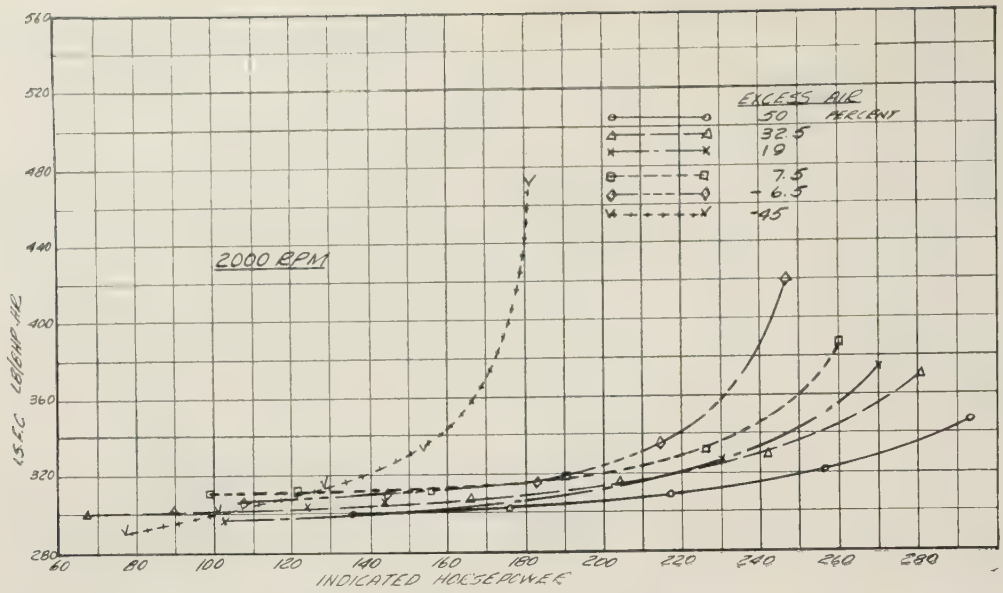

Fig. 9—Effect of reduced airflow on engine indicated performance

Fig. 10—Nozzle of Elliott Model M-10 compressor

speed of the standard blower. Comparative tests showed both methods gave almost identical engine performance.

The blower with shorter rotors presented a serious problem of interchangeability between the turbocharged and nonturbocharged engine components. It was therefore decided to use a blower incorporating a self-contained reduction gear. This permitted changes in blower ratio to be made without disturbing any of the basic engine components. It also appeared desirable, since improvements in turbocharger overall efficiency would necessitate still lower drive ratios.

Variable Nozzle

To match the turbocharger to the engine more accurately an adjustable nozzle ring was designed and built to fit the Elliott Model M-10 compressor. The nozzle area could be varied from 75 to 125% of normal. The nozzle is shown in Fig. 10. This proved a useful tool in checking the optimum nozzle area for any desired rating. In addition, it permitted us to determine the effect of a variable nozzle on engine torque and power characteristics. The torque characteristics of the turbocharged 2-stroke engine are not desirable if high torque at low speed is required. In general, the higher the speed and power of the turbocharged engine, the less desirable the torque characteristics if the application requires a drooping torque curve. The performance with this adjustable nozzle is shown in Fig. 11. The nozzle did not have sufficient range to permit the desired control of the turbine speed. However, this curve does indicate a definite torque improvement in the low-speed range, and with a greater variation in nozzle area even better torque characteristics could probably be obtained.

Although the variable nozzle would be desirable from a performance standpoint, there are both mechanical and economical problems that prohibit its use at the present time.

Other methods of torque control, such as wastegating the exhaust, throttling the compressor intake, and wastegating the compressor outlet, are being considered, but scheduled tests on these items have not been completed.

Fuel Modulating Governor

In connection with the torque control problem we should not overlook the action of the fuel modulating governor designed for use with the turbocharged engine. The natural characteristics of the unit injector are such that the injector fuel output increases approximately 1 cu mm for every 100 rpm decrease in engine speed. Therefore, at wide-open throttle the maximum fuel input occurs at the lowest operating speed. If the air supply is designed to provide for high-speed full-throttle operation, then low-speed operation will be in the excessive smoke range. The modulating governor used is sensitive to airbox pressure and will permit only a fixed amount of fuel to be injected at any given pressure. Since the airbox pressure is a function of engine and compressor speed, the fuel rate can be controlled at or below the smoke limit throughout the entire engine speed range. This system of fuel control also prevents excessive smoke during acceleration. While the modulating governor permits some control of the engine torque characteristics, it is not effective in increasing low-speed torque. The effect of the modulator on torque response appears to be negligible.

Torque response time is sometimes overlooked in

turbocharger installations. In nonturbocharged engines the increase in torque at any fixed speed is practically instantaneous when the throttle is opened. The torque of a turbocharged engine at any fixed engine speed must wait for the turbine to get up to speed. In the case of the 71 engine the torque response time is affected by the Roots blower drive ratio (the availability of excess air independent of the turbocharger) and the mass of the rotating parts of the turbocharger. The lighter the rotating parts the faster the turbocharger accelerates.

The aforementioned tests gave us a fair idea of what could be accomplished with the 6-71 engine and the Elliott M-10 turbocharger. Simultaneously tests were conducted on the 4-71 with the Elliott M-5 turbocharger and a satisfactory combination determined. After this turbocharged engine had been developed, a series of tests was run to evaluate turbochargers of other makes and designs.

The availability of turbochargers in automotive diesel sizes has increased rapidly in recent years. Thus far, tests have been run with six different turbochargers, four of them on the 6-71 engine. Several of these were desirable units from the standpoint of efficiency, size, and weight. Some lacked the mechanical reliability necessary, others were in the experimental stage. The comparative performance is shown in Fig. 12. In each case the turbocharger was matched to the engine as closely as possible. The full-throttle performance is shown in Fig. 13. Though the difference is not excessive it does exist.

It appears that, among the many possible causes for performance differences, the overall efficiency of the turbocharger seems to be the major item that correlates directly with engine performance. The peak overall efficiency on these turbochargers varied from 48 to 60%. The interconnected problems of matching the turbine to the compressor and the Roots blower to the turbocharger and the combination to the engine can become quite complex. However, it is felt that the higher the overall effi-

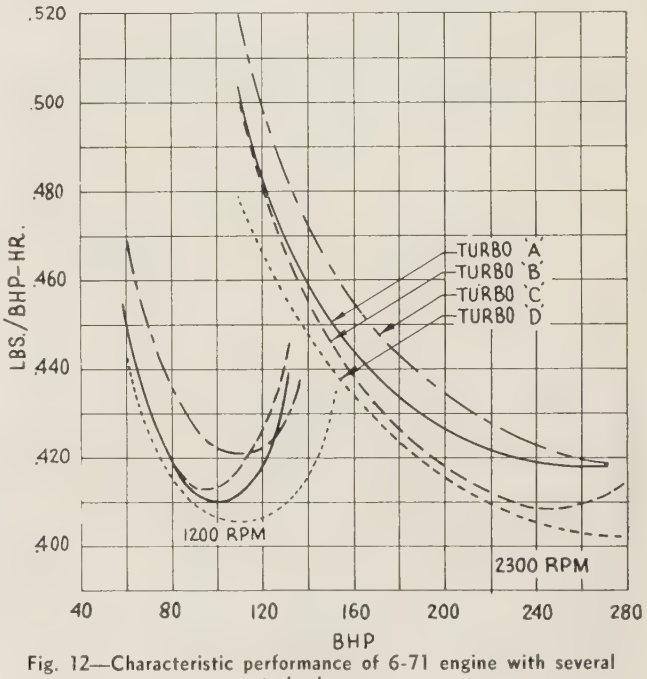

Fig. 12—Characteristic performance of 6-71 engine with several turbochargers

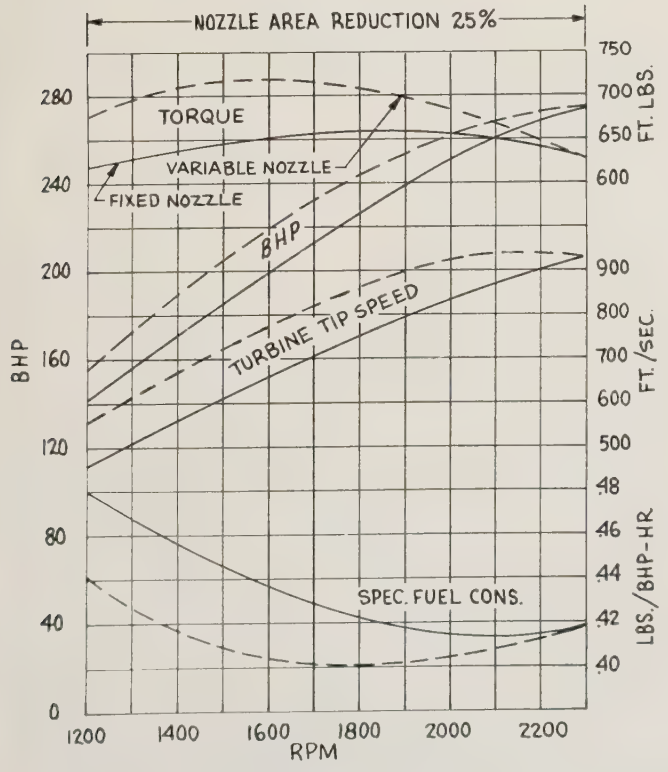

Fig. 11—Effect of turbine nozzle area on fixed-throttle performance of Model 6-71 engine

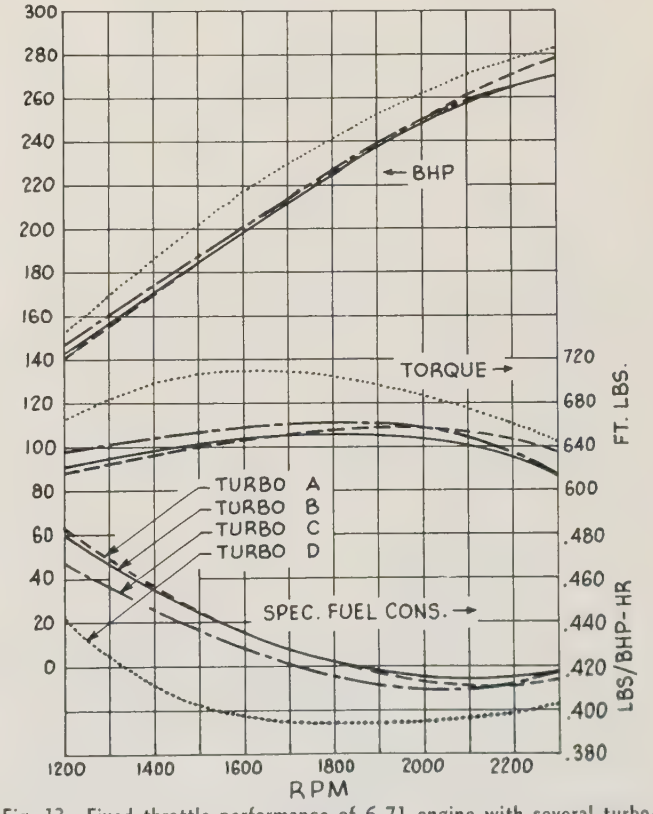

Fig. 13—Fixed-throttle performance of 6-71 engine with several turbochargers

ciency of the turbocharger the greater the possibility of engine performance improvement.

Turbochargers vary considerably. Fig. 14 shows the calibration chart of two types of compressors. One might be considered a high pressure ratio type as compared to a medium pressure ratio type. The major differences are the available flow ranges and the comparative pressure ratios. Each has its desirable characteristics.

Engine Ratings

A turbocharged 2-stroke engine is a difficult one to rate, since the rating possibilities are too extensive. Increased supercharging can be extended to a point where the engine becomes a gasifier with all the power of the engine available to the turbine. The turbocharger can readily be used to improve power and economy and less readily used to improve economy without changing the power output. In early tests we increased the power and engine speed to the extent shown in Fig. 15. This is an output of approximately one hp per cubic inch of displacement with satisfactory fuel economy. It would not be difficult to increase both air and fuel and thus further increase output. Among the factors that finally decided the engine ratings were: engine life, startability, combustion peak pressures, thermal

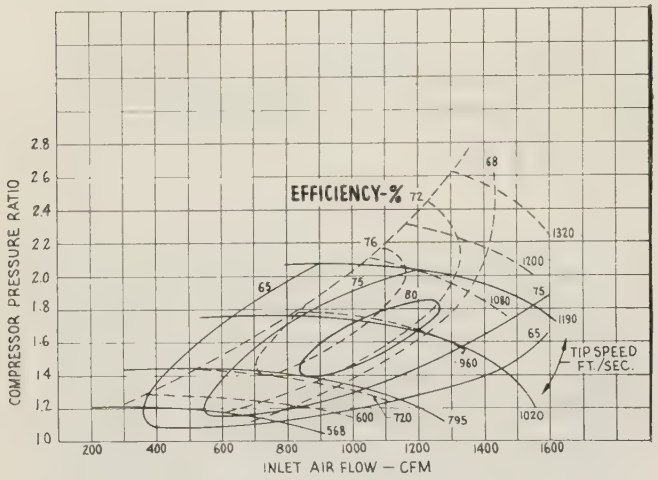

Fig. 14—Calibration chart of typical compressor types

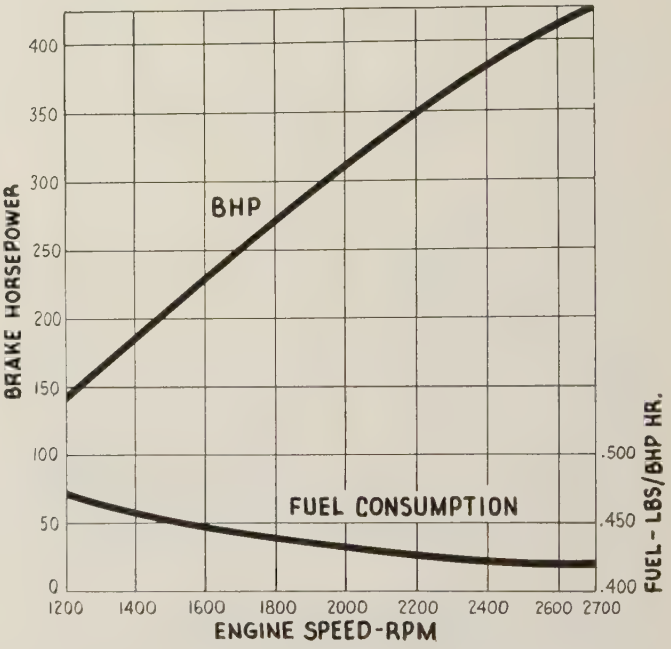

Fig. 15—Model 6-71 turbocharged for power; with 100 cu mm injectors

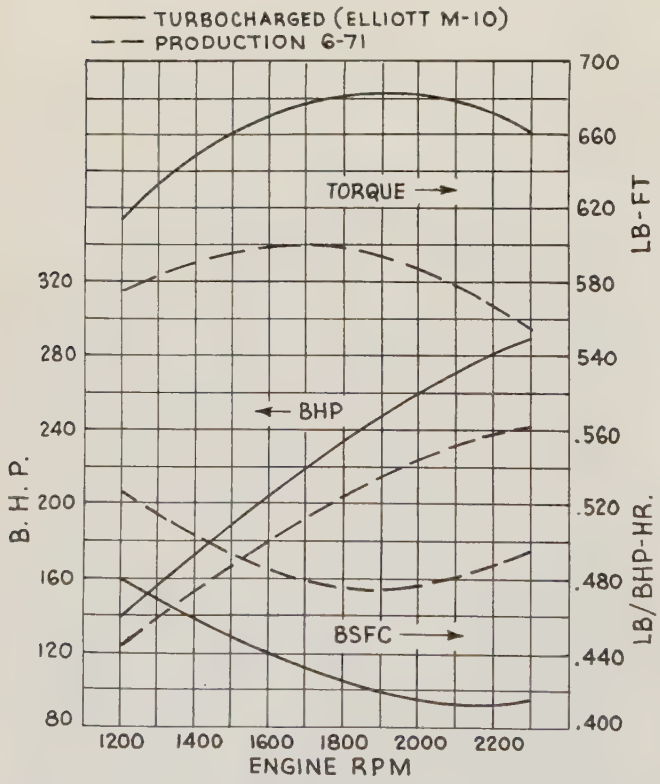

Fig. 16—Model 6-71 at full throttle, standard and turbocharged; with 80 cu mm injectors

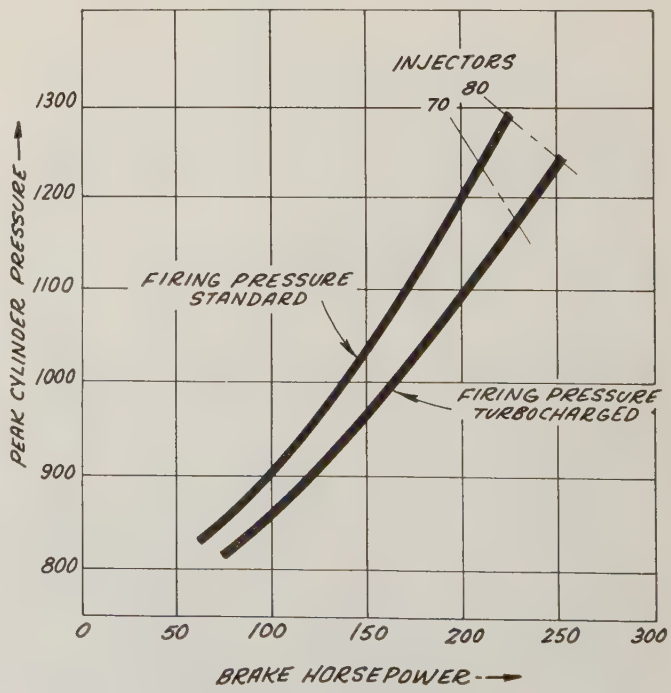

Fig. 17—Improved high-output durability with lower peak pressures

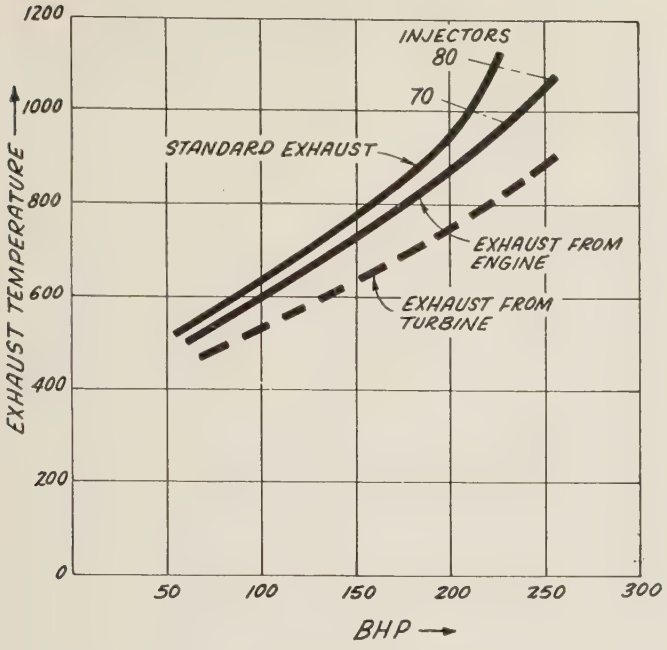

Fig. 18—Improved high-output durability with lower exhaust temperatures

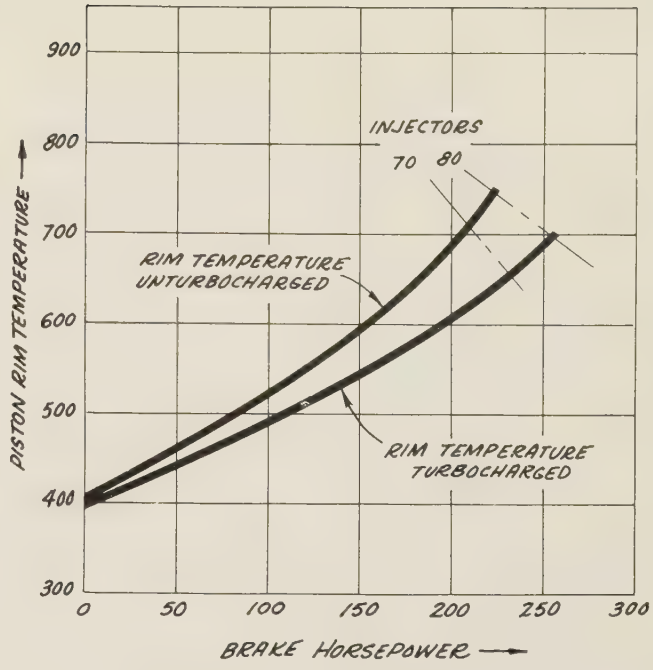

Fig. 19—Improved high-output durability with low piston temperatures

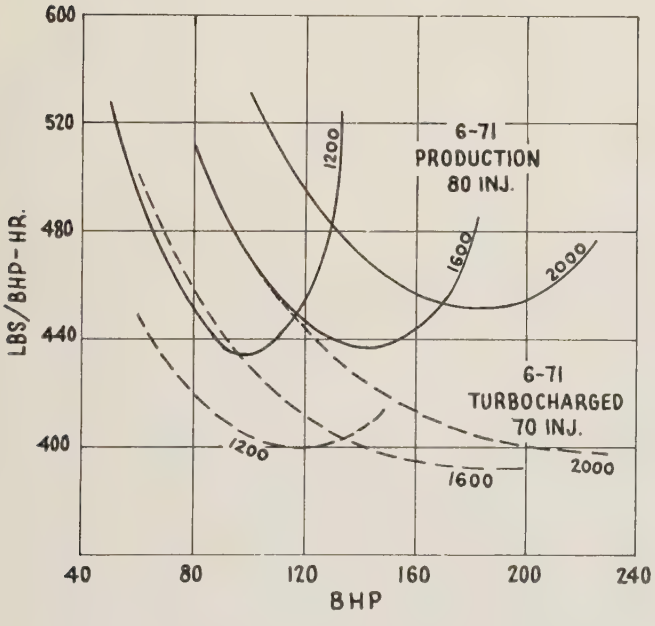

Fig. 20—Turbocharging for economy with Elliott M-5 turbo

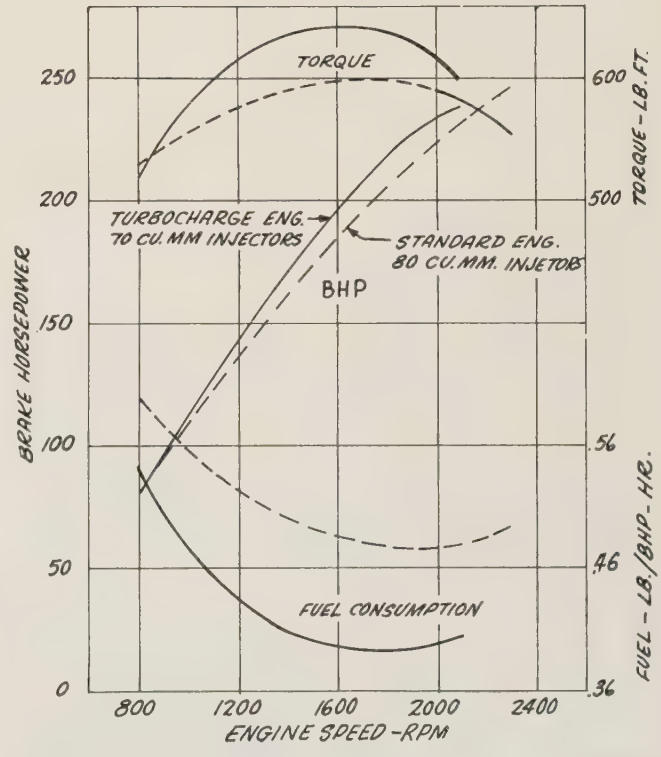

Fig. 21—Power increase and fuel decrease. Preliminary performance with M-5 turbocharger

loading, cost, weight, and available market. Higher engine speed was desirable, since this permitted the use of existing torque converters and clutches whose torque capacity was limited. The maximum rating finally decided on is shown in Fig. 16.

This rating maintained the fuel rate of nonturbocharged engines, provided a respectable improvement in power and economy, and did not destroy the torque characteristic. In addition, we felt there would definitely be no decrease in engine life.

Peak pressures were not increased (Fig. 17).

Exhaust temperatures were lowered (Fig. 18).

Piston temperatures were reduced (Fig. 19).

This may be considered as starting out at a crawl rather than a walk, but time and field experience will decide the optimum rating. It will not be difficult to increase it.

Turbocharging for economy only was somewhat more difficult than turbocharging for both power and economy. After checking several combinations, the Elliott M-5, with a suitable nozzle and a high flow diffuser, appeared to give the best overall results. The performance obtained is shown in Fig. 20. The full-load performance is shown in Fig. 21;

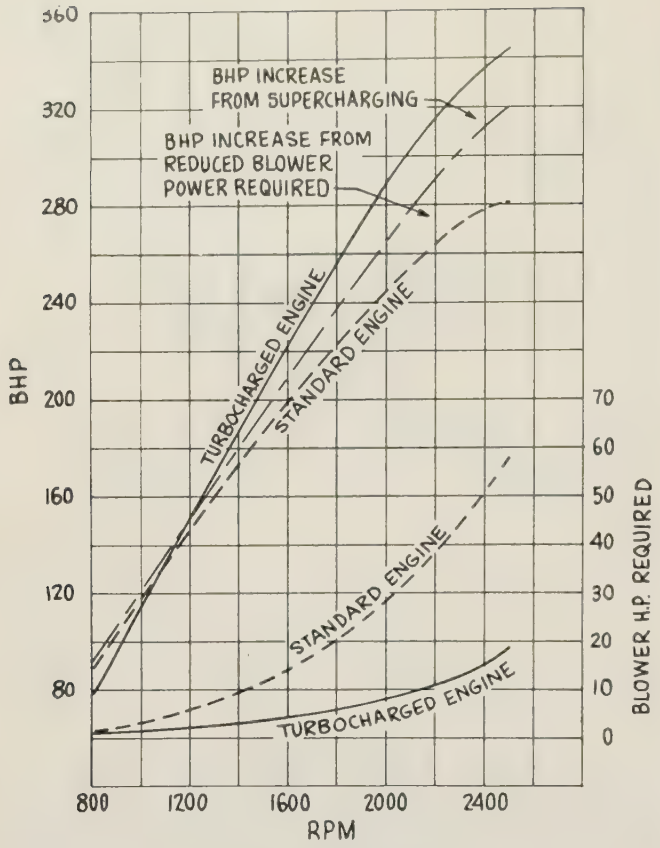

Fig. 22—Full-throttle performance, standard and turbocharged; with 90 cu mm injectors

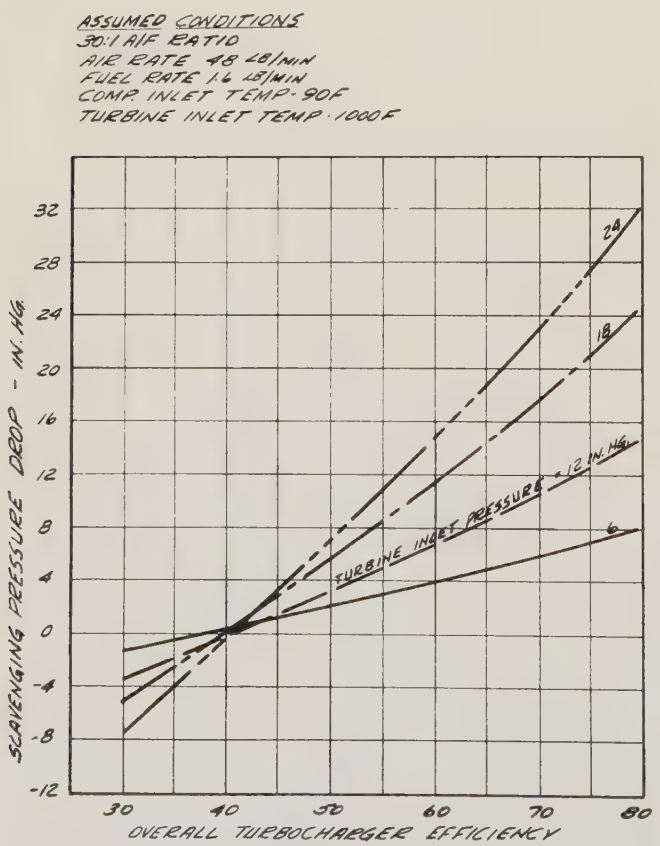

Fig. 23—Effect of turbocharger efficiency and turbine inlet pressure on scavenging pressure drop

the increase in power output is quite small but the improvement in economy is respectable. This model will readily fit in existing applications and should pay for itself in reduced fuel cost. Production unit injectors are used to obtain both ratings.

The higher rating is obtained with 80 cu mm injectors and the lower rating with 70 cu mm injectors. The 80 injector (80 cu mm per stroke at 2000 rpm) is the highest output injector used in commercial applications. Ninety cubic millimeter injectors are used in pleasure craft and for military installations. The question is frequently asked: Where does this increase in power come from? Fig. 22 shows a full-throttle curve with 90 cu mm injectors. The increase in output at top speed is approximately 24%. Of this 24%, 14% is obtained by a reduction in the blower drive ratio and the reduced pressure rise through the Roots blower. The remaining 10% increase in power can be considered the effect of increased supercharging. The effect of operation at a higher pressure level results in increased density of the trapped air, higher effective compression ratios, higher air-fuel ratio, and possibly improved scavenging.

To what degree each of these various factors contributes to the overall gain has not been determined. While much of the increase in power output results from the decrease in power required to drive the Roots blower, a still greater increase in power output would result if the Roots blower could be eliminated. This would be possible if the turbocharger had an overall efficiency sufficient to maintain a high enough pressure differential across the engine throughout its entire load and speed range.

Fig. 23 shows the overall turbocharger efficiency requirements at several turbine inlet pressure levels. It can be readily observed that to maintain a respectable scavenging pressure drop across the engine, a high turbocharger efficiency is necessary. At light loads and low speeds even a very superior turbocharger is not capable of scavenging the engine. Starting, light-load operation, and good acceleration are not possible. This applies, of course, only to a constant-pressure turbocharging system. Using the pulse system, operation without a mechanically driven blower throughout the speed and load range is theoretically possible and has actually been accomplished. The pulse system, however, requires complex manifolding, and it appears that the greater the speed and load range of the engine the more difficult it becomes to eliminate completely the mechanically driven blower. The turbocharger can be engine-driven or driven from an external source and in this way eliminate a separate blower, but this introduces mechanical complications. The pulse system has advantages, although it would require considerable development work before it could be considered satisfactory for 2-stroke automotive diesels.

Heat Balance

Fig. 24 shows a heat balance diagram of a turbocharged and nonturbocharged engine at equal fuel rates. The comparative heat rejection data at 2300 rpm are given in Table 1.

These data show an increase in heat rejection to the exhaust and a decrease in heat rejection to the

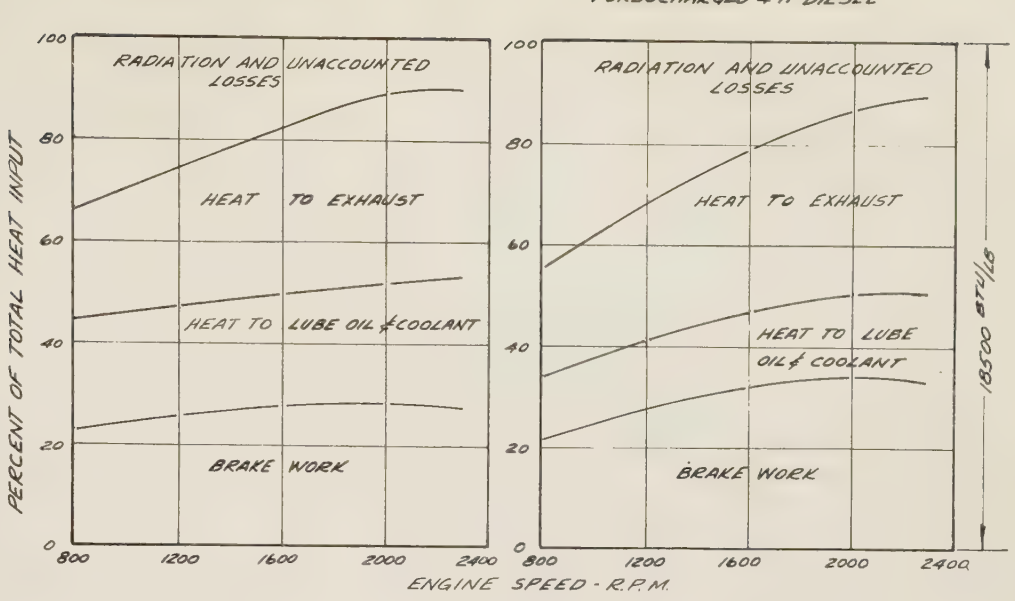

Fig. 24—Comparative heat balance of turbocharged and nonturbocharged diesel

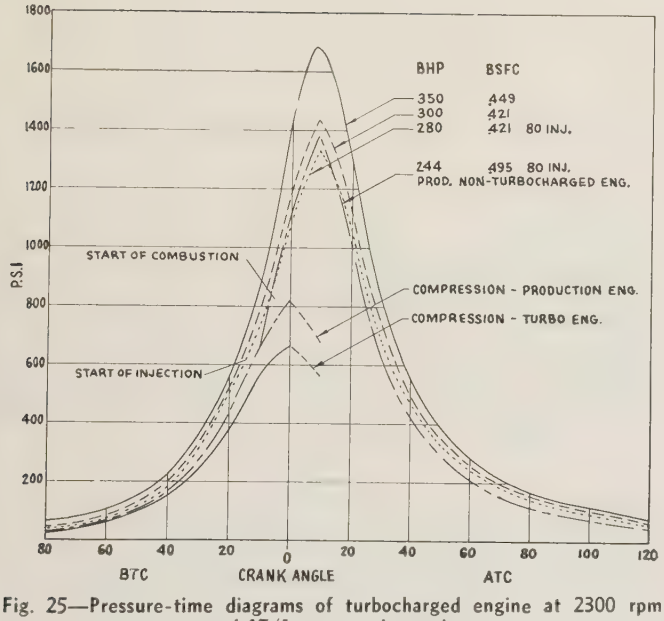

Fig. 25—Pressure-time diagrams of turbocharged engine at 2300 rpm and 17/1 compression ratio

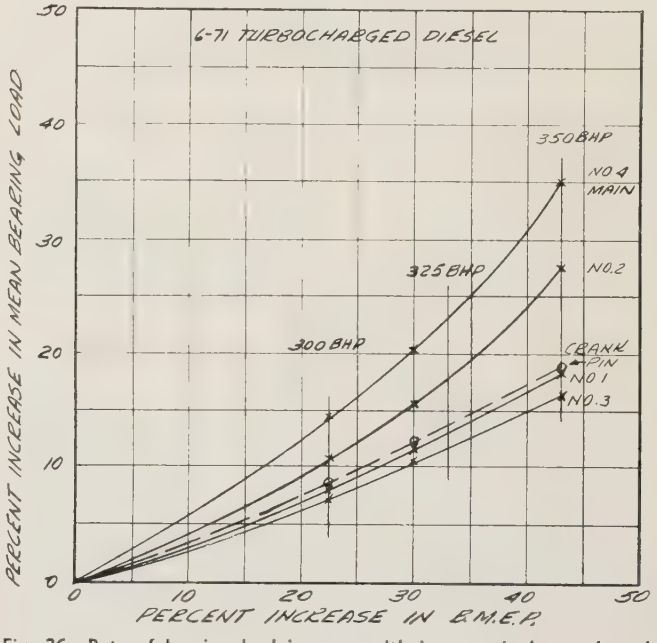

Fig. 26—Rate of bearing load increase with increase in bmep through turbocharging

cooling water. This considerably simplified the problem of cooling the turbocharged engine.

Mechanical Loading

Tests indicated that startability was appreciably affected by a reduction in engine compression ratio. Therefore, the production compression ratio of 17/1 was maintained. A moderate increase in combustion pressures was acceptable since the engine had been operating successfully in the laboratory for a number of years on an accelerated test cycle designed to produce very high combustion pressures. Indicator cards taken on the turbocharged engine at 2300 rpm are shown in Fig. 25. The cards showed that at the selected rating, peak pressures were satisfactory and that higher outputs could be used without excessive pressures.

Table 1—Comparative Heat Rejection Data at 2300 Rpm

	Heat to Exhaust, %	Heat to Oil & Water, %	Brake Work, %
Turbocharged	42.3	23	32.9
Nonturbocharged	37.0	25	28.2

Bearing load calculations indicated that the higher output produced only a moderate increase in bearing loads. Fig. 26 shows how the bearing loads increase with increased bmep. It would appear that No. 4 main bearing load increases rather rapidly

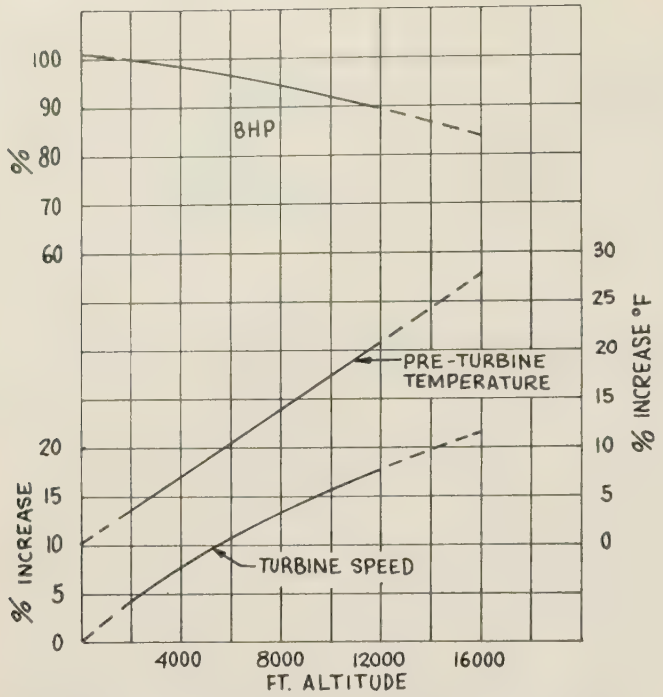

Fig. 27—Effect of altitude on engine power, turbine speed, and temperature at 2300 rpm and with rated fuel input

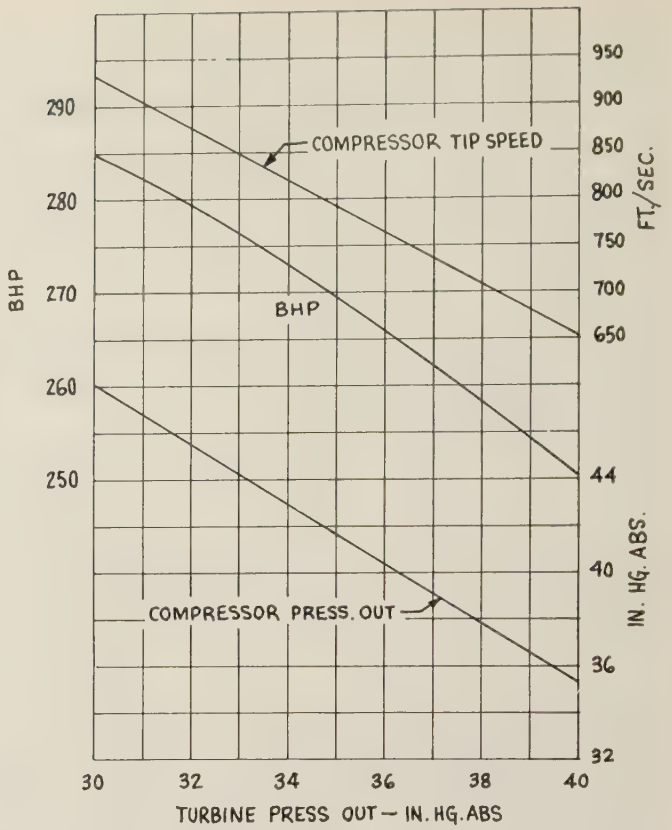

Fig. 28—Effect of turbine back pressure with fixed fuel rate at constant speed

with increased bmep. The crank arrangement is such that the increase in gas load has a greater effect on the No. 4 bearing than on any of the others. However, the actual load on No. 4 is normally low and at 350 bhp is less than 1000 psi. In general, an increase in bmep of 50% would not increase bearing loads beyond accepted limits.

Altitude Effects

Another item that was of definite concern was the effect of altitude on the turbocharger. A test room was equipped to simulate altitude conditions and a series of tests was run. Oversimplified, the results are shown in Fig. 27. This indicates a power output drop of approximately 1% per thousand feet of altitude. There is a definite increase in turbine speed and preturbine temperature with altitude. These factors affect the sea level rating of the turbocharger engine combination. If the turbine is operating at maximum safe speed and temperature at sea level, continuous high-altitude operation can obviously cause trouble. Probably the simplest way to maintain the desired turbine operating conditions is to reduce the fuel input, thus lowering turbine speed and temperature in addition to engine output at sea level. A reduction in the rated engine speed will also prevent overspeeding or overheating of the turbine but also reduces the power available at sea level. Each turbocharged engine application must be considered carefully and rated accordingly.

Exhaust Noise

Although turbochargers tend appreciably to reduce the objectionable noise level of the engine exhaust, the muffler cannot be eliminated. Turbocharger engineers object to any back pressure on the turbine outlet, but in many applications muffling is necessary. Fig. 28 shows the effect of exhaust back pressure on engine output and compressor pressure. While any back pressure is objectionable, the turbocharger does some silencing, so that a straight through type of muffler with minimum restriction provides satisfactory noise control. These curves, however, do indicate the importance of maintaining minimum back pressure on the turbine for optimum engine performance.

Intercooling

All engines are affected by inlet air temperature. In the case of the 71 installation there is an appreciable temperature rise through the turbocompressor and a further temperature rise through the Roots blower. The air entering the cylinder is definitely warm. A gain in performance and a reduction in peak pressures and thermal loading can be obtained by intercooling. This is standard practice where facilities are available. Figs. 29 and 30 show the effect of intercooling on engine performance. The intercooler is located between the compressor and Roots blower. Fig. 31 shows the inlet air temperature variation through the system. The full benefit of the intercooler is not obtained since the temperature differential between the airbox and the inlet of the Roots blower is much greater when an intercooler is used. The airbox is partially surrounded by engine water at approximately 175 F and acts as a heat exchanger, tending to raise the temperature of incoming air when an intercooler is used. With no intercooler the water-jacketed portion of the airbox lowers the temperature of the incoming air. An after-cooler is indicated. The value

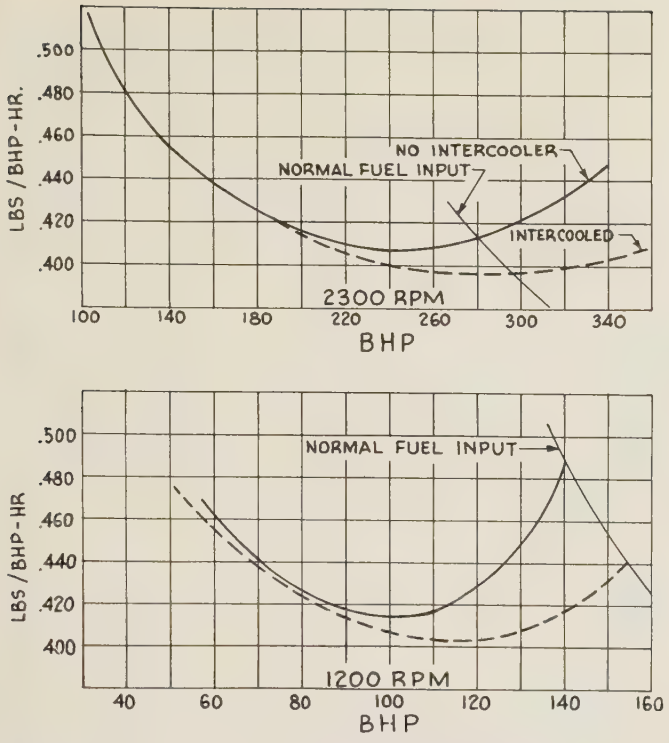

Fig. 29—Effect of intercooler between compressor and Roots blower on economy 6-71 turbocharged engine

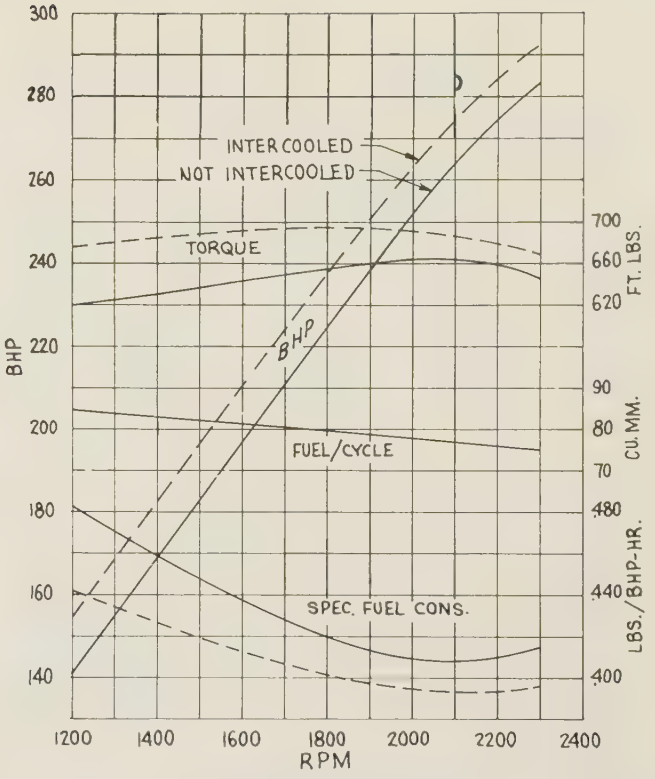

Fig. 30—Effect of intercooling on wide-open-throttle performance of turbocharged 6-71 engine

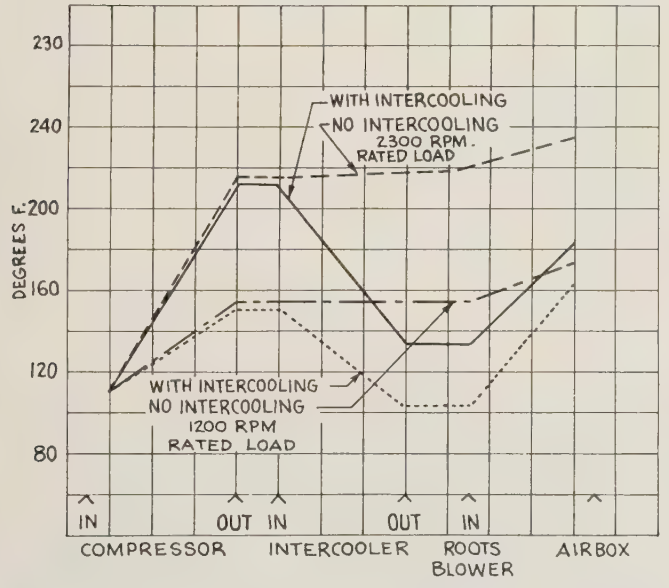

Fig. 31—Effect of intercooling on air temperatures through engine

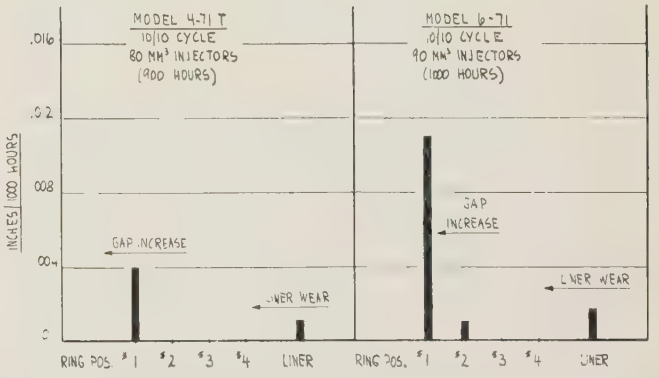

Fig. 32—Comparison of piston-ring gap increase in liner wear for turbocharged and nonturbocharged operation

of intercooling is very definite on marine and other heat exchanger engine models where an unlimited supply of relatively cold water is available. In automotive applications the value of intercooling must be weighed against its added complexity and cost.

Engine Life

To evaluate the effect of turbocharging on the life of the various parts in the Series 71 engine, two types of durability tests were run. Except for load, the turbocharged engines were tested using the same procedure followed by our laboratory for some time to evaluate basic engine components. Some of the engines were run continuously at full-throttle 2500 rpm, with 90 cu mm injectors (300–325 bhp). A second group of engines was run on a cycle consisting of alternate periods of 10 min at an idle speed of 550 rpm and 10 min at 2300 rpm wide open throttle with 90 cu mm injectors. Past experience on nonturbocharged engines indicated that piston and valve life may be considerably shortened by cyclic operation, while ring, liner, and bearing life was not appreciably changed.

The durability tests indicated turbocharging had little effect on the life of the main and connecting-rod bearings. The aluminum coplated, steel-backed bearings had a life considerably in excess of the normal engine overhaul period. Piston-ring life and liner life (as shown in Fig. 32) were also not appreci-

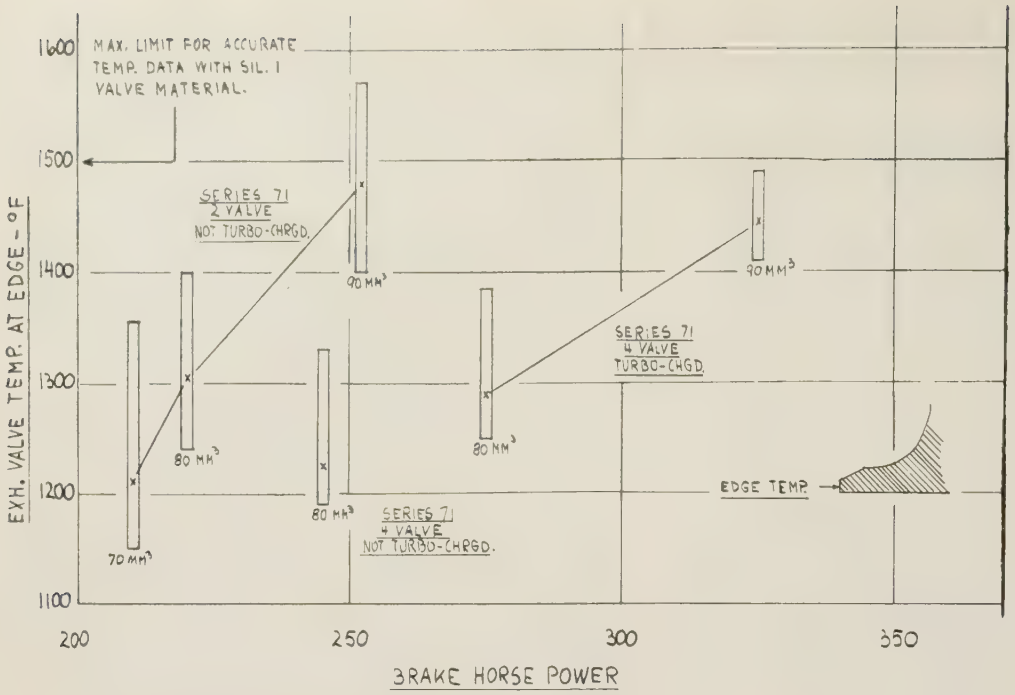

Fig. 33—Comparison of exhaust valve temperatures on Series 71 engines

ably affected by turbocharging.

The most critical item in the life of the turbocharged engine appeared to be the exhaust valve. The life of production exhaust valves made of a jet blade N-155 alloy was considerably shortened in the turbocharged engine. This was somewhat confusing to us at first, inasmuch as our exhaust temperatures were approximately the same as those normally encountered on nonturbocharged engines. A series of valve temperature tests using Silcrome No. 1 alloy valves, which indicate their operating temperature by a reduction in the material hardness, showed that considerably higher valve temperatures existed in the turbocharged engine (Fig. 33). These higher valve temperatures may have been due to the increased density of the exhaust gas resulting from the pressure restriction of the turbocharger. The rate of heat transfer to the exhaust valve during the blowdown period is probably greater with the increased density gas.

A number of high temperature alloy valves were evaluated in the turbocharged engine before valves

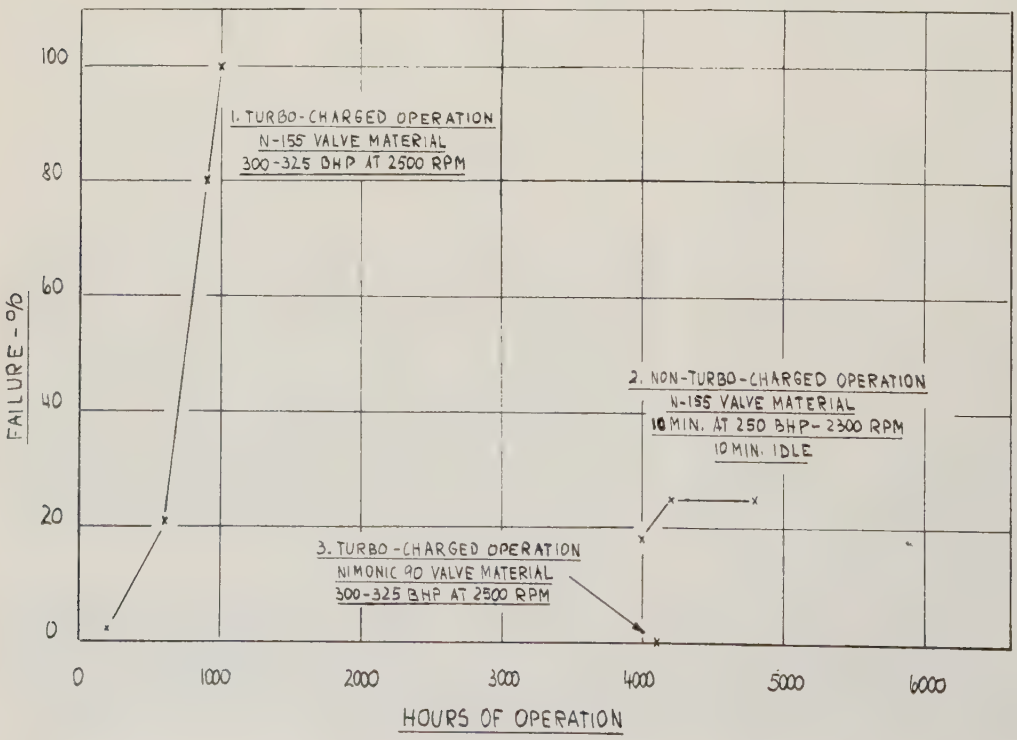

Fig. 34—Effect of turbocharged operation on exhaust valve life in Series 71 engines

made of Nimonic 90 material were released for production engines. Nimonic 90 is a nickel-base alloy developed for gas turbine blades. It has the following analysis:

C-0.10 Cr-19.5 Ni-58.0 Co-18.0 Ti-2.40 Al-1.20

As shown in Fig. 34 valves of this material gave exceptional life in the engine and may be better and more expensive than necessary. Valves of other materials are on test to determine if a less expensive valve can be found which will still provide adequate life.

Except for exhaust valve life, turbocharging appears to have very little adverse effect on the other part of the engine. At the present time a number of turbocharged engines have been operating in the field of periods ranging up to 1500 hr and 100,000 miles. While some failures have occurred during these field tests, practically all were the result of difficulties associated with getting the four-valve head into production.

It is believed the turbocharged Series 71 engine will prove to be an economical and reliable unit for those applications requiring the maximum power with a minimum of engine size and weight. In the future the ratings for the turbocharged engine will continue to increase as improvements are made in both turbochargers and basic engine components.

Applications

Various applications of the turbocharged 71 engines have been made to date. These include trucks, marine, industrial, tractors, and other earthmoving equipment. Fig. 35 shows a cutaway view of an early 6-71 basic engine with an Elliott M-10 turbocharger suitable for large trucks and earthmoving equipment.

Only a few of the problems of the turbocharged 2-stroke diesel have been discussed in this paper. Improved turbochargers with higher overall efficiencies and higher pressure ratios are in the development stage. With them will come engines of higher outputs per cubic inch of displacement and still higher thermal efficiencies.

As yet only a beginning has been made in turbocharging 2-stroke automotive diesels. The possibilities are almost limitless. The number of turbocharged engines in the field is increasing rapidly, and the successful performance of these engines will greatly extend their future use.

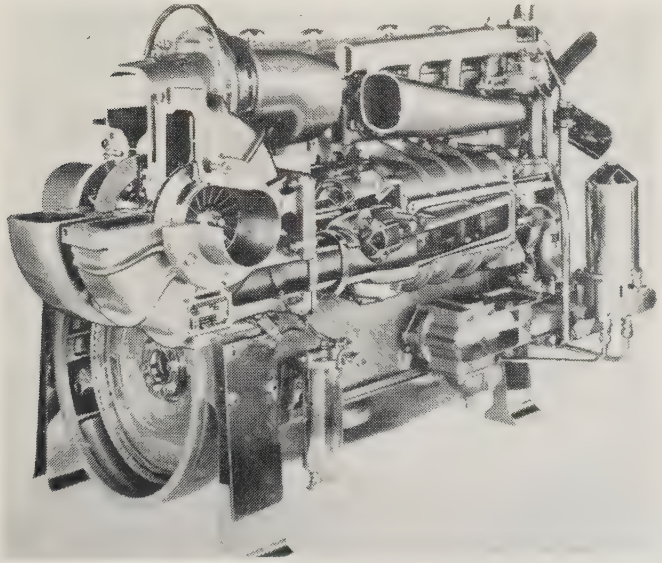

Fig. 35—Cutaway view of early 6-71 basic engine with Elliott M-10 turbocharger. It is suitable for large trucks and earthmoving equipment

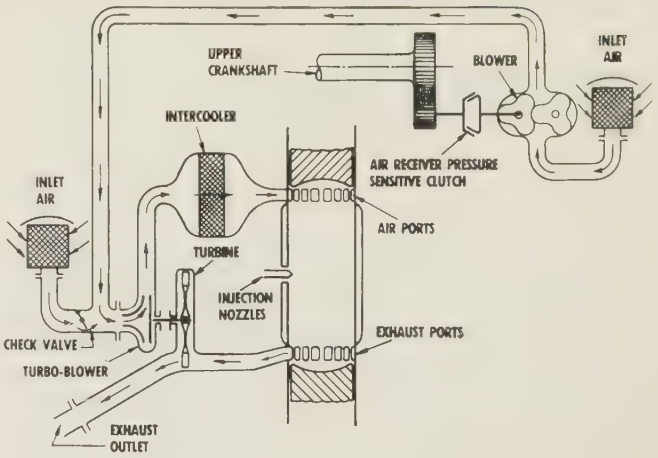

Fig. A—Diagram of auxiliary positive blower arrangement. Discharge into turboblower inlet

DISCUSSION

Advantages of Positive Displacement Blower Discharging into Turboblower Inlet

—Anker K. Antonsen
Fairbanks, Morse & Co

IT IS evident that General Motors and Fairbanks, Morse & Co. have carried out supercharging developments on small and large 2-stroke engines simultaneously and without knowledge of the other's work. The smallest FM engine on which supercharging experiments were carried out is a 5¼×7¼ opposed-piston engine operating at 1200 rpm, which is a considerably larger engine than the General Motor Series 71.

We would like to comment on the various possibilities of turbocharger arrangements which are illustrated by Figs. 1–4 inclusive in the paper. We are wondering if the most advantageous possibility has not been omitted. Up to the present time our experiments have indicated that the most advantageous arrangement consists of the positive displacement blower discharging into the turboblower inlet. This is shown in Fig. A. In such a case, a check valve is controlling the atmospheric admission to the turboblower when its delivery exceeds the delivery of the positive blower. This system automatically completely unloads the positive blower to idle operation at a point which will vary to suit the loads and speeds at which the engine is operating. On our larger engines we have found that the effect of such a system manifests itself on variable-load curves in the way of practically eliminating the upward curve at the high-load end and by a low fuel consumption over a very wide range of operation. We are wondering if the authors have had similar experiences even though not published in their paper.

Perhaps the fact that the exhaust on our engine is controlled by ports instead of valves is responsible for a difference in characteristic performance and therefore the two engines may perform differently relative to supercharging.

In Figs. 29 and 30 it would have been of interest to learn the temperature levels of the inlet air to the turboblower,

the inlet air to the positive blower, and the air in the air box. Presumably, the temperature curves in Fig. 31 are for rated full load only.

Compares Results of Applying Turbocharging To 2- and 4-Stroke Diesel Engines

—E. A. V. Horiak
Hercules Motors Corp.

AMONG the many interesting details presented in this paper, the most outstanding are the improved fuel economy and the increase in power output brought about by the application of a turbocharger on the General Motors Series 71, 2-stroke diesel engines. These features which make turbocharging desirable for the 2-stroke diesel are also found when applying turbocharging to the 4-stroke diesel engines, and a comparison of results obtained with either type of diesel will be of interest.

With the turbocharged Series 71, 2-stroke diesel engine arranged as shown in Fig. 2 in the paper (turbocharger in series with Roots blower), the engine can be classified as follows in terms of 4-stroke engines:

1. Engine equipped with positive displacement blower so geared that there will be no excess of air and no turboblower applied can be readily paralleled with a naturally aspirated, 4-stroke diesel engine of 1.6–1.8 times the displacement of the 2-stroke engine.

2. When the positive blower of the 2-stroke-cycle diesel is speeded up to give an airflow of approximately 50% excess air, the engine is then comparable to a 4-stroke diesel equipped with Roots blower.

3. As far as airflow is concerned, the turboblower in series with the positive displacement blower geared for a scavenging ratio of 1 makes the airflow in the 2-stroke diesel engine like the airflow in a turbocharged 4-stroke engine.

For many years we have been building some of our high-speed, 4-stroke turbulence-chamber type of diesels, naturally aspirated, equipped with Roots blower as well as with turboblower.

Fig. B shows the specific fuel consumption as a function of observed brake mean effective pressure for a naturally aspirated engine (curve A), Roots blower equipped engine (curve B), and a turbocharged engine (curve C). It is to be noted that these curves are approximately the same for a small engine with approximately 47 cu in. piston displacement per cylinder operating at 3000 rpm or 2000 fpm piston speed and an engine with 184 cu in. displacement per cylinder operating at 2000 rpm, which also corresponds to 2000 fpm piston speed.

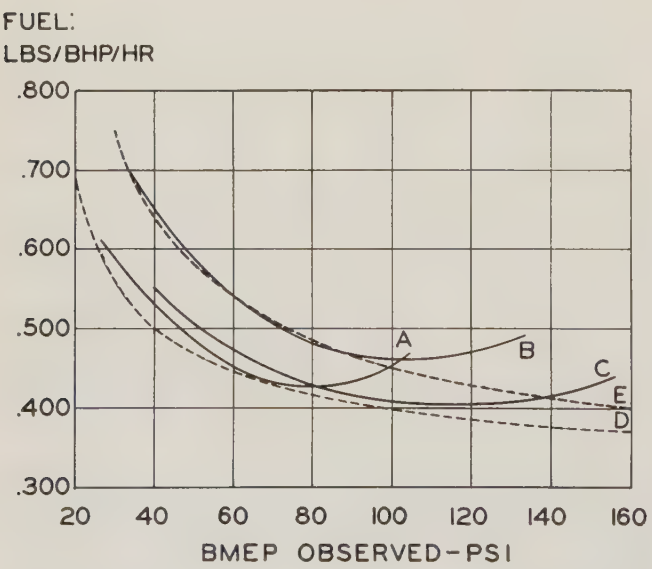

Fig. B—Specific fuel consumption of Hercules diesel engines with turbulence chambers

The dotted curves D and E on the illustration represent specific fuel consumption for a theoretical engine operating with constant fuel economy for the indicated horsepower over the entire load range. A constant loss of 18.5 psi, representing the power required to drive the mechanical blower, was added when computing curve E. Attention is drawn to the fact that curves A and C for naturally aspirated and turboblown engines generally follow curve D, whereas curve B, representing the Roots blower engine, more closely corresponds to curve E. That the actual fuel consumption at increased loads is higher than the values for theoretical engines is due principally to the imperfect combustion with decreased air-fuel ratio.

The maximum brake mean effective pressures at 2000 fpm piston speed of engines as rated for commercial operation is approximately 102 psi for naturally aspirated engines, 140 psi for engines equipped with the Roots blower, and 150 psi for engines equipped with turboblowers. Brake mean effective pressures of 165 psi are quite readily obtained with turboblown engines, especially when intercooling is employed.

It is interesting to note that all the above values closely approximate the values given in the different charts of the paper under discussion, which clearly indicates that the development problems of supercharging the 2-stroke cycle diesel engine are broadly the same as those encountered when turbocharging is applied to the 4-stroke cycle diesel.

Data Obtained from Application of Turbocharger to Navy 64HN-9 Diesel

—J. F. Blose
U. S. Naval Engineering Experiment Station

I WOULD like to supplement the performance data reported by the authors by presenting some of the data we obtained when we applied a turbocharger to a stock Navy Model 64HN-9 diesel engine. This engine was a marine conversion of a 6-cyl 2-stroke engine and was about 12 years old.

The engine was modified in the following respects: (1) 17/1 compression ratio pistons and cylinder liners, chromium-plated piston compression rings, special exhaust valves, and a late production camshaft were installed in place of the parts available from Navy stock. (2) Injector capacity was maintained at 90 cu mm. (3) The scavenge air blower was driven at 80% of its normal speed. (4) A turbocharger was installed with its compressor section as a first stage in series with the engine-driven scavenge air blower. (5) A center outlet manifold was so designed as to minimize the effect of the exhaust pulses from any one cylinder on the scavenging of other cylinders.

Our first test showed that the turbocharged engine developed 24% more power than the stock engine (Fig. C) and fuel consumption was very much improved. Much of the gain in engine performance was attributed to the air-fuel ratios provided by turbocharging. At maximum power, the pressure at the discharge from the turbine-driven compressor was 70% of that in the engine air box. No tests were made to determine the optimum capacity for the engine-driven blower. Use of a four-valve cylinder head did not appear to be warranted when engine speed was limited to 2100 rpm since we obtained excellent performance at this speed when using a two-valve cylinder head. The combined efficiency of the turbine and compressor ranged from 47% at half load to 49% at maximum engine power output.

A tentative rating of 275 bhp at 2100 rpm was assigned the turbocharged engine as compared to a rating of 225 bhp at 200 rpm for the stock engine. Due to the turbine installation, the overall weight of the marine engine with transmission and heat exchangers was increased by 10%. While we were studying the effect of turbocharger and

engine adjustments on engine performance, we found the following changes to be desirable:

(a) A viscous-fluid-type torsional vibration damper was installed in place of the rubber-bonded type used on the stock engine due to failure of the rubber in the rubber-bonded dampers.

(b) The stock copper-lead main bearings were replaced with steel-backed aluminum bearings in order to extend bearing life.

(c) Pistons fitted with special seal rings above the oil control rings were installed to control blowby.

We experienced one exhaust valve failure after less than 100 hr of engine operation, but the remaining valves lasted throughout the test. While the development was terminated before cylinder pressures could be measured, they were believed to be higher on the turbocharged than on the stock engine due to the higher rate of main bearing wear and the torsional damper failures experienced on the turbocharged engine.

Our experience indicates that turbocharging a stock engine offers unexpected problems which are not always easy of solution; however, worth-while gains in both power output and fuel economy were obtained.

(The opinions or assertions made in this discussion are those of the author and are not to be construed as official or reflecting the views of the Department of the Navy or the naval service at large.)

Questions Engine and Altitude Ratings Of Turbocharged Engines

—Hans A. Bohuslav
Dexter Folder Co.

I HAVE a few comments and questions as follows:

1. Variable nozzle versus fixed nozzle: The authors indicate that the variable nozzle would be desirable from a

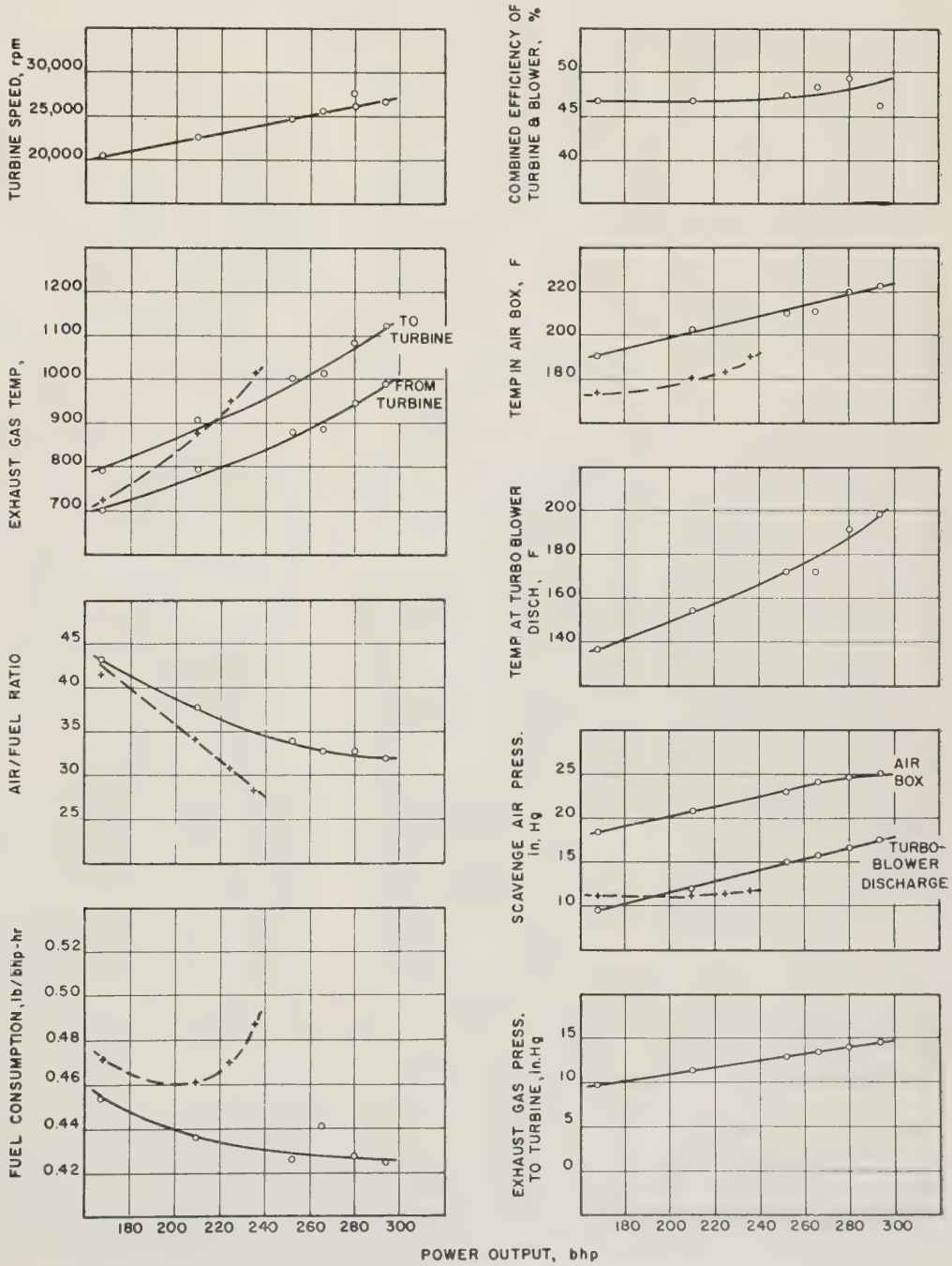

Fig. C—Results of tests of Navy 64HN-9 diesel engine that had been turbocharged.

performance standpoint. They refer to Fig. 11, which admittedly shows a considerable improvement over the fixed nozzle. However, in comparing this curve with Fig. 13, the performance of turbo D shows a good, or possibly better, performance over the entire speed range and with just as much in the way of increased torque, with reduced speed, as that shown for the variable nozzle.

It seems to me that, with a turbocharger of high efficiency, and one which is well matched to the engine, a variable nozzle would not show much improvement over the fixed nozzle. This matter may be somewhat academic, since at least for engines of this type, it is obviously not practical to utilize variable nozzles on production engines.

2. Fuel modulating governor: The paper mentions a modulating governor, which appears to refer primarily to a variable fuel stop, or limit stop, which is responsive to manifold pressure. It also states that the effect of the modulator on torque response appears to be negligible. A torque peak at about two-thirds full engine speed is usually desirable for most automotive applications. This, as the curve in Fig. 13 shows, is largely dependent upon the efficiency and proper matching of the turbocharger.

3. Engine ratings: For the full-throttle performance curves shown in Figs. 15 and 16, it would be interesting to know the exhaust temperatures, before and after the turbo, as well as the pressure level (gas pressure before turbine and air pressure at compressor outlet). There must be an optimum performance of the engine at any of the limiting values of thermal loading and combustion peak pressures. The question I have is: What are the exhaust temperatures and pressures and the compressor outlet pressures which correspond to these limiting values?

4. Effect of altitude: The paper states that the power output drops approximately 1% per thousand feet of altitude. The curve in Fig. 27, which shows the effect of this, indicates a substantial increase in the preturbine temperatures and in the turbine speed. The recommendations made by the Diesel-Engine Mfrs. Association in their "Standard Practices," are 3% per thousand feet of altitude for the turbocharged engines and 3.7 in. for the nonturbocharged engines.

I would like to ask the authors what the amount of derating per thousand feet of altitude is on this particular engine; also, if this derating is done primarily to limit the exhaust temperature before the turbine or whether it is done to limit the turbine speed. In my opinion, the amount of derating for altitudes can be reduced considerably if a turbocharger is used which has a substantial margin in safe overspeed and also is capable of operating at substantially higher exhaust temperatures than those normally encountered in diesel engines.

5. Engine life: The statement is made that the most critical item in the life of the turbocharged engine appeared to be the exhaust valve. This experience is contrary to practically all other cases of supercharging I know of. Exhaust valve life is usually improved when supercharging is adopted. Even in the paper, Fig. 33 shows a generally lower valve temperature for the supercharged engine. This is contrary to the statement made in the paper and should be clarified. I believe that this trouble was due to reasons other than supercharging and the resulting "increased density of the exhaust gas."

Is This Supercharging Or Turbocharging?

—E. T. Vincent
University of Michigan

THE main question raised in my mind is: Is this supercharging or turbocharging? The usual definitions of these terms involve increase of output by supplying more fuel and air to the working part of the cycle. True, a greater airflow is used in the results under discussion, but is there a greater charge weight trapped in the engine cylinder? Several statements throughout the paper, such as the one showing that the main gain is by reduction of the power absorbed by the Roots blower, and so forth, all seem to point to the fact that the results reported have been achieved by the use of a greater excess air coefficient. In other words, the cylinder has been scavenged more efficiently, leaving a cleaner air supply for the combustion process. The result is that the efficiency of combustion has been improved, giving more power output for the same fuel supply. It would be appreciated if the authors could give the relative weights of air trapped in the cylinder at inlet closing for the two cases together with the existing pressure at that time. This, in conjunction with the other data, would place the cause of the improved results in better perspective.

As for some of the details, the results submitted indicate that, with the final selection made of positive and turbocharger, a power increase of approximately 20% occurs with an improvement of about the same magnitude in the specific fuel consumption. Such improvements can be considered a major advance, provided, of course, that the cost of the equipment to do this is not excessive.

The above values compare to corresponding changes in the 4-stroke type of engine, amounting to 35–40% in power output accompanied by 15–20% reduction in fuel consumption. Magnitudes in excess of these have been achieved in special applications of the 4-stroke principle.

If it is assumed that size and weight reduction are the major advantages of the 2-stroke cycle, it follows that the modern supercharged 4-stroke engine has cut into what advantage the 2-stroke engine held in this respect; at the same time it retains its advantage with regard to specific fuel consumption, which in most cases is well below 0.4 lb per bhp-hr, being from 0.35–0.37 per bhp-hr. Would the authors like to predict the possible further improvement to be anticipated in the case of the 2-stroke turbocharged engine to offset this relative reduction in the advantages of the 2-stroke engine?

Another point which I think should be expressed somewhat differently so that the uninitiated can grasp the correct interpretation is that of the data in Fig. 24, showing the heat balance. One does not question the percentage figures given, but it should be pointed out that in general we are dealing with percentages of a larger quantity when the engine is supercharged. The present plot on a per pound of fuel basis is confusing to those not intimately connected with the problem.

The impression is also given that the cooling water losses are reduced and the cooling problem simplified. This should not be taken at face value, since it applies to the selected combination of circumstances for the 71 engine only where the fuel flow in pounds per hour has been kept constant.

I find the data in Fig. 31, showing the effects of intercooling on air temperature, somewhat confusing, despite the authors' comments on heat transfer. Take the curves for 2300 rpm, then without intercooling the positive displacement machine gives a temperature increase of only 16 F; but with an intercooler applied the same blower, presumably, gives a temperature increase of 47 F, indicating a greatly increased work of compression despite a great reduction of inlet temperature from about 219 F to 135 F.

Theoretically, it seems that the work done should decrease with intercooling, since the pressure of the air will not vary much unless a high pressure drop exists through the intercooler. Without some knowledge of the manner in which the pressure ratio of the blower changes under the two circumstances it is difficult to picture the effects presented in Fig. 31.

The authors mention the effect of heat transfer from the air box, but this is questioned, since in one case the air temperature recorded is 235 F. This temperature is higher than that of the cooling medium, which is presumed to be water at, perhaps, 180 F, in which case heat flow would be from air to water. An explanation not mentioned

could be the effect of backflow from the cylinder if the pressure in the cylinder at the point of opening of the scavenge ports exceeded the air pressure. A little hot gas from the cylinder to the air box would easily account for the high temperature recorded.

Fig. 28 shows the engine performance versus turbine back pressure for a fixed fuel rate, according to the heading for the plot, while the abscissa of this diagram says "Turbine Pressure Out," which would be interpreted as being the exhaust pressure on the turbine.

If we assume the caption is correct, then this diagram does indicate that a 2-stroke engine is not a good machine for turbocharging or compounding. In most cases when back pressure is applied to a 4-stroke engine, the bhp will keep constant and sometimes increase a little with back pressure, while the compressor speed and supercharge pressure increase. This appears to be a particularly desirable combination if a compound engine is desired.

Authors' Closure To Discussion

MR. ANTONSEN has asked if we had considered placing the Roots blower ahead of the turboblower. This was considered but, because of the mechanical difficulties involved, was not tested.

In answer to the question concerning operating temperatures of Figs. 29 and 30, the compressor inlet temperature was controlled at 110 F. A family of curves would be required to show all the temperatures requested. However, it can be said that both inlet air temperature to the Roots blower and air-box temperature drop rapidly with load and less rapidly with speed, to the extent that intercooling ceases to be appreciably effective below 60% load.

We can readily agree with Mr. Horiak's comparisons of the 2- and 4-stroke combinations. It must be remembered, however, that the 2-stroke engine must be designed to handle more than twice the volume of air required by a 4-stroke engine of equal displacement.

Mr. Blose's experiments apparently check quite closely with ours. The Model 64-HN9 was modernized with present production Model 71 parts, except for the 4-valve head, and should have given comparative performance. We felt that the performance improvement obtained at high speeds with the 4-valve head, plus the longer life of the smaller exhaust valves used, warranted using the 4-valve cylinder head in production.

Mr. Bohuslav has proposed several questions; first, the value of a variable turbine nozzle. The question of variable nozzles is somewhat academic, as Mr. Bohuslav suggests, since they are not economically practical at this time. The comparison of the torque curves of turbo D (Fig. 13) and the torque curve with a variable nozzle in Fig. 11 shows similar characteristics. Turbo D showed good performance but reached its peak efficiency at a considerably lower engine speed than the other turbos tested. This improved performance in the lower speed ranges with a slight relative sacrifice at higher speeds. This same turbo, when tested with several nozzle areas, indicated that it also would benefit by a variable nozzle and give even better performance throughout the speed range.

The fuel modulator has been designed to eliminate exhaust smoke at low-speed full throttle and the usual puff of black smoke observed on turbocharged engines when going rapidly from idle to full throttle.

The question of exhaust temperatures and pressures and compressor pressures at the limiting value of thermal loading is difficult to answer, since as far as we know this limit has not as yet been reached. The maximum preturbine temperatures obtained in the laboratory have been approximately 1300 F at 60 in. of Hg. absolute pressure. Compressor discharge pressure at this point is slightly higher. At the production rating, peak compressor and preturbine pressures range from 45–50 in. of Hg. absolute. Preturbine temperatures seldom exceed 1050 F. The posturbine temperatures are shown in Fig. 18.

Altitude performance: On this particular engine the power drops with altitude up to 7000 ft, as shown in Fig. 27. The engine is derated by installing 70-cu-mm injectors for continuous operation above this altitude. This is done to limit the combination of preturbine temperature and turbine speed. A turbocharger with both a high safe overspeed plus good resistance to high temperatures would certainly improve high altitude performance; however, the temptation to use these turbocharger characteristics to improve the engine sea level performance would be excessive. The problem of altitude performance would then be unchanged.

Engine life: Fig. 33 shows exhaust valve operating temperatures with both the 2- and 4-valve cylinder heads. A direct comparison of the average valve operating temperatures in the 4-valve head show 1290 F for the turbocharged engine and 1220 F for the nonturbocharged engine.

Prof. Vincent has indicated that he believes some of the increase in power is the result of increased scavenging efficiency and asks about the relative amounts of trapped air in the cylinder under the nonturbocharged and turbocharged conditions. We do not believe that the scavenging efficiency has been greatly improved by turbocharging. Fig. 9 shows that the indicated economy is not greatly changed over a wide range of scavenging air ratios, providing the overall air fuel ratio does not exceed approximately 30/1. If scavenging efficiency were greatly effected by decreased scavenging air ratios, the minimum indicated fuel consumption would have a much wider spread. It also indicates that the trapped air increases with increased scavenging ratio, because more fuel can be burned efficiently as the scavenging ratio increases. The trapped air is increased on the turbocharged engine over that of the nonturbocharged engine. Indicator cards show that cylinder pressures at the point of intake port closing are approximately the same as the air-box pressure. The cylinder and air-box absolute pressures at the time of intake port closing are approximately 50% higher on the turbocharged engine than on the nonturbocharged engine. Since air-box temperatures on both engines are almost identical, the weight of trapped air is increased with turbocharging. This increased weight of trapped air, the lower heat rejection to the water, and the higher effective compression ratio probably account for most of the power gain not attributed to the reduction in Roots blower power requirements.

The question of percentage increase in power output resulting from turbocharging is purely a question of engine rating, of both the basic engine and the turbocharged engine. The basic engine is rated at a maximum of 242 bhp at 2300 rpm, Fig. 16. As shown in Fig. 15, the turbocharged engine could be rated at 365 bhp at 2300 rpm, an increase of over 50% in power with a fuel consumption improvement of approximately 18%. This is by no means the limit either in output or fuel economy. From our point of view, the advantages of the 2-stroke engine have not been disturbed by the turbocharged 4-stroke engine.

Concerning the heat balance and cooling requirements of the turbocharged engine, it is true that if the rating were increased above that now used, increased cooling would be required; however, the present turbocharged engine cools very satisfactorily with the same cooling system used on the basic engine.

Intercooling: The data in Fig. 31 may be somewhat confusing. It must be remembered that air-box temperature is not a measure of air temperature out of the Roots blower. The air-box temperature is the result of temperature rise through the Roots blower, blowback from the intake ports, and radiant heat, all in a container which might be considered an inefficient heat exchanger with jacket water as the coolant. In controlled tests at constant engine speed and fuel input, a reduction in jacket water temperature of 80 F reduced air-box temperature 37 F.

The abscissa caption of Fig. 28, "Turbine Press Out—In. of Hg. Absolute," has apparently been misinterpreted. This is postturbine pressure, pressure downstream from the turbine outlet.

Problems in the Application of High-Strength Steel Alloys in the

THE increase in aircraft speed made possible by the development of efficient jet engines brought with it the problem of kinetic heating. The most serious effect of the increase in temperature associated with high-speed flight is the gradual deterioration of the mechanical properties of the aircraft materials. The concurrent loss of strength and stiffness has to be compensated by added structural weight. In some instances, at the higher Mach numbers, the possibility of cumulative creep deformations must be guarded against by a further reduction of the allowable stresses. Besides, a nonuniform temperature distribution within the structure may add appreciable thermal stresses to those induced by the flight loads.

While the research scientist may concentrate on any particular aspect of the structural problems introduced by aerodynamic heating associated with high speeds, the practical aircraft designer must familiarize himself with the overall picture. Before he can devise satisfactory solutions for the many intricate problems introduced by thermal flight, he should enlarge his engineering knowledge on this subject by studying the recent work of aerodynamics, metallurgists, and research engineers in the structural field; he must acquaint himself with the nature and intensity of the heat loading, the processes of heat transfer, and its effect on individual types of structures. In addition to having at least some practical perception of the significance of convection, conductivity, radiation, specific heat, diffusivity, and thermal expansion, he should acquire an intimate knowledge of the mechanical behavior of the many new materials in terms of elastic stability, plasticity, ductility, fatigue resistance, crack-susceptibility, creep tendencies, and other relevant factors at room and elevated temperatures.

This paper intends to give the practical designer some help in making sound decisions in the application of high-strength steel alloys to aircraft structures flying in the intermediate hypersonic range by describing some of the means available for solving the problems. The various problems he will encounter are presented in three sections: temperature problems, design problems, and production problems.

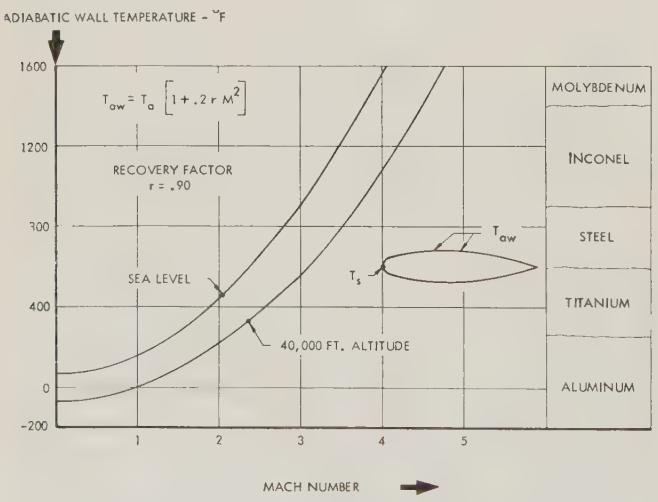

Fig. 1—Aerodynamic heating of surface skins

Aerodynamic Heating

Heat Source—The subject of aerodynamic heating has been discussed in great detail in a series of notable papers by Prof. N. J. Hoff and other leading American and British authorities. (See Additional References.) A few general remarks should, therefore, suffice to refresh the memory.

Our present knowledge of this intricate subject is based mainly on theoretical speculations. Full-scale experimental simulation of thermal conditions theoretically encountered in supersonic flight are just being started in a few research laboratories. Reliable experimental verification of the theoretical studies pertaining to the nature and intensity of heat transfer, thermal loading, and their effect on any but idealized simplifications of actual configurations are still lacking.

When an object travels through the atmosphere the local air-stream flows around its body. Surrounding the moving aircraft is a thin boundary layer of air which is accelerated to the velocity of the vehicle. The heating arising from frictional effects in the boundary layer is rapidly dissipated in subsonic flight. However, in supersonic flight this effect is noticeable, and beyond Mach 2 the consequences become progressively more severe. Ahead of the leading edge of the moving body, the relative airflow comes to rest. At this point, the entire energy of the airflow is transformed by compression

Design of *SUPERSONIC* Aircraft

A. F. Ensrud, Lockheed Aircraft Corp.

This paper was presented at the SAE National Aeronautic Meeting, New York, April 3, 1957.

and friction into kinetic heat. Disregarding thermal losses through conduction and radiation, the resulting stagnation temperature T_s can be expressed by:

$$T_s = [1 + 0.2M^2]T_a \quad (1)$$

where T_a is the ambient temperature corresponding to the altitude and M is the Mach number of the undisturbed flow. The temperatures are in degrees Rankine, that is, degrees Fahrenheit plus 460. The Mach number is the ratio of air speed to sonic speed under ambient conditions. By inserting into this basic formula the recovery factor r, which accounts for the heat loss in the boundary layer and usually is assumed somewhere between 0.85 and 0.90, the adiabatic wall temperature T_{aw} or zero heat transfer temperature in the boundary layer is found:

$$T_{aw} = [1 + 0.2rM^2]T_a \quad (2)$$

This simple relationship is plotted in Fig. 1 for flight at sea level and at an altitude of 40,000 ft. Heat losses due to radiation are not included in this diagram.

Unless an aircraft is protected by an ideal layer of insulation or completely saturated at the temperature of the heat source, heat will be transferred from the source, which in this case is the kinetic heat generated in the boundary layer, to the surface of the moving body. The intensity of this heat exchange, termed the heating rate, is governed by the temperature differential and the surface-transfer coefficient. Actually, the problem is more complex than stated. In a refined analysis, several additional parameters would enter the picture. However, for a practical approach to the subject, these simplified explanations will be considered adequate.

Skin Temperatures—The ambient temperature of the atmosphere through which the aircraft travels varies with altitude. At sea level in this part of the world an average value of 60 F is usually agreed upon, while at altitudes of 40,000 ft and above the ambient temperature of the undisturbed airflow in the stratosphere is taken equal to −67 F. When a body passes through the atmosphere at high speed, an enormous amount of heat is created by a combination of compression and friction in a relatively thin layer of air which surrounds the surface of the vehicle.

The next generation of fighter aircraft will be

PROBLEMS resulting from increased temperature associated with flight at supersonci speeds, the serious effects of aerodynamic heating on material properties, and the ultimate strength of assembled structures are discussed in this paper.

Ways are outlined which will alleviate the intrinsic weight penalties accompanying the use of high-density alloys at elevated temperatures. Primarily, this can be accomplished by the proper selection of materials and the choice of more suitable structural configurations.

Suggestions are made how to lessen the peaks of thermal stresses induced by temperature gradients during the interval of transient heating.

The need for efficient stabilization of compression panels subjected to thermal environment is pointed out in a general way; and recent innovations which might accomplish this purpose are then discussed with special regard to thin wing and fuselage design. Also mentioned are the more serious production problems arising from the change-over to high-temperature alloys.

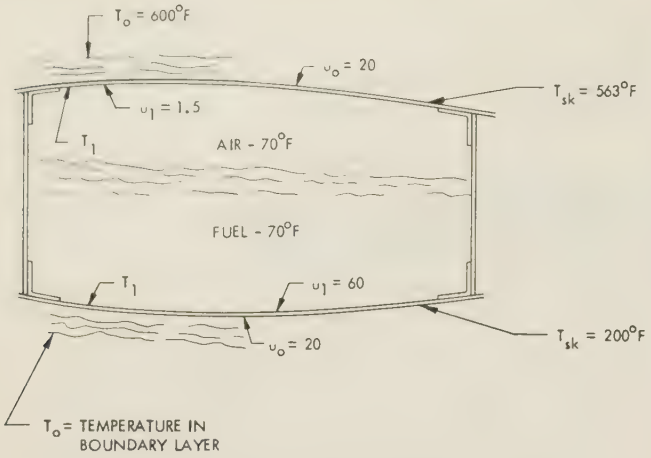

Fig. 2—Skin temperatures in a box beam

supersonic and capable of operating at high Mach numbers in level flight at all altitudes for periods of 10 min or more. Under such conditions, the air in the immediate proximity of the wing surfaces will acquire a temperature considerably higher than that of the aircraft structure before the attainment of a steady state. Consequently, heat will flow from the boundary layer into the surface skins and a little later into the internal members of the wing and fuselage structure.

The general mechanics of this process have been described by Duhamel more than a century ago in his classical memoire, "Theorie du mouvement de la chaleur dans les corpes solides." After the phase of transient heating is past, the steady-state skin temperature can be found from the simple expression:

$$T_{sk} = T_o - \frac{u_i}{u_o + u_i} [T_o - T_i] \qquad (3)$$

where:

T_i = Temperature of medium touching the inner surface of skin

T_o = Equilibrium temperature in the boundary layer

T_{sk} = Temperature of the surface skin

u_i = Inner surface convective heat transfer coefficient

u_o = Kinetic heat transfer coefficient relevant to outer skin surface

This formula strictly applies only to metal skins of high conductivity. However, thin skins of titanium and steel, in spite of their higher conductive resistance, do not retard the heat flux to any appreciable extent.

In the majority of cases, the medium which contacts the inner skin surface is air. The flux from skin to the medium which contacts the inner surface of the skin is governed by the inner surface heat transfer coefficient which, in the case of convection is still air, approximately equals unity.

For altitudes considered for the immediate future, the kinetic transfer coefficient is estimated to vary between 15 and 90. It is obvious, therefore, that natural convection in air only can bring about a very slight drop of the skin temperature below the source temperature for sustained flight at lower levels.

At higher altitudes the kinetic transfer coefficient reduces considerably and, consequently, the picture improves to some extent. Monaghan[1] estimates that in a flight at $M = 4$ at an altitude of 75,000 ft with $u_o = 7$ and a maximum equilibrium temperature of 670 F, the skin temperature would drop to 540 F although the stagnation temperature exceeds 1100 F. These figures are based on an inner surface transfer coefficient of 2, which includes radiation besides natural convection, and on the assumption that the temperature of the interior is held at 70 F. Unless some provisions for internal cooling are made, it takes only a few minutes before thin skins approach the temperature of the boundary layer.

Skins, which form the bottom of integral fuel tanks, are kept at lower temperatures due to the fuel acting as a rather efficient heat sink. Assuming the storage capacity of the fuel compartment is sufficiently large to keep a steady fuel temperature for a short duration of heat loading and taking the transfer coefficient for convection in sloshed fuel equal to 60, the skin temperature remains, according to Equation 3, much closer to the temperature of the fuel, at least at the higher altitudes. Fig. 2 indicates the result of Equation 3 applied to two practical cases.

Transient Heating and Thermal Stresses—The thermal environment encountered in supersonic flight introduces several additional parameters which have to be considered in the design of aircraft structures. These new parameters are temperature, thermal gradient, and time of loading at temperature.

The heat source and the adverse effects of elevated temperatures on the strength and stiffness of structural members are dealt with in another part of this paper. The life-strength parameter, taking account of the duration of the individual load-temperature combinations and the resulting creep tendencies, will be discussed in the next section.

Transient heating of an airplane, resulting in thermal gradients, occurs whenever the airplane changes either its speed or altitude. The temperature differential between the boundary layer and the surface of the airplane induces a heat flux q between the two media which is given by:

$$q = u_o \cdot \Delta T \qquad (4)$$

where u_o denotes the convective heat transfer coefficient and ΔT is the temperature potential. This energy transfer continues until the entire aircraft is completely saturated at the temperature level of the source. During the transient heating period serious thermal stresses may develop in the structural components of an airplane. The magnitude of these stresses depends on the severity of the temperature gradients. In this connection, it is helpful to remember that the thermal response varies with the conductivity of the materials and depends on time and distance from the heat source. To quote a familiar example, it takes 15 min to raise the temperature 50 F in a section of long steel bar located 10 in. from the end, when the temperature of said end is suddenly raised and maintained at 600 F. The slow

[1] "Introductory Notes to the Problems of Aerodynamic Heating," by R. J. Monaghan. Ministry of Supply Report, London, 1954.

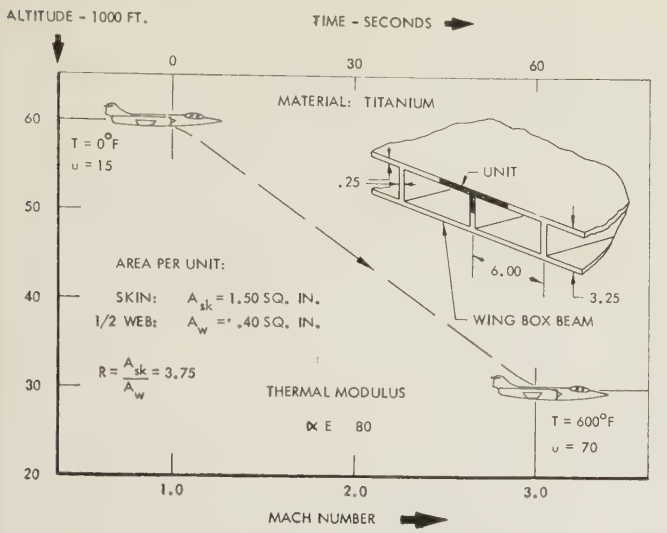

Fig. 3—Flight maneuver: dive from altitude

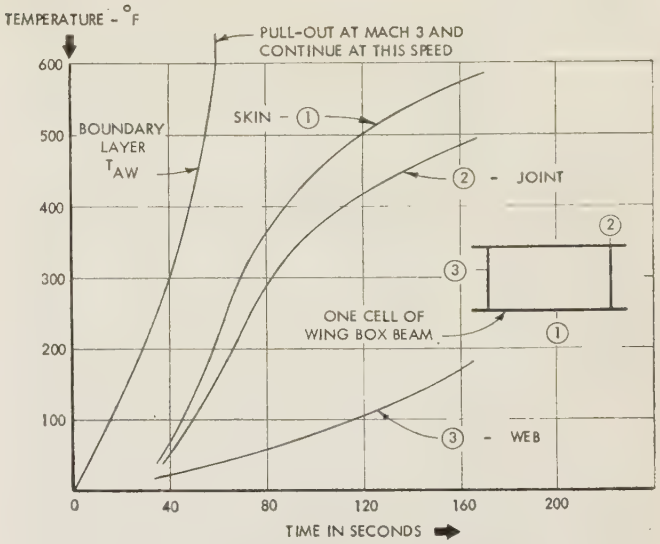

Fig. 4—Temperature history of mission

conduction of heat within most metals and across structural joints is responsible for the severity of thermal stresses in thermal-redundant structures.

A round bar will expand uniformly, without producing thermal stresses in the process, when submerged in a homogeneous medium of even temperature. However, in an airplane wing the surface is heated very fast while the substructure responds only slowly to the temperature change in the skin panels, thereby restraining their free thermal expansion. Consequently, appreciable shear forces may be induced at the junctions of the surface skins with the supporting structure. The magnitude of these redundant forces depends on the geometry of the structure, the material of its components, and, to a greater degree, on the particular flight mission in which the aircraft is engaged. The rates of change of the boundary-layer temperature which can occur in modern aircraft performance are so fast as to be practically instantaneous. Therefore, during certain maneuvers it is possible that the temperature potential between skin and supporting structure approaches the temperature rise in the boundary layer. Selecting a random mission of a modern interceptor, as pictured in Fig. 3, the effects of transient heating will be demonstrated in a realistic example.

After a prolonged high-level cruise at Mach 1, a fighter plane goes into a dive, accelerating to Mach 3 and pulling out at this speed at a lower altitude. Due to the decrease in altitude the kinetic heat transfer coefficient increases from 15 to 70. Fig. 4 indicates that the adiabatic wall temperature rises to 600 F, while the skin temperature at the center between the webs lags behind for about 2 min. It can also be noticed that the largest temperature potential between skin and web occurs about 1 min after the pull-out. The thermal stresses induced by these transient temperature gradients are plotted in Fig. 5. The skin experiences compression, while the spar webs are subjected to tension. The temperature distributions and the resulting thermal stresses during the transient state can be determined analytically with help of well-known equations. However, even for simple idealized con-

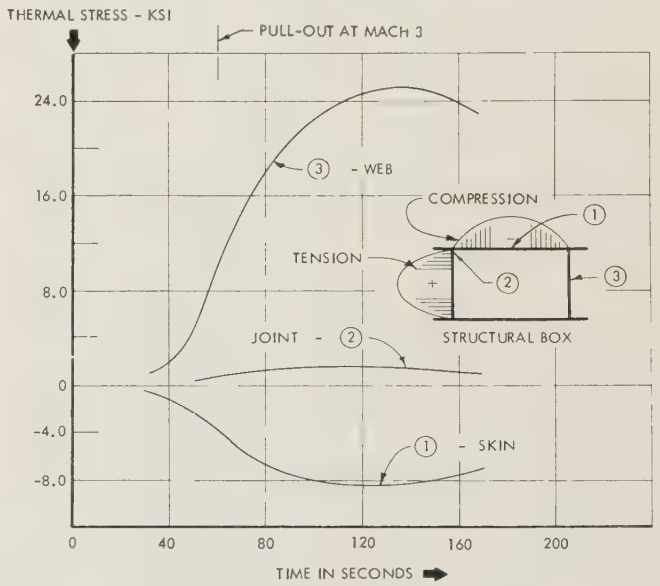

Fig. 5—Thermal-stress history of mission

figurations the analytical procedures are tedious and time consuming. Therefore, approximate methods based on engineering judgment should be resorted to. For example, for the case under consideration, by simple inspection it can be concluded that the maximum thermal potential between skin and web would not exceed 500 F. Should the spars offer perfect restraint, the thermal stress in the surface panels would reach the maximum possible value of:

$$(F_{sk})_{max} = (\alpha E)_{sk} \Delta T \qquad (5)$$

where $(\alpha E)_{sk}$ is the thermal modulus of the skin panel. Evaluating Equation 5 for titanium yields the worst possible thermal stress in the surface equal to 40,000 psi. Since, however, the thermal expansion of the skin pulls the webs along, self-equilibrating stresses are induced in the whole system. From simple equilibrium computations, it

follows that the actual thermal stress in the skin panels would approximate:

$$F_{sk} = -\frac{(aE)_{sk} \cdot \Delta T}{1 + R} \qquad (6)$$

In this equation the geometrical configuration index R is expressed by:

$$R = \frac{(AE)_{sk}}{(AE)_{w}}$$

where:

A_{sk} = Area of one skin panel
A_w = Area of ½ web

Similarly, for the thermal stress in the web one may write:

$$F_w = a_{sk} E_w \Delta T \left[\frac{R}{1+R}\right] \qquad (7)$$

For the example presented in this section, the above formulas yield thermal stresses equal to 8400 psi in the skin and 31,500 psi in the web. Since the actual maximum temperature potential during the mission reaches only 400 F, these stresses should be reduced accordingly. It will be seen that they agree satisfactorily with stresses computed by a more accurate, but for practical design purposes too cumbersome, method which is explained in the outstanding paper by Mar and Schmit.[2]

From the rather elementary discussion of this subject, nevertheless, several important conclusions may be drawn. In multiweb wing beams and in fuselage structures, the cross-sectional area of the supporting members is always much smaller per structural unit than the surface-panel area. This fact is, eo ipso, very beneficial in reducing the surface compressive stresses and it also lessens the magnitude of the redundant forces which are transferred to the substructure during the transient state of aerodynamic heating. However, due to the relatively small cross-sectional areas of the supporting members, the induced thermal stresses in spar webs and fuselage rings may be rather severe. By playing with the configuration index R in Equations 6 and 7, the designer can occasionally work out a satisfactory balance between the thermal stresses in the surface panels and the supporting structure. In the majority of cases, however, this remedy will prove inadequate. Realizing that during flight missions different from the one described above, the induced thermal stresses might be greater and have opposite signs, the necessity of providing strong spar webs or means which will alleviate these stresses becomes obvious, especially since in modern fighter performance the possible decelerations in level flight can be much greater than forward accelerations. Several ideas which would alleviate the thermal stresses have been proposed: sliding joints between surface and substructure; or decreasing the resistance to longitudinal translation of the spar caps by the use of sandwich or Unicore[3] webs, corrugations, or lightening holes. The last suggestion seems feasible for very thin wings only.

Of more practical importance is the proper selection of materials. At a pull-out from a steep dive the steepest temperature gradients and the severest thermal stresses would coincide with the highest aerodynamic loads, which in a modern interceptor plane probably would correspond to an ultimate load factor in excess of 10 g. Even during such maneuvers, the combination of stresses due to applied load and thermal redundancy must be kept low enough to give assurance that no excessive residual stresses or permanent deformations remain in the spar webs after the steady state is reached. A quick inspection of Equation 7 informs the designer that the most effective relief from thermal web stresses is obtained by making as small as possible the cross-product of the thermal expansion coefficient pertaining to the skin panel times the effective modulus of the web material. A combination of precipitation-hardened steel panels supported on aluminum spars does very well in this respect, according to Equation 7. In addition, this combination will be concomitant with a lower temperature potential because the steel skin heats up more slowly due to its lower conductivity and higher heat capacity, while the aluminum spars receive the heat from the skin more readily due to their diffusivity being about 12 times as great as for the steel alloy. The combined effect can be estimated to result in a reduction of about 75% in the magnitude of the thermal web stresses of a typical fighter or missile wing. Of this total reduction, 55% can be attributed to the difference in the materials and the balance would be due to the decrease in the temperature potential.

Another alleviating factor which permits a less pessimistic outlook in regard to the seriousness of weight penalties caused by the thermal environment associated with high-speed flight is the fact that the modulus of elasticity decreases with the higher stresses in the plastic range as well as with temperature. How much one may avail oneself of this remedy depends on the anticipated life span of the aircraft under consideration.

A rigorous determination of the temperature gradients arising during accelerated or decelerated supersonic flight and of the ensuing thermal stresses entails a tremendous amount of computational work for each individual flight path. At this time, solutions are available only for the most idealized reproduction of an actual structure. Available methods confine themselves to the effect of one-dimensional thermal expansion, neglecting chordwise redundancy caused by ribs and other incidental detail requirements and overlooking the effect of spanwise conduction.

The application of a refined thermal analysis to practical design configurations is far beyond the powers of the average engineer. However, the problem lends itself to the same approximate treatments applied so satisfactorily in the analysis of highly redundant aircraft components. After the temperature distribution is determined by judicious guesses as to the heat-sink capacity of the substructure, the computation of the thermal stresses can be achieved by solving a system of homogenous difference equations expressing the shear transfer of the redundant forces. Modified forms of the methods suggested in other studies should be helpful.[4, 5]

[2] "Structural Penalties Associated with Thermal Flight," by J. W. Mar and L. A. Schmit. Paper presented at ASME Symposium on Structures for Thermal Flight, March, 1956.

[3] Unicore construction is a proprietary design configuration developed by Lockheed Aircraft Corp.

[4] *Journal of Aeronautical Sciences*, Vol. 8, April, 1941, pp. 246–255: "Unit Method of Beam Analysis," by F. R. Shanley and F. P. Cozzone.

[5] "Analysis of Redundant Structures by the Methods of Elastic Poles," by A. F. Ensrud. Lockheed Aircraft Corp., Burbank, Calif., July, 1952.

Thermal Buckling—This section will explain the action of an individual plate element which is subjected to a compression load and at the same time prevented from free thermal expansion. The behavior of such a specimen under kinetic heating is of special interest, as it can be shown that under certain circumstances the critical Euler stress does not necessarily indicate failure.

A plate element, initially flat and unstressed, is provided with knife edges at each end and placed in a perfectly rigid testing machine (Fig. 6). The specimen is subjected to a compressive load P and then heated to 500 F. As the plate warms up, it tends to expand, but is restrained from this action by the fixed heads of the testing machine. The thermal expansion of a free element over its length L would be equal to:

$$\Delta L = \alpha T L \tag{8}$$

where α is the coefficient of linear thermal expansion and T denotes the rise in temperature. Because of the restraint, axial thermal stresses are set up in the specimen in addition to the load stresses. The temperature stress F_t is independent of the length of the specimen. From the general expression:

$$F = \frac{\Delta L}{L} \cdot E$$

follows with Equation 8:

$$F_t = \alpha E T \tag{9}$$

The product αE is termed the thermal modulus and may be considered a material property. For the important aircraft materials the pertinent values are shown in Table 1. Since initially the specimen was perfectly straight, it will remain so until the combined load and thermal stress exceeds the critical Euler stress:

$$F_{cr} = 0.914 E_t \left(\frac{t}{b}\right)^2 \tag{10}$$

which in this case happens to be: $F_{cr} = 90{,}000$ psi.

Beyond this stress the plate will buckle and thus automatically relieve additional thermal stresses.

In the example (Fig. 6) the specimen is subjected to an initial compression load of 2500 lb per in. of width, resulting in an axial stress of:

$$F_L = 25{,}000 \text{ psi}$$

Then heat is applied gradually to the plate element. Consequently, the compressive stresses increase until, after a rise in temperature of 340 F, the specimen buckles. At this point, the maximum compressive load has been reached, namely:

$$P_{max} = 9000 \text{ lb/in.}$$

Any subsequent heat input will increase only the amplitude of the buckle. At a temperature rise of 500 F, the deviation from the initial straight configuration will equal 0.034 in. If the specimen had been prevented from bowing, the axial stress would have increased to 120,000 psi. Since the panel was free to buckle, a bending stress of about 110,000 psi is added to the critical buckling stress, resulting in a maximum extreme fiber stress of 200,000 psi, which still is below its ultimate failure stress.

From this simple example, it can be learned that, provided aerodynamic requirements permit a small degree of rippling, occasionally it may be advantageous to profit from the postbuckling strength of plate elements exposed to thermal environment. However, care should be taken that the combined normal and bending stresses do not exceed the yield stress of the material, thus resulting in permanent deformations. Another important point to watch is that the stiffness of the supporting structure does not deteriorate during the process of aerodynamic heating.

Insulation and Cooling—The gravest aspect of supersonic flight is the aerodynamic heating of the airframe and its internal compartments. The thermal potential of the boundary layer is of such magnitude that it may finally impose a barrier to sustained high-speed flight for manned aircraft under atmospheric conditions, unless practical methods of insulation and cooling can be devised.

Raising the flight altitude would aid the aerodynamic heating problem by reducing the heat input and by lowering the steady flight equilibrium temperature, owing to the fact that at the higher altitudes the kinetic heat transfer coefficient is greatly diminished and heat losses due to radiation become important. Other means of alleviating this critical situation are the application of insulation or a resort to the various ways of artificial cooling. The paragraphs which follow should give the designer at least an idea of the practicality and efficiency of such measures.

Heat is transferred in several ways: by conduction, radiation, or convection. Hence, insulation can lessen the intensity of the heat flow by employing materials of low conductivity, by using radiation foils, or by trapping small air spaces within the insulating medium to interfere with the process of natural convection.

Outer skin surface insulation can serve several purposes. Applying a heavy layer of high-thermal capacitance would act as an efficient heat sink dur-

Table 1—Thermal Modulus of Important Aircraft Materials

	At room temperature	At 600 F
Aluminum	130	80–100
Titanium	80	70
Stainless Steel	200	190
Inconel	236	220
Molybdenum (0.5% Ti)	140	140

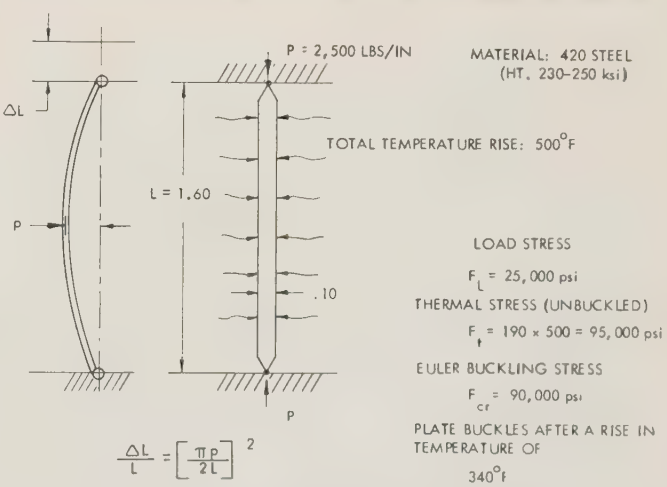

Fig. 6—Thermal buckling of a plate element

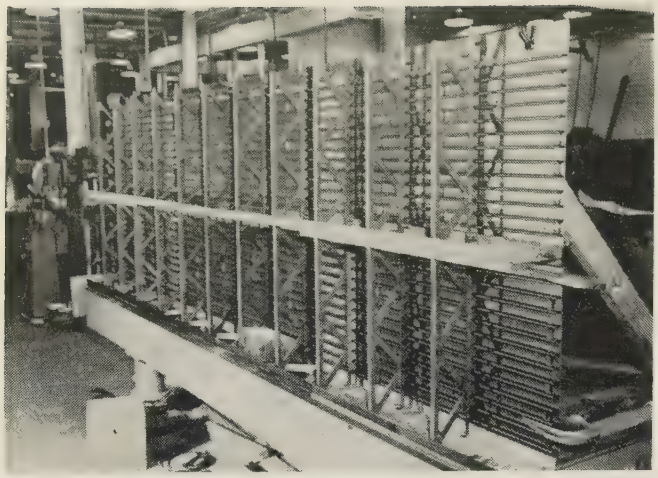

Fig. 7—Test specimen—upper surface of wing box, made of corrosion-resistant 420 steel, heat-treated to 230-250 ksi

ing the transient interim. It could delay as well as reduce the temperature rise in the structural surface. A thin layer of insulation just lessens the intensity of the heat flow but, nevertheless, can be very effective during a short-lived ultrasonic dash.

Without insulation the heat flux between the boundary layer and the structural surface was given by Equation 4 as: $q = u_0 \cdot \Delta T$.

The benefit of an outer layer of low-conductive substance, having a thickness d and a coefficient of thermal conductivity K, is found from:

$$q' = \xi q \qquad (11)$$

where:

$$\xi = \frac{1}{1 + u_o \cdot \frac{d}{K}}$$

For example, using a thin sheet of cellular-type insulation, continuing fine mineral fibers like Thermoflex, would require a thickness of 0.30 in. in order to keep a ¼ aluminum skin below 200 F for 15 min after an instantaneous rise of 500 F in the adiabatic wall temperature. Assuming a density of 3 lb per cu ft for the insulation blanket, this increases the weight of the surface structure by 0.075 psf. To this would have to be added the weight of a suitable covering protecting the insulation against the supersonic airflow.

Thin high-temperature coatings are being seriously considered for ultrasonic-fighter design. Thicker layers cannot be permitted on the outer surface of high-performance aircraft for aerodynamic reasons. However, in the design of larger airplanes a heavy layer of insulation on either side of the structural surface may be provided, preferably on the inside, because of readier space availability.

Inside insulation does not protect the skin against the effects of aerodynamic heating. According to Equation 3, a perfect job of inner surface insulation, attaining zero convection at the inside face of the skin, raises the skin temperature to that of the boundary layer in a very short time. During the transient state this fact might increase local thermal stresses appreciably.

A thick layer of light-weight foamed plastic coupled with mechanical refrigeration is very effective in reducing the cabin temperature to tolerable levels during sustained flight in thermal environment. Without such prevention, after a short time the whole structure would be saturated at the temperature of the boundary layer.

It is a simple matter to determine the requirements for keeping the cabin temperature of a transport plane at a desired level. Computing the heat input into the aircraft, subtracting the amount which can be stored during the transient interim and the amount which escapes by convection and radiation, yields the remaining quantity to be removed by artificial means.

For a large transport plane, traveling at an altitude of 35,000 ft at Mach 3, the required mechanical refrigeration equipment, inclusive of coolant and plumbing would weigh in excess of 100,000 lb. This figure is based on a surface area of 3000 sq ft, a heat input of 10 Btu per sq ft per sec and an installation which weighs 4 lb per Btu per sec. The same aircraft traveling at an altitude of 100,000 ft would require only one-tenth of this weight provided the same efficiency of the equipment could be maintained at the higher level. These theoretical figures clearly show the limitations of such equipment if used without insulating the surface of the aircraft. At lower levels the weight penalties would be prohibitive and at higher altitudes the atmospheric air can no longer be used as an ultimate heat sink.

Another idea proposed by several engineers is transpiration cooling. This system consists of the controlled pumping of gas or liquid through a porous skin, maintaining a continuously regenerated protective film on the surface.

Very little reliable data is available at this time in regard to any type of cooling system. For fighter aircraft performing in the range of immediate interest, it might be advisable to design the structure for the thermal environment to be encountered and, if necessary, just thicken the skin to act as a heat sink.

Structural Configurations for Thermal Flight

General Considerations—Several major aircraft companies are playing with the idea of designing a new generation of fighter-interceptor planes which will be capable of better performance in more severe thermal surroundings, at least for a limited duration of time. It has been pointed out that the practical value of protective measures against the intense heat of the boundary layer has yet to be proven under actual flight conditions encountered at high Mach numbers. Without resort to insulation and cooling, the temperatures developed in the surface structure of an aircraft traveling at the contemplated speeds will be so high that the material strength of light alloys would fall well below satisfactory levels. The replacement of aluminum with denser materials having better heat-resisting qualities seems unavoidable. The individual merits of possible candidates will be discussed in the following section on the basis of their suitability for thermal flight. It will be shown that some of the new super-steel alloys are rather attractive in this respect and probably will be used before titanium because of more assured availability.

The substitution of stainless steel in place of aluminum alloys as structural material for the major components of airplanes operating under thermal conditions is likely to result in many new problems for the designer, the production department, and

the service personnel. A drastic change-over of this nature will be very costly in time and money. It requires the collection of new design data, production know-how, training of personnel, and large expenditures for additional shop equipment. For this reason, such radical steps should not be taken until conventional methods have been fully exploited and all possible alternatives have been thoroughly explored. Some engineers are inclined to believe that aluminum alloys will remain competitive even for interceptors which operate at Mach 3 for very short durations.

One of the major problems facing the structural designer is the possible weight penalties associated with the use of high-density heat-resisting alloys at elevated temperatures.

Potential increases in structural weight are due to:

1. Higher specific gravity of the material.
2. Reduced allowables and lower modulus of elasticity at elevated temperatures.
3. Increased stabilization requirements for compression panels.
4. Thermal stresses due to nonuniform heating.
5. Creep tendencies induced by long-time loading at temperature.

The aircraft engineer has at his disposal several ways which might alleviate some of the critical conditions encountered during thermal flight. Among others, he will help the situation to a great extent by selecting the material most suitable for his particular application, by devising structural configurations which will permit ultimate utilization of the potential strength of the chosen alloy, by keeping parasitic stabilization weight to a minimum, and, last but not least, by blunting the peaks in the transient thermal stress curves.

As a rule, little difficulty is encountered in developing the full tensile strength of a material in the net section of a tension member, provided excessive secondary stresses due to eccentricities or other causes are avoided and fail-safe requirements are omitted. However, great ingenuity and design experience are needed to arrange the material in compression members to its best advantage. This problem is aggravated by the fact that the change to high-strength alloys will result in very thin gages for skin and stiffeners, which at elevated temperatures will loose some of their already low initial strength and stiffness. For this reason, conventional sheet-stiffener combinations are no longer able to develop compressive stresses approaching the tensile strength of the material, unless in the case of high-structural loading indices.

To illustrate this point, attention is called to a wing box-beam test recently conducted at our laboratory. The compression surface of the box failed unexpectedly by buckling into a chordwise wrinkle of rather short wave length. The design consisted of conventional stiffener and skin combinations supported by ribs and spars (Fig. 7). The material was corrosion-resistant 420 steel, heat-treated to 230–250 ksi. Subjected to bending and heated to 500 F, the compression surface of the box beam buckled at an external load stress of 42,000 psi. The thermal stress at time of failure was estimated as 35,000 psi, making the total compressive stress equal to 77,000 psi. The maximum allowable crippling stress for the 0.050 gage plate elements, 1.5 in. wide between rivet lines, was:

$$F_{cc} = 116{,}000 \text{ psi}$$

while the compressive yield of the material at the relevant temperature equaled 188,000 psi. As mentioned, the mode of failure was a chordwise wrinkle in the top cover, which formed between the spars pulling the flexible stiffener flanges along. The cross-section of a single bay of the box beam is shown in Fig. 8. The indicated skin temperatures were reached after an exposure of 7.5 min to radiant heat emitting from infrared quartz lamps.

From this and similar test results the following conclusions may be drawn. In order to develop the compressive yield or even higher stresses in flat-plate elements of superalloys, it is necessary to provide:

1. Unyielding supports.
2. A closely spaced supporting structure.
3. Adequate shear and tensile strength in the

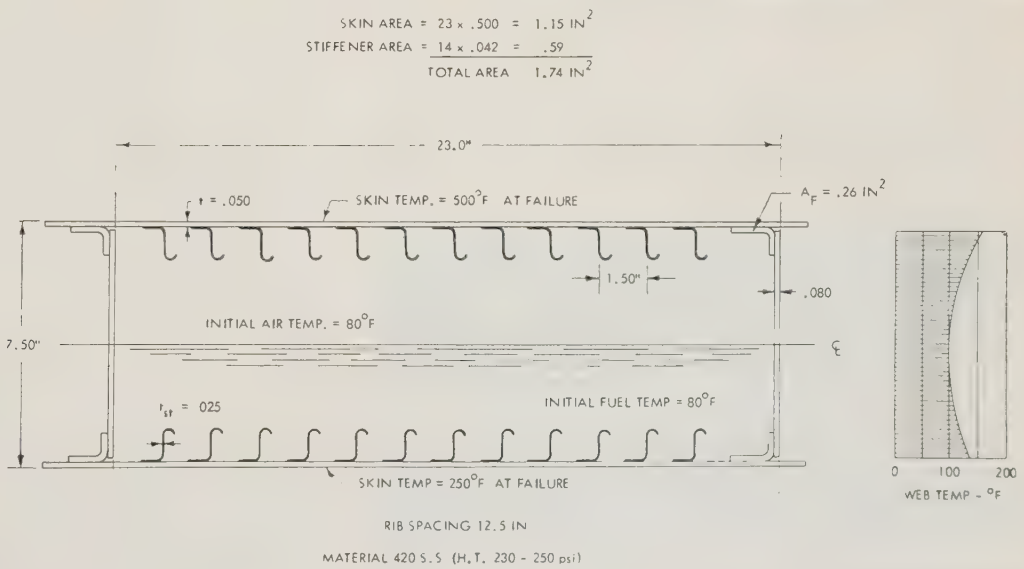

Fig. 8—Cross-section of box beam, one bay

bond between skin and stabilizing medium.

1. *Unyielding support:* The conventional configuration of a multiweb wing divides its compression surfaces into long narrow strips which are attached to the spar flanges. For long skin panels of this type, supported along their unloaded edges and subjected to longitudinal compression, the critical buckling stress is given by:

$$F_{cr} = \frac{\pi^2 \cdot \overline{E}}{3(1-\nu^2)} \left(\frac{t}{b}\right)^2 \qquad (12)$$

The postbuckling strength or crippling stress of such plate elements can be derived from:

$$F_{max} = F_{cc} = 1.6 \left(\frac{t}{b}\right) \cdot (E_s F_{cy})^{\frac{1}{2}} \qquad (13)$$

The above equations are predicated on the assumption of simple and unyielding supports. In case the flexibility of the spar flanges exceeds the permissible limit, the basic buckling and crippling stresses computed from Equations 12 and 13 have to be reduced. Another article[6] treats this subject in detail and presents original expressions for the reduced buckling and crippling stresses due to support deflections normal to the plane of the sheet. These formulas are derived in the quoted reference and are repeated in Fig. 9. It can be noticed that the rivet offset c has a predominant effect on the magnitude of the coefficient β_B and β_C, by which the allowable stresses given by these equations must be reduced on account of yielding supports. It should be obvious that the maximum values these reduction coefficients may assume cannot exceed unity. A high value of the eccentricity index e/t_w together with a low aspect ratio b/t of the cross-section of a plate element indicates that the panel, due to the insufficient spring constant furnished by the supports, may fail by forming a chordwise wrinkle, as shown in Fig. 10.

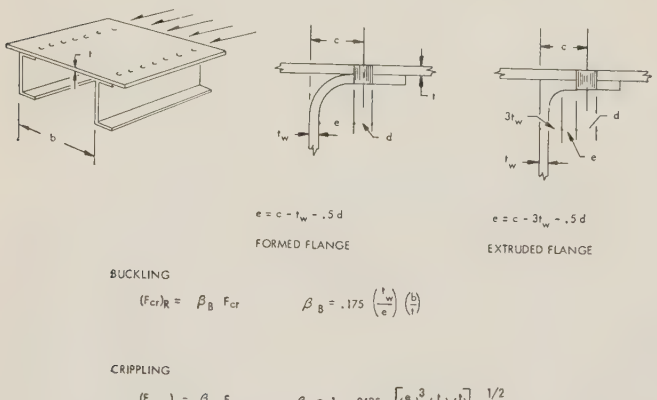

Fig. 9—Reduced compression allowables, flexible supports

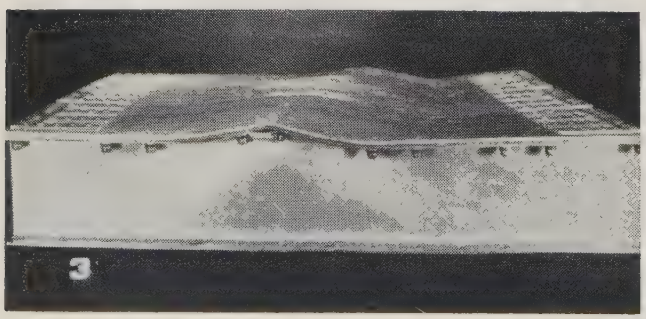

Fig. 10—Chordwise wrinkle in the compression cover of a multispar box beam, due to the flexibility of the intermediate supports

2. *Closely spaced supporting structure:* The continuing improvement in the mechanical properties of high-density alloys could result in greatly increased strength-weight ratios for skin panels, provided they can be stabilized by a light but efficient supporting structure. Unless other than strength requirements determine the skin gage, conventional types of structures cannot be used any longer since in many cases, they are unable to take full advantage of the greatly improved strength of the new superalloys. Especially for low load indices, resulting in very thin gages, an efficient supporting structure must employ very close spacings. This can be accomplished in a most desirable manner by the use of sandwich panels containing cellular cores.

The theoretical advantages of such configurations are obvious. However, fabrication difficulties and unreliable bonding between facing and core structure have up to this time precluded the full exploitation of high-strength steel sandwich panels for primary structural application.

Considering the great expenditure of money and the large amount of development work required to make the use of reliable high-strength steel sandwich panels a reality in any but the simplest secondary applications, the question arises, "Is the use of steel sandwich panels really necessary in the design of surface structures for high-performance aircraft engaged in thermal flight and how great is the advantage in comparison with other possible configurations?"

It is not always a simple matter to give an intelligent answer to such generalized questions. Some academic scribifaxes make it their favorite pastime to engage in theoretical optimum design studies which, based on unrealistic assumptions, usually have scant practical value and at times can even be misleading. The experienced designer, as a rule, knows by intuition which particular configuration will best serve the special needs of his problem. For a given loading and ultimate compression stress of the skin material, the required gage of the facings is easily computed. To this is added the weight of the core structure, which for stainless-steel cores can vary between 6 and 18 lb per cu ft, and also the weight of the bonding, attachments, and joint details. It is then quite a simple matter to determine how much of the weight of the surface skin can be saved by reducing the support spacing. This saving must be offset against possible weight increases in the supporting medium and concomitant details.

In order to help the designer in his comparative weight-strength studies, the relationship between the required cross-sectional aspect ratio of a flat-plate element and the maximum compressive stress which can be realized will now be established for several geometrical boundary conditions.

Taking, for example, a multispar wing surface, one encounters wide column action whenever the skin panels are subjected to chordwise compression, as during transient heating. For this case, the as-

[6] "Comparative Design Study of Thin Fighter Wings," by A. F. Ensrud. Report 10,129. Lockheed Aircraft Corp., Burbank, Calif., October, 1954.

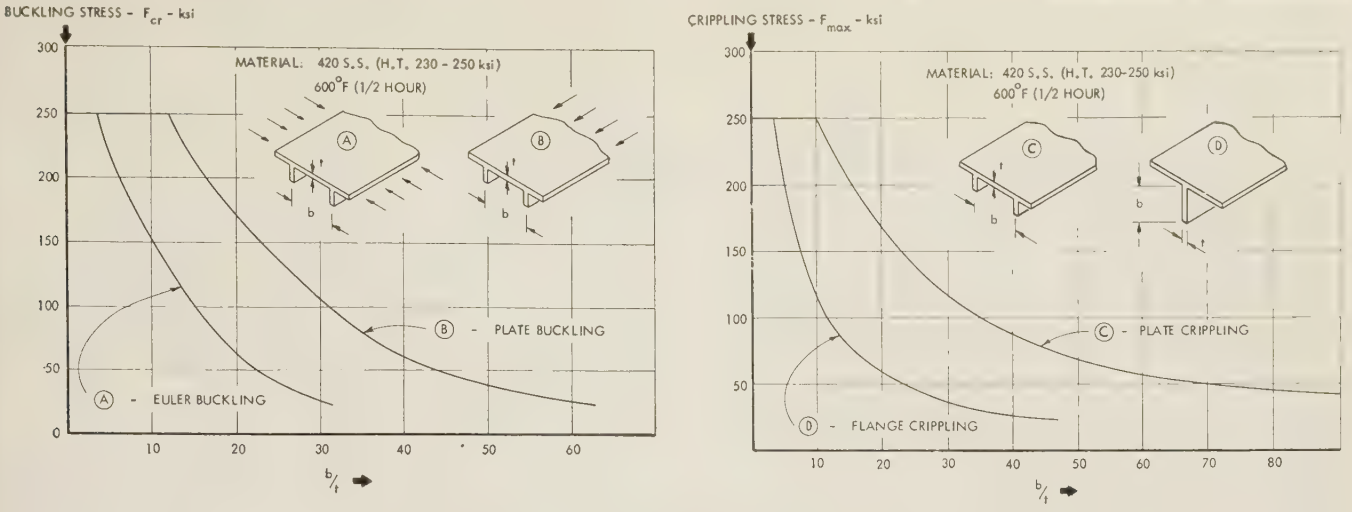

Fig. 11—Aspect ratio versus allowable stress

pect ratio associated with the Euler buckling stress F_E is given by:

$$\frac{b}{t} = \left[\frac{0.914E_t}{F_E}\right]^{\frac{1}{2}} \tag{14}$$

For a wide skin panel (Fig. 11, Case A) compressed in transverse direction, the critical Euler load indicates the maximum stress the element can sustain, since no plate action comes into play. As pointed out in the section on thermal buckling, a sudden increase in temperature will not precipitate immediate failure in this case, since even a small buckle would bring instantaneous relief.

The more important case is the long and narrow strip which is supported along its unloaded edges and subjected to longitudinal compression (Fig. 11, Case B). Here one must differentiate between the initial buckling stress F_{cr} and the ultimate crippling stress designated F_{cc} or F_{max}. The basic formulas pertaining to this case were given by Equations 12 and 13. Assuming rigid supports and solving for the aspect ratio b/t, yields these simple expressions:

Buckling of a plate element—F_{cr}

$$\frac{b}{t} = 1.9 \cdot \eta_t^{\frac{1}{4}} \cdot \left(\frac{E}{F}\right)^{\frac{1}{2}} \tag{15}$$

Crippling of a plate element—F_{max}

$$\frac{b}{t} = 1.6\left[\frac{E_s F_{cy}}{F^2}\right]^{\frac{1}{2}} \tag{16}$$

The above formulas apply to plate elements whose edges are simply supported and not free to move. For the flanges of integrally stiffened panels (Fig. 11, Case D) or for flat-plate elements, one edge free, corresponding equations take the following form:

Flange Buckling—F_{cr}

$$\frac{b}{t} = 0.615\left(\frac{E_s}{F}\right)^{\frac{1}{2}} \tag{17}$$

Flange Crippling—F_{max}

$$\frac{b}{t} = 0.52\left[\frac{E_s F_{cy}}{F^2}\right]^{\frac{1}{2}} \tag{18}$$

In the above formulas the effective modulus of elasticity must correspond to the actual compressive stress in the respective elements. These relationships between the aspect ratio of flatplate elements and the permissible compression stress have been

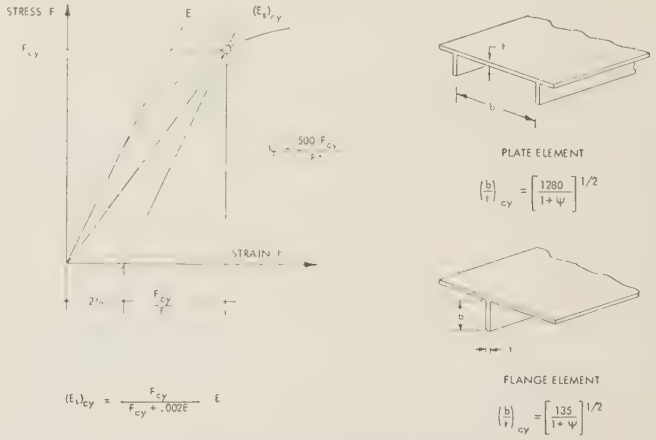

Fig. 12—Aspect ratios associated with yield stress

evaluated for the high-strength steel alloy, which was used in the box beam test mentioned before. The curves plotted in Fig. 11 pertain to 420 corrosion-resistant steel (heat-treated 230 to 250 ksi) exposed to 600 F for a short duration (½ hr). From these diagrams it is apparent how beneficial any reduction in support spacing is in raising the compression allowables.

Before any worth-while optimum design studies can be undertaken, one very important question has to be settled. Assuming adequate stabilization, what is the maximum compressive stress which can be permitted in the surface structure of a steel wing? Should this value be tied to the limit load stress or to ultimate loading? Several other considerations would have to enter the picture, as the anticipated life span of the structure, the creep behavior of the specific material, aeroelastic limitations during thermal flight, and so forth. Some engineers propose that the ultimate compression stress should be set equal to the mean of the compressive yield and the ultimate tensile stress.

For the purpose of a comparative strength-weight evaluation of available aircraft materials it is more convenient to take the compressive yield as the ultimate allowable. From the typical stress-strain diagram of Fig. 12 follows that the secant modulus

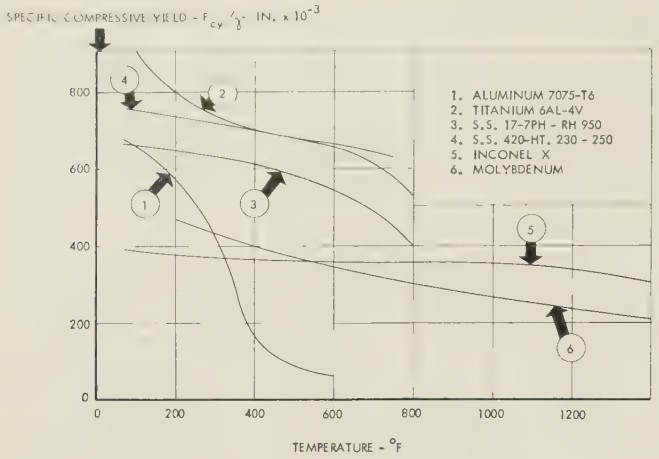

Fig. 13—Effect of temperature on strength-weight ratio of aircraft materials

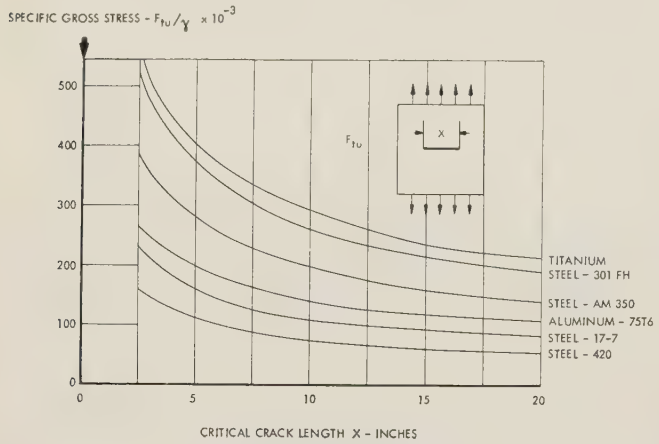

Fig. 14—Strength of cracked sheet

associated with the yield stress of a material can be determined from:

$$(E_s)_{cy} = \left(\frac{F_{cy}}{F_{cy} + 0.002E}\right) E \qquad (19)$$

Substituting this expression into Equations 16 and 18 and setting the actual stress F equal to the yield stress of the material, renders formulas for the aspect ratio b/t of plate elements, which will realize permissible compressive stresses equal to the yield stress of the material. The resulting equations are given in Fig. 12.

3. *Bond strength:* The required bond and shear strength, which will insure the structural integrity of a built-up panel, is a subject which has been treated on several occasions in the current literature. However, practical formulas which agree with test data are not available at this time. In the past, sheet-stiffener combinations of conventional design in aluminum alloy showed, as a rule, more than sufficient strength in their attachments. After the introduction of integrally stiffened panels which permitted the use of higher gross stresses, the flanges occasionally separated from the skin when stressed in the neighborhood of the compressive yield.

A change-over to high-strength steel alloys, coupled with the possibility of appreciable thermal stresses which may induce high-shear loads between skin and substructure, might make this situation more critical.

Many questions still remain unanswered as, for example, what is the effect of repeated thermal shock on the bond strength between the exposed facing, and the core of a sandwich panel. Considerable research on this subject will have to be done before reliable design criteria can be established.

Choice of Air Frame Materials—In order for the engineer to select intelligently among the many aircraft materials available at present or in the near future, he must be familiar with their behavior when subjected to loads at room temperature and under thermal conditions.

The deleterious effect of elevated temperatures on the mechanical properties of aluminum alloys is well-known. Comparing the most popular alloys, it is found that 7075-T6 has better short-time properties at lower temperatures, while at higher levels 2024-T3 is superior. However, after a long exposure at temperatures above 150 F, the room temperature properties of 7075-T6 are greatly decreased and cannot be recovered.

Some titanium alloys have rather attractive features. Besides having excellent corrosion resistance, only a slight loss of strength is noted between 400 and 600 F for the recently improved alloys. However, the unique creep properties of this metal bear watching. The weight-strength ratio of the newer titanium alloys, especially 6AL-4V, is somewhat superior to most stainless steels used at the present time.

The high-strength corrosion-resistant steels can be divided into three main groups:

1. The austenitic stainless steels, which are represented by the 300-series: These alloys are usually called the chrome-nickel steels. They are most widely applied on account of their good formability and the fact their hardness can be increased by cold working. Their tear-resistance properties are quite good, but even in the full-hard temper the compressive yield does not exceed 150,000 psi. Exposed to elevated temperatures they show excellent resistance to oxidation and corrosion, while their strength and stiffness deteriorates rapidly when heated to temperatures above 800 F.

2. The age, or precipitation, hardening stainless steels: This group includes the 17-7 types, stainless W, and Allegheny Metal 350. They are basically chrome-nickel steels which are modified by the addition of small percentages of other elements (aluminum, molybdenum, titanium, and the like). Small additions of silicon at times result in brittleness. These modified alloys respond readily to heat-treating procedures.

3. The straight chromium corrosion-resistant steels which are found in the 400-series: These alloys are martensitic or ferritic. They respond readily to varied cycles of heat-treatments, similar to most low-alloy steels. As a group, they give a good performance at elevated temperatures.

A number of years ago, we came to the conclusion that much could be gained by a fuller exploitation of the potentialities of proven low-alloy steels. By modifying the heat treatment, a large increase in strength could be achieved without loss of integrity. The successful application of 4340 steel (heat-treated 240–260 psi) in landing-gear design is well-

known in the industry. Since this is not a corrosion-resistant alloy, it seems preferable for the use in surface skins to develop new alloys especially tailored to provide even higher yield strength without loss of ductility or danger of embrittlement during heat-treatment. By combining a relatively high carbon content with 2% silicon, the makers of Super Tricent are reaching for a compressive yield strength in excess of 300,000 psi. Only the future can tell how much of this potential strength of the proposed ultra high-strength alloys the structural engineer will be able to use in practical design.

Beyond 800 F better heat-resistant but costlier materials, such as Inconel X or molybdenum (0.5% Ti), will have to be considered.

A comparison of the effect of elevated temperatures on the specific compressive yield of some of the above mentioned materials is shown in the diagram of Fig. 13. The curves presenting the strength-weight ratio of several aircraft materials were obtained by dividing the 0.2% offset yield by their respective density.

On several occasions lately mention has been made of the possible application of beryllium to aircraft structures. It can readily be understood that a material, which has the same density as magnesium when combined with a modulus of elasticity 50% higher than steel, has great potentials for alleviating some of the thermal problems connected with high-speed flight. Even the present price of $100 per lb would not prohibit its use if the more objectionable features could be overcome. The major deterrents are the scarcity of the metal, its toxicity, and, most important, its extreme brittleness. If these obstacles could be overcome, beryllium compression panels employed in aircraft surface structures could save about 50% of the weight of present materials at all temperatures.

The problem of brittleness brings up a topic which lately is attracting increasing attention from the aircraft designers. The tear resistance of an alloy has become an important property to be considered in the final selection of a material. As a rule, the comparison of different metals in this respect is based on the response of a specimen containing an initial crack to tensile loading. Such comparison for presently available materials has been made in Fig. 14. The critical crack length is related to the maximum gross area stress a damaged panel can sustain. The specific gross stress is obtained after dividing this value by the density of the material. As can be noted, Allegheny metal 350 has far superior tear resistance than highly heat-treated 420 steel; however, its yield strength at 600 F is not very impressive.

Fatigue problems do not seem to be aggravated to a great extent by the thermal environment encountered in high-speed flight. Since the fatigue strength of most aircraft materials decreases more slowly at elevated temperatures than their static strength, structures which are adequate fatigue-wise at room temperature should remain so in thermal surroundings.

Creep is a phenomenon which up to this time has not plagued the aircraft engineer very much. Only recent designs will be capable of flying at speeds where aerodynamic heating increases the temperature of the airframe to such an extent that creep might have to be considered.

Creep is the time-dependent plastic deformation of a metal subjected to heat and prolonged loading. It can occur under tension, compression, bending, shear, and combined stresses.

Basic creep data is determined from a tensile test coupon which is placed in a testing machine and heated to a fixed temperature. By subjecting the specimen to a constant tensile load and recording the resulting elongations at successive time intervals, a typical time-strain curve showing three distinct stages of creep is obtained (Fig. 15). The first stage AB shows a decreasing creep rate due to strain hardening, while during the next phase the creep rate is more or less constant and quite low. This is followed by the third stage CD during which the creep rate increases exponentially, ending in sudden rupture. By changing the intensity of the applied stresses a series of time-strain curves can be determined (Fig. 15). Transplotting this information on a stress-strain relationship, diagrams equivalent to the familiar stress-strain curves are obtained (Fig. 16). Since each curve in this diagram pertains to a specified duration of loading, they are labelled isochronous curves.

It is convenient to plot available constant-temperature, constant-load creep, and rupture data pertaining to the material of interest on a log-log graph (Fig. 16) to facilitate extrapolation. The creep rate based on the secondary stage then indicates the magnitude of the constant stress, which is

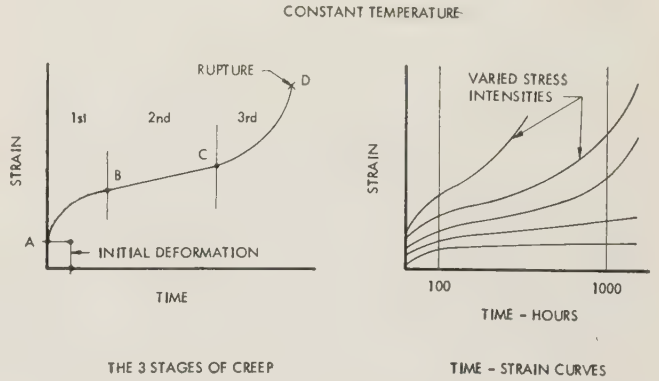

Fig. 15—Tensile creep data of a metal coupon

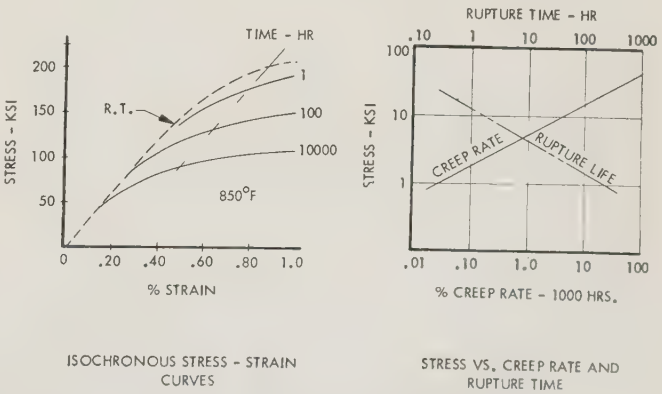

Fig. 16—Required creep design data

Table 2—Nonferrous Materials

	Mechanical Properties						Thermal Properties			
		Room Temperature			600 F (½ hr)					
	Density (γ), lb/in.^{3}	E, 10^6 psi	F_{tu}, ksi	F_{cy}, ksi	E, 10^6 psi	F_{tu}, ksi	F_{cy}, ksi	a, 10^{-6}/ in.-deg F	K, Btu/hr-ft-deg F	Specific heat (c), Btu/lb-deg F	Diffusivity (κ)[a] ft^2/hr
Aluminum 2024 T4	0.100	10.6	65	40	7.9	15	12	12.9	70	0.205	2.00
Aluminum 7075 T6	0.101	10.4	76	68	5.3	8	6	13.1	70	0.205	2.00
Titanium RC130A	0.170	16.0	140	130	13.5	103	82	4.8	6	0.116	0.18
Titanium 6AL-4V	0.160	16.5	180	148	14.7	128	106	4.8	4	0.135	0.10
Inconel X	0.300	31.0	160	115	29.0	135	100	7.6	9	0.105	0.17
Molybdenum 0.5% Ti	0.370	46.0	132	115	45.0	116	104	3.1	68	0.061	1.74
Beryllium	0.066	44.0	125	95	43.0	85	65	6.4	87	0.460	1.66

[a] Formulated as $\kappa = \frac{K}{c\,\gamma}$

Table 3—High-Strength Steel Alloys

	Mechanical Properties						Thermal Parameters			
		Room Temperature			600 F (½ hr)					
	Density (γ), lb/in.^{3}	E 10^6 psi	F_{tu} ksi	F_{cy} ksi	E 10^6 psi	F_{tu} ksi	F_{cy} ksi	a, 10^{-6}/ in.-deg F	K, Btu/hr-ft-deg F	Specific heat (c), Btu/lb-deg F	Diffusivity (κ) ft^2/hr
4130 Steel	0.283	30	188	102	27	162	82	8.0	27.0	0.11	0.50
17-7 Ph (TH1050)	0.276	29	200	160	27	160	130	5.5	9.8	0.12	0.17
17-7 PH (RH 950)	0.276	29	225	180	27	176	150	5.5	9.8	0.12	0.17
AM-350	0.280	29	200	167	29	190	134	7.0	9.4	0.12	0.16
AM-355	0.280	29	220	188	29	208	149	7.0	9.4	0.12	0.16
Stainless W	0.280	30	192	187	28	162	156	5.5	12.1	0.12	0.21
420-Stainless Steel	0.280	29	250	210	27	245	186	5.7	14.4	0.11	0.27

associated with the maximum permissible deformation after a fixed length of time. The rupture life line, on the other hand, specifies the maximum life span during which a structure will sustain a given load-temperature combination before failure occurs.

Full-scale elevated-temperature tests which simulate actual operating conditions extended over the expected service life of the structure are extremely costly and time-consuming. The extrapolation of a simple log-log plot of stress versus rupture time, such as the one pictured in Fig. 16, can quite often be inaccurate and misleading since sudden accelerations in the creep rate cannot be predicted. Efforts were, therefore, made to formulate a time-temperature relationship for rupture and creep stresses which would permit the determination of specific long-time data from comparatively short tests at a higher temperature. Larson and Miller[7] have suggested the use of the following equation:

$$T\ (20 + \log\ t) = \text{contant} \qquad (20)$$

In this well-known formula T denotes the temperature (deg R) and t is the rupture time in hours. From the rupture test of a specimen subjected to a fixed stress for a specified time-temperature combination, it is now possible to compute other combinations which will result in an equivalent rupture stress. The same relationship can be used to determine the time-temperature combinations which are associated with a specific creep rate of a material. By adding the elastic strain, the time-independent slip strain (instantaneous plastic deformation), and the time-dependent creep strain the total deformation of a structure can be determined at any stage of its service life.

Creep can become a very important factor in the life of supersonic interceptors whose flight missions frequently include a speedy acceleration to high Mach numbers and a supersonic dash, followed by rapid decelerations. Care must be taken that after such maneuvers no plastic deformations of appreciable magnitude remain in the supporting structure, which might progressively accumulate and result in sudden catastrophic failure with little or no warning.

The evaluation of the effects of creep in an assembled structure is a very complex problem, due to the high redundancy of aircraft components. A procedure similar to that used in testing the fatigue life of a structure might recommend itself.

Dow[8] claims that the effects of creep will be significant only in rare cases for aircraft designs contemplated for the immediate future, due to intrinsic stress relaxation within the structure.

Mechanical properties and relevant thermal parameters for nonferrous metals and high-strength steel alloys are listed in Tables 2 and 3.

Sandwich and Other Types of Panels—Recent developments have shown that by proper alloying and by using improved heat-treat cycles some steels can be processed to much higher strength than it is customary today. Laboratory research indicates that the increased strength is not necessarily associated with dangerous brittleness and that in a not too distant future satisfactory sheet stock might be available with a guaranteed minimum tensile strength exceeding 350,000 psi. But how can the aircraft designer take advantage of this large increase in strength? The possibility of weight savings in forgings and fittings is obvious. However, a large percentage (about 60%) of the structural weight of the airframe is absorbed by the surface panels of the fuselage and wings, which have to be properly stabilized before they can be subjected to extreme compressive loading.

In the majority of cases, the load indices pertaining to the surface structure of aircraft components are rather low, resulting in thin gages for the skin panels. Conventional structures with stringers or

[7] ASME Transactions, Vol. 74, July, 1952, pp. 765–775: "Time-Temperature Relationship for Rupture and Creep Stresses," by F. R. Larson and J. Miller.

[8] *Aeronautical Engineering Review*, Vol. 15, November, 1956, pp. 61–66: "Re-Evaluation of Some Air Frame Thermal Problems," by N. F. Dow.

ribs spaced sufficiently close to realize maximum compression allowables are likely to prove either costly to make or impracticably heavy. As a matter of fact, their weight becomes prohibitive when dealing with the thin skin gages so frequently associated with the use of ultra-high-strength alloys. One way to overcome the higher density disadvantage of heat-resistant materials by realizing high compression allowables in the skin surface, is the use of sandwich construction which permits the load-carrying material to be distributed so as to provide optimum strength and stiffness for a given weight.

There are many types of sandwich panels either commercially available or in the experimental stage. It is not the intention to give at this time a complete review of the present state of the art. The two principal design configurations, which in the near future are seriously being considered for thermal flight, have either cellular cores (honeycomb, squarcel, and the like) or corrugated cores. The cellular cores are formed from thinly rolled metal foil of 17-7PH steel or similar alloys and welded together at the cell nodes. The bond between core and facing is achieved by furnace brazing or resistance welding. The corrugated cores consist of thin sheets which are formed in sinusoidal or trapezoidal shapes. As shown in Fig. 17, this type of core may be used in one or more tiers and, at times, is preferred because the corrugations contribute to the load-carrying area of the panel. Also shown in the same figure is a recent innovation manufactured by the Ferro-Therm Co. of Cleveland. This sandwich, known as Truss-Core panel, consists of two face sheets which are stabilized by a core of interlaced truss-shaped wires.[9] The individual wire trusses, forming the core matrix are spaced about 1 in. c to c in the longitudinal and transverse direction and are furnace braced to the facings.

Sandwich panels are ideally suited for high-performance aircraft since they preserve an accurate outside contour and are not given to quilting under pressure loads. Weight-wise, a sandwich panel has a large effective thickness due to the low density of the core and thus needs fewer internal supports, making it a better enclosure for fuel compartments. Optimum design studies indicate that it is advisable to use a minimum of supports and to determine the lowest core density which will attain the compressive yield stress in the face sheets. The cell size must be small enough to prevent local buckling of the facing within the confines of the cell boundaries. Good bonding between core and facing should at the least be able to realize compressive yield stresses in the surface skins. Higher loadings in the surface skins usually result in failures, with the sandwich facings buckling into the core by forming a transverse wrinkle.

The major advantages of steel sandwich panels are:

1. The possibility of stabilizing thin sheets at very close intervals in an efficient manner, thus realizing high-compression allowables in the facings without the addition of excessive parasitic weight.

2. The high weight-strength ratio of sandwich panels as compared with solid plates or skin-stiffener combinations.

3. The aerodynamic smoothness and rigidity of the finished assembly.

4. Excellent fatigue characteristics.

In spite of their many good points, the theoretical potentials of high-strength steel sandwich panels have not been fully exploited at this time, because of fabrication difficulties and the reasons mentioned below.

The principal deterrents to the use of high-strength steel sandwich panels at present are:

1. Lack of adequate facilities and production know-how which would guarantee the structural integrity of the final product. No brazing furnaces of sufficient size are available today to accommodate large panels and no company has as yet been successful in fabricating any but the simplest configurations at reasonable cost.

2. Excessive cost of manufactured panels. Present quotations run anywhere from $150 to $1500 per sq ft prior to installation for brazed or resistance-welded steel honeycomb panels.

3. The complicated details required at splices and points of attachment. Satisfactory solutions which will guarantee reliable load transfer at these points have yet to be devised. Present designs are usually too costly, too heavy, or impractical in regard to meeting close tolerances. In making weight estimates of panels, it is necessary to add between 40 and 80% of the facing weight for splices and attachments.

4. The questionable quality of the bond between core and facings. While tests have shown that it is possible to realize yield strength or even higher allowables in the facing material of brazed sandwich panels, a report[10] indicates an alarming inconsistency in the failure loads of test specimens. It seems that out of a series of 12 specimens only one gave satisfactory results, while several others failed at much lower loads, one as low as 15% of the predicted strength.

In spite of the overoptimistic claims of some vendors, high-strength steel sandwich panels, adequate for highly loaded primary applications, are still in the experimental stage. Extensive research and development programs are required before complicated sandwich configurations can be incorporated in actual production designs. For the time being, it seems that other maybe less efficient but pres-

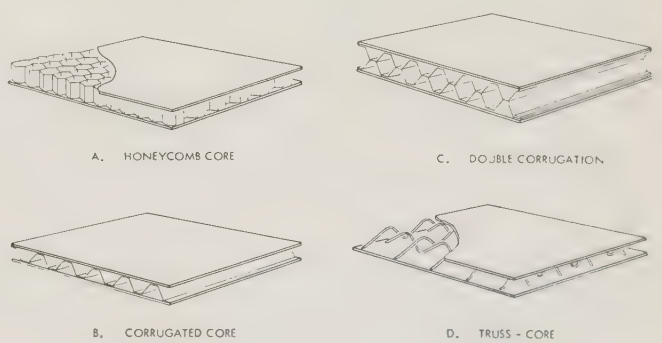

Fig. 17—Types of sandwich construction

[9] "Structural Evaluation of a Truss-Core Sandwich Panel," by A. F. Ensrud. Report 11,318, Lockheed Aircraft Corp., Burbank, Calif., May, 1956.

[10] WADC Technical Report 55-417, September, 1956, "Performance of Stainless-Steel Sandwich Construction at High Temperatures," by V. C. Setterholm and E. W. Vuenzi.

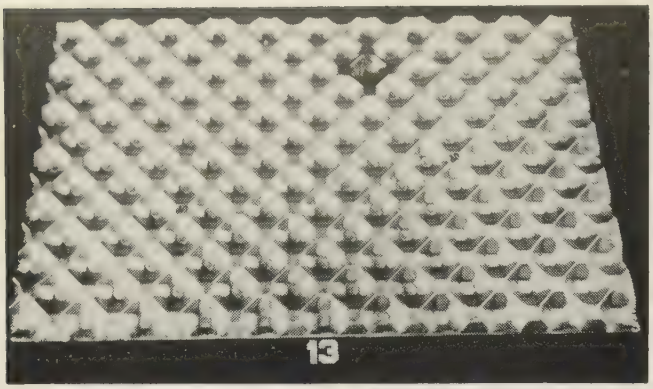

Fig. 18—Waffle pattern of unicore configuration

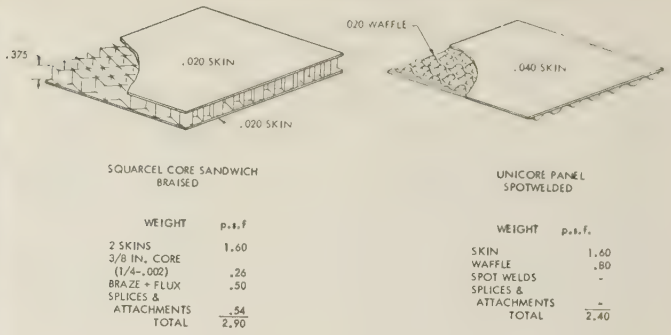

Fig. 19—Weight comparison of steel panel

ently available configurations such as machined waffle-grids or chem-milled panels, will have to be used.

In this connection, it may be of interest to mention the Unicore construction which was developed some time ago by our company. This combination consists of a die-formed wafflelized sheet which is spot-welded at close intervals to a flat or curved skin panel. Fig. 18 shows the pattern of embossing used in the orginal design of the Unicore configuration.

A weight comparison between a brazed sandwich and a similar panel of Unicore construction is shown in Fig. 19. The brazed sandwich is 17% heavier than the Unicore panel, mostly due to the excessive weight of the braze and flux. A resistance-welded sandwich panel would be somewhat lighter due to a saving in the bonding material.

While Unicore panels are not as efficient in regard to overall strength and stiffness as true sandwich panels, their economical fabrication and easy assembly recommend them for immediate application.

Thin Wing Structures—Of foremost interest in the design of future fighter aircraft is the possible application of heat-resistant alloys in the surface structure of wing and fuselage. While many types of design configurations are suitable for wing structure of subsonic airplanes, in thermal flight the choice should be limited to the following surface configurations: integral panels, machined or chem-milled; sandwich panels, brazed or resistant-welded; face to face stabilization by cellular cores or truss-cores; and unicore construction.

A typical example of the last design configuration is pictured in Fig. 20. By combining a chem-milled waffle-grid with a wafflelized Unicore panel, the interattachment buckling stress in the skin panel is greatly increased, making the overall efficiency of the surface structure very attractive. Furthermore, the use of aluminum spars provides additional weight savings by reducing the transient thermal stresses. Assuming instant accelerations to Mach 3 and neglecting probable reductions due to the high diffusivity of the light-alloy spars, the maximum thermal stresses reached during the transient stage are conservatively estimated at the values shown in Fig. 20.

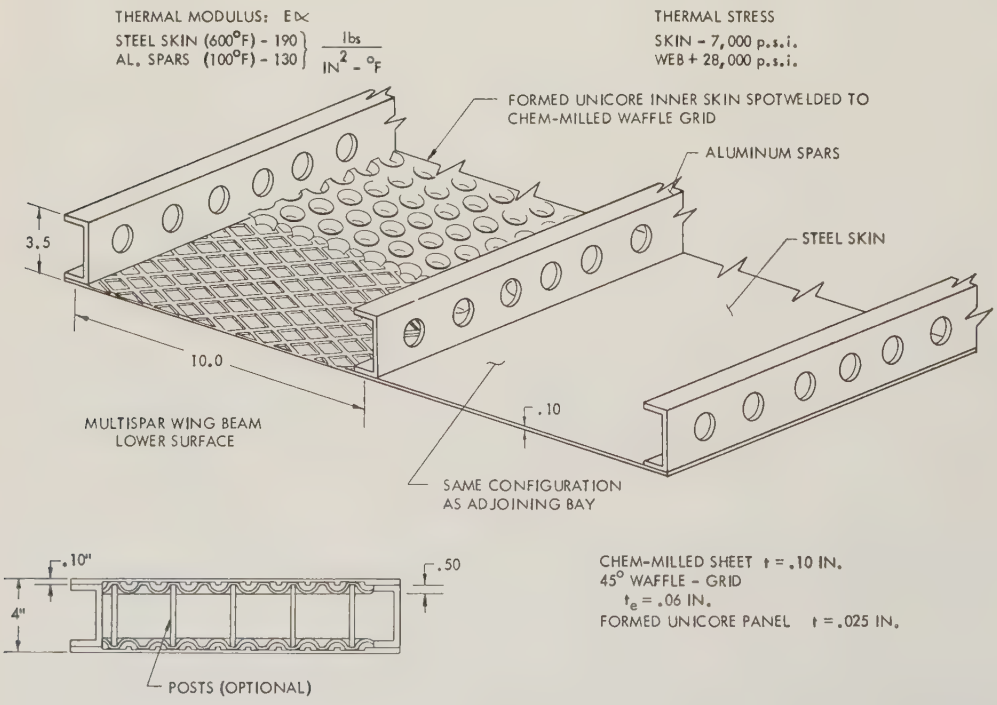

Fig. 20—Unicore construction

CHEM-MILLED SHEET t = .10 IN.
45° WAFFLE - GRID
t_e = .06 IN.
FORMED UNICORE PANEL t = .025 IN.

Fuselage Shells—Stiffened shell structures of conventional design are not suited for fuselages of ultrasonic fighters or missiles, whenever aerodynamic requirements demand a smooth surface contour. Due to the extremely low loading indices encountered in the design of shell structures for the above mentioned vehicles, economical nonbuckling configurations can be realized only by the use of sandwich-type structures. Distributing the small amount of material, required to sustain the bending and shear loadings, around the circumference of the shell results in rather flexible structures, which only by the addition of an appreciable amount of parasitic weight can be prevented from local instability even when constructed from light alloys.

How little material is actually required for a fuselage enclosure can be gathered from the fact that minimum strength requirements for the aft body of the Electra transport airplane call for an average effective shell thickness of only 0.075 in. This value includes the skin thickness to which is added the distributed weight of the stringers and fuselage rings. In steel construction of corresponding weight, the effective skin thickness would equal 0.027 in. Only sandwich construction could try to realize a competitive figure.

Ring-stiffened fuselages for interceptors built from light alloys use, as a rule, skin gages varying between 0.025 and 0.040, supported by Z-shaped rings spaced 6 in. c to c . Here again, only sandwich construction can furnish an economical design whenever thermal and aerodynamic requirements demand a nonbuckling steel shell. During the interval until sandwich panels in double curvature will become available, a resort to Unicore construction might prove worthwhile.

The major features an acceptable fuselage design, suitable for thermal flight at high Mach numbers, should possess are:

1. Light weight.
2. A nonbuckling skin surface.
3. Satisfactory Tear-resistance.
4. An assured overall torsional stability of the fuselage structure.

Fig. 21 shows the application of Unicore configuration in the design of a cylindrical fuselage in contrast with a ring-stiffened sandwich shell. Only actual designs worked out in detail would permit an intelligent weight comparison.

Since loading parameters are usually very low for this type of fuselage, no great difficulty should be encountered in attaching the Unicore panel to the skin in an efficient manner. Bending loads are, as a rule, resisted by longerons, so that only torsional buckling of the skin panels might become critical. The convenient formula given in Fig. 21 should be helpful to check the panel buckling strength under shear for a ring-stiffened fuselage.

Actual tests have proven that the fail-safe characteristics of Unicore construction are far superior to those of conventional design.

The high density of heat-resistant alloys resulting in thinner gages of the structural element makes it mandatory to make a careful check of the overall fuselage structure for torsional instability. Formulas pertaining to the torsional stability of monocoque cylinders and ring-stiffened sandwich shells are given in Fig. 22. A not yet published extension of a simplified method of solving a system of difference equations, which has been[5], explained in detail permits the writing of neat closed-form expressions for this intricate problem.

Production Problems

The change-over from light alloys to any of the denser high temperature materials will be accompanied by a multitude of production problems. The aluminum industry, thanks to extended know-how and tremendous production facilities, was able to supply the airframe constructors with a number of most satisfactory products. Taken for granted are large sheets and plates, 48–72 in. wide and 30 ft or more in length, heat-treated as the source and de-

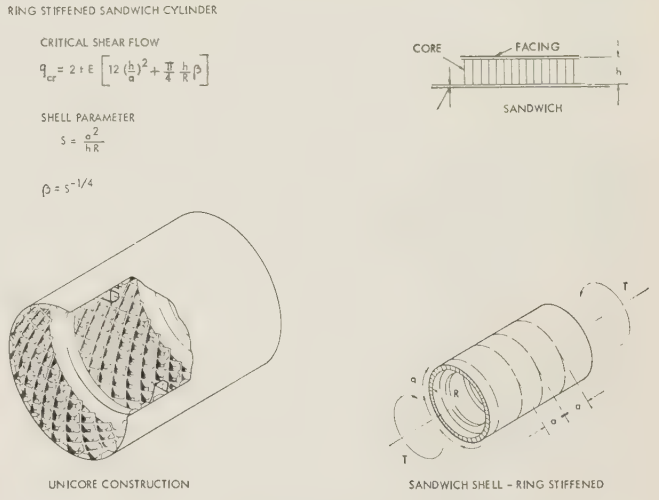

Fig. 21—Bi-lateral stiffened cylinders

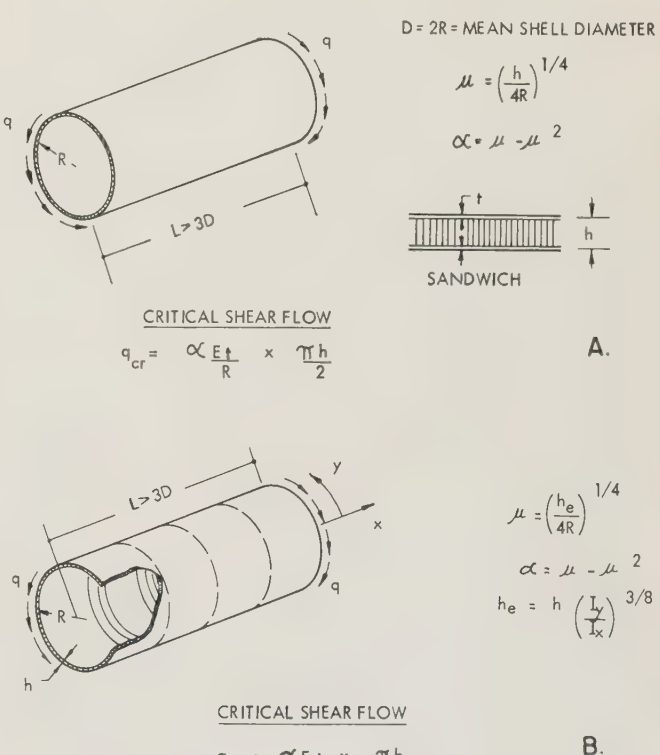

Fig. 22—Torsional instability of:
A—a long cylinder of monocoque sandwich construction
B—a long ring-stiffened sandwich shell

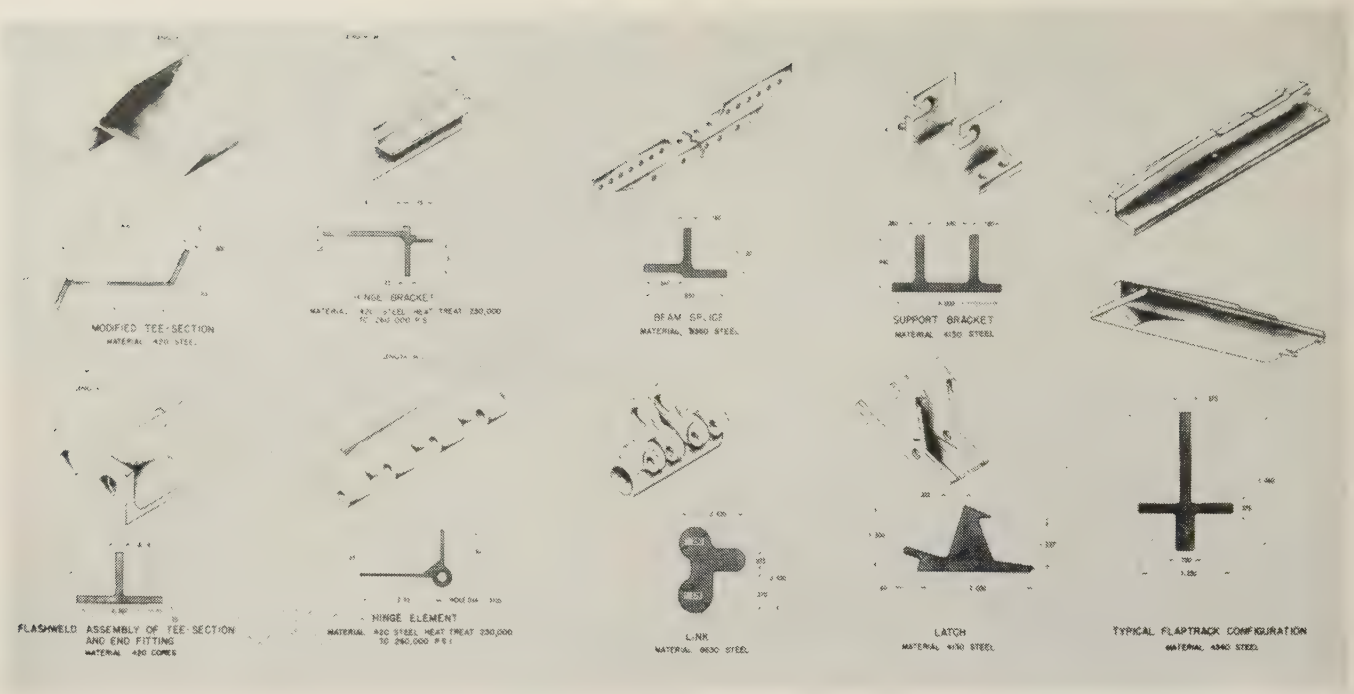

Fig. 23—High-strength steel extrusions, typical extrusion designs

livered to the shop with minimum out-of-flatness tolerances. In addition, there are available large precision forgings and extrusions, as well as accurate dependable castings produced and guaranteed by several large companies in the light-metal industry.

Unfortunately, not any of the heat-resistant alloys has reached this state of the art yet. The steel industry is probably the one exception which in the near future would be able to meet the severe tolerance requirements demanded by the aircraft engineer. Excessive parasitic weight due to too liberal tolerance margins cannot be permitted in our next breed of fighter aircraft, where a single lb of useless weight may require 10–15 lb of additional airframe, fuel, or engines to carry it without change in performance. Based on a realistic cost figure of approximately $100 per lb for the delivered steel airplane, an initial increment of 1 lb of unnecessary weight may increase the cost of the final product by more than $1000. Under these circumstances, it seems justified to spend substantial amounts for improved machine tools which would enable the production department to realize an irreducible minimum of parasitic weight in the final parts. Naturally, similar considerations apply to the products of rolling mills and to the suppliers of forgings, extrusions, and castings.

Aside from the light-alloy industry, only the steel companies have the required experience in manufacture, processing, and fabricating techniques of their material. In addition, sudden demands for large production quantities would tax neither their huge pool of skilled manpower nor their extensive plant facilities.

Another important matter is the development of a suitable alloy which will retain a high-yield strength under sustained thermal exposure without being handicapped by excessive brittleness. A great number of new alloys with highly intriguing names (Hot-Form, Hy-Tuff, USS Strux, Super Tricent) have been devised for special purposes and applications with little regard to the overall picture. It might take the combined efforts of the aircraft companies, the steel industry, and the Government to find proper alloys which would minimize the weight penalties due to higher density and thermal effects. According to present information, many years will pass before titanium can seriously enter the picture. This opinion, however, is not shared by all companies.

Fabrication—After the steel sheets, forgings, castings, extrusions, and other semifinished products supplied by the various vendors arrive at the plant of the airframe constructor, much additional work must be done before they can be joined together into the final airplane. Expensive equipment and advancements in the state of the art are required to accomplish this job in an efficient and economical manner.

Sheets and plates have to be cut to shape, stretched, drawn or joined, then hardened and cleaned prior to the assembly. Tapered sheets may have to be ground or sanded to be economically feasible.

Controlled heat-treatment without resulting warpage and embrittlement poses another serious challenge. New cycles with intermittent stretching operations have shown some promise in this respect. Parts made at our plant from material treated in this manner were very accurate as to contour and fit and could even be dimpled for riveting in spite of a heat-treatment equal to 250,000 psi.

Better and more economical cleaning methods must be developed to remove surface corrosion and oxide film caused by the various heat-treat operations without embrittling the material.

While at present hot extruding of steel aircraft shapes is limited to small sections falling within a 7-in. diameter enclosure, future possibilities are indicated by a few practical applications portrayed in Fig. 23. Further study is required, however, to pro-

duce extrusions with closer tolerances in order to reduce material waste and machining cost.

An extensive program is proposed by our company to investigate the merits of flashwelding in the fabrication of structural angles, tees, integral stiffened panels, or intricate fittings from superstrength steel alloys. Considerable experience is already available in flashwelding larger structural components and it is quite possible that the superior joint efficiency might make flashwelding a significant method of assembling stiffening elements.

Methods of Attachment—1. Rivets and bolts: Because of the higher strength of steel as compared to aluminum, much thinner gages will be used, a fact which adds to the stress concentrations around rivet holes. Thermal redundancy results in the transfer of appreciable shear forces across the surface structure-web junctions, in addition to the thermal stress built up along the length of riveted joints. If small diameter rivets of low shear strength are used to join heavy sections, the thermal stresses alone may fail the rivets.

No wonder an increased number of engineers feel that in future designs of airplanes subjected to sustained thermal flight rivets and bolts are on the way out. In the meantime, however, it still will be necessary to attach highly stressed surfaces adequately to the substructure and to be able to transfer substantial thermal shear loads through the connections. We are presently engaged in studying various ways to upset rivets of high-strength titanium and supersteel alloys. Two methods under investigation are:

1. Instant heating, forming, and cooling of the entire rivet without affecting its temper.
2. Rapid local heating and forming of the end of the rivet shank without reducing the initial strength in the shear plane of the rivet.

2. Adhesive bonding: The primary advantage of adhesive bonding is the simplicity of the process. Satisfactory bonding can be achieved at low temperatures, reducing the possibilities of warpage or change in the material properties of the component parts. The process also permits the joining of dissimilar materials, automatically providing a safeguard against galvanic corrosion. In comparison with riveted or bolted joints, adhesive bonding is leakproof and not susceptible to stress concentrations. The successful application of adhesive bonding technique to cellular-core sandwich panels is well-known. In thermal flight, the major problem is to develop adhesive films which will withstand the ever-increasing temperature to which supersonic aircraft is exposed.

Postcured epoxy-resin adhesives show fair bond strength at temperatures up to 250 F. New adhesives developed in this country by North American Aviation and Minnesota Mining and by Aero Research Ltd. in England promise 50% of room-temperature shear strength at 650 F. At higher temperatures, other methods like riveting, welding, or brazing will have to be used.

Brazing: In spite of the problems which are, by nature of the process, associated with intense furnace heating and subsequent cooling, joining by brazing appears to be the answer to the fabrication of many types of sandwich panels. Theoretically, the process is very attractive; however, many practical problems remain to be solved. To assure at least some degree of success in manufacturing this type of assembly, very careful production and inspection control must be maintained. Separate departments have to be established where the process can be carried out with clinical cleanliness, workmen must wear gloves, and each individual part should be protected against possible contamination. After assembly, the continuity of bond must be ascertained by 100% radiographic inspection. Noting the many additional problems encountered in the manufacture of brazed sandwich panels[11], it is understandable that sometimes out of a batch of 15 panels as few as three pass final inspection. This fact, naturally, is reflected in their present market price. Present plans to start large-scale facilities and experimental operations should be successful in solving many of these problems.

Spotwelding: The cheapest method of joining steel sheets in aircraft structures is by the process of spotwelding, provided proper equipment and monitoring during the process reduces the required radiographic inspection to less than 10% of the spotwelds. Unicore construction lends itself admirably to this process. However, resistant-welded sandwich panels must still be considered in the experimental stage. The John J. Foster Mfg. Co. of Santa Ana, Calif. and the Budd Co. of Philadelphia, are making great strides in developing proprietary designs for resistant-welded sandwich panels. The greatest deterrent to their success is the tremendous cost involved in proving the structural integrity of new configurations when applied to intricate design problems.

Ultrasonic Welding—Ultrasonic welding is a method for joining similar or dissimilar metals by introducing elastic vibratory energy into the area of the components to be bonded. The metallurgical bonds produced by this ultrasonic sheet-to-sheet welding process obtain the same order of shear strength as with the older technique of high-pressure welding. The process is still very much in the experimental stage. Several attractive features associated with this procedure seem to warrant further development of the method. Ultrasonic welding requires no heat and uses lower applied static compression. Hence, the resulting deformations at the surfaces, where the pressure is applied, are relatively small. The internal plastic flow which occurs during the process at the interface and the absence of heat during welding are responsible for less local brittleness in the weldment. Surface cleanness and the absence of surface films are not nearly as important as in resistance welding in obtaining a satisfactory bond.

Conclusions

The material presented in this paper is, to a large degree, the result of studies made at our laboratory. Some theoretical information was taken from scattered sources to be found in current literature in a few instances almost verbatim. (See Additional References.)

Definite progress seems to have been made in the past few years in understanding the problem of aerodynamic heating and the resulting effects on the structural integrity of the airframe. In the

[11] "High-Temperature Sandwich Structure, Present State of Development and Outlook for the Future," by H. M. Rush. Paper presented at SAE National Aeronautic Meeting, Los Angeles, October, 1956.

range of immediate interest, that is, Mach 3 or Mach 3.5, it is most likely that a change to more heat-resistant material will become mandatory. How far the application of heat sinks or a stabilization of the boundary layer can help in retaining the use of light alloys can only be guessed at the present time.

It has been shown that by taking advantage of several alleviating factors and by a prudent choice of more suitable materials and their optimum structural utilization, as in steel sandwiches, some of the problems associated with thermal flight can be greatly reduced. While, in the beginning, there might be a multitude of new problems for the designer as well as the production engineer, all indications point to the fact that they will be mastered in proper time and that, through the combined effort of the aircraft industry and the governmental agencies, the so-called thermal barrier shall gradually be pushed ahead.

APPENDIX I

Terms and Definitions of Heat-Transfer Problems

Adiabatic wall temperature: Actual temperature of the boundary layer at the solid boundary, assuming no heat flow across the interface between the air and surface of moving body.

Ambient temperature: Undisturbed free-stream temperature of the atmosphere at a given altitude based on a ICAO standard day.

Conduction: Heat transfer by molecular agitation, predominantly in solids.

Convection: Heat transfer by circulation or mixing of the medium, exclusively in liquids or gases.

Diffusivity: Thermal conductivity of a substance divided by its capacitance, sometimes called the thermometric conductivity.

Emissivity: Ability of a surface to radiate energy as compared with that of a "black body" which has an emissivity of 1.0 at a given temperature.

Equilibrium temperature: Temperature of the structure when heat input is balanced by amount of heat being removed per unit of time.

Radiation: Heat transfer (electro-magnetic) through a nonabsorbing medium, like a vacuum or gases.

Recovery factor: Coefficient indicating the heat loss within the boundary layer.

Specific heat: Amount of heat required to raise 1 lb of substance 1 F.

Stagnation temperature: Temperature of a moving fluid brought to rest at a solid boundary without exchange of heat.

APPENDIX II

Notation

E = Modulus of elasticity
E = Effective modulus of elasticity
E_s, E_t = Secant, tangent modulus
F = Applied stress or Fahrenheit
F_E, F_{tu} = Euler, ultimate tensile stress
K = Coefficient of thermal conductivity
M = Mach number
T = Temperature

b = Support spacing
q = Heat flux or shear flow
t = Skin thickness or time
u = Convective heat-transfer coefficient
α = Coefficient of linear thermal expansion
η = Plasticity reduction factor associated with tangent modulus

Subscripts refer to:

cy = Compressive yield
i = Inside of surface skin
o = Exposed surface of skin
sk = Surface skin
w = Web of wing spar

Additional References

1. Proceedings of the Third Anglo-American Aeronautical Conference, Brighton, England, September, 1951: "Structural Problems of Future Aircraft," by N. J. Hoff. Also reported in *Engineering,* Vol. 172, Nov. 2, 1951, pp. 573–575.

2. Proceedings of the Third General Assembly of the Advisory Group for Aeronautical Research and Development of the North Atlantic Treaty Organization, London, September, 1953: "Structural Effect of Aerodynamic Heating," by N. J. Hoff.

3. "Thermal Barrier—Structures," by N. J. Hoff. Paper presented at ASME Annual Meeting, New York, November, 1954.

4. *Journal of the Royal Aeronautical Society,* Vol. 60, June, 1956, pp. 402–407: "Engineering Approach to Some Structural Problems Arising from Kinetic Heating," by E. H. Bateman.

5. *Aircraft Engineering,* Vol. 25, February, 1953, pp. 51–53: "Alleviation of Thermal Stresses," by E. W. Parkes.

6. *Aircraft Engineering,* Vol. 25, December, 1953, pp. 373–378: "Transient Thermal Stresses in Wings," by E. W. Parkes.

7. *Materials and Methods,* Vol. 43, March, 1956, pp. 94–98: "Ultra-High-Strength Steels, Present and Future," by J. W. Sands, and O. O. Miller.

8. Rand Corp., Report R-222, July, 1952: "Weight-Strength Analysis of Aircraft Structures," by F. R. Shanley.

9. *Product Engineering,* Vol. 24, October, 1953, pp. 129–141: "Ultra-High-Strength Steel for Aircraft Structures," by M. A. Melcon.

10. *Materials and Methods,* Vol. 44, November, 1956, pp. 120–123: "How to Use Creep Data in Design," by W. F. Simmons.

11. "Problems in the Design of Aircraft Subjected to High Temperatures," by F. R. Steinbacher and L. Young. Paper presented at ASME Annual Meeting, November, 1954.

12. *Journal of the Aeronautical Sciences,* Vol. 23, April, 1956, pp. 289–329: "Some Structural and Aeroelastic Considerations of High-Speed Flight," by R. L. Bisplinghoff.

13. Rand Corp. Report P-489, March, 1954: "Method for Determining the Effects of Elevated Temperature on Structural Design and Weight," by W. R. Micks.

14. WADC Technical Report 55-305, October, 1955: "Structural Design for Aerodynamic Heating," W. H. Dukes and A. Schnitt.

15. "The Hot Airplane Challenges Material Suppliers," by G. W. Papen. Symposium on Manufacturing Problems, Wright-Patterson Air Force Base, April, 1956.

16. Lockheed Aircraft Corp. Report 9655, January, 1954: "Aerodynamic Heating and Aircraft Structures," by L. Young.

The Beam Strength of Modern Gear-Tooth Design

B. W. Kelley and R. Pedersen, Caterpillar Tractor Co.

This paper was presented at the SAE Earthmoving Industry Conference, Peoria, Ill., March 26, 1957.

SINCE the advent and failure of the first wooden gear, designers of power-transmitting equipment have searched for the greater accuracy in their work which would enable them to produce higher capacity gears, capable of keeping machines operating in, on, and off the surface of the earth. The ability of an engineer to design a gear tooth is based on his knowledge of the principles involved in structural failure. Widespread, however, are the opinions of gear engineers who, on the basis of experience, "select" a higher pressure angle, a larger fillet radius, or a longer or shorter addendum ratio with the hope that it will solve the pressing problems of new production models or horsepower increases.

We are familiar with the serious concern of the researcher on such subjects as notch sensitivity, residual stress effect, dynamic loadings, and the like, which all influence the apparent strength of gears. To some degree, the recognition of these numerous factors tends to muffle the interest or curiosity in design accuracy improvement. Fortunately, this is not the case with the engineer who actually has the burden of responsibility in the design. Indeed, disputes have arisen over differences of less than 3% in design calculations; whereas, the unknown values amount to much more than this. This effect of geometry on heat-treatment alone may be sufficient to overshadow these efforts. However, the designers' feelings are not to be underestimated but rather encouraged, for increased accuracy from any standpoint narrows the fields of the general problem of beam strength in gears. Such a design analysis is the subject of this paper.

Present Formulas

About 65 years ago, Wilfred Lewis[1] published the first analytical examination of gear teeth. Even now, his original formula is widely used, not withstanding the investigations of such men as Dolan and Broghamer, R. B. Heywood, H. Glaubitz, and others, who have added much to the subject. Dolan and Broghamer[2] have greatly influenced the use of the Lewis formula by means of a stress-concentration factor or, more properly termed, a stress-correction factor based upon their own photoelastic work of 1942. This combined formula, which is generally referred to as the modified Lewis formula, is the most widely used in the United States today.

The arrangement of the Lewis formula is, or can be, universally applied to all symmetrically shaped projections. However, its inaccuracy became apparent by the work of Dolan and Broghamer, who made corrections for pressure angle, fillet radius size, and other geometrical characteristics. Since their photoelastic work was based on 14½- and 20-deg pressure angle gears, we started a series of photoelastic examinations on gears having higher pressure angles with the object of obtaining another stress-correction formula for 25-deg pressure angle.

This work was done with the encouragement and help of Prof. Broghamer; the mounting of specimens and photoelastic pictures, both isochromatic and isoclinics, were made under his direction at the University of Illinois. We are indebted to him for his exactness, care, and expert advice on photoelastic technique.

Our photoelastic models were made of Columbia Resin CR-39 and had a tooth size of 2 pitch and thickness of approximately ¼ in. Correction for exact thickness was made with a micrometer on each model. They included three teeth, as shown in

THIS paper includes a somewhat critical review of formulas and methods for determining the beam strength of gears now being used.

The authors describe what they consider to be a new, more accurate approach to this problem. It is based on photoelastic work, combining the best features of two existing methods. Some data from actual gear test runs are shown verifying the accuracy of the new solution.

[1] Proceedings of the Engineers' Club, Philadelphia, 1893: "Investigation of the Strength of Gear Teeth," by Wilfred Lewis.

[2] "Photoelastic Study of the Stresses in Gear Tooth Fillets," by T. J. Dolan and E. I. Broghamer. University of Illinois Engineering Experiment Station Bulletin No. 335, 1942.

Fig. 1, and had a single mounting hole. The center tooth was the only one loaded. Restraint for the turning moment was by means of a flat bar following the straight-edge back of the model The mounting hole and the straight-edge mount were sufficiently far from the root radius to avoid fringe influence.

Manufacturing of such models is not accomplished without some difficulty. Ours were band-saw cut to within 1/16 in. of the true profile and finished with a small high-speed rotary file in sufficiently light cuts to avoid heating. The models were examined with polaroid film after finishing to make sure no residual stresses existed. Unfortunately, with such materials the models are affected by time, temperature, and humidity. It was found that the handling of such models on warm, humid days increased the residual-stress formation tendencies. Machining of the models started in the afternoon and left our plant by special delivery, arriving at Prof. Broghamer's office the following morning where they were given an additional residual stress examination and, if found to be free of such stresses, were loaded immediately. Calibration bars were cut close to each model and accompanied them for fringe calibration under pure bending.

Care was taken in loading to assure only elastic straining by restricting load to the development of less than eight fringes and by examining the specimen for residual stresses after each load application. The load arm was pivoted on a bearing some distance from the contact area so that the deflection of

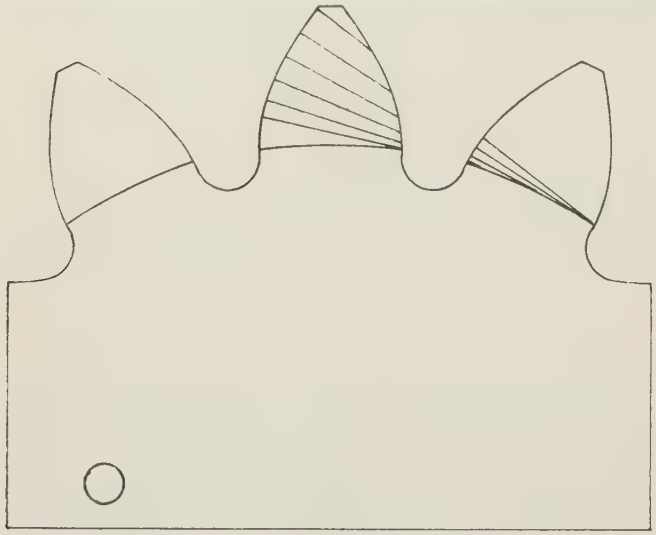

Fig. 1—Caterpillar photoelastic model

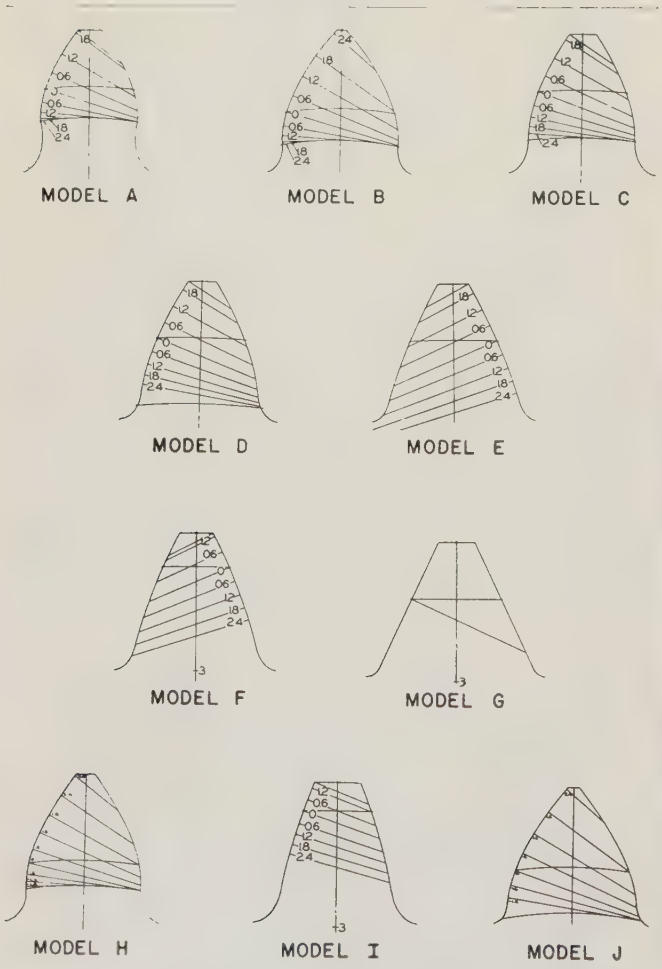

Fig. 3—Tooth shapes of Caterpillar photoelastic models

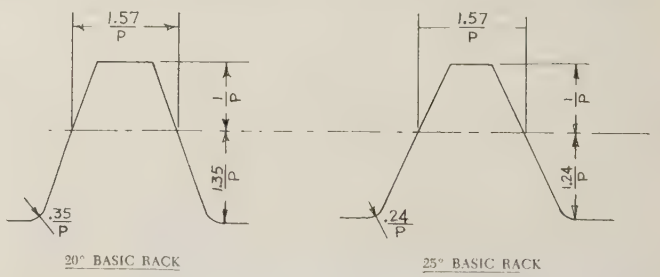

Fig. 2—Generating rack dimensions of models

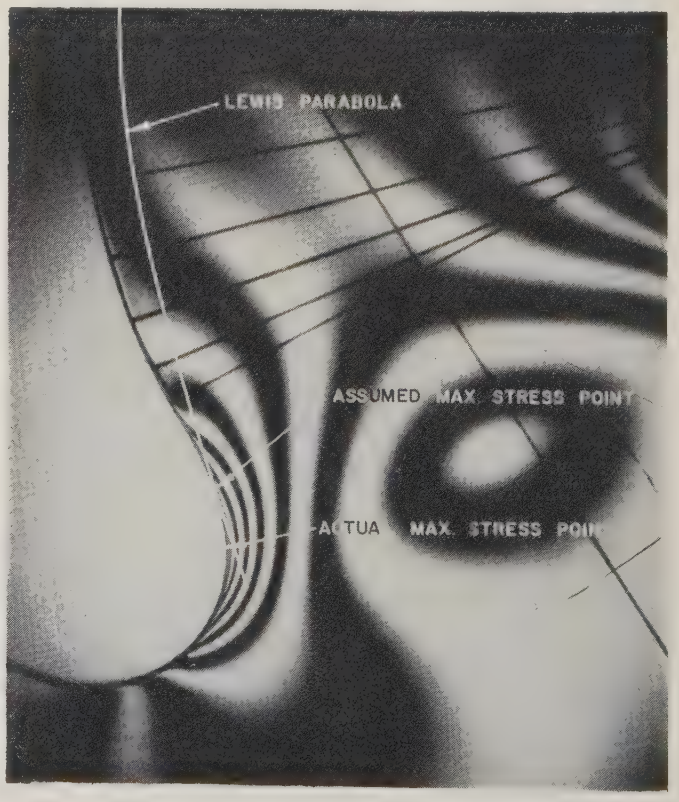

Fig. 4—Error in maximum stress point location

the tooth would not introduce a frictional component of force of any significance on the surface. A small celluloid shim 0.075 in. thick was inserted between the end of the load arm and the model surface to assure reasonable contact area distribution with a well-defined maximum-load application point. The alignment of the model and the load arm were accomplished with the help of accurately scribed lines at each loading point, normal to the surface and, therefore, tangent to the base circle on each model. Upon completion of loading, the photographing of isochromatics, and the drawing of isoclinics, model and data were returned to our research department for analysis.

As will be noted in the data of Table 1, we had purposely selected a variety of addendum ratios for examination. All model shapes were made from generating rack dimensions, as shown in Fig. 2. Our selection of geometries, therefore, included a large number of tooth shapes (Fig. 3).

Since the models were principally of 25-deg pressure angle to start with, our initial attempts were to arrive at a stress-correction factor following the form laid out by Dolan and Broghamer in their work with the 14½- and 20-deg pressure angles. It was found, early in our work, that reasonable correlation of the Dolan-Broghamer type of stress-concentration factor could be developed for a few of the gears, particularly those having the higher numbers of teeth. But the error increased at alarming rates for the smaller numbers of teeth. The conclusion of this attempt was that something was basically missing in the Lewis approach.

The historical use of a method is a strong influence to retain it regardless of its errors, but the discrepancies could not be easily ignored. One of the most serious was found in the position of maximum stress (Fig. 4). Whereas the determination of the weakest section by the Lewis parabola was at one place (Fig. 5) the maximum stress occurs somewhat below. Furthermore, it was noted that the Dolan-Broghamer stress concentration was calculated by use of the minimum fillet radius which occurs at the bottom of the trochoidal fillet of a generated tooth, again some distance away from the maximum stress area. On modern gears with full tip radius of the generating tool, the difference between this radius and the instantaneous generated radius can be quite large. In a way then, Dolan and Broghamer used an ineffective radius in attempting to correct the stresses in the wrong area. This is one of the major reasons for the more proper use of the term "stress correction" instead of "stress concentration."

Detaching ourselves from the method, we learned of the work primarily intended for straight-sided projections by R. B. Heywood.[3] In his paper, a suggested method of inserting an equivalent straight-sided projection in a gear tooth form was presented. Dr. Heywood's formula included all of the necessary components for a more theoretical approach to the

[3] Proceedings of Institution of Mechanical Engineers, Vol. 159, 1948, pp. 384–398: "Tensile Fillet Stresses in Loaded Projections," by R. B. Heywood.

Table 1—Photoelastic Gear Models Used in Tests

Model Designation	Number of Teeth	Pressure Angle, deg	Addendum Diameter Pitch Ratio	Load per In. of face width, lb
		Tested by Caterpillar		
A	12	25	1.0	400
B	12	25	1.4	400
C	18	25	1.0	400
D	25	25	1.0	400
E	50	25	1.0	400
F	50	25	0.6	400
G	Rack	25	1.0	400
H	14	20	1.5	400
I	72	20	0.5	400
J	14	27½	1.4	400
		Tested by M. A. Jacobson		
1	10	20	1.5	750
2	40	20	0.75	750
3	Rack	20	1.0	750
		Tested by H. Glaubitz		
1	34	20		560
2	34	20		560
3	34	30		560
4	34	Concave tooth		560

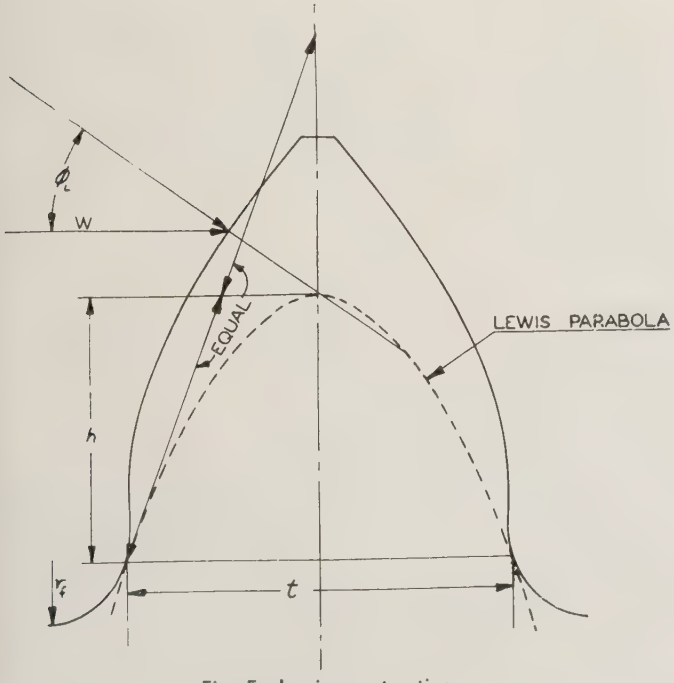

Fig. 5—Lewis construction

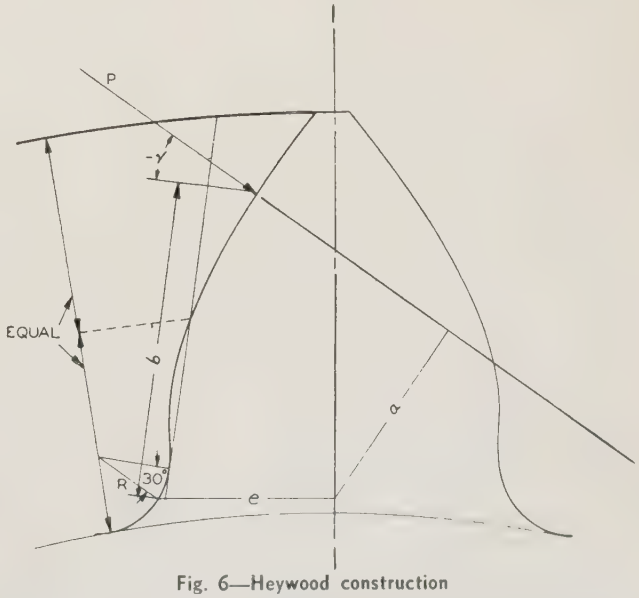

Fig. 6—Heywood construction

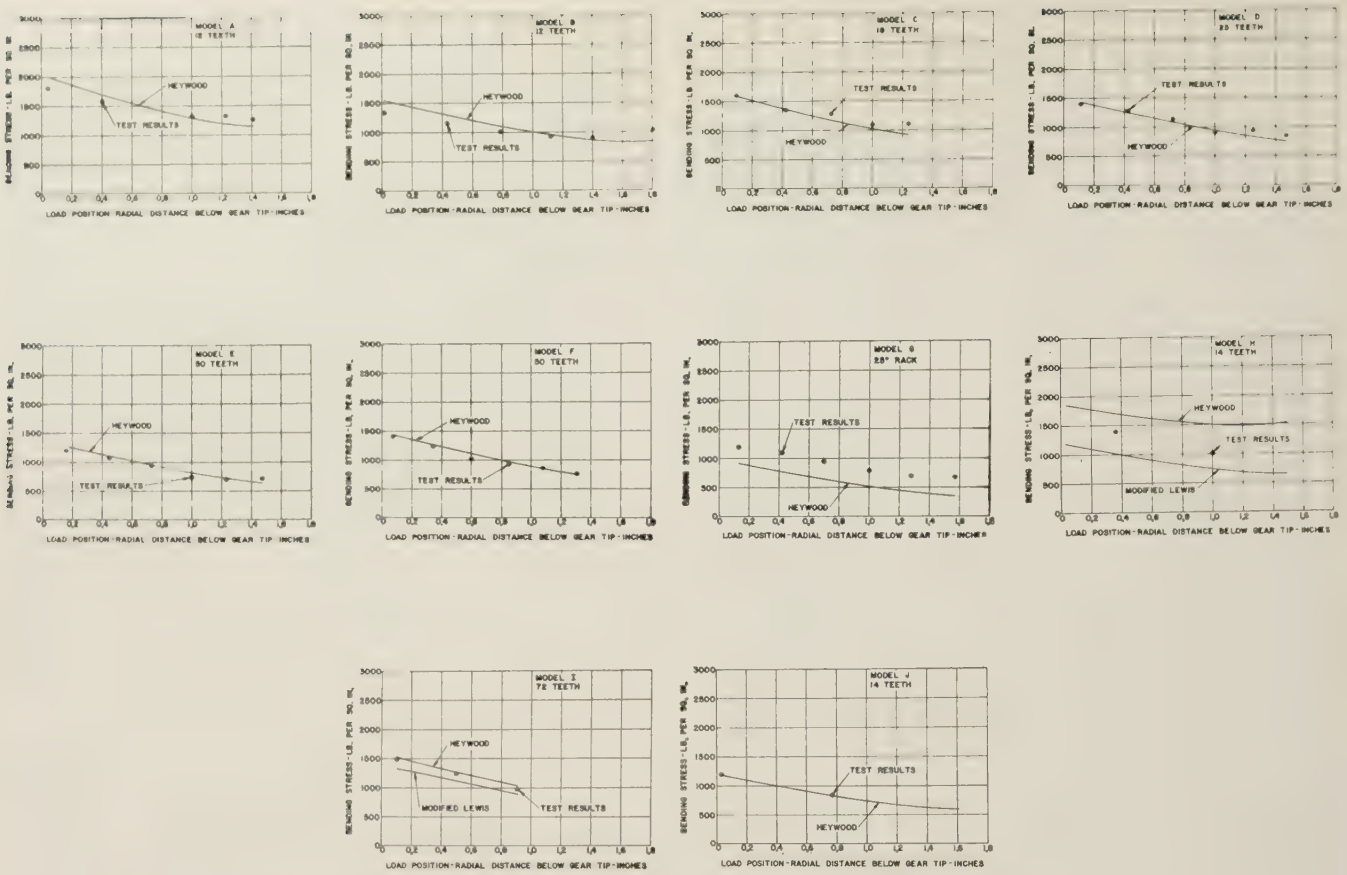

Fig. 7—Comparison of Heywood and modified Lewis formulas with Caterpillar test results

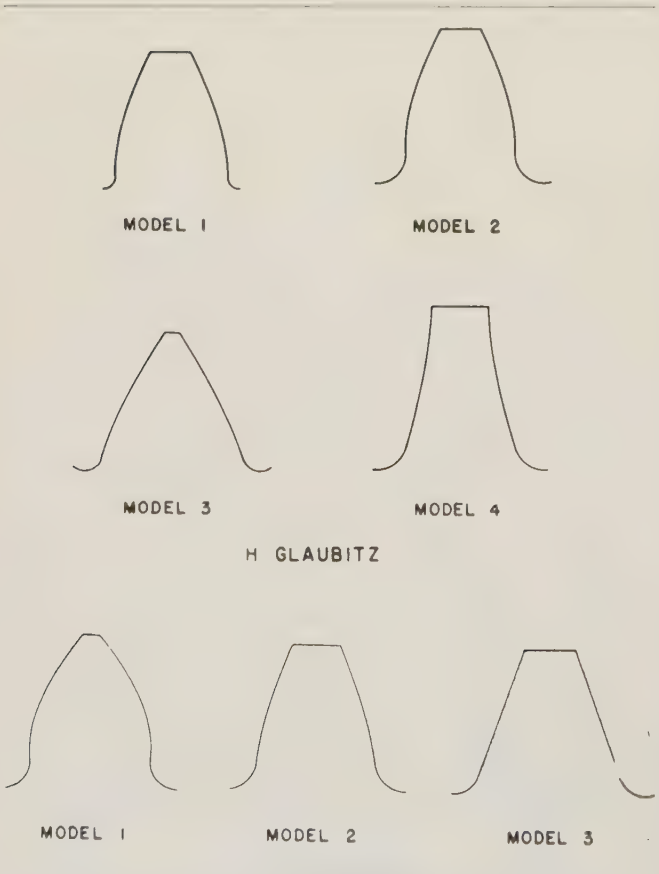

Fig. 8—Photoelastic tooth shapes tested by Glaubitz and Jacobson

problem, and he showed good correlation with his as well as other published photoelastic test results.

It was unfortunate that Dr. Heywood's construction of the equivalent straight-sided projection shape does not lend itself to all generated gear design variations, for the method actually works quite well, being somewhat more accurate than the modified Lewis method for normal gear design. The diagram of Fig. 6 shows the Heywood construction.

The tooth height is divided by two and this measurement transferred radially to the tooth profile. A line through this point tangent to the fillet forms an equivalent straight-sided projection. The remaining values are graphically obvious. Heywood's formula is:

$$S_b = \left[1 + 0.26\left(\frac{e}{R}\right)^{0.7}\right]\left[\frac{1.5a}{e^2} + \left(\frac{0.36}{be}\right)^{\frac{1}{2}}(1 + \tfrac{1}{4}\sin\gamma)\right]\frac{p}{t} \qquad (1)$$

S_b = Maximum fillet stress
a = Moment arm
e = Dimension of resisting material
R = Fillet radius
b = Distance parallel to equivalent section side from the point of loading to the point of maximum stress
γ = Angle deviation of load from normal to the equivalent section
p = Normal load
t = Tooth width

If the tip of the tooth were removed, the geometrical pattern would be changed, which would affect

the position of the assumed weakest section since the equivalent section shape is dependent on the outside diameter. Such removal of the tip down to the point of loading would not actually affect the fillet stress. The value of a and e, will be slightly disturbed, but e and a are often increased or decreased in a somewhat similar proportion, and when applied to his formula the change is not serious in most cases. Somewhat more serious is the changing radius of curvature in the generated fillet: Heywood suggests tranforming the generated fillet into an equivalent semicircular one. Where the trochoidal fillet is extensive, such as in Model A, this becomes very arbitrary. Therefore, the most reasonable approach in the case of a variable radius is to select the radius at the point where maximum stress is assumed to occur. When the tip is removed, the effective radius is changed due to a change in the equivalent section. This may result in an erroneous calculated stress change of 7–8%. It is understandable that if the full depth of the gear is standardized to a given amount, the error will not be large. But increased tooth height, or tooth stubbing to permit clearance between the OD and the housing, removes the universality of such a method, and such changes in modern gear designs are quite common.

With the use of Heywood's equivalent section, which remains the same for a given tooth height and given tooth form, the point of maximum stress does not change with each new position of load on the profile. This is somewhat in error, as was noted by Heywood. Since the actual change in position of maximum stress is not great, particularly with small fillet radii, the method of using a single point for maximum stress does agree fairly well with the *average* position of maximum stress in most cases. The Lewis method, on the other hand, indicates quite a large change in the position of maximum stress.

Another somewhat important problem with both the Lewis and Heywood methods is their lack of applicability to concave-sided projections such as internal gear teeth. We feel that any method should not become limited by such minor geometrical changes.

At this point we come to a comparison of data with the two methods discussed. The graphs in Fig. 7 show our test results in comparison with the Heywood method and modified Lewis formula. Those tooth shapes of 25-deg pressure angle cannot be compared with the modified Lewis equation because of the restriction of the modified Lewis equation to the 14½- and 20-deg pressure angles. Careful scrutiny will show discrepancies of slope and level of stress in both methods, but a decided improvement is seen on the Heywood curves. Main errors occur in the curve slopes for lower numbers of teeth. This is quite natural since Heywood's work on straight-sided projections more closely simulates the higher numbers of teeth. The difference of Heywood's formula and the 25-deg rack results is actually not as severe as it may appear. Because of the small fillet radius to be cut in the model, a certain amount of undercut appeared which, while still producing a uniformly changing radius, did not lend itself to the Heywood construction method which assumes no such radius change.

A definite contribution to photoelastic work has been made by Jacobson[4] and Glaubitz,[5] whose photoelastic experiments were made on tooth shapes shown in Fig. 8. We have compared their test results with the methods also in Fig. 9. Glaubitz in-

[4] Proceedings of Institution of Mechanical Engineers. Vol. 169, 1955, pp. 587–609: "Bending Stresses in Spur Gear Teeth: Proposed New Design Factors Based on a Photoelastic Investigation," by M. A. Jacobson.

[5] "Root-Strength of Straight Toothed Steel Spur Gears," by H. Glaubitz. Sponsored Research Report No. 23, Department of Scientific and Industrial Research, 1950.

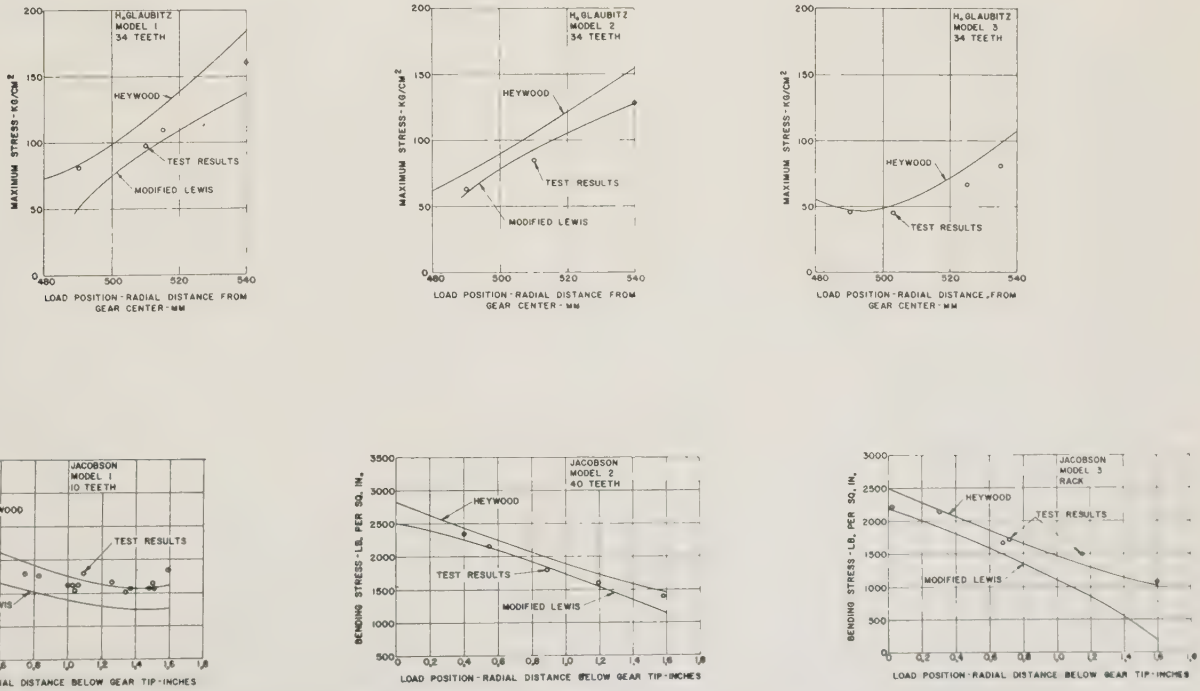

Fig. 9—Comparison of Heywood and modified Lewis formulas with test results of Glaubitz and Jacobson

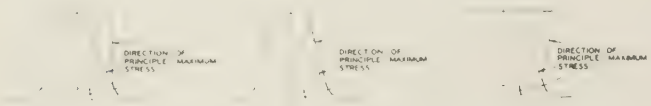

Fig. 10—Influence of projection taper on maximum stress point

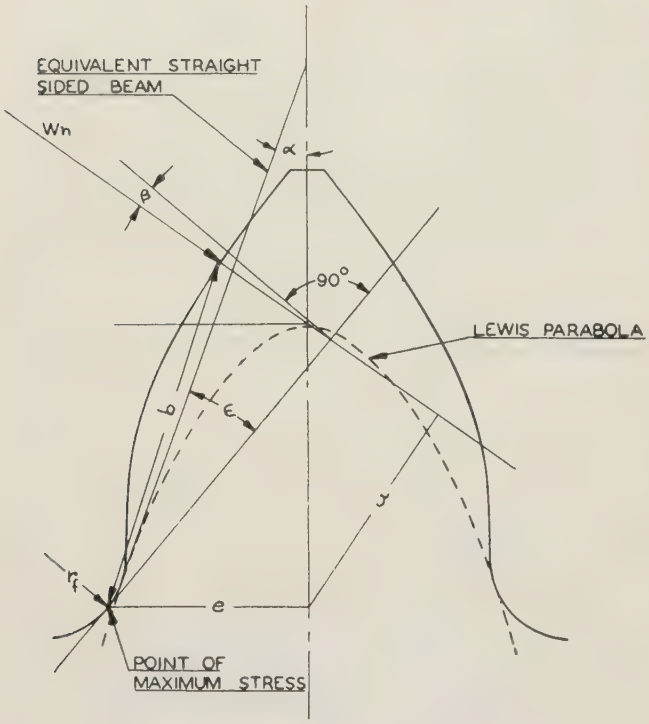

Fig. 11—Construction for values in new beam strength formula

cluded a concave tooth shape in his work which will be mentioned later.

Perhaps because of a difference in experimental techniques unknown to us, Glaubitz's values seem to be consistently low. This is actually of little importance since the insertion of a constant experimental factor K_e can be used to reduce Heywood's results to Glaubitz's test results:

$$\text{Photoelastic results} = \text{calculated stress} \times K_e$$

This in no way effects the comparative results of one model to another in any one investigation. A K_e value of 0.82 would seem to fit Glaubitz's work fairly well when applied to Heywood's formula. Here again, however, the error in slope for those teeth having more curvature of the profile is apparent.

Of particular interest is the number of test points obtained by Jacobson on his 10-tooth model which improves the accuracy of a fitted curve considerably. Another finding of Jacobson's is that the results are practically independent of the radii of curvature of the loading members in the area of contact. This might be expected from an analysis of this distribution of contact stresses beyond the contact area, but experimental verification is always valuable.

In the presentation of this work, Dolan and Broghamer's original data is not used for comparison. It has been brought to the attention of the writer by Prof. Broghamer that a model mounting influence, not previously suspected, could have entered into his work. This is indicated in the isochromatic photographs by the position of the neutral axis, which was located toward the unloaded or compression side of the model from center, whereas the work of Heywood, Jacobson, Glaubitz, and our own test results show it to be toward the load or tension side of center.

Certain features of the Lewis and Heywood formulas are not easily discarded from our study. For instance, the parabolic section used by Lewis as a beam of uniform stress has certain attractive characteristics. It has a sound theoretical background for parallel-sided projections. It also indicates, in most cases, the proper direction of movement of the point of maximum stress in the fillet caused by movement of the point of loading, even though the magnitude of motion for a given change in load positions is largely in error.

On the other hand, the Heywood formula construction is attractive from the standpoint that the stress-concentration factor $\left[1 + 0.26\left(\frac{e}{R}\right)^{0.7}\right]$ follows a form which is more universally accepted by those who have had theoretical and experimental background in notch effects. The proximity factor $\left[\left(\frac{0.36}{be}\right)^{\frac{1}{2}}(1 + \frac{1}{4}\sin\gamma)\right]$ is not particularly desirable but seems to be a necessary correction. Personal communications with Heywood indicate the lack of a truly rational analysis of the factor. Generally, however, its effect is considerably less than the remaining parts of the formula. It will be recognized, of course, that the $\frac{1.5a}{e^2}$ is retained from the flexure formula.

It has been noted from a number of sources that, in addition to being influenced by the position of loading, the position of maximum stress in the fillet is a function of the positive or negative taper in the cantilever projection, such is is shown in Fig. 10 from Dolan-Broghamer's experiments on straight-sided projections. This influence can be seen from the differences of angle θ in the models. It is also evident in Heywood's work, as is shown by his construction of the equivalent section and its control of the point of maximum stress. However, in the Lewis construction, the position of maximum stress is determined solely by the load position and base thickness and is not influenced by the taper of the projection.

This change in stress position, which we shall term here as "stress shift," is perhaps also influenced by other factors having minor importance in our case, such as the completeness of a notch effect by the fillet approaching an included angle over 90 deg due to severe undercut. The stress shift may be either below or above the Lewis point of maximum stress, dependent upon the above factors. Experimentally, we have found the stress shift to be largely controlled by the angle α made by a tangent to the Lewis parabola at the point of contact with the fillet and the centerline of the projection (Fig. 11). The

simple empirical relation developed from our photoelastic work is:

$$\varepsilon = 25 \text{ deg} - \frac{\alpha}{2} \qquad (2)$$

where ε is a stress-shift angle around the fillet. In the case of layout work, this angle can be easily constructed with a drafting machine. The point of maximum stress can be located with rather surprising accuracy in this manner. More rationally, the value of ε should be some more complex function of α, perhaps including the value b. Since for extremely small α angles, which would represent pure bending at the fillet, ε should approach zero. However, this cannot be attained in gear design, and for values of α between 12 and 55 deg, the accuracy of the angle ε has been found to be within 2 deg. (On a gear tooth of 1 diametral pitch having a full generated fillet, this would normally represent an error of 0.035 in. or less.) Actual tooth-fracture patterns from fatigue tests give further verification of this point. Further accuracy is unnecessary and may be undesirable from the standpoint of increased complexity in the actual design; for, in effect, the inaccuracy of calculated stress due to such an error in the formula has shown to amount to less than 1%.

We may consider the tangent to the parabola as the outline of our equivalent straight-sided projection. However, the important angles in our formula should be related to the direction of the principal stresses that are involved which are, of course, parallel to the fillet at the point of maximum stress.

The remainder of our formula appears as:

$$S_b = \frac{W_n}{F}\left[1 + 0.26\left(\frac{e}{r_f}\right)^{0.7}\right]\left[\frac{1.5a}{e^2} + \frac{\sin\beta}{2e} + \frac{0.45}{(be)^{1/2}}\right] \qquad (3)$$

where:

W_n = Normal load

F = Tooth width

r_f = Fillet radius at the point of maximum stress

β = Deviation of load line from direction of principal stress

The factors $\left[\frac{\sin\beta}{2e}\right]$ and $\left[\frac{0.45}{(be)^{1/2}}\right]$ are unanalyzed quantities. One finds a great similarity between them and the Heywood proximity factor, yet we were unable to change the numerical values of the proximity factor within the Heywood arrangement to fit the results. The factor $\left[\frac{\sin\beta}{2e}\right]$ has some rational appeal as a means for determining the effect of the angle of loading on the principal stresses. The $\left[\frac{0.45}{(be)^{1/2}}\right]$ has no such reflection and can be handled here as a proximity factor such as Heywood's. The determination of the fillet radius at the point of maximum stress should be as accurate as possible. On a large scale, carefully constructed layout, it is possible to measure this fillet radius with an accuracy of about 7–8% which will affect the stress calculation only a few percent. Increased accuracy of course will result from automatic computer calculation.

Fig. 12 shows the correlation of the formula with

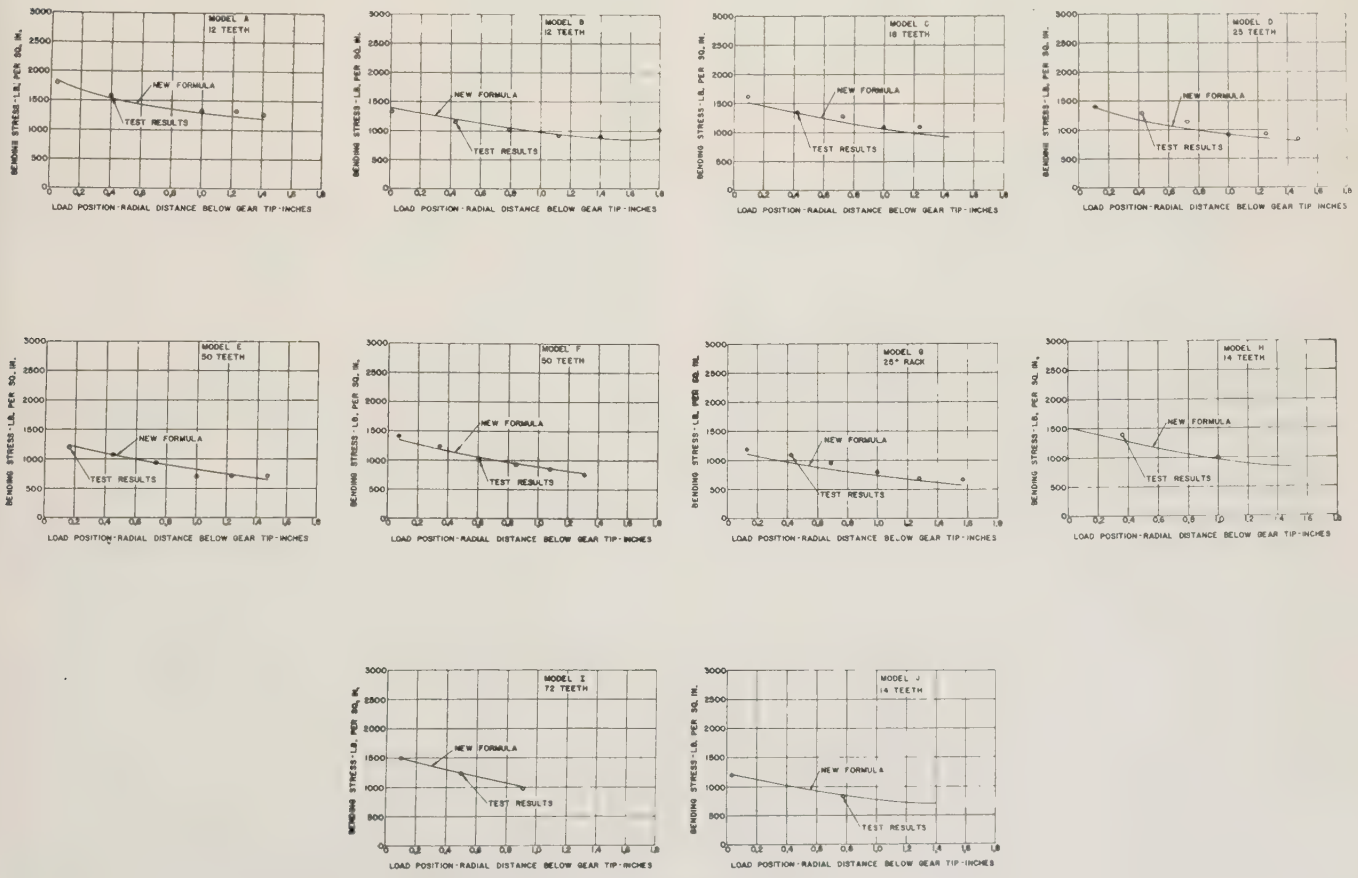

Fig. 12—Comparison of new formula with Caterpillar test results

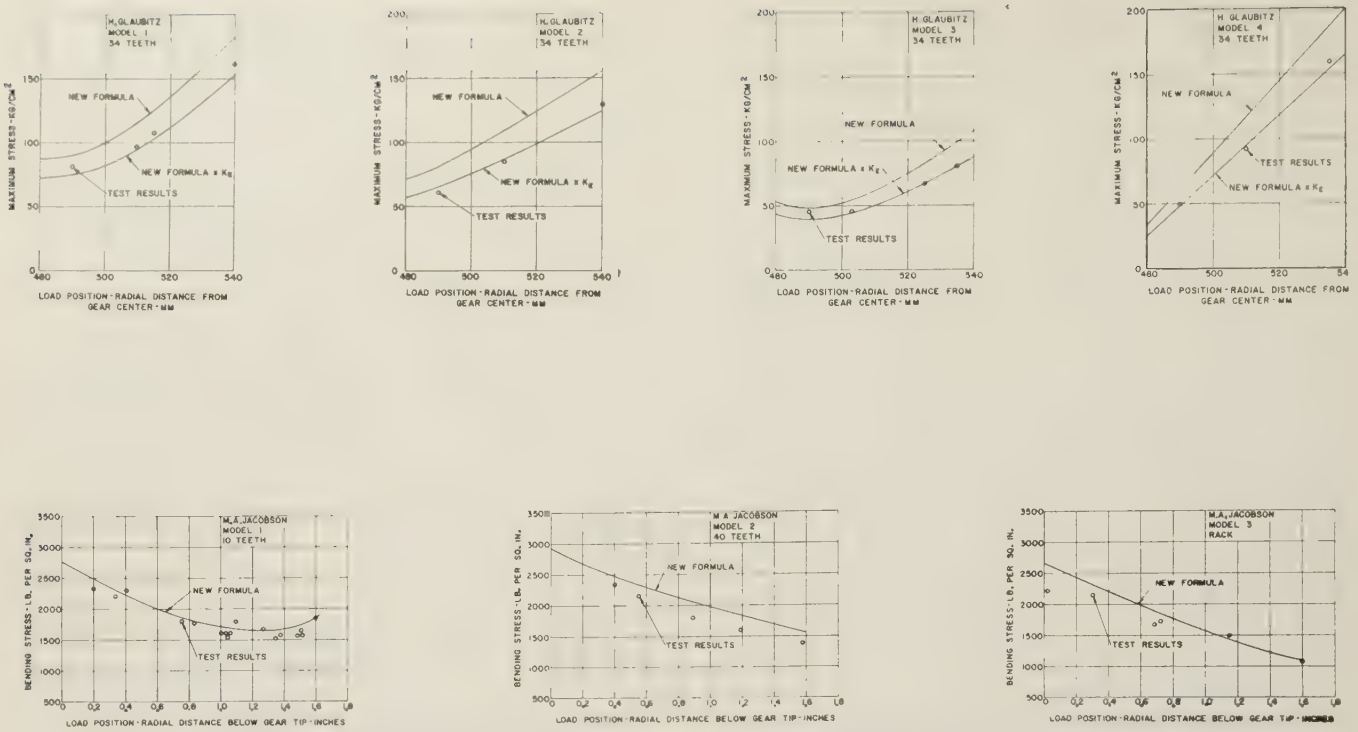

Fig. 13—Comparison of new formula with test results of Glaubitz and Jacobson

our test data and Fig. 13 with that of Jacobson and Glaubitz. As in the case of the experimental factor K_e found necessary in comparing Heywood results with Glaubitz's data, we find it also necessary to use a K_e of 0.82 with our formula. It is interesting to note that the correlation is good even with the concave tooth Model 4.

Some Experimental Evidence

Experimental evidence is always desirable and often necessary for the reliability of design formulas. Directly comparative evidence is the most desirable. As illustration, two designs were made for tests on our single-pair gear test machines. These machines used a locked-up torque principle and are more fully described in a previous publication.[6] The gears were designed to exercise the maximum burden on the formula, as can be seen by the two shapes of Fig. 14. They were manufactured from the same heat of steel and carburized and hardened in one batch. They were checked metallurgically to make sure they were of the same hardness, structure, and the like. The loading point used for calculations of maximum stress was selected as the highest point of single tooth contact. Calculations showed the higher pressure angle gear would actually have, for this design, about 10% less load-carrying capacity than the lower pressure angle design. Within the allowable accuracy of such tests, the experimental results verify the formula amazingly well for values close to the endurance limit.

The fatigue diagram illustrates a fairly significant scatter of results, which is understandable on actual running tests for a number of reasons. Somewhat less scatter would occur on single-tooth fatigue tests where misalignment adjustments could be made for each tooth, and the entire curve could be constructed from teeth broken from one gear. The curve indicates a convergence of the curves approaching the static fracture point. This may suggest minute plastic deformation and redistribution of the actual stresses, causing a reduction in the response to the calculated stress concentration. However, near the endurance limit the 10% difference in capacity becomes more obvious since at the lower loads the actual fatigue strength would more closely respond to theoretical stress concentration values. Furthermore, we have used a material having a surface hardness over Rc 60, which should encourage good response to the theoretical stress concentration. A more ductile material would not perhaps have shown such results.

The existence of residual stress may also effect such data. However, the applied load constitutes a range of stress fatigue condition. Because of the compressive residual stresses that occur in the carburized case, it seems likely that the range of stress may cover, instead of the maximum-tension-to-zero range, a complete reversal, or even maximum compression to zero. There is considerable evidence indicating that, particularly for notched specimens, the range of stress under these conditions is the criterion for fatigue failure.[7, 8]

We do not imply from the fatigue test results that higher pressure-angle gears are weaker than lower pressure-angle gears. These were merely used in

---

[6] SAE *Quarterly* Transactions, Vol. 3, April, 1950, pp. 354–368: "Gear Testing Methods for the Development of Heavy-Duty Gearing," by R. P. Van Zandt and B. W. Kelley.

[7] "Effect of Range of Stress on the Fatigue Strength of Metals," by J. O. Smith. University of Illinois Engineering Experiment Station Bulletin No. 26, 1942.

[8] "Stress Distribution and Strength Condition of Two Rolling Cylinders Pressed Together," by E. I. Radzimovsky. University of Illinois Engineering Experiment Station Bulletin No. 408.

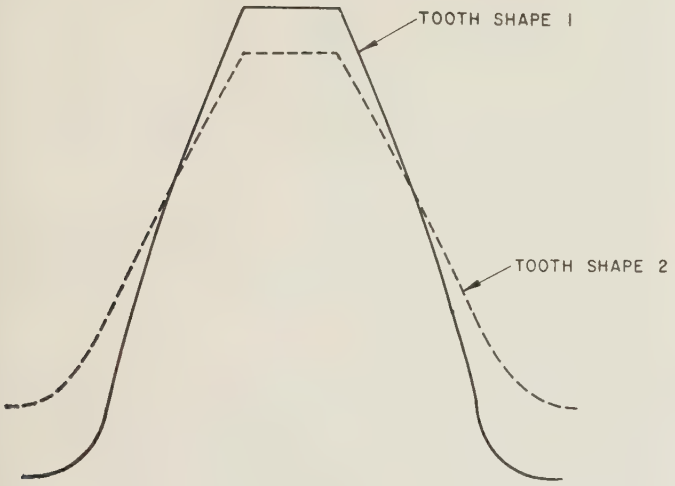

Fig. 14—Tooth shapes of running test gears

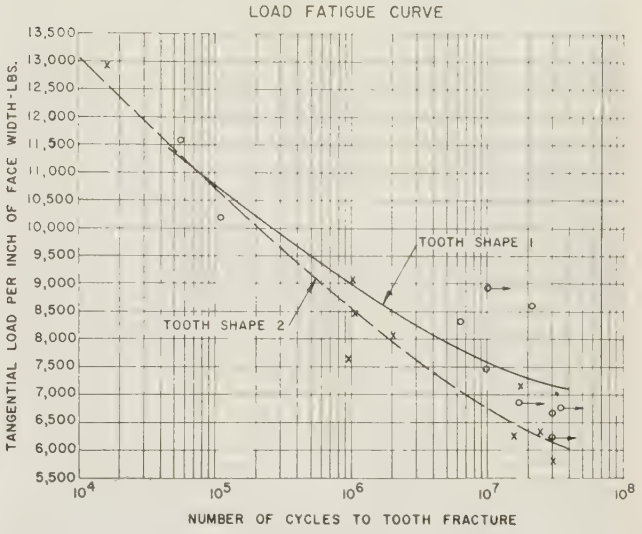

Fig. 15—Fatigue curves of running tests on steel gears having the tooth shape shown in Fig. 14

this case to illustrate the application of the formula, and a number of the factors in the design are different from normal practice.

To summarize, we feel that several things have been accomplished in this analysis. First, the designer can now accurately locate the point of maximum stress. The radius in the area of maximum stress seems to be and should be the controlling factor for stress concentration. Second, we have retained to a certain extent the Lewis theoretical method for obtaining an equivalent straight-sided section, even though the assumed weakest section is not necessarily the point at which the maximum stress occurs as noted by our stress shift factor. Third, we have retained the semi-theoretical arrangement for stress concentration as expressed by Heywood. Fourth, in our comparison of the formula with all existing photoelastic models that we know of, we have found good correlation from the tip of the tooth down to the lowest point at which load might occur even on concave sided projections. Fifth, our experimental evidence using carburized and hardened gears has shown that our photoelastic results may be used as a design tool on such parts.

DISCUSSION

Compares Lewis, Heywood, and Kelley Formulas For Analysis of Gear Stress

—R. B. Heywood
Institution of Mechanical Engineers

THE designer who requires information on gear stresses has been laboring under a difficulty—on the one hand, a precise analysis of stress by use of refined methods, such as the analytical relaxation method of the experimental photoelastic technique, was beyond his reach for everyday use; while, on the other hand, the classical Lewis formula would give him only an approximate solution. Now, however, the designer can escape from this quandary by utilizing a formula of the type that has been discussed by the authors, which neither outrages theoretical concepts of stress analysis nor is too complicated to be of practical use.

I am particularly indebted to the authors for having made a comparison between experimental results as obtained by themselves, Jacobson, and Glaubitz and those calculated from a formula that I have suggested. The comparison shows that general agreement was obtained, even though no degree of fitting by adjustment of constants to suit the new data has been made. Nevertheless, it is to be expected that a semi-theoretical formula is dependent on experimental results for the evaluation of its constants, and I consider that the authors' careful analysis on the new data might well lead to greater accuracy. These points suggest that gear tooth stresses can be assessed with much greater accuracy than has been possible heretofore.

The formulas under discussion are of the type $S = K(A + B + C)$, where the maximum tensile fillet stress S is expressed in terms of a stress-concentration factor K and "nominal" stresses A, B, and C. The term $A \left(= \frac{1.5a\,W}{e^2\,F} \right)$ is the Lewis theoretical bending stress, while the empirical terms $B \left(= \frac{\text{constant}\,W}{\sqrt{(be)\,F}} \right)$ and $C \left(= \frac{\sin \beta W}{2e\,F} \right)$ are stresses associated with the proximity of the point of load contact to the fillet. The justification for the use of these proximity terms requires some explanation, and I have suggested previously three possible causes of boundary stress.

The Lewis bending term takes no account of local stress distribution effects at the point of local contact and, in-

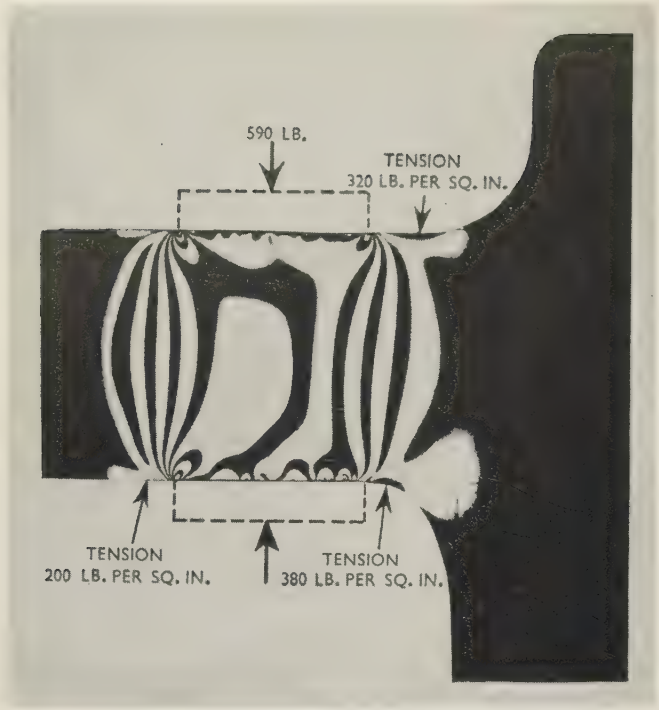

Fig. A—Effect of distributed load applied to boundary of projection

deed, gives the same nominal fillet stress for load applied at any point on its line of action. With load applied close to the fillet, the fillet stress is distributed by the local load effect, and it is the function of the proximity terms to assess this. Theoretically, the uniform application of pressure to a portion of the boundary of a semi-infinite sheet will produce no boundary stresses whatsoever outside the portion of contact. That result can not be achieved in practice, for a nonuniform pressure distribution and also shear forces acting parallel to the boundary are inevitably produced. These departures cause boundary stresses, usually tensile, and their presence can always be observed in photoelastic fringe models.

A second cause of boundary stress arises from the difference in width between the gear tooth and semi-infinite sheet, producing much larger straining actions near the point of load contact in the gear tooth than in the semi-infinite sheet.

Thirdly, the boundary stresses produced by the above actions may be further modified by a general shape factor, which is associated with the relatively large distortions in the tooth as compared with those in the main body of the gear wheel. The magnitude of boundary stresses thereby produced depends upon the fillet radius, the width of the tooth, and the proximity of load to the fillet.

All these effects are dependent on local loading rather than on general bending of the tooth and are assessed by the terms *B* and *C* in the formula, the latter term making only a small contribution to allow for the effect of loading direction. Fig. A demonstrates the effect of a distributed load applied to the boundary of a projection. In spite of the fact that bending moments are avoided, a tensile boundary stress is produced near to the loading pads, the magnitude decreasing with distance from the pads and depending on the proximity to regions of high rigidity, such as occurred particularly in the lower right hand fillet.

I would like to comment on certain characteristics of the formulas. One problem is the conversion of the gear tooth to some equivalent shape in which nominal stresses can be calculated. The solution originally proposed by Lewis was that the tooth could be replaced by a projection of parabolic shape. This gives satisfactory results for stresses predominantly caused by bending, but if proximity stresses are also present the solution is clearly inadmissible, as no allowance for those additional stresses has been made. In the extreme case where the line of action of load crosses the tooth centerline at a point below the fillet, it becomes impossible to construct the Lewis parabola, and so the method fails. Failure is also implied by the authors' remarks in the paper, for not only is it demonstrated that proximity stresses do exist, but also that the point of maximum stress does not coincide with the point at which the parabola touches the fillet. For these reasons, I suggest that the use of the parabola construction for ascertaining stresses be abandoned.

To utilize the principle suggested by Lewis it is necessary to plot the loci of points for which the nominal stress (as derived from the sum of the bending and proximity terms) is constant, and to scale the curve thus produced so that it touches the fillet at one point. Such a procedure is both laborious and cumbersome.

A simpler solution is to employ the equivalent flat-sided projection, having a shape unaffected by the position of loading. The justification for the use of the equivalent projection is that its shape be approximated to that of the gear tooth, especially in the critical regions, and that the maximum fillet stress be calculated by means of an existing formula. Although I have my own suggestions as to its construction, I agree with the authors that the shape is influenced by the region of the tooth outboard of the point of loading. It is probable that the apparently unstressed region in fact influences the fillet stress. The point has been demonstrated by Hetenyi[a] for the parallel case of T heads, where for admittedly somewhat unusual proportions, the stress-concentration factor increased from 4.05 to 5.10 or by 26%, with removal of material from the free end. Much smaller differences would be expected in gear teeth, but it appears that further experimental evidence is necessary before this type of construction can be rejected.

The authors have discussed the question of assessing the effect of fillet radius. I agree that the expression of an equivalent radius is vague, and that a precise definition, such as the radius at the point of maximum stress, is preferable. It should be noted, however, that the point of maximum stress can not always be ascertained from the Lewis parabola, for the reasons that I have already mentioned. Where analysis is made by reference to the flat-sided projection, perhaps the use of the gear fillet radius at say 30 deg to the flank of the projection is a suitable compromise.

The radius at a point has no significance as to its stress-raising effect; it is only when the radius extends over some distance that a stress increase is produced. I have shown elsewhere[b] that a fillet of "streamline" shape, which contained a particular radius at one small region of the fillet, produces a stress which is 37% less than that of a more normal fillet having the **same** radius of curvature. This shows that general shape of fillet is important, while the radius at a point has only a limited, though practical, range of application.

The use of an equivalent flat-sided projection is a device for simplifying the procedure of stress assessment. I would like to suggest an alternative solution, which I believe will overcome certain difficulties, such as that raised by the authors in the analysis of stress in concave-shaped teeth. This is that the same formula can be applied directly to the gear tooth, without any reference whatsoever to the equivalent projection. Broadly, the method of defining dimensions is the same as that given in Fig. 6 and reproduced in Fig. B, but with the following qualifications:

1. The radius is defined as that occurring at the point under consideration.

---

[a] ASME Transactions, Vol. 61, 1939, p. A151 and Vol. 62, 1940, p. A80: "Some Applications of Photoelasticity to Turbine Generator Design," by M. Hetenyi.

[b] "Designing by Photoelasticity," by R. B. Heywood. Pub. by Chapman & Hall Ltd., London, 1952.

Table A—Comparison of Beam-Strength Factors Assessed by Different Methods

Number of Teeth in Gear	Number of Teeth in Mating Gear	Y Value, Determined Photoelastically	Y Value, Based on Lewis Analysis	Difference, %
	20	0.382	0.660	72.8
	30	0.389	0.691	77.7
20	50	0.396	0.728	84
	100	0.403	0.766	90
	Rack	0.408	0.820	101
	20	0.418	0.612	46.3
	30	0.431	0.670	55.5
40	50	0.440	0.782	77.7
	100	0.451	0.851	88.6
	Rack	0.464	0.931	100.8
	20	0.430	0.639	48.5
	30	0.444	0.713	60.5
80	50	0.453	0.814	79.5
	100	0.467	0.894	91.4
	Rack	0.478	1.011	111.5
				Range: 46.3–111.5%

2. The dimension b is the distance from the point under consideration to the point of load contact.

3. The angle α is the angle between the normal to line b and the line of action of load. Alternatively, the angle β, defined as the deviation of load line from the direction of principal stress, can be used as suggested by the authors.

By applying the formula to various points along the fillet, the value of maximum stress, and also its position along the fillet, can be readily ascertained. Only a few points have to be considered since the position of maximum stress was known approximately.

A significant feature of this method of analysis is that both the authors' and my own formulas effectively became identical. All dimensions are defined in the same manner, with the possible exception that some doubt exists as to the simplest method of assessment for the effect of direction of loading, but this has only a small influence on stresses. The use of the angle β will produce stresses identical to those given by the authors' formula, provided the method of ascertaining the position of maximum stress that they used is exact, for otherwise the proposed method will indicate slightly greater stresses at some adjacent point.

The modified procedure appears to rationalize the methods suggested by the authors and by myself; it entails simple measurements of the tooth, is capable of high accuracy, and has a wide range of application with respect to both positions of loading and shape of tooth. Furthermore, the use of the equivalent flat-sided projection or the Lewis parabola becomes incidental, and merely provides a construction for ascertaining the approximate position of maximum stress, but serves no other useful purpose.

Compares Strength Factors Found by Lewis, Kelley, and Jacobson Analyses

—M. A. Jacobson
Austin Motor Co., Ltd.

WHEN considering the beam strength of gear teeth, five component factors come to mind: tooth shape, basic material, machining finish, service, and dynamic load.

The present paper deals with the first only and is a significant contribution to the problem of finding a general solution for all possible gear tooth shapes. It would appear that the semi-empirical formula advanced as a result of a large number of photoelastic tests covers most tooth shapes adequately well. It is, therefore, a great improvement on the older methods.

There are, however, a few observations which we wish to make. As pointed out by the authors, "The historical use of a method is a strong influence to retain the method regardless of its errors, but the discrepancies cannot easily be ignored." The magnitude of these errors is perhaps best illustrated by comparing the strength factors found by different methods. In a recent paper to the Institution of Mechanical Engineers[c] the writer compared beam-strength factors for "uncorreted" gears, having been generated by cutters conforming to the British Standards of 20-deg pressure-angle basic-rack proportions, when assessed by the Lewis formula and by photoelastic stress analysis. (See Table A.)

By definition the beam strength factor Y is:

$$Y = \frac{W_m \times P_n}{F \times S_b} \qquad (a)$$

where:

W_n = Loading normal to tooth face, torque per base radius
P_m = Normal diametral pitch
F = Face width
S_b = Maximum tooth fillet stress

The significant fact is not so much the actual percentage difference but rather that the range varies from +46.3–115.5%. It is, therefore, not possible merely to add a linear correction factor for the old Lewis formula to bring it into line with experimentally determined strength values.

In the face of such discrepancies and such a large variation it appears questionable whether any real defense can be put up for retaining the old Lewis formula. We have, after all, been discarding quite a few well-established methods of strength calculation over the last 65 years or so. The defense repeatedly advanced for the retention of the Lewis formula in some modified form is that it enables us to calculate the stress-concentration effect at the tooth fillet, since the Lewis parabola accurately locates the weakest section. This, however, it does not do, as Fig. 4 clearly shows. We have found in the analysis of some 300 photoelastic fringe photographs of many different gear tooth shapes having widely differing points of application of load, that the maximum tooth fillet stress occurs on the fillet radius within a narrow band, namely $\frac{1}{8P_n}$ to $\frac{1}{6P_m}$ above the root circle. The gears were all cut to conform with gear teeth which could be generated by the British Standard Basic Rack Cutters and incorporated the extremes of addendum modification possible, which avoided undue pointing of teeth on the one hand, and undercutting near the root on

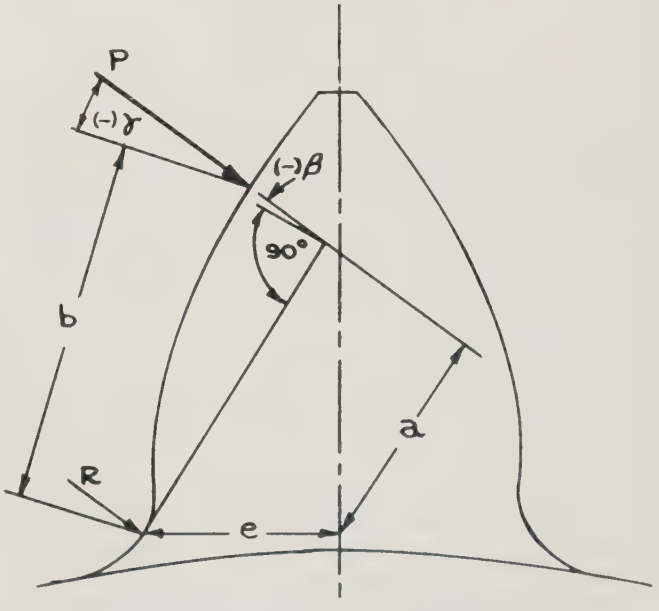

Fig. B—Definition of terms by direct reference to gear tooth

[c] See footnote 4.

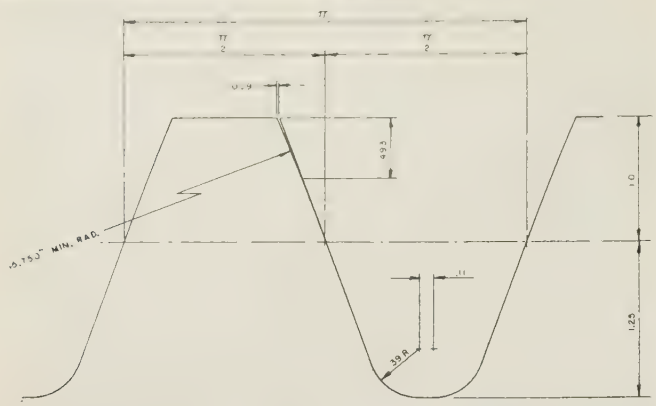

Fig. C—B.S. 436/1940 basic-rack tooth shape with 20-deg pressure angle. Classes A_2 and B precision and high-class cut gears

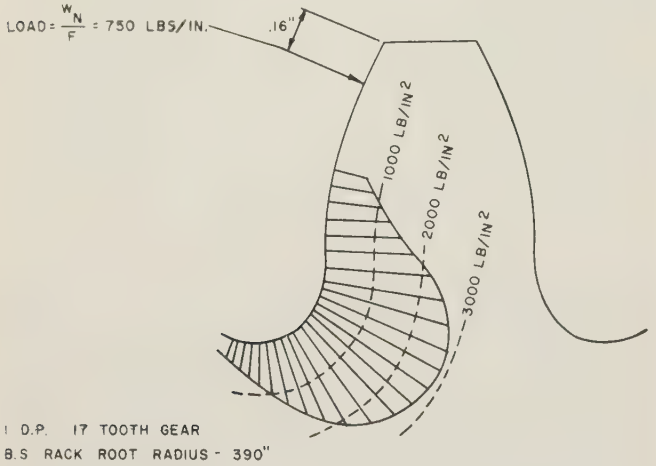

Fig.D—Stress distribution in tensile root fillet of gear tooth

the other hand. The range of addendum modification possible for spur gears is given by:

$$\frac{1+\frac{20}{t}}{2P} \leq \text{addendum} \leq \frac{4-\frac{10}{t}}{2P} \qquad \text{(b)}$$

where: t = Number of teeth in gear
P = Diametral pitch

Fig. C shows the proportion of the 20-deg pressure angle basic rack to B.S. 436/1940.

We maintain that an attempt to arrive at the actual bending stress by means of the construction of the Lewis parabola analysis is likely to lead to an erroneous picture. When we talk of a stress-concentration factor we commonly infer that the stress is locally raised above that calculated easily and accurately by the rigorously mathematical analysis of stress distribution on the section. Only then can it be related in some form to notched bar beam tests and notch sensitivity factors. As can be shown by photoelastic tests the Lewis analysis does not locate the weakest section of the tooth exactly, and moreover, when comparing the location of this weakest section by photoelastic tests and the Lewis analysis we find that for different points of application of load this relative shift is not constant.

This, therefore, means that the basic stress distribution is not determined substantially correctly by the Lewis parabola. However, unless the basic stress can be determined substantially correctly the separation of a photoelastically formed root fillet stress into two component parts, one being the basic stress and the other the theoretical stress-concentration factor K_t becomes meaningless.

Stress concentrations there undoubtedly are at gear tooth fillets, as can quite readily be seen from Figs. D, E, and F, which show respectively root fillet stress distribution for a 17-tooth gear cut with a B.S. 20-deg pressure angle basic-rack cutter of 1 diametral pitch, a 125-tooth gear cut with the same cutter, and a basic-rack cutter of the same proportions but having a 0.098-in. instead of an 0.39-in. rack root radius. The point of application of the load is the same in all cases, being 0.16 in. from the tip of the tooth. The effect of varying the rack root radius in the case of these two selected gears can be clearly seen in Fig. G. From this it is evident that the effect of a variation of rack root radius is more marked for gears having a large number of teeth, since these approach the actual basic-rack dimensions.

It naturally follows from this that the determination of the critical radius r_f in the authors' formula greatly affects the calculated values of root fillet stress and that the accuracy of such calculations depends on the designer's care in laying out his tooth shapes to an enlarged scale. We feel that such a reliance on meticulous accuracy of graphical analysis is introducing another source of error into gear calculations. For this reason, we have avoided the need for any graphical analysis in the case of our own work on the subject and introduced a somewhat different approach. While there may be differences of calculated values between the authors' and our own beam strength analysis, a remarkably close agreement exists with the experimental photoelastic results. This is all the more noteworthy since these large numbers of experiments were carried out independently and unrelatedly, using different techniques in the preparation and loading of their models, different types of polariscopes, stress frames, and mounting methods for the models. This is indeed a most heartening confirmation of the accuracy and repeatability of the photoelastic stress analysis method, when carefully used.

In this connection it may be relevant to refer to the probable errors due to the graphical construction method advocated by the authors. The self same gear tooth beam strength problems were given to two junior designers to do the layout and subsequent calculation work. Their results varied by 8%. Giving the same two problems to one of these designers a few days later the second analysis differed by 8½% from his first findings in one case and 7% in the case of the second analysis. Taking about 12 such analyses and comparing them with the results obtained photoelastically, we have found the calculated values to be from 95–118.5% of the observed values.

In our own analysis we had reported photoelastic results directly in such a way that all the work asked of the designer was to read off beam strength values, requiring at most a linear interpolation of the values obtained from the graphs. While the advantage of such a system is simplicity and ease of application and repeatability, it suffers from

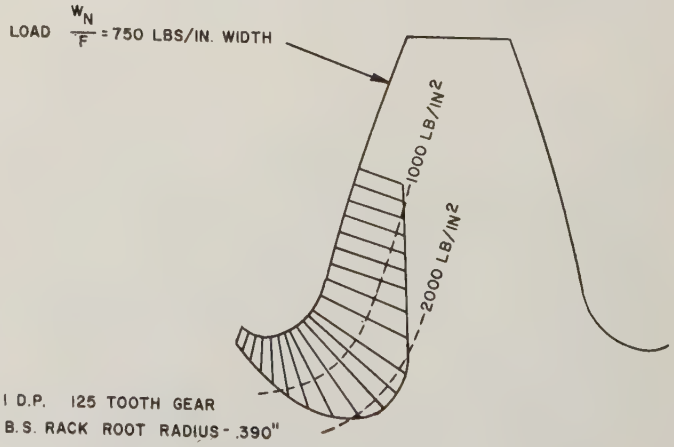

Fig. E—Stress distribution in tensile root fillet of gear

one serious drawback. When contemplating a change of some of the leading proportions of the basic rack (rack root radius, pressure angle, or depth of tooth) fresh series of photoelastic tests are required. The authors' semi-empirical method, on the other hand, enables a forecast of the effect of such changes to be made without any further tests being undertaken, but does not yield the same accuracy.

In this connection we would, however, like to make a special plea to gear designers to refrain from adopting special cutter proportions whenever possible. Just as thread forms have been standardized, now it should be possible and profitable to apply similar standardization in the case of gear cutters for the sake of rationalization. Before abandoning the idea of making a standard cutter do, let us examine just how wide the range of possible variation in spur gears is which might be obtained when using, for example, the basic-rack proportions of the 20-deg pressure angle cutters conforming to B.S. 436/1940. This we feel, should adequately cover most current design problems. It is common knowledge that gear tooth shapes and, hence, effective pressure angles can differ very widely from those of the generating cutter. Fig. H shows that this range of possible effective operating pressure angles is very wide. The smaller the number of teeth in the pinion, the wider the range.

Taking as an example a 10-tooth spur gear pinion, the operating pressure angle is bound to be 20 deg in one case only, namely when in mesh with rack ($T = \infty$) but can be large as 31.5 deg when two 10-tooth gears, both having an addendum of $\frac{1.5}{P}$ are meshed together.

It is obvious, therefore, that in the case of say a 25-tooth gear the beam strength value may vary greatly. In fact, it may vary from $Y = 0.595$ and $Y = 0.32$, which represents a ratio of relative strengths of 1.86/1. The larger Y value is the beam strength of a 25-tooth gear of 1 diametrical pitch, having an addendum of 1.8 in. (gear A) meshing with a rack. The smaller Y value is that of a 25-tooth gear wheel having an addendum of 0.9 in. (gear B) meshing with a 10-tooth pinion, which has an addendum of 1.5 in. (gear C).

Narrowing the field to one specific gear ratio 2.5/1 and selecting a 25-tooth wheel and 10-tooth pinion of the same proportions as before, we find that for the closest center distance when gear C meshes with gear B, $Y = 0.32$ and for the widest center distance when gear C meshes with gear A $Y = 0.44$. This corresponds to a ratio of relative strengths of 1.38/1.

It can be seen from this that by judiciously selecting addendum corrections for any given gearing problem, it is possible to obtain a significant increase in load-carrying capacity without using special cutters.

Discusses Limitations of Kelley-Pedersen Equation

—E. L. Broghamer
University of Illinois

THE designer, when developing an optimum tooth design insofar as beam strength is concerned, is confronted with the necessity of having adequate knowledge regarding conditions of service, dynamic load effects, machining factors, material stress limit factors, and load-stress relationships.

Wilfred Lewis in 1893 published a load-stress relationship, relating tooth load to bending stress, which gained wide acceptance and usage through the years. Since that time various other investigators, such as Timoshenko, Baud, Merritt, Glaubitz, Jacobson, and Heywood, have suggested modifications to the original Lewis equation or other approaches to this load-stress problem. Currently, the most generally used relationship in the United States is the so-called modified Lewis formula, which is the original Lewis equation modified by the addition of a stress-concentration term. The stress-concentration or "stress-correction" factor (as the authors of the current paper suggest it be termed) is an empirical term compensating for the

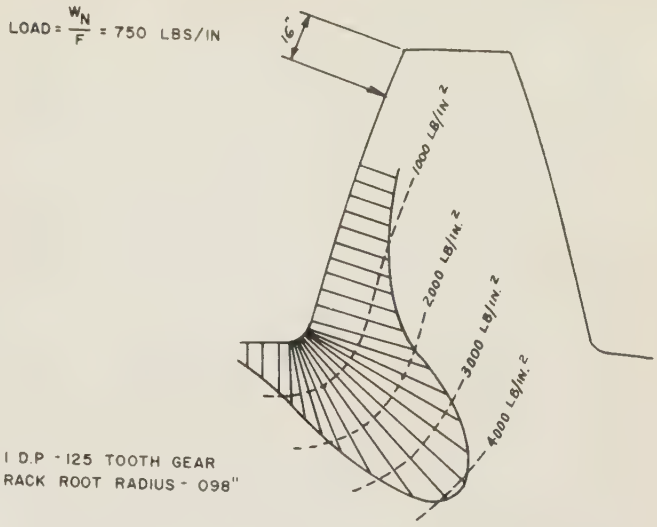

Fig. F—Stress distribution in tensile root fillet of gear tooth

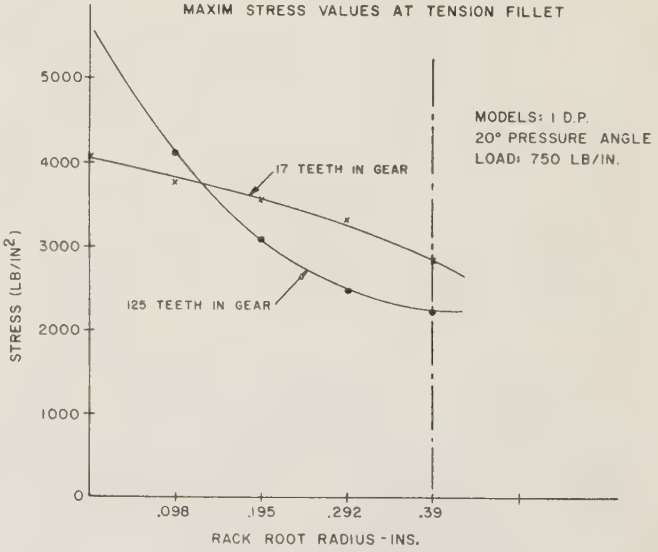

Fig. G—Effect of rack-root radius on tensile fillet stress

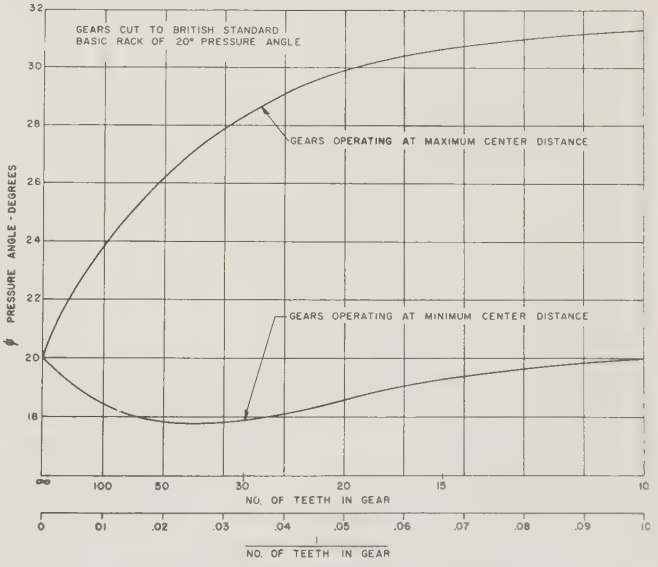

Fig. H—Variation of effective pressure angle

many simplifying assumptions Lewis used when developing his original relationship.

It must be remembered that at the time the Lewis formula was published the state of knowledge relative to changing cross-section, proximity of load to section of calculated bending stress, and the like, was considerably less advanced that now. With current knowledge indicating the importance of such factors, it is rather unrealistic to continue to use an equation which in no way compensates for these factors. Probably this equation has remained in modern use primarily because it has long familiarity, stress values computed by it have through experience been correlated with appropriate limiting values predicated by service experience, and no rather simple form of relationship has been proposed to replace it.

The authors refer to the equation proposed in 1947 by by R. B. Heywood for determining the maximum fillet stress in gear teeth and other loaded projections. As yet, this method has not received widespread acceptance, even though it is more realistic than the Lewis method and shows good correlation with published test results. As noted by the authors, Heywood's equation lacks universality, since it does not take into account shift of location of maximum fillet stress with changing load position and is not applicable to concave-sided projections.

The formula presented by the authors provides the designer with a more advanced and accurate mathematical relationship for evaluating maximum fillet stress in gear teeth. The new equation entails relatively simple measurements of the tooth, is more exact in predicting maximum fillet stress, and covers a much wider range of conditions than that covered by the modified Lewis equation. In addition, the construction associated with it does reflect a variation in location of the section of maximum fillet stress and also is applicable to concave-sided projections. Since it does provide the designer with a much better tool than he has previously had for design use, it is obviously an improvement on present methods and should merit careful consideration for general usage.

There are some observations, however, which should be made in connection with limitations of the proposed equation. The discusser agrees with the authors that it is more realistic to utilize the fillet radius at the point of maximum stress rather than the minimum fillet radius. The minimum fillet radius was used in the equations published by the discusser because it was readily calculated and appeared to be a satisfactory parameter for the stress-concentration factor. It must be remembered, however, that the formula being proposed is based almost exclusively on results of investigations on members having trochoidal fillets. Heywood, presents evidence that the rate of change of fillet radius has an appreciable effect on the stress and, therefore, may be more generally applicable than the radius at a particular point.[b]

The method of locating the section of maximum fillet stress proposed by the authors is more accurate than the parabolic method utilized by Lewis. The authors do utilize the Lewis parabolic method, but provide a compensation for the inaccuracy of the Lewis method by means of the "stress-shift" angle ε. This method, since it does utilize the Lewis method as a controlling factor, has the inherent weakness of the Lewis method in that it cannot be utilized where the line of action of tooth force intersects the tooth centroidal axis below the fillet. In addition, the empirical equation given for the determination of the stress-shift angle is based on investigations covering primarily trochoidal fillets. The above observations should offer no particular hindrance to a general usage of the proposed equation since practically all gear teeth are generated and, therefore, have trochoidal fillets. Also the practical range of load position on current standard gear tooth shapes does not permit attaining the limiting position of utilization of the Lewis parabolic method. The effect of the rate of change of fillet radius on maximum fillet stress and a method of locating the weakest section without the use of the Lewis parabolic method would merit further study.

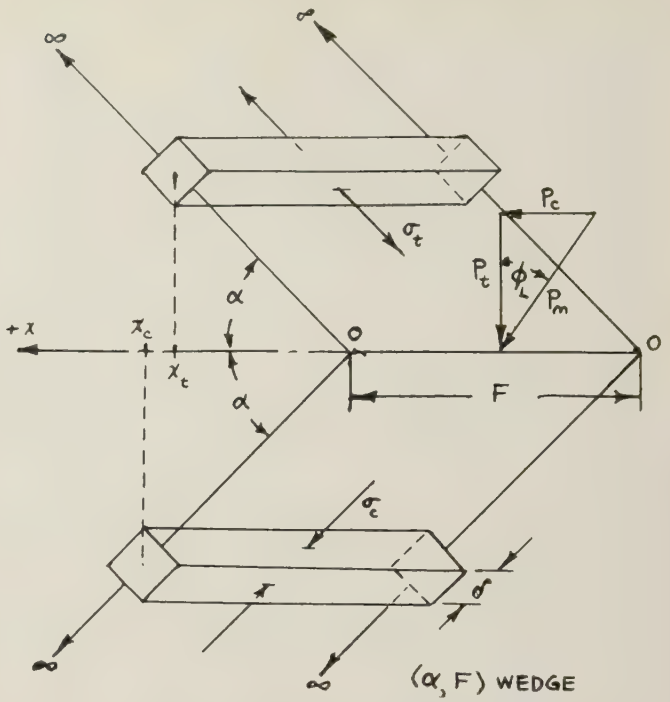

Fig. 1—Demonstration of wedge theorem

Heywood's equivalent straight-sided projection indicates a change in the location of the weakest section in the case where material is removed from the tip of the tooth. The proposed method of locating the weakest section does not produce any change in the location of the weakest section for this case. Whether or not the effect of such a change produces measurable variations of the location of the weakest section and of the maximum fillet stress might also be the subject for some future investigation.

The equation proposed by the authors provides a method for evaluating the maximum fillet stress. This has been true also of all other proposed relationships. There is considerable evidence indicating that the range of stress, rather than the maximum stress, is the criterion of failure under fatigue conditions. The writer has observed that the so-called tensile fillet of an unloaded tooth, on a member having no residual stress, actually experiences compressive stresses due to the transfer of load through the material from the adjacent loaded tooth. This indicates that the tensile fillet is subject to a range of stress greater than from zero to maximum tensile stress. Therefore, it is suggested that another area worthy of more extensive investigation would be the stress range of a fillet section and the factors which control it.

There are without doubt other parameters which influence the maximum fillet stress and whose effect has not as yet been isolated. Continued investigation and analysis will promote improvement in the strength design of gear teeth. In the opinion of the discusser, some of the other factors which exercise an influence on the beam strength of modern gear teeth are: residual stress effects, variation of the tooth to the other, instantaneous load carried by the tooth and the rate of load variation, heat-treatment, and surface finish effects. What effect, if any, each of these factors does have will only be known when experiments directed at these parameters are undertaken.

There is a minor point of difference between the authors and the discusser regarding a statement relative to the Lewis construction. The authors state that in the Lewis construction the position of maximum stress is determined sclely by the load position and base thickness and is not influenced by the taper of the projection. Considering two of the projections shown in Fig. 10, if only load position on

the projection surface and base thickness are the determiners of location of the weakest section, it would be necessary that the apex of the parabola in the parallel-sided projection and that for the projection having sides tapering outward originate at the same location on the line of centers, in order that they be tangent to the fillets at the same location. In order that the apex of the parabola be at the same location in both projections, it would be necessary that the load applied to the surface of the projection having sides tapering outward be applied much closer to the fillet than in the case of the parallel-sided projection.

Leaving facts and dipping into the realm of conjecture, it would appear to the writer that the term $\left[1+0.26\left(\frac{e}{r_f}\right)^{0.7}\right]$ in Equation 1 is a correction factor compensating for the shortcomings of having an actual maximum fillet stress tangent to the fillet and having calculated a maximum stress on a section which intersects the fillet at the same point but is not normal to the fillet surface. Since the term $\left[\frac{1.5\,W_n\,a}{Fe^2}\right]$ represents the flexural bending stress, the terms $\left[\frac{Wn\sin\beta}{2eF}\right]$ and $\left[\frac{0.45\,W_n}{(be)^{1/2}\,F}\right]$ must be representive of stresses having the same direction as the flexural bending stress since they have been added together algebraically. These latter two terms have no rational explanation in themselves, but in combination must be accounting for such factors as the direct load stress effects on the section, the proximity of load application to the section of maximum stress, and the curved surfaces of the tooth.

Gear Strength in Terms of Fatigue Failure

—L. E. Iverson
International Harvester Co.

OUR prime concern in recent years has been gear strength in terms of fatigue failure. The need for more knowledge in this phase of design has been caused by the very evolution of machine design that faces most of us today.

Originally, a certain amount of experience was gained on a company's standardized gears with standardized addendum systems. This experience was finally tabulated and was perhaps presented in a graphical form to enable the gear designer to choose the pitch and face width which would safely carry a specified torque and rpm. This simple method, based on "gear history," is reliable and has given satisfactory results for some time. However, increases in horsepower and engine speed have carried the problem into the science of gearing.

The first problem in the science of gearing, after its geometry had been accurately defined, is to define a gear's relative strength in terms of its geometry. Once this has been accomplished we have the second problem, that of correlating known strength of materials with the relative strength based on this geometry. By strength of materials we mean ultimate yield and fatigue strength. In this discussion, we shall concern ourselves with the bending strength.

Since a gear tooth is a cantilever beam, the proportions of which (although not always beneficial) can be varied at will, we require a general theory for determining the stress in a cantilever beam. We believe such a theory exists in what we shall call the wedge theorem.

Wedge Theorem

We consider a wedge of infinite depth and finite width loaded at its vertex. The solution for the radial stress at any point with the wedge when the load is directed along the wedge centerline or more correctly center plane was given by J. H. Michell.[d] This solution and the solution for vertex loading perpendicular to the centerline at the vertex is listed in Timoshenko & Goodier.[e]

By solving any inclined force into its components normal and parallel to the wedge centerline we can combine the two solutions to give the stress at any point in the wedge. (See Fig. I.) We then have the following equation for radial stress at the wedge surface, where it is maximum for a given X:

$$\sigma_{r'_{t,c}} = \frac{P_n}{F\,X_{t,c}}\left[\cos\phi_L \cdot K_t \mp \sin\phi_L \cdot K_c\right] \qquad (c)$$

where:

P_n = Magnitude of the force in its applied direction

F = Face width

ϕ_L = Angle between the normal to the wedge centerline and the direction of the total force (positive in counterclockwise sense)

$K_t = \dfrac{\sin\alpha\cos\alpha}{\alpha - \sin\alpha\cos\alpha}$ (contributes to tension)

$K_c = \dfrac{\cos^2\alpha}{\alpha + \sin\alpha\cos\alpha}$ (contributes to compression)

α = One half the included wedge angle

X = Coordinate along the wedge centerline of the surface point investigated

Minus sign = Tension side

Plus sign = Compression side

We now apply this to a cantilever beam (Fig. J). We extend the load to the centerline of the beam, the vertex of the wedge. We construct the wedge by drawing lines tangent to the fillet. If we take the ratio of the photoelastic stress at the point to the wedge stress at the point we find: $\frac{\sigma_p}{\sigma_r} = 1.7$ where σ_p is the photoelastic stress. This held promise since any other approach from theories of maximum stress did not give a constant value, especially when the load was applied relatively close to the point of maximum stress. The significance of this ratio is ra-

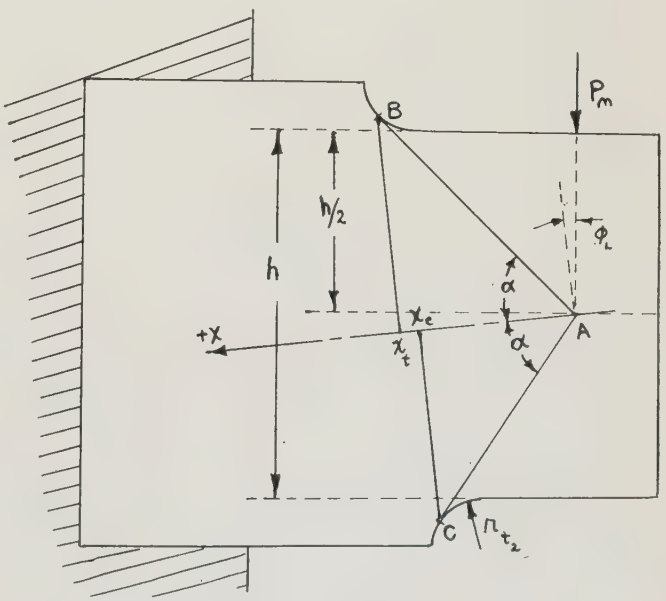

Fig. J—Wedge theorem applied to cantilever beam

[d] Proceedings of the London Mathematical Society, Vol. 34, 1902, p. 134–142: "Inversion of Plane Stress," by J. H. Michell.

[e] "Theory of Elasticity," by S. P. Timoshenko and J. N. Goodier, 2nd ed. Pub. by McGraw-Hill, New York, 1951, pp. 96–99.

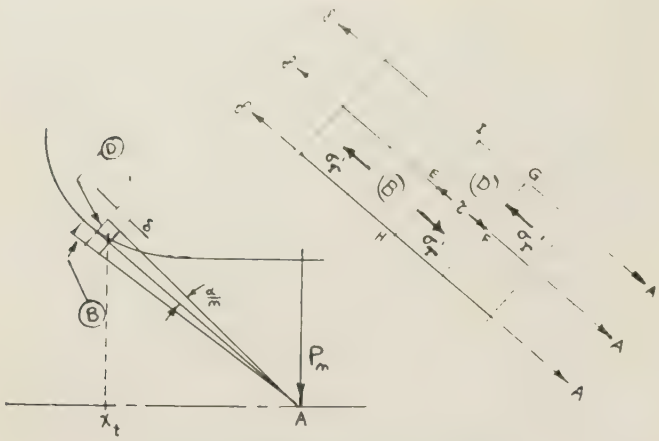

Fig. K—Application of wedge theorem

tionalized in the following manner which leads to some rather important conclusions.

We shall assume, rather than a smooth fillet, one made up of small building blocks (Fig. K).

We divide the wedge angle 2α into $2n$ parts and increment concentric circles by $m\delta = \overline{AB}$ and if we choose the subdivision point B can be represented approximately by a square. We next consider a slighter larger wedge angle of $\alpha^1 = \alpha + \alpha/n$. If the division is fine enough the radial stress on face $\overline{FG}$ of point D will be equal to the radial stress on $\overline{EH}$ of B. Since the wedge was assumed infinite the same force or stress must exist on $\overline{EI}$ to balance the forces in the elementary particle D. But there can be no force on IE since it has no supporting material. We then rationalize the force is dissipated in shear t along EF of D. Since the assumed area was approximately a square ($\tau = \sigma rt$). Converting the shear stress into an equivalent tensile stress by the Henckly-VonMises Distortion-Energy Theory ($\sigma = \sqrt{3} \cdot \tau$) where the normal stresses are zero. We then have:

$$\sigma_{t,c} = \frac{P_n \sqrt{3}}{F X_{t,c}} [\cos \phi_L \cdot K_t \mp \sin \phi_L \cdot K_c] \qquad (d)$$

as the limit where the subdivisions are made arbitrarily small and D approaches B. Actually there may be another point in the direction of D that has a higher stress ($\sigma_{\max.\ t,c}$).

Basic Tooth Models of Dolan and Broghamer[f]

We will consider only the tensile stress in the three models studied (Fig. L) and compare stresses and stress concentration factors applied to the Lewis beam formula from: the measured photoelastic values, the maximum surface wedge stress at wedge tangency, the proposed Kelley stress, and the stress concentration of filleted cantilever beams by Timoshenko and Baud photoelectric data.[g]

[f] See footnote 2.

[g] "Gears," by H. E. Merritt. 2nd ed., p. 204. Pub. by Sir I. Pitman and Sons, Ltd., London. 1942.

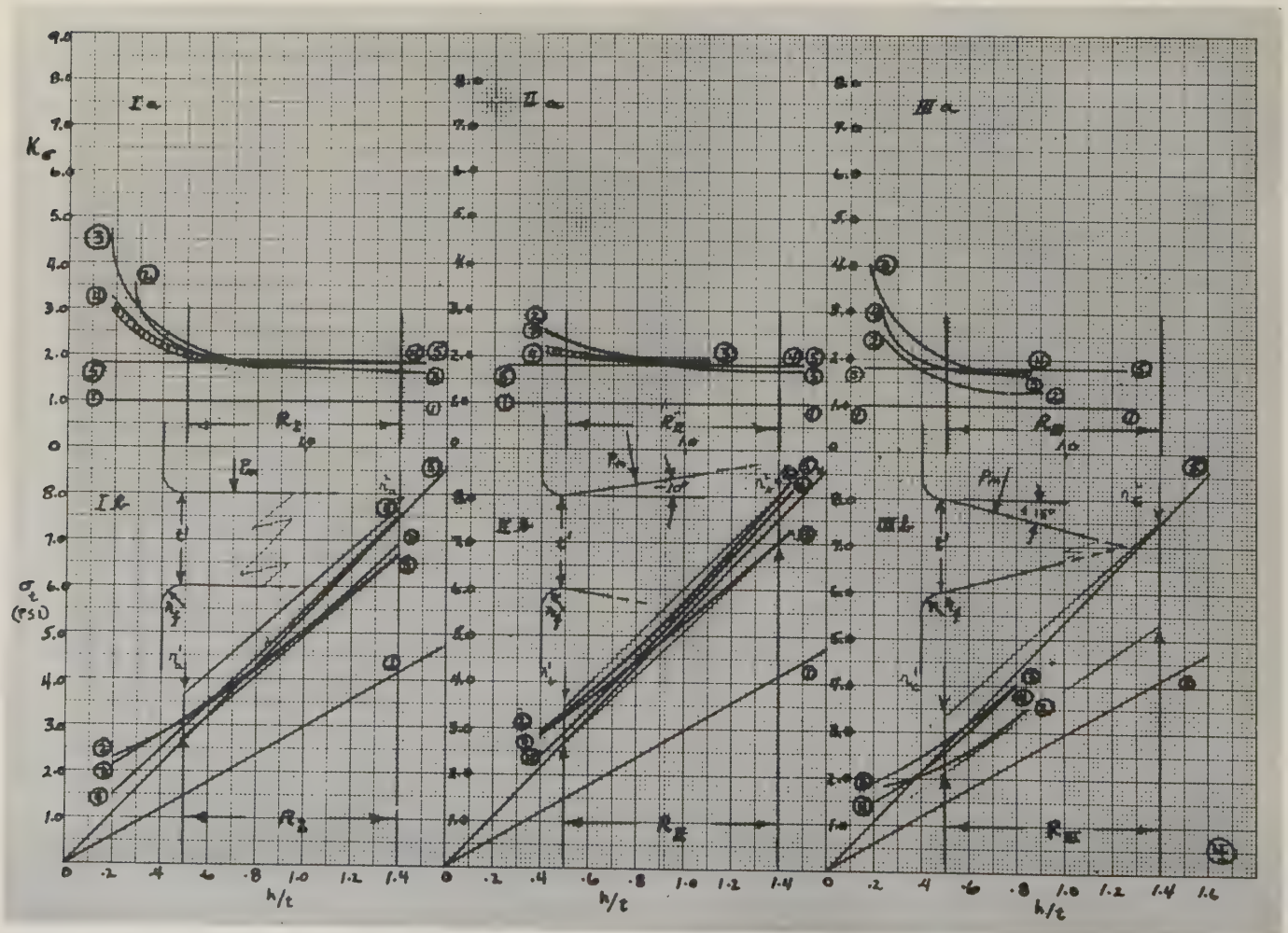

Fig. L—Comparison of actual stress and stress concentration (Pn = 1 lb, unit face, $r_{t/t'} = 0.225$, basic tooth models of Dolan)

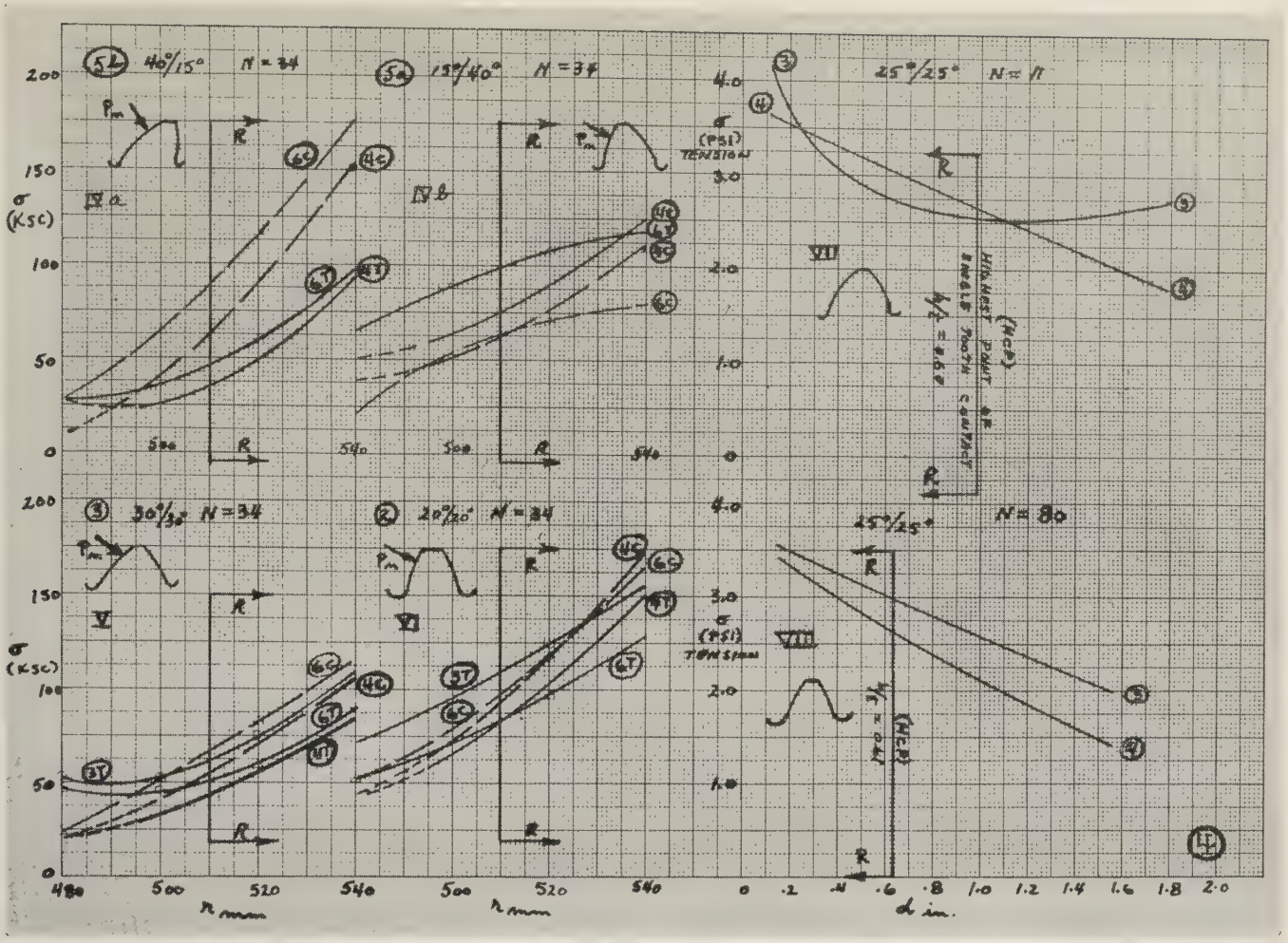

Fig. M—Formate fillet gears of Glaubitz (graphs IV to VI) and Mating pair of 25-deg P.A. generated gears

The numbered curves of Figs. L and M have the following significance:

1 —Based on the Lewis stress
2 —Dolan's measured photoelastic stress
3 —Kelley's proposed stress
4 —Wedge stress
5 —Timoshenko and Baud stress
6T—Glaubitz measured photoelectric tensile stress
6C—Glaubitz measured photoelastic compressive stress
4T—Wedge tensile stress
4C—Wedge compresssive stress

A tolerance band of stress concentration is given in graphs Ia and IIa for the wedge stress. The lower bound is determined by the stress calculated in the manner prescribed above and the upper bound by the maximum wedge stress in the fillet. Since the difference is slight, all following wedge stresses are calculated in the original manner of inscribing a tangent from the assumed vertex and letting the point of tangency be the point of maximum stress.

Stress Concentration and Actual Stress—Since stress concentration in terms of h/t ratio is the most familiar in the literature we present this first. In this analysis $r_f = 0.45$ in., $t' = 2.00$ in. Stress concentration was calculated in the usual manner, as the ratio of a stress to the Lewis stress.

For models I and II (stress concentration in graphs Ia and IIa and stress in graphs Ib and IIb, respectively) the stress concentration was comparable within the range $R = h/t$ between 0.5 and 1.4 for all methods of stress calculation mentioned herein. In model III, calculated stresses were comparable with one another for this range but not comparable with Dolan's measured values. For the range R' less than 0.5 the stresses deviated haphazardly in I and uniformly in II and III.

The important conclusion that can be drawn from this is that all stress concentration factors considered here (excluding, of course, the constant Lewis factor of 1.0) are comparable, especially when the range of h/t is between 0.5 and 1.4. This range is significant since it includes the extreme range for gear-stress calculation when the load is at the highest point of single tooth contact (*HCP*). All the stresses in models I, II and III were comparable, exclusive of the Lewis stress, for h/t between 0.5 and 1.4. By comparable, I mean that if we box off the curves in R such that all the curves are within the box and we find the average stress for $h/t = 0.95$ in the box than the maximum value and the average value have less than 20% difference. Actually it was 9.6% for I, 7.5% for II, and 17.4% for III where in III we have prorated to a region beyond our calculations.

Basic Tooth Models of Glaubitz

Of all previous methods of calculating the true stress we mention a few criticisms:

1. None of them apply to the compression side of the tooth.
2. All of them require construction of an inscribed parabola.
3. None of them fully apply to nonsymetric teeth.

The compression side of the tooth may become a criterion

for failure in extreme pressure angle gears when the compressive stress well exceeds the tensile stress in the zone of *HCP*.

In a nonsymetric tooth we have the problem of defining the tooth centerline. If we consider the usual centerline, the projected load intersects it (in the region of tip loading) at a point where there is no tooth. If we call the tooth centerline the curve made up of the midpoints of all circular tooth thicknesses (as was done in calculating the wedge stresses) we find we can get a parabola tangent to only one fillet and not both at one time. This is probably why Mr. Kelley did not include the unsymetric tooth in his comparison of stress analysis of the Glaubitz models.

The unsymetric gear is rather common place inasmuch as all hypoid gears are gears with unsymetric teeth.

Here again, the Kelley and wedge stresses are comparable on the tensile side for symetric gearing and the wedge stresses are comparable also for the compression side.

In the graphs IVa to IV (Fig. M) r is the radial distance to the point of load and since these are standard addendum gear the important stress range is for r equal or greater than the pitch radius.

Graphs VII and VIII show a mating pair of 25-deg pressure angle extreme ratio gears (11/80 ratio). This is just entered as a final comparison between the wedge and Kelley stress. d is the distance along the centerline of the tooth from the top land. The stresses were comparable to HCP and for any other load position nearer the top land.

Application of the Stress Numbers

We may say from the above we have three methods to calculate tensile stress that compares to the photoelastic stress, namely Timoshenko and Baud's stress concentration applied to the Lewis stress, the Kelley stress, and the wedge stress for symetric teeth. I shall call these stresses, which correspond to the photoelastic stress, stress number for the following important reason: We wish to convert stress into terms of fatigue life.

The greatest amount of fatigue data has been accumulated by rotating beam fatigue machines. A great collection of this material has been presented by R. Cazaud.[h] Much of Cazaud's work was done on rotating cantilever beams of large fillet radius and large h/t ratio of about 12.5. We wish to remark that the rotating beam is of circular section while a gear tooth has rectangular section, or simply a rectangular beam.

In order to convert rotating beam data into wedge data, a cone theorem was developed for circular beams which corresponded to wedge theorem for rectangular beams. If we do not apply the square root of three as factor to the cone theorem we find that as the included cone angle becomes small (large h/t ratio), the cone stress at the fillet surface approaches the Lewis stress as close as we please by taking h/t sufficiently large. As the cone angle becomes larger, the cone stress becomes noticeably larger than the Lewis stress. But the ratio $h/t = 12.5$ in Cazaud's work was well within the range to enable us to say that the cone stress without $\sqrt{3}$ was identical to the Lewis stress. All of the fatigue limits are usually based on the nominal or Lewis type stress and are exclusively so used in Cazaud. This leads to an important conclusion: either (1) we should multiply all existing nominal fatigue limit stresses by the square root of three or (2) we should divide all stress numbers by the square root of three, if we wish to compare gear life to fatigue strength.

Conclusion

1. The above conclusion works for finite, infinite, and staticly[i] failed gears in our four square and single tooth fatigue machines to "within the tolerance band of fatigue results."

2. For almost a thousand gear combinations, including full and standard fillets, four pressure angles, two tooth depths, standard and spread-center gear sets, we have not found a difference greater than 11% between the first wedge stress and the nominal Lewis stress for *HCP* loading as calculated on our IBM machine. This may well explain why the historical method has been so successful by establishing an endurance curve on Lewis stress and why prorating to new fillet radii and addendum systems has at times been misleading. For a majority of investigated gears the first wedge strength factor was very close to the nominal Lewis factor. Sometimes it was greater and sometimes less. When the Lewis factor gave a smaller stress the gear had a chance to fail in half the designed time, since fatigue life is proportional to approximately the 7.5 power of the ratio of the stresses. If the nominal Lewis stress was higher than the wedge stress the design was probably conservative.

Table B—Calculated Beam Stresses

(Mating gears are 1-2, 3-4, 5-6, and 7-8.)

Gear No.	Number of Teeth	Cutter Pressure Angle, deg	Work. Pressure Angle, deg	Diameter Pitch	Lewis Formula and Construction Stress psi	Lewis Formula with Construction Per Paper Stress, psi	Modified Lewis Formula and Construction Stress psi	Proposed Formula and Construction Stress, psi
1	18	20	20.46	4½	27,246	17,047	25,944	31,258
2	34	20	20.46	4½	25,035	18,266	29,190	26,655
3	23	20	23.24	4½	21,401	13,369	20,825	24,491
4	28	20	23.24	4½	21,629	14,266	21,816	25,909
5	15	20	22.44	5	18,481	11,442	17,326	22,819
6	42	20	22.44	5	21,098	15,150	24,198	27,437
7	19	20	23.37	6	34,714	21,503	34,406	43,013
8	31	20	23.37	6	37,587	25,383	42,874	48,916
			Average		25,899	17,435	27,072	31,312
			Per Cent		83%	56%	86%	100%

3. Finally, we wish to briefly review the object and contents of this paper:

There are existing methods of predicting photoelastic stress values in symetric cantilever beams and we wish to describe one more method that is general enough to include unsymetric cantilever beams, namely the stress number calculated by the wedge theorem.

Once we have a stress number, which relates to the stress of the beam, we wish to convert this into terms of fatigue life. This is done by dividing the stress number by the square root of three and comparing this stress with the stress-cycle curve obtained from rotating beam data. In this manner we very closely approximate the number of stress cycles to failure, at least within the tolerance band. It is to be remarked once more that this modified stress number is very close to the nominal Lewis stress but there are times when life-wise it may lead to serious results if we use the Lewis stress and do not heed the modified stress.

Emphasizes the Many Variables About Gear Strength

—H. E. Merritt
Consultant

THE authors' contribution to means for evaluating the actual stress in a loaded gear tooth is most welcome, but it leads to the question of how those results can be effectively applied. The calculation of the maximum bending stress must rest on assumptions in regard to the point of load on the tooth profile associated with the maximum stress. Such assumptions must be arbitrary, because of the uncertain effect of errors of pitch and profile, combined with tooth deflection and the resulting dynamic loading; thus, the ultimate results must be regarded as comparative rather than absolute. It is probable, therefore, that on the basis of any particular set of assumptions of this kind, the authors' results could be reduced to a simplified form.

[h] "Fatigue of Metals," by R. Cazaud. Pub. by Philosophical Library, New York, 1953.

[i] When the ultimate strength is used.

A further question which arises is how the maximum stress thus calculated is related to the endurance limit of any gear material as determined on specimens having only a modest rate of change of section. It would appear probable that not merely the maximum stress, but also the stress gradient near the surface, must be taken into account. It is, therefore, to be hoped that the authors' work will be supplemented by a much larger number of tests on gear teeth of different formations and in various materials. In the absence of such information, the practicing gear designer may well be reluctant to change his techniques.

It may well be that, having regard to the effects of stress gradient and the different notch-sensitivity characteristics of various materials, the best basis may be that adopted by Dolan and Broghamer, in superposing a stress-concentration factor upon the nominal stress along the inscribed parabola.

Finds Original Lewis Formula Best Approach To Gear Strength Analysis

—K. J. Harris
Deere Mfg. Co.

MY FIRST observation is that there seems to be some degree of difference in the test results of the various research groups in the study of photoelastic models as recorded in the paper. Therefore, we have reason to believe that there is some basic difference in the preparation and handling of the test specimens, which throws a shadow of doubt over the formulas derived from them.

In order to evaluate the formula proposed by the authors, I have selected four pairs of gears from our tractors, and analyzed them using the following formulas:

1. Lewis formula as presented in his paper.[j]
2. Lewis formula as described in this paper.
3. Modified Lewis formula as described by Dolan and Broghamer.[f]
4. The new formula presented in the paper that we are discussing.

As you will note I have listed two different Lewis formulae.

In the files of the our research division we have a copy of the transactions of the Engineers Club, which include the original paper by Mr. Lewis. In reviewing this information I found that the formula has been handed down to us correctly, but its application has been distorted, as can be seen in Fig. N, which is a reproduction of the original Plate I of Mr. Lewis' paper.

It seems that in those days engineers were experiencing the same difficulty that we are having today: They couldn't agree on a formula.

You will note that the normal load is shown as applied at the tip of the tooth instead of at the highest point of single tooth contact, as the authors suggest in their paper. Also, the tangential load is taken at the intersection of the line of action with centerline of the gear tooth, as is true in the analysis of the strength of a beam, instead of at the surface of the gear tooth as used in the paper. Mr. Lewis stated that theoretically on perfectly formed and spaced gear teeth, there would be two teeth in contact at the point used in his formula, and the load would be divided between the gear teeth, but that a method of cutting such perfect gears had not been developed to date.

This observation is still true, as even today's best commercial practices allow enough error in gears produced to specifications to permit loading at the tip of a single tooth. Soft gears may wear in after a time and have the desired contact, but we have observed that conditions can exist in a group of samples due to varying material and heat-treatment. Engineers responsible for manufacturing can do much to overcome this complaint, but they can hardly be expected to make perfect gears all the time.

This is the construction that our engineers use in their analysis of gear strength. Since the other formulas used in the calculations have been used in the paper we are discussing, I will not explain them here. Table B shows the results of our calculations.

From the analysis of the formula presented in this paper, I have come to the following conclusions:

1. The calculated static stresses obtained with the new formula are much higher than those obtained with the formulas used by practically all gear designers up to this time.
2. The reason for the increased calculated stress is the "stress shift" described in the paper.
3. The "stress shift" is so dominant in the proposed formula that it even changes the relationship of the stresses as shown in the first pair of gears I examined.
4. Due to the difference in the loads and loading points used, the original Lewis formula and construction will in-

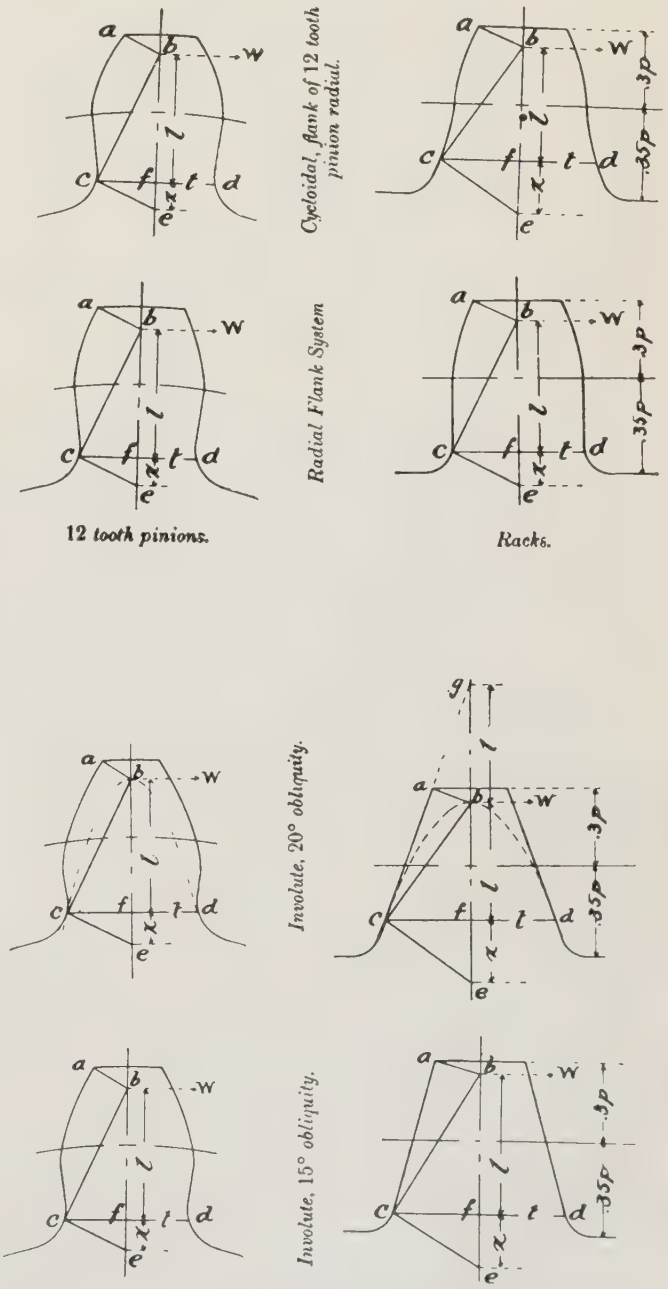

Fig. N—Reproduction of original Lewis construction

[j] See footnote 1.

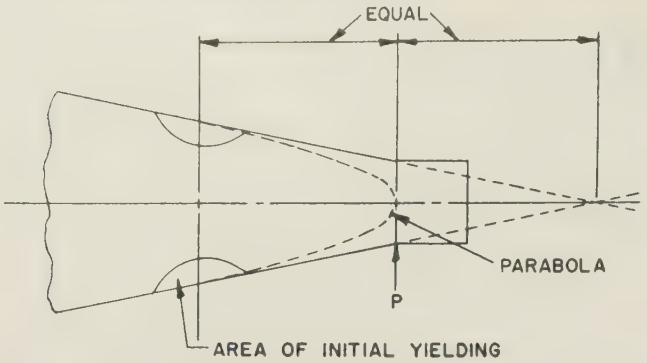

Fig. O—Yield regions found by Steele and Hassan

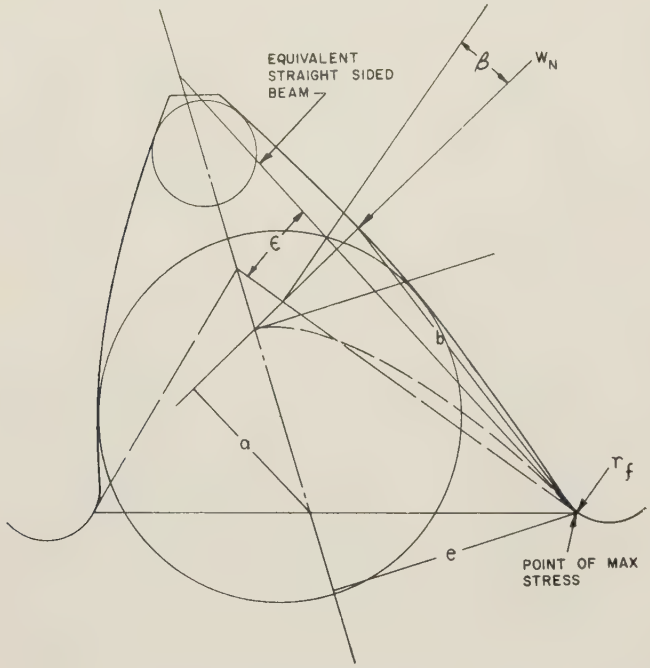

Fig. P—New formula for unsymmetrical tooth

dicate the existence of the same relationship of stresses for a pair of gears as the new formula does.

5. Both the original Lewis formula and the modified Lewis formula show stresses that are nearer those indicated by the new formula, than the spread of data recorded by the other investigators.

6. When we take into account the variations in gear-tooth strength due to materials, heat-treatment, surface finish, imperfections in fillets, mismatching of shaved surface with fillets, and dynamic load factors that have not been covered in this paper, it becomes apparent that the formulas are only approximations, and as such must be modified still farther in order to reflect the true conditions that exist in a vehicle.

It should be noted that in our plant we use tooth forms that are tailor made to accommodate the loads they are required to carry. Therefore, I am unable to make a direct comparison between them and the type of gears used in the analysis reported in the paper.

In conclusion, I want to say that we are able to predict the load-carrying capacity of our gears fairly accurately by using the original Lewis formulas and construction in conjunction with our knowledge of gear strength obtained from locked-up torque gear test machines, similar to those used at Caterpillar. The only variables that we do not allow for in this method of analysis are those due to mountings, deflections, and source of power.

We have found this to be a realistic and satisfactory approach to a very complex problem.

Author's Closure To Discussion

WE are grateful to the contributors who have written formal comments regarding this work and to those who have personally discussed the problem with us. Particular thanks are due to Dr. Heywood since much of our work was based upon the foundation material in his book.[b]

In reply to Dr. Heywood's comments, the authors' selection of the parabola to establish the sides of the equivalent straight-sided beam has additional background other than those points mentioned. In a recent discussion, Prof. J. O. Smith at the University of Illinois pointed out with reference to some work done by Steele and Hassan[k] that such a straight-sided beam as suggested in the paper appears to be the most rational selection that could be made. Briefly, their work concerned a series of mild steel-tapered beams loaded at some distance from the apex as shown in Fig. O. The center of the yield regions that actually occurred in their tests can be located by the insertion of the parabola shown. If a fillet existed close to this area the maximum stresses would be pulled away from the yield region by the amount of the "stress shift" discussed in the paper.

As Dr. Heywood has mentioned, there is no doubt that a large area of the fillet has an effect on the stress concentration. The selection of the radius at the point of maximum stress was used because, with reasonable accuracy, it represents the average value of those radii which play the most prominent role in the actual concentration of stress.

We must agree with Mr. Jacobson about the benefits of using charts, and there is no question but what the accurate use of any formula is subject to the care given by the designer. Of course, as was mentioned in the paper, the use of automatic computers will eliminate the layout stage and the corresponding errors.

It may be well to keep in mind that charts that are constructed strictly from experimental values must invariably be subjected to some adjustment during their construction. A single photoelastic measurement is less likely to be reliable and consistent with other values than a calculated value based on an encompassing formula. One needs only to connect the points of a calculated curve and compare them with the problem of connecting experimental points in a smooth curve to recognize this. Our attitude is that a formula which correlates closely with the mass of data, covering well the extremes of variation, is more reliable for extrapolation and can be more successfully used in the construction of charts such as Mr. Jacobson recommends.

We agree with Prof. Broghamer's comments on the projections shown in Fig. 10 that admittedly the degree of taper will influence the point of intersection of the load extension with the centerline of the projection, which in turn will cause a change in the Lewis position of maximum stress. We also maintain, however, that if the distance from the root to the point of intersection is held constant, then the degree of taper will independently influence the position of maximum stress. A more thorough study of the reasons for and a clarification of the "stress shift" factor is needed, however.

A minor disagreement exists between the authors and Prof. Broghamer with regard to the term $\left[1 + 0.26\left(\frac{e}{r_f}\right)0.7\right]$ in the equation. Although empirical, it is nevertheless, a formula which fits the average of curves for many measured stress concentration values as Dr. Heywood has pointed out in his chapter on "Stress in Particular Notches." If the formula recommended is changed in the future, it is doubtful that this part will be modified significantly.

Mr. Iversen's comments are most interesting, although there are several points of disagreement between the

[k] WADC TN 56-330, Part III: "Effects of Inelastic Action on the Resistance to Various Types of Loads of Ductile Members from Various Classes of Metals," by M. C. Steele and H. A. Hassan.

method and the results proposed by Iversen and the authors' proposed method. We are fully cognizant of the wedge theorem as suggested by Iversen, but we feel that much more work needs to be done before it can be successfully applied. A detailed discussion of the proper application of the wedge theorem cannot be made here.

Mr. Iversen has selected a wedge which, in effect, has empirically given him satisfactory results in the use of a constant stress-concentration factor. Even moderate variations of fillet radii cannot produce the desired results in the formula suggested. In this regard, if Mr. Iversen had included in his work the data from Glaubitz's model 1, we feel sure the results would not have been as satisfactory.

Furthermore, if one compares Iversen's graphs V and VI with each other, ignoring the correction factor K_e described in the paper for Glaubitz's work, we find that, if the gears were loaded at the tip, both our formula and Glaubitz's stress measurements show the 20-deg pressure angle gear to be approximately 40% weaker than the 30-deg pressure angle gear. This ratio of calculated stress parallels the measured stresses on these two models for all points of loading. This is not true with Iversen's application of the wedge theorem, which indicates the 20-deg pressure angle to be 80% weaker than the 30-deg pressure angle gear when loaded at the tip, and the ratios of calculated to measured stresses change drastically at different loading points.

With regard to Mr. Iversen's critcisms, we should first mention that we have yet to see a fracture that has originated from the compression side of the gear tooth. However, as a matter of academic interest, we have tried the formula on the compression side and have found the results excellent. There should be, after all, no physical restrictions to the formula that do not apply to any such formula including the wedge theorem.

Secondly, the construction of an inscribed parabola is a matter of a few seconds and should never be used as a drawback to the use of any formula.

Third, because we were not, at the time, concerned with unsymmetrical gear teeth they were left out of the original paper. Since Mr. Iversen's comments include it, however, we can show that by using the construction of Fig. P the formula can be used with somewhat more accuracy than Mr. Iversen's wedge theorem.

Briefly, the tooth design is divided as close to center as possible by constructing two circles which contact the profiles. The parabola can be constructed for one side through this centerline. True, the complete parabola would not be symmetrical about the centerline but neither would an inserted wedge. The values ε, α, e, β and b are obtained as illustrated and inserted in the formula of the paper.

The results of this and test results are shown in comparison with Iversen's in Fig. Q.

We may also mention that in regard to the comparison between stresses on rotating beam tests versus gear tests of identical heat-treatment, material, and breakage cross-section, we have direct correlation without the use of a correction factor, such as Iversen's square root of three.

Dr. Merritt has expressed the feelings of many engineers concerning the many variables which enter into gear strength. He has very well expressed the reluctance to change that is also expressed by Mr. Harris. There really is no serious harm in remaining with an old tried-and-true method of analysis—providing the engineer is completely familiar with its limitations.

In this regard, Mr. Harris's method of analysis may work well with a strongly standardized, limited range of gear designs. If, however, we apply the "original" Lewis method to the gears in Fig. 10, we find that the high-pressure angle gear is predicted to be 64% stronger than the lower pressure angle gear, which constitutes considerable error since it is 10% weaker.

It is scarcely necessary to review the old problem of where the maximum load occurs on a gear tooth. This has been subjected to convincing analytical and experimental work[1] to prove that for good commercial accuracy the maximum stress occurs when the load is at the highest point of single tooth contact. A comparison relating gear to pinion strengths of the "original" Lewis formula values and the new formula values of Table B, assuming that the "original" values predicted the strength of the gears correctly, prove that the new formula would be of equal accuracy in this case while also being of equal accuracy on "nonstandard" designs.

We have a strong preference for building information of factors such as notch sensitivity and dynamic loads on as solid a foundation as possible. Only in this way can we attempt to extrapolate information, not only in the field of gear design, but from that of other machine parts as well.

[1] SAE *Quarterly* Transactions, Vol. 6, April, 1952, pp. 252–258: "Beam Strength of Spur Gears—Whether to Use the Higher or Lower Strength Factor," by R. P. Van Zandt.

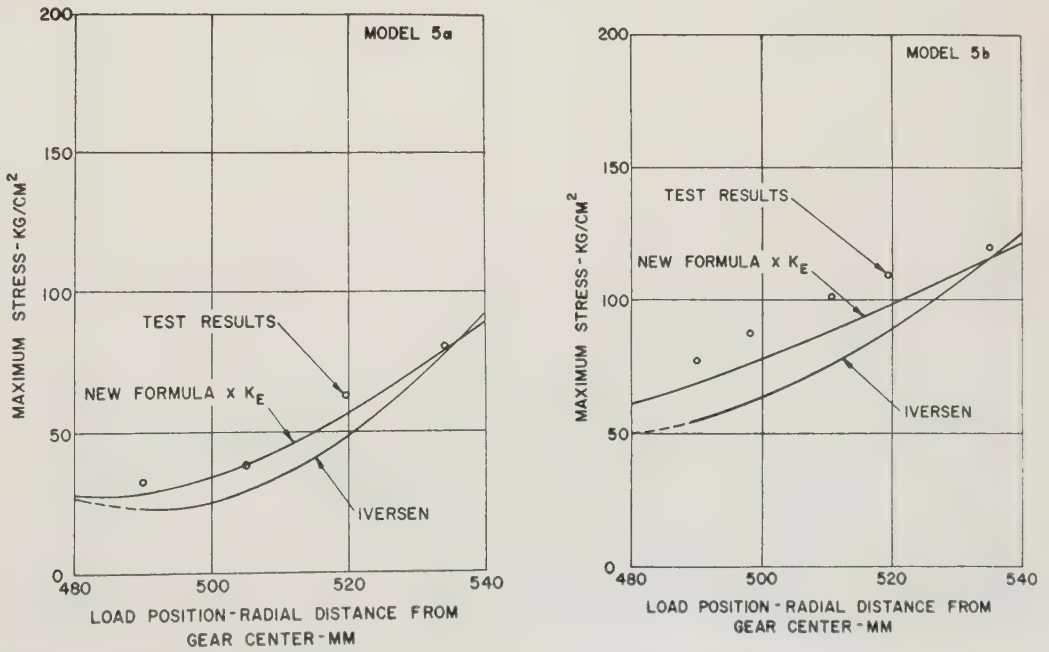

Fig. Q—Comparison of Iverson and author's formulas with test results

THIS paper describes the Chrysler TorqueFlite transmission, a 3-speed unit with torque converter. The discussion includes details of the push-button controls of the automatic transmission, operation of the transmission and hydraulic controls, power transmission through the gearbox, and design of several of the components.

The authors think that the TorqueFlite offers to a greater degree the advantages of automatic transmission: ease of operation and maximum power over a wide range of car speeds.

Chrysler

THERE has been in recent years a marked preference for automatic transmissions, especially in the medium- and high-priced cars. The main reason for this preference is the ease of overall car operation. It also permits the driver to obtain near maximum power for acceleration and hill-climbing ability over a wide range of car speeds.

Among the automatic transmissions offered to the car-buying public, the PowerFlite transmission, first introduced by Chrysler in the 1953 Imperial models, proved to be a successful innovation. This transmission became available on all our 1954 models, and over 2,000,000 units have been built to date.

As a result of the subsequent demand, it became necessary to decide whether to enlarge the existing production facilities for the PowerFlite transmission, or tool-up for a new transmission. Because of the improved car performance made possible by a new transmission design which we had been testing for some time, the latter solution was adopted.

The new TorqueFlite transmission, Fig. 1, was selected after many studies and tests—both in the laboratories and on the road—of several combinations involving a 2-speed transmission with a torque converter, a 3-speed transmission with a torque converter, and a 4-speed transmission with a fluid coupling. Performance and economy data were obtained along with general driver reaction, and this information indicated that the 3-speed transmission with a torque converter was the most desirable unit. It was also found that, for maximum performance, all three gear ratios should be used during every start in drive range. In keeping with Chrysler tradition, emphasis was logically placed upon smoothness of operation.

In our opinion, the TorqueFlite transmission embodies the basic design parameters that result in high performance, quiet operation, smooth shifting,

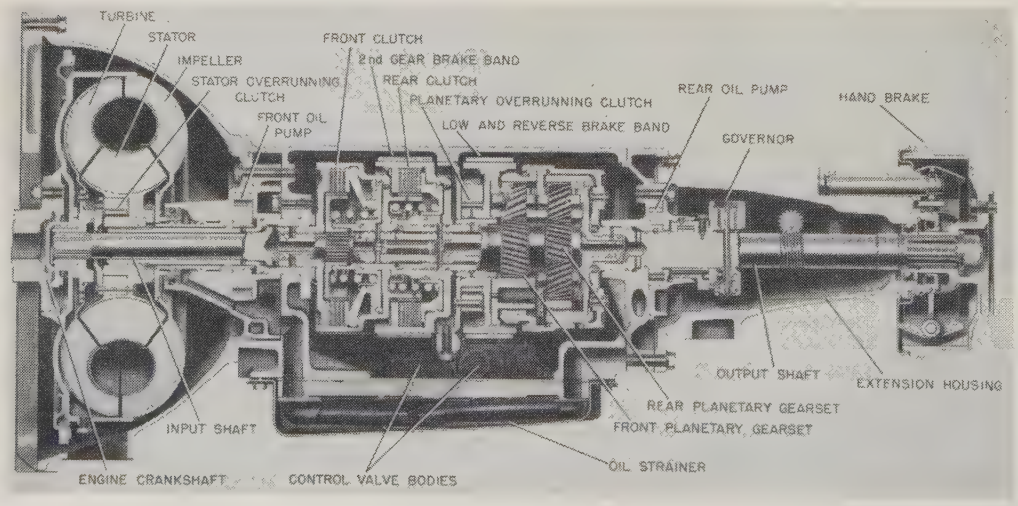

Fig. 1—Chrysler TorqueFlite transmission

TorqueFlite Transmission

S. D. Jeffe and B. W. Cartwright, Chrysler Corp.

This paper was presented at the SAE Annual Meeting, Detroit, Jan. 16, 1957.

and component construction that provides for ease of manufacture on a high-volume basis.

Push-Button Controls

Before discussing the TorqueFlite transmission, it might be well to point out the features of the push-button control system introduced by Chrysler Corp. in the fall of 1955. This was an entirely new and unique automatic transmission control system. It represented the latest step in the logical progression from floor-lever shifting to steering-column lever, then to the dash-selector lever, and finally to push buttons—an important advance toward greater ease of operation.

The shift control unit is made up of three components: the push-button control box located on the instrument panel, the control valve at the transmission, and a flexible cable linking the push-button box with the manual control valve. (See Fig. 2.)

The control box contains the push buttons which are attached to individual slides. The slides limit the travel of the cable and are locked in place through an actuator bar and spring clip mechanism. The spring clip is designed so that one button must be fully depressed to release the previously engaged one.

The control cable extends from the push-button housing on the instrument panel down to the transmission manual valve. The complete cable assembly consists of a rubber-covered steel outer housing encasing a flexible stranded precision steel cable. The outer housing is held stationary at both ends. When a button is pushed, the cable moves within this housing to locate the position of the transmission manual control valve.

The manual valve is accurately held in position in the transmission valve body by a ball and spring detent mechanism. The manual valve directs oil pressure to the proper control circuit in the transmission to obtain the desired range.

The push-button control box incorporates a back-up light switch actuated by the reverse button slide, and on some models, the control box also contains a neutral starting switch. The latter allows the driver to crank the engine by pushing the neutral button beyond its normally applied position, thereby eliminating additional manipulation of the ignition key if the engine should stall.

The push buttons are located to the left of the steering wheel so only the driver can reach them. For night operation, the buttons are illuminated. As can be seen, reliability and simplicity were the prime factors in selecting a purely mechanical system for the push buttons.

Transmission Operation

The TorqueFlite transmission consists of a 3-element torque converter coupled to an automatic 3-speed planetary gearbox. This provides, along with neutral, three forward driving ranges and reverse. The gear ratios are obtained through two compounded planetary gear sets and are controlled

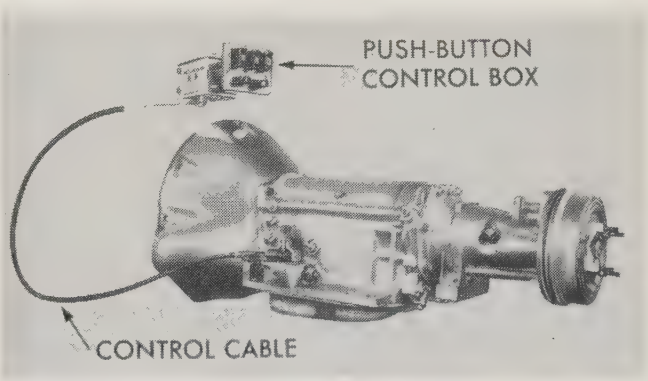

Fig. 2—Push-button control system

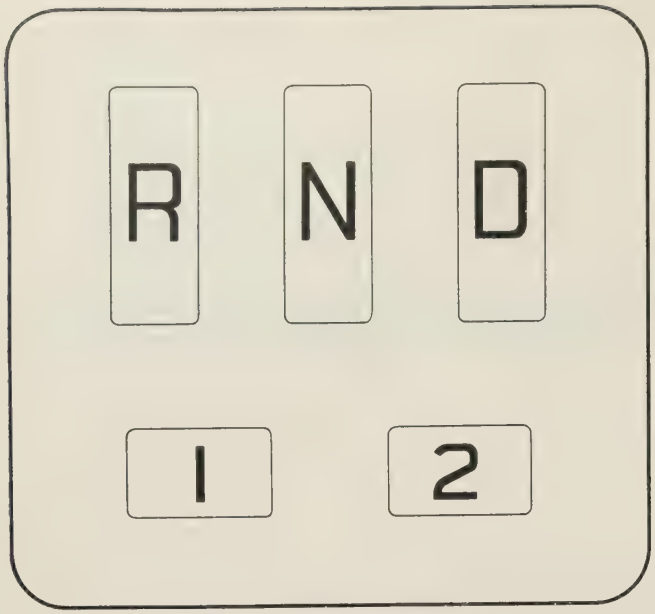

Fig. 3—Push-button panel

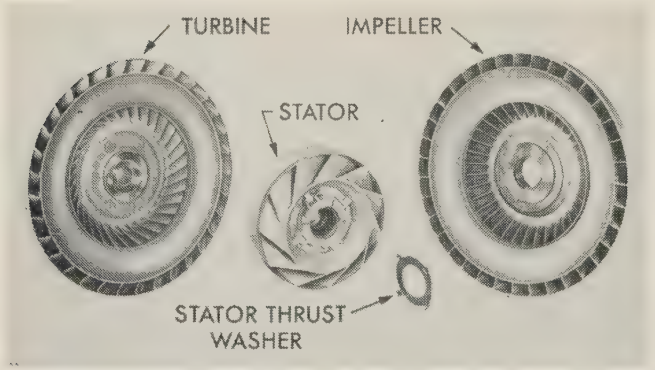

Fig. 4—Torque converter components

by two multiple disc clutches, two bands, and an overrunning clutch. As on the PowerFlite, the complication of a parking position is eliminated through the use of a powerful internal expanding hand brake mounted on the rear of the transmission extension. The hand brake, which is completely independent of the wheel brakes, is a standard feature on all our cars equipped with automatic transmissions.

TorqueFlite is presently used in Plymouth, Dodge, DeSoto, Chrysler, and Imperial models. These vehicles vary in weight from 3700 to 5200 lb, in engine displacement from 301 to 392 cu in., and axle ratio from 2.92 to 3.54. In general, our cars equipped with this transmission contain axles one ratio numerically lower than previous models. A 12½-in. diameter water-cooled torque converter is used with the 392-cu in. engine installations. All other powerplants use 11¾-in. diameter torque converters.

Fig. 3 shows the five push buttons used to select the driving ranges. In addition to neutral ("N") and reverse ("R"), three forward driving ranges are provided:

"D"—Drive—In this position, the transmission always starts in "first" gear and automatically upshifts into "second" and "direct." Kickdown into "second" gear is possible below 65 mph, and into "first" gear below 30 mph. A closed throttle downshift from "direct" to "first" gear occurs at 10 mph.

"2"—Second—In this position, the transmission always starts in "first" gear and automatically upshifts into "second." It will remain in "second" regardless of throttle opening until 70 mph, at which time it will upshift into "direct" to prevent overspeeding the engine. Kickdown into "first" gear is possible below 30 mph. A closed throttle downshift from "second" to "first" occurs at 10 mph. The provision for "second" gear operation allows greater drive control in city traffic and hilly terrain.

"1"—First—In this position, the transmission starts and remains in low gear regardless of car speed and throttle opening. If this position is selected at speeds above 30 mph and below 65 mph, the transmission downshifts into "second" immediately and will remain in "second" until the vehicle speed falls below 30 mph, at which time it will downshift into "first" gear. As will be pointed out subsequently, this is a 2-way drive gear position.

All of the shift speeds referred to are approximate values for a Chrysler New Yorker car with 3.18 axle. The progression through all three gears in "drive" operation obviously results in two automatic upshifts. The upshift from first to second involves a transition from an overrunning clutch to a band. The upshift to direct is completed by the transfer from a band to a clutch in a manner similar to the present PowerFlite upshift. The incorporation of the overrunning clutch has greatly improved the operation of this transmission. During the 1–2 upshift, the overrunning clutch remains engaged until the kickdown band has gained sufficient torque capacity to carry the load; at that time a torque reversal occurs on the "low" reaction member, thereby causing the overrunning clutch to freewheel at precisely the proper instant. The transient capacity of the band is controlled by the kickdown piston and an accumulator. If friction material had been employed as a "low" reaction, the control of the shift would become considerably less accurate. The normal 3–1 downshift involves the transition from the direct clutch to the overrunning clutch. Since this

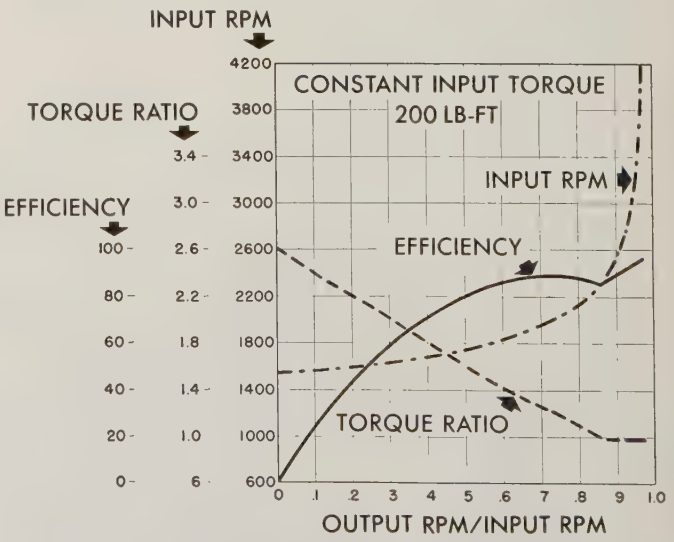

Fig. 5—Performance characteristics for 11¾-in., 2.6 stall ratio converter

downshift normally occurs at closed throttle, the "low" reaction member will rotate forward causing the overrunning clutch to freewheel and thereby will permit an imperceptible downshift.

A forced downshift from 3 to 1 or 2 to 1 is also aided by the overrunning clutch. Good quality in this shift can only be maintained by proper engagement timing of the oncoming element. In the TorqueFlite, the overrunning clutch will always automatically engage at precisely the instant when the engine has made the proper speed change to correspond to the new ratio. In this manner, an extremely smooth kickdown is accomplished.

Torque Converter

Three torque converters are available to cover all Chrysler models employing the TorqueFlite transmission. All of the converters are single-stage, 3-element units containing an impeller, a turbine, and a single stator (Fig. 4).

The turbines and impellers employ stamped blades which are spot-welded to a stamped inner shroud and, in turn, hydrogen-brazed to their individual shells. The stators are die-cast aluminum employing an internal overrunning cam riveted in place. The remainder of the overrunning unit which is incorporated into the stator includes eight individually-energized rollers and a splined free-wheeling hub which mounts on the reaction shaft. The front cover, which is mounted rigidly to the crankshaft, is fastened to the impeller by means of a submerged arc weld about the periphery of the converter.

The three converters available with TorqueFlite are:

1. An 11¾-in. diameter, 2.6 stall torque ratio, air-cooled converter employed in the Chrysler Windsor (Fig. 5); water-cooled in the Chrysler Saratoga.
2. An 11¾-in. diameter, 2.7 stall torque ratio, air-cooled converter employed in all other V-8 installations (Fig. 6), except the 392-cu in. V-8.
3. A 12½-in. diameter, 2.3 stall torque ratio, water-cooled converter employed for all 392 cu in. engine installations (Fig. 7).

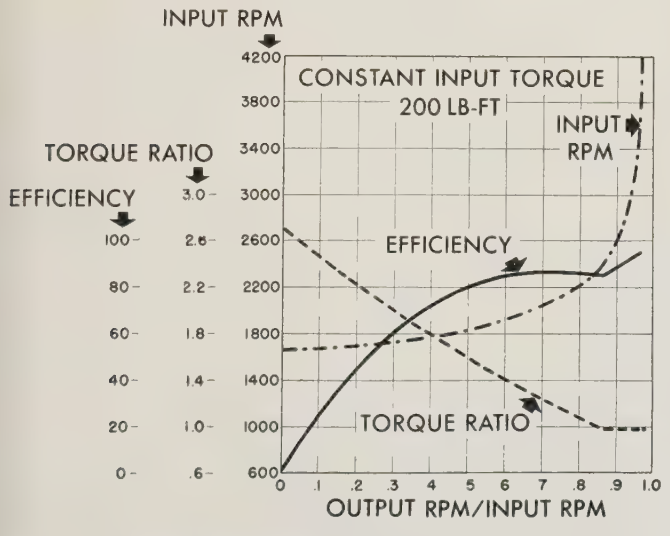

Fig. 6—Performance characteristics of 11¾-in., 2.7 stall ratio converter

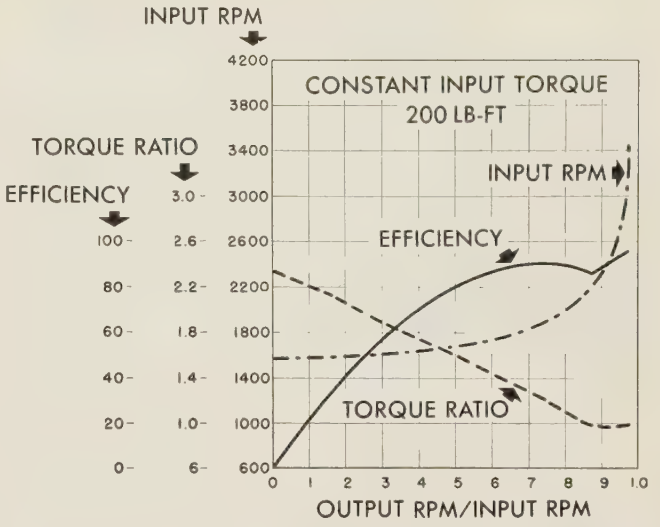

Fig. 7—Performance characteristics of 12½-in., 2.3 stall ratio converter

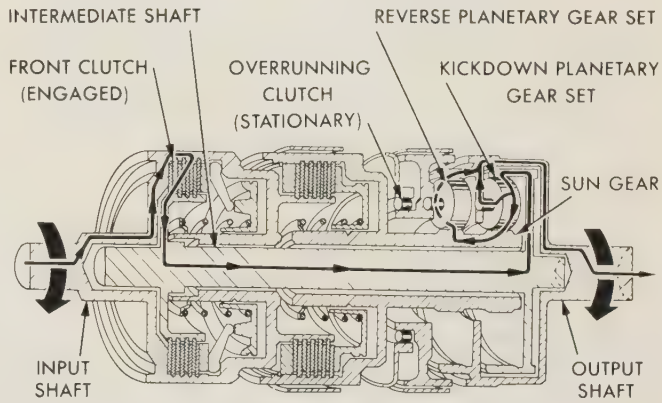

Fig. 8—Power flow—breakway

Both of the 11¾-in. diameter units were available with the PowerFlite transmission, but the 12½-in. diameter converter was developed specifically for the TorqueFlite application. The 11¾-in. diameter converters could further improve car performance with the large engine, but are not used because of the greater torque-capacity requirements of the transmission as well as excessive wheel-skid characteristics with these smaller converters.

The new 12½-in. diameter converter was designed to reduce excessive peak torques that the transmission must handle, but still provide increased performance compatible with engine overrun. The low-speed peak input torque has been reduced with the new torque converter, but the higher torque available in the midrange provides a net gain in overall vehicle performance as compared to the 12½-in. diameter converter previously used with the PowerFlite.

Power Flow

The following section reviews each driving position to show how the power is transmitted through the gearbox.

Drive: Breakaway (Fig. 8)—The power flow is

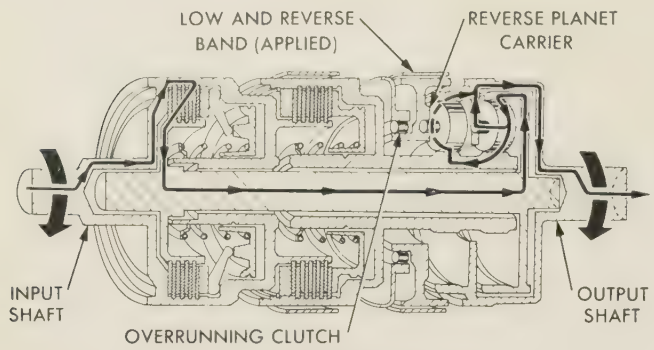

Fig. 9—Power flow—low

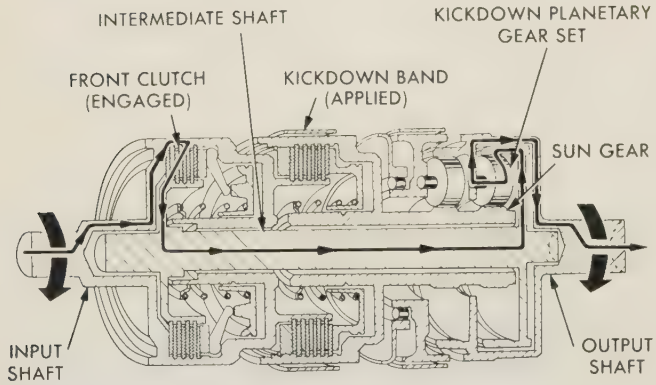

Fig. 10—Power flow—second

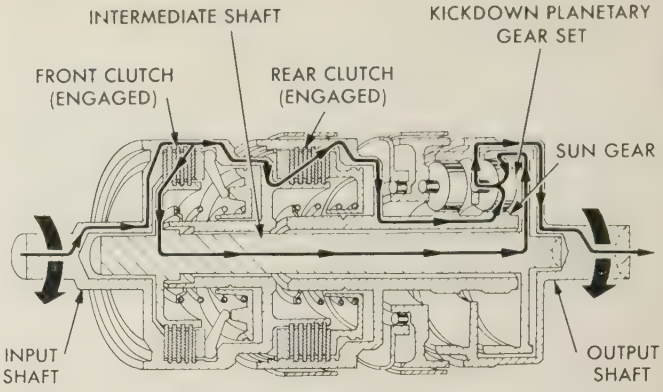

Fig. 11—Power flow—direct

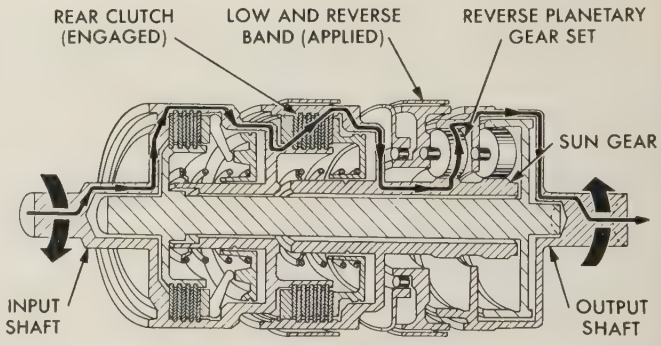

Fig. 12—Power flow—reverse

from the torque converter turbine through the input shaft and front clutch retainer. The front clutch is engaged, and the power is transmitted through the front clutch hub and intermediate shaft to the kickdown annulus gear. The annulus gear drives the kickdown planet pinions which rotate the sun gear in a reverse direction. The sun gear rotates the reverse planet pinions forward and thereby produces a forward rotation of the reverse annulus. The reverse planet carrier is prevented from rotating backwards by an overrunning clutch which becomes stationary during "breakaway." The reverse annulus and kickdown planet carrier combine in the output shaft drive housing to rotate the output shaft forward and produce a torque ratio of 2.45 to 1. For low-range operation (Fig. 9), the overrunning clutch is locked out by the low band.

Drive: Second Operation (*Fig. 10*)—The power flow is from the torque converter turbine through the input shaft and front clutch retainer. The front clutch is engaged and the power is transmitted through the front clutch hub and intermediate shaft to the kickdown annulus gear. The kickdown band is applied and holds the sun gear stationary. The kickdown annulus gear causes the planet pinions to rotate forward forcing the planet carrier in the same direction. The kickdown planet carrier is splined to the output shaft drive housing and rotates the output shaft in the same direction, producing a torque ratio of 1.45 to 1.

Drive: Direct (*Fig. 11*)—In direct drive both clutches are engaged and locked together. Since the kickdown annulus gear is connected to the front clutch through the intermediate shaft and the sun gear is connected to the rear clutch, the kickdown planetary unit is locked, and the entire planetary system rotates as a unit at input shaft speed. This produces a torque ratio of 1 to 1.

Reverse (*Fig. 12*)—The power flow in reverse is from the torque converter turbine through the input shaft and the rear clutch retainer. The rear clutch is engaged and the power flow is through the rear clutch retainer and sun gear. The sun gear drives the reverse planet pinions in the reverse direction. The reverse planet carrier is held by the action of the low and reverse servo and band, and the planet pinions drive the reverse annulus gear in the reverse direction. The reverse annulus gear, being splined to the output shaft drive housing, rotates the output shaft in a reverse direction, producing a torque ratio of 2.2 to 1.

Hydraulic Controls

Fig. 13 shows a diagram of the TorqueFlite hydraulic control system in drive ("D") breakaway.

The hydraulic controls of the transmission have some unique features worthy of mention:

3–1 Downshifts—In most automatic transmissions currently in production, the procedure used in downshifting when stopping the vehicle is the reverse of the upshift sequence. That is, in a 3-speed transmission making automatic upshifts from first to second to third, the closed throttle downshifts have

been made from third to second to first in rapid sequence with resulting undesirable roughness and noise. In the TorqueFlite transmission, the upshift sequence in Drive range utilizes all three ratios, but when the vehicle is brought to a stop, the transmission remains in direct drive until approximately 10 mph, when the downshift at closed throttle is made to low gear without passing through the second ratio. This arrangement results in an imperceptible downshift because the overrunning clutch freewheels and completely eliminates any objectionable bumps or noise. The direct-to-low downshift is accomplished by the 3–1 relay valve, which coordinates the movements of both shift valves.

Shift Pattern—Considerable development effort was spent in establishing the most desirable shift pattern. Several modifications were made to experimental units to vary the speed at which shifts occurred for a given throttle opening, and these units were evaluated by various personnel to establish their preference. In general, they seemed to prefer a shift pattern that places the transmission into direct ratio as early as possible at light and medium throttle openings. The maximum performance shift pattern was limited by engine characteristics and noise. The TorqueFlite transmission control system provides an early pattern for normal driving and what we have chosen to call a "delayed shift pattern" for situations that require optimum performance. The "delayed shift pattern" is obtained by depressing the accelerator pedal through the "detent" to the wide-open throttle position. At wide-open throttle, the 1–2 shift occurs at approximately 40 mph and the 2–3 shift at approximately 70 mph. At the detent, just short of wide-open throttle, the two shifts occur at approximately 25 and 55 mph. This arrangement has met with the widespread acceptance of all who have taken the wheel of a TorqueFlite-equipped car.

Kickdown Control—The use of the shuttle valve for control of kickdown quality in the PowerFlite has proven successful, and this valve was retained in the TorqueFlite controls with certain refinements to provide for smooth engagement of the kickdown band during forced 3–2 downshifts. Below approximately 30 mph, the TorqueFlite will kickdown into low gear, and the overrunning clutch provides a smooth transition without the need for additional hydraulic controls.

Design Features

A number of unusual innovations in transmission design have been incorporated in this new transmission and will be discussed briefly.

Gear Train—The gear train is designed so that both sets have the same numbers of teeth and iden-

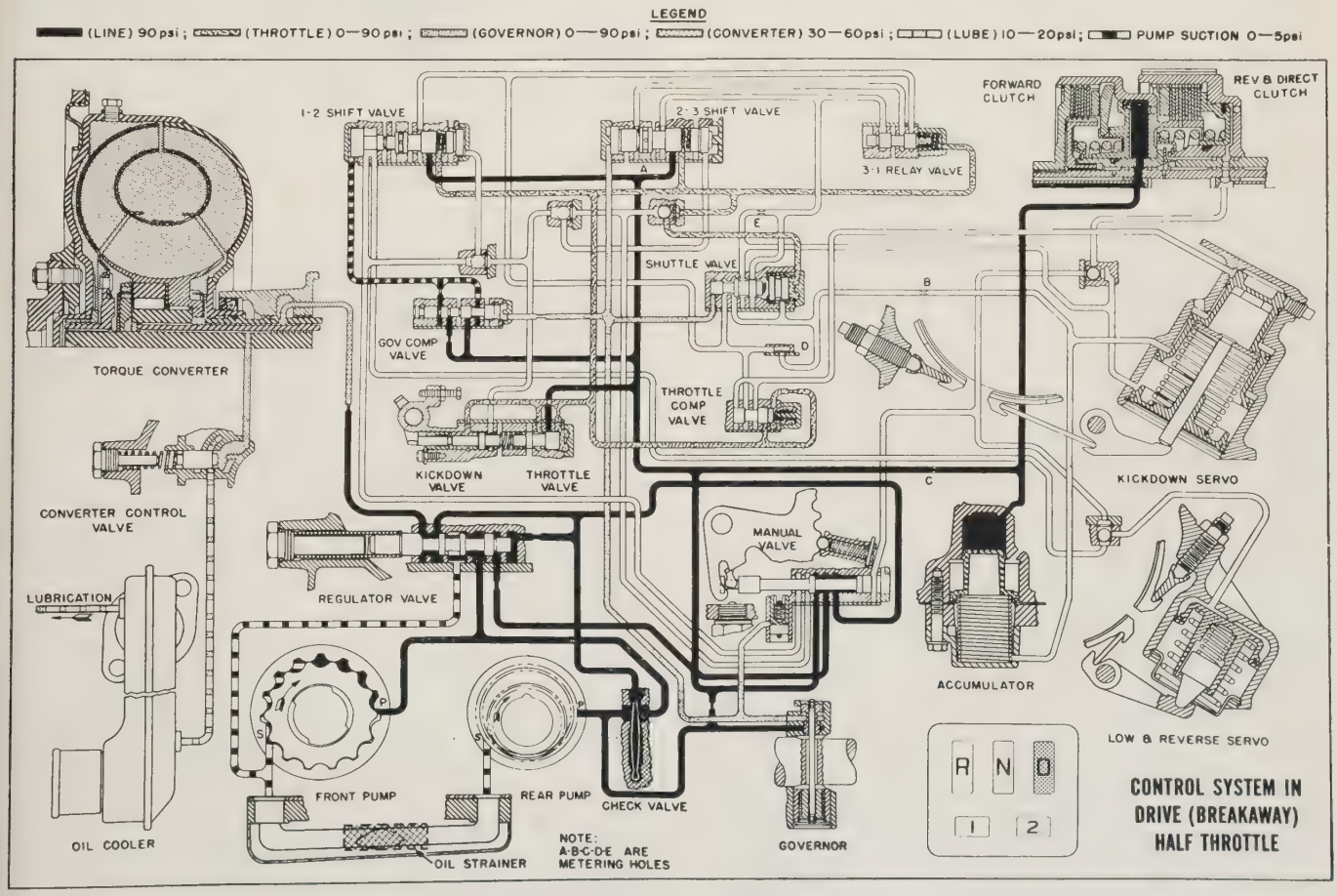

Fig. 13—Hydraulic circuit—breakway

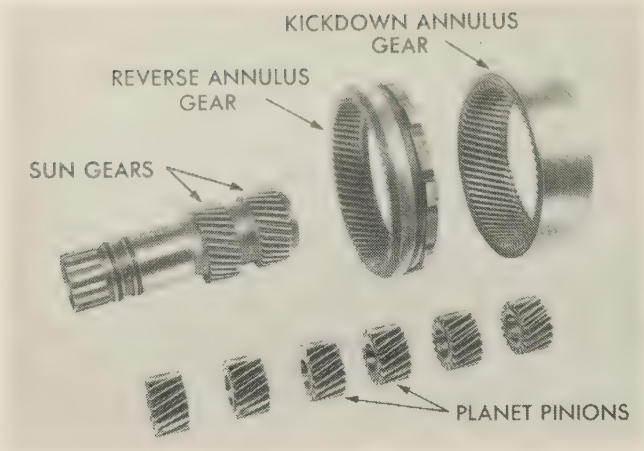

Fig. 14—Gear train components

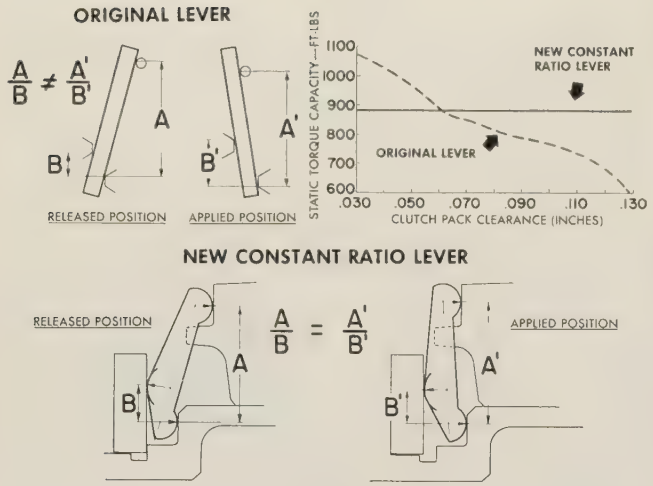

Fig. 15—Front clutch lever operation

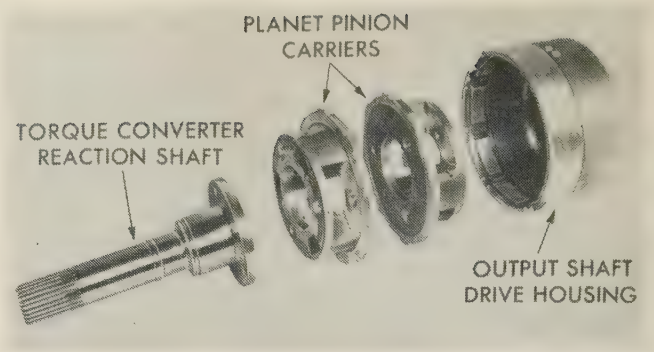

Fig. 16—Aluminum power train members

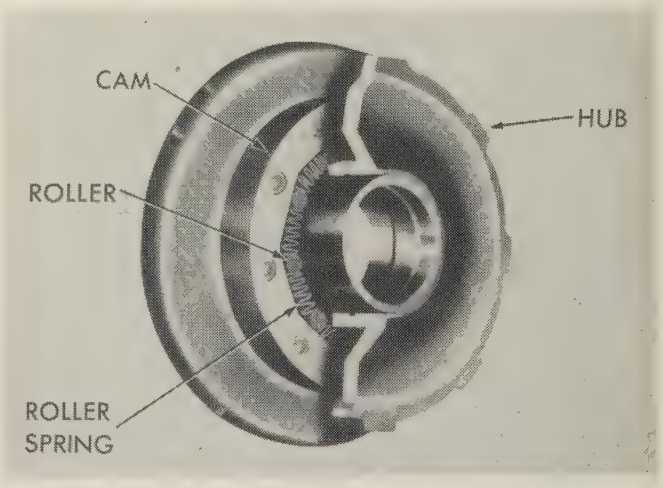

Fig. 17—Overrunning clutch

tical gear data (Fig. 14). The annulus gears have 66 teeth, the planet pinions have 18 teeth, and the sun gears have 30 teeth. The gear teeth are 14 diametral pitch with a 20-deg helix angle and a 20-deg normal pressure angle.

Since both sets are the same, the planet pinions, the carriers, and the planet pinion shafts and needles are interchangeable. The sun gears are both hobbed on a single forging. The annulus gears are made from steel tubing, which is broached to produce the tooth form. This broaching operation on the annulus gears has resulted in a saving in both part and tooling costs.

Front Clutch Levers—The operating levers in the front clutch assembly are interesting, not only from a manufacturing, but from a design viewpoint as well. The initial design utilized eight flat steel stampings to apply the multiple disc clutch, and due to a characteristic of decreasing lever ratio as piston travel increased, five friction discs were required. The latest refinement of this design utilizes only four levers with a shape that provides a constant lever ratio, regardless of piston travel (Fig. 15). Since the lever ratio remains constant, it was possible to reduce the number of friction discs to four, with a subsequent cost saving. The levers are made from powdered metal and require no machining.

Rolled Splines—The use of a rolling operation to form the involute splines on the input and intermediate shaft has proven very satisfactory. Manufacturing time for these operations has been reduced from approximately 4½ min to only 13 sec for the finished spline. The same procedure is used to form the speedometer worm gear, which is integral with the output shaft.

Torque Converter Reaction Shaft—The torque converter reaction shaft (Fig. 16) is made from an aluminum impact extrusion. This method of fabrication has eliminated all semifinishing operations and requires only five operations for a finished part. This shaft must carry torque converter reaction torque, and its strength has proven to be adequate by cycling the shaft under considerable torque overload.

Planet Pinion Carriers—The planet carriers are identical aluminum die castings. Only six machining operations are required to finish the part. Considerable development work was necessary to produce a design in aluminum with sufficient strength to carry the torque load. The results of this pro-

gram have indeed been gratifying. The kickdown carrier is mounted in the output shaft drive housing. This housing, although carrying full transmission output shaft torque, is finish-machined from an aluminum die casting.

Overrunning Clutch—The overrunning clutch assembly shown in Fig. 17 is of the cam and roller type. The unit contains 10 rollers, each of which has its own energizing spring. The outer race is broached to form the cam surfaces and then finish-ground after hardening.

Rear Pump Gear—The rear pump outer gear is made of plastic and operates in an aluminum die-cast pump housing. The gear is accurately molded to size; the only finishing operation is that of grinding to the desired thickness. Considerable development time was spent in finding a plastic which could withstand the effect of type "A" oil at elevated temperatures without excessive growth or wear.

Conclusions

In conclusion, it can be stated that the TorqueFlite transmission meets the objectives for which it was designed:

1. Simplicity of construction resulting in trouble-free operation.
2. High breakaway torque ratio providing good low- and medium-speed acceleration.
3. Controlled low and intermediate gear ratios giving adequate engine braking or hill-climbing ability for moderate or steep grades.
4. Wide range of ratios making possible the use of low rear axle ratios to improve fuel economy.
5. Smooth shifting and quietness of operation.

DISCUSSION

Finds TorqueFlite Design Gives Satisfactory Performance

—H. W. Simpson
Consulting Engineer

I CONGRATULATE the authors and also Teno Iavelli and Gus Syrovy of the Transmission Dept. of Chrysler, for the smooth shifting and quiet transmission they have produced, but I think the authors are too modest and casual about some of the features. For one thing, the use of aluminum for the converter reaction sleeve is a first, to my knowledge, for shafts under high torque. Another first is the use of two identical planetary gear sets with two sets of identical sun gear teeth cut on a single blank in one operation.

Automatic transmissions have many parts but manufacturing can be simplified somewhat by selecting a design in which duplicate parts can be used. In the TorqueFlite there is only one sun gear, one planet pinion, and one carrier to tool up. This not only lends itself to automation but helps by reducing parts inventory and storage space, not to mention elimination of mixups, which often cost more than the parts themselves.

This gear train is inherently well adapted to high torque because tooth loads are kept low by having the input at the ring gear in both low and second gears, instead of at the sun gear.

In the TorqueFlite train the low gear ratio is equal to the second gear ratio plus one. This is true for any number of teeth when both gear sets are alike.

In low the two gear sets are coupled differentially in parallel relationship with the front and rear gear sets producing respectively 1.0 and 1.45 times input torque. The two are added to give a total low gear ratio of 2.45/1.

When shifting from low to second, the sun gear (which was turning backward at 90% of engine speed in low) is held by its brake, and the front gear set drops out of the picture ratiowise and idles slowly while the rear gear set continues to deliver its 1.45 times input torque.

It is unusual to have the input gear at the rear of the transmission. In this case it makes it possible to have identical carriers and also serves to cancel out thrust loads. In low gear, for instance, the thrust of the two ring gears balance each other with only one thrust bearing washer loaded under drive conditions. The thrusts of the two sets of teeth on the sun gear balance each other since one is driving and the other driven in low gear. In second gear there is also only one loaded thrust bearing and in high none. Thrust loads in both forward and reverse are self-contained with none imposed on the housing.

The fact that the input in both low and second gear is at the ring gear also keeps the thrust load itself low.

Since the thrust load at 20-deg helical gears is over 36% of the tangential tooth load, the high torque of the various Chrysler engines would produce excessive thrust loads if the input were at a sun gear.

The main feature contributing to smooth shifting is, of course, the 1-way clutch located between the low gear reaction member and the housing. This gives a self-timing shift for both up and down shifts between one and two, and also provides a smooth forced shift from three to one. Besides it eliminates the "clunk" downshift to low when slowing to a crawl or coming to a stop.

In most gear trains in which the same individual gears are used to produce both forward and reverse speeds the low-gear reaction member turns backward when in reverse, and this prevents use of a 1-way clutch. But in this case, the front carrier is the reaction member for both low and reverse, and consequently it never upsets the applecart by turning backward.

As engine horsepower keeps increasing year after year, we have witnessed the lowering of axle ratios (numerically) without sacrifice of performance. This has been made possible by use of automatic transmissions of three or more speeds. This calls for more use of the kickdown gear (second speed in this case), but when shifts are smooth and gears quiet, the use of second gear is imperceptible to the average person and therefore is not objectionable.

It is interesting to note the part that the TorqueFlite plays in the improving fuel economy. The use of a numerically lower axle ratio is of course the main reason for this. A 3-speed transmission is the best possible tool for improving fuel economy because, if it is quiet and smooth, you can use a numerically low axle ratio and tailor the transmission and converter ratios to obtain desired performance.

I would like to point out that the main reason the second speed of the TorqueFlite is quiet and efficient is that the most efficient gear arrangement known for a planetary re-

duction is used. This is a simple gear set with ring gear input, carrier output and with the sun gear as the reaction member. In this instance only 31% of the power is transmitted by the gear teeth, and therefore, only this 31% is subject to gear tooth and planet bearing friction. The other 69% is transmitted through the gear set by planetation because in second gear the carrier is turning along with the ring gear at 69% of input speed.

This explains why so much power can be pushed through small planetary sets of this type with impunity. That this is recognized is shown by the use of a similar third speed in the Hydramatic and now for second speed in the Chevrolet Turboglide.

The efficiency of the TorqueFlite in combination with a numerically-low axle ratio of 2.92 is undoubtedly the reason the Chrysler Imperial was the sweepstakes winner in the 1956 Mobilgas Economy run by the biggest margin in history with a ton mpg figure of 61.38, and mpg of 21.04.

The TorqueFlite is another automatic transmission to be really used in reduction ratios and not just lugged along for occasional use for starting and passing.

Discusses Chrysler and Chevrolet Improved Transmissions

—H. G. English
Ford Motor Co.

CHRYSLER, in their search for an improved transmission, have followed the more conventional approach by providing added ratio coverage. By means of a 3-speed gearbox and a comparatively high torque ratio converter a general improvement in performance throughout the speed range has been achieved. This has been done, of course, at the expense of one additional shift which might well be considered as a negative factor in terms of pleasing operation. On the other hand, this added ratio coverage permits the use of faster (lower numerical) axle ratios which result in some improvement in fuel economy and general sweetness of the overall automobile.

With the higher power-to-weight ratio of our modern cars there is some question regarding the performance advantages to be gained through the use of converter stall torque ratios in the order of 2.6 or 2.7 to 1 when coupled with a low gear ratio of 2.45 to 1. Such high torque ratios usually result in lower converter efficiencies beyond the 0.6 speed ratio and increased road load slip. As a result, cooling problems are magnified, and power transmitting members in the gearbox are unduly stressed.

The Chevrolet Turboglide transmission represents a rather novel marriage of the torque converter and basic 3-speed planetary gear set to provide no-shift operation with reasonable overall performance. It is in effect a more or less final step in the evolution of the basic principle which Buick has doggedly stood by since 1948 when the Buick Dynaflow transmission was first introduced.

The primary functional advantage of the Turboglide principle is smoothness of operation, which is certainly one of the more important factors from the customers' point of view. Along with smoothness, the principle of parallel gearing provides a distribution of torque which permits a "daintiness of design" so apparent throughout the entire transmission. By "daintiness of design" I do not mean to infer in any way that the design is insufficiently rugged. The complete unit and the majority of the component parts are merely small in comparison with other automatic transmissions in production today.

The manner in which the multiple turbines are coupled to the two planetary gear sets, and the use of 1-way clutches to take the reaction torque, make the unit inherently torque- and speed-responsive. As a result, vastly simplified controls are possible.

The outstanding feature of smoothness is, of course, obtained at the expense of overall performance, when compared with the more conventional arrangement of torque converter and gearbox. Good starting performance is possible with the Turboglide principle; however, since the engine speed is controlled by the converter it is not possible to develop maximum engine horsepower except at top speed of the vehicle. Whereas our modern engines develop maximum horsepower in the area of 4400 to 4600 rpm, a maximum engine speed of approximately 3500 rpm is obtained with the Turboglide installation during the effective range of the transmission. This occurs at the coupling point of the third turbine phase or approximately 65 mph. Lower input horsepower coupled with lower efficiencies due to complete operation in the converter range are factors which are negative to performance, particularly in the 25–40- and 55–70-mph ranges. These negative factors are partially compensated for, of course, by a reduction in rotational acceleration losses.

The inability to operate selectively in a geared ratio at high converter speed ratios and efficiencies would appear to present a rather severe problem in overall transmission and engine cooling under conditions of prolonged severe operation such as encountered on Pikes Peak. Perhaps the author would care to comment on this point.

Although I have not had the pleasure of driving a Turboglide installation we at Ford were fortunate in recently obtaining a Turboglide transmission for observation and dynamometer evaluation. Naturally, there was great interest in the disassembled unit and much comment on such items as the die-cast aluminum case, the 20 pitch gears, and the molded synthetic rubber bypass valve in the oil strainer. The one item, however, which caused the most comment was the direct clutch drum, not because of any apparent design features or manufacturing innovations, but because of these thoughtful words which were etched thereon—"Merry Christmas."

Questions Certain Aspects of New Transmission

—V. C. Moore
General Motors Corp.

I THINK Mr. Jeffe and Mr. Cartwright have done a fine job of explaining their TorqueFlite transmission. I congratulate Chrysler for adding more geared ratio coverage to their new transmission. I am sure that you would expect that opinion from a confirmed Hydra-Matic man.

I am not surprised at the use of a die-cast aluminum carrier of relatively normal size for the kickdown gear; but I am surprised at the use of aluminum for the reverse carrier, which I believe carries over 8½ times engine torque with your 2.7 converter ratio. In describing the number 2 driving range, it is mentioned that there is an automatic upshift to direct at 70 mph to prevent overspeeding the engine. However, it seems that in the number 1 position the transmission remains in low gear regardless of car speed. Why isn't there danger of overspeeding the engine in this range under full throttle conditions?

In respect to the differences between the two 11¾-in. diameter converters, it would be interesting to know if this change of capacity between the two units was brought about by the modification of the pump or stator blade angles or possibly a combination of both. In low gear the rear clutch plates have a differential speed of about 1.9 times engine speed. Did this present any development problems for durability or power loss?

This question may have been covered at some previous time since it applied to the previous transmission as well as the new one, but I would like to ask it again. With your converter welded as a sealed unit how do you handle service of this item? For example, if a thrust surface fails within the converter, it is necessary for a dealer to replace the whole converter. Does the customer have to pay the bill for the whole assembly, or is there an exchange credit given on the used one? If so, are these units returned to the factory and rebuilt?

Oral Discussion of this paper—as well as of the Winchell, Route, and Kelley paper which follows—is to be found on p. 178.

CHEVROLET

TURBOGLIDE

TRANSMISSION

F. J. Winchell, W. D. Route, and O. K. Kelley, General Motors Corp.

This paper was presented at the SAE Annual Meeting, Detroit, Jan. 16, 1957.

THE Turboglide is a nonshifting, concurrent-geared, multiple-turbine, torque-converter transmission with dual stator-blade control. Turboglide has no low gear. It is unique in that it provides a competitive performance factor without manual or automatic shifting. Most important, it is unique in that the transmission performance ratio is available at any throttle position, allowing simultaneous modulation of torque ratio and engine output by depression of the throttle pedal alone.

There are, therefore, no "up-shifted" performance "holes" in city or hill climbing operation, which is characteristic of the conventional-sequence geared turbine. Maximum engine and "normal" transmission performance converge smoothly at wide-open throttle. Further depression of the throttle pedal through a conventional "detent" changes the stator blade from the "normal" or "cruise" angle to the performance or passing angle.

With the Chevrolet 283-cu-in. displacement, 4-barrel carburetor engine, the cruise angle stall torque ratio is 3.8/1 with an engine speed of 1700 rpm. Wide-open throttle coupling is attained at approximately 50 mph and 2700 engine rpm.

Performance angle stall torque ratio is 4.2/1 at 2600 engine rpm. Wide-open throttle coupling is

TURBOGLIDE is the deluxe automatic transmission of the General Motors Chevrolet. One of its most important features is that its performance ratio is available at any throttle position, enabling control of torque ratio and engine output by the throttle pedal. The system includes a five-element torque converter, pump, three turbines, and the dual stator. The entire installed unit weighs 148 lb, a result of the general arrangement and the use of aluminum in the case and bell housing.

The authors discuss the basic operating principle of the transmission, the arrangement, performance, torque distribution, control system, and valve body.

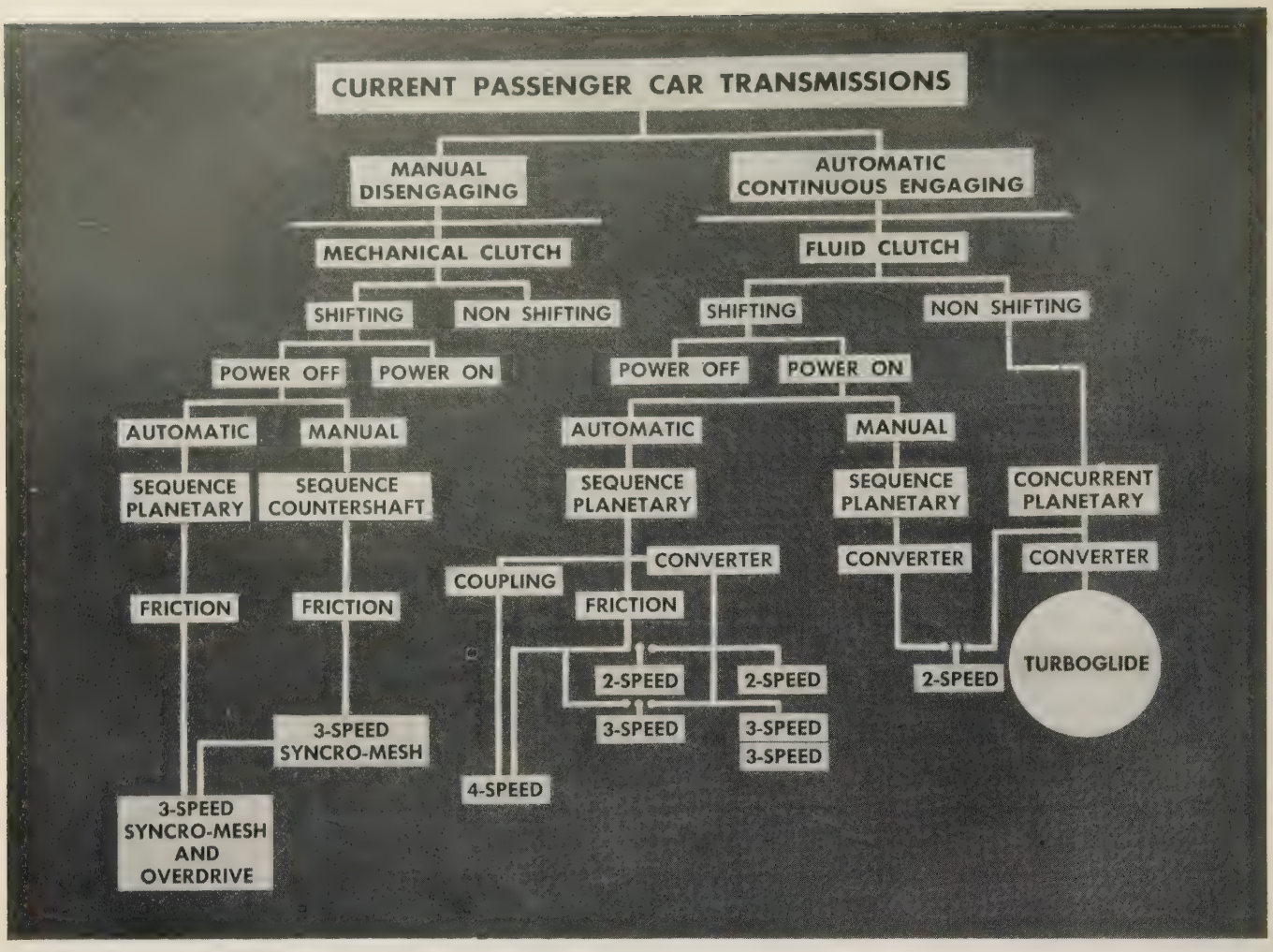

Fig. 1—Types of current passenger-car transmissions

reached at approximately 65 mph and 3200 engine rpm.

Part-throttle starts in cruise angle are "tight" and connected, as a consequence of the low stall speed and high torque ratio. Actuation of the detent permits the blade change and consequent elevated engine speeds for maximum horsepower.

The Turboglide incorporates a five-element torque converter, a pump, three turbines, and the dual stator. The torque converter operates in conjunction with two simple planetary gearsets. The three turbines are connected concurrently to the driveline at ratios of 2.67 for the first, 1.6 for the second, and 1 for the third. The first and second turbine reactions are grounded through one-way clutches to permit inactivation at the limit of their useful speed range.

Since an independent low range is not required, a grade-retarder range is provided by gearing the first turbine at the 2.67 ratio in the conventional manner, while permitting the second and third turbines to run free.

Reverse is accomplished by compounding the two planetary gearsets.

Drive, grade-retarder, reverse, and neutral require the use of three cone clutches, one plate clutch, and two one-way clutches. Park augments neutral with a pawl and gear-type lock on the output shaft. The shift quandrant sequence is P, R, N, D, and GR.

The structural components as well as many functional elements are of die-cast aluminum. The elimination of radial and bending loads through use of clutches rather than bands permits a compact and rigid design with relatively light construction. The absence of "power shifts" eliminates the requirement for calibration and timing functions, thus greatly simplifying the control system and contributing to the overall reliability factor.

The principle, general arrangement, and use of materials have resulted in a total installed weight of 148 lb, as compared to an average weight of 241 lb for the industry's passenger-car transmissions.

Operating Principle

Prior to detailing the physical and functional description it would be well to spot the Turboglide in the family tree of automotive transmissions (Fig. 1) and to explain what is meant by sequence and concurrent gearing.

The major classifications are intended to be in order of their importance to the operator. The first classification identifies the engine coupling mechanism; the continuously engaged fluid clutch has

eliminated the coordinated manipulation of the throttle and clutch in starting and is, therefore, considered to be the major factor toward operational simplicity.

The second major classication identifies the operational characteristics of the gearbox in providing the total forward performance generally accepted as a minimum for current passenger cars. For an equivalent performance factor, a nonshifting transmission is more desirable than a power-shifting automatic, and a power-shifting manual transmission more desirable than a power-off automatic. The remaining portion of the chart classifies the mechanism accomplishing the ratio coverage.

The third classification identifies the type gear train. Conventionally, the input member to a reduction unit (turbine) operates at two or more ratios in sequence as dictated by the performance demand on the vehicle. This has been true whether the drive is mechanical or hydraulic, or the transmission manual or automatic, and has been independent of the number of gear ratios. The Turboglide, however, employs three independently geared turbines which may simultaneously contribute to the output of the transmission as required; thus, the terms sequence and concurrent.

The fourth identifies the "engine drive" as such and not necessarily the engine coupling referred to previously. For example, the transmission may start in fluid drive and later shift into a mechancal drive or a combination of both.

The fifth classification envelopes the number of forward ratios; a general index of the operator's awareness of a transmission.

The open ends of the chart recognize potential developments.

It is clear that, with the exception of one hybrid arrangement, the Turboglide is singular in its class.

For a more detailed understanding of the significance of sequence and concurrent gearing, it would be well to consider the fundamental difference between a typical torque-converter 3-speed transmission and the Turboglide. The evolution of the converter 3-speed is as follows:

With the output member of a typical three-element converter connected directly to the propeller shaft, the resultant speed and tractive effort curves would be as diagrammed in Fig. 2. Experience has shown the performance factor to be adequate for cruise and high speed but deficient for starting and passing.

If a reduction unit is added to offset this disadvantage (Fig. 3), a compromise ratio must be selected; otherwise, the transmission will be conspicuously deficient in either starting or high-speed passing. Regardless, a planetary gearset must be added with a reaction band and a direct-drive clutch. Operation, of course, requires one manual or automatic power shift.

If additional complexities are not prohibitive, a second reduction may be added (Fig. 4). The result is a completely adequate transmission but with the annoyance factor and complexities of two power shifts.

The concurrent principle, while not quite offering the degree of potential extension in wide-open throttle tractive effort of each of the sequence ratios, avoids the annoyance of shifting and the complexities and uncertainties in controls and eliminates high energy-absorbing friction elements; yet it results in superior "after-sequence" or "up-shifted" performance, as explained previously.

For example, at the speed illustrated in Fig. 4, the sequence transmission permits only modulation between "road load" and wide-open throttle third gear or, in some cases, second gear.

The operator is unable to modulate the performance factor between wide-open throttle third and wide-open throttle first without manual shifting. The nonshift concurrent arrangement, as stated previously, does not have this limitation.

The concurrent principle is probably best illus-

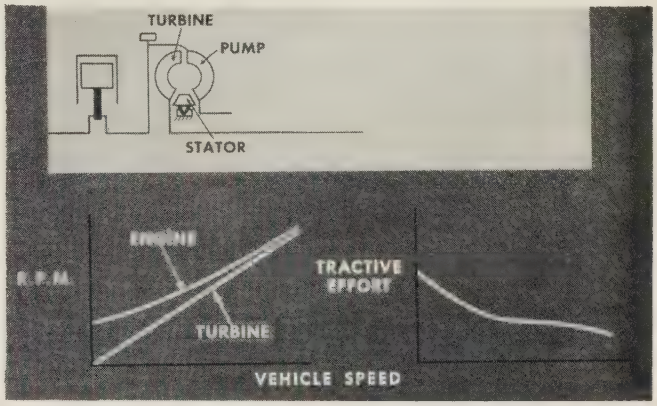

Fig. 2—Three-element torque converter, direct drive

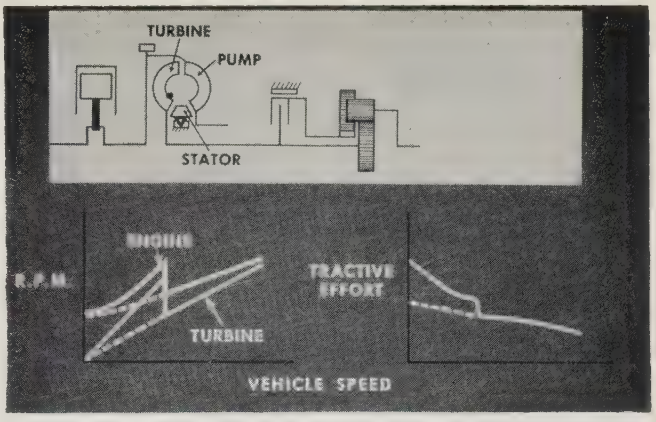

Fig. 3—Three-element torque converter, two-speed drive

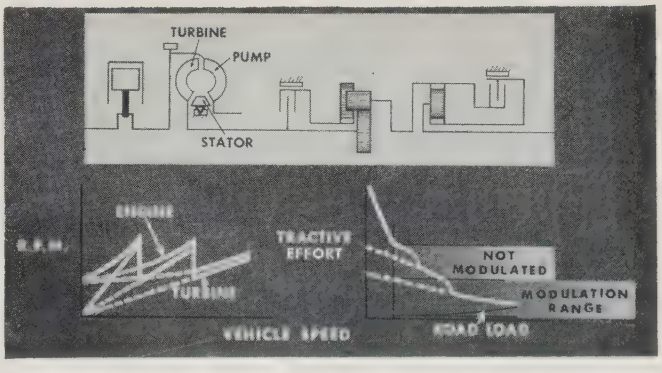

Fig. 4—Three-element torque converter, three-speed drive

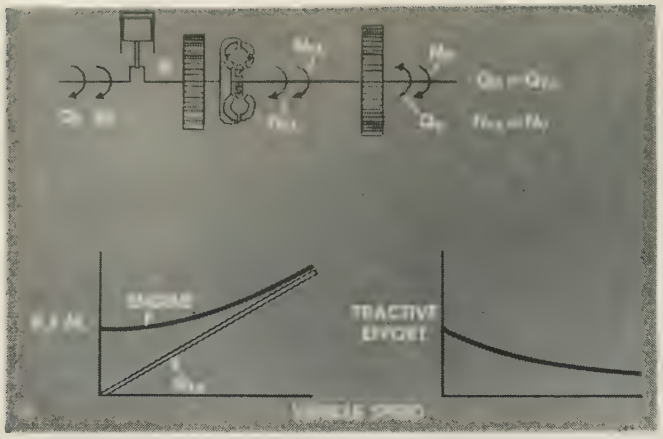

Fig. 5—One transmission

trated by the parallel or countershaft combination of three transmissions as follows:

First, (Fig. 5) shows a single element converter direct drive transmission A and its characteristic performance curves; it is deficient for both starting and passing, adequate for cruise only.

A second transmission B combined with the turbine geared to the output shaft at a ratio R_b through a one-way clutch is shown in Fig. 6. The symbol selected for the one-way clutch is intended to show, by overlapping the shaft with the gear, that the gear may run faster or "overrun" the shaft and turbine assembly.

The individual contribution of the additional transmission is probably best realized by analysis of the speed curve at the lower left of the chart. The total "load" on the engine is the sum of the driving torques of both converters so that with the addition of transmission B the input speed is reduced at stall. As the output load is relieved and accleration begins, the speed of turbine B increases at the rate R_b times the output-shaft rpm. As the turbine B approaches the speed of the engine, the torque required to drive pump B approaches zero, so that at and above the point X pump A alone is controlling the engine speed. From this point, the turbine B no longer is driven and is, thereafter, coasting at approximately engine speed, free of the gear by virtue of the one-way clutch. Turbine B torque is, of course, zero at the freewheel point.

The combined output torque at any point is equal to the output of A, plus the ratio R_b times the output of B. The result is a smooth speed and tractive effort curve uninterrupted by abrupt ratio changes. The arrangement now provides adequate "passing" and "cruising", but is still deficient in "starting" performance.

For starting performance a third transmission operating at a larger reduction R_c may be added. The effect is as illustrated in Fig. 7. The turbine C becomes inactive and freewheels at a lower vehicle speed, due to the larger reduction R_c.

Now, the total output at any point is equal to the output of A, plus the ratio B times the output of B,

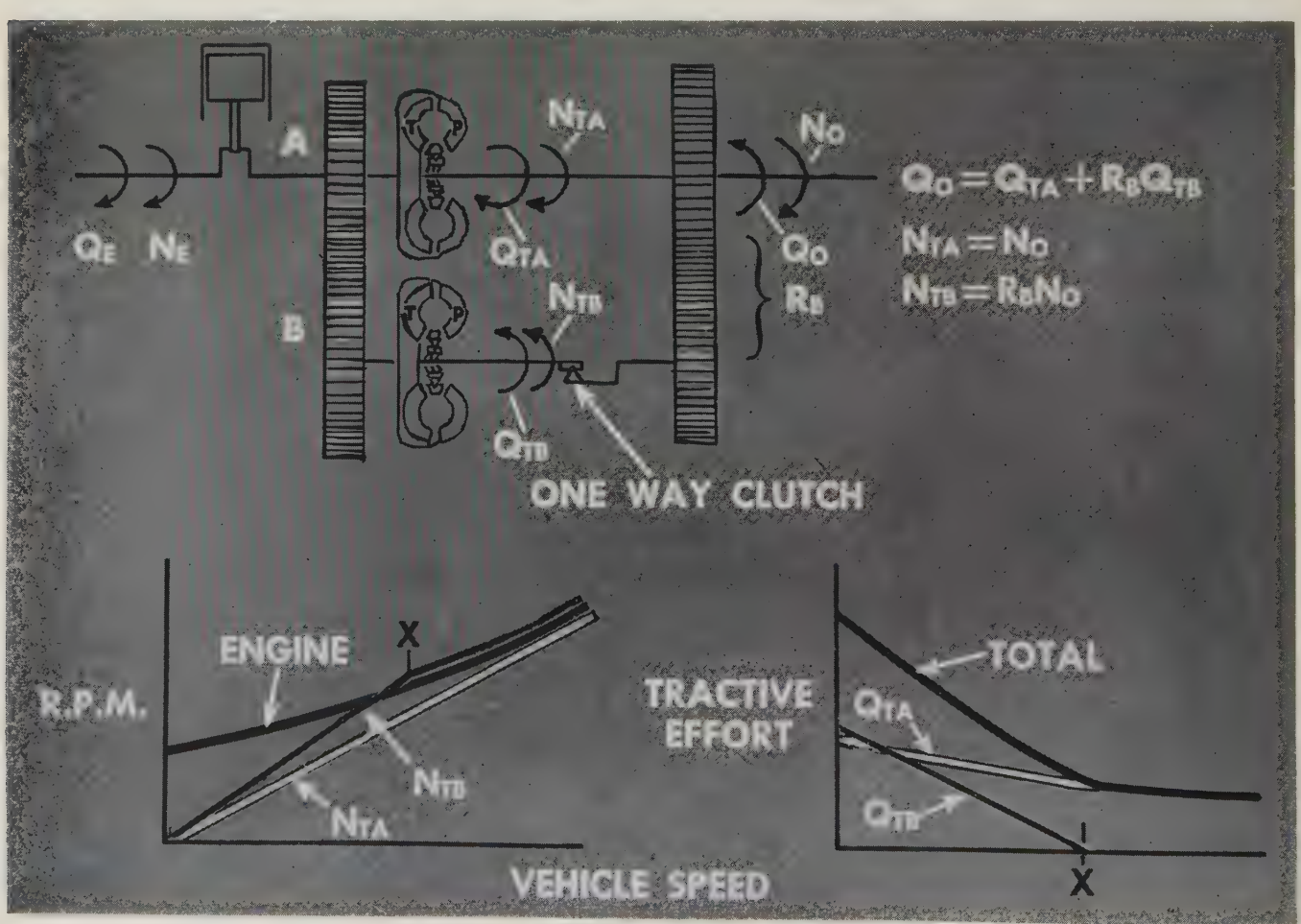

Fig. 6—Two transmissions operating concurrently

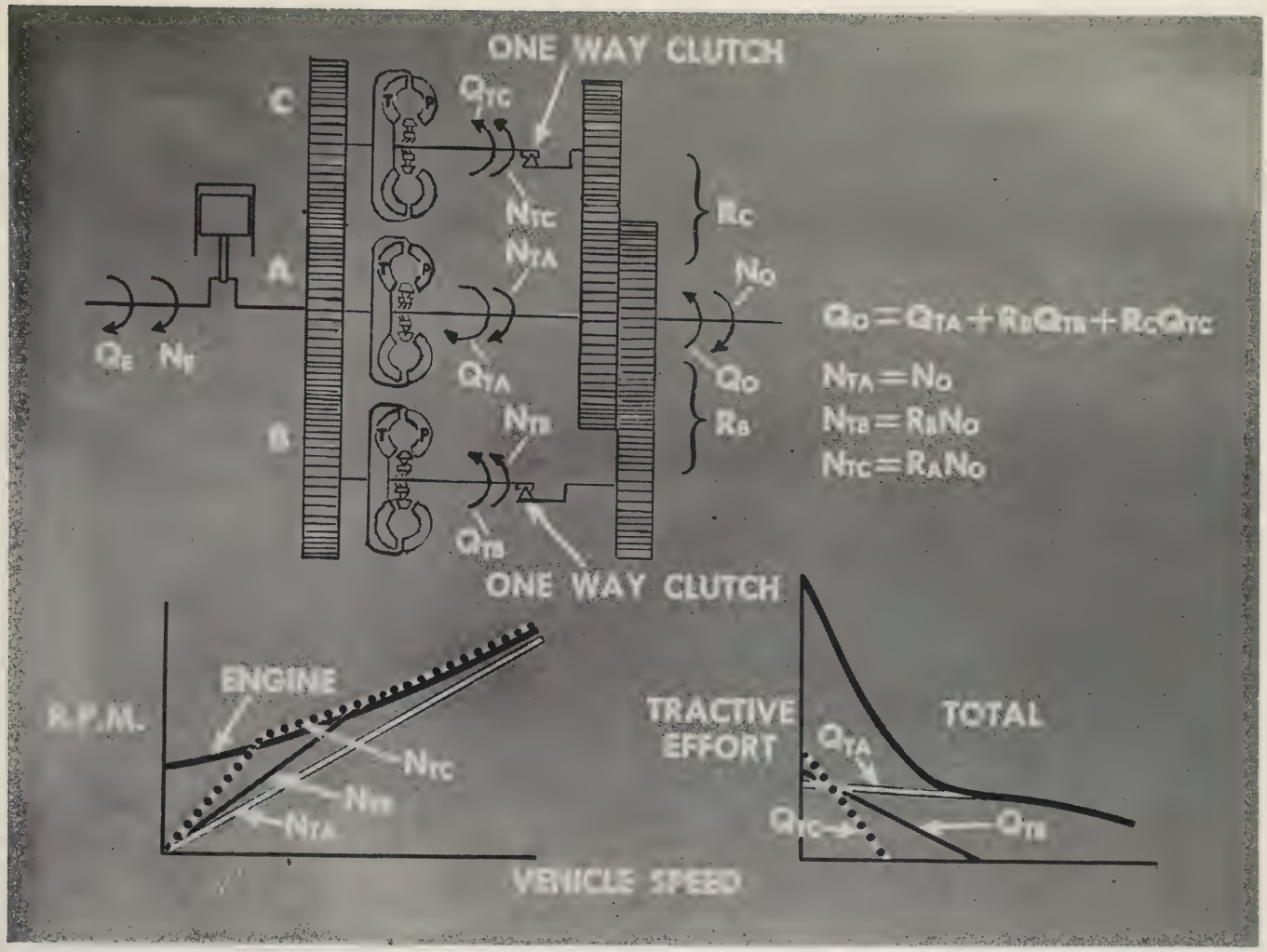

Fig. 7—Three transmissions operating concurrently

plus the ratio C times the output of C. The result again is a smooth and uninterrupted transition of speed and tractive effort.

Selection of optimum blade angles and gear ratios results in a completely adequate performance factor without the addition of a reduction unit or "low gear" on the output shaft.

Turboglide Arrangement

The Turboglide is a coaxial arrangement of this principle requiring, however, only one pump and stator and, of course, no input gearing.

For clarity the arrangement is illustrated function by function as follows:

Turbine A (Fig. 8) is connected directly to the output shaft. The "passing" turbine B (Fig. 9) is

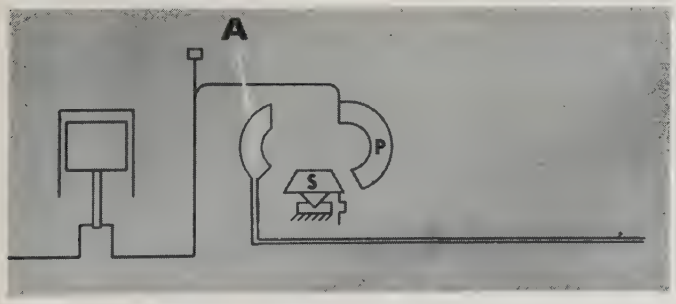

Fig. 8—Turboglide arrangement: turbine A drives the output shaft directly, provides cruising performance

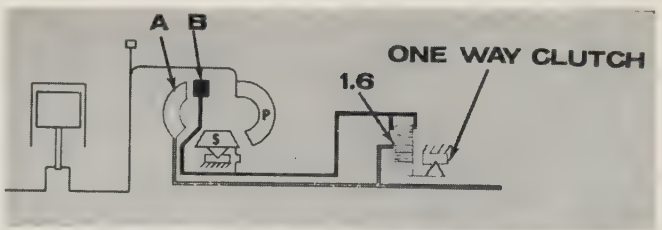

Fig. 9—Turboglide arrangement: turbine B drives through front planetary gearset, predominant in middle or passing ranges

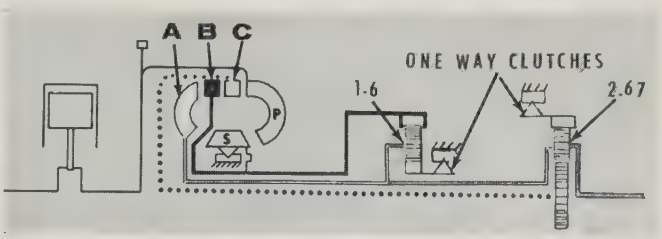

Fig. 10—Turboglide arrangement: turbine C drives through rear planetary gearset, provides starting performance

geared to the output through a simple planetary gearset at a ratio of 1.6/1. The input member is the ring gear with the output as the carrier integral with the T_{11} shaft, while the reaction is the sun to ground through a one-way clutch.

The turbine C (Fig. 10) is geared to the output

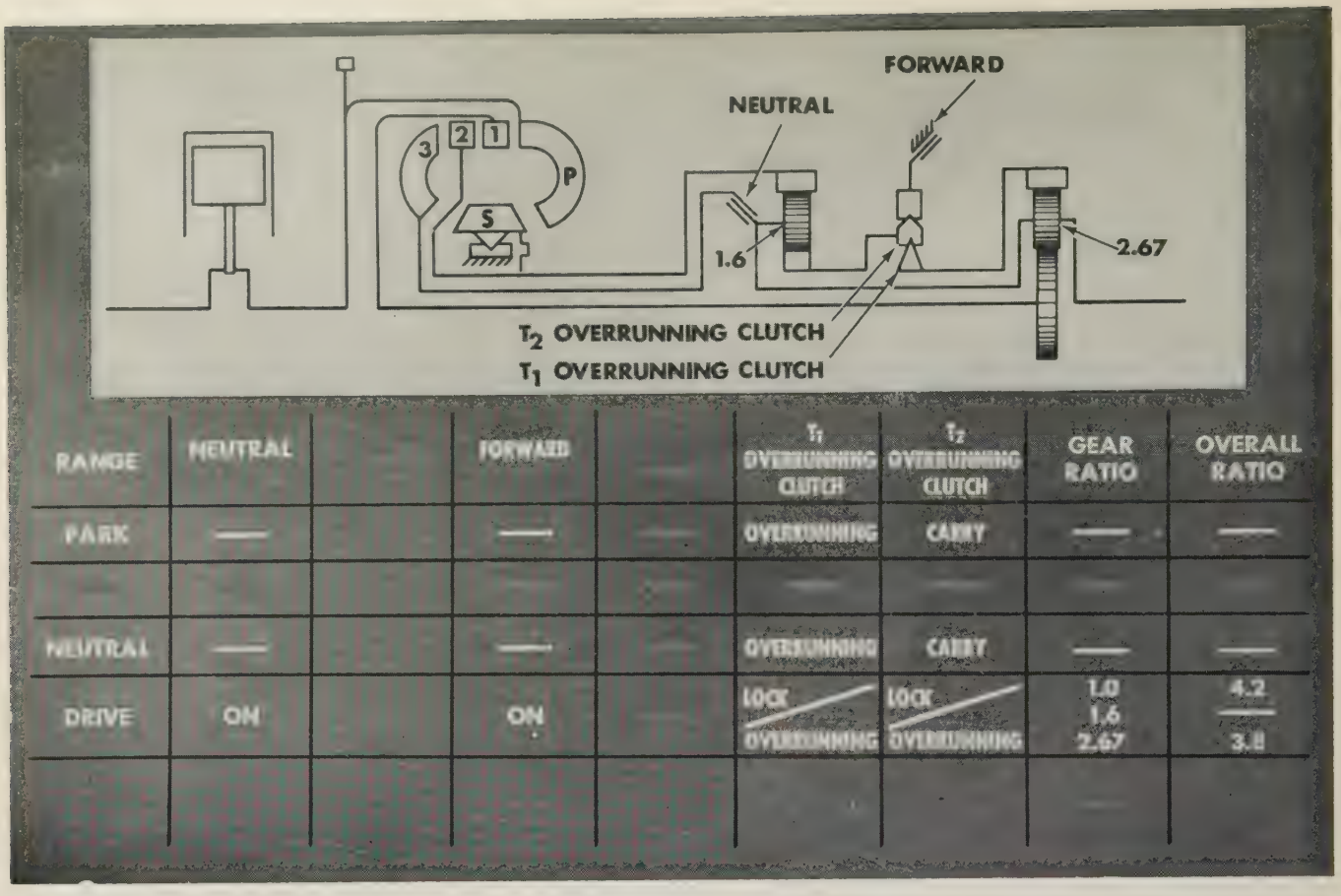

RANGE	NEUTRAL		FORWARD		T_1 OVERRUNNING CLUTCH	T_2 OVERRUNNING CLUTCH	GEAR RATIO	OVERALL RATIO
PARK	—		—		OVERRUNNING	CARRY	—	—
NEUTRAL	—		—		OVERRUNNING	CARRY	—	—
DRIVE	ON		ON		LOCK OVERRUNNING	LOCK OVERRUNNING	1.0 1.6 2.67	4.2 3.8

Fig. 11—Turboglide arrangement: neutral clutches

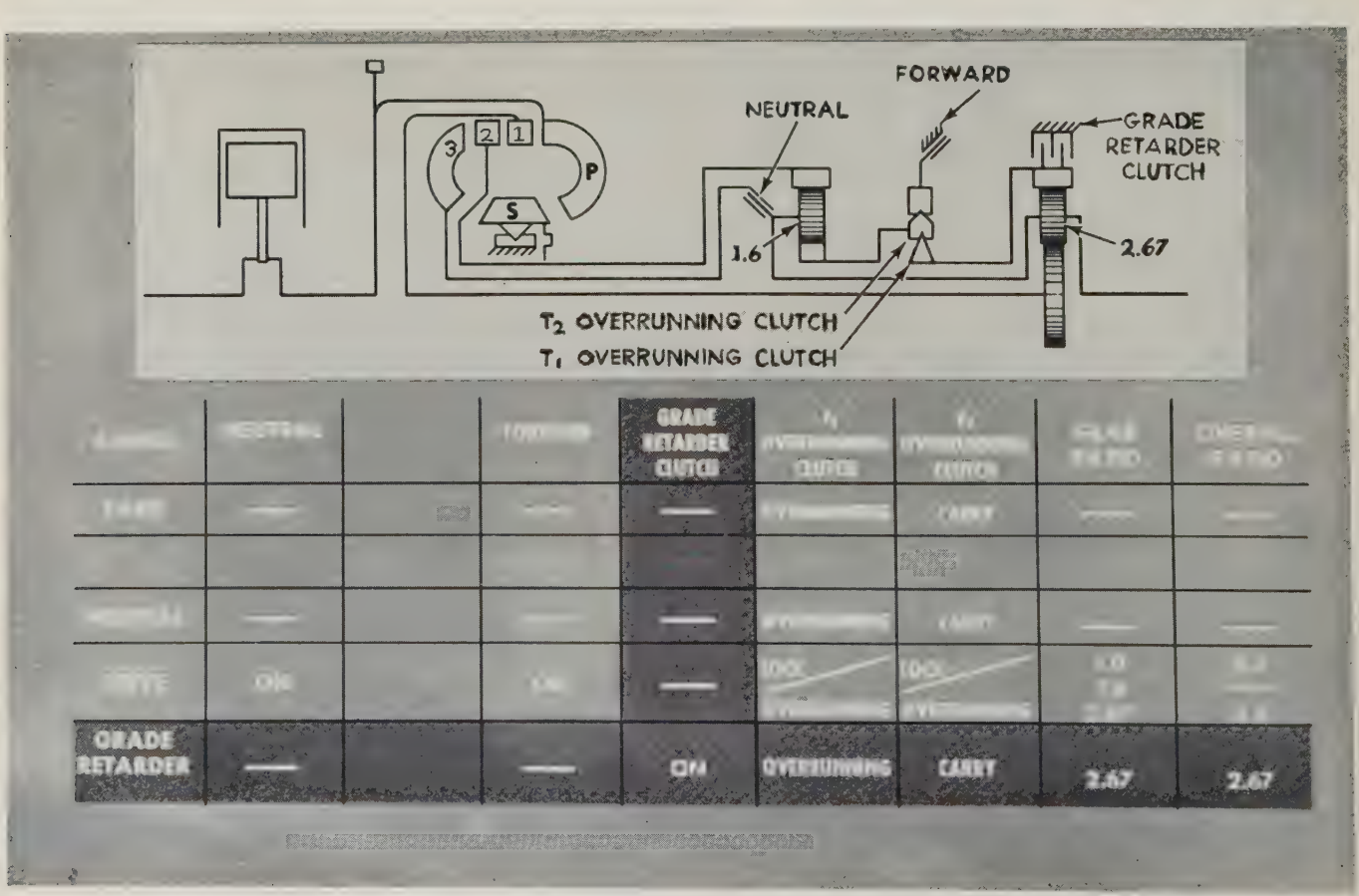

				GRADE RETARDER CLUTCH				
				—				
				—				
				—				
GRADE RETARDER	—		—	ON	OVERRUNNING	CARRY	2.67	2.67

Fig. 12—Turboglide arrangement: grade retarder

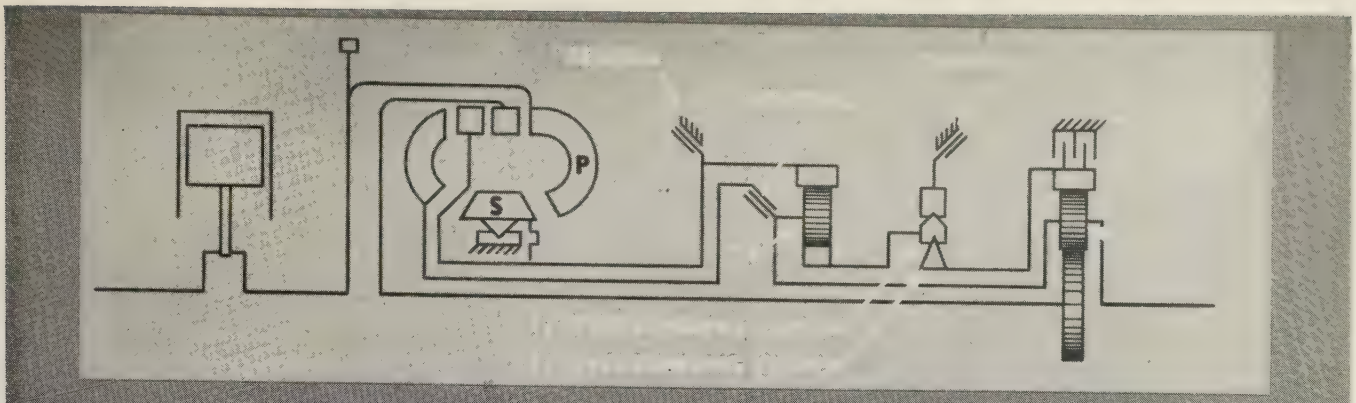

RANGE	NEUTRAL	REVERSE	FORWARD	GRADE RETARDER CLUTCH	T_1 OVERRUNNING CLUTCH	T_2 OVERRUNNING CLUTCH	GEAR RATIO	OVERALL RATIO
PARK	—	—	—	—	OVERRUNNING	CARRY	—	—
REVERSE	ON	ON	—	—	LOCK	CARRY	1.78	3.1
NEUTRAL	—	—	—	—	OVERRUNNING	CARRY	—	—
DRIVE	ON	—	ON	—	LOCK OVERRUNNING	LOCK OVERRUNNING	1.0 1.6 2.67	4.3 — 2.8
GRADE RETARDER	—	—	—	ON	OVERRUNNING	CARRY	2.67	2.67

Fig. 13—Turboglide arrangement: reverse

through an identical planetary gearset at a ratio of 2.67/1.

The input now, however, is the sun; the output is again the carrier and integral with both T_a and the output of T_b. The reaction is the ring to ground again through a one-way clutch. Now that the order of elements in the flow path is established, the turbine will be reidentified according to SAE recommendations, so that T_c becomes T_1; T_b–T_2; T_a–T_3. While now providing the necessary functions for forward operation, the transmission still lacks, for one thing, neutral.

T_3 is disconnected from the output by a cone clutch as shown in Fig. 11. T_1 and T_2 are disconnected by releasing the ground members. This is accomplished through a series arrangement of the one-way clutches and a single cone to ground. Park is provided by a pawl engaging a gear integral with the rear carrier.

Grade retard is accomplished (Fig. 12) by a 4-active-faceplate clutch which grounds the T_1 reaction, while freeing T_2 and T_3 through release of forward and neutral cones. The T_1 is thus geared at 2.67 times the output. Since the stator is freewheeling, the reaction is against the engine only so that the propeller shaft torque is 2.67 times engine torque.

Reverse (Fig. 13) completes the scheme by the addition of a ground cone on the second turbine, compounding the two planetaries for the reversal and reduction (1.78/1). In reverse the third turbine turns in the counterengine direction with the output shaft. The second turbine is stationary and is a reaction member within the torque converter, causing T_3 to be driven in the reverse direction. Thus, it contributes to the total reverse output ratio of 4.1/1.

The first column of the chart (Fig. 13) indicates the order of range selector sequence. The term "carry" in the one-way clutch column is intended to explain that the clutch is not locked in the torque-transmitting sense but is carrying the free outer race in the direction normally prevented by the application of the forward cone.

Fig. 14 is the "true" cross-section of the Turbo-

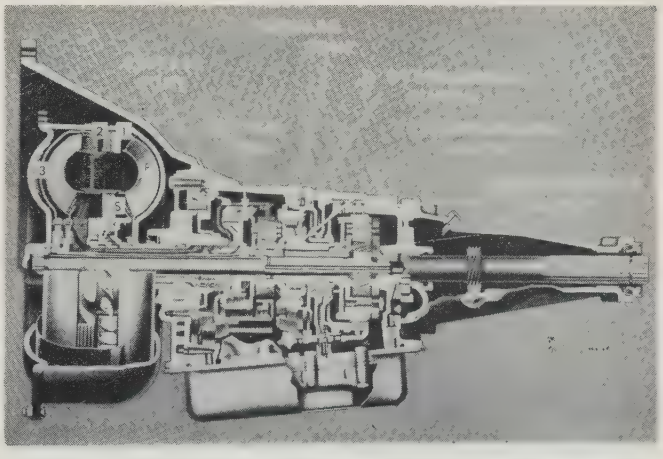

Fig. 14—Turboglide arrangement: power path

glide. The order is consistent with the previous outlines in identifying the turbines and the power paths.

Performance

In the analysis of torque distribution within the torque converter (Fig. 15A), it is clear from the summation of the moments acting on the oil mass that for maximum performance the total available torque should be transmitted through the turbine having the largest gear reduction. This, of course, dictates "sequence" gearing and the resultant power shifts. If shifts are to be avoided, the total available torque must be shared by the individual turbines, with minimum torque to the lowest ratio turbines.

For maximum total output, the direction of the moment or torques should be as shown in Fig. 15, so that the sum of the turbine torques is equal to the sum of the engine and stator torques.

The family of torque curves (Fig. 15B) is arranged to illustrate the direction as well as the relative magnitudes for optimum distribution. For maximum output at stall, the total available torque (engine plus stator) should be arranged to react against the first turbine (the largest gear multiplication). Thus, at stall, T_2 and T_3 torque must equal zero. The engine speed curve is primarily a pump function and is based on a selected stall speed and N/V factor. The curve characteristics between stall and maximum vehicle speed are established by the efficiency factor, so that the engine speed curve may be roughed-in prior to establishing blade angles and gear ratios. It now may be seen that with the first turbine running at 2.67 times the output rpm its useful range is limited by its proximity to engine speed. The limit or freewheel point may be more or less than engine speed, depending on the final selection of blades angles. At the speed shown, the second turbine should carry as much of the available torque as possible. However, since T_3 must start at stall, the available torque at speed X must be split between T_2 and T_3, with T_2 carrying the largest possible share. With the second turbine running at 1.6 times output, its useful range is limited to speed Y. At this speed, T_3 torque must equal engine plus the stator and,

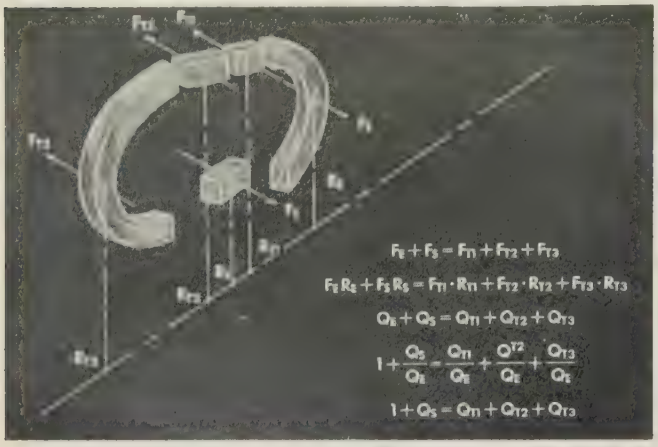

Fig. 15A—Distribution of forces acting on a segment of converter oil

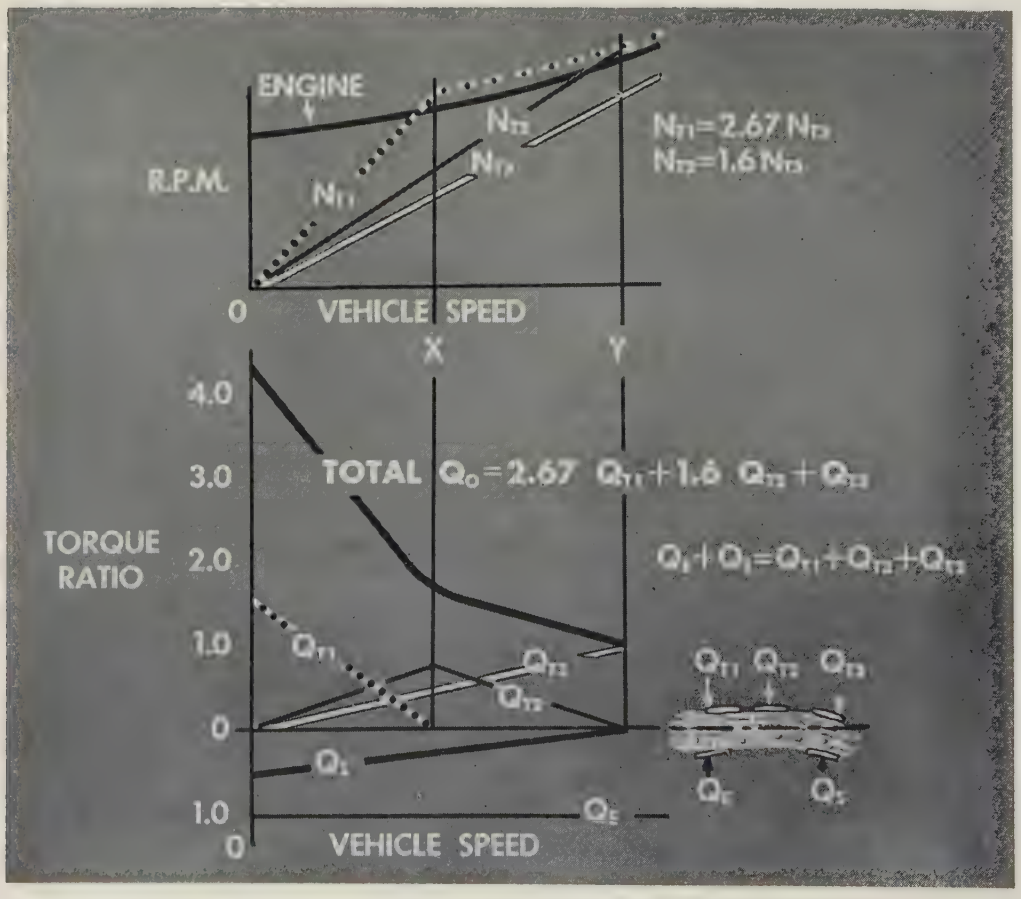

Fig. 15B—Optimum wide-open throttle performance

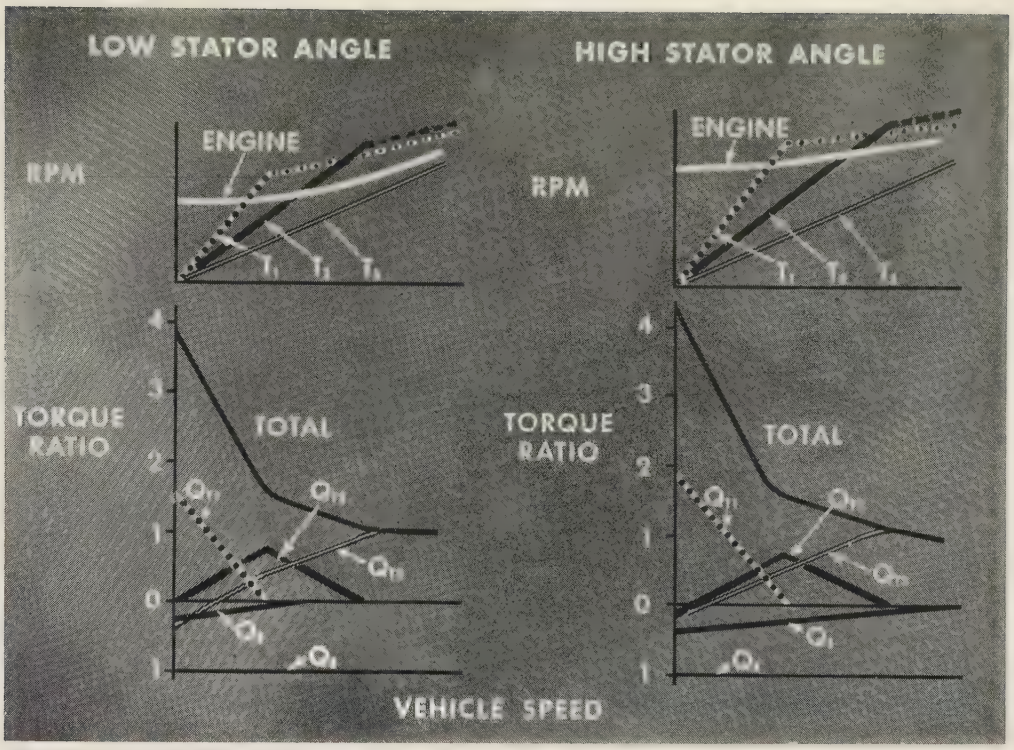

Fig. 16—Turboglide torque distribution

ultimately, engine torque at the freewheel point of the stator. Thus, the total output torque at any speed is obviously equal to 2.67 times T_1 plus 1.6 times T_2 plus T_3 torque.

This torque distribution is optimum, and cannot be improved on by subsequent blade design.

Turboglide Torque Distribution

The selection of a stator angle producing a high stall speed results in maximum output as a consequence of high input horsepower as well as high torque ratio. However, as with all highly regenerative stators, cruising efficiency is down and part-throttle starts have a characteristic "loose" feeling. The dual-blade angle eliminates these deficiencies by providing a low angle for tight connected operation for normal driving, while allowing high angle for maximum performance. Individual and total torque ratio for high and low angle are shown in Fig. 16.

The curve in Fig. 17 is the product of the above distribution and represents the actual wide-open throttle performance of the Turboglide with a Chevrolet 283-cu-in. 4-barrel carburetor engine.

As stated previously, the Turboglide allows simultaneous modulation of both engine and transmission performance. For example, by depression of the throttle alone any performance value is available from road load to wide-open throttle low angle. Further depression of the throttle results in the blade change and maximum performance.

Control System

As stated previously, due to the absence of shifts the control system is relatively simple. (See Fig. 18) It contains the conventional input and output crescent pumps, a main regulator valve providing the necessary pressure for holding the various clutches and allowing the rear pump to by-pass the front for a reduction in parasitic losses. Also in the interest of minimum losses, a vacuum modulator system varies the regulated pressure in proportion to engine torque so that normal cruising is at minimum pressure (90 psi). A manually operated selector valve routes oil pressure to the required clutches.

A detent or stator valve is spring loaded against the throttle linkage, so that on depression oil is exhausted on the forward side of the stator pistons,

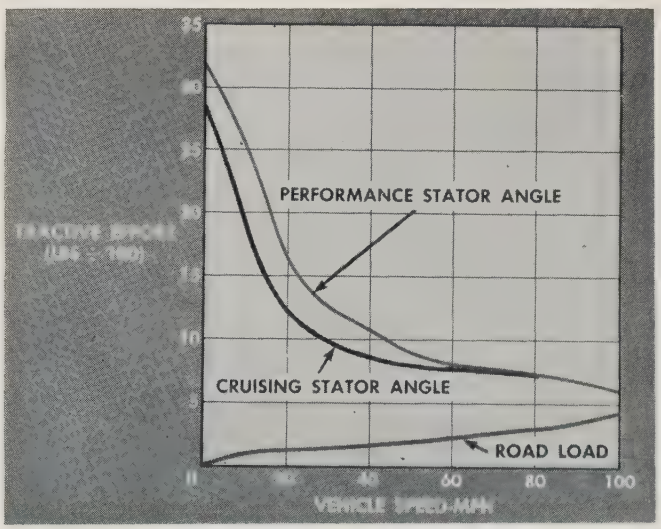

Fig. 17—Turboglide tractive effort

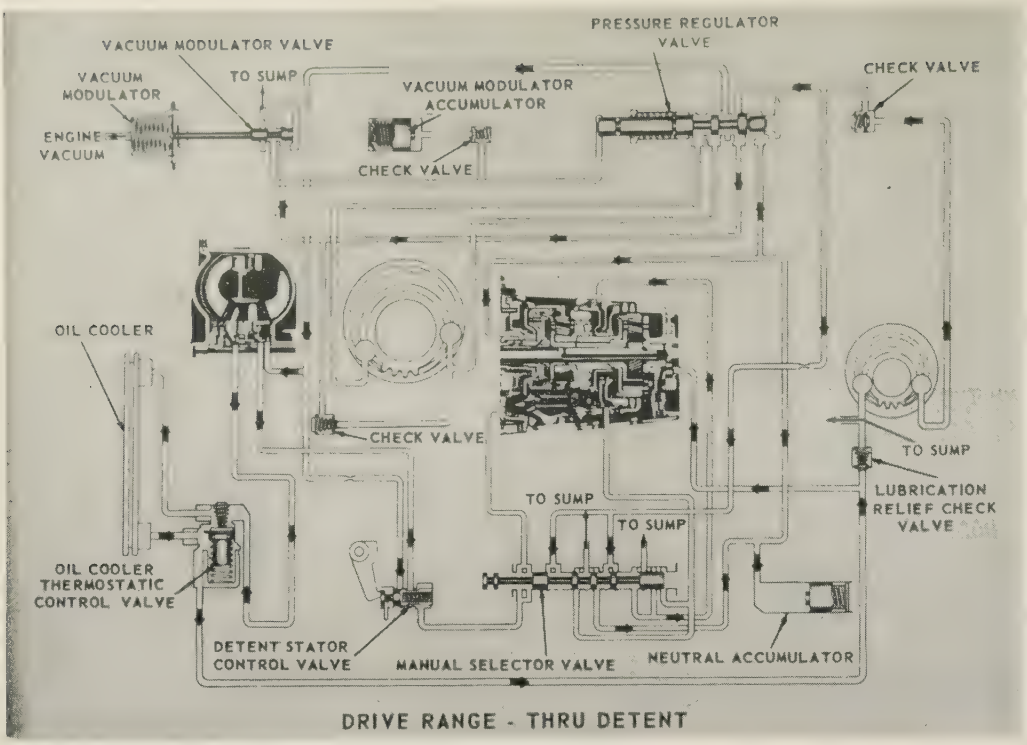

Fig. 18—Hydraulic control circuit

allowing converter pressure to force the piston to the high blade angle position. An accumulator and fixed orifice provide the necessary cushioning of the "garage" shifts. Converter cooling and charging pressure are ported through the main regulator valve with an exhaust restriction to limit the maximum flow. The cooler return is routed to the lubricating passages containing a pressure limiting valve. A time-delay accumulator prevents a sudden drop in line pressure on quick release of the throttle.

Physical Description

Structurally, the transmission consists of a one-piece aluminum die-cast case and bell housing with an attached aluminum die-cast extension (Fig. 19). The cast-iron valve body spans the bottom of the case and is covered by a sheet metal pan. The converter assembly is primarily steel stampings with the converter pump and third turbine of the familiar lance and tab construction (Fig. 20). The first turbine blades are an integral die-cast aluminum ring pinned to a steel stamping. The second turbine is an aluminum die-casting mounted on streamlined spokes to present the least resistance in the oil path. The three spokes are tangentially arranged and transmit torque in compression. An OD serrated armsteel hub is pressed in the aluminum bore, cutting its own drive.

Axial retention to the hub is provided by spinning over the aluminum. The stator blades are magnesium extrusions with serrated crank pins pressed in place for blade control. The crank arms engage an annulus in the control piston for the actuation. A cam and roller one-way clutch grounds the stator in the reaction direction.

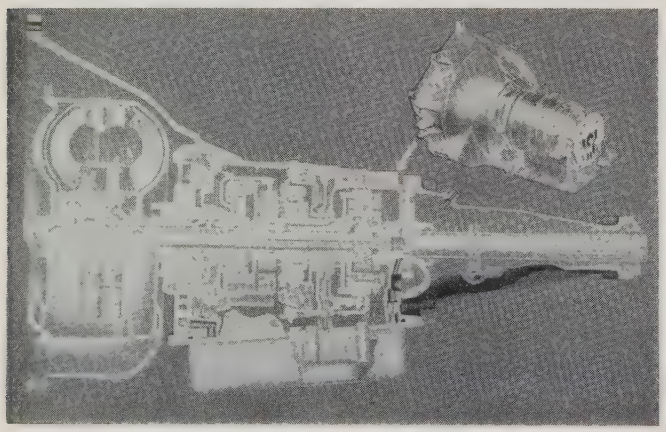

Fig. 19—Die-cast aluminum bell housing, transmission case and extension

Gears

Planetaries are 20-pitch 18.5-deg helix and a 20-deg pressure angle. The suns have 45 teeth, the rings 75, and the planets have 15. Both planetaries contains three pinions. The gear steel is 5130 with 0.007–0.010 carbo-nitride case.

Clutches

The cone clutches are 17 deg., with two active faces. The die-cast aluminum pistons and reaction members are faced with a non-metallic material. In engagement, the cones are free to take their axial and radial position from the outer or reaction member. Both the LD and drive lugs are in clearance. Since all cones are engaged while rotating, squareness is insured through the "ringing-in" process. The apply pistons are axially free by the ring land clearance or approximately 0.015 in. which is adequate due to the small dimensional stack to the ground cone. While running free, the cones rest radially on the inner member and are limited axially by the spring on one end and the reaction member

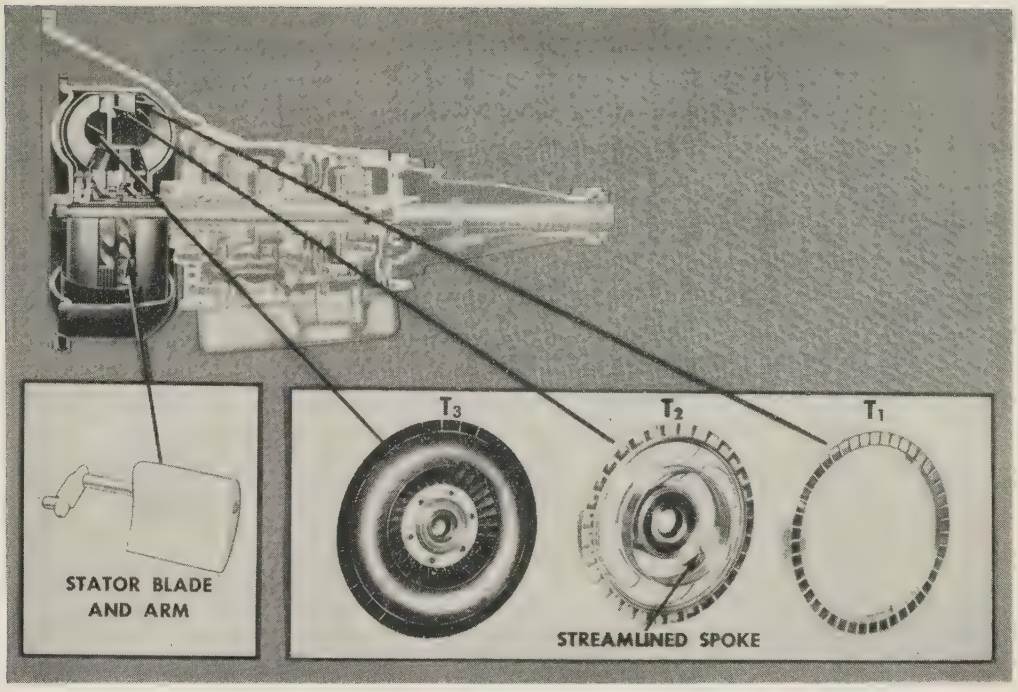

Fig. 20—Five-element torque converter with dual pitch stator

on the other. The wave-type return spring releases the apply piston only. The cones release by virtue of the relationship of the friction coefficient and the tangent of the cone angle. The forward piston is integral with the grade-retarder piston, ensuring that they do not overlap in the shift. Momentary grounding of T_2 through the forward cone in grade retarder would result in a very abrupt shift. The grade-retarder reaction is a 4-active-face cork and aluminum clutch on the T_1 ring gear.

Bearings

The torque converter is supported radially by the crank pilot on the front end and the front pump bushing on the rear. A low axial rate fly-wheel prevents excessive radial loads at the pump bushings and thrust loads on the crankshaft.

The gear train is supported entirely from the inner or T_1 shaft. The T_1 shaft is supported on the forward end through the cover to the engine crankshaft and in the rear through the output carrier to the case. Thrust within the converter and the gear train are absorbed through 11 radial needle thrust bearings. The rear pump is piloted from the output shaft and in turn pilots the extension.

Valve Body

The valve body assembly consists of a cast-iron body, a steel transfer plate, and a die-cast aluminum ditch plate (Fig 21).

The design and arrangement of the valve body assembly and case are such that oil is transferred from front to rear through the ditch plate so that the case passages are short, as illustrated. Oil is routed to the forward and grade-retarder pistons through short "universal" jumper tubes.

An important fact to note is that the arrangement eliminates any machined die-cast aluminum surfaces between pressure oil and the garage floor. With the exception of the converter flange and one gage line, there are no external pressure seals or gaskets. The one gage point, stator control pressure, is accessible from the outside for trouble shooting. Remaining gage points are located in the bottom face of the valve body for quick, easy accessibility for production testing.

The front pump and stator support housing as well as the rear pump are of cast iron, for expansion compatibility with the steel gears and the resulting maintenance of volumetric efficiency at elevated temperatures.

The valve body is cast iron rather than aluminum, for its compatible expansion with the steel valves as well as its superior resistance to dirt imbeddability and sticking valves.

Parking lock mechanism does not employ the

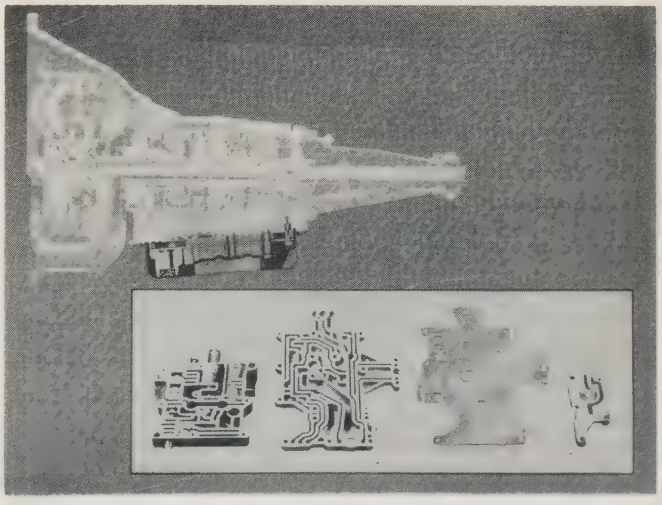

Fig. 21—Valve body assembly

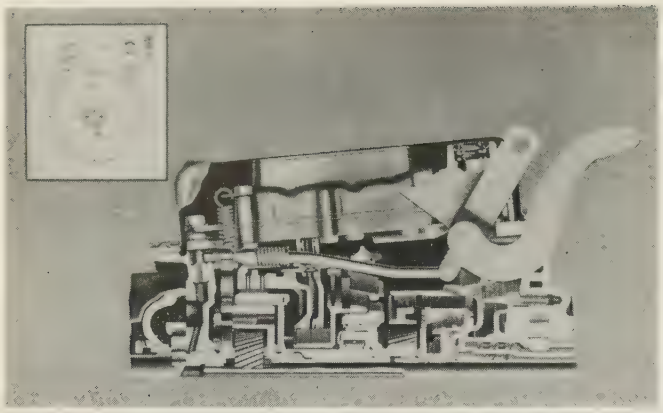

Fig. 22—Parking lock

Table 1—Parts of Turboglide Transmission

	Number	Weight, lb
Different Parts	277	
Total Parts	900	
Aluminum Die Castings	37	23.4
Iron Castings	21	25.3
Steel Parts	823	82.2
Miscellaneous Parts	19	17.1
Total Weight of Turboglide		148.0
Total Weight of Powerglide		256.0

conventional overcenter type of lock (Fig. 22). Instead, the mechanism utilizes a spring-loaded wedge for actuation while locking on a straight or neutral line.

In the case where the parking pawl butts a gear tooth, the selector lever may be locked in the park position while compressing the wedge spring, so that subsequent movement of the car permits actuation of the wedge onto the neutral diameter. The 10-deg. pressure angle ensures an ejecting component, while an ejecting spring releases the pawl when there is no tooth load. The range selecting and stator lever are simple concentric shafts with inner and outer levers.

The number of the transmission parts and weight are shown in Table 1.

DISCUSSION

Points Out Problem of Terminology

—C. J. Lucia
Ford Motor Co.

THE Turboglide unit poses a perplexing problem for the historians. Either the hydrodynamic unit (or units) is assuming more of the total job of multiplying torque and, therefore, might continue to be known as the torque converter or, the terminology may have to be revised to refer to the hydrodynamic unit as the fluid clutching unit. It is difficult to determine which is the primary function of the torque converter in the new Turboglide.

The tractive effort curve still leaves a challenging amount of area between it and the theoretically attainable. I, for one, will be very interested in reading the next paper by the authors on the subject of passenger-car transmissions. Any major tractive performance improvement on this concept will be very exciting reading.

ORAL DISCUSSION

of Jeffe—Cartwright and Winchell—Route—Kelley papers

Reported by B. W. Cartwright
Chrysler Corp.

Oscar Banker, New Products Corp.: The changes in automotive design are very apparent when we compare the present-day engine and transmission with that of 1928. In that year the engine weighed 750 lb, was 48 in. long, and produced 95 hp; today, the average engine weighs 650 lb, is 32 in. long, and delivers 206 hp. The transmission of 1928 weighed 98 lb and was only 18 in. long; today, it weighs 241 lb and is 35 in. long. The engineers of that era felt that transmissions of the future would not be saleable if they:

1. Were any larger.
2. Were heavier.
3. Were of the planetary type. (All present units are of this type.)
4. Wasted power. (Fluid-drive units all tend to be less efficient.)
5. Required special lubricants. (Special type A oil is in widespread use.)
6. Operated with friction elements in the lubricant. (All units operate with friction materials in oil.)
7. Completely eliminated the clutch pedal. (This had been considered a safety feature; however, the elimination of the pedal is one of the present goals.)
8. Increased in price. (All present-day automatics are more expensive.)
9. Were complicated to service. (Service has become one of the major problems.)
10. Automatically changed ratios. (Today's driver does not wish to be burdened with the problem of selecting gear ratios.)

Thus, it would seem that we have completely contradicted all of the limitations set in 1928.

V. C. Moore, General Motors Corp.: Why is engine overspeeding prevented in second gear and permitted in low gear on the TorqueFlite transmission?

Mr. Jeffe: Overspeeding in low is permitted as a safety feature on steep grades.

Mr. Moore: Were there any problems presented by high clutch differential speeds in reverse?

Mr. Jeffe: No, proper lubrication was all that was required.

Mr. Moore: Does the customer have to stand the entire service cost if a thrust washer fails within the welded torque converter unit?

Mr. Jeffe: Yes. However, the number of failures is practically nil due to manufacturing test procedures and a simplified design.

Mr. Moore: Can the axle ratio be reduced by the numerical value of 1.0 by using the TorqueFlite rather than the PowerFlite?

Mr. Jeffe: No, the difference in axle ratio used is one step, from 3.36 to 3.18.

Mr. Moore: Can the shift pattern be varied between closed throttle and the detent position?

Mr. Jeffe: Yes, the shift pattern can be modulated between closed throttle and wide-open throttle.

Mr. H. G. English, Ford Motor Co.: Did the efficiency of the Turboglide present converter cooling problems?

Mr. Winchell: The cooling problems were of sufficient magnitude to justify two separate trips to Pikes' Peak.

Mr. English: Why did the new Turboglide change the selector positions?

Mr. Winchell: It was necessary because of the design of the hydraulic controls.

Mr. Banker: What is the magnitude of the gap loss in the Turboglide with its six transfer points in the fluid circuit.

Mr. Kelley: The shock loss in this unit has been reduced to a value as low as possible.

AUTOIGNITION associated with HOT STARTING

F. W. Bowditch and R. F. Stebar, General Motors Corp.

This paper was presented at the SAE Summer Meeting, Atlantic City, June 6, 1957.

THE several difficulties involved in restarting a hot engine have been recognized for some time. But, perhaps the most important difficulty in modern high-compression engines is the fact that the torque requirement for starting hot engines in many cases exceeds the requirement for starting cold engines. As a consequence, the hot starting torque determines, in a large part, the required starter size in today's modern automobiles.

Despite the knowledge of the existence of the problem, no definite information has been available concerning its origin. For example, when we developed the present strain of high-compression engines in 1949, the phenomenon was observed and termed "Dieseling," but the cause was not known. Since any alleviation of the problem of hot starting would mean a direct saving in starter costs, a program was initiated to identify it and suggest any possible action.

Combustion Terminology

The combustion terms used throughout this paper are as proposed by the Coordinating Research Council[1] with the exception of the term autoignition. Autoignition as used herein includes not only the knock phenomenon, but also any other self-ignition process. It, therefore, includes the ignition phenomenon termed compression ignition in which spontaneous ignition takes place in a few isolated areas from which a normal combustion process proceeds. The heat necessary to produce a sufficient mixture temperature for spontaneous ignition to occur may be produced in three ways: first, by the heat transferred to the mixture from the hot combustion-chamber walls; second, by the heat gen-

USING a high-speed motion picture camera, flame photographs were taken of the combustion process associated with the starting of hot gasoline engines.

Compression ignition at isolated points followed by normal combustion caused peak cylinder pressures to occur prior to top dead-center under some low-speed engine conditions.

In addition, an abnormal combustion phenomenon was observed in the last part of the charge to burn. The reaction rate was appreciably faster than normal for the engine speed and much slower than is usually observed in knocking combustion at normal engine speeds.

[1] *SAE Journal*, Vol. 62, October, 1954, pp. 46–47: "Combustion Terms Defined by CRC."

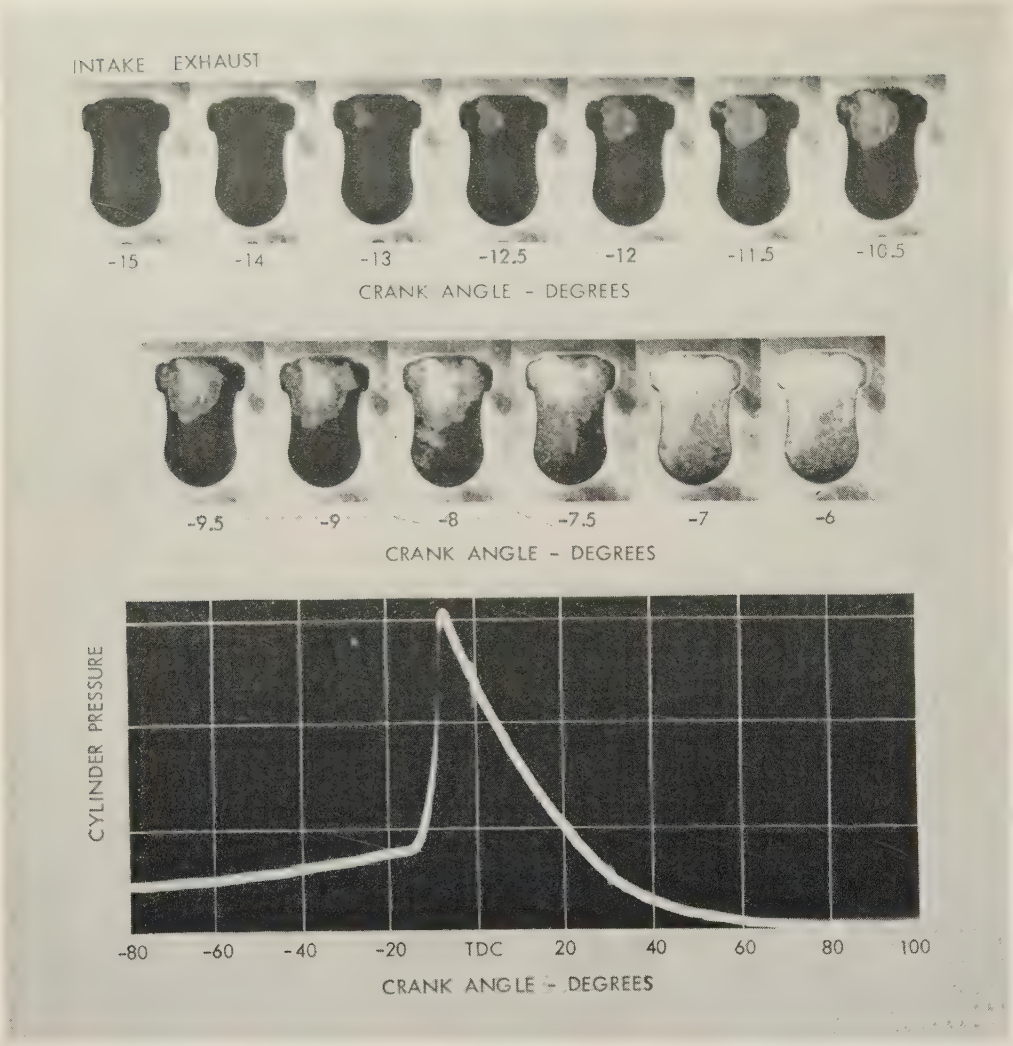

Fig. 1—Flame photographs and corresponding pressure record of a typical explosion occurring with 70 octane primary reference fuel under standard hot starting conditions

erated as the mixture is compressed during the compression stroke; and third, by the heat produced by a combination of these.

Equipment

The engine used for the majority of this investigation was a standard overhead-valve ASTM-CFR knock test engine. A quartz ell head and block of 6.75/1 compression ratio were substituted for the corresponding standard CFR parts when flame photographs were taken. In addition, a few observations were made in a multicylinder engine.

The engine operating conditions taken as representative of those encountered in the hot starting problem will be referred to as standard hot starting conditions throughout this paper and are listed in Table 1.

An unexpected problem was encountered in maintaining a constant rate of revolution of the engine. This is illustrated by the fact that under these standard hot starting conditions the stub end of the CFR crankshaft was twisted off. To alleviate the problem, a 4-speed synchromesh truck transmission was mounted backwards between the engine and the dynamometer in such a manner that the dynamometer speed could be approximately seven times that of the engine. This helped by increasing the inertia of the rotating system and permitted dynamometer controls to work more effectively. With the transmission, the engine speed was held constant within ± 5 rpm during the four strokes of the cycle.

Pressure cards were recorded at the same time flame photographs were taken. The cards were produced with GMR condenser indicators using GMR Capacagages as amplifiers and were displayed on a DuMont 322-A dual-beam oscilloscope. One trace of this oscilloscope was used to display the pressure cards and the other for timing marks generated with a magnetic pickup and flywheel slugs. Oscilloscope photographs were taken with a DuMont 321 oscilloscope record camera.

When flame photographs were not taken, a statistical average time of peak pressure was used to measure the extent of the abnormality of the combustion processes. To obtain this average time of peak pressure, the peak pressure distribution counter described in detail by Weller, Schubring, and Fitch[2] was used. Basically, this instrument takes the signal from a condenser-type pressure trans-

[2] Proceedings of National Electronics Conference, Vol. 12, 1956, pp. 197–211: "Peak Pressure Distribution Counter for Engine Fuel Studies," by E. F. Weller, Jr., N. W. Schubring, and M. E. Fitch.

Table 1—Standard Hot Starting Conditions

Engine Speed	150 rpm	Throttle	Fully open
Coolant Temperature	190 F	Spark Advance	tdc
Oil Temperature	180 F	Air-Fuel Ratio	10% rich

ducer, produces the first derivative of that signal, and furnishes a pulse when the first derivative trace passes through zero (when peak pressure occurs). This pulse is then counted by the appropriate one of 20 counters. For this study each counter covered three crank-angle degrees of crankshaft rotation, the first counter receiving all the pulses occurring between 10 and 7 deg btdc and the last counter receiving all pulses occurring from 57 to 60 deg atdc. The instrument could be preset to count the desired total number of cycles and would automatically stop at the end of this count leaving the distribution of time of peak pressures displayed on the 20 counters.

For the multicylinder engine data a standard V-8 9.75/1 1956 production engine was used under the standard hot starting conditions with a strain gage spark plug pressure transducer in cylinder No. 7. Again, a 4-speed transmission was run backwards between the engine and dynamometer. The operating conditions were the same as those for the single-cylinder engine work except that the air-fuel ratio was controlled by the standard production 4-barrel carburetor and was not measured. In addition, deposits had been accumulated using a commercial fuel and oil.

Data and Discussion

The problem was first examined in a preliminary way on a production 1957 engine. A strain gage spark plug pressure transducer was placed in one of the cylinders and the resulting pressure cards were viewed on an oscilloscope while attempts were made to start the hot engine with the starter. These first results indicated that the cylinder pressure was peaking sometime prior to tdc at cranking speeds and that as the cranking speed slowed, the time of peak pressure advanced until the starter was no longer able to crank the engine. Loud knock-like noises accompanied these conditions.

Analysis by Combustion Photographs—Since it was not possible to maintain a constant cranking speed with the starter motor and since it was deemed advisable to take combustion photographs in order to identify the type of combustion occurring in the engine cylinder, the study was continued with a standard ASTM-CFR single-cylinder knock test engine modified to accommodate a full quartz window as explained previously. Running this engine at the standard hot starting conditions with 70 octane primary reference fuel produced loud noises from the engine and peak cylinder pressures prior to tdc. Apparently, then, the hot starting phenomenon could be reproduced in a single-cylinder engine.

Flame photographs of a characteristic explosion under these conditions together with the resulting pressure card are shown in Fig. 1. The initial ignition occurred at about 14 deg btdc over the intake valve in two different areas. Moreover, additional areas of ignition occurred as combustion proceeded.

Photographs of additional explosions which occurred consecutively with the one shown in Fig. 1 showed that the sources of ignition did not occur at the same places in the combustion chamber in consecutive explosions. However, the spurious initial ignitions usually occurred in the valve end of the combustion chamber.

The spatial rate of flame propagation for the explosion shown in Fig. 1 (relative to the combustion-chamber walls) from the ignition centers was about 25 ft per sec, which is considered to be a normal flame propagation rate at an engine speed of 150 rpm.

Still another observation may be made from these flame photographs. At 9 deg btdc and even more evident at 8 deg btdc a second type of combustion process began. The rate of this process was three to four times greater than that which occurred prior to this time. However, even though the rate of reaction was relatively high, it was still far below that normally associated with knock at higher engine speeds. This relatively high-speed reaction will be called slow knock for want of better terminology.

The pressure record also shows the effects of the abnormal explosion in Fig. 1. For example, it shows the higher rate of reaction which started at 8–9 deg btdc and ended at 6–7 deg btdc. The rate of pressure rise was so rapid that the trace appears almost vertical and can barely be seen due to the low film exposure for this section of the card. As the flame photographs show, combustion is complete at from 6–7 deg btdc with the pressure record also peaking at about this point. The pressure decrease, which occurred after combustion was complete despite the continued minor piston compression, may be attributed to heat loss and gas leakage which have time to play a particularly great part at such low engine speeds.

The pressure scale on the pressure cards is approximately 200 psi per division; hence, peak cylinder pressure was somewhat greater than 600 psi for this explosion. Even though the total work of the cycle may be approximately zero as it was in this case, an automobile starter cranking an engine under these conditions would be required to furnish extra torque in order to turn the engine the last 20 deg btdc of the compression stroke. Hence, the starter requirement would be increased and the reason for the starter stalling is apparent.

The reason for the knock-like noise accompanying this phenomenon is not so apparent. The fact that it is not knock in the usual sense is evident by the lack of oscillations on the expansion side of the pressure card and by the rate of the final reaction, as seen in the flame photographs. A possible explanation for the noise is the fact that if the piston and attached engine parts are considered as a mass and spring system and the application of the gas pressure impulse as an inelastic collision with the mass and spring system, then it can be shown that with a constant impulse, the deflection of this system is an inverse function of the initial momentum of the system.

Surface Ignition as Cause of Early Ignitions—The reason for the early ignition is not apparent from these data. The spots which appear behind

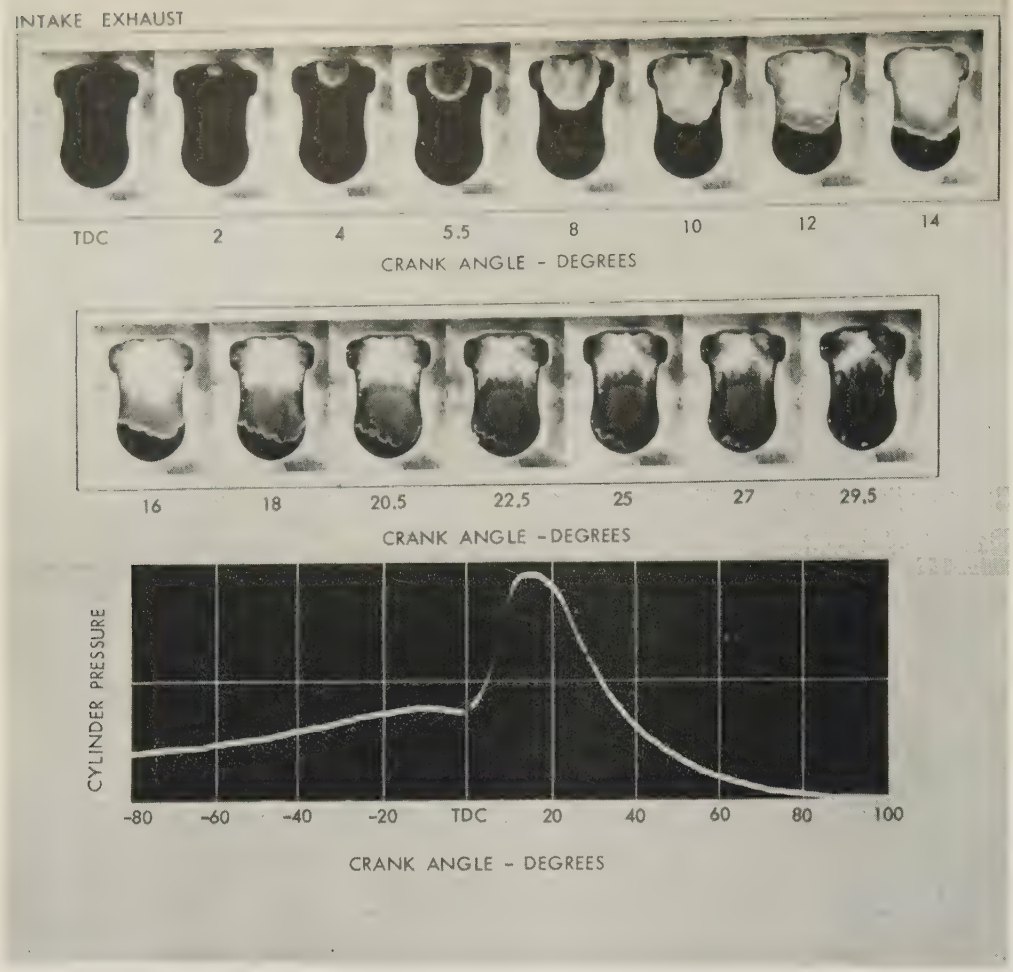

Fig. 2—Flame photographs and corresponding pressure record of normal combustion occurring with benzene under standard hot starting conditions

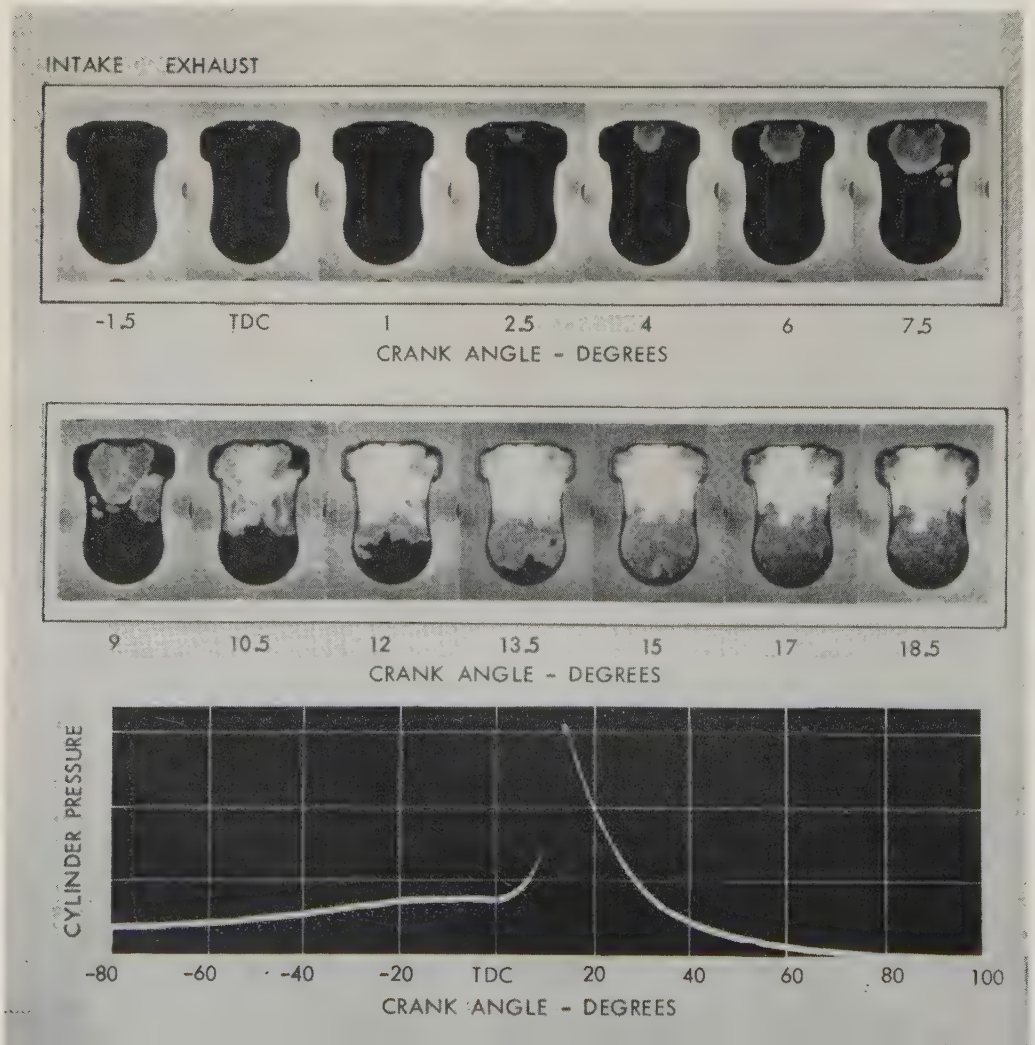

Fig. 3—Flame photographs and corresponding pressure record of a typical explosion occurring with 85 octane primary reference fuel under standard hot starting conditions

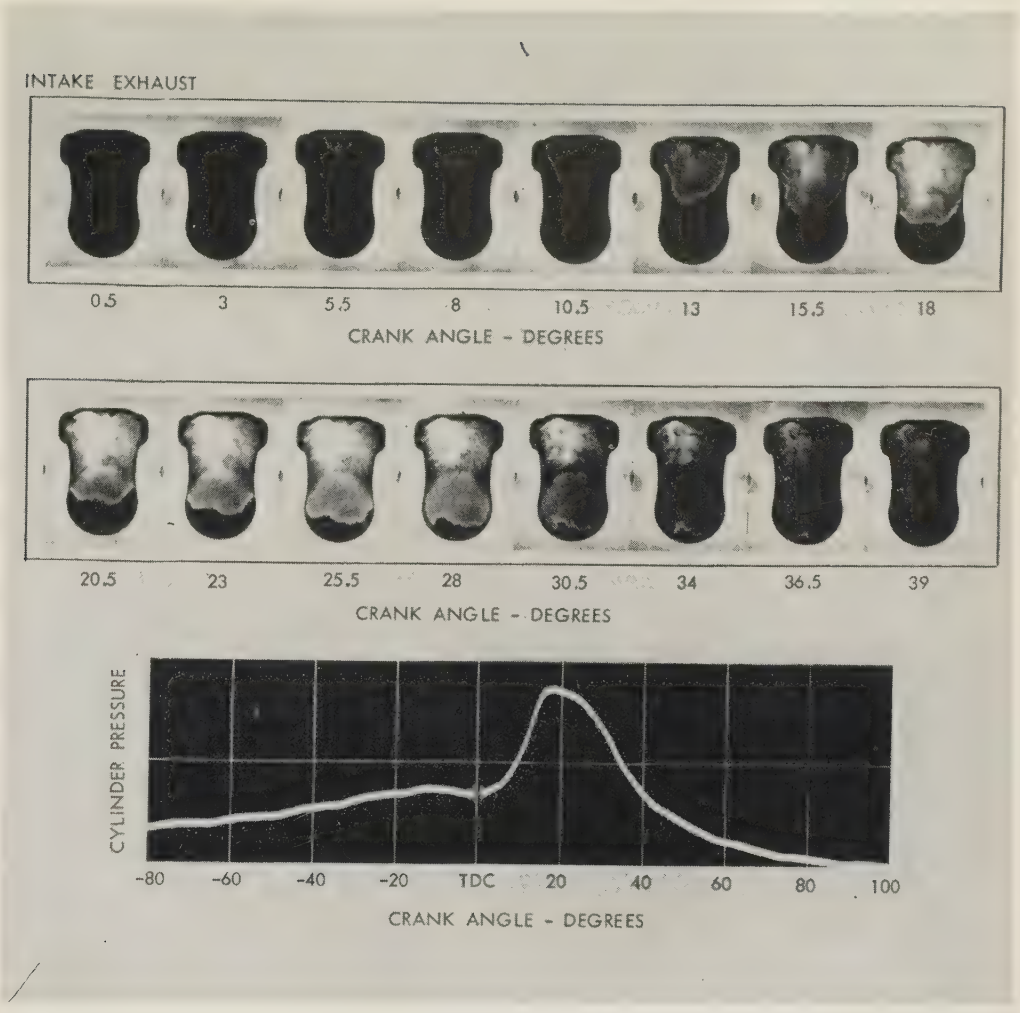

Fig. 4—Flame photographs and corresponding pressure record of normal combustion occurring with isooctane under standard hot starting conditions

the flame front in Fig. 1 suggest that engine cleanliness may be a factor, that is, this phenomenon might be a case of deposit-induced surface ignition. However, these photographs were taken shortly after the engine had been thoroughly cleaned.

In order to see if the ignition phenomenon was some form of particle-induced surface ignition, benzene (a fuel having a very low deposit-induced surface ignition resistance) was run. Fig. 2 shows a typical benzene explosion under the standard hot starting conditions. The explosion was completely normal despite the low surface ignition resistance of the fuel. Combustion of the benzene-air mixture was initiated by the spark discharge at tdc, and the inflammation process continued normally until combustion was complete at about 29.5 deg atdc. The cylinder pressure reached a peak of from 350–400 psi at approximately 15 deg atdc. Since no spurious ignition occurred even with this very sensitive fuel, it appears that the hot starting problem does not involve deposit-induced surface ignition.

Octane Sensitivity of Early Ignitions—To determine if there was an effect of octane quality, the engine was run with 85 octane primary reference fuel with resulting explosions similar to those shown in Fig. 3. In this instance, combustion was initiated by the spark discharge at tdc. Propagation from this point was normal until 7.5 deg atdc at which time two or three spurious ignitions occurred. In the next frame, 9 deg atdc, ignition had occurred at several additional places. Even though the rate of reaction was apparently normal from each source, the number of the sources produced a sharp increase in the overall mass rate of burn. At 12 deg atdc the slow-knock type of reaction began. This reaction completed the combustion process at from 15–17 deg atdc.

The initiation of the slow knock is again apparent on the pressure card with the rate of pressure rise per deg again being so high that insufficient exposure resulted. The pressure peaked at just over 600 psi, slightly less than the 70 octane fuel shown in Fig. 1, but at about 15 deg atdc. In this instance, this phenomenon would probably have assisted a starting motor, but still would have produced some objectionable noise. Therefore, it appears that the ignition phenomenon is octane sensitive. To verify this conclusion, isooctane and normal heptane were used as fuels.

Fig. 4 shows a characteristic explosion with isooctane. Ignition took place from the spark discharge and the flame propagated normally throughout the entire mixture, being completed at about 39 deg atdc. The accompanying pressure card shows no rapid increase in pressure, with the pressure peak of about 350 psi occurring around 18 deg atdc. Evidence for the conclusion that deposit-induced surface ignition is not involved is the fact that

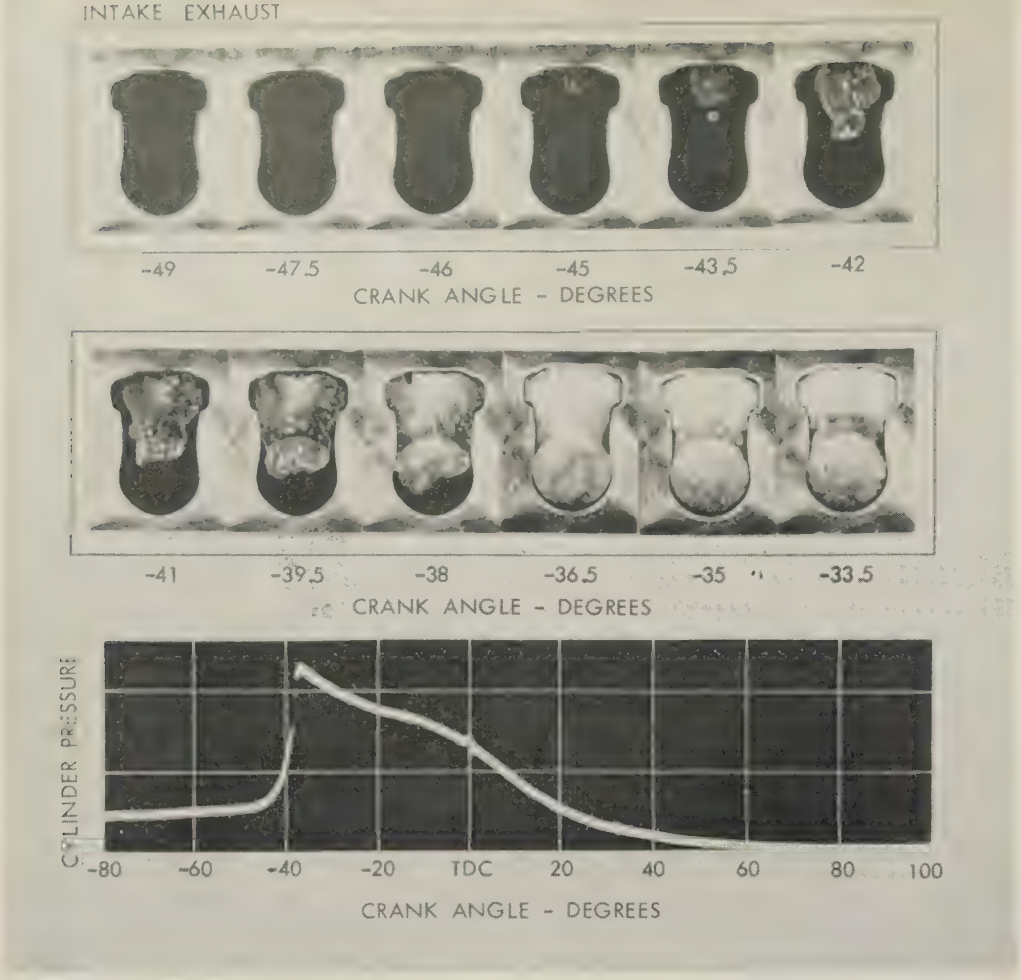

Fig. 5—Flame photographs and corresponding pressure record of a typical explosion occurring with normal heptane under standard hot starting conditions

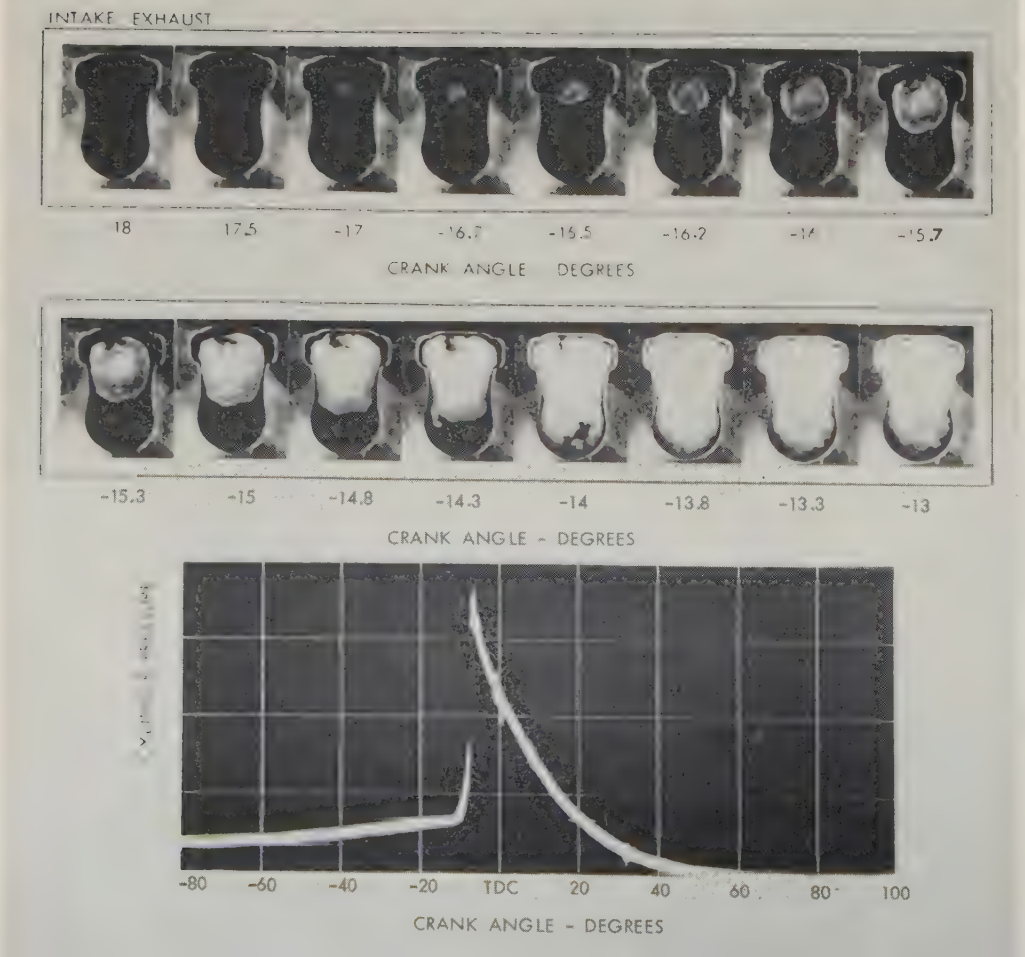

Fig. 6—Flame photographs and corresponding pressure record of typical explosion occurring with acetylene under standard hot starting conditions

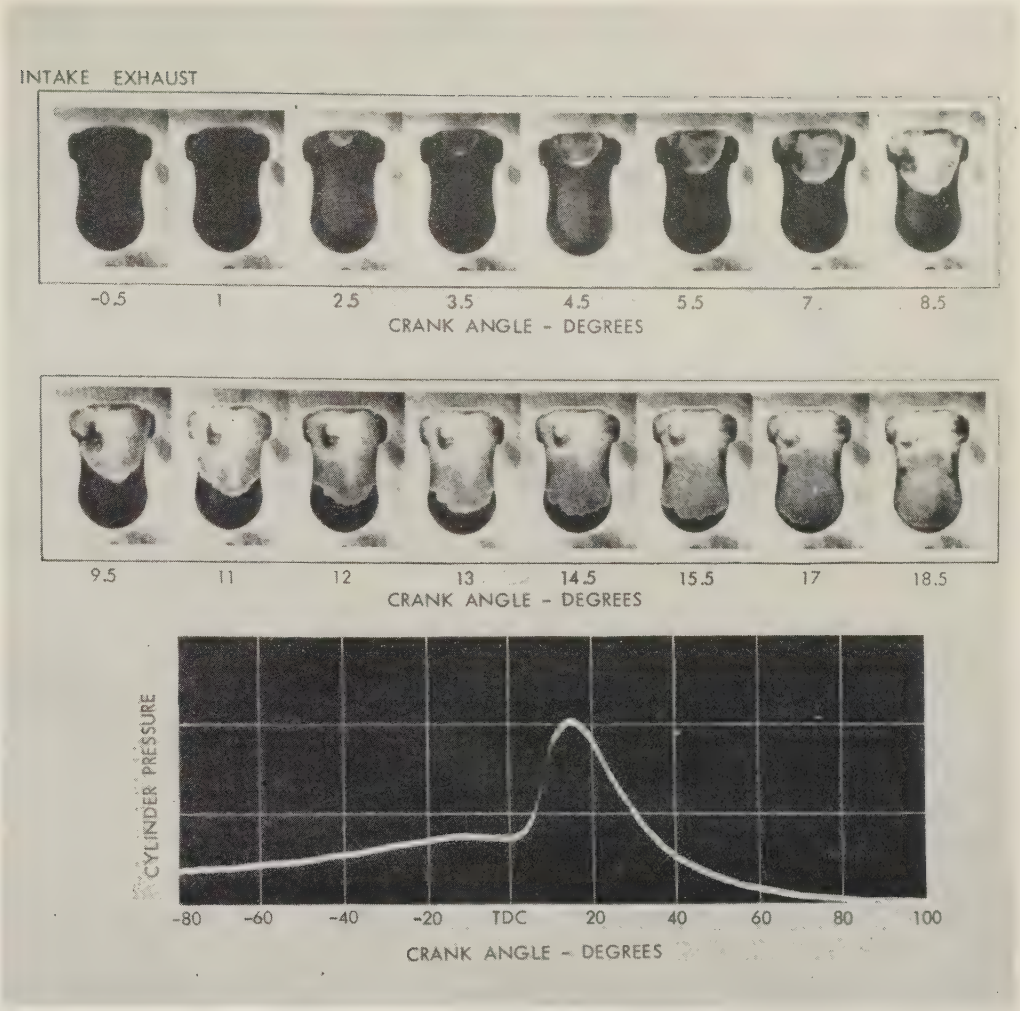

Fig. 7—Flame photographs and corresponding pressure record of normal combustion occurring with ethylene under standard hot starting conditions

benzene explosions were quite similar to those of isooctane. This evidence suggests that antiknock quality rather than surface ignition resistance may be involved.

Fig. 5 shows a normal heptane explosion and the pressure card it produced. Ignition occurred about 46 deg btdc with additional ignitions occurring thereafter. In this instance, the slow-knock reaction started at from 38–39.5 deg btdc and consumed less volume of charge than in the case of the 70 octane primary reference fuel shown in Fig. 1. This may be due to the fact that with normal heptane the end-gas density and temperature are considerably below those occurring with the 70 octane fuel during combustion of the end-gas regions due to the piston positions at the time these final reactions occur.

The pressure card generated by the normal heptane explosion reflects the abnormal combustion process with the peak cylinder pressure of approximately 450 psi occurring at about 35 deg btdc, the same time combustion is complete. It is interesting to note that even though a zero octane fuel was used, knock, in the usual sense, did not occur as evidenced by the lack of pressure oscillations on the expansion side of the card. In this instance, negative total work resulted for the cycle.

Origin of the Luminous Spots—Since the highly luminous spots appearing in some of the previous explosions might be the cause of the spurious ignitions, an attempt was made to find their origin. In order to be sure that incomplete vaporization of the liquid fuels was not a contributing factor, gaseous fuels were used. Acetylene have a Research octane number of about 50, ethylene with a Research octane number of about 100, and mixtures of the two were run under the standard hot starting conditions.

Fig. 6 shows a typical acetylene explosion with accompanying pressure card. The highly luminous spots are also in evidence in the burned-gas region. This explosion is characteristic of the low-speed combustion phenomenon shown in some of the previous figures with a rapid reaction, beginning at about 14.3 deg btdc, completing the combustion process. The pressure card generated by this explosion shows the effect of the abnormal combustion process on cylinder pressure.

With ethylene, no abnormal combustion would be expected because of its high octane number. Fig. 7 shows a typical ethylene explosion. It is completely normal except for a few spots in the burned-gas region and the section of unburned charge in the intake-valve area. All of the explosions photographed with the one shown in Fig. 7 exhibited the same deviations from normal. The reason for

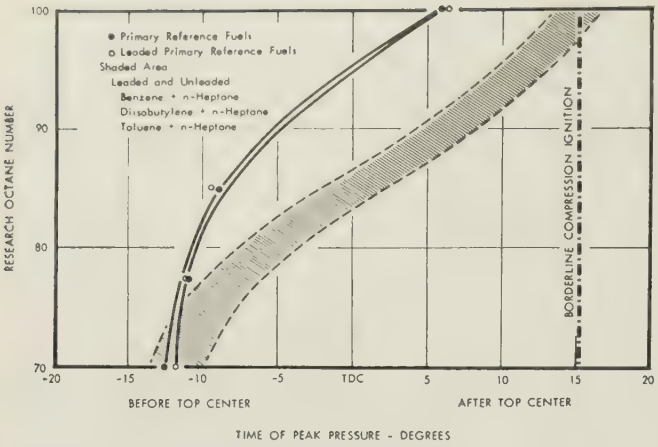

Fig. 8—Effect of Research octane number on time of peak pressure (leaded fuels contain 3 ml tel per gal)

the unburned volume is not known, but may be due to incomplete mixing of the fuel and air.

Due to the higher rate of normal reaction, combustion is complete earlier in the ethylene explosion than in either the benzene or the isooctane explosions even though all three fuels exhibit normal combustion under these standard hot starting conditions. Combinations of acetylene and ethylene produced intermediate amounts of the abnormal combustion phenomenon.

The appearance of the highly luminous spots behind the flame fronts apparently follows the octane quality of the fuels. For instance, this is shown by the fact that the 70 octane fuel experiment (Fig. 1) was run in a completely cleaned engine and immediately afterward the ethylene experiment (Fig. 7) was run. Comparison of the two figures shows the multitude of spots in the case of the 70 octane fuel, and the few spots evident in the ethylene case. Colored movies were taken of the combustion process in which these highly luminous spots appeared. Whereas the majority of the burned gas region appeared blue, the spots were yellow—possibly indicating diffusion-type combustion. Possible sources for these spots would appear to be burning fuel or oil droplets or dust particles.

Accordingly, an effort was made to eliminate these possible causes. The engine was completely cleaned, the oil was drained from the crankcase and removed from operating areas, a 10-micron filter was attached to the intake-air system and gaseous fuels were used. The engine was run for one hour with no lubrication at standard hot starting conditions with ethylene, after which high-speed photographs were taken with both ethylene and acetylene. These explosions appeared quite similar to those shown in Figs. 6 and 7, indicating that the precautions taken did not eliminate the spots.

A much more complete analysis of the cause of bright spots occurring in known cases of explosions initiated by compression ignition has been made by Livengood and Leary.[3] In this investigation the above factors were considered as well as the possible role of radiation, carbon, and hydrogen in the formation of the spots. None of these were found to be factors affecting the formation of the spots. However, the study did reveal that high-temperature areas do exist in the burned-gas area. It would, therefore, appear that the spots are characteristic of explosions initiated by compression ignition.

Autoignition as Cause of Early Ignitions—Flame photographs have been obtained using rapid compression machines in which the compression ignition of the fuel-air mixture is used to initiate combustion. Photographs taken of the combustion process occurring in such a machine at the Massachusetts Institute of Technology have been published by C. F. Taylor and others[4] and Livengood and Leary. These photographs bear a striking resemblance to those shown in this paper where abnormal ignitions occurred. Studies of the combustion process in rapid compression machines have shown that at least some relation exists between the compression ignition phenomenon and knock[3, 4, 5, 6, 7, 8]. Therefore, it might be expected that the ignition phenomenon occurring during hot starting should be octane sensitive if the spurious hot starting ignitions are due to compression ignition. All evidence thus far indicates that such is the case.

The slow-knock reaction such as is shown in Figs. 1 and 3 resembles the usual engine knock in all respects except in the speed of reaction. In no instance was the slow-knock reaction observed to occur without compression ignition initiating the combustion process.) The slow-knock reaction is apparently another variety of autoignition.

Effect of Engine Operating Variables

A continuation of the study was desirable to investigate the magnitude of the effects of engine operating variables on the autoignition phenomena associated with hot starting, in the hope of alleviating the problem through changes in the hot starting engine conditions. Since operation in the window engine limits the operating variables, the standard overhead-valve ASTM-CFR knock test engine was used. As can be seen from the foregoing combustion photographs and pressure-time cards, the time of peak pressure offers an accurate and convenient method of measuring the extent of this abnormal combustion phenomenon. With the aid of the GMR peak pressure distribution counter a statistically accurate time of peak pressure could be determined for each experimental condition. The determination of the statistical average time of peak pressure was readily obtained since the time of peak pressure was more reproducible when the abnormal combustion process occurred than when normal combustion took place.

Octane Number Effect—Octane number was in-

---

[3] *Industrial and Engineering Chemistry*, Vol. 43, December, 1951, pp. 2797–2805: "Autoignition by Rapid Compression," by J. C. Livengood and W. A. Leary.

[4] SAE *Quarterly* Transactions, Vol. 4, April, 1950, pp. 232–274: "Ignition of Fuels by Rapid Compression," by C. F. Taylor, et. al.

[5] *Industrial and Engineering Chemistry*, Vol. 43, December, 1951, pp. 2805–2814: "Two Stage Autoignition of Some Hydrocarbons," by W. J. Levedahl and F. L. Howard.

[6] *Industrial and Engineering Chemistry*, Vol. 46, May, 1954, pp. 1029–1034: "Effect of Preflame Oxidation Reactions on Engine Knock," by C. Walcutt, J. M. Mason, and E. B. Rifkin.

[7] *Fuel*, Vol. 32, July, 1953, pp. 279–309: "Cool Flame Formation in Motored Engine," by D. Downs, J. C. Street, and R. W. Wheeler.

[8] Fifth Symposium (International) on Combustion, 1954, pp. 347–356: "Correlation of Autoignition Phenomena in Internal Combustion Engines and Rapid Compression Machines," by J. C. Livengood and P. C. Wu. Pub. by Reinhold, New York, 1955.

vestigated in the manner described above to augment the information which was discussed earlier in the analysis of the flame photographs. Isooctane, toluene, diisobutylene, and benzene were blended with normal heptane to obtain desired Research octane numbers. To see if differences existed between the fuels with and without lead at the same octane levels, the fuels were also bended with 3 ml tel per gal plus normal heptane to obtain the various Research octane numbers.

The effect of octane number in this instance was studied at 9/1 compression ratio and the standard hot starting conditions with the ASTM-CFR knock test engine. Fig. 8 shows the results of this study. The dashed vertical line in the figure represents the estimated average time of peak pressure if no compression ignition occurred. Therefore, the horizontal distance between the dashed line and the curves for the fuels is a measure of the extent of compression ignition.

In general, the results are consistent with the analysis of the flame photographs. For the results shown in Fig. 8, three of the fuels (benzene, toluene, and diisobutylene) reacted similarly with considerable autoignition occurring at the 70 Research octane level. As a result peak cylinder pressures occurred 10–13 deg btdc or 23–28 deg before the average time of peak pressure in the absence of compression ignition. At the 100 Research octane level these same fuel blends show little or no compression ignition.

The case of the primary reference fuels is different, however. At the 70 octane level, the level of compression ignition severity is about the same as that of the other fuels. At the 100 octane level, however, a considerable amount of compression ignition still persists, causing cylinder pressure to peak about 10 deg early. This indicates that isooctane is considerably more prone to compression ignition than the other pure hydrocarbons of the same Research octane level under these engine conditions.

The addition of tel was as effective as fuel blending in controlling compression ignition. Had tel not been effective in controlling this phenomenon, the validity of the conclusion that the spurious ignition process was compression ignition would have been somewhat doubtful since the effectiveness of tel on knock is well substantiated and similar results would be expected in both instances.

Compression Ratio Effect—The effect of compression ratio is shown in Fig. 9. Compression ratios were varied from 7/1 to 10/1 under standard hot starting conditions using various fuels of 100 Research octane number and a commercial fuel of 94 Research octane number. In this instance, the diisobutylene, toluene, and benzene blends of 100 Research octane number, both leaded and unleaded, had no compression ignition occurring over the engine compression ratio range. Therefore, the shaded portion of the figure represents the time peak pressure should occur in the absence of compression ignition. The isooctane and the isooctane-n-heptane plus 3 ml tel per gal blend of 100 Research octane number again exhibit a sensitivity to compression ignition by producing peak cylinder pressures at about 2 deg btdc at a compression ratio of 10/1. The commercial fuel of 94 Research octane number follows the isooctane curve closely, indicating that the commercial fuel is comparable to isooctane in compression ignition resistance under these engine conditions.

Fig. 10 shows the effect of compression ratio on a series of blends of 78 Research octane number. The dashed line on the right-hand side of the figure denotes the approximate times of peak pressure which would result if no compression ignition occurred. Here the compression ratio effect is considerably magnified for the benzene, diisobutylene, and toluene blends. Only unleaded blends of the pure hydrocarbon blends are shown, since the leaded blends fell quite close to their unleaded counterparts. The difference between the primary reference fuel and the rest of the fuels is not as pronounced as before, indicating perhaps that isooctane is the unusually reactive component. This is in agreement with the data presented in Fig. 8.

The effect of compression ratio is consistent with the known change in knocking requirement with compression ratio. This adds further evidence that the spurious ignition phenomenon is a form of autoignition.

Coolant Temperature Effect—The effect of coolant temperature on the time of peak pressure under the standard hot starting conditions and 10/1 compres-

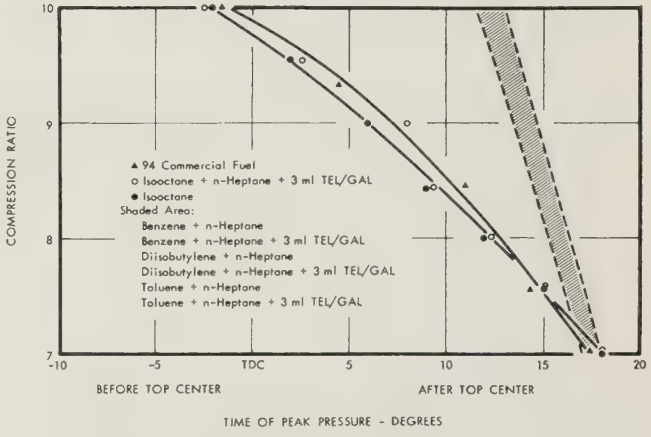

Fig. 9—Effect of compression ratio on time of peak pressure (100 Research octane blends, commercial fuel)

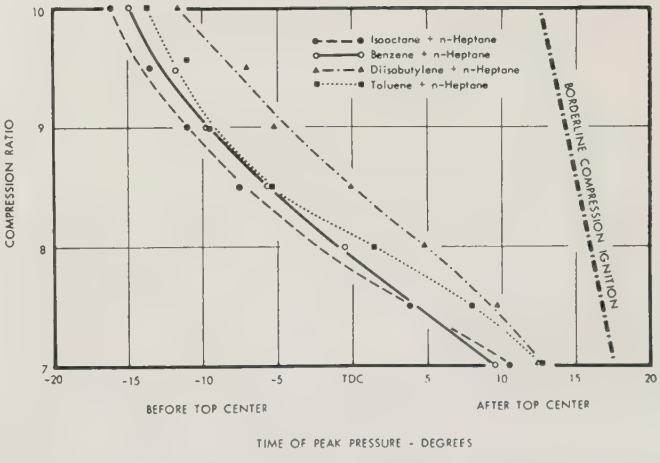

Fig. 10—Effect of compression ratio on time of peak pressure (78 Research octane blends)

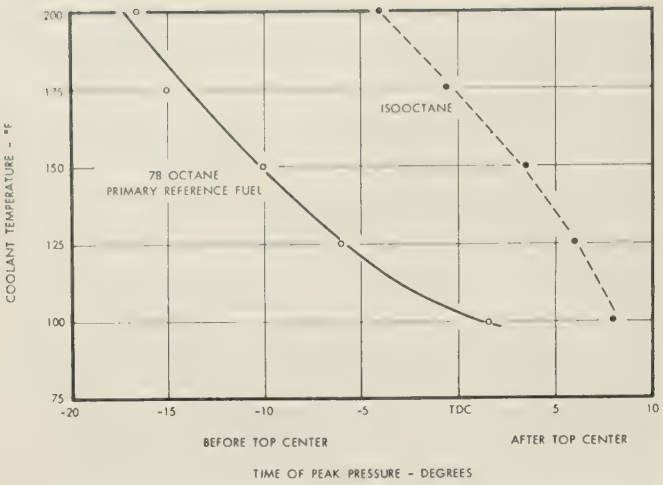

Fig. 11—Effect of coolant temperature on time of peak pressure (10/1 compression ratio)

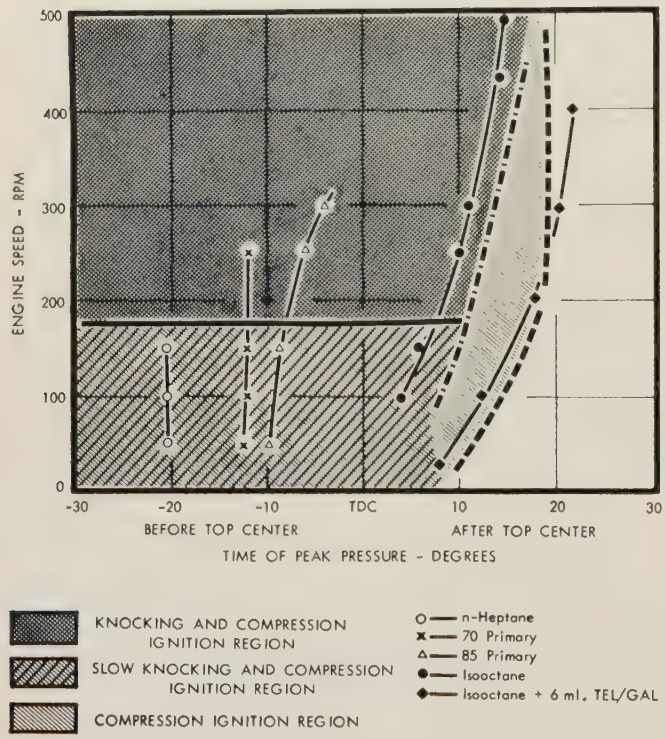

Fig. 12—Effect of engine speed on time of peak pressure (primary reference fuels)

sion ratio is shown in Fig. 11 for isooctane and a primary reference fuel of 78 octane number. At the higher coolant temperatures, peak pressures are considerably advanced due to the spurious ignitions, and markedly more so with the primary reference fuel than with isooctane as shown in Figs. 9 and 10. This again illustrates that any changes in engine operating conditions which increase the normal knock requirement of an engine also increase the extent of compression ignition. The effect of coolant temperature indicates it should be maintained as low as practicable since small changes in this temperature have a pronounced effect on the extent of compression ignition.

Engine Speed Effect—The effect of engine speed on the extent of this low-speed autoignition was determined over the range of 25–500 rpm using primary reference fuels at 9/1 compression ratio and the standard hot starting conditions. Fig. 12 shows the results of this study. The approximately vertical dashed line on the right-hand side of the figure shows the approximate time of peak pressure in the absence of compression ignition, as was shown in Figs. 8 and 10. This denotes that with all the fuels shown, except above 250 rpm with isooctane plus 6 ml tel per gal, compression ignition was occurring. The extent of the occurrence may be approximated by noting the difference in the time of peak pressures between the dashed borderline compression ignition curve and the curves for the rest of the fuels at the same engine speeds. The heavy horizontal line separates the knocking region from the one in which the slow-knock reaction occurs, indicating that the knocking combustion phenomenon changes below an engine speed of 175 rpm. The remaining dashed-dot line separates the knocking from the nonknocking regions on the figure.

It is interesting to note that normal heptane is not as much different from 70 octane primary reference fuel as the 85 is from isooctane. It would appear that there may be some limit to how early the compression ignitions take place or that charge density enters into the picture. The isooctane plus 3 ml tel per gal data has not been included in this figure. However, it was almost the same as the isooctane plus 6 ml tel per gal data indicating that the additional tel did not appreciably affect the time of occurrence of peak pressure. However, a marked difference exists between the leaded and unleaded isooctane.

The particularly interesting information shown in this figure is the fact that knock does not occur below 175 rpm under the standard hot starting conditions regardless of octane number. The absence of knock under these same conditions (with the exception of compression ratio) was apparent in the window engine as has been shown in the flame photographs of Fig. 5. Incidentally, peak cylinder pressure occurs markedly earlier in this case, probably due to the presence of the hot quartz window.

Combustion photographs were taken in the window engine running on 85 octane primary reference fuel at 1000 rpm. A typical explosion is shown in Fig. 13. No autoignition occurred and the explosion appears normal. Comparison of this engine explosion with that shown in Fig. 3 in which engine operating conditions were the same except for engine speed illustrates the fact that the hot spurious ignition phenomenon is speed sensitive.

Fig. 14 shows the effect of speed with a typical commercial reference fuel series. The heavy curves separate the figure into regions as before. The times of peak pressure are advanced due to compression ignition for all of the fuels shown except that of 100 Research octane number above 350 rpm. Again, knock does not occur below speeds of about 175 rpm. There are two points to note in comparing the data shown in this figure and that shown in Fig. 12. The first is that the engine speed separating the knocking and slow-knocking regions remains constant despite the difference in fuels. The second is that the primary reference fuels are more susceptible to the compression ignition phe-

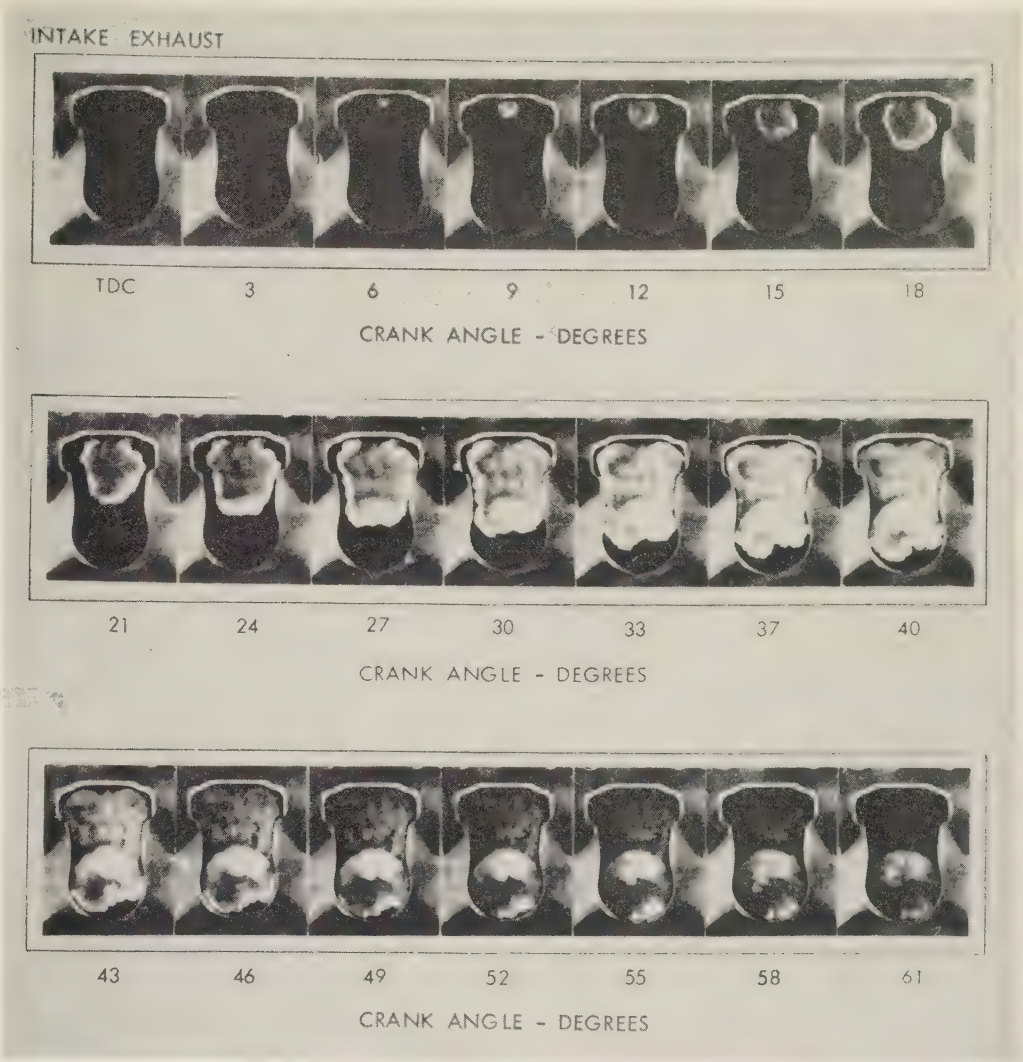

Fig. 13—Flame photographs of normal combustion occurring with 85 octane primary fuel at 1000 rpm

nomenon than commercial fuels at the same Research octane levels. A comparison on the basis of Motor octane numbers magnifies this difference.

The effect of engine speed on the occurrence of compression ignition demonstrates how it is quite possible to stall a starter motor once the cranking speed begins to decrease. The decrease in starter speed increases the severity of the abnormal combustion causing the speed to drop even faster, until the starter stalls. This emphasizes the necessity of keeping the starter electrical system in the best possible condition in cases where starting is borderline. There does not appear to be sufficient help in alleviating the hot starting problem by raising engine starting speeds, since Fig. 14 indicates that it would require approximately a 100% increase in starter speed to retard the time of peak pressure five crank-angle degrees for fuels of 90 Research octane number or greater.

Air-Fuel Ratio, Spark Advance, and Intake Manifold Pressure Effects—The effects of air-fuel ratio, spark advance, and intake manifold pressure on the compression and ignition process are consistent with the effects of these variables on knock, so that only limited data were accumulated for them. The maximum amount of compression ignition occurred at approximately a 10% rich air-fuel ratio. This agrees quite well with the air-fuel ratio for maximum knock. The effect of spark advance was not large; however, complete control of the combustion process could be maintained if the spark advance was earlier than 48 deg btdc or later than 18 deg atdc with isooctane under standard hot starting

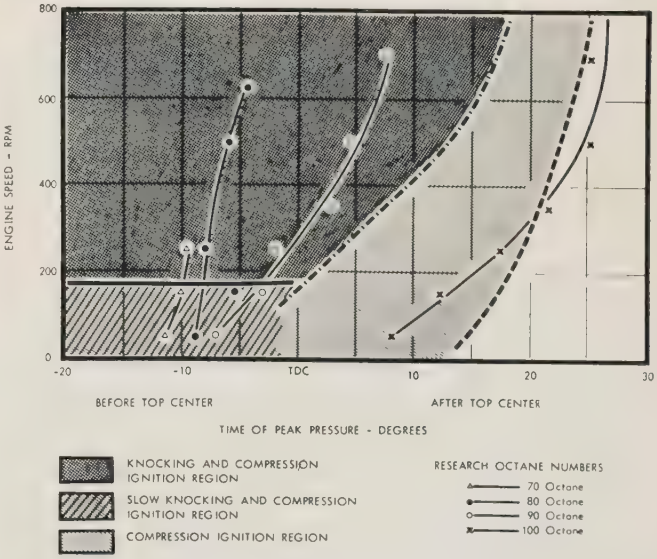

Fig. 14—Effect of engine speed on time of peak pressure (commercial reference fuels)

conditions at 9/1 compression ratio. In the case of the early ignition this means that the combustible mixture will burn to completion without the occurrence of any abnormal combustion condition if ignition of the charge occurs sufficiently early. Obviously, negative work will result from such an early spark advance so that the information is of only academic interest. The late spark advance condition apparently indicates that if combustion is delayed sufficiently in the cycle, mixture temperature will not become high enough to cause compression ignition with the bulk of the heat leaving the engine during the exhaust portion of the cycle.

Intake manifold air pressure was varied over a limited range because of carburetion difficulties at the lower intake air pressures. Over the range of pressures of 20–38 in. of Hg absolute the severity of compression ignition, as measured by the occurrence of the time of peak pressure, increased linearly with intake manifold pressure.

Multicylinder Engine Requirement—In order to indicate the extent of this low-speed abnormal combustion problem in modern automobile engines, a series of typical commercial-type fuel blends was run in a standard production 1956 V-8 engine. The engine was run under the same standard hot starting conditions as used in the single cylinder work. The ratings were made after the engine had accumulated equilibrium engine deposits using a commercial fuel and oil. The deposits raised the compression ratio from a nominal 9.75/1 compression ratio to an average of 10.4/1. As explained previously, a spark plug pressure transducer was used to obtain pressure records and the time of occurrence of peak pressure again used as the criteria of the extent of the low-speed autoignition.

Using a 96 Research octane number commercial-type fuel, the road-octane requirement of this engine, produced peak cylinder pressure at about 2 deg btdc under the standard hot starting conditions. In order to eliminate the low-speed autoignition completely, it was necessary to raise the Research octane number of the commercial-type fuel to 108. Intermediate octane number commercial fuels produced intermediate times of occurrence of peak pressure. Had the engine speed been lower or the coolant temperature higher, or both, the requirement would probably have been higher. (See Figs. 11 and 14.)

Conclusion

The principal purpose of the paper has been to present some of the existing evidence concerning the causes of the high-torque requirement in starting hot gasoline engines. It is hoped that the evidence may clarify to some extent the thinking about this problem and perhaps suggest to equipment designers and others responsible for the use of fuels possible means of alleviating these difficulties.

One of the most important characteristics of the low-speed abnormal combustion problem, as revealed by the flame photographs, is the fact that the spurious ignition process is due to the autoignition of the fuel charge itself. At the low speeds occurring during the starting operation, enough time becomes available for a considerable transfer of heat from the combustion-chamber walls to the gaseous mixture. This heat, plus that generated by the compression of the mixture during the compression stroke, apparently raises the temperature in localized areas above the temperature required for ignition and spurious ignition occurs. Here again, as in the case of deposit-induced surface ignition, once the abnormal ignition has occurred, the combustion process proceeds from the ignition source in a normal manner. Hence, the major problem associated with hot starting is one of ignition, not of the propagation of the combustion process.

The combustion process which replaces the usual form of knock (called slow knock throughout this paper) is quite similar to normal knock but takes place at a much lower rate. The argument as to whether or not the combustion process propagates during knock is equally controversial in the case of this low-speed end-gas reaction. The engine noise resulting from the slow-knock phenomenon is quite similar to that produced by knocking combustion. Due to the relatively low rate of the reaction, the combustion-chamber pressures apparently equalize as the slow-knock reaction proceeds so that very little, if any, excess pressure builds up in the end-gas region and no pressure oscillations result. Despite the lack of the pressure oscillations, the engine noise resulting from both knocking combustion and the slow-knock reaction are strikingly similar. In both cases, vibrating engine parts apparently produce the resulting noise.

Because of the fact that compression ignition, slow knock, and knock are all apparently forms of autoignition, it is somewhat difficult to understand why the compression ignition phenomenon is followed by a normal combustion reaction as it does under these standard hot starting conditions. It would appear that if some small isolated areas reach the temperature at which ignition takes place, most of the rest of the mixture should be approaching this temperature, so that as the combustion process proceeds through this mixture from the localized high-temperature area, the combustion reaction should be greatly accelerated, perhaps at the rate shown for the slow-knock reaction. Such is not the case. This, then, must indicate that temperature gradients exist throughout the mixture just prior to ignition.

The relationship between the luminous spots and the low-speed autoignition process is not known, but the spots do not seem to be the direct cause of the early ignition. Since the spots are known to be of different color than the remainder of the burned-gas region, this might indicate that diffusion combustion occurs in these areas. The source of the illumination would not necessarily have to be carbon[9] at the high pressures and temperatures prevailing in the burned-gas region. Another possibility might be that some heterogeneous product of the premixed combustion process radiates in the yellow region much as the remainder of the burned gases radiates in the blue region at the temperatures of the burned gasses. No further evidence is available for a more complete analysis of the phenomenon.

The reason for the relatively high susceptibility to autoignition of the primary reference fuel series, and particularly isooctane, is not understood. All of the fuels tested, with the exception of these fuels,

[9] Proceedings of the Royal Society of London, Series A, Vol. 236, July, 1956, pp. 89–103: "Spectrographic Examination of Gaseous Flames at High Pressure," by J. Diederichson and H. G. Wolfhard.

showed remarkably similar autoignition susceptibilities at the same Research octane levels. This would seem to indicate that the basis for the octane scale is unsually prone to knock at low engine speeds and is perhaps a poor measure of knock resistance in this range.

Acknowledgments

The authors take this opportunity to express their appreciation: To J. P. Charles of Pontiac Motor Division, General Motors Corp., for calling attention to this important general problem of hot starting; to N. W. Schubring and Wilson Colcer of the Physics and Instrumentation Department for assistance with problems incident with the operation of the peak pressure distribution counter; and to Dr. L. L. Withrow, Dr. W. G. Agnew, and W. A. Daniel for criticism and suggestions during the preparation of the manuscript.

DISCUSSION

Reports Fuels Giving Hot Starting Noise

—W. E. Morris

E. I. du Pont de Nemours & Co., Inc.

I FEEL, along with the authors, that autoignition associated with hot starting is a very interesting phenomenon. Data we have obtained in two 10/1 compression ratio engines are in agreement with the authors' results as to the relative standing of fuels. In both engines isooctane gave hot starting noise, whereas diisobutylene, benzene, and toluene did not.

In one of these engines we found that the engine must be hot but not very hot to give hot starting noise. This engine required 111 octane primary reference fuel to eliminate hot starting noise when completely warmed up. This requirement was reached after only 10 min of idle following start of a completely cold engine. The same engine would give hot starting noise after about 5 min of idle on isooctane and after about 1 min of idle on normal heptane. Even when operating with normal heptane, this 10/1 compression ratio engine did not give hot starting noise on the first start after standing overnight.

Describes Test for Starting Knock

—V. F. Massa

Esso Research and Engineering Co.

WE agree with the conclusions drawn in this paper. Our data confirm that the abnormal combustion phenomenon that occurs during the cranking period is associated with compression ignition and that it is affected by octane number.

The approach of the authors to this problem and the approach that we are making is consistent with our respective backgrounds. As engine builders, the authors want to make sure that their engines can be built so as to start dependably without unduly increasing starting-motor size and cost. As petroleum refiners, we have every confidence that the engine builders will continue to build engines that will start easily. The authors have not, however, told us very much about the noise emanating from the engine during the period of "slow knock." We have called the noise produced by slow knock during the cranking period "starting knock." It is the level of noise produced by this knock which is of special interest to us.

Table A—Starting Knock Test Procedure

1. Car driven 10 miles, shutdown after 5-sec idle.
2. Six starts at 5-sec intervals following 5-sec idle.
3. Ignition-off starting tendency checked.
4. Starting-knock intensity observed during procedures 2 and 3.
5. Procedures 1–4 repeated over required octane-number range.

Table B—Effect of High Octane Quality on Starting Knock

Compression ratio increased to 11/1

Fuel	Research[a] Octane Number	Motor[a] Octane Number	Knock Intensity, ignition on	Number of Starts Possible, key off
Isooctane plus 0.2 cc TEL	102.5	102.5	None	None
Isooctane	100	100	Light minus	10
98 Primary Reference	98	98	Light	20 +
96 Primary Reference	96	96	Light plus	20 +
94 Primary Reference	94	94	Medium minus	20 +

[a] CRC extension above 100 octane number.

For this reason our approach was to study starting knock in cars being operated on the road under normal service conditions. We found, as did the authors of this paper, that jacket temperature was important and that starting knock rarely occurred in a cold engine. Under these conditions, the rich mixture supplied with the choke in operation also probably tends to suppress starting knock. For these reasons, a test for starting knock was developed that consisted of operating the car under normal driving conditions for a period of 10 miles to insure adequate warmup. (See Table A.) The car was then stopped and the engine allowed to idle for 5 sec prior to shutdown. The engine was then alternately started and stopped six times, at half- and full-throttle settings. Following this, three attempts were made to start the engine with the ignition off. When key-off starts were found possible, the engine could be stopped by closing the throttle. By this means the number of key-off starts possible without resorting to spark ignition were counted. As the authors, we found that octane number would control slow knock and, hence, also control the level of noise heard during the starting period.

Table B shows the data obtained with primary reference fuels. As the octane number of the primary reference fuels was reduced, the starting-knock intensity increased. Also the number of key-off starts possible finally exceeded 20.

It was also shown that the Research octane number of commercial-type reference fuels influences starting-knock intensity. In Fig. A it may be seen that a commercial-type fuel of 99.5 Research octane number gave a light plus-knock intensity in a 1957 production model car. Increasing the Research octane number of these fuels to 102.5 in terms of the CRC extension eliminated the knock. This same relationship between starting knock intensity

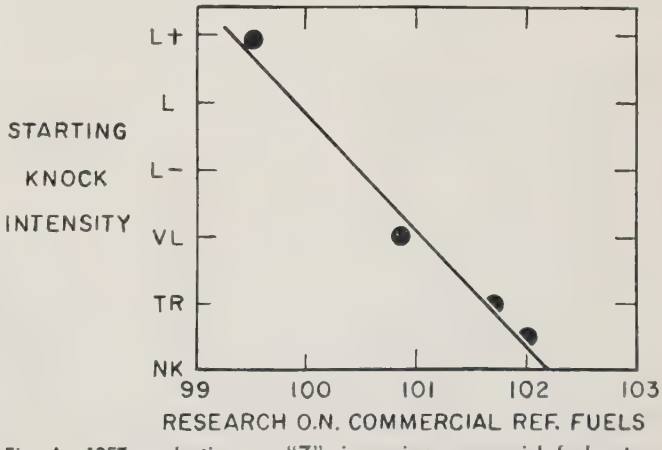

Fig. A—1957 production car "Z", increasing commercial fuel octane number reduces starting knock

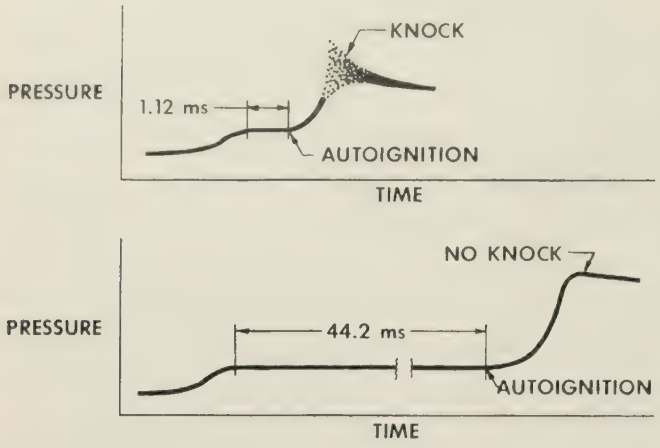

Fig. B—Rapid compression machine data, isooctane

and Research octane number has also been established in several other car makes.

To satisfy ourselves that this phenomenon was compression ignition and not deposit-induced surface ignition, we also tried surface-ignition-prone benzene and other fuels that we had previously compared for surface-ignition tendencies in a laboratory engine. The results obtained under starting conditions again appeared related to octane-number quality rather than the previously established surface-igniting tendencies since benzene gave no starting knock or key-off starts. Isooctane, on the other hand, which had been shown to be superior to benzene in surface-ignition characteristics in the laboratory engine gave a light-minus starting-knock intensity and showed a pronounced tendency to start with the ignition off. These data were obtained in a recent model car raised to 11/1 compression ratio and are shown in Table C. The no-starting noise requirement of this car was 101.5 Research octane number in terms of commercial reference fuels by the CRC extension. Toluene and diisobutylene were above the required Research octane number and gave no noise and showed no tendency to give compression ignition starts.

Based on the results of the road studies that we have made, we feel that the laboratory engine studies and conditions of operation chosen by the authors were very realistic and are quite representative of what may occur under actual operating conditions in the field.

Emphasizes Temperature Factors in Engine Combustion

—Cleveland Walcutt
Ethyl Corp.

WE agree with the authors that the problem of hot starting is concerned primarily with the autoignition tendencies of fuels. In addition, the authors have indicated that, in the case of fuels of equal octane number and, therefore, equal autoignition tendency, aromatic- and olefinic-base fuels give greater trouble than the paraffinic type. This can be understood by reference to earlier work[a] in which measurements were made of the heat liberated by various hydrocarbon mixtures during precombustion reactions. This work shows that extensive reactions occurred in leaded and unleaded primary reference fuels over a wide range of octane number, while mixtures of diisobutylene and normal heptane show markedly decreasing activity as the octane

Table C—Effect of Selected Fuels on Starting Knock

Compression ratio increased to 11/1

Fuel	Research[a] Octane Number	Motor[b]	Knock Intensity, Ignition on	Number of Starts Possible, key off
Toluene	Isooctane + 5.8 (113 +)	Iso + 0.3 (103.5)	No knock	None
Benzene	Isooctane + 1.0 (108.5)	Iso + 2.7 (113 +)	No knock	None
Diiso-Butylene	Isooctane + 0.5 (105)	88.5	No knock	None
Isooctane	100	100	Light minus	10

[a] CRC extension above 100 octane number.

number is raised. Thus, the observed variation among fuels of different types with respect to the time of development of peak pressure is probably related to their tendencies to liberate precombustion energy as well as to their autoignition characteristics. It would be quite interesting to know whether these same differences in fuel type occur in actual attempts to start a hot engine, as contrasted with the information obtained by the authors in their continuously operating engine.

The authors' observations of bright spots in the compressed gases undergoing autoignition ties in nicely with similar observations in the rapid compression machine. The most reasonable conclusion, based on extensive studies in this apparatus, is that the bright spots are due to inhomogeneity of temperature; the supposition being that the points of highest temperature are those which autoignite first, and these probably remain hotter as the remainder of the charge burns. These inhomogeneities would be expected to be minimized under conditions of high turbulence. This concept is supported by the fact that spotty autoignition does not occur in engines operated at normal speeds where the turbulence can be expected to be reasonably large.

Temperature gradients in the engine combustion chamber have been shown to be an important factor in the rate of propagation of autoignition through the fuel-air mixture.[b] It has been proposed that the rate of the autoignition propagation determines the overall rate of pressure rise and, thus, the physical manifestations of knock which accompany the autoignition. In an engine operating at low speeds, the opportunity exists for establishing large thermal gradients which control the autoignition reaction and result in "slow" autoignition without pressure oscillations. Similar effects are obtained in the rapid compression machine operated in such a manner as to have a long delay period, which is representative of engines operating at a slow speed. This is illustrated by Fig. B where large pressure oscillations accompanied the autoignition of isooctane after an ignition delay of 1.15 millisec. Operation of the rapid compression machine in a manner to result in an ignition delay of 44.2 millisec on the same fuel indicated, however, that no pressure oscillations accompanied the autoignition reaction. Consequently it is concluded that the slow-knock reaction observed by the authors is not another variety of autoignition, but simply an autoignition where the rate of propagation is controlled by the thermal gradients within the mixture.

Authors' Closure To Discussion

THE luminous spots seen on the motion picture of compression ignition were yellow as compared to light blue for the burned gas. This could be due to temperature gradients causing different reactions to occur. Precombustion may be a factor in the relatively low resistance of paraffins to compression ignition during starting. However, the paraffins are known to be low-speed knockers, which could also explain their relatively low resistance.

[a] SAE *Quarterly* Transactions, Vol. 6, July, 1952, pp. 472–487: "Early Combustion Reactions in Engine Operation," by E. B. Rifkin, C. Walcutt, and G. W. Betker, Jr.

[b] SAE Transactions, Vol. 65, 1957, pp. 552–566: "Basis for Understanding Antiknock Action," by E. B. Rifkin and C. Walcutt.

High–Temperature Properties of *vacuum-melted* Superalloys

F. M. Richmond, Universal-Cyclops Steel Corp.

This paper was presented at the SAE National Aeronautic Meeting, New York, April 3, 1957.

THE history of high-temperature alloy development in the United States is dotted with several important processing innovations which have played a prominent role in the attainment of higher operating temperatures in jet engines. The use of hot-cold work to increase the strength of Cyclops 17W, the development of precision casting techniques which led to Stellite 21 and 31, and the controlled forging procedures that made S-816 a practical commercial alloy are but a few of the many improvements in processing techniques that have helped to eliminate serious bottlenecks in alloy development. Vacuum-melting is the most recent example of such improvements.

One of the most critical applications of high-temperature alloys in jet engines is the turbine bucket, which must withstand severe combinations of temperature and stress. A great amount of alloy development has, of course, been directed toward improving the properties of materials used for buckets. Fig. 1 is a chronological plot of the temperature ratings of bucket alloys that have been used in aircraft turbines[1] [2] [3] since the advent of the turbosupercharger in 1918. The leveling off of this curve around 1950 was due primarily to the ceiling on hardening additions to nickel- and cobalt-base alloys imposed by the ductility requirements of jet engine turbine buckets. At that time, Howard Scott[3] pointed out that "the strength or temperature rating of present conventional alloys may be improved by an increase in their hardener content if the ductility can be increased by some expedient," and suggested that future research be devoted primarily to discovering new methods for increasing ductility as a prerequisite to increasing the strength or temperature rating.

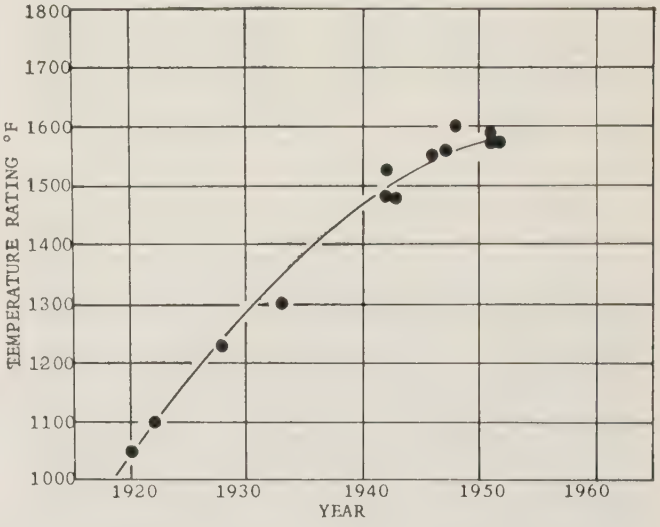

Fig. 1—Chronological increase in temperature rating (100-hr life at 20,000 psi) of turbosupercharger and jet engine bucket alloys

Development of better wrought alloys was also seriously limited by forgeability problems, which are naturally increased as the hardener content goes up. This, of course, is merely another manifestation of the inverse relationship between strength and ductility.

In 1950, the best forged bucket alloys in use were nickel-base alloys, such as Waspaloy (developed by Pratt & Whitney) and M-252 (developed by General Electric.) These alloys are hardened primarily by additions of titanium and aluminum, which promote beneficial precipitation-hardening effects. The highly reactive nature of such alloying additions required the utmost skill in producing alloys of this type by conventional melting techniques, and even then the quality of the material was often less than was desired. Thus, the melting problem was another serious obstacle to increased strength

[1] "1943 Supercharger Symposium Lecture Book," by W. L. Badger. General Electric Co., Riverworks, West Lynn, Mass. 1943.
[2] *Journal of Metals*, Vol. 6, February, 1954, pp. 113–118: "High Performance Jet Engine Design Dependent Upon Metallurgical Ingenuity," by I. Perlmutter.
[3] *Metal Progress*, Vol. 58, October, 1950, pp. 503–511: "Gas Turbine Alloys Ten Years Later," by H. Scott.

IMPROVED high-temperature rupture strength and ductility of nickel-base superalloys has been obtained by utilization of vacuum melting and certain modifications in the nominal chemistry of these alloys.

A brief description of the melting technique and chemistry modifications is given in this page. The tensile and rupture properties of five nickel-base vacuum-melted alloys are reported for the temperature 1000–1600 F.

and ductility of bucket alloys. In fact, it was probably the most important since it was believed that improved melting techniques might be a potent remedy for all three problems—low ductility, poor forgeability, and uncertain quality—which were restricting alloy development.

In an effort to eliminate or reduce some of the melting difficulties, a vacuum-induction furnace was installed at our Bridgeville plant in 1954. This furnace had a capacty of 1000 lb and was the first vacuum furnace of this size in the United States. Since then, its capacity has been increased to 2000 lb and three vacuum arc-melting furnaces, utilizing the consumable electrode technique, are now under construction. The arc furnaces will permit the casting of larger ingots than is possible with the induction furnace. They range in size from 4000–25,000-lb capacity.

It is obvious in reviewing the brief history and current status of commercial vacuum melting, that the melting problems associated with nickel-base alloys containing titanium and aluminum have been nearly eliminated. Improved properties achieved by vacuum melting have resulted in higher service temperatures for existing alloys. Higher ductility, together with the increased forgeability imparted by these melting techniques, has opened the door to new alloy development programs which show promise of significantly extending the temperature ratings of wrought nickel- or cobalt-base alloys. The increase in workability has been so great that many of these alloys are now amenable to fabrication to sheet, which opens new fields of applications for these materials in ram jets, rockets, and the like.

A detailed description of the vacuum-melting process is beyond the scope of this paper, but it should be pointed out that the primary role of these techniques is to lower the total gas content and to reduce sources of contamination, as shown in Fig. 2. In the electric-arc furnace previously used for melting these alloys, there were three obvious sources of contamination—the crucible, the covering slag, and the air. Vacuum-induction melting (Inductovac)[4] eliminates the slag and the air as sources of contamination. Crucible contamination has not been eliminated and is actually more severe than in air melting, due to the lower pressures. Deoxidation is usually carried out by carbon or hydrogen, which produces gaseous deoxidation products that can be drawn off through the pumping system. The vacuum cold-crucible arc furnace eliminates the last of the serious contaminating sources by utilizing a water-cooled copper crucible. It is important to remember that crucible contamination has not been entirely eliminated in vacuum-arc melting, as normally practiced for iron-, cobalt-, and nickel-base alloys, since the electrodes are originally consolidated by melting in furnaces utilizing ceramic crucible materials. When the original melting operation is done in conventional electric-arc furnaces, the product after remelting in the vacuum-arc furnace is known as Duomelt,[4] signifying a double melting operation—one in air and one in vacuum. When the original melting is done in the vacuum-induction furnace, the final product is known as Duovac,[4] signifying a double *vacuum*-melting process. A complete evaluation of the properties of Duomelt and Duovac alloys has not been completed. It appears that these methods of melting should produce material at least equivalent to Inductovac with a much better opportunity for uniformity due to the improved ingot structure from the cold-mold arc melting.

The mechanism by which vacuum melting increases elevated temperature strength has not yet been demonstrated. It is probable that the lower gas contents (up to 90% reduction as compared to air melt), together with fewer oxide and nitride inclusions, play an important part in the mechanism of high-temperature strengthening and, particularly, in increasing the high-temperature ductility of these alloys. In addition to these effects, which are common to both vacuum-induction and vacuum-arc melting, the vacuum-arc furnace has another advantage in that the highly directional solidification—bottom to top—results in a greatly improved ingot structure.

It is quite important to note that all of the improvement in the high-temperature properties of vacuum-melted nickel-base superalloys is not due to the melting process itself but also to several minor but highly significant chemistry modifications of these vacuum-melted alloys. The elimination of manganese and silicon from the nominal composition of these materials has certainly contributed to the overall improvement in high-temperature properties, particularly ductility.[5] The melting of these alloys without manganese and silicon was facilitated by the utilization of vacuum melting, since this process permits thorough deoxidation with C or H_2, and since Mn and/or Si are not required for deoxidation. Another significant chemistry modification, which contributed to the increase in high-temperature strength of some of these alloys, was the increase in total titanium plus aluminum content made possible by the increase in ductility at a given hardener level. Thus, vacuum melting has become the "expedient" which Scott pointed out was required to enable increases in strength or temperature rating of high-temperature alloys.

Still another very important modification in chemistry has been made recently as a result of an intense investigation to determine the cause of variation in properties of vacuum-melted alloys. In the early days of vacuum melting, it appeared that the vacuum-melting technique was incapable

[4] Registered trademark.

[5] *Journal of Metals*, Vol. 6, December, 1954, pp. 1364–1367: "Vacuum Melting Improves Alloy Properties and Workability," by R. D. McKechnie, D. W. Green, and W. F. Moore.

of reproducing consistent properties. In late 1955 Frank Chesnut[6] quoted a maker of automotive and aircraft parts as follows: "We have learned that . . . melting any given alloy in vacuum melting does not assure a miraculous increase in physical properties. . . . improvement is possible only when a proper technique or practice is employed. We can supply stress rupture test data on Waspaloy heats melted in a vacuum which show quite divergent results. . . . since the analyses are comparable, the differences in results can be attributed only to the differences in the melting procedures." Similar experiences were noted by other users of vacuum-melted alloys. This scatter in rupture properties was, of course, of considerable interest to producers of vacuum-melted alloys, and approximately two years ago an investigation into the cause of this scatter was initiated at our research laboratory. It now appears that a large portion of the scatter in early vacuum-melted heats can be accounted for. Although the cause is related to melting practice, it is actually due to a difference in chemistry not noted in routine chemical analyses of these heats.

In June 1956 our laboratory published a report[7] which pointed out that very small residuals of boron (0.002–0.01%) and zirconium (0.05–0.15%) exhibited a tremendous beneficial effect on rupture life and ductility of various superalloys, and that this effect, or at least the level of the elements necessary to produce it, is greatly emphasized in vacuum melting. It was discovered, moreover, that these elements could be introduced accidentally by various sources of contamination, and thus account for a large portion of the scatter in vacuum-melted heats. Zirconium, for instance, could be introduced into a heat melted in a zirconia crucible, and it was supposed that boron found its way into these heats by its presence in small amounts in the raw materials. Decker, Rowe, and Freeman[8] of the University of Michigan have now discovered that boron contents of around 0.002% may be introduced into vacuum-induction melted heats by contamination from magnesia crucibles, and that this level of boron greatly increases the rupture life and ductility of a vacuum-melted nickel-base superalloy.

Both investigations point out a potent interaction between boron and zirconium which, if utilized correctly, can quadruple the rupture life and ductility of vacuum-melted nickel-base superalloys at elevated temperature. Incorporation of these elements into recent chemical specifications for certain such superalloys has resulted in a significant improvement in these qualities. At the same time it has greatly reduced the scatter due to uncontrolled amounts of boron and zirconium at very low levels where the effect of minor variations in these elements is the greatest.

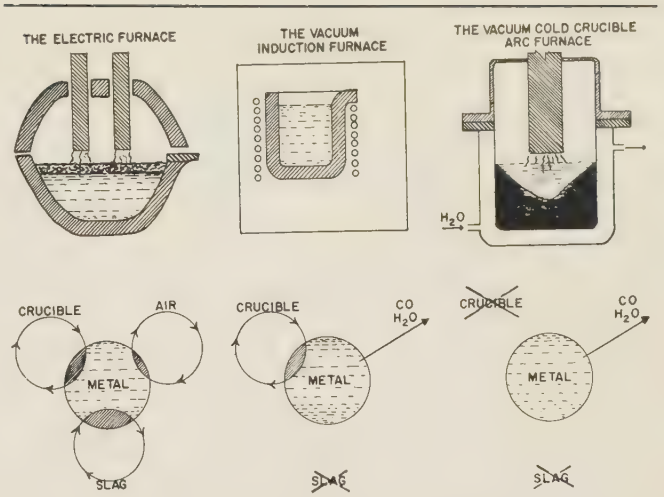

Fig. 2—Schematic comparison of melting techniques, with reference to sources of contamination during melting

Since the above chemistry modifications are being utilized simultaneously with the vacuum-melting techniques, it is rather difficult to determine the exact contribution of the melting process itself as well as the individual contributions of the chemistry modifications. There is no doubt that the process itself does contribute to this improvement; however, the current level of properties being obtained in commercial vacuum-melted alloys should not be considered to be due only to vacuum melting per se. It is true that vacuum melting has enabled the utilization of certain chemistry modifications and has contributed to the discovery of other beneficial alloying additions which may result in an entirely new series of alloys.

Alloy development programs have, of course, continued during the past few years and several new alloys have been developed which show great promise. One of these, GMR-235, is a cast nickel-base alloy containing, in addition to the normal hardeners Ti, Al, and Mo, from 0.025–0.10% B.[9] (The development of this alloy with this particular boron level preceded the work on boron and zirconium at our laboratory and at the University of Michigan.) While not originally developed as a vacuum-melted alloy, it has now recently been shown[10] that vacuum melting significantly increases the rupture life and ductility of this alloy. Two other new alloys are evidences of the new field of alloy development opened up by the increase in ductility associated with vacuum-melting techniques. One of these, Udimet 500, is a vacuum-melted nickel-base alloy developed by the Utica Drop Forge & Tool Corp. This alloy utilizes 3% Ti and 3% Al to attain superior high-temperature properties. The other, J-1570, is a vacuum-melted alloy developed by General Electric and contains about 4% Ti and 7% W.

Since the installation of the first commercial vacuum-induction furnace at our plant, many heats of various nickel-base superalloys have been melted and evaluated. Most of this evaluation has been by stress-rupture and tensile tests at temperatures and stress levels dictated by the pertinent specifications covering these materials. It was considered highly desirable to determine the rupture and tensile properties of some of these alloys over a range of tem-

[6] *Metal Progress*, Vol. 68, December, 1955, pp. 118–123: "Vacuum Melted Metals—An Interim Report," by F. T. Chesnut.

[7] "Effect of Small Amounts of Boron and Zirconium on the High Temperature Properties of Vacuum Melted Super Alloys," by R. W. Koffler, W. J. Pennington, and F. M. Richmond. Universal-Cyclops Steel Corp. Research and Development Report No. 48. Submitted to NACA Subcommittee on Power Plant Materials, June 11, 1956.

[8] NACA TN 4049, June, 1957, "Influence of Crucible Materials on High-Temperature Properties of Vacuum-Melted Nickel-Chromium-Cobalt Alloy," by R. F. Decker, J. P. Rowe, and J. W. Freeman.

[9] SAE *Journal*, Vol. 63, August, 1955, pp. 36–38: "GM Research Labs Develop New Turbine Bucket Alloy," by D. K. Hanink, F. J. Webbere, and A. L. Boegehold.

[10] *Materials and Methods*, Vol. 45, March, 1957, pp. 165, 167: "New Nickel-Base Alloy Has Long Rupture Life."

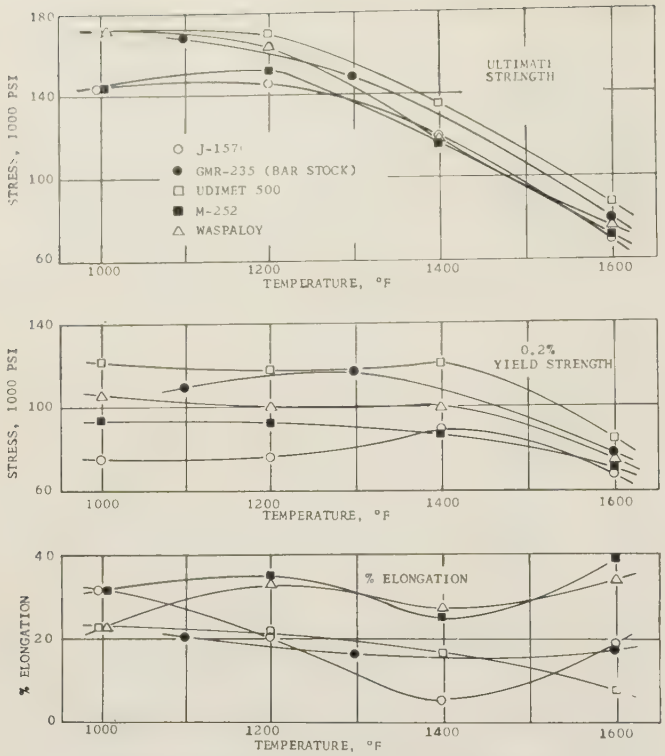

Fig. 3—Tensile properties of vacuum-melted superalloys as a function of test temperature

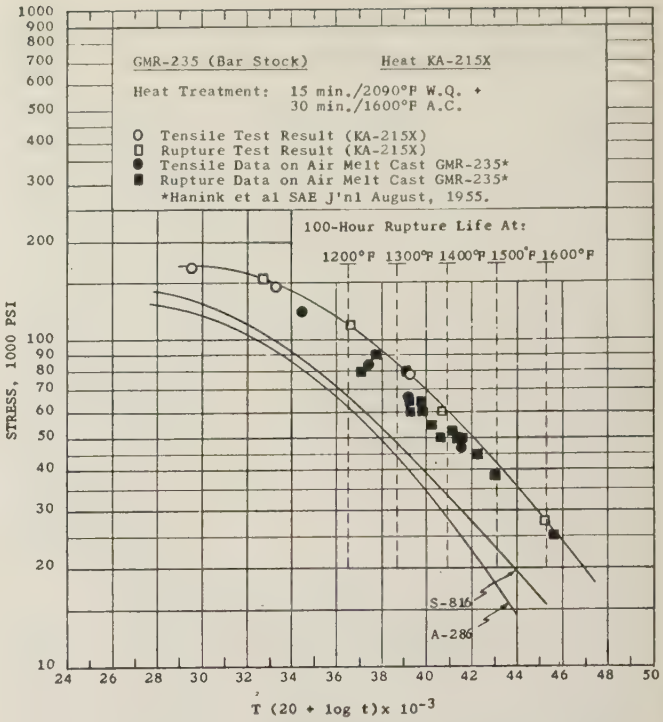

Fig. 4—Parameter plot for GMR-235, including tensile and stress-rupture data

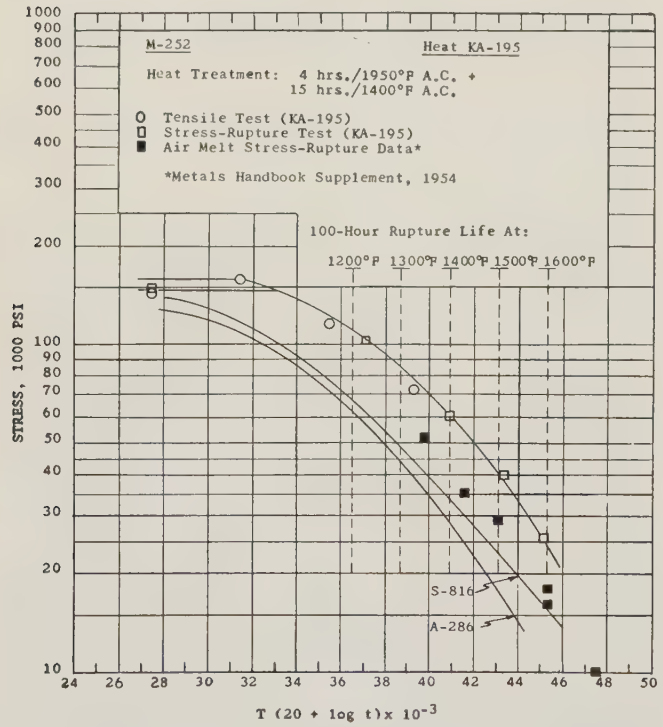

Fig. 5—Parameter plot for M-252, including tensile and stress-rupture data

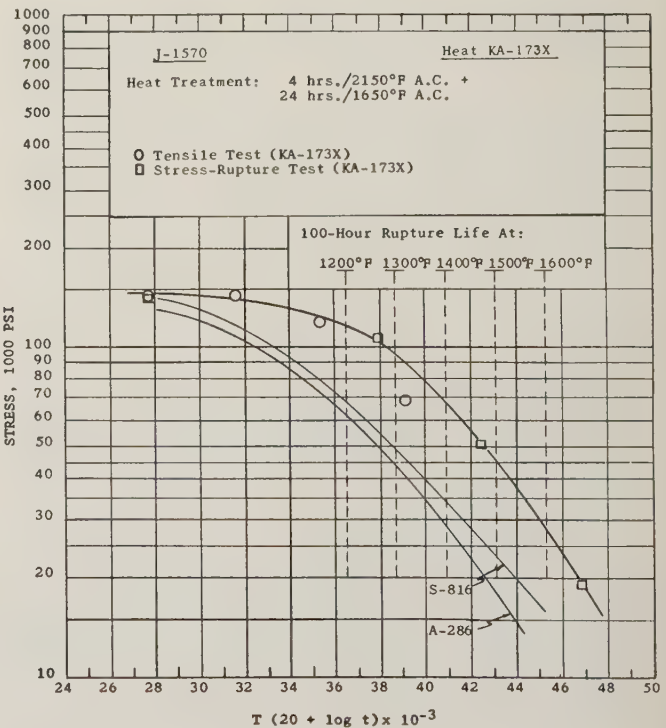

Fig. 6—Parameter plot for J-1570, including tensile and stress-rupture data

Table 1—Chemical Compositions of Five Alloys

Grade	Heat Number	C, %	Cr, %	Ni, %	Mo, %	Co, %	Al, %	Ti, %	Fe, %	W, %	B, %	Zr, %
J-1570	KA-173X	0.14	19.86	29.58	—	36.60	—	4.38	1.65	7.18	0.0018	(0.04)[a]
GMR-235	KA-215X	0.093	15.51	63.85	5.42	—	2.86	2.11	10.59	—	0.10	—
Udimet 500	KA-277X	0.055	16.18	54.30	4.12	17.96	2.84	3.24	1.50	—	0.0025	0.096
M-252	KA-195	0.110	18.98	56.95	9.55	9.99	1.05	2.52	0.52	—	(0.005)	0.048
Waspaloy	KA-175	0.065	20.04	55.85	4.10	14.12	1.26	3.22	0.69	—	0.0062	—

[a] Figures in parentheses are nominal aims; all others are actual analyses.

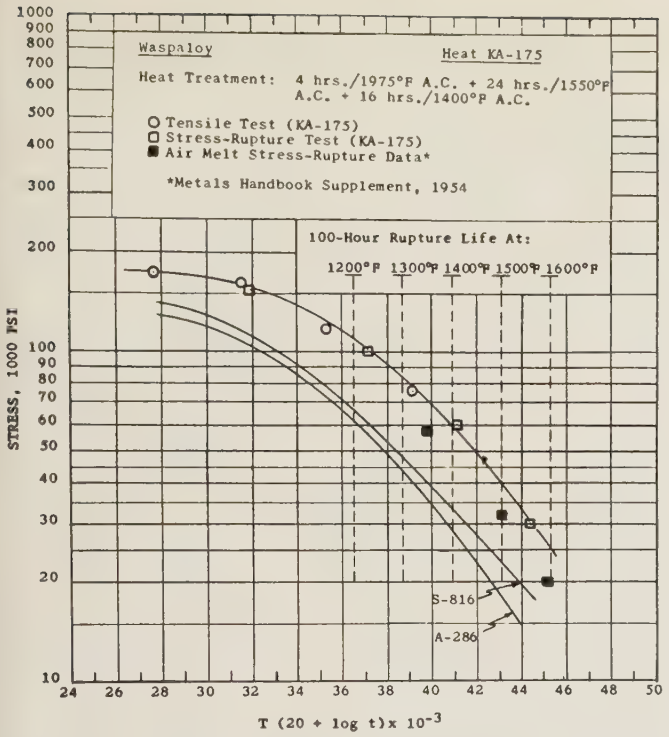

Fig. 7—Parameter plot for Waspaloy, including tensile and stress-rupture data

perature and stresses, in order to obtain design data which might be utilized in applying these new alloys. For this purpose, five alloys—J-1570, GMR-235, Udimet 500, M-252, and Waspaloy—were chosen for an extensive evaluation program. The grade, heat number, and chemical analyses of these heats are shown in Table 1. The manganese and silicon contents of all of these materials were less than 0.02%. The titanium and aluminum contents of the Waspaloy heat were increased consistent with new specifications issued on the basis of vacuum-melting procedures. Boron was added to all heats (0.1% in the GMR-235 and 0.0018–0.006% in the others), and zirconium additions (0.04–0.1%) were made to J-1570, Udimet 500, and M-252.

The heat-treatments used for the various grades are shown in Table 2. All of these tests were conducted on specimens machined from bar stock of approximately ¾-in. diameter. In this regard, it is interesting to point out that although GMR-235 was developed as a casting alloy, vacuum melting enables the material to be forged and rolled with little difficulty This particular heat was fabricated from a 9-in. ingot to 9/16-in. diameter bar stock for this evaluation.

Elevated temperature tests were conducted on the heat-treated specimens utilizing a nominal strain rate of 0.05 in. per in. per min at temperatures of 1000–1600 F. The results of these tensile tests are given in Table 3 and plotted in Fig. 3. Stress-rupture tests were also conducted at various temperatures in this same temperature range at stresses chosen on the basis of the previously determined tensile results. The results of these rupture tests are reported in Table 4, and both the tensile and rupture

Table 2—Heat-Treatments Used for Various Alloys

Grade	Heat-Treatment		Approximate Hardness, Rc
	Solution Treatment, F	Aging Treatment, F, aircooled	
J-1570	4 hr/2150, aircooled	24 hr/1650	32.0
GMR-235	15 min/2090, water quenched	30 min/1600	35.0
Udimet 500	2 hr/2150, water quenched	16 hr/1550	38.5
M-252	4 hr/1950, aircooled	15 hr/1400	33.0
Waspaloy	4 hr/1975, aircooled	24 hr/1550 + 16 hr/1400	36.0

Table 3—Elevated Temperature Tensile Data

(Nominal Strain Rate 0.05 per in. per in. per min)

Test Temperature, F	0.2% Yield Stress, 1000 psi	Tensile Strength, 1000 psi	Elongation, %	Reduction of Area, %
	J-1570 (KA-173X)			
1000	75.0	143.6	32.0	35.9
1200	75.8	145.0	20.3	20.0
1400	88.6	118.7	5.5	11.0
1600	66.5	68.7	19.0	23.0
	GMR-235 (KA-215X)			
1100	109.7	167.5	20.4	31.5
1300	117.1	148.1	16.4	21.8
1600	77.3	79.0	18.0	25.8
	Udimet 500 (KA-277X)			
1000	121.7	171.4	22.8	22.6
1200	117.8	169.5	21.9	19.2
1400	121.3	134.5	17.1	19.1
1600	84.4	86.4	8.3	7.6
	M-252 (KA-195)			
1000	94.2	144.4	31.7	36.2
1200	91.8	151.9	35.5	27.0
1400	87.2	115.0	25.2	30.5
1600	70.5	71.2	39.5	55.5
	Waspaloy (KA-175)			
1000	106.0	172.0	22.7	24.1
1200	100.2	163.4	33.4	32.0
1400	99.8	117.2	27.8	40.8
1600	75.7	76.2	34.7	54.0

Table 4—Stress-Rupture Data

Test Temperature F	Rupture Stress, 1000 psi	Rupture Life, hr	Elongation, %	Reduction of Area, %
	J-1570 (KA-173X)			
1000	141.3	0.1	31.3	36.9
1200	105.0	590.3	16.5	13.0
1400	51.0	609.2	6.9	9.0
1600	19.0	507.8	27.3	39.4
	GMR-235 (KA-215X)			
1000	152.5	67.2	18.3	24.1
1200	110.0	115.9	5.0	9.8
1400	60.0	75.5	7.7	39.3
1600	28.0	85.3	12.0	29.4
	Udimet 500 (KA-277X)			
1000	162.0	251.9	22.7	22.4
1200	120.0	105.7	4.5	10.7
1400	75.0	34.6	3.1	3.0
1600	30.0	64.9	8.7	11.4
1650	25.0	38.8	26.2	25.7
1650	25.0	36.0	20.2	26.9
	M-252 (KA-195)			
1000	145.9	0.1	30.0	38.7
1200	102.0	219.6	11.1	16.1
1400	60.0	90.6	38.3	42.9
1600	26.0	65.2	35.0	46.1
	Waspaloy (KA-175)			
1000	155.0	73.0	25.3	21.6
1200	102.0	235.5	13.0	19.1
1400	60.0	127.4	17.0	29.4
1600	30.0	39.5	24.9	38.4

strengths are plotted parametrically in Figs. 4–8. Where available, results[11] on air-melted heats of these same grades are incorporated in these plots. Parameter curves for air-melted A-286 and S-816 are shown for convenience in comparing the alloys, and a supplementary scale has been included to facilitate determination of the 100-hr rupture strength of these alloys at temperatures of 1200–1600 F.

The parameter curves for M-252, Waspaloy, and GMR-235 illustrate that vacuum melting, plus the pertinent chemistry modifications, has resulted in a significant improvement in rupture properties over the entire temperature range investigated.

The effect of vacuum melting on the ductility of

[11] ASM Metals Handbook, 1954 Supplement, pp. 42–48: "Heat-Resisting Alloys," American Society of Metals, Cleveland, 1954.

Table 5—Effect of Boron and Zirconium Variations on Rupture Properties of M-252 at 1500 F and 40,000 PSI

Heat	Boron, %	Zirconium, %	Rupture Life, hr	Elongation, %
Effect of Nominal Additions of 0.01% B and 0.10% Zr				
KA-161	0.00	0.00	48.6	5.4
KA-162	0.01	0.00	77.5	18.7
KA-163	0.01	0.10	88.0	17.6
Effect of Nominal Additions of 0.005–0.10% B and 0.05–0.10% Zr				
KA-193	0.005	0.05	80.9	19.1
KA-199			88.0	20.1
KA-194	0.005	0.10	71.6	27.8
KA-195			89.4	19.2
KA-197	0.01	0.05	66.0	31.3
KA-200			92.6	19.5
KA-196	0.01	0.10	71.2	22.6
KA-198			91.4	17.8
Average of Low-Boron Heats			82.4	21.5
Average of High-Boron Heats			80.3	20.3
Average of Low-Zirconium Heats			81.8	20.0
Average of High-Zirconium Heats			80.9	21.8
Average of All Heats			81.4	22.2

Table 6—Temperature Ratings of Vacuum-Melted Alloys, Based on 100-Hr Rupture Life at 20,000 PSI

Grade	Temperature Rating[a], F	
	Air Melted[b]	Vacuum Melted
J-1570	—	1650
GMR-235	1640	1670
Udimet 500	—	1670
M-252	1570	1625
Waspaloy	1570	1630

[a] Based on parameter plots of rupture data.
[b] Air-melt rupture data sources:
GMR-235—Materials & Methods, March, 1957, pp. 165, 167.
M-252 and Waspaloy—ASTM, STP No. 170.

M-252 and Waspaloy is shown in Fig. 9 in which the 1500 F tensile strength, tensile ductility, 100-hr rupture strength, and ductility of air and vacuum-melted material are compared. These results are based on average values for these alloys as melted in air and vacuum.

Fig. 10 illustrates the increase in stress-rupture specifications for Waspaloy as a result of vacuum melting and chemistry modifications. The first specification for air-melt Waspaloy required a rupture life of 23 hr at 1500 F and 27,500 psi. After considerable melting experience, this stress level was increased to 32,500 psi. There was no ductility requirement in the air-melt specification. Even so, it was very difficult for the air-melt producers to consistently meet the specification. As a result of first vacuum-melting efforts, it was possible to increase this specification to 40 hr at 1500 F and 37,500 psi and to incorporate a minimum elongation of 5%. Later on, the stress was increased to 40,000 psi, the rupture life to 55 hr, and the elongation to 10%; and still more recently, primarily as a result of the development of controlled boron and zirconium additions by our laboratory, the minimum rupture life under these same conditions of 1500 F and 40,000 psi has been increased to 75 hr.

It should be pointed out that the tensile and rupture properties of superalloys intended for bucket materials are generally based on fabrication and heat-treatment practices which have been tailored to produce the best combination of tensile strength, rupture strength, and ductility. Variations in either forging practice or heat-treatment can be used to emphasize any of the these properties at any given temperature. Grain size, for instance, can be quite easily controlled to maximize either high- or low-temperature properties. At temperatures below 1350 F, optimum tensile properties can be obtained with a fine grain size; whereas, at higher temperatures or for longer times as in a rupture test, larger grain size is an advantage.

Fabrication and heat-treatment also have an important role in determining the combination of rupture life and ductility produced in these materials as shown in Fig. 11, where ductility and rupture life are plotted schematically to show the usual inverse relationship. The right side of this diagram illustrates the effect of increasing solution temperature and grain size in increasing rupture life and decreasing ductility. Increasing amounts of cold work or hot-cold work prior to solution treatment appear to lower the ductility for a given rupture life—by increasing the solution temperature required to obtain a given grain size—as indicated by the arrow pointing downward in the center of this figure. This diagram can also be used in an attempt to explain the higher rupture strengths of vacuum-melted alloys by considering the major effect to be one of increased ductility. As shown on the left hand portion of this figure, increased incongruous or hardening additions can increase the rupture life but generally result in a rapid decrease in rupture ductility. Vacuum melting with no changes in chemistry can be considered to increase the rupture ductility with a minor improvement in rupture life. (In this scheme, it has been assumed for simplicity that there is no primary effect of vacuum melting on rupture life.) At this higher ductility level, it is possible to then incorporate increased alloy content and obtain a net result of both increased rupture life and ductility. The incongruous elements in this example have been considered to be elements such as titanium and aluminum. Boron and zirconium are elements which have the facility for increasing both rupture life and ductility. Utilization of these latter elements results

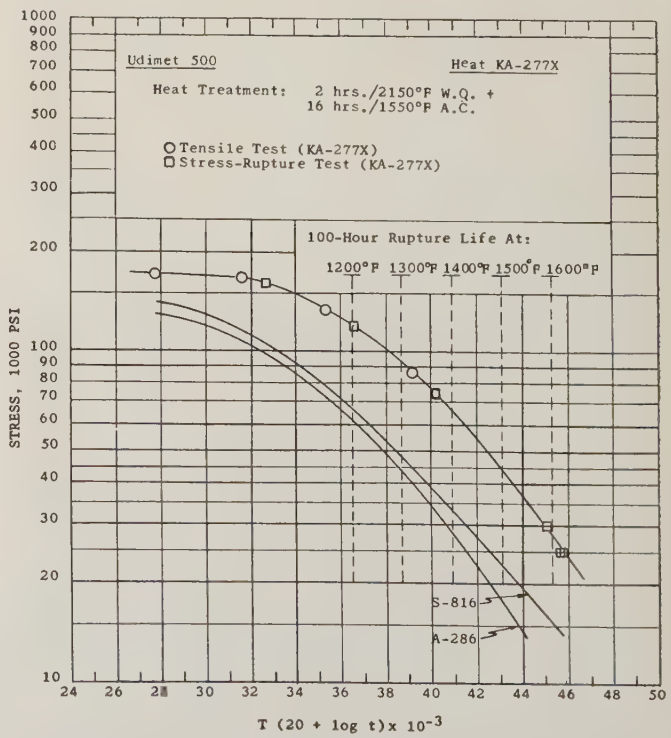

Fig. 8—Parameter plot for Udimet 500, including tensile and stress-rupture data

in still higher rupture life and ductility than possible with vacuum melting and increased hardening additions alone.

Due to the potent effects of small quantities of boron and zirconium, the question has been raised concerning the variation in properties due to uncontrollable variation in boron and zirconium content. As mentioned previously, the effect of the first small amounts of boron and zirconium is quite potent, but at higher levels the increase in properties levels off somewhat so that the scatter due to variations in these elements is minimized. This is shown in Table 5. In Part I of this table, the effect of 0.01% boron compared to a 0%-boron heat can be clearly seen, and the addition to 0.1% Zr has a slight effect on rupture life. Part II illustrates the consistency of rupture life and ductility in several heats of M-252 in which the boron was varied intentionally from 0.005–0.01%. These are the maximum variations that should be encountered in vacuum melting this type of alloy with controlled boron and zirconium additions. Comparison of the average rupture life and ductility of the low- and high-boron and low- and high-zirconium heats illustrates that variations in these elements in the ranges studied should have no significant effect in inducing scatter.

Table 6 gives the temperature ratings based on 100-hr rupture life at 20,000 psi (as determined from the parameter plots) for the vacuum-melted materials studied in this investigation. Comparing these values with the chronological plot of Fig. 1 illustrates the upturn in temperature rating due to vacuum melting and new chemistry modifications. These properties are merely an indication of what can be expected in the next few years as a result of the intensive alloy development programs now underway. It appears entirely possible that forged nickel- or cobalt-base alloys can be developed which will have a 100-hr rupture life of 20,000 psi at temperatures approaching 1800 F. Further increases in service temperatures of jet engines will probably require the use of refractory metals such as molybdenum for the critical bucket application. When this occurs, the overall increase in engine temperatures will dictate the use of nickel- and cobalt-base alloys as turbine wheel—or even compressor wheel—materials. The new fields of ram jet and rocketry will also find many uses for these alloys in sheet form. These factors portend a continued growth of the vacuum-melting industry.

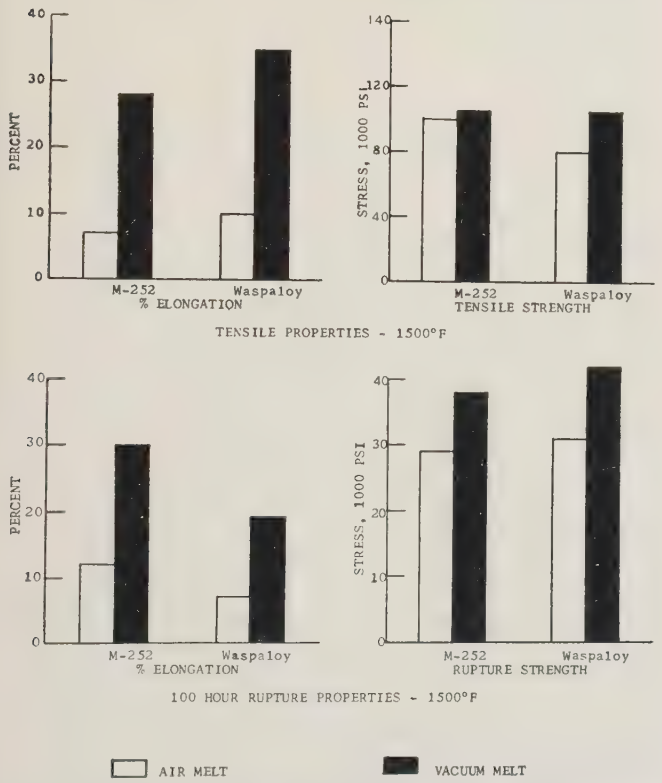

Fig. 9—Effect of vacuum melting (incorporating beneficial modifications in chemistry) on properties of two nickel-base superalloys

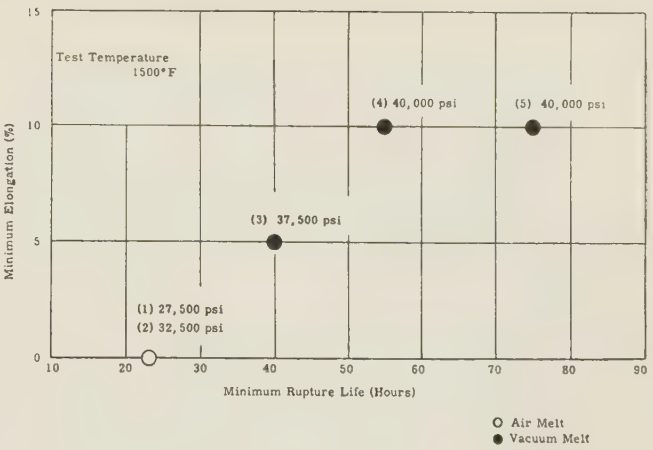

Fig. 10—History of Waspaloy stress-rupture specifications

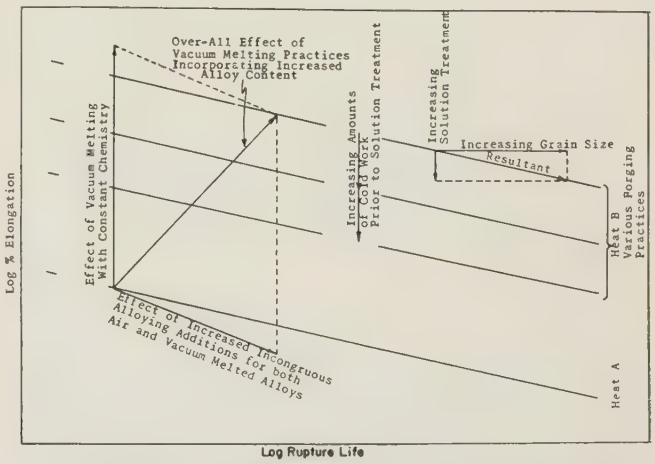

Fig. 11—Schematic diagram illustrating effects of melting practice, composition, solution treatment, and fabrication practice on a commercial superalloy at constant test temperature and stress

Summary

This new processing technique has increased the high-temperature properties of existing superalloys; it has enabled metallurgists to utilize more efficiently and in larger quantities the alloying elements known to improve high-temperature strength, and it has indirectly resulted in the discovery of pronounced beneficial effects of some trace elements. In combination, these results have permitted increased operating temperatures in present-day jet engines, and will undoubtedly contribute to the growth of new fields of aircraft propulsion.

TORQUE CONVERTERS

THE paper points out the principal basic differences between hydraulic torque converters of various types.

The following designs are described and compared in terms of fundamental design and operating characteristics when combined with a typical power source for the internal-combustion engine:

1. Three-stage converters.
2. Single-stage converter couplings.
3. Single-stage outflow stator type.
4. Single-stage inflow stator type.
5. Single-stage stationary housing high utility ratio converter.

The subjects discussed include: basic theory, vane velocity vectors and their influence on torque absorption characteristics, utility ratio, counter head, shutoff, torque equation factors affecting capacity, speed effect on capacity, effect of impeller absorption curve shape on engine speed, split torque effect on engine lug down, converter cooling, push-start devices, and cranking and braking characteristics.

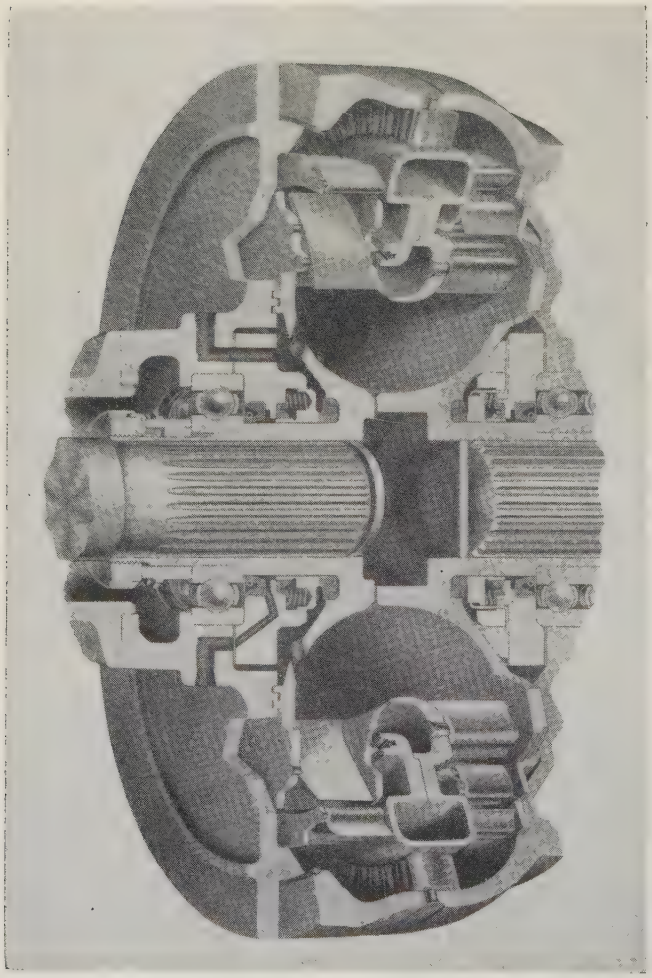

Fig. 1—Twin Disc three-stage converter

THE ART of hydraulic torque converter design has progressed during the last 20 years to the point where the industrial equipment manufacturer is now faced with a more or less bewildering array of torque converter types. Each type has its own set of operating characteristics inherently imbeded in its physical design. The discerning manufacturer, desiring to produce equipment which will transmit the greatest amount of available horsepower, is faced with the problem of determining the relative merits of all the industrial types of converters on the market.

This process of evaluation is accomplished most efficiently when the manufacturer sets up a design group within the engineering department to prepare a detailed mathematical analysis of output performance with the cooperation of the various torque converter manufacturers. These studies include the calculation of output horsepower, output torque, engine rpm, efficiency, heat-rejection requirement, drawbar pull, and other performance factors over the whole operating range. From these studies, comparative performance curves can be drawn for the various types of converters which are invaluable in immediate and long-range planning.

This combined technical exchange between the vehicle design engineer and the converter engineers has proved to be extremely successful. The vehicle designer has begun to master the torque converter as a tool in the same sense that he has learned to use the internal-combustion engine, the transmission, and the final drive to translate power into work accomplished on the ground. At the same time, the converter engineer has been put into closer association with the performance problems of the ultimate users, who operated vehicles varying from the trac-

CAN BE DIFFERENT

J. B. Black and M. W. Dundore,
Twin Disc Clutch Co.

This paper was presented at the SAE Earthmoving Industry Conference, Peoria, Ill., March 26, 1957.

tor to the shovel to the end-loader to the off-highway truck.

This paper, therefore, has been written to attempt to show some of the many considerations facing these joint analysis groups as they view the various types of converters on the market and to attempt to explain the reasons behind the performance characteristics peculiar to each.

In the early years—the 1940's—of American industrial converter application there were only two major types of converters. One was the three-stage converter of the Lysholm-Smith design, which consisted of one impeller wheel, a turbine wheel made up of three separate vane stages, and a fixed or stationary housing containing two sets of stator vanes (Fig. 1). The second was the single-stage converter with a single impeller, turbine, stator or stators, and a rotating housing (Fig. 2).

Now, however, other single-stage converters making their way into the American and the world markets have such radically different performance characteristics that by analysis and examination we can demonstrate most of the principles of converter operation and thereby prove that converters can be different.

In the past few years, we have all been made aware of the more or less obvious differences by the many papers that have been presented before SAE and other technical groups. These have included the single-stage, two-stage, and three-stage converters, which are identified by the number of turbine stages. We have been introduced to the terms "single-phase" and "polyphase." A single-phase converter is one in which the impeller is fixed to the input shaft, while the turbine stage or stages are fastened permanently to the output shaft. The stator stage or stages are fixed to the ground through a housing or ground shaft attached to the housing. The polyphase, by contrast, has one or more blade stages attached to its respective shaft or the housing by means of a freewheel or some other type of clutch mechanism and may include gearing. This element fixes the motion of the blade stage with the housing or shaft during part of the performance cycle and allows it to float freely or to turn in a geared relation during the remainder of the cycle.

Examining the various types of single-stage converters, we will bring to your attention the more subtle differences which will affect directly the overall picture of performance, especially when these units are applied to the diesel or gasoline engine.

Basic Theory

To understand the manner in which the torque converter functions, it will be helpful to review a few basic hydrodynamic principles. First of all, the basic converter element is a rotating wheel with vanes attached which operates submerged in fluid. Forces are transmitted from an impeller connected to a source of power to the fluid or from the fluid to the turbine by force components which lie in the direction of the runner motion, that is, components that are in a peripheral direction. A hydrodynamic transmission must have at least two of these elements, in which the transfer of power between the input and output runners is by means of the mass effects of the fluid. In general, the passages between the vanes are fairly large and continuous; thus, the pressure differences within the runner are not due to positive displacement action. Also, the fluid passages are large enough to eliminate the possibility that viscosity effects will have a deciding influence on the forces acting on the runners.

The controlling forces are due primarily to the mass effects of the fluid and, thus, the following well-known formula applies:

$$F = MA \tag{1}$$

In turbomachinery, this law is expressed in the form:

$$F = M\frac{dv}{dt} \text{ or } F\,\Delta t = M\,\Delta v \tag{2}$$

Since the principal motion of the runners is rotational, the forces that cause a transfer of power between the runner and the fluid lie in the direction of motion or tangential. Consider the diagram

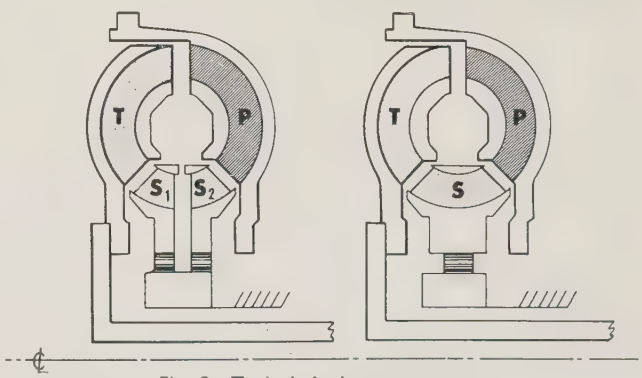

Fig. 2—Typical single-stage converter

for a radial flow impeller in Fig. 3. As the fluid is propelled from R^1 to R, the flow velocity changes from V^1 to V. The tangential components or torque producing components change from S^1 to S. The vectors shown for V and the others represent velocity in fps:

U—Peripheral velocity at the outlet tip of the vane, identified as the radius R times the angular velocity, w.

W—Approximate exit relative velocity direction of a fluid particle leaving the vane and being influenced by the vane angle itself.

V—Absolute velocity of the particle or the resultant of the peripheral and relative velocity vectors.

S—Tangential component of the absolute velocity or the vector component lying in the direction of runner motion.

F—Torus flow velocity or transportation of flow.

The direction of relative velocity is determined, in general, by the vane angle while its magnitude depends on the flow Q passing through the vane. If the channel between two vanes is considered as a form of a rectangular pipe, it is obvious that the flow and velocity will then vary with the flow area.

If no vanes are present in the flow channel and only a change in radii takes place, the product of the tangential component S times the radius R remains constant. This is referred to as the law of constant angular momentum. Now, if a torque is applied to the fluid by means of a vane or set of vanes, a change in the angular momentum takes place. The torque absorbing capacity of the vane element depends on the net change in the angular momentum and the mass of fluid to which this change is made. The torque equation for an impeller (pump), therefore, becomes: $T = M\Delta SR$

or

$$T = M\ (S_pR_p - S_p{}^1R_p{}^1) \qquad (3)$$
$$\text{outlet} - \text{inlet}$$

where:

$$M = \frac{Qd}{g} = \frac{\frac{\text{cu ft}}{\text{sec}} \times \frac{\text{lb}}{\text{cu ft}}}{\text{ft/sec}^2} = \frac{\text{lb sec}}{\text{ft}}$$

Q = Flow in cu ft per sec

d = Weight of fluid in lb per cu ft

g = Gravitational constant, 32.2 ft per sec per sec

Therefore:

$$\text{Torque } T = \frac{\text{lb sec}}{\text{ft}} \times \frac{\text{ft}}{\text{sec}} \times \text{ft} = \text{lb ft}$$

$$T = \frac{Qd}{g}\ (S_pR_p - S_p{}^1R_p{}^1) \qquad (4)$$

Power, then, is equal to Tw, where w is the angular velocity in radians per sec or 2πrpm $\div$ 60:

$$Tw = \text{Power} = Q\,\frac{d}{g}\,w\ (S_pR_p - S_p{}^1R_p{}^1)$$

$$\text{or } P = Q\,\frac{d}{g}\ (S_pR_pw_p - S_p{}^1R_p{}^1w_p{}^1)$$

Then, since rw = peripheral velocity U, substituting we have

$$P = Q\,\frac{d}{g}\ (S_pU_p - S_p{}^1U_p{}^1) \qquad (5)$$

The head of fluid developed in terms of ft per lb of fluid flowing is:

$$\text{Head } H = \frac{P}{Qd} = \frac{1}{g}\ (S_pU_p - S_p{}^1U_p{}^1) \qquad (6)$$

Equation 5 is the standard Eulers equation and as written would represent the theoretical head imparted to the fluid by a centrifugal impeller. This head is made of three major parts:

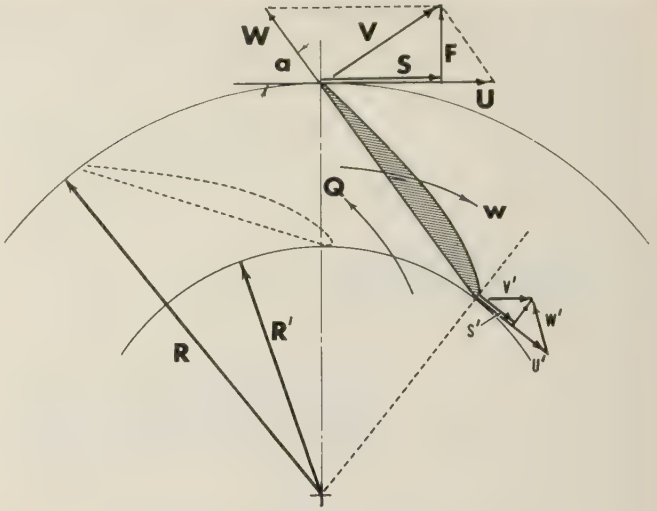

Fig. 3—Typical radial flow impeller vane

1. The pressure rise due to the centrifugal forces acting on the fluid particles.

2. The pressure rise due to the velocity change of the fluid flowing within the vane channels relative to the vane surfaces.

3. The change in kinetic energy represented by the change in direction and magnitude of the absolute fluid velocities.

The similar equation for the torque absorbed by a turbine is

$$T_t = \frac{Qd}{g}\ (S_t{}^1R_t{}^1 - S_tR_t) \qquad (7)$$
$$\text{inlet} - \text{outlet}$$

Equation 5 can be rewritten as follows:

$$P = Qd\,\frac{1}{g}\ (S_pU_p - S_p{}^1U_p{}^1)$$

Thus, horsepower $P = \dfrac{QdH}{550}$

We also know that horsepower = $\dfrac{\text{torque} \times \text{speed}}{5252}$

Equating the horsepower equations:

$$\frac{QdH}{550} = \frac{TN}{5252}$$

Solving for T:

$$\text{T} = \frac{5252}{550}\ \frac{QdH}{N}$$

or in simplified form:

$$T = kQH \qquad (8)$$

where:

k = Constant terms

H = Ft per lb of fluid

Equation 8 is one of the most fundamental and important equations in torque converter design. It states that if we compare two hydrodynamic machines, using the same fluid at the same temperature and input speed and which give the same torque capacity (that is, the input runner or impellers of both machines absorb the same torque), then the product of flow times head must be equal. To expand this still further, we see that the head, which represents the change in momentum that we stated was a function of the vanes, and the flow representing the mass of fluid moved could vary widely in

their individual values as long as their product was equal.

In other words, one converter could have a greater vane effect with a correspondingly lower flow than its comparative unit. This idea has lead to the generalized reference to a specific converter as a high head-low flow or a low head-high flow unit. The importance of this relationship to the designer will be explained later.

To separate the hydraulic torque converter, which implies the ability to multiply torque, from any hydrodynamic machine requires the presence in the circuit of a fixed stator stage. This stage fastened to the ground does for the converter what the fulcrum does for mechanical advantage in a lever, that is, it gives the unit something to push against. Without the fixed stage, the torque transmitted by the output runner would be equal to that absorbed by the input runner. The fixed reaction stage provides torque which is transmitted through the turbine wheel to the output and is equal and opposite to the reaction torque. Thus, the equation for the output torque becomes:

$$T_{out} = T_{in} + T_{reaction} \qquad (9)$$

Torque ratio of the machine becomes:

$$\text{Torque ratio} = \frac{T_{out}}{T_{in}} = \frac{T_{in} + T_{reaction}}{T_{in}} \qquad (10)$$

The torque ratio possibilities of any given unit, then, are a function of the amount of torque the unit will transmit compared to the amount it absorbs from the prime mover. Also, the torque ratio depends on the effectiveness of the stator stage or stages. We have seen that the amount of torque that can be absorbed and transmitted is a function of the flow times the head.

Performance Characteristics

To understand what these conditions imply to the torque converter designer, we must first consider the characteristic performance of this type of hydrodynamic machine.

Assume for this example that the input speed of the prime mover remains constant as the output shaft varies in speed from zero rpm or stall to a racing speed equal to that of the input runner. Then, consider Fig. 4 representing the turbine vane following the pump. To preserve the direction of rotation, that is, to have the output shaft rotating the same direction as the impeller, the turbine vane must have a reactive force in the same direction as the rotative motion of the impeller. The vane would be positioned as shown, and the resultant force of the V^1 inlet and V outlet must be in the direction shown by w_t. Since the turbine is increasing in speed from zero rpm to 1.0 speed ratio, the peripheral velocity U^1_t increases as shown. It can be seen that the relative inlet velocity W^1 changes direction with speed ratio, its angle of attack moving around the vane nose by a considerable number of degrees. The characteristic of each vane is that at some angle approximately in line with the vane physical inlet angle (that is, a line tangent to the mean camber line) the vane will perform with maximum efficiency. Attack angles on both sides of this optimum angle will cause some increasing inefficiency. At adverse attack angles, the fluid has a tendency to break away from the vane surface with resultant energy-absorbing swirls. This breakaway is aggravated by roughness or other irregularities on the vane surface at the inlet nose and results in serious loss in performance. Most converters use a basic pressure of 20–60 psi supplied by an external positive displacement pump to suppress this separation.

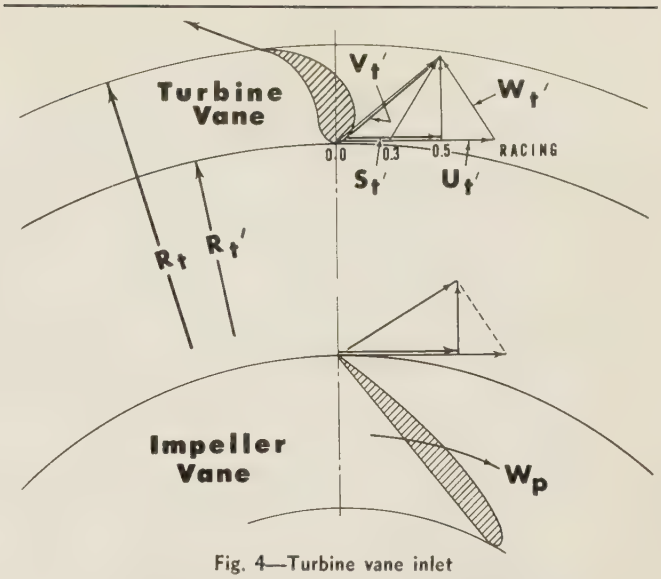

Fig. 4—Turbine vane inlet

As the speed ratio changes, it can also be seen that the bending of the fluid by the vane becomes less as we move away from stall until, at a point where the relative inlet velocity equals the outlet blade angle, the vane is completely unloaded and will not transmit torque. These two actions can produce the performance characteristics shown in Fig. 5, depending on the basic unit.

The input torque shown is the torque-absorbing characteristics of the impeller at some given input speed held constant as the output shaft and turbine vary from stall (0.0 speed ratio) to racing runout, shown as 1.0 speed ratio in this example. The shape of the input curve depends on the stage preceding the impeller and will be explained in detail later.

The efficiency curve varies from zero at stall to a peak when flow conditions are at the design point and back to zero at racing. The runout speed ratio of the efficiency curve depends on the speed ratio at which the turbine vanes are completely unloaded and zero torque is transmitted. This point can occur below, at, or above 1.0/1 depending on the converter design. The stator vane attack angles vary in a manner similar to those of the turbine vane. At a speed ratio where the relative inlet attack angle into the stator equals the stator vane outlet angle, the stator ceases to produce a reaction torque and the hydrodynamic torque converter becomes a hydrodynamic coupling where input torque equals output torque (Fig. 5). At speed ratios greater than the coupling point, the force on the stator vane is no longer opposite to the normal impeller and turbine forces and the stator is in the way, reducing the efficiency of the unit. For this reason, it is possible to increase the efficiency above the coupling point by mounting the stator on a one-way clutch or freewheel. Thus, when the force on the stator changes from reactive to the same direction as impeller rotation, the stator will automatically float with the general fluid rotation. This would be the second phase of a two-phase converter.

Fig. 5 shows graphically how the output torque

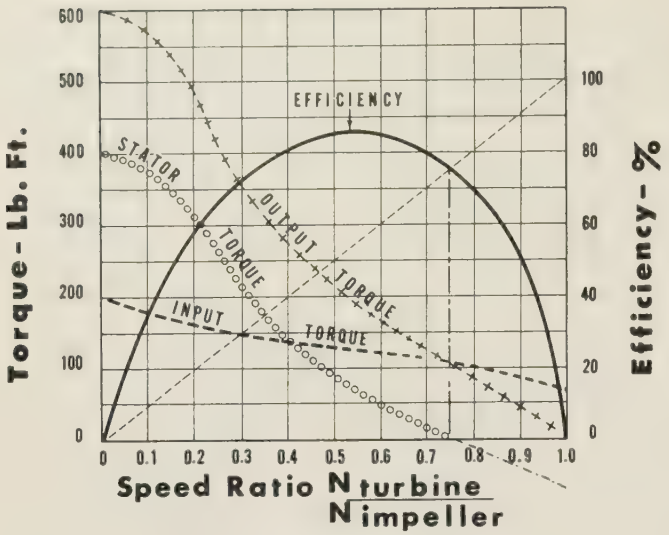

Fig. 5—Possible performance curve

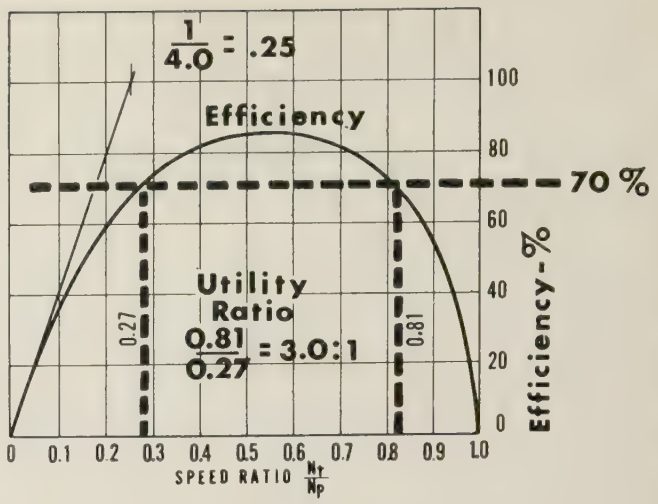

Fig. 6—Utility ratio

consists of the input torque added to the reaction or stator torque. It also shows the importance of stator stage design in the multiplication of input torque at low speed ratios.

Stator torque can also be expressed in terms of the general torque formula:

$$Ts = \frac{Qd}{g}(S_s{}^1 R_s{}^1 - S_s R_s) \qquad (11)$$

inlet – outlet

Another method of increasing the torque capacity and efficiency in this range is to shift into direct drive; in other words, to lock the turbine and the impeller together by means of a clutch. This would give engine torque out of the converter at nearly 100% efficiency. The converter would be operating at 1/1 speed ratio. At this time, the maximum efficiency of power transfer will be realized if the stator stage is mounted on a freewheel and allowed to float.

Utility Ratio

Converter performance tests have shown that the slope of the low speed ratio portion of the efficiency curve can be represented by a line drawn from the zero torque, zero speed ratio point of the performance curve, to a speed ratio point on the 100% efficiency line that is equal to the reciprocal of the stall torque ratio (Fig. 6). This fact is important when considering what is normally the most important single converter characteristic, utility ratio. We will arbitrarily define utility ratio as the ratio of the speed ratios where the efficiency of power transmission through the converter is 70% or more. This utility ratio is equal to the highest speed ratio at which the efficiency crosses the 70% efficiency line divided by the lowest speed ratio at which the curve again crosses 70%.

For most industrial applications, be it shovels, tractors, or end-loaders, there is a constantly changing load demand which causes the output speed to vary over a wide range, from near stall to racing. The chief justification for any hydraulic torque converter is its ability to adjust automatically output torque to load demand variations without any conscious effort on the part of the operator. This ability can be fully realized only if the converter has a sufficiently broad operating range so that the number of transmission shifts behind the converter can be reduced to a minimum.

A measure of the usable output horsepower is represented by the area under the curve of output horsepower plotted versus output speed. This evaluation should, of course, be tempered by the time interval spent in each portion of the curve during the work cycle. Using this yardstick of overall usable power, peak converter efficiency could be second in importance to the total efficiency curve that rises above a predetermined efficiency level, such as 70%.

In terms of vane shapes, this means that with the wide dispersion of the approach velocity attack angles into the various converter stages, the design trend has been toward those shapes that will efficiently pass the flow at the widest possible variance from the optimum attack angle. This accounts for the bulbous or bluntly rounded vane noses encountered in converters of wide utility ratio.

In the constant struggle to obtain higher utility ratio, a major design consideration has become obvious. (See Fig. 7.) Assume a converter having an efficiency curve with a utility ratio of 2.0/1.0. The high end of the curve crosses 70% at 0.8 speed ratio while the lower end crosses at 0.4. If it is desired to improve the ratio to 3.0/1.0 mathematically, we could hold the low end at 0.4 speed ratio and attempt to develop blading with good high speed-ratio performance characteristics. The crossover point for the high end would have to move out to 1.2 speed ratio. A second alternative would be to hold the high end 0.8 point and use blading with good low speed ratio characteristics. We would have to move the lower crossover point back to 0.267 speed ratio. It is readily apparent that a much smaller gain in low speed-ratio performance will produce greater utility than a much larger increase in the high end. It is also apparent by the slope of the efficiency curve that the stall torque ratio will increase considerably when the low speed-ratio blading is used. Usually, you will find that converters with wide utility ratios have high-stall torque ratios.

It has been a standard axiom that if an application requires peak performance at the high speed-ratio end of the curve and the time element in ar-

riving at this speed ratio is small, such as in the automotive field, the converter blading can be designed for a narrow high-efficiency range at high speed ratios at the sacrifice of good low-speed performance and stall torque performance. However, at the present time, we are witnessing a mighty struggle within the automotive converter transmission field to extend the useful range of the converter, by such modifications as multiple turbine stages and stator stages that freewheel out of the way under adverse attack angles, variable pitch stator vanes, and multiple turbine stages that multiply torque through the use of planetary gear sets.

Full understanding of converter operation requires an examination of the torque-absorption curve of the converter impeller.

To understand the influence of blading on the torque curve, we must return to the basic torque equation (Equation 4) and to the statement that the whirl SR remains constant in a vaneless space. This means that this outlet whirl SR of the stage immediately preceding the impeller is equal to the inlet whirl of the impeller:

$$SR_{\text{preceding}} = S^1R^1{}_{\text{impeller}}$$

Thus, the torque equation could be rewritten:

$$T = Q\frac{d}{g}(SR_{\text{impeller}} - SR_{\text{preceding stage}}) \qquad (12)$$

This makes the preceding stage a critical one in terms of impeller performance. If the preceding stage is a rotating one, that is, a turbine, the torque curve will rise from racing to stall. If the preceding stage is a stationary one, such as a stator, the torque characteristic will be more or less flat. Fig. 8a shows in its simplest form how a constant whirl would leave the stator at all speed ratios, assuming a constant flow condition which actually does not exist, as will be pointed out later. Assuming also that the impeller remains at a constant speed at all speed ratios, which could be achieved in a dynamometer test, the impeller-absorbed torque will tend to remain constant, giving a flat curve. Under the same assumption, Fig. 8b shows the effect of a variable speed turbine vane "feeding" the impeller. At stall with zero peripheral velocity and a backward curved vane, the resultant tangential component of the absolute velocity S is in the opposite direction to the normal rotation and is considered negative. The whirl SR is, therefore, negative and when entered in the torque equation gives a plus value to the inlet whirl. This results in the maximum possible value for the torque. As the turbine begins to rotate, the whirl changes from negative to positive and increases in magnitude, thereby decreasing the value for torque. This gradual and continuous unloading of the impeller results in a torque curve (Fig. 9b). This is somewhat the shape of the curve of our three-stage converter. Fig. 9a shows the flat curve of the stator preceding the impeller.

In actual practice, the flow of the three-stage is comparatively constant as the speed ratio changes. However, the flow through certain types of single-stage converters decreases rapidly from stall to racing.

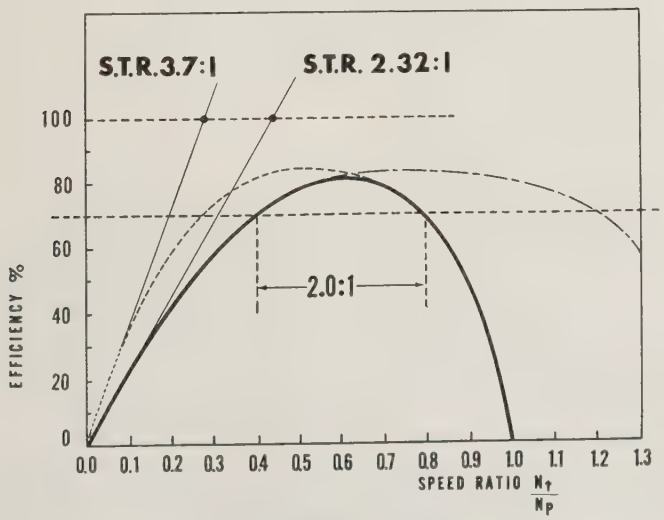

Fig. 7—Utility ratio increase

Turbine Counter Head

This brings up another major consideration in design of any single-stage converter, namely the position and the size of the turbine stage relative to the impeller. We have stated previously that a vane system rotating builds up a head which tends to propel the fluid outward by the centrifugal forces acting on the fluid particles. This force depends entirely on the rotational speed. In converters of the inward flow turbine type, such as those shown in

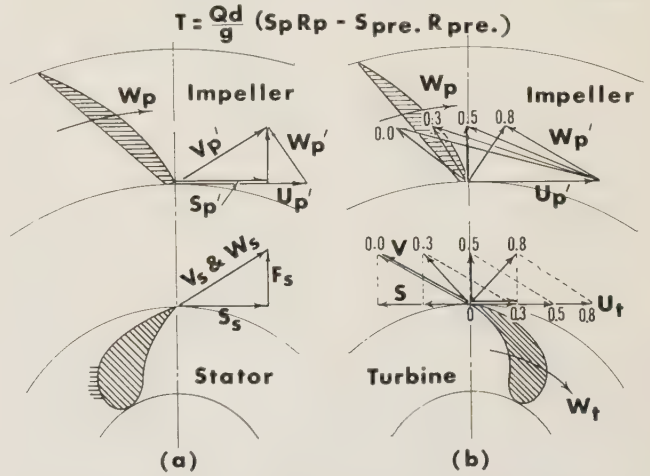

Fig. 8—Effect of speed on stator and turbine

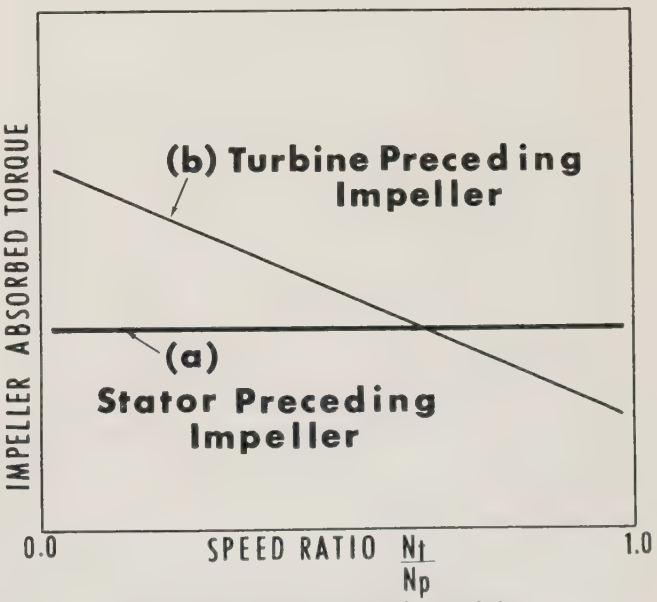

Fig. 9—Comparative torque characteristics

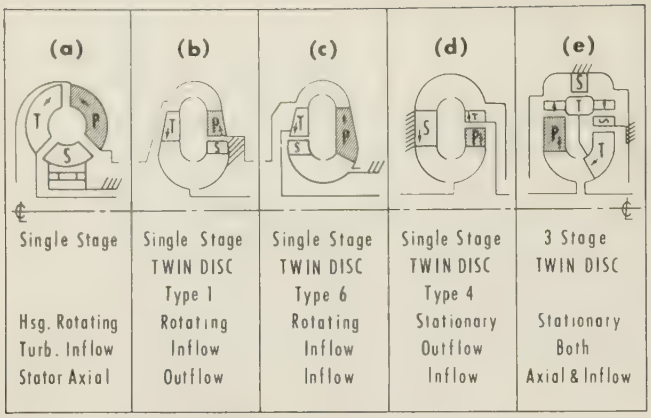

Fig. 10—Some typical converter basic types

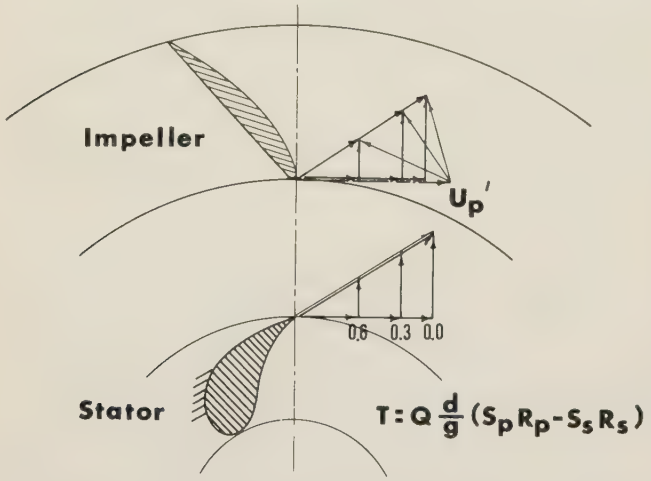

Fig. 11—Stator preceding impeller

Fig. 10 a, b, and c, although the flow is being forced through the turbine inwardly, the turbine, as it picks up speed, builds up a counter centrifugal head which opposes this inward flow. The maximum flow occurs when the turbine is stalled and it gradually decreases with increasing turbine speed until the turbine head equals the impeller head and the flow ceases. This decreased flow tends to *reduce* the torque absorption of the impeller. However, as the flow decreases (Fig. 11) so does the absolute velocity leaving the stator stage. This means that the impeller inlet whirl will decrease, tending to *increase* the impeller torque. As this decreasing plus increasing tendency varies in net effect, the theoretical flat input curve is modified approximately as shown in Fig. 12. At the stall end, the curve can fall off (a) or actually rise (b). The actual characteristic will depend on the converter design.

Shortening the impeller vanes and changing the stator from basically axial to radially outflow (Fig. 10b) decreases the centrifugal head of the pump relative to the turbine counter head. The rotating mass of oil contributing to turbine counter head extends down to the center of the circuit and not just to the vane inner diameter. This causes the flow shutoff to occur at a much lower speed ratio and results in a sudden drop in both input-torque absorption and in output torque shortly after passing the clutch point or 1/1 torque ratio point. This rapid unloading of both the prime mover and the

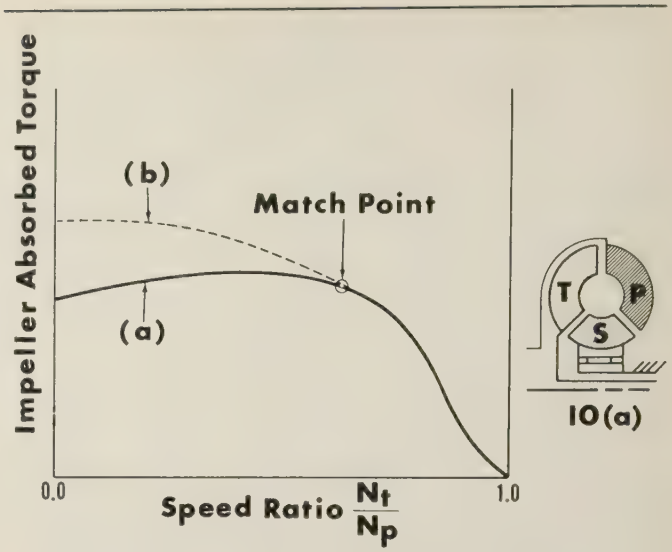

Fig. 12—Typical torque curve of single-stage coverter

output shaft can be useful in certain applications, where it is desired to limit the top speed under light load conditions without the use of an output-shaft governor. In contrast to an output-shaft governor that has to sense an overspeeding condition and then reduce engine output by closing down the throttle, which takes some time, the sudden unloading of the output shaft which occurs based on speed ratio corrects the overspeeding as soon as it occurs by reducing the high torque causing the overspeeding.

Moving the stator to the other side of the circuit (Fig. 10c) reduces the turbine counter head by increasing the inner diameter of the rotating oil mass. At the same time, if the impeller vanes are lengthened, the centrifugal head effect of the impeller is increased. Thus, the angular velocity of the turbine must now exceed that of the impeller by some amount before shutoff can occur. This increases the runout rpm and, therefore, the delivered horsepower at high speed ratios. The comparative characteristics of these two types is shown in Fig. 13.

The importance of the converter characteristics can be understood better when a combination of the engine and converter is considered. For a given engine, we would need a converter whose impeller would absorb the engine net full-load rated torque at the matching speed ratio point. The engine curve itself would resemble that shown in Fig. 14. This is the normal diesel engine curve of torque plotted against engine rpm.

Capacity Factors

To provide a converter whose impeller absorbs or matches this torque, we can again return to Equation 4. We have already seen how the vane stage ahead of the impeller can affect the impeller's torque absorbing capacity through its influence on the $S_p{}^1R_p{}^1$ whirl value.

Analyzing the equation, we can see several other factors which could affect capacity. They are the quantity of flow Q, the weight of the fluid d, the outlet velocity component S; and the radius R.

In general, weight and viscosity go together and since fluid friction losses within the blade channels increase with increasing viscosity, it is to our advantage to use the lightest possible fluid with the

greatest possible specific gravity. This immediately suggests water, but water has too low a boiling point which, if used in a converter, would give severe cavitation losses in low-pressure areas of the circuit in spite of converter basic pressure. Incidently, one of the earliest applications of a hydraulic torque converter, as described to us by Prof. Wilhelm Spannhake, was a ship propulsion converter for the Kaiser's yacht which used sea water for the fluid medium. However, a major requirement which water cannot fill is that of lubrication.

In many converter designs, the converter circuit, the clutches, and the transmission and cooling are tied together with a common fluid (SAE 10 or transmission fluid type A). When the fluid circuit is separated from the lubrication system by means of face-type seals (usually carbon rings running against steel rings), a light fluid such as kerosene or a special torque converter fluid can be used. Since the overall weight difference between the lightest and the heaviest of the customary fluids is relatively small and a given design might not be flexible enough to use a choice of fluids, the weight factor in matching a converter to an engine can be eliminated.

Control of the vane channel area giving various flow rates Q could be used for changes in torque capacity. However, all areas in the circuit must be changed to maintain some given area relationship which has been determined as giving the optimum overall operating characteristics in the test model. Also, this type of change can greatly affect unit tooling costs unless the unit is predesigned to enable the flow area to be modified. A converter of this type produced in this country uses a laminated pattern which enables a unit of a given size to be cast in three different capacities, maintaining the same identical vane angles and shapes but varying the flow areas proportionally in each stage. This variation covers a horsepower range of about 1.6/1.

The outlet velocity component S_p is one of the major control items. This value can be affected (Fig. 15). For the same peripheral velocity, that is, at the same rotative speed, the greater the outlet angle of the vane, the larger the tangential component S will become. Thus, once a unit size is tooled up for manufacture, a range of unit capacities can be provided by supplying several pump wheels with different vane angles which are interchangeable in the basic unit.

Normally, good performance characteristics can be produced over a torque capacity range of just slightly less than 2/1 using this method.

The two most important factors influencing capacity are the outlet radius of the impeller R_1 and the rotational speed N. The effect of these two can be seen from the following analysis.

Velocity of fluid flow V is proportional to the flow Q divided by the flow area A. Since area is equal to $D \cdot 1$ (1 being the width of the channel at diameter D) and the ratio of 1 to D is always fixed for similar units, A can be considered proportional to πD^2 or just D^2, as: $V :: Q \div D^2$

Peripheral velocity $U :: ND$ and the ratio of fluid velocity to peripheral velocity must remain a constant. Therefore:

$$\frac{V}{U} = K_1 = \frac{Q/D^2}{ND} \text{ or } Q :: ND^3$$

Head H can be expressed as a constant times

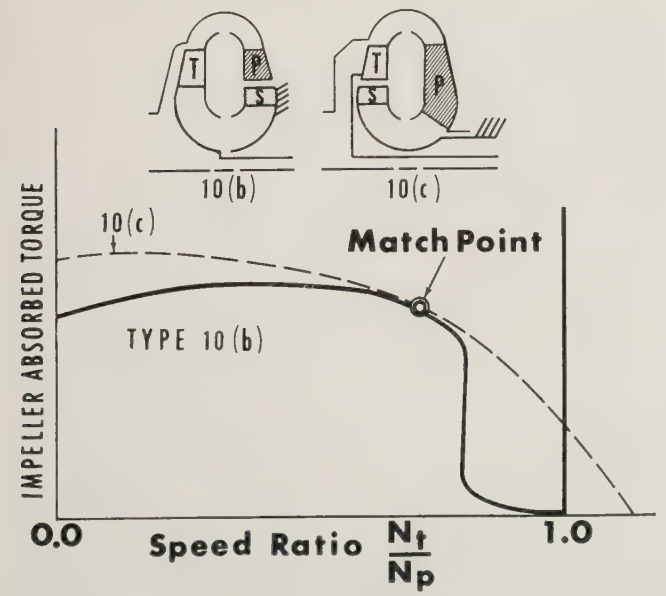

Fig. 13—Typical torque curves of single-stage Twin Disc converters

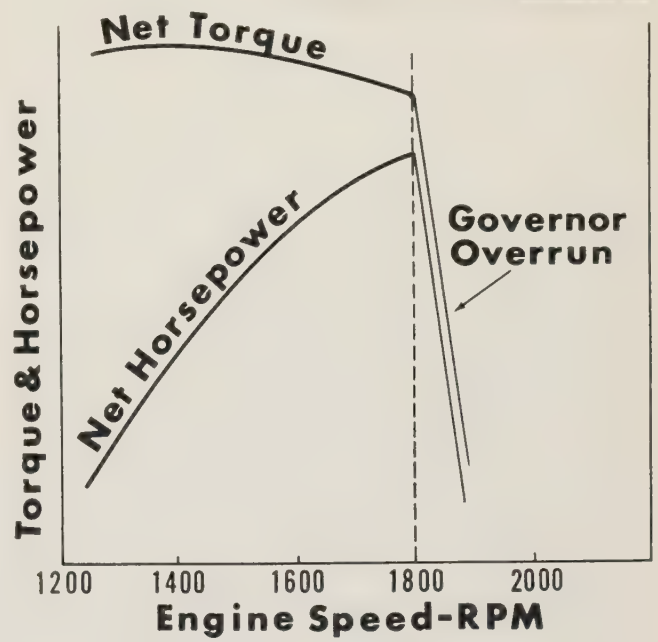

Fig. 14—Typical engine curve

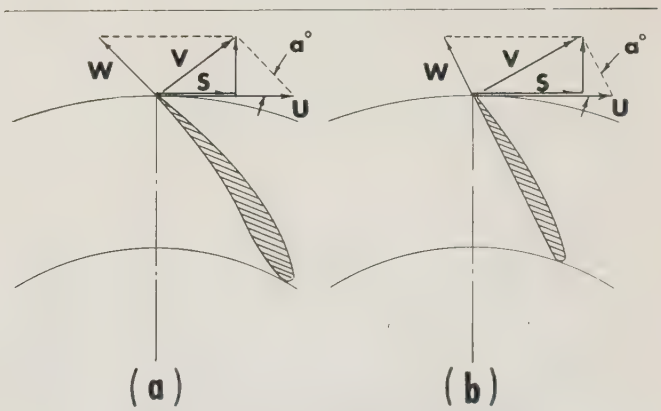

Fig. 15—Effect of impeller outlet angle

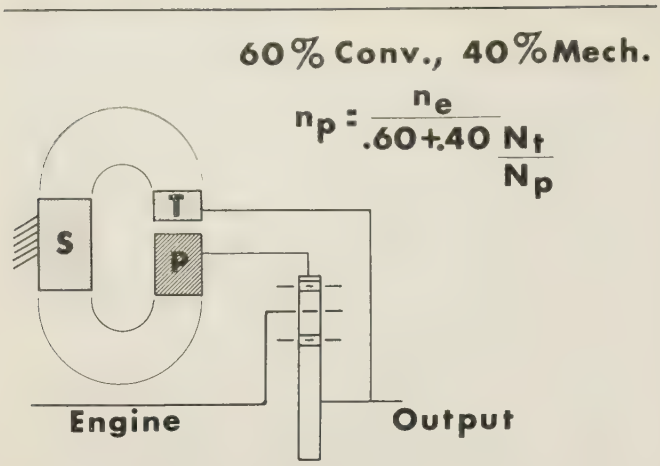

Fig. 16—Split torque converter

$V^2/2g$. Since V and U are proportional,

$$H :: \text{Constant} \times \frac{U^2}{2g} :: \frac{N^2D^2}{2g} :: N^2D^2$$

Substituting in the abbreviated torque equation $\left(T = \frac{kQdH}{N}\right)$:

$$T :: \frac{QH}{N} :: \frac{ND^3N^2D^2}{N} :: N^2D^5 \qquad (13)$$

Since power $P = Tw$ and $w = \frac{2\pi N}{60} :: N$

$$P :: (N^2D^5)\ (N) :: N^3D^5 \qquad (14)$$

From this, it can be seen that the torque capacity will vary as the square of the speed or the fifth power of the diameter of the impeller. Power varies as the cube of the speed and fifth power of the diameter. It is, of course, understood that to maintain model similarity, all linear dimensions must be modified in the same proportion as the diameter change. From this consideration, it is quite obvious that chief matching factor will be unit size and the next most important one will be speed.

This means that for a given engine horsepower, the higher the speed of operation, the smaller the converter will have to be to match the engine torque. A given engine speed and horsepower must be matched with the correct converter capacity to produce satisfactory results. Too large a converter will keep the engines lugged down, reducing the potential delivered horsepower. Too small a converter will result in considerable operation on the governor overrun, again losing horsepower. Once the proper size is selected to match the engine closely, accurate tailoring can be accomplished by varying the impeller vane setting. Often, slight adjustment of the governed speed of the engine of 50 or so rpm will bring an engine and converter into better match and thereby deliver more useful work.

Input Curve Versus Engine Pulldown

Referring again to Fig. 12, let us assume that we have a single-stage converter which matches the engine-governed torque at a point shown on the converter curve. The converter curve shown is the torque absorption curve for the converter impeller at one given speed. Any change in the input speed to the impeller will result in a change in the absorbed torque, which varies as the square of the speed change. As the speed ratio of the converter decreases towards stall, the converter will absorb more torque than that at the engine-governed speed and the engine will be lugged down to balance the impeller-required torque. This process of lugging down will continue until the peak of the converter torque curve is reached. Then, as the output speed is reduced farther toward stall, the converter-absorbed torque requirements fall off and the engine will be unloaded until the engine speed returns to governed speed at the stall point in this example. If the converter torque should drop below that at the match point at stall, the engine would be unloaded to some point on the governor overrun curve. Thus, the actual stalled output torque, which equals the input torque times the converter stall torque ratio, would be reduced by the loss in input torque.

To an equipment operator, this means that as the load forces his vehicle closer to stall, instead of the usual heavy lug down to near stall out that would be experienced in a mechanical drive or more moderate lug down with the three-stage, he finds the engine speeding up. This type of action meets with varying degrees of acceptance. The operator who is used to working by engine tone has to adapt himself to new sounds. Some engine flywheel inertia effects are lost, which could be transmitted up to the stalled torque capacity of the converter. However, in some applications, such as end-loaders, it is advantageous to allow the converter to unload the engine at stall which can then produce maximum speed and capacity of engine-driven pumps for operating the hydraulic cylinders on the bucket.

Split Torque Versus Engine Pulldown

In most industrial applications, practice has shown the desirability of some engine pulldown as the load increases. One method of producing a gradual loading of the engine as the speed ratio of the converter is reduced from racing to stall is to modify the relatively flat torque absorption curve of the single-stage converter by means of a split torque planetary either ahead of or behind the converter. One possible application is shown in Fig. 16. In this example, the engine drives the planet carrier. The ring gear of the planetary drives the torque-converter impeller. The turbine is attached to the sun gear and the output shaft. In this system, the engine power is divided into two paths. Part of the power is transmitted through the converter and part mechanically through the gears. Thus, during general operation, the two parts are simultaneously transmitting constantly varying portions of the engine output power. The engine output torque, however, at all times is split between the converter and mechanical at a definite ratio determined by the gearing. Since only part of the power goes through the converter, only that part is subject to the hydraulic losses of the converter. The remainder, going through the mechanical drive, passes with normally low gearing losses. The net result is a generally higher efficiency for the system. However, only that part of the torque going to the converter can be multiplied by the torque multiplying ratio of the converter. The torque ratio for the system in the converter torque multiplying range tends to be lower than for the converter alone. Therefore, even though the split system produces high speed ratio ranges of efficiency operation, much

higher than the converter alone could produce, the torque output at stall is reduced as is the utility ratio. A successful application of split torque on equipment, where wide utility ratio is required, depends on using a converter with the widest possible utility ratio and the maximum possible stall torque ratio. Units of this type have been produced and are in operation in Europe at the present time.

Since only a part of the engine power has to be carried by the converter, use of a smaller converter could result in lower initial cost if the cost of producing the planetary could be held low enough.

The basic formula for the planetary shown in Fig. 16 can be expressed as:

$$N_p = \frac{N_e}{\frac{\%\ \text{converter}}{100} + \frac{\%\ \text{mechanical} \times Nt/N_p}{100}} \quad (15)$$

where: N_p = Speed of the impeller, rpm
N_e = Speed of the engine, rpm
Nt/N_p = Speed ratio of the converter

From Equation 15 it can be seen that, as the converter speed ratio comes down, the total value of the divisor becomes smaller and the speed of the converter impeller rises. It is also evident that the speed of the converter impeller is always faster than the engine speed. Since the impeller-absorbed torque goes up by the square of the input speed, the normally "flat" single-stage torque curve has been modified in such a manner that it appears to the engine to have a rising characteristic as the output shaft is slowed down by the increasing load. This lugs the engine down at stall in much the same manner as the rising torque curve of the three-stage converter.

Combinations of planetary gearing, clutches, and brakes with various converter types are infinite and the study of the resultant engine-converter combined characteristics is a formidable one at best. However, it is one which the manufacturer cannot afford to ignore in his search for the ultimate in performance of his piece of equipment.

High Speed Ratio Characteristics

Referring again to Fig. 12, the high speed ratio portion of the torque absorption curve for a typical single-stage converter of the type shown in Fig. 10a reveals a gradually falling characteristic due to the flow shut-off characteristics of the circuit as the turbine wheel approaches the speed of the impeller. Some converters of this type have freewheeled stators which, in this range, float with fluid rotation. In this phase, the unit is operating as a hydraulic coupling at efficiencies approaching those of couplings. This efficiency is equal to the speed ratio. As the speed ratio in the coupling range increases, the falling torque characteristic unloads the engine down the governor overrun curve. In spite of the fact that the converter is operating at high efficiency, very little torque is transmitted, due to the rapid loss of torque supplied by the engine.

In most cases, a much less efficient unit than the converter coupling can actually transmit more output horsepower if the converter has a sustained torque absorption characteristic at racing. The circuit of Fig. 10c, whose performance is shown in Fig. 13, was designed to maintain this torque capacity at higher speed ratios and to prevent the loss of theoretical stalled output torque by actually pulling the engine down slightly at stall due to its rising torque curve. Fig. 13 also shows the comparison between the characteristics of the outflow stator converter of Fig. 10b and the inflow stator of Fig. 10c.

High Utility Ratio Single-Stage

Fig. 10d shows another type of single-stage configuration consisting of an outflow turbine and an inflow stator, in addition to the impeller wheel.

This type of converter does not have a flow shut-off characteristic because of the outflow turbine and stationary stator, neither of which can produce a counter haed to that of the impeller. At the high speed ratio end of the curve (Fig. 17) when the unit has zero efficiency at runout, the converter still absorbs torque in much the same manner as the three-stage converter. This torque absorption characteristic is not the only unique feature of this particular type of single-stage unit. Tests have shown that this converter is capable of producing stall torque ratios up to 7/1 and utility ratios between 3.6–4.0/1 and operating at efficiencies up to 86%. This is quite an achievement when it is realized that the normal single-stage converter produces stall torque ratios from 2.0/1 to 3.8/1 and without polyphase operation rarely exceed 2.5/1 in utility ratio. The runout over 1/1 is typical of the higher capacity units in a given size.

Flow-Head Relationships

To understand the basic differences between these converters and their characteristics, we must return to Equation 8. This equation shows that two units having the same torque capacity could have quite different flow and head characteristics as long as the products of the two were equal. To evaluate the given specific types of converters covered in this paper, it has been necessary to build or obtain samples of each type and, after a complete dynamometer test, calculate their flow characteristics. Using the physical dimensions of vane diameters, vane channel areas, and vane angles, and the performance data, the flow in cubic feet per second and the head

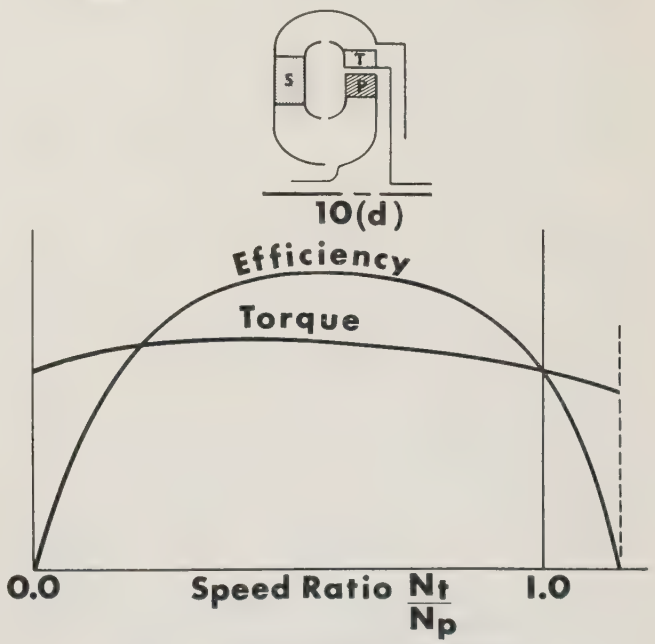

Fig. 17—Typical performance characteristics

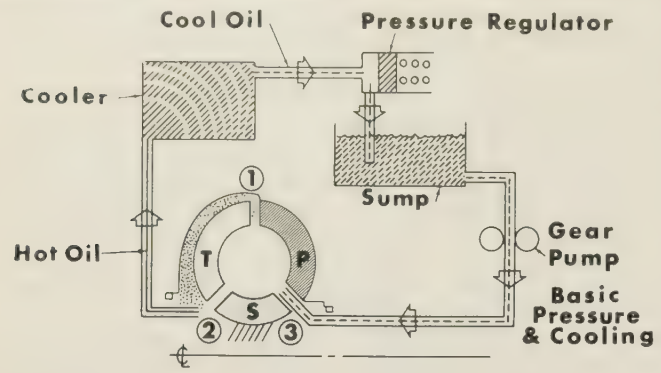

Fig. 18—Typical cooling circuit, positive or forced cooling

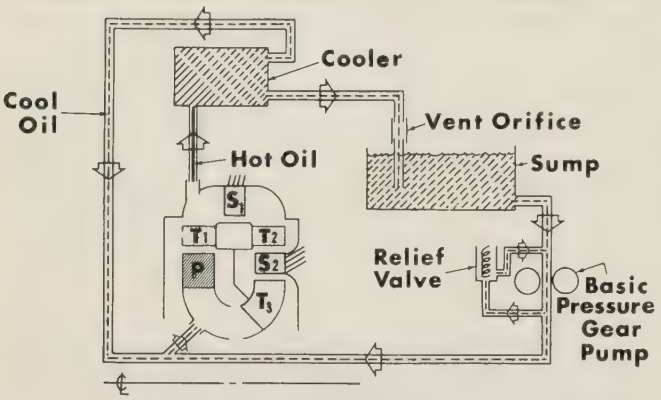

Fig. 19—Typical cooling circuit, natural cooling

in feet were calculated on the basis of design path flow at a common input speed. Naturally, these units varied widely in size and capacity. Therefore, to compare them on a common basis, all units were mathematically corrected to a given input requirement of 1000 lb-ft at 1700 rpm at the coupling or 1/1 torque ratio point. This meant that first the impeller diameter necessary to absorb 1000 lb-ft had to be determined on the basis that the torque would be changed by the fifth power of the impeller outer diameter. Flow then was modified by the cube of the ratio of the 1000 lb-ft diameter to the test diameter, and head by the square of this ratio.

The data obtained from this analysis enabled us to divide the converter types into three definite major groups in terms of head and flow. These groups could be labeled as follows:

Low flow-high head	Fig. 10a, 10b, 10c
Medium flow-medium head	Fig. 10e
High flow-low head	Fig. 10d

The flow in the medium group ran about 66% of that in the high-flow group. The low-flow group had only 25% as much flow as the high.

It is necessary for the converter designer to consider the amount of flow in a certain type when the method of production is determined. High flow leads to high losses due to viscosity changes in a given fluid operating at low temperatures or in fluids of high viscosity at normal operating temperatures. The surface finish and vane nose contours in the high-flow unit must be of excellent quality to minimize the fluid friction losses and the losses due to local separation of fluid from the vane surfaces and resultant energy loss.

Specifically, this means that units of the low-flow type can be produced from cast aluminum by sand, plaster, or shell-mold methods with their inherently rougher surfaces and can be operated on fairly high viscosity oil such as SAE 10 and still produce efficiencies between 86–90%. Substituting a low-viscosity fluid, such as kerosene or diesel fuel, in these circuits will not significantly improve their performance.

Medium-flow units of our three-stage type require surface finishes as good as practical to produce the maximum performance. At the present time, surface finishes of not higher than 125 rms are specified on all circuit parts. This can be accomplished with good machining practices, fabricated stages of rolled or extruded vane shapes, and stampings.

To realize maximum performance from units of the high-flow group, better finishes are required, probably in the range of 60–85 rms acquired by some grinding, polishing, and buffing procedures.

Converter Cooling

One of the major problems of torque converter application is that the power lost in the inefficiency of the converter results in heat. Referring to the performance curve in Fig. 5, the efficiency curve represents the percentage of power transmission through the converter. At stall under heavy load, the efficiency is zero; therefore, the power of the engine is trapped in the converter and must revert to heat. It is also obvious that under zero load with the turbine runout speed determined by the blading, the efficiency is again zero and any power from the engine entering the converter must be transferred into heat.

From this, it is also obvious that the engine speed at stall and racing, determined by the converter impeller characteristics, will in turn determine the amount of input power and, therefore, the amount of heat to be handled in a cooling system.

Fortunately, in most earthmoving converter applications, it is virtually impossible to stall the converter because of wheel or track slippage. Also, extremely low speed ratio operation is only intermittent, thus overheating very rarely occurs.

However, the other end of the curve is a different story and one which is most often misunderstood by the layman. Under very light load conditions or when using an oversized converter, that is, one which matches the engine far to the right, it is possible to be putting in considerable engine power but operating at low efficiency at the high speed ratios.

In Fig. 5, assume the converter and full-throttle engine-governed torque match at 0.75 speed ratio. This occurs at a converter efficiency of 76%, a normal matching point for this type converter. Now assume the load on the wheels or tracks decreases. The turbine rpm rises. The impeller absorbed torque decreases, unloading the engine down the governor overrun curve. Assume the output shaft is completely unloaded, such as would occur if the transmission following the converter was shifted to neutral. At this point, the input-torque requirement of the converter equals the drag torque of the stator and the engine reaches its minimum horsepower output on the governor overrun, matching the input and stator torque. Using a converter performance, such as that shown in Fig. 5, the heat generated under this no-load racing condition is usually

the governing factor in calculating the cooling capacity requirements for continuous operation. The heat developed during downhill braking can also dictate the size of cooling capacity.

If the converter torque-absorption requirements drop to near zero in this range, either by virtue of hydrodynamic flow shutoff or freewheeling the stator, the cooling requirement under racing conditions will be greatly reduced.

The heat trapped in the converter must be dissipated in a radiator or heat exchanger. In order for this cooling to take place, fluid from the converter circuit must be moved to the cooler and returned to the converter. Here again, the basic design of the converter can make this problem cheap and simple or costly, both in initial expense for an adequate pump and in loss of available horsepower to drive the pump.

To demonstrate the basic differences between converter types, we refer to Fig. 10. It has been mentioned that one of the so-called byproducts of a rotating centrifugal impeller is pressure. Therefore, if we can tap the converter system providing a path from the higher pressure through the cooler and back to the low-pressure side, we can make use of pressure differential to push the cooling oil through the cooling circuit. If we cannot tap a sufficient pressure differential, it is necessary to use a positive displacement pump driven by the engine.

The converters shown in Figs. 10a, b, and c are rotating housing converters. That is, one element, either the impeller or the turbine, is attached to a cover which surrounds the other members of the circuit and forms a casing in which the fluid is contained. The rotating casing is then mounted inside a fixed housing attached to the flywheel housing or the transmission case which acts as a cover for the rotating parts, a sump for the excess oil supply, and a means of supporting the rotating members.

Ordinarily, piston-ring seals are used to seal the fluid in the converter circuit. These rings are usually kept to the minimum possible diameter to reduce friction loss and subsequent wear. Thus, the cooling oil must move radially inwards from the high-pressure impeller outer diameter 1 (Fig. 18), through the space between the cover and the internal wheel, under the sealing rings at 2 to the exit passage provided in the fixed outer housing, and thence to the cooler and back to the inlet side of the impeller 3. The oil in the space 1 to 2, between the internal wheel and the cover, builds up its own counter centrifugal head, which reduces the high pressure potential existing at the impeller outlet. The external cooling circuit senses only the pressure differential remaining between points 2 and 3. Generally, this differential is close to zero by the time the fluid has emerged from its rather devious path to the housing mounting pads where the fluid cooling hoses can be attached. Thus, this type converter will normally require an engine-driven pump for a positive or forced cooling system.

Assuming that it would be necessary to cool 30% of the engine horsepower under the worst conditions in which the converter will be operated for extended periods of time, and assuming the use of economical heat exchanger design, the cooling requirements would normally be between 10–15 gpm per 100 hp. It is easy to see that this external pump could be quite a sizeable one in some applications.

Figs. 10d and e show converters of the stationary-housing type in which all wheels rotate within the converter housing and in which the stator vanes are attached directly to the housing. In this type of unit, it is possible to tap the housing at almost any desired point (Fig. 19) and to make use of virtually all the available pressure drop the impeller can provide. Varying with the speed of operation and the physical size of this type of unit, the available cooling flow depends entirely on the size of the lines and the resultant pipe friction, bend, entrance, and exit losses. A 1-in. line system with a radiator and about 20 ft of piping would have flows in the range of 30–50 gpm at 20–40 psi differential. This cooling flow bleed from the circuit is a negligible loss when the total output of the centrifugal impeller is considered. A converter with an impeller outlet diameter of about 13¾ in. running at 1700 rpm in our three-stage converter is circulating fluid at the rate of 8–10 cu ft per sec within the circuit. This amounts to 3600–4500 gpm.

Push Starting

Since the fluid is the only connection between the input shaft and the output shaft in the hydrodynamic transmission, it is often necessary to supply a mechanical lockup for push starting the vehicle. A direct-drive clutch between the impeller and the turbine driveshafts can be engaged by means of hydraulic pressure from a gear pump driven from the tracks or wheels. In units which do not normally have a direct-drive clutch, a freewheel is installed between the impeller shaft and the turbine shaft. This freewheel operates at differential speeds during the normal working cycle from zero to 1.0 speed ratio. The freewheel locks up when the turbine reaches impeller speed, thus preventing the converter from operating over 1/1 speed ratio. Here also the resultant performance varies with the converter design characteristics.

Fig. 20(a) shows the efficiency and torque absorbing characteristics of a high-runout converter with sustained torque characteristics. Without the freewheel, the turbine at 1/1 speed ratio still has potential output torque. The freewheel prevents the turbine from attaining zero torque output over 1/1 and the excess torque over that required to operate at 1/1 returns through the freewheel to the impeller;

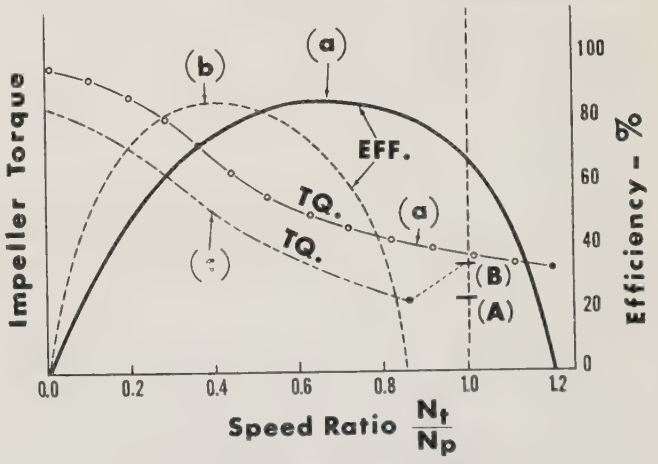

Fig. 20—High runout versus low runout

since the impeller can absorb only a given amount of torque at a given speed, the torque supplied by the turbine reduces that required of the engine and the engine is unloaded further down the overrun curve. Under no output shaft load conditions, the engine speed will rise until the engine output matches the stator torque.

The power absorbed by the stators and supplied by the engine is determined by the inefficiency of the converter at the 1/1 speed ratio point. Thus, the more efficient the converter at 1/1, the less cooling will be required.

Fig. 20(b) represents a converter with sustained torque requirements, but which runs out under 1/1 speed ratio. In this case, even though the unit contains a push-start freewheel, it can never engage the freewheel under its own power. Thus, the impeller torque at runout determines the output torque of the engine and also the cooling requirement. A push-start freewheel in a rotating housing-type converter whose shoutoff condition occurs at or prior to 1/1 will not affect the heat problem, as the engine is more or less completely unloaded.

Cranking Characteristics

Periodically, there develops the question of the cranking characteristics of different converter types without a direct lockup clutch or a push-start freewheel.

A torque converter can be run in the laboratory by driving the turbine and measuring the torque delivered at the impeller shaft at different speeds. Under these operating conditions, the fluid in the circuit is at ambient temperature, seldom lower than 70 deg unless a special cold room is provided. The fluid is in a fairly thin state, compared to normal push-start operations at temperatures well below zero. These conditions will produce torque-transmitting flow characteristics and the unit designed as the best hydraulic coupling will theoretically give the greatest cranking torque.

Several factors in actual practice tend to affect the actual cranking torque during the cold start. Units of the rotating-housing type normally drain down to somewhat less than half full after a shutdown, because of the piston-ring seals. The full cranking potential then will not be realized until the cold thick oil is forced into the converter and a flow pattern set up.

Converter cranking requires comparatively high ground speed which would depend on the footing for and capacity of the pushing vehicle. Successful field push starts have been accomplished with converter types that theoretically have poor push-start characteristics. This was probably due to a shearing action in the thick cold oil rather than a fluid flow condition.

The general conclusion seems to be that push-start cranking with a converter only is uncertain at best. For positive cranking at lower ground speed, a freewheel or lockup clutch is more dependable.

Braking Characteristics

Many vehicle applications require braking for certain operating conditions. Braking occurs at a high speed ratio when the turbine wheel is being driven by the tracks or wheels and the power supply is coming from the inertia of the vehicle and load. If a push-to-start freewheel is used, part of the braking is supplied by the engine compression. If the converter is the rotating-housing shutoff type, it can supply little or no braking effort. This requires the use of an auxiliary hydrokinetic brake, which consists of an impeller attached to the output shaft and fixed vanes attached to the vehicle frame through a housing and is in essence a stalled hydraulic coupling. In the normal working range, this coupling must be dumped to prevent power loss. If the converter is the sustained-torque type with fixed stator vanes, the flow of oil against the stator vanes will supply an additional braking force equal to the ability of the vanes to absorb torque, which varies about as the square of the speed. Therefore, the braking ability of any converter at 1/1 is closely allied with the heat characteristics discussed under cooling. Fig. 20 showed that in a high-runout converter, the higher the efficiency at 1/1, the lower the heat load. Similarly, the higher the efficiency, the lower the stator torque and, therefore, the lower the braking.

The regenerative feature of the high-runout turbine wheel (Fig. 20a) sends part of its power to the impeller wheel which reduces the net braking effect. The unit which has a runout under 1/1 (Fig. 20b), would provide more braking than the former unit since it requires external effort from the wheels to drive the turbine wheel up to 1/1 lockup.

For example, a high-runout unit of our three-stage converter with a 13¾-in. impeller and a push-to-start freewheel could supply 290-lb-ft braking torque at 1700-rpm output shaft speed in a unit whose match-point torque would be 390 lb-ft at 1700 impeller rpm. A similar low-runout unit would have a braking torque of 330 lb-ft at 1700 rpm with a match-point capacity of 200 lb-ft at 1700 impeller rpm.

When converter braking of this type unit is combined with the engine braking, no auxiliary hydrokinetic brake type of device is normally required.

Conclusion

The performance characteristics that have just been discussed are some of the major ones that must be taken into account in the evaluation of equipment performance and design. When the hydraulic torque converter is understood and used to its maximum degree, its use can offer some tremendous advantages to the ultimate user. In order to recognize its maximum utility, it must be designed as an integral part of the power train. An educated, planned approach to its use can influence the choice of engine characteristics, the number of gear shifts, and the reduction ratio of the mechanical portion of the drive train.

The converter types discussed here are by no means the final answer to the torque-converter design problem. Future developments in industrial equipment will include the combination of converters and planetaries which are capable of modifying converter characteristics in many different ways.

The converter will continue to play an integral role in the development and use of the power-shift transmission, as the heavier earthmoving vehicles continue on their design path toward the ease of handling that rivals the passenger car.

In keeping step with this revolutionary phase of development, it is the duty of the engineer to produce a proper marriage of the converters that can be different to the jobs that are different.

THE AUTHOR compares aircooled and liquid-cooled diesel engines from the several points of view, including: Plumbing difficulties, anti-freeze requirements, bulk (hp per cu ft), weight (lb per hp), fan power and quantity of cooling air required, noise, costs, operation and maintenance.

Present-day aircooled diesel engines can be divided into four categories: those for industrial installations, small sized engines for agricultural applications, medium sized multipurpose engines, and large engines for military uses. Several examples of each type are discussed.

The author reports that because of their advantages in space utilization and adaptability to a wide range of temperatures, the aircooled engine is coming into greater and greater use.

AIRCOOLED DIESEL-ENGINE APPRAISAL

C. F. Bachle, Continental Aviation and Engineering Corp

This paper was presented at the SAE National West Coast Meeting, Seattle, Aug. 12, 1957.

EVER since Rudolph Diesel invented the combustion cycle that bears his name, engineers have been striving to design better and better versions of this engine. Many designs of diesel engines have been built and tested and many facets of these designs have been thoroughly covered by the literature; notably combustion, lubrication, intake and exhaust systems, and the like. One subject, however, has received relatively little attention during the more than 50 years of diesel-engine development and this is the question of aircooling versus liquid cooling of diesel engines. (See Additional References.)

When this subject is put forth the question naturally arises: "Why aircooling?" Admittedly, there are several applications where aircooling is obviously not practical. In general, these are marine installations or industrial installations alongside of free water supplies where liquid cooling is inexpensive and, therefore, desirable, and where at the same time the heat can be disposed of without capital cost in coolers. Likewise, there are applications such as motorcycles, aircraft, and military vehicles where aircooling has become the accepted standard, since it is the logical choice in the existing environment. Aircooling also becomes very attractive where nature has given us either extreme temperatures to contend with or reduced the available water supply to practically nil, such as in desert or arctic areas. For 25 years we have been building aircooled gasoline engines for use by Army Ordnance in track-laying military vehicles. These engines have been highly successful in meeting the special requirements of combat vehicles, namely:

1. Minimum bulk for the total power package, including all cooling of the engine and transmission.
2. Minimum power losses for cooling.
3. Adequate cooling of the power package buried in an engine compartment with all openings on top and with considerable airflow restrictions from ar-

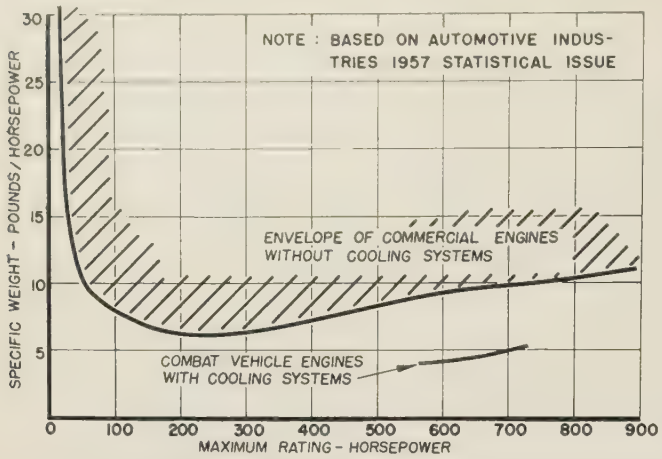

Fig. 1—Weight comparison, combat vehicle versus commercial engines

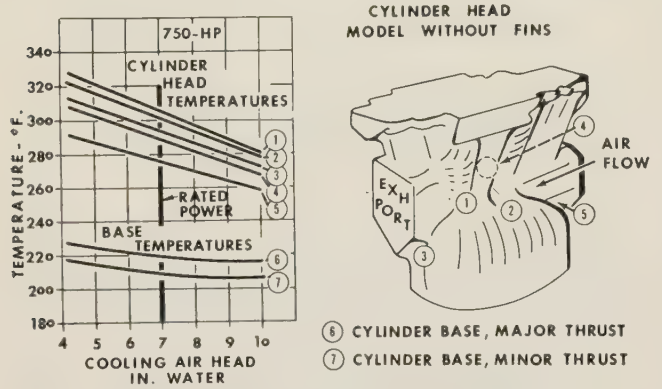

Fig. 2—5¾-in. bore diesel cylinder cooling

Table 1—Comparison of Aircooled and Liquid-Cooled Engines

	Military Vehicles, Advantage for		Commercial Vehicles, Advantage for	
	Air	Liquid	Air	Liquid
Plumbing Difficulties	X		X	
Antifreeze Requirements	X		X	
Bulk, hp per cu ft	X		Equal	
Weight, lb per HP	X		Equal	
Fan Power and Quantity of Cooling Air Required	X		Equal	
Noise		X		X
Costs	Equal		Equal	
Operation and Maintenance	X		X	
Lubricating Oil Cooler	Equal		Equal	
Lubricating Oil Cleanliness	X		X	
Net Specific Fuel Consumption	Equal		Equal	
Cylinder Wear	Equal		Equal	

mored bulletproof airflow grilles.

4. Operation under the extreme climatic conditions of desert and arctic.

5. Improved logistics due to elimination of two items of supply—water and antifreeze.

We have recently developed an aircooled diesel engine as a replacement for the aircooled gasoline engines.[1] It was a relatively small step from gasoline to diesel in the technical sense, but one that paid dividends in reduced fuel consumption compared to the gasoline predecessor.

The military turned to the diesel principle as a replacement for the gasoline engine[1] since this type of engine would contribute substantially to the overall logistic problem. Miles per gallon for a diesel engine have been well-established at 60% more than that of a gasoline engine; hence, a reduced supply problem or a larger radius of action is possible. The change involves the addition of one extra item of fuel supply; but the possibility of a diesel engine running on gasoline or turbine fuel, which is already being supplied for other purposes, is being examined.

Liquid Cooled versus Aircooled Engines

Table 1 summarizes the more apparent items in the comparison of liquid-cooled and aircooled engine principles and states an evaluation based on our experience.

Plumbing Difficulties—Elimination of plumbing difficulties is an obvious advantage of aircooled engines. Liquid-cooled engines for military purposes have as many as 40 hose clamp connections (the average V-8 passenger car or truck engine has about 12, each a potential point of leakage. In addition, liquid-cooled engines have cylinder head and liner gaskets which are potential trouble spots. These items, together with the water pump, plugs, and other gaskets constitute hundreds of places for leakage troubles. Service department records show that about 20% of all engine failures in liquid-cooled engines are caused by cooling system faults. Nearly all of these are of a type which can be eliminated by the aircooled engine. Offsetting the leakage disadvantage of liquid-cooled engines, there is a sheet metal problem with aircooled engines. This sheet metal does not require tight joints, however. The attachment and stiffening methods must be carefully worked out to obtain long life and ease of assembly.

Antifreeze—Antifreeze problems are listed in Table 1 as a separate item, since they do become quite severe in a great many regions of the world. Some fleet operators are so concerned with the uncertainty of ordinary antifreeze protection that they prefer to completely drain the cooling system in cold weather rather than risk a freeze-up. Others use an equally undesirable procedure of allowing the engine to idle for hours so that it never can cool down. In addition to the freezing problem, liquid-cooled engines suffer from corrosion and clogging of the radiator and cooling system as a result of decomposition of the antifreeze with scale and rust forming in the jackets. The initial incentive to the use of aircooled engines is normally this one item in conjunction with the plumbing problem, and there is no doubt that the aircooled engine has the advantage in this feature without an offsetting disadvantage.

Bulk—Ordinarily cylinder spacing is dictated by the thickness of the cylinder walls and the liquid-cooling space between cylinder bores. Aircooled engines require considerably more space between cylinder bores because of the necessary height of the fins and this means that the overall length of the engine is greater. This length differential between the two types is being reduced by modern trends to high bmep because the large boost in specific output demands stiffer and, therefore, larger crankshafts in proportion to cylinder bores. The net result of these modern trends toward high specific output is that cylinder spacing of both aircooled and liquid-

[1] SAE Transactions, Vol. 65, 1957, pp. 641–656: "Continental 750-Horsepower Aircooled Diesel Engine," by H. H. Haas and E. R. Klinge.

cooled engines is now dictated by crankshaft and crankcase structure rather than space between cylinder bores.

Three classifications of usage can then be discerned:

1. High-performance packages, such as armored fighting vehicles. For these applications, the liquid-cooled engines themselves may be slightly smaller, but the power package turns out to be considerably larger than the aircooled package when the cooling system and ducts are added for desert cooling in the restricted space of armored hulls.

2. Moderate performance applications, such as trucks and earthmoving machinery. In these cases, the more compact liquid-cooled designs are often selected where package bulks may be similar between aircooled and liquid-cooled installations.

3. Low output industrial uses where the aircooled package is undoubtedly larger, but it is also likely that bulk considerations are not very important weighed against such matters as trouble-free running, availability of coolant, and the like.

Weight—General statements regarding comparative weights of liquid-cooled and aircooled engines are difficult to support, as the predominant influence is the objectives of the design and the applications intended. There is a tendency for aircooled engines to be lighter because of the necessary extensive use of aluminum. But this margin partially disappears if liquid-cooled engines are designed with a similar policy and material usage. Because of the need to include radiators and coolant in the weight analysis, liquid-cooled engines are usually found to be at a slight disadvantage on weight compared to an aircooled engine. Fig. 1 shows published weight information of both aircooled and liquid-cooled types presently available, but makes no attempt to evaluate future types. It shows that the demands of military usage leads to engines of lower weight than does the commercial types.

Fan Power and Cooling Air Quantity—It is a comman misconception that aircooled engines use more power for cooling and a higher quantity of air than do the liquid-cooled types. The reverse is usually found in military applications while commercial applications of aircooled engines are usually about equal to the liquid-cooled engines.

Fig. 2 shows typical temperatures measured on one of our 5¾-in. bore aircooled diesel cylinders. If a median temperature of the fins is taken as 260 F and the ambient air on a hot day is 125 F, the temperature differential between the metal and the cooling air is 135 F. This compares with a differential of only 55 F between the radiator (180 F) and the cooling air of liquid-cooled military engines if no pressure system is used. Fig. 3 is a pictorial representation of these conditions, showing the extra equipment required by the liquid-cooled engine.

There are advantages to operating a liquid-cooling system under pressure, in which case the temperature differential between the coolant and air is increased. In general, the military are opposed to pressure systems because of the greater problems of sealing and the danger of losing all of the coolant in cases where the pressure valve pops open. In certain commercial applications it is common practice to use pressure systems of 4–7 psi (corresponding to temperatures of 224–232 F), in which case the airflow and cooling power for the liquid-cooled system approaches the values of the aircooled type.

Fig. 4 gives a group of examples from the combat military field of liquid-cooled and aircooled vehicle installations with the airflow and cooling power compared on the design basis of 125 F cooling air for aircooling and 90–100 F cooling air for liquid-cooling. In this illustration the unshaded extension at the upper part of the liquid-cooled engine bars represents the magnitude to which the airflow and power for cooling would reach for a 125 F day if additional space were available, as would be the case in a normal installation for nonmilitary use. These examples are chosen because the installations were particularly comparable in that vehicle horsepower requirements and other factors were nearly identical. This experience shows that the average power and airflow are down about 50% for the aircooled type under desert conditions. In the commercial field where radiator size is not a factor, these gains are not shown.

There are additional benefits in the case of military vehicles with buried power plants, because concurrently with the reduction in fan power, the reduced airflow permits a saving in grille sizes and duct work necessary for handling the cooling air.

The military vehicle, as opposed to the industrial engine, is designed with wide ambient temperature in mind, since the standard hot day is specified at

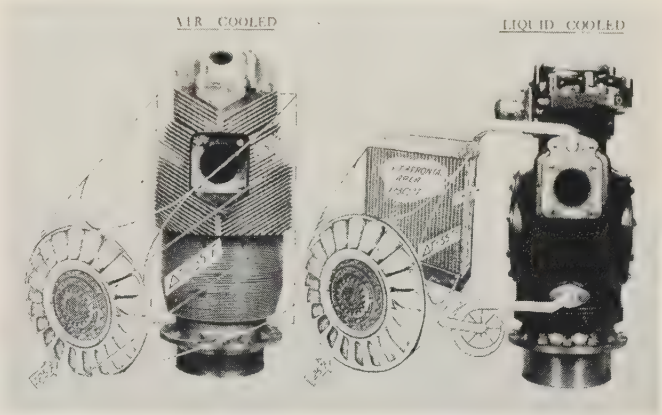

Fig. 3—Comparison of typical cooling systems

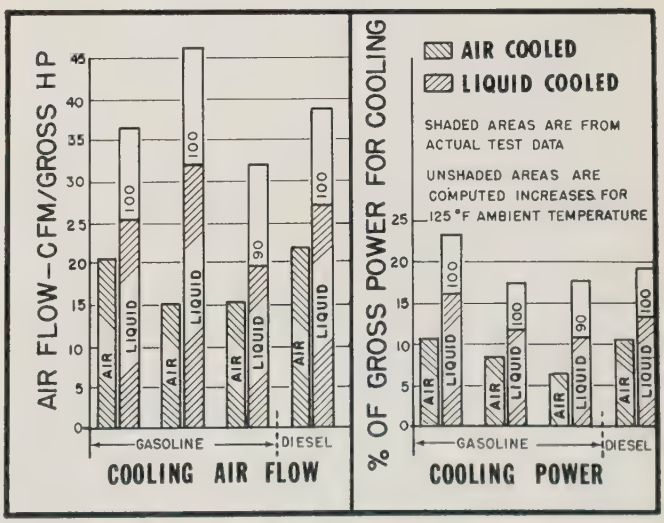

Fig. 4—Military vehicle cooling test results

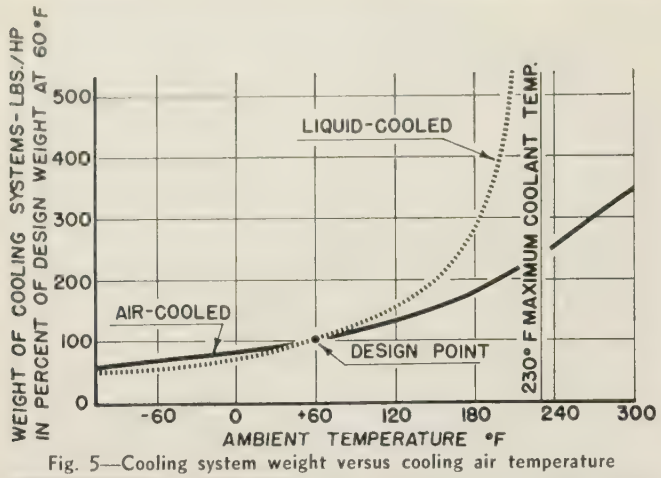

Fig. 5—Cooling system weight versus cooling air temperature

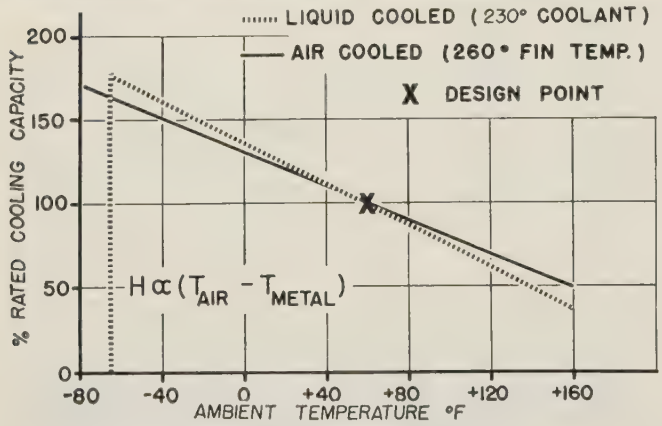

Fig. 6—Cooling system capacity

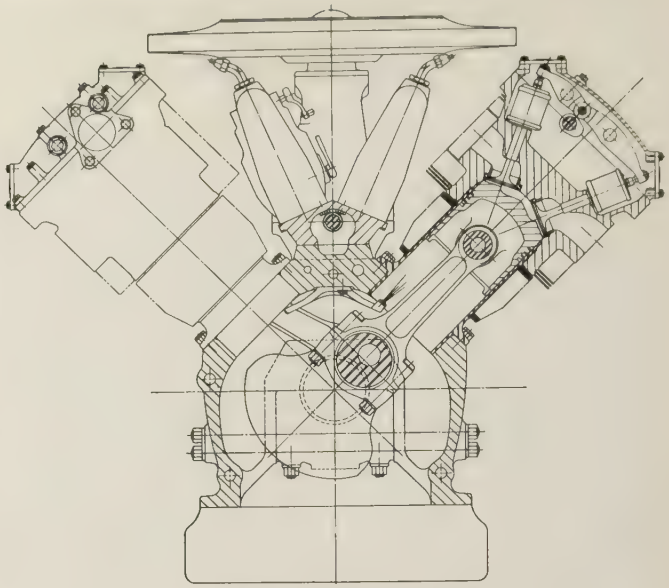

Fig. 7—Fan arrangement on V-type aircooled engine

Table 2—Comparison of Coarse and Fine Finning

	Coarse Finning	Fine Finning
Bore, in.	4.33	5.75
Stroke, in.	4.33	5.75
Displacement, cu in.	63.8	149.1
Hp per Cyl	12	80
Speed, rpm	1800	2400
Hp per Cu In Displacement	0.188	0.536
Bmep	83	177
Cooling Surface, sq ft	3	36
Cooling Surface Internal Cyl and Head Surface	5.85	39.8

125 F ambient and the engine compartment temperature can then be 140 F but with modern airborne equipment this same vehicle could, inside of a few hours, be transported to the arctic with temperatures of – 65 F or lower. It is of interest, therefore, to compare the two types of cooling on the basis of such a range of ambient temperatures. Fig. 5 shows the relative change in weight of cooling system for an engine of constant output as the coolant temperature is varied for each type of coolant, based on each being called 100% at the design point of 60 F. It is apparent that for temperatures below 60 F the liquid-cooled system has advantage over the aircooled engine. Full advantage cannot be taken of this point in practice, however, since even present-day antifreezes will begin to slush at – 65 F.

On the high temperature side, an increase in weight of about 50% occurs in the liquid system if an ambient temperature of 120 F is to be encountered. The aircooled engine requires only about 30% increase in weight of the cooling system for the same ambient temperature.

Another feature of the two types of engines, which is worthy of discussion, is their response to variations in ambient temperatures. Fig. 6 shows the variation in cooling capacity of aircooled and liquid-cooled engines from the standard design day of 60 F ambient to the extremes of cooling air ambient temperature of – 65 to 120 F. It is very apparent that if both cooling systems are designed for 100% capacity at the same ambient temperature, the one having the highest metal temperature in contact with the cooling air will also have the highest reserve when the cooling air temperature increases. The liquid-cooled engine with its maximum temperature of 230 F (pressurized system) at the radiator can cool only at 65% of its designed capacity on a 120 F day, while the aircooled engine still has 70% of its capacity. It may also be noted that these figures are not extreme conditions by any means. Our practice is to design engines with adequate cooling capacity for ambient temperatures of 140 F. Even though this increase in capacity is small, there are installations where it can become quite important.

A natural question to ask at this point is, "Does not this condition penalize the aircooled engine under conditions of arctic operation, when the ambient temperatures are extremely low?" The answer is found in a variety of ways, such as to install a thermostat providing for recirculation of the cooling air in the same manner as liquid is recirculated in the liquid-cooled type. Likewise, shutters to control or limit the flow of cooling air are used, similar to devices used on many liquid-cooled vehicles. The best method, however, is to provide for speed-control mechanism to stop or control the speed of the cooling fan. This method not only maintains a correct engine operating temperature but also reduces the fan power losses; also, it is coming into use for liquid-cooled engines as well.

The ideal coolant should have a high specific heat, a freezing point well below the lowest operating temperature, a boiling point of at least 300 F, be chemically inert, and be available in unlimited

quantities throughout the world. Except for its high specific heat, water does not meet these qualifications; neither does any other liquid. However, air does more nearly meet the requirements of the ideal coolant.

Aircooled engines, particularly V-type engines, lend themselves to utilization of otherwise wasted space for installation of the fans and fan drives (Fig. 7). With this type of arrangement there is no increase in bulk to accommodate the cooling system. Liquid-cooled engines, on the other hand, must be supplemented by large radiators, fans, fan drives, and a piping system. These items add materially to both the bulk and weight of the complete power package. In addition, there is the weight of the coolant itself, which is no mean item.

The two cylinders (Fig. 8) illustrate the difference made in cylinder finning and the resultant change in performance made possible by better finning. The sectional view showing the coarse finning represents a type which is in harmony with the service required and illustrates a very useful class of engine. This engine and the fine finned cylinder are compared to show what is necessary in the way of cooling fin design to make a high output type cylinder. Many other features, such as supercharging and high-strength materials, are necessary in addition to fine finning to achieve the high output shown. The fine finned type is admittedly more expensive, but the increase in power permitted more than offsets the cost increase, so that the result in terms of cost per horsepower is in favor of the fine finned construction. (See Table 2).

Fig. 9 shows the variation of relative cooling power required with the variation of relative weight of the cooling equipment. Marine engines may be considered special cases in that their cooling plant weight becomes very large by comparison with other engines, since these units may be thought to have a whole ocean or lake at their disposal as part of their cooling system. Aircooled military engines are a compromise between cooling power sacrificed on the one hand and bulk increase in an effort to reduce cooling power losses on the other.

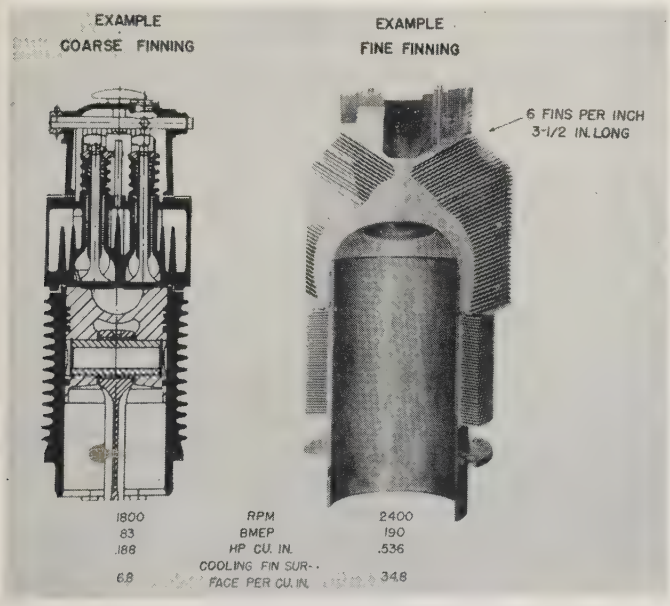

Fig. 8—Comparison of extremes of aircooling cylinder design

Commercial vehicles are different than high-performance military engines since civilian economy dictates quite a different sort of compromise, because relative bulk of the cooling unit is not as important for trucks by comparison with military engines. In general, low relative cooling power means high relative size of cooling system and vice versa.

A description of a typical aircooled engine fan performance is included to show that use of high pressure drops in cooling air systems does not imply low performance fans. This typical assembly (Fig. 10) is a 25-in. tip diameter fan with a 15½-in. hub, or a hub-tip ratio of 0.62. It operates at 5600 rpm and moves 15,000 cfm of 240 F air against 13 in. of water static pressure. The maximum axial width of

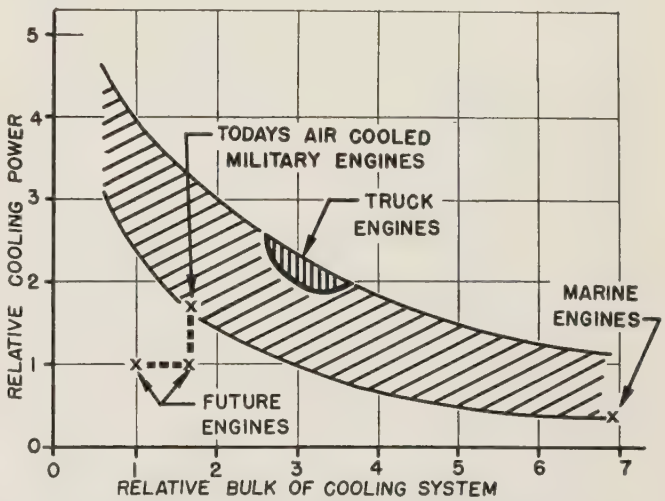

Fig. 9—Effect of size of cooling system on power requirements

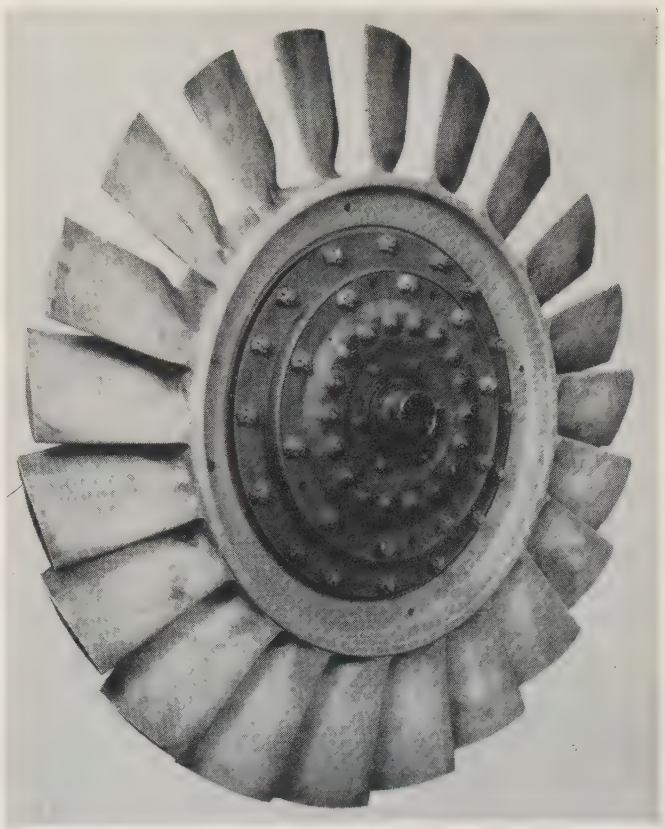

Fig. 10—Aircooled engine fan and clutch

the fan rotor is 2.4 in. Fig. 11 shows the typical fan test wind tunnel performance of this fan rotor at 5600 rpm. The comparatively flat static pressure performance curve at the design point is noteworthy, since this means that operation off design conditions is feasible.

The dimensions of this rotor and its stator were chosen physically to maintain a minimum overall engine height with an airflow velocity about 115 fps through the fan annulus and to allow the mounting of a centrifugally actuated clutch which will unload during water immersion. If increased fan efficiency is required, increase in stator height to improve diffusion is effective.

Noise—Aircooled engines are often more noisy than liquid-cooled designs and frequently this is because of fan noise. Military installation of aircooled engines ordinarily use half of the fan pressure differential in overcoming the duct system resistance and the other half for pressure drop across the cylinders. This demands high tip speed for fans, which in turn is conducive to high noise. A way of greatly reducing sound from the fan is by uneven spacing of the fan blades.

Fig. 12 shows the sound spectra of three fan rotors having 21, 22, and 24 blades. On the 21- and 24-bladed fans, the blades are unevenly spaced around the hub; the 22 blades are evenly spaced. Fig. 12 shows that the energy peaks are higher for the 22 evenly spaced blades in comparison with the unevenly spaced blade fans, and this reduction of sound energy is very noticeable to the human ear. In addition, prominent fan noises have been dispersed and masked by sound hash in the place of distinct reinforcing harmonics. It is the dispersion and masking of predominant frequencies that makes the unevenly spaced design an improvement.

Additional noise considerations are those sounds produced by the valve gear, piston slap, and fuel injector, which are essentially equal in the two types. Minor advantage for the liquid-cooled principle results from some damping of sound by the water layer and extra metal wall.

Costs—As manufacturers of both aircooled and liquid-cooled engines, we have found that there is little, if any, cost differential between liquid-cooled and aircooled engines, given identical conditions. Fig. 13 gives relative sales price of engines in three industries. No attempt is made in this chart to compensate for variation in accessories, materials, life requirements, or other factors which affect cost as indicated in the explanatory table included. The point to be made from this chart is that aircooled types are not greatly different from liquid-cooled engines in cost per horsepower.

Since 50% of the weight of the aircooled engine is of parts of the same type and workmanship as on liquid-cooled engines, this much of the comparison will show equal cost. The accessories comprise an additional 10% of the engine weight and the same type of accessories may be used on either engine. This leaves 40% of the weight to be compared for costs. Our aircooled engine uses aluminum for the cylinder head and crankcase as compared to cast iron for the liquid-cooled engine. Examination of the cost of these materials shows that there is no reason to claim extra cost because aluminum is more expensive on a per pound basis. Aluminum parts of equal strength to cast iron are usually lighter and aluminum is generally more economical to machine so that the net result is often a lower cost. Also, scrap losses are usually less, since the individual cylinder construction of the aircooled engine does not condemn five good cylinders because of one defective spot. The size and design of many aircooled engine parts permits casting by permanent

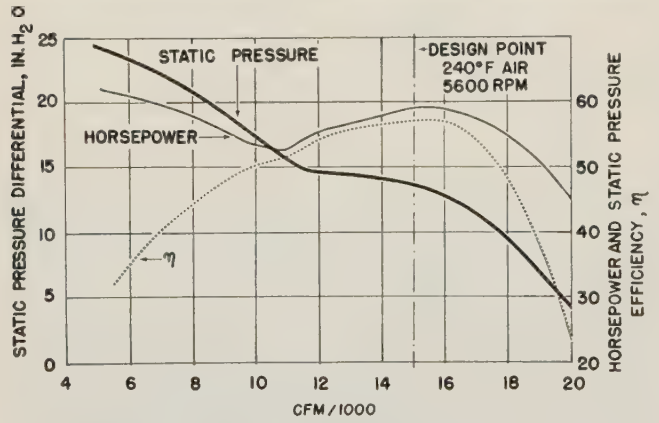

Fig. 11—Performance of typical aircooled engine fan

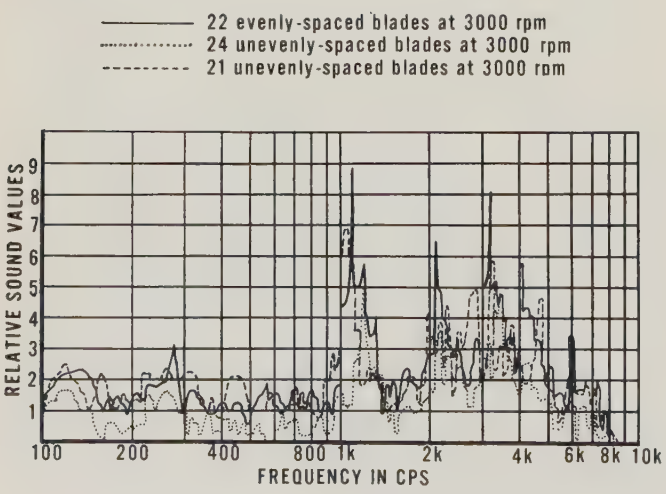

Fig. 12—Sound spectra of typical aircooled engine fans

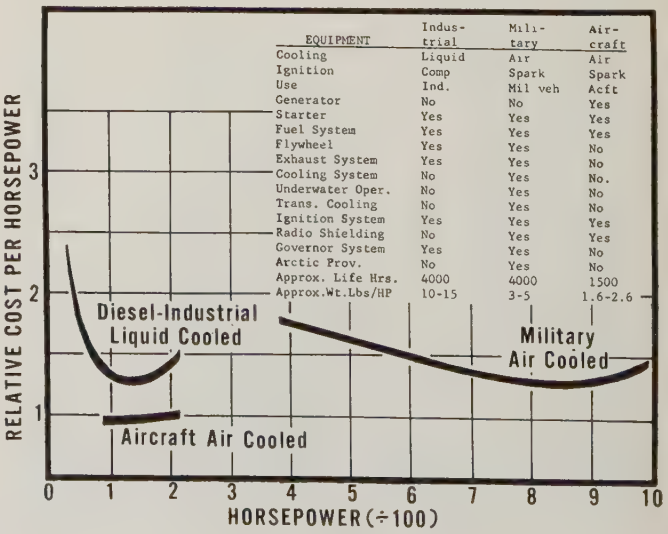

EQUIPMENT	Industrial	Military	Aircraft
Cooling	Liquid	Air	Air
Ignition	Comp	Spark	Spark
Use	Ind.	Mil veh	Acft
Generator	No	No	Yes
Starter	Yes	Yes	Yes
Fuel System	Yes	Yes	Yes
Flywheel	Yes	Yes	No
Exhaust System	Yes	Yes	No
Cooling System	No	Yes	No.
Underwater Oper.	No	Yes	No
Trans. Cooling	No	Yes	No
Ignition System	Yes	Yes	Yes
Radio Shielding	No	Yes	Yes
Governor System	Yes	Yes	No
Arctic Prov.	No	Yes	No
Approx. Life Hrs.	4000	4000	1500
Approx.Wt.Lbs/HP	10-15	3-5	1.6-2.6

Fig. 13—Relative sales price

mold or die casting methods which can give still further economies.

Because of the individual cylinder construction, the automation system of production can be economically applied at a smaller engine unit rate than would be the case with an enbloc design. Combined with the smaller size of the individual cylinder unit, this leads to automation with all of its benefits.

It is concluded that the cost of aircooled vehicle engines when produced at low yearly rates may be equal to and, at high yearly rates, less than the cost of an equivalent liquid-cooled engine with its cooling system on a dollars per horsepower basis.

Operation and Maintenance—The usual experience is that aircooled engines warmup quicker and operate with higher cylinder wall temperatures at light load than do liquid-cooled engines. The reduced warmup period is beneficial as far as cylinder bore wear is concerned and helps to reduce the possibility of fuel or condensation contaminating the lubricating oil and forming acid or sludge. This characteristic is especially valuable when it is necessary to operate with fuels which contain a high percentage of sulphur.

Many test comparisons of aircooled and liquid-cooled engines show that the fuel consumption is unaffected by the cooling type. Fuel consumption is more importantly influenced by combustion principles and friction losses.

It is obvious from an operator's point of view, that it is advantageous to omit the water pump, radiator, and many coolant seals and gaskets. Not only do these parts never cause an interruption in service, but no spares for them need to be carried in stock, and they never need to be maintained nor replaced. The omission of water and antifreeze are of obvious benefit when applied to engines that are operating in unattended stations, where the operators are inexperienced, or where more than one crew operates the same piece of equipment.

The basic design pattern for most aircooled engines is the individual cylinder. This feature makes for smaller parts to store as spare parts and reduces the amount of money invested in spare parts.

Aircooled Diesel Engine

Over the years there has been a considerable background of aircooled diesel experience, especially in Europe, and some previously published data on the results are included here for ease of reference.[2]

The small and medium size high-speed diesel engine was fostered in Europe after World War I due to the need for economical and low cost power plants in automotive and industrial applications. In 1927, Austro Daimler in Austria offered the first aircooled diesel engine for public sale and since that time other companies have provided a continuing program of engine development.

During World War II, the aircooled engine was used to a rapidly increasing extent by the ground forces of both parties. The German Army operated aircooled gasoline and diesel engines in cars, trucks, tractors, and tanks, and the U. S. Army in tanks only. During this period, the outstanding reliability of the aircooling system under the most severe conditions in the arctic, as well as in the desert, was proved most conclusively.

[2] Prepared by Dr. H. H. Haas, Chief Engineer, Diesels, Continental Aviation and Engineering Corp.

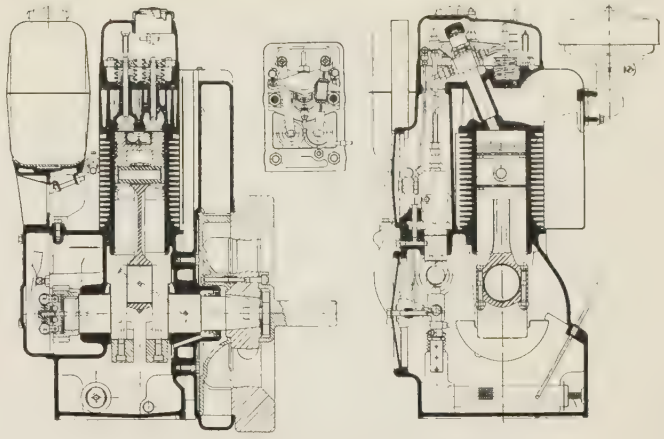

Fig. 14—Lister 6-hp, 1-cyl engine

Table 3—Average Characteristics of Aircooled Diesel Engines

	Industrial[a]	Small Size Tractor[b]	Medium Size Multipurpose[c]	High Performance Military[d]
Bore, in.	3.0–4.5	2.7–3.4	3.5–4.7	5.1–6.1
Stroke, in.	3.0–4.5	3.5–3.8	4.4–5.5	5.5–6.9
Displacement per Cyl, cu in.	21–80	20–33	47–90	113–204
Horsepower per Cyl	2.5–12	6–12	12–28	27–62
Number of Cyl	1–8	1–2	1–12	9–16
Horsepower per Engine	2.5–96	6–24	12–330	245–750
Speed, rpm	1200–1800	2000–3000	2000–2500	2000–2400
Horsepower per cu in.	0.12–0.19	0.26–0.36	0.23–0.32	0.24–0.42
Lb/Horsepower	106–20	19–13	49–9	7–2.9
Bmep, psi	60–85	43–65	78–122	86–138
Piston Speed, ft per min	750–1300	1350–1850	1650–2120	2000–2300
	Characteristic of Type			
Cycle	4-stroke	2-stroke	4-stroke	4-stroke
Illustration Figs.	14 and 15	16–19	20–24	25–29
Combustion Chambers	Divided or open-chamber combustion systems used in all classes.			

[a] Low output, low cost engines for industrial installations.
[b] Small Size, light weight engines, principally for agricultural applications.
[c] Medium Size, large production engine families for a wide range of automotive, agricultural, and industrial applications.
[d] Large Size, high performance engine families essentially for military applications.

After World War II a sequence of aircooled diesel engines appeared on the European market. Because of the unusually wide diversity of design, any comparison of different models produces confusion. However, it seems that intended use and characteristic features permit a classification which may lead to a better evaluation of the various models. The distinguishing features of the four classifications are given in Table 3.

A more detailed description of the features common to each category follows, illustrated by representative engine models of various makes.

Low Output, Low Cost Engines for Industrial Installations—The characteristic features are:

1. Four cycle.
2. Three to twelve hp per cyl.
3. Low bmep (60–85 psi).
4. Low Speed (1000–2000 rpm).
5. One to eight cyl.
6. Long life (5000 hr minimum, without overhaul).
7. Simple, sturdy, but rather bulky and heavy structure.
8. Wide use of cast iron for cylinder head, cylinder liner, crankcase, and other parts.

Engines of this kind show wide acceptance overseas, where their reliability and ease of maintenance are appreciated. Most British aircooled diesel engines belong to this group. The Lister engine (Fig. 14) built in Great Britain, is a typical representa-

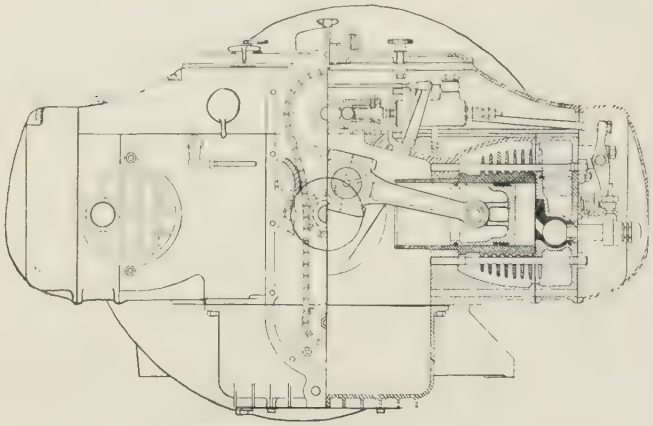

Fig. 15—Enfield 13.3-hp, 2-cyl engine

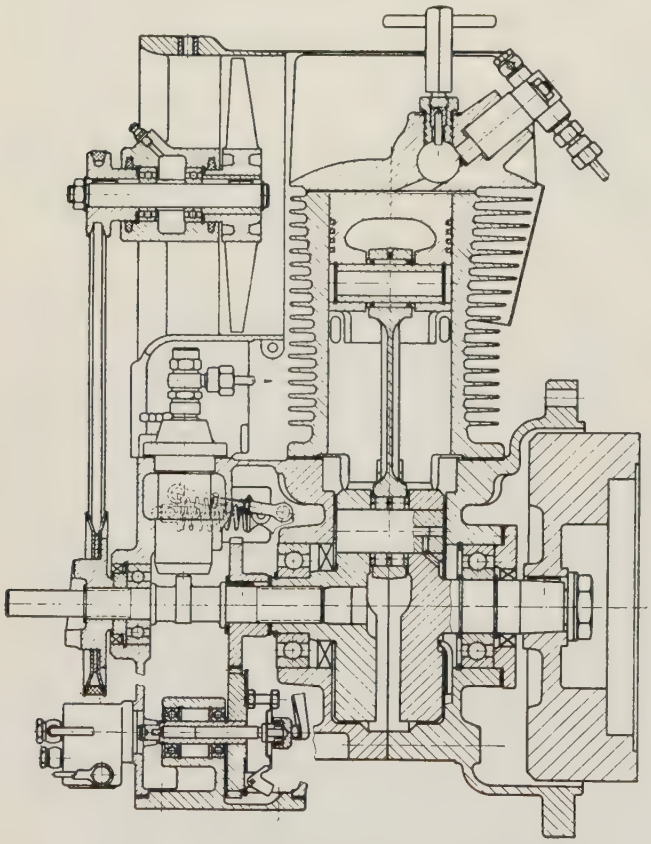

Fig. 16—Two-cycle Hirth 7-hp, 1-cyl engine

tive. Its specifications are:

Bore and stroke—3 × 3½ in.
Displacement—25 cu in. per cyl
Maximum speed—1800 rpm
Maximum net output—3.5 hp
Weight of complete single cylinder package—250 lb

The Enfield engine (Fig. 15), likewise built in Great Britain, represents another version of the same category. Aluminum is used to a somewhat wider extent for cooling fins and shrouds, thus improving performance and reducing weight. Much emphasis is laid on a neat appearance. The opposed

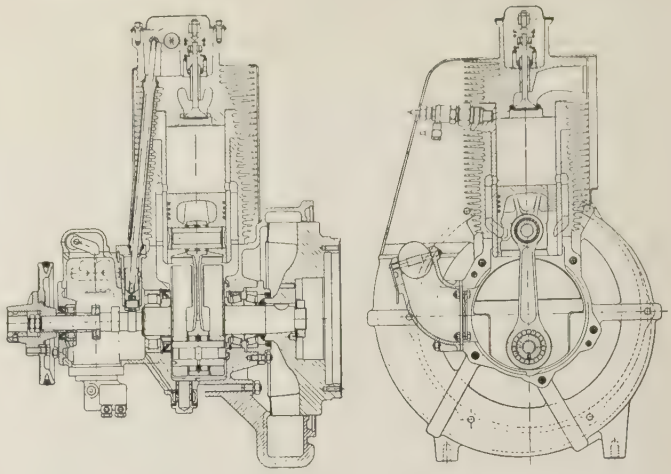

Fig. 17—Two-cycle Stihl 12-hp, 1-cyl engine

cylinder configuration of the twin results in a well-balanced, short engine:

Bore and stroke—3.35 × 3.9 in.
Displacement—34 cu in. per cyl
Maximum speed—1800 rpm
Maximum net output—6.5 hp per cyl
Weight—200 lb single, 310 lb twin

Small Size Air-Cooled Diesel Engines—The need for mechanization of the small farms in Europe led to the development of a special kind of small diesel engine, primarily of German origin. The common features of nearly all of these new engine types are:

1. Two cycle.
2. Six to twelve hp per cyl.
3. Single and twin cyl.
4. Approximately 30 cu in. per cyl.
5. Bmep, 43–65 psi.
6. Speed, 2000–3000 rpm.
7. Crankcase scavenged.

These engines use aluminum die castings to a wide extent and are thus light, simple, and easy to maintain. They are usually designed into a neat, compact power package. Resulting from the employment of crankcase scavenging, the crankshaft is built up from several individual pieces to facilitate space filling counterweights; and the use of antifriction bearings for crank and main bearings to permit metered fresh oil lubrication.

The Hirth engine (Fig. 16) is possibly the most simple design of all. Cylinder head, crankcase, and shrouds are aluminum die castings. The combustion chamber is of the swirl type, and the power package is distinguished by its neat appearance:

Bore and stroke—3.0 × 3.8 in.
Displacement—27 cu in. per cyl
Maximum speed—2200 rpm
Maximum net output—7 hp
Weight, including flywheel, filter, and cleaners—130 lb

The Stihl engine (Fig. 17) is characterized by its uniflow scavenge system. The combustion air enters through an automatic inlet valve in the crankcase. The exhaust gas leaves through an exhaust valve located in the center of the cylinder head.

The cylinder unit is of a rather unconventional design and comprises three parts:

1. A cast-iron cylinder liner, which has cooling fins around the combustion chamber and carries the injection nozzle.
2. A finned aluminum muff which is shrunk on the cylinder liner and includes the scavenging ducts from the crankcase to the cylinder liner.
3. An aluminum cylinder head which carries the exhaust valve and the disk-like combustion chamber.

This design, although more complicated and expensive, improves the scavenging efficiency and avoids the critical exhaust ports controlled by the piston crown. A higher than average continuous output is the result. Also, on this engine all major housings are aluminum die castings leading to a clean outline. The engine is built in single and twin cylinder type:

Bore and stroke—3.35 × 3.7 in.
Displacement—33 cu in. per cyl
Maximum speed—2200 rpm
Maximum net output—12 hp per cyl
(corresponding to 65 psi at 1600 ft per min)

The Triumph engine (Fig. 18) did hold a particular position in the range of these small engines insofar as it was of the so-called "semidiesel" type. It was characterized by the low compression ratio of 11/1 combined with a sufficiently high surface temperature of the combustion chamber located in the cylinder head to initiate combustion. For this purpose, the aluminum cylinder head had a comparatively thick wall with restricted heat dissipation, except at the nozzle seat, which was surrounded by fins to keep the fuel injector cool. The combustion pressure did not exceed 750 psi, thus permitting a light weight structure. Combined with the comparatively high speed of 3000 rpm, a specific unit weight of 13 lb per hp was achieved. The engine had to be started with gasoline until the required temperature of the cylinder head was obtained. A small carburetor and a spark ignition system were provided for this purpose. Recently this engine has been modified to a normal diesel engine with a 16/1 compression ratio to eliminate the carburetor system. It is noteworthy that at the same time the output has been reduced to 10 hp at 2800 rpm. The Triumph's specifications are:

Bore and stroke—3.35 × 3.7
Displacement—33 cu in. per cyl
Maximum speed—3000 rpm
Maximum output—12 hp per cyl
Weight of complete power package—155 lb

The Gutbrod engine (Fig. 19) is another sample of small high-speed engines, shown in the 2-cyl version. The use of crankcase scavenging requires that the crankcase compartments be completely separated, leading to a rather expensive crankshaft and bearing configuration. There are four crankshaft bearings and the crankshaft is built up from seven parts. The engine is built in 1- and 2-cyl models. Its specifications are:

Bore and stroke—2.7 × 3.5 in.
Displacement—20 cu in. per cyl
Maximum speed—2700 rpm
Maximum output—6 hp per cyl
Weight of one cylinder—105 lb

Medium Size, Large Production Engine Families for a Wide Range of Applications—This is by far the predominant group of all aircooled diesel engines; certain families are produced in numbers up to 50,000 engines per year. It is characterized by:

1. Four cycle.
2. Good performance.
3. High speed.
4. Moderate weight.
5. Low price.
6. Ultimate standardization with families of one to twelve cylinders.
7. Aluminum cylinder head secured to the crankcase by necked-down cylinder attaching studs, using

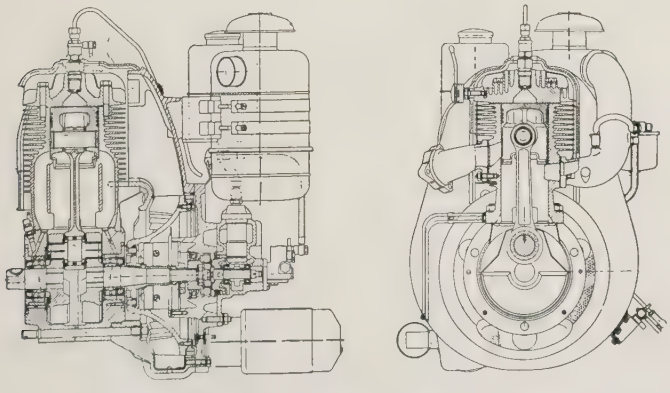

Fig. 18—Two-cycle Triumph 10-hp, 1-cyl engine

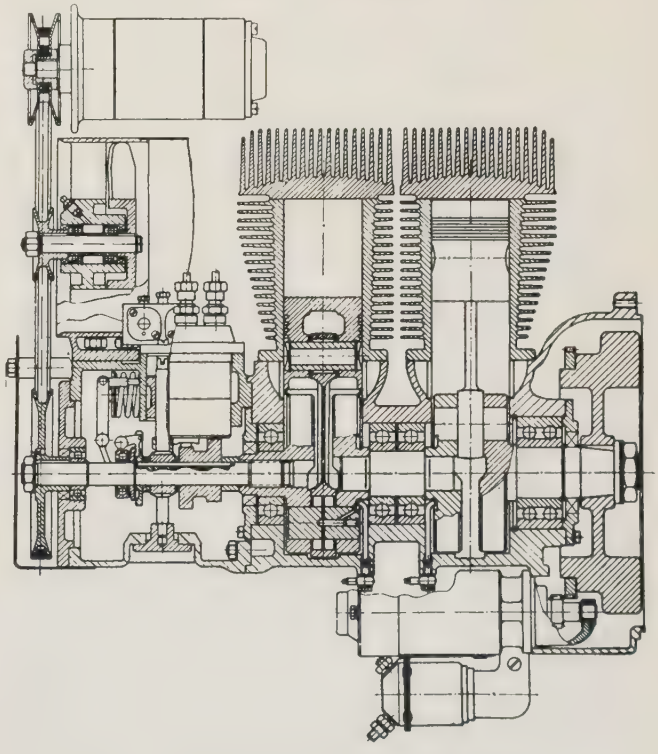

Fig. 19—Gutbrod 12-hp, 2-cyl engine

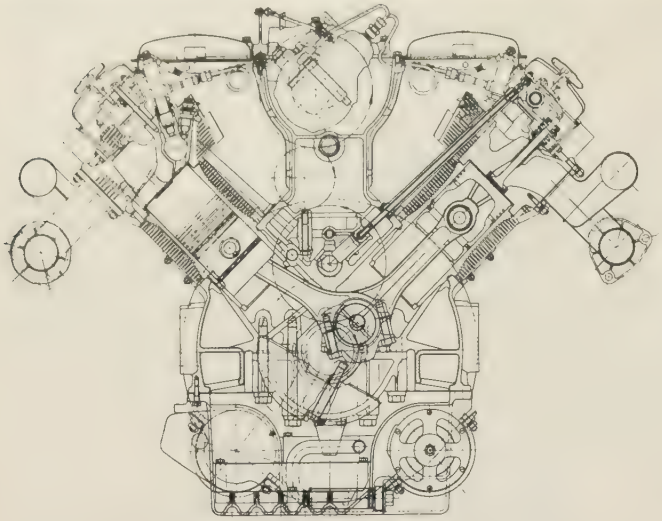

Fig. 20—Deutz V-style 6, 8, and 12-cyl engine

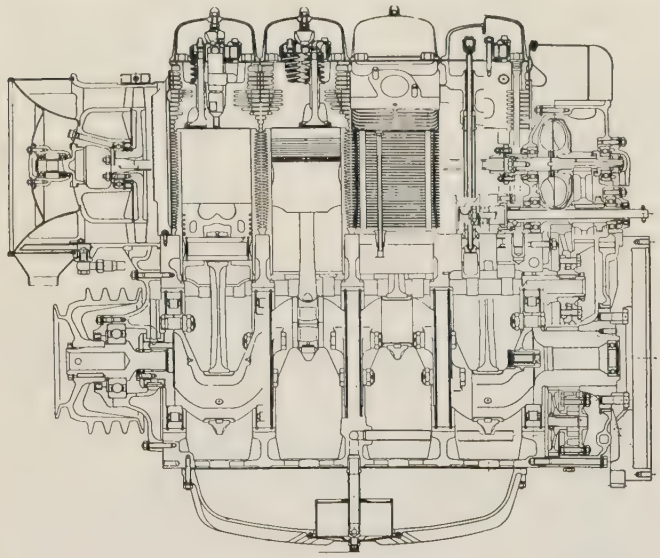

Fig. 21—Tatra 95-hp, 4-cyl engine

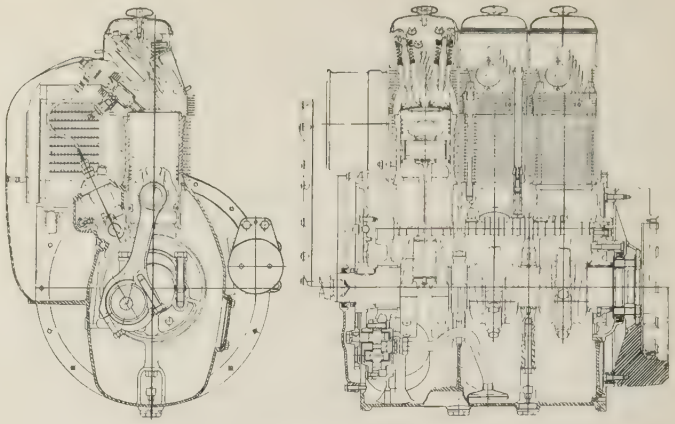

Fig. 22—Kaelble 60-hp, 3-cyl engine

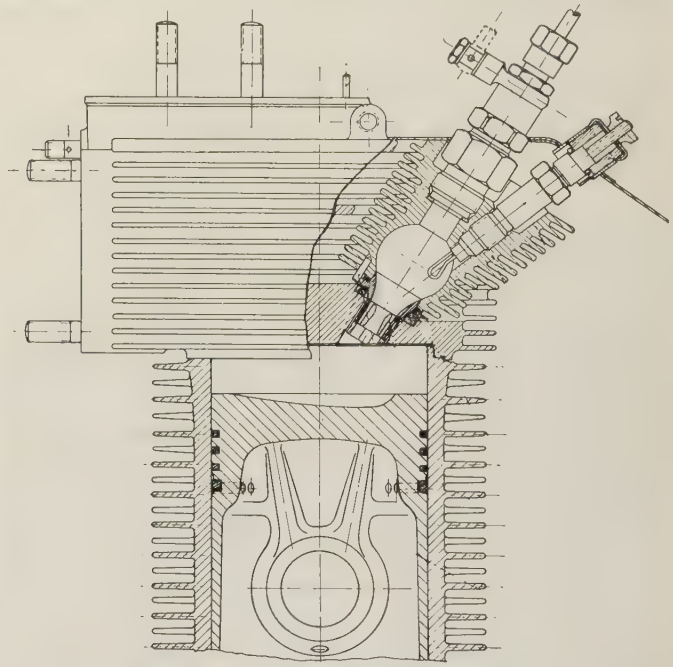

Fig. 23—MWM cylinder head section

the cast-iron cylinder barrel as a spacer under compression.

Typical for this group is the well-known family of Deutz in Germany (Fig. 20). All Deutz engines use a whirl-type combustion chamber, made from stainless steel and cast in the aluminum alloy cylinder head. The engines are designed with a view to low cost and high production volume:

Bore and stroke—4.4 × 5.5 in.
Displacement—81 cu in. per cyl
Maximum speed—2300 rpm
Maximum net output—21 hp per cyl
Turbocharged V-12—26 hp per cyl

Simple machining, wide use of sheet metal parts, and permanent mold castings serve this purpose. It is obvious that the same cylinder parts are used in engines with various numbers of cylinders. This family consists of 1-, 2-, 3-, 4-, and 6-cyl in-line configuration; 6-, 8-, and 12-cyl V-style configuration. The weight varies widely with the number of cylinders from 45 lb per hp for the single cylinder with 16 hp at 1800 rpm to 9 lb per hp for the turbocharged 12-cyl with 310 hp at 2300 rpm. These weight ratios illustrate clearly the influence of the number of cylinders and how carefully specific data must be evaluated if valid conclusions are to be drawn.

Tatra (Fig. 21), in Czechoslovakia, is another pioneer of aircooled engines. Its line of aircooled diesel engines presents many worthwhile features beyond those mentioned in the group specification. Tatra uses an open-chamber combustion system with direct injection. The aluminum crankcase is shaped as a tunnel housing with roller main bearings. The crankshaft is built up from individual cast-steel crankpin units, which are secured together by bolts, clamping the main roller bearings between crankcheeks. This construction results in a short power package, a stiff structure which is essential for aircooled diesel engines, and gives an exceptionally high degree of standardization using two crankshaft units for all in-line and V-style engines.

Another remarkable feature of the Tatra engines

is the control of the cooling air fan and supercharger drives by means of fluid couplings which are automatically operated by the cooling air temperature and engine load, respectively. The considerable fuel savings at part load and protection against overcooling obtained with such an arrangement will probably lead to general acceptance of this feature by other manufacturers. The family includes 1- and 4-cyl in-line and 6-, 8-, and 12-cyl V-style configuration. The two latter ones are also built with a mechanical blower. The engine's features:

Bore and stroke—4.7 × 5.1 in.
Displacement—90 cu in. per cyl
Maximum speed—2000 rpm
Maximum net output—23 hp per cyl
8 and 12 cyl—28 hp per cyl

The Kaelble engine (Fig. 22), manufactured in Germany, is another example of this category. The engine is interesting because of its fin arrangement across the valves and the tunnel crankcase with plain main bearings mounted in special bearing carriers. The combustion system is of the antichamber type with the antichamber cast in the aluminum head. The engine is built in 1-, 2-, 3-, and 4-cyl in-line models:

Bore and stroke—4.5 × 5.1 in.
Displacement—83 cu in. per cyl
Maximum speed—2300 rpm
Maximum net output—20 hp per cyl

Motoren-Werke Mannheim (Fig. 23), another German make, uses a particular antichamber design which permits operation on a wide range of fuels. An interesting feature is the separation of the combustion chamber from the cylinder head, thus simplifying the cylinder head casting. This engine model is planned to be built in 1-, 2-, 3-, 4-, 6-, 8-, and 12-cyl versions:

Bore and stroke—3.86 × 4.72 in.
Displacement—55 cu in. per cyl
Maximum speed—2200 to 2500 rpm
Maximum net output—12 hp to 15 hp

Fig. 24 shows the Swiss Locomotive Works 12-cyl opposed cylinder engine. Although still in the experimental stage, this design demonstrates the potential of the aircooled engine with regard to compactness of the power package. Engine is planned to be built in 4-, 6-, 8-, and 12-cyl models:

Bore and stroke—4.4 × 5.5 in.
Displacement—81 cu in. per cyl
Maximum speed—2200 rpm
Maximum net output—21 hp per cyl

Large Size, High Performance Engine Families, Primarily for Military Applications—The characteristic features of this group are:

1. Four cycle.
2. High performance.
3. Minimum weight.
4. Minimum bulk.
5. High speed.
6. Supercharged.
7. 27–60 hp per cyl.
8. Bmep up to 140 psi.
9. Piston speed 2300 fpm.
10. High standardization, families of 6-, 8-, and 12-cyl.
11. Design characteristics influenced by aircraft engine practice as: Use of aluminum wherever possible; use of high strength materials; cylinder unit, consisting of aluminum cylinder, head shrunk on steel cylinder barrel, secured to the crankcase by flange connection.

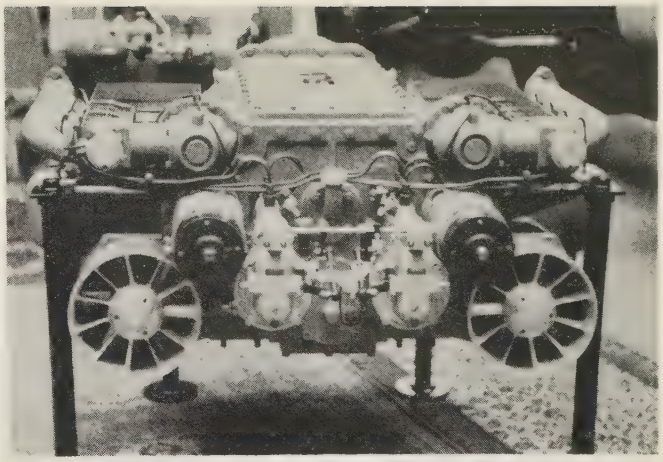

Fig. 24—Swiss Locomotive Works 250-hp, 12-cyl engine

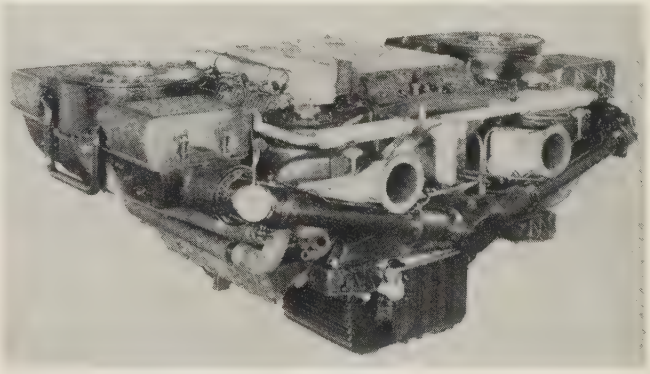

Fig. 25—Simmering Graz Parker 750-hp, 16-cyl tank engine, Austria

It is obvious that such features lead to a higher price per weight unit but not necessarily to a higher price per horsepower. However, the high ratings require periodical overhaul at shorter intervals than the engines for industrial uses and the medium sized engines. Because of the very specific military requirements, widely different engine models have been developed of which the following four examples may demonstrate the diversity of possible approaches.

Figs. 25 and 26 show a 750-hp, 16-cyl, turbocharged tank engine developed by Simmering Graz Pauker in Austria during World War II. The cylinders are arranged in four banks with 135- and 45-deg V-angle, respectively. Two vertical turbochargers provide the combustion air, two suction fans supply cooling air to the cylinders and oil coolers. The crankcase is fabricated steel. Three link connecting rods are attached to one master rod. The crankshaft has four cranks and five main bearings. The combustion system is of the antichamber type, the antichamber mounted separately on the cylinder head to facilitate the cylinder head finning. The engines features are:

Bore and stroke—5.3 × 6.3 in.
Displacement—2240 cu in.
Maximum speed—2000 rpm

Continued on page 224.

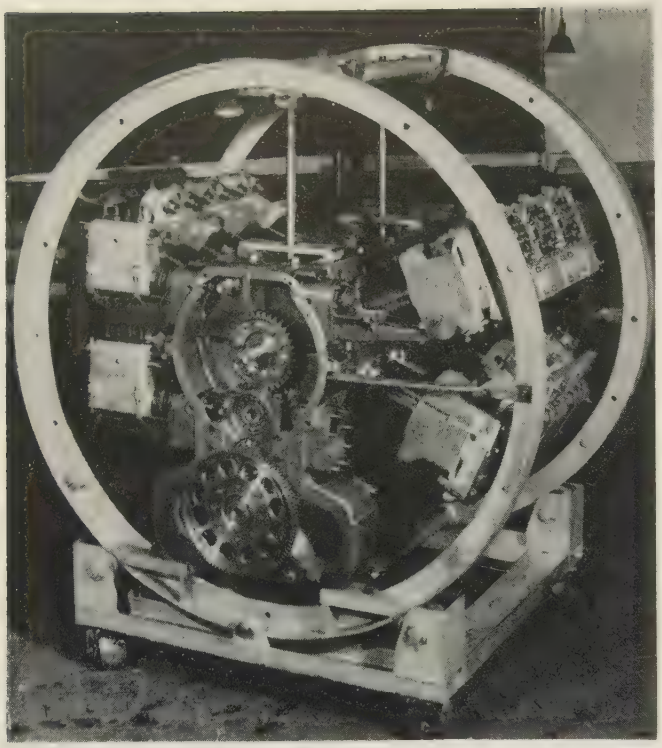

Fig. 26—Simmering Graz Parker 750-hp, 16-cyl bare engine, Austria

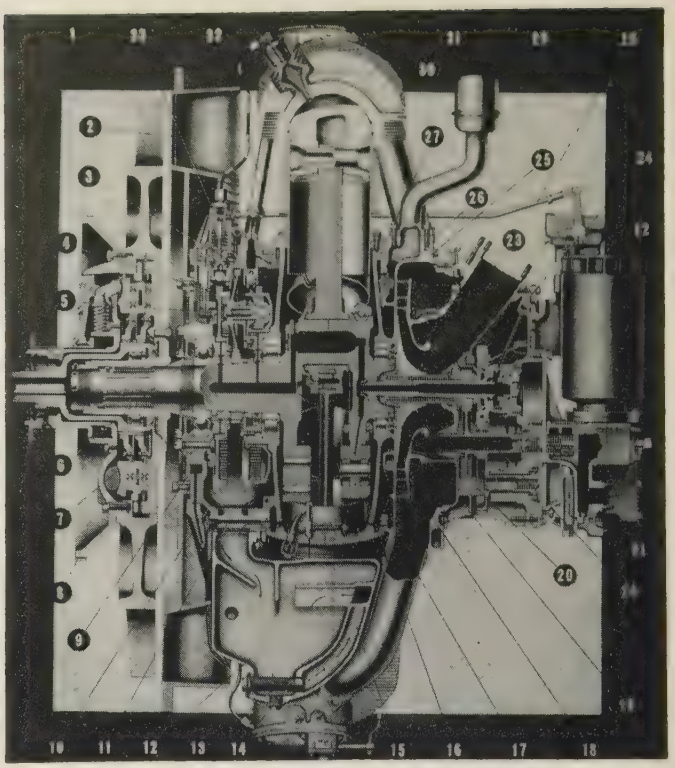

Fig. 27—Caterpillar 450-hp, 9-cyl radial

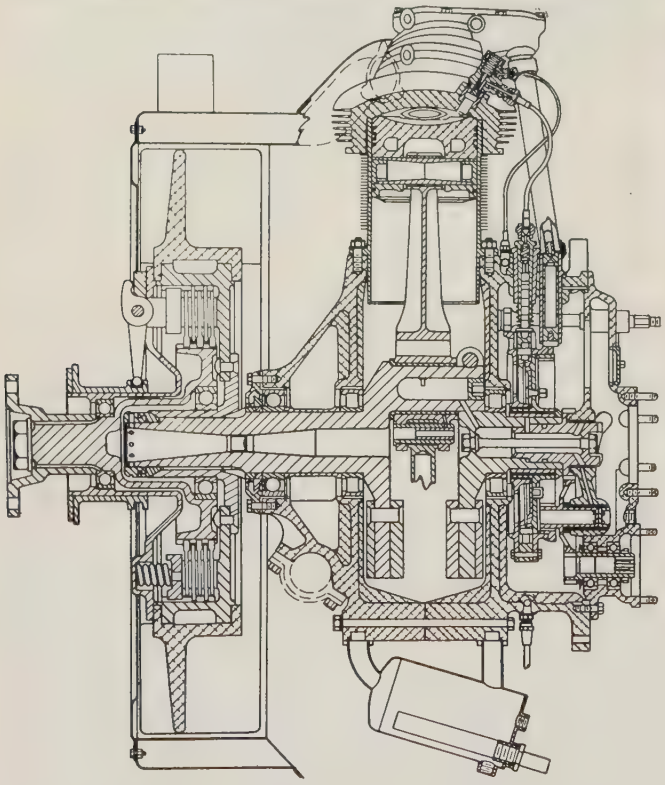

Fig. 28—Guiberson 245-hp, 9-cyl radial

Maximum gross output[3]—750 hp
Net weight—5300 lb (use of aluminum was limited to cylinder head and piston)

The Caterpillar radial tank engine (Fig. 27) was likewise developed during World War II. The engine design follows the usual pattern of radial aircraft engines, increasing the proportions according to the higher combustion loads of the diesel engine.

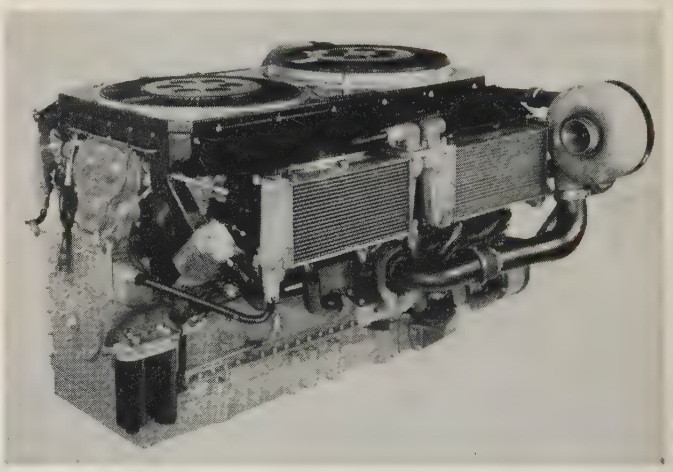

Fig. 29—Continental 750-hp, 12-cyl V-style engine

A finned precombustion chamber is screwed in the cylinder head. The engine is supercharged by a mechanically driven compressor. Its specifications are:

Bore and stroke—$6\frac{1}{8} \times 6\frac{7}{8}$ in.
Displacement—1823 cu in.
Maximum gross output[3]—520 hp
Maximum speed—2000 rpm
No. of cylinders—9
Total weight (approximately)—3200 lb

The Guiberson 9-cyl radial diesel engine (Fig. 28) was produced in small quantities before World War II for United States light tanks and undoubtedly would have been continued but for the policy decision to discontinue supply of diesel fuel for combat vehicle use. Its features were:

Bore and stroke—$5\frac{1}{8} \times 5\frac{1}{2}$ in.

[3] For tank engines gross maximum ratings are given because the required cooling horsepowers are widely dependent upon the particular installation.

Displacement—1020 cu in.
Maximum gross output[3]—245 hp at 2200 rpm
Weight—700 lb

The new Continental 750-hp tank engine (Fig. 29) has been described thoroughly in a recent SAE paper.[1] The engine is listed here as a representative of the V-style configuration which leads to a particularly compact power package with 5 lb per gross hp and 10 hp per cu ft of volume occupied by the power package:

Bore and stroke—5.75 × 5.75 in.
Displacement—1790 cu in.
12-cylinder
Maximum speed—2400 rpm
Maximum gross output[3]—750 hp
Weight of complete package—3800 lb

Summary

Aircooled diesel engines are coming into increased usage commercially and continued military applications of the principle can be expected because of the special demands of this service. Aircooled diesel engines are built with a great variety of features showing that most of the well-proved designs from liquid-cooled engine development may be used when applied carefully. The aircooled principle shows advantages in space utilization and in ability to handle hot and cold ambient temperatures. The liquid-cooled engines may be expected to continue their present commercial popularity until more extensive service records prove that the aircooled principle is superior.

Additional References

1. *The Engineer,* Vol. 191, April 6, 1951, pp. 457–460: "Aircooled Deutz Diesel Engine."
2. *Product Engineering,* Vol. 23, January, 1952, pp. 150–151: "Diesel Engine Cooled by Forced Air."
3. SAE Transactions, Vol. 61, 1953, pp. 422–441: "Contemporary European Aircooled Diesel-Engine Practice," by W. H. Worthington.
4. *Automotive Industries,* Vol. 112, Jan. 1, 1955, pp. 92, 106: "Aircooled Automotive Diesels Introduced in England," by David Scott.
5. *The Engineer,* Vol. 199, May 6, 1955, pp. 643–645: "Air- and Water-Cooled Diesel Engines," by Helmut Meyer.
6. "The High Speed Aircooled Diesel Engine—Past and Present," by Richard Kloss. Paper presented at SAE New England Section Meeting, March 6, 1956.
7. *Oil Engine and Gas Turbine,* Vol. 24, January, 1957, pp. 346–347: "Aircooling for Vehicle Engines."
8. "European Developments in Small Aircooled Engines," by W. E. Meyer. Presented at SAE Summer Meeting, Atlantic City, June 2, 1957.

DISCUSSION

Describes Advantages of Aircooling on Military Vehicles

—Capt. Richard H. Sawyer
Ordnance Tank-Automotive Command, U. S. Army

DESPITE the technical advantages which are more or less easily shown to accrue on aircooling, as far as the Army is concerned the basic advantage is reduction of logistic burden by the elimination of the fluids required by more conventional cooling systems.

This advantage is emphasized when one considers that military vehicles must be expected to operate in deserts and in Arctic areas without essential changes to meet different climatic conditions.

With the advent of very high output conventional engines or where high output is to be achieved through the use of unusual engine configurations to gain high displacement in a relatively small volume, aircooling appears to be put to a severe test. The army is attacking its dieselization program through parallel approaches involving aircooling and liquid cooling.

Military requirements for multifuel operation consider the ability to burn 83/91 octane gasoline, as well as JP-4 or conventional diesel fuels, as an essential criterion. Operation on gasoline must be achieved at a reasonably high power level and obtain a temperature range whose lowest value must be in the neighborhood of 0 F.

ORAL DISCUSSION

Reported by E. R. Donner

Standard Oil Co. of California

Wallace M. Brown, Pacific Car & Foundry Co.: Present design of the chassis makes it almost impossible to install aircooled engines in present day trucks.

Dr. F. W. Lohmann, Kloechner-Humboldt-Deutz AG and Diesel Energy Corp.: It is true that present-day design does not lend itself to installing aircooled engines where frames are designed for liquid-cooled engines.

W. P. Eddy, 1957 SAE President: What in your opinion has been done to develop a suitable liquid to operate as a coolant at 250 F?

Mr. Bachle: The coolant now available is ethylene glycol cooling up to 275–300 F. Trouble is encountered in the plumbing to handle these elevated temperatures.

Robert Niels, J. Niels Lumber Co.: We have a starting problem with fuels and lubricants at – 40 F. Lubricants that are conducive to starting at low temperatures do not lend themselves to a safety factor at higher ambient temperatures.

Capt. Sawyer: The Army calls for fuels and lubricants to have a usable range from – 65 to 125 F ambient temperatures.

Henry Ard, Potlatch Forests, Inc.: How is wear rate affected by aircooled engines?

Mr. Bachle: Aircooled engine fins can be tailored so as to give a maximum of cooling to all points.

Lloyd E. Johnson, Caterpillar Tractor Co.: We have trouble keeping dust and the like from clogging radiator. How do you control this in aircooled engines?

Dr. Lohmann: Aircooled engines have high velocity of air passing through the fins, thereby assisting to keep the fins clean. However, this does not help too much with straw and sticks, tumbleweed, and the like.

Mr. Bachle: Engines with a long fin design set up vibration which assists in keeping fins free from dust. However, on landing boats salt spray and/or water will clog fins very rapidly.

Fred H. Dodson, Division of Forestry Fire Control, State of California: How do you eliminate sand blasting in some sandy soil operations?

Mr. Bachle: Sand does no damage to cylinders, only to the fan. There are coatings on the market that will protect the fan.

Mr. Eddy: Fatigue failure from vibration is a problem in large aircooled engines. How do you compensate for this in the engines you refer to?

Mr. Bachle: The fins on the large engines are machined, whereas the fins discussed in my paper are cast. This gives them a larger and sturdier base.

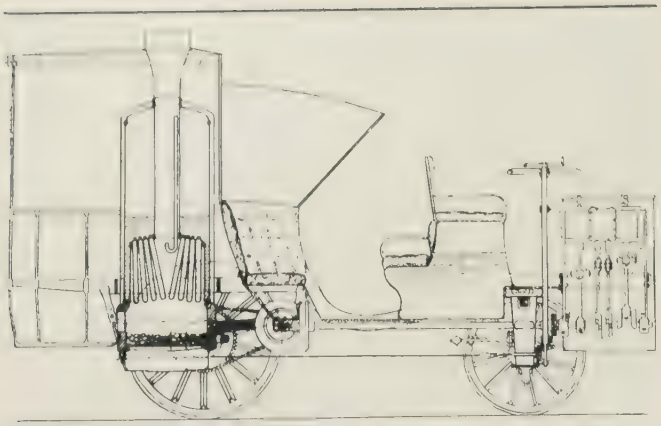

Fig. 1—Longitudinal section of "La Mancelle," 1875

REAR-ENGINE

The

Fernand Picard, Regie Nationale des Usines Renault

This paper was presented at the SAE National Passenger-Car, Body, and Materials Meeting, Detroit, March 5, 1957.

THE development of the rear-engined motor car which has taken place in Europe during the past 10 years may be surprising to many persons, but it is not to those engineers who know the history of the industry. Rear-engined cars have always been built, and if their numbers remained relatively small during the first half century of the motor car, it is because its degree of evolution did not permit drawing on all the advantages of the rear-engine formula.

In the "prehistoric" days of the motor car, that is, the years preceding 1880, only the steam powerplant was used. As it did not comprise a single unit, its constituents were divided on the vehicle—the engine on one end and the boiler on the other. The "Mancelle (Fig. 1), one of Amédée Bolée's first cars, had the boiler at the back and the engine in front with a longitudinal driveshaft and bevel gears. The Bollée prototypes, such as the "Rapide" in 1881, reversed the position of the units in order to simplify the mechanism by eliminating the driveshaft and bevel gears. Further, the steam engine needed no gearbox, and it was simpler to place the engine close to the wheels (which it drove almost directly) when the size and weight of the boiler did not require another arrangement.

With the internal-combustion engine operating on gas or liquid fuel, the requirements for the grouping of the mechanical units changed. The engine became more compact; there was no longer any boiler. However, a gearbox became a necessity. As an inheritance from the horse-drawn vehicle, the front wheels were used for steering, so it was natural to place the engine as close as possible to the rear

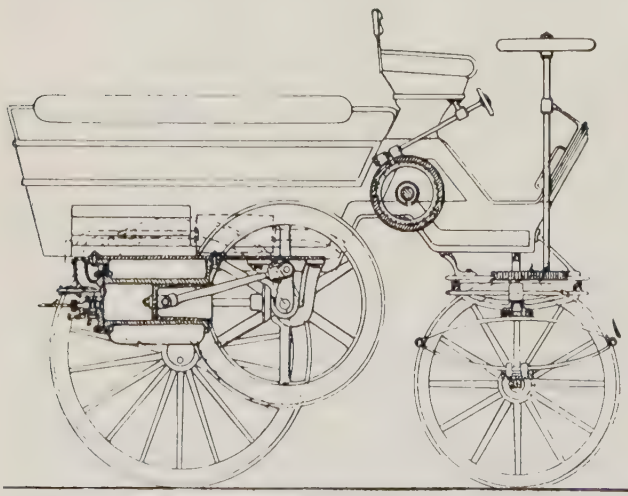

Fig. 2—Hunting Brake of Edouard Delamare-Debouteville, 1883

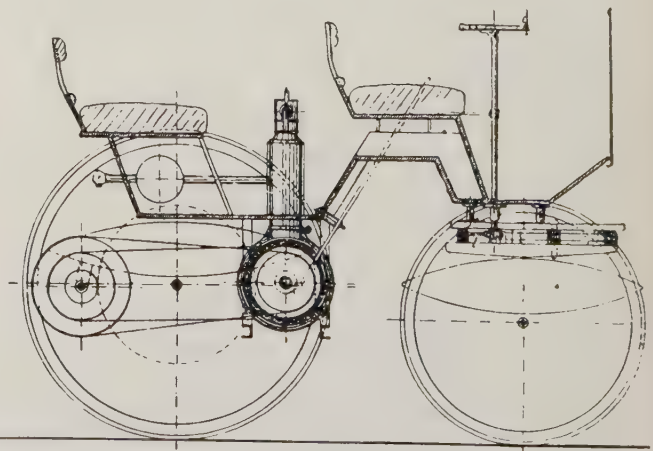

Fig. 3—Gasoline Victoria of Gottlieb Daimler, Germany, 1886

MOTOR CARS

European Point of View

wheels, which did the driving. The problem of the gearbox itself was most easily solved by mounting the engine so that its axis was parallel to the rear axle and by driving the rear wheels by a system of belts and pulleys or chains and sprockets of different diameters. Conforming to this disposition of units, nearly all of the cars built between the years 1880 and 1895 had the engines at the rear: the "Break de Chasse" (Hunting Brake) with gas fuel built by Edouard Delamare-Debouteville in 1883 (Fig. 2), the gasoline Victoria by Gottlieb Daimler in 1886 (Fig. 3), and the gasoline motor car of Karl Benz in 1886 (Fig. 4).

Only a few of these cars were built. However,

THE author traces the history of the rear-engined motor car, from Amédée Bollée's first car in 1875 to Dr. Porsche's present-day Volkswagen. He then discusses the advantages and disadvantages of the design, describing the solutions on the Volkswagen, Fiat, and Renault of the present.

Emphasizing that the rear-engine arrangement is most successful on the small car of less than 1300-cc piston displacement, the author mentions the following advantages: simplicity of design, light weight, economy of fuel consumption, ease of parking, excellent road holding, less danger from collision. Among the difficulties of the construction are weight distribution, engine cooling, air filteration, limited baggage space, and operation of clutch, throttle, and starter.

The production of rear-engined passenger cars in Europe has increased from 2.6% of total European production in 1947 to 26.6% in 1956, an indication of the expanding demand for the small economy car.

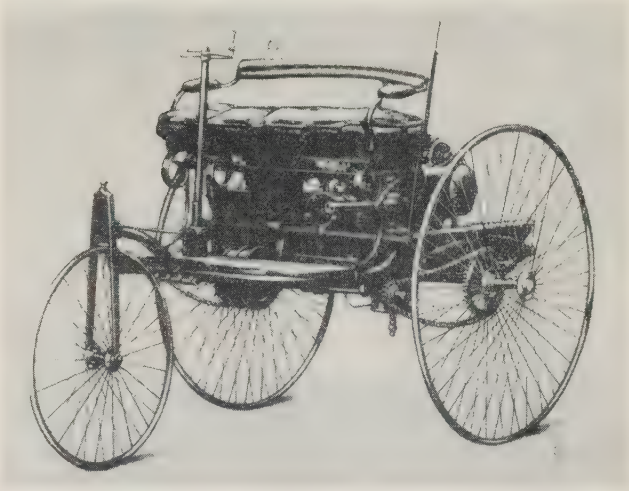

Fig. 4—Benz little gasoline car, Germany, 1886

Fig. 5—Rear-engined Panhard quadricycle, France, 1893

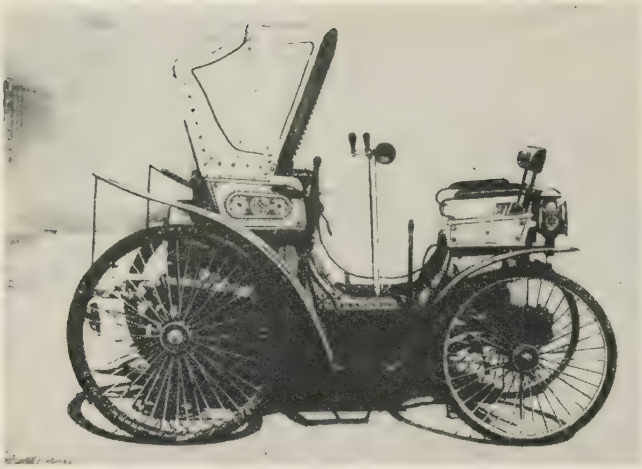

Fig. 6—Peugeot car with 2¾-hp Panhard engine, 1894

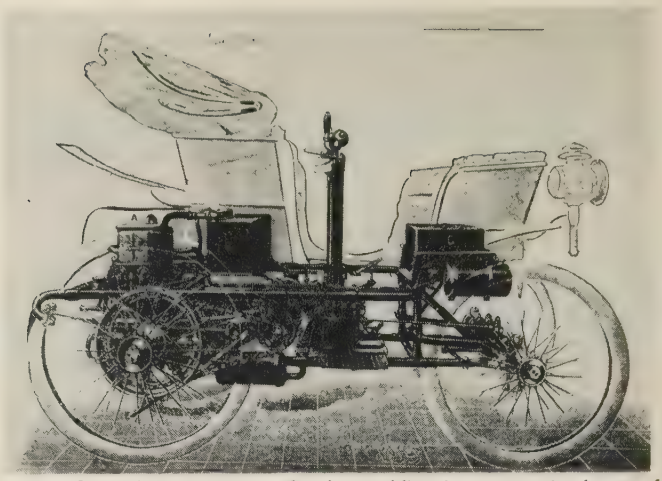

Fig. 7—General arrangement of subassemblies in rear-engined car of Rochet, 1896

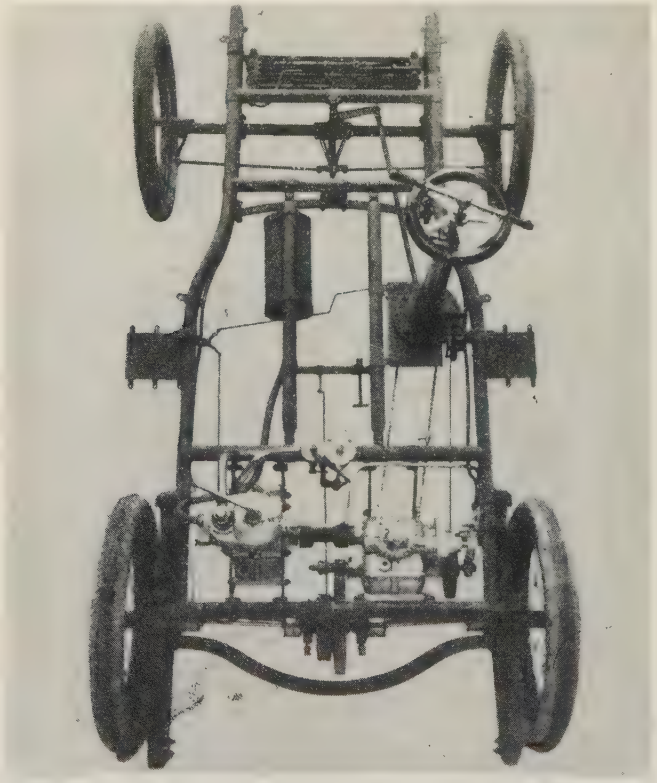

Fig. 8—Chassis for 3½-hp de Dion Bouton car, 1899

soon the motor car was being produced in quantities for the public. The rear-engine arrangement was usual and continued to the end of the century.

This was the case with Panhard who continued it in his light car until 1893 (Fig. 5), of Peugeot with his 2¾-hp car in 1894 (Fig. 6), and of Rochet in 1896 (Fig. 7). On these cars one finds the same disposition of units as found today, made possible by the creation of a real gearbox, the lengthwise placement of the engine, and the placement of the gearbox, bevel gear, and differential in front of the engine. However, because the engine did not overhang the rear wheels a chain drive to the wheels was needed. This also provided the necessary gearing.

In spite of the gearbox, de Dion in 1899 kept the initial placing of the engine with its crosswise axis, and inaugurated the formula of the de Dion rear axle in which the wheels were carried on a dead axle and driven by universally jointed shafts from a chassis-mounted differential (Fig. 8).

This same disposition of units is found in the United States on the curved-dash Oldsmobile in

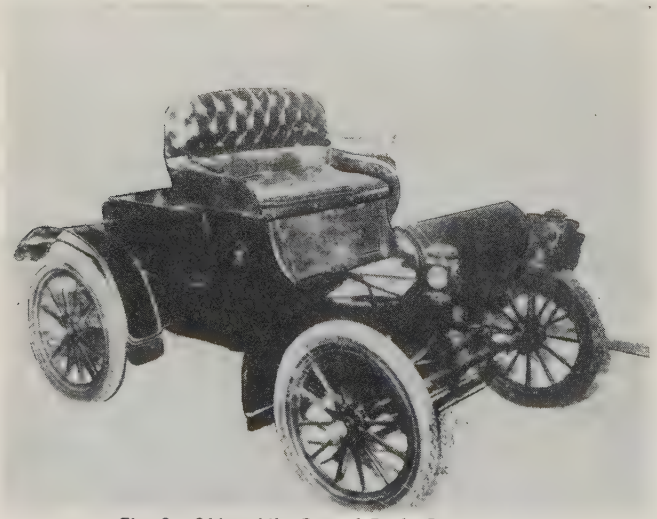

Fig. 9—Oldsmobile Curved Dash, Detroit, 1901

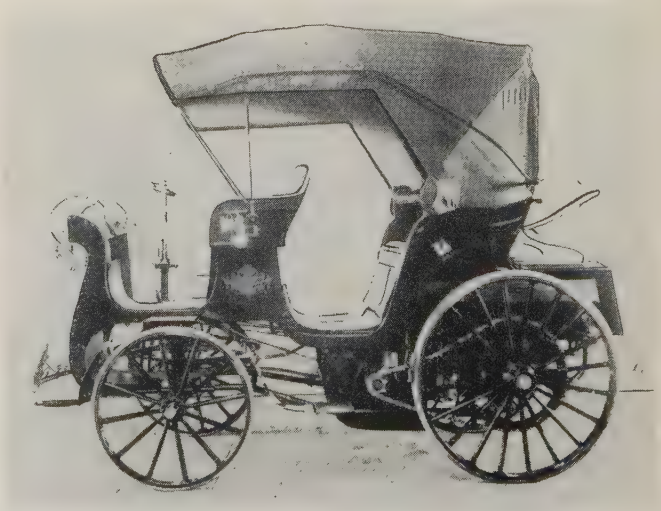

Fig. 10—Tatra car with rear engine, 1897

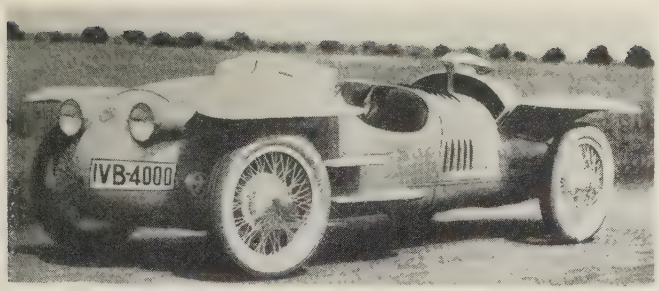

Fig. 11—Benz Tropfenwagen racing car, 1923

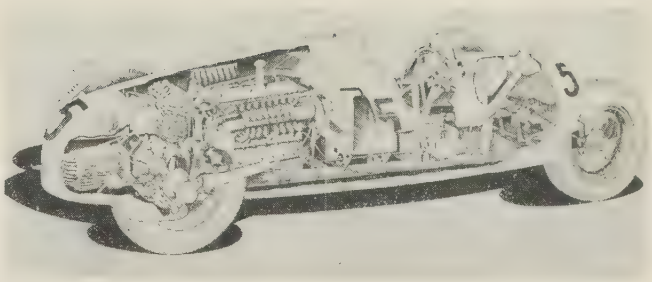

Fig. 12—Auto Union racing car, 1934

1901 (Fig. 9). We note that Tatra, who was to remain faithful to the formula for a long time, built rear-engined cars in 1897 (Fig. 10).

Post-1900 Development

This Golden Age for rear engines, which had also been uniformly adopted by the steam cars with the boilers in front, ended with the century. In the great races—Paris–Berlin 1901, Paris–Vienna 1902, Paris–Madrid 1903—front placement of the engine became general. A number of factors seem to have played a role in this change. The gearbox and the development of gearing in general (making the gearbox capable of both transmitting and increasing torque) gave a greater facility and choice in the location of units. It was natural, then, to try to divide the dead weight between the two axles. The control of the gearbox and of the clutch was easier and simpler when these units were placed near the driver. Cooling was also more efficient in front, and it was natural to place the radiator in the open air. However, none of these arguments would have been decisive without the general increase in power, the result of heavier engines. This meant that part of the weight had to be carried on the front end, which in turn posed a cooling problem. At this period when the motor car was a luxury or a competition vehicle, such evolution was dictated by logic, simplicity of structure, and economy.

We have to await the period between the two world wars to see the rear-engined motor car reappear. Among the numerous experimental cars, of which there were more than 30 prototypes in the world, there were three distinct groups. First was that of racing cars (which we will not discuss in this paper) which sought in the "everything at the rear" formula either an increase in driving-wheel adherence and traction or a larger housing for the powerplant. In fact, this usually was rather a "between-the-axles" mounting than a true rear-engine placement. We cite only the 1923 Benz Tropfenwagen and the 1934 Auto Union and the Alfa Romeo 512 derived from it (Figs. 11 and 12).

The second group comprised vehicles or prototypes of large deluxe or finely finished medium-sized cars. In France we find only the 1936 Dubonnet Narval with a V-8 engine (Fig. 13). However, in Britain we note the Mastra with a 6-cyl opposed engine, the 13-hp Crosley, and above all the celebrated Damistown Burney, a 3-liter piston displacement car in which the Prince of Wales made a trip through Canada (Fig. 14). In the United States there were the Sterkenburg (Fig. 15), the body of which was created by Briggs and was used on the 1933 Lincoln Zephyr; and the Stout Scarab, a few

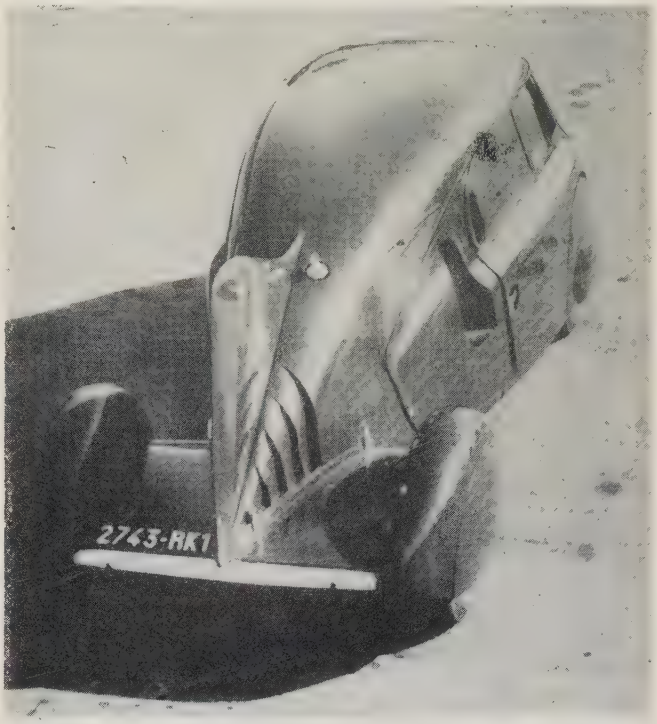

Fig. 13—Dubonnet Narval, 1936

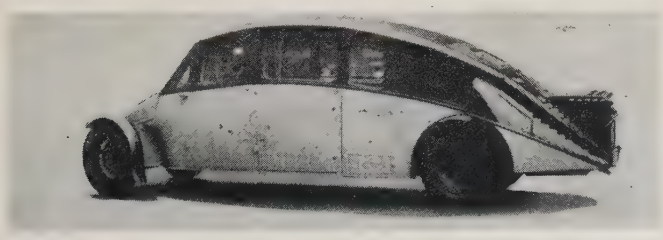

Fig. 14—Rear-engined Damistown-Burney, 1935

Fig. 15—American rear-engined Sterkenburg, 1933

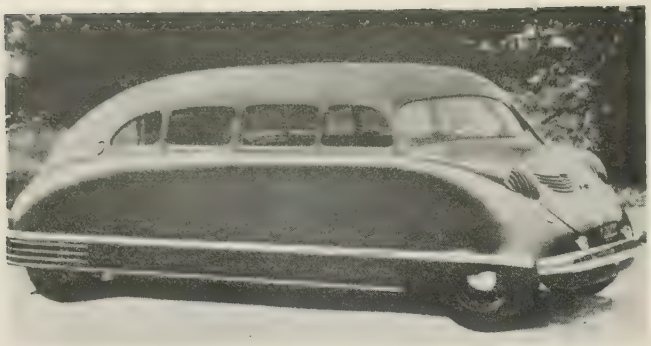

Fig. 16—American rear-engined Stout Scarab, 1936

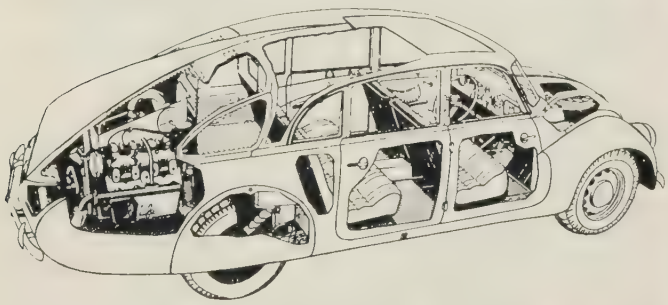

Fig. 17—Tatra with rear 4-cyl V-type engine, 1938

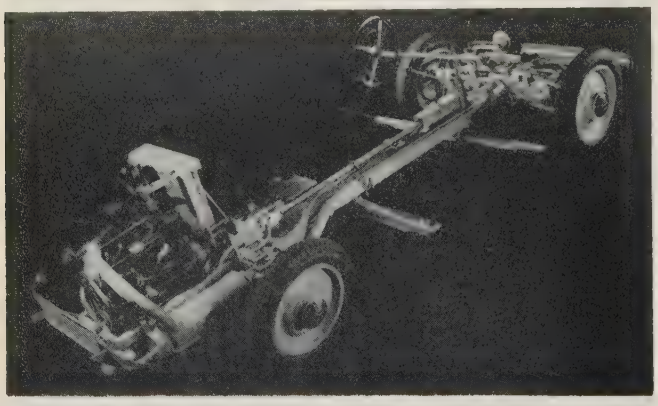

Fig. 18—Chassis view of Mercedes 170H with rear 4-cyl in-line type engine, 1938

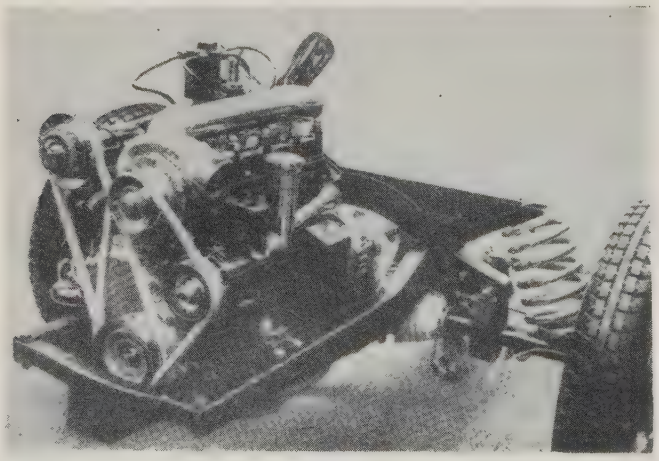

Fig. 19—Rear-driving unit of Mercedes 170H

of which came out in 1936 (Fig. 16). Neither of these cars was developed commercially. The only rear-engined cars of this group which were actually placed on the market were two Continnental types, the Tatra 77 (Fig. 17) and the 4-cyl, 1700-cc displacement Mercedes 130, which afterwards became the model 170H. It is interesting to note that the disposition of the mechanical units of this car (Figs. 18 and 19) have become classic on the Volkswagen and the Renault—motor overhanging the rear wheels, the gearbox and differential casing forming a unit with it and pointing forward, the differential being between the engine, and the gearbox with the wheels being carried on swing axles.

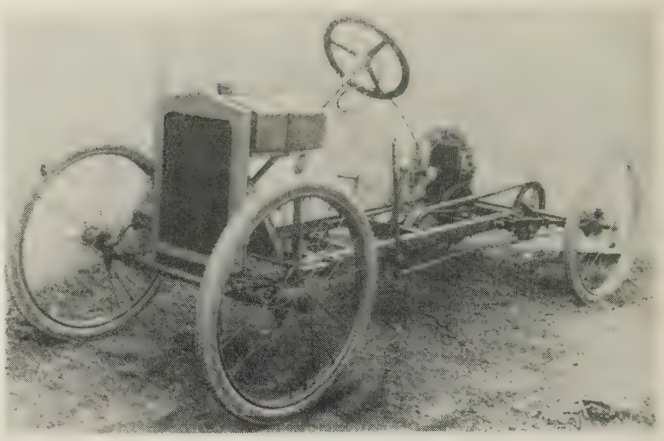

Fig. 20—Rear-engined Autocyclette cyclecar, France, 1923

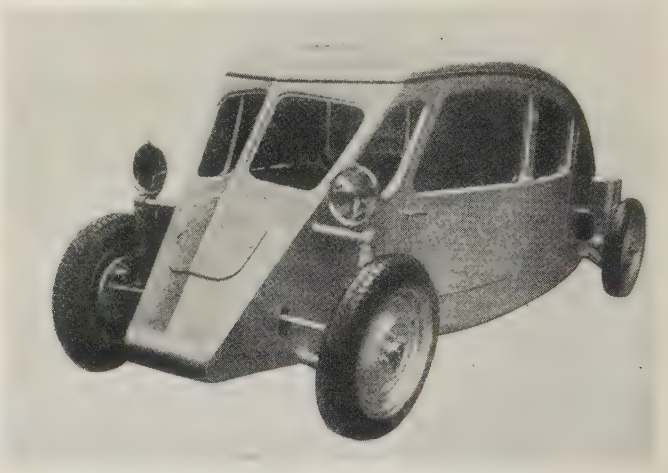

Fig. 21—Claveau Regina, France, 1925

The third group is the most interesting because the rear-engined European economy cars descend directly from it. Here we find a whole line of tiny cars, often prototypes without any commercial future. However, from time to time bold attempts were tried in an effort to make them commercially successful. These required a rear-engined layout as the solution to lower manufacturing costs. The Autocyclette (Fig. 20) was one of many models of the cyclecar which flourished immediately after World War I. However, the time was not right economically to make a place for this type of motor car, the basic idea of which is now found in the scooter.

Designs and models between the bicycle and deluxe motor car, aimed at in-between clientele, had greater success. In France there were only prototypes: Claveau showed a well-designed and well-built series during 1923–1927, of which the Regina was put on the market in 1924–1925 (Fig. 21). However, it was in Germany and in Britain that the most successful small cars were developed and pro-

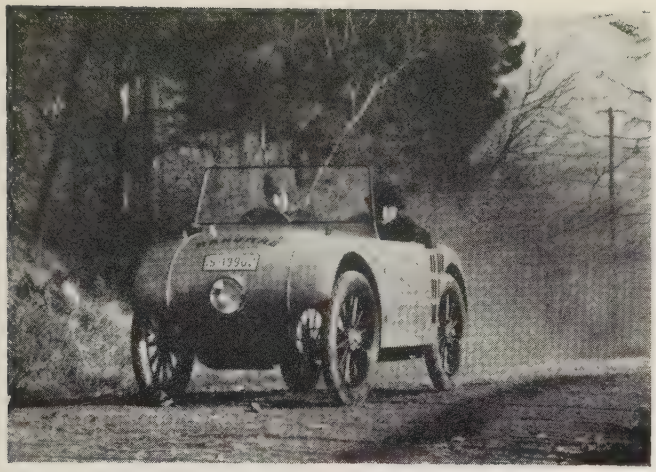

Fig. 22—Popular Hanomag rear-engined car, Rollende Kommisbrod, Germany, 1925

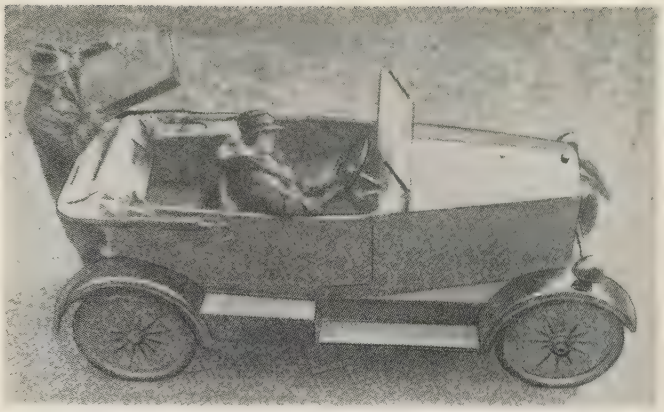

Fig. 23—Leyland-built rear-engined Trojan, with 1100 cc displacement, Britain, 1922

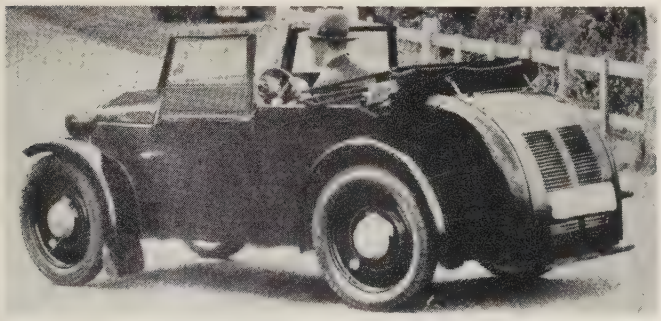

Fig. 24—Rear-engined Rover, Britain, 1936

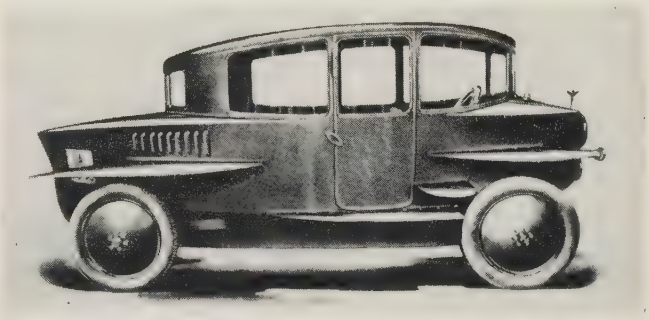

Fig. 25—German Rumpler with W-type engine, used as taxi in Berlin, 1920

duced. About 1925 the Rollende Kommisbrod was put into production by Hanomag. It was powered by a single-cylinder engine placed in front of the rear axle (Fig. 22) and showed the way for the modern economy rear-engine passenger car. Its name, meaning "People's Bread," indicates the market at which it was aimed. In England, the 1100-cc displacement, 2-stroke Trojan (Fig. 23) enjoyed six years of commercial success, and the 1-liter displacement Rover (Fig. 24) was also built in quantity. To complete the story we must also cite the Rumpler (Fig. 25) which in 1920 were the taxicabs in Berlin and which by its original design (six cylinders in a W arrangement) soon proved in this arduous service the value of the rear-engine placement.

The great industrial expansion of the rear-engine mounting began in 1938 with Dr. Porsche's Volkswagen, first shown under the name of the K.D.F. As one can see from the folder printed in that year, little has been changed since then (Fig. 26).

Not only have many prototypes of the rear-engined cars appeared in Europe during the past 10 years but a large-scale, widely distributed production model, first the 4CV Renault and then the 5CV Dauphine, were developed. We should also note the Porsche sports cars, derived from the Volkswagen (Fig. 27), with a piston displacement as high as 1600 cc; the very small cars such as the Maico and the Goggomobil, brought back by scooter technique and corresponding more to the cyclecar than anything else, the production of which reached 10,000 cars in 1955. In Italy since March, 1955, Fiat has

Fig. 26—First advertising folder for Volkswagen, Germany, 1938

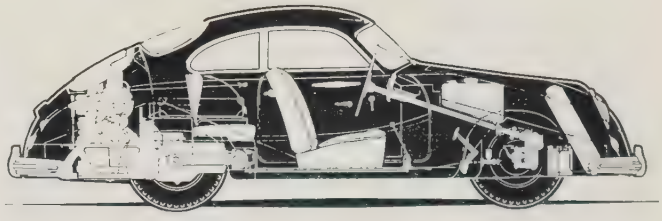

Fig. 27—Porsche, 356 type, 1950

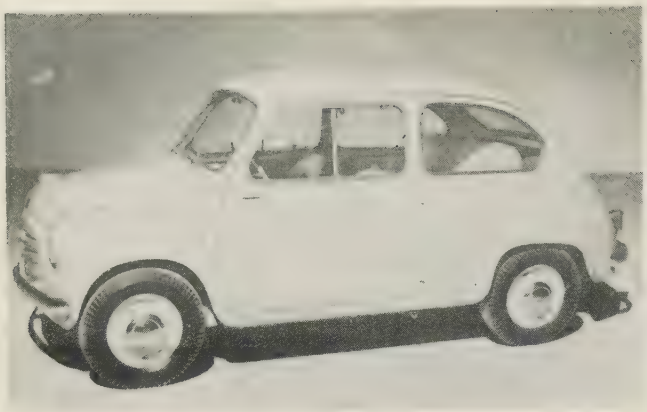

Fig. 28—Fiat 600, 1955

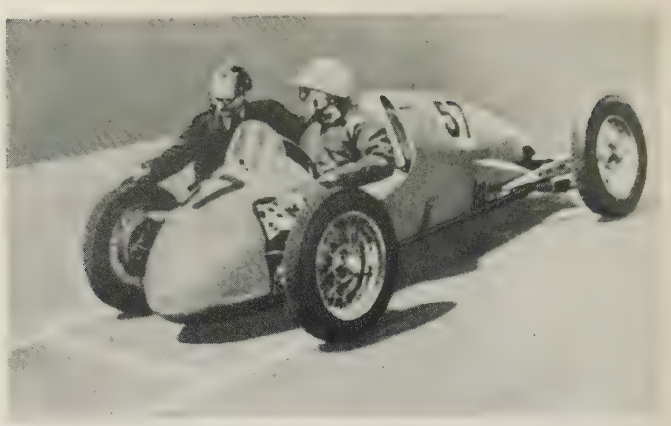

Fig. 29—Kift racing car with small-displacement rear engine, Britain, 1950

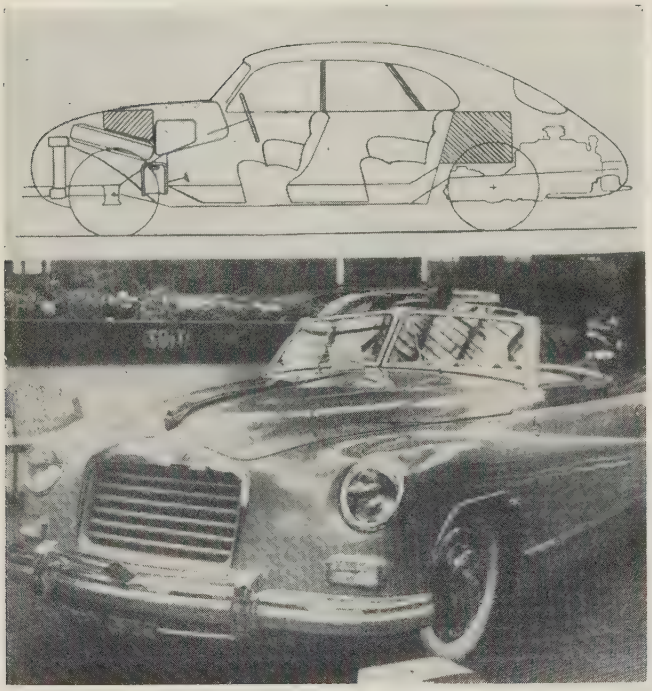

Fig. 30—Isotta Fraschini with rear V-8 engine, Italy, 1950

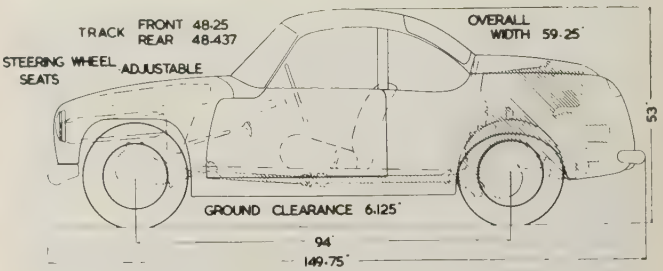

Fig. 31—Rover T3 with rear turbine engine

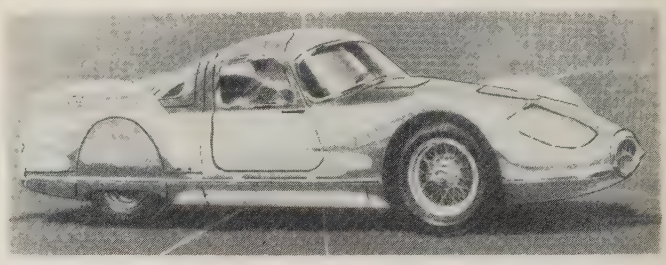

Fig. 32—Experimental prototype of Fiat with rear turbine

Table 1—European Production of Rear-Engined Passenger Cars as Compared with Total Passenger-Car Production

	1947	1948	1949	1950	1951	1952	1953	1954	1955	1956
European Passenger-Car Total Production	382,389	509,257	769,400	1,089,769	1,182,543	1,230,732	1,478,221	1,919,186	2,393,154	2,532,792
Rear-Engined Passenger-Car European Production	9780	41,852	116,754	168,086	194,532	218,524	248,569	327,701	508,543	673,258
Ratio Rear Engine/Total Production, %	2.6	8.2	15.2	15.4	16.5	17.75	16.8	17.1	21.25	26.6
Less than 1300 Cc Passenger-Car European Total Production	188,794	305,537	446,273	641,169	739,906	812,497	935,693	1,265,559	1,525,741	1,755,654
Rear-Engined Passenger-Car European Production	9780	41,852	116,754	168,086	194,532	218,524	248,569	327,701	508,543	673,258
Ratio Rear Engine/1300-Cc Production, %	5.2	13.7	26.2	26.2	26.3	26.9	26.6	25.9	33.3	38.35

also rallied to the rear-engine formula with the Fiat 600 (Fig. 28) and the Fiat Multipla.

Aside from these successes, many attempts to build such cars have failed: in France Rosengart's Marathon Corsaire, the downfall of which was caused by insufficient means for its manufacture. A dozen prototypes show that the minds of numerous "engineers" have been applied with enthusiasm to this problem. The best known of these Rovin, Julien, and Charles Mochet. It is the same in Germany with many tiny cars shown at each motor-car show. In Britain and in Italy the tendency is somewhat different but one still finds a few enthusiasts with rear-engined racing cars, notably Kift (Fig. 29), Cooper, and Siata. Is it a result of natural evolution that these cars are usually racing machines of small size and low fuel consumption? On the other hand, among the big displacement cars, a few deluxe models such as the Isotta Fraschini, with its V-8 engine overhanging the rear wheels (Fig. 30), appear and soon disappear. The rear-engine formula has a decisive advantage only for small-displacement engines.

To round things out, let us remember that all of

Table 2—Dimensional Comparisons of Some European Cars

	Volks-Wagen	4CV Renault	600 Fiat	Dauphine Renault
Piston Displacement, cc	1192	747	633	845
Engine Maximum Output, hp	36	26	21.5	30
Engine Maximum Torque, ft-lb		5.9	4	6.7
Vehicle Weight (Unladen), kg	720	600	585	630
Weight Distribution: Front Axle, kg	305	190	228	240
Rear Axle, kg	415	410	357	390
Vehicle Weight, kg	1045	920	893	1000
Weight Distribution: Front Axle, kg	455	360	338	420
Rear Axle, kg	590	560	555	580
Wheelbase, mm		2100	2000	2270
Overall Length, mm	4050	3627	3215	3945
Front Tread, mm	1250	1216	1150	1250
Rear Tread, mm	1250	1220	1154	1220
Overall Width, mm	1540	1430	1345	1520
Number of Doors	2	4	2	4
Main Body Work Interior Dimensions, mm				
Pedal to Front Seat Back	900–1005	885–1015	880–1000	910–1040
Distance Between Front Seat Back and Rear Seat Cushion	110–240	170–290	115–235	200–320
Depth of Rear Seat Cushion	450	450	450	455
Elbow Room at Front	1150	1260	1200	1240
Elbow Room at Rear	1315	1200	1190	1220
Height above Front Seat	925	915	900	900
Height above Rear Seat	915	880	820	860
Luggage-Loading Capacity, cu dm		150	70	200

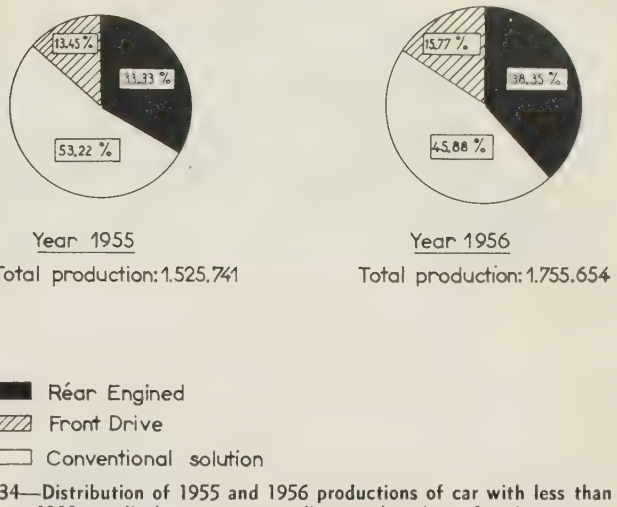

Fig. 34—Distribution of 1955 and 1956 productions of car with less than 1300-cc displacement, according to location of units

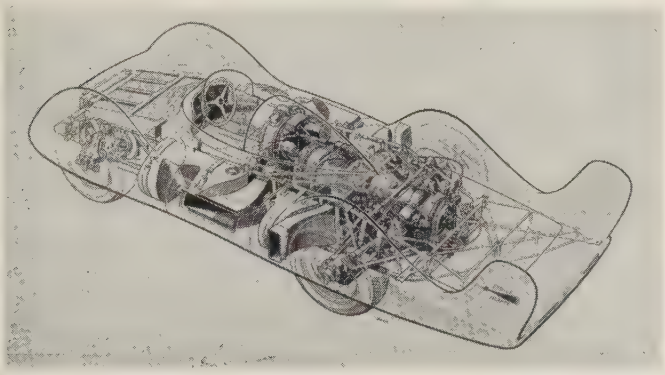

Fig. 33—Etoile Filante, Renault's experimental car with rear engine

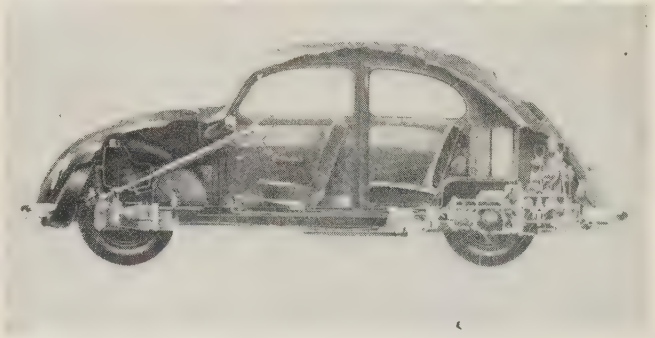

Fig. 35—Volkswagen

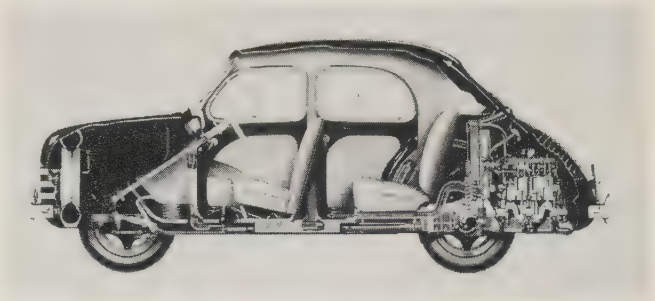

Fig. 36—Renault 4CV

the European turbine cars which hold international speed records for this class whether it be the Rover (Fig. 31), the Fiat (Fig. 32), or the Renault Etoile Filante (Fig. 33) have the engine at the rear.

Statistics from 1945 to 1956

It is interesting to follow, through the statistics of European production over the last 10 years, the progress of the rear-engined car as compared to the other arrangements.

Table 1 compares the European production of rear-engined passenger cars and cars of less than 1300-cc piston displacement versus the total European production. Fig. 34 shows the comparison for production of passenger cars of less than 1300-cc piston displacement. This shows in a striking manner the progress made with a percentage increase from 5.2% in 1947 to 38.3% in 1956. You will also note that this progress is still more marked when one considers only those cars having a very small piston displacement.

Why Has This Technique Succeeded?

To have achieved such a development in European mass production, this technique must have marked advantages for both the customer and the manufacturer.

This is what we wish to examine now. The discussion will be in three parts:

First, we will outline the principal characteristics of the four cars actually being mass produced by the big European manufacturers.

In the second part, we will enumerate the known advantages of these cars.

Third, we will study the technical problems which this type of construction presents and how they have been solved by Volkswagen, Renault, and Fiat, with special reference to the Dauphine, which we know particularly well.

Principal Characteristics of the Four Best-Known European Cars—It seemed to us that an easily read table giving a resumé of the principal specifications of these cars would be of interest to our readers (Table 2). These four cars are: Volkswagen, of which 1,400,000 had been built by the end of 1956 (Fig. 35); Renault 4CV, of which 870,000 were running as of the same date (Fig. 36); Fiat 600, of which

Fig. 37—Fiat 600

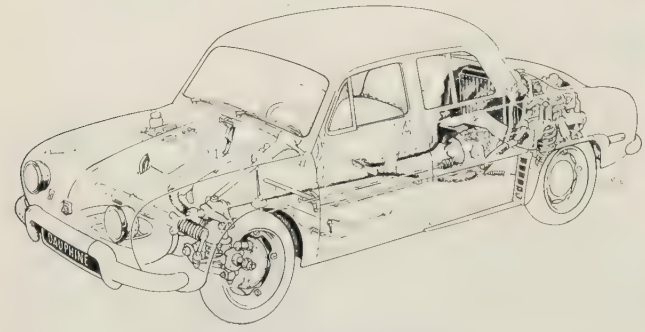

Fig. 38—Renault Dauphine

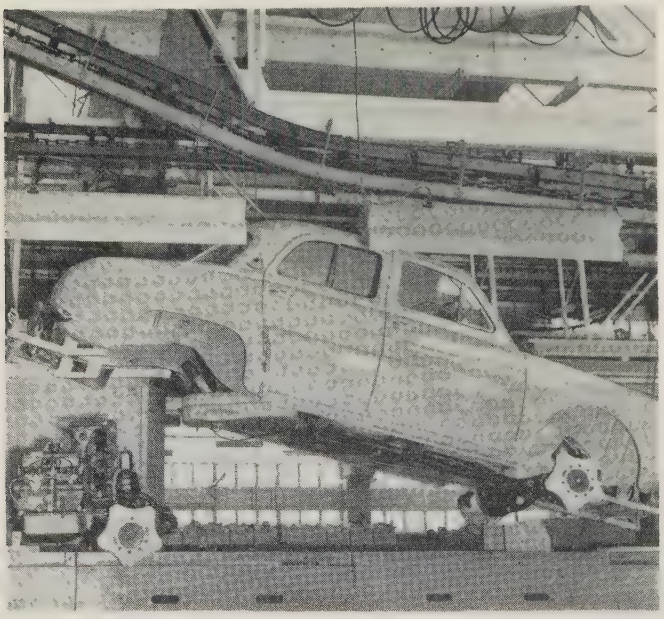

Fig. 39—Assembly of engine and chassis of Renault Dauphine

230,000 had been produced (Fig. 37); and Dauphine Renault, first produced on March 6, 1956, of which more than 100,000 have been delivered (Fig. 38).

The Advantages of This Design—1. Simplicity of construction is due to the simplicity of the structure of the car. The true rear-engined car is composed of a closed passenger package (the body) at the rear of which is fixed the mechanical propulsion unit (Fig. 39). The other mechanical units are small in number (Fig. 40) and are self-contained subassemblies easy to install on the body unit as it passes down the assembly line. The body is a self-contained unit which comprises the body proper with stiffeners in the floor making a true one-piece

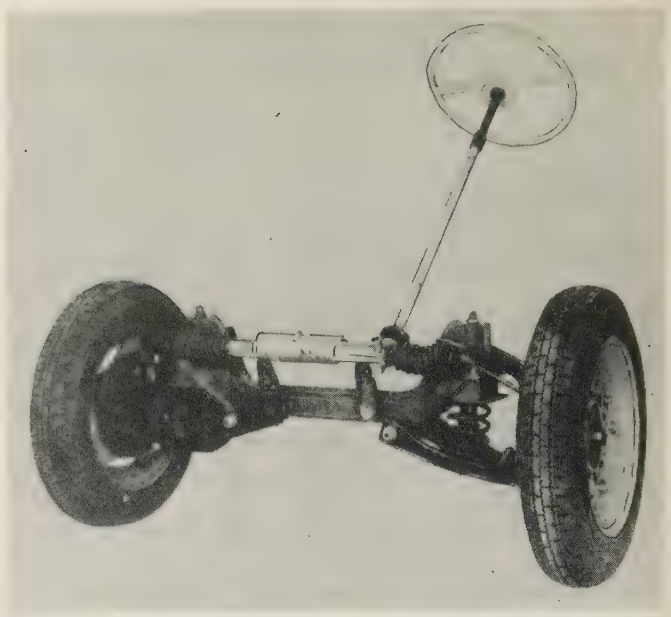

Fig. 40—Front axle and steering subassembly of Dauphine

stressed-skin body and frame. This construction lends itself particularly well to the one-piece body structure which is now common in Europe.

Naturally, in this case the transmission is the shortest and simplest possible. The swing axle needs but one universal joint per wheel axle, placed at the exit of the differential housing. The driving wheels are not used for steering and thus do not require the double constant speed universal-joint assemblies of front-wheel drive.

2. The overall length of the body is the minimum for a given passenger space. In effect, it allows the front-seat passenger's feet to go to the front wheel centers while the powerplant's farthest unit is located under the rear seat. This gives the minimum possible wheelbase and length for a given passenger space. Fig. 41 compares this on the Dauphine Renault with the front-wheel drive and the usual type of car with front engine and rear-wheel drive.

3. Light weight is the first result of the two foregoing qualities. In the classic design the engine, gearbox, driveshaft, and differential housing (with independent rear wheels) are all carried by the body. In the rear-engined car the body carries but part of the weight (which can be very small) of the powerplant and propulsion mechanism which literally pushes the car through a small number of points of attachment (Fig. 42). Naturally, the crankcase walls, the transmission, and differential housings all carry weight plus the driving and braking loads.

The compact design of the unit (engine, gearbox, and differential housing) allows the use of a minimum number of housing walls, ball and roller bearings, and seals. The shafts are short, so the quantity of transmission lubricant is held to a minimum.

On front-drive vehicles, the front-suspension units are usually more generously dimensioned in comparison to those of the rear suspension because they are calculated to carry maximum braking loads. In the rear-engined car, the braking load at the front (Fig. 43) compensates only for the much smaller difference of the static loads between the front and rear of the vehicle. This gives great di-

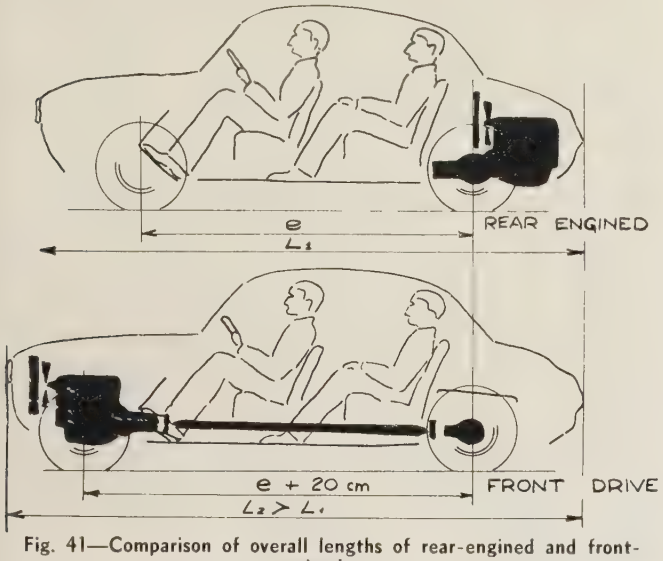

Fig. 41—Comparison of overall lengths of rear-engined and front-engined cars

mensional homogeneity (using the same design factors back and front). It also results in a lightening of the whole, the advantages of which will be shown in the following paragraphs and clearly seen in the tables.

The Dauphine could not afford the comfort it gives for 1386-lb curb weight, unless it had the engines at the rear.

4. Reduction of price results from the optimum use of material through light-weight design (Fig. 44) and the simplicity of construction. This permits an economy in tooling for the manufacture of parts, the number of which is reduced as compared to the usual design. Finally, the ease of assembly reduces the length of the assembly lines and, thus, the money invested in buildings and labor. All of this results in a reduction of cost of manufacture as compared to the conventional design of the front-wheel drive.

5. There is a possibility of a better drag coefficient (C_x). Generally, a rear-engined car suffers less from aerodynamic resistance or drag than a front-engined car having the same lines and cross-sectional area. This is a result not of the aerodynamic characteristics of the car itself, but of the nature of the flow of cooling air and that which supplies the engine. In consequence, this advantage cannot be seen during model trials in the wind tunnel.

Trials of an actual car were conducted in the large wind tunnel at Chalet Meudon. Drag was observed on a masked car with the air intakes closed and the engine stopped, and on a car in running condition with unmasked air openings and engine operating at a speed corresponding to the airspeed of the wind tunnel. It was noted that for the front-engined car the drag increased from 10 to 40% and for rear-engined cars it always diminished. For the 4CV and the Dauphine this lowering of the drag was approximately 8%.

Detailed explanations of this phenomenon can be derived from the body of this paper. Let us note that in the case of the front engine the airflow lines are strongly deflected (the air usually being deflected below the floor), but that in the case of the

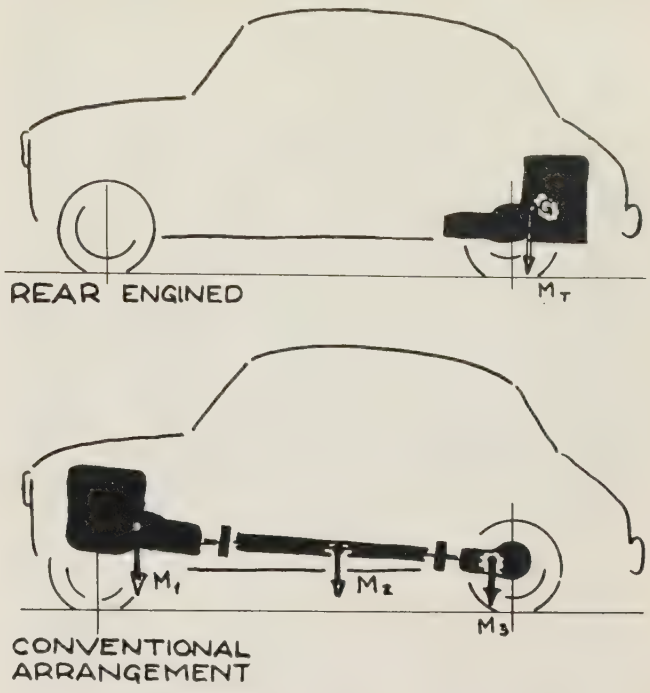

Fig. 42—Distribution of weights of mechanical units

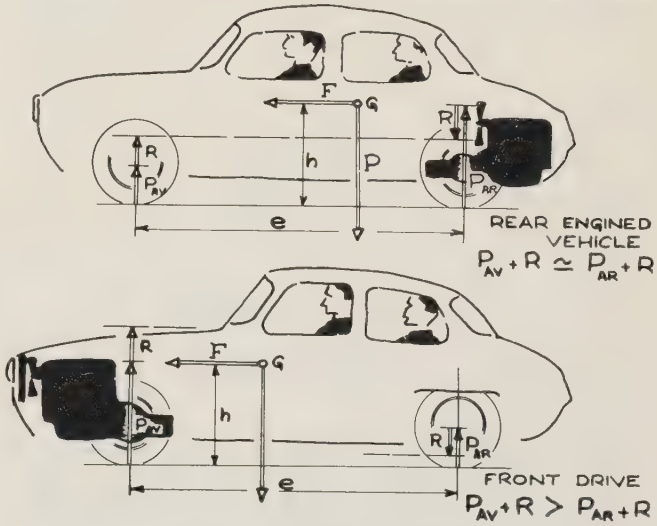

Fig. 43—Overload on braking action $\left(R = F \times \frac{h}{e} \right)$

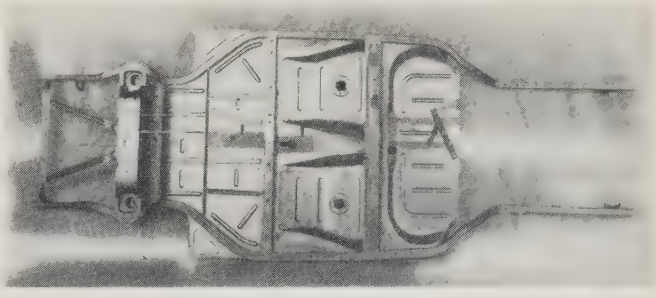

Fig. 44—Dauphine floor, stripped

rear engine the aspiration of air through the side intakes tends to retard the breakaway of the air and the formation of eddy currents caused by frontal projections and also to smooth out the airflow.

We also find that the aerodynamic forces involved

tend to produce lift at the front of a front-engined car and to give negative lift or aerodynamic loading in the rear-engined car. Felt only slightly on a heavy car, these aerodynamic forces work favorably to help road holding in the rear-engined car where the front suspension is more lightly loaded.

6. There is economy of power and of fuel consumption. The preceding considerations of its lightness of construction and the increase in its aerodynamic efficiency forecast that the power necessary for given accelerations and maximum speed are less for this type of passenger car than for cars of conventional design (Fig. 45). Experience confirms this. In average running on normal roads the fuel consumption of this car is but 6–6.5 liters of fuel per 100 km (36.2–39.2 mpg).

7. The rear-engined car has a short turning radius. The short wheelbase and short overall length, combined with the sharp angle at which the front wheels can be turned (thanks to the free space between them), results in a short turning radius. This means easy handling which is much appreciated for parking the car in crowded cities. One can easily park either the Dauphine or the 4CV alongside the curb with a few maneuvers in a space not more than 8 in. longer than the overall length of the car (Fig. 46).

8. There is also the possibility of easy steering. The light weight on the front permits installation of a rack and pinion steering gear connected directly to the wheels, while the presence of an engine in front forces other designs to employ a greater number of steering rods and connections. This gives a steering gear which is light and precise at the same time.

9. The stiffness of the front structure provides excellent road holding. The baggage compartment (Fig. 47) is formed by the firewall, the front-wheel cutouts, the rigid front structure of the body, and the floor which goes to the extreme front of the car. In conventional cars it is necessary to open the underpart of the front in order to lodge the engine and offset the radiator grill in order to provide the cooling air for the radiator and the oil pan of the engine.

Good road holding in the rear-engined car is thus assured, absolute rigidity of the front of the body structure being one of the essentials for the maintenance of the steering geometry and front-wheel alignment.

10. Better ride is given by the advantageous location of the seats between the front and rear suspensions, which reduces the amplitude of the suspension movement at passenger levels and thus permits the diminution of the vertical accelerations to which they are subjected.

11. There is excellent road holding on slippery roads. The importance of the ratio:

$$\frac{\text{Weight on the driving wheels}}{\text{Total weight}}$$

insures a maximum of control of slippery surfaces.

12. There is road holding in the mountains. The transfer of weight to the rear due to grade increases the adherence of the driving wheels already carrying an important percentage of the total weight of the vehicle (Fig. 48). Experience shows that antiskid chains are rarely used on this type of car in the mountains in the winter.

13. Front seat and compartment space is provided. The toe board has a great deal of free room because it is not necessary to provide for the gearbox (hump). This results in a flat floor that is particularly advantageous in a small car (Fig. 49).

14. Absence of engine heat in the summer is provided by the placement of the engine at the rear

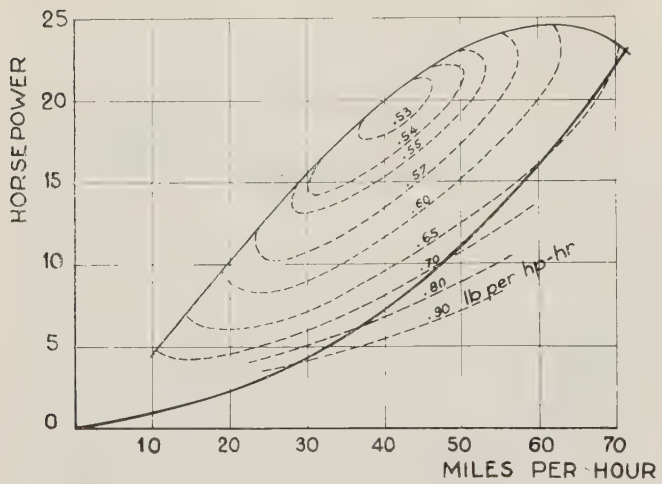

Fig. 45—Adapting engine to desired performances of car

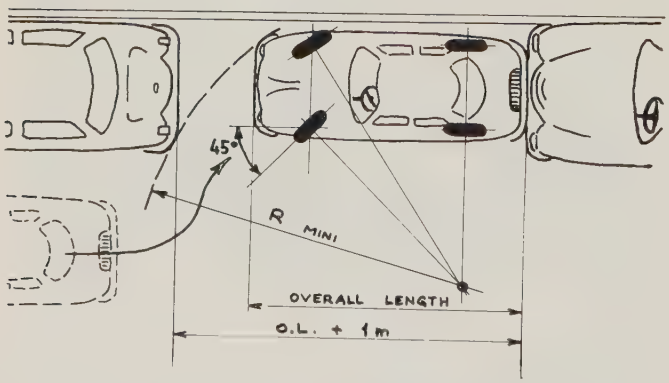

Fig. 46—Parking ability

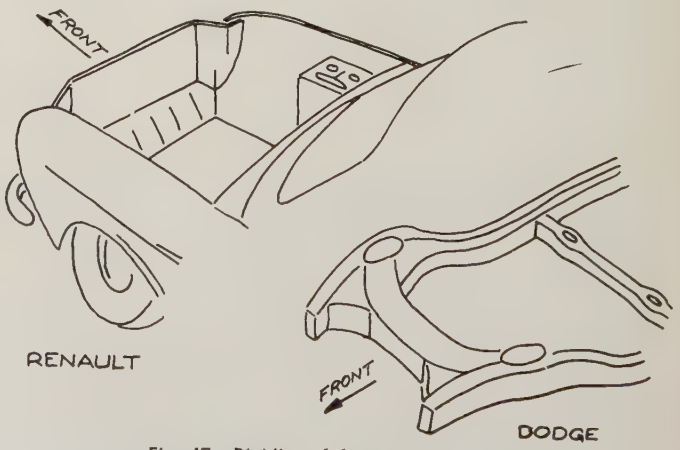

Fig. 47—Rigidity of front-end structure

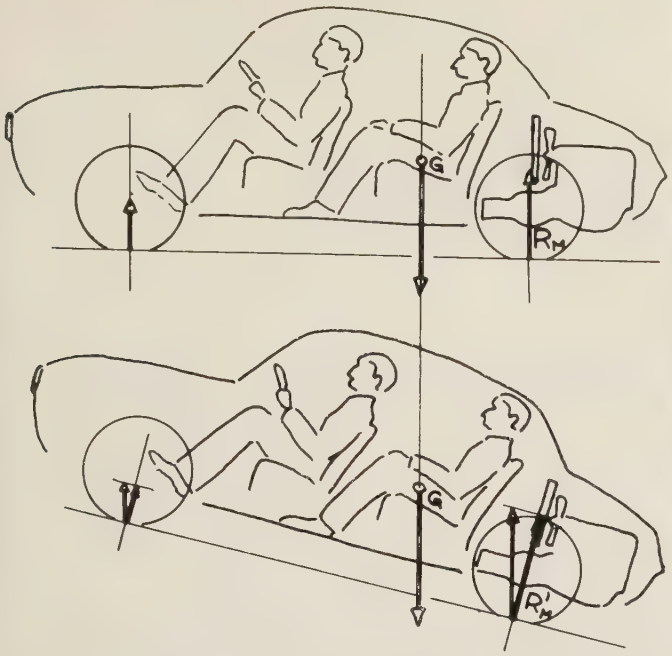

Fig. 48—Overload on rear axle due to slant

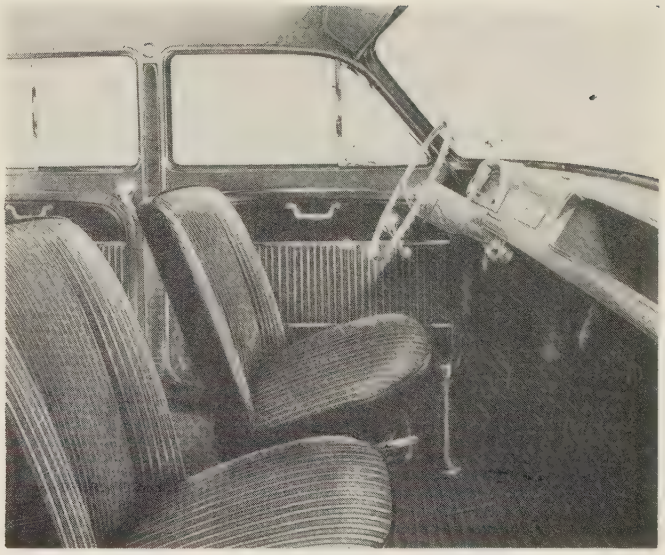

Fig. 49—Front seat arrangement of Dauphine

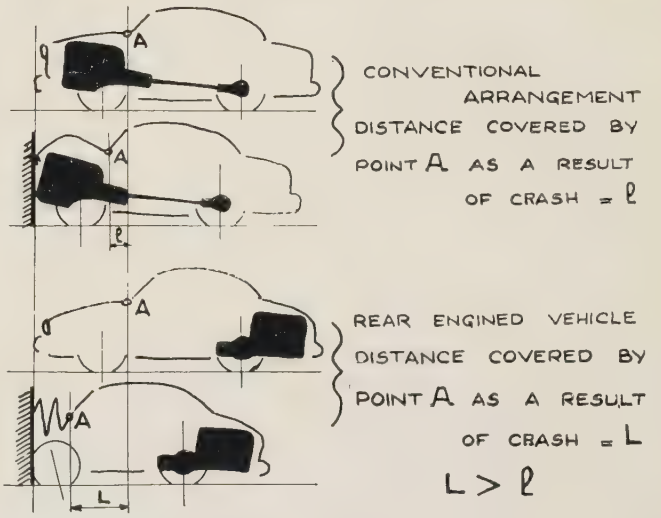

Fig. 50—Effect of crash on front end of car against stationary obstacle

outside of the passenger compartment, totally isolating the passengers. Thus, the heated air does not flow over the floor of the body as it does in the front-engined car.

15. There is no exhaust pipe or muffler below the car. With the unit type of body and a flat floor, forward placement of the engine necessitates hanging the exhaust pipe and muffler below the floor of the car, thus radically lowering the road clearance as well as making these elements particularly vulnerable in deep snow or mud.

16. Less danger exists in case of collision. Accident statistics show that 75% of all collisions involve the front or sides of a motor car. We have shown in Point 9 that the front construction of the unit body gives it great strength and rigidity, which helps road holding, and that there is no group of units having excessive massed weight (such as the engine, clutch, and gearbox) mounted on closely spaced sections (chassis frame). This rigidity, which is that of a thin-walled beam of great depth and width, provides for a change of shape under shock loads which is superior to that of cars fitted with the ordinary frame.

The result is that in the most common types of accidents the deceleration of the car at passenger level is less violent and the passengers have a lower momentum at the instant they strike the front of the passenger compartment (windshield, dash, and the like). Because of this the danger of serious injury is greatly diminished (Fig. 50).

17. The spare wheel acts as a shock absorber. On the Dauphine, the spare wheel is placed horizontally under the luggage space in the front compartment. This protects the passengers from shocks at the front of the car, while in the front-engined car a frontal impact sends the engine into the inside of the body like a battering ram.

18. The windshield is placed favorably. In a rear-engined car it is much easier to bring the passengers close to the windshield. This has several advantages: better all-around visibility without recourse to expensive wrap-around windshields (Fig. 51), and prevention of the passengers from attaining in collision a relative momentum significantly higher than that of the windshield and its mounting.

19. Danger of poisoning from fumes decreases. The infiltration of carbon monoxide, hydrocarbon gases, or their derivatives in the passenger compartment is less to be feared than in the front-engined car because, in motion, the gases from the engine compartment of any car pass to the rear—that is, toward the passenger compartment of the front-engined car and the exterior of the rear-engined car. The absence of an exhaust pipe and muffler below the floor of the car, where it would be in the front-engined vehicle, shelters the passengers from leaks in these parts due to corrosion of gases on the inside or salt on the outside.

20. Vapor lock is at a minimum. The placement of the gasoline tank on the Renault 4CV and the Dauphine in front of and below the engine compartment puts it in the coolest part of the car, protected from engine heat and the sun. This also provides

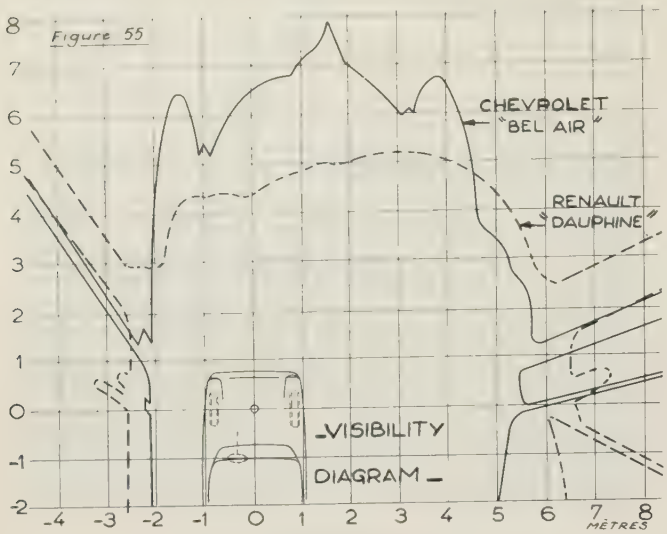

Fig. 51—Visibility diagram

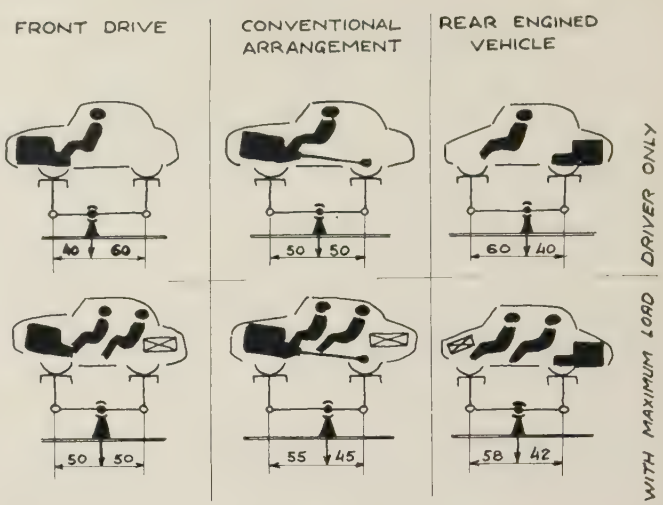

Fig. 52—Distribution of weights on axles

for a short, straight pipe between the fuel tank and the fuel pump, so that cool fuel comes directly to the fuel pump with a minimum of depression. Therefore, the danger of vapor lock is kept to a minimum. Only the rear placement of the engine allows this to be done.

21. Noise is carried to the rear. Finally, the rear-engine compartment forms a sort of "engine room" which is isolated from the rest of the car. The rear bulkhead, or fire wall, is also duplicated by the back of the rear seat, making extremely good sound insulation.

Difficulties of This Technique—These advantages, although numerous and important, should not allow us to forget the proved difficulties in the application of this construction.

1. The distribution of weight is a problem because of the concentration of the essential mechanical units and the engine at the rear. Fortunately, the weight of the driver and a passenger, which is the average loading, improves the weight distribution between the front and rear wheels. For a long time this objection was the principel drawback of the rear-engine design. It was criticized as giving poorer road holding than the conventional design and the front-wheel drive. Experience has shown that it is possible to provide weight distribution which is acceptable under all conditions of loading.

Fig. 52 shows that for the Dauphine the ratio:

$$\frac{\text{Weight on the front wheels}}{\text{Total weight}}$$

remains 40–42% under any loading condition, while it may vary 45–50% with the conventional design and 48–58% with the front-wheel drive.

2. Engine cooling is more difficult. With the rear-engined car it is more difficult to profit by the favorable action of the dynamic pressure of the car airspeed to get proper circulation across the radiator fins of the liquid-cooled car, or across the engine fins of the aircooled car. The problem was solved by working on the ensemble of the radiator and fan and by directing the airflow in front and in back of the radiator in such a manner as not to waste the dynamic pressure which is present (Fig. 53).

Once solved for maximum road speed, this answer to the problem was found satisfactory for the lower gears (mountain driving) because the ventilation system which utilizes but a small dynamic pressure is practically independent. The car will, therefore, operate at a temperature which is practically constant under these different conditions, while the front-engined car will cool too much driving on the level in third and fourth gears and overheat in the mountains running in the lower gears.

The fan is somewhat larger than that of a front-engined car. It takes little more power to drive it, however, because it cools under the conditions cited. We estimate that, at most, ½ hp is needed for the Dauphine. Finally, the radiator is not directly exposed to clouds of dust and insects.

3. Dust is more dangerous. If there is a real disadvantage in this design it is the difficulty of protecting the engine against dust. In many regions of the world dirt roads still exist, over which the passage of the front wheels raises a cloud of dust.

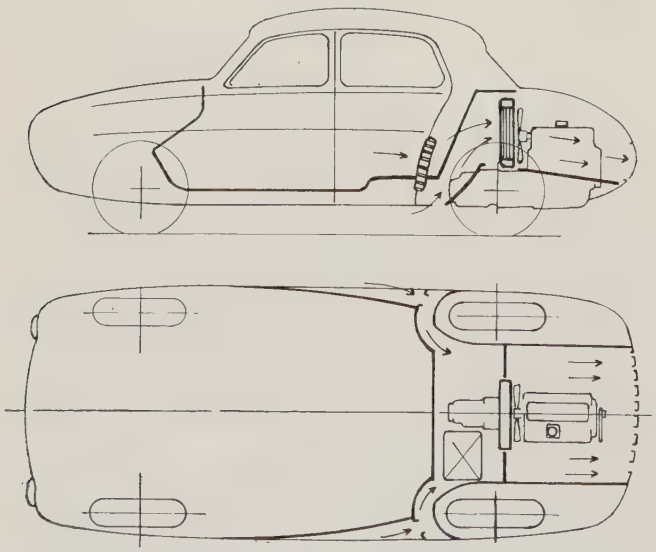
Fig. 53—Cooling system on rear-engined car

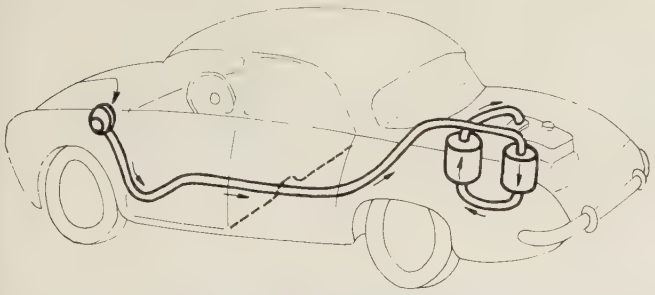

Fig. 54—Air filtering with air inlet at front

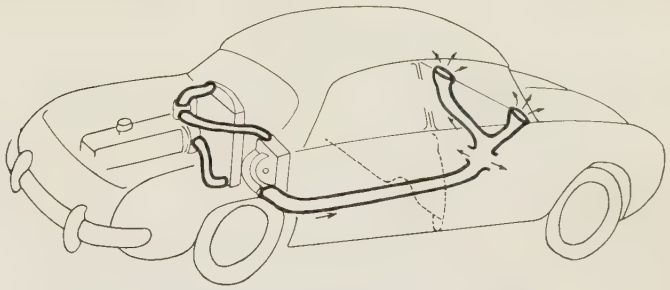

Fig. 55—Heat and demisting (hot airflow)

Thus, the air which comes into the rear compartment to cool the engine and to supply it with air is loaded with very fine dust, the chemical composition of which varies from silicon to almost pure clay, depending upon the region.

In countries with modern roads, this problem does not exist. The use of a properly dimensioned oil-bath filter suffices. On the other hand, cars destined for use in countries having dustry roads are fitted with a compound filtering system (an oil bath and a dry filter in series) fed by a tube taking its air from the baggage compartment located in the front of the vehicle. This gives even more favorable conditions than the front-engined car, as the baggage compartment acts as a settling chamber (Fig. 54). This does not prevent the engine from operating in a dustry atmosphere. To avoid deterioration of the mechanical elements we have provided airtight ignition distributors and seals at the exits of the crankshaft and camshaft.

Numerous trials on the African desert have proved the efficiency of this solution, the cost of which is very reasonable. The life of engines before overhaul is about that when operating on normal roads in the temperate zone, that is to say 100,000 km or 62,000 miles.

4. The heating of the car and defrosting of the windshield are more difficult. The rear placement of the engine is also less favorable for heating.

With the aircooled engine it is necessary to carry warm air forward through a fairly long conduit. With a water-cooled engine, it is also advantageous to place the heating radiator close to the engine. In both cases the transfer of the air necessary for warming the front-seat passengers and the defrosting of the windshield causes a loss of pressure and volume, which necessitates an increase in the capacity of the heater fan. The heat losses demand a carefully designed and insulated system. As a solution, a larger conduit having a cross-section about 50% greater (about 25% greater in diameter), which is within acceptable design limits and insulated by a coating of sponge rubber, is used.

With this arrangement (Fig. 55) the loss of pressure in the conduit is about 2 mm of water and the temperature drop (with an outside temperature of 14 F and a speed of 44 mpg) is but 11 F. The efficiency of the heater is, therefore, comparable to that of the front-engined systems and has the advantage of taking its air from a zone which is not contaminated by the exhaust gases of the cars in front of it.

5. The long rods and cables required are more delicate. The long distance from the driver's seat to the engine and the drive requires longer and more complicated control rods or cables to assure the operation of the throttle, the starter, clutch, and gearbox. If the gearshift lever is located on the steering column below the steering wheel, there is a further rise in the complication and cost.

These annoyances were serious for a long time but developments in the manufacture of accessories have eliminated them. The perfection of cable and conduit controls, especially those for the clutch and throttle, solved most of the problem by permitting them to take the most torturous paths.

In low-priced cars, the floor-mounted gearshift lever is acceptable, making this control easy to design.

Finally, the development of automatic chokes and solenoid-operated starters have eliminated the distant controls of these accessories. The use of an electromagnetically operated clutch, such as the Ferlec, is rapidly gaining ground and resolves the problem of the clutch control.

6. It is difficult to make one basic body serve as a basis for several types of cars. This problem applies particularly to Europe where a number of manufacturers have come to use the same basic mechanical structure in order to increase production of cars destined for different tasks: for example, sedan, panel truck, station wagon, and even a platform truck or pickup.

The rear placement of the engine makes the design of commercial bodies difficult as the space required for the powerplant prevents locating any opening at the rear. This difficulty is very real. Volkswagen has partially resolved it by building special bodies with very wide side openings to compensate for the absence of a rear opening (Fig. 56).

However, the best solution of this problem lies in

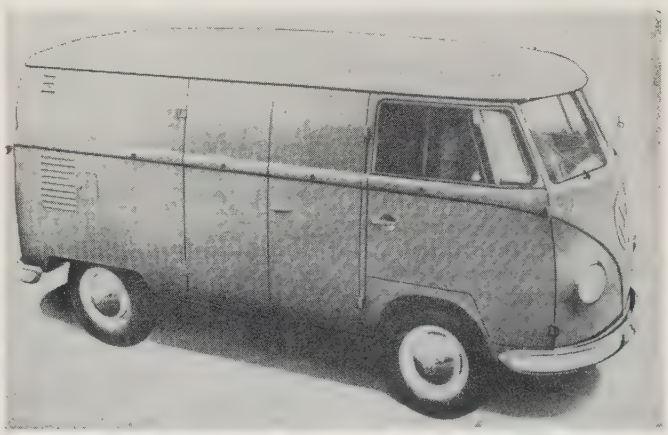

Fig. 56—Volkswagen 1.7-ton rear-engined light van

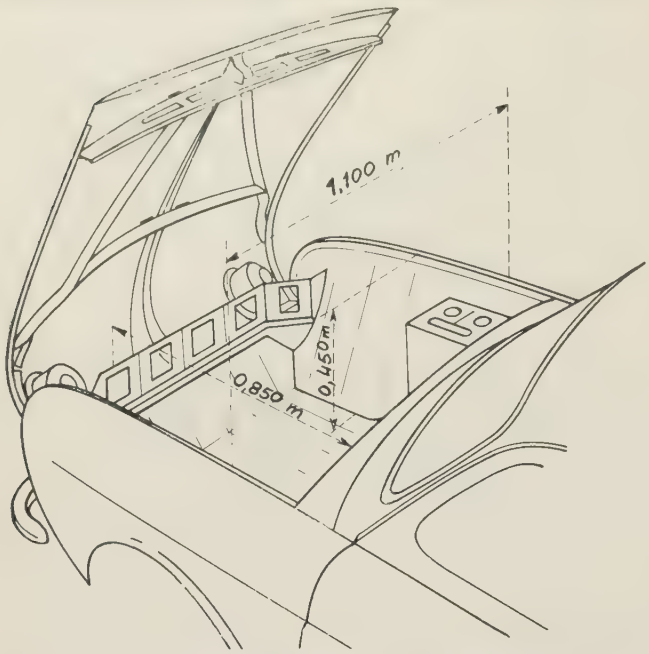

Fig. 57—Luggage compartment on Renault Dauphine

the fact that mounting daily output will permit the manufacturers to drop the all-purpose body very rapidly and to design each vehicle specifically for the service for which it is intended.

7. Baggage space is limited. The forward position of the baggage compartment makes the designing of it troublesome and limits its capacity. Nevertheless, one can pardon a roof rack on a widely distributed, low-priced economy car to give additional luggage space for those short periods when a great deal of baggage must be carried (vacation time, carrying skis, fishing tackle, or camping equipment).

This objection was real and still is for some cars. On the Dauphine Renault the builder has lengthened the front "hood" in order to provide a maximum of baggage space. This design, plus the fact that the spare tire is stored in a place unsuitable for any other use, has given the car a trunk space and capacity equal to and often greater than that provided on numerous front-engined cars of greater piston displacement (Fig. 57).

Conclusion

Has the rear-engined design a good chance to continue its victorious comeback? We believe that it has, in the same measure as low-priced cars extend their market. There is absolutely no doubt that this technique, which has now found an equilibrium in both design and manufacture, is particularly adaptable to economy cars, the development of which never ceases to expand in Europe.

We have seen that the advantages of this design are numerous; we have studied the difficulties which it presents; and we have been able to note the technical progress in the last 10 years which has solved the problems.

The numerous successes in over-the-road competitions, such as the very difficult races—Liege-Rome-Liege, Tour de France, Tour de Corse, Mille Miglia (1000-mile road race)—where rear-engined cars of less than 1-liter piston displacement often win over front-engined cars of much greater displacement, proves that on the basis of road holding and safety they do not have to fear the competition of other types of construction.

Customer acceptance is no longer a problem, now that 2,500,000 of these cars are being driven on all continents and in all climates. They are no longer a novelty.

We can, therefore, conclude that for piston displacements of less than 1500 cc, the rear-engined car will not only maintain its present position but improve it.

DISCUSSION

Discusses Problems Of Handling Stability

—R. N. Janeway
Janeway Engineering Co.

THE first broad question is just what does the rear engine have to offer us from a basic functional and economic standpoint. I can see the following possible incentives:

1. If overall cost reduction is possible in American size cars, as Mr. Picard has found in European practice, there will be a strong economic justification for the rear engine. Certainly, present car costs to the public are getting out of hand.

2. Redistribution of weight toward the rear will relieve the present excessive concentration of braking energy absorption at the front wheels and improve the tractive ability. Both items have become serious limitations to the high-performance trend which shows no sign of abating. It is quite clear that front drive is not the answer to these problems, because of the unfavorable weight transfer both on acceleration and braking.

3. Elimination of the floor tunnel. This has always been a nuisance and present low car heights have already made it an abomination.

4. If gas-turbine power plants materialize, the large exhaust duct required will make a rear installation attractive. The much greater air consumption may also make it desirable for aerodynamic reasons brought out by Mr. Picard.

5. Greater safety to passengers in head-on crash can very likely be achieved by sound structural design. I agree completely with Mr. Picard's analysis of this point. However, I am inclined to discount the seriousness of possible adverse public psychological reaction regarding the safety of rear-engine cars.

The next question is what are the fundamental engineering problems that must be solved to make the rear engine feasible in cars that will meet requirements in the United

Table A—Specifications for Ideal Weight Distribution

Wheelbase—126 in.
Road weight—3360 lb
Powerplant weight—750 lb
Powerplant located wholly forward of the rear axle
Two passengers front, three passengers rear
Front body overhang—43 in.
Rear body overhang—51 in.
Ample luggage space both front and rear

States. Here we can start and finish with handling characteristics. If these can be licked, the rest is just detail.

The trouble originates with the slip angle which a wheel and tire must assume relative to the direction of vehicle motion in order to develop lateral thrust, as required to oppose centrifugal force on a curve. The front-wheel slip angle can, of course, be controlled by the driver through the steering gear. However, if the rear-wheel spindles are held in fixed relation to the car frame, they can assume a slip angle only if the vehicle as a whole adopts a similar attitude to the direction of motion. The rear-wheel slip angle requirement is thus imposed on the front wheels as well. Unless the front wheels require at least as great a slip angle as the rear wheels, the driver finds that he must reverse the steering wheel after the car has entered the curve. This disconcerting experience is known as oversteering. It is generally and wisely held in American industry that this characteristic is hazardous and can not be tolerated in any degree in cars intended for our mass market. Instead, some degree of understeer, which is the reverse charactristic, is generally aimed for under all load conditions. It is unfortunate that tires, at their rated inflation pressure, do not develop cornering thrust in proportion to load at a given slip angle. If they did, there would be no problem. But since they don't, greater load on the rear wheels than on the front leads to greater slip angle at the rear and, inevitably, oversteering. There is one possible corrective expedient: namely, to provide automatic rear-wheel steering relative to the car frame and in proportion to required thrust.

It has been common practice for as long as Hotchkiss drive has been in use, to provide a certain amount of rear roll understeer. By suitably arranging the geometry of the equivalent linkage of leaf springs and axle, the roll of the car induces an angular displacement of the rear axle in the direction of the required slip angle. A significant indication of the American demand for a safe margin of understeer is that some rear roll understeer is virtually a standard feature of American designs. This is so in spite of greater weight on front wheels and inherent understeering of independent front suspensions.

However, roll understeer holds no promise for the rear-engine car. In fact, it is a vanishing effect, diminishing as roll stability continues to be increased by lowering of center of gravity and by suspension improvements. Moreover, a high degree of roll understeer cannot be tolerated because it boomerangs in the form of severe wander, induced by rear-end steering on straight but uneven roads and in crosswinds. Consequently, other means must be found to produce rear understeer to offset any important shift of weight to the rear.

Another obstacle in this connection is that rear-engine mounting demands a sprung differential; hence, a de Dion axle or some form of full independent rear suspension is a must. Suspension systems of this type have almost invariably shown inherent oversteering tendencies; yet, what is needed is a positive degree of understeering.

An important additional requirement for handling stability has to do with the transient conditions in entering or leaving a curve. Here the relation of radius of gyration (about the vertical axis) to wheelbase and center of gravity location should not exceed the ratio $\frac{i''}{ab}=1$; in other words, the center of percussion about the front-suspension center should not extend beyond the rear-suspension center. If the moment of inertia exceeds this limit, a greater steering force at the front wheels is required to accelerate the car angularly into a curve than is necessary after the steady state has been reached. Here again, the initial steering angle must be cut back and oversteering is introduced. The action in leaving the curve can be even worse because the car will tend to require positive steering out of the curve rather than merely the straightening of the front wheels. If this condition is superimposed on a car which normally oversteers, the result is a real, handling "pig." These dynamic considerations are fundamental to the design of a rear-engine car because they show that it is undesirable to augment the radius of gyration by overhanging the powerplant beyond the rear axle. This is aside from its tendency to exaggerate the proportion of total weight on the rear wheels.

The importance of the handling problem in connection with rear-engine mounting has been correctly emphasized. Yet it is felt that a 45–55 weight distribution might be workable. However, the weight of evidence is very much against this expectation, barring some entirely new and successful approach to rear-wheel steering. It would be far safer to set 50–50 as a working limit for a rear-engine design under the most unfavorable loading condition. Some rather extensive design studies of my own have shown that this objective can be realized, given the certain specifications (Table A).

A powerplant of the indicated weight and size is clearly the missing link in this enticing picture. This is right in line with the conclusion that the rear-engine car must wait for a compact, light-weight powerplant with present high output. The size of the job to be done is brought out by comparing the 750-lb figure with the 1150 lb now required for a typical 300-hp, internal-combustion engine with automatic transmission and all accessories including cooling. The present trend toward ever greater performance results in a vicious circle in which each increment of power and torque output generates a geometric progression of weight increases throughout the vehicle, requiring still further output to reach the performance goal. A reversal of the powerplant weight trend will start a similar chain reaction of weight reductions that can have far-reaching consequences.

The light-weight powerplant is far from visionary. For example, serious work is already underway on die-cast aluminum engine blocks. Moreover, the new types of powerplant under development, such as gas turbines and free piston, if successful will drastically reduce present weights, especially if heavy transmissions can be eliminated. Against these competitive threats, I venture to predict that the internal-combustion engine will not give up without a real struggle.

A discussion of handling cannot omit at least some mention of aerodynamics. To paraphrase Mark Twain, automobile aerodynamics is like the weather—everybody talks about it but nobody does anything about it. I think it is safe to say that the precise location of the center of side wind pressure is an unknown quantity for any American automobile. However, there is good reason to believe, as a matter of observation, that the center of pressure is typically quite far forward of the center of gravity. As a matter of fact, that is where it should be, within reason, for stability in a cross wind. Here again, the force distribution should favor the front wheels, so as to demand a greater slip angle at front than at rear. Therefore, I see nothing serious in this regard for a rear-engine car that the stylist could not compensate for with a little more rear fin.

In conclusion, I should like to submit the thought that the rear-engine car, if it is to win wide acceptance in the United States, will do so not because of any engineering brainstorm that will suddenly solve all the technical problems. Rather, it will come only through an evolutionary process. Even then, it will prevail only if the basic trends dictated by economics, styling, and powerplant developments, all lead unmistakably toward rear-engine mounting.

VALVE TRAIN WEAR

AS AFFECTED BY----Metallurgy,

WEAR has been the subject of much study by lubricant suppliers and engine manufacturers since the early days of the automobile. The many factors which influence wear have made it extremely difficult to reach any general conclusions which might be applicable to the variety of conditions existing on the many rubbing surfaces in engines.

During 1953 and 1954 a number of car manufacturers and oil companies reported field service problems arising from excessive wear of tappets and cams. Several papers appeared presenting both field data and laboratory test results. However, the conclusions reached were not in general agreement. A realization of the large number of variables involved and the need for duplication of tests to attain reasonable statistical significance in wear tests made it appear that a cooperative effort would discover the facts most effectively. The CLR Camshaft and Valve Tappet Wear Group was, therefore, formed with the long range objective of developing techniques for evaluating the compatability of oils with valve gear of different designs and metallurgical combinations.

After considering the data available in the fall of 1954, this group concluded that more extensive field test information was essential before their goal could be attained. A field test program was planned immediately and put into operation in the spring of 1955. Cam and tappet wear, spalling, and scuffing in field service have all been investigated as functions of valve-gear design, metallurgy, lubricant properties, and type of operation. This test program was completed during 1956 and this paper is based upon the results obtained.

Test Program

Sixteen car makes were selected, representing a wide range of cam and tappet design. Eight different combinations of cam and tappet materials were employed. These were not all in production during 1955 but all have been recently. They were selected to provide information on as many variables as

Table 1—Design and Metallurgy Characteristics of Cars Used in Tests

Car	Camshaft			Valve Tappet				Maximum Compression Stress
	Material	Taper	Surface Treatment	Type	Crown	Material	Surface Treatment	
1	S	None	None	Hydraulic	None	CCI	Ferrox	161,000
2	HCI	6–7 min	None	Hydraulic	50–80 in. Radius	S HCI	Lubrite [a] Lubrite	160,000 141,500
3	HCI	4–7 min	Lubrite	Hydraulic	50–80 in. Radius	HCI	None	173,000
4	HCI	None	Lubrite	Hydraulic	None	HCI	None	———
5	S	None	Lubrite	Hydraulic	None	CCI	Lubrite	100,000
6	HCI	8–10¾ min	None	Hydraulic	0.003–0.005 in.	HCI CCI	Lubrite Ferrox	162,500 177,000
7	HCI	5–8½ min	None	Hydraulic	0.003–0.005 in.	HCI CCI	Lubrite Ferrox	162,500 177,000
8–9	HCI	7–10 min	None	Hydraulic	0.003–0.005 in.	HCI CCI	Lubrite Ferrox	162,500 177,000
10	CI	6–8 min	Phosphate	Solid	50 in. Radius	S	None	135,300
11	CI	6–8 min	Phosphate	Solid	50 in. Radius	S	None	119,800
12	CI	6–8 min	Phosphate	Hydraulic	50 in. Radius	CCI	None	129,000
13	HCI	0.001–0.002 in. per in.	Lubrite	Solid	50–70 in. Radius	CCI ACCI-1 ACCI-2	Lubrite	105,000
14	HCI	6–8 min	Lubrite	Hydraulic	30–40 in. Radius	HCI	Lubrite	145,000
15	HCI	6–8 min	Lubrite	Hydraulic	30–40 in. Radius	HCI	Lubrite	163,500
16	S	6–8 min	Lubrite	Solid	0.0024–0.0036 in.	CCI	[b]	102,000

[a] Also grit blasted.
[b] Steam tempered, lubrite optional.

Driving Conditions, and Lubricants

Report of the Field Survey of the Camshaft and Valve Tappet Wear and Corrosion Group of the Engine Lubricants Division of the Coordinating Lubricant and Equipment Research Committee of the Coordinating Research Council, Inc.

V. Ayres, Eaton Mfg. Co.; J. B. Bidwell, General Motors Corp.
A. C. Pilger,Jr., Tidewater Oil Co.; R. K. Williams, Lubrizol Oil Co

This paper was presented at the SAE Annual Meeting, Detroit, Jan. 18, 1957.

possible. More than one tappet material was used in some engines to obtain direct comparisons of these materials. The pertinent design and metallurgy characteristics of the cars used are summarized in Table 1.

Previous work by several investigators had demonstrated the importance of oil-additive composition upon cam and tappet performance. For this reason, four reference oils were compounded which differed only in this respect. A Midcontinent base stock with V.I. improvers added to produce a 10W-30 viscosity grade was used to permit the use of one grade for both winter and summer operation. Though the oils were not commercial oils, they were compounded with commercial additive materials. The additive level, as measured by sulfated ash, was about Supplement 1 level. Typical inspection data are given in Table 2. The following is a general description of the additive compositions:

Oil 1—(REO-128-54) Base oil, V.I. improvers, and barium phenate.

Oil 2—(REO-129-54) Base Oil, V.I. improvers, zinc dialkyl dithiophosphate to provide 0.2% zinc, and barium sulfonate.

Oil 3—(REO-130-54) Base oil, V.I. improvers, one-half the barium sulfonate in oil 2, one-half the barium phenate in oil 1, and zinc dialkyl dithiophosphate to provide 0.05% zinc.

Oil 4—(REO-131-54) Same as oil 3 except that 0.5% of sulfurized olefin replaced the zinc dialkyl dithiophosphate.

Thirty laboratories representing the oil and automobile industries operated 295 cars for approximately one year on this program. These participants installed new measured cams and tappets at the start of the test, serviced the cars during the test period in accordance with an established schedule, and supplied the Inspection Panel with the wear measurements and test parts at its conclusion. No restrictions were placed on the type of operation during the test period. Consequently, operating conditions were an additional variable. The Inspec-

Table 2—Laboratory Inspection of Test Oils

CRC Oil Code No.	Base	128–54	129–54	130–54	131–54
IBM Oil Code No.	Oil[a]	1	2	3	4
Tests					
Gravity, deg API	31.4	29.6	28.8	29.4	29.4
Viscosity, SUS					
At 100 F	310.0	341.0	319.0	332.0	331.0
At 200 F	60.1	62.2	60.0	61.0	61.0
Viscosity Index	132.8	130.7	130.0	129.6	129.8
Neutralization No. (D-664)	0.04	0.16	–	0.48	0.20
Flash, O.C., F	445	–	–	–	–
Sulfated Ash, weight %	–	1.10	1.50	1.20	1.02
Phospphorous, weight %	–	–	0.20	0.05	–
Barium, weight %	–	0.67	0.52	0.62	0.62
Zinc, weight %	–	–	0.22	0.05	–
Sulfur, weight %	0.11	0.32	0.64	0.39	0.46

[a]A 95 V. I. solvent-treated Midcontinent stock, plus V. I. improvers.

THIS paper is a report of tests performed in 1956 by the Camshaft and Valve Tappet Wear Group of the Coordinating Research Council. Cam and tappet wear, spalling, and scuffing were studied as functions of valve-gear design, metallurgy, lubricant properties, and type of operation.

Some of the results announced by the Group are:

1. Oil composition had considerable effect on cam and tappet wear when chilled-cast-iron or steel tappets were used, and on the spalling of the former.

2. Only chilled-cast-iron tappets showed appreciable spalling tendency.

3. Tappet scuffing was more dependent on metallurgy-design than on oil composition.

4. Tappet spalling tendency seemed to be related to the rate of wear.

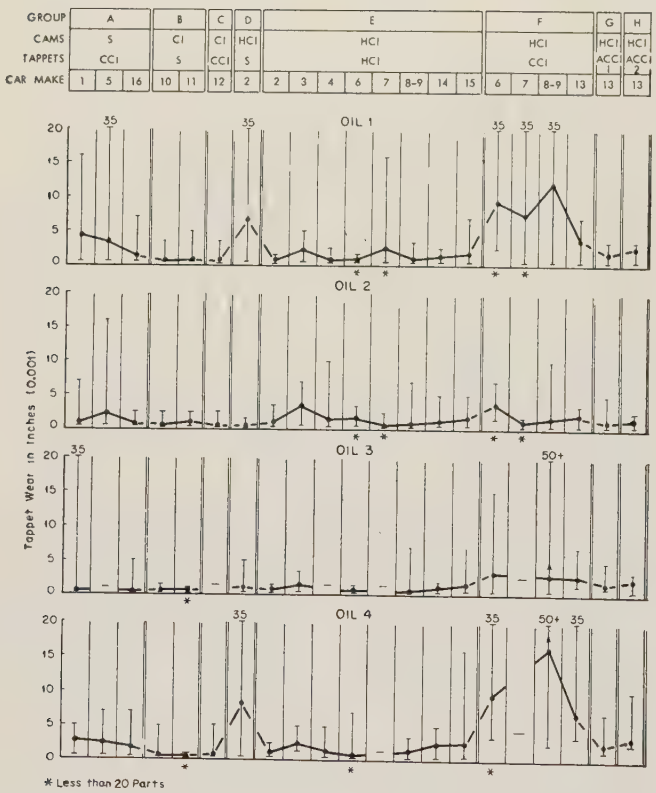

Fig. 1—Summary of tappet wear

tion Panel made subjective observations on the condition of all of the test parts and supplied this data along with wear measurements to the Analysis Panel. The large amount of information collected necessitated the use of punched cards to permit thorough analysis. To aid participating laboratories in the conduct of their own analyses, each was supplied with a set of these cards.

Table 3—Abbreviations Used in Paper

		Material
Cams	S	Carburized steel
	CI	As-cast cast iron
	HCI	Hardened cast iron
Tappets	S	Carburized steel
	HCI	Hardened cast iron
	CCI	Chilled cast iron
	ACCI-1	Alloy chilled cast iron-1
	ACCI-2	Alloy chilled cast iron-2

Table 4—Effect of Tappet Metallurgy on Tappet Wear in Cars Using HCI Cams

Car	Tappet Material	Average Tappet Wear (0.001 in.) Oil				Maximum Tappet Wear (0.001 in.) Oil			
		1	2	3	4	1	2	3	4
2	S	6.6	0.6	1.1	8.3	35	1.5	5.0	35.0
	HCI	0.9	1.5	1.0	1.1	1.5	3.5	1.5	2.5
8–9	CCI	12	1.9	3.8	16.5	35	10	50 +	50 +
	HCI	1.2	1.2	0.8	1.8	3.5	7.0	7.0	3.5
	CCI	3.9	2.1	2.8	6.6	7.0	3.5	7.0	35
13	ACCI-1	2.0	1.3	1.8	2.8	3.5	5.0	5.0	7.0
	ACCI-2	2.5	1.5	2.4	3.5	3.5	2.5	3.5	10.0

In discussing the results, we will be concerned primarily with combinations of variables that produced large effects, since these are the ones which might be expected to cause service problems and also will be the most useful in establishing correlation with laboratory tests. Distribution of values for individual parts as well as averages are considered in evaluating the results, since these provide a means of estimating variability and significance.

In order to shorten the discussion of results, abbreviations have been used to describe cam and tappet material. These are shown in Table 3.

Tappet Wear

Fig. 1 summarizes all of the tappet wear data. Cars utilizing the same metallurgical combinations are grouped together so that effects of the variables may be most readily separated. Average tappet wear and the observed spread in wear is shown for each car make-metallurgy-oil combination. Several general observations can be made. Considering all of the cars designs and metallurgies, oil 3 seems to provide the best overall wear protection. Groups B (CI cams and S tappets), C (CI cams and CCI tappets), E (HCI cams and HCI tappets), and G and H (HCI cams and ACCI tappets) appear to be least affected by oil composition. It should be noted that the trend in recent models has been toward the use of these metallurgical combinations. The metallurgical combinations which are most sensitive to lubricant effects are groups A (S cams and CCI tappets), D (HCI cams and S tappets), and F (HCI cams and CCI tappets).

It is quite difficult to evaluate design effects independent of metallurgy unless comparisons are made between cars in the same group. For example, rather large differences are apparent between cars 1, 5, and 16 when all are operated on oil 1. These differences may be considered to result primarily from design differences. Similarly, large design effects are found with the cars of group F, especially when operating on oils 1 and 4. It is likely that the most and the least severe designs do not employ the same metallurgy and, therefore, are not directly comparable. Thus, the range of design effect is not

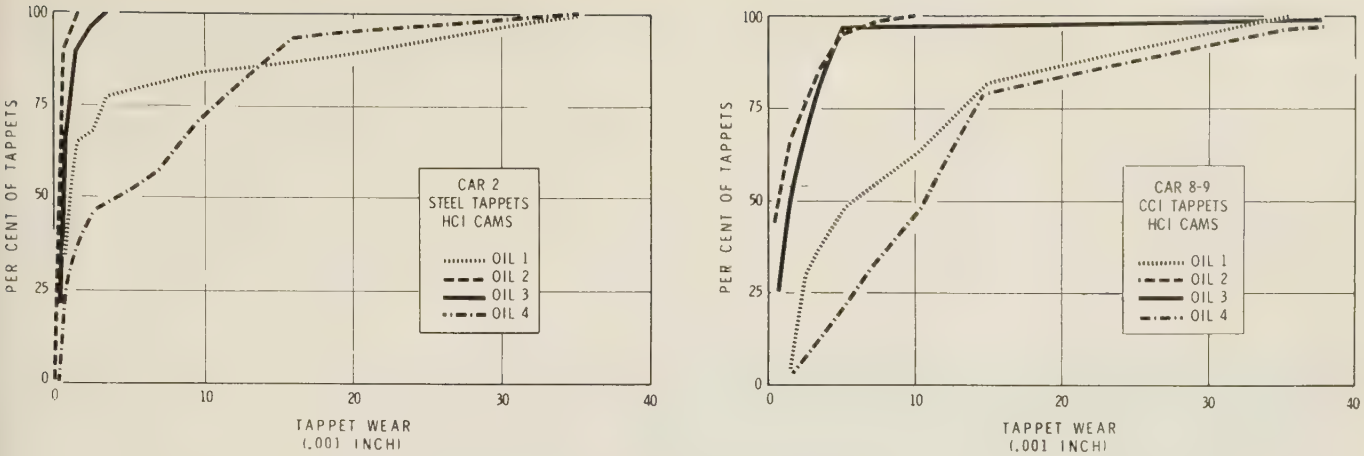

Fig. 2—Tappet wear distribution

very well-established but it is clearly quite a large one.

The influence on tappet wear of tappet metallurgy alone can be seen most directly in cars which used more than one tappet material. This was done in cars 2, 6, 7, 8–9, and 13. All of these cars used HCI cams and, therefore, the tappet material variable alone can be evaluated. Tappet wear data are summarized in Table 4 for cars 2, 8–9, and 13. Low average and maximum wear resulted in car 2 with all oils when HCI tappets were used. However, the least wear (both average and maximum in car 2) was obtained with S tappets and oil 2, even though this tappet material experienced extensive wear when oils 1 and 4 were used. This observation points out the strong interaction between oil and metallurgy. Both CCI and HCI tappets were used in car 8–9. Again the wear of the HCI tappets was affected only slightly by the oil composition. Though the CCI tappets exhibited a wide range of wear with oils 1, 3, and 4, the results with oil 2 are comparable to the wear of the HCI tappets. Wear differences with all oil and tappet material combinations in car 13 are not outstanding. Only oil 4 produced significant differences and here the CCI tappets suffered greater wear than either of the other materials.

The distribution of tappet wear encountered in car 2 with steel tappets and car 8–9 with CCI tappets is shown in Fig. 2. In this figure, the ordinate corresponding to any point on each curve represents the fraction of all tappets which wore less than the wear given by the abscissa of the point. In addition to illustrating the wide spread in wear data, this type of plot gives a graphic illustration of the large influence of oil with these metallurgy-design combinations. For example, only 25% of the steel tappets operated in car 2 with oil 2 wore more than 0.0005 in. This same metallurgy-design resulted in wear exceeding 0.0100 in. for 25% of the tappets when oil 4 was used. This is an increase of 20 times. Similar large lubricant effects can be seen in car 8–9.

Cam Wear

Cam wear data is summarized in Fig. 3 in a manner similar to that employed for tappet wear. It will be seen that the same general trends are shown

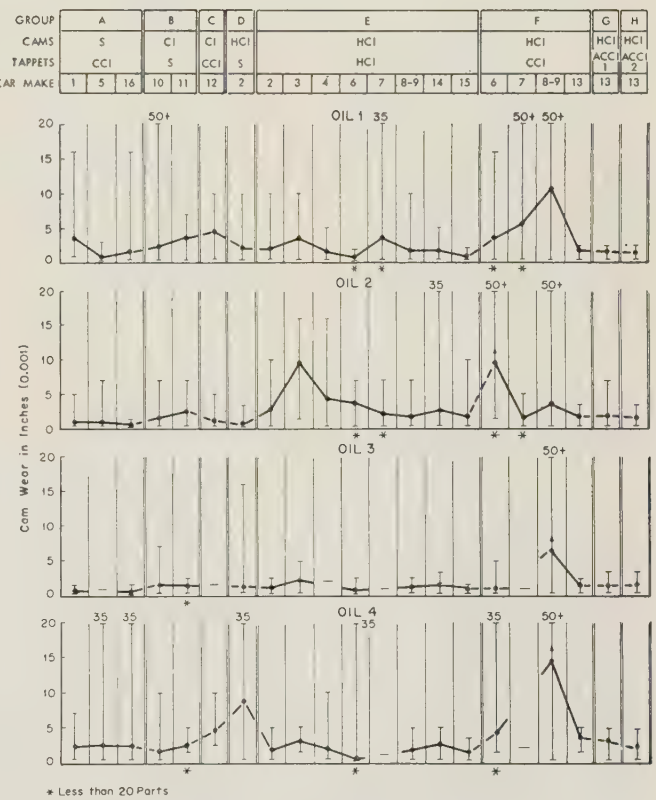

Fig. 3—Summary of cam wear

concerning the influence of the variables as were found in the case of tappet wear. Oil 3 provides adequate wear protection for all of the metallurgy-design combinations employed in this program. Comparison of cars within a single group permits study of design effects. For example, in group E, cars 3 and 8–9 operating with oil 2 exhibit rather large differences in average cam wear—car 3 wearing three times as much as 8–9. Similarly, in group F car 8–9 suffered about 6 times the wear of car 13 when both are operated on oil 1. These wear differences indicate that design variations may influence cam wear as much as do metallurgy and oil composition. Again, the influence of tappet metallurgy alone can be seen directly only in cars which utilized split sets of tappets. This effect is shown for

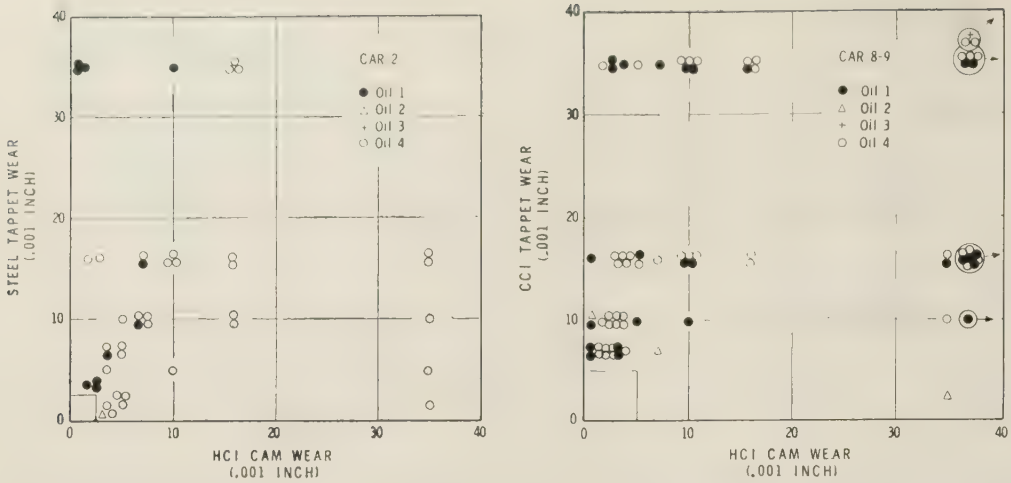

Fig. 4—Relation between cam and tappet wear

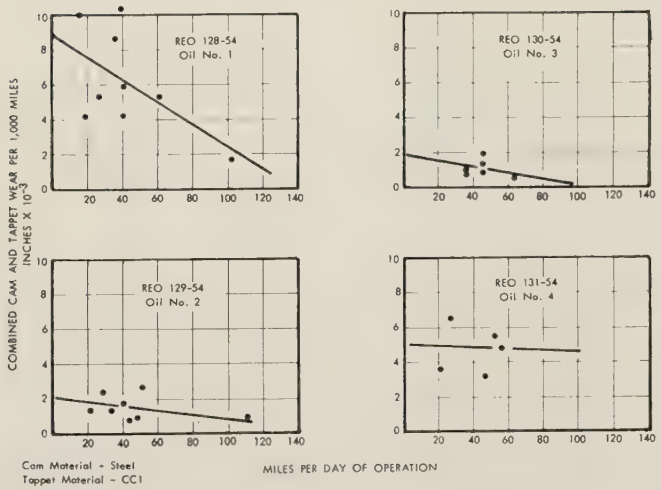

Fig. 5—Variation of combined cam and tappet wear with miles per day of operation, Car 1

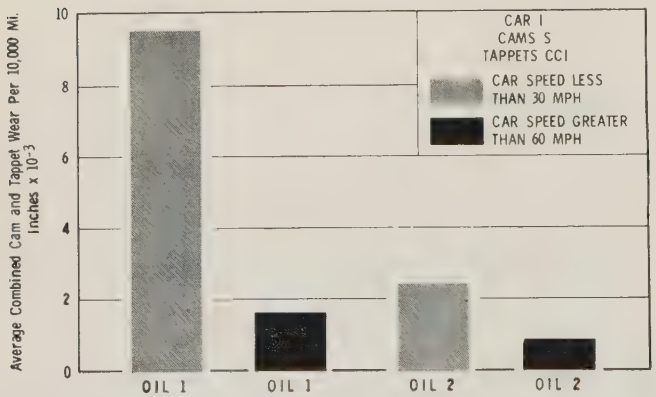

Fig. 6—Effect of type of driving on combined cam and tappet wear in highly controlled test at extremes of operation

Table 5—Effect of Tappet Metallurgy on Cam Wear in Cars Using HCI Cams

Car	Tappet Material	Average Cam Wear (0.001 in.) Oil				Maximum Cam Wear (0.001 in.) Oil			
		1	2	3	4	1	2	3	4
2	S	2.0	0.8	1.4	8.7	10	3.5	16	35
	HCI	3.5	2.8	1.1	1.9	10	10	2.5	5.0
8–9	CCI	10.8	3.0	5.0	13.4	50+	50+	50+	50+
	HCI	1.7	1.9	1.4	2.9	10	7.0	3.5	5.0
	CCI	1.8	1.7	1.5	3.7	2.5	3.5	2.5	7.0
13	ACCI-1	1.5	2.0	1.5	3.3	2.5	7.0	3.5	7.0
	ACCI-2	1.6	1.6	1.4	2.3	2.5	3.5	3.5	7.0

cars 2, 8–9, and 13 in Table 5. As was the case with tappet wear, in cars 2 and 8–9 it appears that on cams operating with HCI tappets wear is generally less than the wear experience by cams operating with S or CCI tappets. This is especially apparent from the maximum wear values. Only a small effect of metallurgy can be seen in car 13 where relatively low wear was observed with all oils and tappet materials.

Relation Between Cam and Tappet Wear

The similarity in effect of lubricant on tappet and cam wear in cars 2 and 8–9 suggests that there might be some correlation between cam and tappet wear. Fig. 4 shows plots of corresponding cams and tappet wear for individual mating parts. That is, each point represents the wear of one tappet and its mating cam. Points where both cam and tappet wear were less than 0.0025 in. for car 2 and 0.0050 in. for car 8–9 have been omitted for clarity. It can be seen that extremes of either cam or tappet wear can occur without excessive wear of the mating part. This indicates that a cause and effect relationship does not exist between cam and tappet wear. However, the fact that there is some correlation between average cam and average tappet wear suggests that both may result from the same cause. It is also evident that most of the bad wear of both cams and tappets occurs with oils 1 and 4, since only a few points are shown representing results with oils 2 or 3. Finally, in the case of 2, it appears that oil 1 tends to produce large S tappet wear but relatively low HCI cam wear while the use of oil 4 results in generally lower tappet wear but high cam wear. Similar conclusions are not possible in car 8–9 where CCI tappets operate with an HCI cam.

Influence of Operating Conditions

Since no restrictions were placed on the operation of the test cars, it was possible to separate out to a limited extent the influence of driving conditions on cam and tappet wear. Determination of this effect was limited by the fact that in most groups the majority of the cars were operated in mixed service and extreme variations in service were not attained. Cars of make 1 can, however, be used to illustrate the effect since there were a larger number of these on each oil than other makes and relatively large differences in operation and wear were observed. One of the problems encountered in this correlation was that of defining the service condi-

tions. Two methods were used. Data supplied by the test participant concerning the relative amount of trip and city driving for each car resulted in the same conclusions reached using the second method described here. Since it had previously been suggested that engine speed has an effect on valve train wear, this speed effect was approximated for each car by assuming average engine speed to be proportional to the total miles the car operated during the test divided by the length of time the car was on test. This implies that cars driven greater average distances per day also operate at higher average speeds. This is an imperfect assumption but not completely unreasonable. In Fig. 5 the average combined wear rate of tappets and cams is plotted for each car of make 1 as a function of the miles driven per day. The wear rate has been used rather than total wear due to relatively large differences in total mileage on these cars. In spite of the scatter of points, it is possible to draw some conclusions re-

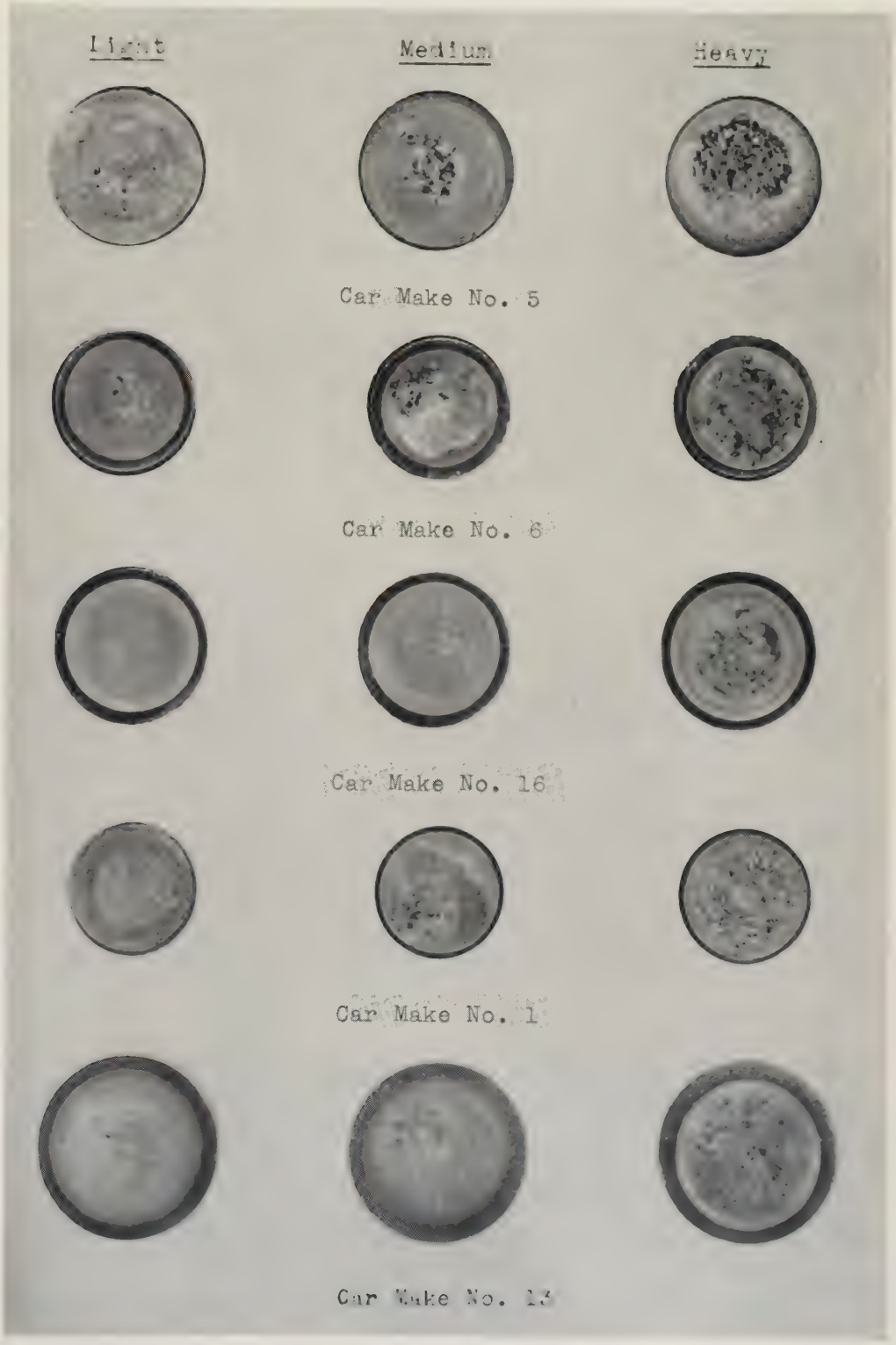

Fig. 7—CLR-ELD camshaft and valve tappet wear and corrosion field test program. Lifter pitting reference parts

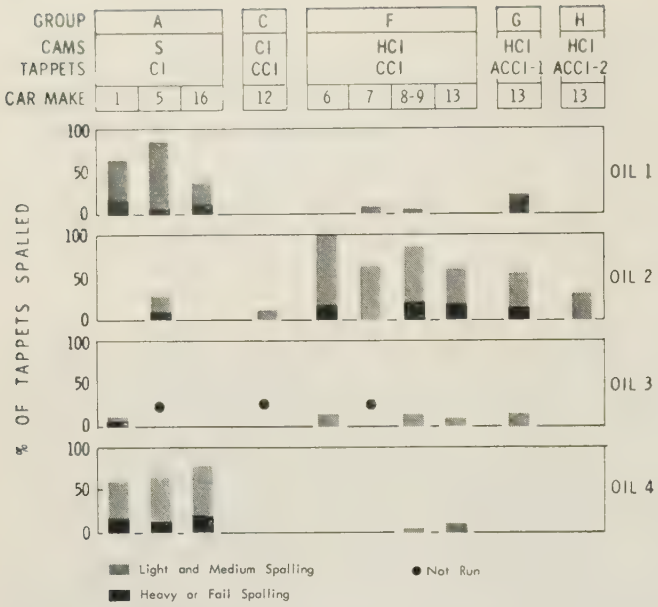

Fig. 8—Tappet spalling, interrelation between metallurgy and lubricant

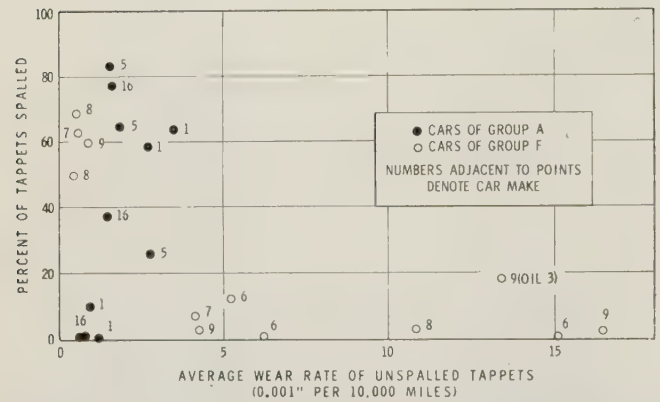

Fig. 9—Tappet spalling as affected by tappet wear (chilled-cast-iron tappets)

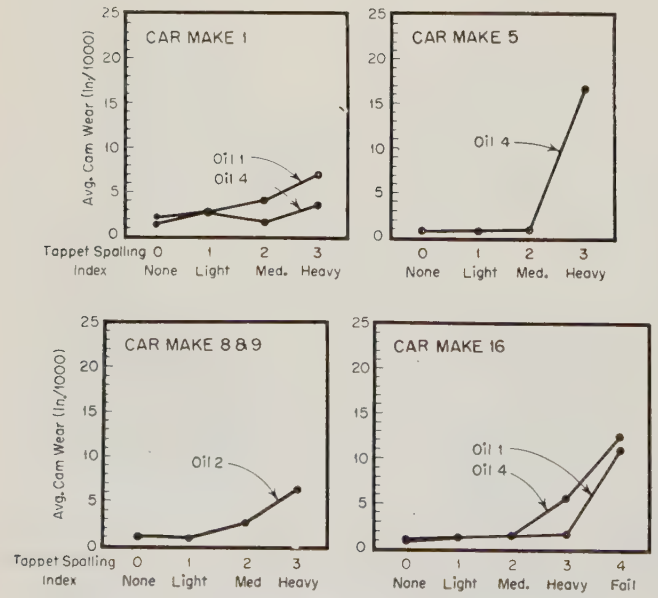

Fig. 10—Cam wear as affected by tappet spalling severity

garding trends. The wear rate seems generally to be most severe for low daily mileage. This trend is most noticeable with oil 1 where large differences in operation occur and where the wear is relatively large. The trend is less apparent when the wear level is low or where the variation in driving conditions is small. These same conclusions may be reached from the results of four tests which were run under more controlled conditions. Two cars of make 1 were operated for one year in shuttle service at speeds below 30 mph. Two other cars of make 1 were operated in trip service only. In these cars the speed exceeded 60 mph most of the time. One car in each type of service used oil 1 and the other oil 2. The results of these tests are given in Fig. 6. The marked effect of operating conditions on wear is apparent. Using oil 1 the low-speed wear rate is six times that of the high speed. With oil 2 this ratio is 2.7. It also appears that oil differences are more pronounced in low-speed operation. In low-speed service the wear rate of oil 1 is about four times that of oil 2, but in high-speed service this ratio is only about 2/1.

Tappet Spalling

The extent of spalling of each tappet was observed and rated by the Inspection Panel. This was done by selecting test parts from those submitted by the participants to serve as reference standards. The parts selected are shown in Fig. 7. Each tappet was then rated by comparison with the standards established for that make. Those which were worse than heavy were arbitrarily designated failures.

The influence of metallury-design combinations on spalling is shown in Table 6. From this tabulation it is clear that only groups A, C, F, G, and H using CCI or ACCI tappets experience significant spalling. The effect of lubricant upon spalling in these groups is shown in Fig. 8. The most important observation to be made is that there is an interaction between lubricant and metallurgy effects. This is illustrated by the fact that oils 2 and 3, which permitted the least spalling with group A cars (S cams), caused the greatest spalling in the remainder of the groups which used CI and HCI cams. Considering all of the metallurgy-design combinations, oil 3 gave the least tappet spalling.

A study was made to determine whether any relation exists between tappet wear rate and spalling tendency. Fig. 9 is a plot of the per cent of all tappets spalled in cars 1, 5, and 16 of group A and 6, 7, and 8–9 of group F as a function of tappet wear. Each point represents the tappet spalling and corresponding tappet wear for a particular car make and oil. In determining the tappet wear for each oil and car, only the unspalled tappets were averaged, since the loss in length due to spalling is not wear in the usual sense. Points for cars of group A have been distinguished from those for cars of group F. It can be seen that for all cars in group A there is little difference in wear. Evidently spalling is independent of wear for this group. The situation is somewhat different in the case of group F. The CCI tappets in these cars did not experience appreciable spalling when the wear exceeded about 0.004 in. per 10,000 miles. The most extensive spalling appeared with the lowest wear. This general relation fits the data for all oils.

It might be expected that the roughened tappet face resulting from spalling would seriously affect cam wear. Fig. 10 illustrates the average cam wear associated with tappets of different degrees of spalling found in cars 1, 5, and 16 using steel cams and CCI tappets and in car 8–9 using HCI cams and CCI tappets. Though there is a decided increase when the tappets are heavily spalled, there is relatively little effect when the spalling is light or medium. This would indicate that cam wear is not the result of sliding on the roughened tappet until extensive spalling damage has occurred.

Tappet Scuffing

Scuffing of tappets was observed in a large number of cases and was evaluated by the Inspection Panel. A rating scheme similar to that employed for spalling severity was utilized. The standards employed are shown in Fig. 11. Only three degrees were distinguished. Table 7 is a tabulation of the scuffing observed. Although some scuffing was found with all metallurgy-design combinations except groups C and H, only car make 1 of group A evidenced a significant number of tappets with heavy scuffing. This design used S cams and CCI lifters, which are intended not to rotate during operation.

In cars using two or more tappet materials, it was possible to evaluate the influence of this variable on tappet scuffing independently. Split metallurgies were used only in cars with HCI cams. With this material HCI tappets suffer much less scuffing than do either steel or CCI tappets.

Though some scuffing was observed with all oils, oil 2 is the only one which exhibited no heavy scuffing with any of the metallurgy-design combinations used in this test program.

It has been suggested that scuffing and spalling of tappets are related. Cars 1 and 5 both exhibited appreciable scuffing and spalling and the relation between these factors is shown in Table 8. Both the per cent of scuffed tappets which were also spalled on each oil and the per cent of spalled tappets which were also scuffed are shown. From these results it is clear that these are independent phenomenon.

Cam Damage

Spalling and scuffing of the cam noses was also observed and rated by the Inspection Panel. Spalling was evident in any degree only in cars of groups B, C, and F. Groups B and C utilize CI cams and S and CCI tappets, while those of group F have HCI cams and CCI tappets. Little influence of lubricant was observed except in makes 6, 7, and 8–9 using CCI tappets. However, it appears that the incidence of spalling is reduced with oils 3 and 4. In these cars a significant amount of cam spalling occurred only with oil 2, but with this oil 54–88% of the cams spalled. Cam spalling has a small but consistent tendency to increase cam wear in the case of all of the makes which exhibited spalling. In the case of makes 10 and 11, the data showed that medium spalling on one oil gave less wear than a case of no spalling on another oil. There is no consistent effect of cam spalling on tappet wear, however.

Cam scuffing was observed only in a relatively few cases and then primarily with oils 3 and 4 in car makes 2 (using S tappets) and 8–9 (using CCI tappets). Though this type of damage did not occur often, its effect upon cam wear was very large when it was found. In car 8–9 using CCI tappets, a marked increase in tappet wear was associated with scuffed cams. This was also the case in car 2 when oil 4 and S tappets were used, but oil 3 maintained tappet wear about the same whether the cams scuffed or not.

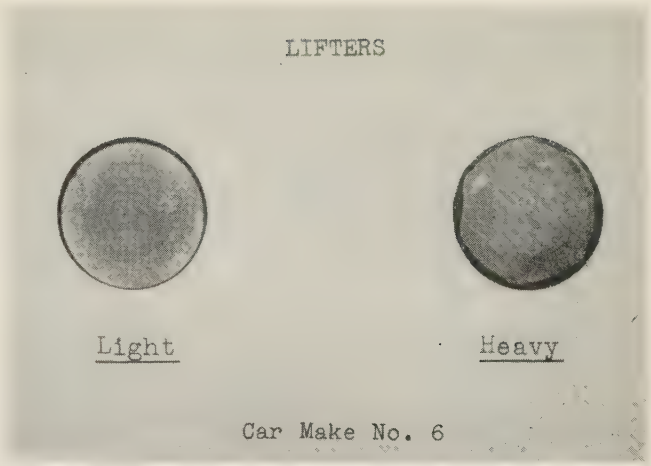

Fig. 11—CLR-ELD camshaft and valve tappet wear and corrosion field test program. Scuffing reference parts

Table 6—Effect of Metallurgy Design on Tappet Spalling

Group	Cams	Tappets	% Tappets Spalled on All Oils				
			Light	Medium	Heavy	Fail	Total
A	S	CCI	19	9	7	0.7	35.7
B	CI	S	–	–	–	–	0
C	CI	CCI	1.7	2.9	–	–	4.6
D	HCI	S	–	–	–	–	0
E	HCI	HCI	0.4	0.1	–	–	0.5
F	HCI	CCI	8.3	11.7	4.0	–	24
G	HCI	ACCI-1	8	11.4	2.3	–	21.7
H	HCI	ACCI-2	4.5	2.3	–	–	6.8

Table 7—Effect of Metallurgy Design on Tappet Scuffing

Group	Cams	Tappets	% Tappets Scuffed on All Oils		
			Light	Heavy	Total
A	S	CCI	31.9	6.5	38.4
B	CI	S	10.4	0.1	10.5
C	CI	CCI	–	–	0
D	HCI	S	11.2	0.1	11.3
E	HCI	HCI	3.7	0.1	3.8
F	HCI	CCI	4.8	1.5	6.3
G	HCI	ACCI-1	8	–	8.0
H	HCI	ACCI-2	–	–	0

Table 8—Relation between Tappet Scuffing and Tappet Spalling on Cars with CCI Tappets and S Cams

Car	% Scuffed Tappets Also Spalled[a]			
	Oil 1	Oil 2	Oil 3	Oil 4
1	54(73)	0(13)	3(63)	53(88)
5	82(39)	3(55)	[b]	66(83)
Car	**% Spalled Tappets Also Scuffed[c]**			
	Oil 1	Oil 2	Oil 3	Oil 4
1	65(102)	[d]	8(13)	79(66)
5	37(61)	62(16)	[b]	8(39)

[a] Number of scuffed tappets in parentheses.
[b] None tested.
[c] Number of spalled tappets in parentheses.
[d] None spalled.

Tappet Rotation

Extent of tappet rotation was also observed and recorded at the time of inspection. Analysis of this data indicated that design and metallurgy were the

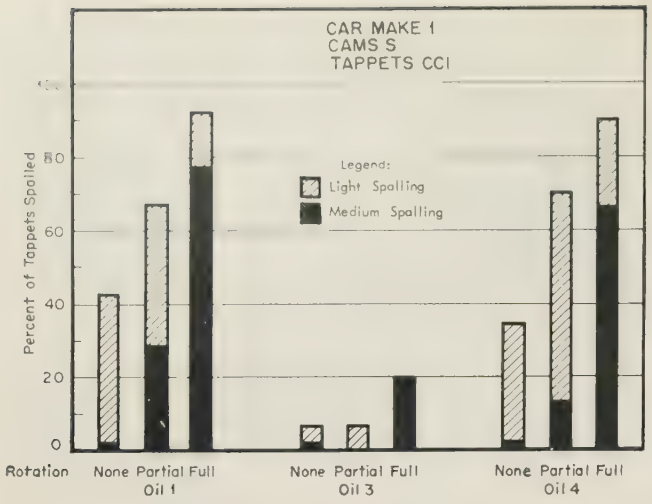

Fig. 12—Effect of tappet rotation on tappet spalling

principal factors influencing rotation. Car 1 which is designed to avoid rotation had, of course, a large percentage of nonrotating tappets on all oils. Only makes 10, 11, and 13 also had any appreciable number of tappets which did not rotate fully. The data for cars 1, 10, and 11 were utilized to evaluate the effect of tappet rotation upon cam and tappet wear. Though the differences are small, there appears to be a trend toward higher cam and tappet wear when tappets rotate than when they do not.

It has been postulated that tappet rotation may be related to tappet spalling. Car 1 provides sufficient data to evaluate this relation. Fig. 12 illustrates this effect. Oil 2 is not shown since no spalled tappets occurred with this oil. It is clear that more spalling is observed with rotating tappets than with nonrotating for car 1 where the design is such as to discourage rotation. This trend is especially marked for heavily spalled tappets.

Correlation between tappet scuffing and rotation was also investigated for makes 1, 10, and 11. A consistent trend toward reduced scuffing with increased rotation is apparent with all oils.

Conclusions

The following summary and conclusion are quoted directly from the CLR Report.

Thirty laboratories submitted data on a total of 295 cars having a variety of camshaft and tappet metallurgy-design combinations and operated on four different test oils. Results of this study have shown that oil composition, metallurgy, and design all have independent as well as related effects in controlling the degree of wear, scuffing, and spalling. Wide differences in these phenomena were observed with certain combinations of oil compositions, metallurgy, and engine design. However, even in cases of extreme wear, spalling, or scuffing, the vehicles were able to complete the test. Detailed observations of the survey are:

1. The differences in performance among the oils, metallurgies, and design were great enough to provide suitable background for developing a laboratory test or tests to correlate with camshaft and valve lifter performance in service.

2. Oil composition had considerable effect on cam and tappet wear when chilled-cast-iron or steel tappets were used. With these tappets the two oils containing zinc dialkyl dithiophosphate gave considerably less wear than the two oils which did not contain this chemical.

3. Oil 3 gave the least wear in most of the car makes. Oil 2 gave higher wear in some makes than oil 3 and also contained a much higher concentration of zinc dialkyl dithiophosphate than oil 3. This indicates that excessive quantities of this chemical may have an undesirable effect on wear with some metallurgy-design combinations.

4. Oil 2, containing a heavy dosage of zinc dialkyl dithiophosphate, appeared to minimize tappet scuffing severity. In one car group, oil 2 increased cam spalling and provided the greatest resistance to cam scuffing.

5. Oil composition had a marked effect on spalling of chilled-cast-iron tappets. The effects differed noticeably depending on metallurgy-design. For example, oils 2 and 3, which virtually eliminated spalling in cars utilizing steel cams, greatly increased tappet spalling in the cars of a group employing hardened-cast-iron cams. The opposite effect was noted with oils 1 and 4.

6. Unhardened-cast-iron cams in combination with steel or chilld-cast-iron tappets gave negligible tappet wear; but most of the wear occurred on the cams. With all other combinations the average tappet wear was approximately the same as the average cam wear. However, where individual tappets showed high wear the contacting cam did not necessarily do so and vice versa.

7. In combination with hardened-cast-iron cams, chilled-cast-iron, or steel tappets showed considerably more wear than hardened-cast-iron tappets with oils 1 and 4 in cars 2, 6, 8, and 9.

8. Only chilled-cast-iron tappets showed an appreciable spalling tendency. With these tappets some spalling occurred with all types of cams tested, but was least prevalent with unhardened-cast-iron cams. In one make where three types of chilled-cast-iron tappets were distributed evenly among the cams, one type was significantly superior to the other two.

9. Appreciable cam spalling was observed only with unhardened-cast-iron cams and was more severe with steel than with chilled-cast-iron tappets. With these combinations, the cam spalling was accompanied by a slight increase in cam wear but had no effect on tappet wear. The effect of oil composition on cam wear can be greater than the effect of cam spalling, as evidenced by the fact that the cams of make 12 showing medium spalling with one oil wore less than the unspalled cams with another oil.

10. Tappet scuffing is more dependent on metallurgy-design than on oil composition. Only one make evidenced tappet scuffing to a serious degree but the scuffing appeared to cause no objectionable cam distress.

11. In car 1, designed to prevent rotation of tappets, nonrotating tappets gave the least cam and tappet wear. Nonrotation was usually associated with the greatest scuffing tendency in these cars and spalling tendency was greatest for rotating tappets.

12. Most cars in the survey were operated in mixed long and short trip service and no clearcut

effect of driving conditions could be detected. As a result, it is concluded that the type of driving should not affect the conclusions reached above. Results in controlled tests with four cars of make 1 indicate higher wear for two cars operated exclusively on short trips than for two identical cars operated exclusively in high-speed service.

13. There were indications that tappet spalling tendency was related to the rate of wear. In general, a reduction in wear rate was associated with increased spalling tendency. This effect was most clearcut among designs where the wear was sensitive to oil composition.

14. Cam scuffing was not a widespread problem. It occurred to a limited extent in certain combinations of oil and metallurgy-design. When observed, it was generally associated with a many-fold increase in cam and tappet wear.

DISCUSSION

Piston-Ring and Connecting-Rod Bearing Wear With Four Types of Oil

—G. K. Malone
General Motors Corp.

I AM going to present some additional data on piston-ring wear and connecting-rod bearing wear with the same four reference oils. In fact, the data was obtained from 40 cars operating in the program described in the paper.

I would like to emphasize two conditions which should be considered in interpreting the data:

1. The initial measurements on the piston rings and connecting-rod bearings were made after a run-in of 1000 to 2000 miles with the factory installed run-in oils. This means that the rapid wear which may occur during the break-in of new parts is not included in the data.

2. The sample size is small. Duplicate cars of each make were run on each of the four reference oils. We are considering here an average of 16 top piston rings and 16 connecting-rod bearings.

Fig. A shows the relationship of top compression-ring wear to the four reference oils with each of five car makes. The wear, expressed in milligrams of weight loss per 10,000 miles of operation, is plotted on the ordinate. There is a separate bar for each of the four reference oils with each of the five car makes. Cars A, B, and E use chrome-plated cast-iron top compression rings. Car C uses a chrome-plated steel-top compression ring, and car D a lubrited-cast-iron ring.

We would note four observations concerning this plot:

1. There appears to be an indication that oils 2 and 3 offer better wear protection than oils 1 and 4. This is true of all cars except car C, where the wear is relatively low and roughly equivalent with oils 1, 2, and 3.

2. In general, oil 3 with the lower concentration of zinc dithiophosphate appears to give the best protection.

3. In general, oil 4 with the sulphurized olefin treatment appears to give the poorest protection.

4. The difference in the level of wear with a single oil among the five car makes indicates that engine design factors, ring composition, and surface treatment are also important factors in controlling ring wear.

Fig. B relates connecting-rod bearing wear to the four reference oils with the five car makes. The connecting-rod bearing wear expressed as weight loss per 10,000 miles of operation is plotted on the ordinate. There is a separate bar for each of the five car makes. Cars A, B, and E use Durex 100 A connecting-rod bearings. Cars C and D use Moraine 400 connecting-rod bearings.

We would make two observations concering this plot:

1. The weight loss is low for all of the oils and all of the cars.

2. There does not appear to be any consistent oil composition effects on the amount of wear obtained.

We would conclude from this limited amount of data that some extreme pressure agents, such as zinc dithiophosphate, may be quite important in minimizing piston-ring wear. There does not, however, appear to be any comparable oil composition effect on connecting-rod bearing wear.

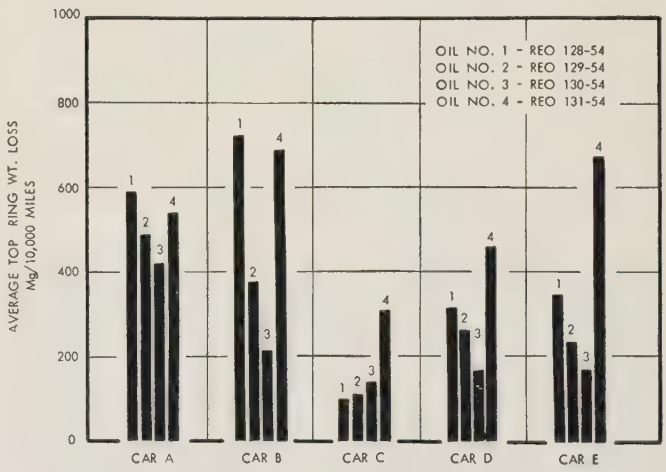

Fig. A—Average top ring weight loss per 10,000 miles of operation

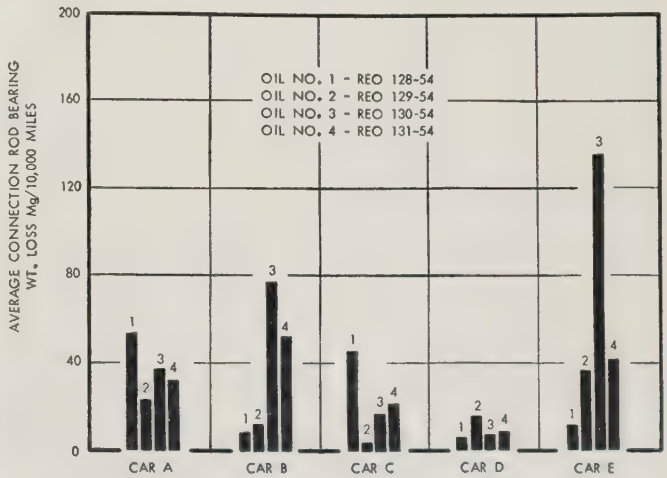

Fig. B—Connecting-rod bearing weight loss per 10,000 miles of operation

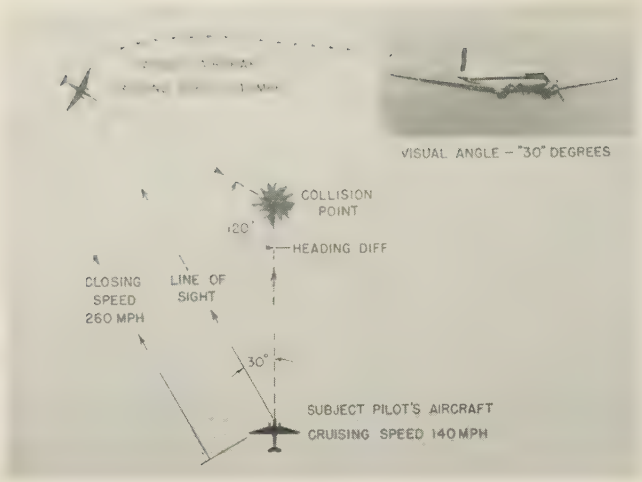

Fig. 1—Conditions of Collision Case III

Visual Avoidance

W. D. Howell and R. B. Fisher,
Civil Aeronautics Administration

This paper was presented at the SAE National Aeronautic Meeting, New York, April 4, 1957.

WE at the Civil Aeronautics Administration's Technical Development Center in Indianapolis are, and have been, continually searching for a solution, or possible solutions, to the mid-air collision problem.

In the past few years the mid-air collision hazard has grown enormously. Prior to World War II, little or no thought was given to the seriousness of congestion in airspace by aircraft. The airplane manufacturer was oblivious to the existence of such a condition; the commercial aircraft operator refused to admit to himself, or to others, that such a condition could never occur in the vast, unlimited airspace; and the airport manager and private pilot either deliberately ignored the developing situation, or they were unaware that the day was near when flying would be hazardous because of saturation of the airspace. However, the situation is now completely reversed and the aviation industry, from designer to pilot, recognize the problems involved with steadily increasing air traffic. We are all vitally interested in a workable solution, even though it be only an interim system or procedure, that will reduce the mid-air collision hazard.

Realizing the magnitude of the groundwork required to develop an adequate solution to the ever-increasing problem, the Technical Development Center initiated basic studies in 1948 by investigating the various factors relating to the mid-air collision problem. Since this start, reports of Airline Pilot Questionnaire Studies, Pilot Eye Movement Studies, Flight Path Studies, and Windshield and Cockpit Visibility Studies have been published. From these studies we established recommendations on cockpit visibility standards for transport-type aircraft. We feel that these standards will improve the visual angles available and should raise the present safety level; however, they will not afford 100% protection. The studies that I am presenting in this paper, therefore, are further steps toward helping us to arive at a solution that will afford substantial collision protection.

In our search for scientific data related to the mid-air collision problem, measurements were taken during daytime flights of distances at which pilots became aware of DC-3 aircraft, normally painted and equipped, as they approached from various angles on courses that would result in collision.

The study was broken up into two phases, the uninformed and the informed. In the former, we tried to simulate the actual cockpit environmental conditions that are present during cruising flights between cities. We informed the subject pilot only that he was to fly the same course twice, first using the VOR course-deviation indicator, and then using VOR and DME with a CAA Type IV pictorial computer. Since we were going to photograph his eye movements during each run, we told him this analysis was being made to compare the amount of eye fixation time spent on the course-deviation indicator while performing normal in-flight duties, as compared to the fixation time spent on the pictorial computer. So the pilot would not overconcentrate on the flight instruments, we told him it was strictly a VFR flight, and in the interest of safety, he should point out to our CAA copilot any airplanes in the vicinity. Thus, the uninformed subject pilot was unaware that he was flying a collision course.

The informed phase of the project was intended to simulate actual cockpit environmental conditions that are present when aircraft are flying in a terminal area. The subject pilot was completely informed of what we were trying to accomplish. He was well-aware that he was on a collision course with another aircraft, but he did not know from which direction the other aircraft were approaching. Most of the subject pilots that performed tests in the uninformed phase were available a second time in the informed phase.

# of Mid-Air Collisions

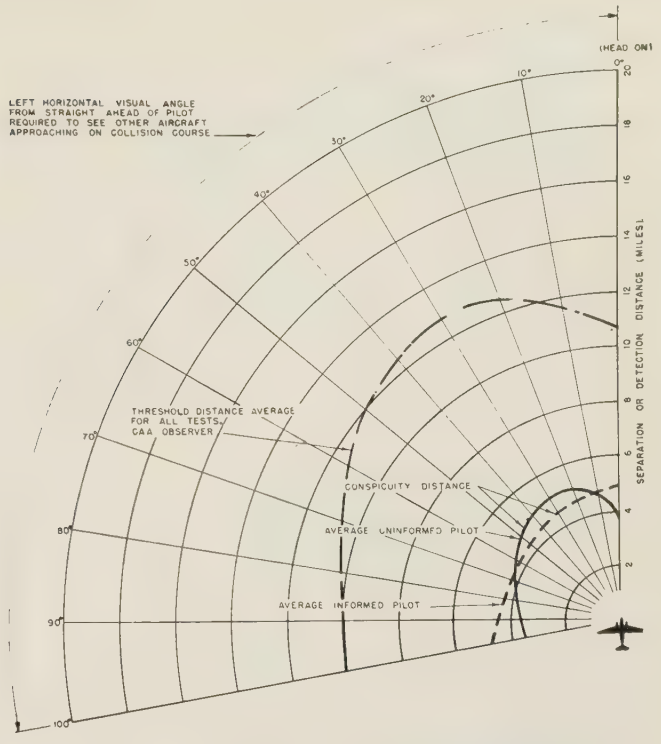

Fig. 2—Conspicuousness of present-day aircraft

Table 1—Conditions of Collision Test Runs

Collision Case No.	Visual Angle, deg left	Subject Aircraft Speed, mph	Target Aircraft Speed, mph	Closing Speed, mph
I	100	120	150	60
II	60	140	140	140
III	30	140	140	260
IV	0	140	140	280

Through the excellent cooperation of the Air Pilots Association, we were able to obtain 64 subject airline pilots. Forty-three pilots participated in the uninformed phase and 21 pilots in the informed phase. Each pilot flew two collision runs, making a total of 128 test runs.

Four different collision cases were investigated. The aircraft speeds and visual angle, or angle from straight ahead required for the subject pilot to see the target aircraft, are listed in Table 1. Fig. 1 illustrates Collision Case III.

The target aircraft was painted white on top with a blue stripe along the side of the fuselage, simulating the paint schemes used by most standard commercial aircraft today. In our tests, we tried to simulate standard conditions on every item possible.

Accuracy of running each collision course was maintained by the following method:

The flight paths of both the subject pilot's aircraft and the target aircraft contained 10 ground check points. Our CAA copilot flying with the subject pilot would notify the target airplane every time the subject pilot's airplane passed over a check point. If the target airplane was not over its corresponding check point at the same instant of time, the pilot of the target aircraft would vary his speed accordingly. In this manner, the constant closing rate and constant relative bearing angles that are present between aircraft during a level cruise collision condition were sustained. Each flight was synchronized on a time basis. Time that the subject pilot spotted the target aircraft was recorded and distance of separation between the aircraft was computed. A CAA engineer flying in the same airplane as the subject pilot and knowing exactly from what visual angle the target airplane was approaching, kept constant vigil until his eyes perceived the target aircraft. This time of detection was recorded and used to compute threshold distance.

All tests were run under approximately the same brightness conditions; that is, time of day (for relative sun location) and prevailing weather conditions (which were CAVU). Tests were held during VFR weather, since 84 out of 86 mid-air collisions during a period of five years (1948–1953) occurred during daylight or twilight hours, with visibility in excess of three miles.

Fig. 2 shows the overall results obtained from the study. Noting the outside curve, you can see that the average threshold obtained at the four visual angles investigated is as follows: head on or 0 deg (11 miles); 30 deg (13 miles); 60 deg (11 miles); and 100 deg (10 miles). The two smaller curves are average detection distances obtained from subject pilots in the uninformed phase and the informed phase. Looking first at the average uninformed pilot curve, you can see that the pilot, on an average, detected the other aircraft at 3.5 miles, head on; 5 miles at 30 deg, 4.5 miles at 60 deg, and 3.5 miles at 100 deg. The average informed pilot curve shows

SINCE World War II the danger of mid-air collision of aircraft has increased enormously, as the number and speed of planes has increased. The Civil Aeronautics Administration has been studying the problem for several years in an effort to develop new safety standards and procedures.

This paper presents the results of some of these studies. Among the findings are: the need for a collision warning device to alert the pilot of the presence and direction of approach of other aircraft, and the need for more conspicuous paint pattern on planes.

Studies of past collisions show that many were caused by one plane overtaking another from the rear, that 90% occurred within 5 miles of the airport, and that over 50% happened at or below an altitude of 500 ft.

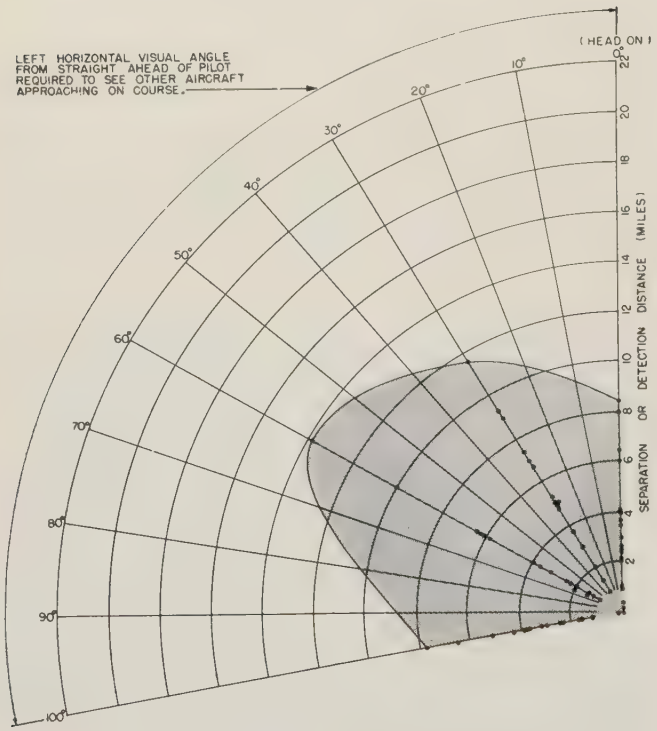

Fig. 3—Detection distances (uninformed pilot phase)

five miles at head on, 4.5 miles at 30 deg, 4.5 miles at 60 deg, and 4.75 miles at 100 deg.

A very surprising result was the fact that the uninformed subject pilot's average curve and the informed subject pilot's average curve were almost identical. Informing the pilots that they were flying a collision course seemed to make a difference only at the head on and at 100 deg. The ratio of average threshold distance (the ultimate distance that a DC-3 can be seen with the naked eye) to the average pilot detection distance, is almost 3 to 1 in every case. Therefore, if a collision warning device were developed which could detect an airplane at threshold distance and indicate its direction of approach, the present average pilot detection curve could effectively be extended threefold.

The detection distances obtained from the subject pilot and the threshold recorder in both the informed and uninformed phases varied considerably.

Fig. 3 shows within the shaded area the distribution of all the detection distances obtained in the uninformed phase. The detection distances varied from a maximum of 13½ miles at 60-deg visual angle to no detection. Seven pilots in this phase failed to detect the approaching aircraft—four at 100-deg visual angle, two at 60 deg, and one at 30 deg.

Fig. 4 shows the distribution of all the detection distances obtained in the informed phase. The detection distances varied from a maximum of 10½ miles at 30-deg visual angle to no detection. Two pilots in this phase failed to detect the aircraft approaching from 100-deg left visual angle.

Fig. 5 shows the distribution of the detection distances obtained from the threshold recorder during all collision runs. Threshold distances varied from a maximum of 22 miles at 30-deg visual angle to a minimum of 4 miles. These figures show that there was more deviation from the mean in threshold distance recordings than in subject pilot detection distance recordings. Threshold recordings were much more easily affected by slight changes atmospheric conditions, such as background, lighting conditions, or the presence of haze, because the aircraft at this distance appears so small as compared to the size of the aircraft at subject pilot detection distance. The aircraft at threshold could be visible for one instant of time and then suddenly disappear, due to a sudden change in conditions. The wide variance in detecting distances obtained from the subject pilots was caused primarily by the differences in their search habits. Some pilots were very deliberate and efficient while searching for other aircraft, and consequently detected the target aircraft at a greater distance than the subject pilot who in most cases was spending as much time in looking but not as efficiently. In a few cases in the uninformed phase, the subject pilot spent the majority of his time looking at the instruments, which resulted in a very near or no detection distance. It is felt that each individual collision run made in this study, regardless of whether the pilot detected the aircraft at distances beyond the average or even failed to detect the other aircraft, is representative of situations that could occur or are occurring in everyday flying.

Some sample pilot eye movement studies of two of the subject pilots indicated that the first pilot, who was informed, oversearched his visual area and was one of the few subjects who failed to spot the target aircraft. The second pilot, who was uninformed, undersearched his visual area and allowed the target airplane to get so close that he was really startled when he finally spotted it at a distance of less than one-half mile.

The following conclusions were drawn from this study:

1. Aircraft can be seen farthest under negative contrast conditions (dark aircraft against a light background) when there is present a very high overcast.

2. Pilots could improve their ability to detect

other aircraft on a collision course by developing better search habits, but, due to cockpit work load and other factors, the pilot could not be expected to detect an aircraft at threshold.

3. There is a need for a collision warning device to aid the pilot in searching for other aircraft. A device that would detect an aircraft approaching on a collision course at threshold and indicate the direction of approach, could effectively extend the present average pilot detection curve. Informing a pilot only that an airplane within a certain proximity is a potential hazard is insufficient information to aid effectively in visual detection. He must be given the direction of approach.

4. The results obtained in this study give a definite indication of expected average pilot performance in detecting aircraft approaching on a collision course while performing normal cockpit duties.

5. Since aircraft used in this study were of relatively slow speed, the average pilot detection distance can be expected to be much less in similar tests involving aircraft of much higher speeds and smaller profile area, such as jets. This indicates that as the speeds of aircraft become greater, the rate of closure of converging aircraft will exceed the limits within which human visual capabilities can insure collision avoidance.

6. Aircraft need to be made more conspicuous.

This study, in showing the need for a device to aid the pilot in searching for other aircraft, prompted us to make a further investigation of the factors related to mid-air collisions.

In an effort to establish a background for the operational requirements and limitations of a collision avoidance system, a study of 50 mid-air collisions was conducted. We wanted to determine, if possible, what factors, sets of conditions, and patterns had been most prevalent in past collisions.

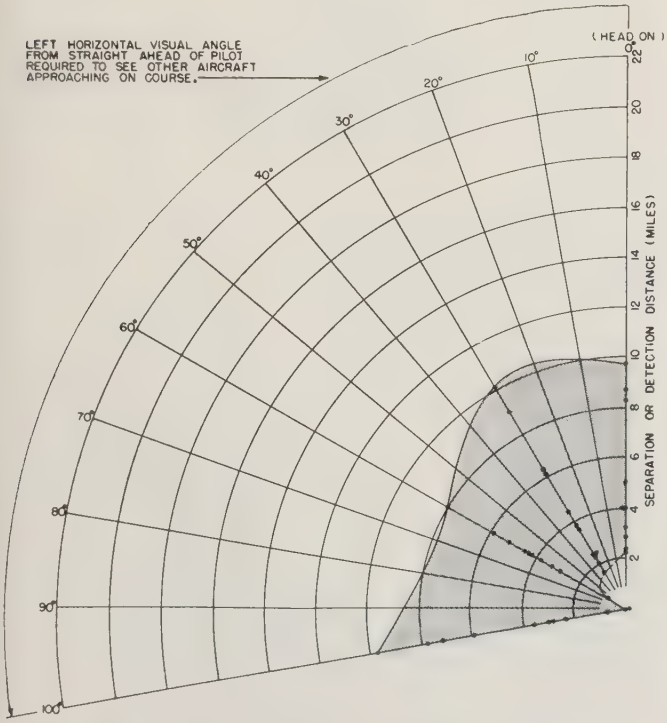

Fig. 4—Detection distances (informed pilot phase)

A collection of 92 reports covering the period from 1949 to 1954 was selected as a basis for this analysis.

The primary consideration at the start of this analysis was the relative separation between two colliding aircraft or their difference in headings prior to or at the time of collision. Types of aircraft involved, type of operation, altitudes, visibility, and the like were not considered when the initial 50 reports were selected.

The summary of convergence angles for the 50 mid-air collisions selected for study is shown by Fig. 6 and tends to contradict a popular belief, and

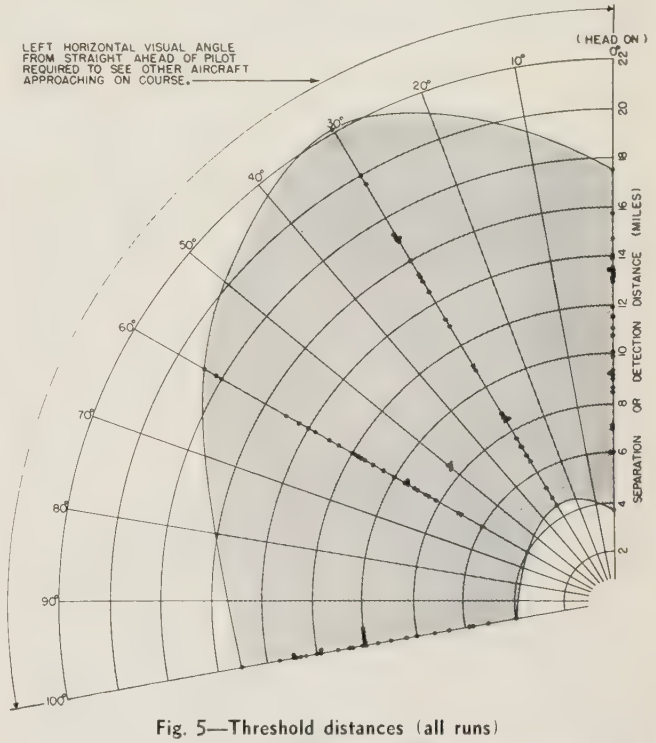

Fig. 5—Threshold distances (all runs)

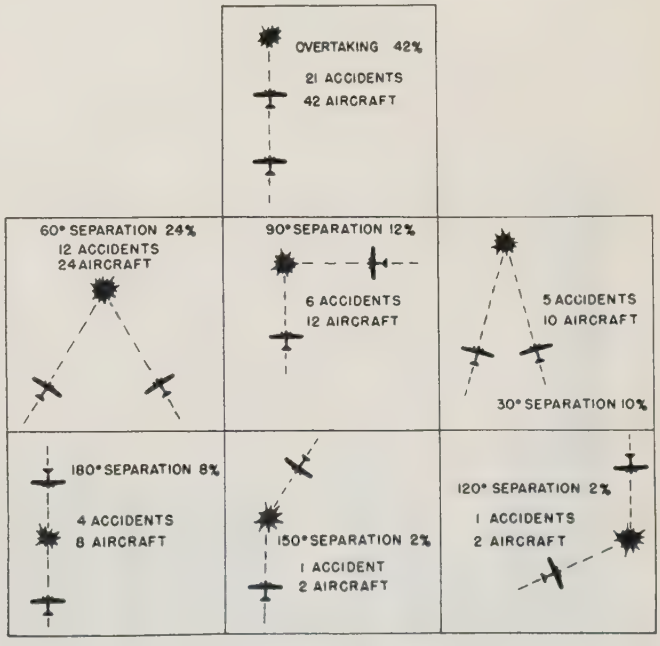

Fig. 6—Summary of 50 mid-air accident investigation reports 1949–1954, selected at random

one of which we were also guilty, that the forward hemisphere contains the greatest danger, by head-on approach, to aircraft in flight. Actually, as shown by this summary, the greatest cause of collision accidents has been overtaking, in which one aircraft approaches another from the rear.

This revelation then led us into a study of why, and what factor of procedure, pattern, performance, and structure, was most at fault. First, we summarized visibility. By averaging visibility cutoff angles of various cockpits in popular aircraft (Fig. 7) it was apparent that the majority of airplanes in use today have little, if any, rear hemisphere visibility, and practically no visibility below the horizon in the forward hemisphere (Fig. 8). It was then quite clear that one airplane can easily approach another from the rear hemisphere with very little altitude separation, and neither pilot will be aware of the presence of the other aircraft.

Next, we asked ourselves, "Where have these collisions been occurring, what distance relation have they had to airports, and at what altitudes?" Further analysis, shown by Fig. 9, revealed that 90% of these collisions were within five miles of an airport, and that 54% were within one mile.

The altitudes at which the aircraft collided are shown by Fig. 10, indicating that over 50% of those collisions for which an altitude could be established happened at or below 500 ft.

From this analysis the following conclusions were drawn:

1. The rear hemisphere and below the horizon forward are the areas in which practically all aircraft have poor or no visibility.

2. The overtaking of one aircraft by another has been the type of convergence in the greatest percentage of past collisions.

3. More collisions hapened at an altitude of 500 ft and below than at all other altitudes combined.

In conclusion, I should like to state that the data presented in this paper have fulfilled a definite need for basic information on the subject. It has helped us to gain a better understanding of the collision problem by showing what is confronting the pilot as he searches his immediate area for other aircraft. Also, it has shown the trend of past accidents and the areas where collision protection is needed. These overall results, therefore, will serve as a guide or tool in helping us to solve the mid-air collision problem.

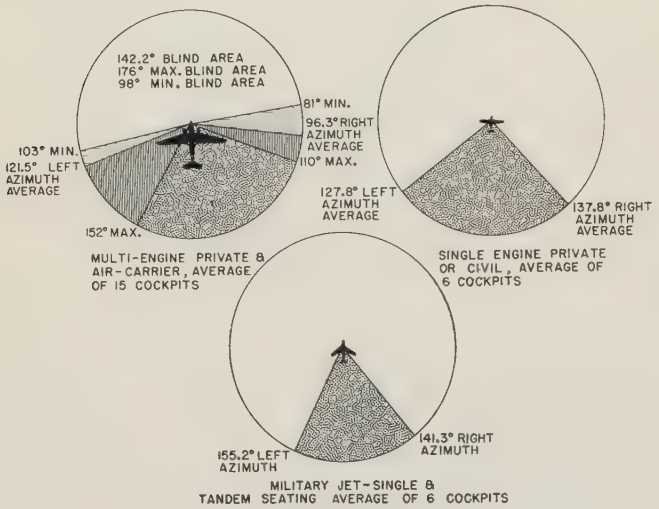

Fig. 7—Pilot vision right and left, azimuth cutoff angles

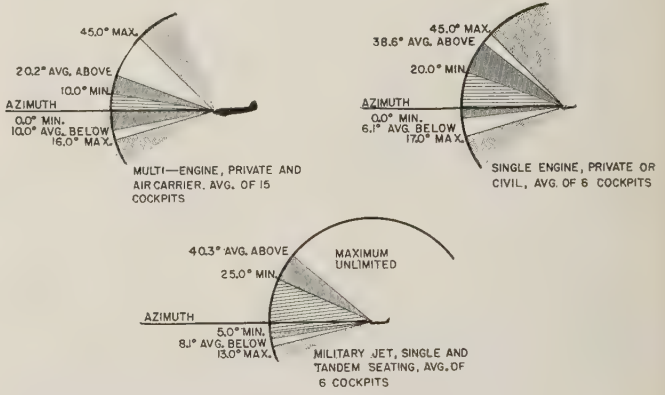

Fig. 8—Pilot vision forward, vertical cutoff angles

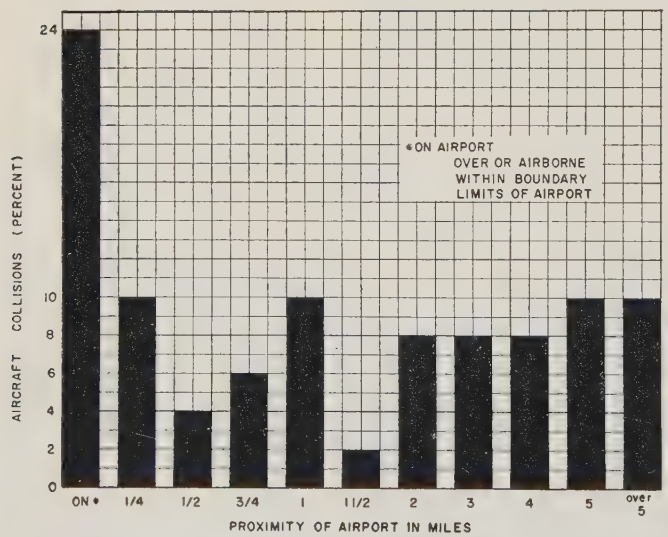

Fig. 9—Distance relationship to airport, summary of 50 mid-air accidents

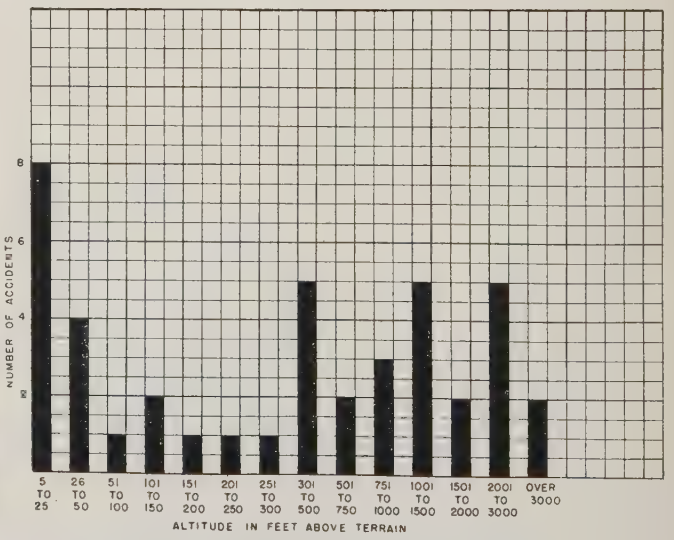

Fig. 10—Number of accidents and altitudes of 42 mid-air collisions within 5 miles of airport, 1949–1954

Design Features of the New Ford Axle

Bain Griffith, Ford Motor Co.

This paper was presented at the SAE Passenger-Car, Body, and Materials Meeting, Detroit, March 7, 1957.

EARLY in 1955 our engineering staff recommended a new design of rear axle for use on the 1957 Ford and Mercury cars and ½-ton truck. It incorporated a straddle-mounted pinion for improved rigidity of structure and potentially greater torque capacity and life (Fig. 1). Our familiarity and experience with this design in truck axles had left us with the opinion that this type of axle would be, in the long run, the most successful, pound for pound, and we hoped eventually the easiest to manufacture.

Further chassis design studies indicated the possibility of continued use with a single propeller shaft on the 1957 passenger cars if the axle design could be revised to an increased pinion offset. (See Fig. 2.) Such a change introduced added weight and cost in the axle assembly and placed us in an unexplored area of hypoid gear development. Elimination of the originally planned 3-joint driveshaft with its added cost and potential problems was unquestionably of sufficient value to justify an intensive development program to determine the feasibility of the proposed 2¼-in. offset axle.

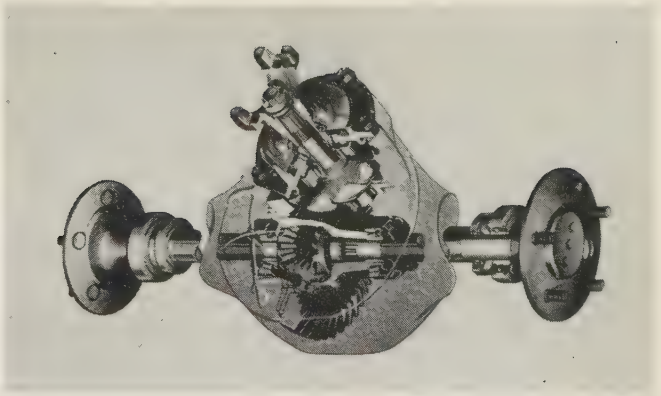

Fig. 1—1957 Ford-Mercury rear axle

After a brief but intensive period of gear development work and testing, the practicability of the 2¼-in. offset axle was indicated and the 1957 car development program was committed to the design.

The new axle housing was designed especially to obtain flexibility of tread width and maximum manufacturing efficiency.

Through the use of the straddle-mount arrangement with pinion gear cradled between bearings, the new differential carrier was designed to hold deflections under load to a minimum and, thereby, to maintain a more consistent tooth contact pattern than practically obtainable with the conventional overhung pinion design.

Tests on 1957 carriers indicate a substantial reduction in deflection as compared with 1956 Ford and competitive axles. The axle carrier is of typical truck design, with horizontal ribs and substantial pedestal skirts to obtain rigidity and an oil deflection pattern to lubricate the differential bearings. The carrier was made of cast iron, contrary to previously used malleable iron.

The differential case is of 2-piece design, more or less spherical with small holes for lubricant, to ob-

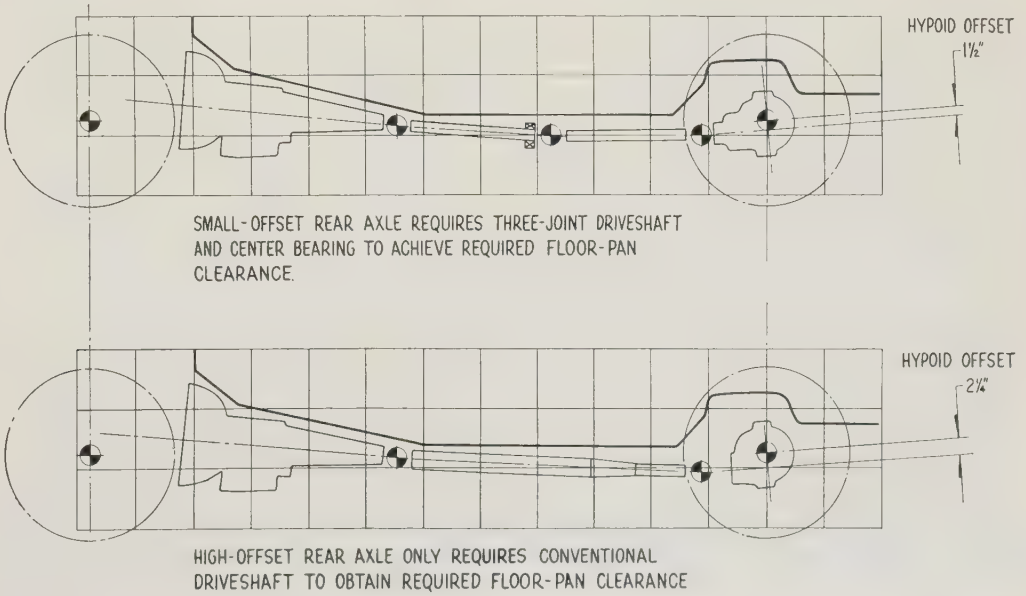

Fig. 2—Sketch of vehicle drive line, showing effect of hypoid offset

IN 1957 Ford introduced in its passenger cars a new rear axle incorporating a straddle-mounted pinion. This paper describes the development and features of the 2¼-in. offset axle.

The author thinks the most interesting feature of the development problem was the design of the hypoid gears. The 1957 gears were designed with the deepest possible teeth to give maximum fatigue strength. They maintained the conventional scheme of 50 deg on the pinion and about 15 deg on the gear.

tain maximum stiffness with a minimum of metal. The differential case is of malleable iron.

The pinion and differential bearings were selected to insure adequate life and reasonably balanced loadings, and were based on the classic roller-bearing formula of long standing. Pinion bearings are relatively small, high in angle, and are the same in all applications. Two sizes of differential bearings are used, the smaller in the Ford passenger cars. It is interesting to note that the five bearings in the 1957 axle cost about as much as the four bearings previously used in the 1956 rear axle.

The practical advantage of the three pinion bearings becomes evident in performance. Designing with an independent radial bearing for the pinion and separate drive and coast-thrust bearings results in more latitude of bearing preload. Therefore, gear performance is less critical. Well-made hypoid gears can tolerate some "lameness" from drive to coast which is immediately associated with thrust-bearing preload. The loosening of these bearings will induce a relatively small amount of radial deflection, while vertical gear deflections are held to a minimum. This vertical gear deflection develops high, short tooth contacts at the heel of the gear teeth. Gears in this running condition are noisy.

Perhaps the most interesting feature of the entire problem has been the design of the hypoid gears. Development of the wide range of gear ratios from 2.9/1 to 5.8/1 for acceptable noise characteristics has been somewhat difficult. Previously used assumptions in gear calculations and manufacturing techniques required modifications and redevelopment.

Increased pinion offset from 1½ in. in the 1956 axle to 2¼ in. in the 1957 design was, to us, a new problem in new territory. This increased offset results in larger diameter pinions with some increase in size of the assembly. Reduced tooth pressures combine with increased pitch-line sliding velocity of the gear teeth; the lower tooth pressures compensate for some of the higher sliding velocity. However, in our opinion, the relative importance of the two features cannot be accurately evaluated. We have not fully studied an analysis of the two factors combined that permits us to design better gears.

The ratio of offset to gear diameter was relatively larger than in any conventional designs. Axle engineering's problem is to create the design, make samples, and complete the necessary tests proving the extreme offset was commercial. At the same time, our gear development laboratory had to explore the new design sufficiently to prove the manufacturing feasibility. Our knowledge of the gear cutting industry and automotive rear axles indicated gears had never been produced in substantial quantities with this more severe offset. There are no reference textbooks in a problem of this nature: Can severely offset hypoid gears be made commercially?; would these gears be adequate in an automobile?

To understand the problem, we restate that all gears slide to a degree in the profile action; hypoid gears also slide along their face. Extreme pressure lubricants are mandatory to successful performance. Scoring or welding caused by the lubricant being wiped clean of the tooth surfaces is a matter of extreme concern.

The measure of pitch-line sliding along the face of hypoid gears (Fig. 3) is recognized as the difference in the tangents of the spiral angles of gear and pinion. The advantage of reduction of normal tooth loading is obtained simultaneously with a substantial reduction in gear spiral angle, all other design factors remaining equal.

Hypoid gears produced in quantities in the last 25

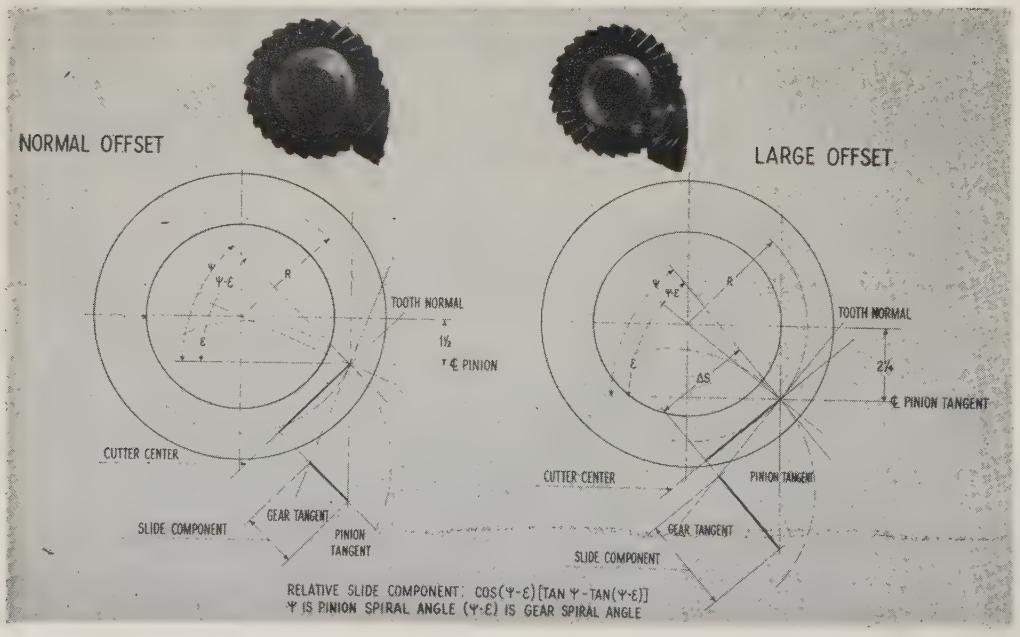

Fig. 3—Relative slide component, hypoid gears

years have been designed with 45- or 50-deg pinion spiral angle and the offset angle (difference in spiral angle) varied from 10 deg in truck application, with relatively small offsets, to 25 deg in the lighter passenger-car application. The maximum endwise sliding factor with commercial experience, and recognized to be successful because it has worked, is the tangent of 50 deg minus the tangent of 25 deg. It has been generally presumed that exceeding this quantity might induce scoring with commercially available lubricants. Slide components not exceeding this quantity with 2¼-in. offset gears dictated a maximum pinion spiral angle of 40 deg and around 5 deg on the gear. With this as a starting place, gears were designed in ratio of about 3/1 and 4/1 as design scheme trials to avoid scoring or unusual lubrication requirements.

The engineering of a set of hypoid gears is time consuming.[1] Our own designers worked in close collaboration with the development people who manufactured the gears. A 20-year old formula was used with no basic change in design technique. Some revisions were found necessary as work progressed to obtain realistic machine settings.

If relatively deep teeth in the coarsest possible pitch are designed with the wrong pressure angle, the pinion teeth will undercut and develop impossible tooth forms. Pressure angles are not arbitrarily selected. We find deep coarse pitch the most satisfactory to manufacture accurately and to assemble for quiet performance.

Hypoid gear teeth "lean over," and the variation in pressure angle in the two sides must be properly established. Gear cutting is a real problem because the leaning over condition of the teeth becomes very substantial as the pinion offset increases.

Again referring to Fig. 3, it is evident that in the pitch plane, gear and pinion teeth are simultaneously moving in two different directions. The tops of the pinion profiles on the drive side are engaging larger gear-tooth elements as they roll out of mesh; conversely, the profiles have to shrink on the coast side, going out of mesh in reverse rotation. The instantaneous rate of change in size of tooth profile establishes the so-called "limit pressure angle" which is talked about so much in the design of hypoid gears; this is the quantity that must govern the lean over of the gear teeth. By merely changing the pinion offset, with all other conditions remaining equal, the limit pressure angle increases rapidly. Fig. 4 is a "virtual" section of the pinion tooth and the radial distance to the inner ends of the two pinion profiles is about equal, if the projection of the pressure angles themselves are equal from the projection of the limit pressure angle. The maximum depth of a pinion tooth from the pitch point that will develop no undercut on either profile can be determined with fair accuracy. This undercutting condition will not necessarily remain constant from end to end across a relatively long tooth face. Gear teeth designed on this basis can be expected at the outset to be reasonably free of undercut.

From studies of this nature, all of our 1957 gears have been designed with deepest possible teeth to give a maximum of manufacturing latitude for

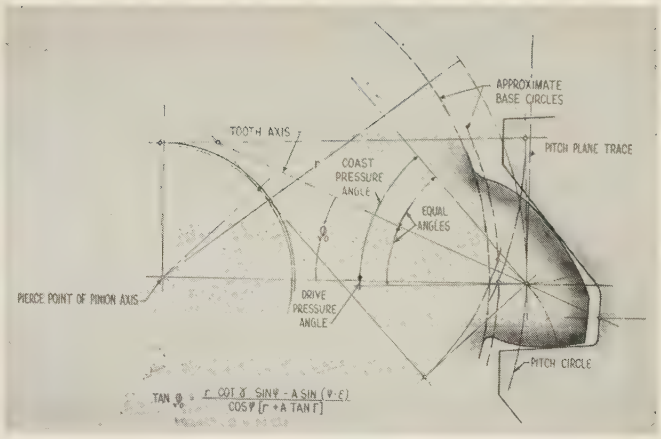

Fig. 4—Transverse pinion profile showing tooth axis

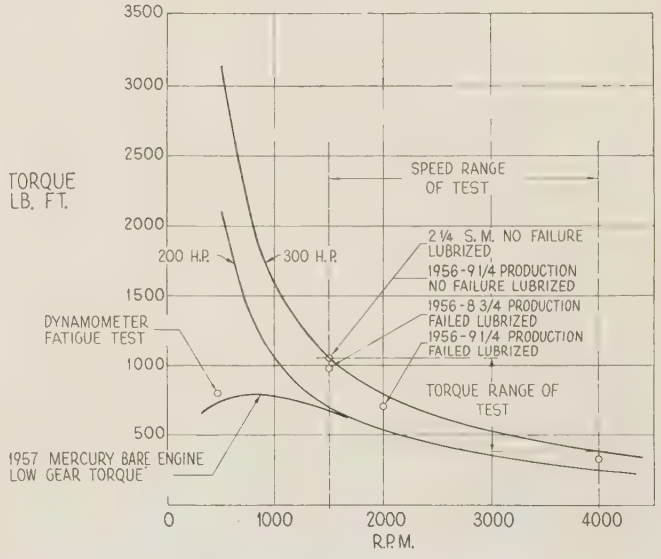

Fig. 5—Critical p-v test chart

lameness, shim selection, and very likely a maximum of fatigue strength. Designing the gears was a relatively easy task; setting the machinery to cut the gears was more difficult.

Our first gears which looked right and rolled well were designed with the 40-deg pinion spiral angle, but the lack of tooth overlap was evident with noise and roughness. Gears of this type, of course, must operate smoothly and silently; discriminating manufacture would be impossible if they were rough and noisy prior to assembly.

At the suggestions of our gear development people who must maintain the quality in production, new gears were designed to the conventional scheme of 50 deg on the pinion and about 15 deg on the gear. The endwise sliding was expected to be disastrous. However, from the cutting standpoint, these designs were entirely satisfactory. In the gear laboratory, they looked and sounded right, and they reacted to manufacturing methods of long-standing. These were gears that could be made commercially.

Scoring was expected to be the major problem, but dynamometer efficiency factors of 96 and 97% are identical in axles with normally offset hypoid gears or bevel gears. The design appeared reasonable.

An indication of the effect of tooth pressures and endwise sliding velocity was obtained by comparing assemblies of known characteristics (Fig. 5). To see

[1] Our new digital computer now replaces the tedious calculation process; in 5 min the required one thousand sequential calculations are obtained and three copies printed in manifold forms. The computer can be set up in about 5 min.

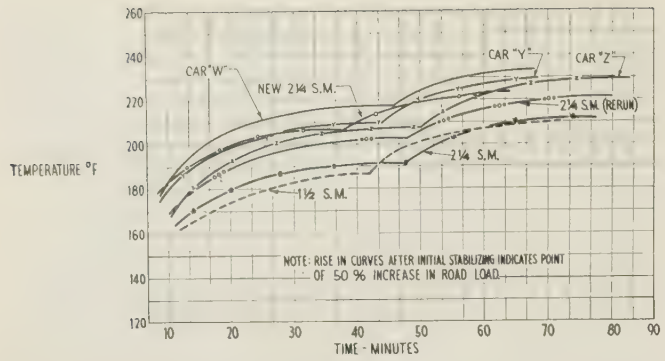

Fig. 6—Rear axle temperature comparison, 90 F tunnel air temperature and 70 mph vehicle speed

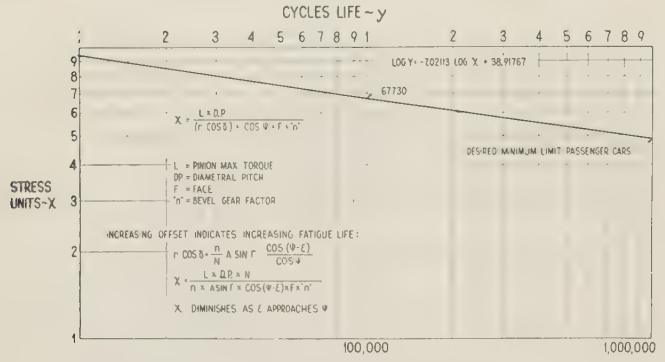

Fig. 7—Life cycle curve hypoid gears

if scoring developed, axles designed to transmit about 150 hp were subjected to 300 hp at various speeds for short periods of time; starting at 4000 rpm of the pinion and the appropriate 395 lb-ft torque, speeds were reduced at 5-min intervals by 1000 rpm with torque increases to maintain the 300 hp. Of three conventionally designed axles, two successfully survived the test and one failed at 2000 rpm before the full 790 lb-ft torque had been introduced. The 2¼-in. offset axle survived the test quite satisfactorily. It was concluded that the increased rate of endwise sliding of the teeth was not the problem that it had been presumed to be. This test has been repeated many times with different ratios to establish the soundness of the progressively different gear designs required.

The scoring character of the gears was further established in many car tests using untreated gears, active sulfur lubricant, and the best grades of inactive lubricant with lubrized gears. Bump score tests and high-speed score tests were successful, and with lubrized gears score tests were repeated after 1500 miles of durability with inactive oil.

Performance with sustained high speed was checked with automobiles driven at an average of 95 mph, 85 F ambient air temperature. After a few laps of the track, oil temperature stabilized at 195 F, which is lower than the temperature of many axles of conventional design. Furthermore, in our "Operation Left Turn" the 1957 axles withstood the continuous high-speed operation, evidenced no distress, and remained entirely serviceable after being removed from the test cars.

Additional competitive temperature readings were obtained with axles of conventional design and recognized successful in performance. Chassis dynamometer was used, permitting 90 F air temperature and 70 mph maximum speed, overloaded 50%. Oil temperatures with the new design axle were consistently the lowest recorded. The results of these tests are shown in the graph in Fig. 6.

Our original formula relating dynamometer life experience and structural fatigue of hypoid gear teeth indicated that severely offset gears were structurally superior to conventionally offset gears of the same size. The formula in graphic form is shown in Fig. 7. The validity of the formula with the extreme change in tooth proportion was questioned, but endurance tests were performed with gratifying results. Testing at the present time indicates definite fatigue strength advantages. The tabulation in Series 1 of Table 1 shows the input torque and tooth loading data that has resulted in an average of a million pinion cycles with successful fatigue life.

There are currently in production 16 different ratios with no change in gear mounting distance. All ratios are interchangeable in the same differential carrier with the same differential case. Spiral angles on the gears, however, vary from 45 deg on the fastest ratios to 60 deg on the slowest. Table 1 indicates the design quantities of the entire range.

It is interesting that the design strength and the flexibility with respect to fatigue life, ratios adapted, and possible future requirements for added gear capacity have been obtained with modest assembly weight. Our 1956 assembly weighed 57 lb and the 1957 assembly weighs 65 lb. All but ½ lb is directly attributed to the increased offset in forging and casting requirements. The range of gear ratios is also much broader. Minimum competitive assembly weighs 64.25 lb and the balance of 1957 production in the field range heavier to 80 lb.

Noise and durability characteristics of our experimentally built axles indicated that we should expect highly satisfactory results in customer operation. Of course, it was not until the axle was produced in high volume that we were able to establish how well the overall job had been done.

It can be reported that our quality experience to date, after having produced approximately 750,000 axles, is very satisfactory; the percentage of rejects through constant sampling that represents the customers' reaction is far less than our previous best record last year. Our warranty expense is at a low level, and the durability experience in the hands of the customer is satisfactory.

Table 1—Design Values, 1957 Ford Motor Co. Axle Gears
(8.75 pitch-diameter gear, 1.375-in. face, 2.25-in. offset down)

	Ratio	Number of Pinion Teeth	Number of Gear Teeth	Pinion Spiral Angle	Gear Spiral Angle	Torque Input lb-ft	Pinion Speed, rpm
	2.91	11	32	47° 30′	15° 21′	970	500
	3.10	10	31	50°	17° 19′	970	500
Series 1	3.22	9	29	50°	17° 2′	970	500
Regular	3.56	9	32	50°	16° 21′	875	500
Production[a]	3.70	10	37	50°	16° 7′	840	500
	3.89	9	35	50°	15° 47′	840	500
	4.11	9	37	50°	15° 30′	730	500
	3.40	10	34	50°	16° 38′		
	4.29	7	30	55°	20° 14′		
	4.57	7	32	55°	19° 57′		
Series 2	4.72	7	33	55°	19° 45′		
Special	4.86	7	34	55°	19° 38′		
Production	5.14	7	36	60°	24° 7′		
	5.43	7	38	60°	23° 57′		
	5.67	6	34	60°	23° 50′		
	5.83	6	35	60°	23° 46′		

[a] Includes dynamometer loading; average life exceeds 1,000,000 pinion cycles.

BENDIX AVIATION CORPORATION RESEARCH LABORATORIES LIBRARY

The Improvement of Welded Structures by Subsequent Forging Operations

W. R. Wollering and E. H. Lundby, Ladish Co.

This paper was presented at the SAE Summer Meeting, Atlantic City, June 5, 1957.

THIS PAPER describes a new technique of utilizing the subsequent forging of welded structures. The method results in the development of physical properties in welded sections of alloy materials approaching those of the wrought parent material.

The authors think that the process offers several advantages, including: Weight reduction in dynamically stressed wrought-steel assemblies, increase in design factor values, and conservation of critical alloy materials.

The authors have drawn the following conclusions from their work thus far: Definite economies can be effected by the forged weldment approach; parts formerly impossible to forge can be fabricated by the method; and forged weldments can be obtained with the same chemical and mechanical properties as the parent material.

OUR investigation of a technique utilizing the subsequent forging of welded structures has resulted in the development of mechanical properties in welded sections of alloy materials approaching the properties of the wrought parent material.

This production process may be considered an intermediate step between a weld fabrication and a one-piece forging, where forging in one piece is not possible due to its geometric shape. However, it is without the compromising factors of strength, ductility, and design frequently associated with structures fabricated by welding methods.

Dynamically stressed, wrought parts forged from alloys such as SAE 4340, (AMS-6415) heat-treated to hardness levels resulting in ultimate tensile strengths approximating 150,000 psi, have ductility values of approximately 20% elongation and 55% reduction of area. However, sections in the same alloys welded with electrodes having similar properties, when heat-treated to the same ultimate strength will disclose ductility values substantially inferior to the wrought parent material.

To utilize the forging and welding processes to the fullest advantage in higher strength alloy components subjected to dynamic stresses in service operating conditions, it is necessary to improve the ductility of the weld material. Enhancement of the ductility values in welds may be effected by heating to a temperature in the plastic range and subjecting the structure to a hot-forging operation.

Some of the many advantages that may accrue to designers and users of this forging technique are:

1. Ultimate reduction in weight in dynamically stressed wrought-steel assemblies.
2. Increase in design factor values.
3. Reduction in the amount of expensive machining operations.
4. Conservation of critical alloy materials.
5. Production of integrally forged geometric shapes heretofore not possible by conventional forging methods.
6. Enhancement of mechanical properties and microstructure of the forged weld compared to the unforged weld section of such nature that the forge-welded section exhibits properties comparable to the parent forged material.
7. Exclusion of a percentage of the weld material from the finished forged part in certain forging operations subsequent to welding.
8. Use of integrally forged metals of varying com-

Table 1—Mechanical Properties of Tensile Specimens Removed Transversely Through Weld Zone

Specimen Identity	Section Reduction by Forging %	Ultimate Strength, psi	Yield Strength 0.2% Offset, psi	Elongation, %	Reduction of Area, %	Hardness, Bhd
	Welded (No forging)	131,800	124,200	6.0	12.9	3.45
1A	9.0	119,200	101,000	13.0	54.8	3.65
1B	12.5	140,700	123,700	18.0	58.1	3.65
2A	25.0	141,900	123,100	18.0	54.5	3.55
2B	33.0	139,800	122,800	18.0	58.8	3.60
3A	43.0	142,600	124,800	17.5	57.1	3.60
3B	No test	—	—	—	—	—
4A	58.5	140,200	124,200	18.0	59.4	3.55
4B	66.0	141,100	126,700	16.5	58.7	3.55
Parent Metal		136,000	125,000	20.0	58.6	3.60

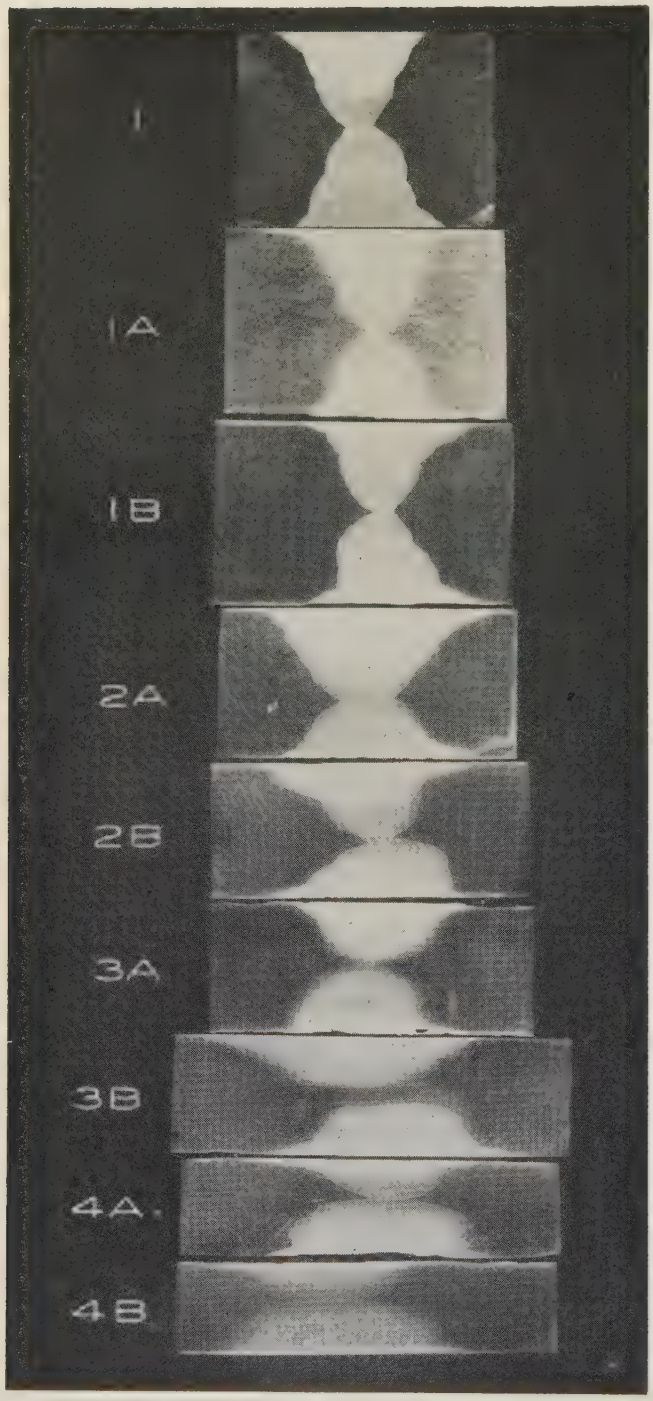

Fig. 1—Macrophotograph of welded AMS-6415 test section and sections subsequently forged to reductions indicated in Table 1

Table 2—Mechanical Properties of Specimen Removed Transversely Through Weld Zone After Heat-Treating

Specimen Identity	Ultimate Strength, psi	Yield Strength 0.2% Offset, psi	Elongation, %	Reduction of Area, %	Hardness, Bhd
Welded (No Forging)	141,600	125,400	14.0	36.3	3.50
Welded and Forged	141,500	125,500	17.0	56.4	3.50
Parent Metal	143,900	127,700	20.0	61.4	3.50

positions, such as carbon steel and SAE 4340, as well as combinations of stainless steel.

9. Production of forgings heretofore impossible due to limitations in size of raw material.

10. Deposition of a weld metal with a chemical composition identical to the parent material, heretofore prohibitive due to elongation values substantially lower than parent metal.

Our initial investigation consisted in forging two welded plates which conformed to AMS 6415. The weld material was deposited manually and conformed to AWS Class E12016. The forging operations permitted hot-work in the weld zone in successive reductions to a maximum of 66% (Fig. 1). After forging, the test pieces were heat-treated to a hardness of 285–321 Bhn (3.40–3.60 mm Bhd). The results of tensile specimens removed transversely through the weld zone are shown in Table 1.

It is noted that the mechanical properties of the welded (no forging) specimen exhibit low ductility, which is characteristic of cast structures. As the cast weld material is hot-worked by forging, a wrought structure is developed (Fig. 2). The mechanical properties have been enhanced by the hot-working and transition from a cast structure to wrought structure to a degree where they are comparable to the properties developed in the parent material.

The second phase of this investigation comprised forging a welded disc and rim assembly in contour dies. Fig. 3 shows the welded section at the top and the forged welded section at the bottom. It will be noted that in this particular case, the remaining weld metal in the finished part was reduced to a very small order.

The mechanical properties of a specimen removed transversely through the weld zone after heat-treating to 285–321 Bhn hardness (3.40–3.60 mm Bhd) are shown in Table 2. It is to be noted that the ductility determined in the cast weld metal is substantially lower than that developed in the welded and forged

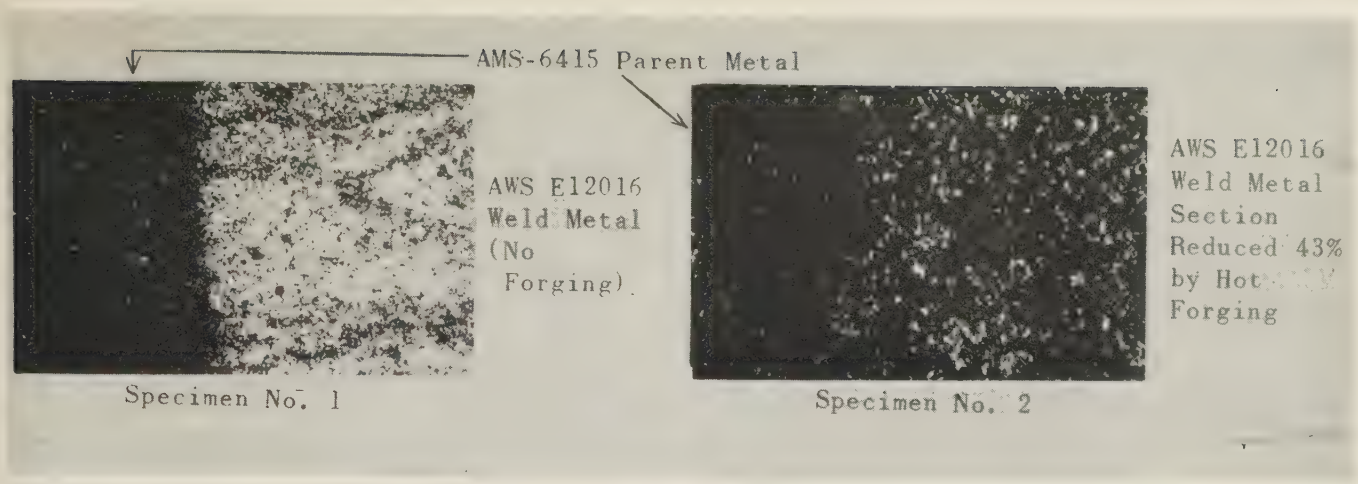

Fig. 2—Comparison of cast weld material section with no forging and section reduced by hot forging (500x magnification, 2% Nital etchant)

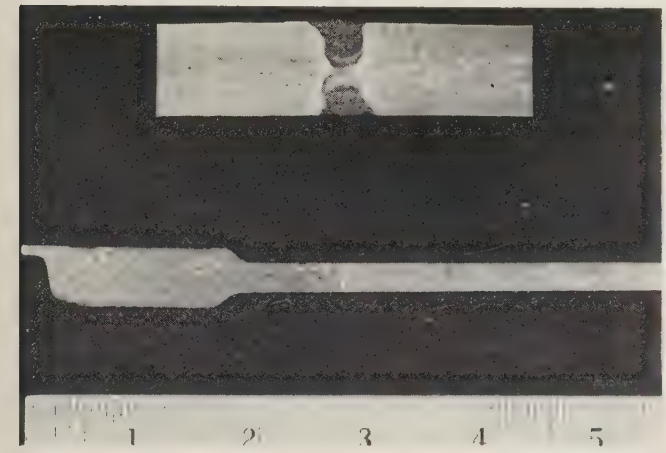

Fig. 3—Macrophotograph of section through weld joining ring to web before (top) and after (bottom) forging

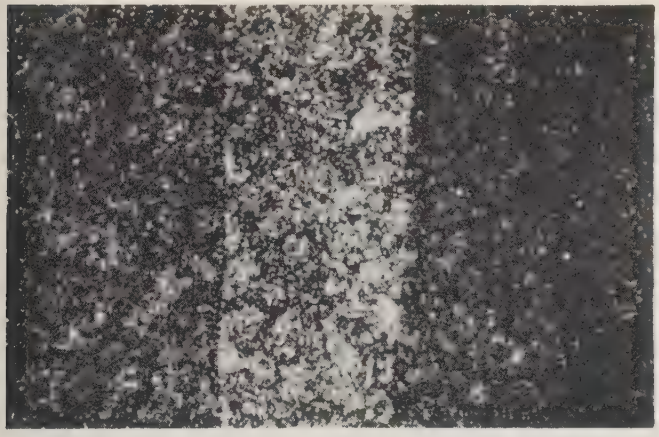

Fig. 4—Wrought structure developed by forging in weld zone (100x magnification, 2% Nital etchant)

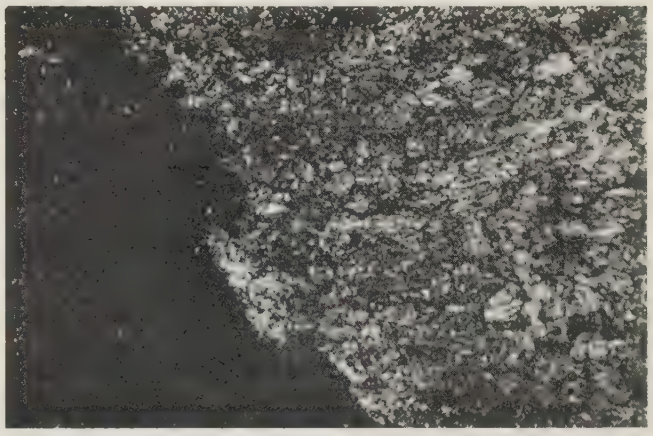

Fig. 5—Cast dendritic structure of weld (100x magnification, 2% Nital etchant)

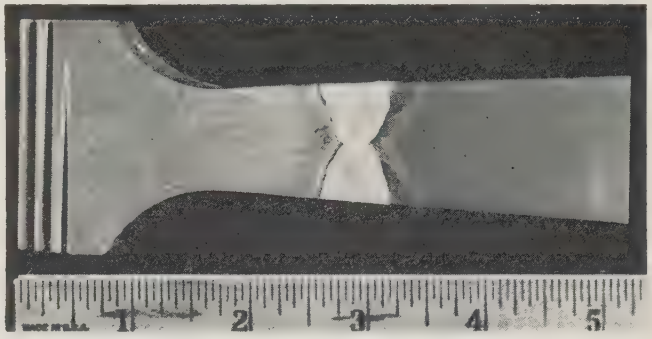

Fig. 6—Macrophotograph of section through turbine wheel weldment of ring (16% Cr, 25% Ni, 6% Mo) to 4340 hub exhibiting large weld and heat-affected zone

specimen which has a ductility comparable to that of the parent metal. The wrought structure developed by forging the weld zone is shown in Fig. 4 and the cast dendritic structure of the weld is shown in Fig. 5.

A typical turbine wheel manufactured by conventional methods is shown in Fig. 6, in which the large weld and heat-affected zone have been revealed by a macroetch process.

The foregoing discussion illustrates a successful approach to improving mechanical properties of a low alloy weldment. However, with more complex alloys, it must be recognized that solution of the forged weldment problem is not so simple. Experimentation is required to develop proper welding and forging procedures.

The problem, in this instance, involved a forging the weight of which required the specified material in a size greater than was manufactured in a single piece. This forged weldment method provided a means of accomplishing the part manufacture otherwise not possible and providing the requirement of no cast structure in the finished product.

The material was 440A stainless steel of a vacuum-

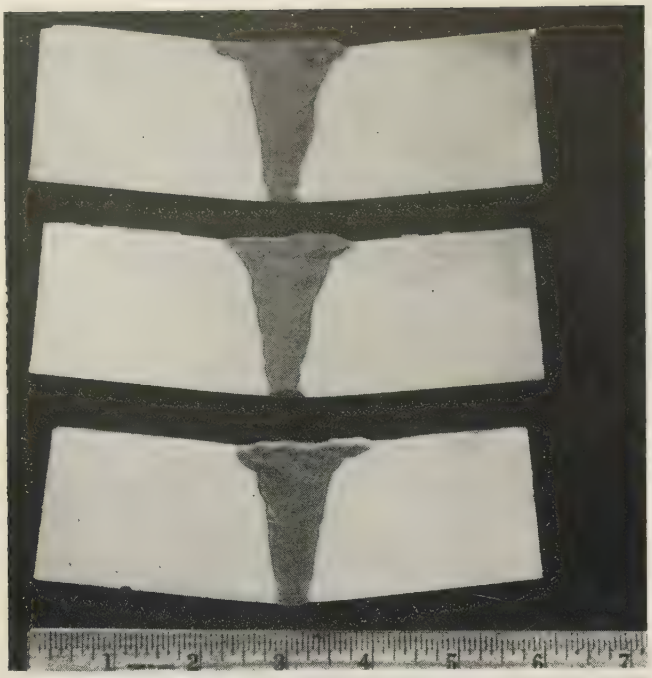

Fig. 7—Macrophotograph of 440A stainless steel sections welded with inert-gas processes

Fig. 8—Macrophotograph of welded 440A stainless steel sections forged with increasing reductions

melted Consutrode grade.[1] The cleanliness of the deposited weld was required to be equal to that of the parent material.

It was found that with the maintenance of the proper preheat and interpass temperature that the material was weldable using either of three processes. These processes were the shielded inert gas with tungsten electrode, the shielded inert-gas consumable electrode, and the submerged-arc process.

To obtain maximum cleanliness we thought that the inert-gas shielded processes would show an advantage. Consequently, the initial experiments were conducted by welding a portion of the test plate by the consumable-electrode process and the balance of the plate by the tungsten-electrode process with a manual deposition of the required filler metal.

Metallographic inspection of these weldments revealed that the cleanliness obtained was equal to the parent metal with very little difference in the microstructure and the cleanliness obtained with either inert-gas processes. Macroexamination of the welded test sections prior to forging revealed a uniform structure produced by both processes. One small interbead crack was discovered in the weld made with the consumable electrode (Fig. 7). Sectioning and macroetching after forging revealed some minor porosity in the deposit produced by both processes (Fig. 8).

The forging of the initial test bars was accomplished using heating and forging procedures normal for material of this type. All test bars were cycle annealed after the forging operation.

The physical testing was accomplished in this annealed condition to evaluate the effects of forging on the ductility of the material. Table 3 shows the results of the tensile testing.

It can be seen that the expected improvement had failed to materialize. Fig. 9 shows tensile specimens which exhibit the brittle nature of the fractures attendant with the low ductility values attained.

Metallographic examination at this stage gave no clues determining the reasons behind our failure to achieve the desired improvement in the mechanical properties. However, the results of this metallographic examination indicated that the desired refinement in the weld metal structure had been achieved.

Further efforts included the comparison of weld quality and cleanliness between the consumable-electrode inert-gas process and the submerged-arc process (Fig. 10). Radiographic inspection and sectioning revealed that some difficulty would be encountered in depositing a completely sound weld with the inert-gas process. The submerged-arc process, however, produced a sound weld free from cracking or porosity. A metallographic examination revealed that the cleanliness of the deposit by the submerged-arc process was well within the rating of the parent material.

Forging of this second set of tests was accomplished by modifying both the thermal control and the forging technique so as to give the greatest protection possible to the weld deposit. The results of the new approach are shown in Table 4. A review of these results shows that the desired improvements to the physical properties had been achieved.

A metallographic survey reveals that the cast structure of the weld deposit is virtually eliminated at approximately 45% of forging reduction (Fig. 11). Subsequent heat-treating of the material produces a structure which satisfies all the requirements listed as primary objectives in this investigation. Also, subsequent production of a part by the developed

[1] Trade name for product resulting from a consumable-electrode vacuum-remelting process.

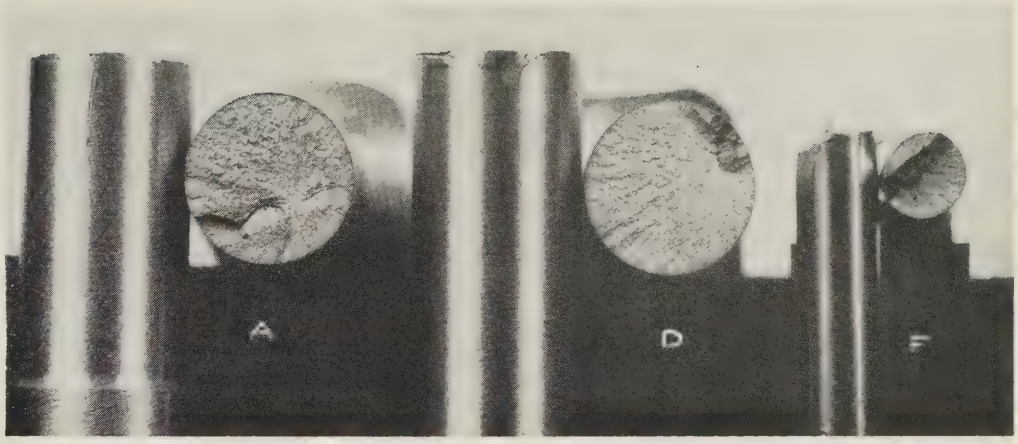

Fig. 9—Brittle type, tensile test fractures of improperly forged inert-gas-welded 440A stainless steel

technique has met with the customer's requirements in all respects.

Improvement of flash butt welds has been accomplished by subsequent forging operations. This development is advantageous when the properties of the weld can be made equivalent to the parent metal. Flash butt welds in aircraft parts are governed by specifications which require the weld to have minimum properties 90–95% of the strength of the parent metal and elongation 50% that of the parent metal. These types of parts are restricted for use as static rings in turbine-type engines. The dynamic rings require seamless forged properties. Use of another process, such as welding, can expand design flexibility and effect economics in production of required ring contours, providing parent metal properties can be achieved.

Results in Table 5 show required ductility for a flash butt weld in a 6% Al–4% V titanium alloy to AMS-7498 specification. However, subsequent forging operation has restored the ductility of the weld

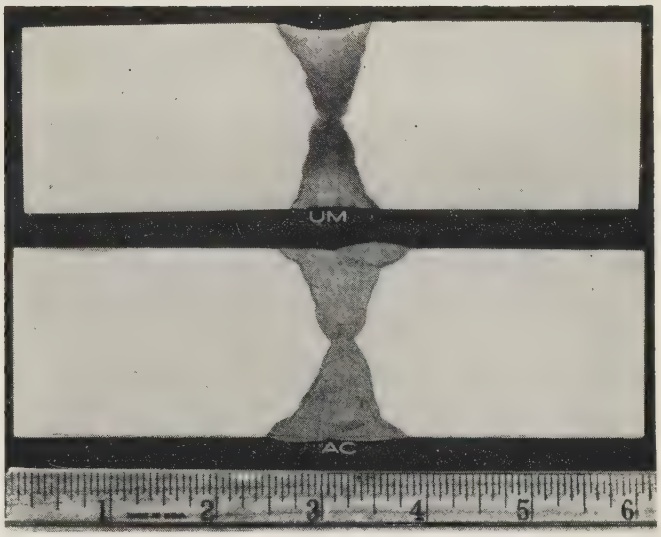

Fig. 10—Macrophotograph comparing submerged arc-welded 440A stainless steel with inert-gas-welded sections

Table 3—Physical Properties of Forged Inert-Gas Welded 440A Stainless Steel

Forging Reduction	Bar Identity	Ultimate Tensile, psi	Yield Strength, 0.2% psi	Elongation, %	Reduction of Area, %	Tag No.	Remarks
As-Welded	AW	102,200	46,600	9.5	25.7	S234	Fractured in parent metal
To 1 5/8 in.	A	105,150	55,400	5.5	7.45	S228	Fracture exhibits brittle-type failure; two small areas resembling flaking.
To 1½ in.	B	104,750	49,090	7.0	6.8	S229	Brittle-type fracture; one small gas hole
To 1⅜ in.	C	107,740	47,650	10.5	14.2	S230	Brittle-type fracture; no visible discontinuities
To 1¼ in.	D	86,000	52,625	4.5	4.3	S231	Brittle-type fracture; small area exhibits dendritic-type structure, slight discoloration
To 1⅛ in.	E	69,000	50,900	—	4.72	S232	Compound shear-type fracture with an excessive side lip; shear portion extremely smooth and regular
To 1 in.	F	86,740	47,640	3.5	5.9	S233	
Parent Material	—	105,250	54,750	19.0	24.4	S235	Shear-type fracture with fibrous quality

Table 4—Physical Properties of Material Welded by Submerged Arc Process

Weld type	Force Reduction, %	Ultimate Tensile, psi	Yield, 0.2%, psi	Elongation, %	Reduction of Area, %	Fracture Occurred	Type of Fracture
Inert Gas Shielded Arc	65	102,000	47,800	20.0	42.6	Center weld	Cup-cone
Subarc	25	105,300	53,500	19.3	39.8	Parent metal	Cup-cone
Subarc	45	103,000	52,600	20.7	48.6	Center weld	Cup-cone
Subarc	65	102,000	50,600	20.7	49.4	Center weld	Cup-cone
Parent Material		105,250	54,750	19.0	24.4		Shear-type Fracture with fibrous quality

Table 5—Physical Properties of Flash Butt Welded Titanium Alloy (6% Al - 4% V)

	Ultimate Tensile, psi	Yield Strength 0.2% Offset, psi	Elongation, %	Reduction of Area, %	Bhn	Fractured
AMS-7498 Requirement	130,000 minimum	120,000 minimum	10.0 minimum	30.0 minimum	321 maximum	
Parent Material	144,690	133,270	15.0	41.5	311	
As-Welded and Heat-Treated[a]	144,270	135,000	11.0	29.3		In weld area
Welded, Forged, and Heat-Treated	144,290	135,470	15.0	40.1		In weld area

[a] Heat-Treatment: Heat to 1300 F, hold at color for 2 hr, and aircool.

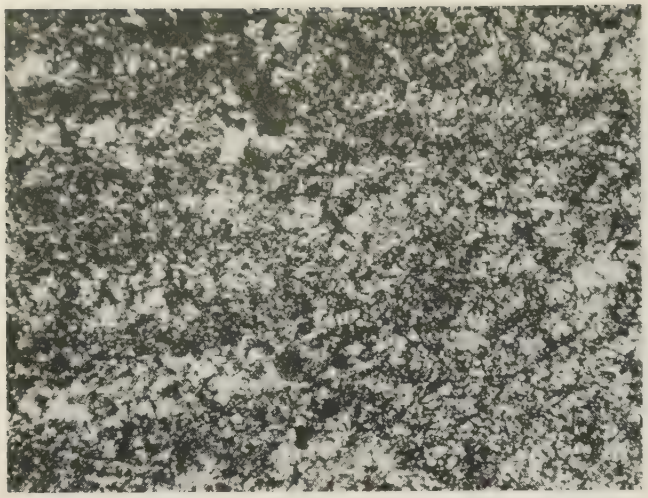

Fig. 11—Metallographic survey of cast structure of weld deposit. (A) Welded, forged 25%, and annealed

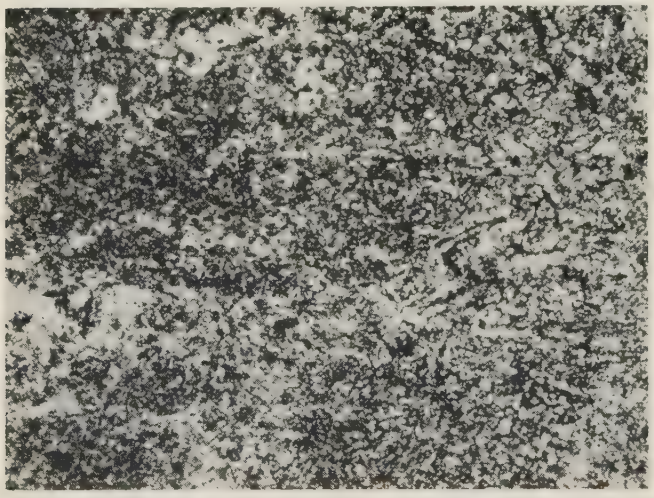

Fig. 11B—Welded, forged 45%, and annealed

Fig. 11C—Welded, forged 45%, quenched, and tempered

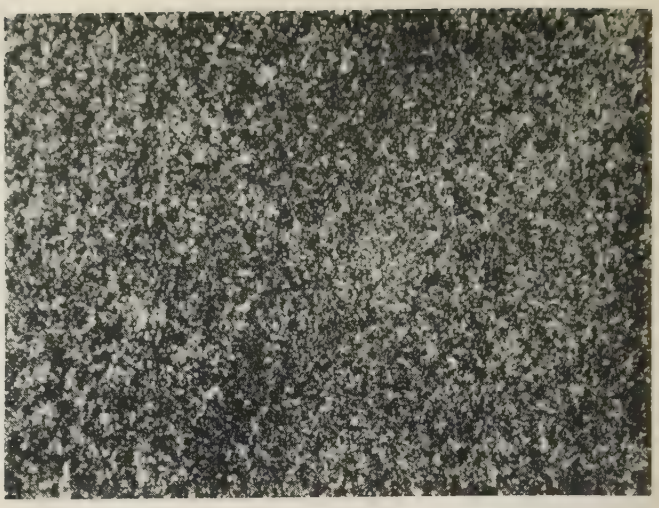

Fig. 11D—Welded, forged 65%, and annealed

Fig. 11E—Welded and annealed

area so as to equal that of the parent material. Room-temperature strength of the weld has been elevated by forging to equal that of the parent metal. Room-temperature stress rupture properties were found to meet specification.

It is recognized that there is no cast metal in a properly executed flash weld. The improvement is one of reorienting the transverse grain flow produced in a flash weld to a grain flow orientation having greater ductility. The designer should recognize this more favorable orientation in relation to operating stresses.

In correlating the results of the work thus far accomplished, the following conclusions have been drawn:

1. Definite economies can be effected by proper application of the forged weldment approach.
2. Many parts heretofore impossible to forge can now be fabricated by the use of forged weldment.
3. Weldments can now be obtained with the same chemical composition as the parent material and having comparable mechanical properties. In many cases, this was not possible in the past, due to the necessity for adjusting the alloy composition to provide adequate physical properties in the as-cast weld deposit.

Acknowledgement

The early work on forged welds in SAE 4340 (AMS 6415) was inspired by C. A. Furgason, Vice President in charge of Research & Metallurgy at the Ladish Co. and executed by F. E. Dowling presently a metallurgical engineer in the Custom Forging Sales Division.

DESIGNING MATERIALS for FUTURE AERIAL VEHICLES

N. E. Promisel, Department of the Navy

This paper was presented at the SAE National Aeronautic Meeting, New York, April 3, 1957.

MANY years ago, Rudyard Kipling wrote this about aircraft: "We are at the opening verse of the opening page of the chapter of endless possibilities." It is not the purpose of this paper to contemplate our current whereabouts, but this is clear: Regardless of our specific position design-wise, we appear to have covered a substantial portion of this "chapter of endless possibilities" with respect to materials.

This is not to imply that major progress in materials development will not be forthcoming. Viewed from the present state of the art, however, and pending major developments in our technology and fundamental understanding of the behavior and compositions of materials, it does appear that the possibilities are by no means endless for aircraft materials, that in many areas we are in fact on the outer fringes of possibility, that the more obvious and merely difficult advances have already been or are being made, and that future technical breakthroughs in aircraft materials will require a far greater degree of ingenuity, initiative, perseverance, uninhibited thinking, logic, time, and effort. It is now evident that future aircraft design depends directly on progress in the development and design of new or greatly improved materials. Structural-design requirements and concepts of future aerial vehicles have outstripped our thinking and accomplishments in the materials fields. Materials engineers need not feel completely guilty, however. In the first place, it is often easier to conceive a new vehicle than it is to provide the materials and processes with which to build it. Second, unfortunately, the basic importance of materials has too often been recognized too late, in aircraft research, development, and planning, in spite of repeated warnings and protestations by materials engineers.

To comprehend more clearly the materials problems now facing us, it would be desirable to examine first the anticipated flight regimes of future vehicles. Since this cannot be done with any precision in this paper for security reasons, let us consider, instead, a few factors contributing to materials problems in these vehicles. For simplicity, we shall not consider satellites (with one exception) nor the so-called space-travel vehicles.

1. Speed. Aerodynamic heating is one of the major results of speed. Erosion of entrant surfaces, such as nose radomes and wing-leading edges, is another deteriorating effect. It can be of significance after minutes of flight even at subsonic speeds and increases in severity exponentially with speed and as a function of time; the nature of this latter function depends considerably on the specific material and the atmospheric contamination. Another important effect of speed at very high Mach numbers is the creation of a viscous flow or a plasticity in many solid surfaces, even metals, appearing as a surface flow below their melting point.

2. Temperature. Fig. 1 shows the now-familiar increase in vehicle surface temperature with increasing Mach number, which will be discussed in greater detail later. Other sources of heat are the

IN this paper a few of the many materials problems facing engineers in the aircraft field are discussed.

Factors involved in these problems include speed of the vehicle, temperature, altitude at which the plane or missiles will operate, noise and its accompanying vibration, deteriorative chemicals of fuels and fluids, and the use of nuclear power and radiation.

The author describes several new tools of technology in melting, shaping, and joining such as levitation melting, extrusion-molding, ultrasonic welding, and an inert-gas room for fabrication of refractory metals. Also, he discusses the nature and philosophy of developments in light nonferrous metals, Thermenol, superhigh-strength and high-temperature materials, as well as related aspects of nonmetallic structural materials and the functional components such as transparents, elastomers, and lubricants.

The importance of designing and synthesizing materials specifically to meet complex requirements is emphasized, an invaluable approach being composites (heterogeneous combinations).

powerplant, both chemical and nuclear; electrical, electronic, and hydraulic equipment; internal cooling systems; exposure to external nuclear explosions for even extremely short times and, under some conditions, radiation in the upper atmosphere. At the other end of the scale are the low temperatures of the upper atmosphere and the low ground temperatures of certain geographic areas. Also, there must be considered the many problems of thermal shock and thermal cycling as the vehicles or components thereof are subjected to rapid temperature changes.

3. Altitude. In addition to the temperature effects, at the very high altitudes at which some vehicles will operate (100,000 ft and higher) the environment will change significantly. Ozone, ionized gases, and cosmic radiation become destructive influences. As the filtering effects of the atmosphere at high altitudes diminish, ultraviolet and infrared radiation intensities increase, with increased deterioration of exposed organic and transparent materials.

4. Noise. Air intake, rotating equipment, and the turbulence created by high-velocity exhausts and the accompanying pressure differences create sound effects which, through induced vibration in materials, can be very destructive.

5. Deteriorative chemicals. Included in this category are new fuels; rocket propellants; heat-transfer media, such as liquid salts and metals, for nuclear-powered aircraft; synthetic lubricants such as the di-ester type; high-temperature hydraulic fluids (particularly in their effect on organic components such as seals, packings, and hoses).

6. Availability of materials. Although some of the metals formerly in short supply are now more readily available (for example, columbium), it remains necessary to minimize use of critical and strategic materials (such as cobalt and nickel) whenever possible. Quite often, financial economies also accrue from such conservation.

7. Nuclear power. In addition to the nuclear effects mentioned above, the use of nuclear power

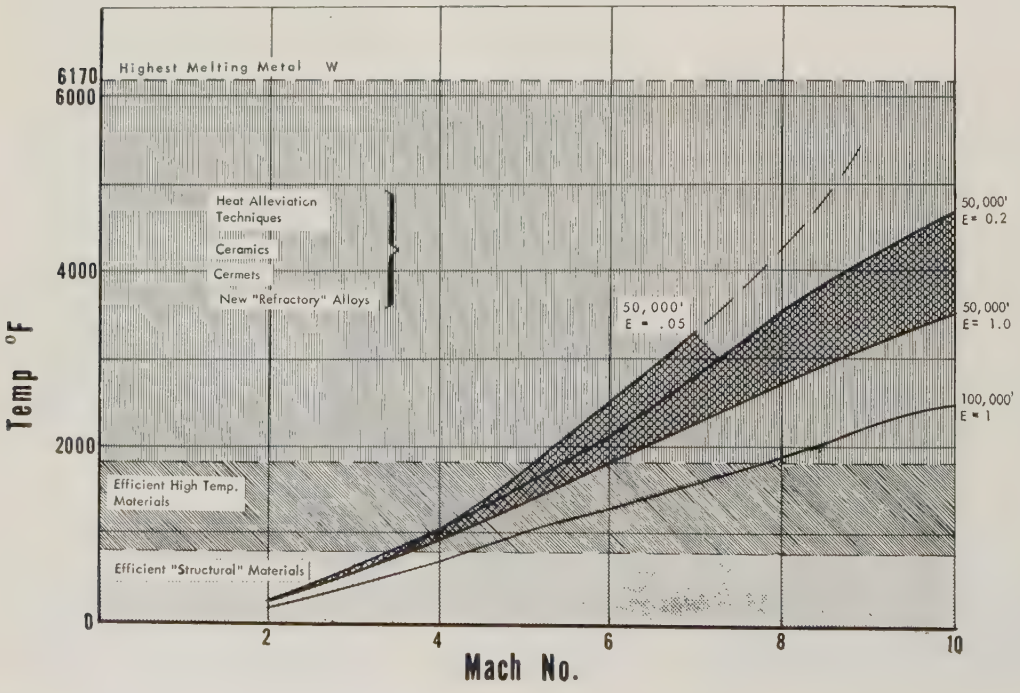

Fig. 1—Skin temperature versus speed, recovery factor 0.9

in vehicles creates two additional material problems: The possible damaging effect of radiation on material properties and the need for satisfactory nuclear properties, such as low neutron capture cross-section, and low level and half-life of induced radioactivity, not to mention the special category of radiation shielding.

We could also discuss the effects of combinations of these factors, such as lowered "ignition" temperatures of metals; the ever-growing importance of reduced weight, or of higher strength-to-weight and stiffness-to-weight materials, to avoid the penalty of severe growth of multiplying factors and their disastrous minimization of payload or performance; the problem of complexity engendered by the growing reliance on design (at extravagant cost) to circumvent materials' limitations, such as cooling devices to maintain materials at safe operating levels; the problem of limited space, as in thin wings of supersonic aircraft; the problem of thermal stresses (sometimes reaching and even exceeding 75,000 psi) resulting from use of materials with dissimilar thermal properties or from nonuniform temperature distribution. It becomes evident that it is very unlikely that materials can be developed with such broadly satisfactory properties that they can adequately resist all these destructive influences. It becomes necessary, therefore, to consider carefully each new difficult application and define the requirements such that a material can be designed for that particular application, or more often to design a combination or composite of individual materials such that each element thereof contributes to certain requirements, the summation of which satisfies the overall needs of the application.

To illustrate some of the materials problems resulting from the above factors, I have selected a number of difficult areas for more detailed discussion. Fortunately, new or improved tools of technology have appeared in recent years, some of which I will briefly recall first. No attempt will be made to cover the whole gamut of materials and processes.

New Tools in Processing and Fabrication

In the melting field, the use of vacuum has introduced a capacity for freedom from extraneous contaminants not previously available. Vacuum is being used in connection with many different types of melting operations, ranging from the zone refining of ultra-pure metals in small laboratory sizes to the 4000 lb consumable-arc titanium-melting furnaces. Vacuum melting is not always advantageous in the practical sense. Its advantage accrues along two major lines. Reduction in gas content during melting may improve the material by reducing the content of undesirable inclusions which, in turn, can improve certain properties (Fig. 2). In addition, reduction in oxygen and nitrogen in the atmosphere may make possible beneficial composition changes, by permitting the increase of hardener elements like titanium and aluminum. This has been demonstrated by the marked improvement in properties attained in a nickel-base high-temperature alloy through composition changes made possible by vacuum melting.

The technique of zone refining developed in connection with single-crystal work has raised the level

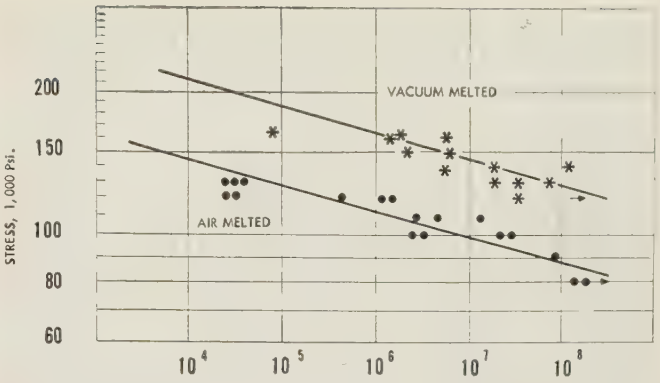

Fig. 2—Cycles to rupture, effect of vacuum melting on fatigue strength SAE 52100

of purity of materials attainable in a reasonably practical manner, although still limited to about ½-in. diameter bar. For example, hyperpure silicon is now being produced for electronic applications having less than one part impurity in a billion. This level of impurities lies well below the sensitivity of normal methods of analysis. In operation, a narrow zone of bar is melted (for example, by a surrounding induction coil) and the heat source or the bar is moved continously so as to advance the narrow melt zone along the bar length. As melting and freezing proceed, the high-melting constituents or alloy phases are concentrated in the end of the bar initially heated and the low-melting constituents in the other end. The process is repeated until the necessary separation of impurities is achieved.

In levitation melting, a solid can be literally suspended without mechanical support in an electromagnetic field and melted in whole or in part by induced current. High-melting reactive elements, such as titanium, zirconium, uranium, and other metals, have been thus melted without physical contamination of a surrounding support. Another interesting melting technique for reaching extremely high temperatures for a short time makes use of a coaxial-capacitor discharge. Depending on the nature of the surrounding gas, its pressure, and restriction of spark channel, a gas temperature close to a million degrees K has been claimed in deuterium. The author has seen a 2-in. piece of steel with a 1-in. hole melted in approximately 3 sec by related techniques. Somewhat more practical at the moment, and of increasing application to the study of materials, is the solar furnace, which in a limited area can reach about 4000 C. With this type furnace, extremely high-melting-point materials can be melted in such a localized manner that the nonmolten surrounding material serves as its own crucible, thus avoiding contamination reactions.

The subject of melting leads to other consolidating and shaping techniques. For example, vapor-phase reactions open new approaches to producing metal (pure or alloyed) and "vapor-forming" it to shape, without going through a melting phase. New techniques for producing submicron powders and for pressing and sintering increase the versatile potentialities of powder metallurgy. Even in the more conventional operations such as casting, important improvements are coming. Thus, in light

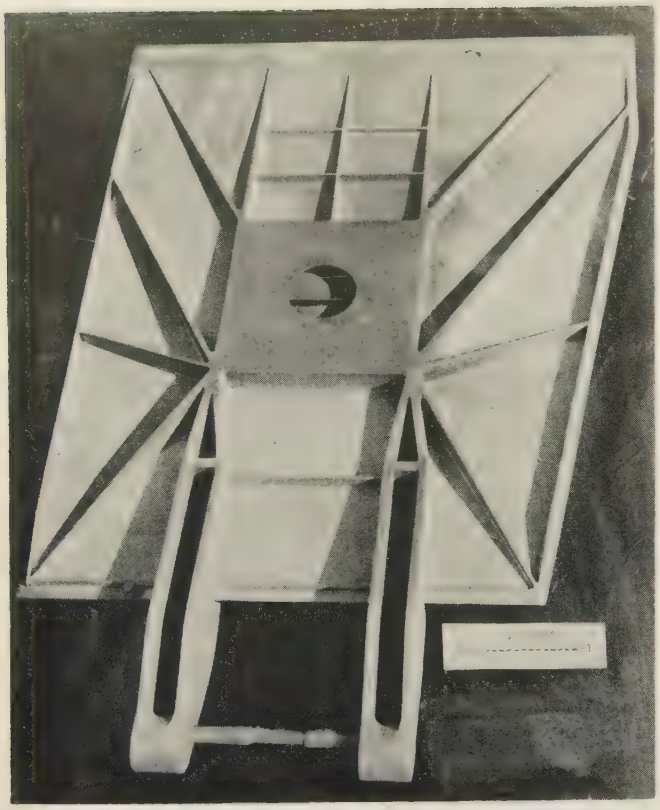

Fig. 3—Cast magnesium alloy dive brake (Courtesy of Osbrink Mfg. Co.)

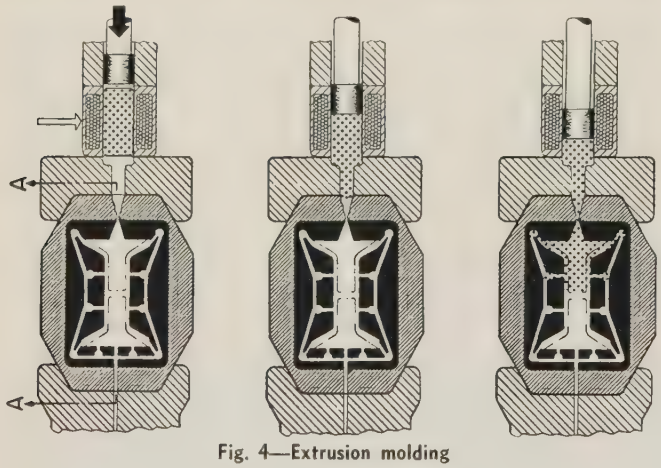

Fig. 4—Extrusion molding

alloys the use of new mold materials, such as aluminum metal and high-conductivity plasters, together with more exacting control of temperatures, composition and atmospheres, and attention to detail in casting design and mold practice, have afforded considerable advances in the properties and shapes available. Large-area thin-section magnesium sand castings of the type shown in Fig. 3 are already in service. Table 1 lists the properties of specimens cut from experimental aluminum-alloy bell-crank castings. These castings were completely free of observable radiographic defects. Experiments are now in progress on a high-purity 3% copper–7% silicon aluminum alloy aimed at 60,000-psi tensile strength, 45,000-psi yield strength, and 3% elongation in 2 in.

A machine is now under construction to evaluate the practicability of "extrusion molding" of light

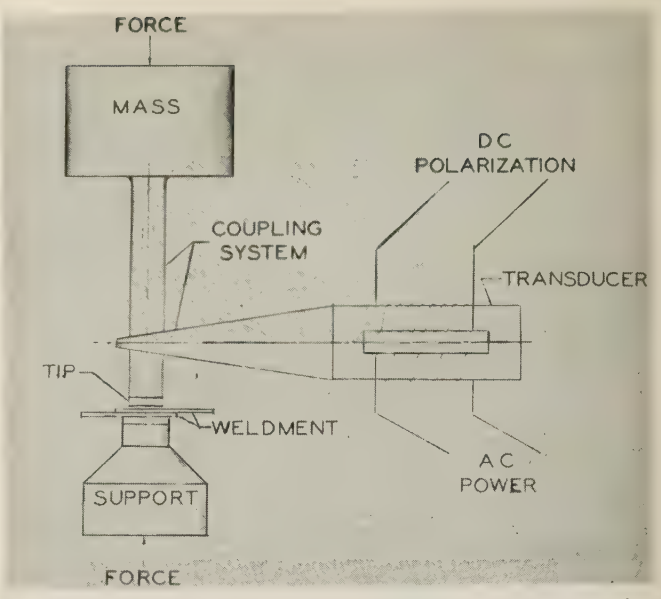

Fig. 5—Transducer-coupling system (Courtesy of Aeroprojects, Inc., West Chester, Pa.)

Table 1—High-Strength Aluminum-Alloy Castings
(tensile specimens machined from castings)

Alloys	Tensile Strength, psi	Yield Strength, 0.2% Offset, psi	Elongation—1-in. Gage, %	Reduction of Area, %
Special Process C355-T62	55,100	38,200	10.7	11.0
	55,900	45,800	3.0	5.9
	51,900	40,800	5.0	9.5
Typical Sand Cast 355-T6	35,000	25,000	3.0	
Special Process A356-T61	39,600	28,500	21.5	28.3
	40,400	33,100	15.0	17.3
	39,100	30,200	21.5	28.3
Typical Sand Cast 356-T6	29,000	24,000	3.0	

alloys. In this process, which is somewhere between forging and casting, a cast or wrought extrusion billet is forced in a semiplastic state into a split-metal mold under carefully controlled pressure conditions. Fig. 4 is a diagrammatic illustration of the proposed machine. The properties anticipated in parts made in this manner approximate those of forgings, with the advantages of freedom from anisotropy and elimination of many of the forging shape and alloy restrictions and with lowered die and operation cost.

In the joining field a new method of welding, using ultrasonic energy instead of heat, is being developed. In this process, the pieces to be joined are clamped together under low pressure (40–300 lb) between two welding members. Ultrasonic energy is applied to the weld area through the welding members. Fig. 5 shows the transducer-coupling system used in Navy-sponsored work at Aeroprojects, Inc. A metallurgical bond is produced in 1–2 sec with negligible deformation of the pieces being welded (less than 5%) and with no apparent disruption of crystal continuity. Fig. 6 illustrates the continuous transition in an ultrasonic weld in clad aluminum alloy 2024 compared with the nugget discontinuity in a spot weld in the same material.

The fact that excessive heating and melting are avoided in ultrasonic welding makes this approach very attractive. In many materials such as the high-strength aluminum alloys, molybdenum, titanium alloys, and in making welds which extend over appreciable areas, lowered ductility, strength,

and corrosion resistance result from a heat-welding operation. Elimination of these unsatisfactory effects will make possible advantageous use of welding. For example, this technique should enable the welding of area joints in high-strength aluminum alloys of the type used in bonded construction, without the temperature limitations of the organic adhesives now in use and without the drop in strength and corrosion resistance in high-strength aluminum alloys caused by multiple spot welds or seam welds.

Structural Materials for Use 400-1000 F

It is in the approximate range of 400–1000 F that many of our current and future problems in so-called "structural" materials lie. In this range, the old standbys in efficient aircraft structural materials, the aluminum and magnesium alloys, begin to fail us occasionally. Some years ago, the threatened necessity of converting to steels with a density increase of 250% and more was cause for considerable anguish. Fortunately, titanium appeared on the scene and offered at least temporary alleviation of this difficulty. I will review briefly recent advances in the magnesium and aluminum fields; indicate some activities and aspirations in titanium; and discuss some trends in high-strength steels which bring them again into the aircraft structural field.

Starting with the lowest density structural material, magnesium, the new major contributor to improved elevated-temperature properties is the addition of 2–3% thorium to previous contents of zinc, zirconium, and manganese. One such alloy, HK31, contains nominally 3% thorium and 0.7% zirconium and is available both for cast and rolled forms. HZ32 is approximately the same alloy with an addition of 2% zinc and is used for castings. Another new casting alloy is ZH62A with 6% zinc, 1.6% thorium, and 0.7% zirconium. HM31, still somewhat experimental, contains 3% thorium and 1% man-

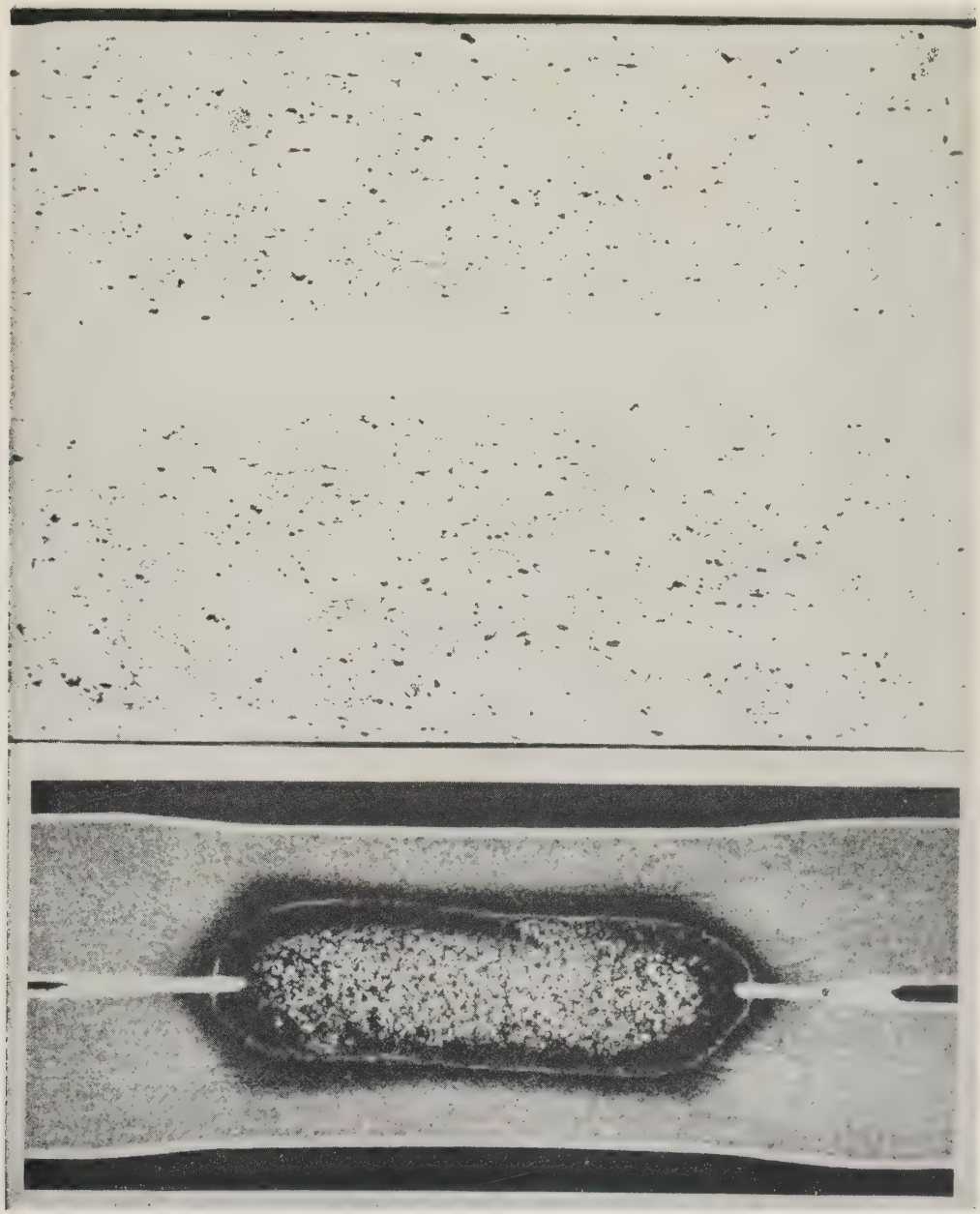

Fig. 6—Comparison of structure in ultrasonic and spot welded alclad 2024 aluminum alloy (Courtesy of Aeroprojects, Inc., West Chester, Pa.)

ganese and is intended for sheet and extrusions. Fig. 7 shows, for castings, how these thorium types compare in tensile and yield strength at various temperatures, with the older aluminum-zinc type (AZ92) and cerium types (EZ33 and EK30). Fig. 8 shows tensile properties after various exposure times at different temperatures. It is interesting to note that at 400 F the HK31 alloy increases in strength with time, while a number of the other curves remain relatively flat.

How much further magnesium alloys may be increased in strength at elevated temperatures is difficult to predict; but it appears that conventional alloying techniques will yield only marginal improvements. Powder-metallurgy techniques may permit addition of different types of hardening agents and thus prove to be more profitable for future investigation. Some activity has already been initiated in this direction.

With respect to aluminum alloys, it has long been recognized that the heat-treated alloys which are best for high strength at room temperature do not show to advantage even below 400 F. This is illustrated in Fig. 9, showing the rapid drop in 7075-T6 and 2014-T6 between 300 and 400 F. On the other hand, 2024 alloy in the T86 temper, that is, cold-worked about 6% and then artificially aged, shows superior characteristics and, in fact, is still of value in our present so-called "high Mach number" aircraft. Better characteristics are also shown by 2618-T61 alloy (a forging alloy with about 2% copper, 1% iron, 1.6% magnesium, 1% nickel, and 0.07% titanium), by X2219-T6 alloy (for all wrought forms, with 6% copper, 0.3% manganese, 0.1% vanadium, and 0.15% zirconium), by M-237 which is unlikely to appear in production, and by the powder-metallurgy products (APM) designated M257 and M276. The latter type of product, as in the case of its original Swiss counterpart, Sintered Aluminum Powder (SAP), contains only aluminum and its oxide (in the range about 8–16%) and shows very flat temperature curve characteristics. Unfortunately, these products tend to be more brittle than desired, though they have some applications. For castings, a fairly new alloy, XA140, with 8% copper, 6% magnesium, and 0.5% each of manganese and nickel, is markedly superior to other aluminum-casting alloys at 600 F.

As mentioned above for magnesium, the degree of future improvement of aluminum alloys by conventional approaches, although worthwhile, appears to be becoming marginal. The new concept of dispersion hardening by powder metallurgy, particularly with new design concepts which would recognize the apparently inevitable downward trend of ductility, in time may well pay good dividends.

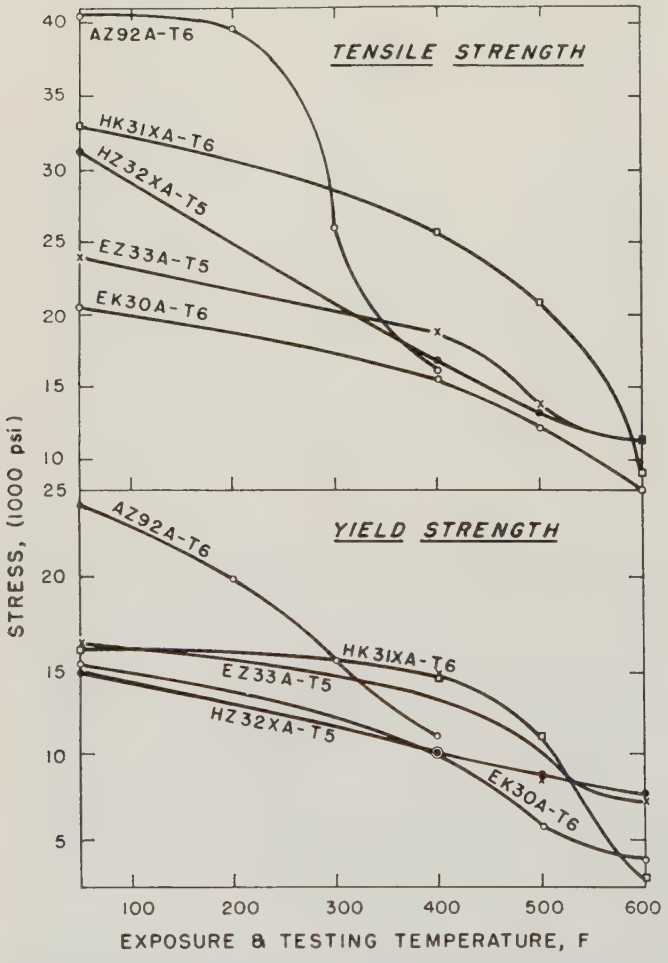

Fig. 7—Tensile and yield strength at temperature, 1000-hr exposure at that temperature, of alloys with thorium (Courtesy of Dow Chemical Co.)

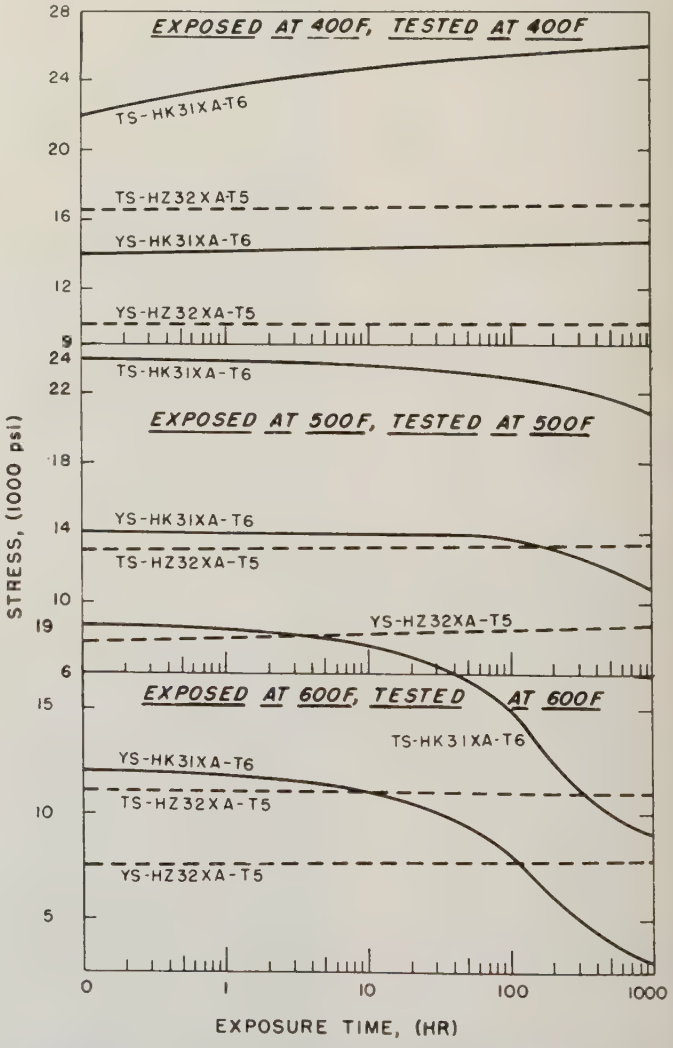

Fig. 8—Effect of exposure at elevated temperatures on tensile properties of alloys containing thorium (Courtesy of Dow Chemical Co.)

Table 2—Titanium Sheet Rolling Program

	Properties in Solution-Treated Condition, Room Temperature				Short-Time Properties in Heat-Treated Condition					
					Room Temperature			800 F		
	Ultimate Tensile Strength, psi	Yield Strength, psi	Elongation in 2 in., %	Bend Duct[a]	Ultimate Tensile Strength, psi	Yield Strength, psi	Elongation in 2 in., %	Ultimate Tensile Strength, psi	Yield Strength, psi	Elongation in 2 in., %
Target Properties[b]	120,000	—	15	2T	180,000	160,000	10	130,000	105,000	15
Selected Alloys										
3% Al-6% Mo[c]	135,000	—	15	2.5T	180,000	160,000	7	130,000	105,000	15
4½% Al-3% Mo-1%V[c]	150,000	125,000	15	3T	170,000	150,000	10	100,000	80,000	15
6% Al-4%V[c]	130,000	120,000	10	6T	170,000	155,000	7	100,000	80,000	—
2½% Al-15% V[c]	100,000	—	15	2T	180,000	160,000	6	130,000	105,000	10

[a] Minimum 105-deg bend without cracking with radius of bend expressed as multiples of the thickness of the sheet.
[b] These properties were specified on the basis of information furnished by the airframe industry.
[c] Hydrogen shall not exceed 150 parts per million.

So much has already been written on the subject of titanium that I shall treat it only briefly. The development of ductile titanium has opened a fertile field of potentialities, at least up to about 1000 F, which is second to none. Perhaps no better expression of faith and expectation in the future of this material can be cited than the fact that about a billion dollars has been invested in it by both government and industry in only 10 years. Present alloys, produced in almost every desired commercial form, have strengths equal to what was not long ago considered fairly high-strength steel, weigh approximately 40% less, and have generally phenomenal corrosion resistance. Fig. 10 shows one of the many interesting comparisons for various high-strength sheets.

The most important current program likely to push titanium to new usefulness, particularly in future airframes and missiles, is a high-strength, elevated-temperature sheet program. In this program, being conducted by the Bureau of Aeronautics but applicable to the entire Department of Defense, four alloys have been selected as showing the most promise of meeting or approaching certain target properties, based on limited exploration and production by the leading titanium producers. These target properties, extensively coordinated with the aircraft industry, and the selected alloys with their tentative compositions are shown in Table 2.

The program itself consists of three main phases:

Through Bureau of Aeronautics contracts with the titanium-alloy producers, Phase 1 will attempt to determine the significant variables incident to melting, rolling, and processing the selected alloys. The emphasis will be on establishing production procedures, inspection methods, and acceptability criteria required for the production of reliable, uniform, reproducible alloy sheets.

Phase 2 will develop design data on those alloy sheets successfully produced in Phase 1. These data will be obtained by government laboratories, the aircraft industry, and other research and testing laboratories. In order to obtain agreement in tests performed, uniform testing procedures are being developed.

Phase 3 deals with the fabrication and application of the titanium alloys. In this phase, the alloys that have successfully demonstrated they can meet the established requirements will be evaluated by the aircraft industry.

At the present time, some 75,000 lb of material have been melted and are in various stages of developmental processing under a carefully designed and controlled experimental plan aimed at producing completely identified, "pedigreed" sheet for use in Phases 2 and 3. By the end of 1957, many thousands of pounds of this pedigreed material should be in numerous laboratories and aircraft companies undergoing final evaluation, fabricating studies, and demonstration of suitability.

What lies ahead for titanium? Many things could be listed, but perhaps some of the more important implications are: (1) progress made toward development of alloys for use at 1000 F; (2) interesting possibilities developed for alloys with room-temperature tensile strength in the neighborhood of 200,000 psi; (3) encouraging possibilities for significant reduction in cost of titanium (a factor which has been a serious deterrent to more extensive use of this material) including electrolytic refining and electrolytic processing of raw material, melting improvements, recovery and use of scrap, and improvement of fabricating equipment, techniques, and processes; (4) significant further progress expected in extrusion and casting; (5) exploitation of high-strength, light-weight titanium fasteners.

The excellent oxidation resistance of iron-aluminum alloys has been recognized for many years, but their lack of ductility discouraged serious consideration of compositions containing more than 6–8% aluminum until the Naval Ordnance Laboratory, employing vacuum-melting and planetary-rolling mill techniques, succeeded in producing thin

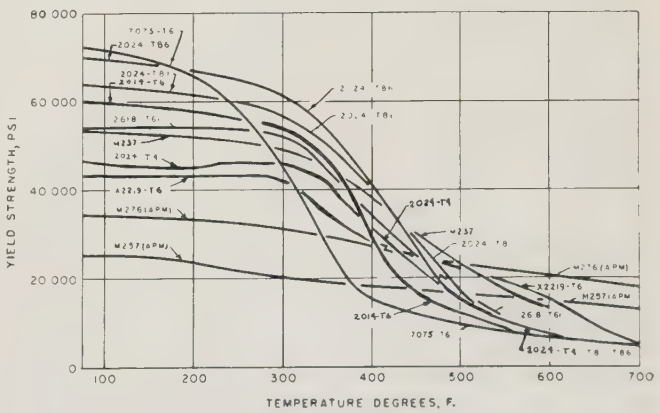

Fig. 9—Yield strength of wrought alloys at elevated temperatures after 100 hr at temperature (Courtesy of Aluminum Co. of America)

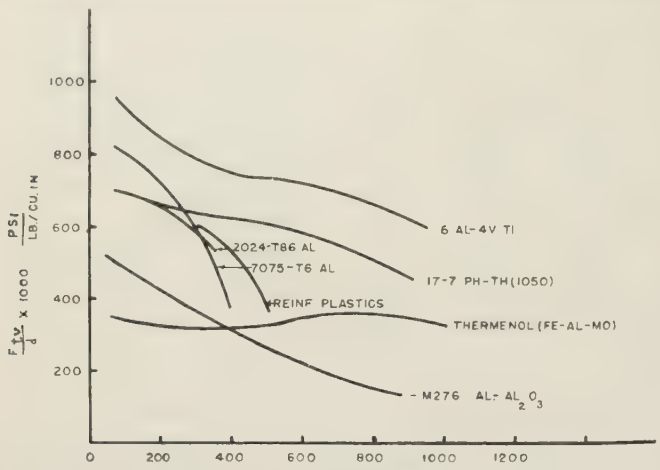

Fig. 10—Strength density comparison of titanium and other alloys versus temperature

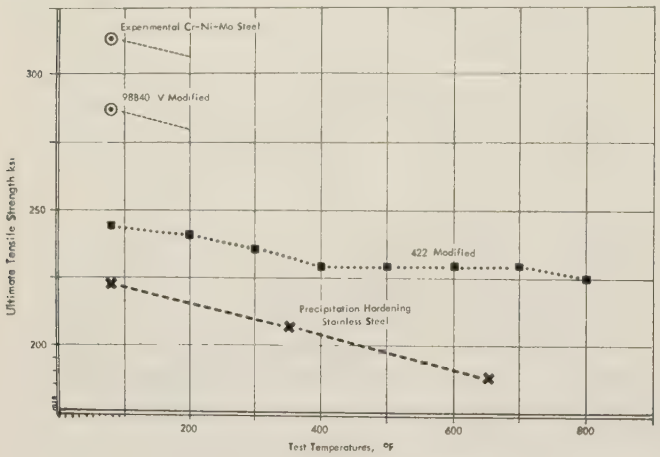

Fig. 11—High-strength steels

sheets of iron-16% aluminum alloy for use as magnetic material. Addition of 3% molybdenum to enhance the elevated temperature strength resulted in a product called Thermenol.

A comparison of the properties of Thermenol and other materials is given in Table 3. Thermenol has excited considerable interest because of the absence of critical materials from its composition, its low density compared to the corrosion-resisting steels, its good strength to 1000 F and somewhat higher (Fig. 10), and its impressive resistance to oxidation. It is being considered for a variety of applications ranging from compressor blading to combustion chambers for auxiliary gas-turbine engines. Because of its still marginal ductility, forming must be performed warm and in small steps. However, the use of vacuum-arc melting with added grain refiners followed by controlled heat-treatment has been found to result in a simultaneous doubling of strength and ductility.

This brings us to steels for this intermediate temperature range. Steel developments for aerial vehicles appear to fall into two major categories: (1) increasing the strength in large sections around room temperature to values in the neighborhood of 300,000 psi tensile strength, for applications such as landing gear, and (2) improving the strength and other properties for use up to about 1000 F, primarily for sheet and other flat-rolled products.

In the first case, steels with design values between 260,000 and 280,000 psi tensile strength are already in use in fairly large sizes, as for landing gear parts. It should be recalled that steel in small cross-section, well over 300,000 psi in wire, is by no means new. The higher strength in larger sizes has been based on low tempering temperatures of carefully controlled chrome-nickel-molybdenum steel or by juggling these elements and silicon with minor additions of vanadium, boron, aluminum, and titanium. For example, one such steel developed at the National Bureau of Standards for the Bureau of Aeronautics contains nominally 0.4% carbon, 0.75% manganese, 1.60% silicon, 0.85% chromium, 0.30% molybdenum, 1.80% nickel, 0.10% titanium, and 0.002% boron. Other compositions are the modified 98BV40 and the relatively new Inco steel. Fig. 11 shows the tensile properties at approximately room temperature of two of these. There is reason to believe that increases in strength can be made slowly through the years, particularly with improvement in ductility and transverse properties. Several approaches to such improvements are already being investigated with promising indications, for example, rare-earth additions. If successful, this could raise the general design level of super high-strength steel compositions already known or in use.

The second case dealing with rolled products for use up to about 1000 F emphasizes problems of the lower temperature materials. In addition to the usual strength properties, there are creep, stress-corrosion, temperature stability, fabricability, weldability, tolerance control, magnetic permeability, simplicity of heat-treatment, and other factors to consider more sensitively. Several interesting compositions may be mentioned. The two that have received most attention in the aircraft industry, and about which much has been published, are two chrome-nickel stainless steels, 17-7PH and AM350, containing about 1% aluminum and 3% molybdenum, respectively. Both depend on transformation from austenite to martensite, followed by precipitation and tempering, respectively, with resulting tensile strength to about 225,000 psi, depending on details of heat-treatment. Both have interesting elevated temperature properties and good corrosion resistance and formability. Even higher strengths, but with sacrifice in the latter properties, may be obtained by heat-treatment of "martensitic stainless" steels, such as type 422 modified. One such steel has a composition of approximately 0.25% carbon, 12% chrome, 0.75% nickel, 1% molybdenum, and 0.25% vanadium. The carbon and nickel were selected to achieve a completely martensitic structure with high strength; the molybdenum and vanadium minimize stress-corrosion cracking and the former also increases ductility. Aircooling from the austenitizing temperature of 1875 F, followed by tempering between 800 and 1100 F gives room-temperature strengths of about 250,000 psi ultimate tensile, 200,000 psi yield, and 5–6% elongation in 2 in. Fig. 11 shows properties as they vary with temperature after tempering at 1125 F, from United States Steel Corp. data.

At least two other approaches to improved aircraft steels are being made. Age-hardenable austenitic steels, such as one with 0.60% carbon,

15% manganese, 14% chrome, and 2% vanadium, depending on precipitation of vanadium carbide for hardening, offer one possibility. Another is the cold-working of austenitic steels. In all these types of steel, the needs of specific applications must be considered for the properties enumerated above vary with the steel type and, unfortunately, no one steel is superior in all respects. In addition, one must always keep in mind the need for avoiding, if possible, critical materials such as nickel.

There are other interesting possibilities under consideration for the future. The tool and die steels with about 5% chromium offer good promise at both room and elevated temperatures. In an entirely different direction, beryllium and its alloys are of interest, for the combination of unusually high modulus of elasticity (approximately 43,000,000 psi) with low specific gravity (1.8) is extremely intriguing and would fill one of the outstanding gaps in present light alloys, namely, lack of stiffness. Some of the high-density refractory elements must also be considered, since their modulus to density ratios are at least competitive with those of the light alloys. In turn, these elements will necessitate further concentration on fundamentals; for example, further dependence on studies of the physics of the solid state to clarify and point the way to eliminating the brittle behavior of beryllium. Some day, it should be possible to reach more closely the theoretical structural strength of materials. The already achieved attainment of fine filaments or whiskers of metals having tensile strength in the order of 1,000,000 psi is an encouraging step in this direction.

Materials for Use Above 1500 F

The need for materials giving satisfactory operation above 1500 F, and extending certainly to 5000 F, arises primarily from the requirements of gas turbines, nuclear powerplants, rockets, and long-range guided missiles. Some of the highest temperatures anticipated occur on the nose of long-range missiles, after re-entry into the atmosphere at speeds of 10,000–20,000 mph. For example, the boundary-layer temperature on the nose of a missile flying at Mach number 18 and an altitude of 85,000 ft can reach the neighborhood of 12,000 F. The actual surface temperature in this case would be, of course, substantially lower, depending on the ingenuity of the designer and the materials engineer. On the other hand, although the temperatures in jet-engine blades are currently below 2000 F, the high stresses, long operating times, and criticality of dimensions make this application one of the most difficult to satisfy. For the latter and similarly critical applications, the nickel-cobalt-base alloys now are used, but their temperature limits for efficient use at high stresses appear to be 1700–1800 F. Aside from cooling, with which I shall not deal in this paper, there are three major approaches to breaking through the thermal limitations: chrome-base alloys, refractory metal-base alloys, and cermets.

The Bureau of Aeronautics has been studying chrome-base alloys at the Massachusetts Institute of Technology for many years. Results to date point toward alloys of the general composition 40–45% chromium, 45–50% nickel, 2–10% iron, 2% molybdenum, and 2% niobium. The 1800 F rupture life for alloys of this type, 100 hr for 7000 psi, is superior to that of current nickel-base alloys hardened with aluminum and titanium. Recent improvements have resulted in several possible alloys which appear to be superior to the best cobalt alloy at this temperature. Vacuum melting and other advanced techniques are being employed to obtain further improvements both in the 45% chromium area and in alloys containing 60–90% chromium. While ductility at room temperature continues to be a problem, the confirmed inherent ductility of the pure metal encourages continuing efforts in this important field.

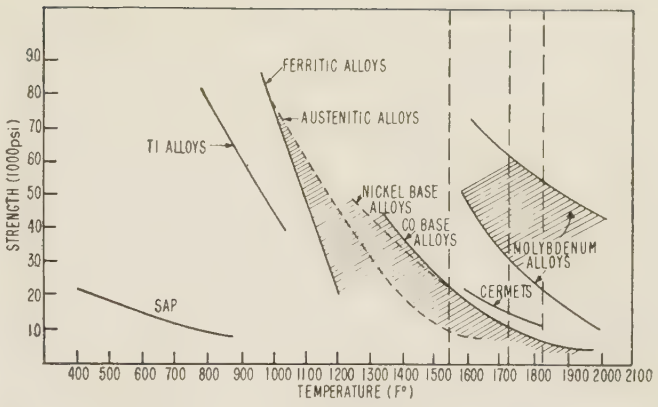

Fig. 12—Comparison of stress-to-rupture properties (100 hr) of various materials

Table 3—Comparative Properties of Thermenol and Other Materials

	Thermenol	Stainless 302-½ H	Titanium Commercially Pure	Aluminum 2024-T4	Magnesium AZ31
Modulus of Elasticity	24×10^6	29×10^6	16×10^6	10.3×10^6	6.5×10^6
Density, gm/cm³	6.58	7.93	4.5	2.77	1.78
Resistivity, microhm cm	160	72	54	5.7	9.3
Relative Corrosion Resistance, Sea Water	Good	Excellent	Excellent	Good	Poor
Relative Oxidation Resistance, 1600 F	Excellent	Good	Unusable	Unusable	Unusable
Relative Weldability	Good	Excellent	Fair–Good	Fair–Good	Good
Relative Machinability	Fair	Fair	Fair	Excellent	Excellent
Relative Workability	Poor	Good	Good	Good	Fair
Maximum Permeability	130,000		Nonmagnetic	Nonmagnetic	Nonmagnetic
Cost of Sheet per Pound	$3.00	$0.50	$20.00	$0.50	$0.75

Table 4—Refractory Metals

	Melting Point, F	Density, g per cc	Modulus of Elasticity, psi
Tungsten	6170	19.3	50×10^6
Rhenium	5740	20.0	42×10^6
Tantalum	5425	16.6	27×10^6
Osmium	4900	22.5	80×10^6
Molybdenum	4760	10.2	45×10^6
Iridium	4450	22.5	75×10^6
Niobium	4380	8.57	19×10^6
Chromium	3430	7.19	36×10^6
Zirconium	3380	6.5	14×10^6
Titanium	3140	4.5	16×10^6
Vanadium	3125	6.11	$21–22.5\times10^6$
Hafnium	3100	11.4	20×10^6

Table 4 shows the elements generally listed among refractory elements. Many of these have been investigated for one reason or another; for example, titanium, niobium (columbium)—because of its desirable nuclear properties—chromium, zirconium, and vanadium. In spite of all this work, however, no integrated effort has been made to explore this group as a whole, for development of more general-purpose high-temperature alloys. The Navy Department has such a plan outlined and hopes to begin attacking this problem soon.

Molybdenum has received extensive study over the past 10 years with excellent results. Fig. 12 shows

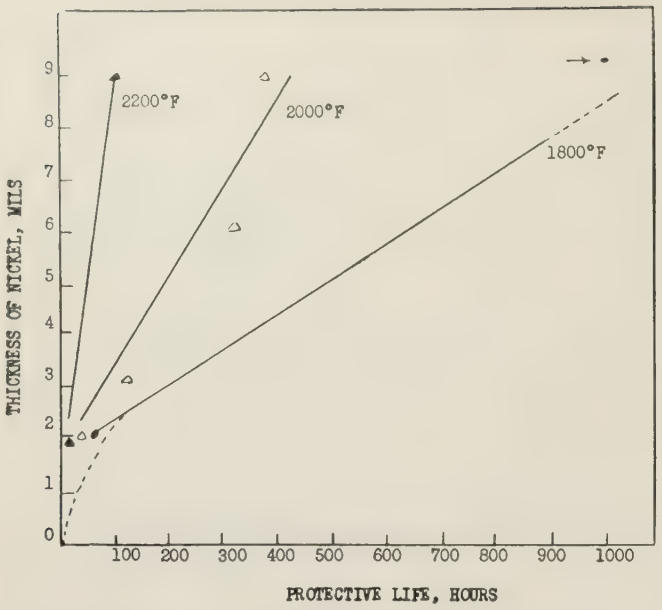

Fig. 13—Effectiveness of varying thicknesses of nickel over 0.001 in. of chromium for the protection of molybdenum against oxidation

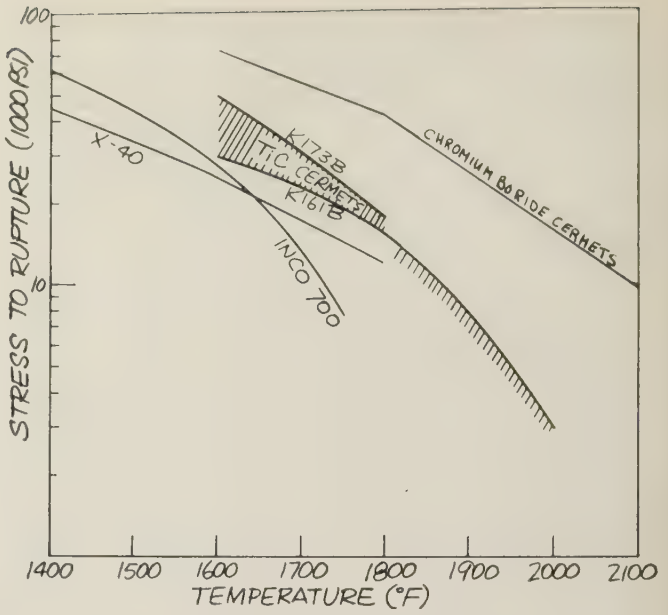

Fig. 14—Creep-rupture properties (100 hr life)

one comparison of molybdenum with other competitive materials. The only real deterrent to more extensive use of molybdenum is the absence of a reliable coating to prevent oxidation at high-temperatures, unless the time at temperature is so short that this oxidation can be tolerated. The applications which are of outstanding importance are turbine blades and guide vanes of gas turbines where higher temperatures, such as 1800–2000 F, are sought but where suitable materials are lacking because of the high static and vibratory stresses present, the need for thermal and shock resistance, and the need for long life under these conditions. Molybdenum is currently the most promising material to fill these needs and, therefore, coating development has been directed to this type of application.

These requirements dictate that the coating, and its method of application, not deteriorate the molybdenum alloy as by recrystallization. Also, the coated blade must resist oxidation for hundreds of hours at temperature; resist many cycles of rapid heating to temperature and cooling in an air blast; resist fracture of the coating under impact of a foreign body, such as a small steel shot fired at its edge at high velocity from an air rifle; resist erosion, for example, from a controlled blast of hot abrasive particles while at temperature; and not develop unhealed surface defects under creep conditions or when elongated a few percent in a hot-tensile test. Obviously, some of these illustrations comprise empirical tests being applied to present products.

Many approaches have been taken to solving this problem, (See Table 5). Of these, cladding has been quite successful where it can be used, for example, with the obvious limitation that it cannot be applied to a finished object. Though there have been varying degrees of success with the other approaches, one of the most promising is the electrodeposition of chromium, in a thickness of 1 mil, followed by electrodeposited nickel, 5–10 mils thick, applied under controlled conditions. Fig. 13 shows the results of some work performed for the Navy Department at the National Bureau of Standards.

One interesting side light on molybdenum development may be mentioned briefly. Because of the oxidation problem and the need for exploring fabrication and working techniques for molybdenum and other refractory metals at temperatures far higher than ever before, the Navy is sponsoring facilities at the Universal-Cyclops Steel Corp. for the creation of a large, inert-gas-atmosphere chamber, large enough to contain fabricating equipment such as a rolling mill, a forging impactor, and welding equipment. At this stage, final details of intriguing problems are being resolved, such as control of impurities in the chamber atmosphere to about 100 parts per million and breathing suits for operating personnel.

Graphite should be mentioned as a nozzle material for rockets and ram-jets or for similar application where extremely high temperature is accompanied by relatively low stress. Its sublimation temperature, though not accurately known, is perhaps in the neighboorhood of 7000 F, placing it as high as or above the melting or sublimation temperature of any other refractory material. Graphite does not melt, except under simultaneous conditions of extremely high temperature (exceeding its sublimation temperature) and high pressure (in excess of 3500 atmospheres). Other properties of value are its very low density of 2.25 grams per cc, its high thermal conductivity of 98 Btu per hr per sq ft per F per ft, its machinability, and its high availability. However, its resistance to erosion under oxidizing conditions requires improvement. This can be done in one of several ways: (1) Alloying with other refractory materials; (2) use of protective surface layers; (3) impregnation with materials which reduce porosity and, consequently, improve immunity to attack.

Alloying techniques have produced excellent results. For example, work by the Stanford Research Institute for the Air Force has resulted in very in-

teresting combinations of silicon, molybdenum, carbon, titanium, and boron. Work by the same Institute on protective layers has produced graphite impregnated with refractory metal capable of resisting oxidizing atmospheres at temperatures well over 4000 F without dimensional change in torch tests.

The third area under consideration for temperatures above 1500 F is cermets, a combination of metal and ceramics. It is evident that the number of possible combinations of these two constituents is tremendous. The binders must be designed to have high melting point, high temperature strength, ductility at low and high temperatures, thermal shock resistance, oxidation or environment resistance, and ability to "wet" the refractory or ceramic portion of the cermet. In practice, metal binders to date have been limited primarily to nickel and cobalt alloys with current grades running 50–70% binder content for improved ductility, impact resistance, and thermal shock resistance of the cermet. It is evident, however, that some of the refractory metals shown in Table 4 offer interesting possibilities and, in fact, must be considered if only because of the need for increase in melting point. Rhenium, for example, would be a very interesting possibility from a technical point of view, although economic and availability problems must be considered.

On the ceramic or refractory side of the cermet, the possibilities lie in carbides, borides, oxides, silicides, nitrides, and the like. These types of compounds are, in general, extremely hard, brittle, and temperature resisting. For example, boron carbide is second only to diamond in hardness. Hafnium and tantalum carbides are probably the highest melting materials known, melting at over 7000 F. One of the molybdenum borides, melting at over 3500 F, is very useful for brazing molybdenum, tungsten, and tantalum. Less is known about beryllides, phosphides, rare earth sulfides, and some others. In general, the same desiderata as for the binders are important in these refractory compounds, but those related to toughness are difficult to achieve, which is the main reason for using a metal binder. Interesting constituents are titanium carbide, silicon carbide, zirconium boride, silicon boride, and molybdenum disilicide. For use up to about 1800 F, the oxidation-resisting, nickel-base titanium-carbide cermets have received most consideration, with binder content 50–70% for reasons given above. With designs which avoid severe notch-stress concentrations, they offer promise for some turbine blade, nozzle guide-vane, and small turbine disk applications. Fig. 14 shows stress-rupture properties of some of these titanium-carbide materials, such as K161B and K173B, compared with two of the best nickel- and cobalt-base alloys, Inco 700 and X-40, respectively. Fig. 15 shows a titanium-carbide wheel, simulating a design for small turbines, which was satisfactorily spun-tested at 1600 F. A similar wheel will soon be tested at 2000 F at the Naval Air Material Center. Low impact strength remains the greatest deterrent to use, mainly because of risk of serious damage if struck by foreign objects.

Other cermets to about 1800 F include chrome-alumina, molybdenum disilicide, nickel aluminide, and metal-bonded Cr_2Ti types. A relatively new group of cermets based on chrome-molybdenum reinforced chromium boride shows significant promise up to at least 2100 F, or alternatively, much higher strength than the carbide cermets at lower temperatures (Fig. 14). Still another relatively new type which has shown impressive results in preliminary rocket nozzle tests is zirconium boride in a boron binder.

Since ductility and resistance to impact are the serious deficiencies in cermets, a technique has been designed by the Sintercast Corp. for improving this situation by overinfiltrating a skeleton of titanium carbide with an Inconel binder in such a way as to produce a metal-rich ductile protective surface, relatively low in carbide. In specimens prepared for the Bureau of Aeronautics, the impact results shown in Table 6 were obtained, indicating that overinfiltration produced substantial improvement in toughness on the impact side only. It is conceivable that pre-metal-coating each ceramic particle, controlled in shape and size, would also improve matters.

Even aside from the above potential and increment improvements, one cannot say that the prospect of obtaining these materials with a significant

Table 5—Protective Coating Types

1. Ceramic Coatings
2. Molybdenum Disilicide Coatings
3. Metallic Coatings
   a. Cladding
   b. Sprayed Metal Coatings
   c. Electroplated Coatings
   d. Diffusion Coatings (Cementation)
   e. Hot-Dipped Coatings
   f. Vapor-Deposited Coatings
   g. Chromizing

Table 6—Unnotched Impact Strength of TiC Infiltrated with Inconel, ft lb

	Room Temperature	1600 F	1800 F
Not overinfiltrated	1.2	2.0	1.5
Overinfiltrated all over	0.5	1.0	0.7
Overinfiltrated on impact side only	—	6.6	3.7

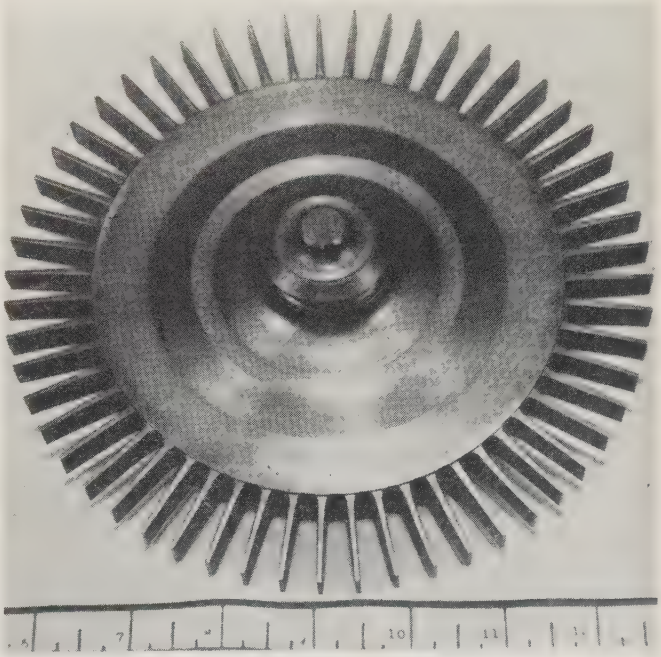

Fig. 15—Cermet wheel

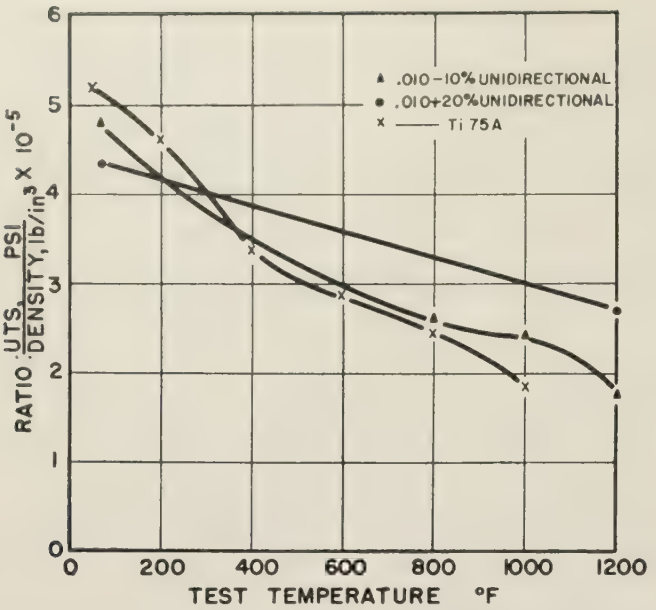

Fig. 16—Strength-to-density ratio of fibrous structures compared to unalloyed titanium at various temperatures

degree of inherent ductility is hopeless. For example, some inorganic crystalline materials normally considered brittle, like salt, can be made to behave in a ductile manner under certain conditions. The "why" of this behavior is not clear, though apparently related to surface changes. It would appear that concentrated effort in the physics of solid state and in fundamental studies of plastic deformation, with the solution of this problem clearly in mind as an objective, could pay dividends, in the long run transcending by far the results of our almost exclusively empirical efforts to date.

Surface Modifications

The aerial vehicle of the future will present a large number of problems of accomodation of the structural materials to the environment in which they must operate. Many ingenious design and materials modifications are being explored to lower surface temperatures as an alternative to attempting to develop new complex materials. I will cite two examples to indicate what might be accomplished.

As is indicated in Fig. 1, the heat balance of materials in very high temperature environments is significantly affected by the surface emissivity of the body concerned. Development work on surface coatings is now being directed toward a requirement for emissivity control. Low-emissivity (0.05) surfaces, sometimes desired, are produced with lustrous metal coatings protected with thin, transparent ceramic coatings, such as silicon monoxide. At the other extreme, high-emissivity (0.9) surfaces may be produced by formation of black metal oxides. Intermediate values may be obtained with selected ceramic coatings.

A requirement for thermal insulating coatings for applications, such as ram-jet combustion-chamber liners in which flame temperatures over 4000 F and material temperatures over 2000 F are encountered, has also necessitated a rather extensive development program. Since the thermal insulating power of such coatings is a function of thickness, coatings of up to about ¼ in. are being emphasized. Coatings of Al_2O_3 and ZrO_2 have shown excellent adhesion and resistance to thermal shock on austenitic stainless steel in cycle tests of direct flame heating to 2500 F, followed by forced aircooling. Equilibrium thermal drops of 250–800 F have been obtained by using coating thicknesses of 0.020 in. with Al_2O_3 to 0.190 in. with ZrO_2. Unfortunately, thick coatings bring with them increasing problems of adhesion and resistance to flaking and cracking. A recent approach to overcoming these difficulties has been the reinforcement of the coatings with metal fibers.

Composite Materials

For our purposes, composite materials may be considered as heterogeneous combinations of two or more different materials to achieve a particular set of characteristics. Not only are they classic examples of materials design, but collectively, with an inherent capacity for unlimited variations, they offer a still largely unexploited approach to the solution of many of the materials problems confronting us. As indicated previously, since it is unlikely that we can develop general-purpose materials to meet our increasingly complex requirements, we must in many cases redesign our applications and design materials to meet the specific requirements of these applications.

Composite materials are not new, of course. The ancients used laminations of wood and rawhide to achieve desired elastic properties in their hunting bows. Prestressed concrete, which has received considerable attention abroad for aircraft structures with a good measure of success, is a prime example. The lamination of glass with a rubbery interlayer to prevent the scattering of lethal splinters results in the widely known "safety glass". Reinforced plastics, which will be discussed in connection with radomes, comprise a class of composite materials of unique importance in modern aviation.

What are some of the problems to which the composite materials approach seems to lend itself best?

One such problem discussed in more detail later under transparent materials is that of extending the excellent toughness of stretched acrylics further up the temperature scale by overlaminating more heat-resistant materials, taking advantage of a thermal gradient to maintain the stretched component at a compatible temperature. Also discussed below, are the composites of glass fiber and resins, an extremely important application where composites of some type may prove to be irreplaceable.

Helicopter rotor blades furnish another area, where the major design considerations of strength, weight, modulus of elasticity, damping properties, and fatigue resistance indicate the use of composite construction. Considerable success has been achieved in blade design through exploitation of composite construction in bonding multilayers of metal, and also in bonding layers of metal with honeycomb core, as a sandwich.

The various types of sandwich construction, in fact, comprise one of the most thoroughly exploited classes of composite materials. High stiffness at

low weight, combined with the surface smoothness and excellent fatigue characteristics available in sandwich construction, have accounted for its wide acceptance in the airframe industry for wing and control surfaces, flooring, bulkheads, and a number of lesser applications. Although a number of configurations are possible, the most popular type of structural sandwich utilizes a honeycomb core fabricated of 1–3 mil foil, between two face sheets. To date, most aircraft sandwich has utilized aluminum alloys assembled with structural adhesives. This construction is suitable for long exposures up to 400 F, and for higher temperatures at much shorter times. However, as heat-resistance requirements have mounted, increased attention has been given to brazed or welded sandwich constructions based on stainless steel, already in use to a limited extent in engine shrouds and other parts subjected to engine-generated heat in the range of 500–600 F. At the same time, questions of corrosion in brazed steel and of fatigue strength are stimulating consideration of inorganic adhesives for these higher temperatures. As other alloys, including titanium, become available in foil form, they most certainly will be exploited in sandwich construction, particularly for applications involving exposures to temperatures up to about 1000 F. The relatively inferior efficiency of the higher density alloys, such as steel and nickel, in columnar buckling and shear emphasizes the importance of resorting to sandwich-type construction where the use of these materials is indicated. Some applications may altogether preclude other type structures. In addition, sandwich construction in integrally stiffened design offers some of the better prospects for insulation from heat and noise, thus serving to protect the balance of the structure.

Although sandwich construction solves many problems, its use is not unattended by difficulties. Better methods of producing large sections are needed. More simple, reliable nondestructive inspection methods and simple effective field repair methods will be required. The use of a heat-pulse to create a local thermal stress for proof testing against weak bonds and a hot-melt-type adhesive for repair purposes offer some promise in these areas and will be investigated further.

In spite of the many useful applications already established for composite materials of the types and trends indicated above, strength characteristics of materials as currently used place a ceiling on design, unless their properties can be greatly enhanced or a method devised for their efficient and safe use at their highest attainable strength.

For example, it is well known that steel may be heat-treated and/or cold-work to tensile strengths in excess of 400,000 psi. However, in this condition in sizes representative of normal parts, the sensitivity of the material to crack propagation deters its exploitation. Composite construction offers an approach to solving this problem by bonding music wire of about 450,000 psi tensile strength into high-density laminates with organic adhesives. It is hoped that, if successful, the very high strength and satisfactory modulus of elasticity of steel will be combined with the good damping characteristics of laminates and the good fatigue strength of bonded construction. In this case, the crack-propagation problem is being solved mechanically, for example, by separating the steel into discrete wires or strips so that a crack in one will not propagate through the remainder.

An analogous approach is being explored as an additional alternative to solving the problem of preventing oxidation of molybdenum. Molybdenum wires have been impedded in a chrome-nickel matrix on the premise that even if the outer layers fail, repeated layers of protected molybdenum will appear, acting as so many inner "lines of defense." Silicide-coated wires are also being tried in this manner, since previous work has established that silicide coatings are very effective in preventing oxidation, provided they contain no pores and are not subjected to stresses which introduce cracks or other discontinuities.

With somewhat the same philosophy, molybdenum and other refractory wires are being incorporated into titanium by powder metallurgy, in an effort to create a composite with improved elastic and strength properties at elevated temperatures and in an attempt to obviate the current high-temperature limitations of titanium. Fig. 16 illustrates very early results in this effort and indicates, as anticipated, that materials can be produced which, although somewhat lower in strength-weight properties at room temperature due to the higher density of molybdenum, show definite superiority at higher temperatures.

Another promising composite material which the Navy Department has been developing is an aluminum-coated glass fiber in an aluminum matrix. Preparation of the laminate has been accomplished by both vacuum injection and hot pressing. Glass contents vary 20–60% depending on the process used. Although the room-temperature tensile strength of this composite is currently low, the material is of interest because of its very nearly constant strength at temperatures up to 900 F (Fig. 17).

Still another approach to higher temperature titanium materials through the use of composites of dissimilar materials, although perhaps not strictly a composite as we have defined it, is the use of finely dispersed refractory particles in a titanium matrix, analogous to the SAP material already described.

A similar approach is being used with matrices of

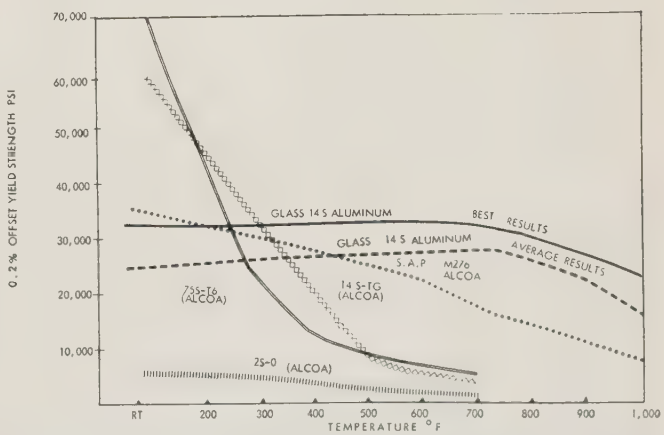

Fig. 17—Comparison of strengths of aluminum alloys with glass-fiber reinforced aluminum alloys

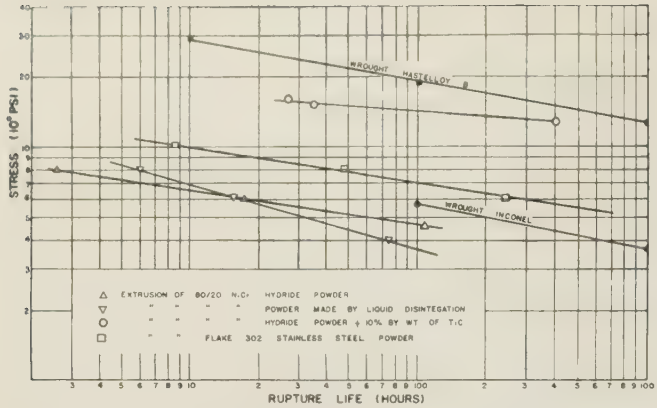

Fig. 18—Stress-rupture curves of extruded powder-metallurgy products. test temperature 1500 F

molybdenum, nickel-chrome alloys, and others. For example, work sponsored by the Air Force at Battelle Memorial Institute, indicates improvements of at least 20% in stress-rupture strength of molybdenum attributable to the addition of 0.1% zirconium oxide by powder-metallurgy methods. Preliminary Navy-sponsored work at Sintercast Corp. indicates that titanium-carbide additions increase the rupture life of 80/20 nickel-chrome at 1500 F (Fig. 18).

Eventually, due to heat limitations of organic compounds, nonmetallic inorganic materials must be considered as replacements in applications described above. After years of reliance on the ductility of metallic structural alloys to help obviate the significance of the flaws and other stress raisers inevitably present in both materials and structures of any complexity, the need for dealing with materials exhibiting marked brittle-failure characteristics poses a problem of truly major proportions. One classical approach to the problem of brittle materials is, of course, to obviate tensile stresses of any appreciable magnitude by prestressing the structure in compression. One technique for accomplishing this would entail the use of high-strength metallic reinforcement protected from the thermal environment by the insulating properties of the matrix material. The thermal expansion coefficient of ceramics and glasses can often be varied over fairly wide ranges and, therefore, could be exploited to lessen thermal stress levels. Another technique might be thermal treatments to produce compressive stresses at the surfaces, much in the manner in which plate glass is tempered to produce a 3-or 4-fold increase in effective strength. Perhaps these two techniques could be combined to advantage. While the thought of a ceramic wing may seem abhorent at first glance, from a weight standpoint, it should be noted that as a result of the work conducted abroad on prestressed concrete, it has been concluded that the weight penalty, compared with steel, would be no more than 10% in a highly loaded structure. The concrete structure, incidentally, offers a very substantial increase in rigidity, besides obvious economic advantages.

Transparent Materials

As long as aircraft remain manned, it is likely that there will be a requirement for transparent openings in the aircraft structure to provide vision for pilot and crew, although some argue their replacement with television arrangements. With transparent material as with others already discussed, advancing speeds place an increasing premium on heat resistance and, combined with higher altitudes, emphasize the importance of shatter-resistance. Although the high-temperature problem will eventually force reliance on glass constructions, use of glass will be shunned as long as possible because of excessive weight and vision penalties. Con-

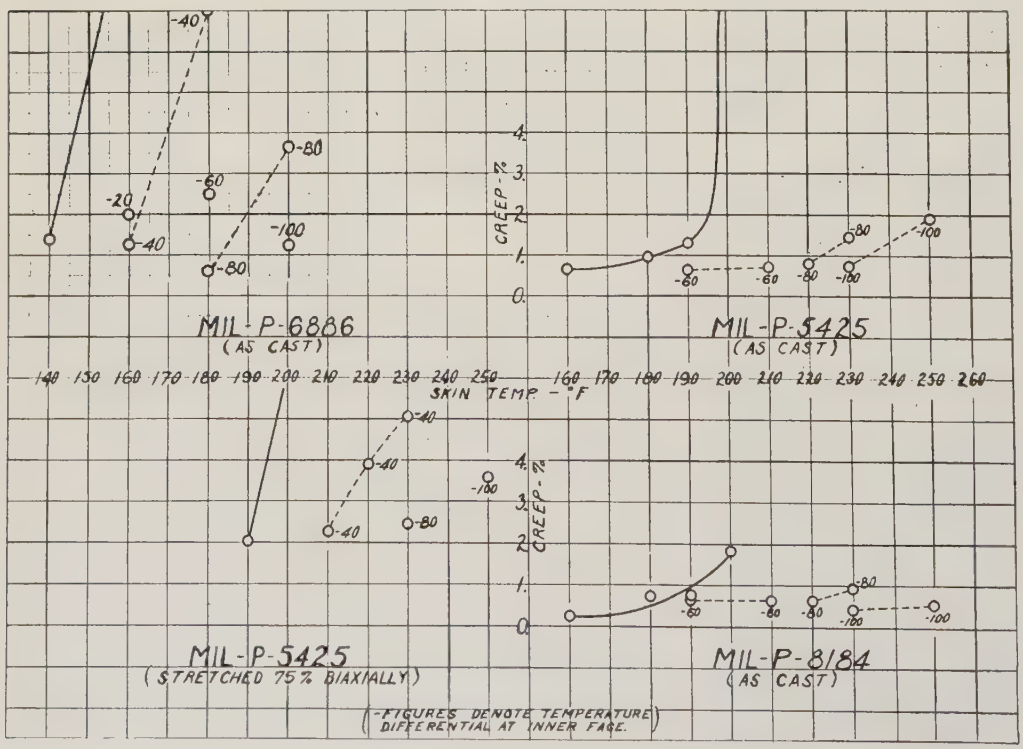

Fig. 19—Creep of acrylic sheet materials at 50 hr and 1000-psi stress

sequently, it has been advantageous to exploit the much more efficient transparent plastics to extend their usefulness as far as possible. A three-pronged approach is being followed.

It is generally agreed that with the most popular plastic glazing materials, the thermoplastic acrylics, creep would prove to be the limiting design factor at elevated temperatures. When uniformly heated, the standard grades of acrylic sheet are severely limited in this regard, the limiting temperature of the best of them being little better than 200 F. But what is the influence of thickness-wise thermal gradients? Because of the need for maintaining occupied spaces at a reasonably comfortable level, inside surface temperatures lower than the outer surface or skin temperature must prevail when the latter temperatures reach much above 100 F, that is, a downward temperature gradient from outside to inside surfaces. What are believed to be the first creep studies ever understaken entailing a thermal gradient have shown that appropriate temperature differentials do indeed exhibit a marked influence on creep and can be used effectively to increase the temperature tolerances of acrylic glazing materials. Typical results obtained in this work conducted for the Bureau of Aeronautics at the National Bureau of Standards with the conventional acrylic sheet materials are summarized in Fig. 19. The solid lines show creep versus skin (hot face) temperature at zero gradient. The remaining plots are points only; the connecting dotted lines serve merely to quickly identify points of identical gradient. The pronounced effect of gradient as a creep deterrent is immediately apparent. For example, with MIL-P-8184 material, a modified methylmethacrylate sheet, it will be seen that the creep is still well within tenable bounds at a skin temperature of 250 F when coupled with a 100 F gradient, while in the uniformly heated condition the creep is fast approaching a limiting value at only 200 F. This work is continuing with emphasis on new materials as they become available.

Another prong of our attack on the transparent materials problem has been devoted to the subject of shatter resistance. Here, a project at the Naval Research Laboratory in collaboration with industry and the Air Force, is exploiting the toughness advantages of stretched acrylics. When stretched hot under appropriate conditions, by large amounts (75–100% in both directions), acrylic-sheet materials develop ductile-like characteristics accompanied by a remarkable increase in toughness. These changes are attributed to planar orientation of the normally randomly coiled molecules to produce a structure characterized by planes of weakness, which are akin to the cleavage planes of mica. These tend to divert and absorb some of the energy necessary for crack propagating. Ability to carry stress in the presence of a notch without catastrophic crack propagation is increased 300–400% by this stretching. This improvement is illustrated in Fig. 20 showing relative performance of as-cast and stretched materials under gunfire. Whereas the as-cast window shattered at a load of 5 psi, the stretched panel resisted penetration without shattering to 6½ psi. The ability of a full-scale, full-pressurized stretched fighter canopy to withstand 20 mm gunfire without shattering has been reported. The Navy's contribution in this field has included the development of the now widely recog-

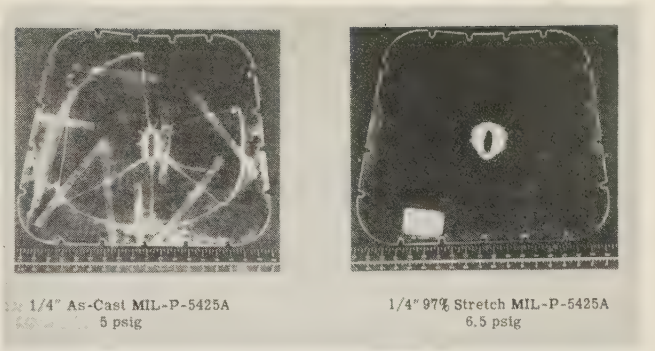

Fig. 20—Toughness of as-cast versus stretched acrylic. Shot with 0.50-in. diameter yawed dart, at 2000 ft per sec and 72 F (Courtesy of Swedlow Plastics Co.)

nized dG/dA test, which measures the crack-energy absorption rate at the onset of fast fracture and which has become the basic criterion for the design of stretched components now being specified in new aircraft.

The prospects of radically extending the thermal capabilities of thermo-plastics are very dim. Other approaches must, therefore, be sought if we are to capitalize on their advantages in the higher thermal environments now confronting us, and forestall acceptance of the heavy penalties attending all-glass constructions. One possibility entails composite laminates in which the superior heat resistance of thermosetting polymers, or even glass, or both, are combined with the superior toughness of stretched thermoplastics, using thermal gradients to preserve the shatter-resisting function of the latter. In addition to heat resistance, the thermosetting materials (and glass even more so) would provide protection against abrasion and resistance to the deleterious effects of fuels and other solvents to which the thermoplastics are susceptible. Composites would be specifically designed to satisfy in an optimum manner the requirements and fabricating problems peculiar to particular transparent components. Although only preliminary experiments have been performed along these lines, thus far the results have proved encouraging.

Radome Materials

With the steadily increasing dependence on electronics for detection, guidance and communication, radomes and other antenna housings have become essential components of most aerial vehicles. Materials for such housings must first, of course, be transparent to electromagnetic radiation, so electrical properties and their control are prime requisites. They must be amenable to precise fabrication over a wide range of sizes and configurations. Perhaps the epitome thus far achieved in this respect is the radome for the Navy WV-2 airplane. This umbrella-like structure of reinforced plastic sandwich construction is 38 ft in diameter and 6½ ft deep. Because it rotates for increased search efficiency, it is called a rotodome. The use of radome materials externally—often in integral components of the airframe such as the nose, wing tip, or tail surfaces—places a premium on structural efficiency and resistance to flight environments, with heat resistance now a major problem. Concurrent problems include still better structural characteristics

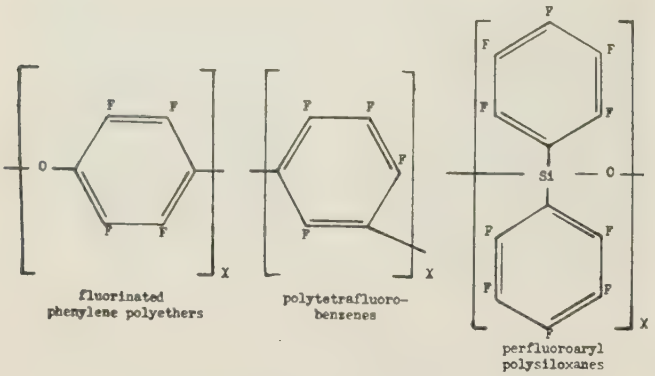

Fig. 21—Prospective perfluoroaromatic-type structures.

$$xCF_2CF_2 + yCF_2O \xrightarrow{\lambda} (CF_2CF_2)_x(CF_2O)_y$$

Teflon + carbonyl fluoride → perfluoropolyether

to accommodate higher flight loads, closer control of electrical properties and dimensions of the fabricated item for greater functional accuracy of the electronic equipments involved over wider temperature ranges, and improved rain-erosion resistance.

Because of their impressively higher structural efficiency, glass-fiber-reinforced plastics are now being used to the virtual exclusion of other possible radome materials, such as clear or unreinforced plastics, glass, and ceramics. Although they may be used in solid-wall configurations, reinforced plastics are normally employed for increased rigidity in the form of sandwich construction consisting of low-density reinforced plastic honeycomb or foamed plastic cores between reinforced plastic skins.

Notwithstanding rather severe deficiencies in rain-erosion resistance, it has been considered that reinforced plastics will continue to be preferred to the much less structurally attractive alternatives previously mentioned, such that their fuller exploitation remains an important approach to future radome materials requirements. This limitation is today being alleviated to a tenable, if not ideal, degree by the use of optimum laminating techniques and replaceable coatings. In addition to the requirement of being inherently resistant to the erosive effects of rain, which become pronounced above 250 knots and increase exponentially with speed, such coatings must be electrically compatible with the radome. They should be capable of being easily and safely applied, adhere well to the substrate, be aerodynamically smooth, be resistant to temperature increases and to solvents and other fluids with which they might come in contact, and not affect adjacent metallic components. Although a wide variety of materials have been evaluated as coatings, none surpassing neoprene have yet been found for current speeds and for the bulk of environments thus far encountered. Polysulfides and polyurethanes have shown promise of some superiority. Neoprene coatings, however, when applied over a sound, void-free reinforced plastic laminate are many times better in erosion resistance than the bare plastic. Although these coatings will, with higher speeds, become increasingly limited with respect to both heat and erosion resistance, their relative ease of replacement will facilitate acceptance of higher attrition rates and, therefore, continued use of reinforced plastics in arriving at the best design compromise. Beyond the range of organic films, glass or ceramic coatings with their inherently superior heat and erosion resistance may find use short of the regime where radome structures made completely of glass or ceramic will have to be used.

One of the items in the Navy's program on radome materials is the development of an inorganic silicate-base foam material for sandwich construction. Although not yet fully evaluated, it is thermally stable at 1000 F and when teamed with glass-fiber silicone-resin faces is expected to develop useful properties for radome use up to 750 F, as compared with current values of 500 F, and substantially higher temperatures for short-term exposures as in some missile applications.

Another facet of the Navy's program has been directed toward boosting the structural capabilities of reinforced plastics through the development of a high modulus glass fiber. Experimentally, moduli of 20×10^6 psi have been achieved, about twice that of the presently used fiber, and work is now proceeding on the development of optimum production techniques. This development, when reduced to practice, should go far toward alleviating the growing need for greater rigidity in radome design. It should also pave the way for wider use of these materials in other airframe structures in order to realize their advantages with respect to ease of fabrication, freedom from corrosion, improved aerodynamic characteristics, reduction in critical materials consumption, and security against radar detection.

With an eye to longer range requirements, an investigation of the fundamental aspects of reinforcement has been undertaken to define more precisely the relationship between fiber and binder that should prevail for an optimum marriage of the two in terms of the properties of the composite material. Because of the elemental importance of adhesion in the fiber-binder relationship, much effort has been directed toward checking various hypotheses on adhesion, calling for data such as contact angles, surface tension and related energy constants, adsorption and monolayer properties. So far, technical difficulties encountered in devising reliable test methods and techniques have precluded the accumulation of data from which positive results can be derived. However, a number of improved tests have been adopted, such as a bubble pressure technique for surface tension studies, the use of a light-scattering microphotometer for adsorption measurement, and a satisfactory film spreading technique for monolayer work.

For prolonged service at temperatures much above 750 F, neither the present glass fiber nor resinous binder system will suffice. While the prospects of finding substantially higher temperature fibers coupled with high moduli are good, the inherent thermal limitations of organic materials clearly suggest that the best approach to a high-temperature binder lies in the inorganic field. Such a binder might be an inorganic polymer or it might be a ceramic that can be fired at temperatures low enough to preserve the fibrous structure of the

reinforcement. Although both these possibilities will receive attention, the latter is considered to offer somewhat more promise at the present time.

The major portion of this paper has been devoted to what might be called structural materials or materials of construction. There are many other types serving vital operating functions, which pose problems as difficult in their field as any described thus far. However, only two categories of these functional materials will be discussed.

Elastomers

Conventional types of synthetic elastomers, employed in the fabrication of seals and other mechanical goods and used extensively in aircraft sealing compounds, do not satisfy some of the more rigorous operating requirements. Major problems at this time are the result of the inability of solvent-resistant types (neoprenes, nitriles, and liquid polysulphides) to withstand adequately the deteriorating effects of fuels and lubricants at temperatures above 275 F, in such applications as seals, hose, and integral fuel-tank sealants. Elastomeric compounds having improved heat resistance (above 275 F) are now required for such dry applications as structural sealing and encapsulating. Use of a variety of fluorinated polymers, recently developed and not yet fully evaluated for specific applications, may alleviate the above problems to some extent. Their most serious limitation appears to be their very poor low-temperature characteristics. No elastomeric polymer known will withstand expected temperatures of 600 F and higher, except for such short intervals of time as to be useful only in very limited applications. Furthermore, it is probably safe to say that there is little likelihood of developing such elastomers, at least in the near future, because very extensive research in the field has failed to develop promising leads.

The most promising solvent-resistant materials developed to date for the 275–600 F range are the fluorinated polymers. A current Bureau of Aeronautics program has the two-fold objective of correlating heat and cold resistance with chemical structure and the synthesis of new fluorinated polymers having improved thermal resistance. With respect to the first objective, the relationship of the second order transition (glass-transition temperature) to copolymer composition and to the side groups in the methacrylate polymers is being studied, through synthesis and evaluation of copolymers of ethylene with styrene and carbonyl fluoride, and methylmethacrylate copolymers with carbonyl fluoride. The second phase of the program, that is, the synthesis of more heat-stable polymers, has to date been primarily directed toward the preparation of perfluoroethers. At the moment, polytetrafluoroethylene (Teflon) most nearly meets the desired high-thermal stability. Unfortunately, it has no rubbery properties. It is probable, on a theoretical basis, that a related perfluoropolyether would have comparable thermal stability and a higher degree of "rubberiness" than Teflon. As shown in Fig. 21, attempts are being made to prepare perfluoroether by the copolymerization of Teflon and carbonyl fluoride, initiating the reaction by means of gamma radiation. Preliminary analytical data indicate that small amounts of polymer have been formed. Several prospective polymers, shown in the lower portion of Fig. 21, are also of interest on a theoretical basis. These structures, all having perfluoroaromatic nuclei, should be elastomeric and heat-stable. Their synthesis, however, depends upon the availability of intermediates yet to be made. Here again is an illustration of the need for more fundamental work and understanding of material behavior to permit these complex organics to meet specified requirements.

Preliminary results from another investigation indicate that the useful temperature limit of certain room-temperature-curing silicone rubber polymers may be raised significantly by a special compounding technique involving the incorporation of glass beads approximately 40 microns in diameter, primed with a titanium ester. The resultant material exhibits greatly reduced shrinkage during curing and increased resistance to oxidation. This development is of particular interest in connection with the production of heat-resistant sealing compounds.

The pessimistic outlook for elastomers at relatively high temperatures naturally raises the question of what can be done to satisfy future requirements. A partial answer is to design to eliminate the need for elastomers wherever possible. Serious consideration must be given to this approach, recognizing that some increase in expense, design complication, and weight may have to be tolerated. Applications which demand materials having elastomeric properties not now available could conceivably be treated on a mechanical basis. The concept of a "mechanical rubber," although not new, has perhaps not received the attention it deserves. By way of illustration, a vibration isolator in which the rubber core was replaced with a roll of loose-mesh steel fabric has many of the resilient properties associated with rubber. It is emphasized, however, that this is only a partial answer to many elastomer problems. Another complexity will be the required resistance to radiation effects in nuclear-powered aircraft, particularly in the engines and the oil and fuel systems. Without such resistance, the need for frequent replacement would, in effect, shorten engine operating life.

Specialty Fluids and Lubricants

Another important class of functional materials are the grease-type lubricants and the hydraulic fluids. Except for the few cases where preheating is possible, these greases and hydraulic fluids must be capable of use at very low temperatures as well as at any elevated temperature which may exist locally in any part of the vehicle structure. The low-temperature requirements, in general, must be met by the inherent properties of the materials. To an increasing degree, there are very few cases where a low-temperature limit above – 65 F can be tolerated. Some helicopter transmissions are among the applications where inadequate low-temperature properties must be tolerated. Therefore, helicopter operation is limited to temperatures higher than – 40 F as the result of inability to combine low-temperature properties with the extreme pressure and other requirements of the gear lubricant. On the other hand, flying boat aircraft are a case where

the ambients preclude the necessity for very low-temperature properties.

With respect to high-temperature requirements, at present the general requirements for greases for inhabited aircraft are well under control through use of petroleum and diester fluids incorporated in various lithium, sodium, and calcium soaps developed prior to or during World War II. The situation with respect to hydraulic fluid is, however, quite critical at elevated temperatures. Oxidation resistance, corrosion behavior, and thermal stability are important characteristics. The conventional petroleum-base fluid is in most general use up to 275 F, but at this relatively high temperature there is increasing leakage and fire hazard, shortening of pump life, and more rapid deterioration of rubber components. No entirely satisfactory replacement fluid is available at present, although organo-silicates, phosphates, and variations thereof are being used with a limited degree of satisfaction in some of the latest fighter-type aircraft, at the risk of inferior fluid performance due to effects on rubber, high-shear breakdown, poor lubricity, and other qualities. In general, silicones and chlorinated aromatic hydrocarbons are among the more thermally stable materials.

Requirements for greases in pilotless aircraft in the low Mach range at present can, in general, be satisfied by use of the diester-lithium soap greases mentioned above for piloted aircraft, or by the combination of silicone or other materials. Judicious additions of molybdenum disulfide or graphite to various lubricants serve to increase load-carrying ability and life when operating conditions approach or exceed the limits which can be withstood by these conventional greases. In the hydraulic systems these fluids can in many cases be used, but a need exists to a greater degree than above for suitable fluids for higher temperatures. However, the necessity for preheat of some equipments to permit operation may allow the use of fluids whose low-temperature properties might be unsatisfactory for conventional systems. Chlorinated and fluorinated materials with relatively good properties up to 700 F are becoming available for use under this circumstance.

The use of organic lubricants and fluids in anticipated high Mach number vehicles is not yet well-defined. As stated above, inherent limitations in some vehicles and presence of components containing materials subject to degradation at elevated temperatures will make possible continued use of available lubricants and fluids in some cases. Further development of solid or gaseous lubricants and recourse to liquid metals or salts for the extreme temperature associated with high Mach numbers and heat output of propellents are being considered to fulfill the need. An additional advantage of certain solid lubricants is their resistance to radiation damage in nuclear-powered aircraft. Indications point to solids like MoS_2 being effective to 1000 F in rolling contacts, and various gas mixtures and air may also support successfully loads to about this temperature. Finally, design of lubricant and hydraulic systems may have to be such as, for example, to exclude air or otherwise take advantage of whatever degree of oxidation and heat resistance become available, if necessary with more frequent replacement of lubricant or fluid. Bearing material and design are also, of course, important factors.

Conclusion

This paper has covered many materials fields and has necessarily omitted many. Nothing has been said of the closely related problems of testing and inspection; of facilities for evaluating the new materials under simulated conditions of operating temperatures, speeds, pressures, and environment; of the needs and developments in materials for vital components such as electronic, electrical, and magnetic equipment. It is hoped that it is evident, however, from the examples given, that future aerial vehicles are posing requirements for materials of such increasing complexity that, in spite of the wealth of research and development being done and the excellent progress being made, it is extremely doubtful how many of these will be satisfied with individual materials. Emphasis must, therefore, be placed on designing materials to meet the major specific requirements for particularly difficult applications, in many cases requiring composites to attain these goals. Nor should there be overlooked the need, in many cases, for revision of current structural design concepts to circumvent deficiencies in otherwise valuable materials, thus preventing what could be a partial vacuum of efficient materials application. The intensified coordination and mutual cooperation of design and materials engineers has now become an indispensable necessity, and to these must be added, for optimal results and progress, the aerodynamicist, physicist, chemist, and others.

Acknowledgments

The opinions expressed above are those of the author and not necessarily those of the Department of Defense or specific groups therein. Although most of what has been presented is based on investigations and studies made in or sponsored by the Bureau of Aeronautics, or as otherwise specifically indicated, incidental information is related to too many sources to permit detailed acknowledgment in all cases. The author is particularly grateful, however, for the very helpful cooperation of his associates in the Materials Branch of the Bureau of Aeronautics and of Julius Harwood of the Office of Naval Research.

ORAL DISCUSSION

Reported by F. C. Smith

National Cylinder Gas Co.

Jerome Strauss, Vanadium Corp. of America: Can you give me further information about the "Cinderella" alloy, 6% aluminum and 4% vanadium; 2.5% aluminum and 15% vanadium; and the ductility of Thermenol alloy, especially with various percentages of beryllium?

Mr. Promisel: The 6% Al-4% V alloy is showing good results in forgings and sheet, even in the heat-treated conditions.

In the 2.5% Al-15% V alloy, ductility is a problem, although the results show: 160,000–180,000 psi with 6% elongation at room temperature and 135,000 psi with 10% elongation at 800 F.

Thermenol alloy is showing considerable improvement by vacuum melting and the addition of grain refiners such as 0.5% ZnO_2. The strength has been raised from 80,000 psi to over 100,000 psi and the ductility from 4–5% to about 10%. These results are based on preliminary laboratory tests.

COMBUSTION-CHAMBER DEPOSITS— A RADIOTRACER STUDY

L. B. Shore and K. F. Ockert, Esso Research and Engineering Co.

This paper was presented at the SAE Summer Meeting, Atlantic City, June 6, 1957

COMBUSTION-CHAMBER deposits in gasoline engines remain an important problem in the development of fuels and lubricants that will better satisfy automobile owners' needs. These deposits can cause uncontrolled ignition of the fuel-air mixture and may cause the spark plug to misfire occasionally; their most important effect, however, seems to be their tendency to raise an engine's spark knock octane requirement. While it is true that the numerical size of the octane-requirement increases caused by deposit formation is going down as compression ratio goes up, it appears that the noise-producing tendency of these increases remains as great as ever[1]. This is mainly due to the nonlinearity of the octane scale. An octane number near the 100 level is worth more for knock suppression than one at the 90 level. Because of the increasing cost of making higher octane numbers, it is essential that every effort be made to develop clean-burning gasolines that will keep down engine octane requirements. To accomplish this, further information is needed on the qualities that make for a clean-burning fuel. This report discusses a new approach to this problem. By using radiotracer techniques, much has been learned about the relative deposit-forming tendencies of many of the individual hydrocarbons commonly found in gasoline. In fact, the information presented in this report permits the evaluation of the combustion-chamber deposit-forming tendency of gasoline without engine testing.

A brief survey of the voluminous literature on combustion-chamber deposits will emphasize the need for this kind of information and why it was not obtained earlier. Three general fields of interest have been covered in the literature:

1. The ways in which deposits, from whatever source, raise engine octane requirements seem to be fairly well understood. Because of their low thermal conductivity, the deposits impede the flow of heat from the combustion chamber; they also can act as uncontrolled sources of ignition. These phenomena can lead to increased octane requirements.[2 3 4 5]

2. The mechanism by which lead salts form and are deposited on the surface of the combustion chamber has been thoroughly studied. Our knowledge in this field is largely the result of a series of theoretical and experimental papers by investiga-

[1] "Fuel Quality Requirements of High Compression Ratio Engines," by J. K. Appledoorn. API preprint, Detroit, Feb. 28, 1956.
[2] SAE *Quarterly* Transactions, Vol. 5, October, 1951, pp. 577–583: "Effects of Combustion-Chamber Deposits on Octane Requirement and Engine Power Output," by J. B. Duckworth.
[3] SAE Transactions, Vol. 62, 1954, pp. 582-594: "Combustion-Chamber Deposits and Octane-Number Requirement," by Joel Warren.
[4] "Effect of Simulated Surface Ignition on Engine Performance," by L. B. Shore and J. F. Kunc, Jr. Paper presented at SAE Summer Meeting, June 6–11, 1954.
[5] "Ignition Temperatures of Lead Compound Carbon Mixtures," by G. J. Nebee and P. L. Cramer. ACS preprint, Cincinnati, April 4–7, 1955.

AN IMPORTANT effect of combustion-chamber deposits is their tendency to raise the engine's need for higher octane fuels; also, they may cause uncontrolled ignition of the fuel-air mixture and misfiring of spark plugs. This paper describes a new approach to this problem.

By means of radioactive hydrocarbons, present in tracer amounts, the authors have been able to conclude the following about the effect of gasoline hydrocarbon composition on deposit formation in the combustion chamber:

1. The deposit-forming tendency of hydrocarbons goes up strongly with increasing boiling point.

2. Aromatics are considerably worse deposit formers than paraffins. Olefins are intermediate.

3. The carbonaceous part of combustion-chamber deposits appears to form via a mechanism involving condensation followed by carbonization.

4. Careful control of the back-end is needed to make a clean-burning gasoline.

Table 1—Effect of Hydrocarbon Composition on Combustion-Chamber Deposits

	Two Car Averages—Controlled Field Test			
	Deposit Weight, grams	Deposit Volume, cc	Equilibrium Octane Requirement	Weight of Pb in Deposits, grams
High-Quality Commercial Fuel – 2 cc tel per gal	61.8	19.17	88	42
Isooctane + 2 cc tel per gal	39.3	9.35	77	27

Table 2—Inspections of Base Fuel

Research Octane Number	98.0
Motor Octane Number	87.5
Sulfur, %	0.032
Tel, cc per gal	2.8
Hydrocarbon Content	
Aromatics, %	34.8
Olefins, %	26.1
Saturates, %	39.1
ASTM Distillation	
Ibp	97 F
10% D + L	127
50% D + L	232
90% D + L	325
Fbp	396

Table 3—Engine Operating Conditions

Compression Ratio	8/1
Speed	900 rpm
Jacket Temperature	155 F
Oil Sump Temperature	160 F
Intake Air Temperature	120 F at full throttle
Ignition Timing	Tdc
A/F Ratio	13.4 at full throttle 12.6 at idle
Cycle	150 seconds at full throttle 50 sec at idle

tors of the E. I. du Pont de Nemours Co.[6 7 8 9] and the Ethyl Corp.[10 11 12]

3. Many papers have tried to answer the question, "What hydrocarbon constituents of the fuels and lubricants used in engines are responsible for the majority of the deposit harm?" It is almost impossible to summarize this work except by saying that there are differences among hydrocarbons and that there seems to be a general feeling that higher boiling constituents of fuels and lubricants are the worst performers from this point of view. This work has been of two kinds: pure compounds have been studied or selected refinery streams have been blended to make test fuels. It is at once obvious, we think, why the results are ambiguous. The first method gives results which may bear no relationship to what happens when a commercial fuel or lubricant is used, and the second gives results which are almost impossible to interpret to develop fundamental information because of the enormous complexity of even the most carefully controlled refinery stream. It is a tribute to the diligence and ingenuity of the many investigators in this field that their work has led to the improved fuels and lubricants now being marketed. Of particular value has been the introduction and wide acceptance of the multigrade oils made from a low viscosity narrow cut neutral distillate thickened with a suitable V.I. improver rather than with bright stock. Such an oil can give an equilibrium octane requirement significantly lower than that obtained with a conventional lubricant.[13]

It seems clear from this survey that of all the combustion-chamber deposit problems, there is a special need for more information on how changes in gasoline hydrocarbon composition affect deposit formation. It is also clear that further progress requires the use of new techniques. Radiotracers have provided such a new method, one that has proved quite productive. The results presented in this report were obtained in a series of engine tests using C^{14} labeled hydrocarbons to determine the deposit-forming tendency of the various hydrocarbon components of a gasoline. The technique consists of adding, to a typical gasoline, a very small amount of a radioactive hydrocarbon labeled in one or more positions. The radioactivity of the fuel is measured and the fuel is then burned in a single-cylinder engine. The deposits are collected and their radioactivity is measured. The ratio of the specific activity of the deposits to that of the fuel has been called the "concentration ratio." (Specific activity is the activity per unit weight of carbon.) The concentration ratio is a measure of a component's deposit-forming tendency. The higher the concentration ratio, the worse the component. The concentration ratio is the most important measurement obtained in these studies.

This technique has several advantages when compared with conventional methods:

1. It measures the deposit-forming tendency of a component in the concentration in which that component actually is present in the gasoline. The gasoline is not unbalanced by the addition of large amounts of the material to be studied. There is no assurance, for example, that toluene when present in 50% concentration will behave the same way as when present in 2% concentration. In the radiotracer technique, the labeled material is added in such small amounts that the concentration of the component is unaffected.

2. It is possible, by varying the labeled position, to differentiate not only among compounds but even among carbon atoms in the same molecule.

3. The results are expressed directly as deposit-forming tendency and not as some other property from which deposit-forming tendency must be inferred.

4. The test is reproducible.

Before discussing the experimental technique in detail, some information on the importance of controlling the hydrocarbon composition of the gasoline may prove instructive. Since, normally about 80% of the deposits, when using a leaded fuel, is composed of lead salts it might appear that the gasoline hydrocarbons would be of little importance. This is not true. Cleaner burning hydrocarbons in

[8] SAE *Quarterly* Transactions, Vol. 5, October, 1951, pp. 565–576: "Possible Mechanisms by Which Combustion-Chamber Deposits Accumulate and Influence Knock," by L. F. Dumont.

[7] "Mechanism of Combustion-Chamber Deposit Formation with Leaded Fuels," by W. E. Newby and L. F. Dumont. ACS preprint, Atlantic City, Sept. 14–19, 1952.

[8] "Investigation of Combustion-Chamber Formation and Scavenging Using Tetraethyl Radiolead," by H. P. Lander and B. M. Sturgis. ACS preprint, Los Angeles, March 15–19, 1953.

[9] "Combustion-Chamber Deposits and Their Effects on Engine Fuel Requirements," by J. J. Mikita and W. E. Bettoney. Preprint for Western Petroleum Refiners Assoc., San Antonio, March 23–25, 1953.

[10] *Analytical Chemistry*, Vol. 23, October, 1951, p. 1388: "Formation of Engine-Deposit Compounds by Solid-State Reactions," by F. W. Lamb and L. M. Niebylski.

[11] *Journal of American Chemical Society*, Vol. 71, November, 1949, pp. 3709–3720: "Studies in Lead Chloride-Lead Bromide System," by G. Calingaert, F. W. Lamb, and F. Meyer.

[12] *Journal of American Chemical Society*, Vol. 75, Feb. 5, 1953, pp. 511–518: "Phase Study of PbO-$PbBr_2$ System by X-Ray Diffraction," by F. W. Lamb and L. M. Niebylski.

[13] SAE Transactions, Vol. 62, 1954, pp. 228–242: "Effect of Lubricant Composition on Combustion-Chamber Deposits," by J. G. McNab, L. E. Moody, and N. V. Hakala.

the gasoline lead to a substantial reduction in deposit weight and deposit harm. (See Table 1.)

Replacing the commercial gasoline with leaded isooctane lowers the deposit weight substantially, cuts the deposit volume in half, and lowers the equilibrium octane requirement by 11 units. Moreover, even though the same amount of lead passed through the engine in both tests, there was much less present in the deposits when isooctane was the fuel. This indicates that the carbonaceous part of the deposit is important not only in itself but also because it acts as a matrix to which the lead adheres. It is quite possible that if the carbonaceous part of the deposit could be eliminated the entire deposit might disappear. It is apparent from this that an improvement in the deposit-forming properties of the gasoline hydrocarbons would be of great value in all aspects of engine performance affected by combustion-chamber deposits.

Experimental Method

The purpose of the radiotracer studies was to measure directly the deposit-forming tendencies of hydrocarbons in a typical gasoline. The gasoline used was a leaded, high aromatic, full-boiling experimental gasoline described in Table 2.

In each run 0.5–1.0 millicuries of a single labeled hydrocarbon was added to the base gasoline. The concentration of the labeled material was always too small to affect materially the concentration of the component in the original fuel. In other words, the labeled material was used only as a tracer. For example, when toluene was studied the radioactive toluene represented only about two parts per million of the total amount of that compound in the gasoline.

The labeled gasoline was then used to operate an L-head CFR engine for 35–50 hr. The operating conditions in this engine are shown in Table 3. The same lubricant was used for all the tests. It was a high quality commercial 10W-30 motor oil containing no bright stock but with conventional V.I. improvers and detergents. In each run the total amount of fuel consumed ranged from 15–20 gal.

At the completion of each engine test the deposits were collected separately from the head, block, piston top, intake valve, and exhaust valve areas. Also, in some runs the head was removed at intervals during the test and patches of deposit were removed to investigate the effect of time on deposit composition. After collection, the deposits from the various engine areas were weighed and homogenized separately by thorough grinding. No further treatment was given the deposits before analysis.

The analytical method used was that developed by Van Slyke and his coworkers.[14] Although designed for the analysis of pure organic compounds, it was found that the Van Slyke method works quite well for the analysis of the mixture of carbonaceous and inorganic material found in engine deposits. Carbon contents calculated from the wet Van Slyke analysis agreed with values found from conventional Pregl dry oxygen combustions. The Van Slyke procedure depends upon the wet oxidation of the carbonaceous portion of the deposit by a mixture of potassium dichromate and potassium iodate in concentrated phosphoric acid and fuming sulfuric acid. The CO_2 evolved is measured manometrically after it has been freed of extraneous gases. It is then diluted with methane and used as the filling gas for a gas-filled Bernstein-Ballentine counting tube. A Nuclear-Chicago Ultrascaler was used for counting the radioactive CO_2. The method yields the carbon content of the deposit and from the measured activity and known amount of CO_2 in the counting tube, the specific activity of the deposit is calculated as counts per minute per milligram of carbon.

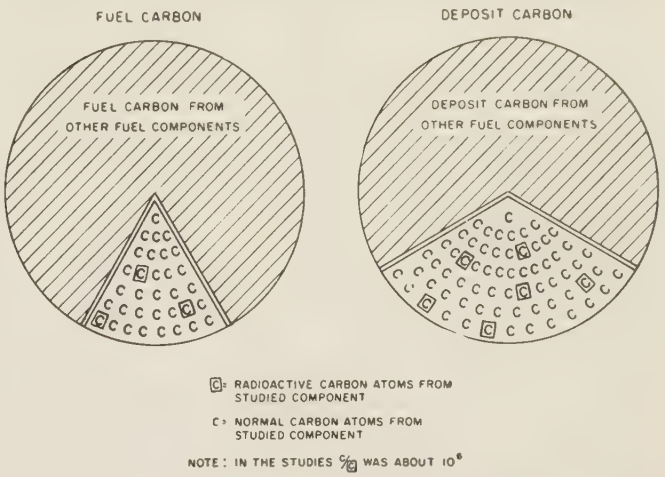

Fig. 1—How concentration ratio is determined

Since the Van Slyke method is unsuitable for use with very volatile materials, the labeled fuel in each case was analyzed by means of a dry combustion in oxygen. The evolved CO_2 was trapped in strong KOH solution and later liberated in the Van Slyke apparatus, measured, and quantitatively transferred to the counting tube. The specific activity is again calculated as counts per minute per milligram of carbon. The specific activities of the deposits and of the fuel blends were the primary measurements obtained in these tests and from them the deposit-forming tendency of the labeled hydrocarbon could be calculated as concentration ratio.

As was stated earlier, the concentration ratio is the fraction that any hydrocarbon contributes to deposit carbon divided by its contribution to fuel carbon. Fig. 1 makes clear how this is equal to deposit specific activity divided by fuel specific activity. The ratio of normal carbon atoms from the tested component to radioactive carbon atoms from the tested component is the same in the deposit as in the fuel. This depends only on the assumption that C^{14} and C^{12} behave in the same way, which is substantially true. Then, since the specific activity measures the concentration of radioactive C in the deposit and the fuel, it also measures the concentration of normal hydrocarbon from the same source. Thus:

$$\frac{\text{(Specific activity) deposit}}{\text{(Specific activity) fuel}} = \frac{\text{(Fraction } C^{14}\text{) deposit}}{\text{(Fraction } C^{14}\text{) fuel}} = \frac{\text{(Fraction normal carbon from tested component) deposit}}{\text{(Fraction normal carbon from tested component) fuel}} = \text{Concentration Ratio} \quad (1)$$

If the concentration ratio for a gasoline compo-

[14] *Journal of Biological Chemistry*, Vol. 192, October, 1951, pp. 769–805: "Determination of Total Carbon and Its Radioactivity," by D. D. Van Slyke, R. Steele, J. Plazin.

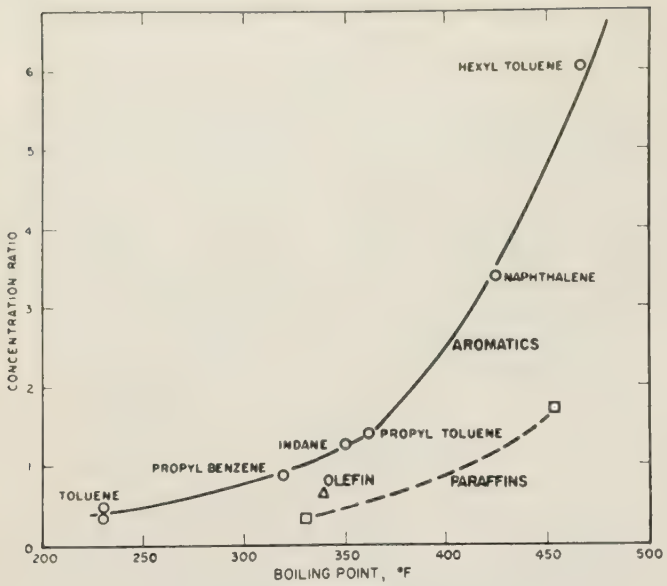

Fig. 2—Deposit formation goes up with boiling point

Table 4—Deposits Formed by Aromatics and Paraffins

	Concentration Ratio		
Boiling Point, F	Paraffin	Aromatic	Aromatic/Paraffin
330	0.35	0.95	2.7
453	1.70	4.90	2.9

Table 5—Olefins as Deposit Formers

(Concentration Ratio at 340 F)

Aromatic	Olefin	Paraffin	Aromatic/Olefin
1.07	0.63	0.40	1.7

Table 6—Effect of Time on Concentration Ratios

Time, hr	Run A—Toluene Head Deposit	Run B—Naphthalene Head Deposit
10	0.38	2.98
20	0.54	—
30	0.54	3.63
40	0.52	—
50	0.48	3.44

nent is less than 1, it means that the component is diluted in the course of forming deposits and, therefore, has a lower deposit-forming tendency than the rest of the gasoline. If the concentration ratio is greater than 1, the component is enriched in the process of making deposits and, therefore, has a greater deposit-forming tendency than the average of the rest of the gasoline. These statements depend on the assumption that virtually all of the deposit carbon is derived from the fuel. That is, there is very little lubricant contribution. As will be shown later, this assumption is essentially correct.

Results

1. The deposit-forming tendency of hydrocarbons goes up strongly with increasing boiling point. This is especially obvious for aromatics. This effect is so striking and so pronounced that it is probably the most important consideration in the design of a clean-burning gasoline. Fig. 2 shows the average concentration ratios throughout the combustion chamber at the end of the runs. For example, isohexyl toluene boiling at 465 F has a concentration ratio of 6.06 and forms almost 14 times as many deposits at a given fuel concentration as toluene that boils at 213 F. The increase in concentration ratio becomes especially large at a boiling point just below 400 F (Fig. 2).

2. At a given boiling point, aromatics are more harmful than paraffins, while the olefins appear to be intermediate. This has long been suspected but this is probably the first time that quantitative data giving the magnitude of the differences have been available. The results in Fig. 2 indicate that the concentration ratio of paraffins goes up with boiling point in the same way as the concentration ratio of aromatics. At a given boiling point the aromatics are nearly three times worse than paraffins. There is little change in their relative harm as the boiling point increases. (See Table 4.)

Another way of looking at the same data is at constant concentration ratio. A paraffin boiling at 420 F is no more harmful than an aromatic boiling at 340 F. Naphthenes will probably behave in the same way as paraffins.

Only one olefin was studied. It fell almost midway between the paraffins and the aromatics as summarized in Table 5.

3. Boiling point is not merely an important factor in determining the deposit-forming tendency of aromatics; it seems to be the only factor. That is, as long as a compound contains at least one aromatic ring, its deposit-forming tendency can be predicted from its boiling point alone. Four kinds of aromatics were evaluated. These include toluene and two of its derivatives; one benzene derivative; indane, an aromatic alicyclic compound; and naphthalene, a condensed ring aromatic. When plotted against boiling point, the concentration ratios all fall on the same smooth curve with almost no scatter.

4. In an aromatic, all carbons in the molecule are equivalent with regard to their tendency to make deposits. Fig. 3 shows the structure of each of the aromatics studied, with the C^{14} boxed. The location of the labeled atom varied widely. In the toluene derivatives the labeled carbon was in the ring adjacent to the methyl group. The propyl benzene was randomly labeled throughout the ring. The indane was labeled in the 5-membered alicyclic ring. If there were any striking differences among the deposit-forming tendencies of the various carbon atoms in the molecule, it is extremely unlikely that the concentration ratios would fall on a smooth curve as they do. The effect of location of the labeled atom would be super-imposed on the boiling point effect, causing scatter. Since there is no scatter, it is inferred that there is no effect of carbon atom location.

5. On any one surface the concentration ratios do not change systematically as the deposits build up. In several of the tests, the head was removed from the engine at intervals and small amounts of deposit were removed and analyzed. No systematic differences were noted in concentration ratio. (See Table 6.) For the small samples analyzed for these results it is probable that these differences for a given hydrocarbon are within experimental error. It should be understood, however, that the 20-hr results are a mixture of the layer formed during the first 10 hr plus the layer formed during the second 10 hr. Thus, the deposits formed toward the end of the test could be substantially different from those formed earlier without materially affecting

the results. This is especially true since less material is formed per unit time as the test continues because of the increasing surface temperature as the deposit accumulates. For these reasons, it is not possible to be absolutely certain that the deposits formed on old deposits are identical in their sources with those formed on clean surfaces.

6. There is an effect of deposit location on concentration ratio. Probably this effect is caused mainly by the differences in surface temperature throughout the engine. When deposits were analyzed from separate locations throughout the engine, it was found that those deposits having a high per cent of carbon had a generally lower concentration ratio (Fig. 4.) It is felt that per cent of carbon in the deposit is not in itself the important variable but that it is rather a measure of the average temperature of the surface on which the deposit is formed. The higher the per cent of carbon in a deposit the lower its temperature. On very hot surfaces, such as the ceramic of the spark plug or the exhaust valve, there is almost no carbon present and, of course, analyses are not possible. The results shown in Fig. 4 suggest that of those locations where carbon did form, the intake valve had the lowest average temperature and the piston top had the highest average temperature. The head and the block surfaces had about the same temperature which was somewhere between that for the intake valve and the piston top. These results are reasonable. The piston, being only oil-splash cooled, is quite hot. The intake valve is exposed to the cooling action of the fresh charge for a long period of time and its average temperature is low. The head and block are both water-cooled and would be expected to have similar temperatures. Fig. 4 shows that for each of the materials plotted the concentration ratio goes down with increasing per cent carbon, that is, decreasing surface temperature. The concentration ratio is almost invariably lowest on the intake valve and highest on the piston top. Some implications of these results will be discussed in detail later.

Mechanism of Deposit Formation

Some of the results discussed above shed important new light on the way combustion-chamber deposits are formed. It is very significant that all aromatics of the same boiling point have the same deposit-forming tendency and that all the carbon atoms in the molecule are equivalent in this property. These facts could probably be explained in one of two ways. The less likely explanation is that the carbon may be formed after the molecule has entirely broken down into some much simpler and uniform state; for example, acetylene, carbon monoxide, or carbon dioxide. The intermediate must be some material which *all* carbon atoms pass through on their way to complete oxidation. On the face of it, such an explanation appears to be very unlikely thermodynamically and it does not explain the differences between aromatics and paraffins. Also, it does not explain the strong effect of boiling point on deposit formation. The other, and much more likely, possibility is that the deposits are formed via a liquid phase. The molecules are first liquefied followed by complete carbonization in that phase. This mechanism explains the strong effect of boiling point on deposit formation. Boiling point will directly govern the tendency of a compound to liquefy. This is much more satisfactory than assuming that boiling point is merely a measure of some other property that governs deposit formation. Boiling point is not an accidental variable but is really controlling. There is at present no way of knowing whether the liquid phase consists of droplets in the main volume of the combustion chamber or of liquid condensed or

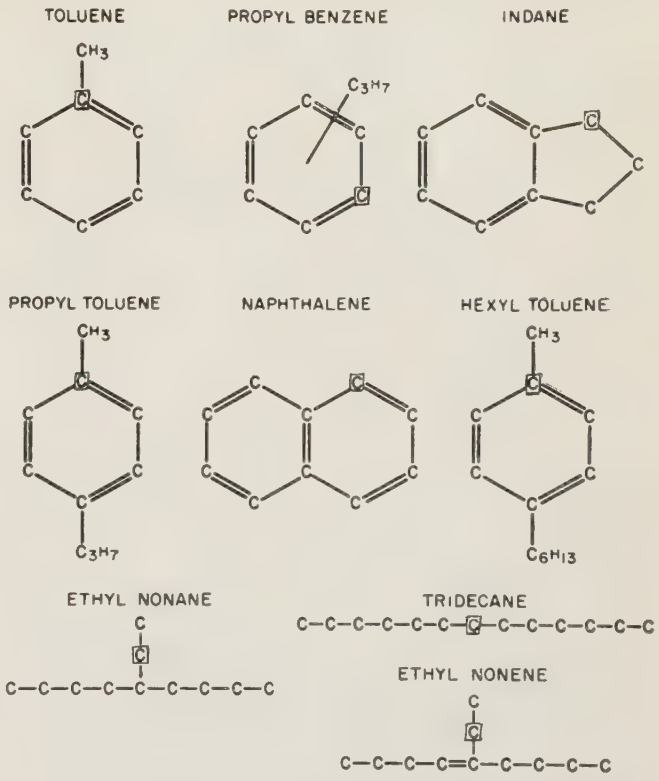

Fig. 3—Structures of compounds studied

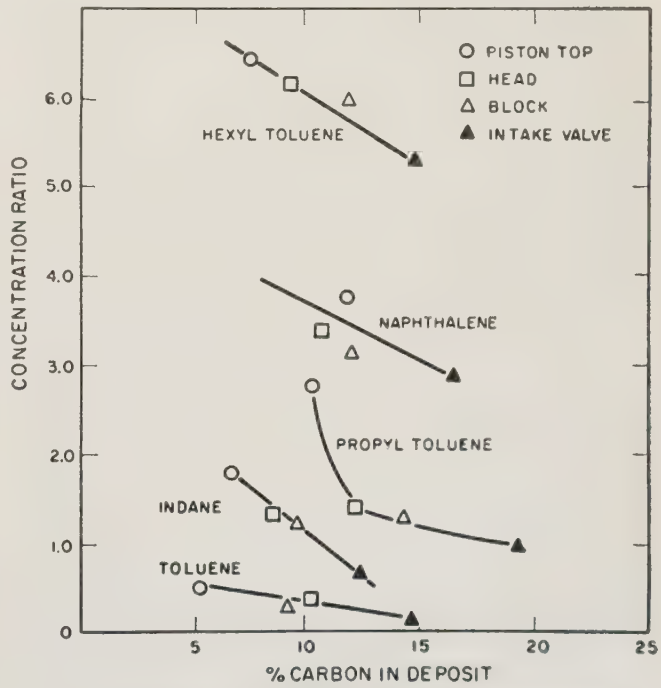

Fig. 4—Concentration ratio varies throughout combustion chamber

Table 7—Calculation of Deposit-Forming Tendency

	Components	Concentration Ratio	Deposit-Forming Tendency
Gasoline 1	20% Toluene	0.44	0.088
	70% Naphthalene	3.40	2.380
	10% Propyl Benzene	0.86	0.086
		Total Gasoline =	2.554
Gasoline 2	60% Toluene	0.44	0.264
	10% Naphthalene	3.40	0.340
	30% Propyl Benzene	0.86	0.258
		Total Gasoline =	0.862

Table 8—Lubricant Contribution of Benzene

Combustion Chamber Area	Concentration Ratio
Head	0.95
Intake Valve	0.71
Block	0.89
Piston	0.92
Weighted Average	0.92

Table 9—Gasoline Hydrocarbon Constituents

Cut Number	Boiling Range, F	Fuel, %	Aromatics, %	Olefins, %	Paraffins, %
Light Ends	To 78	6.13	0	60	40
1	78–127.4	18.0	0.9	59.0	40.1
2	127.4–186.8	12.9	8.4	42.4	49.2
3	186.8–237.2	17.3	24.1	27.7	48.2
4	237.2–287.6	20.0	40.7	18.1	41.2
5	287.6–338	16.0	57.5	12.9	29.6
6	338–388	6.13	79.0	6.4	14.6
Bottoms	Undistillable at 50 mm Hg	1.73	67	3.0	30
	Average Molecular Weight:		Olefins—290 Paraffins—290 Aromatics—178		

absorbed on the chamber walls. Perhaps both occur.

This hypothesis also assumes that the difference in deposit-forming tendency of aromatics and paraffins lies in the difference in their tendency to carbonize once they are in the liquid phase. There is a competition between the rate of re-evaporation and the rate of carbonization or coking. It is known that liquid aromatics will carbonize more readily than liquid paraffins, possibly because of their higher carbon/hydrogen ratio.

If the hydrocarbons form deposits by first condensing on the wall, increasing the wall temperature should cut down the condensation rate and, therefore, the deposit formation. A number of studies have supported this. In this work, the engine variable studies included air/fuel ratio, spark advance, compression ratio, and engine speed. Invariably when one of these factors was changed so as to increase combustion-chamber wall temperature, deposit formation went down. While this does not prove the importance of condensation, it is at least compatible with that mechanism.

This mechanism of carbon formation via the liquid phase is probably substantially correct. It does not, however, appear to explain all the facts. The results shown in Fig. 4 are quite puzzling. Here it is shown that, for all the aromatics for which there is sufficient information, there is a regular variation in concentration ratio throughout the engine: the higher the per cent of carbon in a deposit, the lower the concentration ratio. If per cent of carbon is a measure of deposit temperature, this means that for these materials concentration ratio drops with decreasing deposit temperature.

For any one run, concentration ratios may be looked on as being measures of the per cent of carbon in the deposit derived from the compound studied. The data are, therefore, in the peculiar position of indicating that the percentage of everything goes up with increasing surface temperature. This is an impossible situation. As the per cent of some things goes up, the per cent of others should be going down. There are several possible explanations for this.

First it could be an isotope effect. That is, due to the difference in mass, it is theoretically possible for the C^{14} to behave differently from the C^{12} and this difference in behavior could depend on surface temperature. However, this is unlikely. In one run, as will be discussed later, labeled benzene was evaluated using leaded benzene as the base fuel. If there were an isotope effect, it would show up here as well as in the runs with gasoline. In this run, however, a plot of concentration ratio versus per cent of carbon is horizontal.

Secondly, it is possible that some material not in the gasoline is diluting the carbonaceous part of the deposits and that the dilution decreases with increasing wall temperature. The diluent represents a smaller fraction of the deposits when the wall temperature is high. While this cannot be ruled out, it is hard to see what the diluent could be. It will be shown later that, in this engine, the lubricant contribution was small. This hypothesis is, therefore, unlikely.

While the mechanism of carbon formation in engines seems clear in outline, it is apparent that further work is required to establish the details.

Relative Tendency of Gasolines To Form Deposits

The principal object of this work was to obtain information that would permit a quantitative evaluation of the clean-burning characteristics of gasolines. Obviously, the deposit-forming tendency of the hydrocarbon part of an entire gasoline can be determined from the deposit-forming tendencies of the individual components. The weighted average of the concentration ratios of the components will give a number proportional to the deposit-forming tendency of the hydrocarbons in the fuel. The example in Table 7 means that the hydrocarbon part of gasoline 1 will form about three times as many deposits as the hydrocarbon part of gasoline 2.

While this technique seems to be quite straightforward, it does contain one implicit assumption: that deposit-forming tendency is independent of concentration. The need for the assumption is made clear in the course of the mathematical proof of the validity of the averaging technique described above.

$$X^1_A = \alpha^1_A C^1_A D^1 \tag{2}$$

$$\frac{X^1_A}{C^1_A} = \alpha^1_A D^1 \tag{3}$$

where:

α_A = Concentration ratio for component A

$$\alpha_A = \frac{\%\text{ C from component A in the carbonaceous deposit}}{\%\text{ C from component A in the gasoline}}$$

C_A = Fractional of component A in the gasoline

X_A = Weight of deposit from component A

D = Total weight of deposit

Superscripts:

[1] = Gasoline used in this test

[2] and [3] = Gasolines not yet tested

(Note: This derivation applies only to the carbonaceous part of the deposit.)

It is now necessary to assume that the weight of deposits from any one component is directly proportional to the concentration of that component in the gasoline. This assumes that the tendency to form deposits is independent of the concentration. According to this assumption, doubling the concentration of a component in the fuel will double the amount of deposits it forms. This is borne out by the fact that the materials tested were in concentrations ranging from trace amounts to 5% and gave consistent results.

Now if the assumption is true:

$$\frac{X^1{}_A}{C^1{}_A} = \frac{X^2{}_A}{C^2{}_A} = a^1{}_A D^1 \tag{4}$$

And:

$$X^2{}_A = a^1{}_A D^1 C^2{}_A \tag{5}$$

But

$$D^2 = \Sigma X^2 = D^1 \Sigma a^1 C^2 \tag{6}$$

In the same way:

$$D^3 = D^1 \Sigma a^1 C^3 \tag{7}$$

So that:

$$\frac{D^2}{D^3} = \frac{D^1 \Sigma a^1 C^2}{D^1 \Sigma a^1 C^3} = \frac{\Sigma a^1 C^2}{\Sigma a^1 C^3}$$

This equation merely states mathematically the conclusions drawn earlier in this section. The deposit-forming tendency is directly proportional to the sum of the concentrations times the concentration ratios. The concentration ratios a may be read directly from Fig. 4, or more conveniently, from a semilog plot to be shown later. The concentrations C may be determined by conventional analytical techniques. This means that the relative deposit-forming tendencies of gasoline can be readily calculated without expensive engine testing. It does not necessarily follow, however, that there will be a direct one to one correlation between deposit-forming tendency as calculated above and octane-requirement increase. First, all who have run many engine tests know that there is not a complete correlation between deposit weight and octane-requirement increase even if the composition of the deposits is the same. There is certainly a general correlation, but it is not perfect. Second, there are other materials that form deposits besides the gasoline hydrocarbons. These are mainly the lubricant and the lead salts. It is obvious that, if 75% of the carbonaceous part of the deposit comes from the lubricant, then doubling the deposit-forming tendency of the fuel will have only a small effect on total deposit weight and octane-requirement increase. It is known, however, that gasoline hydrocarbon type does play an important role in octane-requirement increase. These techniques should, therefore, be quite useful in making comparisons of different gasolines.

Source of Deposits

In the calculations of the previous section, it was assumed that the lubricant contribution to deposit weight was low. To check this assumption, a run was made using leaded benzene as a base fuel. A small amount of labeled benzene was added to this fuel. The fuel was then run in the L-head CFR engine using the same technique as previously described. If there were no contributions from the lubricant, the concentration ratio of the deposits would be 1.00 exactly. Any lubricant contribution would make the concentration ratio lower than 1.00. The results in Table 8 show that there was only a slight lubricant contribution.

Table 10—Fuel Deposit Formation

	Aromatic Fraction		Olefin Fraction		Paraffin Fraction		Total
Cut Number	a	Σac	a	Σac	a	Σac	Σac
Light Ends	Negligible		Negligible		Negligible		Negligible
1	0.30	—	0.10	0.01	0.10	0.01	0.02
2	0.35	0.004	0.15	0.01	0.13	0.01	0.02
3	0.40	0.02	0.20	0.01	0.18	0.01	0.04
4	0.54	0.04	0.30	0.01	0.25	0.02	0.07
5	0.90	0.08	0.51	0.01	0.32	0.20	0.11
6	1.80	0.08	1.0	0.004	0.64	0.006	0.09
						Total	0.35

This means that in the run with leaded benzene only 8% of the carbonaceous part of the deposits came from the lubricant. Moreover, in the benzene run the total deposit weight was 1.9 grams. The average deposit weight for the runs with the fuel shown in Table 2 was about 9 grams. If it is assumed that the lubricant contribution is independent of the fuel contribution then the per cent of the deposit due to lubricant in the majority of the runs is:

$$8\% \times \frac{1.9}{9} = 1.7\%$$

This implies that the lubricant contribution with the full-boiling gasolines is probably around 2%; at most, it is 8%. It can therefore, be neglected in this discussion. This is not necessarily the case in automotive engines under typical operating engines. CFR engines are designed for very low oil consumption. The engine used in this study was carefully maintained to give very low flow of oil into the combustion chamber. Also, the lubricant used was of high quality (had low deposit-forming tendency). In automotive engines, the lubricant contribution might certainly be substantial and should not be neglected without good reason.

Since the lubricant contribution was small, essentially all of the carbonaceous part of the deposit in the tests had to come from the fuel. This means that for the test gasoline the ΣaC must equal 1. This is a simple material balance. Also, the ΣaC for any part of the gasoline represents the fraction of the deposit carbon coming from that part of the gasoline. It should be understood that this sum will equal 1 only for the particular gasoline on which these tests were run.

To check this relationship, the base gasoline used was cut into fractions and each fraction was analyzed separately for hydrocarbon type. (See Table 9.)

To calculate ΣaC, it is necessary to pick values of a for each type of material in each cut. This is simplified by use of the semilog plot in Fig. 5. This is a replot of the data in Fig. 2. All the aromatics fall on a straight line except toluene. The reason for the deviation of toulene is not known. It is interesting that a straight line connecting the two paraffin points is almost parallel to the aromatic line. A line for olefins was drawn parallel to the paraffin line. The a chosen will not be at the average boiling point but two-thirds of the way toward the maximum boiling point of a cut. This arbitrary choice will partly compensate for the fact that the higher boiling part of a cut gives the majority of the deposits. Table 10 presents the results for all but the bottom 1.73% of the gasoline.

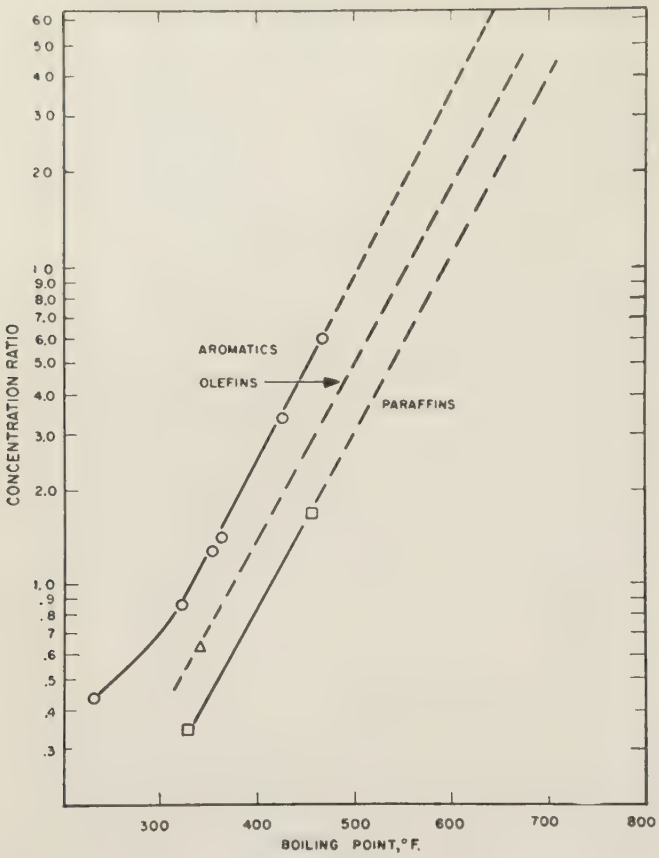

Fig. 5—Concentration ratio

This means that the top 98.3% of the gasoline contributes only 35% of the carbonaceous part of the deposits and that 65% of the deposit must come from the bottom 1.73% of the gasoline. This is difficult to check. The greatest difficulty lies in estimating the boiling point of the aromatic fraction of the bottoms. An aromatic of a molecular weight of about 178 can have a boiling point anywhere from 507 F for a normal alkyl benzene to 672 F for anthracene. It is also necessary to extrapolate the curves in Fig. 5 well beyond the experimental data. Nevertheless, the value of 0.65 does not appear unreasonable for the gasoline bottoms. By estimating the boiling point from the molecular weight, the paraffin contribution is calculated to be about 0.16 and the olefin contribution about 0.02. If the aromatics are alkyl benzenes, the aromatic contribution is 0.13. If the aromatics are all polynuclear, the aromatic contribution is about 1.1. Therefore, the aromatics are probably a mixture of alkyl benzenes and polynuclear materials and the 1.73% bottoms *can* cause 65% of the carbonaceous part of the deposits.

It is apparent that these results have profound implications on gasoline quality and on the processing needed to make a good gasoline. The moral is quite clear: To make a clean-burning gasoline, look to the bottoms and keep the heavy material out of the gasoline. With the aid of these precepts it is possible to make an exceptionally deposit-free gasoline simply by keeping a careful check on its hydrocarbon constituents.

Summary

1. The deposit-forming tendency of hydrocarbons goes up strongly with increasing boiling point.
2. Aromatics are considerably worse deposit formers than paraffins. Olefins are intermediate.
3. The carbonaceous part of combustion-chamber deposits appears to form via a mechanism involving condensation followed by carbonization.
4. Careful control of the back-end is needed to make a clean-burning gasoline.

Acknowledgment

The authors are indebted to Dr. A. S. DeMartini and M. H. Edson of the Esso Research and Engineering Co. for their help in obtaining some of the data presented in this report and also for their assistance in interpreting the results.

DISCUSSION

Describes Surface-Ignition and Deposit-Forming Effects of Fuels

—Joel Warren
Ethyl Corp.

THE authors are to be complimented on their use of radiotracers in the study of the combustion-chamber deposit problem. These deposits are one of the limiting factors in the utilization of higher engine compression ratios because of their tendency to increase the octane number requirement for the suppression of knock and to ignite the fuel-air mixture erratically, producing uncontrolled combustion (surface ignition).

The radiotracer technique employed gives information concerning two related factors, the origin of the carbon that is present in the deposits and the deposit-forming tendencies of fuel components. This information in itself is of value and it substantiates previous work which by more indirect means indicated that the fuel is a large contributor in deposit formation. However, the radiotracer work does not relate fully the two factors concerned to either the octane-requirement increase or the surface-ignition effects of the deposits.

The octane-requirement increase effects of individual leaded hydrocarbons as fuels have been described in an earlier paper.[a] This work showed that there was a marked tendency for requirement increase to become greater with paraffinic, naphthenic, and aromatic fuel types as the boiling point of the fuel was increased. However, the effects of olefin volatility were not so clearly defined.

Surface-ignition studies have been carried out using individual leaded hydrocarbons[b] as well as two-component

[a] SAE Transactions, Vol. 61, 1953, pp. 361–377: "Combustion-Chamber Deposition and Knock," by H. J. Gibson, C. A. Hall, D. A. Hirschler.
[b] SAE Transactions, Vol. 62, 1954, pp. 40–49: "Deposit-Induced Ignition—Evaluation in a Laboratory Engine," by D. A. Hirschler, J. D. McCullough, C. A. Hall.

blends. This work was done in a CFR L-head engine under an almost identical deposit accumulation procedure as that used by the authors in their work except that the compression ratio of the engine was 7/1. Surface ignition was measured by means of an ionization gap and associated electronic instrumentation. The data in Fig. A indicate that increasing the boiling point of the aliphatic hydrocarbons had very little effect on surface ignition. However, the same change in boiling point more than doubled the surface-ignition effects of the aromatics and the lowest boiling aromatic produced many times more surface ignitions than the highest boiling aliphatic. Also of importance, however, is the fact that generally as much as 40% of the blend could be composed of aromatics, regardless of the boiling point, before the number of surface ignitions began to increase at an excessive rate. (Light ends were added to the highest boiling blends to improve ignitibility.) This nonlinearity of blending behavior probably explains why it is generally difficult to predict the engine performance of fuels in respect to deposit effects simply from their hydrocarbon-type composition. Deposit weight data from these tests are shown in Fig. B. Application of the authors' concentration-ratio data to the fuels used in Fig. B forecasts deposit weight effects for the aromatics which are in agreement directionally with those which actually occurred. However, there is a definite lack of agreement between the concentration-ratio forecasts and the actual weights of deposits when either the wholly aromatic materials are compared with the nonaromatics or when some intermediate blends of the two components are considered. Here again, as with surface ignition, there is a nonlinearity in depositweight effects as increasing amounts of the aromatic component are present in the blend.

In addition to the nonlinearity effects, there is also reason to doubt that the measurement of the amount of deposited carbon will necessarily relate directly to the harm caused by the deposits. Three high molecular weight solvents used as fuel additives produced some interesting deposit effects (Fig. C). Although deposit weight was reduced drastically by all three additives, their influence on the weight of carbon in the deposits was not uniform. Two of the additives caused increases in the amount of carbon while the third caused a decrease. In spite of these changes in both total deposit weight and weight of carbon, there was essentially no change in requirement increase by any of the additives, but surface ignition was increased to different degrees by all three. These results indicate that a lack of correlation existed between deposit weight and either requirement increase or rate of surface ignition. Therefore, some factors other than carbon-forming tendency alone must be important in influencing the amount of harm caused by the deposit.

The authors showed in Table 7 how concentration ratio could be used to predict the deposit-forming tendencies of two gasolines made up of different amounts of the same components. By a somewhat similar method they calcu-

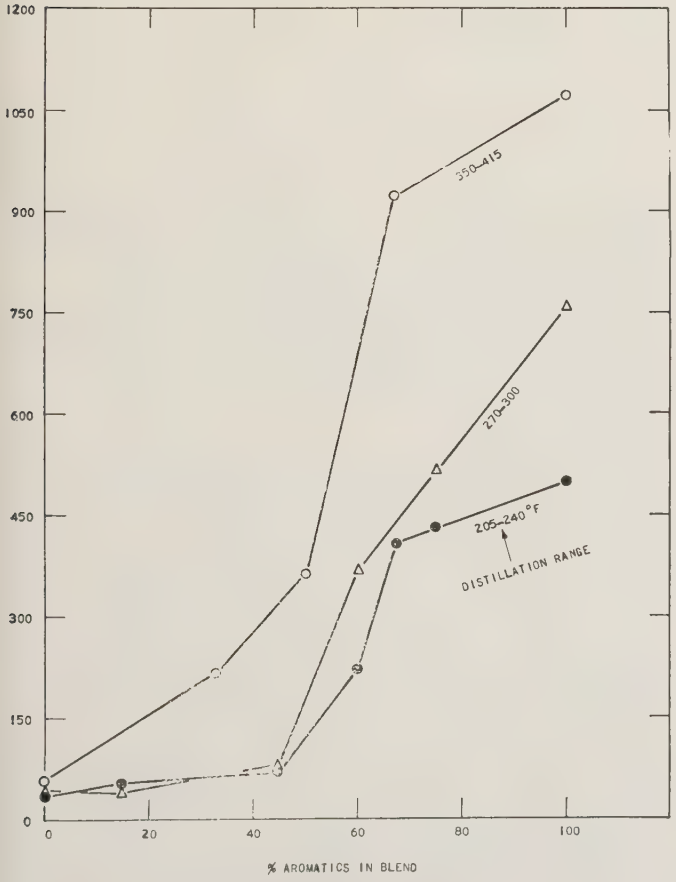

Fig. A—Surface-ignition tendencies of aliphatic-aromatic blends (blends contain 3.0 ml tel per gal, CFR L-head engine)

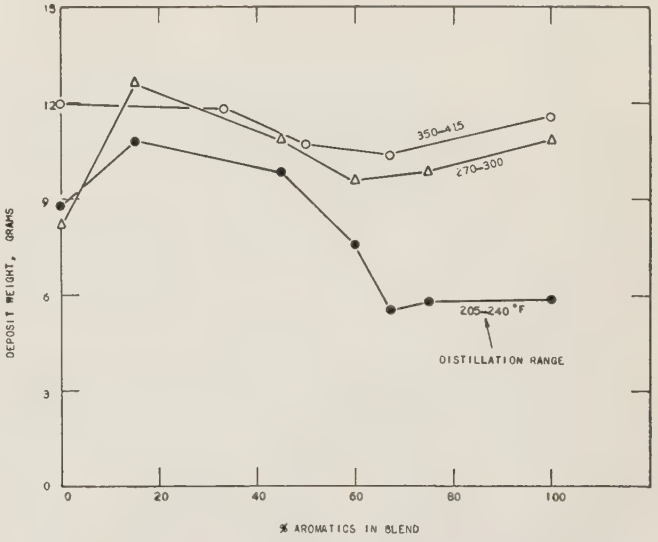

Fig. B—Deposit-weight effects of aliphatic-aromatic blends (blends contain 3.0 ml tel per gal, CFR L-head engine)

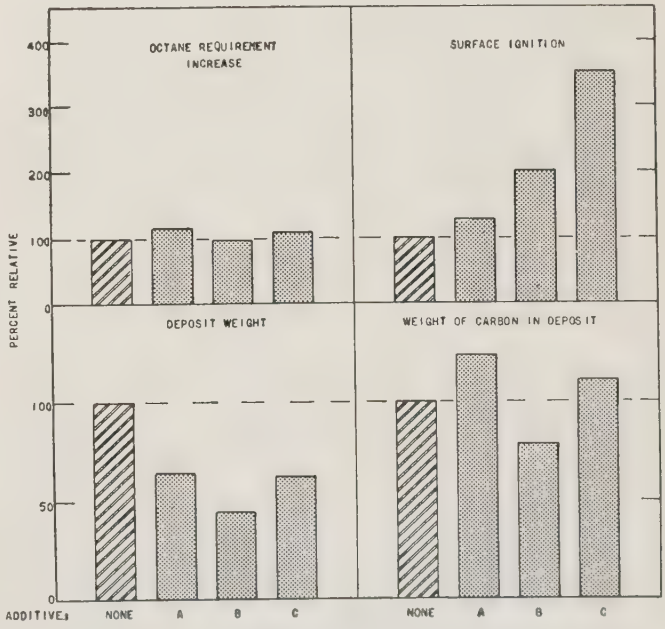

Fig. C—Effect of fuel additives (blends contain 3.0 ml tel per gal, CFR L-head engine)

lated that 65% of the carbonaceous portion of their base fuel deposits came from the bottom 1.73% of the base gasoline. Since the data presented in Figs. A and B have suggested that concentration effects of aromatics are not linear, it would be of interest to know if actual engine tests were made by the authors with the fuels on which their calculations were made. Such engine data would be very useful in proving that the deposit-forming tendencies of fuels can be predicted by their method.

The technique used by the authors presents an interesting approach to the complex problem of engine deposits. Knowledge such as this represents another step toward the complete understanding of the ways in which deposits form and exert their harmful effects.

Emphasizes the Effect of Boiling Point on Deposit Formation

—W. E. Newby

E. I. du Pont de Nemours and Co., Inc.

THE authors are to be congratulated on their definitive approach to this problem and the firm concise answers they obtained.

It is interesting that this paper dealing with fuel contribution points sharply to the importance of fuel boiling point. The work of McNab, Moody, and Hakala and others dealing with the lubricant contribution also points sharply to boiling point as a critical factor in formation of carbonaceous material in engine deposits.

In phenomena which are dependent upon boiling points the importance of the environment temperature cannot be overlooked. Some work at the du Pont Petroleum Laboratory by J. C. Burke and L. F. Dumont deals with the effect of deposit surface temperature on carbonaceous deposit formation from lubricating oil.

These experiments were conducted in a single-cylinder COT engine with a controlled temperature plug inserted in a spark-plug hole. Cooling by water or air, or resistance heating, was used to hold the plug temperature at 200, 400, or 800 F. The deposit temperatures were held close to plug temperatures by allowing only thin deposits to grow in short 15-hr tests. The engine was operated under mild steady duty conditions. The carbon content decreased with increasing temperatures, both in amount and per cent, from about 6% at 200 F to zero at 800 F. (See Fig. D.)

The carbonaceous material was derived from the oil in these experiments with a clean-burning fuel, isooctane. The results are the same as the authors obtained when the effect of only labeled fuel components was considered.

A stimulating question remains unanswered. The gasoline boils between 100 and 400 F. Lubricating oil boils above 700–800 F. In spite of this wide separation in boiling ranges both of these hydrocarbon sources can contribute significantly to carbonaceous material in deposits;

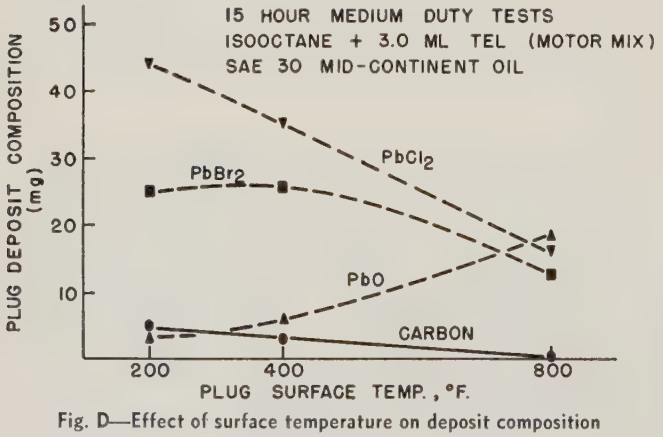

Fig. D—Effect of surface temperature on deposit composition

both are quite crictical with respect to their highest boiling components; and both are equally sensitive to surface temperature for the formation or retention of deposits. Furthermore, the carbon-containing material must face the same environment once it is on the surface, regardless of the original source. One would suspect that the route from the carburetor, or the crankcase, to the combustion-chamber walls includes some chemical reactions to equalize the original wide differences in molecular weight.

The route followed by a hydrocarbon from the original liquid state to a carbonaceous combustion residue has been studied in much more detail for jet fuels, which represent still another boiling point range for hydrocarbons. The excellent data by the authors are so similar to those from studies of jet fuel components that it is hard to believe that this is a coincidence. Consideration might well be given to information on carbonaceous deposit formation from jet fuels in further efforts to unravel the question of carbonaceous deposits from gasoline in internal-combustion engines.

Authors' Closure To Discussion

WE should like first to comment on Joel Warren's interesting and informative discussion. Several points should be made:

1. The surface ignition data shown in Fig. A, while interesting, are probably not very pertinent to the discussion. These data measure two independent factors, the deposit-forming tendency of the fuels and their ease of ignition by deposits. Since the second factor may vary as much as the first and since in this paper we are concerned only with deposit formation, some differences in results are to be expected.

2. The reason for the new techniques used in our study was our reluctance to accept data obtained with mixtures of pure components. None of our hydrocarbons were present in more than 5% concentration and all were tested in the complex base of hundreds of hydrocarbons present in a real gasoline. Surely mixtures of relatively pure components in very high concentration would behave somewhat differently. As a matter of fact, we are gratified by the general similarity of our results compared with those of the Ethyl Corp. Our example in Table 7 is a sample used to explain simply how calculations could be made. The answers shown probably would not be quantitatively accurate considering the simplicity of the mixtures.

3. There is certainly not a one-to-one correlation between deposit weight and deposit harm. There are other important factors, but the amount of deposit must be important though at times it may be overshadowed by other changes.

Now we have one general comment. Mr. Warren says, ". . . it is generally difficult to predict the engine performance of fuels in respect to deposit effects simply from their hydrocarbon-type composition." We agree. It is difficult, but not impossible. By judicious application of the ideas and data presented here, we feel quite confident of our ability to predict the relative deposit harm caused by two fuels differing only in hydrocarbon composition. These ideas have been checked by large scale field testing in many cars with many full-boiling gasolines and have been of great assistance to us in designing exceptionally clean-burning gasolines.

Regarding the question of the lubricant raised by W. E. Newby, we too are puzzled by the small lubricant contribution. The test, however, seems straightforward and the result unambiguous. As mentioned in the paper, the most reasonable explanation is simply that not much lubricant got into the combustion chamber. The possibility that pre-reactions are altering boiling points is an intriguing one, but we would hesitate to draw any conclusions without further data.

CHRYSLER TORSION-AIRE SUSPENSION---------Across The Board

O. D. Dillman and R. R. Love, Chrysler Corp.

This paper was presented at the SAE National Passenger-Car, Body, and Materials Meeting, Detroit, March 7, 1957

THE modern passenger car has evolved by eras. The decade before World War II was the streamlining era. The past six or seven years might be termed the era of the V-8 engine, and the last few years that of the automatic transmission—now found on some 80% of all new cars. With the advent of the 1957 models, began another period of modern passenger-car development—the era of suspension systems.

It has been said, by some of the men who have seen the passenger car develop over the past 25 years, that when we had plenty of hills to climb in the days gone by, we didn't have enough engine power or transmission ratio. Yet now that freeways and expressways are here and we pass through mountains instead of over them, our modern cars have engines and transmissions capable of negotiating hills with ease. And along the same line of reasoning, now that superhighways have little more than the permissible roughness tolerance of a pool table, we are accelerating our search for perfection in car ride.

With the majority of driving being done on such smooth-surfaced roads, it sounds as though sus-

IN 1951 Chrysler Corp. began working on a new torsion suspension. In this paper the authors describe details of the development and design of the suspension, now available on 1957 cars.

The authors claim the Torsion-Aire suspension has the following advantages: reduced high-speed float, boulevard harshness, impact harshness, road noise, body roll, nose dive, and acceleration squat; better directional stability and cornering ability; fewer lubrication points; and a better balanced ride.

The main feature of the front suspension is the use of torsion bars. One of the principal advantages of torsion bars is their weight: 10 lb as compared to 15.8 lb for a 1956 production coil spring.

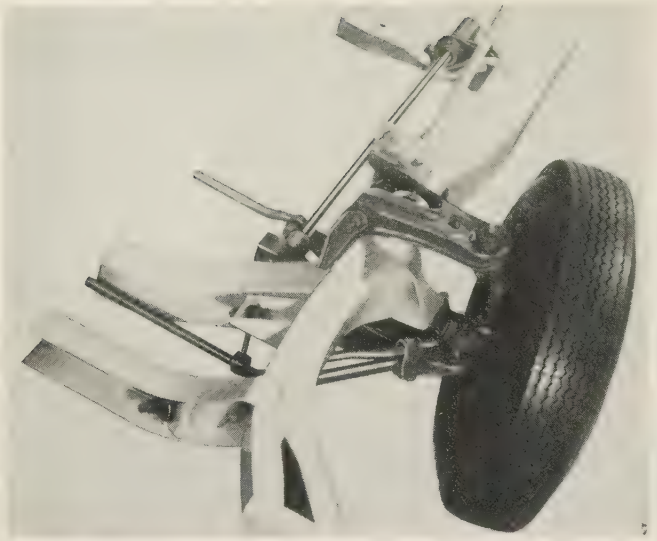

Fig. 1—1957 Plymouth and Dodge front suspension, front view

Fig. 2—1957 Plymouth and Dodge front suspension, rear view

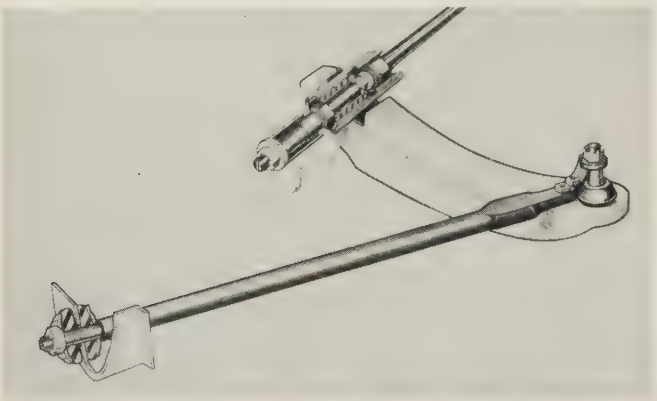

Fig. 3—Lower control arm and front strut mounting assembly

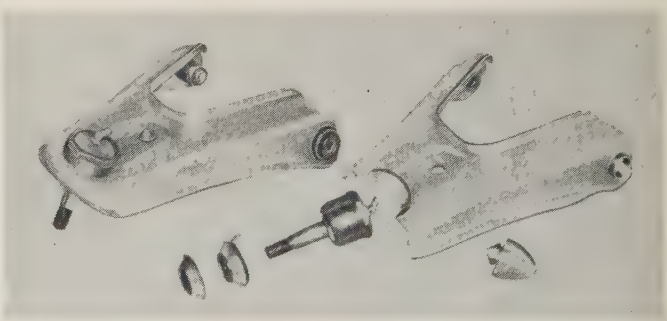

Fig. 4—Ball joint and upper control-arm assembly

pension engineers should have an easy job of providing a cloud-like ride for six passengers in a 4,500-lb modern automobile. While that's how it might seem, the following discussion is a look at what was actually done to bring about our "Torsion-Aire Suspension-Across the Board," that is, to all production models from Plymouth through the Imperial.

Development of Torsion-Aire Suspension

If this were a motion picture, we could fade out and flash back to a drafting room located at our Engineering Center in the year 1951. Our management had set goals of new engines, brakes, transmissions, and suspensions as prime chassis features for cars of the "Forward Look." But in this particular drafting room, a group of chassis designers were commissioned to develop a new suspension system that would readily adapt itself to a complete line of volume-production cars To rework or doctor-up a current suspension is one thing, but to have the opportunity to start with a clean board is just short of delight to the chassis designer.

If a car owner had been asked at that time to name items he would like improved in automobile ride, the list would probably have looked a great deal like ours. Our goals were:

1. We must do something about high-speed float.
2. Harshness during boulevard ride must be minimized.
3. Steering effort must be reduced.
4. Let's cut down on road noise.
5. More high-speed directional stability required.
6. Stop the front end from doing a nose dive on braking.
7. Help production to maintain car heights on the line.

8. Let's have a chassis that doesn't require lubrication.

9. How about a flat ride?

Production Version

There are two basic torsion-bar suspension units in production to fit the correct weight and dash-to-centerline-of-front-wheel requirements. One unit is used on the Plymouth and Dodge lines and a second larger suspension is used on the DeSoto, Chrysler, and Imperial lines. As a point of interest, the steering knuckle for the Imperial is special, mainly to take the large wheel bearings required for the additional weight. Since the principle of operation is the same in both the large and small front suspension designs, we will examine the Plymouth and Dodge design which was called the A-518 production unit.

Figs. 1 and 2 show views of the A-518 mockup covering all attachments. Starting at the ground and working up, we are now able to see the "Aire" in Torsion-Aire: a new 14-in. wheel and 22-psi tire. This combination of smaller diameter wheel and lower pressure tire was introduced for the purpose of adding to the softness and quietness of this system.

The lower control arm is made up of two main pieces, the load-carrying arm and the front strut (Fig. 3). The pivot point of the strut lies on the inner axis of the lower control arm. The front attachment is a large mass of rubber that makes two pillows upon assembly, one on each side of the inner front frame member. In addition to this rubber mounting, each of the additional attaching points of the suspension is isolated from the frame by rubber. The use of rubber in these points accomplishes two objectives: elimination of a previously lubricated point and elimination of the breakaway friction problem which was characteristic of these points when they were mounted steel-on-steel. The latter we considered a major accomplishment. Finally, the use of rubber contributes to the reduction of front-end harshness.

As the wheel strikes an object, the wheel and lower control-arm assembly retreats to the rear approximately ⅛ in. to reduce the gravity force build-up. The strut has a forged rear end that allows the proper metal section to carry offset loads around the corner to the 2-bolt attachment and, incidentally, provides a permanent wheel stop. The inner pivot of the load-carrying arm is cantilevered on the inner pivot bar that mounts in the lower-arm housing within a rubber bushing. This assembly is held in place by a safety check washer, nut, and lock wire. The rest of the housing extends rearwards and has a hexagonal hole broached in it to accept the torsion bar that is simply slid into place at assembly.

The upper ball joint deserves some attention, due to its different type of attachment. After eliminating forged and stamped ball-joint housings as too expensive or bulky, the simple method of attachment illustrated in Fig. 4 was developed. As shown, the entire ball joint is built around one common centerline. The outer surface of the housing is threaded with a flat-pitch thread, similar to that used on the now outmoded steel bushing. By drawing and reaming a hole in the outer end of the control arms, it is possible to have the hardened

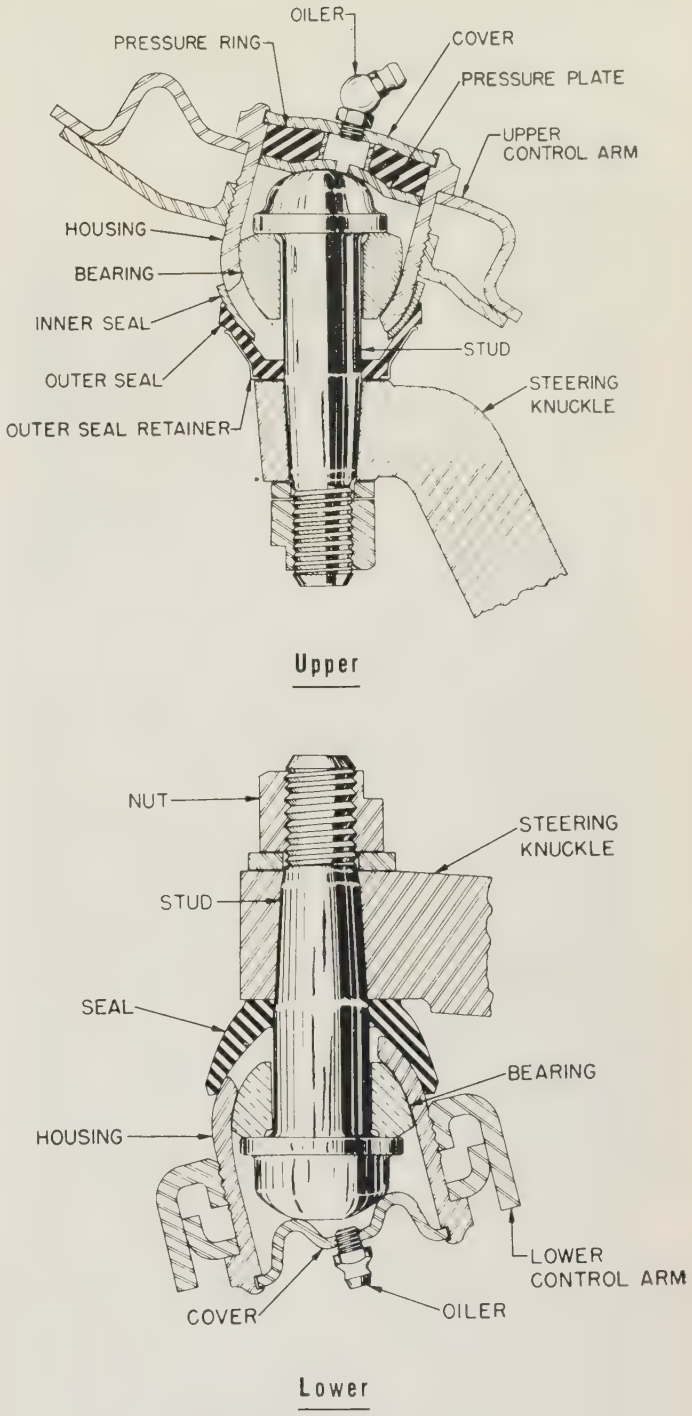

Fig. 5—Front-suspension ball joints

flat threads on the ball-joint housing cut their way into the control arm and, at the same time, lock themselves in place. Fig. 5 is a cross-section of the upper and lower ball joints showing the rubber spring-loading member in the upper joint as well as the permanently lubricated SuperOilite hardened bearing.

Again, the upper arm, like the lower, is a stamping and uses a snap-in type rubber rebound bumper. The inner pivots are straddle-mounted rubber-shouldered bushings using the double-shear prin-

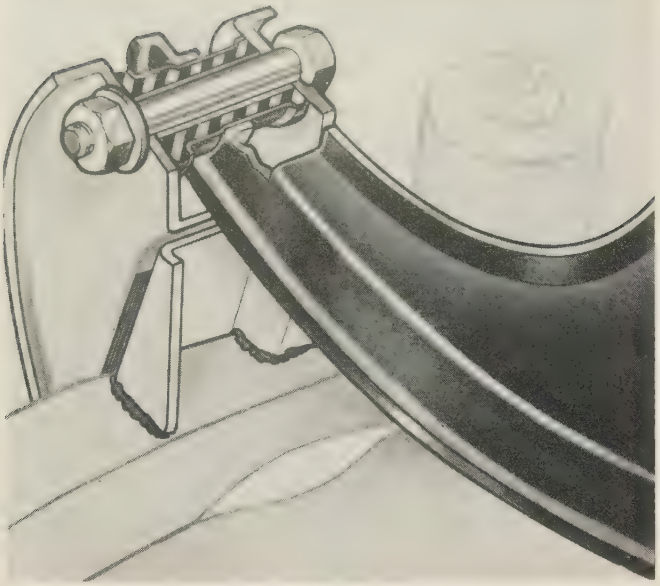

Fig. 6—Upper control rubber inner pivot mounting

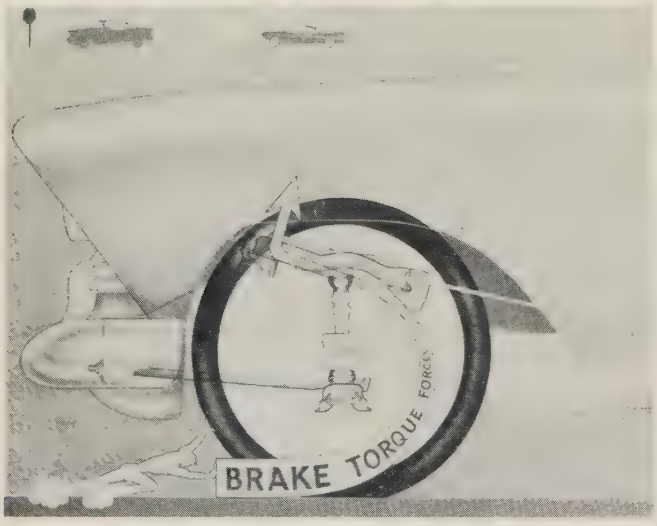

Fig. 7—Antidip braking principle of load application

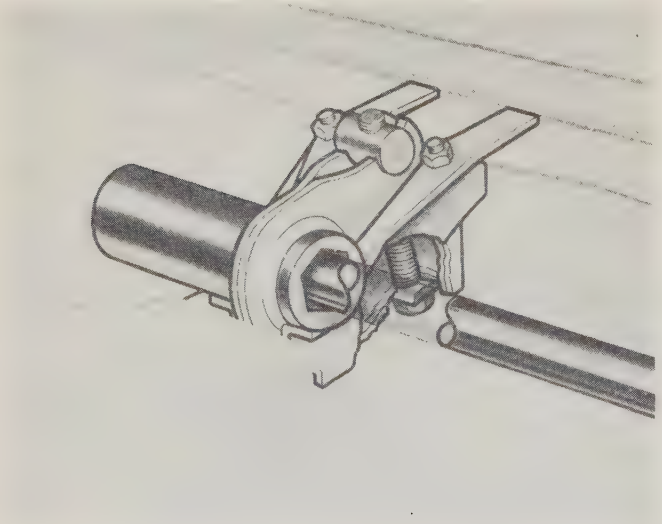

Fig. 8—Adjustable rear torsion bar anchor

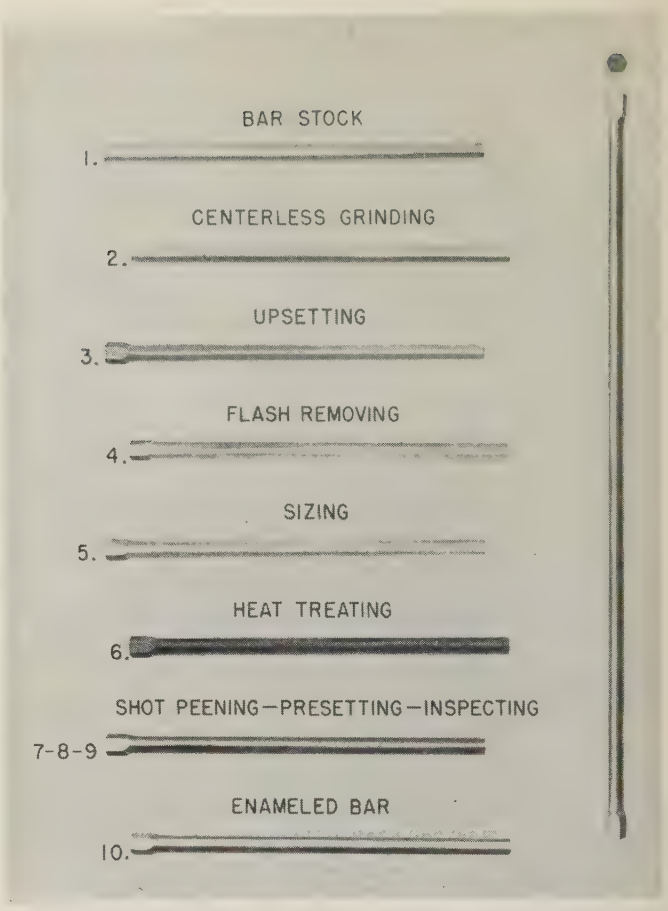

Fig. 9—Manufacturing steps of front-suspension torsion bar

ciple on their mounting bolts (Fig. 6). We chose this method to keep additive wheel rate down as compared to a larger single-cantilever mounting system. Each bushing is attached to the frame by a stamped inner pivot bracket that is spaced away from the frame by a stack of 1/16-in. shims. With a ball-joint outer pivot, wheel caster and camber can be adjusted by adding or subtracting the proper number of shims under the front or rear control-arm bracket.

As mentioned, one of our original goals for this suspension was to keep the front end from doing a nose dive on braking, which is referred to as "antidip" braking. The elimination of braking nose dive was accomplished by the diversion of the braking forces through the use of an upper control arm inclined to the chassis structure. Fig. 7 indicates the manner in which the braking force is transferred into the steering knuckle and upward to the ball joint of the upper control arm, which is inclined at 17 deg to the horizontal. Simplified, an engineer would say that the rearward braking force is divided into two components through the use of the inclined upper control arm: a horizontal braking force to stop the car and a vertical force to lift the car. Thus, as a car is stopped with a nominal braking force of 1,000 lb applied to one front wheel, 212 lb (which is a portion of this load) is diverted into counteracting the weight-shift forces which would normally cause the front end of the car to dip.

The main feature of this front suspension is, of course, the use of torsion bars. The torsion bar is one of the most efficient ways that we know to use expensive spring steel. A 1956 production coil spring

weighed 15.8 lb as compared to 10 lb for a torsion bar. The major saving is in the elimination of dead coils for seating.

The rear of the torsion bar is fixed in an anchor housing that is cradled in the engine rear-frame cross member (Fig. 8). The adjustable height feature of the torsion bars allows us to insure that all front-end car heights are uniform as the cars come off the assembly line and permits further field adjustment, if necessary.

In addition, torsion bars permit us to transfer the loading point of the suspension more exactly to the portion of the frame structure which can best handle these loads. By eliminating the previously used bulky coil springs, the torsion bar gave us more usable space in the engine compartment—a major consideration with today's low car silhouettes.

The major factor in the design of high-production torsion bars is to keep operating stresses down and thus permit normal automotive production methods. Fig. 9 shows each of the 10 steps that a piece of bar stock goes through in becoming a Torsion-Aire torsion bar.

Moving to the rear, Fig. 10 shows the modified Hotchkiss drive rear suspension. In order to allow as low a tunnel as possible for reduced car heights, this standard unit was once more called upon to give a little more performance than usually demanded of it. By using a 1/3–2/3 offset in the position of the rear axle with respect to spring length, a stiffness ratio of 8.4 for the front section to 1.0 for the rear section was obtained by stubbing or clubbing the front ends of the spring leaves. In effect, a trailing arm of sorts is produced which has an instant center such as to allow a pleasant rise to the rear of the car on maximum acceleration and also work as a member of the suspension team in controlling braking dip. Additional advantages are roll control and increased stability.

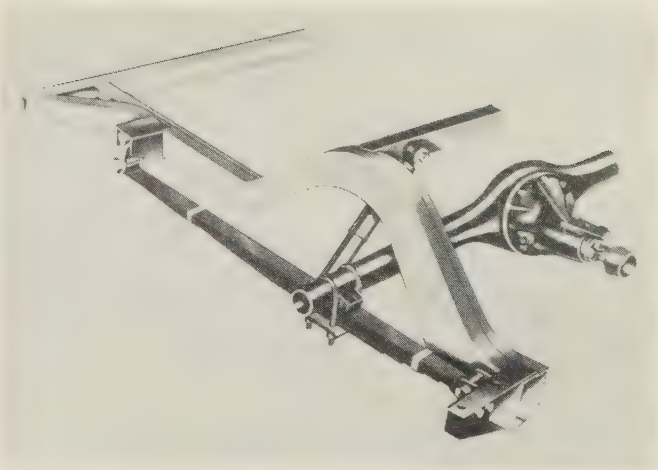

Fig. 10—1957 modified Hotchkiss rear suspension

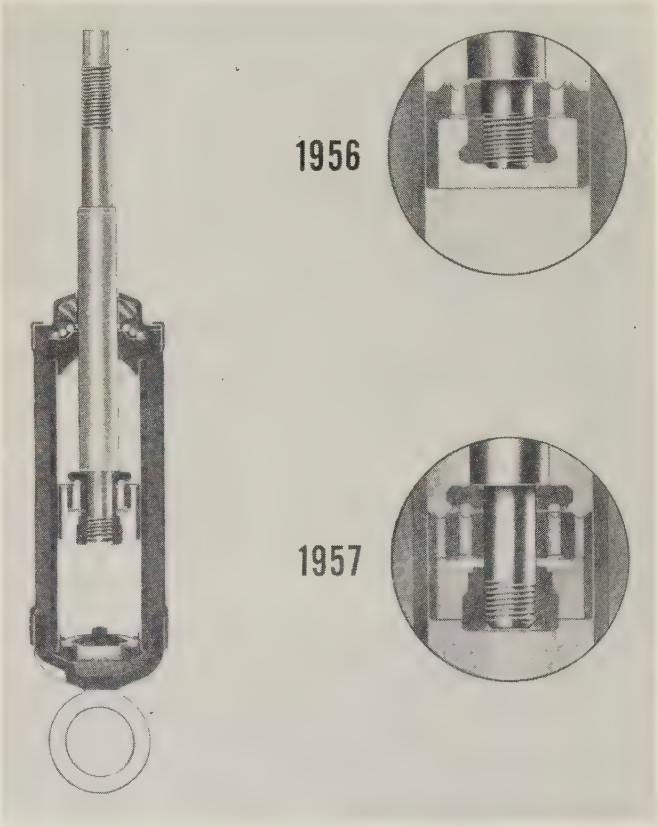

Fig. 11—Front shock absorber

Results

During the development of the Torsion-Aire suspension, design engineers and laboratory engineers built and tested countless laboratory setups as well as nearly 100 different partial suspensions in experimental automobiles. Before the final version of this new suspension was placed in production, it was tested and proved reliable on over 50 experimental cars. Tests on these cars were not only conducted at our proving grounds under every conceivable condition, but tested also in every weather condition from the biting cold of Minnesota to the baking heat of Texas. During this time the experimental cars equipped with Torsion-Aire suspension were driven over 750,000 miles. These tests showed the following effects on our list of objectives.

Reduction in High-Speed Float—The phenomenon known as high-speed float is characterized by a bobbing motion of the front end of the car when it is driven over an undulating road. Under this condition, shock absorber control appears to be completely lacking. The control of this front-end float at highway speeds has long been a major concern of the suspension engineer. His problem is one of providing sufficient shock-absorber resistance to eliminate float and yet avoiding the harshness of a stiff-legged ride.

While the Torsion-Aire suspension was being developed, shock-absorber development engineers were perfecting a modification in the valving of the Oriflow shock absorbers. Their goal was to provide greater damping at low-shock-absorber piston velocities without sacrificing the excellent rough road control and absence of harshness of the Oriflow. Their work resulted in the release of a new shock absorber for the front suspension on all models (Fig. 11). The additional set of valve disks and orifices provides greater shock-absorber resistance at low piston velocities while maintaining all the other desirable characteristics. This shock absorber played a large part in making it possible to eliminate the sway bar on the Plymouth and most of the Dodge models. The first objective was, therefore, quite successfully fulfilled.

Reduced Boulevard-Ride Harshness—Boulevard-ride harshness is best described, we believe, as the

effect produced by greatly over-inflated tires riding over small road irregularities. This harshness is caused by suspension friction or stiff suspension springs; in traversing small bumps, therefore, the car ride is determined principally by the high spring rate of the tires. Obviously, then, the direct approach to the problem is to use lower tire pressures. If lower pressures are to be used, the tire cross-sectional area must be increased to carry the same load. Thus the Plymouth tire was changed from a 6.70 x 15 tire carrying 24 psi to 7.50 x 14 carrying 22 psi. On the other extreme, the Imperial tire was changed from 8.20 x 15 to 9.50 x 14 with the same reduction in air pressure. These 14-in. diameter tires have a considerably greater enveloping power (Fig. 12) with rates in the order of 10% less than their 15-in. diameter counterpart.

The other important factor in boulevard harshness is the static friction of the suspension. Suspensions with low friction will deflect under small road surface irregularities and allow the car to ride on the suspension springs rather than on the tires. The fact that the rate of the tires is approximately eight times that of the suspension springs indicates the importance of reducing static friction. In the Torsion-Aire suspension friction has been reduced 20% over its predecessor. This was made possible by virtually eliminating sliding friction of the pivot points and replacing it with rubber deflection. We found that the fore-and-aft movement of the front suspension (also made possible by rubber deflection) made a significant contribution to the reduction of single bump impact harshness, a more severe phenomenon than boulevard harshness.

It is extremely difficult to measure accurately boulevard harshness by instrumentation. Ride juries using the time-honored"seat-of-the-pants" method are still, we believe, the best way to evaluate a suspension's performance under this particular ride condition. Every jury that tested the Torsion-Aire suspension for boulevard harshness brought in a verdict of "substantial improvement."

Reduced Steering Effort—Larger and softer tires, increased front-end weight, and smaller diameter steering wheels in the new cars made increased steering effort a possibility, if not a probability. With such conditions clearly established, the only remaining means of counteracting their adverse effect (short of releasing power steering as standard equipment) was an increase in steering ratio or a

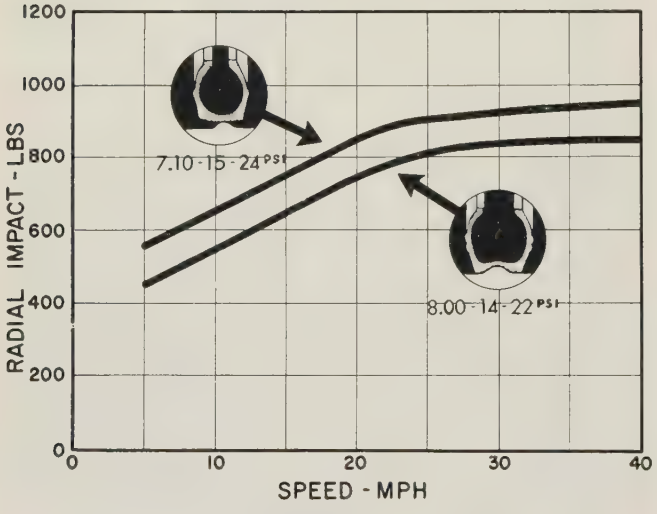

Fig. 12—Tire enveloping power comparison

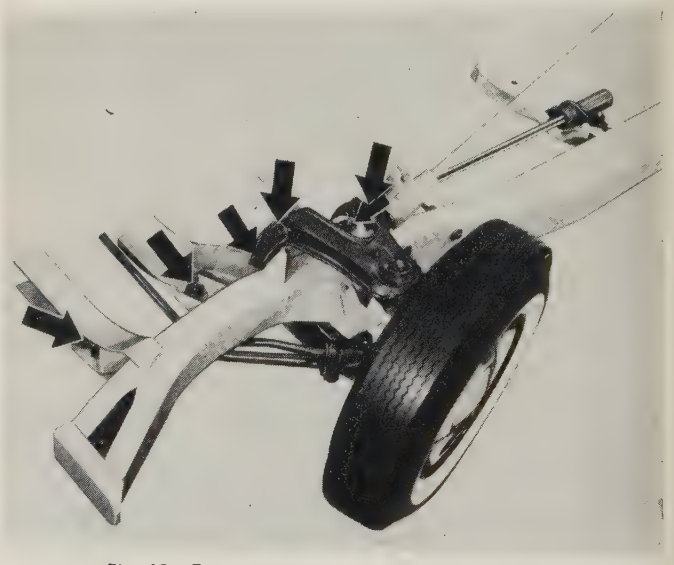

Fig. 13—Front suspension rubber isolation points

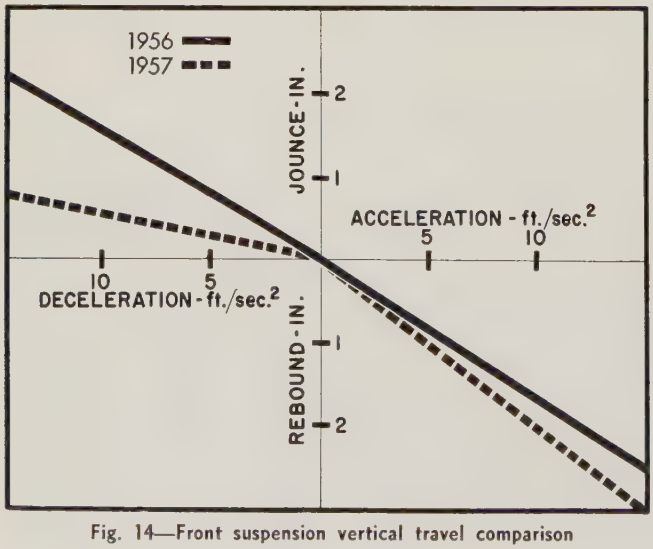

Fig. 14—Front suspension vertical travel comparison

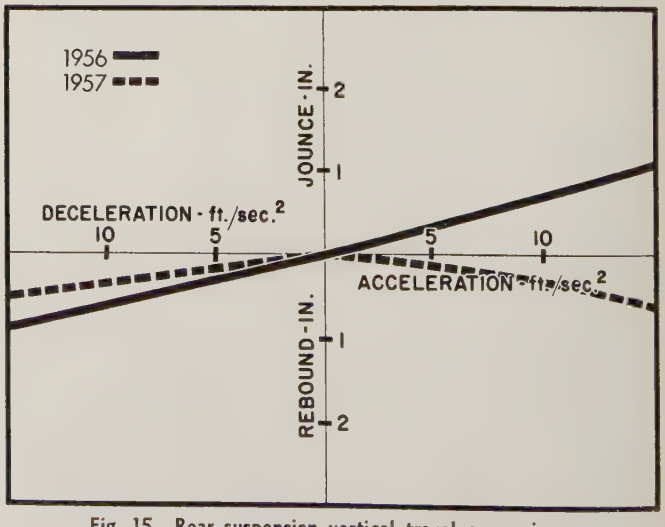

Fig. 15—Rear suspension vertical travel comparison

reduction in the friction of the several pivot points. Since we proposed to maintain steering ratios, the latter approach was the one we took. Major friction points in the steering system are the ball joints and steering linkage.

The upper ball joint is preloaded by a rubber spring. The load and rate of this spring was selected to keep the stud engaged with the bearing at all times. The bearing, which is made of Super-Oilite, has grease grooves on top and on the inside diameter to provide lubrication for free steering action.

The lower ball joint also utilizes a SuperOilite bearing with grease grooves. The weight of the car is supported by this joint. It is, therefore, not necessary to preload this bearing since there is no reversal of load. Early in the development stages, needle bearings and ball bearings were used below the head of the stud. It was found that turning friction with SuperOilite was sufficiently small that needle or ball bearings were not required.

A rubber idler-arm bushing and nylon bearings in the ends of the transverse steering link provide less friction at these points.

The net result was a steering effort approximately equal to that of previous models. At the outset, it thus might appear that our original objective was not completely attained, but considering the obstacles involved, we felt that maintaining the same steering effort was an accomplishment.

Friction in the pivot points has on occasion been used as a means of damping out wheel fight on cars with manual steering. The design of Torsion-Aire steering and suspension geometrics is such that they do not fight each other. The result is that wheel fight is no problem even with these low-friction pivot points.

Reduced Road Noise—Transmission of road noise into the car has been greatly reduced by completely isolating the front suspension from the frame by means of rubber at every point of contact (Fig. 13). In some of our previous development work where rubber pivot bushings were used in conjunction with a conventional coil spring, it was discovered that the car became more sensitive to unbalance disturbances.

The permissible unbalance in the front-wheel assembly of the Torsion-Aire suspension, however, has been increased by 40%. Conversely, a given amount of unbalance will disturb this new suspension considerably less than the same amount of unbalance disturbed the conventional coil-spring suspension.

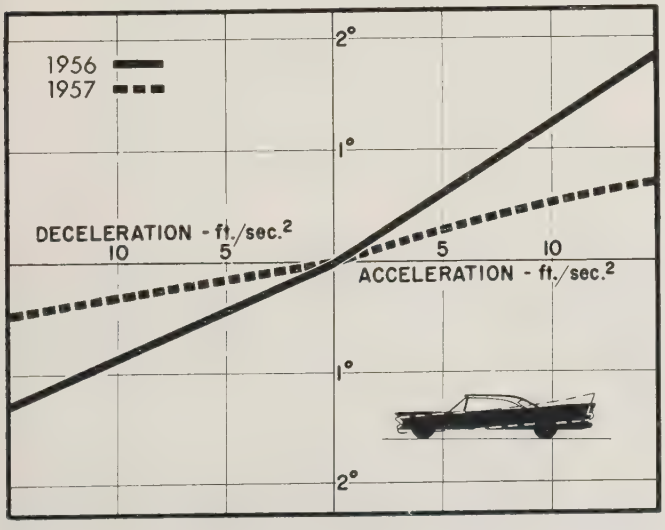

Fig. 16—Car attitude comparison

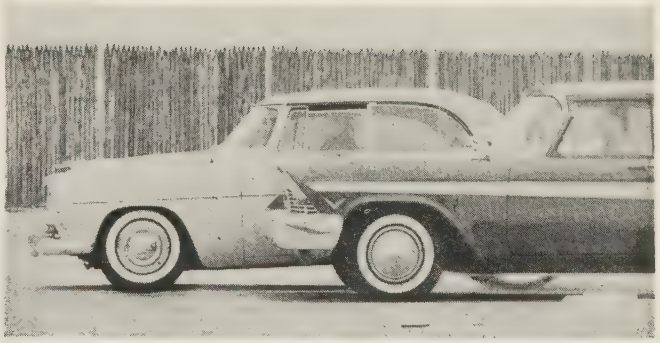

Fig. 17—Brake dive comparison

Road noise is another item that is difficult to measure with instrumentation, but our tests and observations indicate that it has been substantially reduced in cars equipped with the Torsion-Aire suspension.

More Directional Stability Required—Two of the outstanding characteristics of the Torsion-Aire suspension are its directional stability and its cornering ability. Nearly everything connected with the suspension and steering design helped contribute toward these desirable results, but the following factors were of major importance:

1. Rear suspension geometry. Considerable roll understeer was introduced in the geometry to counteract the loss in roll steer due to the increased roll stiffness, and to offset increased rear-tire slip angle caused by a greater percentage of the roll couple taken at the rear.

2. Steering geometry. We found that a neutral toe pattern (no change in toe setting through jounce and rebound movements) was the best overall compromise for cornering ability and directional stability.

3. Caster setting. The caster was increased over that on previous models. Manual steering cars were changed from -2 to $-\frac{3}{4}$ deg, and power steering cars from zero to $\frac{3}{4}$ deg positive caster.

4. Wheels and tires. Rim widths are $\frac{1}{2}$–$1\frac{1}{2}$-in. wider than those used on previous models, thus increasing tire lateral stiffness.

Reduced Braking Dip and Acceleration Squat—Antibraking dip and antiacceleration squat are dependent upon the design of both the front and rear suspensions. As seen in Fig. 14, the acceleration attitude of the 1957 Chrysler New Yorker as dictated by the front suspension is very little different from that of the 1956 model. However, during deceleration the amount which the suspension goes into jounce is reduced some 65%, due to the inclined upper control arms which provide a lifting component on the front suspension to offset the weight shift. Fig. 15 indicates the contribution of the highly unsymmetrical leaf-spring rear suspension. During deceleration the rise in the rear of the car is reduced by 40% while during acceleration the rear, instead of squatting, actually rises somewhat. The resultant effect is shown in Fig. 16. The change in car attitude is now sufficiently small that it is difficult to perceive any change during either acceleration or deceleration. Fig. 17 shows the difference

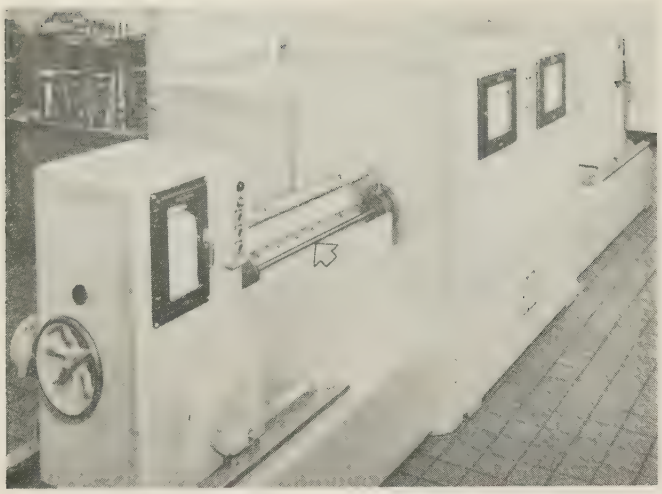

Fig. 18—Torsion bar fatigue test machine

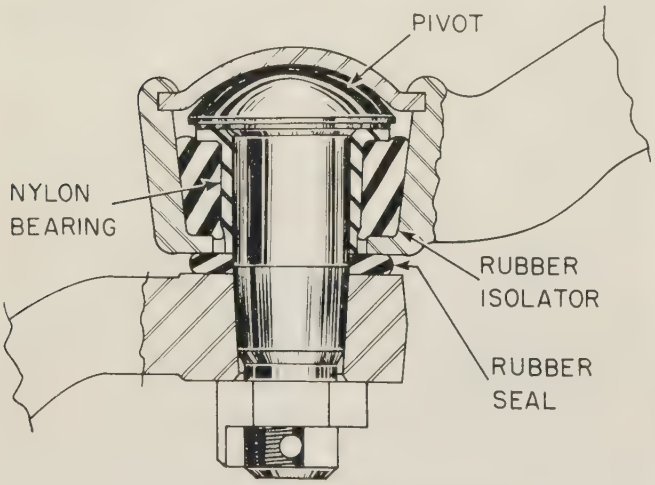

Fig. 19—Transverse steering link bearing

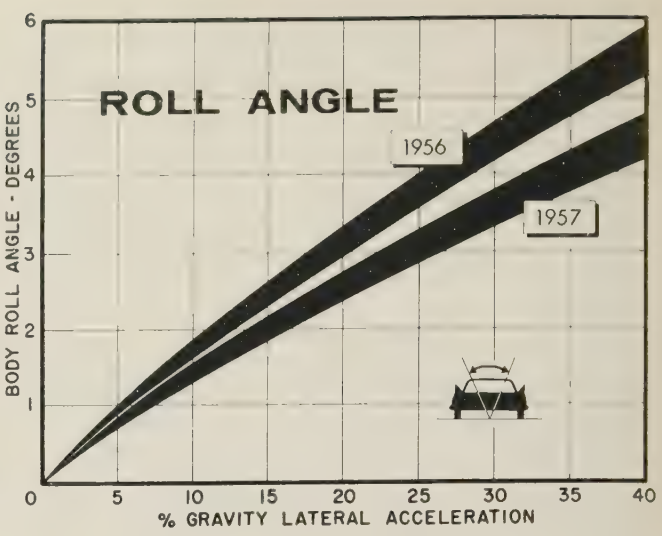

Fig. 20—Roll angle comparison

in brake dive between a 1956 and a 1957 Plymouth at 15 ft per sec^2 deceleration

Help Production Maintain Car Heights on Line—As already mentioned, the ability to adjust the height of the front suspension by winding up the torsion bar is one of the features of Torsion-Aire. This feature, of course, provides the advantage of permitting rapid adjustment in the field if the springs should settle. Actually, we have not been able to realize this advantage simply because the torsion bars have been designed with stresses that are low enough to preclude settling. The extensive testing necessary to develop these torsion bars began in 1954, at which time there was very little data available to determine a correlation between laboratory test and service life, and no laboratory test machine was readily available to conduct these tests. Fig. 18 shows the laboratory torsion bar fatigue test machine which was designed and built specifically to test the torsion bars for this new suspension. In the laboratory, the bars are cycled at stresses between 35,000 and 135,000 psi. This stress range is held constant automatically by the loading arm at each end of the machine which winds up one end as the spring begins to settle. A life of 100,000 cycles over this severe stress range is considered satisfactory. In order to establish this correlation, car tests were run simultaneously with laboratory tests on springs from the same production run, even to the extent of putting defective bars on cars to induce failures.

Let's Have a Chassis that Doesn't Require Lubrication—Front-end lubrication points have been reduced from as many as 23 to 8—four tie rod ends and four ball joints. Again, the rubber bushings play a very important part in eliminating lubrication fittings by replacing the metallic joints which require lubrication. Fig. 19 shows a cutaway of one end of the transverse steering link showing the use of nylon and rubber. We find we're a little short of our goal of eliminating all the lubrication fittings, but development work still continues.

Desired—A Flat Ride—One aspect of flat ride is the amount which the body rolls during cornering. From the standpoint of how the driver feels it is desirable to keep the roll angle at a minimum. Although in reducing roll we are making what is actually a rather small angle still smaller, the reduction appears to have a greater effect on one's feelings than the change would indicate that it should. As seen in Fig. 20, at 30% gravity-lateral acceleration, which is a moderately severe side thrust, the body roll has been reduced 25%. The reduction in roll angle resulted from:

1. Lower center of gravity. The center of gravity was lowered 1–3 in. over previous models.

2. Higher front roll stiffness. The roll stiffness was increased 30%.

3. Increased rear roll stiffness. The roll stiffness of the rear suspension was increased 35%.

Some improvements in pitch rate have been made by better selection of spring rates, front versus rear, by better shock-absorber control, and by a somewhat higher radius of gyration.

Conclusion

To summarize, the Torsion-Aire suspension has given our 1957 cars:

1. Reduced high-speed float by the use of new

front shock absorbers with better control.

2. Reduced boulevard harshness through the use of lower pressure tires and reduced front-suspension friction.

3. Reduced impact harshness by introducing fore-and-aft flexibility of front suspension.

4. Reduced road noise through ample use of rubber bushings.

5. Better directional stability brought about by additional rear-suspension roll understeer, wider wheel rims, neutral toe pattern, and additional positive caster.

6. Reduced nose dive and acceleration squat due to inclined upper control arms and unsymmetrical rear springs.

7. Fewer lubrication points through the use of rubber pivot points.

8. Reduced body roll due to lower center of gravity and higher roll stiffness.

9. A better balanced ride because of better spring balance front to rear, higher radius of gyration, and better balanced shock-absorber control.

Probably our most effective summary came from one new Plymouth owner who said, in effect, that "I don't see anything so spectacular about this Torsion-Aire suspension. I admit it has no front-end dip on braking, it doesn't sway on curves as before, it's softer on rough bumps, and at highway speeds it's as stable and quiet a car as I've ever driven, but that's about all you're getting out of it."

We had to admit that that was about all.

DISCUSSION

Describes Instrument for Measuring Car Attitude

—G. E. Adams
Ford Motor Co.

IT appears to us that the Torsion-Aire workout has provided an excellent solution to the space problems associated with lower hood lines and the width of V-8 engine installations while attaining excellent interchangeability throughout their wide range of car models.

The quoted saving of 5.8 lb of steel per coil spring appears greater than could be associated with the elimination of "dead coils," however, and I would be curious as to the comparison of the coil spring and torsion bar design stresses employed.

The use of an adjustable anchor for the torsion bar, which permits adjustment of car height on the production line and in the field, is something that I am sure would be appreciated by any suspension engineer who has had to cope with production variations in spring height, variations in car weight due to variations in optional equipment installed, and the nasty basic habit that cars have of varying in weight throughout a model run. There have been times when I would have put this as the first item on the authors' list of nine design goals.

In regard to the braking "antidip" feature incorporated, it should be pointed out that the trends in overall car design since the introduction of independent front suspension have tended to reduce the amount of forward braking front-end drop, front suspension linkage geometry notwithstanding:

1. Vehicle center-of-gravity height from the ground has been reduced and wheelbases increased, both of which reduce the actual "weight transfer" to the front wheels during forward braking.

2. Vehicle centers of gravity have moved forward somewhat and, therefore, for a given front-end frequency, spring rates become slightly stiffer, tending to reduce the actual drop at the front for a given weight transfer.

Some years ago our testing department developed instrumentation for the measurement of car attitude during braking maneuvers. Fig. A shows an arm carrying a small rubber-tired wheel which contacts the road surface directly under the bumper. This arm is mechanically coupled to operate a slide wire resistor in an electrical circuit feeding a recording oscillograph. Fig. B shows a car undergoing test, with the units installed front and rear. The oscillograph information can then be plotted in terms of height change at the front wheel or bumper centerline, height change at the rear wheel or bumper centerline, or vehicle tilt angle. A plot of vehicle tilt angle during forward braking for various deceleration rates on three 1957 cars recently tested is shown in Fig. C.

One humorous unexpected effect of an antidip front geometry we observed is that a pedestrian watching a car

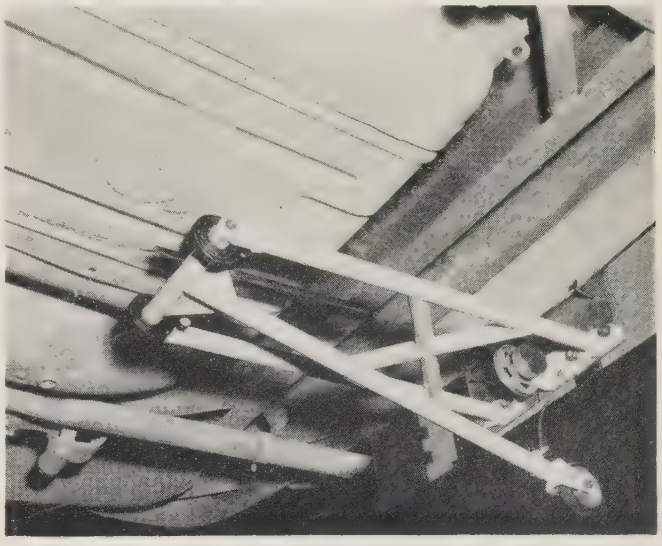

Fig. A—Bumper motion gage

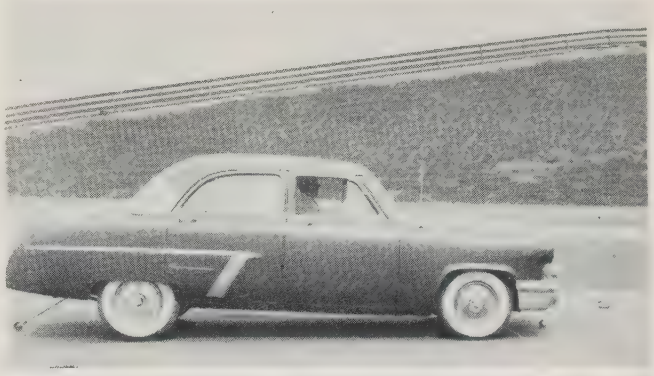

Fig. B—Test measuring car attitude during braking

approaching a stoplight has less confidence the car is really decelerating since the car lacks "dip"—an increase in the pedestrian "fright factor," if you will.

In conjunction with the design goal of a completely greaseless chassis, I might caution that going too far in this direction will eliminate the very popular Powr-Luber accessory and would ultimately deprive the dealer of his chance to spot additional maintenance work required while his customer's car was on the grease rack. As a long term objective, it is considered a sound one.

In connection with steering efforts, I would like to ask the authors if their kingpin inclination and scrub radius was changed appreciably in the 1957 design.

In closing, since by tradition every discussion is supposed to pose some sneaky question, I would like to ask Messrs. Dillman and Love if they would care to make any comments relative to the cost of their new front suspension compared to their previous design?

Compares Torsion Bar Spring and Coil Spring

Bernhard Sterne
Chrysler Corp.

SINCE Mr. Dillman in his paper and Mr. Adams in his discussion raised the question of weight comparison between the torsion-bar spring and the coil spring, the following observations may be helpful.

The spring is an elastic body which deflects under load and which recovers its original shape when released after being deflected. In this process the external work imparted to the spring by the product of the two factors "load" and "deflection" is first stored by the spring as potential energy and then substantially recovered as kinetic energy.

With deflection F proportional to load P, the spring has a constant load rate $(R = P/F)$. In the case of the torsion-bar spring, R is the linear rate for the load P acting at the end of the control arm or lever (of length A) which is attached to the spring. Within certain limits the deflection F at the end of the lever equals the product of A and of the windup angle ϕ of the torsion-bar spring.

With these definitions, the energy E stored by the spring at deflection F or load P can be expressed as follows:

$$E = \frac{PF}{2} = \frac{P^2}{2R} = \frac{F^2R}{2} \qquad (a)$$

The energy capacity of every spring is limited by the maximum stress S to which any fiber of its material can be safely subjected. The magnitude of the stress is substantially identical for the two spring types since they are both torsionally stressed. When the energy to be stored by the spring is due to static loading, the maximum stress is expressed in the following formula for the torsion bar spring:

$$S = \frac{\phi dG}{2L} \quad \frac{FdG}{2AL} \qquad (b)$$

And for the coil spring:

$$S = \frac{FdG}{\pi D^2 N} \quad \frac{FdG}{DL} \qquad (c)$$

In both springs the bar or wire diameter is d, the active bar or wire length is L, the volume of active spring material is $V = \frac{\pi d^2}{4} L$, the modulus of elasticity in torsion is G. In the coil spring the mean coil diameter is D, the number of active coils is N, and consequently $L = \pi DN$.

These stress formulas serve to express the deflection factor in the energy equation. The rate factor is expressed as follows for the torsion bar spring:

$$R = \frac{P}{A\phi} = \frac{P\pi d^4 G}{A32PAL} = \frac{Vd^2G}{8A^2L^2} \qquad (d)$$

And for the coil spring:

$$R = \frac{P}{F} = \frac{Pd^4G}{8PND^3} = \frac{Vd^2G}{2D^2L^2} \qquad (e)$$

The energy equation $\left(E = \frac{F^2R}{2}\right)$ can then be written for the torsion bar spring:

$$E = \frac{4A^2L^2S^2Vd^2G}{2d^2G^2 8A^2L^2} = \frac{S^2V}{4G} \qquad (f)$$

And for the coil spring:

$$E = \frac{D^2L^2S^2Vd^2G}{2d^2G^2 2D^2L^2} = \frac{S^2V}{4G} \qquad (g)$$

Therefore, under static loading and identical maximum stress both spring types have identical energy capacity and both require the same volume of active spring material.

But under dynamic or fatigue load (as in a suspension spring) the coil spring is at a disadvantage. The higher stresses near the inside of the coil due to wire curvature and direct shear are then more critical and become the limiting factor for the energy capacity of the coil spring. This is taken into account by using a "corrected stress." The "uncorrected" stress S' is computed from the standard formula and is then multiplied by the (Wahl) stress correction factor K, resulting in the corrected maximum stress $(S = S'K)$ for the coil spring.

While the volume of active spring material required under dynamic loading remains $\left(V = E\frac{4G}{S^2}\right)$ for the torsion bar spring, it becomes $\left(V = E\frac{4G}{S'^2} = E\frac{4G}{S^2}K^2\right)$ for the coil spring.

Since the factor K was in excess of 1.20 for all the suspension coil springs we used prior to Torsion-Aire, it follows that their active material had to weigh about 50% more than that of the torsion bar springs used for comparative models and subjected to the same maximum stress.

The comparison of total weight involves also the inactive material at both ends of both spring types. Using approximate average values, it can be stated that in our suspension coil springs the inactive end coils added 20% to the weight of the active material, while in the torsion bar springs the upset hexagon ends add 12%. Consequently, the total weight of the coil spring was about 60% greater than the total weight of the comparable torsion-bar spring subjected to the same maximum stress.

This discussion is confined to a comparison between the torsion-bar spring and the coil spring. It shows why, pound for pound, the torsion-bar spring is more efficient under fatigue loading conditions. Still, it should be remembered that there are other spring types which are nearly twice as efficient as the torsion-bar spring. This is particularly true of the ring springs in which all fibers of the material are under equal stress. This discussion also does not touch upon the comparative weight of the attachment parts which are needed to make the springs function in assembly.

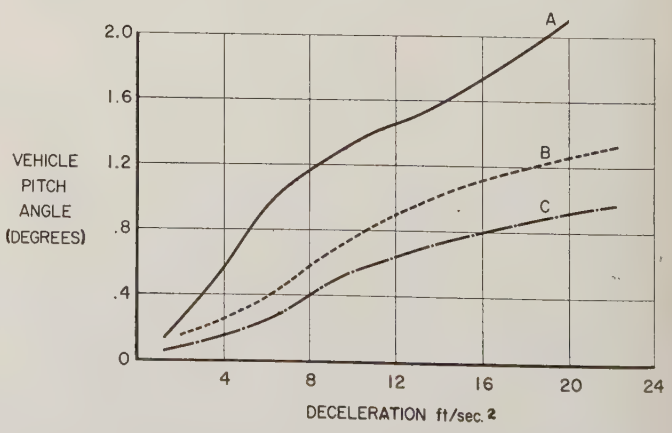

Fig. C—Dynamic pitch angle, forward braking on 1957 cars

The Future of the FREE-PISTON ENGINE in Commercial Vehicles

O. B. Noren and R. L. Erwin, Ford Motor Co.

This paper was presented at the SAE Summer Meeting, Atlantic City, June 7, 1957.

THIS paper describes the development and utilization of a new Ford free-piston powerplant, the model 519. Mr. Noren traces the development of the engine from the initial idea to the point where commercial utilization could be considered.

Mr. Erwin describes one commercial use: in the Typhoon tractor. The ratio of size and weight to horsepower is favorable for farm tractors, being smaller and lighter than equivalent diesel engines. The performance of the tractor has been satisfactory thus far, operating smoothly and being practically vibration-free, with little noise.

The advantages of the free-piston gasifier, as reported by the authors, are: flexibility, fuel economy, no need for auxiliary starting engine, economical manufacture of a wide range of engine sizes, adaptability to a wide range of fuels, and good torque characteristics.

Free-Piston Tractor Powerplant

by O. B. NOREN

OUR company's Free-Piston Engine Program was started in February, 1954. The objective of the program was to obtain basic thermodynamic and design information on small high-speed free-piston engines as a basis for designing an industrial or automotive size powerplant. This objective has been realized.

The first Ford free-piston engine (Fig. 1) had a

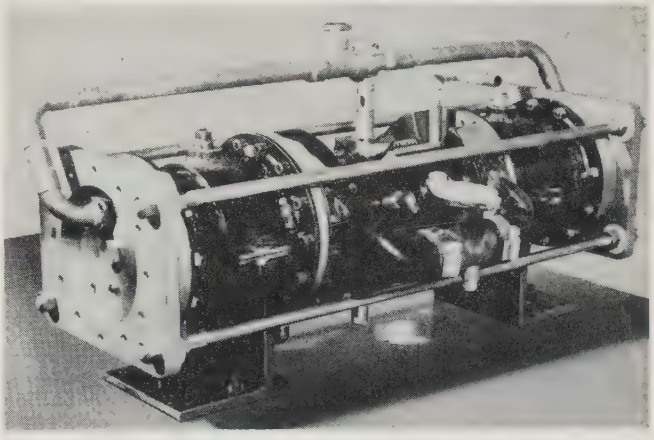

Fig. 1—First Ford free-piston engine

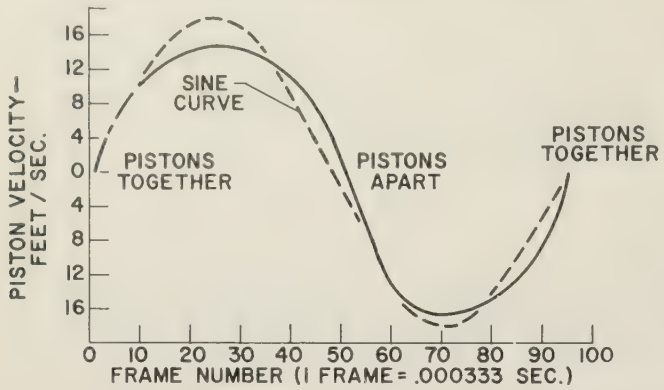

Fig. 2—Free-piston engine, piston velocity versus time of one complete cycle of operation

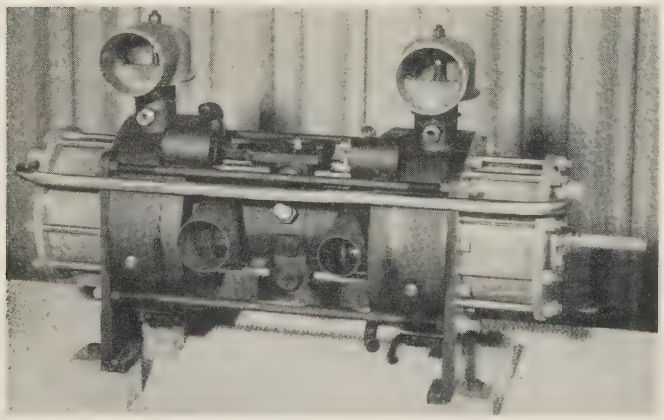

Fig. 3—Second Ford free-piston engine

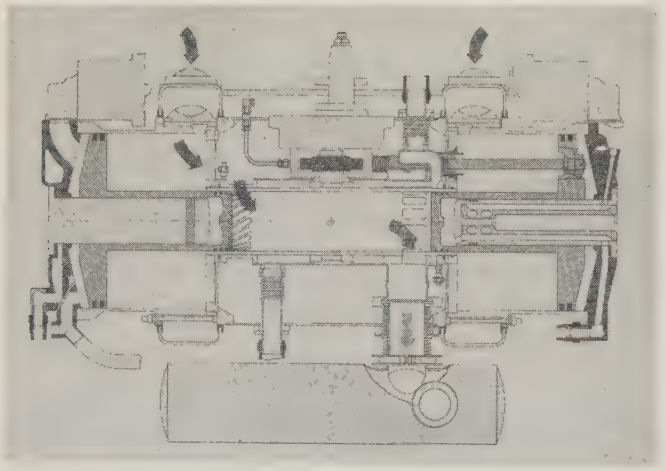

Fig. 4—Model 519 free-piston gasifier

2-in. power cylinder and 5-in. compressor, and operated at frequencies up to 3600 cpm, according to piston weight, and developed up to 16 ghp. Complete measurements were made on this test engine, establishing the piston motion diagram and the pressure-volume relationships in the three working chambers. The engine was run on many different hydrocarbon fuels, on 0–100 octane number gasoline and on gaseous fuels such as propane. Operation was successful with either carburetion or fuel injection, and with either spark or compression ignition.

This program emphasized the almost complete insensitivity of the free-piston engine to fuel ignition quality. Fig. 2 is a curve of piston motion as a function of time, for the small free-piston engine. Fig. 3 is a photograph of a second version of this engine which incorporated structural changes.

This program verified an opinion that successful, small free-piston engines could be built, and many of the design features of these small engines were incorporated in the present model 519. The use of one pair of synchronizing racks was one of the design features carried over directly to the 160-hp version. Work on the model 519 engine described in this paper was started in November, 1955.

The program was a dual effort. One concentrated approach was directed toward determining the thermodynamic relationships for the 519 engine which would establish the proper engine geometry. From this analysis, the bore, stroke, port relationships, and area ratios as well as cyclic frequency were obtained.

The second effort was concerned with the mechanical design of the 519 powerplant, determining synchronizing means, injection pump actuation, valve design, piston design, power cylinder construction, engine materials, and a multitude of small but important design features.

During the preliminary phase, performance calculations were made by hand, establishing the basic geometry to which the engine was built. Concurrently, a complete and detailed performance anaylsis was programmed for the IBM 702 computer. Applying this analysis to a number of basic engine configurations, the computer verified the results of the hand calculations and justified the basic engine geometry.

The outboard equation of the Model 519 is:

$$\frac{1}{n_1-1}P_1(A+1)(e-x)\left[\left(\frac{e-x}{y}\right)^{n_1-1}-1\right]$$
$$-P_2A\left[\frac{\pi_1(x+c)}{n_2-1}\left\{1-n_2\pi_1^{\frac{1}{n_2}}\right\}+(e+c-y)\right]$$
$$-\pi_2(e-y-g)-\frac{1}{n_4-1}\left\{g\pi_2\left(\frac{g}{x}\right)^{n_3-1}+\frac{R}{C_v}F\right\}$$
$$\left\{1-\left(\frac{g}{x}\right)^{1-n_4}\right\}+P_3(e-x-y)=0 \qquad (1)$$

The inboard equation is:

$$\frac{1}{n_1-1}P_1(A+1)(e-x)\left[\left(\frac{e-x}{y}\right)^{n_1-1}-1\right]$$
$$-P_2A\left[\frac{(e+c-y)}{n_2-1}\left\{n_2\pi_1^{\frac{n_2-1}{n_2}}-1\right\}-\pi_1(x+c)\right] \qquad (2)$$
$$-\pi_2\left[e-y-g+\frac{q}{n_3-1}\left\{\left(\frac{g}{x}\right)^{n_3-1}-1\right\}\right]-P_3(e-x-y)=0$$

Under all circumstances the outboard energy must equal the inboard energy.

As soon as the 519 gasifier was running, test data were fed into the computer program to reconcile the computer results to the test stand results. This reconciliation involved programming adjustments for actual scavenging efficiency, port losses, valve

losses, combustion efficiency, temperatures in the working chambers, and other related factors, so that test data and computer results were essentially the same over the load range of the engine. With the basic analysis locked in with the gasifier test program, it became possible to make changes in engine geometry on the computer with the expectation that the engine would faithfully reproduce the results. This expectation has been realized in practice. With the programming adjustments derived from practice, changes in the performance characteristics of the engine could be evaluated on the computer. This practice saves time and money, and accelerates engine development.

The mechanical design posed a difficult and complex problem. In common with any new powerplant design, there was the necessity of avoiding a bulky package. The primary problem was restricting the overall engine length to 37 in. Fig. 4 is a cross-sectional view of the 519 free-piston engine. Fig. 5 shows the engine with the intake manifolds removed, and Fig. 6 the complete engine with the manifolds in place.

Prior to the actual design work, some preliminary research was done on compressor valves. It was recognized that the compressor inlet and exhaust valves had to be as foolproof as possible, offer minimum pressure drop, and have adequate life expectancy. Experience dictated the selection of a reed-type valve (Fig. 7).

A test rig was built which simulated the valve operation as closely as could be predicted by calculation. The valve was operated at engine frequency against calculated back pressure and temperatures (Fig. 8). The 519 engine has 144 intake valves mounted in 24 pads, 12 for each compressor cylinder. The compressor discharge valve plates have 40 valves per cylinder.

The development of this valve included establishing the proper clearances, determining the material, developing the back-up plate shape, and determining the flow restriction. The particular valve design chosen was characterized by low flow restrictions. During testing, the valve life was progressively improved until valves were developed which would run 1000 hr without failure at conditions approximating full-load engine operation. The real worth of this valve program has been realized in the engine development period, during which there have been no valve failures of any type.

Of equal importance with the valve problem was the problem of fuel injection. Every new diesel engine must have a fuel-injection system tailored to the engine's particular requirements. It was, therefore, necessary to study the limitations on fuel

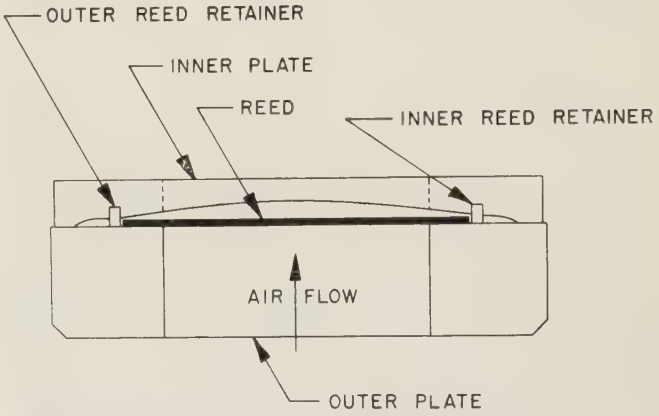

Fig. 7—Section through reed-type valve

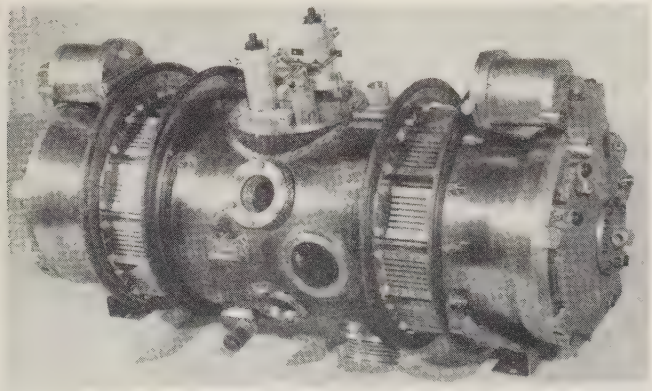

Fig. 5—Model 519 with intake manifolds removed

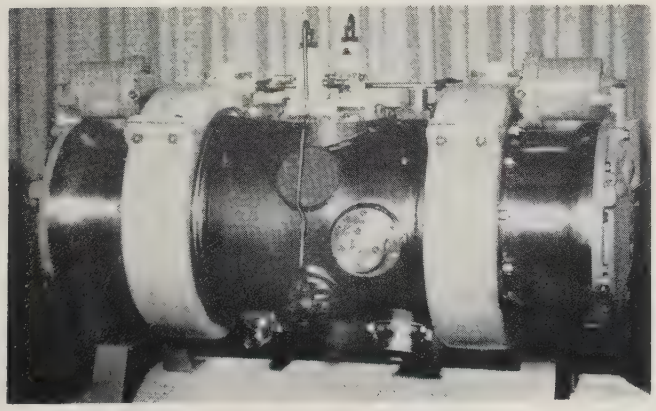

Fig. 6—Model 519 with intake manifolds in place

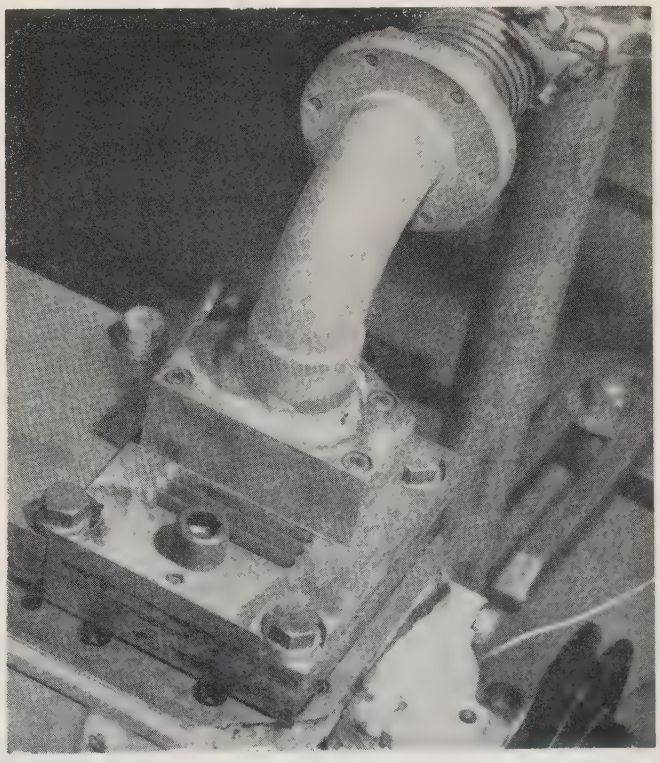

Fig. 8—Valve test rig

injection imposed by the configuration of the 519 engine. The lack of a finite stroke and clearance volume, and the absence of rotating parts to actuate the injection pumps posed two of the most difficult problems.

In an effort to minimize the shock loading on the cams and followers, linear cams with equivalent cycloidal contours were selected. Mounted on the synchronizing rods, these cams move exactly as the pistons move, creating a timing problem. There is no motion at inner dead point (idp) when injection should be taking place. To be satisfactory, injection should occur from about 30-deg bidp to 10-deg aidp. As another step toward minimizing cam loading, one larger pump has been replaced by two smaller pumps of equivalent combined delivery. Work is continuing, to determine if one pump and nozzle can be eliminated without impairing cam and follower life, engine efficiency, and dependability.

The major difference between pumps is in the configuration of the plungers, which are upper, lower, or double helix. Most of the engine development has been with a lower helix plunger pump which starts delivery at the same cam position in each stroke, and varies the termination of injection by the position of the helix relative to spill port.

In conjunction with this configuration, it was found necessary to use an 84-in. delivery or delay line to time the injection to the desired position in the cycle. Experiments with a pump in which the retraction piston had been removed from the delivery valve to increase displacement demonstrated longer injection duration, shortening the discharge line to 20 in. Further work is planned with an upper helix pump, since preliminary analysis indicates that this pump should regulate timing and reduce the duration of injection to suit engine requirements. Figs. 9 and 10 show the timing and injection duration characteristics of upper and lower plunger helix pumps, without retraction pistons. Injection pressures are in the order of 6000 psi.

Much work has gone into finding the correct atomization, penetration, and distribution of the fuel spray to yield optimum combustion performance in the 519 combustion chamber. A 3-hole tangential nozzle has resulted in the longest nozzle life, while a 7-hole fan appears to give slightly better engine performance. The search continues for a spray pattern which will improve both performance and nozzle life. Fig. 11 shows the spray pattern of the 3-hole tangential nozzle. The present injection system is reliable and reasonably efficient, but there are modifications yet to be made before the system is adequate.

A third major problem in the design of the 519 engine was the development of the starting system. Most commercial starting systems studied were cumbersome, unreliable, and costly. Our small free-piston engine was started by positioning the pistons near the idp, filling the combustion chamber with a fuel-air mixture, and igniting the charge with a spark. This system served its purpose on the

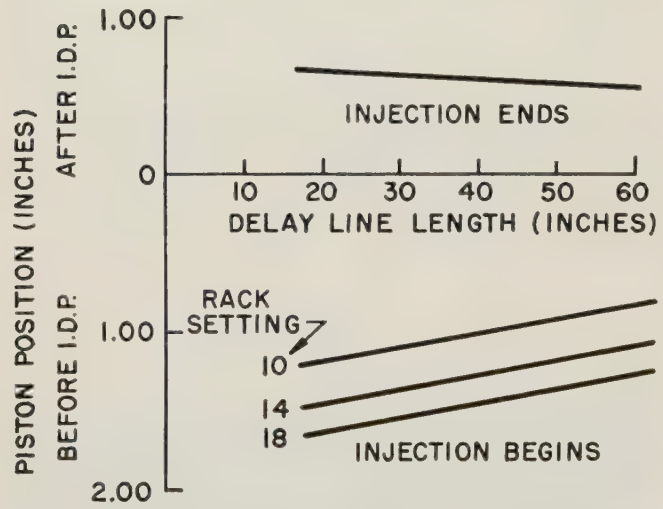

Fig. 9—Upper helix injection characteristics versus delay line length (2000 cpm)

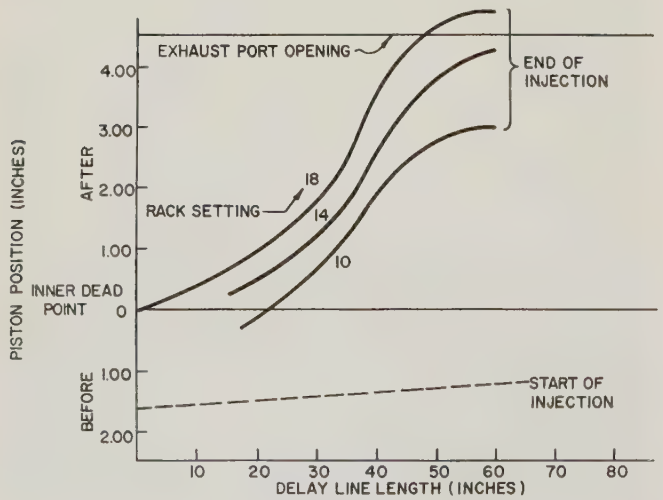

Fig. 10—Lower helix injection characteristics versus delay line length (2000 cpm)

Fig. 11—Spray pattern of 3-hole tangential nozzle

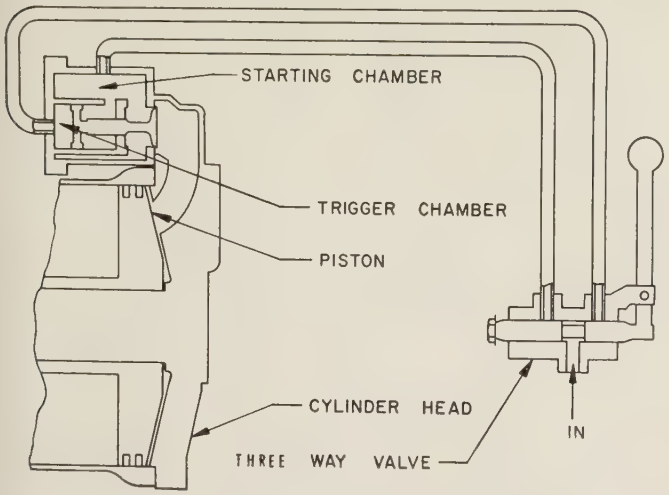

Fig. 12—Diagram of Model 519 starting system

small engine, but was unsuitable for the 519 gasifier for obvious reasons.

Unlike conventional engines, the free-piston engine cannot be motored through a repetitive cranking cycle. It must start on the first stroke of a starting cycle. The pistons must be brought together with sufficient energy to compress the air in the power cylinder to a pressure and temperature which will ignite the fuel as it is injected. Many systems were tried before the present system was evolved, which works as follows:

1. The pistons are retracted to their outermost position by means of a vacuum pump or an air piston.
2. The starting cans are filled to about 300 psig from an air bottle.
3. The starting valves are triggered by admitting bottle pressure into the trigger chambers.
4. The starting valves open, allowing the stored air to expand into the bounce chamber, driving the pistons together.
5. As the pistons travel inwards, the control ports are opened and the excess air in the bounce chamber is allowed to escape.
6. The starting valves close and the engine runs.

The entire starting operation is accomplished in a simple and direct manner. Fig. 12 is a schematic diagram of the starting system showing the 3-way valve and the pressure-operated trigger valves. The starting system may be actuated by a solenoid, or manually as shown. The pressure supply for the starting system may be unregulated if a gage is available for the operator. The starting bottle is automatically recharged by the engine, through a tapping valve in the combustion chamber.

Stub shaft piston supports on the bounce-cylinder head perform two important functions. They provide a means of supplying cooling oil to the underside of the piston crowns. Oil is directed by a nozzle within the piston guide; the return flow is removed from the guide by a scavenge pump driven by the turbine. This oil is used to cool the power pistons and to lubricate the compressor pistons through a controlled leakage path. To lubricate the power pistons oil is applied directly to the ring belt through four small holes, being supplied by a

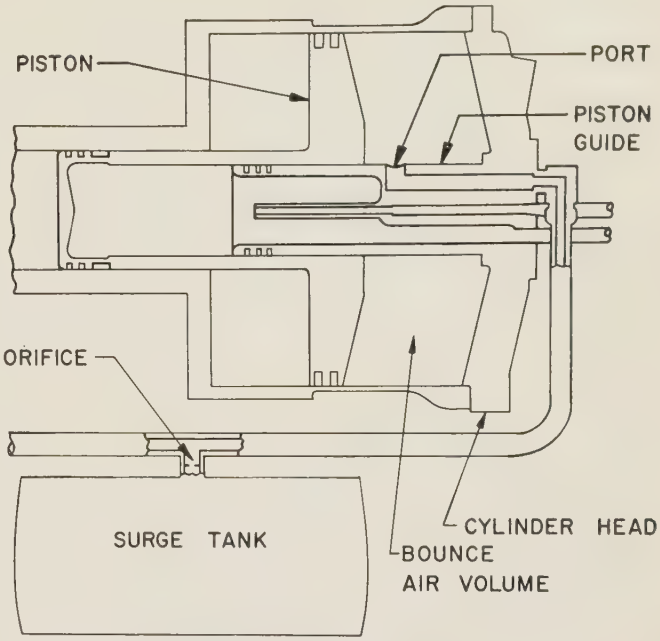

Fig. 13—Diagram of Model 519 stroke control system

metering pump. The total consumption is regulated to 1/200 of full-load fuel flow.

The stub shaft piston guides serve a second important function by providing means for stroke control. Fig. 13 is a schematic diagram of the stroke control system showing the bounce-control ports located in the stub shafts. These ports are opened on the inward stroke of the pistons at about the mid-point of the piston travel, and are connected to the surge tank which is at turbine inlet pressure. At a predetermined point in the bounce-chamber cycle, the bounce pressure is adjusted by the action of the control ports. When the bounce volume has been properly selected in relation to the position of the control ports, automatic stroke control is maintained over the full-load range of the engine. An orifice in the connecting passage allows air to flow between the bounce chamber and the surge tank according to the relationship between turbine pressure and the pressure in the bounce chamber while the ports are open.

As the power level is increased, the bounce pressure and turbine inlet pressure increase. This pressure change effectively changes the mass of trapped air in the bounce volume and provides the control-medium. The control system is self-compensating and has no moving parts. Throttle response is instantaneous and positive.

Load control of the engine is accomplished by a single link to the compressor inlet throttles, which are mechanically connected to the fuel-injection pump racks through an adjustable ratio linkage. This system provides air and fuel metering to the gas generator in predetermined proportions dictated by the gas horsepower required. There is no control connection between the turbine and the gas generator except as provided by the turbine speed governor.

The philosophy behind this control system is based on the independence of the gas generator and turbine. Though the pressure-flow relationship

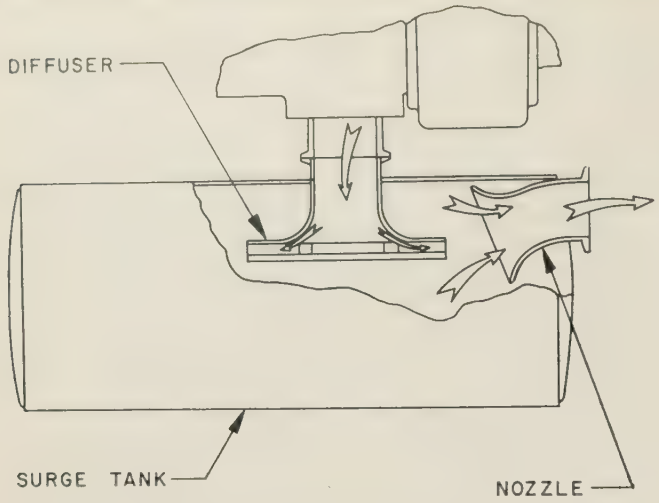

Fig. 14—Cross-section of Model 519 turbine surge tank

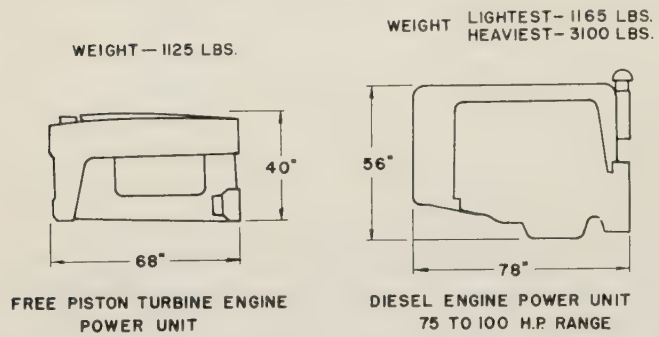

Fig. 15—Comparison of power units of free-piston and diesel engines

changes slightly with turbine speed, this change is negligible. Therefore, aside from governor influence, the gas generator is independent of turbine speed and the gasifier may develop its maximum gas horsepower in conjunction with any speed of the turbine.

When the throttle-rack linkage is properly adjusted, the fuel-air ratio follows a predetermined schedule over the load range of the engine. A primary criterion of proper adjustment is turbine inlet temperature. The better adjustments appear to be those which result in an increase of temperature with load. The turbine inlet temperature range is 600–900 F. Rated turbine speed is 43,000 rpm, and at full load, the turbine inlet pressure is 60 psia.

The present 519 engine has no provision for recirculation. Compressor inlet throttling provides the necessary control and maintains air-box temperatures through thermodynamic processes quite similar to recirculation, but with the added advantages of simplicity and directness.

Basically, compressor inlet throttling increases the pressure ratio of the compressor when the power level of the engine is decreased. This provides high air-box temperatures to insure compression ignition even at low compression pressures. With reduced airflow to the compressor, total flow losses are small. This control system works well in actual practice and provides simple, complete, and positive control of the powerplant.

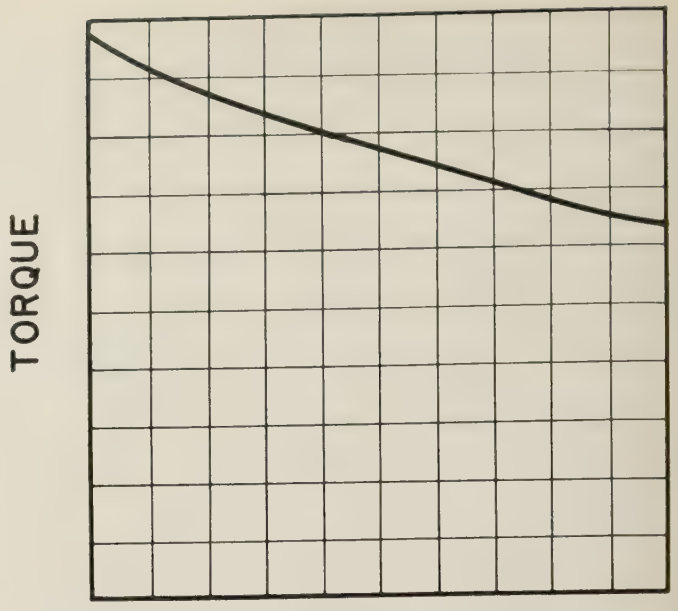

Fig. 16—Turbine engine torque characteristics

During the development of the 519 engine, many difficulties were encountered: Piston-ring life was initially very short, flow losses from the gasifier to the turbine were unusually high and, occasionally, unreasonable temperatures were encountered. Most of these problems have been solved. Piston-ring life has been greatly extended by proper material selection and ring design. A chrome-plated steel ring, which has shown acceptable durability, is used in the power cylinder.

Flow losses from the gasifier to the turbine have been reduced by the use of a flat-plate diffuser in the surge tank inlet and a rounded edge nozzle in the outlet. Fig. 14 is a cross-sectional view of the turbine surge tank. Scavenge ports have been materially improved during the engine development program. The basic problem with scavenge ports is the perpetual fight between low flow losses and high combustion-chamber turbulence. Fortunately, the 519 power cylinder lends itself well to efficient scavenging. This is primarily due to the favorable L/D ratio. The power cylinder has a 3.75 in. bore and is 9.6 in. between the inner edges of the inlet and exhaust ports.

In the present state of development, the 519 engine has reached 80% of its design point power. Fuel consumption has been reduced to 0.45 lb per ghp-hr with expectations for further reduction. The engine is reliable, starts well, and provides a foundation for the development of a commercial free-piston powerplant.

Free-Piston Turbine Power for Farm Use

by R. L. ERWIN

After a study of the characteristics of the free-piston turbine engine during its early development phases, it seemed that it would be an ideal powerplant for the farm tractor. As reported in the previous section of this paper, it has economy equiva-

lent to, or better than, a diesel-piston engine, and the response and flexibility of a gasoline engine. An auxiliary starting engine is not required, such as those necessary with most diesels of equivalent size in mobile use. A wide range of engine sizes can be economically produced from the same manufactured parts. It is adaptable to a wide range of fuels. And last but most important, the torque characteristics are ideal.

The physical size and weight to horsepower ratio of the free-piston engine is favorable for farm tractors or industrial power. The size and weight of the power package used in the Typhoon tractor is compared with a typical diesel power unit of equivalent power rating in Fig. 15. The outlines shown and weights quoted are for an industrial power package with all accessories, less skids.

The free-piston turbine engine fits well into a tractor where a long, low silhouette is desirable. More freedom for configuration and mounting is allowed with the free-piston powerplant. The gasifier, the major determining factor in the size of the power package, is approximately 37 in. long and 16 in. in diameter.

The free-piston power unit with all accessories and auxiliary gear box is 40 lb lighter than the smallest equivalent tractor diesel power unit, and 1975 lb lighter than the heaviest—a 100-hp engine.

There is a growing trend toward the diesel engine for farm tractor powerplants, particularly in the larger sizes. Industrial users have been taking advantage of the diesel engine, with its good economy and lugging characteristics, for many applications. Preliminary tests have shown that the free-piston turbine engine may equal or surpass the diesel in economy. Also, its adaptability to a wide range of hydrocarbon fuels may be an important consideration in the future.

Much design time and engine development work is done on reciprocating engines to get a flat torque curve. The best of these cannot approach the torque curve of the turbine engine in its application to farm tractor work (Fig. 16). Due to the varying load encountered in fieldwork with the farm tractor, this is a very important characteristic and one that gives the free-piston turbine engine a big advantage over conventional farm tractor engines.

To achieve best economy with a farm tractor it must be worked near its peak drawbar pull. Only the part of the engine power reaching the implement through the drawbar is converted to useful work. The two largest losses are the rolling resistance of the tractor and the slip of the drive wheels. The rolling resistance of the tractor is practically the same, regardless of the drawbar pull. The losses due to slip can be excessive if the drawbar pull is too great. On the other hand, if the drawbar pull is too low, the loss due to rolling resistance is a large percentage of the total power output. The proper balance between the two is necessary to achieve maximum efficiency, and tests have shown that with heavily weighted wheels the maximum tractive efficiency is obtained when the tractor is worked at 75–80% of the maximum drawbar pull (Fig. 17).

An 80% drawbar pull would be easily maintained if the soil and the implement loads were constant. However, this is not likely in most farming conditions. If traction conditions are good and the tractor is being worked at its most efficient loads, an increase in drawbar pull will slow down the engine. When the speed reduction is enough to pull the engine speed down on the descending part of the curve, either the engine will stall or a gear ratio change must be made. Usually the reduction in ground travel does not reduce the load enough to compensate for the reduction in torque delivered to the rear wheels.

For purposes of comparison, engine torque has been converted to drawbar pull delivered as torque at the drive wheels for the turbine engine and a conventional tractor engine (Fig. 18). Thus, it can be seen that the turbine engine will deliver in-

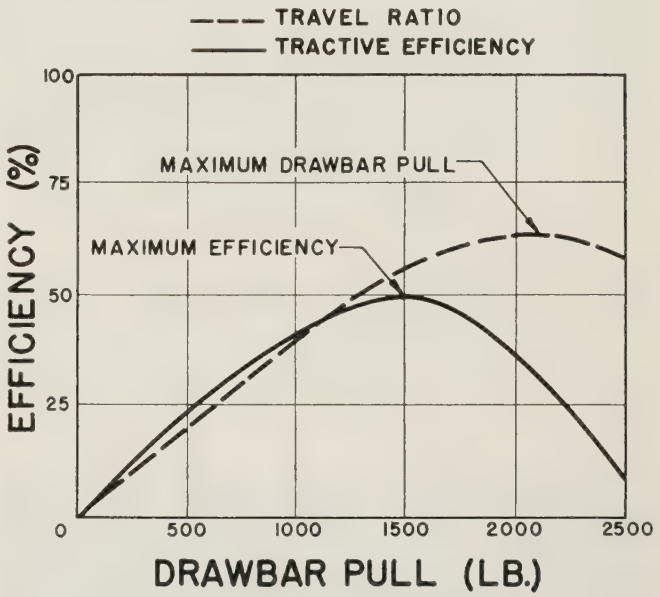

Fig. 17—Comparison of efficiency and drawbar pull of tractor (tractive surface of tilled soil, 12 ply rubber tires, 340 lb weight per wheel)

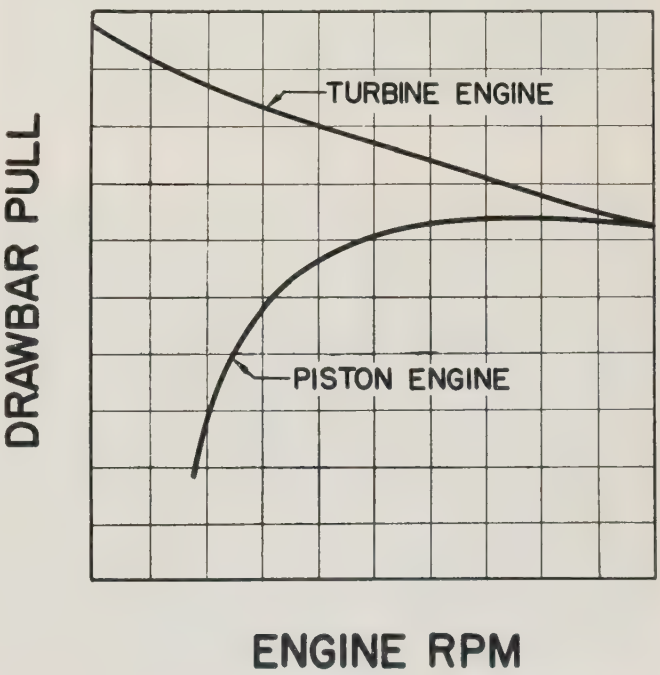

Fig. 18—Comparison of engine torque of turbine and piston engines

creasing drawbar pull up to stall speed. However, for most practical applications the increased drawbar pull would allow the tractor to move through the conditions in the field causing the increased load, without a change in gear ratio or without stalling the engine.

The cost of the free-piston turbine engine has not been fully determined. However, it lends itself well to farm tractor production where it is necessary to produce a variety of sizes with a small tooling investment. As previously mentioned, the gasifier unit shown can be used to produce from 50 to 150 hp. With a minimum number of changes, several different size engines can be assembled from the same manufactured parts or from parts made on the same tooling. This would allow economical manufacture of several sizes of tractors.

When it was decided to install a free-piston turbine engine in a tractor, a conventional tricycle configuration (Fig. 19) was selected because it is typical and easily adaptable to the free-piston engine powerplant. Also, the tricycle tractor could be used with a large variety of production farm implements, desirable because the engine is to be tested in as many different farm operations and conditions as possible.

Many standard tractor parts were used in building the Typhoon tractor. Due to the size and horsepower potential of the engine, the tractor was made larger than our other tractors. Larger rear tires were used. A power shift feature was provided in the transmission to keep the turbine connected to the load at all times.

Fig. 20 shows the arrangement of the gasifier, turbine, gearbox, and accessories in the tractor. The tractor specifications are shown in Table 1.

The turbine power unit used in the Typhoon tractor is a package consisting of a 5½-in. turbine wheel and a 7.17 reduction gear. An overspeed cutoff, a governor, and turbine gearbox oil pump are incorporated into this unit. The oil cooler that was furnished with the power turbine was removed and attached to the tractor radiator; a second oil cooler is provided in the radiator to cool the gasifier oil.

Fig. 21 shows the power turbine attached to the tractor accessory drive gearbox. This gearbox has a 3/1 reduction gear, making an overall reduction of 21.5 between the turbine and transmission input. The standard turbine speed of 43,000 rpm is reduced to 2,000 rpm transmission input.

From this gearbox are also driven the gasifier scavenge and oil pressure pump, the tractor hydraulic system pump, and the generator and power steering pump (not shown in Fig. 21). These are gear-driven from the transmission input gear. A belt drive from the upper shaft in the accessory gearbox drives the fan, water pump, fuel pump, and tachometer. Fig. 22 shows the gearbox with the tractor hydraulic system pump and the generator in place. Fig. 23 shows the belt-driven units mounted on top of the gearbox.

The air consumption of the free-piston turbine

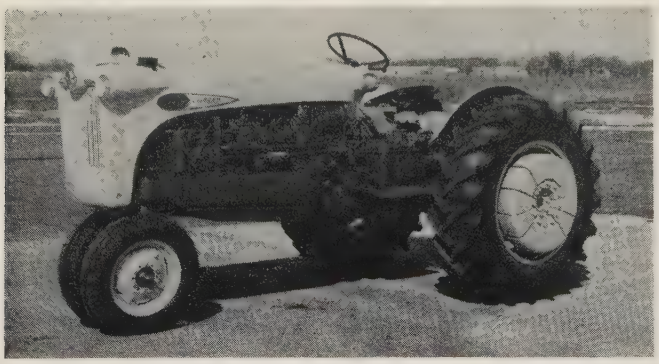

Fig. 19—Tractor with conventional tricycle configuration

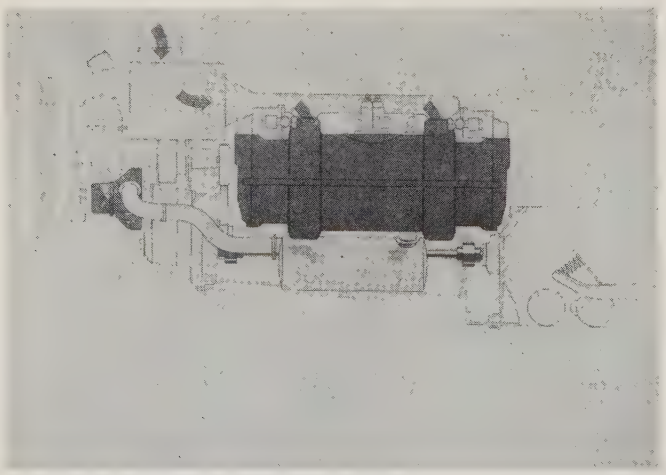

Fig. 20—Arrangement of gasifier, turbine, gearbox, and accessories in tractor

Table 1—Specifications of Typhoon Tractor

Wheelbase	99 in.
Rear Tread, Adjustable	60–84 in.
Weight, Dry	4,200 lb
Tire Size, Rear	13 × 30
Front	6:00 × 16
Front Axle	Tricycle
Steering	Power steering
Engine, Type	Free-piston turbine engine
Rated Speed	43,000 rpm
Fuel	Diesel
Transmission, Type	Full power shift
Speeds	10 forward, 2 reverse
Overall Height	70 in.
Overall Length	144 in.

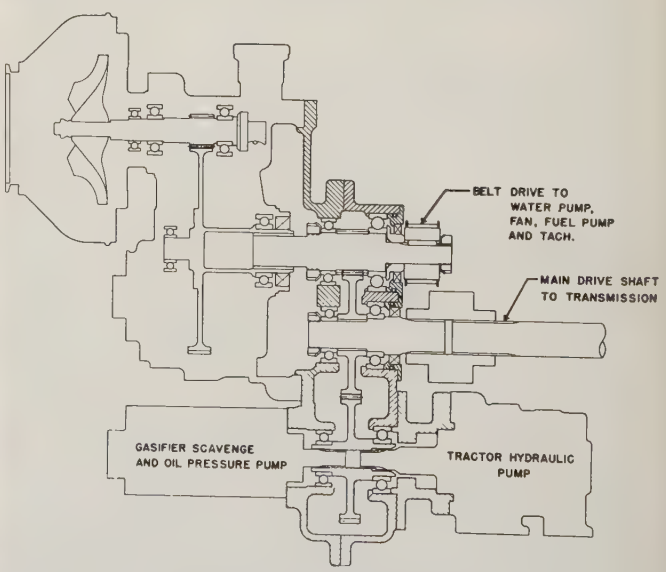

Fig. 21—Power turbine and accessory gearbox

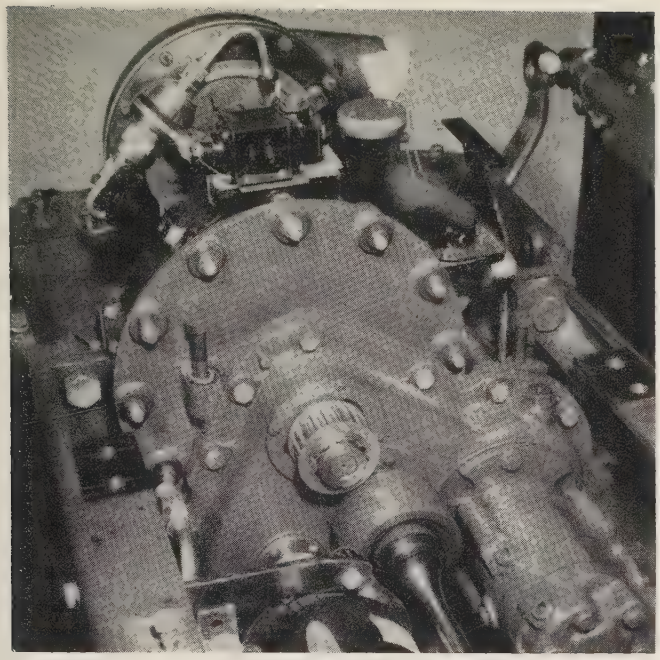

Fig. 22—Tractor accessory drive gearbox with turbine unit, generator, and tractor hydraulic system pump

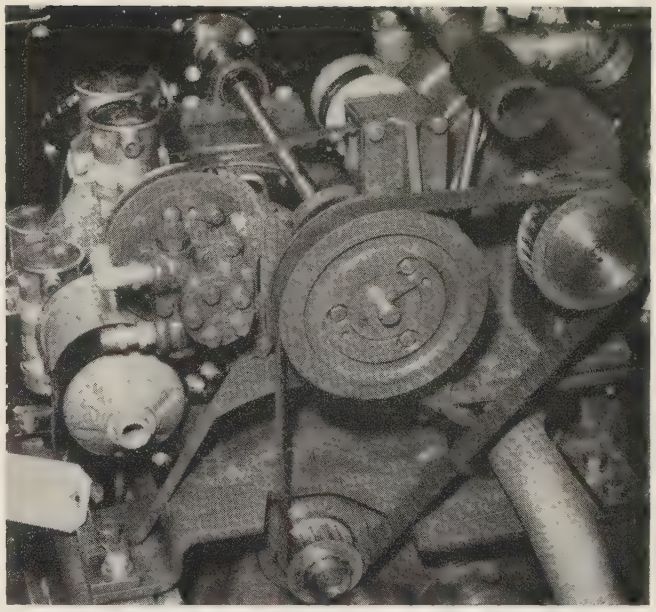

Fig. 23—Accessory gearbox with belt-driven water pump, fuel pump, and tachometer generator (electric fuel pumps used for starting have been reduced to one unit)

engine is two to three times that of an equivalent diesel. The air cleaner provided for this tractor used six paper air filters, 8-in. OD by 2-in. thick; and air was drawn through a scoop on top of the sheet metal near the forward end of the tractor.

Another accessory unique to the free-piston engine is a high-pressure air bottle used to provide starting air for the gasifier. This was located alongside the fuel tank under the sheet metal.

The performance of the tractor power unit has been satisfactory in tests to date. The engine operates very smoothly and is practically vibration free. Mufflers are not necessary, as the noise level is low. A turbine whine is perceptible at idle speeds but is not audible at working speeds.

The Typhoon tractor with the free-piston turbine engine opens many new possibilities for better application of power to farm operations. There is still much work to be done, and we have not made even a beginning on the possibilities of future designs based on the free-piston turbine powerplant. Like any other new development, the greatest advantages of this powerplant may not be realized if it is used as a substitute for a gasoline or diesel engine, but will be realized only when tractors are designed to take advantage of all of its possibilities.

DISCUSSION

Free-Piston Turbine Power Dispels Smog, Vibration, Engine Knock, Backfire

—J. G. Coutant
Phoenix Iron & Steel Co.

THE long accepted evils inherent in automotive power will pass into oblivion with free-piston turbine power, currently being studied by the leading automobile manufacturers.

The Free-Piston Engine Program at the Ford Motor Co. has already achieved enough trial information to be a guide to future automotive power. The program has realized several objectives and emphasizes the almost complete insensitivity of free-piston engine to fuel-ignition quality and temperatures without the aid of an electric spark.

Fig. A includes a curve of piston motion as a function of time, showing the freedom of pistons to gain initial speed. This permits the burning of 70% of the fuel in a fixed volume or say 12% of the effective engine cylinder volume. This feature allows for greater expansion of working gases and more time for the recombination of most of the dissociated gaseous products; and avoids the inherent evils of the crank-engine.

At the bottom of Fig. A is a cross-sectional view of the 519 free-piston engine, the figure includes an analysis for the thermodynamic relationships and develops several values for the engine.

Fuel-Air Ratio—The theoretical quantity of free air to burn fuel is 1 cu ft for each 100 Btu of fuel. The maximum fuel burned in a free-piston limited by the practical engine cylinder pressures and temperatures is 50 Btu of fuel per cu ft of free air.

The 3.6 atmosphere supercharged air intake per power

Table A—Dimensions of Model 519 Engine

Length, in.	37
Height, in.	16
Power cylinder bore, in.	3.75
Compressor cylinder bore, in.	11
Maximum stroke, in.	6.8
Minimum stroke, in.	4.2
Power cylinder effective volume, cu ft	0.095875

stroke is equivalent to 0.208 cu ft of free air, sufficient to burn 10.4 Btu. Assuming 27% engine efficiency and 2400 power strokes per min the engine would develop 159 hp.

From general dimensions shown in Table A, it has been possible to conclude the following values:

Scavenging air pressure, lb per sq. in. abs	58.8
Supercharge air pressure, lb per sq in. abs	52.5
Turbine gas pressure, lb per sq in. abs	52.5
Compression ignition pressure, lb per sq in. abs	700.0
Maximum thermo-compression pressure, lb per sq in. abs	1706.0
Maximum engine discharge pressure, lb per sq in. abs	157.7
Supercharge air, F	320
Supercharge air engine heat recovery, F	100
Compression ignition temperature, F	1263
Thermo-compression temperature, F	3496
Maximum cylinder gas temperature, F	4121
Engine discharge gas temperature, F	2052
Scavenging air temperature, F	420
Surge tank gas temperature, F	1201
Weight of cylinder air per power stroke, lb	0.0156
Weight of turbine gas per power stroke, lb	0.0312
Maximum fuel injected per power stroke, Btu	10.4
Combustion chamber volume, maximum, cu ft	0.0139

For the large capacity power output units operating under every climatic condition (desert, tropical, marine, frigid) this type of power has established the longest continuous operation and maximum fuel economy while supervised by unskilled men of many tongues.

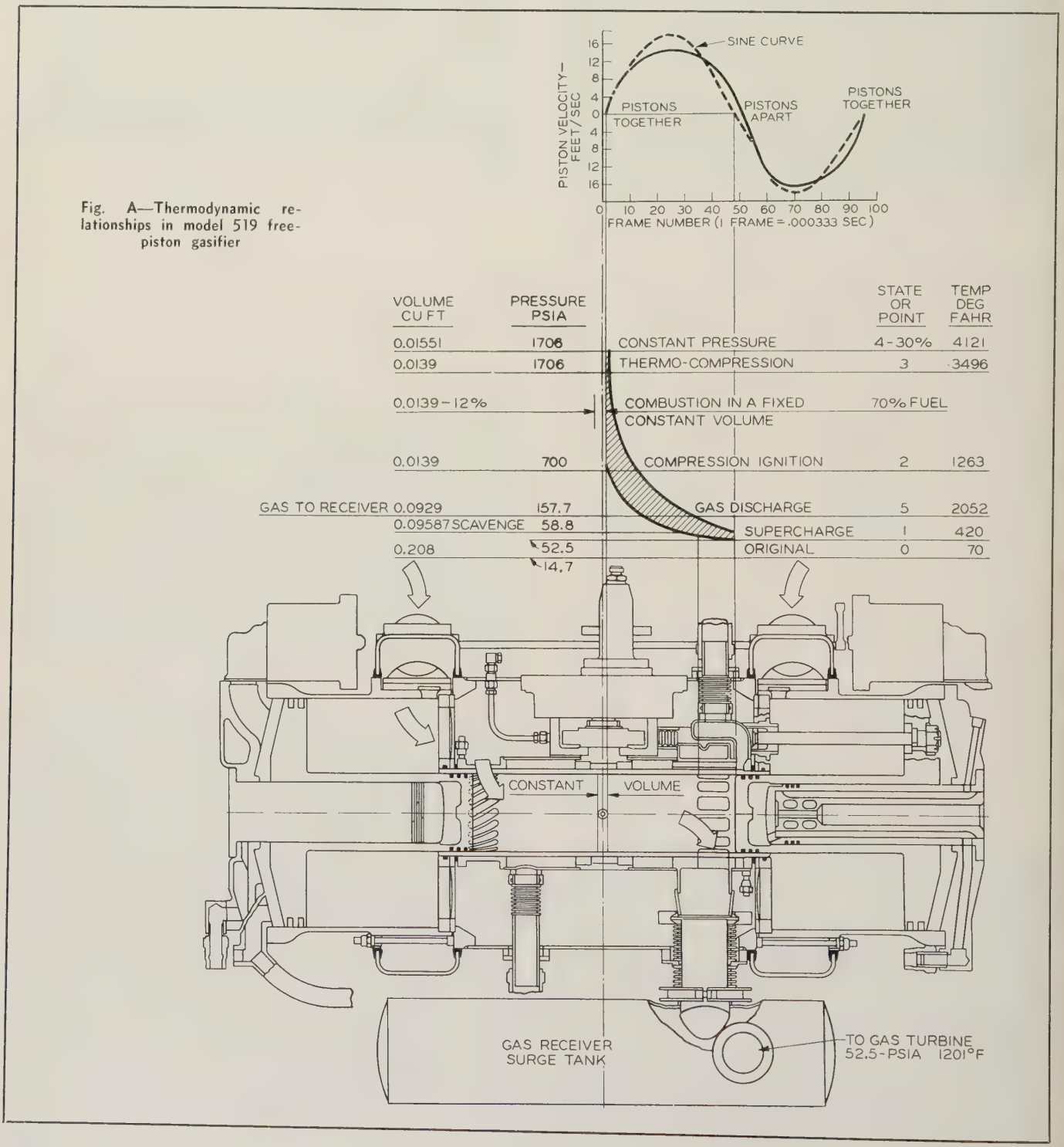

Fig. A—Thermodynamic relationships in model 519 free-piston gasifier

Large Lightweight Turbojet Engines

C. A. Grinyer, Orenda Engines, Ltd., Canada

This paper was presented at the SAE National Aeronautic Meeting, New York, April 3, 1957.

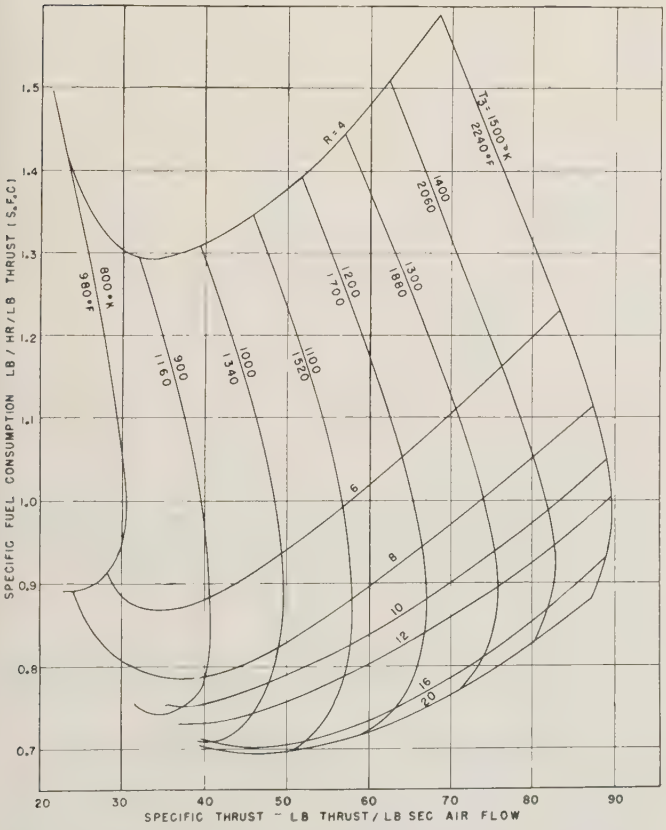

Fig. 1—Jet engine performance, specific fuel consumption versus specific thrust: Sea-level static, $T_i = 288$ K (59 F), no afterburning, no intake loss, full expansion, fuel JP4

THE importance of low engine weight in its effect on the range of a given aircraft or on the weight of an aircraft to accomplish a certain mission has been adequately emphasized by previous writers. It is particularly important in short-range aircraft.

In this paper we will first review the performance characteristics and requirements of turbojets, with particular regard to operation at high Mach numbers. The problems associated with the design of turbojets required to operate over a wide speed range and possible implications with respect to aircraft range are discussed. Brief commentary is made on the current controversial topics, "bypass versus turbojets" and "large versus small engines." We will also examine the effect of titanium on the mechanical design of large engines and the work directed towards engine operation at higher turbine temperatures.

General Performance Characteristics of Turbojets

While the general performance characteristics of turbojets have been previously discussed several times and are fairly well-known, a review is not considered to be out of place at this time in the light of interest in higher speeds.

Figs. 1–6 show the effect of compression ratio and turbine inlet temperature of specific thrust and specific fuel consumption at sea-level static and Mach number 0.9 and 2.5 in the stratosphere. Additional effect of afterburning is shown at Mach 2.5.

Briefly, at sea-level static and Mach 0.9, to attain high specific thrust, we require high turbine inlet temperatures irrespective of compression ratio, while to attain low specific fuel consumption requires high compression ratio and moderate turbine inlet temperatures of about 1000 K (1340 F). We will see that the performance requirements of the aircraft considered are such that only moderate specific thrusts are required at these flight conditions, which is compatible with low specific consumption.

At Mach 2.5 without afterburning, high turbine inlet temperatures are, of course, still required to attain high specific thrusts; however, much lower compression ratios are required to attain minimum specific fuel consumption. While the minimum specific fuel consumption which can be attained is of the order of 1.35, the maximum specific thrust, even at the turbine inlet temperature of 1300 K (1880 F), is only about 35 lb per lb per sec.

At Mach 2.5 with afterburning, both maximum specific thrust and minimum specific fuel consumption are attained by the use of high turbine inlet temperatures and low compression ratios of the order of six. Most noticeable, of course, is the tremendous increase in specific thrust possible when using afterburning at this speed. While specific thrusts of the order of 110 lb per lb per sec should be attainable with stoichiometric afterburning and theoretical full expansion—since they would require final nozzle throat and exit diameters considerably greater than those of the main engine—it is probable that in practice, specific thrust at this speed will be limited to about 70 lb per lb per sec with consequent increase in specific fuel consumption.[1] Nevertheless, the specific thrust attainable with afterburning at this speed is about twice that available without afterburning, so that afterburning en-

[1] *Canadian Aeronautical Journal*, Vol. 2, November, 1956, pp. 322-328: "Choice of Design for an Advanced Turbojet," by F. H. Keast.

THIS paper deals with the general performance of turbojet engines in both subsonic and supersonic flight in relation to aircraft requirements.

The advantages and disadvantages of the bypass engine and small turbojet in relation to the large straight jet engine of 18,000-lb thrust are examined. Also discussed is the improvement in the thrust-weight ratio of large engines made possible by the use of titanium, and the potentialities of ejector nozzles and turbine-blade cooling.

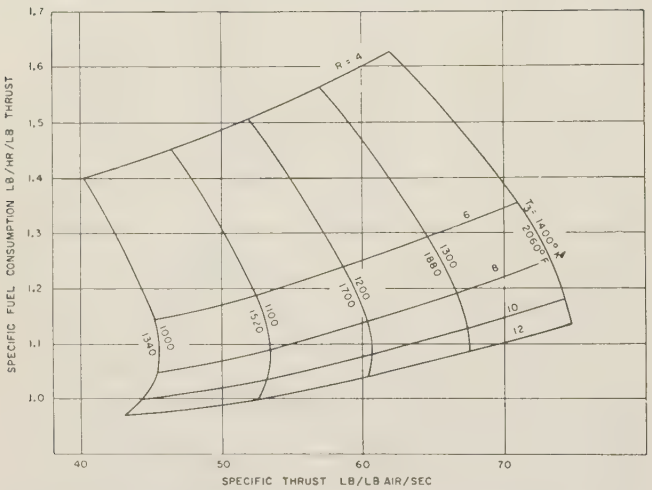

Fig. 2—Jet engine performance, specific fuel consumption versus specific thrust: Mach 0.9 stratosphere, no afterburning, no intake loss, full expansion

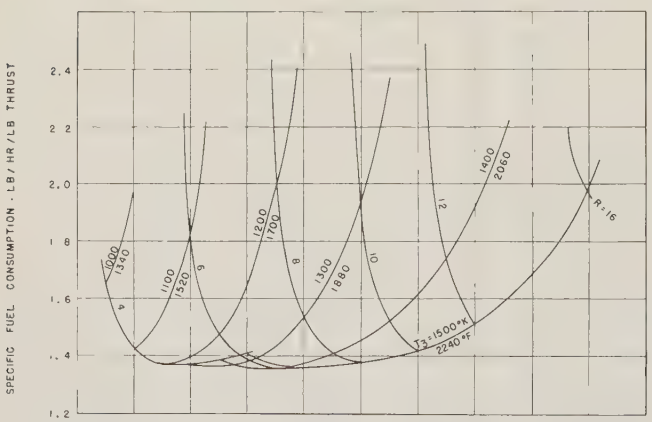

Fig. 3—Jet engine performance, specific fuel consumption: Mach 2.5 stratosphere, no afterburning, intake efficiency, 0.81, full expansion

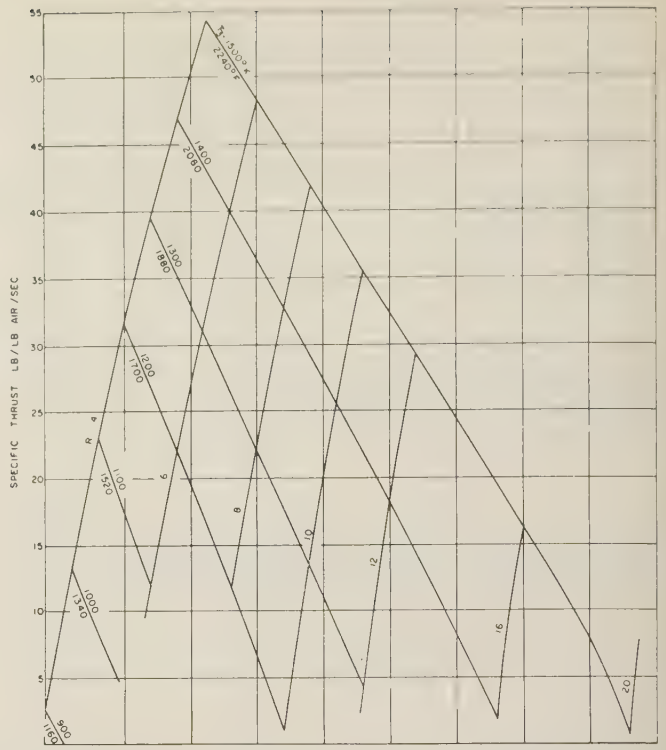

Fig. 4—Jet engine performance, specific thrust: Same conditions as Fig. 3

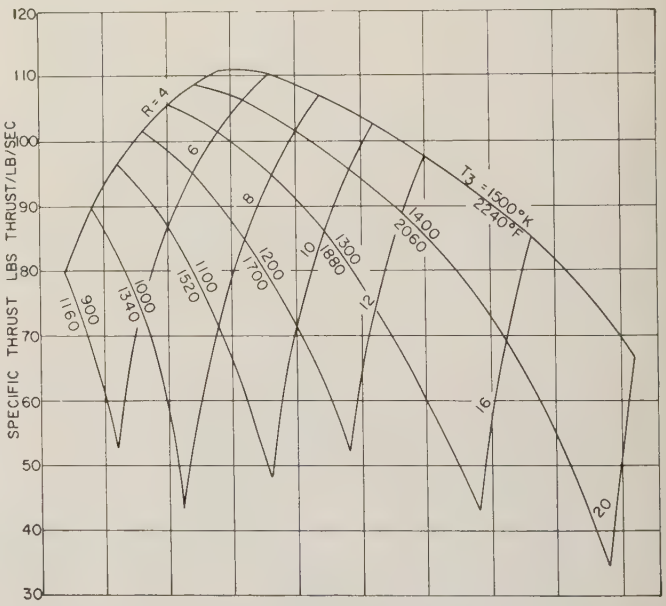

Fig. 5—Jet engine performance, specific thrust: Mach 2.5 stratosphere, afterburning to stoichiometric limit (total $f/a = 0.06105$), full expansion, intake efficiency 0.81, afterburner combustion efficiency 0.85, A/B outlet temperature 2265-2090 K (3617-3302 F)

gines would need have only half the airflow of non-afterburning engines and should be considerably lighter. This is only achieved at the expense of a 50% increase in fuel consumption for a given thrust.

The relationship between engine weight and aircraft weight will be considered later.

Effect of Forward Speed on Engine Operation

Using the simple assumptions given in Appendix I, we can predict approximately the effect of forward speed at constant mechanical rpm on compression ratio and nondimensional flow. The results are plotted in Fig. 7 for an engine of 12/1 pressure ratio under standard NACA atmosphere conditions.

Two curves are shown, one assuming constant turbine throat area and turbine inlet temperature and the other assuming constant compressor temperature rise.

The assumption of constant compressor tempera-

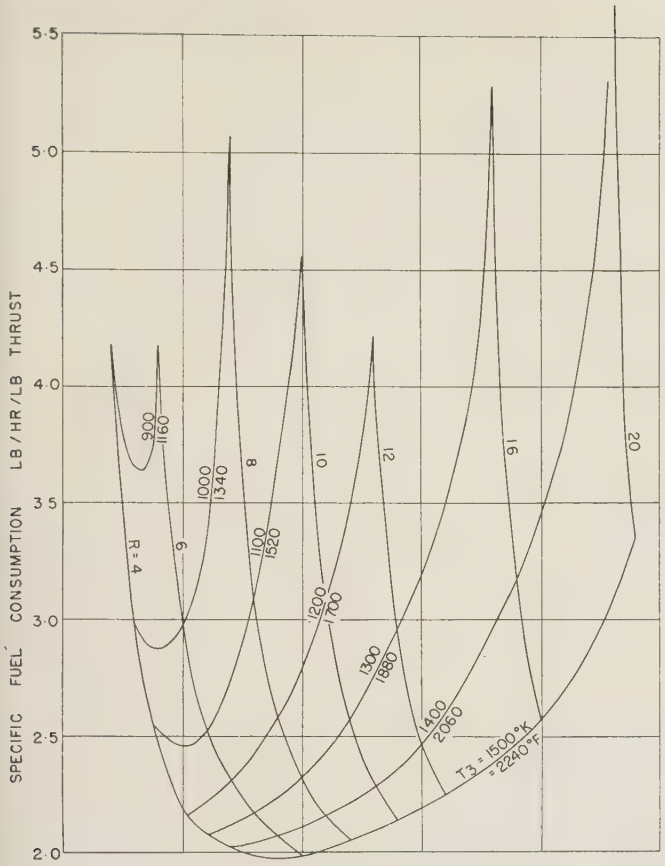

Fig. 6—Jet engine performance, specific fuel consumption: Same conditions as Fig. 5

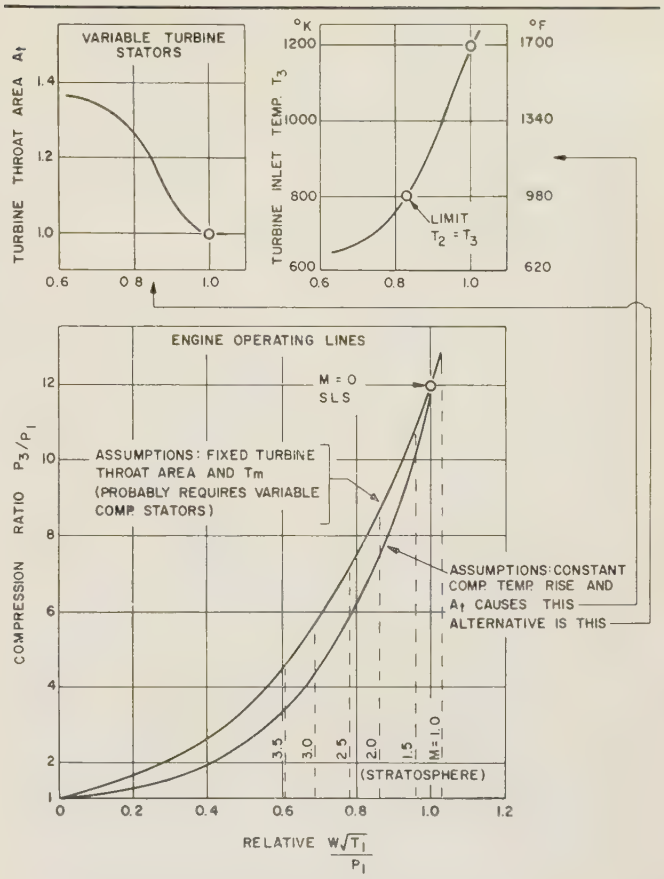

Fig. 7—Effect of forward speed on turbojet operation at maximum rpm

ture rise at constant rpm necessitates a fall-off in turbine inlet temperature with constant throat area or an increase in turbine throat area with constant turbine temperature at temperatures greater than 15 C. Therefore, we use the first assumption of constant turbine throat area and turbine inlet temperature as the basis of approximate prediction of the change in pressure ratio and flow of a turbojet. Using general performance curves such as Figs. 1–6, we can obtain the variation in thrust and specific fuel consumption with forward speed (Fig. 8).

It is emphasized that the above method gives only the approximate performance of an engine. Accurate performance prediction can be obtained only by the use of appropriate compressor and turbine characteristics.

As to the problem of surging at high forward speeds, no conclusions can be drawn from Fig. 7.

In general, the operating line at constant rpm and turbine inlet temperature will lie slightly below that associated with part-rpm operation at constant inlet temperature.

In any high compression ratio engine with fixed turbine geometry, some variable geometry, such as variable angle stators or two spooling, will be required in the compressor for normal test-bed accelerations.

Effect of Forward Speed on Turbojet Performance

Fig. 8 shows the effect of forward speed on turbojet performance. Here we have considered an engine of compression ratio of 12 at sea-level static and assumed constant turbine inlet temperature of 1200 K (1700 F) operation. It will be seen that the

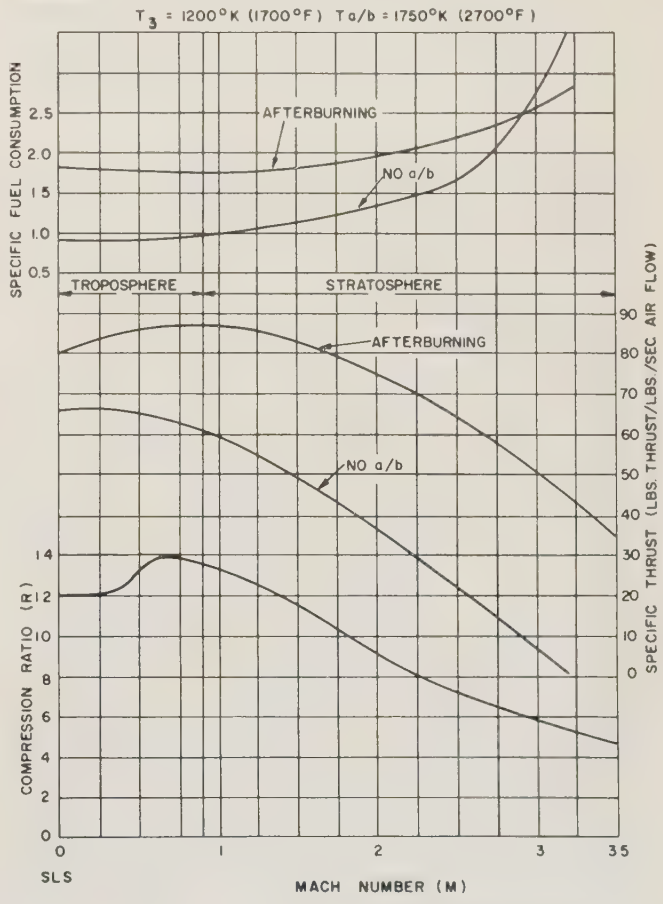

Fig. 8—Effect of forward speed on turbojet performance

compression ratio decreases with forward speed, in a manner compatible with the requirements of maximum specific thrust. With no afterburning, the specific thrust becomes zero at about Mach 3. With afterburning 1750 K (2700 F), the afterburner contributes a large proportion of the thrust with increasing speed. At Mach 2.5 a specific thrust of about 65 is available with full expansion and in subsonic flight the engine is capable of the same specific thrust of 65 without afterburning.

Performance Requirements of Turbojet Engines

It is, unfortunately for the engine designer, impossible to talk about the performance requirements of turbojet engines without some reference to aircraft characteristics. Fig. 9 shows typical maximum lift-drag ratios likely to be attained.[2] For the purpose of the following discussion it has also been assumed that the maximum lift-drag ratio of a particular aircraft over its speed range follows this curve. It is known that in practice this is not quite the case, particularly with aircraft designed for very high supersonic speed, because a compromise is necessary in high-speed performance if reasonable low-speed performance is required, and vice-versa. The extent of this compromise obviously depends on the mission, and values must be substituted for any particular case. Also shown are the assumed values of lift coefficient occurring at these values of lift-drag.

Now the altitude corresponding to these values of maximum lift-drag is a function of wing loading, lift coefficient, and Mach number (Appendix III). In Fig. 10 the altitude corresponding to maximum lift-drag is shown for wing loading of 50 psf. A value of 50 psf seems to be reasonable, at least for some current aircraft,[3] and gives values of cruise altitude which appear to be of the right order. Using the values of engine intake efficiency shown in Fig. 10 it is, therefore, possible to determine the variation of engine intake pressure with Mach number at the best cruise altitude (Appendix III). This, together with the variation of intake temperature, is also shown in Fig. 10. Since a supersonic fighter will sometimes have to operate at altitudes lower than these best altitudes, the intake pressures may be considered as minimum values.

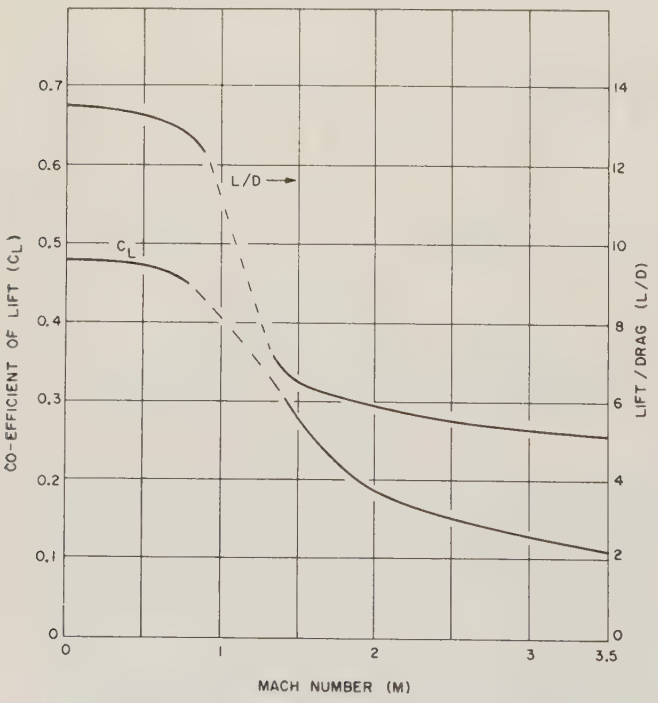

Fig. 9—Coefficient of lift and lift-drag at maximum lift-drag ratio

If we assume that the ratio of sea-level static airflow to engine weight is about 0.060 lb per sec per lb weight for an afterburning engine, it is possible to determine (Appendix III) the ratio of engine weight to aircraft weight required for any flight speed using the aircraft characteristics of Fig. 9. We find, in general, that with nonafterburning engines the weight of engine to aircraft weight reaches a very high value of about 0.5 for level supersonic flight and, therefore, it appears that afterburning engines are necessary for high supersonic speeds, notwithstanding the higher fuel consumption. Employing afterburning engines, the engine weight required is almost constant at about 16% of aircraft weight for all speeds. With respect to the specific thrust required for the subsonic cruise of a supersonic aircraft, we find that quite a low value of the order of only 40–50 is required, which would require a high-temperature engine to be throttled back even without afterburning.

It is apparent from the foregoing that the design of an engine optimized for both subsonic and supersonic operation poses quite a problem. At high speeds we require afterburning and high turbine inlet temperatures, while at subsonic speeds we require high compression ratio and moderate turbine inlet temperatures. Apart from the previously mentioned difficulty of designing aircraft to fly efficiently over a wide speed range, it is apparent that there is some difficulty in designing engines to do likewise.

In this respect, we might consider the question of range. For a fixed ratio of fuel load to aircraft weight, the range of an aircraft is directly proportional to the lift-drag ratio and Mach number and inversely proportional to the specific fuel consumption (Appendix III). Comparing values at Mach 0.9 and 2.5, taking data from Fig. 9, we find that the range factor at Mach 0.9 is 10.8 and that at Mach 2.5 it is 6.25. While this indicates that maximum range will be obtained by keeping some portion of the mission subsonic, a study of particular aircraft and engines may indicate that continuous supersonic flight will give maximum range. This would happen if, in optimizing for supersonic flight, the aircraft lift-drag and engine specific fuel consumption were both 30% worse at Mach 0.9 than the best possible at this speed.

Ejector Nozzles

We have already seen the growing importance of the final nozzle of the engine, both on its performance at high speeds and also on the weight of the engine. To be capable of satisfactory performance both at subsonic and supersonic speed and of using afterburning when desirable, an engine would ideally require a Laval-type nozzle with a fully variable throat in order to accommodate afterburning and a fully variable exit diameter to give correct expansion at every engine rpm and forward speed. Such

[2] "High-Speed Aerodynamics," by W. F. Hilton, pp. 95 and 214 et seq. Pub. by Longmans, Green and Co., New York, 1951.

[3] *Canadian Aeronautical Journal*, Vol. 2, December, 1956, pp 358–363: "Some Performance Problems Associated with the Mach 2 Fighter," by J. Morris.

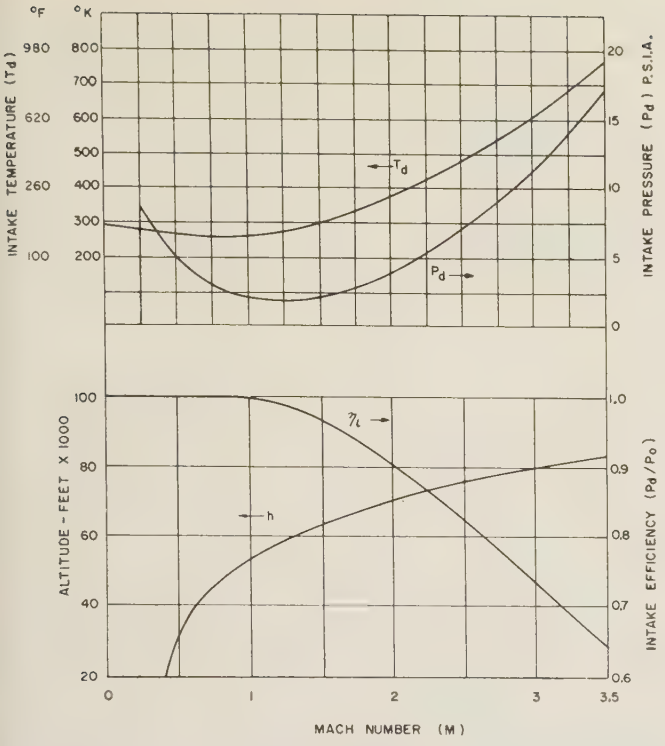

Fig. 10—Engine intake conditions at maximum lift-drag for wing loadings of 50 psf

a nozzle is an extremely heavy and mechanically complex device. Moreover, in actual aircraft practice we have to deal not only with the main engine flow but also the cooling airflow which passes around the engine, plus whatever bypass flow is necessary for intake matching. It is, therefore, apparent that the final nozzle of an engine must have ejector characteristics in order to scavenge adequately the engine compartment and cool the afterburner during take-off when the ram pressure ratio is low.

Fortunately, the flow phenomenon in the simple ejector-type nozzle used on subsonic aircraft is such as to allow a certain amount of divergent expansion of the main jet. This idea can be developed in order to obtain divergent expansion at high speeds with considerable weight saving.

Figs. 11 A and B show ejector-type nozzles for use at Mach numbers up to about 1.5. In A without afterburner, it will be seen that as the secondary flow is accelerated through the final nozzle, the annulus which it occupies diminishes in area thus allowing the main jet to expand. In B with the afterburner in operation, since the throat area of the main jet (D_p) is now greater, a correspondingly greater diameter (D_j) must be allowed for its expansion. This is achieved by throttling the secondary flow.

This basic principle can be extended to engines required to fly up to Mach numbers of 2.5 as shown in Figs. 11 C and D. At low speeds, it may be necessary to bring in some of the secondary flow from outside of the aircraft in order to fill the final nozzle when the main-jet pressure ratios are low and divergent expansion is not desirable. This would be done by means of bleed doors. At high speeds the bleed doors are automatically closed, allowing the main jet to expand to the full diameter of the exit nozzle. An alternative method of obtaining the

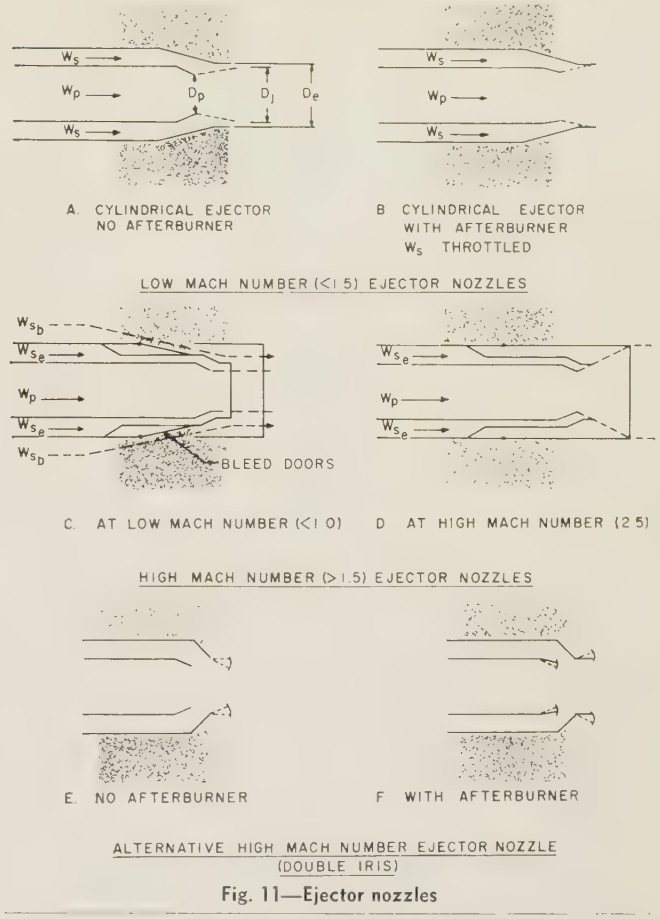

Fig. 11—Ejector nozzles

necessary amount of divergent expansion at high speeds would be to equip the shroud as well as the primary-jet nozzle with an iris-type nozzle, as shown in Figs. 11 E and F.

Bypass Engine

No paper dealing with large lightweight turbojet engines would be complete at this time without some comments on the advantages and disadvantages of the bypass engine. In the bypass engine, the diameters of the first stages of the compressor are greater than that of the latter stages. Some of the compressor airflow is bled off, bypassing the combustion chamber and turbines, and can either be exhausted separately or remixed with the turbine exhaust stream, the whole exhaust flow then being ejected through a single final nozzle.

In Fig. 12 a comparison has been made between the design point performance of straight-jet and bypass engines of the same overall compression ratio. The flight conditions assumed were Mach 0.85 in the stratosphere. The overall compression ratio of 12 relates to this flight condition. To permit mixing of the bypass air and turbine exhaust gas with minimum pressure loss, it was arranged for the bypass delivery pressure and turbine exhaust pressure to be equal. For all turbine inlet temperatures investigated, the bypass flow was assumed to be 33% of the total flow. Thus, we are considering a different bypass engine at each turbine inlet temperature, in that the compression ratio of the bypass air increases with turbine inlet temperature. A bypass airflow of 33% of the total airflow was assumed since this value seems likely to permit satisfactory

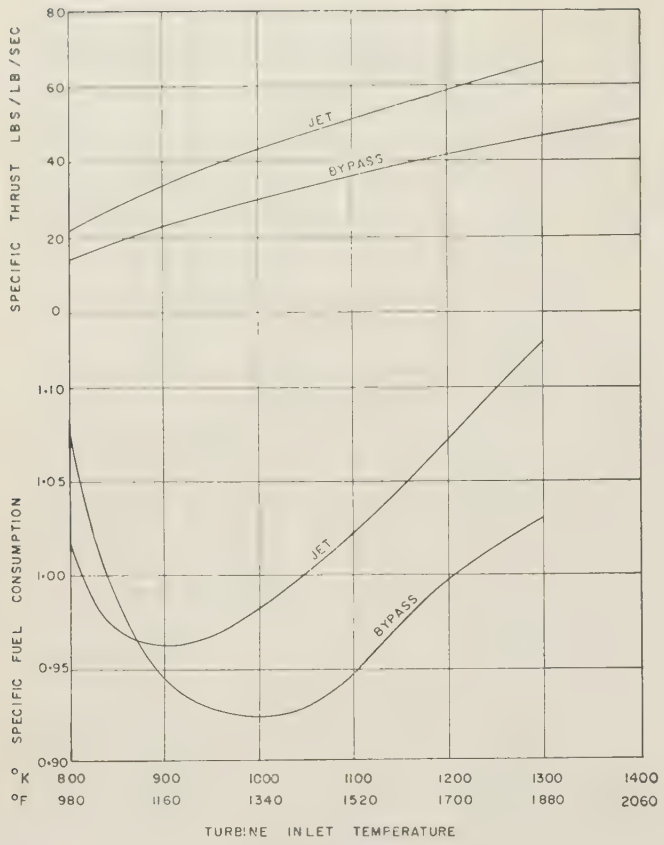

Fig. 12—Comparison of design point performance, straight-jet versus bypass engines. Conditions: $R = 12$ at Mach 0.85 stratosphere, 33% of total flow bypassed and bypass pressure equals main flow exhaust pressure

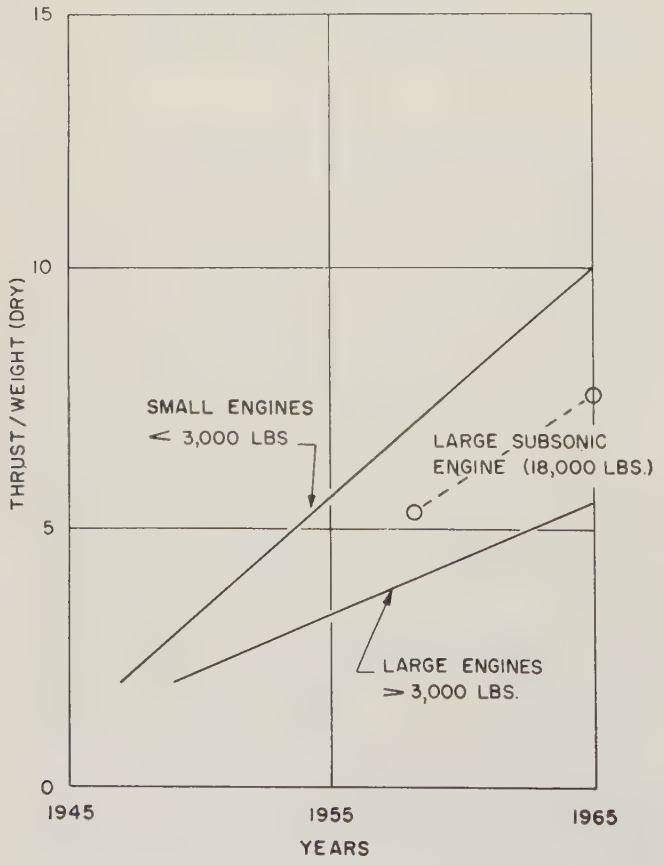

Fig. 13—Thrust-weight ratio (dry)

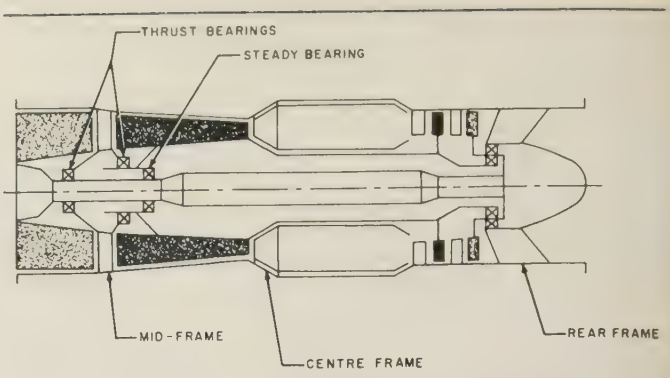

Fig. 14—Four main bearing arrangement of 2-spool jet engine

engine operation at reduced rpm by using a 2-spool arrangement and without the additional complication of variable compressor stators which may be necessary, by analogy with a turboprop, at higher bypass flows.

On the basis of these detailed assumptions, the following conclusions can be drawn from the results shown in Fig. 12. At a given specific thrust, the bypass engine requires a higher turbine inlet temperature than the straight-jet engine. As the bypass flow is increased, the bypass engine has to operate at higher and higher turbine inlet temperatures in order to achieve a reasonable specific thrust. The bypass engine, for the example shown, has a minimum specific fuel consumption at a turbine inlet temperature of about 1000 K (1340 F). It gives a specific thrust of about 30 lb thrust per lb of airflow per sec. At this same specific thrust, the straight-jet engine has a specific fuel consumption about 4% higher, but operates with a turbine inlet temperature of only 900 K (1160 F). At a specific thrust of 47 lb per lb per sec the situation is reversed, the straight-jet engine having a specific fuel consumption about 3% better which does not allow for the blade cooling losses which would be required at the turbine inlet temperature of 1400 K (2060 F) for the bypass engine at this specific thrust. Thus, for a given specific thrust there is probably very little to choose between the straight-jet and bypass engine, as far as fuel consumption is concerned. Consideration of the reduced rpm performance of a given engine may modify this conclusion somewhat, but probably not to any great extent, provided the bypass engine uses separate exhausts.

If we consider a straight-jet engine and bypass engine of the same specific thrust, it would also seem reasonable that they would have the same specific thrust at take-off at the same rpm. Since specific thrust is a direct function of jet velocity, we would, therefore, expect both engines to emit the same amount of noise at take-off. The jet engine has an advantage in that, because of its lower inlet turbine temperature, it can be overspeeded at take-off (if suitably stressed), and the extra thrust (30–40%) can be used to get a greater load airborne within a given distance or alternatively would prove useful under hot-day conditions. Only when overspeeded, however, will it be noisier than the bypass engine.

While much has been said about bypass engines in terms of better propulsive efficiency, it appears that the only real advantage of the bypass engine lies in higher thrust-weight ratio. A comparison has been made between a straight-jet engine and a bypass

engine of the same thrust, both having 2-spool arrangements and the same intake diameter. In the bypass engine the high-pressure portion of the compressor can be made smaller in diameter. With respect to the turbines, the low-pressure turbine power per lb of turbine flow is greater in the bypass engine, necessitating a turbine diameter somewhat larger than in the straight-jet engine if the same number of turbine stages are to be employed. Another important point is that the high-pressure compressor, combustion chamber, and high-pressure turbine are shorter, leading to reduced shaft lentghs. This reduction in length may be offset somewhat by the necessity for reasonable distance between the low-pressure compressor outlet and high-pressure compressure compressor inlet to accommodate changes in bypass ratio at reduced rpm operation.

Nevertheless, an overall reduction in engine length would appear to be possible in the bypass engine.

In conclusion, it appears that the application of the bypass principle offers the possibility of a certain reduction in engine weight for a given thrust, at the expense of higher turbine operating temperatures. Against this, the straight-jet engine, while perhaps slightly heavier, affords the advantage of a reserve in thrust and longer turbine operating life.

With regard to application, since the advantages of the bypass principle diminish with forward speed, the bypass engine shows to best advantage at low speed. Because of low specific thrust, both the bypass and low-temperature straight-jet engines require pod-type installation, since high airflows are an embarrassment in buried installations.

Mechanical Design

Fig. 13 shows the trend in thrust-weight ratio of large and small turbojets as predicted by Gregory[4]. Our work indicates the possibility of an 18,000-lb thrust engine with a thrust-weight ratio which lies about midway between the trend for small and large engines. How is this large thrust-weight ratio achieved?

With the introduction of new materials, such as titanium, the weight of rotating components of turbojet engines can be reduced considerably. The weight of a compressor stage in titanium is only about 45% of the same stage designed in steel, while the density of titanium is about 60% that of steel. This considerable reduction in the weight of dynamic parts in turn allows us to use a very much simplified rotor-bearing system as shown in Fig. 14 with even further weight reduction. Fig. 14 shows a 4-bearing arrangement for a large 2-spool engine. In order to keep the low-pressure shaft as light as possible, a steady bearing has been added where the low-pressure shaft passes through the high-pressure thrust bearing. Nevertheless, there are only two oil sumps, one at the front of the engine where the thrust bearings are located and one within the tail-cone bullet. The usual center bearing associated with turbojet construction, together with its oil sump and supporting structure, has been completely eliminated. In a 2-spool engine this leads to further simplification, since the couplings and other components are unnecessary, and to a comparatively low-cost engine.

[4] "The Future of Small Turbojet Engines," by A. T. Gregory. Fairchild Engine Division. November, 1956.

Fig. 15 shows the type of vibration pattern likely to be obtained with this type of rotor system. The usual design practice is to assume rigid bearing supports and to design both shafts to have critical speeds above maximum speed. Because of the flexibility of the bearing supports, we find that both critical speeds will lie within the engine speed range. However, the damping capacity of the engine frame is such that the amplitude of shaft vibration at this critical speed does not attain any appreciable magnitude and, moreover, the amplitude of vibration of the engine frame itself is well within the allowable tolerances.

Fig. 15 was obtained with the shaft-weight distribution and joint efficiencies as designed. In the case of compressor blade failures, weight distribution can vary considerably, providing out-of-balance forces

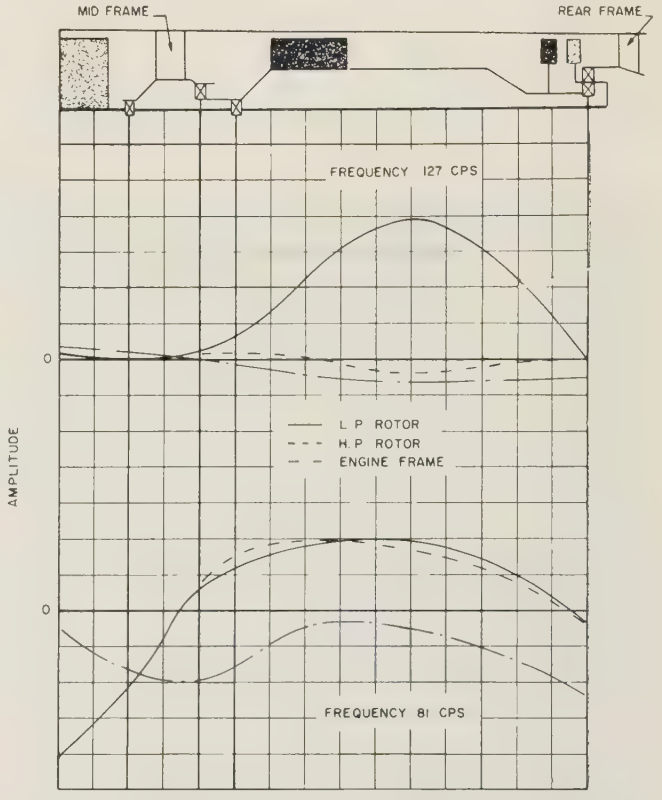

Fig. 15—Vibrational patterns of 5-bearing, 2-spool jet engine

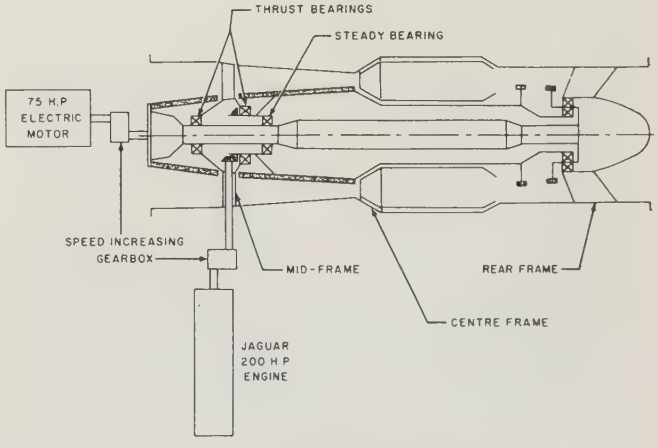

Fig. 16—Whirling speed test rig

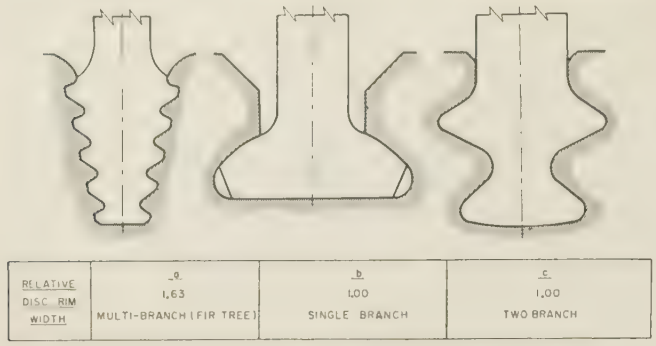

Fig. 17—Development of turbine blade root fixings for equal load

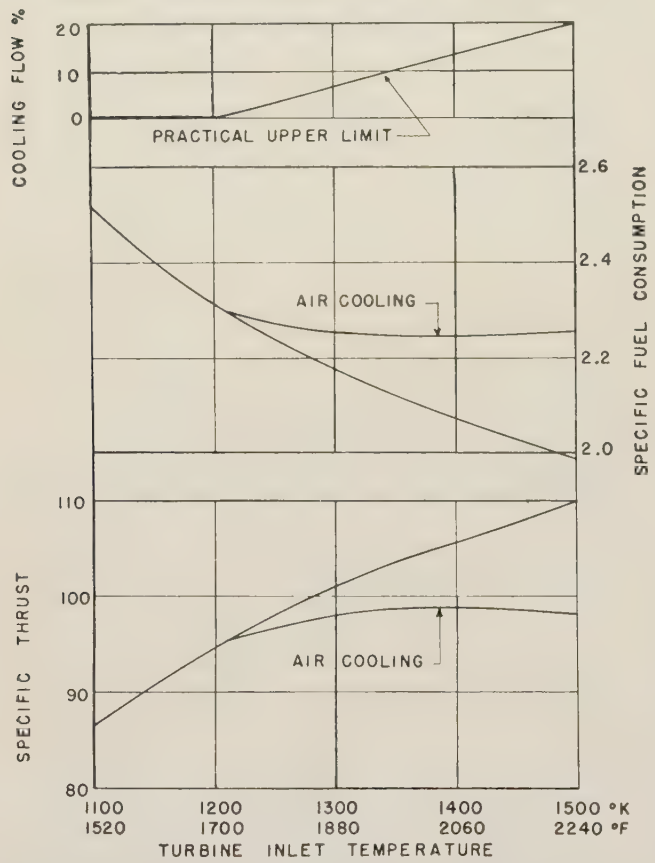

Fig. 18—Effect of aircooling of turbine blades on performance: Stoichiometric afterburning, Mach 2.5, compressor outlet temperature = 875 K (1115 F), $R = 6.0$, 3-stage turbine, full expansion

that may increase the amplitude at the critical speed leading to permanent distortion at the shaft joints, rotor instability, and failure.

To check that this condition did not arise, an engine has been built with rotor-weight distribution as designed but without blades in the compressors or turbines. Each rotor was driven from external sources at rpm well above maximum design speed. When normal vibration characteristics had been obtained, out-of-balance was introduced equivalent to the worst case likely to arise. Dimensional checks subsequently disclosed no movement of the rotor joints and that complete stability had been achieved. Fig. 16 shows the engine and external drives used for this investigation.

In order to reduce the weight of rotating components so that the engine structure can be correspondingly lightened, stress studies require particular emphasis when dealing with a new material such as titanium. The low modulus of elasticity, for example, presents difficulties in load distribution when designs approach ultimate values.

Turbine Design

Fig. 17 shows the development of turbine-blade fixings. The well known "fir-tree" type of foot (A) was one of the earliest types of turbine-blade fixing. This type of design was necessitated by the large number of blades required in the single-stage turbines of early turbojets, which were highly loaded.

With engine development to higher compression ratios it was eventually necessary to use a 2-stage turbine. This immediately gave reduced blade loadings and permitted consideration of the simplest form of fixing, namely the single-branch shown in B. This fixing is the simplest possible to manufacture and inspect and permits a rocking motion, thereby giving some damping. Nevertheless, the width of the stub between blades is undesirably narrow and in the event of shear of a branch the complete blade could leave the disc. This, in turn, would permit all blades to be shed.

A compromise between ease of manufacture and safety is, therefore, attained by the use of a two-branch fixing (C).

With regard to the permissible limit of output of a turbine stage, it has been our experience that a 2-stage turbine of the same total output as a single-stage turbine at its maximum output is only slightly heavier but has greater efficiency, leading to lower specific fuel consumption.

Turbine Disc Materials

The development of new turbine disc materials is also contributing to the reduction of weight in turbines. In changing from H-46 to A-286 it is possible to achieve a reduction in disc weight of about 50%. Further decrease should be possible when Inconel 901 is used. Since the turbine of a turbojet accounts for something like 10% of its total weight, it will be appreciated that any reduction which can be effected in weight of this rotating component will be extremely beneficial towards reducing the total engine weight.

Turbine Blade Cooling

With the continuous improvement of turbine-blade materials, up to the present time there has been very little interest in attaining even higher temperatures by the use of turbine-blade cooling, the advantages and disadvantages of which are still subject to controversy. As we saw in Figs. 3 and 4 for nonafterburning engines, while higher turbine inlet temperatures do not give very much benefit as regards specific fuel consumption they can considerably increase the specific thrust and thus avoid the use of afterburning except at very high speeds and during maneuver. In Fig. 18 the effect of aircooling of turbine blades on the performance of an afterburning engine is shown. In this example a 3-stage turbine is employed and, in view of the high compressor delivery temperature at Mach 2.5, very high cooling airflows would have to be employed. Assuming that it is possible to pass these airflows through the blades, it will be seen that the quantities which

have to be bled from the compressor and, therefore, perform very little useful work in the turbine, are such that the improvement in performance is only slight. In actual practice with a 3-stage turbine, about 10% is probably the maximum airflow which could be used, which would give an upper limit of turbine inlet temperature of about 1350 K (1970 F). In addition to this aerodynamic limitation of air-cooling blades, the difficulty of fabrication is quite considerable. Fig. 19 shows some early types of fabricated turbine blades which were run in engines for the purpose of evaluating different methods of construction and fabrication. While all three types of blade completed a 150-hr qualification test with a turbine inlet temperature of 1200 K (1700 F), cracks occurred in the cover plates or in the joint in all cases. The results of fatigue tests in the laboratory at room temperature indicated that blades A and B have an endurance limit of about 40% of that of a solid blade in the same material. Blade type C, made of two machined blade forgings joined on the convex surface near the neutral bending axis, was slightly better. Improvement is expected with development.

When the cooling airflow exceeds about 2% per stage, it appears that it will be necessary to increase the pressure of the cooling air over that of the compressor cooling air, in order to obtain the necessary pressure drop to drive the air through the blades.

To summarize the position as we see it, it appears possible to attain turbine inlet temperatures of about 1350 K (1970 F) at forward speeds up to about Mach 1.5. This requires cooling airflow of about 2% per stage.

It is apparent from the foregoing that if we wish to achieve higher turbine inlet temperatures or even moderate increases in turbine inlet temperature at speeds of the order of Mach 2.5, we will have to use methods other than aircooling. Considerable development has already taken place in Canada on alternative methods of cooling. Ideally, of course, it would be desirable to obtain these higher temperatures without cooling. The properties of molybdenum with its tremendous improvement in creep are receiving attention; however, use of this material is dependent upon the development of satisfactory methods of "cladding" the molybdenum blade to prevent high-temperature corrosion to which the bare material is very susceptible. It should not be forgotten, of course, that the use of higher inlet turbine temperatures also imposes combustion development problems.

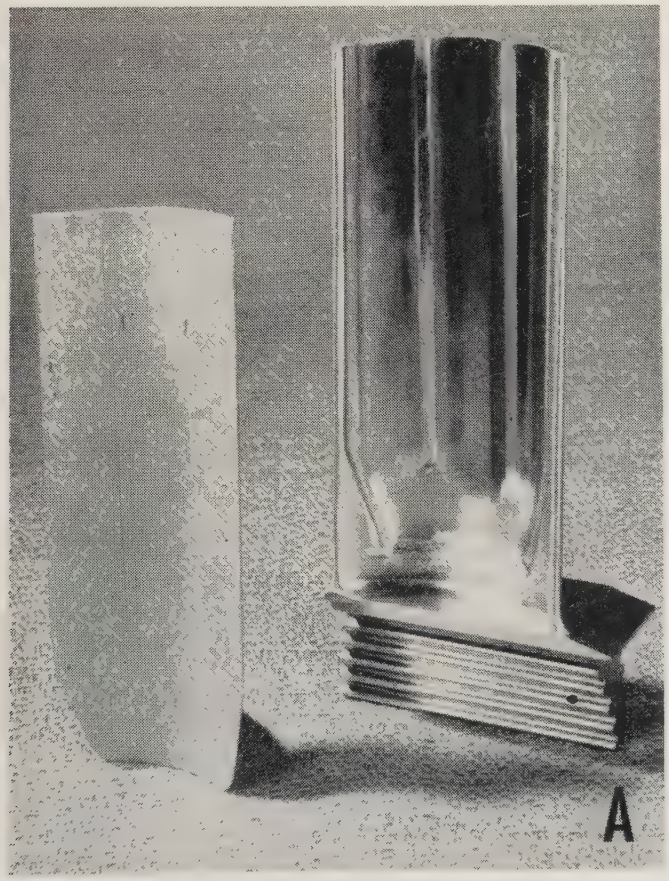

Fig 19A—Single-cover plate joined at leading and trailing edge

2250-Lb and 18,000-Lb Thrust Engines in Large Aircraft

As we have seen in Fig. 13 Gregory predicts that small jet engines of simple construction with about 2000-lb thrust will be available in 1960 with a thrust-weight ratio of 7.5. This agrees with our own esti-

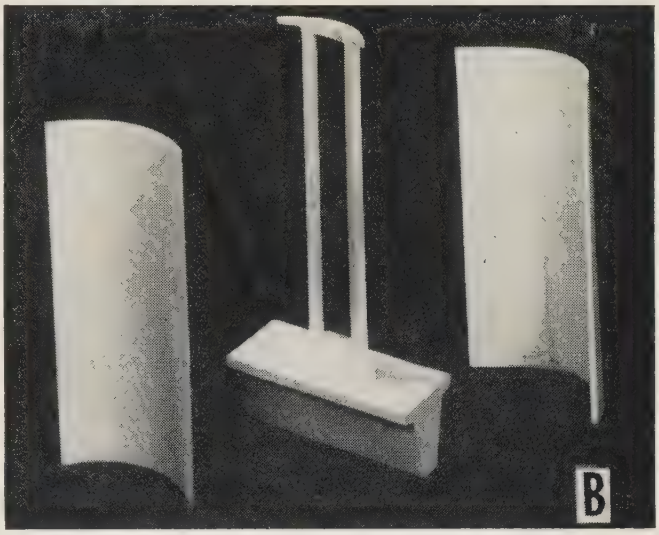

Fig. 19B—Double-cover plate joined at leading and trailing edge

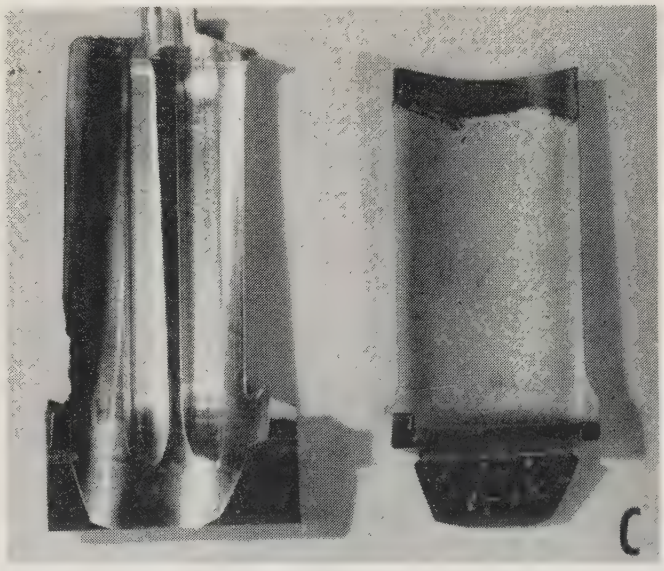

Fig. 19C—Two machined blade forgings joined on convex surface near neutral bending axis

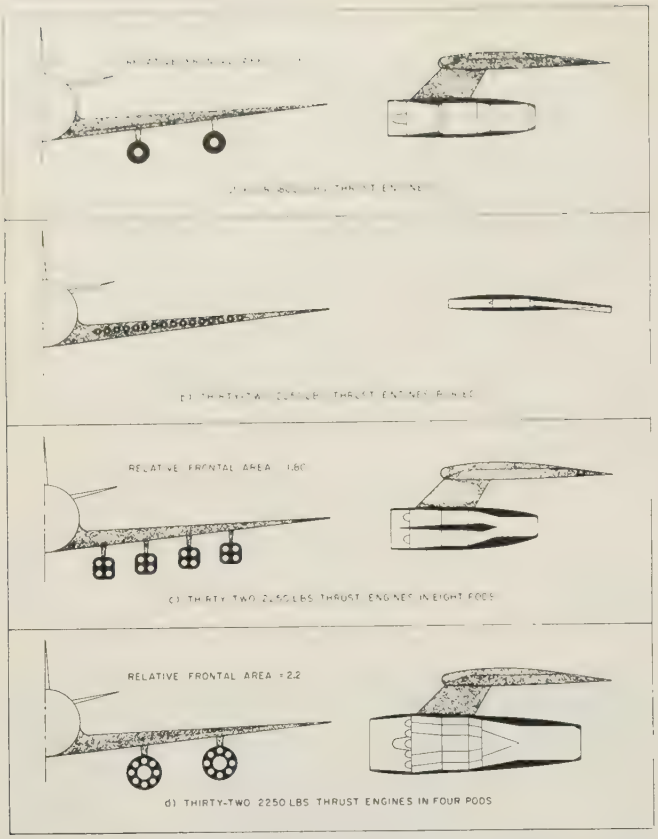

Fig. 20—Comparison of 2250-lb and 18,000-lb thrust engines in large aircraft

mates. We have also shown that large subsonic engines of 18,000-lb thrust with a thrust-weight ratio of 6.0 should be available at that time. This seemingly large weight advantage of the small engine is, however, considerably diminished, as far as use in large aircraft is concerned, when we come to consider the installation and control problems associated with small engines. In Fig. 20 we have considered the installation of both types of engine to an aircraft requiring 72,000-lb take-off thrust. This aircraft would require four 18,000-lb engines, or alternatively, 32 small engines. Since an aircraft of this size would probably have a wing chord of the order of 25 ft, it will be seen that the buried installation (Fig. 20B) necessitates very long intakes and jet pipes. Thus, with 16 engines in each wing, the wing structure would be penalized and space which might conceivably be used for fuel tanks would be considerably reduced. No value of relative frontal area has been given for this installation but it is apparent that if the frontal area required to swallow the air approaches that of the wing, the engines cannot be buried. At the cruise altitude of such an aircraft, the engine performance and intake efficiency will certainly deteriorate due to Reynolds-number effect.

In Fig. 20C we have considered a podded arrangement of small engines. The largest number of pods which one can use in order to avoid interference drag effects is probably eight. Thus, each pod will contain four engines. Nevertheless, making allowance for external piping and control systems the frontal area of such a pod will be approximately 1.8 times that of the 18,000-lb engine pod. In order to attain a satisfactory aerodynamic shape for the pod and to obtain good flow into the engines and avoid base drag, the pod would probably have to be about the same length as for a single-engine pod.

If interference effects demand the use of only four pods with eight engines in each, the relative frontal area increases to 2.2. Again the overall length of the pod will be equal to or greater than that of an 18,000-lb engine pod.

With regard to the problem of the control and supply of fuel to a large number of engines, it is presumed that a single control system would be used to control at least all the engines in one pod. Each engine would have to contribute an equal share of bleed air for driving the single-turbine pump to avoid overtemperature on any one engine. Satisfactory fuel distribution, although necessitating extensive piping, could probably be achieved in podded engines. But it would be very difficult with buried engines, particularly at high altitude when fuel flows and burner pressures are very low.

In considering the application of small engines to interceptor aircraft which today, ignoring the lightweight fighter, appear to require take-off thrusts of 18,000 lb or greater, clusters of small engines appear undesirable because of frontal-area considerations.

In comparing large and small engines, another consideration which cannot be ignored is the matter of cost. While it is unlikely that the small engine can incorporate the necessary degree of aerodynamic refinement to achieve the performance possible with large engines, if we assume that it could, then it would contain approximately the same number of parts. Because of the finer tolerances required on the parts for the small engine, the manufacturing cost, even though the amount of machining is less, would probably be equal to that of the large engine. The cost of the large engine would, therefore, be greater only by the amount of the increased material cost. Therefore, it is difficult to avoid the conclusion that eight 2250-lb thrust engines would cost several times that of one 18,000-lb engine.

We conclude that the small jet engine is not competitive with the large engine as the main power plant for large aircraft, since it will be deficient in performance by reason of its necessarily simpler construction and Reynolds number effects. While its installed weight will be about the same, its frontal area will be greater and its cost per pound of thrust several times greater.

Conclusions

The use of titanium in turbojet engines has permitted an improvement in thrust-weight ratio of a greater magnitude than is to be expected by straight material substitution. This is because the use of titanium in rotating parts permits the use of a 2-bearing rotor system with elimination of center bearings. Furthermore, with smaller dynamic forces the engine structure can be correspondingly lighter.

Small turbojet engines, despite their slightly higher bare thrust-weight ratio are not competitive with large engines for large aircraft, for one or more of the following reasons: higher installed weight, inferior performance, installation and control complication, higher cost per pound of thrust.

A bypass engine and turbojet of the same specific thrust have about the same specific fuel consumption. In addition to having a lower turbine operat-

ing temperature, the turbojet at the same specific thrust is no noisier. Moreover, the turbojet can be overspeeded, giving a thrust reserve of about 30%.

In order to operate over a wide speed range at maximum rpm with maximum combustion temperature indicates, a small compromise in subsonic performance appears to be the desirable alternative to variable turbine geometry.

High-speed aircraft using afterburning have to accommodate bypass flow for intake matching and cooling flow for the afterburner. The use of a lightweight ejector nozzle fulfills this purpose; and also permits satisfactory divergent expansion within the range of exit diameter to engine diameter likely to be used in practice.

Higher turbine inlet temperatures are most beneficial in nonafterburning engines. For high speeds because of high compressor delivery temperatures, the use of aircooling of turbine blades becomes limited and the development of other methods of cooling or of materials which do not require cooling is necessary.

Acknowledgments

I wish to thank Orenda Engines Ltd. for permission to give this paper and to my colleagues for their help; in particular to W. H. Gibson, who was responsible for preparation of much of the detail.

APPENDIX I

Nomenclature

A = Area
A_t = Turbine throat area
C_L = Aircraft lift coefficient
D = Aircraft drag, diameter
$F = SF_n$ net specific thrust
L = Aircraft lift
M = Mach number
N = Rpm
P = Total pressure, absolute
p = Static pressure
q = Dynamic pressure
R = Compression ratio
rf = Range factor
S = Wing area
sfc = Specific fuel consumption, lb/hr/lb thrust
T = Total temperature, deg absolute
t = Static temperature, deg absolute
W = Air weight flow
w = Weight
w_a = Aircraft weight
w_e = Engine weight
Δ_t = Compressor temperature rise, deg
γ = Ratio of specific heats for air
η = Efficiency
η_i = Intake efficiency
η_{poly} = Polytropic compressor efficiency

Other subscripts (not defined in text)

1 = Compressor inlet
3 = Turbine inlet

APPENDIX II

Effect of Forward Speed on Engine Operation

If we assume that the flow $\frac{W_1\sqrt{T_1}}{P_1}$ into the compressor is a linear function of $N/\sqrt{T_1}$ then for constant rpm (N):

$$\frac{W_1 T_1}{P_1} = \text{constant} \qquad (1)$$

If we further assume that the turbine nozzles are choked, then: $\frac{W_1\sqrt{T_3}}{A_t P_3} = \text{constant}$

Therefore:

$$\frac{\sqrt{T_3}}{T_1} \times \frac{P_1}{P_3} \times \frac{1}{A_t} = \text{constant} \qquad (2)$$

Hence, for fixed A_t and T_3 $\frac{P_3}{P_1} \propto \frac{1}{T_1}$ the compression ratio is inversely proportional to the inlet temperature. Alternatively, we may assume that the compressor temperature rise Δ_t remains constant giving:

$$R \propto \left(\frac{T_1 + \Delta_t}{T_1}\right)^{3.5 \eta_{poly}}$$

Substituting in (2) we can obtain variation of T_3 for constant A_t or vice versa.

APPENDIX III

Relationships Between Engine and Aircraft Performance

1. Best cruise altitude (h):

Let $\frac{(w_a)}{S}$ = aircraft wing loading.

Then $\frac{(w_a)}{S} = C_{Lq} = C_{L\frac{\gamma}{2}p_a M^2}$

Therefore:

$$\text{Altitude ambient pressure } (p_a) = \frac{\frac{(w_a)}{S}_2}{\sigma_{L_\gamma M^2}} \qquad (1)$$

2. Engine intake pressure (P_d):

$$P_d = P_o \times \eta_i$$
$$= p_a(1 + 0.2M^2)^{3.5} \times \eta_i \qquad (2)$$

3. Engine intake temperature (T_d):

$$T_d = t_a(1 + 0.2M^2) \qquad (3)$$

4. Ratio engine weight/aircraft weight (w_{e/w_a}):

Let subscript s refer to sea level static condition and d to design conditions. Then:

$$\frac{W_s T_s}{P_s} = \frac{W_d T_d}{P_d} \text{ (Equation 1 of Appendix II)}$$

$$\text{or } W_s = W_d \frac{P_s}{P_d}\frac{T_d}{T_s}$$

Let SF_n = specific thrust.
Then:

$$W_d = \frac{w_a}{L/D\ (SF_{nd})}$$

Giving: $$W_s = \frac{w_a}{L/D\ (SF_{nd})} \times \frac{P_s}{P_d} \times \frac{T_d}{T_s}$$

and taking $\frac{W_s}{w_e} = 0.06$ lb airflow per sec per lb weight for an afterburning engine at sea-level static we obtain:

$$\left(\frac{w_e}{w_a}\right) = \frac{0.55}{L/D\ (SF_{nd})} \times \frac{T_d}{P_d} \qquad (4)$$

for: $P_s = 14.7$ psia
$T_s = 288$ K (59 F)

NOTE: The value of $\frac{W_s}{W_e}$ of 0.06 is for an engine of compression ratio 12 stressed for supersonic flight.

5. Ratio of specific thrusts for given engine at dif-

ferent flight speeds:

Let M_1 and M_2 be the two speeds and assume as in Appendix II that a constant rpm:

$$\frac{W_1 T_1}{P_1} = \frac{W_2 T_2}{P_2}$$

$$\text{or } \frac{w_a}{(L/D)_1 (SF_n)_1} \times \frac{T_1}{P_1} = \frac{w_a}{(L/D)_2 (SF_n)_2} \times \frac{T_2}{P_2}$$

Therefore:

$$\frac{SF_{n1}}{SF_{n2}} = \frac{(L/D)_2}{(L/D)_1} \times 2 \frac{P_2}{P_1} \times \frac{T_1}{T_2} \qquad (5)$$

Example: Let $M_1 = 0.9M$, $M_2 = 2.5M$, then from Fig. 8 for $\frac{w_a}{S} = 50$ psf, $T_1 = 260$ K, $T_2 = 480$ K,

$$P_1 = 2.5 \text{ psia}, P_2 = 6.5 \text{ psia}$$

$$(L/D)_1 = 12, (L/D)_2 = 5.5$$

Therefore: $\frac{SF_{n1}}{SF_{n2}} = \frac{5.5}{12} \times \frac{6.5}{2.5} \times \frac{260}{480} = 0.65$

Therefore, if the maximum specific thrust at Mach 2.5 was 70, then the specific thrust required from the same engine for subsonic cruise at Mach 0.9 would be $0.65 \times 70 = 45.5$.

6. Range factor:

$$\text{Range factor} = \left(\frac{L}{D}\right) \times \frac{\text{Mach no.}}{\text{specific fuel consumption}} \qquad (6)$$

Example: At $0.9M$, $L/D = 12$, (Fig. 7) and sfc = 1.0 (Fig. 6) at $2.5M$, $L/D = 5.5$ and sfc = 2.2

Hence:

$$\text{rf}_{0.9} = \frac{12 \times 0.9}{1.0} = 10.8$$

$$\text{rf}_{2.5} = \frac{5.5 \times 2.5}{2.2} = 6.25$$

Suppose, however, that in order to attain $L/D = 5.5$ at $2.5M$ the maximum L/D at $0.9M$ was only 9 and that in order to attain a specific fuel consumption of 2.2 at $2.5M$ the exhaust was over-expanded and compression ratio lower than 13 at $0.9M$ giving a specific fuel consumption of 1.3, then $\text{rf}_{0.9} = 6.25$.

ORAL DISCUSSION

Reported by R. A. Cole,
Sanderson & Porter

Harry Pearson, Rolls-Royce Ltd.: I question the effect of the compression-ratio compromise outlined in the section on "Effect of Forward Speed on Engine Operation." Also, I think that the limits cited for turbine-blade cooling are very conservative.

Mr. Grinyer: As shown in Appendix II we can derive a simple relationship between nondimensional engine flow and compression ratio at constant mechanical engine speed with increasing intake temperature. This assumes that the compressor characteristics are such that the nondimensional flow is a linear function of the nondimensional speed along the operating line. Such an assumption for the compressor characteristics is not strictly correct. Nevertheless, the derived relationships provide a rapid means of obtaining the high-speed performance of a turbojet at 100% rpm given the sea-level static compression ratio and flow and design point performance curves at various intake temperatures without recourse to actual compressor characteristics. Moreover, in preliminary design studies of new engines, suitable compressor characteristics are sometimes not available.

The relationship between nondimensional flow and compression ratio on this simplified basis has been plotted in Fig. 7 for an engine of a sea-level static compression ratio of 12.

We also thought it would be interesting and instructive to see what sort of operation was necessary if we assumed constant compressor temperature rise. It will be seen in Fig. 7 that this assumption would require a fall-off in turbine operating temperature or necessitate variable turbine stators.

We, therefore, adopted the first method for purposes of rapid estimation of turbojet performance at high forward speeds as being more typical, since variable turbine stators are undesirable and a fall-off in turbine temperature is not acceptable.

Now considering operation at high forward speeds with respect to the problem of surging. It is not intended that any conclusion in this respect be drawn from Fig. 7. As Mr. Pearson pointed out, the operating line at constant mechanical speed and turbine temperature will lie slightly below and be steeper than the sea-level static operating line. However, because a fixed geometry high pressure ratio compressor of pressure ratio 12 as used in the example in Fig. 7 will almost certainly have a "kink" in the surge line, it will be necessary to use some variable geometry in the compressor to achieve satisfactory operation both at high forward speeds and for normal test-bed acceleration of the engine. The variable geometry in the compressor may consist of variable angle stators or "two spooling."

A. T. Gregory, Fairchild Engine Division: It is a mistake to expect the small engine to do the same job as a large engine. The small unit has its own particular field of application.

"Clusters" or multicylinder engines were promising from some viewpoints but introduced a number of new problems. They may be designed so that failure of any one will not affect the others but it is now more customary, in the interest of saving weight, to treat the cluster as a multicylinder engine with common accessories.

One proposal used a common combustion chamber with several cans or annular burners, so that all compressors and turbines operated at the same pressures; however, much remains to be done in the development of this type of engine.

Mr. Pearson: The advantage of the small engine is supposed to be low weight per pound of thrust, but the cost is the most important factor to the commercial operator. In this respect, I think that the fundamentals of fatigue were being overlooked; the small engine, operating at higher rpm than the large engine, accumulates fatigue cycles faster and should, therefore, have shorter life and cost more to operate.

Raymond Capiaux, Curtis-Wright Corp.: The small turbojets can use much shorter blades with aspect ratios as low as 2, which reduced the vibration problems.

Richard Opsahl, Grumman Aircraft Engineering Corp: Can data be given for specific fuel consumption versus weight for combined range or 0.9 Mach-number cruise conditions?

Mr. Ginyer: A study has been made but I can not quote the figures.

D. Q. Marshall, General Electric Co.: How is intake distortion accommodated?

Mr. Grinyer: We have not yet investigated intake distortion in flight but we expect to start in a B47 aircraft within a month and to have a complete picture by the end of 1957. Ground tests of the compressor indicate that the distortion will have to be considerable before the effect became serious.

Mr. Capiaux: Such distortion has not been checked by my firm; however, a similar design was tested by the NACA but the data has not yet been released.

Vapor-Locking Tendencies of Fuels

A Practical Approach

J. D. Caplan and C. J. Brady, General Motors Corp.

This paper was presented at the SAE Summer Meeting, Atlantic City, June 6, 1957.

THIS paper describes what the authors consider to be a simplified method of determining the vapor-locking tendencies of gasolines.

The study of vapor lock was undertaken after they found the Reid vapor pressure method to be inadequate. The result of their work was the development of the General Motors vapor pressure, a single number which predicts vapor-locking tendency.

The authors point out the following advantages of the new method: It allows direct comparisons of vapor-lock test results of different reference fuel systems; establishes distribution curves of volatility requirements of cars for vapor-lock free operation and of vapor-locking tendencies of gasolines; is a common reference value for both petroleum and automotive engineers. Finally, it more realistically evaluates the effects of small weathering losses on vapor-locking tendency than does Rvp.

THE most recent ASTM publication[1] concerning the significance of petroleum product tests states, "The Reid vapor pressure of motor gasoline is the best single criterion of freedom from vapor lock in automotive equipment." It is the contention of the authors that this is an instance where the best is not good enough.

As early as 1930 Wilson[2] indicated his surprise that there was no test which measures directly the volatility of a fuel under conditions similar to those prevailing in service. In this respect, it should be pointed out that the Reid method for determining vapor pressure originated[3] as an improvement of an Interstate Commerce Commission method (vapor tension) concerned with the safe transportation of dangerous articles and not as an index of volatile fuel performance in passenger-car fuel systems.

In 1930 the use of a vapor-pressure method such as Reid vapor pressure had adherents as a suitable

[1] "Significance of ASTM Tests for Petroleum." STF No. 7-B, American Society for Testing Materials, Philadelphia, 1955.

[2] SAE Transactions, Vol. 25, 1930, pp. 151–160: "Significance of Tests for Motor Fuels," by R. E. Wilson.

[3] *National Petroleum News*, Vol. 20, Aug. 29, 1928, pp. 25–27: "National Gasoline Association Adopts Reid Vapor Pressure Test."

Fig. 1—Modified vapor pressure bombs

criterion for vapor-lock performance in passenger cars. For example, the literature contains the following statement by two of the foremost authorities in the field,[4] "The experimental work, just summarized, shows that the gas-free vapor pressure is essentially the only property of a gasoline which is of interest as regards vapor lock in a well-designed fuel feed system." However, by 1953 these same authorities had altered their viewpoint and they state,[5] "Such values (Rvp) lack significance for application to vapor lock in modern passenger cars unless suitably interpreted."

The problem of improving the methods of both measuring and expressing fuel volatility as related to its vapor-locking tendencies has been the subject of numerous studies in the period 1930–1957. Perhaps the most important of these have been concerned with the elucidation of the temperature-vapor/liquid ratio relationships of gasoline and their application to the interpretation of vapor-lock performance. Of equal importance, from a practical standpoint, have been attempts to develop empirical equations involving both Reid vapor pressure and ASTM distillation data which could be used to express the tendency of a fuel to cause vapor lock. (see Additional References.)

In reports covering these studies, time and time again one conclusion has been either expressed or implied by the authors when interpreting their test results. This conclusion is that for engineering purposes we need a greatly simplified and more direct method of determining and expressing the vapor-locking tendencies of gasolines.

The study being reported was undertaken to satisfy this need.

Practical Considerations in Selection of Approach

Before undertaking these studies, certain ground rules were established to ensure that any resultant method would be acceptable for use in engineering work. These were:

1. The method should give a single number to a gasoline which will reflect its tendency to vaporize and cause vapor lock.

2. The best measure of this tendency to vaporize and cause vapor lock is the integration performed by actual passenger cars. Such an integration inevitably considers all factors of gasoline volatility and fuel system characteristics in their proper proportions.

3. Any measurement performed by a secondary device must agree with the primary integration in passenger cars.

4. The method should be based on a single experimental measurement and the equipment should be of such design as to minimize the time required for a measurement.

With these rules established, it was apparent that the most logical approach to this assignment would be to measure the volatility of the gasoline under conditions corresponding closely to those existing in the fuel system of the car.

Consideration was first given to the use of a dynamic (nonequilibrium flow) system. For example, a system composed of passenger-car fuel system components involving fuel flow rate, pressure, and temperature controls could be used.[6] For measurement of vapor-locking tendency a method of quantitatively detecting transient vapor formation would be required. As indicated, in attempting to devise such a system it became apparent that it would violate ground rule 4 in that the time requirements for a single measurement would be excessive and the equipment would, of necessity, be complex. Consequently, consideration was given to changes that could be made in the Reid method to make it more comparable to the conditions experienced by the

[4] SAE *Journal*, Vol. 27, July, 1930, pp. 93–110: "Properties of Gasoline with Reference to Vapor Lock," by O. C. Bridgeman and E. W. Aldrich.

[5] "Fuels and Fuel Systems—A Petroleum Viewpoint," by T. W. Legatski, O. C. Bridgeman, E. W. Aldrich, and R. Rohde. Paper presented at SAE Summer Meeting, Atlantic City, June 7–12, 1953.

[6] SAE Transactions, Vol. 65, 1957, pp. 567–578: "Automotive Fuel Pumps—A Fundamental Study of Their Performance," by R. A. Randall.

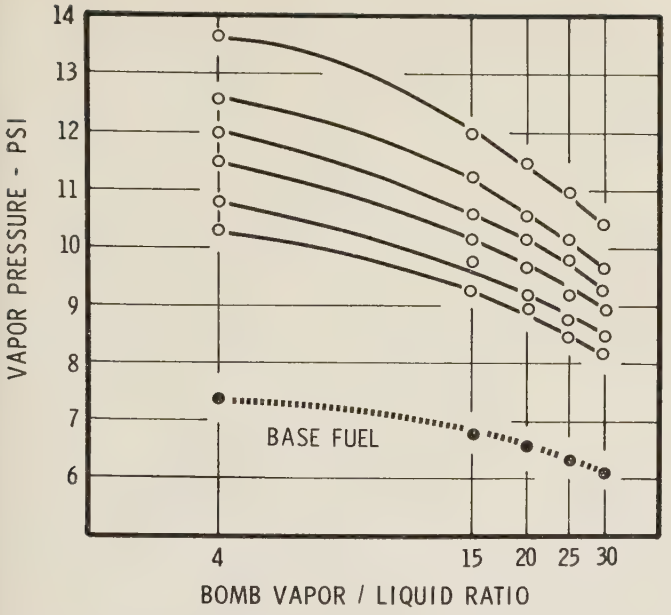

Fig. 2A—Variation of vapor pressure with V/L ratio—base fuel plus progressively greater quantities of butane (100 F)

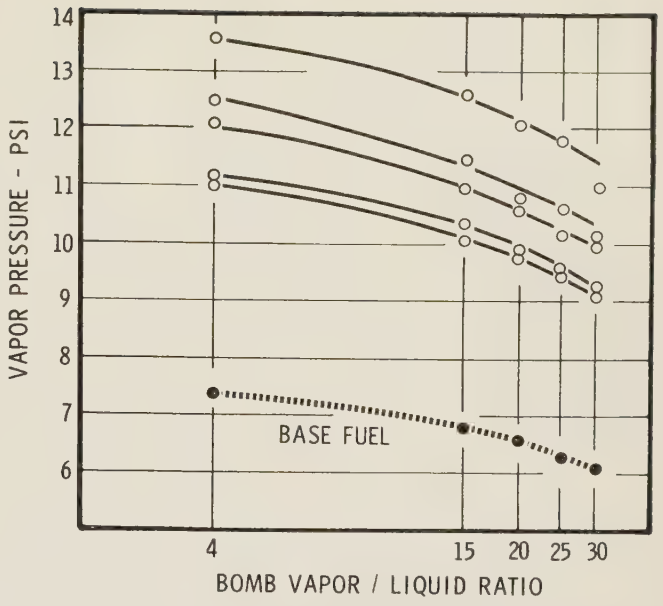

Fig. 2B—Variation of vapor pressure with V/L ratio—base fuel plus progressively greater quantities of natural gasoline (100 F)

gasoline in a passenger-car fuel system. Two changes were contemplated:

1. Increasing the V/L ratio of the "bomb."
2. Increasing the gasoline temperature.

Modifications of Conventional Reid Vapor Pressure Bomb and Bath

Bomb V/L Ratio Modifications—Although a number of investigators have reported the apparent specific V/L ratios existing in fuel systems at time of vapor lock, the authors decided to study a wide range of ratios. Consequently, modifications were made to the Reid bomb to provide ratios of 10, 15, 20, 25, and 30 to 1 in addition to the conventional 4/1. These modifications were made by two techniques:

1. The gasoline-chamber volume was decreased by filling part of the original volume with Woods metal.

2. The gasoline-chamber volume was decreased by machining off the base, machining off part of the remaining cylinder wall, and resoldering the base to the machined cylinder. Fig. 1 illustrates a conventional gasoline chamber and modifications thereof made by this technique.

Calibration of the exact V/L ratio of the modified bombs was made by determining either the weight or the volume of water that could be contained by the gasoline and air chambers.

Constant Temperature Bath Modifications—Inasmuch as passenger-car fuel system temperatures during vapor lock are at least 40–50 deg higher than the 100 F temperature used in the Reid method, it appeared desirable to increase the temperature at which the vapor-pressure measurements were made. Therefore, studies were made of the effects of elevated bath temperatuers on the vapor pressures measured with the various modified bombs.

Variation in Vapor Pressure with Bomb V/L Ratio

In Figs. 2A, B, and C are shown families of curves for the same base gasoline with three different pressurizing agents. These curves were obtained by plotting the vapor pressure at 100 F as a function of bomb V/L ratio. A logarithmic scale was used for the abscissa to provide equal percentage changes in the ratios. It is evident that the slopes of these curves are sensitive to both the composition of the pressurizing agent and the quantity of agent added. Other studies have indicated that the composition of the base gasoline also influences the slope of these curves.

A more informative presentation of the effect of bomb V/L ratio on vapor pressure is obtained by crossplots of the vapor pressures at various V/L

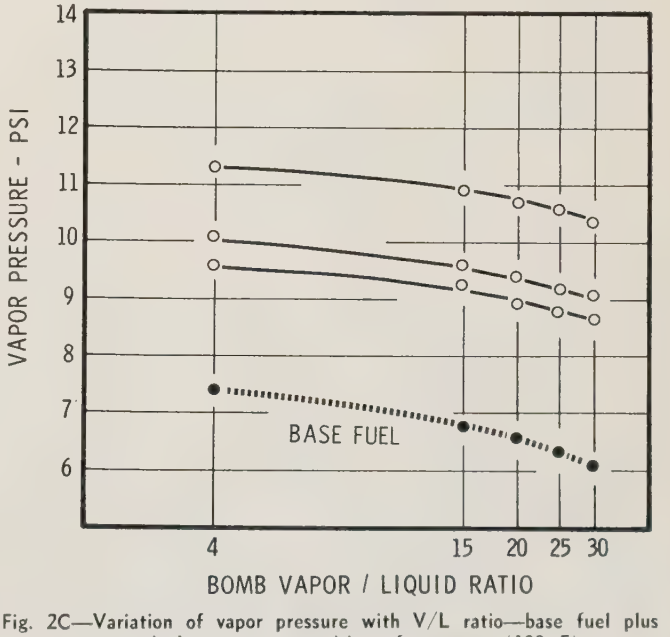

Fig. 2C—Variation of vapor pressure with V/L ratio—base fuel plus progressively greater quantities of pentane (100 F)

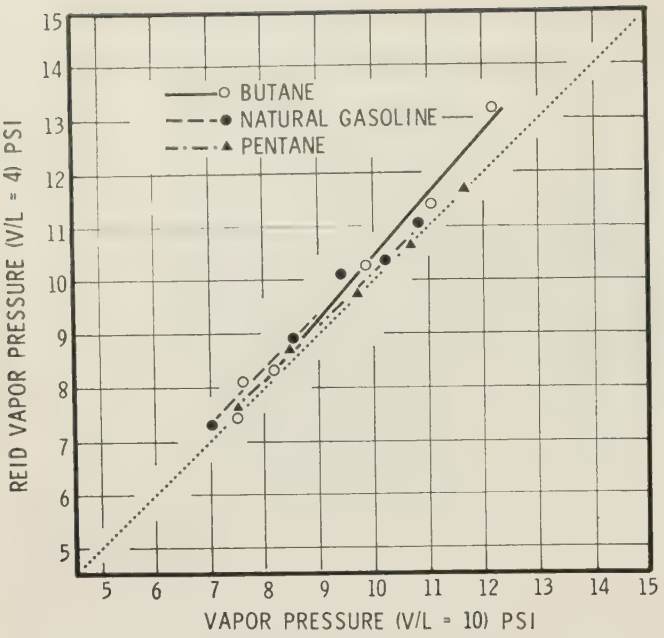

Fig. 3A—Rvp versus vapor pressure at V/L = 10

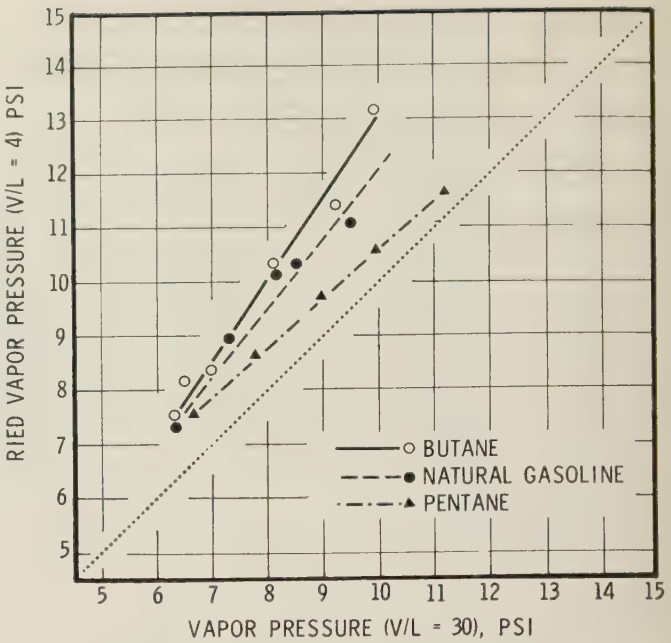

Fig. 3C—Rvp versus vapor pressure at V/L = 30

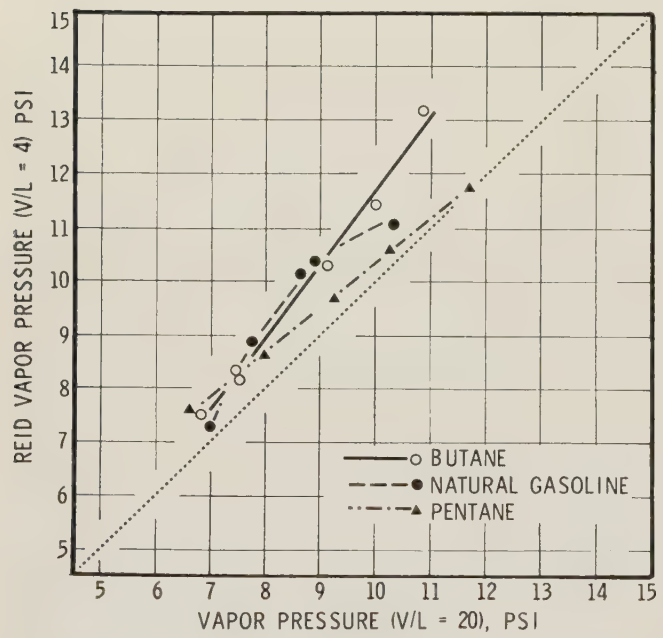

Fig. 3B—Rvp versus vapor pressure at V/L = 20

Table 1—Precision of Vapor Pressure Measurements

Reid Vapor Pressure (V/L = 4)	
Mean	13.4
Standard Deviation	0.09
Vapor Pressure (V/L = 30)	
Mean	10.9
Standard Deviation	0.13

Table 2—Comparison of Modified Bombs and Temperature-V/L Apparatus

Parameter	Modified Bombs	Temperature-V/L Apparatus
V/L ratio	Independent variable	Dependent variable
Pressure	Dependent variable	Held constant (atmospheric)
Temperature	Held constant (100 F)	Independent variable
	(Both equilibrium systems)	

ratios. Figs. 3A, B, and C present such crossplots for the three pressurizing agents in a base fuel which was different from that used in Figs. 2A, B, and C. These figures clearly indicate the large differences in the vapor pressure of the remaining liquid gasoline at the various ratios as well as the ability of the modified bombs to give single numbers to the vapor-forming tendencies of gasolines that are markedly different from the Reid vapor pressures.

Variation of Vapor Pressure with Bath Temperature—Both experimental and theoretical studies of the effect of bath temperature on vapor pressure indicated that it was not necessary to increase the temperature. This is due to the fact that the vapor pressure-temperature curves for most hydrocarbons are of nearly identical slope. Thus, an increase in temperature only increases the magnitude of the vapor pressure for all gasolines without altering their relative rankings. Substantiating data for this statement are presented in Fig. 4, where the variation in vapor pressure with temperature is shown for bomb ratios of 4/1 and 25/1. It is evident that changes in temperature have very little effect on the relative vapor pressures of the three diverse types of fuels.

Since increasing the bath temperature makes it difficult to manipulate the bombs, the use of a 100 F bath temperature was continued. This has the additional advantage of permitting both Rvp and modified bomb vapor pressures to be determined simultaneously in the same bath.

Corrections, Precision, and Overall Accuracy—In determining the modified bomb vapor pressures, the corrections for the difference in temperature of the air in the chamber at time of fill and in the bath on both the water vapor pressure and dry air pressure are made in a manner identical to that for Reid vapor pressure. (See ASTM D-323.) As an alternative the "100 F initial air temperature" procedure can be used.

Table 3—Relative Ratio of Moles of Vapor

Rig	Volume of Vapor	Temperature of Vapor, F	Pressure of Vapor	Molar Vapor Ratio, Bomb to V/L Apparatus
Bomb	Same (1)	100	8.05	0.57
V/L Apparatus	Same (1)	139	14.7	

The results of a study of the precision of measurements in the 30/1 V/L ratio bomb in comparison to the Reid vapor pressure bomb made on the basis of groups of 10 replicate tests are summarized in Table 1. These studies indicate that the random error (precision) of the two methods are comparable and that the 30/1 bomb has adequate precision for its application.

An important advantage of the modified bomb is not evident from the precision study. This is that small weathering losses occurring either in sampling or in sample transportation result in only small changes in vapor pressure in the modified bomb, but in large decreases in Reid vapor pressure. This is an extremely important consideration from the standpoint of overall reliability of the method.

Modified Vapor-Pressure Bombs versus Temperature V/L Ratio Apparatus

Experimental curves relating the temperature-V/L ratio characteristics of gasolines have been used for a number of years for describing fuel volatility. In 1944 a correlation was developed which permitted calculation of these curves from Rvp and ASTM distillation data. However, recent studies by Sheppard and Withers[7] have shown that this correlation does not have as general application as had been assumed. Consequently, it is again necessary to resort to experimental determination of temperature-V/L ratio curves. These measurements, in comparison to the modified bomb, are more time consuming and the apparatus is much more complex.

It is of considerable interest to examine the relationship between results obtained in the modified bombs and the temperature-V/L ratio apparatus. As indicated in Table 2, the major difference in these two methods is the dependent variable used to bring the system to equilibrium as the independent variable is varied.

It is important that the adjective "volumetric" be used to modify V/L ratio since at the same volumetric ratio a smaller per cent of the mass of gasoline is vaporized in the bombs than in the V/L apparatus. To clarify this concept, the data presented in Fig. 5 are most useful. These curves were obtained for each of the gasolines by plotting the modified bomb vapor pressure versus the calculated V/L apparatus temperatures for the same volumetric ratios. Consider the point obtained for the butane blend at a ratio of 30/1. The relative ratio of moles of vapor in the bomb to that in the V/L apparatus at equilibrium is shown in Table 3. If it is assumed that the molecular weight of the vapor is the same in both cases, then the relative mass ratio will also be approximately 0.57.

A series of similar calculations indicate that for this particular fuel, a modified bomb with a volumetric ratio of 30/1 will have the same weight per cent of fuel vaporized as the V/L apparatus at a ratio of 18/1. The importance of these calculations is that they indicate that the V/L ratios in the modified bombs and V/L apparatus are not directly comparable with respect to the per cent of the original fuel vaporized. Further, it can be shown that the comparable ratios will vary with the characteristics of the gasoline. Although it is generally accepted that vapor lock is due to the formation of vapor in the fuel system, it is not always the volume of this vapor per se that is objectionable; it is rather the effect of this vapor on

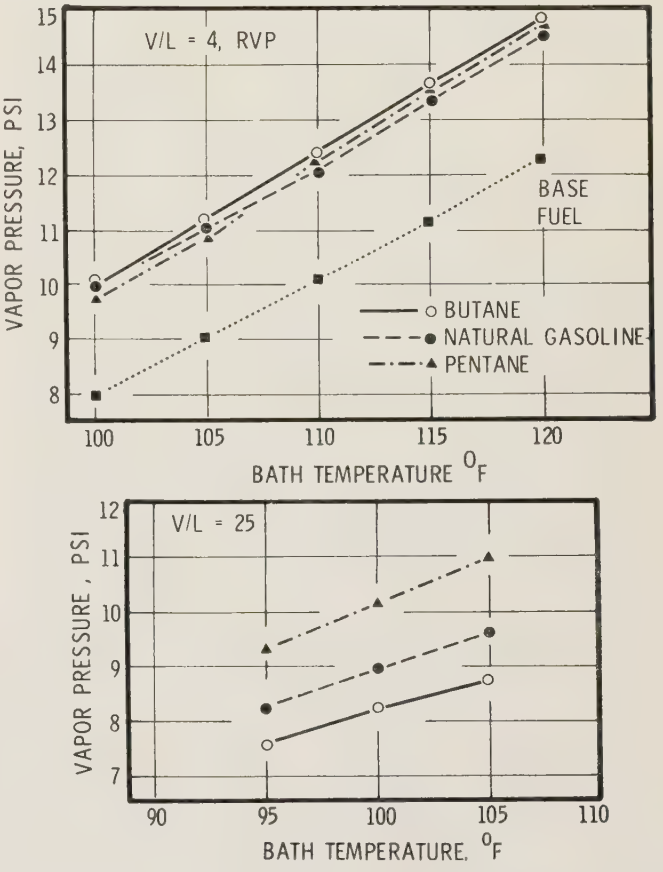

Fig. 4—Effect of bath temperature on vapor pressure at V/L ratios of 4/1 and 25/1

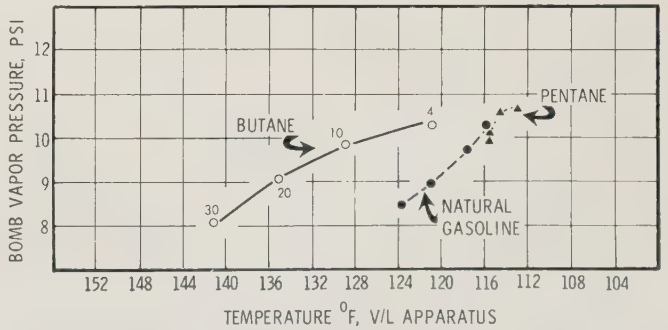

Fig. 5—Comparison of bomb vapor pressures and temperatures from V/L apparatus at corresponding V/L ratios of 4, 10, 20, and 30/1

[7] Institution of Mechanical Engineers Proceedings, Automobile Division, No. 7, 1954–1955, pp. 187–198: "Assessment of Car and Fuel Factors Affecting Vapour-Locking Tendency," by G. F. Sheppard and J. G. Withers.

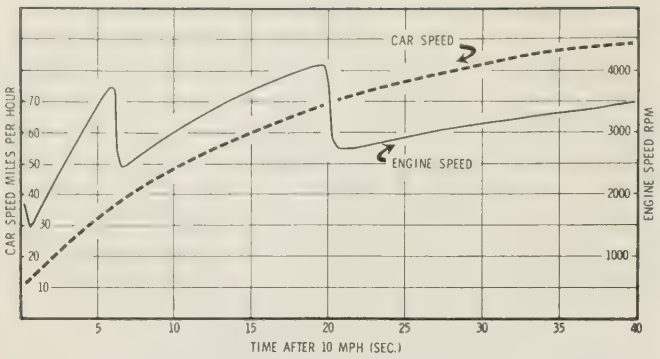

Fig. 6—Typical performance curves during vapor-lock test acceleration

Table 4—Passenger-Car Evaluation of Vapor-Locking Tendencies of Fuels

Experimental Arrangement

Passenger Car	Fuel Network	Ambient Temperature, F
A	1	100 ± 2
B	2	100 ± 2
C	2	95 ± 2
D	3	73 ± 2

Passenger Cars

Code	Carburetor, bbl	Transmission	Model Year
A	2	Torque Converter	1955
B (Air Conditioning)	2	Hydra-Matic	1956
C (Air Conditioning)	4	Torque Converter	1956
D	4	Hydra-Matic	1957

Fuel Networks

(Base fuel pressurized with butane, 26 lb natural gasoline, or pentane to provide a series of fuels with each pressurizing agent ranging in Rvp from base Rvp to 14 lb)

Code	Base Fuel Characteristics					
			Temperature for Given Per Cent Evaporated			
	Rvp	lbp	10	20	30	50
1	8.0	85	121	143	163	213
2	7.1	101	132	149	169	227
3	7.4	94	131	152	—	227

Table 5—Fuel Blending Proportions for Rvp

(Bomb ratio 4/1, 7.0 psi Rvp base fuel, percent by volume)

Rvp	Butane	26 psi Natural	Pentane
7.0	—	—	—
8.0	1.5	5.3	11.1
9.0	2.9	10.5	22.2
10.0	4.4	15.8	33.3
11.0	5.9	21.1	44.4
12.0	7.4	26.3	55.6

the "bulk" density of the fluid being handled. Consequently, comparisons between the bombs and V/L apparatus are not rational on a vapor/liquid volume basis.

One fundamental aspect of any method of characterizing the vapor-locking tendencies of gasoline should be clarified. It is well-established that a given fuel system will tolerate a rather large reduction in bulk density of the fluid before the engine is starved. Consequently, for a sensitive measure of the tendency of different gasolines to cause vapor lock, it is desirable to measure the vapor-forming tendency of the *remaining liquid gasoline* after the major portion of the vapor tolerated by the fuel system has been formed. In the case of the modified bombs, this means that the V/L ratio of the bomb should be lower than the critical ratio of the fuel system if the results are to be used to predict the tendency of the *liquid* gasoline to undergo the further vaporization which will result in vapor lock. This fundamental concept should be kept in mind when comparing the V/L ratio for predicting vapor-locking tendency and the V/L ratio existing at time of vapor lock.

Vapor-Locking Tendencies of Gasoline as Measured by Passenger Cars and Modified Bombs

It has been shown that the modified vapor pressure bombs will differentiate between the vapor-forming characteristics of gasolines and that the relative results depend upon the volumetric vapor/liquid ratio. It has also been shown that the precision of the results obtained with the modified bombs and the Reid bomb are comparable. *However, as with any bench test, adequate ability to separate products with precision is of no importance if the results do not bear a direct relationship to the performance of the products as measured in an actual passenger car.*

To determine the relationship between vapor-locking tendency as measured in the modified bombs and in passenger cars the following study was undertaken:

1. A fuel network consisting of three series of fuels having diverse vapor-forming characteristics was evaluated in the various modified bombs.
2. The same fuel network was evaluated in a particular passenger car.
3. The above two steps were repeated, using a different fuel network, a different passenger car, and a different temperature for the car tests.
4. In total, three different fuel networks, three different ambient test temperatures, and four different passenger cars which encompassed a wide range of fuel system geometry, fuel pumps, transmissions, and the like, were investigated.

The inclusion of a wide range of variables in this study was desirable in order to ensure that any correlation developed between the bombs and the car tests would be generally applicable. Table 4 presents a summary of the experimental arrangement.

Fill versus Soak Samples—Two distinct, yet equally important applications must be considered when contemplating fuel volatility measurements and vehicle performance:

1. From the standpoint of the petroleum technologist, the performance of the fuel based on its volatility characteristics when dispensed from the service station pump is of prime importance.
2. From the standpoint of the automotive engineer, when evaluating changes in fuel system components, the performance of the fuel based on its volatility characteristics in the vehicle's tank at time of test is of prime importance.

Due to the unequal effect of weathering losses in the vehicle tank on the Reid vapor pressure of different gasolines, these two applications are not compatible when using Rvp as a criterion of gasoline vapor-lock performance. This fact presents a dilemma in vapor-lock testing when using Rvp by itself or any of the various empirical volatility expressions in which it is included as a factor.

The dilemma is whether to use the value of Rvp measured on the fill sample or on the soak sample.

In Table 5 are shown the volume percentages of three pressurizing agents required to increase the Rvp of a 7-psi base fuel in 1-lb increments to 12 psi. This table, coupled with the fact that roughly 1.5% weight of the liquid gasoline is vaporized in the Reid bomb in contrast to 8.6% in a 30/1 bomb permits some interesting observations concerning fill and soak samples:

1. If it is assumed that 1–2% of the fuel is weathered from the vehicle tank during testing, then the Rvp of the soak sample with butane pressurized base fuel will be markedly lower than the Rvp of the fill sample. In contrast, the soak sample Rvp will differ only slightly from the fill sample Rvp with pentane pressurized fuel.
2. Making the same assumption of weathering loss but considering the 30/1 V/L bomb, the change in vapor pressure due to weathering with the butane pressurized fuel will not be as great as in the case of Rvp. This follows in that the fill sample vapor pressure at 30/1 V/L will be based upon the vapor pressure of the remaining liquid gasoline after a considerable portion of evaporation of butane has occurred in the bomb.

As a consequence of these observations, it follows that even though weathering losses result in appreciable differences between the Rvp of the fill and soak samples, the differences due to these losses will be considerably smaller at the higher V/L ratios.

In the present study samples of the test fuel were collected both at the time the tank was filled and during the soak period of the test. Comparisons of the vapor pressures at the various bomb ratios of these two types of samples indicated that the pressure differences due to weathering losses were considerably smaller at the higher ratios than at the 4/1 ratio used in the Rvp method.

The foregoing observation is important as it emphasizes a further advantage of the modified bombs. Whereas during vapor-lock tests the Rvp method gives undue weight to small weathering losses, the modified bombs more realistically reflect the effects of these losses on the vapor-locking tendencies of different gasolines.

Passenger-Car Evaluation Technique—The most difficult portion of this study was the evaluation of the vapor-locking tendencies of the fuels in the passenger cars. In general, what was required was the determination of the changes in vehicle performance with changes in fuel volatility. Specifically, it was desired to determine for each car which specific fuel in each of the three series of the fuel network would give "borderline" vapor lock. These three specific fuels were, therefore, of equal vapor-locking tendency. It was also desired to determine the three specific fuels giving equal vapor lock at levels of performance impairment more severe than "borderline."

In brief, the vapor-lock testing procedure was of the soak-acceleration/idle-acceleration type and was performed on a 5-mile circular track at our desert proving ground. Warmup runs were made at 70 mph and accelerations were continued for a period of 40 sec after attaining 10 mph initial speed. Vehicle performance was recorded (both car speed and engine speed) with a recording oscillograph. Idle and hot-starting performance were also observed.

Fig. 6 presents a typical set of curves of performance data obtained during an acceleration after soak. Similar performance curves were obtained with each test fuel in each car both after a 15-min soak and a 5-min idle. From curves of this type, the ratings of the fuels were established.

For comparison of vehicle performance on the

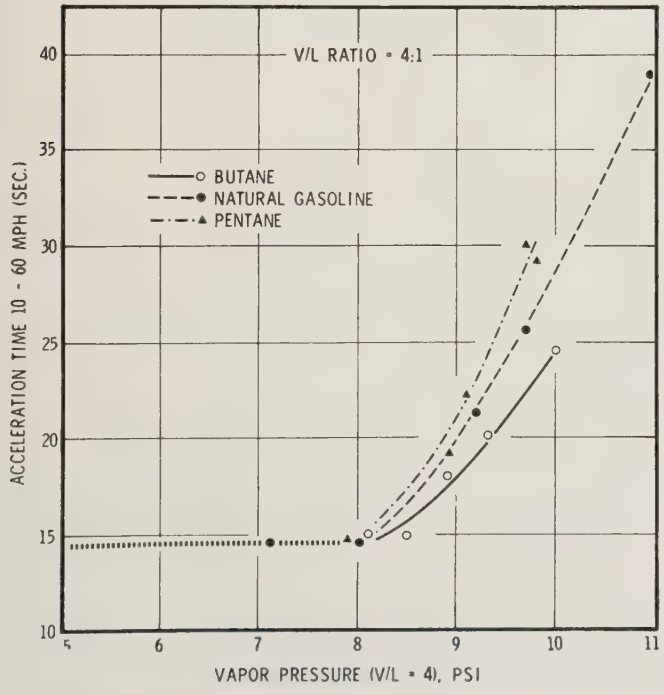

Fig. 7A—Vapor-lock severity versus V/L = 4 vapor pressures, Car B

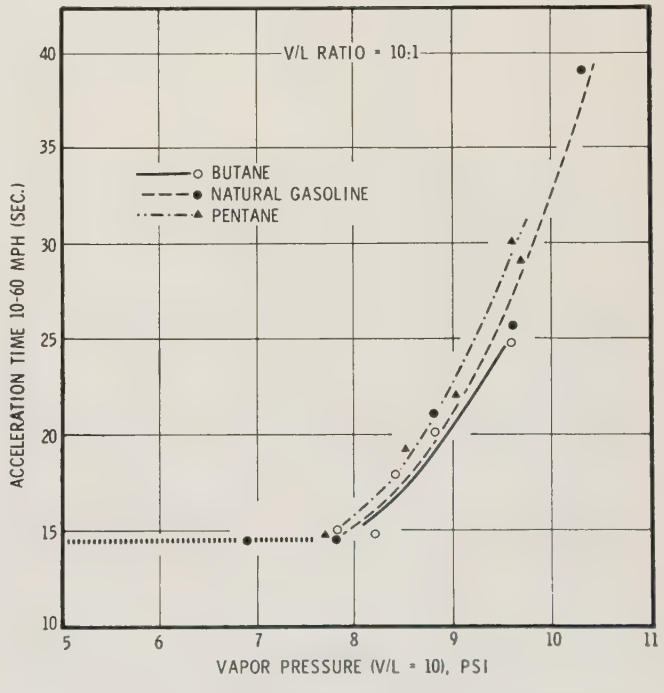

Fig. 7B—Vapor-lock severity versus V/L = 10 vapor pressures, Car B

various fuels it was necessary to make different analyses depending on the transmission and carburetor characteristics of the car. For example, in the case of the car equipped with a torque-converter-type transmission and 4-barrel carburetor, the difference between the car speeds at the 40-sec point on the performance curve was determined for the test fuel and for a fuel of low front-end volatility. In the case of a car equipped with a Hydra-Matic transmission and 2-barrel carburetor, it was found that nearly equal degrees of vapor lock could produce widely different 40-sec speed differences when operating on the edge of the Hydra-Matic shift range. Consequently, for this latter type car, comparisons were made of the elapsed time from 10 mph to various terminal speeds (60 mph, 70 mph) for the two fuels.

In making these tests it is extremely important that all comparisons of fuels be made at the same ambient temperature in a particular car. If this is not done, it is necessary to attempt to correct the results to a given ambient temperature. Unfortunately, the methods of correction available require a number of assumptions that are known to be seriously in error. Consequently, any such correction procedure is entirely indefensible in a study of this type. Therefore, all the test work in a particular car was performed at a temperature within ± 2 F of the standard.

Summary of Results—The most informative method of displaying the results of passenger-car and modified bomb evaluations of the same fuels are plots of car performance as a function of bomb vapor pressures for each of the various bomb ratios. Since data were obtained in four cars at two conditions (soak and idle acceleration) and at six bomb ratios, 48 such plots would be required to present all of this information. Consequently, it is necessary to summarize by the use of a limited number of representative plots.

Figs. 7A, B, C, D, and E are the data obtained with car B during soak accelerations for bomb ratios of 4, 10, 20, 25, and 30 respectively. Two conclusions are evident from these plots:

1. Fig. 1A strikingly supports the contention that as a criterion of vapor-locking tendency, Reid vapor pressure is not satisfactory.

2. Bomb ratios of 20 or 25 result in a satisfactory correlation between vapor-locking tendency as predicted by the modified bomb and as experienced by the car.

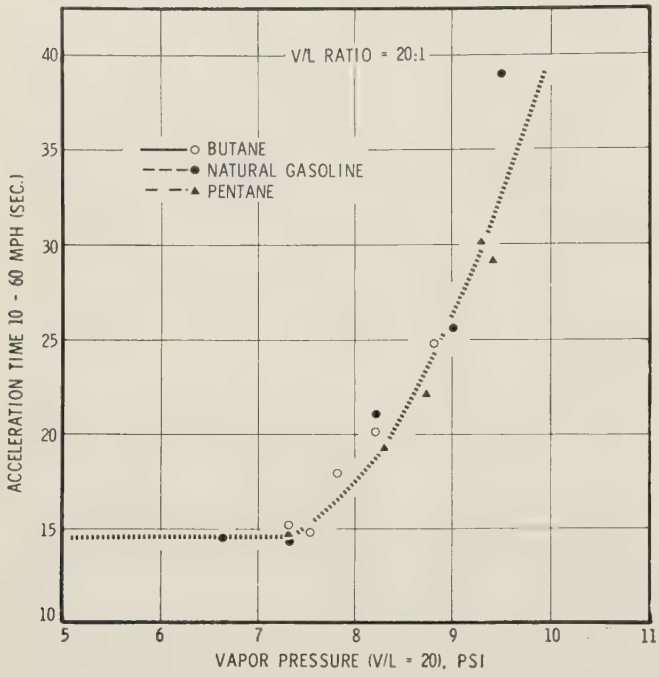

Fig. 7C—Vapor-lock severity versus V/L = 20 vapor pressures, Car B

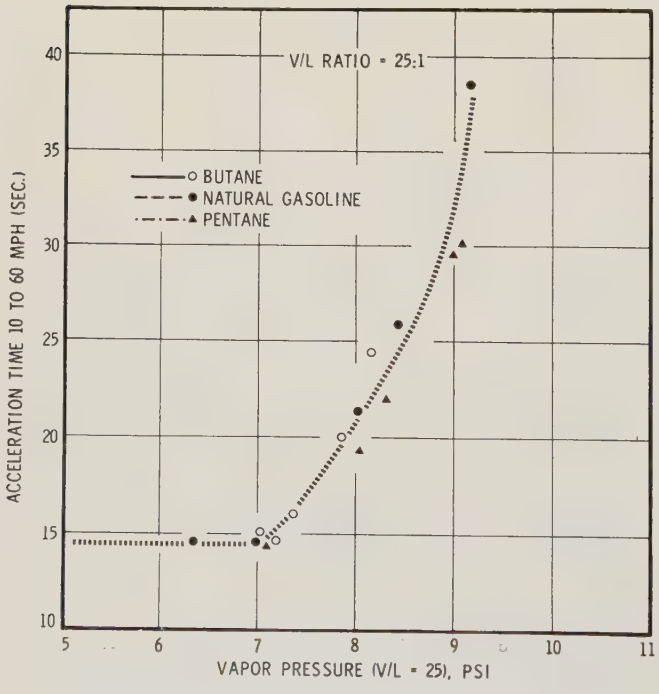

Fig. 7D—Vapor-lock severity versus V/L = 25 vapor pressures, Car B

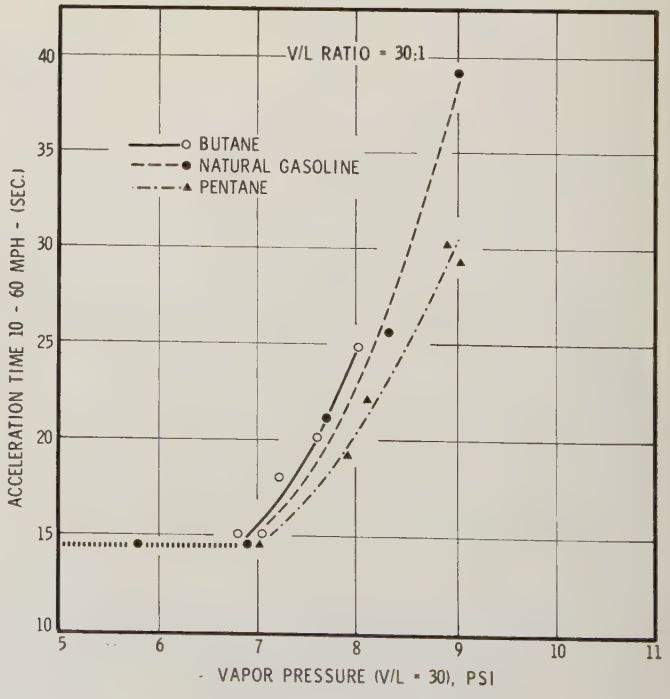

Fig. 7E—Vapor-lock severity versus V/L = 30 vapor pressures, Car B

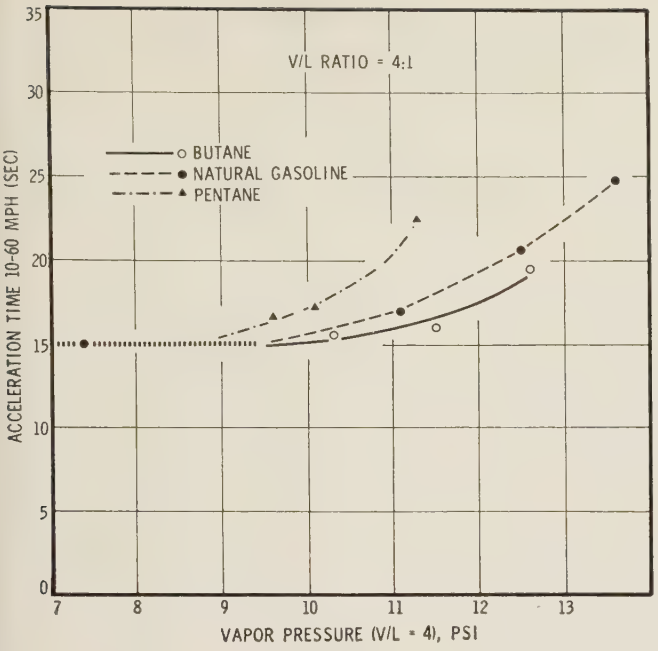

Fig. 8A—Vapor-lock severity versus V/L = 4 vapor pressures, Car D

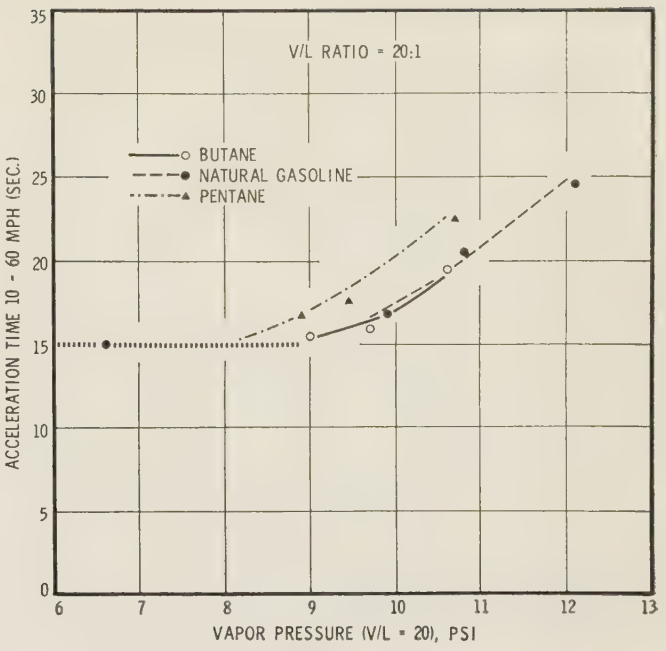

Fig. 8B—Vapor-lock severity versus V/L = 20 vapor pressures, Car D

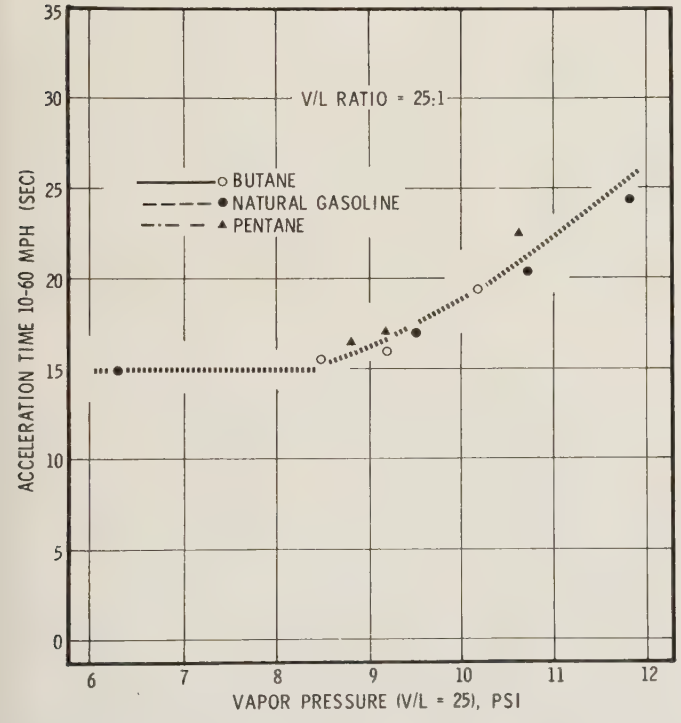

Fig. 8C—Vapor-lock severity versus V/L = 25 vapor pressures, Car D

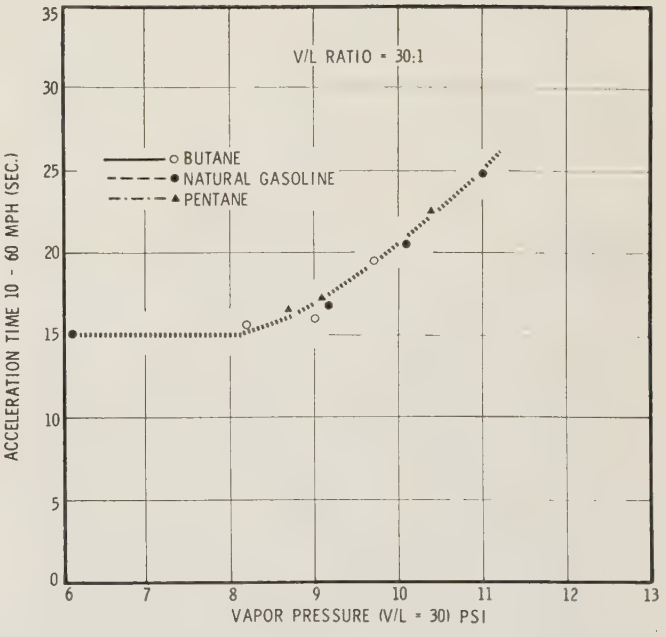

Fig. 8D—Vapor-lock severity versus V/L = 30 vapor pressures, Car D

An analysis of the idle acceleration data for this same car confirms the fact that a ratio of 20 to 25 gives a satisfactory correlation between predicted and measured vapor-locking tendencies. The observation that the bomb ratio of best correlation is the same in both types of accelerations for a particular car has been confirmed for each of the cars tested.

A similar series of plots for car D is shown in Figs. 8A, B, C and D for bomb ratios of 4, 20, 25, and 30 respectively. In this instance, the data are for the idle accelerations rather than the soak accelerations. Again, it is evident how poorly Rvp predicts vapor-locking tendency. However, note that for car D it appears that best correlation is with bomb ratios of 25 or 30 in contrast to 20 or 25 for car B.

The observation that the ratio which gives the best correlation varies slightly from car to car is not unexpected since it is known that the relative vapor-handling capabilities of cars vary. However, the important observation is that by the use of a higher bomb ratio, irrespective of the car, a great improvement can be made in the ability to pre-

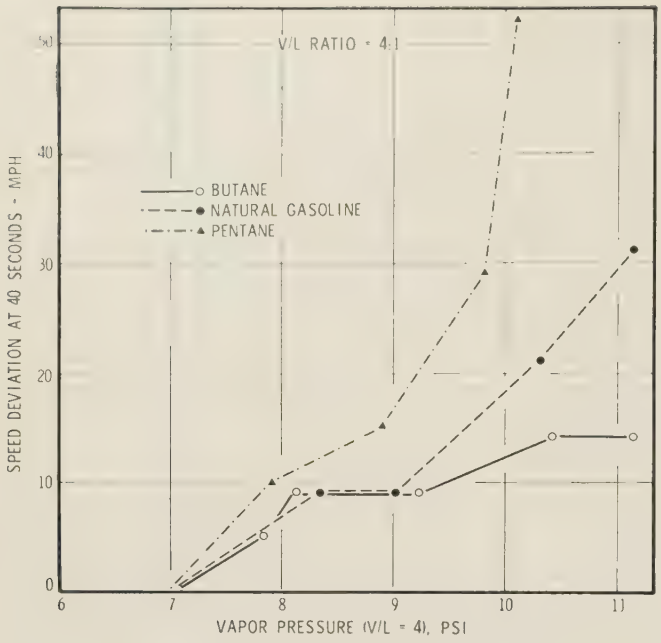

Fig. 9A—Vapor-lock severity versus V/L = 4 vapor pressures, Car C

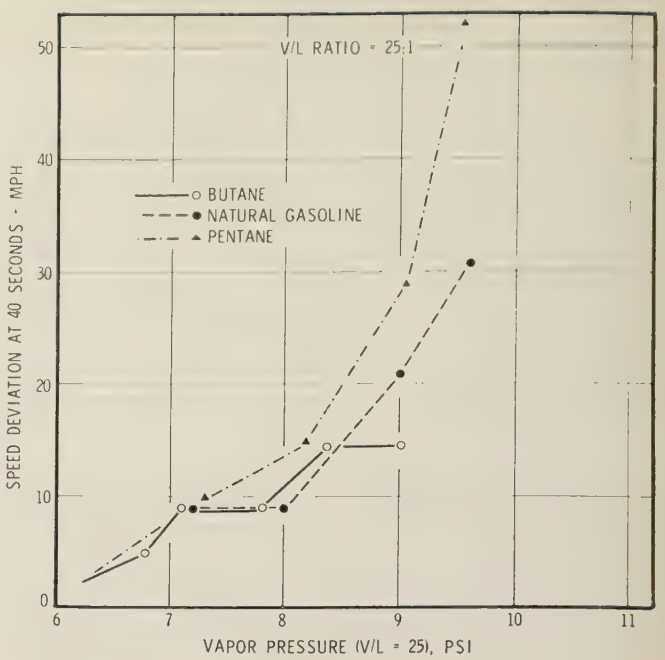

Fig. 9B—Vapor-lock severity versus V/L = 25 vapor pressures, Car C

dict vapor-locking tendency over that obtainable with Reid vapor pressure.

The preceding two sets of data were for different cars, but each was equipped with a Hydra-Matic transmission. Fig. 9A and B present similar data for car C which had a torque-converter-type transmission. In this case, only data for bomb ratios of 4 and 25 are shown. The 25/1 ratio gave the best correlation of the ratios studied. Note that with this car, at performance impairment levels greater than borderline lock, flat spots are observed on the curves. These flat spots as well as the erratic performance at severe levels of lock are characteristic of certain fuel system-engine-transmission combinations. The reasons for these characteristics are not well understood. A logical possibility is that the carburetor metering systems in these vehicles have greater vapor-handling capabilities than in those vehicles not exhibiting these characteristics. Consequently, vapor formation in excess of that causing borderline look is not as deleterious in terms of performance impairment as in metering systems of lower vapor-handling capabilities.

In spite of the different performance behavior observed with car C at severe levels of lock, it is evident from Fig. 9 that at the border-line level (10 sec or less speed deviation) the use of the 25/1 ratio bomb gives a satisfactory correlation of vapor-locking tendencies and that the 4/1 ratio bomb does not. Although consideration of severe levels of lock are of interest in understanding the interrelation of the fuel system-vehicle combination, it is the borderline level of lock that is of more practical importance.

In Fig. 10 are shown crossplots of some of the data from Figs. 7, 8, and 9. For each car, only the fuel from each series which gave approximately borderline lock (that is, same performance impairment) is considered. The curves relate the vapor pressures of these specific fuels as a function of bomb ratio. This illustration, therefore, compares fuels which have the same vapor-lock rating in the cars with the vapor pressure at the various bomb ratios. When the precision of both road vapor-lock testing and bomb vapor pressure determinations are considered, the coincidence of the points for the different fuels at the higher ratios is excellent. It is the authors' belief that these data provide sufficient incentive and adequate justification to use a vapor pressure bomb modified to provide a higher V/L ratio as a practical method of measuring the vapor-locking tendencies of gasolines.

Standardization of Bomb Ratio at 25/1

For practical application of the modied bomb, it is necessary to select a specific single V/L ratio. A ratio of 25/1 is recommended based upon the following considerations:

1. A ratio anywhere in the range 20–30 will provide a satisfactory prediction of vapor-lock performance which will be a radical improvement over the use of Rvp.

2. Of the four cars tested, the best correlation was obtained for two of the cars in the range 20–25 and for one of the cars in the range 25–30. For the fourth car, sufficient data over a narrow temperature range were not obtained to indicate which specific ratio between 20 and 30 would give the best correlation.

3. It is expected that the vapor handling capacity of car fuel systems are more likely to increase than decrease. Consequently, a ratio of 25/1 provides a suitable compromise between immedate and future applications. In this connection, it should be noted that present-day cars will still be in operation 10–15 years from now.

4. Radical changes in fuel systems which result in marked increases in vapor-handling capacity will require an upward change in the ratio and a re-evaluation to determine the ratio of best compromise. The possibility of such changes is inherent

in any bench test which is designed to predict the performance of a product in a mechanism such as a passenger car, which is continually being improved.

The modified bomb with a V/L ratio of 25/1 is now in use in our corporation for characterizing gasoline volatility. This vapor pressure is designated "General Motors vapor pressure (GMvp)."

Practical Applications of GM Vapor Pressure

The availability of a single number which predicts the vapor-locking tendency of gasoline has a number of very practical applications. First and most important, it permits volatility studies to be performed and comprehended by individuals who have not been exposed to the considerable "lore" that has become associated with the volatility of gasoline.

Another important application of the GMvp is in interpreting the significance of vapor-lock test results. In the past it has been common practice to carry out vapor-lock tests with either a base fuel and a single pressurizing agent or with blends of high and low Rvp fuels of the same distillation characteristics. When the limiting Rvp of a vehicle was found with this fuel, the results could be compared to those obtained on another vehicle only when using the same system of reference fuels. Also, there was no reliable method available to predict from the test results the performance in the vehicle of a group of commercial gasolines of volatility characteristics differing from those of the reference fuels. Further, if the volatility characteristics of the reference fuels were changed from year to year, there was no reliable method available for comparing the vapor-locking tendencies of vehicles tested in different model years.

With the utilization of GMvp the situation has radically changed in that:

1. Irrespective of variation in test fuel from year to year or even test to test, the use of GMvp permits direct comparison of test results.
2. Based upon the GMvp of commercial gasolines marketed, it is possible to develop a curve relating GMvp versus per cent of gasoline marketed. By plotting the limiting GMvp of a specific passenger car on this curve, a prediction can be made as to the per cent of available gasolines that will permit vapor-lock free operation under the test conditions. Further, it is possible to determine from curves of this type what additional vapor-handling capacity must be built into the car to handle satisfactorily under the chosen test conditions any given percentage of the gasolines marketed.

Limiting GMvp of passenger cars can also be used advantageously by the petroleum industry. By reversing the second procedure outlined above, a curve can be constructed of limiting GMvp versus per cent of cars on the road. From this curve, estimates can be made of the maximum allowable GMvp which can be marketed to provide vapor-lock free performance for any given percentage of the motoring public.

Summary

A practical method of measuring and expressing the vapor-locking tendencies of gasolines has been developed. This method utilizes a modification of the Reid vapor pressure apparatus.

The development work was based upon measuring the vapor pressure of gasoline under conditions similar to those occurring in the fuel systems of passenger cars. The final selection of these conditions was made on the basis of vapor-locking tendencies of gasolines as measured by passenger-car performance.

The method has a number of advantages among which are:

1. It provides a single number which realistically predicts the vapor-locking tendencies of gasolines. This number is easily and rapidly determined.
2. It more realistically evaluates the effects of small weathering losses on vapor-locking tendency than does Rvp.
3. It allows direct intercomparisons of vapor-lock test results to be made when using different reference fuel systems.
4. It makes it possible to establish distribution curves of the volatility requirements of the car population for vapor-lock free operation and of the

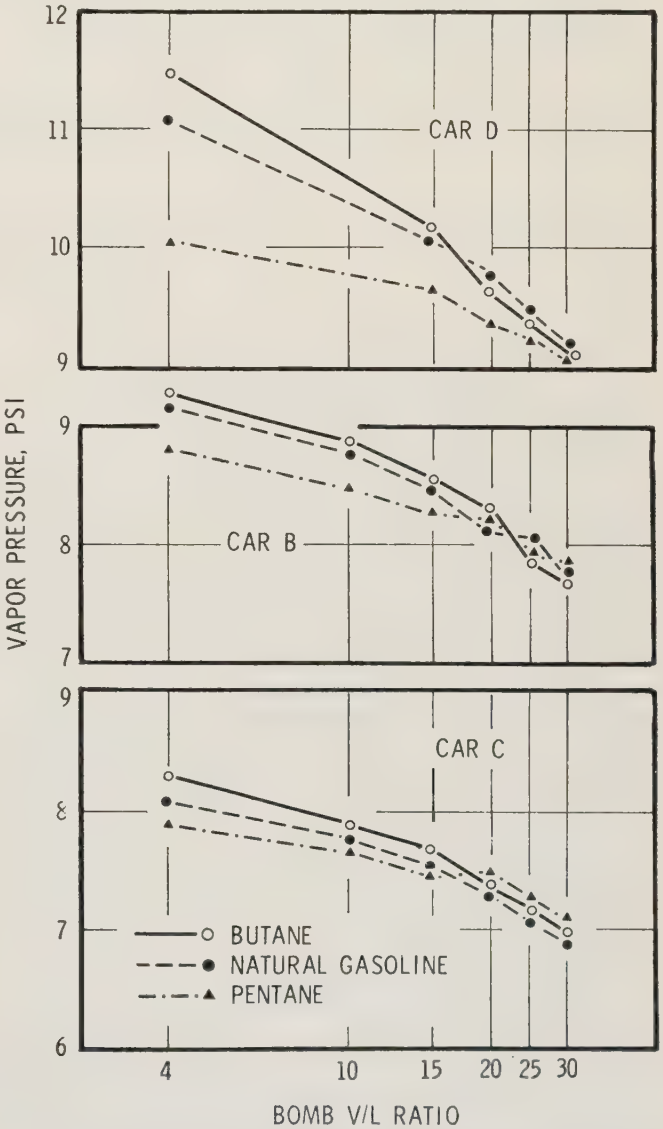

Fig. 10—Comparison of three fuels giving borderline vapor lock, vapor pressure versus bomb V/L ratio

vapor-locking tendencies of gasolines marketed.

5. It permits comprehension of the vapor-locking tendencies of both passenger cars and gasolines by both petroleum technologists and automotive engineers.

The method is designed as General Motors vapor pressure (GMvp) and is now in use throughout our corporation for measuring and expressing gasoline volatility.

Acknowledgment

The authors would like to express their appreciation to Dale R. Johnson for his invaluable help in completing this study and to the General Motors Engine-Fuel Relationship Subcommittee and General Technical Committee for their encouragement and support.

Additional References

1. SAE *Journal*, Vol. 39, 1936, p. 345: "Direct Measurement of V/L Ratio Indicates Discrepancies," by J. M. Campbell, W. G. Lovell, and M. J. Mulligan.

2. *Petroleum Engineer*, Vol. 10, February, 1939, pp. 51–54: "Special Vapor-Pressure Bomb for Demonstration of Vapor-Liquid Relationships," by J. A. Campbell.

3. SAE Transactions, Vol. 53, 1945, pp. 392–402: "Occurrence of Vapor-Lock as Related to Temperature—V/L Characteristics of Motor Gasolines," by E. W. Aldrich, E. M. Barber, and A. E. Robertson.

4. SAE *Journal*, Vol. 52, August, 1944, pp. 364–367: "Correlation of Temperature—V/L Characteristics of Motor Gasolines with Inspection Test Data," by E. W. Aldrich, E. M. Barber, and A. E. Robertson.

5. "Evaluation of CRC V/L Apparatus." Coordinating Research Council, New York, 1951.

6. API Proceedings, Vol. 33, 1953, Sec. 3, pp. 112–116; "Effect of Gasoline Volatility on Performance of Passenger Cars," by C. J. Domke, C. B. Tracy, and H. R. Taliferro.

7. "Vapor-Locking Characteristics of Passenger Cars," by R. E. Barnum, P. J. Clarke, and J. P. Hamer. Paper presented at the SAE Summer Meeting, Atlantic City, June 6–11, 1954.

8. "Passenger-Car Vapor Lock," by D. P. Heath, R. H. Thena, and G. Way. Paper presented at SAE Annual Meeting, Detroit, Jan. 10–14, 1955.

9. "Fuels and Fuel Systems." National Gasoline Association of America, Tulsa, 1955.

10. "Weather or Lock, Vapor-Lock Study, Road and Laboratory," by D. P. V. Barnard, R. B. Fell, E. H. Scott, and G. Way. Paper presented at SAE National Fuels and Lubricants Meeting, Tulsa, Nov. 8–9, 1956.

DISCUSSION

Favors Higher V/L Ratio

—L. E. Hebl
Shell Oil Co.

I THINK Messrs. Caplan and Brady have brought forth a very sound idea in proposing that the vapor space of the Reid vapor pressure bomb be increased sufficiently to eliminate the discrimination of the present test against certain types of gasoline blends.

At the present 4/1 ratio of vapor volume to liquid, the Reid test favors pentanes relative to butanes at the expense of the automobile. With a much larger vapor-to-liquid volume ratio, the test could be made to penalize pentanes and favor the lighter hydrocarbons, which I believe the cars and customers would like.

Not only can present-day cars handle much more vapor than the 4 volumes per volume of liquid as now tested in the Reid apparatus, but some of the lightest vapors escape from the fuel tank before reaching the fuel intake system. Thus, the 25 or 30/1 ratio that is shown to give best correlation when testing fresh samples should probably be increased to 40 or even 50/1 in order to correlate best in practice, using actual filling station gasoline blended with the residue left from previous purchases.

I rather feel that a ratio of 25/1 is a short step in the right direction, and that pentanes will still be slightly favored over butanes because of the additional vapor volume actually tolerable besides that of the fuel system alone.

Compares Vapor Pressure Data with That of Authors

—D. P. Heath
Socony Mobil Oil Co.

THE authors deserve much credit for taking an idea that has been talked about for years and doing something useful with it. Since we are among those who have proposed this approach, we thought it would be interesting to compare some of our data with that presented by the authors.

In Fig. A we show a plot of Rvp versus vapor pressure at V/L = 20. These were obtained in a bomb very similar to that used by the authors. The pressuring agents were propane, butane, and pentane.

As they noted, the vapor pressures at V/L = 20 are lower than at V/L = 4. They also commented that the change in vapor pressure with handling losses are smaller at V/L = 20 than with Rvp. We confirm this point for propane and butane fuels, but with pentane fuels both our data and that of Messrs. Caplan and Brady show a greater change at the high V/L ratios than with the Reid method. Thus, the authors' conclusion is true for the general case, but there will be exceptions.

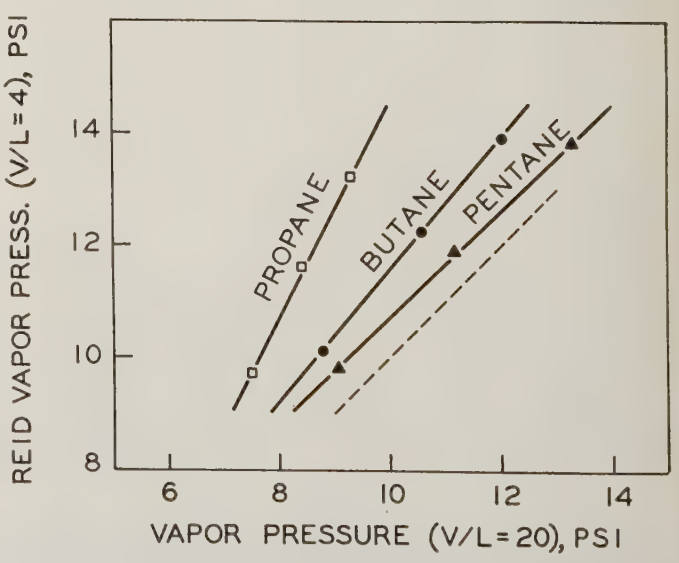

Fig. A—Relationship between vapor pressure at V/L = 4 and V/L = 20

The authors also conclude that the temperature at which the bomb vapor pressure is run is not important, since the relative rating of the fuels does not change with temperature. Some of our data on temperature are shown in Fig. B. Here, vapor pressure at V/L = 20 is plotted against temperature for a fuel pressured with propane, butane, or pentane. As the authors noted, the ranking does not change with temperature; the temperature range shown is much wider, 100–140 F, than what they show, 95–105 F.

Being interested in utilizing this approach to volatility from the petroleum refiners' viewpoint, we find that it is easily adaptable to refinery operation. Taking some liberties, we have composited some of the authors' data and re-present them in Fig. C. You will note that the Rvp increases linearly as butane is added, making it easy to adjust the Rvp of different batches of fuel. Since the authors did not provide a chart for a V/L = 25, we could not accurately present the variation of General Motors vapor pressure (GMvp) with butane addition. However, as an illustration of how this approach could be utilized, we plotted the variation of vapor pressure at V/L = 20 with butane addition. The refiner then can easily determine how much butane to add to obtain a desired change in the vapor-locking tendency of each batch of fuel being blended. With this simplified method of control, he would no longer have to worry about the 10% slope, the Rvp, the 50% point, the per cent off at 158 F, or whatever combination of controls with which he has been previously concerned and confused.

While our vapor pressure data confirm the GM information, there is still one area where we feel that more data are required. This is information on cars to support the choice of V/L = 25 as the point of best correlation. The data presented on three cars support this choice, but we would like to see a wider range of vehicles included and are looking forward to the results of the 1957 CRC program on about thirty vehicles of ten different makes.

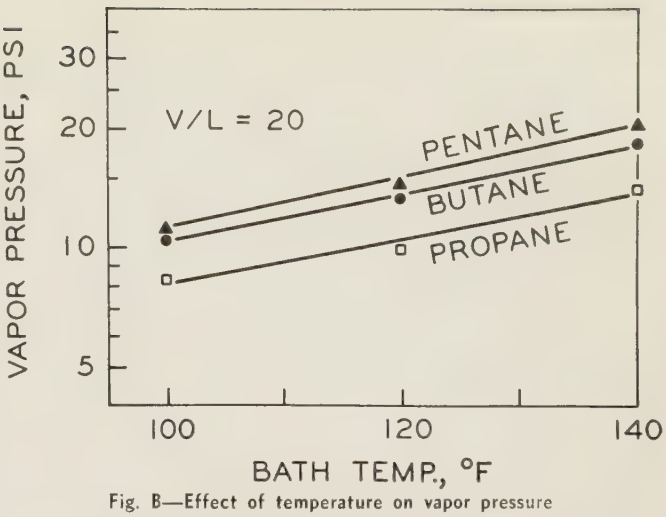

Fig. B—Effect of temperature on vapor pressure

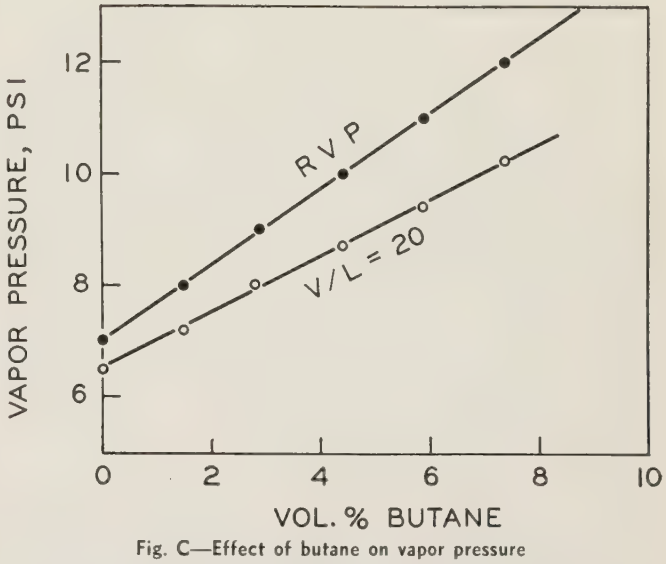

Fig. C—Effect of butane on vapor pressure

Describes Isovapor-Lock Concept

—T. W. Legatski
Phillips Petroleum Co.

THE paper presented is of special interest to us, since our studies of the vapor-lock problem in the past several years have been based on vapor pressures at a V/L ratio of 30 and a fuel temperature of 130 F. The difference between our V/L of 30 and the value of 25 employed by the authors is of relatively minor importance. The temperature difference (130 versus 100 F) is of greater significance since the higher value approximates fuel system temperatures more closely. However, the generalized vapor pressure relations, based on the work of the National Bureau of Standards, permit transformation of the vapor-pressure values from one temperature level to the other.

Laboratory vapor-pressure values obtained under either of the above sets of test conditions have practical value only if they can be interpreted in terms of the values with which we are all familiar, namely, the Reid vapor pressure. This is essential if consideration is to be given to the voluminous vapor-lock information obtained over the past 25 years, and if consideration is to be given to the characteristics of fuels which have been marketed or are currently being marketed. It is for these reasons that we introduced the isovapor-lock concept, that is, a line relating Reid vapor pressure and 10% point slope for constant vapor-locking tendency. Each isovapor-lock line is equivalent to a *single* vapor pressure value at V/L = 30 and at 130 F, and in fact is derived therefrom by means of the generalized vapor-pressure relations. Similar derivations can be made from other chosen values of V/L ratio and of temperature.

The authors emphasize the desirability of running check vapor-lock tests at constant ambient temperature, and question the validity of the methods which have been employed by others for making correction for changes in ambient temperature. It is agreed that more precise information on this temperature coefficient would be helpful, but until such information becomes available, there is no choice but to use the best methods currently available. From the standpoint of marketing practices, the petroleum industry has employed the current methods with marked success in their endeavor to maintain a uniform degree of protection against vapor lock regardless of season.

It is possible that the GMvp would serve as a useful screening tool to simplify the testing of prototypes of new model cars as regards their vapor-locking tendency. Use of these GMvp data, however, as a guide to vapor-pressure levels for commercial fuels introduces the same uncertainties as in the past. Thus, all cooperative vapor-lock test programs follow the same historic pattern. Data are obtained on a variety of cars, and on analysis it is found that the cars should encounter serious vapor lock on most commercial fuels. The facts are, however, that these cars in the hands of their owners show almost entire freedom from vapor lock. Therefore, a correction is applied to the cooperative road test data to make them conform to fuel marketing practices. Experience has shown that the safest guide for the petroleum industry is a study of vapor-pressure levels of marketed fuels, relative to their distillation characteristics. On the other hand, the car manufacturer needs the best type of test methods available and obtainable in order that he may keep pace with the steadily increasing vapor pressure and front-end volatility of motor fuels.

Mathematical in Removed

DETERMINATION of subsurface residual stresses by X-ray diffraction and layer removal requires correction in the stresses as measured. The significance of the correction is proportional to the magnitude of relieved stress in the layer and to the depths involved.

Correction formulas are developed for the solid circular cylinder, the hollow cylinder or tube, and the flat plate. Symmetric and nonsymmetric peripheral stresses are taken for the solid cylinder. Examples are shown and limitations and applications of the formulas are discussed.

PREVIOUS papers[1,2] have discussed the application of modern X-ray diffraction techniques for the determination of residual stresses. Because X-rays are diffracted from surface layers only, a determination of stress distribution with depth requires removal of material to the depths desired. When stressed layers are removed, the successively measured stresses at depths below the surface must be corrected by an amount proportional to the relaxation created by the removed layers. This means that all determinations except the initial value at the surface must be corrected in order to obtain the true stress distribution that existed before the layers were removed.

These corrections can be determined by the "theory of elasticity" and are expressed as functions of the successively measured stresses. Several geometric shapes will be considered

Theoretical Development

Case 1, Solid Cylindrical Bar, Rotationally Symmetric Stresses—We consider a solid bar of radius R in the form of a right circular cylinder (Fig. 1), and we first assume that its residual stress pattern has both rotational and longitudinal symmetry. The stresses, then, are functions only of the distance r from the axis, and do not depend on the angle θ measured around the cylinder or on the distance z taken parallel to its axis. We avoid taking points near an end of the bar since, otherwise, we could expect to encounter end effects depending on z.

By repeatedly removing thin concentric shells from our cylinder and measuring the stresses on the surfaces of our remaining cylinders, we obtain the transverse and longitudinal measured stresses $\sigma_{\theta m}$ and σ_{zm} to be used to determine the original stresses σ_θ, σ_z, and σ_r.

The theory of elasticity provides us with nine partial differential equations, the three equations of equilibrium and the six of compatibility. These have unique solutions for properly specified boundary conditions.

The compatibility equations, expressed in rectangular coordinates, are:

$$(1+\nu)\nabla^2\sigma_x+\frac{\partial^2\Theta}{\partial_x{}^2}=0 \qquad (1+\nu)\nabla^2\tau_{yz}+\frac{\partial^2\Theta}{\partial_y\partial_z}=0$$

$$(1+\nu)\nabla^2\sigma_y+\frac{\partial^2\Theta}{\partial_y{}^2}=0 \qquad (1+\nu)\nabla^2\tau_{xz}+\frac{\partial^2\Theta}{\partial_x\partial_z}=0 \qquad (1)$$

$$(1+\nu)\nabla^2\sigma_z+\frac{\partial^2\Theta}{\partial_z{}^2}=0 \qquad (1+\nu)\nabla^2\tau_{xy}+\frac{\partial^2\Theta}{\partial_x\partial_y}=0$$

where: $\nabla^2=\dfrac{\partial^2}{\partial_x{}^2}+\dfrac{\partial^2}{\partial_y{}^2}+\dfrac{\partial^2}{\partial_z{}^2}$

$\Theta=\sigma_x+\sigma_y+\sigma_z$

These are based on certain simple geometric assumptions, along with the usual linear relationships between stress and strain for isotropic, homogeneous bodies. They do not hold for residual stresses, but they do hold for superimposed stresses produced by outside forces. We readily see that, in particular, constant values of the six stresses, $\sigma_x=\tau_{xy}$ and the rest, satisfy all six equations. We shall be especially interested in the situation, in cylindrical coordinates:

$$\sigma_r=\sigma_\theta=\text{Constant}$$
$$\sigma_z=\text{Constant}$$
$$\tau_{r\theta}=\tau_{rz}=\tau_{\theta z}=0 \qquad (2)$$

where the compatibility equations are satisfied, because $\sigma_x=\sigma_y=\sigma_r=\sigma_\theta=\text{Constant}$, and $\tau_{xy}=\tau_{yz}=\tau_{xz}=0$.

Equations 2 also satisfy the equilibrium equations:

$$\frac{\partial\sigma_r}{\partial r}+\frac{1}{r}\frac{\partial\tau_{r\theta}}{\partial\theta}+\frac{\partial\tau_{rz}}{\partial z}+\frac{\sigma_r-\sigma_\theta}{r}=0$$

$$\frac{\partial\tau_{rz}}{\partial r}+\frac{1}{r}\frac{\partial\tau_{\theta z}}{\partial\theta}+\frac{\partial\sigma_z}{\partial z}+\frac{\tau_{rz}}{z}=0$$

$$\frac{\partial\tau_{r\theta}}{\partial r}+\frac{1}{r}\frac{\partial\sigma_\theta}{\partial\theta}+\frac{\partial\tau_{\theta z}}{\partial z}+2\frac{\tau_{r\theta}}{z}=0 \qquad (3)$$

These are based on the ideas of statics and hold for residual stresses as well as for other stresses.

At the surface of a cylinder of radius r, the residual stress $\sigma_r=\tau_{r\theta}=\tau_{rz}=0$. Since all stresses are independent of θ and z, we then have from Equations 3:

$$\frac{\partial\tau_{rz}}{\partial r}=\frac{\partial\tau_{r\theta}}{\partial r}=0 \qquad \frac{\partial\sigma_r}{\delta r}=\frac{\sigma_\theta}{r} \qquad (4)$$

On removing a thin outer shell, the only force we have removed from each square unit of surface of the remaining cylinder is, then, the small outward force $(-\sigma_\theta)\ dr/r$, where dr is the thickness of the shell. The radial and transverse stresses throughout the remaining cylinder are then reduced by this same constant quantity, as our discussion of Equation 2 indicates.

By repeatedly removing thin shells, we may then use integration to find the total stress removed be-

---

[1] "Structures of Metals," by C. S. Barrett, Chap. 14. Pub. by McGraw-Hill, New York, 1952.

[2] Transactions of American Society for Metals, Vol. 45, 1953, pp. 638–676; "X-Ray Measurement of Residual Stress in Hardened High Carbon Steel," by A. L. Christenson and E. S. Rowland.

Correction for Stress Layers in X-Ray Diffraction Residual Stress Analysis

M. G. Moore, Mathematics Department, Bradley University
W. P. Evans, Caterpillar Tractor Co.

This paper was presented at a meeting of the SAE Residual Stress Committee, Pittsburgh, Aug. 7-8, 1956.

fore we reach some value $r = r_1$ in which we are interested. We thus obtain the formula:

$$\sigma_r(r_1) = -\int_{r_1}^{R} \frac{\sigma_{\theta m}(r)\,dr}{r} \qquad (5)$$

where:

R = Radius of the entire cylinder
$\sigma_r(r_1)$ = Radial stress at a distance of r_1 from the axis
$\sigma_{\theta m}(r)$ = Transverse stress actually measured when the part of the cylinder which remains has a radius r.

Since the removal of a thin shell has the same effect on transverse stresses as on radial, we also know that:

$$\sigma_\theta(r_1) = \sigma_{\theta m}(r_1) + \sigma_r(r_1) \qquad (6)$$

The longitudinal component of stress has not entered our equations. However, in Equation 2 we noted that the removal of a thin shell modifies σ_z by a constant. To determine the constant, we need only note that the sum of all longitudinal forces exerted by one end of the bar on the other must still vanish after the removal of a thin shell. The stress which has been removed is, then:

$$(-\sigma_z)\,(2\pi r dr)/\pi r^2 = (-2\sigma_z dr)/r$$

We thus obtain the formula:

$$\sigma_z(r_1) = \sigma_{zm}(r_1) - 2\int_{r_1}^{R} \frac{\sigma_{zm}(r)\,dr}{r} \qquad (7)$$

In practice, each of these integrals is evaluated as an area under the smooth curve which seems best to fit the finite number of measurements taken.

Case 2, Solid Cylindrical Bar Varying σ_θ Stresses—If the stresses in a cylinder are independent of z (Fig. 2), it is natural and convenient to assume that $\tau_{\theta z} = 0$. We then make the two assumptions together. On the curved surface (where $\sigma_r = \tau_{r\theta} = \tau_{rz} = 0$) the equilibrium Equations 3 give the results:

$$\frac{\partial \sigma_r}{r} - \frac{\sigma_\theta}{r} = 0 \qquad \frac{\partial \tau_{r\theta}}{\partial_r} + \frac{1}{r}\frac{\partial \sigma_\theta}{\partial_\theta} = 0 \qquad \frac{\partial \tau_{rz}}{\partial_r} = 0 \qquad (8)$$

The removal of a shell of small thickness dr will then remove forces on the remaining cylinder in both the radial and transverse directions, but none in the longitudinal. We thus have a two-dimensional stress pattern produced by the radial force $(-\sigma_\theta)\,dr/r$ and the tangential force $(\partial\sigma_\theta/\partial_\theta)\,(dr/r)$ per square unit of surface area.

Such problems have been solved by complex variable methods, and I. S. Sokolnikoff[3] does this by taking X_ν and Y_ν as the rectangular components of the surface force per unit area, taking with $i = \sqrt{-1}$:

$$f_1 + if_2 = ir\int_0^\theta (X_\nu + iY_\nu)\,d\theta$$

and expanding $f_1 + if_2$ in a complex Fourier series.

In cylindrical coordinates, we write, then:

$$f_1 + if_2 = ir\int_0^\theta (\sigma_r + i\tau_{r\theta})\,e^{i\theta}d\theta$$

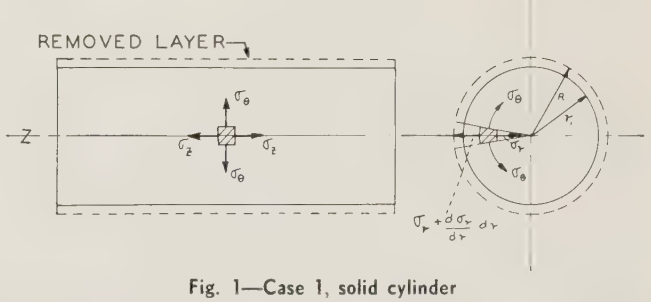

Fig. 1—Case 1, solid cylinder

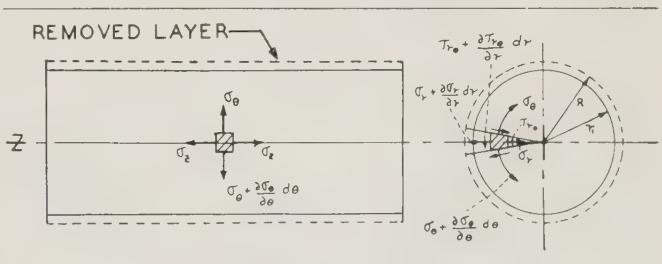

Fig. 2—Case 2, solid cylinder with varying σ_θ stresses

[3] "Mathematical Theory of Elasticity," by I. S. Sokolnikoff, Chap. 5. Pub. by McGraw-Hill, New York, 1956.

for σ_r and $\tau_{r\theta}$ at the surface of our inner cylinder. From Equation 8 it then follows that:

$$f_1 + if_2 = (-idr)\int_0^{\theta}(\sigma_\theta - i\frac{\partial\sigma_\theta}{\partial\theta})e^{i\theta}d\theta \qquad (9)$$

where σ_θ is at the surface and, so, is identical to $\sigma_{\theta m}$.

Expanding $\sigma_{\theta m}$ in a Fourier series as:

$$\sigma_{\theta m} = \sum_{n=-\infty}^{\infty} g_n e^{ni\theta} \qquad (10)$$

it follows that:

$$f_1 + f_2 = (-idr)\int_0^{\theta}\sum_{\infty}^{\infty}(n+1)g_n e^{(n+1)i\theta}de$$

$$= (-dr)\sum_{\substack{-\infty \\ n\neq 0}}^{\infty} g_{n-1}(e^{ni\theta}-1) \qquad (11)$$

Sokolnikoff gives the stresses in terms of two functions $\phi'(z)$ and $\psi'(z)$, where $z = x + iy = re^{i\theta}$. Expressed in our notation, they are:

$$\phi'(z) = (-dr)\left[\frac{g_c}{2r} + \sum_2^{\infty}\frac{nz^{n-1}g_{n-1}}{r^n}\right]$$

$$\psi'(z) = (-dr)\sum_1^{\infty}\frac{nz^{n-1}}{r^n}[\bar{g}_{-n-1} - (n+2)g_{n+1}] \qquad (12)$$

He now obtains the stresses from the equations, using "*Re*" to indicate the real part:

$$\sigma_r + \sigma_\theta = 4Re\phi'(z)$$

$$\sigma_r - i\tau_{r\theta} = \phi'(z) + \bar{\phi}'(\bar{z}) - [\bar{z}\phi''(z) + \psi'(z)]\,e^{2i\theta} \qquad (13)$$

Since our chief interest is in the case for which $g_n = 0$ except when $n = -1, 0, 1$; we now restrict ourselves to this case, although the mathematics does not compel us to do so. We then have $\psi'(z_1) = 0$ and $\phi'(z_1) = -(\frac{1}{2}g_0/r + 2g_1r_1e^{i\theta}/r^2)$, where r_1 and z_1 refer to a point in our cylinder, and r is the outside radius.

Proceeding in the same way as in Case 1, and taking $g_n(r)$ as a function of r determined from $\sigma_{\theta m}$:

$$\sigma_r(r_1,\theta) = \int_{r_1}^{R}\{g_0(r)/r + 2r_1/r^2 Re[g_1(r)(\cos\theta + i\sin\theta)]\}\,dr, \qquad (14)$$

$$\sigma_\theta(r_1,\theta) = \sigma_{\theta m}(r_1,\theta) - \int_{r_1}^{R}\{g_0(r)/r + 6r_1/r^2 Re[g_1(r)(\cos\theta + i\sin\theta)]\}\,dr \qquad (15)$$

If the stresses are always symmetric with respect to the X-axis, the above formulas may be simplified by dropping the *Re* and the $i\sin\theta$, for $g_1(r)$ will be real. The equations are then:

$$\sigma_r(r_1,\theta) = -\int_{r_1}^{R}\{g_0(r)/r + 2r_1/r^2 g_1(r)\cos\theta\}\,dr \qquad (16)$$

$$\sigma_\theta(r_1,\theta) = \sigma_{\theta m}(r_1,\theta) - \int_{r_1}^{R}\{g_0(r)/r + 6r_1/r^2 g_1(r)\cos\theta\}\,dr \qquad (17)$$

We also have:

$$\tau_{r\theta}(r_1,\theta) = -Im\int_{r_1}^{R} 2r_1/r^2 g_1(r)(\cos\theta + i\sin\theta)\,dr \qquad (18)$$

which, with $g_1(r)$ real, becomes:

$$\tau_{r\theta}(r_1,\theta) = -\int_{r_1}^{R} 2r_1/r^2 g_1(r)\sin\theta\,dr \qquad (19)$$

The value of $\sigma_z(r_1,\theta)$ will be handled in a way similar to that employed in Case 1. The removal of a thin shell must not change the fact that the sum of all longitudinal forces exerted by one end of the bar on the other must vanish, and the sum of the moments of force must also vanish. For:

$$\sigma_{zm}(r,\theta) = h_0(r) + h_1(r)e^{i\theta} + h_{-1}(r)e^{-i\theta} \qquad (20)$$

We are then led to the formula:

$$\sigma_z(r_1,\theta) = \sigma_{zm}(r_1,\theta) - \int_{r_1}^{R}\{2h_0(r)/r + Re[8r_1h_1(r)/r^2(\cos\theta + i\sin\theta)]\}\,dr \qquad (21)$$

If the stresses are symmetric with respect to the X-axis, we have:

$$\sigma_z(r_1,\theta) = \sigma_{zm}(r_1,\theta) - \int_{r_1}^{R}\{2h_0(r)/r + 8r_1h_1(r)/r^2\cos\theta\}\,dr \qquad (22)$$

If we make stress measurements at points $\theta = 0$, 90, 180, and 270 deg, and, if we call these $\sigma_{\theta m_0}$, $\sigma_{\theta m_1}$, $\sigma_{\theta m_2}$, $\sigma_{\theta m_3}$, the quantities g_0 and g_1 in our formulas can be obtained as follows:

$$g_0(r) = \tfrac{1}{4}[\sigma_{\theta m_0}(r) + \sigma_{\theta m_1}(r) + \sigma_{\theta m_2}(r) + \sigma_{\theta m_3}(r)]$$

$$g_1(r) = \tfrac{1}{4}[\sigma_{\theta m_0}(r) - \sigma_{\theta m_2}(r) - i(\sigma_{\theta m_1}(r) - \sigma_{\theta m_3}(r)] \qquad (23)$$

Similarly

$$h_0(r) = \tfrac{1}{4}[\sigma_{zm_0}(r) + \sigma_{zm_1}(r) + \sigma_{zm_2}(r) + \sigma_{zm_3}(r)]$$

$$h_1(r) = \tfrac{1}{4}[\sigma_{zm_0}(r) - \sigma_{zm_2}(r) - i(\sigma_{zm_1}(r) + \sigma_{zm_3}(r)] \qquad (24)$$

Case 3, Hollow Cylinder, Rotationally Symmetric Stresses—Let R_1 and R be the inner and outer radii of a long cylindrical pipe, as shown in Fig. 3 We suppose that the residual stresses are independent of θ and z for portions sufficiently distant from the ends. Repeatedly removing thin cylindrical shells from the outer surface, we obtain stress measurements $\sigma_{\theta m}(r)$ and $\sigma_{zm}(r)$, as in Case 1.

The equilibrium Equations 3 again lead to the Equation 4, so that the removal of a thin shell from a hollow cylinder of outer radius r again removes the

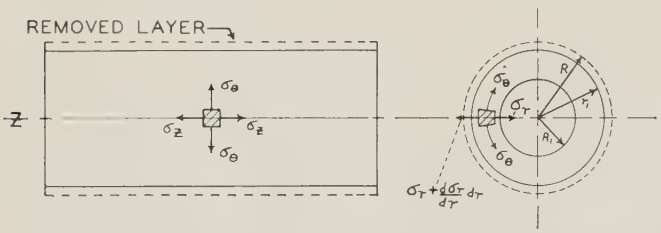

Fig. 3—Case 3, hollow cylinder

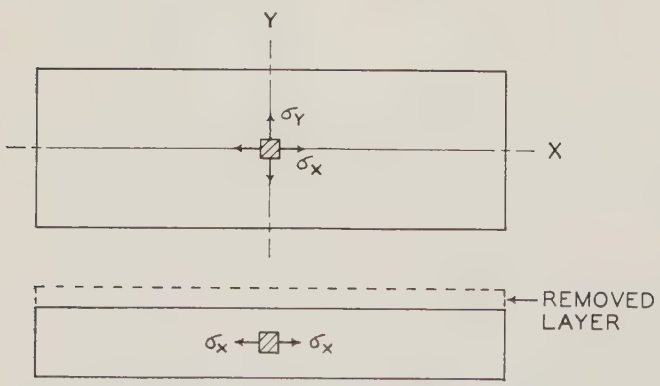

Fig. 4—Case 4, flat plate

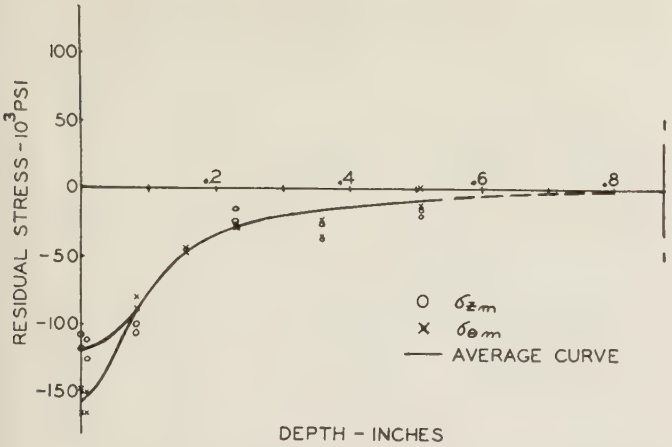

Fig. 5—Solid bar, Case 1 measured data, SAE 1049 induction hardened steel, 0.125-in. depth of case

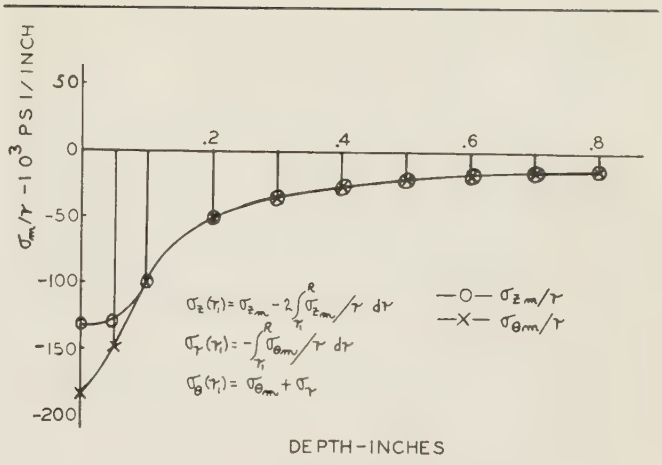

Fig. 6—$\sigma m/r$ for numerical integration, Case 1

small outward force $(-\sigma_\theta)\,dr/r$ from each square unit of curved outer surface of the remaining cylinder.

Employing the known solution to the stress problems of a hollow cylinder subject to uniform external pressure,[4] we find that the removal of the shell removes along with a constant longitudinal stress, a radial stress at r_1, of: $$-\frac{\sigma_{\theta m}(r)}{r}\cdot\frac{r^2}{r^2-R_1^2}\cdot\left(1-\frac{R_1^2}{r_1^2}\right)dr$$

and a transverse stress of:

$$-\frac{\sigma_{\theta m}(r)}{r}\cdot\frac{r^2}{r^2-R_1^2}\cdot\left(1+\frac{R_1^2}{r_1^2}\right)dr$$

Our final formulas, then, are:

$$\sigma_r(r_1) = -\left(1-\frac{R_1^2}{r_1^2}\right)\int_{r_1}^{R}\frac{r\sigma_{\theta m}(r)\,dr}{r^2-R_1^2} \qquad (25)$$

$$\sigma_\theta(r_1) = \sigma_{\theta m}(r_1) + \frac{r_1^2+R_1^2}{r_1^2-R_1^2}\,\sigma_r(r_1) \qquad (26)$$

$$\sigma_z(r_1) = \sigma_{zm}(r_1) - 2\int_{r_1}^{R}\frac{r\sigma_{zm}(r)\,dr}{r^2-R_1^2} \qquad (27)$$

Case 4, Flat Plate—We suppose that the residual stresses in a flat plate of uniform thickness depend only on the distance from one of the flat surfaces of the plate except, of course, near the edges. We suppose at first, also, that the principal stresses are σ_x, σ_y, σ_z, with the Z-axis perpendicular to the flat surfaces of the plate (Fig. 4).

From our assumptions and the equilibrium equation:

$$\frac{\partial\tau_{xz}}{\partial_x}+\frac{\partial\tau_{yz}}{\partial_y}+\frac{\partial\sigma_z}{\partial_z}=0 \qquad (28)$$

it follows immediately that: $$\frac{\partial\sigma_z}{\partial z}=0 \qquad (29)$$

and, since σ_z must vanish on the surface, for all points sufficiently distant from the edges of the plate: $$\sigma_z = 0 \qquad (30)$$

In removing a layer of small uniform thickness from the top surface of the plate, we remove a tension (or compression) and a bending moment in the rest of the plate for each of the two principal stresses σ_x and σ_y. If z is the thickness of the plate, and z_1 the distance from the lower surface to a point in which we are interested, the removal of a layer of thickness dz from the top surface will, if we neglect the bending movement, remove a compression in the direction of the x-axis of $\sigma_{xm}(z)\,dz/z$.

For each unit of plate width in the direction of the y-axis, it will also remove a bending moment of $\frac{1}{2}z\sigma_{xm}(z)\,dz$. This produces a tension at the point in which we are interested, $z^3/12$ being the moment of inertia of the rectangular cross-section with respect to the neutral axis:

$$\frac{(z_1-\frac{1}{2}z)\cdot\frac{1}{2}z\sigma_{xm}(z)\,dz}{z^3/12}$$

Correcting the measured stress, we then find that, if H is the original thickness of the plate, $\sigma_x(z_1)$ must be:

$$\sigma_{xm}(z_1) - \int_{z_1}^{H}\frac{\sigma_{xm}(z)\,dz}{z} - \int_{z_1}^{H}\frac{(z_1-\frac{1}{2}z)\,\frac{1}{2}z\sigma_{xm}(z)\,dz}{z^3/12}$$

which simplifies to:

$$\sigma_x(z_1) = \sigma_{xm}(z_1) + 2\int_{z_1}^{H}\frac{\sigma_{xm}(z)\,dz}{z} - 6z_1\int_{z_1}^{H}\frac{\sigma_{xm}(z)\,dz}{z^2} \qquad (31)$$

The similar formula also holds:

$$\sigma_y(z_1) = \sigma_{ym}(z_1) + 2\int_{z_1}^{H}\frac{\sigma_{ym}(z)\,dz}{z} - 6z_1\int_{z_1}^{H}\frac{\sigma_{ym}(z)\,dz}{z^2} \qquad (32)$$

If σ_x and σ_y are not principal stresses, Equation 30 still holds, as do the equations $\tau_{xz}=\tau_{yz}=0$. Our stress pattern is then produced by the superposition of τ_{xy} on σ_x and σ_y. But τ_{xy} is the difference of two equal principal stresses making angles of 45 and 135 deg with the X-axis. Separate consideration of the four stresses again lead to Equations 31 and 32, as well as to a new similar equation:

$$\tau_{xy}(z_1) = \tau_{xym}(z_1) + 2\int_{z_1}^{H}\frac{\tau_{xym}(z)\,dz}{z} - 6z_1\int_{z_1}^{H}\frac{\tau_{xym}(z)\,dz}{z^2} \qquad (33)$$

Discussion

Case 1 considers a solid cylindrical bar with rotational symmetry of stress with regard to r, θ, and z at points away from the ends. Fig. 5 shows the measured stresses of an induction hardened bar (1¾-in. diameter) in the θ and z directions as successive layers are removed. An average curve of measured stress was taken except for the initial values near the surface where some difference was noted. It is seen that no tensile stresses were meas-

[4] "Theory of Elasticity," by S. Timoshenko and J. N. Goodier, pp. 59–60. Pub. by McGraw-Hill, New York, 1951.

ured whatsoever, which is a condition that could not exist in an equilibrium state before the layers were removed.

Fig. 6 shows an intermediate step in the calculation of the correction. As is indicated by the equation on the figure, evaluation of the definite integrals of (σ_m/r) are required. This is accomplished by plotting the integrand as shown and determination of the areas with a planimeter corresponding to the individually removed surface layers. Having evaluated this integral, which is the negative of the σ_r stresses removed, the σ_θ and σ_z stresses are easily obtained.

Fig. 7 shows the corrected principal stresses and comparison to the initially measured values. It is apparent that the correction is directly related to the magnitude of the stresses removed and to the depth. For shallow examination, that is, less than 10% penetration, the correction might well be neglected; for greater depths, however, it becomes increasingly significant.

Case 2 considers the solid cylindrical bar above, except that no rotational symmetry is assumed. Fig. 8 shows a hypothetical plot of measured stresses at four positions, 90 deg apart. A single plane of symmetry is assumed through 0 and 180 deg (making the stresses at 90 and 270 deg equivalent) although this is not necessary in theory as previously mentioned. This type of symmetry would usually exist particularly in bending or straightening operations or many types of heat-treatment. The 90 and 270 deg positions were taken equivalent to the mean of the two extremes at 0 and 180 deg for ease in computation, although, here again the mathematics does not require this to be so.

The corrected θ stresses are shown in Fig. 9. The required equations are indicated and again the integrals are easily evaluated by numerical means. The integrands are functions of g and cos θ, the angle referring to the peripheral position under consideration. The g is evaluated by the relations shown in terms of the four measured θ stresses. If a plane of symmetry exists (as in the case assumed), the 1 and 3 positions are equivalent and the complex part of g is zero, which simplifies the calculation somewhat. The r and z stresses (not shown) can be evaluated in a similar manner.

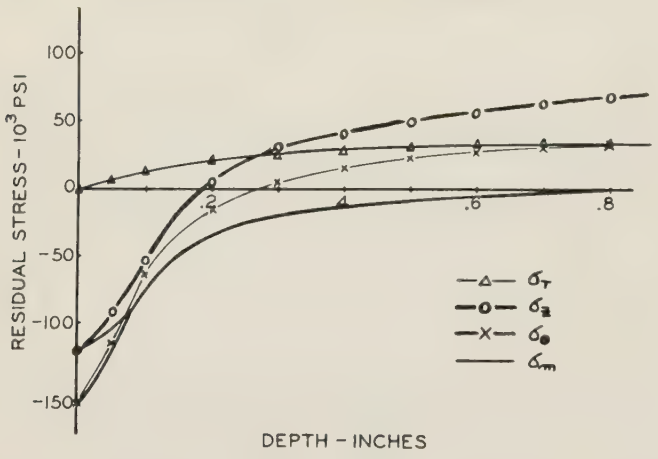

Fig. 7—Corrected stresses, Case 1

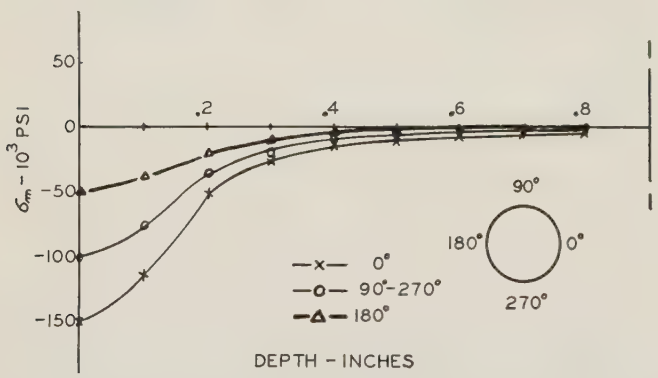

Fig. 8—Solid bar, Case 2, hypothetical σ_m measured stresses

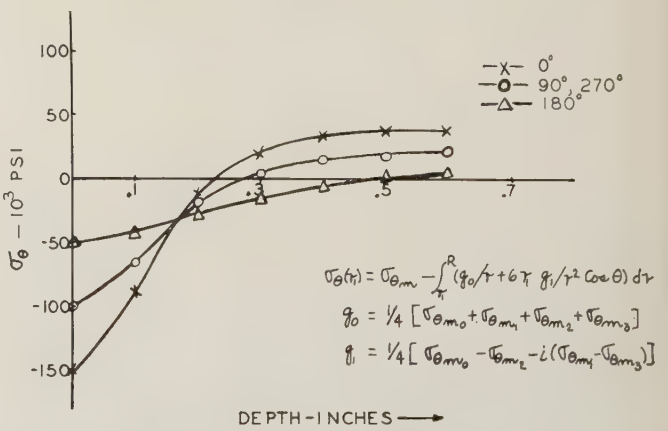

Fig. 9—Solid bar, Case 2, corrected σ_θ stresses

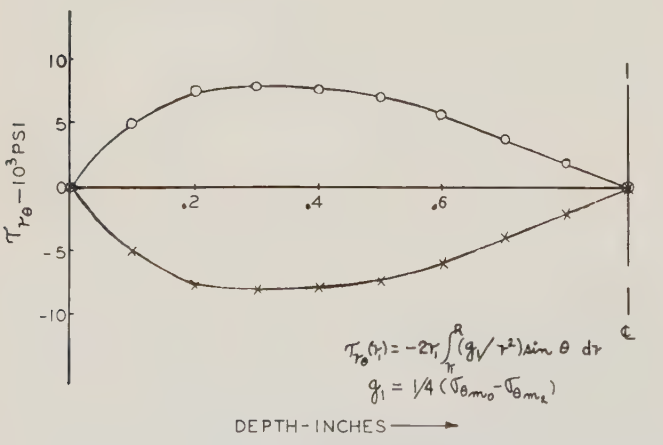

Fig. 10—Solid bar, Case 2, calculated $\tau_{r\theta}$ shear stresses

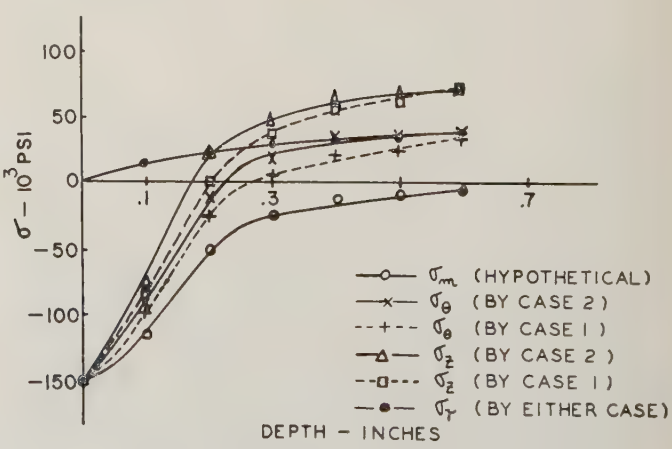

Fig. 11—Solid bar, Cases 1 and 2, hypothetical σ_m 0-deg position

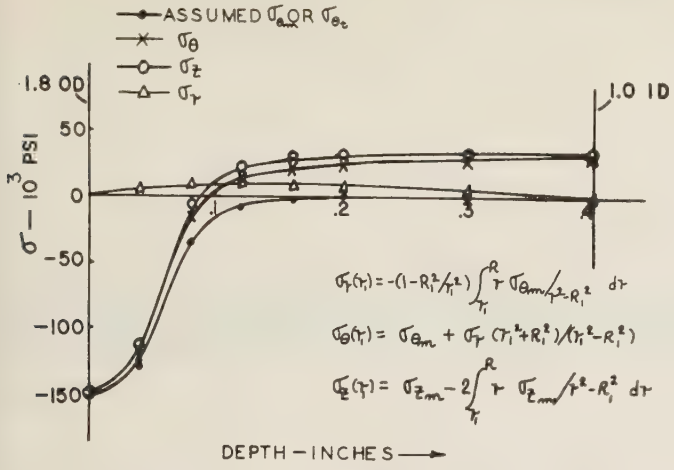

Fig. 12—Hollow bar, Case 3, hypothetical σ_m corrected stresses

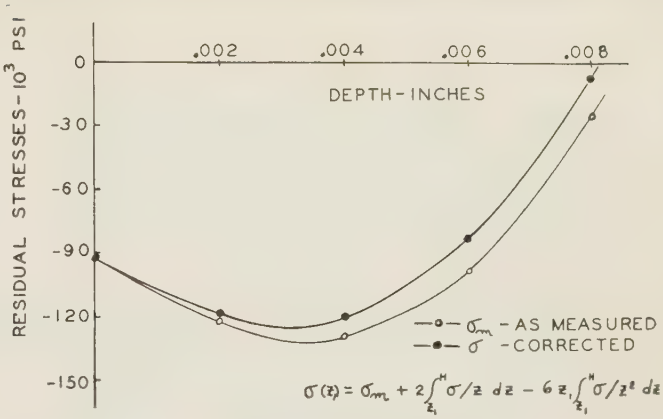

Fig. 13—Flat plate, Case 4, shotpeened leaf spring, SAE 5160 steel (0.192 × 1½ × 12 in.)

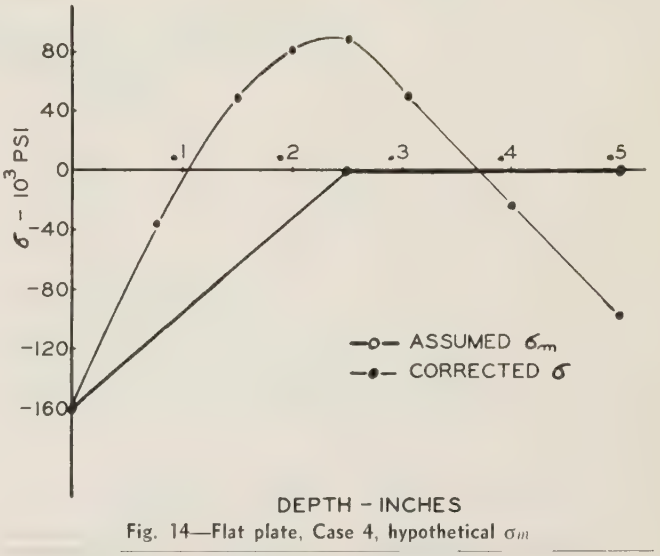

Fig. 14—Flat plate, Case 4, hypothetical σ_m

A salient feature of this case is the residual $r\theta$ shear stress that exists as a result of the asymmetry of the θ stresses. Fig. 10 shows a plot of this shear as a function of depth and position. It is noted that the 90 and 270 deg positions are equal but opposite in sign, while the 0 and 180 deg positions feel no shear at all. This obtains from the sin term in the integrand which vanishes for 0 and 180 deg. This equation can also be evaluated numerically, although IBM or other machine methods would be applicable for this entire work.

Fig. 11 shows Case 1 applied erroneously to the measured stresses at 0 deg, ignoring the effects of the asymmetry existing. The appropriate dotted curves (by Case 1) correspond to the respective solid curves (by Case 2). Depending upon the degree of accuracy desired, this may very well be a practical approximation. The degree of asymmetry is the main factor and, if very great, would not justify the simplification. The $r\theta$ shear, however, can only be found by application, at least for that part, of Case 2. It is interesting to note that the equations of Case 2 revert to Case 1 under conditions of symmetry.

Case 3 considers a hollow cylinder or tube. Again, hypothetical data is assumed for illustrative purposes of method only (Fig. 12). The applicable equations are indicated and the three stress components can be calculated in terms of the measured σ_m. As can be seen in the equations, this case also reverts into Case 1 of the solid bar when the inside radius R_1 becomes zero.

Case 4 of the flat plate is illustrated in Fig. 13. Measurements of stress were obtained from a shotpeened leaf spring as layers were removed from the peened side only. The correction equation involves the evaluation of two integrals of the form σ/z and σ/z^2 which can best be done numerically as previously mentioned. The correction in this case is hardly justifiable inasmuch as the depths involved are relatively shallow. This correction, as are the others, is related to depth, increasing in direct proportion to material removed.

A hypothetical case in Fig. 14 illustrates the significance when greater depths are removed. A stress σ_m, is assumed to be measured from the surface decreasing linearly to zero at a point in the center of the plate and remaining zero from there to the other side. Except for the linear form of σ_m, this stress could exist as a result of deep hardening on one side only, flame hardening of one side, and the like. The corrected stress is shown extending into appreciable tension near the center, which would be entirely missed had the correction been ignored. In this example, the true stresses and apparent measured stresses are widely different everywhere except at the single point on the surface where the measurements were begun.

Conclusions

Corrections of measured stresses are important whenever significant removed layers are involved. Increasing magnitude of the stresses in removed layers is a factor which tends to increase the correction. Stress gradient governs the depth of any one removed layer. Obviously, a minimum number of cuts are desired, but the number should be great enough to ascertain changes in sign through the stresses involved. The stress equations give an integrated correction through the removed layers, but cannot supply missing stress reversals through transition zones, if such are missed in the original measurements.

We do not feel that we know at this time the significance of subsurface residual stresses. But, whenever these stresses are desired, corrections are generally necessary if the true state of stress is to be found.

PART I of this paper describes the basic research and experimental development program of the air-spring suspension, Part II details the application of the principle to the 1957 Cadillac Eldorado Brougham.

The authors think that the final design successfully met the development program criteria of cost, size, life, adaptability, and rate characteristics. This design, in turn, offered the features of constant height, smoother ride, and better handling, which appealed to the design engineers working on the Cadillac.

Cadillac's for the

Part I

by V. D. Polhemus and L. J. Kehoe, Jr.

Experimental Development of the Air Spring

WE have been striving continually to effect an appreciable ride improvement in our cars by trying such devices as torsion bars, single leaf, and other types of steel springs. We have managed some minor improvements, but always wind up facing the fact that steel springs have definite limitations.

In 1953 Fox and Labelle[1] listed six undesirable features present when steel springs are used. However, the limitation which causes passenger-car engineers the most concern is that steel springs are not readily adaptable to increased static deflections without affecting the relationship between curb standing height and full-load ride clearance. This is probably the most controversial suspension problem today. The industry's trend, with lowered roof heights bringing lower floors, has intensified the chassis engineer's search for a solution which would permit maintaining soft ride without undesirable compromise.

Some years ago, feeling that a fundamental change was necessary, we began a development program which produced the type of air spring now in production for the Cadillac Eldorado Brougham.

To use air as a suspension medium is no new idea. It was proposed over 50 years ago but, as with many other ideas, practical application has been delayed.

At the beginning of our air-spring development program, we established certain criteria: reasonable cost and size; long life; adaptability to any type of suspension; its fundamental concept should permit any desired length of stroke being obtained without altering other design features; and last and most important, it should have correct rate characteristics.

In Fig. 1 is shown what we feel is the best shape of load-deflection curve. Considering first A-B, the curve for a considerable distance on either side of normal position is a straight line, neither gaining nor losing rate. This characteristic, when coupled with some form of standing height adjustment, permits a consistently balanced ride over major road irregularities. Second, the spring should have (at C) a high end load to reduce any sensation of "crash-through" over ruts and pot holes. Third, there should be a gradual blend (B-D) between the center (low rate) section and the high end rate (D-C) portion of the curve. Without a gentle transition, those abrupt swells, known variously as "donkey backs" or "thank you ma'ams," can upset an otherwise excellent ride. The last factor, while not a necessity, is very desirable. We feel that on rebound (at point E) a considerable reduction in load is worth seeking, both to reduce lift on braking and accelerating and to prevent excessive input to the frame and suspension members. Of course, a gradual blend (A-E) should be provided.

Somewhat over 10 years ago we investigated the double-convolution air spring and have retained an

[1] "Motor Coach Suspensions," by H. B. Fox and D. J. LaBelle. Paper presented at SAE National Transportation Meeting, Chicago, November 2–4, 1953.

Air Suspension *Eldorado Brougham*

V. D. Polhemus, L. J. Kehoe, Jr.,
F. H. Cowin, S. L. Milliken, General Motors Corp.

This paper was presented at the SAE Passenger-Car, Body, and Materials Meeting, Detroit, March 7, 1957.

eager interest in it. This form of air spring has much to recommend it for certain applications. It has proved itself as a heavy vehicle supporting device, having an excellent record of durability in its use on the General Motors Coach.

Certain basic problems led us to bypass the double-convolution bellows approach to passenger-car applications. As you are well-aware, scaling down an otherwise satisfactory device is not always a solution to an enginering problem. To appreciate the problems involved in using the double-convolution bellows in a passenger car, let us examine a familiar unit, one used on the GM Coach as a front-suspension spring. It has an outside diameter of 9 in. and has a stroke of 8 in.

At normal height it would have a load carrying capacity of 2000 lb at 65-psi operating pressure and might be used as a passenger-car front spring, if applied through a wishbone linkage. However, obtaining the necessary 300 lb per in. spring rate would involve using an additional 700-cu-in. reservoir. For long-stroke direct-acting rear-axle applications, the picture becomes more critical. A reduction in diameter to bring loads to, let us say, 1200 lb at 60-lb operating pressure means that we have reduced stroke to an unsatisfactory amount. Dynamic stability is, as with a coil spring, a function of spring rate, spring length, and spring diameter. It is apparent that it would be difficult to obtain longer stroke by increasing the number of convolutions because instability would result, and could be overcome only by guiding the bellows in some fashion. Even assuming that these difficulties could be solved, the load-deflection curve does not have the shape that we have previously determined to be the optimum.

In brief, with the double-convolution bellows, un-

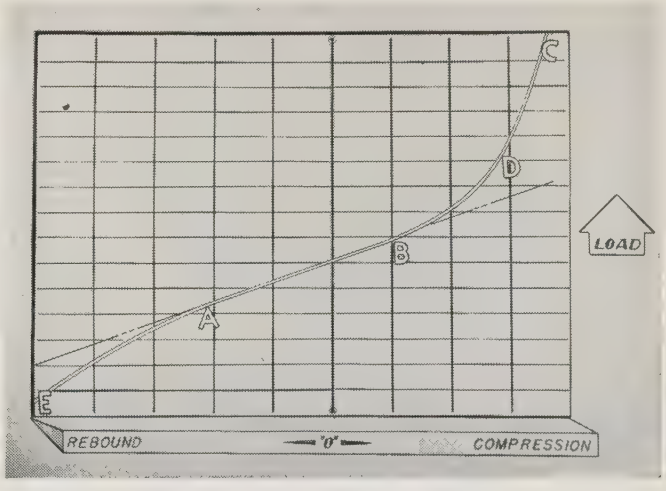

Fig. 1—Ideal load-deflection curve

desirable factors are present to a greater degree than we feel can be tolerated.

A piston compressing air in a chamber is a simple form of air spring. The load-carying capacity of this spring is a matter of simple mathematics: area of piston X gage pressure = load. Applying the tight-fitting piston and chamber principle immediately presents certain practical problems. It would be difficult to obtain a 100% seal against air leakage without paying an excessive penalty, both in dollar cost for precision machining and in friction.

Our next step was to increase the piston clearance and install a rolling seal (Fig. 2). At one stride we have solved two problems: minor size variations of the piston and cylinder are inconsequential, and friction is eliminated. We still retain the virtues of the original piston concept.

The diaphragm will present no unusual problem of manufacture, a backlog of experience in tire making having solved most of the difficulties connected with making a rubber-impregnated fabric which can withstand flexing to a practical degree. No air springs were ever made, of course, with the diaphragm in the shape shown in the model.

It will be recognized that this still represents the basic concept of the straight piston and cylinder, and that we have not as yet satisfied the conditions laid down in the original graph which indicated the ideal spring. We obtain the long low rate, but gentle buildup and the high end load are missing. What is required is a variable-area piston (Fig. 3). This we obtain by increasing the outside diameter of the diaphragm and adjusting the piston and retainer to permit a regulated adjustment of effective piston area.

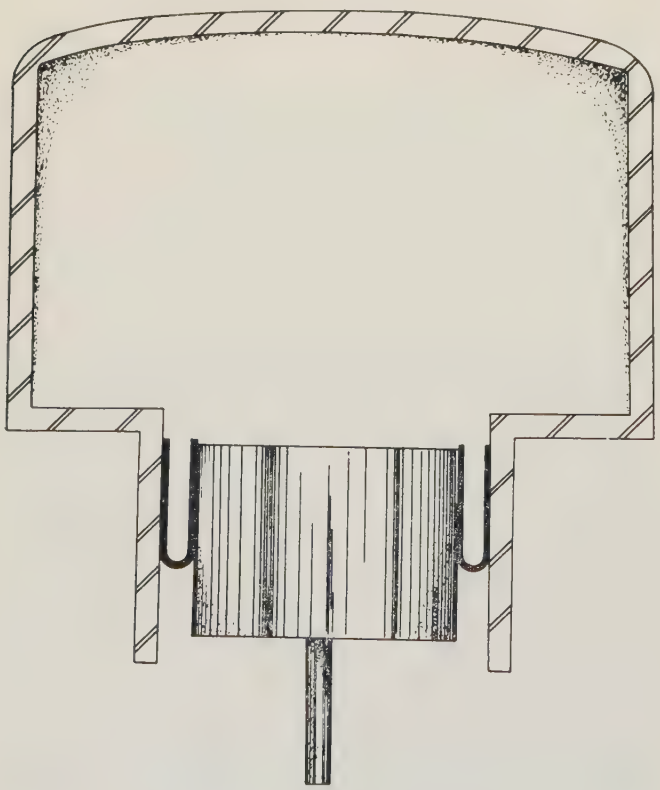

Fig. 2—Frictionless rolling seal

With this early hypothetical spring, the diaphragm is restrained between the piston and the outer skirt (diaphragm retainer), thus the effective diameter is fixed for some distance below and above the normal position. As can be seen from the upper piston position, when the diaphragm is lifted up and out of its previously restrained stations, an increase in effective diameter (and hence an increase in effective working area) is obtained. Looking at the view of the piston in its lowest position, it can be seen how the diaphragm, lifting away from the piston, produces greatly reduced effective diameter. In all positions the length of a horizontal line, tangent to the meniscus, determines the effective diameter. It will be noted the percentage increase in effective area in the full-compression position is less than the decrease in full rebound. This is necessary due to the fact that air pressure increase, as the piston enters the chamber, tends to assist in load buildup, while in rebound the air-pressure drop requires a more rapid reduction of effective piston area.

With our basic theory of design for an air spring established, the next step was developing a method of attaching the diaphragm to the piston and chamber. Two methods have been employed, both equally acceptable. The first, as shown in Fig. 3, used a circular wire bead ring encased in rubber, which sealed with a clamp plate to the piston and between the skirt and chamber at the outer rim. This forms a very satisfactory connection, and was used for some time in the early stages of the program.

Concurrent with our theoretical and design studies, an intensive program of car-building and road-test evaluation was instituted. It seemed quite obvious, at the time, that the best way of obtaining the air-chamber volume was to use the interior of the frame cross members. The first road car used aluminum cross members, front and rear. It presented seeming advantages which were not borne out in practice. We were troubled with porosity before installation, and in spite of a multitude of attaching screws, a reduction in frame stiffness was experienced in comparison with the conventional all-steel frame.

Drawing on this experience, a second car was built using integral-steel cross members containing the air chambers. This car was sent through our standard 25,000-mile durability test primarily to obtain information on cold-weather operation over gravel, freezing slush, ice, and snow. The chambers were built to simulate what could be expected from production tooling, with production limits, with the intention of introducing a sealant similar to that used in aircraft fuel cells. Again practical difficulties arose: The sealant was unpredictable in its adhesion; frame motions tended to cause leaks; we were unable to devise a suitable method of field repair; and, probably the greatest hurdle of all, there was inflexibility of chamber size alteration between models.

With the foregoing in mind, the next step was individual pots (Fig. 4). Advantages of this system are:

1. Simple shapes with reduced amount of welding.
2. Structural stresses removed from chambers.
3. Bench testing is possible.
4. Ease of installation and field service.

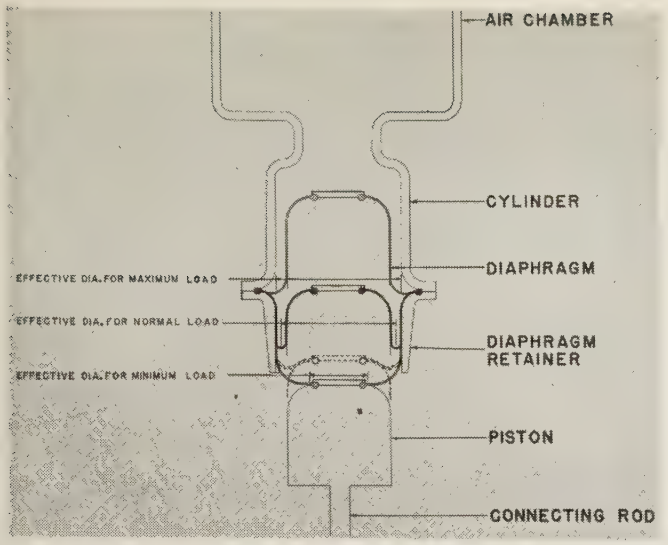

Fig. 3—Variable-area piston

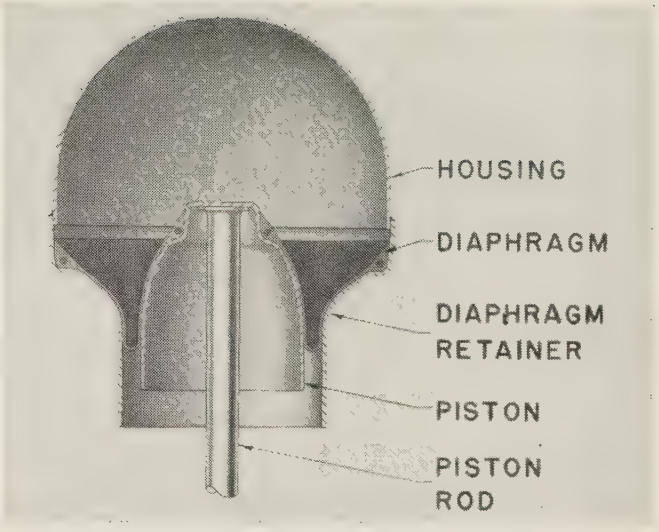

Fig. 4—Individual air spring

5. Interchangeability with optional steel springs.

At present, we see no better method.

Fig. 4 also shows the second method of attachment developed for connecting the diaphragm to the piston and the retainer. The steel bead rings are still used, but a wedge shaped rubber lip surrounds each ring. The internal air pressure on the rubber lips forms a seal much the same as does the tubeless tire to its rim. The diaphragm is installed in the retainer by temporarily deforming the normally circular outside bead into an oval shape that will pass up through the circular opening of the retainer.

In development work with its constant changes, of course, we cannot justify draw-die costs, in either time or money. Retainers and housings are usually made by spinning, and we find the surface obtained is adequate for sealing without any machining.

Selection and application of the suspension is the prerogative of the division using it and will be covered in Part II of this paper. However, brief mention might be made of some road-test cars used in the experimental development by engineering staff.

No serious problems are encountered when adapting air springs to a torque-tube rear suspension, so this type of installation was used to good advantage all during our development program.

Cars using a Hotchkiss suspension do not lend themselves to air-spring installation as readily as the torque-tube type. In Fig. 5 is shown the basic 4-link suspension we have used on cars originally equipped with Hotchkiss rear suspensions. We have made the minimum of frame changes, retaining the outer frame members. It will be noted that the piston rod is connected directly to the axle and piston stroke is the same as vertical wheel movement.

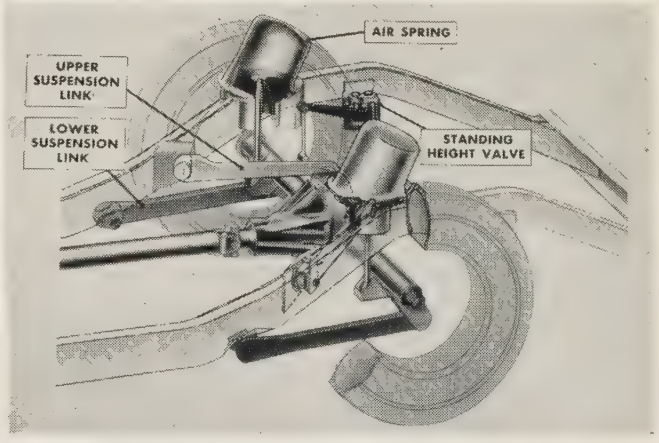

Fig. 5—Air springs as applied to 4-link rear suspension

Spring Design

As previously mentioned, the desired load-deflection curve is the basis of preliminary design (Fig. 1). Knowing the load, operating pressure, and desired rate, the effective piston diameter is readily calculated, with clearance between the piston and retainer being established at a figure that has been found, from tire building experience, to be satisfactory for long life. Volume of the chamber is obtained from the formula:

$$R = \frac{\gamma \cdot Pa \cdot A^2}{V} \qquad (1)$$

This of course, applies only to the derived A-B section of the curves, from the basic equation:

$$R = \frac{dw}{dh} = (Pa - 14.7)\frac{dA}{dh} + A\frac{d\,Pa}{dh} \qquad (2)$$

Gamma is accepted as being 1.4, the usual adiabatic factor for diatomic gases, but caution should be exercised since under certain conditions the spring may function in a region approaching isothermal operation, with the attendant lower rate.

When we first began developing the diaphragm spring we felt that the curve should show (in the B-C section) a constant rate of acceleration and so calculated it. With more experience we now use a simpler method. When the straight section of low rate A-B is established, the desired end load is placed on the graph. We have a family of curves which we recognize as giving a desirable blend and end rate. The same procedure is followed on the

Fig. 6—1956 Cadillac Eldorado Brougham

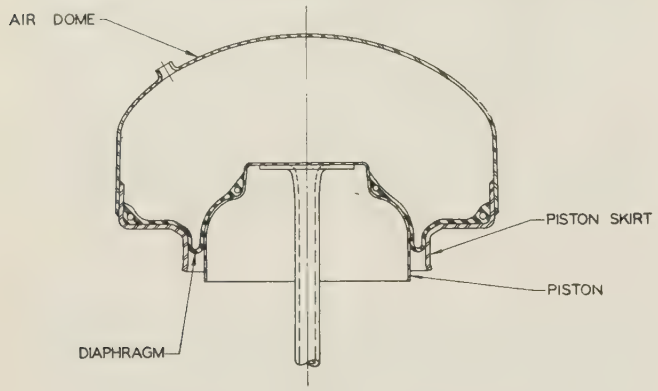

Fig. 7—Early design of front air spring

unloading portion A-E of the curve.

In the example shown, the upper curve is calculated and found to be a fifth-order equation:

$$(W = 1227 + 163.6\ h + 1.80\ h^5) \qquad O \leq h < 3.66 \tag{3}$$

For the unloading portion of the curve the equation is:

$$(W = 1227 - 163.6\ h - 2.4\ h^3) \qquad O \leq h < 4.91 \tag{4}$$

With the values fed into an IBM No. 704, the profiles necessary for the piston and retainer can be established in 10 min. Before the programming was established it required two mathematicians two days to complete one calculation series.

We feel that with the diaphragm type of air spring we have met the conditions we laid down at the beginning of our development work regarding cost, size, life, adaptability, and ease of "tailoring" rate characteristics.

Part II

by F. H. Cowin and S. L. Milliken

THE advantages of air springing had been interesting to us for some time and when the Eldorado Brougham was proposed, the air spring seemed to be particularly attractive. The preliminary studies and experimental testing with Cadillac modifications of the engineering staff designs increased our liking for the springs.

1. The car was to be only 55½ in. high (Fig. 6) which was 3½ in. lower than our standard sedan for 1957 and 6½ in. lower than the sedan of 1956. All of these are measured at the standard five-passenger load conditions, of course.

Air suspension offered a constant-height feature, with the car at the same height whether at curb weight or under full-load conditions. Between these extremes of loading, the car would stand at the same height as in the design studio or on the showroom floor. Even with the trunk filled with luggage, the styled appearance would be retained.

2. The height available for ride clearance between the axle and the frame could be used more efficiently.

Air-spring suspension would insure a constant ride clearance under all load conditions and permit a ride rate and balance that would not change from minimum to maximum load.

3. The air suspension would permit lower ride frequencies, thus giving us greater latitude in choosing the best characteristics for both ride and handling. The constant height gives constant-ride travel so the ride rate could be lower without excessive bottoming. It would give the ideal boulevard ride without compromising the handling characteristics.

With these promising advantages of the air spring, supported by our experimental testing on modified production cars, the following design parameters were established for the new Eldorado Brougham springing:

1. The ride frequencies would be approximately 55 cycles per min, or about 15% lower than those with our steel springs. This was a good compromise, we felt, for handling and ride. Ride rates lower than this might introduce problems in handling, and we did not want to impair those important characteristics for the sake of basic ride.

2. The diaphragm type of air spring would be used. The amount of development work and the experience up to that time with experimental installations favored the diaphragm type, rather than the type that is used on large passenger-bus suspensions.

3. The pressure in the air domes at normal passenger load would be approximately 75 psi. This pressure would permit a piston of reasonable size that would not necessitate a larger air dome than we could conveniently accommodate in the chassis. This air pressure would not be too demanding on the rubber diaphragms.

4. The front suspension would be a modification of our basic parallel-link design, with air springs replacing the usual coil springs. This would permit considerable interchangeability of frame and suspension parts with the standard line of cars, which would continue with coil-spring front suspension.

5. The rear suspension would be of the so-called 4-link type with a rigid axle. This would be entirely new and different from the leaf-spring and Hotchkiss-drive design used on the standard line of cars. The 4-link design would permit independent control of roll center, lateral stiffness, and acceleration squat.

The roll center could be raised and established definitely to assure proper car handling with the proposed lower spring rates.

Lateral stiffness could be increased to reduce rear-end sway and steer. Understeer could be set and depended on as the suspension height would not change with the load.

The swing arm for the rear axle could easily be set for the best performance between rear-end rising or lowering on acceleration; a latitude that was not possible with the leaf-spring design.

This type of suspension would give better control of rear-axle pinion windup under both braking and acceleration torque.

6. The air system would be of the "Open-type," with inlet air for the compressor being drawn from the atmosphere. Air vented from the air springs would be discharged to the atmosphere.

The engineering staff installations had used a "closed" system, with the used air returned to a low-pressure tank from which it was drawn by the air compressor for re-use in the air spring. The proposed "open" system, in conjunction with our leveling-system controls, would use only small amounts of air which could be supplied by a small, electrically-driven compressor requiring little current. The "open" system would not require a low-pressure tank or the associated plumbing.

With these major parameters established, serious design work was started to adapt the basic design to the chassis requirements of the Brougham body. The design work was done concurrently with that for the 1957 standard cars.

Front Suspension

The adaptation of the engineering staff's basic design to our Eldorado Brougham naturally brought many changes in detail. Mounting the air spring in the frame-front cross member is a good example.

It was desirable that the frame-front cross member be common to both the air-spring and the coil-spring suspensions.

With the spring rate established at approximately 85% of our 1956 rate, and the air-spring position determined, the volume required in the air dome was fixed at 450 cu in. The normal working pressure was to be 75 psi. But the original design of piston, diaphragm, and air dome (Fig. 7) resulted in an air dome that was too large for the space available in our frame-front cross member.

This led to a basic redesign of the piston. It was made with a hollow shape and a 3-in. diameter hole at the top. The 126-cu-in. volume in the piston reduced the volume required in the dome by 36%. The smaller-sized air dome would then fit into the space available in the front cross member. The piston and diaphragm are shown in the normal-height position (Fig. 8).

The first design of the piston (Fig. 7) relied upon air pressure in the dome to hold the inner bead of the diaphragm against the piston. And the bottom of the piston was held into a spherical depression in the lower control arm by the same pressure.

But experience showed the desirability of having the piston mechanically retained, so it could not jump out of position if the pressure was lost during car repairs or improper jacking. Mechanical retention to the diaphragm was obtained by adding a narrow strap, or clip, (Fig. 8) that twists into the top opening of the piston and extends over the inner bead of the diaphragm.

At the bottom of the piston, a stud was added, which bolts into the lower control arm tray. The head of this stud is encased in a phenolic resin cover that has a spherical shape to match the seat in the bottom of the piston.

In the first designs of the air dome, (Fig. 7) the dome was welded to the piston skirt. This made it necessary to install the diaphragm through the smaller opening in the skirt and then spring the outer diameter to its proper seat in the air dome. Experience showed that a separate skirt, bolted to the dome after the diaphragm was in position, would be better (Fig. 8). This permits a stiffer wire in the diaphragm's outer bead and a slight interference between the bead and the dome for better sealing.

The separate dome and piston skirt design also permitted an improvement in the skirt, for it could now be tailored to its particular task. The first skirts were made of fairly light steel, but laboratory tests revealed deflections in the skirt, and the two-piece design made it possible to: increase the gage of the steel used, add reinforcing sections, and add additional flanges.

This change to separate dome and skirt was also an aid to the production department in that the assembly of the dome, piston, and diaphragm was simplified. Also, the bead seat in the dome was exposed and could be better controlled for size and finish.

Diaphragms—The all-importance of the diaphragm in this suspension is apparent. The early diaphragms, made by the U. S. Rubber Co., showed promising durability, both on the cycling tests and in experimental installations. Fig. 9A shows the front diaphragm.

It is of two-ply nylon construction and has solid

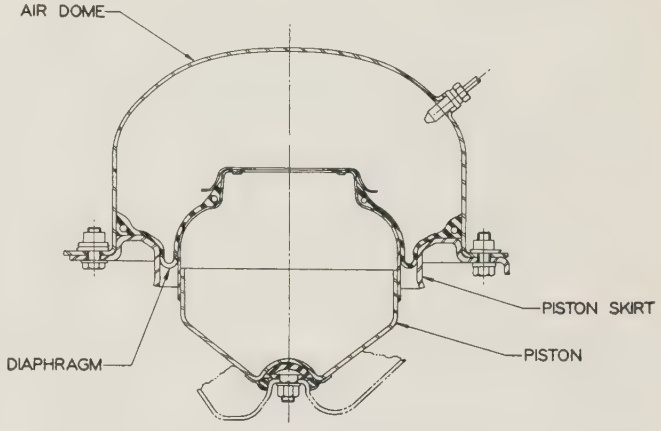

Fig. 8—Final design of front air spring

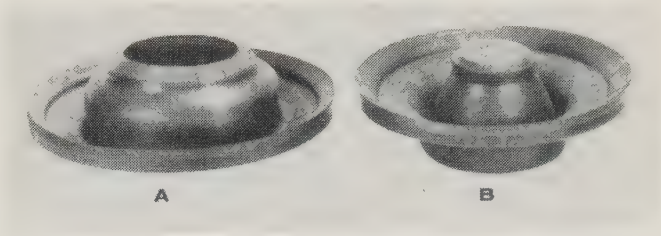

Fig. 9—(A) Front diaphragm (B) Rear diaphragm

Fig. 10—Test apparatus used to evaluate sealing qualities

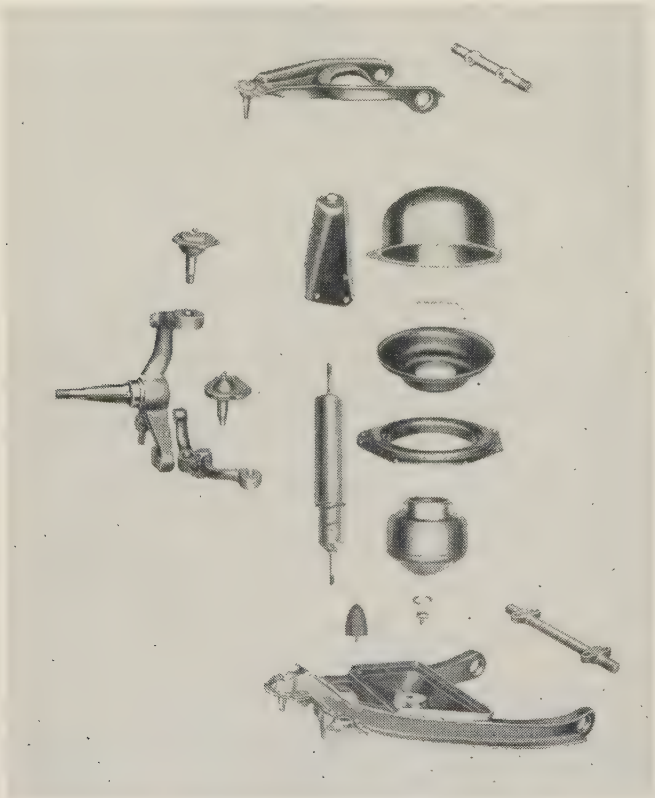

Fig. 11—Exploded view of front suspension parts

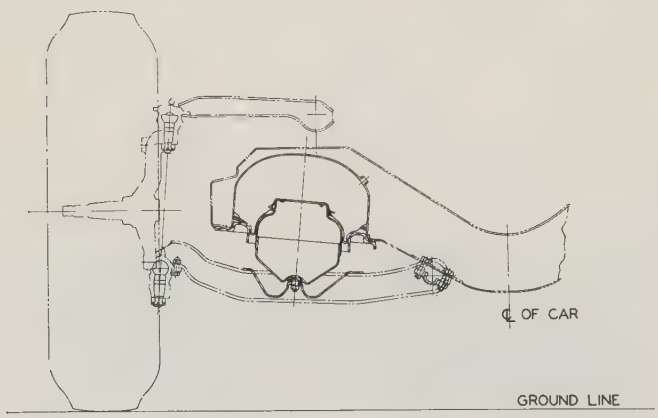

Fig. 12—Front suspension

wire beads. Early diaphragms had braided bead-wires, but tests proved that solid bead-wires are stiffer and assure a better seal. The solid bead-wire was possible after the air dome and piston skirt were changed from one-piece to bolted construction. Natural rubber is used for the covering because of its good flex life. It is compounded for ozone resistance.

As the Cadillac designs developed, changes were required in the size of the diaphragms, and this introduced some new problems. The cord pattern, and resultant strength of the diaphragm, is satisfactory if the diameter of the inner bead is at least 30% of that of the outer bead. This influenced the proportions of the spring. The cords must be well-secured around both beads, and the beads must be precisely located to prevent any movement of the bead on the seat. Movement would result in bead chafing and possible leaks.

The early diaphragms were built under laboratory conditions and it was possible to have thin wall sections, with each cord covered with rubber. Because it was realized that it would not be practicable to hold these close tolerances on the production diaphragms, much laboratory and road testing was done.

This resulted in a section that allows enough rubber to insure good coverage of the cords, even if they float toward one side of the membrane during the moulding cycle. Wall thickness is still thin enough to insure low strain in the outer skin of the membrane during the stroke cycle. The wall is approximately ⅛ in. thick for all of the area between the beads.

At first, radial grooves were moulded into the diaphragm for venting during the moulding operations, but this sometimes exposed the cords and caused air leaks. Development work resulted in a change to radial lands that provide mold venting but do not expose the cords.

Careful laboratory work, followed by extensive testing under extreme conditions, has resulted in diaphragms with a life of 1,000,000 cycles on the test rig.

Diaphragm Sealing—Early tests, both on the road and in the laboratory, showed the need and the difficulty of maintaining a good air seal between the diaphragm bead and the dome and piston.

The original diaphragms had tapered bead seats that necessitated a reverse draft in the air-dome bead-seat area. This was changed to a vertical bead seat that allowed a normally drawn sealing diameter in the air dome. This, along with the separate-piston-skirt construction and the stiffer bead-wire mentioned earlier, allows a slightly oversize diameter on the diaphragm and a light interference at the seal.

The surface finish of the air dome at the bead-seat area is most important. We thought, at first, that this would be comparable to the sealing of a tire bead to the rim, but development work in the laboratory showed a marked difference. While a tire rim is formed by rolling, the air dome and piston are drawn in a die and the resultant surface is not as good for sealing.

The apparatus shown in Fig. 10 was devised to evaluate the sealing qualities of different surfaces. Rubber suction cups, 3 in. in diameter, were attached to each specimen. Springs, loaded to a 4-lb

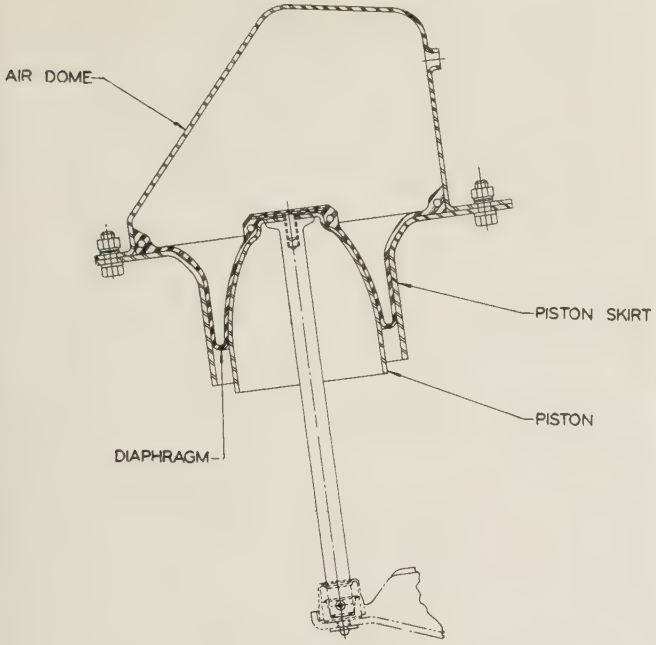

Fig. 13—Rear air spring

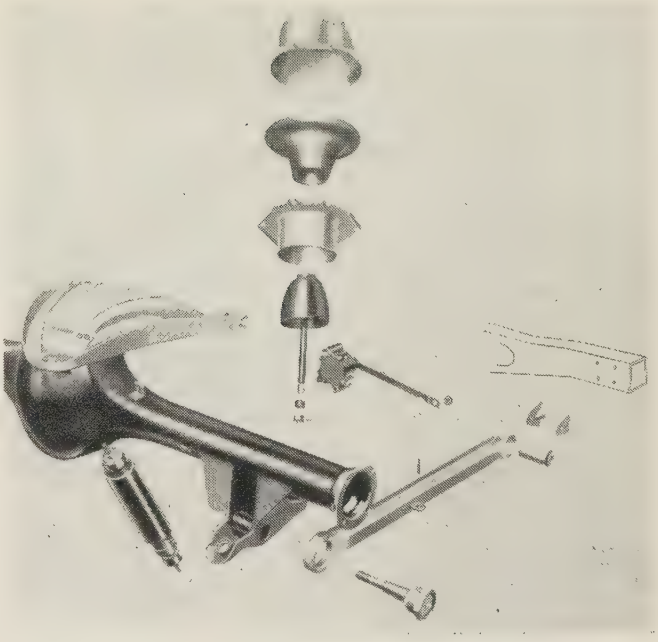

Fig. 14—Exploded view of rear suspension parts

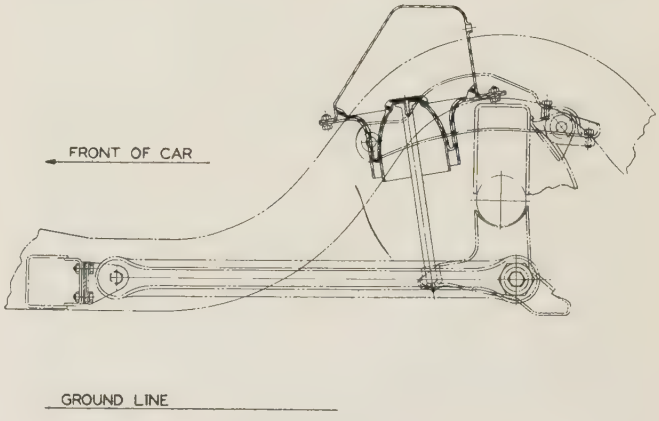

Fig. 15—Rear suspension

pull, attempted to pull the suction cup from the steel surface. The time required to do this was a measure of the airtightness of the seal between the rubber and the steel surface.

Many methods of finishing, plating, and sealing the steel surface were investigated. This resulted in the following specification for the air domes and pistons:

1. Use mill-run 1008 cold-rolled satin-finish steel with surface of 45-micro-in. maximum.
2. After forming, buff the sealing areas to remove die marks.
3. Apply a rust-preventive phosphate coat.
4. Apply black primer paint to the same area.
5. Cover sealing areas with Silicone grease #4.

The relation of the air dome, diaphragm, and piston to each other and to the suspension parts is shown on this exploded view (Fig. 11). The shock absorber works between a bracket on the lower control arm and a bracket which is bolted to the frame side bar.

Fig. 12 shows the relation of the air-spring assembly to the lower arms of our parallel-link front suspension. The air dome is bolted to the underside of the frame cross member. The locating and retaining stud at the bottom of the hollow piston bolts into the lower control-arm tray.

Rear Suspension

The parts for the rear air springs are not interchangeable with those at the front (Fig. 13). The piston is of smaller diameter, as dictated by the air pressure, spring position, and geometry for the 4-link suspension. The top is closed and has a bullet-nosed shape. A rod is anchored in the piston and connects it to a bracket on the rear-axle housing.

The lower end of the rod is domed and bears in a steel cup that is attached to the axle bracket. The rod is loosely pinned to the cup to prevents its jumping out of position at any time.

A rubber seal around the cup and the rod retains the grease and insures long-life lubrication for the bearing.

The shape of the dome was determined by the volume required (300 cu in.) and the space available. The attachment to the piston skirt is the same as at the front spring.

The rear diaphragm (Fig. 9B) is of the same type as the one used at the front spring, but is not interchangeable. The center of the diaphragm is solid and has a steel washer vulcanized in place. A stud on the underside of this washer screws into the tapped head of the piston to give a mechanical tie between the diaphragm and the piston.

Fig. 14 shows the relation of the components to each other, along with the lower arms and the upper yoke that form the 4-link suspension.

Fig. 15 shows the relation of the air spring to the complete rear suspension. The lower control arms are parallel to the centerline of car. The front end of the arms anchor to the same frame outriggers

that are used for body mounting bolts. Rubber bushings are used at this point.

Ball joints attach the rear ends of the arms to the same bracket on the axle housing as carries the lower end of the air-spring piston rod.

The upper control arm of the so-called 4-link suspension is in the form of a yoke, as this gives a better mounting to our "Tubular Center-X" frame. Rubber bushings are used between the front end of the yoke and the frame cross member. At the rear of the yoke a ball joint is used for the mounting to the axle housing. The length of the upper yoke and of the lower links, along with the height of their attachments to the frame and to the axle, gives the desired geometry for the proper swing-arm length, rear-end steering, roll center, and rear-end lowering on acceleration.

The combination of bushings and ball joints in the arms and the yokes gives freedom in roll, desired noise isolation, and good durability.

Considerable design and development work was required on the upper yoke to insure sufficient strength to handle the lateral, fore-and-aft, and tramp forces exerted by the axle.

Testing at our proving grounds disclosed fatigue failures in the ball-joint mounting bracket on the axle housing. Strain gages were mounted on the bracket and the axle housing to determine the transverse and fore-and-aft loads during Belgian Block and other road driving. The loads were found to be high (3400-lb maximum) and about equal in magnitude. A laboratory set-up was then evolved to permit controlled testing of the mounting and to determine the necessary strength.

Fig. 16 is a picture of the Eldorado Brougham chassis showing the suspension components mounted in the frame. The lower arms and the upper yoke that form the so-called 4-link suspension at the rear axle are shown. The air-spring installation, plus the control arms and new frame parts that were required in our design, added about 45 lb to the weight of the car.

Leveling System

As mentioned previously, the leveling system used on the Cadillac Brougham is of the "open" type, in which the air is compressed from atmosphere and is exhausted to atmosphere after being used.

Many systems of valve control were studied and tested in the search to find the best control for the wide range of conditions that affect car height. The system found best for all the conditions of loading and operation combines simplicity and dependability. Four solenoid-controlled valves in one package meter the flow of high-pressure air to the leveling valves at the wheels.

The first pair of valves allow pasage of air only when a car door is open or the ignition is on. Of this pair, one valve controls the inlet air to the leveling valves, with the other valve controlling the outlet air. When the car doors are closed and the ignition is off, there is no passage of air and the leveling system is locked out. This provides for all conditions of jacking, shipping, and parking.

The second pair of solenoids control the flow of air under operating conditions. When any door is opened, there is an unrestricted flow of air to the leveling valves and any change in car height, due to entrance or egress of passengers is corrected quickly. This occurs with the ignition on or off.

During all driving, there is a restricted flow of air through a coined orifice in the solenoid valve. This permits constant adjustment of car height during running to compensate for loss of weight (as with the consumption of fuel) or for added weight (with an accumulation of mud or ice). And it allows a correction in height when the car is driven away after having been parked on a side hill, or with one wheel on a curb or in a deep hole. This leveling can be done without excessive use of air.

Severe drops in temperature during overnight parking will, of course, reduce the pressure in the air dome and, consequently, lower the car height. This is corrected as soon as a car door is opened.

Briefly, the car height is quickly adjusted to a new load condition when a door is opened and is constantly adjusted when the car is in motion, but at a much slower rate. During jacking, parking, and shipping, the levelizing system is locked out.

Leveling Valves—The leveling valves control the pressure in the air spring at each wheel to keep the horizontal plane of the car parallel to, and a fixed distance above, the ground. The valve is mounted on the frame, and connected to the wheel control arm with a mechanical linkage. Any change in height of the frame actuates the valve, and high-pressure air is admitted to or exhausted from the air spring to restore the normal height of the car.

There are two leveling valves at the rear suspension, one at each air spring. At the front, one leveling valve serves both of the front springs. This arrangement of the three valves establishes the plane for the car and avoids the fight effect that would accur with a leveling valve at each of the four wheels.

Our leveling valves are made by Delco Products Div. and are the result of much experimental testing and development with that division. The only valves available at the start of the program were too large, too heavy, and too complicated for our needs. (Leveling valves of the electrically controlled type were tested during the development program, but did not have the durability of the mechanically actuated valves.)

Each leveling valve has two tire-type valves (one for intake, one for exhaust). They are operated directly by the linkage from the lower control arms. The composition of the rubber seal of the core has been changed to assure long life in this use.

Each leveling valve has a delay mechanism to prevent leveling action during wheel-hop frequency.

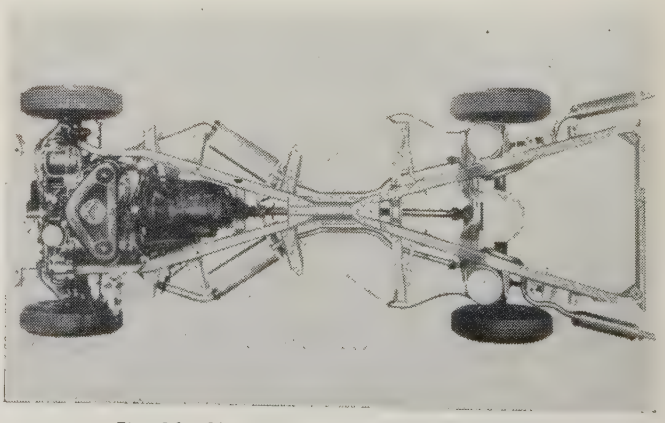

Fig. 16—Chassis of 1956 Eldorado Brougham

This prevents a pumping-up or a bleeding-down of the air spring due to small differences in the inlet and outlet restrictions. Levelizing action takes place at all frequencies below approximately 10 cps. Fig. 17 shows a typical leveling valve. This one is mounted on the front cross member and, as mentioned before, it controls the two front springs.

The tee fitting in the air-line connection between the two springs also incorporates a special check valve that permits fast flow of air during leveling, but a restrained flow through a 0.012-in. orifice during roll. This prevents the mushy handling that would result during cornering if there was an unrestricted flow of air between the two front springs.

The threaded portion at the lower end of the valve linkage allows manual adjustments for height of body in relation to the suspension. This provides for precise trimming of car height if there is any variation in production parts.

The enlarged view shows the details of the special joint used for all the air-line fittings. A shoulder is upset near the end of the air line. At assembly, the threaded nut forces this shoulder down against the bottom of the tapped recess in the body. This assures a fixed compression of the special rubber "O" ring and insures a leak-free joint. This joint allows minor misalignment of parts at assembly without leaks.

Compressor—The compressor is of the piston type, with 0.276-cu-in. displacement and a capacity of 600 cu in. per min against a 100-psi head. It is electrically driven and is mounted atop the generator in the engine compartment. This mounting and location was found best for noise isolation, oil supply, and plumbing. An integral thermal switch protects the motor from overheating.

The inlet side of the compressor is piped to the engine air cleaner to insure a clean supply of air.

The compressor is lubricated from the engine's oil system. The high-pressure oil line from the engine is restricted at the compressor to meter the oil flow to slow drops onto the crankshaft bearing. A standpipe in the crankcase returns the overflow to the engine oil pan by gravity.

The compressor normally runs only about 30% of the car operating time. However, at high altitudes the compressor runs about 80% of the time.

A pressure switch, integral with the compressor, starts and stops it to maintain pressure in the air reservoir at 120 to 130 psi. A blow-off valve on the outlet side of the compressor is set at 160 psi to protect the compressor and the air system from excessive pressure.

The compressor can run only when the engine is running. This insures that there will always be adequate lubrication for the compressor.

Air Reservoir—A cylindrical tank, of 500-cu-in. capacity, is mounted just forward of the radiator top tank. This provides a reservoir of high-pressure air more than sufficient to level the car from curb to five-passenger load without additional air from the compressor. It also serves as a trap for any oil or water, and has a manual valve to allow periodic draining of any fluids.

If for any reason the pressure in the air reservoir drops below the 75 psi required for car leveling, a light on the instrument panel (similar to the oil-pressure warning light) notifies the driver that the pressure level should be restored. This can be done by starting the engine, which permit the air compressor to start. There is a tee fitting in the air-reservoir line that can be used with an air hose during any service work on the car or to check air pressure in the system.

The general arrangement of the chassis components is shown in Fig. 18.

All of the air lines are 3/16-in. OD copper tubing. This diameter of pipe was found to be the smallest that would allow the fast leveling we wanted when a car door was opened. Further experience and testing may allow us to use less expensive steel or plastic lines.

Assembly—The design and location of the components was developed with constant consideration of the making and the ultimate assembly of the parts into the chassis. As a result, the air-spring suspension has caused no unusual problems on the production line.

The vital importance of a leak-free system was realized from the first consideration of the idea of air suspension so the design, the manufacture, and the assembly of the components has been tailored to that result.

After the complete assembly of springs, pipes, and controls into the chassis, there is a snifter test for leaks and a final check with soapy water on the tubing connections. Experience gained with air-conditioner installations has helped with the air sus-

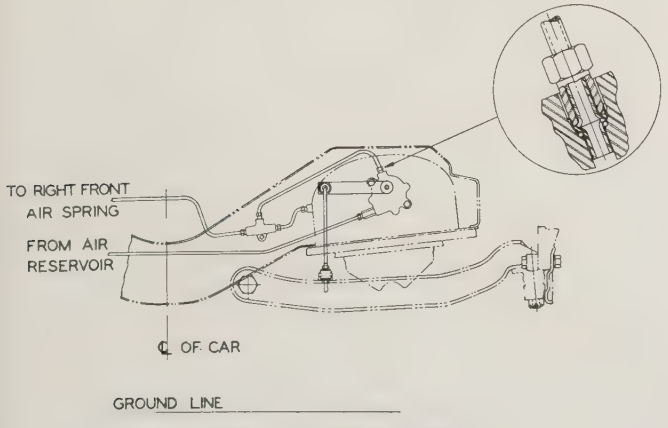

Fig. 17—Leveling valve

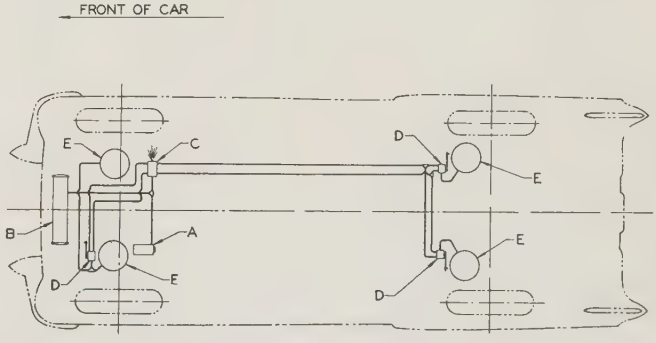

Fig. 18—Air-spring suspension: A—compressor, B—air reservoir, C—control solenoid package, positioned between air reservoir and leveling valves, D—three-wheel leveling valves, E—air springs

pension, as the leak problems are similar.

The manufacturing and assembly divisions have done an excellent job in devising new methods and procedures to insure a trouble-free car that will give the better ride that is inherent to this design. The men in those departments deserve much credit.

The suspension system was subjected to an extensive testing program after the final design was determined. Tests at Pikes Peak and other high-altitude areas showed that the compressor had adequate capacity for the suspension at any operating altitude.

Many thousands of miles on the Belgian Block roads at our proving grounds and on road tests have shown satisfactory life for all of the components.

John Hoban, Cass Cislo, and Dick Nietert of our department carried along the design and development work and surmounted the many new problems that cropped up so frequently.

Summary

In summary, Cadillac's air suspension on the Eldorado Brougham gives a new and a better ride.

1. The ride is of slower frequency, with slower body motions that are pleasing to the passengers.
2. The ride characteristics are constant. With the driver alone in the car or with a full passenger load plus baggage, there is no change from the designed ride.
3. The air suspension gives a damping quality that cannot be obtained with conventional springs or with shock absorbers.
4. The combination of a low center of gravity and the high roll center, that is obtained with the 4-link rear suspension, results in an exceptionally good-handling car.
5. The constant-height feature improves the appearance of the car, as it is always at show-room height regardless of the load.

We feel that the air-suspension principle has even greater potential and that, as we gain more experience with it, we will be able to design and build further advantages into the car for the benefit of our customers. Acceptance of the air ride has been gratifying, and we suspect that in the future many more people will be "riding on air."

DISCUSSION

Describes Experiments in Air-Spring Development

—Charles J. Smith
Monroe Auto Equipment Co

WE, at Monroe, have been engaged in air-spring development to a limited degree for approximately three years. During this time we have experimented with a number of different systems, the majority of which perhaps represented an effort toward the ride problem but did not necessarily take care of the handling problem. Due to this experience, however, we do feel that we are qualified to recognize the right approach and we are convinced that the Cadillac design is a step in the right direction.

Most of our preliminary work was done on a Nash car, which could quite easily be converted from coil springs to air springs. This consisted of several types of metal cylinders and also various rubber assemblies; in all about 10 different types. With this combination we invariably found that when we lowered the oscillating rate, the riding qualities improved, but the handling of the car became unsatisfactory. This would indicate that the features of high-roll center and low center gravity incorporated in the Cadillac design are major contributing factors which insure good-handling characteristics. While we feel that 55 cycles may not be the optimum frequency and that an even lower frequency might be desirable, the afore-mentioned problem remains a challenge which chassis designers will accept. The proper leveling system will be a definite factor in solving the problem. The system described in the paper can readily be seen as a necessity for good handling. On several occasions we have had difficulty with a 4-valve system where one front wheel and the opposite rear wheel supported the load and handling became extremely poor. The feature of rapid leveling when doors are opened or ignition is turned on, combined with controlled rate of leveling when the car is in operation, is very good.

One problem which confronted us in our development work, and which apparently was not of major significance in the Cadillac design, was a definite feeling of "harshness" in the ride. Experimentation showed that proper location of the units to relieve loads on suspension bearings reduced friction. Lower oscillating rates gave us the best results for harshness and ride. Although the diaphragm-type unit appears ideal from a frictional standpoint, it is rather surprising that a compromise design which would lend itself to the installation of either coil springs or air springs would show any improvement as far as harshness was concerned.

The paper does not indicate the wheel travel obtainable on either front or rear wheels. We feel that, in spite of the feature of constant ride height, a wheel travel of about 8" in the front and about 10" in the rear would be desirable. It is possible, however, to cut this down somewhat by the varying rate of the springs.

It is our belief that, when the ultimate design in air suspension is reached, an improved type of shock absorber will be required. The elimination of friction in the suspension system will mean that this unit will be required to do more of the damping. Existing designs with 4-coil springs have already pointed up this fact. We feel that units with greater piston displacement will provide the required damping without increasing harshness, provided proper mounting location giving good displacements can be obtained.

The approach to the rear-suspension problem with the 4-link design would appear to have considerable merit and, since this is a very complex problem, I shall not attempt any detailed discussion at this time. Several other designs have been tried, among which are: Packard type, conventional torque-tube type, and dedion type. There are many features of the latter type which we feel would merit serious consideration.

Some advantages of the constant-level air-suspension system not mentioned in this paper are improved lighting and vision out of the rear window.

We feel, as do the authors, that the air-suspension principle has a great potential and that, as soon as the public has the opportunity to become acquainted with its advantages, the demand will be even greater than that which we have witnessed in the case of automatic transmissions, power steering, power brakes, power windows, and the like.

Thrust Measurement for Jet Transport Operation

M. J. Saari, National Advisory Committee for Aeronautics

This paper was presented at the SAE National Aeronautic Meeting, New York, April 4, 1957.

SUPPOSE it is an exceptionally hot day in Denver. A jet transport lines up with the runway, all engines are brought up to rated speed, and the airplane gains momentum. Somewhat beyond the halfway mark down the runway the pilot, realizing that he cannot become airborne in the remaining length of runway, frantically cuts the engine and applies the brakes. As the airplane slithers beyond the end of the runway the pilot's mind is filled with unkind thoughts about engineers in general. A more rational thought might follow in the form of a question, "Why can't the jet transport be provided with an accurate thrust-measuring device so that the take-off distance can be predicted under all operating conditions?" The example may be bad, but the question is perfectly legitimate. The following discussion is concerned with some of the general aspects of the problem.

A viewpoint on thrust measurement can be developed by finding answers to four questions:

1. What type of thrust measurement is of significance for jet transport operation?
2. When and why is the measurement of thrust important?
3. What are the limitations and accuracies of current methods of evaluating thrust?
4. What other method might be used to better satisfy the requirement of thrust measurement?

While many other considerations are conceivable, it is felt that answers to these questions will provide a general insight into the problem.

Definition of Thrust

In considering the significant type of thrust measurement, it is necessary to define the expression "thrust." The installed thrust of a turbojet installation (Fig. 1) can be defined as either jet thrust or net thrust. The jet thrust represents the gross reaction force of the gases issuing from the exhaust nozzle and can be expressed as:

$$F_j = m_2V_2 + A_2(p_2 - p_0) \qquad (1)$$

The term m_2V_2 denotes the momentum of the exhaust gases at the exhaust-nozzle exit and $A_2(p_2 - p_0)$ represents the excess pressure force acting on the exhaust-nozzle exit projected area when the exhaust nozzle operates supercritically (choked). When the exhaust nozzle operates subcritically (unchoked), the excess pressure force becomes zero and the jet thrust is merely a function of the nozzle-exit momentum.

Net thrust is defined as the total change in momentum of the gases passing through the engine and represents the net propulsive force acting on the aircraft. In its simplest form, net thrust consists of two terms, the jet thrust and the inlet or free-stream momentum drag, which can be expressed as: $F_n = F_j - m_1V_0$ (2)

The term m_1V_0 is the free-stream momentum drag and represents the force required to accelerate the mass airflow entering the engine from ambient conditions to the flight velocity of the aircraft. Although there can be several components of the inlet momentum term chargeable (with discretion) to either the airframe or the powerplant installation, the general definition of net thrust is adequate for the purpose of this discussion.

A graphical illustration of the relative variation of jet thrust and net thrust with flight speed at a given altitude is presented in Fig. 2. At static conditions ($V_0 = 0$) the net thrust and jet thrust are equal. As flight speed increases, the engine-inlet total pressure and total temperature (at a given altitude) increase in a unique manner. With the engine operating at maximum mechanical rotative speed, the effect of increased flight speed is an in-

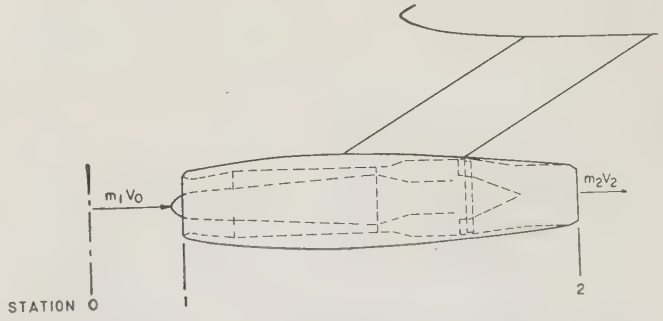

Fig. 1—Definition of jet thrust and net thrust for turbojet engine installation

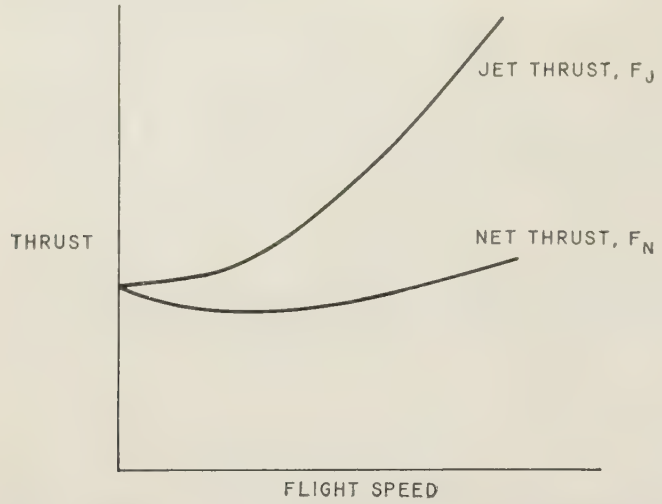

Fig. 2—Typical variation of jet thrust and net thrust with flight speed

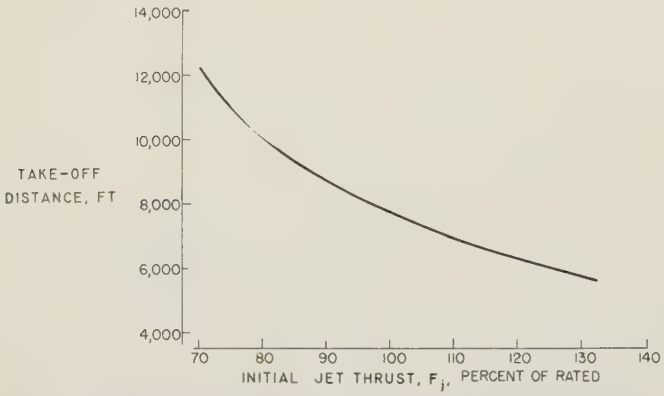

Fig. 3—Variation of take-off distance with initial jet thrust for 4-engine jet transport, 250,000-lb take-off gross weight, 40,000-lb rated total jet thrust, wing loading of 100 psf

crease in mass flow through the engine. Consequently, jet thrust increases continuously as flight speed increases. Net thrust, on the other hand, decreases gradually during the initial rise in air speed simply because the inlet momentum drag in Equation 2 increases more rapidly than does the jet thrust. Above a certain air speed, the jet thrust begins to increase more rapidly than the inlet momentum drag; and net thrust begins to rise and continues to rise at the higher air speeds. But jet thrust is higher than net thrust at all air speeds.

Net thrust is the yardstick used in evaluation of overall turbojet engine performance since it represents the useful propulsive thrust developed by the powerplant and, when related to the rate of fuel consumption, defines the operating efficiency or economy of the engine installation. Net thrust is also required in the evaluation of overall airplane drag in flight, since the total drag force is equal to the net propulsive thrust at a given flight speed. A description of the instrumentation and techniques involved in the accurate measurement of net thrust in flight is beyond the scope of this discussion, except to mention that the instrumentation required would be prohibitive with regard to an operational-type aircraft. Furthermore, in rationalizing the type of thrust measurement suitable for jet transport operation, net thrust is not a vital prerequisite since the overall airplane performance and operating procedures are generally defined in the experimental or prototype stages of development.

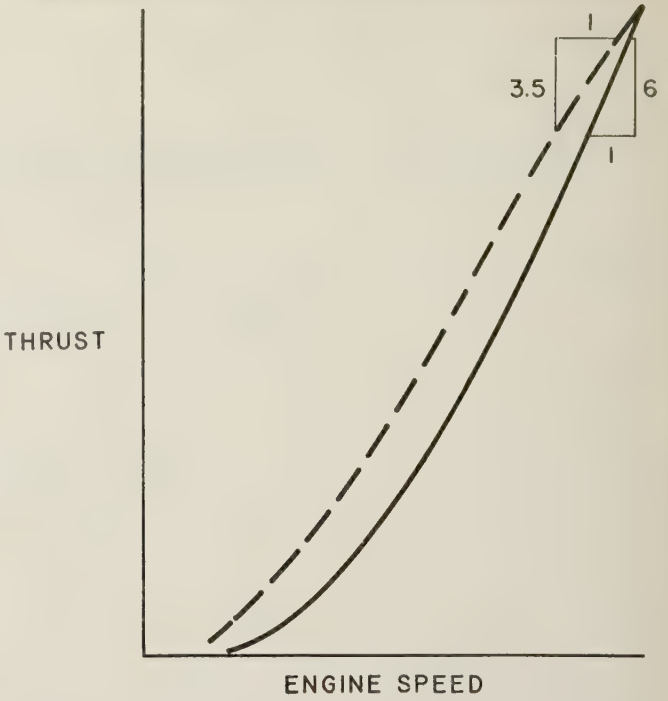

Fig. 4—Variation of thrust with engine speed

From an operational viewpoint, an accurate, direct, and continuous measurement of jet thrust would provide the pilot with an adequate assessment of condition and output of each of the aircraft's powerplant units.

Importance of Thrust Measurement

When and why is thrust measurement important? A typical flight plan might be broken down into six operations: take-off, climb to cruise altitude, cruise, letdown from cruise altitude, holding during stacked landing conditions, and landing. Prior to and during the take-off operation, a knowledge of the total thrust available is extremely important in predicting the ability to become airborne within a given runway length. Fig. 3 shows a typical variation of take-off distance with initial jet thrust for a 4-engine transport having a gross weight of 250,000 lb and a rated total static thrust of 40,000 lb. At thrust levels higher than rated thrust (100%), a 10% increase in thrust decreases take-off distance by about 6%. However, at thrust levels lower than rated thrust, a 10% reduction in thrust increases the take-off distance by as much as 17%. Thus, where runway lengths are marginal for rated thrust, an accurate indication of thrust prior to take-off would be highly desirable to predict the go or no-go odds. Except under rare conditions, an initial thrust evaluation would eliminate the "point of no return" during take-off when the pilot must decide whether to continue or to abort the operation.[1]

During all other operating phases of the flight plan, a direct thrust measurement is of secondary importance since the flight operating conditions can be predicated on a prescheduled air speed-altitude program. Nevertheless, a direct thrust measure-

[1] NACA TN 3252, November, 1954, "Description and Preliminary Flight-Investigation of Instrument for Detecting Subnormal Acceleration During Take-Off," by G. J. Morris and L. J. Lina.

ment in flight would provide an accurate method of power trimming for multiengine aircraft and of sorting in-flight operating problems as to whether the engine or airframe is responsible for performance deficiencies.

Existing Method of Estimating Thrust

At the present time, the predominant method of estimating the thrust output of a turbojet engine installation depends on engine speed and exhaust-gas temperature measurements. In setting up rated engine speed and rated exhaust-gas temperature prior to take-off, probable errors in engine speed of ±1–2% and in exhaust-gas temperature of ±2–3% can exist due to instrument and reading errors in aircraft instrumentation.

In a gross sense, the jet thrust is a function of mass flow and jet velocity. The mass airflow through a turbojet engine is a function of engine-inlet total pressure, total temperature, and engine rotative speed. The exhaust-nozzle exit jet velocity is a function of total pressure and temperature of the gases in the tailpipe. In modern high-pressure-ratio engines, the mass flow and exhaust-nozzle total pressure and temperature change rapidly with engine speed; therefore, thrust output is very sensitive to engine speed (Fig. 4). In general, a 1% change in engine speed can result in 3–6% change in thrust, depending on the design compressor-pressure ratio. Therefore, small errors in the indication and reading of engine speed can result in sizeable errors in judging the thrust output of an engine. Similar errors in estimating thrust can be attributed to errors in indicating and reading exhaust-gas temperature. Shifts in radial and circumferential temperature profiles at the turbine exit, distortion of exhaust-nozzle area, or engine deterioration may result in false indication of the average gas temperature. In general, for a high-pressure-ratio engine operating near rated conditions, a 1% error in temperature indication would cause about a 2.5% error in estimated thrust.

Two factors that directly affect the critical take-off operation are ambient temperature and ambient pressure. The effect of ambient temperature on engine thrust is shown in Fig. 5 for an engine having a moderate-rated compressor-pressure ratio of about 8/1 and another having a high-rated pressure ratio of about 12/1. With the engines operating at 100% rated mechanical speed, both engines develop 100% (rated) thrust at sea-level standard-day temperature (60 F). For a constant mechanical engine speed the thrust increases as ambient air temperature decreases below standard-day conditions. However, at ambient temperatures above 60 F the thrust for 100% mechanical engine speed decreases so that on a 100 F day the thrust developed by the moderate-pressure-ratio engine is 92% of rated thrust, while the high-pressure-ratio engine develops only 81% of rated thrust.

The high-pressure-ratio engine is probably the more representative engine type for jet transport application from consideration of cruise efficiency. The ambient temperature effect, on the high-pressure-ratio engine, translated into take-off distance is shown in Fig. 6 for the same airplane configuration described in Fig. 3. The standard-day reference take-off distance is 100%. The thrust increase at ambient temperatures lower than 60 F shortens the take-off run so that at 0 F the distance is reduced by about 30%. Conversely, on a 100 F day it is 30% greater than the standard-day distance.

The effect of ambient pressure on engine thrust is shown in Fig. 7 for constant ambient air temperature. For the range of pressure variation considered

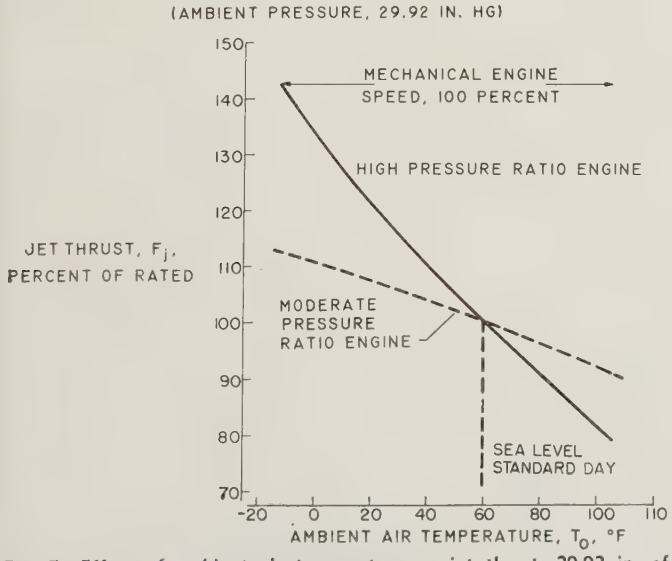

Fig. 5—Effect of ambient air temperature on jet thrust, 29.92 in. of Hg ambient pressure

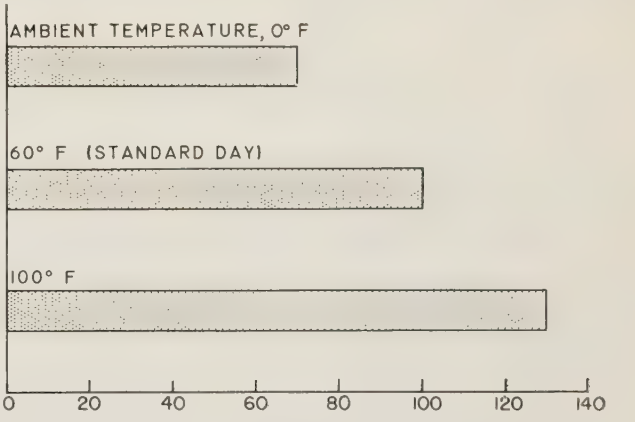

Fig. 6—Effect of ambient air temperature on take-off distance of 4-engine jet transport

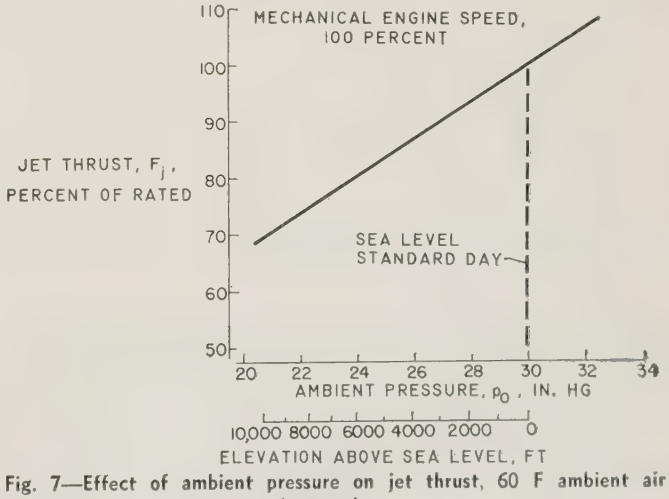

Fig. 7—Effect of ambient pressure on jet thrust, 60 F ambient air temperature

here, the effect of ambient pressure would be the same for all engines regardless of compressor-pressure ratio, since it affects only the density of the air swallowed by the engine. At sea-level standard-day conditions ($p_0 = 29.92$ in. of Hg) the engine develops 100% (rated) thrust at 100% (rated) engine speed. At ambient pressures of 26.8 and 24.0 in. of Hg, corresponding to airport elevations of 3000 and 6000 ft, the jet thrust at 100% engine speed is reduced to 90% and 80% of sea-level rated thrust, respectively. The effects of these thrust reductions on take-off distance is shown in Fig. 8. Relative to sea-level standard-day conditions, the take-off distances for ambient pressures corresponding to airport elevations of 3000 and 6000 ft would be about 14% and 31% greater, respectively. Since the effects of ambient pressure and ambient temperature on engine thrust are additive, a take-off from the "mile-high city" of Denver, for example, on an 80 F day would require a 52% longer ground run than one from New York on a standard day. It is, therefore, evident that estimation of total thrust output from engine speed and exhaust-gas temperature indications could lead to considerable difficulty during the take-off operation. Other factors that affect the thrust output include: (1) nonuniformities in total-pressure distribution at the engine inlet caused by changes in air-induction characteristics or by ice formations; (2) Reynolds number effects on engine components, particularly the compressor; and (3) general engine deterioration.

Thrustmeter Principle

Now, the final question can be raised, "What other method might be used to satisfy the requirement of thrust measurement?" Much of the credit for the answer to this problem must be attributed to W. Hesse of the United States Naval Air Test Center for his proposal and research on the thrustmeter principle.[2,3] An extension of the principle has evolved from full-scale engine investigations at the NACA Lewis Laboratory. An understanding of the thrustmeter principle can be obtained by examination of the jet thrust equation:

$$F_j = C_F[m_2V_2 + A_2(p_2 - p_0)] \qquad (3)$$

This expression is different from ideal thrust Equation 1 in that a nozzle-thrust coefficient is introduced, which accounts for pressure losses between the instrumentation station and the nozzle exit as well as differences between actual and measured velocities, areas, and pressures that inevitably result from use of limited instrumentation. The variation of thrust coefficient C_F with nozzle-pressure ratio for a typical simple fixed-area convergent exhaust nozzle is shown in Fig. 9. The thrust coefficient is constant for choked-nozzle operation, that is, at nozzle pressure ratios (P_2/p_0) above 1.89, with a general value of 0.97 ± 1%.

The momentum term m_2V_2 of Equation 3 implies the necessity of an accurate measurement of engine airflow and exhaust-gas temperature which is difficult to accomplish without a complex of instrumentation. In order to eliminate the necessity of measuring these variables the momentum term can be expanded and simplified and the jet thrust can be written as: $F_j = C_F[\gamma_2 A_2 p_2 M_2^2 + A_2(p_2 - p_0)]$ (4)

This expression of jet thrust could be further simplified if the exhaust-nozzle exit Mach number could be deleted. Examination of characteristics of current high-pressure-ratio engines indicates that the pressure ratio across the exhaust nozzle P_2/p_0 is critical (choked) at take-off, climb, and cruise conditions. The minimum corrected engine speed at which the exhaust nozzle is choked is shown in Fig. 10 as a function of flight Mach number for a typical turbojet engine. The range of engine speeds for choked-nozzle operation is smallest at static conditions; however, even on a 100 F day the exhaust nozzle of a high-pressure-ratio engine operates in a choked condition. As Mach number increases the minimum speed for choked-nozzle operation decreases because of the rise of engine inlet total pressure. Thus, for the range of operating conditions where thrust measurements are required, the exhaust nozzle is choked and the Mach number term M_2^2 of Equation 4 is unity.

Also, when the exhaust-nozzle exit Mach number is unity, the static pressure at the exhaust-nozzle exit p_2 can be expressed as a function of the nozzle-exit total pressure and the ratio of specific heat γ_2:

$$p_2 = P_2\left(\frac{2}{\gamma_2 + 1}\right)^{\frac{\gamma_2}{\gamma_2 - 1}} \qquad (5)$$

Substituting this expression into Equation 4 and

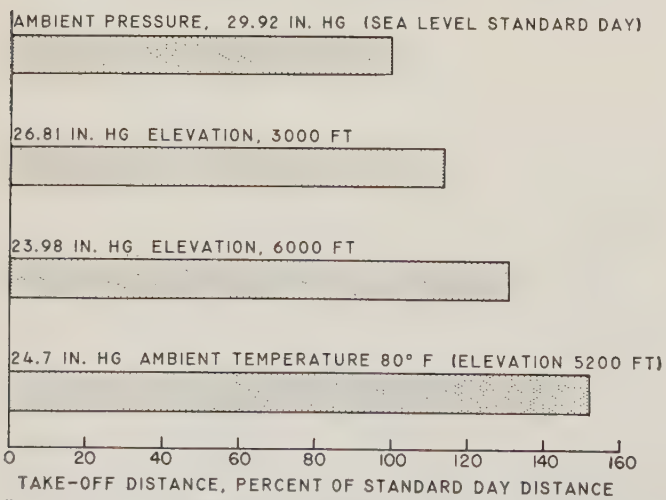

Fig. 8—Effect of ambient pressure on take-off distance of 4-engine jet transport

[2] Technical Report 2–52, Test Pilot Training Division, U. S. Naval Air Test Center, Maryland, April 3, 1952, "Simple Gross Thrust Meter Installation Suitable for Indicating Turbojet Engine Gross Thrust," by W. J. Hesse.

[3] Project TED-PTR-PP-343 Test Pilot Training Division, U. S. Naval Air Test Center, Maryland, July 18, 1951, "Analysis of Turbojet Engine Thrust in Flight," by W. J. Hesse.

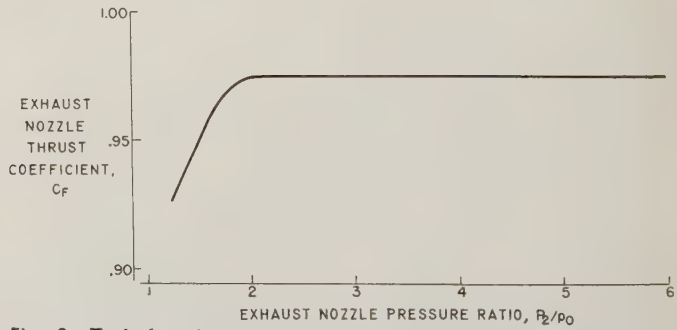

Fig. 9—Typical variation of exhaust nozzle thrust coefficient with nozzle pressure ratio

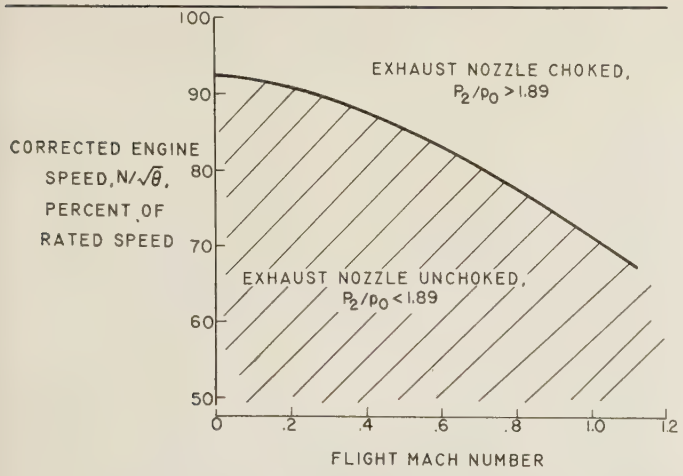

Fig. 10—Typical variation of minimum engine speed at which exhaust nozzle is choked with flight Mach number

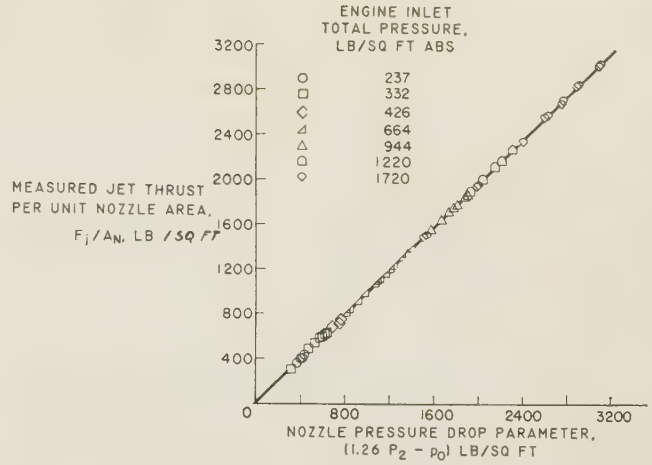

Fig. 11—Typical correlation of measured thrust per unit of measured exhaust-nozzle area with nozzle pressure drop parameter

recalling $M_2 = 1.0$ yields:

$$F_j = C_F A_2 \left[(\gamma_2 + 1) \left(\frac{2}{\gamma_2 + 1} \right)^{\frac{\gamma_2}{\gamma_2 - 1}} P_2 - p_0 \right] \qquad (6)$$

The terms including γ_2 can be replaced by a constant without appreciable error. The term $(\gamma + 1)\left(\frac{2}{\gamma + 1}\right)^{\frac{\gamma}{\gamma - 1}}$ varies only 0.24% for an exhaust-gas temperature range of 600–1300 F. Using an average value of γ_2 the constant becomes 1.26 Equation 6 can be written as:

$$F_j = C_F A_2 (1.26\ P_2 - p_0) \qquad (7)$$

The quantity $(1.26\ P_2 - p_0)$ is defined as the nozzle pressure drop parameter.

The nozzle thrust coefficient C_F was shown earlier to be constant in the range of engine operation where the exhaust nozzle is choked and, therefore, is also constant for the applicable range of thrust expression of Equation 7. The exhaust-nozzle exit area, which is measured cold and corrected for thermal expansion by use of an appropriate average metal temperature and expansion coefficient, can be considered essentially constant for the range of metal temperatures encountered in flight operation. Consequently, the only variables to be measured in evaluating jet thrust are exhaust-nozzle exit total pressure and ambient or free-stream static pressure. The jet thrust equation, therefore, indicates that for a fixed-area convergent exhaust nozzle a correlation of jet thrust with nozzle pressure drop parameter should be possible for all flight conditions, provided the exhaust nozzle is choked and the thrust coefficient remains constant.

Correlations of actual jet thrust, measured by balance scale systems, with nozzle pressure drop parameter have been made for a large number of different types of turbojet engines in NACA altitude facilities and other test installations. A typical correlation of jet thrust per unit of exhaust-nozzle area with nozzle pressure drop parameter is shown in Fig. 11 for a wide range of engine-inlet total pressure. In all correlations such as this it has been found that the variation of jet thrust with nozzle pressure drop parameter is linear and, moreover, is independent of flight condition. The slope of the correlation line is equal to the nozzle thrust

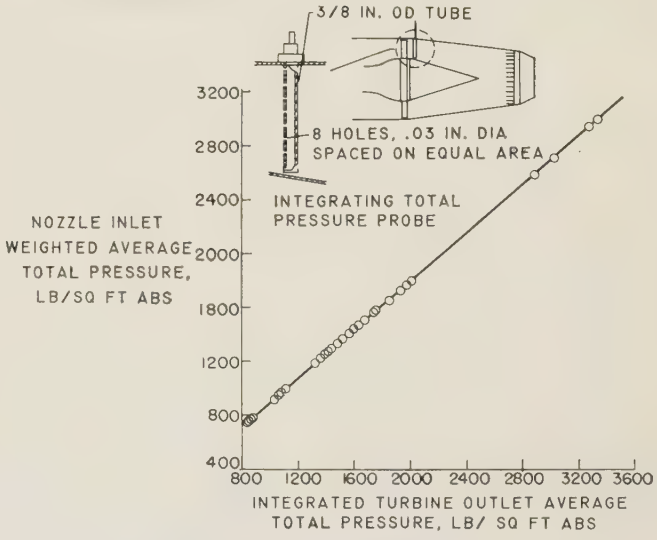

Fig. 12—Correlation of nozzle inlet weighted average total pressure with integrated turbine outlet total pressure

coefficient. The consistent linearity of the data indicates that the slope of the correlation line can be determined from a single data point obtained at rated engine speed at sea-level conditions, thereby eliminating extensive engine calibration tests.

In many cases it is difficult to obtain an accurate measurement of exhaust-nozzle exit total pressure P_2 with a minimum of instrumentation due to radial pressure gradients. On the other hand, average turbine outlet total pressure can be measured accurately with a simple integrating probe. Usually the total pressure ratio between the turbine outlet and exhaust-nozzle exit are known from manufacturer's engine calibration tests. Consequently, the turbine outlet average pressure can be used in Equation 7 in place of nozzle-exit total pressure by adjusting the constant 1.26 by the tailpipe total-pressure loss.

A correlation of average turbine-outlet pressure measured by an integrating probe with the average total pressure at the exhaust-nozzle inlet measured by a detailed weighted survey rake is shown in Fig. 12. The relationship of the two total pressure measurements is linear and the slope of the correlation line is equal to the tailpipe total pressure ratio. In order to minimize possible errors, the

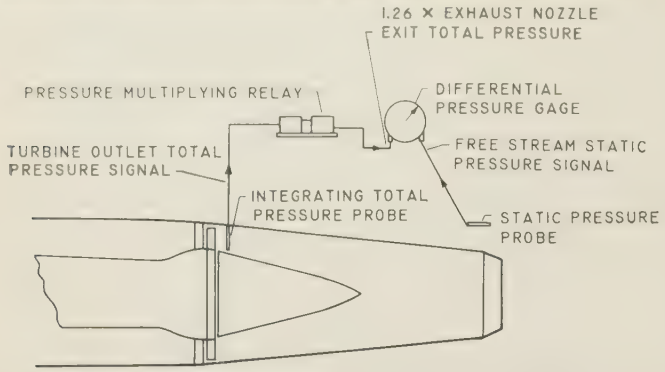

Fig. 13—Schematic diagram of thrustmeter installation

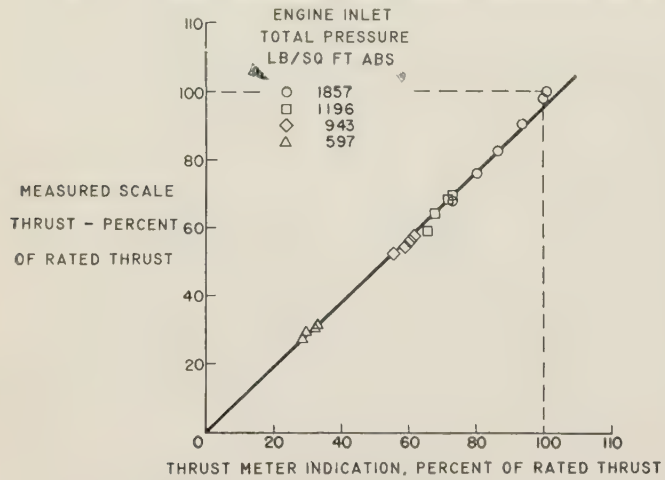

Fig. 14—Thrustmeter calibration

integrating probe should be located in a region where the radial pressure gradient is not greater than about 15%.

Experimental Thrustmeter

An experimental thrustmeter incorporating the nozzle pressure drop parameter was designed and installed on an engine (Fig. 13). An integrating total pressure probe was used to sense the total pressure at the turbine outlet. This signal was fed into a pressure multiplying relay that produced an outlet pressure of 1.26 times exhaust-nozzle inlet total pressure which, in turn, was fed to one side of a sensitive differential pressure gage. (It should be noted that, in this case, the multiplying relay was adjusted to account for the pressure drop between the turbine-outlet and exhaust-nozzle inlet stations.) Free-stream static pressure was sensed in the plane of the exhaust-nozzle exit and was fed into the case vent of the differential pressure gage.

A calibration of the thrustmeter is shown in Fig. 14, where the percent of rated thrust measured by balance scales is plotted against thrustmeter indicated thrust. The maximum variation from the linear correlation line was about 2% and the slope of the line again is equal to the thrust coefficient of the exhaust nozzle. In an operational-type thrustmeter the scale of the differential pressure gage would be adjusted by the product of $C_F A_2$ so that the gage would read directly in pounds of actual jet thrust. It is conceivable that with development of a very accurate pressure multiplier and by discrete selection of the total pressure measuring station for a particular engine, accuracies in order of 0.5–1.0% could be achieved.

The installation of a thrustmeter in a jet transport, therefore, requires only the definition of the relationship of measured jet thrust with the exhaust-nozzle pressure drop parameter for the particular type of engine to be used. As mentioned earlier, this relationship can be established from a single data point of static sea-level conditions. The exhaust-nozzle thrust coefficient and measured nozzle-exit area would be used as constants in deriving the scale on the thrustmeter dial. If exhaust-nozzle geometries other than the simple circular convergent nozzle (such as special geometries dictated by jet noise suppression requirements) are used, the thrust coefficient must be obtained from nozzle calibration data or the thrustmeter correlation must be established for the particular engine-nozzle combination in a test stand calibration. Thus, with reasonable care in selection of representative total and static pressures, in measuring the quantities to be used as constants, and attention to the accuracy of pressure multiplying equipment, it is felt that this principle of thrust measurement will satisfy the requirement for an accurate, simple, and reliable assessment of jet thrust for jet transport operation. It is emphasized that the thrustmeter principle discussed herein is valid for all engine operating conditions at which the exhaust nozzle operates in a choked condition.

Conclusions

1. In lieu of net thrust, an indication of jet thrust would provide the pilot an adequate assessment of the power output of each powerplant unit.
2. While thrust measurement is of particular importance prior to and during the take-off operation, it would also observe many useful purposes during other phases of flight plan.
3. Because of the many factors that influence the thrust output, existing methods of evaluating thrust from indications of engine speed and exhaust gas temperature are inadequate.
4. The utilization of the thrustmeter principle based on the nozzle pressure drop parameter provides an accurate measure of jet thrust and is valid for all operating conditions at which the engine exhaust nozzle operates in a choked condition.

APPENDIX

Symbols

A = Area, sq ft

C_F = Nozzle thrust coefficeint, $\frac{\text{actual thrust}}{\text{ideal thrust}}$

F_j = Jet thrust, lb

F_n = Net thrust, lb

M = Mach number

m = Mass flow, slugs per sec

N = Engine rotative speed, rpm

P = Total pressure, lb per sq ft

p = Static pressure, lb per sq ft

V = Velocity, ft per sec

γ = Ratio of specific heats

θ = Ratio of engine-inlet total temperature to standard sea-level day temperature $\left(\frac{T_1}{519}\right)$

Subscripts: 0 = Free-stream conditions
1 = Engine inlet
2 = Exhaust-nozzle exit

ORAL DISCUSSION

Reported by E. C. Breinig
Bendix Aviation Corp.

Harry Pearson, Rolls-Royce, Ltd., England: I have several comments to make. First, there was too much emphasis on this place called Denver. Besides all airports have a thermometer and barometer so that the pilot is aware of atmospheric conditions and could, therefore, estimate thrust and take-off distance. Second, the thrustmeter must provide an indication that the pilot can understand so that at altitude, as engine thrust decreases, the thrust reading lacks reference as to how well or poorly the engine is developing thrust. Also, the accuracy of the thrustmeter would decrease as altitude increases.

Third a system using engine pressure ratio would be better. The thrust-measuring device should be more reliable than the engine. Because it is not necessary for the pilot to know the thrust exactly, existing engine instruments are adequate.

Mr. Saari: I didn't expect the subject to be controversial. The purpose of the presentation was to suggest a proved principle of thrust measurement providing a method of indicating thrust that is independent of the many factors which affect thrust estimation from engine speed and exhaust-gas temperature measurements. The control tower can inform the pilot of ambient pressure and temperature but it is doubtful that he can be enlightened as to whether the compressor bleeds are closed completely, inlet guide vane settings have slipped a little, or some inlet flow distortion has been introduced due to foreign objects stuck on inlet screens, or the engine has deteriorated performance wise. Even if he could be supplied with this information he would need a catalog of correction charts to estimate thrust. A thrustmeter, on the other hand, would tell the pilot at a glance what thrust the engine (or engines) are developing.

It is, of course, possible to modify the thrustmeter system to provide a reference so that the pilot can read a thrust indication that is relative to a value or number with which he is familiar. For example, by finding the ratio of engine-inlet total pressure and the nozzle pressure drop parameter $(1.26\ P_2 - p_0)$ and applying the necessary constants, a thrust indication referred to sea-level rated thrust can be obtained. The principle is valid and results are consistent. The accuracy depends on how well the variables are evaluated.

Many attempts have been made to develop thrustmeters, most of which have correlated thrust with nozzle pressure drop $(P_2 - p_0)$ or nozzle pressure ratio (P_2/p_0). However, to date, these systems have lacked generality and deviations in correlations exist because the basic concepts deviate from the parameter suggested by the jet thrust equation. Engine pressure ratio may be used as a thrust indication if a good average engine-inlet total pressure can be measured without entailing a complexity of instrumentation.

There is no reason why the thrust indicator should not be as reliable as the engine, if it is kept simple.

As to the necessity of thrust measurement, I don't think that we can deny the pilot the right to have the best possible indication of engine power output; and it seems logical that the direct method is better than an indirect method which involves many improbables.

Ralph S. White, Civil Aeronautics Administration: The measurement and effects of humidity were omitted. It is generally considered to have no effect, but this opinion is not shared by all.

Mr. Saari: The effects of ordinary variations in humidity are negligible in comparison to the other factors that affect thrust such as ambient pressure and temperature, flow distortion, and the like. Therefore, it is not an important factor in thrust measurement. It is the 5–10% error in estimating thrust that causes concern at take-off, for example.

H. H. Wakeland, Sperry Gyroscope Co.: If the accuracy of measuring other parameters such as engine speed and temperature were improved, could not some other approach to thrust measurement have promise?

Mr. Saari: The improvements in measuring instrument accuracies is, of course, desirable since the error in estimating thrust from speed-temperature indications would be cut correspondingly. However, even if the pilot had perfect speed and temperature indications, he would still be faced with many other unknown factors and not sure of the actual thrust being developed by the engines. A thrustmeter would put him on solid ground. So as not to be misunderstood, the tachometer and temperature indicators are still important for indicating how close to mechanical limits the engine is being operated.

Mr. Wakeland: Are there other parameters that might be used to indicate what the engine is doing relative to rated performance?

Mr. Saari: There may be, since investigation of this problem area is by no means exhausted. A compressor discharge pressure indication might be used, since, ordinarily, the major factors that affect thrust also affect the compressor. However, considering the changes in flow profiles and distributions at the compressor discharge, the instrumentation might be more complex. The best way to look at the thrust measurement problem is to consider the engine as a gas generator. The thrust is basically a function of the pressure and temperature of gas supplied by the gas generator to the tailpipe. The problem of providing a direct-thrust measurement is one of translating the tailpipe conditions into a recognizeable indication of thrust force.

Edward A. Rock, Boeing Airplane Co.: I am involved with thrust measurements on the B-52. I agree that tailpipe pressure is a good reading to get, but it is very inconsistent. The single probe (compressor discharge pressure) does not give a good average reading.

Mr. Saari: An accurate indication of average turbine outlet pressure is necessary for thrustmeter application. If a steep radial pressure gradient exists, a more elaborate integrating method should be used. However, for most engines an integrating probe is adequate. For the thrustmeter principle, the measurement of tailpipe temperature is not required.

Mr. Rock: I agree that something consistent and reliable is needed for take-off. However, rather than a pressure-ratio device, a straight pressure reading one is needed. The results would then be considered more reliable. During climb the rpm measurements are reasonable and accurate, during cruise the tailpipe readings are all right. As far as four engines are concerned, the four readings have to be consistent.

Mr. Saari: A straight pressure reading device would not indicate thrust level any better than rpm and temperature indications. The thrustmeter readings would be consistent from engine to engine only if the thrust developed is consistent.

J. B. Butler, Bristol Engineering Corp.: The reproducibility of data is the worst problem. What accuracy is required?

Mr. Saari: The thrust of a turbojet engine installation can vary from engine to engine of a given make and from one run to another. A thrustmeter indication of $\pm 1\%$ might be a good accuracy to think about. This is far better than the accuracy we might expect from engine speed and gas temperature indications in an operational-type installation.

ON THE basis of laboratory and field tests of passenger-car and light-truck rear axles, the authors conclude:

1. The capacity of present axles can be increased, without increasing axle size, when greater load-carrying antiwear and antiscore lubricants are available.
2. Gear noise will always be a major problem because axle gears are operating at varying speeds and loads whenever a car is in motion. Many gear noise problems can be overcome by proper tooth development and by testing in the actual car model under which the axle will be used.
3. The only reliable basis for torque-capacity rating is the tractive effort (wheel-slip torque).
4. The limited-slip type of differential will eventually become standard equipment on all passenger cars, if only to improve car handling and stability during high-speed driving under varying traction conditions.

REAR

Today's Axles

General Design

EARLY in the 1930's the requirements and principles of rear-axle design and construction became generally recognized. The art of axle design and manufacture since that time has become primarily one of improvement to provide increased capacity and a better product, as required by the improvement in the automotive vehicle itself.

Three general types of axles are prominent in the automotive field today.

The first is called the "trumpet-type," as shown in Fig. 1. In this design the ribs can be carried to the supporting bearings and the gears can be very rigidly supported. This type, is difficult to manufacture and service, and, therefore, is gradually being replaced in general use.

Fig. 2 shows the "banjo-type" axle, probably the most commonly used today. This axle lends itself to high-production manufacture. However, it has definite limitations in rigidity and lubrication features. It may be that, as these requirements become more exacting, the banjo-type axle will have to undergo some major design changes.

The "carrier-type" design is shown in Fig. 3. In the early 1930's, we selected the carrier-type as the best axle from both design and production standpoints. The design permits a full rib to extend between the pinion bearings and the differential bearings, supplying excellent support of the gear teeth at the mesh point. It also permits the use of oil channels to direct lubricant to each of the pinion and differential bearings. It is easily adaptable, for the center section may be common and only the tubes and shafts have to be changed to fit a particular vehicle. This carrier is not any more difficult to machine than the banjo-type and, in addition, it supplies support to the differential bearings and has oil circulation features not possible with the latter. The prime function of an axle is to support the gears and bearings properly. Once this is accomplished and parts are properly manufactured, quiet operation over the life of the vehicle is practically insured and service is reduced to a minimum.

The hypoid gear has become a standard in passenger-car axles and is being used more and more in truck axles. Improved lubrication has largely overcome the limitations of the hypoid gear and is providing the means to maintain minimum axle size with maximum loading. The larger hypoid

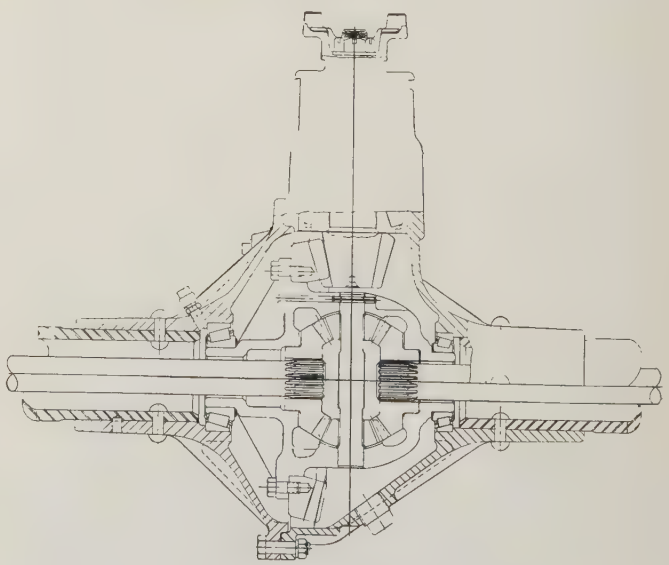

Fig. 1—Trumpet-type axle

AXLES—Today—Tomorrow

R. P. Lewis and L. J. O'Brien, Dana Corp.

This paper was presented at the SAE National Passenger-Car, Body, and Materials Meeting, Detroit, March 7, 1957.

pinion provides a gear set with as much as 20–30% more capacity in a given size than the conventional spiral-bevel gear. In the early use of hypoid gears, strength was an important factor in that the rigidity of axles was not adequate to support gears. Today, with improved axle designs strength is not the important consideration; therefore, we may direct gear design to provide more flexibility. By increasing the number of teeth in contact, we provide a gear which is easier to make and inherently quieter in its operation.

Tapered roller bearings have become practically a standard in axle design throughout the world. This bearing provides the most rigid mounting for bevel or hypoid gears. Thus, there is less change over the life of the axle.

In addition to general construction, axles are classified as to the type of wheel end used. The semi-floating wheel end in passenger cars and the full-floating one in heavier trucks are in general

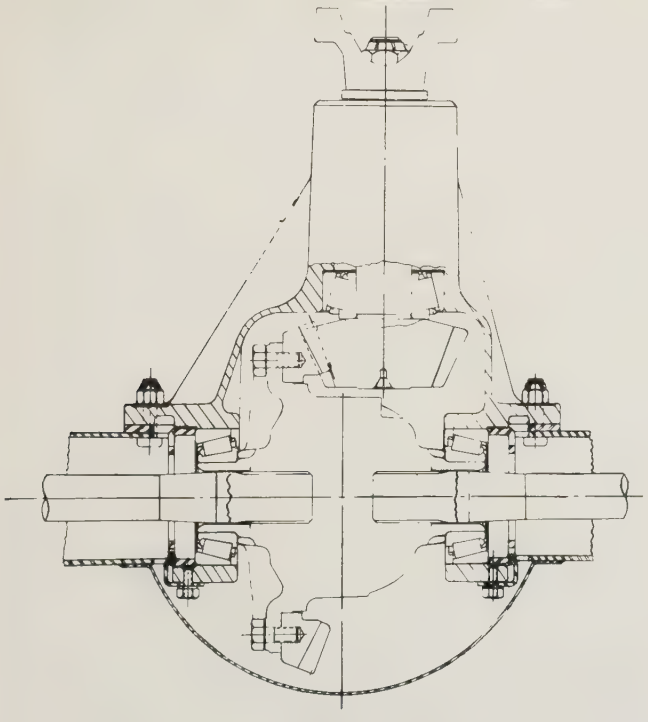

Fig. 2—Banjo-type axle

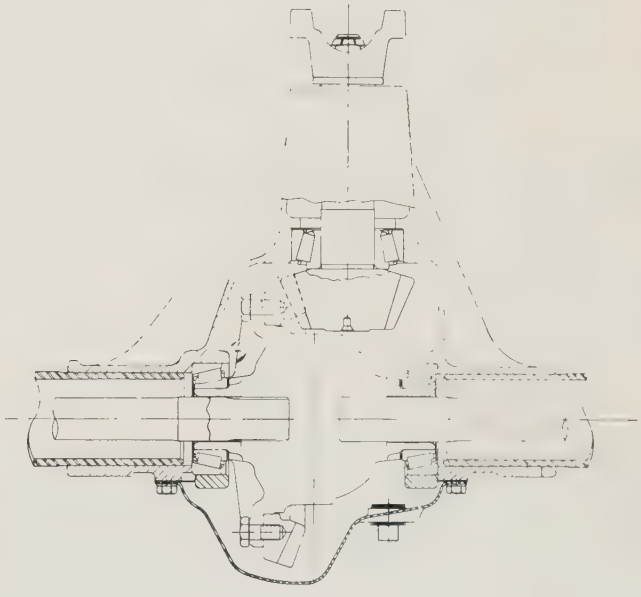

Fig. 3—Carrier-type axle

use. Fig. 4 illustrates two types of the semi-floating wheel end. The wheel is supported directly on the axle shaft which, in turn, is supported by a bearing inside the axle housing. The weight of the vehicle is, therefore, transmitted through the axle shaft to the axle housing. The axle shaft must withstand a bending load imposed by the weight of the vehicle, as well as the torsion load imposed by the driving force between the axle gears and the wheel. This design is used with both the tapered and ball-type wheel bearings. The tapered-bearing construction generally employs a tapered-axle shaft to which is attached a separate wheel hub; while the ball-bearing construction is used with a flanged shaft (Fig. 4).

Fig. 5 illustrates the full-floating type axle. In this design the wheel is supported on the axle housing through the wheel bearings. The axle shaft floats in the housing and merely transmits driving force from the axle gears to the wheel hub. There is no bending load on the axle shaft. This axle is commonly used in trucks of approximately ¾ ton and heavier.

The materials used in axle construction have also become standard. The carrier and differential case in any of these three types are usually made of gray cast iron or malleable iron. The gears are all made of carburizing-type materials. The main requirement of the gear material is that it provide a hard surface with a minimum of distortion. Axle shafts are made both from oil-hardened alloy steels and induction-hardened straight carbon steels. Since World War II, the induction-hardened shaft has been coming into greater general use. The induction-hardened shaft has proved to offer more strength at a lower cost due to the use of cheaper material. Axle housings and spring seats are generally made of low-cost straight carbon steel stampings. The use of forged spring seats, housings, and the like is now generally limited to the heavier trucks.

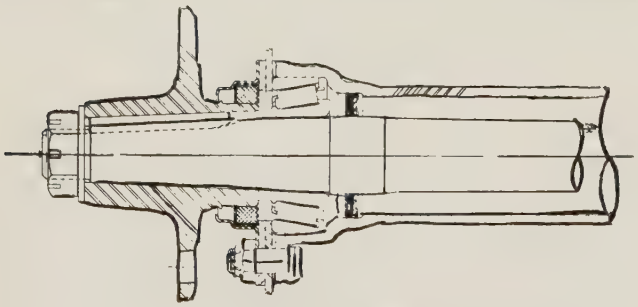

TAPERED BEARING CONSTRUCTION

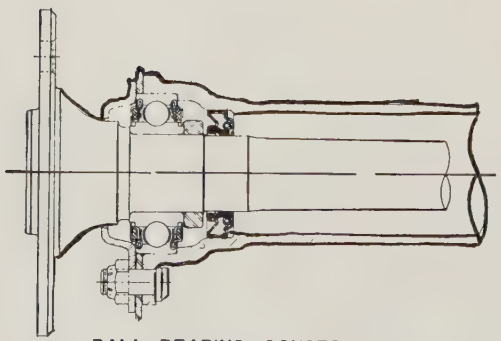

BALL BEARING CONSTRUCTION

Fig. 4—Semi-floating wheel end

Lubrication

With improvements in the design of the axle, lubricants and lubrication have become limiting factors in load-carrying capacity. In order to provide more surface capacity, various active and inactive additives have been used in the compounding of lubricants. The active-type lubricant offers more load-carrying capacity; but it is not as good from the wear and lubricity standpoints. The trend to the use of more active lubricants in passenger-car axles has reversed in the past few years to the use of the inactive-type lubricant with some treatment to obtain the same surface capacity. With continued development of inactive lubricants, it may be that in the future we will have a lubricant which will have all of the load-carrying advantages of the active lubricants and the desirable antiwear and lubricity features of the inactive lubricants.

The use of some surface treatment is now common. Lubrizing, an iron-manganese-phosphate coating, has been found to offer an initial resistance to scoring and to result in the same load-carrying capacity as that previously obtained with the active lubricants. After a gear set has been broken in, of course, its lubricant requirements are much less severe. By applying an appreciable amount of load, a gear set may be broken in within a few hundred miles; however, with light loads and very careful driving, a few thousand miles may be required. It has been found by field experience that proper lubrizing of the gear set will eliminate field failures due to scoring during the break-in period. Lubricity has become a more important factor with the increased loading at low speeds introduced by automatic transmissions, lower numerical axle ratios which these transmissions require, and the increased sliding due to the use of hypoid gears. Several of our present-day passenger cars have low-speed noises which have been corrected only by the use of lubricants having greater lubricity.

Noise

Noise is the major problem in axle design and manufacture. In the design of passenger-car axles, rigidity is much more important than strength. The gears and bearings must have as little deflection as possible under all conditions of loading. The actual load on the gears and bearings is limited by practicality with the particular design of axle determined from a noise rather than a breakage standpoint. Gears must have several teeth in contact to provide quiet operation. Bearings must be properly aligned to prevent bearing noises. Consideration in allowable loading must also be given to manufacturing requirements. The introduction of gear cutting and heat-treating errors reduces the load-carrying capacity of an axle more from a noise than a strength standpoint. Because noise in an axle cannot be controlled by design alone, the development of the gear set is of prime importance. Assuming that we have an axle of practical design, the gear set must be developed to provide a tooth bearing that can be controlled in cutting, heat-

treating, and lapping, and which will meet all requirements of loading under a particular vehicle. This is one phase of axle manufacture which is often overlooked.

The analysis of the noise problem is important in that it may save work in redesign to fix some condition not directly connected with the axle itself. The use of noise or vibration analyzing equipment will generally give a clue to the problem. We have found very few noise problems that could not be overcome. Different vehicles will have different noise characteristics which will change with manufacturing changes. The only known method of determining whether an axle will be satisfactory from a noise standpoint is to check the unit in the particular vehicle. Our procedure is to run at least one axle of every ratio from every shift in the vehicle in which it will be used. A change in the manufacture of the vehicle will often require a change in our noise requirements on the axle, thus, controls in its manufacture are of extreme importance. In order to maintain satisfactory quality, it is necessary to process each heat of steel separately throughout the various steps of manufacturing and heat-treat, to control the accuracy of the carriers and component parts, and to assemble the parts properly. The control of these items is a major factor in design consideration of the use of a particular axle under a given vehicle.

The use of some artificial means of correcting a noise problem is not generally satisfactory. It is a rare case when a combination of vibrations in a vehicle may be corrected by the introduction of rubber at the axle. The use of rubber at the axle may reduce road noises; however, it is very seldom that the introduction of rubber will correct an axle noise problem in itself.

Testing

We would like to go over some of the test procedures used to determine whether an axle is satisfactory from the design, manufacture, and loading standpoints. A deflection test is generally used first to check a new design, determining the relative movements of all parts. Indicators measure the lift, end movement, and side movement of the gear and pinion, bending and movement in various sections of the housing, and the alignment of the bearings under various conditions of loading. In analyzing the results it should be remembered that the relationship of assembly parts under various conditions of loading is more important than the actual deflection of parts. The dynamometer test is used to determine the fatigue life of an axle or its load-carrying capacity from a gear tooth surface standpoint. Although, the fatigue test is important in truck axles, in passenger cars, where strength is not the determining factor, the gear tooth surface capacity test becomes of prime importance. This test is connected with the lubricant used in the particular application.

Strain-gage equipment is used in a vehicle to obtain actual load requirements under various conditions of driving. In the past few years we have had good success in correlating the loads actually encountered in the vehicle with actual test work in the laboratory. An oil flow test shows how much lubricant must be supplied to the gears and bearings under various speeds. The actual temperature at which an axle will operate, however, depends more on the vehicle in which it is used than on the axle itself. An axle must receive an adequate air supply underneath the vehicle for proper cooling. The axle shaft test determines fatigue life. This test is used not only to check the initial capacity of a new axle, but also to maintain production quality.

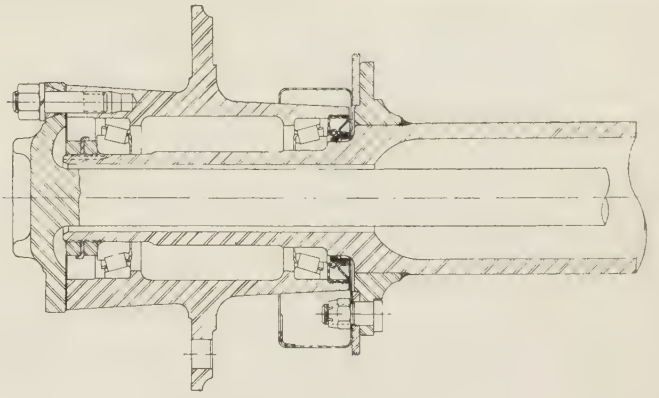

Fig. 5—Full-floating wheel end

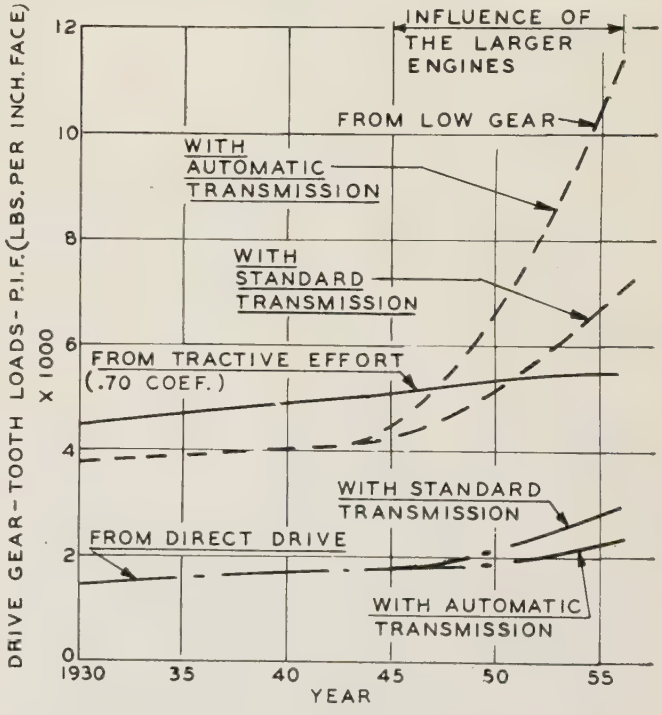

Fig. 6—History of rear-axle drive loads

Axle Loading

In Fig. 6 we show the loading on axles in use since 1930. There has been little change in allowable loading from tractive effort or wheel-slip torque. However, there has been a considerable change in loading in low gear due to automatic transmissions and in direct drive due to larger engines. Actually, axle size has remained somewhat constant. We have much less trouble today with the axle than we had in the 1930's, especially from a breakage

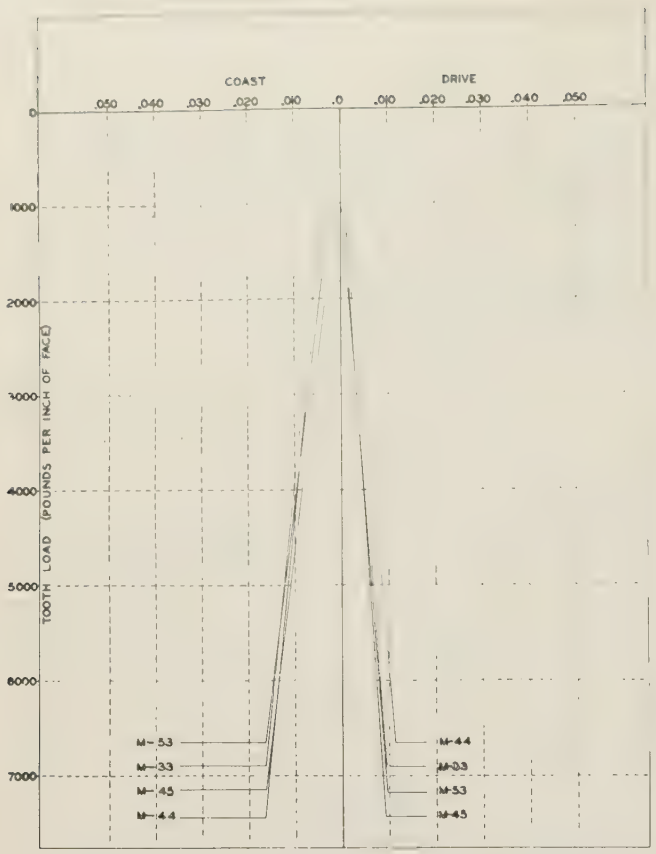

Fig. 7—Deflections, relative lift

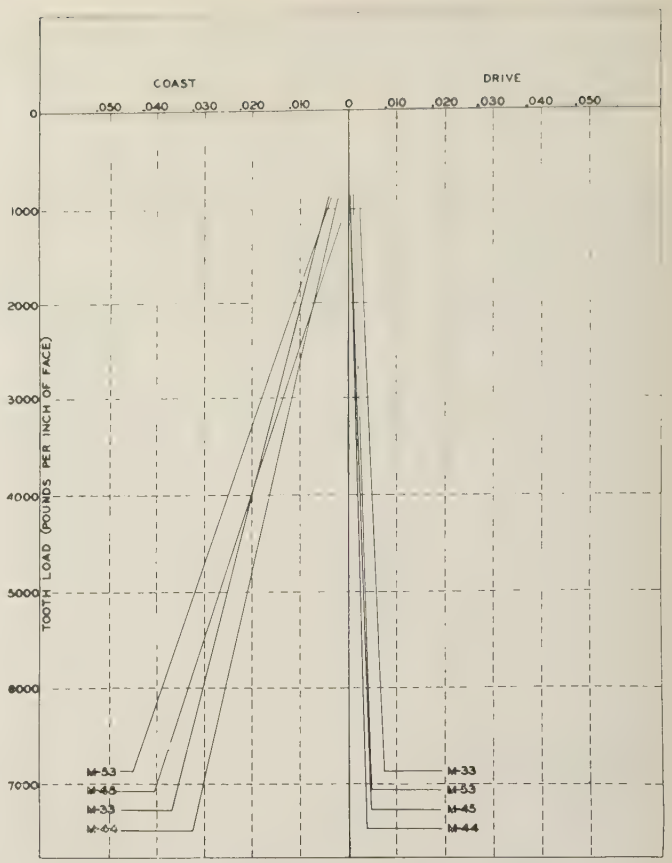

Fig. 8—Deflections, relative side movement

standpoint. In this connection, we mean primarily the passenger-car axle.

It will be noted that sometime between 1945 and 1950 we reached a point where the tractive effort or wheel-slip torque was no longer the maximum load. Due to the larger engine and the increase in low-gear ratio in the transmission, we now have a low-gear loading which may be several times the wheel-slip torque. Considering this a few years ago, we decided that we needed a better basis of comparison of axle loading for these reasons.

1. As axle manufacturers, we had to provide the most economical-size axle for each application.
2. We were not taking full advantage of design improvements and the features of the carrier-type design.
3. Conventional methods of calculation were out-of-date. Cars had much more horsepower; the low-gear transmission ratio had approximately doubled; and allowable loading was still based on low-gear torque, while wheel-slip torque definitely determined the maximum load that could be applied to the axle.
4. Allowable loads on gears and bearings will vary with rigidity and accuracy of the axle being used. The limits which had been set up did not provide for this or for improvements in manufacture.
5. We needed a better method of correlation with field experience.
6. In order to take full advantage of experience on all units, it was necessary to provide a method that would disregard size.
7. We required a basis of qualifying the selection of an axle size based on field experience as well as laboratory tests. We know that the load-carrying capacity of a gear set depends directly on the way the gear set is held in position in the assembly. Therefore, we plotted the major deflections of the gear set against the actual loading used in the field on all models of axles which we build. The allowable loading on a bearing depends on the mounting of the bearing, its alignment, and lubrication. We again plotted the loading used in actual application in the field for each bearing in each model axle.

For the past few years all improvements in design, the design of new axles, and the selection of an axle for a given size have been based on these factors. We believe that we now have a method which will accomplish our objectives. The variety of vehicles for which we build axles provides a wide field for obtaining experience. When design changes are contemplated, we have been able to check our laboratory test results with field experience by putting the changes in the most critical spot. For example, when a design change to reduce noise was contemplated, it was first tested in a make of vehicle that was more critical to noise than others. When a change to improve differential gear capacity was considered, the tests were made in cab service where differential requirements are more critical.

When a change has been worked out successfully in the initial application, we incorporate it in all units. To illustrate, we will analyze a proposal for a new axle, the Model 45. Comparisons of the relative lift (Fig. 7), the relative side movement (Fig. 8), and the relative end movement (Fig. 9) of the

gear and pinion plotted against pounds per inch of face for Model 45 axle and our other production models reveal similar patterns.

Loading on the Model 45 is not excessive, when compared with other production models for direct drive (Fig. 10), tractive effort (Fig. 11), low gear (Fig. 12), and axle bearing (Fig. 13). There is a large variation in the allowable loading used on various axles in the different applications due to a lack of knowledge as to actual requirements, which we hope to overcome with the new method of analysis. Of course, there is also a big variation because the requirements of vehicles differ considerably. In analyzing these charts and the history of axle loading, it is fairly obvious that the only consistent load that could be used for passenger-car axle design is the wheel-slip torque. In the same vehicle the requirements with different transmissions and axle ratios will vary considerably. It is also reasonable to expect that wheel-slip torque will offer a good design requirement, in that it indicates the load which will propel a vehicle of a given weight under various conditions.

We recognize that the careful analysis of bearing loads and the selection of the proper bearings is as important as the gears; and, therefore, we work closely with the bearing engineers. Knowing that they were faced with the problem of the effect on bearing loads due to the larger passenger-car engines, we asked a chief engineer of one of the large bearing manufacturers how they met this challenge. Quoting directly from his reply, it is inter-

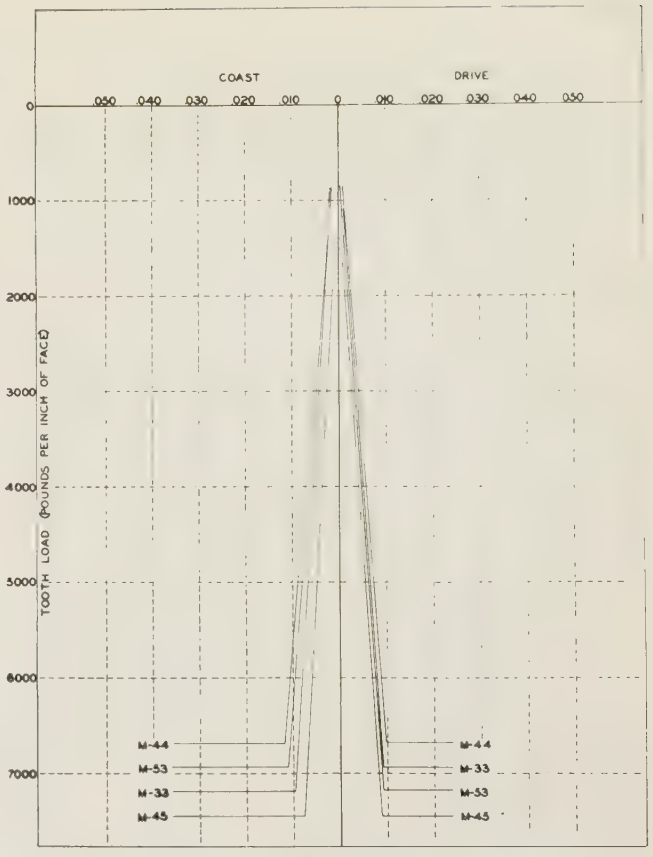

Fig. 9—Deflections, relative end movement

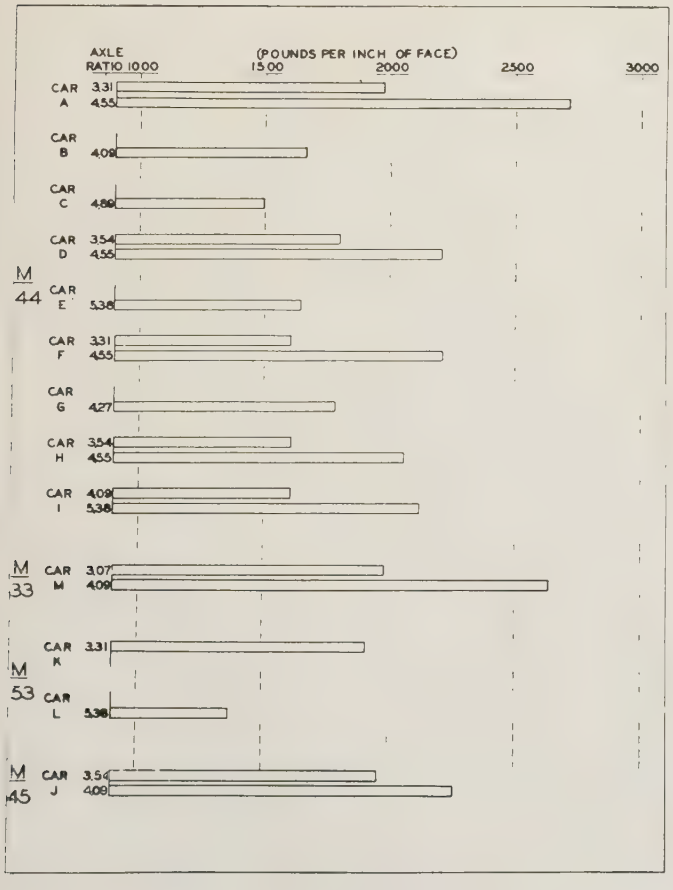

Fig. 10—Direct-drive tooth loading

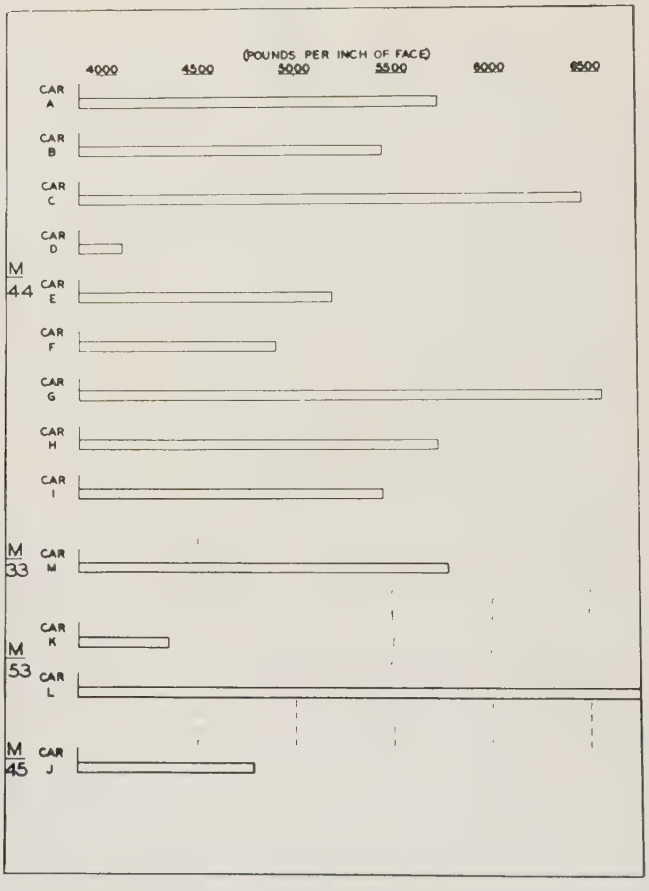

Fig. 11—Tractive-effort tooth loading

esting to note how closely it follows our own axle and gear analysis:

"To meet the performance demands of the new cars, it was felt that larger bearings would have to be used in the rear axles. A complete analysis, however, demonstrated that the additional horsepower did not increase bearing loads under slip torque, if car weights remained the same.

"Due to the much faster acceleration of the new cars, further study was given to bearings use in different applications or rear axles.

"To improve the performance of tapered roller bearings in all uses, The Timken Roller Bearing Co. did several things. The steel mill made improvements that enabled the production of a more uniform and higher quality alloy steel. Facilities in the Timken bearing plant were developed, making it possible to produce an even more uniform bearing. Since the geometry of a bearing is important, new gaging methods and instruments had to be found and used.

"These developments provided improved, more uniform tapered roller bearings. Laboratory tests also showed a definite improvement in bearing life.

"In the final analysis, it was determined that not only are the present sizes of bearings perfectly satisfactory for use in cars with higher horsepower, but in certain applications it is possible to reduce bearing sizes."

We have attempted to cover some of the general considerations used in today's axles. We will now point out some of the things we believe will be introduced in axles in the future.

Tomorrow's Axles

Locking Differentials

The conventional differential used in today's passenger cars and trucks offers limitations to performance under a variety of driving conditions. As the performance characteristics of cars and trucks improve with larger engines, owners will become more dissatisfied with the lack of performance under adverse conditions. We can, therefore, expect that it will be necessary to provide some form of limited slip differential to overcome these objections. The fact that the conventional differential has disadvantages is evident in the efforts that have been extended to overcome its limitations. There are over 300 patents of devices to improve the conventional differential. In the past 8–10 years we have had an extensive program to obtain a differential which would overcome the limitations of the conventional differential and yet provide a unit which could be used satisfactorily at a reasonable cost in today's vehicles. We made a careful study of all types, including full locking, bias or power dividing, overrunning, hydraulic, and the like. This covered all methods of construction, variable leverage, bastard teeth, eccentric pinions, cranks, shoe, and band brakes, cams and sliding pins, spirals, cross-helical, and worm gears, overrunning clutches, ball, roller, and sprag escapement clutches, also hydrostatic and hydrodynamic arrangements.

This work established a number of requirements for a good locking differential. It must:

1. Maintain differential action.

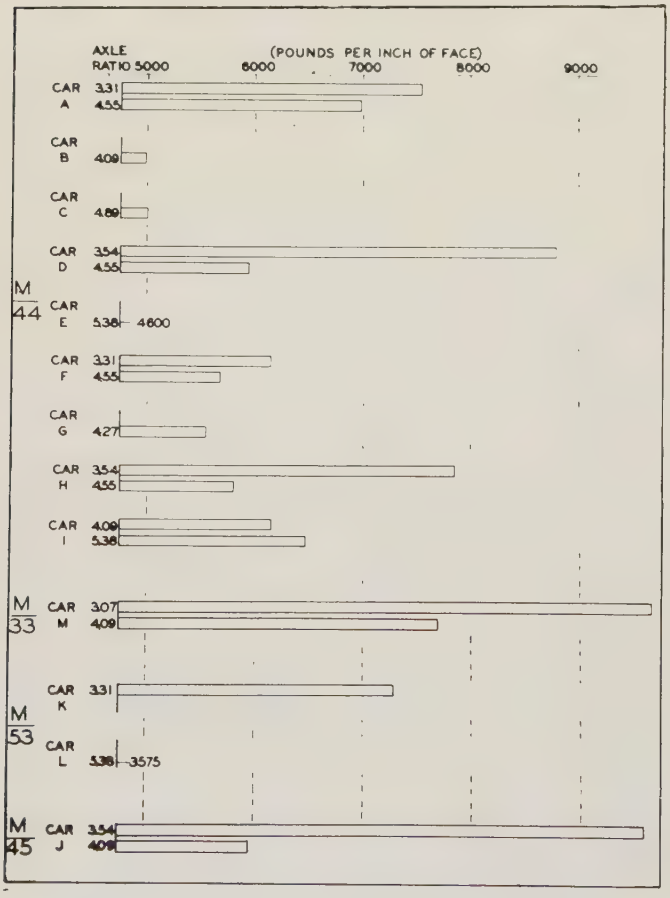

Fig. 12—Low-gear tooth loading

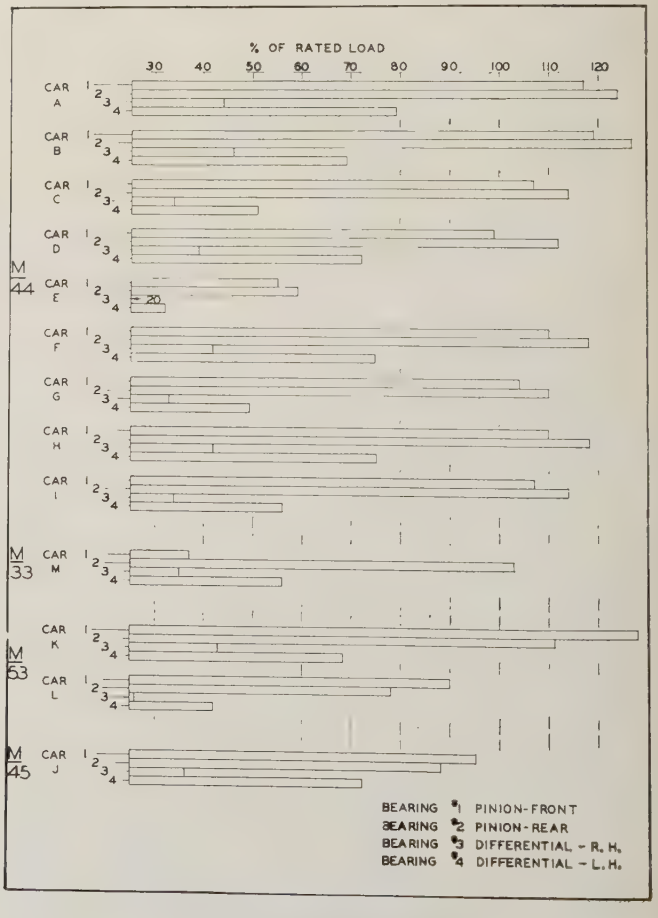

Fig. 13—Axle bearing loads

2. Prevent shock loads and the transfer of full-engine torque to one-axle shaft, so must not be of the full-locking type.

3. Provide sufficient traction torque to the non-spinning wheel at all times and under all operating conditions.

4. Not interfere with steering.

5. Be of long life and not subject to abnormal loads of wear.

6. Continue to function efficiently, regardless of the amount of wear.

7. Be quiet in operation.

8. Be of minimum cost, size, and weight

9. Be a unit that could be used without major design changes in today's axles.

During this period of development we tested approximately 25 devices of different design and construction. We found that the Thornton Powr-Lok differential fulfilled all of our requirements and, in addition, had several worthwhile features: The capacity is increased over conventional differentials as the load is divided between the gear teeth and the clutches; action is the same for both drive and coast loads and forward and reverse driving. Fig. 14 shows a Thorton Powr-Lok unit as we are now building it in production. The torque is transmitted from the differential case to the cross-pins and from differential pinions to the side gears as torque is applied in the conventional differential. The driving force moves cross-pins B up the ramp of the cam surface C, applying a load to the clutch rings D, and thus restricts the turning of the differential through the friction surfaces of the clutches at E. This provides a torque ratio between the axle shafts which is based on the amount of friction in the differential and the amount of load being applied to the differential.

When turning a corner this process is, in effect, partially reversed. The differential gears become a planetary gear set with the gear on the inside of the curve becoming a fixed gear of the planetary. The outer gear of the planetary overruns as the outside wheel on the curve has a further distance to travel. With the outer gear overrunning and inner gear fixed, the pinion mates A are caused to rotate. Inasmuch as they are restricted by the fixed gear, they first must move the pinion mate shafts B, back down the cam surface C, relieving the thrust loads on the clutches E when turning the corner.

The Thornton Powr-Lok differential, for all practical purposes, is similar to a conventional differential and the wheels are free to rotate at different speeds. The engagement of the clutches provides many features in this unit that are not common in other types of locking differentials. On straight driving, the clutches are engaged and thus prevent momentary spinning of the wheels when leaving the road or when encountering poor traction. Turning the corner, the load is relieved from the clutch surfaces, so that wear is reduced to a minimum. Field experience with the differential has indicated that shock loads are less severe than with the convential differential, because wheel spinning is reduced to a minimum. For the same reason, shock loading on the axle and the drive train is also reduced. Experience with the Thornton Powr-Lok unit in production has also indicated that this type of unit is probably here to say. Some of the automotive manufacturers who are now using this unit have increased their orders to as much as 50% of their vehicle sales.

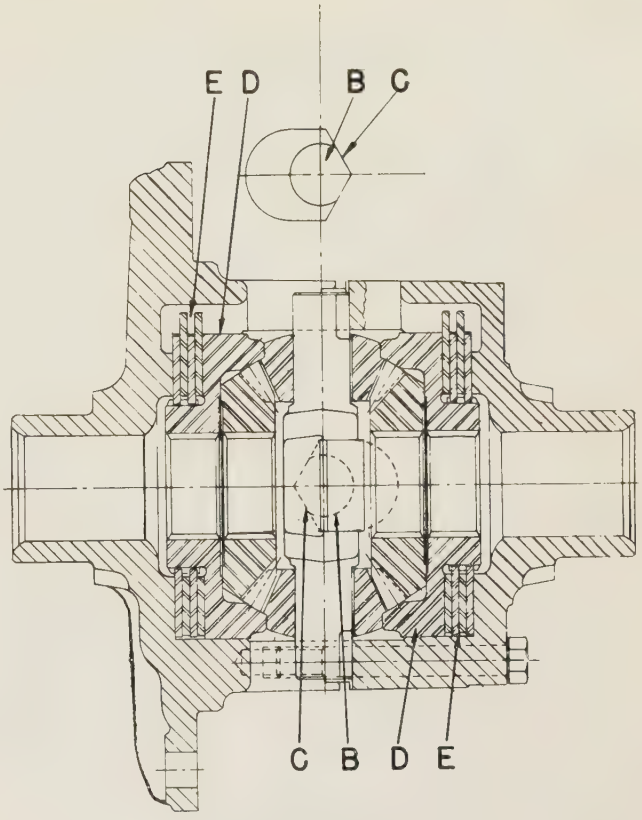

Fig. 14—Powr-Lok differential

High Offset Axles

The design trend to the lower car may require a higher offset between the ring gear and pinion in the very near future. This requirement introduces some new axle problems. One is more sliding between the ring gear and pinion. In an axle which is already on the borderline as to load-carrying capacity, this requirement might become quite serious. The higher offset also introduces some problems in gear manufacture itself. Today's gear-cutting equipment will definitely limit some desirable changes with a higher offset. New machines are being developed which will overcome these factors; however, considerable investment is required to replace equipment which is already available. The higher offset will also increase the weight of the axle, unless improvements are made so that unit loading can be increased to a point where present weight can be maintained. In connection with the high offset, we are also faced with the requirement of lower numerical ratios in a gear set. We believe that the combination of the higher offset and the low ratio may require some drastic changes in axle design in the near future.

Independent Rear Suspension Axles

Independent rear suspensions now appear to be on the horizon in the not too distant future for American cars. We feel that these suspensions offer many advantages that cannot be obtained by any other means and therefore, should be considered in connection with the future rear-axle designs. Several improvements have been adopted

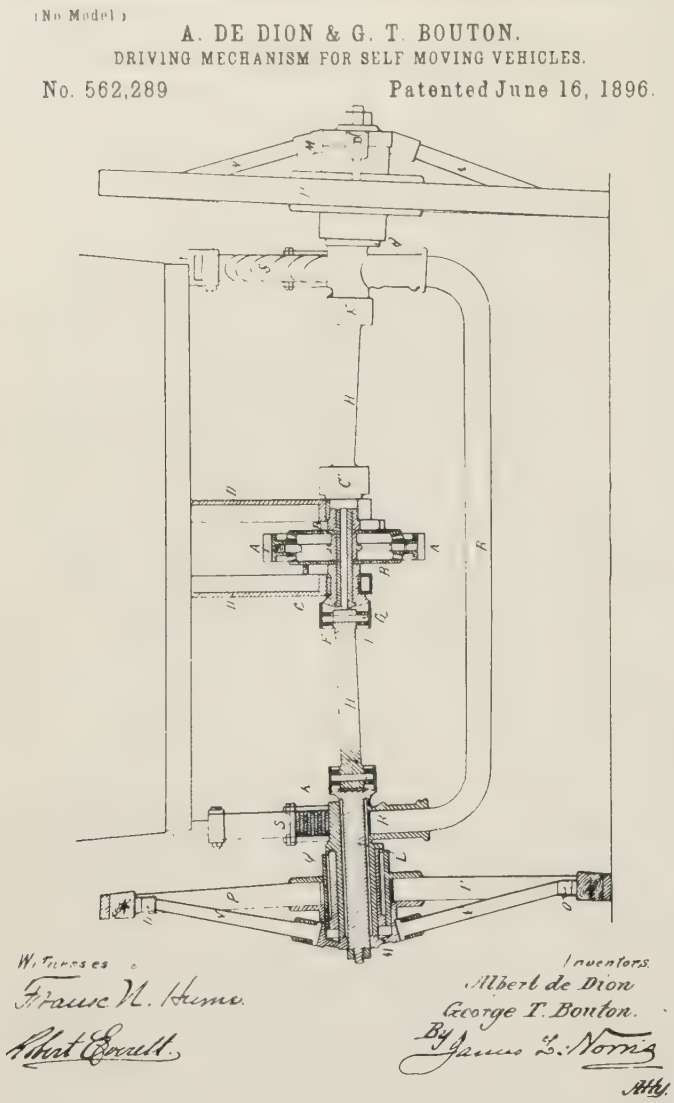

Fig. 15—First de Dion rear axle

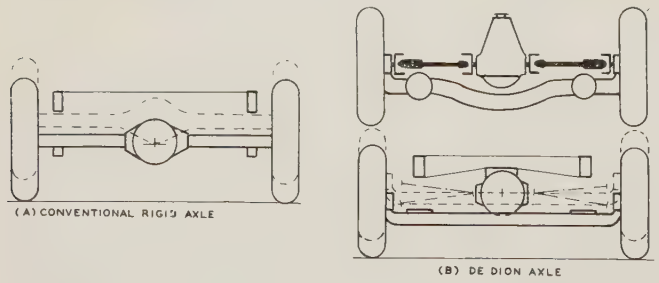

Fig. 16—Present-day axle compared with de Dion axle

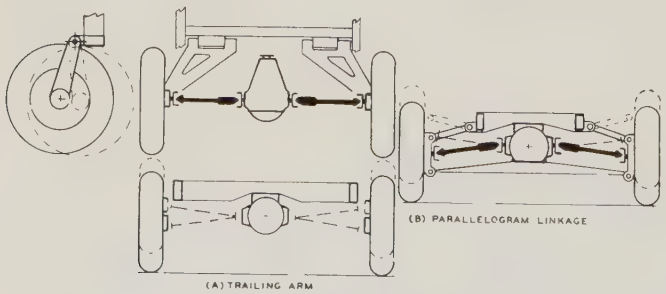

Fig. 17—Parallel axles

for the conventional rear suspensions in recent years that have made it more attractive to incorporate independent rear suspensions. This includes the use of torsion bars, coil springs, or air springs, thereby eliminating the variable friction element and thus providing savings in unsprung weight. The addition of a leveling means makes it possible to maintain a constant height, regardless of variation in the sprung mass or number of passengers. Thus, the universal joints at the wheel shafts work at much smaller and more constant angles with less movement required of the slip spline, resulting in much smoother and quieter operation and longer wear life.

Independent rear suspensions are not new. They were used on a few of our very early cars; and some makes of European cars have used them continually since the early 1920's and 1930's. In fact, the de Dion type of rear suspension was patented by de Dion in France in 1893 and in the United States in 1896. A copy of the American patent is shown in Fig. 15.

Table 1 shows the different features of independent rear suspensions now being used. We have selected only those that have been in use for some time, are well-known, and have already proved satisfactory. We have purposely not included (as being of no great interest to the axle designer) the "dead" type of this axle which is used on many of the front-drive cars in Europe. It is interesting to note that they are being used on both small and large cars, on the lower priced cars as well as on some of the most expensive. The final type to be selected must not only give satisfactory performance, but also be of economical design and manufacture.

Independent rear suspensions are divided into two general classes, parallel and swing axles. On the former the wheels move parallel to each other without affecting the tread or the camber angle. On the latter the wheels swing about a fixed pivot point, constantly changing the wheel angles and tread. Several variations of each of these as shown by Figs. 16, 17, and 18.

Fig. 16A shows the conventional rigid axle, a typical conventional rear axle used today on all American cars. The dotted lines show movement and indicate the wasted space under the trunk. Although the de Dion axle (Fig. 16B) is not truly an independent suspension, it is included as it has many of the same advantages and problems. The gear unit is independently suspended on the frame; both wheels are supported by a single tubular beam and move together.

Parallel Axles are shown in Fig. 17. The pivot axis for the trailing arm type is transverse of the car and parallel with the centerline of the axle, causing the wheels to move parallel to each other. This results in no change in tread or wheel angle, but a slight change in wheel base. By using a parallelogram arrangement (B) the wheels remain approximately parallel during movement. Arms may be separate beams, leaf springs, or a combination of beams and springs.

Fig. 18 shows swing axles:

Center pivot—The axles and wheels swing about a single pivot point located at the center of the gear unit.

Side pivot—Each axle and wheel swings about its

own pivot point on each side of the gear unit.

Diagonal pivot—The pivot axis is placed diagonally each side of the gear unit to improve some steering or handling conditions.

Articulated center pivot—The gear unit is mounted rigidly with one of the half axles, and swings about the single pivot point with the axles. Although this adds slightly more to the unsprung weight, the mass is located close to the pivot point. Only one universal joint is required and no slip spline is necessary with the center pivot.

Articulated low pivot—This is similar to the center pivot except that the pivot point is placed below center to improve handling and cornering conditions. This also makes it necessary to use a slip spline on the axle-drive shafts as there is some variation in length during movement.

There are also several modifications of each of these types, such as the possibility of putting the brakes inboard or outboard.

Because rear axles must be designed for use with each of these types, we believe a general knowledge of the advantages and features of independent suspension will be of value to the axle designers:

1. Lower silhouette and lower center of gravity. The better utilization of the space at the rear of the car possible when using a combined transmission and axle and a fixed propeller shaft results in a lower silhouette, a reduced shaft tunnel, and lower center of gravity.

2. Better ride. Depending upon the type used, the unsprung weight can be reduced by 25–50%. In some designs a reduction of as much as 100 lb. per wheel has been possible. This results in an improved and more easily controlled ride. In addition, there is less load and wear on the shock absorbers.

3. Improved handling and greater safety. Independent suspension eliminates various kinds of wheel hops, shakes, and tramp of the rear axle; and the difference in handling (under power) between right and left turns. It reduces rear steering effects, and sideway thrust with single rear-wheel bump or rebound. The result is better road holding, particularly when cornering and braking. Further improvement can also be made by using the Powr-Lok differential to prevent wheel spinning.

4. Improved traction. The lack of propeller-shaft torque effect results in improved and more uniform traction at both wheels in extreme conditions. Here also, the Powr-Lok differential can be used to improve traction.

5. Improved braking. The system provides better cooling by using inboard brakes, eliminates brake hop, reduces suspension loads as brake-torque reaction is taken directly by the frame, and makes it easier to connect mechanical hookup.

The Lagonda Saloon, which has used independent rear suspension for a number of years, is one of England's high-quality cars. It has a curb weight of 3700 lb. and 113-in. wheelbase. It is reported to handle well with a combination of good-steering and road-holding qualities, plus good cornering power and traction. This uses a swing axle and torsion bar springs (Fig. 19), with diagonally located pivots (Fig. 20) and inboard brakes (Fig. 21). Four cardan joints are used.

The Lancia car made in Italy was one of the first to adopt independent suspension. The car is in the

Table 1—Independent Rear Suspensions

Car	Suspension[a]	Gear Unit[b]	Springs[c]	Brake Location	No. of Universal Joints
England					
A.C.	PL	A	SET	Outboard	4
Allard	d	A	C	Inboard	4
Aston Martin	d	A	B	Inboard	4
Frazer-Nash	d	A	B	Outboard	4
Lagonda	SD	A	B	Inboard	4
Czechoslovakia					
Skoda	SD	A	SET	Outboard	2
Tatra	SC	ATE			0
Germany					
Borgward	d				
Mercedes-Benz 190SL	SS	A	C	Outboard	2
220A	SAL	A	C	Outboard	1
300SC	SS	A	C	Outboard	2
Porsche	SS	ATE	B	Outboard	2
Volkswagon	SS	ATE	B	Outboard	2
France					
Renault—Fregate	PA	A	C	Outboard	4
Dauphine	SS	ATE	C	Outboard	2
Italy					
Alfa Romeo	d				
Lancia—Aurelia	SD	AT	C	Inboard	4
Flaminia	d	AT	SE	Inboard	4
Fiat 600	SD	ATE	C	Outboard	2
Spain					
Pegaso	d		B	Inboard	4

[a] Type of suspension:
d—de Dion.
P—Parallel.
A—Trailing arm.
L—Linkage.
S—Swing
A—Articulated.
C—Center Pivot.
D—Diagonal pivots.
L—Low pivot.
S—Side pivots.

[b] Type of gear unit:
A —Axle gears only.
AT —Combined axle and transmission.
ATE—Combined axle, transmission, and engine.

[c] Type of springs:
B —Torsion bar.
C —Coil.
SE —Semi-ellipic.
SET—Semi-ellipic transverse.

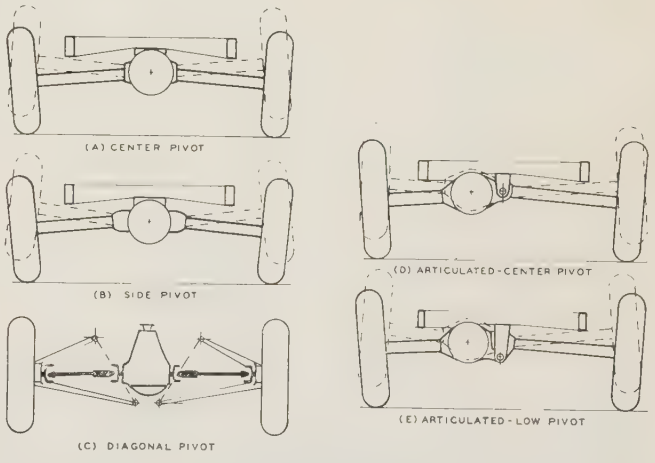

Fig. 18—Swing axles

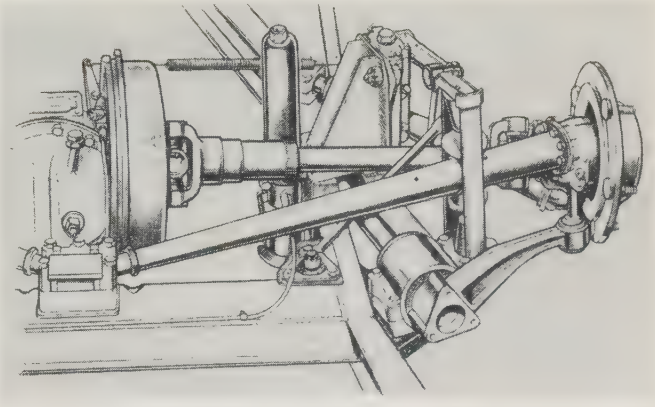

Fig. 19—Lagonda rear suspension

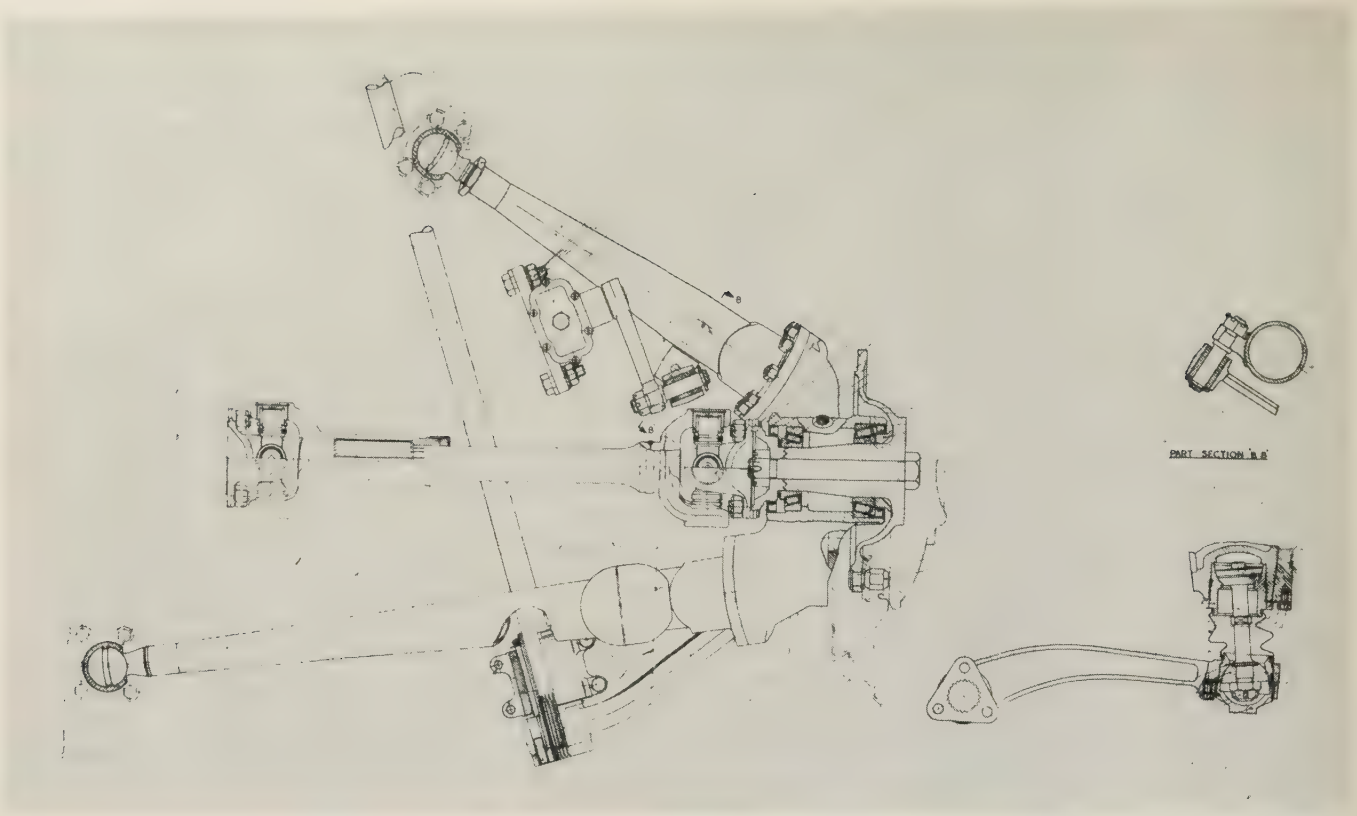

Fig. 20—Lagonda diagonal swing arms

Fig. 21—Lagonda gear unit

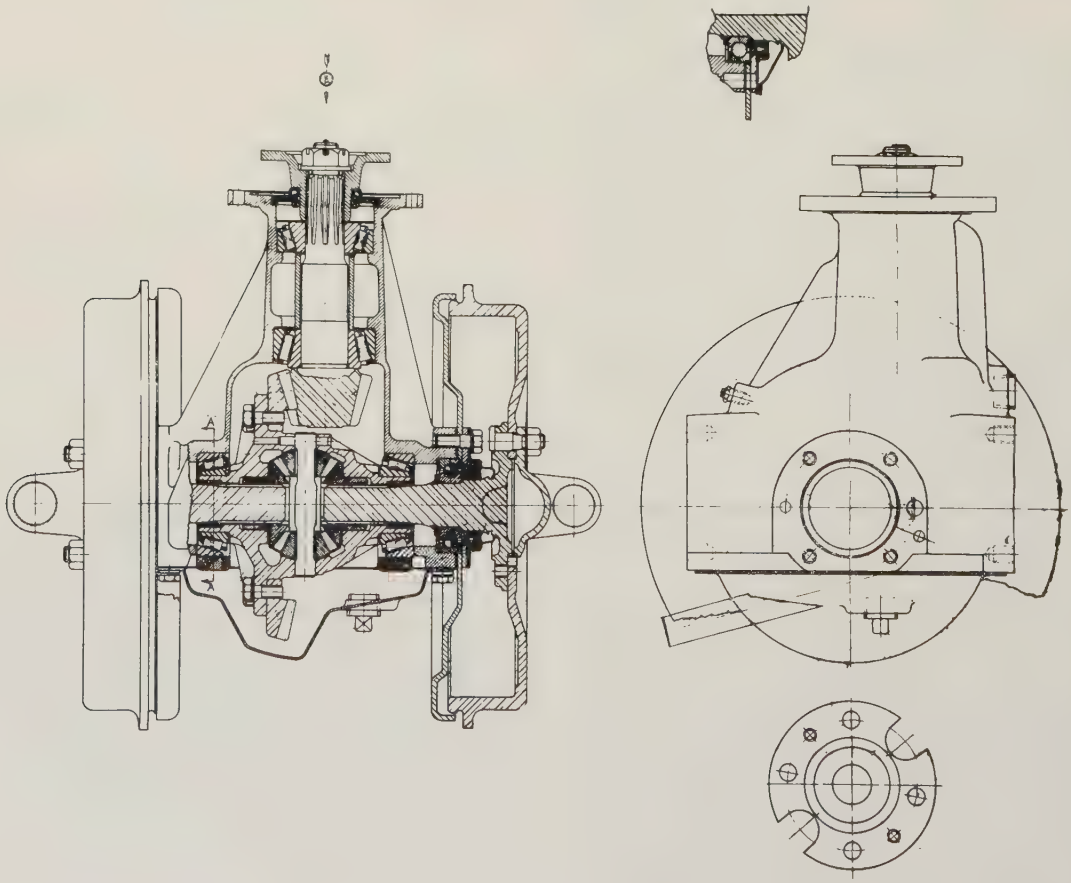

medium class, weighing 2400 lb. with integral body construction. The original suspension (Fig. 22) was the diagonal-swing type with vertical coil springs. Four cardan joints are used, the outer joints being located outside the wheel hubs to keep the operating angles as small as possible. The clutch and transmission are combined with the axle gear unit (Fig. 23), making it possible to lower the floor, reduce the propeller shafts tunnel, and remove the floor bumps usually necessary to clear the clutch housing and transmission. Inboard brakes are used, as shown in Fig. 24. The complete gear unit is supported by rubber mountings, providing a four-point suspension to the frame, and is connected to the propeller shaft with a rubber coupling rather than conventional cardan joint. For the more recent models, the de Dion type axle with semi-elliptic springs (Fig. 25) is being used, still keeping the combination gear box and other features.

In the Renault we have an example of the same manufacturer using two types of construction, possibly because of the difference in size, weight, and price of the cars and the performance and operation expected of each. The Frégate model is the larger six-passenger car weighing 2400 lb with 110-in. wheelbase. The suspension (Fig. 26) is the trailing-arm-parallel type with coil springs and outboard brakes. The Daphine model is a small rear-

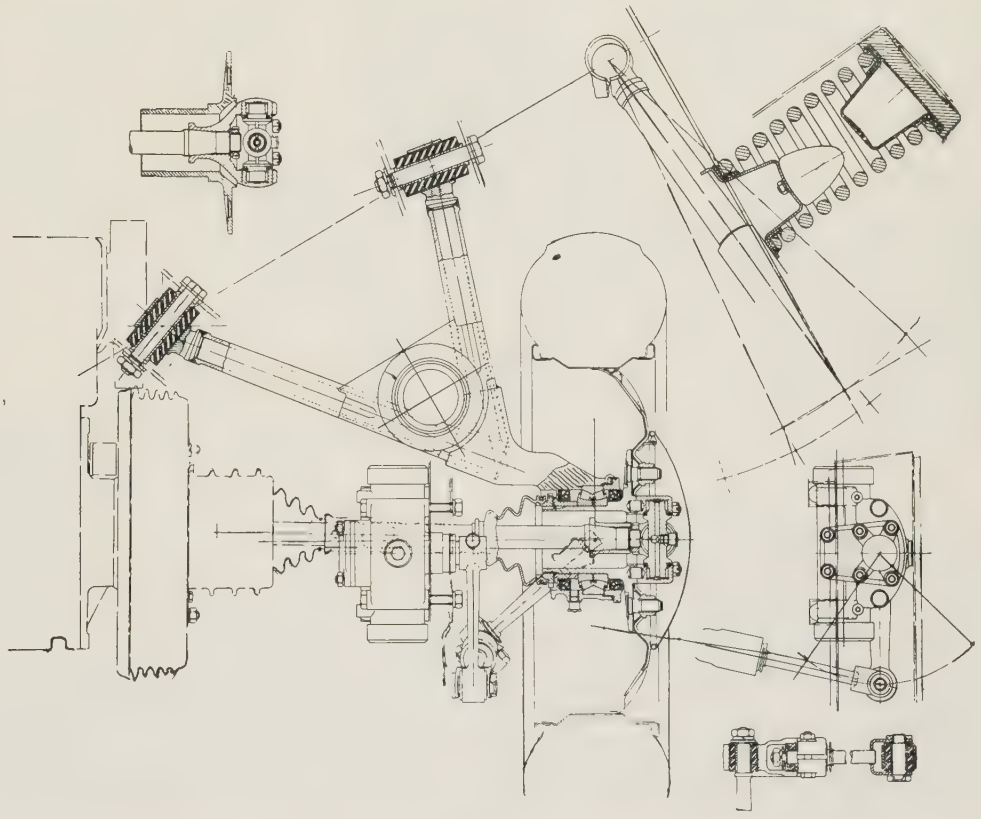

Fig. 22—Lancia rear suspension, diagonal swing

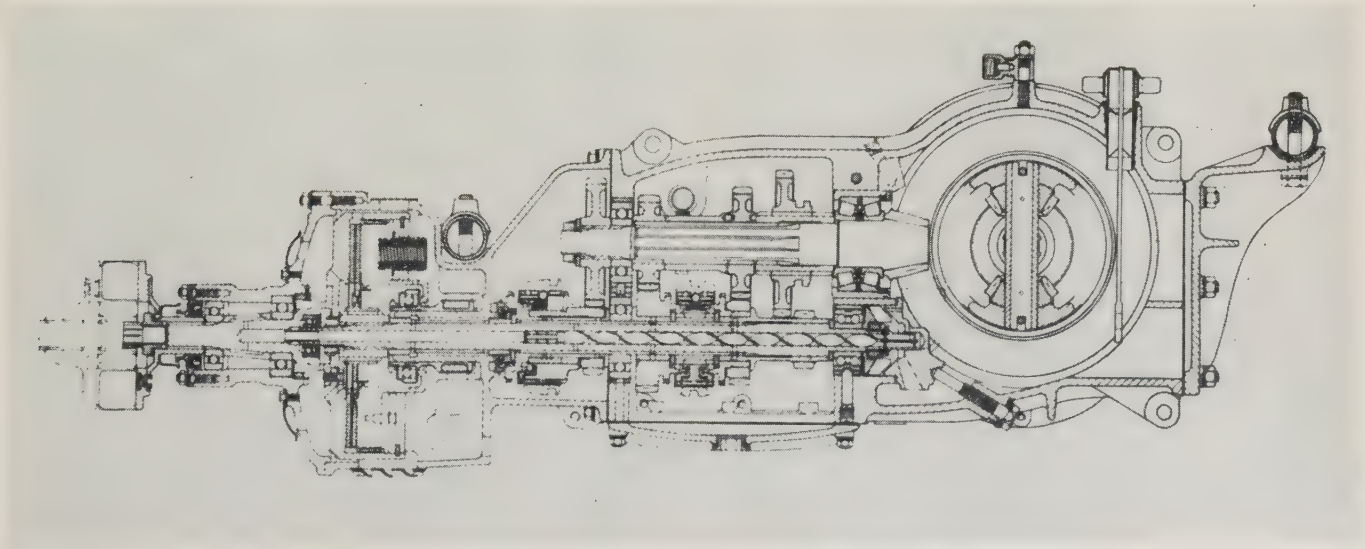

Fig. 23—Lancia combined clutch, transmission, and rear axle

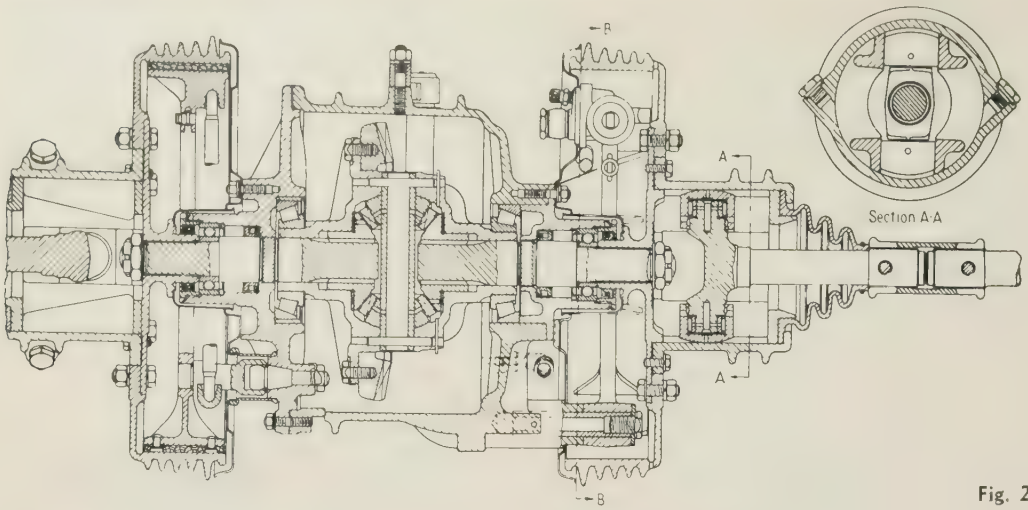

Fig. 24—Lancia gear unit and mounting

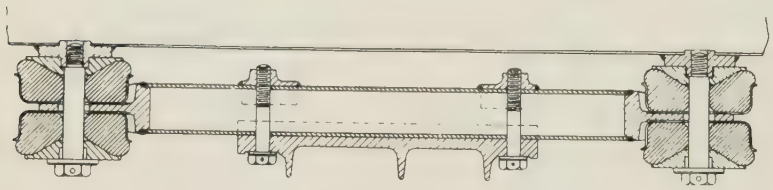

Mounting of final drive assembly

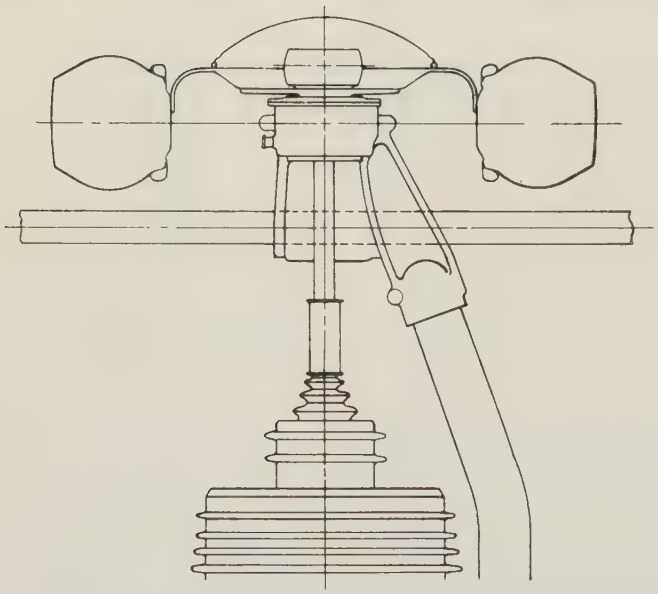

Fig. 25—Lancia de Dion rear axle

engine car with 89-in. wheelbase, weighing 1400 lb. This uses a swing axle (Fig. 27), with side pivots, coil springs, and outboard brakes. The axle gear unit is combined with the transmission and rear engine.

The Daimler-Benz Co. was one of the first to recognize the many advantages of independent rear suspension and have used some form of it on their cars for over 25 years. Their most recent development and most interesting design is the type which they refer to as the "one joint swing axle with low pivot" (Fig. 28). This is the articulated type with the pivot point located below the centerline. Originally used on their race cars, it was placed in production on Model 220A, a 2900-lb car with a 107-in. wheelbase. This type has proved so satisfactory that it is now being installed in all the passenger-car models. The entire axle has a three-point suspension (Figs. 29 and 30). The gear unit is pivoted around a single vertical mounting, suspended on a transverse frame member by an extra large rubber mounting. In order to keep the lateral movements of the axle within controllable limits, support is carried out over adjustable rubber buffers. The axle is held in the longitudinal direction of the vehicle by two guiding bars, which also carry the springs. The construction of the gear unit, the low pivot, and single cardan joint are shown in Fig. 31. The pivot point, being located below the cardan shafts, makes it necessary to provide a slip spline or other means because the length of the shaft is constantly changing with the springing action. This has been solved by using a roller-bearing spline at this location.

One of the most recent designs to arouse great interest and admiration is the small Fiat 600. This four-passenger rear-engine car weighs only 1234 lb and has a wheelbase of but 78 in. The independent rear suspension is the swing type with diagonal pivots using coil springs (Fig. 32). The axle gear unit (Fig. 33) is combined with the transmission and rear engine. The unit is very compact with the center of the universal joints on the axle shafts located very close to the center of the differential, thereby keeping the angle of operation as small as possible. A rubber coupling is used at the wheel end instead of the usual cardan joint (Fig. 34).

During recent years our engineers have designed, built, and tested 25–30 prototypes of many different forms and sizes of independent rear suspension

axles. At the present time, we are experimenting with a de Dion axle in our Studebaker test car (Fig. 35). This is a plain de Dion with outboard brakes, semi-elliptic springs, and four cardan joints. We selected this particular type for our test work because it could be applied more readily to one of our standard test cars. Since we were not involved with the suspension design, it has answered our purpose very well in working out axle and universal joint problems that are generally common for all types.

One of the first projects was to eliminate or reduce greatly the friction of the sliding splines on the cardan axle shafts and so reduce interference with the riding quality. Our universal joint engineers after considerable development work came up with a very satisfactory answer: a rolling spline (Fig. 36). This has the following features:

1. Greatly reduced friction. (It is approximately one-tenth that of the sliding spline.)
2. Greatly increased capacity.
3. Any length of movement easily provided for.
4. Compactness, small in size and swing diameter.
5. Light weight.
6. A self-contained unit, easy to assemble and

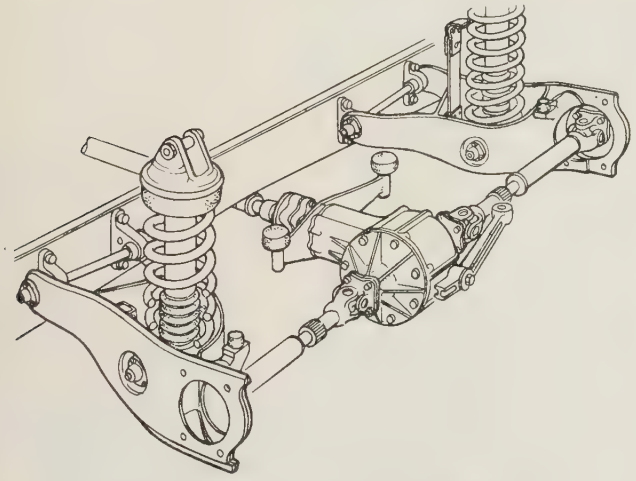

Fig. 26—Renault Frégate rear suspension

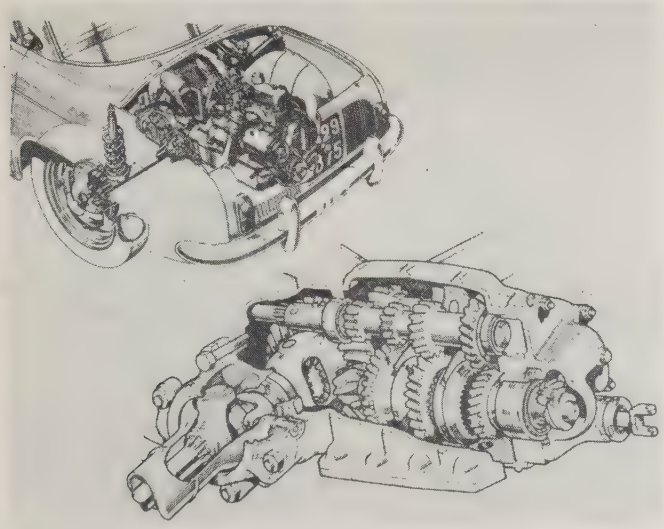

Fig. 27—Renault Dauphine combined rear-engine axle and transmission

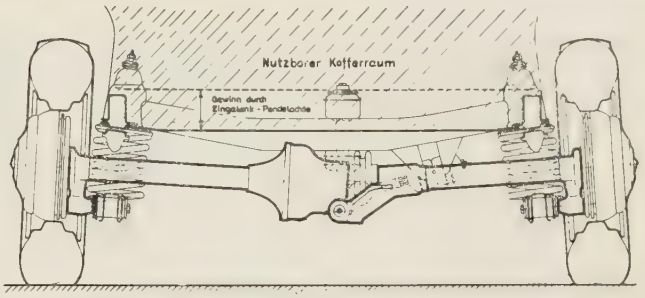

Fig. 28—Daimler-Benz pendulum swing axle

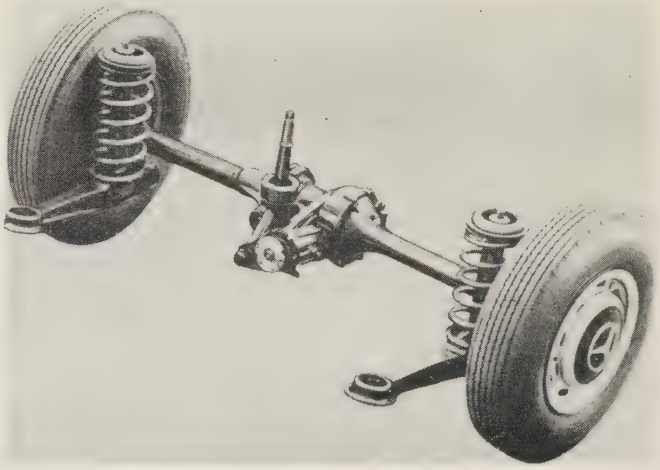

Fig. 29—Daimler-Benz pendulum axle, Model 220A

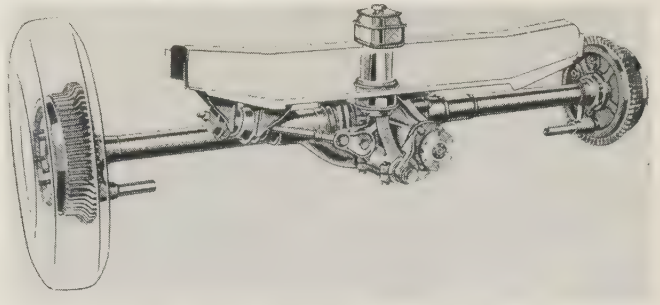

Fig. 30—Daimler-Benz pendulum-axle installation

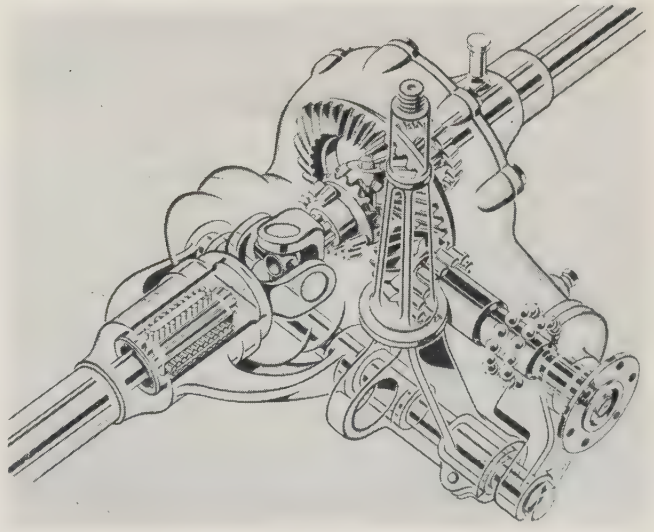

Fig. 31—Daimler-Benz pendulum-axle gear unit

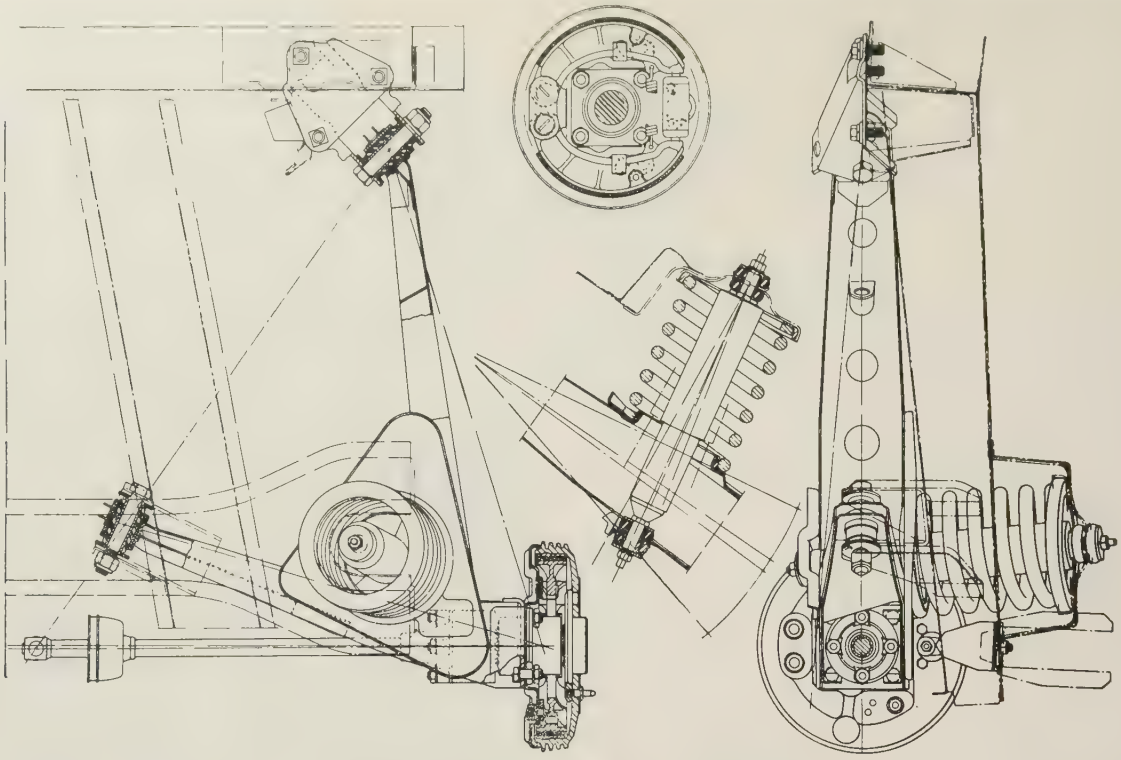

Fig. 32—Fiat rear suspension, diagonal swing

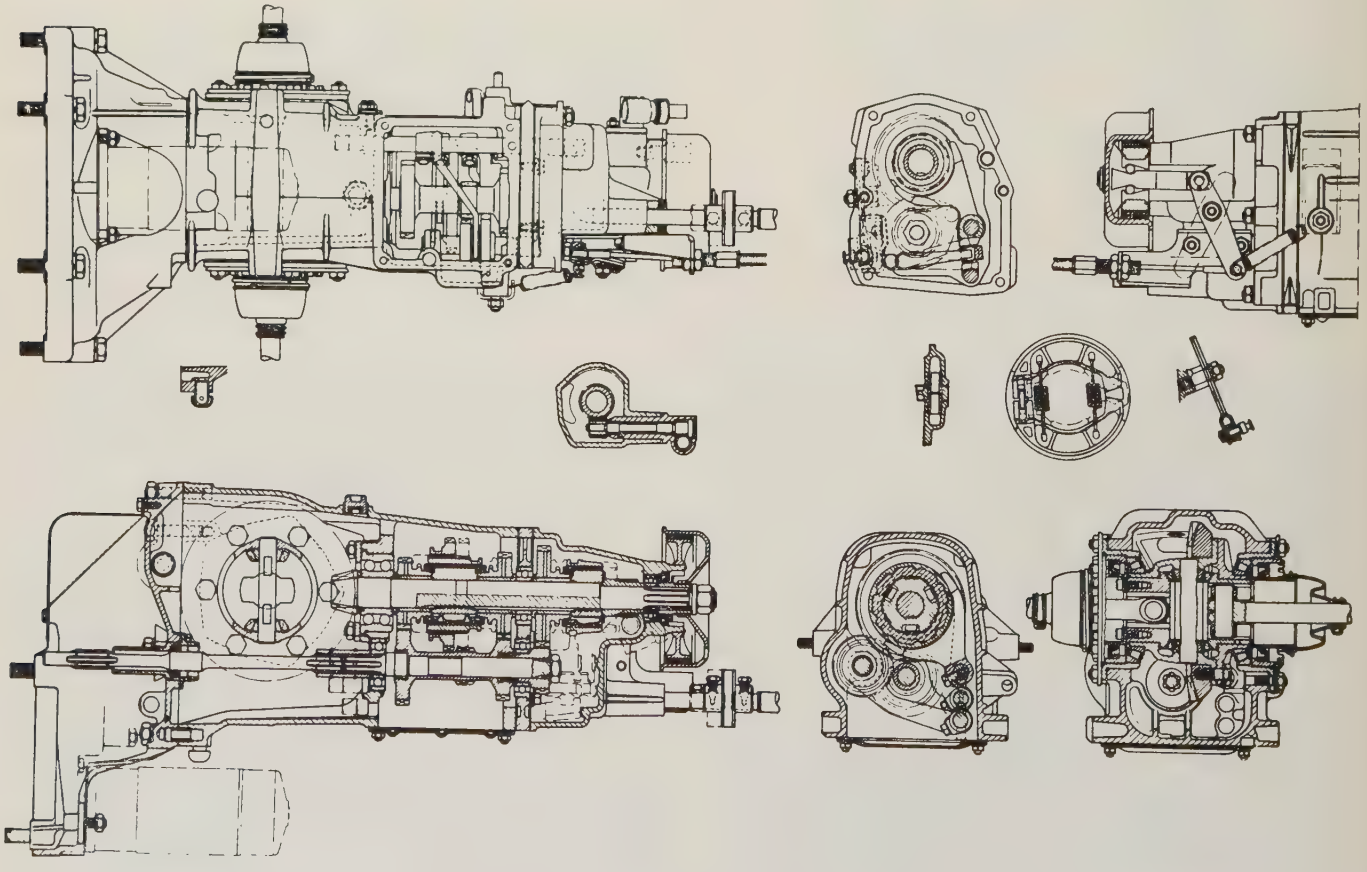

Fig. 33—Fiat combined axle gear unit and transmission

disassemble. (Rollers are held in place as a package by the retainer.)

7. Recirculating rollers.
8. Very small lubrication requirements.
9. Low cost.

Careful study and testing has indicated that the following problems must be considered and worked out satisfactorily if performance is to be successful. The limited space and complex construction complicate solving these problems.

1. Noise: With the gear unit more closely confined under the body, the noise problem becomes more acute. The use of rubber mountings for the gear unit to the frame is an absolute must. These must be carefully designed as to number, size, shape, location, material, frequency, deflection, and then thoroughly tested. They must also support the gear unit, absorb shock loads, and take the torque and thrust reactions under all driving conditions. This includes braking loads if inboard brakes are used.

Rubber couplings will probably be used instead of cardan joints for the fixed type of propeller shaft because they will be required to operate only at small constant angles with independent rear suspensions. Some are already being used in Europe.

The design, being more compact than a conventional axle, makes it more difficult to provide sufficient rigidity to prevent excessive deflections caused by the gear loads. However, this can be accomplished by providing satisfactory stiffening ribs.

2. Lubrication. The main lubrication problem is that of cooling, as the air circulation is badly restricted. This is particularly true when inboard brakes are used, as some of the braking heat is transferred to the gear unit. This problem can be solved by the proper circulation of the lubricant and, if necessary, by redirecting the air circulation with small deflectors attached under the car.

The gear unit must be properly ventilated to prevent the build up of internal pressure and resulting leakage. Both the type of vent and its correct location must be determined by actual tests.

3. Suspension friction. Every precaution must be taken to keep to a minimum all friction which would interfere with the proper functioning of the suspension and riding quality. For example, excess friction of the sliding spline under full-torque load at the universal-joint shaft to the wheel badly interferes with the so called "boulevard" ride of which we are so proud in our American cars. One method of overcoming this is by using the spicer rolling spline previously described (Fig. 36). Swing axles with the pivots located at the center of the universal joints do not require a slip spline and, therefore, this condition does not exist.

4. Increased weight. Although considerable reduction can be made in the unsprung weight, the total or overall weight is increased by the added number of parts and additional material required. As noted by Table 1, from one to four additional universal joints will be required along with the gear unit mounting and the revised frame structure. The amount of this increased weight will depend upon the type of independent suspension used and how carefully it is designed. It has been our experience that this will vary from 25 to 50 lb.

5. Increased cost. The amount of the increased weight and the new parts involved gives some indication of the additional cost of the system. But, surely the increased cost would not be out of line with so many of our recent automotive improvements, such as automatic transmission, power steering, and power brakes, which the public as accepted and now demands.

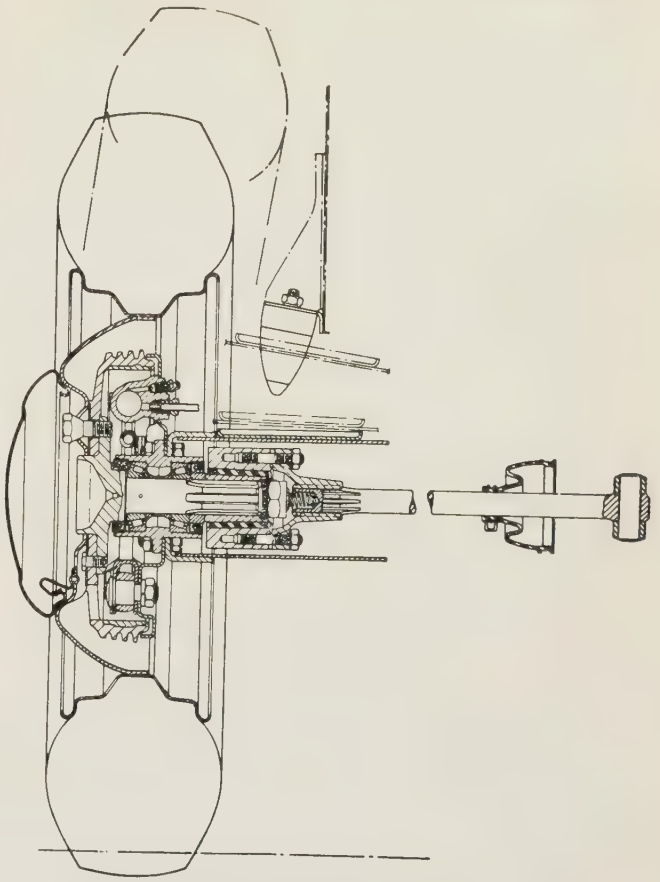

Fig. 34—Fiat rear-axle wheel end and rubber coupling

In the early 1930's the entire industry adopted independent front suspensions to overcome the very serious problem of front-wheel stability and "shimmy." Although, at present, we do not have such a serious or urgent need for independent rear suspensions, we believe that this is the one remaining major change that offers the greatest possibility to improve the ride, handling, and safety of American passenger cars.

Front Drive Axles

Low, sleek, good-looking body lines are the number one sales item for American automobiles, thereby putting the stylist in the driver's seat. His demands for a lower silhouette still continue, and must be accomplished with little or no raised tunnel or obstruction in the floor. Automotive engineers have resorted to all forms of design gymnastics to approach this in our present rear-drive cars: 3-joint propeller shaft, lower hypoid pinion, smaller wheels, engine and axles set at rakish angles, and the like, until we have about reached the limit. If we must go further we might have to consider the front-drive or rear-engine car. Either would permit the lowest possible silhouette and uninterrupted floor surface.

There are 12 front drive cars being made in

Europe, including such cars as the Citroen, Panhard, Hotchkiss Gregoire, D.K.W., and Gutbrod. Although most of these are much smaller than American cars, front-drive axle design features and problems are similar and should offer no great difficulty if we decide to adopt it.

1. Rigid type. This is similar to the conventional rigid rear axle except that steering knuckle and universal joints have been added. It is the type used for jeeps, 4-wheel drive trucks, and the like. It is not satisfactory for passenger cars due to the increased unsprung weight, steering and handling instability.

2. Beam or "dead" axle type. This is similar to a de Dion rear axle with steering knuckles added. Both wheels are supported by a single crossbeam with the gear unit mounted on the frame, usually in combination with the transmission and engine. This type was used on the last American front-drive cars, the Ruxton and Cord. Today, it would not be considered satisfactory for passenger cars due to handling instability.

3. Independent suspension type. The parallel type of independent suspension is best suited for front-drive passenger-car axles. Either the trailing-arm or wishbone-linkage type is used on all those now being made.

The use of rigid front-drive axles has increased considerably in this country with the advent of the jeep and light 4-wheel drive truck. A satisfactory front-drive axle can be designed for American passenger cars if and when needed. However, we believe that other problems might prevent serious consideration of a front-drive car, for example, driving habits. The performance and handling of front-drive cars is excellent once the new driving technique is mastered. However, it is questionable whether the appeal for the ultimate in the low silhouette and clear floor is strong enough to overcome this handicap to give serious consideration for the use of front drives on American cars.

Axles for Rear-Engine Cars

The rear-engine car also appeals to the stylist as a further challenge on body intrigue, still lower silhouette, and the like.

At the present time, there are five rear-engine cars being made in Europe, including such well-

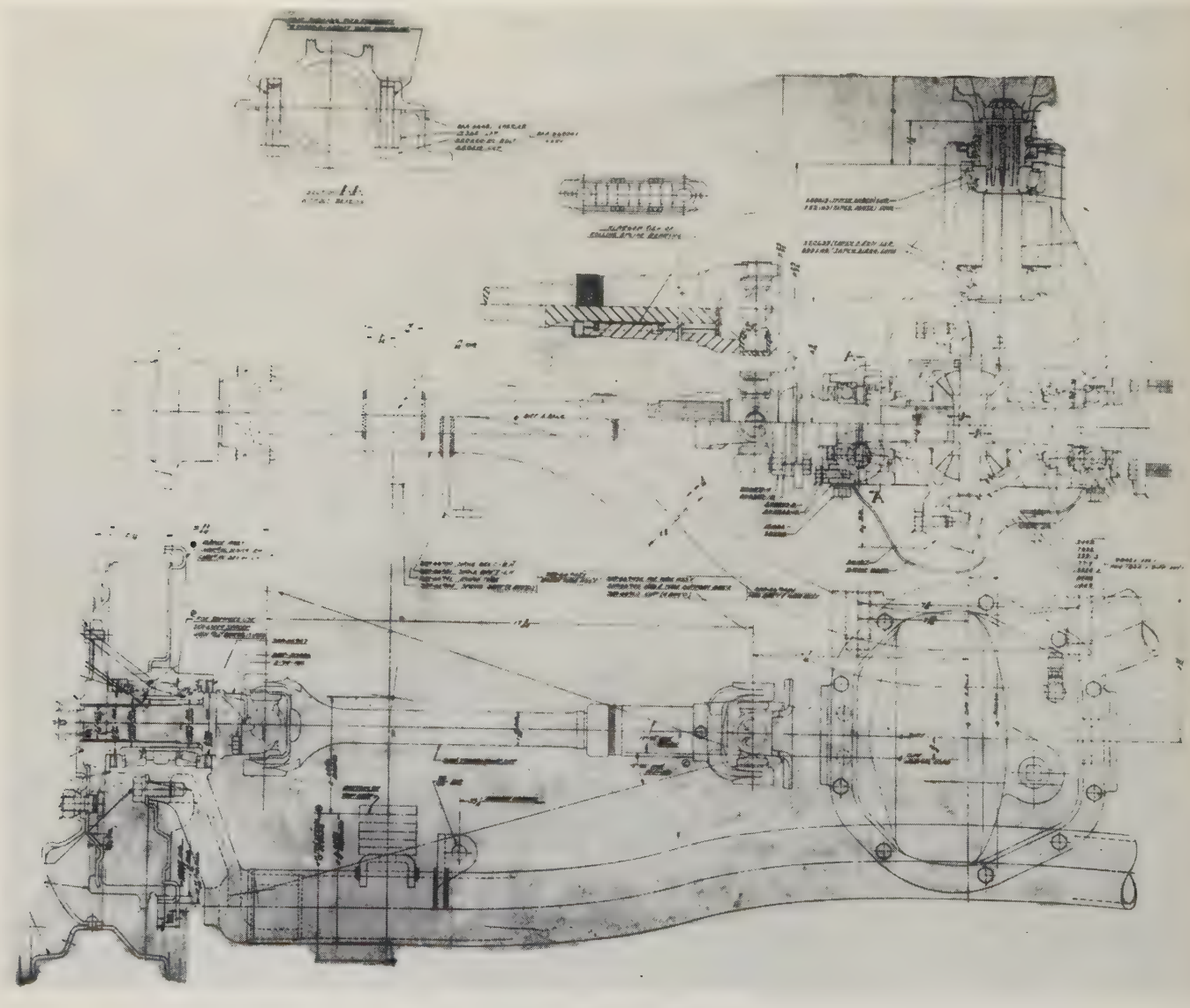

Fig. 35—Dana experimental de Dion axle

known makes as Volkswagen, Porsche, Renalt, and Fiat. These have proved very satisfactory and popular, not only in Europe but also in the United States and Canada.

The independent suspension rear axle is a natural for rear-engine cars, because it is possible to combine the engine, transmission, and axle gear unit in one compact assembly. For these small cars the rear-engine location appears well-adopted, providing additional weight and better traction on the driving tires.

It is questionable whether or not the rear-engine application can be worked out well enough to suit our larger American cars with such problems as weight distribution, handling, and steering ability.

Conclusions

1. The axle engineer has met the challenge to deliver the power of the larger passenger-car engines without increasing the size of the axle.
2. The only reliable basis for torque-capacity rating, load, and stress analysis of passenger-car rear axles is the wheel-slip torque (tractive effort), not the maximum engine torque, horsepower, or low-gear torque.
3. The capacity of passenger-car hypoid gears is controlled by the allowable tooth surface loading, antiscoring and antiwear qualities, and lubrication; not by bending fatigue or failure of the gear teeth.
4. The capacity of present axles can be increased still further without increasing size when greater load-carrying, antiwear, and antiscore lubricants are available. Dry or solid lubricants might play an important part.
5. Extreme rigidity of the gear and bearing mountings is the first requisite of good rear-axle design and satisfactory performance insurance.
6. Axle gears are operating under varying speeds and loads whenever the car is in motion; therefore, gear noise will always be a major problem.
7. Ninety-five percent of all gear noise problems can be overcome by proper tooth development, combined with testing in the actual car model under which the axle will be used.
8. The limited-slip type of differential will eventually become standard equipment on all passenger cars, if only for the purpose of improving car handling and stability during high-speed driving under varying traction conditions (icy and slick spots, rough and bumpy roads, and the like).
9. Independent rear suspension axles is the one remaining major change to improve the ride, handling, and safety of American passenger cars. It will come about as soon as one of the car manufacturers needs another important feature to boost sales.
10. The new development of the rolling spline eliminates the friction factor previously so objectionable with independent rear suspensions.

Acknowledgements

We want to acknowledge and thank those who have so kindly contributed to this paper.

Dana Axle Engineering and Testing Departments.
R. M. Riblet, Timken Roller Bearing Co.
T. Marek, David Brown (Lagonda), England.
T. H. Millward, Salisbury Transmission Ltd., England.
Lancia Co., Technical Department, Italy.
Dr. F. Nallinger, Dr. H. Scherenberg, R. Uhlenhaut, and J. Muller, Daimler-Benz Co., Germany.
Iliffe and Sons Ltd. (*Automobile Engineer*), for permission to republish Figs. 22–24, 26, 32–34.
The Autocar, London for permission to republish Fig. 19.
Sports Cars Illustrated, for permission to republish Fig. 27.

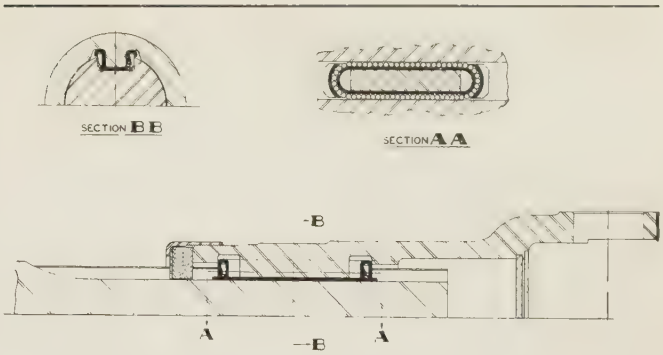

Fig. 36—Spicer rolling spline

References

1. *Automobile Engineer,* Vol. 29, February, 1939, pp. 37–41: "Rear Suspension," by Maurice Platt.
2. *Automobile Engineer,* Vol. 41, February, 1951, pp. 43–51: "Lancia 'Aurelia'."
3. "Renault-Frégate-Automotive Industries," by W. F. Bradley. May 1, 1951.
4. Proceedings of Institution of Mechanical Engineers, 1951–1952, Part II, pp. 35–58: "Independent Rear Suspension," by Donald Bastow.
5. SAE Transactions, Vol. 61, 1953, pp. 503–528: "European Postwar Cars," by Maurice Olley.
6. *Automobile Engineer,* Vol. 45, November, 1955, pp. 467–478: "Fiat 600."
7. *Sports Cars Illustrated,* October, 1956: "Renault Dauphine."
8. *The Motor* (London), Vol. 110, Dec. 19, 1956, pp. 836–839: "Motor Road Test No. 31/56 (Continental)—The Lagonda 3-Litre Saloon."

DISCUSSION

Comments on Gear Wear and Rear-Axle Noise

—J. S. Voigt
American Motors Corp

IT would be redundant to discuss this paper without some disagreement. About two years ago, in cooperation with The Timken Roller Bearing Co., we ran a number of tests in rear axle bearings on roll end wear, particularly of pinion bearings with consequent loss of preload. Timken furnished measured bearings and after the tests they were returned to them for evaluation. Tests were run on the road and bench. As nearly as possible, axles were assembled surgically clean. Before and after each test, bearing torque was recorded, as well as end movement under load. New assemblies were tested, after which the bearings only were replaced and the test repeated. Generally, roll end

wear was definitely less with the second set of bearings.

These tests were run with production gears, both lubrited and nonlubrited. Most of the tests were run with production axle oil, which is an active sulfur type. However, when run with inactive-type lubricant we could not distinguish any appreciable difference in roll end wear.

Our conclusions were that a minor amount of gear wear occurred initially which acted as a lapping agent, causing this condition. For the most part, bearing standout change was in the low ten-thousandths.

Commenting on rear-axle noise, I am in complete agreement. When we originally installed the Hydramatic transmission with our 6-cyl overhead valve engine, we used 11/39 gears which had been in limited production on the 1942 model. In the 1942 model these gears were questionable for noise, and quite satisfactory with the Hydramatic. Our gearshift transmissions were equipped with a solid propeller shaft, ball-bearing supported at its center, mounted in the torque tube; the first Hydramatics were also so equipped. With the Hydramatic it was necessary to increase the stiffness of our propeller shaft due to low-gear start groan, which was commonly labeled G string. This was accomplished by using a tubular propeller shaft and U joint assembly having a female spline at its rear end, which mated with the male spline of an extension shaft coupled to the rear-axle pinion, ball-bearing supported immediately behind the spline joint. It was necessary and difficult to keep this spline lubricated to avoid fretting. Later, we developed a long tubular shaft at considerably less cost which had welded to its rear end a short 1 in. diameter section with integral flange which coupled to the pinion flange. This was entirely satisfactory as regards axle gear noise with both an 11/39 or a 13/41 gear set.

On our V-8 with automatic transmission and torque converter, the 11/39 gear combination was noisy at approximately 60-mph drive coast and float, and had a frequency which coincided with axle gear tooth engagement. The 13/41 ratio was hardly passable. By resorting to the propeller shaft assembly as first used on the Hydramatic, gear noise was cured. Mr. O'Brien is entirely familiar with this condition on a later V-8 and the Flashaway transmission for which his company furnished axles.

As regards the rear axle-rating formulas, I agree where this is used with automatic transmission. With conventional clutch and gear shift, inertia loads far in excess of slip torque can be instantaneously applied; and where the latter are used, I would suggest careful test.

I am intrigued with the authors' explanation of unloading the Powr-Lok differential when cornering. With the outer wheel free-wheeling, does the car speed increase? Also what happens when the driver, as I am in the habit of doing when on the highway, slowing down going into the curve and accelerating in the curve?

These authors point up what to expect unless we can come up with some checkmate on the stylists' desire to emulate the lowly worm—long, lean, and with its belly on the ground.

Discusses Problem of Axle Noise

—J. T. Conwell
General Motors Corp.

ONE of the greatest problems existing for the axle manufacturers today is noise. This is becoming increasingly more and more important as the engine-transmission combinations require more work from the rear axle, while styling dictates that the axle remain at its present size. An important facet of the noise problem is the difficulty involved in obtaining a true evaluation of gear noise short of installation of the axle in a vehicle followed by a road test. The procedure which is industry-wide has already been outlined by Mr. O'Brien: "The only known method of determining whether an axle will be satisfactory from a noise standpoint is to check the unit in the particular vehicle". In this manner it is possible to test a very few axles produced each day. Quality control of the axle noise then resolves into a matter of statistics. It would be extremely advantageous if we could satisfactorily test 100% of the axles produced each day in an environment which would correlate with the picture which the customer receives in his automobile. In this area lies the greatest gain to be made in control of axle noise.

Noise test facilities now in use range from telephone-booth type shacks (with a production rear axle and production brakes used as a power-absorbing device) to the almost full-scale axle dynamometer with flexibility of speed and load. Neither of these types have yielded a completely satisfactory analysis of the noise as encountered in the automobile. Herein lies a fertile field for the development of a vital tool for axle builders.

ORAL DISCUSSION

Reported by E. L. Jones
Chrysler Corp.

J. S. Voigt, American Motors Corp.: How does the Powr-Lok differential free itself when turning corners under torque application?

Mr. O'Brien: Powr-Lok differential actually does partially unlock when the vehicle is making turns. This has been proved by strain-gage measurements, and appears to be related to the amount of backlash in the unit.

C. L. Burton, Aluminum Co. of America: Would you comment on the general level of axle and transmission noise present in foreign cars?

Mr. O'Brien: I can see no reason why foreign cars should be noisier than domestic cars. It should be possible to make them just as quiet. The United States automotive industry benefits primarily from experience gained through mass production, which affords more opportunity for refinement through development.

Mr. Lewis: The European public will accept more noise; hence, there is less pressure to develop quieter components.

W. C. Allison, Motor Research Corp.:

Sprung final-drive units add complication with resulting cost penalties, so we must have very real and sound reasons for their adoption. Conventional "live" axles are virtually trouble-free. Sprung units would have to give comparable dependability.

With the large engines advertised today, combined with high-performance transmissions, the torque applied to the rear axle tends to lift the right wheel off the road. The right wheel spins, limiting the performance of the vehicle. Independent or modified independent rear suspension provides a means for keeping equal load on both rear wheels during acceleration.

With independent rear suspension, it is possible to design in a feature whereby the rear of the car is lifted physically during forward acceleration. This causes a momentary increase of the rear-wheel reactions when torque is applied, and helps keep the wheels from breaking traction. Elimination of torque roll is another advantage to be gained from independent rear suspension.

Future suspension may be expected to be substantially frictionless, with the exception of the shock absorbers and a few rubber bushings. Better road adhesion is obtained by providing some lateral flexibility between the axle and frame rather than by connecting these members rigidly.

Oversteering associated with swing axles is considered to be a function of tread changes rather than camber changes on turns. This may be thought of as a change that causes the rear end of the car to "ratchet" itself toward the outer side of the turn. It should be possible to design swing axles without objectionable oversteering by recognizing this principle and designing the geometry in such a way as to minimize tread changes on turns.

The de Dion type of rear axle provides good handling.

Automotive Exhaust Hydrocarbon Reduction During Deceleration by . . .

Induction System Devices

Induction System Task Group,* Automobile Manufacturers Association

This paper was presented at the SAE National West Coast Meeting, Seattle, Aug 16, 1957.

EARLY in 1955 the Automobile Manufacturers Association created the Induction system Task Group to build, test, and evaluate devices for the reduction of unburned hydrocarbon emission from vehicles by induction system methods. This paper is a progress report of the work performed to mid-1957 by the group.

Two types of devices are described: those which stop the flow of fuel from the carburetor during the deceleration cycle and those which maintain burnable mixtures during deceleration. However, the effectiveness of such devices is limited. Los Angeles traffic survey data have indicated that the hydrocarbon emission during deceleration is considerably less than reported by early investigators and that relatively low speed decelerations predominate in traffic.

In addition, the wide variety of carburetors and engine installations in use today make it unlikely that any one device is entirely suitable for universal adaptation. The Induction System Task Group found that the principle of the vacuum limiting type of device appears to be the best approach to this requirement.

IN 1952, A. J. Haagen-Smit of the California Institute of Technology proposed the theory that smog is largely formed by the action of sunlight on hydrocarbons and nitrogen oxides. Later tests have confirmed this theory.

Work by the Los Angeles County Air Pollution Control District indicated that the hydrocarbons came from industry, automobiles, backyard incinerators, and the like, with about one-third of the hydrocarbons coming from automobile exhaust in the form of unburned fuel. The results of tests by various groups have shown that a considerable portion of the unburned hydrocarbons from automobile exhaust is produced during deceleration.

Data presented by the AMA Data and Analysis Task Group in April, 1956, showed the relative hydrocarbon emission during different phases of typical Los Angeles area driving (Table 1). Later survey data indicate some changes in this information; however, these data have not been officially confirmed.

In a program planned to do everything possible to reduce the exhaust emissions which might be contributing to the smog problem, the automobile industry through AMA sent a group of technical men

* H. H. Dietrich, General Motors Corp.; C. E. Burke, American Motors Corp.; R. E. Clark, Chrysler Corp.; N. R. McManus, Ford Motor Co.; W. J. Pelizzoni, Mack Trucks, Inc.; R. D. Randall, Stewart-Warner Corp.; A. Rudolph, Ford Motor Co.; J. L. Smith, Studebaker-Packard Corp.; J. T. Wentworth, General Motors Corp.; and E. P. Wise, Chrysler Corp.

Table 1—Relative Hydrocarbon Emission in Los Angeles

	Time, %	Total Hydrocarbon Emission, %
While idling	18	5
During acceleration	18	30
During cruising	46	32
During deceleration	18	33

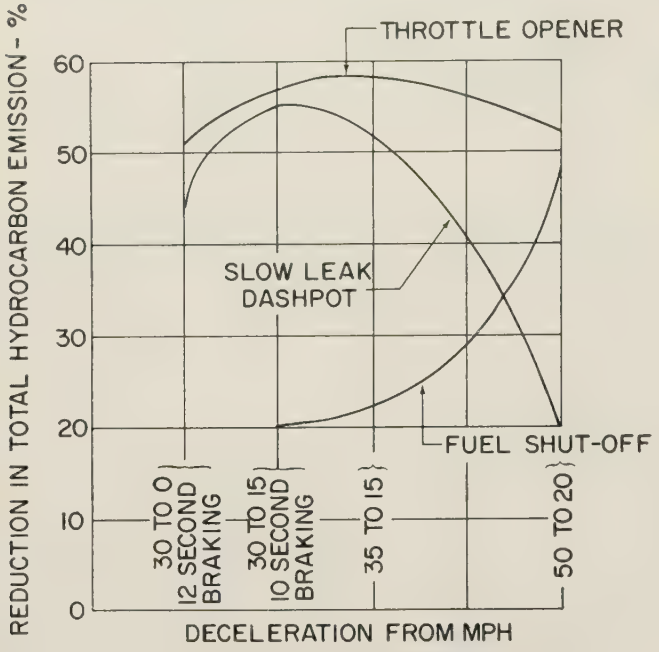

Fig. 1—Typical reduction in hydrocarbon emission from principal types of devices

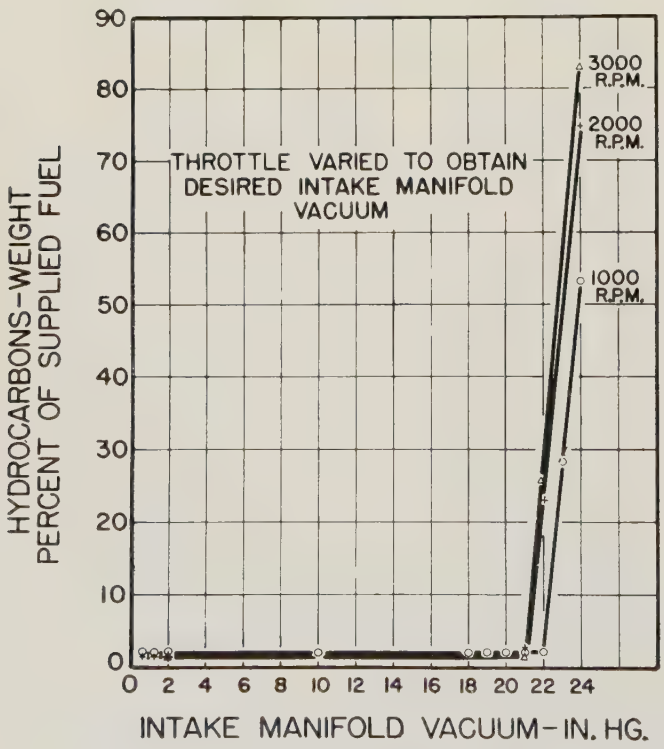

Fig. 2—Effect of intake manifold vacuum on hydrocarbon emission

to Los Angeles early in 1954 to study the situation. The AMA at that time formed the Vehicle Combustion Products Committee to work on the reduction of unburned hydrocarbon emissions from automobiles. Task groups were appointed by this committee to attack various phases of the problem, including field surveys and development of instrumentation to measure hydrocarbons and to develop means of reducing hydrocarbon emissions from automobiles. Specifically, the Induction System Task Group was assigned to develop and evaluate induction system devices for the reduction of hydrocarbons.

This group studied the available information on hydrocarbon emission. Experience of the members on engines and carburetion was utilized. It did not appear that appreciable reductions in the idle, acceleration, and cruise phases of operation could be made by readily applicable design changes.

It was concluded, therefore, that for more immediate results, and from a practical standpoint in application to current automobiles (existing and new), a device to operate during the deceleration cycle would be the most promising way of reducing hydrocarbon emissions.

Approximately 30 different types of corrective devices were designed, tested, and evaluated for their overall effects. The three devices shown in the curves (Fig. 1), were the only types of devices remaining under consideration at the time this paper was originally published. Since that time the throttle opener remains the only corrective device under active consideration. The illustration shows the effect of this device in the reduction of vehicle hydrocarbon emission for various types of deceleration. However, in the evaluation of these devices, other factors such as the following were actively considered:

1. Effect of device on driveability of vehicle.
2. Adaptability to old and new cars.
3. Cost of device.
4. Ease of maintenance and reliability of device in service.

Unburned Hydrocarbon Theory

It is interesting to consider the question: Why are hydrocarbons found in the exhaust? Superficially, one might expect that the high temperatures and pressures in the engine cylinders would ensure complete burning of the fuel. Unfortunately, this is not the case. Any engine will exhaust a certain amount of unburned fuel under the best conditions. It has been found that the unburned hydrocarbons are a result of two phenomena occurring within the engine cylinders. One, residual-gas dilution, has been known by automotive engineers for years. The other, wall quenching, is comparatively new to automotive engineers although it has been studied for years by combustion theoreticians. It is residual exhaust-gas dilution that causes most of the unburned hydrocarbons that are emitted during deceleration.

Let us consider residual-gas dilution first. In an otto cycle engine the amount of burned gas carried over from one cycle to the next depends, among other things, on the intake manifold vacuum. As vacuum increases, residual-gas dilution increases until at 21 in. of Hg (slightly above the usual idle

vacuum) the residual gas amounts to approximately one-fourth of the mixture in the cylinder. At this level of dilution, the mixture is on the verge of failing to burn. Any higher vacuum will prevent portions of the mixture from burning, and the higher the vacuum, the larger will be the unburned portion.

Fig. 2 has been reprinted from a paper by Chandler, et al.[1] and illustrates the problem very nicely. In this graph the amount of hydrocarbon in the exhaust is expressed as a weight per cent of the supplied fuel and is plotted against intake manifold vacuum for three engine speeds. The abrupt rise in hydrocarbon concentration at 21 in. of vacuum is due to excessive residual-gas dilution as just described. It should be realized that vacuums above 21 in. are possible only during deceleration. A more detailed explanation of this subject is given by Wentworth and Daniel.[2]

During the other three driving conditions (cruising, accelerating, and idling) the per cent of unburned fuel is much lower, but still significant. Daniel[3] has shown that the hydrocarbon present in the exhaust during these driving conditions is due to wall quenching. The flame in the cylinders approaches the wall surfaces within thousandths of an inch, but does not actually burn right up to the wall. Thus a thin layer of quenched fuel-air mixture covers all of the combustion-chamber wall after flame propagation is completed. This occurs every time a cylinder fires and is believed to account for the concentrations of hydrocarbon that have been found in automotive exhaust with manifold vacuums under 21 in. of Hg.

Goals and Methods of Measurements

One of the first acts of the Induction System Task Group was to decide on its goals. These evolved from discussions during the first few meetings and were recorded as follows:

1. Only devices for control of hydrocarbons during deceleration would be studied.

2. A reduction of hydrocarbon emission of 70% during deceleration would be sought. The per cent reduction would be based on the difference in emissions from a car in good condition with and without a device. Tentative operating conditions were: Deceleration from 50 to 20 mph on level ground, closed throttle, engine braking only.

3. Practical devices of reasonable cost would be sought for both old and new cars with manual and automatic transmissions.

4. Applications to both passenger cars and commercial vehicles would be considered.

It was recognized that these goals were arbitrary, but it was believed that they established a basis for constructive work. It was agreed that the goals could be modified as new information developed.

Of the four goals only the second was materially changed. The Traffic Survey Group indicated that decelerations from 35 or 30 mph, with some braking, were more typical of city driving. Further, it was found by the Induction System Task Group members that evaluations made from 50–20 mph would not necessarily correspond to evaluations made from 35 mph. Some devices gave a good reduction for the short decelerations, but not for long ones. Other devices behaved in an opposite fashion. Therefore, as the development work progressed, it became common to make evaluations both from high speeds and low speeds, with increasing emphasis being given to the low-speed decelerations. It was found that the requirements for a good functioning device differed between manual transmission cars and automatic transmission cars.

At the beginning of the group's work the equipment and techniques necessary for detecting and measuring hydrocarbons in exhaust gas were generally not well-developed. However, late in 1955 three of the participating laboratories acquired continuous-reading instruments. These were Liston-Becker nondispersive, infrared analyzers[4] designated Model 15A. The instruments were equipped with 2½-in. sample cells and the detectors were charged with either n-hexane or n-heptane. The group's work was aided considerably by the use of these instruments, which permitted rapid analysis of transient conditions. Having been charged with n-haxane or n-heptane, it was found that the instruments had little response to one- and two-carbon atom hydrocarbons and somewhat reduced response to olefins and aromatics. Thus, the instrument was not an ideal indicator of total hydrocarbons. However, the group had confidence in the ability of the instrument to compare devices and rank them according to their relative effectiveness in reducing hydrocarbon concentration in the exhaust.

One of the most recent developments is the Integrator, an instrument which electronically and continuously integrates the product of airflow and per cent hydrocarbon emission, thus furnishing a measure of total hydrocarbon emission.[5]

During the 2½ years the group has been active, the methods of testing and the instruments for measuring have been gradually changing. Naturally, this makes it difficult to compare tests, but the improvements brought about by the changes have been worthwhile with the result that now all of the participating laboratories have similar equipment.

Devices

As has been pointed out, the work of this task group has been concentrated on developing and investigating devices intended to reduce the exhaust hydrocarbon emission during the deceleration cycle. It should be emphasized at this point that the illustrations in this paper are only typical examples of the many devices considered by the different members of this group. Before describing them we would like to draw attention to the fact that the "normal" emission, on which comparisons and reduction figures are based, may vary greatly for different engine conditions and adjustments and for

---

[1] *Journal Air Pollution Control Association*, Vol. 5, August, 1955, p. 65: Paper by J. M. Chandler, W. A. Cannon, J. C. Neerman, and A. Rudolph.
[2] SAE Transactions, Vol. 63, 1955, pp. 602–619: "Flame Photographs of Light-Load Combustion Point Way to Reduction of Hydrocarbons in Exhaust Gas," by J. T. Wentworth and W. A. Daniel.
[3] Sixth Symposium (International) on Combustion, 1956: "Flame Quenching at the Wall of an Internal Combustion Engine," by W. A. Daniel.
[4] "Application of Infrared Spectroscopy to Exhaust Gas Analysis," by Twiss, Teague, Bozek, and Sink. Air Pollution Control Association, Detroit, 1955.
[5] "Integrator for Determining Total Emission of Automotive Exhaust Gas Components," by R. L. Dennis, J. D. Jenks, S. B. Smith, and R. T. VanDerveer. Paper presented at SAE National West Coast Meeting, Seattle, Aug. 16, 1957.

different modes of driving. Factors influencing the normal emission during deceleration are:

1. The idle adjustment. As seen in Fig. 3 a lean idle adjustment produces considerably less hydrocarbon emission during deceleration than a rich idle adjustment.
2. The type of transmission used. Due to slip, automatic transmissions will turn the engine over more slowly during deceleration, thereby producing less manifold vacuum with resulting less hydrocarbon emission (Fig. 4).
3. The engine load prior to the start of deceleration. The greater the load, the greater is the emission (Fig. 5).

Prior to all device evaluation tests, engines were tuned according to recommended practice with particular attention being given to proper idle adjustment. Tests were made on level roads from constant speeds under both free and braking decelerating conditions. It should be noted that due to normally greater hydrocarbon emission, the effectiveness of various devices on manual transmission cars normally was higher than on automatic transmission cars.

Carburetor Throttle Controls

Since engine combustion efficiency is good at values of manifold vacuum below 21–22 in. of Hg even under deceleration conditions, one method of reducing emission of unburned hydrocarbons during the deceleration phase is to prevent high manifold vacuum. Of course, this must be done in such a manner that normal fuel-air mixture is delivered to the engine. Therefore, merely admitting extra air into the manifold is not sufficient; a proportionate amount of fuel must also be added.

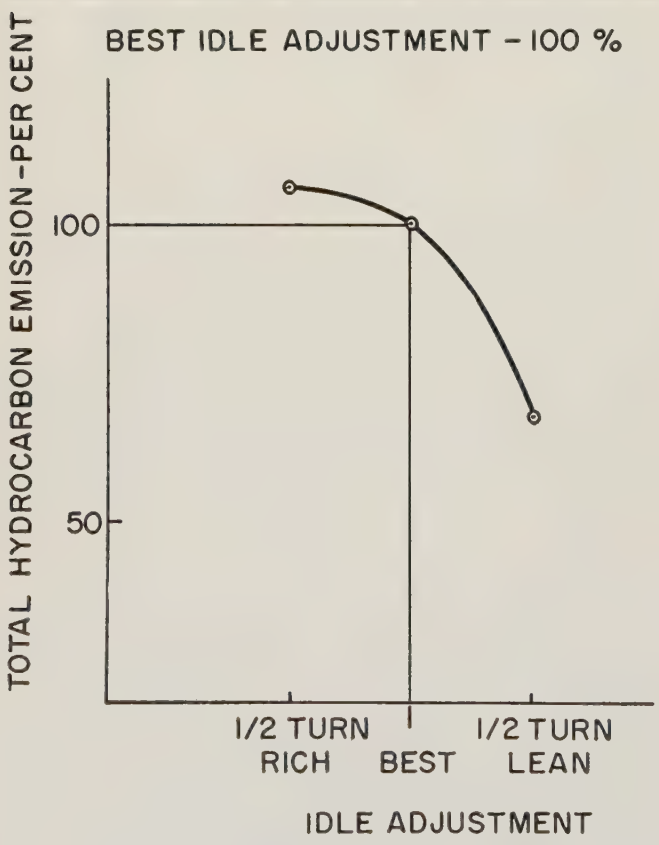

Fig. 3—Effect of idle adjustment on exhaust hydrocarbon emission during deceleration

A straightforward way of accomplishing reduced vacuum with controlled mixture ratios is to prevent complete throttle closing during deceleration. It has been found that even though the total amount of fuel and air entering the engine is thereby increased, a significant decrease is effected in the total weight of hydrocarbons released. From the standpoint of effectiveness, driveability, and ease of application, this approach to the problem has been found to be the most promising of all methods tested by the automotive industry to date.

Two major types of throttle controls have been developed and tested, both of which are under active consideration at the present time. One, the slow throttle return dashpot, makes the throttle return slowly during the last few degrees of travel to idle. This results in reduced manifold vacuum during most of the traffic deceleration periods encountered. The second, called the vacuum control throttle opener, holds the throttle open slightly as the manifold vacuum tends to exceed a predetermined amount.

Slow Throttle Return Dashpot—Fig. 6 shows the principle of operation of the slow throttle return dashpot. It is seen that as the throttle reaches a point near closed position, a lever on the throttle shaft engages the dashpot plunger. Air or liquid is trapped behind the diaphragm of the dashpot, slowing the throttle closing. The rate of closing from this point is determined by the rate of bleedout of the trapped fluid. After the throttle is opened, the return of the dashpot plunger is accomplished by an internal spring. The return action (resetting) can be speeded up by a check valve which opens into the compression chamber during the return stroke, or it can be slowed through use of a simple orifice into the chamber. The advantages and disadvantages of each will be discussed later.

The slow throttle return dashpot was one of the first devices considered by the Induction System Task Group. However, the initial goal was a 70% hydrocarbon reduction with a manual transmission car decelerating from 50 to 20 mph. The time duration of such a deceleration was so great (20–30 sec) that a dashpot to control hydrocarbon emission makes the car undriveable at lower speeds. Consequently, work was discontinued on the device in order to concentrate on the idle fuel cutoff principle. However, later field information indicated that short decelerations from around 35 mph are more typical of Los Angeles traffic than the 50–20 mph type. In the 35-mph area of operation and for short decelerations (less than 10 sec) the dashpot does a good job of hydrocarbon reduction, so work was resumed on its application.

As has been stated, the reason for installing a carburetor throttle control is to prevent high manifold vacuum. Since the dashpot is a preset, nonfeedback type of device, it cannot accurately control throttle position to obtain optimum manifold vacuum under all decelerating conditions, but must be tailored to be effective for the conditions most frequently encountered. This tends to allow excessively high vacuum at high speed, while a deceleration initiated at low speed will suffer from excessive throttle opening. Installation variables that must be considered

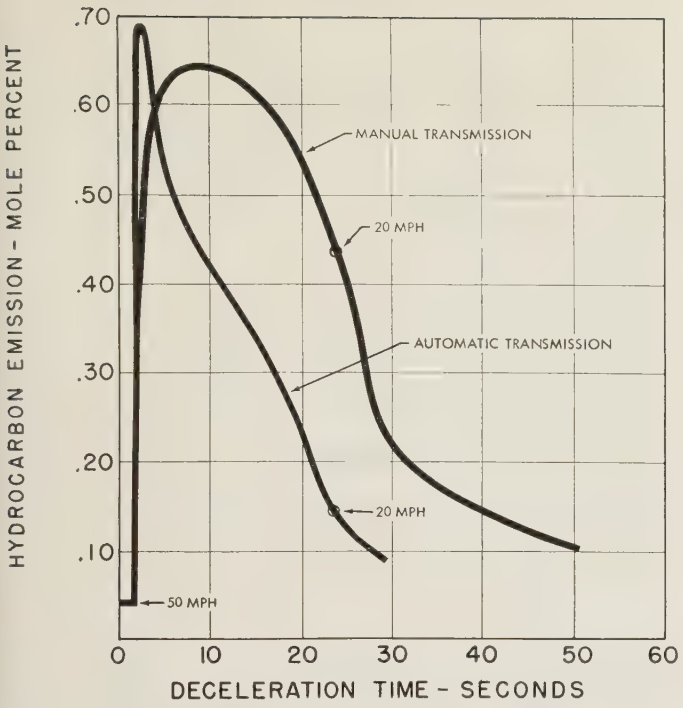

Fig. 4—Exhaust hydrocarbon emission during deceleration from 50 mph, effect of transmission type

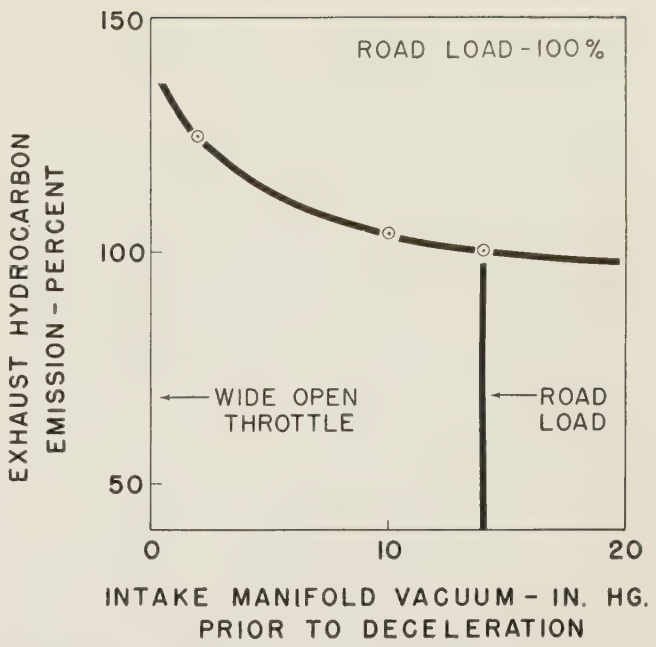

Fig. 5—Effect of engine load prior to deceleration from 50 mph on exhaust hydrocarbon emission

in striking the best compromise are effective stroke, throttle return pressure, dashpot force versus travel characteristics, deceleration speed and duration, engine vacuum versus throttle opening characteristics, transmission type and characteristics, and the like.

As a result of increased engine power developed during deceleration of a dashpot equipped car, decreased engine braking is obtained. This adversely affects driveability, so it is desirable to limit the dashpot bleeddown time to a minimum while maintaining good effectiveness. Since most traffic decelerations last less than 10 sec, it is generally considered unnecessary to exceed this figure in bleeddown time. It appears likely that 6 sec may give acceptable results, though additional testing is desirable to establish this.

If the dashpot is of the fast-reset type, it is always ready to catch the throttle return stroke, even if the throttle has been open only a short time. This causes a serious driveability difficulty when maneuvering the car for parking or when driving in slow traffic. Consequently, a slow-reset type dashpot is considered preferable or even necessary. Some loss in effectiveness occurs because the dashpot controls a smaller portion of the time, but the gain in driver control is very much improved.

The effectiveness of the slow throttle return dashpot in reducing unburned hydrocarbon emission cannot be represented by only one set of tests, since so many variables are involved. Table 2 summarizes the many tests of different cars.

The effectiveness of the device on manual transmission cars is much greater than on automatic transmission cars simply because the car "motors" the engine during deceleration more efficiently through the solid coupling provided by the manual transmission, therefore, creating a greater intake manifold vacuum. The result is poorer combustion for the manual transmission car without a device,

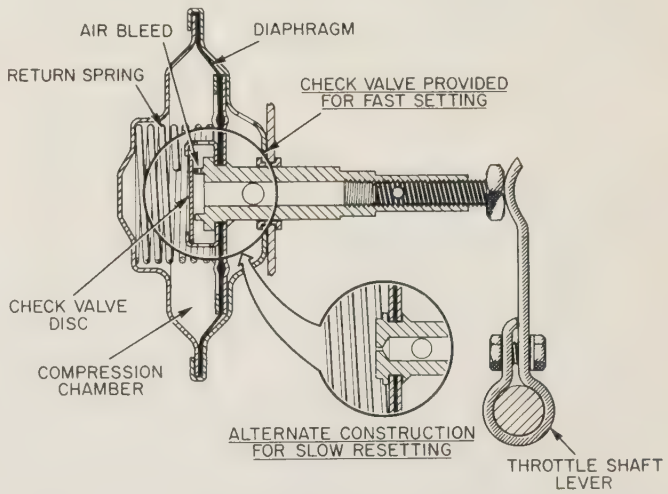

Fig. 6—Slow throttle return dashpot

Table 2—Effectiveness of Slow Throttle Return Dashpot

(Short decelerations from 35 mph or less)

	Hydrocarbon Reduction, %		
	Minimum	Maximum	Average
Automatic Transmission	12	66	46
Manual Transmission	46	75	61

providing more opportunity for improvement. One type of automatic transmission car emits roughly one-third of the hydrocarbons that its manual transmission counterpart does under typical traffic deceleration conditions (no device).

Some data have been obtained that show the overall effectiveness of the dashpot during a traffic run. The figures in this case represent the percentage reduction of total unburned hydrocarbons emitted during all portions of the driving cycles, not just deceleration periods. An automatic transmission car was used.

The fast-reset dashpot effected a 22% reduction,

while the slow reset dashpot resulted in a 14% reduction. Much additional data with other installations are needed in order to firmly establish these results.

To summarize the Task Group experience with the slow throttle return dashpot, the following may be said:

1. Hydrocarbon reduction is good during short low-speed decelerations typical of traffic driving, while long high-speed decelerations are helped considerably less.
2. Installation is simple and inexpensive on old and new cars.
3. A slow resetting dashpot does not affect driveability to an objectionable degree and is preferred over a fast resetting dashpot in spite of a loss of effectiveness.
4. A fairly large diameter dashpot is preferred because the volume of trapped fluid is greater and the bleed orifice can be correspondingly large. However, it should be noted that, at best, orifices will be so small as to present a possible maintenance problem.
5. An inspection procedure would be necessary to insure proper installation and adjustment of dashpots. Maintenance of proper throttle return mechanism friction will be a problem. Owners might be tempted to remove the dashpot entirely if annoyed by maintenance and driveability problems.

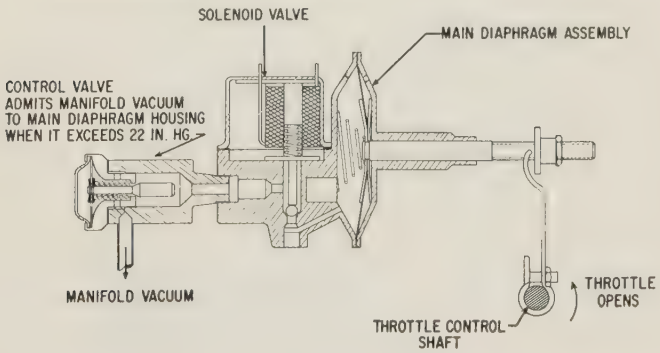

Fig. 7—Vacuum control throttle opener

Vacuum Control Throttle Opener—An improvement in the accuracy of control of manifold vacuum during deceleration can be achieved with a closed loop servo throttle opener, sensing and controlling manifold vacuum. Such a system eliminates many of the variables that reduce the effectiveness of the simple dashpot, including deceleration speed, time, throttle return spring force, friction, and dashpot variables.

The type of throttle opener tested by the Task Group is shown by Fig. 7. This device automatically opens the throttle when necessary and desirable to reduce and regulate manifold vacuum to a predetermined value. The device consists basically of two units, a vacuum operated throttle opener which acts against a lever on the throttle shaft and a pilot control valve to evacuate the throttle opener as required to obtain any necessary reduction in manifold vacuum to maintain the desired limit.

In operation, manifold vacuum acts on the control valve diaphragm. When this vacuum exceeds the value required to overcome the control valve spring, the control valve opens and vacuum is allowed to act on the main diaphragm. This controls the throttle opening through the throttle control shaft lever, thereby reducing manifold vacuum to the desired limit as determined by the control valve setting.

The electric solenoid valve makes the device inoperative except when its action is desired (basically, decelerating in direct drive). A circuit diagram showing operating options is shown in Fig. 8. On automatic transmission cars, a pressure switch can be located in the transmission hydraulic line associated with direct drive, or on the shift linkage. On manual transmission cars, switch interlocks prevent operation except when the clutch is engaged and the transmission is in direct drive. These controls prevent engine idling at high speed at the control vacuum when in neutral, and they permit full engine braking in the lower gears. The device is also inoperative when maneuvering at low speed, such as parking.

Since the basic control will have an adverse effect on engine braking in high gear, and since this is

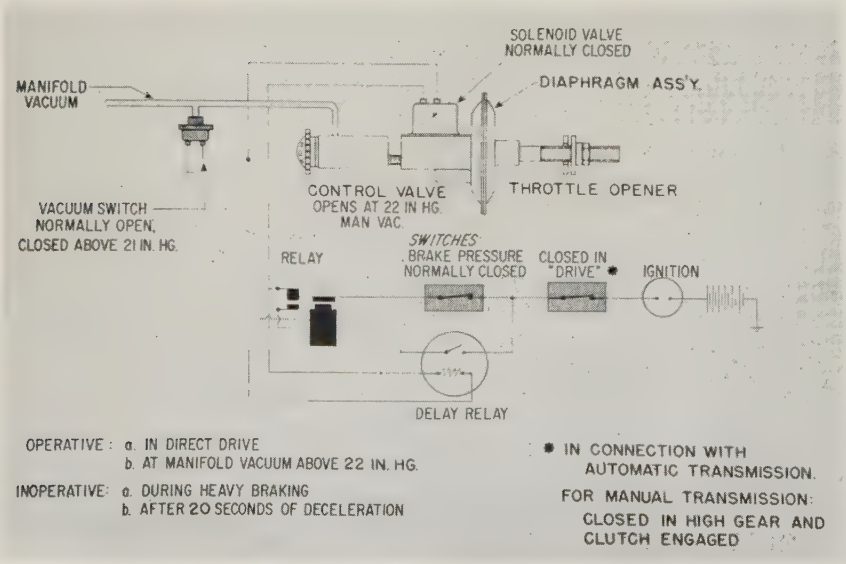

Fig. 8—Control circuit diagram vacuum control throttle opener

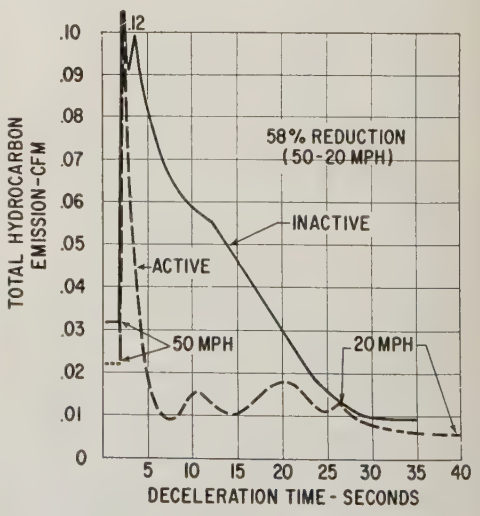

Fig. 9—Effect of vacuum control throttle opener on exhaust hydrocarbon emission during deceleration from 50 mph

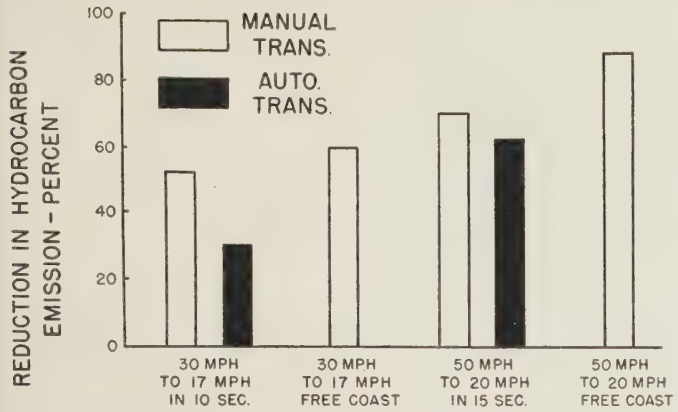

Fig. 10—Unburned hydrocarbon reduction using vacuum control throttle opener with manual and automatic transmissions

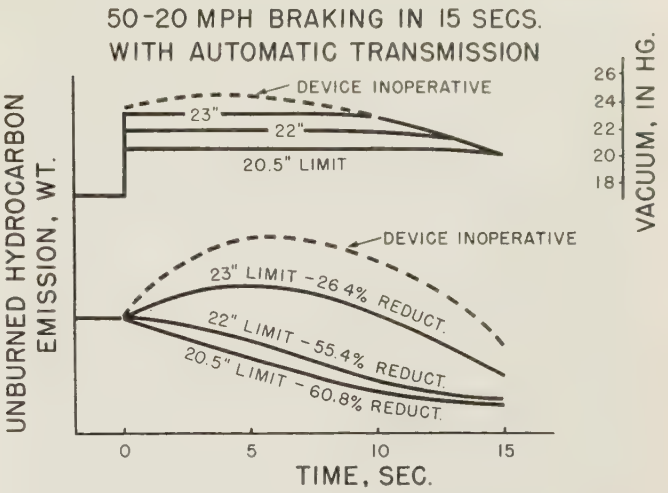

Fig. 11—Effect of vacuum limit values on exhaust hydrocarbon emission

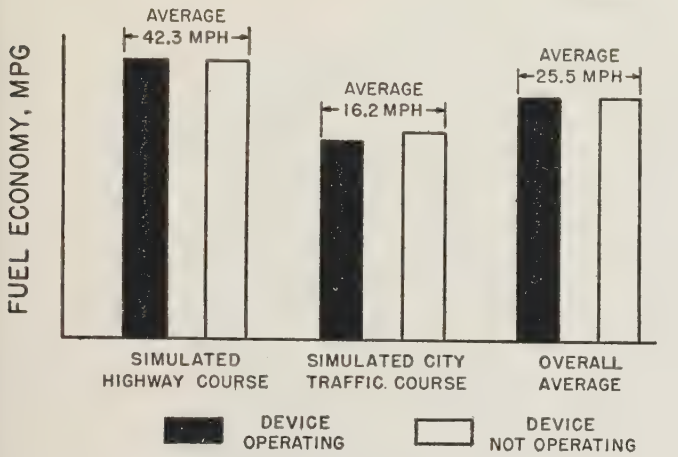

Fig. 12—Fuel economy with vacuum control throttle opener

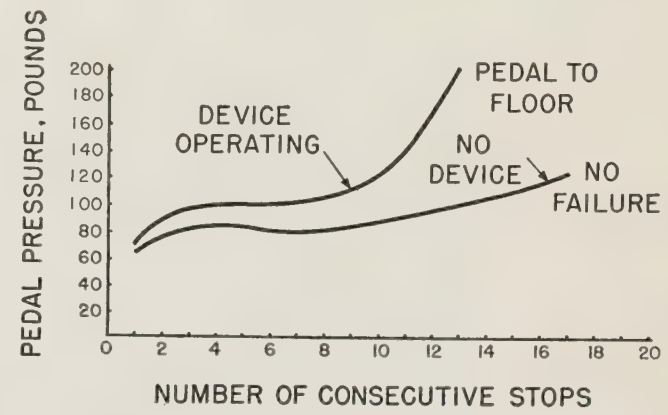

Fig. 13—Brake fade tests with vacuum control throttle opener at 22 in. of Hg, 18 fps² braking stops from 50 mph, repeated with minimum cycle time

not a temporary condition as it is with a dashpot, it is felt that some means should be provided to limit the time that the device will operate without resetting. One such method is shown in Fig. 8. Also shown is a means of making the device inoperative during heavy braking through the use of a brake line pressure switch.

Fig. 9 shows a sample measurement of unburned hydrocarbon emission during deceleration with and without a vacuum control throttle opener.

Typical reductions in unburned hydrocarbons are shown by Fig. 10 for manual and automatic transmission cars. It is seen that the reductions are appreciable for all deceleration conditions. The biggest gain is, of course, obtained with the manual transmission cars because the unaltered deceleration vacuums are highest with these cars.

A preliminary survey to determine the best vacuum limit value was run and results are shown by Fig. 11. Though about 20.5 in. of Hg produces the best results under the conditions tested, no great loss is incurred in raising the vacuum limit to 22 in. of Hg and the car driveability is considerably improved.

During a traffic run the overall level of hydrocarbon emission from cars with and without the vacuum control throttle opener was determined. Results indicated 25% overall reduction with manifold vacuum set at 22 in. Again much additional data are needed to firmly establish such a figure.

In order to determine what effect the throttle opener has on economy, both deceleration economy and traffic economy tests were run using automatic transmission cars. Test results indicate that although a 21% increase in fuel consumption was noted in deceleration from 60 to 10 mph in gear (44.7 versus 54.3 mpg during deceleration, device on an off), the amount of additional fuel used per mile of deceleration was only about 0.004 gal. The customer economy comparison of Fig. 12 shows no essential difference.

The loss in engine braking during deceleration with the vacuum control throttle opener is serious. Decreases of 24 and 31% in engine braking at 40 and 50 mph respectively were measured on one car with the device operating at 21 in. of Hg. Though a setting of 22 in. of Hg helps reduce this loss, the effect on braking lining wear is significant. From a safety standpoint, it is necessary to add a brake hydraulic pressure switch to cut out the device when severe braking is required. Without such a cutout, ability to make repeated high speed stops was reduced 25% on one car tested. In order to make direct gear engine braking available when descend-

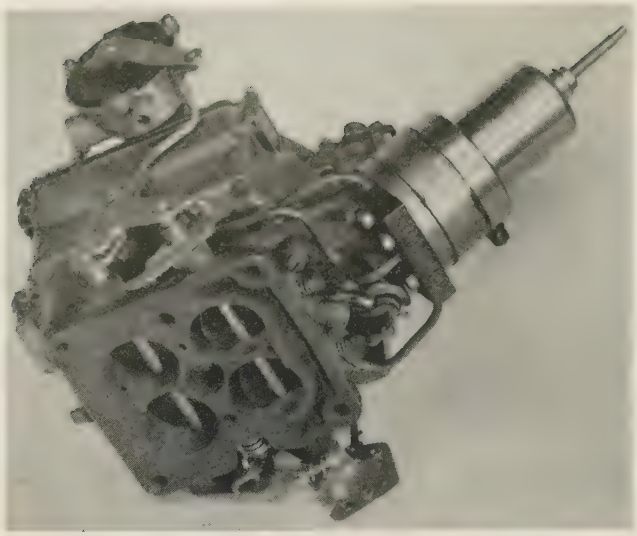

Fig. 14—Example of idle fuel shutoff device, air-bleed type

ing long, moderate grades (second gear not required), a time delay circuit is necessary to prevent operation of the throttle opener for longer than is necessary for traffic-type decelerations (up to about 20 sec). This circuit and the brake pressure cutout are shown by Fig. 8.

Fig. 13 shows the results of another test, repeated 18 fps^2 stops with and without the device set at 22 in. of Hg. It is seen that the number of stops without the device is essentially unlimited, while that with the device operating is limited.

With the vacuum control throttle opener set to control at 22 in. of Hg and operating in direct drive only for a maximum of 20 sec at a time, driveability is not affected to a noticeable degree. The car has a feeling equivalent to "free wheeling" in normal traffic nonbraking decelerations, and there is always a more than normal need for brake application. This effect is no more pronounced, however, than is experienced in the transition from manual to automatic transmission cars, and it is expected that most

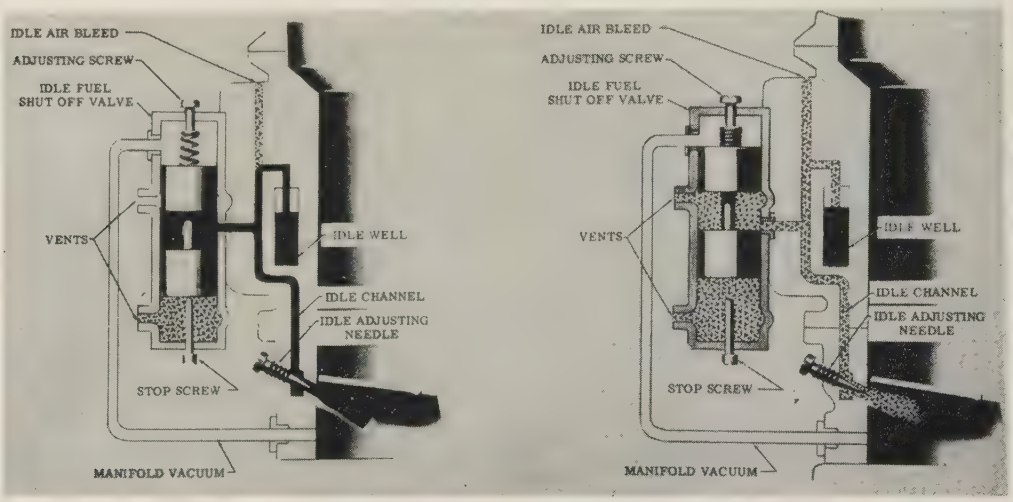

Fig. 15—Air-bleed type idle fuel shutoff device

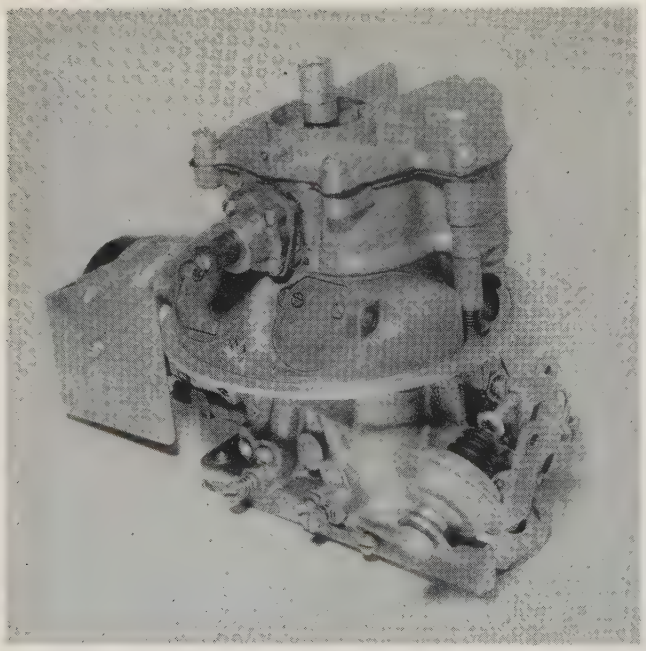

Fig. 16—Built-in air-bleed idle fuel shutoff device

drivers would become accustomed to it.

Experience with the vacuum control throttle opener has shown the following:

1. Reduction in unburned hydrocarbon emission is good under all deceleration conditions. Overall effectiveness is better than with any other practical device tested.
2. Installation is not difficult either in production or in the field. However, the number of controls required makes installation time considerably greater than the simple dashpot.
3. Cost of the package is within an acceptable range and no extensive tooling is required.
4. Driveability is affected by the requirement for increased brake use.
5. Brake wear in traffic is substantially increased, but the amount involved is not yet known. This is a major objection to the adoption of this device.
6. Fuel economy is affected to a negligible extent.
7. The vacuum throttle opener can probably be depended on to maintain accurate control of unburned hydrocarbon emission. Functional inspection can be reliable. Inactivation by the owner is

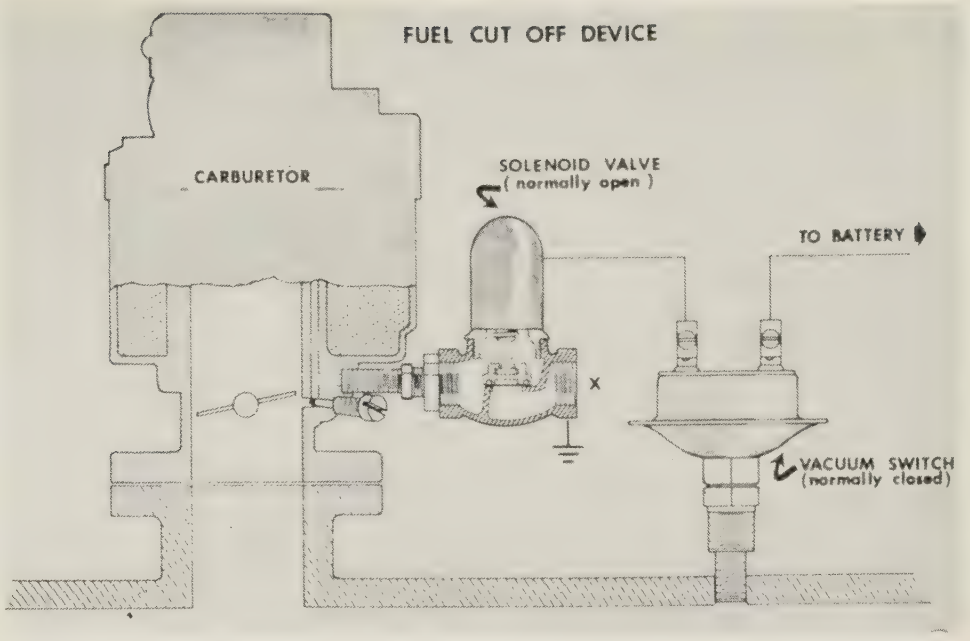

Fig. 17—Idle fuel shutoff air-bleed device with solenoid valve and vacuum switch control

relatively simple, however, and policing methods will have to be developed.

Idle Fuel Shutoff Devices

At closed throttle, as during idling and deceleration, fuel is normally supplied to the engine through the carburetor idle system only. Shutting off the idle fuel flow during deceleration was, therefore, considered promising as a means for substantially reducing hydrocarbon emission. A device to accomplish this is usually operated by the increased manifold vacuum existing during deceleration. If, for example, the manifold vacuum is 19 in. of Hg at idle and rises to 25 in. of Hg during deceleration, the device may be set to cut in and out at 21.5 in. of Hg. The range from 25–21.5 in. of Hg covers most of the deceleration period.

Various idle fuel shutoff devices representing a wide range of concepts have been developed and tested.

Air-bleed Type Idle Fuel Shutoff—Such a device admits air into the idle system under high-vacuum conditions, thus cancelling the suction head that normally causes fuel to flow through the idle system. At the left of Fig. 14 the device is shown inactive. The idle system is then functioning in its normal manner. At the right the piston is raised by the increased manifold vacuum of deceleration, thereby admitting atmospheric air to the idle channel and stopping the fuel flow.

Air-bleed type devices of various designs were built and tested by the different participating companies. Commercially available air-bleed devices were also tested on various cars. Typical examples are shown in Figs. 14–16. Instead of using a piston as shown in the diagram, it was generally preferred to use diaphragms as operating members.

Fig. 17 shows an idle fuel shutoff air-bleed device consisting of a solenoid valve and a vacuum switch. This arrangement has the advantage of reducing hysteresis with resulting improved effectiveness and recovery characteristics.

Typical exhaust hydrocarbon emission curves ob-

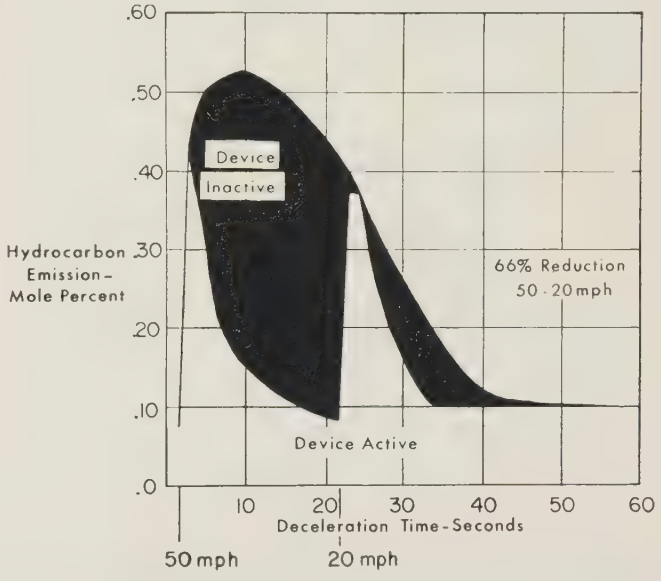

Fig. 18—Hydrocarbon emission during deceleration 50-20 mph, manual transmission, with idle fuel shutoff

tained during a free deceleration from 50 mph with an air-bleed type device first active and then inactive are shown in Fig. 18. In this particular example, a 66% reduction in hydrocarbon emission was obtained, which is a typical value for numerous test runs with various manual transmission cars. The values were obtained with a continuously recording Liston-Becker infrared exhaust analyzer. Although fuel is shut off immediately after the start of deceleration, a substantial increase in hydrocarbon emission takes place before it gradually fades out. This shows that it takes considerable time to clear the induction tract of fuel which was trapped after the sudden cessation of the preceding road load operation. A second hump indicates the rise in hydrocarbon emission after idle fuel flow is reestablished. If this cut-in point is set too low, a momentary lack of fuel exists, causing the engine to stall, particularly when declutching, braking, or

during a period of free-wheeling in connection with overdrive or some automatic transmissions.

Fig. 19 shows how the reduction becomes less impressive during a deceleration from speeds more typical of city driving (37% reduction). Better results could be obtained when the device was readjusted to operate at low manifold vacuum. But driveability problems were substantially increased. Typical results on both manual and automatic transmission cars are summarized in Fig. 20.

Best results with regard to effectiveness and general driveability were obtained with a solenoid valve and vacuum switch idle bleed arrangement installed on a small compact engine. During decelerations from 50 mph the device gave reductions of 70–90%. Effectiveness of this magnitude, however, was obtained only with this particular engine. The intake manifold was short and cast into the cylinder head. The small volume and absence of wall wetness due to water heating resulted in quick removal of the evaporated fuel after deceleration began. By the same token it took less time for the normal idle fuel flow to be reinstated.

It is understandable that with no fuel flowing during deceleration, no combustible mixture will be available when normal operation is suddenly demanded. Under many driving conditions the accelerating pump apparently was capable of supplying sufficient fuel to re-establish engine operation. In other cases a perceptible lag or flat spot was felt. Idling after a particularly long deceleration posed a more serious problem. A "drooping" of the engine or even stalling was experienced, particularly during or sometimes after an extended deceleration period when the clutch was disengaged just before the idle fuel flow resumed. Engine flywheel inertia, in such a case, is generally not sufficient to keep the engine motoring at speeds required for restarting.

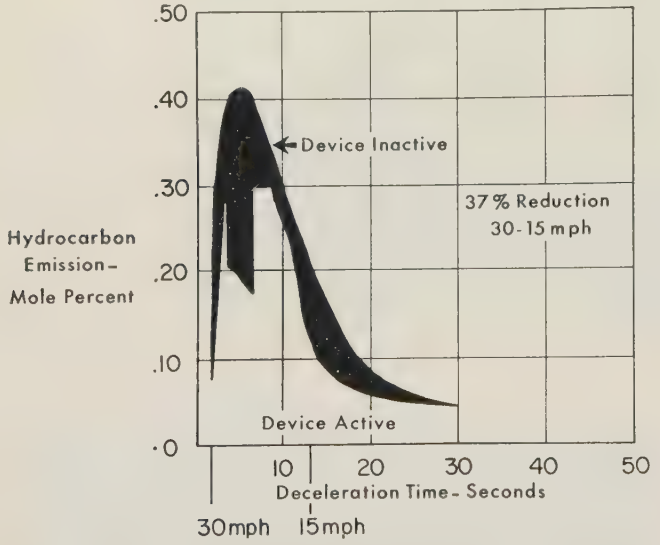

Fig. 19—Hydrocarbon emission during deceleration 30-15 mph, manual transmission, with idle fuel shutoff

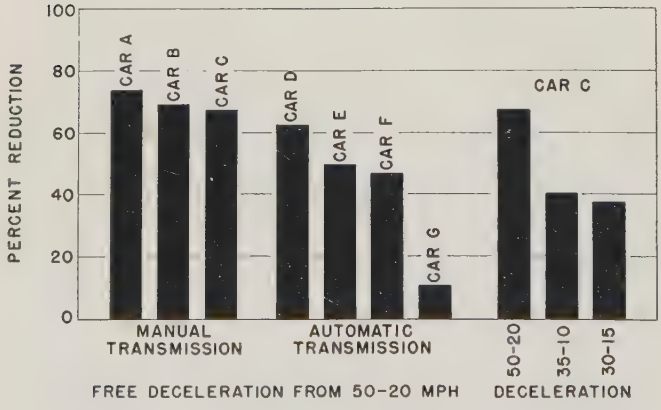

Fig. 20—Reduction in exhaust hydrocarbon emission with idle fuel shutoff devices, air-bleed type

The time of recovery after deceleration consists of two periods:

1. The time necessary for the fuel to travel from the float bowl fuel level in the idle channel to the idle outlet at the adjusting needle.
2. The time for the mixture to travel from the carburetor to the cylinders.

The recovery time within the carburetor was found to be in the order of 0.6 sec; this, however, varied somewhat with the length of the idle system and its design characteristics. The second period of recovery, the time it takes for the mixture to fill the cylinders for the first combustion, was calculated as the ratio of total induction system and cylinder volumes over the idle airflow in cfm at idle depression. This time is in the order of 0.8 sec. The total time of approximately 1.4 sec was found to be long enough in many cases to cause either engine stalling or stumbling. Although small improvements in idle system recovery were made, these changes did not materially reduce the inherent problem of engine recovery.

Complete idle fuel shutoff by air bleed depends on a sufficiently large air-bleed passage. It was also found that a greater passage length resulted in a smaller effective area. In adapting devices to existing carburetors, in particular those with multiple barrels, long passages cannot always be avoided. In addition, quantities of fuel would collect in these passages and be drawn into the engine with the device operating, thus reducing the amount of the total fuel reduction.

In some cases fuel was consumed even when the idle channel was completely blocked off. Fuel spillage from the main nozzle or from other fuel outlets must be expected. Fuel may frequently leak past the float needle valve due to road vibrations. This leakage, normally consumed by the idle fuel flow, can cause an increase in float level height until this fuel spills over into the main venturi. Valves in the carburetor fuel inlet lines were used with some devices to overcome this problem.

It may be summarized that even when the idle shutoff device effectively shuts off idle fuel flow a significant hydrocarbon emission results from the normal manifold "dry-out" period and from the period after fuel flow is re-established. In addition, any small amount of fuel emerging from the idle system, bowl vents, or other sources will appear fully as unburned hydrocarbons.

The adaptability of an air-bleed type idle fuel shutoff to old carburetors appears difficult unless the device can be sandwiched between the carburetor and intake manifold or between the carburetor throttle body and main body (Fig. 21). This will normally increase carburetor height, which usually is at a premium. Furthermore, most existing carburetor idle systems are generally inaccessible and

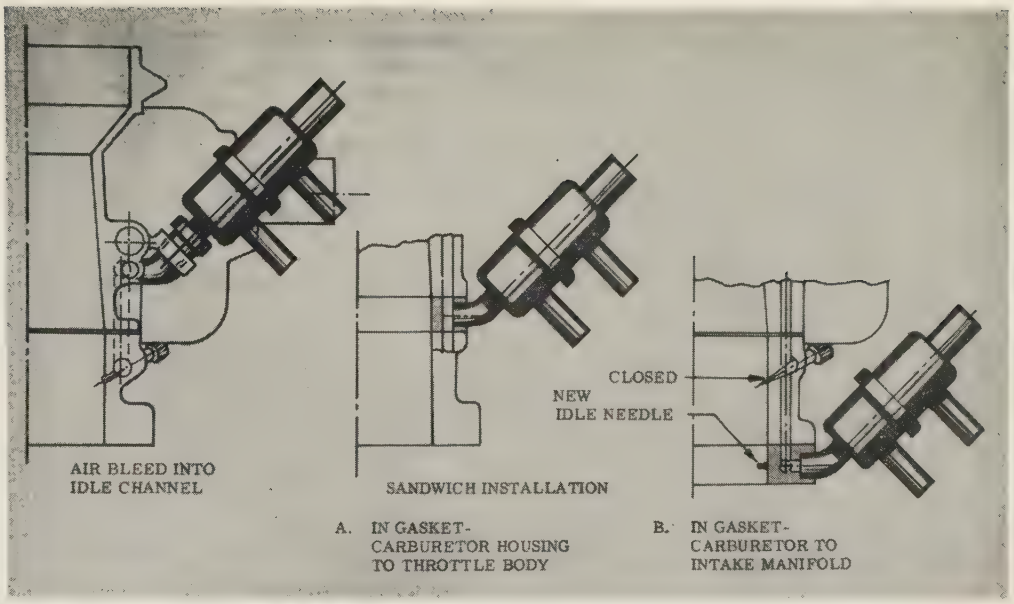

Fig. 21—Installation of idle fuel shutoff valve, air-bleed type

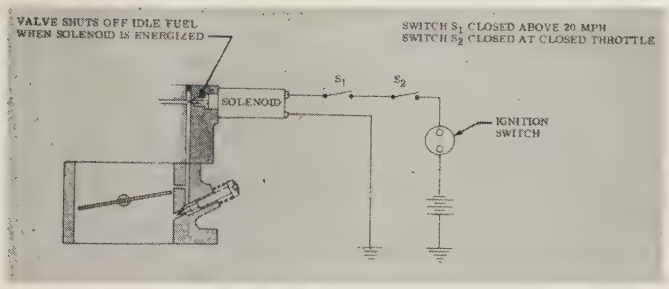

Fig. 22—Positive idle fuel shutoff valve, solenoid operated

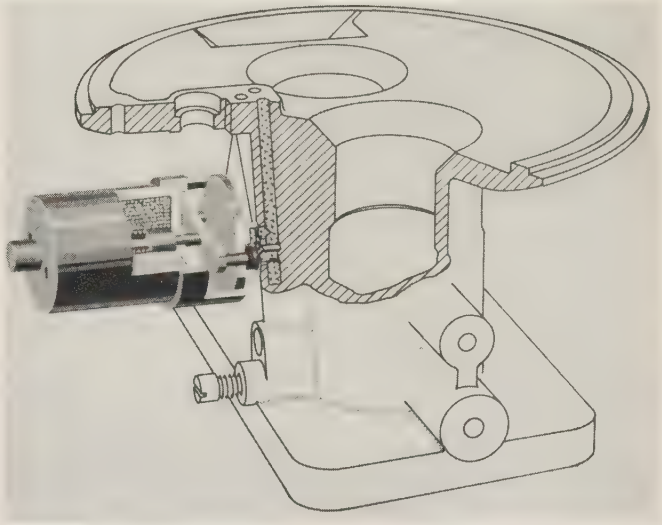

Fig. 23—Solenoid-operated positive idle fuel shutoff installation

seldom permit a simple connection to a device. Most carburetors used today would require use of multiple devices with long connecting air-bleed passages to prevent interference with air cleaner and other engine components.

In many cases, the installation of an air-bleed type device could be made more conveniently on some new design carburetors where a fitting and passage could be provided leading directly to the idle system. In other cases, it may be possible to build the device integral with the carburetor body (Fig. 16). Extreme difficulties arise in connection with new design, low-built multi-barrel carburetors, especially when they incorporate four separate idle systems.

Positive Idle Fuel Shutoff—A valve which mechanically shuts off the idle fuel flow during deceleration should, if properly constructed, leave no doubt about a complete stoppage of idle fuel flow. Fig. 22 shows such an arrangement schematically, Fig. 23 illustrates an installation on a 4-barrel carburetor with two separate idle systems. Two valves were operated simultaneously by one solenoid, energized by a vacuum switch. A 60% reduction in hydrocarbon emission was obtained during deceleration from 50 to 20 mph. In spite of the apparent complete fuel shutoff there remains the initial peak of hydrocarbon emission during the manifold dry-out period, and a further peak when the device cuts back in. The recovery, except after very severe braking, was generally satisfactory.

Various forms of positive idle fuel shutoff valves combined with the idle mixture adjusting screws

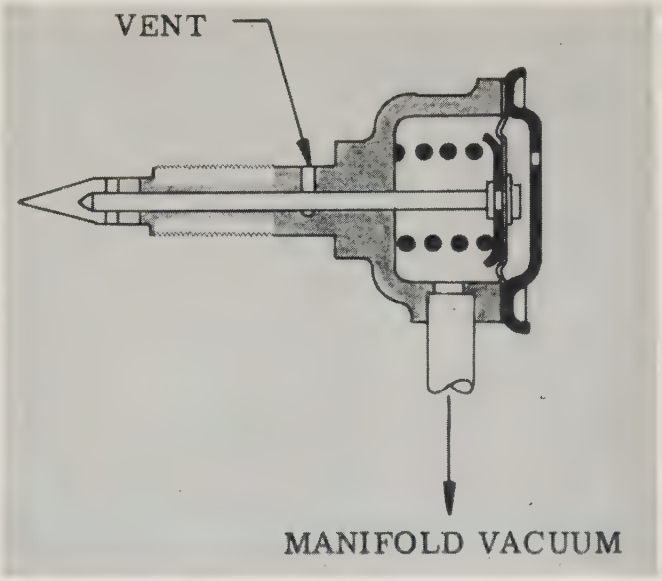

Fig. 24—Positive idle fuel shutoff combined with idle adjusting screw

have also been under consideration (Fig. 24). The ease with which this device could replace the original adjusting screw on some carburetors made it very attractive. The major problems encountered with this device were:

1. Incomplete fuel shutoff. If the idle discharge hole is closed, in most carburetors some fuel will flow from the idle transfer holes.
2. Possible misalignment of valve and seat.
3. Problem of maintaining idle mixture adjustment with a movable needle valve.
4. Space lack on new design, low-built carburetors.

Other Methods of Shutting Off Idle Fuel Flow—1. Overtravel throttle plate. If the carburetor throttle plate could be rotated further in the closed direction from its normally closed position such that the idle feed ports would be completely exposed to atmosphere, all idle fuel flow would be effectively stopped (Fig. 25). During deceleration a vacuum-operated throttle stop would be retracted to allow the throttle plate to move past the idle discharge hole. At manifold vacuums below 21 in. of Hg the throttle stop would not retract and would position the throttle plate in the normal idle position. With this arrangement, however, the car accelerator pedal has free travel in the closed throttle position prior to actual opening of the throttle. This combined with the tendency of the fully closed throttle to stick gave unsatisfactory driving feel.

2. Back suction method. Flowstand tests were made to determine whether the application of vacuum to the carburetor float bowl would effectively shut off the idle fuel by overcoming the pressure differential causing fuel to flow (Fig. 26). The necessary back suction was found quite critical in that it caused violent bubbling in the float bowl; also, in some carburetors, slightly increased vacuum would cause fuel flow to resume.

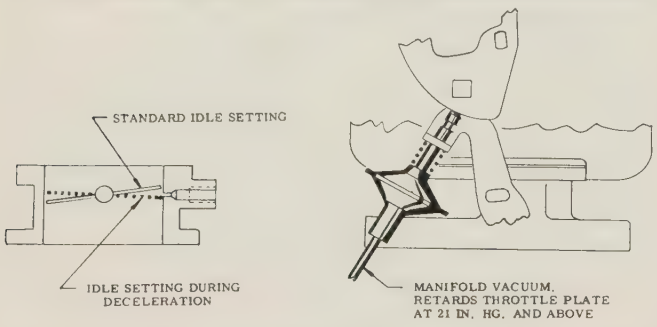

Fig. 25—Idle fuel cutoff during deceleration by override throttle plate

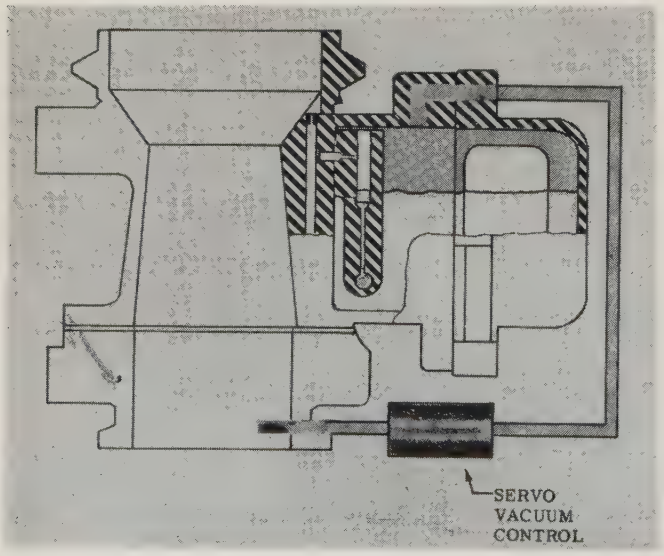

Fig. 26—Back suction method of idle fuel cutoff during deceleration

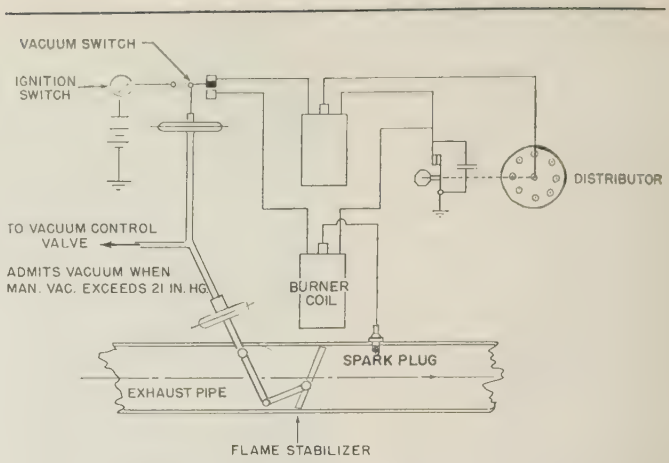

Fig. 27—Wiring diagram of ignition cutoff burner

In summary, promising hydrocarbon reductions were obtained with many idle fuel shutoff devices tested during decelerations from road speeds in the 50-mph range. Less promising results were obtained with short decelerations from 35 mph or less. Since more recent traffic surveys have indicated that the lower speed and shorter duration decelerations are the more common, this basic device approach has been de-emphasized in preference to others which are more effective at lower speeds.

Of the idle shutoff devices, the air-bleed type was the most favored mainly due to the fact that the device itself did not have to be located directly in the idle system passages. Its effectiveness and tendency to introduce driveability problems, like all of the idle shutoff devices tested, varied widely depending upon carburetor design, installation, engine, and car used. Even with the flexibility of location provided by the air-bleed type device, no simple universal method of adapting such a device to the multitude of of carburetor makes and models now on the road or being produced has been conceived. Major redesign is required for incorporation of such devices on even future model carburetors, considering the increasing use of multibore multiple-idle systems and trends toward extremely low compact designs.

Ignition Cutoff Burner[6]

In July, 1956, work was started on a new device called the ignition cutoff burner. As the name implies, the ignition was interrupted during deceleration and a spark in the exhaust pipe was fired. The purpose of this device was to eliminate residual gas dilution problem existing in the engine. It was hoped that during deceleration, combustion in the exhaust pipe would be more complete than combustion in the engine cylinders (Fig. 27).

In tests on three different makes of cars, the reduction for decelerations from 50 to 10 mph was 0–80%; from 30 to 10 mph, the reduction was up to 45%. However, there was some noise associated with

[6] Also reported in: "Automobile Exhaust Gas Treatment—An Industry Report," by G. J. Nebel, et. al. Paper presented at SAE National West Coast Meeting, Seattle, Aug. 16, 1957.

the operation of the device that was obviously caused by explosions of accumulated fuel-air mixture in the exhaust pipe and muffler. While these explosions apparently did a good job of burning up the fuel, the noise was not acceptable.

It was expected that a flame stabilizer, which would anchor the flame to a fixed point in the exhaust pipe, would eliminate the cyclic burning process and also the noise associated with it. Accordingly, efforts were made to achieve this end. But, it was found that the environment in the exhaust system was not favorable for steady burning. All attempts to obtain continuous burning failed.

Another consideration, entirely apart from the failure to perfect the device, prompted its abandonment: The fact that no economical means was known to make the device fail-safe. It was feared that malfunctioning of the igniter or other parts could cause destructive explosions in the muffler.

Other Devices

In the design and experimental development of any device, there are usually many requirements that the device must meet to be satisfactory for application to a vehicle. For example, the device might have good capability of hydrocarbon reduction but be unsatisfactory with respect to driveability of the vehicle. Also, it may become a driving safety hazard because of some peculiarity of its operation. It may require additional vehicle braking means. It may by its nature be a difficult device to service properly and, in the case of a device for hydrocarbon emission purposes, to police and enforce properly. A very major limitation in designing any device is the requirement that it must be adaptable to existing vehicles in service. At times during this development, this limitation existed but overall it has not hampered the various developments to any appreciable extent. Any device can be only as good as its ability to meet the overall requirements of its application.

Sandwich Butterfly Valve Fuel Cutoff Device—system consists of or employs four units in its operation (Figs. 28 and 29):

1. A vacuum-actuated diaphragm arrangement controlling an auxiliary butterfly, which is built into a sandwich flange located between the carburetor and the engine intake manifold. The unit is adjusted to close the auxiliary butterfly above 21 in. of Hg manifold vacuum and fully open below 21 in. manifold vacuum. This unit has an operating hysteresis of about 1½ in. of Hg.

2. Double-throw, single-pole throttle switch, actuated by the carburetor throttle lever at the time the throttle reaches the curb idle position. It is adjustable and set to operate in the last 2 deg (approximately) of throttle travel.

3. Solenoid valve, normally open, used as a quick air bleed to the vacuum diaphragm which operates the auxiliary sandwich butterfly.

4. Voltage regulator of generator with reverse current relay set to operate at about 150 rpm above normal curb idle speed.

In operation, the vacuum diaphragm is preset to close the auxiliary sandwich throttle at manifold vacuum values above 21 in. of Hg and to be fully open at values below 21 in. of Hg. Thus, during a drift-down against closed throttle at road speeds above approximately 12 mph, the auxiliary throttle is tightly closed, cutting off all airflow and consequently all fuel flow.

In road operation, two conditions of operation must be taken care of to make a driveable unit from the device as described. One is the ability to resume operation from a point in drift down prior to 12 mph or the 21 in. manifold vacuum operating point of the vacuum diaphragm. This is accomplished through the throttle switch and solenoid valve. Moving the throttle from its idle position actuates the throttle switch, de-energizing the solenoid. This bleeds air into the vacuum diaphragm, which in turn quickly opens the auxiliary butterfly. The new carburetor throttle position sets up a vacuum in the manifold below 21 in. of Hg; consequently, the auxiliary sandwich butterfly remains open and normal car operation is resumed.

The second special condition that causes engine stalling unless anticipated is the situation in which the engine is accelerated in neutral and then let drift down against the closed throttle to its normal curb idle. Without a quick air bleed to the actuating diaphragm, its operation is too slow, resulting in the engine arriving at its normal idle speed with the auxiliary butterfly still closed. The result is engine stalling. To overcome this, an electrical signal is picked up from the generator at the reverse current relay when set approximately 150 rpm above normal idle speed. This signal de-energizes the solenoid valve, bleeding air to the vacuum diaphragm and opening the auxiliary throttle.

The alternate to using the generator as a means of obtaining an engine speed signal would be to drive a separate mechanical governor that would make or break the electrical circuit to the solenoid valve at the desired time.

Vacuum Form of Sandwich Thottle Device—This device was designed, built, and tested in several

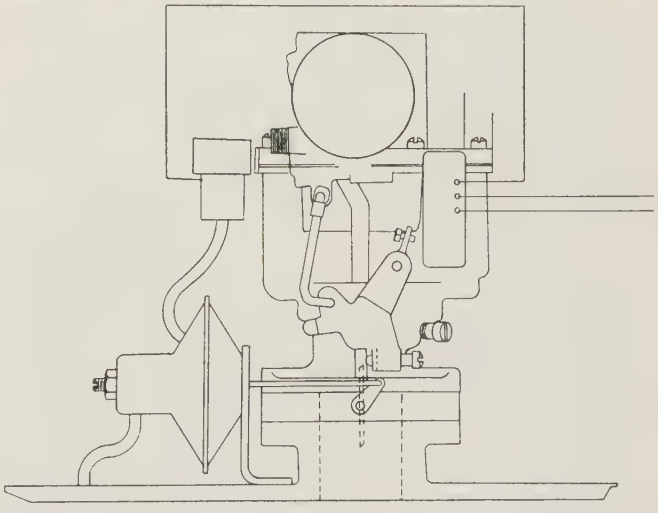

Fig. 28—Sandwich butterfly valve fuel cutoff device

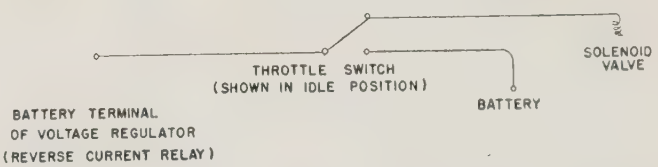

Fig. 29—Wiring diagram of sandwich butterfly valve fuel cutoff device

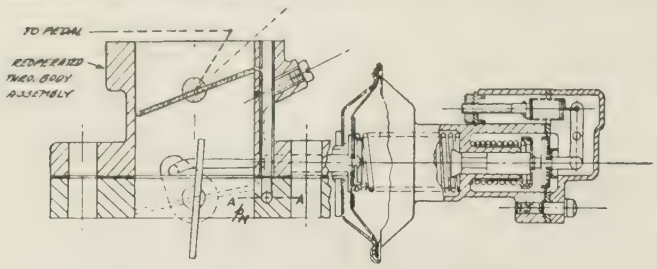

Fig. 30—Vacuum form of sandwich throttle device

forms. Basically, it is a pilot valve actuated by manifold vacuum to act upon a power diaphragm, and is located between the carburetor and the intake manifold. The latter positions a throttle valve posterior to the regular carburetor throttle to close off tightly the air and fuel flow into the intake manifold when the normal manifold vacuum is higher than a predetermined set value. (See Fig. 30.)

These various auxiliary butterfly throttle arrangements were considered impractical because of the inability to shut off airflow completely by any type of standard throttle control means. At this high value of pressure drop, an air leak as low as 0.005 lb per min will completely scavenge a normal size of intake manifold in 1.18 sec. Thus, during this period any fuel already in the manifold will gradually be drawn into the cylinders of the engine (in a state too lean to burn) and thus 100% of this fuel will emerge from the engine as a hydrocarbon emission to atmosphere. Depending upon the type and characteristics of the intake manifold and of the engine, reduction in hydrocarbon emission as high as 79% (grab sampling methods) were obtained. However, for most engines the percentage reductions would be considerably less. Because of the complication of the structure and general low effectiveness, work on this type of device was discontinued.

Air and Fuel Regulator with Fuel Augmentation—This device bypasses the normal carburetor throttle and provides an additional air supply with a predetermined amount of fuel added to promote good burning during the deceleration cycle.

This type of regulator controls air and fuel individually to some desired value in about the same manner as the later developed vacuum-controlled throttle opener type of device. Efforts along this line were discontinued in favor of the throttle-opener type of device.

Idle Fuel Shutoff by Manifold Vacuum Means and Idle Fuel Delivery Directly at Engine Ports—In various fuel cutoff devices, considerable difficulty was encountered in recovery of the system sufficiently fast to prevent unstable transient engine operation when the system returned to normal operation following a deceleration. As a potential means of preventing this, it was believed that better performance might be obtained if the engine received a nonreversing idle flow directly at the engine ports.

However, the engine with this system had poor idling, so this approach was discontinued.

Extra Electrical Energy Ignition System to Burn Fuel During High Vacuum Engine Operation—Increased electrical energy did not promote better burning, so development of this device was discontinued.

Device to Change Ignition Advance During Vehicle Deceleration—Optimum spark advance during deceleration (about 30-deg btdc) produced slight reductions in hydrocarbon emission on a vehicle during road test, but the improvement was not significant enough to warrant the necessary complication.

Carburetor-Poppet Device in Carburetor-Throttle Valve—This type of device was designed, built, and tested in a number of variations and consisted of a poppet type of valve located directly in the carburetor-throttle valve. The poppet valve was spring-loaded and set to open when manifold vacuum exceeded a predetermined value. When the valve opened, manifold vacuum was reduced because of additional airflow into the engine, and fuel flow was increased but to a lesser extent, resulting in an increased air-fuel ratio.

This type of device is limited to carburetors having a special type of idle system and it was found that the poppet-valve principle would not apply to the majority of carburetors being made, which led to discontinuance of this approach.

Effect of Closing Off the Exhaust System on Idle Fuel Flow—A proposal was made to stop the flow of idle fuel by having a valve in the exhaust pipe completely shut off the exhaust system during the coast period. It was theorized that this would stop practically all airflow through the engine, reduce the intake manifold vacuum to a low level, and thereby stop fuel flow from the carburetor.

Tests indicated that with the exhaust completely shut off, the high back pressure produced so much leakage past the exhaust valve guides, piston rings, and other parts of the system that a fairly high airflow still existed. Since this air with the large amount of fuel would be expelled through the crankcase vents or other openings, no effective hydrocarbon reduction was obtained by this method.

Intake Manifold, Air-Bleed Device—The effect of intake manifold vacuum on hydrocarbon emission has been previously discussed and is shown in Fig. 2. The effectiveness of combustion-chamber burning depreciates rapidly in terms of unburned hydrocarbon emission when the intake manifold exceeds 21 in. of Hg depression.

From this it was reasoned that if manifold vacuum could be maintained at values less than the above, better combustion and a lesser percentage of unburned hydrocarbons would result.

A device of this type appeared to be impractical and was discontinued for two reasons:

1. To reduce manifold vacuum to less than ½ in. of Hg, which is required to stop idle flow at closed throttle, very large openings in the intake manifold are necessary. A simple valve cannot do this because the signal required to actuate the valve opening is destroyed by the action of the valve when it opens. A mechanism actuated by some independent signal arrangement, such as engine rpm and throttle position, would be required. However, the overall result of this type of device is to sweep unburned fuel into the combustion chambers in a condition too lean to burn and thus 100% of this amount of fuel emerges as unburned.

2. If manifold vacuum is partially reduced, the amount of air added to the intake manifold will always be too great, such that the air-fuel ratio will be too lean to burn and 100% of the fuel charge will emerge unburned.

TRUCK PERFORMANCE —

Computed versus Measured Data

A. F. Stamm, Chrysler Corp.

This paper was presented at the SAE Annual Meeting, Detroit, Jan. 17, 1958.

THE purpose of TR-82[1] is to provide a method of estimating those phases of truck ability performance dealing with the relation between vehicle resistance and engine horsepower. With the aid of the forms, tables, and charts contained in that report, it is possible to calculate solutions to problems pertaining to speed, grade ability, and acceleration from readily available specification data and with the minimum amount of effort.

Fundamental to every application discussed in that report is the equation expressing the difference between net engine horsepower and the sum of the power absorbed by rolling resistance, air resistance, and chassis friction as available for grade climbing and/or acceleration. Since it is impossible to solve any ability problem without knowledge of vehicle resistance, TR-82 includes what is believed to be the best data presently available, but also cautions that results from a computed performance sometimes differ appreciably from the actual performance.

Several examples are contained in TR-82 showing good agreement when the actual road performance is compared with computed performance. Only the end result is given, which is sufficient for the purpose of verification, but measured grade ability by itself does not furnish sufficient data to permit a study of the individual vehicle resistance components. Test results allowing a separation of the various resistances should be of considerable interest.

This paper deals with some recent test data which, unfortunately, could not be broken down without first making certain assumptions. Moreover, all three of the variables considered could not be segregated from the data available for any one vehicle. Test information for four vehicles was selected and, as far as possible, compared with results computed from TR-82.

In all computations some uncertainty existed as to the actual net engine horsepower, as this was not contained in the reports on the individual vehicles. What appeared to be the most appropriate curves of advertised net certified horsepower were used. A further, rather unsuccessful effort also was made to derive the best possible generalized expressions for resistances for this group of test vehicles. These also were used to compute ability perform-

THIS paper outlines tests made to verify the SAE recommended practice for estimating truck ability performance described in TR-82.

The author has collected data on four vehicles and compares it with the results computed in TR-82 and with a Method X. The data includes information on air and rolling resistance, effect of wind velocity, chassis friction power, grade ability, and the like.

The author concludes that the SAE method of TR-82 is at the present time the most reliable method for computing truck ability.

[1] SAE Technical Report 82, August, 1957, "Truck Ability Prediction Procedure."

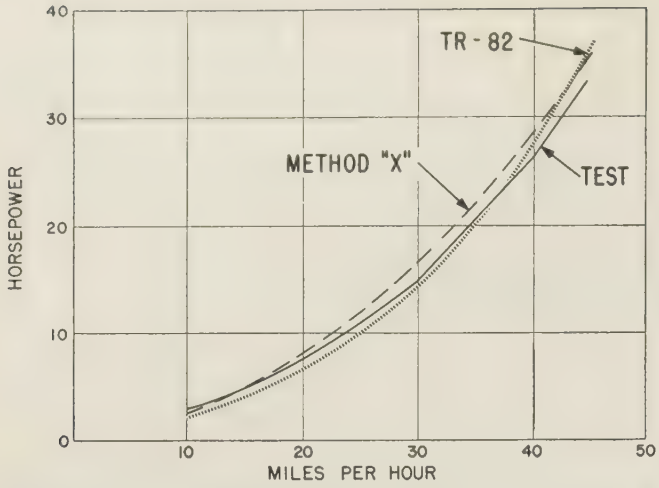

Fig. 1—Sum of air and rolling resistance hp, vehicle A tractor of 8433 lb (gross weight)

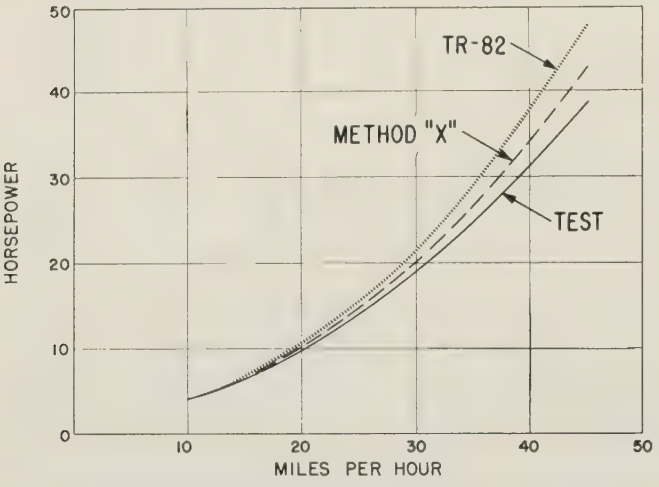

Fig. 2—Sum of air and rolling resistance hp, vehicle A tractor weighted to 16,163 lb (gross weight)

Table 1—Sum of Air and Rolling Resistance Horsepower, Vehicle A

Speed, mph	Tractor only, 8433 lb			Tractor only, 16,163 lb			Combination, 16,163 lb			Combination, 34,016 lb		
	Test	TR-82	Method X	Test	TR-82	Method X	Test	TR-82	Method X	Test	TR-82	Method X
10	2.7	2.2	2.5	3.7	3.9	3.8	4.4	3.9	4.1	8.0	8.0	7.2
15	4.8	3.9	4.9	6.7	6.7	6.8	8.2	6.7	7.6	13.5	13.1	11.2
20	7.5	6.4	7.9	9.8	10.3	10.5	13.1	10.3	12.5	20.0	19.2	18.6
25	10.8	9.8	11.7	13.9	14.9	15.0	19.1	14.9	18.6	27.1	26.6	26.2
30	14.8	14.3	16.4	18.5	20.7	20.3	26.3	20.7	26.1	36.2	35.4	35.3
35	20.6	20.4	22.0	24.2	28.4	26.6	36.2	28.4	36.1	47.7	46.8	46.7
40	26.9	27.6	28.4	30.9	36.8	33.7	46.7	36.8	46.1	60.3	58.1	58.2
45	34.0	36.7	36.0	39.0	47.4	41.8	60.0	47.4	58.5	75.0	72.4	72.2

ance by the procedure of TR-82 and the results are shown under a heading designated as Method X.

Vehicle A

The first truck, called vehicle A in this discussion, was subjected to four tests, each time measuring the combined rolling and air resistance over a speed range from 10 to 45 mph. (Wind effect was included and reported data are the average of two runs in opposite directions.)

The significant point in relation to these tests is that all four were made with the frontal area, as

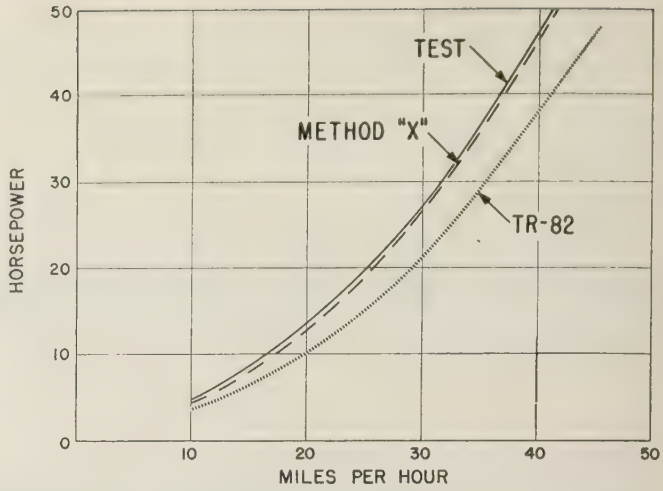

Fig. 3—Sum of air and rolling resistance hp, vehicle A tractor plus trailer of 16,163 lb (gcw)

used for air resistance computation in TR-82, unchanged. A set of test runs was made with the bobtail tractor at its normal weight of 8433 lb. The weight was then increased to 16,163 lb, corresponding to the train weight of this tractor coupled to an empty trailer, and another set of data was obtained. The tractor coupled to the empty trailer was also tested, as was the combination loaded to 34,016 lb.

Table 1 indicates the results of these tests with corresponding values computed by applying TR-82 and also by Method X, using resistance equations derived from the test data for all four vehicles investigated. Three curves result for each of the four cases as plotted in Figs. 1–4. There appears to be good agreement of the test data for the bobtail tractor at 8433 lb and loaded combination at 34,016 lb, with results computed by both TR-82 and Method X. With the tractor loaded to 16,163 lb, TR-82 tends to give a higher value of resistance, as the speed increases, than was observed. Although there is some improvement for Method X, the same trend exists. At a combination weight of 16,163 lb, representing the empty trailer coupled to the tractor, TR-82 does not give enough resistance so the condition becomes reversed. Method X is also low but to a significantly lesser degree, for it can be considered in good agreement with the test results.

An increment of rolling resistance power was separated from the data. Tests for the tractor alone and for the tractor in combination with the trailer were, in each case, conducted at two loads. The increase in resistance power observed by changing the tractor weight from 8433 to 16,163 lb, and by changing the combination weight from 16,163 to 34,016 lb, in each case was assumed to represent an increment due to greater rolling resistance only.

With the same assumption made in TR-82, namely that rolling resistance power varies directly with weight, a rolling factor was calculated for each test speed. This separation of variables was made for the tractor bobtail and the tractor-trailer combination; the results are found plotted in Fig. 5. The data for the combination gives a fairly good curve; that for the tractor is less consistent at higher speed. The best single curve for this data was judged to be given by the equation: Rolling factor = 0.017 mph. It is plotted as Method X. Rolling fac-

tor as given in TR-82 is also plotted and shows poor agreement with the test data. If the data and the method of analysis used are valid, TR-82 must give values of rolling resistance horsepower which are much too high. The correlation is much poorer than would be expected from the results of the combined resistance observed and plotted in Figs. 1–4.

Quite obviously, the air resistance horsepower calculated from TR-82 cannot agree with the test data, because combining the calculated air and rolling resistance horsepower seems to compensate to a considerable degree for the observed variation in each. With the corollary assumption that air resistance of either the tractor or the combination is unchanged when the load is varied, the air resistance power for each was determined by subtracting a rolling resistance loss as indicated by the test data, but adjusted for the two respective load conditions. Air resistance horsepower, as plotted in Figs. 6 and 7 is the result. As appears logical, although contrary to the recommendation of TR-82, air resistance horsepower of a combination is considerably greater than for the bobtail tractor, even though the frontal area was not increased by adding the trailer. In both cases the deduced air resistance power is greater than TR-82 indicates. It is also impossible to fit a third degree equation to either of the curves. Equations for approximate curves drawn for the test data are shown as Method X on Figs. 6 and 7.

Vehicle B

The second vehicle considered in this study is designated as vehicle B. It was a 2½-ton tractor-trailer combination loaded to 50,000 lb, gross combination weight (gcw). Two sets of measured test data of interest here were recorded: excess drawbar pull (dbp) and the combined rolling and air resistance. Excess drawbar pull is readily converted into an equivalent test grade ability. TR-82 was applied to find the calculated grade ability. Method X grade ability was also calculated from the derived resistance equations. All results are shown in Table 2. Method X appears to be in better agreement with the test grade ability than TR-82. The absolute grade ability error by TR-82 is greatest in the lowest gear, amounting to over 2%, decreasing as faster transmission speeds are used until in direct (sixth) gear the error is about one-fifth of 1%. If the correlation is checked on the basis of percentage deviation from the test result, TR-82 is roughly equally accurate in all gears with the deviation being around 20%. TR-82 gave a higher value of

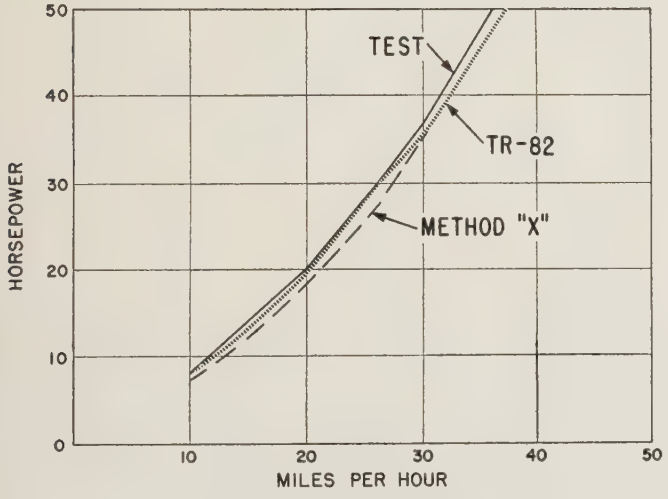

Fig. 4—Sum of air and rolling resistance hp, vehicle A tractor plus trailer weighted to 34,016 lb (gcw)

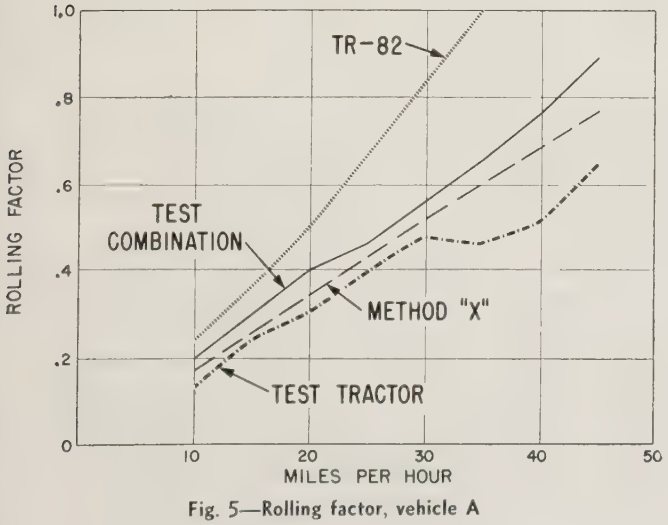

Fig. 5—Rolling factor, vehicle A

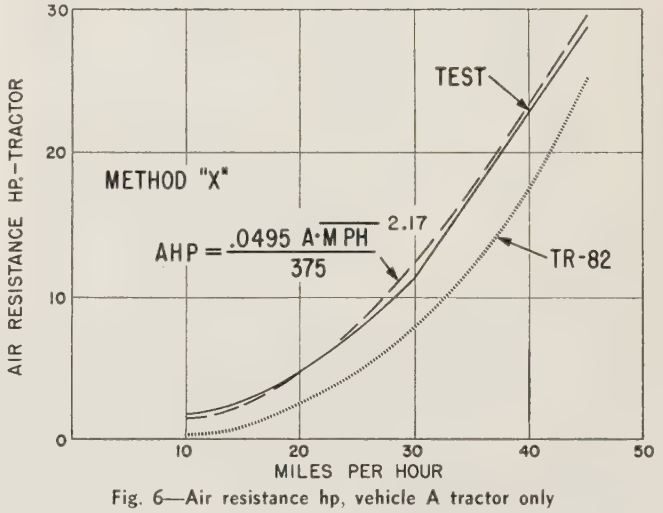

Fig. 6—Air resistance hp, vehicle A tractor only

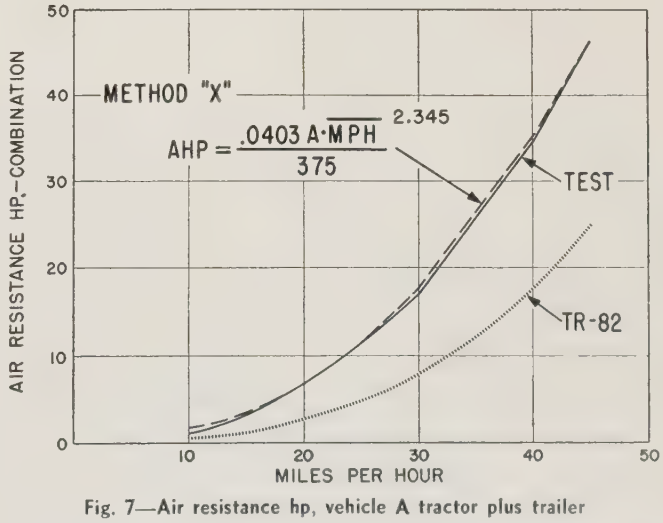

Fig. 7—Air resistance hp, vehicle A tractor plus trailer

grade ability for this vehicle than was observed from the tests.

Excess drawbar pull can also be converted into what is described in TR-82 as reserve horsepower. This, subtracted from the net engine power taken from the curve, results in the test level road horsepower. The sum of rolling and air resistance power was determined from measured data contained in the test report for vehicle B. Taking this from the test level road horsepower resulted in chassis friction horsepower. These three sets of data are to be found in Table 3, which contains determinations of friction horsepower as found from test data, by calculation according to TR-82, and by applying Method X. This is tabulated for the various transmission gears and road speeds used in testing.

Chassis friction horsepower is plotted in Fig. 8. The test results show a much higher chassis friction power than given by the equation in TR-82. Additional data on friction power loss was obtained from the tests on vehicle C, which was also considered in drawing the curve labeled Method X. Vehicle B gave three points in direct gear which might indicate a lower power loss in direct than in lower gear. This trend was not noted for vehicle C and it appears impossible to draw a definite conclusion. Caution is further indicated by noting an apparently out-of-line point in fourth gear. There does seem to be an approximately linear relation between engine rpm and chassis friction power which is independent of road speed. On the other hand, the data are totally inadequate to attempt any correlation of the relation implied in TR-82 between gvw rating and chassis friction. The sum of rolling and air resistance was determined independently of other variables for vehicle B. Results are plotted in Fig. 9, and show a remarkable agreement with calculations made by TR-82. Method X suffers in this comparison, giving values which are too low. It should be noted that vehicle B was operated as a combination and the correlation for air plus roll-

Table 2—Comparison of Grade Ability, Vehicle B

Gear	Mph	Rpm	Net Hp	Excess Dbp	Grade (Test), %	Grade (TR-82), %	Grade X, %
1	6	2020	116	5075	10.1	12.4	10.6
	10	3360	174	4450	8.9	10.9	9.1
	12	4040	188	3875	7.8	9.6	7.9
2	10	2420	140	3525	7.1	8.7	7.5
	12	2900	162	3325	6.7	8.3	7.1
	14	3390	175	3025	6.1	7.6	6.3
	16	3870	185	2625	5.2	6.8	5.6
3	14	2390	139	2325	4.6	5.9	5.0
	17	2905	162	2175	4.3	5.5	4.7
	20	3420	176	2025	4.0	4.9	4.1
	22	3760	183	1775	3.5	4.5	3.7
4	20	2460	142	1525	3.0	3.8	3.3
	25	3070	167	1325	2.6	3.4	2.9
	30	3690	182	1100	2.2	2.9	2.3
	32	3930	186	975	1.9	2.6	2.1
5	30	2650	152	950	1.9	2.3	1.9
	35	3090	168	825	1.6	1.9	1.6
	40	3530	178	650	1.3	1.6	1.2
6	45	2850	160	325	0.65	0.85	0.66
	50	3175	170	175	0.35	0.59	0.43

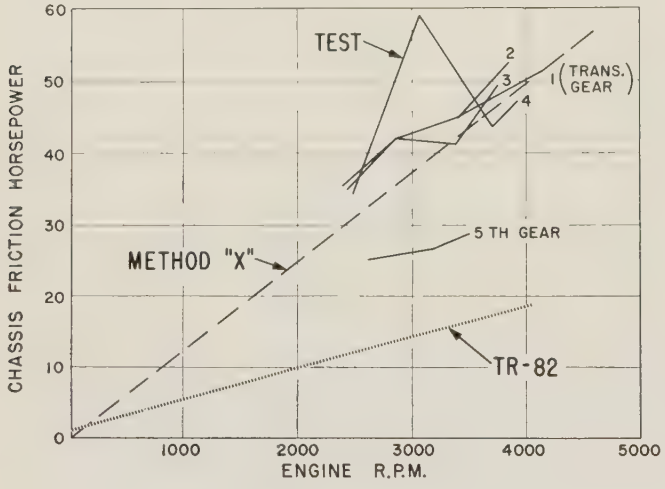

Fig. 8—Chassis friction hp, vehicle B

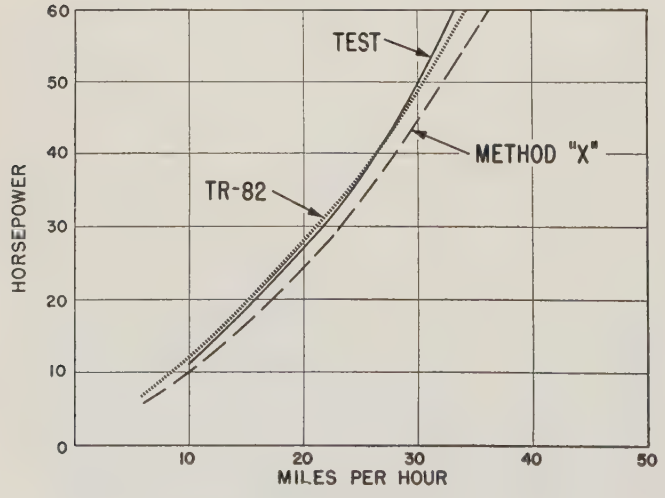

Fig. 9—Sum of air and rolling resistance hp, vehicle B

Table 3—Resistance Horsepower, Vehicle B

Gear	Mph	Rpm	Level Road Hp			Air plus Rolling Hp			Friction Hp		
			Test	TR-82	Method X	Test	TR-82	Method X	Test	TR-82	Method X
1	6	2020	34.9	16.8	30.7	—	6.5	5.5	—	10.3	25.2
	10	3360	55.3	28.1	51.9	11.0	11.7	9.9	44.3	16.4	42.0
	12	4040	64.0	34.0	62.2	13.5	14.4	11.8	50.5	19.6	50.4
2	10	2420	46.0	23.7	40.1	11.0	11.6	9.9	35.0	12.1	30.2
	12	2900	55.7	28.7	48.0	13.5	14.4	11.8	42.2	14.3	36.2
	14	3390	62.1	33.8	57.2	17.0	17.2	14.9	45.1	16.6	42.3
	16	3870	73	39.3	66.0	20.0	20.4	17.7	53	18.9	48.3
3	14	2390	52.3	29.2	44.8	17.0	17.2	14.9	35.3	12.0	29.9
	17	2905	63.5	36.4	55.6	21.2	22	19.3	42.3	14.4	36.3
	20	3420	68	43.9	66.7	26.4	27.2	24.0	41.6	16.7	42.7
	22	3760	79	49.3	74.3	30.5	31	27.3	48.5	18.3	47.0
4	20	2460	60.8	39.5	54.7	26.4	27.2	24.0	34.4	12.3	30.7
	25	3070	96.4	52.2	71.2	37.3	37.1	32.9	59.1	15.1	38.3
	30	3690	94	66.6	89.1	49.9	48.6	43.4	44.1	18.0	45.7
	32	3930	102.8	72.8	97.2	55.0	57.3	48.1	47.8	19.1	49.1
5	30	2650	76	61.8	76.5	49.9	48.6	43.4	26.1	13.2	33.1
	35	3090	90.9	77.0	94.8	64.1	61.8	56.2	26.8	15.2	38.6
	40	3530	108.6	94.5	113.2	80.2	77.3	69.1	28.4	17.2	44.1
6	45	2850	125.4	108.9	120.0	—	94.8	84.4	—	14.1	35.6
	50	3175	146.7	130.4	141.3	—	114.8	101.6	—	15.6	39.7

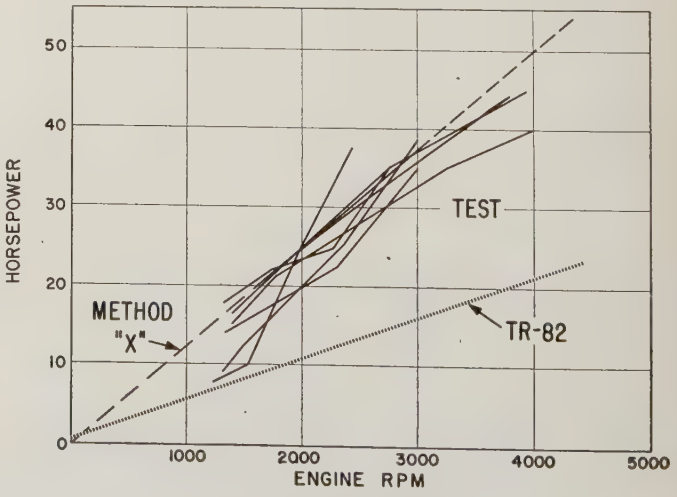

Fig. 10—Friction hp, vehicle C

Table 4—Data for Vehicle C

Gear	Axle	Mph	Rpm	Net Hp	Excess Dbp	Grade Ability			Level Road Hp			Air Hp		Rolling Hp		Friction Hp			Air plus Rolling. Hp		
						Test	TR-82	A	Test	TR-82	B	TR-82	C	TR-82	D	Test	TR-82	E	Test	TR-82	F
1	9.01	3	1715	97	9060	16.6	19.0	16.5	25	13.1	24.4	0.0	0.1	3.5	2.8	22	9.6	21.5	2.7	3.5	2.9
		5	2860	161	8640	15.8	19.0	16.3	46	21.2	40.7	0.0	0.3	5.9	4.7	41	15.3	35.7	4.7	5.9	5.0
		7	4010	187	6960	12.7	15.2	12.6	57	29.6	57.3	0.1	0.6	8.5	6.6	50	21.0	50.1	7.0	8.6	7.2
1	7.33	3	1400	76	7020	12.8	14.5	12.7	20	11.5	20.4	0.0	0.1	3.5	2.8	17	8.0	17.5	2.7	3.5	2.9
		5	2330	135	7560	13.7	15.7	13.7	34	18.5	34.1	0.0	0.3	5.9	4.7	29	12.6	29.1	4.7	5.9	5.0
		8	3730	182	6108	11.2	12.9	10.7	52	29.5	55.0	0.1	0.8	9.8	7.5	44	19.6	46.7	8.0	9.9	8.3
2	9.01	4	1320	70	4872	8.8	9.8	8.5	18	12.3	20.5	0.0	0.2	4.7	3.8	14	7.6	16.5	3.7	4.7	4.0
		7	2320	135	5358	9.7	11.1	9.6	35	21.2	36.2	0.1	0.6	8.5	6.6	28	12.6	29.0	7.0	8.6	7.2
		9	2980	164	4998	9.0	10.3	8.8	44	27.3	46.8	0.2	1.1	11.2	8.5	35	15.9	37.2	9.2	11.4	9.6
		12	3970	187	4074	7.4	8.5	7.0	57	36.7	63.0	0.5	2.1	15.4	11.3	44	20.8	49.6	12.8	15.9	13.4
3	9.01	7	1265	66	2362	4.3	4.8	4.2	22	15.9	23.0	0.1	0.6	8.5	6.6	15	7.3	15.8	7.0	8.6	7.2
		10	1810	102	2664	4.8	5.4	4.7	31	22.8	33.4	0.3	1.4	12.5	9.4	21	10.0	22.6	10.3	12.8	10.8
		14	2530	146	2752	5.0	5.5	4.7	43	32.7	47.8	0.8	3.0	18.3	13.2	28	13.6	31.6	15.2	19.1	16.2
		18	3260	172	2408	4.4	4.9	4.1	56	43.4	62.9	1.6	5.2	24.5	16.9	35	17.3	40.8	20.7	26.1	22.1
		22	3390	187	2046	3.7	4.1	3.3	67	55.0	79.2	2.9	8.6	31.1	10.7	40	21.0	49.9	27.0	34.0	29.3
4	9.01	12	1340	71	1236	2.2	2.7	2.3	31	23.6	29.6	0.5	1.6	15.4	11.3	18	7.7	16.7	12.8	15.9	12.9
		16	1790	102	1452	2.6	3.0	2.5	40	32.3	41.5	1.1	4.1	21.3	15.0	22	9.9	22.4	17.7	22.4	19.1
		20	2240	130	1530	2.8	3.0	2.6	48	42.1	53.8	2.2	7.0	27.7	18.8	24	12.2	28.0	24.0	29.9	25.8
		25	2800	159	1376	2.5	2.8	2.4	67	55.6	70.2	4.3	11.7	36.3	23.5	35	15.0	35.0	31.8	40.6	35.2
		30	3360	174	1284	2.3	2.3	1.9	71	70.7	88.1	7.4	17.9	45.5	28.2	31	17.8	42.0	40.3	52.9	46.1
		35	3910	186	966	1.7	1.9	1.5	96	87.7	108.3	11.7	26.5	55.5	32.9	45	20.5	48.9	50.7	67.2	59.4
5	9.01	15	1130	58	836	1.5	1.4	0.88	25	27.3	31.7	0.9	3.5	19.8	14.1	9	6.6	14.1	16.5	20.7	17.6
		20	1510	82	839	1.5	1.5	1.2	37	38.4	44.7	2.2	7.0	27.7	18.8	13	8.5	18.9	24.0	29.9	25.8
		30	2265	131	831	1.5	1.5	1.3	65	65.2	74.4	7.4	17.9	45.5	28.2	25	12.3	28.3	40.3	52.9	46.1
		40	3020	166	619	1.1	1.1	1.0	100	99.7	110.4	17.5	35.1	66.1	37.6	38	16.1	37.7	62.4	83.6	72.7
5	7.33	20	1230	64	595	1.1	0.42	0.78	32	37.1	41.2	2.2	7.0	27.7	18.8	8	7.2	15.4	24.0	29.9	25.8
		25	1540	84	632	1.1	0.95	0.81	42	49.3	54.5	4.3	11.7	36.3	23.5	10	8.7	19.3	31.8	40.6	35.2
		30	1840	105	564	1.0	0.95	0.81	60	63.1	69.1	7.4	17.9	45.5	28.2	20	10.2	23.0	40.3	52.9	46.1
		35	2150	125	486	0.9	0.89	0.75	80	78.9	86.3	11.7	26.5	55.5	32.9	29	11.7	26.9	50.7	67.2	59.4
		40	2460	142	402	0.7	0.77	0.66	99	96.9	103.5	17.5	35.1	66.1	37.6	37	13.3	30.8	62.4	83.6	72.7

ing horsepower is applicable to this condition only. Of course Method X gives good agreement for vehicle A for both bobtail and combination operation, but this is no proof of validity because this vehicle was the source of data for the rolling factor and air resistance equations developed. The test on vehicle B, and as will be seen later for vehicles C and D, leads to the conclusion that the results from Method X are probably no more reliable when applied to a combination for determining the sum of rolling and air resistance horsepower than is the application of the equations given in TR-82.

Vehicle C

Test data for vehicle C also permitted separation of chassis friction horsepower. A greater volume of data was available for this vehicle combination because it was equipped with a 2-speed rear axle and tests were made in seven gear selections. Results derived from these tests are: grade ability, level road horsepower, friction horsepower, and the sum of air and rolling resistance horsepower. Corresponding calculations were made according to TR-82 and Method X. All results are presented in Table 4.

Friction horsepower results are plotted in Fig. 10. Except for a few points at lower engine rpm, the friction is considerably greater than given by TR-82. Method X was adjusted to be in fair agreement with this data, although its curve falls on the high side. This is because the data for vehicle B was also considered in determining the slope of the friction equation. Vehicle C is actually in a somewhat higher gvw class than vehicle B. The generally slightly lower observed values of friction for the heavier vehicle indicate that it is not completely safe to assume a direct relation between gvw rating and friction horsepower.

The three sets of results for the sum of air and rolling resistance horsepower are plotted in Fig. 11. TR-82 gives results which are considerably high. Even though Method X gives lower values, they also are too high and cannot be considered in accurate agreement with the test result.

Fig. 12 gives the level road horsepower required for vehicle C in fifth gear, low axle range, where the results calculated from TR-82 are in almost exact agreement with the tests. However, exam-

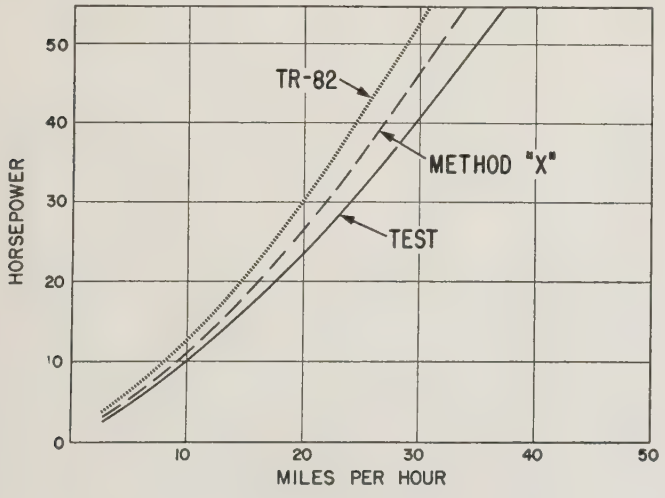

Fig. 11—Air plus rolling resistance hp, vehicle C

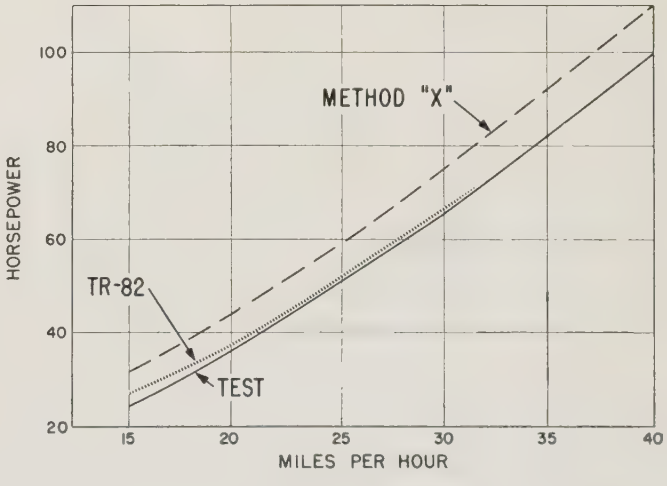

Fig. 12—Level road hp, vehicle C, fifth gear and 9.01 axle

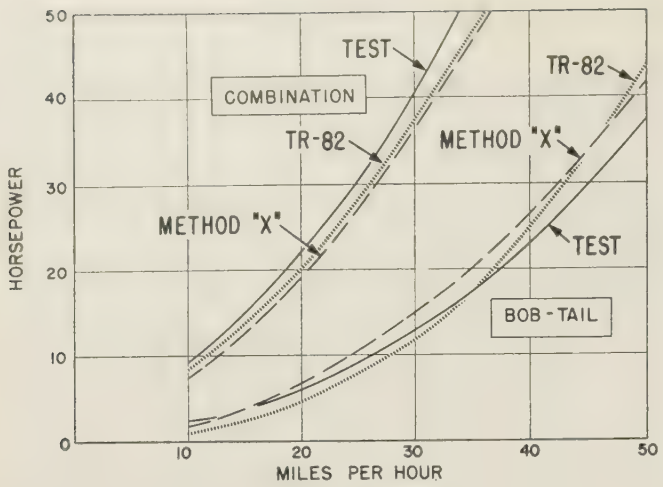

Fig. 13—Sum of air and rolling resistance hp, vehicle D

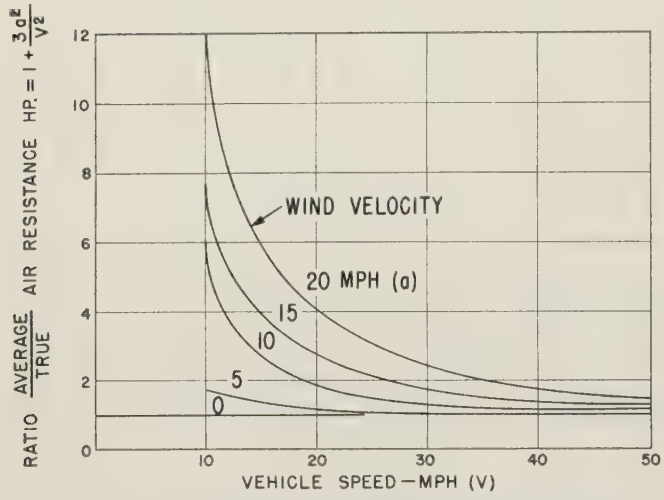

Fig. 14—Ratio of average to true air resistance hp, relative wind direction 0 and 180 deg

ination of Table 4 will reveal that there is considerably more divergence in the lower gears.

Vehicle D

Another 2½-ton tractor-trailer combination investigated is vehicle D. The data are given in Table 5. Insufficient testing was done to permit other than determination of the sum of rolling and air resistance horsepower. Fig. 13 compares results in graphical form. When operated in combination, the actual resistance measured was greater than determined by either TR-82 or Method X, with both sets of calculated data being practically identical. Results for the tractor-operated bobtail are only in rough agreement with calculations. TR-82 gives a curve crossing the test results at higher speed, but showing resistance required to increase at a higher rate than the tests. Method X gives high resistance values but there is somewhat better agreement in the general shape of the curve.

Effect of Wind

All data used in this discussion were taken from proving ground reports which state that the results given are the average of two runs in opposed directions. Three out of the four reports drawn on for information contained statements as to wind velocity and direction prevailing at the time of testing, but nothing was found about the direction of vehicle travel. In the absence of this information, it was necessary to neglect the effect of wind in making the comparisons discussed above, even though wind velocity ranged from 2½ to as much as 24½ mph.

The lower value probably had little effect, but at 24½ mph the resistance due to wind can be the governing factor in the air resistance, particularly at lower vehicle speeds, and at higher vehicle speeds this wind velocity is in the order of one half the road speed—certainly not negligible. Even though the analysis of test data made above seems in contradiction, air resistance horsepower varies as the cube of the speed. With a possible air speed of 1½ times the vehicle speed of 40 mph, the air horsepower would be high by a factor of about 3-1/3. In order for the effect of wind to be truly negligible, the ratio of vehicle to wind velocity must be a large number.

Finding that air resistance appeared to vary at a rate lower than the cube of the speed and that its magnitude was also considerably higher than expected raised two questions, namely: (1) Do averaging runs in two directions actually cancel out the effect of wind, assuming that it remains constant throughout both runs, and (2) how can such an average result be expected to compare with that which would be obtained in still air?

According to TR-82 ambient wind influences the air resistance horsepower because the effective air speed is different from the vehicle speed except when the wind direction is at 90 deg to the direction of vehicle motion.[2] With this exception, the effective speed may be greater or less than the vehicle speed. The two velocities and their relative directional orientation also produce an angle of yaw, changing the magnitude of the air resistance coefficient; this is true even when the wind direction is 90 deg and the resulting effective speed is equal to the vehicle speed. With the wind head on at 0 deg (or following at 180 deg), the angle of yaw is 0 deg, but the effective air speed is a maximum (or a minimum), being the sum (or difference) of the vehicle speed and wind velocity. As the angle of yaw increases from 0 to about 25 deg the air resistance coefficient may increase appreciably unless the vehicle is well-streamlined. With still further increases in yaw angle the coefficient decreases, going through zero and finally becoming negative.

Take, for example, the simplest case where the yaw angle is zero. The test runs are made respectively directly into the wind, that is at 0 deg relative the wind and then down wind at 180 deg. For the two cases the relative air speed will be $(V+a)$ and $(V-a)$, where V is the vehicle speed and a the air speed. The average of $(V+a)$ and $(V-a)$ is equal to V. This does not mean that the effect of wind has been cancelled because air resistance horsepower varies as the cube of the speed. It is true that the average relative velocity between vehicle and air is V, but the average air resistance horsepower is proportional to:

$$\frac{(V+a)^3+(V-a)^3}{2} = V^3 + 3\,V\,a^2 \qquad (1)$$

[2] Ibid., p. 63.

Table 5—Sum of Air plus Rolling Resistance, Vehicle D

Mhp	Combination, 35,350 lb gcw				Bobtail, 5590 lb gvw			
	Air plus Rolling Resistance lb (Test)	Air plus Rolling Resistance Hp			Air plus Rolling Resistance lb (Test)	Air plus Rolling Resistance Hp		
		Test	TR-82	Method X		Test	TR-82	Method X
10	339	9.0	8.3	7.4	82	2.2	1.6	2.0
15	382	15.3	13.6	12.5	102	4.1	2.9	4.1
20	415	22.1	19.9	19.0	116	6.2	5.0	6.9
25	456	30.4	27.5	26.7	135	9.0	8.0	10.5
30	510	40.8	36.5	35.9	164	13.1	12.0	15.0
35	561	52.4	47.1	47.5	186	17.4	17.3	20.3
40	617	65.8	59.7	59.1	213	22.7	24.2	26.5
45	—	—	—	—	242	29.0	32.7	33.6
50	—	—	—	—	280	37.3	43.3	41.5

The ratio of the average air resistance horsepower measured in this manner to the air resistance horsepower which would be observed if there were no wind is equal to $1+\frac{3a^2}{V^2}$. This shows quite clearly that the effect of wind cannot be cancelled by two runs in opposite direction. Also, the results of the average will be higher than the true air resistance and the average will increase at a rate which is less than the cube of the speed. All these conclusions seem to be reflected in the test results shown in Figs. 6 and 7. The relation just derived is plotted for several wind velocities in Fig. 14. From this it is evident that a large ratio between vehicle and wind speed must exist if reasonably accurate data for air resistance are desired. For the inherent error of the average to be less than 10% the wind velocity cannot exceed 5 mph; neither may the vehicle speed be below 30 mph.

TR-82 also contains some information about the effect of yaw on the air resistance coefficient. In order to obtain a better understanding of this and at the same time see if it would further confirm the deviation observed, a hypothetical analysis of relative air resistance horsepower was made for three wind directions. Wind speed was taken constant at 10 mph while vehicle speed varied from 10–50 mph. Figs. 15 and 16 summarize the results in graphical form. Case A is for the wind "on the beam" (at 90 deg). The lower of the two curves is the same for all three cases and is replotted in B and C. It is the actual still air resistance horsepower calculated as $HP_xF = 0.002\ V^3$. Factor F is the same throughout, including effective area and dimensional conversions. It is clear that in case A a beam wind results in increasing the air resistance horsepower. The curve is somewhat flatter and does not change for either direction of vehicle operation. Also, the average of the two runs is equal to the horsepower observed for either direction of operation. (Effective air speed is the same as the vehicle speed but the angle of yaw decreases with speed, causing the air resistance coefficient to drop in value. Consequently, the average observed air resistance horsepower increases at a lesser rate than the cube of the speed.)

Case B is the second example, where the two runs are into the wind and then down wind at 180 deg. With a tail wind the measured power is greatly decreased and conversely, when heading into the wind, air resistance increases. Yaw angle is, of course, zero for both directions. The average of the two runs gives an air resistance power which is higher than the still air reference curve.

The last analysis made is shown as case C. The wind is assumed at 45 deg in one direction of operation. This becomes a following wind at 135 deg when the travel direction is reversed. Only a small reduction in horsepower is noted for the following wind, but the increase is quite large with the heading at 45 deg relative to the wind. Averaging the two runs gives a curve considerably higher than the still air reference. Although it may not be readily apparent from an inspection of the curves, the values of average air resistance do not follow the third power law accurately at low to moderate speeds.

With the wind at 90 deg, the departure results from a change in the resistance coefficient as the angle of yaw varies. In case B the coefficient remains constant but the error of the average at lower speeds is quite large as explained earlier. The error for the average of case C is influenced by both considerations. Thus, the averaging of air resistance tests in the presence of wind introduces errors of two kinds, the result is too high and the exponent appears less than its true value.

Conclusions

While the analysis of the tests data for the four vehicles just reviewed entailed the expenditure of

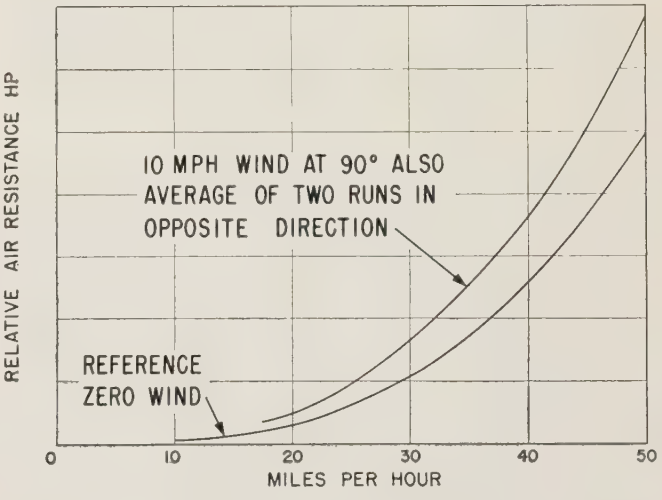

Fig. 15—Calculated effect of wind on air resistance hp, case A

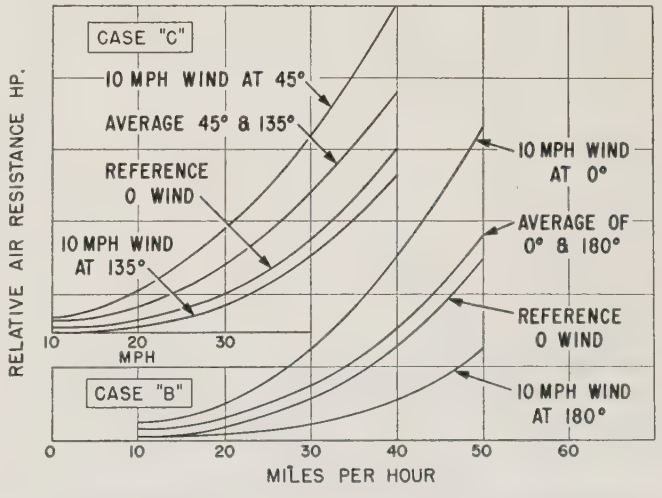

Fig. 16—Calculated effect of wind on air resistance hp, cases B and C

some effort and considerable time, the conclusions can be stated quite briefly.

1. A valid separation of air and rolling resistance was not accomplished.
2. The effect of wind velocity and direction on air resistance may be significant.
3. Averaging runs in opposite directions does not cancel the effect of wind.
4. Chassis friction power appears to be roughly related to engine rpm.
5. Grade ability calculated from TR-82 was generally higher than determined from the test data.
6. Even though deviations in the order of 20% (tolerance, not grade) were noted between observed and calculated performance, this by no means indicates that all this error is inherent in TR-82.
7. TR-82 remains the most reliable method available for computing truck ability.

DISCUSSION

Emphasizes Correlation Between TR-82 and Measured Data

—M. C. Horine
Mack Trucks, Inc

MR. STAMM has again made a real contribution to the art of performance prediction; but it will require more actual testing of vehicles to warrant positive conclusions.

Despite numerous instances in which Mr. Stamm's full-scale tests showed considerable divergence from the predictions obtained from TR-82, it is encouraging to those of us who fathered the procedure that close correlation is conspicuous in Figs. 1, 2, 4, 9, 11, 12, and 13. These cover the sum of air rolling resistance. That Fig. 3 appears to favor Method X would be more understandable if Mr. Stamm had explained just what Method X is.

It is certainly true, as Mr. Stamm observed, that it is difficult to separate rolling resistance from air resistance; but we are fortunate that their sum seems to be fairly well predictable by the TR-82 method. This points up the desirability of actual full-scale testing of the air resistance of commercial vehicles, for once this element is isolated the problem of evaluating rolling resistance becomes greatly simplified.

Particularly interesting is Mr. Stamm's work relative to the effect of wind upon air resistance. As shown in Fig. 16, full headwinds or tailwinds seem to add or subtract air resistance about as we have always assumed. Thus, a vehicle capable of 60 mph in still air would be able to make 40 mph against a 20-mile headwind; while with a 20-mile tailwind, it could go 80 mph.

Crosswinds, on the other hand, appear to produce erratic results, as shown in Figs. 14–16. This is not difficult to understand, however, when we consider that even at 90 deg, the wind, combined with the forward motion of the vehicle, produces an angular airflow. Such a flow will have aerodynamic effect similar to that about an airplane wing, producing a yawing effect as noted by Mr. Stamm.

Here we have two component forces combining to produce a resultant which is the vector and greater than either component. The resulting yawing effect is resisted, of course, by steering, which means that the front tires are deflected from a true rolling path, and thus produce increased friction. With the added component of the sidewind acting aerodynamically on the bulk of the vehicle, we can hardly expect a 90-deg sidewind to have a neutral effect.

Approaching the problem of chassis friction, we are faced with more serious uncertainties, though fortunately of less magnitude. Mr. Stamm's observations confirm the soundness of the TR-82 approach in that it appears that engine speed, rather than vehicle speed, is the principal coefficient.

This may be understood when we consider that modern antifriction bearings, gear design, and finish have reduced outright mechanical friction to a minimum with the efficient lubricants available today. Principal losses in transmission are, therefore, oil churning and seal friction. Unavoidably, different designs of transmissions and driving axles vary widely in these respects. Despite a great deal of laboratory testing of components, too little is known about the magnitude of these losses or how they are affected by differences in input and output speed and by temperature.

Perhaps the most serious lack of correlation appears in Mr. Stamm's results on grade ability, which is all the more surprising in view of the good correlation as regards rolling and air resistance. Grade resistance is where we have always considered ourselves on the surest ground, since it amounts to no more than a vertical lift of a known weight at a known rate. Grade ability must be in direct proportion to reserve horsepower; therefore, for its accurate determination we must know the reserve horsepower. Since this is what is left of the input net horsepower after rolling, air, and chassis friction resistance are estimated, we know only to the extent that we have correctly estimated these others.

Practical trials of grade ability do not necessarily reveal the full grade ability of the vehicle, since the potential as predicted by TR-82 is possible to produce only with a total gear reduction precisely adapted to the vehicle's gross weight and engine characteristics. Prevailing step-gear transmissions, unfortunately, do not always provide this.

Noticeable in the results obtained respecting level road horsepower, is the fact that whereas in Fig. 12 test results in high gear coincide very closely with the TR-82 predictions, in the lower gears they indicate considerably higher horsepower requirements than predicted. This leads to the conclusion that the friction losses in the lower gears are much higher than generally supposed. Without much more test data, however, this conclusion is not warranted. In many laboratory tests, the opposite has been found to be the case, namely, that the transmission losses are sometimes lower in the slower ratios than in the faster ones, particularly where the top ratio is overgeared.

It has been the experience of many of us that the performance predictions based upon TR-82 generally coincide very closely with actual performance, except at speeds in excess of 50 mph, where they tend to understate rather than exaggerate performance potentials.

Cites Data Confirming TR-82 Procedures

—Hoy Stevens
U.S. Department of Commerce,
Bureau of Public Roads

AS Mr. Stamm's paper primarily is a discussion of the TR-82 method of predicting truck ability, my comments, also, will be a discussion of some results from using the TR-82 procedures and data.

Insofar as highway freight transportation is concerned, there has been some acceptance of 400 lb per net engine hp as rule-of-thumb measure of desirable weight-horsepower ratios for practical line haul freight combinations for use on other than mountainous roads. I recently was confronted with the problem of predicting the engine requirements for a wide range of gross combination weights at some given speed on a level road at a given altitude. The TR-82 procedures can be used for such predictions, and the following data are based on these procedures.

After some trial calculations using 55 mph as a theoretical desirable maximum level road speed and after finding the horsepower requirements too high, I settled on 50 mph on level road at sea level as representing a practical performance specification for highway freight combinations. The combinations assumed were trailer combinations with van bodies 8-ft wide by 12½-ft high and with tires of a size appropriate to each rated axle loading.

Thirty-five performance problems were calculated for a

series of gross combination weights and a series of actual engines. For gross weights below 76,800 lb, the data represent a sampling of vehicles listed in manufacturers' data books. Above 76,800 lb the engines are assumed selections for the gross vehicle weights, but the engine data are from manufacturers' data books.

For each vehicle, a rear axle ratio was calculated which would give 50 mph in direct gear at manufacturers' recommended net horsepower engine speed. This calculation was to check to be sure that the rear axle ratios were within the range of available rear axle ratios. Of course, actual rear axle ratios seldom match precisely this requirement, but practically the degree of lack of match is not great because of the variety of axle ratios and transmission ratios offered by the manufacturers.

Four examples of these calculations are shown in Table A. As you can see, the TR-82 calculations predict that vehicles A and D will not run 50 mph because the level road horsepower is more than the engine net horsepower. The level road horsepower of vehicle C is nearly matched with its net horsepower, so that it probably will run 50 mph. Vehicle B has more net horsepower than the required level road horsepower. However, from some performance results reported by Carl C. Saal,[a] it appears likely that all four of these combinations would do 50 mph on a level road paved with class 1 good pavement.

Fig. A shows the calculated data of 35 trailer combinations with a range of gross combination weights from 30,000 to 130,000 lb. Each x mark shows a vehicle's net engine horsepower at the manufacturers' recommended engine speed. The dots and curve show the level road horsepowers as calculated by TR-82 for each trailer combination, using both standard and optional engines. According to TR-82, high-speed engines have greater chassis friction horsepower losses than equivalent power slower speed engines. As a result, we can get two or more different level-road horsepowers depending upon the engine selected. Where the level road horsepower is greater than the engine net horsepower, TR-82 predicts that the combination will *not* run 50 mph on level road.

Next, I computed the level road speeds for a number of these same combinations using the graphic method with Fig. 6 of TR-82. With this method, the predictions in regard to ability to run 50 mph on 0% grade were the same as were indicated by the longer calculations just described and, in addition, one obtains estimates of possible road speeds. While the authors have some reservations about the graphic method because it omits certain refinements which are discussed on page 20 of TR-82, nevertheless the series of charts beginning with Fig. 6 appear to be useful tools for the preliminary analyses of the speed capabilities of vehicles.

Fig. B shows gross weight-horsepower ratios for the two kinds of horsepower—TR-82 level road horsepower and net engine horsepower. The dots and curve show the weight-horsepower ratios based on TR-82 calculated level road horsepower for the same series of trailer combinations as was shown in Fig. 2. The x marks show the weight-horsepower ratios for standard and optional engines. Because of the scatter of these latter ratios, no attempt was made to draw a curve, but the arrangement of the x marks indicates a trend towards more pounds per horsepower as the gross weights increase. The lighter gcw combinations show weight-net-engine horsepower ratios much below 400 lb per hp.

Looking at the curve and dots showing the weight-horsepower ratios calculated from TR-82 level road horsepower, you will note the wide range from 257 lb for the 30,000 lb gross combinations to 388 lb for the 130,000 lb combination. From this viewpoint of level road horsepower, it is evident that weight-horsepower ratios are not constant across the board when we want a uniform level road speed performance. Also, if we wish to calculate the level road horsepower by TR-82 and use this horsepower in calcu-

[a] SAE *Quarterly* Transactions, Vol. 5, January, 1951, pp. 18–25: "Truck Road Performance—Actual vs. Computed," by Carl C. Saal.

Table A—TR-82 Data for 50 Mph on Level Road at Sea Level

Vehicle	A	B	C	D
1. Gross Combination Weight, lb	30,000	55,000	85,000	120,000
2. Engine Net Horsepower	126.5	184.0	235.0	283.0
3. Recommended Maximum Rpm	3600.0	2600.0	2100.0	2100.0
4. Pounds per Net Engine Hp	237.0	299.9	362.0	424.0
5. Rear Axle Ratio for 50 Mph	7.83	6.27	5.1	5.7
6. Rolling Resistance Hp	48.4	88.7	137.1	193.6
7. Air Resistance Hp	62.7	62.7	62.7	62.7
8. Chassis Friction Hp	22.4	29.6	36.6	51.4
9. Level Road Hp	133.5	181.0	236.4	307.7
10. Pounds per Level Road Hp	225.0	304.0	359.0	390.0

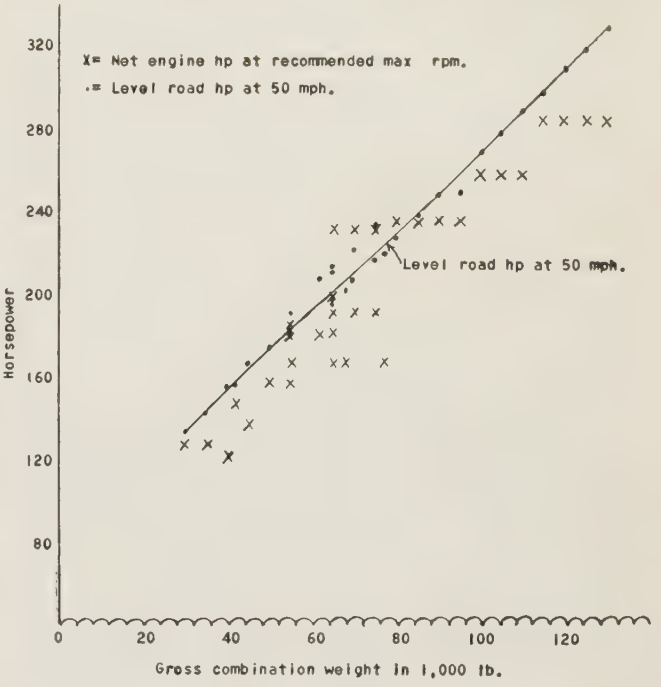

Fig. A—Comparison of TR-82 level road hp at 50 mph and net engine hp

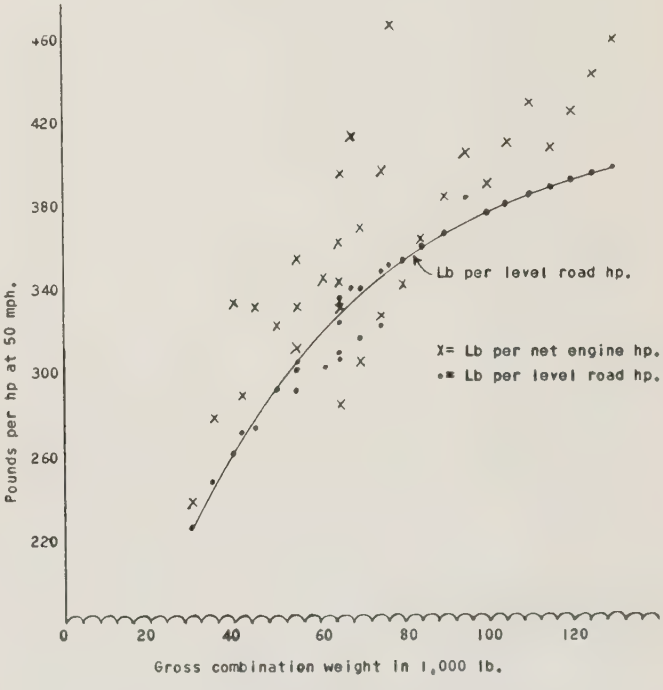

Fig. B—Weight-hp ratios at 50 mph

lating a weight-horsepower ratio, we must expect the weight-horsepower ratios to vary on the order of that shown by the curve and to be less than 400 lb per hp.

As a further commentary on the TR-82 procedures, I will report the results of actual runs on a number of van-type tractor semitrailer combinations. These field data were obtained last fall by R. L. Douglas of Eastern Express, Inc. The calculations were made by Carl C. Saal.

Table B shows the level road performance of nine diesel engine tractor-semitrailer combinations on a level stretch of the Pennsylvania Turnpike east of Bedford. Performance is reported from trips in both directions with similar models of power units but with different loads, as these runs were part of the regular freight operation. The readings were made with speedometers and tachometers.

Table B shows the gross weights, the actual road speeds, and the TR-82 calculated speed for level road. There are 15 runs with loads over 47,500 lb and three runs with loads of 46,000 lb or less. In the two cases of the 43,300- and the 40,000-lb loads, TR-82 predicts significantly faster speeds than were observed. Because these light loads do not require the horsepower to move them, it is likely that the engine governors were cutting in to control the road speed. For the 46,000-lb load the prediction was only slightly above the observed speed. Of the 15 runs with gross weights above 47,000 lb, the TR-82 speed predictions for 11 of the runs were less than the observed speeds, while in three of the runs the TR-82 predictions were higher than the observed speeds and in one run the predicted speed was the same as the observed speed.

On Table C are shown 10 runs of a similar series of diesel engine tractor-semitrailer combinations on an approximate 3% grade on the Pennsylvania Turnpike. The observed data has been corrected to 3% grade for use in this discustion. Of the 10 runs shown the TR-82 speed predictions were less than the observed speeds on eight of the runs, and were more than the observed speeds on two.

Comparing the predictions for the level road runs and the 3% grade runs it is apparent the proportion of underpredictions to overpredictions is about the same for both sets of circumstances, and the former predominate.

I agree with Mr. Stamm that the TR-82 procedure is the best prediction method now available, not alone because of its close predictions, but because its use will enable everyone using the procedures to obtain consistent results. However, judging from both my calculations and from Mr. Douglas's data it appears that the TR-82 predictions are conservative insofar as road speed performance of van tractor-semitrailers combinations are concerned. Also, when one uses the TR-82 method for level road speeds of 50 mph, one must expect that the resulting weight-horsepower ratios, using calculated level road horsepowers, will be less than 400 lb per hp.

Slight errors of underprediction are more desirable than errors of overprediction in a prediction method such as TR-82. On the basis of the few examples I have presented it appears that the contents of the last edition of the TR-82 truck ability prediction procedure are reasonably valid for van tractor-semitrailer combinations.

Table B—Actual Performance on Level Road Compared with That Predicted by TR-82

Eastbound			Westbound		
Gcw, 1000 lb	Speed, mph		Gcw, 1000 lb	Speed, mph	
	Actual	TR-82		Actual	TR-82
49.5	50.8	50.0	46.0	50.8	51.2
49.0	50.8	50.1	56.0	50.8	47.6
47.5	50.8	50.6	56.9	50.8	47.3
43.3	50.8	52.1	54.0	52.1	48.4
40.0	50.8	53.3	56.5	50.8	47.4
54.6	49.6	48.1	56.6	50.8	47.4
52.0	48.3	48.9	52.2	49.6	48.9
53.6	48.3	48.5	48.0	50.8	49.6
48.5	48.3	50.0	54.0	48.3	48.3

Table C—Actual Performance at 3% Grade Compared with that Predicted by TR-82

Gcw, 1000 lb	Speed, mph	
	Actual	TR-82
51.6	25.8	22.9
47.6	24.6	26.0
51.0	24.6	23.5
52.1	24.0	22.4
50.7	24.6	23.7
54.3	27.0	27.4
58.9	27.0	23.3
48.5	30.8	28.8
37.0	38.6	33.2
50.0	30.8	27.5

Comments on Author's Conclusions

—B. Frank Jones
White Motor Co.

FIRST, let me compliment Mr. Stamm on a very thorough and comprehensive analysis of several tests of vehicles in actual operation and his effort to correlate these tests to the computed data contained in TR-82. Having had occasion to observe the operation of vehicles in an attempt to determine their performance based on the TR-82 calculation, I can say that in my opinion the results are closely allied to the calculated figures.

With the great number of variables required to compute grade ability road speed and the number of speed changes involved as well as variations in the net and friction horsepower developed by individual engines, it is not surprising that variations in results are observed. The best answers can be obtained by averaging the factors and this results in a percentage of error that must be "lived with" until more accurate data is available.

Having had the privilege of working with the members of the Committee on TR-82 I can say that while we have come a long way toward producing an accurate measuring device still there are a great many refinements that can be added as we progress toward our goal of greater accuracy in the prediction figures.

I would like to comment on Mr. Stamm's conclusions as given at the close of his paper.

Conclusion 1—Until a greater depth of factual data on the horsepower required to overcome rolling resistance is developed the present figures can be assumed to be approximately correct. Tire tread patterns have a considerable influence on rolling resistance, tending to increase this factor. The resistance caused by brake drag and tight bearings can be considered part of the cause of increased drag horsepower. Air resistance in actual operation is a constantly variable factor which, classed as wind resistance, can materially increase the loss in effective horsepower. At the present time, therefore, Mr. Stamm's statement regarding the difficulty of separating rolling and air resistance must be accepted.

Conclusions 2 and 3—It is almost impossible to allow for the constantly variable pressure due to the gusty nature of free air in motion. Some automotive companies, in giving the top speed of a vehicle under certain load conditions, also state that this is calculated and certified in reasonably still air preferable under an air motion of less than 5 mph. On the plains the steady push of a current of air can retard the top speed of a vehicle to a marked degree, especially on a straight road where no advantages can be gained from turning away from the direct force of the wind.

Conclusion 4—An accurate chassis dynamometer can verify this fact; however, extensive tests should be engaged in to establish if possible a more accurate factor.

Conclusions 5 and 6—Although Mr. Stamm concludes that this error is not all inherent in TR-82, this is indicative of the additional work necessary to perfect our factors pointing toward an ultimate correlation between actual practice and data procedure.

Conclusion 7—The presently accepted methods of computation are a great advance over the former more or less inaccurate methods of predicting truck performance but as indicated a number of cooperative tests must be made before an absolutely satisfactory result can be attained.

BELL AVIATION
CORPORATION
RESEARCH LABORATORIES
LIBRARY

Designing with STEEL for Lighter Aircraft

Bruce Mitchell, Ryan Aeronautical Co

This paper was presented at the SAE National Aeronautical Meeting, Los Angeles, Oct. 3, 1957.

A STUDY of airplane structure with good stiffness and good elevated temperature characteristics was started at my company in the summer of 1954. A weight penalty was expected and considered justifiable in order to achieve satisfactory structure for supersonic aircraft. This study investigated honeycomb, foam, posts, and closely spaced stiffeners as means of achieving the desired rigidity.

Any one of these methods is quite satisfactory from a stiffness standpoint and the temperature limitations are easily established. However, because the weight penalty seemed to be too severe in every case, the study rapidly turned into a weight battle. If the weight is to be minimized all of the structure must be considered. All joints and attachments add weight, all nonstructural material such as glue and excessive core material add weight. For example, a single glue line is equivalent to a sheet of aluminum 0.006 in. thick.

All of these things were considered, tested, and analyzed from a weight and strength efficiency standpoint. A great deal of time and effort was spent trying to develop satisfactory resistance-welded honeycomb. We also developed a sandwich with cone-shaped posts that looked very promising. They were all discarded when we applied our criteria that the material must work to a stress near its yield point in the lightly loaded areas and carry the same basic design into the high-load structure.

Discussion

Choosing the most efficient material is not easy when you combine practical considerations with the theoretical weight advantages. We found that much of our material had to be extremely thin and that steel is the only high-strength material presently available in extremely thin sheet. Steel can be rolled into sheets as thin as 0.001 in. and still be heat-treated to develop the same high strength as before. It has exceptionally good welding and forming characteristics. Its properties at elevated temperature make it the number one material for structure in hot areas. It is relatively cheap and should be used almost exclusively for airframe construction.

One of the better steels for lightweight aircraft structure is 17-7PH. It is particularly desirable for thin sheet applications because it can be heat-treated without scaling. It is annealed at 1750 F in order to prepare it for transformation at low temperatures. The annealed material has a yield strength of 45,000 psi and elongation of 35%. It is transformed at −100 F after which it has a room temperature yield strength of 110,000 psi. The final aging treatment is given at 950 F. It then has a room temperature yield strength of 200,000 psi and an ultimate tensile strength of 240,000 psi, with elongation of 5%. In Fig. 1, this steel is compared on a strength, weight, and temperature basis with 6AL-4V titanium alloy, 75ST aluminum alloy, and HK31XA magnesium alloy. This comparison is made with compression yield as a limit because that is the major design limitation. The diagonal lines cross the vertical lines at points of equal weight.

This chart shows a required yield strength of 250,000 psi if the steel is to match the strength to weight value of the titanium at room temperature. This difference is less as the temperature increases until they are about equal at 700 F, where the steel has a yield strength of 160,000 psi. Much of the theoretical advantage of the titanium at room temperature is lost because of practical considerations. The titanium alloy is unavailable in sheets thinner than 0.025 in., it is not easily welded or formed and is initially a very expensive material.

The theoretical strength-to-weight advantage of steel over aluminum and magnesium at room temperature as well as at elevated temperatures can be a practical advantage if we use the full available strength of the steel. The room temperature yield strength of 17-7 steel is 200,000 psi which means that a piece of this steel 1 in. wide and 0.001 in. thick can carry an axial load of 200 lb. In order to

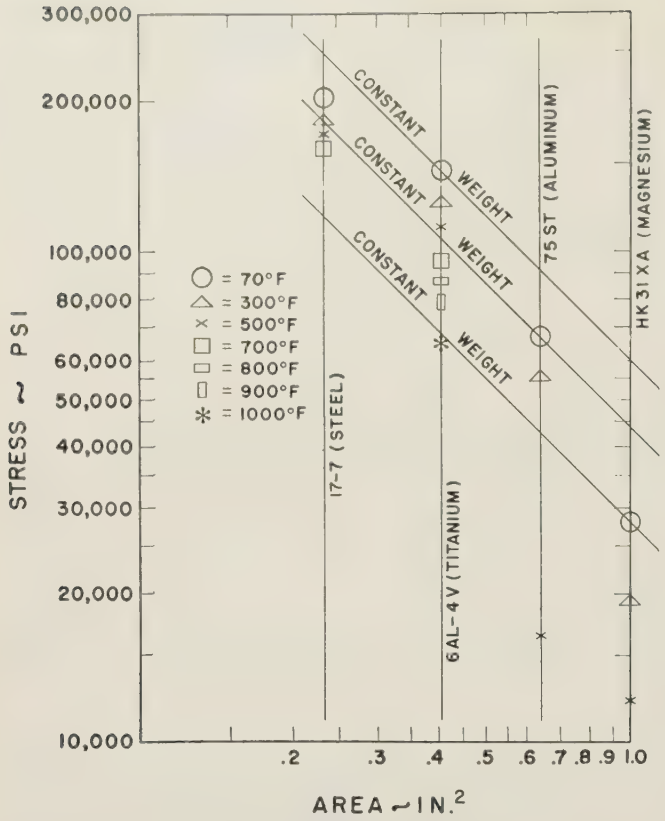

Fig. 1—Compression yield, strength-to-weight comparison chart for elevated temperatures

Table 1—Properties of Corrugations Alone

	t_c	Pitch	A per in.	I per in.	ρ	F_c (Cap)	F_c (Web)
No. 1	0.001	0.152	0.00185	0.000001508	0.0285	32,000	24,000
	0.002	0.152	0.00368	0.000002945	0.0283	128,000	100,000
	0.003	0.152	0.00548	0.000004340	0.0281	290,000	200,000
No. 2	0.001	0.227	0.00215	0.00000618	0.0536	21,000	15,000
	0.002	0.227	0.00424	0.00001221	0.0536	85,000	22,000
	0.003	0.227	0.00633	0.00001800	0.0533	191,000	50,000
	0.004	0.227	0.00840	0.00002360	0.0530	200,000	90,000
	0.005	0.227	0.01042	0.00002900	0.0527	200,000	143,000
	0.006	0.227	0.01243	0.00003415	0.0524	200,000	200,000
No. 3	0.001	0.324	0.00210	0.0000123	0.0767	17,000	2,300
	0.002	0.324	0.00419	0.0000243	0.0762	67,000	9,300
	0.003	0.324	0.00626	0.0000362	0.0760	151,000	21,000
	0.004	0.324	0.00832	0.0000477	0.0757	200,000	38,000
	0.005	0.324	0.01040	0.0000591	0.0754	200,000	60,000
	0.006	0.324	0.01240	0.0000704	0.0753	200,000	87,000
	0.007	0.324	0.01440	0.0000811	0.0750	200,000	119,000
	0.008	0.324	0.01640	0.0000916	0.0748	200,000	156,000
	0.009	0.324	0.01868	0.0001047	0.0748	200,000	199,000

exploit this high strength we must devise ways of stabilizing this sheet for compression loads of this magnitude or of collecting the load and concentrating the material until stabilization is possible.

We have found that the buckling formula:

$$F_c = KE\left(\frac{t}{b}\right)^2 \qquad (1)$$

holds true for thicknesses at least as low as 0.002 in. Fig. 2 is a plot of the allowable buckling stress of steel panels with a K factor of 3.6. This figure indicates a required stiffener spacing of 0.50 in. for 0.022 skin or 0.10 for 0.0045 skin if we wish nonbuckling at a stress of 200,000 psi. Practical considerations rule out the use of individual stiffeners that are spaced closer than $\frac{3}{8}$ in. This forced the consideration of miniature corrugations as a practical means of obtaining closely spaced stiffeners.

The design of the miniature corrugations shown in Fig. 3 was a compromise between theoretical and practical considerations. These corrugations are

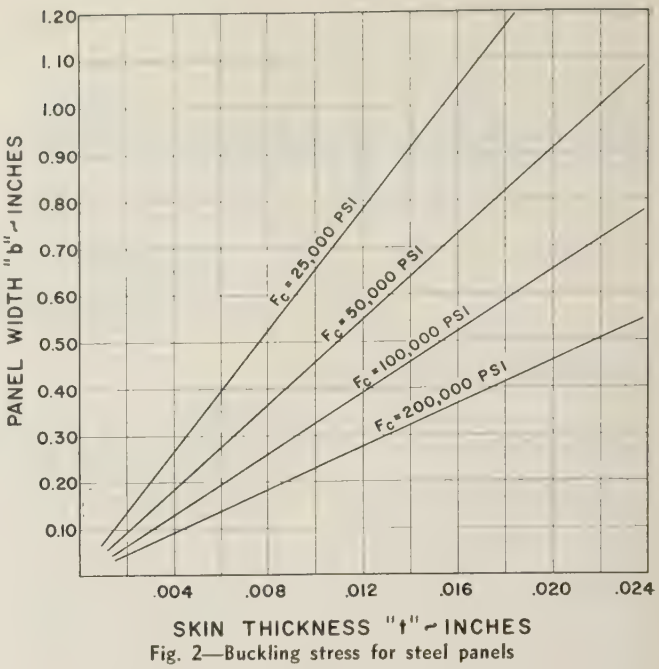

Fig. 2—Buckling stress for steel panels

symmetrical because this is necessary for the details of structural assembly. The 0.050 dimension of the flat face of the corrugation was dictated by welding requirements. Tests indicated enough fixity in the corners to permit a K factor of 5.3 in the buckling formula. Nonbuckling up to a stress of 200,000 psi established the corrugation depth. The pitch was based on the nonbuckling limits of a skin of twice the thickness of the corrugation material. Practical considerations required a limitation of the number of standard sizes. The three sizes shown in Fig. 3 were finally arrived at after careful consideration of all of the factors involved. Corrugation No. 1 has a top gage limit of 0.003 in. No. 2 has a top gage limit of 0.006 in. and No. 3 of 0.009 in. Corrugations larger than No. 3 are not desirable because individual stiffeners become practical for stiffening sheet above 0.016 in. The section properties and the calculated buckling allowable of the webs of these three standard corrugations are given in Table 1.

Design of Structure

The structural design of the complete airplane should follow a smooth pattern of gradual transition from lightly loaded structure to high-load structure. Excess material must be avoided wherever possible with strength and stiffness as the sole reason for putting it in. The designer must condition his thinking in terms of stress and develop a feel for design with extremely thin sheet.

Miniature corrugations when welded to thin skin can provide a very rigid surface covering for the airplane. This combination is rigid in one direction only and locally very strong. The corrugations are too shallow, however, to have good column characteristics. It is not practical, in most cases, to attempt to provide enough supports to get the column length down to the short column needed for high stress. This corrugation-skin combination has good bending stiffness in one direction and can be used very effectively to beam the pressure loads to the spars. The section properties and skin buckling allowable of the various skin-corrugation combina-

tions are given in Tables 2–4. These properties were used in calculating the allowable pressure loading of Figs. 4–9. This pressure loading is based on a unit width of beam parallel to the corrugations and passing over many supports. The maximum moment at midspan and over the supports is:

$$M = \frac{WL^2}{12} \qquad (2)$$

Suppose we have a pressure loading of 10 psi. The required spar spacing for No. 1 corrugation is 6 in. for a skin gage of 0.005 in. and corrugation gage of 0.003 in. (Figs. 4 and 5). The required spar spacing for No. 2 corrugation is 12 in. for a skin gage of 0.007 in. and corrugation gage of 0.006 in. (Figs. 6 and 7). We could have used a spar spacing of 4 in. with 0.004-in. skin and 0.002-in. corrugation for the No. 1 combination. Since the total weight of the structure must include the spar and rib weights many trials are necessary to find the best combination.

In order to use high-strength steel efficiently we

Table 2—Properties of No. 1 Corrugation with Skin

t_s	t_c	A per in.	e	e'	I_{x-x} per in.	ρ_{x-x}	F_c (Skin)
0.001	0.001	0.00285	0.0268	0.0533	0.00000257	0.0300	4,500
0.002	0.001	0.00385	0.0207	0.0595	0.00000313	0.0285	18,000
0.002	0.002	0.00568	0.0275	0.0529	0.00000512	0.0300	18,000
0.003	0.002	0.00668	0.0243	0.0560	0.00000580	0.0308	41,000
0.004	0.002	0.00768	0.0221	0.0583	0.00000634	0.0287	72,000
0.003	0.003	0.00848	0.0284	0.0519	0.00000768	0.0301	41,000
0.004	0.003	0.00948	0.0263	0.0541	0.00000842	0.0298	72,000
0.005	0.003	0.01048	0.0247	0.0558	0.00000907	0.0294	113,000
0.006	0.003	0.01148	0.0237	0.0569	0.00000964	0.0290	163,000
0.007	0.003	0.01248	0.0227	0.0580	0.00001016	0.0286	200,000

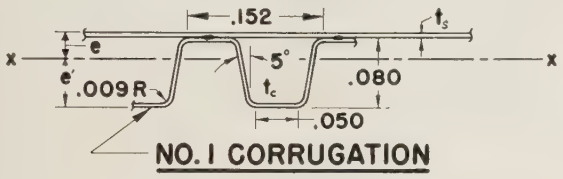

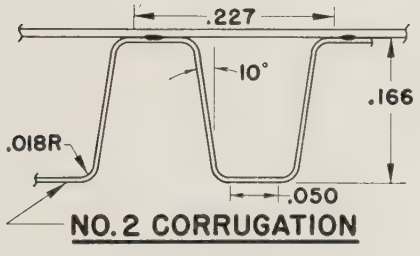

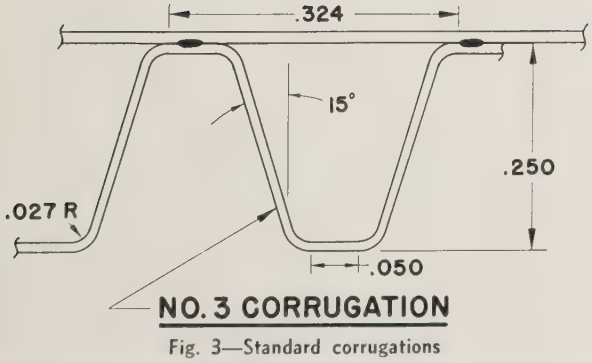

Fig. 3—Standard corrugations

Table 3—Properties of No. 2 Corrugation with Skin

t_s	t_c	A per in.	e	e'	I_{x-y} per in.	ρ_{x-x}	F_c (Skin)
0.001	0.001	0.00315	0.0575	0.1095	0.0000108	0.0585	2000
0.002	0.001	0.00415	0.0445	0.1235	0.0000132	0.0565	8100
0.002	0.002	0.00624	0.0581	0.1099	0.0000224	0.0600	8100
0.003	0.002	0.00724	0.0510	0.1180	0.0000245	0.0582	18,000
0.004	0.002	0.00824	0.0457	0.1243	0.0000267	0.0570	32,000
0.003	0.003	0.00933	0.0589	0.1101	0.0000324	0.0590	18,000
0.004	0.003	0.01033	0.0541	0.1159	0.0000363	0.0591	32,000
0.005	0.003	0.01133	0.0502	0.1208	0.0000387	0.0584	51,000
0.006	0.003	0.01233	0.0472	0.1248	0.0000408	0.0575	73,000
0.004	0.004	0.0124	0.0584	0.1116	0.0000446	0.0600	32,000
0.005	0.004	0.0134	0.0549	0.1161	0.0000459	0.0585	51,000
0.006	0.004	0.0144	0.0519	0.1201	0.0000489	0.0583	73,000
0.007	0.004	0.0154	0.0495	0.1235	0.0000515	0.0578	99,000
0.008	0.004	0.0164	0.0473	0.1267	0.0000539	0.0573	130,000
0.005	0.005	0.0154	0.0603	0.1107	0.0000537	0.0590	51,000
0.006	0.005	0.0164	0.0577	0.1143	0.0000572	0.0590	73,000
0.007	0.005	0.0174	0.0552	0.1178	0.0000604	0.0589	99,000
0.008	0.005	0.0184	0.0532	0.1208	0.0000633	0.0596	130,000
0.009	0.005	0.0194	0.0514	0.1236	0.0000660	0.0583	164,000
0.010	0.005	0.0204	0.0499	0.1261	0.0000699	0.0585	200,000
0.006	0.006	0.0184	0.0609	0.1111	0.0000641	0.0590	73,000
0.007	0.006	0.0194	0.0588	0.1142	0.0000677	0.0590	99,000
0.008	0.006	0.0204	0.0569	0.1171	0.0000710	0.0589	130,000
0.009	0.006	0.0214	0.0552	0.1198	0.0000742	0.0588	164,000
0.010	0.006	0.0224	0.0537	0.1223	0.0000771	0.0586	200,000
0.012	0.006	0.0244	0.0513	0.1267	0.0000825	0.0581	200,000

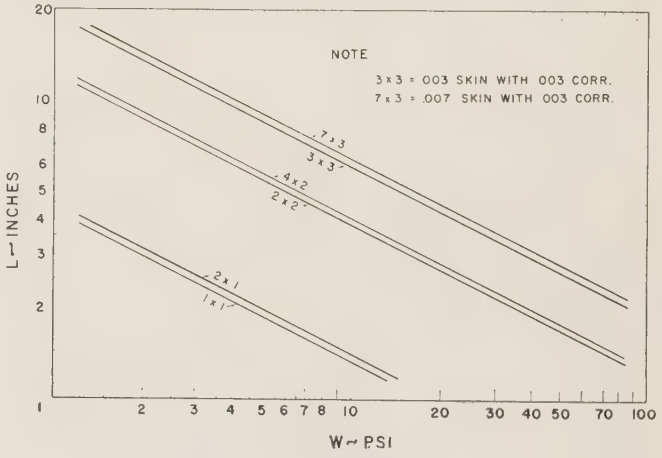

Fig. 4—Allowable pressure loading for No. 1 corrugation with skin (corrugation critical)

Table 4—Properties of No. 3 Corrugation with Skin

t_s	t_c	A per in.	e	e'	I_{x-x} per in.	ρ_{x-x}	F_c (Skin)
0.001	0.001	0.00310	0.0855	0.1655	0.0000230	0.0862	1000
0.002	0.001	0.00410	0.0652	0.1868	0.0000286	0.0835	4000
0.002	0.002	0.00619	0.0863	0.1657	0.0000458	0.0860	4000
0.003	0.002	0.00719	0.0754	0.1776	0.0000523	0.0854	9000
0.004	0.002	0.00819	0.0672	0.1868	0.0000573	0.0837	16,000
0.003	0.003	0.00926	0.0871	0.1659	0.0000687	0.0861	9000
0.004	0.003	0.01026	0.0796	0.1744	0.0000756	0.0858	16,000
0.005	0.003	0.01126	0.0735	0.1815	0.0000814	0.0850	25,000
0.006	0.003	0.01226	0.0683	0.1877	0.0000864	0.0840	36,000
0.004	0.004	0.01232	0.0876	0.1664	0.0000914	0.0861	16,000
0.005	0.004	0.01332	0.0820	0.1730	0.0000985	0.0860	25,000
0.006	0.004	0.01432	0.0771	0.1789	0.0001049	0.0855	36,000
0.007	0.004	0.01532	0.0732	0.1838	0.0001104	0.0848	49,000
0.008	0.004	0.01632	0.0695	0.1885	0.0001155	0.0840	64,000
0.005	0.005	0.0154	0.0887	0.1663	0.0001141	0.0862	25,000
0.006	0.005	0.0164	0.0842	0.1718	0.0001214	0.0860	36,000
0.007	0.005	0.0174	0.0802	0.1768	0.0001281	0.0858	49,000
0.008	0.005	0.0184	0.0769	0.1811	0.0001344	0.0855	64,000
0.009	0.005	0.0194	0.0740	0.1850	0.0001400	0.0850	81,000
0.010	0.005	0.0204	0.0713	0.1887	0.0001452	0.0844	100,000
0.006	0.006	0.0184	0.0892	0.1668	0.0001367	0.0862	36,000
0.007	0.006	0.0194	0.0858	0.1712	0.0001442	0.0862	49,000
0.008	0.006	0.0204	0.0825	0.1755	0.0001513	0.0862	64,000
0.009	0.006	0.0214	0.0795	0.1795	0.0001578	0.0858	81,000
0.010	0.006	0.0224	0.0769	0.1831	0.0001638	0.0855	100,000
0.012	0.006	0.0244	0.0727	0.1893	0.0001751	0.0847	144,000
0.007	0.007	0.0214	0.0900	0.1670	0.0001588	0.0861	49,000
0.008	0.007	0.0224	0.0868	0.1712	0.0001666	0.0863	64,000
0.009	0.007	0.0234	0.0841	0.1749	0.0001740	0.0863	81,000
0.010	0.007	0.0244	0.0817	0.1783	0.0001808	0.0860	100,000
0.012	0.007	0.0264	0.0775	0.1845	0.0001935	0.0856	144,000
0.014	0.007	0.0284	0.0738	0.1902	0.0002048	0.0850	196,000
0.008	0.008	0.0244	0.0906	0.1674	0.0001811	0.0863	64,000
0.009	0.008	0.0254	0.0882	0.1708	0.0001891	0.0864	81,000
0.010	0.008	0.0264	0.0858	0.1745	0.0001965	0.0863	100,000
0.012	0.008	0.0284	0.0815	0.1805	0.0002106	0.0862	144,000
0.014	0.008	0.0304	0.0781	0.1859	0.0002232	0.0857	196,000
0.016	0.008	0.0324	0.0755	0.1905	0.0002372	0.0855	200,000
0.009	0.009	0.0277	0.0918	0.1672	0.0002066	0.0864	81,000
0.010	0.009	0.0287	0.0896	0.1704	0.0002148	0.0865	100,000
0.012	0.009	0.0307	0.0857	0.1763	0.0002302	0.0865	144,000
0.014	0.009	0.0327	0.0824	0.1816	0.0002441	0.0864	196,000
0.016	0.009	0.0347	0.0804	0.1856	0.0002572	0.0860	200,000
0.018	0.009	0.0367	0.0773	0.1907	0.0002694	0.0856	200,000

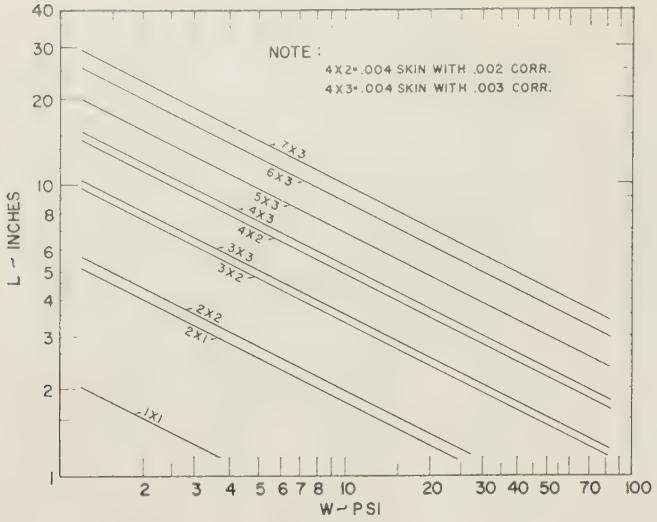

Fig. 5—Allowable pressure loading for No. 1 corrugation with skin (skin critical)

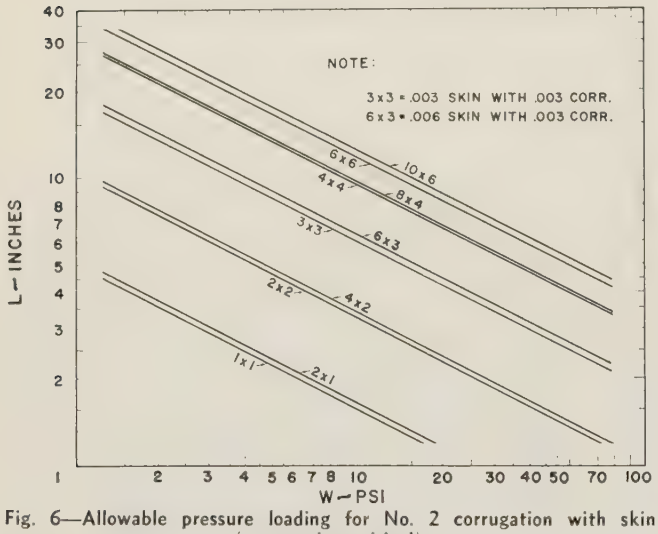

Fig. 6—Allowable pressure loading for No. 2 corrugation with skin (corrugation critical)

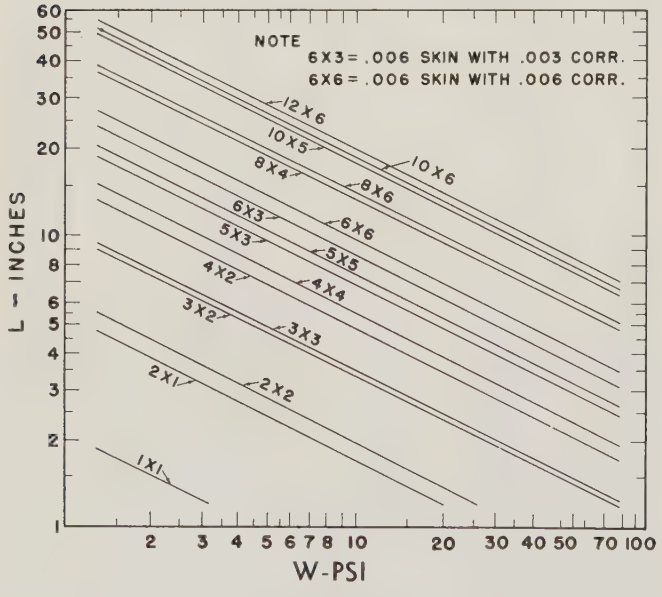

Fig. 7—Allowable pressure loading for No. 2 corrugation with skin (skin critical)

must carry this stiffened foil construction into all of the supporting structure. This can be demonstrated by looking at a typical spar shown in Fig. 10. At the spar tip the shear load is practically nil and the bending moment is zero. The shear web will start as a corrugation made from 0.001 in. gage. It is attached to the spar cap by two attach angles for stability. As we follow it inboard the shear load increases and forces an increase in the corrugation gage or the addition of a sheet or both. A further increase in shear may require the second sheet shown in Fig. 12, and finally for extremely high shear loads the corrugation may give way to individual stiffeners. Similarly, the spar cap may be the doubler corrugation plus the skin and skin corrugation. As the moment builds up, the axial load will increase to where the beam cap shown in Fig. 10 is required. This beam cap can start at about 0.004 in. thick and 0.50 in. wide and increase in

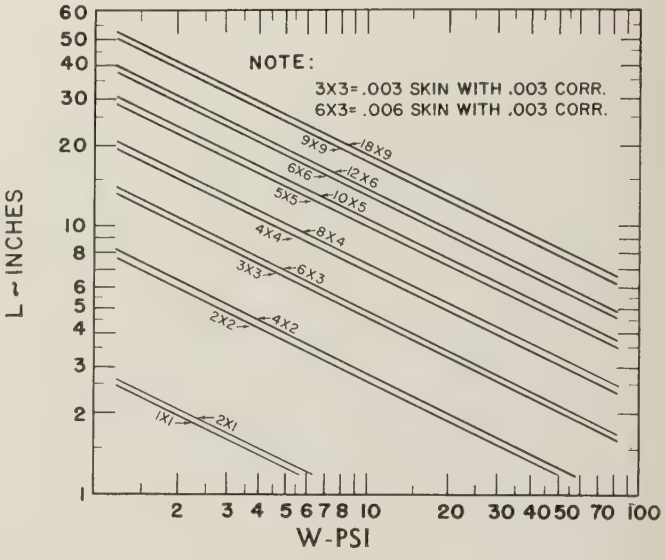

Fig. 8—Allowable pressure loading for No. 3 corrugation with skin (corrugation critical)

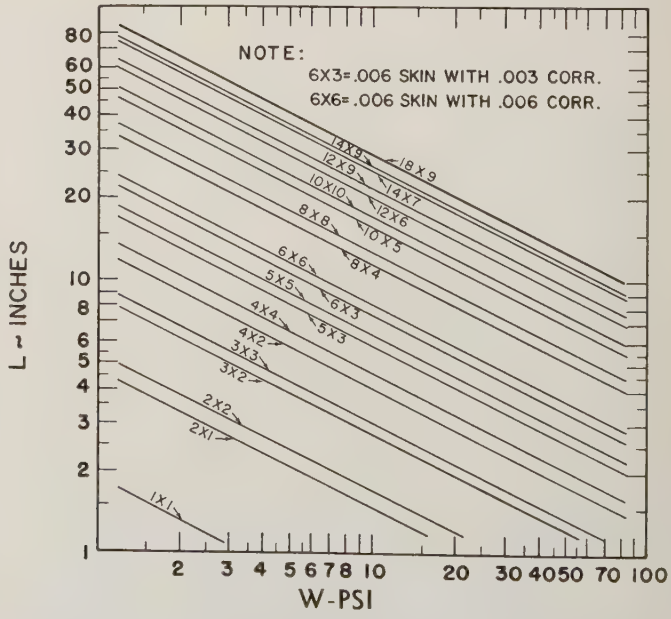

Fig. 9—Allowable pressure loading for No. 3 corrugation with skin (skin critical)

thickness and width as the load requires. This cap is well-stabilized and can work at a stress of 200,000 psi. If the axial load should increase to 200,000 lb there is a full inch of material in the spar cap.

There are cases where there may be a relatively low shear load and a high bending moment. In such cases the beam deflection will put a compressive load into the shear web that must be accounted for. The caps may be curved geometrically and require additional stiffening in the shear web to offset the directional change of the cap load. After both of these things are accounted for there is one more stabilizing force to consider. This stabilizing force is given by the empirical curve of Fig. 11, where the spar cap is considered to be made up of a series of short columns whose length is determined by the radius of gyration of the cap and the column stress in the cap. This stabilizing pressure alternates in direction from one node of the column to the next. It is given as a pressure because it is a uniform force across the full width of the cap. At a cap stress of 195,000 psi this stabilizing pressure is 100 psi and is critical only for the attachment and buckling of very thin webs. A narrow cap width will reduce this pressure and is recommended where the strength of the attachment of the web to the cap may be critical.

This type of structure is readily adaptable to integral fuel tanks. Seam welds or overlapping spots make a fuel tight joint. Multiple spar construction will keep the tension loads on the spots within safe limits and final closure of the tank can be made by external fusion welding as shown in Fig. 12.

Assembly of structure built up from sheet has not presented serious difficulties even though the gages range from 0.001–1.00 in. These assemblies are easily

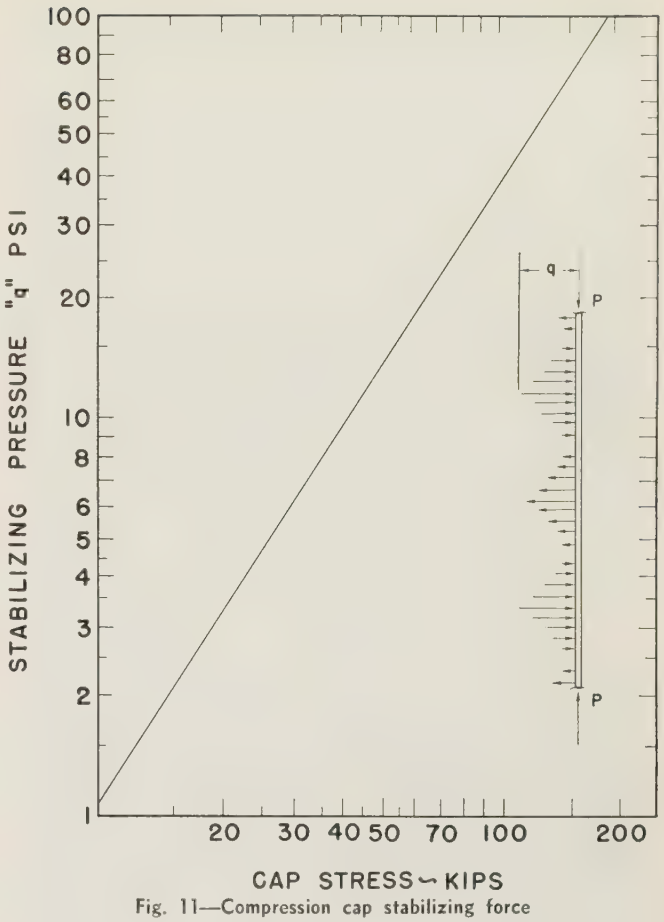

Fig. 11—Compression cap stabilizing force

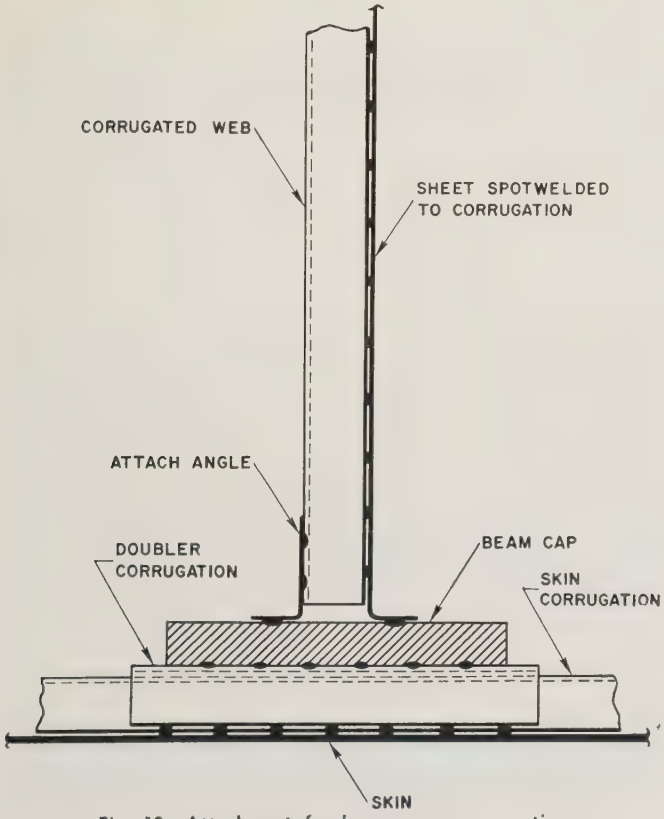

Fig. 10—Attachment for beam across corrugation

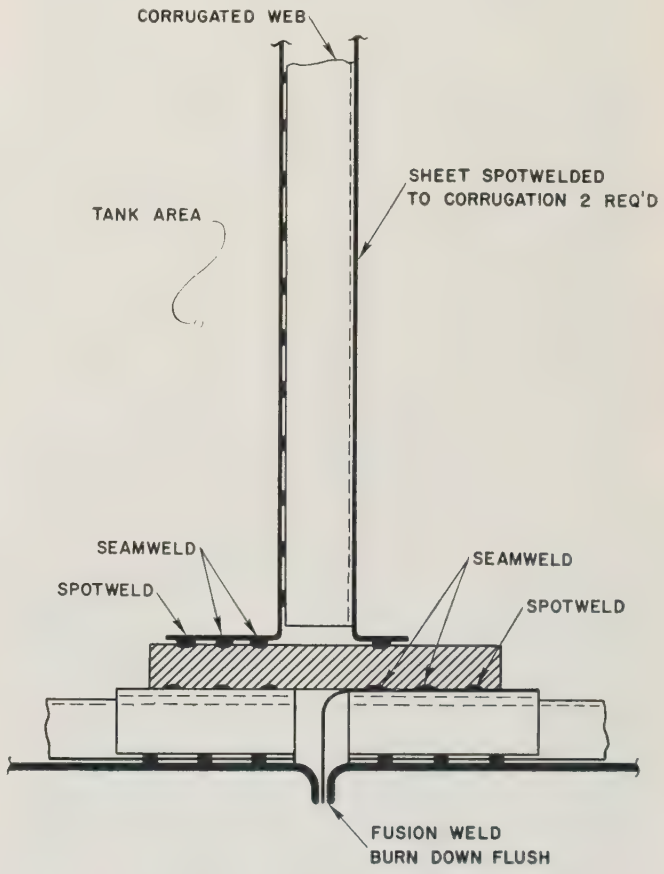

Fig. 12—Fuel tight tank section

built up from smaller subassemblies with the only limitation on size being accessibility for welding. Production spot welding of the corrugation to the skin can be done with multiple welding units with a roller running in each corrugation. Fig. 13 shows a setup of this nature that will make six rows of spots at one time. A certain amount of handwork is required for final assembly. This can be simplified by careful design. A variety of tips can be made for the poke type welder shown in Fig. 14 for use in touch-up work or for welding in places that are hard to reach. Good welds are consistently made as long as clean, matched surfaces and correct machine settings are used. Some typical welds are shown in Fig. 15 where micrographs of three combinations are shown. The upper view shows two sheets of 0.016 in., the middle view shows 0.002 in. to 0.002 in., and the lower one shows 0.002 in. welded to 0.016 in. The problem of welding thin sheet to heavy bar was successfully solved by our weld laboratory with one limitation; the thinnest sheet must be less than 0.016 in. thick. The thicker one can be an inch or more thick. Fusion welding of 0.002 in. foil has been accomplished but better equipment will be required before it becomes regular shop practice.

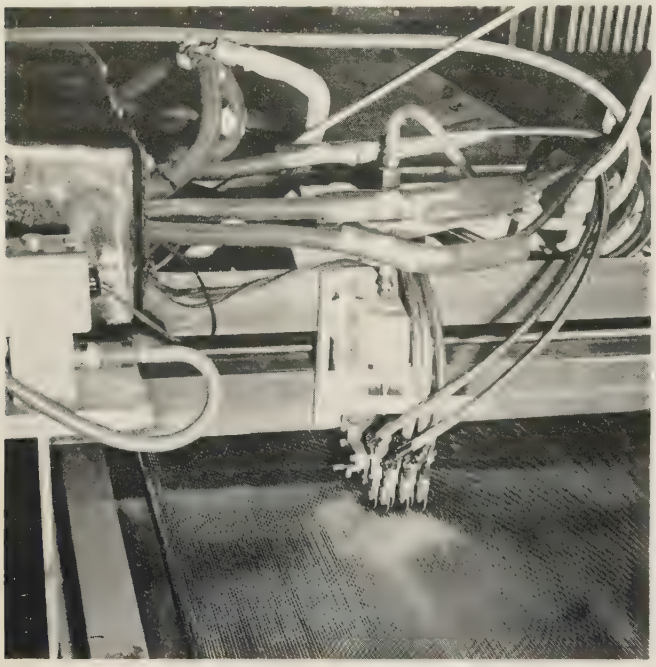

Fig. 13—Six-wheel spot welder welding corrugation to skin

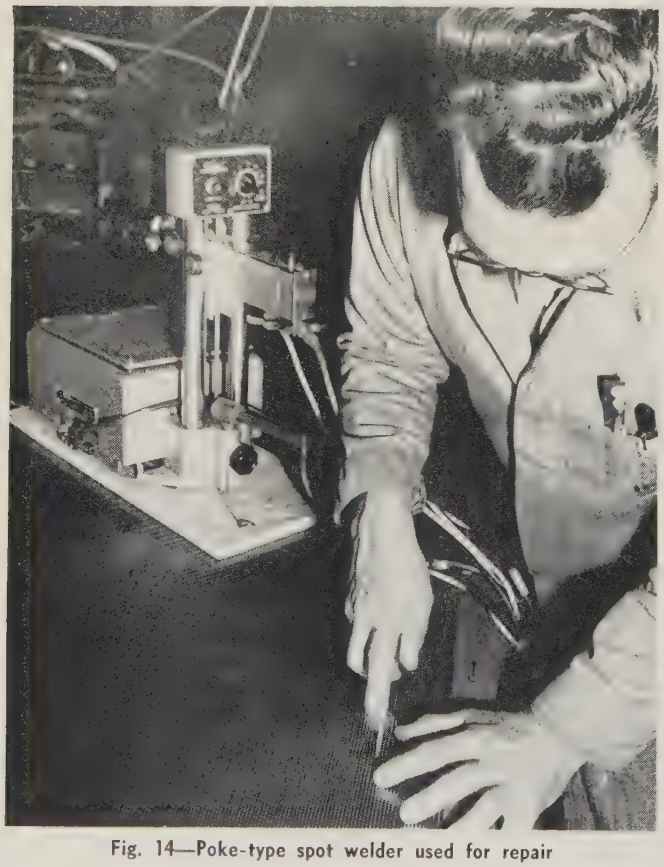

Fig. 14—Poke-type spot welder used for repair

We have not tried to anticipate or solve all of the problems that may be encountered in designing and building with high-strength steel foil. These problems are better handled on specific designs than as general solutions. There is no good way of making a weight comparison between this type of design and the more conventional skin-stringer or honeycomb design, except by comparing direct calculations of the total material used in comparable designs intended for the same purpose. The designer can be sure his weight is a minimum if he has achieved a taper effect in material that matches the applied load for his primary structure and if his supporting structure contains the least possible material needed to prevent buckling of the primary load members. He must also use a material with a high strength-to-weight ratio and be able to develop stresses near the yield strength of the material.

Fabricated Parts

We have made many design studies on existing structure where we followed the design methods outlined here. In every case, a large saving in weight

Fig. 15—Typical spot welds. Top—0.016 to 0.016 in., middle—0.002 to 0.002 in., bottom—0.002 to 0.016 in.

Fig. 16—Sandwich panels with separate stiffeners

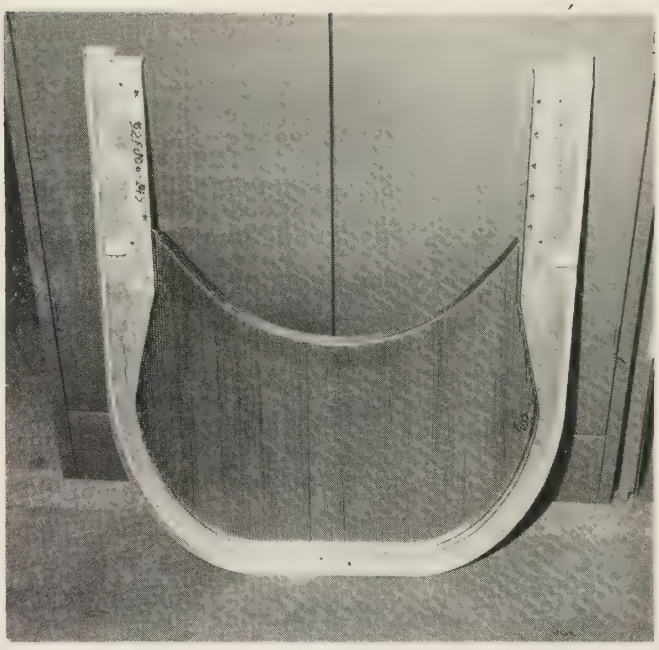

Fig. 17—Corrugated firewall

was easily made. In several cases the weight was cut in half. These studies included structure formerly designed for aluminum, titanium, and steel. Some of these parts have been built. Fig. 16 shows left and right panels that were formerly made with brazed honeycomb. These panels now have Z stiffeners made from 0.006-in. 17-7 steel. The Z's are welded to 0.010-in. 17-7 steel skins at spacings of 0.625 to 1.25 in., representing an 18% weight saving.

Fig. 17 shows a firewall made from 0.002-in. type 321 steel sheet welded to No. 1 corrugation made from the same material. This represents a weight saving of 60% over the 0.016 in steel firewall originally planned for this job.

Fig. 18 shows a lightweight steel tailpipe that is 14 in. in diameter and 12 ft long. It is made from type 321 steel sheet 0.002 in. thick welded to No. 1 corrugation of the same material. This cylinder is stiffened radially by ring bands of steel that are 0.030 in. thick and 0.375 in. wide. These bands are approximately 2 ft on centers. The total weight of this tailpipe is 14.7 lb. It replaces a design that would have weighed 35 lb. Fig. 19 shows the welded corrugation sheet assembly of this tailpipe before it was rolled into the cylinder of Fig. 18.

Fig. 18—Lightweight steel tailpipe

Conclusion

The design philosophy discussed and illustrated here leads logically to the use of very thin sheet; the problem of stiffening this thin sheet leads logically to miniature corrugations; and the requirement of a great many points of attachment leads logically to spot welding for production assembly.

High-strength steel can be used for both structural and nonstructural parts with a resulting saving in weight of more than 25% over past design with aluminum, titanium, or steel. This saving is possible because the full strength of the material can be utilized. If high-strength steel and this method of design is used for the complete airplane its structure can be either 25% lighter or it can withstand aerodynamic heating up to 750 F with no increase in weight.

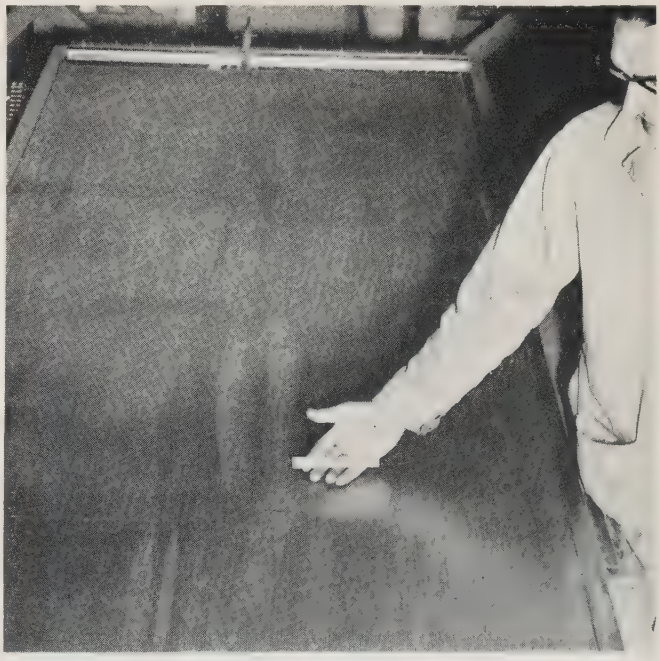

Fig. 19—Tailpipe skin assembly

Mercedes-Benz Racing Design and

H. Scherenberg, Daimler-Benz AG, Germany

This paper was presented by J. E. Witzky at the SAE National Passenger-Car, Body, and Materials Meeting, Detroit, March 6, 1957

THE automobile is not only a means of transportation but also an expression of technical progress, a subject of fashionable taste, and last but not least, an implement of sport. We have been active in racing competition since March, 1899: 38 victories in Grand Prix racing were earned between 1906 and its suspension in 1939.

After World War II the international regulation for formula-I racing cars was based on an engine of 750 cc supercharged, or 2.5 liter naturally aspirated. We decided to use for this new development the naturally aspirated engine of 2.5-liter displacement.

The Racing Car W 196

Fig. 1 shows the car after the top half of the body work has been removed. The frame is of the space-tube type, calculated by means of the Cremona plan and designed so that the individual tubes are stressed only in compression or tension. This type of frame is also used on the 300 SL sports car, which is in production today. It provides exceptional advantages of stiffness with low weight and is, therefore, particularly suitable for sports and racing cars.

The water and oil radiator can be seen in front. To save space, the torsion bars of the front suspension pass through them. Just behind the radiators are the inboard front-brake drums.

The engine is tilted on its side, the V of the cylinder head being inclined to the right; the inlet manifold with its eight ports is at the top, and below this is the injector pump.

The propeller shaft runs alongside the driver's seat to the rear. The rear-brake drums are also inboard. A 5-speed gearbox forms a unit with the rear axle. The fuel and oil tanks are mounted behind the rear axle.

The decision to use the 2.5-liter engine was determined after extensive experiments. From the many supercharged engines developed over several decades, we know the various effects which influence the output of an engine. The most important ones are boost pressure, rpm, degree of cylinder filling, and engine compression. Another means is the injection of alcohol into the inlet tracts before the supercharger. This factor was included in the calculations. If, for a 750-cc supercharged engine, a maximum revolution limit of 10,000 rpm is assumed, and the compression ratio is reduced proportionally to the increased boost pressure (this in view of peak loading—that is knock limit), then under certain further premises a curve is produced, giving the obtainable power output relative to boost pressure.

The output obtainable from the 2.5-liter unsupercharged engine was reasonably easy to foresee: It could be calculated that an output of about 115 bhp per liter, which means that about 290 bhp at 8000 rpm could be expected. It appeared, however, that to obtain the same result from the 750-cc blown engine, an exceptionally high boost pressure of the order of 3.4 atmospheres or 48.35 psi would have to be provided. Our racing cars before the war had a boost pressure of about 1.4 atmospheres or 19.91 psi. A supercharge of 48.35 psi would necessitate multi-stage compressors. A 290-bhp engine would require 400 bhp per liter and a bmep of 525 psi. The super-

Cars

Experience

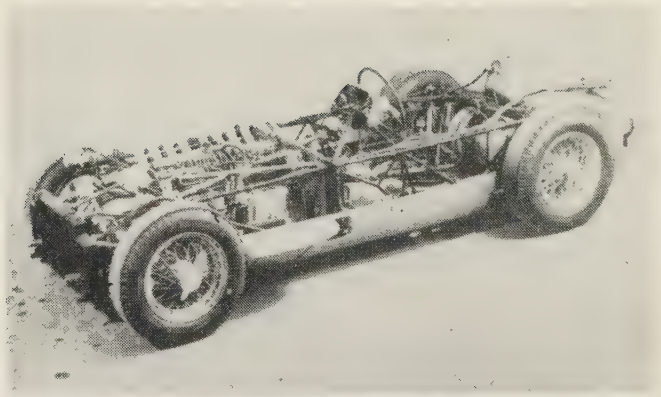

Fig. 1—Mercedes-Benz racing car W 196 with 2.5-liter engine

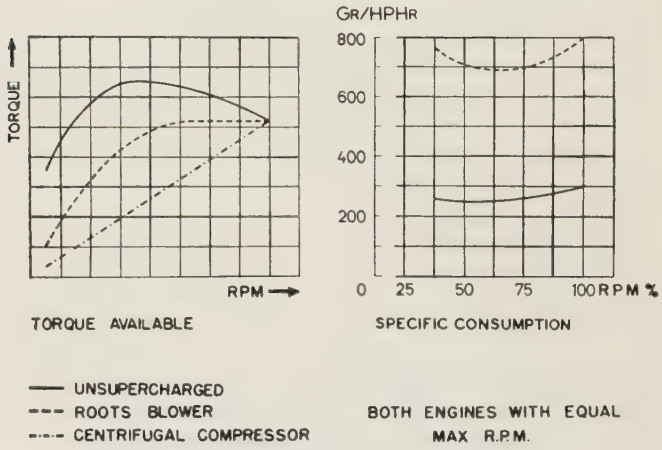

Fig. 2—Comparison of 2.5-liter unsupercharged and 0.75-liter supercharged engines

charger alone would absorb 100 bhp, so that the imep at an engine output of 290 + 100 (390) bhp would be of the order of 700 psi. As a comparison, a bmep of only 195 psi is required from the naturally aspirated 2.5-liter engine.

But even if the 750-cc supercharged engine gave 290 bhp, relative torque curves would still show the advantage of the unblown engine (Fig. 2). The highest curve on the left-hand graph indicates the atmospheric engine, the middle curve shows a Roots-blown engine, and the lower a centrifugally supercharged one. The latter is the most unfavorable because of its "square" characteristics in relation to rpm. The naturally aspirated engine has, therefore, a much better torque curve and, therefore, better acceleration than a supercharged engine.

The estimated fuel consumption figures shown on the right-hand graph of Fig. 2 also speak for the unblown engine.

If one considers further that the experience gained on supercharged engines cannot be applied so easily to the production engine, then the decision to adopt the unblown 2.5-liter engine can readily be understood.

Having settled this question, the design of the engine itself had to be decided. The first problem was the number and arrangement of the cylinders.

With an unblown engine the highest possible degree of cylinder filling is of paramount importance, so particular design attention must be paid to valve timing and cross-section areas.

To get a maximum of cross-section areas, we de-

DEVELOPMENTS in racing cars often indicate future trends in passenger-car design. This is indicated in the description of the Daimler-Benz racing car W 196.

The car has a 2.5-liter naturally aspirated engine with an output of 115 bhp per liter, or 290 bhp at 8000 rpm, making it far more efficient than the 750-cc blown engine. A new valve-gear arrangement permits higher rates of acceleration and deceleration, and higher speed ranges.

The 300 SL sports car offered an opportunity to compare outputs of an engine with carburetor and one with fuel injection. The latter increases output by 10%, permits higher compression ratios, reduces fuel consumption, and eliminates flat spots. Therefore, fuel injection was put on the W 196. Finally, improved design of brakes and axles brought about better spring and road holding.

veloped a new valve-gear arrangement. With this it became possible to arrive at generous valve openings, which never could be obtained with a normal valve-gear arrangement.

Fig. 3 is a basic layout sketch showing the difference between normal and controlled (desmodromic) valve actuation. The left-hand portion illustrates the usual layout with cam, valve, valve spring, and cotter. In this arrangement, the valve is opened by the cam, while the valve spring is compressed at the same time. On closing, that is when the cam has moved on, the spring closes the valve against the cam. The strength of the spring is, therefore, the deciding factor for the closing operation.

A photograph of the desmodromic valve gear with the cam cover removed shows a camshaft with two cams per valve (Fig. 4). One cam is directly above the valve and is responsible for the valve opening; the other closes it via the rocker-arm.

The desmodromic valve gear enabled acceleration values to be obtained, the extent of which had never been known before. Fig. 5 gives direct comparison values of a racing engine with spring-operated valves, calculated on the basis of present experience, and the new desmodromic actuation.

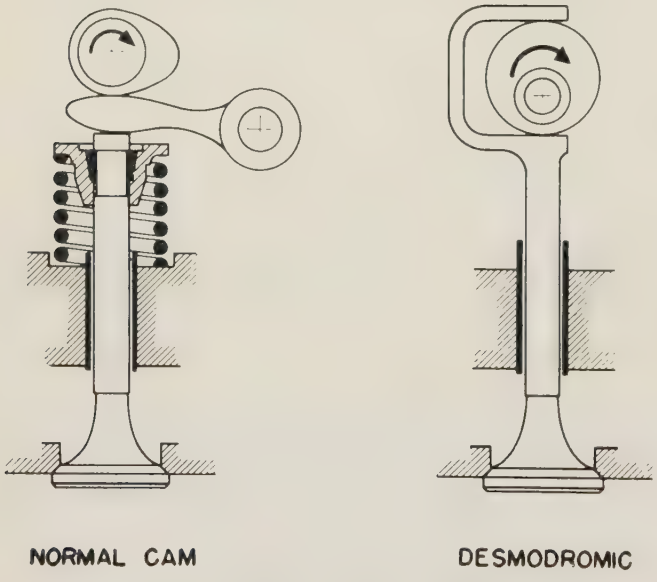

Fig. 3—Scheme of valve actuation

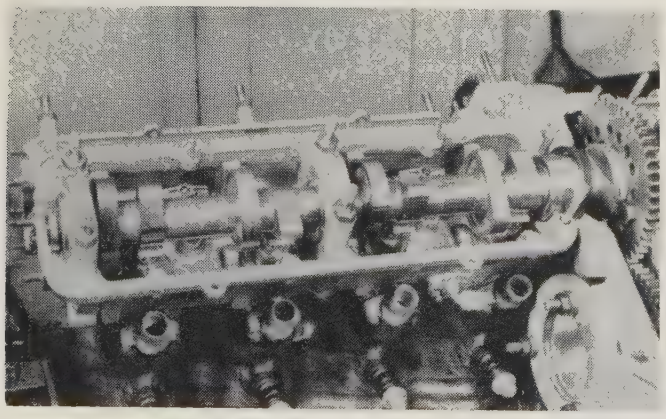

Fig. 4—Valve actuation of 2.5-liter racing engine

The acceleration curves show that higher rates of acceleration and deceleration are possible with the new system, and this enables the angle of opening to be kept relatively small and, therefore, comes close to the ideal situation.

Further increases permit engine development to even higher speed ranges without hindrance by valve-gear limits. How the drivers liked the willingness of their engines to speed-up could be clearly seen after the various races, when the maximum tachometer needle reading was checked. The one in Fangio's car usually showed over 9000 rpm.

The choice of crank-throw sequence, the firing order, and drive take-off was preceded by much theoretical research. It was found that the 8-cyl in-line engine offers considerable advantages if the drive is taken from the middle of the crankshaft.

Fig. 6 shows the scheme of the crankshaft and drive. In fact, this layout provides a 4-cyl engine on each side of the power take-off. Calculations have shown that, in an 8-cyl engine with normal drive at the end of the crankshaft, the dynamic stresses would be so high that a vibration damper could cope with them only under difficulties. The engine arrangement with central-drive take-off has, however, additional advantages in regard to torsional vibration, as shown in the lower half of Fig. 6.

The central-drive take-off has the advantage of dispensing with the flywheel, and the two small vibration dampers at each end of the crankshaft are sufficient. The propeller shaft is also moved so far to the side that it can lie alongside the driver's seat. Thus, the vehicle acquires a lower center of gravity.

In view of our experience in the field of fuel injection and the possibility of easy comparison between carburetor and fuel injection in the 300 SL sports car, we decided to apply fuel injection.

Fig. 7 shows comparisons between carburetor and fuel injection on the 300 SL engine. After extensive experimentation, a maximum of about 200 bhp was obtained from this engine with carburetor; however, the output of the fuel-injected engine in our regular production cars is in the region of 220 bhp.

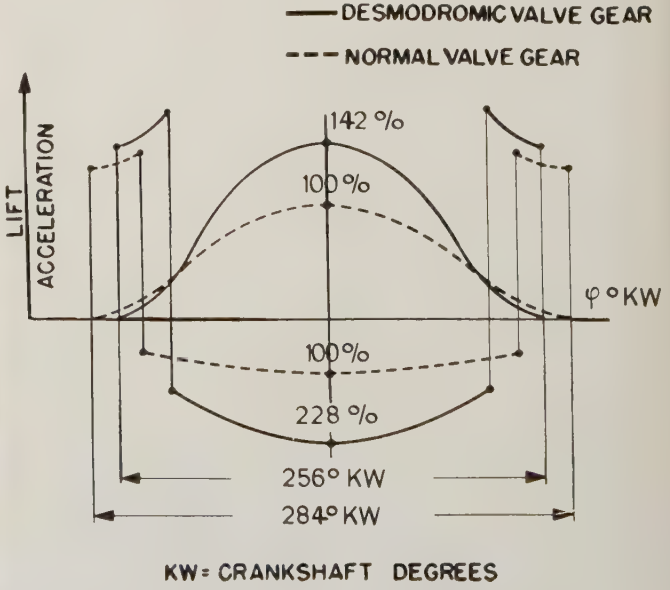

Fig. 5—Comparison of lift and acceleration curves

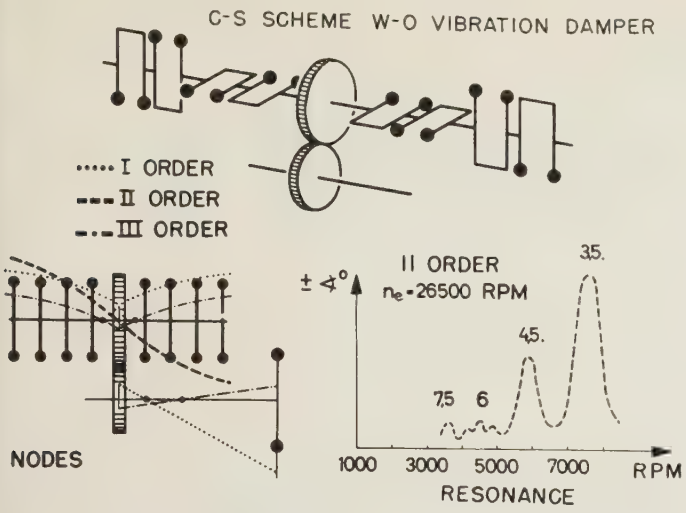

Fig. 6—Vibration chart and crankshaft scheme of 2.5-liter racing engine

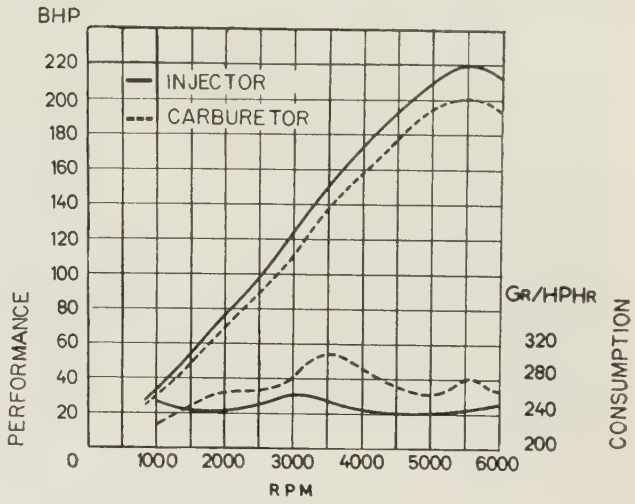

Fig. 7—Comparison of performance with carburetor and fuel injection on 300 SL engine

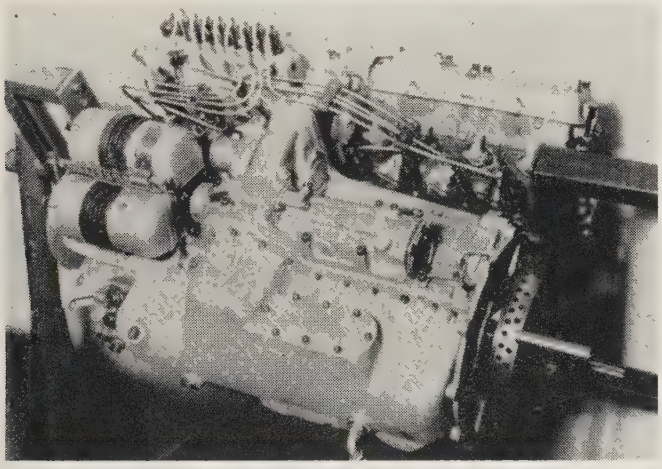

Fig. 8—W 196 racing engine with fuel injection

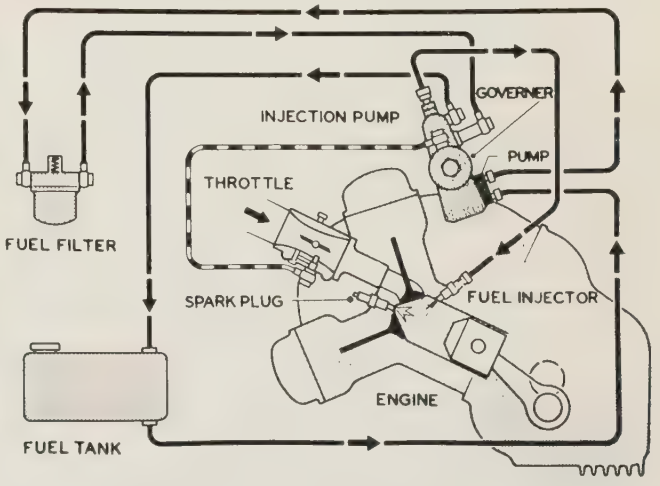

Fig. 9—Fuel injection system used on 2.5-liter racing engine

In other words, the output is increased by about 10%. This performance gain with fuel injection is proportionally similar in all engines. It stems chiefly from the reduction of choke losses by omitting the carburetor. Furthermore, higher compression ratios are possible because the knock limits are higher. Increased performance is also obtained by a more favorably shaped inlet manifold with better use of pulsation, so that over 100% filling can be obtained.

Fuel injection has other advantages, too. The reduction of fuel consumption, a major factor in racing cars, is particularly noteworthy. The refueling stops in races, when tires were usually also changed, are a thing of the past. Sufficient fuel for the entire race has to be carried. The elimination of pit stops was possible through performance reduction, due to change of the international racing formula and the considerable improvement in tires. Fuel consumption also enters into the question of starting weight of the car, which in turn influence acceleration and braking.

A further advantage gained from fuel injection is the elimination of flat spots. Sports engines often present difficulties when the throttle is opened wide from idling speeds; but the 300 SL sports car can be driven without difficulty in top gear at 15–20 mph and be accelerated without a gear change to its maximum speed of about 160 mph. There are other advantages of fuel injection, but their description is beyond the scope of this paper.

Fig. 8 shows the W 196 racing car engine with fuel injection. The injection pump, designed by Robert Bosch, is of the 8-cyl in-line type, driven from the central power take-off of the engine. Extensive experiments were necessary to determine the optimum position and direction of the jet itself and the shape of the spray. A schematic view of the injection system is shown in Fig. 9. A low-pressure pump brings fuel from the tank to the filter and from there to the injection pump. A certain quantity of fuel returns to the tank after passing a blow-off valve. Its function is purely to scavenge the inlet chamber to prevent vapor lock and to guarantee equal filling. The sucked-up fuel is then sprayed into the cylinder by way of the jets.

The quantity of fuel injected in relation to the inlet-manifold pressure is governed from the rear of the butterfly throttle. Under partial load a correction is made by means of differential pressure

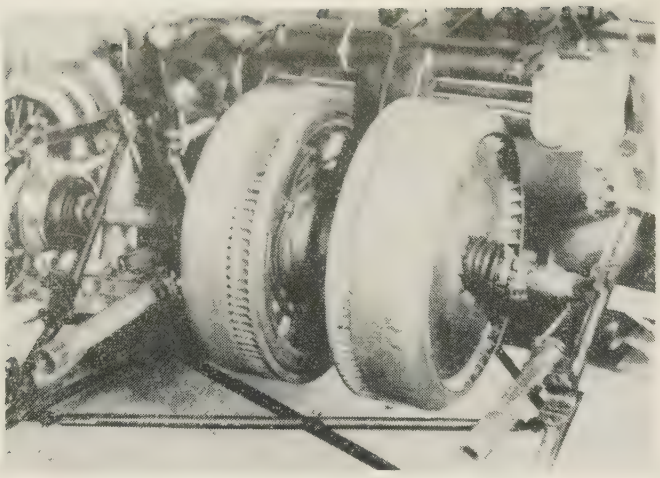

Fig. 10—Front axle of 2.5-liter racing car

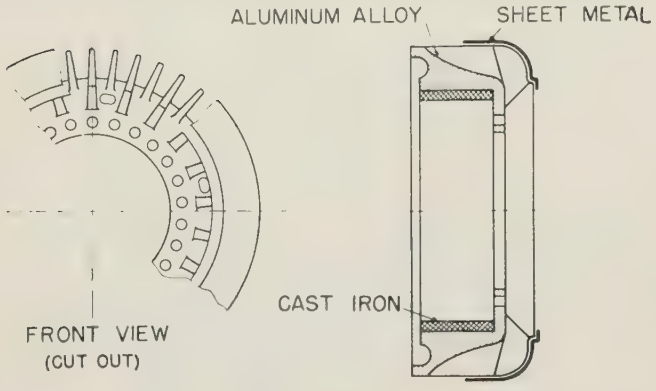

Fig. 11—Brake drum of 2.5-liter racing car

across the throttle.

Since 1932, we have used independent 4-wheel suspension on passenger cars. This resulted in particularly good springing and consequently good road-holding. Therefore, we decided to apply this method to the racing car.

Fig. 10 shows the front axle with the brake drums and the shafts to the front wheels. This construction made it possible to keep unsprung masses at a minimum. The brake drums could, therefore, be kept large, which was important on the front axle because of the particularly high brake forces on the front wheels. The joints of the shafts are contained in sleeves. Wishbone-arms support the wheels. Torsion bars are used as springs.

The brake drums conform to a system developed for the 300 SL and have, in the meantime, been applied in similar form to the 300- and 220-series of passenger cars. Fig. 11 shows a section through the front drum of the racing car. The inner cast-iron ring is bonded directly to a Silumin light-alloy drum by means of the Al-Fin process. The outer drum carries radial fins, which simultaneously cope with heat dissipation and air disposal.

For better ducting, a light metal-alloy cover is fitted over the drum. The effect of this brake construction is excellent. It prevents brake fading, because the generated heat under repeated sharp brake application is quickly dissipated. Consequently, wear and tear on brake linings is small.

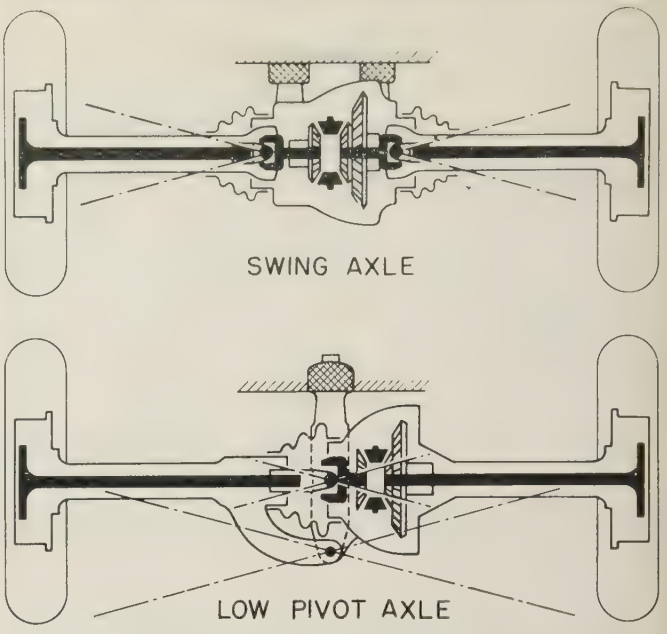

Fig. 12—Comparison of rear axles

Particular attention was paid to the rear axle because its development and arrangement have considerable influence not only on springing but also on road-holding when cornering. Fig. 12 shows the essential difference between the normal swing axle and the single-joint, low-pivot swing axle as applied to the 220 passenger car. The rear axle of the racing car follows essentially the latter system.

On the normal swing axle the casing is fixed to the chassis through the medium of rubber bushings. The two half-shafts are joined to the casing, the outer-axle shaft joints being mounted coaxially with the inner shaft. On the single-joint system there is only one common, low-mounted pivot, which is attached to the frame, and only one joint connects the two half-shafts. Therefore, the casing swings with the right-hand axle shaft.

This lowering of the pivot of the swing axles and the simultaneous extension of the swinging arms affects cornering. If one drives a car with understeering tendencies into a corner at high speed, it is necessary to turn the steering wheel further than would be commensurate with the radius of the bend, in order to compensate for the understeering characteristics of the vehicle. Such a vehicle displays steering reluctance. In borderline cases, even maximum lock is not sufficient. The vehicle will slide straight on to the opposite side of the road or even beyond.

The oversteering car displays steering willingness. In borderline cases, it will steer into the bend through the rear wheels sliding and, therefore, a little steering lock must be taken off. But beyond the limit, even paying-off steering, which is contra-lock, will not be enough and the vehicle will begin to revolve, sliding diagonally across the direction of travel.

This diagonal turning motion slows the car considerably and it is generally easier to correct than in understeering, which can easily lead to collision in serious cases.

Therefore, we strive to build a car in such a manner that it over- and understeers as little as possible, which means it follows the steering as accurately as possible. In borderline cases, however, it is our view that there should rather be a slight oversteering tendency.

Our procedure enables us to calculate the cornering behavior of a vehicle. These calculations must contain not only the constructional data, but also data ascertained by experiment in relation to tires, their treads, road surface, the humidity of the latter, and so forth.

The rear-axle layout of the 2.5-liter racing car is given in Fig. 13. The two half-shafts, joined to one pivot, are mounted low under the center of the rear-axle housing. Also shown are the inboard brake drums, the two joints on either side, and the construction of the hub.

From the section through the hub (Fig. 14), one can see weight has been minimized as far as possible. Stress calculations were made for the various sectional areas.

Particular stresses appeared at the inner hub. This turns with the wheel and must, therefore stand considerable bending stresses. The lateral forces that bear upon the tire, together with the wheel loading, are increased by shocks and applied power, and provide combined and particularly unpleasant stresses at the point where the inner part leads to the bell-shaped portion. The shape, described in Fig. 14, keeps the maximum stress at the most critical cross-section down to 21 tons per sq in. Test runs on a specially built test rig indicated beforehand that the construction was sound. This was subsequently proved in racing.

Body Shape

We were able to deduce from prewar experience with record cars and afterwards from the 300 SL sports car that fully enclosed bodywork would be advantageous in fast races. A one-fifth scale model was thoroughly investigated in the small wind tunnel of the Automotive Research Institute at the University of Stuttgart and, by cooperative work, a good air penetration factor was achieved.

Then a complete racing car was subjected to tests with a view to finding improvements. Fig. 15 shows the car standing on two streamlined bearers which hang on wires. If wind is directed against the vehicle, it yields in the way of a pendulum and this yielding potential can be balanced by way of another wire. The air resistance can thereby be measured.

It can be seen that in this experiment the cooling air intake has been closed. By comparison with an open air intake, the influence of air passage through the radiator and engine compartment can be measured. It became obvious, in accordance with previous tests, that the passage of air through the radiator ducts and cooling intake creates considerable resistance and, therefore, it is necessary to be extremely careful with air for cooling purposes.

We also developed a nonaerodynamic monoposto-type of body, which has advantages on circuits with many corners. The driver sees the front wheels and can aim the car into the corners. From the weight point-of-view, this type of body is also advantageous because it results in better acceleration. Although the monoposto-type has less frontal area than the aerodynamic body, its coefficient of air resistance C_W is so much worse that an air resistance difference

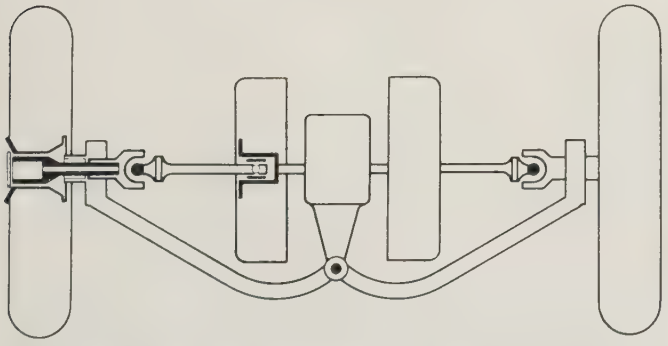

Fig. 13—Rear-axle construction of 2.5-liter racing car

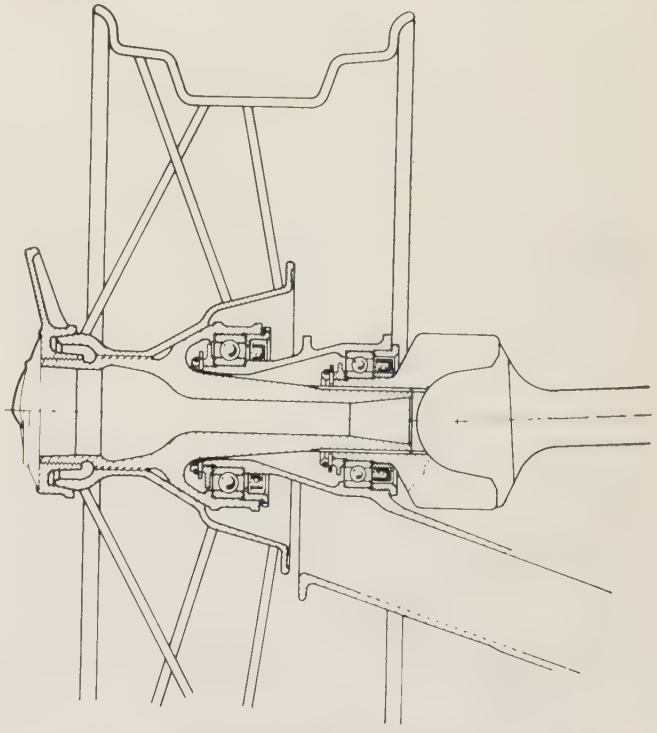

Fig. 14—Rear-axle wheel hub of 2.5-liter racing car

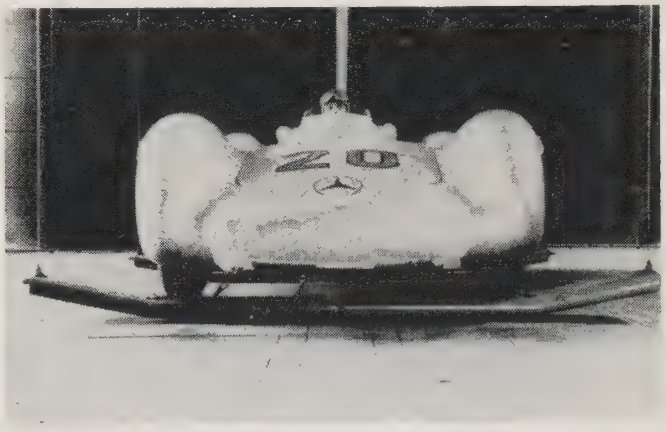

Fig. 15—Windtunnel test

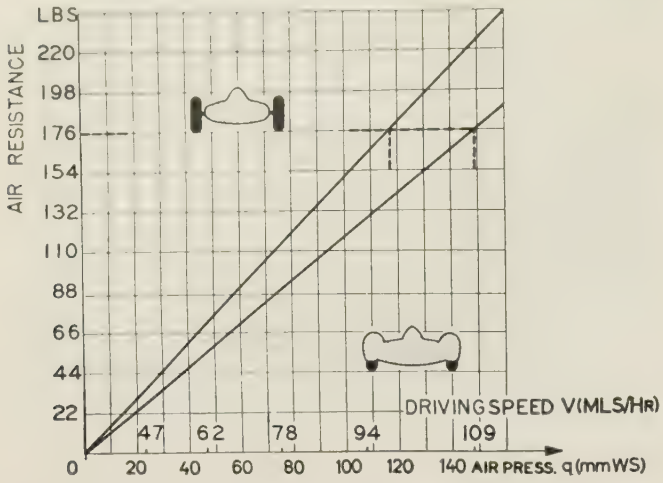

Fig. 16—Comparison of air resistance of monoposto-type body and aerodynamic body

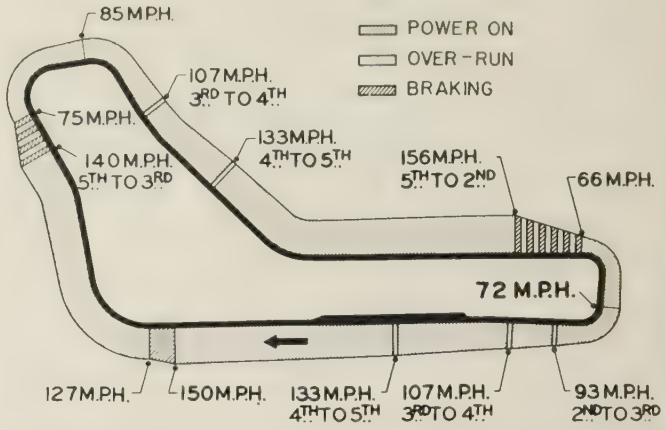

Fig. 17—Racing circuit of the Monza track in Italy

arises. Fig. 16 shows the resistance of both body shapes (which can be fitted to the same chassis) according to speed and degree of pressure buildup.

Comparison shows that the enclosed car, in spite of its greater sectional area, has 20% less air resistance than the monoposto type. The dotted example is valid for an air resistance of 175 lb. Therefore, with a corresponding engine output, the unenclosed car would reach 98 mph and the enclosed one 109 mph. The small influence of rolling resistance is disregarded in this instance. In very fast races, such as Rheims, the fully aerodynamic car has unquestionable advantage.

Our mathematics department established exact calculations for each given circuit, so that we know which type of body work and gear ratio will be most suitable for each race. With the aid of the circuit map and various plotted graphs for acceleration and braking of the vehicle, diagrams are established and comparisons made to show the type of body form and the rear-axle and gearbox ratios which will be most effective. Naturally these findings are tested during racing practice; but almost always calculations have provided the correct values.

The result of such calculations as applied to the Monza track in Italy are shown in Fig. 17. Around the track the shadowed portion shows the speeds; on the finishing straight, for instance, speeds of 150 mph are attained. The crosshedged lines show the individual braking distance before the corners. The first corner required braking to 127 mph and then accelerating to 140 mph before the next bend. The sharp radius here necessitates slowing to 75 mph with simultaneous shifting from fifth to third gear. Thus, we provide a complete driving diagram of the racing circuit before the race.

We have endeavored to provide insight into design and calculation of the 2.5-liter Mercedes-Benz racing car. The results of the development are known.

To win a race, enthusiasm and collaboration of all concerned are absolutely necessary from the engineers in the drafting rooms to the experimental and construction departments to the last pipe fitter, and from the organizers to the driver.

Motor-car racing provides the engineer not only with new ideas, but also stimulates the everlasting efforts for the best technical solution. Therefore, it is a powerful impact for improved automobiles to the automobile industry.

ORAL DISCUSSION

Reported by Lloyd E. Muller
General Motors Corp.

P. O'Shea, 1955 U. S. Sports Car Champion: In order to prevent driver fatigue, Mercedes-Benz cars were tailor-made to the driver's dimensions. This allows the driver to maintain a greater sustained speed with less chance of accident.

H. Pringham, General Motors Corp.: The conventional car design gives a high moment of inertia, that is, principal masses such as engine, transmission, and axles are divided and placed at opposite ends of the car. Why does Mercedes use this design instead of the Auto Union design, which places its 600-hp, 400-lb engine to the rear of the driver thus giving the car a relatively smaller moment of inertia?

Mr. Arkus-Duntov, General Motors: The lower the moment of inertia of a car, the faster the car will turn—other things being equal. However, this is not the proper criterion by which to judge a car's handling characteristic. The proper moment of inertia is that giving a turning rate which is in proportion to the driver's reflexes. The rate or moment of inertia of the Mercedes is such that any good driver can handle it, while the moment of inertia of the Auto Union is such that only one driver can handle it. I personally favor the higher inertia of the Mercedes.

F. R. McFarland, General Motors Corp.: Also to be considered is the question of the relation of the center of air resistance to the center of gravity of the car with respect to stability, the center of air resistance ordinarily being very much forward.

Use of

TEMPERATURE-DENSITY

for Measuring Antiknock Quality

Bruno R. Siegel, Sinclair Research Laboratories, Inc.

This paper was presented at the SAE Annual Meeting, Detroit, Jan. 17, 1957.

FUEL-ENGINE adaptation work can be simplified by describing both fuel and engine behavior on the basis of compression temperature and compression density (T-D) since these two factors predetermine the combustion characteristics of fuels as well as engine fuel requirements. Since it is difficult to obtain instantaneous measurements of these factors, calculated values were used.

Use of the T-D parameters has the potential of replacing all present ASTM engine test methods and CRC road testing techniques. A critical examination of past and present testing and analytical techniques shows that many engine performance characteristics are unsuitable as variables for forcing fuels into the knocking zone. That is, such relationships as spark advance, rpm, air-fuel ratio, or compression ratio, which plot parabolically against power or efficiency, do not permit description of fuel quality over a large enough range of operating temperatures and pressures. In contrast, knock-limited manifold air pressure relationships plot hyperbolically and, therefore, permit rectification of data by extending graphical treatment to logical termini. This, in turn, results in the development of stable mathematical formulas for rigid classification of pure hydrocarbons with respect to their knocking behavior.

It is demonstrated that the fundamental limitations of existing test methods can be eliminated by operating the laboratory engine at constant fuel-air ratio and peak power spark and by using manifold air pressure to stress fuels into the knocking zone. Data obtained in this manner can be analyzed to describe fuel antiknock or antipreignition quality at an infinite number of combinations of compression ratio, inlet temperature, and manifold pressure by a single curve or formula.

Fuel additives, especially tetraethyl lead, produce bulges in the curves of the base fuels. These secondary curves emanate from and return to the

THIS paper explains the temperature-density concept used to measure the antiknock quality of fuels. In this method a laboratory engine is operated at constant fuel-air ratio and peak power spark, with manifold air pressure being used to stress fuels into the knocking zone.

According to the author, the data obtained can be analyzed to give a single curve or formula expressing antiknock quality or preignition resistance at any combination of compression ratio, inlet temperature, and manifold pressure.

The paper summarizes 14 practical applications, including suggestions for new control and auxiliary test methods for studying knock and autoignition behavior on a much broader basis than is possible with ASTM methods.

curve of the base fuels, depending on the T-D response of the additive. There are strong indications that the effect of a given amount of tetraethyl lead in a fuel over the realistic compression temperature range assumes a parabolic relationship easily expressed by formula.

Tests in progress at our laboratories have covered a range of 1000 R in compression temperature. They have demonstrated the feasibility of constructing T-D frameworks of blends of pure hydrocarbons. These frameworks can be superimposed on one another to show the relationship of their combustion characteristics. The intersections of the T-D lines of pure hydrocarbons are also used to calibrate the laboratory engines for exact agreement with published frameworks.

Fuel requirements of full-scale engines on the test stand or on the road (on a T-D basis) are established by operating the engine under well-specified sets of operating conditions and determining the exact blends of various types of reference materials which knock. The combination of temperature and density at which the laboratory engine has to be operated to rate these same blends equal is then ascribed to the full-scale engine as its "T-D requirement."

Byproducts of the tests were the discoveries that (1) the existing octane-number scale can be utilized by use of a linear relationship which also permits logical extension in both directions; (2) the earlier findings of D. B. Brooks that the absolute end of the octane-number scale is 130 "octane" could be substantiated; (3) it would be ill-advised to associate an extended octane-number scale with only one other set of reference materials, such as isooctane plus tetraethyl lead; and (4) the differences in the shapes of the T-D curves of leaded and nonleaded fuels offer a plausible explanation of the long-standing paradox that engines become milder as compression ratio is increased, while physical law says this cannot be true.

Present Test Methods Inadequate

The acceptance of knock measurements made by the four ASTM knock-testing methods both here and abroad is chiefly the product of two factors: reliability of ever-improving test equipment and excellent reproducibility of test results. The significance of test results has been a questionable factor.

Critical examination of the reasons for the present dignified status of the methods focuses attention on the laboratory equipment—the single-cylinder, variable-compression-ratio test engine used without basic modification since early in the second quarter of this century. This is a tribute to the individuals, technical committees, and companies responsible for its creation and continued improvement. It is, likewise, a particular tribute to the Waukesha Motor Co. which has been the sole manufacturer of the test unit. It is concluded that it is the enviable, nearly three-decade record of a manufacturer's full cooperation with technical societies; it is the assumed continuation of such cooperation and not the particular breed of numbers delivered which merits consideration of the methods as international standards for knock measurement.

The other factor is the excellent reproducibility obtained. But here again, it is the equipment, instrumentation, reference fuel system, operating manuals, and years of experience which are responsible for the fact that the ratings delivered can be used confidently in specifications. It is not that particular operating conditions are sacred to repeatability and reproducibility.

The history of knock testing raises an important question. The ASTM has four highly standardized test methods for measuring the antiknock quality of gasoline, all using the same basic laboratory equipment. The CRC has as many methods for rating fuels in vehicles and still others for obtaining stationary and vehicular engine fuel requirements. Why cannot all these methods be related mathematically or graphically?

The answer seems to lie in the fact that every additional road or laboratory method was developed without sufficient regard for the systematic handling of the operating conditions most important to antiknock measurement, namely, manifold pressure, inlet temperature, spark advance, fuel-air ratio, and compression ratio. It is believed that this, plus the fact that by far most of the effort for both road and laboratory methods has been expended in the direction of improving reproducibility, has unnecessarily complicated the field of knock testing.

The complex fuel-engine adaptation problem manifested by knocking and preignition can be simplified by describing both fuel and engine behavior on the basis of compression temperature (T_c) and compression density (P_c). These parameters can be applied in all areas of the problem. Therefore, they have the potential of modifying or replacing all of the ASTM and CRC engine test and analytical procedures related to knock testing.

The paper explains the physical and analytical mechanisms whereby these parameters might be applied to routine testing. It is demonstrated that the fundamental limitations of existing test methods can be eliminated by operating the laboratory engine at constant fuel-air ratio and peak power spark and by using manifold air pressure to stress fuels into the knocking zone. Data obtained in this manner can be analyzed to describe the antiknock or antipreignition quality of a fuel at an infinite number of combinations of compression ratio, inlet temperature, and manifold pressure by a single curve or formula. Curves of this type are being developed on a variety of fuels in our laboratories. They cover the temperature range 800–1800 R, which amply brackets the compression temperatures developed in cars on the road.

Other investigators will recognize the type of data presented as being strikingly similar to that contained in many technical papers. Even the fuels used have often been used before to show the effect of various engine operating conditions on detonation. The only innovations were the use of peak power spark at all operating conditions, the use of standard ASTM equipment, and the fact that a larger combination of compression ratio, mixture temperature, and manifold air pressure was covered.

While the data have been used to inject a note of caution into the presently popular idea of extending the octane-number scale by assigning a value of 120 octane number to isooctane +6.0 cc tel per gal and while they have been used to discuss the effect of

temperature on the decomposition and antiknock action of tel, these studies were byproducts of the data.

Development of Hypothesis

It is recognized that although the four ASTM methods for rating gasoline enjoy worldwide acceptance, they leave much to be desired when they are compared to each other and to full-scale engine operation. It was recognized also that redesigned cylinders, new instrumentation, or other modified laboratory equipment may be forthcoming but that such modified equipment by itself will not result in the delivery of more significant knock ratings. It will still be the particular operating conditions selected which dictate the relative order in which fuels are rated. It was realized also that, to be practicable, any new scheme must be so simple that data can be obtained and fully analyzed on an engine operator level and that such test results must be interpretable to the layman. It follows without question that, for results to be significant, operating conditions, test technique (criteria), and the manner of expressing results have to be tied to the basic variables—time, temperature, density, rather than to one symptom of the engine syndrome.

The approach was based on the proposition that the combustion environment of the full-scale engine can be recreated in the laboratory engine, thus capitalizing on the great versatility of the present ASTM laboratory engine. Not only can this engine be operated over an extremely wide range of compression temperatures but any particular compression temperature may be obtained by any number of combinations of compression ratio and mixture temperature.

The chief objective of the project was to determine whether or not conventional T_c and P_c formulas could be used as more fundamental parameters in evaluating antiknock quality.

This objective in no way questioned the validity of the theory, but there *was* conflicting evidence regarding the practical application of these parameters. The theory and supporting data of Rothrock[1] held that there is a temperature-density (T-D) relationship for knocking conditions which can be expressed as a single curve. The other fundamental variable, time, was still considered a nebulous factor. While the study concerned itself with end-gas conditions, later work of Rothrock and his associates held that a similar relationship existed even if the T-D relationships of the compressed but unburned charge of fuel and air were considered. The analysis of the data obtained by the Armed Services/Industry Cooperative Group on Fuel Rating[2] (ASI) supported this; in fact, it demonstrated among other things that a single test unit could be used to obtain reliable predictions of aviation fuel behavior under both take-off and cruise conditions. The altitude chamber tests,[3] on the other hand, showed that the formulas could not be applied to solve the barometric pressure rating variation problem then existing with the ASTM Motor and Research Methods; so empirically developed operating conditions based on the theory had to be found to solve the problem. In this case, however, it was reasoned that other fundamental limitations of the methods prevented the formulas from being applicable. Shortly thereafter, work with a small-scale knock-testing engine developed by the Waukesha Motor Co. for possible use in the Quartermaster Corps Mobile Petroleum laboratory demonstrated that operating conditions could be selected which would result in this engine delivering both Motor and Research Method ratings.[4] This latter project proved that equipment design is not sacred to the type of numbers delivered.

The hypothesis developed from a critical examination of the aforementioned test programs was that the formulas are applicable provided ignition timing is adjusted for peak power or at a constant advance or retardation from peak power at every operating condition at which data is to be recorded, and provided that fuel-air ratio and engine speed is held constant. It was reasoned that any series of T-D curves will have to be studied independently by cross-plotting and interpolation. It was considered that these innovations would in large measure overcome the fundamental limitations of the four ASTM test methods for rating fuels.

At the onset of the test program it was anticipated that, if the hypothesis were proved true, a new "control" method as well as several auxiliary methods for determining fuel sensitivity would suggest themselves automatically from the location of modern engines on the T-D charts. For this reason the bulk of the data were obtained at the more realistic operating conditions. For example, thus far data have been obtained at only 0.078 F/A (12.8 A/F). It is at this point that the curve describing power output across the F/A range reaches its peak.

The same anticipation influenced the decision to concentrate testing time on the 1000 rpm engine speed. This choice results from several compromises. The torque curve on this engine peaks at 1800 rpm. It seems consistent with the contention that in fairness to the refiner the rating number assigned to his product should be obtained at those operating conditions desired by the test engine for peak performance. That is, peak power spark, peak F/A, peak torque, and the like, so that ratings might confidently be expressed in terms of "peak performance numbers." On the other hand, sampie size is a factor to be considered for a routine method and from this standpoint a speed of 600 rpm is attractive. Ultimate decision, therefore, should consider smoothness of operation and sample size.

Engine speed per se was not considered to be critical to correlation. The concept recognized that rigid classification of fuels on a temperature-density basis eventually would have to be tied to combustion time. Since combustion time, and hence end-gas residence time, changes with both temperature and density, it would be highly impractical to keep the time factor constant. The alternative is to recognize that any T-D chart represents a curved surface in the T-T-D cube and that the level of this curved

---

[1] SAE Transactions, Vol. 48, February, 1941, pp. 51–65: "Fuel Rating—Its Relation to Engine Performance," by A. M. Rothrock.

[2] Department of Defense Report FL205/24: "Final Report, Background and Organization of ASI."

[3] ASTM Special Technical Publication No. 186, July, 1956: "Methods for Reducing the Effect of Barometric Pressure in Measurement of Octane Number," by Bruno R. Siegel.

[4] "Project Log—QMC Engine Tests." Transmitted by Bruno R. Siegel to Harold A. Stiles, chief, Fuels and Lubricants Handling Equipment, Branch of QM R & D Center, Natick, Mass., April 18, 1954.

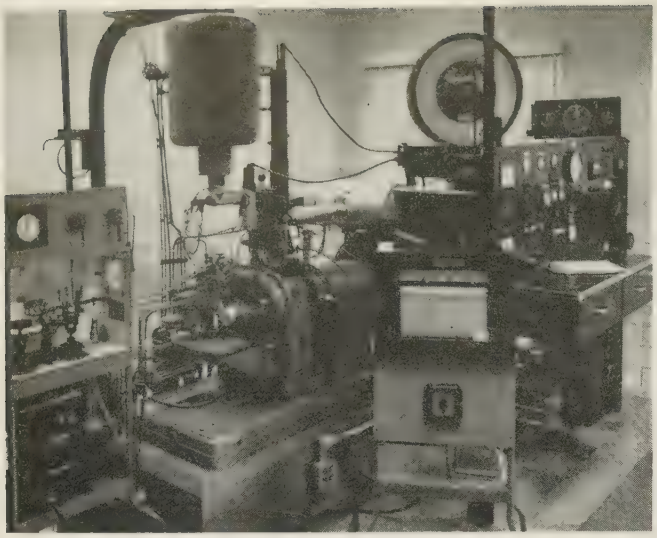

Fig. 1—Test unit, consisting of slightly modified standard equipment used in ASTM supercharge method tests

surface can be changed by changing turbulence. Since turbulence can be changed more effectively by valve shrouding or combustion-chamber configuration than by engine speed, it was reasoned that any desirable speed could be used. Future correlation work will establish whether the decision to concentrate testing time on 1000-rpm operation without valve shrouding has resulted in the combustion time factor being too long. If this should be the case then the remedy would be either valve shrouding or cylinder redesign.

The program was so designed that, if the hypothesis could not be proved the data could still be used to explore other methods of expressing antiknock quality on a two-dimensional basis as suggested in an earlier discourse.[5] As indicated, the program was begun with the deep conviction that the whole field of knock testing needs simplification both in the laboratory and on the road. This line of reasoning automatically developed into secondary hypotheses: (1) The four present ASTM test methods using different test units can be replaced by one standard unit operated over a series of conditions which can be related graphically and, perhaps, mathematically; and (2) a revision to road-testing techniques and full-scale aviation piston engine requirement techniques should make it possible to relate present and future engines to the new laboratory methods.

Test Unit

All data were obtained using the SRL constant temperature test methods for rating fuels.[6] These were developed chiefly from knowledge gained from Rothrock, Barber, et al.,[7] the work of the ASI, the API/ASTM/NBS altitude chamber tests and the QMC small-scale correlation tests. The test unit was composed essentially of standard equipment used with the ASTM supercharge method (D-909). The only modifications of the equipment were the use of a variable speed dynamometer and a slight change in piston rings. The test unit was completely described in a previous report[8] and is shown in Fig. 1.

It was considered unnecessary to use the shrouded inlet valve. Cyclic variation is considered to be much less than that encountered with the supercharge method. This may be due largely to the increased turbulence and resulting improved vaporization and mixing of the charge afforded by use of the standard mixture heater between the injection nozzle elbow and inlet port.

Table 1—Calculated Compression Temperatures at Various Compression Ratios and Mixture Temperatures

Compression Ratio	Compression Temperature, R Mixture Temperature		
	100 F	200 F	300 F
4/1	889	1048	1207
5/1	957	1129	1300
6/1	1018	1200	1381
7/1	1071	1261	1453
8/1	1120	1320	1520
9/1	1163	1372	1580
10/1	1207	1421	1638
11/1	1246	1469	1691
12/1	1280	1511	1740
13/1	1315	1551	1786

While an oscilloscope with various pickups was used early in the program, it was felt that audible incipient knock served equally well as the criteria. A stethoscope with pickup rod placed on the spark-plug gasket served remarkably well as an aid to the ear.

Operating Conditions and Test Technique

The following operating conditions were used:

Fuel-air ratio: 0.078 ± 0.004

Engine speed: 1000 rpm (some data obtained at 600, 2000, and 3000 rpm)

Spark advance: variable with compression ratio and manifold pressure as described by formula presented

Spark-plug gap: 0.020 ± 0.003 in.

Breaker-point gap: 0.020 in.

Valve clearances: 0.008 ± 0.0005 in., measured with engine hot and running at equilibrium under these conditions, Isooctane fuel; 7/1 compression ratio; manifold air pressure, 30.0 in. of Hg abs; F/A, 0.078

Crankcase lubricating oil: SAE 50 viscosity grade

Oil pressure: 60 ± 5 psi

Oil temperature: 175 ± 5

Coolant temperature: 212 F

Fuel-pump pressure: 15±2 psi in the gallery

Fuel-injector opening pressure: 1200 psi ± 100 psi

Mixture temperature: 100, 200, and 300 F

Air temperature: Commensurate with mixture temperature. It was controlled so that the mixture temperature being used was obtained by supplying no more than 4.0 amp to the mixture heater.

Intake air humidity: 70 (maximum) grains of water per pound of dry air

Standard knock intensity: Light knock as determined by ear

Temperature-density response curves were developed by first establishing relationships between knock-limited manifold air pressure and compression ratio (K-L MAP/CR). That is, the engine was

[5] "1-D Octanes: 3-D Minds," by Bruno R. Siegel. Address to Chicago Regional ASTM-DCC Group, Chicago, Sept. 11, 1953.

[6] Sinclair Research Report No. 54-12, March 26, 1954: "Elements of the SRL Constant Temperature Engine Test Methods for Rating Fuels," by Bruno R. Siegel.

[7] API Proceedings III, June 2–3, 1947: "Some Characteristics of Combustion in the ASTM-CFR Knock Test Engine," by E. M. Barber, L. E. Endsley, Jr., and T. H. Randall.

[8] Sinclair Research Report No. 55-44, Sept. 23, 1955: "Laboratory Apparatus for the SRL Constant Temperature Engine Test Methods for Rating Fuels," by R. G. Moser.

operated at various compression ratios, and at each compression ratio the fuel was made to knock by increasing the manifold air pressure. The K-L MAP/CR points thus obtained were plotted and a smooth curve drawn. Curves of this type were developed at mixture temperatures of 100, 200, and 300 F. The faired K-L MAP values were converted to density values by use of the formulas presented. The K-L density values were then plotted against compression temperature. The points described singular, reasonably smooth curves even though separate and differently shaped K-L MAP/CR curves were obtained at each mixture temperature.

Definitions and Formulas

Compression Temperature—Compression temperature is that temperature which is assumed to exist when the piston is at tdc at the end of the compression stroke. It is a calculated value and is expressed in degrees Rankine. By definition, it is the value obtained by multiplying the fuel-air mixture temperature (in R) by the compression ratio raised to the one-third power. This formula yields values for the 30 specified combinations of T_m and CR given in Table 1. The tabulated values are shown graphically in Figs. 2 and 3.

While many factors not considered by the formula are known to affect compression temperature, it was assumed that they counteract one another to the extent that they could be ignored.

Compression Density—Knock-limited compression density is a term used to describe the density of the fuel-air mixture as it is assumed to exist when the piston is at tdc at the end of the compression stroke and when the engine is operating on a fuel which is producing an audible knock. It is a calculated value and is expressed in terms of lb per cu ft. By definition, it is the value obtained by using the formula:

$$\text{K-L } P_c = \frac{W\ (\text{CR} - 1)}{nD} \qquad (1)$$

where:

K-L P_c = Knock-limited compression density (lb per cu ft)
W = Weight of air being consumed when fuel is knocking (lb per hr)
CR = Compression ratio
n = Number of intake strokes per hour
D = Displacement (cu ft)

At 1000 rpm the formula is:

$$\text{K-L } P_c = \frac{W\ (\text{CR} - 1)}{500 \times 60 \times 37.33} = \frac{W\ (\text{CR} - 1)}{648.09} \qquad (2)$$

The formulas for various compression ratios are shown in Table 2.

It is apparent from the nature of the P_c formulas that knock-limited weight of air plays an important part. Accurate air measurement, therefore, is mandatory. Since conventional means of airflow measurement leave much to be desired from this standpoint, it was considered more reliable to use average values of accumulated data. That is, it was decided to develop formulas from the linear relationship which exists between manifold air pressure and airflow. However, when the lines defining this relationship were drawn through the data and extended to zero air consumption, it was found that

Table 2—Compression Density Formulas for Various Compression Ratios

Compression Ratio	Formula
3.5/1	K-L $P_c = 0.003860W$
4.0/1	K-L $P_c = 0.004630W$
5.0/1	K-L $P_c = 0.006172W$
6.0/1	K-L $P_c = 0.007715W$
7.0/1	K-L $P_c = 0.009258W$
8.0/1	K-L $P_c = 0.010801W$
9.0/1	K-L $P_c = 0.012344W$
10.0/1	K-L $P_c = 0.013887W$
11.0/1	K-L $P_c = 0.015430W$
12.0/1	K-L $P_c = 0.016973W$

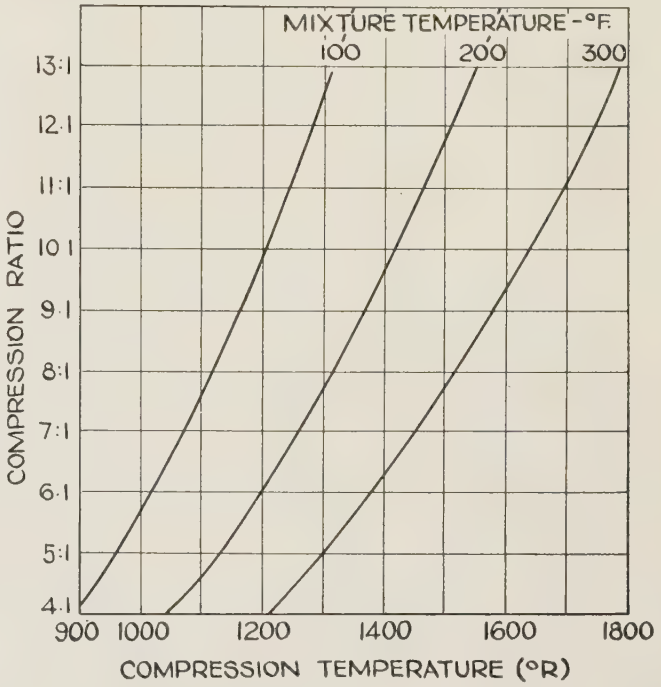

Fig. 2—Calculated compression temperatures at various compression ratios and at given mixture temperatures

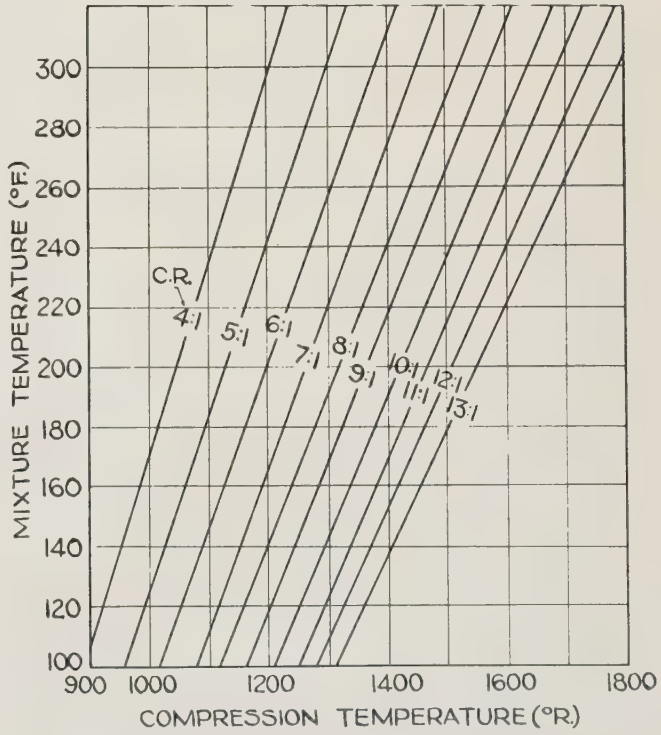

Fig. 3—Calculated compression temperatures at various mixture temperatures and at given compression ratios

Table 3—Formulas for Computing Air Consumption at Various Compression Ratios and Mixture Temperatures

(ASTM engine, 1000 rpm, 0.078 F/A, 212 F jacket, plain intake valve)

Compression Ratio	Mixture Temperature, F	Formulas[a]
3.5/1	100	AC = 1.718 MAP − 9.449
4/1	100	AC = 1.667 MAP − 8.335
	200	AC = 1.488 MAP − 7.440
	300	AC = 1.342 MAP − 6.710
5/1	100	AC = 1.585 MAP − 6.499
	200	AC = 1.422 MAP − 5.830
	300	AC = 1.290 MAP − 5.289
6/1	100	AC = 1.527 MAP − 5.345
	200	AC = 1.376 MAP − 4.816
	300	AC = 1.250 MAP − 4.375
7/1	100	AC = 1.476 MAP − 4.384
	200	AC = 1.336 MAP − 3.968
	300	AC = 1.216 MAP − 3.612
8/1	100	AC = 1.439 MAP − 3.598
	200	AC = 1.304 MAP − 3.260
	300	AC = 1.190 MAP − 2.975
9/1	100	AC = 1.406 MAP − 2.953
	200	AC = 1.277 MAP − 2.682
	300	AC = 1.170 MAP − 2.457
10/1	100	AC = 1.389 MAP − 2.778
	200	AC = 1.263 MAP − 2.526
	300	AC = 1.156 MAP − 2.312
12/1	100	AC = 1.364 MAP − 2.690
	200	AC = 1.252 MAP − 2.490
	300	AC = 1.148 MAP − 2.220

[a] AC = Air Consumption (lb per hr)
MAP = Manifold air pressure (in. of Hg. abs)

Table 4—Formulas for Converting Manifold Air Pressure to Compression Density at Various Compression Ratios and Mixture Temperatures

(ASTM engine, 1000 rpm, 0.078 F/A, and plain intake valve)

Compression ratio	Mixture Temperature, F	Formula[a]
4/1	100	$P_c = 0.00772$ MAP − 0.039
	200	$P_c = 0.00689$ MAP − 0.034
	300	$P_c = 0.00621$ MAP − 0.031
5/1	100	$P_c = 0.00978$ MAP − 0.040
	200	$P_c = 0.00878$ MAP − 0.036
	300	$P_c = 0.00796$ MAP − 0.033
6/1	100	$P_c = 0.01178$ MAP − 0.041
	200	$P_c = 0.01062$ MAP − 0.037
	300	$P_c = 0.00964$ MAP − 0.034
7/1	100	$P_c = 0.01366$ MAP − 0.041
	200	$P_c = 0.01237$ MAP − 0.037
	300	$P_c = 0.01126$ MAP − 0.033
8/1	100	$P_c = 0.01554$ MAP − 0.039
	200	$P_c = 0.01408$ MAP − 0.035
	300	$P_c = 0.01285$ MAP − 0.032
9/1	100	$P_c = 0.01722$ MAP − 0.036
	200	$P_c = 0.01564$ MAP − 0.033
	300	$P_c = 0.01433$ MAP − 0.030
10/1	100	$P_c = 0.01929$ MAP − 0.039
	200	$P_c = 0.01754$ MAP − 0.035
	300	$P_c = 0.01605$ MAP − 0.032
12/1	100	$P_c = 0.02315$ MAP − 0.046
	200	$P_c = 0.02125$ MAP − 0.042
	300	$P_c = 0.01949$ MAP − 0.038

[a] P_c = Compression density (lb per cu ft)

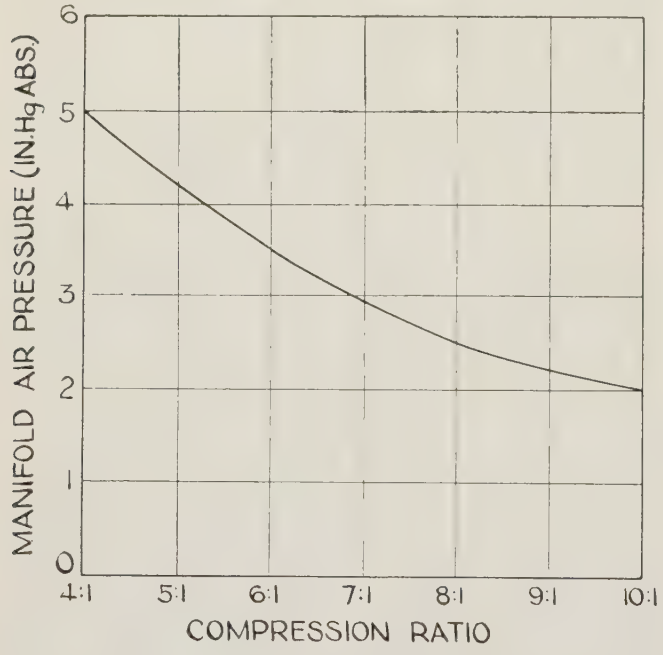

Fig. 4—Manifold pressure at zero air consumption at various compression ratios

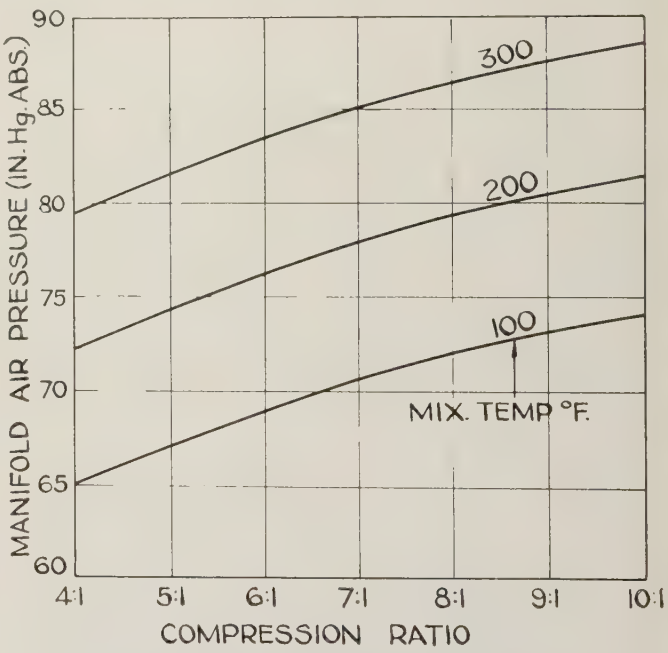

Fig. 5—Manifold pressure required to deliver 100 lb per hr of air to engine at various compression ratios and mixture temperatures

manifold air pressure (MAP) varied with compression ratio, as shown in Fig. 4. While there would be no temperature effects at zero air consumption, of course, and while it was fully realized that the motored engine cannot develop zero MAP, it was not realized that there would be 3-in. MAP difference at zero air consumption between 4/1 and 10/1 compresion ratio. Experiments, therefore, were made which confirmed these findings. The individual air consumption versus MAP lines as established at the seven compression ratios and three temperatures were then extended to 100 lb per hr air consumption. The 21 lines crossed the 100 lb per hr mark as shown in Fig. 5. Formulas for 3.5/1 and 12/1 compression ratio were obtained by extrapolating the slopes and constants of the other formulas. The complete set of formulas as derived from these data are given in Table 3.

Elaborated tables were developed in increments of 0.1 in. of Hg between 10 and 80 in. of Hg MAP. These tables are not reproduced here because of their bulk but prints of them are obtainable from our laboratories. The tables are necessary for maintaining a fuel-air ratio of 0.078 if continuous air measurement is foregone.

It is considered that the development of reliable tables of this sort would greatly simplify development of a control method based on this concept since the induction system could be limited to that portion of the standard ASTM Supercharge Method induction system which is downstream of the MAP regulating valve inlet. This also eliminates the leakage problem since MAP is not materially affected by external leakage.

Substitution of the respective formulas given in Table 3 for W in the preceding formulas permits direct conversion of MAP to P_c. These reduced formulas are given in Table 4.

Peak Power Spark Advance—By definition, peak power spark advance is the lowest spark advance required for the engine to deliver its maximum power at a given set of operating conditions. It is assumed that this value is unaffected by fuel type or mixture temperature at 1000 rpm. However, it does vary with compression ratio and manifold air pressure. The following general formula describes ignition timing for the operating conditions specified:

$$\text{Spark advance} = \frac{121.9}{(CR-1)\ (MAP)} + \frac{1}{0.0025\ CR + 0.0275} \quad (3)$$

At various compression ratios this formula reduces to the quantities shown in Table 5.

Test Fuels

Test data were obtained on blends of the primary reference fuels isooctane in n-heptane, isooctane with additions of 0.5, 1.0, 2.0, 3.0, and 6.0 cc tel per gal, diisobutylene in n-heptane, and diisobutylene in isooctane.

Presentation of Data

A total of 68 data points were obtained on isooctane, covering a compression ratio range of 3.5/1 to 12/1. Repetitious ratings were obtained since it was felt that if the hypothesis could not be proved on isooctane it could not be proved at all. An analysis of about a fourth of these points (available at the time) was made early in 1954 and upheld the hypothesis. Subsequent tests were made to verify the earlier conclusions. Also, it was considered advisable to combine all data obtained over a three-year period with two cylinder assemblies with various operating hours on the cylinders and to reanalyze all data using averaged air consumption tables. A summary data tabulation on isooctane is given in Table 6. Segregated data tabulations of all the individual observations are not reproduced here, but in the latter part of 1956 they were made available for critical review to both the CRC-MFD Group on Fundamental Expressions of Antiknock Quality and to ASTM RD-1 Section F on Test Method Development.

Less numerous data points were obtained on the isooctane/n-heptane blends. However, the data lend themselves admirably to various types of cross-plots which aid averaging and also make it possible to interpolate accurately. The averaged K-L MAP framework is shown in Fig. 6. The manner in which

Table 5—Spark Advance Formulas for Various Compression Ratios

Compression Ratio	Formula[a]
4/1	$SA = \frac{406}{MAP} + 26.7$
5/1	$SA = \frac{305}{MAP} + 25.0$
6/1	$SA = \frac{244}{MAP} + 23.5$
7/1	$SA = \frac{203}{MAP} + 22.2$
8/1	$SA = \frac{174}{MAP} + 21.1$
9/1	$SA = \frac{152}{MAP} + 20.0$
10/1	$SA = \frac{136}{MAP} + 19.1$
11/1	$SA = \frac{122}{MAP} + 18.2$
12/1	$SA = \frac{111}{MAP} + 17.4$

[a] SA = Spark advance

Table 6—Summary Sheet T-D Data on Isooctane

Compression Temperature, R	Compression Ratio	Mixture Temperature, F	K-L MAP	Air Consumption, lb/hr	K-L Compression Density
804	3.5/1	80	72.7	115.45	0.446
889		100		92.69	0.429
1048	4/1	200	60.6	82.73	0.383
1207		300		74.62	0.346
957		100		65.62	0.405
1129	5/1	200	45.5	58.87	0.364
1300		300		53.41	0.330
1018		100		50.24	0.388
1200	6/1	200	36.4	45.27	0.349
1381		300		41.13	0.318
1071		100		40.34	0.374
1261	7/1	200	30.3	36.51	0.338
1453		300		33.23	0.308
1120		100		33.82	0.366
1320	8/1	200	26.0	30.64	0.331
1520		300		27.97	0.302
1163		100		28.96	0.358
1372	9/1	200	22.7	26.31	0.325
1580		300		24.10	0.298
1207		100		25.28	0.351
1421	10/1	200	20.2	22.99	0.319
1638		300		21.04	0.292
1280		100		19.82	0.337
1511	12/1	200	16.5	18.17	0.309
1740		300		16.72	0.284

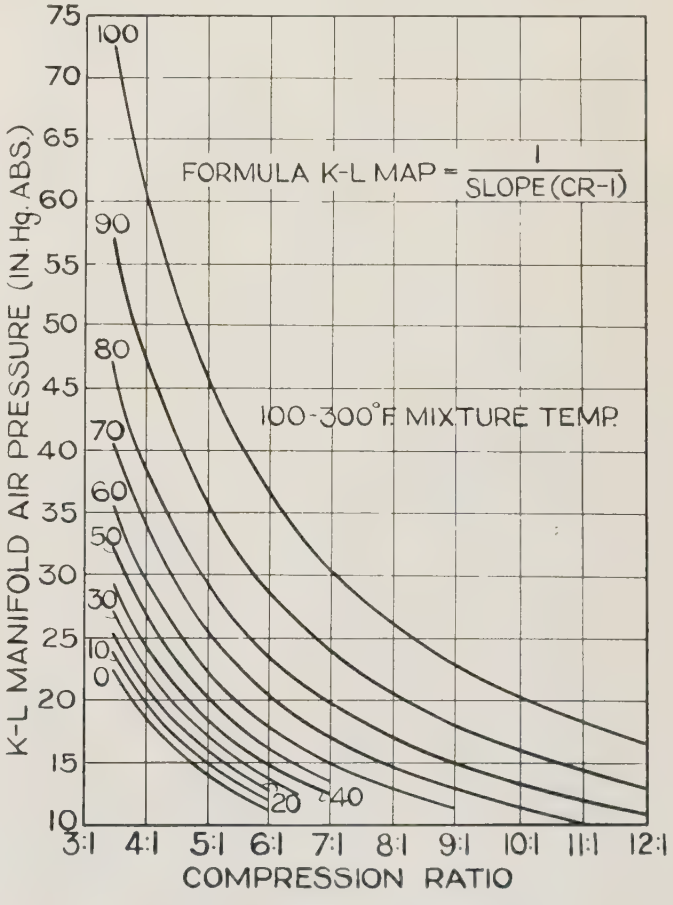

Fig. 6—Knock-limited manifold air pressure of isooctane and normal heptane blends at various compression ratios

observed MAP values differed from the averaged and rectified values is shown in Table 7.

Limited data were obtained on 80, 90, and 100 octane primary reference fuels at 600, 2000, and 3000 rpm and two compression ratios and at several mixture temperatures. At 100 and 200 F mixture temperature the trend was toward higher MAP as speed was increased. At 300 F mixture temperature the trend was reversed but there was considerable discrepancy between the observations on 90 and 100 octane. Since the data were too meager and too inconsistent to be decisive, they were not analyzed beyond the comparative values given in Table 8. This tabulation indicates the K-L MAP differences obtained when the 600, 2000, and 3000 rpm values are compared to the average values obtained at 1000 rpm.

Sixteen data points were obtained on diisobutylene at various compression ratios and at three mixture temperatures as indicated in Table 9. A similar series of observations were made on blends of diisobutylene and n-heptane (Table 10) and on blends of diisobutylene and isooctane (Table 11).

Anticipated increased interest in antiknock ratings above 100 octane prompted the development of K-L MAP versus CR curves on isooctane plus 0.5, 1.0, 2.0, 3.0, and 6.0 cc tel per gal. The surprising shape of these response curves (as discussed in the next section) in turn prompted use of a larger experimental range. The observed and faired values obtained are given in Table 12.

Data Analysis

In general the data obtained at 1000 rpm were analyzed by segregating the K-L MAP points with respect to mixture temperatures and plotting them against compression ratio. These average curves were plotted against reciprocal MAP and rectified. Values extracted from the three curves describing the K-L MAP-CR-relationship of a given fuel at the three mixture temperatures (100, 200, and 300 F) were converted to T-D values. These were plotted and cross-plotted several ways as will be described. Final rectification was on the basis of those plots and cross-plots in which the curves could be extended to logical termini. This analytical procedure revealed some interesting details and unexpected relationships.

Table 7—Deviation of Average Manifold Air Pressure from Faired Values for Blends of Isooctane in Normal Heptane

Octane No.	Compression Ratio (in. of Hg abs) 3.5/1	4/1	5/1	6/1	7/1	8/1	9/1	10/1	12/1
0	−0.7	+0.5							
20	−0.8	−0.1		+0.3					
50	−2.3	−0.9	−0.2	+0.4		+1.0			
60		−0.8		+0.1					
70		−1.0		+0.1					
75		−0.7		+0.3					
80		−1.7		+0.3					
82						+0.3			
82.5		−1.7		+0.1					
84						−0.1			
85		−2.7		−0.1		−0.3			
86						−0.3			
87.5		−2.5		−0.2		−0.3			
90		+0.1	−3.2	−1.9	−1.7	−1.1			
92				−0.1		+0.1			
92.5		−2.8		+0.4		−0.3			
94				−0.3		0.0			
95		−1.8		−0.3	−1.2	−0.9			
96				+0.7	−1.4	+0.8			
97.5		+4.0		+1.1		−0.4			
98				+0.3		+1.4			
100	−8.7	−2.4	0.0	−0.2	+0.3	+0.1	−0.5	0.0	+0.4

Table 8—Deviations in Knock-Limited Manifold Air Pressure of Various Isooctane/n-Heptane Blends

(from respective values accepted for 1000 rpm for mixture temperatures between 100 and 300 F)

Octane Number	Engine rpm	Compression Ratio 6/1 Mixture Temperature 100 F	6/1 200 F	8/1 200 F	8/1 300 F
80	600	−1.5	−2.5	–	–
	2000	–	–	–	–
	3000	–	+0.5	–	–
90	600	−2.1	−1.6	+1.1	–
	2000	+5.4	+5.4	+2.6	−0.4
	3000	–	–	+5.1	−0.4
100	600	−1.9	−0.9	+1.0	–
	2000	+8.6	+8.1	+1.5	−4.0
	3000	–	–	+3.0	−4.0

Table 9—Summary Data on Diisobutylene (SR-10)

Operating Conditions: Compression Temperature, R	Compression Ratio	Mixture Temperature, F	Faired Values: 1/K-L MAP	Air Consumption lb/hr	K-L Compression P_c	1/K-L P_c	K-L MAP	Observed: K-L MAP	Deviation
1048	4/1	200	1.69	119.82	0.555	1.80	85.6	89.0	+3.4
1207	4/1	300	1.51	82.25	0.381	2.62	66.3	59.5	−6.8
957		100	1.39	107.67	0.665	1.50	72.0	76.0	+4.0
1129	5/1	200	1.76	74.97	0.463	2.16	56.8	–	
1300		300	2.43	47.77	0.295	3.39	41.1	36.0	−5.1
1018		100	1.69	76.43	0.590	1.69	53.6	53.5	−0.1
1200	6/1	200	2.50	50.26	0.388	2.58	40.0	45.0	+5.0
1381		300	3.66	29.79	0.230	4.35	27.3	26.5[a]	−0.8
1071		100	2.41	56.89	0.527	1.90	41.5	42.0	+0.5
1261	7/1	200	3.38	35.62	0.330	3.03	29.6	31.0	+1.4
1453		300	5.26	19.54	0.181	5.52	19.0	19.5	+0.5
1120		100	3.05	43.67	0.472	2.12	32.8	30.0	−2.8
1320	8/1	200	4.48	25.81	0.279	3.58	22.3	20.0	−2.3
1520		300	7.52	12.86	0.139	7.19	13.3	14.5	+1.2
1163		100	3.76	34.41	0.425	2.35	26.6	24.5	−2.1
1372	9/1	200	5.81	19.27	0.238	4.20	17.2	–	
1207		100	4.59	27.49	0.382	2.62	21.8	20.0	−1.8
1421	10/1	200	7.41	14.54	0.202	4.95	13.5	–	

[a] Average of two points.

The first of these concerned the unreliability of continuous air measurement. At the onset of the program the relationship between K-L MAP and CR was not considered significant or even particularly interesting. Test results, therefore, were put directly on a T-D basis by use of the unsimplified density formula and by using individual air measurements. Plots of such values indicated that the formulas successfully resolved the effects of mixture temperature. That is, the three K-L MAP versus CR curves on a given fuel which had been obtained at 100, 200, and 300 F mixture temperature respectively would plot as a singular T-D curve. However, the data were inconsistent.

In order to establish whether data point scatter was due to poor test reproducibility or to formula inadequacy, knock-limited air consumption was plotted against compression ratio. It was found that the data on some fuels plotted smoothly but on others it was either quite divergent at the same mixture temperature or else it would not cross-plot smoothly against temperature. This was attributed to poor reproducibility until it was discovered that almost all data plotted smoothly against K-L MAP. This, in turn, led to the development of the air consumption tables already described and to the presented reduced formulas for calculating K-L P_c.

Effect of Mixture Temperature on Primary Reference Fuels—It was quite surprising to learn that

Table 10—Knock-Limited Manifold Air Pressure Data on Diisobutylene/N-Heptane Blends

Diisobutylene in n-Heptane, %	889 R T_c (4/1 CR 100 F Mixture)			1018 R T_c (6/1 CR 100 F Mixture)			1120 R T_c (8/1 CR 100 F Mixture)			1200 R T_c (6/1 CR 200 F Mixture)			1320 R T_c (8/1 CR 200 F Mixture)			1520 R T_c (8/1 CR 300 F Mixture)		
	Faired MAP, in. of Hg abs	Observed MAP, in. of Hg abs	Deviation	Faired MAP, in. of Hg abs	Observed MAP, in. of Hg abs	Deviation	Faired MAP, in. of Hg abs	Observed MAP, in. of Hg abs	Deviation	Faired MAP, in. of Hg abs	Observed MAP, in. of Hg abs	Deviation	Faired MAP, in. of Hg abs	Observed MAP, in. of Hg abs	Deviation	Faired MAP, in. of Hg abs	Observed MAP, in. of Hg abs	Deviation
30	25.7	26.5	+0.8	–	–	–	–	–	–	–	–	–	–	–	–	–	–	–
50	34.1	35.0	+0.9	20.5	21.0	+0.5	13.9	17.0	+3.1	18.7	21.5	+2.8	–	–	–	–	–	–
60	36.0	40.0	+4.0	24.7	24.5	−0.2	–	–	–	21.9	24.5	+2.6	–	–	–	–	–	–
70	–	–	–	30.0	30.0	0.0	19.7	20.0	+0.3	25.5	28.0	+2.5	15.7	17.5	+1.8	11.2	14.5	+3.3
80	–	–	–	–	–	–	23.9	24.5	+0.6	–	–	–	–	–	–	–	–	–
90	–	–	–	45.2	41.5	−3.7	28.4	28.0	−0.4	35.3	37.0	+1.7	20.1	18.5	−1.6	12.6	15.5	+2.9

Faired Compression Density Values of Diisobutylene/n-Heptane Blends at Various Compression Temperatures

Compression Temperature	Diisobutylene in n-Heptane										
	0%	10%	20%	30%	40%	50%	60%	70%	80%	90%	100%
900	0.098	0.115	0.135	0.158	0.186	0.223	0.278	0.355	0.475	0.600	0.740
1000	0.090	0.104	0.122	0.142	0.167	0.202	0.255	0.320	0.410	0.508	0.610
1100	0.085	0.096	0.110	0.127	0.150	0.182	0.224	0.276	0.345	0.420	0.494
1200	0.080	0.090	0.101	0.116	0.135	0.161	0.198	0.235	0.285	0.339	0.388
1300	0.076	0.082	0.089	0.100	0.116	0.139	0.165	0.195	0.228	0.262	0.295
1400	0.073	0.077	0.083	0.091	0.102	0.120	0.136	0.155	0.175	0.195	0.217
1500	0.070	0.071	0.075	0.082	0.089	0.098	0.108	0.118	0.129	0.140	0.151
1600	0.068	0.068	0.069	0.071	0.073	0.076	0.079	0.082	0.086	0.090	0.096

Table 11—Knock-Limited Manifold Air Pressure Data on Diisobutylene-Isooctane Blends

Diisobutylene in Isooctane, %	889 R T_c (4/1 CR 100 F Mixture)			1071 R T_c (7/1 CR 100 F Mixture)			1320 R T_c (8/1 CR 200 F Mixture)			Diisobutylene in Isooctane, %	1381 R T_c (6/1 CR 300 F Mixture)			1520 R T_c (8/1 CR 300 F Mixture)		
	Faired	Observed	Deviation	Faired	Observed	Deviation	Faired	Observed	Deviation		Faired	Observed	Deviation	Faired	Observed	Deviation
10	63.1	–	–	31.1	36.0	+4.9	25.4	28.0	+2.6	10	35.8	38.5	+3.0	25.1	–	–
20	66.3	62.5	−3.8	31.8	–	–	25.2	27.0	+1.8	20	35.2	37.5	+2.3	24.3	20.0	−4.3
30	68.8	–	–	32.6	–	–	25.0	27.0	+2.0	30	34.6	37.0	+2.4	23.4	–	–
40	72.3	68.0	−4.3	33.3	–	–	24.8	27.0	+2.2	40	34.1	35.5	+1.4	22.4	18.5	−3.9
50	75.4	–	–	34.1	–	–	24.5	25.0	+0.5	50	33.3	34.0	+0.7	21.5	–	–
60	79.0	–	–	35.2	–	–	24.2	23.0	−1.2	60	32.6	33.0	+0.4	20.4	17.0	−3.4
70	80+	–	–	36.2	–	–	23.9	22.0	−1.9	70	31.6	32.0	+0.4	19.1	–	–
80	80+	–	–	37.6	41.5	+3.9	23.4	–	–	80	30.5	30.5	0.0	17.7	15.5	−2.2
90	80+	–	–	39.0	40.0	+1.0	22.8	20.0	−2.8	90	29.1	29.0	−0.1	15.9	–	–

Faired Compression Density Values of Diisobutylene/Isooctane Blends at Various Compression Temperatures

Compression Temperature, R	Diisobutylene in Isooctane									
	10%	20%	30%	40%	50%	60%	70%	80%	90%	100%
900	0.444	0.466	0.487	0.510	0.534	0.561	0.593	0.634	0.682	0.740
1000	0.407	0.421	0.436	0.451	0.466	0.486	0.510	0.537	0.570	0.610
1100	0.376	0.384	0.392	0.400	0.409	0.421	0.433	0.450	0.469	0.494
1200	0.350	0.352	0.354	0.357	0.360	0.363	0.367	0.373	0.380	0.388
1300	0.328	0.325	0.323	0.321	0.318	0.315	0.313	0.307	0.301	0.295
1400	0.309	0.302	0.296	0.289	0.282	0.273	0.263	0.252	0.236	0.217
1500	0.294	0.284	0.273	0.262	0.250	0.237	0.221	0.204	0.181	0.151
1600	0.280	0.266	0.252	0.236	0.221	0.205	0.182	0.160	0.133	0.096

Table 12—Knock-Limited Manifold Air Pressure Data

Operating Conditions: Compression Temperature, R	Operating Conditions: Compression Ratio	Operating Conditions: Mixture Temperature, F	Faired Values: K-L Compression Density, (Lb/cu ft)	Faired Values: K-L MAP, in. of Hg	Observed: K-L MAP, in. of Hg	Observed: Deviation in MAP, in. of Hg
			Isooctane + 0.5 cc Tel/gal			
889	4/1	100	0.442	62.2	60.0	− 2.2
1018	6/1	100	0.455	42.1	42.5	+ 0.4
1163	9/1	100	0.455	28.3	28.0	− 0.3
1200	6/1	200	0.448	45.7	44.5	− 1.2
1207	10/1	100	0.447	25.2	25.0	− 0.2
1320	8/1	200	0.414	31.9	33.0	+ 1.1
1372	9/1	200	0.394	27.1	25.0	− 2.1
1421	10/1	200	0.370	23.1	24.0	+ 0.9
1520	8/1	300	0.327	27.9	25.5	− 2.4
1580	9/1	300	0.310	23.5	22.5	− 1.0
			Isooctane + 1.0 cc Tel/gal			
889	4/1	100	0.459	64.4	64.0	− 0.4
1018	6/1	100	0.490	45.1	45.5	+ 0.4
1163	9/1	100	0.500	30.9	30.5	− 0.4
1200	6/1	200	0.492	49.8	47.5	− 2.3
1207	10/1	100	0.490	27.4	27.5	+ 0.1
1320	8/1	200	0.457	34.9	35.0	+ 0.1
1372	9/1	200	0.433	29.5	28.0	− 1.5
1421	10/1	200	0.402	24.9	26.0	+ 1.1
1520	8/1	300	0.347	29.5	26.5	− 3.0
1580	9/1	300	0.322	24.4	24.5	+ 0.1
			Isooctane + 2.0 cc Tel/gal			
1018	6/1	100	0.533	48.7	48.0	− 0.7
1163	9/1	100	0.555	34.1	33.5	− 0.6
1200	6/1	200	0.543	54.6	52.5	− 2.1
1207	10/1	100	0.542	30.1	30.5	+ 0.4
1320	8/1	200	0.502	38.1	37.5	− 0.6
1421	10/1	200	0.447	27.5	29.0	+ 1.5
1520	8/1	300	0.379	32.0	28.5	− 3.5
1580	9/1	300	0.342	25.8	26.0	+ 0.2
1638	10/1	300	0.315	21.6	20.5	− 1.1
			Isooctane + 3.0 cc Tel/gal			
889	4/1	100	0.498	69.5	70.0	+ 0.5
1018	6/1	100	0.557	50.8	51.0	+ 0.2
1120	8/1	100	0.580	39.8	39.5	− 0.3
1163	9/1	100	0.579	35.4	35.5	+ 0.1
1200	6/1	200	0.572	57.3	56.0	− 1.3
1207	10/1	100	0.570	31.5	32.0	+ 0.5
1320	8/1	200	0.530	40.1	40.5	+ 0.4
1372	9/1	200	0.503	34.0	32.5	− 1.5
1381	6/1	300	0.498	55.1	55.0	− 0.1
1421	10/1	200	0.472	28.9	30.0	+ 1.1
1520	8/1	300	0.405	34.0	35.0	+ 1.0
1580	9/1	300	0.361	27.1	27.5	+ 0.4
1638	10/1	300	0.324	22.2	21.5	− 0.7
			Isooctane + 6.0 cc Tel/gal			
889	4/1	100	0.517	72.0	71.5	− 0.5
1018	6/1	100	0.594	53.9	58.5	+ 4.6
1163	9/1	100	0.630	38.4	38.5	+ 0.1
1200	6/1	200	0.625	62.3	61.0	− 1.3
1207	10/1	100	0.624	34.3	34.5	+ 0.2
1320	8/1	200	0.575	43.3	46.0	+ 2.7
1372	9/1	200	0.545	36.6	36.0	− 0.6
1381	6/1	300	0.540	59.5	58.5	− 1.0
1421	10/1	200	0.512	31.2	32.5	+ 1.3
1520	8/1	300	0.439	36.6	35.0	− 1.6
1580	9/1	300	0.391	29.2	30.5	+ 0.7
1638	10/1	300	0.345	23.5	23.5	0.0

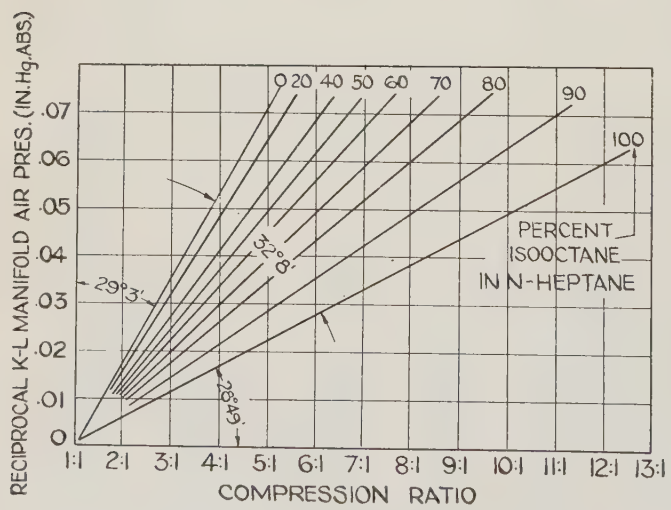

Fig. 7—Reciprocal knock-limited manifold air pressure of isooctane-heptane blends at various compression ratios

mixture temperature had no effect on the K-L MAP of any of the isooctane/n-heptane blends at these operating conditions. The K-L MAP versus compression ratio framework on the primary reference fuels shown in Fig. 6, therefore, is considered valid for the 100–300 F mixture temperature range. It should be remembered, of course, that air consumption varies with inlet temperature and if the same test observations were plotted against air consumption instead of MAP, a separate framework would result for each temperature. It is strictly coincidence that this peculiar relationship between MAP and air consumption exists. In the final analysis, it is the density (in terms of lb per cu ft) that the fuel will recognize and it just happens that several factors apparently balance out on primaries at these conditions. This was not true for other fuels investigated.

Analysis on Basis of Reciprocal Manifold Air Pressure—A plot of the data on the basis of reciprocal MAP confirmed the fact that the primary reference fuel framework is perfectly hyperbolic. This plot is shown in Fig. 7. It will be noted that the relationship is linear and that the lines can be extended to the origin. It seems theoretically sound to say that at 1/1 compression ratio all fuels are equal since all would require infinite supercharging to make them knock. It is believed that this characteristic imparts a rigorism not found in previous reference-fuel frameworks.

Fig. 7 illustrates that it is possible to use polar coordinates to compare various test methods and full-scale engines with respect to their knocking behavior on primary reference fuels. Considerable importance is placed on the fact that a rigorous vectorial angle can be assigned to any isooctane/n-heptane blend. This means that the compression ratio scale can be used as a polar axis with either reciprocal K-L MAP or knock-limited compression ratio used to assign a radius vector to an engine. The knocking characteristics of any reciprocating engine, therefore, can be described over the entire MAP range by the particular type of wedge it creates in this quadrant.

Octane-Scale Extension and other Rating Scales—The fact that the wedge describing the primary-reference-fuel framework shown in Fig. 7 covers only one-third of the quadrant area gives rise to the question of octane-scale extension. The use of polar coordinates gives a somewhat stronger im-

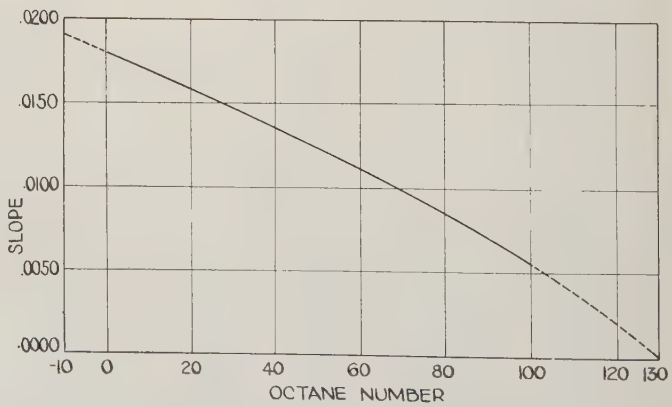

Fig. 8—Slopes of reciprocal manifold pressure versus compression ratio lines of isooctane in n-heptane blends

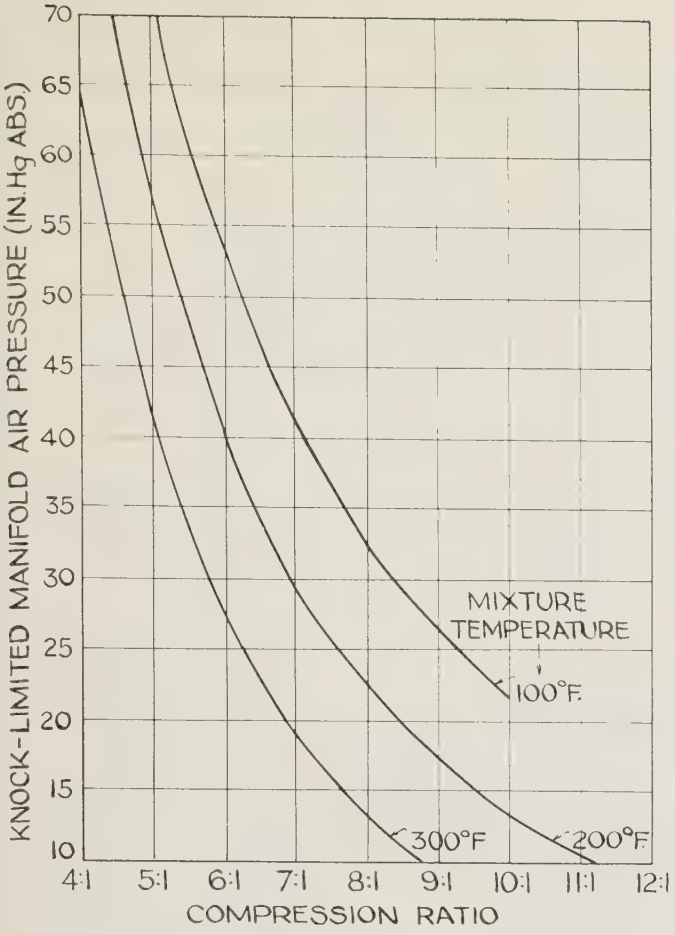

Fig. 9—Knock-limited manifold air pressure of diisobutylene at three mixture temperatures

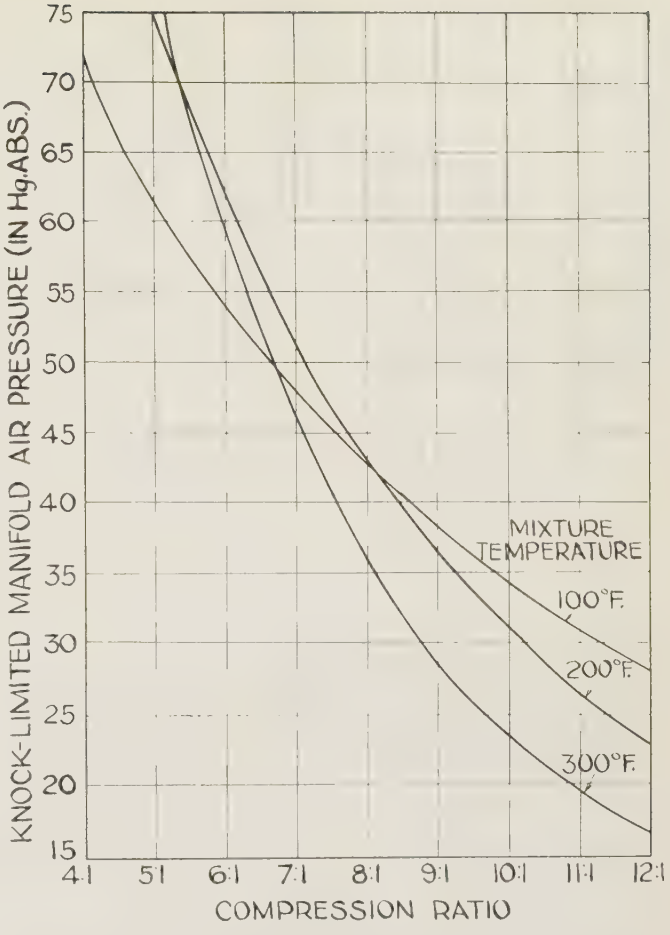

Fig. 10—Knock-limited manifold air pressure of isooctane plus 6.0 cc tel per gal at three mixture temperatures

pression of the reasoning which must be satisfied in this respect. Thus, if the angles (or slopes) of the isooctane/n-heptane framework are considered rigorous it must be possible to assign some "octane number" to any line in the quadrant. This is important since engine operation is in no way limited to the area defined by these hydrocarbons. While experimental data exceeds these bounds in both directions, imaginary engines cover the quadrant and some dispensation regarding their octane-number requirement must be made. The plot gives concrete evidence of the increasing size of octane numbers. They become infinitely small as a 90-deg angle is approached; they become infinitely large as the x-axis (or zero slope) is approached. This means that the scale is hyperbolic and is asymptotic to the scale itself below n-heptane. Fig. 8 shows that it is assymtotic to 130 "octane number" above isooctane.

Fig. 8 is a plot of the slopes and shows that the curve, when extended, assigns an "octane number" of 130 to a line of zero slope. (See Fig. 7). The extrapolation of these data on this basis completely substantiates the earlier findings of Brooks[9] in these respects.

The coordinates used in Fig. 7 suggest a mechanism for an antiknock quality scale or scales. One or more of such charts could be tied to well-chosen operating conditions in a given test engine. The 90 deg of the quadrant could be divided into any desirable parts. The lines arbitrarily drawn in the quadrant would become the "antiknock scale." It would be adequate for present and future engines since the entire MAP and compression ratio ranges are covered and it would have the advantage of not being tied to a particular reference fuel system. However, the scheme is not pursued further because use of temperature-density offers many additional advantages.

Effect of Mixture Temperature on Other Fuels—Data obtained on blends of diisobutylene in isooctane and in n-heptane and the data on leaded isooctane were analyzed in a similar manner. In all cases a separate K-L MAP versus compression ratio curve was obtained at each mixture temperature. This, of course, made it possible to refair the curves on the basis of cross-plots against temperature.

The nature of the K-L MAP versus compression ratio response curves of all blends containing diisobutylene was as expected. That is, the curves developed at the three temperatures formed an orderly series such as shown for diisobutylene in Fig. 9. The lines do not cross; with unleaded fuels, lowering the mixture temperature always requires higher manifold air pressure to produce knock. This was not the case with the leaded primaries. Fig. 10 shows

[9] "Basis for Extension of Octane-Number Scale," by D. B. Brooks. Memorandum to CFR Detonation Subcommittee, Oct. 21, 1933.

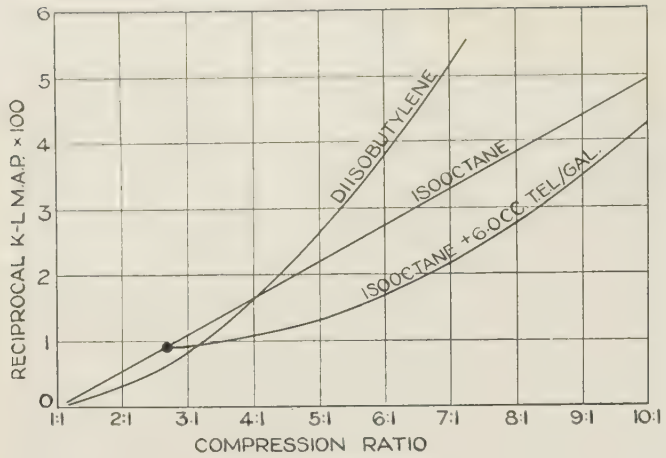

Fig. 11—Reciprocal knock-limited manifold air pressure of three fuels at 300 F mixture temperature

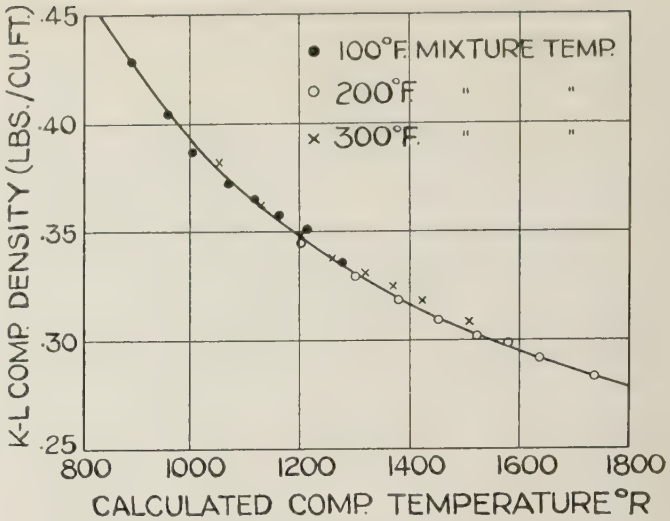

Fig. 12—Knock-limited compression temperature-density curve on isooctane

the response curves obtained on isooctane plus 6.0 cc per gal tel at the three mixture temperatures. The peculiar crossing of these curves seemed to make no sense at all. It could not easily be attributed to experimental error since the curves obtained with other amounts of lead followed the same pattern.

The data, therefore, were subjected to various graphical treatments in an effort to explain the extraordinary differences existing between the behavior of leaded and unleaded fuels. None of these offered reasons why mixture temperature would have opposite effects on leaded fuels at various compression ratios. When the data on the leaded fuels were plotted on the basis of reciprocal manifold air pressure, it was found that the curves could not be extended to the origin. Instead, they seemed to level out at the lower compression ratios and intersect the straight line defining isooctane neat. Fig. 11 compares three diverse fuels on this basis.

Application of Fig. 7 to Test Method Development —The coordinates used in Fig. 7 can be used to compare the knocking behavior of fuels in a given engine or to compare engines with respect to their treatment of given fuels. Fig. 7, which rigorously describes the behavior of the primary reference fuels in a highly standardized test engine, can be used as a basis for comparing: (1) The behavior of other pure hydrocarbons which, when blended with one another, may be used as reference materials; (2) the behavior of refinery components, additives, and finished commercial fuels; (3) the effect of other operating conditions in this same engine; (4) the effect of equipment design changes at various operating conditions; and (5) the degree to which "mechanical octanes" have been built into commercial engines.

The linear relationship between reciprocal manifold air pressure and compression ratio permits rigid establishment of so-called "standard knock intensity guide curves" for a large number of test methods. In the ASTM Motor and Research Methods curves of this type stipulate the compression ratio at which a given octane-number blend should produce "standard" knock intensity at a given manifold air pressure (corrected for barometric pressure). Such guide curves are required for any method and since any number of methods could be adapted by using various combinations of compression ratio and mixture temperature (T_m), Fig. 7 automatically prescribes the MAP at which any octane-number fuel should knock if engine condition is satisfactory. The guide curve for any combination of compression ratio and T_m, therefore, could be described by a general formula developed by combining the equations of the straight lines of Fig. 7 and the equation of the curve of slopes shown in Fig. 8. While the latter equation has not been developed, the lines of Fig. 7 are described by the formula:

$$\text{K-L MAP} = \frac{1}{\text{Slope } (\text{CR}-1)} \qquad (4)$$

where the slope is related to a given octane number. This formula, of course, reduces to dividing a constant by the (CR-1). A number of these constants, related to various octane number blends, are given in Table 13.

An enlightening graphical picture is obtained when the four ASTM knock testing methods are drawn on Fig. 7. On this basis the methods appear "disorderly" and the reasons why they cannot be related or correlated with each other become obvious. At the same time, such an examination points up the advantages which could be gained by designing test methods which acquire their various "severity" levels by more carefully considered differences in operating conditions.

Here again, the scheme is not pursued further because it is felt that use of temperature-density is superior. While the coordinates of Figs. 7 or 11 have the slight advantage of being more readily understood, T-D has a much greater advantage in that it resolves the effects of mixture temperature. True, the lines defining the octane-heptane scale on a K-L MAP versus compression ratio basis remained unchanged between 100 and 300 F T_m at these conditions. But, as explained, this was *coincidence* and it did not hold true for other fuels. Useful as such charts might be, they nevertheless would have to be

labeled with respect to temperature. From the discussion to follow it will be seen that T-D can be used to relate fuels and engines; to develop new or extend the old rating scales; to compare the old or to develop new test methods in the same manner that the K-L MAP versus compression ratio relationship can be used. But the T-D charts do not have to be labeled with respect to inlet temperature.

Analysis of Primary-Reference-Fuel Data on a T-D Basis—The averaged data obtained at 1000 rpm were analyzed on a T-D basis. This consisted of assigning compression temperatures to the various combinations of mixture temperature and compression ratios used as given in Table 1. In other words, the values which the formula yields for these combinations are used as an arbitrary "engine severity" scale.

It is interesting to note the extent to which one of these variables counteracts the other. Near 1200 R the formula says that the temperature effects of six compression ratios can be offset by a 200 deg change in mixture temperature. For example, the following combinations of compression ratio and T_m yield about the same T_c: 4/1 and 300 F, 6/1 and 200 F, or 10/1 and 100 F.

It follows that a given T_c can be obtained by an infinite number of combinations of compression ratio and T_m. While any of these combinations might produce the same T_c, at a given manifold air pressure each would, of course, produce a different compression density (P_c) because air consumption varies with T_m and compression ratio and because pressure (or P_c) varies with compression ratio. A given fuel, then, would require a different air consumption to knock at all of these combinations of conditions.

If the T_c scale is arbitrarily accepted as a good severity scale, the search must be for a formula which resolves the effects of the differences in air consumption and compression pressure existing at any of the various combinations of compression ratio and T_m which might have been selected to produce a certain T_c. This is necessary to prove the theory that a fuel will knock at certain combinations of temperature and density and the fuel cannot distinguish between the infinite number of engine operating conditions which might have been used to create these T-D combinations. Many factors are present which influence each other but the net result is that, in combination, they produce T-D combinations which the fuel recognizes.

The search for such a formula began and ended with the one presented. Table 14 (extracted from Table 6) compares the P_c values which the formula yielded on data obtained on isooctane at the three sets of conditions mentioned earlier and which produces about the same T_c.

As shown, at 1207 R T_c, isooctane knocked at essentially the same P_c even though compression ratio differed by six ratios, manifold air pressure differed by 40 in of Hg, and air consumption differed by 50 lbs per hr. It was concluded that these three data points proved the hypothesis. It was considered significant that the P_c values shown were calculated from *faired* MAP values. This meant that values derived from the formula describing the linear relationship between reciprocal K-L MAP versus compression ratio were convertible to reasonably valid T-D values. It was not a comedy of experimental errors.

This conclusion was substantiated by the analysis of all 68 observations on isooctane. First, it was established that the density values derived from the MAP formula for isooctane across the entire experimental range would plot as shown in Fig. 12. Then, reverse calculations showed that points exactly on the line would require MAP values within experimental error of the faired values shown in Table 6.

The entire primary-reference-fuel framework shown in Figs. 6 and 7 were converted to the T-D parameters by the same mechanism. This resulted in the T-D framework, shown in Fig. 13. Further

Table 13—Formula and Table of Constants for Calculating Knock-Limited Manifold Air Pressure of Various Isooctane/n-Heptane Blends

$$\text{Formula: K-L MAP} = \frac{\text{Constant}}{\text{CR-1}}$$

Octane Number	Constant	Octane Number	Constant
0	55.55	80	117.65
10	59.17	82.5	121.95
20	63.29	85	128.21
30	68.02	87.5	135.14
40	73.53	90	142.86
50	80.65	92.5	149.25
60	89.29	95	158.73
70	102.04	97.5	169.49
75	107.53	100	181.82

Conditions: ASTM engine
1000 rpm
0.78 F/A
212 F jacket
Peak power spark advance
Plain intake valve

Table 14—Comparison of P_c Values from Equation 2

Compression Ratio	T_m, F	K-L MAP	Air Consumption, lb/hr	P_c	T_c, R
4/1	300	60.6	74.6	0.346	1207
6/1	200	36.4	45.3	0.349	1200
10/1	100	20.2	25.3	0.351	1207

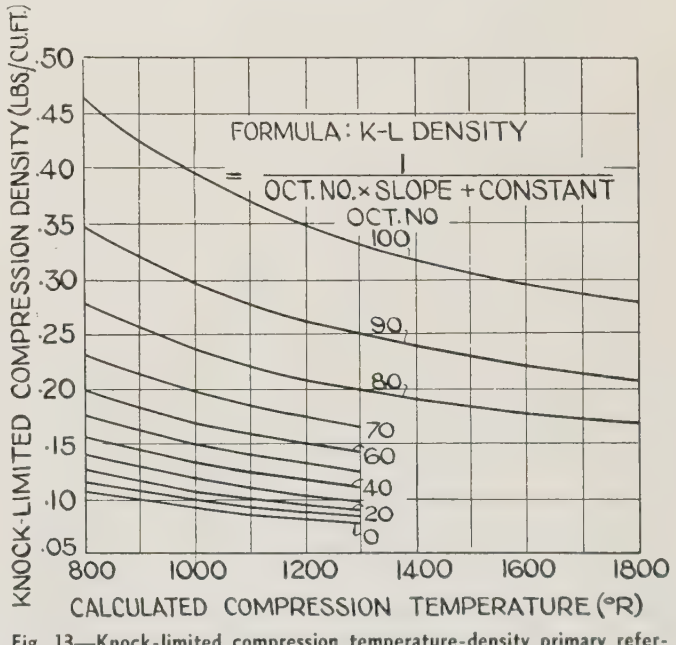

Fig. 13—Knock-limited compression temperature-density primary reference fuel framework

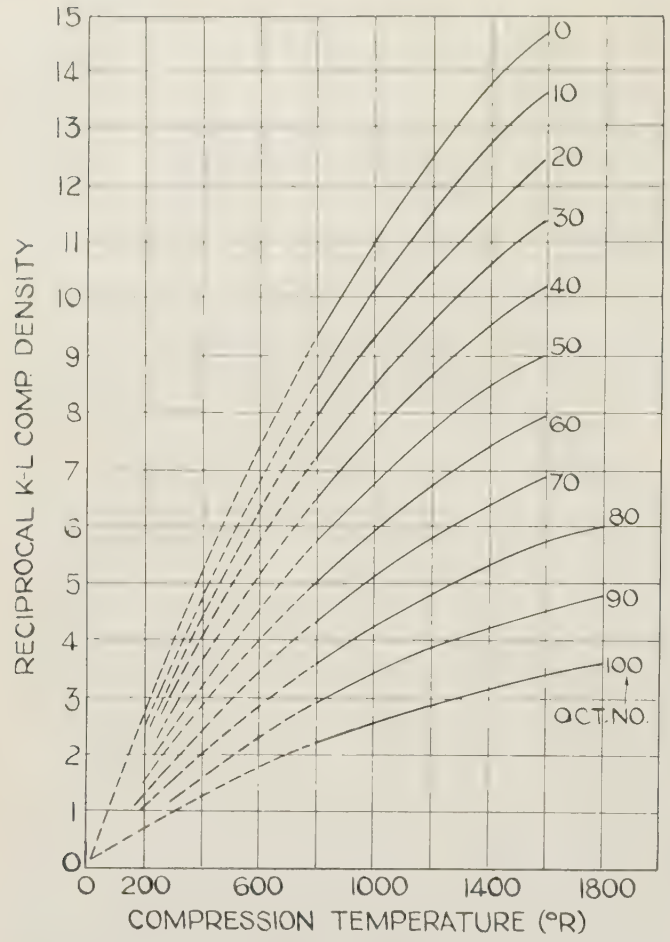

Fig. 14—Reciprocal knock-limited compression density at various compression temperatures

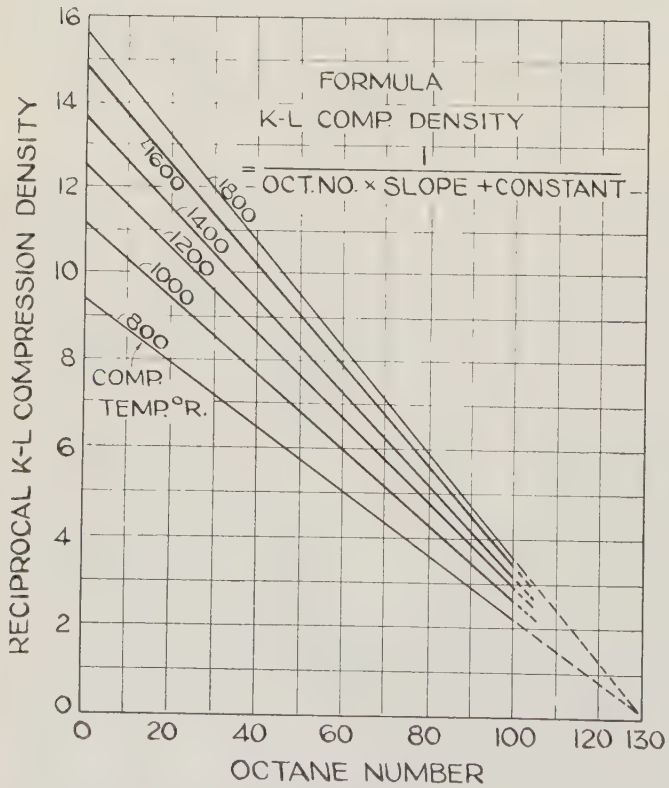

Fig. 15—Reciprocal knock-limited compression density at various octane numbers

Table 15—Slopes and Constants for Calculating Knock-Limited Compression Density of Isooctane/n-Heptane

Formula: $P_c = \frac{1}{\text{Octane No.} \times \text{Slope} + \text{Constant}}$

where: P_c = K-L compression density

Compression Temperature, R	Slope	Constant
800	− 0.0720	9.360
900	− 0.0787	10.231
1000	− 0.0850	11.050
1100	− 0.0907	11.791
1200	− 0.0957	12.441
1300	− 0.1007	13.091
1400	− 0.1050	13.650
1500	− 0.1093	14.209
1600	− 0.1133	14.729
1700	− 0.1167	15.171
1800	− 0.1200	15.600

examination of this framework revealed some attributes which seemed to impart rigorism. When reciprocal P_c values were plotted against T_c, an orderly family of curves was obtained which seemed to emanate from the origin as shown in Fig. 14. Linearity was obtained when the same values were cross-plotted against octane number. As can be seen from Fig. 15, the relationship is linear at any T_c and all of the lines meet the x-axis at 130 octane number. The K-L P_c of any octane-number blend, at any T_c, therefore, can be determined by the formula and the slopes and constants given in Table 15.

Application will entail the construction of large scale segments of the T-D chart. For this reason IMB tables have been prepared using the formula and tabulated slopes and constants. Copies of these tables may be obtained from our laboratories. They cover the 1000 R temperature range in increments of 100 R and cover the octane-number scale in convenient increments.

T-D Response of Diisobutylene Blends—The data on the diisobutylene blends were averaged by the various types of plots described. In addition, the K-L MAP versus CR frameworks could be cross-plotted against T_m. Conversion of these averaged frameworks to T-D values resulted in the construction of Figs. 16 and 17.

Reverse calculations were made to judge the degree to which the data had been rectified. The K-L MAP values so extracted are given and compared to the observed values in Tables 9, 10, and 11. The latter two also include tabulations of averaged T-D values for various blends at even 100 deg T_c increments to facilitate construction of large-scale sections of the frameworks.

Although not reproduced here, Figs. 16 and 17 were subjected to various cross-plots. When extended to the origin, to infinite supercharging, or to conversion points, some of them might be considered academic but, nevertheless, interesting to test method and rating scale development. All were illustrative of the approach which might be used toward the ultimate rigid classification of pure hydrocarbons with regard to their knocking and autoignition propensities.

T-D Response of Leaded Isooctane—It was surprising to learn that a singular T-D response curve could be constructed from values extracted from the three perplexing curves shown in Fig. 10. Where the peculiar crossing of the K-L MAP versus CR curves (as obtained on isooctane plus 6.0 cc tel gal) could not be understood, the singular T-D curve

Table 16—Faired K-L Compression Density Values of Isooctane with Various Additions of Tetraethyl Lead

Compression Temperature, R	Tel in Isooctane, cc/gal					
	0.0	0.5	1.0	2.0	3.0	6.0
800	0.463	0.463	0.463	0.470	0.478	0.487
900	0.424	0.442	0.460	0.485	0.501	0.524
1000	0.392	0.454	0.485	0.526	0.550	0.585
1100	0.368	0.460	0.502	0.551	0.578	0.625
1200	0.349	0.448	0.492	0.544	0.572	0.625
1300	0.331	0.421	0.465	0.511	0.540	0.586
1400	0.317	0.380	0.416	0.460	0.486	0.526
1500	0.305	0.333	0.358	0.394	0.419	0.454
1600	0.294	0.305	0.315	0.331	0.346	0.375
1700	0.286	0.286	0.286	0.288	0.291	0.305
1800	0.278					

on this fuel offered plausible explanation of the antiknock action of tetraethyl lead. The K-L MAP response curves obtained at 100, 200, and 300 F T_m on isooctane with other amounts of tel added were similar in nature to those shown for isooctane + 6.0 cc tel per gal in Fig. 10. Conversion of all of these averaged K-L MAP versus CR curves to T-D values resulted in the construction of the leaded isooctane framework shown in Fig. 18. Reverse calculations again were used to determine the MAP which would be required for the data points to be exactly on the lines of the rectified framework. The values so obtained are compared to the observed values in Table 12. Table 16 lists the faired K-L P_c values of the framework in more convenient T_c increments.

Discussion

A study of the four T-D frameworks presented opened many new avenues of thought along the lines of the following discussions. The 235 data points left little room for doubt concerning proof of the hypothesis. The tests had covered a T_c range of nearly 1000 deg which had been obtained in the compression ratio range of 3.5/1 and 12.0/1 and at T_m of 100, 200, and 300 F. A P_c range of .07 to 0.70 had been covered by varying MAP from 10 to 80 in. of Hg abs. In all areas and with all fuels the T-D formulas had successfully resolved the various K-L MAP/CR curves into singular T-D response curves. This meant that the T_c scale could be used as a practical engine severity scale and that the P_c scale was a better scale of knock-limited power than imep because the P_c formulas resolved the effects of T_m.

The range of experiments had amply bracketed the operating range of past, present, and future engines. The fact that such a large experimental range had been covered made it relatively safe to extend graphical treatment to logical termini. While this imparted a rigorism not often present in conventional analytical schemes, the chief interest in the T-D charts stemmed not only from rigorism but from contrast.

A new appreciation of contrasting fuel behavior was obtained by superimposing one or more of the frameworks on each other. While somewhat academic, the same charts converted to reciprocal P_c reflected great contrast in the types of formulas required to describe fuel quality across the realistic range and into the theoretical areas.

By superimposing charts of this type and by ex-

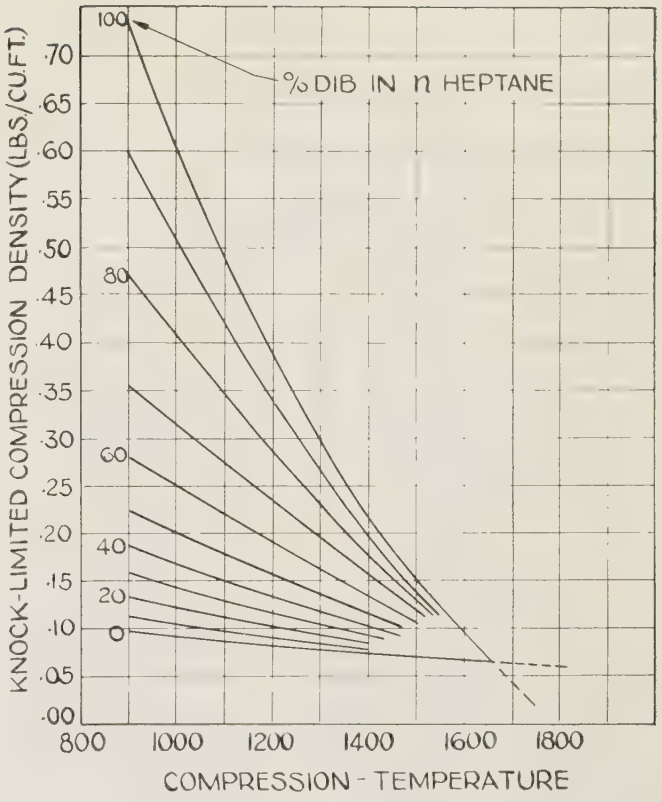

Fig. 16—Knock-limited compression temperature-density framework of diisobutylene in n-heptane

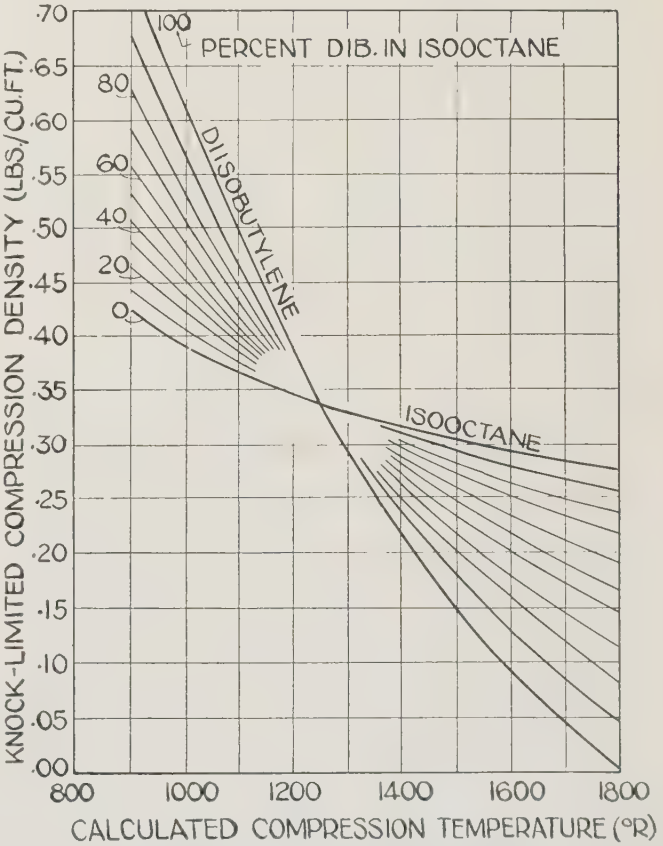

Fig. 17—Knock-limited compression temperature-density framework of diisobutylene in isooctane

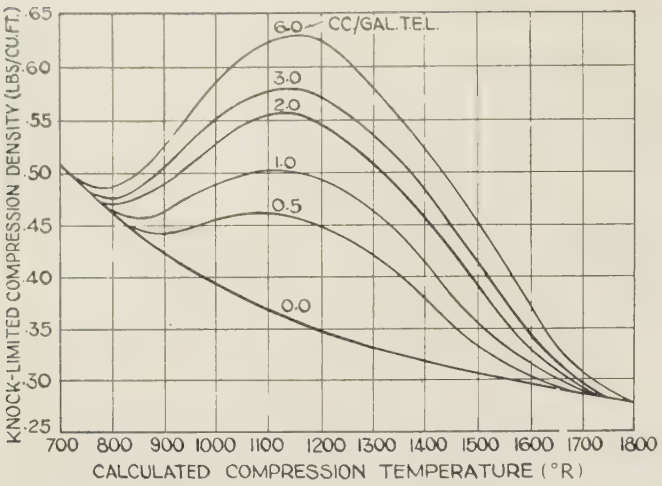

Fig. 18—Knock-limited compression temperature-density curves of leaded isooctane

amining the contrasting types of stable mathematical formulas involved, a new approach to problems in any area of fuel-engine adaptation or fuel-quality evaluation was obtained. Full exploration of such topics is not possible here, but the following discussions illustrate the extent of potential applications.

Effective Use of Tetraethyl Lead and Other Additives—One of the most interesting facets of the use of T-D for measuring antiknock quality concerns the evaluation of fuel additives, especially antiknock compounds and tetraethyl lead. The data available on leaded fuels furnishes plausible explanations to classic and sometimes frustrating paradoxes concerning the "road ratings" of leaded and nonleaded fuels as compared to their laboratory ratings. They also show the factors limiting the use of tel in any reference fuel or "octane scale extension" scheme. While these are areas of great current interest and will be discussed later, perhaps the most important guidance which the data can give concerns the effective use of tel.

From the test data it is concluded that the T-D curves of pure hydrocarbon fuels—such as n-heptane, isooctane, toluol, and diisobutylene—are hyperbolic and easily expressed by formula. Additions of a temperature-sensitive pro- or antiknock compound produces a bulge in the curve of the base fuel. This distortion, of course, is downward if proknock and upward if antiknock. The temperature sensitivity of the additive determines the length and shape of the bulge.

Fig. 18 illustrates the varying degrees to which specific amounts of tel distort the curve of isooctane. It also shows that tel is highly temperature sensitive. It was surprising to learn that the laboratory engine may be operated at compression temperatures either so low or so high that tel is not an antiknock agent. From a practical standpoint the ineffectiveness of tel at low temperatures can be forgotten since these temperatures exist only with compression ratios below 4/1. The high-temperature region, however, should be considered seriously, since any engine with a compression ratio of 10/1 will, after the deposits build up, be well into the region of diminishing benefits of tel.

Isooctane is considered to have a relatively high lead susceptibility. However, Fig. 19 shows the "susceptibility" of isooctane (or any other fuel) is entirely dependent on the compression temperature at which it is measured. Thus, at 800 or 1800 R susceptibility approaches zero. On the other hand, it is evident that tel is most effective in the 1100–1300 R T_c range. While its effectiveness is greatly reduced by operating the engine at lower or higher temperatures, it is noted that none of the curves obtained in the 1000–1600 R T_c range "level off" between 3.0 and 6.0 cc per gal concentration—at least, not to the degree usually shown by other test methods. In other words, if the engine is operated at favorable temperatures, the antiknock action of tel is not limited to 6.0 or even 10.0 cc per gal.

The nature of the leaded isooctane framework led to the supposition that tel has to be decomposed to be antiknock and that temperature during any part of the time history preceding ignition affects such decomposition. While this may not completely explain the antiknock action of tel, the recent work of Rifkin and Walcott[10] apparently substantiate this conclusion.

Acceptance of this conclusion raises many questions. Among them is one concerning the lead susceptibility of other fuels as determined at given compression temperatures and flame propagation rates. The question is enhanced by the strong indications that the T-D response of any additive or impurity, either pro- or antiknock, can be expressed in a formula which will be applicable throughout the operating range of present and future engines. At first thought it appears strange that this was not done long ago. But it must be remembered that the ASTM Motor, Research, and Aviation Methods rate fuels at increased T_c with increased antiknock quality level. Thus, the benefits derived by adding 3.0 cc per gal tel to an 80 octane number base fuel is measured at one T_c while the benefits derived by adding an equal amount of tel to a 90 octane number base fuel is determined at quite another. It is not usually questioned whether either of these temperatures is the one desired by tel for maximum benefit or whether either temperature is in the range developed by commercial engines. This distorted picture of lead response is then compounded by the various ways in which fuel-air ratio, knock intensity, spark advance, engine rpm, and jacket temperature is handled by these methods.

Since the use of T-D promises much in the way of more orderly and realistic fuel and additive evaluation, a hasty and limited examination was made of the approach which might be used to reduce the available data to a formula describing the rate at which tel gains or looses its effectiveness with T_c.

From the framework, it was noted that the highest K-L density (and, therefore, the greatest power) on isooctane + 6.0 cc per gal tel was obtained at a compression temperature of 1150 R. However, the greatest gain in density over isooctane neat was obtained at 1200 R. Since the extreme ends of the curves were in doubt anyway, an attempt was made to rectify the curves so that the gain in K-L density

[10] SAE Transactions, Vol. 65, 1957, pp. 552–566: "Basis for Understanding Antiknock Action," by E. B. Rifkin and C. Walcutt.

of the various lead curves over isooctane neat (across the compression temperature range) would describe perfect parabolas. For isooctane + 6.0 cc per gal tel, parabolas somewhere near the two given below came close to describing this:

$$P_c = 0.28 - a(1200 - T_c)^2 \quad (5)$$
$$\text{or } P_c = 0.28 - b(1200 - T_c)^2$$

where:

$$a = 1.12 \times 10^{-6}$$
$$b = 1.389 \times 10^{-6}$$

However, when the original data are spotted on true parabolas of this type it becomes apparent that the directrixes of the respective lead curves are not in the exact center of the region bounded by the data. According to these particular data the directrixes are 50 – 100 R to the left of true center. In other words, the rate at which tel increases in effectiveness with an increase in T_c (up to 1200 R) is somewhat greater than the rate at which it recedes.

It is immaterial, of course, whether or not the behavoir of tel can be reduced to mathematical formulas since both fuel and engine designer can obtain all necessary information from graphs. Since it has been shown that a given fuel with a given amount of tel can be described by a single curve over a range of 1000 deg or more, it follows that the same can be done with other additives, with or without tel being present in the fuel. The increased understanding of their behavior, singly or in combination, should aid their effective use.

Octane Scale Extension and Potential of other Rating Scales—Since it has been shown that T-D response of such pure hydrocarbons as paraffins and olefins is hyperbolic and that an additive such as tel is parabolic, it follows that it is impossible to extend the octane-number scale on the basis of tel in isooctane without having such a scale tied to one compression temperature in a given engine, at one combination of fuel-air ratio, spark advance, jacket temperature, and one engine rpm.

For strictly scientific purposes it would be ideal to describe the combustion characteristics of fuels by the basic variables—time, temperature, and density. If it were possible to measure these variables, it would be possible to develop true roughness, knock, and autoignition fuel-quality scales; thus, near perfect correlation with engine fuel requirements would be obtainable. Such three-dimensional scales would not have to be related to reference materials or engine variables.

Long before a theory regarding the basic variables was developed it became customary to base rating scales, test methods, and correlation schemes on "reference fuels." For many years "secondary" reference fuels were used which had to be calibrated against the "primaries," isooctane and n-heptane. It was a cumbersome scheme because each test method and each car would rate them differently. A separate calibration was made for each laboratory method and one or the other was arbitrarily used for road ratings. Needless to say, knock testing was greatly simplified when the primaries became available in commercial quantities.

A slight departure of this scheme has been made for rating aviation fuels above 100 octane number. As its name implies, the "performance-number"

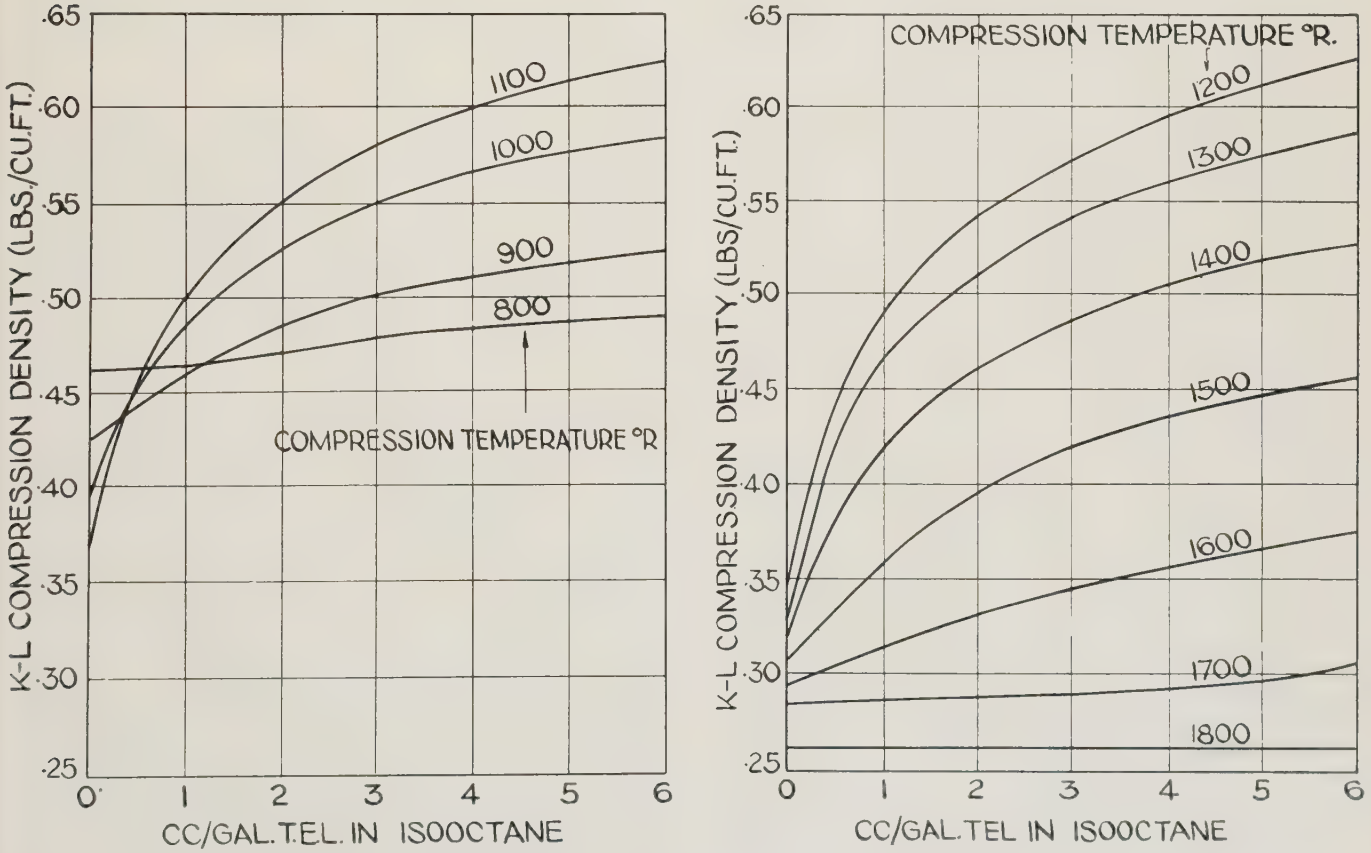

Fig. 19—Compression density lead response curves of isooctane at various compression temperatures

scale is based on the percent increase in K-L power which now antiquated engines supposedly gave with various amounts of tel added to isooctane over that which could be obtained on isooctane. The scale itself does not recognize the temperature sensitivity of tel. This shortcoming is overcome, in a measure, by using two engine test methods. One of these uses a T_c highly favorable to tel. The other uses variable T_c but in a higher area which, of course, is very unfavorable to all temperature sensitive materials. Regardless of the arguments which so often have been advanced against the scale and the methods, their hasty wartime adoption was a step in the direction of divorcing antiknock quality scale numbers from octane numbers.

A similar scheme could be adopted for motor fuels. Fig. 20 illustrates how the T-D framework of leaded isooctane appears when converted to percentage proportionality. The performance number scale assigns a value of about 160 to isooctane + 6.0 cc per gal tel. It will be noted that the laboratory engine may be operated so that an 80% increase is obtained. This occurs in the 1200–1300 R T_c range which is believed to be the T_c area of modern cars before deposit accumulation. Adoption of a scale extracted from the center portion of Fig. 20 would be quite realistic. This supposition could be easily confirmed Moreover, the scale could be easily changed as engines change and the record could be kept orderly by associating any such scale with the T_c at which it is derived. From the discussion to follow it will be seen that such a performance number scale would not be restricted to use of leaded isooctane as reference fuels. Other additives or pure hydrocarbon fuels can be described and used in like manner.

Another and more attractive choice would be to tie test methods, rating scales, and their extensions directly to engine variables by use of T-D. The logic here is that fuel behavior can be associated with given T-D conditions in a highly standardized test engine in the same manner that physical phenomena are associated with (and relate) various temperature scales. In this case, the T_c/P_c points at which various pure hydrocarbons are equal would be used as pseudo physical phenomena.

For commercial reasons it may be desirable to retain the octane scale. This scale reenters the picture and is associated directly to engine variables via the framework presented in Fig. 13. It can be extended in either direction on a linear basis as already shown in Fig. 15. Likewise, it fixes the absolute end of the octane-number scale at 130 "octane." Thus, where the cross-plot shown in Fig. 14 extended the data to make graphical sense to zero T_c and infinite P_c at any octane-number level, Fig. 15 extends the data to make graphical sense to infinite P_c at any temperature. The connotation here is that any engine which can be infinitely pressured requires "130 octane number fuel" at any temperature. Another way to express this is to say that the T-D curves of the primary reference fuels form an orderly family of true hyperbolas since all are asymptotic to the T-D parameters.

The fact that the formulas assign density values to hypothetical octane numbers up to but not including 130 makes it possible to construct T-D lines for such hypothetical fuels. This may be done as well for fuels below zero octane. The cross-plots of

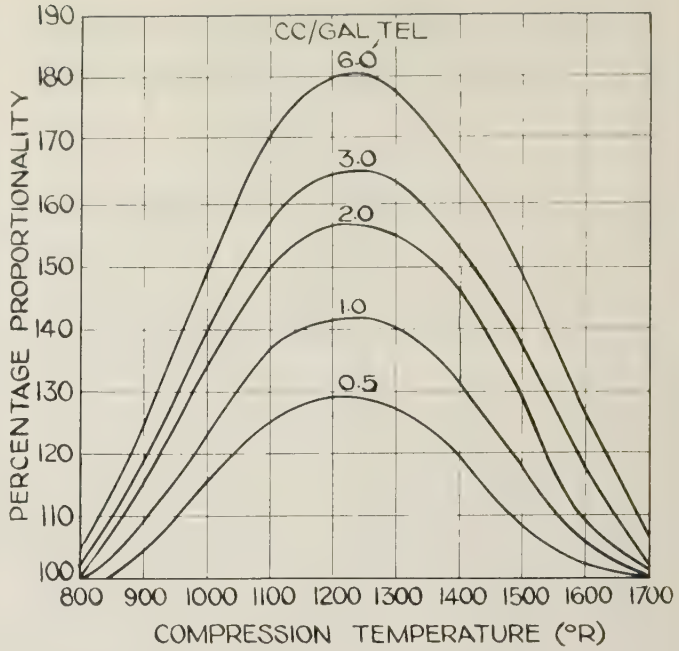

Fig. 20—Percentage proportionality knock-limited compression density of leaded isooctane to isooctane

these octane numbers, below zero and above 100, all fall on a perfect hyperbola at each compression temperature. These curves, of course, are also asymptotic to the octane scale (below zero) and to 130 octane number. A common curve and formula may be used to relate all of these so-called octane-scale extensions. It follows that the T-D curve of any fuel which exceeds the boundaries of the octane scale (below or above) can be assigned octane numbers by the intersection of the T-D lines of these fuels with the hypothetical higher or lower octane-number T-D curves.

Interest in the T-D octane-scale extension increases when the T-D curve of a fuel such as diisobutylene is superimposed on the T-D extended octane-heptane framework along with the leaded isooctane curves. This is done (for only the upper portion of the framework) in Fig. 21. It will be noted that the chart assigns a different octane number to diisobutylene at different compression temperatures. Below 1253 R, it assigns equivalent values of isooctane plus tel and it likewise assigns "T-D extended" octane numbers above 100. These values may now be plotted. Fig. 22 shows that the real and T-D extended octane number of diisobutylene plot smoothly across the compression temperature range. While the chart does not illustrate it, this hyperbolic curve remains smooth for values below zero octane as well as above 100. This means that the octane number of diisobutylene could be expressed by an equation which would hold true throughout the experimental range and which would be stable from zero air consumption to infinite pressure.

Since the chart also gives equivalent values in terms of leaded isooctane, these can be converted to octane numbers by the tables circularized by ASTM. A plot of these values is also shown on Fig. 22. This curve not only has a definite break at 100 but it changes direction and "runs out of numbers" even in the experimental range.

Appraisal of the scale extension based on these

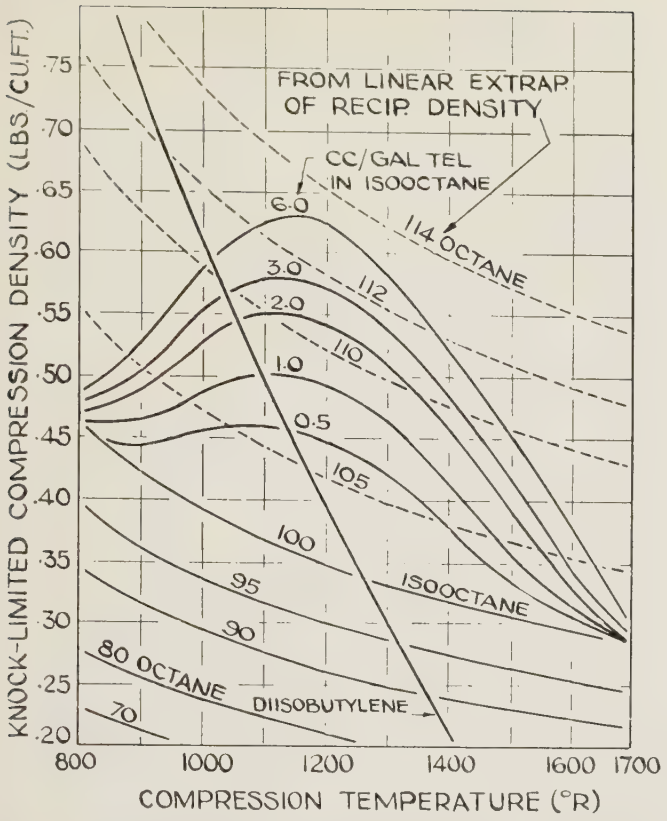

Fig. 21—Temperature-density chart, leaded isooctane and diisobutylene superimposed on extended octane-number scale

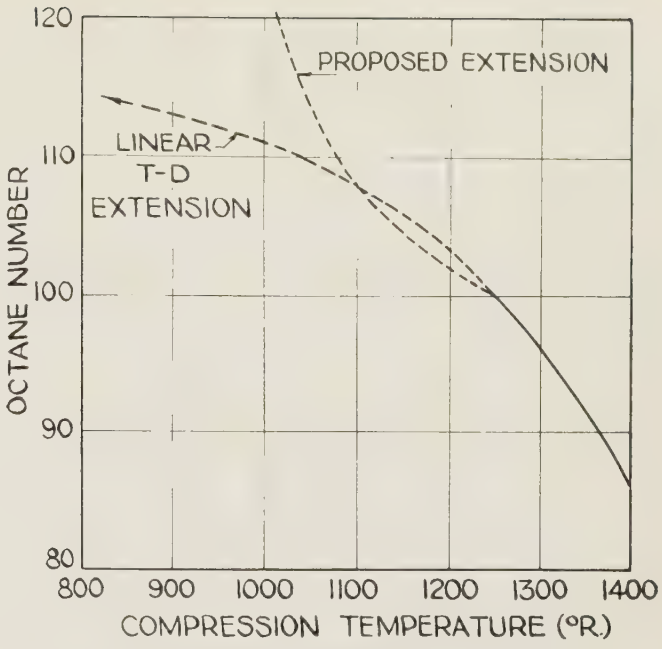

Fig. 22—Octane number of diisobutylene at various conditions

data indicates that it would be based on the combined and harmonic effect of infinite combinations of compression ratio, mixture temperature, and manifold pressure in the accepted laboratory equipment at a given speed, fuel-air ratio, and jacket temperature. Although such a scale would have its limitations, it has more to offer than the one now being considered by technical committees. It would be a step toward more fundamental expression of anti-knock quality instead of a retroversion to the complexities of using secondary reference fuels. Moreover, it could be used with any other reference fuels.

As mentioned, the use of T-D makes possible the consideration of entirely different sets of reference fuels. While such a study may be academic, superimposing the various frameworks demonstrates that the antiknock quality of a fuel can be expressed in terms of other reference fuels. Such T-D charts calibrate various hydrocarbons in terms of each other over the entire experimental range. Since this range is so large, all frameworks can be extended to logical termini and all pure hydrocarbons, therefore, can be related mathematically. The graphical pictures so obtained reveal many contrasting attributes of particular fuels. The nature of the scales which would result if blended with one another are also illustrated.

For example, by superimposing the curve of one pure hydrocarbon upon the other it is found that some meet only in the theoretical and infinite regions while others cross in the experimental region. Diisobutylene, for example, will cross the curves formed by isooctane with 6.0 cc tel per gal, isooctane neat, and n-heptane. All of these intersections form anchor points of engine severity and they also become the zero points of the various chemical scales.

In this light the octane-heptane scale is a "good" one since these two fuels have equal antiknock quality only in infinity and, since they apparently have equal temperature response, they maintain a uniform increase in scale unit size at any temperature. From Fig. 16 it is apparent that a scale based on diisobutylene-heptane would have entirely different and undesirable characteristics.

The T-D attributes of a possible but impractical diisobutylene-octane scale (Fig. 17) are interesting in view of the fact that this scale would have its zero point in the center of the experimental region. Positive scale numbers would be possible only at temperatures below 1253 R. At higher temperature fuel quality would have to be expressed in terms of negative diisobutylene numbers. On the other hand, the intersection of these two fuels offers an excellent anchor point regarding severity and, therefore, merits consideration in the development of a new control method. This T-D point takes on added significance if it is fully realized that it can be created in the laboratory engine by an infinite number of combinations of compression ratio, MAP, and mixture temperature.

Needless to say this type of study becomes more interesting when naphthenes and aromatics are included. Toluol is an interesting example since its T-D curve is steeper than that of diisobutylene and, like diisobutylene, it has a T_c sensitivity of far over 100 octane numbers. Limited and unpresented data indicate that, in its pure state, toluol can be rated with high reproducibility. This holds true even in the region above isooctane + 6.0 cc per gal tel. However, blends of Toluol with blends of lower antiknock quality fuels are difficult to rate.

Considered in the aggregate, the frameworks give a new understanding of the temperature sensitivity of fuels and additives. Mass data will confirm that

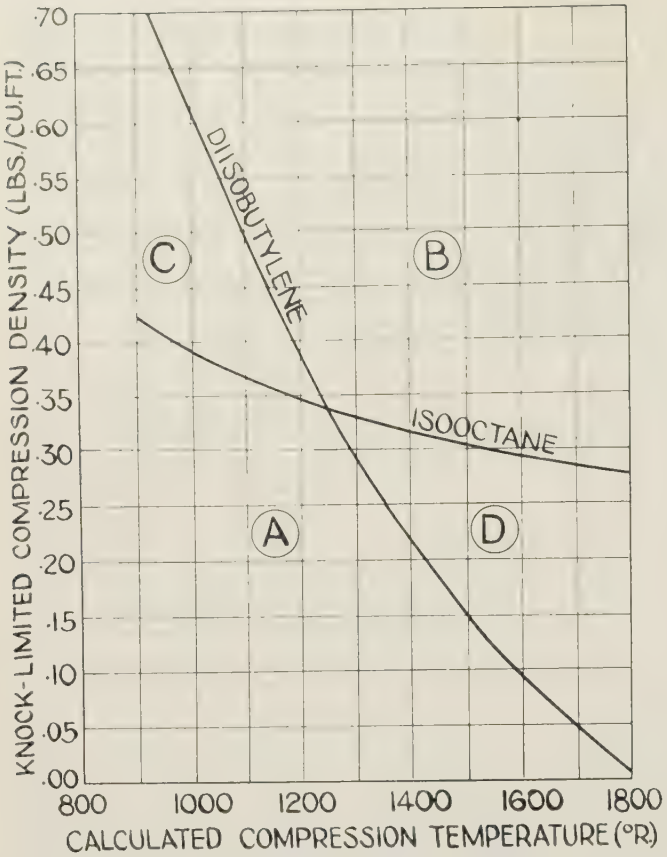

Fig. 23—Engine treatment of two fuels decides its general location on temperature-density chart

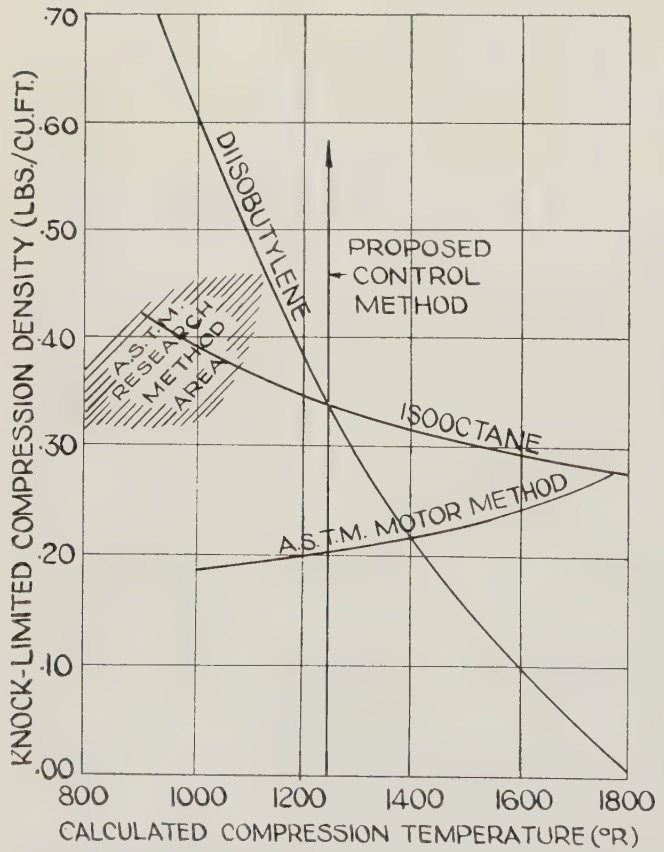

Fig. 24—Relative temperature-density location of present and proposed control methods

any number of reference fuel scales and their extensions can be used interchangeably since they are all mathematically related by the T-D parameters. This, in turn, means that expressions of antiknock quality need not be tied to any of them for the "T-D number" describes it in terms of all of them.

Road-Laboratory Correlation—The T-D parameters may be applied to road-laboratory correlation by considering them pseudo scales. Numerical values or factors thereof may be assigned to the scales by the methods set forth and then applied without questioning whether they are absolute values. It is not even necessary to call them by these names—the T_c scale could be used as an index of relative severity and some factor of P_c could be used to develop a new antiknock number scale. Another alternative is to retain the octane scale but associate octane numbers with a numerical severity scale (such as T_c) instead of method names such as Motor or Research.

The superimposed reference fuel frameworks offer the media for establishing the fuel requirements of full-scale engines on the basis of any of these numerical scales. Since the T-D lines of various fuels have entirely different shapes and slopes, clear-cut intersection points are formed. These intersections, of course, define the T-D points where the laboratory engine rates various fuels equal to each other. Fig. 23 shows that the curves of isooctane and diisobutylene can intersect at only one T-D combination and the two lines create four distinct areas in the quadrant.

It is important to know the area in which critical cars are operating. This can be established by operating them alternately on these two fuels at specified conditions. If an engine does not knock on either isooctane or diisobutylene, it must be in area A. If it knocks on isooctane but not on diisobutylene, its requirement would be in area C. It would be in area D if it knocks on diisobutylene but not on isooctane. Since it is necessary to specify requirements more exactly, they must be determined in terms of blends of pure hydrocarbons or segregated batches of commercial-type reference materials for which T-D frameworks have been constructed.

If the engine, at constant speed and manifold pressure produces incipient knock on both isooctane and diisobutylene, the answer is simple: The engine's fuel requirements on a T-D basis must be 1253/0.337—the intersection point of the curves of these two fuels. In other words, if two or more fuels are rated as "equal to each other" in a full-scale engine, the T-D conditions required by the laboratory engine to rate them equal would be ascribed to the full-scale engine as its T-D requirement." It follows that any commercial fuel whose T-D response line falls below this point will knock in this engine under those conditions. It is no guarantee that the engine will or will not knock on this commercial fuel at other conditions.

While the laboratory technician might find it expressive to say the T-D requirement of this engine is 1253/0.337, it seems more meaningful to say its requirement is 100 octane at 1250. But regardless of the mode of expression, Fig. 23 points up the need for expressing engine fuel requirements and antiknock quality two-dimensionally.

The question is raised whether the T-D curves of other fuels which also produce incipient knock in

this engine would all intersect in the same general location. This will have to be decided by mass data obtained in cooperative test programs. Whether or not this will be the case, it is intended to develop similar charts at other speeds and fuel-air ratios. It is reasoned that this course of action eventually will offer the mechanism for near perfect road-laboratory correlation.

It is believed that the majority of present cars operate at compression temperatures between 1200 to 1400 R. The compression temperature of those late model cars which have been operating without benefit of combustion-chamber deposit modifiers and which autoignite on modern premium fuels can be assumed to be operating at considerably higher temperatures.

Proposed Control Method—The fact that the relative compression temperature of cars can be established by this technique gives rise to the proposal to adopt a control method which, on a T-D basis, cuts through the region of car population. (Fig. 24). It would rate diisobutylene equal to 100 octane which is also the severity region where tel is most effective. Several other auxiliary sets of operating conditions could be used for studying the T-D response of fuels over a larger temperature range.

Fig. 24 also shows the relative locations of the ASTM Motor and Research Methods. While cars apparently are located in the region lying between these two methods, it is technically impossible to spot them accurately by conventional methods of handling road and laboratory data. As previously pointed out, the curves of leaded and unleaded fuels have different shapes. Attempts to relate road data to the laboratory methods by using straight lines to describe fuel behavior in engine severity regions falling between the two methods can give extremely misleading results.

This can be more easily understood by referring again to Fig. 22. It will be noted that leaded fuels will rate the same octane number at two compression temperatures. This two-valued curve might well explain the paradox that engines become "milder" as compression ratio increases while the usual interpretation of physical law says this cannot be true.

Summary of Practical Applications

The T-D concept may be applied in many areas of fuel-engine adaptation. The following specific applications are described in this paper:

1. Mathematical and graphical expression of knock-limited manifold air pressure across a large compression ratio range.
2. Mathematical and graphical expression of knock-limited or preignition-limited density across a large compression temperature range.
3. Creation of pseudophysical phenomena to relate any number of chemical scales in the same manner physical phenomena are used to relate temperature scales.
4. Use of the mathematical expression of T-D response for the preparation of elaborated tables by electronic computers, rigidly classifying the behavior of various combinations of pure hydrocarbons and blends of the chief commercial fuel components.
5. Use of the analytical techniques for rectifying limited data on the supposition that even limited data have to produce stable equations, make graphical sense, and/or satisfy theoretical reasoning when such data are extended to absolute zero compression temperature, 1/1 compression ratio, infinite manifold pressure, or zero air consumption.
6. Use of the T-D parameters for defining the absolute limits of chemical scales of antiknock and anti-autoignition quality.
7. Use of the superimposed T-D frameworks for locating the relative positions of full-scale engines by their respective behavior at various well-defined conditions on the fuels covered by the frameworks.
8. Use of the intersections of the various pure hydrocarbons (pseudophysical phenomena) for tuning laboratory engines in the same manner that physical phenomena are used to check temperature indicating instruments.
9. Use of the T-D charts for relating the Sinclair constant temperature test methods to each other and to full-scale engines.
10. Use of T-D correlation of laboratory and full-scale engines in the selection of adequate routine methods for control and specification purposes.
11. Use of the standard laboratory engine and T-D methods or of the T-D concept with other engines for the development of more reliable screening and proof tests.
12. Evaluation of proposed modifications to laboratory equipment on the basis of their improvement of, or disturbance of, the T-D relationships of pure hydrocarbons already established.
13. Use of the laboratory created T-D charts as a base line for evaluating the relative mechanical octanes built into full-scale engines.
14. Use of surveys of T-D requirements of full-scale engines for more adequate description of general trends and the impact of specific innovations. Particularly, will increased underhood temperature, further increases in compression ratio, and the use of fuel injection or supercharging, singly or in combination, move the engines into T-D areas not satisfied by current fuels?

Acknowledgments

The author expresses thanks to the many technical committee associates who will have recognized this paper as being a recapitulation and extension of knowledge gained in several cooperative test programs mentioned in the text. These groups crystallized many facets of the complex problem, solved some of them, and laid the groundwork for the solution of others. They have been patient audiences to many previous discussions of the tests in progress at Sinclair and have been generous in their moral support.

The author also thanks his associates, especially J. McWilliams, for obtaining all the data herein reported; R. G. Moser, for adapting the standard equipment; Prof. Herbert W. Best of Yale University, for constructive criticism concerning analysis; and the management of Sinclair Research Laboratories, Inc., for permission to present this paper.

Discussion of this paper will be found on pp. 442-443.

Time Factor May Be Necessary In Temperature-Density Studies

—Harold H. Trimble
Phillips Petroleum Co.

IT IS NOTED in Fig. 24 that the Research Method is indicated by a crosshatched area, whereas, the Motor Method is shown as a line. In searching for a reason for this, I thought that possibly the time factor was entering the picture in the Research Method. This reasoning was based on information obtained by us some time ago on fuels being studied on the road and in the laboratory.

The tests concerned two fuels, one of low and one of high sensitivity. On the road, the fuel of low sensitivity was consistently giving ratings higher than its Research rating; whereas the high-sensitivity fuel gave ratings less than its Research rating. It was, therefore, decided to vary the Research Method conditions and determine the effect on the ratings of these two fuels. First, the intake air temperature was varied and the compression ratio adjusted to give constant knock intensity. Under these conditions the high-sensitivity fuel showed the greatest variation with respect to the primary reference fuels, and the low-sensitivity fuel was similar to the reference fuels. While by going to high intake air temperatures the low-sensitivity fuel could be made to rate higher than the high-sensitivity fuel, it rated less than its Research rating.

It was then decided to vary the spark instead of the compression ratio to maintain constant knock intensity. Under these conditions the low-sensitivity fuel showed the greater variation with respect to the reference fuels; whereas, the high-sensitivity fuel acted more like the primary reference fuels. Under these conditions the low-sensitivity fuel could be made to rate higher than its Research rating as well as higher than the high-sensitivity fuel under the same conditions. This suggested to us the possibility that the time factor needed to be adjusted in the Research method. A graphical representation of these test condition effects in the Research engine are shown in Fig. A.

Such data also suggest that the time factor may have to be reckoned with in these temperature-density studies. Further work will be needed before we can be sure we get the complete story as simply as the author has shown it. In this connection, a CFR group is working on the project. They are obtaining full-scale data on several series of fuels, and Mr. Siegel is supplying the temperature-density data on the same fuels. It is hoped these data will aid in the understanding and use of this concept.

Engine Operating Condition May Be Located by Fuel Curves

—Otto Enoch
Ford Motor Co.

WE cannot yet measure end-gas temperature and density and so must use calculated compression temperature and compression density as questionable substitutes. Mr. Siegel, realizing this deficiency suggests the use of pseudo-scales for practical application of the T-D graph: for instance, numbers for the *T* ordinate and letters for the D abscissa.

We assume that such scales still would be based on T-D values. But possibly we could eliminate T-D calculations or measurements altogether by applying an old trick and use reference fuel parameters to express engine conditions.

In Fig. B we have superimposed the primary reference and diisobutylene-heptane blend networks on the T-D graphs in Figs. 13 and 16 of Mr. Siegel's paper. These two reference fuel systems, because they have different sensi-

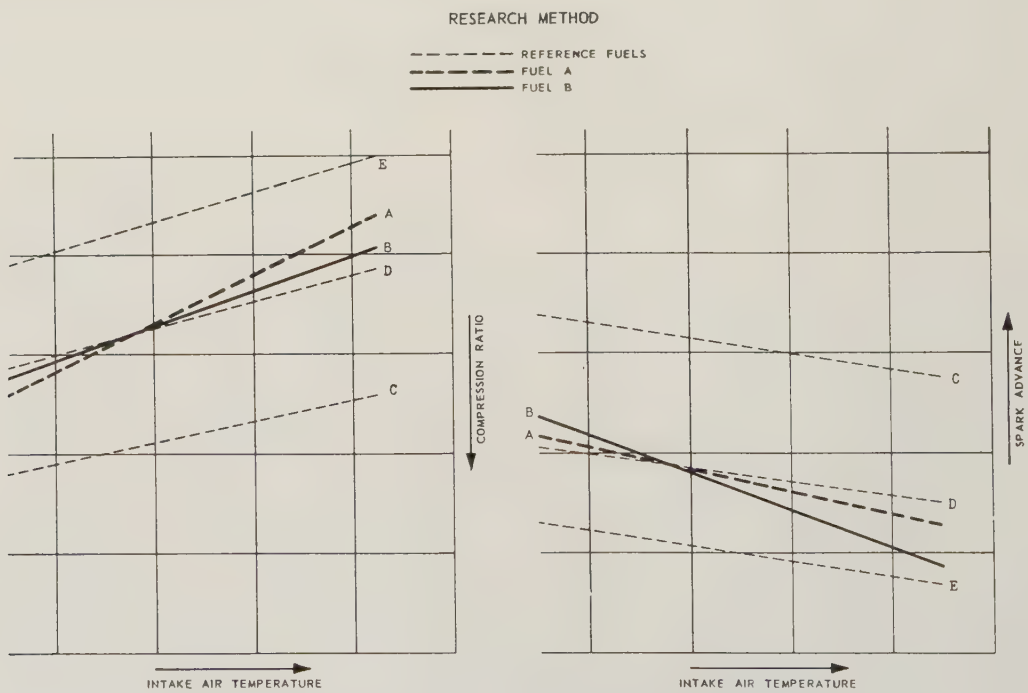

Fig. A—Effect of intake air temperature, compression ratio, and spark advance on Research method antiknock ratings

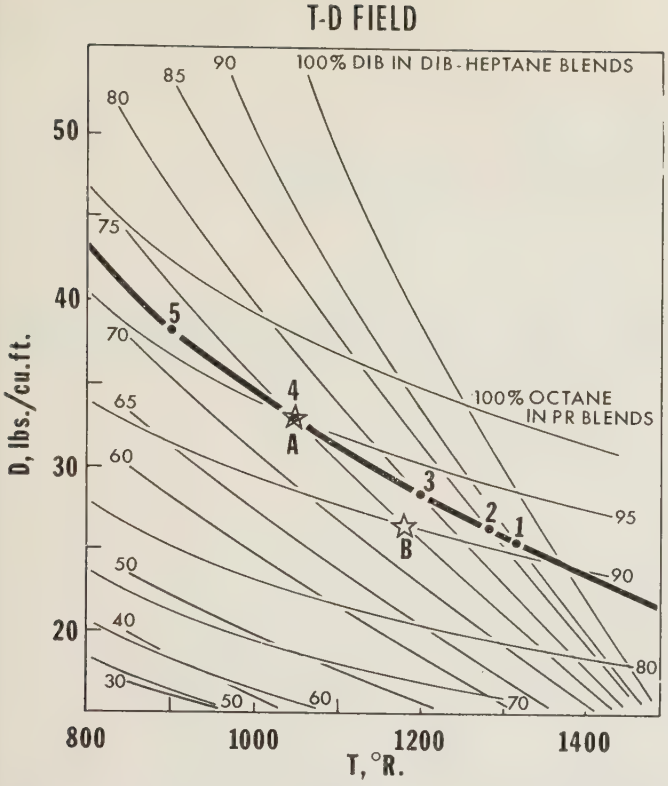

Fig. B—Primary reference and diisobutylene blend networks superimposed on Figs. 13 and 16

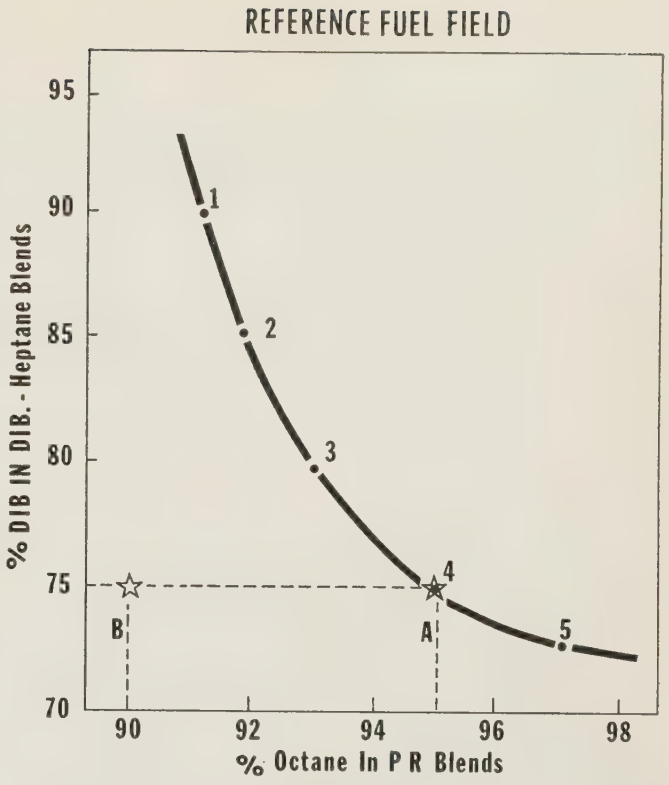

Fig. C—Engine operating condition located by matching two reference fuels instead of by temperature-density coordinates

tivities, intersect each other. Each intersection marks a definite engine operating condition in regard to temperature and density. Therefore, each engine operating condition can be defined by two or, in the case of fishhook fuel curves, by three, intersecting reference fuel blends instead of temperature and density.

For instance, a particular operating condition for engine A could be defined as the intersection of the 95 octane primary reference and the 75% diisobutylene-heptane blend. This intersection means that both blends are on borderline knock. Also T-D conditions 1, 2, 3, 4, and 5 mark the path of an arbitrary commercial gasoline borderline knock curve (the heavy line in Fig. B) in terms of intersecting reference fuels. Point 4 is shown coinciding with the operating condition for engine A, which means that this commercial fuel would borderline knock in that engine at that operating condition. Or, for instance, a particular operating condition for engine B can be defined by the intersection of the 90 octane primary reference and the 75% diisobutylene-heptane blend. The commercial fuel would not knock in this engine at that particular operating condition.

Since each T-D combination in the T-D field thus can be defined by a pair of reference fuels and each fuel borderline knock curve can be defined by a series of such reference fuel pairs, we might forget the T-D coordinates and instead plot engine operating conditions and fuel borderline knock curves in a reference fuel coordinate system as shown in Fig. C.

In Fig. C the abscissa represents primary reference fuel blends, the ordinate diisobutylene-heptane blend. Points 1, 2, 3, 4, and 5 of the commercial gasoline borderline knock curve are obtained as before by applying five different engine operating conditions. But we do not have to determine these conditions in terms of T-D coordinates. All we have to do is to match each condition by two reference fuels. Point 4, for instance, is located by the 95 octane primary reference blend abscissa, and the 75% diisobutylene-heptane blend ordinate. Engine B operating condition is located by the 90 octane primary reference blend abscissa and the 75% diisobutylene-heptane blend ordinate.

Fig. C shows as clearly as Fig. B that the commercial gasoline will not knock in engine B, but will borderline knock in engine A.

I suggest that this method be given a try in further studies to apply the T-D concept for knock rating.

Suggests Time Factor Should Be Introduced

—E. M. Barber
Texas Co.

MR. SIEGEL'S approach seems to stand the best chance of freeing us from the empiricism at the root of our present problems in matching fuels and engines.

There are two points, however, on which I quibble with Mr. Siegel. First, I would like to have seen him point out that the temperature and density values that he measures are approximations to or pseudovalues of temperature-density parameters of reaction rate theory.

Second, I think it would be helpful to introduce an approximate reaction time as a specific factor. Mr. Siegel's practice of using maximum power spark timing is a desirable simplification of testing which also provides data that can be used to estimate a relative reaction time. This time can be calculated from 4/3 P_{max} (where P_{max} is the maximum power spark advance in crankshaft degrees) and is to be expressed in seconds.

Such a time factor will be helpful in dealing with the antiknock problem over a wide range of engine speeds. Also, it will provide time to go with temperature and density to round out the three parameters of temperature, density, and time that are needed to identify the antiknock problem with reaction rate theory. The recognition and development of this identification, even in terms of approximate values of the temperature-density-time parameters will enhance the power of the technical tools that can be brought to bear on the antiknock problem.

LOOP SCAVENGING versus THROUGH SCAVENGING of

C. F. Taylor and A. R. Rogowski, Massachusetts Institute of Technology
A. L. Hagen, J. J. Henry Co., Inc., J. D. Koppernaes, Nova Scotia Technical College

This paper was presented at the SAE National Diesel Engine Meeting, Cleveland, Nov. 5, 1957.

FOR as long as the 2-stroke engine has been in existence, the relative merits of loop scavenging versus through scavenging have been a subject of controversy. On the other hand, few, if any, investigations of this subject have been made where other conditions were controlled in such a way that the difference in scavenging method alone was measured. The purpose of this investigation was to compare the two methods of scavenging under conditions which would measure their relative merits as objectively as possible.[1]

THIS paper reports the latest investigation of the relative merits of loop scavenging versus through scavenging. The authors hope that the conditions of the work permitted an objective evaluation of the two types of engines.

The results of the study may be summarized as follows:

1. With symmetrical timing, neither cylinder shows significant advantage in trapping efficiency.
2. With symmetrical timing, the best ratio of exhaust-port to inlet-port effective area seems to be about 0.6.
3. Unsymmetrical timing is an effective method of improving trapping efficiency.
4. The value of net indicated fuel economy shows no significant difference between the two cylinders.

The authors point out that because the areas were equal it is unlikely that the optimum port design of each type was used in comparing the cylinders. If optimum porting had been used, the two types might have shown more difference.

Methods of Evaluation

The criteria by which a scavenging system can be judged may be stated as follows for a given quantity of fresh air[2] supplied per stroke:

1. Maximum quantity of fresh air should be retained in the cylinder after the ports (or valves) close.
2. The work required to supply the fresh air should be minimum.
3. The work lost between exhaust opening and the end of the expansion stroke should be minimum.
4. The mechanical system involved should be simple, reliable, and have small weight and bulk compared to that of the cylinders which it serves.

Retention of Air in Cylinder—The first criterion is usually tied in with a set of definitions involving an assumed ideal scavenging process. Such definitions are now under study by the Committee on Nomenclature of the SAE. Pending adoption of SAE standards in this field, we will use a set of definitions which have been described and explained in a previous SAE paper.[3] These definitions form a consistent system and can express comparative results in convenient form.

The ideal scavenging process on which these definitions are based consists of filling the entire cylinder volume at bottom dead-center with fresh air

[1] This investigation was carried out under the direction of the senior author as a thesis submitted for the degree of Master of Science at M.I.T. by Messrs. Hagen and Koppernaes. The experimental work was done in the Sloan Laboratories for Aircraft and Automotive Engines during the spring and summer of 1956.

[2] For engines scavenged with a mixture of fuel and air, read "fresh mixture" for "fresh air."

[3] SAE Transactions, Vol. 62, 1954, pp. 486–502: "Scavenging the 2-Stroke Engine," by A. R. Rogowski and C. F. Taylor.

TWO-STROKE ENGINES

(or fresh mixture) at inlet temperature and exhaust pressure. In accomplishing this result no fresh air (or mixture) would escape from the exhaust ports until the quantity supplied was sufficient to fill the cylinder as above indicated.

With the above idealized process in mind, the following definitions are used.

1. Scavenging Ratio[4] (R_s)

$$R_s = \frac{M}{V\left(\frac{r}{r-1}\right)\rho_s} \qquad (1)$$

where:

M = Mass air (or mixture) flowing into the cylinder during one scavenging process

V = Piston displacement

r = Compression ratio, defined as in the case of 4-stroke engines

ρ_s = Density of air (or mixture) computed at inlet temperature and exhaust pressure

R_s = Controllable variable, dependent on how much air (or mixture) is forced through the inlet ports during one scavenging process

2. Trapping Efficiency (Γ)

$$\Gamma = \frac{M'}{M} \qquad (2)$$

where:

M' = Mass of fresh air (or fresh mixture) retained in the cylinder after ports close

The value of Γ in the *ideal* scavenging process is 1.0, as long as R_s is 1.0 or less.

3. Scavenging Efficiency (e_s)

$$e_s = \Gamma R_s \qquad (3)$$

The ideal value of e_s is $1.0 \times R_s$ up to the point where $R_s = 1.0$. When R_s exceeds 1.0, $e_s = 1.0$ in the ideal process.

Fig. 1 shows e_s versus R_s for the ideal scavenging process and includes a curve of e_s versus R_s constructed under the assumption that the fresh air (mixture) mixes continuously and completely with the residual gases in the cylinder during the scavenging process.[3]

In the case of real engines Γ is always less than 1.0 (except at very low values of R_s). It is evident that, from the point of view of scavenging only, at a given value of R_s the higher the value of Γ, the better is the scavenging system.

Mep Required to Scavenge—With a given mass flow of air (or mixture) through the engine, the work required to deliver air will increase with increasing ratio of p_i, the scavenging pressure, to p_a, the ambient pressure.

Assuming that the engine exhausts to the atmosphere, the exhaust pressure p_e can be substituted for p_a. In cases where an exhaust turbine is used, p_e will not equal p_a, but the resistance through the *cylinder* will still be measured by p_i/p_e.

The pressure ratio required for a given flow through a cylinder is an inverse function of a flow coefficient C defined as follows:

$$C = \dot{M}/\dot{M}_t \qquad (4)$$

where:

$\dot{M}$ = Measured mass flow per unit time of air (or mixture)

M_t = Theoretical mass flow through an ideal orifice whose area is the piston area, with the same values of T_i and p_i/p_e

Thus C describes the effect of port design on the resistance to flow through a cylinder. It is evident that, from the point of view of work required to

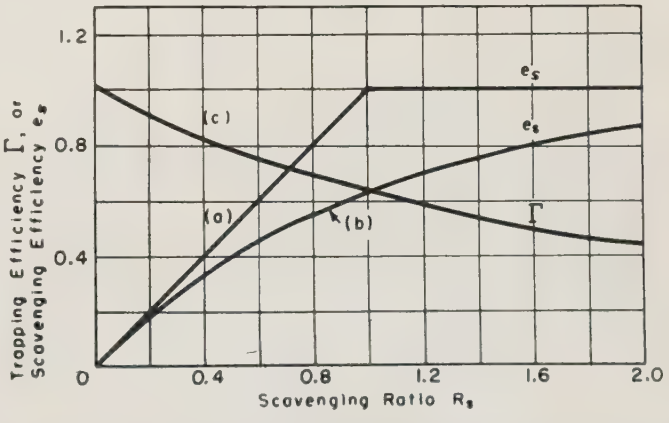

Fig. 1—Theoretical relationships between scavenging efficiency, trapping efficiency, and scavenging ratio (a—perfect scavenging; b—perfect mixing, $e_s = 1 - \varepsilon^{-Rs}$; c—$\Gamma$ with perfect mixing)

[4] Sometimes called the delivery ratio and often based on piston displacement. In that case, $(r/r-1)$ is omitted.

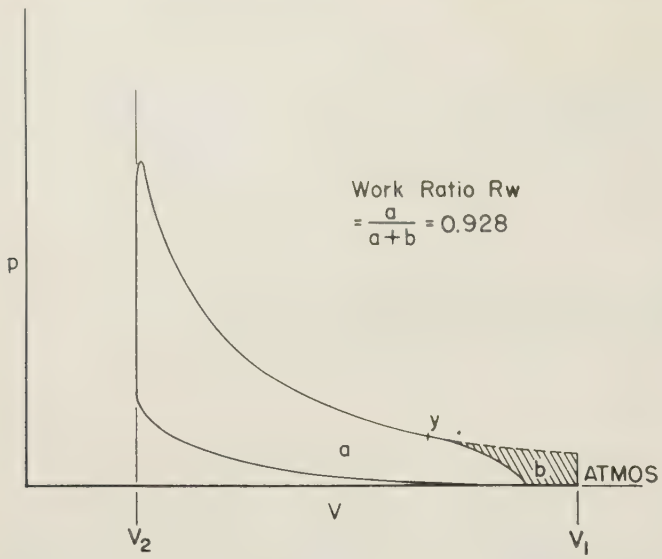

Fig. 2—Lost work during blowdown, loop-scavenged engine configuration A (piston speed 1200 fpm, $R_s = 1.2$)

Table 1—Indicated Efficiency of 4-Stroke CFR Engine

Engine	Configuration	Compression Ratio	Fuel-Air Efficiency	Mean, R_w	Indicated Efficiency[a]
Loop	A, B, C	5.43	0.30	0.94	0.240
Poppet	A, B, C	6.8	0.33	0.94	0.264
Poppet	D	6.8	0.33	0.895	0.248
Poppet	E	6.8	0.33	0.860	0.242
Poppet	F	6.8	0.33	0.850	0.238

[a] Indicated efficiency = fuel-air efficiency × 0.85 R_w

scavenge, the higher the value of C the better is the scavenging system. Typical values of C for 2-stroke engines range between 0.02 and 0.04, depending on design and operating conditions.[3]

Lost Work During Blowdown—Fig 2 shows a p-v indicator diagram from a 2-stroke engine. The exhaust port starts to open at y, at which point the cylinder pressure starts to fall rapidly.

An ideal case might be taken as an exhaust system which could reduce the cylinder pressure to exhaust-system pressure instantaneously at bottom center. The resultant diagram indicated by the dotted line, would have isentropic expansion from point y to bottom center.

The work ratio will be defined as follows:

$$R_w = \frac{a}{a+b} \tag{5}$$

where:

a = Area of the p-v diagram
b = Shaded area in Fig. 2

In the ideal case $R_w = 1$ and in the actual case, the greater is R_w the more satisfactory is the scavenging system from the lost-work point of view.

Mechanical Qualities—It is obviously difficult to measure simplicity and reliability numerically. On the other hand, the weight and space qualities of a cylinder assembly, including valve gear, can be measured by such ratios as the following:

$$R_v = \frac{\text{Cubic volume occupied}}{\text{Displacement volume}} \tag{6}$$

and:

$$R_m = \frac{\text{Mass of cylinder assembly}}{\text{Displacement volume} \times \text{reference density}} \tag{7}$$

For convenience, the reference density may be taken as 1 in the second expression.

Test Equipment

The equipment used consisted of two CFR-size cylinders, 3¼-in. bore by 4½-in. stroke, each mounted on CFR crankcases and coupled to cradle dynamometers with complete measuring equipment.

The engines were each scavenged with a gaseous mixture consisting of 100-octane gasoline vapor and atmospheric air, thoroughly mixed in an inlet tank whose walls and contents were held above the mixture dew point at all times.

The scavenging air at the controllable pressure was supplied from the laboratory mains. An inlet surge tank and an exhaust surge tank were connected to the cylinder by large, short pipes. Inlet and exhaust pressures and inlet temperature were measured in these tanks. In all cases the tank volume was greater than 50 times cylinder volume.

Test Procedure

As far as possible, the engines were run at four scavinging ratios ($R_s = 0.6$, 1.0, 1.2, and 1.4) over a range of mean piston speeds from 675 to 1500 ft/min (900–2000 rpm).

Spark advance was adjusted for best power in every case.

Indicated power was taken as equal to brake power plus motoring power. This assumption was spot-checked by means of indicator diagrams and found to be of very satisfactory accuracy. The indicator diagrams were made with the M.I.T. balanced diaphragm indicator[5]. Table 1 gives the values of friction mep measured by motoring and Fig. 14 compares indicated mep as measured by the two methods.

Trapping efficiency was measured by the imep method, discussed more fully by Rogowski, and Taylor.[3] This method is based on careful estimates of indicated thermal efficiency based on experience with the CFR 4-stroke engine whose trapping efficiency is 1.0.[6]

The estimated indicated efficiency was taken as the corresponding fuel-air cycle efficiency times 0.85, multiplied by the average value of R_w as measused from the indicator diagrams. The ratio 0.85 is based on experience with the 4-stroke CFR engine. The values used are shown in Table 1.

Air flow was measured by means of standard ASME sharp-edged orifices and fuel flow by calibrated rotometers. Speed was measured by a tachometer and monitored by a 60-cycle flash lamp illuminating 36 evenly spaced stripes painted on the flywheel. Brake load was measured by hydraulic torque scales.[7]

Test conditions held constant in all tests were as follows:

Inlet temperature, T_i	160 F
Oil temperature	160 F
Water jacket outlet temperature	180 F

[5] NACA TN 1896, June, 1949, "Improvement of Accuracy of Balanced-Pressure Indicators and Development of Indicator Calibrating Machine," by J. C. Livengood.

[6] "Comparison of Actual Engine Cycle with Theoretical Fuel-Air Cycle," by J. J. Van Deun and J. G. Bartas. Thesis, M.I.T., June, 1950.

[7] "Hydraulic Scale for Measurement of Engine Dynamometer Forces." Bulletin No. 6, Jan. 3, 1949, Diesel Engine Manufacturers Assoc., Chicago.

Fuel-air ratio, F,	0.08 = 1.2 × stoichiometric
Spark advance	adjusted for maximum power
Compression ratio:	
loop-scavenged cylinder	5.43[8]
through-scavenged cylinder	6.80
Fuel	100-octane gasoline
heat of combustion	Q_c = 19,000 Btu per lb

Cylinder Design

Assembly drawings of the two cylinders used are shown in Figs. 3 and 4.

The looped-scavenged cylinder was of the Curtis (Sulzer or Schnurle) type, that is, the inlet ports were arranged so as to direct the incoming air to the side of the cylinder away from the exhaust ports. A flat-head piston was used. The port arrangement in planes intersecting the cylinder axis was that which found optimum in experiments by Rogowski and Bouchard.[9]

Inlet Ports—The through-scavenged cylinder had rectangular inlet ports and two poppet valves in the head. No attempt was made to introduce a tangential component of motion, or "swirl," by means of the inlet ports. (It has been found by many investigators that high swirl is detrimental to scavenging.)

The inlet ports of the through-scavenged engine were designed to have the same timing and the same effective area at each crank angle as those of the loop-scavenged engine. Effective area is defined as the product of port area and a port flow coefficient measured in steady flow at various piston positions

[8] In comparing indicated performance (Figs. 12 and 13), imep of the loop-scavenged engine was corrected to 6.8 compression ratio by assuming that the efficiency was increased in proportion to the theoretical fuel-air-cycle increase (10%) from 5.43 to 6.80.

[9] NACA TN 674, November, 1938, "Scavenging a Piston-Ported Two-Stroke Cylinder," by A. R. Rogowski and C. L. Bouchard.

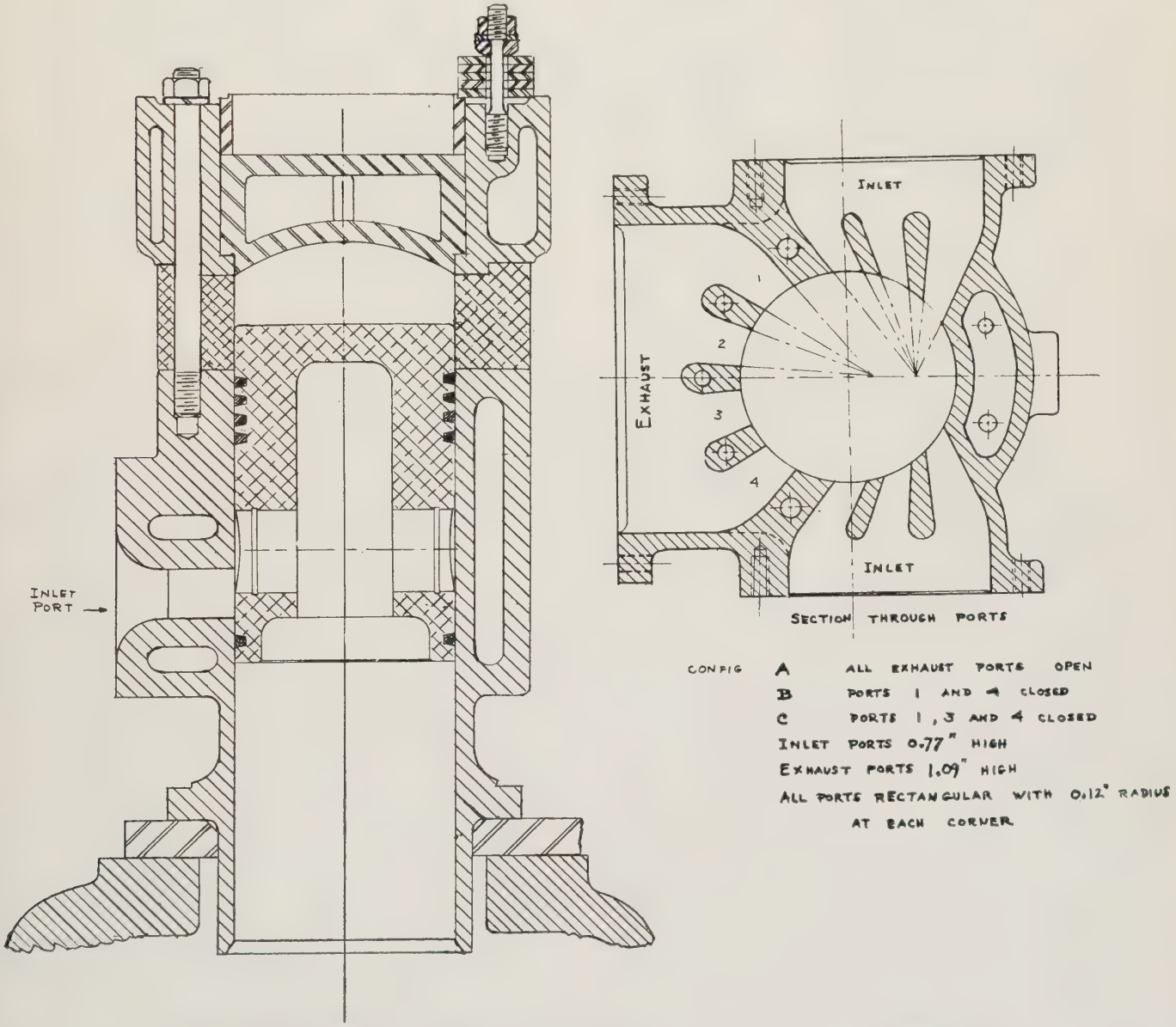

Fig. 3—CFR loop-scavenged 2-stroke cylinder (3.25-in. bore, 4.5-in. stroke, 37.5-cu-in. displacement)

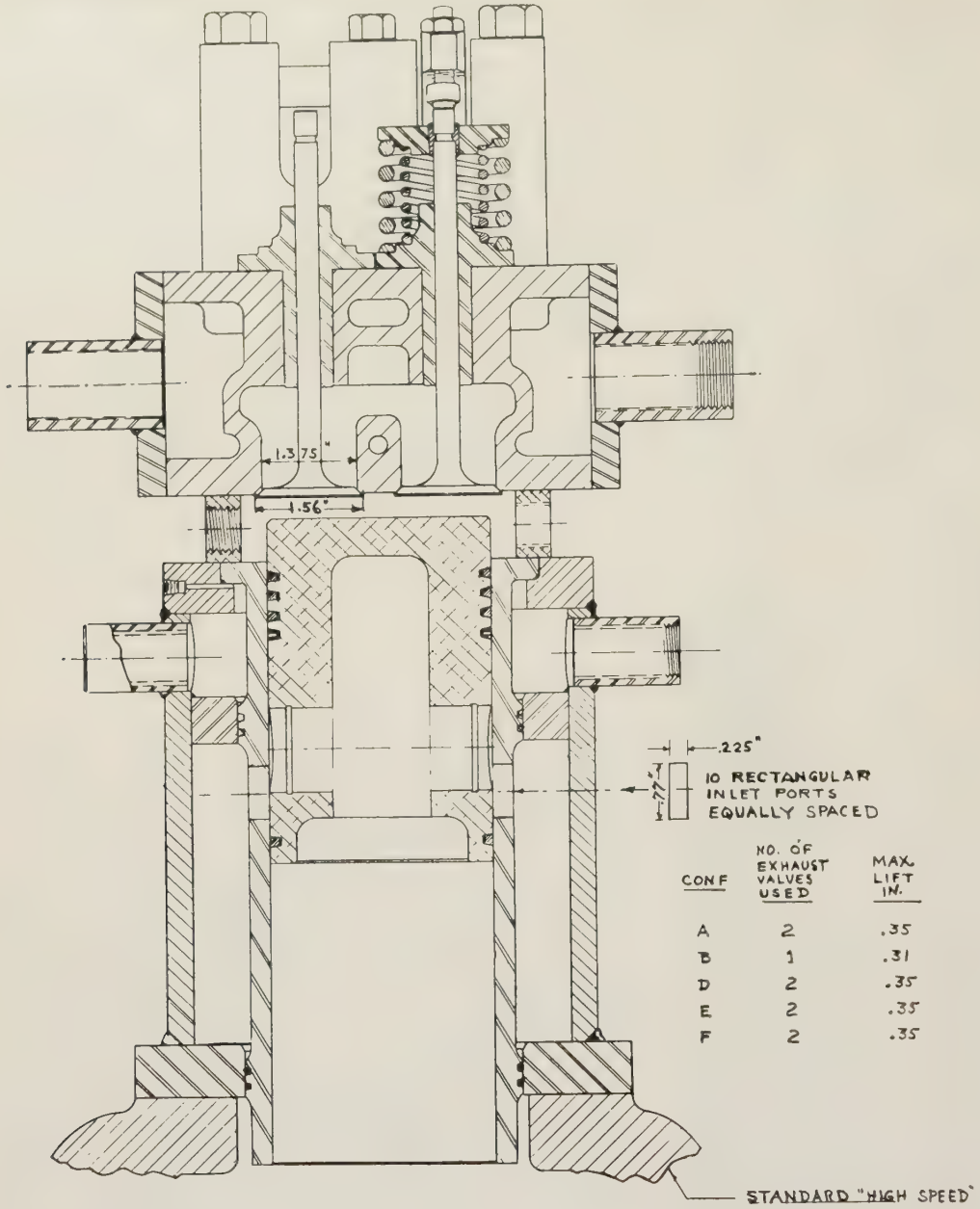

Fig. 4—CFR poppet-valve 2-stroke cylinder (3.25-in. bore, 4.5-in. stroke, 37.5-cu-in. displacement)

corresponding to known crank angles.

Exhaust Ports—The loop-scavenged engine had four exhaust ports of equal height. Exhaust-port area in this engine was varied by blocking off two or three of these ports. In the first case the two outer ports were blocked. For the second case one of the central ports was also blocked off. This method left the timing of the exhaust ports unchanged.

In the case of the through-scavenged engine, exhaust-port area was changed by adjusting the rocker arm ratio of the exhaust valves. This method varied the lift but left the timing unchanged.

Flow Factor—The effective area of ports at a given crank angle, divided by the piston area, is called the flow factor (FF) and is defined as follows:

$$FF = \frac{AC}{A_p} \tag{8}$$

where:

A = Port maximum area (subscript i for inlet, e for exhaust)

A_p = Area of piston

C = Port flow coefficient (subscript i for inlet, e for exhaust)

Values were measured at each crank angle in a steady flow apparatus.

Configurations—In order to identify the various arrangements used, a system of configuration letters was adopted.

Fig. 5 and Table 2 give valve opening diagrams for configurations A, B, and C for both engines, in terms of flow factor versus crank angle. The following relations should be noted:

1. Configurations A, B, and C differ from each other only in exhaust-port flow factor.
2. For each configuration A through C, the effec-

Table 2—Flow Factor Measurements of Poppet-Valve and Loop-Scavenged Engines

Configuration	Poppet-Valve Exhaust Valves				Loop-Scavenged Exhaust Ports			
	Number	Maximum lift, in.	Mean Flow Factor	Flow Factor Ratio[a]	Number	Maximum area, in.^{2}	Mean Flow Factor	Flow Factor Ratio
A	2	0.35	0.050	1.29	4	2.5	0.048	1.25
B	1	0.31	0.023	0.60	2	1.2	0.023	0.60
C	1	0.19	0.014	0.36	1	0.6	0.013	0.33

Inlet ports, all configurations

Poppet-Valve			Loop-Scavenged		
Number	Maximum area, in.^{2}	Flow Factor	Number	Maximum area, in.^{2}	Mean Flow Factor
10	1.73	0.039	6	2.15	0.038

[a] Flow factor ratio = Mean exhaust flow factor/mean inlet flow factor

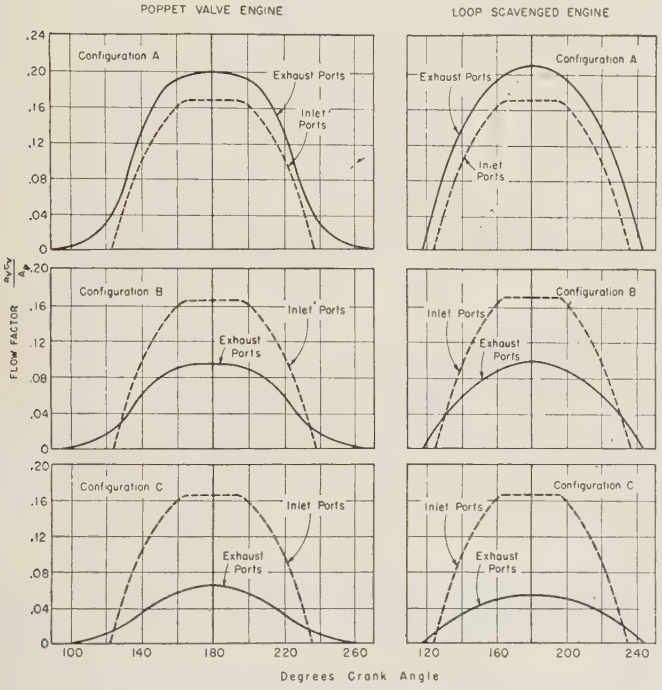

Fig. 5—Valve-opening diagrams with symmetrical timing (See Table 2)

tive port openings and port timings were essentially the same for the two engines.

3. In configurations A, B, and C the timing is symmetrical.

Configurations D, E, and F (used on the through-scavenged engine only) were the same as configuration A except that the exhaust-valve timing was set 7, 14, and 21 deg, respectively, ahead of the symmetrical position.

Test Results

The results of this investigation are summarized in Figs. 6–13.

Fig. 6 shows e_s versus R_s for the loop-scavenged engine for configuration A, B, and C. Reduction of the ratio exhaust-to-inlet flow factor from 1.29 to 0.60 gives a substantial increase in e_s at the higher piston speeds. Further reduction to 0.36 seems to offer no improvement in scavenging, but reduces C as indicated later.

Fig. 7 shows e_s versus R_s for the poppet-valve engine for configurations A and B. Configuration C was not tested with this engine.

Again, the reduction of exhaust-port to inlet-port

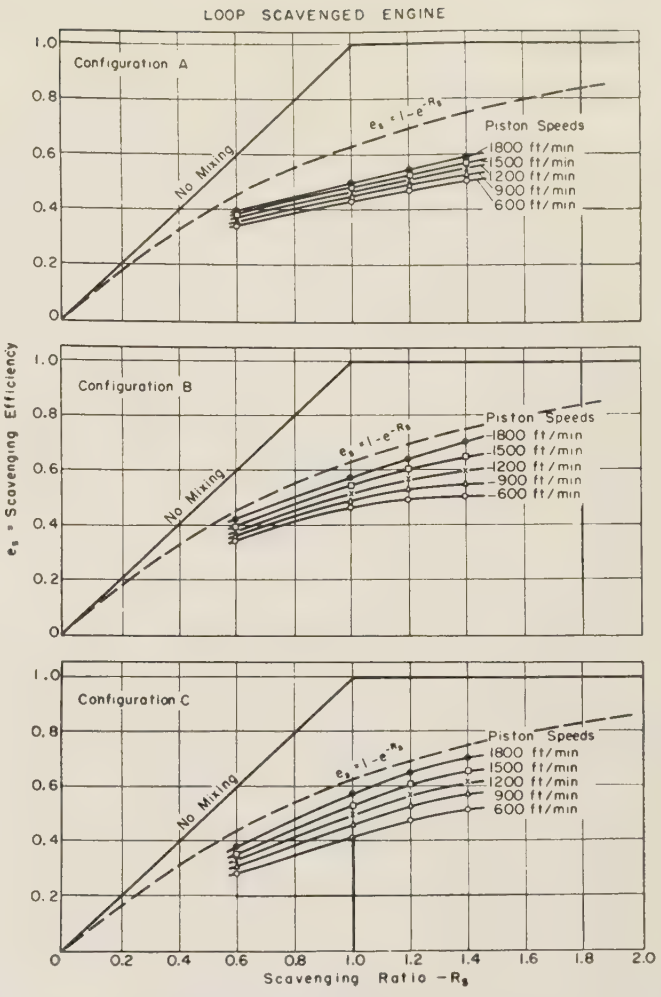

Fig. 6—Scavenging efficiency versus scavenging ratio, loop-scavenged engine configurations A, B, and C (ratio exhaust-port to inlet-port mean flow factor: A—1.25, B—0.60, C—0.33)

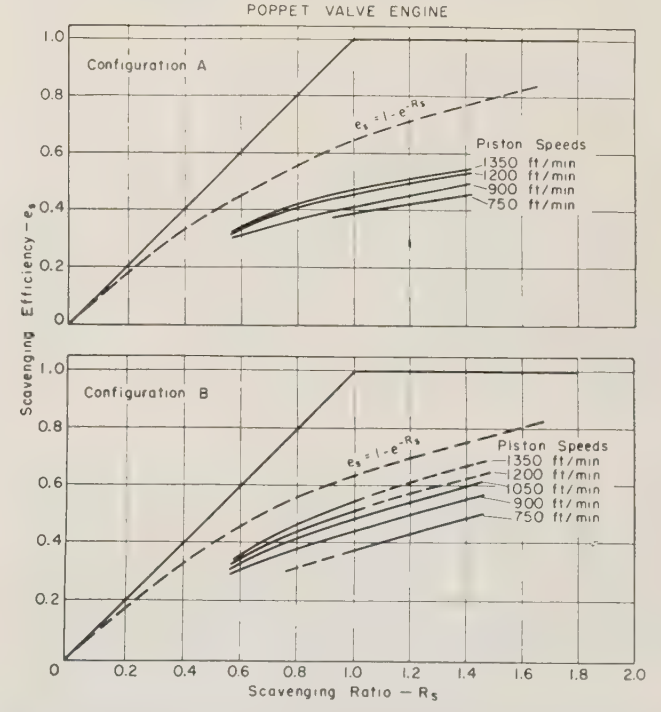

Fig. 7—Scavenging efficiency versus scavenging ratio, poppet-valve engine configurations A and B (ratio exhaust-port to inlet-port mean flow factor, A—1.29, B—0.60)

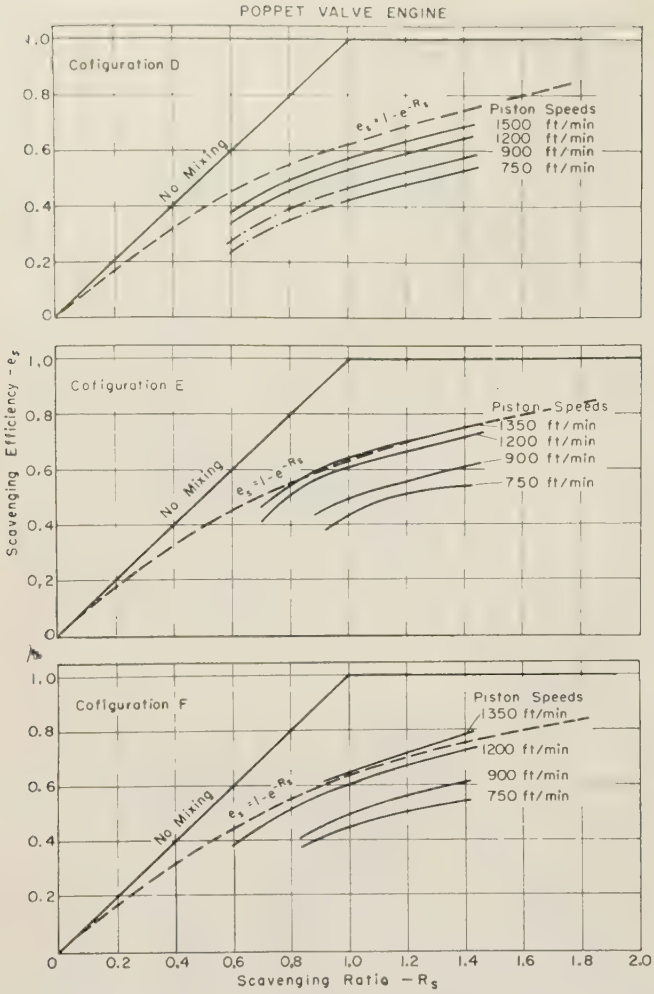

Fig. 8—Scavenging efficiency versus scavenging ratio, poppet-valve engine, configurations D, E, and F (See Table 3)

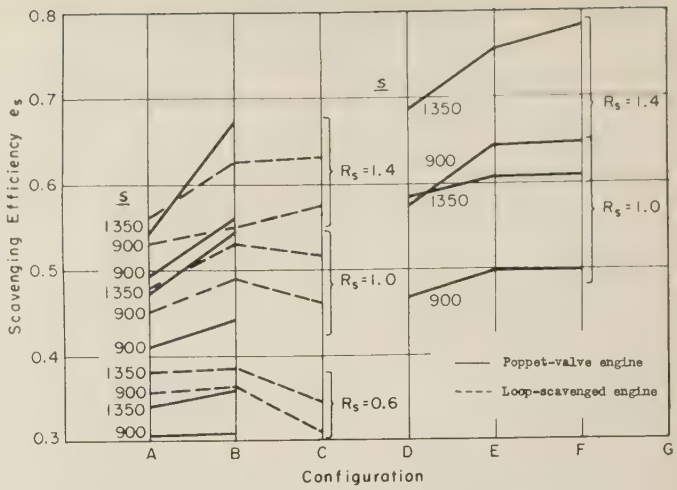

Fig. 9—Effect of configuration on scavenging efficiency

Table 3—Flow Factor Ratios on Poppet Valve Engine

Configuration	Exhaust Advance, deg	Exhaust/Inlet Flow Factor
D	7	1.29 (as in configuration A)
E	14	
F	21	

Table 4—Values of R_v and R_m for Loop-Scavenged and Poppet-Valve Cylinders

	Loop-Scavenged	Poppet-Valve
Approximate volume occupied by cylinder assembly and valve gear (excluding parts inside crankcase), in.^{3}	355	459
$R_v \frac{\text{in.}^3}{37.5}$	9.5	12.2
Weights		
Cylinder Barrel[a]	24.00	24.00
Cylinder Head	17.56	26.75
Valve Gear	---	4.75
Connecting Rod and Piston	6.80	6.80
Assembly Total	48.36	62.30
$R_m \frac{\text{lb}}{37.5}$	1.29	1.66

[a] NOTE: The actual cylinder barrels used were quite different in weight, but since these differences were not necessary, the weight of the lighter barrel was used for both cylinders.

mean flow factor ratio from 1.25 to 0.60 gives a substantial increase in e_s versus R_s at the higher piston speeds.

Fig. 8 and Table 3 show e_s versus R_s for configurations D, E, and F on the poppet-valve engine. Except for exhaust-port timing, the port flow factors used were the same as in configuration A. Comparing D, E, and F with configuration B (best arrangement with symmetrical timing) of Fig. 7, it is evident that advancing the exhaust timing 14 deg effects a substantial rise in e_s versus R_s, especially at the higher piston speeds. Further advance to 21 deg seems to afford little improvement.

Comparison of Engines

1. Scavenging Efficiency—Fig. 9 shows the range of e_s versus R_s for both engines at the various configurations tested.

Allowing for experimental error, with symmetrical timing, (configurations A and B) the loop-scavenged cylinder appears about equal to the poppet-valve cylinder at the higher scavenging ratio, and better at $R_s = 0.60$. However, when the exhaust-valve timing is advanced by 14 deg or more on the poppet-valve engine (configurations E and F), the highest values of e_s versus R_s are reached.

2. Engine Flow Coefficients—Flow coefficients C for the two engines in various configurations are shown in Fig. 10.

Since the flow factors and timing of the individual ports were the same for both engines in configurations A and B, the lower flow coefficient for the poppet-valve engine, measured under running conditions, must be due to differences in the dynamic characteristics of the inlet and/or exhaust systems. While every effort was made to minimize dynamic factors by using short inlet pipes and large surge tanks, the two engines had quite different inlet and exhaust systems due to their differences in port configuration. Further study of this question is planned by making instantaneous pressure measurements in the inlet and exhaust systems of the engines.

In the case of the poppet-valve engine, the change of flow coefficient due to advancing the exhaust timing is indicated by comparing configurations A, D, E, and F. This change appears to be negligible.

3. *Lost Work Due to Blowdown*—Fig. 11 shows indicator diagrams for the two engines in various configurations, operated under otherwise similar conditions at 1200-fpm piston speed. The lost-work ratio, R_w, is shown in each case.

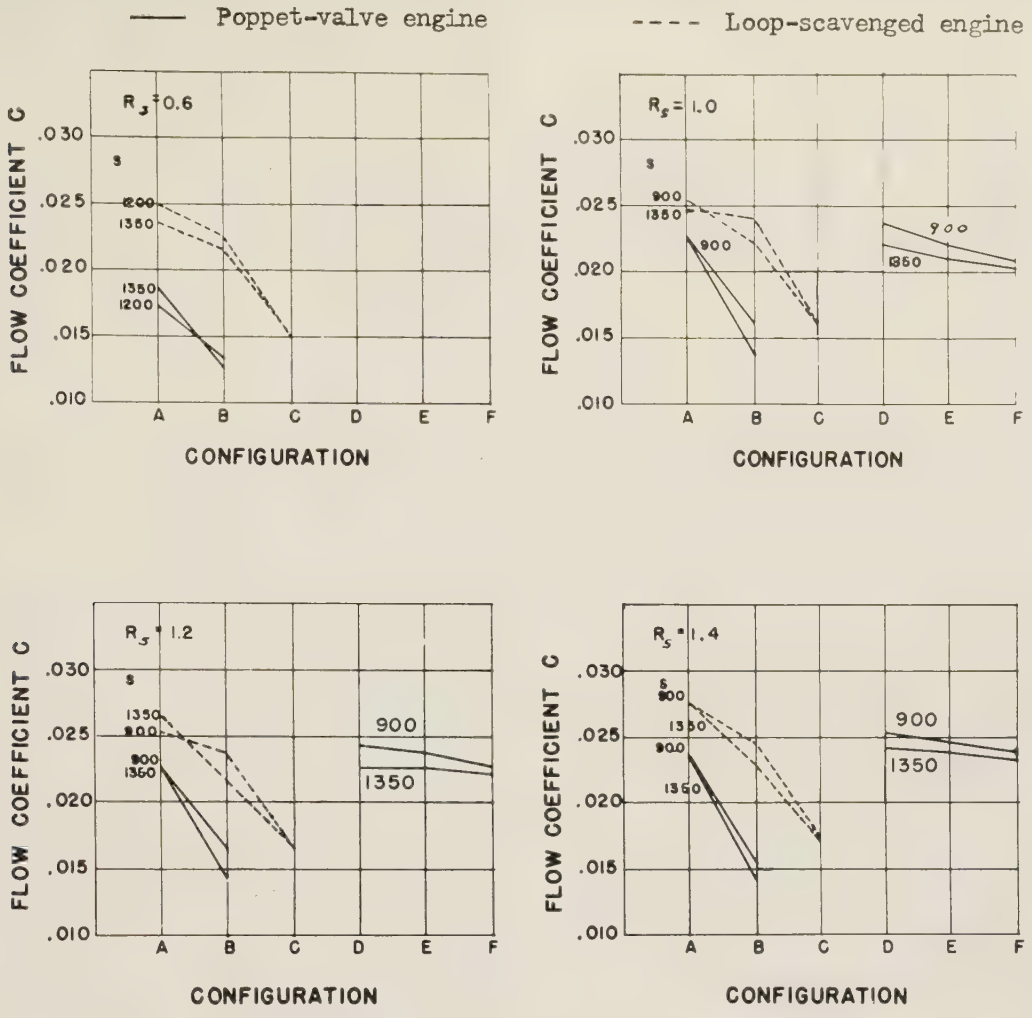

Fig. 10—Effect of configuration on overall engine flow coefficient under operating conditions

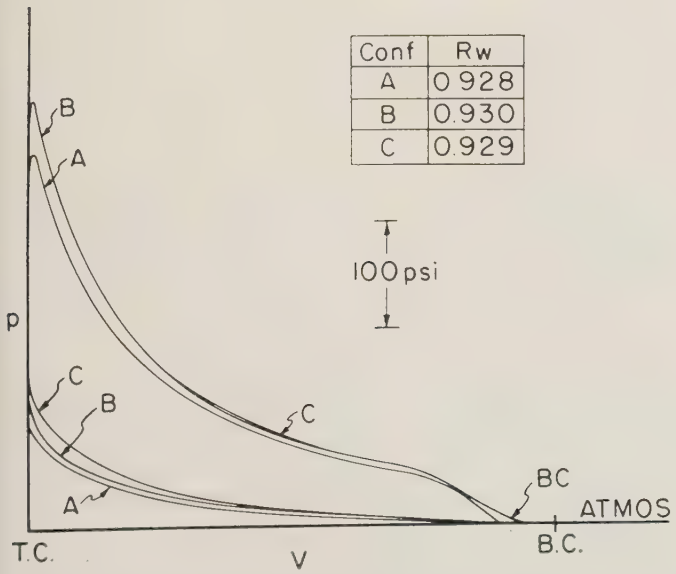

Fig. 11A—Effect of configuration on indicator diagram, loop-scavenged engine (R_s = 1.2, s = 1200 fpm, symmetrical timing)

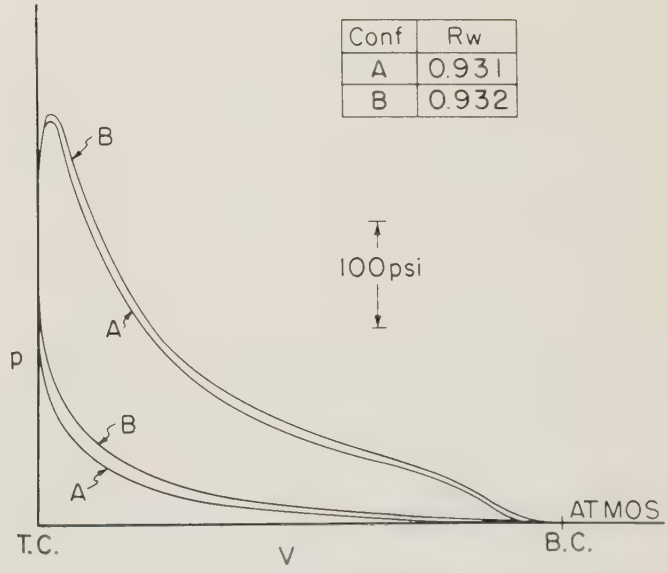

Fig. 11B—Effect of configuration on indicator diagram, poppet-valve engine (R_s = 1.2, symmetrical timing, piston speed: A—1200 fpm, B—1050 fpm)

Table 5—Friction Mep from Motoring Tests[a]

(lb per sq in., all scavenging ratios)

Piston Speed, ft per min	Loop			Poppet Valve				
	A	B	C	A	B	D	E	F
600	13	12	13					
750				11	10.3	12.0	12.2	12.0
900	16	15.8	16.5	11.5	11.2	12.7	13.1	13.0
1200	18.7	18.9	19.6	12.4	13.0	14.0	15.0	15.2
1350						15.0	16.0	16.8
1500	21.4	23	22.7	14.2	15.3	16.2		
1800	24.3	27	27					

[a] "Influence of Exhaust-Port Design and Timing on the Performance of Two-Stroke Engines," by A. L. Hagen and J. D. Koppernaes, Figs. 19, 23, and 24. Thesis, M.I.T., August, 1956.

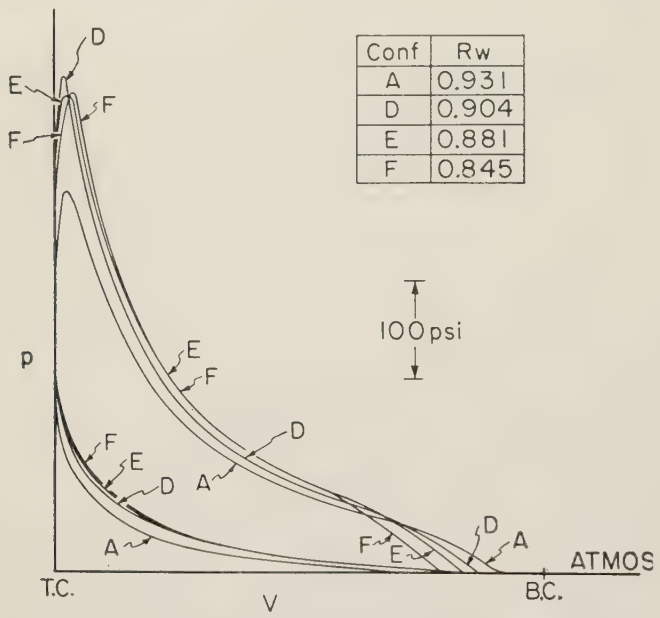

Fig. 11C—Effect of exhaust valve lead on indicator diagram, poppet-valve engine ($R_s = 1.2$, $s = 1200$)

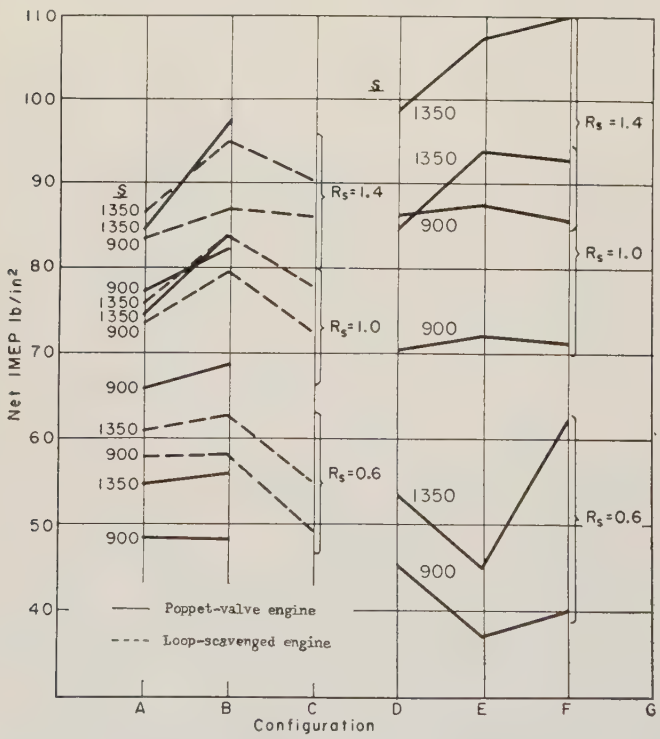

Fig. 12—Effect of configuration on net imep, corrected to $r = 6.8$

The lost-work ratio will increase with increasing piston speed, since the blowdown process takes place largely at sonic velocity. Hence, the pressure will fall more slowly as a function of crank angle as speed increases. Lost-work measurements are not yet available at piston speeds other than 1200 fpm.

Fig. 11C shows that the lost-work ratio decreases appreciably as exhaust timing is advanced, with no change in inlet timing.

4. Bulk and Weight—The values of R_v and R_m were measured for these two cylinders. and are shown in Table 4. (See Equations 6 and 7.)

Indicated Mep—Fig. 12 shows net imep versus configuration.

Imep is taken as the measured brake mep plus the friction mep determined by a motoring test at each speed and scavenging ratio with each configuration. On account of the scatter of motoring friction readings, faired values of fmep versus piston speed were used. These values are shown in Table 5, while Fig. 14 compares such measurements with imep measured from indicator diagrams.

Net imep is defined as the imep determined above, corrected to 6.8 compression ratio in the case of the loop-scavenged engine (correction factor was 1.10), less the mep which would be required to drive a compressor of 0.75 adiabatic efficiency giving the required scavenging ratio. The method of computation is explained in Rogowski and Taylor.[3]

Under the conditions of these tests, the only significant advantage in net imep of the through-scavenged arrangement occurs when the exhaust valves are advanced 14 deg or more ahead of symmetrical timing with scavenging ratio of 1.0 or more.

Specific Fuel Consumption—Net indicated specific fuel consumption, shown in Fig. 13, is the observed fuel flow divided by the power computed from speed and net imep.

Net indicated specific fuel consumption for fuel-injection engines is the observed net indicated specific fuel consumption multiplied by the trapping efficiency. This value of indicated specific fuel consumption would be that obtained with the same fuel-air ratio and scavenging ratio if no fresh fuel escaped from the exhaust ports during scavenging. In practice, this result could be accomplished by scavenging with air and injecting the fuel after the ports close. It may be assumed that high-performance 2-stroke engines would be designed for fuel injection, whether operated on the spark-ignition or the diesel cycle.

Summary—Comparative figures for the two types of cylinder, each with its optimum porting, are shown in Table 6. Absolute values may not be typical because the cylinder designs used may not be typical in regard to weight and volume.

Discussion of Results

One of the most interesting results is the observation (Fig. 9) that, with equal effective port areas and the same (symmetrical) timing, the through-scavenged cylinder shows no significant advantage over the loop-scavenged cylinder in respect to trapping efficiency (Γ).

Another important indication for both cylinders is that, with symmetrical timing, the best ratio of exhaust-port to inlet-port effective area appears to lie in the neighborhood of 0.6 (Figs. 6 and 7).

A third significant observation is that unsymmetrical timing is an effective method of improving trapping efficiency (Fig. 9). Whether the added mechanical complication necessary to achieve unsymmetrical timing is justified will depend on particular circumstances.

Allowing for experimental error, the values of net indicated fuel economy with fuel injection (Fig. 13) show no significant difference between the two cylinders, with symmetrical timing (configurations A and B). With the poppet-valve engine, the small

Table 6—Comparison of Loop-Scavenged and Poppet-Valve Cylinders with Best Porting

Configuration	Loop-Scavenged B	Poppet-Valve E
Piston Speed, fpm	1350	1350
Best Net Imep at $R_s = 1.4$ (Fig. 12), lb per in.^{2}	95	107.5
Net Ihp	16.6	18.8
Cylinder Weight, lb	48.36	62.3
Overall Cylinder Volume, in.^{3}	355	459
Weight per Net Ihp, lb per hp	2.92	3.31
Volume per Net Ihp, in.^{3} per hp	21.4	24.4
Net Indicated Specific Fuel Consumption with Fuel Injection (Fig. 13)	0.57	0.59

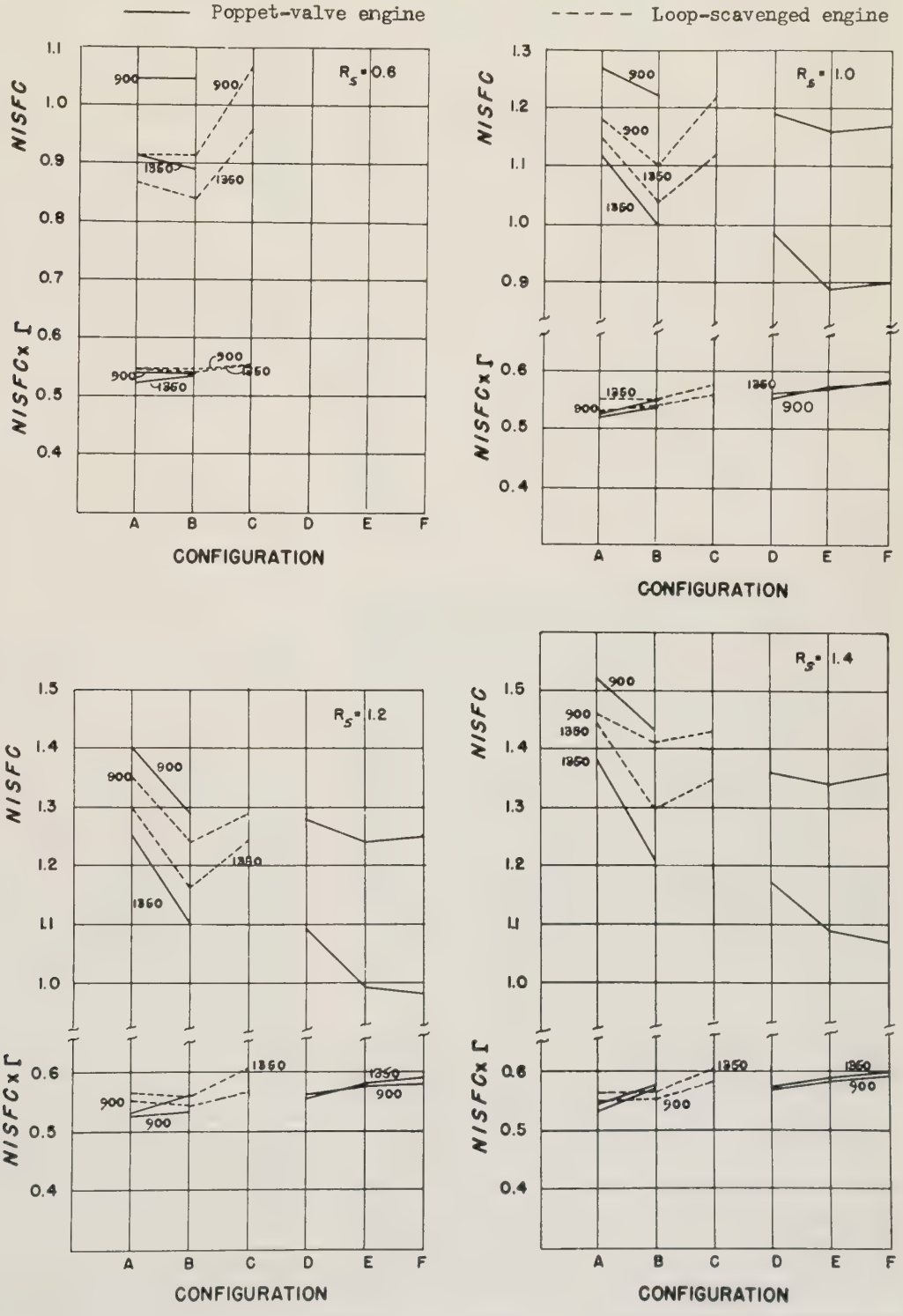

Fig. 13—Effect of configuration on net indicated specific fuel consumption (numbers on curves refer to piston speed fpm)

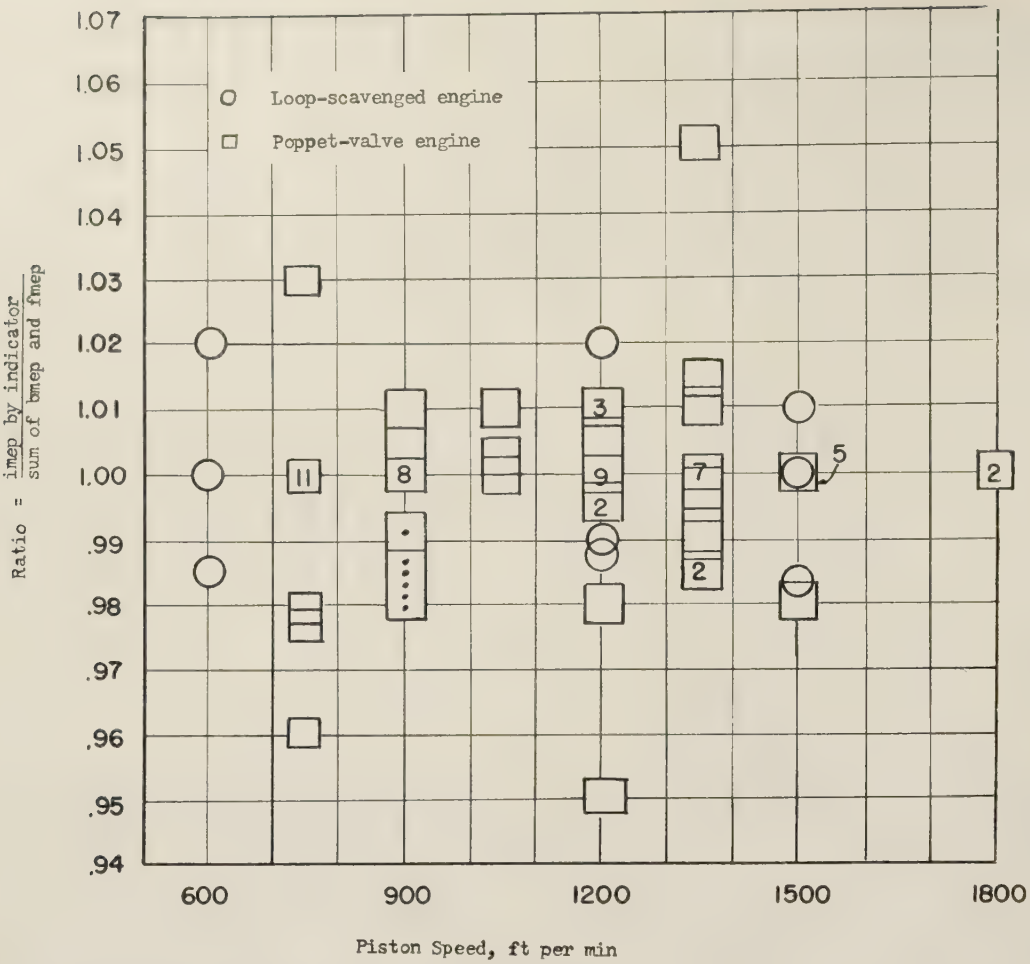

Fig. 14—Ratio of imep by indicator to sum of bmep and motoring mep (numbers indicate number of readings at one point)

change in net isfc × Γ as the exhaust-port timing is advanced (configurations D, E, F) is perhaps also within experimental error. It will be recalled (Fig. 10) that the flow coefficient was not reduced by the advance in exhaust-valve timing and, therefore, the apparent decrease in fuel economy cannot be attributed to greater scavenging mep.

Diesel engines, in general, would have lower imep at the same operating conditions, which would make differences in flow coefficient more important. However, the comparison between types should be nearly the same.

Brake results will, of course, depend on engine friction. Since the friction mep of the CFR crankcase is not typical of that of multicylinder engines, the measured brake output of these engines is of academic interest only.

Future Work

In the work reported here, the principal objective was to compare the two cylinders when their port areas were substantially equal. It is improbable that the optimum port design was used in either case.

It is hoped that support can be obtained for further experiments with these cylinders, in which the object would be to determine the optimum porting for each type and then to compare their performance.

It is possible that, if optimum porting were used in each case, the two types would show differences greater than those here reported.

DISCUSSION

Says Loop-Scavenged Engine Penalized in Authors' Experiments

—P. H. Schweitzer
The Pennsylvania State University

THIS paper is a distinct contribution to our knowledge of scavenging of 2-stroke engines. The authors subjected to rigid experiment questions which have been answered only speculatively before, sometimes right and sometimes wrong. But those guesses were based only on hunches and scattered observations.

It is comforting to have authentic answers based on well-controlled series of experiments to such questions as:

1. Is the performance of the uniflow scavenging superior to loop scavenging? The authors say no. The scavenging and charging efficiencies of the uniflow engines are usually higher than those of the loop-scavenged engines, but only because the former generally have unsymmetrical timing (exhaust lead) while the latter usually do not. If a rotary valve is used in the exhaust duct to make it close earlier, a good loop-scavenged engine can be as efficient in scavenging as any uniflow engine. A small Saurer engine of such design has 105 psi maximum bmep.

2. Does it pay to increase the exhaust area of the 2-stroke cycle engine beyond 60% of the inlet area? The authors' answer is again no. From the scavenging standpoint it is wrong to increase the exhaust flow area beyond 60% of the inlet area.

3. Does a 2-stroke cycle engine behave with regard to airflow as a fixed orifice? If it were, the "flow coefficient" of the authors or my "scavenge factor" would be independ-

ent from air-box pressure, exhaust back pressure, and piston speed (rpm). No explicit answer was given to this question by the present paper but Messrs. Taylor and Rogowski have given tentative answers in their previous papers: In the practical range of 1.5–6 psig air-box pressure and 500–1800 fpm piston speed the engine does behave substantially as a fixed orifice when it is motored. Under firing conditions the flow coefficient does change with speed and pressure ratio which can be explained by the powerful effect of tuning on the gas dynamics of the exhaust process.

4. I would like to draw an additional conclusion from the results of the authors. While their tests have shown that the loop-scavenged engine is not inferior to the through-scavenged one in scavenging performance, the comparison should have come out still more favorably to loop scavenge if the authors had not penalized the latter unnecessarily. The M.I.T. loop-scavenged engine had four exhaust ports with a maximum area 1.25 times inlet port area. This proved to be too much. To reduce it the authors closed the two outer ports and left open the two inner exhaust ports. Thus, they reduced the exhaust port area to about one-half (0.60 times inlet port area) and obtained optimum results.

What they did is equivalent to reducing the port width and leaving the port height alone. The proper way to reduce the port area is to reduce the port height and leave the width alone. Then, the effective blowdown can be preserved and the trapping efficiency still increased by restricting the outflow of fresh air from the cylinder.

Inlet ports in most 2-stroke engines go down to bottom center position of the piston while the exhaust ports often end a little above that line. Judging from Fig. 7, it was the other way in the M.I.T. engine. What was the reason?

Efficiency of Through-Scavenged Engine Can Be More Effective

—K. C. Karde
Dexter Folder Co

THE authors are certainly to be complimented for their fine work on the important subject of evaluating the 2-stroke scavenging process. The results of their engine tests are leading to the conclusions that obtainable mep is about the same for the loop-scavenged and the through-scavenged 2-stroke engine.

The experience with some actual production diesel engines shows in some instances a somewhat different picture in favor of the through-scavenged engines. Some of these engines, whether the exhaust poppet-valve type or the opposed-piston type, are far superior in comparison to the loop-scavenged engine, even if this engine is equipped with a rotary exhaust valve which makes an unsymmetrical timing diagram possible.

A review of Figs. 3 and 4 indicates that a good porting design apparently has been used for the evaluation of the loop-scavenged system. The through-scavenged system is represented by a rather inefficient port design.

In order to see this more clearly, let us take a look at Fig. 3. The scavenging air is excellently guided at the inlet ports and covers in its flow about half of the piston area after entering the cylinder. On its return to the exhaust ports, the air covers the other half of the cylinder cross-section area. Port area and flow direction indicate the tendency of covering the entire area of the cylinder cross-section during the scavenging process.

Porting of the through-scavenged engines (Fig. 4) is designed to have the same area at each crank angle as the ports of the loop-scavenged engine. This results in rather wide bridges between the 10 inlet ports, so that a relatively high percentage of dead space (not covered by the flow of the incoming scavenging air) exists above the piston crown. In such a manner, favorable conditions for mixing the incoming air with the combustion gases are created at the inlet side of the cylinder.

What can be achieved with the through-scavenging system is best illustrated by reviewing the development of a well-known 2-stroke diesel engine. Table A shows engine data at the beginning of production and seven years later:

Table A—Comparison of 2-Stroke Diesel Engine, First Year of Production and Seven Years Later

	First Year	Seven Years Later
Hp	500	1000
Rpm	2050	3000
Bmep psi	94	131
Bmip psi	124	166
Inlet Porting	Rectangular	3 rows of round holes
Scavenging Ratio	1.50	1.25
Scavenging Blower		
Pressure Ratio	1.46	1.73
Adiab Efficiency	0.60	0.78

These data clearly indicate the trend in the development of the through-scavenging system. It seems very desirable that such highly effective porting systems are included in the future work on the through-scavenged 2-stroke engine.

Divides the Scavenging Process Into Four Components

—D. S. Sanborn
Consulting Engineer

THE nicely correlated series of scavenging tests executed and reported on by Prof. Taylor and his associates should provide the basis for speculation and discussion by 2-stroke engine zealots for years to come.

It is somewhat unfortunate that it was not possible to run the tests of the loop-scavenged cylinder at the same compression ratio as the through-scavenged cylinder. Analysis of the test data by this discusser (of somewhat smaller engines, both air-cooled and water-cooled) has consistently shown only about half of the expected theoretical air-cycle response in the range of about 5–8 compression ratio. Do the authors have any test data on the cylinders studied which would substantiate the extrapolation of the loop-scavenged cylinder results to 6.8 compression ratio?

It is believed that typical scavenging trends, as those so graphically illustrated in Figs. 6, 7, and 8, can be more easily understood (especially in the case of unsymmetrical timing) by subdividing the rather loosely termed "scavenging process" into four components:

1. Cylinder blowdown.
2. The actual scavenging process itself.
3. The supercharging or compressibility effects.
4. The postscavenging loss of charge thru the exhaust ports.

Inspection of Fig. 8 shows that for the regions of low piston speeds and low scavenge ratios, where cylinder pressures are only slightly above atmospheric during scavenging, there is not very much difference between configurations A and B. At higher piston speeds, especially when combined with high scavenging ratios, the greater exhaust restriction of configuration B increases the trapping efficiency by reducing the actual cylinder scavenging ratio due to the compressibility effect. In addition, it appears that the postscavenging charge loss is reduced by the smaller exhaust ports. Were any low-pressure indicator cards taken during these tests which might be used to determine the scavenging ratio at actual cylinder conditions and the pressure at exhaust-port closing? Is there any difference in the efficiencies of the actual scavenging processes of configurations A and B or are the differences due to the other effects that are not truly part of the scavenging process?

If the exhaust is restricted too much, as in Fig. 8 configuration C, the pressure differential across the inlet ports will be small compared to that across the exhaust ports. The resultant low inlet velocity may then be too small to give the required high scavenging and short circuiting will result. Such a deterioration of the actual scavenging process in configuration C might be expected to show up most in the regions of low piston speeds and/or low scavenging

ratios where it is not offset by improvements due to the other effects.

Step by step analyses of similar cylinder designs indicate that the post scavenging loss of charge from the cylinder may amount to 20% of the maximum fresh charge that is in the cylinder prior to inlet closing (in a symmetrically timed engine). This loss phase encroaches so much on the end of the scavenging period, however, due to the displaceing effect of the piston, that exhaust closing might have to be earlier than those of configuration F in Fig. 10, in order to eliminate the fresh charge loss completely. It is probable that the greatest potentialities of asymmetrical timing would be gained by exploiting the possibilities of the supercharging effect, which for maximum net gain may require high scavenge pressures and exhaust closing only shortly after btdc. Contemplation of Figs. 8, 9, and 10, especially in view of the difficulties of providing sufficient poppet-valve area for high-speed operation, should presage great specific output advantages for the simple loop-scavenged engine supplemented by an equally simple rotary exhaust valve.

Discusses Scavenging Efficiency in Relation to Engine Speed

—Dr. B. L. Sheaffer
McCulloch Motors Corp

THIS paper presented a thorough comparison under similar test conditions of the scavenging efficiencies of a loop-scavenged engine. More work of this nature is needed to remove some of the mysteries surrounding the scavenging process of 2-stroke engines.

Of great interest were the statements that with equal port areas and the same symmetrical port timing the trapping efficiencies of the two engines were equal, and that an unsymmetrical exhaust timing was found to be an effective means of improving trapping efficiency (tested only on the through-scavenged engine). It is hoped that the authors will consider extending their work to include a loop-scavenging engine with a rotary exhaust valve. Such an engine would still be simpler in construction that the poppet-valve, through-scavenged engine and would not be speed limited due to cam dynamics.

Figs. 6, 7, and 8 of the paper indicated that the scavenging efficiency increased with engine speed. In tests conducted at Purdue University[a] on a GMC 1-71 diesel engine converted to spark ignition and gasoline injection (with a flat-top piston and a bathtub-shaped combustion chamber), the writer found that at a constant scavenging ratio the scavenging efficiency decreased slightly as the engine speed increased from 1100 to 1500 rpm. Have the authors found any indications that the scavenging efficiency will peak in value and thereafter decrease as the engine speed is increased?

Concerning the effects of swirl, it was also found that at the two speeds tested identical values of scavenging efficiency were obtained with either radially drilled inlet ports or with the ports drilled at an angle of 25 deg from the radial direction.

The writer feels that the information regarding the optimum ratio of port areas should not be construed as being applicable to crankcase-scavenged engines. For a given port timing and engine speed, tests on small crankcase-scavenged engines have shown that increasing the port time areas above a certain size will not increase the power output of the engine at that speed and below, but will increase the power output at all higher engine speeds. As is well-known, the scavenging ratio of a crankcase-scavenged engine is profoundly influenced by flow restrictions, whether they appear in the inlet system, the exhaust system, or the ports. Hence, the scavenging efficiency is increased more by an increase in scavenging ratio for this type of engine than by an increase in trapping efficiency caused by port reduction.

[a] Study of Certain Aspects of Two-Stroke Cycle Spark-Ignition Engine with Gasoline Injection," by B. L. Sheaffer. Purdue University thesis, 1957.

Authors' Closure To Discussion

WE are not as sure as Prof. Schweitzer seems to be that the results show the loop-scavenged cylinder to be superior. To be sure, the port configuration of the loop-scavenged cylinder was probably not optimum, but neither was that of the poppet-valve cylinder. The configurations used were those available at the time. Without outside support for this kind of work (which is rather expensive), we cannot afford to build and test many cylinder configurations. We would certainly like to try a loop-scavenged cylinder with the more conventional exhaust porting that Prof. Schweitzer suggests, and will do so if and when funds become available.

The views of Mr. Karde are opposite to those of Prof. Schweitzer, in that he feels we were unfair to the through-scavenged cylinder, while Prof. Schweitzer feels we slighted the loop-scavenged one. If we were equally unfair to both types, our results have excellent comparative value!

In answer to Dr. Sanborn, we had hoped that this paper would reduce, rather than increase, the areas for speculation about 2-stroke engines. Regarding his remarks on the correction for compression ratio, we find that within the small range involved (5.43–6.8), correction by the air-cycle ratio is in excellent agreement with experimental measurements. We were not able to take light-spring indicator diagrams, but hope to do so in the future. Some of the questions he raises would be answered, at least in part, by such diagrams.

Replying to Dr. Sheaffer, we will be glad to extend our tests to include rotary valves, and the like, whenever sufficient financial support is obtained. We have not found any indication as yet of a peak in scavenging efficiency versus speed, as speed increases. We agree that the crankcase-scavenged engine may be a special case for which porting requirements may differ from those for a steady scavenging pressure at the inlet ports, as used in our tests.

With regard to Mr. May's discussion, his first sentence applies only to the case where equal port areas and symmetrical port timing are used.

ORAL DISCUSSION

Reported by T. E. Kartisek
Christensen Machine Co.

Robert Cramer, Nordeberg Mfg. Co.: The type of engine (4-stroke or 2-stroke) is not too important, but the design details are what count. Prof. Taylor did not settle which was the better, uniflow or loop-scavenged. He also brought out that it is not the quantities that are important but the form in which results are obtained. A 17-in. bore engine which had a 1-in. difference in the size of the opening in the block to exhaust header gave an improvement in fuel consumption from 0.42 to 0.37 due to a change in the block flow path.

J. J. May, General Motors Corp.: The scavenging efficiency of loop or uniflow engines are the same. Prof. Taylor's measuring of scavenging efficiencies was done with gas vapor to indicate characteristics. The results of a 2-stroke spark-ignition engine tend to increase the compression ratio above the actual designed ratio.

Laskar Wechsler, Bureau of Ships, U. S. Dept. of the Navy: The Taylor paper is a point for argument that is not to be settled soon, but building of all types of engines is to continue. The Navy has no loop-scavenged engines in the small size. The large loop-scavenged and uniflow engines both perform very well. Before World War II 105 bmep was the maximum, after the War 160–200 bmep was obtained from the same size 2-stroke engines. The turbocharged 2-stroke engine will gain in size factor temporarily, but the 4-stroke engines will catch up. The most important point in the design of engines is the "detail of design."

Behavior of . . . Aircraft Structures under Thermal Stress

G. H. Sprague, Martin Orlando,
and P.C. Huang, Martin Baltimore

This paper was presented at the SAE National Aeronautic Meeting, Los Angeles, Oct. 3, 1957.

THE design of structures for high-speed flight must reflect the consequence of aerodynamic heating. The design philosophy may be to live with the heat, utilizing heat sinks and mass configurations to minimize thermal stresses, or to insulate or cool the structure to reduce the thermal effect. In either case, a knowledge of the structural behavior under the combined effects of load induced and thermal stresses is essential to define limiting criteria and safety factors on design loading.

The presence of a temperature gradient in a structure produces complex stress distributions due to varying degrees of restraint. While such complex stress patterns must be considered in specific detail design conditions, the primary, one-directional stress system is of most general significance to the designer. Basically, a temperature gradient produces a nonlinear stress distribution in a structure which might otherwise be analyzed for uniform stress conditions. A study of the structural behavior under axial loading in the presence of a stress-producing temperature gradient is considered to portray the typical significance of the thermal effects. The analyses are based on the structural configuration and temperature distributions of Fig. 1 and the material property data of Fig. 2. Only very short-time loading conditions (which do not include the effects of creep) are considered, although the phenomena of creep must be accounted for in design for high temperature and stress levels under sustained loading.

A basic consideration in the design for aerodynamic heating is the fact that structures, which might otherwise be analyzed for uniform end-loading conditions, are subject to nonlinear stress patterns due to the temperature gradients in the structure.

The significance of such nonlinear stress systems, when combined with external loading, on the inelastic behavior and buckling characteristics of structures is presented. The effect of residual stresses, resulting from inelastic behavior under nonlinear stress systems, on subsequent structural behavior is considered.

Experimental verification* of the basic analytical procedures for predicting inelastic tensile behavior and critical buckling load is shown.

Inelastic Behavior

Several authors[1, 2, 3] have previously applied inelastic analysis methods to stress systems produced

* Work sponsored by the Mechanics Research Branch of the Aeronautical Research Laboratory WADC under Contract No. AF-33(616)-3617 to The Martin Co. To be published as WADC TR 57-442.

[1] WADC TR 55-350, September, 1956: "Analytical and Experimental Investigation of Stress Distribution in Long Flat Plates Subjected to Longitudinal Loads and Transverse Temperature Gradients," by G. H. Sprague and P. C. Huang.

[2] Air Force Institute of Technology Tech Report 56-16, December, 1956: "Determination of Inelastic Stresses at Elevated Temperatures by Strain Analysis," by B. E. Gatewood.

[3] *Aircraft Engineering*, Vol. 26, December, 1954, pp. 402–406: "Wings under Repeated Thermal Stress," by E. W. Parkes.

by thermal effects combined with external loading. In general, the conventional simplifying assumptions of beam theory are observed and the approach to the solution on the basis of a strain analysis is not novel. The difference among authors lies in their techniques of arriving at the unique stress distribution associated with any given loading condition.

Method of Analysis—The method of analysis used in these studies has been previously presented by the authors.[1] Using the equations of equilibrium and the equations of compatibility of strain with the concept of stress equal to the product of secant modulus E_s and effective strain e' two governing equations are obtained as follows, based on the geometric presentation given in Fig. 3:

$$\phi = \frac{Pe}{E_B I_{kk}} + \frac{\int_b^a k_e k_p \alpha \Delta T z dA}{I_{kk}} \qquad (1)$$

$$\varepsilon_B = \frac{P}{E_B}\left(\frac{1}{A_{kk}} - \frac{ec}{I_{kk}}\right) + \frac{\int_b^a k_e k_p \alpha \Delta T dA}{A_{kk}} - \frac{c\int_b^a k_e k_p \alpha \Delta T z dA}{I_{kk}} \qquad (2)$$

Hence, the stress at any point can be easily calculated by:

$$\sigma = E_s \varepsilon' = E_s [\varepsilon_B + \phi(z + c) - \alpha \Delta T]$$

where:

E_s = Secant modulus

ε' = Effective strain, that is, strain associated with stress in any fiber

E_B = Modulus of elasticity at bottom edge of plate

k_e = Modulus of elasticity at any point/E_B

$k_p = \dfrac{\text{Secant Modulus}}{\text{Modulus of elasticity}} = E^{s}/_{E_B}$

A_{kk}, I_{kk} = Total effective area and moment of inertia of effective area about centroidal axis.

The values of ϕ and ε_B are functions of the effectivity factors k_e and k_p, which vary with the temperature and the degree of plasticity over the cross-section. They cannot be solved directly, but must be determined by either a trial and error technique or some iterative procedure. The authors employed the following iterative procedure: Assign initial values to ϕ and ε_B and then determine the resulting stress distribution using the known stress-strain relationships; determine the compatibility with the external loading by use of the equilibrium equations; adjust any unbalance by making corrections to the values of ϕ and ε_B based on the stress-strain relationships in the range of strain resulting from

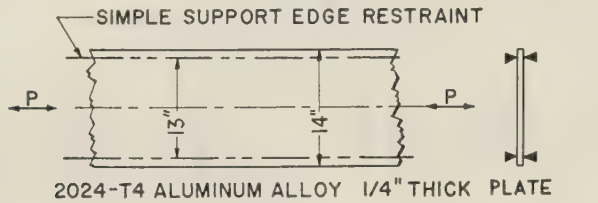

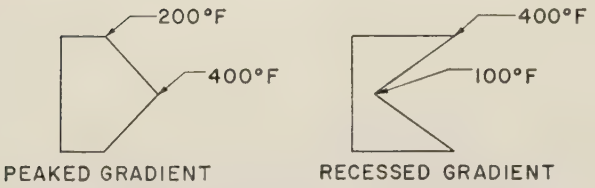

Fig. 1—Structural configuration and temperature gradients

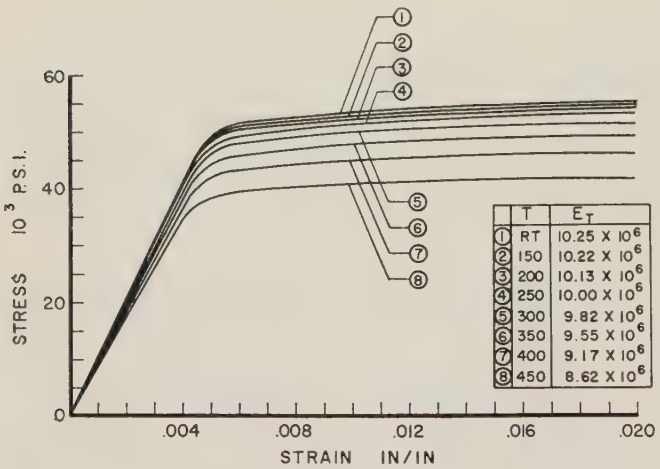

Fig. 2—Stress-strain curves at various temperatures (material 2024-T4 aluminum alloy)

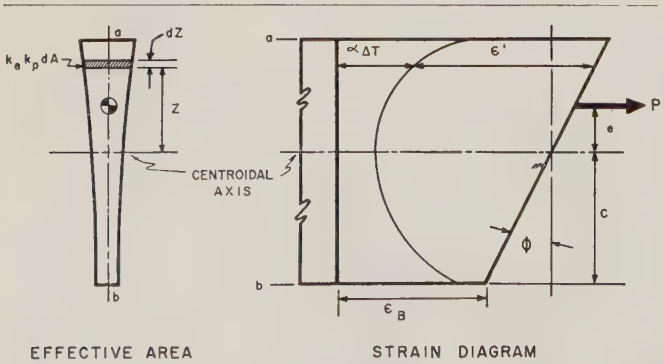

Fig. 3—Strain diagram

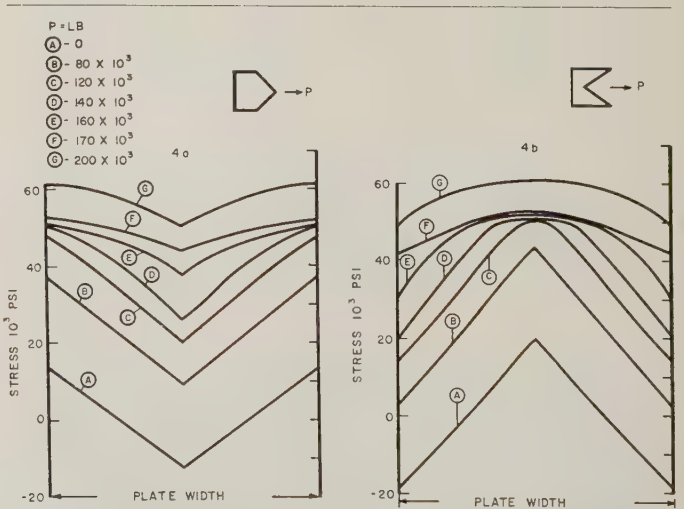

Fig. 4—Longitudinal stress distribution under tensile loading

the previous iteration. The procedure will converge on the unique stress distribution for the given loading condition in only a few iterations. By assuming elastic property behavior in determining the initial values of ϕ and ε_B, the first iteration will give the correct answer if the solution is entirely elastic.

This method of analysis is readily adaptable to high-speed digital computation over the full range of stress-strain relationship up to failing load.

Stress and Deformation—Under conditions of inelastic behavior, the most highly stressed fibers deform plastically and produce a variation in the shape of the stress distribution over the cross-section. Studies of the transverse distribution of axial stress, for the structural configuration and temperature distribution of Fig. 1, are shown in Fig. 4 for varying magnitudes of axial loading. In each condition there is a gradual smoothing out of the nonuniform stress distribution and, consequently, a diminishing of the thermal-stress pattern.

The essential elimination of thermal stresses at high deformations indicates that thermal stresses do not influence the static tensile failing load in a structure. Boukidis and Doman[4] have shown experimentally that the failing load of structures under elevated temperature conditions can be predicted on the basis of the stress due to external loading only by using the temperature dependent material strength properties.

On the other hand, comparison in Fig. 5 of the unit deformation for the condition involving thermal stress with that of a uniform average temperature condition (ignoring thermal stresses) shows the reduced load level at which inelastic behavior occurs in the presence of thermal stress.

It is significant, however, that although the inelastic behavior starts at a much reduced load level, the total deformation, and hence the permanent set, does not increase abruptly. Thus, an appreciable increase in applied loading can be permitted before excessive permanent set occurs.

Residual Stresses—Although the inelastic behavior of a structure subject to a temperature gradient produces an alleviating effect on the thermal stresses in the design for failure under external loading, the deformation characteristics may be a much more significant factor in design. As a result of the nonlinear stress distribution in the inelastic range, a system of residual stresses is developed in the subsequent unloaded condition. If the load history is of such magnitude that the thermal-stress pattern is completely diminished, the subsequent residual-stress pattern in the unloaded and cooled condition will be essentially equal in magnitude, but opposite in sign to the initial elastic thermal-stress pattern.

The residual stresses of a plastically deformed structure under nonlinear temperature distribution can be calculated by using Hooke's Law and the principle of superposition. First, the load is released by applying an equal but opposite force, and the corresponding stress distribution is calculated. The temperature is removed by applying a set of equal and opposite thermal strains ($\alpha\Delta T$). Again the corresponding stresses can be calculated elastically. The residual stress can then be obtained by adding these two stress distributions algebraically to the original inelastic system. Since the load-temperature history will affect the stress distribution, the residual stresses arrived at by different unloading procedures may not be identical.

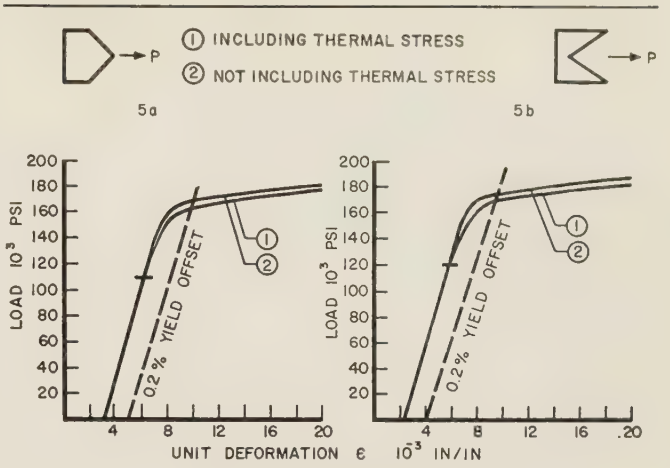

Fig. 5—Load-deformation curve

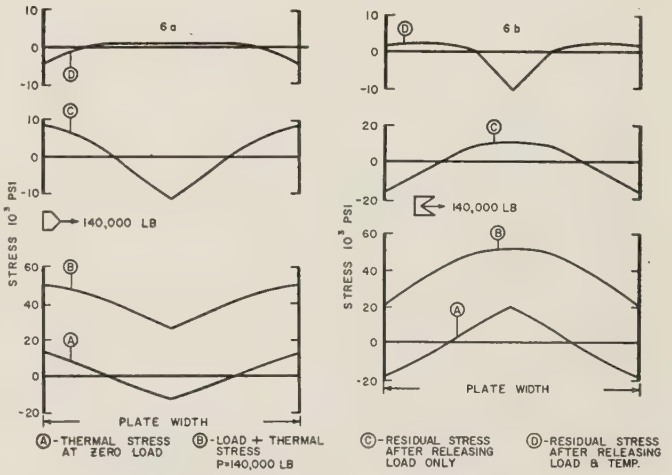

Fig. 6—Development of residual stresses during loading cycle

An illustration of the residual stresses developed in the flat plate structural configuration of Fig. 1 is shown in Fig. 6 for both the heated and cooled condition subsequent to inelastic tensile loading. The loading for the conditions shown in Fig. 6 was selected to represent a practical limit load application. With respect to Fig. 5 the load of 140,000 lb is greater than the actual load level which produces inelastic behavior, but is still within the range of practical design loading based on permanent deformation of the structure. It can be seen from Fig. 6 that the shape and magnitude of the residual stress pattern varies greatly with the temperature gradient.

For the condition of Fig. 5B, this 140,000 lb load represents:

$$\frac{140{,}000}{225{,}000} = 62\% \text{ of tensile failing load}$$

$$\frac{140{,}000}{120{,}000} = 117\% \text{ of actual load which produces plasticity}$$

The maximum residual stress for this condition (Fig. 6B) is approximately 10,000 psi, or roughly

[4] ARDC Tech Report 57-46, Vol. 2, ASTIA No. 113004: "Proceedings of Florida Conference on High-Speed Aerodynamics and Structures."

20% of the permissible yield strength of the material. This residual-stress system can significantly effect the stress pattern and structural behavior under subsequent loading conditions. Such effects will be pointed out in the discussions of compression loading and sequential loading effects.

Inelastic Design Criteria—Two basic requirements of design are the required strength and allowable deformation. A safety factor on the design loading condition is used primarily to ensure that in an overload condition neither of these limiting criteria will be exceeded.

In normal design procedure, a factor of safety—usually 1.5—is applied to the design load. The structure is then designed for this loading on the basis of full elastic behavior up to failing load. Conversely, the actual critical fiber stress under design limit load does not exceed two-thirds of the failure stress of the material. This concept has proved satisfactory in previous designs, such as a wing cover in which the stress distribution has been of a more uniform nature. Thus, a high structural efficiency is obtained on the basis of a limiting elastic stress. Inelastic analyses have generally been considered only in special structures under nonuniform bending stress conditions.

Under nonuniform thermal stress conditions the limitations to critical peak stresses result in a very low structural efficiency since many fibers are not significantly loaded. Thus, for the design of structures subject to combined load and thermal stress, the direct addition of the separate stress fields (with the requirement that the maximum fiber stress not exceed a prescribed elastic-stress level) imposes a severe weight penalty on the structure. Under these conditions of nonlinear stress it appears mandatory that advantage be taken of the beneficial effects which result from inelastic behavior.

Using the structural configuration and temperature distribution of Fig. 1, a study has been made to establish the structural behavior in terms of the failing load of the structure. For the purpose of this study the following assumptions were made:

1. The ultimate fiber stress was taken as the failing stress obtained from material coupon tests.

2. The ultimate strain was arbitrarily assumed as 0.20 in. per in. strain.

3. The ultimate load of the structure was taken as that load which produced ultimate stress in any fiber.

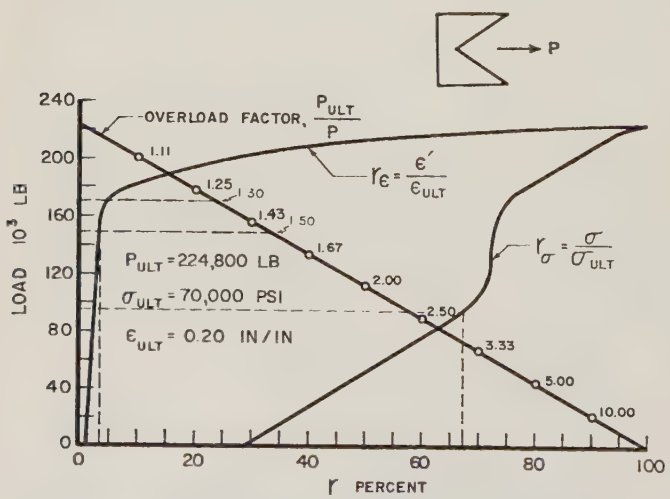

Fig. 7—Structural performance curve

The structural behavior in terms of failing load is shown in Fig. 7 (in which the stress and strain are expressed as per cent of ultimate values). The overload factor represents the increase in applied load required to produce failure.

For design based on a maximum allowable fiber stress of two-thirds of ultimate, that is, a safety factor of 1.5, the design loading would be approximately 95,000 lb and the actual safety factor or overload factor 2.5. Thus, based on elastic design, this structure has nearly twice the required strength.

If, on the other hand, the limiting design load is based on a 1.5 safety factor, (that is, overload factor) on failing load, the structure would support approximately 150,000 lb. Under this condition the critical fiber stress would be approximately 75% of ultimate. Also, the unit deformation of the structure as shown in Fig. 5B is less than the 0.2% offset yield point which satisfies usual deformation criteria.

For conditions in which limiting deformation is not critical, the strain ratio curve of Fig. 7 can be used to select an allowable loading based on the rate of increase of critical fiber strain. On this basis a limiting load of approximately 170,000 lb, with an overload factor of 1.30, might be selected.

Thus, for each design condition, a plot of the structural performance can be used to select the allowable load which will satisfy both deformation and failure criteria as limiting conditions. However, for design in which sequential loading is anticipated, a study of the effect of subsequent loading conditions would be required.

Panel Buckling in Compression

Due to the structural configuration and the rates of heating and cooling in flight, a uniform temperature distribution rarely exists in the structure. Thus, the allowable load which a structure can sustain without buckling when subject to a stress-producing thermal gradient is critical for a vehicle flying at high speeds. Not only does the critical buckling load of a panel drop off due to the reduced material properties, but the stress pattern produced by a thermal gradient can significantly affect the buckling behavior of the panel and, in some cases, buckling can be produced by the thermal gradient alone. The effects of nonlinear temperature gradients on the buckling behavior of structures have been discussed by several authors.[5, 6]

Method of Analysis—A simplified method of calculating the critical buckling load based on the energy method has been developed by P. C. Huang for a simply supported long flat plate with nonlinear end-load variations. Temperature-dependent material properties are easily included in the solution. For a more or less symmetrical case, a simple equation was derived from the above method with satisfactory accuracy. From that equation, the critical

[5] NACA TN 2771: "Thermal Buckling of Plates," by M. L. Gossard, P. Seide, and W. M. Roberts.

[6] PIBAL Report No. 240: "Structural Effects of Aerodynamic Heating," by N. J. Hoff.

stress σ_{CR_T} under the influence of thermal stresses and variable material properties can be expressed as follows:

$$(\sigma_{CR})_T = C(\sigma_{CR})_T \tag{3}$$

where:

$$C = \frac{2}{b}\int_o^b \left\{[\mu k_e - S]\sin^2\frac{\pi y}{b} + \frac{(1-\mu)}{2}k_e\right\} dy \tag{4}$$

$$(P_{CR})_T = A(\sigma_{CR})_T \tag{5}$$

$(P_{CR})_T$ = Critical buckling load
$(\sigma_{CR})_{RT}$ = Critical stress of the plate at room temperature
A = Geometric area of the plate
b = Width of the plate between edge restraints
μ = Poisson ratio
k_e = Ratio of flexural rigidity $\frac{D_T}{D_{RT}} = \frac{E_T(1-\mu^2_{RT})}{E_{RT}(1-\mu^2_T)}$

if $\mu_T = \mu_{RT}$ then $k_e = \frac{E_T}{E_{RT}}$

S = Ratio of thermal stress at each element to the critical stress at room temperature
y = Distance from the top supporting edge to an elemental area

In the buckling equation, the terms k_e and S, which reflect the temperature effects in the material and the effect of the thermal-stress distribution, are the factors that govern the buckling behavior of the panel. A study of the behavior of panels under temperature gradients shows that up to the point of panel buckling, the stress ratio S is much more significant in producing the buckling behavior than the rigidity ratio k_e.

Effect of Shape of Temperature Gradient—The magnitude and shape of the thermal-stress pattern in a compression panel plays a dominant part in determining the external axial loading a panel can sustain. A temperature gradient which produces compression thermal stresses in the middle of the panel reduces the allowable external loading. On the other hand, a gradient which produces tensile thermal stresses in the middle of the panel will increase the external loading required to produce buckling.

A study of the effect of the shape and magnitude of the transverse temperature gradient on the external buckling load for the structural configuration shown in Fig. 1 is presented in Fig. 8. The curves are based on symmetrical temperature gradients which are both peaked and depressed at the middle of the panel. In all cases, the average temperature of the panel is taken at a constant value of 300 F (that is, a temperature differential, ΔT, of 200 F represents a temperature distribution varying from 200 F minimum to 400 F maximum).

The general increase or decrease of buckling load produced by recessed or peaked gradients respectively is evident. In addition, it is seen that gradients with only a slight curvature produce the greatest variation in buckling load from the uniform temperature value, while those with the greater curvature produce results which approach a uniform temperature or stress condition. This variation is due to the fact that the nearly triangular gradients produce high-magnitude thermal stresses

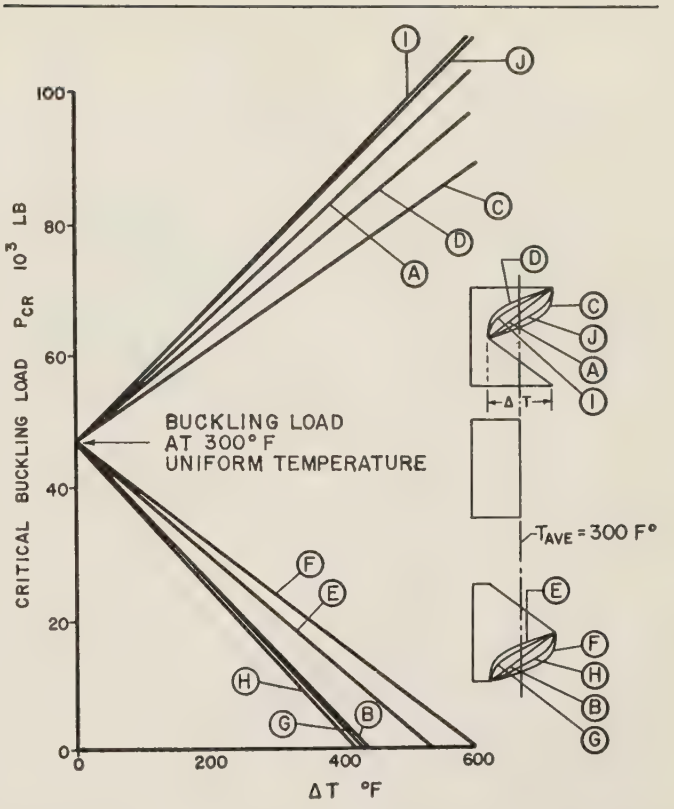

Fig. 8—Variation in critical buckling load with temperature gradient

in the center of the panel which affect the panel instability. The highly curved gradients, on the other hand, produce thermal stresses which are both of a lower magnitude at the center of the panel and more evenly distributed over the cross-section.

From the standpoint of general design considerations, it is apparent that the buckling behavior is quite sensitive to the temperature gradient shape and resultant stress distribution. Detail analysis of the panel buckling behavior should be made for all critical design conditions.

In establishing the safety factor for panels subject to buckling, if the temperature gradient is small the critical parameter will be the applied load; while, if the temperature gradient is large, the temperature becomes the critical parameter.

It should be pointed out that the curves of Fig. 8 are based on a uniform thickness plate in which the shape of the thermal-stress pattern is very similar to that of the temperature gradient. In design application the structural mass distribution is such that the stress pattern may vary appreciably for a given temperature gradient. Thus, while the curves of Fig. 8 do not provide specific design values, the general conclusions for corresponding types of thermal-stress distributions are applicable.

Effect of Residual Stresses—The thermal stress system produced by a temperature gradient is essentially a transient residual stress. Thus, any induced system of permanent residual stress, such as that resulting from inelastic loading as discussed previously, will combine with the thermal-stress system to further affect the buckling behavior of panels.

In the extreme condition in which the thermal stress has been essentially diminished due to inelastic loading, the system of residuals is such that

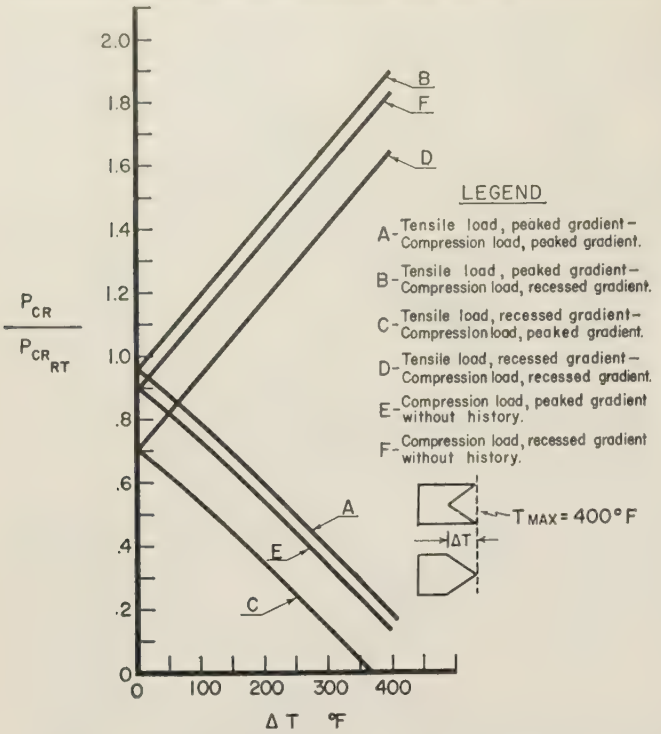

Fig. 9—Effect of residual stresses on critical buckling load

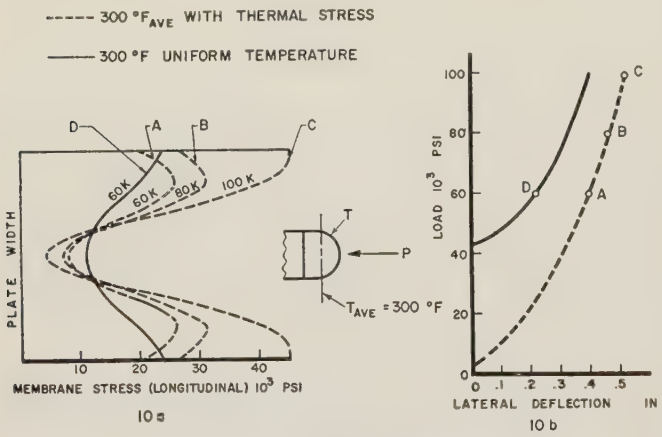

Fig. 10—Post-buckling behavior

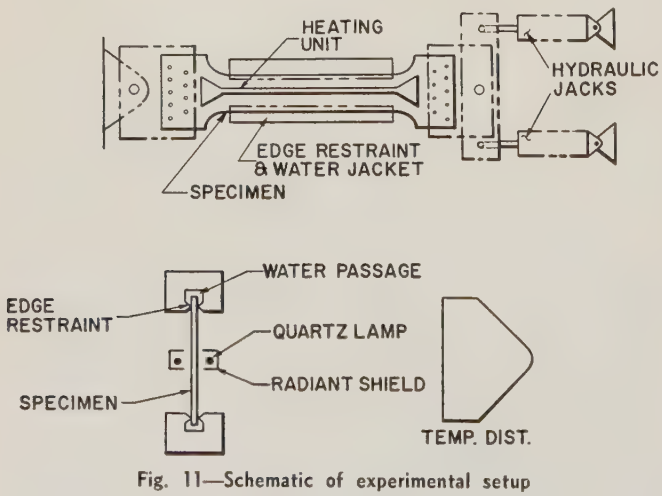

Fig. 11—Schematic of experimental setup

upon removal of the external loading, the residual stress will tend to cancel out the thermal-stress pattern. This results in a stress distribution which will be essentially nil over the cross-section, while still subject to the temperature gradient. Under these conditions the buckling load would be similar to that of a panel under uniform stress conditions. Also, were the temperature gradient removed, the residual-stress pattern would produce a change in the critical buckling load similar to that which occurs in the presence of a thermal gradient. Furthermore, if after the inelastic loading the temperature gradient were changed from "peaked" to "recessed" at the middle of the panel the resulting nonuniform stress system would be more pronounced than that due to the thermal stress alone. Consequently, a more significant change in the buckling behavior would be produced.

The effects of previous load history and reversal of temperature gradient on the critical buckling load are shown in Fig. 9 for the structural configuration and temperature distributions of Fig. 1. The critical buckling load was calculated by the buckling formula (Equation 3) in which the residual stresses produced by the inelastic loading were added algebraically to the thermal-stress system to obtain the stress ratio S. The level of previous tensile loading was taken as 140,000 lb, which has been shown previously to be within the range of practical design consideration and yet produces significant residual stresses.

It is seen from Fig. 9 that previous inelastic tensile behavior in the presence of a peaked temperature gradient will increase the critical buckling load of a panel while inelastic behavior in the presence of a recessed gradient will reduce the critical buckling load. Thus, as a general design consideration, tensile loading is critical in decelerating flight conditions, which produce recessed-type gradients in a panel, since any inelastic behavior will reduce the critical buckling load in subsequent flight conditions.

Post Buckling Behavior—A compression panel will, in general, exhibit an appreciable reduction in stiffness and increase in panel deformation after the critical buckling load is exceeded. However, in many cases, limited buckling of the structure may be permissible. A study using the structural configuration of Fig. 1 was made to show the effect of the thermal stress on the post-buckling behavior. The analyses were based on the theory of large deflections, using the energy method discussed by Bisplinghoff.[7] The post-buckling stress distribution is shown in Fig. 10A, with the lateral deflection curve in Fig. 10B.

Experimental Verification

Experimental results have been obtained to show the validity of the methods of inelastic and buckling behavior discussed in this paper.[8]

Tests were conducted on long flat plate 2024-T4 aluminum alloy specimens with a structural con-

[7] Chap. 11 of "Notes for Special Summer Program in Aerodynamic Heating of Aircraft Structures in High-Speed Flight," by R. L. Bisplinghoff. Department of Aeronautical Engineering, Massachusetts Institute of Technology.

[8] The experimental program was conducted by The Martin Co., under contract AF33(616)—3617 sponsored by the Mechanics Research Branch of the Aeronautical Research Laboratory at Wright Air Development Center.

figuration as shown in Fig. 1. The specimen was uniformly heated along the longitudinal centerline with radiant heat using General Electric quartz lamps controlled by a saturable reactor. The specimen edge temperature was maintained by circulating water at a controlled temperature through ducting in the simple support edge restraint at the longitudinal edges of the specimen (Fig. 11).

Since the stress and temperature levels considered for the tension tests encompassed the range where creep becomes significant, the tests were performed under controlled loading conditions to produce a constant strain rate. The selected rates were chosen on a rather arbitrary basis, being within a range which could be easily controlled and for which the time at load would be sufficiently short to preclude significant creep effects at high load. An additional and important feature is that the constant rate condition permitted successive tests, as well as material coupon tests, for material property data to be performed under similar conditions to provide consistent data.

The temperature was measured by use of iron-constantan wire thermocouples spotwelded to the specimen. The data were recorded by a Bristol recorder. The strain measurements were made by means of temperature compensated bakelite type (EBD-1D) gages and the data were recorded by oscillograph. Proper calibration and compensation factors were considered in the reduction of the test data.

Very satisfactory agreement was obtained between the theoretical and experimental results.

A comparison of theoretical and experimental results of inelastic behavior is shown in Fig. 12. The transverse variation in longitudinal stress for various load levels is shown. The experimental results were limited to total strains of approximately 1% maximum due to the limitation of the strain gages. However, since the theoretical and experimental results agree in the early inelastic range, it is considered as verification over the full range of behavior.

The test specimens were not carried to failure and so no experimental data on failing load was obtained. However, it has been pointed out previously that the failing load condition has been successfully investigated by other authors.

The experimental verification of the theoretical buckling analysis is presented in Fig. 13. Experimental results were obtained for three different temperature gradient conditions. Since the test gradients could not be produced to a prescribed shape for the varying magnitudes, the theoretical results are shown only as specific points calculated for each of the three test conditions. The curve shown in Fig. 13 is the theoretical behavior for a temperature gradient shape which varies linearly between a temperature of 400 F at the centerline and the specified edge temperature.

Sequential Load-Temperature Effects

In those cases where only a single application of high load level is anticipated, the inelastic behavior produces favorable results due to the increased allowable loading. However, the effect of the residuals so produced on any subsequent loading condition can be significant. The effect of such load induced residuals on the buckling behavior has already been shown in Fig. 9.

The condition of structural behavior under cyclic temperature application for a wing structure subjected to differential heating has been discussed previously by Parkes.[3] He has shown four conditions to exist:

1. Permanent elasticity—no inelastic behavior.

2. Shakedown to elastic state—inelastic behavior occurs in one cycle only followed by elastic behavior.

3. Alternate plasticity—inelastic behavior occurs alternately in tension and compression.

4. Incremental collapse—repeated inelastic be-

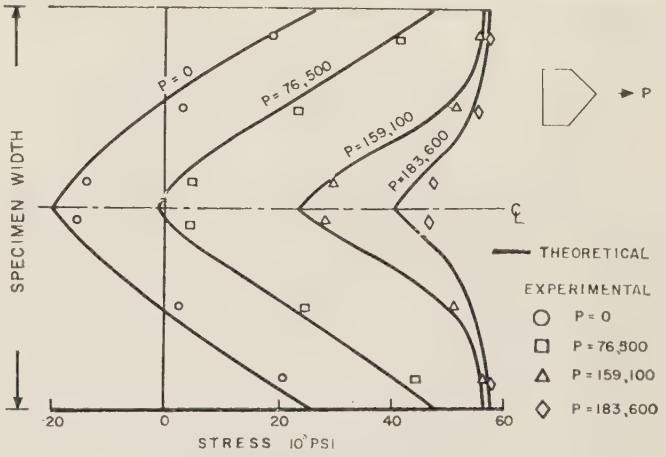

Fig. 12—Theoretical-experimental comparison, inelastic behavior

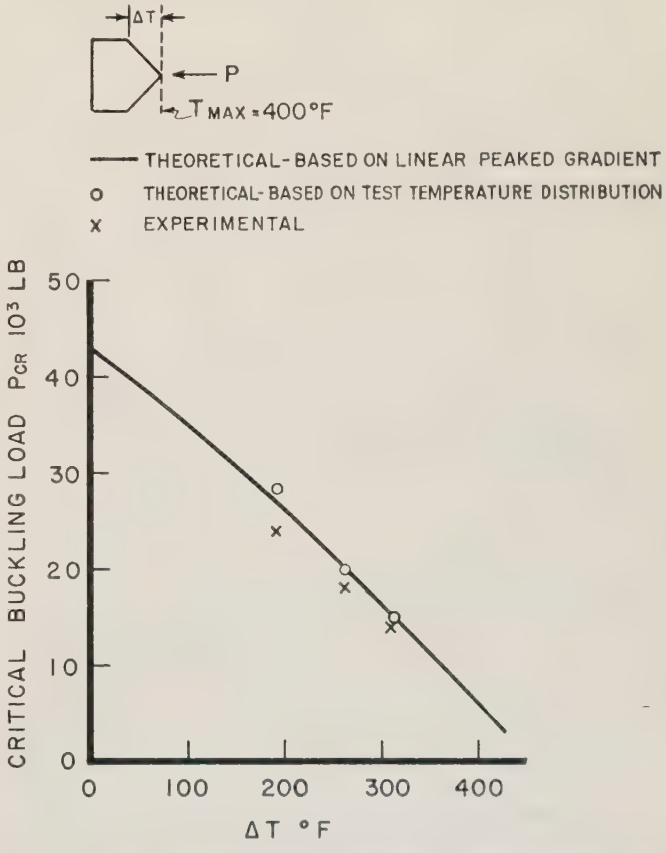

Fig. 13—Theoretical-experimental comparison, critical buckling load

havior producing continued deformation in one direction.

To more fully determine the design significance of sequential loading in the presence of thermal stress, a study was made of the effects of the simple arbitrary mission of Fig. 14 on the structural behavior of the panel configuration of Fig. 1. The behavior is evaluated in terms of stresses, unit deformation, permanent set, critical buckling load, and failing load.

The mission is assumed to consist of the following phases: acceleration O-A, steady supersonic flight A-B, deceleration B-C, and steady subsonic flight C-D. It is assumed that the mission is repeated; however, the study has been carried only through the second acceleration phase D-E which is similar to the first acceleration phase O-A. For simplicity, the peaked and recessed gradients of Fig. 1 were assumed to exist during the acceleration and deceleration phases, while uniform temperature distributions are assumed to exist during the steady flight conditions.

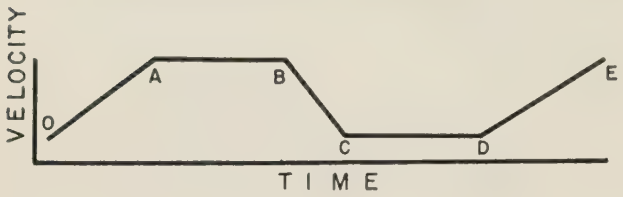

MISSIONS	TRANSVERSE TEMP.	LOAD
O A	200 °F / 400 °F	140,000 LB TENSION
A B	400 °F	140,000 LB TENSION
B C	400 °F / 100 °F	140,000 LB TENSION
C D	ROOM TEMPERATURE	140,000 LB TENSION
D E	200 °F / 400 °F	140,000 LB TENSION

Fig. 14—Sample mission

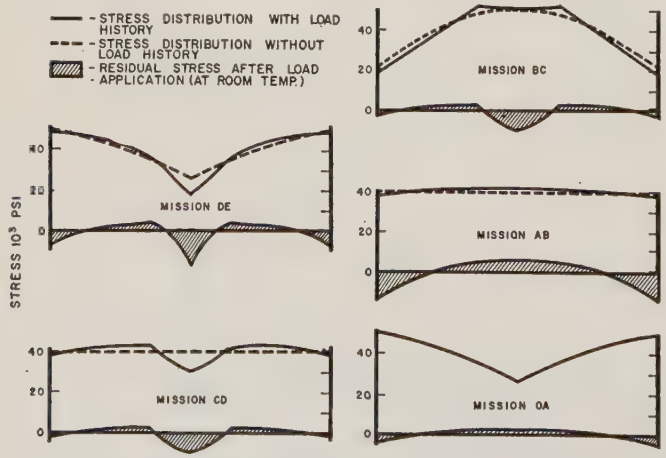

Fig. 15—Effect of load-temperature history on stress distribution

During each phase of the mission a single short duration loading of 140,000 lb was assumed to occur. This loading, which might correspond to limit load as shown in Fig. 7, is sufficient to produce inelastic behavior at the first application during phase O-A. However, such inelastic behavior does not necessarily occur in all phases of the mission.

The variation in the stress distribution at maximum load is shown for each phase in the mission profile in Fig. 15. For comparative purposes the stress distribution is shown for the similar load-temperature condition without previous history. In addition, the accumulated residual-stress pattern at room temperature is shown for each phase subsequent to the load application.

Although there is a progressive variation in the stress distribution during the mission, the full significance of the structural behavior is not apparent from the stress distribution patterns of Fig. 15. However, it is apparent that there is a fluctuation in the residual-stress pattern during the mission. Such a variation and continued reversal of stress may have a significant effect on the fatigue life of the structure.

The variation in the unit deformation and permanent set in the structure following each phase of the mission is shown in Fig. 16, with a comparison

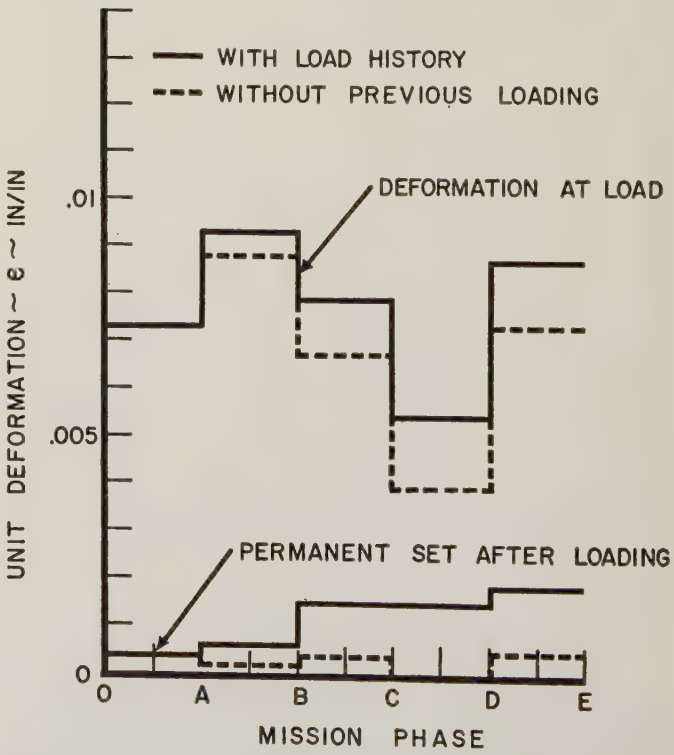

Fig. 16—Effect of load-temperature history on unit deformation and permanent set

to the result which would have been produced by the respective load-temperature condition without any previous history. It is seen that there is a continual increase in the total deformation and permanent set in the structure which amounts to approximately 19% at the beginning of the second cycle, phase D-E. Further study is required to determine the exact behavior in subsequent cycles; however, the continued increase in deformation should be more gradual. This variation in total deformation can be used by the designer as a quantitative measure of the degree of inelastic behavior to be permitted in a structure, since the deformation is usually a primary design criterion.

In a further attempt to evaluate the effect of sequential loading, a study of the strucutral behavior over the full load range up to failure was made in the second acceleration cycle D-E. A comparison of the load-deformation curve during phase D-E with that of the intial condition, phase O-A (as shown in Fig. 5A), indicates very little significant overall change. The curve is displaced horizontally due to the permanent set in the structure, and there is some change in shape at the knee of the curve due to the strain hardening in the material. Both of these changes are reflected in the previous discussion of deformation and permanent set. However, the change in deformation under load is very slight in terms of total deformation at failure. Thus, the sequential loading effect of the load-temperature history appears to have an insignificant effect on the static failing load in the structure.

A final basis for comparison of the structural behavior is the variation of the critical buckling load.

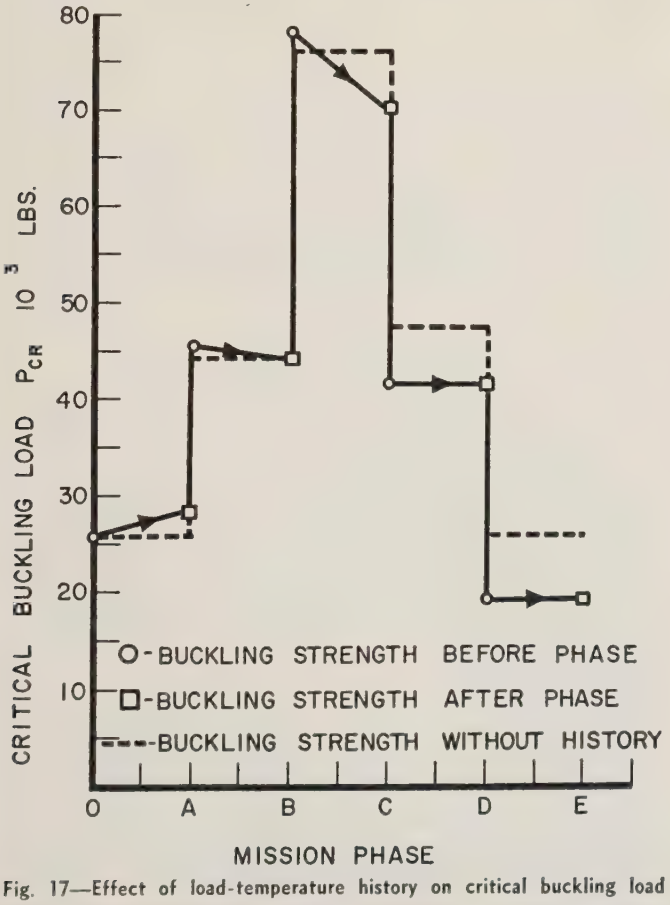

Fig. 17—Effect of load-temperature history on critical buckling load

Fig. 17 shows the variation in critical buckling load at various points during the mission, including the effects of both residual and thermal stresses. This is compared to the buckling load for the same condition without previous history. It is seen that although the residuals tend to produce some fluctuation in the buckling load, there is a very significant reduction in the allowable buckling load during the mission cycle. In fact, by the end of the second acceleration phase, a total reduction of approximately 25% is evident.

In general, any of the four conditions as described by Parkes and discussed previously can occur at random, dependent on the specific load-temperature conditions. Although, there appears to be no specific limiting boundaries of structural behavior, there are several points which are of significance to the designer:

1. The static failing load does not appear to be affected appreciably.
2. There is a continual change in the total deformation and permanent set.
3. The critical buckling load is reduced continually.

While inelastic behavior appreciably minimizes the problems of thermal stress for single applications of high load level conditions, a detailed analysis of the structural behavior under subsequent loading conditions must be made for design conditions involving a repeated load-temperature spectrum. Thus, in missile design, where relatively few applications of high-level loading are encountered, a greater degree of plasticity can be considered than would be permissible in the design of an aircraft with its long service life.

Conclusions

The following design considerations have been established from a study of structural behavior under nonuniform stress systems produced by combined thermal effects and external loading:

1. A considerable increase in design tensile loading can be achieved by permitting inelastic behavior to occur, without incurring excessive structural deformation.
2. Both the nonuniform thermal stresses produced by a temperature gradient and the residual stresses produced by inelastic behavior affect the structural deformation and critical buckling load, but do not affect the static tensile failing load.
3. The selection of maximum design load can be more effectively determined by considering the structural performance in terms of overload factor, unit deformation, and rate of change in strain than by considering critical fiber stress.
4. Panel buckling is most critical during accelerating flight conditions, which produce peaked temperature gradients and, hence, a reduction in the critical buckling load.
5. Tensile loading is most critical during decelerating flight conditions, which produce recessed temperature gradients, because any residual stresses produced will reduce the critical buckling load in subsequent flight conditions.
6. The basic methods of analyses used for inelastic and buckling behavior have been satisfactorily verified by test.

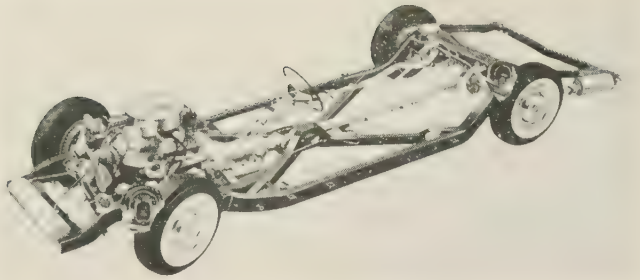

Fig. 1—Air-Poise suspension chassis

THE BUICK

Air Poise

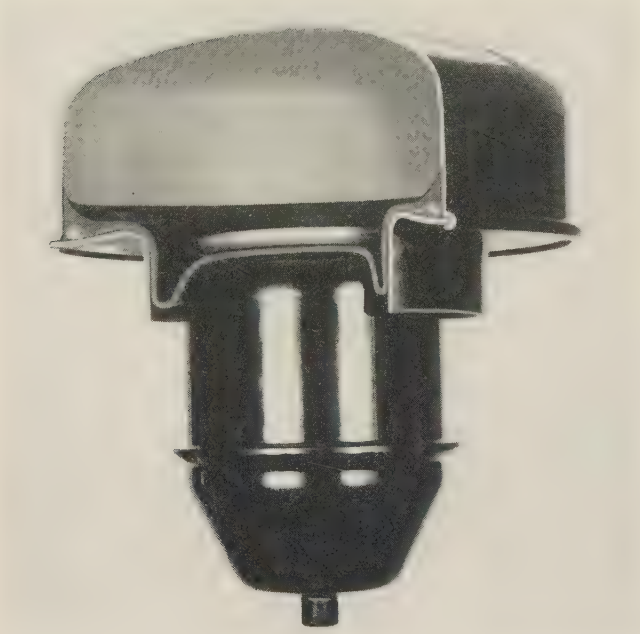

Fig. 2—Air spring, front

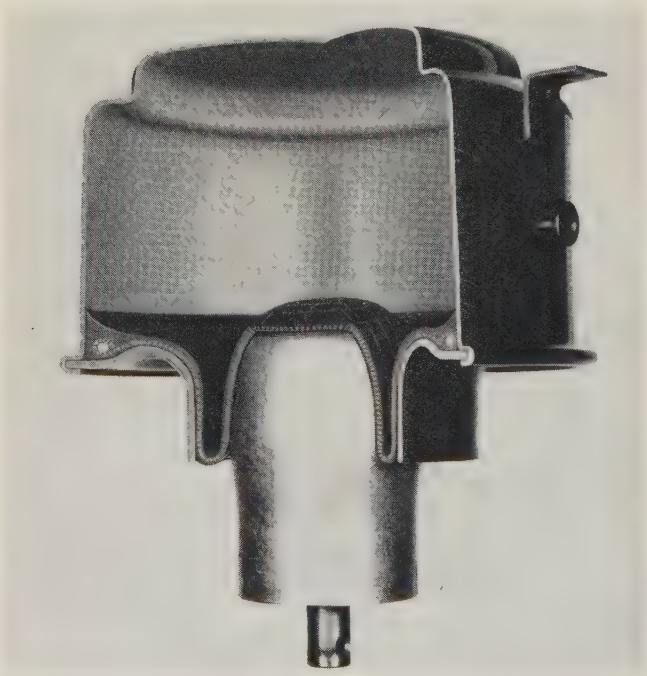

Fig. 3—Air spring, rear

WE are now in an era of suspension development similar to previous eras of engine and automatic transmission development. This is a fortunate situation, as American passenger-car suspensions in general have changed little in basic design in the 20 years since the introduction of independent front suspensions in the early and middle thirties. We are certainly overdue for something outstanding in ride improvement.

Since our company has laid emphasis on a soft and comfortable ride for years, it is only natural that development of any systems embodying a definite improvement in ride would be of great interest. It has long been known that low spring rates would assist greatly in giving a good "boulevard" ride, but under normal circumstances the low rate has been considered by many as giving an unstable highway ride. Air suspensions have characteristics which overcome this latter objection and "wed" these presumed opposing characteristics. This fact coupled with other advantages has led to the introduction of the Air-Poise suspension on the 1958 Buick.

General Description and Air Springs

Fig. 1 shows a view of the chassis. It will be seen that the previous front and rear coil spring suspensions with the torque tube drive permitted installing air springs with a minimum of change.

Enlarging the openings slightly in the frame front spring cross member where the springs were previously located has permitted installation of the front air springs with the general linkage arrangement of the suspension unchanged. Enlarging the openings slightly in the frame rear spring cross member has likewise permitted installation of the rear air springs.

One height control valve is located in the center of the front spring cross member and is controlled by a lever clamped to the middle of the front stabilizer bar. Two additional height control valves are located just ahead of the rear axle on the frame rear spring cross member and are connected to the rear axle assembly inboard from the wheels through levers and links.

SUSPENSION

Forest R. McFarland, E. G. Peckham, and Eric Dietrich, General Motors Corp.

This paper was presented at SAE Annual Meeting, Detroit, Jan. 14, 1958.

THIS paper describes the springs, control system, and ride of the air suspension system on the 1958 Buick.

The system is a semiclosed one, providing a variable-rate suspension, automatic leveling and trim control, and manual lift. The latter feature is a knob below the instrument panel which can be operated when necessary to cope with unusual clearance conditions. The car remains at the same height with loads of up to five passengers and 500 lb in the trunk.

The authors describe the road-holding ability of a car with this suspension system as excellent.

The air compressor is located on the engine and is driven by the engine through a belt. It supplies air to a pressure tank, which in turn delivers air through the pressure regulator valve in the manual control valve to the three height control valves. Air from the height control valves returns to the manual control valve, and is then routed back to the air compressor inlet. The entire operation described above is routed through copper-clad steel tubing except for the lines from the compressor to tank, tank to manual override valve, and from this valve to compressor inlet and air cleaner, which are rubber hoses.

Let us now describe these elements, taking the air springs first. Various forms were considered, the final design decided upon being illustrated in Fig. 2, which shows the front member. This construction embodies a diaphragm of 2-ply nylon cord design, rubber-coated inside and outside. This member fits into the outer rim of the metal container. The lip on its outer periphery seals it to the container in a manner similar to the sealing of a tubeless tire. The inner ring of the front diaphragm is clamped to the top of a piston-like member, which in turn has a flat bearing at its lower end contacting a spherical bearing located in the lower "A" frame. This bearing arrangement reduces friction to a minimum.

Fig. 3 shows a section through the rear member which is similar in construction to the front. The inner portion of the rear carries a plug snapped into a hole in the top of a piston-like member carrying a bearing similar to the front.

At normal design height the front air springs have an area of 25 sq in. and a volume of 300 cu. in. and the rear air springs have an area of 12 sq in. and a volume of 235 cu in. These sizes have resulted from extensive development work which started with 715 cu in. in front and 800 in the rear. Operating pressures, which vary with load, are in the neighborhood of 100 psi for a five-passenger load, depending upon the model of the car. Because the front air springs act through a linkage of approximately 1.9 to 1 and the rear air springs act directly, these sizes result in wheel rates of 71 lb per in. front and 81 rear, or less, depending upon the model of the car at normal design height front and rear. This rate varies as shown in Fig. 4 for each front spring and Fig. 5 for each rear spring. The

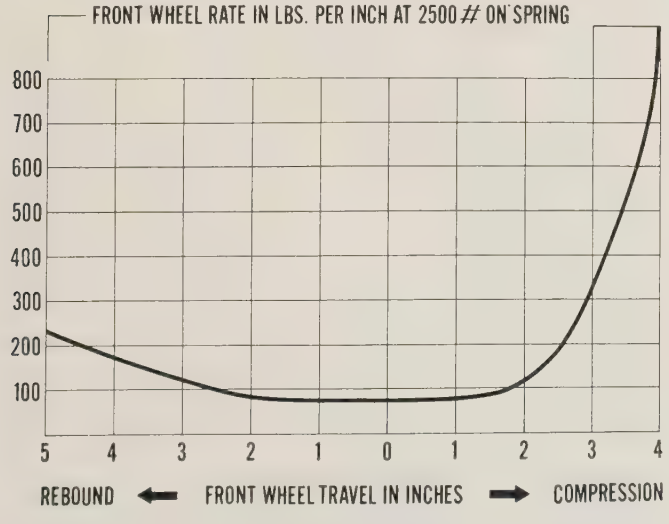

Fig. 4—Front rate curve

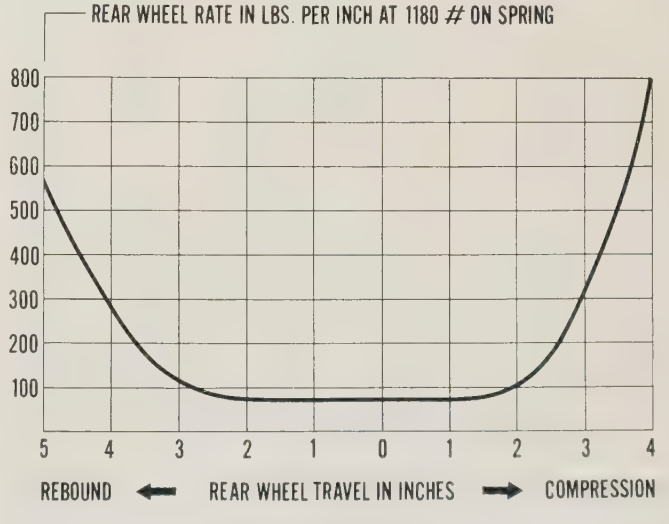

Fig. 5—Rear rate curve

variation is due to the air compression curve characteristic of approximately $pv^{1.3} = K$, plus the change in size of the inner piston and outer container diameters through the stroke, plus a slight effect due to cord angle. The change in effective diameter of the piston and diaphragm at positions above and below the design height is illustrated in Fig. 6. It will be noted that the effective diameter is established at the lowest point of the rolling diaphragm.

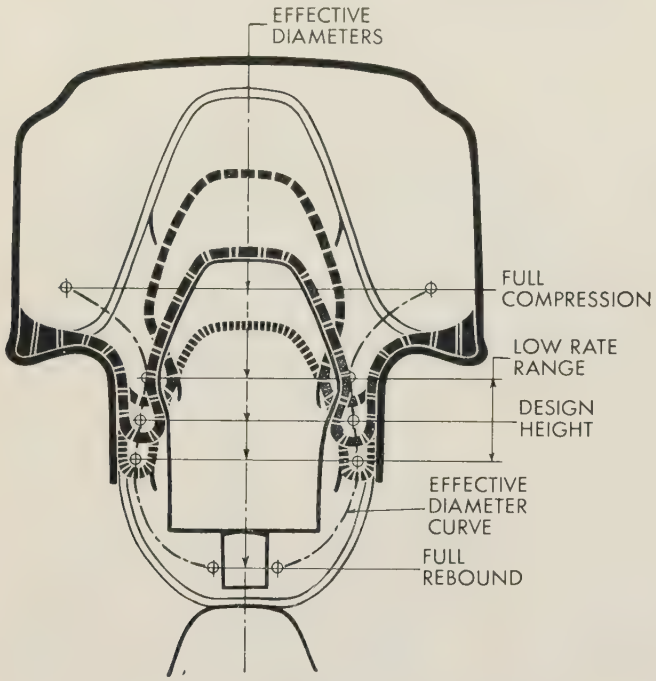

Fig. 6—Air spring effective diameters

It can also be seen that there is a certain amount of stretch in the diaphragm as it passes from the inner diameter to the outer, resulting in a lowering of the cord angle measured from the horizontal. Experience to date has indicated the length of the curve giving low rate either side of normal design height is desirable for boulevard smoothness.

This change in rate permits a soft boulevard ride, but a definitely increased rate either side of the normal design height gives increased ride stability on rough roads.

The development of the air diaphragm and the effect of the cord angle on rate would make an interesting story in itself, too long to be included in this paper.

The sizes arrived at have resulted in a frequency of 43 cpm front and 52 rear, regardless of load with the car in the vicinity of design height. This is due to the fact that a greater load causes a higher pressure in the air spring, resulting in a higher rate curve. Since the frequency is proportional to the square root of the stiffness of the air springs divided by the mass, the product is substantially constant.

To increase roll stability the roll center at the rear wheels has been raised slightly, being a little over 1 in. above the center of the rear wheels.

The torque tube drive permits the use of lower rate rear springs without rear-end "squat" under acceleration. The front end rises slightly under this condition. A certain amount of antilifting effect is also obtained at the rear under braking. This, together with the antidive front suspension, keeps the car reasonably near level under even severe braking.

Control System

The control system is shown diagrammatically in Fig. 7. Air is furnished by a 2-cyl compressor driven

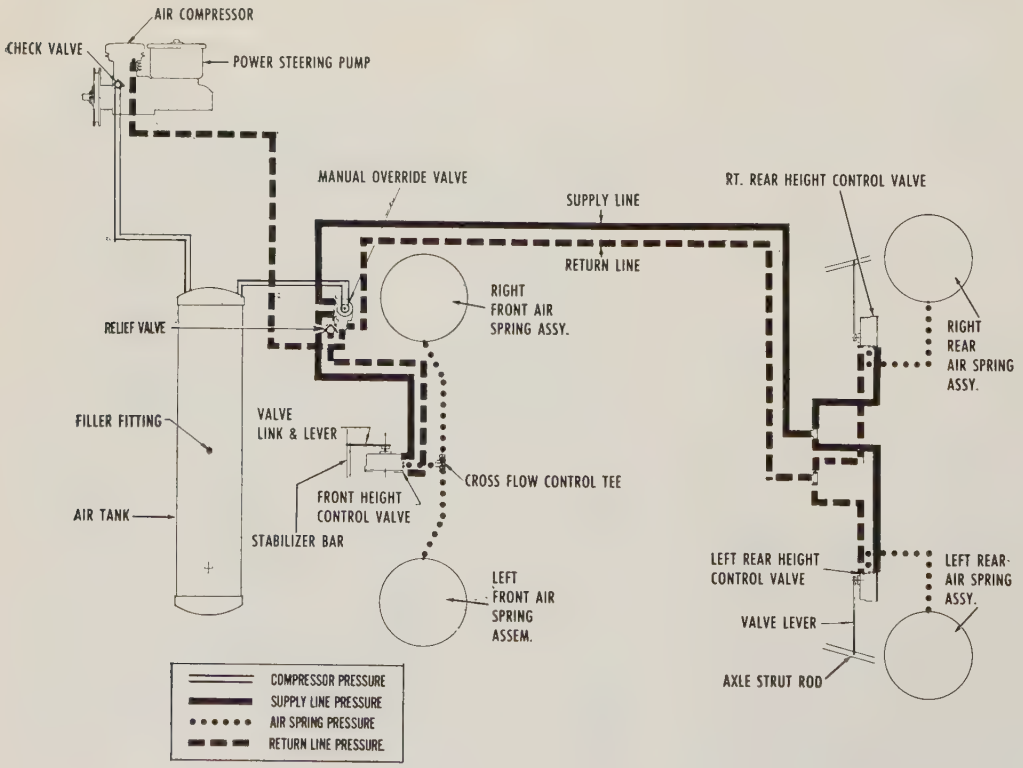

Fig. 7—Air-Poise control system

by the engine through a V-belt at 1.15 times crankshaft speed, delivering air up to 290-lb-per-in. stall pressure. Air from the compressor passes through a check valve to a high-pressure storage tank of approximately 820-cu-in. volume, located at the front of the chassis. From the storage tank, the air is conducted to a reducing valve in the manual override valve set at 145 psi to maintain a constant pressure supply which controls the rate of response of the air springs. The manual valve and its overriding function will be detailed later.

From the manual override valve, air is piped to a front height control valve through a check valve. The height control valve is operated by the lever from the center of the stabilizer bar to obtain the average of the car height at both front wheels. This valve permits air to flow to the air springs when the car is below design height or to escape from the air springs when the car is above it. The air from the front height control valve to the air springs passes through a crossflow valve, which consists of a double check valve permitting unrestricted flow to either but restricted flow from each to minimize cross flow from one air spring to the other under roll.

Air flows to the rear right and left control valves, controlling the height of the car at both air springs in the same manner as the front except that each wheel is controlled separately. The configuration of one valve at the front and two at the rear was reached after a preliminary setup was made at the beginning of the development employing four valves —one at each wheel. Lack of stability of this arrangement immediately led to the arrangement shown. Each of the two valves at the rear maintains pressure in each of the air springs in accordance with the load on that air spring, maintaining levelness of the car laterally and helping to maintain constant frequency by increasing the rate of the spring in the vicinity of the increase in load.

Air from the three height control valves returns to the manual override valve and then to the compressor inlet or to the air cleaner, depending on whether or not the compressor is running. Any "make-up" air required by the compressor when the air springs are not exhausting is drawn in through the air cleaner connection. This results in a semi-closed system. Results to date under a wide range of temperature and humidity conditions have not disclosed a condensation problem. The air from the storage tank is drawn from the center of the tank, utilizing the tank as a moisture accumulator. Any casual water collected is drained on the lubricating schedule.

Fig. 8 shows a section through the compressor which is assembled ahead of the steering pump and combined with it, both units operating from a common oil reservoir. This unit has two cylinders 90 deg apart, operating on a plain crankshaft. This type of unit was chosen after considerable study taking into account compactness, crankshaft stiffness, torque variation, cooling, and other factors. It has a 1.875-in. bore by 0.906-in. stroke, giving a displacement of 5 cu in. per revolution. The cylinders and heads are aluminum, with cast-iron sleeve inserts in the cylinders. Valves are the familiar reed type. A small vane pump provides lubrication to all bearings and also scavenges the compressor sump. The size of the compressor was established

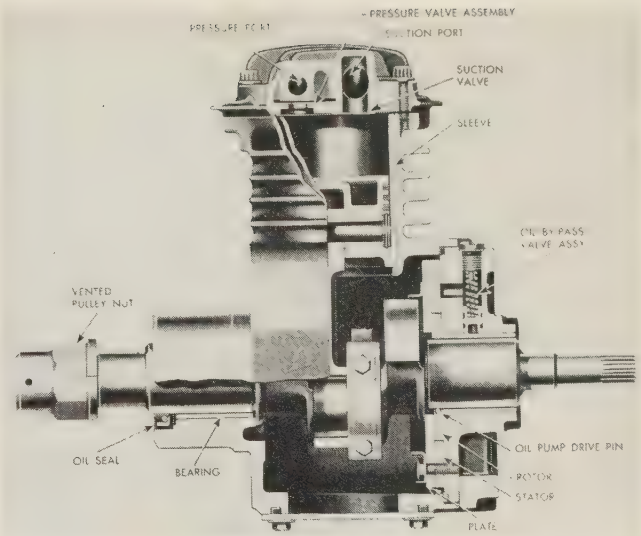

Fig. 8—Air compressor

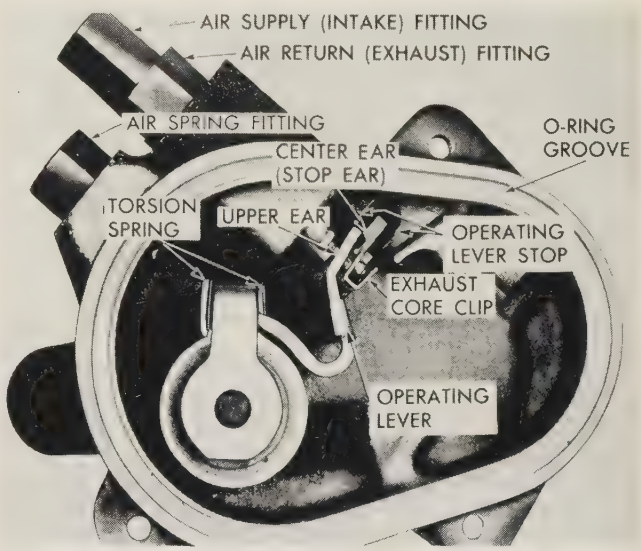

Fig. 9—Height control valve

by test runs under all conceivable conditions to determine capacity under most demanding conditions. These tests included "grocery store" runs between Colorado Springs and Manitou Springs, making a considerable number of stops with passengers getting out the car and then entering the car after it had "leveled" empty to obtain demands at over a mile altitude. A considerable number of runs were also made up Pikes Peak, which is one of the extreme limiting conditions.

The height control valve shown in Fig. 9 is the result of extensive development work in throwing away devices we didn't feel were necessary. The height control valve, in detail, consists of two spring-loaded, rubber-sealed valves, one inlet and one exhaust, operated by an arm connected to a shaft to the exterior. On the front valve this shaft carries an arm connected to a link fastened to an arm on the stabilizer bar at the front. On the rear valves these shafts are attached to arms and then to links, which in turn are attached to the rear axle strut rods. When the car is too low, the inlet valves are opened; when too high, the exhaust. The free play

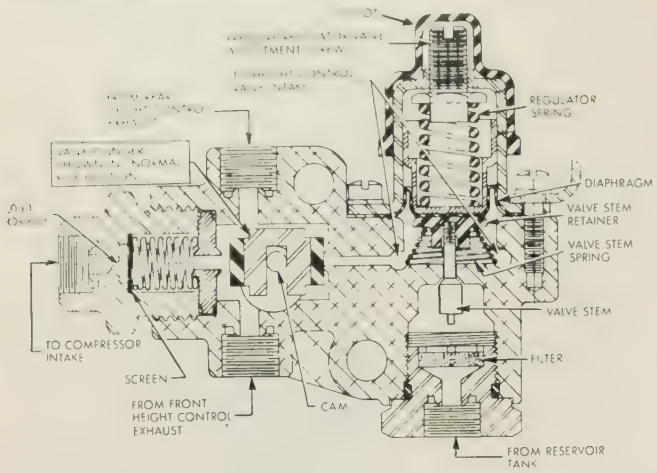

Fig. 10—Manual override valve

in the lever between the two valves permits ± ¼ in. variation in car height at front and rear before the valves operate.

Control pressures are adequate to maintain levelness of car with loads up to five passengers in the car and 500 lb in the trunk. During development, various airflow control mechanisms were incorporated in the controls: for instance, one design had the opening of the doors operate solenoids to increase airflow to speed up leveling of the car, yet retain air-saving restrictions for leveling when the car was in motion. We also tried pressure switch operating solenoids to cut off airflow from the height control valves under extreme acceleration and braking. Various types of delays were built into the valves. We believe several of these ideas have merit, but our weighing of the advantages and disadvantages of the units developed to date led us to the design adopted.

The design finally accepted consisted of flow restrictions through 0.025-in. orifices protected by screens immediately ahead of them. The screens were mainly a precaution, as considerable running was done without clogging the orifices. These orifices gave satisfactory control of the air system while traversing winding roads with a variety of curves. With the rate of flow established for this condition, the restrictions were found to be satisfactory for rough road travel or leveling when passengers enter or leave the vehicle.

The manual override valve shown in Fig. 10 receives air from the high-pressure reservoir tank. Incorporated in this unit is the pressure regulator valve set to limit air pressure past it to 145 psi. Air flows from this valve to the respective leveling valves and air springs, returning through the leveling valves to the low-pressure chamber and then through a 0.030 in. orifice to the compressor intake.

The manual override valve has another function —that of raising the car over 4 in. when a knob under the instrument board is pulled. This operation causes a valve plunger in the override valve to shut off the exhaust line to the compressor and open the exhaust lines of the height control valves to the 145 psi air normally reaching the valves through the inlet lines only. The air through the exhaust lines raises the exhaust valves off their seats and fills the air springs with 145 psi air, overruling the height control valves' normal function. This causes the air springs to lift the car up against the rebound bumpers over 4 in. in front and approximately 5½ in the rear.

This function is useful for abnormal conditions such as pulling through mud holes, deep snow, high crowned roads, or loading the car on unusual lift hoists. While the ride is, of course, not comparable to normal, this function can be very helpful. While driving over one of the trails in the Rocky Mountains during development, our drivers used this device to get through one bad spot. A tourist, seeing our cars go through, attempted to follow and ended up stuck in the middle of the spot. After pulling him out, our people left him wondering how we were able to get through so easily.

Included in the low-pressure line is a pressure relief valve, set at 150 psi minimum, to act as a safety valve should the air pressure become too high in the override position of the valve due to possible leakage of the 145 psi reducing valve. This has not been a problem, but is an additional precaution to insure reliability.

The compressor check valve is located adjacent to the compressor in the high-pressure line. This valve simply prevents air from the storage tank backing up into the compressor and leaking down slowly when the car is parked.

Summary

This suspension offers the following advantages:

1. Car is at same height at all times regardless of passenger load.
2. Ride is soft on boulevard, yet controllable on rough roads.
3. Ride is level with no perceptible pitch.
4. Frequency of front and rear suspensions is substantially constant regardless of load.
5. Ability of suspension to remain level at constant height keeps headlights on road, a valuable safety feature.
6. Car can be raised by operation of a knob below the instrument panel to cope with unusual clearance conditions.

Ride and Handling

The combination of boulevard and highway ride obtained by the system described will give the motorist an experience new to him. The fear expressed by those in the past that frequencies as low as described could not be employed has now been shown to be groundless. The reason is that we do not operate in them, as they are only in the center band of the ride; and even if we should, the shock absorber control would prevent repetition of cycles at these frequencies. The characteristics of the air spring curves are felt to account for the superior road-holding ability of these vehicles.

Acknowledgment

We wish to take this opportunity to express our appreciation to our associates in General Motors Engineering Staff for their help, to the Buick Engineering team for its splendid performance, and to our suppliers for their energetic participation in this program. Their combined efforts have made this development possible.

THE AIR COIL SPRING — —

A New Factor in Rambler Suspension

W. S. Berry, American Motors Corp.

This paper was presented at the SAE Annual Meeting, Detroit, Jan. 14, 1958.

AIR springs for passenger cars, while not new, have been the subject of considerable research and testing by various rubber companies during the past 20 years. Ralph Isbrandt[1] was active in air-suspension development when this program was in its infancy, and demonstrated an air ride car to the writer in 1938. The advantage of riding on air was obvious even then, particularly for cushioning severe bumps, but independent front suspension had just come into general use and seemed to fulfill the need for improvement in the ride of cars of that era.

Recently, however, requirements of the engineer and stylist to lower the center of gravity of the passenger car as much as possible have again aroused interest in the air spring. The air spring offered several intriguing possibilities: first, the height of the car would be substantially the same regardless of load; second, the air spring could be designed to have a low rate for the boulevard-type ride and a high rate for rough roads which produced maximum axle movement. This feature of an increasing rate would reduce the axle travel required under all load conditions—a definite advantage to the designer in keeping the car low.

As a result of this interest in air springs, we undertook a long-range program involving extensive development and testing of a variety of systems. The use of coil springs in both front and rear suspensions presented a ready-made structure for supporting air springs. Our familiar torque tube drive rear suspension guided the rear axle in the proper path and imposed no loads on the rear springs except that of supporting the unit body. Because of this adaptability of our cars to air springs, it was possible to test and evaluate a considerable number of air-spring systems.

Some air suspensions tested did not materially improve the soft ride inherent in our 4-coil suspension system. Our desire to avoid too much side roll in turns and excessive bump-through on rough roads eliminated air suspensions with extremely soft springing. Therefore, it became apparent that the most important advantages of air springs were, first, the ability to maintain the car at a constant level under all load conditions and, second, the characteristic of a rate which varies with the load so that the desired ride quality was maintained for both empty and loaded vehicles.

The effect of passenger load upon the weight distribution between front and rear wheels is typified in the 1958 Rambler Ambassador with a 117-in. wheelbase and powered by a V-8 engine of moderate size and weight. The curb weight of this vehicle is 3558 lb of which 55.5% is on the front wheels and 44.5% on the rear. When a 6-passenger load totaling 900 lb is added, 31% or 279 lb of this load is on the front and 69% or 621 lb is on the rear. The total weight of the vehicle so loaded is almost equally split between the front and rear wheels. Furthermore, an additional load in the trunk reduces the weight on the front wheels and places the entire

THE air suspension offered by Rambler employs a rolling lobe air spring, designed to go inside a coil spring. The combination coil and air springs are utilized on the rear wheels only.

This arrangement enhances the 4-coil spring suspension by using the air spring for leveling and for maintaining essentially the same ride characteristics whether the car is empty or loaded.

The author considers the simplicity of the system to be one of its outstanding features. Reliability and ease of service were goals in the design.

[1] Director of Engineering, American Motors Corp.

weight of the trunk load, plus the amount reduced from the front, on the rear wheels. It is very evident that the rear springs are most critically affected by extreme loads, while the front springs are affected to a much lesser degree.

The experience gained with the various air-spring systems and the foregoing analysis of the effect of extreme load on weight distribution resulted in the decision to concentrate on the development of a system in which air springs are used at the rear wheels only. It was felt that such a system would enhance our 4-coil spring suspension by utilizing the air springs to the best advantage for leveling, and for maintaining essentially the same riding characteristics with the car either empty or fully loaded. In addition, the system would be less complex and would enable a significant reduction in the number of parts—resulting in maximum interchangeability with the standard coil spring suspension, greater ease of manufacture and servicing, and, most important, less cost to the ultimate purchaser. The air-suspension system (Fig. 1) which is now available on all Rambler models, is the final result of a development program based on this approach.

A rolling lobe air spring was designed to go inside the rear coil spring, thus paralleling the characteristics of the air spring with the steel coil spring (Fig. 2). Most of the weight of the empty car is carried by the steel springs having a relatively low rate of 60 lb per in. for the sedan and 96 lb per in. for the station wagon. These rates are approximately 30% lower than the rates used on the same models without air suspension. The rear coil spring rates are lower because the air spring contributes the additional rate necessary for good ride and stability.

A single leveling valve is mounted near the center

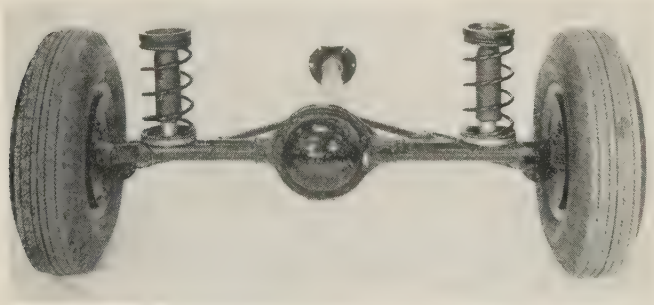

Fig. 1—Axle components of Rambler air-suspension system

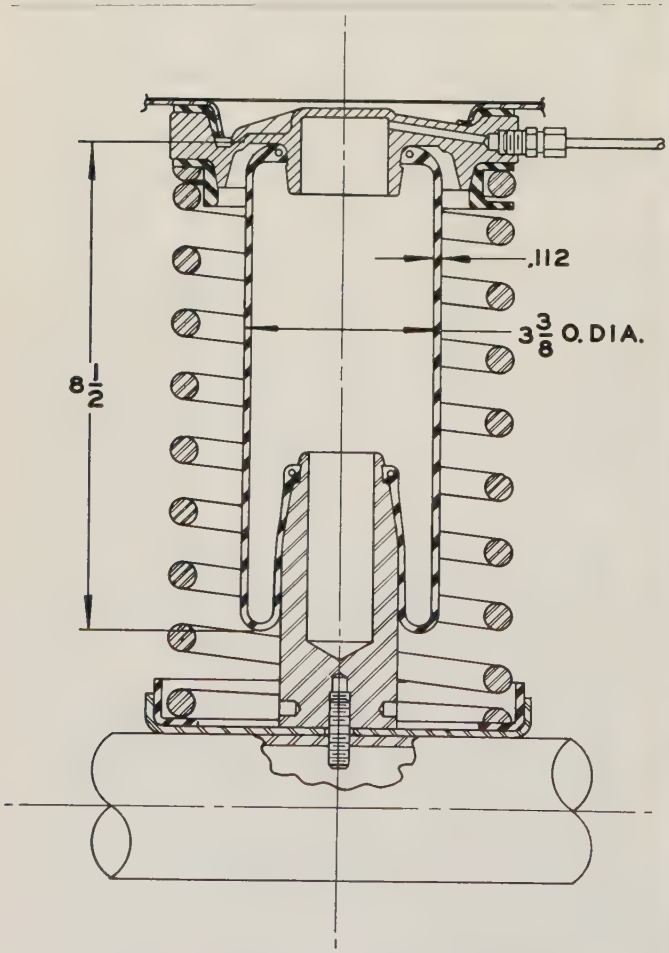

Fig. 2—Air spring and coil spring arrangement

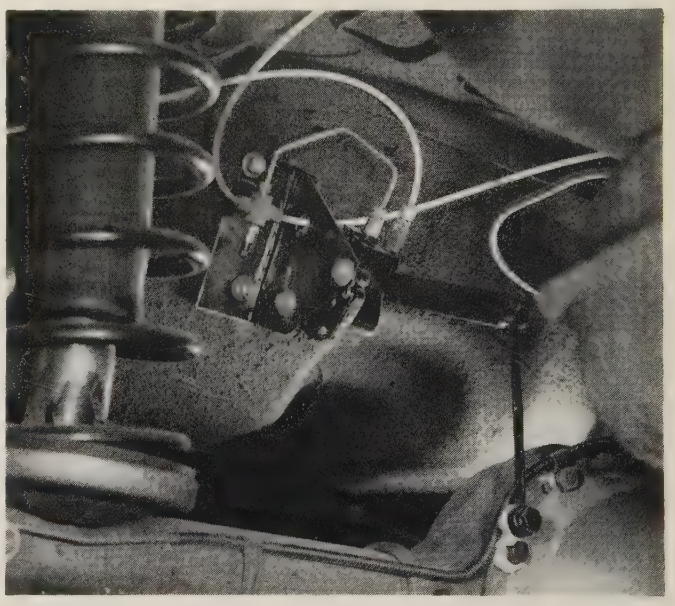

Fig. 3—Single leveling valve link-connected to rear axle housing

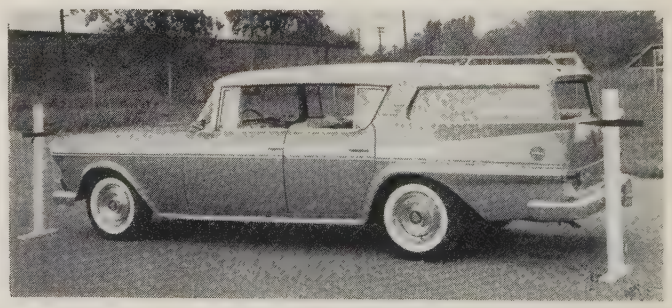

Fig. 4—Height of empty 1958 Rambler station wagon

Fig. 5—Height of 1958 Rambler station wagon with 5-passenger load

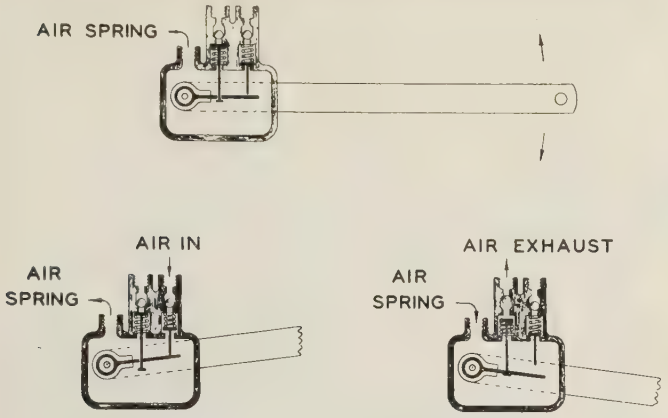

Fig. 6—Leveling valve schematic

of the body above the rear axle (Fig. 3). With the car empty, 20-psi pressure exists in the air spring and each air spring supports about 100 lb. The steel spring supports 500 lb. As load is added, a leveling valve senses the change and increases the air pressure so that the air spring carries the additional weight of passengers and baggage. In a loaded station wagon, the air pressure in the springs may be over 100 psi.

Fig. 4 illustrates the height of the air ride Rambler Ambassador station wagon empty, Fig. 5 shows the same vehicle loaded with five passengers. The height gages indicate that there is little difference between the empty and loaded conditions.

The principal function of the leveling valve (Fig. 6) is to admit air to the air springs when the load in the car is increased and also to exhaust air from the springs when the load is decreased. The leveling valve contains ball check restrictions to limit the flow of air so that very little air is used when driving over bumps in the road at normal speeds. The duration of the suspension disturbance caused by these bumps is so short that the small amount of air admitted or exhausted by the leveling valve does not affect the height of the car.

The exhaust port of the leveling valve is connected to a pressure limiting valve which keeps the pressure in the air spring from getting below 18 psi. This prevents the spring from being entirely deflated if the body is jacked up to change the tire or to lubricate the chassis components. In shipping new cars the air is released from the system. Since most of the load is on the coil springs, the car can be transported without any air in the system. In an emergency, the car can be driven without any air supply. Running the engine for approximately ½ min supplies ample air pressure for normal operation of the car.

The rolling lobe air spring is made with neoprene because of its excellent air-holding properties and resistance to oil and ozone. The air spring is built up in layers somewhat similar to the method of building tires. Over an inner layer of neoprene, two layers of fabric are applied. The fabric is then protected with an outside cover of neoprene. This fabric is made of nylon cord. The cord angle is accurately controlled to give the air spring the necessary 520 psi burst strength and physical characteristics.

The air-spring testing machine as shown in Fig. 7 is arranged to simulate the rear suspension geometry of the vehicle. The vibrating load is varied to equal

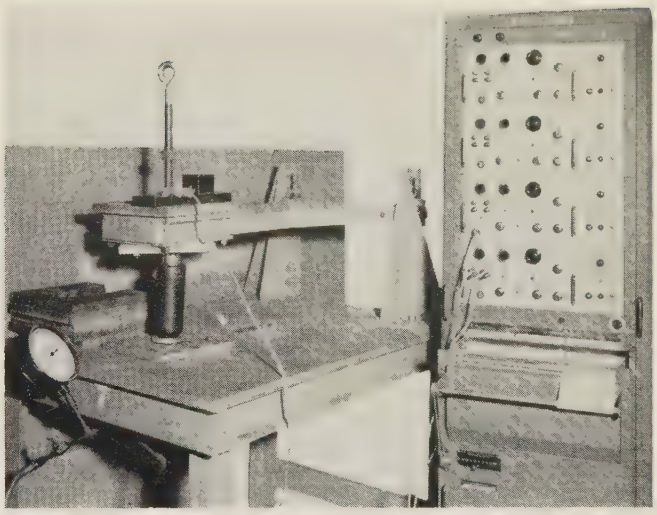

Fig. 7—Dynamic testing machine for air spring

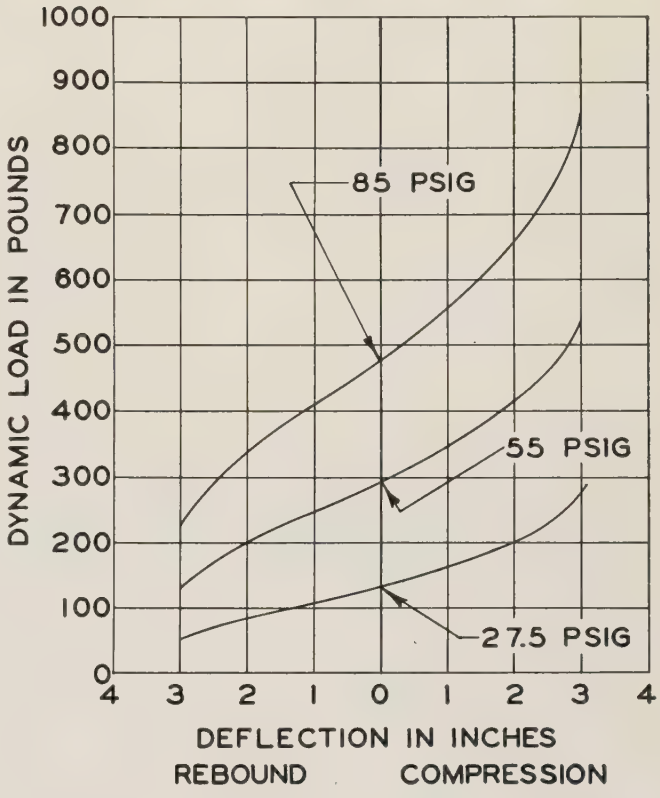

Fig. 8—Air spring dynamic load versus deflection

the sprung mass of the car carried on each air spring. The mass is vibrated through the range of the spring travel and a continuous record of the load, deflection, pressure, and acceleration is taken on a 6-channel electronic anaylzer. This data is then used to plot the dynamic characteristics of the suspension. The characteristics of the steel coil spring are mathematically added to those of the air spring and the riding qualities of the car predicted.

The dynamic spring load is shown in Fig. 8, the three curves represent three different loads on the air spring. The air pressure designated is the initial pressure corresponding to the load at the zero ordinate on the curve. Note that the curves show an increasing dynamic rate as the springs are compressed. This explains why there is almost no bump-through

with these air springs, although a conventional rubber bumper is provided to limit the rear axle travel. The design of the air spring permits 4-in. travel in compression and 4-in. travel in extension. The rear axle rubber bumper is effective during the last inch of the 4 in. of axle travel in compression.

Fig. 9 shows the testing of the rolling lobes. They are being flexed at the two most critical positions, full-rebound and full-jounce. On this testing machine the air springs are being flexed at approximately wheel hop frequency, 600 cpm, and at a 2¼-in. stroke. The upper spring is being tested at full-rebound position at light-rebound air pressure. The lower spring is being flexed in the full-jounce position and at maximum jounce pressure.

Fig. 10 is a schematic arrangement drawing showing the simplicity of the system. A Bendix-Westinghouse compressor having a piston displacement of 2.7 cu in. supplies 1 cu ft. of air per min at 150 psi at 50 mph. This compressor is driven from the engine by a belt and runs 1.1 times engine speed on the V-8 engine and 0.85 times engine speed on the 6-cyl engine. The maximum pressure occurs when there is no requirement for air and is controlled by the compression ratio of the compressor. This maximum pressure is approximately 300 psi. The compressor is lubricated with oil from the engine oil system.

A 280-cu-in. supply tank is located under the left front fender. The piping from the supply tank to the air springs is by means of 3/16 heavy wall nylon tubing connected with selfalign fittings. The total volume of both air springs is 110 cu in. This relatively small volume means that there is no problem in supplying sufficient air for leveling.

In conclusion, many thousands of miles of testing have shown that the air spring, as used in the rear suspension of the Rambler, is a direct and effective solution to the problem of achieving the benefits of air suspension. The designed ride and height is maintained regardless of load. A rising rate curve is used to minimize any tendency for rear axle to bump through on rough roads. The increase in rate improves the handling and stability of the vehicle when heavily loaded and is particularly effective for station wagons. Furthermore, the headlamp beams are not deflected upwards with a full load in the car.

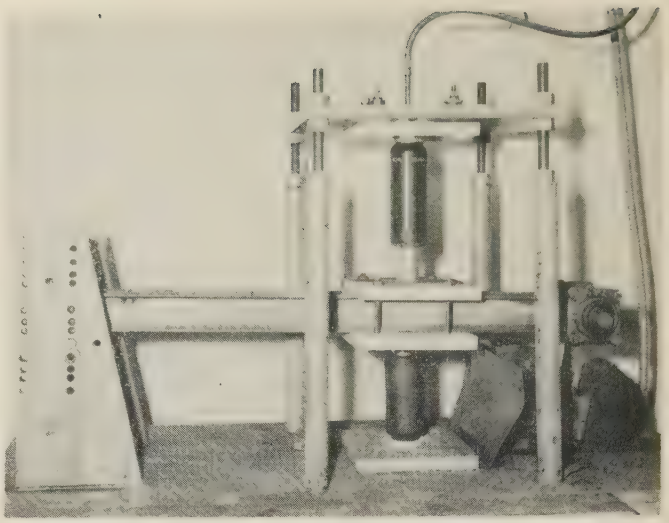

Fig. 9—Fatigue testing machine for two rolling lobe units

These advantages are obtained with only 16 air connections and a minimum of working parts. There are no electrical solenoids and wiring to complicate the system. Reliability and ease of service have been prime consideration in combining the principal benefits of air springs with the existing features of the unique configuration of coil spring suspensions used on our cars.

Acknowledgments

The author wishes to express appreciation to A. B. Hirtreiter of the Goodyear Tire and Rubber Co. who directed development of the rolling lobe air spring.

We also acknowledge the contribution of many people at American Motors Research and Engineering Department where the Rambler Air-Suspension project was under the direction of W. J. Zechel, Chief Design Engineer, and C. E. Burke, Chief Development Engineer.

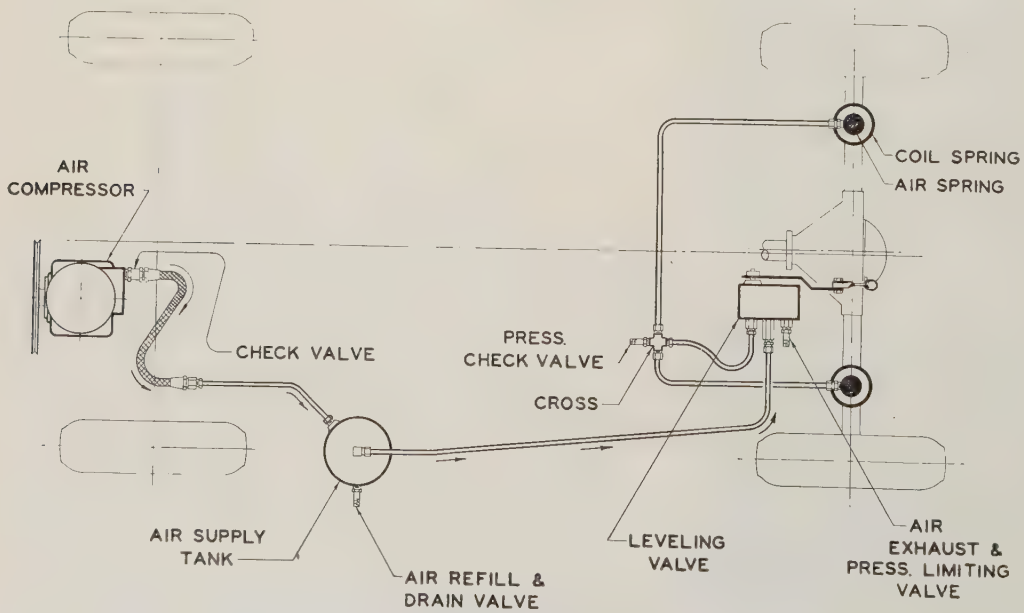

Fig. 10—Air ride schematic

The Ford Approach to AIR SUSPENSION

C. F. O'Shea, Ford Motor Co.

This paper was presented at the SAE Annual Meeting, Detroit, Jan. 14, 1958.

OUR company's suspension engineers have been constantly searching for means of improving car ride. It was obvious that lower spring rates and lower ride frequencies were required to give the soft, luxurious riding qualities desired.

The design or manufacture of conventional steel springs with very low rates can be readily accomplished. To apply them to our cars, however, where the trend has been to lower and lower vehicles, placed a sharp limitation on their use due to available wheel travel space limitation.

With low-rate coil springs and torsion bars the problem is essentially space. In addition, with appreciably lower rate leaf springs, torque windup becomes a problem. In any instance, with lower rate springs, more and more wheel travel must be provided. Cars designed to carry a normal load of five passengers with adequate compression ride clearance are, under light loads, almost on the rebound stops and look much too high. Also, since steel springs are essentially constant rate devices, satisfactory cushioning at the compression and rebound extremities becomes increasingly difficult. Thus, it is obvious why the ride improvements over the past several years with conventional steel spring suspensions have been limited since they were in large measure the result of other minor design changes without significant change in spring rates.

The limitations of steel springs, as we know them, made it necessary for our engineers to look for a

FORD'S answer to the air suspension problem is a system of the "open" type in which the air is exhausted from the springs to the atmosphere. It features a 2-speed automatic height and leveling control to handle differing load conditions.

In adapting the air springs to the suspension arms, the front suspension was modified only slightly, while the rear was completely redesigned.

The author reports that a significant improvement in passenger comfort has been achieved with the new suspension, especially for the rear seat passenger. Also, the car height remains constant under all loadings—a contribution to the car's appearance.

suspension system with fundamentally different characteristics. The desired system should provide:

1. A spring that could be fitted into the space provided for a normal rate coil spring.

2. A spring system that was readily adaptable to automatic leveling to insure a constant ride clearance under all load conditions. The leveling system must provide for rapid leveling under load changes and yet provide slow leveling with a car in motion.

3. A spring medium with a constant low rate and frequency in the ride range and with sufficient buildup of rate in the compression and rebound positions to provide adequate cushioning and satisfactory handling characteristics.

The curves in Fig. 1 depict wheel travel plotted against dynamic wheel rate for typical automotive suspension springs in use today, revealing that the air spring offers excellent potential for ride improvement. Both coil and torsion bar springs have a higher constant rate with no buildup in compression or rebound. The leaf spring is shown to have a high rate with some buildup in compression and rebound, but this is due to shackle effect and can be modified only slightly. However, the air spring shows all of the desired rate characteristics. It has an essentially constant low rate thru the normal ride range with very pronounced rate increase at both the compression and rebound ends of the curve.

When we decided to offer an air suspension system for the 1958 Ford car, it was decided to adopt the system which is the basic air system for all 1958 Company cars. This system was a composite of a considerable number of systems which were studied and evaluated in our Advance Car, Product Study, and Research Development Areas. The best features were selected from each in conformance with major design and performance objectives to provide:

1. Maximum improvement in riding comfort on all types of roads.

2. Steering and handling characteristics equivalent to our standard suspension cars.

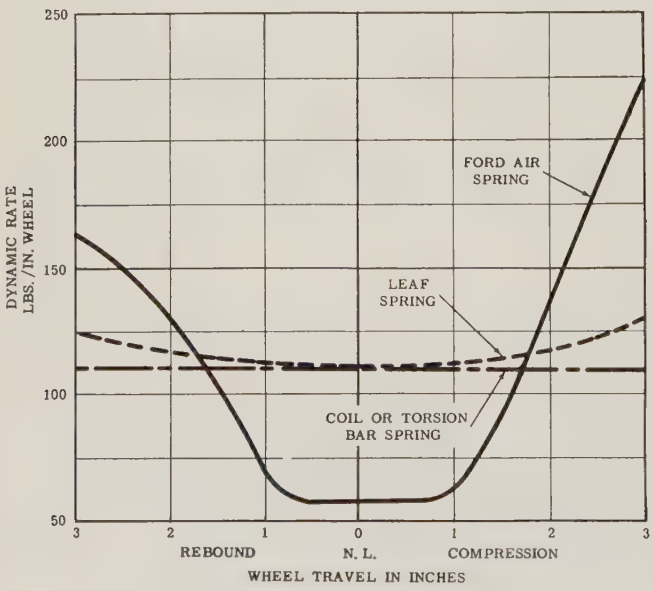

Fig. 1—Typical spring rate curves

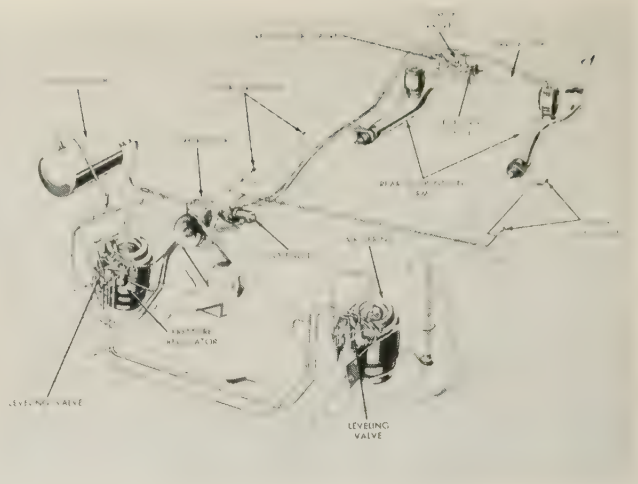

Fig. 2—Ford air suspension system

3. Continuous 2-speed automatic height and leveling control.

4. Harshness and road noise reduction.

5. A practical, trouble-free system requiring minimum maintenance readily adaptable to conventional production and service requirements.

The system selected to meet these objectives is shown in Fig. 2. It can be broken down functionally into four categories, comprised of components as indicated:

1. *Air Supply System*
   - Air compressor and check valve.
   - Air reservoir.
   - Pressure regulator.
   - Filters.
   - Connecting lines.
2. *Control System*
   - Leveling valves.
   - Solenoid and door actuating switches.
   - Restrictor valve.
   - T-check valves.
3. *Air Springs*
4. *Suspension Structural Components*
   - *Front*—Conventional suspension.
   - *Rear*—Trailing arms and attaching parts to frame and axle assembly, conventional rear axle and wheel assembly, and track bar.

Air Supply System

Figs. 3 and 4 are schematic diagrams of the air supply system. The function of the air supply system is to maintain the air requirements of the springs and to be a triggering agent for the fast-leveling mechanism in the valves.

The air system is of the "open" type in which air is taken from the atmosphere and after use is exhausted to the atmosphere. This system was chosen instead of a closed system, which reuses the exhausted air, because it eliminates the complications of a low-pressure tank and its attendant air lines.

Briefly, the system operates as follows: Air from

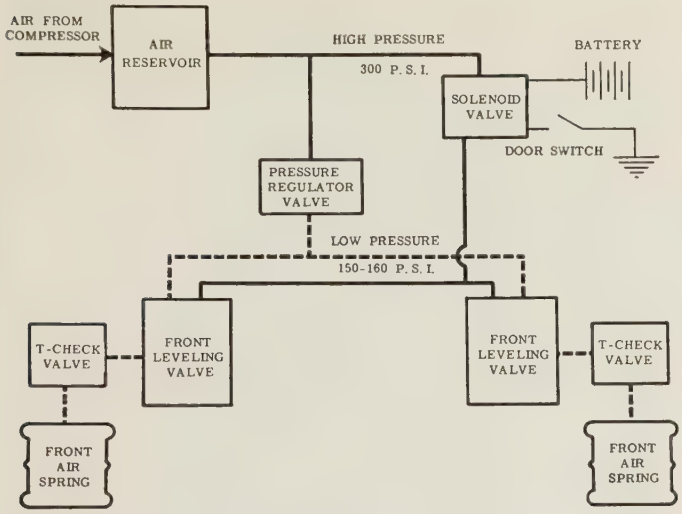

Fig. 3—Ford-Aire front suspension schematic diagram of air system components

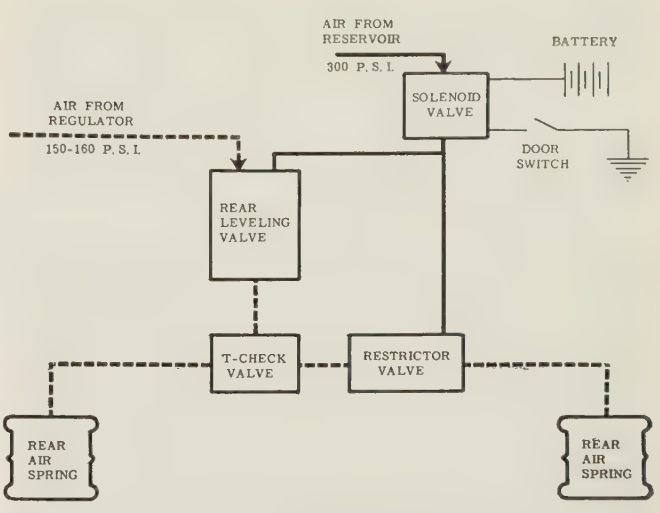

Fig. 4—Ford-Aire rear suspension schematic diagram of air system components

the compressor is supplied to a reservoir which is maintained at approximately 300 psi. High-pressure air is routed to a pressure regulating valve which reduces the pressure to 150–160 psi. At this pressure, air is routed to the leveling valves, thence through low-pressure T-check valves to the air springs. High-pressure air is also routed from the air reservoir to the solenoid valve, thence to the fast-action mechanism of the leveling valves and the restrictor valve between the rear air springs.

Compressor—The compressor is a specially developed single-cylinder aircooled pump. It is belt driven by the engine at approximately engine speed and is lubricated by engine oil. Its piston displacement is 2.71 cu in. Balance pressure is approximately 300 psi and maximum power requirement is 1 hp. It is a quiet, smooth-running mechanism with adequate capacity.

Air Reservoir—The 400 cu in. air reservoir is mounted in the right front fender and is connected to the compressor by a flexible hose. A one-way check valve prevents flow of air from the reservoir to the compressor when the engine is not running. A manual drain valve is provided at the low point of the reservoir for the removal of any accumulated moisture. The reservoir provides air to operate the system when the compressor is not running.

Regulator Valve—The diaphragm-type regulator or reducer valve performs the following functions:

1. Maintains a lower system pressure than that in the air reservoir (300 to 150–160 psi) so that the reservoir provides an air supply sufficient to operate the system when the compressor is not running.

2. Maintains the required balance between the fill (air system-to-spring) differential pressure and the exhaust (spring-to-atmosphere) differential pressure. The balance requirement will be explained later when the air springs are discussed.

Air Lines and Filters—Copper tubing is used for all lines which are constantly under pressure due to our greater experience in sealing metal lines. Nylon tubing is used for those lines which are under pressure only intermittently, the solenoid-to-leveling-valve lines and the solenoid-to-restrictor-valve line.

All lines are connected to the various units of the system by special fittings with rubber "O" rings to prevent leakage.

Design specifications require that all elements in the air system operate satisfactorily from –40 to 200 F without malfunctioning or leakage resulting.

Filters are incorporated in the following units of the system to prevent entry of foreign material: air compressor inlet, air reservoir outlet, air line and air spring inlets to leveling valves, and leveling valve atmosphere outlet.

Control System

The control system is designed to keep the car at a predetermined height and in a plane parallel to the road. It is a continuous 2-speed system. It provides fast leveling when the doors are opened and load changes are likely to occur, and slow leveling when the car is in motion with the doors closed.

The leveling control is obtained through three leveling valves which control the attitude of the car with respect to three points on the road. There is a leveling valve at each of the two front springs and a common leveling valve to control the two rear springs, mounted on the chassis frame as shown in Figs. 5 and 6. The actuating levers are attached by adjustable links to the upper suspension arms in the front and to the rear axle housing in the rear. Since the actuating levers are attached to the unsprung mass, any deviations in car riding height at these points of attachment result in the levers rotating the leveling valve cams.

Leveling Valves—The leveling valves are the "brain" of the Ford-Aire system. They provide dual or "slow-fast" type of leveling control. When the car is being driven, or is standing with the doors closed and a height adjustment is required, air is directed to or from the springs through highly restricted passages in the leveling valves so that height changes occur slowly. However, when the doors are opened for passengers to enter or leave the car, a solenoid valve is actuated. This pneumatically opens a relatively unrestricted bypass in

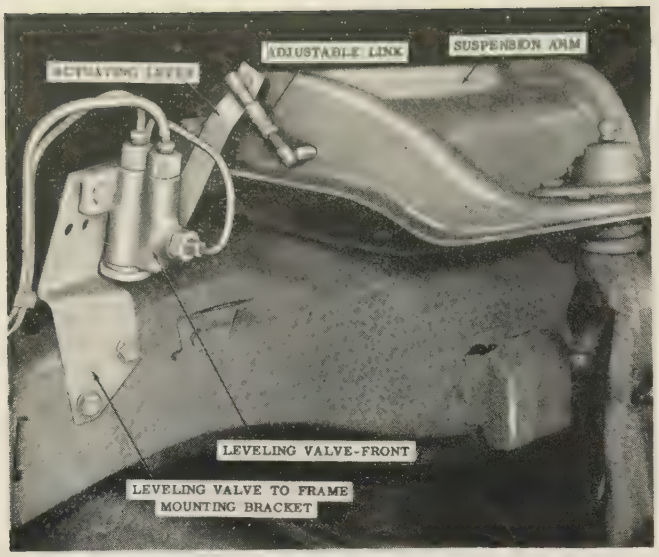

Fig. 5—Installation of front leveling valve

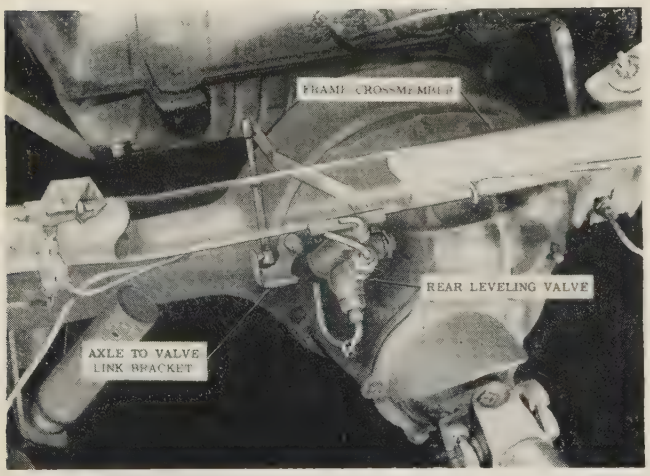

Fig. 6—Installation of rear leveling valve

each leveling valve through which the springs are filled or exhausted depending on the attitude of the car. Fig. 7 is a cross-section of the leveling valve showing the component parts. The left portion of the valve controls normal slow leveling. The right side controls fast leveling.

For the slow-leveling operation, air from the regulator enters the valve as shown by the cutaway view (Fig. 8), passes the intake check valve, passes around the intake and exhaust valve which is lifted from its seat by the leveling cam, goes through the passage to the metered orifice valve and out of the leveling valve to the check valve, and thence to the air spring. For slow-leveling exhaust the intake and exhaust plunger is moved down by the leveling cam. Air from the spring and check valve enters the leveling valve, passes through the metered orifice valve, through the passage, and out of the valve through the center of the intake and exhaust plunger as indicated by the arrows.

When fast leveling is required, the passage of air through the valve to the spring is the same as described for slow leveling, with this exception: High-pressure air from the solenoid actuates the fast-leveling piston which moves the metered orifice valve from its seat. Moving the valve from its seat permits

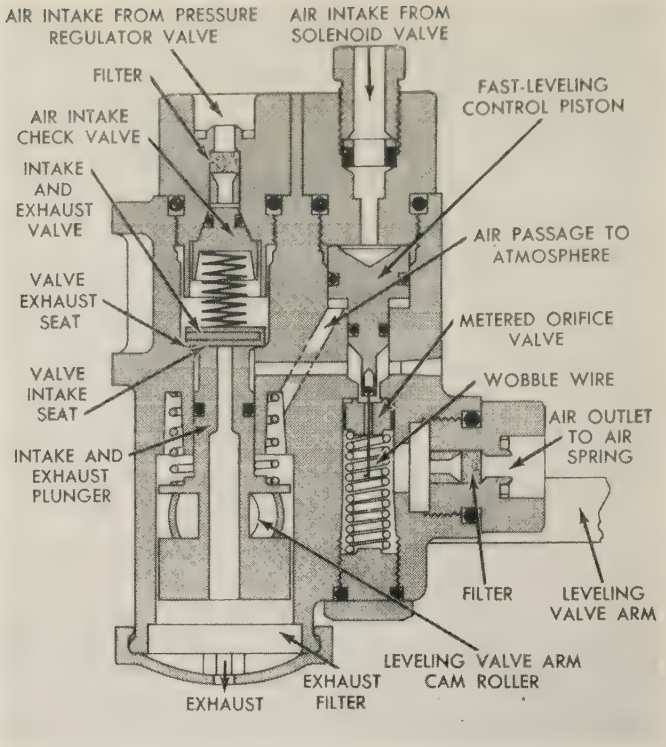

Fig. 7—Cross section of leveling valve

air to flow around the valve rather than through the orifice, and permits fast fill or exhaust action depending on the position of the leveling valve cam. The only use of the air directed by the solenoid is to provide a triggering action to permit faster movement of air through the normal fill or exhaust passages. (See Fig. 9.)

The development of the leveling valve posed many interesting problems in materials and dimensional control of parts. A 25-hr laboratory bench stroking test was established which, through correlation with actual rough road operation, corresponded to the required life of the valve on the car. In this test, the valve was cycled under full-operating air pressure at a controlled temperature of 200 F at 800 cpm. The fast-leveling mechanism was actuated twice each min.

This test provided a convenient and fast means of developing the required dimensions and material specifications for the seals, pistons, valves, and other components and adequate leak-free life of the parts. In addition, other tests were conducted in the refrigeration rooms at temperatures as low as –40 F to insure satisfactory functioning and leak resistance under extreme cold weather conditions.

Road tests included operation in dust, mud, slush, and snow.

The valve body is an aluminum die-cast part and all of the pistons are of coated steel. This combination was found to give excellent life and a minimum of wear and scuffing. All of the seals are made of specially developed, durable, leak-proof, synthetic rubber materials. It was found convenient from a manufacturing standpoint to make the metered orifice valve of nylon with the 0.012-in. metering hole molded into the part. A fine wire 0.009-in. in diameter passes through the 0.012-in. hole. This not only serves to reduce its effective area but also acts as a

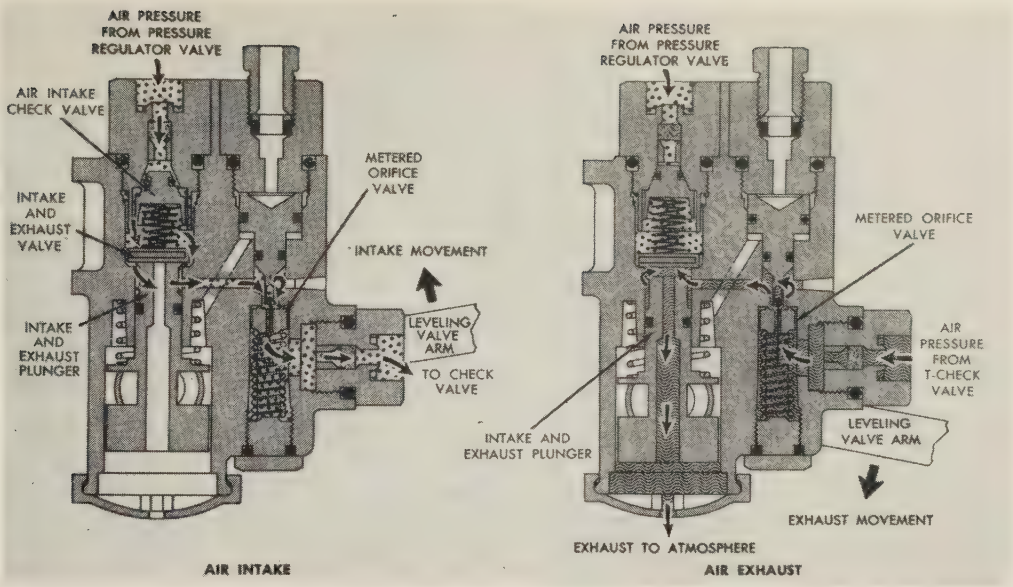

Fig. 8—Slow-leveling control

cleaning means.

Solenoid Valve—The solenoid valve is actuated by the dome light switches mounted in the door hinge pillars. As noted in the discussion of the leveling valves, its purpose is to provide air at reservoir pressure (300 psi) to the fast-action mechanisms in the three valves when the doors are opened and any appreciable load change occurs. It also acts as a high-pressure relief valve for the system and will open at 400 psi if the system pressure should become abnormally high.

Restrictor Valve, Rear Air Spring—In order to provide adequate rear suspension roll resistance, the two rear springs are isolated with regard to air transfer by a restrictor valve. This valve functions as follows:

Normally, with a single rear leveling valve, the two rear air springs are interconnected by a common air supply line. During roll, if the restrictor were not installed, unrestricted air transfer would take place between the rear air springs so that they would contribute no roll resistance. However, by incorporating the restrictor in the supply line to the right rear spring (Fig. 4) airflow between the two springs is severely inhibited so that the individual springs act to increase roll resistance.

The restrictor valve is also triggered by high-pressure air from the solenoid so that, when fast leveling action is required, the high restriction orifice is temporarily bypassed.

T-Check Valves—The T-check valves between the leveling valves and air springs are low-pressure limiting devices which prevent the springs from exhausting below a set minimum value (55–65 psi front

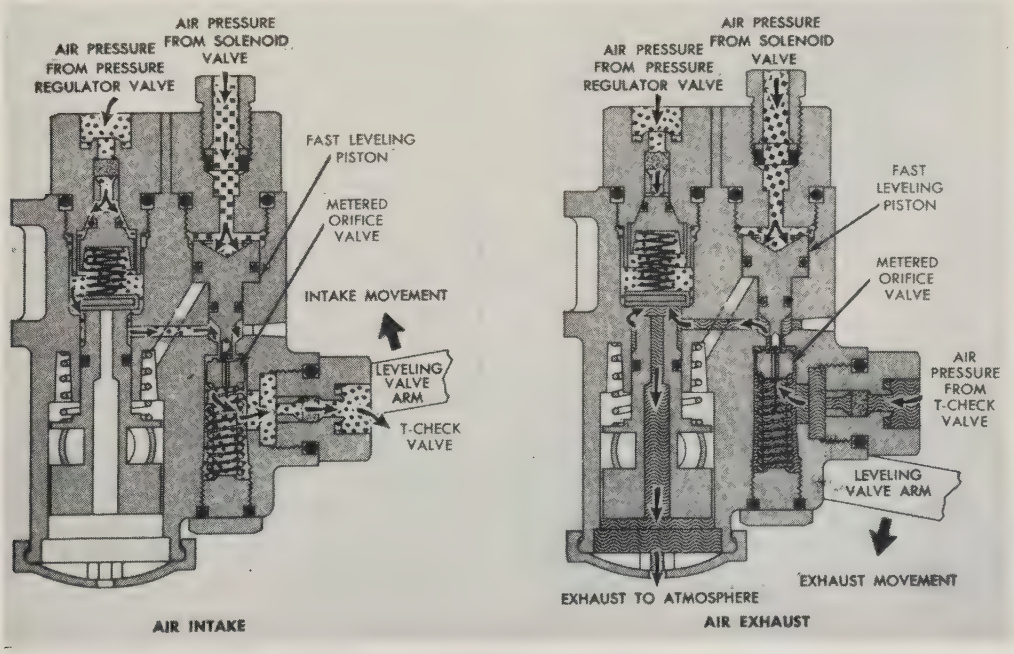

Fig. 9—Fast-leveling control

and 25–35 psi rear). They prevent extreme leveling action which would otherwise occur when one wheel is jacked up for tire changing, and they prevent complete loss of air from the springs if a leak develops elsewhere in the system.

Air Springs

The heart of any suspension system is its springs; they are the most important of all the factors which influence a vehicle's ride and to a lesser degree its handling. The air springs were chosen and developed in line with major design objectives to take the utmost advantage of the ride potential of ultrasoft springing without sacrificing good handling qualities.

The front air spring unit shown in Fig. 10 consists of four basic parts: the rubber diaphragm, the support sleeve or girdle, the piston or pedestal, and the upper seat and air pipe assembly. In addition, the rear unit (Fig. 11) has retainers at both upper and lower seals to prevent unseating if the shock absorbers are removed or disconnected while the car is on a hoist.

This air spring design was selected for two reasons:

1. It requires minimum air volume and installation space to provide exceedingly low rates in the normal ride range.

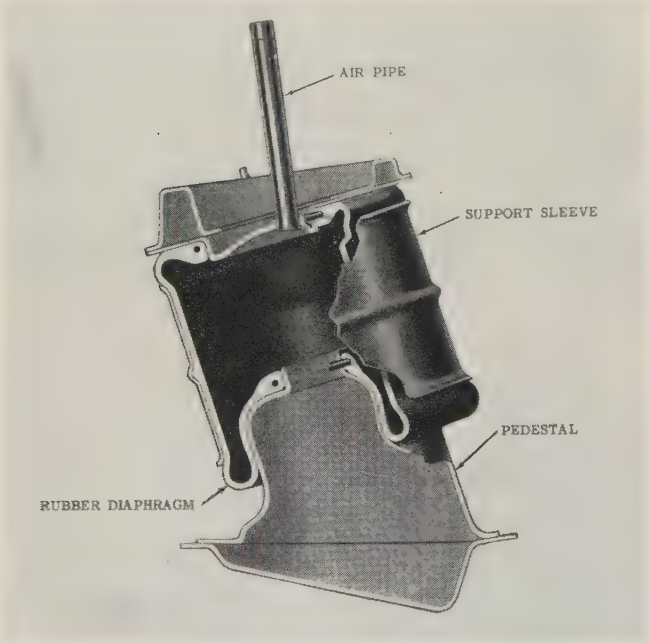

Fig. 10—Front air spring unit

2. It permits maximum flexibility in attaining any desired rate deflection pattern.

It is evident that as the piston travels up and down within the diaphragm, its effective area varies considerably. The character of this area variation depends primarily upon the shape of the piston and determines the shape of the load-deflection and rate curves. Fig. 12 shows a typical static load-deflection curve having the characteristic pattern which was sought and achieved. Also shown is a corresponding dynamic load-deflection curve for the same spring, obtained electronically at approximately 100 cpm. A comparison shows that the static and dynamic curves bear a strong general resemblance to each other, but dynamic rates in the neutral ride range are very much higher than static rates. In a vehicle, the dynamic wheel rate may be four or five times the static wheel rate.

The load-deflection curves describe ride characteristics of a vehicle. The shape of the air spring curve which we adopted provides some important information. The flat slope of the middle portion of the static curve (indicating a considerable movement for a small load change) shows that the car is exceedingly "soft" in normal ride movements. Smooth transitions followed by steep slopes toward both ends of the curve not only are necessary for acceptable handling but provide excellent rough road cushioning in jounce and rebound.

The manner in which the desired rate characteristic was achieved is worthy of note. First, it was necessary to establish the working volume for which space was available and the effective piston area which at reasonable working pressures would support the vehicle over the loading range. With these fundamentals determined, the remaining factors governing performance had to be manipulated to obtain the desired results. Chief among these factors were the cord angles in the fabric layer of the rubber diaphragm and the shape of the piston. If a straight piston were employed with horizontal cords in the diaphragm (Fig. 13), an almost linear load-deflection curve similar to that of a leaf spring would result. As the cord angles are increased toward the vertical the curve acquires an "S" shape. If vertical cords were to be used with a straight piston, an almost ideal curve would result (Fig. 14). However, this is prohibited by practical limitations such as strength and folding characteristics of the diaphragm. Contouring of the piston and using diagonal cord angles was adopted to approach the ideal curve and to obtain ample diaphragm strength in all directions. By contouring the piston it is possible to change the effective area, which is the major

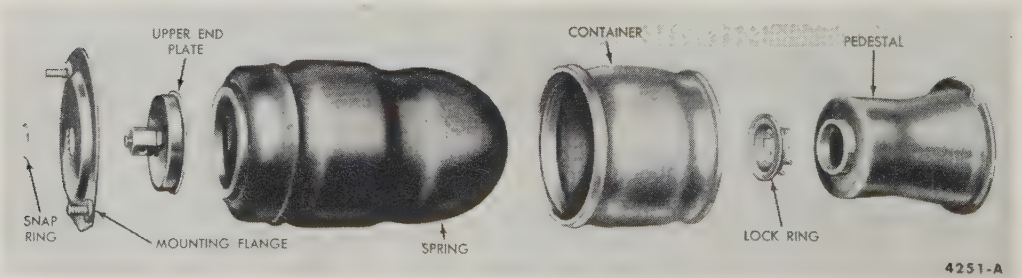

Fig. 11—Components of rear air spring unit

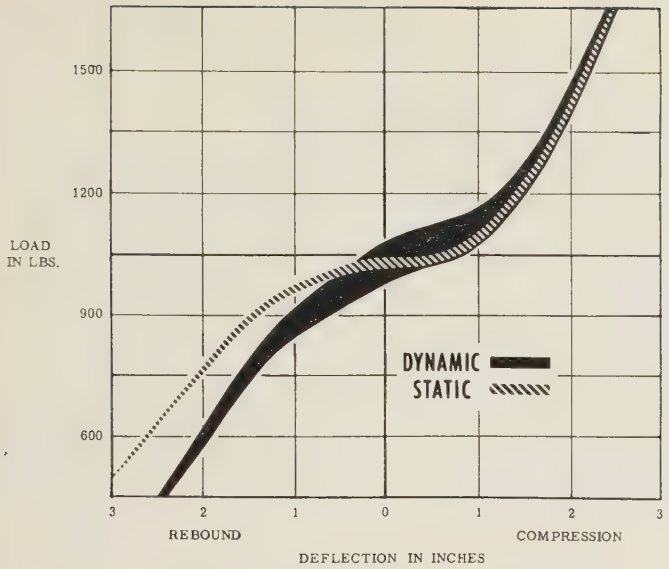

Fig. 12—Load-deflection characteristics, static versus dynamic

factor in determining the rate characteristics as the piston travels up and down in the rubber diaphragm. The piston was modified by giving it an hour-glass shape which changes the area-pressure relationship to give a low ride rate in the center of the ride range (Fig. 15). Below the center portion of the piston the area, which increases with compression, provides the compression buildup shown in the curve. In the enclosed diaphragm type of spring with rolling lobes, the hour-glass type piston also gives a rate buildup in rebound, as shown. As full-rebound is approached, the diaphragm lobe becomes larger and is forced out to increase the effective area, while the pressure is decreasing because of increasing volume. Both of these factors result in marked rate buildup.

Other less influential factors, such as container configuration, molded diaphragm shape, thickness, cord modulus, and rubber compounding were tailored to secure the final shape of the load-deflection curve providing optimum performance with acceptable durability.

For satisfactory performance of the springs on the car, it was found important to maintain the air pressure as it enters the spring at 150–160 psi. The pressure regulator performs this function. It was found that if the system were operated at the normal 300-psi reservoir pressure with a rear spring pressure of 80 psi, for example, there would be approximately a 220-psi differential to fill the rear springs and an 80-psi differential to exhaust them to atmosphere. On a long stretch of rough road, especially washboard, far more air would be admitted during jounce motions than could be exhausted during rebound motions. This soon caused the car to ride hard against the rebound stops. Pressure regulation to 150–160 psi, on the other hand, provides an approximate balance of fill and exhaust differentials of equal value (80 psi) and the car remains in trim regardless of road condition.

Suspension Structural Components

In adapting air springs to the Ford front suspension it was possible to use conventional upper and lower arms with minor modifications, and to use them for either coil springs or air springs. Changing the upper arm involved only the addition of a hole for the leveling valve link.

Changes to the lower arm included the addition of holes for attaching the air spring to the arm and provision for attaching the lower end of the shock absorber to the lower arm near the ball joint (Fig. 16). The upper end of the front shock absorber is attached to a bracket, mounted aft of the spring pocket, and attached to the frame side rail.

A completely new rear suspension was used. Fig.

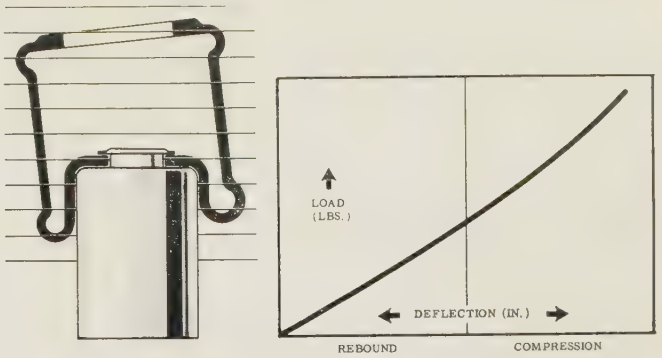

Fig. 13—Air spring horizontal cords-cylindrical piston

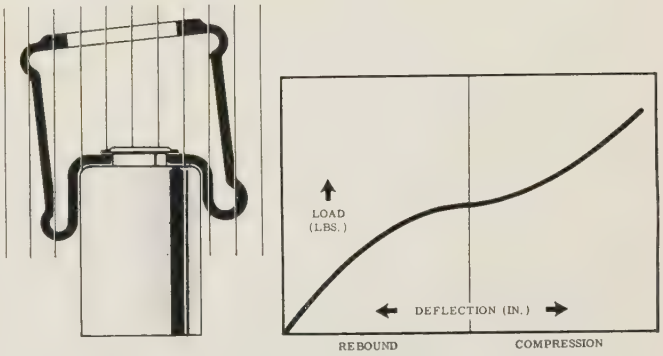

Fig. 14—Air spring vertical cords-cylindrical piston

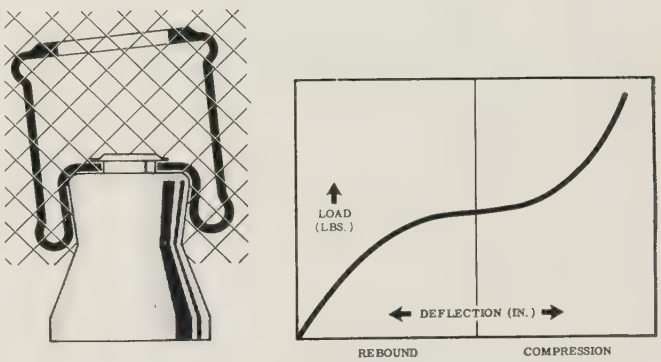

Fig. 15—Air spring diagonal cords-hour-glass piston

17 shows the design which was finally adopted. It is a trailing-arm type with several rather unusual features. One is the forward attachment of the trailing arm to the frame; instead of the usual transversely mounted rubber journal bushing, it uses a large spike-end rubber mount, similar to those often found in shock absorber ends. This particular design serves several purposes. It practically eliminates torsional loading in the trailing arm. It permits rather large axial, but only small radial deflections. This contributes very greatly to the reduction of harshness without adversely affecting rear end steering.

The trailing-arm rear mounting consists of an arm attached to the axle by means of a pair of transverse rubber bushings (Fig. 18) whose axes are spaced approximately 5 in. apart. This arrangement gives effective isolation, yet ties the axle and trailing arms together in such a way that they constitute a roll stabilizing unit, with the axle housing acting as the torsion member. Some roll resistance is obtained in this manner. However, the major portion of the rear roll resistance is provided by the restrictor valve mentioned previously.

In order to provide lateral stability in the rear suspension, a track bar has been incorporated. This bar is attached to the left frame side rail behind the rear axle and to the right side of the rear axle housing near the right air spring. Both ends of the track bar are attached to brackets by means of rubber insulators similar to those used for trailing-arm-to-frame attachment.

The rear suspension structural components were developed and proved by car durability and laboratory fatigue tests. Laboratory testing was based on stress values and frequency of occurrence electronically measured with strain gages during rough road durability operation. These same stress values and frequencies were duplicated in the laboratory on a complete rear suspension assembly which was cycled on a motor-driven test fixture. This test gave a quick and convenient method to study and develop efficient designs, prior to final road testing.

Combined with the geometrically conventional front suspension, the rear air suspension provides excellent cornering and general handling qualities.

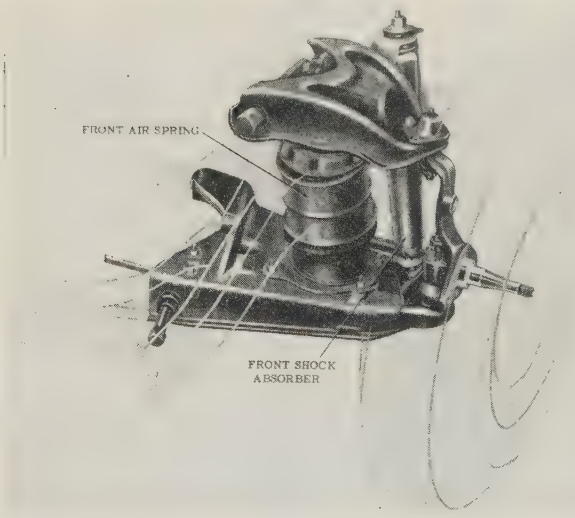

Fig. 16—Air springs installed on front suspension

Conclusions

In conclusion, by complementary tailoring all of the components of the air suspension system in our ride development program, a very significant improvement in overall passenger comfort was achieved. The result was a very soft boulevard ride with an outstanding rough road ride. The rear-seat ride is remarkably free from pitch and there is a noticeable reduction in harshness and road noise. These gains have been made without sacrifice of acceptable steering and handling qualities. A very definite aesthetic gain has been made in that the car height appearance remains constant under all loading conditions.

Our experience after thousands of miles under every conceivable type of climatic and road condition has clearly indicated that the Ford-Aire suspension has more than met our established objectives.

Acknowledgments

Ford Division Product Engineering wishes to acknowledge the important contributions of other Ford Motor Co. engineering departments in the design and development of the air suspension systems. These include Engineering Staff Product Study and Research Areas, Edsel Division Product Engineering, and Lincoln-Mercury Division Product Engineering.

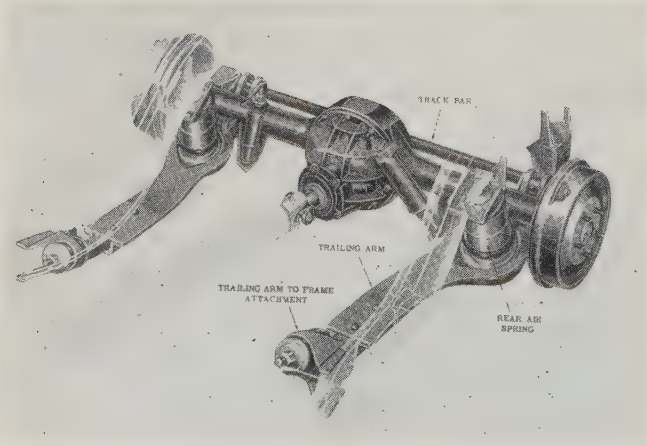

Fig. 17—New rear suspension with air spring

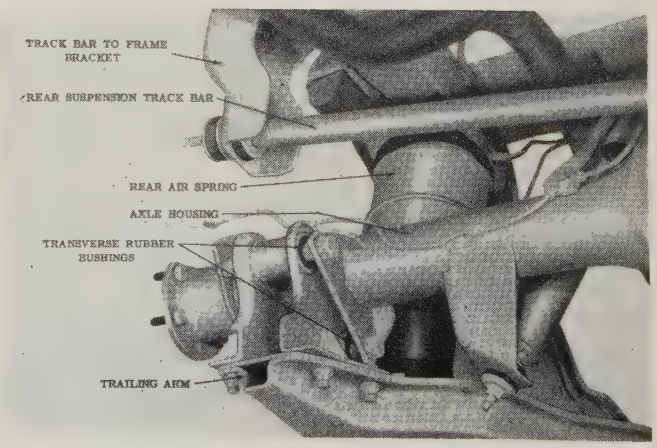

Fig. 18—Air spring mounted on rear axle

CHEVROLET has made its new air-suspension system easily interchangeable in production line assembly with standard full-coil suspension by adopting a 4-link-type rear suspension with short and long arms.

A feature of the system is the mounting of the leveling valves within the air-spring assemblies. These valves correct riding height continually at a moderate rate, regardless of whether the springs are leveling or operating in ride motion.

The system provides constant frequency ride—ride comfort remains the same whether the car is occupied by the driver alone or is fully loaded.

1958 Chevrolet LEVEL AIR SUSPENSION

K. H. Hansen, J. F. Bertsch, and R. E. Denzer, General Motors Corp.

This paper was presented at the SAE Annual Meeting, Detroit, Jan. 14, 1958.

THE air-suspension system on the 1958 Chevrolet represents a major step forward in achieving ride comfort much superior to that attainable in a vehicle with conventional steel springs. With this system, known as Level Air Suspension, it has been possible to reduce the spring rate considerably, while maintaining the same high degree of ride comfort whether the car is fully loaded or occupied only by the driver. This phenomenon is known to the automobile engineer as a constant frequency ride. Even with this softer air springing, the excellent handling and stability of conventional coil springs have been maintained.

Using air as a medium, we have developed a suspension with self-dampening qualities for a gentle boulevard ride, as well as the proper absorption characteristics for high impact forces encountered on secondary roads.

A fundamental design requirement was a high degree of production interchangeability with our conventional steel-spring suspension so that the lowest possible cost to the customer could be realized. To accomplish this a full coil suspension was adopted as regular equipment, with the air-spring assembly having the same approximate shape and fastening as the conventional springs. In other words, to simplify assembly operations, the suspension mounting must be equipped to receive either coil or air spring equally well.

The well-known short and long arm independent front suspension lends itself to use of either air springs or coil springs (Fig. 1). For the rear suspension, a departure was made from the formerly used leaf springs to a new link type with short and long arms, making the installation very similar to the front suspension (Figs. 2 and 3).

For many years the stylists have been confronted with the problem of making a car look as attractive when fully loaded as when lightly loaded or not loaded at all. The Level Air suspension system with its automatic constant height maintenance feature solves this problem. It also makes optimum wheel travel and optimum geometry available at all times.

General Description

Four air-spring assemblies are used in the Level Air suspension system (Fig. 4). Integral with each of three of the units is a leveling valve which automatically controls vehicle height at all times. Since three points define a plane, only three points may

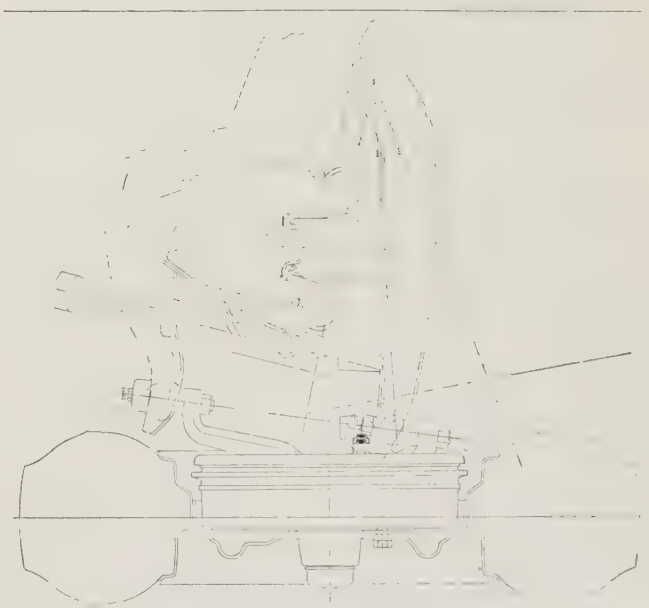

Fig. 1—Front suspension

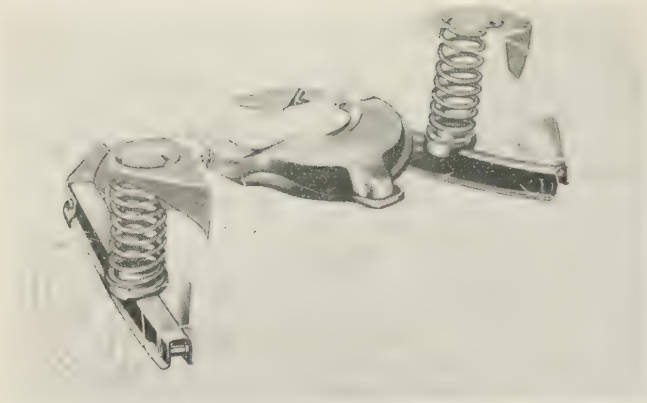

Fig. 2—Conventional coil-spring installation (rear suspension)

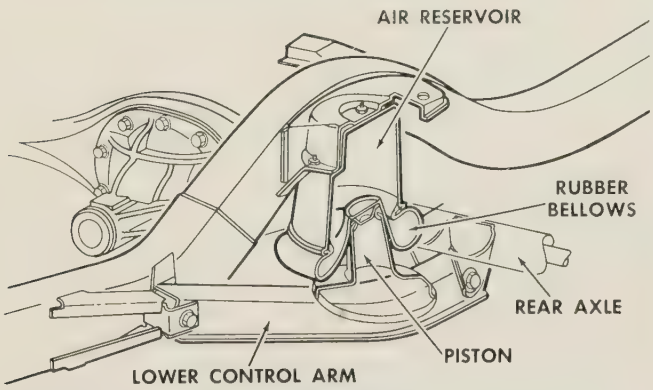

Fig. 3—Air spring

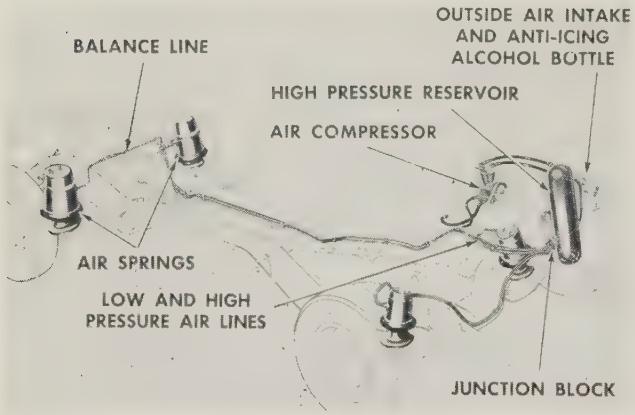

Fig. 4—Level Air Suspension

be used to establish the attitude and height of the car. Therefore, two leveling valves are used in the front, one in each spring, and a single valve is installed in the left rear. The left rear spring is cross-connected to the right rear spring by a balance line. In order to keep unrestricted cross-flow between the two from interfering with the vehicle's handling, a 0.020-in. orifice is included in the balance line.

A single-cylinder compressor, belt driven from the crankshaft, supplies air to the system, directly charging the high-pressure reservoir when the engine is running. A complete circuit of supply and exhaust lines to each leveling valve is provided for air circulation. These lines connect to a junction block mounted on the frame. A manual valve in the junction block prevents the exhaust of air from the system. Thus, the entire air suspension can be as-

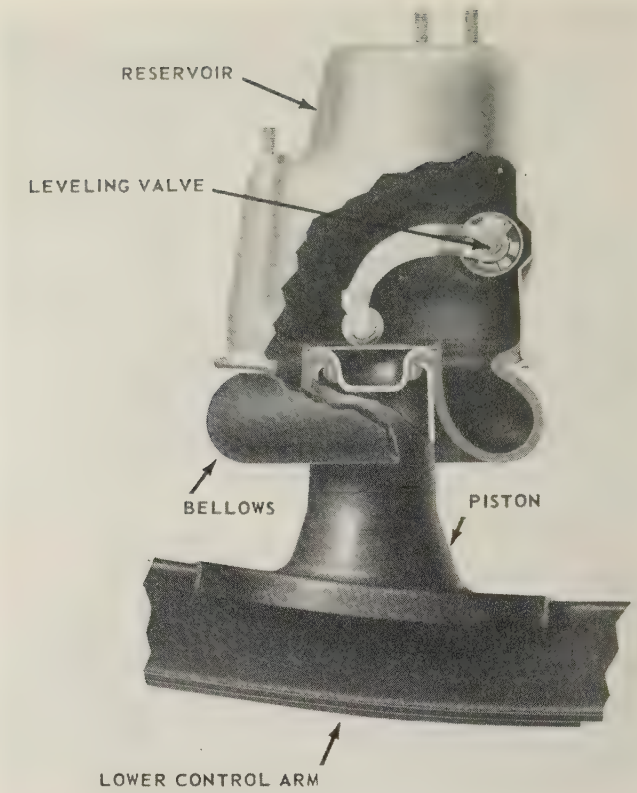

Fig. 5—Air-spring assembly

sembled and inflated prior to installing the body and the front sheet metal which mounts the reservoir.

Air Spring

The air-spring assembly consists of an airtight reservoir, a leveling valve, a single convolution rubber bellows, and a piston (Fig. 5). The lip of the bellows fits into a flange in the reservoir and is self-sealing in much the same manner that a tubeless tire seals to the rim of a wheel. The bellows is made of rubber with two plies of nylon fabric.

When the spring is inflated with air, it will support a load. When the spring is compressed, the pressure of the enclosed air is increased and the spring carries a greater load. A plot of the resulting load versus deflection gives a curve similar to that of a coil or leaf spring, but with several exceptions.

For an air spring, the slope or rate of the load-deflection curve differs depending on whether the spring is cycled at ride frequencies or is tested under extremely slow or static conditions. When the spring is cycled at ride frequencies, the heat of compression and the cooling of expansion cause the pressure to change more rapidly than when the spring is stroked slowly and the temperature of the air in the spring remains relatively constant. This means that dynamic test equipment must be provided in the laboratory to measure the adiabatic (constant heat) spring rate. The isothermal (constant temperature) rate obtained by normal static methods is of very little significance when considering ride and handling on an air-suspended car.

The dynamic testing fixture we used for air-spring development work is shown in Fig. 6. Its cycling speed can be varied between 30 and 90 cpm. A hand crank is provided for isothermal testing. A linkage capable of wide adjustment holds the air-

spring assembly. The arrangement shown simulates the lower control arm of the 1958 rear suspension, with the air-spring reservoir in its proper relationship to the pivots.

The vertical load required to move the linkage is applied through the crankshaft mechanism. The magnitude of the vertical load is measured by the four load cells which support the entire operating assembly. Vertical displacement of the pivot is sensed by a helipot installed on the base of the test fixture. The resistance changes of the helipot and the load cells are translated into voltage on a calibrated oscilloscope as direct reading plots of load versus deflection.

Fig. 7 is a curve of the dynamic load deflection at the outer pivot of the rear suspension linkage. Each vertical square is equivalent to 100-lb load, and two horizontal squares equal 1 in. For convenience in investigating various wheel-to-spring ratios, we chose to measure the rate of the outer pivot, which is easily converted to wheel rate.

There are several things to notice on the load-deflection curve. One is the relatively low constant rate, ± 2 in. from design. As the bump region is approached, the rate increases smoothly and rapidly. This characteristic smooths the transition into the very high rate of the rubber bump stops. Thus, the energy absorption required when hitting a severe bump is accomplished smoothly and with far less incidence of "crash through," an annoyingly familiar characteristic of conventionally suspended cars.

Another property to note on this curve is the hysteresis due to the air spring. This gives the air suspension an inherent damping quality, or the ability to absorb road irregularities and reduce the amount of shock-absorber control required for normal ride motions. A coil spring stroked in this same fixture exhibits no hysteresis.

Effective area is defined as the load divided by the pressure in the spring. If the load at the wheel is used, the effective area at the wheel is obtained. Considering the values at the wheel:

$$\text{Load} = \text{Pressure} \times \text{Effective Area}$$

$$\frac{d\,(\text{Load})}{d\,(\text{Travel})} = \text{Pressure}\,\frac{d\,(\text{Effective Area})}{d\,(\text{Travel})} + \text{Effective Area}\,\frac{d\,(\text{Pressure})}{d\,(\text{Travel})}$$

It may be seen that to obtain a low rate of change of load, the rate of change of effective area and the rate of change of pressure should be kept low. With pressure in the 80–90 psi range and effective area in the 10–12 sq in. range, it can also be seen that effective area change is more critical than pressure change for a given travel.

It is easy, in theory, to control pressure change by increasing the volume of the spring reservoir. An infinite volume of air would have zero pressure change. In practice, however, there are severe space limitations on the air-spring unit size. Effective area variation is a function of the chord angle in the bellows, the molded shape of the bellows, the piston contour, the linkage arrangement, and to a small extent, the pressure in the bellows.

Effective area curves for the front and rear suspensions of the 1958 Chevrolet are shown in Fig. 8. It can be seen that the rate of change of effective area is very low, even negative, near the design region. Because of this, it is possible to obtain a low-rate air suspension in a unit of a size that conveniently replaces coil springs in the front and rear.

The familiar two-convolution bellows which has been used for several years on buses has an effective area curve with a large positive rate of change. Experimental cars were built as early as the 1930's using this type of bellows, but the relatively large reservoirs required to obtain low rates made the spring assemblies unacceptable for production consideration on passenger cars.

The calculated suspension frequencies of the 1958

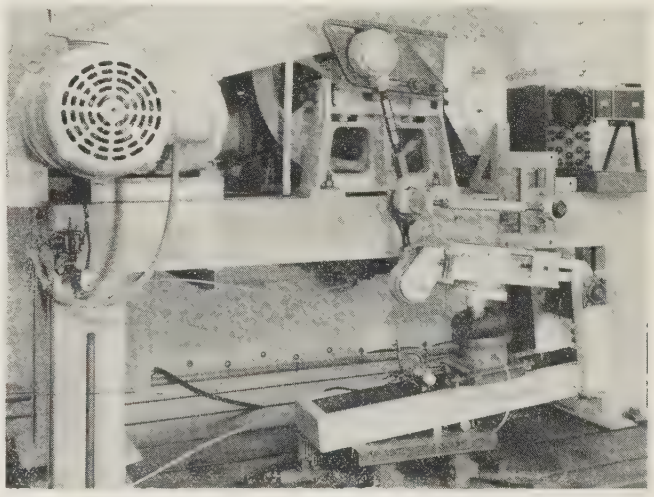

Fig. 6—Dynamic testing fixture used for air-spring development work

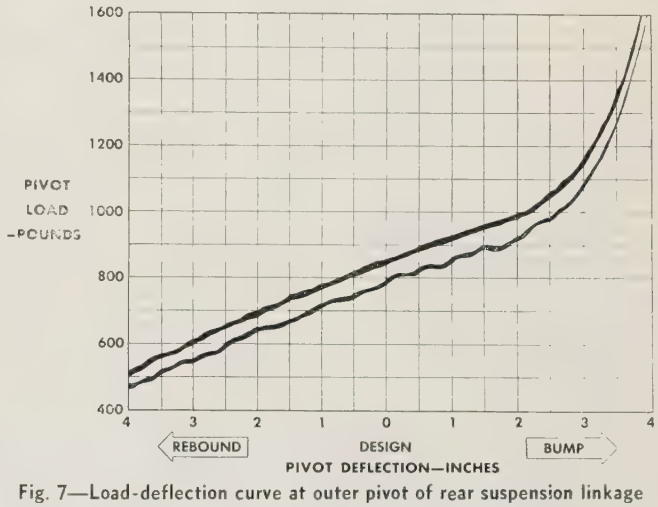

Fig. 7—Load-deflection curve at outer pivot of rear suspension linkage

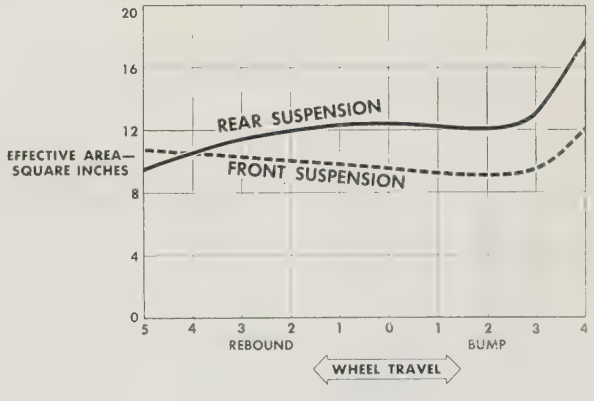

Fig. 8—Effective area curves

Chevrolet are based on the wheel rates (Fig. 9). Since the frequency varies as the square root of the rate, the air-suspension car has much lower rates than the coil-spring car. The relatively constant frequency due to leveling of the air suspension is also evident here. This means that ride smoothness in an air-suspended car will be relatively consistent regardless of load.

Shown in Fig. 10 is the air-spring assembly at its top and bottom extremes of travel, and at the design position. The area marked by the arrow is shown going through the full-stress cycle from the large diameter at full-rebound to the diameter of the piston at full-bump.

The bellows is similar to a coil spring so far as endurance testing goes—the larger the stroke, the more severe the test. If the bellows is moved ± ½ in. about the design position, the area goes through a much smaller stress cycle. This is not the case with diaphragm-type springs where the complete stress cycle occurs during normal ride motions.

A durability test fixture rig used to test air bellows is shown in Fig. 11. Current practice calls for rejection of any group of bellows where test samples do not satisfactorily exceed 100,000 full-stroke cycles on the machine without failure. Results obtained from durability test cars at the General Motors proving ground show that the air-spring bellows are fully as reliable as present-day coil or leaf springs. This statement of reliability also considers the possibility of leakage in the air-spring assemblies. One of the requirements specified for the assembly is that it must not lose more than 1 psi per day over a 3-day period when inflated to 75 psi. The air-spring assemblies have been able to satisfy this specification after 35,000 miles of durability testing.

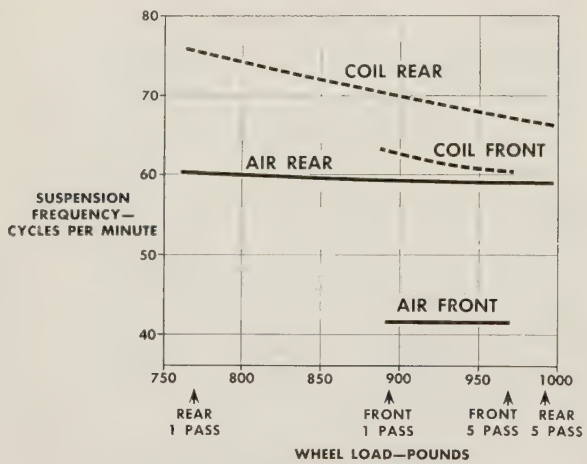

Fig. 9—Variation of suspension frequency with load

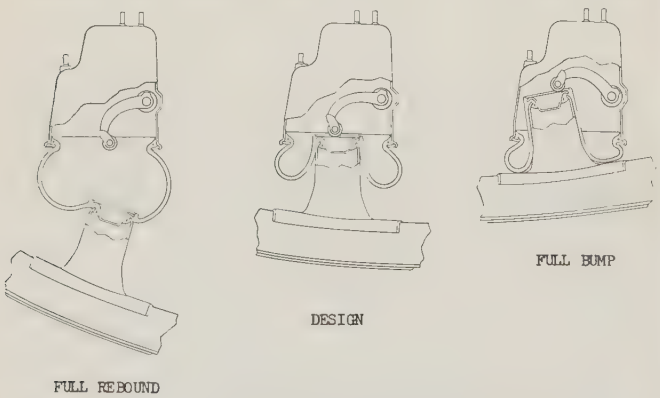

Fig. 10—Air-spring travel

Control System

The control system of an air-suspension system must automatically maintain the car at a constant height regardless of load, and correct for gasoline load and for temperature and altitude changes while the car is in motion. The correction for a change in loading must be made rapidly enough to furnish proper ride clearance before the vehicle is driven. These requirements are currently being met by either of two basic types of control system:

1. A dual-rate system, which permits air to flow rapidly to the air springs under loading conditions, and shuts off or highly restricts the airflow rate under ride conditions.

2. A moderately restricted control system in which the restriction of airflow remains substantially unchanged, regardless of whether the springs are leveling a load or operating in ride motion.

Our first attempt to solve the problem was to make the leveling valves inoperative while the car was in motion by introducing a time-delay action into the leveling valves. This was done to permit the use of a very small compressor, and to have the air springs act in the same manner as conventional coil springs during cornering. In other words, transfer of air to and from the air springs would not occur. It was found that in order to have low airflow rates through the system, the delay had to be close to 15 sec. During testing of the system under continuous cornering, such as in mountainous driving, the car quite frequently would come out of a series of curves in an unlevel attitude and remain that way for the duration of the delay time of the valve before correction to normal occurred.

We gradually reduced the delay time in the leveling valve in a series of tests, down to as short a time as 1–2 sec. In reducing the delay time, we found a more reliable delay system could be achieved by using restrictions in place of delay dashpots.

Several other ideas to make the leveling valve

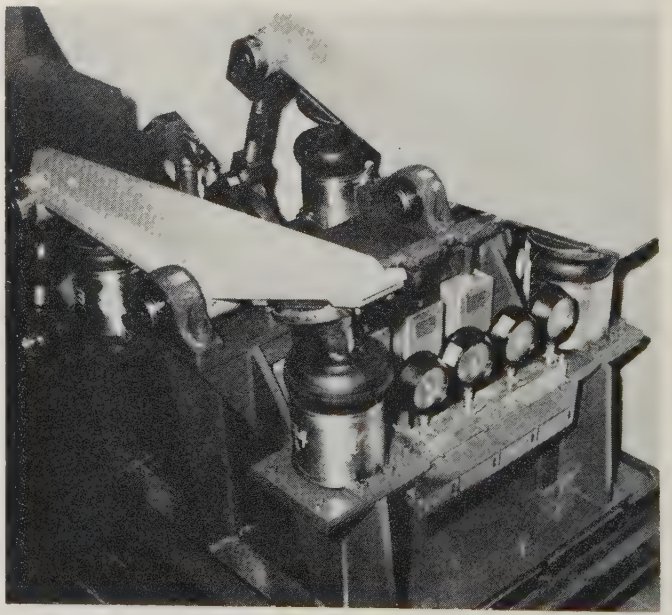

Fig. 11—Four-station air bellows stroking machine (test setup)

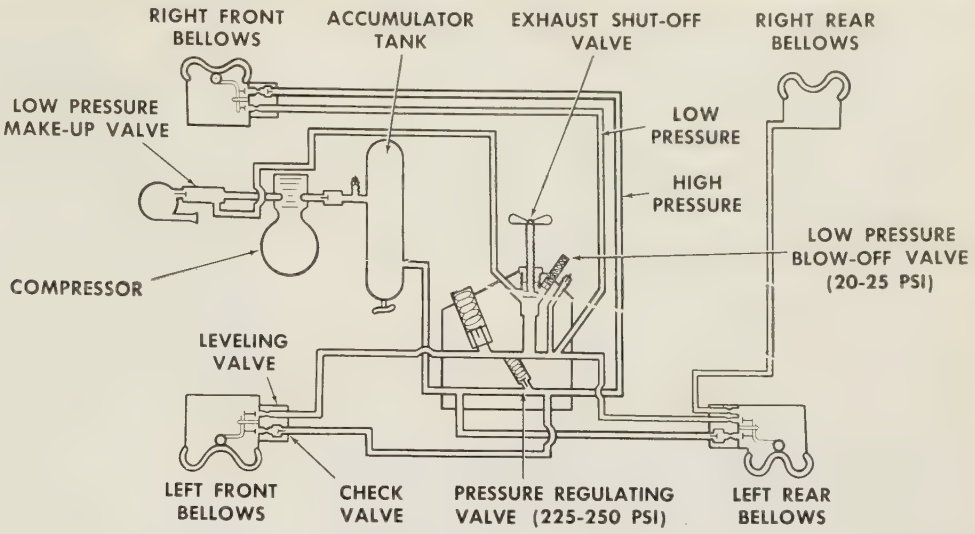

Fig. 12—Air-suspension schematic

practically inoperative when the car was in motion were tested. This included auxiliary control valves which would operate in response to an open or closed door, acceleration of the car, or simultaneous flow in both intake and exhaust lines. Each of these ideas had its shortcomings. For example, we found that dual-rate systems, when leveled on a rutted surface, would be misleveled for a considerable time after driving onto a smooth road. It was extremely difficult in the highly restricted systems to make the car ride at its correct height.

The Chevrolet "moderately restricted" system continuously corrects riding height at a controlled rate. Even though faster leveling time may be produced by the dual-rate system, we feel that our system is the most satisfactory compromise to meet the widely varying conditions encountered in road operation. This system also is the least complex, having fewer parts.

Under certain conditions, it is not desirable to make a suspension system level too rapidly. The rate at which a moderately restricted system should be made to level (assuming adequate compressor capacity) is dependent upon: (1) acceptable rate of change in attitude of the car during ride motions and (2) acceptable leveling time for load changes.

It must be of a slow enough rate so that the leveling action in roll, that is, the rate of transition from the rolled attitude to a level straight ahead position, produces no perceptible feel on the handling of the car. In addition, leveling action due to weight transfer in braking must be minimized so that the car does not noticeably level after each brake stop. These conditions are satisfied, and at the same time an acceptable leveling time for load changes is provided for in the Chevrolet system.

Air Distribution

Shown in Fig. 12 is the complete control circuit.

The compressor maintains compressed air in the system, taking in outside air only when required through the low-pressure make-up valve. Air pressure in the reservoir tank is limited to 225–250 psi by the high-pressure regulating valve. Any excess is bypassed to the low-pressure system.

Compressed air is supplied to the three leveling valves through the high-pressure lines, and exhaust air from the springs returns to the compressor inlet through the low-pressure lines, forming a closed system for any given load.

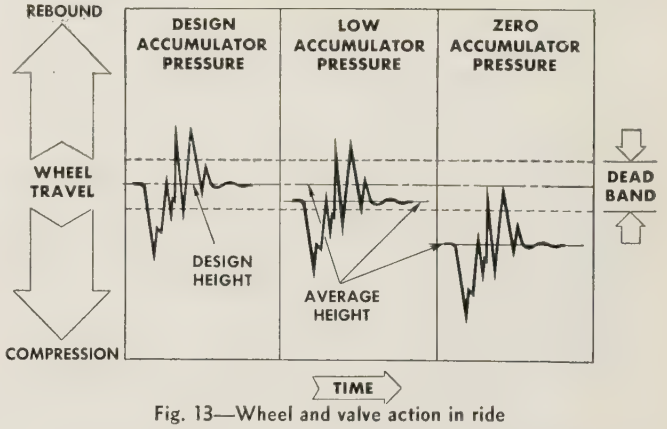

Fig. 13—Wheel and valve action in ride

The rate of airflow to the springs is controlled by orifices in the leveling valves. The inlet and exhaust orifices in the front leveling valves are 0.020-in. diameter. In the left rear, the inlet orifice is 0.031-in. diameter, and the exhaust orifice 0.042-in. diameter. Because a single leveling valve controls both rear air springs, the larger orifices are necessary to permit the rear springs to level at approximately the same rate as the front springs. These valves are position sensitive and operate either to admit or exhaust air from the springs as the spring length changes from design height. When the engine is shut off and air is exhausted, as in passenger unloading, the air escapes from the system through a low-pressure blow-off valve set at 25 psi. This blow-off pressure is sufficiently high to prevent the escape of air during ride motions. A check valve is built into each leveling valve to prevent back flow into the air supply line. This prevents deflation of the spring should the car be inadvertently loaded with zero pressure in the reservoir.

Leveling Valve

As previously outlined, the rate of air circulation in the system is controlled by the sizes of the orifices in the leveling valves. The diagram shows, in chart form, how the leveling valve functions when the car is in motion (Fig. 13). It illustrates the action of

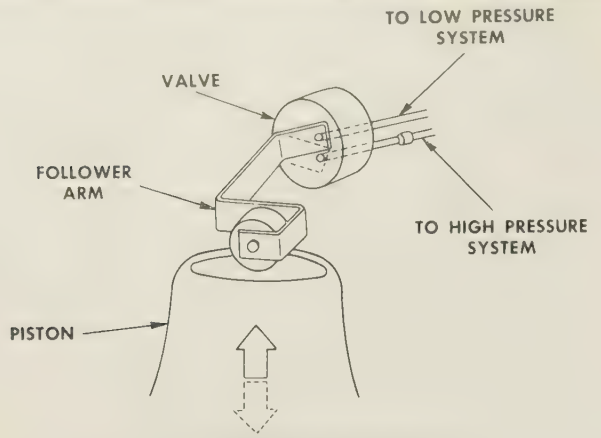

Fig. 14—Schematic of leveling valve

Fig. 15—Leveling valve

the suspension under various reservoir pressures which might vary from suspension pressure to a maximum of 250 psi.

The action of the leveling valve with reservoir design, or normal pressure, is considered in column (a). In order to remain at the design height position, the leveling valve must admit as much air in bump as it exhausts in rebound. This means that the time intervals during which the valve is open in bump and rebound, multiplied by the corresponding pressure differentials, must be approximately equal. If the springs change length during ride motions, the leveling valves automatically act to return themselves to the dead band denoted by the distance between the two dotted lines. For instance, when a spring is extended, the leveling valve remains open a longer time in exhaust with each subsequent body movement until bump and rebound movements of the valve are again equalized.

When the car is brought up to full-load the reservoir pressure under certain conditions can drop to slightly above suspension pressure. Column (b) illustrates the leveling action that takes place until the reservoir is fully recharged. The suspension tends to ride on the low side of the dead band, below the normal height. The valve must remain open a longer time in bump to take in as much air as it exhausts in rebound because of the lower pressure differential between the reservoir and the spring.

An interesting phenomenon, shown in column (c), is the action of the suspension under zero reservoir pressure. A condition of that nature may occur with either a belt or compressor failure. The suspension does not become completely deflated, as at first may be expected, but only deflates to a point where the air exhaust valves do not open during vehicle motions. The car then rides slightly low on the air trapped in the bellows.

In the Chevrolet Level Air suspension, the design of the leveling valve is very simple. A spring-loaded lever rides on top of the piston in the air spring. Through linkage, the lever opens and closes the orifices in the valve, as determined by the position of the piston. At design position, both orifices are closed. The metering orifices are incorporated in the valve seats (Fig. 14).

The leveling valve has a zinc die-cast body and two stamped sheet metal valve levers (Fig. 15). A common spring loads both valve levers against their seats. The orifices are incorporated in the valve seats, and because their diameters are small only a slight spring force is required to hold the valves

Fig. 16—Roller in contact with top of piston

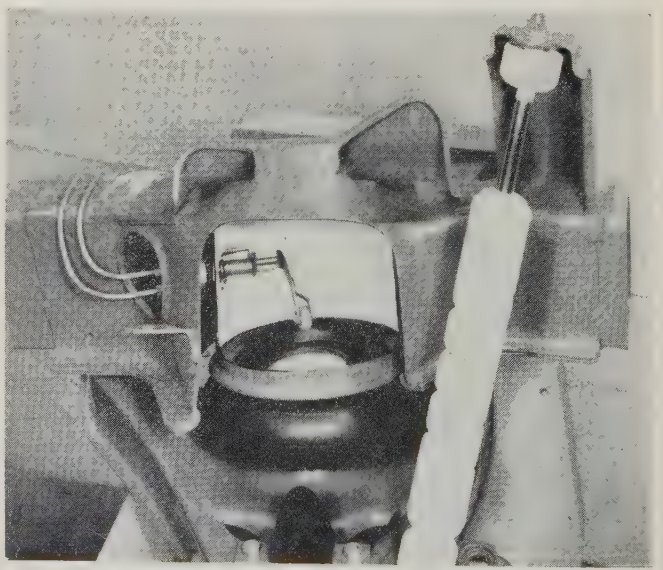

Fig. 17—Position of follower and piston after 1½ in. of wheel travel in rebound

closed against air pressure in the line. Lugs on the inner end of the follower lever pick up tabs on the valve levers to open the valves around a common shaft. These tabs can be bent during manufacture to adjust the "dead band" or inactive portion of the leveling-valve travel. This type of action is far superior to a close tolerance cam mechanism with its sliding action and attendant hysteresis due to friction and wear.

A spring on the follower keeps the roller in contact with the top of the piston during ride motions (Fig. 16). In order to reduce the travel requirement of the valve levers, the follower is prevented from following the piston beyond 1½ in. of wheel travel in rebound, since more than 1½ in. is beyond the normal wheel amplitude (Fig. 17). The roller and piston normally remain in contact. The natural frequency of the lever is high enough to maintain contact during wheel hop. This feature also disconnects the leveling-valve linkage from the suspension arm and thus averts accidental damage to the valve if the rebound stops of the axle are removed in service.

A number of advantages have been gained from this integral air spring and valve construction. Several air seals are eliminated, simplifying the design of the valve and the connecting air lines. The valve operating linkage can be made relatively simple and light in weight since it is completely protected from exterior environment such as road splash, snow, and ice. The spring design can be set to length and checked as a complete subassembly prior to installation in the vehicle in a manner very similar to that for a conventional spring.

In addition to the plus features of having the air valve installed in the reservoir, as previously listed, the design is relatively simple to service. This has been accomplished by designing the valve so that it can be installed or removed through the mounting boss on the side of the air-spring assembly (Figs. 18 and 19).

A key in the mounting boss locates the valve to set the spring to design length. This service operation can be performed by merely disconnecting the leveling-valve lines, unscrewing the gland nut, and removing the complete valve assembly.

The high-pressure air reservoir has a volume of 360 cu in., and when fully charged operates at 250 psi. Enough energy is stored in this tank to quickly level a 5-passenger load, with the engine shut off. This tank is of welded construction and has a minimum burst pressure of 1000 psi.

It was early realized that making the air suspension leak free was one of our most immediate problems. As a result, a modified rubber O-ring-type fitting was developed for use in all connections.

Compressor

The engine-driven air compressor is designed for high production. It has a steel liner in a die-cast

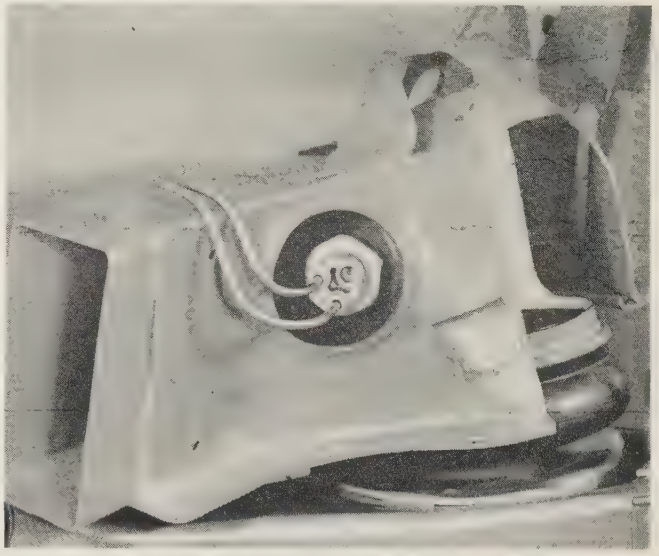

Fig. 19—Location of removable leveling valve

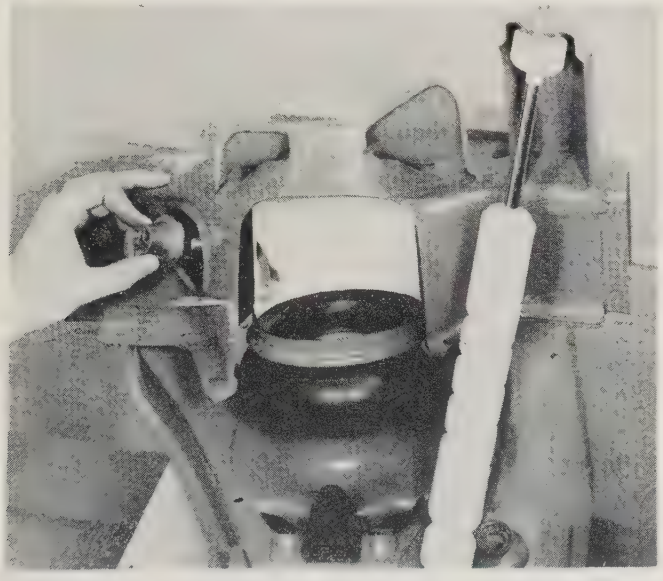

Fig. 18—Leveling valve being removed for servicing

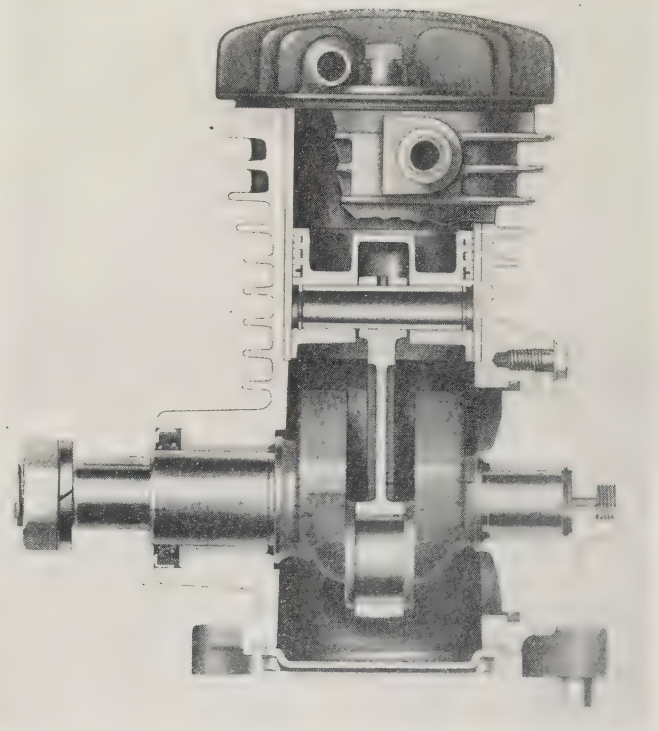

Fig. 20—Air compressor

aluminum cylinder block, and a die-cast head. The intake valve is a reed valve, and the exhaust valve is a disc-type poppet. This construction eliminates the valve plate normally used in reed-valve compressors. One advantage of this arrangement is a cooler exhaust valve because the heat in the plate does not have to pass through a gasketed surface to be dissipated by the fins of the head (Fig. 20).

Leveling Operation

The rate of air circulation in the system is controlled by the sizes of the orifices in the leveling valves. The orifices, in turn, control the rate at which the suspension will level when taking on or discharging a load. Selection of orifice size then, becomes dependent upon a compromise between a satisfactory leveling time and a practical compressor size. Experimentally we determined that if the car would level a 5-passenger load in approximately 10 sec, that elapsed time for leveling would be most satisfactory. For simplicity, we felt a single-cylinder design compressor was desirable. The practical size of the compressor is limited by two factors: vibrational disturbances, due to inherent mechanical imbalance, must be kept down to an acceptable level; and a simple belt drive must be capable of starting the compressor under high torque without slip.

A diagram of compressor performance at altitude, as related to airflow in cu in. per min, is shown in Fig. 21. It shows, as may be expected, that the most severe operating condition for the air-suspension system is at high altitude. This is due to the decrease in volumetric efficiency of the compressor as altitude increases. Taking 180 psi for a reference line, since that is the minimum pressure required for the system, it will be noted that compressor output falls off from 2000 cu in. per min at slightly above sea level, to about 750 cu in. at 11,750 ft. This reflects about 62% reduction in compressor output in comparison to operation at sea level.

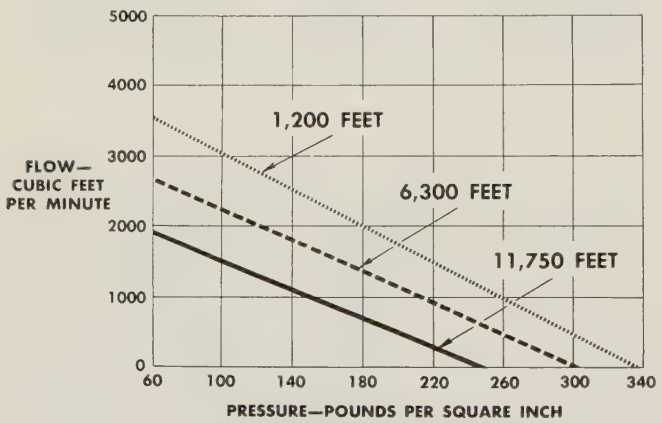

Fig. 21—Compressor performance at altitude

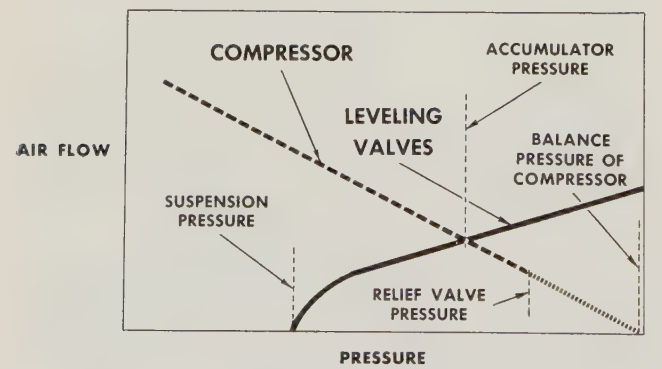

Fig. 22—Air consumption versus compressor capacity

Our experimental development program for setting up specifications for the compressor took place in Leadville and Cripple Creek, Colo., which are at approximately 10,000-ft elevation. Ample provision was made for adequate performance at the top of Pike's Peak, which is 14,000 ft above sea level.

The first requirement of the air compressor is that it have enough pumping capacity to operate the system without loss of system air to atmosphere under severe cornering and rough road operation. This requirement is shown by a curve of leveling-valve air requirements versus compressor capacity (Fig. 22). The intersection of these two curves represents the system pressure which can be maintained under the speed conditions plotted.

One of the design requirements of the air suspension is that there should always be enough air stored in the high-pressure reservoir to level a 5-passenger load. This requires a minimum pressure of 180 psi. After leveling a load, the compressor must have ample capacity both to maintain the rate of air circulation and to take in air from atmosphere to recharge the reservoir.

It was felt that if the compressor could recharge the reservoir in 5 min while the vehicle was being driven over a very rough road, its capacity would be ample. The air system would then satisfactorily handle a frequency of loading of five passengers every 5 min at extreme altitudes.

If the frequency of loading were greater than five passengers every 5 min the results would not be disastrous. For instance, assume that five passengers were loaded with suspension pressure only in the reservoir. Since the compressor is required to pump only to 100 psi to supply air to the springs at any given speed, its rate of flow is approximately doubled (Fig. 22). Furthermore, since the suspension under this condition is low, it is not exhausting air into the exhaust lines. The compressor will take in air continuously, and the suspension will level in a very short time. To achieve those results the required capacity of the air compressor was determined by a test of the complete system under the most extreme conditions.

The Trans-Canada Highway, between Port Arthur and Toronto, was one of the roads used for testing the air-suspension system. Temperatures which dropped as low as −30 F indicated a need for preventing icing of moisture introduced with make-up air. The addition of a simple alcohol evaporator at the air intake has provided the needed protection.

Conclusion

In its development, the Chevrolet air-suspension system was thoroughly tested at the General Motors proving ground, in our engineering laboratory, on roads from northern Canada to Florida, and in the mountainous country of the western states.

Air suspension is probably the greatest advancement in passenger-car springing to be introduced in recent years. It is a novelty to the motoring public but has tremendous pontential. We are convinced air suspension is here to stay.

OLDSMOBILE NEW-MATIC RIDE

R. W. Perkins, General Motors Corp

This paper was presented at the SAE Annual Meeting, Detroit, Jan. 14, 1958.

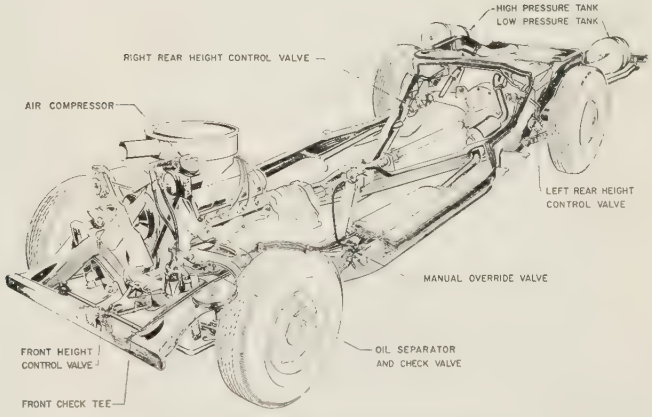

Fig. 1—Oldsmobile New-Matic Ride.

MANY months of testing in all parts of the country were necessary to develop and perfect the Oldsmobile air suspension system, New-Matic Ride.

In New-Matic Ride, where steel springs are replaced by springs operating on compressed air, we are able to produce a more pleasing ride with slower body swing motions, less tendency for pitch, and more nearly constant static deflection regardless of load in the vehicle, all of which greatly enhance passenger comfort. Cars equipped with New-Matic Ride are better able to carry heavy passenger and luggage loads without the problem of excessive "pound-through," yet without load it is the same height as when fully loaded. Air suspension with its variable rate springs and constant height control make this possible.

Components of System

The New-Matic Ride chassis (Fig. 1) includes in addition to a new frame (not interchangeable with that used on steel-spring cars), the following major components in the suspension system:

1. Four-link rear suspension.
2. Diaphragm-type air springs.
3. Height-control valves.
4. Air compressor, mounted integrally with the power-steering pump.
5. Oil and moisture separator.
6. High-pressure tank of extra large volume.
7. Low-pressure tank.
8. Pressure regulator and elevator valve unit.
9. Copper air lines throughout the system.

A rubber insulated 4-link suspension (Fig. 2) is used at the rear to hold the rear axle in position, a function normally performed by rear leaf springs. The rear air springs are mounted on the axle housing independent of the suspension links and are in this manner used solely to control ride. The upper suspension links are diagonally mounted to provide lateral control of the axle; together with the lower links they absorb drive and braking torque and control fore-and-aft motions. The lower links are adjustable to permit optimum setting of the differential pinion angle. The 4-link suspension provides a high rear roll center and is designed to minimize rear "squat" and brake lift.

The diaphragm-type air springs are designed to operate at 100 psi. While the basic design is the same front and rear, the configuration is necessarily different to suit space limitations and to provide the necessary spring stroke. Spring volume at design height is 295 cu in. in front and 240 cu in. in the rear.

The springs have a variable rate as shown by the heavy line of the load-deflection curve (Fig. 3). In the normal ride range slow movements are possible because the air-spring rate is approximately 60% of the conventional steel spring, but as the wheel travels farther into compression and rebound the spring rapidly builds up rate to absorb the energy created by severe bumps or dips in the road. Thus, greater passenger comfort is provided.

In the diaphragm-type spring, rate is a function of effective area and is controlled by mechanically guiding the diaphragm between the lower ring of the air-chamber assembly and the piston (Fig. 4). The letters A, B, and C represent the spring in its normal position, full-compression and full-rebound positions, and the change of effective areas which determine the rate characteristics of the spring.

Three height-control valves maintain the car at constant trim height regardless of passenger load. Two valves are used at the rear, one located near each rear spring, with the actuating arm connected to the suspension by a short rubber-insulated link (Fig. 5). Rear height adjustment is made by turning an eccentric in the actuating arm. One valve, centrally mounted at the front of the chassis (Fig. 6), is actuated by a linkage arrangement from the front stabilizer bar. This linkage also has the eccentric design for height adjustment. Small orifices in each valve restrict the flow of air to and from the springs, thereby permitting the inlet and exhaust valves to function without a delay mechanism or "dashpot" effect.

A check valve tee (Fig. 7) is used in conjunction

with the single front height valve that controls the two front springs. The check tee permits full flow of intake air to the springs as the ball checks move from their seats; however, exhaust air from the springs must pass through small orifices in the ball check seats. This feature prevents free flow of air from spring to spring which would be detrimental to car handling, but does provide a restricted intercommunication between front springs to enable them to equalize in pressures in a short time.

The air compressor is a 2-cyl V-block design having a displacement of 5 cu in. It is driven from the engine with a pair of matched belts; and the compressor crankshaft end is extended to the rear to drive the power-steering pump rotor. A lubrication pump is incorporated into the design, its oil coming from the power-steering pump reservoir (Fig. 8).

The oil and moisture separator (Fig. 9) is mounted on the chassis below the compressor, and connected to it by flexible high- and low-pressure hoses. All other pipes and tanks are chassis mounted, the high- and low-pressure system pipes originating at the separator assembly. This unit contains a high-pressure check valve and low-pressure cutoff valve designed to prevent loss of air back through the compressor when the engine is not running. The flexible high- and low-pressure hoses may be disconnected if necessary while performing service work on the engine without losing air from the system.

High-pressure air from the compressor flows into the separator past the high-pressure check valve, through the filter bowl and filter where oil particles and moisture are removed before passing on to the high-pressure storage tank.

Additional features of this unit are the low-pressure system blow-off valve, and filtering valve at the fresh-air intake port. A sediment drain at the bottom of the separator bowl provides for ease in servicing this unit.

An extra large high-pressure tank is mounted on the right rear of the chassis. Its function is to store the filtered air from the compressor until needed by the height-control system to maintain car standing height. A tire valve fitting is located at the rear of the tank (Fig. 10) to permit recharging of air in the system and pressure checking in service. This tire valve also connects to a rubber hose inside the tank which acts as a siphon to drain off any moisture that may collect in the high-pressure tank.

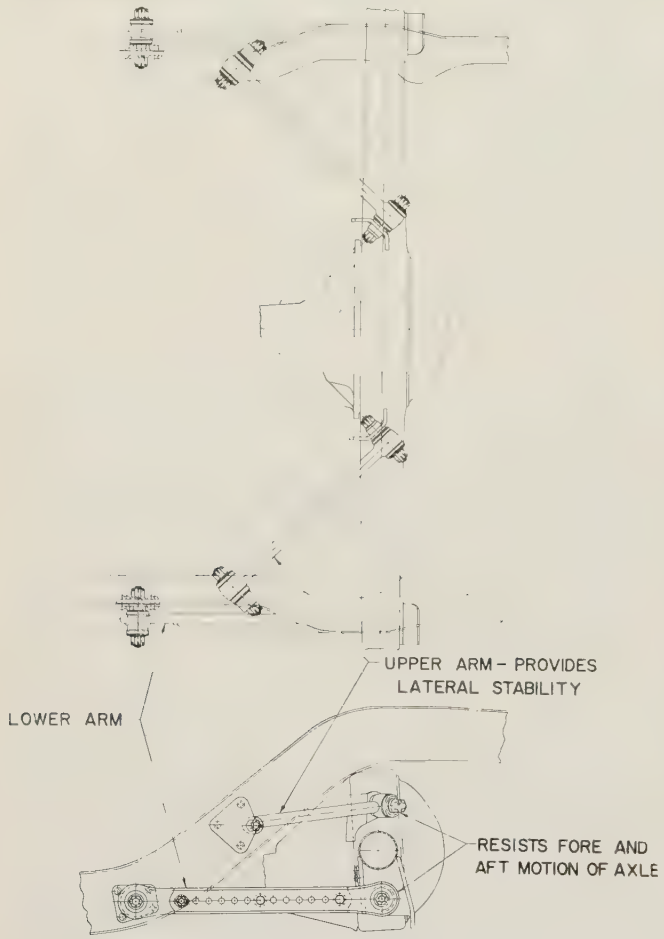

Fig. 2—Four-link suspension.

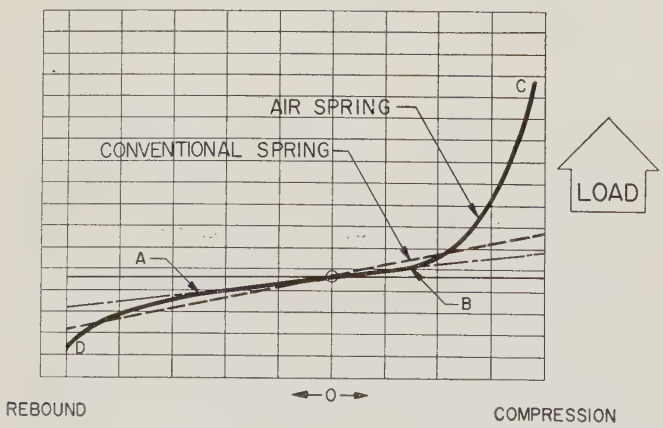

Fig. 3—Load-deflection curve.

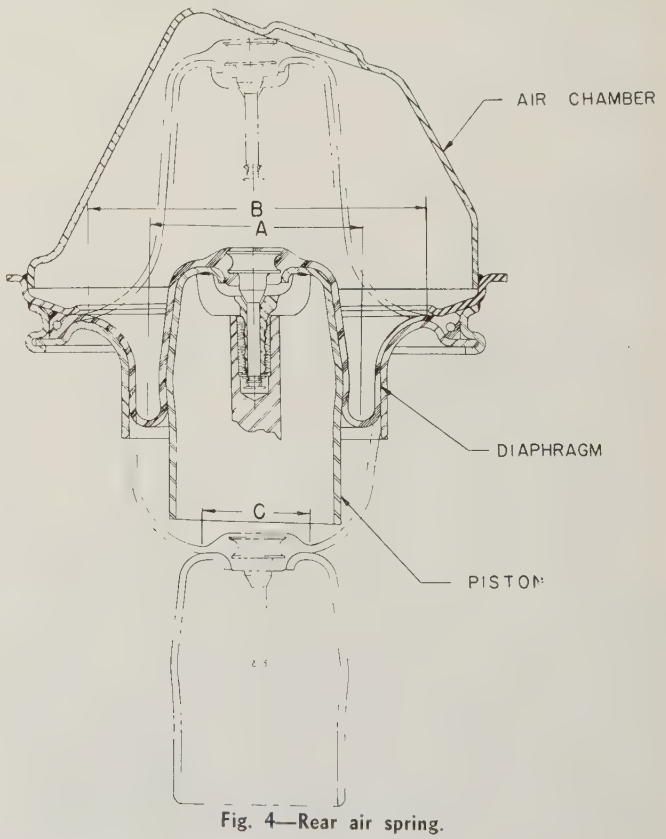

Fig. 4—Rear air spring.

The closed system has a low-pressure tank which collects air exhausted from the springs and stores it for re-use in the high-pressure system. This minimizes the need for fresh-air make-up in the system and, consequently, reduces liability of contamination from moisture and dust. Maximum pressure in the low-pressure system is limited to 70 psi by the blow-off valve in the oil separator.

Protection against overinflation of the air-spring assemblies is assured by limiting the high pressure to 150 psi through the pressure regulator valve in the elevator valve assembly.

The elevator valve assembly provides a manual control that allows the driver to raise the car approximately 4 in. higher than normal if this should become necessary to clear steep ramps or difficult driveway approaches. The elevator lever on the instrument panel must be held out to maintain this 4-in. elevation; and as soon as it is released, the car automatically returns to normal height.

All air pipes in the system are made of copper for maximum rust protection. Fittings are sealed in rubber to prevent leaks from shock and vibration.

Performance

When air suspension became a production possibility, our engineering management set up several requirements as to performance of the system, its durability, and ease of manufacture and assembly.

Realizing that high-pressure air is difficult to seal, the first goal was to produce a leak-free air-suspension system that would maintain the car at its design height over long periods of time. It was felt that the average passenger-car owner would not tolerate a system that fell short of the performance of the conventionally sprung car.

Secondly, the control system would have to perform satisfactorily under all conditions of temperature, altitude, and humidity, and must never be

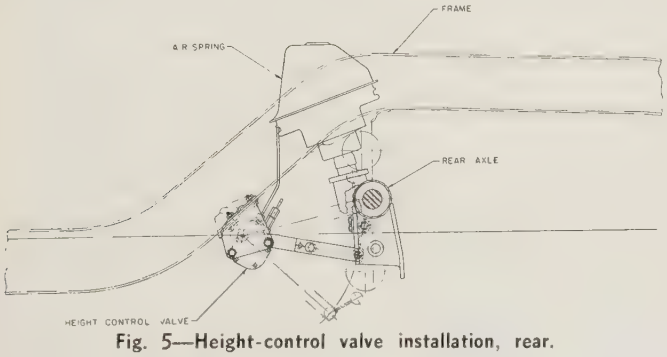

Fig. 5—Height-control valve installation, rear.

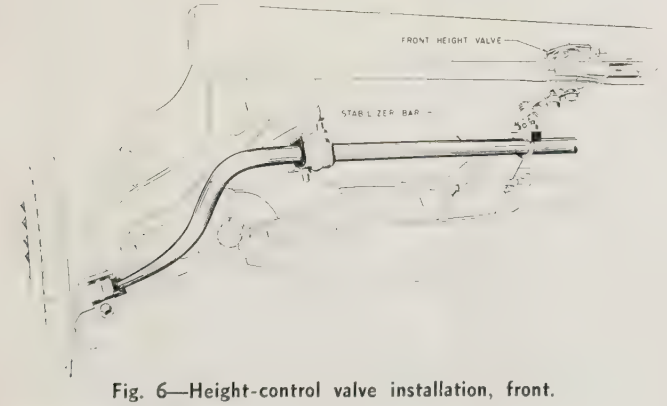

Fig. 6—Height-control valve installation, front.

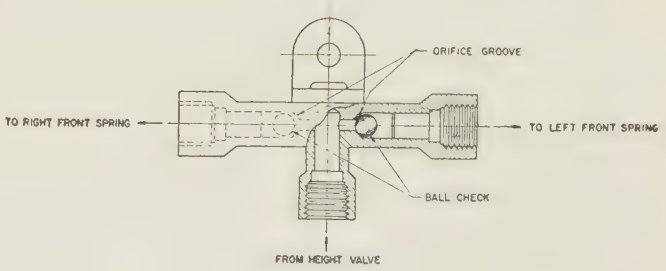

Fig. 7—Front check tee.

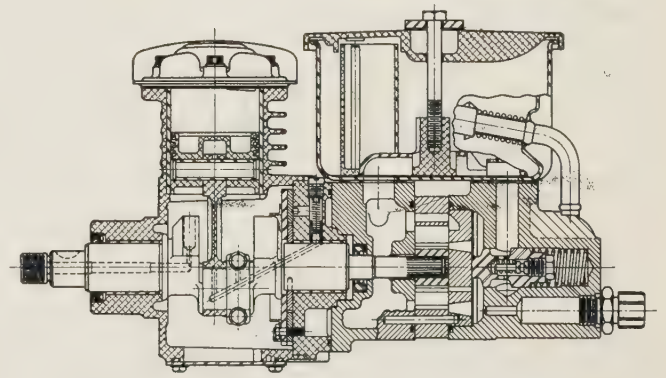

Fig 8—Air compressor assembly.

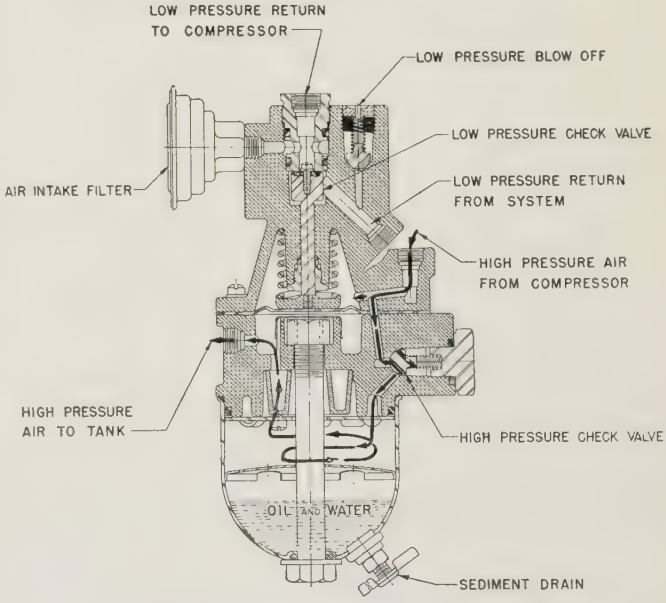

Fig. 9—Oil separator and check valve assembly.

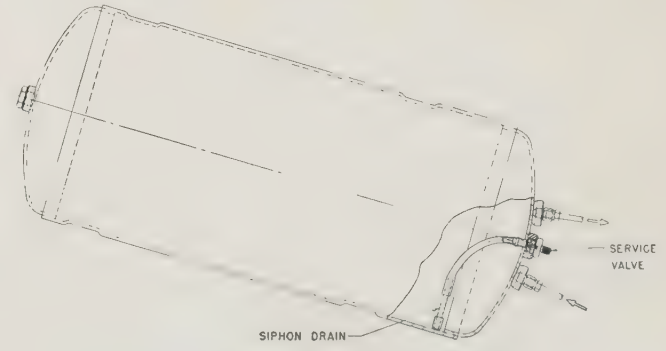

Fig. 10—High-pressure tank assembly.

"tricked" by unusual conditions of road or loading.

Durability of the air springs should be equivalent to or better than the life expected from leaf springs. Spring assemblies, storage tanks, and other components of the system should be given maximum anti-rust protection to insure long life.

Design of the suspension components had to be such that the parts could be easily manufactured, would be practical to assemble on an assembly line and would be easy to service.

To make the car sustain itself over long periods of time even though the engine was not started to replenish the high-pressure air, it was decided to use an extra large high-pressure tank to store potential energy to overcome the effect of small air leaks and of repeated temperature drop night after night. In addition, a maximum allowable leak rate was established at 4 cu in. of free air per hr for any component of the system. Theoretically, this meant that the car would sustain itself for over three weeks without compressor assist.

During early testing of air springs, the most frequent problem was air loss, either at the spring or in the numerous connections of the pipe system.

Self-sealing type diaphragms were found to give inconsistent sealing results from day to day, to be somewhat sensitive to cold temperatures, and to require extra smooth metal surfaces. It was found that the bead seal was easily broken and required extreme care on installation to assure a leak-free spring. To overcome these difficulties, the spring tank and diaphragm assembly was designed so that it would withstand all normal pressures without the support of the piston (Fig. 11). The center bead area was closed in and the outer bead designed to seal by rubber compression. The spring-tank assembly forms half of the outer bead seat; the crimped ring positions the lower diaphragm retainer, forming the other half. When these parts are assembled in place, the outer bead area is compressed into a positive seal. Ordinary tire-bead lubricant is applied to the outer bead area before assembly to allow the rubber to flow into the cavity during compression.

Double-flared compression-type pipe fittings leaked high-pressure air during tests and occasionally had to be re-tightened. Flaws or scores in the flared pipe ends were a source of leaks. Also, the problem of cross-threading fittings was ever present, so this type of air connection was discarded for production use. Our engineers designed a new type fitting (Fig. 12) using a rectangular section "O" ring on the end of a beaded tube with a cavity in the fitting to receive it. Internal air pressure on the ring makes the seal more positive. Engagement of the pipe end into the fitting is extra long, providing a long pilot to minimize cross-threading.

Numerous height-control systems were tested; lock-out systems, electrical controls, 2-speed levelizing, electrical and mechanical delay systems, and several others. These were all finally abandoned in favor of a simple nondelay mechanical height system. At first, there was the mistaken idea that a car should adjust itself for height in 3–4 sec; however, it was later proved that the best was a slower rate of levelizing and a system that could levelize at any time required. Systems having instantaneous leveling action could be "tricked" more easily, and were more sensitive to deceleration and acceleration motions of the car. Three height-control valves, two in the rear and one in front, gave the most satisfactory action. The front valve, being mounted at the center of the car, ignores body roll motions and does not tend to change car height when cornering. The two rear valves quickly sense changes in passenger load distribution and make prompt height correction. Because passenger load has a greater weight effect on the rear axle and very little effect on front weight, it was decided to control the two front springs through a single line and height valve arrangement to make the car levelize more evenly front to rear.

Testing of experimental models revealed that moisture and contamination of the system were serious problems if the cars were to operate under all conditions of temperature and humidity. A closed system having capacity to collect air exhausted from the springs and to store it for re-use in the system appeared to be a partial solution. Later, it was decided to add the oil and moisture separator with a low-pressure system check valve and blow-off designed into it. As a further means of protection against moisture getting into the height-control valves, a siphon-type drain was added to the high-pressure tank.

Copper air lines were released for production for positive insurance against rust. Steel pipes with different types of coating all showed signs of rust in a relatively short time.

The air-spring tanks, and high- and low-pressure tanks are coated with a special zinc chromate paint. The air-spring pistons (Fig. 13) and lower diaphragm retainer rings are cadmium plated. All internal parts of functional units, such as separator and height valves, are of noncorrosive materials or are plated.

As more experience was gained with air-suspension cars, it became apparent that there were more items that might prove troublesome on a car in ordinary use. Since the air springs normally exhaust air when a car is jacked for tire changing, towing, or ordinary maintenance service, there was a possibility of the air-spring diaphragms and pistons becoming unstable when spring pressures were near zero. Therefore, designs were modified to secure the spring parts together to prevent misalignment of parts when a car was lowered from a hoist or jack (Fig. 14).

The suspension system was designed to mount completely on the chassis with no connections to the body or front sheet metal. The oil separator unit is the origin of all pipes; thus, having high- and low-pressure check valves integrally designed into this unit meant that the complete buildup and leak checking procedure could be made in a separate area or on the main car assembly lines. It was decided to schedule and build air-suspension cars on the main assembly line to avoid double operations.

Provisions were made for complete leak and functional tests of each component and subassembly prior to installation on the chassis. Dirt plugs were specified for all pipes and units. Special equipment was designed to check the operational characteristics of functional units of the system.

Air-spring diaphragms are checked for rate on a special test machine before being assembled and

crimped into a spring tank. Completed spring assemblies are also checked in the same equipment. This test fixture oscillates the spring piston at its natural frequency by applying a load on the free ram equal to the design load of the spring, after pressure and height of the piston have been adjusted to design conditions. Load versus deflection is read on an oscilloscope and travel of the pip is observed in relation to the rate slope lines on an overlay chart.

Leak testing of subassemblies for external leaks is accomplished mainly by the fixture-cavitation method whereby the part to be tested is totally enclosed within a cavity having approximately ⅛–¼ in. clearance between girth of part and cavity volume. The part being tested is pressurized with an air and nitrous oxide mixture and a stream of air is drawn from the cavity past the part into a nitrous oxide analyzing unit. Should a leak occur, the presence of nitrous oxide is quickly detected. Each testing unit is calibrated to detect the maximum allowable leak rate.

Methods engineers devised a unique method of subassembling the pipe system, valves, junction blocks, and allied brackets. These parts are assembled on jigs which clamp units in their proper location with respect to each other so that pipes can be applied and fittings tightened. Cross-threading and pipe damage are practically eliminated by this method. The jig, with its harness-like subassembly of pipes and units, is then lowered onto the chassis frame at the beginning to the assembly line. Clamps on the jig are released and the transfer of this assembly to the frame is made with all parts fitting into their proper location.

The spring assemblies and pressure tanks are mounted on the frame and air pipes to these units are connected. Then, the system is pressurized to 30 psi with a mixture of air and nitrous oxide.

Leak test is performed using nitrous oxide analyzer and probe. Each fitting in the system is individually checked.

Car height is preset on the assembly line:

1. A pointer on each height valve, previously assembled during checking operations, marks the position of neutral.
2. Rear axle assembly is clamped to its proper height.
3. Height valve links are assembled to valve actuating arms, and by means of the eccentric adjustment the pointer is moved to indicate neutral.
4. Front height is set by the same method as the chassis passes over the caster and camber checking fixture, since at this station the front suspension is held at correct height.

Prior to body drop on the assembly line, the high-pressure tank is inflated to 250 psi through the tire-type valve in rear of tank. The elevator valve is blocked open and body installation accomplished with the chassis in the elevated position.

Other assembly operations are similar to those for standard cars.

During final checking operations, the drive shaft angle to differential pinion is gaged and adjusted if necessary by moving the adjustable rear suspension lower arms.

Every feature of the New-Matic Ride system has a definite purpose, all found necessary during an extended test period of over two years.

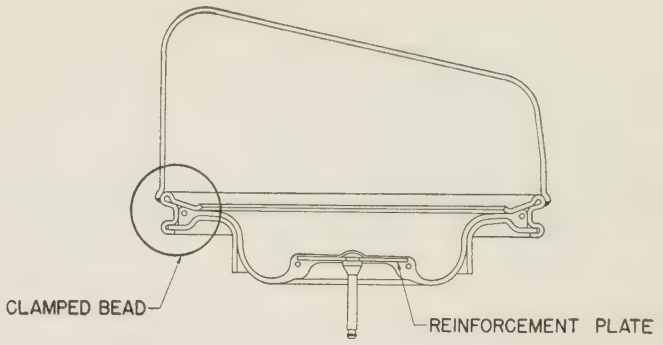

Fig. 11—Spring tank and diaphragm assembly.

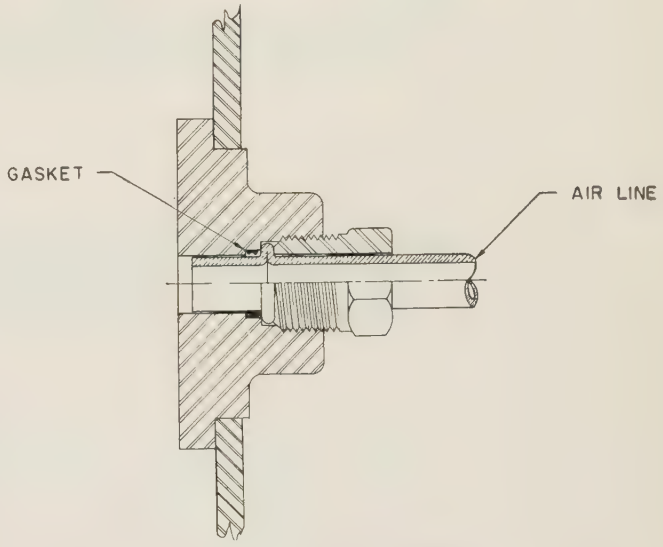

Fig. 12—Air line connection.

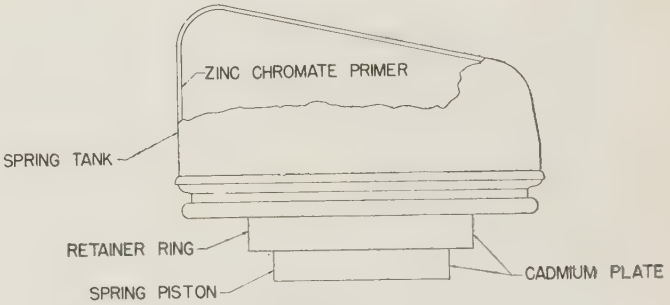

Fig. 13—Air-spring piston.

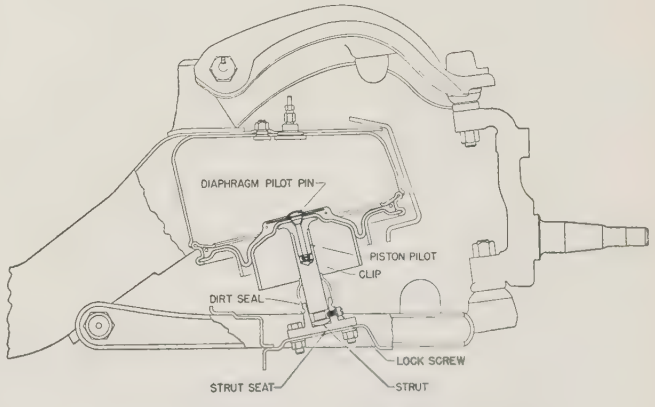

Fig. 14—New-Matic front suspension installation.

Requirements, Parameters, and Design PNEUMATIC INLET

CORRECT matching of inlet ductwork to jet engine demands and accurate control of variable inlet geometry are prime requirements for maximum thrust under all operating conditions. The first step is to design a variable inlet to meet changing speed, altitudes, airplane attitudes, and power requirements.

Efficient designs will have a large number of shock waves of equal strength to minimize the total pressure loss across the shocks. The geometry of the inlet, its boundary layer control, and bypassed air must be varied with changing flight conditions to meet the efficiency objective.

External shock inlets have simple internal flow patterns but can starve the engine if their shock pattern does not intersect the cowling. Internal shock inlets are not bothered with this problem but require careful compression surface control to prevent expelling the shock. The authors describe two methods of inlet controls, the closed-loop and scheduling types.

The authors of this paper were awarded the 1957 Manly Memorial Medal.

THE role of air-induction systems, or inlets, in the development and operation of aircraft with air-breathing engines is becoming more and more critical as we design for greater supersonic speeds. In the flight regime of Mach 2.0, poor management of air induction to the engines can result in decreases in net thrust up to 20% and increases in total aircraft drag up to 8%. Furthermore, the magnitude of these penalties increases with higher speeds. A rough indication and comparison of these values and trends is shown in Figs. 1 and 2 for three inlet systems which represent the range of effort which can be extended on inlet design and development. System A is an open inlet, commonly called a normal-shock inlet, which represents a minimum effort and a minimum performance system. System B is a reverse De Laval nozzle inlet with variable entrance and throat area which theoretically would give maximum performance. System C represents inlet systems which would give the inlet pressure recovery that has been proposed by the AIA (Aircraft Industries Association) as a standard. The corresponding total pressure recoveries and net thrust coefficients for a typical high-speed turbojet engine application are shown in the curves of Fig. 1. At a flight speed of Mach 3.0, a potential increase in net thrust of about 30% exists between the reverse De Laval nozzle inlet and an inlet system performing in accordance to the AIA standard. The shaded areas represent typical ranges of performance for future applications. The upper curves of

BENDIX AVIATION
CORPORATION
RESEARCH LABORATORIES
LIBRARY

Considerations for CONTROL SYSTEMS

R. E. Matzdorff and C. F. Newberry, Marquardt Aircraft Co.

This paper was presented at the SAE National Aeronautic Meeting, Los Angeles, Oct. 4, 1957.

Fig. 2 show the free-stream capture area required by the engine operating with the different inlet systems. The lower curves represent typical operational and installation drag that is chargeable to the different engine inlet installations. Again, an appreciable reduction in drag can be realized with advanced inlet designs. It is apparent then why increasing emphasis and effort are being made and must continue to be made in the design and development of air-induction systems.

The primary function of any inlet system is twofold: (1) the conversion of the supersonic velocity head of the air entering the inlet into subsonic flow with a maximum pressure energy and (2) the deflection or bypassing of the air not required by the propulsion system with a minimum drag penalty to the aircraft. The efficiency of the reduction in velocity is measured in terms of total pressure recovery. This is defined as the ratio of the total pressure of the flow at the engine face to that which is theoretically possible with an isentropic process. In addition, there are secondary items which re-

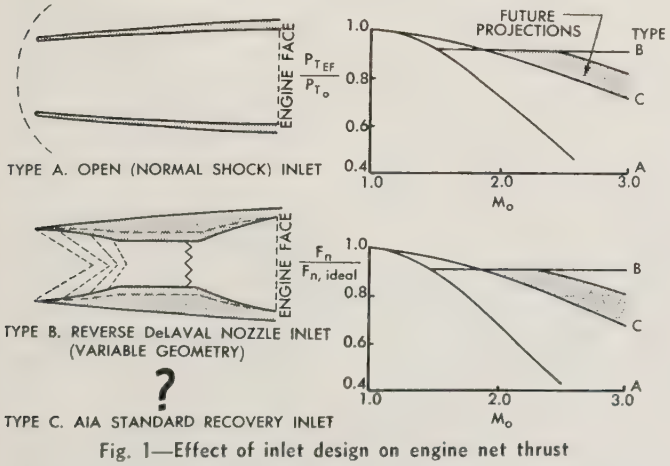

Fig. 1—Effect of inlet design on engine net thrust

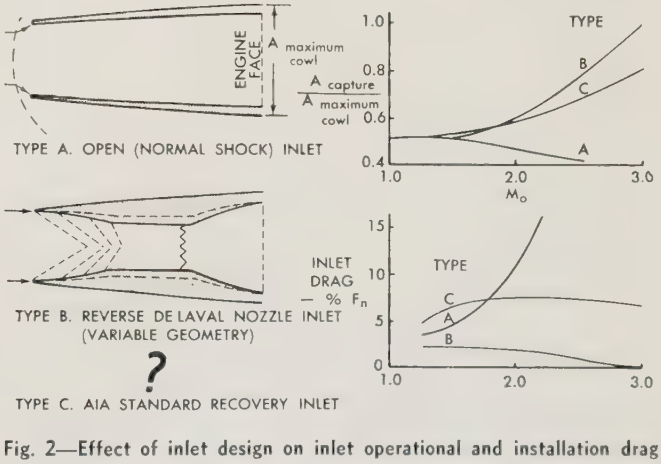

Fig. 2—Effect of inlet design on inlet operational and installation drag

quire consideration, such as velocity distribution at the engine face, stability of airflow, weight, and the like.

Types of Inlets—Inlet systems generally can be described as being one of two types, depending upon the method used in reducing the relative velocity of the captured air from supersonic to subsonic speed—external compression or internal compression.

The more familiar type is the external compression inlet wherein the reduction in velocity to subsonic values occurs before the air enters into the inlet. A reduction in the relative supersonic velocity takes place through one or more oblique shocks which are caused by deflection or compression surfaces extending ahead of the inlet entrance. Final reduction to subsonic velocity occurs through a normal shock at or near the inlet entrance. Fig. 3 shows schematics of three common types of external compression systems. Inlets A and B are known as one oblique and two oblique shock inlets. The fact to be remembered here is that the use of additional oblique shocks allows smaller reductions in velocity across each shock. This results in a more efficient conversion of the velocity head to pressure head. Inlet C is called an isentropic system because the solid field of infinitesimal shock waves theoretically reduces the flow velocity with a 100% efficiency.

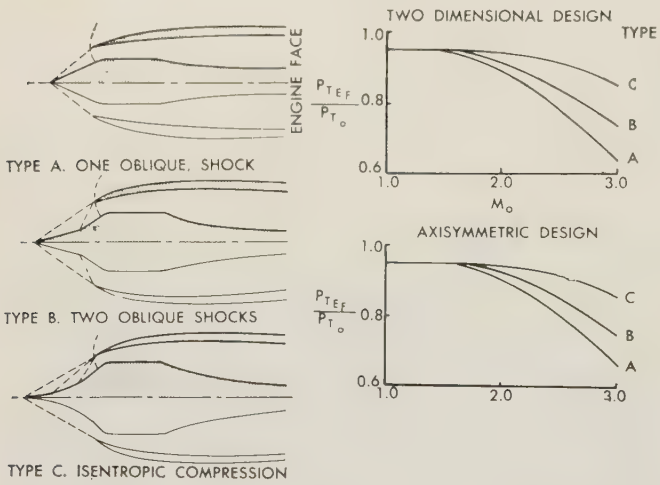

Fig. 3—Comparison of external compression inlets (variable geometry)

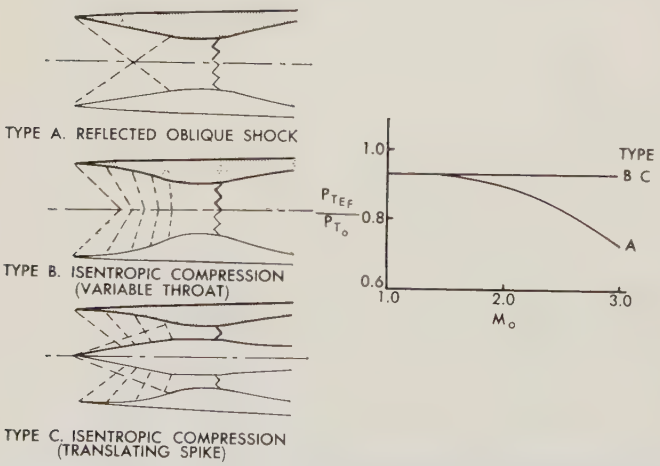

Fig. 4—Comparison of internal compression inlets (variable geometry)

Unfortunately, the more efficient shock systems require higher initial slopes on the external cowl surfaces which produce drag increases to nullify some of the gain in engine thrust achieved with the increased pressure recovery. This factor plus machanical design complexities and complications in preventing the boundary layer from separating on the compression surfaces has caused inlet designers to use one or two oblique shock compression systems in current applications.

The second type of inlet system is the internal compression inlet wherein the reduction of the relative velocity of the captured air occurs after the air has entered the inlet. The internal surfaces of the inlet cowl serve as compression surfaces to generate finite oblique shocks or isentropic compression waves. Fig. 4 shows schematics of three possible systems. It will be noted that the final step in reduction of the supersonic flow to subsonic flow occurs through a normal shock downstream of a minimum area. Nature does not permit a normal shock to exist in the converging section of the inlet. The shallow initial external cowl slope, which is inherent with this inlet system, creates a negligible cowl pressure drag. This offers a large advantage over the external compression system. In addition, the efficiency of the conversion of the velocity energy to pressure energy is potentially greater, especially for the flight speeds of the future. Conversely, the operational problems of the internal compression inlets are much more severe. Considerable difficulty is encountered in keeping an attached boundary layer in the presence of the rapid

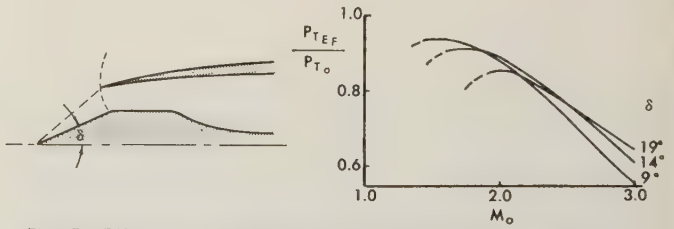

Fig. 5—Effect of compression surface angle on pressure recovery

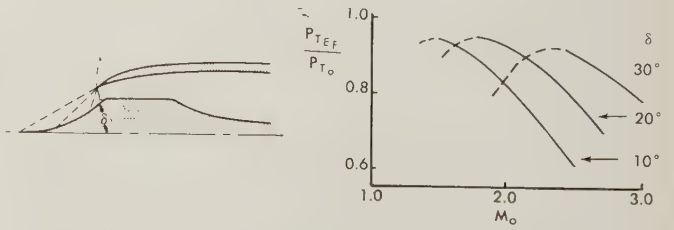

Fig. 6—Effect of total turning angle on pressure recovery

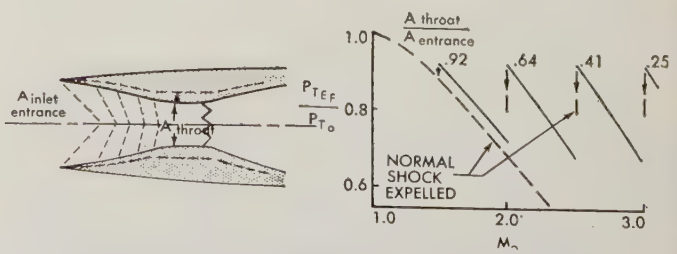

Fig. 7—Effect of contraction ratio on pressure recovery

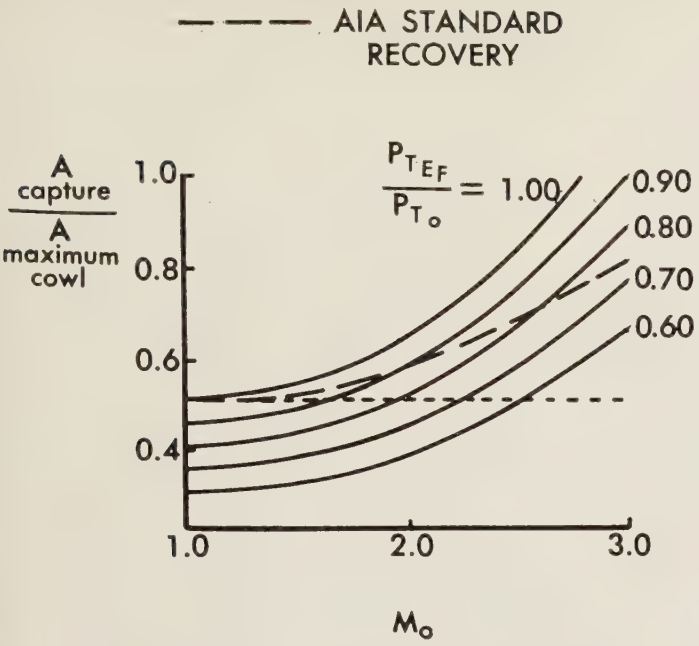

Fig. 8—Effect of pressure recovery on required engine airflow

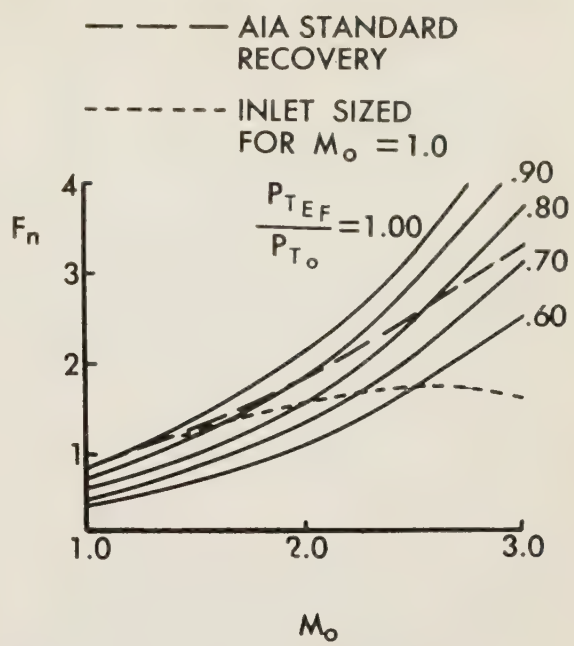

Fig. 9—Effect of pressure recovery on engine net thrust

pressure rise and shock interactions. The efficiency suffers badly with increasing angle of attack. Large and rapid variations in the physical geometry are necessary for establishing and maintaining the desired internal flow pattern throughout present-day flight profiles. Because of these operational problems, the aircraft designer has been hesitant to consider the internal compression inlets.

It is reasonable to suspect that some sort of hybrid inlet design may well provide the optimum system by incorporating both external and internal compression features. The foregoing discussion is applicable for our purposes to inlet systems using two or three dimensional compression surfaces and flow fields.

Factors Affecting Inlet Pressure Recovery—It was stated previously that the pressure recovery obtained from an inlet system was proportional to the number of shock waves used in decelerating the flow. This was only part of the truth for obtaining maximum efficiency. A further requirement is that the strength of the shock waves be controlled so that equal total pressure loss occurs across each shock wave. The strength of any shock wave is a funtion of the flow deflection angle determined by the compression surface from which the shock originates. Hence, the deflection angle should increase with increasing flight speed so that the strength of each shock may increase uniformly and, therefore, maintain maximum pressure recovery. Fig. 5 shows the variation of pressure recovery with Mach number for several fixed angles of the ramp or wedge with one oblique shock system. The advantage of a variable ramp angle is obvious, since the pressure recovery for a fixed angle falls off very rapidly from the design Mach number. This trend is similar for the two or three oblique shock system.

For a somewhat different reason, the external isentropic compression inlet also requires a variation of the compression surface, since there are no finite oblique shocks. The reduction of velocity along an isentropic surface is a function of the total turning angle. If the flow is to be reduced to the same Mach number prior to the normal shock at the inlet entrance, the higher flight Mach numbers will require greater turning angles. Fig. 6 shows theoretical pressure recoveries for several inlets with compression surfaces of different total turning angles. There are several factors that limit the total allowable turning angle. Their explanation, however, is outside the realm of this paper.[1] The effect of exceeding the allowable turning angle is to cause a normal shock to move forward into the network of compression waves. This substantially reduces the inlet efficiency. This condition is shown on the curves by the dashed lines.

In summary, large engine thrust losses will result at off-design Mach numbers with fixed compression surfaces because of the reduced total pressure recovery. The first advantage of variable compression surfaces for external compression inlets is apparent.

The pressure recovery of internal compression inlets is primarily a function of the Mach number at the inlet throat. The closer the throat Mach number is to one, the better the pressure recovery will be. A practical value of minimum throat Mach number is dependent upon various empirical factors. For example, if proper boundary layer removal is employed, a value of 1.35 may be obtained. Any attempt to reduce the throat Mach number below the minimum value will result in breakdown of the supersonic flow into the inlet and the inlet will operate as a normal shock inlet. A reduction in flow area is necessary to reduce the velocity of captured air to a desired throat Mach number. This required reduction in flow area, however, must increase with higher flight speeds if the throat Mach number is to be kept constant. Fig. 7 shows the

[1] For further information see NACA TN 3589, January, 1956; "Design Criteria for Axisymmetric Inlets and Exits," by J. F. Connors and R. C. Meyer.

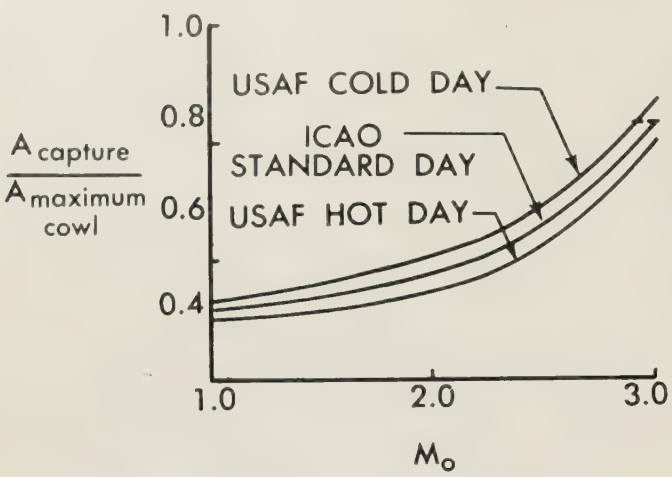

Fig. 10—Effect of nonstandard atmospheric temperature on desired engine airflow. Assumptions: AIA standard recovery, 45,000 ft altitude, inlet sized for standard day at $M_o = 3.0$

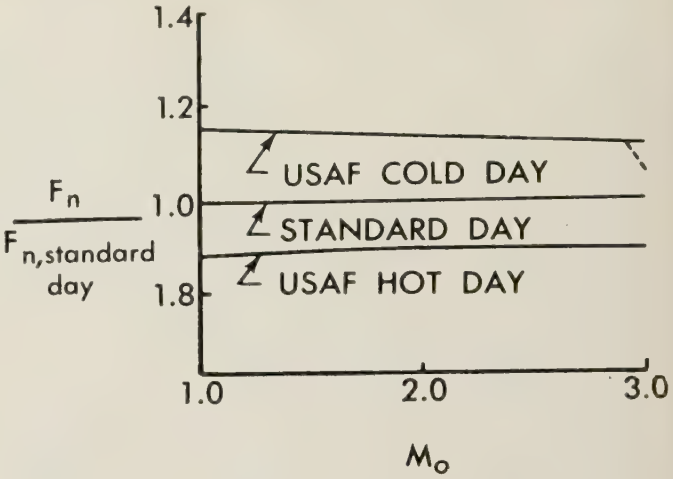

Fig. 11—Effect of nonstandard atmospheric temperature on engine net thrust. Assumptions: Same as Fig. 10

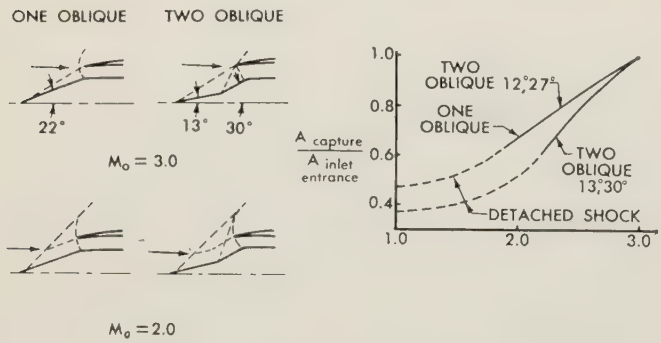

Fig. 12—Capture area characteristics of fixed inlets

variation of pressure recovery with flight Mach number for inlets with fixed area contractions. In computing these curves, the normal shock location was assumed at the throat and the minimum obtainable throat Mach number was set at 1.35.

A study of these curves shows that excellent pressure recoveries are theoretically obtainable for the design Mach number and also for associated off-design Mach numbers with this type inlet when variable area contraction is used.

Matching of Airflows Between Inlets and Engines —We will first review some typical characteristics of a turbojet engine so that we may study the problem of designing and operating an inlet system with a turbojet engine. The designer must optimize the complete propulsion system for high performance throughout the flight envelope. We will assume a maximum flight speed of Mach 3.0. Fig. 8 shows the effect of the inlet efficiency on the air consumption of the engine. It will be noted that the captured tube area increases with Mach number and with pressure recovery. The long dashed line represents the AIA standard pressure recovery. Assuming that the inlet produces this pressure recovery, the inlet entrance area would be sized for the Mach 3 condition where the capture area is the greatest. Then, at lower speeds this would require some sort of deflecting or bypassing of the surplus air which will be contained in the stream tube approaching the inlet opening. This requirement will be discussed later. Fig. 9 shows the effect of the inlet efficiency on the net thrust of the engine. Here again, the thrust increases with the Mach number and with pressure recovery. The long dashed line represents performance corresponding to the AIA standard pressure recovery. Referring again to Fig. 8, let us assume that the inlet opening was sized on the AIA recovery curve at Mach number of 1.0. Then, at the higher flight speeds, the engine would not receive the amount of airflow that it is capable of consuming. This "starving" of the engine forces additional losses to occur within the inlet so that the inlet efficiency is reduced. The short dashed line on Fig. 9 shows the resulting effect on thrust with a substantial penalty occurring at the maximum Mach number.

A second factor affecting the airflow consumption of the engine is the atmospheric temperature. Figs. 10 and 11 compare this effect for Air Force hot days and cold days with ICAO standard days. The AIA pressure recovery has been assumed for this comparison. If the inlet opening is sized for the standard-day operation at Mach 3.0, the inlet will starve the engine during cold-day operation, reducing the thrust as shown by the dotted line in Fig. 11. In addition, operation on a hot day requires less captured air with the attending problem of deflecting or bypassing greater amounts of air in the stream tube approaching the inlet.

In conclusion, the free-stream tube of air consumed by a typical turbojet engine at normal operating conditions varies as a function of free-stream Mach number, atmospheric temperature, and inlet recovery. In passing, recognition must be made of the fact that captured air is also affected by reduced engine speed. Also, the angle of attack and yaw condition of the aircraft may change the pressure recovery of the inlet. To a general degree,

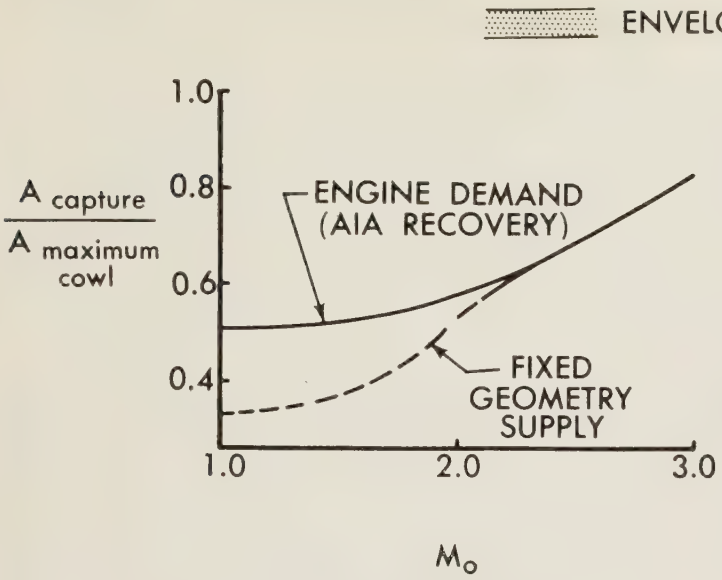

Fig. 13A—Mismatch of airflow characteristics of engine and fixed geometry inlet sized for maximum flight speed

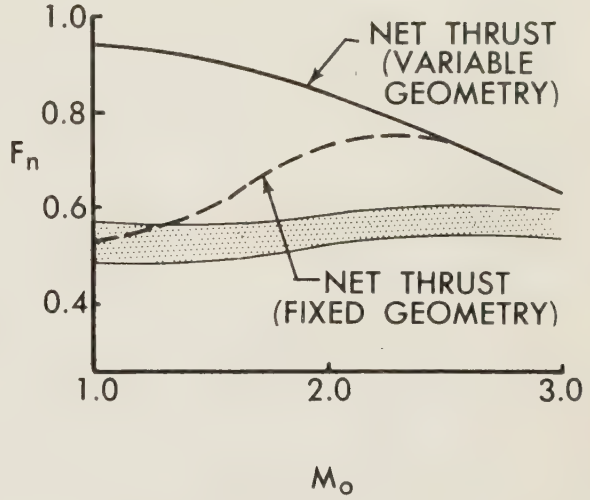

Fig. 13B—Effect of mismatch on engine thrust

other engines such as the ramjet, ducted fan, turbo-rocket jets, and the like, exhibit the same characteristics as the turbojet.

The angle of an oblique shock generated from a deflection or compression surface steepens as the approach Mach number decreases. Fig. 12 illustrates this fact for two fixed geometry external compression inlets at different Mach numbers. Since the airflow is turned outward when passing through the oblique shocks, spillage or deflection of the airflow will occur for those cases where the oblique shocks do not fall on or within the inlet cowl leading edge. Thus, the maximum free-stream tube of air that can be captured by fixed geometry inlets will decrease with decreasing Mach number. The curves in Fig. 12 show the ratio of this maximum capture area to the projected inlet entrance frontal area for several fixed geometry inlets. The capture area characteristics of an inlet with a single 22-deg compression surface and an inlet with double compression surfaces of 12 and 27 deg are nearly identical and are shown as a single curve. These curves show the large decrease in capture with decreasing Mach number that is inherent with fixed geometry inlets and, as will be shown later, produces a mismatch with required engine airflows. The "intercept" Mach number, which is the flight velocity at which the oblique shocks intercept the inlet cowl lip, is controlled by the compression surface angles and their axial location with respect to inlet entrance.

The free-stream tube of air captured by an internal compression inlet necessarily must always be the maximum when the inlet is operating properly, since the flow enters the inlet at free-stream velocity. The transient and steady state behavior of this type of inlet is complex when supersonic flow has not been established in the converging part of the duct. A complete discussion of this condition is available in several textbooks and reports.[2,3,4,5] The important point to be made here is that severe penalties in thrust and drag will exist if the internal compression inlet is not capturing the maximum air tube.

Now that the basic airflow characterisitcs of jet engines and fixed geometry inlets have been reviewed, a brief study will be made of their combined operation. Fig. 13A presents a comparison of the airflow characteristics of an engine and a two oblique shock inlet with 12- and 27-deg compression surfaces to be operated at a maximum Mach number of 3.0. The inlet is sized so that it delivers the airflow required by the engine at Mach 3.0. Therefore, it will not supply the necessary airflow at lower Mach numbers. This "starving" of the engine will cause a reduction in pressure recovery and, hence, a reduction in available thrust. This is shown in Fig. 13B. Since the shaded area represents a band of typical airplane drag curves, we see that this engine-inlet combination would have marginal or possibly no acceleration thrust during transonic flight.

On the other hand, if the inlet was sized so that the engine airflow demand was satisfied at Mach 1.0, considerable spillage would be necessary at the higher Mach numbers as shown in Fig. 14A. Nature accomplishes this spillage by moving the normal shock forward from the inlet entrance. The high static pressure behind the normal shock serves to deflect the unwanted air very sharply. Spillage of the air in this manner results in a substantial penalty to the engine net thrust. This penalty is commonly referred to as "additive drag" and is equal to the integration of the pressures along the streamline of the spilled air from the normal shock to the inlet cowl lip. Considerable amount of confusion is associated with additive drag, since it ap-

[2] NACA Wartime Report ACRL 5020, May, 1945: "Preliminary Investigation of Supersonic Diffusers," by A. Kantrowitz and C. Donaldson.
[3] Chap. 5 of "Dynamics and Thermodynamics of Compressible Fluid Flow," by A. H. Shapiro, Vol. 1. Pub. by Ronald Press Co., New York, 1953–1954.
[4] Chap. 9 of "Elements of Aerodynamics of Supersonic Flows," by Antonio Ferri. Pub. by Macmillan Co., New York, 1949.
[5] Chap. 2 of "Supersonic Inlet Diffusers and Introduction to Internal Aerodynamics," by Rudolf Hermann. Pub. by Minneapolis-Honeywell Regulator Co., Minneapolis, 1956.

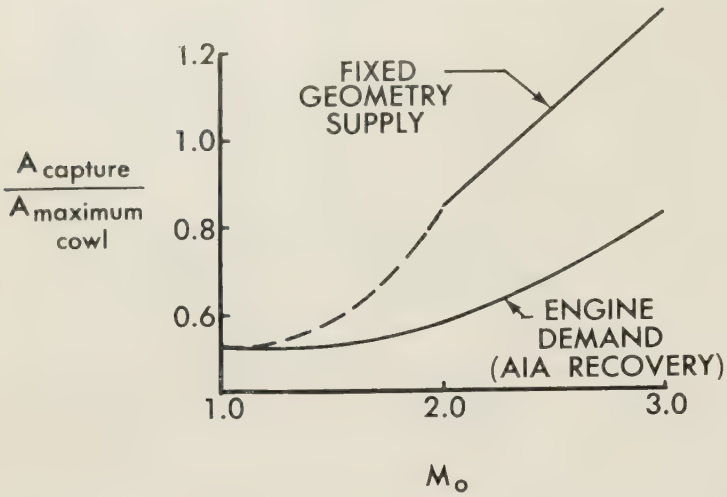

Fig. 14A—Mismatch of airflow characteristics of engine and fixed geometry inlet sized for Mach 1.0

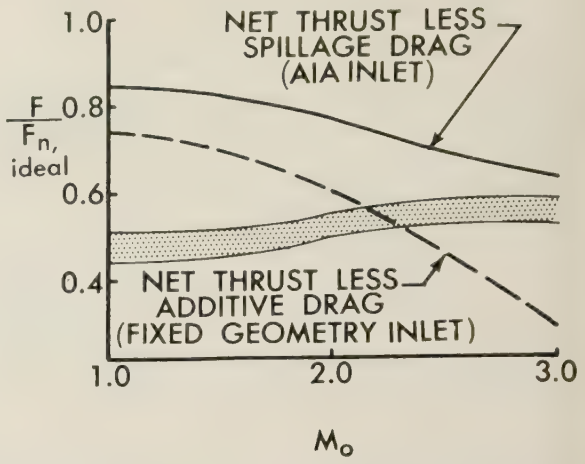

Fig. 14B—Effect of mismatch on corrected engine thrust

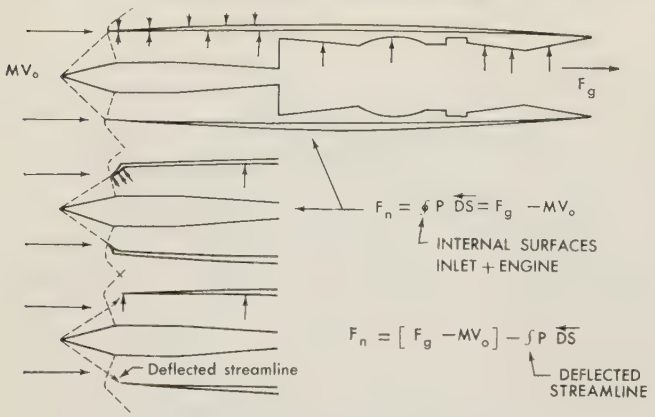

Fig. 15—Diagrammatic explanation of additive drag

pears that we are penalizing ourselves for something that an aircraft does not feel. A simple explanation can be made by referring to the three sketches of Fig. 15. The first sketch has an inlet entrance just equal to the capture area required by the engine. The air approaching in the projected annular area of the cowling is deflected by the shallow external surface of the cowl with a small increase in static pressure. The cost of deflecting the air is a relatively small increase in cowl drag. The net thrust of the engine is defined as the net forward force produced by the action of pressures on all the internal surfaces of the engine *and the inlet.* By using the momentum equation it can be shown that this summation of internal pressures is identical to the gross thrust of the engine minus the momentum of the free-stream tube of captured air, or, $F_N = F_G - MV_0$. Note that considerable thrust is due to the pressures acting on the internal forward cowl surface. The second sketch shows the forward part of the inlet cowl deformed in a manner such that considerable diffusion and static pressure rise occur immediately after the air enters the inlet. However, the contribution of the internal cowl pressures to the net thrust has not changed from that of sketch 1 so that the total net thrust remains unchanged. Sketch 3 shows the deformed part of the cowl in sketch 2 removed so that we now have an inlet which is oversized and spilling air by means of a normal shock. Note that the airflow pattern in sketches 2 and 3 has been kept the same. In computing the net thrust for this configuration, aircraft practice uses the same equation as for the other sketches, that is, $F_N = F_G - MV_0$. It can be seen that this equation is now in error because the thrust producing segment of the cowl adjacent to the captured stream tube is nonexistent. Hence, the true net thrust of the engine and the inlet must be reduced by the integration of the pressures over the projected forward area of the missing segment or the streamline of the deflected air as we refer to it. Perhaps this correction should be called "subtractive thrust" rather than additive drag.

Referring now to the curves in Fig. 14B, we may compare the effective net thrust obtained for an inlet with normal shock spillage to the thrust of an inlet which will deflect or bypass the excess air by a more efficient method. The additive drag shown here would be offset somewhat by a reduction in drag on the external cowl surface, since the projected area is less. Nevertheless, this penalty is very great and could result in a limitation on the maximum flight speeds as indicated by the band of typical aircraft drag curves.

A study similar to the foregoing could be made for the mismatch problems attending the variation in engine airflow demand for nonstandard temperature days. The results would be the same. If an inlet was designed to give the required engine airflow for a standard day, it would choke or starve the engine with the attendant thrust loss on cold days and spill the excess air with high additive drag on hot days.

There are four basic methods by which inlet systems can be designed to deliver the required engine airflow with maximum efficiency and deflect or bypass excess airflow at relatively low cost in drag.

Two methods apply to external compression inlet

systems wherein the oblique shock or shocks are used to spill excess airflow. One method translates the compression surface fore and aft. Fig. 16 shows sketches of the inlet with the compression surface positioned to satisfy the demand engine airflow at three Mach numbers. The dashed line shows the airflow which would be delivered to the engine for the compression surface fixed in the maximum Mach number position.

The second method varies the deflection angle of the compression surface. Fig. 17 shows three sketches with the compression angle at different values to satisfy the demand airflow at three Mach numbers.

In using both methods one must remember that the strength of the oblique shocks and, hence, inlet pressure recovery are related to the compression angle. Care is required so that efforts to reduce drag do not cause a greater loss in thrust due to lowered inlet pressure recovery. A combination of both methods would insure best inlet efficiency and minimum additive drag. Of course, the mechanical design and operation complexities of the inlet would be more severe.

A third and fourth method apply both to external compression and internal compression inlets. The method which is finding considerable usage in inlet designs is the bypass system. This system allows the inlet to take aboard the maximum free-stream capture area. The air not required by the engine is bypassed from the diffuser through slots or doors ahead of the engine face. The desirable feature of this system is that the compression surfaces can be varied to produce maximum inlet efficiency since no compromises need be made to spill excess air. The drag penalty of bypassing excess air in this manner is about equal to the additive drag attending oblique spillage in the flight regime around Mach 2.0. However, for higher Mach numbers the drag advantage of the bypass system becomes increasingly greater. In some powerplant installations the bypassed air can be used as the secondary airflow in the ejector nozzle of the engine. This can result in a gross thrust increase of the engine that may completely cancel the bypass drag.

The fourth method which may be employed is an adjustable inlet entrance. The inlet cowling is varied to capture the desired engine demand airflow. What would normally be excess airflow is now deflected around the inlet by the external cowl surfaces. This probably represents an optimum inlet design system from the standpoint of deflecting air with minimum drag. Once again, this method will allow variation of the compression surfaces for maximum pressure recovery.

Fig. 18 compares for two flight speeds the typical drag penalties of the four methods for deflecting or bypassing excess air. The additive drag incurred with normal shock spillage is included. The spillage drag for the variable entrance inlet is shown as the incremental increase in the external cowl drag.

The drag coefficients are based upon the maximum cross-sectional cowl area. The ratio of inlet entrance area to the maximum cowl area for these comparisons is 0.78.

These plots point out the definite advantage of using a variable geometry configuration to match the inlet and engine airflow characteristics. Somewhat ironically, the lowest drag values are obtained with the most mechanically complex systems.

Requirements for Inlet Controls

Factors Affecting Control Design—Once the inlet system has been developed and documented, the inlet designer will want a control system that will

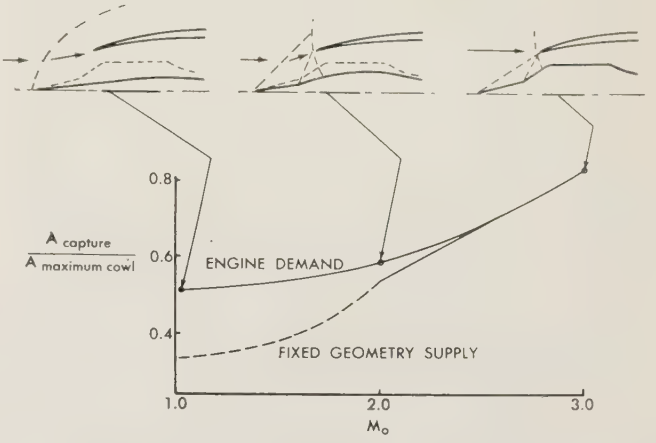

Fig. 17—Engine-inlet airflow matching by varying compression surface angles

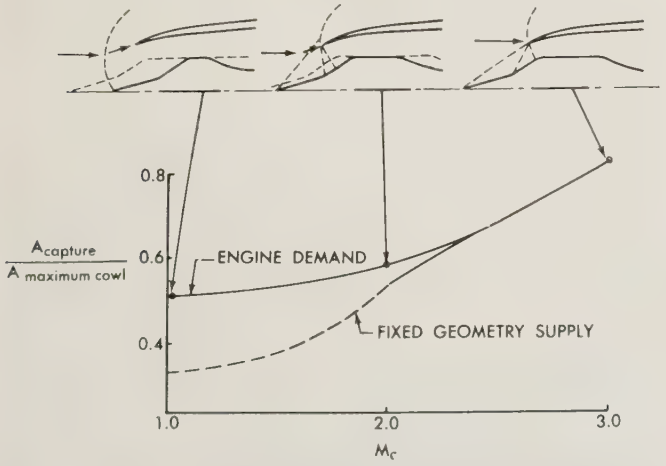

Fig. 16—Engine-inlet airflow matching by translating compression surface

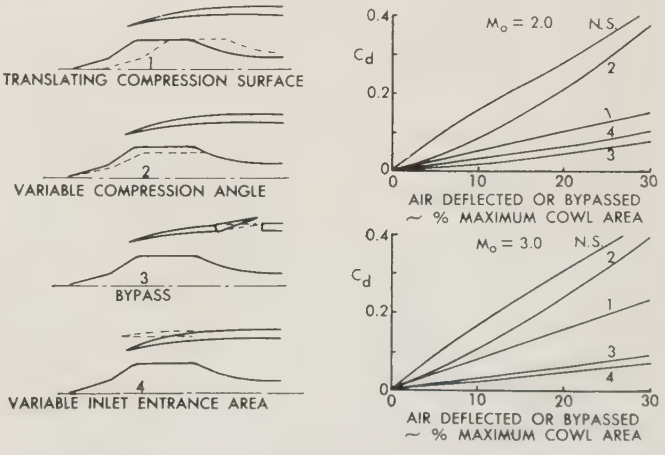

Fig. 18—Comparison of methods of deflecting or bypassing excess air

extract maximum performance from the inlet at all normal flight conditions and airplane altitudes. After all, an inlet system can be no better than the control system.

A control system must meet many requirements. In addition to extracting maximum performance under normal operating conditions, it must maintain safe and stable operation of the inlet under abnormal flight conditions such as high "g" maneuver and engine flameout. It must be light, small, durable, simple to maintain, insensitive to high "g" shocks and temperature variations, and meet other specifications of the aircraft manufacturer. Also, it must display good dynamic characteristics and have no tendency to produce interaction with either the engine or airframe controls.

Establishing Variable Geometry Requirements for Maximum Performance—The first step in the analysis of an inlet control is the determination of the settings of the variable geometry inlet which produce the maximum net propulsive thrust of the powerplant installation. Net propulsive thrust is defined as the net engine thrust minus the sum of the drag of spilled or bypassed excess air and the pressure drag on the external surface of the inlet cowl and powerplant nacelle. Optimum settings must be established for all pertinent operational points in the aircraft flight envelope.

An example of the determination of an optimum net propulsive thrust setting is shown in Figs. 19, 20, and 21. The inlet system for this example has a variable external compression ramp and bypass doors near the engine face. For each study graph the flight Mach number, aircraft angle of attack and angle of yaw, the corrected airflow of the engine, and the corrected airflow of any auxiliary systems are all held at a constant value representative of an operational point in the aircraft flight envelope. The only variables are the compression surface angle and the opening of the bypass doors. The various parameters affected by geometrical settings are plotted against the bypass area for a family of ramp angle values.

In Fig. 19 the upper curve shows the effect on inlet total pressure recovery of the different settings. The pressure recovery curve becomes the basis for computing the net engine thrust, which is shown in the lower curve. Note that the right side of the curves represent conditions where the engine is being "starved" because too much air is spilled or bypassed. The left side of each curve represents conditions where the normal shock is moving upstream from the inlet entrance to supplement the spillage of excess air not required by the engine.

In Fig. 20, the upper curve shows the additive drag which occurs when the oblique shock and/or the normal shock move upstream of the inlet entrance. The middle curve shows the momentum drag of the bypassed air which is dumped through the bypass doors. The lower curve indicates the change in pressure drag on the external surfaces of the inlet cowl and powerplant nacelle. The sum of these curves is representative of the total drag of the powerplant installation.

The upper curve of Fig. 21 repeats the net engine thrust curve from Fig. 19. The middle curve is a summation of the three drag curves developed in Fig. 20. The bottom curve is the difference between the thrust and drag which yields the net propulsive effort of the powerplant installation. From this curve, we arrive at the ramp angle and bypass opening which produce optimum performance for this flight point.

The process described above is repeated for a network of important flight conditions in the aircraft flight envelope. In this manner the optimum settings of the variable geometry are prescribed. These settings become requirements which the control designer must strive to satisfy.

Aerodynamic Parameters for Control Intelligence

Definition of Parameters—The second step in the analysis of an inlet control is the establishment of methods for monitoring the inlet operation to determine whether the variable geometry elements are at the optimum setting for powerplant performance and, if not, to indicate corrective action. Our experience to date has been that this can be done almost exclusively by sensing static and total pressures of the airflow which is approaching or passing through the inlet system. In isolated cases, a means of sensing airflow temperature has been required in addition to pressure sensers. These signals are referred to collectively as "aerodynamic control parameters."

The operation of a control unit requires pressures from two independent sources. One source of pressure must reflect the condition of inlet operation in relation to the net propulsion thrust. We shall refer to this pressure as the "signal pressure." This pressure is always obtained from the inlet compression surfaces or within the inlet.

The second source of pressure is not used directly, but it supplies an airflow which is used to establish a "demand" or "forcing" pressure. For want of a better name, this source shall be referred to as a "reference pressure." It can be located within or outside of the inlet system.

The demand pressure is generated by a "pressure divider" in the control unit. This pressure divider operates to reduce the pressure of the air from the reference pressure source to a value desired for the demand pressure. A detailed explanation of the pressure divider and its operation will be made later. The purpose of the demand pressure is to provide a reference against which the signal pressure can be compared by the controller. The demand pressure is set at the value which the signal pressure will have when optimum setting of the variable geometry is achieved. The demand and signal pressures may be said to provide the intelligence for the control system.

Characteristics of Signal Pressure Parameters—The location of a suitable signal pressure source must be chosen so that two essential requirements are met. First, the signal pressure must undergo a variation in pressure with movement of the variable geometry. This variation in pressure should be single valued, that is, the same pressure should not occur for two or more geometrical settings. Second, a substantial rate of change in pressure must occur when the variable geometry is being moved past or away from its optimum setting. Furthermore, the signal pressure ideally must possess these characteristics at all operational points within the flight envelope.

Signal Pressures for Matching Engine and Inlet

Airflows—To illustrate the method of establishing the signal pressures, we shall continue with the example inlet system and the net propulsive curves of the previous figures. The net propulsive thrust curve is reproduced at the top of Fig. 22. First, we shall investigate several methods of providing a signal pressure for bypass control. We shall assume that the compression ramp angle remains constant at its optimum setting while the effects of bypass variation are studied. The operation is represented by the solid line on the propulsive thrust curve. One method would be to place a static pressure probe in the region of the normal shock, as indicated on the sketch. A high value of signal pressure would be obtained with the normal shock positioned upstream of the pressure port. A low value would be obtained as the shock moved downstream of the pressure port. A rapid change in pressure would occur as the shock passed over the pressure port. The lower curve of Fig. 22 illustrates the variation of signal pressure for different bypass settings with three different locations of the pressure port. The pressure port on the probe must be located so that the high rate of change in signal pressure occurs

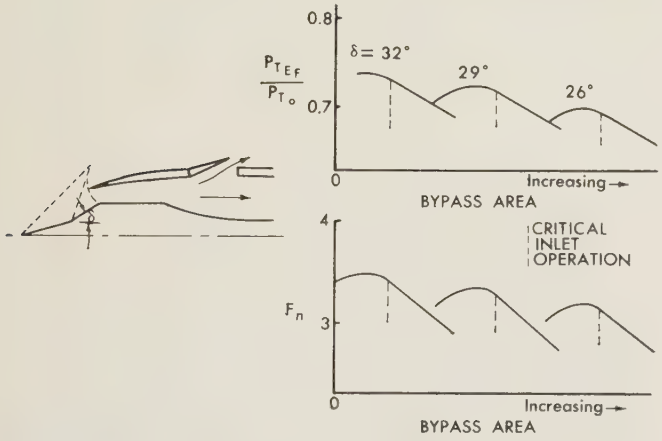

Fig. 19—Typical effect of ramp angle and bypass area variation on pressure recovery and net engine thrust

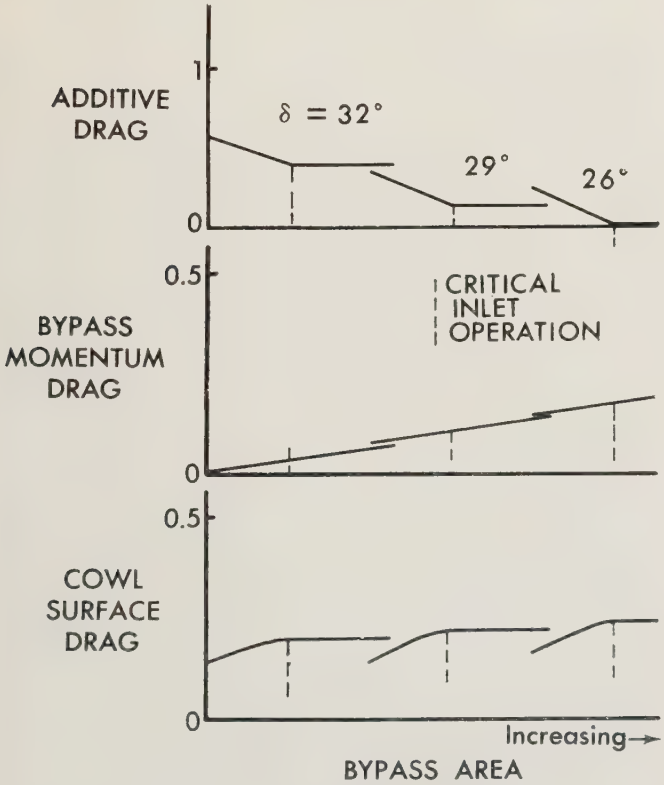

Fig. 20—Typical effect of ramp angle and bypass variation on drag parameters

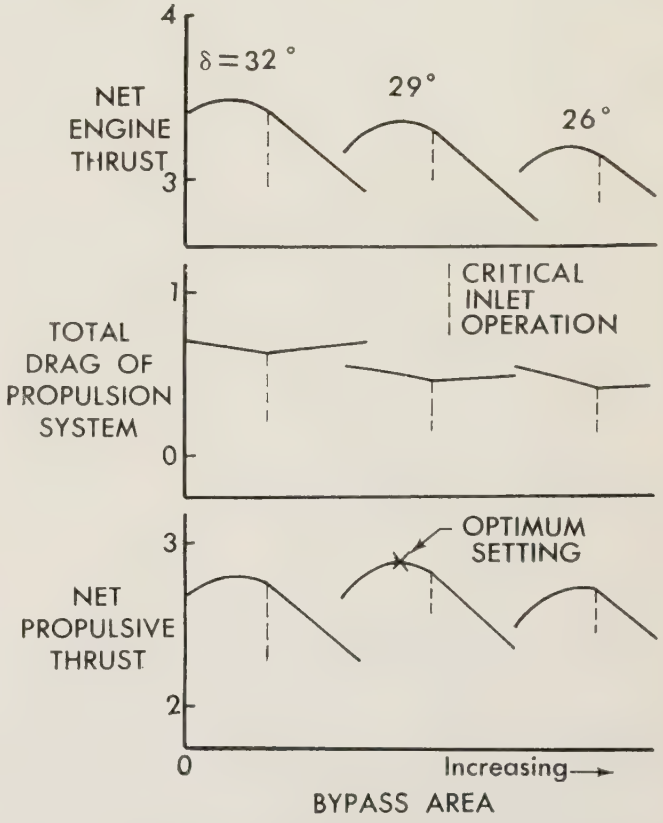

Fig. 21—Typical effect of ramp angle and bypass variation on net propulsive thrust

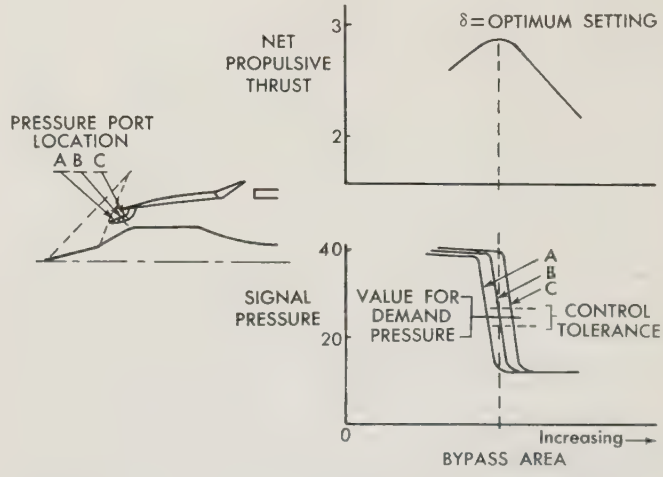

Fig. 22—Control of bypass variation with normal shock position

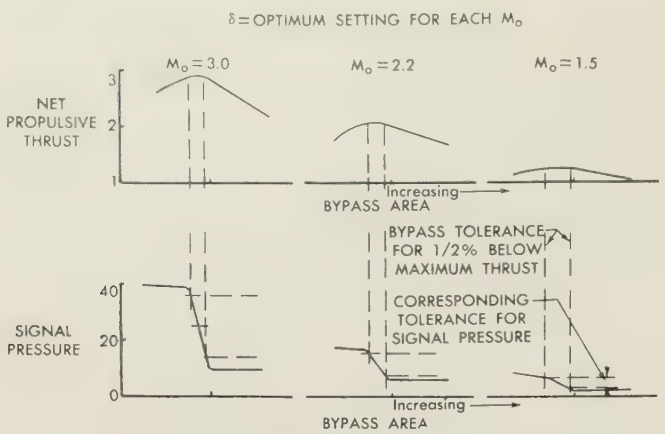

Fig. 23—Determination of tolerance band of signal pressures to maintain thrust within desired margin

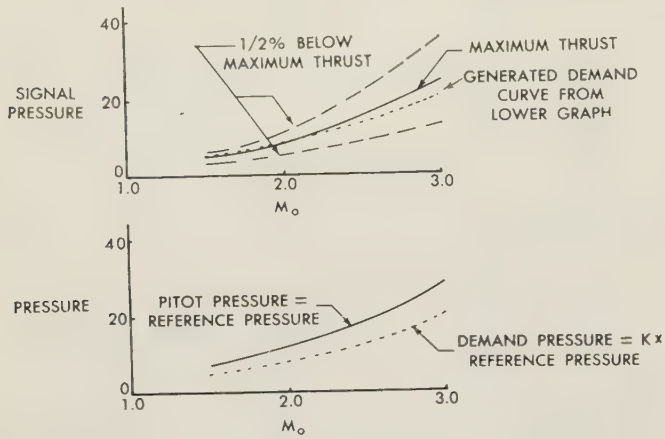

Fig. 24—Method of establishing a demand pressure that follows allowable signal pressure band

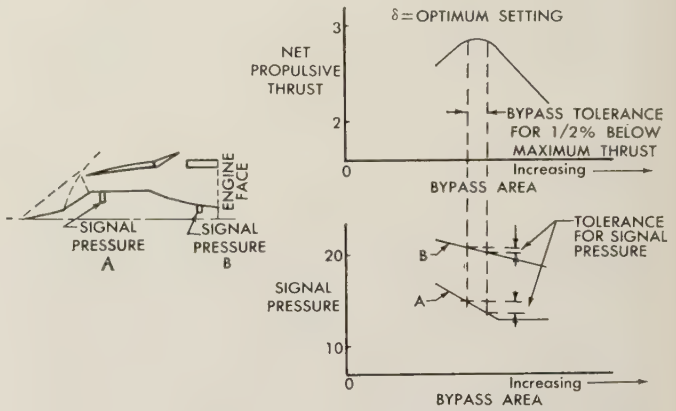

Fig. 25—Control of bypass variation with diffuser Mach number

at maximum net propulsive thrust. In this illustration the pressure port at location B will serve to satisfy this requirement. Therefore, not only has the requirement of pressure port location on the probe been established, but so has the signal pressure value which must exist for maximum net propulsive thrust. We will discuss a little later how a demand pressure is generated to equal this value. When the bypass is open too far, the signal pressure will be less than the demand pressure. This will cause the control to close the bypass until the pressures are equal. The converse would occur if the bypass was closed too far. Note that the tolerance or accuracy band of the control has negligible effect on the net propulsive thrust. The width of the band has been exaggerated for clarity.

This method of control presents some difficulty with decreasing supersonic flight Mach numbers when the strength of the normal shock diminishes and becomes nonexistent. The upper graphs of Fig. 23 show the net propulsive thrust curves for three different flight speeds. The lower graphs show the corresponding signal pressure curves. Although the normal shock no longer exists for the Mach number, the signal pressure does undergo a small change because of the changing entrance velocity. Tolerance bands are shown on the allowable variation in signal pressure that would maintain net thrust within one-half per cent of maximum, for example. The tolerance band decreases with decreasing flight speed, as is shown in the upper graph of Fig. 24, because of the diminishing pressure rise across the normal shock. The final requirement is to generate a demand pressure which will fall within the allowable tolerance band and, ideally, coincide with the maximum net propulsive thrust line.

The reference pressure from which the demand pressure will be generated must have the same trends that the signal pressure has a maximum thrust. In this example, the reference pressure must decrease with flight Mach number at the same rate that the signal pressure at maximum thrust is decreasing, as shown in the upper graph of Fig. 24. A pitot tube placed on the external cowl surface has produced a satisfactory reference pressure in several actual applications. The solid line in the lower graph of Fig 24 shows the variation of a typical pitot tube pressure with flight speed.

The dotted line represents the demand pressure that is generated as a constant fraction of the pitot pressure or reference pressure. This demand pressure is superimposed on the signal pressure band shown in the upper graph of Fig. 24. It is apparent that satisfactory operation of the bypass doors will be maintained for the flight range indicated, since the control will keep the signal pressure equal to the demand pressure.

A large variety of demand pressure curves can be generated by locating the pitot tube on the compression surfaces, within the inlet, or on other areas of the aircraft. Also, the pitot tube can be placed in diverging or converging shrouds or mounted with a small shock-producing surface of its own. Considerable other "tricks-of-the-trade" can be used in tailoring the demand pressure to have the charcateristics desired for different flight speeds and aircraft angle of attack or yaw.

A second possible method of controlling the bypass would utilize a static pressure probe or pressure port somewhere within the inlet. This would preferably be at the minimum area section where

the largest change in flow Mach number, and hence signal pressure, would occur (Fig. 25). The line labeled location A on the lower graph shows a typical signal pressure trace for bypass variation between full-closed and full-open. Note that at some point near full-open and on to full-open, the signal pressure does not change. This is due to either choking of the inlet when Mach 1.0 exists at the minimum area or the normal shock being swallowed. A value of signal pressure can be determined for the maximum net propulsive thrust setting.

The somewhat undesirable characteristic of constant signal pressure when the inlet chokes can be eliminated by placing the static pressure probe or pressure port sufficiently downstream within the inlet diffuser so that an internal normal shock will not pass over it. The characteristic signal pressure trace would then appear as shown in Fig. 25 for location B. Although the pressure is continuously changing, the rate of change is much less than for location A, because the flow Mach number at location B is much less and undergoes a smaller variation for the range of bypass setting. For a given accuracy of thrust control, location B results in a more severe restriction on the allowable tolerance of the signal pressure band. Note that the normal shock probe control discussed in Fig. 22 is inherently much more accurate than the internal pressure or duct Mach number control. However, on certain inlet systems a duct Mach number control may be required to take over the inlet control at the lower supersonic flight speeds where the normal shock control becomes inadequate.

The foregoing discussion of signal pressure sources utilized by the control in bypassing the optimum amount of air can also be applied to other methods of matching the engine and inlet airflows. These would include systems that translate the compression surface as in a conical inlet with a moving spike tip; or systems which vary the compression surface angle for airflow matching only; or systems which have adjustable inlet entrances. In the case of internal compression inlets, where the normal shock must be maintained within the inlet, the same principles for control of the normal shock will apply although the tolerance on the signal pressure band and response of the control system becomes much more critical.

Control Parameters for Maintaining Optimum Shock Patterns over Compression Surfaces—Reference is again made to our example inlet system to illustrate several methods of controlling the compression surface angle. Fig. 26 shows the sketch of the inlet and the net propulsive thrust curve for three flight Mach numbers. The curves are plotted against compression ramp angle for the constant optimum bypass setting at each Mach number. One method of obtaining a signal pressure would be to place a static pressure tap on the surface of the compression ramp. The lower graph of Fig. 26 shows the variation of surface pressure as a function of ramp angle. The dashed portion of the curves indicates detachment of the oblique shock from the compression surface. The values of signal pressure for optimum ramp positions can then be established for all three flight speeds. Note that considerable tolerance or allowance can be permitted in controlling the signal pressure before any appreciable reduction in maximum net propulsive thrust occurs.

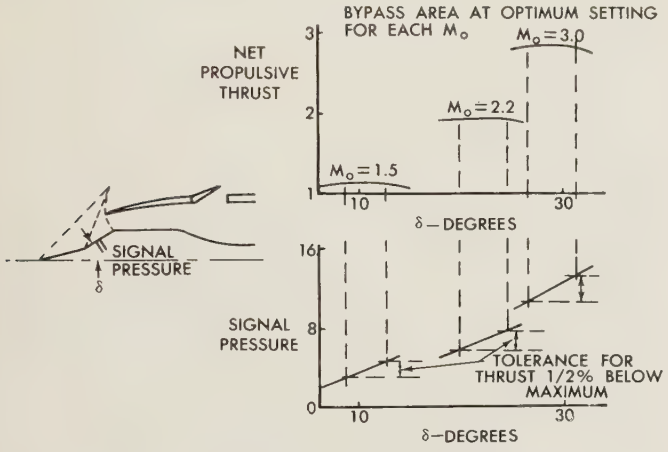

Fig. 26—Control of compression surface angle variation with static pressure on compression surface

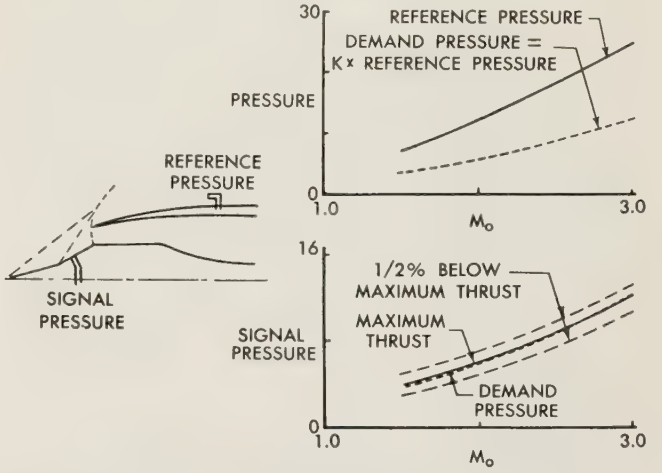

Fig. 27—Method of establishing demand pressure that follows allowable signal pressure band

A method of generating demand pressures having values corresponding to the signal pressures for optimum compression angle settings is shown in Fig. 27. The top curve of the upper graph presents the total pressure felt by a pitot tube placed on the outside cowl surface. The lower curve of the graph represents a demand pressure generated by taking a constant value of the pitot tube pressure or reference pressure. In the bottom graph, this demand pressure is superimposed on the allowable band of signal pressures for optimum compression angle. It is evident that this demand pressure is acceptable for controlling the compression surface angle of the example shown. As previously stated, the demand pressure curve can be tailored to satisfy any other signal pressure band by using different location and configuration of the pitot tube.

Another possible method of controlling the compression surface angle would be to maintain the oblique shock at a constant angle or a constant posi-

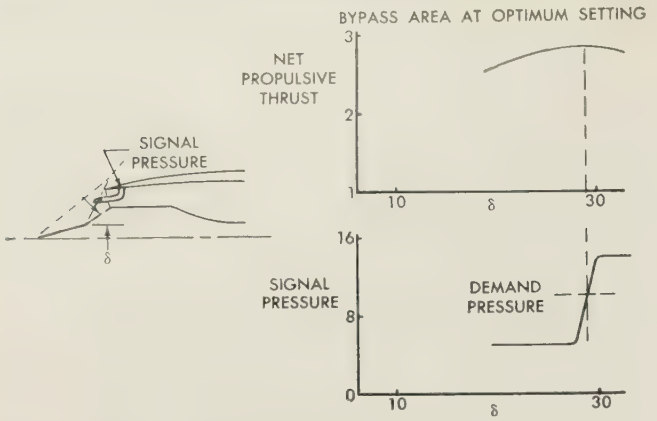

Fig. 28—Control of compression surface angle variation with oblique shock position

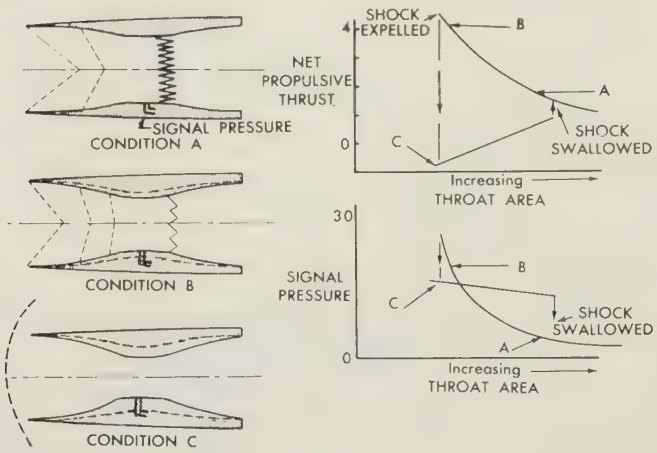

Fig. 29—Behavior of internal compression inlet with varying throat area

tion with respect to the inlet cowl lip. This would be done by placing a static pressure probe in front of the inlet entrance so that the oblique shock would fall across the pressure port (Fig. 28). The variation in the pressure signal with compression surface angle is plotted in the lower curve. If the ramp angle is too large, the oblique shock would be ahead of the pressure port, causing a high value of signal pressure. Similarly, for a low angle the oblique shock is behind the pressure port and a lower value of signal pressure occurs. The control would function to keep the signal pressure midway between the maximum and minimum value and thereby maintain the oblique shock on the pressure port. The exact location of the pressure port on the probe would be determined by the angle of the oblique shock necessary for maximum net propulsive thrust. One must be cautious in the use of this method, since the optimum shock angle may be substantially different for different flight speeds with a particular inlet configuration. The generation of the demand pressures would be accomplished by the same methods already described for the normal shock control and compression surface control.

In passing, the two methods just described for controlling compression surface angle of external compression inlet systems also tend to compensate automatically for relatively large changes in inlet angle of attack and still maintain optimum settings. This feature is difficult to obtain with control systems that maintain the compression angles as a scheduled function of the aircraft flight parameters.

The control of the compression surfaces of internal compression inlets would be done by a manner similar to the first method described above for external compression inlets. However, since there is an oddity associated with these inlet systems, a brief study will be presented. Fig. 29 includes sketches of an internal compression inlet with variable throat and bypass doors. The first curve shows the typical effect of throat area on the net propulsive thrust parameter. In this study, we are assuming that the bypass door control is acting to keep the normal shock at a fixed position downstream of the throat as the throat area is varied. For large values of throat area as represented in sketch A, the throat Mach number is at a relatively high supersonic value and considerably in excess of what is known as the minimum stable throat Mach number. Also, the Mach number at the normal shock is high, producing a large total pressure loss and a low net propulsive thrust. As the throat area is reduced, the increased compression of the air reduces the Mach number at the throat and before the normal shock, thereby resulting in better net propulsive thrust (sketch B). Further reduction of the throat area will produce "choking" at the throat, largely due to separation of the boundary layer, and a complete breakdown of the supersonic flow pattern within the inlet (sketch C). Experimental data shows that the value of the minimum stable throat Mach number appears to be between 1.3 and 1.5, depending upon the extensiveness of boundary bleed systems and the rate of compression of the flow. The net propulsive thrust decreases in a discontinuous manner when the flow breakdown occurs, since severe pressure losses now exist across the strong "expelled" normal shock ahead of the inlet. In order to re-establish desired flow conditions, the throat area must be opened considerably beyond the area when the breakdown occurred. After the shock "swallows," or the inlet is "started," the throat area can be reduced along the line AB to some desired value near maximum thrust. The reason for this hysteresis effect will not be discussed herein. The arrow heads on the dashed lines indicate the direction of the irreversible steps in the cycle.

The lower graph of Fig. 29 shows the static pressure existing at the throat plotted for the throat area variation cycle just described. The pressure is seen to increase slowly as the throat area is reduced and drop discontinuously with flow breakdown. The pressure remains essentially constant as the throat area is increased during the "inlet starting" part of the cycle. When the normal shock is swallowed by the inlet and the supersonic flow pattern established, the static pressure drops abruptly to the normal operating line AB.

Use of the throat static pressure as a signal pressure does not appear feasible at first glance because the curve is not single valued. However, a demand pressure can be generated which displays the same characteristics as the throat pressure during flow breakdown and the restart cycle. This demand pressure may be obtained very simply by placing a total pressure tube at the throat of the inlet. The

solid curve of the upper graph in Fig. 30 shows the variation of the throat total pressure as the throat area is cycled from point A through point C and back again to A. The similarity of the throat total pressure curve to the throat static pressure is important. The dashed curve on the upper plot will be obtained if a demand pressure is generated by taking a constant fraction of the throat total pressure. In the lower plot of Fig. 30, the demand pressure is superimposed on the signal pressure. The demand pressure has been tailored to cross the signal pressure at point B. If the throat area is less than that required for point B, the signal pressure will be greater than the demand pressure and the control will act to increase the throat area. The opposite occurs if the throat area is greater than required for operation at point B. Of great importance is the fact that this control will automatically start the inlet if the supersonic flow should break down. This is evident since the signal pressure will always be greater than the demand pressure with an "unstarted" inlet, which will cause the control to increase the throat area until starting occurs. When the inlet starts the signal pressure will fall below the demand pressure, thus causing the control to reduce the throat area until point B is reached.

The diffcult task in controlling this inlet is readily apparent. It is desirable to operate as near as possible to the maximum net propulsive thrust. However, allowance must be made for the danger of some transient disturbance from the engine, aircraft, or atmosphere causing possible flow breakdown before the control can sense and correct for it.

Closed-Loop Versus Scheduling Controls

In considering an automatic control for a variable geometry inlet, the controls can be generally placed into one of two classes, either a closed-loop control or a schedule control. The former senses the inlet flow conditions and holds the inlet at a predetermined setting. The parameter used for this setting could either be duct Mach number or shock position. A scheduling control is one which will schedule the geometry of the inlet as a function of certain external input parameters, usually airplane Mach number and attitude. Fig. 31 shows a pressure recovery curve as a function of inlet duct Mach number for an inlet with internal compression. As the duct Mach number is decreased, the normal shock will move forward to or near the throat of the inlet and then it is expelled suddenly from the inlet resulting in a high loss of pressure recovery. It is desirable to operate the inlet as near to the "knee" of the curve as possible without expelling the shock under airplane maneuver conditions. If a scheduling control is used, it will be necessary to degrade the inlet and schedule the control for a lower pressure recovery in order to accommodate the manufacturing tolerances necessary to fabricate airplanes. These tolerances normally result in considerable variation between inlet geometry. The inlet will then operate somewhere within the area shown on the curve illustrated by the cross-hatched lines. If a closed-loop control system is utilized, the inlet conditions will be sensed; therefore, even though the inlets vary due to manufacturing methods, the control will still maintain the inlet at or near the optimum condition. The shaded area illustrates the dead band associated with a closed-loop control and, as can be seen, results in a set point that consistently gives higher pressure recovery. Another advantage of the closed-loop control system is the automatic restarting of the inlet should the shock be expelled. This was discussed earlier under the inlet discussion.

Inlet Dynamic Considerations

Once the parameters to be controlled are established, it then becomes necessary to define the dynamic requirements before continuing with the design of the control components. Usually the inlet control can be separated into two distinct functions, that of controlling the compression surface and that of controlling the compression surface and that of regulating the amount of spillage air. In some inlets these two functions are performed by the same controller but for the purposes of this paper they will be considered separately.

As pointed out earlier, the compression surfaces are varied as a function of the airplane attitude and flight speed. (This is generally true regardless of whether a closed-loop or a scheduled control is employed.) Therefore, the dynamic requirement of this control loop is dictated by the aircraft response rates. If the surface varies only as a function of Mach number, the control can be relatively "slow." If angle of attack and yaw considerations are made, the speed of the control system must be

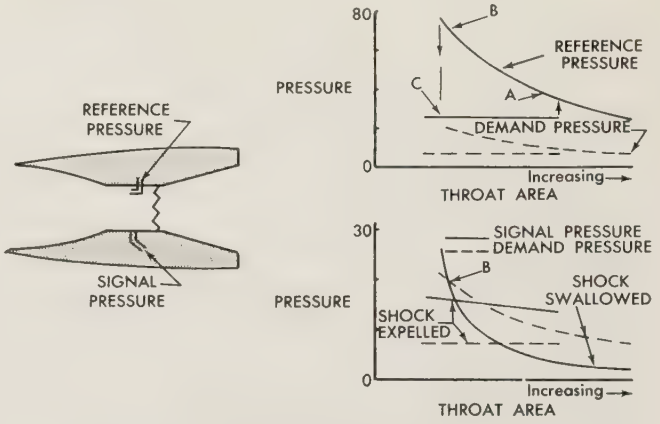

Fig. 30—Method of establishing demand pressure used in control of throat area

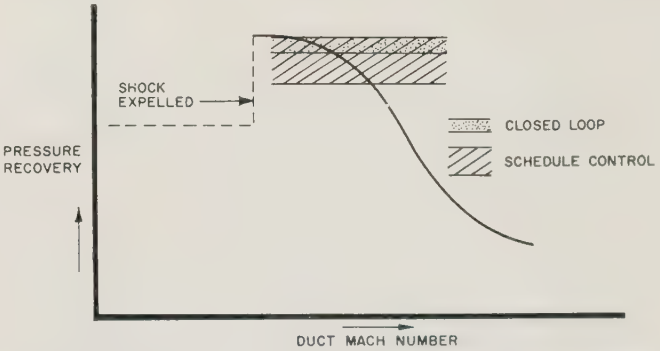

Fig. 31—Comparison of closed-loop and scheduling control systems

increased to be compatible with the vehicle.

As stated previously, two methods may be employed to control the spillage of excess air: changing the inlet geometry or bypassing the excess air after is has been taken aboard. If the terminal shock is controlled at the lip of the inlet, the inlet is said to be operating critically; if it is downstream of the diffuser throat, the inlet is said to be operating supercritically. Subcritical operation (that is, shock ahead of inlet) is usually not desirable and, therefore, will not be given any further consideration. An earlier portion of the paper also dealt with the subject of controlling the shock location or controlling the duct Mach number and it can be seen that regardless of the method used, the control information is in the form of a signal pressure and a reference pressure. This section will deal with the control of the normal or terminal shock; however, the arguments apply equally as well to a duct Mach number control system. Furthermore, this paper will be restricted to the discussion of superficial inlet operation using bypass air spillage. The dynamic considerations which follow can be applied to subcritical inlet operation as well, with an additional term appearing in the continuity equation to account for the air spilled ahead of the inlet. This term increases with increasing to subcritical operation.

Fig. 32 is a block diagram of a typical closed-loop bypass control system. The system shown here is in a general form and various refinements can be added if detailed analysis is to be performed. A schedule control system would not have the feedback portion of the diagram and would receive its inputs from external sources. A detail breakdown of the diagram is as follows:

Block 1 contains the controller and actuator and in a pneumatic system the controller is a single item. In an electrical system, this block would consist of a pressure transducer, signal mixer, amplifier, electrical servo valve and an actuator. The pneumatic controller will be discussed in a later portion of this paper.

Block 2 is the gain of the mechanical linkage between the actuator and the bypass area. This is established by the air frame designer and need only be considered when studying the overall loop stability.

Block 3 deals with the effect of the bypass area upon the compressor face static pressure and is obtained by writing the airflow continuity equation in the diffuser. This is also referred to as the filling time of the duct. For the purpose of simplification, assume that the diffuser can be divided into a subsonic diffuser section (section 3) and an engine inlet section (section 4) as shown in Fig. 33.

As further aid to analysis an average pressure P_3 is assumed to be present from the normal shock to the bypass opening. An average pressure P_4 is considered between the bypass and the compressor face. With these assumptions, it can be found that P_3 is related to P_4 in the following manner:

$$P_3 = CP_4 \tag{1}$$

where:

C = constant = f(bypass opening)

Airflow through the diffuser may be written in the form:

$$W_{TH} = W_E + W_B + W_S \tag{2}$$

where:

$$W_{TH} = \frac{P_{T_0} f(M_{1H}) A_{TH}}{\sqrt{T_{T_0}}} \tag{3}$$

$$W_E = \frac{P_{T_0} f(\mathrm{M}_4) A_E}{\sqrt{T_{T_4}}} \tag{4}$$

$$W_B = \frac{P_{T_4} f(\mathrm{M}^*) A_B}{\sqrt{T_{T_4}}} \tag{5}$$

(Flow out bypass assumed choked.)

$$W_S = \frac{V_3}{RT_3}\dot{P}_3 + \frac{P_3}{RT_3}\dot{V}_3 - \frac{P_3 V_3}{RT_3^2}\dot{T}_3 + \frac{V_4}{RT_4}P_4 + \frac{P_4}{RT_4}\dot{V}_4 - \frac{P_4 V_4}{RT_4}\dot{T}_4 \tag{6}$$

$\dot{V}_3$, $\dot{V}_4$, $\dot{T}_3$ and $\dot{T}_4$ are negligibly small and may be neglected in Equation 6. With this assumption, Equations 3–6 are substituted into Equation 2 and linearized. The static pressure P_4 may then be related to the total pressure P_{T_4} in the following manner:

$$P_{T_4} = \left(1 + \frac{\mathrm{M}_4^2}{5}\right)^{\frac{7}{2}} P_4 \tag{7}$$

Equations 1 and 7 are then substituted into the linearized equation and the Laplace transformation is performed. The proper arranging of the terms will yield a transform function of the form:

$$\frac{\Delta P_4(s)}{\Delta A_B(s)} = -\frac{K_a}{\tau_A s + 1} \tag{8}$$

where:

$$K_a = \frac{f(\mathrm{M}^*)P_{4_0}}{f(\mathrm{M}_4)A_E + f(\mathrm{M}^*)A_{B_0}} \qquad \tau_A = \frac{\frac{P_4}{P_{T_4}}\left[\frac{V_3 C}{RT_3} + \frac{V_4}{RT_4}\right]\sqrt{T_4}}{f(\mathrm{M}_4)A_E + f(\mathrm{M}^*)A_{B_0}}$$

The dead time (or transport delay time) for transmitting upstream the effects of P_4 on the control signal pressure P_X is due to two things: (1) the time for the pressure wave to travel upstream to the shock and (2) the lag time required for the shock to travel to the control probe. This lag time depends upon the initial distance between the shock and the probe. In a closed-loop control, the shock will be maintained at or near the probe; therefore, the lag time is negligibly small. The time for the pressure wave propagation from the bypass to the shock is computed by dividing the length of the travel by the difference between the speed of sound and the fluid Mach number downstream. Since the diffuser Mach number variation with area ratio is small, an average value of Mach number can be used. Another approach that can be used to determine wave propagation time is to obtain Mach number as a function of area ratio. By making simplyfying assumptions about the diffuser geometry, it is possible to integrate over the range of the area ratios in terms of Mach number to obtain the dead time.[6] (See block 4, Fig. 32.)

The probe gain (block 5) is a function of the

[6] NACA Research Memorandum Report E55 D22, June, 1955: "An Analysis of Ramjet Engine Time Delay Following a Fuel Flow Disturbance," by F. Wilcox and A. R. Anderson.

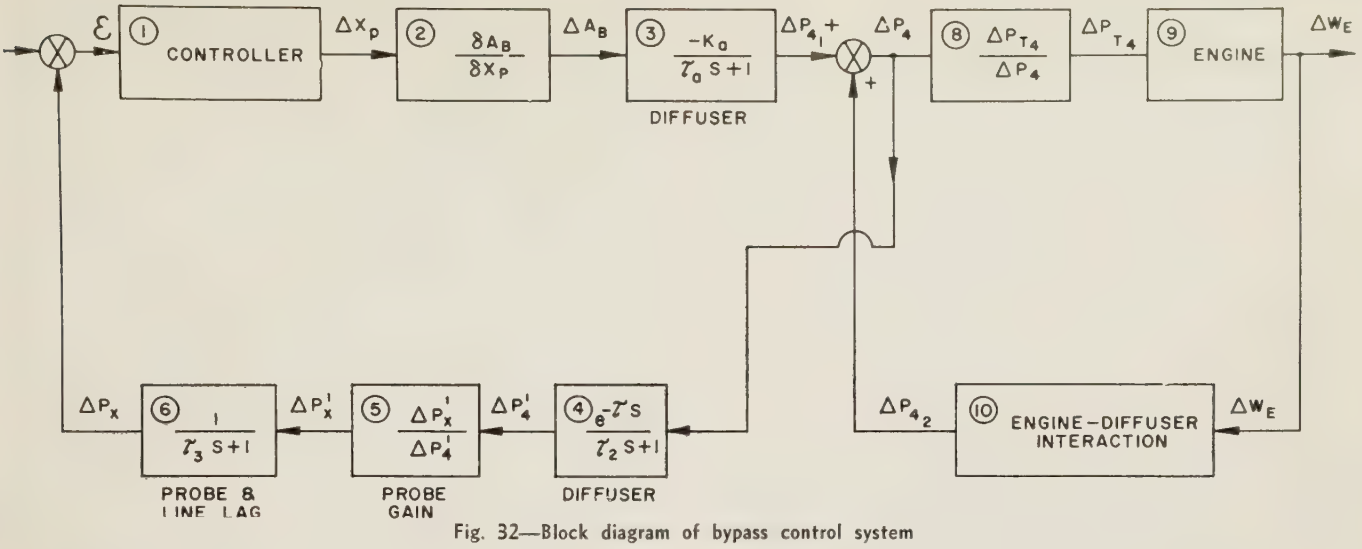

Fig. 32—Block diagram of bypass control system

probe geometry and the signal pressure being sensed. In general, a static probe placed on the diffuser wall sensing the pressure through the boundary layer results in low gains. A static probe placed in the free-stream usually results in a higher gain. However, this gain can be adjusted by varying the probe geometry. The probe can be designed in such a manner that amplification of the signal is obtainable when necessary.

The lag time of the signal being transmitted from the probe to the controller is represented by block 6. This can be computed by considering the volume of the line and controller cavity, the inertia of the column of air within the line, and the length of the line. For a typical pneumatic system using ¼-in. diameter line, a 15-ft length would result in a delay of about 0.007 sec.

The engine dynamics (block 9) are not a part of the considerations of this paper. However, many reports are available on this subject.

The problem of engine interaction with the control operation depends greatly on the effective time constant of the engine. The transfer function of the engine air flow in terms of its variable parameters would take the following form:

$$\Delta W_E = \frac{\delta W_E}{\delta N}\Delta N + \frac{\delta W_E}{\delta W_F}\Delta W_f + \frac{\delta W_E}{\delta P_{T_4}}\Delta P_{T_4} \qquad (9)$$

From this equation it is possible to determine the dynamic effects on diffuser static pressure P_4 as a function of change in engine airflow. In general, it is sufficient to state that with the larger engines being employed in the supersonic flight regime, the engine time constant is such that the interaction is negligible.

Control Design Considerations

The pneumatic control must sense an inlet condition, which is represented by some pneumatic pressure, compare this information with a predetermined demand signal, and initiate a corrective action in the event of an error in the signal pressure. The pneumatic controller transduces directly from the signal pressure to the controller output.

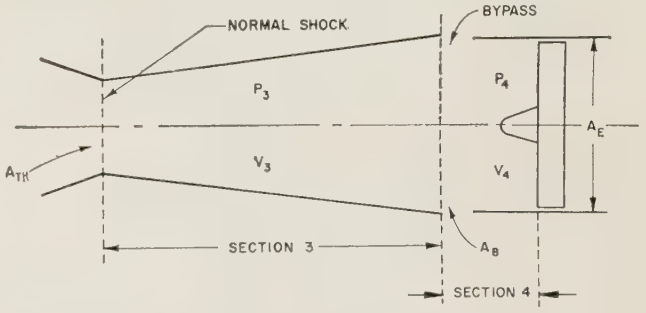

Fig. 33—Schematic of engine induction system

In the case of a pneumatic-hydraulic system, the output would be hydraulic and this transition from pneumatics to hydraulics is accomplished with the minimum number of steps. The output could be electric or pneumatic. If an electrical output is desired, the hydraulic servo valve would be replaced by an electrical potentiometer. In the case of a pneumatic output requirement, the servo valve would be of the pneumatic variety or a pneumatic pressure divider. The pneumatic pressure divider will be discussed later in conjunction with another application. For the purposes of this discussion only, hydraulic outputs will be considered.

The process of controlling the variable geometry bypass of a supersonic inlet usually is accomplished by shock positioning or controlling a duct Mach number. In the case of shock positioning, it was shown earlier that the signal pressure for desired shock location can be related to a constant percentage of some reference pressure. In the event of controlling a duct Mach number, the desired signal pressure is equal to a constant percentage of the duct total pressure. Therefore, in addition to the signal pressure the controller must sense a reference pressure and divide this pressure to the proper percentage so that a demand pressure is obtained. The signal pressure is compared against the demand pressure across a flexible diaphragm. An unbalance between the pressures causes a movement of the diaphragm. This diaphragm motor is then used to drive the servo valve. In generating this demand pressure, a device commonly referred to as a pres-

sure divider is used. Fig. 34 shows a schematic drawing of this device. As can be seen by the illustration, the pressure divider consists of two choked orifices placed in series with a reference pressure used as the supply pressure. If the continuity equation is used to evaluate the mass flow passing through the pressure divider, it can be shown that:

$$P_{\text{Reference}}\, A_1 = P_{\text{Divided}}\, A_2 \qquad (10)$$

where:

A_1 = Flow area of upstream orifice
A_2 = Flow area of downstream orifice

Therefore:

$$P_{\text{Divided}} = \left(\frac{A_1}{A_2}\right) P_{\text{Reference}} \text{ or } KP_{\text{Reference}} \qquad (11)$$

The divided pressure, or demand pressure, is then placed on one side of a diaphragm with the signal pressure acting against the other side of the diaphragm. In order to get a diaphragm movement proportional to the error in the signal pressure, the diaphragm must act against a spring. A mechanical spring would be good for a single signal pressure and demand pressure level. However, as the pressure level is varied, which occurs when the airplane altitude or Mach number is changed, the displacement of the diaphragm will no longer be a function of the per cent error in the signal pressure but a function of absolute error. In order to make the displacement proportional to the percent of signal pressure error, it is necessary to have a spring force which will vary directly with the signal pressure level. This is accomplished with an "air spring." The air spring is generated by varying either the upstream or downstream orifice of the pressure divider as a function of the diaphragm displacement. As the error in signal pressure displaces the diaphragm, the area of ratio of the pressure divider varies until the demand pressure has changed sufficiently to produce a balance across the diaphragm and stop the movement. Note that the balanced pressures are not at the desired value with the diaphragm displaced. The change of area ratio of the pressure divider is proportional to the diaphragm displacement. Therefore, the greater the per cent error in signal pressure the greater must be the displacement to change temporarily the demand pressure to balance the displaced signal pressure. As can be seen, this action is identical to that of a mechanical spring. However, as the signal level increases or decreases, the spring force from the air spring will also increase or decrease accordingly. The diaphragm is also coupled to a servo valve which will result in a fluid flow that is a direct function of the per cent error in the signal pressure.

In some applications the flow required may be of such magnitude that a considerable force is required to modulate the servo valve, or it may be necessary to have a shaft displacement that is a function of the error in the signal. This can be accomplished if the output from the servo valve of the unit described above is ported to an actuator which not only has a shaft output but also varies the upstream orifice of the demand signal pressure divider as a function of its displacement. As the signal pressure increases, the hydraulic fluid from the servo valve entering the actuator will displace the actuator to the right, increasing the upstream area to the pressure divider which further increases the demand pressure and returns the diaphragm and servo valve to its null position (Fig. 35). The resultant action will be a shaft displacement as a function of the per cent error in the signal pres-

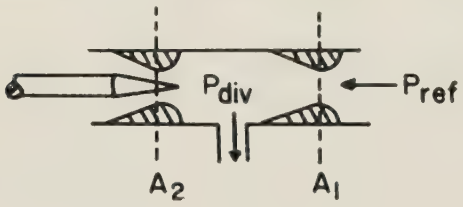

CONTINUITY EQUATION

$$m = P_{ref}\, A_1 \frac{f(M_1)}{\sqrt{T_1}} = P_{div}\, A_2 \frac{f(M_2)}{\sqrt{T_2}}$$

WITH ORIFICES CHOKED

$$P_{ref}\, A_1 = P_{div}\, A_2$$

$$\text{OR} \quad P_{div} = \frac{A_1}{A_2} P_{ref} = K\, P_{ref}$$

Fig. 34—Pressure divider

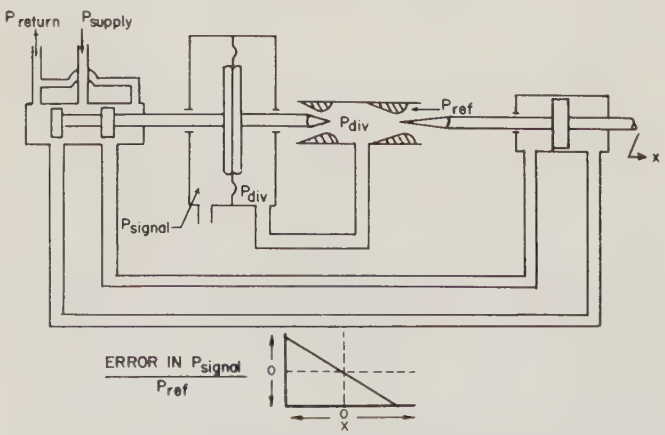

Fig. 35—Pneumatic pressure ratio controller

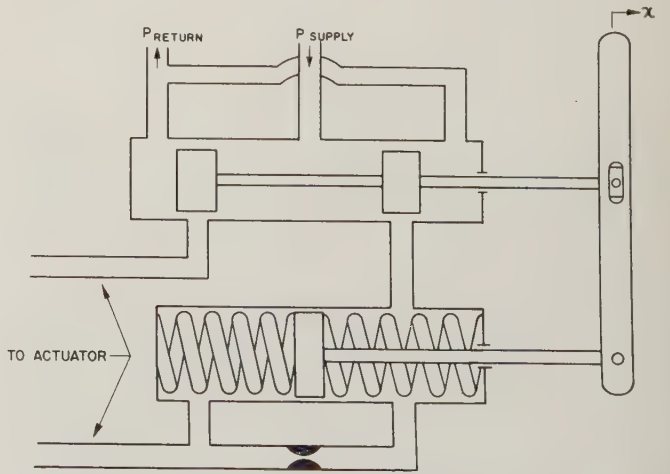

Fig. 36—Flow rate computer

sure. This is illustrated by the curve shown on the insert of Fig. 35. The shaft output can then be used as mentioned above either to drive a control surface of the inlet or to drive a servo valve where a high force level is required. The amount of hydraulic fluid entering and leaving the actuator dictates the rate of movement of the actuator. The hydraulic flow can be represented by the following equation:

$$Q = CA\sqrt{\Delta P} \qquad (12)$$

where:

Q = Fluid flow
A = Valve opening area
ΔP = Pressure drop across servo valve

The actuator output is dictated by ΔP across the actuator piston. Therefore, it can be shown that:

$$\Delta P_{SV} = P_S(P_R + \Delta P_A + \Delta P_{SVR}) \qquad (13)$$

where:

ΔP_{SV} = Pressure drop across the servo valve
P_S = Hydraulic supply pressure
P_R = Hydraulic return pressure
ΔP_A = Pressure drop across actuator piston
ΔP_{SVR} = Pressure drop across the return port of the servo valve

Equation 13 shows that as the load changes on the actuator the pressure drop across the actuator piston will vary. This is reflected into a varying rate of hydraulic flow for a given servo valve displacement. If the unit is designed for the load conditions, the system may become unstable when the load decreases. Some means of resetting the valve opening is, therefore, required as the rate tends to increase. Fig. 36 shows a method of accomplishing this. The output of the servo valve is ported to one side of a spring-balanced piston, through a restriction, and to the actuator. The pressure downstream of the restriction is placed to the other side of the piston. As the fluid flow rate increases, the pressure drop across this restriction increases, thus causing the piston to be displaced in the direction tending to close the servo valve and thereby maintaining a constant flow rate. This device can be driven by the controller described above utilizing its shaft output.

Another parameter that often becomes important in inlet control applications is the sensing and computing of inlet total temperature. This may also be accomplished pneumatically by using a bimetal temperature probe wherein two metallic tubes are placed concentrically. One end of the outside tube is fastened to the orifice of a pressure divider and the other end is attached to an end of the inside tube. The free end of the inside tube translates a needle within the orifice of the pressure divider. As can be seen from the schematic in Fig. 37, increasing temperature varies the relative position of the needle and orifice in accordance with the differential expansion rates of the bimetal tubes. This results in a variation of the divided pressure within the pressure divider. The pneumatic signal from this device can be used directly. In applications where an amplification of the signal is desired, the senser-amplifier described above can be used. The shaft displacement from the amplifier will then become a function of the temperature being sensed.

In establishing parameters to control the variable

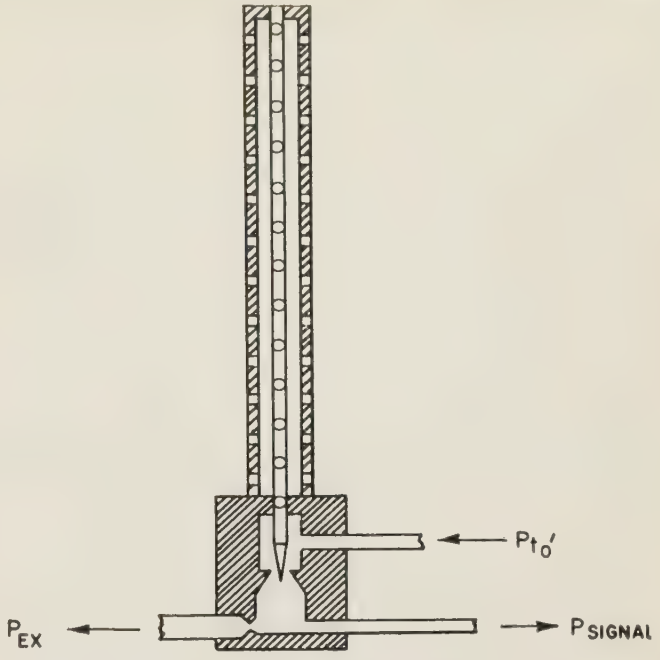

Fig. 37—Temperature senser

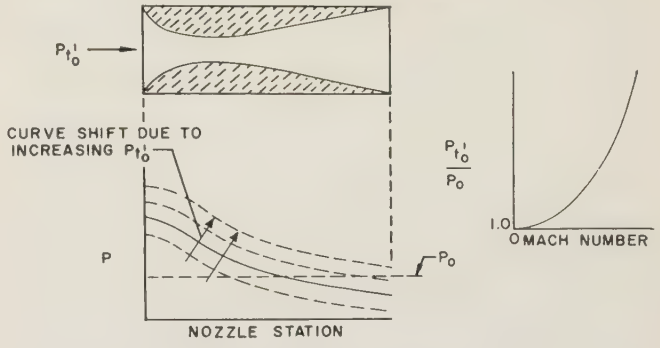

Fig. 38—Nozzle Characteristics

geometry of an inlet it sometimes becomes necessary to sense two pressures whose ratio is varying with flight conditions and to have an output as a function of this changing pressure ratio. One such application would be to sense a total to static pressure ratio in an airstream and compute the flow Mach number. This device can compute either free-stream or duct Mach number. Fig. 38 shows a nozzle in which air is passed through the nozzle with pressure ratio suffcient to maintain supersonic flow throughout the downstream portion of the nozzle. If the pressure source supplying the airflow through the nozzle can be made a function of the free-stream Mach number, it can be shown that a definite relationship exists between the pressure within the nozzle and the free-stream Mach number. Such a reference pressure may be obtained by placing a total pressure pickup in the free-stream flow. The relationship between the nozzle and free-stream Mach number can be correlated by finding a static pressure in the nozzle that matches the free-stream static pressure. This may be accomplished by placing a movable static pressure pickup in the nozzle and porting this pressure to one side of a diaphragm motor. The diaphragm motor will

have the free-stream ambient pressure ported to the other side of the diaphragm. The diaphragm motor will then be used to drive a servo valve, pressure divider, or electrical potentiometer. As the Mach number increases, increasing the static pressure throughout the nozzle, the pressure pickup must be moved to a new location in order to balance this sensed pressure against the free-stream static pressure. This will result in a shaft displacement which is a function of Mach number. A pressure divider which has a variable area orifice can be driven off the same diaphragm motor. Fig. 39 is an illustration of such an arrangement. As the Mach number increases, the area ratio of the pressure divider will vary changing the divided or demand pressure from the pressure divider. This pneumatic output can be used to bias another pneumatic control, or the pressure divider can be replaced with an electrical potentiometer or hydraulic servo valve.

In the event a hydraulic output is required, the diaphragm motor can be connected directly to a hydraulic servo valve and a flow rate from the servo valve will be obtained directly proportional to the displacement from a single pressure ratio or Mach number condition. However, for this application it is the usual practice to use a single pressure ratio controller. If the shaft displacement is required to indicate Mach number or to drive a variable inlet surface as a function of Mach number, the hydraulic flow from the servo valve can be ported directly to an actuator and the actuator in turn to the nozzle. As the Mach number increases, thereby increasing the static pressure throughout the nozzle, the diaphragm is displaced allowing hydraulic oil to flow to the actuator. The actuator translates the nozzle which changes the relative position of the pressure pickup in the nozzle until the pressure sensed by the pickup allows the diaphragm and servo valve to return to its nulled position. The summarized action is a shaft displacement as a function of the pressure ratio across the device and hence free-stream Mach number. The above described device can also be used to measure pressure ratio across such things as turbojet compressors, exhaust nozzles, and the like. Many applications of this device have been used at our plant in the past for such things as compressor pressure ratio, free-stream Mach number in ramjet engine controls, and free-stream Mach number to schedule variable geometry inlet surfaces.

The above devices described will sense and control pressure ratios to a single point value or to a multipressure ratio value. With these functions it is possible to mechanize any inlet geometry control system. Therefore, by utilizing the parameters available in the inlet such as described earlier it is possible to go directly from pneumatic pressures to the output of the working media used to drive the variable geometry surfaces. Any elimination of unnecessary steps between the sensing of the inlet parameters and the output of the control inherently increases the reliability of the system. As vehicle speeds steadily increase further and further into the supersonic regime, it becomes increasingly apparent that a rugged and reliable control system must be utilized, as the failure of the inlet control system can be catastrophic.

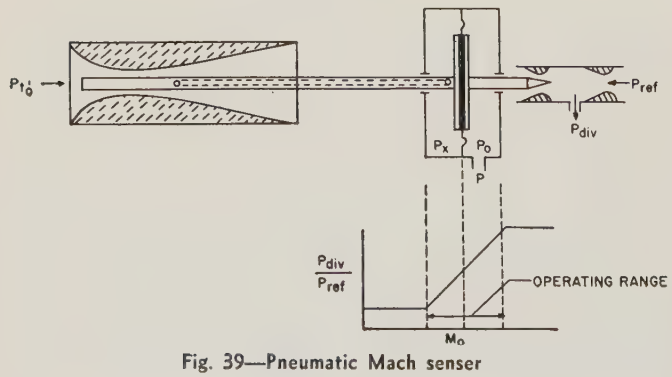

Fig. 39—Pneumatic Mach senser

APPENDIX

Nomenclature

A_B = Bypass flow area, sq in.

$A_{capture}$ = Area of free stream tube of air captured by the inlet, sq in.

A_E = Compressor face flow area, sq in.

$A_{inlet\ entrance}$ = Area within projection of inlet cowl leading edge, sq in.

$A_{maximum\ cowl}$ = Maximum cross-sectional area of powerplant cowling, sq in.

A_{throat}, A_{TH} = Minimum flow area within the inlet sq in.

AIA standard recovery = Standard total pressure recovery curve proposed by the Aircraft Engine Committee on the Aircraft Industries Association

C_D = Drag coefficient based on maximum cowl area

DS = Area of integration projected in direction of engine thrust, sq in.

$F(M)$ = Mass flow parameter = $\frac{W\sqrt{T_T}}{A\,P_T}$, $\left(\frac{\text{Sec }\sqrt{\text{R}}}{\text{ft}}\right)$

$F(M)^*$ = Mass flow parameter for choked flow, $\left(\frac{\text{Sec }\sqrt{\text{R}}}{\text{ft}}\right)$

F_G = Engine gross thrust, lb

F_N = Net engine thrust = $F_G - MV_0$, lb

F_N, F_{ideal} = Net engine thrust at 100% pressure recovery, lb

M = Mach number

M_o = Free stream or flight Mach number

MV_0 = Free stream momentum of engine airflow, lb

N = Engine rpm

Net Propulsive Thrust = Net engine thrust minus operational drag of inlet and installation drag of inlet and engine cowling, lb

P = Static pressure (absolute pressure except for additive drag calculations when gage pressure is required), lb per sq in.

P_T = Total or pilot pressure, lb per sq in.

$P_{T_{EF}}$ = Average total pressure at the engine face, lb per sq in.

P_{T_0} = Free-stream total pressure, lb per sq in.

R = Universal gas constant, ft lb per lb R

S = Laplace transform operator

T_T = Total temperature, R

V = Volume, cu in.

W = Mass flow, slugs per sec

W_F = Engine fuel flow

PRINCIPLES OF NOISE REDUCTION

L. M. Ball, Chrysler Corp.

This paper was presented at the SAE Annual Meeting, Detroit, Jan. 13, 1958.

THIS paper explains a few of the basic principles of the character of sound and the mechanism of human hearing. The author describes some simple experiments which demonstrate the relationship between intensity and loudness and the nature of harmony.

He also points out the difficulties of accurately analyzing sound electronically, and the resulting importance of combining the finest electronic equipment with sharp, attentive human faculties.

Five basic ways to reduce noise and the mechanics of each are described. The effect of these methods on the work of the sound engineer is indicated.

THIS discussion of the principles of sound reduction will explain a little of the scientific background of the subject by means of a few simple experiments. We shall explore the loudness of sounds and develop a suitable system of units to explain how sounds combine. We shall observe certain aspects of the character of sound and the mechanism of hearing. The five basic means available in the solution of all noise reduction problems will be demonstrated.

A simple sound of 500-cps frequency is called a pure tone because it contains no other components and its wave form is a pure sine wave. As the volume is turned up and down, the amplitude of the wave rises and falls and, of course, the loudness of the sound increases and decreases. What we would like to have is some sort of relation between the *physical intensity* of the sound and the *psychological loudness.* We can measure the *intensity* with instruments, but we must ask you to measure the *loudness* on a personal basis. Before this experiment can be performed, a set of coordinates should be worked out on which to plot the results.

In Fig. 1, the abscissa are loudness units, and for our purposes these units may be quite arbitrary. All we will need to use is the fact that a sound of 50 loudness units seems half as loud as one of 100 loudness units, and so on. The scale of ordinates—the physical sound intensity as measured with instruments—must cover quite an extended range to include all the sounds that can be heard from the weakest to the loudest. A scale for intensity units is shown in Fig. 2. If we don't want to spend the

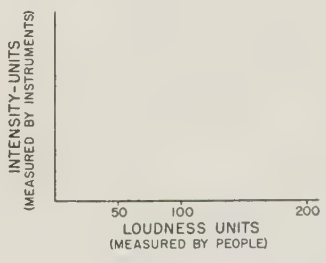

Fig. 1

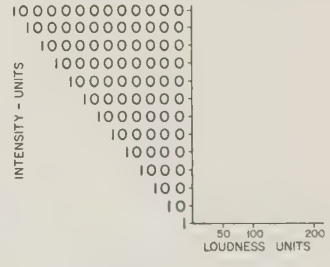

Fig. 2

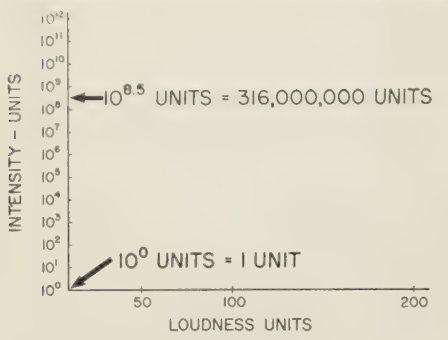

Fig. 3

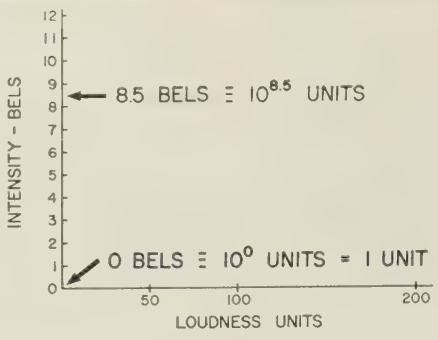

Fig. 4

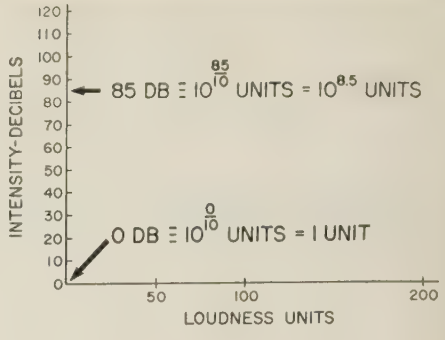

Fig. 5

rest of our lives writing zeros, we will have to use some other type of nomenclature. The physicists, of course, would write this as shown in Fig. 3. Note here that the point halfway between 10^8 and 10^9 represents $10^{8.5}$, which is approximately 316,000,000 units. Also, since any number raised to the 0 power is equal to *one*, 10^0 units is equal to 1 unit.

The telephone people decided not to bother with all this formality, so they just write down the exponents and give them a special name—bels—as shown in Fig. 4 Here, the point halfway between 8 and 9 represents 8.5 bels, which is equivalent to $10^{8.5}$. Likewise, 0 bels is equivalent to 10^0 units.

A bel is a pretty large measure. Increasing any quantity by 1 bel is equivalent to multiplying it by 10, and increasing it by 2 bels is equivalent to multiplying by 100. Consequently, most engineering work would involve small fractions of a bel. It is convenient to multiply these exponents by 10 and call them decibels as shown in Fig. 5. The point halfway between 80 and 90 represents 85 db, which is equivalent to $10^{\frac{85}{10}}$ or $10^{8.5}$ which, as we have shown before, is approximately 316,000,000 units. Zero db is one unit.

Sound Intensity Related to Loudness—Now we are in a position to plot a relationship between sound intensity and loudness. A sound of 80 db intensity (100 loudness units) is represented by the point shown in Fig. 6. A vast majority of participants in an experiment indicate that this sound has been reduced to one-half its original loudness at the point shown in Fig. 7.

If we now start with the original 80-db sound and by a similar method *increase* the volume so that it appears to be twice as loud, we get another point to plot. The results indicate that the loudness has been doubled at the point plotted in Fig. 8. These points are replotted in Fig. 9, indicating several important things. In the first place, the three points are equally spaced on the vertical scale, and each reduction of 50% in loudness occurs when the intensity has been reduced 9 db.

Conversely, increasing the intensity of the sound by 9 db doubles its loudness. This is a fairly accurate representation in the range which has been covered and has been confirmed by numerous experiments on large numbers of people under very carefully controlled conditions. This simple relationship does not hold throughout the entire range of audible sound intensity but is sufficiently accurate for most practical purposes.

Decibel Arithmetic—It is now necessary to develop a little simple mathematics in order to make use of the relationship just discussed. We know that:

$$316{,}000{,}000 = 10^{\frac{85}{10}}$$

To be a little more general, let's say:

S = Strength of sound in intensity units

N = Number of db corresponding to S

$$S = 10^{\frac{N}{10}}$$

Taking the common logarithm of both sides:

$$\text{Log } S = \frac{N}{10} \qquad (1)$$

or

$$10 \text{ Log } S = N$$

Suppose we add two equal sounds so the strength is $S + S$ intensity units. How many db will that be? In mathematical form: 10 Log $(S + S)$ = ?

$$10 \text{ Log } (S + S) = 10 \text{ Log } 2S = 10 \text{ Log } S + 10 \text{ Log } 2$$

(Log 2 = 0.30)

$$10 \text{ Log } (S + S) = N + 3 \qquad (2)$$

This is true regardless of the size of S, so whenever two equal sounds are added, the db increase by 3.

The following table conforms with this law, although it may look a little odd at first glance:

$$N + N = N + 3$$
$$50 + 50 = 53$$
$$80 + 80 = 83$$
$$95 + 95 = 98$$

and even $0 + 0 = 3$

With this new arithmetic, we can now try to determine the effect of adding several sources of sound. To make it easy we shall say that each source has an intensity of 80 db. Adding two of these sounds together we have $80 + 80 = 83$. If we add to these another *pair* of 80-db sounds, we would in effect be combining two 83-db sounds, and the sum would be 3 db greater, or 86 db. Thus, the combined effect of four 80-db sounds is a sound of 86 db. If we now take another set of four 80-db sounds, this set also would have an intensity of 86 db and, consequently, the intensity of the two sets acting together would be 89 db.

Need Seven-eighths Intensity Drop to Reduce Loudness by Half—Suppose now we decide that this amount of sound is intolerable and we desire to cut the loudness in half. It is easy to see that by cutting out half of the sources, the intensity would drop from 89 to 86 db. However, we have already shown in our earlier experiment that this is not

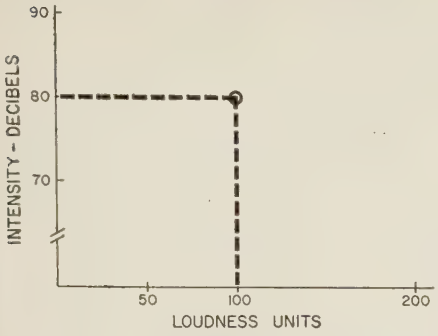

Fig. 6

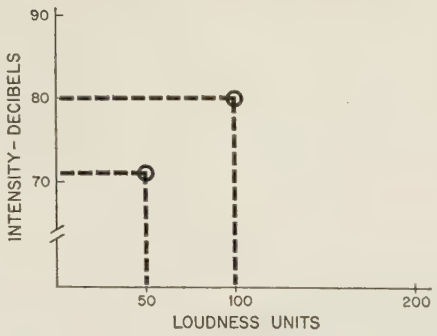

Fig. 7

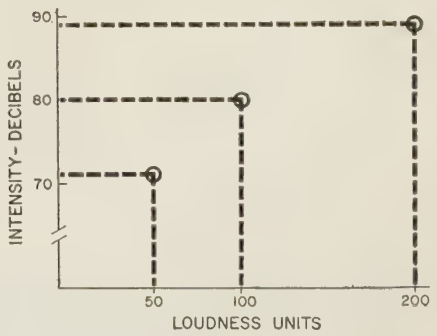

Fig. 8

enough to reduce the loudness 50%. Let us, therefore, cut off two of the remaining four sources. This maneuver of cutting the number of remaining sources in half accomplishes another 3-db reduction, and the sound intensity drops from 86 to 83 db. So with six of the eight equal sound sources cut off, the intensity has decreased from 89 to 83 db, a decrease of 6 db, and still not enough to reduce the loudness 50%.

In order to achieve the 50% reduction in loudness which demands a 9-db reduction in intensity, we see that we must cut off one of the two remaining sources. Thus, in order to reduce the loudness to one-half, we must remove seven-eighths of the sound.

This is one of the things that makes sound reduction so very difficult. Since it is a built-in characteristic of the human hearing system, we have no choice but to comply.

Incidentally, cutting off only one of the eight equal sources of sound makes only an inconsequential reduction in either loudness or intensity. As a matter of fact, in db arithmetic: $89 - 80 = 88.4$.

Putting Character into Sound—Let us now turn our attention to the *character* of sound. A pure tone having a frequency of 500 cps, is a pure sine wave. If we mix in a little sound having a frequency of 1,000 cps (physicists call this second harmonic and the musicians call it the octave), the wave shape is distorted, the upward peak somewhat sharpened and the downward peak somewhat flattened. Also, it is very easy to detect the presence of the octave or second harmonic by merely listening to the sound.

Another combination is a mixture of some 500-cps and some 750-cps sound. The ratio of these frequencies is 3:2, and in musical notation this is called a perfect fifth. Adjacent strings on the cello or violin are tuned in this ratio. The next combination is a mixture of 500 and 667 cps. The ratio between these frequencies is 4:3, and in musical notation this is known as a perfect fourth. Incidentally, all the nice sounding pairs of musical tones can be expressed as ratios of integers smaller than six.

It is interesting to note that we have not only the sensation of hearing the combination itself, but also hear and can recognize the tones of which it is composed. This is called analyzing ability and it is much more highly developed in the mechanism of hearing than in the sensation of sight. While we cannot distinguish the separate frequencies in mixed light, as revealed by the well-known experiment of the spinning color wheel, we can hear separate frequencies in mixed sound.

A mixture of 500 cps with 501 cps produces a periodic rise and fall in intensity called "beats." The variation in intensity is repeated at a rate equal to the difference between the two frequencies, which is one variation per sec in this case. In mechanical systems, such a phenomenon always suggests a cause involving two elements running at slightly different speeds.

Another important aspect of the character of sound is commonly called the "signal-to-noise ratio." A vocal statement is referred to as intelligence (within the broad meaning of the word), and the reproduction of a voice transmitting the intelligence is called the signal. If a lot of other noise is present on a tape recording the signal is unintelligible, or, in other words, the intelligence cannot be abstracted from this complex sound. Even after an increase in the volume by amplification, it is still unintelligible. Of course, when the whole sound is amplified the signal and the background noise are amplified equally; consequently, the "signal-to-noise ratio" is not improved.

When the relative intensity of the background noise is reduced so that the "signal-to-noise ratio" is much higher the signal is perfectly intelligible.

The Human Ear, A Very Sensitive Organ—A most important consideration is the *sensitivity* of the average human ear, and it is particularly enlightening to discuss this in terms of the amplitude of mo-

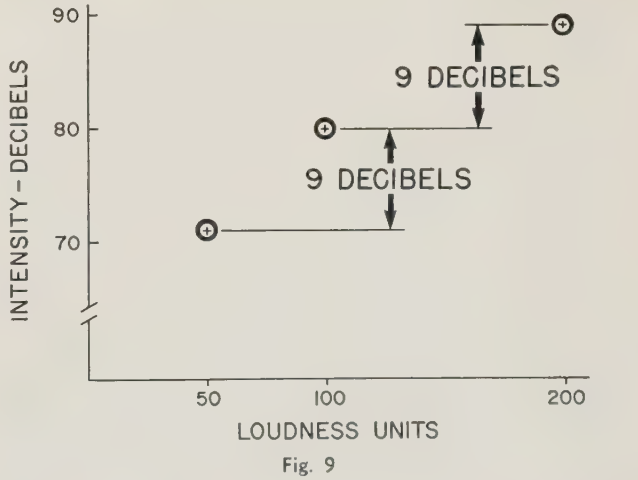

Fig. 9

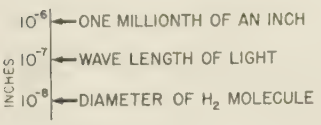

Fig. 10

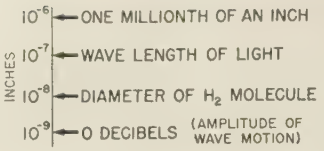

Fig. 11

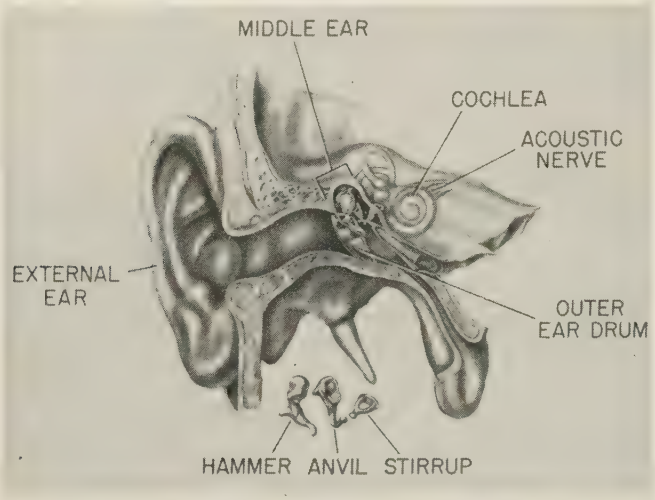

Fig. 12

tion of air particles in the sound wave which stimulates the sensation of hearing. The scale in Fig. 10 follows the nomenclature of the physicists.

People with normal hearing acuity can detect a sound having an intensity of 1 unit (0 db) and the corresponding amplitude of wave motion is as shown in Fig. 11. Thus, we see that an ordinary human ear is so fantastically sensitive that it can detect motions much smaller than the diameter of a hydrogen molecule.

It is a fact that certain persons with especially acute hearing can detect sounds having intensities 10 db lower than 1 unit; that is, sounds having an intensity of 1/10 unit. The molecules of air are always moving to and fro in a random motion called thermal agitation, the violence of which is a direct function of the absolute temperature. This random motion produces noise (called white noise by analogy with white light, since it is a mixture of all frequencies). When the intensity of this white noise is calculated for normal temperatures it is discovered that any further increase in the sensitivity of the human ear would not improve the ability to hear significant sounds, since the human ear is already so sensitive that the "signal-to-noise ratio" is a limiting factor. We thus conclude that the design of the human hearing system is optimum for creatures living in air at normal temperatures.

Fig. 12 is a cross-section of the human ear. The *outer ear* includes the visible external part which collects sound waves and directs them into a channel terminated by the outer eardrum. Sound waves impinging on this membrane set it in vibration, and the vibrations are transmitted through the three little bones of the *middle ear* to the *inner ear*. The inner ear is a long tube filled with fluid and separated into two channels by the basilar membrane which extends almost, but not quite, to the end of the tube. This tube communicates with the middle ear through two windows or diaphragms, one above the basilar membrane and one below it.

Thus, sound waves can enter the upper window, pass along through the fluid above the basilar membrane, and return under the membrane to the lower window which accommodates the pressure variations in the fluid. The basilar membrane supports the nerve endings which are stimulated by the fluid vibrations and give rise to the sensation of hearing. This tube is coiled into a spiral of about 2½ turns and is called the cochlea.

The three little bones of the middle ear—the hammer, the anvil, and the stirrup—form a chain which terminates in the upper window of the cochlea. They transmit vibrations of the outer eardrum through this window or inner eardrum into the cochlea. These bones deserve further comment, but let us first digress a moment to mention a principle of electrical engineering.

When a generator delivers power to a load, as shown in Fig. 13, maximum efficiency is obtained when the impedance of the load Z_2 is equal to that of the generator Z_1. When this is not the case and the impedances are not equal, the generator may work harder but deliver less power, as shown in Fig. 14. Under such conditions, the delivery of power can be optimized by introducing a transformer as shown in Fig. 15. Here n is the ratio of the number of turns in the secondary to the number of turns in the primary and should be equal to the square root of the ratio of the connected impedances.

In the human ear the outer eardrum is relatively large, thin, and flexible, and is in contact with air on both sides; in other words, its impedance is low. The inner eardrum, on the other hand, is relatively small, thick, and inflexible, and is in contact on one side with a fluid having a density much higher than that of air. Its impedance is high, and, as a matter of fact, the ratio of the two impedances is of the order of 400:1.

If we now carefully examine the three little bones of the middle ear, we discover that they form a mechanical lever system. They perform a function exactly analogous to that of the transformer in an electrical circuit. It is interesting to realize that the ratio of this mechanical lever system is about 20:1, which turns out to be equal to the square root of 400, the impedance ratio of the two eardrums. Here again, the design of the ear embodies the very best scientific principles.

Methods Being Used to Analyze Sounds

We now return to the subject of analyzing sounds to discuss some of the more practical aspects. We have at our disposal various oscillographic devices which can record the actual wave shape of the motions involved in a sound. In Fig. 16, two such oscillograms are shown and the striking correspondence between the traces produced by the two different sounds is readily apparent.

They appear to have about the same duration, amplitude, and frequency. The initial rise in amplitude, the sudden decay, and even the fine structure are about the same for both oscillograms. According to the oscillographic analysis, it would certainly appear that there is little, if any, signifi-

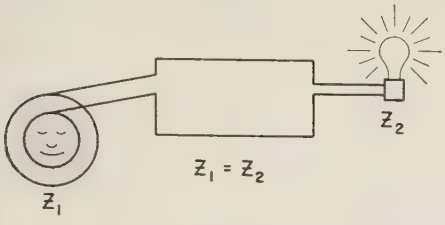

Fig. 13

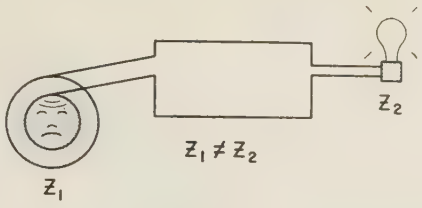

Fig. 14

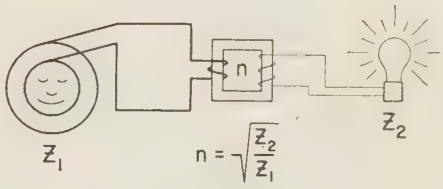

Fig. 15

cant difference between these two sounds.

The same sound "A" recorded on tape consists mainly of a repetition of the word "white, white, white." Sound "B" is a similar repetition of the word black. It is hard to see how we could be misled any further if, using an oscillograph, we cannot tell black from white. Consequently, it behoves us to use oscillograms with great caution when it comes to analyzing sound.

There are sound analyzing devices which can be tuned to respond only to a sound of a specified frequency in much the same way as a radio can be tuned to receive only signals of a specified frequency; that is, the signals from a particular radio station. These devices are certainly helpful, but we so often find that they "hear" and respond to sounds which may be entirely extraneous to the problem under investigation and thereby give false and misleading clues.

A good analyzer, of course, would be one which you could direct to respond to a certain specified disturbance in such a way that you could, for example, say "Now pay no attention to this road noise or the wind whistle . . . but when I step on the gas like this . . . wait a minute until that truck goes by . . . now! that is the sound I mean . . . what frequencies does it contain?"

Fantastic as it may seem, this is not impossible. In fact, I have used such an analyzer (Fig. 17). This young lady happens to be blessed with absolute pitch, and can indeed analyze complex sounds as described, with attention being directed towards certain specified combinations of tones while other interfering sounds are deliberately ignored.

I do not mean to be frivolous in any way, but I merely wish to lay great emphasis on the fact that in sound work it is of the utmost importance to make the fullest possible use of human faculties. It is almost always unwise to entirely replace human reactions with electronic instruments. It is far preferable to use electronics to extend and supplement human faculties. An electronic analyzer is abysmally stupid and has no conscience whatsoever. It will lead you astray at the slightest provocation and it should be constantly monitored and checked by intelligent listening.

With the rapid development of electronic arts, the field of acoustics has been immensely enriched. Today, the sound engineer has many powerful tools and sophisticated techniques.

Basic Ways to Reduce Noise

We shall now review briefly a few experiments which demonstrate the five basic means available for the solution of all noise reduction problems.

Fig. 16

Fig. 17

They are:

1. Reduction at the source.
2. Mechanical isolation.
3. Damping of resonant elements.
4. Enclosure (sound insulation).
5. Sound absorption.

Reduction at the Source—In an electric buzzer, for example, which produces a moderately complex sound, we can reduce the noise at its source by inserting soft bumpers to modify the sharp metal-to-metal impacts. In more intricate machines, noise can usually be reduced by balancing rotating parts, reducing clearances, and generally improving the excellence of mechanical design and manufacture. This is an important step which should never be overlooked, since it is often more rewarding than merely loading on acoustic treatment.

Mechanical Isolation—It is a matter of common experience that a mechanism may transmit vibrations through its supports and telegraph them to other parts of the structure which seem to amplify and radiate the sound. A well-designed vibration-isolating mounting can produce spectacular reductions in transmitted vibrations and noise. The theory of such mounting systems has been treated

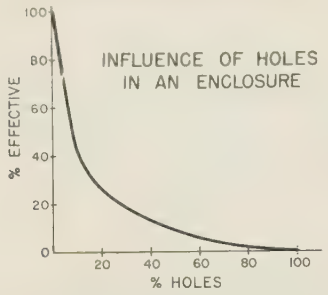

Fig. 18

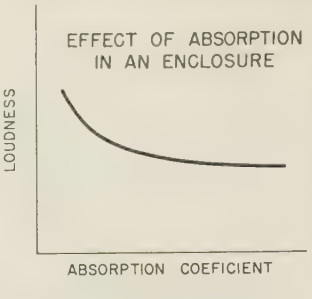

Fig. 19

exhaustively in papers before this Society and elsewhere in the literature.

Damping of Resonant Elements—When a frequency of the noise source is "tuned in" with a natural frequency of some relatively large flexible panel, the resonant vibrations produced may radiate large quantities of sound. Some treatment of the panel which produces hysteresis damping or converts vibrational energy into heat can greatly reduce the amplitude of motion at resonance and thereby reduce the sound radiated. If the panel is excited impulsively, say by an impact such as slamming a car door, then the damping shortens the duration of the sound emitted, eliminating ringing or rumbling and giving the sensation of a dull thud or thump which is generally considered more agreeable. Asphalt with sand filler and asphalt-saturated felt are commonly used to provide damping of metal panels. This method can be demonstrated by using a panel which can be caused to vibrate by plucking a rope attached to the center of the panel. As a little sand is poured on the panel, the sound becomes softened, muffled, and deadened.

Enclosure (Sound Insulation)—Although the term sound insulation is frequently used to include any and all kinds of acoustic treatment, it is more properly restricted to those constructions designed to prevent or reduce the transmission of airborne sound.

By experiment, we shall demonstrate how the noise transmitted from a source is reduced by surrounding it with an enclosure. A box made from one of the finest sound-absorbing materials is placed over the source, giving a remarkably disappointing reduction in noise. This explodes a very popular misconception that sound enclosures should be made from light, fluffy sound-absorbing materials.

That the contrary is the case can easily be demonstrated by covering the source with a heavy steel box. The sound then appears to be completely eliminated. Analysis predicts and experience confirms that, in general, the effectiveness of sound-insulating materials is directly proportional to the weight.

A factor of the utmost practical importance and one which is often overlooked is the degree of completeness of the enclosure. A few leaks or holes which amount to an insignificant percentage of the total area of an enclosure can almost completely nullify its effectiveness. Fig. 18 shows this in a graphical way. It indicates, for instance, how a poorly fitted grommet in the dash could easily rob the dash liner of a dollar's worth of sound-insulating value.

Sound Absorption—When the sound level within an enclosure has been reduced by reasonable application of the methods discussed, it is often possible to make a further reduction by applying sound-absorption materials. The sound level in a space is determined by equilibrium between the rate at which sound energy enters the space and the rate at which it leaves. If, for example, the strength or output from a noise maker is increased, the sound level will rise just enough to force the increased energy out of the space at the rate at which it is being generated. Conversely, if the rate at which sound energy leaves the space be enhanced (for example, by increasing the amount of sound absorption within the space), then equilibrium of energy rates will be reached at a lower sound level.

If the rate of energy absorption is great enough, when a noise maker is placed inside an elongated box lined with sound-absorbing material, the sound level will be so low that even at the open face of the box the noise will be inaudible. As the amount of sound absorption within an enclosure is increased, the effectiveness follows a law of diminishing returns. This is depicted in Fig. 19 for a typical case; as a matter of fact, the shape of this curve is characteristic of the law of diminishing returns for all types of acoustic treatment in general.

Application of this curve explains certain experimental results which might otherwise seem quite paradoxical. Consider the case of two alternative car components: A and B. Fig. 20 shows that "B" is inherently quieter than "A" (and we shall assume that, as is usually the case, "B" costs more than "A"). Suppose we perform experiments to evaluate the effect of adding acoustic treatment to "A" and plot the results as shown in Fig. 21. It is seen that in order to reduce the sound level of "A" to that of "B" we must add $5 worth of acoustic treatment. In this case, if the cost penalty of "B" is less than $5, it would be more economical to use "B" rather than to add acoustic treatment to "A."

However, an alert cost-conscious management might well ask: On the assumption that the noise level of "A" is acceptable, how much money might we *save* by using "B" and *removing* enough acoustic treatment to bring the sound level up to that of "A"? If suitable experiments were performed and it were reported that the cost saving in acoustic treatment amounted to only $0.70, there might be some question as to the competence or objectivity of the acoustical department. How can it be true that we must add $5 worth of acoustical treatment to *reduce* the sound level a certain amount while we can remove only $0.70 worth of insulation to *increase* the sound level by the *same amount?*

As previously indicated, the explanation of the paradox is revealed by the law of diminishing returns. In this case, this can be demonstrated by extending the curves as in Fig. 22. It can be seen that the result is an inevitable consequence of the fact that each additional increment of acoustic treatment produces a diminishing increment of sound reduction. In other words, no matter where we start, the cost penalty for an increment of sound reduction is always greater than the cost saving for an equal increment of sound increase.

The curve of diminishing returns also operates in reverse. Let us assume that the acoustic treatment of a vehicle comprises a large number of equivalent pieces. Working backwards along the curve, we see

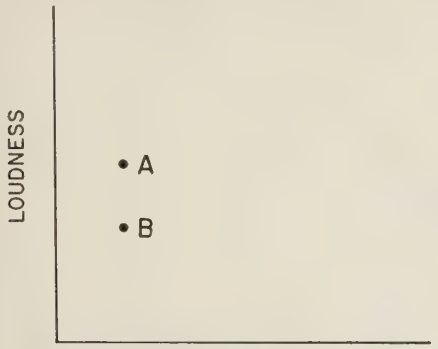

Fig. 20

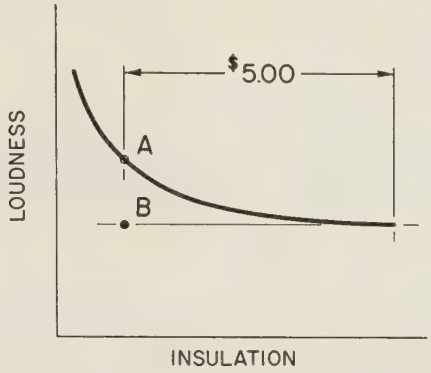

Fig. 21

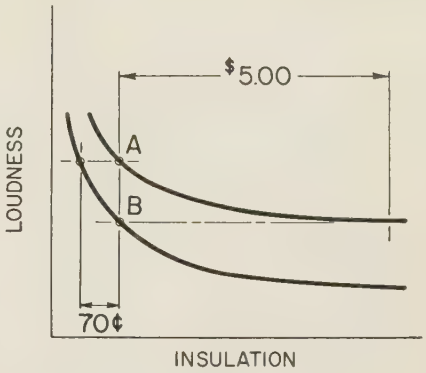

Fig. 22

that removal of the first piece does not do as much harm as removal of the second piece. An overzealous cost expert interprets this to mean that he wasn't getting his money's worth out of the first piece because, although it cost just as much as the second piece, it wasn't doing as good a job. Unfortunately, this is quite true. Furthermore, because of technical difficulties in the precise measurement of sound, a test to demonstrate the effect of removing a small piece of acoustic treatment might very well show that the sound level doesn't increase at all, whereas the cost expert can always show a cost saving.

If we do indeed remove the first piece of acoustic treatment, a very interesting situation develops. The second piece is not doing as good a job as the third piece. The argument presented above now applies just as well to the second piece. This "divide and conquer" approach, if employed with diligence, should result in removing all but the last piece of acoustic treatment. The science of acoustics offers no ready-made solution to this problem.

Conclusion

From what precedes, it can be seen that because of physiological factors inherent in our hearing system, and because of the peculiar relationship between *sound intensity* and *loudness perception*, noise reduction in mechanical systems presents real problems to the sound engineer. While economic factors must be taken into account and the law of diminishing returns imposes a certain restriction upon a noise reduction program, the sound engineer has at his disposal five basic means to achieve the desired results. In summary, these means are:

1. Reduction of noise at the source by avoiding mechanisms which produce large impulsive forces and by general refinement of mechanical design and fabrication.
2. Use of vibration isolating mountings to reduce the disturbances transmitted to other parts of the assembly where the configuration may be conducive to the radiation of sound.
3. Damping of resonant elements to reduce vibration and consequent radiation of noise and to quench the ringing or rumbling which might otherwise be prolonged.
4. Enclosure of the noise source in a heavy barrier which is free from cracks and openings through which noise may escape.
5. Use of sound-absorbing materials to reduce the sound level at which noise energy dissipation is in equilibrium with noise energy generation.

These are the resources of the sound engineer, and the success of any noise reduction program depends upon his astuteness in blending these ingredients into a well-balanced recipe.

DISCUSSION

Points Out Noise Reduction Properties of Butyl Tires

—R. F. Neu
Enjay Laboratories

IN considering this paper, I have been trying to relate Mr. Ball's five basic principles of noise reduction to some specific techniques available to the design and materials engineers in the automotive industry—particularly in the reduction "unpitched noise."

The choice of elastomer for various automotive parts seems quite important in reduction of noise (1) at the source, (2) by vibration isolating materials, and (3) by damping of resonant elements.

For example, recent road tests in Florida have shown that the use of butyl nylon tires instead of SBR nylon tires can reduce average noise level at the source (that is the road) by 50%. Similar noise reductions are obtained when comparing rayon tires. These tests were run on coarse macadam and were evaluated by human ear and by instruments. Furthermore, tire squeal on cornering has been substantially eliminated through the use of butyl tires.

As Mr. Ball points out, the use of rubber is common in reducing noise by isolating vibration and damping. The unique shock-absorbing and damping properties of butyl may be of special interest here. R. E. Morris and coworkers at the Navy's Mare Island Rubber Laboratory have shown that natural rubber exhibits three resonant peaks over the frequency range of 0–1400 cps, while over the same range butyl exhibits no such peaks because of its high damping factor.

Thus it would appear that by judicious choice of the elastomer to be used in the tire and various shock-absorbing, mounting, and insulating assemblies on a car, the automotive engineer can effect still further reductions in noise and vibrations beyond those attained with today's complex suspension and acoustical systems.

Diesel Cylinder

THE problem of this study was:

1. Can a method of analysis be found which adequately predicts the heat-transfer and cyl-wall temperature phenomena in diesel engines?
2. Are there criteria for the design of diesel engine cyl that give the limits of reliable practice as found in typical diesels?

Such a method of analysis is detailed in this paper. Design criteria were also found which appear applicable to broad classes of diesel engines. It was determined that the method was useful in prediction of the thermodynamic performance of a diesel insofar as the influence of cyl heat transfer on efficiency, power, and cooling load were predictable.

THE development of the Orion engine[1] called for unusually stringent diesel cylinder[2] cooling limitations. As a result, criteria were sought for the thermal design requirements of diesel engines. It was anticipated that there would be a limiting cyl-wall temperature at which lubrication would break down, possibly due to fractional distillation of the lubricating oil from the cyl walls as described by Nutt, Landen, and Edgar.[3] Such a phenomenon would explain the ability of laboratory engines to achieve high ratings for short bursts which were far beyond the capability of a reliable hard-working engine. The position on the cyl wall reached by the highest travel of the piston ring would be most critical due to its continuous exposure to gas.

A second area wherein criteria were needed was that of cooling capacity. Water-cooled engines generally have adequate cooling capacity. However, the aircooled engine requires detailed design effort to assure that the supply of coolant is adequate and its distribution is effective.

A third limitation is the thermal stress problem. Insight into this problem may be gained through detailed analyses of the heat input into the cyl wall from the cyl gases. This problem is aggravated by complex structures which make an analysis less exact and more necessary.

In the thermodynamic analysis of a new engine design, the gross cyl heat loss represents a penalty to engine efficiency and output. Early assessment of this loss may point to design modifications which can prevent excessive cooling in unnecessary regions. The analytical method outlined results in reasonable cyl heat loss and indicates its variation in a manner consistent with physical expectations.

Factors Influencing Cyl Heat Transfer

It has been a common experience that thermocouples measuring exhaust temperature at the cyl head of diesel engines read 100 F lower than the temperature recorded at the exhaust manifold outlet. Such a difference can be rationalized on the basis of the physics of heat transfer. The initial gas which blasts out of the cyl is at a very high temperature. The high velocity of this gas as it rushes past the first thermocouple reduces the boundary layer thickness and, consequently, promotes rapid heat transfer from that gas to the thermocouple. However, the total heat transferred to the thermocouple during blowdown is small compared to the mass of gas causing that heat transfer. The gas which remains in the cyl is at reduced temperature as a consequence of the continued gas expansion resulting from the outburst of the blowdown gas. When this residual gas is displaced from the cyl it moves at a relatively languid velocity by the thermocouple. The heat-transfer rate from the hotter thermocouple to this relatively cooler gas is reduced, due to a thicker gas boundary layer. However, the thermocouple continues to be cooled by this gas during the working strokes which comprise approximately half the time. The exhaust gas thermocouple in the cyl head, therefore, comes to a temperature which favors the cooler residual gas. In contrast, the rate of gas flow over the exhaust manifold thermocouple is more uniform and it records an energy mean temperature which should be higher. From this example it can be seen that in the use of gas temperature as a potential for heat transfer, consideration must be given to the variation of heat-transfer coefficient and the duration of exposure to heat transfer.

The gas in the cyl of the diesel engine experiences continuous changes of state. For this reason, it must be expected that temperatures and heat-transfer coefficients for the cyl gas will vary drastically. The physics of heat transfer demands that the following influences should be an integral part of cyl heat-transfer correlations.

Piston speed or gas velocity within the cyl must

---

[1] SAE Transactions, Vol. 65, 1957, pp. 293–330: "Orion—A Gas-Generator Turbocompound Engine," by R. J. Hooker.
[2] Abbreviated as cyl throughout paper.
[3] SAE Transactions, Vol. 63, 1955, pp. 694–703: "Effect of Surface Temperature on Wear of Diesel Engine Cylinders and Piston Rings," by H. V. Nutt, W. W. Landen, and J. A. Edgar.

Heat Transfer Design Criteria

D. H. Brown, General Electric Co.

This paper was presented at the SAE National Diesel Engine Meeting, Cleveland, Nov. 6, 1957.

influence heat transfer. As the speed increases, a thinner boundary layer must result and resistance to heat transfer decrease. As a result of higher piston speed, heat transfer must be expedited and a greater thermal load will be experienced by the engine. In this context rpm should not be confused with piston speed. The actual velocity in such units as fpm is the index of the generation of turbulence and a measure of the boundary layer condition.

The density of the gas must be an influential factor. The rarer the gas, the greater the resistance to heat transfer. This is of importance when consideration is given to supercharging of the engine to higher levels. In addition, variation of the compression ratio will be influential. The initial cyl charge as determined by scavenging in 2- and 4-stroke diesels will effect the mass of gas trapped in the cyl and, thus, the gas density. Since the greatest amount of heat will be transferred when the density is greatest, the more influential measure of density will be that when the piston is on tdc during the working stroke.

The instantaneous gas temperature is, of course, a prime variable in regard to heat transfer. It must be expected that the mean temperature which gives the potential for heat transfer from the cyl gas must be more representative of the peak temperatures in the cycle than of the lower temperatures. The peak temperatures will be determined by the combustion processes and the initial cyl charge. Reduction of cyl charge while maintaining the same fuel input will greatly increase peak cyl temperatures and heat transfer.

Cyl-wall thickness and material does not appear to greatly influence the rate of heat transfer. However, it is of prime importance in determining the cyl-wall surface temperature and its adequacy to maintaining a lubricated surface.

The coolant heat-transfer phenomenon is important with regard to avoidance of hot spots and insuring cyl-wall lubrication. This is particularly true of air as a coolant. In a liquid-cooled engine the condition of the water coolant is of importance in regard to the likelihood of nucleate boiling. Also, the presence of antifreeze solutions drastically reduces the heat-transfer coefficients. In searching the literature for means of analytically evaluating diesel-cyl conditions, satisfaction of these criteria was required. In addition, it was deemed necessary that the analytical method should stem from actual engine measurements and tests. It was further hoped that the method employed would be applicable to a wide spectrum of engine size and speed. The Eichelberg method of analysis[4] showed promise of meeting these requirements, so it was applied to data from the technical literature and found to be

[4] *Engineering*, Vol. 148, Oct. 27, 1939, pp. 463–466; Nov. 17, 1939, pp. 547–550; Dec. 1, 1939, pp. 603–605; Dec. 22, 1939, pp. 682–686; Vol. 149, March 22, 1940, pp. 297–299: "Some New Investigations on Old Combustion Engine Problems," by G. Eichelberg.

Fig. 1—Single Orion cyl

consistent with the method of thermodynamic analysis used and the engine test results reported.

Orion Engine

The Orion engine was unique in that it comprised an opposed-piston engine driving only a supercharging air compressor and a high-pressure cooling air compressor. The diesel exhaust and the heated cooling air were mixed at turbine inlet pressure and then expanded through the drive turbine. The operating characteristic was similar to a torque converter drive in that the diesel followed a propellor-type load and supplied only hot pressurized gas to the turbine; variations in load torque were met by the turbine without influencing the diesel. The critical consideration was whether a supercharged 2-stroke diesel could be adequately cooled by relatively high-temperature air. The engine cyl had the injector hole at the center, the finned surface on either side of the injector hole surrounded the clearance volume, and the top piston ring on either side advanced only to the section where the fins are interrupted (Fig. 1). This interruption of the airflow was designed to promote air turbulence and enhance the cooling heat transfer at this critical section. Since this is the hottest cyl-wall surface, and the point where greatest wear occurs, particular attention must be paid to liner-wall temperature on the gas side where adequate lubrication must be maintained.

Cyl Heat Transfer

The determination of temperatures would be very easy if steady heat flow existed. (See Fig. 2). The temperature drop through the gas to the cyl wall is visualized as occurring in a thin gas film that adheres to the wall. Due to the poor thermal conductivity of the gas a steep temperature drop is portrayed. The conduction of heat through the cyl-wall metal would require but a small temperature drop due to the high metal thermal conductivity. On the coolant side a film is again envisioned through which only conduction occurs. It is important to remember that the idea of a film or a stagnant boundary layer is a figment of the imagination which successfully yields engineering solutions in many instances. All studies of boundary layers reveal that they are physically much more complex than the simple model of a stagnant film. It is this degree of approximation that leads to good heat transfer correlations in simple apparatus like long straight tubes, and much more divergent results in complex apparatus like the diesel engine.

While the concept of thermal conductivity through films and metal follows typical heat-transfer nomenclature, it leads to unnecessarily cumbersome mathematics. The reciprocal of thermal conductivity is the resistance to heat transfer. As illustrated by the right hand portion of Fig. 2, such a measure straightens out the abrupt variations in temperature gradient and gives the heat-transfer rate as the slope of the temperature-resistance curve. As in any series flow situation:

$$\bar{q} = \frac{T_{GA} - T_{WG}}{R_G} = \frac{T_{WG} - T_{WC}}{R_W} = \frac{T_{WC} - T_C}{R_C} = \frac{T_{GA} - T_C}{R_G + R_W + R_C} = \frac{T_{WG} - T_C}{R_W + R_C} \qquad (1)$$

Since the thermal resistance of the cyl wall and the coolant are readily determined and coolant temperature is generally known, it is evident that only the effective gas temperature and gas film resistance are needed for a solution. In this instance,

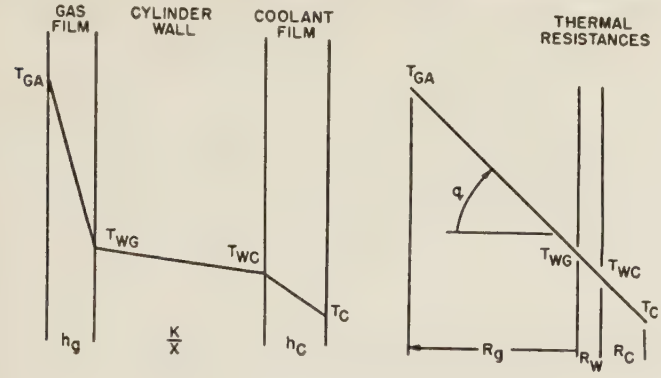

Fig. 2—Cyl-wall heat transfer

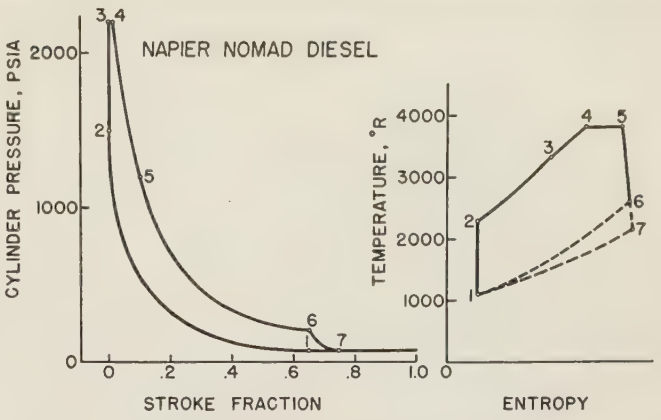

Fig. 3—Cyl thermodynamic processes

the engine can solve the problem somewhat more easily than the engineer.

The gas temperature and gas film resistance are not constant in an engine; they fluctuate greatly in each cycle. The cyl wall comes to such a gas side temperature that it continually drains off heat at a rate equal to the integrated input from the gas each cycle. The thermal capacitance of the cyl-wall metal is sufficiently great that temperature fluctuations are in evidence only within a mm or less of the cyl-wall gas side surface. The small cyclic variation in cyl-wall temperature was not evaluated. Since the engine constitutes a high-speed computer in this phenomenon, it appeared imperative that a computational procedure be similar to that within the engine. This required the evaluation of instantaneous values for gas temperature and gas film resistance over a complete engine cycle—one revolution for a 2-stroke and two for a 4-stroke diesel. Thereafter, the integration of these values reveals the effective values which would produce the same results by acting continuously.

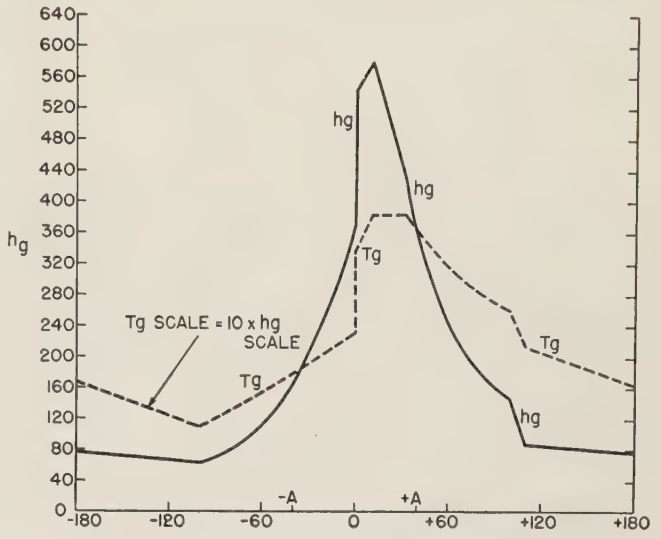

Fig. 4—Instantaneous gas properties for one cycle

Eichelberg Method of Analysis

The method of analysis presented by Eichelberg was derived by measurements on actual engines. It meets the necessary standards that have been outlined. In addition, the necessary values for determination of the instantaneous gas heat-transfer coefficient stem from the thermodynamic pressure-volume data which are needed for evaluation of mechanical loads on the engine and its crankshaft as well.

$$h_G = K(PT)^{1/2} \qquad (2)$$

The influence of speed is incorporated in the constant through use of the average piston speed in fpm.

$$K = 0.0147 \text{ (piston speed)}^{1/3} \qquad (3)$$

To illustrate the application of this method the Napier Nomad diesel has been analyzed.[5] This choice was based on the unusual operating conditions with high air manifold pressure and temperature and low compression ratio. Similar analyses were made for the General Motors 567B diesel,[6] the Alco 244 diesel, and the MAN highly supercharged diesel.[7] The thermodynamic processes within the Nomad cyl are illustrated in Fig. 3. The cyl condition at the end of scavenge and at the end of blowdown was determined by use of transient thermodynamic analysis.[8] The energy release by combustion was reduced in proportion to cyl cooling to avoid establishing an unattainable performance standard.

The events from Fig. 3 were then replotted on the basis of crank angle which is a suitable time basis. The resulting gas film heat-transfer coefficient is seen to vary greatly over one revolution of the engine. It is notable that the value is 10 times as great during combustion as it is during scavenge. Since gas temperature peaks simultaneously, it would appear that the sequence of events over the combustion process influences the ultimate heat transfer far more than that at the low pressures represented by the exhaust and scavenging events. The time average value for the film coefficient, *hg* was determined from Fig. 4.

The sequence of events is depicted in a manner

[5] SAE Transactions, Vol. 63, 1955, pp. 107–131: "Napier Nomad Aircraft Diesel Engine," by H. Sammons and E. Chatterton.

[6] "History and Development of 567 Series General Motors Locomotive Engine," E. W. Kettering. ASME paper 51-A-72, 1951.

[7] *American Society of Naval Engineers Journal*, August, 1952, pp. 512–538: "New MAN Engine," by G. Eichelberg and W. Pflaum.

[8] Proceedings of Second Nuclear Science Congress, 1957, pp. 526–534: "Transient Thermodynamics of Reactors and Process Apparatus," by D. H. Brown.

illustrative of the heat transfer in Fig. 5. The instantaneous heat-transfer rate would be represented by the slope of the line from the value of cyl-wall temperature at the axis to that at any instant of time. It may be noted that q_3 is of the order of 80 times as large as q_1. The value of q_1 is usually negative for diesels more conventional than the Napier Nomad, indicating that heat is transferred from the cyl walls to the gas during scavenging.

Since the thermal resistance is greatest during scavenging, effective cyl cooling should not be expected as a result of direct heat transfer to a copious scavenge airflow. Effective scavenging reduces the net heat transfer by increasing the cyl charge so that gas temperature is reduced throughout the cycle. Decreased temperatures during combustion are most influential in reducing heat load. Variation of supercharge changes the beginning of compression 1 only slightly. Variation of cyl fuel-air ratio or of cyl peak pressure can drastically alter the location of points 3, 4, and 5 with large effects on heat transfer.

Mean Effective Gas Temperature

Although the equations for heat transfer foretell a method of determining the effective gas temperature for heat transfer, a mathematical approach lacks the physical conviction required by most engineers. In order to realize that same reality in a physical approach it is necessary to engage in a momentary excursion. Let us seek to determine, "What temperature would a thermocouple suspended in the clearance volume of the diesel indicate?" At any instant the heat inflow to the thermocouple which is at T_T would be:

$$q_T = h_G(T_G - T_T) = h_G T_G - h_G T_T \qquad (4)$$

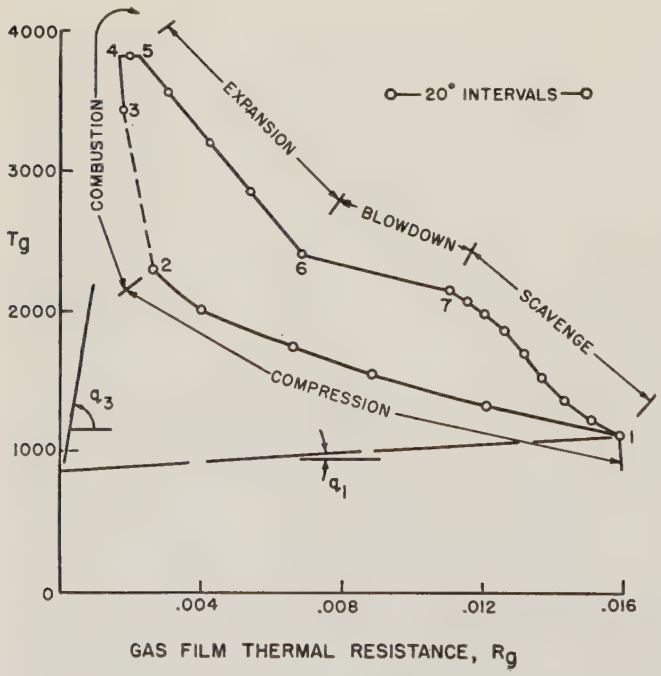

Fig. 5—Cyl gas heat-transfer cycle

Table 1—Calculated Values for Clearance Volume at Cylinder-Wall Section of Highest Piston Ring Travel

Engine	t_{GA}	t_{WG}	t_{WC}	t_C	R_G	R_W	R_C	e
MAN	1520	460	240	170	0.0147	0.00305	0.0010	70,000
Alco	1680	445	260	170	0.0133	0.00195	0.0010	90,000
GM 567B	1745	425	260	170	0.0143	0.00175	0.0010	90,000
Orion	1800	450	380	220	0.0095	0.0005	0.00115	145,000
Nomad	2255	400	270	170	0.00575	0.0004	0.0003	320,000

The values for gas resistance and effective temperature apply to the entire clearance volume. The cyl-wall resistance and coolant thermal resistance are only applicable to the cylinder wall at the level reached by the highest travel of the piston ring.

If the heat conducted away along the leads of the thermocouple is negligible, then the time average heat transfer would be zero:

$$\overline{q_T} = 0 = (\overline{h_G T_G}) - \overline{h_G}\, T_T \qquad (5)$$

Now if the heat capacity of the thermocouple bead is sufficiently large, its temperature will appear to be constant. It is this constant temperature of the thermocouple itself that is indicated by the electrical voltage output. Considering the geometry of the thermocouple it is evident that its unique thermal property is thermal isolation from everything but the gas surrounding it. The word "adiabatic" describes such isolation, so adiabatic wall temperature has been used to describe this resulting thermocouple temperature. Eichelberg and others prefer to call it "residual" temperature. Since it is a temperature derived from the gas by virtue of the particular sequence of temperature and gas film conductance, it is herein termed T_{GA} to indicate its relation to the gas and to the thermal isolation needed to attain it.

$$T_{GA} \equiv \frac{\overline{h_G T_G}}{\overline{h_G}} \qquad (6)$$

The value of h_G which is a time mean value was determined from Fig. 4. Fig. 6 presents the instantaneous values of $h_G T_G$ over one cycle as derived from Fig. 4. The units are those for heat-transfer rate. From the mean value of the $h_G T_G$ plot T_{GA} was computed by Equation 6. As visual evidence of its meaning, the values for $h_G T_{GA}$ were plotted. The vertical distance between these two plots is the instantaneous rate of heat exchange between an isolated body and the cyl gas. It is visually evident that for one cycle the net total heat exchanged is zero. Then it is evident that T_{GA} is the mean effective gas temperature for heat transfer and $\overline{h_G}$ is the mean effective film heat-transfer coefficient.

Cyl-Wall Temperature

The instantaneous heat transfer to a body such as the cyl wall follows the dictates of heat transfer and is represented on Fig. 6 by the vertical distance between the respective functions.

$$q = h_G(T_G - T_{WG}) = h_G T_G - h_G T_{WG} \qquad (7)$$

The average heat-transfer rate will be determnied through evaluation for one or more complete cycles.

$$\overline{q} = \overline{h_G T_G} - \overline{h_G} T_{WG} \qquad (8)$$

For convenience the mean value $\overline{h_G T_G}$ may be

expressed in terms of the value T_{GA} from Equation 6.

$$\overline{q} = \overline{h_G} T_{GA} - \overline{h_G} T_{WC} = \overline{h_G}(T_{GA} - T_{WC}) \qquad (9)$$

Thus, T_{GA} assumes the importance of the mean effective gas temperature for heat transfer. It is significant that the value is independent of the constant of Equation 3 and is thermodynamically determined through the mean values for one cycle of:

$$T_{GA} = \frac{\overline{P^{1/2} T^{3/2}}}{\overline{P^{1/2} T^{1/2}}} \qquad (10)$$

The value for R_G, mean effective gas film resistance to heat transfer, is the reciprocal of the mean effective heat transfer coefficient:

$$R_G = (\overline{h}_G)^{-1} \qquad (11)$$

It was initially stated that values of these two properties with known values for other design parameters would permit determination of cyl-wall temperature. For such evaluation the resistance of the cyl wall will vary directly as the thickness, and inversely as the thermal conductivity of the metal.

$$R_W = X/K_W \qquad (12)$$

The most important temperature was deemed to be that on the gas side of the cyl wall at the point of highest travel of the top piston ring. From data in the literature evaluation for mean effective gas temperature and mean effective gas film resistance were undertaken. In each instance synthesized P-v, T-S, T_G-θ, h_G-θ, and $h_G T_G$-θ curves were plotted. Table 1 presents the calculated data, the resulting values of cyl-wall gas side and coolant side temperature, and the rate of heat transfer. Fig. 7 presents the evaluation, in that coolant temperature and the sum of wall and coolant resistance were plotted on the left and values of mean effective gas temperature and thermal resistance on the right. The resulting straight line connecting these points for any given engine has a slope equal to the rate of heat transfer, and its intercepts at the cyl-wall resistance give the temperatures which were the goal of the evaluation.

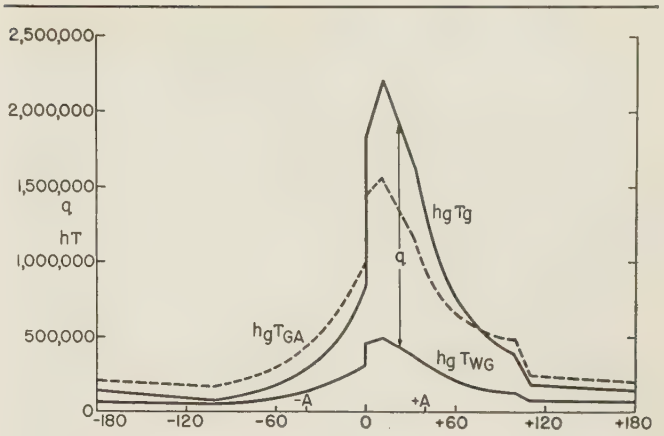

Fig. 6—Instantaneous heat-transfer rates

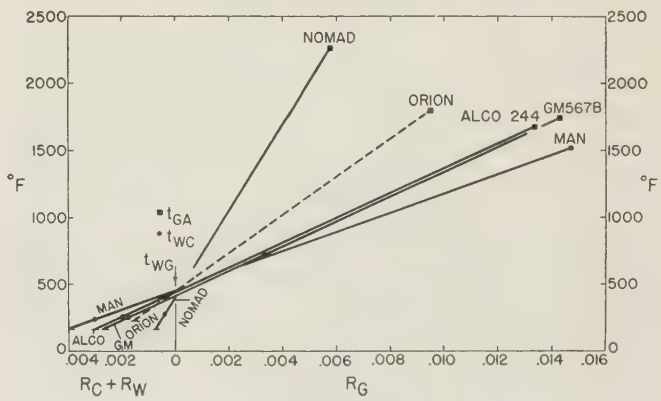

Fig. 7—Mean effective heat transfer

Design Criteria

The wide range of values in Fig. 7 for the mean effective gas temperature and thermal resistance indicates that there are no unique values for these parameters. However, engines of similar construction and design such as Alco, GM, and MAN are grouped closely together. This grouping indicates that correlations such as those of Taylor and Toong should prove valid and useful when a new design corresponds to the class of data correlated.[9] Extreme variations such as the Nomad diesel should not be expected to conform to such generalizations.

The narrow range for cyl-wall gas side temperature is instructive. The greatest value was 460 F while the least value was 400. It was pointed out by Nutt, Landen, and Edgar[2] that lubrication of the top piston ring would be lost when the cyl-wall temperature became so high that the fractional distillation of oil from the surface resulted in insufficient lubrication. The criterion gained from these limited samples indicates that cyl-wall temperatures less than 500 F are desirable. The Orion design was accordingly set at 450 F.

An additional design criteria for liquid-cooled engines results from scrutiny of the cyl-wall waterside temperature for the MAN, Alco, GM, and Nomad diesels. These are all between 240 and 280 F. With the exception of the Nomad diesel, the rate of heat transfer is such that nucleate boiling in the water film would be avoided with reasonable water circulation. However, the Nomad presents an interesting exception. At the high rate of heat transfer indicated, nucleate boiling cannot be avoided. This phenomenon should be clearly distinguished from bulk boiling. The steam formed is only short lived. It does not remain as steam and blanket the cooling surfaces. Instead the minute steam bubbles formed on the wall detach and project themselves into the otherwise stagnant water film like projectiles. They are immediately condensed by the surrounding water which rushes in to fill the void left by the steam. As a result the water reaching the cooling surface is exceedingly turbulent, and at saturation or boiling temperature rather than at average coolant temperature. The agitation of the liquid film due to nucleate boiling far exceeds the modest turbulence due to the normal flow of liquid. The surface temperature need be approximately 30 deg greater than the fluid boiling temperature for this to be the governing phenomenon. Thereafter, increases of the rate of heat transfer of two or three times require

[9] "Heat Transfer in Internal-Combustion Engines," by C. F. Taylor and T. Y. Toong. ASME paper 57-HT-17, 1957.

only a few deg rise in surface temperature.

The Alco, GM, and MAN engines appear to operate just below the temperature for the inception of nucleate boiling. Cavitation on the waterside of the cyl should be avoided by such a design choice. It should be noted that for nucleate boiling heat transfer the apparent resistance of the water is a consequence of the rate of heat transfer and appears to be far less than that resulting for normal forced convection as indicated in McAdams.[10]

The Orion design used a thin-walled cyl with high thermal conductivity and extensive finning to achieve adequate cooling with high-temperature air. Thermocouple measurements of cyl-wall temperature indicated that the predictions achieved by use of the Eichelberg calculation of temperature are reasonable.

Additional Applications

This paper has concerned itself with determination of cyl-wall temperature at one specific point, namely that which experiences the full cycle of clearance volume events. The resulting effective gas temperature and thermal resistance are applicable to the piston and cyl head as well as the exposed wall. If a point further down the cyl wall were selected as represented by exposure to gases through all of the cycle except from – A to + A in Figs. 4 and 6, lower mean values would result. For that portion of the cycle when the piston covers the wall the gas heat transfer coefficients would be effectively zero. Evaluation of the mean values of $\overline{h_G}$ and $\overline{h_G T_G}$ would be unaltered in method. By this means the heat-transfer effective temperatures on all surfaces may be found. From this knowledge heat-transfer rates, cyl-wall temperatures and thermal stresses may be determined. In addition, the heat transfer to the coolant from the entire cyl and head may be found. Cyl thermodynamic processes may be altered to conform with these additional processes so that a more realistic prediction of potential performance levels is attained.

Conclusion

In conclusion, a method of analytically simulating the diesel engine by computation of heat transfer and cyl temperatures has been presented. A design criteria derived from published data on a variety of engines appears to limit the lubricated cyl-wall temperature to less than 500 F. A design criteria for the cyl coolant side indicates that with water cooling the normal cooling regime is slightly below the inception of nucleate boiling.

The diesel engine is in itself a remarkable computing machine. It requires an integration of various parameters to determine what the mep will be, what the peak bearing pressures will be, and what torsional vibrations the crankshaft may experience. The determination of the mean effective gas temperature requires similar effort. It is neither more complex nor more simple. It should not surprise or dismay the engineer that he has to imitate what the engine does physically if he is to analytically achieve similar results. On the other hand, a good theory is of value only insofar as it relates what should transpire in a wide range of practical experience. Within such experience and through the insight of such broad theories, we may hope to discover design criteria that will serve as guideposts or limits until we discover how to surmount or break through these barriers.

APPENDIX

Nomenclature

q = Heat-transfer rate, Btu per sq ft per hr
T = Absolute temperature, R
t = Temperature, F
P = Absolute pressure, psi
h = Heat transfer-coefficient, Btu per sq ft per hr Δ F
R = Thermal resistance to heat transfer, Δ F per Btu per sq ft per hr
θ = Crank angle, deg atdc

Subscripts:

GA = Gas adiabatic, mean effective gas temperature for heat transfer
WG = Cyl wall, gas side surface
WC = Cyl wall, coolant side surface
T = Thermocouple
G = Gas
W = Cyl wall
C = Coolant

Bar above quantity represents mean value on a time basis for one or more complete cycles of cyl events, for example:

$$\overline{h_G} = \oint_{-180^\circ}^{+180^\circ} h_G d\theta \Big/ \oint_{-180^\circ}^{+180^\circ} d\theta$$

DISCUSSION

Confirms Author's Approach To Heat-Transfer Problem

—E. T. Vincent
University of Michigan

THIS subject for some time has interested me, arising from efforts to decide the various limitations that might be imposed upon the performance of any form of internal-combustion engine, by mechanical, cycle, or heat-transfer limitations.

A method was worked out for the first two without much difficulty whereby on allowing for an estimated heat transfer, the engine performance as regard to cycle pressures, power output, and specific fuel consumption could be calculated with considerable accuracy (about ±5%) of that actually obtained in operation.

The problem of heat loading of the wall and heat-transfer coefficients followed naturally from this work and a doctoral candidate at the University of Michigan, Naeim A. Henein, under my direction undertook the investigation. The results were published in 1957.[a]

---

[10] Figs. 14–21 and 14–22 of "Heat Transmission," by W. H. McAdams. Pub. by McGraw-Hill Book Co., New York, 3rd edition, 1954.

[a] "Thermal Loading and Wall Temperature as Functions of Performance of Turbocharged Compression Ignition Engines," by Naeim A. Henein. Doctoral dissertation, 1957, University of Michigan.

The approach employed followed the author's very closely inasmuch as the Eichelberg paper formed a starting point. The major difference is perhaps in the employment of a special thermocouple to record the fluctuation of the wall temperature throughout the cycle, thus providing a continuous checking the calculated results. The couple had a response time of 4.5 microsec during which the crank of the engine rotated 0.034 deg at a speed of 1200 rpm.

The oscillographs of cyl pressure and wall temperature followed one another so closely that the above estimated lag is considered fairly accurate.

The records of this work would make a paper by themselves and no attempt will be made to indicate the interesting relationship achieved between fuel-air ratio supercharge, intensity of thermal loading, and the like.

The main result of interest here is that I can confirm the usefulness of Mr. Brown's approach to the heat-transfer problem.

Substantiates Usefulness Of Author's Method

—R. J. Hooker
General Electric Co.

THE basic concepts of the Eichelberg method of calculating cyl-wall temperatures has been known for several years, but it has not become the useful tool of the engine designer that is warranted by its strength. I believe that this paper will help to publicize it to the extent that designers will be encouraged to use it more freely. The data for making a temperature survey of a cyl wall can be obtained from cycle computations with which the designer is already familiar. There will be objections to using this very simple and useful method by engineers who are better versed in the more elegant theories of heat transfer, but I argue that if a simple relation can serve a useful purpose and its accuracy is within reasonable values, then as a design engineer I would use it. It is not enough to know what the gross heat rejection from an engine is; I want to know in detail where the heat comes from, where it goes, and what it does in passing through the wall.

In order to substantiate the usefulness of this method, many calculated flux plots of the temperature distribution in the cyl wall and cooling fins of a single-cyl opposed-piston engine were studied to determine the design of the Orion cyl. The calculated inner cyl-wall temperature (Fig. A) are for two values of imep. The measured cyl-wall temperatures from tests performed at about the 157 imep value of the above curves are given on Fig. B. It is evident that the agreement between the calculated and measured results are very real.

By this demonstration of the accuracy of predicting wall temperatures, it is my observation that many piston ring scuffing problems could be analyzed by extending the present method to include the piston ring. It would seem that by lowering the ring, some drop in temperature (that the ring sees) could be accomplished—provided that the hot gas in the clearance space could not transport an amount of heat required to maintain the temperature profile. Here can be written the theorem—that the clearance between the piston and cyl wall above the top ring should be as small as possible—consistent with other mechanical requirements.

This statement can be further expanded into the thought that by shielding the cyl wall from exposure to the hot gases less heat will be transferred to the wall and then out to the coolant. Both measurements and calculations show that fully half of the heat transferred through the cyl wall is done so in about the top 10% of piston travel. Therefore, it would seem most appropriate to suggest removing the stationary cyl head, which sees the entire range of the hot gas temperature and replace it with another moving piston, if an engine with minimum cyl cooling is required.

The opposed-piston and free-piston engineers will approve of this statement, but the cyl-head engine designer will object. In order to soften the blow, free-piston engines still have a strip of cyl wall exposed to the hot gas because they are forced to use a flat-topped piston crown. The

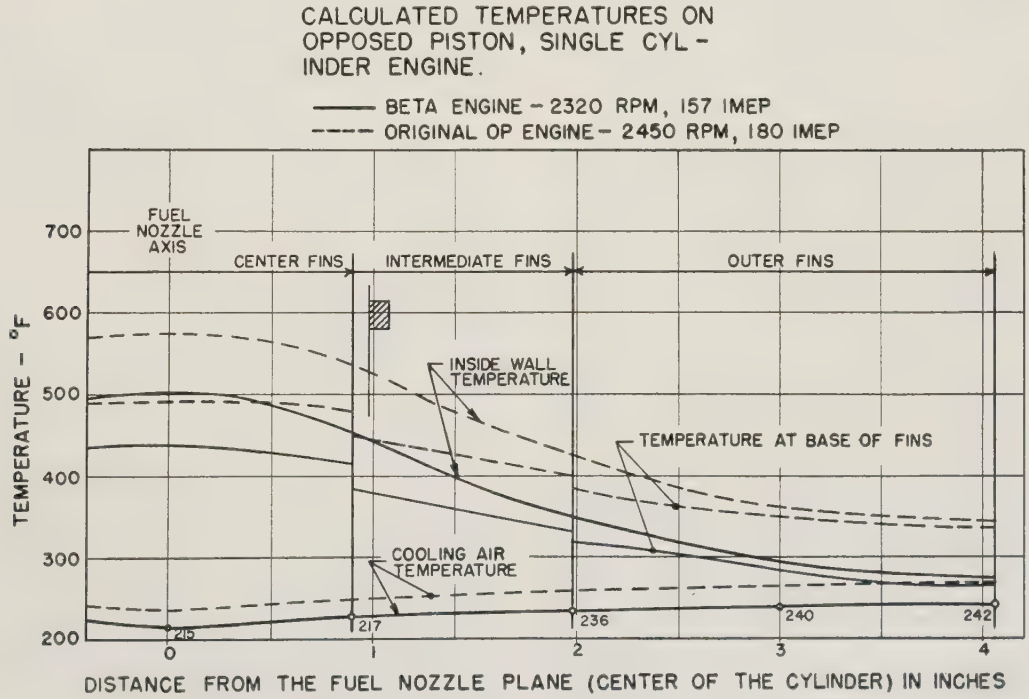

Fig. A—Calculated temperatures on opposed-piston, single-cyl engine

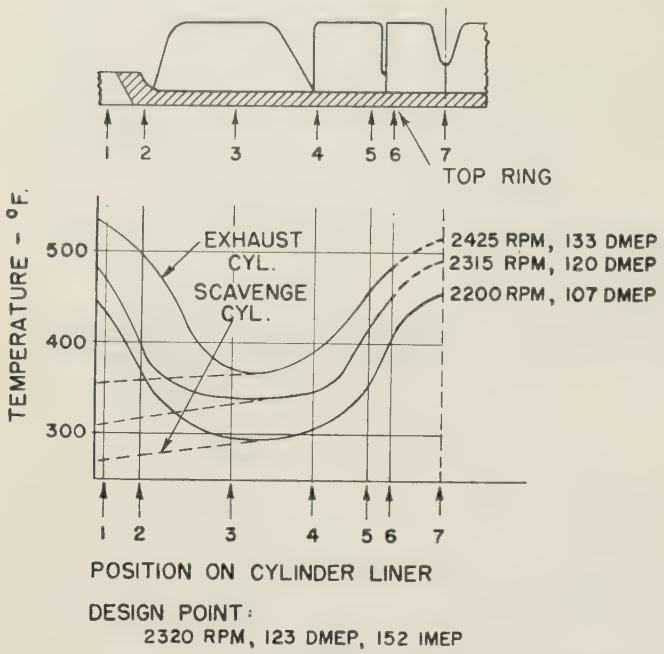

Fig. 8—Temperature distribution at inner surface of beta engine cyl liner (design point: 2320 rpm, 123 dmep, 152 imep)

opposed-piston engineers are more fortunate, in that the piston crown can be made to nearly cover the entire cyl wall at tdc.

In the 1940's I was project engineer on the Pratt and Whitney Aircraft free-piston project where both the problems and the magnitude of the heat rejection through the combustion-chamber walls were recognized, but the project ended before anything could be done about it. This knowledge laid dormant for several years until it was used in the design of the Orion cyl, where a "heat shield" was incorporated in the combustion chamber to reduce the heat rejection through the cyl wall to the cooling air. These are the uses this method can be put to in studying the problems of heat transfer in an engine cyl and what can be done about them.

The phenomenon of "nucleate boiling," as a means of cooling engine cyl was mentioned. The connotation of the word "boiling" will be misunderstood, and knowing the deadly objections that many engineers have of "steam" cooling diesel engine cyl, I want to conclude my remarks by asking Mr. Brown if he would not explain this very interesting theory in somewhat more detail.

Correlates Test Data With Author's Calculations

—Ralph Miller
Consultant Engineer

AMONGST diesel-engine designers I have stood alone in using thermal load as a criteria for engine loading so let me congratulate the author on his treatment of this subject and on pointing out the importance of controlling cyl-wall temperatures.

In my work I have used heat flow per unit time to cooling water as a measure of thermal load and I have found it interesting to correlate such test data with the author's calculations.

A 3600-bhp 1000-rpm 11×12-16 cyl 4-stroke engine recently developed for the U.S. Navy was tested at this load with various manifold temperatures. The engine operates on the Miller system of supercharging. Air manifold pressure and compression pressures were held constant at all manifold temperatures. When the latter was raised from 100 to 160 F the heat flow to the water jackets increased from 2.28×10^6 to 2.62×10^6 btu per hr. The corresponding compression temperatures of 1365 and 1510 R respectively show that the heat flow to water jackets is proportional to the compression temperature to the power of 1.35. (Heat flow is also proportional to the mean temperature of the cycle or the absolute air manifold temperature to the same power.)

In Fig. 7 the heat transfer is shown proportional to the mean effective gas temperature minus the temperature where R_G is zero. I should like to ask the author whether there exists a determinable relationship between the author's mean effective temperature, T_{GA} and the mean temperature of the cycle or the compression temperature.

The air manifold temperatures of the Alco 244 and GM 567B should give a clue to the high mean temperature shown for the former.

The standard Alco 244 operating without intercooling would have a manifold temperature of about 700 R while the GM 567B with its lower scavenging pressure would have an air box temperature of about 590 R

Reducing the manifold temperature in the Alco engine to 590 R lowers the heat-transfer rate q from 90,000 to 71,000 btu and the wall temperature from 445 to 388 F. To be of any value the relative thermal load or cyl-wall temperature of 2- and 4-stroke engines must be compared on the basis of equal air manifold temperatures. With a manifold temperature of 590 R (130 F) the Alco engine operates with a compression temperature of 1560 R (compression ratio of 12).

The two engines compared here are standard locomotive engines and it may be reasoned that intercooling is not practical in this service. However, the author shows in Table 1 for comparison, the MAN engine which is intercooled although air temperature is not stated.

A 4-stroke engine such as the Alco engine operating on the Miller system of low temperature supercharging would have the same compression temperature, namely, 1560 R and compression pressure with an air manifold temperature of 180 F by increasing the supercharging pressure from 2 to 2.75 atmospheres absolute. The wall temperature T_{WG} would then be 388 F as in the standard Alco engine intercooled to 130 F.

Intercooling the Alco engine to 180 F, which is practical in locomotive service, would lower the wall temperature from 445 to 415. The operating records of the engine in the past without intercooling shows that both the engine and turbocharger suffers from excessive thermal load.

The author's selection of a 4-stroke engine operating on an obsolete supercharging system to show the relative wall temperature of 2- and 4-stroke engines might be questioned.

Question Usefulness Of Eichelberg Relations

—C. Fayette Taylor
Massachusetts Institute of Technology

MR. Brown's paper presents a direct method of attack on the problem of heat flow at a given point, through the walls of a diesel cyl. The method is based on the Eichelberg relations given in Equations 2 and 3.

The Eichelberg relations appear to have been obtained from a limited number of observations over a limited range of operation conditions. These relations do not conform to the Nusselt equation for convective heat flow, which most other investigators have found to hold very well for internal-combustion engines.[b, 8] If the Nusselt relations

[b] Work by Nusselt, National Advisory Committee for Aeronautics.

had been used as a basis, the analysis would stand on firmer ground.

In the area chosen for consideration, that is, the cyl wall under the piston rings at tdc, the heat-transfer process is complicated by piston motion and by ring friction. For this area I am not convinced that either the Eichelberg or Nusselt relations apply. Has any attempt been made to measure actual temperatures and rates of heat flow at the point in question?

Author's Closure To Discussion

FIRST, I wish to thank each of the discussors, for in addition to a critical review of this work each has drawn from his own experience to make additional contributions. Mr. Hooker expresses an engine designer's point of view—if a simple theory works, use it. Professor Vincent has described experimental work done under his direction at the University of Michigan that substantiates this simple Eichelberg correlation. The achievement of a cyl-wall thermocouple with a response time constant of 4 microsec or a delay of only 0.03 crank deg is a notable advance of the art. These discussions indicate that more elegant theory is unnecessary. Mr. Hooker further presents data on actual test results compared to the Eichelberg calculated wall temperature for the aircooled highly supercharged Orion opposed-piston diesel cyl. He then shows how use of theoretical insights can lead to more astute design of particular engine components. It is my conviction that any theory has validity only insofar as it produces answers of sufficient accuracy to permit design or to guide development of apparatus. These discussions indicate that a more elegant theory is not appropriate.

In answer to Mr. Hooker's question: the phenomenon of nucleate boiling occurs above a limiting threshold of heat-transfer rate. The metal surface in contact with the water coolant must be approximately 35 deg hotter than the temperature appropriate for boiling the liquid at the existing pressure. The bulk of the liquid is and remains cooler than the boiling temperature. However, in the boundary film at the cyl wall a most dynamic exchange of heat takes place. Minute steam bubbles are formed at the metal surface and then project off into the liquid. As these bubbles move they exchange heat with the liquid and heat it locally up to the boiling temperature. In the process, the bubbles of steam are condensed so that there is no steam bulk conveyed along with the coolant.

The importance of this phenomenon of boiling arises from the response to increased rates of heat transfer. As the heat transfer increases, the number of bubbles projected from the wall into the liquid mass increases. This stirs the liquid, creating great turbulence, and thus expediting heat transfer. The wall temperature would rise only 25 F to accommodate a 10-fold increase in heat transfer. It is thus apparent that a doubling of the heat-transfer rate would require only a 5 deg increase in wall temperature. This phenomena is most important in the cooling of water moderated nuclear reactors. In high output diesels it should have similar importance. This mode of cooling will aggravate waterside erosion problems. However, hard coatings such as the chrome-plated outer surface of the Junkers Jumo 205-D cyl liner should gain immunity from this latter trouble. The MAN diesel cyl head and the Napier Nomad cyl both utilized this mode of cooling.

Professor Taylor points out that the Eichelberg analysis is not so general an approach to heat transfer as that of Nusselt. However, the results obtained using common heat-transfer theory require use of an artificial Reynolds number and give rise to an overall heat-transfer coefficient that is meant to average out all effects due to compression ratio, fuel-air ratio, variation of exposed cylinder area throughout a cycle, and variation of heat-transfer path resistance from place to place, as well as influences of charge variation due to cyl charging. If all engines and conditions of operation were exactly similar such correlations might prove valuable. However, these correlations have been presented with logarithmic plots wherein variations of $\pm 50\%$ from the mean are common. It is my conviction that the internal-combustion engine is not comparable to a simple heat exchanger and that only through the rigors of integration over a complete cycle and examination of each cyl-wall position may the designer foretell the adequacy of his design. Rules of thumb may serve well for initial layout, but whether our concern is for mechanical stress, vibration analysis, or heat transfer, we should expect to trace out the cyclic processes.

Mr. Miller merits special recognition for his contribution in this regard. He was the earliest in this country, and certainly the most forceful, to proclaim the necessity of finding a mean effective gas temperature by integration throughout a complete cycle. It is typical that we build on the contributions of others, and it is well to consider wherein his work and this work differ. First, I have found no direct relationship between the mean effective temperature for heat transfer T_{GA} and the average cyl gas temperature on a time basis. However, it is apparent that both participate in the same trends. It is for this reason that Mr. Miller so quickly detects and puts numbers on the advantage to be gained through cooling of the manifold air for the 4-stroke diesel. The author is impartial to the question of 4- or 2-stroke diesels. However, it is notable that the cyl-wall temperature at the hottest position reached by the piston rings was virtually the same for the Alco at 250 F, the MAN at 90 F, the Nomad at 400, the GM at 115, and the Orion at 210 F manifold temperatures. Thus this study revealed that all of these diesels participated in a common design limitation whatever their degree of refinement or cycle of operation. This method of analysis is useful for comparison of different engines. The insights gained are in accord with Mr. Miller's assertion that for a given engine the heat rejection is a measure of thermal load.

The data given by Mr. Miller indicate a variation of heat rejection as the 1.35 power of manifold temperature for a particular 4-stroke diesel. For the Eichelberg analysis the fundamental parameter is charge temperature and not manifold temperature. Modification for volumetric efficiency and charge heating must be made. On the basis of charge temperature the exponent will be found from equations 1, 2, 10, and 11:

$$\text{Exponent} = \frac{T}{q}\frac{dq}{dT} = \frac{T_{GA}}{T_{G\,t} - T_c} + \frac{R_G}{2(R_G + R_W + R_C)} \qquad \text{(a)}$$

The contribution due to temperature alone varied from 1.30 to 1.46 for the diesels presented. The additional contribution due to the influence of temperature on the gas film resistance varied from 0.46 to 0.39. Thus, the Eichelberg analysis results in a variation of heat transfer as the 1.75 to 1.83 power for the cyl wall. The difference may well result from the influence of the cooling of the exhaust passages through the cyl heads. If this cooling burden is large it may mask the cyl cooling variation. If the heat-transfer coefficient in the exhaust passages were constant, then that portion of the heat transfer would vary directly with temperature. The net result could be a gross variation as a power less than the 1.8 power appropriate for the cyl walls.

In closing I wish to reiterate that the mean effective temperature, T_{GA}, has physical significance. It is the temperature that would be reached by a thermocouple suspended in the space.

I should like to acknowledge the stimulation provided me by Dr. R. A. M. Toesca who first introduced me to the Eichelberg analysis, E. L. Lustenader and A. E. Kakretz who subsequently shared in the labors of its application, and Dr. F. J. Neugebauer, Thermal Systems Consulting Engineer, who has aided and encouraged the author in this and other technical work.

the effects of . . .

Machine and Foundation Resilience

on the Isolation Provided

IN the simplest approach to the problem of estimating the effectiveness of a vibration mount[1], it is customary to assume that the machine or equipment to be isolated is a rigid mass M_M, that the mount is a massless mechanically paralleled spring and dashpot of stiffness K_m and resistance R_m, and that M_M, K_m, and R_m are constants independent of frequency.[2]

For the case of foundation-excited machine vibration,[3] one assumes that the vibratory foundation velocity is not effected by the machine, whether rigidly or resiliently attached.[4] The ratio of the vibratory velocity amplitude of the isolated machine to the vibratory velocity amplitude of the foundation is calculated; and this ratio, *transmissibility,* is used as a criterion for isolation prediction.

The complex transmissibility of a rigid machine, massless spring-dashpot mount system is given by:[5]

$$T = \frac{R_m - \frac{jK_m}{w}}{R_m + j\left(wM_M - \frac{K_m}{w}\right)} \qquad (1)$$

THE effects on the transmission of vibration through isolation mounts of machine and foundation resilience, and of wave propagation are investigated. The prediction of the effectiveness of mounts is discussed, and curves are presented for estimating their effectiveness under certain conditions.

A number of conclusions are drawn relevant to the problems of mount design and selection.

where:

$j = \sqrt{-1}$

$w = 2\pi f$, the frequency of the exciting disturbance in radians per sec

The magnitude or modulus of T can be written:

$$|T| = \left\{ \frac{1 + \left[\frac{w}{w_o}\frac{w_o R_m}{K_m}\right]^2}{\left[\left(\frac{w}{w_o}\right)^2 - 1\right]^2 + \left(\frac{w}{w_o}\frac{w_o R_m}{K_m}\right)^2} \right\}^{\frac{1}{2}} \qquad (2)$$

where:

$w_o = 2\pi f_o = \sqrt{\frac{K_m}{M_M}}$, the natural frequency of the machine-mount system in radians per sec

$\frac{wR_m}{K_m}$ = Loss factor of the mount at the circular frequency w

Transmissibility modulus in db is plotted in Fig. 1 as a function of frequency ratio $\frac{w}{w_o}$ with $\frac{w_o R_m}{K_m}$ as a parameter.

$$|T|_{db} = 20 \log_{10}|T| \qquad (3)$$

---

[1] This paper considers only steady state vibration problems in which all vibratory forces and velocities are colinear.

[2] Throughout the rest of the text, the word machine will be used to describe whatever equipment is to be isolated.

[3] The problem of reducing machine-excited foundation vibration has been discussed by the author in a parallel paper, "Theory of Sound Transmission in Isolation Mounts," presented in March, 1957, at the Office of Naval Research sponosred symposium, "A Decade of Basic and Applied Science in the Navy." It was published by ONR in October, 1957.

[4] This assumption is equivalent to assuming the foundation is infinitely stiff and massive.

[5] Pp. 176–186 of "Vibration and Shock Isolation," by Charles E. Crede. Pub. by John Wiley and Sons, New York, 1951.

and of Wave Propagation

by Vibration Mounts

A. O. Sykes, David Taylor Model Basin

This paper was presented at the SAE National Aeronautic Meeting, Los Angeles, Oct. 2, 1957.

From Equation 2 and Fig. 1, one can conclude that:

1. A mount magnifies the vibratory velocity of the machine for frequency ratios $\frac{w}{w_o} < \sqrt{2}$.

2. A mount reduces the vibratory velocity of the machine for frequency ratios $\frac{w}{w_o} > \sqrt{2}$.

3. For frequency ratios greater than $\frac{w}{w_o} = \sqrt{2}$, the isolation a mount provides increases with increasing $\frac{w}{w_o}$; for $\frac{w_o R_m}{K_m} = 0$, the isolation increases in proportion to $\left(\frac{w}{w_o}\right)^2$.

4. Increasing the resistance in a mount will decrease its effectiveness for frequency ratios $\frac{w}{w_o} > \sqrt{2}$ and increase it for $\frac{w}{w_o} < \sqrt{2}$.

These conclusions and the assumptions made in deriving them are not always correct, however.

The assumptions that R_m and K_m are constants independent of frequency are wrong for many rub-

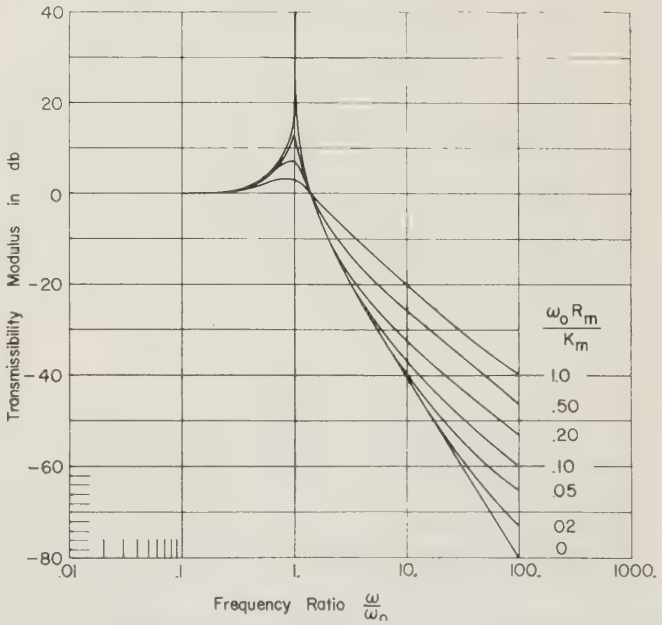

Fig. 1—Transmissibility modulus in db versus frequency ratio, R_m and K_m are constants independent of frequency

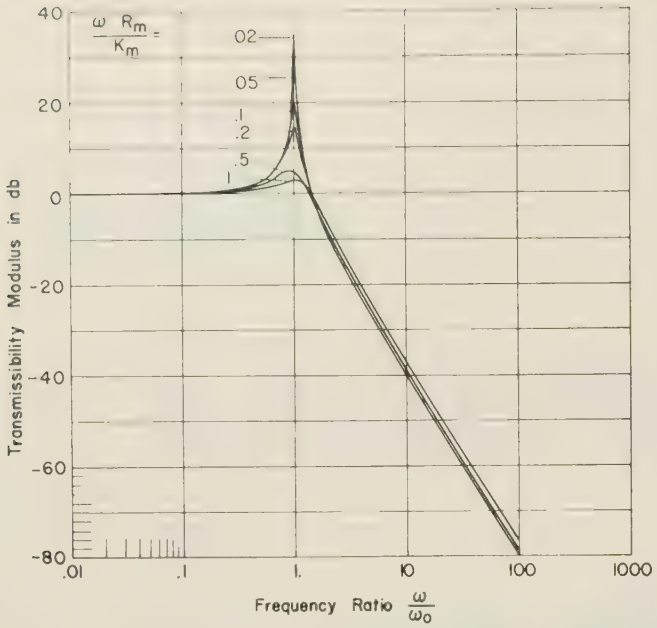

Fig. 2—Transmissibility modulus in db versus frequency ratio, loss factor $\frac{wR_m}{K_m}$ is a constant independent of frequency

ber mounts.[6] At frequencies above a few hundred cps, machines, particularly large ones, do not act like rigid masses; foundation structures (for example, air frames or ships' hulls) are neither infinitely stiff nor massive; and wave effects occur in the mounts.

Isolation of Nonrigid Machines from Nonrigid Foundations

Since transmissibility, as defined by Equation 1, cannot be used for predicting the isolation a mount will provide when isolating a nonrigid machine from a nonrigid foundation, a new criterion must be selected.[7]

Such a criterion is effectiveness.[8] This quantity can be defined in terms of two hypothetical experiments illustrated in Fig. 3. In the first experiment, the machine is attached directly to the vibrating foundation and the resulting vibratory velocity amplitude $\dot{x}_{12}$ of the machine-foundation juncture is measured. In the second experiment, the machine is attached to the same point on the vibrating foundation by a resilient mount, and the vibratory velocity amplitude $\dot{x}_{22}$ of the machine-mount juncture is measured. The ratio of the first to the second velocity amplitude defines the effectiveness of the mount. In the notation of Fig. 3, the complex effectiveness of a mount is:

$$E = \frac{\dot{x}_{12}}{\dot{x}_{22}} \tag{4}$$

It is the magnitude of E which is of interest.[9] If it is greater than unity, the mount reduces the machine vibration; if it is less than unity, the machine vibration is increased.

Effectiveness of Massless Spring-Dashpot Mounts Isolating Nonrigid Machines from Nonrigid Foundations—The effectiveness of a mount can be calculated most easily by the application of mechanical network theory.[10]

Consider the first experiment illustrated in Fig. 3. By Norton's theorem:[11]

$$\dot{x}_{12} = \frac{Z_F}{Z_M + Z_F}\dot{x}_{12}{}^f \tag{5}$$

where:

$\dot{x}_{12}$ = Vibratory velocity amplitude of the machine-foundation juncture when the machine is directly attached to the foundation

$\dot{x}_{12}{}^f$ = Vibratory velocity amplitude of the foundation at the point at which the machine is to be attached, before the machine is attached

Z_F = Mechanical impedance of the foundation, looking into it at the point of attachment of the machine

Z_M = Mechanical impedance of the machine, looking into it at the point of attachment to the foundation.[12]

Now consider the second experiment as illustrated in Fig. 4.

By Norton's theorem and the rules for combining mechanical impedances:

$$\dot{x}_{23} = \dot{x}_{12}{}^f \frac{Z_F}{\frac{Z_m Z_M}{Z_m + Z_M} + Z_F} \tag{7}$$

where:

Z_m = Mechanical impedance of the mount

Since:

$$\frac{\dot{x}_{22}}{\dot{x}_{23}} = \frac{Z_m}{Z_m + Z_M} \tag{8}$$

it follows that:

$$\dot{x}_{22} = \frac{Z_m}{Z_m + Z_M}\,\dot{x}_{23} = \frac{Z_m}{Z_m + Z_M}\,\frac{Z_F}{\frac{Z_m Z_M}{Z_m + Z_M} + Z_F}\,\dot{x}_{12}{}^f \tag{9}$$

Consequently, the effectiveness E of the mount is

---

[6] For rubber mounts, R_m usually decreases with frequency and K_m increases. For some mounts, the lost factor $\frac{wR_m}{K_m}$ is nearly constant independent of frequency. The assumption loss factor constant independent of frequency has been used with Equation 2 to plot Fig. 2, which shows that the transmissibility of mounts with constant loss factors is essentially independent of loss factor at frequency ratios $\frac{w}{w_o} > \sqrt{2}$, and that the loss factor of the mount is important only in that it determines the transmissibility at the natural frequency f_o of the machine-mount system. (See Additional References.)

[7] The words, machine and foundation, are used loosely to refer to whatever structures are attached at the machine and foundation ends of the mount. It is assumed that the metal components of the mount can be considered massless and infinitely stiff.

[8] Effectiveness in mechanical network theory corresponds to insertion loss in electrical network theory.

[9] Effectiveness has been defined in terms of foundation-excited machine vibration. It might also have been defined in terms of machine-excited foundation vibration. It has been proved that the effectiveness of a mount at a given frequency is the same whether isolating foundation vibration from the machine or machine vibration from the foundation. (See Additional Reference 3.)

[10] Mechanical network theory as used in this paper is reviewed in Additional Reference 3.

[11] Norton's theorem in mechanical terminology states that if $\dot{x}_p{}^f$ is the vibratory velocity amplitude at any point p on a vibrating structure, the vibratory velocity amplitude $\dot{x}_p$ at that point after attaching an additional mechanical structure is given by:

$$\dot{x}_p = \dot{x}_p{}^f \frac{Z_p}{Z_p + Z_a} \tag{6}$$

where:

Z_p = Mechanical impedance of the original vibrating structure looking into it at p

Z_a = Mechanical impedance of the added structure looking into it at its point of attachment to p

[12] Mechanical impedance as used in this paper is defined as the quotient of vibratory force and velocity amplitudes, taking account of phase. Mechanical resistance is indicated by R, mechanical reactance by X. The convention chosen is that masslike reactance is positive, springlike reactance negative.

given by:

$$E = \frac{\dot{x}_{12}}{\dot{x}_{22}} = \frac{Z_M + Z_F\left(1 + \frac{Z_M}{Z_m}\right)}{Z_M + Z_F} \tag{10}$$

If the foundation impedance is much larger than the machine impedance, that is, $Z_F \gg Z_M$, Equation 10 reduces to:

$$E = 1 + \frac{Z_M}{Z_m} \tag{11}$$

The effectiveness in this case is independent of foundation impedance and, if the machine acts like a rigid mass, is equal to the reciprocal of the transmissibility (Equation 1). The mount will be effective if its impedance is much less than the machine impedance.

If the machine impedance is much larger than the foundation impedance:

$$E = 1 + \frac{Z_F}{Z_m} \tag{12}$$

The effectiveness in this case is independent of machine impedance. The mount will be effective if its impedance is much less than the foundation impedance.

The machine, mount, and foundation impedances, expressed in terms of their resistive and reactive components, are given by:

$$Z_M = R_M + jX_M \tag{13}$$

$$Z_m = R_m + jX_m = R_m - j\frac{K_m}{w} \tag{14}$$

$$Z_F = R_F + jX_F \tag{15}$$

These quantities can be nondimensionalized by dividing them by the magnitude of the mount reactance $|X_m|$:

$$\frac{Z_M}{|X_m|} = \frac{R_M + jX_M}{|X_m|} = r_M + jx_M = z_M \tag{16}$$

$$\frac{Z_m}{|X_m|} = \frac{R_M + jX_M}{|X_m|} = r_m - j = z_m \tag{17}$$

$$\frac{Z_F}{|X_m|} = \frac{R_F + jX_F}{|X_m|} = r_F + jx_F = z_F \tag{18}$$

If Equation 10 is nondimensionalized by dividing numerator and denominator by $|X_m|$ and is then expressed in terms of z_M, z_m and z_F, one can show that the effectiveness modulus is:

$$|E| = \left[\frac{[r_m(r_M + r_F) + x_M + x_F + r_M r_F - x_M x_F]^2}{[r_m(r_M + r_F) + x_M + x_F]^2 + [r_m(x_M + x_F) - r_F - r_M]^2} + \frac{[r_m(x_M + x_F) - r_M - r_F + x_M r_F + x_F r_M]^2}{[r_m(r_M + r_F) + x_M + x_F]^2 + [r_m(x_M + x_F) - r_F - r_M]^2}\right]^{\frac{1}{2}} \tag{19}$$

where:

$r_m = \frac{wR_m}{K_m}$, loss factor of the mount

This equation can be used to estimate the effectiveness of any massless spring-dashpot mount isolating any nonrigid machine from any nonrigid foundation, if the system of interest can be represented by Fig. 4 and if the mechanical impedances of the machine, mount, and foundation are known.

Since Equation 19 is unchanged if machine and foundation are interchanged, it follows that subscript M can refer to either the machine or foundation, likewise subscript F. For this reason, subscripts M and F will be replaced by 1 and 2 in subsequent discussion, and it should be understood that if, for example, subscript 1 refers to the machine, subscript 2 refers to the foundation. With this notation, Equations 16 and 18 become:

$$z_1 = \frac{R_1 + jX_1}{|X_m|} = r_1 + jx_1 \tag{20}$$

$$z_2 = \frac{R_2 + jX_2}{|X_m|} = r_2 + jx_2 \tag{21}$$

Effectiveness calculations have been made from Equation 19 for r_m constant independent of fre-

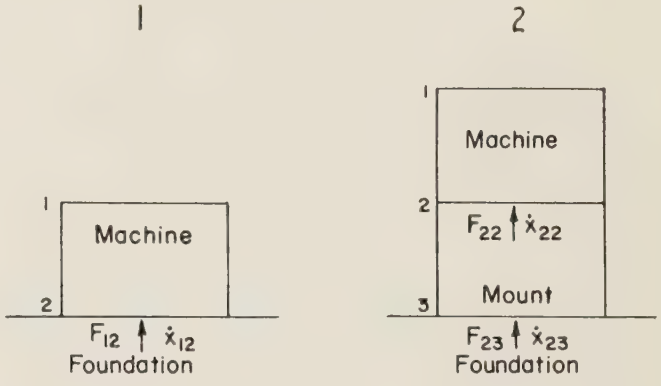

Effectiveness $E = \frac{\dot{x}_{12}}{\dot{x}_{22}} = \frac{F_{12}}{F_{22}}$

$|E|$ in db $= 20 \log_{10} \frac{|\dot{x}_{12}|}{|\dot{x}_{22}|}$

Fig. 3—Definition of effectiveness

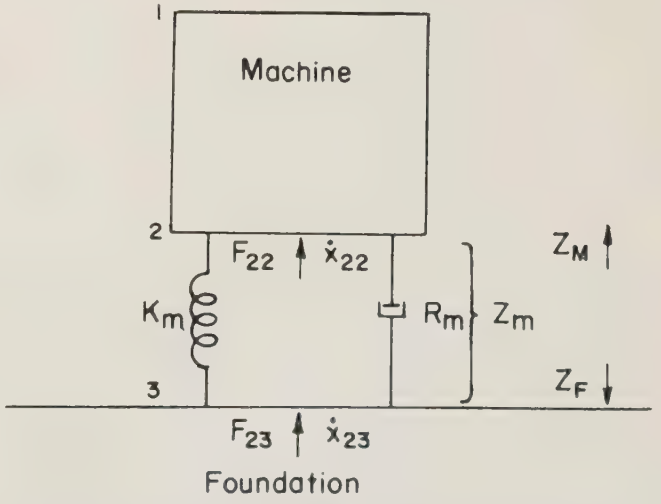

Fig. 4—Machine spring-dashpot mount foundation system

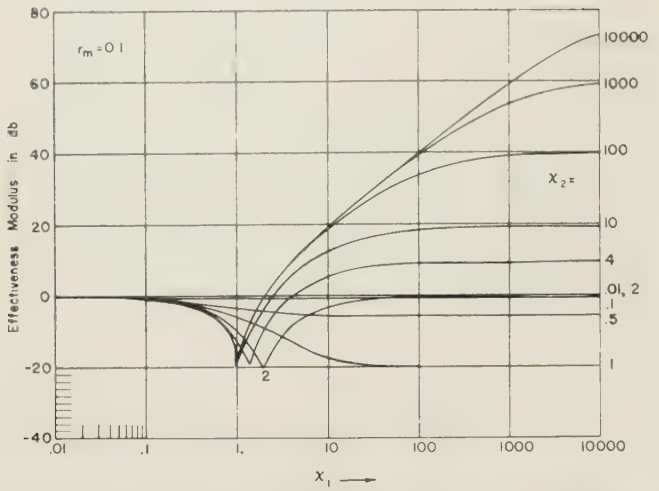

Fig. 5—Effectiveness modulus in db versus x_1 with x_2 as a parameter; x_1 and x_2 masslike

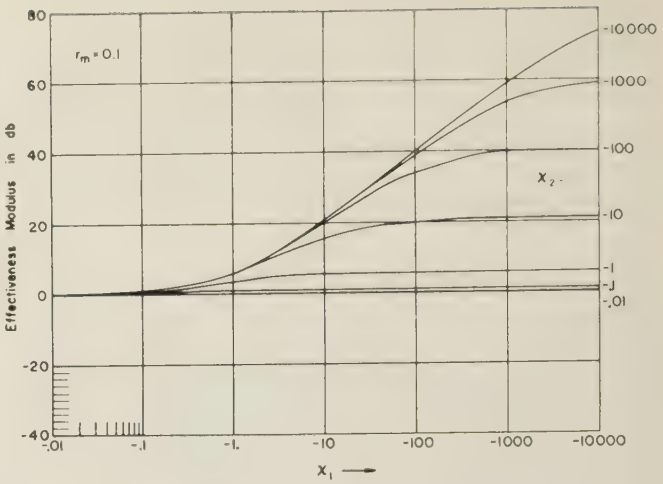

Fig. 6—Effectiveness modulus in db versus x_1 with x_2 as a parameter; x_1 and x_2 springlike

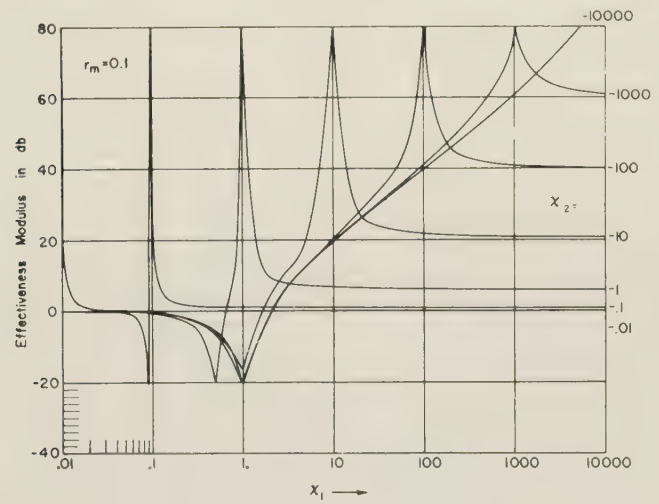

Fig. 7—Effectiveness modulus in db versus x_1 with x_2 as a parameter; x_1 masslike, x_2 springlike

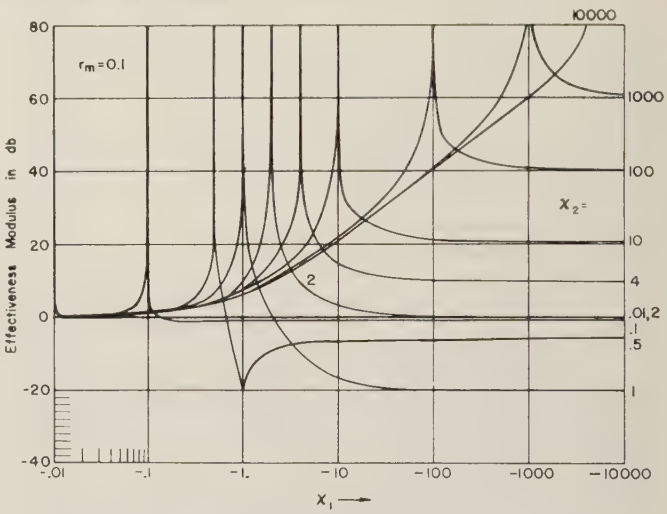

Fig. 8—Effectiveness modulus in db versus x_1 with x_2 as a parameter; x_1 springlike, x_2 masslike

quency ($r_m = 0.1$) for a variety of machine and foundation conditions, namely:

1. z_1 and z_2 reactive:
   - x_1 and x_2 masslike
   - x_1 and x_2 springlike
   - x_1 masslike, x_2 springlike
   - x_1 springlike, x_2 masslike
2. z_1 reactive and z_2 resistive:
   - x_1 masslike, r_2 resistive
   - x_1 springlike, r_2 resistive
3. z_1 and z_2 resistive.

The results of these calculations are presented in Figs. 5–11 where effectiveness modulus in db $|E|_{db}$ is plotted versus z_1 with z_2 and r_m as parameters.

$$|E|_{db} = 20 \log_{10} |E| \qquad (22)$$

Two conclusions valid for every case studied are:

1. The softer a mount is, (that is, the larger z_1 and z_2 are) the more effective the mount is provided that z_1 and z_2 are both greater than about 2.[13]

2. For z_1 and z_2 both much greater than unity, and for z_1 much greater than z_2, the effectiveness of the mount will be determined by z_2; in fact:

$$|E| \cong |z_2| \qquad (23)$$

For z_1 and z_2 respectively both masslike, masslike and springlike, or masslike and resistive, depending on their magnitudes, use of a mount can cause vibration magnification. (See Figs. 5, 7–9). The minimum in effectiveness—corresponding to the maximum magnification that can occur—is controlled by the loss factor of the mount used, and is given by:

$$|E|_{min} \cong r_m \qquad (24)$$

If z_1 and z_2 respectively are both masslike, or masslike and springlike, the effectiveness minimum occurs near the values of x_1 and x_2 for which:

$$x_1 + x_2 - x_1 x_2 = O \qquad (25)$$

provided that $r_m \ll 1$. For z_1 and z_2 both masslike, the minimum corresponds to resonance of the mount with the equivalent masses of x_1 and x_2. For z_1 masslike and z_2 springlike, the minimum corresponds to resonance of the equivalent mass of X_1, with com-

[13] A trivial exception occurs for z_1 masslike and z_2 springlike, in which case, for $|z_1| = |z_2|$, the effectiveness is infinite without regard to mount stiffness.

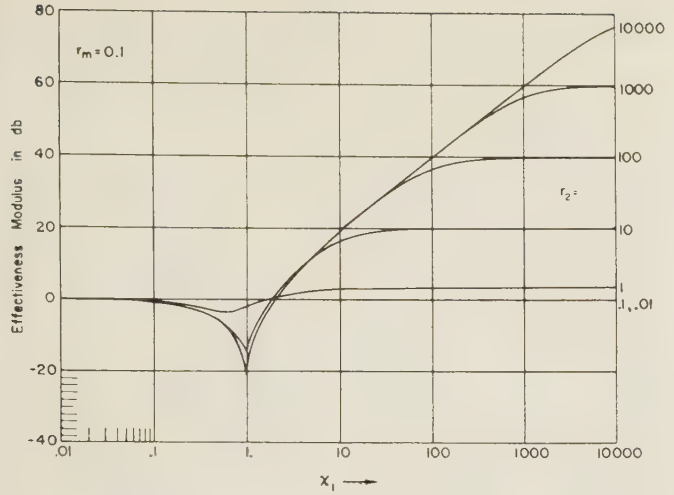

Fig. 9—Effectiveness modulus in db versus x_1 with r_2 as a parameter; x_1 masslike, r_2 resistive

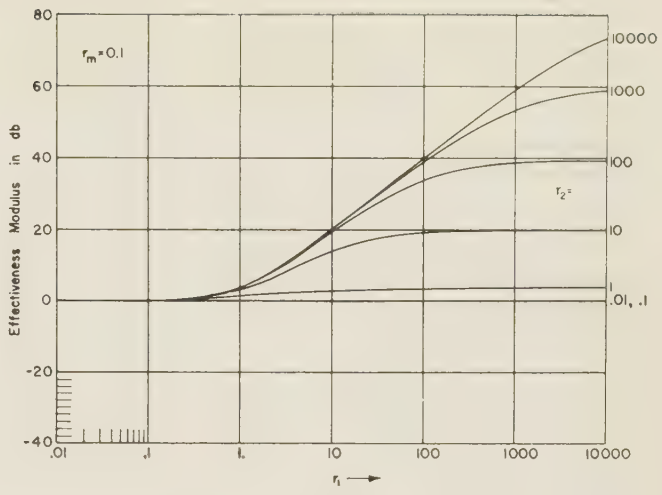

Fig. 10—Effectiveness modulus in db versus x_1 with r_2 as a parameter; x_1 springlike, r_2 resistive

bined stiffness of the mount and X_2 mechanically in series.

If z_1 is masslike, z_2 is resistive, and $x_1 \ll r_2$, the minimum occurs near $x_1 = 1$. This minimum corresponds to resonance of the equivalent mass of X_1 with the mount.

For z_1 and z_2 respectively both springlike, springlike and resistive, or both resistive, the effectiveness of a mount is always unity or greater, and magnification of the vibration does not occur. (See Figs. 6, 10, and 11.)

For z_1 masslike and z_2 springlike, an infinity in effectiveness occurs for $x_1 = |x_2|$. This reflects the fact that when a mount is used, the machine and foundation no longer resonate for $X_1 = |X_2|$ as they do if directly connected. In a practical case, the effectiveness is not infinite because both machine and foundation are somewhat damped. From Equation 19, the effectiveness for $x_1 = |x_2|$ is given by:

$$|E| = \left\{ \frac{\left[r_m + \frac{r_1 r_2}{r_1 + r_2} + \frac{x_1^2}{r_1 + r_2} \right]^2 + \left[-1 + \frac{x_1 (r_2 - r_1)}{r_1 + r_2} \right]^2}{1 + r_m^2} \right\}^{\frac{1}{2}} \tag{26}$$

For $r_m \ll 1$ and for r_1, $r_2 \ll x_1$ this equation reduces approximately to:

$$|E| = \frac{x_1^2}{r_1 + r_2} = \frac{X_1}{|X_m|} \frac{X_1}{R_1 + R_2} \tag{27}$$

It follows that for $x_1 = |x_2|$ the softer the mount is, the more effective it is.

Effectiveness of Massless Spring-Dashpot Mounts Isolating Rigid Machines from Nonrigid Foundations —Although the curves of Figs. 5–11 are valid for both nonrigid and rigid machines, the isolation of rigid machines will now be given further consideration since a different and more familiar representation of the effectiveness data is possible.

If the machine is rigid, its mechanical impedance is given by:

$$Z_M = jwM_M \tag{28}$$

where:

M_M = Its mass

Substituting Equations 14 and 28 in Equation 10, defining some new symbols, and taking the modulus

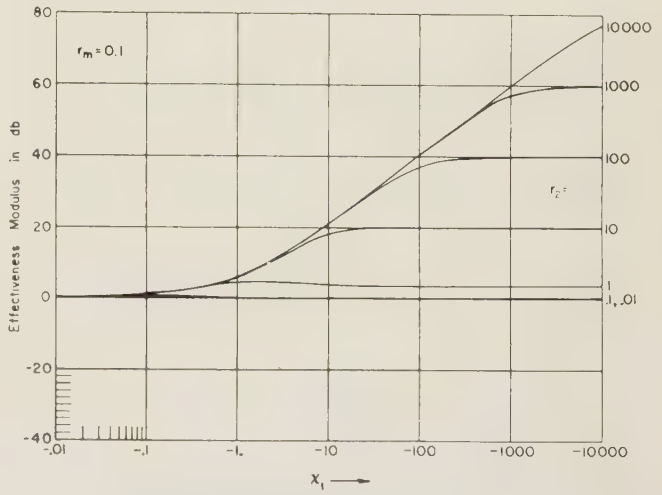

Fig. 11—Effectiveness modulus in db versus r_1 with r_2 as a parameter; r_1 and r_2 resistive

of the resulting expression, one can show that:

$$|E| = \left[\frac{[f_r^2 (1 - f_r x_{FO}) + f_r r_{FO} r_m + f_r x_{FO}]^2}{[f_r r_{FO} r_m + f_r^2 + f_r x_{FO}]^2 + [r_m (f_r^2 + f_r x_{FO}) - f_r r_{FO}]^2} + \frac{[r_m (f_r^2 + f_r x_{FO}) + f_r r_{FO} (f_r^2 - 1)]^2}{[f_r r_{FO} r_m + f_r^2 + f_r x_{FO}]^2 + [r_m (f_r^2 + f_r x_{FO}) - f_r r_{FO}]^2} \right]^{\frac{1}{2}} \tag{29}$$

where:

$$f_r = \frac{w}{w_o}$$

$$w_o = \sqrt{\frac{K_m}{M_M}}$$

$$x_{FO} = \frac{w_o X_F}{K_m}$$

$$r_m = \frac{w R_m}{K_m}$$

$$r_{FO} = \frac{w_o R_F}{K_m}$$

This equation has been plotted in Figs. 12–14 as

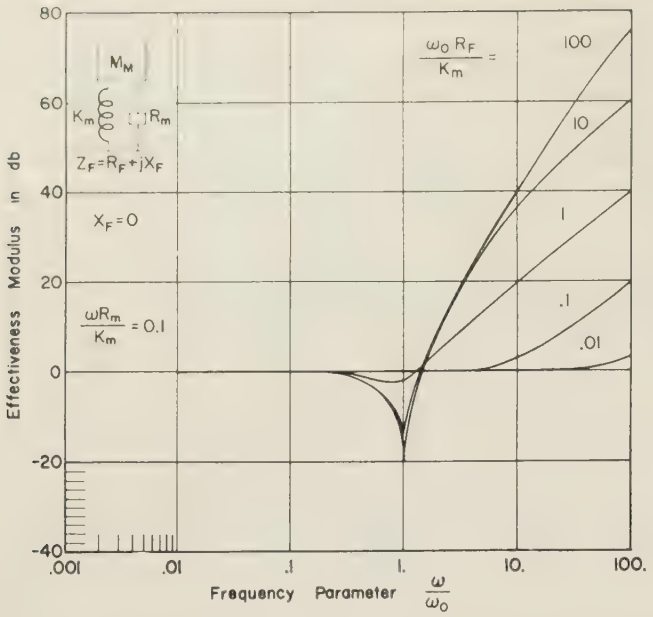

Fig. 12—Effectiveness modulus in db versus frequency ratio $\frac{w}{w_o}$; rigid machine, spring-dashpot mount, resistive foundation

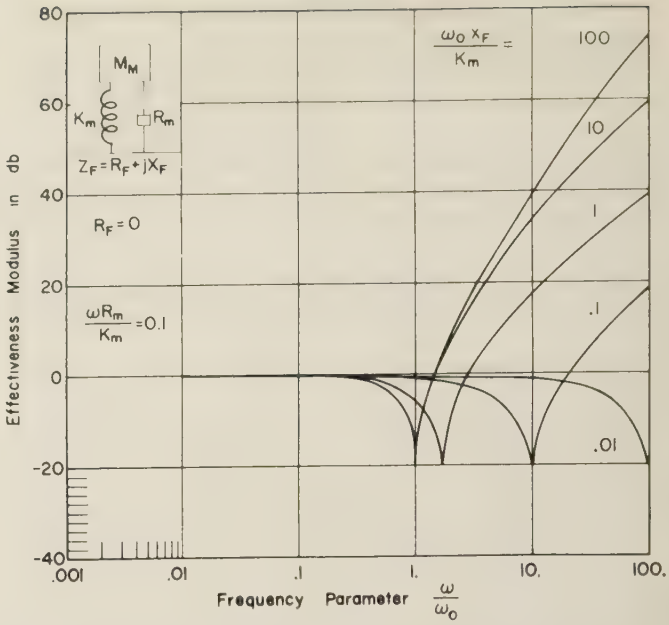

Fig. 13—Effectiveness modulus in db versus frequency ratio $\frac{w}{w_o}$; rigid machine, spring-dashpot mount, masslike foundation

a function of frequency ratio $\frac{w}{w_o}$, with the parameter r_m constant independent of frequency ($r_m = 0.1$), for resistive, masslike, and springlike foundations.

From Fig. 12 it is evident that for $\frac{w}{w_o} \gg 1.5$, the greater the foundation resistance, the more effective a mount will be. For $\frac{w_o R_F}{K_m} \gg 1$, the effectiveness is minimum near the natural frequency of the machine-mount system ($\frac{w}{w_o} = 1$); at the minimum, the effectiveness is controlled by the damping factor of the mount, and is given by Equation 24.

From Figs. 13 and 14 for reactive foundations, it is evident that an effectiveness minimum occurs for each value of the parameter $\frac{w_o X_F}{K_m}$. This minimum corresponds to the natural frequency of a system composed of the rigid machine, spring-dashpot mount, and a hypothetical foundation whose reactance X_F is constant independent of frequency. For $R_F \ll X_F$, the frequency ratio of the effectiveness minimum is given by:

$$\left(\frac{w}{w_o}\right)_{\min} = \frac{\frac{1}{x_{FO}} + \sqrt{\left(\frac{1}{x_{FO}}\right)^2 + 4\left(\frac{r_{FO} r_m + x_{FO}}{x_{FO}}\right)}}{2} \qquad (30)$$

The effectiveness at $\left(\frac{w}{w_o}\right)_{\min}$ is determined by the loss factor of the mount and is given once again by Equation 24.

For $r_m \ll 1$, it can be shown from Equation 30 that for masslike foundations:

$$\left(\frac{w}{w_o}\right)_{\min} \gtrsim 1 \qquad (31)$$

and that the smaller $|x_{FO}|$, the higher $\left(\frac{w}{w_o}\right)_{\min}$ will be; for springlike foundations:

$$\left(\frac{w}{w_o}\right)_{\min} \lesssim 1 \qquad (32)$$

and the smaller $|x_{FO}|$, the lower $\left(\frac{w}{w_o}\right)_{\min}$ will be.

For masslike foundations, the mount will isolate only for $\left(\frac{w}{w_o}\right)$ greater than about 1.5 $\left(\frac{w}{w_o}\right)_{\min}$. For springlike foundations, the mount will isolate only near $\left(\frac{w}{w_o}\right)_{\infty}$ given by:[14]

$$\left(\frac{w}{w_o}\right)_{\infty} = -x_{FO} \qquad (33)$$

and for frequency ratios $\frac{w}{w_o}$ greater than 1 or 2.

Effectiveness of Continuous Mounts Isolating Rigid Machines from Nonrigid Foundations—The use of a massless spring-dashpot model for an isolation mount is possible only at frequencies for which inertia forces associated with the mount can be neglected. At higher frequencies, the mount must be considered an extended mechanical system with distributed mass and elasticity, through which mechanical energy can be propagated by elastic waves.

The effects of wave propagation on the transmissibility of mounts were investigated several years ago at David Taylor Model Basin.[15, 16, 17] The trans-

[14] $\left(\frac{w}{w_n}\right)_{\infty}$ corresponds to resonance of a rigid machine and a foundation whose purely reactive impedance, specified by x_{FO}, is constant independent of frequency.

[15] DTMB Report 766 (Revised), August, 1952: "Wave Effects in Isolation Mounts," by M. Harrison, A. O. Sykes, and M. Martin. David Taylor Model Basin.

[16] DTMB Report 818, February, 1952: "Use of Helical Springs as Isolation Mounts," by A. O. Sykes. David Taylor Model Basin.

[17] DTMB Report 845, October, 1953: "Study of Compression Isolation Mounts Constructed from Cylindrical Samples of Various Natural and Synthetic Rubber Materials," by A. O. Sykes. David Taylor Model Basin.

missibility of compression and shear mounts with simple shapes was determined both theoretically and experimentally, and it was demonstrated that:

1. The transmissibility of mounts having certain simple configurations can be accurately predicted if the properties of the mount material are known.
2. The transmissibility of a mount can be increased at standing wave resonances by 5–20 or more db over what lumped spring-dashpot mount theory predicts.
3. For minimum transmissibility, the wave propagation velocity (the phase velocity) in a mount should decrease with frequency.
4. For minimum transmissibility at standing-wave resonant frequencies, the damping factor for a mount should be high.

Recently, the effects of wave propagation on the effectiveness of mounts have been investigated.

Consider the mechanical system of Fig. 15. The machine and foundation are considered nonrigid and are characterized respectively by the impedances Z_M and Z_F looking into them from their junctures with the mount.

If the mount, pictured as a vertical cylinder, is a long thin rod[18] or a thin disc[19] in tension or compression or torsion, a shear sandwich, or a helical spring in tension or compression, it can be shown that the approximate equation of motion of a cross-section of the mount which is normal to the direction of wave propagation is:[20]

$$G\frac{\delta^2 x(y)}{\delta y^2}+\mu\frac{\delta^3 x(y)}{\delta^2 y\delta t}=\rho\frac{\delta^2 x(y)}{\delta t^2} \qquad (34)$$

where:

$x(y)$ = Instantaneous displacement of the cross-section from its equilibrium position
y = Coordinate of the cross-section measured from one end of the mount
G = Real part of the appropriate elastic modulus of the mount
μ = Appropriate viscosity coefficient
ρ = Density of the mount material

If Equation 34 is solved for $\dot{x}(y)$—the dot indicates the time derivative of $x(y)$—subject to the boundary conditions existing at the junctures of the machine and foundation with the mount, the velocity amplitude $\dot{x}_{22}$ (See Fig. 3) at the machine-mount juncture can be computed.

If this result and Equation 5 for $\dot{x}_{12}$ are substituted in Equation 4, one can show that the complex effectiveness of the mount is given by:

$$E=\cosh\ \gamma\iota+\left(\frac{SZ_o+\dfrac{Z_MZ_F}{SZ_o}}{Z_M+Z_F}\right)\sinh\ \gamma\iota \qquad (35)$$

where:

$\gamma=\alpha+j\beta$, the complex progagation constant of the mount

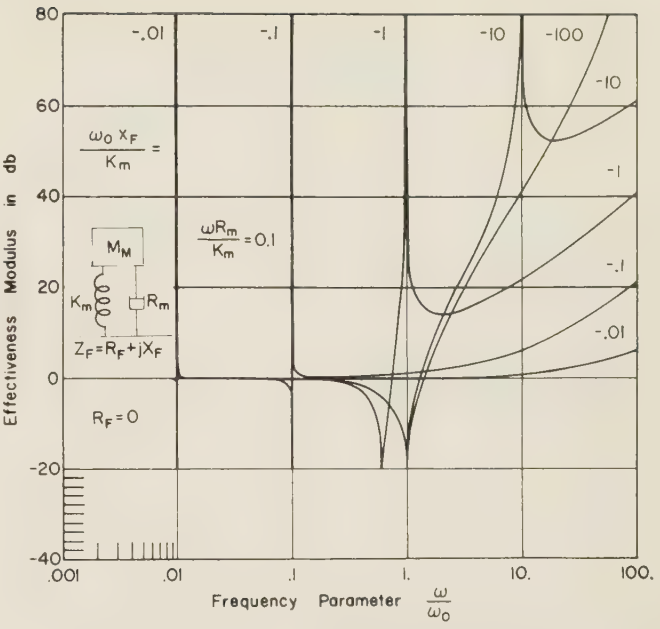

Fig. 14—Effectiveness modulus in db versus frequency ratio $\frac{w}{w_0}$; rigid machine, spring-dashpot mount, springlike foundation

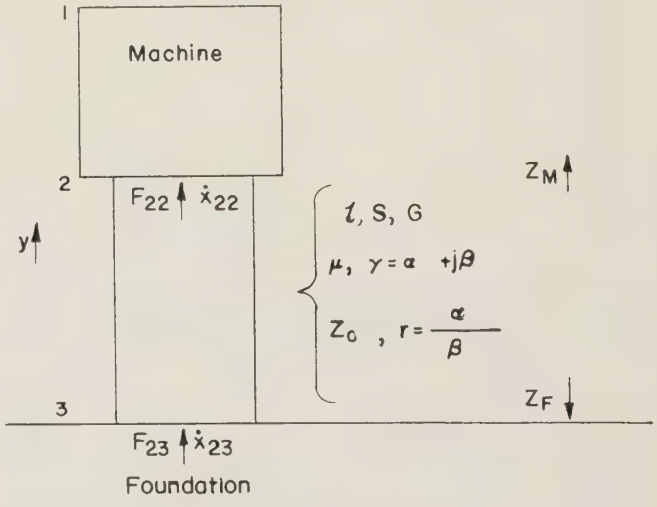

Fig. 15—Machine continuous mount foundation system

α = Attenuation per unit length in the mount
$\beta=\frac{w}{c}$, the phase constant of the mount
$j=\sqrt{-1}$
$w=2\pi f$
f = Frequency in cps
c = Phase velocity in the mount
ι = Length of the mount
S = Cross-sectional area of the mount
Z_o = Complex characteristic impedance per unit area of the mount (SZ_o is referred to as the characteristic impedance)
Z_M = Complex machine impedance looking toward the machine from the machine-mount juncture
Z_F = Complex foundation impedance looking toward the foundation from the

[18] By a thin rod is meant a rod whose diameter is much smaller than the wave length of the vibration in the rod at the highest frequency of interest.
[19] By a thin disc is meant a disc whose edges are constrained so as to prevent motion perpendicular to the direction of wave propagation.
[20] The damping stresses in the mount have been assumed proportional to the time rate of strain $\frac{\delta}{\delta t}\left(\frac{\delta x(y)}{\delta y}\right)$.

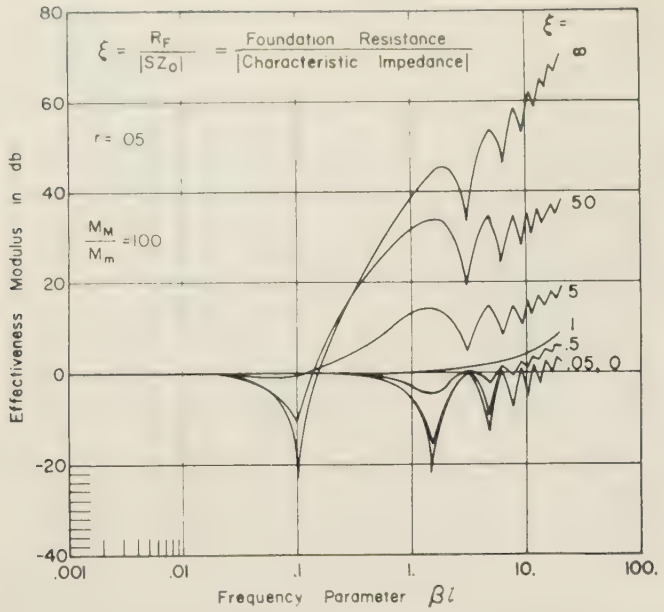

Fig. 16—Effectiveness modulus in db versus frequency parameter βι; rigid machine, continuous mount, resistive foundation

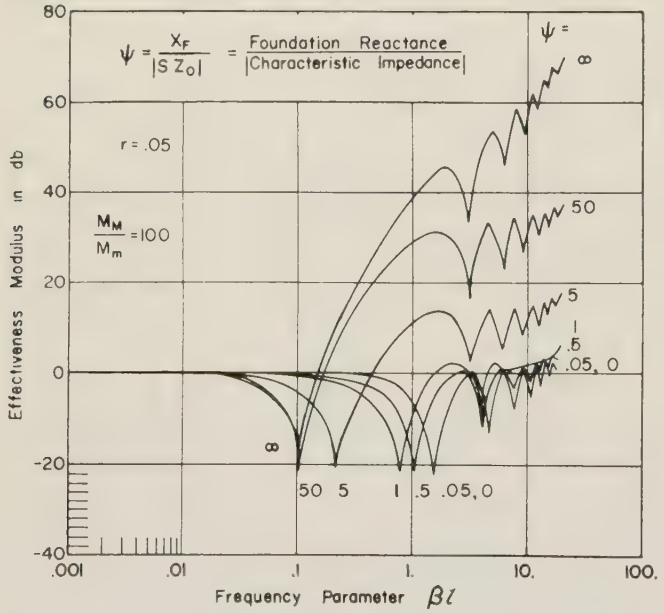

Fig. 17—Effectiveness modulus in db versus frequency parameter βι; rigid machine, continuous mount, masslike foundation

foundation-mount juncture

The modulus of this equation can be written:

$$|E| = [(1 + A_1)\sinh^2 r\beta\iota + \cos^2 \beta\iota + A_1 \sin^2 \beta\iota + A_2 \sin 2\beta\iota + A_3 \sinh 2r\beta\iota]^{\frac{1}{2}} \quad (36)$$

where:

$r = \frac{\alpha}{\beta}$, the damping factor of the mount

If the machine is rigid, its impedance is given by Equation 28, in which case:

$$A_1 = 1 + \frac{4r\xi m\beta\iota}{\sqrt{1+r^2}} - \frac{2(1-r^2)m\psi\beta\iota}{\sqrt{1+r^2}} + (\xi^2+\psi^2)(m\beta\iota\sqrt{1+r^2})^2 \Big/ \xi^2 + (\psi + m\beta\iota\sqrt{1+r^2})^2$$

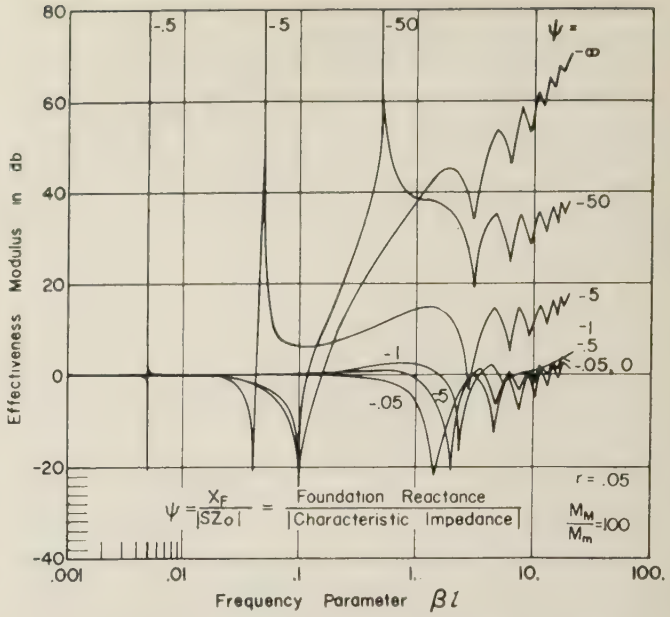

Fig. 18—Effectiveness modulus in db versus frequency parameter βι; rigid machine, continuous mount, springlike foundation

$$A_2 = \frac{m\beta\iota\sqrt{1+r^2} + \psi - r\xi + (m\beta\iota\sqrt{1+r^2})^2(r\xi - \psi)}{[\xi^2 + (\psi + m\beta\iota\sqrt{1+r^2})^2]\sqrt{1+r^2}} - \frac{(\xi^2+\psi^2)m\beta\iota}{\xi^2 + (\psi + m\beta\iota\sqrt{1+r^2})^2}$$

$$A_3 = \frac{\xi + r(m\beta\iota\sqrt{1+r^2} + \psi) + (\xi + r\psi)(m\beta\iota\sqrt{1+r^2})^2}{[\xi^2 + (\psi + m\beta\iota\sqrt{1+r^2})^2]\sqrt{1+r^2}} + \frac{rm\beta\iota\,(\xi^2+\psi^2)}{\xi^2 + (\psi + m\beta\iota\sqrt{1+r^2})^2}$$

where:

$$m = \frac{M_M}{M_m}$$

$$\xi = \frac{R_F}{|SZ_o|}$$

$$\psi = \frac{X_F}{|SZ_o|}$$

M_m = Mass of the mount

$Z_F = R_F + jX_F$, the mechanical impedance of the foundation

$|SZ_o| = \frac{\rho cS}{\sqrt{1+r^2}}$, the magnitude of the characteristic impedance of the mount

Examination of Equation 36, for $Z_F \to \infty$ and $r^2 \ll 1$, shows that an effectiveness minimum will occur near:

$$\beta\iota = \sqrt{\frac{M_m}{M_M}} \overset{\text{def.}}{=} (\beta\iota)_o \quad (37)$$

if $\beta\iota \ll 1$. This minimum corresponds to resonance of the machine and mount at the natural frequency f_o of the machine-mount system. Additional minima will occur for:

$$\beta\iota \cong n\pi$$

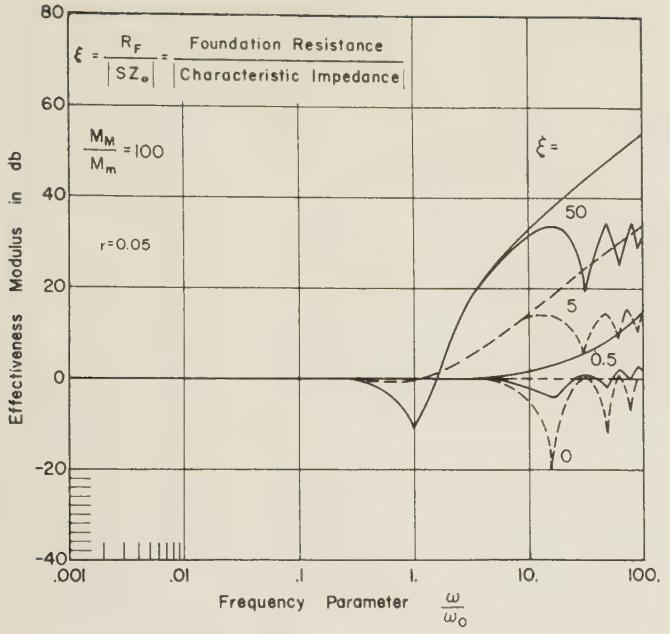

Fig. 19—Effectiveness modulus in db versus frequency ratio $\frac{w}{w_0}$; rigid machine, spring-dashpot and continuous mounts, masslike foundation

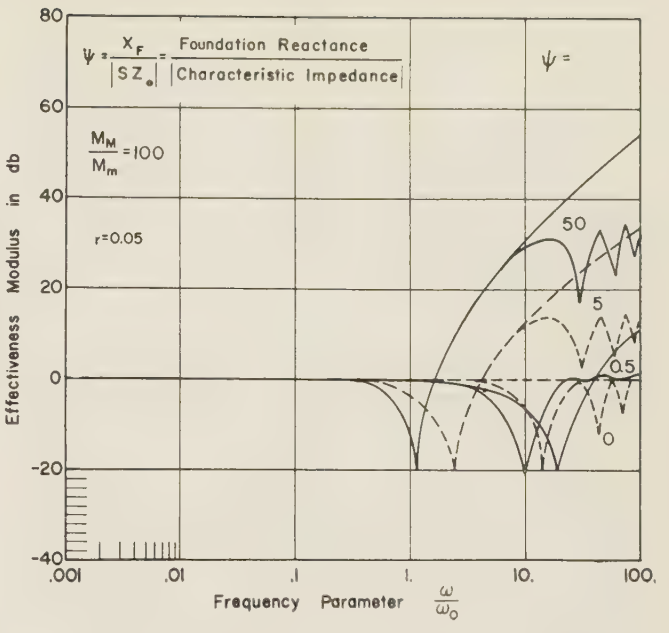

Fig. 20—Effective modulus in db versus frequency ratio $\frac{w}{w_0}$; rigid machine, spring-dashpot and continuous mounts, springlike foundation

where:

$$n = 1, 2, 3 \tag{38}$$

These minima occur at the standing-wave resonant frequencies f_n of the mount:

$$f_n = \frac{nc}{2\iota} \tag{39}$$

for which the length of the mount is an integral number of half wavelengths.

Examination of Equation 36, for $Z_F \to 0$ and $r^2 \ll 1$, shows that effectiveness minima will occur for:

$$\beta\iota = (2s+1)\frac{\pi}{2}$$

where:

$$s = 0, 1, 2 \tag{40}$$

These minima occur at the standing-wave resonant frequencies f_s of the mount:

$$f_s = \frac{(2s+1)}{4}\frac{c}{\iota} \tag{41}$$

for which the length of the mount is an odd integral number of quarter wavelengths.

Equation 36 has been plotted in Figs. 16–18 as a function of the frequency parameter $\beta\iota$ for r constant independent of frequency ($r = 0.05$), for a machine-mount mass ratio $\frac{M_M}{M_m} = 100$, for resistive, masslike, and springlike foundations.

These continuous-mount effectiveness curves have been compared with spring-dashpot mount curves in Figs. 19–21 by making use of the transformations:

$$\frac{w}{w_o} = \frac{1+r^2}{\sqrt{1-r^2}}\sqrt{\frac{M_M}{M_m}}\beta\iota \tag{42}$$

$$\frac{w_o R_F}{K_m} = \sqrt{\frac{(1+r^2)\ M_m}{(1-r^2)\ M_M}}\frac{R_F}{|SZ_o|} \tag{43}$$

$$\frac{w_o X_F}{K_m} = \sqrt{\frac{(1+r^2)\ M_m}{(1-r^2)\ M_M}}\frac{X_F}{|SZ_o|} \tag{44}$$

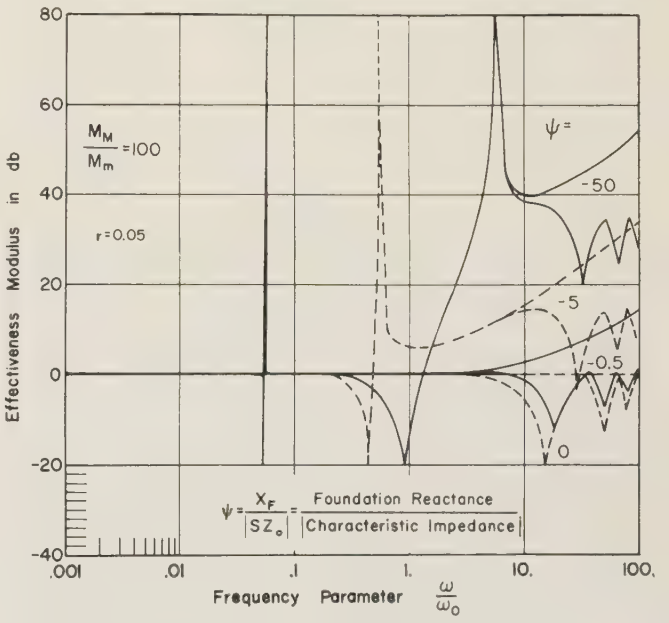

Fig. 21—Effectiveness modulus in db versus frequency ratio $\frac{w}{w_0}$; rigid machine, spring-dashpot and continuous mounts, springlike foundation

$$\frac{wR_m}{K_m} = \frac{2r}{1-r^2} \tag{45}$$

From these curves and Equations 38–41, it follows that the behavior of continuous mounts is quite accurately described by spring-dashpot mount theory, if the wavelength in the mount of the exciting vibration is approximately 10 or more times the length of the mount. On the other hand, if the wavelength in the mount of the exciting vibration is less than about six times the mount length, the mount effectiveness can be considerably lower than spring-dashpot mount theory predicts. Particularly large reductions in effectiveness occur at the lower standing-wave resonances of the mount, irrespective

of the magnitude of the foundation impedance and whether it is resistive or reactive. In fact, if the foundation impedance is predominantly resistive or reactive, and if the impedance ratios $\frac{R_F}{|SZ_o|}$ and $\frac{X_F}{|SZ_o|}$ are less than unity at any of the exciting frequencies, the mount will magnify the vibration at those frequencies.

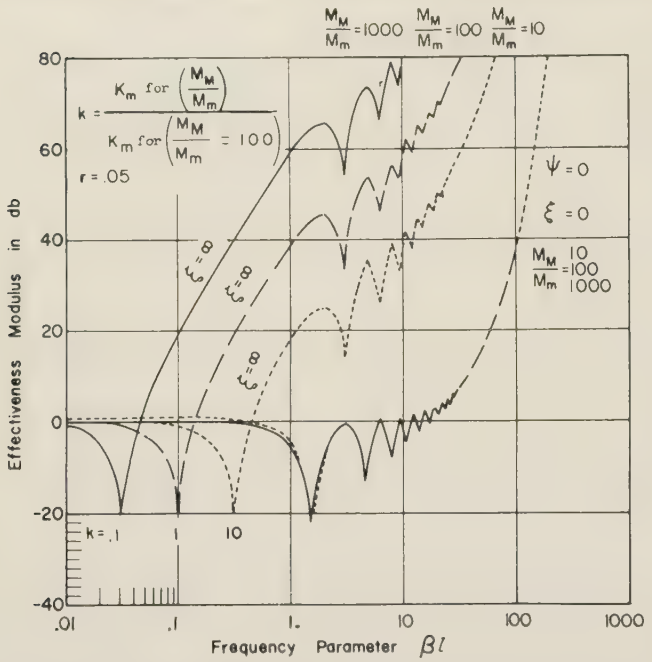

Fig. 22—Effectiveness modulus in db versus frequency parameter $\beta\iota$; rigid machine, continuous mount, zero and infinite impedance foundations; mount length fixed, cross-sectional area varied

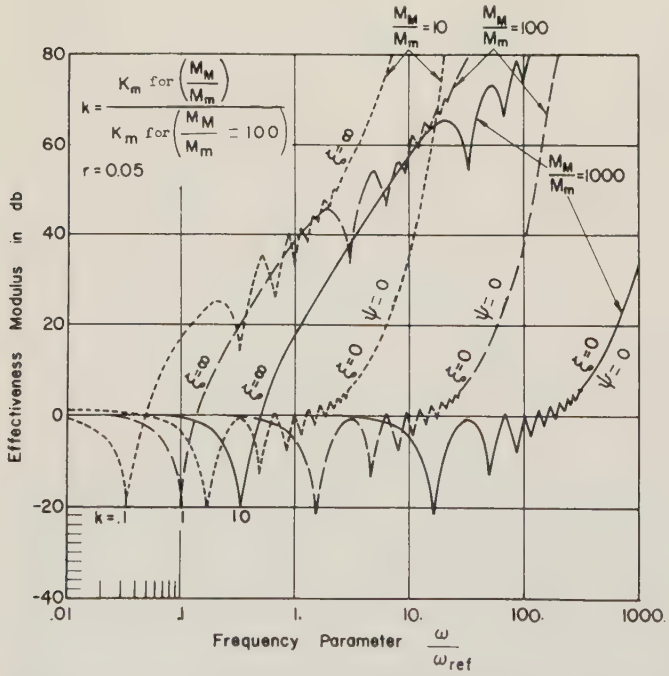

Fig. 23—Effectiveness modulus in db versus frequency ratio $\frac{w}{w_{ref}}$; rigid machine, continuous mount, zero and infinite impedance foundations; mount length varied, cross-sectional area fixed

For ξ and $|\psi| > 1$, the standing-wave resonant frequencies are more or less independent of foundation impedance, and are given approximately by Equation 39. If the foundation impedance is resistive and is of such magnitude that $\xi < 1$, the standing-wave resonant frequencies are given approximately by Equation 41. If the foundation impedance is reactive such that $|\psi| < 1$, the standing-wave resonant frequencies will depend on the magnitude of X_F and on whether it is masslike or springlike. If $|\psi| \ll 1$, the standing-wave resonant frequencies will be near the quarter-wave frequencies given by Equation 41. If the foundation is masslike, the lowest resonant frequency will decrease as ψ increases from zero, until for $\psi \gg 1$ it will coincide with f_o, the natural frequency of the machine-mount system; the higher resonant frequencies will decrease as ψ increases, until for $\psi > 1$ they nearly coincide with the half-wave resonant frequencies (Equation 39). If the foundation is springlike, the natural frequency of the machine-mount-foundation system will increase from zero as $|\psi|$ increases from zero, until for $|\psi| \gg 1$ it also coincides with f_o; the frequencies of the standing-wave resonances will increase as $|\psi|$ increases from zero, from the quarter-wave resonant frequencies given by Equation 41 to the half-wave resonant frequencies given by Equation 39.

Influence of Mount Characteristics on Effectiveness

Spring-dashpot mount theory describes a mount in terms of its stiffness K_m and resistance R_m. Experiment has shown that this description is reasonably adequate for most mounts provided that the dynamic strains in the mount are small enough for it to act as a linear spring, and the frequencies of the exciting forces are low enough for wave effects in the mount to be unimportant.

Continuous-mount theory (for small strains) can describe a mount in terms of its propagation constant γ, length ι and characteristic impedance SZ_o (Equation 35), or in terms of various combinations of related properties. It can be shown from Equations 50, 52, 57, and 62 that a mount can be described by specifying its damping factor r, and any two of the quantities mount stiffness K_m, mass M_m, frequency constant $\frac{c}{\iota}$, and characteristic impedance SZ_o, which themselves can be expressed in terms of the density ρ of the mount material, the phase velocity c in the mount, the damping factor r, the length ι, and cross-sectional area S.

These physical characteristics are determined by various factors:

ρ depends only on the mount material.

c and r depend not only on the material but on what isolation mechanism is chosen, that is, compression, shear, dilation, or some combination thereof and, to a small degree, on the shape (c and r may be somewhat different for thin round rods and thin square rods).

ι and S are determined by design requirements such as, for example, static load.

The effects on effectiveness of varying certain mount characteristics will now be investigated. It

will be assumed that the machine to be isolated acts as a rigid mass M_M, and that the behavior of the mount is described by Equation 36.

For the following discussion, it will be assumed also that the mount material, mechanism of isolation, and shape have been selected, and that this selection has fixed the phase velocity c in the mount and its damping factor r.

Mount Dimensions and Effectiveness—Suppose, for example, that a thin cylindrical rod has been selected as a compression mount. Excluding density, phase velocity, and damping factor—which have been fixed by selection of the mount material, isolation mechanism, and shape—the mount characteristics important in determining its effectiveness can be changed by changing its length, or cross-sectional area, or both.

1. Mount length fixed and cross-sectional area varied.

Fixing the length of the mount fixes its frequency constant, since the phase velocity in the mount has been fixed. Changing its cross-sectional area changes its stiffness, mass, and characteristic impedance in direct proportion.

The effects on effectiveness of varying mount cross-sectional area, with mount frequency constant fixed, are illustrated in Fig. 22 where effectiveness in db is plotted versus $\beta\iota$ for three mount cross-sectional areas, for $r = 0.05$, $\xi = \infty$ and ξ, $\psi = 0$.[21] The area changes are indicated by the changes in mass ratio $\frac{M_M}{M_m}$, and stiffness ratio k defined by:

$$k = \frac{K_m \text{ for } \left(\frac{M_M}{M_m}\right)}{K_m \text{ for } \left(\frac{M_M}{M_m} = 100\right)} \qquad (46)$$

For $k = 0.1$, the cross-sectional area of the mount has been reduced by a factor of 10 from the area for $k = 1$; for $k = 10$, the area has been increased by a factor of 10.

For $\xi = \infty$, it is evident that the mount is effective for all exciting frequencies $(\beta\iota)_i$ greater than about 1.5 $(\beta\iota)_o$ (Equation 37); further, if a mount is effective at a particular frequency, a mount with smaller cross-section—a softer mount—will be more effective.

For ξ and $\psi = 0$, the mount magnifies the vibration except for $\beta\iota \gg \frac{\pi}{2}$; its effectiveness is essentially independent of cross-section.

2. Mount length varied and cross-sectional area fixed.

Fixing the cross-sectional area of the mount fixes its characteristic impedance, since the mount's density and phase velocity have been fixed. Changing its length changes its mass in direct proportion, and its stiffness and frequency constant in inverse proportion.

The effects on effectiveness of varying mount length, with mount characteristic impedance fixed, are illustrated in Fig. 23 where effectiveness in db is plotted versus $\frac{w}{w_{\text{ref.}}}$ for three mount lengths, for $r = 0.05$, $\xi = \infty$, and ξ, $\psi = 0$. $w_{\text{ref.}}$ is defined by:

$$w_{\text{ref.}} = \frac{c}{\iota_{100}} \qquad (47)$$

where:

$$\iota_{100} = \text{Length of the mount for } \frac{M_M}{M_m} = 100$$

The length changes are indicated by changes in $\frac{M_M}{M_m}$ and k. For $k = 0.1$, the mount length is 10 times that for $k = 1$; for $k = 10$, the length is 1/10 that for $k = 1$.

Both for $\xi = \infty$ and ξ, $\psi = 0$, the effectiveness is length dependent. Increasing the length of the mount decreases both the frequency at which the mount first begins to provide isolation, and the standing wave resonant frequencies; it may either increase or decrease effectiveness depending on the exciting frequencies.

Phase Velocity and Effectiveness—It has been established experimentally that the dynamic elastic moduli of many viscoelastic materials are frequency dependent. (See Additional Reference 2.) Below a few hundred cps, they usually increase with frequency. The increase in elastic modulus results from an increase in phase velocity in the mount.

The effects on effectiveness of phase velocity increasing with frequency are illustrated in Fig. 24 for $\frac{M_M}{M_m} = 10$, $r = 0.05$, $\xi = \infty$.

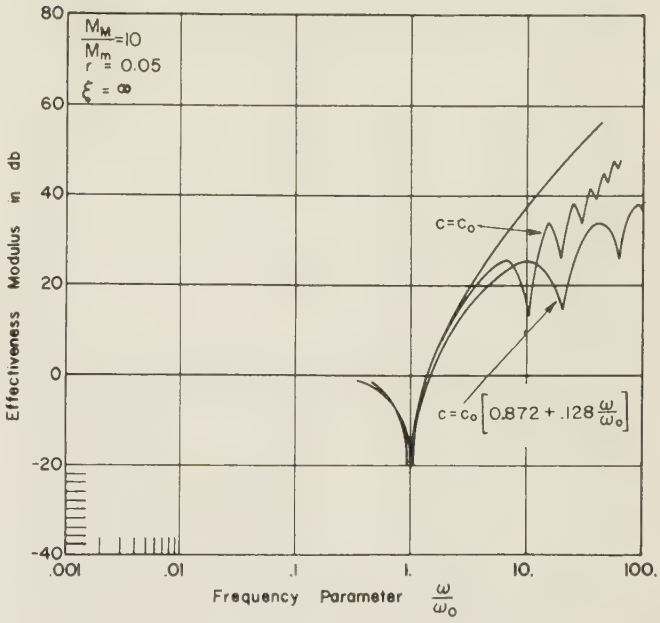

Fig. 24—Effectiveness modulus in db versus frequency ratio $\frac{w}{w_o}$; rigid machine, continuous mount, infinite foundation impedance; mount phase velocity increasing with frequency

Increasing phase velocity with frequency results in reduced effectiveness of the mount, and increases the standing-wave resonant frequencies.

Damping Factor and Effectiveness—The effects on

[21] If the foundation impedance is infinite, the effectiveness of a mount is the same whether the foundation impedance is resistive, reactive, or resistive and reactive.

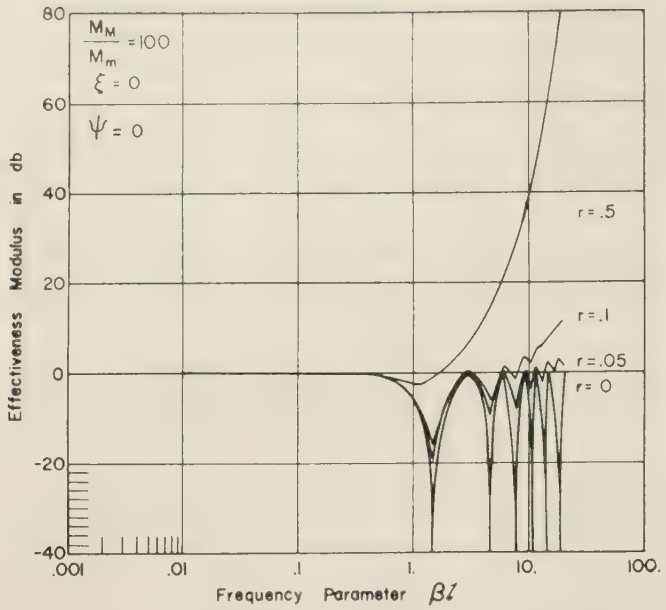

Fig. 25—Effectiveness modulus in db versus frequency parameter $\beta\iota$; rigid machine, continuous mount, zero foundation impedance; mount damping factor r as a parameter

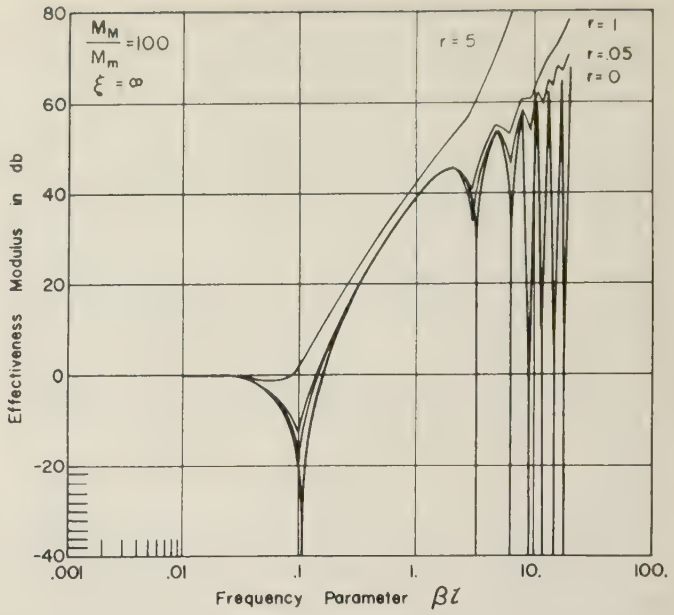

Fig. 26—Effectiveness modulus in db versus frequency parameter $\beta\iota$; rigid machine, continuous mount, infinite foundation impedance; mount damping factor r as a parameter

effectiveness of mount damping factor are illustrated in Figs. 25 and 26 for:

$$\frac{M_m}{M_M} = 100$$
$$r = 0,\ 0.05,\ 0.1,\ 0.5$$
$$\xi = \infty$$
$$\xi,\ \psi = 0$$

For both $\xi = \infty$ and ξ, $\psi = 0$, increasing r increases the mount effectiveness at effectiveness minima and at very high frequencies for which the mount length is many wavelengths.

One can infer that increasing damping factor with frequency should increase the effectiveness of a mount. That this inference is correct is demonstrated in Fig. 27.

Characteristic Impedance and Effectiveness—The characteristic impedance of a mount can be changed by changing the mount material, isolation mechanism, or mount geometry. If mount mass and frequency constant are allowed to change, mount characteristic impedance can be changed without changing the mount stiffness.[22]

Effectiveness curves have been computed for continuous mounts, having the same stiffness but different characteristic impedances, isolating a rigid machine from a resistive foundation. The results are presented in Fig. 28.

It is evident that increases or decreases in characteristic impedance can either increase or decrease effectiveness depending on the frequency ratio. What characteristic impedance is best can not be decided without knowledge of the machine vibratory output spectrum.

Mount Design

Design Parameters—As mentioned in the previous section, a mount can be described in terms of its damping factor r and any pair of the quantities mount stiffness K_m, mass M_m, frequency constant $\frac{c}{\iota}$ and characteristic impedance SZ_o.

The most convenient pair for design purposes are stiffness and frequency constant, since the mount stiffness determines its behavior over the frequency range for which it can be treated as a massless spring-dashpot, while its frequency constant is indicative of the frequency at which wave effects become important.

Design Procedure—Considering only vibration isolation and excluding problems involving shock, static load, drift, and the like, to design a mount for a specific application, one should know:

1. The blocked force or free velocity frequency spectrum of the exciter (whether machine or foundation).

2. The machine and foundation impedances, as functions of frequency, looking into them at the terminals which attach to the mount.

3. Acceptable vibration levels.

From the first two can be calculated the vibratory velocity amplitude as a function of frequency that would occur at the point of contact of machine and foundation if they were directly connected. These data, with the third, define what mount effectiveness is required.

If the exciting frequencies are low enough, it may be possible to design a mount which acts as a massless spring-dashpot over the entire frequency range. The mount stiffness required can be determined from the effectiveness requirement and the machine and foundation impedances, by using Equations 19 or 29 or one of Figs. 5–14, whichever is appropriate. The frequency constant required can be determined from the blocked force or free velocity frequency

[22] For $r^2 \ll 1$, it can be shown from Equations 50, 52, and 57 that:

$$M_m = \frac{|SZ_o|^2}{K_m} \quad (48)$$

$$\frac{c}{\iota} = \frac{K_m}{|SZ_o|} \quad (49)$$

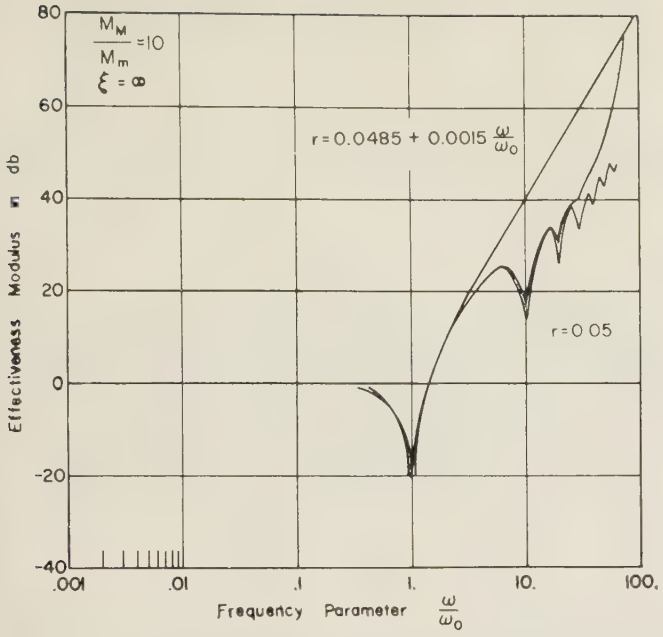

Fig. 27—Effectiveness modulus in db versus frequency ratio $\frac{w}{w_o}$; rigid machine, continuous mount, infinite foundation impedance; mount damping factor increasing with frequency

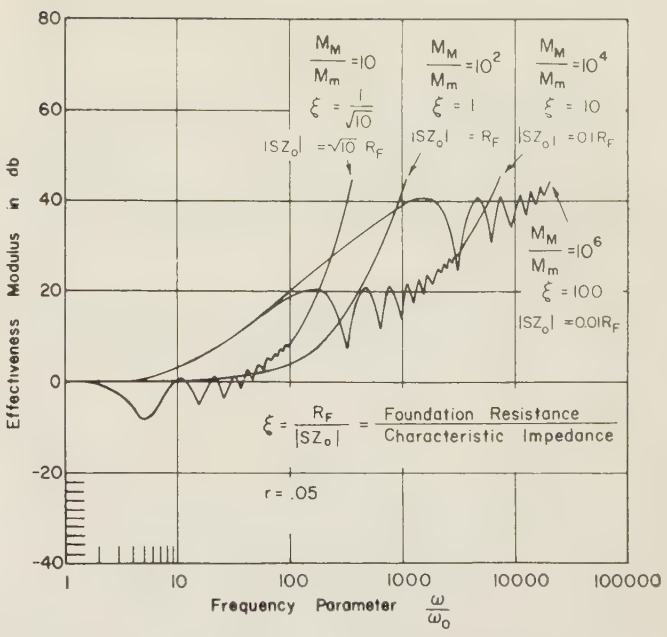

Fig. 28—Effectiveness modulus in db versus frequency ratio $\frac{w}{w_o}$; rigid machine, continuous mount, resistive foundation; machine mass constant, mount stiffness constant, effectiveness varied by varying mount characteristic impedance

spectrum of the exciter, since to assure spring-dashpot mount performance, the frequency constant should be about 10 times the highest exciting frequency. Once these numbers are known, the design can be started. Mount material, isolation mechanism, and mount dimensions should be selected to meet the stiffness and frequency constant requirements, in addition to those of static load, deflection under shock, drift, temperature, oil resistance, and the like.

If the frequency constant requirement for spring-dashpot mount performance can not be met in a realistic design, an attempt should be made to choose $\frac{c}{\iota}$ to avoid coincidences between exciting and standing-wave resonant frequencies.[23]

If the exciting frequencies are all very high, it may be possible to use the high-frequency, high-effectiveness range of a mount. (See curves in Fig. 22 for $\frac{M_M}{M_m}=10$ for $\beta\iota > 20$.) In this case, the mount should be designed so that $\frac{c}{\iota}$ is much lower than the lowest exciting frequency.

In either case, the mount damping factor should be as high as possible, commensurate with mount phase velocity fairly constant or decreasing with frequency.

Conclusion

The evaluation of massless mechanically paralleled spring-dashpot mounts isolating rigid and nonrigid machines from nonrigid foundations has been investigated using the concept of mount effectiveness.

Curves have been presented for estimating the effectiveness of spring-dashpot mounts isolating rigid and nonrigid machines from nonrigid foundations, provided that:

1. The machine-mount-foundation system is such that it can be represented by the model in Fig. 4, where all vibratory forces and velocities are colinear.

2. The machine, mount, and foundation impedances are known as functions of frequency.

3. The machine and foundation impedances are predominantly resistive or reactive.

4. The mount loss factor $\frac{wR_m}{K_m}$ is near 0.1.

Analytical expressions for computing effectiveness in cases for which the curves are inadequate are also presented (Equations 13–33).

The effectiveness of certain types of continuous mounts (Equation 34) isolating rigid machines from nonrigid foundations has also been investigated.

The spring-dashpot mount investigations show that:

1. The softer a mount is, the more effective it will be, if coincidences (or near coincidences) do not occur between exciting frequencies and the natural frequencies of the machine-mount-foundation system.

2. If the machine and foundation impedances are predominantely resistive or reactive and if the magnitude of one is much greater than the magnitude of the other, the effectiveness of the mount will be determined by the ratio of the smaller impedance to the magnitude of the mount reactance, if this ratio

[23] The most important factor in determining standing-wave resonant frequencies is the mount's frequency constant $\frac{c}{\iota}$; however, machine and foundation impedances influence these frequencies and must be considered in computing them.

is greater than about 4. (See Figs. 5–11 and Equation 23).

3. Vibration can be magnified by a mount if machine and foundation impedances are both masslike, or if one is masslike, and the other springlike or resistive (Figs. 5, 7–9); vibration is never magnified by a mount if both machine and foundation impedances are springlike or resistive, or if one is springlike and the other resistive (Figs. 6, 10, and 11).

4. The maximum magnification of vibration that a mount can cause is controlled by its loss factor (Equations 19, 24, and 29; Figs. 5, 7–9, and 12–14).

The investigations of continuous mounts show that:

1. A continuous mount acts like a massless mechanically paralleled spring-dashpot mount at frequencies whose wavelength in the mount is 10 or more times its largest physical dimension.

2. The effectiveness of a continuous mount at its lower standing-wave resonant frequencies can be 5–20 or more db less than spring-dashpot theory predicts, depending on the mount's damping factor; the higher the damping factor, the more effective the mount.

3. The effectiveness of a continuous mount at its lower standing-wave resonant frequencies is less than spring-dashpot mount theory predicts, whether the foundation impedance is large or small relative to the mount characteristic impedance.

4. A continuous mount will either provide no isolation or will magnify the vibration in the frequency range containing its lower standing-wave resonant frequencies, if the foundation impedance is resistive or reactive and if its magnitude is less than the magnitude of the mount characteristic impedance.

5. The effectiveness of a continuous mount, depending on its damping factor, can be much higher than spring-dashpot mount theory predicts at exciting frequencies much higher than the mount frequency constant. (See curves in Fig. 22 for $\frac{M_M}{M_m} = 10$).

6. The standing-wave resonant frequencies of a machine-mount foundation system depend not only on the characteristics of the mount, but also on the machine and foundation impedances. For a rigid machine isolated from a resistive or reactive foundation by a continuous mount, whose characteristic impedance is much lower than the foundation impedance, the standing-wave resonant frequencies will be those frequencies for which the mount length is an integral number of half wavelengths; if the mount characteristic impedance is much larger than the foundation impedance, the standing-wave resonant frequencies will be those frequencies for which the mount length is an odd number of quarter wavelengths. Other relationships between foundation impedance and mount characteristic impedance give intermediate standing-wave resonant frequencies.

The problem of mount design has also been discussed briefly and the need for specifying, in addition to mount stiffness and damping factor, a quantity which determines at what frequency wave effects become important has been pointed out. The use of frequency constant $\frac{c}{\iota}$, the ratio of phase velocity in the mount to mount length, has been suggested for this purpose for the simple types of mounts discussed here.

Acknowledgment

This paper is based on investigations performed at the David Taylor Model Basin, which were sponsored by the Noise Shock and Vibration Section of the Applied Science Division of the Bureau of Ships under Bureau of Ships Project NS-713-017.

The author would like to express his appreciation to Morris Engineering, Inc., of Washington, D. C., for performing the effectiveness calculation and for preparing the figures and text.

Additional References

1. *Journal of Polymer Science,* Vol. 5, January, 1950, pp. 1–54: "Dynamic Mechanical Properties of Rubberlike Materials," by A. W. Nolle.

2. *Industrial and Engineering Chemistry,* Vol. 43, November, 1951, pp. 2540–2547: "Transmission of Mechanical Vibrations through Rubbers," by R. E. Morris, R. R. James, and H. L. Snyder.

3. Shock and Vibration Instrumentation, ASME, June, 1956, pp. 1–39: "Evaluation of Mounts Isolating Nonrigid Machines from Nonrigid Foundations," by A. O. Sykes. Also, DTMB Report 1094, September, 1957, David Taylor Model Basin.

APPENDIX I

Summary of Mount Formulas

A number of equations, most of which are not given in the text, but which are useful in dealing with mounts described by Equation 34 are listed below.[17]

1. Real part G of the elastic modulus:

$$G = \rho c^2 \frac{1 - r^2}{[1 + r^2]^2} \tag{50}$$

2. Viscosity coefficient μ:

$$\mu = \frac{\rho c^2}{w} \frac{2r}{[1 + r^2]^2} \tag{51}$$

3. Mount stiffness K_m:

$$K_m = G\frac{S}{\iota} \tag{52}$$

4. Mount resistance R_m:

$$R_m = \mu\frac{S}{\iota} \tag{53}$$

5. Complex elastic modulus $\overline{G}$:

$$\overline{G} = G + jw\mu \tag{54}$$

6. Magnitude of the complex elastic modulus G:

$$|G| = \sqrt{G^2 + (w\mu)^2} = \frac{\rho c^2}{1 + r^2} \tag{55}$$

7. Complex characteristic impedance per unit area:

$$Z_o = -j\frac{\overline{G}\gamma}{w} = \frac{\rho c}{1+r^2}(1+jr) \qquad (56)$$

8. Magnitude of the complex characteristic impedance per unit area:

$$|Z_o| = \frac{\rho c}{\sqrt{1+r^2}} \qquad (57)$$

9. The driving point impedance Z_D of a mechanical transmission line of complex characteristic impedance SZ_o and complex propagation constant γ terminated by a mechanical impedance Z_T:

$$Z_D = SZ_o\frac{SZ_o \sinh \gamma\iota + Z_T \cosh \gamma\iota}{SZ_o \cosh \gamma\iota + Z_T \sinh \gamma\iota} \qquad (58)$$

10. The complex transmissibility T_m of a continuous mount:

$$T_m = \frac{1}{\cosh \gamma\iota} \qquad (59)$$

11. The complex transmissibility T of a machine-continuous mount system:

$$T = \frac{1}{\cosh \gamma\iota + \dfrac{Z_M}{SZ_o}\sinh \gamma\iota} \qquad (60)$$

12. The magnitude of T:

$$|T| = [(1+B_1)\sinh^2 r\beta\iota + \cos^2 \beta\iota + B_1 \sin^2 \beta\iota + B_2 \sin 2\beta\iota + B_3 \sinh 2r\beta\iota]^{-\frac{1}{2}} \qquad (61)$$

where:

$$B_1 = \frac{|Z_M|^2}{|SZ_o|^2}$$

$$B_2 = \frac{SZ_o{}^i R_M - SZ_o{}^R X_M}{|SZ_o|^2}$$

$$B_3 = \frac{SZ_o{}^R R_M + SZ_o{}^i X_M}{|SZ_o|^2}$$

$$SZ_o = S(Z_o{}^R + jZ_o{}^i)$$

$$Z_M = R_M + jX_M$$

13. Mount mass M_m:

$$M_m = \rho S\iota \qquad (62)$$

14. Complex effectiveness E:

$$E = \cosh \gamma\iota + \left(\frac{SZ_o + \dfrac{Z_M Z_F}{SZ_o}}{Z_M + Z_F}\right)\sinh \gamma\iota \qquad (35)$$

15. Magnitude of E:

The magnitude of E is given by:

$$|E| = [(1+B_1)\sinh^2 r\beta\iota + \cos^2 \beta\iota + B_1 \sin^2 \beta\iota + B_2 \sin 2\beta\iota + B_3 \sinh 2r\beta\iota]^{\frac{1}{2}} \qquad (63)$$

where:

$$B_1 = 1 + \frac{\dfrac{4r}{1+r^2}(\phi\psi + \xi\sigma) + 2\left(\dfrac{1-r^2}{1+r^2}\right)(\phi\xi - \sigma\psi)}{(\phi+\xi)^2 + (\sigma+\psi)^2} + \frac{(\xi^2+\psi^2)(\phi^2+\sigma^2)}{(\phi+\xi)^2 + (\sigma+\psi)^2}$$

$$B_2 = \frac{\sigma + \psi - r(\phi+\xi) + (\phi^2+\sigma^2)(r\xi - \psi)}{[(\phi+\xi)^2 + (\sigma+\psi)^2]\sqrt{1+r^2}} + \frac{(\xi^2+\psi^2)(r\phi - \sigma)}{[(\phi+\xi)^2 + (\sigma+\psi)^2]\sqrt{1+r^2}}$$

$$B_3 = \frac{\phi + \xi + r(\sigma+\psi) + (\xi + r\psi)(\phi^2+\sigma^2)}{[(\phi+\xi)^2 + (\sigma+\psi)^2]\sqrt{1+r^2}} + \frac{(\phi + r\sigma)(\xi^2+\psi^2)}{[(\phi+\xi)^2 + (\sigma+\psi)^2]\sqrt{1+r^2}}$$

16. Mount frequency constant $\frac{c}{\iota}$ in terms of mount stiffness K_m and M_m mass:

$$\frac{c}{\iota} = \left[\frac{(1+r^2)^2}{1-r^2}\frac{K_m}{M_m}\right]^{\frac{1}{2}} \qquad (64)$$

17. Ratio of the frequency constant $\frac{c}{\iota}$ to the natural frequency f_o of the machine-mount system:

$$\frac{\dfrac{c}{\iota}}{f_o} = 2\pi\sqrt{\frac{M_M}{M_m}\frac{1+r^2}{1-r^2}} \qquad (65)$$

where:

ρ = Density of the mount material

c = Phase velocity in the mount

$\gamma = \alpha + j\beta$, the propagation constant of the mount

$j = \sqrt{-1}$

α = Attenuation per unit length in the mount

$\beta = \dfrac{w}{c}$, the phase constant of the mount

$r = \dfrac{\alpha}{\beta}$, the damping factor of the mount

ι = Length of the mount

S = Cross-sectional area of the mount

$Z_M = R_M + jX_M$, the machine impedance looking toward the machine at the machine-mount juncture

$Z_F = R_F + jX_F$, the foundation impedance looking toward the foundation at the foundation-mount juncture,

$$\phi = \frac{R_M}{|SZ_o|}$$

$$\sigma = \frac{X_M}{|SZ_o|}$$

$$\xi = \frac{R_F}{|SZ_o|}$$

$$\psi = \frac{X_F}{|SZ_o|}$$

APPENDIX II

Effectiveness in Terms of Mobility

Equation 10, the effectiveness equation for a spring-dashpot mount isolating a nonrigid machine from a nonrigid foundation, was derived using the concept of mechanical impedance. Mobility, that

is, reciprocal impedance, might have been used as well.

Defining the mobilities of the machine, mount, and foundation respectively by:

$$Y_M = \frac{1}{Z_M} \tag{66}$$

$$Y_m = \frac{1}{Z_m} \tag{67}$$

$$Y_F = \frac{1}{Z_F} \tag{68}$$

one can show from Equation 10 that the effectiveness in terms of mobility is given by:

$$E = \frac{Y_M + Y_m + Y_F}{Y_M + Y_F} \tag{69}$$

Equation 69 may be simpler to use for computational purposes than Equation 10.

APPENDIX III

Notation

c = Phase velocity in the mount
E = Mount effectiveness
f = Frequency in cps
f_o = Natural frequency of machine-mount system;
G = Real part of the elastic modulus
$\overline{G}$ = Complex elastic modulus;
$j = \sqrt{-1}$
K_m = Mount stiffness
k = Stiffness ratio
ι = Mount length
M_M = Machine or equipment mass
M_m = Mount mass, that is, mass of resilient element in mount
m = Mass ratio, $m = \frac{M_M}{M_m}$
R = Mechanical resistance
R_F = Foundation resistance
R_M = Machine resistance
R_m = Mount resistance
r_F = Ratio of the foundation resistance to the magnitude of the mount reactance, $r_F = \frac{R_F}{|X_m|}$
r_M = Ratio of the machine resistance to the magnitude of the mount reactance, $r_M = \frac{R_M}{|X_m|}$
r_m = Ratio of the mount resistance to the magnitude of the mount reactance, $r_m = \frac{R_m}{|X_m|} = \frac{wR_m}{K_m}$
r_1, r_2 = Ratio of the machine or foundation resistance to the magnitude of the mount reactance
S = Mount cross-sectional area
T = Transmissibility of a machine-mount system
T_m = Transmissibility of a mount
X = Mechanical reactance
X_F = Foundation reactance
X_M = Machine reactance
X_m = Mount reactance
x_F = Ratio of the foundation reactance to the magnitude of the mount reactance, $x_F = \frac{X_F}{X_m}$
x_M = Ratio of the machine reactance to the magnitude of the mount reactance, $x_M = \frac{X_M}{|X_m|}$
x_1, x_2 = Ratio of the machine or foundation reactance to the magnitude of the mount reactance
$x(y)$ = Instantaneous displacement of the mount cross-section from its equilibrium position
Y_F = Foundation mobility
Y_m = Mount mobility
Y_M = Machine mobility
y = Coordinate of the mount cross-section measured from one end of the mount
Z = Mechanical impedance, $Z = R + jX$
Z_F = Foundation impedance
Z_M = Machine impedance
Z_m = Mount impedance
Z_o = Mount characteristic impedance per unit area
z_F = Ratio of the foundation impedance to the magnitude of the mount reactance, $z_F = \frac{R_F + jX_F}{|X_m|}$
z_M = Ratio of the machine impedance to the magnitude of the mount reactance, $z_M = \frac{R_M + jX_M}{|X_m|}$
z_m = Ratio of the mount impedance to the magnitude of the mount reactance, $z_m = r_m - j$
z_1, z_2 = Ratio of the machine or foundation impedance to the magnitude of the mount reactance
α = Attenuation per unit length in the mount
β = Phase constant, $\beta = \frac{w}{c}$
γ = Propagation constant; $\gamma = \alpha + j\beta$
μ = Viscosity coefficient
ξ = Ratio of the foundation resistance to the magnitude of the mount characteristic impedance, $\xi = \frac{R_F}{|SZ_o|}$
ρ = Density of the mount material
σ = Ratio of the machine reactance to the magnitude of the mount characteristic impedance, $\sigma = \frac{X_M}{|SZ_o|}$
ϕ = Ratio of the machine resistance to the magnitude of the mount characteristic impedance, $\phi = \frac{R_M}{|SZ_o|}$
ψ = Ratio of the foundation reactance to the magnitude of the mount characteristic impedance, $\psi = \frac{X_F}{|SZ_o|}$
w = Frequency in radians per sec, $w = 2\pi f$
w_o = Natural frequency of machine-mount system, $w_o = \sqrt{\frac{K_m}{M_M}}$

Investigating Combustion Phenomena in Unmodified Engines

J. A. Robison, M. D. Behrens, R. G. Mosher, and J. M. Chandler, Ford Motor Co.

This paper was presented at the SAE National Fuels and Lubricants Meeting, Cleveland, Nov. 8, 1957.

IN studies of combustion and engine-fuel relationships, both the research investigator and the engine development engineer are often forced to rely on engine noise alone to detect abnormal combustion. In the past, characteristic metallic "pinging" noise signaling autoignition and the more erratic "thudding" noise of surface ignition have been easily identified audibly by the trained observer. In fact, no instrumentation has ever proved adequate to replace the human ear of the trained observer in establishing borderline knock in multicylinder engines. However, investigations at higher compression ratios using higher octane level fuel compositions have indicated that engine noise resulting from both normal and abnormal combustion has changed to such an extent that the value of engine noise as the criterion of abnormal combustion is questionable.

Some combustion phenomena and resulting noises now being encountered include: autoignition of the end gas manifested as knock ranging in noise quality from thudding to pinging; high-speed autoignition; surface ignition manifested as a pressure rap or a knock; and high rates of pressure rise which may result in rumble. Unfortunately, these noises are sometimes indistinguishable from one another and, under the conditions of high ambient car or engine noise, may be quite difficult to detect. Moreover, the fact that the different combustion phenomena may occur on successive cycles or in different cylinders complicates an already confused situation. Thus, it appears that the accepted method of relating and assigning different noises to different combustion phenomena must be reconsidered.

In research studies, it must be remembered that the basic item being investigated is the actual combustion process—whether normal or abnormal—and not the audible manifestations emanating therefrom. If the combustion event results solely in spark knock, the major factor to consider is customer objection to the noise since autoignition does not seem to be too harmful in today's engines. A problem which arises, however, is the detection and treatment of combustion phenomena which may remain unobserved from a noise standpoint, but which may prove quite deleterious to the engine. It appears, therefore, that evaluation of the actual combustion process by more analytical means is required for fundamental studies, and may even be required as an aid to the conventional audible method for knock rating as now used throughout the automotive and petroleum industries.

Instrumentation Development

Instantaneous pressure-time indicators and rate-of-pressure-rise indicators can be relied on to categorize abnormal combustion. The defining of various types of abnormal combustion by pressure indicators is not new. For single-cylinder engine tests in the laboratory, it is standard practice to instrument the combustion chamber with a pressure indicator. In cylinder-head and combustion-chamber development work, however, the investigator is always concerned about the adverse effect on combustion-chamber cooling that such an indicator installation might have. In full-scale multicylinder engines, installation of pressure indicators in each cylinder is impractical because of space limitations as well as changes in combustion-chamber cooling. The only practical solution to such problems is to consolidate the pressure indicator and spark plug.

The use of spark plugs incorporating strain gages appears to be a step in the right direction. However, these instruments have certain undesirable characteristics. In most instances, the required changes or additions to the spark plug result in a modification to the combustion chamber and could change pressure development and the occurrence of abnormal combustion. Unless the spark plug remains as it was designed for the chamber, there is no absolute guarantee that the combustion process will not be altered. Nevertheless, assuming that strain gages could be successfully installed in standard spark plugs, there still remain the problems of durability and accuracy. Our experience indicates that the durability and accuracy of strain-gage spark-plug combinations leave much to be desired. Moreover, investigations of destructive types of abnormal combustion are particularly hazardous to its life.

The development of a spark-plug pressure-indica-

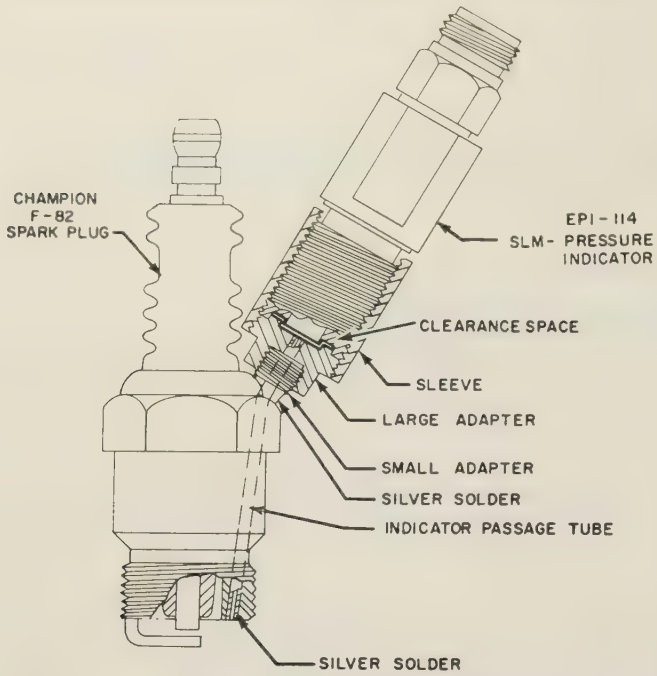

Fig. 1—Cross-sectional view of spark-plug pressure-indicator combination

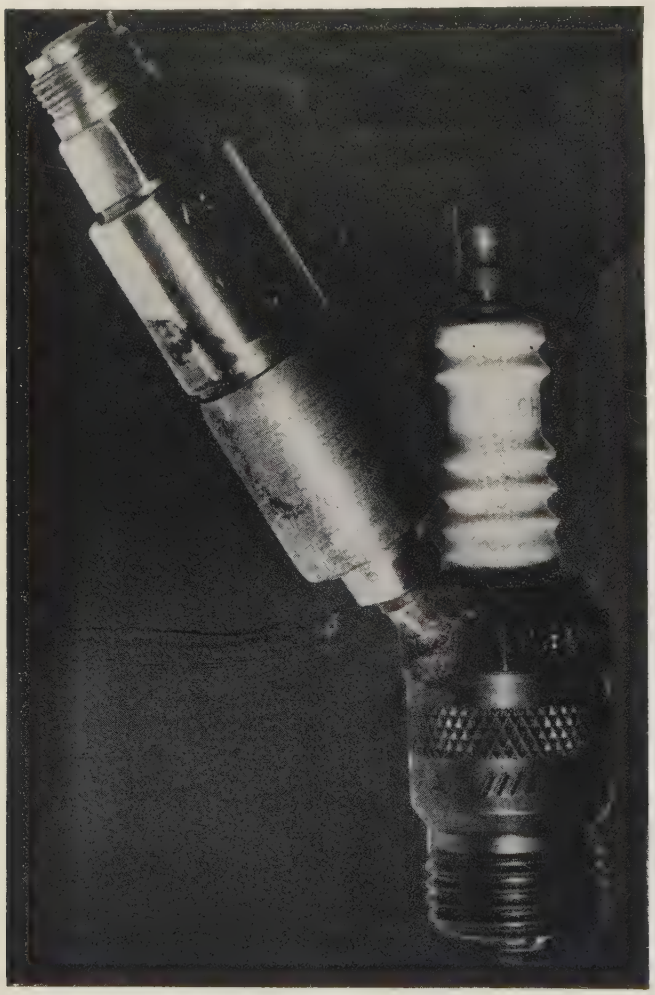

Fig. 2—Spark-plug pressure-indicator combination using Champion F-82 spark plug and SLM EP1-114 pressure indicator

tor combination which would provide a high degree of versatility, good endurance characteristics, and low-cost maintenance without introducing any variable which could affect the combustion process was deemed vital to any study of combustion. To meet the above requirements, it was obvious that standard spark plugs had to be used and that the temperature of the pressure transducer had to be reduced. It was felt that these two objectives could best be accomplished by the use of indicator passages in standard spark plugs. A program was initiated which culminated in the development of a spark-plug pressure-indicator combination that features the use of expendable spark plugs and satisfies all of the preceding requirements.

Fig. 1 shows a cross-sectional view of the spark-plug pressure-indicator combination in its present state of development. Basically, it consists of a spark plug containing a passage leading from the combustion chamber to a pressure-sensing element. Development work has centered about Champion F-82 spark plugs due to their current use in combustion-chamber research at high compression ratios.

The combination is constructed in two units to facilitate the replacement of damaged or fouled spark plugs and to maintain a fixed clearance at the indicator end of the passage. The spark-plug unit, which can be produced at low cost, consists of a standard spark plug, stainless-steel tube, and a small brass adapter. The shell of the spark plug is drilled to accept the tubing. The tubing and adapter are silver soldered in place. Application of the indicator passage principle on virtually any spark plug appears feasible since it is permissible to allow the indicator tube to pass outside the spark-plug shell above the spark-plug seat. The indicator unit consists of a pressure indicator, large brass adapter, and brass sleeve. The pressure indicator used in these investigations is a Kistler SLM quartz crystal pickup, model EPI-114. The large brass adapter is machined to follow the contour of the end of the pressure indicator with a minimum clearance. The sleeve joins the adapter to the indicator. The indicator unit remains intact with fixed clearance until maintenance is required.

Fig. 2 shows the present spark-plug pressure-indicator combination. This instrument has a somewhat limited application due to the mounting angle required by the large indicator to clear the spark-plug ceramic. Fig. 3 shows another spark-plug pressure-indicator combination also under development which employs a smaller indicator. This combination has more universal application due to its smaller size and more ideal mounting on the spark plug.

The spark-plug pressure-indicator combination type shown in Fig. 2 was used to investigate the effects of indicator passage design and indicator-to-adapter clearance space on pressure development. Several investigators[1, 2] have reported the effect of indicator passages on measurements of combustion-chamber pressure development. These investigations have shown that variations in pressure development occur due to lag, dampening, and pressure oscillations in the passage. We have confirmed these find-

[1] *The Engineer*, Dec. 16, 1955: "Effects of Indicator Passages on Accuracy of Indicator Diagrams," by J. G. Withers.
[2] SAE Transactions, Vol. 61, 1953, pp. 557–573: "Engine Cylinder Pressure Measurements," by J. D. McCullough.

Fig. 3—Spark-plug pressure-indicator combination using Champion F-82 spark plug and SLM PZ-6 pressure indicator

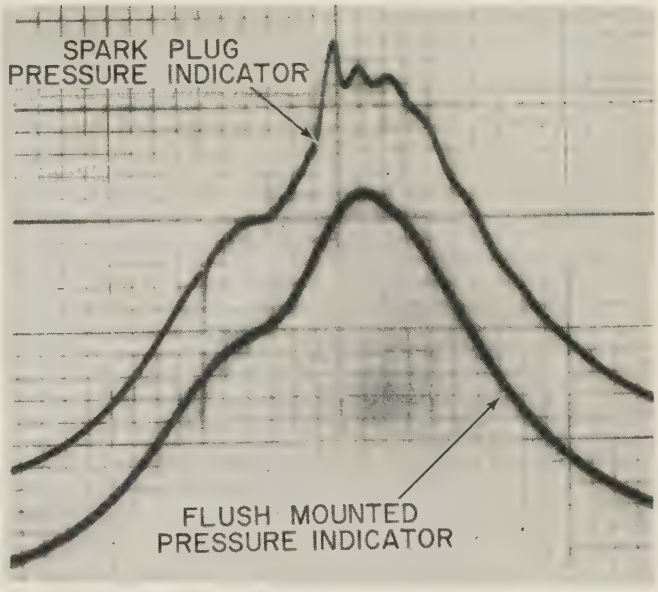

Fig. 4—Pressure oscillations due to excessive clearance space

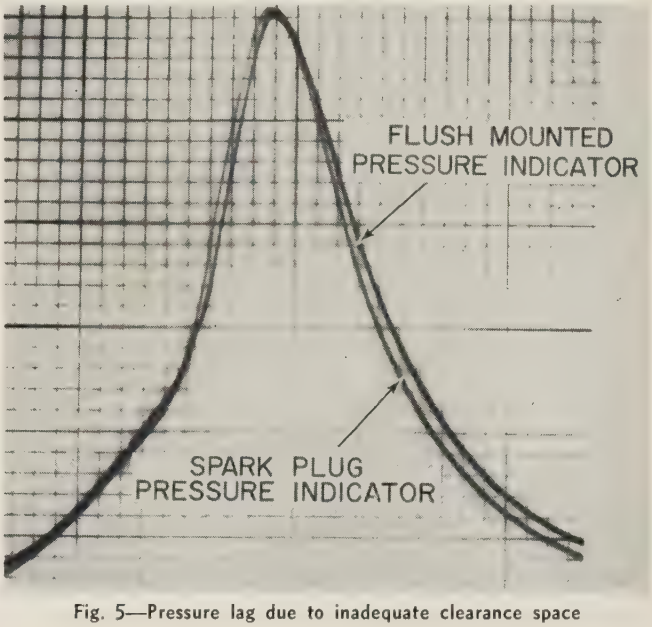

Fig. 5—Pressure lag due to inadequate clearance space

ings for the most part but have discovered that the clearance space at the indicator end of the passage is critical as far as dampening and pressure oscillations are concerned. In the investigations of clearance space and indicator passage design, an 11/1 compression ratio single-cylinder engine was used which was built of experimental parts installed on a Waukesha CFR-48 crankcase. The effects of indicator passage and clearance space were determined by noting the difference in instantaneous signals from an indicator mounted flush with the combustion-chamber wall and from the spark-plug pressure-indicator combination. Observations of these signals were made on a linear dual-beam oscilloscope. The two indicators used were previously established to be identical in dynamic response when operated flush in the chamber.

Effect of Indicator-to-Adapter Clearance Space—In the initial investigations to determine the effect of indicator passage dimensions on pressure development measurements, sufficient adapter-to-indicator clearance height was built into the indicator units to guarantee free movement of the pressure-sensitive element. In addition to the space resulting from this clearance height, the clearance space included the volume in the annular ring between the indicator diaphragm and the adapter. The results obtained with these clearance space conditions showed excessive pressure oscillations and dampening. The results were also inconsistent depending on the amount of clearance space built into each unit. It was eventually determined that a minimum clearance was necessary to eliminate oscillations and dampening. This minimum clearance condition also included filling in the annular ring space between the indicator diaphragm and adapter. Fig. 4 shows the signal of a flush-mounted indicator compared to the signal from a spark-plug pressure-indicator combination with excessive clearance space. Conversely, too small a clearance space may interfere with the normal actuation of the pressure-sensitive element. Fig. 5 shows a lag in pressure devel-

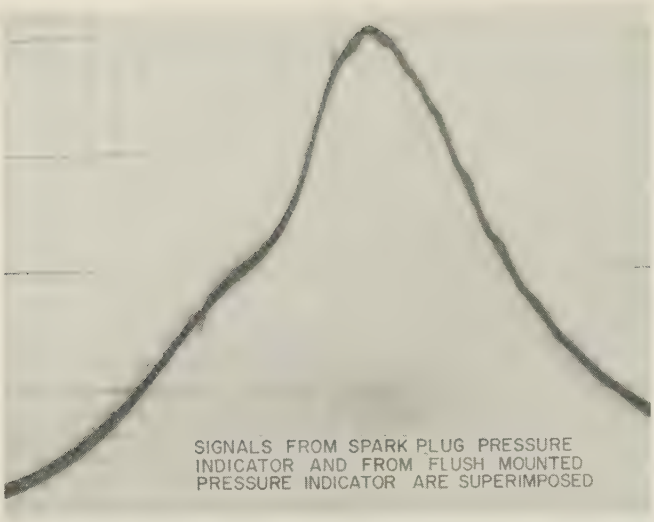

Fig. 6—Pressure oscillations due to excessive indicator passage volume

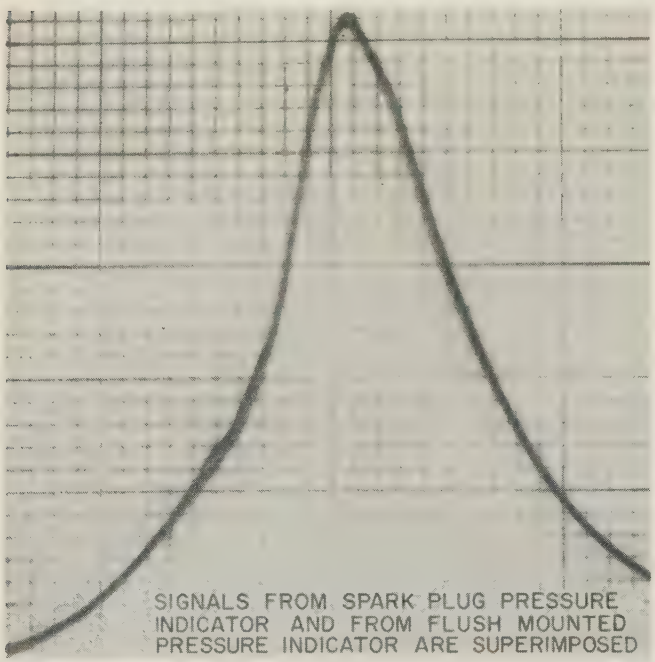

Fig. 7—Pressure-time signal with optimum passage design

opment caused by binding between the adapter and pressure-sensitive element. It was found that approximately 0.001-in. clearance at ambient temperatures was necessary to compensate for metal growth at firing temperatures and to permit free operation of the pressure-sensitive element. There have been instances where deposits have accumulated in the clearance space to the point that action of the pressure-sensitive element was hampered.

Effect of Indicator Passage Dimensions—The effect of indicator passage diameter was determined over a range of engine conditions, including variations in speed, throttle, spark timing, fuel flow, and during autoignition. Spark-plug units with 1½-in. length passages and 0.040-, 0.032- and 0.025-in. diameters were tested. The same indicator unit was used throughout the test. Use of the 0.040-in. diameter passage resulted in pressure oscillations and pressure lag as shown in Fig. 6. These oscillations occurred regardless of engine operating conditions and were most pronounced at peak pressures. Pressure oscillations were eliminated by the use of the 0.032- and 0.025-in. diameter passages. Pressure lag was present in these two passages to the same degree as when the 0.040-in. diameter passage was used and varied with the engine speed on the basis of a maximum of one-half of a crankshaft deg for each 900 rpm. Fig. 7 shows this lag for the 0.032-in. diameter passage at 2800 rpm. For qualitative measurement, maximum cycle pressure and rate of pressure rise as determined by either the 0.032- or 0.025-in. diameter passage are the same as obtained with the flush indicator. The first indication of autoignition occurred simultaneously with the flush-mounted indicator and with either 0.032- or 0.025-in. diameter passages. Pressure oscillations present in the 0.040-in. diameter passage made the determination of autoignition difficult. It appeared that the 0.040-in. diameter indicator passage tended to dampen the pressure rise due to autoignition.

It thus appears that for the length of passage used (1½ in.) it is necessary to use less than 0.040-in. diameter passage to eliminate pressure oscillations and dampening. A pressure lag will be present regardless of the passage diameter selected, but for qualitative types of analyses the magnitude of this lag is insignificant. Either the 0.032- or 0.025-in. diameter passage will suffice for qualitative analyses of pressure development during combustion.

The indicator tube has also been installed into the spark-plug cavity. Tests conducted with this type of indicator-tube installation have indicated that additional variables have not been introduced by leading the indicator tube into the spark-plug cavity. Convenience of installation is apparently the only factor to be considered in choosing between the two methods of indicator-tube installation.

In addition to improper clearance space and too large a passage diameter, signal distortion can result (1) from pressure leakage between the indicator and adapter, (2) from burred passage edges, and (3) from deposits in the passage and clearance volume. The first two can be eliminated by reasonable precautions during assembly and the last by disassembly and cleaning when necessary.

Thus, an instrument has been developed which provides a means of qualitatively measuring cylinder-pressure development of both normal and abnormal combustion in unmodified engines. It also provides a more fundamental means of categorizing the various types of abnormal combustion. Although both peak pressures and maximum rates of pressure rise can be accurately measured, the instrument in its present state of development, cannot be used to determine imep due to the varying time lag introduced by the indicator passage.

Detection of Abnormal Combustion

The development of the spark-plug pressure-indicator combination has provided a research tool which facilitates studies of abnormal combustion in unmodified engines. In subsequent investigations employing this tool, attention has been paid to detection of autoignition and surface ignition and the correlation of these combustion phenomena with engine noise. Table 1 outlines test fuel specifications.

Autoignition Studies—The change in pressure development signaling autoignition of the end gas is easily detectable on the pressure-time trace. Autoignition usually occurs, timewise, at a point just

past peak pressure. Fig. 8 shows a series of pressure development signals from the spark-plug pressure-indicator combination with engine conditions set to give the slightest indication of autoignition. This combustion condition is arbitrarily classified as "borderline autoignition." As would be expected, borderline autoignition is not usually audible. Fig. 9 shows the severity of autoignition resulting from advancing the spark timing several crankshaft degrees to "borderline knock" as it would be defined by the presently used standards of audible knock rating.

The problem of poor knock rating reproducibility was encountered during high compression ratio combustion-chamber development work. The development work was conducted in the laboratory on a multicylinder engine converted to single-cylinder operation. On many of the chambers, particularly those with extremely turbulent design, there was no clearcut division between normal engine noise and spark knock. There was a tendency toward poorer reproducibility of results as the engine speed was increased. Therefore, it was decided to supplement the questionable borderline knock ratings (normal audible rating technique) with borderline autoignition ratings (using the spark-plug pressure-indicator combination) whenever necessary.

Fig. 10 shows a typical primary reference fuel (and leaded isooctane) framework constructed of borderline knock and borderline autoignition spark timings. This particular combustion chamber was one that was extremely difficult to rate. Borderline knock ratings above 2800 rpm are not shown because of poor reproducibility of results at the higher speeds. The differences in borderline knock and borderline autoignition spark timings range from 1 to 3 crankshaft deg. The differences in engine knock rating and engine autoignition rating of the test fuels range from 0.2 to 0.7 octane number. Other combustion chambers which presented no difficulty in knock determination resulted in a closer correlation between borderline knock spark timing and borderline autoignition spark timing and in a closer correlation between engine autoignition rating and engine knock rating of the test fuels. It is felt that good correlation of knock and autoignition ratings has been established and that autoignition ratings as obtained with the spark-plug pressure-indicator combination are justified in this particular type of combustion-chamber development work.

It has been observed at higher compression ratios that as the aromatic content of fuel blends is increased, the noise quality of its knock becomes lower in frequency. It is felt that these variations in the noise quality of knocking fuels could lead to significant errors in borderline knock settings, inasmuch as the thudding type of knock is often indistinguishable with the pressure rap encountered during normal combustion with high rate of pressure rise. These variations in knocking-noise quality were first noted during fuel-rating tests on the CFR F-1 knock-rating engine. The differences in knocking-noise quality of various fuels were investigated by suspending a microphone near the engine and analyzing total engine noise by means of a panoramic

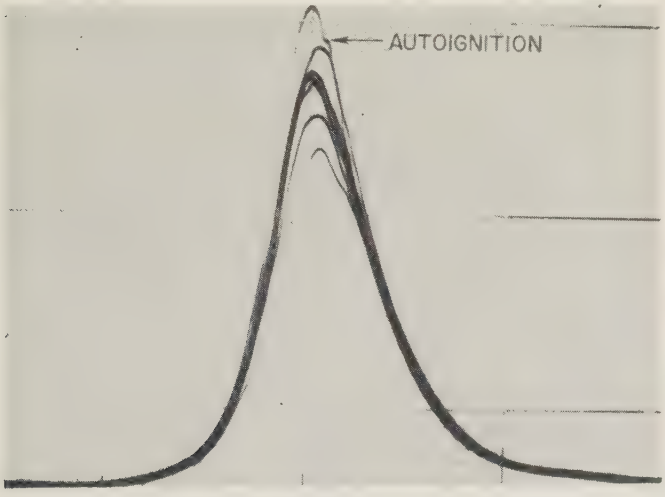

Fig. 8—Borderline autoignition

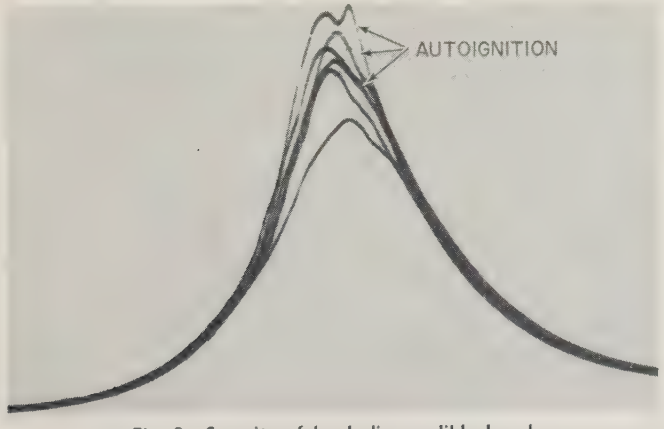

Fig. 9—Severity of borderline audible knock

Table 1—Test Fuel Specifications, Antiknock Quality and Flourescent Indicator Adsorption

	Octane Number		Fluorescent Indicator Adsorption		
	F-1	F-2	Saturate, %	Aromatic, %	Olefin, %
Diisobutylene	101.6	84.3	0	0	100
Toluene + n-heptane	102.6	94.3	14.9	85.1	0
Toluene + n-heptane	106.0	98.8	10.7	89.3	0
Prototype A	104.3	97.5	50.2	36.0	13.8
Prototype B	106.0	97.3	50.8	34.7	14.5
Prototype C	104.8	92.8	45.8	31.4	23.4
Indolene 30 (1957)	102.5	92.9	47.0	41.2	11.2
Indolene 10 (1957)	100.7	91.4	47.0	41.2	11.2
Indolene Clear (1956)	90.4	78.8	47.5	31.5	21.0
115/145 Aviation	106.8	102.4	100.0	0	0

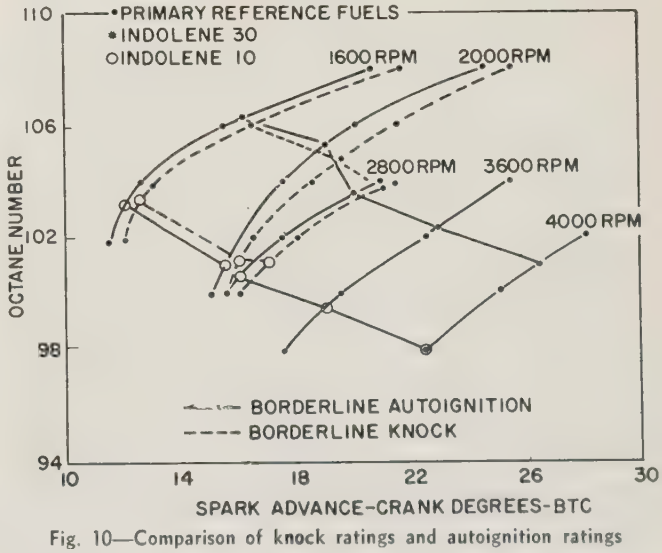

Fig. 10—Comparison of knock ratings and autoignition ratings

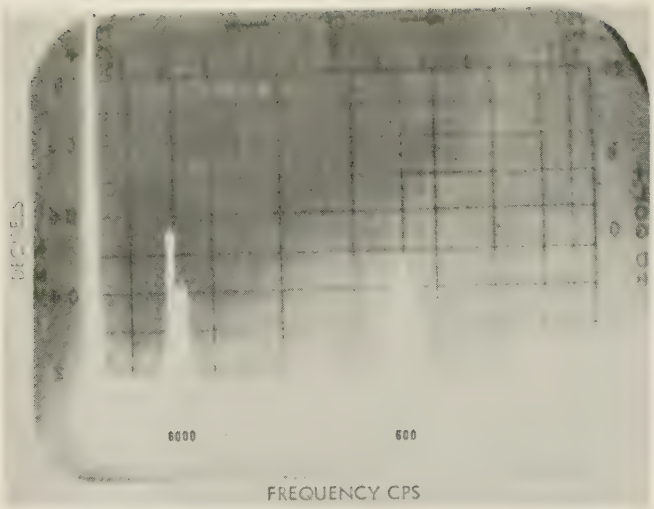

Fig. 11—Noise quality by panoramic sonic analyzer

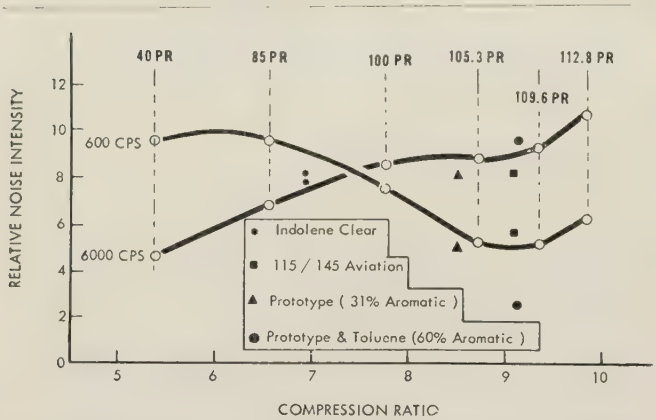

Fig. 12—Noise quality of various fuels, F-1 rating method (standardized at 100 octane number)

sonic analyzer. Fig. 11 shows the screen of the sonic analyzer. The analyzer plots noise intensity in terms of decibels versus noise frequency in cps. When the engine was motored, there was a low noise intensity indicated in the low-frequency range. A slight peak occurred at 600 cps. There was no indication of high-frequency noise. With the engine running on a nonknocking fuel at the same compression ratio, the peak at 600 cps increased slightly. There were still no indications of high-frequency noise. At the same compression ratio, a knocking fuel was run. The peak at 600 cps increased even more. At 6000 cps, a peak of considerable amplitude occurred. With this method of analyzing noise quality and with particular attention to the 600- and 6000-cps frequencies, analyses were made of the noise quality of various fuels.

Fig. 12 shows noise intensity plotted against compression ratio. The noise intensity of the primary reference fuels at a 55 knockmeter setting is shown for the two knock critical frequencies, 600 and 6000 cps. As the compression ratio is increased and octane level raised, low-frequency noise intensity of primary reference fuels decreases. As the compression ratio is raised and the octane level increased, the high-frequency noise intensity increases. The first test fuel, indolene clear, matches very closely the noise quality of its matching primary reference fuel. The 115/145 aviation gasoline also matches very closely the noise quality of its matching primary reference fuel. Prototype gasoline "C" and the prototype "C"-plus-toluene blend show a complete reversal in noise quality in comparison with their matching primary reference fuels. They have considerably more low-frequency noise and considerably less high-frequency noise. The addition of toluene to the prototype apparently made this reversal even greater. These results substantiate previous audible observations made of knocking aromatics on the F-1 engine.

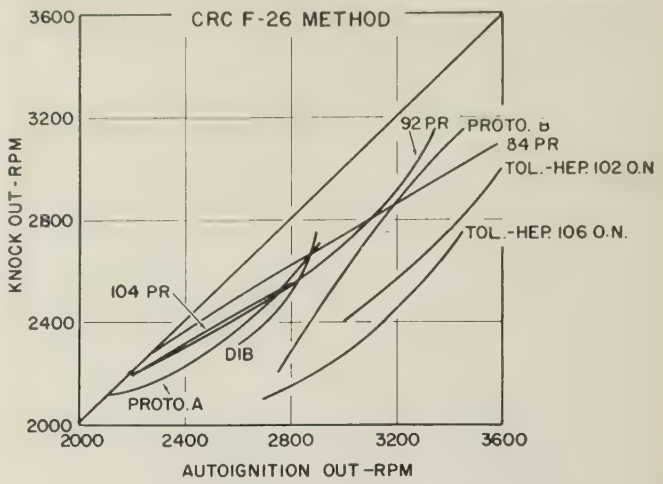

Fig. 13—Comparison of knock-out and autoignition rpm

The differences in knocking-noise quality that result as aromatic content of fuels is increased might be attributed to differences in the rate of pressure release during autoignition. Observations of rate-of-pressure-rise traces of autoigniting aromatics and other fuel types indicate a possible slower pressure development during autoignition for aromatic fuels. It is felt that a relatively rapid pressure development will expend most of its energy at the combustion-chamber level because of the inertia forces of the piston, connecting rod, crankshaft, and the like. The resulting vibrations of the cylinder head (and possibly piston dome) would result in more high-frequency noise. If the rate of pressure development were decreased, possibly more of the energy would be transferred down to the lower engine parts and result in more low-frequency noise.

It is felt that these differences in knocking-noise quality of various fuels as encountered during severe knock at F-1 engine conditions may also exist during borderline knock in full-scale engines. It is conceivable that lower frequency knock may be more difficult to separate from normal engine noise and thus contribute to poor knock-rating reproducibility. The latter problem is being investigated on the road in full-scale engines using the spark-plug pressure-indicator combination.

For example, a 1957 production car with the spark timing of one cylinder advanced 5 crankshaft deg over the timing of the other seven cylinders was audibly rated by the CRC designated F-26 method. Simultaneously, borderline autoignition was determined in the overadvanced cylinder using the spark-plug pressure-indicator combination. Fig. 13 shows the differences in "knock out" (determined audibly) and "autoignition out" (determined by the pressure indicator) while operating on various fuels. There is a general tendency for differences in knock-out

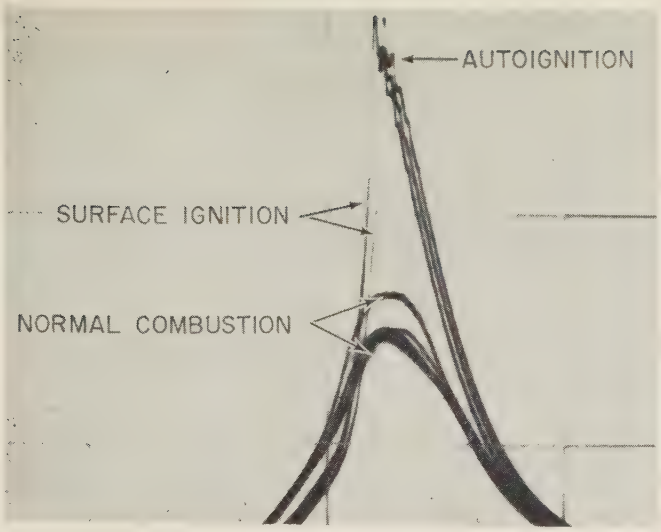

Fig. 14—Surface ignition with audible knock

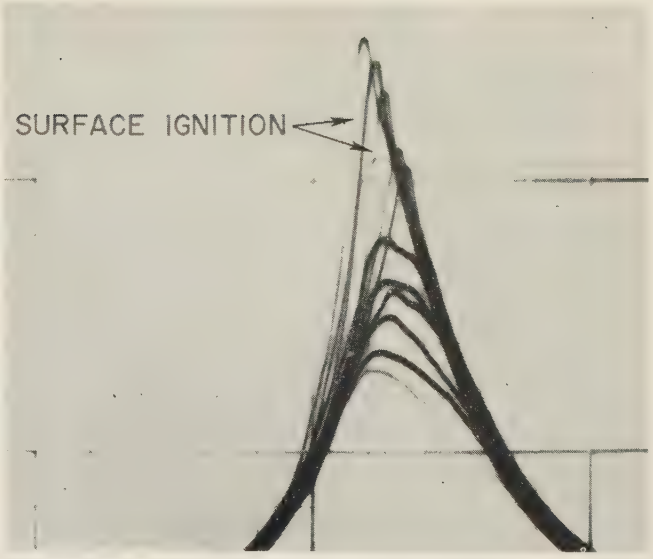

Fig. 15—Surface ignition without knock

and autoignition-out speed to increase as engine speed is increased. This speed effect is much more pronounced than is found in laboratory ratings and may be one of the reasons for poor correlation of laboratory and road ratings. The fact that the two highly aromatic toluene + n-heptane blends show the greatest spread between autoignition-out and knock-out speed may indicate that difficulty in knock determination was encountered on these fuels. The data shown is only one of many tests to be evaluated before making definite conclusions.

Surface Ignition Studies—Surface ignition is distinguished from normal combustion by its increased rate of pressure rise, increased peak pressure, and earlier peak pressure timing. Surface ignition noise may manifest itself either with knock or without knock, the latter producing only a thudding type of noise. Spark-plug pressure-indicator signals of these two phenomena are shown in Figs. 14 and 15.

Inaudible surface ignition was detected by the spark-plug pressure-indicator combination while operating a 1957 production car on pure benzene using CRC F-26 test methods. During accelerations, engine surge was experienced. No unusual engine noise signaling abnormal combustion was observed, however. Analysis of the pressure time trace, obtained with the spark-plug pressure-indicator combination using strip film as recorded during the test, indicated that severe surface ignition was present and that the surging condition was caused by backfiring into the manifold at the end of the induction stroke. Fig. 16 shows a section of the strip film taken during the test and indicates that the two succeeding cycles after the backfire were nearly complete misfires. Finally, a fresh charge reached the cylinder and mild surface ignition occurred which built up in severity on succeeding firings. This cycle of increasing severity of surface ignition, backfiring, and misfiring repeated itself five or six times during the acceleration. An examination of all spark plugs after the test, including the spark plug used with the indicator, showed severe burning of the center electrode and surrounding porcelain. The sources of surface ignition were obviously the spark plugs. However, the indicator was undamaged and easily removed from the damaged spark plug.

In our studies of abnormal combustion we have

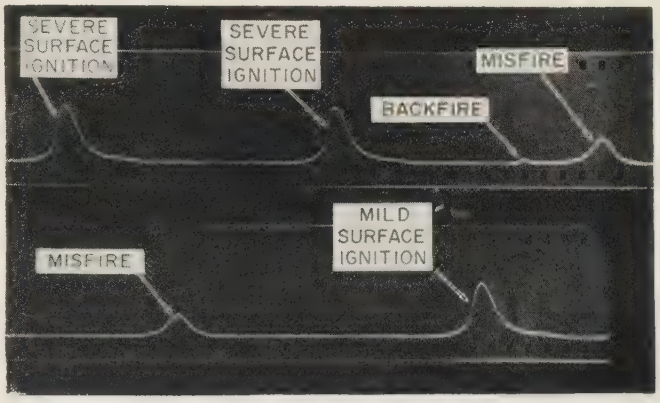

Fig. 16—Strip film showing surface ignition

thus been able to obtain information with the spark-plug pressure-indicator combination in unmodified engines that would have been impossible to obtain in any other manner. The combination has also proved extremely useful in other applications such as determination of peak pressure and rate of pressure rise during normal combustion.

Conclusions

1. Engine noise by itself can no longer be considered adequate for identifying specific types of abnormal combustion.

2. Observation of cylinder-pressure development provides an analytical method for categorizing various types of abnormal combustion that are inaudible or indistinguishable to the ear.

3. A research tool has been developed which provides qualitative analysis of combustion development in unmodified engines. This instrument has other advantages of providing protection for expensive pressure indicators by exposing only inexpensive, replaceable parts to the combustion chamber.

4. Investigations of knock-rating problems encountered on high-compression-ratio engines have been aided by the development of instrumentation, providing a means of separating knock from other combustion phenomena in unmodified engines.

Discussion of this paper will be found on p. 556.

Points Out The Penalty Of Poor High-Frequency Response

—J. D. McCullough
Ethyl Corp.

THE obvious advantages of utilizing an existing opening into the combustion chamber to study engine cylinder pressure phenomena have encouraged many attempts to combine the functions of spark plug and pressure transducer.

Such multipurpose devices have, in general, exhibited one or more of the following flaws: (1) poor accuracy, (2) poor durability, and (3) incompatibility with engine spark-plug requirements.

The instrument described in this paper should certainly satisfy current requirements for durability and spark-plug performance.

However, the very configuration which guarantees these desirable features contains an inherent penalty. This penalty has been paid in the form of poor high-frequency response. As a consequence, pressure diagrams recorded in the presence of surface-ignition, autoignition, or detonation must be interpreted with reservations.

In spite of these reservations there are many types of studies in which such a device can provide useful qualitative data where its ruggedness, convenience, and heat range will outweigh other considerations.

Certainly, instrumenting all cylinders of a road vehicle, where the acoustic coupling to the observer is poor, should be rewarding. It should be possible to tighten the confidence level of road octane ratings, to determine which cylinders are limiting the engine, to determine the percentage of cycles which are surface-ignition limited, and to study fuel system dynamics during cold start, warmup, shifting transients, and full-throttle accelerations.

Many such studies not have been attempted largely because the investigator could not conveniently "Investigate Combustion Phenomena in an *Unmodified* Engine."

Discusses Audible Abnormal Combustion Phenomena

—R. A. Hoffman
E. I. du Pont de Nemours & Co., Inc.

APPARENTLY many of us have followed the same road of instrumentation. We have also endeavored to use strain gages as combustion-chamber pressure transducers and have arrived at the same conclusion: their accuracy and durability leave much to be desired. Present work is being conducted with piezoelectric pressure transducers, similar to those used by the Ford Motor Co. This paper enhances our already optimistic outlook regarding this type pickup. Two questions come to mind: First, just how critical is the 0.001-in. clearance between the pressure-sensing element and the adapter? Second, what is the operating time between cleanings? The authors have mentioned the problems of deposits; to what extent are they a problem?

No doubt, considerable testing was conducted to determine the optimum indicator passage tube size. But Figs. 8 and 9 do not show the pressure oscillations normally associated with knock. Is this due to a dampening out of the pressure oscillations in the tube, giving a distorted signal?

In discussing the audible manifestations of abnormal combustion, the authors have referred to the "erratic thud of surface ignition" and "thudding autoignition." We would like to hear a more complete description of these.

The sonic analyzer studies are of real interest; particularly the observation of a 600-cps frequency and the effect of fuel type on this frequency. These data not only may point the way to a better understanding of abnormal combustion but may help to explain some of the present inadequacies of the Research method knock test procedure.

In an engine with abnormal combustion pressure waves are present in the combustion chamber with knock. These waves set up a forced vibration of the engine having the same frequency as the pressure waves. Therefore, the knock frequency is heard. With the "rap" or "thud" usually associated with aromatic fuel, the engine is in effect subjected to a single blow due to a rapid rate of pressure rise. The end result is analogous to striking a tuning fork —and the tuning fork vibrates at its natural frequency. In the same way, the engine tries to vibrate at its natural frequency, but due to many restraining forces the vibration is dampened out. If this is the 600-cps frequency that has been discussed, engines of various configurations may give frequencies other than 600 cps under these conditions.

We have heard a noise in our test cars which may be similar to the low-frequency noise described by the authors. This rapping noise, which is not covered by the CRC definitions of abnormal combustion, can be obtained on widely different fuels. An example of this is a test conducted in a high compression ratio fuel test car using 106 primary reference fuel and benzene. The rapping sound was heard on both fuels with no apparent difference in noise quality. Knock was also heard on both fuels as judged by the familiar pinging sound. It may be possible that the low-frequency noise described by the authors, the "rap" of a rapid rate of pressure rise, nonknocking audible surface ignition, and the rapping noise heard in our test cars are all due to a rapid rate of pressure rise.

This discussion has dealt primarily with audible abnormal combustion but the possible destructive results of inaudible abnormal combustion certainly cannot be overlooked. The instrumentation presented here looks very promising for studies of inaudible abnormal combustion.

In closing I wish to re-emphasize a point made by the authors. The time has arrived for all interested parties to get together, not only to reconsider, but to bring up to date the CRC definitions of abnormal combustion. Wouldn't it be convenient if everyone called the audible sounds of abnormal combustion by the same name?

Authors' Closure To Discussion

THE poor high-frequency response of the instrument as pointed out by Mr. McCullough is undeniable. During the investigation of indicator passage effects, it was discovered that the high-frequency vibrations following autoignition were not the same as those obtained with the flush-mounted indicator. During severe knock, the high-frequency vibrations following autoignition were dampened and distorted when the indicator passage was used. At less severe knock conditions, the indicator passage completely dampened the high-frequency vibrations. However, the instrument still performed the function it was designed for—to detect and categorize the various types of abnormal combustion. Borderline autoignition is detectable with or without high-frequency vibrations, as illustrated in Fig. 8.

In reference to Mr. Hoffman's inquiry, the minimum clearance space is determined by the clearance between the pressure-sensing element and the adapter at firing temperature. This clearance was found to be approximately 0.001 in. at ambient temperature. The maximum clearance space permissable before oscillations occur is not known to the authors. Possibly 0.002 or 0.003 in. is permissable. In any event, 0.001-in. cold clearance always gave good results and no difficulty was encountered in machining that clearance into any adapter-indicator combination.

Operating time between cleanings will depend on engine operating conditions, fuel type, and chamber deposit condition. Deposits may form in the clearance space or in the indicator passage. Our experience shows that the time between cleanings may vary from 1 to 20 or 30 hr. The actual cleaning time involves only a few minutes of engine shutdown. Incidentally, the indicator passage can be cleaned by removing the indicator unit and inserting a flexible wire into the passage.

ENGINEERING THE EDSEL

N. L. Blume, Ford Motor Co.

This paper was presented at a meeting of the SAE Milwaukee Section, Oct. 4, 1958.

THIS is the engineering story of the newest car introduced to the American public by a major automotive manufacturer in 19 years. The Edsel is new but actually it's the germination of an idea conceived by Edsel Ford who thought years ago that the company should have greater representation in the medium-price range. This idea was furthered by his son, Henry Ford II, in 1948 when another car was proposed to keep abreast of things in the automotive market.

With the decision to enter a new car in the medium-price field, attention was directed to the engineering and styling phases. Basic objectives were for the car to be entirely new but not to the extent of being radical; to be individually distinctive and yet maintain the traditional reliability and ruggedness characterized by the company's vehicles. The style was to be crisp and clean enough to warrant consideration of the more discriminate buyers who were looking for the extras in a medium-price car.

Body Structure

At this point, the engineering staff began advanced package studies and established design objectives. The first consideration in package development was room to provide the maximum seating comfort, adequate entrance room, and convenience and safety for passengers. Edsel package studies resulted in establishing basic dimensional limitations required to fulfill adequately engineering and styling needs and desires. Working from the ground up, it was ascertained that 6–7 in. should be provided for ground clearances; 5–7 in. for mechanical components such as driveshaft and frame members; 4–6 in. for seat deflection to provide seat comfort; 38–40 in. effective head room to accommodate passengers; and ½–1 in. roof thickness providing for headlining and sound-deadening material.

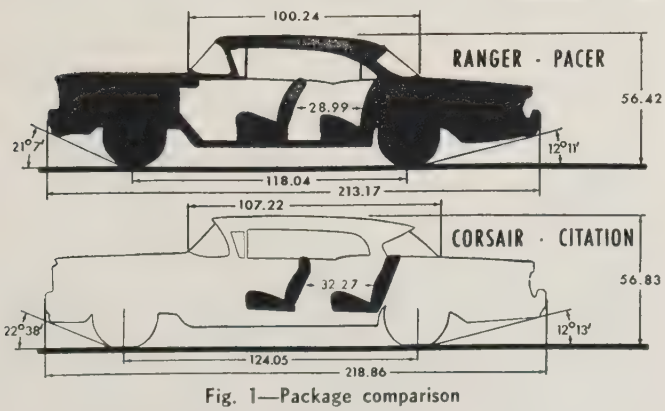

Fig. 1—Package comparison

Layouts were prepared to investigate wheelhouse clearances for wheel jounce, rebound, and tire chains, and to finalize placement of the exhaust system, spare tire, and fuel tank.

Studies resulted in two basic concepts: the 118-in. wheelbase Ranger-Pacer series and the 124-in. wheelbase Corsair-Citation series. A comparison of these packages reveals an overall length of 213.17 compared to 218.86 in., an overall height of 56.42 as compared to 56.83 in. and a greenhouse length of 100.24 on the Ranger-Pacer series as compared to 107.22 in. on the Corsair-Citation series (Fig. 1).

Proposed styles were under consideration simultaneously with advanced package development. With the dimensions set, the styling section proceeded to cut clay. The vertical grille theme evolved from comparison studies of horizontal and vertical arrangements. The vertical grille was a styling feature but not a styling problem alone. Adequate engine cooling, allowance for an air conditioning condenser, as well as structure to support the center impact ring were paramount considerations.

As styling designs progressed, the engineering staff worked hand-in-hand on the engineering im-

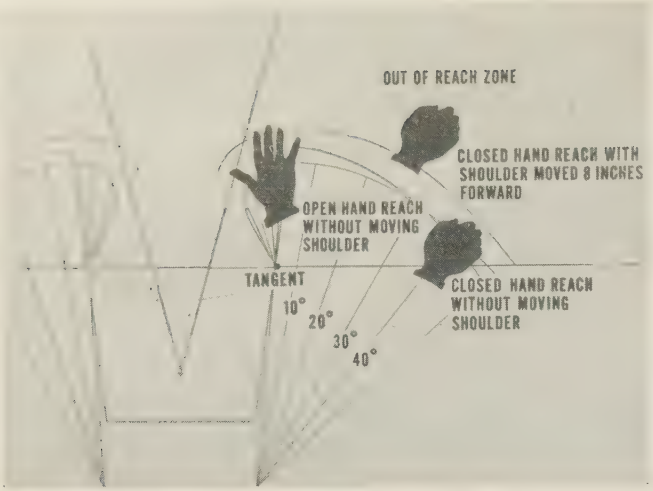

Fig. 2—Instrument panel motion study

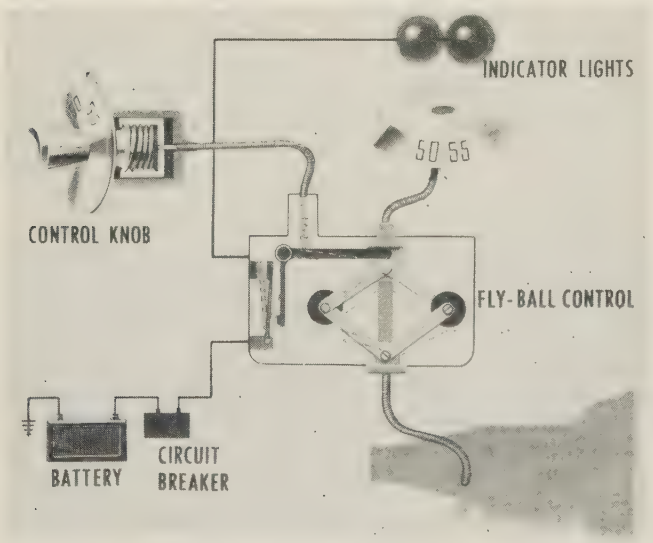

Fig. 3—Speed warning light operation

plications. Consideration was given to clearance for tire removal, particularly on the rear wheels, and turning clearances on the front wheels. Formed areas and sections were designed to please the eye and facilitate manufacturing. You can imagine the consternation when the styling section proposed beautiful varieties of rear-quarter treatment only to be told "it's too deep a draw to be practical." Other problems as the Edsel exterior took shape were bumper heights, angles of approach and departure, and the legal requirements for such items as head lamps, tail lamps, and license plate location.

Lower, longer, and wider bodies, featuring increased glass areas with longer and thinner framework, provide less opportunity to induce loading in the roof. The "dog-leg" characteristic of the roof supports, which is part of the price of the wrap-around theme, adds to this problem. Thus, the tendency is for the roof to carry, as the upper chord member, less than its potential share of the loads imposed on the body truss. These loads, incidentally, are steadily increasing along with car size and weight. All this would seem to imply a tendency toward either much heavier construction or less rigidity.

Actually, and fortunately, neither of these trends

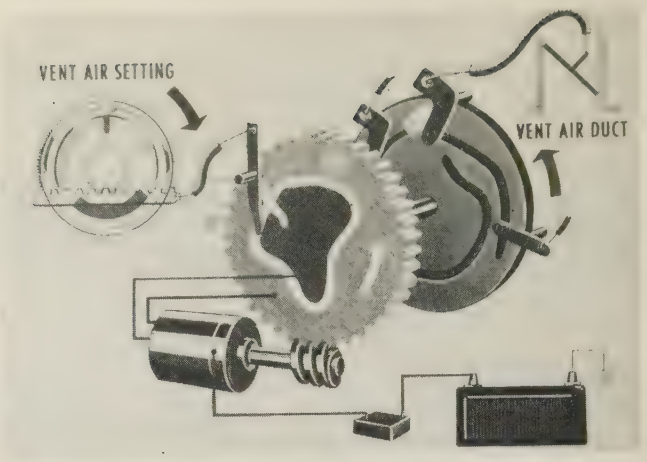

Fig. 4—Dial-Temp operation

has prevailed to any alarming extent. True, the weight of frames and other load-carrying structures has increased, but not out of proportion to the concurrent increase in useable space for passengers and luggage. Nor has there been any disposition to accept low standards of safety or comfort. After all, the acid test of a car's construction is its ability to filter out disturbances such as shake and harshness and to stand up in crash and rollover tests. It is fairly evident that as a result of increasing emphasis and concentrated effort over the past few years, today's cars are safer than ever. In the matter of shake, a vast amount of data has been obtained in our organization by the well-known ESTA[1] (Electronic Selected Threshold Analyzer) technique. Shake readings of recent car models show a definite tendency to decrease.

As each new styling feature makes its appearance, means must be found to minimize any adverse structural effects. Stiffness of the underbody has been one of the most productive countermeasures; the use of heavy box sections in the sills (often aided by increased chassis frame sections) has helped to make up for the loss or partial loss of center pillar structure. Heavier stock in front and rear pillars, a liberal use of gussets and bulkheads, plus boxing of the roof rails has largely offset the effect of dog-legs and thinner framing accompanying wrap-around windshields and rear windows. At the same time, manufacturers have developed means of dealing with increasingly intricate parts and assembly, thus promoting structural efficiency.

As a matter of interest, our laboratory results show that in overall car torsional stiffness, today's Edsel 4-door hardtop is practically equal to the standard 4-door and is only slightly less rigid in bending.

The front seats are somewhat different. (We attempted to have something different—but with increased utility and improved comfort.) We divided the seat into 1/3—2/3 proportions to more individualize the driver's area and to eliminate the split in the area of the third passenger.

The cushion back was constructed as follows: two formed-wire springs were used to provide pressure variance; a heavier, firmer spring in the lower section where pressures were greater and a lighter,

[1] "Measuring Car Shake," by R. J. Saxon. Paper presented at the SAE National Passenger-Car, Body, and Materials Meeting, Detroit, March 4, 1954.

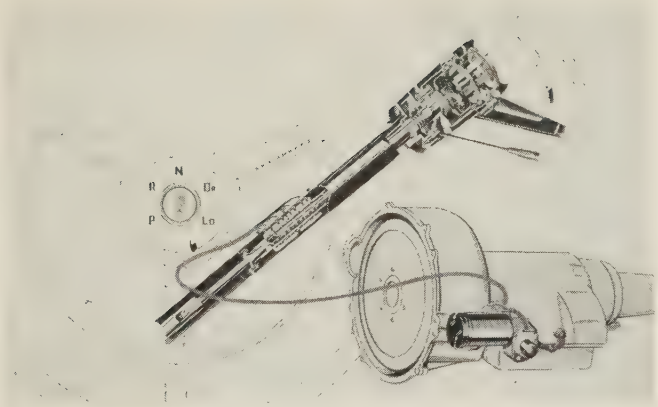

Fig. 5—Teletouch transmission selector

softer spring in the upper section where less resiliency was required. This sectional pressure development resulted after extensive studies to determine the best pressure distribution from the comfort and health standpoints.

Instrument Panel

The interior presented a challenge of a different nature to both the styling and engineering staffs. For example, safety considerations dictated replacement of sharp corners with rounded styled sections, and a great deal of effort went into analyzing motion studies to be sure that controls and instruments were as conveniently located as possible. From these studies, every effort was made to locate major controls in the most accessible area and major instruments in the most visible area. The key engineering problems, in styling any instrument panel, are finding a place for each desired item on the panel surface and providing sufficient space for the mechanisms, motors, bowden cables, and electric wires behind the panel (Fig. 2).

The most often referred to instruments are arranged in the upper portion of the instrument cluster. A speed-warning device has been incorporated in the floating drum-type speedometer as a visual driver aid and a definite safety feature. A selected maximum operating speed is preset by a dial just below the odometer; when the maximum operating speed is exceeded, a switch turns on a lamp and the speedometer face glows red. To accomplish this, a flyball-type governor is connected to the speedometer drive cable. The calibrated control knob on the instrument panel sets the spring tension on the flyball system, determining the speed at which the switch can be actuated. At low speeds, the flyball governor is held from operating the switch by the spring. As the speed increases, the force on the governor equals the spring tension, the contacts close, and the circuit is completed to light the lamps in the speedometer dome. This glow is readily visible and can be seen without diverting the eyes from the road. (See Fig. 3).

Ventilating System

Included in the instrument cluster is the Dial-Temp control for the heating and ventilating systems. The once-complicated, difficult-to-operate multiple lever controls have been eliminated. Heat or fresh air is brought into the car by simply turning a single control. The knurled bezel of the dial is the actual control and when rotated for a desired function brings into play an electric servo unit that actuates the valves for heating, defrosting, or ventilating. This servo mechanism is mounted behind the instrument cluster.

The heart of this system is the gear-driven control plate with preprogrammed cam grooves on one side and electrical contact surfaces on the reverse side. Rollers, connected to actuating arms and bowden wires, ride in the cam grooves and provide the necessary effort to operate the appropriate controls for the dialed function. These rollers are positioned in their proper location in the grooves, by the clockwise or counterclockwise rotation of the control plate. The direction of rotation is determined by a pressure arm which rides on the electrical contact surfaces of the plate. Fig. 4 shows how the servo operates the control for vent air.

When the knurled knob is manually rotated to the selected point of operation, the pressure arm is moved by means of a rack and pinion and a bowden cable. The pressure arm makes contact on one side of the contact plate causing current to flow through one field of the servo motor, thus rotating the motor in one direction and operating the control plate. When the knurled bezel is rotated to another selected point, the pressure arm makes contact on the other side of the contact plate causing current to flow through the other field coil of the motor, rotating the motor in the other direction and operating the control plate in the opposite direction.

The rotation of the motor is always such that the pressure arm seeks and finally comes to rest on the dead band of the contact plate.

Drive Controls

Drive controls for the Edsel "Teletouch" push-button shift are located in the center of the steering wheel. This location provides optimum accessibility for either the right or left hand. The various ranges—park, reverse, neutral, drive, and low—are selected by depressing the appropriate button. This closes the respective circuit that is continued through slip rings and brushes mounted in the steering column. These control circuits operate relays that actuate the motor mounted on the converter housing (Fig. 5). A powerful motor is used to provide the same ease of operation of disengaging the "park" position as the other functions. The control system has been carefully studied and fail-safe features incorporated throughout. A positive feed is used in contrast to a grounding system as customarily incorporated in horn circuits. This positive feed causes the system to remain in whatever position selected, even in the case of accidental grounds. Thus, there is no fear of a failure in the system causing the transmission to go into an unwanted gear accidentally. A dual switch, operated by transmission hydraulic pressure, inhibits the selection of "reverse" above 15 mph and inhibits the selection of "park" above 3 mph. This allows for sufficient "reverse" speeds to permit rocking the car out of mud holes and snow banks, but effectively prevents the transmission from being engaged in "reverse" at high forward speeds. The 3-mph inhibition in "park" prevents damage to the transmission by accidentally pressing the "park" button at high forward speeds. As an added safety feature, the "park" position can be actuated after the ignition is turned off, but it is impossible to actuate any

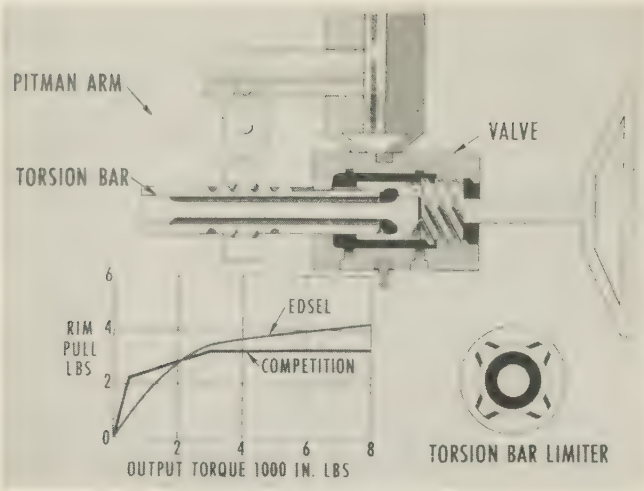

Fig. 6—Power steering operation

other position until the ignition switch is again turned on.

The "Teletouch" buttons are depressed below accidental strike distances in the center of the wheel. In case of major accident, an additional feature is the rubber rim around the controls to absorb any abnormal impact.

To maintain the push-button assembly in a stationary position, a unique planetary gear system is used. One sun gear is fixed to the stationary part of the steering column and another sun gear is fixed to the push-button assembly. A pair of planet gears revolve about these two sun gears with the rotation of the steering wheel. This assembly permits a direct drive from the steering wheel down through the steering column.

Power Steering

Throughout the automotive industry, the tendency is toward the integral-type power steering gear. The reasons for this trend are quite apparent: this type of unit permits neatness of installation, reduced vulnerability to damage from road obstructions, and improved returnability. The new integral-type steering gear in the Edsel cars features a torsion-bar type of hydraulic valve actuation to provide road feel.

The steering gear consists primarily of a gear reduction unit (the recirculating ball and nut type embodied in the standard steering gear), a power cylinder, and a hydraulic servo-control valve. The hydraulic valve, valve sleeve, and torsion-bar assembly are mounted on the end of the worm shaft and operated by the twisting action of the steering shaft on the torsion bar.

The torsion bar is restrained from twisting more than 9 deg either side of normal position to prevent overstressing the bar and permit manual steering. The valve spool moves 0.004 in. for each deg of twist of the torsion bar and approximately 0.036 in. for maximum 9-deg twist. The valve must move 0.008 in. resulting in a 2-deg twist of the torsion bar for intitial power assist. In normal straight driving, approximately ½–1 lb of pull is required on the steering wheel to control the car. Cornering effort is approximately 2–3 lb and maximum parking effort is 4–5 lb. Particularly noteworthy is the smooth transition from no power to full power with the torsion-bar action as compared to other systems.

On a right turn, for example, the valve spool moves up, allowing oil from the pump to enter the right side of the power piston. The oil on the left side of the piston is returned through the valve to the pump. Consequently, the power assist is to the right side of the piston, pushing it to the left and providing assistance in turning of the sector shaft. Restricting the oil flow to one side of the piston increases the oil pressure proportionally to the reaction of turning the front wheels. The action is reversed on a left turn. (See Fig. 6.)

A new concept in pump mounting and drive is introduced on the E-475 engine for power steering. The pump is integrally mounted on the engine front cover and driven directly by the crankshaft. The arrangement eliminates the conventional drive pulleys, belt, and pump mounting bracket. The use of a large diameter rotor in the pump makes possible adequate pressures even though the pump operates only at crankshaft speed. This results in increased durability of the pump. A large-capacity reservoir is used in conjunction with the integral pump; the reservoir is mounted higher than the pump which precludes aeration of the oil and improves accessibility.

Engine

Each of the two series of Edsel cars is powered by an engine designed specifically for it. The E-400 engine is in the Ranger-Pacer series and the E-475 engine in the Corsair-Citation series; both of these are 90-deg V-8 overhead valve engines with 10.5/1 compression ratios. The displacement on the E-400 is 361 cu in.; bore diameter is 4.05 in. with a stroke of 3.50 in., giving a bore-stroke ratio of 1.16. The maximum brake horsepower is 303 at 4600 rpm and the maximum torque is 400 lb-ft at 2800 rpm. The E-475 is a larger engine with a displacement of 410 cu in. The bore diameter is 4.20 in. and stroke is 3.70 in., giving a bore-stroke ratio of 1.135. Maximum brake horsepower of this engine is 345 at 4600 rpm and the maximum torque is 475 lb-ft at 2900 rpm.

The E-400 engine has cylinder heads with machined combustion chambers of the wedge design which provides accurate compression control. The combustion chambers in the E-475 engine are in the cylinder block and are machined at the same time as the cylinder bores. This was accomplished by designing the cylinder deck at a 10-deg angle to the top of the piston. The resulting wedge-shaped cavities form combustion chambers virtually free from pockets in which harmful deposits might accumulate.

A new innovation on the E-475 engine is the water-warmed intake manifold replacing the conventional exhaust-heated manifold. This results in better control of the fuel-air mixture temperature and, thus, improved distribution. It is accomplished by running the engine water from the rear of both heads under and along the intake manifold passages. These intake passages are large and smooth to allow unrestricted flow of the fuel-air mixtures. The manifold is so designed as to eliminate sharp turns or obstructions. Quick warmup is accomplished by the circulating system.

The water-warmed intake manifold is the first stage of the three-stage, parallel-flow cooling sys-

tem in the E-475 engine. In this system, the water is circulated only through the cylinder heads and intake manifold during the first stage. Circulation is confined until the water temperature reaches approximately 140 F and thermostats in each bank of the cylinder block open. Cooling is now in the second stage; coolant is circulated through the manifold, cylinder heads, and block. The third or final stage comes into play when the water temperature rises to 180 F and the thermostat in the water outlet connection opens. Water is now circulated through the whole cooling system, the intake manifold, the cylinder heals, the cylinder block, and the radiator. In all three stages, the major portion of the coolant is circulated through the cylinder heads for greatest scrubbing action at the point of highest heat generation. (See Fig. 7.)

Transmission

With the introduction of the dual-range transmission, the Edsel driver will enjoy greater flexibility of control along with the advantages of greater performance, better fuel economy, and smoother shifting.

The new transmission allows the option of starting in first or second gear and provides for smoother shifts into high gear automatically at speeds which are dictated by throttle opening. The forced downshift feature, the hill-braking ability in low range, and the usual neutral, reverse, and park ranges are retained.

The advantages of first-gear starting are evident. The transmission is automatically in first gear and performance at wide-open throttle is thus better than in previous model transmissions where the throttle had to be depressed past the detent for a downshift to first gear. In city driving, the same acceleration is achieved at a lower throttle opening, providing better fuel economy and the comforting feeling of power in reserve in the form of unused accelerator pedal travel. Also, the high break-away torque, available in first gear through the transmission, allows the use of lower ratio axle and, consequently, improved fuel economy at cruising speeds.

The transmission is basically a 3-element torque converter in combination with a Ravegnaux (compound) planetary gear set that will provide three speeds forward and one speed reverse. The major innovation is the substitution of a sprag-type one-way clutch to be the reaction member of the planetary gear set in the first gear. The shift from first to second gear can be made smoothly since a shift off a one-way clutch is basically smoother than one in which two bands are involved. With the one-way clutch, the timing problem of two bands disappears. A further aid to smooth 1-2 shifting is the addition of a hydraulic accumulator to the front servo that assists in smooth application of the front band. (See Fig. 8.)

Air Suspension

Why an air suspension? It is more complex and costly than conventional types. It requires a staggering expenditure of time, talent, and money for development. Is there, apart from competitive pressure, a compulsive reason for offering it to Edsel customers? Briefly, yes: it offers, for the first time, a practical means of attaining the full ride benefit of very soft springing.

To design or manufacture conventional springs with very low rates, is not at all difficult. To apply them to a car, however, is quite another matter. In leaf springs, for example, torque windup becomes a prohibitive consideration. Leaf springs lost out in front suspensions for this reason many years ago. In coil springs and torsion bars, the problem is space—with lower rates, they become larger; more significantly their operating space (wheel travel) requirements increase. More and more wheel travel is wasted in providing for load changes. Unloaded cars begin to look ridiculously high while heavily loaded cars practically ride on the compression bumpers; net jounce travel approaches zero. Moreover, mechanical springs are essentially constant-rate devices and adequate cushioning at the jounce and rebound stops becomes increasingly difficult with softer springing.

It is in these respects that the use of air as a spring medium has three important advantages: (1) a very low-rate air spring can be fitted in the space vacated by a normal-rate coil spring; (2) air systems necessarily incorporate automatic leveling and a car can have a pleasingly low curbside appearance yet at maximum load, full-jounce travel remains available; (3) the rate pattern of an air spring can be precisely tailored to make the best

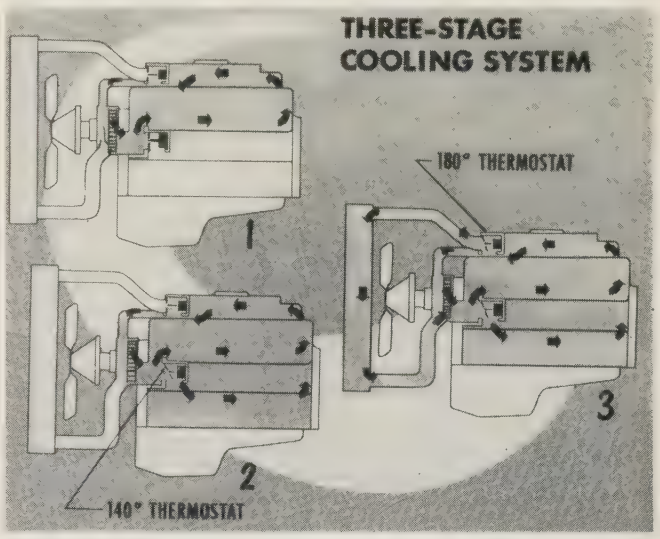

Fig. 7—Three-stage cooling system

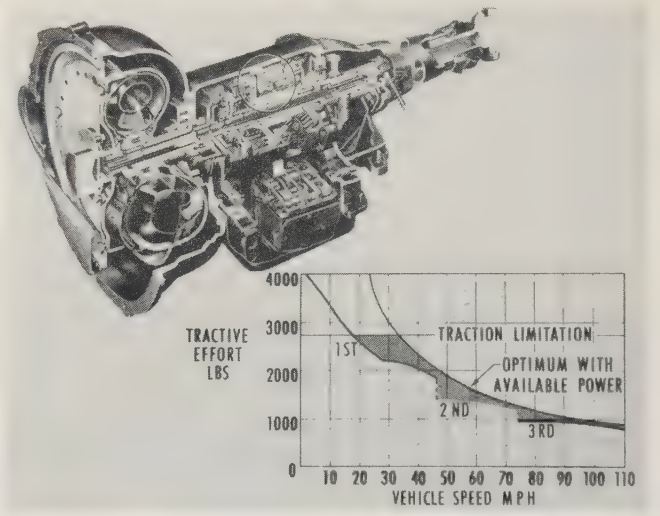

Fig. 8—Dual-range transmission

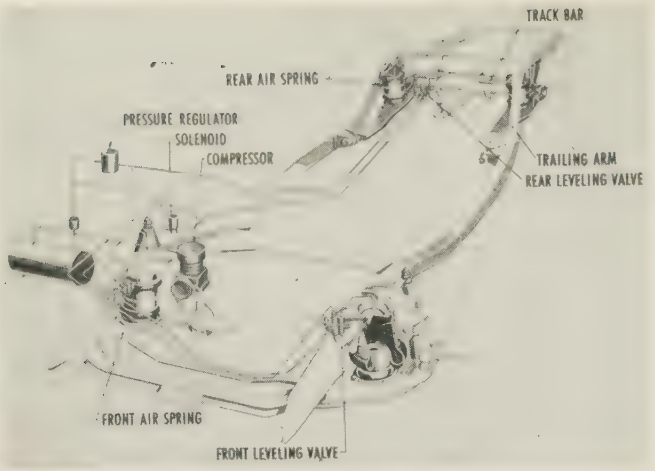

Fig. 9—Air suspension

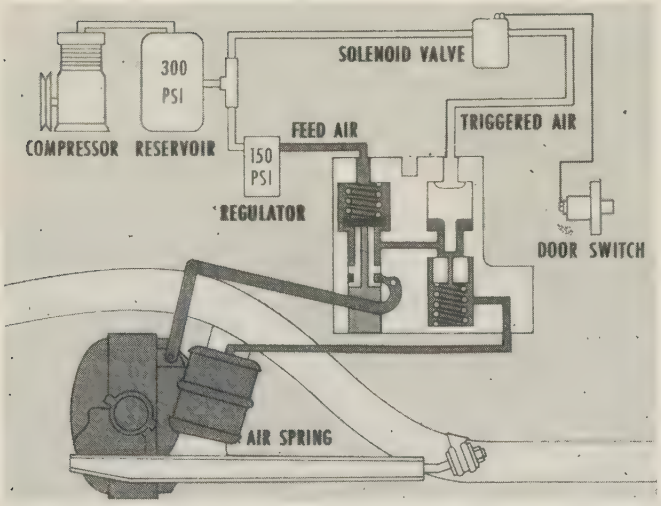

Fig. 10—Leveling operation

possible use of available wheel travel.

Three principal air level ride features are: the air springs, leveling valves, and trailing arm rear suspension. Briefly, the system works as follows (Fig. 9): Compressed air, used both as the spring medium and as the means of height control, is supplied by a specially developed compressor. This is a single-cylinder unit belt driven at approximately engine speed and lubricated by engine oil. Its piston displacement is 2.71 cu in. Balance pressure is approximately 300 psi, maximum power requirement approximately 1 bhp. It is a quiet and smooth running device with adequate capacity. The compressor delivers air through a flexible hose and a check valve to a 400 cu in. reserve tank mounted in the right fender just aft of the headlamp. A manual drain valve, for removal of any accumulated moisture, is installed at the low point of the tank and a filter is placed in the outlet line.

From the reservoir, which is normally at 300 psi (balance pressure of the compressor), air is used for two distinct purposes. Most of it is consumed in supplying the springs; air for this function proceeds through a copper line to a regulator valve, thence at reduced pressure (150–160 psi), to the three leveling valves (two front, one rear), and from these to the springs. Air at reservoir pressure is also supplied for a control, or "triggering" function; in this case, it is fed to a door-controlled solenoid valve and from there by nylon lines to fast-action mechanisms in the three leveling valves.

This arrangement brings about a dual, or "slow-fast" continuous height control. When the car is being driven (or is standing still with the doors closed) and a height adjustment is required, air is directed to or from the springs through highly restricted passages in the leveling valves so that height changes take place slowly. But as passengers enter or leave the car and a door is opened, the solenoid valve is actuated; this pneumatically opens a relatively unrestricted bypass in each leveling valve, through which springs are filled or exhausted. Thus, the leveling process is quite rapid as long as any door remains open. (See Fig. 10.)

The system includes several minor components which require a few words of explanation. The T-check valves between the springs and the leveling valves are low-limit devices which prevent the springs from exhausting below a set minimum pressure. They inhibit extreme leveling action, which could cause difficulties in jacking.

The pressure regulator or reducer valve maintains an approximate balance between the system-to-spring (fill) differential pressure and the spring-to-atmosphere (exhaust) differential pressure. This balance is required in rough road operation where the leveling valve is working continually. If the system were operated at the 300 psi reservoir pressure, for example, there would be perhaps a 220 psi differential to fill the rear springs and an 80 psi differential to exhaust them. On a long stretch of rough road, especially washboard, far more air would be admitted during jounce motions than could be exhausted during rebound motions. Even though the slow leveling passages were in use, the car would soon be riding high against the rebound stops. Pressure regulation at 150–160 psi keeps the car in trim regardless of road conditions.

A restrictor valve is used in the Ranger and Pacer models and is located between the right rear spring and the rear leveling valve. This valve contains a very small orifice, together with a bypass triggered by the solenoid valve in the same manner as the bypasses in the leveling valves. Thus, the orifice is effective only in the slow leveling mode. The reasons for using this restrictor will be made apparent in the discussion dealing with the rear suspension.

The leveling valve might be called the "brain" of the system. Its operation is fairly straightforward. Flow of air to and from the air springs is governed by a small rubber-covered seal disc. Each of the three valves in the system is mounted on the chassis frame; its actuating lever is linked to the unsprung mass, so that when the car riding height at that point deviates from normal, the lever shaft is rotated, and a cam on the shaft causes the plunger to move—up if the car is too low, down if it is too high. An upward movement of the plunger lifts the seal disc off its peripheral seat, admitting air at 150 psi to the passage. If at this time the car doors remain closed (slow leveling cycle), the air passes through the restricted orifice to the appropriate air spring or springs. Similarly, if the car is too high, the plunger moves downward away from the seal disc and exhausts air from the spring via the orifice and passage and then through the vertical

hole in the middle of the plunger to the atmosphere.

The fast leveling fill and exhaust cycles differ from the slow cycles only in that air flows around the circumference of the nylon piston instead of through the orifice. This is accomplished by high-pressure (triggering) air from the solenoid valve which opens whenever a door is opened. The triggering air depresses the plunger and unseats the nylon piston, thus opening the comparatively unrestricted circumferential bypass around the latter.

An interesting feature of the valve is that the orifice, although severely restricted, is not actually very small in diameter. A fine wire passing through the orifice greatly reduces its effective area, and at the same time acts as a cleansing means. Another feature is the small amount of lever movement required to bring about leveling—the valve has a very narrow "null" band. The entire mechanism is compact, simple, and durable.

The heart of any suspension system is its springs; they are probably the most important of all the factors which influence a vehicle's ride and, to a lesser degree, its handling. The Edsel air springs were chosen and developed in line with a major design objective: to take advantage of the ride potential of ultra-soft springing without sacrificing good handling qualities.

The air-spring design, which can be described as a girdled rubber cell with a variable area piston, was selected for two reasons. It requires minimum air volume and installation space to provide exceedingly low rates in the normal ride range, and it permits maximum flexibility in attaining any desired rate pattern.

The production front and rear air spring units consist of four basic parts: the rubber air cell, the retainer band or girdle, the piston or pedestal, and the upper seat. In addition, the rear units include clamps at both upper and lower seals to prevent unseating if the shock absorbers are removed or disconnected while the car is on a hoist.

It is evident that as the piston travels up and down within the cell, its effective area varies considerably. The character of this area variation depends primarily upon the shape of the piston. Since area is a factor in the rate equation, the shape of load-deflection and rate curves can be controlled by piston design. This can be seen on a typical static load-deflection curve having the characteristic pattern which was sought and achieved; also, a corresponding dynamic load-deflection curve for the same spring, obtained electronically at approximately sprung mass resonant frequency. A comparison shows that static and dynamic curves bear a strong general resemblance to each other, but dynamic rates in the neutral ride range are very much higher than static rates. In a vehicle, the dynamic wheel rate may be 4 or 5 times the static wheel rate.

This points out one of the major pitfalls to be avoided in the development of low-volume air springs. In an effort to minimize dynamic rates, it is all too easy to arrive at a suspension with a strong negative rate at normal ride height. A very mild negative rate for the spring itself may be permissible (provided the effect of suspension bushings or other spring elements cumulates in a positive overall suspension rate) but a negative wheel rate is not tolerable. Among other antics which it performs, a vehicle with a negative wheel rate is likely to cycle slowly between full-jounce and full-rebound while standing at the curb.

In the Edsel cars, dynamic rates in normal ride are sufficiently low to provide bounce and pitch frequencies in the neighborhood of 50 and 55 cpm, respectively. This, of course, is a major factor in the attainment of luxurious riding qualities. Static wheel rates are sufficiently positive to provide good stability at the curb, in approaching and emerging from curves, in braking, in accelerating, and other maneuvers. The smooth but strong rate buildup characteristics in both jounce and rebound, combined with automatic leveling, allow maximum utilization of the space available for suspension travel and result in excellent rough-road behavior. In addition, the rate buildup contributes toward good cornering and general handling.

Over and above the springing, first-class suspension geometry is requisite to good handling. In adapting air springs to the Edsel cars, it was possible to retain the standard coil spring front suspension geometrically intact. It was only necessary to move the shock absorbers aft of the control arms. But, of course, a different rear suspension was required and finally adopted. It is a trailing arm type with several rather unusual features. One is the forward attachment of the trailing arm to the frame; instead of the usual transversely mounted rubber journal bushing, it uses a large spike-end rubber mount similar to those often found in shock absorber ends. This particular design serves several purposes. It almost eliminates torsional loading in the trailing arm. It permits rather large axial, but only small radial deflections; this contributes very greatly to harshness reduction without adversely affecting rear end steering.

The trailing arm rear mounting is also interesting; each arm is attached to the axle by means of a pair of transverse rubber bushings whose axes are spaced some 5 in. apart. This arrangement gives effective isolation yet it ties the axle and trailing arms together in such a way that they constitute a roll stabilizing unit, with the axle housing acting as the torsion member. A considerable amount of rear end roll resistance is obtained in this manner.

Because of frame differences, the Corsair and Citation rear end geometry varies slightly from that of Ranger and Pacer models; in the former, the trailing arms run almost straight fore-and-aft; in the latter, the forward pivots of the trailing arms are somewhat further inboard. This reduces the twisting effect on the rear axle housing during roll; consequently, the Ranger and Pacer cars require rear roll resistance, which is provided by the restrictor valve mentioned previously. Normally, with a single rear leveling valve, the two rear springs are interconnected by a common air supply line; during roll, unrestricted air transfer takes place between them and they contribute no roll resistance. However, since Ranger and Pacer cars incorporate restriction in the supply line to the right rear spring, airflow between the two springs is severely inhibited in normal running with the doors closed, so that the individual springs act to increase roll resistance.

Combined with the geometrically conventional front end, the Edsel rear air suspension provides very satisfactory cornering and general handling qualities. There is, of course, a transient "feel"

which differs slightly but not objectionably from that of Hotchkiss drive vehicles; driver consciousness of it quickly disappears.

Braking

Full braking reserve is very important, especially with today's high-speed vehicles. The automatic brake adjuster, designed for this Duo-Servo brake assembly, maintains approximately 0.010-in. clearance at all times by adjusting the brakes whenever lining wear exceeds 0.005 in. All adjustments are made on reverse braking to eliminate the possibility of overadjustment that could be caused by drum distortion on panic stops in forward braking.

The installation consists, mainly, of a control cable fastened to the anchor pin at one end, and to the adjusting lever at the other end. This cable is routed over a guide, which is attached to the shoe web, so that any shoe movement, beyond the predetermined brake adjustment, will lift the adjusting lever. When lining wear exceeds 0.005 in. the shoe movement will raise the adjusting lever until the next tooth is engaged on the adjusting sprocket. After releasing the brakes, the adjusting spring will rotate the screw resulting in the brake adjustment. (See Fig. 11).

An additional advantage of the automatic brake adjuster, aside from eliminating conventional periodic brake adjustments, is to allow the lowering of the brake pedal to a closer relation with the accelerator pedal.

Test Program

In the initial stages of planning, it was decided that as much time as possible would be allowed for testing. The actual test program had its start in the early part of 1955 when several Mercury and Lincoln automobiles were modified to incorporate contemplated Edsel components. These first test cars enabled us to answer preliminary questions regarding package, suspension geometry, and brakes.

Cars were assigned for specific test purposes and the engineers equipped them with latest design components for severe and extensive road tests throughout the country. The test trips were so numerous and the locales so widespread that our test progress boards began to resemble arrival and departure schedules of a busy bus terminal.

Test engineers assigned to brake development piled up miles on the hills and mountains in the vicinity of Jennerstown, Pa., where we have garage and test facilities. Tests were conducted on brakes and related components; master cylinders, wheel cylinders, hydraulic lines, and brake drums were checked and rechecked. Brake lining wear was measured and carefully recorded to cover thousands of durability miles.

Chassis engineers had taken their cars and were headed south on ride, handling, and evaluation trips through Kentucky, Tennessee, and Georgia. Testing procedures and techniques were combined and modified to provide data such as highway fuel and oil economy.

Air conditioning engineers headed into Florida and Texas for their phase of testing. Vero Beach may be a prominent playground but to the test engineers, it was a proving ground. Condensers, evaporators, and compressors were installed and compared.

Other crews were at work testing in various areas from Dearborn to San Francisco: carburetion, vapor lock, fuel handling, and percolation tests were conducted at Pikes Peak, our proving ground in Arizona, Death Valley, and even on San Francisco's Telegraph Hill. The induction engineers tested until they were certain the carburetor that functioned so beautifully on the plains of Kansas served equally as well on Pikes Peak. In many areas, main highways were bypassed and the rough, deep-rutted, cross-country trails were used to get frame durability data.

Inclement weather was no deterrent to our program; in fact, it was made a part of the program. Test cars were driven up into the severe cold of northern Michigan and Minnesota where cold starting, automatic choke, and heater evaluation tests were conducted in sub-zero weather. Heaters were called upon to thaw out semifrozen engineers in –30 F weather.

The Edsel test program was one of the most extensive conducted; well over a million and a half test miles have been driven. Tests at the Dearborn Test Area alone accounted for 779,000 of those miles. The Dearborn test area is our 360-acre backyard with 14 miles of road, including multisurface roads, high-speed track, and a test hill with 17 and 30% grades. Having these facilities so close at hand was a tremendous asset in our development tests. Many times preliminary test data was made available in a day or two. The conference room—where the decision to try a component was made; the machine shop—where the component was fabricated; the garage—where the component was installed; and the test track—where the preliminary tests were conducted—were conveniently located in one compact area. 480,200 test miles were driven at our 3880-acre Michigan proving ground, where we have 30 miles of test roads, hills with grades varying from 7 to 60%, and one of the finest high-speed tracks in the country.

The first Edsel frames were tested at our Arizona proving ground, where the test vehicles were driven over the rough terrain, through dried out river beds, over desert trails, and across arroyos testing frame welds and body mounts. The continuous +90 F temperatures also made this an ideal place to conduct engine cooling and other tests requiring high ambient air temperatures. Tests conducted at this proving ground accounted for an additional 265,800 test miles.

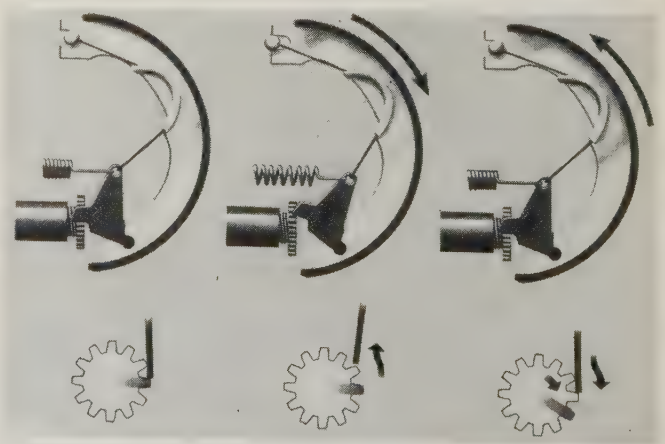

Fig. 11—Automatic brake adjuster operation

Metallurgical Design Considerations for

PRECIPITATION-HARDENING STEELS UP TO 1200 F

F. K. Lampson, Marquardt Aircraft Co.

This paper was presented at the SAE National Aeronautical Meeting, Los Angeles, Oct. 3, 1957.

A NEW group of steels known as the PH, or precipitation-hardening, grade has been added to the family of materials available to the aircraft or missile designer. The aircraft designer has long been accustomed to specifying aluminum or aluminum alloys for his products, but the increased speed of many of his creations has resulted in operating temperatures beyond which the use of the light alloys is feasible. The usage of the 400 series stainless steels results in adequate strength levels but presents many problems with regard to fabrication and corrosion protection, while the 300 series stainless steels, which possess desirable fabrication and corrosion resistance properties, have inherently low physical properties. The new group of materials, the precipitation-hardening stainless steels, by virtue of their adjusted chemical composition provide a class of alloys which possess the forming and corrosion resistance characteristics of the 300 series, and which may, by selected heat-treatments, be endowed with physical properties similar to those of the 400 series stainless steels.

THE latest development in materials for high-speed aircraft and missiles in precipitation-hardening steel. This paper describes in detail five of the new alloys: 17-7PH, 17-4PH, AM 350, AM 355 and A-286. The materials are designed for use up to 1200 F, although long exposure is not feasible above 800 F.

The author discusses the chemistry of each alloy and the effect of heat-treatment on them. He points out that although the new alloys are weldable, the metallurgical characteristics must be realized to assure consistent crack-free weldments.

Careful handling and control of the alloys during fabrication and treatment are essential.

There are many of the precipitation-hardening steels available today, so to discuss each of them individually would be impossible. For purposes of brevity, I have selected 17-7PH, 17-4PH, AM 350, AM 355, and A-286 for treatment in this paper but will point out other alloys which have just recently been made available and for which actual production information is extremely limited. It may be argued that A-286 alloy does not rightly belong in the group since its mechanism of precipitation is of an entirely different type than the other alloys mentioned; I have included it because we are discussing materials which are to be considered for usage up to 1200 F. Alloy A-286, which obtains its excellent properties by precipitation of a complex compound from an austenitic matrix, represents about the maximum in available iron-base materials for usage

Table 1—Ft_u versus Temperature times 1000 psi

Alloy	Condition	Temperature, F						Typical Hardness at Room Temperature
		70	400	600	800	1000	1200	
17-7PH	RH 950	235	205	190	175	100	—	Rc47
	TH 1050	193	177	163	147	123	~70	Rc43
AM 350	Set[a] (RH 850) Double aged (TH 850)	213	201	200	190	124	—	Rc47
		200	180	185	185	124	—	Rc42
AM 355	Set (RH 850) Double aged (TH 850)	225	215	215	210	144	—	Rc48
		—	—	—	—	—	—	—
17-4PH	H900	195	179	170	157	100	58	Rc43
A-286	Solution treat at 1800 F Age 16 hr at 1325 F	154	142	139	137	132	103	Rc29

[a] Subzero cooled and tempered.

Table 2—Ft_y versus Temperature

Alloy	Condition	Temperature, F						Typical Hardness at Room Temperature
		70	400	600	800	1000	1200	
17-7PH	RH 950	220	190	175	150	80	—	Rc47
	TH 1050	182	165	155	130	100	50	Rc43
AM 350	Set[a] (RH 850) Double aged (TH 850)	179	146	140	130	94	—	Rc47
		160	140	140	140	105	30	Rc42
AM 355	Set (RH 850) Double aged (TH 850)	190	165	155	130	97	—	Rc48
		—	—	—	—	—	—	—
17-4PH A-286	H900 Solution treat at 1800 F Age 16 hr at 1325 F	182	170	151	130	75	43	Rc43
		110	100	100	100	98	100	Rc29

[a] Subzero cooled and tempered.

Table 3—Percent Elongation versus Temperature

Alloy	Condition	Temperature, F						Typical Hardness at Room Temperature
		70	400	600	800	1000	1200	
17-7PH	RH 950	7	5	6	9	15	—	Rc47
	TH 1050	10	7.6	4	6.2	10	—	Rc43
AM 350	Set[a] (RH 850) Double aged (TH 850)	15	7.5	8.5	8.5	9.5	—	Rc47
		11.5	8.5	11.5	10.5	—	—	Rc42
AM 355	Set (RH 850) Double aged (TH 850)	19	16	13	10	16	—	Rc48
		—	—	—	—	—	—	—
17-4PH	H900	15	11	10	10	12	15	Rc43
A-286	Solution treat at 1800 F Age 16 hr at 1325 F	24	19	16	16	16	23	Rc29

[a] Subzero cooled and tempered.

up to 1200 F, and considerable tonnage of this material is being used in today's turbojet engines. Therefore, it is included in this discussion.

The temperature ranges for which the various classes of materials are particularly suited, with regard being taken as to the type of loading to be carried by the material, are shown in Fig. 1.

It is not the intent of this paper to present a detailed discussion of the physical properties which are obtainable from each of the alloys. To do so would be extremely time consuming and unnecessary since the manufacturers have provided such information freely and have cooperated extremely well with the consumers of the materials in order to give them the specific property data which they require for their end item product. It is, however, my intent to present information relative to the metallurgical phenomena which have been or which must be taken into consideration for the optimum properties to be obtained. It is hoped that by bringing this type of information to the attention of the designer and the metallurgist, closer cooperation between these men and the fabricator will result in a better realization of the problems which can occur with the use of these alloys.

Mechanical Properties

While it is not intended to present detailed mechanical properties of the materials under discussion, a glance at Tables 1–3 will illustrate the excellent properties which are available. It can be seen that ultimate strengths at room temperature of the order of 210,000 psi and yield strengths of the order of 175,000 psi are readily obtainable. Contrast these to the strength of type 310 stainless steel which has nominally 100,000 psi ultimate and 35,000 psi yield at room temperature. It is obvious that these newer materials present very attractive properties. Note that the PH grades which obtain their excellent properties by virtue of a precipitation mechanism from a martensite-like lattice (that is, 17-7PH, 17-4PH, AM 350, and AM 355) all retain their strengths at a respectable level up to 800 F, but lose them rapidly above this temperature. It is this rapid rate of strength loss above 800 F which limits their usage to about this temperature for long-life vehicles. The missile people will undoubtedly use them at higher temperatures where the times at temperature are much shorter than for the turbojet engine applications.

Alloy A-286, as seen in the Tables 1 and 2, has room temperature properties much lower than those obtainable from the 17-7PH and AM 350 alloys, but retains its properties at 1200 F and slightly above. It is common practice in the turbojet engine industry to limit the usage of this alloy in the form of turbine wheels, compressor blades, and the like to 1350 F. Above this temperature the alloy overages rapidly and the strength properties decrease at a rapid rate.

Chemical Composition

The chemical composition of all of the truly precipitation-hardening class of alloys are adjusted in such manner as to render the materials soft and ductile in the annealed state, with the ability to be strengthened by subsequent or supplementing heat-treating operations. The discussion of the precipitation-hardening alloys requires use of terms which may not be familiar to even some of the metallurgists since these terms are unique to these materials. Therefore, we will define these various terms.

Terms Used for PH Stainless Steels—The following definitions are submitted to allow a common terminology and understanding of the heat-treat process terms which tend to become somewhat confusing because of synonymous terminology for the same process.

Anneal—Thermal treatment usually above 1800 F followed by rapid cooling to homogenize the structure and dissolve prior transformation products and precipitates. Designated "A."

Transformation—Crystallographic change resulting from cooling below the start of Martensite formation (*Ms* temperature). This crystallographic change involves the formation of tetragonal mar-

tensite from the face-centered cubic (austenite) lattice.

Transformation treatment—Thermal treatment of annealed material near 1400 F to precipitate the carbon allowing transformation to occur upon air cooling. Designated "T."

Metastabilization—Thermal treatment of annealed material near 1750 F to precipitate the carbon to a lesser extent, such that completion of transformation requires refrigeration to −100 F. Designated "R." This term has been referred to by many fabricators as a "trigger" anneal operation, since the austenite formed by this treatment is very unstable and transformation to brittle martensite structures occurs easily.

Hardening—Thermal treatment of transformed or metastabilized material between 900 and 1100 F to relieve stress simultaneously or to temper the transformation product and precipitate an intermetallic compound with a cumulative hardening effect. Designated RH 950 and TH 1050, or SCT (subzero cool and temper).

Cold reduced—Mechanical straining of material to cause transformation. Designated "C."

Cold reduced hardened—Thermal treatment of cold reduced material near 950 F.

Austenite—The face-centered phase of the annealed condition in equilibrium with 5–20% delta ferrite. This definition does not apply to A-286 alloy, where the delta ferrite phase is absent.

Delta ferrite—The second lamellar phase in equilibrium with austenite in the annealed condition. This material is body-centered cubic and is normally considered to be the type of ferrite which forms at extremely high temperatures, as differentiated from alpha ferrite which normally forms from austenite in low-alloy or plain carbon steels at temperatures in the 1300–1400 F range.

Transformation product—The martensite-like phase of transformed austenite. The martensite formed from the austenite in these unbalanced steels is a high-alloy lowcarbon medium-hardness product from which precipitation of intermetallic compounds occurs at temperatures in the 950–1050 F range.

Table 4—Chemical Analysis of Several PH Steels

Element	17-7PH	17-4PH	AM 350	AM 355	A-286
C	0.09 max.	0.07 max.	0.08–0.12	0.10–0.15	0.08 max
Cr	16.00–18.00	15.50–17.50	16.00–17.00	15.00–16.00	13.50–16.0
Ni	6.50–7.75	3.00–5.00	4.00–5.00	4.00–5.00	24.0–27.0
Al	0.75–1.50	—	—	—	0.50 max
Mo	—	—	2.50–3.25	2.50–3.25	—
Ti	—	—	—	—	1.9–2.3
Cu	—	3.00–5.00	—	—	—
N_2	—	—	0.07–0.13	0.07–0.13	—
B	—	—	—	—	0.001–0.010
Zr	—	—	—	—	—
Fe	Balance	Balance	Balance	Balance	Balance

Carbides—Precipitates of chromium and carbon which are formed normally during the pretransformation thermal treatment (1400 F). It is believed that the depletion of the carbon from the austenite by combination with the chromium during the 1400 F treatment results in raising the *Ms* temperature of the remaining austenite with a martensite transformation occurring during cooling to 60 F. Subsequent aging treatments at temperatures in the 1000 F range result in the submicroscopic precipitation of complex intermetallic compounds.

Effect of Chemistry Variables

The chemical analysis of the five alloys being discussed are given in Table 4, with only the significant elements being shown. All have the normal restrictions on phosphorus, sulphur, silicon, and manganese; restrictions which are based upon well-recognized melting practices.

Chemistry of 17-4PH—This alloy is relatively simple in composition. The nickel content of the standard type 301 stainless steel has been reduced and copper added as a precipitation-hardening element. This material, available in the form of bars, plate, forgings, and casting, work hardens so rapidly that it does not lend itself to sheet rolling practices. For this reason, sheet stock to 17-4PH chemistry is

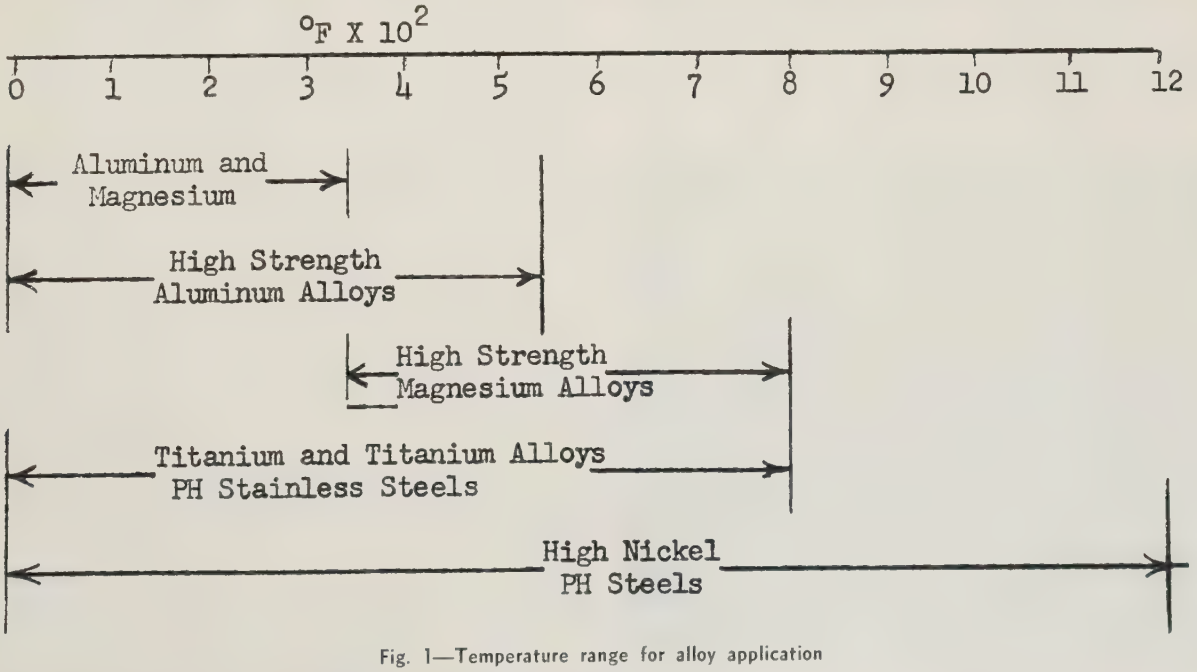

Fig. 1—Temperature range for alloy application

not readily available. Castings have been produced in quantity from this alloy, with the only major difficulty being noted when attempts were made to produce parts by the shell molding process. The organic resin used as a binder for the shell burns to carbon during casting, with the result that a carburized layer exists at the surface of the casting to a depth as great as 0.030 in. It is believed that recourse to inorganic binders will be required before shell mold castings free from the carburized layer will be successfully produced. Fig. 2 depicts this carburized layer.

A glance at the chemical composition of 17-4PH alloy will show that the copper is allowed to vary from 3 to 5%. It has been observed that where fabrication required welding the copper must be held to the low side of the range. Several companies have issued internal material specifications detailing copper ranges for specific applications.

Chemistry of 17-7PH—The chemical analysis of 17-7PH alloy is adjusted such that in the annealed condition the material is fully austenitic, but is sufficiently unbalanced that the austenite can be made to transform to martensite by suitable thermal treatments. There are two factors regarding the chemistry of 17-7PH alloy which come under consideration during this discussion. The first is the fact that the chemical analysis as specified allows a wide range of analyses within the limits, and the second is the tremendous influence of aluminum upon the behavior of the material.

The wide range allowed for each element creates problems for the fabricator of parts from this alloy, particularly where the parts are to be welded and heat-treated. The hardenability is sufficiently wide that fabricators have found it expedient to separate the material by heats or at least by heat-treat response prior to processing through their manufacturing shops. There have been cases where material with all of the elements on the high side of the range has been welded to material with the elements on the low side of the range, with the result that cracking has occurred during subsequent heat-treatment because of the differential response to the hardening operations.

The aluminum content of this material has been a subject of much discussion throughout the industry, with most consumers of the material wanting to control this element far more closely than the producer wishes. Aluminum, a strong ferrite former, creates an austenite with a secondary delta ferrite phase, with the amount of delta ferrite varying 5–20% depending upon composition. Because aluminum is such a potent element, the control of this element has been under discussion by a panel consisting of representatives from 17 aircraft manufacturers. It was their consensus that specifying the aluminum content more closely than now specified would be very desirable in AMS 5528 or MIL-S-25043 from a fabricators standpoint so that a more uniform heat-treatment response could be affected. However, it was felt that this would create an undesirable restriction upon the producer of the material since the aluminum is an extremely hard element to control due to its tendency to oxidize during addition to the melt. The producer is of the opinion that the present range 0.75–1.50% is as close as he can economically control this element, at least with the air-melting practices now being used to produce the alloy. Since they could not control the aluminum by specifying a restricted range of analysis, the representatives attempted to control the heat-treat response by recommending that the materials specifications be revised to include maximum properties after heat-treatment as well as minimum mechanical properties. The latter proposal has been rejected by the parent panel as being impractical.

The discussion of the chemical analysis requirements of 17-7PH, while brief, has been presented to show that this material, by virtue of its very analysis, must be closely controlled within the shop in order to assure successful utilization of the inherent capabilities of the alloy.

Chemistry of AM 350 and 355—AM 350 and AM 355 alloys, as noted in the chemical analyses of Table 1, have the elements controlled within very close limits, differentiating them from the 17-7PH grade of precipitation-hardening steels. AM 350 and 355 have their analyses adjusted such that they are austenitic in the annealed condition, but are capable of being transformed to a martensite-like lattice by subsequent thermal treatments. In this respect, these alloys are identical to 17-7PH and, in fact, the temperatures which are used in the heat-treatment are very similar to those used for the 17-7PH alloy.

The mechanism of hardening for AM 350 and 355 does not appear to be entirely that of precipitation of submicroscopic particles from a martensite-like lattice. Rather, it appears that hardness, per se, is achieved by a straight austenite-to-martensite reaction with the martensite hardness being achieved by a carbon-nitrogen interaction. The role of nitrogen in contributing hardness to the as-quenched structure of a chromium-bearing stainless steel has been recognized of late, as denoted by the inclusion of requirements for nitrogen in a proposed Aeronautical Materials Specification for type 431 stainless-steel investment castings, the inclusion of definite requirements for controlling this element in AM 350 and 355, and in the technical literature of recent years. Nehrenberg et al of Crucible Steel Co. have proposed a mathematical relation between carbon and nitrogen contents and as-quenched hardness for chromium-bearing stainless steels which ap-

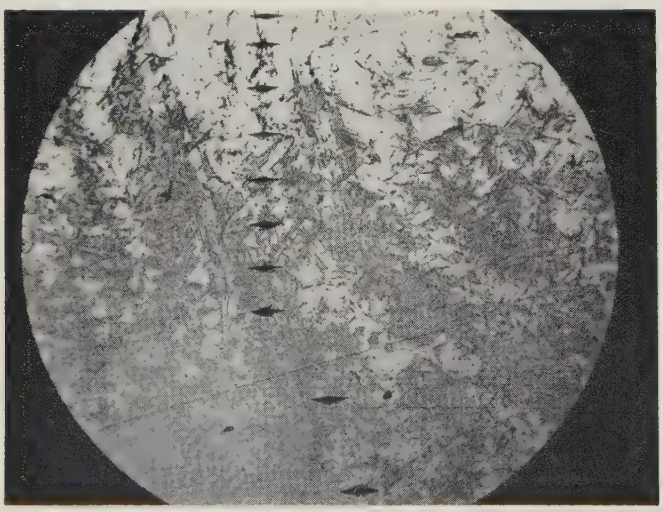

Fig. 2—17-4PH shell molded (original taken at 100× magnification)

pears to be valid for the materials under discussion.

AM 355, containing nominally 1% less chromium than AM 350, is capable of producing slightly higher mechanical properties than the latter alloy, due to the increased amount of austenite which will subsequently transform to martensite during heat-treatment and the higher carbon content of this material. The reduction in chromium, however, is reported to result in the AM 355 material being more subject to stress corrosion than is AM 350.

One important fact for the fabricator of PH steels to consider is the close range of chemistry to which AM 350 and AM 355 are produced, and the lack of elements such as aluminum which can create problems during welding and/or brazing. The extremely close control of the elements results in a material which is uniform in its response to heat-treatment and which would not appear to require segregation by heat-treatment response prior to being released to the shop. AM 355 alloy has not been accepted to the degree that AM 350 has, but both materials are now in the process of having Aeronautical Material Specifications prepared for them, indicating that there are at least two major consumers of these materials.

Chemistry of A-286—Alloy A-286, by virtue of its high nickel content, is fully austenitic at all times and achieves its properties by precipitation from solid solution of complex compounds not fully identified. This alloy is basically different from 17-7PH and 17-4PH, Am 350 and AM 355 alloys in that its composition is balanced such that one crystallographic form, (γ) or austenite, is stable at all times, whereas the true PH grades have their chemistry unbalanced so as to permit a definite allotropic transformation to be achieved by heat-treatment.

Alloy A-286 has found wide acceptance in the turbojet engine field in the form of wheel forgings, buckets, and the like where superior mechanical properties in the 1200 F range are required. There have been recent developments in the melting practices which will have a profound effect upon the properties of the alloy and which should be discussed in the chemistry section since the changes will be chemical in nature.

It has been found that substantial increases in reliability and reproducibility of stress rupture properties at 1200 and 1350 F can be achieved by producing this alloy by the vacuum consummable electrode process wherein an electrode of A-286 composition, which has been produced either by the air-melt process or by a vacuum-melting process, is remelted under vacuum to ingot rolling form. This method of ingot production produces a high-quality product which is free from center segregation and oxide/nitride inclusions. It is believed that the utilization of such a melting process, resulting in greater cleanliness of product, will increase the stress level to which the material may be operated. The maximum operating temperature should not be materially affected, since it is controlled by the temperature at which the precipitation action occurs. Several of the large producers of this alloy are now in the process of installing new facilities for the production of this and other "super" alloys under vacuum.

It has been proposed recently that the chemical analysis of A-286 alloy be amended to specify that boron be required in the amount 0.001–0.01%. Addition of this element in the amount specified is reported to increase the stress rupture life and ductility to a marked degree. Freeman et al of the University of Michigan have published an article stating that boron is present, unless specifically added, as a "tramp" element from the magnesia crucible which is frequently used in vacuum melting. The boron is present in MgO as a borate and is reduced to metallic boron by the reaction:

$$BOx + C \rightarrow CO + B$$

It is quite evident that the beneficial effects of boron additions have been recognized by the producers for some time, but that only recently have these people been reporting the results of chemical analyses of their materials.

The element zirconium has been under discussion in the recent months, with the result that considerable interest has been expressed in controlling this element in the high-temperature alloys. It appears that zirconium, which is present as a tramp element from zirconia fire bricks, up to 0.002% results in increased rupture life and ductility. The effects of zirconium additions above 0.002% are not fully understood, but it appears that amounts in excess of this amount result in decreased rupture life.

It is very obvious that the interrelated effects of boron and zirconium additions upon the properties of high-temperature alloys warrant investigation.

Effect of Heat-Treatment Variables—The heat-treatment of the PH grades of stainless steels can, in the case of 17-7PH, AM 350, and AM 355, be accomplished by two methods, with the choice being dictated by the fabrication procedures to be used. The first method consists of subjecting the mill annealed material to a low (1400 F) austenite-conditioning temperature, followed by cooling to a temperature below the *Ms* of the austenite formed at 1400 F. A crystallographic change from austenite to martensite is accomplished with this operation with an accompanying increase in hardness of the product. Subsequent exposure to temperatures within the range 750–1050 F results in tempering of the martensite and precipitation of complex compounds from the martensite-like lattice. For the materials under discussion, this type of treatment results in a final hardness of Rc40–45, and strength levels in the 165,000–185,000 psi range.

To achieve strength levels higher than those obtainable with the "double-aging" treatment described above, it has been reported that subjecting the material to a "trigger" annealing operation in the vicinity of 1700–1750 F followed by cooling to −100 F results in higher hardnesses and higher strength properties. Subsequent exposures in the range 850–950 F results in tempering of the martensite formed from the triggered austenite and submicroscopic precipitation of complex compounds from the martensite lattice. The effect on the hardness of the 750–950 F tempering operation is one of a slight increase, caused by the precipitation from the martensite. Material heat-treated in this manner exhibits ultimate tensile strengths in the 210,000 to 230,000 range, accompanied by adequate ductility for mild forming operations.

To understand the mechanism of hardening of the PH steels and to get an idea of the reasons for the temperatures which are selected for the heat-

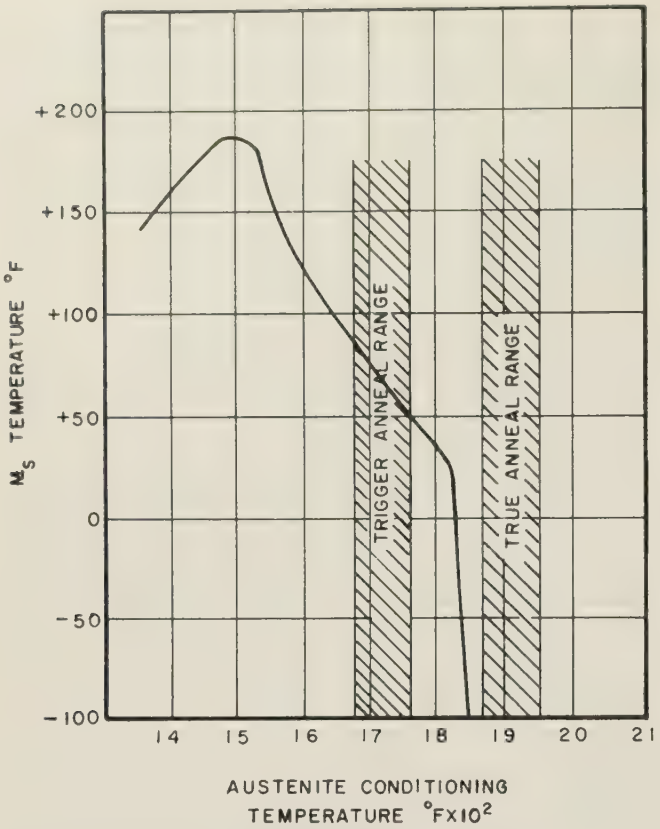

Fig. 3—Effect of austenite-conditioning temperature on start of martensite transformation

treating operations, a discussion of Fig. 3 will be beneficial. The chart depicts the effect of the austenite-conditioning temperature upon the *Ms* of the PH steels in question. This chart appears to be valid for 17-7PH, AM 350, and AM 355, since they are all capable of being hardened by either the double-aging treatment or the "refrigeration" (−100 F) treatment. Alloys 17-4PH and A-286 appear to be fairly straight forward in their heat-treatment operations, requiring principles of heat treating which are well-recognized by metallurgists and fabricators. The heat-treating of the 17-7PH and AM 350 grades involves some fairly complex operations which need to be thoroughly understood for reproducibly successful fabrication.

The chart showing the effect of austenite conditioning temperature upon the *Ms* of the PH steels can be used to explain the reasons for the increased mechanical properties of materials processed by the refrigeration method. Austenite-conditioning temperatures in the 1400 F range result in the precipitation from the austenite-delta ferrite matrix of chromium carbides, leaving the austenite depleted of carbon. This has profound effects: the austenite, being lower in carbon, transforms to a low-carbon martensite which is weaker than a higher carbon martensite. The graph shows that the *Ms* temperature for material conditioned at 1400 F is approximately 160 F. Raising the austenite-conditioning temperature has the effect of lowering the *Ms* temperature and increasing the solubility of carbon in austenite. Thus, where the ability to transform to martensite remains, that martensite which is formed from austenite at higher temperatures is stronger than that formed at 1400 F, due to the strengthening effect of the higher carbon. It can be seen that material subjected to an annealing temperature of 1950 F will have its *Ms* temperature well below −100 F, with the result that annealed material is full austenitic at all times, or until a lower austenite-conditioning temperature is used to achieve subsequent transformation to martensite. Experience has indicated that austenite-conditioning temperatures in the vicinity of 1700 F, where the *Ms* temperature is approximately 60 F and where the transformation is essentially completed at −100 F, result in maximum mechanical properties and ductility.

With this discussion in mind, the variables which must be recognized for each of the materials under consideration will be presented in detail below. The specific heat-treating cycle for each alloy is presented in Table 5.

Heat-Treatment of 17-4PH—Alloy 17-4PH has been classed as a single martensitic reaction material, since its heat-treatment consists simply of a conventional quench and draw operation, similar to that used for the 400 series stainless and the low-alloy steels. While the heat-treating operations are more or less conventional for this material, the metallurgy of the reactions are basically different for this material than for the 400 series stainless steels in that in the annealed condition the matrix consists of pools of delta ferrite in a low-carbon martensite. Hardening at 900 F results in the precipitation of a copper-rich complex from the martensite-like matrix. It is the precipitation of this copper-rich compound that results in the increased mechanical properties of this material.

Heat-Treatment of 17-7PH—The transformation heat-treatment, which consists of conditioning the austenite at 1400 F followed by cooling to 55 ± 5 F and then subjected to an aging treatment at 1050 F, warrants discussion first since it was the original treatment suggested by the producer. There are certain variables with this heat-treatment which must be recognized or serious difficulty will be encountered during the fabrication of parts.

First, the cooling operation to 55 ± 5 F from the austenite conditioning temperature (1400 F) must be accomplished within one hour. Otherwise, the residual austenite becomes stable and complete transformation to martensite is not affected.

The temperature range 55 ± 5 F must be controlled very closely in order to achieve maximum properties inherent with this type of heat-treatment. Cooling to temperatures lower than 50 F will result in increased mechanical strengths but will have the deleterious effect of reducing the ductility significantly. There have been instances reported where fabricators have ignored this requirement and have cooled the conditioned material in conventional freezing boxes where the temperature was down to 0 F. These fabricators could not understand why their material had a tendency to be brittle after this treatment, and it was not until this phase of the operation was corrected that they were successfully producing parts from this material. Conversely, cooling to temperatures above 60 F results in incomplete transformation and erratic physical properties.

It has been reported that the time of exposure at 55 ± 5 F or the interval of time between this treatment and the subsequent aging treatment at 1050 F

are not critical. However, there have been cases where the heating operation from room temperature to 1050 F has been found to be time dependent, in that microcracking of the martensite has occurred when the heating operation was done slowly. It is believed that the heating operation from room temperature to 1050 F must be accomplished rapidly to prevent sensitization or microcracking of the martensite, with an accompanying decrease in mechanical properties of the material.

The aging time at 1050 F does not appear to be critical, but the ± 10 F restriction placed on the temperature of 1050 F indicates that this temperature is extremely critical. It can be shown that the strength level falls rapidly when the aging temperature exceeds 1050 F and that the temperature tolerance of ± 10 F is justified, since there is a difference in strength levels of 4,000 psi within the ± 10 F range. Temperatures in excess of the ones recommended will result in inferior strengths. Because of this, strict furnace temperature control is an absolute necessity with this material. It should be pointed out that the 1050 F aging treatment is preferred by the producer for material previously conditioned at 1400 F, and that recommendations for other aging temperatures have been discontinued.

The refrigeration treatment consisting of exposing "trigger annealed" material to – 100 F temperature, which has been announced only within the past year for this alloy, results in properties which are higher than those obtained with the double aging treatment. This can be explained readily by the concept that the martensite formed with the refrigeration treatment is a higher carbon material and, therefore, is inherently stronger. About the only variable which has come under discussion with this treatment is that of the austenite-conditioning temperature. Initially, the producer specified that this temperature should be 1750 ± 25 F. The consumers of the material have, however, through experience, dictated that superior properties and increased uniformity of heat-treatment responses are achieved when the temperature is lowered to 1710 ± 15 F. The latter temperature is that currently specified in the Aeronautical Material Specification for this material.

Heat-Treatment of AM 350 and AM 355—These alloys, while differing slightly in chemical composition, are heat-treated identically. Alloy AM 355 because of its higher carbon content and lower chromium content exhibits mechanical strengths slightly higher than its companion alloy, but does not have corrosion properties as good as the latter material.

Alloys AM 350 and AM 355 are not truly precipitation-hardening materials, but achieve their excellent mechanical properties through an austenite-to-martensite transformation similar to a 400 series stainless or a low-alloy steel. These alloys, however, are capable of being hardened by the double-aging treatment similar to that of 17-7PH alloy, even though the chemical composition does not appear to support this fact. The hardness which is achieved from these alloys is a function of the carbon-nitrogen ratio, and it is apparent that the precipitation from a martensite-like matrix which occurs during the final aging treatment, must be connected to the molybdenum. At any rate, the tempering temperature of 850 F results in a slight increase in the as-quenched hardness, evidence conclusive that a precipitation mechanism is occurring during this treatment.

An interesting sidelight to these materials is the importance of the correct austenite-conditioning temperature being chosen for specific applications. Austenitizing at 1950 F followed by rapid quenching results in a soft, formable, austenite plus delta ferrite matrix which is ideal for forming and welding operations. Austenitizing at 1710 F creates an austenite which is severely unbalanced and unstable, with the result that material processed with this "trigger" annealing operation is very prone to transform to martensite at a later time. There are cases on record where the material has been shipped from the producer's plant in the 1710 F annealed condition and found to have transformed to a hard, relatively nonformable martensitic structure during shipment. This is particularly true when the material was shipped by air or during the winter months when the ambient temperatures were sufficiently low to create the transformation of austenite to martensite. In this situation, where the metal fabricator was forced to re-anneal the material prior to processing it through his plant, such a phenomenon is disconcerting, time consuming, and costly. The producers, recognizing such a possibility, have found it necessary to inform their customers that it may become necessary for them (the customers) to re-anneal the material if partial transformation occurs during shipment. It would appear however, that where forming or welding operations are to be performed on the material the material should be shipped in the 1950 F annealed

Table 5—Heat-Treating Cycles for PH Steels

Alloy	Annealing Operation	Double Age Treatment					Refrigeration Treatment		
		γ Condition Temperature, F	Time at Condition Temperature min	Cooling Condition	Final Age Temperature, F	Condition Temperature, F	Time at Condition Temperature, min	Cooling Condition	Final Temperature, F
17-7PH	1850–1975 F for 90 min, thick rapid quench	1400 ± 25 F	90	Cool to 55 ± 5 F within 1 hr	1050 ± 10	1710 ± 15	10	Cool to – 100 F, 8 hr	950 ± 10, 60 min
AM 350	1850–1975 F for 30 min, rapid quench	1710 ± 25 F 1375 ± 25 F	30 60	Rapid quench Aircool	850 ± 25, for 3 hr	1710 ± 25	30	Cool to – 100 F, 3 hr	850 ± 25, 3 hr
AM 352	1850–1975 F for 30 min, rapid quench	1710 ± 25 F 1375 ± 25 F	30 60	Rapid quench Aircool	850 ± 25, for 3 hr	1710 ± 25	30	Cool to – 100 F, 3 hr	850 ± 25, 3 hr
17-4PH	1900 ± 25 F for 30 min, rapid quench	—	—	—	—	1900 ± 25	30	Rapid quench	900 ± 10, 60 min
A-286	1800 ± 25 F for 1 hr, rapid quench	1800 ± 25 F	60	Rapid quench	1400 for 16 hr	—	—	—	—

condition where the possibility of partial transformation does not exist.

Heat-Treatment of A-286 Alloy—Alloy A-286 does not rightly belong in the discussion of PH steels since it remains fully austenitic regardless of heat-treatment, whereas the true PH steels have the capability of undergoing an allotropic transformation from austenite to martensite. However, alloy A-286 represents about the maximum in iron-base alloys for use up to 1200 F, the temperature range being discussed. By virtue of its high nickel content, A-286 is austenitic at all times, it is strengthened by taking aluminum and titanium into solution during the solution treating cycle at 1800 F and expelling them along the grain boundaries and slip planes during the precipitation treatment at 1325 F. It is obvious that the major difference between A-286 and the other alloys under discussion is that in the A-286 the precipitation occurs from an austenite matrix, while in the other group of alloys precipitation occurs from a martensite matrix.

The heat-treatment of A-286 alloy does not appear to present too many production problems since the mechanism of solution treating and aging are well-understood, at least on the gross scale encountered in the commercial heat-treater's shop. However, there has been a tendency of late on the part of several large consumers of this alloy to lower the solution treating temperature from 1800 to 1650 F. The proponents of the lower temperature claim that superior stress rupture properties are obtained from specimens processed in this manner, and they have introduced evidence to support this supposition. But, there are other large consumers who claim that many years of successful processing with the 1800 F solution treating temperature preclude the need of going to the new solution treatment temperature.

The fabricators of sheet metal and cold-headed end items from A-286 alloy sheet materials have been plagued within the past year with the occurrence of a lamellar precipitate at the grain boundaries a condition which is undesirable since it results in decreased mechanical properties and ductility of the material. The lamellar precipitate, believed to be $TiFe_2$, appears to be related in some manner to the method used to process the material, and does not appear to be affected in any way by the chemical composition, at least within the range of composition allowed by specification. In certain instances the lamellar precipitate can be reproduced by cold working the material after the solution treatment and before aging. However, this has not been conclusively proved to be the cause for the occurrence, since there is also evidence that performing all heat-treating operations in a protective atmosphere will reduce the incidence of precipitate occurrence. There is reason to believe that recent boron additions to the chemistry will not prevent the formation of the lamellar precipitate, but that it will reduce the effect of this phase upon the mechanical properties of the material. To the best of my knowledge, the problem of the occurrence of the lamellar precipitate in A-286 alloy has not been completely solved.

Welding and Brazing Considerations

The welding and brazing of the PH steels differ from the ordinary 400 series stainless steels in that they can be joined in the austenitic condition, where the susceptibility to cracking is decreased. Linnert of the Armco Steel Co. presented in the 1956 Adams Lecture (American Welding Society) an excellent discussion of the problems to be encountered in the fusion and resistance welding of the precipitation-hardening stainless steels, with particular attention being paid to the 17-7PH grades of steels produced by his company. The consensus of Mr. Linnert's paper was that the precipitation-hardening grades are readily weldable, but that the metallurgical characteristics of the material must be recognized in order to assure crack-free weldments. Also, there seems to be an inherent problem of low weld metal ductility, which has not been fully resolved.

Categorically, it appears that 17-7PH, AM 350, and AM 355 should be fusion welded in the annealed condition, followed by the heat-treating operations in order to achieve maximum weld efficiency. For tungsten inert gas arc processes, which are ideally suited for these materials, the filler metal should be of the same nominal composition as the base metal. In those cases where the material may be required to be welded in the hardened condition, or where the strength of the weldment is secondary, it is permissible to fusion weld these materials using filler metal of the same type used for welding the austenitic stainless steels.

One problem which is inherent with the 17-7PH grade is that of the danger of loss of aluminum by oxidation during the welding process. The problem of aluminum oxidation is decreased in the tungsten inert-gas-welding process by using of slightly higher argon gas coverage than normally used for austenitic stainless steels. The argon provides a protective gas coverage which prevents oxygen from the air from coming in contact with the aluminum of the steel. Metallic arc welding of 17-7PH is normally accomplished using flux-covered electrodes of 17-4PH composition. Metallic arc electrodes to 17-7PH composition are not normally manufactured because the flux coating does not provide sufficient protection to prevent oxidation of the aluminum.

The fusion welding of A-286 alloy should be performed upon material in the annealed, or solution treated, condition, since this alloy is verp susceptible to cracking during welding in the fully aged condition. Considerable success has been achieved using filler metal to Hastelloy W (Ni base-Cr-Mo) composition where the technique is adjusted to require favored dilution of the base metal. Several large consumers of this material have reported considerable success using filler metal to the base metal composition, a situation which is to be preferred where the part is to be heat-treated after welding.

Brazing of 17-7PH steels with brazing materials of the silver-manganese type has been widely accepted, primarily in the fabrication of honeycomb panels and structures.

It has been reported, however, that the silver-manganese brazed joints are subject to crevice-corrosion, and that considerable effort is being expended to correct this condition. Additions to the composition of such elements as lithium and/or nickel have been attempted with varying degrees of success. The brazing cycles are normally coordinated with the double-aging type of heat-treatment, with the result that this material provides about the ultimate in high-strength low-density

structures for use up to 800 to 1000 F, depending upon the time of exposure. Here again, however, the aluminum presents problems with regard to oxidation, with the result that the brazing operations are carried out in dry hydrogen atmospheres. There have been cases reported where the brazed assembly was covered with a white powder after the brazing cycle, with the white residue being identified as aluminum oxide. This condition is indicative that the aluminum content of the base metal has been depleted, a condition which is dangerous because the austenite becomes stable and full response to heat-treatment is not realized. Naturally, this results in a weakened structure. It is believed that dry hydrogen atmosphere with dew points lower than –50 F are required to prevent oxidation of the aluminum during the brazing cycle.

There has been very little production brazing of the AM 350 and 355 steels, but the composition would indicate that little difficulty would be encountered using the convential brazing filler materials. This has been verified by several of the large airframe manufacturers.

The nickel alloy brazing of A-286 alloy presents many problems due to the presence of aluminum and titanium. These elements are not reduced by hydrogen, with the result that normal brazing techniques performed in a dry hydrogen atmosphere are not sufficient to achieve reproducibly satisfactory bonds. To support the theory that it is the presence of titanium and aluminum that create the difficulty when brazing A-286 material, it has been shown that as-forged parts, with one surface finish machined, have been found to bond perfectly along the as-forged surfaces but not along the machined surfaces. It is believed that aluminum and titanium, which are easily oxidized, are depleted from the as-forged surface, a condition which results in satisfactory bonding due to the increased wettability of the nickel alloy brazing alloy and the base metal. In our plant, we have found the following procedure for nickel alloy brazing to work very well:

1. Subject the part to the brazing temperature and atmosphere in the absence of braze filler metal.
2. Vapor blast the parts.
3. Braze at 1950 F using AMS 4778 filler metal with a dew point of –60 F or better.

The vapor blasting operation, which removes the surface layer of titanium and aluminum leaves a surface which is "metallurgically clean" to the brazing filler metal. Recourse to AMS 4778 filler metal in lieu of the more familiar AMS 4775 filler metal was required for our particular operation, but AMS 4777 has been found to work very well. Both AMS 4777 and 4778 appear to have greater wettability than AMS 4775 material, and are considered better for the brazing of A-286 alloy material.

Conclusion

The alloys discussed in this paper represent the precipitation-hardening materials which are being used on a production basis in many of today's engines and airframes and which are not merely laboratory scale development alloys. The producers of these materials, not content to "rest upon their laurels," have continued to work to develop newer and better materials. Some of the newer alloys which could have been discussed, but for which there is very limited production experience, are Universal-Cyclops' Unitemp 212, Armco Steel's 15-7 Mo, and International Nickel's Inco 901. All of these represent improvements over the PH steels discussed herein, but so far, they are not available in large quantities. No doubt these new alloys, and others not announced as yet by their producers, will find their place in industry in those areas where superior properties in the 1000–1200 F range are required for successful operation of the product.

The conclusions which can be drawn with regard to the usage of the PH steels (17-4PH, 17-7PH, AM 350, and AM 355) are that these materials fill a very definite need for high-strength materials for use in engines and airframes up to 800 F, with very short time exposure to slightly higher temperatures being feasible. However, these materials must be handled carefully within the fabricator's shop and closer control of heat-treating and welding operations must be exercised in order to assure maximum realization of the potential properties of these materials. A thorough understanding of the metallurgical properties of these materials must be recognized or costly and time consuming reworks may be required.

ORAL DISCUSSION

Reported by R. H. Sparling
Convair Division, General Dynamics Corp

Wesley W. Safee, Douglas Aircraft Co., Inc.: Why do you show two aging temperatures for AM-350 and only one for 17-7?

Mr. Lampson: For brazed applications, where double aging is required, material is bought with properties guaranteed for the 1400 F treatment. But for parts where the RH condition is desired, we must use the 1710 F treatment. Therefore, we want manufactures to guarantee properties resulting from the 1710 F treatment. (This 1710 was formerly 1750; it was recently changed to 1710.)

Leo Gatzek, Bendix Aviation Corp.: Have you had any experience with 17-4PH casting being rejected by magnetic particle analysis for indications which look like cracks? Annealing at 2150 F made the indications disappear. Further inspection showed that segregation of copper had caused the indications. We have rejected as much as 80% of a lot of 17-4PH castings on magnetic inspection.

Mr. Lampson: We have heat-treated a great deal of 17-4PH, even with the carburized case, but have not experienced any trouble of this sort. You don't heat-treat in dissociated ammonia, do you?

Mr. Gatzek: No, we are afraid of the nitrogen.

G. N. Dollar, Armco Steel Corp.: We are selling material to guaranteed minimum properties rather than a narrow range of chemistry. We have produced thousands of tons with no complaints. The case you mentioned where it was necessary to separate 17-7PH by heats, the fabricator was trying to get a 2 point Rockwell spread, which is hard to do with any material. What aluminum range do you suggest?

Mr. Lampson: The present range of 0.75 to 1.50 for aluminum is all we can reasonably expect to get. I would like to make the point that I personally feel that steels like 17-7PH, AM 350, and the like, are very fine materials. However, our experience (similar to that of other aircraft companies) is that if you are going to use these steels, you must control all practice in the shop. They should be used correctly or not at all.

In regard to the aluminum range, one suggestion has been $1\% \pm 0.2$. This is rather impractical. It arose from trouble in brazing; however, where aluminum varies, it can cause lots of trouble in brazing.

Mr. Dollar: The mill is now working to a 0.35 spread in aluminum.

FUMIGATION KILLS SMOKE — — IMPROVES DIESEL

M. Alperstein, W. B. Swim, and P. H. Schweitzer, The Pennsylvania State University

This paper was presented at the SAE National Diesel Engine Meeting, Cleveland, Nov. 6, 1957.

THE outstanding advantage of the diesel engine—its fuel economy—derives from two facts: The compression ratio of the diesel is roughly double of that of a modern automobile engine, and the diesel can burn a lean mixture which a spark is unable to ignite. In most other respects, however, the diesel is inferior to the otto engine. In the latter the fuel and air are mixed *before* they enter the cylinder, so most of the fuel is in vapor phase at the time of ignition; a rather rich mixture can, therefore, completely be burned without thermal decomposition; hence, carburetor engines generally do not smoke. Secondly, the spark plug is able to ignite fuels of low ignition quality which in a compression ignition engine would ignite too late or not at all.

Fumigation described in this paper represents a little step away from the diesel engine in the direction of the otto engine, a step which preserves all the diesel advantages and alleviates two disadvantages: incomplete mixing of air and fuel and late combustion caused by long ignition lag.

The method broadly consists of introducing part of the fuel in the form of a fine mist or fume into the intake manifold while the rest is introduced in the conventional manner through the high-pressure injection system into the cylinder near tdc position of the piston.

History

Manifold introduction of fuels into a compression ignition engine was experimented with at Penn State as early as 1941 and is reported in the master

Table 1—Fuel Properties

	Chemical Constitution	Specific Gravity (60/60) F	Kinetic Viscosity, cs at 100 F	Boiling Point, F	Octane Number	Cetane Number	Latent Heat of Evaporation, Btu per lb	High Heating Value, Btu per lb	Low Heating Value, Btu per lb	Stoichiometric Air-Fuel Ratio
Normal Hexane	C_6H_{14}	0.659	0.41	155	26		156	20,900	19,432	15.2
Normal Heptane	C_7H_{16}	0.684	0.52	209	0		155	20,850	19,408	15.1
Ethyl Alcohol	C_2H_5OH	0.785	1.11	172	99		367	12,780	11,604	9.0
Diethyl Ether	$(C_2H_5)_2O$	0.714	0.28	94.3			165	15,840	14,560	11.1
Amyl Nitrate	$C_5H_{11}NO_3$	1.000	0.80	297			150	10,600	9810	7.48
Isopropyl Nitrate	$(CH_3)_2CHNO_3$	1.058	1.82	216			137	8210	7580	5.55
90 Octane Primary Reference Fuel Blend	90% C_8H_{18} 10% C_7H_{16}	0.701	0.58	211	90		155	20,600	19,184	15.1
Diesel Fuel, WCN	H/C = 0.154	0.850	2.7	680 end point		43.6		19,610	18,260	14.5
Diesel Fuel, CCD	H/C = 0.156	0.836	2.75	623 end point		52.4		19,780	18,430	14.5
JP-5	H/C = 0.134	0.883	1.27	504 end point		22.9		19,380	18,075	14.3

THE effects of introducing a portion of the fuel charge of a diesel engine into the intake manifold in the form of a fine mist are reported in this paper. Laboratory tests with swirl-chamber and open-chamber engines resulted in smoke reduction up to 80%, increase in smoke-limited power output up to 18.5%, decrease in specific fuel consumption up to 9.8%, shorter ignition lag, lower maximum rate of pressure rise, and smoother operation. In running on good-grade diesel fuel approximately 15% of the main fuel proved to be as good a manifold fuel as any. It was also found that a diesel engine could operate satisfactorily on substandard fuels down to zero cetane number when fumigation was employed.

Maximum benefits from fumigation accrued when inducting fuel in the form of a very fine mist (not over 4 microns) produced by Micro-Fog. As yet an economical method of producing this finely atomized fuel spray in large quantities has not been found. However, significantly improved performance was also obtained by the use of inexpensive pneumatic spray nozzles that require only a small amount of low-pressure air for operation.

PERFORMANCE

thesis of C. W. Van Overbeke.[1] Vaporization and carburetion were used for introducing auxiliary fuels such as hexane, heptane, five different diesel fuels, white gasoline, hydrogen peroxide, benzoyl peroxide, methyl alcohol, benzene, cetane, and diethyl ether. Ether, cetane, hexane, and low boiling point diesel fuels were found to be most effective; acetone, benzene, and ethyl alcohol were least effective or detrimental when introduced into the intake manifold It was pointed out then that slow oxidation and preflame reactions were believed to be responsible for the effect of the manifold-introduced fuels on ignition.

McLaughlin, Pinotti, and Sigworth[2] used manifold introduction of fuels, mostly gasoline and liquid petroleum gas, to kill smoke and/or boost power, as was also done by Derry et al[3] and by Lyn[4] in England.

In all these researches the main fuel was injected into the diesel cylinder in the conventional manner and a small amount of auxiliary fuel was introduced into the intake manifold as an aid to combustion Havemann et al[5], on the other hand, carburetted alcohol as a main fuel and injected a small amount of diesel oil and various vegetable oils to ignite the compressed air-alcohol vapor mixture. In this manner they successfully burned alcohol which otherwise could not be ignited by compression ignition. A similar scheme was used in the last war by the German Air Force. They developed the "R Fluid," a less volatile ether, which they used in place of a spark plug. Ignition was produced by the injection of "R Fluid" btdc into the compressed air-gasoline vapor mixture. Still earlier, a pilot spray of diesel fuel was used in dual-fuel gas engines in the same manner.

In the last three instances the main fuel was inducted through the intake manifold and a relatively small amount of auxiliary fuel injected. But ignition was always released by the injected fuel. In fact, without the injection of a *liquid* jet the gaseous main fuel would not ignite at all, except at a very high compression ratio.

Most recently Arnold et al[6] used fumigation of high ignition quality fuels to help burn low ignition quality fuels which without fumigation would burn only sluggishly or not at all. Their work partly overlapped our work and constitutes a confirmation of the results to be presented in this paper.

Previous investigators used injection nozzles or carburetors to introduce the supplementary fuel into the intake air. Such devices give rather coarse sprays with a mean drop size of 20 microns or more. The present investigation employed an apparatus (Micro-Fog) which produces a very fine mist consisting of droplets under 4 microns. This gave amazingly good results. The investigation was subsequently extended to cover a variety of auxiliary fuels and several methods of introduction. The properties of the fuels used are listed in Table 1.

Tests

Most tests were performed on a single-cylinder CFR cetane test engine and some on a single-cylinder Petter AVA-1 diesel engine. The CFR engine

[1] "Manifold Introduction of Hydrocarbons as an Aid for Starting," by C. W. Van Overbeke. Thesis, The Pennsylvania State University, August, 1942.
[2] SAE *Journal*, Vol. 60, June, 1952, p. 42: "Power Booster Fuels for Diesel Engines," by E. J. McLaughlin, P. L. Pinotti, and H. W. Sigworth.
[3] Proceedings of Institution of Mechanical Engineers, Vol. 168, No. 9, 1954, pp. 280–286: "Effect of Auxiliary Fuels on Smoke-Limited Power Output of Diesel Engines," by L. D. Derry, E. M. Dodds, E. B. Evans, and D. Royle.
[4] Proceedings of Institution of Mechanical Engineers, Vol. 168, No. 9, 1954, pp. 265–270: "Experimental Investigation into Effect of Fuel Addition to Intake Air on Performance of Compression-Ignition Engine," by W. T. Lyn.
[5] *Automobile Engineer*, Vol. 44, June, 1954, pp. 256–262: "Alcohol in Diesel Engines," by H. A. Havemann, M. R. K. Rao, A. Natarjan, and T. L. Narasimhan.
[6] SAE Transactions, Vol. 66, 1958, pp. 54–64: "Bi-Fuel Approach to Burning Residual Fuels in Diesel Engines," by W. C. Arnold, R. H. Beadle, R. L. Logelin, and H. D. Young.

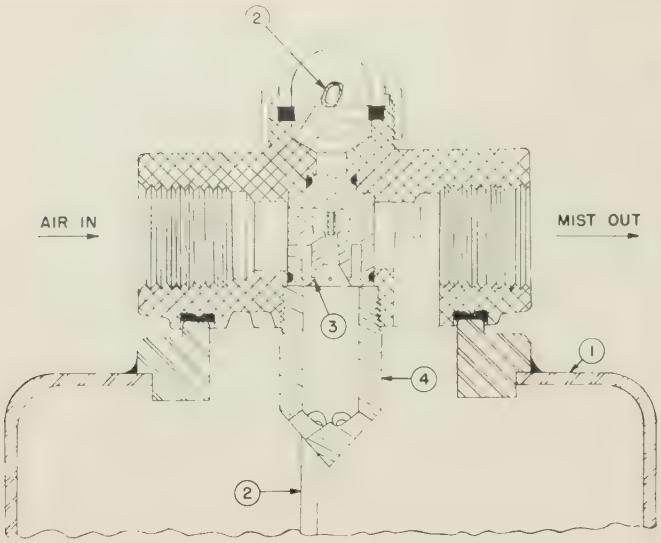

1. FUEL TANK
2. FUEL RISER
3. ATOMIZER HOLES (4)
4. DIFFUSION PLUG

Fig. 1—Cross-section of Norgen Micro-Fog

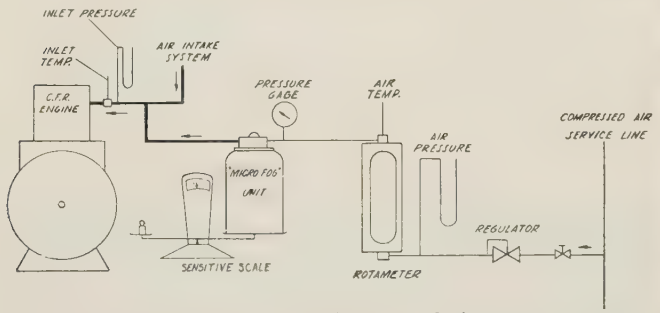

Fig. 2—Micro-Fog supplementary fuel system

Fig. 3—Micro-Fog installation on CFR engine

had a Ricardo Comet type swirl-chamber head and a fixed compression ratio of 17/1, the Petter engine was of the open-chamber type with a compression ratio of 16.5/1 and aircooled. The standard operating conditions of the two engines are listed in Tables 2 and 3.

Supplementary fuel was introduced by four different methods: mist generator, commercial pneumatic spray nozzle, carburetor, and vaporizer The mist generator was an experimental model of the commercial Micro-Fog lubricator made by C. A. Norgren Co., a cross-section of which is shown in Fig. 1. In operation, liquid passes through air jets issuing from four atomizer holes. The atomized liquid is then carried by the air through a series of separator passages where the heavier droplets are removed. The remaining mist is then conveyed by the air stream with controlled pressure into the manifold. This mist (drop sizes all under 4 microns) is so fine that it does not wet the hand or a glass surface held in front of it.

The pneumatic atomizing nozzle used in the test program was made by Spraying Systems Co. The fuel rate was controlled by means of a needle valve feeding to a constant head fuel reservoir. Air at pressures ranging from 10–15 psi passed through an annulus around the fuel nozzle and impinged upon the fuel, thus atomizing it. Airflow requirements were less than 1/40 that of the Micro-Fog, but the mass median droplet size was 59.5 microns, a rather coarse spray.

The carburetor was adapted from a Briggs and Stratton 2½-hp engine carburetor. It consisted of a venturi, metering orifice, and a constant head fuel reservoir. Fuel was introduced into the fuel reservoir from a fuel tank by a needle valve controlling the supplementary fuel rate. The carburetor was mounted in a bypass of the primary air-supply line. In operation, a constant percentage of the engine air requirement passed through the carburetor. The atomized fuel, carried by this bypassed air, joined the primary air supply and was admitted to the engine. To ensure adequate airflow through the carburetor, throttling of the primary air line was necessary.

The vaporizer consisted of a metal container through which all the air to the engine was fed. The bottom of the container was electrically heated above the boiling point of the supplementary fuel so that the fuel would flash immediately into vapor upon hitting it. The fuel was fed to the vaporizer from a gravity feed tank and controlled by a needle valve. This resulted in high intake air temperatures (depending upon the supplementary fuel used).

Instrumentation included: strain gage type and

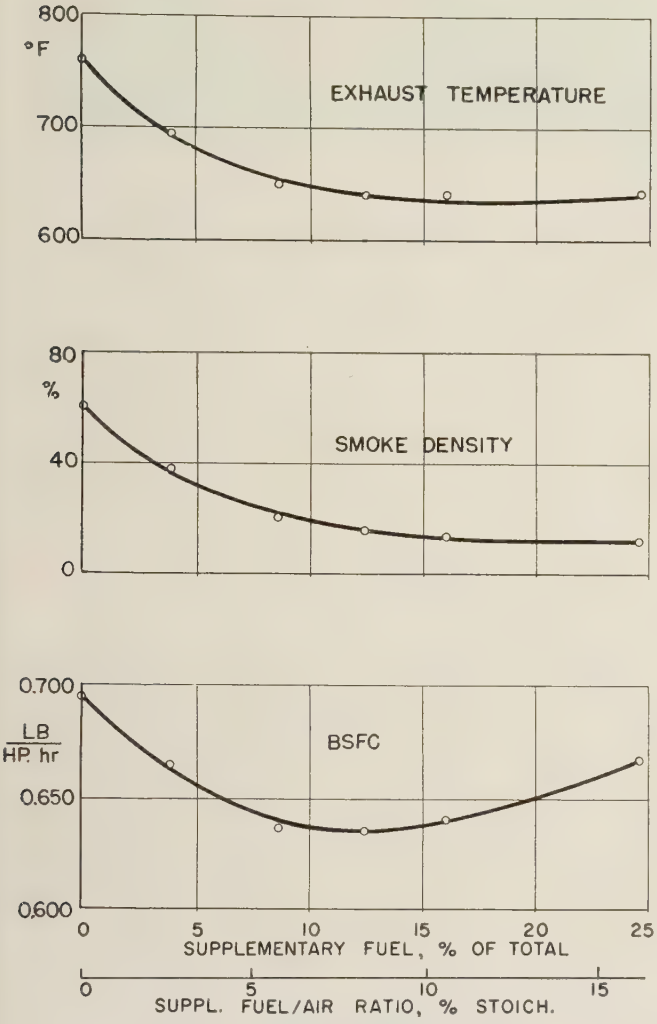

Fig. 4—Effect of fumigation on diesel engine performance. Conditions: constant brake load, bmep = 57.7 psi, both fuels—44 cetane number diesel fuel, supplementary fuel introduced by Micro-Fog, CFR engine, 900 rpm, injection begins 13-deg btdc

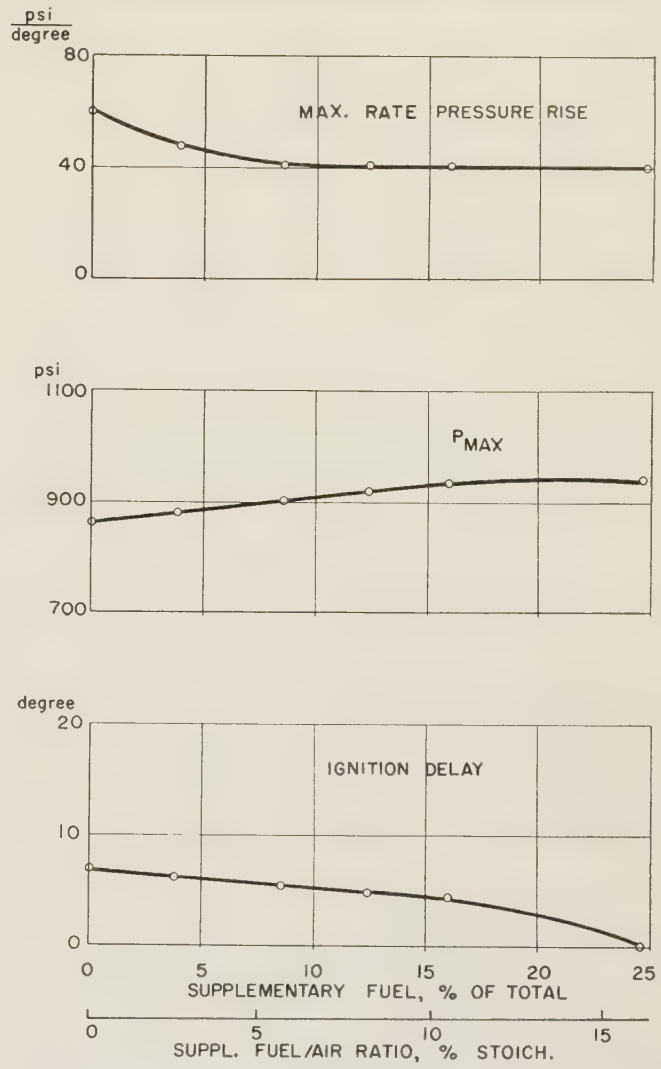

Fig. 5—Fumigation cuts ignition lag and rate of pressure rise. Conditions same as Fig. 4

piezo-electric pressure pickups and oscilloscope with camera to record pressure-time traces, stroboscopic timer, flowraters to measure primary and supplementary airflow, electric air heater, exhaust gas and inlet air thermocouples, CRC and Von Brand smokemeters, and General Radio noise-level meter.

The majority of the tests were conducted with either the exhaust-smoke density or the brake load held constant. Figs. 2 and 3 show the arrangement with the CFR engine and Micro-Fog.

Normal Fuels

Results of constant brake load tests are shown in Figs. 4 and 5. A good-grade 44 cetane number diesel fuel was used for both the primary and supplementary fuels. Micro-Fog was used to introduce the supplementary fuel. It can be seen from Fig. 4 that the addition of the supplementary fuel caused a reduction in smoke density from 60% (full-load starting point) to 12%. A significant decrease in the fuel consumption (8.6% at 11% supplementary fuel) was also noted with a marked decrease in exhaust-gas temperature. Fig. 5 shows that the ignition lag drops to zero at 24% supplementary

Table 2—CFR Standard Engine Conditions

3¼-in. bore, 4½-in. stroke, 900 rpm, 17/1 compression ratio
Lubricating Oil: SAE 30
Lubricating Oil Temperature: 135 ± 1 F
Lubricating Oil Pressure: 25–40 psig, depending upon speed
Water-Jacket Temperature: 210 ± 1 F
Injection Angles: 6 deg btdc for 600 rpm
7 to 13 deg btdc for 900 rpm, depending upon the test
15 deg btdc for 1200 rpm
Inlet Air Temperature: 100 ± 2 F[a]
Inlet Air Pressure: Atmospheric ± 0.3 in. of Hg[b]
Exhaust-Gas Pressure: 1 ± 0.5 in. of H_2O

[a] Inlet air temperature was above 100 F in the tests run with the vaporizer unit, and the actual value for the temperature depended on the fuel used and the rate of introduction.
[b] A series of tests were run under supercharged conditions in which the inlet pressure was maintained at 5 in. of Hg gage.

Table 3—Petter AVA1 Standard Engine Conditions

3.15-in. bore, 4.33-in. stroke, 1200 rpm, 16.5/1 compression ratio
Lubricating Oil: SAE 30[a]
Injection Angles: Not adjustable
24-deg btc up to 1500 rpm
28-deg btc 1500–1800 rpm
Inlet Air Temperature: Room temperature
Inlet Air Pressure: Atmospheric – 0.6 in. of H_2O at 900 rpm
– 0.9 in. of H_2O at 1200 rpm

[a] SAE 10 lubricating oil was used for the nonfiring tests.

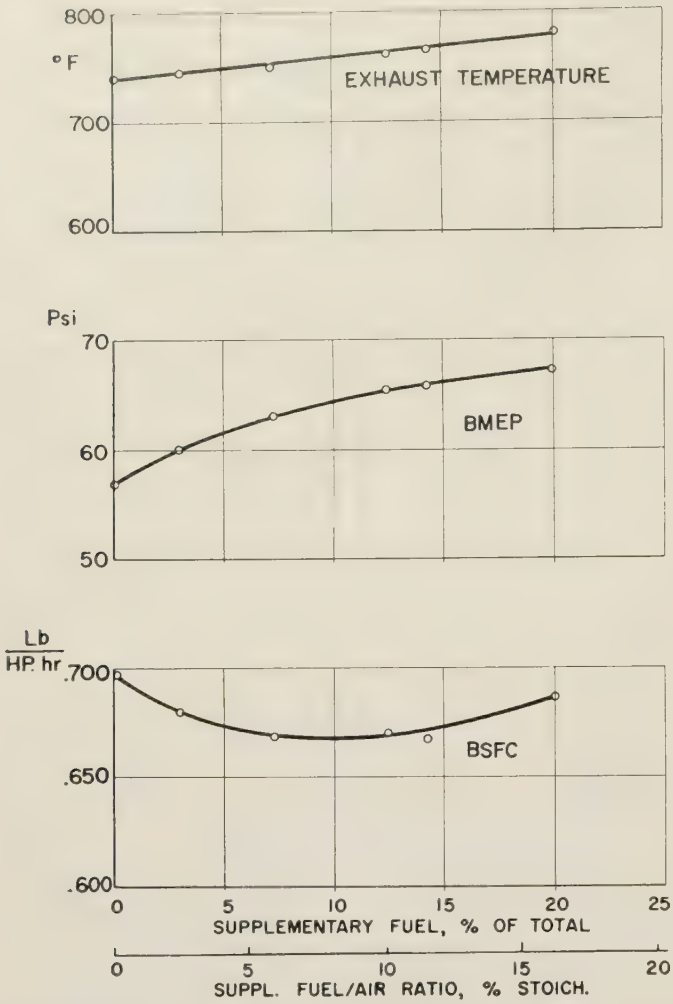

Fig. 6—Fumigation boosts power and improves fuel consumption. Conditions: constant smoke density (60%), both fuels—44 cetane number diesel fuel, supplementary fuel introduced by Micro-Fog, CFR engine, 900 rpm, injection begins 13 deg btdc

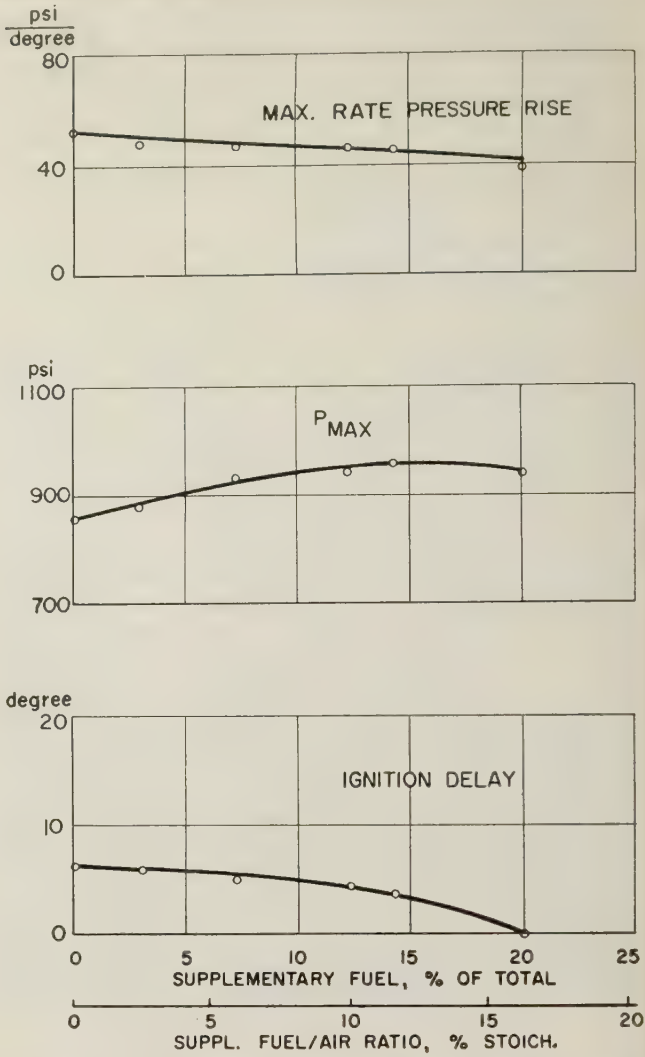

Fig. 7—Other effects of fumigation at constant smoke density. Conditions same as Fig. 6

fuel rate. Then preignition occurs. Smoother, quieter operation was obtained due to the lower rate of pressure rise although the maximum pressure increased.

Figs. 6 and 7 portray results when the smoke density was kept constant at 60% CRC smokemeter reading, which is barely visible exhaust. The bmep was found to increase about 18.6% when 20% of the total fuel was supplied with the intake air. The fuel consumption was found to decrease only about 4.3% when approximately 10% of the fuel was fumigated.

Firing pressures and rates of pressure rise change as before, ignition delay becomes zero at 20% supplementary fuel rate. An indicator diagram picturing this condition and one without fumigation are shown on Fig. 8.

Fig. 9 shows superimposed pressure diagrams. The higher compression pressure of the fumigated engine over the standard engine indicates the presence of exothermic preflame reactions. It shortens the ignition lag and decreases the maximum rate of pressure rise.

The tests illustrated in Figs. 4–9 were performed with an injection advance of 13-deg btdc which was the optimum injection angle for an unfumigated engine. From the pressure traces, it appeared that later injection would further improve the engine performance.

Tests with variable injection angle have indeed shown that specific fuel consumption decreased with retarding injection and optimum was reached at 7-deg advance. The specific fuel consumption was then 9.8% better with 14.5% fumigation than with no fumigation.

In a conventional engine, a slight advance of injection usually makes the engine rougher but improves the fuel consumption; however, in a fumigated engine it is the opposite effect:

Injection Advance		13 deg	7 deg
Bsfc, lb per bhp-hr	No Fumigation	0.635	0.655
	10½% Fumigation	0.624	0.591

The smoke density was kept constant at 60% dur-

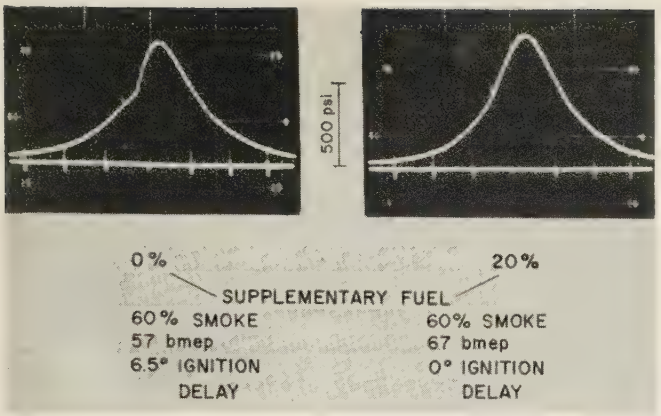

Fig. 8—Cylinder pressure diagrams with and without fumigation (base pips every 20-deg crank angle, trace pip marks actual injection)

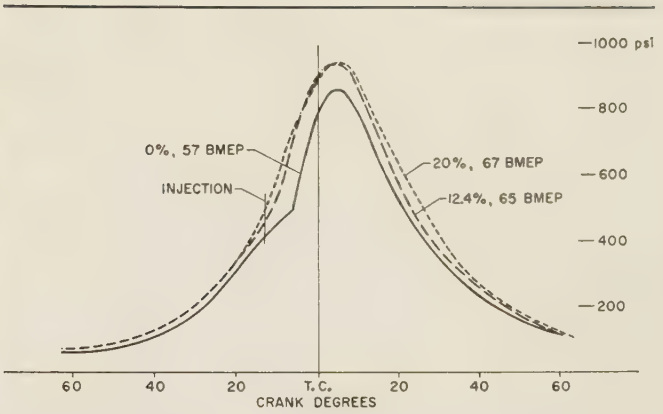

Fig. 9—Pressure diagrams at constant smoke density. Conditions: both fuels—44 cetane number diesel fuel, supplementary fuel introduced by Micro-Fog, CFR engine, 900 rpm, 13 deg btdc injection angle (numbers mark percentage of total fuel introduced through intake air)

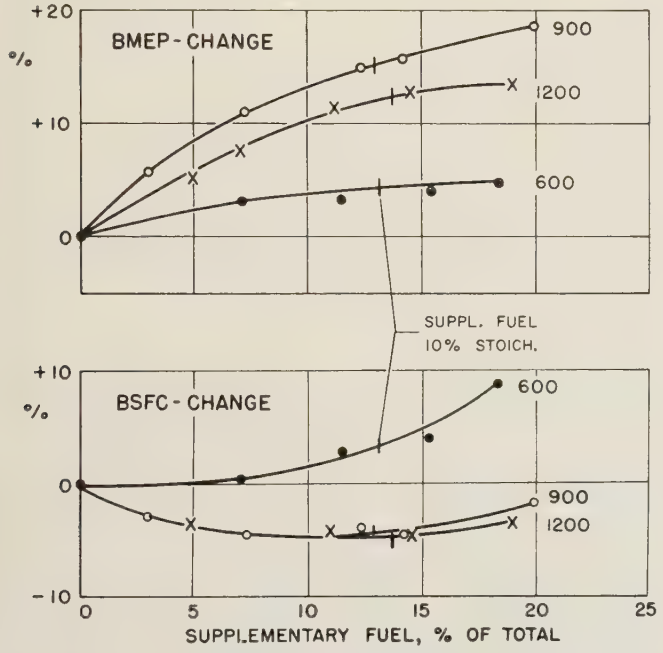

Fig. 10—Effect of speed on supplementary fuel addition at constant smoke density (60%). Conditions: CFR engine, both fuels—44 cetane number diesel fuel supplementary fuel introduced by Micro-Fog, injection angles—6 deg btdc at 600 rpm, 13 deg btdc at 900 rpm, and 15 deg btdc at 1200 rpm

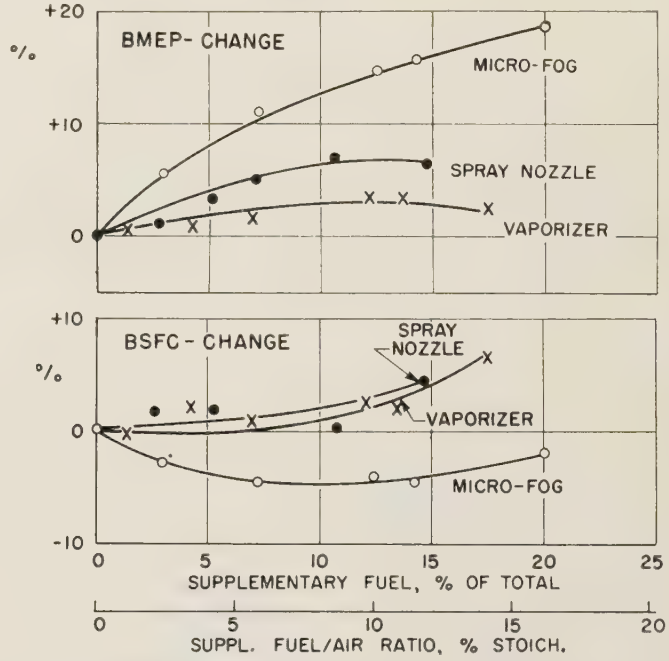

Fig. 11—Method of introduction at constant smoke density (60%). Conditions: both fuels—44 cetane number diesel fuel, CFR engine, 900 rpm

ing these tests.

In Fig. 10 test results with 600, 900, and 1200 rpm are shown at constant brake load. At higher speed the gain is higher.

The test results of three methods of introduction of the supplementary fuel are shown in Fig. 11. Performance in these constant smoke tests was improved by any one of the three methods, but the largest improvement was achieved using the mist generator. The vaporizer unit was penalized by the higher inlet air temperature necessary to operate the unit (250 F compared to 100 F). This was inherent in the operation of the vaporizer as the plate used to vaporize the fuel also heated the inlet air. To avoid separation of the fuel from the air stream, no provisions were made to cool the inlet air prior to induction.

Fig. 12 shows superimposed indicator diagrams of

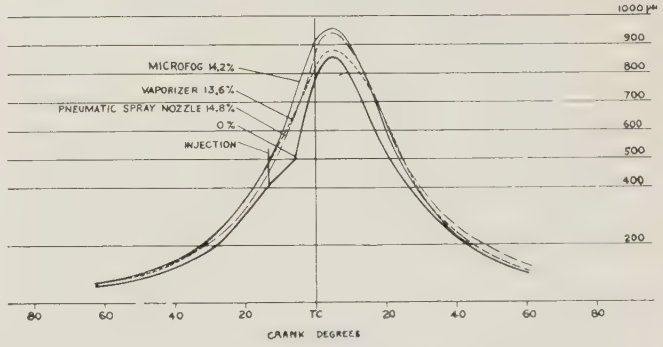

Fig. 12—Pressure diagrams with three different methods of introduction of supplementary fuel at constant smoke density (60%). Conditions: both fuels—44 cetane number diesel fuel, CFR engine, 900 rpm 13-deg btdc injection angle (numbers mark percentage of total fuel introduced through intake air)

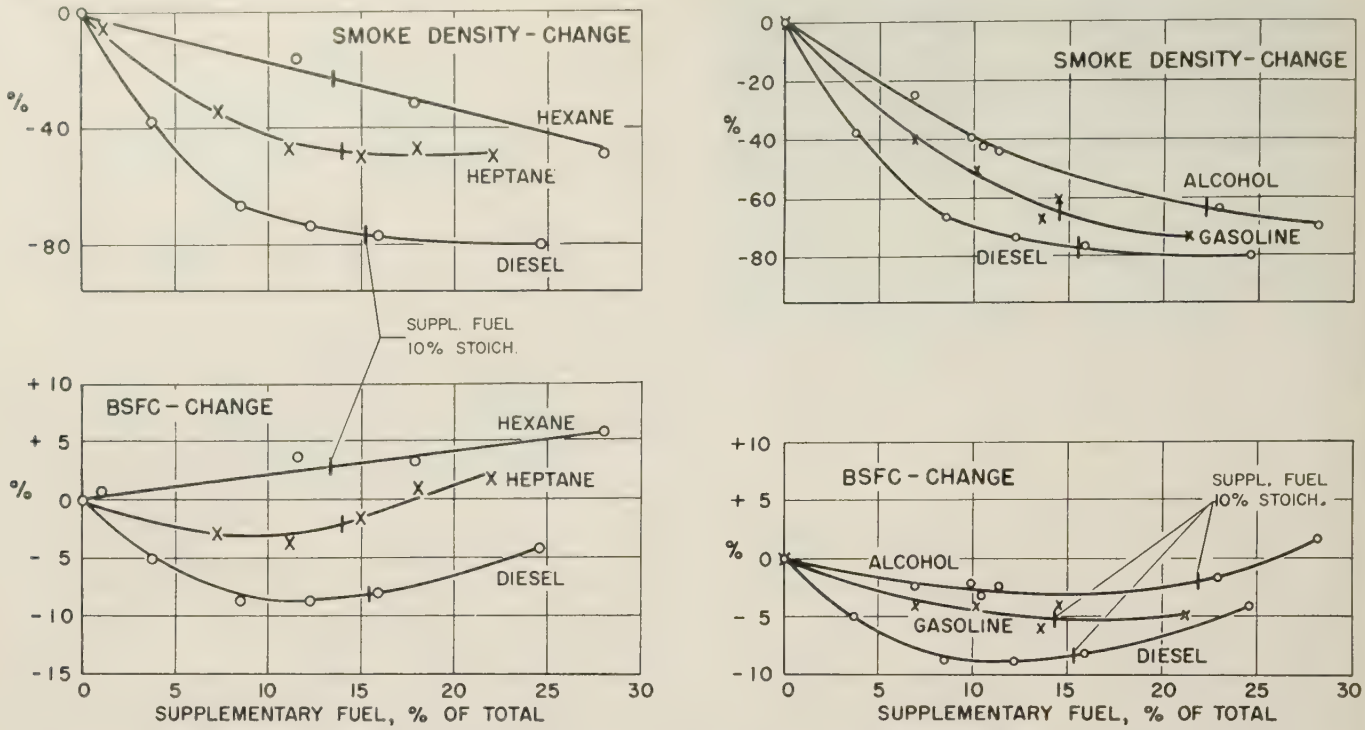

Fig. 13—Effect of various supplementary fuels on engine performance at constant brake load. Conditions: constant brake load, bmep = 57.7 psi, primary fuel—44 cetane number diesel fuel, supplementary fuels introduced by Micro-Fog, 900 rpm

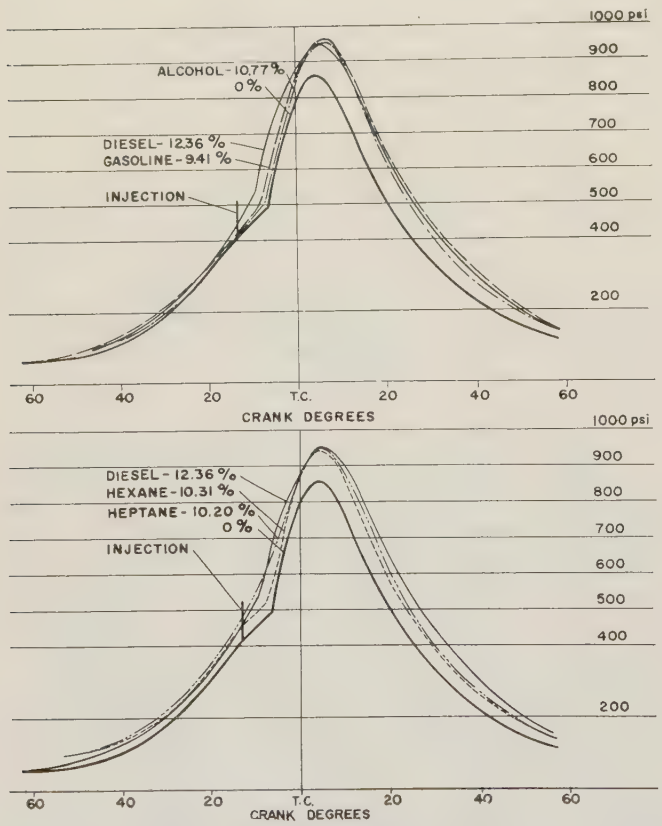

Fig. 14—Five supplementary fuels introduced by Micro-Fog, constant smoke density (60%). Conditions: primary fuel—44 centane number diesel fuel, 900 rpm, 13-deg btdc injection angle (numbers mark percentage of total fuel introduced through intake air by Micro-Fog

unfumigated and fumigated cycles with the three different methods of fumigation. It will be noted that for the greater part of the compression stroke the pressure increase caused by the vaporizer and Micro-Fog are practically equal but the Micro-Fog becomes more effective during ignition and combustion. The pneumatic spray nozzle trails the pressure increase produced by the vaporizer before ignition but exceeds it after ignition.

Tests were run using three introduction methods and five different supplementary fuels (n-heptane, n-hexane, alcohol, gasoline, and diesel fuel) in combination with various primary fuels. The mist generator gave the best results when fumigating diesel fuel. As more volatile supplementary fuels are used, the method of introduction becomes less critical. Fig. 13 shows the results of a series of constant brake load tests using the five different supplementary fuels introduced by the mist generator while injecting a high-grade diesel fuel. The fumigation of diesel fuel brought the greatest improvement.

This is equally true if the tests are run at the maximum load corresponding to 60% smoke (CRC). Fig. 14 shows superimposed indicator diagrams for the five supplementary fuels.

Tests on the Petter AVA1 engine were conducted to determine the effect of fumigation in an open-chamber diesel engine. A pneumatic spray nozzle was used. The engine had a constant geometric injection timing of 24-deg btdc. It was found that engine performance with neat 52 cetane number fuel leaves little room for improvement. Constant heavy load tests (Fig. 15) gave smoke density and fuel consumption reductions of 33 and 4% respectively. With a low-cetane (31 cetane number) injected

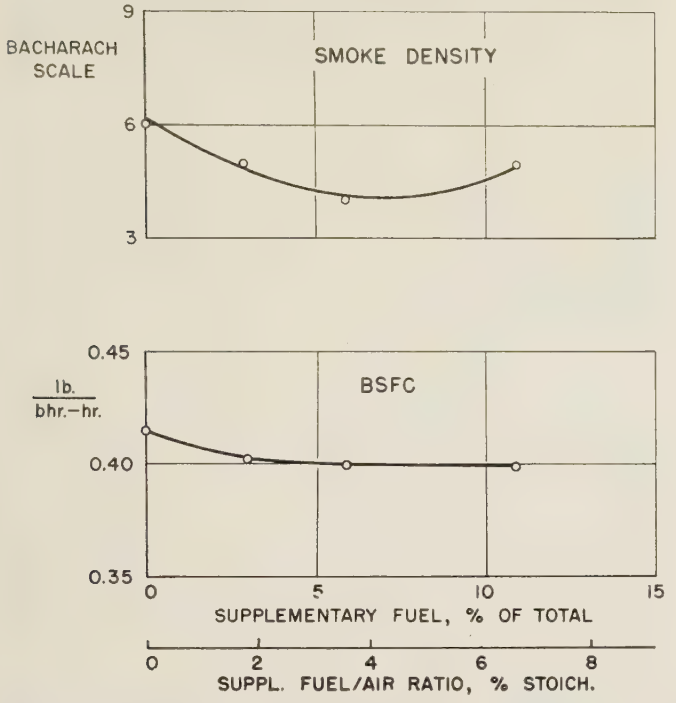

Fig. 15—Fumigation of high-cetane diesel fuel. Conditions: constant brake load, bmep = 97 psi, both fuels—52 cetane number diesel fuel, supplementary fuel introduced by spray nozzle, Petter AVA1 engine, 1200 rpm, 24-deg btdc injection angle

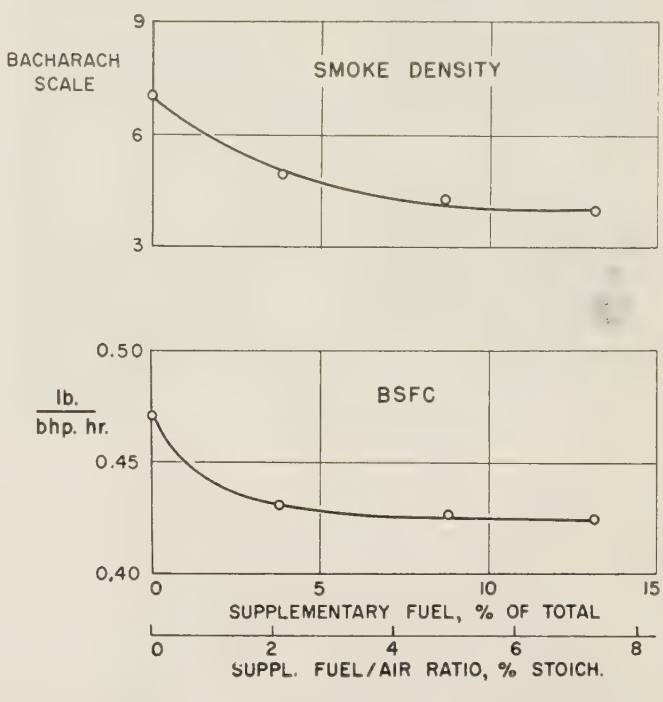

Fig. 16—Fumigation of low-cetane diesel fuel. Conditions: constant brake load, bmep = 86 psi, both fuels—31 cetane number diesel fuel, supplementary fuel introduced by spray nozzle, Petter AVA1 engine, 1200 rpm, 24-deg btdc injection angle

fuel, the engine showed a greater reduction in smoke and fuel consumption (43 and 10% respectively). (See Fig. 16.)

Supercharge Tests

The previous tests were run with 0-in. gage pressure in the inlet manifold. By using shop air the inlet manifold pressure was raised to 5 in. of Hg gage and under those conditions indicator diagrams such as shown in Fig. 17 were obtained. The corresponding bmep and brake specific fuel consumption (bsfc) values are marked on the curve and show that with supercharge the optimum amount of fumigation is less than with natural aspiration. The optimum was actually obtained with 8.7%, when the bmep was 89.2 psi, and the bsfc 0.581 lb per bhp-hr, an improvement of 9.4 and 5.4% respectively.

Substandard Fuels

The reason for the unsatisfactory combustion of low-cetane fuels in a diesel engine is their long ignition lag. Since fumigation shortens the ignition lag, it was to be expected that it would facilitate the combustion of low-cetane fuels.

A 90-octane gasoline (mixture of 90 % isooctane and 10% n-heptane) was tried first. Without fumigation the engine refused to run at low load and was erratic at high load. With Micro-Fog fumigation of approximately 20% of the same fuel the engine ran steadily. Smoother operation was obtained, however, by the fumigation of 12% of 44-cetane diesel fuel which cut the ignition lag from 20 to 10 crank-angle deg and the rate of pressure rise from 90 to 20 psi per deg. The injection advance was 9-deg btdc in these tests. Even so, the operation was far from

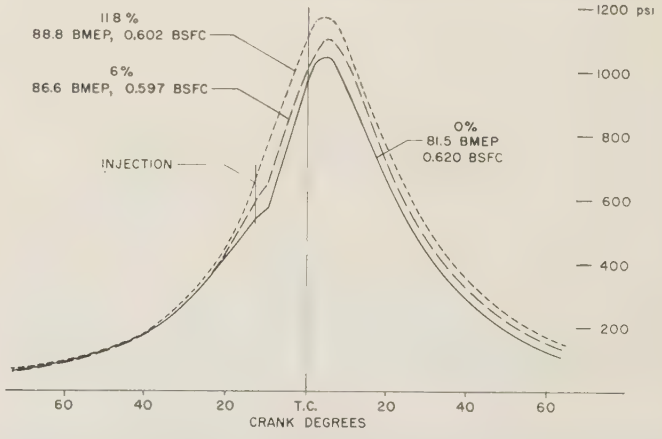

Fig. 17—Pressure diagrams of supercharged engine at constant smoke density (60%). Conditions: both fuels—44 cetane number diesel fuel, supplementary fuel introduced by Micro-Fog, CFR engine, 900 rpm, 13-deg btdc injection angle, inlet manifold pressure—5 in. of Hg, (numbers mark percentage of total fuel introduced through intake air)

ideal and the fuel consumption excessive (0.73 lb per bhp-hr).

The next primary fuel tested was a JP-5 fuel of 23 cetane number. Without fumigation operation was unsatisfactory at light load and impossible at idle. When straight amyl nitrate was used as supplementary fuel introduced by a carburetor at a rate of approximately 1/800 lb per pound of air, there was improvement (Fig. 18). Steady and smooth operation was obtained down to idle, although the fuel consumption was high. N-propyl nitrate and isopropyl nitrate gave similarly favorable results.

A constant amount of isopropyl nitrate carburet-

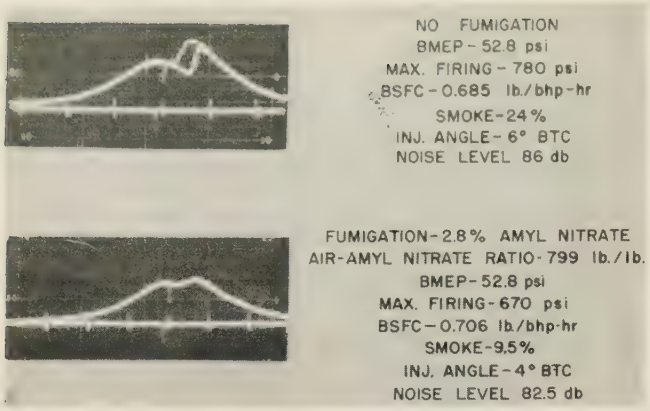

Fig. 18—Combustion of jet engine fuel JP-5 (23 cetane number) improved by fumigation of amyl nitrate through carburetor. Conditions: CFR engine, 900 rpm

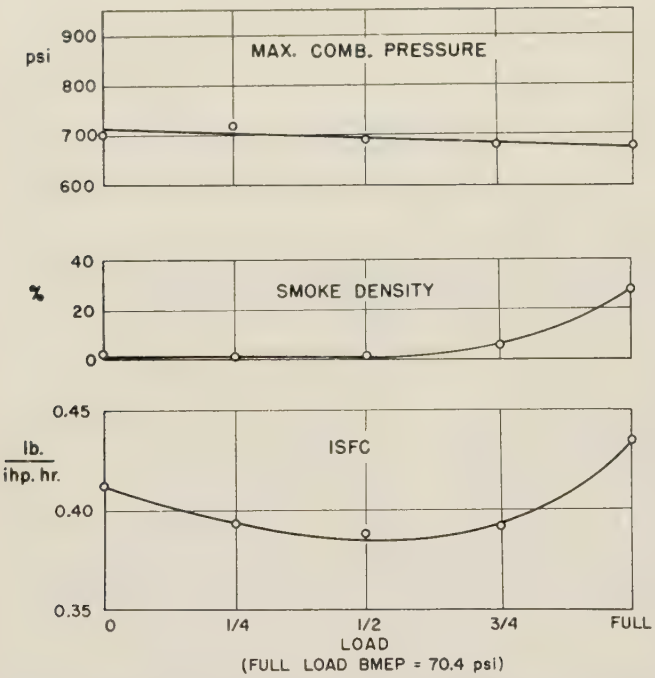

Fig. 19—Fumigation of isopropyl nitrate, low-cetane main fuel. Conditions: primary fuel—23 cetane number diesel fuel, supplementary fuel—isopropyl nitrate, carbureted at constant air/isopropyl nitrate ratio of 587/1 lb per lb, CFR engine, 900 rpm, injection begins as indicated

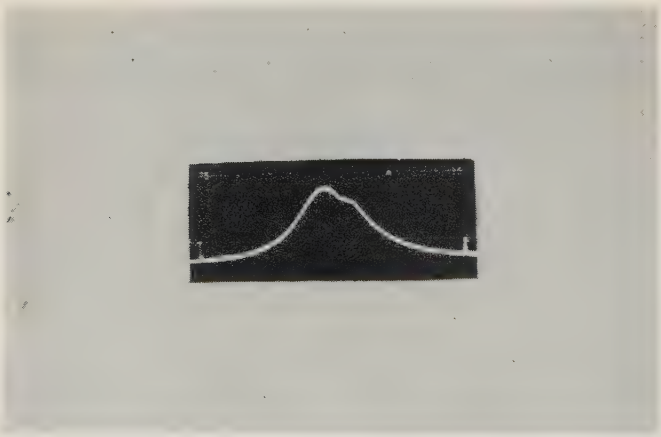

Fig. 20—Light-load cylinder pressure diagram with injection of 29 cetane number fuel. Conditions: Supplementary fuel—52 cetane number diesel fuel and 2.5% amyl nitrate, 22.6% of total fuel introduced by spray nozzle, Petter engine, 1200 rpm, bmep = 15.5 psi, no smoke

ted into the intake manifold gave the results shown in Fig. 19 with JP-5 primary fuel in the CFR engine.[7] Even alpha-methyl naphthalene (0 cetane number) could be burned with this scheme. High-cetane diesel fuel introduced by a pneumatic spray nozzle gave similarly good results.

Low-load operation with low-cetane fuel was still more difficult with the Petter engine. However, the engine could be made to operate satisfactorily on low-cetane injected fuel if the proper fuel was fumigated. Tests revealed that the type of the fumigated fuel had a marked effect on the engine operation; also, the higher the cetane number of the supplementary fuel, the smaller the amount required for acceptable performance. Table 4 shows the minimum rates of supplementary fuel for several different types required to obtain steady combustion when running on 29 cetane number fuel. Excessive amounts (upwards to 50%) of *low-cetane* supplementary fuel were required to achieve stable operation, and even then the performance was relatively poor.

Fig. 20 shows the indicator diagram of the lightly loaded (15.5 bmep) Petter engine running on 29 cetane number fuel and fumigated with 52 cetane number fuel doped with 2.5% amyl nitrate at the rate of 0.23 lb per hr.

It was envisioned that the addition of low-viscosity supplementary fuel to the engine would result in poor lubrication of the cylinder walls by the action of the supplementary fuel washing the lubricant off the rubbing parts. Because of this, piston blowby was watched continuously and an accurate record kept of the engine wear. The CFR engine has been run, using supplementary fuel, approximately 375 hr between overhauls. The blowby did not increase appreciably during the course of the test program, indicating that the rings were operating properly. Measurements of the rings, cylinder, and piston made during the overhaul period revealed no abnormal wear.

How Does Fumigation Work?

It was shown that fumigation of ordinary diesel fuel in an amount of approximately 15% of the total had the effect of increased smoke-limited power output and increased thermal efficiency. Fumigation can be imagined to help diesel combustion in two ways: Better air utilization due to premixing and more complete combustion due to the chemical effect of fumigation. Of the earlier investigators, McLaughlin, Derry, and Havemann, and their coworkers attributed the improvements mainly to better air utilization, while Lyn emphasized the beneficial effects of preflame reactions on diesel combustion.

To analyze the factors contributing to improved engine performance on supplementary fuel and to determine the relative effect of each, Fig. 21 was prepared using the data from a constant smoke test in which both the fuel and air rates were measured. The increase in bmep may have resulted from: (1) the ability of the engine to burn more pounds of fuel per pound of air for the same degree of smoke density (better air utilization); (2) an increase in the

[7] Total fuel consumption was plotted and the lower heating value of isopropyl nitrate disregarded.

thermal efficiency of the engine resulting from decreased ignition lag and faster combustion; and (3) a combination of both. It certainly was not caused by the supercharging effect of the fumigation air because pressure and temperature were strictly kept at their standard values (atmospheric ± 0.3 in. of Hg, 100 ± 2 F) during these tests except when using a vaporizer.

The power increase due to improved air utilization can be estimated on the assumption that the fumigated fuel is perfectly mixed with the air before combustion.

With an excess air factor of λ and a stoichiometric air-fuel ratio of 14.5 the theoretical bmep of the engine is:[8]

$$\text{bmep} = 180 \frac{\text{Brake thermal efficiency}}{0.325} \cdot \frac{\text{Volumetric efficiency}}{\lambda} \quad (1)$$

With $x\%$ fuel fumigated that portion of the fuel needs no excess air ($\lambda = 1$), therefore, the increased bmep will be:

$$\text{bmep}' = (1-x)\,180 \frac{\text{Brake thermal efficiency}}{0.325} \cdot \frac{\text{Volumetric efficiency}}{\lambda} + x \cdot 180 \cdot \frac{\text{Brake thermal efficiency}}{0.325} \cdot \frac{\text{Volumetric efficiency}}{1} \quad (2)$$

The relative boost figures from this:

$$\frac{\text{bmep}' - \text{bmep}}{\text{bmep}} = x(\lambda - 1) \quad (3)$$

Under standard conditions the bmep was 56.8, the brake thermal efficiency was 0.1856, the volumetric efficiency 0.85, the excess air factor 1.54; therefore, the relative boost would be $0.54x$ or roughly one half of the percent of the fuel fumigated.

The bmep plot shows two curves, one the experimental curve and the other computed using a constant brake thermal efficiency. From this it can be seen that both factors contribute to the improved performance.

In general, it is correct to say that if the power boost would come from better air utilization alone, it would amount to less than the percentage of fumigated fuel, while actually the power increase was generally greater than the percentage of fumigated fuel. Improved combustion efficiency must obviously have played its part. This becomes obvious by noting the great differences between the effects of fumigation fuels of different chemical composition.

Preflame reactions can improve combustion in at least two ways: First, by shortening the ignition lag; second, by helping combustion after ignition has set in.

Fig. 22 shows the ignition lag by fumigating with Micro-Fog and with a vaporizer increasing amounts of supplementary fuel (alcohol, 90-octane gasoline, hexane, heptane, and 44-cetane diesel fuel). It will be noted that the effect of alcohol and high-octane gasoline on the ignition lag is almost zero, while that of hexane, heptane, and diesel fuel is very pronounced. But the effect on performance was not in that order. As seen from Fig. 13, hexane reduced the smoke the least amount and actually increased the fuel consumption. Alcohol and high-octane gasoline were, on the other hand, far from without effect on combustion. They must then act through a mechanism other than shortening the ignition lag.

The manifold-introduced fuel obviously exerts an influence on combustion in several ways. First, during the relatively long period of compression it is subject to slow oxidation which, being an exothermic process, must raise the pressure and temperature of the cylinder charge more than if pure air were compressed. For this to happen, the hydrocarbon and oxygen molecules must be in contact, which can effectively take place only if the hydrocarbon is in gaseous state. Volatile fuels could be expected to excel in this effect. In this process of slow oxidation,

Table 4—Minimum Rates of Supplementary Fuels for Stable Operation on 29 Cetane Number Main Fuel

Supplementary Fuel	Minimum Rate (approximate, %)
Neat 52 cetane fuel	25
97.5% 52 cetane and 2.5% amyl nitrate	23
95% 52 cetane and 5% amyl nitrate	18
90% 52 cetane and 10% amyl nitrate	14

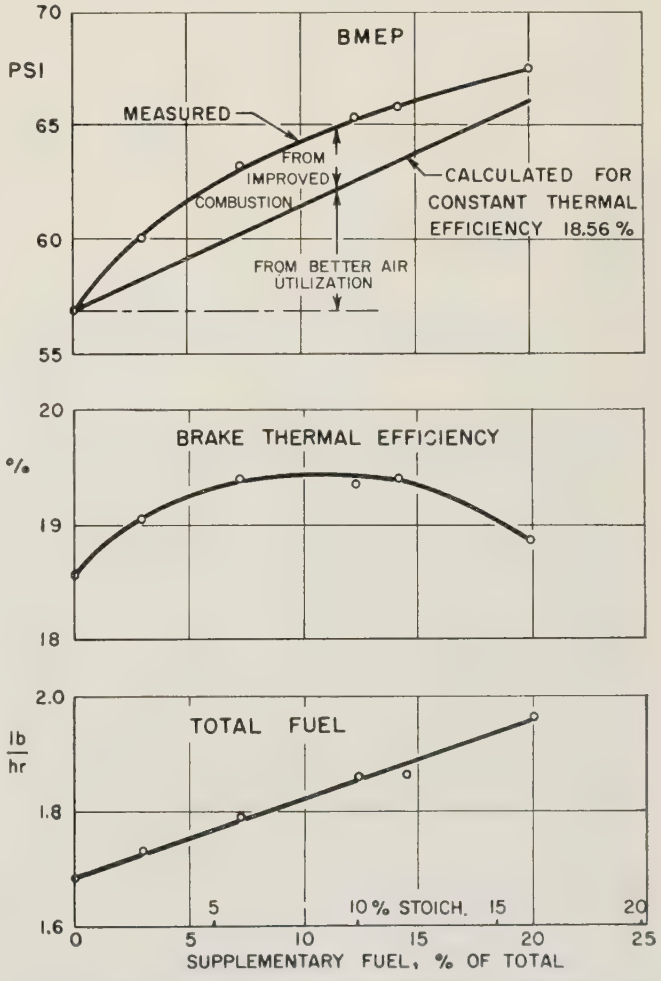

Fig. 21—Source of power increase with fumigation. Combustion analysis at constant smoke density (60%). Conditions: both fuels—44 cetane number diesel fuel, supplementary fuel introduced by Micro-Fog, CFR engine, 900 rpm, 13-deg btdc injection angle

[8] ASME Transactions, Vol. 63, No. 3, April, 1943: "Excess Air and Brake Mean Effective Pressure," by P. H. Schweitzer.

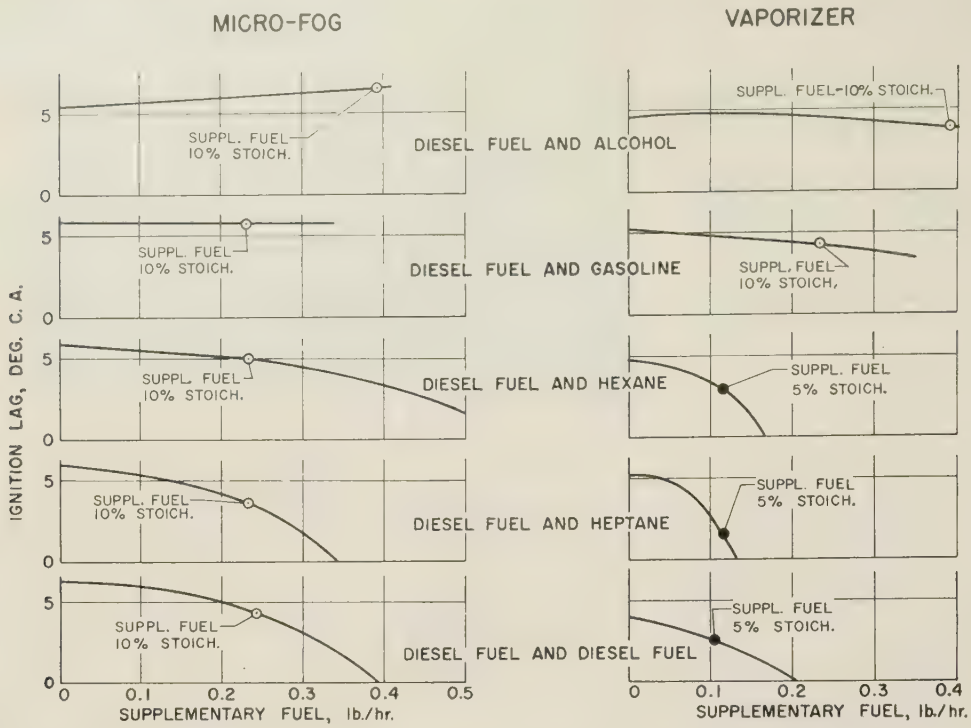

Fig. 22—Ignition lag versus rate of supplementary fuel at constant smoke (60%). Conditions: CFR engine, 900 rpm

Table 5—Nonfiring Test Results, with CFR Engine and Micro-Fog

	Fuel-Air Ratio, lb per lb[a]	Stoichiometric, %	Imep, psi	Exhaust Temperature, F	Maximum Cylinder Pressure, psi
Air Alone	0	0	0	120	520
Ethyl Alcohol	0.01197	10.8	0.8	120	520
90-Octane Primary Fuel Blend	0.00938	14.2	1.7	127	525
44-Cetane Diesel Fuel	0.01072	15.5	7.6	137	565
N-Heptane	0.00863	13.1	6.4	150	570
N-Hexane	0.01129	17.2	22.0	185	640

[a] No main injection, fuel introduced by Micro-Fog, 900 rpm, 100 F inlet air temperature, 0 in. of Hg gage inlet air pressure.

however, few if any of the carbon molecules combine directly with O_2 molecules into CO_2 or the H_2 molecules with oxygen molecules into H_2O. Rather, most go through intermediate combustion products such as peroxides and aldehydes. The heat generated in such reactions is less but these intermediate combustion products react more rapidly with oxygen than the original hydrocarbon.

Slow oxidation may, therefore, shorten the chemical as well the physical portion of the ignition lag.

Parallel to this oxidation process another process is going on—that of pyrolysis or thermal decomposition, commonly called cracking. Under the influence of heat and pressure the hydrocarbon molecule breaks up into smaller simpler molecules. This process is endothermic. It takes 80 kcal per mole to break a C—C bond, 100 to break a C—H bond, 150 to break a double bond C=C, and 200 to break a triple bond C≡C. For this reason, such thermal decomposition may never take place if conditions of easy oxidation are present. Thermal decomposition can, however, take place in the absence of oxygen. The hydrocarbon need not be vaporized to crack.

Thermal cracking has been identified [9, 10] as being responsible for soot deposits and exhaust smoke. But from the standpoint of ignition quality, hydrocarbons which crack easily (long-chain paraffins) are the best diesel fuels and those which crack hard (ring-chain aromatics) are the worst. No matter how undesirable cracking is after ignition, it probably is very helpful, perhaps essential, before ignition. R. O. King[11] has put forth the theory that ignition generally is initiated by solid nuclei like carbon flakes. If the combustion air is free from such nuclei, a thermal decomposition of the fuel is needed to produce such carbon particles that can act as nuclei to initiate combustion.

If the influence of fumigation on combustion is through early oxidation, the volatile fuels of few carbon atoms should be best. If the effect is by speeding up ignition through thermal decomposition, the high-cetane fuels containing many carbon atoms should be best. Fumigation could easily open a little peephole into the mystery of combustion.

Nonfiring Tests

In order to gain better insight into the mechanism of preflame reactions, tests were conducted with a nonfiring engine. Injection was completely eliminated. Introduction of fuel into a motored CFR engine (900 rpm) took place only into the intake manifold.

With some fuels autoignition occurred when the fumigated amount exceeded a certain quantity,

[9] SAE Transactions, Vol. 64, 1956, pp. 250–272: "Evaluation of Reaction Kinetics Eliminates Diesel Knock—The M-Combustion System of MAN," by J. S. Meurer.

[10] *Automotive Industries*, Vol. 114, June 15, 1956, pp. 66–67: "New Concept of Diesel Combustion," by P. H. Schweitzer.

[11] *Canadian Journal of Research*, November, 1947; January, February, May, June, September, and October, 1948; April, September, and November, 1949; May, June, and August, 1950; January, 1951; February–March and September, 1952; January and May, 1954; pp. 220–241, 1954; pp. 335–347, 388–407, and 445–469, 1955; pp. 10–20 and 316–334, 1956; pp. 442–454, 1957: "Oxidation, Ignition, and Detonation of Fuel Vapors and Gases," by R. O. King and others.

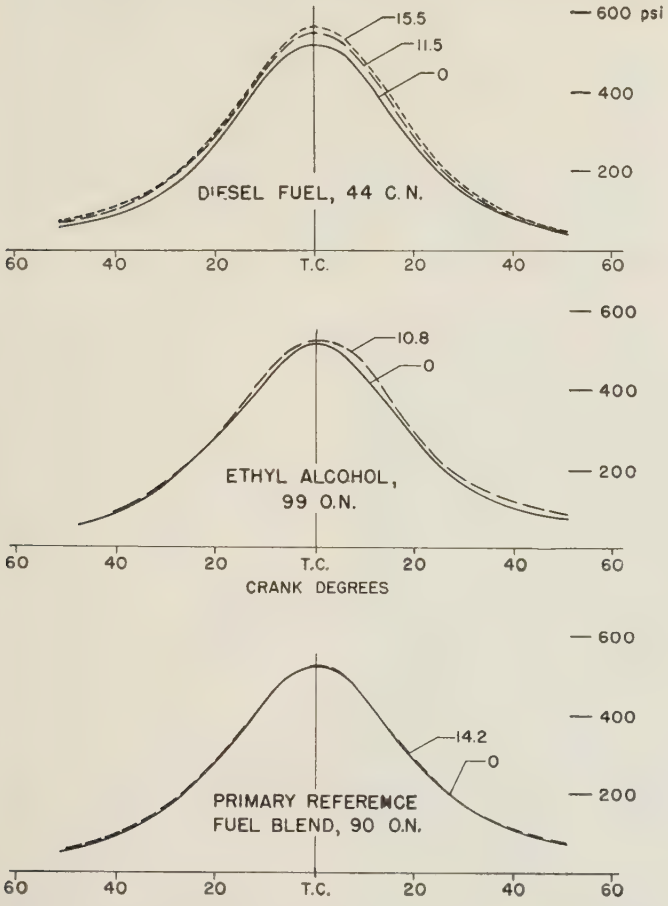

Fig. 23—Nonfiring pressure diagrams of several fuels (numbers indicate percentage of stoichiometric fuel-air ratio)

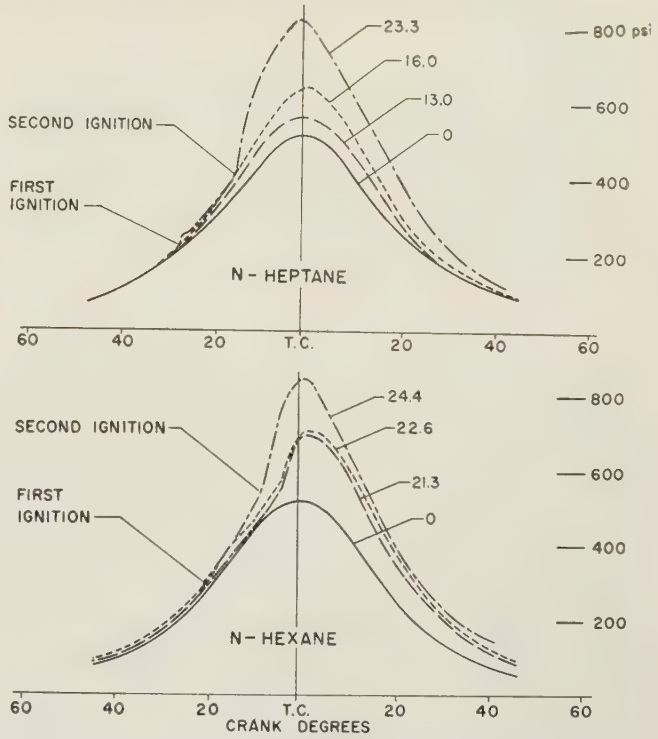

Fig. 24—Nonfiring pressure diagrams of normal heptane and normal hexane (numbers indicate percentage of stoichiometric fuel-air ratio)

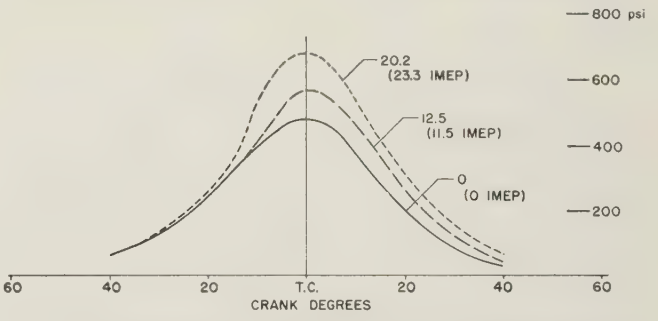

Fig. 25—Nonfiring pressure diagrams of 52 cetane number diesel fuel introduced by vaporizer. Conditions: CFR engine, 900 rpm (numbers indicate percentage of stoichiometric fuel-air ratio)

others did not autoignite at all. Fig. 23 shows pressure traces with 44-cetane diesel fuel, 90-octane gasoline, and alcohol; and Fig. 24 with heptane and hexane. On each, the solid line shows the air compression-expansion line without fumigation. On the hexane and heptane traces the dashed line shows fumigation in the amount which previous tests with diesel fuel injection gave best power output, the dotted lines where incipient ignition set in, and the dash-dotted lines fully developed spontaneous ignition.

Table 5 shows the tabulated observations on maximum cylinder pressure, exhaust temperature, and computed imep. They place the five fuels in a certain order, hexane being the most effective, alcohol the least, and diesel fuel in the middle. This is in marked contradiction to the supplementary fuel fumigation tests which showed diesel fuel the best and hexane the poorest of those tested (Fig. 13).

A significant difference between the two tests was that in the nonfiring tests there was no ignition. The shortening of the ignition lag, therefore, could have no part in the process. What obviously played a decisive part was the heat generation during compression due to slow oxidation of the manifold-introduced fuel. This caused an amazing rise of pressure and temperature and an appreciable indicated power output even though most of the heat introduction took place during the compression stroke.

Inasmuch as in these tests the fuel was introduced by Micro-Fog in small liquid droplets and oxidation on any appreciable scale can take place only in the gaseous state, the fuel had to vaporize before it was oxidized. Volatility, therefore, must have played an important part in the process. This would explain the good showing of hexane but fail to explain the poor showing of alcohol. On the other hand, the presence of thermal decomposition during the compression would result in the creation of lighter molecules, some of which would oxidize at a faster rate than the original heavier molecules.

If this speculation is sound, the thermally unstable high-cetane fuels should again assume top positions if the volatility factor is eliminated. The previous series of tests was performed with Micro-Fog. It was then repeated with vaporizer. The fuel was in vapor state when it entered the cylinder and fuel volatility no longer could have an effect.

Fig. 25 shows the indicator diagrams obtained under such conditions. It will be noticed that rise in

pressure and imep then becomes considerable and compares favorably even with hexane introduced by Micro-Fog.

Fig. 26 shows a series of indicator cards obtained on the Petter engine without injection, all the fuel being fumigated into the intake air by Micro-Fog. Again alcohol and high-octane gasoline showed little activity, but hexane, heptane, ether, and isopropyl nitrate developed so much power that in addition to overcoming engine friction they could carry load. It was not always easy to tell whether the engine was firing because the transition was gradual from non-firing to firing operation, but with the three last fuels the engine could at least surely idle without firing.

Increasing the feed slightly the engine could run steadily on fumigation alone and only the ether caused rough running when the fuel feed exceeded 1.0 lb per hr (23.6% stoichiometric). With acceptable knock the engine developed 25.4 psi bmep with a bsfc of 0.772 lb per bhp-hr. Heptane was not worse with 24.0 bmep and 0.607 bsfc. Hexane was again tops with 40.2 bmep and 0.385 bsfc!

The last figure is better than any we have meas-

	FUEL	FUEL RATE lb./hr (STOICH.)	FIRING	IMEP (BMEP) psi	MAX. CYL. PRESSURE psi	EXH. TEMP. °F	BSFC lb./bhp-hr
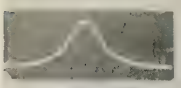	n-HEPTANE	0.369 (12.1%)	NO	8.9	590	165	—
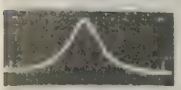	n-HEPTANE	0.481 (15.8%)	NO	13.3 (0)	680	205	—
	n-HEPTANE	0.714 (23.5%)	STEADY	37.3 24.0	880	325	0.607
	DIETHYL ETHER	0.389 (9.1%)	NO	7.9	600	146	—
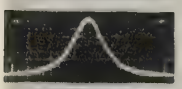	DIETHYL ETHER	0.611 (14.3%)	NO	11.6 (0)	710	210	—
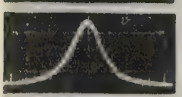	DIETHYL ETHER	0.794 (18.6%)	BORDERLINE	11.6 (0)	820	280	—
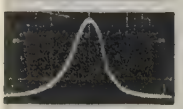	DIETHYL ETHER	1.005 (23.6%)	MAX. WITH TOLERABLE KNOCK	37.0 (25.4)	990	390	0.722
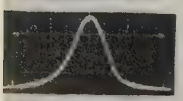	ISO-PROPYL NITRATE	1.467 (17.8%)	STEADY	12.4 (0)	930	345	—
	AIR ALONE	—	NO	0	520	104	—
	ETHYL ALCOHOL	0.966 (18.3%)	NO	0.2	520	105	—
	90 OCTANE PRIMARY FUEL BLEND	0.689 (21.9%)	NO	1.74	520	118	—
	44 CETANE DIESEL FUEL	0.494 (15.1%)	NO	2.91	520	110	—
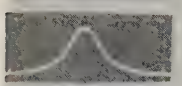	n-HEXANE	0.512 (16.9%)	NO	8.5	600	156	—
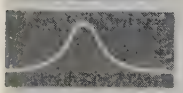	n-HEXANE	0.592 (19.6%)	NO	10.4 (0)	630	215	—
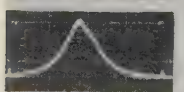	n-HEXANE	0.709 (23.5%)	BORDERLINE	31.0 (20.6)	720	282	0.673
	n-HEXANE	0.810 (26.8%)	STEADY	51.6 40.2	890	355	0.385

Fig. 26—Fumigation without injection. Conditions: Petter engine, 1200 rpm, supplementary fuel introduced by Micro-Fog

ured on this little engine with regular injection, in fact, so good that it may raise doubts as to its accuracy. Some people even have the fallacious idea that heat converted during the compression stroke produces negative work and reduces the thermal efficiency. It is easy to see, however, that (aside from secondary influences) a thermal unit introduced a deg btdc is converted with the same thermal efficiency as a thermal unit introduced a deg atdc. An inspection of the good indicator diagram of hexane shows that most of the pressure rise takes place near tdc. This combined with 16.5/1 compression ratio and relatively high mechanical efficiency results in the good fuel consumption observed, which corresponds to an *indicated* thermal efficiency of 39.7%.

With heptane and ether ignition occurred too early and the indicated thermal efficiencies were 32.5 and 30.3%. Diesel fuel, on the other hand, ignites too late at 16.5/1 compression ratio without injection and its indicated thermal efficiency figure is 3.9%. For hexane the compression ratio and heat transfer were ideal, hence the spectacular fuel consumption. A concocted fuel with the combustion characteristics of n-hexane fumigated into an engine such as this Petter would make a handsome pumpless diesel.

Applications

The study of preflame reactions brought us closer to understanding autoignition. A true understanding of the mechanism through which ignition accelerators work could easily lead to clearer concepts of combustion in both spark and compression-ignition engines including the role of knock-suppressing agents. What during normal combustion occurs in a fraction of a millisecond can by such technique be stretched out and studied in steps. But instead of indulging in theoretical speculations which would necessitate the review of considerable literature, at this time we prefer to point out some practical applications of the fumigation technique to diesel engines.

The most obvious use of fumigation is for reduction of exhaust smoke or increase of smoke-limited power output. Both from the standpoint of convenience and of effectiveness, normal diesel fuel, same as the primary fuel, is recommended for normal fumigation. The complication of the two-fuel system is thereby avoided. True, a low ignition quality fuel such as gasoline used in quantities of 30–40% of the total fuel rate could bring higher power boosts[2,3] but intake pipe induction of diesel fuel in such quantities would cause preignition under certain operating conditions and control over the engine would be lost. When restricting the amount of supplementary fuel to 10–15% of the total, regular diesel fuels are superior to gasoline, provided a fine spray is used in both cases.

Another promising use of fumigation is to reduce fuel consumption. Apparently all types of diesel engines could improve their fuel consumption by its judicial use. Regular diesel fuel, 10–15% of the main fuel, should serve as supplementary fuel and fumigation should cut out whenever the load drops below an established percentage (75–85%) of full load. For best fuel economy it is essential that a mist generator or equivalent be used. With Micro-Fog, full-load fuel economy could be improved some 10% while with an ordinary pneumatic spray nozzle only about 5%.

The saving in fuel consumption will be less in 2-stroke engines where much air is used for scavenging the cylinder. Assuming that the short-circuited air mounts to 25%, which is a good average figure for diesel engines with unsymmetrical timing, one quarter of the fumigated fuel would pass unburned into the exhaust.. With 15% fumigation, this represents a loss of 3.75%. This reduces the saving obtainable with fumigation considerably. In order to minimize it, a reduction of the short-circuiting (smaller exhaust-time area) and a reduction of the fumigation rate seems desirable.

The same holds, but to a much lesser degree, for supercharged 4-stroke cycle engines with considerable valve overlap. However, the valve overlap is never so large that it would materially effect the economy of fumigation.

At present three factors are in the way of using the Micro-Fog mist generator on commercial engines: cost, bulk, and air consumption. The largest capacity Micro-Fog, the experimental model shown in Fig. 3, has a capacity of 0.2 lb per hr with an airflow rate of 4.4 standard cfm. Assuming a diesel specific fuel consumption of 0.4 lb per bhp-hr and fumigation ratio of 15%, 0.06 lb of fumigation fuel is needed per hr; therefore, the pictured device is barely adequate for 3½ hp. An air pressure of 18 psig is needed to produce this flow which requires 0.26 theoretical hp or approximately 0.35 actual hp. This means that all of the fuel saving would be spent to drive the air compressor to furnish the air needed to operate the Micro-Fog. Furthermore, the present Micro-Fog equipment is very bulky.

The reason the Micro-Fog is so large and eats up so much horsepower is that only about 2% of the total amount of atomized liquid is discharged as a mist with drop sizes under 4 microns and the other 98% with larger drop sizes is returned to the tank.

A less extravagant atomizer is an ordinary pneumatic spray nozzle which also operates with compressed air but uses only about 2 lb of air per pound of liquid, roughly 1/50th as much as the Micro-Fog. A 1000-hp engine burns approximately 400 lb of fuel per hr at full load, of which approximately 60 lb per hr would be fumigated which takes about 120 lb of air per hr. The compression of that much air to 50 psig costs about 3.3 effective hp, or 0.33% of the engine output.

Still another application of the fumigation techniques is to be able to burn fuels of low ignition quality in compression-ignition engines. The use of such fuels may offer economic advantage due to the price differential, or may be forced upon us by the nonavailability of regular diesel fuels in an emergency.

High-speed diesel engines have difficulty in burning diesel fuels of about 35 cetane number at light load or idle, although operation may be satisfactory at heavier loads. In such a case, fumigation of part of the main fuel at light loads will allow satisfactory operation at all loads.

If the main fuel has still lower ignition quality, as motor gasoline (approximately 20 cetane number), the fumigation of the main fuel helps some but better results are obtained by the fumigation of a higher cetane fuel eventually doped with a cetane-improving additive. The ignition quality of the injected fuel ceases to limit its use in a diesel engine

if the fumigation fuel is properly selected. Twenty-nine cetane diesel fuel could be satisfactorily used in a small high-speed open-chamber engine with a supplementary fuel of 44 cetane number doped with 2½% amyl nitrate.

The fuel consumption at light load is always poor with fumigation; therefore, it should be used only when necessary and at the lowest possible rate that will insure steady running.

Accessory benefits of fumigation are lower exhaust temperature, smoother combustion, reduced cylinder deposits, and probably reduced bearing wear.

A good field for fumigation is in diesel-driven trucks. They are ordinarily equipped with an air compressor for furnishing compressed air for braking. That should be adequate to supply air to the pneumatic spray nozzle mounted in the intake manifold. A tee in the main fuel line conducts fuel to the spray nozzle. The airflow is controlled by the fuel rack of the injection pump in such a manner that it begins to operate at around ⅞ load and both airflow and fuel flow increase with the rack setting up to an acceptable overload. This would enable diesel trucks to take grades without smoking. Neither the fuel bill nor the maintenance cost would be increased in so doing.

An equally promising field for fumigation is in railroad locomotives. Here smoke reduction may be secondary to the saving in fuel costs that can be achieved. The nature of locomotive operation is such that they run at full load and idle much of the time and at medium load less often. This is favorable to fumigation. All locomotives are equipped with good sized air compressors which can furnish all the air needed. Finally, fumigation will permit the use of an economy fuel, a residual-distillate blend with a cetane number of 25–35, which now costs at least ¾ of a cent less per gallon than the standard No. 2 diesel fuel ordinarily used.

If such a low-cetane fuel is used for main fuel, it is advantageous to fumigate a higher cetane fuel (doped or undoped) when the engine idles but just the main fuel when the engine runs at high load. Inasmuch as the fuel consumption is low at idle and fumigation constitutes a small portion of this, a relatively small additive fuel tank, not more than 40 gal, is adequate for the longest trips to feed the additive spray nozzle. The full-load fumigation is effected by a second spray nozzle which is supplied with fuel from the main tank. At 0, 1, and 2 notch or load position of the engineer's control wheel, additive fuel is fumigated through the additive spray nozzle; at 7 and 8 notch main fuel is fumigated through the main spray nozzle; and at 3, 4, 5, and 6 notch no fuel introduction into the intake air takes place. The operation is completely automatic, requiring no attention from the locomotive personnel. In this way the railroad can have the benefit of two-fuel operation without having a two-fuel system with two large tanks or mixers. In addition, it has the benefit of lower fuel consumption, more miles per gallon. The two savings would add up to 5–10% total savings in fuel costs. The savings will be higher when an economical mist generator becomes commercially available.

The Pennsylvania Railroad has tests in progress for the application of fumigation to its park of diesel locomotives.

Acknowledgments

The work described herein was done in the Department of Engineering Research, The Pennsylvania State University, under the sponsorship of the U. S. Department of the Navy, Bureau of Ships with the active support of Harry F. King, Chief, Fuel and Lubricant Division. E. Mitchell and C. Birnie, Jr., were part of the team in the early tests. The interest and help of the C. A. Norgren Co. is gratefully acknowledged. Dr. W. E. Ranz and C. Hofelt conducted the drop size determination tests on the atomizers.

Details of the equipment were described by C. Birnie et al[12], in May, 1956, and previously by Cummingham et al[13] in August, 1954.

DISCUSSION

Wonders about Distribution Problem of Fumigated Fuel on Multicylinder Engine

—Walter Penzias
Allis-Chalmers Mfg. Co.

THE paper is an interesting one, especially since increased attention is being focused on diesel fuel economy and freedom from smoke. It would have been interesting to see the experiments extended to a good multicylinder engine, representative of current practice. The writer believes that this would have brought to light a distribution problem with the fumigated fuel not considered by the authors. Also, it becomes progressively more difficult to improve combustion as the basic efficiency of the engine tackled is increased.

Fig. A shows performance curves for a European truck diesel on a fixed-rack power curve. This was plotted to see how the formula quoted for theoretical bmep would check out on an actual test. As may be seen, the results are some 15–19% high, but this would depend on the value of the constant chosen. It would be interesting to have the authors' opinions regarding the possibility of a 10% improvement in thermal efficiency by using fumigation on such an engine.

Under the section titled "How does fumigation work?" it is claimed that an increase in thermal efficiency is obtained by faster combustion. This is hard to reconcile with a claim of smoother operation, which is usually linked with the magnitude of dp/dt.

There is a link-up between this and the question of negative work from heat released on the compression stroke. Early and gradual heat release, while helping to smooth combustion, "fattens" the indicator diagram before tdc. Work opposing normal rotation is produced. While this shows no ill effect on an idealized diagram, in an actual engine the secondary effects mentioned are by no means negligible. In short, if a high brake thermal efficiency is the

[12] "Effect of Supplementary Fuel Addition by Fumigation Through Inlet Manifold on Diesel Engine Performance," by C. Birnie, Jr., W. B. Swim, M. Alperstein. The Pennsylvania State University, Department of Engineering Research, Technical Report, 1956.

[13] "Diesel Combustion with Artificial Inlet Atmospheres," by R. G. Cunningham, C. Birnie, Jr., R. M. Law, and E. Micthell. The Pennsylvania State University, Department of Engineering Research, Final Report, August, 1954.

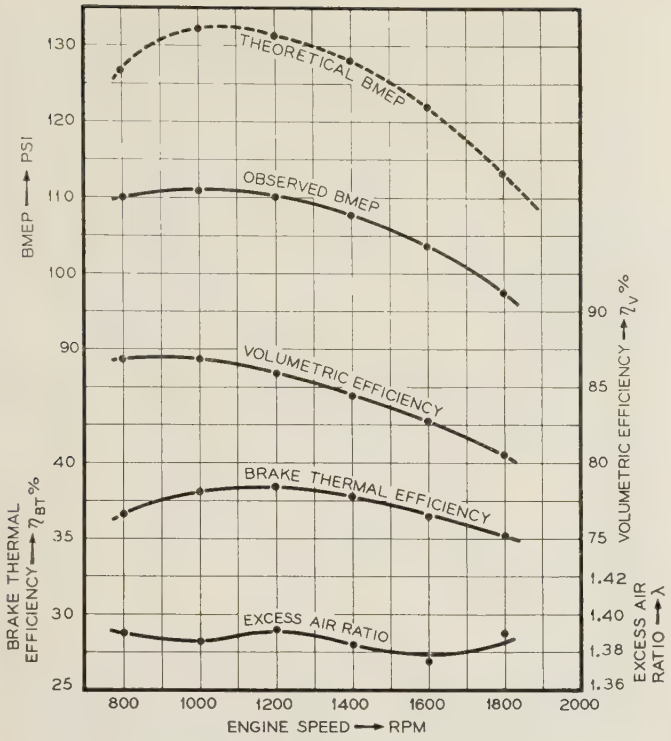

Fig. A—Performance curves for 150 bhp, 6 cyl, direct-injection 4-stroke automatic diesel engine (theoretical bmep = $180 \frac{\eta_{bt} \times \eta_v}{0.325 \times \lambda}$ where: η_{bt} is based on LCV of 18,000 Btu per lb, η_v on air conditions between flow meter and engine inlet manifold, and λ on stoichiometric air-fuel ratio of 14.5/1)

aim, one cannot move heat release far from tdc in either direction.

Turning to the tests on the Petter engine using fumigated fuel only, the run with n-hexane gave a reported 40.2 psi bmep and 51.6 psi imep at 1200 rpm. This yields a friction fmep of 11.4 psi. On a 6-cyl direct-injection engine of lower compression ratio, motored hot without fan, the lowest figure obtained by the writer at a corresponding piston speed is 45% higher than this. A single-cylinder engine will invariably give a higher friction loss than the corresponding 6 cyl version. Can the authors say if an attempt was made to confirm this friction loss by motoring the engine, and what were the test conditions?

Bearing in mind that no fuel injection pump was used, the figure of 0.385 lb per bhp×hr obtained with this fuel is certainly impressive.

There is attraction in the idea of using fumigation to help an engine digest a cheap fuel which would otherwise be unsuitable, but the aim should be to avoid a dual-fuel system.

Mentions Problem of Distribution of Fumigated Fuel to Cylinders

—Grover C. Wilson
Ethyl Corp.

THE paper is very timely in that it presents a system for improving two major weak points in the diesel engine; namely, smoke and relatively low power output for its size and weight. Also, the "fumigation method" offers a means for improving the outstanding feature of diesel engines—fuel economy. The survival of any type of power unit will depend upon improvements for competition in the coming years is going to be keen.

Further evidence of the timeliness of this report is the fact that, recently, in the western part of the United States, many trucks and buses have been converted for the use of LPG as "Power Booster Fuel." This use for LPG was investigated and reported by McLaughlin and others.[2] Undoubtedly, the drive against air pollution has encouraged operators to make such changes.

Much credit is due the authors for making an extensive investigation and a comprehensive report of the project. If combustion can be as greatly improved in multicylinder engines in service, as is indicated from the single-cylinder test data, it would be worthwhile to make any required modifications in engine design. With the present public attitude toward air pollution, it is doubtful if operators would be allowed to bypass any fuel to the atmosphere, such as could occur with fumigated fuel in an engine with large valve overlap.

In order to obtain similar combustion improvements in the multicylinder engine, some additional problems need to be solved. Probably, the most important one is that of accomplishing equal distribution of the fumigated fuel to all cylinders. Besides, field service will require operation over wide ranges of speeds and loads. I would like to ask the authors how critical is the timing for matching the fuel injection with the preflame reaction of the fumigated fuel. From previous test work, one would be led to believe that zero ignition delay is undesirable, because of a lack of time for mixing the fuel and the air. Also, how greatly are the preflame reactions affected by large changes in inlet air temperatures?

Operators of automotive equipment always have shown a reluctance towards adopting a dual-fuel system. The objection most generally stated is that both fuel tanks rarely require filling at the same time. A most desirable feature of the fumigation system is that it shows promise for development for operation on a single fuel. In cases where an ignition improver is required, consideration should be given to the possibilities of applying it to all of the fuel. Fig. 20 shows that smooth combustion was obtained by the addition of 2.5% of amyl nitrate to a fuel for fumigation. Applying the same amount of amyl nitrate to 100% of the fuel would increase its cetane number about one-third of the amount of the cetane number gain for the 15% fumigated fuel. Test data for a 33 cetane number fuel are as follows:

1. 2.5% amyl nitrate in 15% of the fuel would equal 0.375% amyl nitrate in all of the fuel.

2. 2.5% in 33 cetane number fuel will raise its cetane number to 53, while 0.375% would raise it to 40.

Thus, 40 cetane number fumigation fuel with 40-cetane injected fuel might give as good performance as 52 cetane number fumigation fuel with 33-cetane injected fuel. At least, it would avoid the use of a two-fuel system and it would improve the light-load operation without fumigation.

Suggests a Method of Phased Preinjection

—Dr. H. A. Havemann
M. W. Kellogg Co

THE authors were kind enough to mention my name as having contributed to the history of developments aiming essentially at improving the diesel engine by features which have hitherto been characteristic of the otto engine. It may, perhaps, be pertinent to record here briefly findings of work which has been undertaken as a continuation of the investigation which the authors have cited.[5]

In accordance with the conditions in India where the investigation was carried out[a], the principal objective was to substitute (as far as practicable) for the scarce and expensive mineral fuels others which are easily and cheaply available there. Thus, power alcohol was chosen. Because the costs of the changeover had to be kept to a minimum, a

[a] Department of Internal Combustion Engineering, Indian Institute of Science, Bangalore, South India.

carburetor appeared to be a suitable means to induce the supplementary fuel to the intake air of, at first, small high-speed diesel engines. It was expected that possibly lower grade fuels might become acceptable for injection on the grounds of a first (though admittedly incomplete) conception that the highly compressed and heated air-alcohol vapor mixture would somehow assist towards a more complete and faster combustion of a larger than normal amount of fuel. Power alcohol was retained as secondary fuel in all experiments, but different primary fuels were tried and it was only in keeping with the aim of the investigation that an effort was made to increase gradually the alcohol percentage. In the end it became the primary fuel with a value of up to 95% of the total fuel requirements. A vegetable fuel was injected in this case.

In connection with the conceptions of the authors and perhaps even in a wider sense, it is worth noting that a very considerable increase of the effective power of the engine accompanied the rise of alcohol participation: 45% was achieved with Grade A, and 40% with Grade B diesel fuel at constant speed runs. The small engine operated thereby with up to 113 lb per sq in. bmep.

This, as the authors have correctly quoted, was then attributed to a higher air utilization and, perhaps, a closer approximation to the ideal thermodynamic cycle by shortening the duration of heat liberation accompanied by lower heat losses due to the lower level of cycle temperatures. The experiments of the authors and the conclusions drawn by them allow a much closer look at the other factors which account for the higher mep, higher combustion efficiencies, and lower smoke densities.

The tests in Bangalore were undertaken with two engines, one (Petter AVI Series II) with open chamber and the other (Ricardo E6/R) with Comet MKII combustion chamber. The open-chamber engine showed a considerably higher capacity for overloading by higher alcohol manifold induction than was possible with the latter engine. This was thought to be due to the higher level of flow intensities in the engine with precombustion chamber which would lead to too high values of the rate of pressure rise and, finally, to unacceptable operation . A different interpretation was then received from M. H. Howarth, of Ricardo and Co., who had found that the hot plug of the E6 engine was likely to cause considerable preignition. It could be argued that, with a gradual approach to an otto-type of combustion process, details of the combustion-chamber geometry might loose the significance they carry in "pure" diesel operation. However, it appears that physical effects may still play a part in determining the working and success of manifold fuel induction. The compression ratio has surely an influence and much may depend on the mode of flame propagation and accompanying factors such as flame-created or primary turbulence.

This is, perhaps, an occasion to propound an idea which occurred to me as a possible further step in supplementary fuel utilization. The conclusion of the authors that the use of one and the same fuel—though in different ways—carries valuable economic and operational advantages is thereby fully upheld. The peculiar effects of the inducted fuel, that is, better air utilization and preflame reactions, appear also to be assured. This could be obtained in the following way:

Part of the fuel, playing the role of the previously manifold-inducted fuel, is injected separately and directly into the cylinder at a time which is most conducive to achieving its objectives, preferably during the compression stroke. The elevated temperature of the air would help toward its speedy vaporization, the elevated pressure would assist atomization and limit penetration, the timing would allow far-reaching distribution and premixing. The intimate contact with air at the high temperatures would encourage preflame reactions. Details of this "preinjection" could be adjusted to meet requirements of different fuels. Autoignition is, of course, carefully avoided. It need hardly be mentioned that the full amount of air is available in the cylinder unimpaired by fuel vapors carried otherwise through the manifold.

The injection of the second portion of fuel, starting after the completion of "preinjection" with a delay which allows the preinjected fuel enough time to undergo the intended physical and chemical processes, can occur in conventional manner. This would ultimately initiate combustion which would, in all essential aspects, occur under the same propitious auspices as were valid for methods of supplementary manifold induction to the intake air.

It is admitted that the system proposed here calls for two fuel injection systems, or an ingenious design of a double-stroke single-pump element. It would, however, also allow the 2-stroke engine to enjoy the considerable advantages of the now established methods of manifold fuel admission. A closer investigation would have to struggle against a multitude of variables and difficulties of design. However, preliminary tests initiated at the Indian Institute of Science confirmed the fundamental premises and expectations of the method of phased preinjection.

Interested in Effect of Nuclei-Forming Mechanism on Ignition

—R. O. King
Canadian Defense Research Board

THE experiments described by the authors are of interest because of the effect of finely divided material to promote the nuclear ignition at relatively high temperatures of fuel vapors and gases, as shown in our series of publications to which reference has been made.[11] The necessary high temperatures are obtained in the diesel engine by compression and in the end gas of the spark-ignition engine at lower compression ratio. This igniting effect is the fundamental cause of the improved engine performance described by the authors.

When nuclei or small quantities of nuclei-producing substances are not used as additives, they must be formed by thermal cracking of the fuel or of its initial oxidation products. Otherwise, ignition by compression will not occur. This is illustrated by the results of the author's experiments with alcohol as compared with those with hydrocarbon fuels.

Our interest lies in the determination of the nuclei-forming mechanism. The fact that improved performance has been obtained by adding nuclei as a mist encourages us to continue with the somewhat difficult experiments required to determine the nuclei-forming mechanism.

Indicates Improved Efficiency of Aspirated Fuel Due to Improved Cycle Efficiency

—Dr. W. T. Lyn
C. A. V. Ltd.

IT IS gratifying to know that Prof. Schweitzer's work has in the main confirmed my own work and has extended it in a number of places where I have not fully explored. I am referring particularly to the various methods used in introducing the auxiliary fuel and the attempt to differentiate the relative contribution to the improved performance by better air utilization and improved "combustion efficiency." I should like to dwell a little on these two points.

From my previous investigations I have concluded that the main cause of the loss of efficiency at part load is due to the incomplete combustion of the aspirated fuel. This contention is brought into focus again when we consider the behavior of the various methods of introducing the auxiliary fuel. It has been suggested that the auxiliary fuel, being well under the inflammability limit, can only undergo slow oxidation and not flame propagation. This

assumes complete vaporization and mixing of the aspirated fuel and is perhaps nearest to the case when a vaporizer is used. With droplets this state of affairs may not be realized, depending, of course, on droplet size; the fuel properties and the stratification effect may reduce the loss from this source. An improved performance is, therefore, observed with the Micro-Fog technique. When the droplet size is still larger, as in the case with pneumatic spray, the loss due to the arrest of the heavier droplets on the wall during their travel to the chamber may outweigh the benefit mentioned above and performance is once again made worse. This may be only a speculation but it is consistent with the observation that within the hydrocarbon series, as the volatility goes up the difference between Micro-Fog and pneumatic spray disappears (gasoline) and eventually the coarser spray becomes optimum (hexane and heptane at constant smoke level). It may also explain why with the Micro-Fog both alcohol and gasoline fumigation give better efficiencies than the authors' views on this point.

The analysis in Fig. 21 is most instructive. It clearly shows that there is an improvement in efficiency as well as in air utilization. Recent investigations on fuel injection and heat release at C.A.V. indicate that the improved efficiency with aspirated fuel is more likely due to the improved cycle efficiency than to improved combustion efficiency. The improved cycle efficiency is brought about mainly by replacing the last part of the injected fuel, which burns generously at the latter part of the cycle and hence with a lower efficiency, with the aspirated fuel which gives up its heat nearer tdc. It is now clear that the major part of the injected main fuel follows that of the diffusion flame process and the rate-controlling factor is mixing rather than kinetics of chemistry. Preflame reaction, while most powerful in shortening the delay period, will be of little avail in "helping combustion after ignition has set in" as the authors have suggested. By the same reasoning, advancing the ignition by shortening the delay period without changing injection timing will not advance the whole heat release period bodily and, hence, will have little effect on the cycle efficiency. In this respect my own view has changed somewhat and the authors' comments would be welcome. Incidentally, the method by which delay period is determined has not been mentioned. With fumigation, it is clearly impossible to detect this from the pressure diagram because of the pressure rise due to slow oxidation of the auxiliary fuel. In my own work I have used a photocell. With this method the reduction in delay period is not as spectacular as the authors have shown and zero delay was certainly not recorded, although the cylinder pressure diagrams were as smooth as those shown by the authors.

On the question of application, the view does not appear to have changed since my own work was published. The most attractive fields are power boosting from ¾ loads onwards for transport engines and full-load bi-fuel application (one of lower grade) in industrial installations. The light-load smell and smoke due to the incomplete combustion of the fumigated fuel remains the most serious drawback of the system. I am, therefore, particularly interested in the railroad experiment and ask if complaints from this source have been reported due to locomotives idling at stations.

Emphasizes that Ignition Lag Most Important Factor in Improving Combustion

—Julius E. Witzky
White Motor Co

AS ALREADY mentioned in the paper, the introduction of secondary fuel into the intake manifold of a diesel engine is by no means new. Tests by Daimler-Benz of Germany were performed during the World War II to ignite in an aircraft gasoline engine a fuel-air mixture by injecting ignition fuel. The main purpose of these tests was to avoid spark-plug fouling at high altitude. The performance of this engine was really excellent. The maximum output could be considerably improved; especially remarkable was the extremely smooth idling. The injected ignition fuel ignited the mixture in many places. As a result, the one spark of the plug was substituted by a great number of sparks. We called this combination the dies-otto cycle"; it is an abbreviation of "diesel-otto." However, the necessity to carry two types of fuel was killing this project.

A second attempt to boost the horsepower by introducing a secondary fuel in the intake manifold of a diesel engine was made again by Daimler-Benz of Germany during World War II, on a 2000 hp light-weight diesel engine used in all German PT boats. This engine was equipped with a mechanically driven supercharger. No attempts were made to atomize the fuel; the fuel was simply poured in in front of the supercharger impeller. I assume the impeller atomized the fuel, because the result obtained was similar to results reported in this paper. The output could have been considerably increased without increasing the smoke. However, the engine was originally designed for 2000 hp, and the additional horsepower gained (higher peak pressure) was too much for the engine structure; therefore, we had to abandon this very promising experiment.

The ignition of liquid fuel in a compression ignition engine is dependent upon the following basic factors: temperature of the air, density of the air, and cetane number of the fuel.

The common fuel for a compression ignition engine is diesel fuel with a high cetane number. The high cetane number indicates that, when fuel is injected in a high temperature and dense air, the fuel will start to burn after a relatively short delay; or, in other words, after a small amount of fuel is injected, it starts to burn with relatively little pressure rise, then the following fuel burns as quickly as it leaves the injection nozzle. This means that we are pretty much in control of the combustion process and are able to influence the combustion by adjusting the injection characteristic.

To ignite gasoline in a diesel engine with a high octane but a low cetane number fuel, the picture is quite different. The gasoline is designed to avoid in a spark-ignition engine knock as a result of compression ignition of the end gasses. By burning high-octane gasoline in a compression-ignition engine, the ignition lag is getting long and, in most cases, all the fuel is injected until inflammation occurs. This means there will be a violent detonation and we are losing the control of combustion. By using high-octane gasoline with its high ignition temperature in a compression-ignition engine, we are asking for something it is not supposed to do. Whether we burn fuel of high or low cetane rating, a reduction of the ignition lag is certainly the most important single factor to improve combustion. Fumigation is one means to reduce the ignition delay.

At this point, it may be worthwhile to mention some other means to reduce the ignition lag as, for instance, tests conducted in a single-cylinder engine where the intake air was heated. This single-cylinder test proved that, by heating the intake air to about 200 F, ideal constant pressure diagrams could be produced. The peak pressure was about the same as the compression pressure, indicating that the ignition delay was practically reduced to zero.

It is my belief that a similar effect could be obtained if we would be able to revise the injection characteristic. At this time all of our present injection equipment starts with a high rate of injection. If we would be able to change the injection characteristic in a manner where we would first inject a small amount of fuel similar to pilot injection, the pressure diagram could be improved. On a pumpless diesel system tested at The Pennsylvania State University, a diagram quite similar to the one shown in this paper could be obtained. In this system, the introduction of fuel started with a low rate, progressively increasing to the top

of the piston stroke. This indicates that, by changing the injection characteristic, similar diagrams as shown in the paper without fumigation could be produced.

In the nonfiring pressure diagrams, the authors show an increase of compression pressure by fumigation of fuel in the intake air. In combustion, the temperature is of importance—not only the density. Therefore, I would like to ask whether the temperature increase was ever measured during this test work. Secondly, by applying fumigation to a multicylinder engine, maybe we will encounter the same problem as in a gasoline engine whereby one cylinder receives a richer mixture than the other. This means that the gain in a multicylinder engine will not be as great as has been proved in the single-cylinder test engine.

Compares Data on Isooctane with Authors' on Fumigated Diesel Fuel

—D. R. Jones
California Research Corp.

A UNIQUE method for increasing power and reducing smoke of diesel engines is proposed by the authors in this excellent paper. In addition to the obvious practical application of fumigation, the authors have presented data indicating the value of this technique for fundamental combustion studies. Further work along these lines certainly appears warranted.

The authors referred to our early investigations in which volatile, high-octane fuels, called power-booster fuels, were added to the intake air of diesels to improve performance. In this work, we found that high-octane (low-cetane) supplementary fuels gave greater improvements in smoke and power than low-octane (high-cetane) fuels. This result differs from the authors' data which showed that a moderately high (44) cetane number diesel fuel gave optimum performance when added to the intake air in finely atomized form. Lower cetane fuels (gasoline and alcohol) gave poorer performance as did higher cetane fuels (n-heptane and n-hexane). Differences in engines, operating conditions, and method of applying the auxiliary fuels could account for the different effect of cetane number in these two investigations. In our laboratory tests, we used a Cummins HB 600 diesel engine and a modified CFR diesel engine with an open, pear-shaped combustion chamber located on top of the piston. Practically all of our tests were conducted at relatively rich fuel-air ratios (0.05–0.09) which produced heavy smoke and high bmep. The authors' tests were carried out in an open-chamber Petter engine and in a modified CFR diesel with a Ricardo swirl-chamber cylinder head. These engines were operated at a fuel-air ratio, smoke level, and bmep much lower than in our tests.

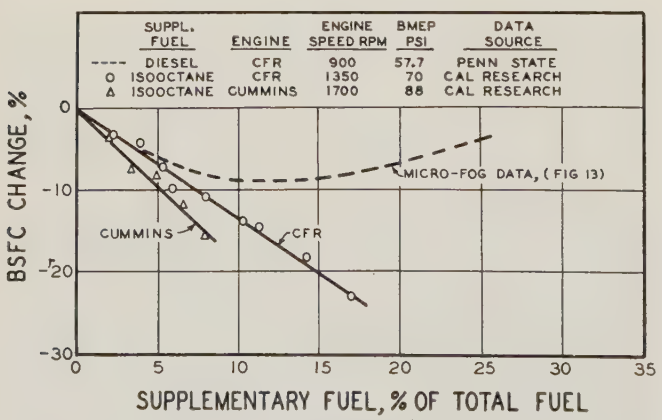

Fig. B—Comparison of diesel fuel and isooctane as supplementary intake air fuels, constant bmep

It occurred to us that it might be of interest to compare results we obtained on isooctane with the authors' data on fumigated diesel fuel. To accomplish this, we have replotted our original data in the exact form of Fig. 13. (See Fig. B.) The figure shows the relative improvement in brake specific fuel consumption (bsfc) with increasing amounts of supplementary fuel under conditions of constant bmep. It will be seen that adding isooctane to the intake air produced larger relative reductions in bsfc in our Cummins HB 600 and modified CFR diesel engines than did fumigated diesel fuel in the authors' modified CFR diesel. It will also be noted that bsfc reduction reached a maximum at 10–15% fumigated diesel fuel; whereas, isooctane gave increasing bsfc improvement up to 15–20% added fuel.

We believe the difference in performance of these two supplementary fuels can be explained largely on the basis of operating conditions. Our modified CFR diesel tests were run at an output (70 bmep, 105 imep) which approached maximum power with straight injected fuel. Under these conditions, large increases in amount of injected fuel were required to effect small gains in power. These same power outputs could be achieved by replacing a portion of the injected fuel with appreciably smaller amounts of carbureted isooctane, resulting in proportionate improvements in bsfc. The Cummins HB 600 was operated under similar conditions, and it also responded exceptionally well to carbureted isooctane. We would estimate from the bmep level that the authors operated their modified CFR diesel under relatively efficient conditions for straight-injected fuel which would explain the relatively smaller bsfc improvement when a portion of the injected fuel was replaced by fumigated fuel.

Describes Applying Authors' Work To Railroad Diesel Engines

—Dr. M. A. Pinney
The Pennsylvania Railroad Co.

THE work done by the authors is very interesting and may be a major contribution to our knowledge of the mechanism of combustion in a diesel engine. Of particular interest to me is how this knowledge may assist the user of diesel engines to burn satisfactorily a wider range of fuels in the higher speed engines which today require high-grade fuels having minimum cetane requirements in the order of 40.

This railroad is sufficiently interested in this work that it has authorized a development program to determine whether the benefits noted in the small laboratory engines can be obtained in the larger diesel engines used in railroad locomotives.

Investigations are already under way, with the assistance of Dr. Schweitzer, to develop adequate spray nozzles which will produce a very fine spray at minimum air consumption. An engine has been prepared for tests which will be conducted initially on our block test stand. When we are satisfied that apparatus suitable for the purpose has been developed the tests will be extended to road operation.

It is anticipated, although we hope to avoid such work, that we may have to experiment with injection and/or valve timing to obtain optimum economy conditions. We do not anticipate that smoke reduction will permit taking higher ratings out of our engines as other factors (particularly the capacity of electrical apparatus used in the locomotive drive) place a maximum limit on this. However, we do believe that reduction in smoke will be an additional advantage, particularly when poorer fuels more prone to producing smoke may be burned or where heavily populated communities object to present smoke levels. Reduction in maximum rate of pressure rise may reduce shock loading on bearings and be beneficial in some classes of engines where bearing failures are not a problem.

Fig. 13 shows a maximum reduction in bsfc of about 9% when fumigating diesel fuel with constant brake load, and when using Micro-Fog and the CFR engine. Spray nozzles will not do this well but we are hopeful of realizing about 5% reduction in fuel consumption in our railroad diesel engines when operating at or near full load. We also believe that with fumugation of a cetane improver such as amyl nitrate at idle and low loads we can burn fuels having cetane numbers as low as 25 at all loads, including idling.

Two schemes have been considered for applying the authors' work to our railroad diesel engines used in road service. These are:

1. Continue using 40 minimum cetane fuels and use fumigation at loads above 80%. Fumigate with fuel from the main storage tank on the locomotive.

2. Use low-cetane fuel (having a minimum of 25 cetane) and fumigate with this fuel at loads above 80% and fumigate with a mixture of 97½% high-cetane fuel and 2½% amyl nitrate at idle and low loads.

It is not considered economically attractive to use fumigation in our switcher locomotives.

Studies have been made of the time our diesel engines operate in each notch or load position of the throttle. Based upon these time studies and the fuel consumption rates in each throttle position we estimate that the following percentages of the total fuel burned are burned in the seventh and eighth notch of an 8-notch throttle locomotive:

Through freight	67%
Through passenger	34%
Other freight	59%
Other passenger	25%
All road service	57%

Based upon a total fuel consumption of about 205 million gal annually in road locomotives a 5% reduction in fuel burned in the seventh and eighth notches would be approximately 5,840,000 gal. Preliminary estimates are that the cost of apparatus installed will be about $1,390,000 for 993 units. Allowing for the cost of fuel to generate the required compressed air and for fixed charges on the cost of the apparatus we estimate a net annual saving of about $454,000.

For the second scheme using fumigation of diesel fuel in the high notches and of a cetane-improved blend in diesel fuel in the low notches and idling, and applying heat exchangers to burn residual-distillate blends we estimate the total cost of apparatus installed to be about $2,768,000 for 1016 units. Based on utilizating a fuel costing in the neighborhood of ¾ of a cent per gal cheaper than our current fuels and allowing for increased engine maintenance, cost of fuel to generate compressed air, cost of cetane improver, and fixed charges, we estimate an annual net saving of about $1,750,000.

Both these schemes offer attractive savings if our test work indicates the expected 5% reduction in fuel consumed at high loads can be realized. Actual tests to determine this have not yet been completed but we have sufficient confidence in the work done by the authors to justify our proceeding with this test and development program.

Points Out That Effect of Fumigation Varies with Speed

—Dr. Siegfried Meurer
MAN, Werk Nürnberg

THE possibilities of injecting fuel into the induction manifold of the diesel engine have had the attention of several investigators. We consider it a very valuable addition to our knowledge that the effect of such fuel injection can be improved considerably by intensifying atomization (Micro-Fog). So far, the tendency of heavy volatile fuel particles to condense in the induction manifold and the cylinder has been the greatest difficulty in the practical application of this method. The very fine atomization ensured by Micro-Fog also helps considerably to reduce this drawback. It would appear that the complications of the present configuration do not make it an economical proposition for commercial applications (high air requirements for Micro-Fog).

It seems that the amazing increase said to be achieved in the mep at the smoke limit does not hold for all applications but is dependent on the utilization of the air ensured by the mixture formation system adopted in the diesel engine. The two experimental engines showed an air-fuel ratio at the smoke limit which is about 18% lower than that obtained in modern diesel engines.

Another important point is that the effect of the fumigation process varies considerably with the speed. In the CFR engine it was at a speed of 900 rpm that the ignition time lag was such that the optimum conditions were obtained. At 600 rpm the increase in mep is already less, even if an appreciable sacrifice is made in fuel economy (Fig. 10). The effective ignition lag measured in crank-angle deg until reactions start in the fuel introduced in the induction manifold is not constant. At 600 rpm the preliminary reactions occur too early; this negatively affects the indicator diagram and also influences mixture formation in the engine adversely (increase in specific fuel consumption). Conversely, it appears that at 1200 rpm the timing of the preliminary reactions is far from what would give optimum results so that the obtainable increase in mep decreases. It is a well-known fact that in the case of such spontaneous reactions the ignition time lag does not decrease in direct proportion to the increase in speed.

A multifuel property—as it is obtained today in special mixture formation processes in diesel engines (such as the "M" system) in the sense that the engine may be run on any one single fuel of a large range including high-octane fuels—is obviously not obtainable by the Micro-Fog process in the two experimental engines of the conventional type. These engines require at least two types of fuel, and sometimes three, for satisfactory operation. As a matter of experience, the difficulties to ensure correct and sufficiently intensive ignition become greater for the lower loads and the higher speeds. The latter was very low in the two experimental engines.

The reason for the success of fumigation by Micro-Fog may be explained by a better utilization of the air fractions which in other systems are not directly involved in the mixture formation. Furthermore, it is likely that there is increased turbulence because the exothermic preliminary reactions, which take place prevailingly in the cylinder space, are apt to cause a greater amount of gas to enter the combustion chamber or turbulence chamber at a higher speed during the compression stroke.

Describes Auxiliary Fuel Aspiration

—N. H. Rickles
Esso Research and Engineering Corp

THE authors have given us an excellent report on the extensive tests they have conducted in the laboratory on the aspiration of auxilary fuels in single-cylinder diesel engines. These tests show that under certain conditions aspiration can reduce both smoking and fuel consumption. It also permits the use of lower quality diesel fuels. As they point out, a considerable amount of engine test data have been published which indicate that aspiration of auxiliary fuels can reduce smoking. All the laboratory tests, however, have been conducted under steady running conditions, while in service acceleration is also a factor. Certainly acceleration smoke from diesel engines is a major

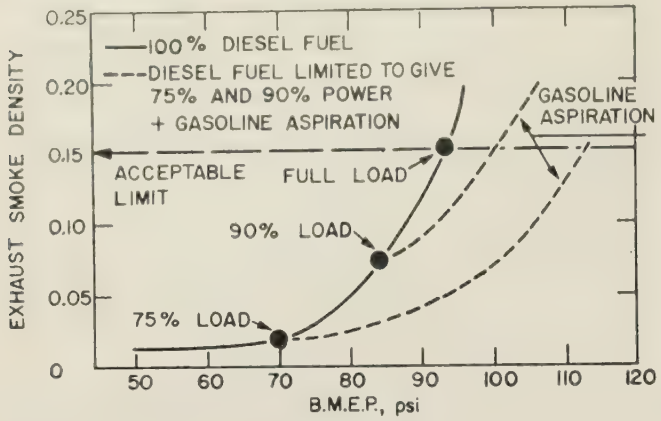

Fig. C—Effect of gasoline aspiration on exhaust smoke at engine speed of 1800 rpm

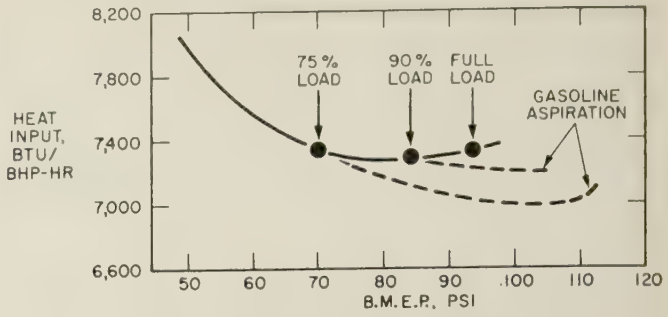

Fig. D—Effect of gasoline aspiration on specific heat input

Table A—Smoke Limited Maximum Power, Diesel Fuel Supply Restricted and Gasoline Aspirated

	Smoke Density, Rated Load 100% Reference	Maximum Power at 0.15 Smoke		Gasoline Consumption, % OF Total Fuel
		Bmep, p.s.i.	% OF Reference	
100% Diesel Fuel	0.15	93	100.0	0
90% Load on Diesel + Gasoline Aspiration	0.11	100	107.5	10
75% Load on Diesel + Gasoline Aspiration	0.05	112	120.5	23

problem in our cities. Perhaps, auxiliary fuel aspiration could aid in alleviating this problem. It would seem that engine builders would want to try this out under full-scale commercial operating conditions.

We have done a considerable amount of work on auxiliary fuel aspiration and believe the results have been encouraging. This work was performed by our affiliate in England, Esso Research Ltd. The results of this work were published in England.[3] Since many of you may not be familiar with it, I would like to summarize some of the principal points indicated by our studies.

The tests were conducted on a direct-injection, 6-cyl, 4-stroke diesel engine rated at 98 bhp at 1800 rpm. The auxiliary fuels tested included 71 octane number (Motor method) gasoline, 55 cetane number diesel fuel, and kerosene. The three methods used in supplying auxiliary fuel to the engines were:

1. Aspiration directly into air intake manifold, gear pump, 60 psi, simple nozzle.

2. Aspiration from vaporizer into air intake manifold, vaporizer fastened to exhaust manifold, part of intake air passed through vaporizer.

3. Injection directly into cylinder, separately mounted and timed 6-cyl injection pump.

Fig. C shows what happened to the exhaust smoke when gasoline aspiration was introduced at the 75 and 90% load points at the rated engine sepeed of 1800 rpm. Smoke measurements were obtained with the photoelectric cell type CRC smokemeter. The limiting value of 0.15 smoke density is equivalent to 30% smoke. You can see that for equivalent power less smoke is obtained, while for equivalent smoke more power can be obtained.

Table A summarizes these results. You will note that at rated load diesel fuel gave 0.15 smoke density. This was reduced to 0.11 and 0.05 when gasoline was aspirated at the 90 and 75% load point, respectively. When operating at maximum power to give 0.15 smoke density, aspiration introduced at 90 and 75% load points permitted 7.5 and 20.5% power increases, respectively. The amount of gasoline used was 10 and 23%, respectively, of the total fuel consumed.

Fig. D shows the effect of gasoline aspiration on thermal efficiency. A fuel consumption improvement of as much as 10% is indicated. As would be expected, lower exhaust gas temperatures were also obtained. The reductions are of the order of 50–100 F.

When diesel fuel and kerosene were aspirated in the same manner as the gasoline, the "exhaust smoke-load curves" were identical with those obtained with 100% diesel fuel operation. When using kerosene, piston seizures occurred on two occasions at 96 bmep. These failures were ascribed to the washing away of lubricating oil from the cylinder walls. Perhaps if we had used the fogging method of aspiration described by the authors, our results would have lined up with theirs. However, the commercial practicability of the fogging apparatus is certainly questionable at the present time.

In our tests using aspiration from a vaporizer, little or no improvement was obtained. We felt this was due to reduced volumetric efficiency because of the higher mixture temperatures caused by this method.

When using a separate injection pump, only small gains in smoke limited power were obtained but these were accompanied by large increases in fuel consumption. This also caused a lubricating oil dilution problem.

Authors' Closure To Discussion

IN answer to Mr. Penzias, fumigation is now being tested by the Pennsylvania Railroad on a 12-cyl locomotive engine. With fine atomization no serious distribution problems are anticipated. The thermal efficiency of a very efficient engine running on good fuel should not be expected to improve 10%, but fumigation should improve performance on substandard fuels and should increase the smoke-limited output with any fuel. Faster combustion produced by fumigation does not necessarily mean an increase in the maximum rate of pressure rise. Our measurements of indicator diagrams generally showed a decrease of the maximum rate of pressure rise, but the rise started earlier and lasted longer. Late heat release was thereby reduced. The measured friction of the Petter engine was exceptionally low.

In answer to Mr. Wilson, injection timing is not too critical with fumigation, but a slight delay relative to the normal operation is helpful. With up to 15% fumigation no zero ignition delay is anticipated. Preflame reactions are naturally intensified by high inlet-air temperatures, but we have no numerical data to offer. When a 2-fuel system

is objectionable, a moderate doping of the entire fuel, as Mr. Wilson suggests, combined with fumigation will satisfactorily take care of operation on low-cetane fuels.

It is true that the introduction of supplementary fuel into the intake manifold of 2-stroke engines or 4-stroke engines with large valve overlap will allow a small amount of raw fuel to pass into the exhaust. But the effect of this upon air pollution on the highways would be infinitesmal compared to the amount of unburned fuel the gasoline engines emit over the same highways.

Dr. Havemann's studies on alcohol carburetion were inspiring to our work. The preinjection he suggests is equivalent to a very early pilot injection, and should have effects similar to fumigation unless the droplets are so large that many of them precipitate on the cylinder wall. Yet phased preinjection or fumigation may be worth their complications in 2-stroke engines.

We also thought that our observations lent support to Mr. King's theory of nuclear ignition. Just *how much* cracking is taking place before ignition in a compression-ignition engine would be a valuable thing to know.

We have no substantial disagreement with the views expressed by Dr. Lyn. In our use of the term, "improved combustion efficiency" included cycle efficiency. Without the use of advanced types of chemical analysis, there was no way to tell whether a given fuel particle burned late in the cycle, or only partially, or not at all. The effect on the indicated work is the same. Dr. Lyn's theory that the loss of efficiency at part load is due to "incomplete combustion" of the aspirated fuel is supported by the observation that in a spark-ignition engine very lean mixtures can only be burned by a very hot spark. In a fumigated engine a big flame is needed, which obtains at heavy load. We realize that we did not explain why combustion at part load was incomplete. The answer would be of great theoretical interest.

Dr. Lyn wants to know how we have measured ignition lag. Injection point was determined by a stroboscope triggered by the nozzle needle lift. With little or no fumigation, the step in the indicator card was sufficiently distinct to spot the ignition point. With increased fumigation, the ignition point gets earlier and more indistinct. Plotting ignition lag against supplementary fuel feed, we have no points for big supplementary fuel feed. But we get a point for zero ignition lag in the following manner. While we increase the supplementary fuel feed in small increments, we periodically cut out the main injection by pushing back the fuel rack for one cycle or two. If the amount of fumigation is not excessive, this will cause misfire for one or two cycles. With an excessive amount of fumigation, cutting out the injection will cause no misfire. The minimum amount of fumigation which avoids complete misfire during the cutout is said to correspond to zero ignition lag. Misfire can, of course, be heard and seen in the color of the exhaust. Having a few points at no fumigation and moderate fumigation and one on the abscissa line permits the drawing of a curve like our Fig. 22.

We have no answer to Mr. Witzky's question on the compression temperature in the nonfiring tests, but the exhaust temperatures were measured and some of them are listed in Table 5. On multicylinder operation the answer given earlier applies.

Messrs. Jones and Rickles offer evidence that aspiration of gasoline or other high-octane fuels resulted in greater improvement than when diesel fuel was aspirated, and exceeded in many ways the results presented in this paper. We do not question their results and could even reproduce some of them. Nevertheless, we maintain that under normal circumstances the fumigation of diesel fuel is more beneficial than fumigation of gasoline. We make the comparison on three accounts.

The first is merely a practical aspect. The 2-fuel system is unattractive to the truck operator and to many other operators. In most cases this alone would decide the matter. Secondly, cylinder and piston scuffing and crankcase oil dilution have been reported by some with kerosene, by others with gasoline. With diesel supplementary fuel there should be no undue wear; and we did not find any over prolonged tests.

Now we come to performance. We have tested combinations of a variety of supplementary fuels and methods of introduction. We have found that the fumigation of finely atomized diesel fuel gave the best results in every respect under normal operating conditions. We found also that the method of introduction was more important with diesel fuel than with gasoline. Best results were obtained with a fog generator, next best with a pneumatic atomizer.

Let us elaborate on "normal" operating conditions. The load was near and up to full load, the fuel one of medium cetane number, the compression ratio not very high. At part load with "normal" fuel and "normal" compression ratio, no fumigation should be used. At overload and/or with very high-cetane fuel and/or higher than normal compression ratios, gasoline may give better results, especially if large quantities (25–30% of the total) are used. Diesel fuel in such quantities would cause preignition.

How does this check with the California Research and Esso results? In both investigations the emphasis was on what we would call the overload region. There the combustion with straight injection is so poor that the results with addition of supplementary fuel to the intake air are quite spectacular. Relatively high-cetane main fuel (relative to the compression ratio) would naturally call for a lower cetane supplementary fuel, just as a very low-cetane main fuel needs very high-cetane supplementary fuel. Optimum combinations cannot be expected all the time, but we believe that an ordinary engine running on 35–40 cetane number fuel between three-quarters and full load would perform better with fumigation of 10–15% of the very same fuel in as fine a spray as possible.

Diesel fuel cannot be well carbureted. Mechanical injection produces a coarse spray, and vaporization is awkward and impairs the volumetric efficiency. It is apparent that in the hands of the investigators mentioned, diesel fuel never had a break because they did not introduce it properly.

Mr. Pinney's analysis of the savings that can be expected from fumigation in railroad operations is most interesting. On that basis the nation's railroads could save approximately $4.5 million or $17.5 million (net) respectively by fumigation on their main-line locomotives. In the case of locomotives, Mr. Wilson's question — Shall we dope moderately all the substandard fuel, or dope the supplementary fuel highly and the main fuel none? — is legitimate.

As we understand it, the railroads do not object to the 2-fuel system as such, but they object to two large fuel tanks, both of which have to be accommodated under the cab between the wheels. If the supplementary fuel tank is not more than 40–50 gal, it can be placed conveniently inside the cab and need not be refilled except at the end of a run. Then performance alone should decide the choice, and with our present experience a highly doped supplementary fuel is preferable.

Dr. Meurer's points are well-taken. We readily admit that fumigation is not equally beneficial at all speeds and loads. But is this a good reason not to use it?

Fumigation equipment is simple to install, and the operator can cut it out at will or an automatic cutout may be set to act when the operating conditions are such (light load or low speed) that they may make fumigation undesirable. During the rest of the time, fumigation will produce fuel savings, smoke reduction, noise reduction, and increased power. Benefits will be maximum near full load and normal speed; under other conditions they will be less. But performance need never be penalized for the sake of fumigation. Better fuel consumption under certain conditions does not have to be paid for by poorer consumption under other conditions. Power will never be less, smoke and noise will never be increased by the employment of fumigation. Sometimes we'll have to accept half a loaf, but the installation is so simple (especially if compressed air is available) that the benefits to be derived are ample justification.

Protective for High-Temperature

C. H. Bailey, S. S. Sorem, and A. G. Cattaneo, Shell Development Co.

This paper was presented at the SAE Annual Meeting, Detroit, Jan. 15, 1958.

TO operate ball and roller bearings at high temperatures, the bearing is surrounded with a reducing atmosphere to prevent destructive oxidation. Lubricating films are formed on the bearing surfaces by means of reactive compounds added to the reducing atmosphere.

An Air Force sponsored research program is now underway to develop this method further and to determine the range of conditions where it may be usefully applied. It has been found that the lubricating film-forming reaction will not go satisfactorily with certain metals frequently used in high-temperature bearing construction.

However, bearings constructed of all-ferrous metals do work with this method. To date test runs of 100 hr at 700 F and 22 hr at 840 F have been completed without any signs of impending bearing failure.

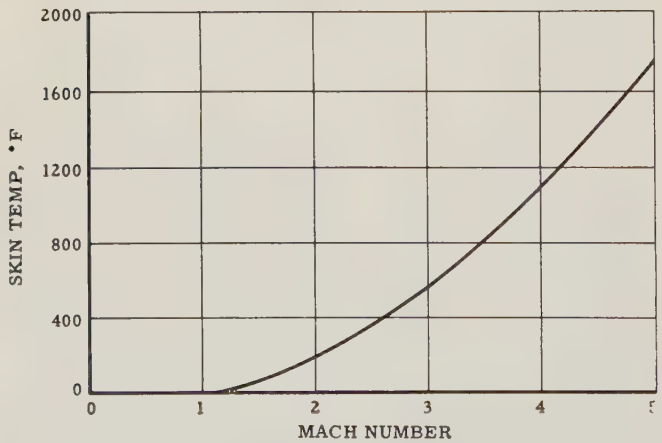

Fig. 1—Skin temperature of high-speed aircraft

IN October, 1955, a new method, which permitted ball and roller bearing operation at high temperatures without the use of liquid lubricants or greases, was reported to the ASME-ASLE Lubrication Conference.[1] Subsequently the Air Force has sponsored a research project to develop this method further and to determine its limitations and the conditions of operation where it may be usefully applied.[2] In this paper the earlier work, which led to the concept of this method, will be reviewed and ensuing progress under the Air Force sponsored program will be reported.

Perhaps the most compelling reason for seeking methods of lubricating mechanical equipment at higher and higher temperatures is illustrated by Fig. 1, taken from a recent paper by George Schairer.[3] This graph shows the skin temperature of an aircraft as a function of its speed. At slow speeds it is quite feasible to transfer sufficient heat to the passing air in order to maintain reasonable temperatures, say below 300 F, in the lubricant and lubricated components. However, as speed increases beyond Mach 1 the temperature of the boundary layer of air adjacent to heat exchange surfaces first approaches and eventually exceeds the permissible temperatures for any of our current lubricants. The passing air ceases to be available as a heat sink. Although the aircraft fuel can be (and in some instances is now) used to absorb unwanted heat, its capacity is limited. Thus, the incentive is large to produce equipment and lubricants which will operate at these higher temperatures.

There appears to be no metallurgical reason why rolling element bearings made of tool steel cannot

[1] *Lubrication Engineering*, Vol. 12, July–August, 1956, pp. 258–260: "High-Temperature Bearing Operation in Absence of Liquid Lubricants," by S. S. Sorem and A. G. Cattaneo.

[2] WADC TR 56-370, March, 1957: "Research in High-Temperature Bearing Lubrication in Absence of Liquid Lubricants." (WADC Contract AF 33(616)-2999.)

[3] *Mechanical Engineering*, Vol. 78, September, 1956, p. 832: "High-Speed Problems of Large Airplanes," by G. S. Schaier.

Atmospheres Bearing Operation

operate satisfactorily up to at least 1000 F. However, organic fluids currently used for lubrication limit the operating temperature to somewhere around 500 F. Further organic fluid research may extend this limit somewhat, but it is not likely to approach the metallurgical temperature limit. Inorganic fluids such as molten metals and solid lubricants (for example, graphite and molybdenum disulfide) are known to be receiving considerable attention as possible high-temperature lubricants. However, the method which is to be described here does not use any such lubricant. It came about as a result of the search for an answer to the question, "Why does a rolling element bearing need a lubricant at all?"

Actually, when considering just the rolling element and race, that is, forgetting the cage for a moment, the reasons for using oil in a rolling element bearing have never been clearly defined. There are, in fact, many everyday examples of steel successfully rolling on steel with no oil present—a railroad wheel on its rail. By analogy then it can be suggested that perhaps no lubrication is required for a steel ball rolling on a steel race. This would be easy to accept if one would assume point contact and, therefore, a complete absence of sliding friction. However, a rolling element and its race deform under load according to the theory of Hertz and, therefore, the contact will be a curved surface rather than a point. Different parts of this contact surface are at different distances from the axis of rotation. For this reason early investigators, such as Reynolds in 1876[4] and Heathcote in 1921[5], concluded that differential slip must take place between the rolling element and its race. They assumed that this accounts for the resistance which accompanied rolling and thus called it rolling friction. Reynolds, however, recognized that lubricants do not have the beneficial effect on rolling friction which one would expect from their usual ability to lower the coefficient of sliding friction.

The work presented by Sorem and Cattaneo[1] led the authors to another view, namely that elastic deformation of the rolling element and its race permits any adjacent surface elements of the contacting surfaces to maintain constant relative position during the period of contact. If this be the case, differential slip does not occur, and there is no sliding friction which lubricants might reduce.

Recently, Tabor[6] has published rather extensive studies of rolling friction. He finds that surfaces in rolling contact do in fact deform elastically without appreciable slip. He further shows that virtually all of the rolling friction is accountable as elastic hysteresis loss incurred by the elastic deformation within the metal of the rolling element and its race.

When considering metal transfer and wear of rolling elements and races, some benefits may be expected from lubrication. Bell and Findlay[7] operated clean ball bearings in a vacuum at elevated temperatures, and observed strong interfacial adhesion and finally seizure between the balls and races. The presence of a lubricant reduced metal transfer between balls and races. There may, however, be ways to prevent such transfer other than by the presence of conventional liquid lubricants.

Sliding contact obviously exists between the cage and the rolling elements. The load at these surfaces has little direct relation to the load supported by the bearing as a whole. In fact, in an accurately made bearing, properly installed in a well-aligned machine, the loading on these sliding surfaces can be very small. For this reason, it seemed logical to consider the cage sliding surfaces as very lightly loaded bearings which might be satisfactorily lubricated by other than conventional liquid lubricants. If the cage rides on one of the races, the load is similarly low.

In the light of this reasoning it appeared worthwhile to try to run a rolling element bearing without lubrication to see what would happen. Some exploratory runs were undertaken on a bearing test

---

[4] Philosophical Transactions, Royal Society of London, Vol. 166, 1876, p. 155: "On Rolling Friction," by O. Reynolds.

[5] Proceedings of Institution of Automobile Engineers, Vol. 15, 1921, p. 569: "The Ball Bearing," by H. Heathcote.

[6] Proceedings of Royal Society of London, Vol. 229, 1955, p. 198: "Mechanism of Rolling Friction," by D. Tabor.

[7] Physical Review, Vol. 59, 1941, p. 922: "Molybdenite as a New Lubricant," by M. E. Bell and J. H. Findlay.

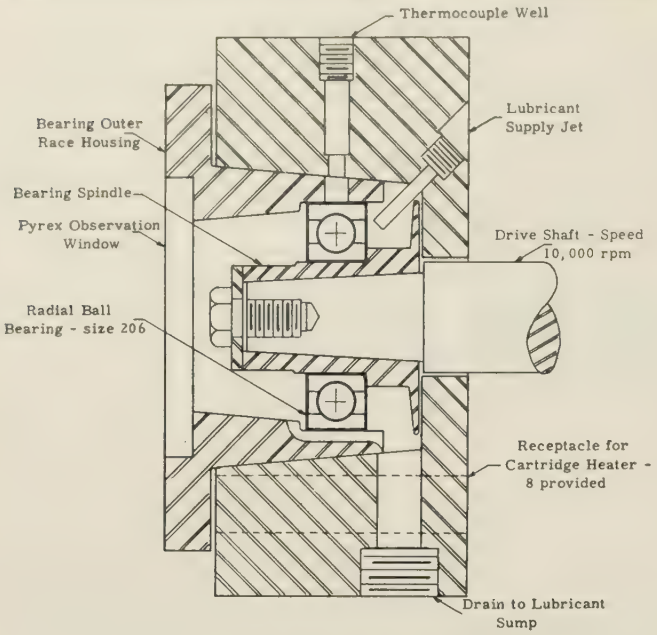

Fig. 2—High-speed bearing assembly

rig which is shown in Fig. 2. The test bearing was mounted on the cantilever end of a 10,000-rpm spindle and held in a housing that could be heated electrically to any desired temperature up to about 800 F. The initial attempts at dry operation, with no external load except the small weight of the housing, produced very erratic results with bearing lives varying from a few sec to a few hr.

It was found that a number of mechanical details had to be carefully controlled before operation in the dry condition could be consistently accomplished. With the bearings then being used it was necessary to "break-in" the bearing surfaces by operating for a period with oil lubrication before the dry run. Bearing fit, alignment, and cage balance were all somewhat more critical when running dry than when running with oil. However, with these mechanical details properly taken care of, short periods of dry operation at 600 F could be accomplished.

Bearing performance then assumed a consistent pattern. After a very short time of dry operation, red iron oxide appeared in the bearing housing. Iron oxide is an abrasive, and wear of all of the bearing parts proceeded from there at a rapid rate. Eventually the bearing failed, usually because of cage breakage at a badly worn section. By removing oxygen from the atmosphere in the bearing or, more conveniently, by maintaining a reducing atmosphere, this destructive oxidation was effectively stopped. It was now possible to operate the bearings many hr without failure of the ball and race surfaces.

Failure did, however, occur as the result of scuffing or metal pickup on the rubbing surfaces of the cage. In boundary lubrication practice, scuffing is counteracted by the use of so-called "extreme pressure" additives, compounds containing sulfur, phosphorus, or halogen. Volatile compounds containing these same elements when added to the reducing atmosphere were found to be effective in minimizing scuffing.

Test results illustrating the progress to this stage of the work are shown in Table 1. These show that the protective functions of a conventional liquid lubricant which permit a rolling element bearing to operate without excessive surface deterioration can be performed at elevated temperatures by a properly designed vapor mixture. This method of bearing operation has been called "protective-atmosphere" operation.

Once the basic ideas of the protective-atmosphere method had been formulated a number of practical questions arose. What atmosphere composition is optimum from the standpoint of protection against oxidation and the formation of lubricating films? What bearing metals work best with the protective-atmosphere method? With optimum atmosphere and bearing, what are the operating limits with regard to speed, load, temperature, and bearing life? Air Force sponsored work during the past 18 months, and still in progress, has provided at least partial answers to some of these questions.

With respect to the prevention of oxidation or rusting, the first reducing atmospheres tried were mixtures of an inert gas and a small quantity of hydrocarbon vapor. It was soon learned that with the hydrocarbon vapor present, it was no longer necessary to remove the last traces of oxygen from the inert gas. If the hydrocarbon could take care of small quantities of oxygen, could it also take care of the 21% oxygen in air? Tests revealed that an air-hydrocarbon mixture was a satisfactory reducing agent from the bearings' standpoint as long as the quantity of hydrocarbon present was considerably in excess of the amount necessary to combine with all the oxygen present or, more simply stated, a rich mixture must be maintained. Air-hydrocarbon weight ratios of about 8 appeared near optimum. Mixture ratios much richer than about 7 would protect the bearings, but would also form considerable quantities of soot and carbon in the bearing housing at the higher temperatures.

The air-hydrocarbon vapor mixture appeared to be practical for aircraft use, because a jet-engine fuel fulfills the hydrocarbon requirement very well. Much of the experimental work has been done using JP-4, a common jet-engine fuel, as the hydrocarbon component of the atmosphere. The hydrocarbon part of the atmosphere is also a convenient carrier for introducing small quantities of various additives, as will be discussed later. Differences have been found in the ability of various hydrocarbons to achieve control of rust formation. For example, an atmosphere based upon benzene, a relatively stable compound, allowed more oxidation than an atmosphere based upon diisobutylene, a much more reactive compound. These results were most noticeable in the 400–650 F temperature range. Above 700 F all hydrocarbon tested seem to be sufficiently reactive. Bearings operated in an atmosphere of air and pure hydrocarbon at high temperature show a bluish film formation. This probably indicates some oxidation is still taking place, but the destructive oxidation, that is, ferric oxide (rust) formation, is prevented.

There are a number of factors involved in the in situ formation of lubricating films which will protect the rubbing surfaces of the bearing cage at high temperature. Not all of the factors were recognized during the early part of the investiga-

tion and test results were sometimes confusing. The initial approach, as has already been mentioned, was to form a sulfide, phosphide, or halide film on the sliding surfaces to prevent contact welding, that is, scuffing. Application methods consisted of adding the appropriate extreme pressure element in organic form, either to the oil used to lubricate the bearing during break-in or to the hydrocarbon component of the reducing atmosphere. All of these procedures led to the formation of scuff-resistant films, but results were frequently unsatisfactory in some respect. Films applied by an additive in the break-in oil had only a limited life. The use of an additive in the reducing atmosphere appeared to require a compromise that was not very satisfactory: If enough additive was applied to take care of the initial startup, excessive chemical attack of the bearing occurred during runs of several hr. The first reasonable degree of success was obtained using a combination of the two application methods. Bearings broken in with an oil containing 1% sulfur could subsequently operate some 40–60 hr in a protective atmosphere consisting of a mixture of air and JP-4 jet fuel. The natural sulfur content, about 0.2%, of the JP-4 furnished the extreme pressure element during the protective-atmosphere operation.

Only limited progress has been made toward the selection of the best extreme pressure compound to use in a protective atmosphere. However, it has been shown that 0.05%v (based on the hydrocarbon content of the protective atmosphere) of tritolyl phosphate, 0.1%v of carbon disulfide, or 0.1%v of carbon tetrachloride will prevent scuffing. Low-volatility high-molecular weight compounds such as a sulfurized C_8 fatty acid are unsatisfactory additives because they tend to crack and form carbonaceous deposits in the bearing housing. Chlorides are objectionable because they promote rusting during periods when the test equipment is idle.

In this additive evaluation work, pure compounds were used as the hydrocarbon component of the protective atmosphere. It was observed that in no case where the protective atmosphere contained pure hydrocarbons plus extreme pressure additive did the bearing performance equal that obtained with JP-4. In an effort to find the material that accounted for its superior performance, the JP-4 was fractionated and the various fractions individually tested as the hydrocarbon component of a protective atmosphere. One of the fractionations involved a percolation procedure in a Florisil-packed column. This treatment selectively removed the resins or gum-forming constituents of JP-4 which amount to about 1% of the total. When these resins were removed the JP-4 atmosphere was no more effective than any of the atmospheres based upon pure hydrocarbons plus conventional extreme-pressure additives. When the resins were added again, the effectiveness of the JP-4 was restored. From previous fuel research work in our laboratories, it is known that the organic compounds that make up these resins fall into three general classifications: nitrogen-base compounds; oxygen-containing compounds, mostly phenols, carboxylic acids, and napthenic acids; and a neutral fraction rich in aromatic olefins.

A few pure organic compounds representative of some of the various types contained in the JP-4 resins have been tested as additives in a benzene carrier, used as the hydrocarbon component of a protective atmosphere. All of the compounds offered some benefit, but m-toluidine was outstanding.

Table 1—Test Results of Dry Run Bearing Operation

Bearing Broken-In	Atmosphere	Test Temperature	Test Duration	Remarks
No	Air	Room	0.1 min	Bearing seized
No	Air	Room to 375 F	2 hr 11 min	Failed due to excessive wear, considerable iron oxide present
Yes	Commercial nitrogen	Room to 375 F	2 hr 20 min	Cage worn out, rust
Yes	Air	Room to 600 F	3 hr 10 min	Cage worn out, rust
Yes	CO_2 + hydrocarbon	600 F	10 hr	No rust visible, considerable soot present, cage severely scuffed
Yes	Air + hydrocarbon	600 F	10 hr	No rust visible, trace of soot present, cage slightly scuffed
Yes	Air + hydrocarbon + Sulfur ep	600 F	40 hr	Bearing in good mechanical condition, but tight due to change of dimensions.

The mechanism by which the JP-4 resins improve protective-atmosphere operation is not yet clear. One hint is contained in the appearance of a bearing operated in a JP-4 atmosphere as compared to an identical bearing operated in an atmosphere of a pure hydrocarbon plus an extreme-pressure additive. The balls and cage contact areas of the former are covered with a dark film that is smooth and shiny, while the latter shows more wear and is not as smooth and shiny. An analysis of the smooth shiny film produced by the JP-4 atmosphere would be interesting and useful, but so far these films have defied removal for analysis. They are insoluble in the common mineral acids and organic solvents, and are not easily removed mechanically.

Studies of the conditions which lead to the best film formation present other clues to the mechanisms involved. In the normal configuration of the test rig, the air and hydrocarbon components of the protective atmosphere are metered at room temperature into a common delivery line leading to the jet in the bearing housing. When the bearing is operated at temperatures below the dew point of the air JP-4 mixture, liquid hydrocarbon arrives at the bearing housing and the bearing operates with liquid lubrication. At temperatures just above the dew point of the mixture (about 450 F) the bearing operates dry, but the films characteristic of most work with JP-4 are not formed. At about 550 F and above, the film formation does take place quite satisfactorily. It was noted that at these higher temperatures the delivery line bringing the mixture to the bearing is quite hot, and exposes the mixture to an appreciable period at elevated temperature before it enters the housing. In another experiment where the hydrocarbon and air components were piped separately to the bearing housing, effective film formation did not occur. Since an appreciable contact period at high temperature is important, the formation of polymers, like gum in fuel, may be responsible for the film. In still another experiment where a long heated delivery line was used, the films again failed to appear. This may be further confirmation of the polymer formation theory, since polymers which normally deposit on the bearing surfaces would in this case have deposited in the hot line. It has been found that with proper preparation and delivery of the protective atmosphere, effective film formation will take place quite rapidly. In fact, the application of an ex-

Table 2—Some Protective-Atmosphere Results at High Temperature

Period of Operation, hr	Bearing Temperature, F	Speed, rpm	Radial load, lb	Bearing Size	Bearing Condition Upon Completion of Test	Run No.
22	840	10,000	87	206	Good, much longer operation possible	HSB 518
100	700	10,000	20	206	Good, much longer operation possible	HSB 498
22	800	10,000	20	206	Good, much longer operation possible	HSB 505
33	700	7200	1000	209	Good, slightly worn	WFB 7

treme pressure film by means of an additive-type break-in oil is unnecessary with such application of the protective atmosphere.

A factor which has delayed some of this work involved the bearing materials. During the course of this investigation many types of bearing construction materials were used. Several different manufacturers supplied their ideas of the best design and materials for the temperature, speed, and load conditions proposed. These several bearing material combinations proved helpful in defining a material limitation for protective-atmosphere operation: the protective-atmosphere scheme will work well only with metals which have a positive oxidation potential. This requirement was illustrated quite emphatically by an unsuccessful attempt to operate a bearing with a bronze cage in a sulfur-containing atmosphere. This atmosphere had previously worked well with a bearing fitted with a steel cage. The difference in performance could be correlated with the appearance of the rubbing surfaces. The bronze surfaces were clean, shiny, and bronze colored, not at all characteristic of a sulfide extreme-pressure film. On the other hand, the steel cage formed dark shiny films on the rubbing surfaces. Even when a bronze cage was precoated with a black sulfide film by operation in a sulfurized oil, subsequent high-temperature operation in a protective atmosphere removed all the black sulfide film, leaving the cage bright and clean again. The reducing atmosphere had taken all sulfur away from the copper in the cage. Other metals were tested also. In all cases the film-forming materials in the reducing atmosphere reacted only with the bearing metals that have a high-oxidation potential, such as iron.

There is another class of metals that does not work well in a protective atmosphere. This includes the corrosion- and oxidation-resistant metals such as monel, inconel, and stainless steel. With this class of metals it is believed that the tenacious and impervious oxide films, which are responsible for their corrosion resistance, also prevent formation of the type of films essential to protective-atmosphere operation. The original oxide films have high frictional characteristics. When bearing components were made of these oxidation-resistant materials and the bearings were operated dry, failures, initiated by ball skidding, usually resulted almost immediately.

Bearings constructed entirely of ferrous alloys have given by far the best results. On the basis of rather limited experience, hard steel or cast iron appears to be preferable to soft steel as a cage material. The various high-temperature race and ball materials that have been tested are SAE, M-2 and M-10 tool steels, Vacuum Metals Corp. Ferrovac-Halmo, Latrobe Steel Co.'s Electrite MV-1, and type 440C stainless steel. All of these, except the stainless steel, seem to be about equally satisfactory from the standpoint of forming effective films in our protective-atmosphere operation.

From the above it may be seen that protective atmosphere presents a potential method for operating equipment in temperature ranges where lubrication is now extremely difficult, if not impossible. Considerably more work will be required to define the optimum combinations of materials and mechanical configurations for use with this method. However, in its present stage, it is sufficiently promising to justify an investigation of its practical limitations with respect to bearing temperature, speed, load, and life. This work which required the installation of variable speed and load test equipment is just getting under way and no limits can as yet be stated. However, a few data listing the test durations and conditions where experimental work has successfully been carried out are shown in Table 2.

To review briefly, the protective-atmosphere method for operating rolling element bearings at high temperature involves the following concepts:

1. Surrounding the bearing with a reducing atmosphere to prevent destructive oxidation during operation.
2. The in situ formation of lubricating films on the bearing surfaces during operation. For best results, these films include both the reaction product of an extreme pressure element, such as sulfur, with the bearing surfaces and an organic film of an as yet undefined composition.
3. The metals of bearing construction must have a positive oxidation potential to accept the films as described in the second concept.

At the current state of this development a protective atmosphere consisting of an air/JP-4 jet fuel mixture (weight ratio 8/1) will permit bearings of all-ferrous construction to be operated at temperatures up to at least 800 F.

DISCUSSION

Protective-Atmosphere Procedure Incompatible with Some Nonscuff Films

—Lawrence D. Dyer
General Motors Corp.

THE purpose of this note is to consider the surface reactions in the authors' work and to suggest modifications in some of their conclusions regarding the concepts involved in bearing operation at high temperatures.

Several phases of the authors' work are diagramed below for the purpose of general consideration. The concepts involved in maintaining a nonscuff film will be commented on particularly. For each phase of work, the object of the work is given, the chemical equation for the surface reaction is written, and the function is singled out which governs the effectiveness of the reaction in accomplishing a beneficial task.

The symbol ΔF, with appropriate subscripts, means the difference between the Gibbs' free energy of the products and the Gibbs' free energy of the reactants (in their standard states) at the temperature in question. Reactions having a negative Gibbs' free energy occur spontaneously, reactions with a positive free energy do not.

Formation of a Working Oxide Film Without Formation of Abrasive Oxide

$$\text{Metal} + O_2 \xrightarrow[\text{Surface broken-in with oil}]{\text{Flowing air, abrasive action, high temperature}} \text{Metal oxide}$$

The function governing effectiveness is:
(Rate of oxidation of metal at the operating temperature) minus (Rate of oxide removal by abrasive action)

Comments:
1. Some metal oxide is needed to avoid high adhesion.
2. Excessive oxidation leads to abrasive oxide formation and wear.
3. $\Delta F_{formation}$ of the metal oxide drives this reaction.

It is negative for all metal oxides except those of the noble metals.

Inhibition of Formation of Excess Oxide

$$\text{Metal oxide} + \text{Reactive hydrocarbons} \xrightarrow[\text{Broken-in surface}]{\text{Air and hydrocarbon flow, abrasive action}} \text{Metal} + H_2O\uparrow + CO_2\uparrow$$

Pertinent function:
(Rate of reduction of oxide by hydrocarbon) plus (Rate of oxide removal by abrasion) minus (Rate of oxidation of metal by air)

Comment:
1. $\Delta F_{reaction}$ need not be negative if the gaseous products are removed by flow.

Maintenance of Nonscuff Film

Two reactions compete:

1. $$[\text{Metal} + \text{Metal oxide} + \text{ep film}] + [CS_2 \text{ or } CCl_4 \text{ or tri toyl-phosphate or mercaptans or JP-4 resins}] \xrightarrow[\text{Broken-in surface, which is an ep film}]{\text{Air, resin, and hydrocarbon flow, abrasion}} [\text{Complex film of metal, metal oxide, resins, unknown combinations}] + [\text{Gaseous reaction products}]$$

2. $$\text{Complex film} + \text{Reactive hydrocarbon} \xrightarrow[\text{Broken-in surface, which is an ep film}]{\text{Air, resin and hydrocarbon flow, abrasion}} \text{Metal} + [\text{Gaseous products: } H_2S, NH_3, HCl, \text{organic materials}]$$

Sum: $$[CS_2, \text{resins, and the like}] + \text{Reactive hydrocarbon} \xrightarrow{\text{Metal surface}} [H_2S, NH_3, \text{etc.}] + \text{Altered hydrocarbons}$$

Comment on Reaction 1—The authors' complex film is an ep film when CS_2, CCl_4, and others, are added, and a dark, shiny film of unknown nature when JP-4 resins are added.

Comment on Reactions 1 and 2—A negative $\Delta F_{reaction}$ is not required because of the removal of the products in the gas flow.

Comment on Reaction 2—The authors' case of a bronze cage which lost its ep film is an example of Reaction 2:

$$\text{Cus} + \text{Hydrocarbon} \longrightarrow \text{Cu} + H_2S \text{ Altered hydrocarbon}$$

There are two separate purposes for which to name the pertinent function in the nonscuff film category:

1. The formation of the film. Pertinent function: (Rate of formation of the complex film) minus (Rate of its removal by abrasion). Monel, inconel and stainless steel have a low value of this function.
2. The maintenance of a film which has already been established. Pertinent function: (Rate of conversion of ep additive to ep film) minus (Rate of conversion of ep film to H_2S, NH_3, or the like) minus (Rate of removal of ep film by abrasion).

From these reactions, it is clear that the action of hydrocarbons as a protective atmosphere for the formation of a useful, but not abrasive, oxide film is in general incompatible with the use of nonscuff films which contain sulfur, nitrogen, or chlorine. The fortunate happenstance is that for the ferrous alloys, the rate of attack on the film by the active hydrocarbons does not exceed the rate of its formation from the ep additive and, therefore, the combination works.

Second, it is a misleading policy to call an atmosphere which contains oxygen, hydrocarbons, and organic substitutional compounds a "reducing" atmosphere when considering these surface film reactions.

Third, the authors concluded that metals of bearing construction must have a positive oxidation potential to accept the antiscuff films. It should be pointed out that this is an empirical observation and that there are reasons for this incompatibility of film with metal beyond the value of the oxidation potential per se. Oxidation potential does not appear to be directly related to either the function which controls the formation of the nonscuff film, or the function which controls maintaining it once it is established. In view of the fact that the nature of the film and the chemical mechanism of its formation are unknown, it behooves one not to settle on a particular chemical-affinity function such as oxidation potential for deciding whether a bearing will retain the nonscuff film.

Authors' Closure To Discussion

WE wish to thank Mr. Dyer for his interesting interpretation of our work. The equations shown are essentially in agreement with the authors' views. Regarding his comments we should note the following:

A "useful, but not abrasive oxide film" is not achieved by the reactions outlined in the first two equations. Our observations indicate that the reactions of the second equation proceed so far to the right as to produce conditions for high adhesion.

Regarding the reactions for the formation and maintenance of nonscuff films, it is recognized that in the dynamic system involved both rate factors and thermodynamic potentials affect the end result. The observation that metals on which nonscuff films can be formed and maintained can be segregated on the basis of oxidation potential from those on which these films are not formed and maintained is empirical, as Mr. Dyer states. The assumption that a thermodynamic driving force is predominant in determining whether or not the desired films are formed is, however, compatible with the above observations and does not appear unreasonable.

CONTINUOUS RADIOTRACER Shows How Piston Rings

THE concept of using radiotracers in wear studies, and particularly the use of radioactive piston rings in gasoline engines, originated about 15 years ago.[1] About 6 years later, a practical way of obtaining radioactive piston rings by exposure to neutron bombardment was developed.[2] The large number of papers published on this subject in the following years is evidence that the technique has been and is being widely used by workers in the field. The quick acceptance of the radiotracer technique for wear measurement arose chiefly from the inherent high sensitivity of the method, which allows a few millionths of a gram of debris in the crankcase oil to be detected and measured. This permitted the use of short tests, resulting in much faster data accumulation than was possible using older conventional techniques of engine measurements and ring weighings. In addition, it was no longer necessary to disassemble the engine to obtain wear data, which allowed wear rates to be obtained without mechanically disturbing the parts under study. Also, the short test times permitted unusual lubricant compositions to be tested with little danger of severe engine damage.

A large part of the ring wear work reported in the literature has been done with single- and multicylinder engines in the laboratory. Wear rates were usually obtained by counting samples of oil withdrawn from the crankcase from time to time. In some cases, by pumping crankcase oil through suitable counting equipment, continuous measurement of the activity in the oil has been used to good advantage to study rapid changes in wear rates caused by frequent changes in engine operating conditions. Continuous wear curves are obtained with this technique rather than discrete points from which smooth curves must be deduced. Where test cars containing radioactive rings have been used, wear measurements were based on the older method of intermittent sampling of the crankcase oil. It was felt that the full benefits of the radiotracer technique would be gained only by adapting the method to a car in the road, and by continuously monitoring the lubricating oil for radioactive debris. A test of this type should be more realistic than laboratory engine tests, and has the advantage of allowing transient wearing phenomena to be observed, which would be either impossible or extremely cumbersome to study using counting methods based on oil drain samples. Equipment to monitor the activity of crankcase oil, adapted to use in an automobile, is described in this paper along with some of the ring wear results obtained.

Test Equipment Used

A passenger car equipped with an overhead-valve V-8 engine was used to obtain the wear data. Two engine modifications were made: (1) The full-flow oil filter was bypassed since the filter would trap radioactive debris and prevent all the activity in the oil from being counted. Frequent oil changes (150 miles maximum) were used to minimize any effect of abrasive wear resulting from solid material that

[1] "Wear Test Method and Composition," by S. W. Ferris. U. S. Patent No. 2,315,845, Oct. 15, 1941. Assigned to Atlantic Refiining Co.

[2] SAE *Quarterly* Transactions, Vol. 3, October, 1949, pp. 634–638: "Application of Radioactive Tracers to Improvement of Fuels, Lubricants, and Engines," by P. L. Pinotti, D. E. Hall, and E. J. McLaughlin.

MONITORING

Wear in Service

J. S. Batzold, J. V. Clarke, Jr., and J. F. Kunc, Esso Research and Engineering Co.

This paper was presented at the SAE Annual Meeting, Detroit, Jan. 16, 1958.

would normally be filtered out of the oil. (2) The chrome-faced top rings used as standard equipment in this engine were replaced by cast-iron rings obtained from the Perfect Circle Corp. (Although counting techniques are available for separate determinations of the amount of radioactive chromium and iron in used oil samples, the equipment required is too complex and bulky for an installation of the type described in this paper). By a 2-week exposure to neutrons at the irradiation facilities of Union Carbide Nuclear Co., Oak Ridge, Tenn., cast-iron rings, each of which contained approximately 1.5 millicuries of Fe^{59}, were obtained. This level of activity was sufficient for 2–3 months work before replacement was required without causing any radiation hazard to personnel involved. Installation of the rings was accomplished with conventional tools having long handles, allowing the mechanics to work from 2–3 ft from the rings at all times. After installation, the head and block provided sufficient shielding to keep the radiation intensity far below hazardous limits.

A cylindrical counting well, shielded with lead 2–4 in. thick, was mounted on the floor of the rear passenger compartment. The thicker 4-in. shielding was located on the side of the counting well which faced the engine block to reduce the background due to the irradiated rings. Lubricating oil was circulated through the well by means of a pump situated in an oil line leading from the bottom of the crankcase. Careful tests showed that the settling of radioactive debris in the crankcase did not introduce errors in the counting. The inlet stream to the counting well came directly from the bottom of the oil pan, and the equipment was such that the total oil charge circulated at least once every 30 sec. This was enough agitation to minimize any effects of settling of radioactive debris.

An aircooled scintillation tube placed in this counting well was connected to a ratemeter and a recorder, also carried in the rear compartment of

THE results of a radiotracer study to obtain a better understanding of the factors governing piston-ring wear in passenger-car engines are presented in this paper. The study was conducted in a passenger-car engine which was equipped with radioactive top compression rings.

The wear rates obtained were of the same order of magnitude as those observed in actual passenger-car service, demonstrating that significant results in terms of field performance can be obtained by running wear tests of relatively short duration with radioactive rings.

The study revealed that a variety of interrelated factors have an important bearing on piston-ring wear in passenger-car service. These include: the operating regimes to which the vehicle is subjected, the temperature of the cylinder walls, the amount of dirt getting into the engine, the kind of fuel burned, and the kind of lubricant used.

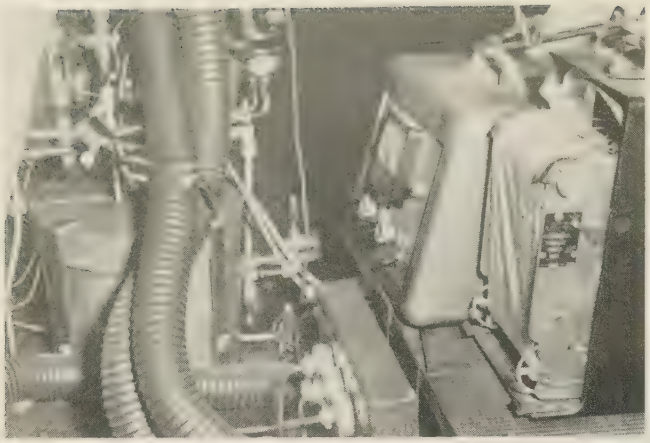

Fig. 1—Continuous counting equipment in test car

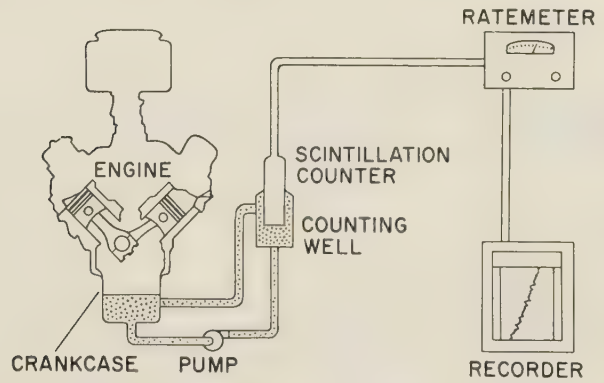

Fig. 2—Schematic diagram of equipment in test car

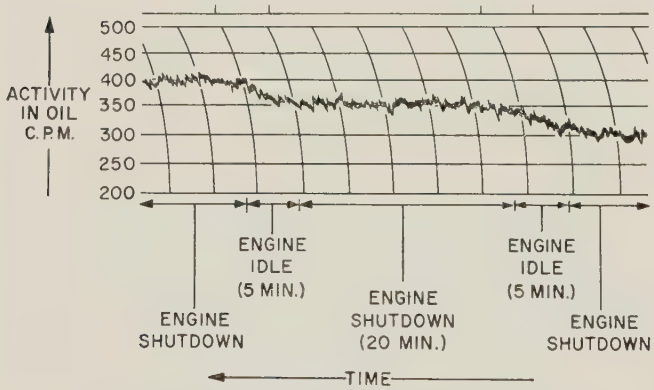

Fig. 3—Typical record, continuous counting system

Table 1—Test Car Ring Wear Correlates With Field Test Results

Type of Operation	Top Ring Wear mg per 1000 miles	
	City-Intercity	Stop-and-Go
Field Test	11	22-38
Test Car	14	29

Table 2—Influence of Operating Conditions on Wear

Type of Operation	Average Jacket Temperature, F	Relative Wear
Highway	150	100
Traffic	150	70
Startup	100	400

the car. When the car was operated over the road, a "Homelite" 2.5-kw motor generator, towed behind the car in a trailer, supplied electrical power to run the counting equipment. Thus, a continuous record of piston-ring wear could be made as the car was run either in the laboratory or on the road. A photograph of the equipment is shown in Fig. 1 and a schematic diagram of it in Fig. 2.

An example of the type of record obtained with this equipment is shown in Fig. 3. Reading from right to left, the trace of the recording pen has charted the radioactivity in the crankcase oil for an operating sequence of shutdown, 5 min of idle, 20 min of shutdown, 5 min of idle, and shutdown. The increase of activity caused by wear during the engine startup and idle is clearly seen and amounts to about 50 counts per min for each operating period.

The validity of the continous counting method was spot checked on a variety of occasions by removing samples of used oil of known volume during the course of tests being run with the continuous method and determining the amount of radioactive iron which they contained by using a scintillation tube and a scaler.

No hazard existed in the day to day use of the car, since the engine block and head provided an efficient radiation shield. In addition, careful checking of the exhaust gas while the car was running failed to reveal any radioactivity.

The weight of iron in a given sample of used oil was calculated, using a standard solution containing a known amount of active piston-ring material. The standard solution was always made up from a piece of piston ring which had been irradiated along with the eight rings normally used in the engine.

Test Car Ring Wear Correlates with Field Test Results

The utility of any wear test, whether radioactive or not, is determined by its ability to correlate with known field results. Unless a correlation exists, the test is of little value for predicting lubricant or fuel quality. The question of correlation is perhaps even more critical with radiotracer work, since there is a certain inherent reluctance to accept results obtained with so much less engine operating time than is required with other wear testing techniques. The data obtained in the test car have been compared wherever possible with ring wear data accumulated by our company in field tests, and the results of the comparisons show very good correlation between the radioactive test and the field. Examples of this agreement are shown in Table 1, where fleet test results under two types of driving conditions, moderate-speed suburban-type driving and low-temperature stop-and-go type driving, are compared with test car results obtained under nearly the same conditions. The field test results involved nearly one-half million miles of operation, while the test car results were extracted from the data obtained during the first 5000 miles.

Since the test car overall wear rates were consistent with field studies, results obtained with the test car could be used with some confidence both in predicting the performance of fuels and lubricants in service, and in studying the effect of engine operating variables on ring wear. Some of the test results obtained with the continuous counting

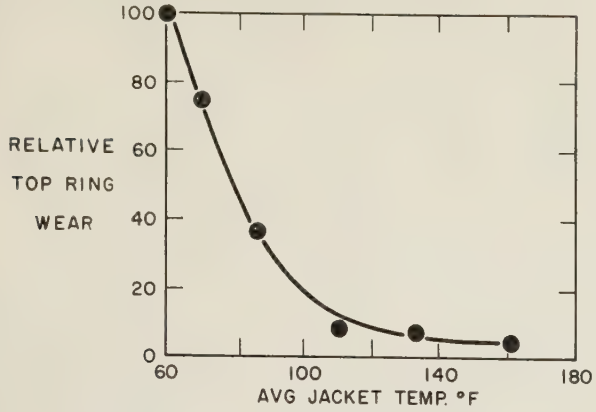

Fig. 4—Running wear increases with decreasing jacket temperature

Table 3—Fuel Additives Affect Ring Wear at 70 F Jacket Temperature

(Commercial 10W-30 Lubricant)

Additive in Isooctane	Relative Wear Rate
None	100
1 Theory Et Br_2[a]	150
1 Theory Et Cl_2 + ½ Theory Et Br_2[a]	180
0.05% Sulfur	460
3.0 cc Tel per Gal[b]	120

[a] No lead present; concentration based on hypothetical 3 cc tel per gal.
[b] As aviation mix (tel + 1 theory Et Br_2).

Table 4—Wear is Decreased by Warmup

Operation	Relative Wear
20 miles of traffic driving starting with cold engine	180
Engine warmup followed by 20 miles of traffic driving	100

equipment are presented in the remainder of this paper. Unless otherwise stated, all work was done using a commercial premium fuel containing 2.5 cc tel per gal.

Vehicle Operating Conditions Influence Ring Wear Rate

Type of Driving—The wear rates prevailing in the test car during typical highway and traffic driving were compared with results obtained from a series of engine starts followed by 5 min of idle and 30 min of shutdown. The comparisons were made on the basis of the same number of engine revolutions. As may be seen from Table 2, wear during engine startups was four to five times as high as it was during highway or traffic driving. In addition, nearly constant speed highway driving was slightly more severe than traffic driving.

The lower jacket temperature during the startup operation was undoubtedly a major contributor to the high wear rate. A separate investigation of this variable is described in the next section. No satisfactory explanation has been evolved for the slightly higher wear observed during highway driving as compared to traffic driving.

Wear Greatest at Low Jacket Temperature—The effect of jacket temperature on the rate of top ring wear was studied at continuous idle. In this work, the jacket temperature was kept at the desired level by adding a controlled amount of cold water to the cooling system. The range of jacket temperature studied was between 60 and 150 F, using an SAE 10W-30 mineral oil in the crankcase and a leaded gasoline containing 0.045% sulfur as fuel. As the jacket temperature was reduced below 110 F, the rate of wear increased markedly. As shown in Fig. 4, the wear rate at 60 F was ten times as high as it was at 110 F. These data agree well with other published results on jacket temperature effects.[3,4]

The sensitivity of the ring wear rate to jacket temperatures below 110 F suggests that a chemical mechanism is responsible for this wear. A postulate suggested earlier[5] that fits the experimental data obtained in the present study is that water- and fuel-derived inorganic acidic materials (SO_2, SO_3, HCl, HBr, and the like) formed as products of combustion are able to condense on the ring surfaces at low temperatures, causing corrosion which ultimately results in loss of metal or wear. In this connection, it is of interest to note that the jacket temperature at the inflection point of the curve in Fig. 4 approximates the dew point of the combustion gases which is in the range of 130–135 F.

To test the postulate of chemical attack, a number of fuels were used in the engine under conditions of continuous idle, where the individual fuels could be burned in sequence without any engine shutdowns. The work was carried out at a controlled low jacket temperature (70 F), using as fuel isooctane both alone and containing sulfur, tel, and lead scavengers. Concentrations of the additives were chosen to approximate the amounts encountered in typical gasolines. The data obtained are shown in Table 3.

On the basis of these results, low-temperature ring wear appears to result from attack in the ring area by corrosive materials formed as products of fuel combustion. Although neutralization would appear to be a logical way of preventing chemical attack by materials of this type, this route by itself was not effective, as will be shown later in this paper.

Warm-up Reduces Low Temperature Ring Wear—The instrumented test car provided an excellent opportunity to answer the question of whether warming up an engine by idling it before starting on a trip is beneficial from the standpoint of ring wear. The study was conducted in cold weather so that the jacket temperature at the beginning of each of the two tests run was about 32 F. In one case, the test car was started from a cold condition and immediately driven 20 miles in traffic. In the second case, a 10-min warmup period at idle preceded the same 20-mile trip. It was found that operating the car with a cold jacket immediately upon starting gave nearly double the wear obtained when the car was allowed to warm up by idling the engine before driving, as shown by the data in Table 4.

Wear Is a Function of Shutdown Time—If low-temperature wear does proceed by a corrosive mechanism, the length of time an engine is shut down between operating periods should influence the overall wear rate. To check this hypothesis, tests were carried out where the length of shutdown

[3] SAE Transactions, Vol. 61, 1953, pp. 221–223, 230: "How Engines Wear," by J. F. Kunc, Jr., D. S. McArthur, and L. E. Moody.
[4] *Lubrication Engineering*, Vol. 11, July–August, 1955, pp. 238–241: "Atoms Trace Wear," by W. R. Miller and H. R. Jackson.
[5] SAE Transactions, Vol. 61, 1953, pp. 378–385: "Lubricants—The Surface Savers," by J. F. Kunc, Jr. and J. P. Hamer.

between 5-min periods of idling was varied from a few sec to 24 hr. In all tests, the engine was actually run for the same length of time. As the shutdown time increased, the amount of wear obtained in the test increased as shown in Fig. 5. The first few min of shutdown appear quite important as regards top ring wear on the subsequent startup, since a 20-min shutdown resulted in over half the increase in wear obtained with a 24-hr shutdown. The wear rate for continuous operation and for shutdowns of very short duration were almost equivalent. Apparently, the physical act of shutdown had little effect on top ring wear.

These data imply that the wear obtained on first starting a cold engine is a function of the conditions which existed in the cylinder during the previous shutdown. It appears that, on startup, corrosion products formed on the engine surfaces during the previous shutdown are removed quickly by the rubbing action of the moving parts. The amount of these corrosion products depends both on the engine wall temperature during shutdown and on the time of shutdown, with a given fuel, lubricant, and jacket temperature. Although the jacket temperature was kept constant at 70 F during these experiments, the metal temperature in the ring zone area would be higher during the shorter shutdowns. As the shutdown times become longer, these metal temperatures would more nearly approach the jacket temperature. Both temperature and time can affect the amount of corrosive materials condensed, and also the extent of reaction between these corrosive materials and the metal surfaces in the ring zone area. Since data relating wall temperature to shutdown time are not available, the relative importance of these two variables in the series of experiments conducted cannot be assessed.

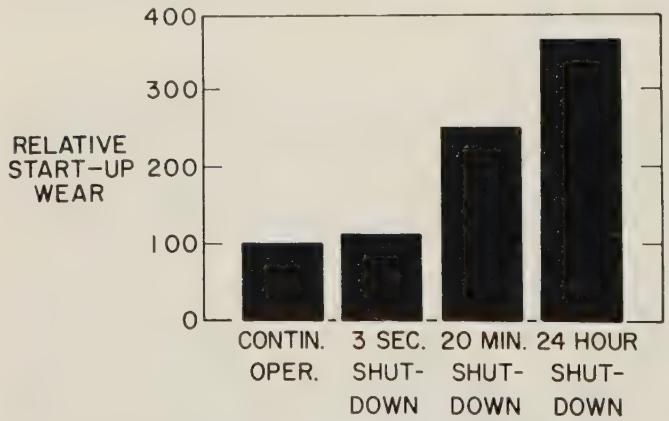

Fig. 5—Startup wear increases with shutdown time

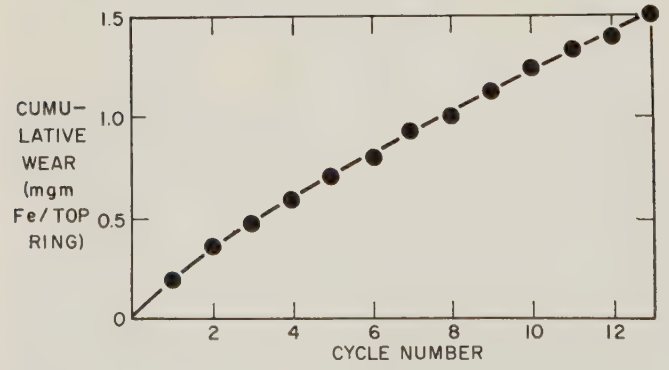

Fig. 6—Startup wear becomes linear with time

These data do not mean that no wear occurs during engine operation except that due to corrosion during shutdown. However, this type of wear can be appreciable, especially under stop-and-go driving at low jacket temperature.

Abrasives in Intake Air Greatly Increase Ring Wear—A limited amount of data was obtained on the effect of oil-born abrasives on ring wear by operating the car for a few miles on a dusty road with the air cleaner removed. The work described in this section where neither oil nor air filter was used is far outside the severity level to be expected in normal operation, but does give an insight into the large role that could be played by abrasives in ring wear, especially in the case of poor equipment maintenance.

The test was carried out in sequential fashion and can be broken down into the following periods of operation: (1) Highway driving with and without the air cleaner in the absence of excessive dust; (2) highway driving with no air cleaner under dusty conditions; (3) highway driving after dust exposure with the air cleaner replaced; and (4) highway driving after an oil change to remove the contaminated oil. The wear levels obtained during this work (Table 5) demonstrate the astronomical rates of wear possible under these very severe conditions. Even after the contaminated oil was changed, extremely high wear rates were obtained. This is felt to be due to a combination of two factors:

1. Ring surface and cylinder wall damage, caused by the abrasive, having to heal by a break-in effect.
2. Corrosion during the shutdown at the time the oil was changed.

These results do not agree with those reported by Watson et al.[6] where the wear caused by road dust was found to decrease with time after the application of the dust was stopped. This was attributed to the relatively low internal strength of the dust causing the particles to become progressively smaller until they were too small to cause appreciable wear. Abrasives of high internal strength, for example, diamond dust, continued to cause high wear as long as they were allowed to remain in the engine. The differences from the results obtained here may be due to the much higher concentration of dust causing considerable surface damage to the ring area, or to differences in the kind of dust involved.

Engine Knock Had No Effect on Ring Wear—An investigation was made to see what effect engine knock might have on ring wear. Rates of wear were measured during both knocking accelerations and nonknocking accelerations, the knock being obtained either by using fuels of insufficient octane quality to satisfy the engine or by advancing the spark. Although knock intensities up to "heavy" were investigated, no appreciable effect on piston-ring wear could be found (Table 6).

Although no increase in ring wear was found in this study when the engine was allowed to knock for a relatively short time it should not be implied that knock cannot damage rings and other engine

[6] SAE Transactions, Vol. 63, 1955, pp. 717–728: "Abrasive Wear of Piston Rings," by C. E. Watson, F. J. Hanley, and R. W. Burchell.

Table 5—Abrasives Can Cause Extremely High Wear

(Commercial SAE 10W-30 Lubricant)

Air Cleaner	Type of Driving	Average Speed, mph	Miles Driven	Relative Ring Wear Rate per Mile[a]
Off	Highway	30	10	100
Off	Dusty Road	30	10	100
On	Dusty Road	30	4	2800
On	Highway (following dusty road)	40	50	3800
On	Highway (after oil change			
	First 10 miles	40	10	6200
	10–30 miles	40	20	3000
	30–99 miles	40	70	1000

[a] Rate per mile of highway driving with air cleaner on was arbitrarily chosen as 100.

parts if allowed to persist for longer periods of time. Bearings in particular might be harmed by even short periods of knocking operation.

Other investigators have reported[4] an increase in piston-ring wear as a result of engine knock. The effect was shown during extended operations in two cars under service conditions. It may be that knocking occurring over an appreciable time interval could increase ring wear by causing local overheating in the ring zone area. Alternatively, increased ring wear might result from removal of deposits caused by knock with subsequent abrasive action occurring between the rings and cylinder walls. Any effect on wear due to knock would then depend on previous deposit buildup in the combustion chambers rather than on the effect of knock itself.

Lubricant Composition Influences Low-Temperature Wear

The results obtained in the work on operating conditions showed that jacket temperature and shutdown time are two important variables in passenger-car service. Conditions for lubricant test work were, therefore, chosen to consist of a cyclic-type test alternating 5 min of idle and 20 min of shutdown. Jacket temperature was maintained at 80 F for most of the work with an external supply of cold water. The wear occurring in each startup cycle was measured using the continuous counting equipment and an average value of wear per cycle was used to compare lubricants. A single test consisted of 10–13 individual cycles of the type indicated. After every two tests, the car was driven for at least 100 miles to restore satisfactory engine performance. Without this period of driving, valve sticking was occasionally experienced due to the cumulative effect of long periods of idling at low jacket temperature. The test conditions used are outlined in Table 7.

The results of a typical test using the conditions outlined are shown in Fig. 6. During the first few cycles, the wear rate is seen to be relatively high. After 4–5 cycles, the wear rate becomes linear with time. This constant linear rate was taken as a measure of the performance of lubricants, poor lubricants exhibiting a wear rate line of greater slope than good lubricants. In this work, it was found essential to have the continuous record of activity as given by the built-in counting system. The high rate of wear at the beginning of the test was not reproducible and oil samples taken at the beginning and end of a test, which included this nonreproducible portion, did not generally give the same results as the test method employed. The high rate of wear at the beginning of the test was dependent on the quality of the previous test oil, and on the length of shutdown between tests, as would be expected. The above test method was found to give results which were repeatable within ±10% for any given lubricant.

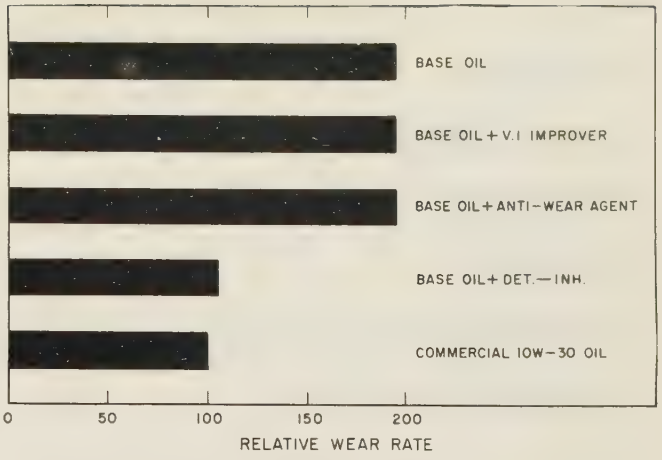

Fig. 7—Detergent inhibitor reduces startup wear

Table 6—Engine Knock Did Not Affect Ring Wear Rate

Type of Operation	No. of Accelerations[a]	Relative Ring Wear Rate
No Knock Accelerations	10	100
Knocking Accelerations	10	85

[a] 20–60 mph, full throttle.

Table 7—Lubricant Test Conditions

Jacket Temperature, F	80
Oil Sump Temperature, F	80
Intake Air Temperature, F	Ambient
Engine Speed, rpm	450
Cycle Length	
Engine Idling, min	5
Engine Shutdown, min	20
No. of Cycles per Test	10–13

Conventional Detergent-Inhibitor Additives Reduce Startup Wear—The additives normally used in compounding a representative SAE 10W-30 motor oil were evaluated separately for their effects on ring wear using the test outlined above. These additives included a detergent inhibitor, V.I. improver, and zinc dialkyldithiophosphate which is used both to reduce valve train wear and as an inhibitor for oxidation and bearing corrosion. As the data in Fig. 7 demonstrate, the detergent inhibitor was the only additive that had any effect on startup wear at low temperature. The presence of the V.I. improver or the zinc dialkyldithiophosphate had no effect on the amount of ring wear obtained.

The failure of zinc dialkyldithiophosphate to reduce wear under low-temperature operating conditions is in contrast with results published by Brenneke[7] on piston-ring wear and with results obtained in valve-lifter wear studies[8] where this same additive has proved very effective in reducing wear. Apparently, the mechanism of piston-ring wear at low temperatures is quite different from the mechanism operating at the higher temperatures studied by Brenneke and also different from that operating between valve lifters and the cam lobes. Further evidence of this latter difference is illustrated by autoradiographs of the cam shaft from an engine used

[7] "Heavy-Duty Oil—Slow Run in Question," by A. M. Brenneke. Paper presented at meeting of SAE North California Section, Jan. 23, 1957.

[8] SAE Transactions, Vol. 63, 1955, pp. 349–361: "New Look in Lubricating Oils," by J. B. Bidwell and R. K. Williams.

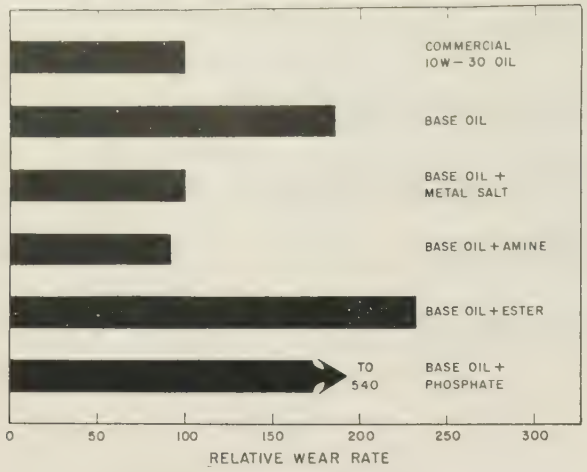

Fig. 8—Some rust preventives reduce startup wear

Table 8—Small Advantage for Lubricant Additives under Highway Driving

(50–55 mph Driving)

Lubricant	Relative Wear Rate
Base Oil	100
Commercial 10W-30	85

for valve lifter wear studies[9] which showed metal transfer from the radioactive valve lifters to the nonradioactive cams. On the other hand, no transfer from the radioactive piston rings to the cylinder wall was found in the test car. This implies that friction or scuffing is much more important in valve-lifter wear, a fact that probably accounts for the effectiveness of the zinc dialkyldithiophosphate additive in this service.

The reason for the effectiveness of the detergent inhibitor is not understood completely. Because of its polar nature, it may adsorb on the metal surfaces and provide a stronger protective coating than the base oil itself. It is well-known that materials of this type are capable of preventing rust formation, at least under certain conditions. Acid neutralizing power alone is probably not sufficient to provide protection, based on results obtained by injecting an acid neutralizing material, ammonia, into the cylinders on shutdown. It was found that ammonia injection, in combination with the use of an oil containing detergent inhibitor, reduced the wear some 40% below the detergent oil alone. However, in the absence of any detergent inhibitor in the oil, ammonia addition had absolutely no effect on the wear rate. Thus, while acid neutralization may play some part in corrosive-wear reduction, some other property of the detergent inhibitor, perhaps film formation, appears to be controlling.

Some Rust Preventives Reduce Startup Wear—A number of conventional materials known to inhibit rust formation under various conditions were tested for their effects in controlling startup wear. These materials can be classified in four main types: a metal salt of an oxidized petroleum fraction, an amine, an ester, and a phosphate. As shown by Fig. 8, the metal salt and the amine were as effective as the detergent inhibitor in their ability to reduce startup wear. On the other hand, the ester and the phosphate were not only ineffective, but actually detrimental in the ring wear test. A phosphate very similar to the one tested here was found very effective in reducing valve train wear. This is another indication that completely different mechanisms are involved in low-temperature piston-ring wear and valve train wear. The effective materials probably act by the same mechanism as the detergent inhibitor, most likely by adsorption on the metal surface to provide a protective film.

Conventional Additives Show Small Advantage under Highway Operation—Wear rates obtained under highway operation (steady 50–55 mph driving) are much lower than for startups at low jacket temperature. The amount of iron worn off the rings in one engine start at 70 F jacket was found to be approximately equivalent to the amount worn off in 10 miles of highway driving. Data have been published by Jackson[10] which imply that a large part of the wear associated with this type of operation must be due to abrasives, and only a small amount due to friction wear. This may explain why only a small and perhaps insignificant benefit was found for the presence of conventional additives under highway driving conditions as shown in Table 8.

If most of the wear occurring at the higher jacket temperatures is indeed due to abrasives in the oil, it is difficult to see how much reduction can be obtained from improvements in lubricants. More efficient filters, combined with frequent oil changes, have the best chance of minimizing abrasive wear. It should be emphasized that the detergent inhibitor contained in the 10W-30 oil referred to in Table 8 is effective in reducing wear under the operating conditions where the wear rate is greatest, namely at conditions of low jacket temperature.

Conclusions

Continuous monitoring of lubricating oil in a car containing radioactive rings is a very useful and flexible tool for use in the study of ring wear. Data can be accumulated rapidly and easily, with more confidence than is afforded by discontinuous sampling, since a continuous record of rate of wear allows instant recognition of the effect of any operating variable chosen for study. Some of the conclusions arrived at during the development of this equipment are:

1. Under conditions of low jacket temperature, very severe piston-ring wear has been found to occur due to corrosive action by products of combustion. The importance of this type of wear in the field will depend on the amount of engine operation occurring at low jacket temperature.
2. The magnitude of low-temperature ring wear is influenced by fuel components capable of producing acidic material on combustion.
3. Present-day compounded motor oils are effective in reducing this type of wear, although the results indicated that further improvement is possible.
4. Wear rates under normal jacket temperature conditions are very low.
5. Some but not all rust preventives are effective in reducing low-temperature wear.
6. Zinc dialkyldithiophosphate is not effective in reducing low-temperature ring wear.

[9] "Radiotracer Approach to Study of Engine Valve Train Lubrication," by M. J. Furey and J. F. Kunc, Jr. Paper presented at 131st meeting of American Chemical Society, Miami, 1957.

[10] "Why Does Your Car Wear Out?" by H. R. Jackson. Paper presented at SAE Annual Meeting, Detroit, Jan. 14–18, 1957.

DISCUSSION

Claims Error in Wear Rate Data Of Radioactive Method

—James J. Gumbleton
General Motors Corp.

THE use of radioactive tracers as an effective tool in measuring engine wear has again been demonstrated by the authors. They have also pointed out that it is through the study of transient engine operation where this tool can be most advantageously used, since no other method can be adapted to continuously monitor engine wear. Moreover, the periods of transient engine operation account for the majority of the wear and are, therefore, obvious areas for intensive study.

Working with similar continuous monitoring equipment on a single cylinder engine in the laboratory, our engineering and research staffs have shown, in concurrence with the authors, that cold engine startups account for a large portion of the ring wear. Typical wear of a piston ring after a cold engine start (Fig. A) shows that 75% of the total wear which occurs during a 2 hr run at 2500 rpm may occur during the first 6 min. This test was repeated numerous times and the curve shown is an average of various tests. Thus, the transient wear during startup, where engine conditions such as speed, load, and temperatures are changing, is significant.

The effect of engine transients is again shown during a ring break-in. Continuously recorded data for a typical ring (Fig. B) shows that the wear rate at the beginning of the break-in period is high. The engine was cold when started and was operated at maximum power for the speeds indicated. The jacket temperature was 180 F and the oil temperature was 190 F when equilibrium was established. After each speed change, the wear rate increased suddenly. A noticeable decrease in slope occurred between 50 and 200 min. operating time. This indicated a decrease in wear rate which was due to better fitting of the ring to the cylinder wall. After 212 min the oil was changed because the counting rate of the activity in the oil was so high that new wear particles were a small fraction of the total activity in the oil. During the oil change the engine cooled. When the engine was started and the speed set at 2500 rpm, the rate of wear was increased over previous trends; however, the total wear during the transient period after starting was not as great as initially because of better seating. After the engine speed was increased to 3000 rpm, the wear rate increased as anticipated.

Thus, it is seen that periods of rapid and radical changes in engine operation, as frequently occur in normal service operation, are times of high engine wear. The authors state that a "continuous record of rate of wear allows *instant* recognition of the effect of any operating variable chosen for study." The ability to instantly record changes in wear with a reasonable degree of accuracy is more complex than pointed out by the authors. We feel that the limitations of the radioactive method should be pointed out as well as its many obvious advantages. Due to the randomness of the nuclear disintegration process which is being detected as an indication of wear, the effect of counting statistics on wear measurement error becomes important. Two fundamental factors enter into the error. One is the time delay in the counting rate meter which in turn feeds the recorder. The other is concerned with the relative counting rate of the background radiation (or previous wear) and the new radiation which is constantly arriving at the detector as an indication of changes in wear rate.

In a counting rate meter each pulse from a counter is converted electronically into a charge which is stored in a tank condenser shunted with a resistor. This produces an electronic system of scanning time, that is, the counts for a short period of time, or time constant, are totaled and then averaged over this time period and displayed on a meter. To determine the effect of this averaging circuit

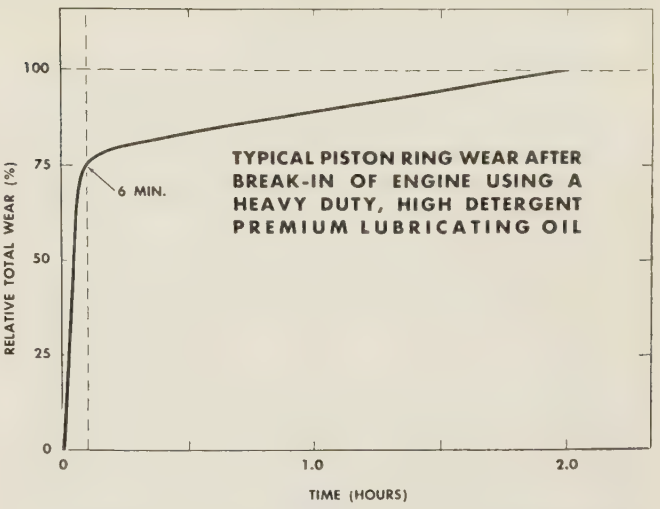

Fig. A—Typical piston-ring wear after break-in of engine using heavy-duty, high-detergent premium lubricating oil

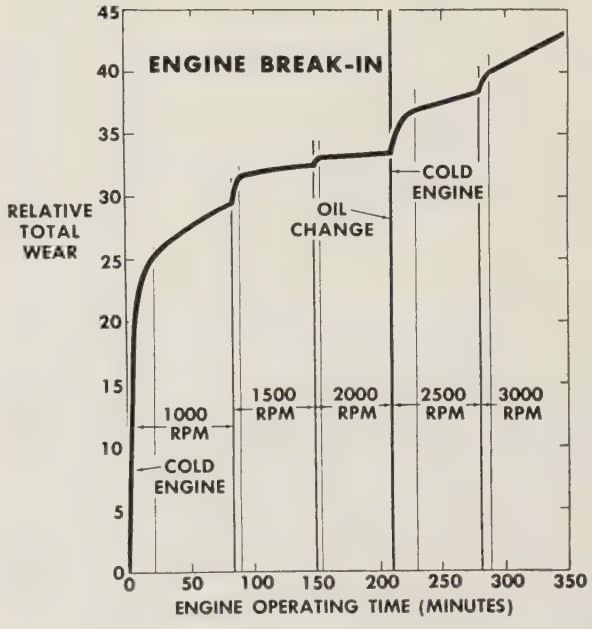

Fig. B—Engine break-in

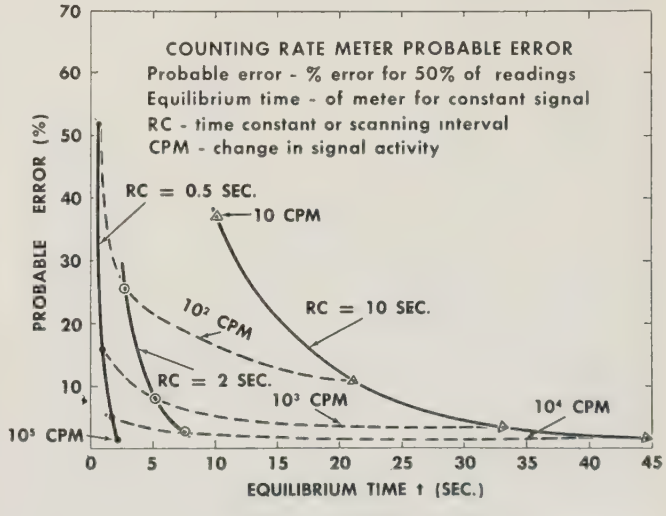

Fig. C—Counting rate meter probable error

on count rate error requires special statistical theory. A more complete development of this problem will be found in a paper by Gumbleton and Green.[a]

To appreciate the effect of the counting rate meter on wear rate error while studying rapid transients, we must interpret this seemingly complicated graph (Fig. C). The ordinate is probable error, which you recall from statistics is the percent error for 50% of the readings and thus equal probability that the error will be greater than this percentage. The abscissa is equilibrium time which is the time required for the meter to reach equilibrium when a constant amount of activity is being detected. *Rc* is the time constant of the rate meter or the time interval of the electronic scanning system. *Cpm* is the change in counts per minute or signal activity required. Relations are shown for various counting rates and for various time constants. An important observation is that one must sacrifice time for low error (high accuracy); in turn, high counting rate is required. Thus, it is evident that instead of instant measurement of changes in wear, we are limited to a time factor; and the continuous method becomes a batch process on an accelerated time basis. The limitations of continuous counting can be illustrated by noting that to measure a transient in less than 30 sec, which is much longer than the time required for changes in many normal engine conditions, to be within 5% probable error we must choose an *Rc* time constant of 10 sec and have a change in count rate of 10^3 *cpm* in the 30-sec interval. The authors showed a change in count rate of only 50 *cpm* in 5 min or 10 *cpm* in 1 min. Thus, to reduce their error, a long time constant and a long equilibrium time was necessary. Moreover, as noted from the author's wear recordings, they depended on averaging the count rate over a period of time, or thus statistically averaging a large number of batch samples taken at short time intervals. Therefore, instead of an instant record of wear, a period of at least a few min without any further transients was required to determine wear with any degree of accuracy. It is evident that to measure the effects of rapid transients, as often occur in service, piston rings of much higher activity than those currently in use are necessary. As seen from the data presented by the authors, only a total change in wear of at least 5-min interval was reproducible and although the continuous counting method seems more attractive upon cursory survey, the same data could have been obtained more simply and with greater accuracy by a batch process with samples taken as frequently as necessary, perhaps every 5 min or less. However, if the personnel protection problems incurred with more active piston rings can be adequately handled, the continuous monitoring method will allow more accurate observations of rapid transients.

Points Out Need for Radiotracer Studies Of Chrome-Plated Piston Rings

—A. G. Cattaneo
Shell Development Co.

THE authors have presented a paper that very clearly demonstrates the value and practicability of radiotracer techniques in studying engine wear. They have contributed an interesting link between laboratory research and long-time field tests by adapting the required instrumentation to use in an automobile on the road. It is encouraging to hear that the results obtained in short-time tests with the mobile unit bear out the results previously obtained in long-term field tests. Our experience would indicate that short-time radiotracer tests made on engines in the laboratory also correlate very well with practical field experience, but we quite agree that a mobile unit can greatly help in solving specific problems which might be difficult to duplicate in the laboratory.

We note that wear was measured in the test car on a cast-iron top piston ring, which replaced the now usual chrome-plated ring. In our experience the authors would as a consequence have found a wear rate about 3–4 times greater for most conditions that would prevail in the

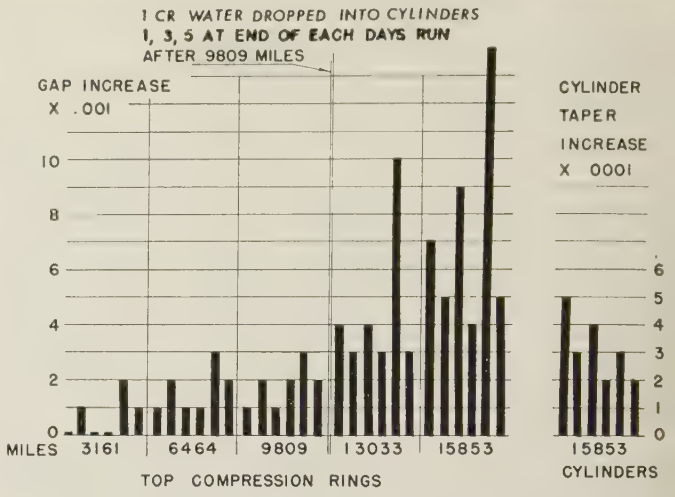

Fig. D—Effect of water leakage on wear

standard engine. This raises the question whether the field test data, with which their test car results agree so well, were also obtained with unplated rings. If so, the validity of the conclusions for engines with chrome-plated rings would still require demonstration, as well as their practical significance at the very much lower wear levels. Incidentally, we have found Cr^{51} quite as suitable an isotope for wear measurements as Fe^{59}.

In comparing the overall wear rates under traffic and highway driving conditions, the authors expected a lower rate on the highway but found a slightly higher one. We offer as a possible explanation our observation that the wear rate at steady speeds increases linearity with the engine power output. Thus, while at low and medium speeds the corrosive- or startup-type wear generally predominates, the high-load type of wear may overshadow it under some high-speed conditions.

The authors certainly settle the old question whether one should warmup a cold engine by prolonged idling. Driving the car without this idle gave twice as much wear. Could this be a tribute to the benefits we derive from good thermostatic control of cooling water circulation? If it is, it would be interesting to know whether the conclusion still applies when the thermostat is not functioning properly, as I suspect may occasionally happen in older cars.

There is no doubt that such techniques as the authors describe permit the oil industry to gain detailed insight into mechanisms of wear which limit engine life, and to find ways to slow them down. There has already been progress through the use of special lubricating oil additives for wear reduction, and more is undoubtedly to come.

Supports Authors' Data on Effect of Water And Combustion Products on Corrosive Wear

—A. M. Brenneke
Perfect Circle Corp.

ESSO Research has made an important contribution to our knowledge of the mechanism of piston-ring wear. Not only have they developed a valuable technique, but they have also accumulated factual data which should put an end to some popular superstitions about the wear behavior of fuel and oil additives.

We are not surprised and certainly not offended by the failure of the authors to corroberate our wear data on zinc dithiophosphate. Our tests were made at 170 F coolant temperature on 100-hr continuous dynamometer runs and, as they point out, this probably explains the disagreement. If we needed further alibis, we could plead variation in

[a] "Transient Piston Ring Wear in Automotive Engines Using Fe-59," by J. J. Gumbleton and F. L. Green. Paper presented before the American Nuclear Society, 1957.

susceptibility of different engines, blame it on Ethyl Corp.'s choice of reference oil, or the kind of fuel we used. It is probably worth mentioning, however, that the engine we used had low susceptibility to low-temperature corrosion and was quite susceptible to the scuffing type of wear.

While we are at a loss for critical comment on this paper, we can offer one interesting bit of evidence supporting the author's data on the part played by water and combustion products on corrosive wear. Fig. D is the result of some work we did in 1955 to see if water seepage after shutdown might contribute to cylinder-to-cylinder variation in ring wear. A total of only 45 grams of water over a period of 6044 miles produced results that were both drastic and gratifying, since so small an amount of water could easily pass as an undetected gasket leak. So, now we are a little less mystified when we find cylinder-to-cylinder wear variation in the order of 10:1.

We congratulate the authors on a fine paper and hope they will continue their work. We particularly hope they will investigate chrome-plated rings since they are so universally used. We suspect interesting differences will be found between them and cast-iron rings.

Emphasizes Need for Data on Wear Of Chrome-Plated Piston Rings

—Richard Abowd, Jr.
Ethyl Corp.

THE authors have presented an interesting and varied study of piston-ring wear in vehicle operation. This discussion will be confined to two of the many relationships outlined in the paper.

We agree with the authors that engine knock has no effect upon top piston-ring wear. Our observations were made using a single-cylinder engine, operating at 1800 rpm, full throttle, with maximum power ignition timing, and with a fuel which induced medium to heavy knock. Continuous monitoring of the radioactive wear debris in the crankcase oil showed that in 20-hr tests the wear rate was no higher than that observed with a fuel providing no-knock. Before these observations, all combustion-chamber deposits were removed in order to eliminate the possibility of deposit-induced ignition. By means of suitable instrumentation it was ascertained that no preignition did occur.

Subsequent modification of the fuel composition (from 100% paraffin to 25% toluene 75% paraffin base) allowed observation of the onset of continuous autoignition simply by increasing the engine operating severity. This phenomenon induced catastrophically high top ring wear. Initially, this abnormal combustion was observed at 26-deg btdc (maximum timing). It progressed to as early as 100-deg btdc. Continuous surface-induced ignitions, which were produced by glowing spark-plug electrodes, gave the same catastrophic wear pattern. It appears, therefore, from our laboratory experiences that the investigation of the effects of these abnormal combustion phenomena upon top piston-ring wear must be conducted in a manner which precludes occurrences of combined processes, such as knock-induced preignition.

Results reported in the literature which show that engine knock adversely affects top ring wear may have been caused by a combined process such as knock-induced preignition.

Inducing knock by over-advancing the ignition timing may very well be the synthesis of a preignition process. This method of producing knock, it seems to us, should be used with caution when the effects are to be related to ring wear.

Under a heavy-duty operating schedule in our single-cylinder research engines the addition of zinc dialkyldithiophosphate (zddp) to the lubricating oil could increase or decrease the iron top ring wear, depending upon how much was added. By using a concentration determined experimentally to yield a minimum amount of wear on a cast-iron top ring, the wear results were still significantly less than that experienced with another oil formulation not containing zddp. These effects were reversed in order when a chrome-plated top ring was substituted. These results seem to have a sobering effect upon the wear performance conclusions we formulated during the years our piston-ring wear studies were limited to radioactive cast-iron rings. It seems to us that the difficulties of using chrome-plated rings must be overcome since their use in wear work is no longer an option but a necessity.

Flexibility and economy of the radiotracer technique has been overwhelmingly demonstrated by the authors. This, I believe, is the first paper to describe a continuous-flow monitoring system mounted in the vehicle.

Reports Effect on Nonbasic Film-Forming Compounds on Low-Temperature Wear

—H. R. Jackson
Atlantic Refining Co.

THE authors have written an interesting and technically sound paper, and it is to their credit. The use of flow-counting equipment over the road seems to be the last word in radioactive counting techniques.

The mechanism by which certain additives can reduce low-temperature piston-ring wear is a point on which we can offer additional information. We agree that film formation and alkalinity both can affect this low-temperature corrosive wear. Since alkalinity is depleted as it protects, an oil offering film formation protection should have greater "staying power" or continued protection with use, compared to one which relies solely on alkalinity.

My company investigated a series of nonbasic film-forming compounds as oil additives to control low-temperature wear. These included several types of carboxylate esters; phosphate esters; isobutylene, styrene, and silicone polymers; phenols, condensation products of alkyl phenols and alkylene oxides, disulphides and neutral metal salts of alkyl sulfonates as examples. The best of the more than 30 such compounds evaluated was not nearly as effective as the normal alkaline detergents.

In a laboratory low-temperature ring wear test, uncompounded mineral oils gave wear rates of 3–4 mg per hr, the nonbasic film-forming compounds reduced this to 1.5-3.3 mg per hr, and the highly alkaline additives reduced this to 0.2–0.4 mg per hr. Since the authors show that nonfilm-forming basic materials by themselves (ammonia) are not effective, it appears that this particular field has been well studied.

ORAL DISCUSSION

Reported by James Lunan
Chrysler Corp.

A. K. Hannum, Thomson Products Corp.: In measuring cold wear there are cases where it is hard to isolate causes. A study of, say, oils may fail to take into account all of the engine wear processes. For instance, face and side wear on piston rings appeared to be separate processes, not necessarily occurring simultaneously. In looking only at side wear, sporadic high side wear was found to occur when the piston rings rotated, usually at high engine speeds. This could not be readily determined in a multicylinder test engine, yet would have quite an effect on the overall results. In order to isolate face wear and side wear it might be necessary to refine the test possibly by measuring ring rotation.

R. D. Best, Southwest Research Institute: The authors' work parallels some that we had been doing. The same high wear rate at starting has been noted. I think that it might be necessary to consider the type of service to which piston rings and other parts are subjected—the relatively constant operation in locomotive and industrial engines, or the start-and-stop short-term operation in automobiles. Also, a need exists for a means of continuous measurement of the various wear rates over much longer periods.

C. K. Murphy, General Motors Research Staff: Has any consideration been given to wear particle hang-up?

Dr. Batzold: This has been considered, and sampling of flushing oil indicated hang-up is not a factor.

THIS paper outlines the advantages and disadvantages of present-day hydraulic systems.

Included in the discussion are: the blocked return line system for single-acting cylinders, the blocked pump inlet, and the basic open-center-valve system. More advanced designs mentioned are: open-center-valve systems with cylinders in series and with parallel cylinders, close-centered valve systems with pressure regulator, and the central hydraulic and accumulator systems.

The author points out that the advantages and disadvantages of each system depend to a great extent upon the design in which it is used.

TRACTOR *good field*

G. L. Hershman, International Harvester Co.

This paper was presented at the SAE Farm, Construction, and Industrial Machinery Meeting, Milwaukee, Sept. 12, 1957.

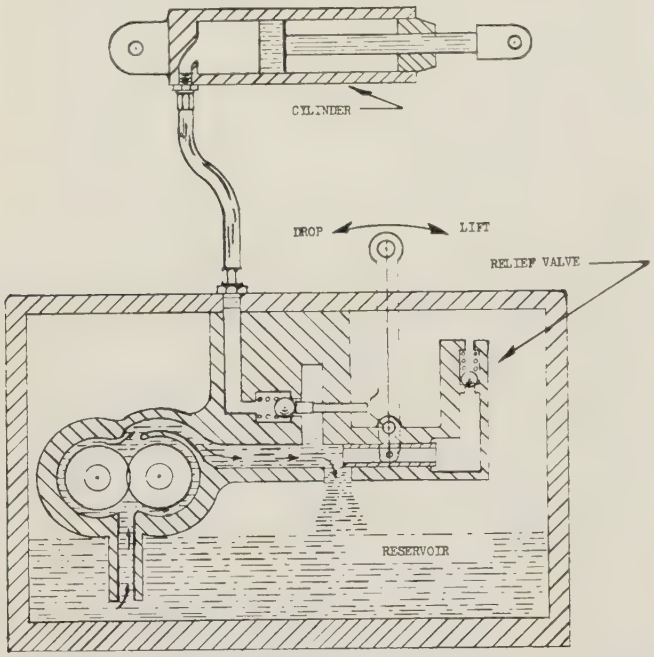

Fig. 1—Blocked return line system

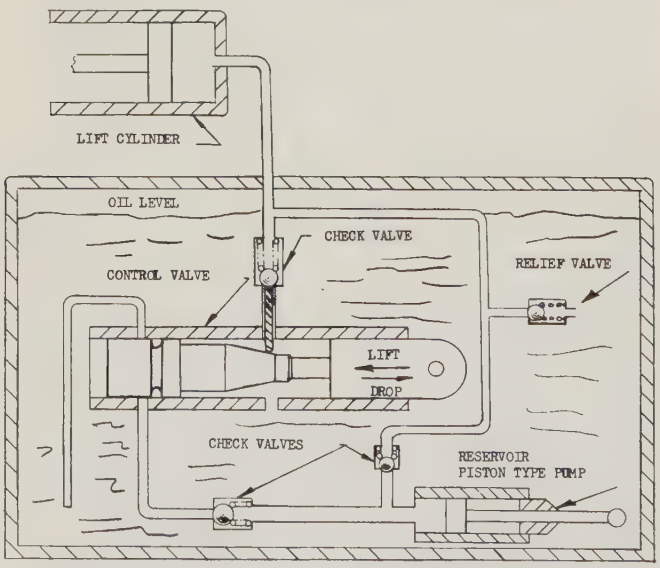

Fig. 2—Blocked pump inlet system

MANY years ago baseball's Mike Gonzales, a non-playing manager and scout with the St. Louis Cardinals, made famous the remark, "Good field, no hit." He was, of course, speaking of a player's ability to perform on the ball field. The quotation intimates that the player should have all-around ability and that there are pros and cons where a person's activities are concerned. Tractor hydraulic systems can perhaps be placed within the realm of this quote, for there are several facets reflecting the action of a hydraulic system. Scout Gonzales left much to be desired in the way of semantics for the words may not mean the same thing to all persons, principally because the words GOOD and NO have such a broad expression and concept. Hydraulic systems are not entirely good or all we desire, and yet, they are not entirely bad. It is the function of this paper to stroll visually and verbally through the various systems that are found on tractors and to point out a few fundamental characteristics, both the good and the not so good.

Historically, Pascal formed the foundation of modern hydraulics in 1653 when he discovered that pressure on a liquid acts equally in all directions, and at right angles to the containing surfaces. He expressed this in the theorum: "If a vessel full of water, closed on all sides has two openings, the one, a hundred times as large as the other, and if each is supplied with a piston that fits it exactly, a man pushing the small piston will exert a force that will equilibrate that of one hundred men pushing the large piston and will overcome that of ninety-nine."[1]

The big problem, then as today, was to *make the*

[1] "Hydraulic and Pneumatic Power for Production," by H. L. Stewart.

HYDRAULICS

. . . no hit

piston fit exactly, and it wasn't until Joseph Brahmah invented the cup packing a hundred years later that the theorum was accepted.

The early tractor hydraulic systems were comprised of a pump or power unit, a valve or directing unit, a relief or safety valve, and a cylinder or motor. These systems quickly progressed to more complex units and it is with these present-day systems that we wish to deal, first touching lightly on those simpler basic systems.

Simple Basic Unit-Type Systems

Blocked Return Line Systems (for Single-Acting Cylinders—Essentially, nearly all systems are of a blocked return line nature (Fig. 1); however, in the simpler systems there is a type that depends strictly on blocking off the return line to cause the oil to back up into one or possibly more single-acting cylinders. Normally, once in the cylinder, the oil is held by a ball-check valve while the blocking valve is moved back to neutral. To release the oil, a mechanical ball-unseating device forces the ball from its seat.

The system is simple in design and low in cost, but effective for minor control operations where the cylinder or cylinders (single-acting type) are positioned in either fully extended or fully collapsed condition. The system lacks adjustment of fine control and it is limited strictly to single-acting cylinders. Additions can be made to this system to gain some control, but it then becomes a more complex system resembling the open-center type to be discussed later.

Blocked Pump Inlet System—This system, made up of basic units, provides operational control by restricting the suction side of the hydraulic pump. The control valve in neutral position blocks the oil from the suction side of the pump, and check valves block the oil return from the cylinder. Moving the valve to the left allows the oil to flow into the suction line to the pump; and in the dropping position (valve to the right) the cylinder return port check valve is mechanically opened, allowing oil to return to the reservoir.

Here again is a simple system that has a cost advantage and can be used for some operations. It has the advantage that speed of operation can be controlled by metering the oil into the suction line. This feature is used in some of the more elaborate systems to control the speed of hitch cylinders. The limitation on the valve pictured is that it can be used only with single-acting cylinders; however, the blocked suction feature could be used with more advanced control valves. The control is rather poor and because there is possible aeration of the oil the system may become spongy in operation.

To prevent air from being introduced through the valve and pump they should be submerged in oil. The cavitation set up by restricting the suction side of a gear-type pump can be detrimental to the pump parts, causing erosion and material displacement. However, there are some systems in use today that apparently have satisfactory pump life. Fig. 2 shows a piston-type pump, which is sometimes used with this system.

Basic Open-Center System—Comparable to the previous two basic unit systems is the simple version of the open-center system (Fig. 3). Advanced from the blocked return line system, the control valve can

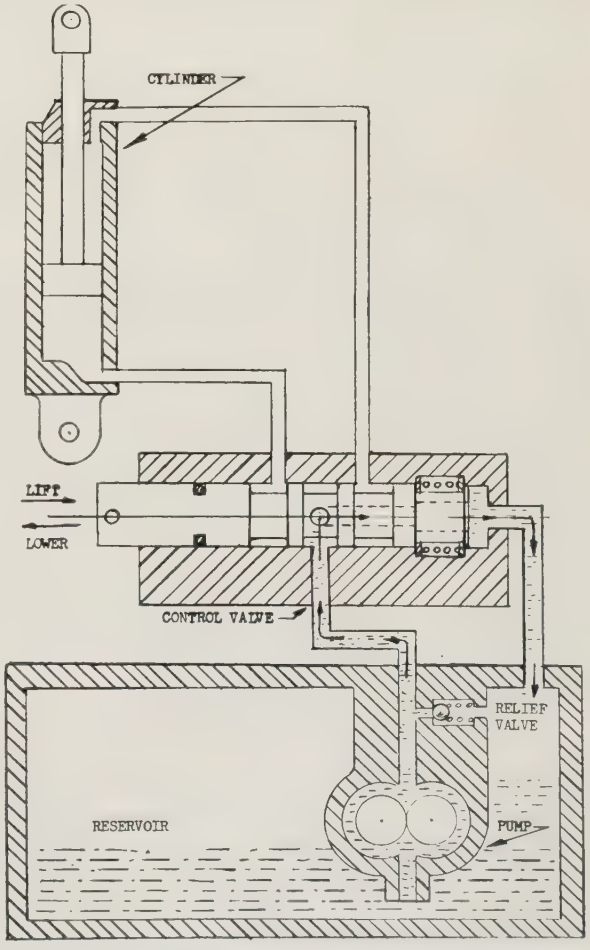

Fig. 3—Basic open-center-valve system

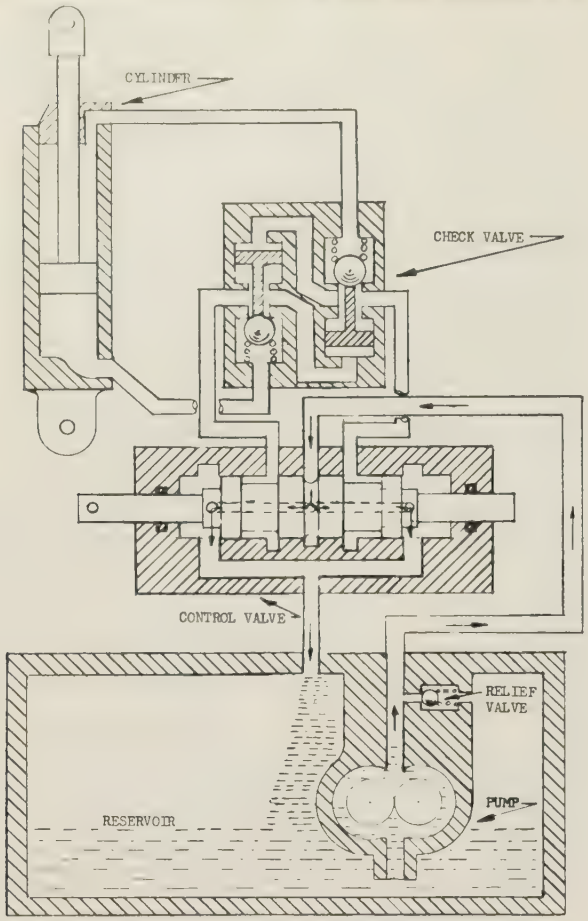

Fig. 4—Open-center-valve system, 4-way valve

direct oil to a particular selected port; therefore, it can operate single-acting or double-acting cylinders. It has better control of operation and, by use of chamfers or slots on the valve spool, has fine control and adjustment features.

This basic version has oil flow from the pump through the center of the valve and then back to the reservoir. This circuit does preclude the use of more than one valve in the system, because of the return line location. Where the oil moves through the valve center to the reservoir, any back pressure in the return line will cause the valve to be unbalanced, tending to drive it to the left. When a second valve sandwiched between this one and the reservoir is operated, high back pressures are created and valve 1 is out of control.

There are always problems of valve clearance with spool valves, and this valve is no exception. The leakage of oil can be controlled by use of check valves mechanically or hydraulically actuated, keeping oil in the cylinders in a positive fashion.

Advance Stage Hydraulic Systems

The use of the early basic hydraulic systems brought a recognition of their limitations. Through development, they were added to and modified. Although the present systems are much improved, there are still characteristics to be found that account for the continued designing toward the ultimate in performance.

Open-Center-Valve Systems—Probably the system used most for tractor hydraulic units is the open-center-valve system. Considered here will be the two common versions:

1. Open-center valve with a series cylinder circuit.
2. Open-center valve with a series—parallel cylinder circuit.

First consideration will be given to the open-center-valve system with the series cylinder circuit. This system is adaptable to hydraulically operated hitches, remote-control cylinder applications, and even on power-steering circuits where a special version of the valve is used. The normal required components designed into the system are the open-center valve (either 3- or 4-way), a relief valve, a pump or fluid power source, a reservoir, and an activated unit such as a cylinder (single- or double-acting). (See Fig. 4).

In the illustration note that the open-center valve is designed so that the cylinder ports are closed off and the inlet or pressure port is open when the valve is in neutral. The oil from the pump moves in through the inlet port across the valve and out through the return port to the reservoir. This is the circuitry when the system is on low pressure. On high pressure the oil moves into the inlet port and out to the cylinder. Oil from the opposite side of the cylinder returns through the valve and back to the reservoir. Such a circuit can handle two control valves (Fig. 5). However, the two must be connected in series, in which the oil passes from the first valve to the second. This means the oil returning from the first cylinder is ported to the pressure port of valve 2, and thence to the second cylinder. The oil from the opposite side of the second cylinder is then returned to the reservoir via the second open-center valve. When in simultaneous valve operation, the two cylinders must both move at the same time. It is evident that stacking this type of valve is possible but simultaneous valve operation is limited.

Advantages of the Open-Center-Series System—

1. Simple valve-closing action is used to activate the system.
2. System receives a minimum of hydraulic shock loads.
3. Hand lever control is flexible.
4. System can be easily modified for additional features.
5. System pressure is developed only enough to accommodate the load.
6. System oil temperature is readily controlled.
7. Simultaneous cylinder action is possible with multiple valves.

The open-center valve is so designed that the lands cover and overlap the cylinder ports, and oil from the pump is directed through the valve to the return port and thus to the reservoir when the valve is in neutral. When moving the valve in either direction, the return port is closed off gradually as the clyinder port is opened. This timed valve action tends to meter the oil to the cylinder and then close off the return passage. In this manner, the cylinder picks up the load gradually, and the maximum dynamic pressure developed in the system is only that required to move the load. The advantage of such action and timing is that shock loading the system and parts is minimized. The importance of this is reduced wear and breakage of parts, reduced design safety factor, and lower costs initially and in regard to maintenance.

The control of hydraulic systems is of prime im-

portance, for in any operation, be it a lathe or a loader even the best operator cannot perform better than his controls will allow. Variations in spool valve contour and land form can be made to provide fine metered control. Timing of the open-center valve can be good even with wide tolerance. Special chamfers and grooves can be added to give fine control.

The use of gravity drop for implements such as cultivators is possible and recommended for open-center systems. Valve land timing of the exhausting oil can be set up to control the light cultivator gangs as well as the loader boom cylinders, without compromising on the load-raising operation.

Modification and building on to the open-center-valve system gives it the unique position of being a simple but complex system. The basic system can be improved by adding hydraulic or mechanically operated check valves to keep the valve cylinder ports from allowing leak back. Linkages added to the valve and its cylinder can make it a follow-up system, and by adding a separate set of linkages, a load-sensing feature can be made available for traction controlled implement hitches. The nudging valve for remote operations can have detenting features when the inner valve is modified by adding valve spool holding and releasing devices.

The timing of the valve is also important in handling the raising of loads. When the control valve is moved to lift, there is a gradual closing off of the return port and a backing up of the oil to produce pressure at the cylinder. With this circuit and timing, only the pressure required to move the cylinder load is developed. This is in contrast to the closed-valve circuit where full maximum saftey valve pressure is reached twice during each stroke, and if slow metering is effected, full safety valve pressure can be continuous.

The open-center valve normally works at pressures less than safety valve and, therefore, does not impart peak loads to the parts of the system. The advantage being that the system not encountering heavy loads will be less subject to wear and deformation.

The direct result of continuous high-pressure operation is, of course, high oil temperature.

The open-center system less likely to be at continued high pressure will tend to have cooler operation. This is to the advantage of the system, for heat tends to break down the rubber seal rings, reduce the viscosity of the oil and thus system efficiency, and cause expansion of parts operating one within the other. All of these are detrimental.

Simultaneous series cylinder action can be considered an advantage, particularly where such action is required. However, it is not always so considered, as will be discussed later. On the good side of the ledger, we find that some operations require simultaneous action mixed with individual action. For example, the front cultivator gangs are individually controlled as the operator travels down the row, and normally on a rectangular field will be raised simultaneously at the end of the field. Such action is possible with this system. The simultaneous series cylinder action is quite rapid, for both or all cylinders begin and complete their stroke as one.

Disadvantages of Open-Center-Series Cylinder System—1. Spool valve fits are critical.

2. Valves must have large ports to maintain low bypass pressures.

3. Stacking of valves is limited.

4. Series cylinder operation cannot be used under all conditions.

5. Simultaneous series cylinder operation divides the available pressure.

The fit of any spool valve is critical, for excess clearance means excess leakage and loss of efficiency. Because the open-center valve depends on blocking off the oil from the return passages, there must be a select fit of bores to valves, even after careful machining. Leak back can be dangerous in that on nudging valve applications the load can drop completely, causing damage; and where follow-up linkage is concerned, the system in trying to re-establish its controlled position will stay on pressure and cause heat buildup.

The open-center valve must be designed with large intake and exhaust passages for the oil circulation, because any restriction will cause high bypass pressures. The heat of normal oil circulation is also detrimental in that the valves are kept at about the same temperature as the oil. Additional leakage can be accounted to hot spots in the valve and the fact that the heat from the valve transfers to the oil at the cylinder port, making the oil thinner and more liable to leakage.

The simultaneous action of series cylinders cannot always be used to advantage. Many implements demand independent operation of cylinders. This may be due to sequence or to speed and load.

Stacking of series system valves is limited due to the simultaneous action of the cylinders. The difficulty, if not in operation sequence, can be due to the dividing of the available force when cylinders are in series. The pressure required to lift loads on each individual cylinder when operated simultaneously

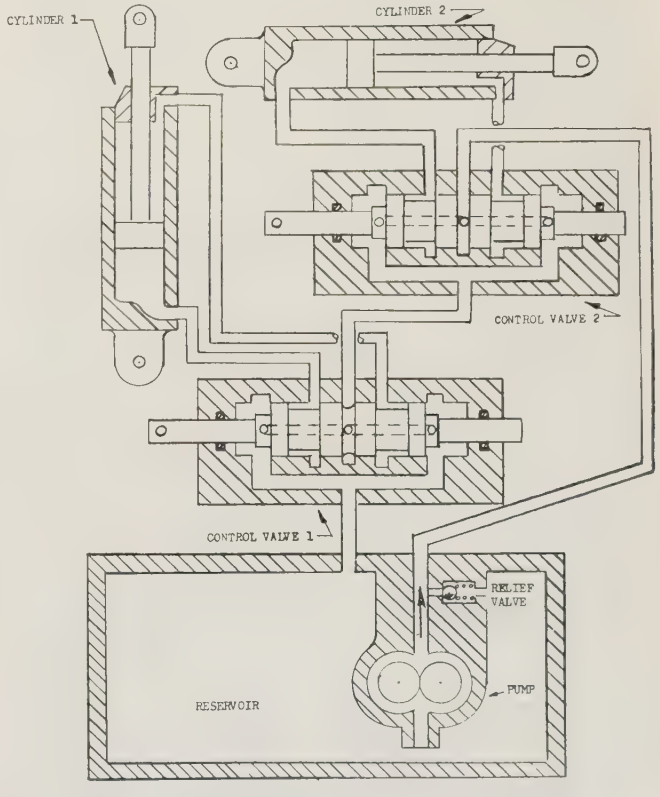

Fig. 5—Open-center system, series valves stacked

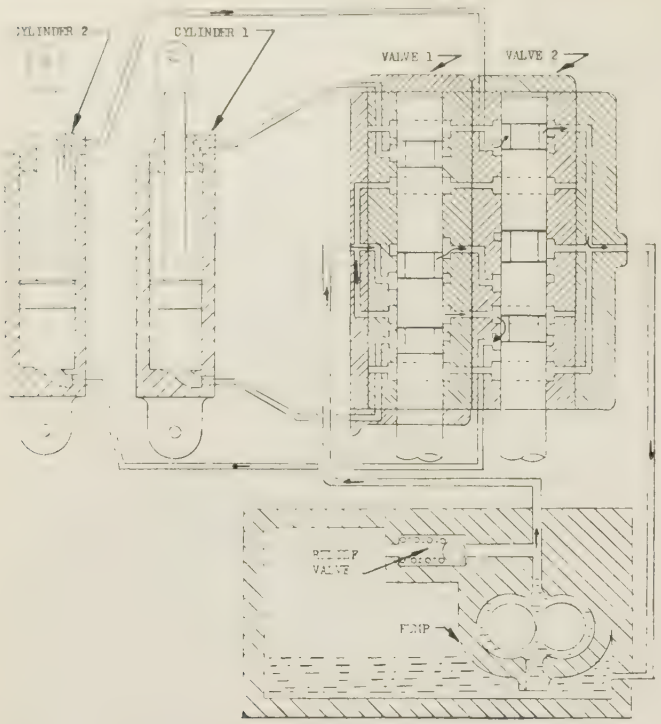

Fig. 6—Open-center system, series-parallel circuit

must equal a pressure less than maximum safety valve pressure or none of the loads can be raised. This quickly limits these systems to one or possibly two valves and cylinders, a decided advantage. This difficulty has been remedied by the alternate open-center system—the series-parallel valve arrangement.

Open-Center-Valve System with Series-Parallel Circuit—Overcoming some of the shortcomings of the open-center valve with series circuit is the series-parallel type open-center-valve system. The main valves are so designed that several of them can be stacked together but they can still be used independently to operate cylinders, motors, or other hydraulic mechanisms (Fig. 6).

This circuit directs the oil from the pump to the center of valve 1; when the valve is in neutral the oil continues through valve 1 into the second valve, on into the third, and so forth. The oil enters the center port, moving through the valve and out to return. If, however, valve 1 is in an operating position, the oil takes a passage to the right or left, depending on direction of valve 1's movement and delivers the oil to valve 2 at a point where its movement will be operative in either direction. This would hold true for a third or fourth valve as well. Valves in the circuit can be either 3- or 4-way models, depending on the requirements.

The system is complete when a simple relief valve is added to the circuit along with the pump and cylinders. The cylinders, of course, can be of single- or double-acting type and are independently operated in the system. When more than one valve is positioned at one time, the cylinder with the lightest load operates until it reaches the end of its stroke before the next heaviest loaded cylinder is raised. This goes on until all cylinders are in position.

Advantages of Series—Parallel Open-Center Circuit—The advantages of this circuit are the same as the first six of the series circuit with one additional feature:

1. Valves mounted in series—parallel circuit can operate cylinders independently when valves are used singly or stacked and connected to one system.

This is an important feature, having opened the way for such equipment as loaders and backhoes where several cylinders must operate simultaneously at varied speeds and pressures.

Because of the parallel circuit, each cylinder can lift a load using maximum high system pressure. There are no additive pressures in this system. The speed of a group of cylinders is equal to sum total of time it takes each one to complete its stroke. This varies from the series-cylinder action where the collective group of cylinders had a time requirement for moving all cylinders when operating simultaneously of only that time needed to fill one cylinder.

Disadvantages of Open-Center Series—Parallel Circuit—In addition to first three disadvantages of the series-open-center system are the following:

1. Simultaneous operation of several cylinders each with its respective valve is accomplished only by expert manipulation of the controls.
2. The valve porting is more complex and subject to valve timing difficulties.
3. Added ports and passages mean added material and size and therefore, increased cost.

Compromise usually is the result when certain requirements are to be met, and so it is when independent action of cylinders is gained, simultaneous action is forfeited. Of course, the operational requirements are the basis for system selection; therefore, the designer can pick the system that will do his particular job the best. To overcome lack of series action of cylinders he may use fine valve control and achieve the same action by manual metering of oil to the cylinders.

Three passages for oil movement from the pump provides a parallel circuit but adds considerably to the porting and timing problems. Matching of valve lands to body grooves becomes more difficult with tolerance buildup, and in general, the valve spools and bodies become more complex. All of these collectively can be handled, but will be reflected in either the cost or quality.

Closed-Center Valve (with Pressure Regulator) Systems

A prominent tractor system we should consider is one that uses a closed-center valve and has an auxiliary pressure-regulating valve, sometimes called pilot-operated bypass valve.

The control or directional valve is a closed-center type with all ports blocked off. In neutral, the pressure port passage is blocked at the valve spool, and the return passages and cylinder passages are blocked by the spool valve. With all passages blocked a second unit must take on the function of maintaining the system on high pressure or on bypass. This second unit triggered by the control valve is the pressure-regulating valve. (See Fig. 7.)

This valve functions at the signal from the main control valve, at which time its action places the system on high pressure or low pressure, as the case may be. This action is accomplished by using an orifice placed in the circuit to allow oil (greatly restricted) to flow to the top end of a regulator piston, which in turn forces a spring-loaded ball check from its seat,

opening the ball-check bypass valve.

A special land in the control valve is needed to cover the relief port that triggers the pressure-regulator valve piston into action.

When the small port is uncovered, the regulator piston drops back because the oil pressure behind it is relieved. This sends the ball-check valve to its seat, and the pressure can build up in the system.

The closed-center valve can be either a nudging-type or a follow-up type, depending on the needs of the unit being operated. The two types of valves can be used simultaneously in a parallel circuit very satisfactorily. The nudging-type valve would be used for remote control cylinder, rotary motors, or cylinders. These valves can be stacked together to allow multiple use; and because of the parallel circuit each can operate its respective load-carrying units independently.

Advantages of Closed-Center Pressure-Regulated Hydraulic Systems—1. Valves can be of 3- or 4-way design.

2. Valves can be stacked together, the number limited only by the needs of particular machines.

3. Nudging valves and follow-up type valves can be used in parallel on the same system without affecting each other.

4. Each cylinder operated can utilize full system pressure; therefore, no compromise on pressure occurs when there are several cylinders operating at the same time.

5. The bypass pressure regulator valve can be so designed as to keep bypass pressures quite low.

6. The use of a pressure-regulating valve allows the use of overlapping and timing arrangements.

7. Fine control and sensitivity of control are features of metering-type valves.

The ability of having 3- or 4-way valves in one circuit is of importance here, although some previously described systems have this feature. Valves can be stacked together, using parallel-type circuits, each operating independently and triggering the regulator valve independently. The number of valves in one stack is limited only by space or requirements.

The valves used can be of the nudging type for remote control, or they can be equipped with follow-up linkage and be of position-controlled design. Each valve operating a cylinder can utilize full maximum safety valve pressure. There are no additive pressures, as were found in the series systems. Cylinders will operate in sequence of lightest loads first, unless specifically controlled by metering oil through the valve via hand lever manipulation.

The bypass regulator can be designed to accomodate large volumes of oil. By specific arrangement of keeping the regulator valve close to the pump and reservoir, short passages can be maintained, thus reducing line loss in the bypass circuit. This in turn keeps bypass pressures low and reduces pump load and hp requirement at bypass. This is accomplished by having a large ball-check opening so that oil from the pump can circulate through it without undue restriction. The pump delivers oil to the regulator valve only and ports oil directly back to the reservoir. Because the oil at bypass does not move through the directional valves, their passageways can be somewhat smaller, in as much as back pressure during short periods of operation is normally not as critical. But, there are limitations.

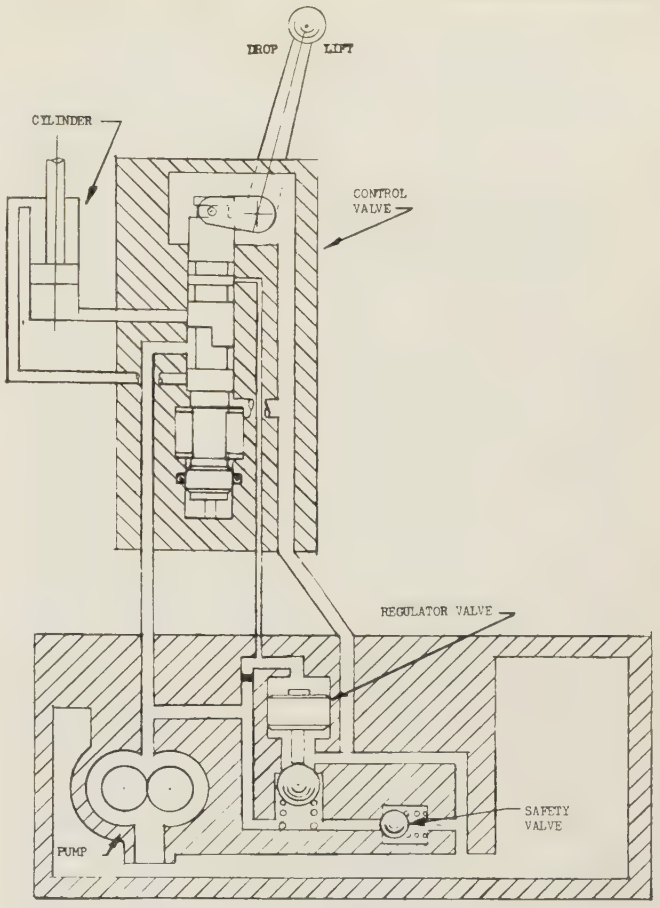

Fig. 7—Closed-center valve with pressure regulator

The use of pilot-operated pressure-regulator valves permits special overlapping timing arrangements. It is possible to elevate the system to maximum high pressure prior to opening the cylinder ports, thus allowing a metering of oil for fine control. This is effective where cylinders are maintaining heavy loads in a particular position and these loads are to be inched up into another position. The metered high-pressure oil prevents the load from dropping instantaneously before the load is supported by the high-pressure oil. Of course, to offset the advantages, there are some disadvantages.

Disadvantages of Closed-Center Pressure-Regulator Hydraulic Systems—1. Spool valve and bore clearances must be held to close tolerance and select fit.

2. Additional parts are required above and beyond the basic units for open-center systems.

3. Additional lines and passages are required.

4. Spool valve leakage must be controlled especially where closed-center valve is used with follow-up.

5. High-pressure loading of system is more common, thus requiring higher factor of safety for componenents relative to maximum system pressures, and as compared to open-center systems.

6. Metering can cause high temperatures.

Wherever spool valves are used close fits and tolerances are required, but here special care must be taken to keep spool valve fits so that the regulator triggering port is not allowed to release oil except with valve movement.

Additional parts, including the closely machined

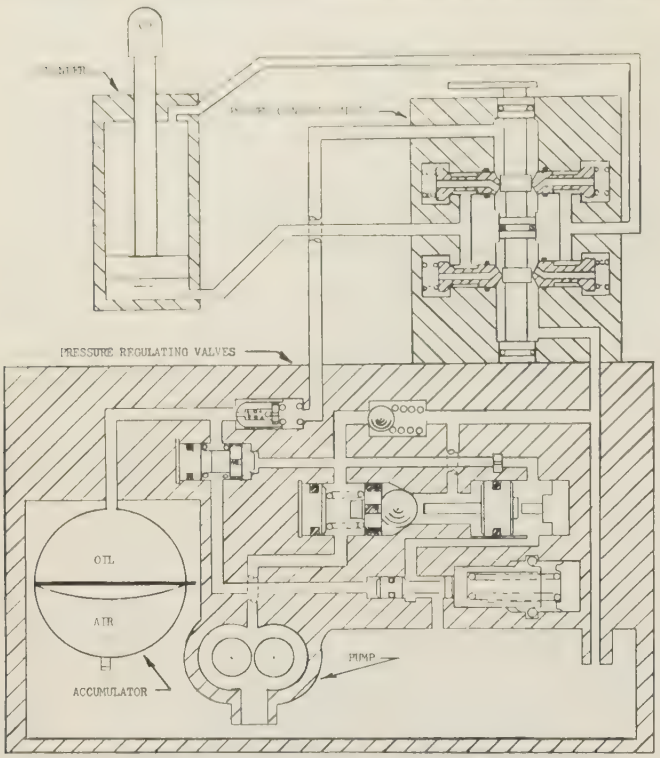

Fig. 8—Central hydraulic system with accumulator

regulator assembly, mean additional wear, initial added cost, and more maintenance. Feeding these parts are extra oil passages and hydraulic lines.

When triggered, the regulator valve places the system on pressure that is dependent on the load to which it is applied. However, where metering is used extensively, the overlap is used to control application of the oil to the load, this type of system can be subjected to shock loading to maximum safety valve pressure more frequently than the open-center-valve system. Because shock loading affects the life of parts, more costly shock-resisting components must be used. When the operations do not require this extra sensitive action and metering, these parts will, however, have long life expectancy.

The metering of high-pressure oil not only loads component parts to a greater extent, but causes heating of the oil. This heat can affect the rubber seals and cause expansion of component parts. As the oil heats, the system's efficiency will tend to drop off compared to normal operating conditions.

Central Hydraulic Systems and Accumulator System

A central hydraulic system doesn't necessarily include an accumulator. However, in general, the accumulator is pressed into service with central systems to help keep the power supply in line with the demand by spreading the work performed by the pump over a longer period of time. A small capacity pump operating over a longer period when used in conjunction with the accumulator can equal in work output the larger capacity short period pump operation found on systems we have previously discussed. (See Fig. 8.)

Central systems using variable delivery pumps and those that have a high-capacity pump or fluid power supply (capacity sufficient to carry out all jobs simultaneously) are normally made up of open-type or close-type valve units.

The variable volume pump unit can operate efficiently and effectively, producing its maximum output when called on to do so. However, if several jobs are to be accomplished at one time, the hp required instantaneously to do these jobs simultaneously can be rather high. It is necessary then, of course, to provide a fluid power supply large enough to do all the jobs that may occur at any one time. Such a power supply could be large, costly, and require considerable hp for operation.

The constant delivery pump when used on a central system should at all times provide a sufficient amount of fluid power to do all the work required at the desired speed. Although at the bypass condition a greater part of the time, the hp requirement of the pump will be large when a function which requires only a small per cent of the pump capacity is performed. On demand of the system the whole pump capacity is elevated to the pressure required for the function. In addition to high hp requirement, the speed of the operation will exceed that required. As an example, should a particular cylinder require and be so operated as to require 5 gpm at 1000 psi, and the main power supply is a 25-gpm pump, then the full 25 gal would be pumped at a 1000 psi pressure, and the cylinder would move a speed relative to the 25 gpm (or five times required speed). This means extra power and speed are used unnecessarily. Because of the obvious difficulties of these two variations of the central system, we believe the accumulator central system is the one that should be considered and evaluated here. In this type system we find the pump and accumulator working together to provide fluid power to the system. They provide constant high pressure on the system, and one supplements the other to feed the various operations as oil is called for. The pump is usually designed to provide a minimum of delivery sufficient to fill the accumulator over a length of time, the design being such that all periods of operation are programmed so that pump plus accumulator volume are equal to required system volume. Such operations as power steering will normally be nearly continuous when tractor is moving, while braking, clutching, or attachment control would instantaneously require small fixed amounts.

Remote cylinder on hitch cylinder operation would require only large volumes at the time of full raise to transport. In traveling through the field, such as in plowing with hydraulically operated hitch, only small amounts of oil would be required. Under these conditions the pump feeds the accumulator a supply of oil which is stored for use when the complete lifting cycle requires a large volume of oil. At that point the accumulator and pump can supply oil simultaneously, maintaining the pressure and speed required. By programming the various operations, the pump delivery can be kept to a minimum.

Advantages of Accumulator-Type Central System

1. Smaller pump unit can be used.
2. Instantaneous engine hp requirement is low.
3. System shock loads are at a minimum.
4. Added speed of operation due to accumulator action.
5. Ability to perform after main power source has failed or is inoperative.
6. Hydraulic holding action for static applications.

7. Low bypass pressures.
8. Smaller oil-carrying lines from pump to reservoir and return.
9. Control valves of poppet type.
10. Operations when engine is at low idle have the same speed as when engine is at high idle.

The most important advantage is the reduction in volume of oil required from the pump. Reduced pump capacity means extra hp for use in other endeavors, such as extra drawbar pull. This is especially true where hitch operations are concerned. Adding hp to the engine then removing it by using high-volume high-pressure pumps does not spell efficiency.

The system with stored energy can more easily overcome emergency situations. For example, when plowing with a hydraulically operated hitch and a very soft spot in the field is encountered, the wheels spin and the control valve is actuated. The tractor engine already pulled down because extra load is called to supply additional work in the form of pump delivery under pressure. With the accumulator system the hitch-lifting action would take place. Then later, when out of trouble, the accumulator oil would be replenished by the pump.

The pressure when using an accumulator remains relatively constant, and because the pump pulsations are dampened by the accumulator there are no pulsations from the pump which would tend to produce shock loads. In addition, when the pump does get into action, it is usually working against pressures of the accumulator which buff out the shock. Thus, again the shock on the system valves and lines and the pump are appreciably reduced.

The accumulator will provide rapid action and will speed the operation, depending, of course, on the size of lines leading from it. The system has the relative speed of a high-output pump unit.

Of some importance as a safety measure is the ability of an accumulator system to perform when the main fluid power source is dead. Because of stored energy, operations such as braking, clutching, or steering can be continued after the engine has stopped turning over and the pump has ceased delivery. Other operations, of course, could also be accomplished but probably would not come under the heading of an emergency.

In operational advantages, there is the use of the accumulator pressure as a holding device. Because the pressure is maintained through a working range, such mechanisms as clamping or loading devices can be connected into the system. The pressure will continue to hold the device while the valve to the system is open.

Because of the low-delivery pump, the suction and pressure lines can be much smaller than open-center system of comparable volume and speed. The lines from the accumulator will remain large to carry oil from the accumulator to the system with the minimum line loss.

Disadvantage of Central Hydraulic System with Accumulator—1. Accumulators are bulky and large if they are to accomplish a large job in a specified length of time.
2. Accumulators add cost to the unit.
3. An unloading valve must be provided to separate the valve circuit from the accumulator circuit.
4. Valves must be leakproof and preferably of poppet type.
5. Timing of the poppets can be critical where follow-up is concerned.
6. High-pressure air for changing the accumulator with air is not always handy when required.
7. Safety difficulties when handling high-pressure air.

The first difficulty is to accomodate a large bulky accumulator somewhere on the tractor. In present-day tractor design there seems to be little available space and fitting in an accumulator is no easy task. The accumulator can be also an expensive unit, and although the cost is offset by use of a low-capacity pump, the total cost may be more than the large capacity pump that they replace.

The accumulator system requires an unloading valve of some sort. This is an additional part and cost, if compared with the simple open-centered-valve system that has only the bare necessities.

The valves used in an accumulator system must be of a type that is leakproof. This means that the rotary or sliding-spool-type valves normally cannot be used. The clearance between the valve and its bore tends to allow oil to escape, causing the pump to cycle more rapidly to keep the accumulator filled. The valves for an accumulator system are usually of the balanced poppet type. These valves when seated are oil tight, thus providing the efficiency required. There are also some difficulties that may be experienced in the timing and leakage with the poppet-type valves. When follow-up mechanisms are used, leakage of the poppet valves would cause excessive pump cycling.

Keeping the accumulator filled with high-pressure air or nitrogen is certain to be difficult even though sealing is much improved during the last few years.

The danger of having a can or tank (accumulator) filled with 1500–2000 psi pressure is not one of small consequence. The container must be designed with safety foremost in mind. The accumulator must be protected from excess heat and should have a type of thermal relief valve that will kick off if high pressures are generated in the unit.

It must be securely fastened to the tractor and the filling stem should be of a safety type. Should a fitting be broken off the air end, the jet effect of the escaping air could send the tank scooting across the field.

Filling an accumulator would be inconvenient for the operator, and although the design should be such that periods between filling are quite long, the equipment for filling would be expensive for the servicing group and would also have to be maintained within the code of safety.

Conclusion

Concluding this summation of hydraulic systems we should remember that engineering is a tool of compromise, and where a design has weak characteristics it usually has favored other factors to provide a strong feature. Therefore, it is necessary to weigh characteristics and determine what effect they have on a particular application.

Many so-called disadvantages can be made into advantages by the opportunist designer. It is this approach as well as inventive approach that has led hydraulic design at a fast pace the last few years. New design, improvement, and rigid test are the watchwords of the hydraulic engineer.

considerations of some

JET-DEFLECTION PRINCIPLES

U. H. von Glahn and J. H. Povolny, National Advisory Committee for Aeronautics

This paper was presented at the SAE National Aeronautic Meeting, Los Angeles, Oct. 3, 1957.

THE performance characteristics of various devices applicable for jet directional control, lift augmentation, and VTOL-STOL studied at the NACA Lewis Laboratory are discussed, including jet deflection devices applicable to the conventonal round nozzle and novel nozzle configurations.

The results indicate that many of the deflection devices applicable to conventional nozzles can readily be used for directional control or lift augmentation. Other deflection devices, such as movable plug, internal flap, cylindrical thrust reverser, swiveled primary with fixed shroud, and 90 deg side-bleed nozzle, are limited in application to jet directional control or aircraft trim because the loss in axial thrust for a given deflection force is prohibitive or the maximum deflected force obtainable is limited.

The novel configurations studied consisted of an annular nozzle with the jet directed perpendicularly to the ground and a Coanda nozzle which deflects the jet over a surface attached to the nozzle.

Many of the directional control and lift augmentation devices for use with conventional nozzles can be applied directly to existing aircraft. The more bizarre deflection devices (annular and Coanda nozzles) will require novel air craft configurations in order to realize optimum performance.

DURING the past 15 years considerable attention has been focused on aircraft configurations utilizing the propeller thrust for vertical lift to support the aircraft at zero ground speed, thereby constituting a vertical take-off and landing aircraft (VTOL). The areas of usefulness for VTOL and STOL aircraft have been discussed and evaluated in previous technical papers and publications.[1, 2, 3, 4] Only recently have serious efforts been made to develop jet-engine-supported VTOL aircraft. These latter aircraft, developed by Bell and Ryan, are still in the experimental flight test phases; however, their capabilities for VTOL and transition abilities to conventional flight attitude have been demonstrated convincingly. The apparent lag in the development of jet-supported VTOL aircraft has been due in part to the relatively low thrust-to-weight ratio of the previously available jet engines. Within the past two years, however, jet engines with more favorable ratios have become available. So, interest in jet-supported VTOL and STOL aircraft has grown.

Jet-supported VTOL aircraft can be categorized into three primary types: (1) tail-sitters, such as the Ryan X-13; (2) aircraft that take off and land in a horizontal attitude, such as the Bell experimental VTOL; and (3) aircraft that are compromises between the first two (inclined attitude). (See Fig. 1.) The horizontal-attitude type can be further divided according to the means by which VTOL is achieved: (1) directed thrust, wherein the complete engine is rotated to yield an upward thrust and wherein additional lift may be obtained by auxiliary jet engines mounted vertically for use only during VTOL; and

---

[1] SAE Transactions, Vol. 65, 1957, pp. 159–174: "Some General Considerations Concerning VTOL Aircraft," by Charles H. Zimmerman.

[2] *Interavia*, Vol. 11, January, 1956, pp. 27–34: "Technical Aspects of Steep-Gradient Aircraft," by M. A. Garbell.

[3] "Safety Thorugh Steep Gradient Aircraft," by R. M. Woodham. Cornell-Guggenheim Aviation Safety Center, Cornell University, May, 1956.

[4] "Reverse Thrust, Vertical Lift, and Jet Side Force by Means of Controlled Jet-Deflection," by Leonard Meyerhoff and Stanley Meyerhoff. Eastern Research Group, January, 1956.

for — — directional control

— — lift

(2) deflected thrust, wherein the jet engine is fixed with respect to the aircraft and jet-stream deflection devices are used to obtain an upward component of thrust and, hence, lift.

In addition to providing the required VTOL or STOL propulsive support, jet-deflection devices will probably have to provide directional control forces during take-off and landing when the air speed is too low for aerodynamic surfaces to be effective. Another region where the aerodynamic surfaces will probably lose their effectiveness and jet directional control be required is at the increased altitudes (and lower density air) made possible by the high thrust-to-weight ratio of these types of aircraft. In general, the application of jet deflection for control purposes will require only partial deflection or turning of the jet.

As a consequence of the wide application of jet-deflection devices to aircraft, a two-phase program of research was instituted at the NACA Lewis laboratory in 1955 to study: (1) the application of jet directional control devices to conventional circular exhaust nozzles and (2) novel means of achieving propulsion support for VTOL and STOL aircraft. These studies were conducted with small-scale setups (primary nozzle throat diameter less than 4 in.) using unheated air and operating at nozzle pressure ratios up to 3.0. All data were obtained by exhausting the jet into still air at approximately sea-level atmospheric conditions.

This paper will discuss some principles and means of achieving jet-stream deflection with various devices and their performance characteristics, without necessarily arriving at optimum jet directional controls or VTOL configurations. The principles included herein that can be used to produce jet deflection for directional control and/or lift are:

1. Swiveled nozzle configurations.
2. Jet deflecting surfaces.
3. Auxiliary jets normal to the exhaust nozzle.
4. Lift-augmenting nozzle.

The swiveled configurations include both shrouded and unshrouded nozzles with rotation of the tailpipe shroud and/or primary nozzle producing jet deflection. The deflecting surfaces include internal and external flaps, deflecting surfaces utilizing the Coanda effect, and a cylindrical thrust-reverser segment. The lift-augmenting nozzle consists of an annular nozzle utilizing ground effect on a large base for producing lift in excess of the jet thrust. All the performance data shown herein are for a nominal nozzle pressure ratio of about 2.0.

Conventional Nozzles for Directional Control and Lift Augmentation

The primary objective of this phase of the program was to explore the jet directional control possibilities of devices that could be applied to conventional sonic and supersonic exhaust nozzles; however, it was recognized that several of these devices may have jet lift application as well. Only devices providing yaw and pitch (or lift) forces were considered since it was assumed that required roll control forces would be relatively small and could be handled by devices such as wing-tip jets.

For use in directional control or augmenting lift, a deflection device should achieve maximum deflected force (side, pitch, or lift depending on the particular application) with minimum reduction in axial jet thrust. Theoretically, this relationship follows the cosine law. The performance data for the deflection devices applied to conventional noz-

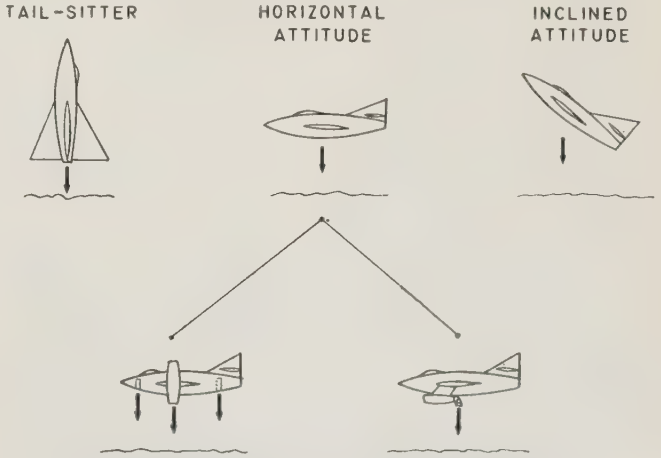

Fig. 1—Jet-supported VTOL aircraft configurations

zles are, therefore, presented in these terms and compared with the cosine curve.

The devices included in the conventional-nozzle studies may be classified by exit configuration, unshrouded and shrouded or ejector type.

Unshrouded Nozzle Configurations—The unshrouded jet-deflection devices investigated include a swiveled nozzle, a swiveled tailpipe (or engine or nacelle), an auxiliary bleed nozzle normal to the tailpipe, and a plug-type nozzle with movable plug (Fig. 2).

The swiveled primary nozzle (convergent) consisted of a spherical segment which was swiveled essentially as indicated by the sketch in the upper left corner of Fig. 2. It is possible to obtain both yaw and pitch (or lift) forces with this device and, because of nozzle symmetry, the performance is the same in either direction. This method is directly applicable to a nonafterburning turbojet, but for the afterburning case (requiring nozzle-throat-area variation) would probably require the use of two pairs of spherical eyelids, mounted one over the other but rotated 90 deg circumferentially with respect to each other. One pair would be used for yaw control and the other for pitch (or lift) and a differential control on one or both pair would permit throat area variations.

The swiveled tailpipe was investigated by a series of fixed configurations similar to that shown schematically in the upper right corner of Fig. 2. For each of these configurations the performance at a specific deflection angle was studied. Symmetry and equivalent yaw and pitch (or lift) performance also prevail for this configuration. In an actual installation, this deflection device would require either a flexible leakproof joint in the high-temperature, high-pressure tailpipe or a swiveled engine. If the engine were swiveled, the nacelle fairing also must swivel. In either case, the external aerodynamics could be considerably affected at high flight speeds.

The performance of an auxiliary nozzle bleeding gas from the tailpipe was studied using a single-bleed nozzle as shown in the lower left sketch of Fig. 2. The bleed nozzle was mounted normal to the tailpipe. Such a single-bleed nozzle would suffice if lift were the objective of this deflection device. For combined yaw and pitch control forces, four such nozzles located circumferentially 90 deg apart would be required. In either case, the bleed nozzles would have to be adjustable or incorporate some means of flow control in order to provide modulated control with constant tailpipe conditions.

The performance of a plug nozzle with movable plug (shown in the lower right sketch of Fig. 2) was obtained by translating the plug perpendicular to the axis of the tailpipe. Although this device can provide pitch (or lift) or yaw forces, considerable mechanical complication may be required to provide forces in both directions with a single device.

The jet-deflection performance of the unshrouded configurations studied is presented in Fig. 3 in terms of the ratio of axial to jet thrust F_a/F_j as a function of the ratio of deflected (lift or side) to jet thrust F_d/F_j. The value of F_j used in these ratios is that measured before the jet was deflected. All performance values are based on the assumption that the forces are acting at the center of the primary nozzle exit. Included in the figure for comparative purposes is the theoretical curve for the swiveled devices (cosine law).

The data for both the swiveled nozzle (circle symbols) and the swiveled tailpipe (square symbols) fall on the curve representing the cosine law. This indicates that with these devices a maximum deflected force can be obtained with a minimum loss in axial thrust and that both devices would be equally efficient in producing directional control or lift. Although convergent (sonic) nozzles were used in these tests, similar results should be obtained for supersonic nozzles. For directional control purposes, the moment produced by the swiveled tailpipe about the center of gravity of the airplane may not be as great as that produced by the swiveled nozzle (Fig. 4) because the moment resulting from displacement of the axial force vector counteracts that obtained from the deflecting force vector. The moment produced by the axial force vector is a function of the length of that part of the tailpipe that is swiveled, and its effect is reduced as the swiveled length is reduced or the distance to the center of gravity is increased. For the swiveled nozzle, however, the moment obtained from the axial force vector may be considered negligible because the vector displacement from the initial jet thrust axis is generally very small. It is evident that either of these devices is capable of producing

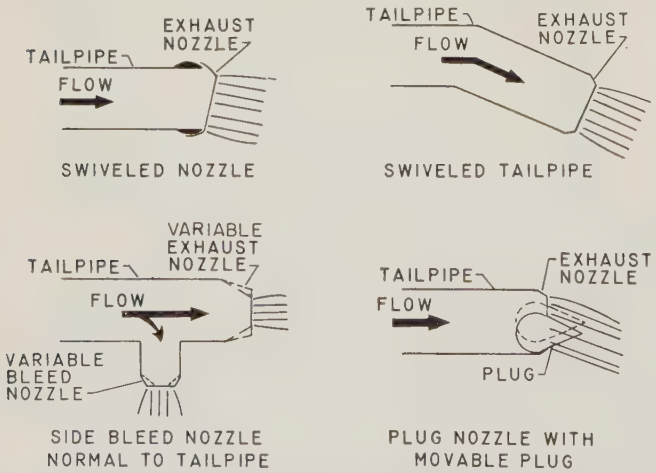

Fig. 2—Jet-deflection devices studied with unshrouded nozzles

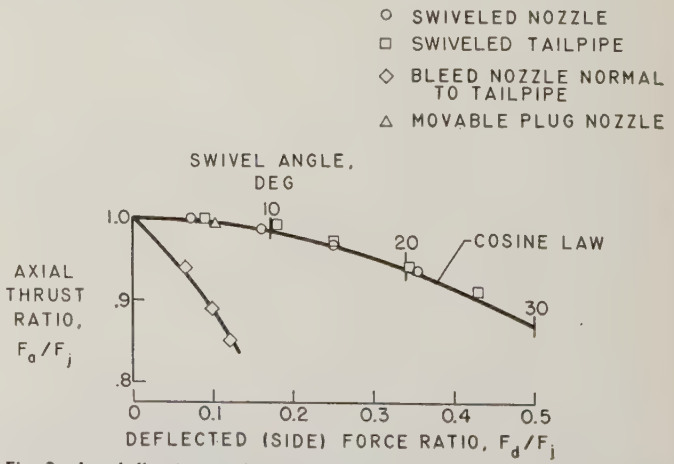

Fig. 3—Jet-deflection performance of unshrouded nozzle configurations, pressure ratio 2.0

adequate control forces; but, whereas the swiveled tailpipe (or engine) is theoretically capable of producing lift up to 100% of the jet thrust, a swiveled nozzle of the type shown in Fig. 2 will probably be limited by geometry to a maximum lift (deflected thrust ratio) of about 35% of the available jet thrust.

From analytical considerations it can readily be seen that the performance of an auxiliary bleed nozzle normal to the tailpipe is far inferior to that obtained by turning the entire jet. Theoretically, the reduction in axial thrust for a bleed nozzle is directly proportional to the ratio of flow through the bleed nozzle to that in the primary nozzle. For example, with a F_d/F_j value of 0.12 the theoretical value of F_a/F_j using a bleed nozzle would be 0.88. This latter value compares to about 0.99 for a swiveled nozzle. Fig. 3 shows that the experimental data (diamond symbols) are less than those predicted analytically. This reduction in performance is attributed to losses incurred by the flow in turning the corner from the tailpipe into the bleed nozzle and could be largely eliminated by use of turning vanes. Although its performance characteristics are considered poor, this device may have some jet directional control uses because of possible ease of application.

Translation of the plug in a plug nozzle (Fig. 2) provided a maximum deflected thrust ratio of about 10% with only a small reduction in axial thrust ratio (Fig. 3, triangle symbol). This device, therefore, has application only where the required directional control forces are small, such as for aircraft trimming. It should be noted that attempts to provide deflected thrust by pivoting the plug were also made but with negative results.

Shrouded or Ejector-Type Configurations—The shrouded-type devices investigated (Fig. 5) comprise conical ejectors with: (1) swiveled shroud, (2) fixed shroud and swiveled primary nozzle, (3) fixed shroud and movable internal flaps, and (4) fixed shroud and movable external flaps. Also included is a thrust reverser that becomes a cylindrical ejector when retracted. These exits are capable of performing as a supersonic nozzle; for the present investigation the ejector-shroud diameters and lengths were set at values typical of those that would be used at flight speeds up to Mach 2.0. Although the performance of these jet-deflection devices was evaluated on ejector-type devices, it is possible that some of them (for example, the external-flap and thrust-reverser configurations) are applicable to nonejector nozzles as well.

For the swiveled shroud configurations, the conical shroud (7-deg cone half-angle) was swiveled approximately as shown in the upper left sketch of Fig. 5 by using a series of fixed configurations covering a range of swivel angles. For practical application, the shroud could be built in four equal sections with opposite pairs being used to control pitch (lift) and yaw, or perhaps a practical flexible joint could be devised. External flow would undoubtedly affect the performance at the higher flight Mach numbers.

The swiveled primary nozzle with a fixed outer shroud (15-deg cone half-angle) is shown by the sketch in the upper center portion. It is similar to

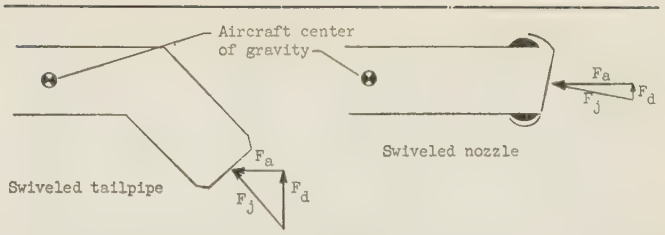

Fig. 4—Moments produced about aircraft center of gravity by swiveled tailpipe and nozzle

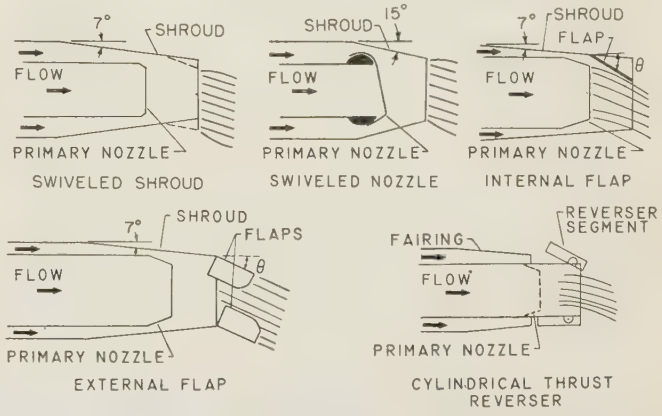

Fig. 5—Jet-deflection devices studied with shrouded (ejector-type) nozzles

the previously discussed swiveled primary nozzle except for the addition of the fixed ejector shroud. The presence of the shroud, however, causes the deflected force to act in a direction opposite to that for the swiveled nozzle alone.

The ejector with internal flap is sketched in the upper right corner of Fig. 5. Each flap would encompass 90 deg of the circumference, thus four flaps are required for complete pitch and yaw control. For lift augmentation a single flap would suffice. Because of symmetry the performance was determined with only one flap installed. Variations in the deflected (side) force were obtained by lengthening and shortening the flaps at each of a series of fixed flap angles θ.

The ejector configuration with external flaps is illustrated by the sketch in the lower left corner of Fig. 2. In this case each flap encompasses 180 deg of the circumference and thus only pitch (or lift) or yaw forces can be obtained. The performance was determined with both flaps installed and variations in deflected force were obtained by pivoting the flaps as indicated on the sketch. External flow would probably also affect the performance of this device.

For the cylindrical thrust reverser a continuously variable configuration was built and patterned after one of the more promising ejector-thrust reversers investigated in a previous program.[5] The method of operating this device when producing a deflected (side) force is shown in the lower right corner of Fig. 5. For directional control only one of the thrust reverser lobes is actuated, whereas for reverse thrust they are actuated together. Obviously, this device will provide only pitch (or lift) or yaw depending on its orientation on the aircraft.

The performance of the swiveled shroud shown in Fig. 6 is presented for D_s/D_p values of 1.1 and 1.4 and a S/D_p of 0.8. The data (circle and square symbols) indicate that, for a given deflected force

[5] NACA RM E55I29, 1956: "Performance Characteristics of Cylindrical Target-Type Thrust Reverser," by Fred W. Steffen and Jack G. McArdle.

ratio F_d/F_j, the axial thrust ratio F_a/F_j is reduced from that indicated by the cosine law. At a F_d/F_j value of 0.12, the F_a/F_j value is about 0.95 compared with the cosine law value of about 0.99. The jet-deflection performance for this configuration, therefore, falls about midway between that indicated by the cosine law and the 90-deg bleed nozzle discussed previously. The effect of varying the D_s/D_p ratio from 1.1 to 1.4 on the performance was quite small, with the F_a/F_j value for a D_s/D_p of 1.4 being slightly higher than that for a D_s/D_p of 1.1. As D_s/D_p was increased, however, it was possible to obtain higher deflected-thrust ratios without having to "close off" the secondary passage to prevent back flow. The close-off point varied from a F_d/F_j of about 0.10 for a D_s/D_p of 1.1 to a F_d/F_j over 0.20 (maximum investigated) for a D_s/D_p of 1.4. At the latter value, the secondary flow was reduced about 30% below that obtained with no jet deflection. The primary flow for these configurations, however, did not vary more than 2% over the range of conditions investigated. Inasmuch as the swiveled shroud is capable of deflected-thrust ratios up to 33%, it may have application possibilities for jet-augmented lift as well as for directional control.

The performance of the swiveled primary nozzle with a fixed shroud (diamond symbols) is shown in Fig. 6 for a D_s/D_p of 1.2 and a S/D_p of 1.0. The reduction in axial thrust ratio with deflected force ratio is much greater for this device than for the swiveled shroud configurations. At an F_d/F_j of 0.12,

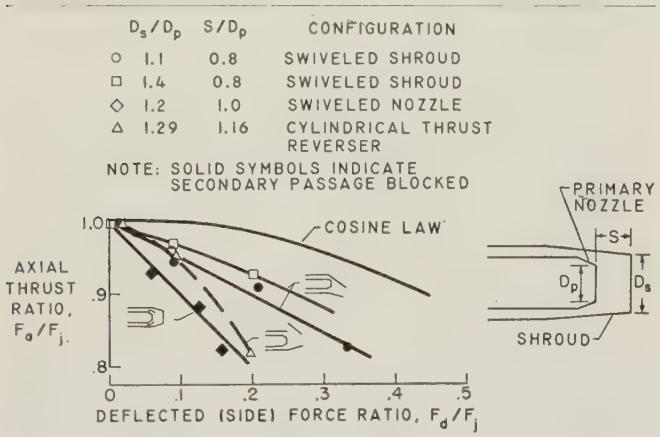

Fig. 6—Jet-deflection performance of shrouded nozzle configurations, pressure ratio 2.0

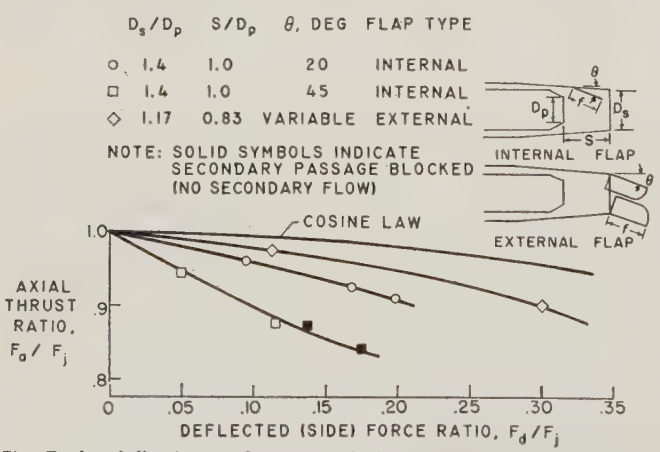

Fig. 7—Jet-deflection performance of shrouded nozzle configurations with flaps, pressure ratio 2.0

the F_a/F_j value for this configuration is 0.87 compared with 0.95 for the swiveled shroud. This larger reduction in F_a/F_j is caused by the side-force component resulting from the reaction of the primary nozzle which opposes that resulting from the jet impinging on the shroud. In all cases tested, it was necessary to operate this model with the secondary passage blocked in order to prevent backflow. This backflow characteristic is unlike that found for the corresponding swiveled shroud and probably results from the higher shroud angle (15-deg half-angle compared to 7 deg) that was used for the swiveled nozzle configuration. Another unfavorable characteristic of this configuration was a reduction of about 7% in primary nozzle flow that occurred over the range of conditions investigated. Inasmuch as the performance of the swiveled nozzle with fixed shroud is about the same as that for the auxiliary bleed nozzle, it may have directional control possibilities, but would be a poor jet lift device.

The performance of the cylindrical thrust reverser (triangle symbols) as a jet-deflection device is also shown in Fig. 6 for an effective D_s/D_p of 1.29 and S/D_p of 1.16. The axial thrust ratio of this device falls off at an increasing rate with increasing deflected-force ratio. For F_d/F_j values less than 0.10, the F_a/F_j ratio is comparable to those obtained with the swiveled shroud configurations and, thus, in this range this device may have application in providing directional control or trim forces. At F_d/F_j values of about 0.20, the performance of the device is comparable to that for the swiveled nozzle with fixed shroud or the auxiliary bleed nozzle and, thus, in this range this device would probably have application only for directional control. No measurements of the secondary flow characteristics were made for this device.

The performance of a shrouded configuration using an internal flap (circle and square symbols) for deflecting the jet is shown in Fig. 7 for a D_s/D_p of 1.4, a S/D_p of 1.0, and flap angles of 20 and 45 deg. It is readily apparent that the jet-deflection performance of these configurations is a function of flap angle, with the lower flap angle giving the better performance. Although not shown, a similar performance trend was observed when the ratio of D_s/D_p was decreased from the 1.4 value indicated in Fig. 7. With a flap angle of 20 deg, the flap length in terms of the nozzle diameter f/D_p varied from values of 0.87 for a F_d/F_j of about 0.10 to 1.45 for a F_d/F_j of 0.20. With a flap angle of 45 deg, the ratio of flap length to nozzle diameter was varied from 0.37 at a F_d/F_j of 0.05 to 0.60 at a F_d/F_j of 0.175. The performance of the 20-deg flap is about the same as that of the swiveled secondary shroud, whereas the performance of the 45-deg flap is only slightly better than that of the 90-deg auxiliary bleed nozzle. It is, therefore, improbable that internal flap angles greater than 45 deg would be used. Increasing the flap angle also increased the tendency of the secondary flow to reverse, so that it was necessary to block off the secondary passage at lower values of deflected thrust ratio F_d/F_j as the flap angle was increased. For fixed flap size and deflection angle, decreasing the diameter ratio D_s/D_p had a similar effect. For all these tests, however, the primary nozzle flow did not vary more than 2%. Inasmuch as the jet-deflection performance of the low-angle (up to 20 deg) internal flap is quite good, the device

		CONFIGURATION	$(F_d/F_j)_{max}$	POSSIBLE APPLICATION
1		SWIVELED NOZZLE	0.35	CONTROL OR LIFT AUGMENTATION
2		MOVABLE PLUG	.10	CONTROL OR TRIM
3		SWIVELED TAILPIPE	~1.00	CONTROL OR LIFT
4		EXTERNAL FLAP	.40	CONTROL OR LIFT AUGMENTATION
5		SWIVELED SHROUD (HI DIA. RATIO)	>.30	CONTROL OR LIFT AUGMENTATION
6		INTERNAL FLAP (LOW ANGLE)	.20	CONTROL OR TRIM
7		SWIVELED SHROUD (LOW DIA. RATIO)	.35	CONTROL OR LIFT AUGMENTATION
8		CYLINDRICAL THRUST REVERSER	.20	CONTROL OR TRIM
9		INTERNAL FLAP (HI ANGLE)	.17	CONTROL
10		SWIVELED PRIMARY, FIXED SHROUD	.16	CONTROL
11		90° SIDE BLEED NOZZLE	~1.00	CONTROL

Fig. 8—Deflection devices in order of decreasing efficiency (least axial thrust loss for given deflected force)

could have either directional control or jet lift application but would probably be lift-limited to trimming because of the low maximum value of F_d/F_j attainable. The performance of the high-angle (45 deg and over) internal flap, on the other hand, is such as to preclude the possibility of jet lift, although directional control application appears feasible.

The performance of the shrouded configuration with external flaps is presented in Fig. 7 (diamond symbols) for a D_s/D_p of 1.17 and S/D_p of 0.83. For these studies the flap length was equal to the primary nozzle diameter. The performance of this device was quite good, with relatively high values of axial thrust ratio being obtained for F_d/F_j values slightly greater than 0.30. Primary flow was unaffected by flap position, and secondary flow did not decrease more than 15% up to a deflected force ratio of 0.40 (maximum investigated). Inasmuch as external flaps are capable of deflected force ratios of at least 40%, this deflecting device has good possibilities for jet lift as well as directional control.

Comparison of Conventional Nozzle Jet Deflectors—A listing of the conventional nozzle jet deflectors in order of decreasing efficiency (least loss in axial thrust for a given deflected force) with an indication of possible applications is presented in Fig. 8. Configurations 1, 3, 4, 5 and 7 produced reasonable efficiencies and are considered to have possible lift augmentation application as well as directional control. The plug nozzle with movable plug (2) and the low-angle internal flap (6) were limited in the maximum deflected force ratio that they could produce (0.10 for the plug and 0.20 for the low-angle internal flap) and thus are probably suitable only for trimming as far as lift application is concerned. The cylindrical thrust reverser, which produced quite high efficiencies at small deflected thrust ratios (about 0.10), is considered also to be suitable for directional control or for limited use for trim application. The remaining configurations (9 to 11) are probably limited primarily to direction control applications because of their low efficiencies and/or low maximum deflected thrust ratios attainable.

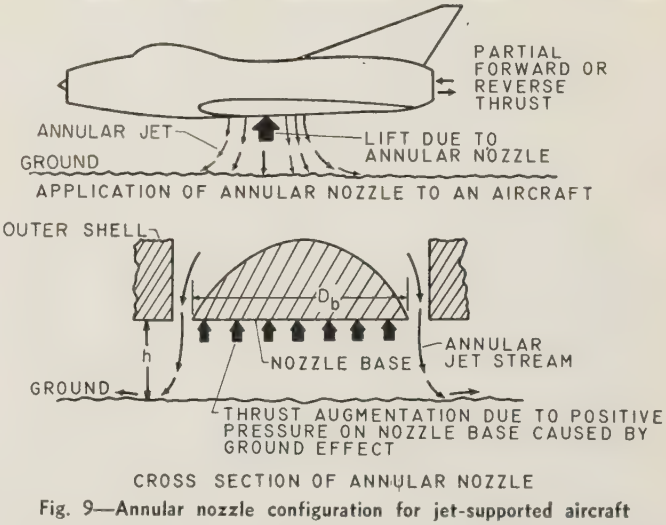

Fig. 9—Annular nozzle configuration for jet-supported aircraft

Unconventional Nozzles for VTOL

VTOL and STOL aircraft, in many cases, will have an unconventional airplane configuration in order to achieve optimum performance. It is of interest, therefore, to consider deflection devices that are best applied using other than circular exhaust nozzles. As part of the NACA jet-deflection program, two unconventional nozzle configurations were studied. The first, consisting of an annular nozzle with the jet directed perpendicularly to the ground, made use of ground effect to obtain thrust augmentation for take-off and landing.[6] The second configuration,

[6] NACA TN 3982, April, 1957: "Exploratory Study of Ground Proximity Effects on Thrust of Annular and Circular Nozzles," by Uwe von Glahn.

classed as a Coanda nozzle, consisted of a rectangular or square nozzle to which a deflecting surface was attached over which passed the entire jet exhaust.

Annular Nozzle—The annular nozzle (Fig. 9) consisted of a nozzle base enclosed by a flow annulus. When this nozzle comes close to the ground, the pressures on the nozzle base become greater than the atmospheric pressure because of ground effect. These positive pressures produce an upward thrust on the nozzle. The total thrust for an annular nozzle near the ground, therefore, consists of the jet thrust and the thrust augmentation obtained from the pressure reaction on the nozzle base. The thrust augmentation increases as the nozzle comes closer to the ground. The magnitude of the augmentation also depends on the nozzle's physical dimensions.

The thrust augmenation obtainable with an annular nozzle will permit a vertical-rising aircraft to have a larger gross weight than that possible by the use of only the direct jet thrust. However, an aircraft using an annular nozzle for lift cannot be considered a true VTOL, since its vertical-rising ability at take-off is very limited. Furthermore, the aircraft would require two exhaust nozzles. The first would be the annular nozzle for obtaining lift during take-off and landing and the second would be a conventional nozzle for obtaining axial thrust. Such an aircraft would rise off the ground for a limited height and then slowly accelerate by means of a small part of the available engine thrust until the aerodynamic lifting surfaces could support its weight. Thereafter, the aircraft would use an exhaust nozzle similar to that of a conventional jet aircraft. Landing techniques would be similar to those for take-off except that some thrust reversal would be required to stop the aircraft.

The thrust augmentation obtainable from the pressure increase on the nozzle base is shown in Fig. 10. The thrust increases are referenced to the thrust obtainable from a circular nozzle of equal flow area and are shown as a function of the ratio of the ground-to-nozzle distance to the nozzle base diameter h/D_b. (This ratio will be referred to as "ground-height ratio.") The data are shown for three values of the nozzle-area ratio A_j/A_t (jet area divided by the sum of the base and jet areas). As the nozzles approach close to the ground (denoted by decreasing h/D_b values), the thrust augmentation increases and for the largest nozzle-area ratio (0.31) reaches a value of about 62% at a ground-to-nozzle distance about 0.2 times the nozzle base diameter. A decrease in the nozzle-area ratio produces two effects: the thrust augmentation at any h/D_b value is somewhat increased, and the thrust augmentation begins closer to the ground. The thrust augmentation, ground-height ratio, nozzle-area ratio, and nozzle-pressure ratio are correlated to a single curve by use of empirical equations.[6]

The thrust augmentation for an annular nozzle is reduced with increasing ground incidence angle. The thrust augmentation for a nozzle with an A_j/A_t ratio of 0.31 is shown in Fig. 11 as a function of h/D_b for ground incidence angles of 90, 85, and 75 deg and a nozzle-pressure ratio of 2.1. (The value of h for the data at a ground incidence angle is the vertical distance from the center of the nozzle base to the ground.) The data show that for a ground incidence angle of 85 deg the thrust augmentation at a h/D_b value of 0.2 is about 3% less than that for an angle of 90-deg. At an incidence angle of 75 deg, the thrust augmentation at this same h/D_b value is about 19% less than that at 90 deg.

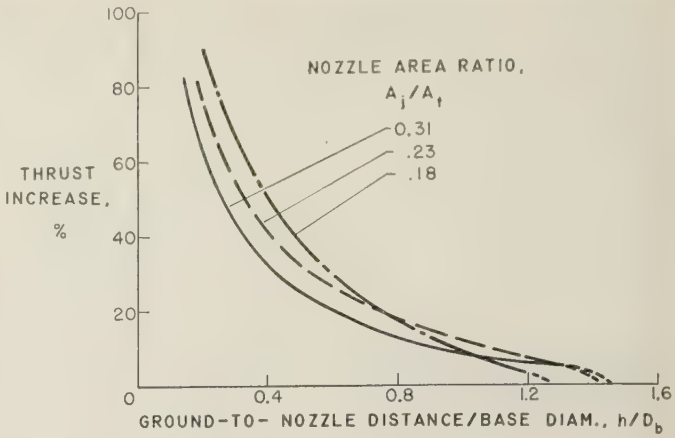

Fig. 10—Thrust augmentation with annular nozzle, pressure ratio 2.1

The thrust augmenation obtained with a fixed-area annular nozzle was accompanied by an increase in jet total pressure, which for an airplane configuration would constitute a back pressure on the engine. This back pressure would result in a change in the operating curve for an engine. The increase in jet total pressure due to ground proximity increased with a decrease in nozzle-to-ground distance. At a h/D_b value of 0.2 where the thrust augmentation for a nozzle with an A_j/A_t ratio of 0.31 was 62% (Fig. 10), the increase in jet total pressure (absolute) amounted to about 3%.

In addition to the increase in total pressure, the static pressure in the nozzle was also affected by the proximity of the ground. As the nozzle approached close to the ground, the jet exit velocity decreased owing to the change in static pressure and became less than sonic; however, the mass flow through the nozzle remained substantially constant.

In the application of an annular nozzle to novel aircraft in which the jet stream supports the aircraft weight during take-off or landing, all the annular-nozzle characteristics just discussed must be taken into account. In order to elevate and support the aircraft a reasonable distance above the ground, perhaps 4–8 ft, a nozzle with a large base and a relatively small annular slit would be required. Such a nozzle configuration could be achieved by utilizing the lower half of the fuselage for the nozzle base or by using delta- or circular-wing platform aircraft that provide sufficiently large base areas to meet these requirements. A variable-area exhaust nozzle or an increase in fuel flow would alleviate the problem of back pressure on the engine, at some cost in thrust augmentation, however. For the same engine thrust an aircraft supported by an annular jet could conceivably take off from an improved landing strip (such as a lightweight steel mesh runway) with a greater payload or fuel capacity than could some other types of VTOL aircraft, provided the incorporation of an annular nozzle for take-off and landing did not make the weight of the aircraft prohibitive.

Coanda Nozzle—The phenomenon by which the proximity of a surface to a jet stream will cause the jet to attach itself to and follow the surface con-

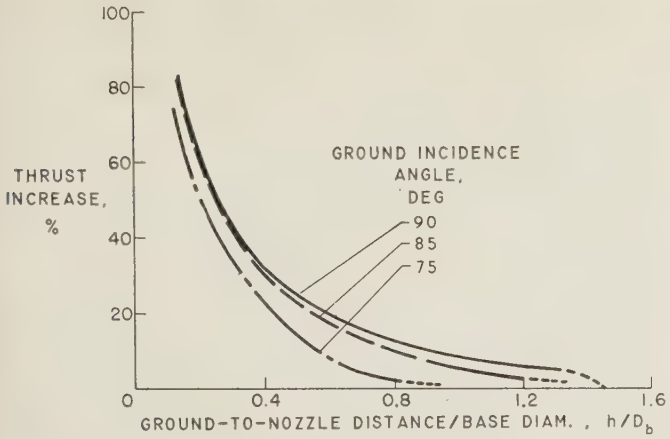

Fig. 11—Effect of ground incidence angle on thrust augmentation with annular nozzle, pressure ratio 2.1

tour is known as the Coanda effect.[7] If the surface is placed at an angle to the original jet axis, the jet will be deflected.

Use of the Coanda effect has been made in studies of the jet flap and supercirculation devices for augmenting the lift of airfoils.[8, 9] These studies have been concerned with large-aspect-ratio nozzles (nozzle aspect ratio is defined as the ratio of nozzle width to height). Research conducted at the NACA Lewis laboratory has been directed toward evaluating nozzle-aspect ratios less than 10 and approaching 1.0. With low-aspect-ratio nozzles, the Coanda effect could perhaps be applied advantageously to pod-mounted jet-engine installations. Since in its practical applications the deflecting surface should be small, the NACA studies were concerned not only with the basic flow phenomenon over various deflecting surfaces but with means of obtaining the maximum lift-to-thrust ratio with minimum size of the deflecting surface.

A typical nozzle-plate configuration, herein called a "Coanda nozzle," is shown in Fig. 12. This Coanda nozzle is rectangular in cross-section and has a flat deflecting plate attached to its lower side. Side plates are used to obtain two-dimensional flow, and their need for low-aspect-ratio nozzles is discussed later. From theoretical considerations the local pressure on the deflecting surface of a Coanda nozzle reaches a maximum negative value relative to the atmospheric pressure near the beginning of the surface and, if the surface is flat, decreases with surface length. If the deflecting surface is directed downward, these negative pressures result in a lift component. A drag component constituting a reduction in axial thrust is also obtained. Also, analysis shows that if the jet could be deflected 90 deg by one or more such deflecting plates, the axial thrust could be reduced to zero by the drag component.

Earlier unpublished studies at the NACA have shown that a Coanda nozzle with low aspect ratio (width-to-height) of the order of 1–10 requires the use of side plates (Fig. 12) to attain the best performance. Without side plates the lift is reduced as

[7] WADC-AMC, (Translation) Rept. No. F-TS-823-RE, February, 1948: "Method of Increasing Fluid Stream by Diverting It from Its Axis of Flow, Coanda Effect," by A. R. Metral.

[8] NACA TN 3364, 1955: "Investigation of Effectiveness of Large-Chord Slotted Flaps in Deflecting Propeller Slipstreams Downward for Vertical Take-Off and Low-Speed Flight," by Richard E. Kuhn and John W. Draper.

[9] NACA TN 3693, May, 1956: "Preliminary Investigation of Effectiveness of Sliding Flap in Deflecting Propeller Slipstream Downward for Vertical Take-Off," by Richard E. Kuhn and Kenneth P. Spreemann.

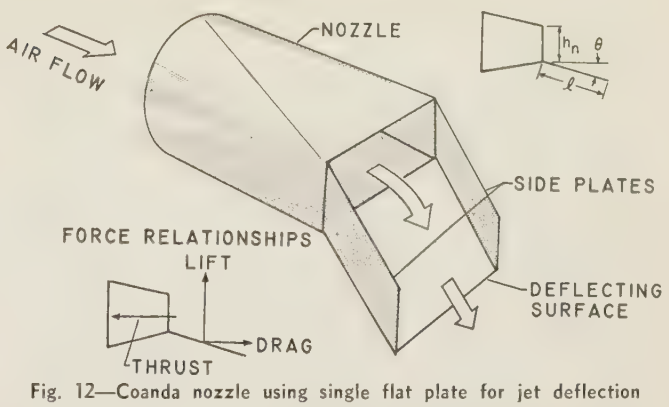

Fig. 12—Coanda nozzle using single flat plate for jet deflection

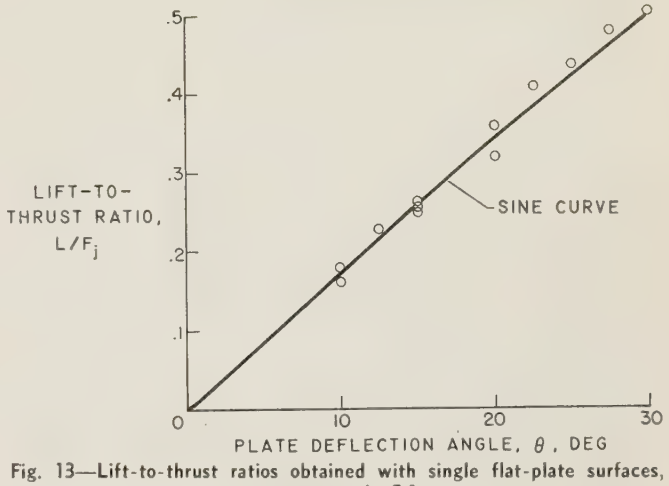

Fig. 13—Lift-to-thrust ratios obtained with single flat-plate surfaces, pressure ratio 2.1

compared with that for a nozzle with side plates. Although some data on the required vertical height of side plates were obtained in the present studies, the results were erratic and inconclusive; consequently, most of the tests were conducted with side plates equal to the nozzle height and extending along the entire length of the deflecting surface.

The initial studies on the Coanda nozzle were conducted with single flat plates hinged at the nozzle exit. These studies were intended to determine the the effect of plate length l, nozzle dimension (height h_n, deflection angle θ, and nozzle-pressure ratio P_n/p_o on the lift-to-thrust ratio L/F_j. (F_j is the jet thrust without a deflecting plate.) The variation of L/F_j ratio with angle of deflection for single flat plates having optimum negative surface pressure coefficients over most of the plate length is shown in Fig. 13 for a nozzle pressure ratio of about 2.1. Also shown is a sine curve which represents the L/F_j values obtained by rotating an engine to a prescribed angle. The experimental data for the Coanda nozzle correlate well with values for the sine curve. These experimental data were obtained with several nozzles and plate sizes. The correlation of plate length, nozzle height, deflection angle, and lift-to-thrust ratio is beyond the scope of this paper; consequently, the various nozzle-plate combinations are not identified in Fig. 13. It appears sufficient to indicate that, for the range of nozzles and plates studied, plate length-to-nozzle height ratios of the order of 1.0 were identified with deflection angles near 15 deg, and ratios up to about 5.0

were identified with deflection angles near 30 deg. Reducing the respective plate length-to-nozzle height ratios at these deflection angles resulted in jet detachment from the plate and a large loss in lift. Increasing the plate length-to-nozzle height ratio at these deflection angles also caused a reduction in lift.

When the deflecting surface, at a given deflection angle, is large compared with the nozzle height, the optimum lifting potential resulting from the negative pressures on the upstream end of the surface is offset by positive pressures on the aft regions of the surface. A typical pressure distribution curve over a flat plate is shown in Fig. 14 (2-in. nozzle height, 2.1 pressure ratio, 10-deg deflection angle, 2.5- and 11.75-in. plate length). In this figure the ratio of the pressure difference between the surface and the atmosphere to the jet total pressure is shown as a function of surface distance along the flat plate measured from the nozzle. Only the negative pressures contribute to lift, while the positive pressures reduce lift. The surface pressures for both plates reach similar negative pressures for the same surface location and become positive at about 1.70 in. from the nozzle. However, the long plate has a much greater length subject to positive pressures than the short plate; consequently, at this deflection angle (10 deg) the L/F_j ratio for the long plate is about 60% of that for the short plate and the sine curve.

In order to achieve high L/F_j ratios with flat surfaces for deflection angles greater than about 30 deg, it is necessary to use a multiple-plate configuration. The Coanda effect is such that large negative pressures are established with every angle increase of the surface relative to the jet stream. Hence, referring to Fig. 14, deflecting the plate an additional 10 deg at 1.7 in. from the nozzle will result in another negative pressure region of approximately equal surface-wise extent to that on the initial plate. The magnitude of negative pressures on this second plate, however, will be somewhat less than those on the initial plate. This procedure can be repeated until the desired total deflection angle or lift is obtained.

The L/F_j data for single and two- and three-plate surfaces having negative pressures over most of the plate surfaces are shown in Fig. 15 as a function of the total deflection angle θ_T. Pertinent dimensions and the sine curve for the configurations are noted in the figure. The relative deflection angles for adjacent plates are not identified because the correlation with other parameters is beyond the scope of this paper. Both the two-plate data (square symbols) and the three-plate data (diamond symbols) fall increasingly below the sine curve with increasing deflection angles. The maximum L/F_j value of 0.68 for the three-plate configurations shown is attained at a deflection angle of about 60 deg. This L/F_j value compares with a value of 0.866 for the sine curve.

From analytical considerations the reduction in the L/F_j ratio from the sine curve by using plates to deflect the jet through large angles (up to 90 deg) is to be expected. In fact, for a 90-deg deflection angle the last plate of a three-plate configuration contributes only to thrust reduction in the axial direction and nothing to lift. Of significance, however, is the fact that the jet can be deflected through essentially 90-deg by using the Coanda effect.

Further analysis of these data leads to the conclusion that use of a large number of small flat plates or a curved surface would achieve larger L/F_j values than those shown in Fig. 15. Tests in progress at the present time verify these conclusions, as shown by the data for such plates in Fig. 16. In this figure the L/F_j ratios for the sine curve and the multiple-plate data shown in Fig. 15 are repeated together with data for: (1) a six-plate surface designed to deflect the jet through 75 deg (2.0-in. nozzle height), (2) a nine-plate surface designed to deflect the jet through 90 deg (0.5-in. nozzle height), and (3) a curved surface designed to deflect the jet through 90-deg (1.1-in. nozzle height). The six- and nine-plate surfaces each consisted of equal-length flat-plate segments (2.0 and 0.6 in., respectively) and equal deflection angles for the adjacent segments (12.5 and 10 deg, respectively). The curved plate consisted of a modified circular arc (approximately 4-in. radius). It should be noted at this point that the effective jet-deflection angle is somewhat less than the plate-deflection angle, the difference increasing with large deflection angles. Consequently, the total plate angle to achieve an effective jet deflection angle of 90 is about 95 deg. For convenience, however, the data for a 90-deg deflection of the jet are plotted at a plate deflection angle of 90 deg. The nine-plate surface and the curved surface configurations both at-

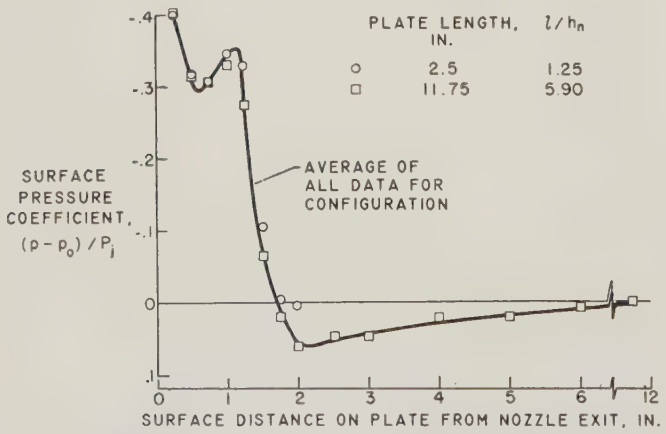

Fig. 14—Pressure distribution over deflected flat plate ($P_N/p_o = 2.1$, $h_n = 2$ in., $\theta = 10$ deg)

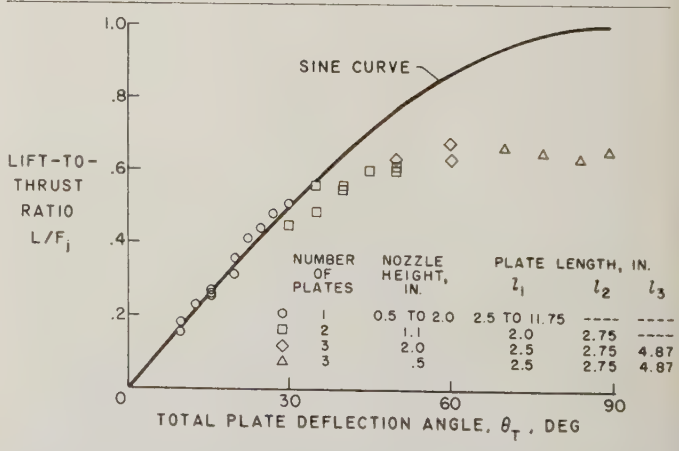

Fig. 15—Lift-to-thrust ratios obtained with 2- and 3-flat plate surfaces, pressure ratio 2.1

tained a L/F_j value of about 0.83 at a deflection angle of 90 deg. This compares with a L/F_j value of about 0.65 for the three-plate configuration.

It is of interest to note that large discontinuities in the plate surfaces had no apparent effect on the L/F_j ratio or the angle to which the plate could be deflected for maximum L/F_j values. Leaks between the side plates and the deflection plate, however, could cause large reductions in the L/F_j ratio. If these leaks were located near the peak negative pressures on a deflection plate, however, immediate jet detachment would occur.

In view of the L/F_j value of 0.83 obtained with a 90-deg deflection angle in this exploratory study of several Coanda nozzles, this type of jet-deflection device may be applicable to certain VTOL configurations. A Coanda nozzle may also be utilized effectively for directional control (pitch or trim) and lift augmentation. The latter use may create external aerodynamic problems if the necessary deflecting surface is large. For VTOL and other uses the hardware problems and the dimensional aspects of providing a retractable jet-deflection plate pose a challenge to the aircraft designer. In the studies discussed, the minimum plate length that would deflect the jet through an angle of 90 deg was about seven times the nozzle height. The vertical distance from the nozzle to the end of the plate was about five times the nozzle height. The aircraft configuration, however, can reduce the plate length requirement for a particular nozzle height. For example, the jet stream of an aircraft having a 30–45 deg attitude with respect to the ground need be deflected only 60–45 deg, respectively, to achieve vertical lift. This reduction in the required jet-deflection angle for VTOL reduces substantially the required plate length. Utilization of nozzles having aspect ratios up to 10 also should be considered as a means of reducing the physical dimensions of the deflection plate.

The application of data from these studies to jet flaps and associated devices is apparent. Also, the need is indicated for additional information on the fundamental compressible-flow considerations associated with the Coanda effect, including the evaluation of side-plate requirements, scale effects, effect of a moving air stream on the lift obtained with a Coanda nozzle, and the problems caused by the use of a heated jet.

Conclusion

In summary, the results of investigations of jet-deflection devices applied to both conventional round nozzles and unconventional exhaust nozzles indicate that there are several devices which are capable of providing jet lift or directional control forces with a minimum of losses. In general, devices which turn or deflect the entire jet rather than a portion thereof are the more efficient. For the conventional nozzles, such devices include the swiveled nozzle or tailpipe, movable plug, and both internal and external flaps; for unconventional configurations, the Coanda nozzle has proved effective.

Many of the jet-deflection devices applicable to conventional round nozzles for directional control or lift augmentation can be applied to existing aircraft. By augmenting the lift of an aircraft during takeoff or landing, the required length of the run can

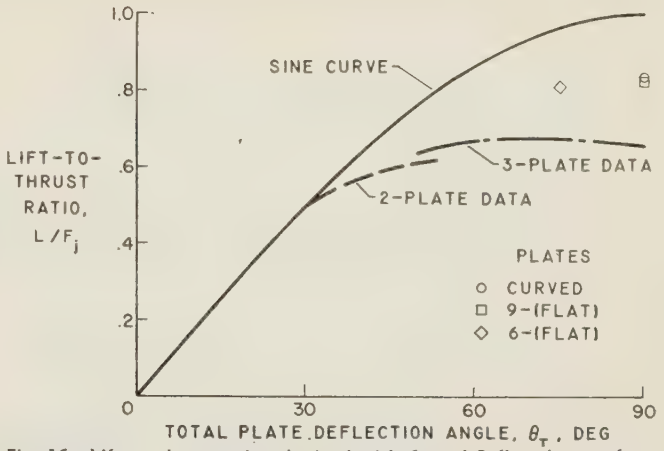

Fig. 16—Lift-to-thrust ratios obtained with 6- and 9-flat plate surfaces and curved flat plate, pressure ratio 2.1

be reduced. Futhermore, by deflecting a portion of the jet thrust in flight for augmenting the normal lift of the wing the altitude capability of the aircraft can be enhanced without serious loss in forward speed. At high altitudes the use of jet directional controls can improve the maneuverability of aircraft over that available with conventional aerodynamic controls.

Best utilization of unconventional jet-deflection devices, such as the Coanda nozzle, can be achieved by designing the aircraft with due consideration for the unique characteristics of the device rather than attempting to incorporate the device in an existing aircraft configuration.

APPENDIX

Symbols

A_j = Annular jet flow area, sq in.
A_t = Total annular nozzle area, nozzle base plus flow annulus, sq in.
D_b = Diameter of annular nozzle base, in.
D_p = Diameter of primary nozzle, in.
D_s = Diameter of shroud exit (ejector-type nozzle), in.
F_a = Axial thrust force, lb
F_d = Deflected (side, pitch, or lift) force, lb
F_j = Initial jet thrust without deflection device, lb
f = Flap length, in.
h = Nozzle-to-ground distance for annular nozzle, in.
h_n = Nozzle height (Coanda nozzle), in.
L = Lift obtained from deflection device (Coanda nozzle), lb
l = Surface length for Coanda deflecting surface, in.
p = Surface static pressure on Coanda deflection plate measured relative to atmospheric pressure, in. of Hg
p_0 = Atmospheric pressure, in. of Hg abs
P_j = Jet total pressure, in. of Hg gage
P_n = Jet total pressure, in. of Hg abs
S = Distance from primary nozzle exit to shroud exit, in.
θ = Deflection angle for device, deg
θ_T = Total deflection angle for multiple and curved plate used on Coanda nozzle, deg

Subscripts 1, 2, 3 denote particular plate for multiple-plate Coanda nozzle.

Bio-Technical of Driver Safety and

R. A. McFarland and R. G. Domey, Harvard School of Public Health

This paper was presented at the SAE Annual Meeting, Detroit, Jan. 16, 1958.

DRIVER safety and comfort depend largely upon the degree of integration achieved among the three major subsystems involved in highway transportation: (1) the vehicle and its dynamic properties, (2) the tracking and other conditions provided by the highway, and (3) the human operator whose dynamic properties are the most intricate of all. Close examination will reveal that not all accommodations built into the vehicles coincide with the variations of anatomical structure and functional characteristics of the humans who must operate them. The bio-technical study of man-vehicle-highway relationships constitutes an analysis of the most advantageous ways to integrate these three subunits into one efficient system.

The interlocking nature of the man-highway-vehicle transportation "system" leads in a very logical way toward one important possibility, namely, that the vehicle-highway segments of the system should be designed as a unit around the variable capacities of the operators. This point of view is being favorably accepted, although coordination of the highway engineer's skills, the vehicle designer's art, and the biological and social sciences remains to be achieved.

For instance, the overall picture has been expressed in the following way by Millikin, Whitcomb, and Segal.[1]

> . . . it may be estimated that present knowledge of automobile handling is on a par with that available to the aircraft designers of the early 1920's. . . .
>
> For the automobile, the slope of progress remains far lower with an expanded scale of events. . . .
>
> This appraisal must conclude, and this is said with great deference to those pioneering efforts already described, that the ability to predict behavior and call out desirable characteristics are yet to become a part of the practicing automotive engineer's facility.

It is precisely the unsystematic factor inherent in empirical design which has impeded development of equipment which would facilitate maximum human efficiency. This assumption has recently been expressed as follows by the automotive engineers just cited:

> Another basic consideration is the response time of the vehicle in relation to that of the human driver, determining, as it does, the degree of closed-loop operation and the possibility of interference between the dynamics of vehicle and driver in transitionary manoeuvers. Unlike that of large ships, the response time of conventional automobiles (on the order of 1 second or less) is sufficiently close to that of the human operator (¼–½ second) that matching problems of the type encountered in automatic controls may be expected, and indeed have been actually encountered in rapid or successive (overlapping) manoeuvers. There is evidence that the human has contributed to an overall system instability, *and the designs of our vehicles would ideally consider the dynamic responses of the human driver.* (Italics ours)

[1] "Research in Automobile Stability and Control and in Tyre Performance," by W. F. Millikin, D. W. Whitcomb, L. Segal, et al. Reprinted by Institute of Mechanical Engineers on behalf of Cornell Aeronautical Laboratory, Inc. of Cornell University.

Aspects Comfort

A STUDY has revealed that few truck cabs are designed with the comfort of the driver in mind. All too often, cabs were found to be far below the minimum standard in dimension, equipment, ease of operation, adjustability, and visibility. This situation interferes with the efficiency of the driver, causing at various times inconvenience and discomfort which eventually has an effect on the safety of operation.

This paper reports the findings of this study and suggests criteria for a more efficient and comfortable cab.

The study was undertaken at the Harvard School of Public Health.*

Further consideration of the idea that the human operator "contributes to an instability of the overall system" leads to a second point: perfect stability of the machine is a highly desirable objective when it is considered as one condition of the man-machine system, but the man-machine "loop" is different from, and more important than, the machine subsystem by itself. However, the contribution to overall system instability is not limited solely to factors of human reaction time. Even if we could assume that the operator of a vehicle had complete control over the rate of his responses, the fact is that he is still dependent upon cues from his surroundings which will influence the actual form and place, as well as the time of initiating and completing his actions.

It might be possible to demonstrate an ideal dynamic vehicular system. However, in order to maintain the theoretical level of efficiency of the system it would be necessary to assume that the human operator was perfectly integrated with the machine. Since in many instances time constants as small as 1 sec or less are involved, any design features which increase this time interval would be highly undesirable. Thus, reference to the time of operation would be one objective way to define some types of design defects, or desirable design features, and to delineate the magnitude of either one in these terms. It is necessary to observe a great many seemingly unimportant design arrangements, and then the significance of these must be interpreted in terms of human factors.

The characteristics of the human operator must not be disregarded. Thus far the highway and vehicle have not been jointly engineered so as to encompass the range of static and dynamic properties of vehicle operators as a group. Until human factors are taken into consideration, vehicular dynamics will remain abstractions of physics.

Unfortunately, systems analysis has demonstrated that the physical "perfection" of man's machine environment has not been a very good predictor of the efficiency of the operators. The point is that the man-vehicle-highway combination as a system is the proper unit of analysis. Until this concept becomes central in technical thinking, a disappointing discrepancy between the theoretical efficiency of the system and the obtained efficiency will remain.

Even under the most ideal conditions the complex interrelationships of human functions coupled with vehicular functions produce inherent instabilities merely by the fact of their combination. For instance, in the absence of proper cues the most cautious of operators may overdrive vehicles, and thus move into a man-machine-highway relationship which is beyond the control of the operator with respect to his sensory acuity, perceptual capacities, and response repertoire. It may also be true that on occasion the most sophisticated of operators may not be at all aware of being in jeopardy. In our complex traffic patterns, the unnecessary introduction of even "minor" inconveniences, "slight" delays, or inappropriate responses into the task of the operator may prove disastrous, especially when the man-vehicle-highway combination has been forced to the limit of its potential efficiency. However, a mathematical theory of vehicle dynamics is being developed, and it is now possible to make limited predictions of the points at which the man-machine-highway system becomes unstable. As prediction becomes more definitive, it seems probable that a greater variety of human factors will require technical consideration.

A few of the recurrent conditions which serve to interfere with the integration of man-and-machine are inadequate space, inappropriate location of controls, obstructions which prevent seeing and interpreting the cues provided by dials and gages, uncomfortable and unadjustable seats, excessive noise, unfavorable temperature, and annoying vibration. At the least, all of these together or singly introduce time delays and distractions, and must be consid-

* This study was sponsored by the Commission on Accidental Trauma of the Armed Forces Epidemiological Board and was supported in part by the Office of the Surgeon General, Department of the Army.

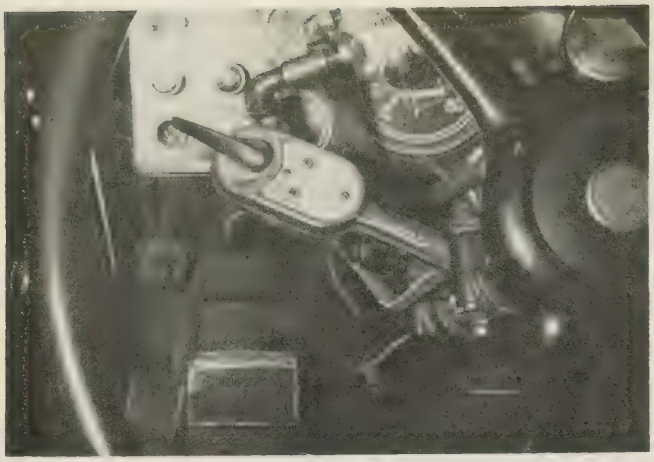

Fig. 1—Trolly brake fixtures and directional signals block the view to the instrument panel (truck issued in 1955)

ered detrimental to the most efficient control over the vehicle.

More specifically stated, the study of vehicle design in relation to biotechnical aspects of operator safety and comfort may be classified into at least three major areas:

1. Design relationships which facilitate or impede sensory input and sensory discrimination.
2. Design relationships which facilitate or impede response output and response differentiation.
3. Design relationships which modify the fundamental physiological states of the operator in favorable or unfavorable ways.

Since 1949 an extensive research program on highway safety has been in progress in the Department of Industrial Hygiene of the Harvard School of Public Health. One of the objectives of this program has been to develop design recommendations for the improvement of safety in the operation of all types of vehicles. Human engineering principles have been applied in the evaluation of current vehicles by a team of scientists with specialized training in the fields of experimental psychology, engineering, physiology, and physical anthropology. The purpose of this approach was to obtain information which, when applied in future models, will result in a more effective integration of drivers with their equipment.

The findings of the first study were published in 1953.[2] In this report detailed evaluations were made of twelve trucks and six buses (1950 and 1951 models) and some preliminary design criteria were formulated. There are three other publications in the series: one presenting the basic approaches of human engineering and the pertinent biological data,[3] and two which condensed much of this material and present specific design recommendations for the drivers workspace.[4,5]

The present study[6] was carried out to evaluate truck models produced in 1956. An analysis was made of the (1) fixed limits of the cab, (2) static dimensions of the seats, (3) range of ajdustability of seats, (4) problems associated with variation in human size, (5) variables influencing visibility of items within the operators' compartment, (6) variables influencing the visibility of the environment outside the vehicle, and (7) ease and convenience in the operation of controls such as pedals, levers, knobs, switches, and cranks. Some measurements of noise level, temperature, humidity, and CO concentration within the operators cab were also obtained. Special notice was taken of design relationships[7] likely to become hazardous under critical conditions of driving. Whenever possible the interpretation of the obtained data was made in conjunction with certain criteria and standards not available at the time of the previous studies.

The findings from the present study will be given in the remaining sections of this paper. Some illustrative principles of bio-technology will be first indicated, together with criteria pertinent for design in terms of human capacities and limitations.[8] The design features of the vehicles studied will be discussed in terms of the sensory input and response output of the operator task. The criteria cited here are considered tentative and will be revised after more definitive experimental study.

Illustrative Criteria and Principles[9]

A few criteria and working principles are listed below. Throughout the text, other criteria will also be given. For example, the criteria proposed by McFarland, Damon, and Stoudt[4] in regard to human sizing will appear in the section devoted to seating and the work space.

Basic Principles—1. Consider the operator.

2. Consider the operator early in the design process.
3. Consider the operator as a crucial part of the man-vehicle-environment system.
4. Consider the physical variablity of men, their size, their strength, and fatigue levels.
5. Consider the variation in the abilities of men.
6. Consider that men are functional.
7. Consider ample margins of safety.
8. Consider that particular installations rather than overall design may cause trouble.
9. Consider that often minor rearrangements will suffice to overcome impediments to safety and comfort.

Some Variables Influencing Efficiency of Operation—1. Controls should be within easy working distance of operator.

2. Controls should be assigned to proper body segments.
3. Important and frequently used controls should

---

[2] "Human Factors in Design of Highway Transport Equipment: Summary Report of Vehicle Evaluation," by R. A. McFarland, J. W. Dunlap, W. A. Hall, and A. L. Moseley. Pub. by Harvard School of Public Health, Boston, 1953.

[3] "Human Body Size and Capabilities in Design and Operation of Vehicular Equipment," by R. A. McFarland, A. Damon, H. W. Stoudt, A. L. Moseley, J. W. Dunlap, and W. A. Hall. Pub. by Harvard School of Public Health, 1953.

[4] SAE Special Publication 142, 1955: "Application of Human Size Data to Vehicular Design," by R. A. McFarland, A. Damon, and H. W. Stoudt.

[5] "Human Factors in Design of Vehicle Cab Areas," by N. C. Kephart and J. W. Dunlap. Pub. by Purdue University, Occupational Research Center, Lafayette, Ind., 1955.

[6] "Human Factors in Design of Trucks, An Evaluation of Models Produced in 1956," by R. A. McFarland, R. G. Domey, et al. Pub. by Harvard School of Public Health, Boston, 1957.

[7] Several photographs of two rough-terrain fork lift trucks will appear in this report. Permission to use these illustrtaions was obtained from Col. James C. Bradford, QMC, Commanding Officer, QM Research and Development Center Operations, QM R and D Environmental Protection Research Division, Natick, Mass. The full text of the operational analysis of this vehicle may be obtained from Technical Report EP-42, January, 1957. The responsible author was Capt. William S. Wolf, QMC, Psychology Branch.

[8] "Layout of Workplaces," WADC TR 56-171, AD No. 110507; and "Design of Controls," WADC TR 56-172, AD No. 118023; by J. H. Ely, R. M. Thomson, and J. Orlansky. (Chapters 5 and 6 of the forthcoming "Joint Services Human Engineering Guide to Equipment Design." These reports are valuable for the specific information and for the extensive selected bibliographies they contain.)

[9] A more detailed analysis may be found in "Human Factors in Design of Trucks—An Evaluation of Models Produced in 1956," by R. A. McFarland, R. G. Domey, et al. Pub. by Harvard School of Public Health, Boston, 1957.

be assigned to preferred locations.

4. Controls and displays should be grouped according to related sequence of use and function.

5. No hand or foot should be overloaded.

6. Distribution of duties should be bilaterally symmetrical if possible.

7. Ease of operation relative to accurate manipulation of controls is a major consideration.

8. Control design should permit "blind" selection.

9. Controls should be identifiable through a number of sensory channels when necessary.

10. Controls should be separated by sufficient distances to accommodate the range of physical variation and the bulk of clothing.

Some Variables Influencing Visual Efficiency—1. The most important and frequently used displays should be located in the line of sight.

2. All displays should be readable from the normal head position allowing for normal head rotation, and for restrictions imposed by goggles and headgear.

3. Miscellaneous equipment should not obstruct sensory intake.

4. Displays used together should be grouped together.

5. The vehicle operator should be able to see the ground at least 10 ft in front of his vehicle.

6. The upward angle of vision should be no less than 15 deg.

7. The downward viewing angle should be no less than 12–15 deg from horizontal.

8. Sideward vision should be as clear as possible through at least 180 deg of arc, preferably through 220 deg of arc.

9. Door posts should be as small as possible.

10. There should be no apparatus which obstructs forward vision.

11. Safety glass should be used throughout.

12. Visual distortion should be eliminated.

13. Cab lighting should be adequate—instrument panels should be equipped with red or violet lights to allow for the most efficient night vision.

14. Interior light switch should be accessible to the operator prior to entering the cab.

Some Variables Influencing Comfort—1. An arm rest should be available.

2. There should be adequate leg room.

3. Accelerator pedals should have heel rest if steeply inclined.

4. The seat should be adjustable horizontally and vertically as a unit. The fore and aft edges of the seat should be adjustable in the vertical plane.

Some Variables Influencing Safety—1. There should be no protuberances in the cab which constitute hazard in case of accident or abrupt deceleration.

2. There should be no impediments to escape from the cab.

3. The vehicle should be equipped with a first aid kit, flares, fuses, hatchet, and other emergency equipment, all in convenient locations.

4. There should be no impediments to mounting and dismounting the cab. Hand grips should be available.

5. The operator and others should not be exposed to CO, aldehydes, or other toxic agents.

6. The operator should be provided with information on the operation of his equipment well in advance of the necessity of taking action.

Variables Influencing Sensory Input

In order to function adequately, the human being must learn to make different appropriate responses at different times and places. He must discriminate sensory input and differentiate response output. Input or sensory cues are extremely complex. Through one or all sensory channels the operator must depend upon such cues as size, location, movement, shape, pattern, duration, frequency, color, vibration, feel sound, temperature, and rate.

Conditions which Interfere with Sensory Input and Sensory Discrimination within the Vehicle—The conditions which interfere with sensory input and discrimination of information-giving dials and gages, or other sources are: (1) inappropriate placement of the object or condition, (2) impediments to activation, (3) delay of delivery, (4) imposition of awkward response necessary to initiate information delivery, (5) insufficient discriminative cues, that is, lack of variation in shape, color, or size, (6) different locations of the same cue systems in different vehicles, (7) glare, (8) parallax, (9) nonrepresentative notation, (10) no provision for night vision, that is, red or violet instrument panel illumination, and (11) no provision for some types of information.

These are not the only conditions possible to include in this list, but they are among those most commonly found. Examples of some problems discovered in one or more trucks are as follows. Dials inappropriately located behind the steering post (Fig. 1) in vehicles with low-hanging instrument panels were not uncommon. In one truck, the oil and the gasoline were indicated by the same pointer. In order to change from on function to the other, it was necessary to press a button on the dashboard. Obviously, information on these items is not readily available to the operator. The problem here is delay of information, and the seemingly unnecessary round-about way of obtaining it.

The tachometer may be selected as another illustration. This dial records engine rpm, and is read principally for determining the proper time to shift gears. Shifting in many of the larger vehicles depends upon a relatively complex sensory-motor, particularly visuo-motor, relationship. One problem observed was the variation among tachometer increments. In one vehicle, the divisions were in 3–6–9–12 . . . 33 units. In another vehicle the units were in blocks of 10, and in another the increments were in actual rpm, 0–500–1000–1500, and so on. Thus, in some instances the dials register symbolic information to which the operator must apply a multiplier for obtaining exact rpm's.

All tachometers do not have an overlay system superimposed upon the dial proper, sometimes in color, to indicate when the engine is overlugging. Included in these systems are zone markings indicating the proper times to shift. Provision for interpretation such as this is commendable practice.

The speedometer and the tachometer were sometimes in different positions in different vehicles. If the tachometer provides the most important information it would seem that it should be given the preferential location. In practice this was not always the case. In one instance, the tachometer was

Fig. 2—Two different dials have figures arranged in opposite directions, one clockwise and one counterclockwise. Also two switches must be manipulated in opposite directions for the OFF position, and in opposite directions for the ON position

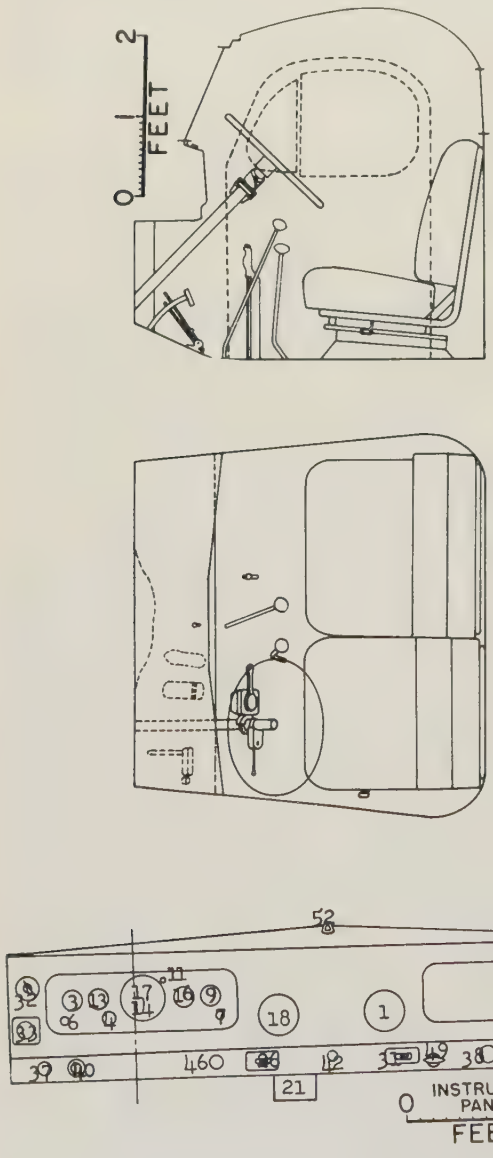

Fig. 3—Scale drawing for vehicle #1801-56

Table 1—Angle of Instrument Panel

Vehicles		Angle of Instrument Panel from Horizontal, deg
Rank	Code	
1	2401-56	90.0
2	1601-56	90.0
3	1801-56	94.0
4	1401-56	96.0
5	2001-56	99.0
6	2801-56	99.5
7	2201-56	102.0
8	1001-56	104.0
9	1201-56	105.0
10	2601-56	137.5

located to the right, out of the direct line of vision of the operator, thus introducing the problem of parallax; also this dial did not have a warning zone overlay. In addition, the pointer rotated in a counterclockwise direction. This feature was found in one other of the tachometers (Fig. 2) seen in the 10 vehicles. Imprudent location and departure from some established or usual expectancy are two conditions which could probably be avoided.

Placing dials and gages in the line of sight of vehicle operators is not an easy matter. That the angle of vision is highly variable is demonstrated in Table 1. The inclinations of the instrument panel in 10 trucks shown in Table 1 are listed in rank order. The angles from the horizontal range from 90 to 137 deg, a difference of 47 deg.

Perhaps of more importance are the wide differences among instrument panels which range from 3½ to 6 feet in length, and the gages, dials, switches, and knobs located upon them. For instance, Figs. 3 and 4 and Table 2 show quite clearly that there are very few standards for the placement of these various objects. Here, eight different dials and gages distributed to the right and in front of the operator in one truck were exactly reversed in another.

The tremendous variation within and among trucks in the size, location, information provided, readability, availability, and interpretability of information systems lead to the conclusion that this area of vehicle design would profit from intensive and definitive research. Developing adequate standards is both possible and practicable. The details necessary to satisfy the bio-technical demands imposed by the operator population would not be too difficult to discover, and in some instances the most that would have to be done would be to extend principles and standards already known. Variability in vehicular design, when it appears, should be in noncritical areas of structure or in applications of design which do not limit the use of gages, dials, or controls.

Design Features which Interfere With Sensory Input and Sensory Discrimination from Outside the Vehicle—A few conditions which interfere with sensory intake and discrimination from outside the vehicle are: (1) total visibility area, (2) filters interposed between the operator and the external environment, (3) curvature of the windshield, (4) number, size, and function of windshield wipers, (5) size, number, composition, location, and shielding properties of the sun visors, (6) unshielded openings, (7) size and location of mirrors, and (8) glare.

One interesting finding concerned the restricted visibility of the ground in front of the truck result-

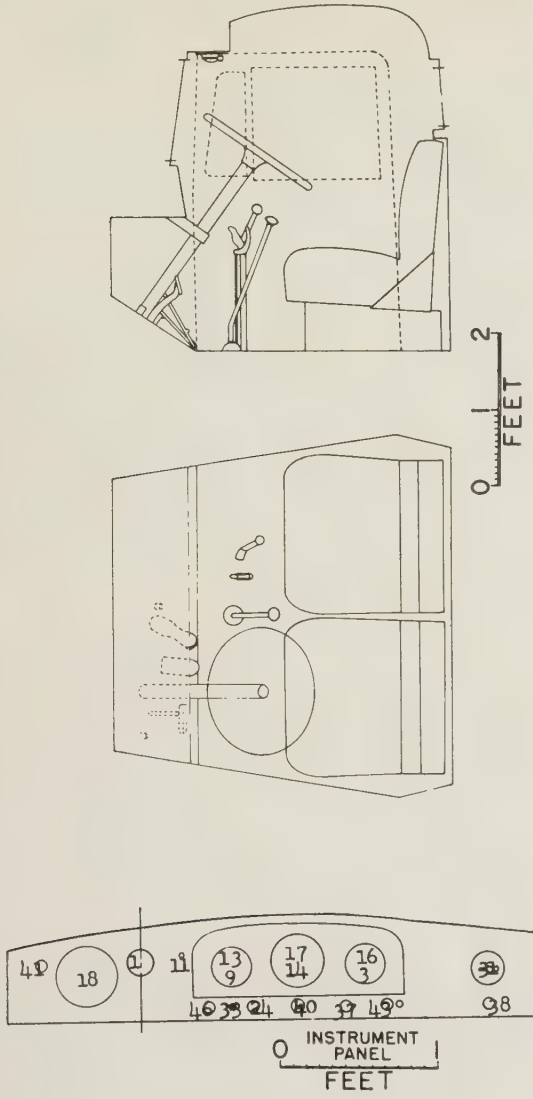

Fig. 4—Scale drawings for vehicle #2801-56

ing from the shape and bulk of its forward structures. A detailed analysis of three of the 10 vehicles was made, selected because they were not extreme in this respect. Using a live manikin in a standard and normal sitting position, the blind area around the side and forward area of each truck was mapped. At ground level, the area of the blind area varied from 700 sq ft for one vehicle, through 1011 sq ft for another. The greatest forward extent of the blind area for the vehicle with the least restriction was 25.5 ft, and the forward extent of the blind area for the vehicle with the greatest restriction was 35.5 ft. Both of these measures are far in excess of the 10 ft minimum forward vision suggested earlier in the discussion. It is possible that in COE vehicles, this criterion may be satisfied or possibly surpassed. Fig. 5 expresses the findings graphically. Figs. 6–8 illustrate related problems of vision associated with vehicle operation.

The curvature of windshields has several annoying results. One of these is distortion, and is found in many modern vehicles. Another is a reduction in transparency because of cleaning difficulties due to the poor fit of wipers on the complex surface of

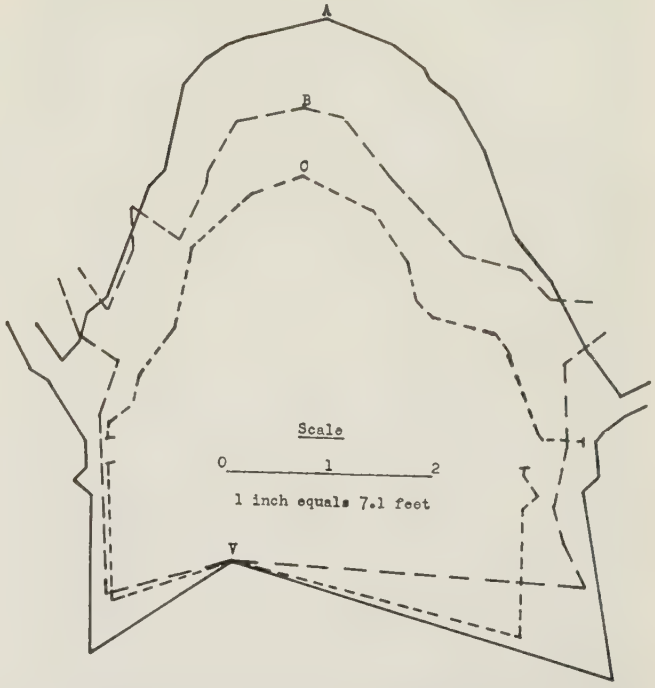

Fig. 5—Forward extent and area of obstructed vision at ground level for three trucks (V—Visual origin; Observer—75th percentile commercial drivers; A, B, C,—Maximum extent of perimeters of three trucks respectively)

V to A—35.5 ft Enclosure A—1011 sq ft
V to B—29.6 ft Enclosure B— 715 sq ft
V to C—25.5 ft Enclosure C— 549 sq ft

Table 2—Reversal of Dial and Gage Location in Two Vehicles

Vehicle, Truck Code No.	Dials Located in Front of Driver	Dials Located to Right of Driver
1801-56	Ammeter Temperature gage Speedometer Mileage indicator Oil pressure Fuel gage	Tachometer Air pressure
2801-56	Tachometer Air pressure	Ammeter Temperature gage Speedometer Mileage inidcator Fuel gage

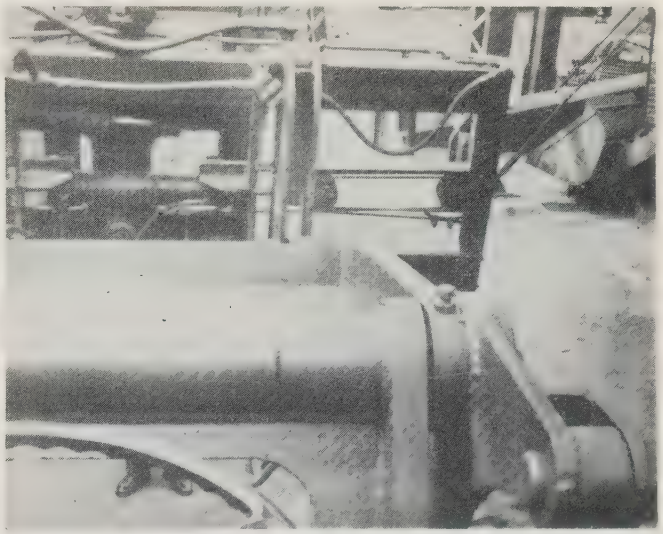

Fig. 6—View from operator's eye level showing what he can see of a 6-ft man standing at work tips with forks in carrying position (new 6000-lb experimental model)

the windshield. Of the two problems, the second may be the more dangerous because of the reduction in light transmission at the most crucial moments, for example, during inclement weather when driving conditions are poor and great demands are made upon the visual capacities of the operator.

The area of the windshield cleaned by wipers was highly variable, ranging from 360 to 815 sq in. Of course, the area cleaned is not necessarily an accurate predictor of the extent to which the outside environment can be seen. Peering through a knot hole at close quarters will reveal more than through a picture window at a greater distance. Some of the cleaned area is useless because vision is obstructed by the motor cowling.

Visors did not always satisfy the purpose for which they were made, especially when their shape was incompatible with the area supposed to be shielded. In some instances there was only one visor in the cab. In several others, light leaked over and around the sides. The single visor and the poorly fitted visor are unfavorable conditions easily remedied.

In one instance, the dispatch box could not be opened unless both visors were down. Therefore, any operator who attempted to open the dispatch box while driving would automatically reduce his forward view virtually to zero. This is an example of incompatable elements of design. The principle of noninterference of one function by another was clearly violated. This is demonstrated in Fig. 9.

Fig. 7—Photograph of operator's error in judging where left front wheel is (old 10,000-lb experimental model)

Fig. 8—Both persons have difficulty in seeing both fork and load. Generally two operators could not coordinate properly in trying to divide work on one vehicle (old 10,000-lb experimental model)

Mirrors were highly variable in size, location, and method of adjustment. Some mirrors could not be adjusted from within the cab. Some were insufficiently supported and subject to vibration, an unfortunate condition that distorts both the shape and the size of reflected objects.

Tinted windshield glass was found in one vehicle. The bio-technical problem of the reduction of visual efficiency by interposing filters between the operator and the objects which he must take into account in his driving during periods of low illumination is still unsettled. Apparently, adequate experimental work was not done to discover the effects of light deprivation upon the driver prior to the manufacture and use of tinted glass. Among the bio-technical conditions important to vehicle operation, the intricate conditions of visual discrimination are probably of special significance.

The above comments illustrate the observations made with regard to the conditions influencing visual contact with the environment. It is obvious that much improvement could be derived from intensive experimental research into this area.

Variables Influencing Response Output

Fixed Limits of the Working Space—There are several fundamental assumptions basic to the present analysis which should be repeated. Vehicles are operated and controlled by a population of persons that cannot be represented adequately by such statistics as the average, and mode, and median measure of a group. Persons in the driving population vary widely in all dimensions. In addition, it is clear that the volume of space required by the operator-in-action is far greater than that needed by a stationary person.

There are also other factors to consider. Some responses do not necessarily exert any direct control over the vehicle. The driver may move because it "pleases" him to do so. He may shift the position of his body and/or its appendages in response to particular conditions such as visual need, thermal changes, tactual and vibratory stimuli, auditory events, dampness, tension, discomfort, and fatigue in general.

If posture change is not possible, then the driver must become resigned to greater or lesser degrees of distress, and endure cramped muscles, reduced circulation, visual restrictions, and the ensuing re-

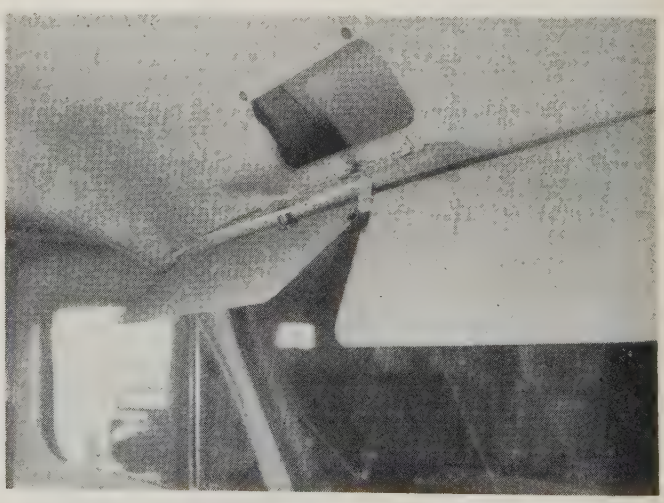

Fig. 9—Use of dispatch box conflicts with location of sun visors

duction of physical efficiency. One may tolerate discomfort for a time, but at a price, which in one form or another has been measured and reported many times.

The concept underlying vehicular design will not be wholly realized as long as the design problem is considered piecemeal. It is not enough to provide space for the arms and legs of the operators, nor is it enough to design a cab that will merely contain all the heterogeneous levers, buttons, dials, knobs, lights, and seats. Nor is it sufficient to design for one static average manikin. The underlying concept implies at the very least that design should be based on a population of varied and active operators making responses to control a vehicle and with a premium placed upon the maintenance of precision for long periods of time.

The fixed limits of the working space are primary considerations because all other aspects of human sizing are either directly or indirectly dependent upon them. The consequences of inadequate space will be summarized below. The following represents a composite picture of certain conditions as found in several vehicles, and can be shown to limit the freedom of the operator in many other situations.

1. Fore, Aft, and Lateral Space.

In general, spatial arrangements found in the 1950 models were still present in 1956. It was common to find the space for the legs and feet somewhat inadequate, not only in relation to stretching and resting, but inadequate for the operation of the vehicle as well. The general impression is that cab space is too shallow (Fig. 10) from front to rear, and with the recent development of the COE (cab over engine) designs, the compression is from either side as well. In some vehicles, the engine housing protrudes into the cab, sometimes as far back as the seat or further at elevations of as much as 18 in. above the level of the floor.

Since this study was completed a new COE has been designed (1958), the so-called "48" cab. This is by far the least adequate of cab designs with respect to fore-and-aft space. Compared with the 1956 models, this cab represents a reduction of space. In some measurements it falls below the least adequate of the 1956 cabs.

In these cabs, the housing cramps the right leg of the operator since the leg cannot easily be pivoted out to rest nor to facilitate rapid responses to the brake pedal. In some instances, this housing rubs against the calf of the operator's right leg when the foot is on the accelerator.

In those vehicles which have the greatest "dog-house" depth, it was observed that the accelerator could not always be depressed unimpeded since there was a repeated tendency for the toe and the right side of the foot to scrape against the inner side of the "dog-house" wall.

In the 1956 vehicles the left side wall of the "dog-house" was already scarred prior to sale. Therefore, these physical restrictions had been forced upon others as well as upon the research observers. In such situations if the operator attempts to compensate for lateral cramping by moving his right foot to the left, it is forced closer to and under the brake pedal. This automatically leads to a foot position which is least efficient for rapid responses to the foot brake. The driver is far more likely to snag his foot under the pedal surface in emergencies. Clearly, those persons with larger feet will encounter greater problems. Winter clothing may be expected to increase the problems arising from limitations on space.[10]

Fig. 10—Clutch pedal tread had been increased in thickness for operator. Trolly brake fixtures are interposed between the operator's eyes and instrument panel. Calf of leg strikes front of seat

There are other consequences of the COE design. The cab has been pushed up and forward over the front wheels as well as over the engine. Since the elevation of the cab does not permit complete wheel clearance, the arc of the fender, and some of the wheel space have been admitted into the left and right forward areas of the cab. These areas on the left are usually used as rest space for the foot, and to locate the dimmer switch, and the hand brake.

2. Vertical Space.

In a sense, the observations related to vertical dimensions belong with the discussion concerned with seating. However, a seat, no matter how adjustable in the vertical plane, will not solve the problem of low ceilings. It will be seen later that if the types of seats generally found in cabs were adequately adjustable in the vertical plane, several cabs would have severely limited the usefulness of this adjustment because the ceilings were too low. There are actually two observations: (1) Vertical

[10] Five specialized reports, EP 39, 41, 43, 48, and 49 concerning the restrictions upon speed and range of motion of certain relevant body segments, and upon certain relevant spatial relationships have been issued by Headquarters, Quartermaster Research and Development Command, Environmental Protection Research Center, Natick, Mass.

Table 3—Seat Depth

1. Pertinent Body Dimension: Buttock to back of calf distance.
2. Purpose: To accommodate both long- and short-legged men with respect to seat depth.
3. Recommendation: A seat depth of not more than 18-19 in.[a]

Human Sizing Data on Buttock to Back of Calf Distance

Buttock-calf distances were not taken on the commercial driver series by McFarland et al.,[4] but comparisons with a group of males measured by Hooten in "A Survey of Seating" indicates that this dimension will closely approximate 17.5 in. for the fifth-percentile driver. Since men rarely drive with the buttocks tightly in contact with the back of the seat but rahter shift them forward varying amounts, the above criterion is recommended.

Rank Order

Vehicle		Seat Depth in.
Rank	Code Number	
1.	1601-56	Adj. 15.50-17.00
2.	1801-56	15.87
3.5	1401-56	16.50
3.5	1001-56	16.50
5.	2001-56	17.00
6.5	1201-56	17.50
6.5	2801-56	17.50
8.	2601-56	17.75
9.	2201-56	18.75
10.	2401-56	Adj. 19.25, 20.5, and 21.75

[a] In this instance the two vehicles falling below the line would be considered borderline.

Table 4—Width of Cab Seat

1. Pertinent Body Dimension: Seat breadth.
2. Purpose: Minimum seat breadth for comfort.
3. Recommendation: Minimum seat breadth, 19 in.

Human Sizing Data on Seat Breadth

	Civilian Drivers	Army Drivers
Number	308	1656
Range, in.	11.42-20.80	11.42-18.90
Median, in.	14.49	13.84
95th percentile, in.	16.34	15.37
5th percentile, in.	13.15	12.65

Rank Order

Vehicle		Breadth of Cab Seat Cushion, in.	Number of Seats in Cab
Rank	Code Number		
1.	1201-56	18.25	2
2.	1001-56	19.50	2
3.	2601-56	19.75	2
4.	1801-56	22.00	1
5.	2401-56	22.50	2
6.	2801-56	24.50	1
7.	1601-56	52.75	1
8.5	1401-56	56.00	1
8.5	2001-56	56.00	1
10.	2201-56	56.87	1

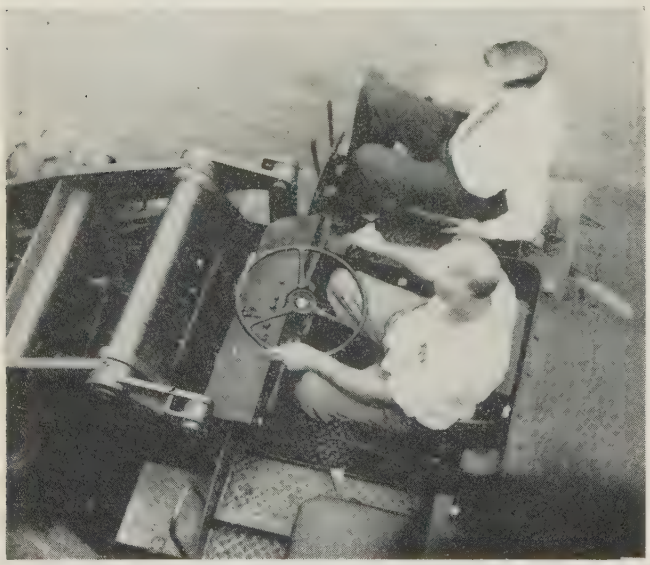

Fig. 11—Operator work space is limited and does not permit much adjustment for different-sized operators. Controls and dials are not visible from normal driving position (new 6000-lb experimental model)

adjustments of the seats were almost always absent, and (2) even if such seats could be adjusted, the ceiling heights in many cabs would have rendered adequate adjustments either impossible, or at least would have imposed a severe restriction.

Seating and Human Sizing—The seat, a structure of prime importance to the driver, should have several attributes. The proper seat is one that can be adjusted to the needs of a vast and heterogeneous driving population. Several important variables to consider are the intricate relationships of the plastic forms of the driver-in-action to the controls of the vehicle, the demands of vision in ordinary and extraordinary situations, and the fact that the driver is encased in a variety of clothing, which play a part in the control over the positions and mobility of the operator. (See Figs. 11 and 12.)

The seat should provide the greatest possible degree of support compatible with the efficient operation of the vehicle. It should possess the latitude necessary to permit the operator to adjust his momentary driving posture to the many sensory input-motor output conditions, and to the demands of the driving tasks characteristic of the first and last hours of trips that vary considerably in duration. The fact that the physiological state of the operator is not "constant" along the time-effort, or time-stress, continuum imposes this particular restriction upon the seat.

Coupled with the physics of movement, the foregoing considerations imply the need for fore, aft, and vertical adjustments, as well as control over the angle and contour of the seat pan and the back rest. There is a need for firm anchoring to prevent swinging, and fore-and-aft rolling during accident and near-accident conditions.

It is assumed that the seat can be easily adjusted in transit. Thus, all adjustment controls should be within the immediate grasp of the operator. They should be physically simple to operate with little effort. Further considerations important to the operator are the protecting and ventilating qualities of the seat.

The McFarland, Damon, and Stoudt[4] criteria have been employed as standards. Accordingly, the following dimensions are considered important, with reference to the anthropometric factors involved; (1) lower leg length and height of seat above the floor, (2) breadth of buttocks and the width of the seat pan, (3) shoulder breadth and the width of the seat back, (4) the length from buttock to the back of the calf of the leg and seat depth, (5) trunk height, height of maximum concavity of the back, and the height of the seat back, (6) abdomen depth and the horizontal distance between the steering wheel and the seat back surface, (7) total leg length and the range of fore-and-aft seat adjustability, and (8) normal sitting eye height and the range of vertical adjustability of the seat.

1. Position.

There were many elements that determined the position of the seats in several cabs. For example, in at least two vehicles, the gasoline tank was located directly behind the driver's seat, and consequently the seat rack was placed forward toward the steering wheel. In at least two vehicles, the construction of the rear wall of the cab was important. In one, the upper section had been tilted forward, and in another there was an arc protrud-

Table 5—Height of Seat Back

1. Pertinent Body Dimension: Trunk height.
2. Purpose: To support part of body weight and to give stable back support for applying pressure to foot controls.
3. Recommendations: 18-20 in. for height of seat back.

Human Sizing Data on Trunk Height

	Civilian Drivers	Army Drivers
Number	311	1671
Range, in.	20.47-26.38	18.50-26.38
Median, in.	23.66	22.96
95th percentile, in.	25.24	24.92
5th percentile, in.	22.01	20.92

Rank Order

Vehicle		Height of Seat Back, in.
Rank	Code Number	
1.	1001-56	17.50
2.	2001-56	18.00
3.	2201-56	18.50
4.	1601-56	19.00
5.	1201-56	19.50
6.	2801-56	19.75
7.	1401-56	20.00
8.5	2601-56	20.50
8.5	2401-56	21.00
10.	1801-56	20.50

Table 6—Width of Seat Back

1. Pertinent Body Dimension: Shoulder breadth.
2. Purpose: To provide adequate lateral space for back and shoulder support.
3. Recommendation: Minimum breadth of 21 in. for seat back.

Human Sizing Data on Shoulder Breadth

	Civilian Drivers	Army Drivers
Number	310	2373
Range, in.	14.94-21.62	14.96-22.05
Median, in	18.34	17.92
95th percentile, in.	19.90	19.66
5th percentile, in.	16.92	16.56

Rank Order

Vehicle		Breadth of Seat Back at Shoulder Level, in.	Number of Seats in Cab
Rank	Code Number		
1.	1201-56	18.25	2
2.	1001-56	18.50	2
3.	2601-56	19.25	2
4.	1801-56	21.50	2
5.	2401-56	22.00	2
6.	2801-56	24.50	2
7.	1601-56	49.50	1
8.	2201-56	55.00	1
9.	1401-56	56.00	1
10.	2001-56	57.00	1

ing several inches directly into the center of the back wall. This also encouraged the forward placement of the seat rack. Had the gasoline tanks been relocated, and the real wall designs modified, the seat frames could have been moved farther back for the very great convenience of the operators who fall in the upper percentiles in both abdomen thickness and height. It will be seen that coupled with other variables, the structure of the cab and the nature of the seats combined to favor the smaller operators and to embarrass the larger operators.

The point to be made is that some human sizing problems, from the standpoint of the proposed criteria, originated with certain restrictions upon the size of the cabs in the first place, and were perpetuated by design features which supposedly had in one instance a structural advantage, and in the other instance a certain aesthetic appeal.

2. Fixed Dimensions of the Seat.

The data collected from the several vehicles are summarized in Tables 3–15 which serve multiple purposes. Each table contains the pertinent body dimension, its purpose, and the recommendation regarding human sizing relevant to the variable under consideration. The range, median, and percentile of physical measurements of a civilian and a military vehicle-driving population are included to allow a comparison of vehicle data with truck driver sizes. The *range* statistic is the primary consideration. Most tables include a horizontal line indicating the departure of the data from the recommendations. Unless otherwise indicated, all dimensions below the line of departure have been considered to satisfy the recommendations. All other measures have been interpreted as questionable dimensions, although some would be considered borderline.

3. Relative Position of Seat.

The horizontal distance between the lower edge of the steering wheel and the seat back is clearly important because this space must be made to fit the operator-in-action. There are two sets of data presented. First, comparative data obtained from 10 vehicles manufactured by 10 automotive concerns are tabulated. Second, a special set of data was obtained from 13 trucks issued by X section of Y manufacturer, and a parallel set of data was ob-

Table 7—Range of Fore-and-Aft Seat Adjustability

1. Pertinent Body Dimensions: Leg length (buttock-knee length and knee height).
2. Purpose: Operation of foot controls.
3. Recommendation: Range of fore-and-aft adjustability of 6 in. in increments of 1 in. or less.

Human Sizing Data on Knee Height

	Civilian Drivers	Army Drivers
Number	301	2376
Range, in.	19.29-25.98	17.72-25.59
Median, in.	21.69	21.56
95th percentile, in.	23.50	23.42
5th percentile, in.	20.08	19.78

Human Sizing Data on Buttock-Knee Dimensions

	Civilian Drivers	Army Drivers
Number	310	2353
Range, in.	21.26-27.56	19.29-27.56
Median, in.	23.78	23.33
95th percentile, in.	25.79	25.16
5th percentile, in.	22.05	21.49

Rank Order

Vehicle		Range of Fore-andAft Adjustability, in.	Number of Seat Positions	Increments, in.
Rank	Code Number			
1.0	1001-56	0.00	0	0.00
2.5	2201-56	3.50	5	0.87
2.5	1401-56	3.50	6	0.50
4.5	2001-56	3.75	8	0.47
4.5	1201-56	3.75	7	0.52
7.0	2401-56	4.00	9	0.50
7.0	1601-56	4.00	6	0.60
7.0	1801-56	4.00	9	0.50
9.0	2601-56	4.12	9	0.50
10.0	2801-56	6.00	7	1.00

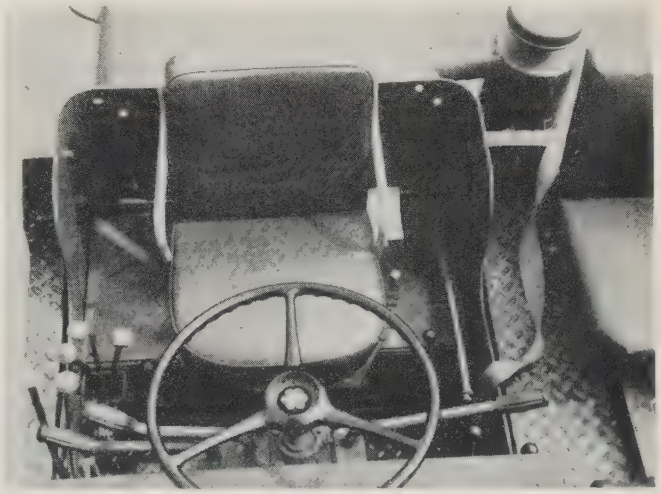

Fig. 12—Unadjustable arm rests limit size of operator or amount of environmental clothing he may wear (new 6000-lb experimental model)

Table 8—Range of Vertical Seat Adjustability

1. Pertinent Body Dimension: Normal sitting eye height.
2. Purpose: Optimum location of operator's eye level.
3. Recommendation: Minimum range of vertical seat adjustability of 4 in. in increments of 1 in. or less.

Human Sizing Data on Normal Sitting Eye Height

	Civilian Drivers
Number	309
Range, in.	26.38-32.68
Median, in.	29.61
95th percentile, in.	31.61
5th percentile, in.	27.72

Rank Order

Vehicle		Range of Vertical Adjustability, in.		Number of Seat Positions		Number and Magnitude of Increments, in.	
Rank	Number	Front Edge	Rear Edge	Front Edge	Rear Edge	Front Edge	Rear Edge
3.0	1601-56	0	0	0	0	0	0
3.0	2001-56	0	0	0	0	0	0
3.0	2201-56	0	0	0	0	0	0
3.0	2801-56	0	0	0	0	0	0
3.0	1401-56	0	0	0	0	0	0
6.0	1201-56	1.00	1.75	2	4	1.00	0.44
7.0	1001-56	1.50	1.50	2	2	1.50	1.50
8.0	2601-56	1.87	1.00	5	2	0.37	− 0.87 to
						1.37	− 1.87
						Above Seat Base	
9.0	2401-56	2.00	1.50	3	3	1.00	0.75
10.0	1801-56	3.36	1.50	4	4	0.87	− 0.50
						1.87	− 1.00
						3.37	− 1.50

Note: The rear edge of the seats in vehicles 1201-56 and 2601-56 could not be independently adjusted. The variations shown here were coincidental with the movement of the front edge of the seats.

Table 9—Distance (Horizontal) from Lower Edge of Steering Wheel to Seat Back

1. Pertinent Body Dimension: Abdomen depth.
2. Purpose: To avoid contact of steering wheel with abdomen, thus reducing possibility of serious abdominal injury in sudden stops or collision and facilitating entrance and exit.
3. Recommendation: Minimum of 15 in. in a horizontal line between rearmost edge of steering wheel (at midpoint of range of fore-and-aft adjustability.

Human Sizing Data on Abdomen Depth

	Civilian Drivers	Army Drivers
Number	311	1665
Range, in.	6.68-13.76	6.69-13.78
Median, in.	9.50	9.03
95th percentile, in.	12.06	10.51
5th percentile, in.	7.84	7.97

Rank Order

Vehicle		Distance (Horizontal) from Lower Edge of Steering Wheel to Seat Back (with seat at midpoint of range of fore-and-aft adjustability)		
Rank	Code Number	Aft	Middle	Fore
1.	1201-56	13.00	11.13	9.26
2.5	2201-56	13.50	11.75	10.75
2.5	2801-56	14.75	11.75	8.75
4.	1401-56	14.00	12.25	10.50
5.	1601-56	14.38	12.38	10.38
6.	1801-56	14.63	12.63	10.63
7.	1001-56	12.75	12.75	12.75
8.	2001-56	14.44	12.87	11.20
9.	2601-56	15.00	12.93	10.87
10.	2401-56	16.25	14.25	12.25

tained from 11 series involving 28 models of Z section of Y manufacturer, all with respect to the dimensions under consideration.

The first set of data shown in Table 9 indicates that one vehicle of the 10 met the suggested criterion. All dimensions at the midpoint of the range of adjustability were too small. If the seats were placed at their greatest possible distance, the maximum of the horizontal range aft, no distance would meet the suggested minimum criterion of 18 in. of horizontal distance between the steering wheel and the seat back. The foremost seat positions tended to favor drivers in less than the fifth percentile.

The within-manufacturer Y data shown in Table 10 indicate precisely the same fact. Thus, the within-manufacturer's values show just about as wide a variation as the values obtained from trucks issued by 10 different manufacturers. It should also be stated that the majority of the cabs of trucks issued by Y manufacturer were "standardized" and were, with very minor modifications, interchangeable among vehicles.

There was one difference found between the Section X data and Section Z data that illustrates an interesting departure from human engineering applications, and demonstrates two mutually exclusive principles of operation practiced within a single industry. It can be seen that the distance between the lower edge of the steering wheel and the seat back was identical in 11 series and 28 models of trucks issued by Z section of Y company. Table 11 shows this relationship. Standardization would have been commendable if the dimension were suitable for seating the driver population. According to the McFarland, Damon, and Stoudt[4] criterion it is not adequate. It can also be seen that this same dimension varied widely in the 13 trucks issued by X Section of Y company.

Therefore, the various sections within the same manufacturing concern have varying standards, not only in the dimensions used in designing, but also divergent principles applying to design for human use. If the dimensions of seat design had been taken from an appropriate human sample then all the seating throughout the company would have been consistent.

Hand and Foot Controls—Controls appear in several forms as small and large hand levers, push-pull buttons, toggle switches, and right and left rotating knobs, all controlling mechanical and electrical sources of energy. Such mechanisms when activated or deactivated perform certain services which are of the utmost importance for the welfare of the

Table 10—Variance in Steering Wheel to Seat Back Dimension in 13 Trucks Manufactured in 1956 by X Section of Y Company

Vehicle	Horizontal Clearance from Steering Wheel to Seat Back in Rearmost Position, in.			McFarland, Damon and Stoudt Minimum Criteria, in.			Differences between Human Sizing Criteria and Actual Cab Dimensions, in.		
	Maximum	Minimum	Range	Maximum	Minimum	Range	Maximum	Minimum	Range
A	13	9	4	18	12	6	− 5	− 3	− 2
B	13	9	4	18	12	6	− 5	− 3	− 2
C	13.25	9.5	3.5	18	12	6	− 5.75	− 2.5	− 2.5
D	13.25	9.5	3.5	18	12	6	− 5.75	− 2.5	− 2.5
E	13.25	9.5	3.5	18	12	6	− 5.75	− 2.5	− 2.5
F	13.25	9.5	3.5	18	12	6	− 5.75	− 2.5	− 2.5
G	14	10.12	3.88	18	12	6	− 4	− 1.88	− 2.12
H	14	10.12	3.88	18	12	6	− 4	− 1.88	− 2.12
I	14	10.12	3.88	18	12	6	− 4	− 1.88	− 2.12
J	14	10.12	3.88	18	12	6	− 4	− 1.88	− 2.12
K	14	10.12	3.88	18	12	6	− 4	− 1.88	− 2.12
L	14	10.12	3.88	18	12	6	− 4	− 1.88	− 2.12
M	14.75	10.75	4	18	12	6	− 3.25	− 1.25	− 2

Table 11—Human Factors in 1956 Design of Vehicle Cab Areas
Z Section, Y Manufacturer

Dimensions 11 Series, 28 Models	Steering Wheel to Seat Back, Horizontal Dimensions, in.	McFarland, Damon and Stoudt Criterion, in.	Difference, in.
Horizontal Adjustment	3.94	6	−2.06
Maximum Distance from Steering Wheel to Seat Back	12.80	18	−5.20
Minimum Distance from Steering Wheel to Seat Back	8.86	12	−3.14

Table 12—Distance (Vertical) from Lower Edge of Steering Wheel to Floor

1. Pertinent Body Dimension: Knee height.
2. Purpose: To help insure lateral freedom of movement between bottom of steering wheel and floor.
3. Recommendation: Minimum clearance of 24.50 in.

Human Sizing Data on Knee Height

	Civilian Drivers	Army Drivers
Number	301	2376
Range, in.	19.29–25.98	17.72–25.59
Medium, in.	21.69	21.56
95th percentile, in.	23.50	23.72
5th percentile, in.	20.08	19.78

Rank Order (Vehicle) Rank	Code Number	Distance (Vertical) from Lower Edge of Steering Wheel to Floor, in.
1.	1601-56	20.50
2.	2001-56	21.00
3.	2201-56	21.50
4.	1801-56	22.50
5.	1201-56	23.75
6.5	2401-56	24.25
6.5	1401-56	24.25
8.	1001-56	24.50
9.	2801-56	25.00
10.	2601-56	27.00

operator and occupants, and for the welfare of the occupants of other vehicles. This is so because no operator performs in social isolation. He communicates with others and responds to others in vehicles, and, therefore, he is an integral part of a complex flow of traffic.

Ultimately, the designs of vehicles are comprehensible only when these facts are taken into consideration. Each control represents a service of some kind, and without the slightest effort no less than 50 such services can be tabulated. Within the 10 vehicles under consideration at least 41 different hand controls were counted and, consequently, as many different functions.

The fixed anatomical structure of operators in any phase of the driver-vehicle relationship forces a certain logic upon any objective analysis. It can be stated with confidence that the important anatomical variables involved are, at the very least: (1) foot breadth, (2) foot length, (3) leg length from the hip, (4) knee height, (5) buttock-popliteal length, (6) hand length, (7) hand breadth, (8) arm length from the shoulder, and (9) the range of angles formed by the leg-foot articulation.

The location, angulation, supporting properties, direction of depression and release, push-pull, articulation, and degree of resistance of controls obviously became important relative to the geometry and function of the operator, both of which are understood to be limited. All objects demanding operator response must be considered extensions of the anatomical structures of the operator-in-action which allow the operator to control the vehicle with maximum efficiency.

In the process of this investigation of 10 trucks,

Table 13—Heights of Seat Front Above Floor

1. Pertinent Body Dimension: Lower leg length.
2. Purpose: To avoid excessive height, resulting in front edge of seat cutting into under part of thigh.
3. Recommendation: Maximum height of 15 in. from front edge of seat to floor (in any position).[a]

Human Sizing Data on Lower Leg Length

This dimension was not taken on the commercial driver series by McFarland et al.,[4] but comparison with other groups indicate it to be slightly over 17.50 in. (including shoes) for the fifth percentile, thus suggesting a seat height of 16.50 in. However, when the legs are extended forward, knee height is reduced, thus requiring a lower seat level.

Rank Order (Vehicle) Rank	Code Number	Height of Seat Front Above Floor, (seat in lowest position), in.
1.	2601-56	17.75
2.	1001-56	17.00
3.	2801-56	16.00
4.	1401-56	15.50
5.	2401-56	15.12
6.5	1201-56	15.00
6.5	2001-56	15.00
8.	1801-56	14.25
9.5	1601-56	13.50
9.5	2201-56	13.50

[a] Had the measurements been taken with the seats in the highest position, the comparison with the criterion would have been more unfavorable.

Table 14—Distance from Seat Bottom to Ceiling of Cab

(This measurement was taken on vertical 4 in. forward from front of seat back)

1. Pertinent Body Dimension: Normal sitting height.
2. Purpose: Accommodation of seated driver to working space with respect to head clearance.
3. Recommendation: Headroom clearance 40¼ in. from seat top to ceiling.

Human Sizing Data on Normal Sitting Height

	Civilian Drivers
Number	313
Range, in.	30.71–37.80
Median, in.	34.65
95th percentile, in.	36.58
5th percentile, in.	32.60

Rank Order (Vehicle) Rank	Code Number	Distance from Seat Bottom to Cab Ceiling, in.
1.	2001-56	36.5
2.5	2201-56	37.5
2.5	1401-56	37.5
4.	1201-56	38.0
5.	2801-56	38.5
6.	1601-56	39.0
7.	1801-56	40.0
8.	2401-56	40.5
9.	1001-56	42.0
10.	2601-56	42.5

Table 15—Number of Vehicles Meeting or Not Meeting 11 Design Criteria

Design Variable	Number of Vehicles Meeting the Criterion	Number of Vehicles Not Meeting Criterion
1. Seat Depth	2	8
2. Seat Breadth	9	1
3. Seat Back Height	9	1
4. Seat Back Breadth	7	3
5. Range of Horizontal Adjustment of Seat	1	9
6. Range of Vertical Adjustment of Seat	0	10
7. Magnitude of Horizontal Seat Adjustment Increments	9	1
8. Distance between Steering Wheel and Seat Back	0	10
9. Seat Height Above the Floor	5	5
10. Distance between Seat Pan and the Ceiling	4	6
11. Distance between Lower Edge of Steering Wheel and Floor	3	7
Total	49	61

This table summarizes 11 human sizing variables. The Acceptable and Not Acceptable criteria will show in general the number of vehicles considered to be satisfactory in each sizing category. It can be seen that the greatest discrepancies were in seat depth, horizontal and vertical seat adjustment, vertical head room, steering wheel to seat back areas, and steering wheel to floor distance.

If the data are summed it can be seen that more than half the dimensions do not meet the McFarland, Damon, and Stoudt[5] criteria. Each variable may be studied in much greater detail in Tables 3–14 which contain the rank order data for all dimensions for all vehicles.

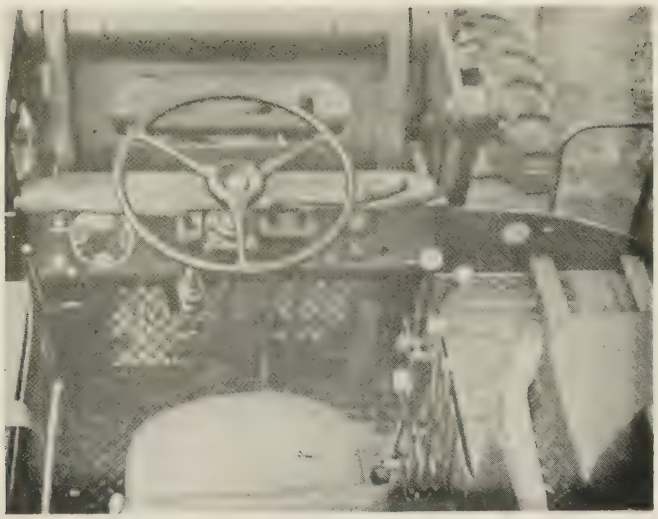

Fig. 13—There appear to be too many controls as well as uneven distribution for right- and left-hand control operations; dials are not easily visible to operator; brake pedal is almost inaccessible behind columns and too close to accelerator; metal controls when too hot or too cold are dangerous to bare skin (new 6000-lb model)

Fig. 14—Picture showing poor distribution of controls for right- and left-hand operation. Distribution of controls remained almost unchanged between the old and new models (old 10,000-lb model)

in addition to parking brakes and shift levers, a total of 118 controls located principally on the instrument panels were observed. The problems associated with some of the controls fall into six related categories, as follows:

1. Reach problems associated largely with the right hand and arm.
2. Obstruction-to-reach problems.
3. Accidental operation of controls.
4. Problems associated with posture distortion.
5. Problems of sensory discrimination.
6. Problems associated with lack of standardization.

1. Control Location.

Since the operator has been assigned an offset position to the left in the cab, the distribution of available space around him is asymmetrical, and the distribution of tasks to each hand is unequal. Also, the distances to be reached vary between hands since controls are mounted along the instrument panel, thus extending the distribution further to the right than to the left. Table 16 indicates the problem under discussion.

Table 16—Comparative Dimensions of Instrument Panels

Vehicle	Horizontal Length of Instrument Panel, in.	Distance between Steering Post Axis and Centerline of Cab, in.
1	70.50	25.25
2	59.25	14.50
3	58.00	13.00
4	55.50	14.50
5	53.63	13.00
6	52.75	14.12
7	50.25	14.75
8	49.50	13.00
9	48.75	15.00
10	44.00	11.87

Table 17—Controls Presenting Reach Problems

Control	Number	Control Location Area		
		Area 1	Area 2	Area 3
Heater	6			6
Defroster	5		1	4
Windshield Wipers	3		2	1
Auxiliary Light Switch	2		2	
Front Brake Control	2	1		1
Headlight Switch	2		1	1
Outside-Inside Fresh Air Control	2			2
Throttle	2			2
Fan Control	1			1
Choke	1		1	
Panel Light	1		1	
TOTAL	27	1	8	18

It can be seen that the variation among instrument panels is very great, the longest panel being nearly 6 ft long, and the shortest panel being about 3½ ft long.

It was found that (1) 25% of all controls were located left of the axis of the steering wheel post, (2) 40% of all controls were located between the axis of the steering wheel and the centerline of the cab, 8% were located at the centerline of the cab, (3) and 27% of the controls were located to the right of the centerline of the cab, occasionally at an extreme distance. This condition is illustrated in Figs. 3, 4, 13, and 14.

2. Controls Located on the Instrument Panel Associated with Reach and Manipulation Problems.

Reach problems may be defined in various ways, depending upon the frame of reference of the observer and the nature of the task to be accomplished.

A reach problem is defined as any demand imposed upon the operator which forces him to reduce his most advantageous visual command over the environment; assume a posture which fails to maintain the greatest mechanical advantage; assume a posture which forces his abdomen, chest, arms, legs, and/or head against some object such as the steering wheel or shift lever; assume a posture which reduces rate of response and control over the vehicle; or encourages taking positions which increase the probability of injury should an accident occur.

As an illustration—objects located to the far right of the operator, and especially those controlled by levers or knobs located below the instrument panel almost always tempt the operator to reach them with his foot. With respect to the demand for exact visuo-motor coordination the disadvantage is obvious, especially when the vehicle is moving. In other instances, the operator must reach with his right arm and hand. The result invariably is a lowering of the head toward the steering wheel and toward the control object, putting the operator at a visual

disadvantage and forcing the thorax or abdomen against the steering wheel, all accompanied by visual scanning for the needed object and therefor removing attention from the road. (See Fig. 15.)

Twenty-seven of 118 controls were considered to present reach problems, or about 22% of all hand controls located on or about the 10 instrument panels. Several controls presented problems merely because they were too far away from the operator. Lesser reach problems were accentuated by the frequency with which the operator had to use a control. This observation was made by professional operators.

Table 17 specifies the controls associated with reach problems of the normally seated driver, and the approximate location of each with regard to three general areas: (1) left or front of the steering wheel column, (2) between the steering wheel column and the centerline of the cab, and (3) right of the centerline of the cab.

3. Operation Problems.

A few illustrations may be given of problems which result in restrictions on efficient operation. Kephart and Dunlap[5] carried out an experiment on vehicle operator efficiency in a vehicle tracking problem which involved 11 variables in regard to human sizing and comfort. These authors pointed out that the efficiency of tracking was associated with the angle of the steering wheel relative to the floor horizontal. They suggested a range within which operator efficiency was greatest.

In an analysis of 59 trucks marketed by one manufacturer, the angle of the steering wheel with the floor horizontal was found to vary 30–90 deg, a range of at least 70 deg in all. In most of these vehicles the vertical adjustment of the seat was negligible, if possible at all. If the concept of a-most-favorable-range-of-angles is valid, such variation does not meet that criterion. The data are presented in Table 18 in a specialized summary to show the variation to be found among vehicles constructed by a single manufacturer. However, other manufacturers seem to follow the same practice as well.

Fig. 15—Hand brake is too far to right of operator. Shift lever tends to interfere with response

It has been shown that the angle of the steering wheel with the floor horizontal preferred by drivers varies with the size of the driver expressing the preference.

Kephart and Dunlap[5] were also able to show that the preferred angle of the steering post is also negatively correlated with the preferred angle of the toe pan ($r = -0.65$). However, when the authors published their recommendations concerning vehicular construction, they did not publish the recommenda-

Table 18—Steering Wheel Angle (1956 Truck Series and Models Sample)

Criterion:
(1) Mean = 45.34 deg.
(2) Range of Acceptability = 42.51–48.17 deg.

Model or Series	Angle of Steering Wheel with Floor Horizontal, deg	Difference from Mean and Range of Acceptability, deg	Model or Series	Angle of Steering Wheel with Floor Horizontal, deg	Difference from Mean and Range of Acceptability, deg
Series 1	48.75	Mean 3.41 Range 0.58	Series 28	37.25	Mean 8.09 Range 5.26
Series 2	48.75		Series 29	36.75	Mean 8.59 Range 5.76
Series 3	48.75				
Model A	48.50	Mean 3.16 Range 0.33	Series 30	36.75	
			Series 31	36.75	
Model B	48.50		Series 32	36.75	
Model C	48.50		Series 33	35.50	Mean 9.84 Range 7.01
Series 4	48.50				
Series 5	44.75		Series 34	35.50	
Series 6	44.75		Series 35	35.50	
Series 7	43.25		Series 36	35.50	
Series 8	43.25		Series 37	33.84	Mean 11.50 Range 8.67
Series 9	43.25				
Series 10	42.50	Mean 2.84 Range 0.01	Series 38	33.84	
			Series 39	33.84	
Series 11	42.50		Series 40	33.84	
Series 12	42.50		Series 41	33.84	
Series 13	42.50		Series 42	33.84	
Series 14	42.50		Series 43	33.84	
Series 15	42.50		Series 44	33.84	
Series 16	42.25	Mean 3.09 Range 0.26	Series 45	33.84	
			Series 46	33.84	
Series 17	42.25		Series 47	33.84	
Series 18	42.25		Series 48	33.84	
Series 19	42.25		Series 49	33.00	Mean 12.34 Range 9.51
Series 20	42.25				
Series 21	42.25		Series 50	33.00	
Series 22	40.75	Mean 4.59 Range 1.76	Series 51	33.00	
			Series 52	33.00	
Series 23	40.75		Series 53	28.00	Mean 17.34 Range 14.51
Series 24	40.75				
Series 25	40.75		Series 54	28.00	
Series 26	40.75		Series 55	28.00	
Series 27	37.25	Mean 8.09 Range 5.26	Series 56	28.00	

Fig. 16—When operator attempts to depress foot brake his knee strikes shift lever. He must learn to compensate to avoid this

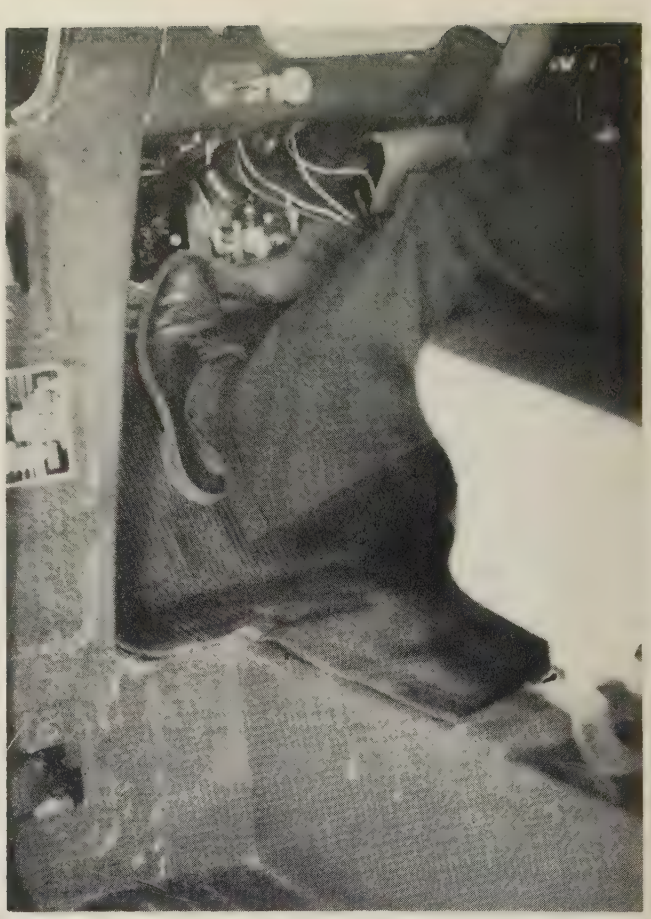

Fig. 18—Copper tubing (part of the compressed air system) is exposed to operator's shoe

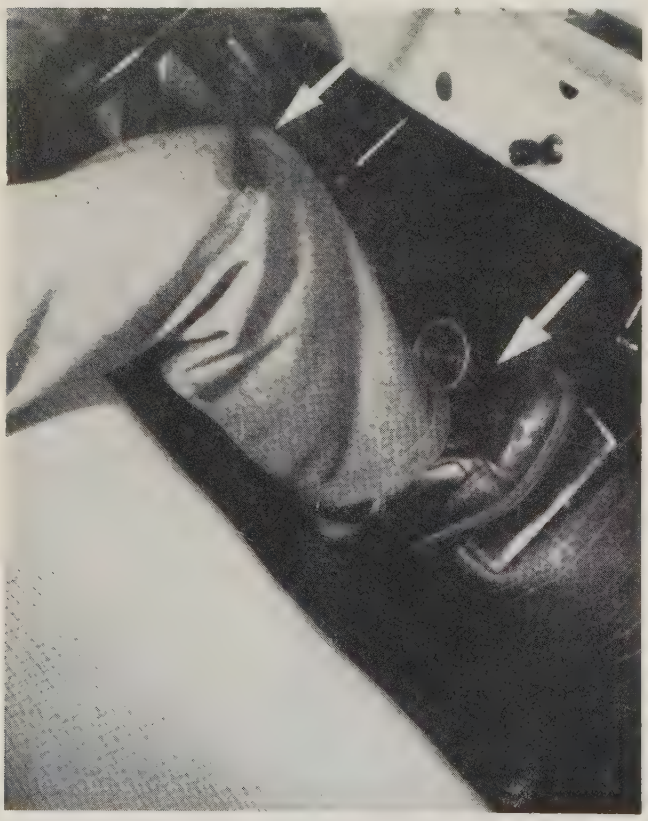

Fig. 17—When the operator raises foot to foot brake, his knee strikes shift lever

tions as steering post angles with the floor horizontal values, but as steering wheel angles with the floor horizontal.

With these experimentally derived recommendations in mind, comparisons can be made among 59 truck steering-wheel angles in the various series and models and the Kephart-Dunlap criteria. It can be seen that angle variability is large, 48.75–28.00 deg, a range of 20.85 deg. To illustrate, the first notation in Column 1, of Table 18, the angle of the steering post is 45.75 deg, and the divergence from the Kephart-Dunlap criterion mean angle is 3.51 deg. This is 0.58 deg in excess of the largest value in the acceptable range of variation as well.

Large angles of the steering wheel with the floor horizontal (henceforth referred to as the steering-wheel angle) can be visualized best by imagining the steering wheel approaching the vertical position by successive steps, and small angles of the stering wheel may be visualized by imagining the steering wheel similarly approaching the horizontal position. Because the tall experimental drivers tended to pivot the movable steering wheel post toward them, and the short experimental operators tended to pivot the steering wheel post away from them, the greater angles of the steering wheel tended to favor the taller drivers and the lesser angles tended to favor the shorter drivers.

Since the Kephart-Dunlap criterion angle (45.34 deg) and the acceptable range of angulation (42.51–48.17 deg) were determined by a sample of operators which ranged from the 5th through 95th per-

Fig. 19—In this position shift lever rubs against knee of operator

centile of military drivers in body height, the upper and lower values of this range represent the experimentally derived extremes of the range. And it is logical to presume that if the steering-wheel angle favors one extreme it cannot simultaneously favor the other, all else being equal. This condition imposes a human sizing dilemma.

Of the 59 vehicles discussed here, 47 have steering-wheel angles which are not only smaller than the Kephart-Dunlap recommended mean angle, but are also less than the lower limit of the range of acceptability. The angles in the remaining 12 trucks all exceed the upper limits of the recommended range of angulation. Hence, the majority of the steering wheel angles favor the shorter driver at or below the fifth percentile. A few of the steering wheel angles favor the taller drivers largely at or above the 95th percentile. The proportion of one angular extreme to the other angular extreme is four to one in favor of the shorter driver.

Among the 10 trucks primarily evaluated in this study, the variation of the steering-wheel angle was relatively great. Table 19 shows that six vehicles had steering-wheel angles which fell below the suggested standard, three within the acceptable range of variability, and one which was above the acceptable standard. What is interesting, however, is that in 10 trucks there was a 35-deg difference between the least and the greatest of the angles. This amount of among-vehicle variation is striking.

The steering wheel may also be used to illustrate other human sizing problems, and problems arising from interference with operator functions.

The distance between the brake pedal surface and lower edge of the steering wheel is an important relationship, since the time of applying the foot brake is increased if the operator is forced to compensate for inadequate room in which to elevate the foot from the accelerator to the brake pedal, whether the mechanism is a conventional hydraulic brake or an air brake. As an extreme example, one vehicle was observed where the shift lever mounted on the steering wheel post was thrown into neutral by the knee when the foot brake was operated. (See Figs. 16 and 17.) This occurred with more than one of the manikins participating in the study. This

Table 19—Angle of Steering Wheel

Recommendation:[a] 45.34 deg
Acceptable Variation: 42.51–48.17 deg

To determine the recommendation and its acceptable variation, three groups of subjects were selected to represent the 5th, 50th, and 95th percentiles of the Army truck driver population in height.

Number	30
5th percentile, in.	64.21
50th percentile, in.	68.23
95th percentile, in.	72.50

Current Data 1956

Vehicle		Steering Wheel Angle, deg
Rank Order	Code Number	
1.	2601-56	20.5
2.	1001-56	30.0
3.5	1201-56	35.0
3.5	2401-56	35.0
5.	2801-56	36.0
6.	1601-56	36.5
7.	2201-56	43.0
8.	1801-56	45.0 (Acceptable Range)
9.	1401-56	46.0
10.	2001-56	55.0

[a] See footnote 5.

Table 20—Distance from Top of Brake Pedal to Lower Edge of Steering Wheel

1. Pertinent Body Dimension: Knee height.
2. Purpose: To give driver sufficient leg room to apply pedals without bumping or trapping knee under steering wheel.
3. Recommendation: Minimum of 26 in. between top surface of foot pedals to bottom of steering wheel.

Human Sizing Data on Knee Height

	Civilian Drivers	Army Drivers
Number	301	2376
Range, in.	19.29–25.98	17.72–25.59
Median, in.	21.69	21.56
95th percentile, in.	23.50	23.72
5th percentile, in.	20.08	19.78

Rank Order	Vehicle	Distance from Middle of Brake Pedal to Bottom of Steering Wheel Rim, in.
Rank	Code Number	
1	2001-56	19.25
2	1601-56	23.50
3	1401-56	23.75
4	2801-56	25.25
5	2601-56	25.38
6	1801-56	26.50
7	2201-56	28.00
8	2401-56	28.75
9	1201-56	29.25
10	1101-56	30.50

type of error could have been avoided by modifying the elevation of the shift lever at the factory, and with little difficulty since no change of basic design would have been involved. A similar condition was common to several vehicles where the operator frequently struck his thigh on the bottom of the steering wheel when placing the foot on the foot brake. This suggests that the space allowances for the operation of pedals by the right leg and foot were not adequate, since both of these illustrations involved manikins who represented approximately the 45th to 75th knee height percentile of the commercial driver population.

Table 20 reveals that in 10 trucks, five of the vehicles met the criterion for the distance required between the surface of the brake pedal and lower edge of the steering wheel. In one vehicle, the distance was too small by about 5 in.

The same observation made in relation to the brake pedal-steering wheel relationship can be repeated when the clutch pedal is concerned. In some vehicles when the taller driver, such as the operator at 75th percentile, raises his left foot to the clutch pedal surface, he strikes his thigh on the lower edge of the steering wheel particularly when making a rapid response. For other illustrations of conflict see Figs. 18–23. Once again such limita-

Fig. 20—Shift lever impedes leg action of driver. Accelerator pedal and air-brake pedal may be depressed simultaneously

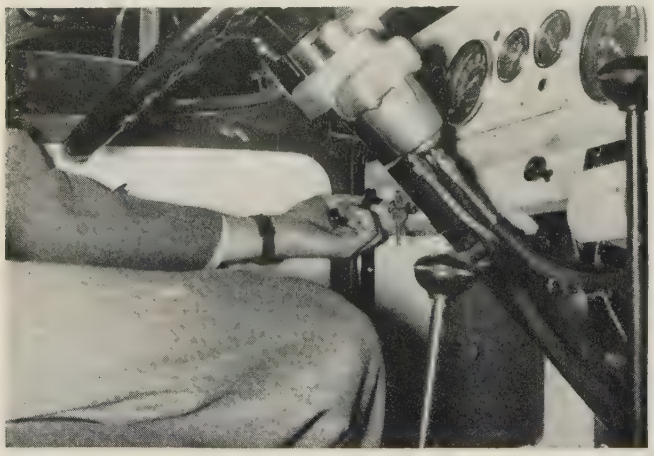

Fig. 21—When operating window crank, operator strikes his fist on protruding light switch

Fig. 22—When reaching for switch on instrument panel, operator inadvertently turns on directional signals

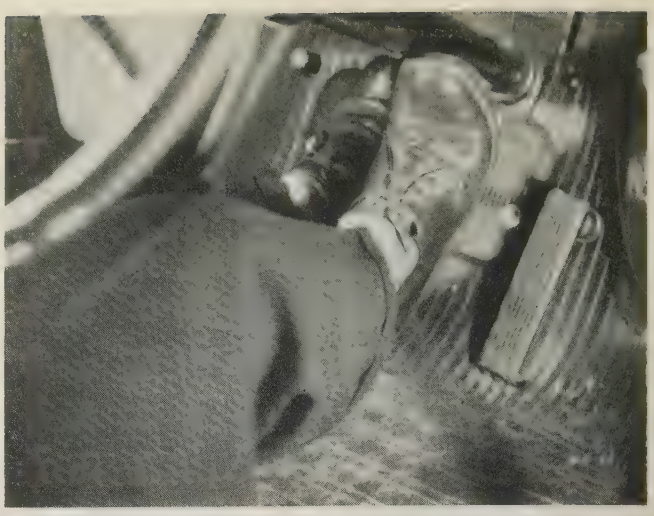

Fig. 23—Foot brake is placed under steering wheel column which acts as impediment to response of operator

Table 21—Distance from Top of Clutch Pedal to Lower Edge of Steering Wheel

1. Pertinent Body Dimension: Knee height.
2. Purpose: To give driver sufficient leg room to apply pedals without bumping or trapping knee under steering wheel.
3. Recommendation: Minimum of 26 in. between top surface of foot pedals to bottom of steering wheel.

Human Sizing Data on Knee Height

	Civilian Drivers	Army Drivers
Number	301	2376
Range, in.	19.29–25.98	17.72–25.59
Median, in.	21.69	21.56
95th percentile, in.	23.50	23.72
5th percentile, in.	20.08	19.78

Rank Order

Vehicle		Distance from Middle of Clutch Pedal to Bottom of Steering Wheel Rim, in.
Rank	Code Number	
1	1201-56	17.00
2	2001-56	23.60
3	1601-56	24.25
4	2201-56	24.50
5	1801-56	24.63
6	2801-56	25.00
7	1001-56	25.50
8	2401-56	25.75
9	1401-56	26.50
10	2601-56	27.63

tion of action represents an impediment to efficient operation.

Table 21 shows that only two vehicles met or exceeded the standard suggested with regard to the distance between the lower edge of the steering wheel and the clutch pedal.

Another unsafe condition may be illustrated by the location of the air-horn fixture in one truck, and interference with the operator's task may be seen in the proximity of the sun visor to the air-horn pull cord. In one cab parts of the horn apparatus were located in a hazardous position because the internal fixture was placed obliquely to the left, behind the operator's head, at no greater distance than 4–6 in., depending upon the sitting height of the driver and his momentary position (Fig. 24). This particular fitting was manufactured of copper and had several sharp edges and protrusions. The location was determined by the manufacturer of the vehicle, although it is considered an auxiliary instrument. It is not originally attached to the cab at the factory, but must be purchased and installed separately. Another dangerous fixture is shown in Fig. 25. The absence of a hand grip out-

side the vehicle is also a safety problem (Fig. 26).

In some vehicles equipped with an air horn, the pull cord or cable was flush with the left wall above the door. This made it difficult to grasp quickly. In other instances, the sun visor was an additional obstacle to efficient operation since it covered the cord when pivoted to the left to protect the peripheral vision of the operator. Reaching for the cord invariably resulted in delayed fumbling behind the visor. (See Fig. 27). In general, the placement of the air horn was not found to be standard. It varied with the type of horn and manufacturer.

Response conflict may be illustrated by describing the relationship of two controls which look alike but have very different functions. One problem that arose concerned discrimination of two levers in two vehicles. Both levers were identical (Fig. 2) and in the normal OFF positions were arranged side by side, each pointing in a direction opposite from the other. Thus, the concept OFF would have to be associated with different locations, but with two different directions of levers as well. The OFF direction for one would mean ON for the other. If one was mistaken for the other, the brake valve

Fig. 24—Air-horn fixture close to operator's head constitutes a hazard

Fig. 25—Coat hanger close to temple and eye of operator constitutes hazard

Fig. 26—Vehicle has no hand grip to assist operator

Fig. 27—Air-horn lanyard is covered by sun visor

would be seen as OFF while the differential lock control would be seen as ON, and vice versa.

When two levers have such important functions, inadvertent activation of one or the other could lead to serious damage, as in the case of the differential lock control. Increasing the discriminative characteristics of these controls, and standardizing the OFF-ON control directions would be important.

Summary

Some of the conditions considered to be impediments to efficient and safe operation of one or more of the ten different trucks studied may be summarized as follows:

1. Fixed limits of driver's cab. With few exceptions the driver's cab was considered to be too small for operators larger than the 65th percentile. For instance, if seats were adequately adjustable it would be impossible to place them most advantageously in most cabs because of space limitations or because of peculiarities of cab shape.

2. Physical dimensions of seats. In some instances the physical dimensions of seats did not meet certain minimum human sizing seating criteria, especially with respect to width and depth of the seat pan, and width and height of seat back.

3. Degree of adjustability of seats. There was not a single instance in which the adjustability available in either the vertical or horizontal plane met minimum criteria. In one vehicle a certain seat could not be adjusted in any direction. At least half the seats could not be vertically adjusted at all. In almost all those seats that could be adjusted in either plane, the range of adjustability was too small.

4. Human sizing accommodations. On almost every truck the placement, static dimensions, and degree and range of adjustability of seats clearly favored the smaller driver. It was also discovered that some of the forward adjustability provided was wasted, since, when the seat was moved forward the space between the steering wheel and seat back became less than the abdomen depth of persons at the 75th percentile. Some improvements could have been made had the seat rack been mounted toward the rear of the cab. As pointed out above, this was usually impossible in view of cab structure.

5. Arrangement of dials and gages on instrument panel. A very wide variation among vehicles was found in both the previous study published in 1953 and the present one as well. There is some evidence that dials and gages have been placed nearer the operator. However, the variation found in the location, placement, size, degrees of visibility, presentation of information, and angle of instruments suggests that displays are not designed to follow any special pattern, nor to depend upon any system related to common human factors. Some gages and dials were wholly or partly hidden behind other instruments mounted on the steering column. Often a certain gage measuring the same thing would be found to vary widely in design in different vehicles. The variation in tachometers would be a specific example.

6. Placement of levers, knobs, and pedals. At least 22% of all hand controls found in 10 vehicles were considered to be located too far away from the operator. Others were placed in disadvantageous positions, such as one important lever which was almost invisible behind the steering column, and was difficult to reach as well. In certain vehicles some operators could not reach pedals without striking their thighs on the steering wheel or shift levers. Some controls impeded the operation of others, and some required excessive effort to operate. It was found that although a great deal of auxiliary equipment was included in some cabs, the additional space required had not been built into the cabs. Thus items of equipment were at times disadvantageously placed.

7. Design of visors, windshields, mirrors, and windshield wipers. The curvature of windshields varied, resulting in different degrees of distortion in vision. In some instances the windshield wipers did not fit the curvature of the windows they were supposed to clean. The size and quality of mirrors were highly variable, and in some instances the mountings were not adequate for preventing vibration. Visors often did not wholly shield the eyes from bright incident light, and there was considerable "leakage" which was uncomfortable. Some vehicles had only a single visor.

8. Temperature, humidity, noise level, and CO concentration in cab. In some vehicles the noise level approaches the discomfort level. Small amounts of CO were found in some cabs, but no cab was considered to have dangerous concentrations. Because of the wide variety of environmental conditions under which the vehicles were studied, only preliminary measurements of temperature and humidity were attempted. In general, humidity levels were not excessive. Temperature was found to be slightly variable. This area of biotechnology in vehicles needs intensive development.

9. Implications of design variation and design standardization. A great many design features of vehicles have been "standardized," for example, seal-beam headlights and standardized cabs that are interchangeable among different types of chassis. In passenger cars the size of the space provided for number plates, and the diameter of steering wheels vary only within a very narrow range. Thus, there is no objection to standardization of design features in principle. The data from this study, however, show that a great many other design features of equal or more importance vary in dimension, size, location, and in many other ways without any discernible relationship to the variation of human factors they are supposed to accommodate. For instance, both within the same manufacturing concern and from one to another, seating arrangements were found to be highly variable. One manufacturing concern has one kind of truck in which the seating arrangements were identical and, therefore, "standardized" for that line. In another line, the seating arrangements were standardized with different dimensions. Thus, each of the two types of trucks, would best accommodate only certain segments of the population of vehicle operators. Also, different manufacturers had seating arrangements which accommodate one segment of the operator population better than another.

It seems doubtful whether vehicle manufacturers have reliable standards available to insure accommodating variations of human body size, or if such standards are available they have not been used to maximum advantage.

DETERMINATION OF TRUE ENGINE FRICTION

R. E. Gish, J. D. McCullough, J. B. Retzloff, and H. T. Mueller, Ethyl Corp.

This paper was presented at the SAE Summer Meeting, Atlantic City, June 3, 1957.

RELIABLE predictions of the improvements in efficiency that can be obtained by raising the compression ratio of spark-ignition engines are of obvious value in the long-range planning of both the automotive and petroleum industries.

New equipment and techniques were developed to measure indicated power by obtaining accurate pressure-volume measurements in each cylinder, thus permitting true friction to be determined as the difference between the indicated power of all cylinders and the simultaneously measured brake power. Tests were conducted on a 4-cylinder engine at compression ratios of 7/1 and 12/1.

Results demonstrate the inaccuracies of the conventional "motoring test" method of measuring friction, reveal the effect of changes in compression ratio on true friction, yield conclusive evidence that the potential gains in thermal efficiency from increased compression ratios are greater on both an indicated and brake basis than earlier studies indicated; and establish empirical thermodynamic relationships which provide a convenient and accurate means of predicting these potential gains in efficiency.

BOTH the automotive and petroleum industries are vitally interested in the future of the spark-ignition engine because of their large investments in the facilities for manufacturing this type of engine and its fuel. Future improvements in efficiency resulting from the use of increased compression ratios will be an important factor in maintaining the favorable competitive position of the spark-ignition engine. Accurate evaluations of the potential improvements in efficiency are, therefore, important to the long-range planning of both industries.

Although many experimental evaluations of potential gains in efficiency at higher compression ratios have been made, those we have seen are questionable and inconclusive because the equipment available to the experimenters did not give sufficiently accurate measurements of one important variable—that of engine friction. Previous experimental evidence[1] supports the belief of many engineers that the method employed to measure friction in these programs, namely the motoring test, gives only an approximation of true friction. Unless friction is accurately known, neither the gains in brake thermal efficiency or indicated thermal efficiency are dependable indications of the potentials that exist.

For example, in an engine having inadequate structural rigidity for increased compression ratios, increased friction could largely offset the greater indicated power developed within the cylinders. The

[1] Automobile Engineer, Vol. 27, 1937, pp. 57 58: "Degree of Error in Relation to Motor Testing," by M. K. McLeod.

brake measurement would then reflect little or no gain, although a potential gain exists and could be recovered by correcting the design. The indicated power (the sum of brake and friction measurements) would not show the true potential either, since the motoring test, which is conducted under nonfiring conditions, would not reflect the true extent of the abnormal friction existing under firing conditions. As a result, the indicated power measurement would be low. Even when abnormal friction is not present the motoring test at full throttle tends to give a low value of friction and, therefore, of indicated power. Thus, the real potentials of higher compression ratios are masked when the true engine friction is not known.

Since the motoring test was considered to be inaccurate for a study of the potentials of higher compression ratios, a different method was employed in this program. It consists of measuring indicated power by obtaining accurate pressure-volume measurements in each cylinder and simultaneously measuring brake power during actual operation of the engine. The true friction, then, is determined readily as the difference between the indicated power of all cylinders and the measured brake power.

The object of the study was to obtain an accurate comparison of motoring and firing friction, to observe the effect of compression ratio on friction in what we consider to be a fairly rigid engine, and to obtain some fundamental data on the potential improvements in power and thermal efficiency that are obtainable by raising compression ratios.

Test Engine and Conditions

Engine—The engine was specially designed and built cooperatively with the Oliver Corp. for an earlier program to explore the potentialities of higher compression ratios, improved combustion-chamber design, and higher volumetric efficiency in tractor engines, since these design characteristics had been successfully exploited in the design of passenger-car engines. Called the XO-121, it is a 4-cylinder, in-line, overhead-valve engine having bore and stroke of $3\frac{3}{4} \times 4\frac{1}{2}$ in. and a displacement of 199 cu in. It is ruggedly built, with five main bearings of 3-in. diameter and connecting rod bearings of $2\frac{5}{16}$-in. diameter.

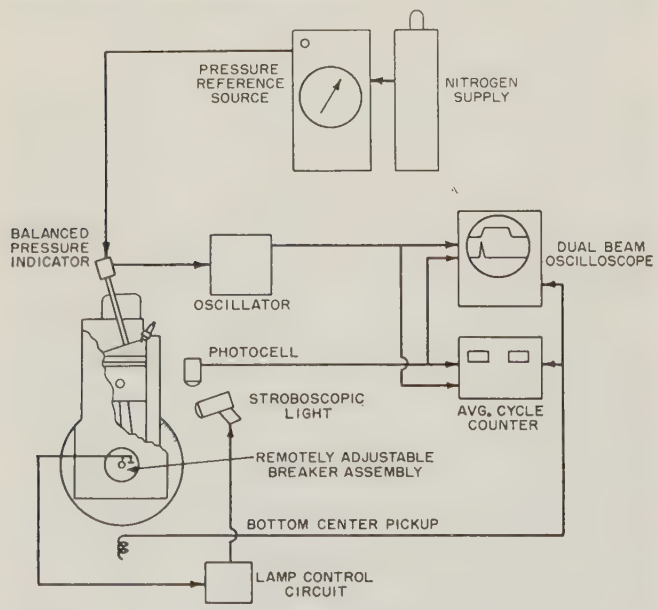

Fig. 1—Balanced pressure indicator system

The engine was well-suited to this program for several reasons. It appeared to have ample structural rigidity to prevent abnormal mechanical losses at high compression ratios, since in the previous program it displayed attractive gains in brake power over the compression ratio range from 7/1 to 12/1. Cylinder heads for this compression ratio range were already available, and the engine had only four cylinders in which to measure pressures rather than the six or eight normally used in commercial vehicle or passenger-car engines. Furthermore, its volumetric efficiency of 82% is reasonably good and was the same for both compression ratios.

Test Conditions—Tests were conducted at a speed of 1600 rpm. This gives a mean piston speed of 1200 fpm which is comparable to speeds of 2000–2400 rpm for engines having strokes in the range 3–3⅝ in. At both 7/1 and 12/1 compression ratios, data were obtained at throttle openings corresponding to loads of approximately 100, 75, 50, 25, and 3%. Thus, friction characteristics were surveyed over the entire load range. Air-fuel mixture ratio at each load was approximately that for maximum economy, except at 3% load. The latter, which is approximately idle load, required a normally rich mixture. Spark timing for each compression ratio was set to give a 1.6% power loss at full load, as the antiknock quality of the test fuel dictated such a setting at 12/1 compression ratio. The timings used at full throttle were also used at part throttle. The aim in selecting engine adjustments was to follow normal practices for tractor engines as well as to maintain comparable conditions between compression ratios. During the tests the engine drove only the oil pump, water pump, and generator, the latter without electrical load. The engine was equipped with an oil bath air cleaner but without muffler, the exhaust being connected directly to the laboratory exhaust system.

Instrumentation

General Description of Instrumentation—The thermodynamic and mechanical relationships reported in this paper hinge upon the careful determination of cylinder-pressure versus volume data from the test engine.

Day-to-day reproducibility of indicated horsepower and indicated mep was within ± ½%. This level of reproducibility was attained by classical procedures using data from two new instruments: (1) a high-sensitivity, contact-free, balanced pressure indicator and (2) an "average-cycle" counter which determined pressure-volume relationships in the presence of large cycle-to-cycle variations in peak cylinder pressures.

Fig. 1 illustrates the functions of the equipment used. The test engine was fitted with a flywheel calibrated in crank-angle degrees and a special cylinder head with auxiliary holes for pressure instrumentation. A reference pressure source supplied accurately known gage pressure and vacuum to a balanced pressure indicator. The balanced pressure indicator provided an electrical voltage indicating when the engine cylinder pressure was greater than, equal to, or less than the reference pressure. A high-

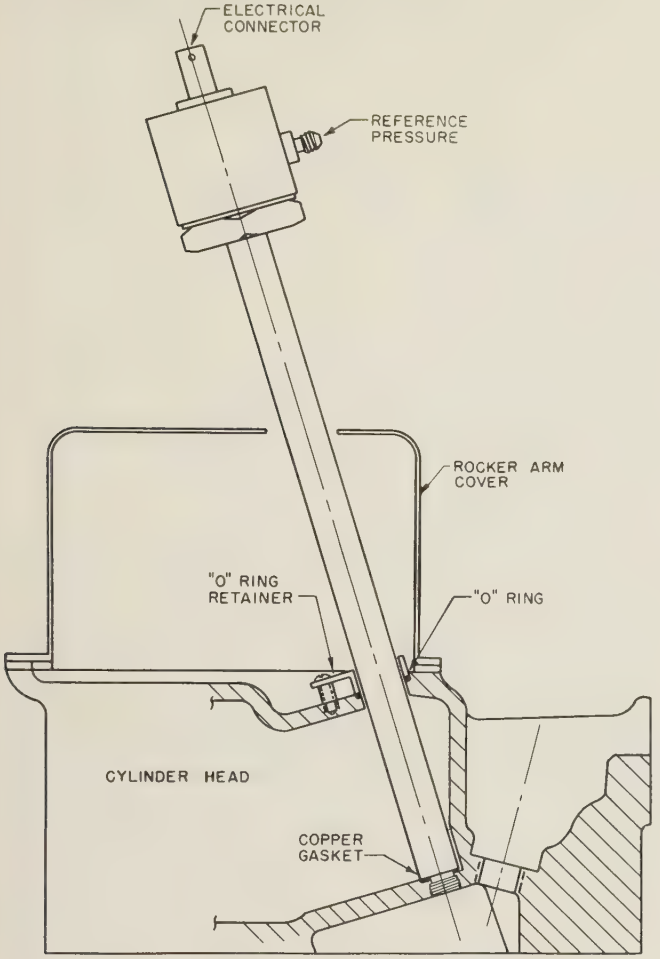

Fig. 2—Balanced pressure indicator installation

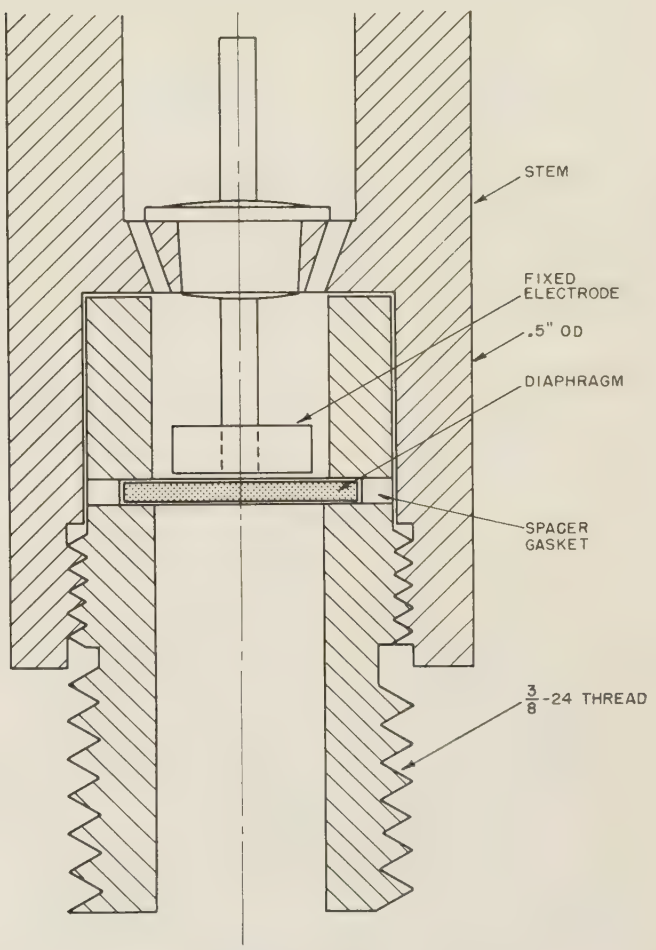

Fig. 3—Balanced pressure indicator

intensity stroboscopic lamp illuminated the flywheel protractor once per engine revolution. The crank-angle at which the lamp flashed was controlled by a set of breaker points driven from the engine crankshaft. The relative timing of these points was done manually by remote control. A photoelectric-cell cathode follower produced voltage proportional to lamp intensity indicating when the lamp flashed.

A dual-beam-cathode-ray oscilloscope simultaneously displayed the output of the balanced pressure indicator and the output of the photoelectric cell. An operator, observing the oscilloscope could remotely position the auxiliary breaker points in such a fashion as to cause the lamp to flash before, simultaneously with, or after the instant of equality of reference pressure with engine cylinder pressure. The average-cycle counter provided statistical data to determine the average pressure-crank-angle relationship during those portions of the engine cycle which exhibited considerable cycle-to-cycle variation in peak cylinder pressures.

Balanced Pressure Indicator—Fig. 2 depicts the balanced pressure indicator. The shape chosen permitted the bulk of the indicator to be placed outside the engine. At the top were located the pneumatic and electrical connections and a toroidal excitation coil. The long shank permitted passage through the engine water jacket to a $\frac{3}{8}$-24 hole tapped in the combustion chamber. At the combustion-chamber end was located a fixed reference electrode (Fig. 3) excited at a frequency of five megacycles by a remote oscillator.[2] An unclamped diaphragm was restrained to permit a maximum motion of 0.003 in. as a result of pressure differences between the combustion-chamber side and the reference-pressure side of the diaphragm. A small surge volume around the fixed electrode communicated with the reference pressure inlet by means of fluted teflon insulators in the long stem. The diaphragm successfully withstood 1500-psi peak cylinder pressures for long periods, yet it required only 0.6 in. of water pressure difference to cause the diaphragm to move from one mechanical limit to the other. Since the diaphragm was not clamped, there was no zero shift due to assembly or thermal stress.

Motion of the diaphragm changed the spacing between the diaphragm and the fixed electrode. This change in capacitance caused the oscillator carrier circuit to produce an electrical voltage proportional to the displacement of the diaphragm. Observation of this voltage on the dual-beam-cathode-ray oscilloscope permitted the operator to observe the first instant of diaphragm motion from either mechanical stop. In this manner, fixed time delays due to diaphragm inertia were minimized.

Reference Pressure—Reference pressures were supplied from nitrogen tanks or a vacuum pump. They were manually set by means of precision pres-

[2] Carrier circuit developed by Wesley Erwin, General Motors Research.

sure regulators. Reference pressures were read on one of three separate precision pressure gages. The 1500- and the 300-psi ranges were read on separate 16-in. pressure gages with a readability of one part per thousand. The ± 15-psi range was covered by a precision aneroid manometer also readable to one part per thousand.

Determination of Crank-Angle Corresponding to Reference Pressure—The first instant of diaphragm motion was related to engine crank-angle by a time-comparison technique. The dual-beam-cathode-ray oscilloscope allowed a direct comparison of the relative time of occurrence of the first instant of diaphragm motion and the time at which the stroboscopic lamp flashed. Fig. 4 illustrates the observer's view of these two phenomena. In this figure, the correct adjustment of the manually set breaker points was effected by placing the peak of the lamp intensity versus time trace at the first discernible departure from the horizontal of the diaphragm displacement versus time trace. The operator then read the desired crank-angle value from the calibrated flywheel. This form of null-balancing technique permitted reproducibility of crank-angle data to ± 0.1 deg.

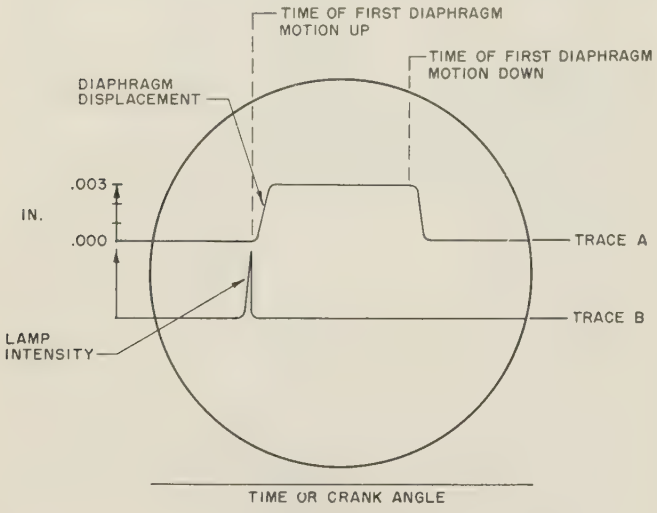

Fig. 4—Scope close-up

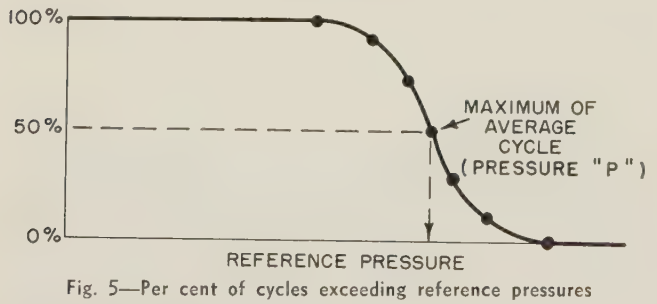

Fig. 5—Per cent of cycles exceeding reference pressures

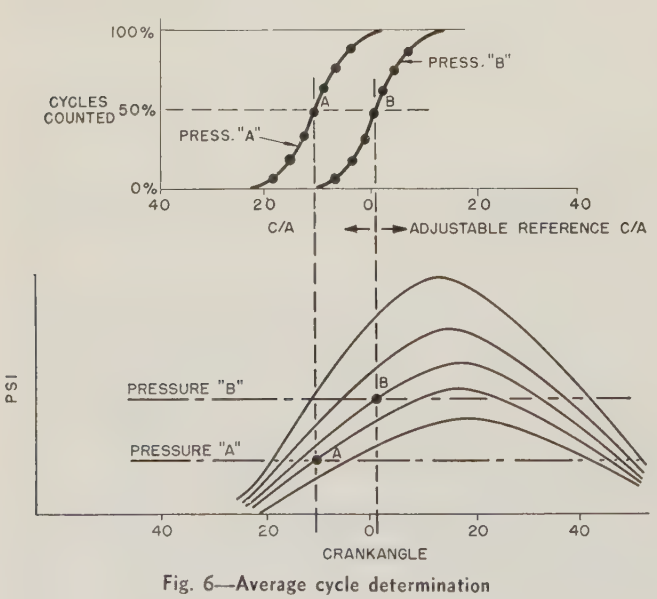

Fig. 6—Average cycle determination

"Average-Cycle" Counter—Most otto-cycle engines exhibit large variations in peak cylinder pressures from one cycle to another. Under these circumstances, the visual comparison of two oscilloscope traces cannot establish a representative pressure versus crank-angle relationship. However, a statistical approach proved valuable.

A survey of the *percentage* of engine cycles which *exceeded* various reference pressures was plotted as a function of reference pressure. Fig. 5 shows that all cycles exceeded the reference pressure up to a certain level. Above that level, a variable percentage exceeded the reference pressure. When Fig. 5 was replotted as a frequency distribution curve, the result was a bell-shaped curve showing a gaussian distribution with no skew. Consequently, the 50% point, indicated in Fig. 5, represented the "average" peak pressure. However this data provided only the

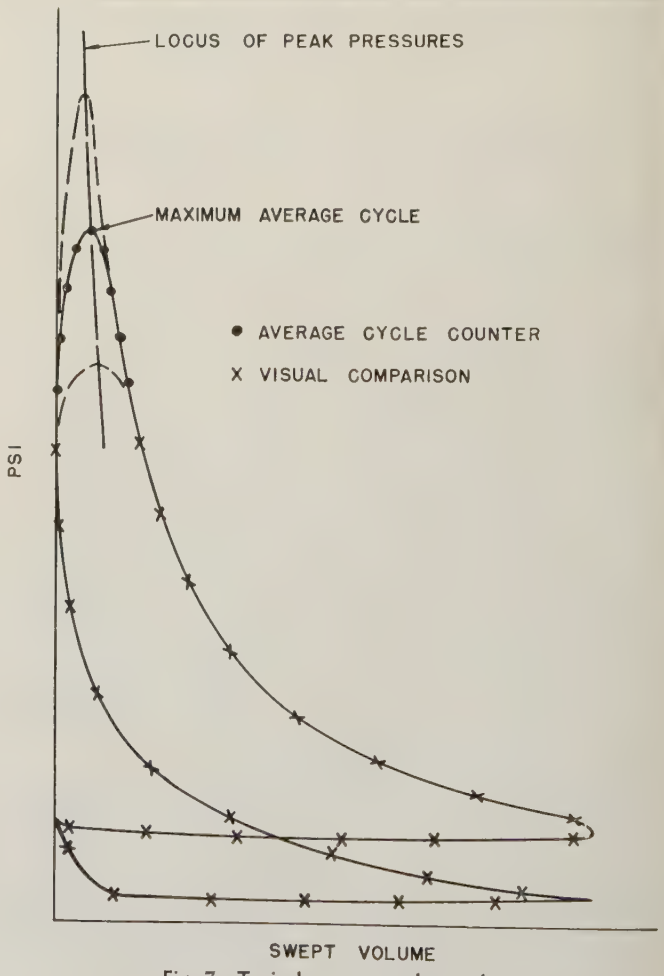

Fig. 7—Typical pressure-volume plot

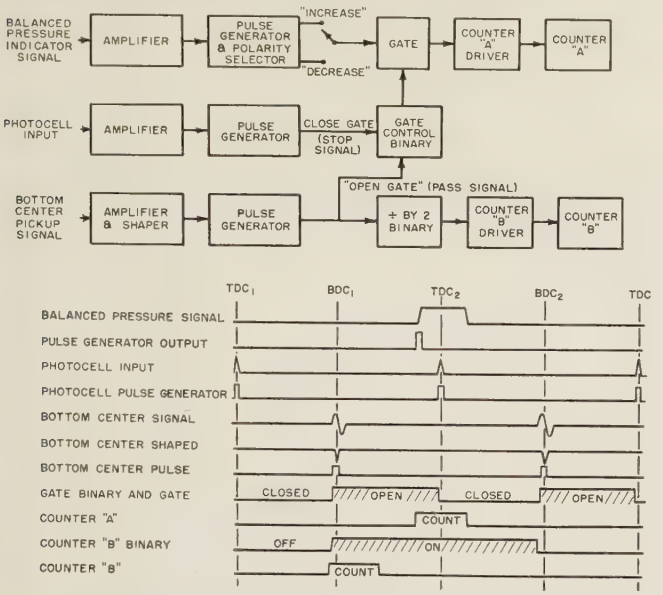

Fig. 8—Block diagram and timing sequence for average cycle counter

value of the peak pressure of the average cycle. The crank-angle corresponding to P, the maximum pressure of the average cycle, was determined by setting the reference pressure to P and waiting for an engine cycle which barely displaced the diaphragm. The crank-angle corresponding to this instant of motion was determined by use of the manually set breaker points and stroboscopic lamp. In this manner, both pressure and crank-angle were defined for one point of the average cycle plot, that is, the peak pressure. Since cycle-to-cycle variations were important over a wide range of crank-angles near peak pressure, many other points were required to establish the path of the average cycle. The additional points were obtained by an extension of the statistical technique.

To this end an electronic counter circuit was devised to furnish additional statistical data. This counter determined the percentage of engine cycles which *exceeded* the reference pressure *before* an adjustable reference crank-angle. The upper portion of Fig. 6 shows the counter percentages plotted as a function of reference crank-angle for two different reference pressures. In each case, at least 1000 engine cycles were sampled per point plotted. The nature of these curves permitted the use of the 50% point as most representative of the average cycle. Point A represents the crank-angle by which time 50% of the engine cycles reached reference pressure A. Point B represents the crank-angle by which time 50% of the engine cycles reached reference pressure B.

Each of the counter percentage plots provided a unique average-pressure crank-angle point which was plotted on the p-v curve. Fig. 7 shows how the visual comparison technique and the statistical technique supplement each other. In this figure, the crosses represent points obtained by the visual comparison technique during those portions of the engine cycle where cycle-to-cycle variations are quite small. The dots represent points obtained from the average-cycle counter during those portions of the engine cycle which exhibited large cycle-to-cycle variations.

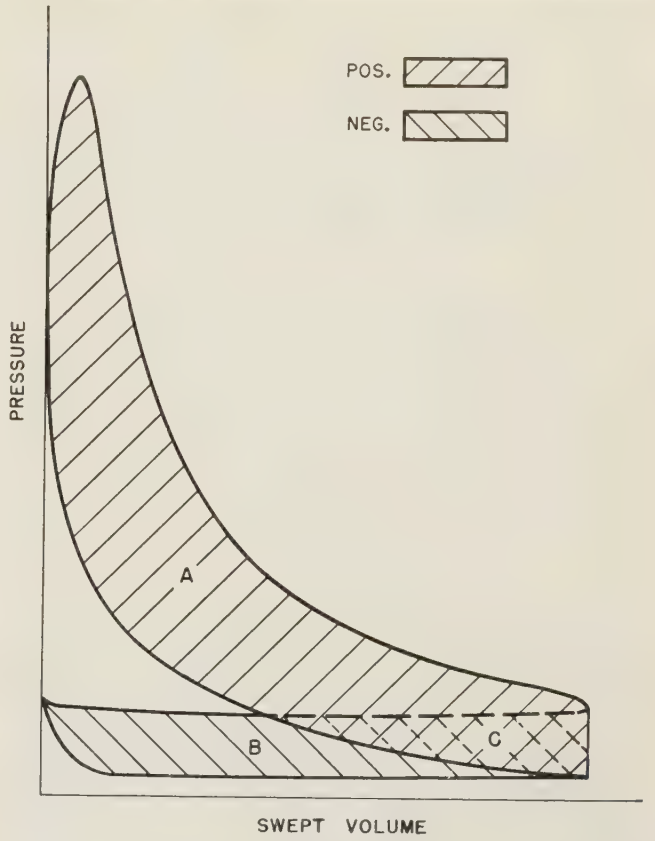

Fig. 9—Pressure-volume diagram showing positive and negative work areas

The block diagram and time sequence chart of Fig. 8 illustrate the action of the average-cycle counter.

Interpretation of Pressure-Volume Diagram

In the interpretation of a p-v diagram (Fig. 7) it is customary to consider the areas enclosed by the upper positive loop and the lower negative loop as being the only ones of practical significance. Although measurement of these areas yields the information needed to calculate indicated power, the meaning of the areas is not readily apparent. Actually, neither area represents any specific phase of the 4-stroke cycle. Each is merely the algebraic sum of various positive and negative work areas, obtained as a result of superimposing the diagrams of all four strokes on the same grid system.

We found in this program that consideration of the two areas illustrated in Fig. 9 leads to a better understanding of the real meaning of a p-v diagram, and reveals important additional information on engine performance. The large area (A + C) represents the net positive work available from the compression and expansion strokes (or working phase of the cycle), while the smaller area (B + C) represents the net negative work expended during the exhaust and intake strokes (or pumping phase of the cycle). Each of the two areas represents not only a specific phase of the cycle but also an important parameter of engine performance which will be defined and discussed later.

The construction of a p-v diagram is such that the two areas unavoidably overlap in the region marked

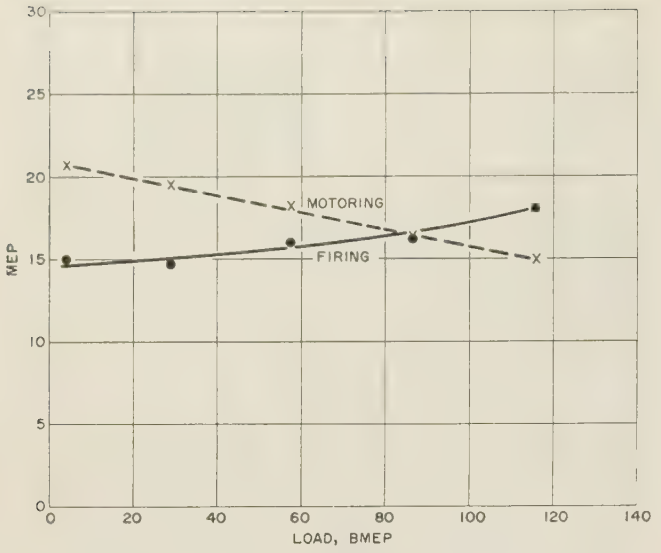

Fig. 10—Comparative results of motoring and firing friction tests, 7/1 compression ratio

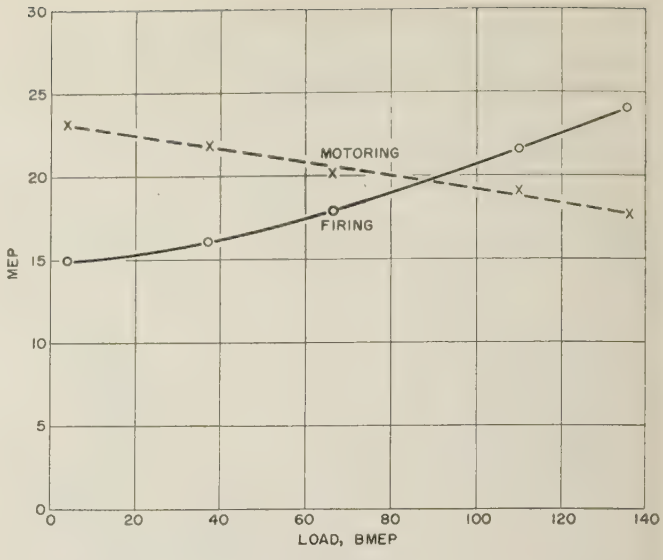

Fig. 11—Comparative results of motoring and firing friction tests, 12/1 compression ratio

C. This overlapping is not significant to the operation of the engine, but serves graphically to cancel out equal positive and negative areas, leaving only areas A and B. Thus the form of diagram shown in Fig. 7 is derived, with the positive loop corresponding to area A and the negative loop to area B. Unfortunately, this form of diagram is often misinterpreted to mean that area A is the positive work developed within the cylinder and area B the negative work expended in pumping. Actually, both areas should be greater by the amount of area C. Although the areas A, B, and C have no real significance as separate entities, they are identified separately in Fig. 9 for purposes of discussion.

It should be pointed out that the p-v diagrams in Figs. 7 and 9 represent operation at very light load rather than at full load. At light load the negative area is relatively large because work consumed in pumping is a large percentage of the available positive work. Under medium to heavy loads, the negative area is so small relative to the positive area that it is usually plotted separately on an expanded scale to permit accurate measurement and analysis. A light-load diagram was used in Figs. 7 and 9 to provide a suitably large illustration of the negative area.

Definition of Terms

Since terms such as friction and indicated power may mean different things to different people, the meanings intended in this paper must be carefully defined. The p-v diagram in Fig. 9 illustrates the work areas referred to in the following definitions:

Friction—By friction or the term true engine friction we mean the mechanical friction that exists in an engine during *actual operation*. By mechanical friction we mean friction between lubricated surfaces as distinct from the negative work required to pump the gases in and out of the cylinder. We were primarily interested in mechanical friction because it is the component most affected by changes in compression ratio, although we were also interested in evaluating the pumping work separately, and could do so with the method employed in this program. Friction is derived from the indicator diagrams and the brake measurements as follows:

$$\text{Positive Work Area} - \text{Negative Work Area} - \text{Brake Work} = \text{Friction}$$

$$(\text{Area A} + \text{Area C}) - (\text{Area B} + \text{Area C}) - \text{Brake Work} = \text{Friction}$$

$$\text{Area A} - \text{Area B} - \text{Brake Work} = \text{Friction} \qquad (1)$$

The difference between the positive and negative areas represents the *net* cylinder work. This net work is available to overcome friction and do useful work. Therefore, the difference between the net cylinder work and the useful (or brake) work is the friction.

The friction measurements obtained in this study include some losses such as generator windage and the work of pumping the crankcase lubricant and cooling water, which are not friction in the above sense. These losses are relatively small but can be determined separately if necessary. For practical purposes, they may be classified as part of the engine friction.

Indicated Work—We learned in this program that the definition of indicated work or power is a controversial subject. After consulting the literature and people engaged in automotive engineering work, we found that at least three different definitions of indicated work were used by reputable authorities. The three in terms of lettered areas on the p-v diagram were:

1. Area A.
2. Area A + Area C.
3. Area A – Area B.

. The third definition, or Area A – Area B, is used in this paper. It defines the net work of the indicator card. During the four strokes of the cycle, the gases in the cylinder do some work on the piston and the piston does some work on the gases, which results in both positive and negative work. The net, or indicated work, is what remains to overcome friction and do useful work. In other words, indicated work = friction + brake work. In a frictionless engine, the brake power would equal the indicated power.

Fortunately, the determination of mechanical friction is not effected by the choice of a definition of indicated power. The reader should know exactly what is meant by the term as used in this paper, however, to understand its significance in some of the subsequent discussions.

Mechanical Efficiency—Since mechanical efficiency is generally defined as brake power divided by indicated power, its value depends on which definition of indicated power is used. To conform to the definition of indicated power selected, mechanical efficiency must be:

$$ME = \frac{\text{Brake Power}}{\text{Indicated Power}} = \frac{\text{Brake Power}}{\text{Brake Power} + \text{Friction}} \quad (2)$$

The mechanical efficiency obtained from the above is that percentage of *available* indicated power that is left after mechanical friction has been overcome. Such a value is exactly what the term "mechanical efficiency" implies. When the conventional motoring test is used to determine friction, the result is unavoidably the combination of friction and pumping work existing under the motoring conditions. Under this procedure pumping work must, therefore, be included as a mechanical loss in the mechanical efficiency determination even though it is not one. Long usage of the motoring test in this manner is probably responsible for common acceptance of pumping work as a factor to be added to the denominator of the mechanical efficiency expression. The method used in this program permits determination of mechanical efficiency on either basis, since friction and pumping work can be determined separately.

Inherent Work—This is defined[3] as the net positive work of the compression and expansion strokes only, and is represented by the area between their curves. In Fig. 9 it is: Area A + Area C.

Some observers call this the indicated work, as shown by the second definition above.

Pumping Work—This is defined[3] as the net negative work of the exhaust and intake strokes only, and is represented by the area between their curves. In Fig. 9 it is: Area B + Area C.

Comparison of Motoring and Firing Friction

The result that was desired in this study was the friction under actual operating conditions. The motoring test could not give this result because it shows the sum of friction and pumping work. Furthermore, these quantities are not the same under motoring conditions as they are during actual operation, for the following reasons:

1. The gas loads on the piston, behind the top rings, and on the bearings are much smaller in motoring operation, which tends to make the friction lower.

2. Piston and cylinder temperatures are lower in motoring operation, which results in greater viscosity of the lubricant and somewhat greater friction. In firing operation, however, the lubrication of the top ring when the piston is near the top of the stroke probably approaches boundary conditions due to exposure of the oil film to the high temperatures of combustion, and to the greater loading resulting from much higher gas pressures behind the ring. The absence of this effect during motoring operation would tend to make friction lower. The lower piston temperatures during motoring provide increased clearances in the cylinder and greater freedom from distortion, which tends to make friction lower. If the structural rigidity of the piston is marginal, the reduction in friction might be very substantial.

3. The absence of exhaust blowdown and gas inertia effects during motoring operation and the greater density of the exhaust result in different pumping work. Although some factors tend to offset others, motoring pumping can be more or less than firing pumping, depending upon operating conditions and design factors. In view of all the variables involved, there appears to be little chance of finding a good general correlation between motoring losses and firing friction. None was found in this study.

Fig. 10 compares true friction with the result of the motoring test over the entire range of throttle openings at 7/1 compression ratio. True friction and motoring losses are expressed as mep and plotted against load expressed as bmep. As the throttle is opened, true friction increases whereas the motoring losses decrease. Relative to motoring losses, true friction ranges from 28% lower at idle throttle to 21% higher at full throttle. The motoring losses exceed firing friction at part throttle because pumping work, which is included in the motoring losses, becomes relatively large as the throttle is closed. Motoring losses are lower than firing friction at full throttle because here the pumping work is relatively insignificant, and the gas loads are much lower than they are during firing operation.

Fig. 11 shows similar results obtained at 12/1 compression ratio. In this case, the relationships are similar but the divergency is greater. Relative to motoring losses, true friction ranges from 35% lower at idle to 36% higher at full load.

Fig. 12 shows friction mep, pumping mep, and the sum of the two for both motoring and firing condi-

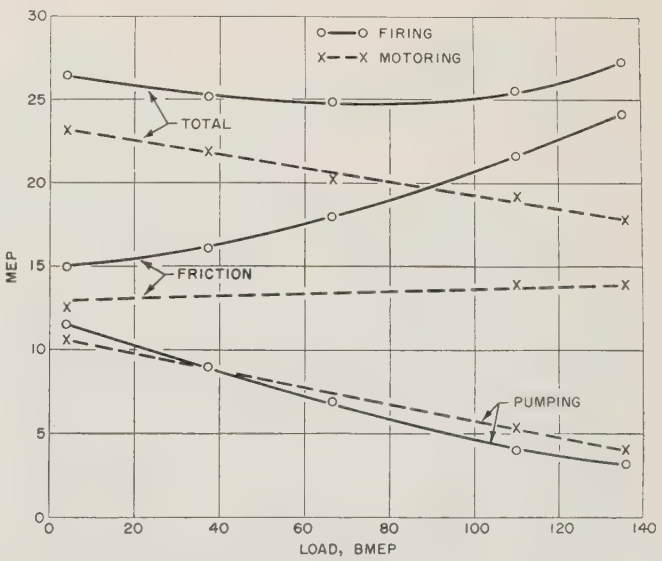

Fig. 12—Friction and pumping work versus load, 12/1 compression ratio

[3] "Internal-Combustion Engines," by L. C. Lichty. Sixth Edition, p. 99. Pub. by McGraw-Hill, New York, 1951.

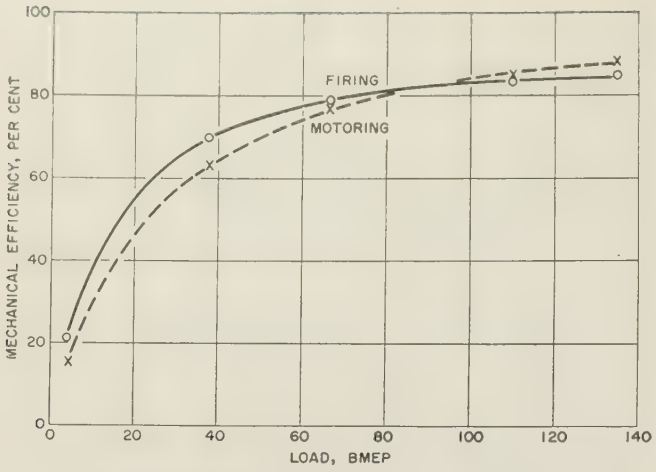

Fig. 13—Mechanical efficiency versus load, 12/1 compression ratio

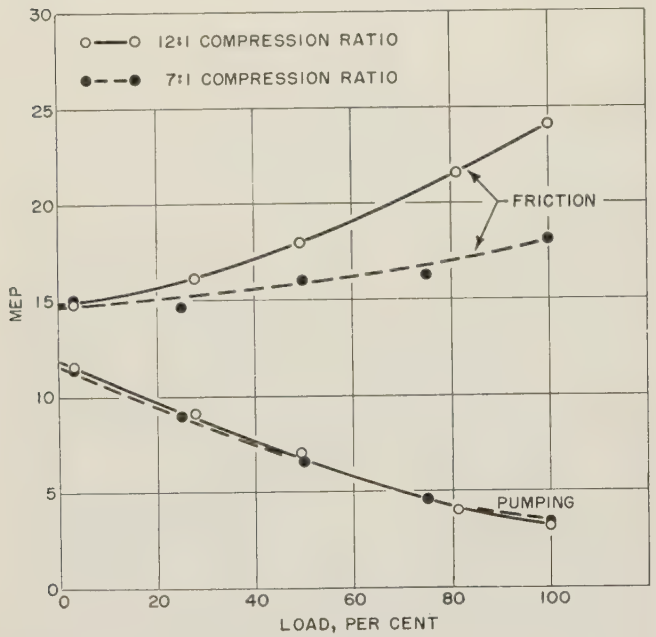

Fig. 14—Friction and pumping work versus per cent load at two compression ratios

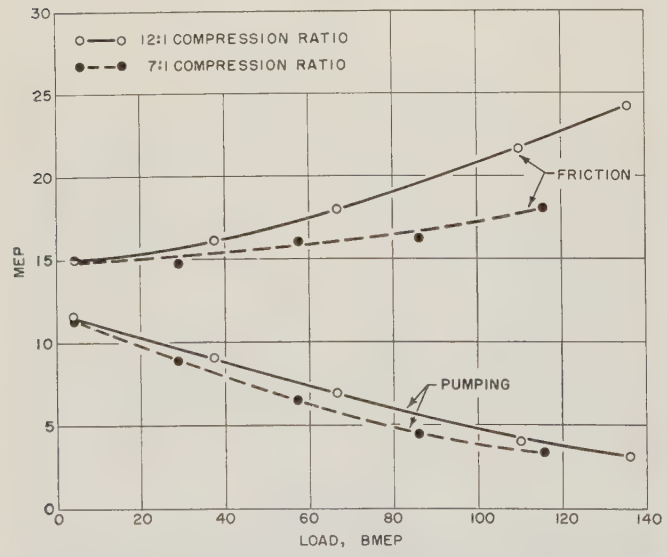

Fig. 15—Friction and pumping work versus load at two compression ratios

tions at 12/1 compression ratio. In order to obtain pumping mep under motoring conditions, indicator cards were taken. It can be seen that pumping is not greatly different under the two conditions, and decreases as the throttle is opened. Friction, on the other hand, may differ widely under the two conditions. Motoring friction remains relatively constant as the throttle is opened, increasing only slightly. Firing friction is only slightly higher than motoring friction at idle load, but increases more rapidly as the throttle is opened. As a result, the two are widely different at wide-open throttle. The sum of the losses under the two conditions is shown by the two top curves. It will be noted that the sum for firing conditions is greater than that for motoring at all throttle openings, with the widest divergence at full throttle. The top curve which represents the sum of friction and pumping under firing conditions is included here to show the result that the motoring test should give. It can be seen that the motoring test does not give good approximation of either this curve or the friction curve.

Fig. 13 compares mechanical efficiencies obtained during motoring and firing tests over the load range at 12/1 compression ratio. It can be seen that mechanical efficiency based on motoring losses is too low at part throttle and too high at full throttle. This is because motoring losses are higher at part throttle but lower at full throttle than true friction, as indicated in the previous figures. At full throttle the mechanical efficiencies are 88.1% motoring and 84.8% firing. In a less rigidly constructed engine, the difference would undoubtedly be much greater.

Effect of Compression Ratio on Friction

The determination of the effect of compression ratio on firing friction was one of the main objectives in this program. Fig. 14 shows how friction mep varies with per cent load for compression ratios of 7/1 and 12/1. At light loads, friction is about the same at the two ratios. As the throttle is opened friction increases, the 12/1 friction increasing more rapidly until at 100% load it is 33% greater than 7/1 friction. Pumping mep for the two compression ratios is also shown in this figure, and is about the same at a given per cent load.

Fig. 15 shows the relationships with load expressed as bmep. This permits comparing the two compression ratios from the standpoint of friction and pumping work at a given bmep. At relatively wide throttle openings, 12/1 friction is greater for a given bmep. Pumping is somewhat greater too because at 12/1 the engine must be throttled more than at 7/1 to produce the same bmep. The fact that 12/1 friction is greater at a given bmep is a significant point. The reason for the greater friction is indicated in Figs. 16 and 17.

Fig. 16 shows p-v diagrams that correspond approximately to equal bmep output for 12/1 and 7/1 compression ratios. In this case, the 7/1 ratio is at full throttle and the 12/1 ratio is at a part-throttle setting which produces the same work area. It will be noted that although the work areas are equal the pressures in the region of tdc are very much higher in the case of the 12/1 compression ratio. This fact suggests that the higher pressures at the 12/1 ratio were probably responsible for the increased friction,

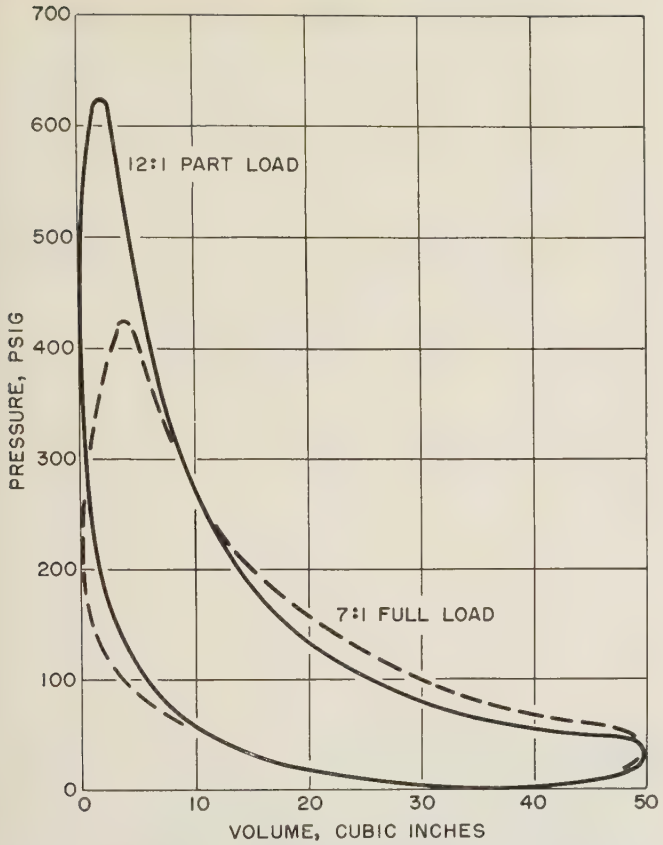

Fig. 16—Pressure-volume diagrams for equal work areas at two compression ratios

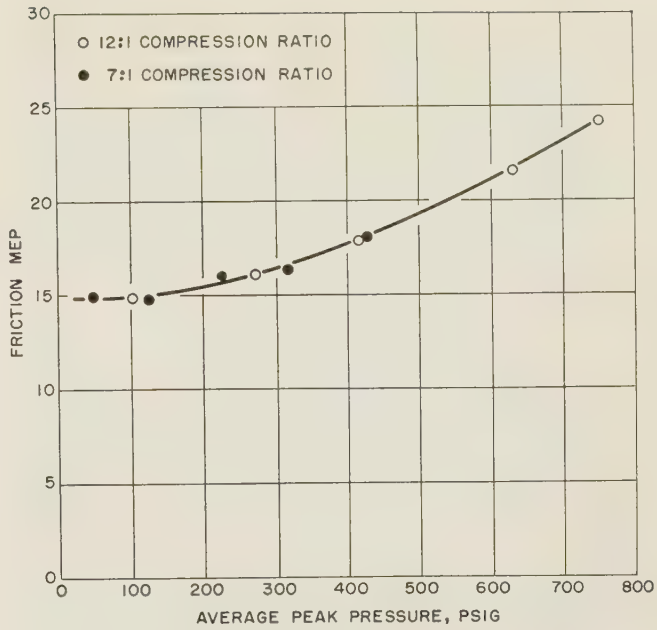

Fig. 17—Friction versus average peak cylinder pressure

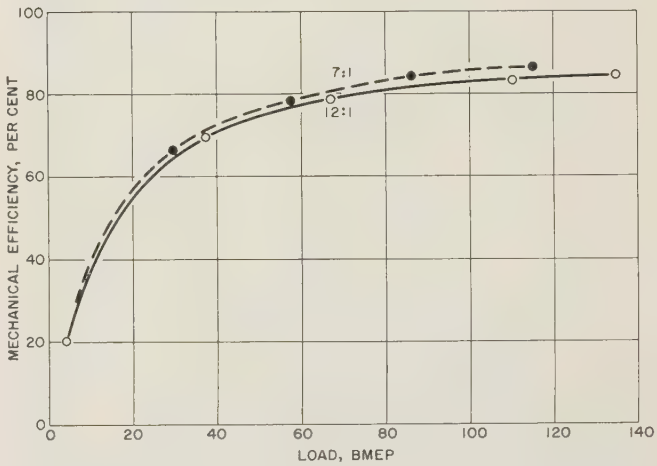

Fig. 18—Mechanical efficiency versus load bmep at two compression ratios

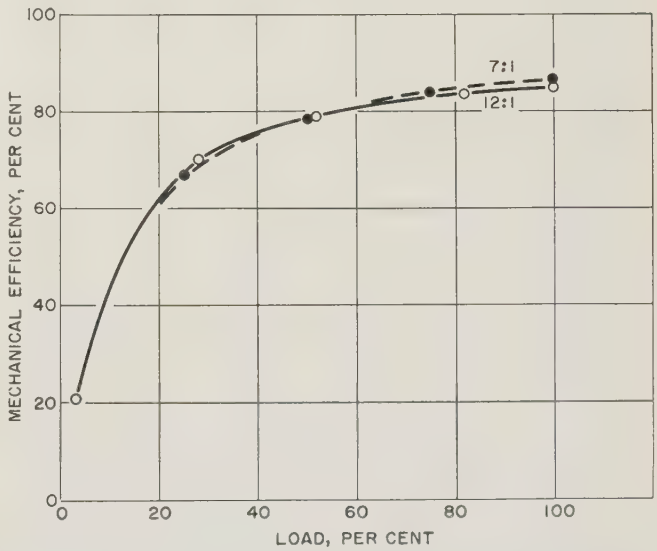

Fig. 19—Mechanical efficiency versus per cent load at two compression ratios

and that there might be a correlation between average peak cylinder pressure and friction.

Fig. 17 shows that such a correlation does exist. The data obtained for all throttle openings at the two compression ratios were plotted in this figure, and it can be seen that a smooth curve fits all points nicely. The data illustrate one of the most interesting relationships developed in the program by showing that the correlation is independent of the compression ratio used. In other words, friction was the same at the two compression ratios if the throttle settings were such as to produce the same peak cylinder pressures. The data also show that if peak cylinder pressures are greater for a given bmep, as was the case for the high compression ratio in Fig. 16, then friction must be greater. It appears possible that the main reason friction increases rapidly with gas pressure is that the high pressures act behind the top compression ring to drive it against the cylinder wall, when the piston is stopped at the top of the stroke or moving very slowly and the lubrication of the top ring is the poorest.

Figs. 18 and 19 show that in spite of the greater friction at the high compression ratio, mechanical efficiency compares favorably with that of the low ratio. Fig. 18 shows mechanical efficiency plotted against bmep for the two compression ratios. It will be noted that 12/1 mechanical efficiency is only slightly lower over the load range. At a given bmep, it is lower because friction is higher. Since mechanical efficiency decreases with load, the high compression ratio must appear at a disadvantage on this plot because at a given bmep it is operating at a lower load factor than the low ratio. Fig. 19 shows

the same relationships plotted against per cent load and provides a somewhat more favorable comparison for the high ratio. The 12/1 mechanical efficiency is again slightly lower at full load but is equal to or slightly greater than 7/1 efficiency at loads of about 50% or less. The actual values at 100% load are 86.3 and 84.8% for the 7/1 and 12/1 ratios, respectively. In view of this small reduction at full load, the attainment of constant mechanical efficiency over the compression ratio range from 7/1 to 12/1 appears possible.

Potentials of Increased Compression Ratios

The results of this program provide a fresh look at the potential improvements in thermal efficiency obtainable from increased compression ratios and permit development of a convenient means of predicting such improvements on a sound empirical basis.

Fig. 20 shows how full-throttle indicated thermal efficiency increases with compression ratio when it is determined by the method employed in this program. The figure also shows the improvements in brake thermal efficiency. The improvement at 12/1 compression ratio relative to 7/1 is 21.1% in indicated efficiency, and 19% in brake efficiency. The smaller improvement on a brake basis, which is 89% of that obtained on an indicated basis, results from the fact that mechanical efficiency is 1½% lower at 12/1 compression ratio. This indicates that a worthwhile improvement in brake gain could be obtained from a relatively small increase in mechanical efficiency. It will be noted, however, that there is no tendency for the brake curve to level off rapidly at any ratio in the range from 7/1 to 12/1. The slope of the brake curve between the two ratios was established in a previous program on the basis of data obtained at compression ratios of 7/1, 9.5/1, and 12/1[4]. This indicates that the compression ratio limit for improvements in brake thermal efficiency is significantly higher than 12/1.

There is a commonly held belief that potential percentage improvements obtainable from increased compression ratios in an engine are defined by the increase in efficiency of the ideal constant-volume air cycle. The theoretical relation between thermal efficiency and compression ratio is: Efficiency = $1 - 1/cr^{n-1}$, where $n = 1.4$ for air. In many experimental programs, however, the actual percentage gains have been greater than those permitted by the air cycle. Fig. 21 shows that greater gains were obtained in this program, not only in indicated efficiency but also in brake efficiency. Based on the air cycle, indicated thermal efficiency is 16.2% greater at 12/1 than at 7/1 compression ratio, but in the engine at full throttle it was 21.1% greater. It appears, therefore, that the ideal air cycle is not a reliable basis for evaluating the potentials of the spark-ignition engine.

The results of this program indicate that a more accurate method of estimating the actual potential gains is to use an empirical value of n, instead of 1.4, in the theoretical equation for air-cycle efficiency. The validity of this approach was established by substituting computed and experimentally determined values of thermal efficiency in the equation, and showing that the calculated empirical value of n remained constant over a wide range of compression ratios.

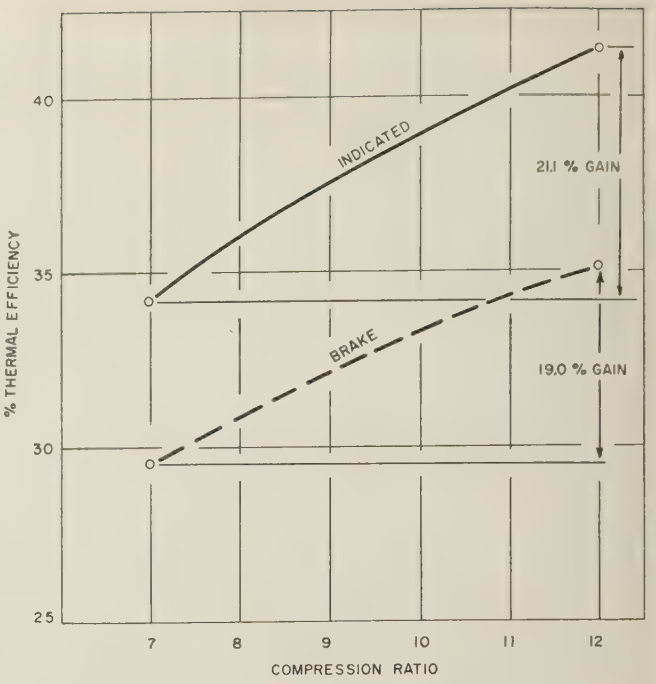

Fig. 20—Thermal efficiency versus compression ratio

The ideal *fuel-air* cycle computed by Goodenough and Baker is a much closer approximation of the actual engine cycle than the ideal air cycle. Taylor and Taylor[5] show that empirical values of n computed from the efficiencies of this cycle remain practically constant over a wide range of compression ratios. Fig. 22 shows that n for a fuel-air cycle with a lean mixture ratio (100% air or stoichiometric) is about 1.282, while n with rich mixture (87% air or approximately maximum power) is 1.245.

Since empirical n for the computed fuel-air cycle remains constant over the compression ratio range, we have reason to expect that n for the actual fuel-air cycle will also remain constant. In computing empirical n for the actual cycle, it should be based on the *inherent work* of the engine, or the area between the compression and expansion curves, since this area is the one considered in the theoretical equation and is the one approximated by the cycle computed by Goodenough and Baker. Fig. 22 shows that n for the actual inherent cycle does remain constant at about 1.221 when the 100% air, or lean mixture-ratio, is used. A value of $n = 1.190$ for the rich mixture at 12/1 compression ratio is shown, and a horizontal line is drawn through it indicating that it remains constant over the compression ratio range. Time did not permit obtaining indicator cards for the rich mixture at 7/1 compression ratio to justify the extrapolation. There is little reason to doubt, however, that n is also constant at the rich mixture. The values for the two mixture ratios are lower than the corresponding values for the computed cycle, because the actual cycle has additional heat losses that are not accounted for in the computed cycle. The real significance of the various re-

[4] SAE Transactions, Vol. 63, 1955, pp. 420–428: "Tractor Engine Design Requirements for Best Fuel Utilization," by H. T. Mueller and R. E. Gish.
[5] "Internal Combustion Engines," by C. F. Taylor and E. S. Taylor, p. 47. Pub. by International Textbook Co. Revised edition, 1948.

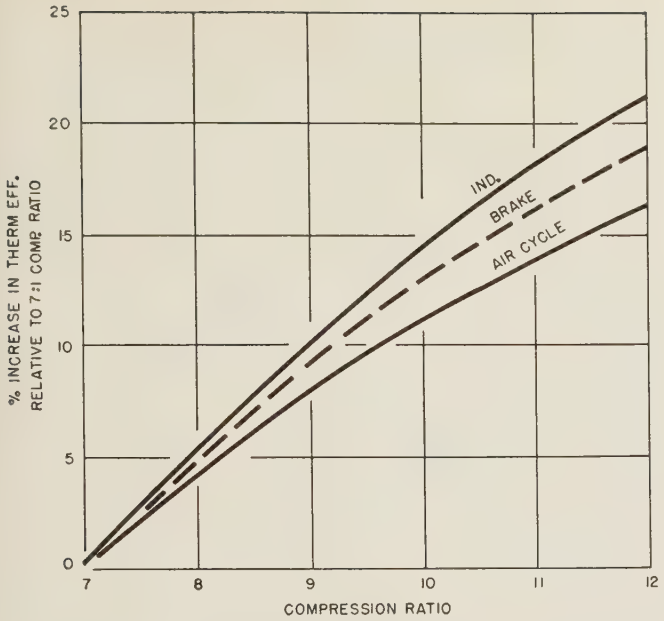

Fig. 21—Increase in thermal efficiency with compression ratio (XO-121 engine versus air cycle)

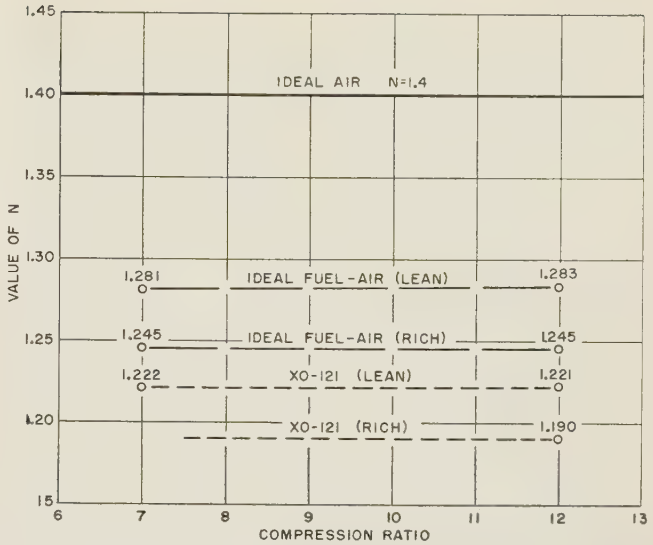

Fig. 22—Variation in exponent n with change in compression ratio (empirical values of n at 7/1 and 12/1 compression ratio computed by substituting known efficiencies in theoretical equation)

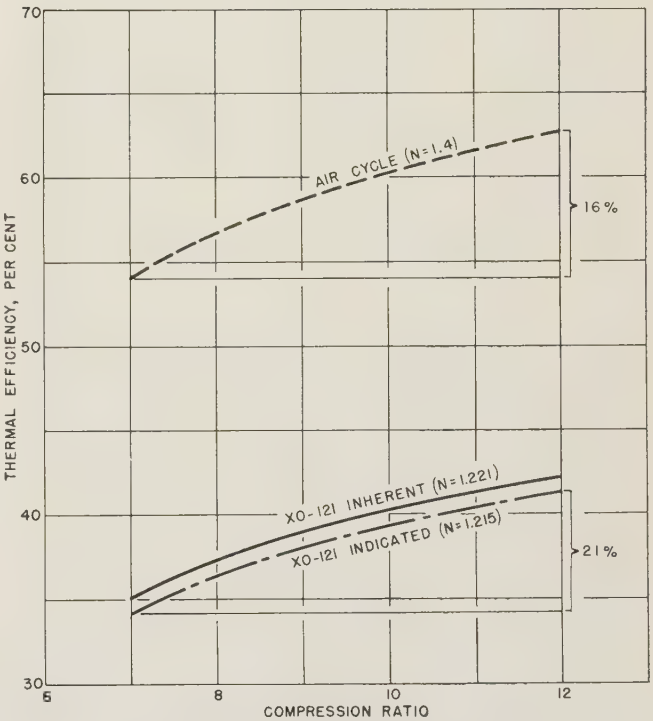

Fig. 23—Relation between thermal efficiency and compression ratio for ideal air cycle and XO-121 engine

lationships, however, is that theoretical analysis leads us to expect empirical n to remain constant with compression ratio change, and the experimental result shows that it does.

Fig. 23 shows the relation between thermal efficiency and compression ratio for both the ideal air cycle and the actual engine cycle, and why greater gains are obtained with the latter. Both the inherent and the indicated thermal efficiencies of the engine at full throttle are plotted. The indicated efficiency is slightly lower because pumping work must be subtracted from inherent work to obtain indicated work. Although the value of n should be based on inherent work, it is interesting to note that when the value is derived from full-throttle indicated work it also remains constant with compression ratio, being 1.215 at both 7/1 and 12/1 ratios. It can be seen that with the low values of n that are representative of actual engine cycles, the curves are in a region of much lower efficiency than in the case of the ideal air cycle, which results in a greater per cent gain for a given increase in compression ratio. The gain at 12/1 relative to 7/1 compression ratio is about 21% for the engine cycle on either an indicated or inherent basis, compared to 16% for the air cycle.

The empirical values of n developed in this study provide a convenient and practical tool for estimating the potentials of increased compression ratios or evaluating the results of an engine development program. The value varies within relatively narrow limits depending on air-fuel ratio, spark timing, speed, cooling, and other factors that govern indicated thermal efficiency. It should and does remain substantially constant with compression ratio, however, if the above factors are reasonably comparable between compression ratios. Notwithstanding changes in these factors, the resulting changes in exponent n for full-throttle indicated thermal efficiency have little effect on the percentage increase in efficiency with increase in compression ratio. The factor having the greatest effect on n in this program was air-fuel ratio. The value of n ranged from 1.183 for the rich mixture ratio to 1.215 for the lean mixture. Yet with either of these values, the per cent improvement in indicated thermal efficiency with compression ratio was about the same.

For estimating the improvements obtainable from increased compression ratios in a multicylinder engine operated at full throttle with maximum power mixture ratio, a value of $n = 1.18$ could be assumed for calculating the per cent improvement in indicated thermal efficiency. If mechanical efficiency is maintained constant, the per cent improvement in brake thermal efficiency would be the same. These data would indicate the amount of gain possible be-

fore a program was undertaken, and would provide a standard for evaluating the gains actually obtained.

The value of n for inherent thermal efficency at part throttle is about the same as at full throttle, and is substantially constant with compression ratio if based on a given percentage of full throttle power. Data indicate that n is no more than about 1% lower at 25% load than at full load for a given compression ratio if maximum power spark timings and maximum economy mixture ratios are used at each load.

On the other hand, the value of n for indicated thermal efficiency at part throttle drops off rapidly as the throttle is closed. Furthermore, it changes with compression ratio and, therefore, does not give a valid empirical relationship between part throttle indicated thermal efficiency and compression ratio. Actually, n becomes larger with compression ratio under these conditions, which means that the increase in thermal efficiency is greater than if n were constant. The greater percentage increase results from the fact that at a given per cent load approximately the same relatively large amount of pumping work is deducted from the inherent work of each compression ratio, and when the two inherent quantities are each reduced by the same amount to obtain indicated work, the percentage difference becomes greater. Thus, percentage gains in indicated efficiency will be larger at part than at full throttle. The percentage gains in brake efficiency will also be larger at part throttle. For example, the brake gain for 12/1 over 7/1 compression ratio was 27% at 25% load compared to 19% at full load. These comparisons are based on a constant percentage of full-throttle power at each compression ratio. If comparisons are based on the same bmep at each compression ratio, however, the part-throttle percentage gains are approximately the same as the full-throttle percentage gains. The lower gain on this basis results from the fact that the additional throttling required at the higher compression ratio not only increases the relative amount of pumping work but also decreases the mechanical efficiency.

With compression ratios of passenger-car engines already in the neighborhood of 10/1, there is considerable interest in the region above 12/1. How far beyond 12/1 the empirical values of n remain constant is not known. This is to be investigated in a continuation of the program.

Fig. 24 shows that measurements of indicated thermal efficiency obtained by adding motoring friction to brake power do not give a reliable indication of potential improvements from higher compression ratios. Per cent improvements relative to 7/1 compression ratio, based on such measurements, are shown for the XO-121 and two other engines as broken curves. In addition, per cent improvement based on measurements reflecting true or firing friction is shown for the XO-121 as the solid curve. All data are for a speed of 1600 rpm. It will be noted that the improvement based on firing friction is greater than that based on motoring friction. The data on the XO-121 indicate that the disparity is due mainly to the fact that as compression ratio is increased true friction increases more rapidly than motoring friction. As a result, indicated thermal efficiency based on true friction must increase more rapidly than that based on motoring friction. The disparity exists in the XO-121 even though the engine apparently has ample structural rigidity to prevent abnormal friction losses at high compression ratios. Thus, the improvements based on motoring friction are inherently low.

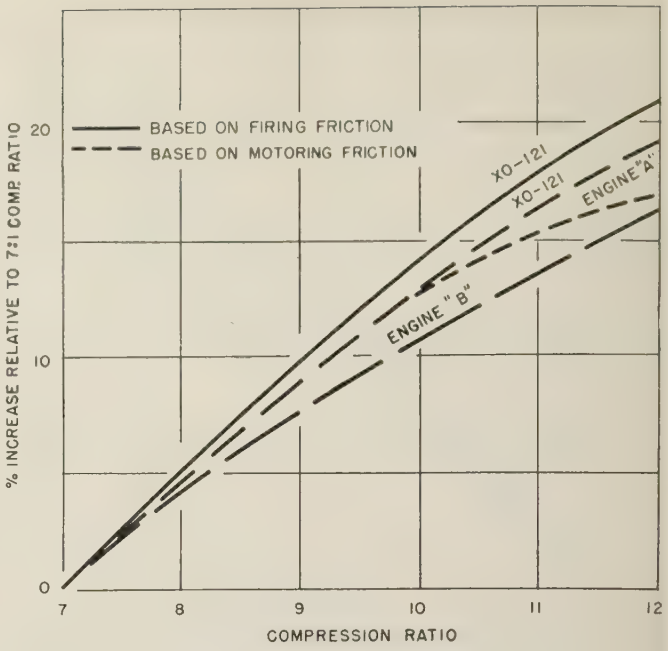

Fig. 24—Increase in indicated thermal efficiency with compression ratio

The curve for engine A illustrates how additional error may be introduced by insufficient component rigidity. It will be noted that curves based on motoring friction for engine A and the XO-121 are in good agreement in the range from 7/1 to about 10/1 compression ratio, but that the curve for engine A falls off more rapidly at higher ratios. Although the two engines have different indicated thermal efficiencies at a given compression ratio, the per cent improvement should be substantially the same for each engine over the whole compression ratio range. In this case, the falling off at high ratios was due to excessive friction resulting from piston deformation. The excessive friction reduced the brake power under firing conditions but was not fully reflected in the friction measurements under motoring conditions. As a result, the addition of brake power to motoring friction gave abnormally low values of indicated power at the high ratios.

The curve for engine B further demonstrates the unreliability of data based on motoring friction and the need for equipment to measure true friction. The data were obtained some years ago before the data on engine A and the XO-121 were available. At that time, the improvements obtained were believed to be truly indicative of the potentials of high compression ratios because they were in good agreement with the gains of the air cycle. The subsequent experimental programs and the theoretical considerations of the potentialities of the fuel-air cycle, however, proved that gains in both indicated and brake thermal efficiencies should be greater than those displayed by engine B. Although the program was conducted in a careful, thorough manner with the same type of test facilities employed in modern laboratories today, the results were misleading. In this case, the reason for the poor response to compression ratio is not known and could not

have been ascertained without equipment of the type described in this paper to determine true friction and indicated power.

Conclusions

1. The equipment and techniques developed in this program provide an accurate means of measuring the friction and indicated power of a multicylinder engine during actual operation.

2. The motoring test method for determining friction can be considered in general to be acceptable for routine test work. It tends, however, to give values too low under some conditions and too high under others. Furthermore, since the result obtained is the sum of the pumping work and friction under nonfiring conditions it does not provide the proper means for exploring true mechanical friction and its effect on the full realization of the potentials of higher compression ratios.

3. Friction at a constant speed correlates with average peak cylinder pressures regardless of whether a given pressure is obtained by throttle opening or compression ratio.

4. Although friction increases with compression ratio, the mechanical efficiency of the engine under full-throttle conditions was only 1.5% lower at 12/1 compresion ratio than at 7/1. Thus, the attainment of constant mechanical efficiency over this compression ratio range appears possible.

5. The potential percentage improvements in indicated thermal efficiency obtainable from increased compression ratios in an engine are greater than those of the ideal air cycle. Improvements can be predicted conveniently and accurately by using an appropriate empirical value of n, instead of $n = 1.4$, in the theoretical relation between air cycle efficiency and compression ratio, namely Efficiency $= 1 - 1/cr^{n-1}$.

6. Potential percentage improvements in brake thermal efficiency are equal to improvements in indicated thermal efficiency if constant mechanical efficiency can be maintained. In the engine used in this program the brake gain at 12/1 compression ratio over 7/1 was 89% of that obtained on an indicated basis, although the mechanical efficiency was only 1.5% lower than at 7/1. This indicates that a worthwhile improvement in brake gain could be obtained from a relatively small increase in mechanical efficiency.

7. Since the curve of brake thermal efficiency versus compression ratio shows no sign of rapid leveling off at high ratios in the range of 7/1 to 12/1, the limiting ratio for improvements in brake power appears to be significantly higher than 12/1.

8. Since it is not presently known how far the relationships developed in this program extend beyond the compression ratio range of 7/1 to 12/1, similar relationships will be investigated not only at higher compression ratios, but also at other engine speeds in a continuation of this program.

DISCUSSION

Describes Motoring Method for Determining Friction

—W. E. Lay
University of Michigan

THE authors of this paper are to be congratulated for an excellent presentation of a difficult and somewhat involved subject—laborious in the obtaining of data and involved as to its analysis.

At the University of Michigan we have been greatly interested in this subject from a somewhat different standpoint. We have felt that undue emphasis has been placed on the maximum power output of the engine and not enough on the road load operation where engine friction has a much greater influence on the efficiency and fuel milage of the vehicle. Recently real gains in efficiency have been made by reducing the friction losses in the engine. These gains are duly appreciated but there is still room for improvement. At low-speed road load operation the engine friction is nearly as large as the engine output.

The friction losses may be determined by either of two methods:

1. By direct measurement, driving the engine with a dynamometer.

2. By calculation from an indicator card and bhp measurements with a dynamometer.

The second method is expressed by the equation:

$$\text{Fhp} = \text{ihp} - \text{bhp} \qquad \text{(a)}$$

Certain discrepancies appeared in the results obtained by the two methods, especially at low-throttle or road load operation. At first it was assumed that the pressure indicator was at fault; however, lately pressure indicators have become available whose accuracy approaches that of our dynamometers and the discrepancy is even more evident.

A general re-evaluation of our ideas as to definition of terms and of test methods was clearly indicated. The theoretical relation of the terms to be considered may be expressed in terms of power as:

$$\text{Ihp} = \text{bhp} + \text{fhp} \qquad \text{(b)}$$

or in terms of pressure as:

$$\text{Imep} = \text{bmep} + \text{fmep} \qquad \text{(c)}$$

The terms bhp and bmep seem to be well-defined and the test methods by which they are determined seem quite unassailable. The other four terms are not so definite and need critical examination.

Ihp is seldom clearly defined by the text books. Sometimes alternate definitions are given. Our preference is to define it as the net power output of the gas cycle or the net power input to the engine pistons.

This ihp should perhaps be termed the net ihp. It is defined mathematiacally by the equation:

$$\text{Ihp} = p\,l\,a\,n/2\;\; N/33000 \qquad \text{(d)}$$

or:

$$\text{Ihp} = p\,N\,D/792000 \qquad \text{(e)}$$

where:

p = Imep, psi
l = Length of piston stroke, in.
a = Area of piston, sq in.
n = Engine speed, rpm ($n/2$ = cpm)
N = Number of engine cyl
$D = laN$ = engine displacement, cu in.

In the above equation there still remains a pressure term (imep) which is not clearly defined except as to the method of measuring it. It is determined from an indi-

Table A—Net Work of Areas Shown in Indicator Card, Fig. 2

	Areas	Sign		Layers	
A	Expansion only	1 positive only		1	1
B	Expansion, compression	1 positive, 1 negative	+1	1	0
C	Expansion, exhaust	1 positive, 1 negative	+1	1	0
D	Expansion, compression, exhaust	1 positive, 2 negative	+1	2	1
E	Expansion, intake, compression, exhaust	2 positive, 2 negative	+2	2	0

Net result (a) = +1 (d) = −1

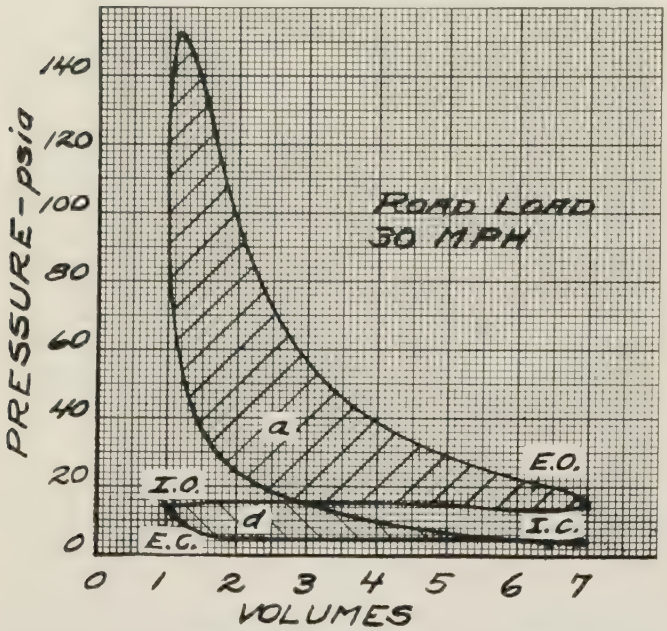

Fig. A—Typical indicator card, absolute pressure versus volume or stroke

cator card such as that shown in Fig. A. This card is a pressure-volume diagram. It is a plot of the absolute pressures in the engine cyl against the piston stroke. Each plotted point is an average value for perhaps some 50 cycles of engine operation. The operation of the engine is carefully stabilized before any pressure readings are taken and a card is obtained from each cylinder. The average values may then be compared to other average data obtained with other test apparatus. The indicator card has an upper positive loop and a lower negative loop, covering a complete 4-stroke cycle. The imep is determined as follows:

$$\text{Imep} = \frac{\text{Positive loop area} - \text{Negative loop area}}{\text{Stroke}} \times \text{Scale Factor (f)}$$

where:

Areas are measured in sq in.
Stroke measured in in.
Scale factor is the ordinate scale in psi per linear in.

Considering the expansion of the gas, it is clear enough that gas pressure in psf multiplied by the changes in volume in cu ft is work in ft lb. Also, with regard to the pistons, the gas pressure in psi multiplied by the piston area in sq in. is a force in lb, which multiplied by the stroke in ft is work in ft lb. This work may then be considered as positive work if the force is acting to aid the normal motion of the piston and negative if it tends to oppose the normal motion.

The piston head is exposed to gas pressure from both above and below. The crankcase pressure is approximately constant. In a 4-stroke cycle it opposes the piston motion during two strokes and aids it during the other two. Therefore, for a complete 4-stroke cycle, the net work due to crankcase pressure underneath the piston is zero. The work done above the piston head is shown in Fig. B for each of the four strokes. First is shown the curve of gas pressure variation during the stroke and the work area beneath the curve. The cross-hatching leaning forward to the right indicates that the work is positive, and leaning backward, that it is negative. Below these are piston diagrams showing the direction of gas pressure and the

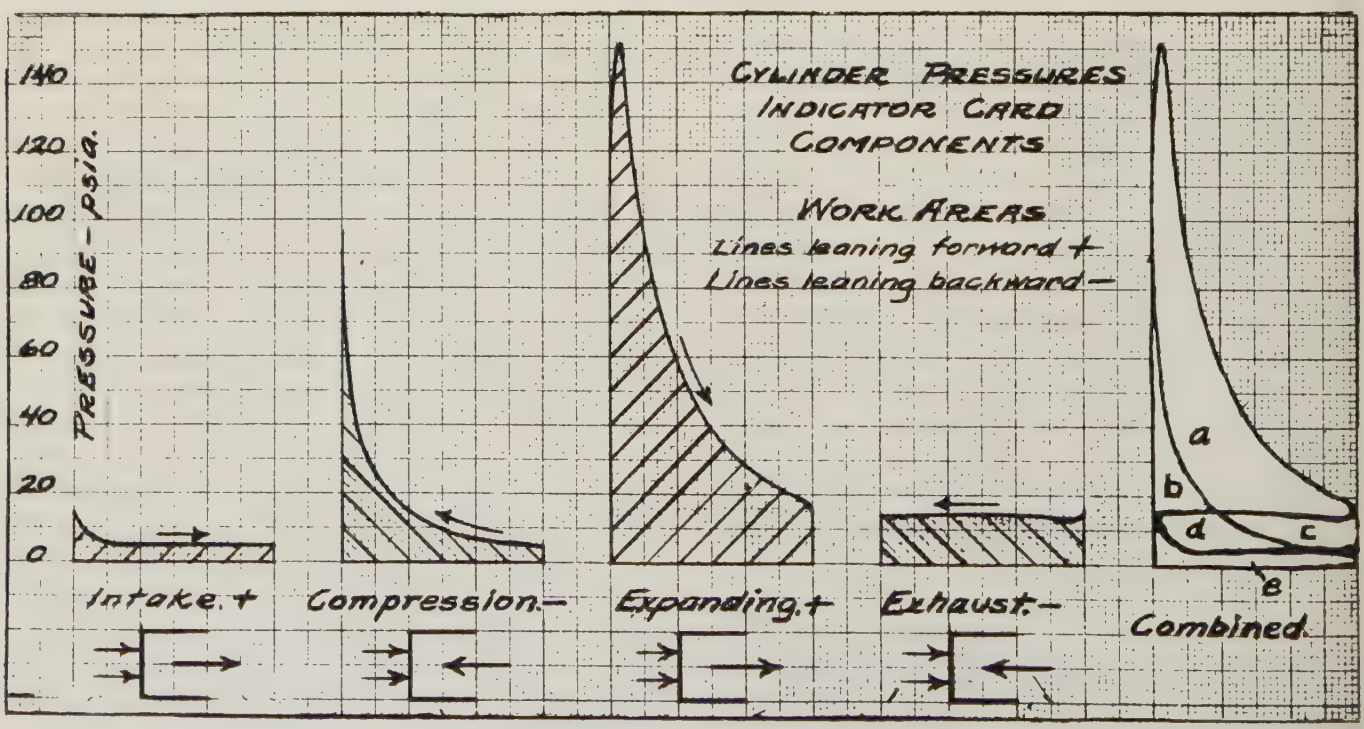

Fig. B—Cylinder pressures indicator card components

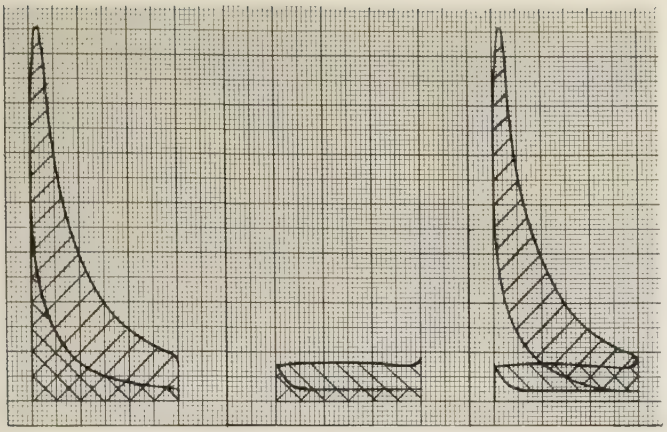

Fig. C—Considering cycle as made up of two phases

direction of piston motion. At the extreme right is a combined diagram with all of the work areas superimposed upon each other. This is the whole indicator card. There are five different areas with one or more work layers. The net work for some areas is positive, some negative, and for some it is zero, as shown in Table A.

Area A is the positive loop of the indicator and represents the net work of the gas on the pistons. Likewise, area D is the negative loop of the indicator card and represents the net work of the pistons on the gas. The net work output of the whole gas cycle is thus the difference (A minus D) which is, of course, the net work input to the piston and the engine mechanism.

The meaning of the work areas may be clarified by dividing the 4-stroke cycle into two phases (Fig. C):

1. The power phase consists of the compression and expansion strokes during which both valves are closed.

2. The pumping phase consists of the exhaust and intake strokes during which one or both valves are open.

In the power phase the work area under the expansion curve represents the work done by the gas on the piston and is clearly positive. In like manner the area under the compression curve is clearly negative since this is work done on the gas by the engine piston. This energy is not lost but goes to increase the temperature and pressure of the gas enclosed or trapped in the cylinder. The net positive area represents the net work done by the gas on the piston during these two strokes. It will be noted that the shape of this net area is very similar to that of the theoretical air cycle shown in Fig. D. For this reason it is sometimes used to determine what is called the inherent ihp. The inherent ihp may be used in making comparisons with the air cycle, but should not be used to determine the mechanical efficiency.

The pumping phase shows the negative area under the exhaust curve and the positive area under the intake curve. The net negative area represents the work done by the piston in moving the charge in through the intake passages and out through the exhaust passages. Both the intake and exhaust operations are best described as throttling processes. The energy taken from the pistons is not returned to the gas cycle but is an irrecoverable loss such as that occurring in the operation of a Prony brake. It might even be called a gas friction loss.

If it is easier to think in terms of gage pressures, a horizontal atmospheric pressure line may be drawn on the diagram of the pumping phase. The area between this line and the exhaust curve represents the negative work done by the piston in pushing the gases out of the cylinder. The area between the atmospheric line and the intake curve represents the work done in sucking the charge into the cylinder. Both areas are negative and taken together represent the pumping work done by the piston.

When the power area is superimposed on the pumping

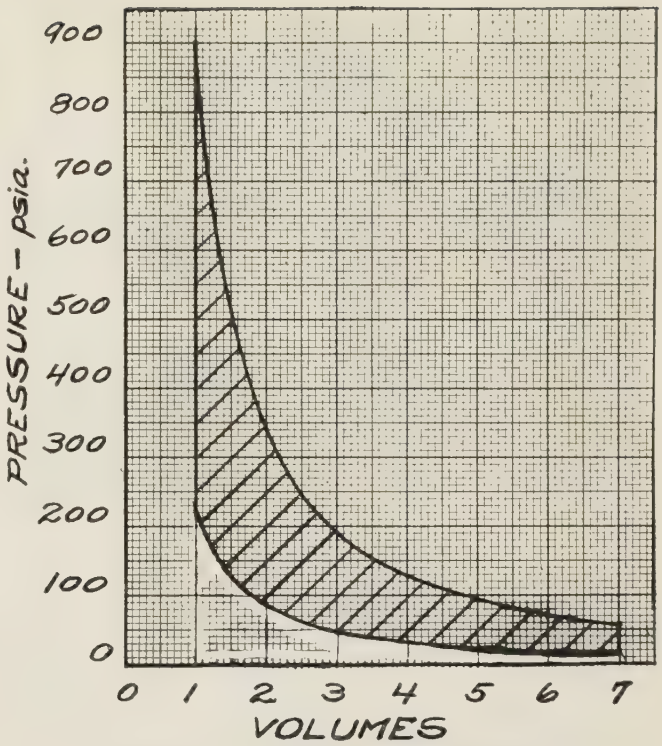

Fig. D—Air cycle pressure-volume diagram

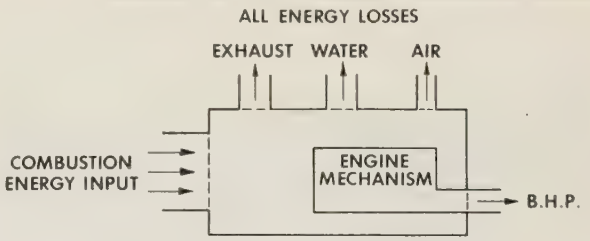

BRAKE THERMAL EFFICIENCY (OVERALL)

$$= \frac{\text{OUTPUT}}{\text{INPUT}} = \frac{\text{HEAT EQUIVALENT OF B.H.P.}}{\text{HEAT FROM COMBUSTION}}$$

Fig. E—Energy flow diagram, whole heat engine

area as shown at the right on Fig. C the area C is cancelled out. The remaining positive area A and the negative area B are the familiar positive and negative loops of the indicator card. The relations may also be represented by energy flow diagrams (Fig. E). The energy flows in from the left and is diminished by the losses which flow upward, leaving the useful power output flowing out at the right of the enclosure. This is the type of thermodynamic enclosure used in determining the brake thermal efficiency (overall thermal efficiency):

$$\text{Brake thermal efficiency} = \frac{\text{Output}}{\text{Input}} = \frac{\text{Heat equivalent of bhp}}{\text{Heat from combustion}} \qquad (g)$$

This overall operation may be divided into the gas cycle operation and the engine mechanism operation. For the gas cycle operation the thermodynamic enclosure is shown by Fig. F. This is used to determine the indicated thermal efficiency:

$$\text{Indicated thermal efficiency} = \frac{\text{Output}}{\text{Input}} = \frac{\text{Heat equivalent of ihp}}{\text{Heat from combustion}} \qquad (h)$$

Fig. G shows a similar enclosure that might be used in

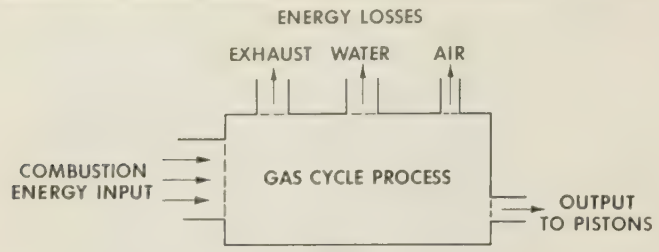

$$\text{INDICATED THERMAL EFFICIENCY} = \frac{\text{OUTPUT}}{\text{INPUT}} = \frac{\text{HEAT EQUIVALENT OF I.H.P.}}{\text{HEAT FROM COMBUSTION}}$$

Fig. F—Energy flow diagram, gas cycle

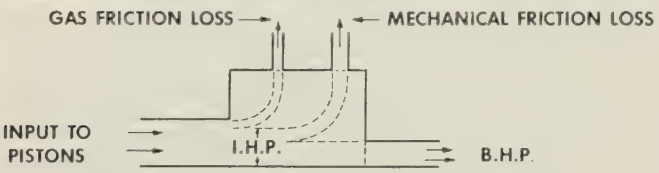

$$\text{I.H.P.} = \text{B.H.P.} + \text{MECH. FRICTION}$$

$$\text{MECHANICAL EFFICIENCY} = \frac{\text{B.H.P.}}{\text{I.H.P.}}$$

Fig. G—Energy flow diagram, engine mechanism

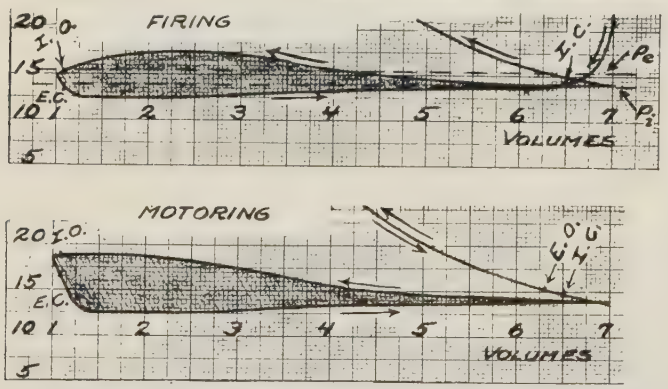

Fig. H—Pumping work shown by low-pressure indicator cards, full-throttle

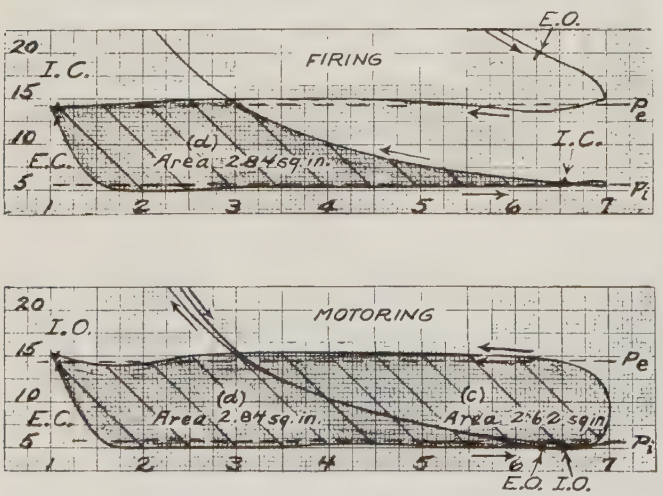

Fig. I—Pumping work shown by low-pressure indicator card, road load

Table B—Values of K for Various Gases

Gas	Formula	Number of atoms	K
Argon	A	1	1.67
Air	—	—	1.40
Carbon dioxide	CO_2	3	1.37
Steam	H_2O	3	1.30
Ethane	C_2H_6	8	1.21
Octane	C_8H_{18}	26	1.04

determining the mechanical efficiency of the engine mechanism.

$$\text{Mechanical efficiency} = \frac{\text{Output}}{\text{Input}} = \frac{\text{Bhp}}{\text{Ihp}} \qquad \text{(i)}$$

Here the input to the piston is the gross input represented by the area of the positive loop of the indicator card. By this analysis the indicated power should be determined from the area of the positive loop alone. It is true that the piston receives this energy but later it gives up part of it by work on the gas. The net work given up by the piston is represented by the area of the negative loop of the p-v diagram of the cycle. It would appear more logical to charge this loss to the gas cycle rather than to the engine mechanism. Therefore, the net input to the piston should be used in the determination of the ihp and the mechanical efficiency.

If the latter procedure is followed, the friction mep when the engine is firing does not include any pressure that is used to pump the charge in and out of the cylinder and the fhp includes only the power used to overcome mechanical friction in the engine mechanism. When engine friction is determined by a motoring test the charge is pumped through the engine in much the same manner as when it is firing. This pumping energy is furnished and measured by the dynamometer. Therefore, the fhp determined by the motoring method includes the work represented by the area of the negative loop and is too large by that amount.

More was learned about the work of the negative loop when a series of indicator cards was obtained showing the negative loops, for the same speed and throttle opening, both with the engine firing and when it was being motored in a friction test. The pressures were indicated on a mercury manometer having least scale divisions of 1/10 psia so that readings could readily be made to the nearest 1/50 psia. The period during which pressure data were obtained was preceded and followed by regular power, fuel, and motoring friction tests. This enabled us to compare friction data obtained from both indicator cards and from dynamometer motoring tests. It also showed whether or not the engine operation had been really stabilized during the test period.

At full-throttle the negative loops when the engine was firing were similar in size and shape to those obtained when the engine was motored (Fig. H). A similar pair of cards for low-throttle operation at the same speed are shown in Fig. I. Here the negative loops are quite different. The area of the motoring loop is about 90% larger than that of the firing loop. The explanation for this oversized motoring loop is quite simple. When the engine is firing, the pressure decreases along the expansion curve until the exhaust valve opens and the cylinder pressure blows down through the valve until it drops to about 15 psia. It then remains fairly constant at this value throughout the exhaust stroke. But, when the engine is being motored, the expansion curve follows very nearly the same path as that traversed in the opposite direction during the compression stroke. At the point where the exhaust valve opens, the pressure in the cylinder may be only 5 psia, while the pressure in the exhaust manifold is about 15 psia. So gas flows from the exhaust manifold into the cylinder until the pressures are nearly equalized, and the exhaust stroke then proceeds at a cylinder pressure of about 15 psia. This accounts for the added area C in the negative loop of the motoring card.

Thus, if the fhp, determined by the motoring method, is accepted, the mistake of including this negative loop work is made. Furthermore, if the operation is at low throttle

a greatly exaggerated value is included. There is still further reason for the discrepancy. The gas pressures increase as the throttle is opened. Therefore, the piston side thrust, piston pin, crankpin, and main bearing pressures should increase and produce an increase in mechanical friction as is born out by Figs 10, 11, and 17.

It appears that the disposition of the work of the negative loop and the definition for ihp and fhp are the items in question. The determination of friction by the motoring method is so simple, compared with the indicator method, that it may be hoped that some kind of a correction factor may be developed.

As was stated earlier in this discussion, the actual engine cycle is often compared to the theoretical air cycle. In my opinion, little is to be learned from such comparisons. The air cycle assumes many things which are not true of the actual working cycle of the engine, for example:

$$K = C_p/C_v = 1.40 \text{ for air} \qquad \text{(j)}$$

This value is not a constant even for air, as shown below:

Temperature, F	Pressure, psia	K
0–200	15	1.40
3000	15	1.30
0	1000	1.58

In the actual cycle gases other than air must be considered. Some are shown in Table B.

It is our hope that this excellent paper will provoke a thorough discussion of definitions and test techniques for the determination of engine friction. It is felt that this is a problem worthy of more investigation, especially at road loads and the normal speeds at which we are allowed to drive. Here a slight reduction in engine friction will bring a sizable increase in fuel mileage.

Points Out Cost and Time Factors in Use of Authors' Method

—J. M. Chandler
Ford Motor Co.

WE are glad to have this opportunity to congratulate the authors on an excellent technical paper. The presentation was particularly interesting since there were really two subjects presented in the same package—one on instrumentation development, one on engine friction.

The method presented by the authors for obtaining engine indicator cards appears to be one of the most accurate methods yet devised. Such accuracy is, however, expensive in terms of time and flexibility. For the theoretical study presented, the cost in engine and man hours would not normally be considered prohibitive. However, for the designer who is interested in evaluating engine design changes, there is still the overwhelming need for a fast as well as accurate means of obtaining indicator cards. As we continue our search for the improved instantaneous dynamic pressure pickup (preferably combined with a standard spark plug, of course) we can be grateful to the authors for what might be an unexpected blessing—a means for calibrating an instantaneous indicator dynamically. Now, using the author's instrumentation, we can find out exactly how nonlinear our dynamic pickups really are.

In regard to engine friction, an engine designer does not particularly like to have it forcibly brought to his attention that rubbing friction increases in proportion to peak cylinder pressure. He would rather just close his eyes and hope that the whole thing will go away. Or he might take refuge in what was our original attitude on reading this paper and prefer to remind the authors that the automobile doesn't really care how the engine's digestive tract functions, it merely wants some amount of shaft hp available in order to obey the driver's whims.

The authors make quite a fuss over engine rigidity and attempt to remove it as a variable by using a sturdy tractor engine for their test program. We frankly have seen little data on true engine friction as affected by rigidity, and, in fact, have seen little data before this paper on true engine friction. While it might be conceded that greater rigidity (in terms of larger bearing areas and larger critical section) would reduce deflections at full-throttle and thus eliminate abnormal rubbing friction, it could also be concluded that the normal friction level would thus be somewhat higher for this more rigid engine. At the same time we must realize that our hard-won part-throttle economy would be penalized by the increased normal friction level of the more rigid engine. Since part-throttle operation in a passenger car still consumes most of the engine operating time, it appears that compromise in engine rigidity is in order so that the engine is not completely overdesigned for most of its operation.

We are hesitant to argue with the authors' data on the potential gains in thermal efficiency obtainable from increased compression ratios. Although much of our data confirms the general trends predicted in this study, direct comparisons become somewhat clouded and obscure because of differences in techniques and objectives. Most of our studies have been conducted on engines of conventional automotive design and have centered around potential efficiency increases obtainable throughout the speed and load range.

We certainly agree, however, with the general philosophy that engine friction should be reduced and the savings passed along to brake power output.

While it is nice to know that indicated power is more than we thought it was because friction is higher than we thought it was, we're still wondering what magic formula the authors suggest for use in obaining the desired friction reduction. Until this formula is forthcoming, we shall be forced to continue measuring brake power, and projecting brake gains from increased compression ratios with existing or projected engine friction levels.

Questions Authors' Findings on Firing Loss

—Edwin E. Nelson
General Motors Corp.

ENGINEERS associated with research, design, and development of automotive engines are familiar with the need for and the desirability of obtaining data on true engine friction. The part of the story that is not known by every engineer is the complexity of this problem. Reliable results can be obtained only after considerable diligence and perseverance are combined with the use of complex and expensive instrumentation. Ethyl Corp. and the authors are to be commended for the effort that was expended on this study and for the helpful conclusions that were produced by their work.

One of the first problems encountered in laboratory testing is that of establishing test conditions. In selecting the engine operating conditions for the determination of engine friction, the authors attempted to simulate normal practice for tractor engine operation. There appear to be two factors here that could cause the magnitude of true engine friction in automotive engines to deviate from true engine friction as found from tests conducted under simulated tractor operating conditions. The first factor is that of constant spark advance over the entire load range. It is obvious that the retarded spark advance which was used for all part-load conditions will cause lower peak pressures and lower average pressures than ignition timing which would give maximum power and economy. Both of these factors, lower peak pressure and lower average pressure, will cause the friction to be lower in the part-load region than if automotive operating conditions were used.

The second condition that may cause friction in automotive engines to deviate from that found by the authors is the use of an air-fuel mixture at full-throttle which will give maximum economy. In automotive engines the general practice is to richen the mixture as full-throttle is approached. Our recent investigations, although not complete at this time, indicate that mechanical friction decreases for conditions of constant load when the air-fuel ratio is changed from lean to rich. Therefore, the difference between full-throttle friction under motoring and fir-

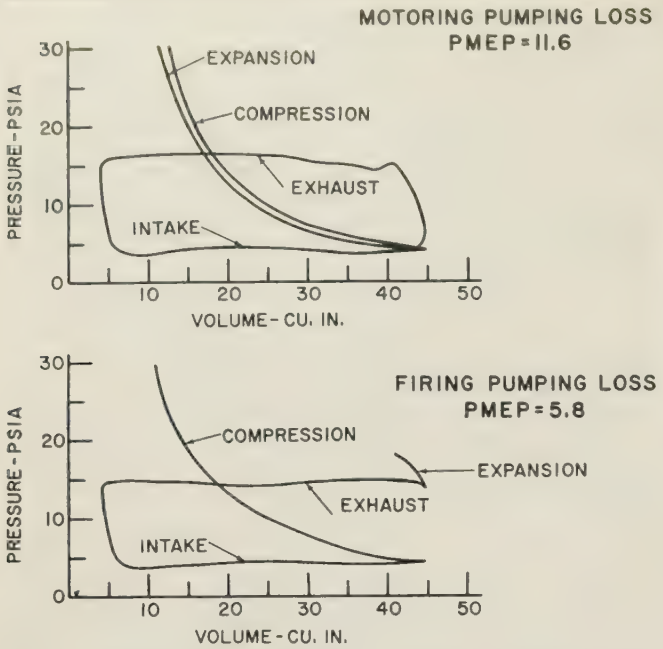

Fig. J—Characteristic pumping loop for part-throttle conditions at 15% load and 2000 rpm

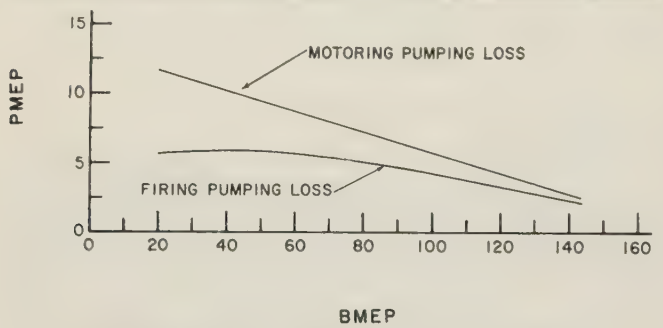

Fig. K—Relationship between motoring and firing pumping losses at 2000 rpm

ing conditions may be less in automotive engines than is indicated by this report.

The problem of establishing appropriate and acceptable definitions of terms for the different portions of the p-v diagram of an engine cycle is very difficult and usually creates considerable controversy. The authors of this paper have done a fine job in choosing suitable definitions. However, there appears to be one place in their paper where rigid use of these definitions has introduced an error. As shown in Fig. 12, the authors have added pumping work under firing conditions to engine friction and call the sum total firing losses. Our contention is that this curve does not represent total firing losses, at least not in the sense of physical losses.

To substantiate this contention we can refer to the author's Fig. 9 and take another look at the areas B and C which constitute pumping work. It must be realized at this time that area C is common to both the area between the compression and expansion strokes and the area between the exhaust and intake strokes. Since one of the latter areas represents the net work done *by* the gas on the piston for two strokes of the cycle and the other represents the net work done *on* the gas by the piston during the other two strokes, the work represented by area C cancels out when one complete cycle is considered. Therefore, the effective pumping loss is represented by area B only. Another way to arrive at this conclusion is to consider that the engine utilizes the work represented by area C during part of each cycle and then is required to expend an equal amount of work during another portion of the cycle; thus,

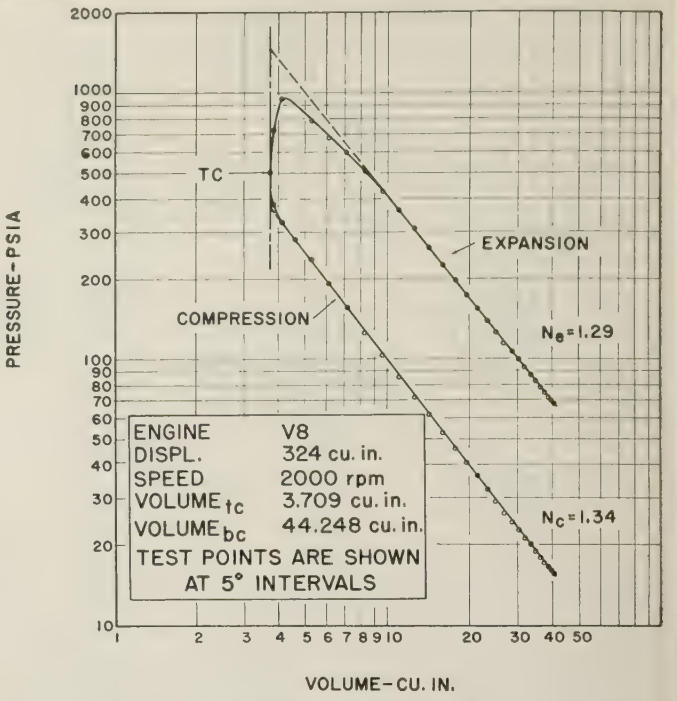

Fig. L—Pressure-volume diagram of compression and expansion processes of 11.9/1 compression ratio engine at full-throttle

area C is not a net physical loss to the engine. It is now clear that the addition of the effective pumping loss, which is smaller than pumping work, to the friction loss will give total engine losses that are lower than those shown by the authors in Fig. 12.

Fig. J shows the effective pumping losses for multicylinder engines as we have defined and measured them under motoring and firing conditions. Fig. K shows a plot of these relationships from light to full load.

Another problem that we would like to discuss is the use of the classical equation for the thermal efficiency of the otto cycle. The authors have modified this equation so that it gives an empirical relationship between compression ratio and indicated thermal efficiency. This empirical relationship is shown to be a convenient means of predicting thermal efficiency and the improvement in thermal efficiency for the range of compression ratios investigated during this study. However, it should be pointed out quite explicitly that the value of n as determined by the method used by the authors is not the exponent of the compression and expansion processes as it is normally considered. The observed exponent n of the compression and expansion processes is considerably higher than the value of n as reported in this paper. Fig. L shows the compression and expansion strokes of a 12/1 compression ratio engine and the values of n that are obtained when these processes are plotted on logarithmic graph paper.

In view of the fact that quite often the arbitrary exponent used to establish an empirical relationship between compression ratio and thermal efficiency is confused with the thermodynamic values of K and n, it is sugested that the arbitrary exponent should be designated by another letter such as a for arbitrary. It is felt that this change would forestall criticism from thermodynamists and at the same time would provide engineers with a suitable equation for predicting the changes in thermal efficiency that result from increases in compression ratio.

This study on the determination of true engine friction has once again emphasized the value of the engine pressure indicator for use in engine studies. The authors, by the use of the balanced-pressure type of engine indicator, have shown that the present method of determining indicated power and indicated thermal efficiency from motoring friction data introduces considerable error.

Authors' Closure To Discussion

PROF. Lay's exhaustive analysis of a typical p-v diagram was prompted by the need for clarification of this rather obscure picture. Although the curves of the diagram clearly trace the pressure path for the four strokes of the cycle, the meaning of the work areas enclosed by the curves is not clear. To understand the work of the cycle it is necessary to examine the individual components of the diagram. Figs. B and C show the work areas representative of individual strokes and phases of the cycle. These help clarify the work of the cycle; Fig. C reveals two important areas, inherent work and pumping work, which are not apparent in the composite diagram. In spite of these clarifications, there can be differences in opinion as to the meaning of the enclosed areas on the composite diagram. Some, including ourselves, differ with Prof. Lay's interpretation of these areas. However, we thing his Figs. B and C present unalterable facts upon which one can judge the correctness of any interpretation.

Mr. Chandler makes the point that if designers have to use larger bearing areas and critical sections in order to reduce deflections at full throttle and thus eliminate abnormal friction, these changes might increase the normal friction level and thereby penalize part-throttle economy. This might be true in some cases. On the other hand, a detailed study of minimum design changes required for ample rigidity will probably show no need for large increases in bearing areas and critical sections in most cases. For example, we are inclined to believe that one of the main causes of abnormal friction at high compression ratios in many engines is piston deformation, and that the necessary stiffness could be incorporated in the piston without unduly increasing the weight.

Mr. Nelson states that from his observations mechanical friction decreases with enrichened air-fuel ratio. Our data at rich mixture ratios, although limited, seem to confirm this. At least, they indicate that at the same peak cylinder pressure friction is slightly lower with rich mixture than with lean mixture. The reasons for this are not too clear at the moment.

In connection with the effect of using fixed ignition timing at all loads, it is believed that this procedure has little effect on establishing a curve of friction versus bmep (Fig. 11). Advancing the ignition timing at part throttle would increase the friction because of the higher cylinder pressure. However, the bmep would also be greater. The coordinates of the new value would, therefore, be displaced not only upward but also to the right of the original point. The displacement to the right would be greater than the displacement upward, since bmep increases more rapidly than friction mep. As a result, the point would probably be located higher on the same curve.

Mr. Nelson has further suggested that values shown by the upper curve in Fig. 12 are too high because we have added **all** of the pumping work to the mechanical friction to obtain these values. He believes only part of the pumping work (area B of Fig. 9) should be added. This area is the familiar negative loop of the customary p-v diagram. He refers to this smaller quantity of work as the "effective pumping loss."

This concept of "effective pumping loss" is shared by many others. It appears in Prof. Lay's discussion and in some text books. We subscribed to it early in our studies but careful consideration of the real meaning of the areas of a p-v diagram convinced us that the area in the negative loop is a meaningless segment of the pumping work area, left after the cancellation of overlapping positive and negative areas. Likewise, we believe the area in the positive loop is a large meaningless segment of the inherent work area.

To substantiate this we refer to Fig. C. In this figure, the p-v diagram is divided into two phases in order to clarify the meaning of the work areas. The area between the compression and expansion curves represents the power phase or inherent work of the cycle, and the area between the exhaust and intake curves represents the pumping phase. In the customary p-v diagram these areas are mutilated by cancellation, and lose their meaning. Fig. C contains all the information needed to analyze the cycle, even though areas such as A and B of Fig. 9 (which are the familiar positive and negative loops) are nowhere to be found. If p-v diagrams had always been plotted like Fig. C, the areas enclosed by the loops would probably never have been recognized and invested with special meaning.

When the two net areas of Fig. C are superimposed on the same coordinate system, we get a diagram similar to Fig. 9. The two areas happen to overlap in the region marked C; however, the overlapping and cancelling out cannot in any way reduce the work required to pump the charge in and out of the cylinders. The cancelling out merely indicates that part of the work expended in the pumping phase is offset by an unequal amount of work generated in the power phase. The amount of pumping work offset by the overlapping of the two areas is of no significance whatever, because **all** the pumping work is offset or cancelled out during the course of one complete cycle, in spite of the fact that the positive power phase does not completely overlap the negative pumping phase on the p-v diagram. We believe the fallacy in the concept of "effective pumping loss" is its assumption that only area C is offset. If we can say the effective pumping loss is area B because area C is offset, we can say just as logically that the effective pumping loss is zero because the pumping phase is completely offset during the cycle. Therefore, we see no justification for assigning such a meaning to area B, and believe Fig. 12 is correct as shown.

Data from Fig. J, showing part-throttle pumping diagrams for motoring and firing conditions, are in good agreement with ours if interpreted the same way. Let us compare total pumping work under the two conditions. If we mentally erect a vertical line on the right side of the firing diagram to enclose the area between the exhaust and intake curves we can see at a glance that the area is practically the same under firing conditions as under motoring conditions. As a result, the firing pumping loss curve in Fig. K would lie very close to the motoring pumping loss curve as in our Fig. 12.

The validity of the firing data in Fig. 12 can be further demonstrated by use of Fig. G. In this diagram we would construe "input to pistons" to mean the net input during compression and expansion strokes as represented by the power phase area in Fig. C. This quantity is the inherent work. The "gas friction loss" is the total pumping work represented by pumping phase area in Fig. C and lower curve in Fig. 12. The "mechanical friction loss" is represented by the middle curve in Fig. 12. If we add the two losses we get the top curve in Fig. 12. According to the energy flow diagram, the sum of the two losses plus the brake work must equal the input or inherent work. When we add the total loss from Fig. 12 to the brake work we do get the inherent work, thus demonstrating the validity of the relations in Fig. 12.

Although we disagree with Mr. Nelson on his concept of effective pumping loss, we are indebted to him for raising an issue which deserves the thorough airing given it here, and the serious consideration of those interested in evaluating the pumping losses of their engines. In road load operation the pumping work is an important loss. We believe that the negative loop is a gross understatement of the loss under these conditions. Fig. J indicates that the negative loop on the firing diagram represents little more than half of what we consider to be the true pumping loss.

In regard to the empirical exponent n that we use in the classical equation for thermal efficiency of the otto cycle, Mr. Nelson is quite correct in pointing out that it is not the exponent of the compression or expansion processes. The equation becomes an empirical relation whose exponent cannot be used to evaluate the compression and expansion curves. We readily agree with his suggestion that the empirical value of n be designated by some other letter such as a, to prevent its meaning being confused with that of the commonly used thermodynamic values of k and n.

SIMULATION OF A FREE-PISTON ENGINE

D. R. Olson, Yale University,
Consultant to Mechanical Development Department, General Motors Corp

This paper was presented at the SAE Annual Meeting, Detroit, Jan. 14, 1958

THE free-piston engine, unlike the crank engine, has pistons that oscillate without direct mechanical control. In this way the pistons transfer energy between the several processes that occur simultaneously in the engine. This is to be contrasted with the crank engine where the crankshaft and flywheel serve to transfer and store energy between the processes that occur successively in the engine. The forces which act on the free pistons to produce the oscillating motion are due mainly to gas pressures in the engine. If the basic engine dimensions are not compatible the gas pressures produce a piston motion that exceeds the limits of operation. In addition, the engine is normally started during a single initial stroke under conditions far different from those used in normal operation. The engine dimensions must also be correct for this starting process.

For these reasons, a thermodynamic study of engine processes is needed to determine the more desirable basic engine dimensions. Such an analysis, if realistic, can also be used to predict the operating characteristics of any engine. Further, some phases of engine operation are difficult to study unless both test and analysis results are available.

Several studies of the free-piston engine process have been presented in this country and in Europe. In some of these studies,[1,2,3] a thermodynamic analysis was made of the process. The object of these studies was the prediction of the maximum efficiency and power that could be expected from a given engine. In this sense they have been useful and in addition they have focused attention upon some of the more important parameters that influence the efficiency of the engine.

For the design and study of a particular engine, however, a more complete analysis must be made. Each process must be studied with respect to the functioning of the engine and the thermodynamic analysis must be augmented with a dynamic study of piston motion. Studies of this latter type have been presented and many of the concepts first shown by Eichelberg[4], Huber[5,6], London and Oppenheim[7] are utilized in this paper.

The purpose of the work presented here was to formulate a general analysis of the free-piston engine process which would realistically "simulate" an operating engine. The analysis was made in terms of variables which, first, allow the basic engine size and configuration to be selected and, second, allow the operating conditions for the hypothesized engine to be arbitrarily fixed. For these conditions, a solution from the analysis gives a numerical description of the performance to be expected of the engine.

The Engine

The basic design of the engine treated in this analysis is termed an "inward compression machine." A cross-sectional sketch (Fig. 1) shows the basic configuration. The engine operates with a back pressure of considerable magnitude and it produces work only in the sense that it supplies high-pressure combustion products to operate the gas turbine. The

[1] ASME Transactions, Vol. 77, February, 1955, pp. 197–210; "Free Piston-and-Turbine Compound Engine—A Cycle Analysis," by A. L. London.
[2] ASME Transactions, Vol. 78, October, 1956, pp. 1757–1764: "Supercharged-and-Intercooled Free-Piston-and-Turbine Compound Engine," by A. L. London.
[3] "Part-Load Characteristics for Free-Piston-and-Turbine Compound Engine," by A. L. London. Technical Report FP-5, Department of Mechanical Engineering, Stanford University, Stanford, Calif., November, 1957.
[4] *Genie Civil*, Vol. 125, November, 1948, pp. 430–434: "Lee générateurs de gaz à pistons libres," by G. Eichelberg.
[5] *Journal of American Society of Naval Engineers*, Vol. 62, May, 1950, pp. 259–274: "Operational Stability of Free-Piston Gasifiers," by R. Huber.
[6] *Journal de la Société des Ingénieurs de l'Automobile*, Vol. 24, December, 1951, pp. 267–274: "Les Générateurs de gaz à pistons libres," by R. Huber.
[7] ASME Transactions, Vol. 74, 1952, pp. 1349–1361: "Free-Piston Engine Development—Present Status and Design Aspects," by A. L. London and A. K. Oppenheim.

WITH A DIGITAL COMPUTER

output is usually measured in terms of gas hp.

Atmospheric air is inducted into the two air compressor cylinders on the outward stroke of the two pistons (the motion of the two pistons is synchronized with suitable linkages). The air is then compressed during the inward stroke and discharged into the air box through valves in the valve plate. As the pistons are pushed outward by the high pressure gases in the combustion chamber, the exhaust ports are uncovered first and a portion of the combustion products flows into the exhaust collector. The inlet air ports are uncovered next and air flows from the air box into the combustion cylinder where it serves to scavenge the remaining combustion products from the cylinder through the exhaust ports. As the pistons move inward again, both the inlet air and exhaust ports are covered and fresh air is trapped in the combustion chamber for the succeeding diesel combustion process. Air trapped in the bounce chambers serves to keep the two pistons in motion.

As the engine-turbine combination is operated over the load range the turbine inlet pressure (engine exhaust pressure) must change from a maximum value at full load down to nearly zero for idling conditions. This is accomplished primarily by controlling the quantity of fuel injected into the diesel combustion chamber. Additional control is needed, however. It is provided in two ways:

1. The mean pressure in the bounce chambers is controlled so that the piston motion tends to remain within the operable limits. As the fuel rate is increased, the outer limit of piston motion (outer deadpoint, odp) moves outward. In order to keep the stroke within limits, additional air is then admitted to the bounce chambers from the air box. For low fuel flow rates the opposite effect must be achieved; air is released from the bounce chambers to ensure that piston motion is greater than the operable minimum, that is, the engine will stall if the ports are not sufficiently uncovered. This control of the bounce chamber air is accomplished by the engine stabilizer. (See Fig. 1.) It is actuated by the pressure in the air box which is directly related to the engine back pressure for most engine operating conditions.

2. The gas flow rate produced by the engine, at

FOR the design of a given free-piston engine, each process must be analyzed with respect to the functioning of the engine. This thermodynamic analysis must then be augmented with a dynamic study of piston motion.

The purpose of the research described in this article was to formulate a general analysis of the free-piston engine process which would realistically simulate an operating engine.

The analysis was made in terms of variables which allowed the basic engine size and configuration to be selected and the operating conditions for the hypothesized engine to be arbitrarily fixed. For these conditions, a solution from the analysis gives a numerical description of the performance that may be expected of the engine.

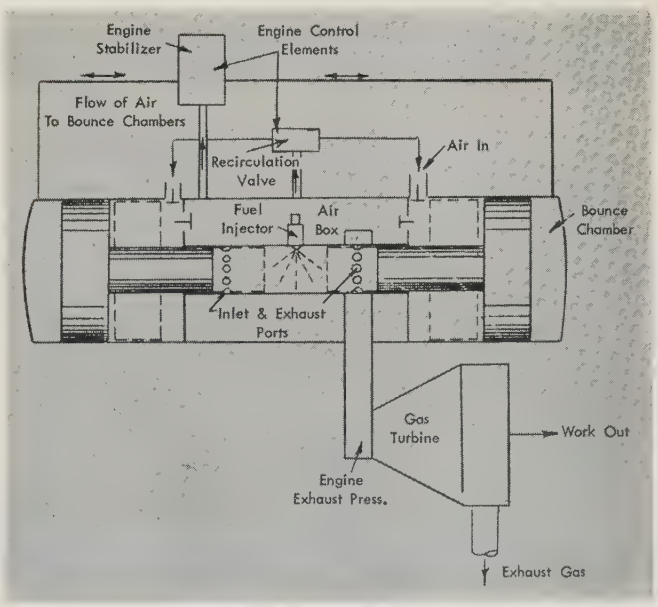

Fig. 1—Free-piston engine gas turbine combination

low engine back-pressures must be drastically reduced to match the flow characteristics of the turbine. This may be accomplished either by restricting the flow of air into the air compressors (throttling) or by recirculation. The latter procedure consists of recirculating a portion of the compressed air from the air box back to the intake of the compressors. (See Fig. 1.)

Engine Processes

During each cycle of piston motion several processes occur simultaneously within the engine:

Bounce Chamber—The air trapped in the bounce chambers is simply compressed and then expanded as the pistons move through a cycle of motion. The process can be represented on pressure-stroke coordinates as shown by the solid curves in Fig. 2. If the compression and expansion occurs without leakage and subject to reversible heat transfer processes, then the processes 1-2 and 2-3 as shown in Fig. 2 would be superimposed. For other engine operating conditions the path of the process (Fig. 2) can be substantially changed. The path A, for instance, would represent the situation when the engine was operated with a higher bounce-chamber pressure. Additional air has been admitted to the bounce chamber to increase the mean pressure and the piston stroke has been increased. Also, the innermost point of piston travel (inner deadpoint, idp) would change, which produces a piston motion over a different portion of the cylinder. Path B represents the opposite effect.

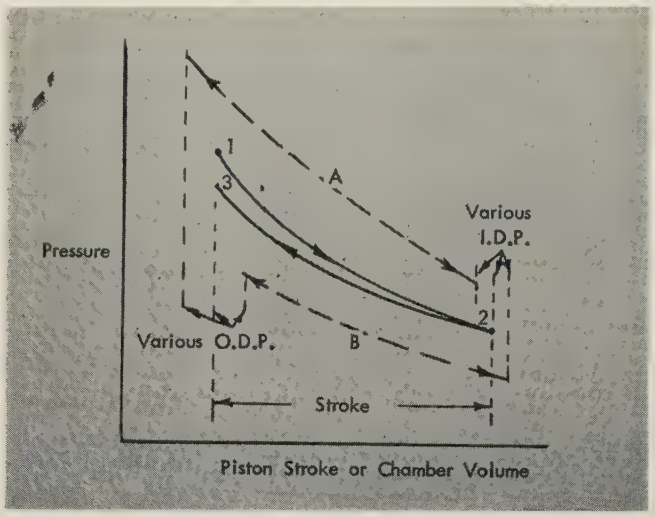

Fig. 2—Bounce-chamber process

Air Compressor—The air inducted into the engine is compressed and then delivered into the air box. The compressor section of the engine operates in a manner similar to an orthodox piston-type compressor but with important differences. For a given operating condition the pressure-stroke history in the air compressor for one cycle of piston motion may be represented as shown by the solid curves in Fig. 3. Process 1-2 represents a simple compression process. Delivery of air into the air box begins at point 2 and this pressure is variable depending upon the engine back pressure. The pressure increases during delivery (process 2-3) because the volume of the air box is relatively small and no air escapes from the air box during the delivery process. Process 3-4 represents a simple expansion process for the clearance air in the compressor and the induction process is represented by 4-1 . This picture of the compression process is somewhat simplified.

Once again for other engine operating conditions this picture of the compression process may be considerably altered. If the engine back pressure is increased, the odp increases and the compression process begins earlier (point 1′, Fig. 3). The pressure when delivery begins changes and idp also changes. (See dashed curves, Fig. 3.) A lowering of the engine back pressure produces other similar changes. If the inlet air is throttled, then the pressure during the induction process is lowered.

Power Cylinder—The processes which occur in the power cylinder are similar to those of a 2-stroke diesel engine but subject once again to important differences. The solid curves (Fig. 4) represent the pressure-stroke history for a given condition. Fresh air is trapped in the cylinder upon the covering of the exhaust ports (point 1, Fig. 4). As the pistons move inward the air is compressed (process 1-2). At point 2 fuel begins to flow from the injection nozzle and injection continues for some period of time (points 2-3). The ensuing combustion combined with further piston motion causes the pressure to rise—finally the pistons stop (idp) and as the pistons move outward the combustion process continues as the products of combustion expand. Upon the uncovering of the exhaust ports, the combustion products flow into the exhaust collector (points 4-5). As

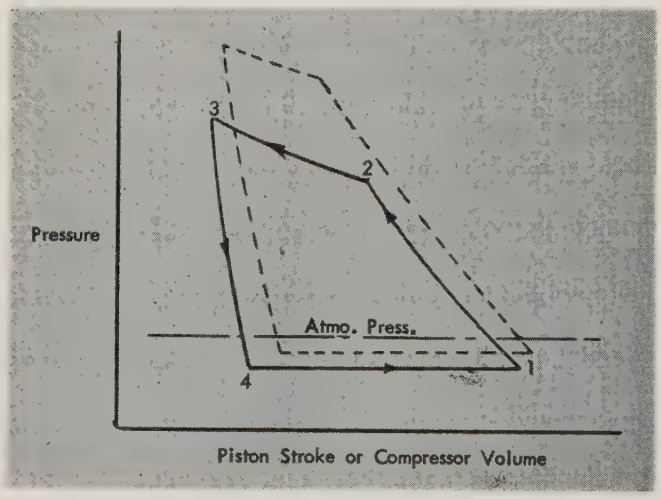

Fig. 3—Air compressor process

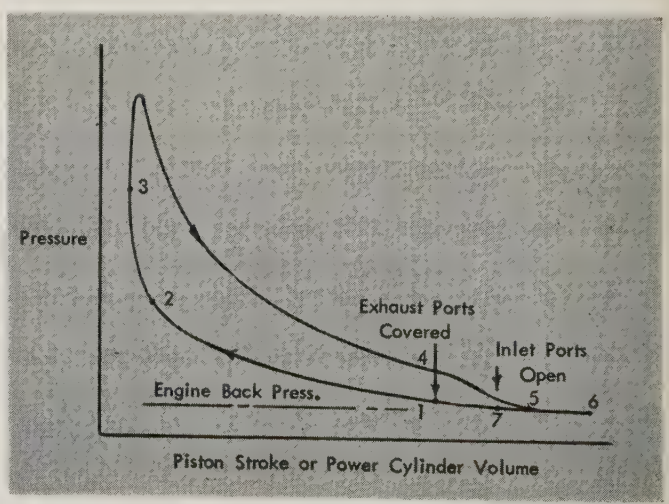

Fig. 4—Power cylinder process

the inlet air ports are uncovered air flows through the power cylinder from the air box, scavenging the cylinder. Scavenging can continue as the pistons move to odp and back to the point where the inlet air ports are again covered (points 5-6-7). As in the previous cases, this picture of the power cylinder changes radically for other operation conditions.

Analysis

The motion of the engine pistons serves as a useful focal point in the examination of engine operation. The energy exchange between the three basic engine processes described above occurs as a result of piston motion. The quantity of air delivered by the air compressor is directly influenced by the piston motion. Indeed, it is found that all of the desired performance results may be computed directly from the piston motion-time history.[8]

One of the pistons may be considered as a mass upon which a variety of forces act. If these forces are not completely in equilibrium, the piston will accelerate according to Newton's Law. The forces considered in this analysis, mainly the result of gas pressures, are indicated in Fig. 5. The forces F_1, F_2, and F_3 represent the forces acting on the piston in the bounce chamber, air compressor, and power cylinder respectively. The forces F_4 and F_5 represent friction effects that depend upon the direction of piston motion. The position of the piston is measured with respect to the fixed x axis (Fig. 5). x is chosen as zero when the piston is near the outer limit of travel and increases as the piston moves inward.

The basic dimensions of the engine may now be notated. The notation refers to a given piston position, that is, $x = 0$. The design of the engine for the analysis may be completely stated in terms of eight design parameters. (See Fig. 5.)

Design Parameters

a = Size of bounce chamber
b = Size of air compressor
c = Size of air box
d = Size of power cylinder
e = Position of exhaust ports
D_1 = Bore of air compressor cylinder
D_2 = Bore of power cylinder
M = Mass of piston assembly

The equations of motion for the piston may be written as:

$$M(d\dot{x}/d\theta) = \Sigma \text{ Forces} = F_1(x) - F_2(x) - F_3(x) - F_4(\dot{x}) \mp F_5 \quad (1)$$

$$dx/d\theta = \dot{x} \quad (2)$$

The gas pressures in the various parts of the engine furnish the means for the evaluation of the force functions. For F_1, F_4, and F_5 single expressions can be used which are valid for all piston positions:

$$F_1 = C_1/(a+x)^{n_1} \quad (3)$$

$$F_4 = C_4\dot{x} \quad (4)$$

$$F_5 = C_5 \quad (5)$$

where the constants C_1, C_4, and C_5 are functions of the operating conditions. (See Table 1.)

For the evaluation of F_2 and F_3, a more complicated situation exists. The pressures in the compressor and the power cylinder cannot be represented with a single expression for a cycle of piston motion. A sketch of F_2 and F_3 for various pistons is shown in Fig. 6. Four separate idealized processes have been used to simulate what occurs in the compressor. The processes are related but the transition from one process to another is discontinuous because of the action of the intake and exhaust valves. A similar situation exists in the power cylinder.

The forces F_2 and F_3 must, therefore, be evaluated differently for various piston positions:

a. $F_{21} = C_{21}/(b-x)^{n_{21}}$ $\quad x_0 \leq x \leq x_2$ for $\dot{x} \geq 0$ (6)
b. $F_{22} = C_{22}/(b+c-x)^{n_{22}}$ $\quad x_2 \leq x \leq x_i$ for $\dot{x} \geq 0$
c. $F_{23} = C_{23}/(b-x)^{n_{23}}$ $\quad x_i \geq x \geq x_3$ for $\dot{x} \leq 0$
d. $F_{24} = C_{24}$

a. $F_{31} = C_{31}$ $\quad x_0 \leq x \leq x_1$ for $\dot{x} \geq 0$ (7)
b. $F_{32} = C_{32}/(d-x)^{n_{32}}$ $\quad x_1 \leq x \leq x_4$ for $\dot{x} \geq 0$
c. $\dfrac{dF_{33}}{d\theta} = \dfrac{1}{(d-x)}\left[kF_{33}\dot{x} + (k-1)AC(\theta^*)\right]$ $\quad x_4 \leq x \leq x_i$ for $\dot{x} \geq 0$ and $x_i \geq x \geq x_1$ for $\dot{x} \leq 0$
d. $F_{34} = C_{31}$ $\quad x_1 \geq x \geq x_0$ for $\dot{x} \leq 0$

where the constants C_{21}, C_{22} and such, and the intermediate limits x_1, x_2, x_3, and x_4 are functions of the operating conditions and design parameters. (See Table 1.)

Except for Equation 7c, the force Equations 3–7

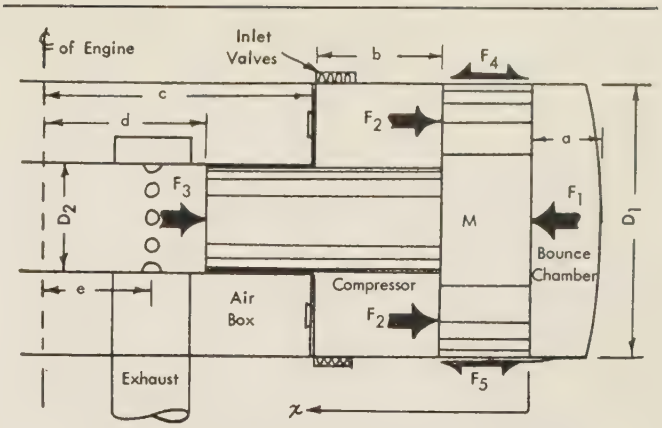

Fig. 5—Sketch of engine showing forces and dimensions considered in analysis

Table 1—Definition of Force Function Constants and Limits

Constant	Definitions
C_1	$(\pi/4)D_1^2P_a b a^{n_1}$
C_{21}	$(\pi/4)(D_1^2 - D_2^2)P_a(1-\Delta P_1)(b-x_0)^{n_{21}}$
C_{22}	$\dfrac{(\pi/4)(D_1^2 - D_2^2)P_b(b+c-x_2)^{n_{22}}}{(1-\Delta P_2)(1-\Delta P_3)}$
C_{23}	$\dfrac{(\pi/4)(D_1^2 - D_2^2)P_b(b-x_i)^{n_{23}}}{(1-\Delta P_2)(1-\Delta P_3)}\left[\dfrac{b+c-x_2}{b+c-x_i}\right]^{n_{22}}$
C_{24}	$(\pi/4)(D_1^2 - D_2^2)P_a(1-\Delta P_1)$
C_{31}	$(\pi/4)D_2^2P_b/(1-\Delta P_3)$
C_{32}	$(\pi/4)D_2^2e^{n_{32}}P_b/(1-\Delta P_3)$
C_4	Coefficient of viscous friction
C_5	Static friction force
$C(0^*)$	Energy release rate function (See Appendix II)
ΔP_T	$(P_a/P_b)(1-\Delta P_1)(1-\Delta P_2)(1-\Delta P_3)$
x_1	$d-e$
x_2	$b[1-(\Delta P_T^{1/n_{21}}) + x_0(\Delta P_T)^{1/n_{21}}$
x_3	$b-(b-x_i)\left[\dfrac{b-x_0}{b-x_2}\right]^{n_{21}/n_{23}}\left[\dfrac{b+c-x_2}{b+c-x_i}\right]^{n_{22}/n_{23}}$
x_4	Point where simulated combustion process begins

[8] In contrast, Frey, Klotsch, and Egli have presented an analysis based on an "energy balance equation for inboard and outboard strokes" of the free-piston engine. SAE Transactions, Vol. 65, 1957, pp. 628–634: "Automotive Free-Piston-Turbine Engine," by D. N. Frey, P. Klotsch, and A. Egli.

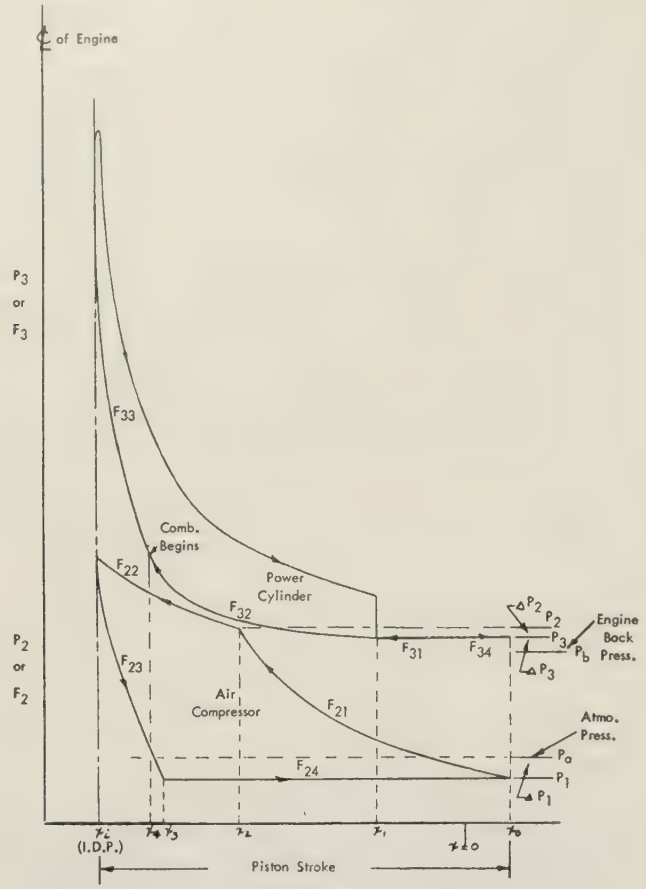

Fig. 6—Sketch of simulated processes used for air compressor and power cylinder

are simple functions which can be substituted directly into Equation 1. They have been obtained with the assumption that the various compression and expansion processes can be suitably represented with polytropic-type expressions.

The combustion process accounts for the differential equation, 7c. The process is simulated by a continuous addition of energy to the contents of the power cylinder. The process begins at x_4 (Fig. 6) upon the start of simulated fuel injection; it continues up to x_i (idp) and on to the time when the exhaust ports are uncovered. (See Appendix II.)

The role of the pressure losses included in the analysis is shown on the right of Fig. 6. The first loss occurs as atmospheric air flows through the compressor inlet valves. This effect is included in the analysis by expressing this pressure loss in terms of the percentage of the upstream pressure which is lost as a result of the friction process. Thus, the pressure at the start of compression P_1 may be written as:

$$P_1 = (1 - \Delta P_1)\, Pa \qquad (8)$$

In a similar manner the pressures, P_2 and P_3, can be obtained in terms of engine back pressure, P_b.

Upon the selection of values for the design parameters and operating conditions to represent a given engine, all of the constants in the force equations may be evaluated and these equations may be incorporated into Equation 1. The equations of motion for the piston may then be written as:

$$dx/d\theta = f_1(x, \dot{x}) \qquad (1)$$

$$dx/d\theta = \dot{x} \qquad (2)$$

$$dF_{33}/d\theta = f_2(F_{33}, x, \dot{x}, \theta), \text{ valid for combustion process} \qquad (7c)$$

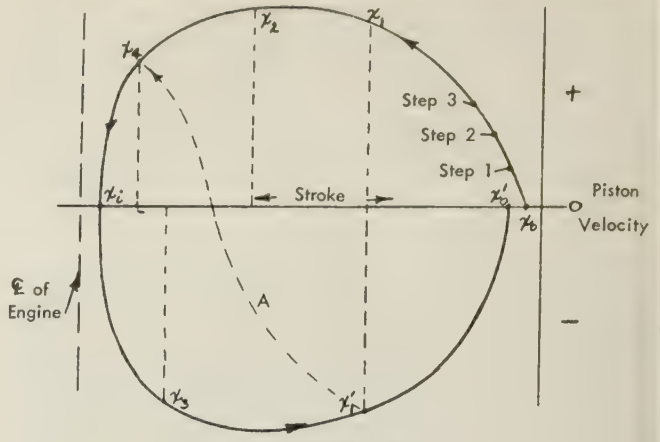

Fig. 7—Piston motion

A solution compatible with the complex nature of f_1 and f_2 may now be contemplated.

Solution

The diverse nature of the expressions obtained for the forces, specifically Equations 6 and 7, thwart any hope for a general solution of the equations of motion. Particular solutions can be obtained, however, with numerical methods. The method of Runge-Kutta was employed and the problem was programmed for the IBM 704 digital computer.

A small time change, $\Delta\theta$, was taken as the independent variable for the calculation of each small step in the development of the solution. The solution was begun at x_0 (Fig. 6) where the initial value of $\dot{x}$ equals zero. The initial value of x_0 must be assumed since the odp for the operating conditions and engine configuration, is not known. Starting from these initial conditions, the piston motion in terms of position, velocity, and acceleration is charted in successive small steps (Fig. 7).

As each of the intermediate limits x_1, x_2, and such is reached the proper force function is substituted, F_{22} for F_{21}, and so forth, in Equation 1. When x_4 is reached, signalling the beginning of combustion, the differential equation 7c is included with the equations of motion 1 and 2 for simultaneous solution. x_i (idp) is located when $\dot{x}$ equals zero.

As the solution is continued x_0 is again reached and a check on the validity of the initial assumption for x_0 can be made. If x'_0 is sufficiently close to x_0, then the solution is complete. If a closer check is desired, then a new solution can be obtained by using x'_0 in place of x_0. This procedure is continued until odp is located with the desired accuracy (Fig. 8). The final checked solution represents the steady state operating condition.

An additional iterative process is required in the course of the solution described above. It concerns the simulated combustion process. In the specification of the $C(\theta^*)$ function in terms of the fuel flow rate, Equation 7c, the total time required for the piston to travel from x_4 to x_i and on to x'_1 must be assumed. During each solution this time interval as predicted by the solution is compared with the assumed value. If a correction is needed, the value of the combustion time constant, A, Equation 7c, is changed and the solution reverts to x_4 for a re-run of the combustion process. This procedure is indicated in Fig. 7 by the dotted path A. In a typical

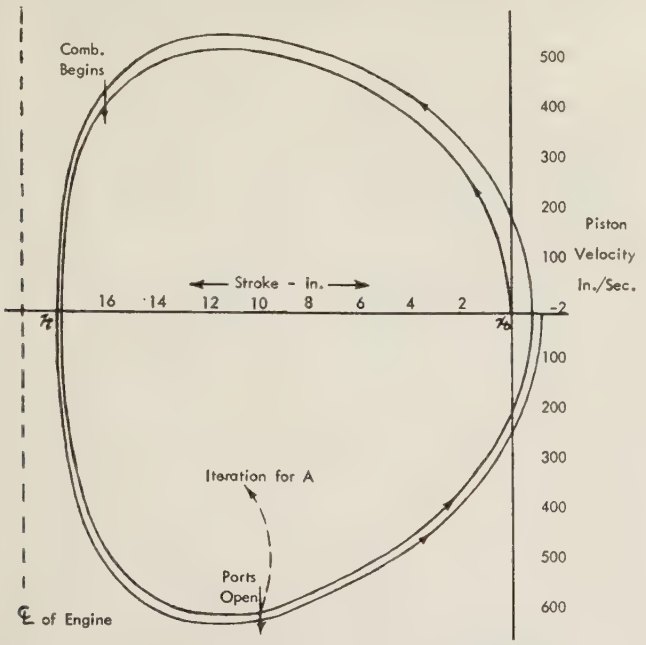

Fig. 8—History of piston motion during solution

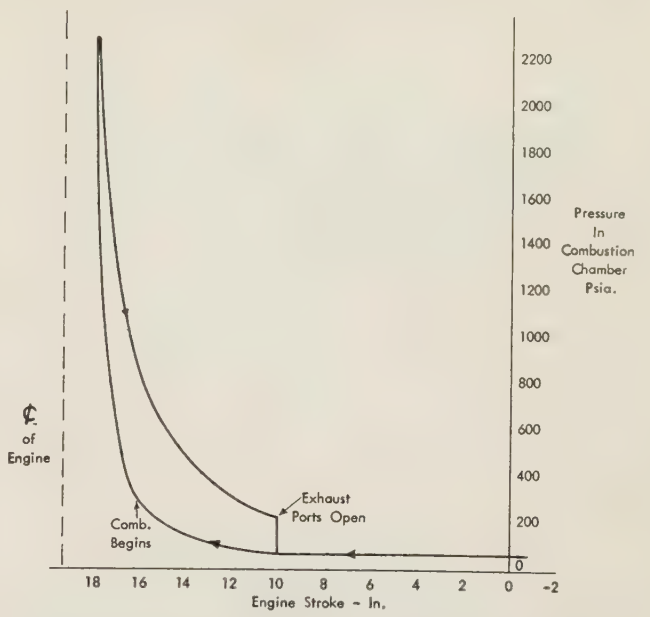

Fig. 9—Pressure-stroke diagram for simulated combustion process

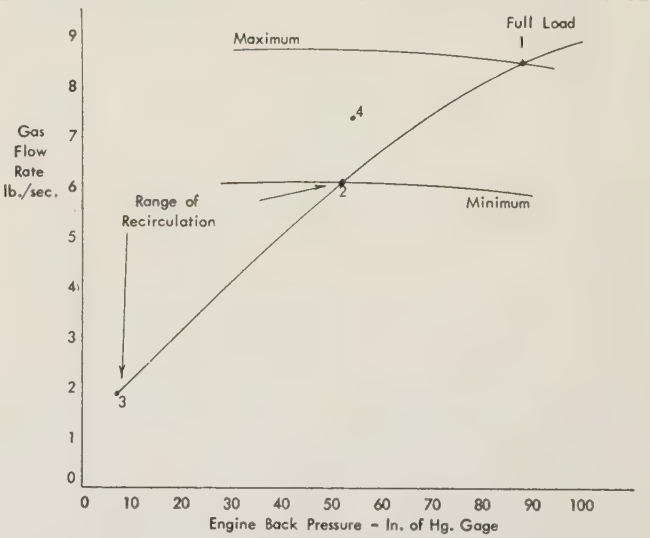

Fig. 10—Flow characteristics for 1000-hp free-piston engine—gas turbine combination

solution three "*A*" loops are required for each simulated combustion process. Obviously, a new combustion process must be simulated for each solution of a cycle of piston motion.

A diagram of the complete history of a single solution of the equations of motion (Fig. 8) illustrates the general nature of the procedure. The pressure-stroke diagram of the power cylinder for the final solution (Fig. 9) illustrates the realistic nature of the simulated combustion process. It is evident that the solution depends upon several factors which might be termed computation constants. The allowable error for x_0 and the step size, $\Delta\theta$, are examples. If these values are made very small the solution will be accurate but the amount of computation required will be very large. If the values are made large, the computation will be greatly reduced and the accuracy will be sacrificed. Solutions in which only these factors are varied, one at a time, enable feasible values to be chosen for computation parameters.

Computed Engine Performance

The solution of the equations of motion provides the necessary information for the evaluation of engine performance. The details of these calculations are shown in Appendix III. The actual calculations are performed by the computer, with two exceptions, from the results obtained for the final checked solution (Fig. 8). The following results are obtained, taking into account any specified amount of recirculation or inlet throttling which may occur.

Performance Results

1. History of piston motion, position, velocity, and acceleration as a function of time.
2. Inner dead point, idp, in.
3. Outer dead point, odp, in.
4. Stroke, in.
5. Speed, N, cpm
6. Gas flow rate, lb per min
7. Air inducted, N_S, lb air per stroke.
8. Air trapped, N_T, lb air per stroke.
9. Scavenging ratio, S, lb air into combustion chamber/lb air trapped.
10. Air temperature prior to release, T_R, deg R
11. Maximum combustion-chamber pressure P_m, psia
12. Fuel flow rate, F, lb per min

Results Computed by Hand

13. Gas hp
14. Gas specific fuel consumption

Comparison of Computed Results with Engine Results

When a gas turbine is connected to the exhaust line of a free-piston engine, the engine must operate under an additional constraint. For now, in addition to the control imposed by the stabilizer and provision for recirculation or throttling, the gas flow rate produced by the engine must be a unique function of the engine back pressure. The turbine flow characteristics establish this function and only small variations for different engine exhaust temperatures are possible. Even these small variations cannot exist, however, for the engine exhaust temperatures are uniquely fixed for given gas flow rates and back pressures. For these reasons an engine-

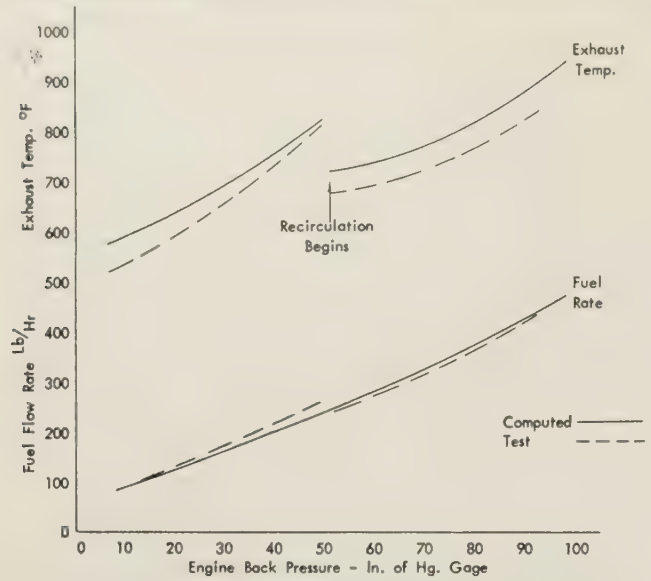

Fig. 11—Comparison of computed results with engine performance

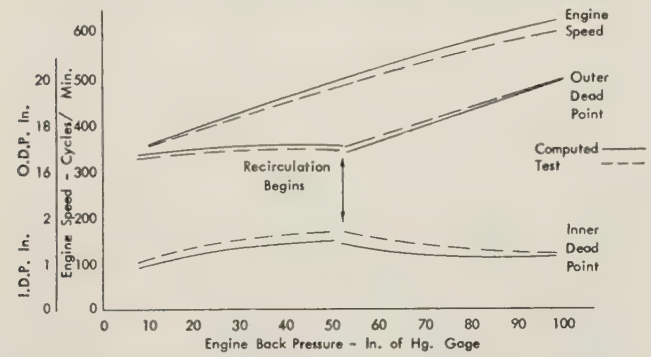

Fig. 12—Comparison of computed results with engine test performance

turbine combination operates over the load range with a unique relationship between the gas flow rate and engine back pressure.

An example of this relationship is shown in Fig. 10 for an operating unit with a rated output of 1000 hp. As the unit operates over the load range from the rated condition (1) to a part load condition (2), the engine stroke varies from the maximum allowable value to the minimum stroke condition. No recirculation is required for this part of the load range. From condition (2) down to (3) recirculation is used in increasing amounts to achieve a compatible flow characteristic between the engine and turbine. Minimum engine stroke is maintained throughout this portion of the load range. A part load condition such as (4), could not be produced with the engine-turbine combination even though the engine could operate under these conditions (Fig. 10).

Now, in order to compare the computed results with engine test results, the control imposed on the actual engine in the form of stabilizer design, turbine characteristics and provision for recirculation must be duplicated in the computed results. The engine simulated with the computer operates with no control save that provided by the values given the operating conditions. The computed results were obtained using representative values for all of the fixed design parameters and operating conditions. These operating conditions controlled the

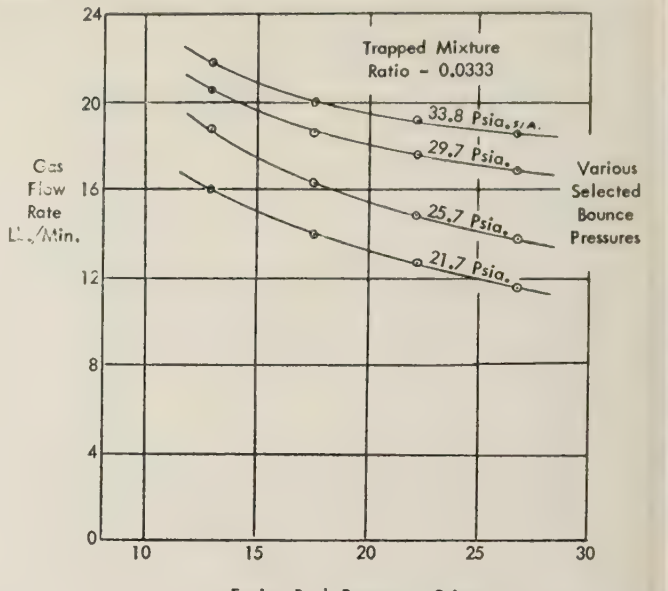

Fig. 13—Computed performance for free-piston engine

computer simulation in a manner identical to the regulation imposed upon the operating engine.

1. The selected bounce pressure, P_{sb}, was made equal to the test value in all cases. This is a function of stabilizer design.

2. The fuel injection timing was used to fix x_4 according to test conditions.

3. The pressure losses attributed to the several values and ports were adjusted from the values used at full load according to the gas flow rates at all part-load conditions.

4. At each of several engine back pressures the flow rate of the fuel was varied in successive simulations until the gas flow rate predicted by the simulation equalled the test value as shown in Fig. 10.

The results of the computer simulation are compared with the engine test results in Figs. 11 and 12.

Prediction of Free-Piston Power Unit Performance

The general problem of using the computer simulation to predict the performance of an engine-turbine combination is complicated by the necessity of control, as the previous section illustrates. The main control elements may be listed as:

1. The turbine—fixes the relationship between the gas flow rate and the engine back pressure.

2. The stabilizer—fixes the relationship between the selected bounce-chamber pressure and the engine back pressure.

3. Recirculation or throttling—can be used to control the gas flow rate independently.

4. Fuel rate—the unit's main independent control.

Disregarding the control imposed by the turbine for the moment, a series of solutions can be obtained which illustrate the nature of the relationship between the selected bounce-chamber pressure and the engine back pressure (Fig. 13).

These results apply to a particular simulated engine and were obtained with the trapped fuel-air mixture ratio maintained constant.[9] Similar results

[9] Equation 7c may be written as follows:

$$\frac{dF_{33}}{d\theta} = \frac{1}{(d-x)}\left[kF_{33}\frac{dx}{d\theta} - (k-1)N_T AC(\theta^*)\right]$$

where the inclusion of the air trapped in the combustion chamber, N_T, permits $C(\theta^*)$ to be specified in terms of the mixture ratio rather than the fuel flow rate.

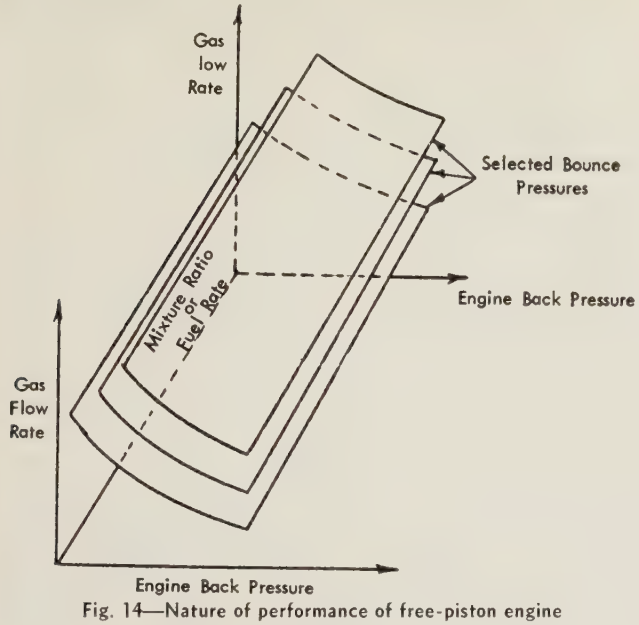

Fig. 14—Nature of performance of free-piston engine

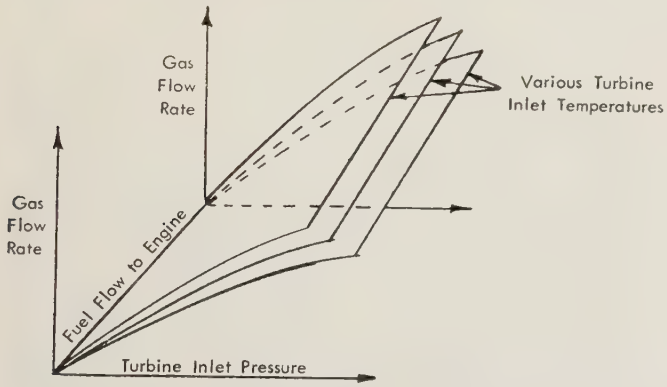

Fig. 15—Flow characteristics of gas turbine

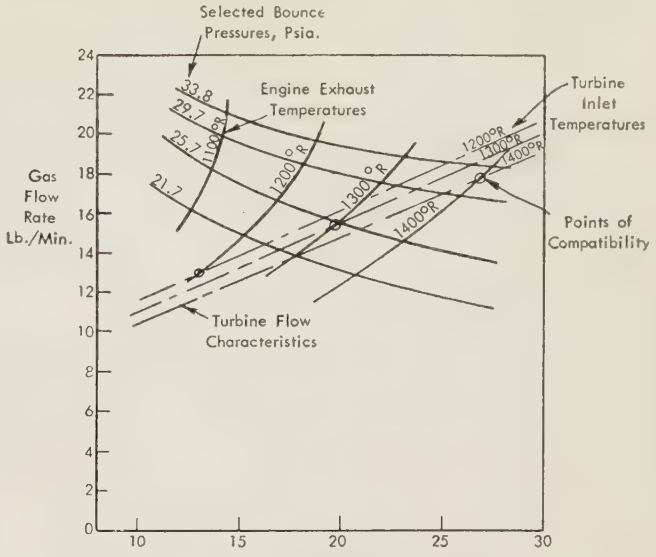

Fig. 16—Combined plot of computed engine and turbine flow characteristics

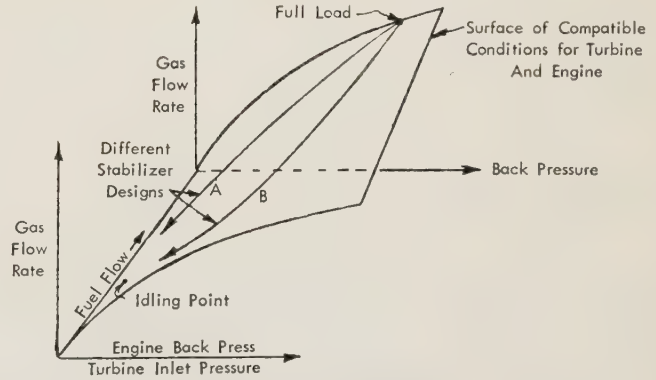

Fig. 17—Nature of region where engine and turbine can operate in combination

could have been obtained for a given fuel flow rate. Obviously, all of the performance results such as, engine stroke, speed, exhaust gas temperatures, specific fuel consumption, and the like, are available from the solution for each of the points shown in Fig. 13. In this particular discussion, however, the gas flow rate is the most important characteristic.

The larger picture may now be obtained by adding another dimension to the results indicated in Fig. 13. This requires results of the same type for various values of the fuel flow rate or mixture ratio, as illustrated in Fig. 14. Each selected bounce pressure now operates to generate a surface. Obviously, other possible surfaces can be shown such as engine stroke, speed, and such, and the surfaces illustrated in Fig. 14 will be bounded by such practical limitations as maximum and minimum possible odp and the allowable minimum idp. Within these practical limitations, however, a given engine may operate at any *point* in the three dimensional space illustrated in Fig. 14. Where it operates will depend upon: (1) back pressure, P_b; (2) rack setting, F; and (3) selected bounce pressure, P_{sb}.

Small variations caused by other engine variables may modify these general characteristics somewhat. Typical examples are the effect of inlet air conditions in terms of pressure and temperature. Another is fuel injection timing which is simulated by the point where combustion begins, x_4.

The control imposed by the turbine can now be added. Fig. 15 illustrates the flow characteristics of a fixed nozzle turbine for various inlet gas temperatures (engine exhaust temperatures). Since the turbine characteristics are not influenced by the fuel flow rate to the engine, the surfaces shown are simple projections of the curves. When the turbine characteristics are superimposed upon Fig. 14, the intersections with the engine characteristics represent conditions that satisfy both machines. A closer view of the intersections is shown in Fig. 16 for a given mixture ratio. The engine characteristics are the same as in Fig. 13 except that the exhaust gas temperature results have been added. The locus of the intersection of the constant temperature curves of equal values for the engine and turbine defines the compatible points of operation.

Returning to the larger picture (Fig. 17) the compatible areas of operation for the combination of the engine and turbine becomes a single surface. As the fuel flow to the engine is reduced from the full-load condition, the unit might follow some curve such as A down to the idling condition. In contrast, the unit might follow some curve such as B. The manner in which it does move down from full load is controlled by the design of the engine stabilizer. As

mentioned above, this device controls the selected bounce-chamber pressure as a function of the engine back pressure. The stabilizer can, therefore, be designed to control the operation of the engine at part load according to certain precepts. These may include operation at maximum fuel economy conditions or at particular part-load power outputs. It is of interest to note that the projections of A and B on a two-dimensional plot of gas flow rate versus engine back pressure will be nearly identical.

Fig. 10 is an example of such a result. Clearly, the details concerning the nature of the stabilizer design are not discernible from this representation.

The recirculation or throttling controls are needed to extend the operating range of the engine-turbine combination. At some point along the path of operation from full load (path A, Fig. 17, and point 2, Fig. 10) the minimum odp condition will be reached (the engine will stall unleses the pistons move out to uncover the ports). From this point downward recirculation or throttling must be used in increasing amounts to reduce the gas flow rate from the engine while the stroke is maintained within operable limits. Since both control devices utilize a throttling process which is irreversible, the control while necessary is undesirable.

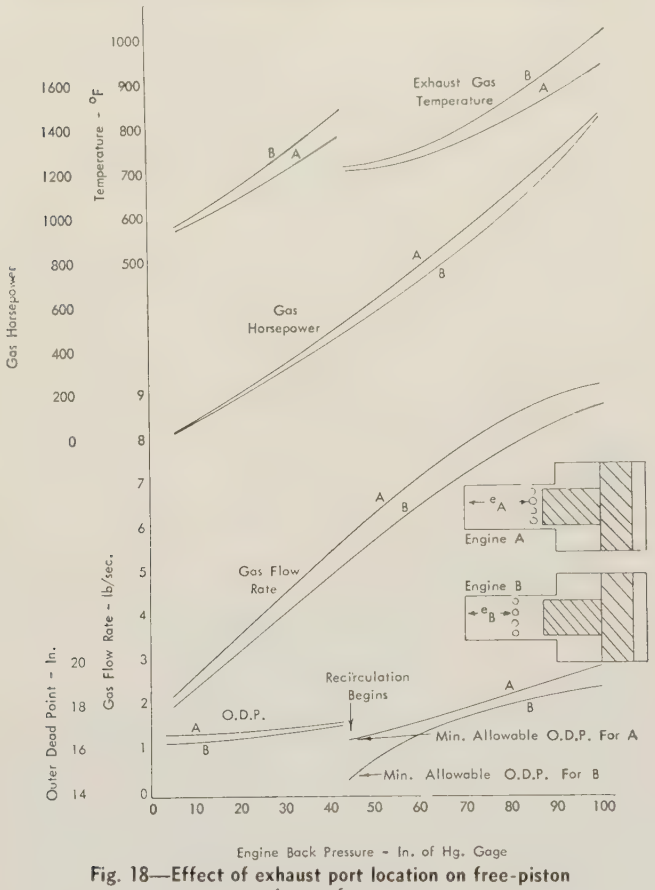

Fig. 18—Effect of exhaust port location on free-piston engine performance

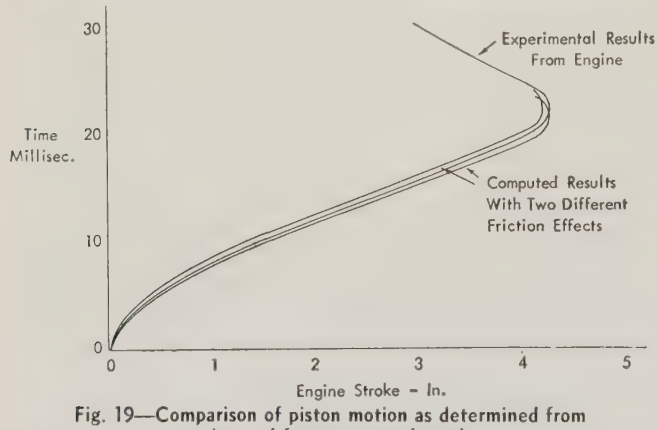

Fig. 19—Comparison of piston motion as determined from engine and from computed results

The performance of a given engine may thus be predicted by constructing a series of plots similar to the one shown in Fig. 13 for a wide variety of fuel flow rates. Upon the selection of the full load condition (represented by a point on one of these plots) the turbine size is essentially fixed. For, to match the engine at this full load point the turbine nozzle size must be selected. The turbine characteristic can now be developed on each of the plots for different fuel rates as illustrated in Fig. 16. In turn, the characteristics of the stabilizer may be selected and the performance of the engine-turbine combination over the entire load range is known. Different full-load conditions can then be selected and the new turbine characteristics and stabilizer designs can be used to investigate a variety of engine-turbine combinations.

Performance Studies

The results of two short-range investigations which were made to show the effect of a design parameter and an operating condition are finally presented to illustrate the use of the analysis.

Effect of Port Location—It can be seen from Fig. 10 that it would be desirable to change the limitation imposed by the minimum stroke condition (point 2). If it could be made to occur at a lower back pressure, then the engine-turbine combination could operate without recirculation over a greater portion of the operating range. Since the exhaust port location fixes the minimum stroke a new port location was simulated by reducing the value of e in the analysis by approximately 20%. All other design parameters and operating conditions were otherwise unchanged to simulate the 1000-hp test unit. Computations were made at several back pressures over the load range. At each back pressure the fuel flow rate was increased in successive computations until the peak pressure during the combustion process was the same as that obtained with the previous port location. The combustion chamber was in this way utilized to the same degree in the two engine designs. The results showed (Fig. 18) that the simulated engine B (with the ports moved in) reached the minimum stroke condition at the same engine back pressure as engine A. In both engines, therefore, recirculation control had to be imposed under comparable conditions. In addition, the exhaust temperatures with engine B were appreciably higher than with engine A, which is undesirable from an engine cooling standpoint. The higher exhaust temperatures are desirable, however, in that the work available from the turbine per lb of gas is increased. This effect is more than offset, however, by the lower gas flow rate available from engine B. The net result was that the gas hp from engine B was less than that shown by the original design (Fig. 18); the specific fuel consumption was higher but not significantly so.

Friction Effects—During the early work with the engine simulation program the proper values for the

friction coefficients included in the analysis were not known. To evaluate these effects special tests were conducted with an engine which could be simulated with the analysis. In this engine (rated output of 200 hp) the piston can be mechanically locked in the outward position in preparation for starting. Upon the charging of the bounce chambers with high-pressure air, the mechanical lock is released and the pistons move inward for the starting stroke. In the tests conducted here no fuel was injected during the starting procedure and a high-speed camera was used to record the position-time history of piston motion (Fig. 19).

The analysis was then used to simulate the comparable situation. Different values of the friction coefficients were used in order to make the computed position-time history of piston motion match the test results. The coefficient of static friction had a predominating influence on the extremes of piston motion (when the velocity was relatively low). The effect of the coefficient of viscous friction was most dominant in the center portion of the stroke when the piston velocity was relatively high. The nature of the computed results is shown in Fig. 19. The friction coefficient determined in this manner are not wholly representative of the operating condition. Since no fuel was injected the effect of the high pressures during the combustion process is not included in the effect of friction on piston motion.

Summary

The analytical simulation of a free-piston engine presented here has shown promise in the investigation of many facets of engine operation. It appears to be sufficiently realistic so that the merit of major changes in engine design and operating conditions can be easily evaluated. It is obviously a relatively cheap tool compared to the construction and test of operating units. However, it cannot be looked upon as a substitute for engine development. Many important aspects of the processes which occur in the engine and greatly influence the performance still defy analytical treatments. The simulation can be considered as a valuable adjunct to engine development. In particular, it can be used to gain a better understanding of the many parameters that influence operating units.

Acknowledgements

The author expresses his appreciation to the many individuals who have aided him during the course of this work. In particular, he wishes to acknowledge the work of Joseph T. Olsztyn who programmed the analysis for the computer, the aid of Dr. Robert Davies in the formulation of the analysis, and the work of Michael Tsou who obtained many of the computer results used here.

APPENDIX I

Symbols

Design Parameters (See Fig. 5 and p. 671.)

Operating Conditions

P_{sb} = Selected bounce pressure, representative pressure at some specified piston position, psia
P_a = Atmospheric pressure, psia
P_b = Engine back pressure, psia
ΔP_1 = Pressure loss for compressor inlet valves, per cent of upstream pressure
ΔP_2 = Pressure loss for compressor discharge valves and inlet air ports, per cent of upstream pressure
ΔP_3 = Pressure loss for exhaust ports and exhaust collector, per cent of upstream pressure
$n_1, n_{21}, n_{22}, n_{23}, n_{32}$ = Polytropic exponents for the various processes.
T_a = Atmospheric temperature, R
C_4 = Coefficient of viscous friction
C_5 = Static friction force, lb
$(HV)_f$ = Heating value of fuel, Btu per lb of fuel
Q_L = Percentage of heating value lost as heat transfer out during combustion
F = Fuel flow rate, lb per cycle or lb per min
x_4 = Point where combustion process begins

A = Combustion time constant (Appendix II)
$C_1, C_{21}, C_{22}, C_{23}, C_{24}, C_{31}, C_{32}$ = Constants in force equations
C = Rate of energy released by simulated combustion process
$C(\theta^*)$ = Rate of energy released by simulated combustion process in terms of θ^*
$C(\theta)$ = Rate of energy released by simulated combustion process in terms of θ
c_v = Specific heat at constant volume of cylinder charge, Btu per mole
$F_1, F_2, F_{21}, F_{22}, F_{23}, F_{24}, F_3, F_{31}, F_{32}, F_{33}, F_{34}, F_4, F_5$ = Various forces acting on piston, lb (Fig. 5)
H = Enthalpy, Btu per lb
k = Ratio of specific heats, c_p/c_v
K = Energy released by a combustion process, Btu
m = Moles of cylinder charge
N = Engine speed, cpm
N_R = Weight of recirculated air per stroke, lb
N_S = Weight of air inducted into compressor per stroke, lb
P = Pressure
P_1 = Pressure in air compressor at beginning of compression, psia
P_2 = Pressure in air compressor when discharge valves open, psia
P_3 = Pressure in power cylinder during simulated scavenging process, psia
ΔP_T = Inverse of overall engine pressure ratio, including pressure losses
P_m = Maximum pressure in combustion chamber, psia
Q = Heat transferred in or out of cylinder walls during combustion, Btu
R = N_R/N_S, percentage of air recirculated
$\overline{R}$ = Universal gas constant, consistent units
S = Scavenging ratio, lb of scavenging air per lb of air trapped
T = Temperature, R
T_1 = Temperature in air compresor at beginning of compression, R
T_2 = Temperature in air compressor when discharge valves open, R
T_R = Temperature of gas in combustion chamber at time of release, R
U = Energy content of cylinder charge, Btu
u = Energy content of cylinder charge, Btu per mole
V = Volume
V_1 = Volume in air compressor at beginning of

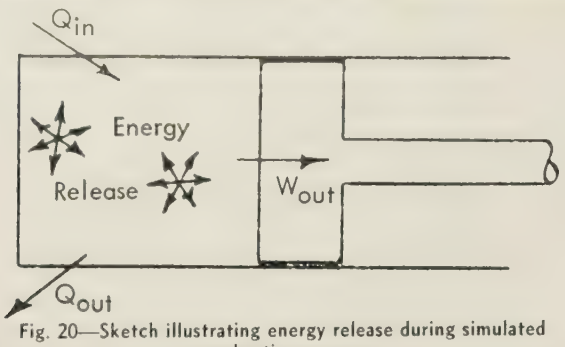

Fig. 20—Sketch illustrating energy release during simulated combustion process

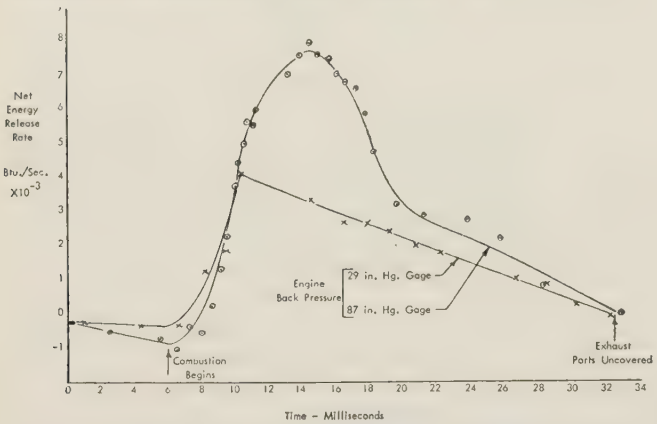

Fig. 21—Computed energy release rate for free-piston engine combustion process

compression, cu ft

V_2 = Volume in air compressor when discharge valves open, cu ft

V_{sb} = Volume in bounce chamber when $P = P_{sb}$, cu ft

W_{out} = Work done on piston by cylinder charge, Btu

x = Measure of piston position, in.

$\dot{x}$ = Velocity of piston, in. per sec

x_o = Position of piston at start of solution, in.

x_o' = Position of piston at end of solution, in.

x_1 = Position of piston when exhaust ports are covered, in.

x_1' = Position of piston when exhaust ports are uncovered, in.

x_2 = Position of piston when air compressor discharge valves open, in.

x_3 = Position of piston when air compressor inlet valves open, in.

x_i = Position of piston at inner dead point, in.

θ = Time as measured in computer solution, sec

θ^* = Arbitrary time used to specify rate of energy release during simulated combustion process, sec

APPENDIX II

Combustion Process

From x_4 up to x_i and then back to the point where the exhaust ports are uncovered, provision must be made to add energy to the air trapped in the combustion chamber to simulate the combustion process in a realistic manner.

Consider the general problem of evaluating the energy released during a combustion process which occurs in an engine cylinder with a moving piston.

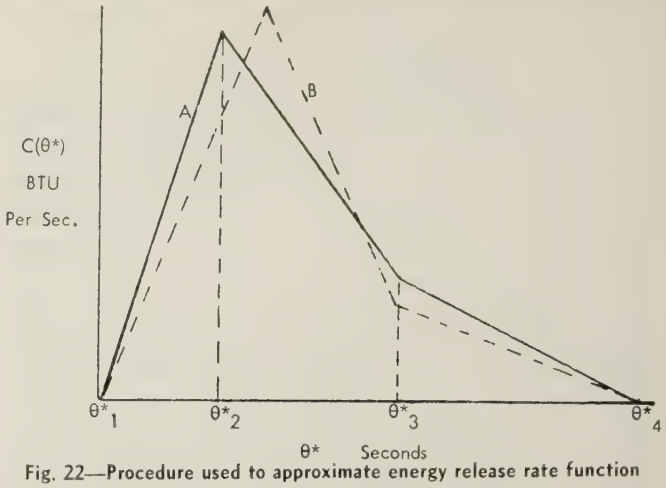

Fig. 22—Procedure used to approximate energy release rate function

The problem will be idealized to the extent that the cylinder charge is assumed to be homogeneous at all times and that the energy is released throughout the entire charge at all stages. A general energy equation may now be formulated (Fig. 20):

δ (energy released) + δ (heat in) = δ (heat out) + δ (work out) + δ (increase in energy content of charge)

or:

$$\delta(K) + \delta Q_{in} - \delta Q_{out} = \delta W_{out} + dU \qquad (9)$$

Now let:

$$\delta(K + Q_{in} - Q_{out}) \equiv C d\theta = \text{Net energy into the cylinder charge from combustion energy release plus the net heat transfer effects} \qquad (10)$$

C is to be considered a time-dependent path function which is the rate of net energy released and is a gross characterization of the combustion process.

Assuming that the cylinder charge is an ideal gas and that the energy content of the charge is solely due to internal energy, Equation 9 may now be written as:

$$C d\theta = P dV + m du = P dV + m\bar{c}_v dT \qquad (11)$$

Using the general gas law and solving for C gives:

$$C = \left(\frac{k}{k-1}\right) P \left(\frac{dV}{d\theta}\right) + \left(\frac{1}{k-1}\right) V \left(\frac{dP}{d\theta}\right) \qquad (12)$$

This equation may now be used to determine the general character of the function C. Indicator diagrams from the power cylinder of a free-piston engine were used to evaluate P, V and $dP/d\theta$ as functions of time, θ. Stroke-time diagrams were used to determine $dV/d\theta$ as a function of time. The results of this evaluation are shown for two different engine back pressure conditions in Fig. 21.

The negative values for C on the left of Fig. 21 indicate that the heat transfer out was the predominating energy effect just before the combustion energy release began. In both of the results shown, energy release continued until the exhaust ports were uncovered.

The area under the curves of Fig. 21 from the beginning to the end of combustion can be interpreted as the portion of the energy released during the combustion process which was manifested as pressure rise. With the assumption that the total energy release can be approximated by the heating value

of the fuel, the area under the curves may be expressed as:

$$\int_{\text{start}}^{\text{finish}} C\,d\theta = (HV)_f(1-Q_L)\ (\text{Fuel rate}) \qquad (13)$$

where:

Q_L = Percentage of $(HV)_f$ lost as net heat out during combustion

The value of Q_L determined from Equation 13 for the two cases illustrated in Fig. 21, accounted for about 80% of the total heat loss from the engine as determined from a heat balance based upon the heating value of the fuel.

Equation 12 may also be used to simulate a combustion process for our need here. Solving for $dP/d\theta$:

$$\frac{dP}{d\theta} = \frac{1}{V}\left[-kP\frac{dV}{d\theta} + (k-1)C\right] \qquad (14)$$

And in terms of F_{33}, Fig. 6:

$$\frac{dF_{33}}{d\theta} = \frac{1}{(d-x)}\left[kF_{33}\frac{dx}{d\theta} + (k-1)C\right] \qquad (15)$$

The force F_{33} can be predicted from this relation provided a suitable procedure can be found to specify the nature of the function C. The general character of the results shown in Fig. 21 were used in the formulation of the procedure used in this analysis.

First, the area under the C function can be specified according to equation 13. In addition, it was assumed that the energy release continued until the exhaust ports were uncovered as is indicated in Fig. 21. Finally, it was assumed that a large part (75–80%) of the energy would be released during the first half of the total time available for the combustion process. These rather general principles were used in the construction of the C function which consisted of three straight lines as illustrated in Fig. 22. Two points should be made clear: A discontinuous derivative in the C function, such as occurs at θ_2^* in Fig. 22, does not produce a discontinuity in the value of F_{33} at this same time. Secondly, an alternate function C, such as B in Fig. 22, will produce an inappreciable change in the pressure-time history compared to path A, provided the areas under the two paths are equal. Both of these characteristics make the procedure valuable and derive from the fact that the derivative is being specified to produce an integrated result.

In order the match the specified $C(\theta^*)$ function (Fig. 22) with the actual time element of the analysis, which is unknown, a scale factor must be applied to the $C(\theta^*)$ function. The basic principle used here is that it will be assumed that θ_4^* coincides with the uncovering of the exhaust ports. The actual time for the simulated combustion process will, therefore, be expressed in terms of the arbitrary time scale used in the specification of $C(\theta^*)$. Thus:

$$(\theta_4^* - \theta_1^*) \equiv A(\theta_{x_1} - \theta_{x_4}) \qquad (16)$$

where the scale factor A will be termed the combustion time constant and will operate in a linear fashion throughout the time interval for combustion.

Therefore: $(\theta_4^* - \theta^*) \equiv A(\theta - \theta_{x_4})$ (17)

which can be used to evaluate θ^* at any intermediate point.

In order to maintain a constant total energy release figure irrespective of the actual time interval, the scale factor must also operate so as to produce the following condition:

$$\int C(\theta^*)\,d\theta^* = \int C(\theta)\,d\theta \qquad (18)$$

This can be accomplished by: $C(\theta) \equiv AC(\theta^*)$ (19)

Equation 15 may now be finally written as:

$$\frac{dF_{33}}{d\theta} = \frac{1}{d-x}\left[kF_3\frac{dx}{d\theta} + (k-1)AC(\theta^*)\right] \qquad (20)$$

The value of A changes for each solution and must be determined by iteration based on Equation 16.

APPENDIX III

Evaluation of Engine Performance

Effects of Recirculation—The provision made in the engine to recirculate a portion of the compressed air from the air box back into the inlet of the air compressor is termed recirculation. Consider N_R lb of recirculated air which mixes adiabatically with $(N_S - N_R)$ lb of fresh air from the atmosphere. The mixture (N_S lb) is inducted into the air compressor at some temperature T_1. The energy equation for the mixing process may be written as:

$$N_R H_{T_2} + (N_S - N_R)H_{T_a} = N_S N_{T_1} \qquad (21)$$

where:

T_a = temperature of atmospheric air

The small rise in the temperature of the air during its delivery into the air box is neglected and it is assumed that the temperature of the clearance air in the compressor at the expanded condition will be equal to T_1. Equation 21 may be written as:

$$RT_2 + (1-R)T_a = T_1 \qquad (22)$$

where:

$R = (N_R/N_S)$ = Percentage of air recirculated

Assuming a polytropic compression process:

$$T_2 = T_1\left(\frac{P_2}{P_1}\right)^{[(n_{21}-1)/n_{21}]} \qquad (23)$$

Combining Equations 22 and 23:

$$T_1 = \frac{T_a(1-R)}{\left[1 - R\left(\frac{P_2}{P_1}\right)^{(n_{21}-1)/n_{21}}\right]} \qquad (24)$$

Air Inducted per Stroke—This process occurs from x_3 to x_o, (Fig. 6). Using the gas law:

$$N_S = \text{Air induced} = \frac{PV}{RT} = \frac{P_1(\pi/4)(D_1^2 - D_2^2)(x_3 - x_o)}{(53.3)T_1(12)} \qquad (25)$$

Air Trapped in Combustion Chamber—It will be assumed that the air trapped in the combustion chamber will be at temperature T_2 as determined in Equation 23. The small rise in temperature during the delivery of the air into the air box is thus again neglected and complete scavenging is assumed. Using the gas law:

$$N_T = \text{Air trapped} = \frac{PV}{RT} = \frac{P_3(\pi/4)D_2^2 e}{(53.3)(12)T_1}\left(\frac{P_1}{P_2}\right)^{(n_{21}-1)/n_{21}} \qquad (26)$$

Scavenging Ratio—The ratio of the air which flows into the combustion chamber to the air which is trapped may be expressed as:

$$S = \frac{N_S - N_R}{N_T} = \frac{N_S}{N_T}(1-R) \qquad (27)$$

Gas Temperature Prior to Release—The gas law

applied to the contents of power cylinder at x_1' gives:

$$T_R \quad \frac{PV}{RN_T} = \frac{(F_{33}@x_1')\,e}{(53.3)\,(12)\,N_T} \qquad (28)$$

where the pressure is evaluated in terms of force F_{33}.

Engine Speed—The engine speed can be determined from the time required for a complete cycle. Since $\theta = 0$ when the piston starts the cycle at x_o, then θ at x_o' after one cycle is a measure of the speed. Thus: $N = 60/\theta_{x'_o} = \text{cpm}$ (29)

Engine Stroke—The engine stroke can be determined from the displacement history of the piston:

$$\text{Stroke} = x_i - x_o' = \text{in.} \qquad (30)$$

Gas Flow Rate—The net gas flow rate through the engine taking into account any recirculation may be expressed as:

$$\text{Flow Rate} = N(N_S - N_R) = NN_S(1 - R) = \text{lb gas per min} \qquad (31)$$

Maximum Combustion Chamber Pressure—The maximum pressure in the combustion chamber will obviously occur during the combustion process. Since F_{33} must be evaluated throughout the process, the maximum value attained by F_{33} gives the maximum pressure. Thus:

$$P_m = \frac{F_{33}\,(\max)}{(\pi/4)\,D_2^2} = \text{psia} \qquad (32)$$

Gas Horsepower—Several assumptions must be made to estimate the gas hp which the engine delivers. The most important of these are the properties of the gas at high temperatures which are needed for the prediction of the power from the gas turbine. Since the best data for this purpose[10] are not easily used in the computer, this result was computed by hand using the necessary results from the solution.

Considering the nonsteady flow process which occurs during the scavenging process, the energy equation may be written for an ideal scavenging process as:

$$N_T U_{T_R} + N_T SH_{T_2} = N_T U_{T_2} + N_T SH_T \qquad (33)$$

where: H_T = Enthalpy of the combustion products and scavenge air leaving the engine, Btu per lb

The value of H_T determined from this expression can be used to evaluate the exhaust gas temperature. In addition, the ideal turbine work can be computed using Keenan and Kaye[10] in which H_T is used as the initial enthalpy. The pressure drop across the turbine is obviously $P_b - P_a$.

Fuel Flow Rate and Gas Specific Fuel Consumption—The fuel flow rate can be evaluated from the specified fuel rate per engine cycle and the engine speed. The gas specific fuel consumption can then be determined.

DISCUSSION

Reported by L. D. Gilmore
International Harvester Co.

Paul Klotsch, Ford Motor Co.: Was the deceleration rate on the inward stroke taken to be less than on the outward stroke?

Prof. Olson: Results at GMC indicate that they are of about the same value and the differences are not as great as suspected.

Robert Cramer, Nordberg Mfg. Co.: Was static friction used in the analysis?

Prof. Olson: The frictions considered were: (1) coulomb (static), (2) viscous, (3) a combination of these.

Theodore M. Robie, Fairbanks Morse and Co.: The forces F_4 and F_5 pertained only to the bounce piston. Was the friction of the power piston neglected?

Prof. Olson: No, the forces F_4 and F_5 were applied to the entire piston assembly.

L. Weschler, Navy Bureau of Ships: How did the amount of fuel introduced account for the heat loss?

Prof. Olson: The area beneath the curve for the rate of energy liberation plotted versus time was made equal to the heating value of injected fuel times the factor (1 – Loss).

Carl H. Meile, International Harvester: While listening to this paper I could not help but think how truly important are the fundamentals of the engineering sciences. My company has made a similar analytical study of the thermodynamics and performance parameters of the free-piston engine. This work was entirely independent of the effort reported by Dr. Olson, yet there is a remarkable similarity in details and display of the interdependence of variables. This shows that the fundamentals of cycle analysis with intelligently applied assumptions will yield valid answers.

Dr. Olson pointed out that analytical simulation is a cheap tool compared to construction and test of operating units. I believe the utilization of electronic computers has awakened us to rediscovering the value of thorough mathematical analysis as a means of design evaluation. In the past the tendency has been to rely heavily upon the experimental test approach. This usually leads to a "cut-and-try" procedure which becomes costly and time consuming—substituting emotional engineering for sound logical engineering thought.

It is true that the solution of many analytical problems are time consuming and wearisome to the calculating engineer; but with the ability to put these problems on an electronic computer, this objection can now be dissolved. It remains only to demonstrate the value of this approach to upper management so that a better balance can be achieved between mathematical analysis and experimental test.

Our free-piston engine design analysis is essentially the same as that presented by Dr. Olson. That is, a thermodynamic description is evolved for the several processes occurring at any given position of stroke. From this we compute the motion and performance data. Our emphasis has been on design parameters rather than simulation of an existing machine. Hence, our input data is the stroke position for a given pressure in the air receiver. Output data is similar to that listed by Dr. Olson, namely: piston motion and frequency, pressures and flow rates, and indicated thermal efficiency. In addition, we are programming calculations for gas hp and specific fuel consumption.

Our problem was programmed for an IBM-650 computer. We have been using the Bell II Interpretive Routine for machine language. A typical problem for free-piston analysis can be solved in a matter of 24 min. By long hand computation, this same problem would require about one man-week, assuming everything had been previously prepared in tabular form. A higher accuracy is obtained with the computer because five times as many increments are used as compared to desk calculation procedure. We are able to punch out and print any variable used or computed in the program.

But it still leaves us with the question, "When should you program a problem for a computer and when should you resort to the desk calculator?" A repetitive problem, using iterative processes, clearly belongs on a computer. But there are some in-between problems that still require a fair amount of calculating time but may not be repetitive. We are attempting to establish some criteria for guidance of our engineering divisions to make this kind of decision.

We have abandoned the concept of a central computing group wherein all engineers can feed their problems and await answers. It appears that a really effective computing group should have all the engineering scientific disciplines represented in order to understand the variety of problems encountered. Following this reasoning, we have resorted to standardized program routines. Our experience shows that

[10] "Gas Tables," by J. H. Keenan and J. Kaye. Pub. by John Wiley and Sons, Inc., New York.

an engineer can learn to program a problem in a matter of 4 to 6 hr, starting from scratch. Once having learned the mysteries of machine language, he can program a problem in half that time. These routines will take care of a large portion of computer problems including disk stresses, shaft vibrations, and test data reduction.

We have a specialty group of two people with engineering background who have been trained fully in the knowledge of computers. The more difficult problems, such as the free-piston engine analysis, are handled by this group.

As you know, the field of computer analysis has grown rapidly. It affords an opportunity to tackle analytical problems undreamed of a few years ago. Just as the dynamometer has become accepted as a necessary piece of equipment in the engine laboratory, I believe a computer of some type will become accepted as a necessary piece of equipment for the analytical design group.

Prof. Olson: Our experience has also been that engineers should program their own problems.

A. R. Bobrowsky, Nucor Research, Inc.: Prof. Olson has done an excellent job in introducing another method for simulation of a free-piston engine with a digital computer. The experimental verification obtained by him and his coworkers is excellent inasmuch as it covers a wide range of loads. His method of analysis is also applicable to specific engine configurations other than those shown.

Many techniques for determining the detailed performance of a free-piston engine begin with Newton's Law applied to a constant mass:

$$F = m\frac{d^2x}{dt^2} \qquad \text{(A)}$$

Integration of Equation A can proceed in either of two directions. When integrated with respect to time, Equation C results, which is the familiar impulse-equals-change-in-momentum.

$$Fdt = md\left(\frac{dx}{dt}\right) \qquad \text{(B)}$$

$$\int_{t_1}^{t_2} Fdt = m\,(v_2 - v_1) \qquad \text{(C)}$$

This formulation is especially suited to the case of velocity-dependent variables—in this paper, the friction and combustion cycle terms. Also, integrating with respect to x yields the usual conservation-of-energy expression for no momentum flows across the boundaries of the system:

$$F\frac{dx}{dt} = m\frac{d^2x}{dt^2}\frac{dx}{dt} \qquad \text{(D)}$$

$$Fdx = mvdv \qquad \text{(E)}$$

$$\text{Work} = \tfrac{1}{2}m\,(v_2^2 - v_1^2) \qquad \text{(F)}$$

This format is valuable since integration between the dead centers results in an expression $\oint$ work = 0. The same results are obtained by any of the techniques listed as Equations A, C, or F. The energy balance used by London and Oppenheim[a] and Bobrowsky[b] makes use of Equation F. This approach is well-suited when the cycle processes are not functions of the frequency. For this reason, a constant value of Coulomb friction was assumed to exist for any individual calculation. This constant value could be adjusted as one progressed from one load point to another. Methods that make use of Equation C are well-suited to processes where frequency enters directly or where its reciprocal dimension, time, enters. Prof. Olson chose to consider a friction characteristic that contained both a Coulomb term and a velocity-dependent component. Integration with respect to time is thus required and a differential-equation technique is indicated.

The following questions then arise: In particular, what is the relative importance of the Coulomb and velocity components? Is the solution appreciably affected by ignoring the viscous components? Is any fraction of the heat of the sliding parts considered to be transferred to the air in the bounce or compressor, or to the gas in the engine? Similarly, to what extent is it necessary to specify the fuel consumption as a rate in order to obtain correlation with experimental results? Is not fuel injection usually a cam-operated and, therefore, a displacement-dependent process, as opposed to a time-dependent process? Of course, heat release may be time-dependent but if heat-transfer coefficients increase with velocity, the rate may become nearly independent of frequency over limited ranges of frequencies. It is necessary to treat the pressure drops as frequency dependent, especially since $\Delta p r v^2$, is a square relation?

The method of solution is an iterated one. Two questions always develop: (1.) Is the solution stable? and (2) is the solution truly obtained close to the correct solution when incremental solutions do not differ greatly from each other, or is it only that a large time constant is involved near this equilibrium point (such as may occur in the usual otto-cycle-powered vehicle as one accelerates in high gear from, say, 6 mph)? The fact that the solutions obtained check the experimental values indicates that no stability test was necessary, and that time constants were not of excessively large magnitude. Is there a guarantee that these points need not be watched with other specific configurations?

It is noted in Fig. 2, which shows a sketch of the bounce-chamber process, that heat transfer is apparent in the cycle 1–2–3. The writer would like to inquire as to how this heat transfer was determined or, equivalently, how the expansion and compression exponents were selected. The same quantitative questions arise with respect to Figs. 3 and 4.

With respect to the eight design parameters listed by Prof. Olson, do dimensionless design parameters assist in scaling the results to engines of other absolute sizes?

In the phase plot of Fig. 7, the usual generalities of phase-plane plots should hold, that is, the path in phase space crosses the displacement axis at right angles. Other figures do exhibit normal intersections. Was there some reason for the lack of orthogonality?

Could one save time by determining the cycle constant for two iterations only, and extrapolating to the equilibrium point? What is the computer time per solution point?

Comparison of three-dimensional plots is cumbersome when comparing performance of different engines. Has the author set up a simplified plot or other criterion to aid in the comparison of performance of a number of engines?

The point should be made that this paper is concerned with a technique for analysis of free-piston engines more than with digital computers. Solutions may be obtained to similar calculations by use of the slide rule. Points obtained in this manner in my paper[b] required no more than one day per point—sometimes less. Simple nomograms reduce the time required to 15–20 min. Of course, digital computers were used also where large amounts of data were required. But it must be emphasized that computer techniques are not completely necessary, and the mechanical engineer should not keep from making such analyses if a computer is not available. It also happens that hand computation requires the engineer to think more deeply of the number of computations required, and to examine results as calculations proceed, and thus can be very beneficial.

Prof. Olson: Although the viscous friction effect is rather small it does need to be included as a time term in the energy release process. The pressure drop effects were included in an elementary way. The coefficients were changed at part load.

The values of the exponents for the expansion and compression processes were initially obtained from the literature for water-cooled reciprocating compressors. Indicator records from the engine later confirmed these values. Slight changes in the values of the exponents give little change in the results.

The proper use of dimensionless design parameters hinges upon a valid correlation between a complete set of dimensionless parameters. Such a correlation or even a complete set of parameters applicable to free-piston engines have not to my knowledge been shown.

David A. Trayser, Battelle Memorial Institute: We were particularly interested in this paper because we also have recently taken the electronic computer into the field of free-

[a] "Free-Piston Gas Generator: A Thermodynamic-Dynamic Analysis," by A. L. London and A. K. Oppenheim. Technical Report FP-1, Navy Contract N6-ONR-251, Task Order 6, Departmnet of Mechanical Engineering, Stanford University, Feb. 15, 1950.

[b] "Analytical Methods for Performance Estimates of Free-Piston Gasifiers," by A. R. Bobrowsky. ASME paper 57-GTP-6, March 18, 1957.

piston engine research.

Several years ago a research program was begun at Battelle to design and develop a gas-fueled free-piston engine-compressor unit for residual air conditioning. The design we selected for development required only a single piston operating in a cylinder with four separate chambers. Practically all free-piston research up to that time had been conducted with opposed piston configurations such as that discussed by Dr. Olson, so it became necessary for us to establish somewhat new patterns for dynamic and thermodynamic analysis.

The small size of our unit and the critical nature of certain component functions necessitated a rather close control over the piston stroke. Before any units were designed and constructed for laboratory tests, it was important to establish the relationships between the piston stroke and the thermodynamic cycles within the various cylinder chambers. The essentialness of the information required plus a desire on our part to experiment in electronic computer applications to research problems led us to the decision to simulate our single-piston free-piston engine with an analog computer.

We chose the analog computer as best suited to the requirements of our program because of its flexibility, ease of control, and methods of data presentation. We had a large number of operating variables and constants to investigate, and extreme accuracy was secondary to simplicity and speed of analysis of results. The particular variables we were interested in included engine operating frequency, piston velocity, acceleration and stroke, starting characteristics, and pressure and energy values in the various cylinder chambers The ability of the analog computer to produce a direct XY plot of any two parameters in the simulation enabled us to change any constant or variable and to observe immediately the results of that change. Just imagine being able to change the clearance volume or the bore size of a compressor with merely the twist of a dial or the flick of a switch, and to observe the effect in a matter of sec. All this without lifting a wrench or turning a lathe.

The circuits of our analog computer were set up to solve the thermodynamic relationship between pressure and volume in a polytropic process, and the dynamic equation of piston motion: force equals mass times acceleration. The instructions which we translated to analog computer language included upper and lower pressure limits in the cylinder chambers, polytropic exponents for the various compression and expansion processes, clearance volumes, piston mass and diameters, and change of state points. Friction forces were simulated both as a function of piston velocity and as a constant. Combustion was simulated by introducing an electrical energy charge in a time-dependent manner into the computer circuit at the proper time in the cycle. For convenience, this energy charge was made proportional to compression pressure resulting in a combustion energy release proportional to compression ratio. Other versions of combustion energy control were also experimented with. The results of our analog simulation were expressed in terms of pressure-volume diagrams, piston velocity-stroke and acceleration-stroke curves, net cycle energy plotted against stroke for each cylinder chamber; also, these and other parameters plotted against time.

The analog computer calculated all the forces acting against the piston and then simulated the resulting piston motion. The simulation was continuous and could be stopped or started at any point. The simulation included a time factor of 100 to 1. If the actual engine were operating at 1500 cpm, the simulated engine would operate at 15 cpm, therefore, requiring 4 sec to complete a cycle. This limitation in computing speed was imposed primarily by the response of the recording instruments. However, we found that at this speed of system operation it was easier to make instantaneous configuration or parameter changes and to observe the results without the intermediate steps of recording and analyzing required in many computer programs. It was possible for us to control completely the operation of the simulated engine from start to stop, introducing load changes, combustion energy variations, and engine misfires or other momentary failures.

Prof. Olson: We seriously considered using an analog computer. However, we were concerned with the uncontrollable accumulation of error, which might reach 10–15%.

S. Chen, International Harvester Co. In the past, we have studied the pioneering Free-piston engine analytical work by Prof. London and Prof. Oppenheim, and the recent work of Ford Co. engineers. There is one common approach to this work—energy balancing equations were used. Today, we listened to an excellent paper by Prof. Olson using force balance as the basis of analysis. Force balance equations possess a unique characteristic in that both thermodynamic and dynamic problems can be solved simultaneously. When energy balance equations are used, force-stroke relationship is still necessary to determine the engine dynamics. But, energy balance equations are convenient for stability study, as Ford's papers have shown.

I have a few questions about this paper:

1. The close correlation between the analytical and experimental results indicates a proper choice of pressure drop factors at design point and at part loads. How are these factors determined experimentally and analytically?

2. How is the friction coefficient used in the computation verified experimentally?

3. Referring to Fig. 11 and looking at the exhaust temperature curves, a definite break is observed on the computed curve as well as the test curve. It is possible to understand the break on the test curve as a result of a finite recirculation valve opening and a large test increment. However, I cannot understand the finite jump on the computed curve unless a fixed opening (not adjustable) recirculation valve opening function is used in the computation.

4. Is throttling better than recirculation for part-load performance?

Prof. Olson: The decision to use throttling or a recirculator valve depends upon the configuration of the engine, bore/stroke, and the like. In Fig. 11, the data were obtained by using a fixed orifice in place of the turbine. The operator actually opened it by too large an increment for the first step. The "finite jump on the computed curve" occurred because the computed engine simulation was based on flow rates obtained from the test curve.

Author's Closure To Discussion

I TAKE this opportunity to thank all of the discussers for their contributions to this session and to answer several of Dr. Bobrowsky's questions which were not covered in the oral discussion. In the friction study illustrated in Fig. 19, it was necessary to include both friction terms in order to predict the experimental results. The effect of the viscous friction term appeared to be fully as important as static friction in this particular engine. The available energy involved in the friction process was not considered to be transferred as heat to the compressor air.

While it is true that the liquid fuel injection rate is a displacement process, the thermodynamic analysis used here depends upon the actual energy release rate produced by the combustion process. This process is largely controlled by mass and energy transfer rates which are time dependent. The time-dependent release rate characteristic will obviously be somewhat affected by the rate of liquid fuel injection in the actual engine. However, as illustrated in Fig. 22, the analysis can tolerate considerable variation in this characteristic with little change in the important result—the pressure-time history.

The stability and convergence of the solution were investigated in terms of the computation constants. The time step size $\Delta\theta$ was taken sufficiently small to give convergence. Convergence to the same value was also obtained when initial values for x_0 were taken on either side of the true solution. The computing time for each operating condition was usually somewhat less than 1 min. For this reason, no special interpolative procedures were used to obtain more rapid convergence.

Dr. Bobrowsky's remarks concerning orthogonality with reference to the sketch shown in Fig. 7 are well-taken. The actual computed results shown in Fig. 8 illustrate his point.

Measurement of — —

Gas Temperature in an Engine by the

VELOCITY OF SOUND METHOD

J. C. Livengood, C. F. Taylor, and P. C. Wu,
Massachusetts Institute of Technology

This paper was presented at the SAE Annual Meeting, Detroit, Jan. 13, 1958.

THE development of the internal-combustion engine, particularly in its earlier phases, was accomplished by cut-and-try methods. Nevertheless, these methods were restrained by sufficient discipline so that steady technological progress was achieved. The consequence of this history is that today we find ourselves in possession of a highly developed machine which has enormous economic significance—but one which is perhaps less perfectly understood than is, for example a nuclear reactor. It is the purpose of this article to show how a part of this gap in knowledge might be filled.

Central to our understanding of the internal-combustion engine is such knowledge as can be accumulated concerning the "cycle" itself, that is, the process occurring in the gases within the cylinder. In recent years study of this process has been greatly facilitated by the development of, and the increasing use of, pressure indicators of quite excellent accuracy.

On the other hand, no direct means have been generally available for measuring the temperature of the cylinder gases, particularly in the period prior to combustion.

As is well-known, conditions during compression have a strong influence on the character of the whole cycle, and especially on the combustion process. It is for this reason that the development of a device which would measure temperature during the compression stroke, as well as at other points, was undertaken. It was expected that knowledge of such temperature would shed important light on questions of charge density (volumetric efficiency), composition (residual gas fraction), and combustion (flame speed and knock).

One great difficulty is the problem of nonhomogeneity of the charge. The cylinder contents are a mixture of fuel, air, and residual products from previous cycles. This mixture is not necessarily homogeneous chemically or physically *before* combustion, and it is most certainly not so during combustion and for some time thereafter.

The chief physical nonhomogeneity is due to the presence of large thermal gradients. These gradi-

THIS paper outlines a new method of measuring end-gas temperatures within the cylinder of an operating engine. The new instrument measures the acoustical properties by the pulse method, transmitting an acoustical impulse through a gas path of known length and measuring the time of propagation through the gas. The method yields a value for the average velocity of sound in the path.

The authors describe the instrument and engine modifications necessary. The results of tests are also discussed, with a detailed description of one series.

The appendixes outline the mathematical steps of finding the sound velocity in gas mixtures and the fuel-air cycle for the detailed series of tests.

ents are the result of incomplete mixing, of heat transfer between the gas and the cylinder walls, and of progressive burning.[1]

It might appear, then, that the concept of "average" temperature of the cylinder charge could be misleading—unless this term were defined precisely and its conditions of measurement described. One obvious way out of this situation would be to make many local measurements of the physical state of the cylinder contents. This would be highly informative, although difficult to achieve.

From a more modest viewpoint, however, there is one region in the combustion chamber which is of especial interest. This region is that which is last to be consumed by the flame front—generally called the "end gas." The unburned mixture in this region has experienced a history of induction, mixing with residuals, heat transfer, compression by the piston, and a further elevation in temperature and pressure by the earlier burning portions of the charge.[2] It is generally agreed that the end-gas region is the place where detonation or "knock" reactions culminate. Also, it has been found that the autoignition processes, which are believed to be responsible for the knock reaction, are extremely sensitive to temperature; in some cases the rates of such reactions may *double* with an increase in temperature of 20 F.[3]

It was for the above reasons that in 1949 the Group on the Fundamentals of Detonation, Motor Fuels Division, Coordinating Research Council, promulgated a requirement for an instrument which would measure the low-temperature portions of an engine cycle, and in particular, the temperature of the unburned end gas. One suggestion was the measurement of the acoustical properties of the gas.[4]

Fundamental Objectives—Preliminary estimates indicated that the unburned end gas might be found in the following physical state:

1. Pressure—from 15 to 700 psia.
2. dp/dt (rate of change of pressure) greater than 2×10^5 psi per sec.
3. Unburned temperature—100–2000 F.
4. dT/dt (rate of change of temperature) greater than 10^5 F per sec.

In addition to functioning under the above conditions, it was desirable that the installation and operation of the measuring apparatus should interfere as little as possible with the normal operation of the engine. A minimum goal for accuracy was set at ± 1% of the absolute temperature.

Basic Principles—Although there are several possible ways for measuring the acoustical properties of a gas, the severe limitations which are imposed by engine operation indicated that a pulse method was easiest to accomplish with the necessary accuracy.

The pulse method involves transmitting an acoustical impulse through a gas path of known length and measuring the time of propagation through the gas. Such a measurement will yield a value for the average velocity of sound in the path. For a perfect gas the temperature is related to the velocity of sound by the classical equation:

$$a^2 = \frac{kRT}{m} \qquad (1)$$

For more precise derivations of temperature from sound velocity the *im*perfect gas behavior must be considered, and this fact complicates the problem somewhat, as is shown in Appendix II.

Sound Generation and Time Measurement—Fig. 1 shows schematically how the pulse method is applied. At a preselected point in the engine cycle a signal (generated by a cam and contact arrangement on the camshaft, for example) is supplied to

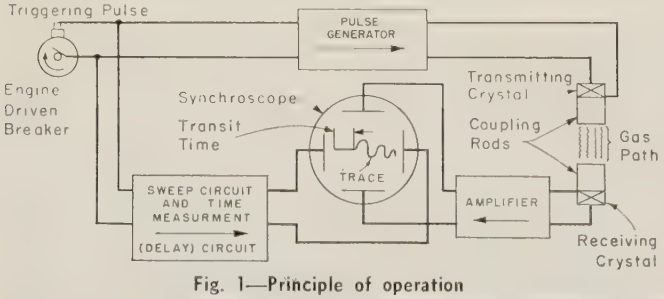

Fig. 1—Principle of operation

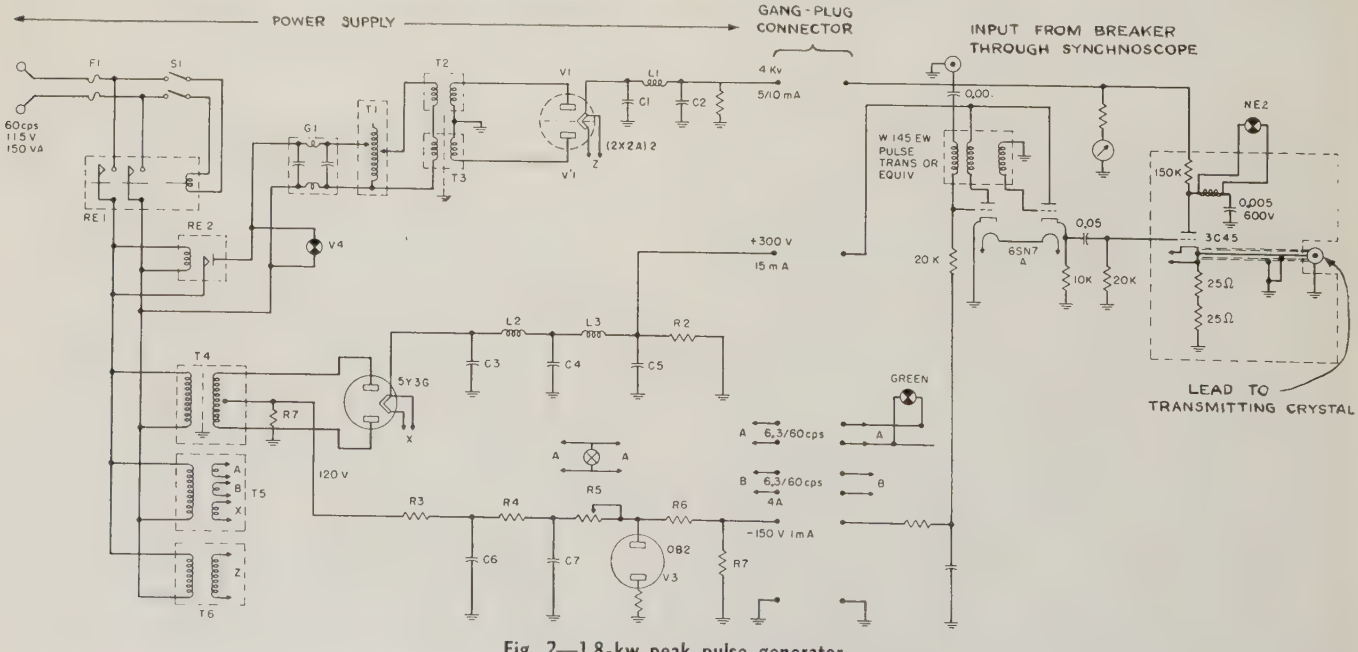

Fig. 2—1.8-kw peak pulse generator

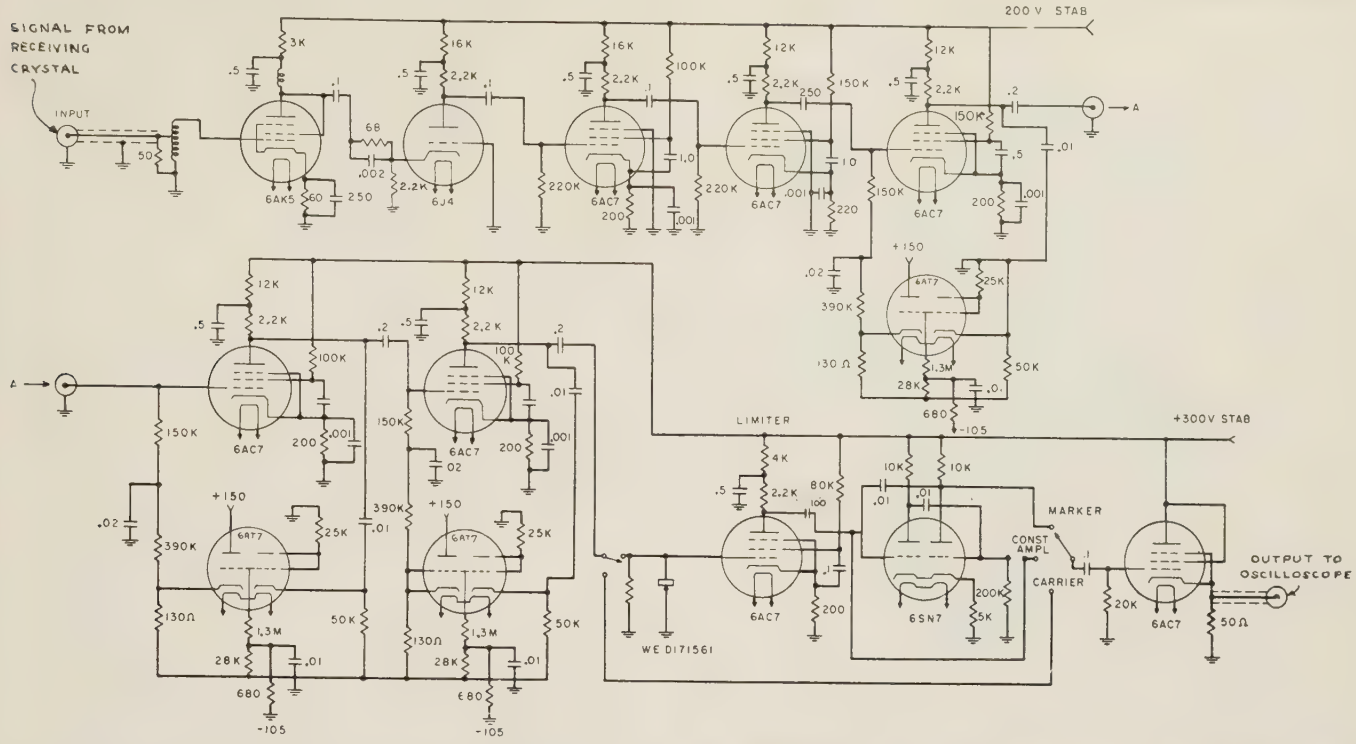

Fig. 3—GC-GG low-noise video receiver

the time-measuring oscilloscope. This scope does two things in response to this signal:

1. It starts the operation of a "delay circuit."
2. It concurrently sends out a pulse which "fires" the transmitter circuit.

The transmitter produces a high-voltage pulse with a very steep leading edge. This pulse excites the piezo-electric crystal (barium titanate), which in turn produces a train of vibrations which travel through the coupling rod and into the gas. Having passed through the gas, the vibration is transmitted through the receiver coupling rod to the receiving crystal, which generates an electrical signal (now reduced to a very small magnitude). This weak signal is amplified and fed to the *vertical* deflection plates of the cathode ray tube.

Meanwhile, the delay circuit (the stop watch of the system) has run its course and has started the horizontal sweep of the cathode ray spot across the screen. The signal on the vertical axis of the tube appears along the sweep at a position which depends upon the time relationship between the delay circuit duration and the total time required for the transmitted impulse to transit the electrical, mechanical (coupling rods), and acoustical (gas) paths in the system. However, it is apparent that if the only *variable* lag is caused by the gas, the *variations* in the horizontal position of the displayed signal are

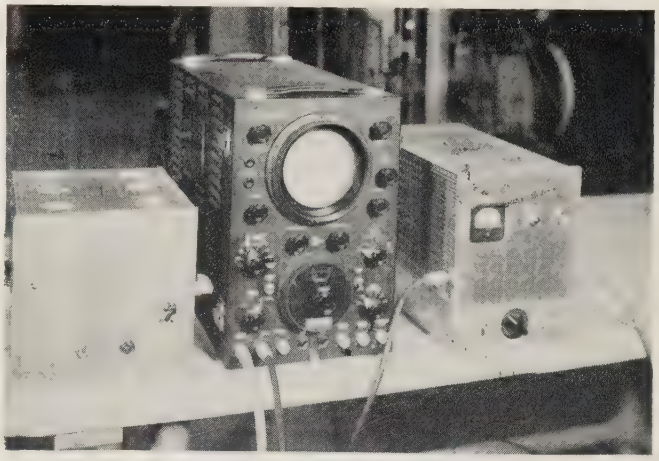

Fig. 4—Electronic equipment

a function of the gas properties and the gas path length (which is known and fixed).

In practice the horizontal location of the received signal is not measured directly, since this measurement cannot be made with good accuracy. Instead, the duration of the delay circuit is changed to make the signal appear at the sweep origin. The duration of the delay can be read on a dial to $\pm$ 0.05 μ sec where 1 μ sec is 10^{-6} sec.

The circuitry which is used to accomplish these measurements will not be described in this paper, but the schematics are included in Figs. 2 and 3. Rona gives further details.[5] A photograph of the equipment is shown in Fig. 4, in order to give some idea as to size and portability.

Description of Engine Modifications—A special combustion chamber was designed to fit a laboratory CFR engine (Fig. 5). This chamber was made by sandwich construction and can be copper brazed so that the three layers form a single unit. Various

[1] P. 60 of "The Internal Combustion Engine," by C. F. Taylor and E. S. Taylor. Pub. by International Textbook Co., Scranton, Pa., 1948.

[2] Ibid, Fig. 33.

[3] Fifth Symposium (International) on Combustion, 1955, pp. 347–356: "Correlation of Autoignition Phenomena in Internal-Combustion Engines and Rapid Compression Machines," by J. C. Livengood and P. C. Wu. Pub. by Reinhold Publishing Corp., New York, 1955.

[4] CRC Report No. 277, January, 1953: "Four Proposed Methods of Measuring End-Gas Properties."

[5] "Gas Temperature Measurements by Ultrasonic Pulse Method," by T. P. Rona. Doctoral dissertation, M.I.T., May, 1955.

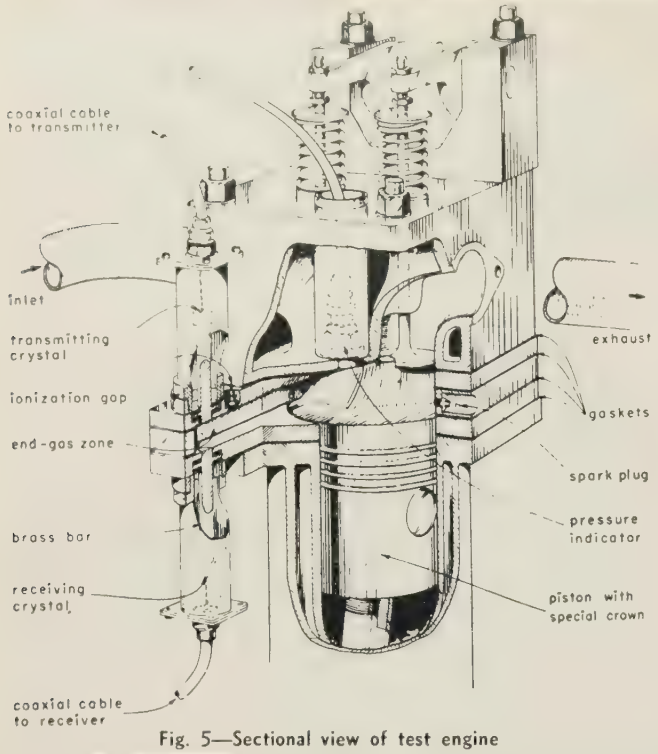

Fig. 5—Sectional view of test engine

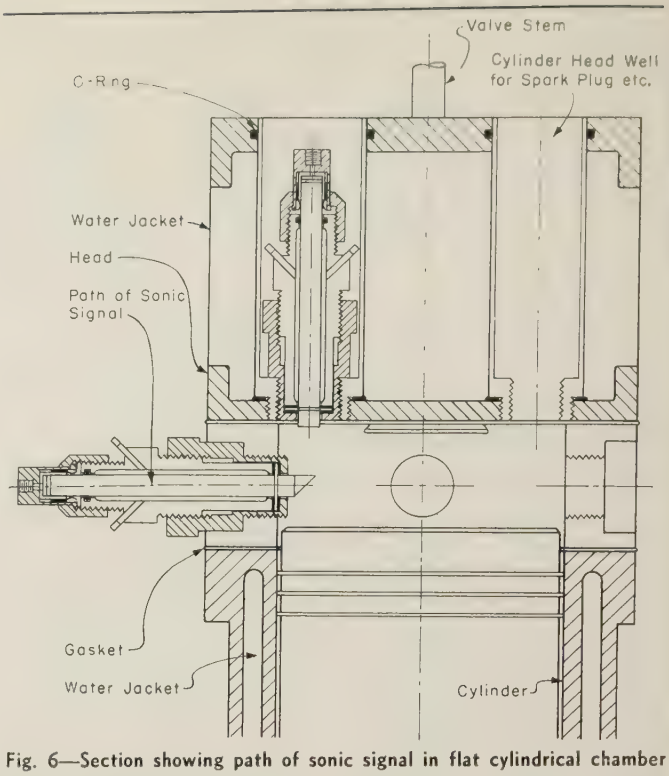

Fig. 6—Section showing path of sonic signal in flat cylindrical chamber

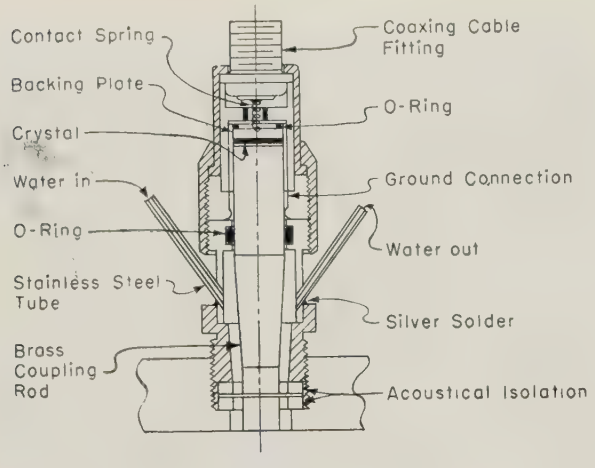

Fig. 7—Transducer assembly

openings can be placed in this sandwich plate, and also several openings can be placed in the cylinder head. In addition to the holes for the transducer coupling rods, as many as seven additional openings at various places have been provided. These may be used for spark plugs, pressure pickups, windows, ionization gaps, and the like. Separate cooling passages surround the pocket which overhangs the cylinder. The coolant in these passages can be held at a temperature different from that in the main cooling system if desired. A partial shroud on the inlet valve directs the inlet gases toward, and aids in scavenging residual gas from, the pocket.

The design in Fig. 5 was adopted in the beginning because the first objective was to measure end-gas temperature. By proper selection of spark-plug position it is easy to operate this type of combustion chamber so that the end gas is consistently in the measuring zone. The side pocket of the chamber overhangs the cylinder sufficiently for the transducer elements to clear the adjacent wall. A later design employs a flat open chamber (Fig. 6).

Fig. 7 shows a section of the sending and receiving transducers. The metal bars, or "coupling rods," in the transducer elements provide the mechanical link between the barium titanate crystals and the inner surfaces of the test zone. They are clamped into position and must be provided with acoustical isolation from the engine structure. This isolation is required to prevent bypassing of acoustical energy through the cylinder walls. The bars are provided with water cooling on their outer portions to keep the barium titanate below its Curie point—about 200 F. The additional requirement for the practical operation of these transducers is that of effective shielding from electromagnetic radiation. The frequency used (about 2 megacycles per sec) is in the radio frequency spectrum—being just above the standard AM broadcast band. Since the transmitting crystal operates in the neighborhood of 1600 v (higher voltage may fracture the crystal), while the receiver operates with signals with values of a few millionths of a volt, great care must be used in the shielding of both the electronic "black boxes" and the transducer units themselves if troublesome "cross-talk" is to be avoided. However, this is not an unusual electronic problem, and it has been managed successfully.

More recently, this system has been applied to a normal CFR combustion chamber (Fig. 6). Here, one transducer is screwed into the top of the combustion chamber and the other into its side. The fact that the receiving transducer is at right angles to the output transducer appears to have little effect on the operation of the system.

Typical Results

Reproducibility of Results—A necessary preliminary to the appraisal of the results of any experiment is the question of reproducibility of replicate

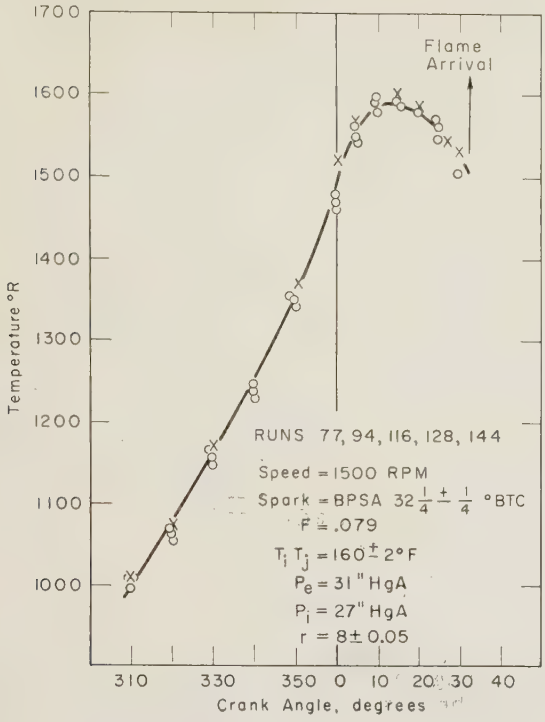

Fig. 8—Reproducibility of end-gas temperature readings

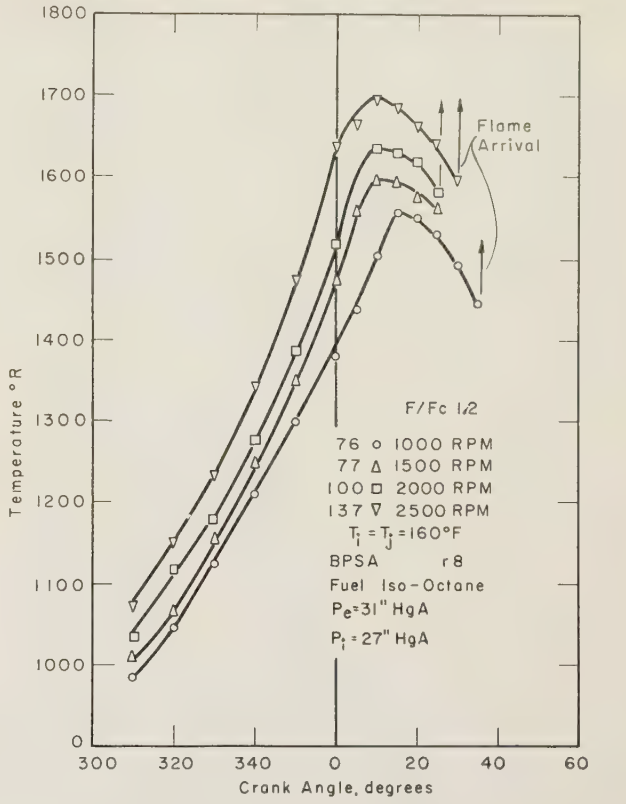

Fig. 9—Effect of speed on end-gas temperature at F/F_c of 1.2

tests. Fig. 8 shows the data from such a series. These particular data came from a whole series of tests designed to explore many engine variables; it was partly by oversight that some of these tests were duplicated and the operators were not aware of this fact until later. It would appear that the original goal of ±1% of the absolute temperature has been met. These data are not unusual, and similar results have been obtained many times under other operating conditions.

However, it must be pointed out that the scatter in Fig. 8 represents not only the inconsistency of the acoustic-electronic equipment and an operator's judgment of its meaning, but also reflects the extent to which an engine can be made to reproduce its own cycle over a period of days or weeks. To achieve this kind of repeatability requires great attention to many small details and rigorous control of important variables. In all fairness it should be remembered that under less than optimum conditions, engines simply will not behave in this nice manner—in fact sometimes they will not run at all!

Accuracy of Results—The "accuracy" or correctness, of the measurements from a new dynamic measuring instrument is always hard to establish. This difficulty arises because there is usually no suitable standard for comparison. In the present instance, it has been estimated[6] that if all the possible errors and uncertainties should conspire to be additive, the deviation from the "true" temperature might be 5%. It is perfectly plain, however, that this situation does not occur (otherwise there would be much greater dispersion in Fig. 8).

The only calibration which has been possible was made in a small steady-flow air tunnel. In this case, the stream temperature (and its gradients) could be checked by thermocouples. Up to 900 R (F abs) the agreement between thermocouples and acoustic device was within ± ½%.

Engine Variables and End-Gas Temperatures

Effect of Speed—Under the conditions of the runs shown in Fig. 9, an increase in speed caused an increase in end-gas temperature. This is caused by two effects:

1. There is a reduction in heat loss per unit mass as speed increases, due to the shortened time for heat transfer.

2. There is an induction work effect which will cause an increase in compression temperature. The temperature of the charge is lowered by the work done on the piston during the inlet stroke. As speed increases, this work decreases, due to increasing pressure drop through the inlet valve.[7] This effect is probably considerably more important than the heat loss effect.

Effect of Fuel-Air Ratio—The effect of fuel-air ratio on compression temperature (Figs. 10 and 11) reflects the well-known effect of fuel-air ratio on combustion and expansion temperatures.[8] The temperatures during compression are affected directly by the influence of expansion temperatures on cylinder-wall and residual-gas temperatures.

Effect of Compression Ratio—As would be expected, end-gas temperatures are higher at higher compression ratios during the whole period from

[6] *Acoustical Society of America Journal*, Vol. 26, September, 1954, pp. 824–830: "Ultrasonic Temperature Measurement in Internal-Combustion Engine Chamber," by J. C. Livengood, T. P. Rona, and J. J. Baruch.

[7] SAE *Quarterly* Transactions, Vol. 6, October, 1952, pp. 617–636: "Volumetric Efficiency of Four-Stroke Engines," by J. C. Livengood, A. R. Rogowski, and C. F. Taylor.

[8] Fig. 25 of "The Internal Combustion Engine," by C. F. Taylor and E. S. Taylor.

310 deg crank-angle to flame arrival (Figs. 12 and 13). This is due to the higher pressures reached at the higher compression ratios.

Effect of Inlet Temperature—Increasing the inlet temperature in general increases the temperature during the compression stroke. Compression and end-gas temperatures vary less than in proportion to inlet temperature due to heat transfer, chiefly from the inlet valve and port. (See Figs. 14 and 15.)

The effect of engine speed on the slope of the end-gas temperature versus inlet temperature curves in Fig. 15 is particularly interesting. At very low engine speeds the freshly inducted charge temperature will approach the jacket temperature, regardless of changes in inlet temperature. As speed increases, the heat-transfer effect grows smaller and the end-gas temperature tends to be more nearly proportional to the inlet temperature.

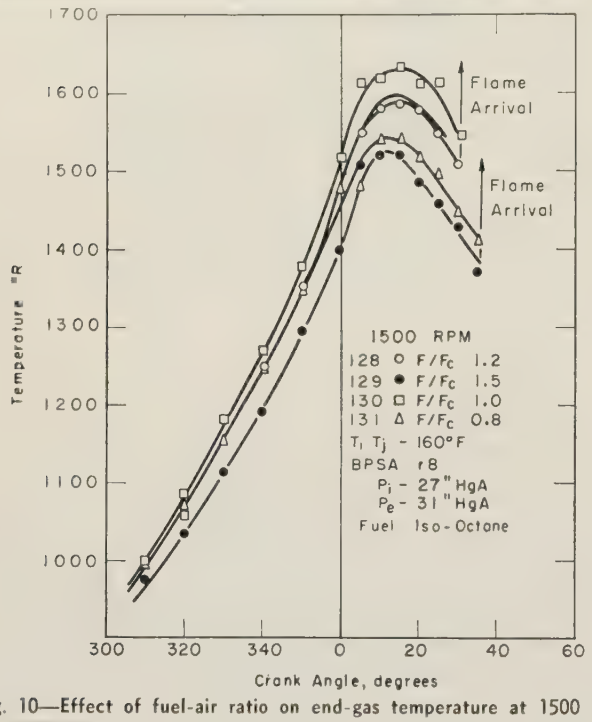

Fig. 10—Effect of fuel-air ratio on end-gas temperature at 1500 rpm

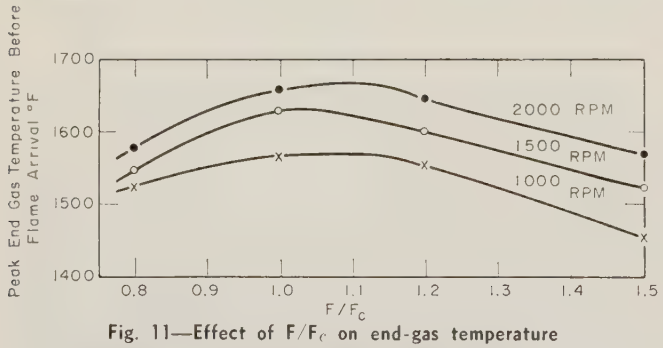

Fig. 11—Effect of F/F_c on end-gas temperature

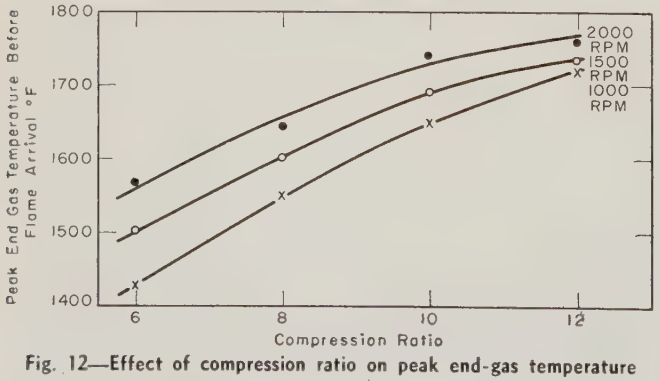

Fig. 12—Effect of compression ratio on peak end-gas temperature

Effect of Spark Advance—The chief differences in the curves of Fig. 16 occur after combustion starts. These differences are of the character to be expected from the fact that the start of combustion occurs at different crank-angles, while the crank-angle occupied by combustion remains nearly constant, except for run 119 where expansion by the piston prevents the flame from entering the measuring zone until later than 80-deg atdc. As would be expected, peak end-gas temperatures are highest when the flame reaches the end gas nearest tdc (Fig. 17).

The trend toward higher temperature *before* ignition, as spark is advanced, is due to the higher wall temperatures caused by advancing the spark. It is a well-known fact that heat loss to the coolant increases as the spark is advanced.

These results show plainly why spark timing has such a powerful effect on octane requirement.

Applications

While end-gas temperature as a function of independent engine variables has been the main objective of the development of the sound-velocity

Table 1—Specifications for Test Run No. 161

Fuel: Isooctane
Fuel-air ratio: 1.2 × stoichiometric = 0.0792
Compression ratio: 8/1
P_i = 16.6 psia p_e = 9.8 psia
T_i = 160 F
T_j = 160 F
Speed: 1500 rpm
Spark advance: 27-deg btdc (best power)

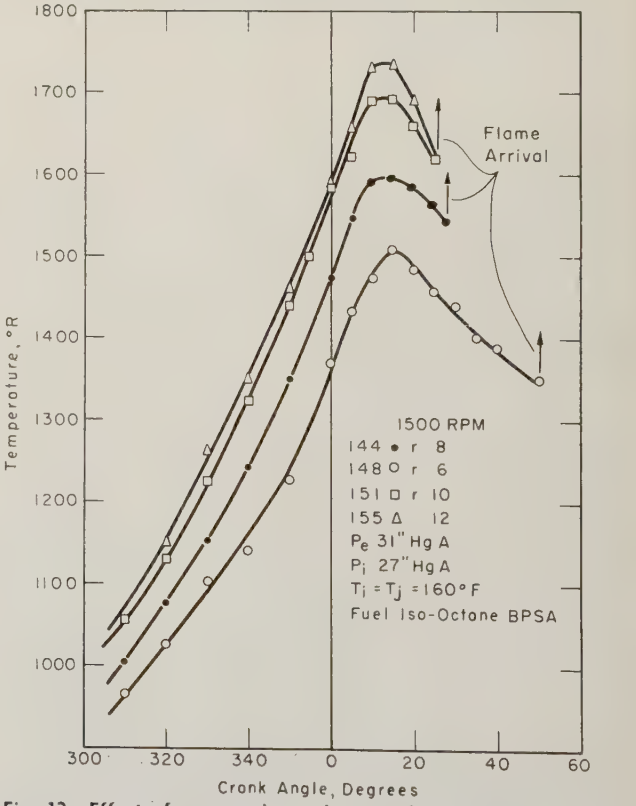

Fig. 13—Effect of compression ratio on end-gas temperature at 1500 rpm

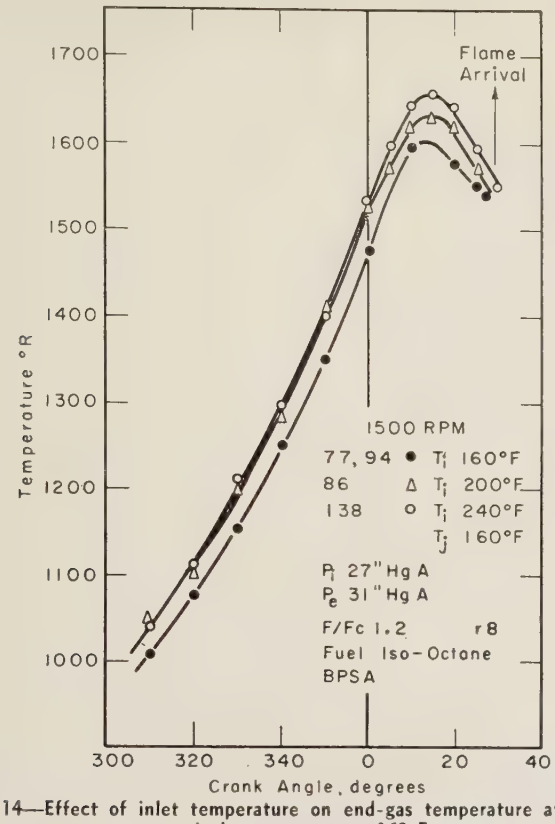

Fig. 14—Effect of inlet temperature on end-gas temperature at 1500 rpm, jacket temperature 160 F

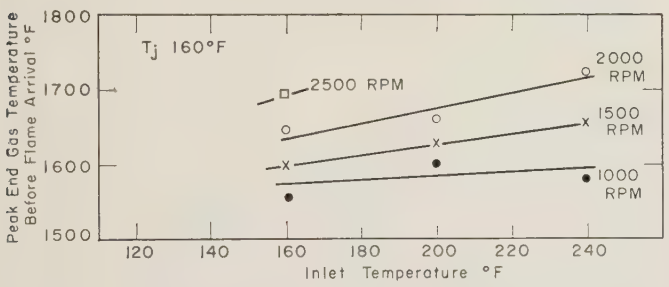

Fig. 15—Effect of inlet temperature on peak end-gas temperature

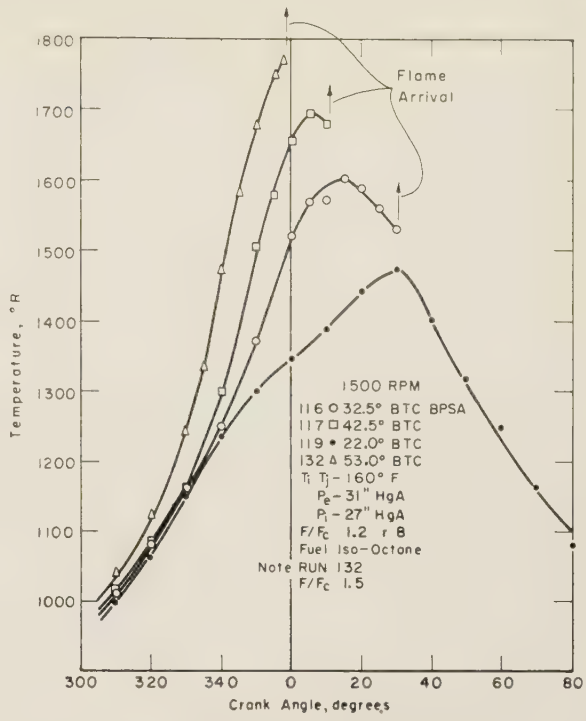

Fig. 16—Effect of spark advance on end-gas temperature at 1500 rpm

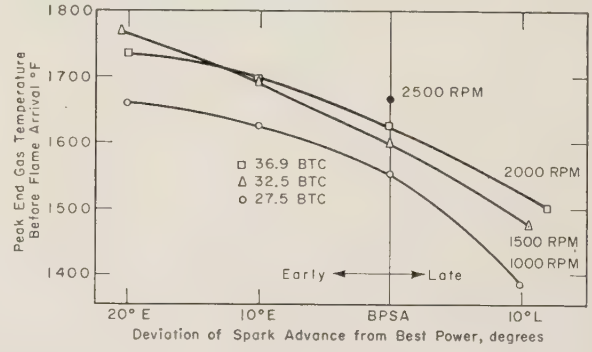

Fig. 17—Effect of spark advance on peak end-gas temperature at 1500 rpm

technique, the temperature data have other important uses. For example, the temperature measurements make possible the evaluation of many quantities which hitherto could only be estimated. Included among these are the extent and character of the heat losses during the several phases of the cycle, and the losses due to noninstantaneous combustion. In general, these losses are evaluated by first constructing an appropriate theoretical cycle with which the real cycle can be compared.

Theoretical Cycles—The usual assumptions for a theoretical cycle include:

1. No heat transfer during the cycle.
2. Combustion occurs at constant volume to full equilibrium conditions.
3. Temperature, pressure, and composition are uniform throughout the charge.

In the past, most computations of theoretical cycles have been based on more or less arbitrary assumptions regarding the composition of the charge and its pressure and temperature at the start of the compression stroke.

Heretofore, pressure measurements on the compression stroke have been possible provided a suitable indicator was available. However, measurement of pressure and temperature during compression makes possible the construction of a more realistic theoretical cycle from which a more accurate evaluation of the losses can be obtained.

An "equivalent" theoretical cycle is defined as one which has the following characteristics in common with a real cycle with which it is to be compared:

1. Fuel-air ratio.
2. Residual-gas fraction.
3. Pressure and temperature at a given fraction of the compression stroke. (This point must be taken after valve closing, but before ignition, in the real cycle.)

Your authors have been using the thermodynamic charts of Hottel et al[9] as the basis for the construction of such theoretical cycles. As an example of the process of constructing an equivalent theoretical cycle, run no. 161 (Figs. 18 and 19) has been used as a basis. The specifications for this run are shown in Table 1.

Details of the method used in constructing the

[9] "Thermodynamic Charts for Combustion Processes," by H. C. Hottel, et al. Pub. by John Wiley and Sons, Inc., New York, 1949.

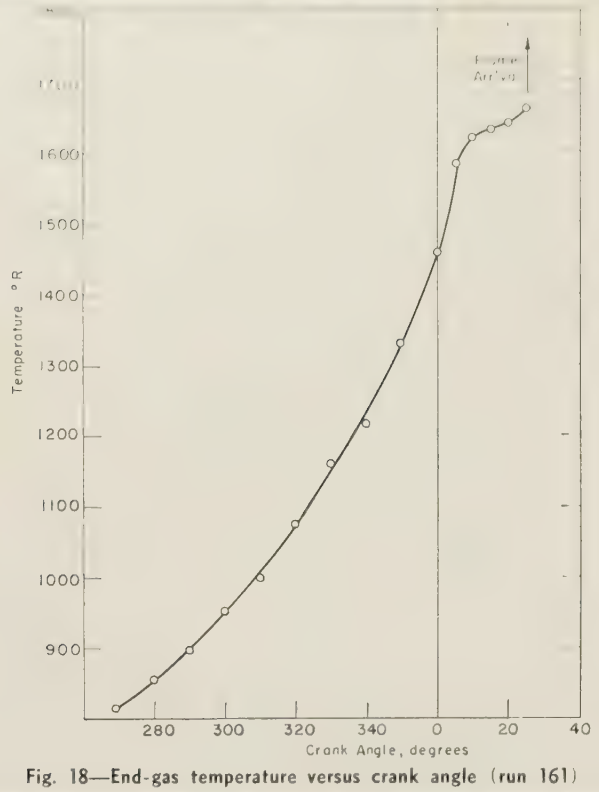

Fig. 18—End-gas temperature versus crank angle (run 161)

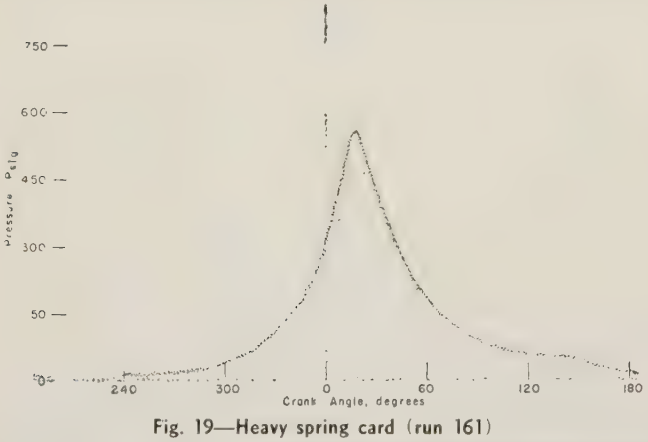

Fig. 19—Heavy spring card (run 161)

equivalent cycle for this run are given in Appendix III. The p-V diagrams for the real and equivalent cycles are plotted together in Fig. 20. Fig. 21 shows temperature versus specific volume for the two cycles.

Since temperatures for the real cycle were measured in the end gas, the specific volume after combustion starts (Fig. 21) goes to smaller values than the minimum of the theoretical cycle.

In the cycle in question (run 161), the accuracy of establishing the conditions for the equivalent cycle at the point of coincidence, and also the accuracy of the residual-gas calculation, depend on how nearly the temperature measured in the end-gas zone represents the average temperature in the cylinder. Sound-velocity measurements in a conventional CFR cylinder (Fig. 26) indicate that before ignition the temperature in the special end-gas chamber is reasonably representative of that of the whole charge.

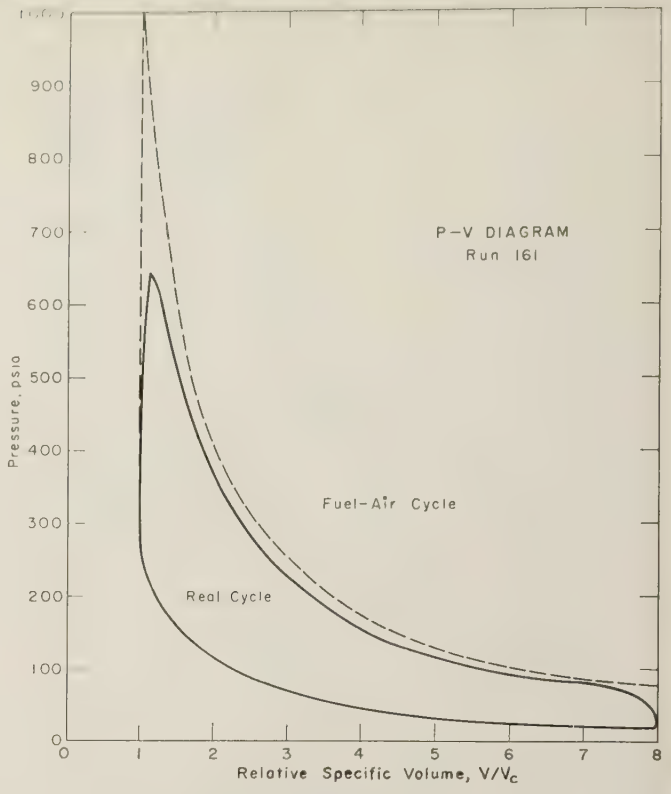

Fig. 20—Cylinder pressure versus volume for real and fuel-air cycle (run 161)

From Figs. 20 and 21 it can be seen that the compression stroke of the real cycle is very nearly isentropic. Assuming leakage negligible, the difference in area of the p-V diagrams of the two cycles represents the power loss due to noninstantaneous burning, and heat loss during combustion and expansion. In run 161, this loss is 22% of the work of the fuel-air cycle, or the real cycle work is 78% of that of the fuel-air cycle. It would be interesting to see how this power loss is related to engine variables such as speed, jacket temperature, and the like. By measuring the indicator card, the real cycle of Fig. 20 has an imep of 143 psi. The corresponding indicated thermal efficiency is 29.6% and the indicated specific fuel consumption is 0.448 $\frac{\text{lb}}{\text{ihp-hr}}$

These values indicate that this engine is comparable to normal spark-ignition engines in indicated power and efficiency, in spite of the unconventional combustion chamber.

p-T Log-Log Plot for Unburned End Gas—For the unburned end gas in an engine, the compression process can be represented by one or more polytropic processes, in which $pV^n = \text{constant}$. It can be shown that for such a process in a perfect gas:

$$\frac{d(\log T)}{d(\log p)} = \frac{n-1}{n} \qquad (2)$$

Therefore, if the temperature and pressure of the end gas are plotted on log-log paper, the slope of the curve is $\frac{n-1}{n}$. If the process is isentropic, $n = k$.

Fig. 22 is such a plot for the unburned end gas in run 161. The curve is very nearly a straight line. From its slope, the value of n is found to be 1.35, which is very nearly the isentropic value for this mixture.

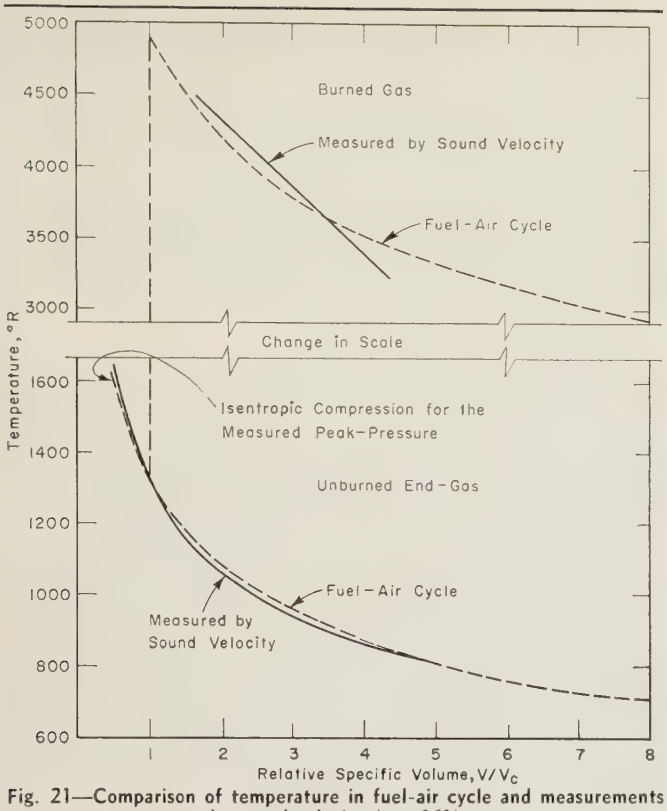

Fig. 21—Comparison of temperature in fuel-air cycle and measurements by sound velocity (run 161)

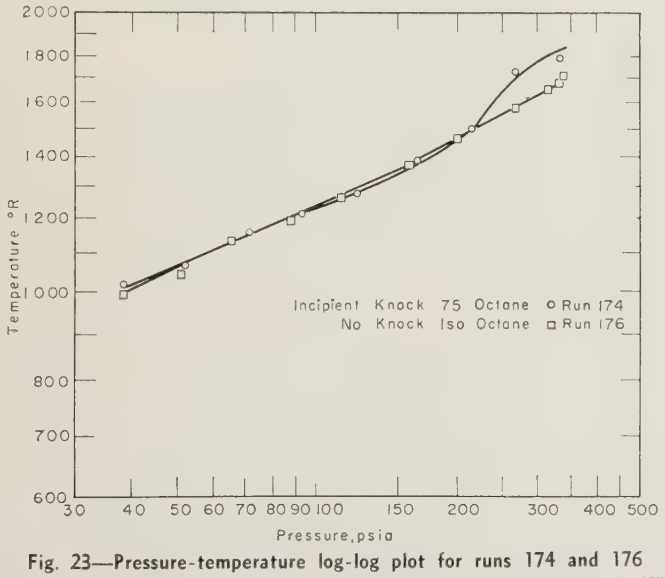

Fig. 23—Pressure-temperature log-log plot for runs 174 and 176

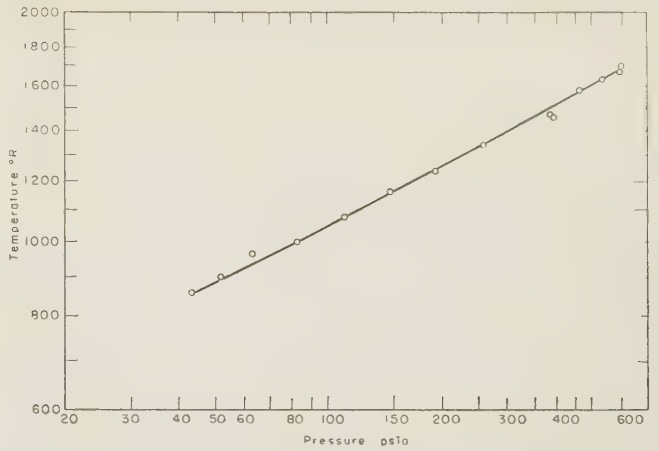

Fig. 22—Log-log plot of pressure versus temperature in unburned gas (run 161)

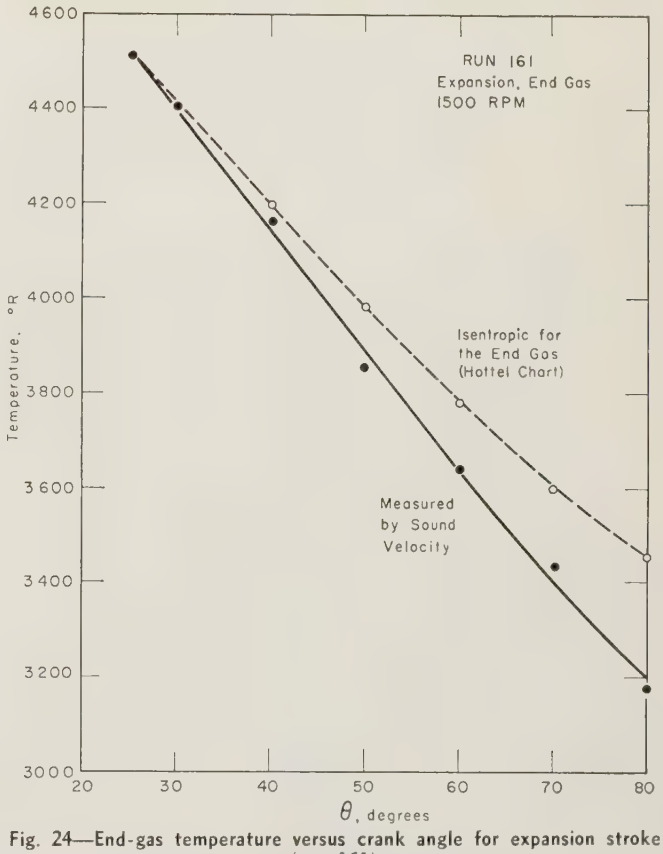

Fig. 24—End-gas temperature versus crank angle for expansion stroke (run 161)

Run 161 was made with isooctane as fuel and was not knocking. In many runs made with lower octane number primary reference blend fuels, with audible knock or near the point of knocking, the p-T log-log plots show a sudden upturn near the high-temperature end. (See Fig. 23, run 174.) At such points, the value of n is too large to be accounted for by heat transfer alone and is due to the heat release in the end gas through the precombustion reactions.

Heat Loss during Expansion Stroke—During the compression stroke, the gas temperatures are relatively low, and hence the heat loss to the cylinder walls is quite small. However, during combustion and expansion, the gas temperatures are several thousand deg R and the heat loss to the walls becomes appreciable. With the sound-velocity technique, it is possible to trace the state of the burned end gas through a good part of the expansion process. If the expansion process is again assumed to be polytropic, then $pV^n = \text{constant}$ and $n > k$ for an expansion with heat loss.

For run 161, the temperature of the burned gas in the end-gas zone is plotted against crank-angle in Fig. 24. An isentropic expansion curve starting from the same point (25-deg atdc) is drawn with the aid of a Hottel chart.[9] Fig. 25 shows the corresponding T-p log-log plot. The isentropic line gives a value for $k_{\text{average}} = 1.25$. The measured line gives $n = 1.33$.

Calculation of Residuals—The percentages of residuals present in the cylinder can be calculated

from the following equation:

$$f = 1 - \frac{M(1+F)RT}{pVm} \qquad (3)$$

The accuracy of this method of calculation of residuals depends not only on the accuracy of measurement of p, V, M and T, but on the assumption that the temperature measured in the end gas is the average temperature in the cylinder. As can be seen from the equation above, if the measured temperature is lower than the average temperature, the value obtained for the percentage of residuals is greater than the correct value.

Fig. 26 shows a comparison of temperatures at several speeds with the unconventional, pocketed chamber (Fig. 5) and similar curves run with the open chamber (Fig. 6). Two things are apparent from Fig. 26. The first is that the open-chamber configuration and the spark-plug arrangement used did not quite place the end gas in the measuring zone. The second point is that, particularly at the higher speeds, the open chamber tends toward higher temperatures of the gases before ignition.

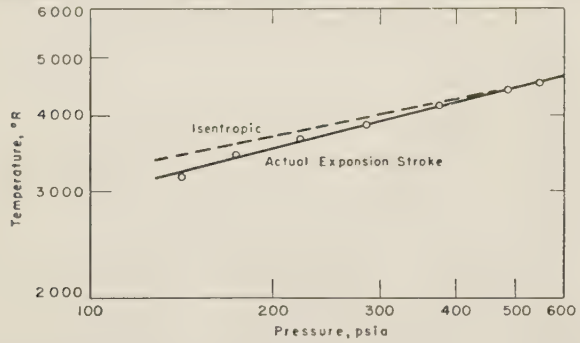

Fig. 25—Log-log plot of pressure versus temperature in burned gas (run 161)

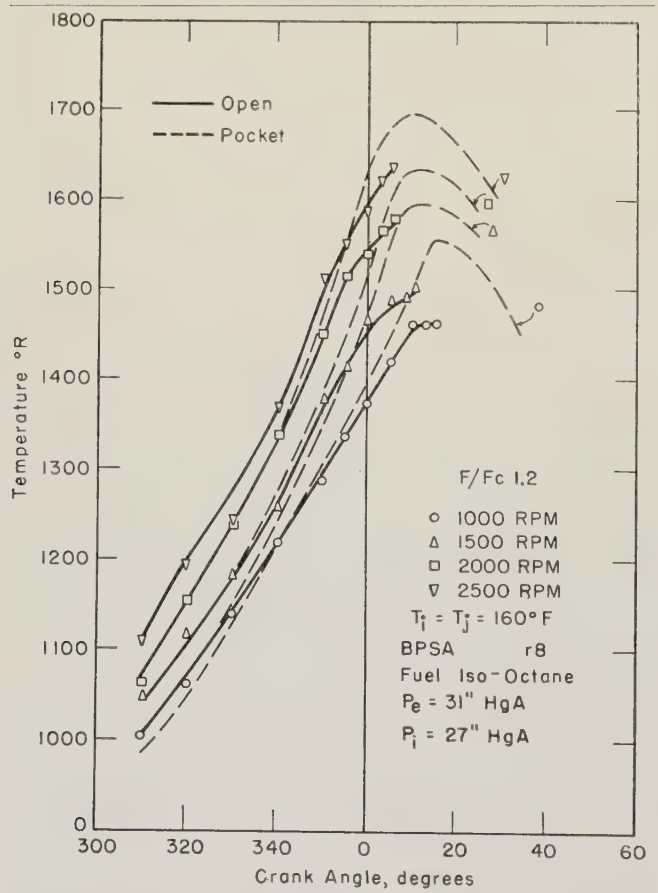

Fig. 26—Effect of speed on end-gas temperature for open and pocketed chambers

The higher end-gas temperatures in the open chamber are probably due to smaller heat loss than in the special end-gas chamber of Fig. 5. It can also be inferred that temperatures measured in the end-gas chamber are probably lower than the average temperatures of the charge and, therefore, tend to yield calculated values of end-gas fraction greater than the real values.

Acknowledgments

This work was instigated by and has been generously supported by the Coordinating Research Council, Inc. In addition to financial aid, this group has provided helpful guidance through the years. At various times financial support has also been provided by the Office of Ordnance Research, U. S. Army, and by a grant from the Shell Oil Co.

This report is a résumé of the work of many minds (and hands). Profs. Jordan Baruch and Thomas P. Rona deserve much credit for development of the apparatus and for interpretation of results. Edwin Jeffery and William Salmon performed the painstaking task of persuading the equipment to provide the data here presented. Professor C. Fayette Taylor has been in general charge of the project.

APPENDIX I

Symbols Used in Illustrations and Text

a = Velocity of sound
bpsa = Best power spark advance
btdc = Before top dead center
C_p = Specific heat at constant pressure
C_v = Specific heat at constant volume
f = Mass residual gas per mass charge
F = Fuel-air ratio (by weight)
F_c = Chemically correct fuel-air ratio
HgA = In. of Hg, abs
k = Ratio of specific heats (in text)
M = Mass of air entering cylinder during one induction stroke
m = Molecular weight
n = Polytropic exponent
p = Absolute pressure
p_e = Exhaust-receiver pressure
p_i = Inlet-receiver pressure
psi = Lb per sq in.
r = Volumetric compression ratio
rpm = Revolutions per min of crankshaft
R = Deg Rankine (deg F abs)
R = Universal gas constant
T = Absolute temperature
T_i = Inlet-receiver gas temperature
T_j = Water-jacket outlet temperature
X = Mole fraction
V = Volume

APPENDIX II

Sound Velocity in Engine Gas Mixtures

Unburned Mixtures—The sound velocity at various temperatures in the mixtures of fuel, air, and residual gas is calculated from the data on thermal properties of the components, considering the effects of composition, variable specific heat, and pressure.

Sound Velocity at Low Pressures—Basic assumptions and derived equations are as follows.

The perfect gas equation is the equation of state. For one mole of the mixture:

$$pV = RT \tag{4}$$

$$C^o_{pm} = \Sigma_i X_i C^o_{pi} \tag{5}$$

where:

X_i = Mole fraction of component i in the mixture
Subscript m = Mixture
Subscript i = Component i
Superscript o = Low pressures

$$C^o_{vm} = C^o_{pm} - R \tag{6}$$

$$a^o = \sqrt{\frac{k}{m} RT} \tag{7}$$

where: a^o = Sound velocity at low pressures

Sources of data:

Composition of mixtures:
Fresh mixture—Stoichiometric equation
Residual gas—Taylor[1], Fig. 32
Specific heat of fuels—National Bureau of Standards[10]
Specific heats of air and residual gas components—National Bureau of Standards[11]

Procedure for calculating sound velocity:

1. Calculate mixture composition, expressed in mole fraction of each component, X_i. Molecular weight of the mixture: $m_m = \Sigma_i X_i m_i$ (8)
2. For each temperature, find C^o_p for each component.
3. Find $C^o_{pm} = \Sigma_i X_i C^o_{pi}$
4. Find $C^o_{vm} = C^o_{pm} - R$
5. Find $k = C^o_{pm}/C^o_{vm}$
6. From the equation $a^o = \sqrt{\frac{k}{m} RT}$, calculate a^o
7. Plot a^o against T for each mixture (Fig. 27.)

Sound velocity in gas mixtures at elevated pressures—Assumptions and derived equations:

The equation of state for the gas mixture is a modified Beattie-Bridgman equation:

$$V = \frac{RT}{p} + \frac{\beta_m}{RT}$$

where: $$\beta_m = RTB_{om} - A_{om} - \frac{RC_m}{T^2} \tag{9}$$

V = Volume of one mole
B_{om}, A_{om}, C_m = Constants

The constants for the mixture are obtained from the constants for the components[12] by using the following formulas:

$$A_{om} = [\Sigma_i X_i \sqrt{A_{oi}}]^2 \tag{10}$$

$$B_{om} = \tfrac{1}{4}(\Sigma_i X_i B_{oi}) + \tfrac{3}{4}(\Sigma_i X_i B_{oi})^{1/3} + (\Sigma_i X_i B_{oi})^{2/3} \tag{11}$$

$$C_m = [\Sigma_i X_i \sqrt{C_i}]^2 \tag{12}$$

The expressions for C_p and C_v, for a gas mixture having the modified Beattie-Bridgman equation of state are, in consistent units:

$$C_p = C^o_p + \left[\frac{2A_o}{RT^2} + \frac{12C}{T^4}\right] p \tag{13}$$

$$C_v = C^o_v + \frac{6C}{T^4} p \tag{14}$$

The velocity of propagation of pressure waves of small amplitude (sound waves) in a substance is:

$$a = \sqrt{\left(\frac{\delta p}{\delta \rho}\right)_s} \tag{15}$$

or, the square root of the rate of change of pressure with respect to density at constant entropy.

For a gas mixture with the modified Beattie-Bridgman equation of state, the above equation can be transformed into:

$$a = \left[\frac{kRT}{m}\left(1 + \frac{2\beta_m}{VRT}\right)\right]^{1/2} \tag{16}$$

where k is the ratio of specific heats at the actual temperature and pressure concerned.

Sources of data: Constants for Beattie-Bridgman equation—Taylor and Glasstone.[12] Specific heat data—National Bureau of Standards.[10, 11]

Procedure for calculating sound velocity:

1. Calculate mixture composition.
2. For each temperature at the pressure in question, calculate C_{pm} and C_{vm}.
3. For each temperature, calculate β_m from the Beattie-Bridgman constants for the mixture.
4. Calculate sound velocity a for each temperature.
5. Plot a versus T for each pressure and mixture.

Approximate Method Used in Converting Sound Velocity into Temperature—Since the calculation of sound velocity at elevated pressures is a tedious task, an approximate method is employed in accounting for the effect of pressure while converting sound velocity into temperature in the unburned mixture. The assumption involved is that the effect of pressure on sound velocity at a given temperature is very nearly the same for air and for fuel-air mixtures. This is a reasonable assumption since pressure effect on sound velocity is an order smaller than the temperature effect. In the end gas of an engine, under the usual operating conditions, the pressure affects the sound velocity by 1.5% at the most. Since the mixture is mostly air, the difference between the pressure effect for the mixture and the pressure effect for air must be of smaller order of magnitude than the pressure effect itself. Thus, this difference would be a negligible quantity when compared with the magnitude of the sound velocity.

The sound velocity in air is tabulated for several pressures from 0.01 to 100 atm.[11] By plotting a^o/a versus pressure for given temperatures, the pressure effect on sound velocity is presented in graphical form (Fig. 28).

Procedure Used for Converting Sound Velocity

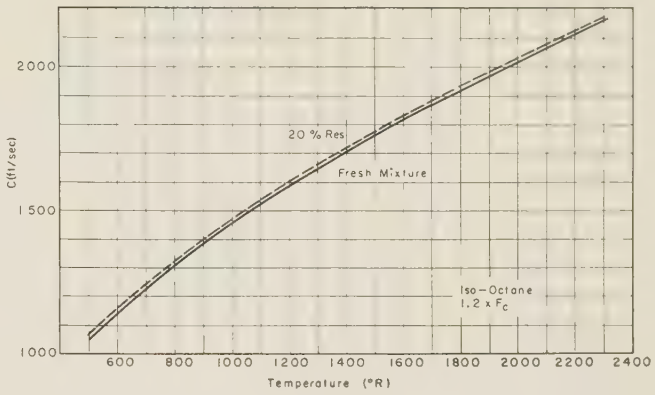

Fig. 27—Sound velocity versus temperature in unburned fuel-air mixture

[10] National Bureau of Standards, C 461: "Selected Properties of Hydrocarbons." Washington, D. C., 1947.
[11] National Bureau of Standards, C 564: "Tables of Thermal Properties of Gases." Washington, D. C., 1955.
[12] Pp. 187–352 of Treatise of Physical Chemistry, Vol. 2, "States of Matter," by H. S. Taylor and S. Glasstone. Pub. by Van Nostrand Co., Inc., 1951.

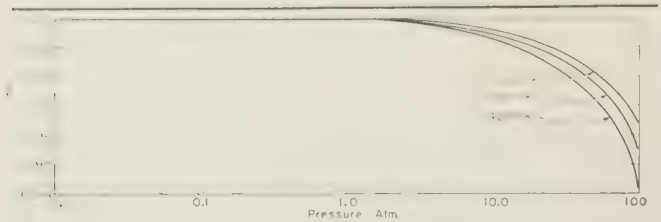

Fig. 28—Pressure effect on sound velocity dry air

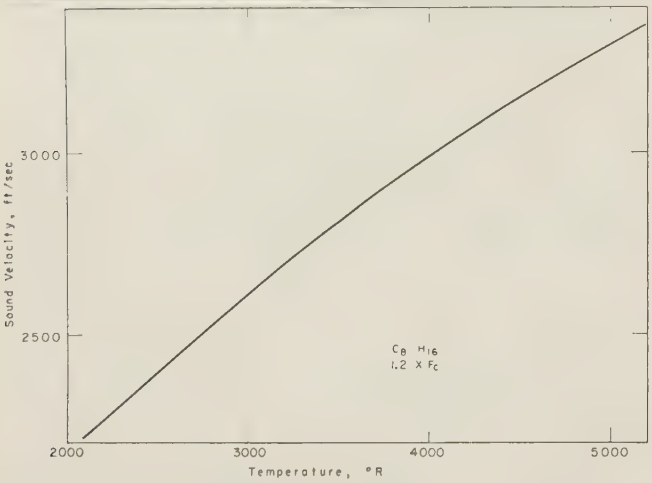

Fig. 29—Sound velocity in burned gas (from Hottel chart)

into Temperature—1. Record the measured sound velocity and pressure.

2. Find a^o/a from Fig. 28 for the measured pressure. It can be seen on Fig. 28 that the a^o/a curves for different temperatures are quite close together.

3. Multiply the measured sound velocity a by a^o/a to obtain a^o, which is the sound velocity at the same temperature if the pressure is very low.

4. Read temperature corresponding to a^o from the chart prepared for low pressures (Fig. 27).

Burned Gas at High Temperatures

Behavior of Burned Gas at High Temperatures and Source of Data—At the high temperatures encountered in the burned gas in an engine, the gas composition is no longer fixed. Chemical equilibrium exists in the hydrogen-carbon-oxygen-nitrogen system. The calculation of the equilibrium composition at various temperatures and pressures is a lengthy task. Fortunately, thermodynamic charts[9] provide the necessary data from which the sound velocity of the gas mixture can be calculated.

Since $a = \sqrt{\left(\frac{\delta p}{\delta \rho}\right)_s}$, it is a straightforward matter to obtain values of p, T, and ρ along a line of constant entropy on the charts prepared for the products of combustion, and calculate the sound velocity.

Procedure for Calculating Sound Velocity in Burned Gas—1. Select a "burned product" chart[9] corresponding to the fuel-air ratio used in the engine. Although these charts are prepared for octene (C_8H_{16})-air mixtures, they can be used for isooctane-air mixtures since the atomic composition of the systems are so close together.

2. Select a line of constant entropy with temperature and pressure approximately corresponding to the conditions expected in the burned gas of an engine. It has been found that as long as the temperatures and pressures along the line appear reasonable, the exact selection of the constant entropy line is unimportant. In other words, different constant entropy lines selected will lead to the same sound velocity versus temperature curves.

3. For each temperature, accurately read the pressure and the volume. These readings are taken at the points of intersection of the constant entropy line with the lines of constant temperature.

4. Calculate the density at each point from the volume reading and the mass basis of the chart.

5. Find Δp between two successive points.

6. Find $\Delta \rho_s$ between two successive points.

7. Find $\left(\frac{\Delta p}{\Delta \rho}\right)_s$.

8. Convert the value obtained for $\left(\frac{\Delta p}{\Delta \rho}\right)_s$ into a quantity having a dimension of the square of velocity. The conversion factor from force into mass × acceleration enters the picture here.

9. Taking the square root of the above quantity gives the sound velocity for an average temperature midway between the two successive points on the constant entropy line.

10. Plot the sound velocity against temperature, as illustrated in Fig. 29.

APPENDIX III

Construction of Equivalent Fuel-Air Cycle for Run No. 161, Fig. 20

Fig. 19 shows the original p-θ indicator diagram for run #161. Fig. 20 shows this diagram translated to the p-V basis, and its equivalent fuel-air cycle.

The equivalent fuel-air cycle is defined as a constant volume (otto-type) cycle having the following characteristics in common with the real cycle: fuel-air ratio, compression ratio, residual-gas fraction, and temperature and pressure at some common point on the compression line.

The fuel-air cycle is assumed to have combustion at tdc, with chemical and physical equilibrium at all points on the compression and expansion lines, and no heat exchange with the cylinder walls.

Equilibrium thermodynamic characteristics are taken from suitable experimental data, such as those of Hottel et al.[9]

The following notation will be used:

E = Internal energy, Btu per lb mole

V = Volume of 1 lb mole, cu ft

Starred values are for a total charge mass of $(1 + F)$ lb

Value with subscript s are thermodynamic values neglecting chemical effects.[9]

For run 161, the equivalent fuel-air cycle is constructed as follows:

1. The first available reading of temperature is at 270-deg crank-angle, where $T = 817$ R (Fig. 18) and the pressure (Fig. 19) is 31.4 psia. The cylinder volume above the piston at this point is 26.09 cu in. or 0.01511 cu ft.

The measured mass M_a of fresh air inducted is 0.001275 lb per cycle and of fuel, 0.000101 lb per cycle. Hence, the fuel-air ratio:

$$F = \frac{0.000101}{0.001275} = 0.079 \qquad (17)$$

The total mass in the cylinder is, by definition:

$$M_{cyl} = \frac{M_a(1 + F)}{1 - f} \qquad (18)$$

From the gas law, for the charge at 270 deg crank angle:

$$pV = \frac{M_a(1+F)}{(1-f)}RT \qquad (19)$$

The charge's molecular weight is close to 30.1.

Substituting known values in the above equation and solving for f, gives $f = 0.15$

The chart for unburned mixture[9] can be entered at $T = 817$ R, $p = 31.4$ psia, $f = 0.15$, and $F/F_c = 1.2$.

From this chart it is determined that at 270 deg crank-angle, $V_{270} = 275$ cu ft per lb-mole mixture.

For this CFR engine at a compression ratio of eight the following ratios of volume are known:

$V_1/V_{\text{clearance}} \equiv r = 8$
$V_{270}/V_{\text{clearance}} = 4.9$
$V_1/V_{270} = 1.63$

Hence, V_2 for the theoretical cycle is:

$$V_2 = V_{270}/4.9 = \frac{275}{4.9} = 56.2 \text{ cu ft per lb-mole} \qquad (20)$$

and: $p_2 = 250$ psia
$T_2 = 1330$ R
$E_2 = 4785$ Btu per lb-mole

Similarly, at point 1 in the cycle:

$p_1 = 17$ psia
$T_1 = 700$ deg R
$E_1 = 800$ Btu per lb-mole

(T_1 is thus about 80 deg above the inlet temperature, which reflects the effects of heat transfer and mixing with hot residuals.)

2. Combustion

Since the charts of thermodynamic properties of the unburned mixture apply to 1 lb mole, and the charts for burned mixture to $(1+F)$ lb, the volumes and internal energies on the burned charts will be $(1+F)/m$ times the corresponding values on the charts for unburned mixture. Values of $(1+F)/m$ are given in Fig. 5 of Hottel.[9]

Hence, the "burned" chart for $F/F_c = 1.2$ is entered at:

$$E_3^* = E_2^* + 1300\ (1-f)(F/F_c) + 336f = 1547 \text{ Btu}$$

where:

$E^{2*} = E_2 y = 4785 \times 0.0358 = 171$
$y = 0.0358$ (Fig. 5 of Hottel)
$V_c^* = V_2 y - 2.01$ cu ft

From the chart for the burned products it can be determined that: $p_3 = 1040$ psia and $T_3 = 4875$ R

By assuming an isentropic expansion $(r = 8)$, the values at the end of expansion for the equivalent cycle are: $V_4^* = 8 \times V_3^* = 8(2.01) = 16.08$ cu ft

$p_4 = 76$ psia
$T_4 = 2930$ R
$E_4^* = 925$ Btu

From these data the theoretical cycles shown in Figs. 20 and 21 can be constructed.

The efficiency of the fuel-air cycle is:

$$\eta = \frac{\text{Work of cycle}}{\text{Heat of combustion}} = \frac{(E_3^* - E_4^*) - (E_2^* - E_1^*)}{(1-f)(1300)F/F_c}$$

where: $E_1^* = E_1 y$ (Fig. 5, Hottel)

$E_1^* = 29$ Btu
$\eta = 0.362$

The mean effective pressure of the cycle is:

$$\text{mep} = \frac{\text{work of cycle}}{(V_1 - V_2)} = \frac{480 \times 778}{(16.08 - 2.01)144}$$

$$\text{mep} = 184 \text{ psi}$$

DISCUSSION

Describes 2-Wavelength Infrared Method For Determining End-Gas Temperature

—Dr. John T. Agnew
Purdue University

THIS discussion will describe preliminary results on another method for measuring end-gas temperature in an engine cylinder—the 2-wavelength infrared method using the water vapor molecules as the "thermometer."

Heated water vapor emits radiation at discrete wavelengths in the infrared region. In order to have a method which would be capable of following the rapid temperature change occurring in an engine cylinder during the period before ignition on the compression stroke, a radiation detector of sufficient rapidity of response must be used. This requirement rules out the use of a thermocouple detector. In the near infrared region, water vapor has six emission peaks when examined with a dispersion system of sufficient resolution. These radiation peaks are grouped into three spectral regions; a pair of peaks at 1.35 and 1.44 microns, a triplet structure at 1.81, 1.86, and 1.95 microns, and a pair at 2.5 and 2.7 microns. The lead-sulfide photoconductive cell has sufficient speed of response and sensitivity in this spectral range to make its use feasible as the detector.

The basic theory behind the 2-wavelength infrared method for determining temperature is that the ratio of the monochromatic intensity of radiation at two specific wavelengths is a function of temperature. However, not only must the intensity of radiation at two specific wavelengths be measured, but also the monochromatic emissivity at each of the two wavelengths must be known. Utilizing Planck's well-known radiation formula, the basic equation used in the temperature determination is:

$$\frac{E_1}{E_2} = \left(\frac{\varepsilon_1}{\varepsilon_2}\right)\left(\frac{\lambda_2}{\lambda_1}\right)\left(\frac{e^{C_2/\lambda_2 T}-1}{e^{C_2/\lambda_1 T}-1}\right) \qquad (a)$$

In order to make a temperature determination, the values of the intensity ratio E_1/E_2 and the emissivity ratio $\varepsilon_1/\varepsilon_2$ must be experimentally determined. The emissivity ratio must be determined by separate calibration experiments in which the temperature of the water vapor is known.

A complicating factor is that the emissivity ratio is a function of the optical depth of the water vapor (product of water vapor partial pressure times the path length). This problem has been investigated at Purdue University[a] and the effects of monochromator slit width and choice of wavelengths have been evaluated.

For end-gas temperature measurements in the temperature range 1000–1700 R large monochromator slit widths must be used in order to obtain sufficient signal intensity at the two wavelengths. This has the effect of giving essentially three radiation peaks from the water vapor near 1.4, 1.9, and 2.5 microns. The peak at 2.7 microns is greatly reduced in intensity by the spectral sensitivity characteristics of the lead sulfide cell. Wavelength settings near the 1.9 and 2.5 radiation peaks have been chosen for temperature determinations in the engine. Using a lithium fluoride prism as the dispersing medium in a Perkin-Elmer infrared monochromator with a slit width of 1000 microns satisfactory intensity readings at these two wavelengths have been obtained from a motored engine.

Preliminary experimentation indicates that the method shows considerable promise, particularly if electronic instrumentation is incorporated into the measurement technique so that the effect of cyclic variations can be evalu-

[a] "The Determination of the Temperature of Water Vapor by Infrared Spectroscopy in the Near Infrared," by Merrill L. Haviland. M. S. Thesis, Purdue University, Department of Mechanical Engineering, January, 1956.

ated. Ultimately it is believed that a two-detector system could be designed so that simultaneous measurement of the radiation intensity at the two wavelengths could be made as a function of crank-angle position. Thus, the temperature-time history of the end gas could be obtained for individual engine cycles.

Comments on Accuracy Of Authors' Method

—Dr. M. E. Gluckstein
Ethyl Corp.

THE observations reported by the authors in measuring end-gas temperatures in engines under laboratory conditions have demonstrated the practicality of this technique, which appears to have been suggested on theoretical grounds by Nernst and Keutel in 1910.[b] The contribution by Mr. Livengood and his coworkers at M.I.T. in developing a device of this type is a most significant accomplishment, and together with some of the data they have presented should arouse interest in the method among others.

In the discussion to follow I would like to present in brief some of the experiences we have had in our Research Laboratories in Detroit in measuring temperatures by this technique and describe some important, although not basic, changes in equipment design.

At our laboratories we are using an instrument which is similar in all respects to that described in the paper, but which has been modified for more convenient operation. In this equipment, breaker points for actuating the signal generator and oscilloscope have been replaced with an electronic counting system. This device counts the number of crank-angle degrees (from tdc) and at a preset point triggers the apparatus. The operator controls the triggering point by means of a simple switching arrangement, and can preset to any point in the cycle in 1 or 2 sec. This counter is also used as a time base for pressure measurements and offers improvement over the mechanical technique (breaker points) both as to accuracy of setting and for operational convenience. This counting equipment is also suitable for other applications where accurate and rugged time base is desirable.

In order to demonstrate the accuracy of this method as a measurement of temperature, a considerable effort was made to verify measurements obtained from the speed of sound by comparison with another technique. We chose as our reference method the direct application of an equation of state for air to measured pressure-volume data in a motored engine, and utilized the equation:

$$pV = znRT \qquad \text{(b)}$$

where z is the compressibility factor and is very near unity for the pressures and temperatures investigated. Its values were obtained from the National Bureau of Standards,[11] as was the relationship between the speed of sound and temperature. By careful calibration of the engine volume-crank angle relation and a closed-loop leakage calibration, it was possible to estimate the order of accuracy of the reference technique and make a direct comparison with the speed of sound method. The agreement between the two methods was within 1% except near tdc. In this range, the reference technique is extremely sensitive to small errors and is not wholly reliable. The speed of sound technique is not subject to these errors in this regime and its is felt that this accuracy may be reliably extrapolated. It would appear that an absolute accuracy of about $\pm 1\%$ can be expected, at least with air as the working fluid. The precision (reproducibility) has been shown to be within the same general limits, if an allowance is made for the rather variable behavior of an engine.

A number of runs made in a fired engine at 1 deg crank-angle increments show a high level of reproducibility both as to the magnitude and shape of the temperature-time curves (Fig. A). It must be remembered that this technique does not give a true point value but is an average over a range of perhaps 0.1 to 0.5 crank-angle deg. If simultaneous pressure measurements are made (as would be desirable if a complete description of the state of the gas is wanted), an additional uncertainty is introduced due to the finite time of response of the pressure transducer and its inherent accuracy. Thus, if one wants a measurement of the temperature, pressure, and crank angle at say 10-deg btc, the measurements obtained are subject to an inherent three-dimensional error. The magnitude of these uncertainties may be estimated and minimized but may not be entirely eliminated. In the discussion to this point it has been tacitly assumed that we have a complete description of the chemical state of the gas in the combustion chamber. This gross oversimplification limits the method when applied to the burned products. But, small variations in the composition do not materially affect the calculated temperatures in the unburned gas.

In Table A, the effect of arbitrary changes in composition on the calculated speed of sound is shown. The method of calculation is somewhat different from that used by the M.I.T. group but, as will be shown later, gives results which are only negligibly different.

The relative insensitivity of the calculated temperatures to composition is due to the large proportion of O_2 and N_2 in the mixture. This would not be the case if the oxidant were oxygen or beneficiated air.

The application of this technique to burned gases may be questionable, since the water vapor and carbon dioxide present may introduce large errors due to sonic dispersion and attenuation. We have demonstrated that it is not possible to propagate an unambiguous signal through a mixture of CO_2 and N_2 (11 mole % CO_2) at room temperature due to peculiarities in the behavior of CO_2. This effect is not entirely unexpected and is in keeping with previous observations. There is some question as to the definition of the speed of sound in a material which is reacting and not in thermodynamic equilibrium, as might be the case in the burned product. The difficulty in obtaining measurements in the burned gas may be attributable to these causes and not to a lowered pressure level.[c]

As our work has been primarily concerned with the end gas prior to the arrival of the flame or completion of the chemical reactions associated with knock, we have calculated our results using a simpler gas law than the M.I.T. group. There has been some question in our minds as to whether the use of the modified Beattie-Bridgeman equation is at all necessary in view of the approximate nature of the derivation, the indifferent quality of the available constants, and the variant nature of a fired engine. While it is certainly correct that the specific heats at constant pressure and volume vary with both temperature and pressure, the former variation is large compared to the latter and is reasonably well-established for most of the gases encountered. Because of the preponderance of the near ideal nitrogen and oxygen in the chamber mixture, it appears that a simplified approach may be justified.

In our work, we have assumed the following:

1. The speed of sound is given by the equation:

$$a^2 = \frac{kRT}{m} \qquad \text{(c)}$$

2. $C_p - C_v = R$ and $k = C_p/C_v$. The specific heats were taken as functions of T only, with a small pressure correction considered by using 7 atm as the base pressure, except for the hydrocarbons where C_p^o was used.

3. The residual composition is computed from stoichiometry and the fraction residuals from engine operating information.

4. Uniform, constant combustion chamber compositions.

5. Chemical equilibrium.

The entire computational procedure has been programmed for a Burrough's E-102 digital computer.

In order to establish the limitations of the assumptions, the temperatures for a motored run with air were com-

[b] "Thesis," by F. Keutel. Nernst Laboratory, Berlin, 1910. Also *Zeit. für Elektrochemie*, Vol. 48, 1942, pp. 62–82. Article by G. Damkohler.

[c] Private communication with C. F. Taylor.

Table A—Effect of Composition on Calculated Temperatures

Crank Angle	All Components	Calculated Temperature, K (neglect residuals)	"Air" + Fuel[a]
140	670	677	679
150	719	727	—
160	761	769	—
170	803	812	—
180	882	891	—
190	980	991	994

[a] Air considered as N_2, molecular weight = 29

puted as above and compared with those values obtained from the tables in Keutel.[b] The maximum error was less than ±1%. Further, the method was applied to some of the data presented by the authors and it was shown that the variation between the two methods is 1% or less for the unburned gas. It appears that the imposition of a complicated calculation technique is unwarranted and results of adequate accuracy may be obtained by simple, direct calculation.

At the present time we are investigating the temperature-pressure history of end gas under knocking conditions and hope to obtain information on the chemical and physical nature of the auto-ignition reactions. When this information is sufficiently developed, it will be published.

C_p = Specific heat at constant pressure
C_p^o = Specific heat at constant pressure in ideal gaseous state
C_v = Specific heat at constant volume
m = Molecular weight
n = Number of moles
p = Pressure
R = Gas constant per mole
V = Volume

Discusses Accuracy of Three Methods Of Measuring End-Gas Temperature

—Shoshi Shimizu and M. C. Burrows
University of Wisconsin

THE authors have presented a noteworthy contribution to a research problem subject to instrumental difficulties, engine vagaries, and innumerable pitfalls. We are particularly aware of the complexity of the problem and the excellent work done at M.I.T. since we are working the same problem under similar sponsorship.

Two other techniques have been under study at the University of Wisconsin, one using the changes in the absorption spectrum of iodine with temperature[d] and the other an infrared technique similar to the sodium line reversal method of temperature measurement except that water vapor is used instead of sodium as the sensing element.

In presenting any new technique, it is essential to evaluate the data obtained with respect to reproducibility, accuracy, and consistency of the data within itself. The authors have evaluated the reproducibility of their instrument and found it to be within ±1% which is appreciably better than that obtained for single cycles by the iodine-absorption technique as evidenced by the scatter in measured temperatures (Fig. B). The infrared technique is not as advanced in its development as the above methods, but present indications are that its reproducibility will be comparable to the sound-velocity technique.

As far as absolute accuracy is concerned, all three techniques face the same problem in that there is no standard of comparison other than studies on a steady-flow system. The authors show excellent agreement with the steady-flow system up to 900 R. Data taken under comparable conditions in a steady-flow system which was operable to 1200 R and using the infrared technique show similar

[d] SAE Transactions, Vol. 62, 1954, pp. 503–513: "Compression and End-Gas Temperatures from Iodine Absorption Spectra," by S. K. Chen, N. J. Beck, O. A. Uyehara, and P. S. Myers.

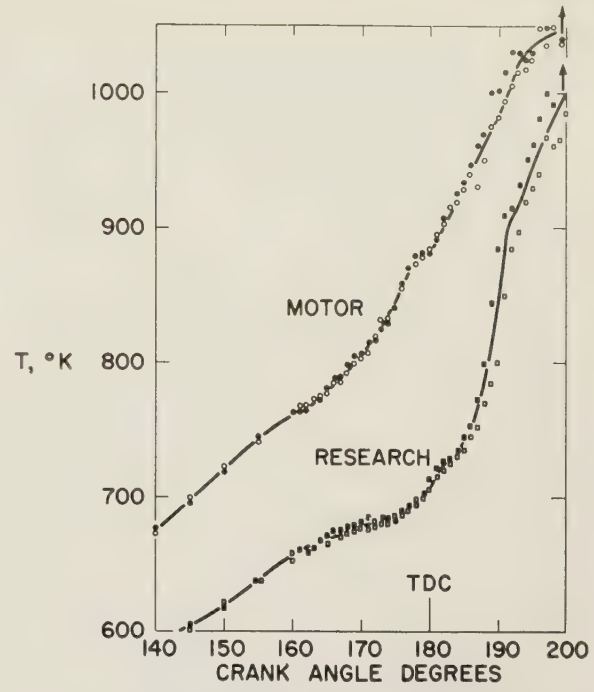

Fig. A—Temperature versus crank angle for 90 prf

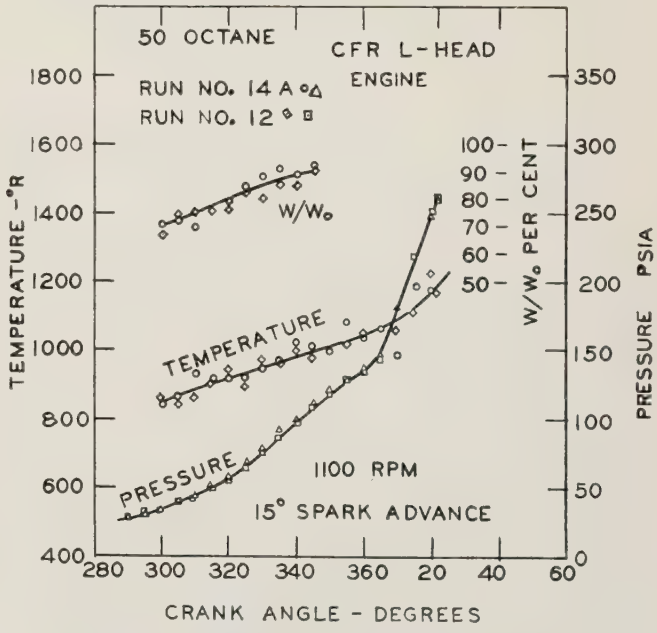

Fig. B—Data obtained with iodine-absorption technique

agreement. No directly comparable data are available for the iodine technique. However, both the 900 and the 1200 R are considerably below the measured peak values of end-gas temperatures presented by the authors.

With respect to the consistency of the temperature data within itself, the paper shows a marked scarcity of pressure data which is essential in determining this consistency. The only pressures given, (run no. 161) are for operating conditions which were unusual when compared with other data presented. In Fig. C temperature data for run 161 are compared with data of Fig. 8, showing the reproduciiblity of the sound-velocity instrument. The only difference in operating conditions between these runs is a small difference in the position of the spark and a large difference in the ratio of inlet-to-exhause pressure, and yet there is a marked difference in the trend of the temperature after tdc. Further inspection of the text will

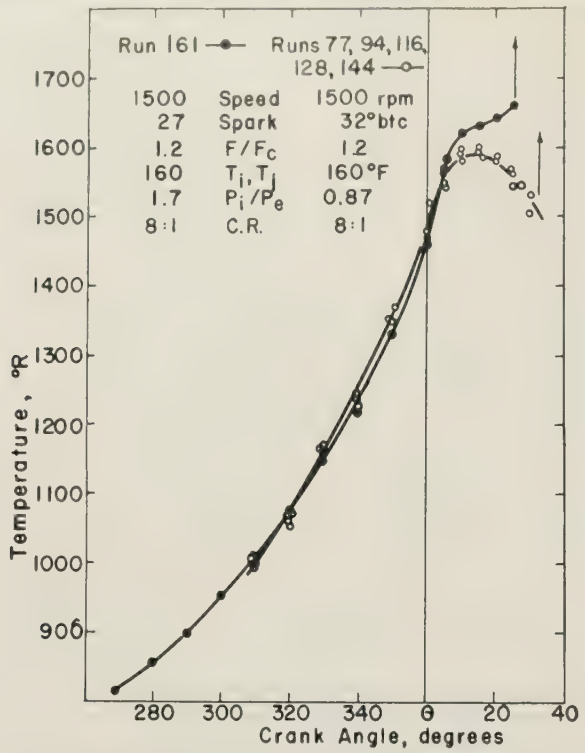

Fig. C—Comparison of run 161 with other data

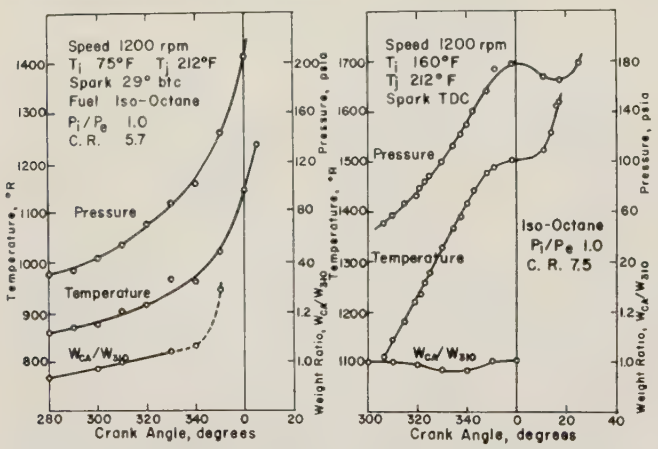

Fig. D—Data by iodine-absorption technique and infrared technique

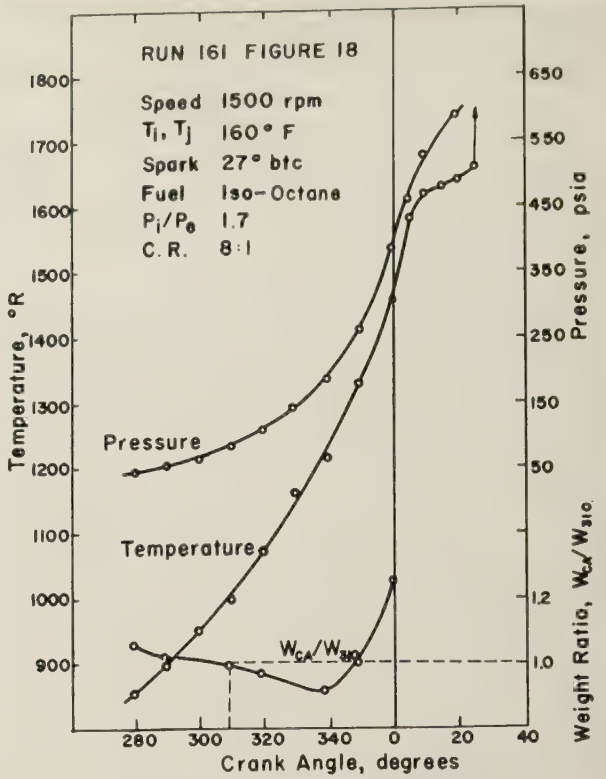

Fig. E—Data by sound-velocity technique

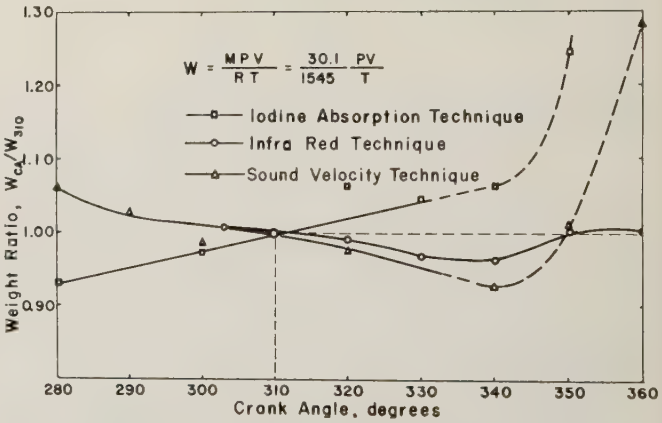

Fig. F—Comparison of weight of charge ratios

show that run 161 is the only data shown that has this upward trend in temperatures after tdc. Inasmuch as run 161 was analyzed in considerable detail it does not seem likely that the choice of this set of data (which had an inlet pressure higher than atmospheric and an exhaust pressure two-thirds atmospheric) was by chance. Perhaps the authors would tell us their reasons for this choice of run 161 for analysis purposes. Is it not possible that the pocketed chamber is poorly scavenged under normal operating conditions and only when the p_i/p_e ratio is high (resulting in better scavenging) does the sound-velocity instrument "see" a reasonably fresh mixture?

One method of checking the consistency of the data within itself is to plot the value of pV/RT as a function of crank-angle using the measured values of p, V, and T. If the entire mixture is homogeneous and the measurements accurate, a straight horizontal line should result up to the point of ignition with a value equal to the weight of gases trapped in the cylinder. In order to compare the consistency of the data directly from the three techniques the weight ratios, defined as the ratio of pV/RT at any crank-angle to pV/RT at 50 btdc, were computed and plotted. Fig. D shows the weight ratios obtained using the iodine-absorption technique and the infrared technique, Fig. E shows weight ratios for run 161, and Fig. F presents a comparison of the weight ratios which compares the consistency of the data from all three techniques. We see from Fig. F that in spite of the better reproducibility of the infrared and sound-velocity techniques, the consistency of all three methods varies by about the same amount, that is, 10%, indicating either inhomogeneities or inaccurate measurements for all three setups. In view of this inconsistency of approximately 10% in the calculated weight in the cylinder it might be appropriate for the authors to comment on the effect of this variation on the validity of the detailed computations which compared the real and theoretical cycle.

Referring next to Fig. 26 which compares the pocketed and open combustion chambers, Fig. G shows the 1500 rpm data as plotted as in the text compared to a log T-log V plot of the same data. For convenience, lines having different values of polytropic coefficients are also shown. It is readily seen in Fig. G that the slope of the log T-log V curve for the pocketed chamber is greater than that for

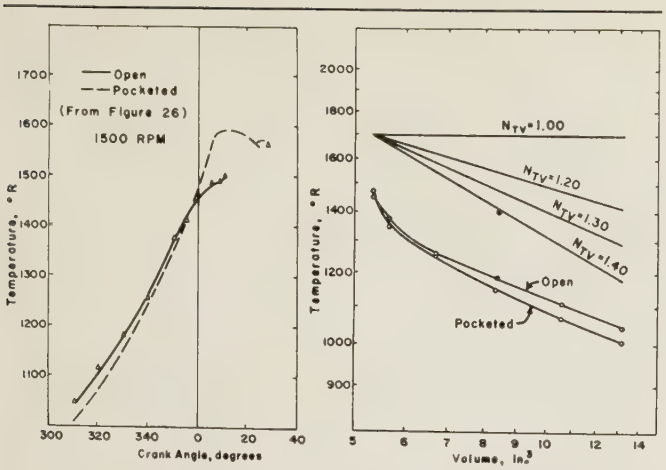

Fig. G—Comparison of open and pocketed chambers

the open chamber, indicating either less heat transfer from the gases or more exothermic prereaction. This same trend is equally evident in the 1000 rpm data but is less evident in the 2000 and 2500 rpm data. Are these results to be expected from surface-volume considerations? How do the authors reconcile the information such as that shown on the log T-log V plot with their statement that "the higher end-gas temperatures in the open chamber are probably due to the smaller heat loss than in the pocketed-chamber engine"?

Traces History of Authors' CRC-Sponsored Project

—J. J. Mikita

E. I. Du Pont deNemours and Co., Inc.

I WAS very pleased to read this paper because, for many years, the measurement of unburned-gas temperatures within an operating engine has been almost a fetish with me. Now that a tool is at hand for doing this job, I am confident that it will help provide valuable data to those men concerned with the further development of internal-combustion engines and the fuels to operate these engines.

In January, 1949, there was presented to the appropriate group, a proposal that CRC sponsor a project aimed at developing a technique for the measurement of unburned-gas temperatures within the cylinder of an operating engine. The proposal was well-received. However, there was considerable question as to whether there was a practical method for accomplishing the objective. The question, "How would it be accomplished and what are the chances for success?," had to be answered. It is a commentary on the authors' technical proficiency that it took longer to answer this question than it did to develop the technique.

I hope that future workers with this technique will elaborate on the data shown in Fig. 23 having to do with gas temperatures for knocking and nonknocking cycles. I believe those concerned with the kinetics of preknock reactions would find further refinement of the data to be very useful. Data on the rate of temperature increase would be of particular value.

Authors' Closure To Discussion

THE information supplied by the discussors helps to support these conclusions:

1. The molecular behavior of the gases in an engine combustion chamber can be interpreted (with some restrictions) in terms of temperature.

2. These restrictions are generally involved with the assumption that equilibrium (chemical and physical) conditions are established.

3. Both optical and acoustical measurements can be applied successfully to a suitably modified engine and the results obtained are more realistic than estimates of temperature derived by purely theoretical methods.

Regarding the choice between optical and acoustical measurements, these practical observations seem to apply:

1. *High gas density* improves the signal-to-noise ratio in both the optical and acoustical systems.

2. *Long path length* is helpful in the optical systems; thus, the measurement of a geometric "average" temperature is easier.

3. *Short path length* is helpful in the acoustical system; hence the measurement of a "point" temperature is favored.

4. The optical systems can be made to operate continuously, whereas the acoustical pulse system yields discrete bits of information, each averaged over a time interval of the order of 25 microsec.

It is gratifying to hear from Dr. Gluckstein that his laboratory has found a good use for the acoustical temperature measuring technique. His approximations for the equation of state are entirely logical. The suggested simplification, plus the use of a computer for data reduction should further encourage the study of engine cycle temperatures. Further investigation of nonequilibrium (both chemical and physical) phenomena should help to outline the limits within which sound velocity (and the temperature concept itself) are unambiguous.

The questions raised by Messrs. Shimizu and Burrows serve to emphasize again the statement made in the fifth, sixth, and seventh paragraphs of this paper: namely, that variations of composition and temperature *do* exist in the charge within the combustion chamber. Thus, it is not surprising to find that the "average" temperatures measured by a long path (optical method) and by the short path (acoustical method) should be at a variance with the corresponding values of $T = \frac{MPV}{Rw}$ for the engine charge (Fig. F).

With regard to scavenging the "pocketed" combustion chamber, it seems likely that had the measuring zone contained an excess of hot residual gas the temperature at, say, 310 deg crank-angle would not have been lower than that found in the open chamber (Fig. G).

Furthermore, it is apparent that the maximum temperature difference between the curves of Fig. G is about 30 F. Since the reproducibility of results is close to this difference (Fig. 8), it seems doubtful whether the conclusion suggested by the log T versus log $\frac{1}{V}$ plot in Fig. G is justified, although the possibility is interesting. Our comment concerning heat transfer in the "open" versus the "pocketed" chamber was based upon the fact that, in Fig. 26, the temperature differences before ignition are greater at high speed than at low speed. In a nearly zero-speed engine, the temperature of the unburned charge will approach the water-jacket temperature regardless of chamber geometry. At higher speeds, differences in chamber geometry, wall thickness, and the like will cause variations in charge temperature. Velocity patterns within the chamber are in general different during different portions of the cycle, that is, inlet stroke as compared to compression stroke. As a consequence, the heat transfer situation is very complex.

Run 161 was used for analysis simply because supercharged operation helps to increase the acoustical signal strength early in the engine cycle, and reduced exhaust pressure enhances the engine's cyclic consistency. Both of these conditions permit measurement of more of the cycle for comparison with the theoretical cycle (Fig. 21). The fact that the peak end-gas temperature is higher in run 161 than in the other runs (Fig. C) is due to the higher p_i. It appears to be unwarranted to turn the curve upward on the basis of the single point at 35 deg at dc (Fig. 18). Unless this peculiarity can be reproduced in additional runs, we believe it should not be taken too seriously.

The application Mr. Mikita suggests is probably the most important area of our ignorance concerning combustion and fuel behavior in reciprocating engines.

Index—Vol. 66, 1958

ABOWD, RICHARD, JR.
Discussion of "Continuous Radiotracer Monitoring Shows How Piston Rings Wear in Service" by J. S. Batzold, J. V. Clarke, Jr., and J. F. Kunc 611
ACCIDENTS AND ACCIDENT PREVENTION
Visual Avoidance of Mid-Air Collisions, W. D. Howell and R. B. Fisher 252
Bio-Technical Aspects of Driver Safety and Comfort, R. A. McFarland and R. G. Domey 630
ADAMS, G. E.
Discussion of "Chrysler Torsion-Aire Suspension—Across the Board" by O. D. Dillman and R. R. Love 303
AGNEW, DR. JOHN T.
Discussion of "Measurement of Gas Temperature in an Engine by the Velocity of Sound Method" by J. C. Livengood, C. F. Taylor, and P. C. Wu 695
AIRCRAFT ACCESSORIES AND EQUIPMENT
Requirements, Parameters, and Design Considerations for Pneumatic Inlet Control Systems, R. E. Matzdorff and C. F. Newberry 496
Thrust Measurement for Jet Transport Operation, M. J. Saari 357
AIRCRAFT DESIGN AND PERFORMANCE
Behavior of Aircraft Structures under Thermal Stress, G. H. Sprague and P. C. Huang 457
Considerations of Some Jet-Deflection Principles for—Directional Control—Lift, U. H. von Glahn and J. H. Povolny 620
Designing Materials for Future Aerial Vehicles, N. E. Promisel 267
Designing with Steel for Lighter Aircraft, Bruce Mitchell 407
Problems in the Application of High-Strength Steel Alloys in the Design of Supersonic Aircraft, A. F. Ensrud 118
Requirements, Parameters, and Design Considerations for Pneumatic Inlet Control Systems, R. E. Matzdorff and C. F. Newberry 496
ALPERSTEIN, M.
Fumigation Kills Smoke—Improves Diesel Performance (Co-authors W. B. Swim and P. H. Schweitzer) 574
ANTONSEN, ANKER K.
Discussion of "Turbocharging the Series 71 Engine" by J. J. May and V. C. Reddy 113
ARNOLD, W. C.
Bifuel Approach to Burning Residual Fuels in Diesel Engines (Co-authors R. H. Beadle, R. L. Logelin, and H. D. Young) 54
AXLES
Bearing Applications For Heavy-Duty Axles, Robert M. Riblet and Charles M. Kitson 5
Design Features of the New Ford Axle, Bain Griffith 257
Rear Axles—Today—Tomorrow, R. P. Lewis and L. J. O'Brien 364
AYRES, V.
Valve Train Wear As Affected By Metallurgy, Driving Conditions, and Lubricants (Co-authors J. B. Bidwell, A. C. Pilger, Jr., and R. K. Williams) ... 242

BACHLE, C. F.
Aircooled Diesel-Engine Appraisal 213
BAILEY, C. H.
Protective Atmospheres for High-Temperature Bearing Operation (Co-authors S. S. Sorem and A. G. Cattaneo) 596
BALL, L. M.
Principles of Noise Reduction 515
BARBER, E. M.
Discussion of "Use of Temperature-Density for Measuring Antiknock Quality" by Bruno R. Siegel 443
BATZOLD, J. S.
Continuous Radiotracer Monitoring Shows How Piston Rings Wear in Service (Co-authors J. V. Clarke, Jr. and J. F. Kunc) 602
BEADLE, R. H.
Bifuel Approach to Burning Residual Fuels in Diesel Engines (Co-authors W. C. Arnold, R. L. Logelin, and H. D. Young) 54
BEARINGS
Bearing Applications For Heavy-Duty Axles, Robert M. Riblet and Charles M. Kitson 5
Protective Atmospheres for High-Temperature Bearing Operation, C. H. Bailey, S. S. Sorem, and A. G. Cattaneo 596
BEHRENS, M. D.
Investigating Combustion Phenomena in Unmodified Engines (Co-authors J. A. Robison, R. G. Mosher, and J. M. Chandler) 549
BERRY, W. S.
The Air Coil Spring—A New Factor in Rambler Suspension 471
BERTSCH, J. F.
1958 Chevrolet Level Air Suspension (Co-authors K. H. Hansen and R. E. Denzer) 483
BIDWELL, J. B.
Valve Train Wear As Affected By Metallurgy, Driving Conditions, and Lubricants (Co-authors V. Ayres, A. C. Pilger, Jr., and R. K. Williams) 242
BLACK, J. B.
Torque Converters Can Be Different (Co-author M. W. Dundore) 200
BLOSE, J. F.
Discussion of "Turbocharging the Series 71 Engine" by J. J. May and V. C. Reddy 114
BLUME, N. L.
Engineering the Edsel 557
BOBROWSKY, A. R.
Discussion of "Simulation of a Free-Piston Engine with a Digital Computer" by D. R. Olson 681
BOGART, H. N.
Shell Molded Cast Crankshafts (Co-author H. C. Grant) 32
BOHUSLAV, HANS A.
Discussion of "Turbocharging the Series 71 Engine" by J. J. May and V. C. Reddy 115
BOWDITCH, F. W.
Autoignition Associated With Hot Starting (Co-author R. F. Stebar) 179
BRADY, C. J.
Vapor-Locking Tendencies of Fuels—A Practical Approach (Co-author J. D. Caplan) 327
BRENNEKE, A. M.
Discussion of "Continuous Radiotracer Monitoring Shows How Piston Rings Wear in Service" by J. S. Batzold, J. V. Clarke, Jr., and J. F. Kunc 610
BROGHAMER, E. L.
Discussion of "The Beam Strength of Modern Gear-Tooth Design" by B. W. Kelley and R. Pedersen.. 149
BROWN, D. H.
Diesel Cylinder Heat Transfer Design Criteria 522
BURROWS, M. C.
Discussion of "Measurement of Gas Temperature in an Engine by the Velocity of Sound Method" by J. C. Livengood, C. F. Taylor, and P. C. Wu 696

CAPLAN, J. D.
Vapor-Locking Tendencies of Fuels—A Practical Approach (Co-author C. J. Brady) 327
CARTWRIGHT, B. W.
Chrysler TorqueFlite Transmission (Co-author S. D. Jeffe) 158
CATTANEO, A. G.
Protective Atmospheres for High-Temperature Bearing Operation (Co-authors C. H. Bailey and S. S. Sorem 596
Discussion of "Continuous Radiotracer Monitoring Shows How Piston Rings Wear in Service" by J. S. Batzold, J. V. Clarke, Jr., and J. F. Kunc .. 610
CHANDLER, J. M.
Investigating Combustion Phenomena in Unmodified Engines (Co-authors J. A. Robison, M. D. Behrens, and R. G. Mosher) 549
Discussion of "Determination of True Engine Friction" by R. E. Gish, J. D. McCullough, J. B. Retzloff, and H. T. Mueller 665
CLARKE, J. V. Jr.
Continuous Radiotracer Monitoring Shows How Piston Rings Wear in Service (Co-authors J. S. Batzold and J. F. Kunc) 602
CONSTRUCTION AND INDUSTRIAL MACHINERY
Resilient Face Seals for Tractor Final Drives, F. S. Engelking and M. C. Keys 75
Torque Converters Can Be Different, J. B. Black and M. W. Dundore 200
Tractor Hydraulics—Good Field . . . No Hit, G. L. Hershman 612
CONWELL, J. T.
Discussion of "Rear Axles—Today—Tomorrow" by R. P. Lewis and L. J. O'Brien 382
COUTANT, J. G.
Discussion of "The Future of the Free-Piston Engine in Commercial Vehicles" by O. B. Noren and R. L. Erwin 313
COWIN, F. H.
Cadillac's Air Suspension for the Eldorado Brougham (Co-authors V. D. Polhemus, L. J. Kehoe, Jr. and S. L. Milliken) 346
CRANKSHAFTS
Shell Molded Cast Crankshafts, H. N. Bogart and H. C. Grant 32

Some Metallurgical Aspects of Pontiac V-8 Engine Pearlitic Malleable Iron Crankshaft, K. B. Valentine ... 81
DENZER, R. E.
1958 Chevrolet Level Air Suspension (Co-authors K. H. Hansen and J. F. Bertsch) ... 483
DEPOSITS, ENGINE
Combustion-Chamber Deposits — A Radiotracer Study, L. B. Shore and K. F. Ockert ... 285
DETONATION
Autoignition Associated With Hot Starting, F. W. Bowditch and R. F. Stebar ... 179
Investigating Combustion Phenomena in Unmodified Engines, J. A. Robison, M. D. Behrens, R. G. Mosher, and J. M. Chandler ... 549
Use of Temperature-Density for Measuring Antiknock Quality, Bruno R. Siegel ... 421
DIETRICH, ERIC
The Buick Air Poise Suspension (Co-authors Forest R. McFarland and E. G. Peckham) ... 466
DIETRICH, N. T., SR.
Discussion of "The Cadillac Frame: A New Design Concept for Lower Cars" by S. L. Millikem and J. R. Parker ... 98
DILLMAN, O. D.
Chrysler Torsion-Aire Suspension—Across the Board (Co-author R. R. Love) ... 295
DOMEY, R. G.
Bio-Technical Aspects of Driver Safety and Comfort (Co-author R. A. McFarland) ... 630
DUNDORE, M. W.
Torque Converters Can Be Different (Co-author J. B. Black) ... 200
DYER, LAWRENCE D.
Discussion of "Protective Atmospheres for High-Temperature Bearing Operation" by C. H. Bailey, S. S. Sorem, and A. G. Cattaneo ... 600
ENGELKING, F. S.
Resilient Face Seals for Tractor Final Drives (Co-author M. C. Keys) ... 75
ENGINES, AIRCRAFT (JET AND TURBINE)
Designing Materials for Future Aerial Vehicles, N. E. Promisel ... 267
High-Temperature Properties of Vacuum-Melted Superalloys, F. M. Richmond ... 193
Large Lightweight Turbojet Engines, C. A. Grinyer 315
Requirements, Parameters, and Design Considerations for Pneumatic Inlet Control Systems, R. E. Matzdorff and C. F. Newberry ... 496
Thrust Measurement for Jet Transport Operation, M. J. Saari ... 357
ENGINES, DIESEL
Aircooled Diesel-Engine Appraisal, C. F. Bachle ... 213
Bifuel Approach to Burning Residual Fuels in Diesel Engines, W. C. Arnold, R. H. Beadle, R. L. Logelin, and H. D. Young ... 54
Diesel Cylinder Heat Transfer Design Criteria, D. H. Brown ... 522
Fumigation Kills Smoke—Improves Diesel Performance, M. Alperstein, W. B. Swim, and P. H. Schweitzer ... 574
Loop Scavenging versus Through Scavenging of Two-Stroke Engines, C. F. Taylor, A. R. Rogowski, A. L. Hagen, and J. D. Koppernaes ... 444
The MWM Balanced-Pressure Precombustion Chamber System for High-Speed Diesel Engines, Hans L. Hockel ... 38
Turbocharging the Series 71 Engine, J. J. May and V. C. Reddy ... 100
ENGINES, GASOLINE
Autoignition Associated With Hot Starting, F. W. Bowditch and R. F. Stebar ... 179
ENGINES, GENERAL
Determination of True Engine Friction, R. E. Gish, J. D. McCullough, J. B. Retzloff, and H. T. Mueller 649
Measurement of Gas Temperature in an Engine by the Velocity of Sound Method, J. C. Livengood, C. F. Taylor, and P. C. Wu ... 683
ENGINES, JET AND TURBINE (NONAIRCRAFT)
Simulation of a Free-Piston Engine With a Digital Computer, D. R. Olson ... 668
The Future of the Free-Piston Engine in Commercial Vehicles, O. B. Noren and R. L. Erwin ... 305
ENGINES, PASSENGER CAR
Automotive Gasoline Injection, C. H. Nystrom ... 65
Continuous Radiotracer Monitoring Shows How Piston Rings Wear in Service, J. S. Batzold, J. V. Clarke, Jr., and J. F. Kunc ... 602
Engineering the Edsel, N. L. Blume ... 557
Investigating Combustion Phenomena in Unmodified Engines, J. A. Robison, M. D. Behrens, R. G. Mosher, and J. M. Chandler ... 549
Some Metallurgical Aspects of Pontiac V-8 Engine Pearlitic Malleable Iron Crankshaft, K. B. Valentine ... 81
Valve Train Wear As Affected By Metallurgy, Driving Conditions, and Lubricants, V. Ayres, J. B. Bidwell, A. C. Pilger, Jr., and R. K. Williams ... 242
ENGLISH, H. G.
Discussion of "Chevrolet Turboglide Transmission" by F. J. Winchell, W. D. Route, and O. K. Kelley 166
Discussion of "Chrysler TorqueFlite Transmission" by S. D. Jeffe and B. W. Cartwright ... 166
ENOCH, OTTO
Discussion of "Use of Temperature-Density for Measuring Antiknock Quality" by Bruno R. Siegel 442
ENSRUD, A. F.
Problems in the Application of High-Strength Steel Alloys in the Design of Supersonic Aircraft ... 118
ERWIN, R. L.
The Future of the Free-Piston Engine in Commercial Vehicles (Co-author O. B. Noren) ... 305
EVANS, W. P.
Mathematical Correction for Stress in Removed Layers in X-Ray Diffraction Residual Stress Analysis (Co-author M. G. Moore) ... 340
EXHAUST SYSTEMS AND EXHAUST GASES
Automotive Exhaust Hydrocarbon Reduction During Deceleration by Induction System Devices ... 383
Fumigation Kills Smoke—Improves Diesel Performance, M. Alperstein, W. B. Swim, and P. H. Schweitzer ... 574
Loop Scavenging versus Through Scavenging of Two-Stroke Engines, C. F. Taylor, A. R. Rogowski, A. L. Hagen, and J. D. Koppernaes ... 444
FERENCE, MICHAEL, JR.
Effects of Radiation on Materials ... 47
FERRELL, W. G.
Discussion of "Some Metallurgical Aspects of Pontiac V-8 Engine Pearlitic Malleable Iron Crankshaft" by K. B. Valentine ... 85
FISHER, R. B.
Visual Avoidance of Mid-Air Collisions (Co-author W. D. Howell) ... 252
FORGINGS
The Improvement of Welded Structures By Subsequent Forging Operations, W. R. Wollering and E. H. Lundby ... 261
FRAMES
The Cadillac Frame: A New Design Concept for Lower Cars, S. L. Milliken and J. R. Parker ... 86
FUELS, MOTOR
Combustion-Chamber Deposits — A Radiotracer Study, L. B. Shore and K. F. Ockert ... 285
Use of Temperature-Density for Measuring Antiknock Quality, Bruno R. Siegel ... 421
Vapor-Locking Tendencies of Fuels—A Practical Approach, J. D. Caplan and C. J. Brady ... 327
GEARS
Design Features of the New Ford Axle, Bain Griffith 257
Rear Axles—Today—Tomorrow, R. P. Lewis and L. J. O'Brien ... 364
The Beam Strength of Modern Gear-Tooth Design, B. W. Kelley and R. Pedersen ... 137
GISH, R. E.
Determination of True Engine Friction (Co-authors J. D. McCullough, J. B. Retzloff, and H. T. Mueller) ... 649
GLUCKSTEIN, DR. M. E.
Discussion of "Measurement of Gas Temperature in an Engine by the Velocity of Sound Method" by J. C. Livengood, C. F. Taylor, and P. C. Wu ... 696
GRANT, H. C.
Shell Molded Cast Crankshafts (Co-author H. N. Bogart) ... 32
GRIFFITH, BAIN
Design Features of the New Ford Axle ... 257
GRINYER, C. A.
Large Lightweight Turbojet Engines ... 315
GUMBLETON, JAMES J.
Discussion of "Continuous Radiotracer Monitoring Shows How Piston Rings Wear in Service" by J. S. Batzold, J. V. Clarke, Jr., and J. F. Kunc ... 609
HAGEN, A. L.
Loop Scavenging versus Through Scavenging of Two-Stroke Engines (Co-authors C. F. Taylor, A. R. Rogowski, and J. D. Koppernaes) 444
HANSEN, K. H.
1958 Chevrolet Level Air Suspension (Co-authors J. F. Bertsch and R. E. Denzer) 483
HARRIS, K. J.
Discussion of "The Beam Strength of Modern Gear-Tooth Design" by B. W. Kelley and R. Pedersen 155

HAVEMANN, DR. H. A.
Discussion of "Fumigation Kills Smoke—Improves Diesel Performance" by M. Alperstein, W. B. Swim, and P. H. Schweitzer 589
HEATH, D. P.
Discussion of "Vapor-Locking Tendencies of Fuels—A Practical Approach" by J. D. Caplan and C. J. Brady 338
HEBL, L. E.
Discussion of "Vapor-Locking Tendencies of Fuels—A Practical Approach" by J. D. Caplan and C. J. Brady 338
HERSHMAN, G. L.
Tractor Hydraulics Good Field . . . No Hit 612
HEYWOOD, R. B.
Discussion of "The Beam Strength of Modern Gear-Tooth Design" by B. W. Kelley and R. Pedersen 145
HOCKEL, HANS L.
The MWM Balanced-Pressure Precombustion Chamber System for High-Speed Diesel Engines 38
HOFFMAN, R. A.
Discussion of "Investigating Combustion Phenomena in Unmodified Engines" by J. A. Robison, M. D. Behrens, R. G. Mosher, and J. M. Chandler 556
HOOKER, R. J.
Discussion of "Diesel Cylinder Heat Transfer Design Criteria" by D. H. Brown 529
HORIAK, E. A. V.
Discussion of "Turbocharging the Series 71 Engine" by J. J. May and V. C. Reddy 114
HORINE, M. C.
Discussion of "Truck Performance—Computed versus Measured Data" by A. F. Stamm 404
HOWELL, W. D.
Visual Avoidance of Mid-Air Collisions (Co-author R. B. Fisher) 252
HUANG, P. C.
Behavior of Aircraft Structures under Thermal Stress (Co-author G. H. Sprague) 457

INJECTION, FUEL
Automotive Gasoline Injection, C. H. Nystrom 65
Fumigation Kills Smoke—Improves Diesel Performance, M. Alperstein, W. B. Swim, and P. H. Schweitzer 574
The MWM Balanced-Pressure Precombustion Chamber System for High-Speed Diesel Engines, Hans L. Hockel 38
IRON AND STEEL
Designing Materials for Future Aerial Vehicles, N. E. Promisel 267
Designing with Steel for Lighter Aircraft, Bruce Mitchell 407
Metallurgical Design Considerations for Precipitation-Hardening Steels up to 1200 F, F. K. Lampson 565
Problems in the Application of High-Strength Steel Alloys in the Design of Supersonic Aircraft, A. F. Ensrud 118
Protective Atmospheres for High-Temperature Bearing Operation, C. H. Bailey, S. S. Sorem, and A. G. Cattaneo 596
Some Metallurgical Aspects of Pontiac V-8 Engine Pearlitic Malleable Iron Crankshaft, K. B. Valentine 81
The Improvement of Welded Structures By Subsequent Forging Operations, W. R. Wollering and E. H. Lundby 261
Valve Train Wear As Affected by Metallurgy, Driving Conditions, and Lubricants, V. Ayres, J. B. Bidwell, A. C. Pilger, Jr., and R. K. Williams 242
IVERSON, L. E.
Discussion of "The Beam Strength of Modern Gear-Tooth Design" by B. W. Kelley and R. Pedersen 151

JACKSON, H. R.
Discussion of "Continuous Radiotracer Monitoring Shows How Piston Rings Wear in Service" by J. S. Batzold, J. V. Clarke, Jr., and J. F. Kunc 611
JACOBSON, M. A.
Discussion of "The Beam Strength of Modern Gear-Tooth Design" by B. W. Kelley and R. Pedersen 147
JANEWAY, R. N.
Discussion of "Rear-Engine Motor Cars—The European Point of View" by Fernand Picard 240
JEFFE, S. D.
Chrysler TorqueFlite Transmission (Co-author B. W. Cartwright) 158
JONES, D. R.
Discussion of "Fumigation Kills Smoke—Improves Diesel Performance" by M. Alperstein, W. B. Swim, and P. H. Schweitzer 592
KARDE, K. C.
Discussion of "Loop Scavenging versus Through Scavenging of Two-Stroke Engines" by C. F. Taylor, A. R. Rogowski, A. L. Hagen, and J. D. Koppernaes 455
KEHOE, L. J., JR.
Cadillac's Air Suspension for the Eldorado Brougham (Co-authors V. D. Polhemus, F. H. Cowin and S. L. Milliken) 346
KELLEY, B. W.
The Beam Strength of Modern Gear-Tooth Design (Co-author R. Pedersen) 137
KELLEY, O. K.
Chevrolet Turboglide Transmission (Co-authors F. J. Winchell and W. D. Route) 167
KEYS, M. C.
Resilient Face Seals for Tractor Final Drives (Co-author F. S. Engelking) 75
KING, R. O.
Discussion of "Fumigation Kills Smoke—Improves Diesel Performance" by M. Alperstein, W. B. Swim, and P. H. Schweitzer 590
KITSON, CHARLES M.
Bearing Applications For Heavy-Duty Axles (Co-author Robert M. Riblet) 5
KOPPERNAES, J. D.
Loop Scavenging versus Through Scavenging of Two-Stroke Engines (Co-authors C. F. Taylor, A. R. Rogowski, and A. L. Hagen) 444
KUNC, J. F.
Continuous Radiotracer Monitoring Shows How Piston Rings Wear in Service (Co-authors J. S. Batzold and J. V. Clarke, Jr.) 602

LAMPSON, F. K.
Metallurgical Design Considerations for Precipitation-Hardening Steels up to 1200 F 565
LAY, W. E.
Discussion of "Determination of True Engine Friction" by R. E. Gish, J. D. McCullough, J. B. Retzloff, and H. T. Mueller 661
LEGATSKI, T. W.
Discussion of "Vapor-Locking Tendencies of Fuels—A Practical Approach" by J. D. Caplan and C. J. Brady 339
LEWIS, R. P.
Rear Axles—Today—Tomorrow (Co-author L. J. O'Brien) 364
LIESMAN, W. E.
Discussion of "The Cadillac Frame: A New Design Concept for Lower Cars" by S. L. Milliken and J. R. Parker 97
LIVENGOOD, J. C.
Measurement of Gas Temperature in an Engine by the Velocity of Sound Method (Co-authors C. F. Taylor and P. C. Wu) 683
LOGELIN, R. L.
Bifuel Approach to Burning Residual Fuels in Diesel Engines (Co-authors W. C. Arnold, R. H. Beadle, and H. D. Young) 54
LOVE, R. R.
Chrysler Torsion-Aire Suspension—Across the Board (Co-author O. D. Dillman) 295
LUCIA, C. J.
Discussion of "Chevrolet Turboglide Transmission" by F. J. Winchell, W. D. Route, and O. K. Kelley 178
LUNDBY, E. H.
The Improvement of Welded Structures by Subsequent Forging Operations (Co-author W. R. Wollering) 261
LYN, Dr. W. T.
Discussion of "Fumigation Kills Smoke—Improves Diesel Performance" by M. Alperstein, W. B. Swim, and P. H. Schweitzer 590

MALONE, G. K.
Discussion of "Valve Train Wear As Affected By Metallurgy, Driving Conditions, and Lubricants" by V. Ayres, J. B. Bidwell, A. C. Pilger, Jr., and R. K. Williams 251
MASSA, V. F.
Discussion of "Autoignition Associated With Hot Starting" by F. W. Bowditch and R. F. Stebar 191
MATZDORFF, R. E.
Requirements, Parameters, and Design Considerations for Pneumatic Inlet Control Systems (Co-author C. F. Newberry) 496
MAY, J. J.
Turbocharging the Series 71 Engine (Co-author V. C. Reddy) 100
McCULLOUGH, J. D.
Determination of True Engine Friction (Co-authors

R. E. Gish, J. B. Retzloff, and H. T. Mueller) ... 649
Discussion of "Investigating Combustion Phenomena in Unmodified Engines" by J. A. Robison, M. D. Behrens, R. G. Mosher, and J. M. Chandler ... 556
McFARLAND, FOREST R.
The Buick Air Poise Suspension (Co-authors E. G. Peckham and Eric Dietrich) ... 466
McFARLAND, R. A.
Bio-Technical Aspects of Driver Safety and Comfort (Co-author R. G. Domey) ... 630
MEILE, CARL H.
Discussion of "Simulation of a Free-Piston Engine With a Digital Computer" by D. R. Olson ... 680
MERRITT, H. E.
Discussion of "The Beam Strength of Modern Gear-Tooth Design" by B. W. Kelley and R. Pedersen 154
MEURER, DR. SIEGFRIED
Discussion of "Fumigation Kills Smoke—Improves Diesel Performance" by M. Alperstein, W. B. Swim, and P. H. Schweitzer ... 593
MIKITA, J. J.
Discussion of "Measurement of Gas Temperature in an Engine by the Velocity of Sound Method" by J. C. Livengood, C. F. Taylor, and P. C. Wu ... 699
MILLER, RALPH
Discussion of "Diesel Cylinder Heat Tranfer Design Criteria" by D. H. Brown ... 530
MILLIKEN, S. L.
Cadillac's Air Suspension for the Eldorado Brougham (Co-authors V. D. Polhemus, L. J. Kehoe, Jr. and F. H. Cowin) ... 346
The Cadillac Frame: A New Design Concept for Lower Cars (Co-author J. R. Parker) ... 86
MITCHELL, BRUCE
Designing with Steel for Lighter Aircraft ... 407
MOORE, M. G.
Mathematical Correction for Stress in Removed Layers in X-Ray Diffraction Residual Stress Analysis (Co-author W. P. Evans) ... 340
MOORE, V. C.
Discussion of "Chrysler TorqueFlite Transmission" by S. D. Jeffe and B. W. Cartwright ... 166
MORRIS, W. E.
Discussion of "Autoignition Associated With Hot Starting" by F. W. Bowditch and R. F. Stebar ... 191
MOSHER, R. G.
Investigating Combustion Phenomena in Unmodified Engines (Co-authors J. A. Robison, M. D. Behrens, and J. M. Chandler) ... 549
MUELLER, H. T.
Determination of True Engine Friction (Co-authors R. E. Gish, J. D. McCullough, and J. B. Retzloff) 649

NELSON, EDWIN E.
Discussion of "Determination of True Engine Friction" by R. E. Gish, J. D McCullough, J. B. Retzloff, and H. T. Mueller ... 665
NEU, R. F.
Discussion of "Principles of Noise Reduction" by L. M. Ball ... 521
NEWBERRY, C. F.
Requirements, Parameters, and Design Considerations for Pneumatic Inlet Control Systems (Co-author R. E. Matzdorff) ... 496
NEWBY, W. E.
Discussion of "Combustion-Chamber Deposits—A Radiotracer Study" by L. B. Shore and K. F. Ockert ... 294
NOISE
Principles of Noise Reduction, L. M. Ball ... 515
NOREN, O. B.
The Future of the Free-Piston Engine in Commercial Vehicles (Co-author R. L. Erwin) ... 305
NYSTROM, C. H.
Automotive Gasoline Injection ... 65

O'BRIEN, L. J.
Rear Axles—Today—Tomorrow (Co-author R. P. Lewis) ... 364
OCKERT, K. F.
Combustion Chamber Deposits—A Radiotracer Study (Co-author L. B. Shore) ... 285
OLSON, D. R.
Simulation of a Free-Piston Engine With a Digital Computer ... 668
O'SHEA, C. F.
The Ford Approach to Air Suspension ... 475
PARKER, J. R.
The Cadillac Frame: A New Design Concept for Lower Cars (Co-author S. L. Milliken) ... 86
PASSENGER CAR DESIGN AND PERFORMANCE
Engineering the Edsel, N. L. Blume ... 557
Rear-Engine Motor Cars—The European Point of View, Fernand Picard ... 226
The Cadillac Frame: A New Design Concept for Lower Cars, S. L. Milliken and J. R. Parker ... 86
PECKHAM, E. G.
The Buick Air Poise Suspension (Co-authors Forest R. McFarland and Eric Dietrich) ... 466
PEDERSEN, R.
The Beam Strength of Modern Gear-Tooth Design (Co-author B. W. Kelley) ... 137
PENZIAS, WALTER
Discussion of "Fumigation Kills Smoke—Improves Diesel Performance" by M. Alperstein, W. B. Swim, and P. H. Schweitzer ... 588
PERKINS, R. W.
Oldsmobile New-Matic Ride ... 491
PICARD, FERNAND
Rear-Engine Motor Cars—The European Point of View ... 226
PILGER, A. C., Jr.
Valve Train Wear As Affected By Metallurgy, Driving Conditions, and Lubricants (Co-authors V. Ayres, J. B. Bidwell, and R. K. Williams) ... 242
PINNEY, DR. M. A.
Discussion of "Fumigation Kills Smoke—Improves Diesel Performance" by M. Alperstein, W. B. Swim, and P. H. Schweitzer ... 592
PISTONS AND RINGS
Continuous Radiotracer Monitoring Shows How Piston Rings Wear in Service, J. S. Batzold, J. V. Clarke, Jr., and J. F. Kunc ... 602
POLHEMUS, V. D.
Cadillac's Air Suspension for the Eldorado Brougham (Co-authors L. J. Kehoe, Jr., F. H. Cowin and S. L. Milliken) ... 346
POVOLNY, J. H.
Considerations of Some Jet-Deflection Principles for —Directional Control—Lift (Co-author U. H. von Glahn) ... 620
PRODUCTION (AIRCRAFT)
High-Temperature Properties of Vacuum-Melted Superalloys, F. M. Richmond ... 193
Metallurgical Design Considerations for Precipitation-Hardening Steels up to 1200 F, F. K. Lampson ... 565
Problems in the Application of High-Strength Steel Alloys in the Design of Supersonic Aircraft, A. F. Ensrud ... 118
PRODUCTION (NONAIRCRAFT)
Shell Molded Cast Crankshafts, H. N. Bogart and H. C. Grant ... 32
PROMISEL, N. E.
Designing Materials for Future Aerial Vehicles 267

RACING
Mercedes-Benz Racing Cars—Design and Experience, H. Scherenberg ... 414
RADIOACTIVITY
Combustion-Chamber Deposits—A Radiotracer Study, L. B. Shore and K. F. Ockert ... 285
Continuous Radiotracer Monitoring Shows How Piston Rings Wear in Service, J. S. Batzold, J. V. Clarke, Jr., and J. F. Kunc ... 602
Effects of Radiation on Materials, Michael Ference, Jr. ... 47
REDDY, V. C.
Turbocharging the Series 71 Engine (Co-author J. J. May) ... 100
RETZLOFF, J. B.
Determination of True Engine Friction (Co-authors J. D. McCullough, R. E. Gish, and H. T. Mueller) 649
RIBLET, ROBERT M.
Bearing Applications For Heavy-Duty Axles (Co-author Charles M. Kitson) ... 5
RICHMOND, F. M.
High-Temperature Properties of Vacuum-Melted Superalloys ... 193
RICKLES, N. H.
Discussion of "Fumigation Kills Smoke—Improves Diesel Performance" by M. Alperstein, W. B. Swim, and P. H. Schweitzer ... 593
ROBISON, J. A.
Investigating Combustion Phenomena in Unmodified Engines (Co-authors M. D. Behrens, R. G. Mosher, and J. M. Chandler) 549
ROGOWSKI, A. R.
Loop Scavenging versus Through Scavenging of Two-Stroke Engines (Co-authors C. F. Taylor, A. L. Hagen, and J. D. Koppernaes) ... 444
ROUTE, W. D.
Chevrolet Turboglide Transmission (Co-authors F. J. Winchell and O. K. Kelley) 167

SAARI, M. J.
Thrust Measurement for Jet Transport Operation 357
SANBORN, D. S.
Discussion of "Loop Scavenging versus Through Scavenging of Two-Stroke Engines" by C. F. Taylor, A. L. Hagen, A. R. Rogowski, and J. D. Koppernaes 455
SAWYER, CAPT. RICHARD H.
Discussion of "Aircooled Diesel-Engine Appraisal" by C. F. Bachle 225
SCHERENBERG, H.
Mercedes-Benz Racing Cars—Design and Experience 414
SCHWEITZER, P. H.
Fumigation Kills Smoke—Improves Diesel Performance (Co-authors M. Alperstein and W. B. Swim) 574
Discussion of "Loop Scavenging versus Through Scavenging of Two-Stroke Engines" by C. F. Taylor, A. R. Rogowski, A. L. Hagen, and J. D. Koppernaes 454
SEALS
Resilient Face Seals for Tractor Final Drives, F. S. Engelking and M. C. Keys 75
SHEAFFER, DR. B. L.
Discussion of "Loop Scavenging versus Through Scavenging of Two-Stroke Engines" by C. F. Taylor, A. R. Rogowski, A. L. Hagen, and J. D. Koppernaes 456
SHIMIZU, SHOSHI
Discussion of "Measurement of Gas Temperature in an Engine by the Velocity of Sound Method" by J. C. Livengood, C. F. Taylor, and P. C. Wu 696
SHORE, L. B.
Combustion-Chamber Deposits—A Radiotracer Study (Co-author K. F. Ockert) 285
SIEGEL, BRUNO R.
Use of Temperature-Density for Measuring Antiknock Quality 421
SIMPSON, H. W.
Discussion of "Chrysler TorqueFlite Transmission" by S. D. Jeffe and B. W. Cartwright 165
SMITH, CHARLES J.
Discussion of "Cadillac's Air Suspension for the Eldorado Brougham" by V. D. Polhemus, L. J. Kehoe, Jr., F. H. Cowin and S. L. Milliken 356
SOREM, S. S.
Protective Atmospheres for High-Temperature Bearing Operation (Co-authors C. H. Bailey and A. G. Cattaneo) 596
SPRAGUE, G. H.
Behavior of Aircraft Structures under Thermal Stress (Co-author P. C. Huang) 457
SPRINGS AND SUSPENSIONS
Cadillac's Air Suspension for the Eldorado Brougham, V. D. Polhemus, L. J. Kehoe, Jr., F. H. Cowin, and S. L. Milliken 346
Chrysler Torsion-Aire Suspension—Across the Board, O. D. Dillman and R. R. Love 295
Engineering the Edsel, N. L. Blume 557
1958 Chevrolet Level Air Suspension, K. H. Hansen, J. F. Bertsch, and R. E. Denzer 483
Oldsmobile New-Matic Ride, R. W. Perkins 491
The Air Coil Spring—A New Factor in Rambler Suspension, W. S. Berry 471
The Buick Air Poise Suspension, Forest R. McFarland, E. G. Peckham, and Eric Dietrich 466
The Ford Approach to Air Suspension, C. F. O'Shea 475
STAMM, A. F.
Truck Performance—Computed versus Measured Data 397
STEBAR, R. F.
Autoignition Associated With Hot Starting (Co-author F. W. Bowditch) 179
STERNE, BERNHARD
Discussion of "Chrysler Torsion-Aire Suspension—Across the Board" by O. D. Dillman and R. R. Love 304
STEVENS, HOY
Discussion of "Truck Performance—Computed versus Measured Data" by A. F. Stamm 404
STRESSES
Behavior of Aircraft Structures under Thermal Stress, G. H. Sprague and P. C. Huang 457
Mathematical Correction for Stress in Removed Layers in X-Ray Diffraction Residual Stress Analysis, M. G. Moore and W. P. Evans 340
The Beam Strength of Modern Gear-Tooth Design, B. W. Kelley and R. Pedersen 137
SWIM, W. B.
Fumigation Kills Smoke—Improves Diesel Performance (Co-authors M. Alperstein and P. H. Schweitzer) 574
SYKES, A. O.
The Effects of Machine and Foundation Resilience and of Wave Propagation on the Isolation Provided by Vibration Mounts 532
TAYLOR, C. F.
Loop Scavenging versus Through Scavenging of Two-Stroke Engines (Co-authors A. R. Rogowski, A. L. Hagen, and J. D. Koppernaes) 444
TAYLOR, C. F.
Measurement of Gas Temperature in an Engine by the Velocity of Sound Method (Co-authors J. C. Livengood and P. C. Wu) 683
Discussion of "Diesel Cylinder Heat Transfer Design Criteria" by D. H. Brown 530
TORQUE CONVERTERS
Torque Converters Can Be Different, J. B. Black and M. W. Dundore 200
TRANSMISSIONS, AUTOMATIC
Chevrolet Turboglide Transmission, F. J. Winchell, W. D. Route, and O. K. Kelley 167
Chrysler TorqueFlite Transmission, S. D. Jeffe and B. W. Cartwright 158
TRAYSER, DAVID A.
Discussion of "Simulation of a Free-Piston Engine with a Digital Computer" by D. R. Olson 682
TRIMBLE, HAROLD H.
Discussion of "Use of Temperature-Density for Measuring Antiknock Quality" by Bruno R. Siegel 442
TRUCK DESIGN AND PERFORMANCE
Bio-Technical Aspects of Driver Safety and Comfort, R. A. McFarland and R. G. Domey 630
Truck Performance—Computed versus Measured Data, A. F. Stamm 397
VALENTINE, K. B.
Some Metallurgical Aspects of Pontiac V–8 Engine Pearlitic Malleable Iron Crankshaft 81
VALVES AND GEAR
Valve Train Wear As Affected By Metallurgy, Driving Conditions, and Lubricants, V. Ayres, J. B. Bidwell, A. C. Pilger, Jr., and R. K. Williams 242
VAPOR LOCK
Vapor-Locking Tendencies of Fuels—A Practical Approach, J. D. Caplan and C. J. Brady 327
VIBRATION
The Effects of Machine and Foundation and of Wave Propagation on the Isolation Provided by Vibration Mounts, A. O. Sykes 532
VINCENT, E. T.
Discussion of "Diesel Cylinder Heat Transfer Design Criteria" by D. H. Brown 528
Discussion of "Turbocharging the Series 71 Engine" by J. J. May and V. C. Reddy 116
VOIGT, J. S.
Discussion of "Rear Axles—Today—Tomorrow" by R. P. Lewis and L. J. O'Brien 381
von GLAHN, U. H.
Considerations of Some Jet-Deflection Principles for —Directional Control—Lift (Co-author J. H. Povolny) 620
WALCUTT, CLEVELAND
Discussion of "Autoignition Associated With Hot Starting" by F. W. Bowditch and R. F. Stebar 192
WARREN, JOEL
Discussion of "Combustion-Chamber Deposits—A Radiotracer Study" by L. B. Shore and K. F. Ockert 292
WILLIAMS, R. K.
Valve Train Wear As Affected By Metallurgy, Driving Conditions, and Lubricants (Co-authors V. Ayres, J. B. Bidwell, and A. C. Pilger, Jr.) 242
WILSON, GROVER C.
Discussion of "Fumigation Kills Smoke—Improves Diesel Performance" by M. Alperstein, W. B. Swim, and P. H. Schweitzer 589
WINCHELL, F. J.
Chevrolet Turboglide Transmission (Co-authors W. D. Route and O. K. Kelley) 167
WITZKY, JULIUS E.
Discussion of "Fumigation Kills Smoke—Improves Diesel Performance" by M. Alperstein, W. B. Swim, and P. H. Schweitzer 591
WOLLERING, W. R.
The Improvement of Welded Structures By Subsequent Forging Operations (Co-author E. H. Lundby) 261
WU, P. C.
Measurement of Gas Temperature in an Engine by the Velocity of Sound Method (Co-authors J. C. Livengood and C. F. Taylor) 683
YOUNG, H. D.
Bifuel Approach to Burning Residual Fuels in Diesel Engines (Co-authors W. C. Arnold, R. H. Beadle, and R. L. Logelin) 54

DATE DUE

GAYLORD

PRINTED IN U.S.A.

3 8198 309 330 452
THE UNIVERSITY OF ILLINOIS AT CHICAGO

TL
1
S6
Vol.66

SAE Transactions

ON
TORIES